



STEPHEN P. RADZEVICH

SECOND EDITION

# THEORY OF GEARING

KINEMATICS, GEOMETRY,  
AND SYNTHESIS



**CRC Press**  
Taylor & Francis Group

# **Theory of Gearing**

## **Kinematics, Geometry, and Synthesis**

**Second Edition: Revised and Expanded**





# Taylor & Francis

Taylor & Francis Group

<http://taylorandfrancis.com>

# **Theory of Gearing**

## **Kinematics, Geometry, and Synthesis**

**Second Edition: Revised and Expanded**

**Stephen P. Radzevich**



**CRC Press**

Taylor & Francis Group  
Boca Raton London New York

---

CRC Press is an imprint of the  
Taylor & Francis Group, an **informa** business

CRC Press  
Taylor & Francis Group  
6000 Broken Sound Parkway NW, Suite 300  
Boca Raton, FL 33487-2742

© 2018 by Taylor & Francis Group, LLC  
CRC Press is an imprint of Taylor & Francis Group, an Informa business

No claim to original U.S. Government works

Printed on acid-free paper

International Standard Book Number-13: 978-1-138-58555-3 (Hardback)

This book contains information obtained from authentic and highly regarded sources. Reasonable efforts have been made to publish reliable data and information, but the author and publisher cannot assume responsibility for the validity of all materials or the consequences of their use. The authors and publishers have attempted to trace the copyright holders of all material reproduced in this publication and apologize to copyright holders if permission to publish in this form has not been obtained. If any copyright material has not been acknowledged please write and let us know so we may rectify in any future reprint.

Except as permitted under U.S. Copyright Law, no part of this book may be reprinted, reproduced, transmitted, or utilized in any form by any electronic, mechanical, or other means, now known or hereafter invented, including photocopying, microfilming, and recording, or in any information storage or retrieval system, without written permission from the publishers.

For permission to photocopy or use material electronically from this work, please access [www.copyright.com](http://www.copyright.com) (<http://www.copyright.com/>) or contact the Copyright Clearance Center, Inc. (CCC), 222 Rosewood Drive, Danvers, MA 01923, 978-750-8400. CCC is a not-for-profit organization that provides licenses and registration for a variety of users. For organizations that have been granted a photocopy license by the CCC, a separate system of payment has been arranged.

**Trademark Notice:** Product or corporate names may be trademarks or registered trademarks, and are used only for identification and explanation without intent to infringe.

---

**Library of Congress Cataloging-in-Publication Data**

---

Names: Radzevich, S. P. (Stepan Pavlovich), author.  
Title: Theory of gearing : kinematics, geometry, and synthesis / Stephen Radzevich.  
Description: Second edition. | Boca Raton : Taylor & Francis, CRC Press,  
2018. | Includes bibliographical references and index.  
Identifiers: LCCN 2018003427 | ISBN 9781138585553 (hardback : alk. paper) | ISBN  
9780429505195 (e-book)  
Subjects: LCSH: Gearing.  
Classification: LCC TJ184 .R326 2018 | DDC 621.8/33--dc23  
LC record available at <https://lcn.loc.gov/2018003427>

---

Visit the Taylor & Francis Web site at  
<http://www.taylorandfrancis.com>

and the CRC Press Web site at  
<http://www.crcpress.com>

eResource material is available for this title at <https://www.crcpress.com/9781138585553>



*This book is dedicated to my grandchildren*



# Taylor & Francis

Taylor & Francis Group

<http://taylorandfrancis.com>

---

# Contents

---

Preface.....	xix
Acknowledgments.....	xxi
Author.....	xxiii
Notation.....	xxv
Introduction.....	xxvii
<b>1. A Brief Overview of the Evolution of the Scientific Theory of Gearing .....</b>	<b>1</b>
1.1 Preliminary Remarks .....	2
1.2 Earliest Designs of Gears .....	6
1.3 Pre-Eulerian Period of Gear Art .....	8
1.4 The Origin of the Scientific Theory of Gearing: Eulerian Period of Gear Art.....	13
1.5 Post-Eulerian Period of Developments in the Field of Gearing.....	17
1.6 Developments in the Field of Perfect Gearings .....	23
1.6.1 Grant Bevel Gearing .....	23
1.6.2 Contribution by Professor N.I. Kolchin .....	24
1.6.3 Novikov Conformal Gearing .....	25
1.6.4 Contribution by Professor V.A. Gavrilenko.....	26
1.6.5 Contribution by Walton Musser .....	27
1.7 Tentative Chronology of the Evolution of the Theory of Gearing .....	29
1.8 Developments in the Field of Approximate Gearings .....	31
1.8.1 Cone Double-Enveloping Worm Gearing.....	32
1.8.2 Approximate Bevel Gearing .....	32
1.8.3 Approximate Crossed-Axes Gearing.....	33
1.8.4 Face Gearing.....	34
1.9 A Brief Summary of the Principal Accomplishments in the Theory of Gearing Achieved by the Beginning of the 21st Century.....	35
1.9.1 Condition of Contact of the Interacting Tooth Flanks of a Gear and Pinion.....	35
1.9.1.1 Condition of Contact .....	35
1.9.2 Condition of Conjugacy of the Interacting Tooth Flanks of a Gear and Pinion.....	36
1.9.3 Condition of Equality of Base Pitches of the Interacting Tooth Flanks of a Gear and Pinion.....	38
1.10 Concluding Remarks .....	38

## Part I Fundamentals

<b>2. Kinematics of a Gear Pair .....</b>	<b>41</b>
2.1 Transmission of Motion by Means of a Gear Pair .....	41
2.2 Vector Representation of Gear Pair Kinematics .....	42
2.2.1 Concept of Vector Representation of Gear Pair Kinematics.....	43
2.2.2 Vector Diagrams of Three Different Types for Spatial Gear Pairs .....	46
2.2.2.1 Vector Diagrams of Rotary-Negative Crossed-Axes Gear Pairs.....	48
2.2.2.2 Vector Diagrams of Rotary-Positive Crossed-Axes Gear Pairs.....	53
2.2.2.3 Vector Diagrams of Rotary-Zero Crossed-Axes Gear Pairs .....	55
2.2.2.4 Analytical Criterion of Type of Crossed-Axes Gear Pair .....	56
2.3 Classification of Possible Types of Vector Diagrams of Gear Pairs .....	57



2.4	Complementary Vectors to Vector Diagrams of Gear Pairs .....	66
2.4.1	Centerline Vectors of a Gear Pair .....	67
2.4.2	Axial Vectors of a Gear Pair .....	68
2.4.3	Useful Kinematic and Geometric Formulas.....	70
2.5	Possible Future Developments in the Theory of Gearing.....	71
<b>3.</b>	<b>Principal Planes and Principal Reference Systems Associated with a Gear Pair .....</b>	<b>77</b>
3.1	Principal Planes Associated with a Gear Pair.....	77
3.1.1	Case of Intersected-Axes Gearing.....	79
3.1.2	Case of Parallel-Axes Gearing .....	80
3.2	Principal Reference Systems Associated with a Gear Pair.....	82
3.3	Coordinate System Transformations.....	86
3.3.1	Transition from the Gear Reference System to the Main Reference System .....	87
3.3.2	Transition from the Pinion Reference System to the Main Reference System.....	88
<b>4.</b>	<b>Conditions for Transmitting a Uniform Rotation Smoothly from a Driving Shaft to a Driven Shaft: Three Fundamental Laws of Gearing .....</b>	<b>91</b>
4.1	Condition of Contact between Interacting Tooth Flanks: The First Fundamental Law of Gearing .....	91
4.2	Condition of Conjugacy between the Interacting Tooth Flanks: The Second Fundamental Law of Gearing .....	94
4.2.1	Pulley-and-Belt Analogy of a Gear Pair.....	94
4.2.2	Camus-Euler-Savary theorem for Parallel-Axes Gearing .....	95
4.3	Condition of Equal Base Pitches (in Parallel-Axes Gearing): The Third Fundamental Law of Gearing .....	100
<b>5.</b>	<b>Permissible Variation of Design Parameters of Pulley-and-Belt Analogy of Parallel-Axes Gearing.....</b>	<b>103</b>

## Part II Perfect Gearing

### Section II-A Perfect Gearing: Parallel-Axes Gearing

<b>6.</b>	<b>Involute Gearing: Kinematics and Geometry .....</b>	<b>113</b>
6.1	Principal Features of Parallel-Axes Gearing .....	113
6.1.1	Kinematics of Parallel-Axes Gearing.....	113
6.1.2	Gear Ratio in Parallel-Axes Gearing .....	116
6.1.3	The Permissible Transverse Pressure Angle Variation.....	120
6.2	Tooth Flank Generation .....	125
6.2.1	Desirable Line of Contact between the Tooth Flanks of a Gear and Its Mating Pinion.....	126
6.2.2	Line of Action and Path of Contact in a Gear Pair.....	128
6.2.3	Operating Base Pitch in a Gear Pair .....	131
6.2.4	Gear Tooth Flank of a Favorable Geometry: General Approach.....	134
<b>7.</b>	<b>A Simplified Approach for Involute Gear Tooth Flank Generation .....</b>	<b>141</b>
7.1	Generation of Involute Tooth Profile in Perfect Parallel-Axes Gear Pair .....	141
7.1.1	Involute Gear Tooth Profile.....	144
7.1.2	Tooth Flanks of a Gear and a Mating Pinion .....	146
7.1.2.1	Spur Involute Gear Tooth Flank.....	146

7.1.2.2	Helical Involute Gear Tooth Flank .....	148
7.1.2.3	Involute Tooth Flank of a Gear with Circular-Arc Teeth in the Lengthwise Direction .....	154
7.1.3	Possible Form of a Gear Tooth in the Lengthwise Direction .....	155
7.1.4	Adopted Gear Terminology .....	158
7.1.5	Euler-Savary Equation .....	160
7.2	Alternative Approach for the Derivation of Equation of the Involute Tooth Flank .....	162
7.2.1	Generating the Straight Line of a Spur Gear .....	162
7.2.2	Length of Involute Tooth Profile .....	166
7.2.3	Generating the Basic Rack of a Spur Gear .....	168
7.2.3.1	Alternative Approach for the Derivation of Equation of Helical Involute Gear Tooth Flank .....	172
7.2.3.2	Generating Basic Rack of a Helical Gear .....	176
7.2.4	Descriptive-Geometry-Based Determination of the Straight Generating Line .....	181
7.2.4.1	Gear Base Helix Angle $\psi_{b,g}$ : General Approach .....	181
7.2.4.2	Base Diameter, $d_{b,g}$ , of an Involute Gear .....	183
7.3	Conical Involute Gears .....	184
7.3.1	Kinematics of Conical Involute Gearing .....	184
7.3.1.1	Geometry of the Tooth Flanks of a Spur Conical Involute Gear .....	184
7.3.1.2	Geometry of Tooth Flanks of a Conical Involute Gear with Helical Teeth .....	192
7.4	Conditions to Be Fulfilled by a Pair of Mating Gears .....	194
<b>8.</b>	<b>Interaction of Tooth Flanks in Parallel-Axes Involute Gearing .....</b>	<b>197</b>
8.1	Interaction of Tooth Flanks in Parallel-Axes Spur Involute Gearing .....	197
8.2	Interaction of Tooth Flanks in Parallel-Axes Helical Involute Gearing .....	199
8.3	Transmission of a Uniform Rotation by Means of Parallel-Axes Involute Gearing .....	201
8.4	Contact Ratio in Parallel-Axes Involute Gearing .....	204
8.4.1	Transverse Contact Ratio in Parallel-Axes Involute Gearing .....	204
8.4.2	Face Contact Ratio in Parallel-Axes Helical Involute Gearing .....	209
8.4.3	Total Contact Ratio .....	211
8.4.4	Transverse Contact Ratio in a Low-Tooth-Count Gear Pair .....	213
8.4.5	Impact of the Elastic Deformation on the Total Contact Ratio in Gear Pairs .....	215
8.5	External Involute Gear Pair .....	216
8.5.1	Main Design Parameters .....	216
8.5.2	Variation of the Tooth Flank Geometry .....	220
8.5.2.1	Normal Curvature of the Gear Tooth Flank .....	221
8.5.2.2	Variation of the Tooth Profile Angle and Helix Angle .....	225
8.5.3	Special Point of Meshing .....	226
8.6	Contact Motion Characteristics .....	227
8.6.1	Sliding Conditions .....	227
8.6.2	Specific Sliding .....	230
8.7	Elements of Dynamics of Perfect Parallel-Axes Gearing .....	232
8.7.1	Forces Acting in a Plane of Action in a Perfect Parallel-Axes Involute Gear Pair .....	232
8.7.2	Forces Acting in a Transverse Section of a Perfect Parallel-Axes Involute Gear Pair .....	240
8.8	<i>Pinion-Gear-to-Rack Mesh</i> as a Reduced Case of External Parallel-Axes Involute Gear Pair .....	241
<b>9.</b>	<b>Internal Involute Gearing .....</b>	<b>245</b>
9.1	Contact Ratio in Internal Gearing .....	245
9.2	Contact Motion Characteristics in Internal Gearing .....	250

9.2.1	Sliding Conditions .....	250
9.2.2	Specific Sliding .....	251
9.3	Conditions to Be Fulfilled by Mating Gears in Internal Gear Pair: Engineering Formulae .....	252
9.4	Tooth Thickness Measurement in Internal Gears .....	254
9.5	<i>Gear Coupling</i> as a Reduced Case of an Internal Parallel-Axes Involute Gear Pair .....	254
<b>10.</b>	<b>High-Conformal Parallel-Axes Gearing .....</b>	<b>257</b>
10.1	A Brief Overview on Conformal Gearing: State of the Art .....	257
10.1.1	The Origin of High-Conformal Gearing .....	257
10.1.2	Power Density in High-Conformal Gearing .....	258
10.2	Conformal Gearing .....	260
10.2.1	Novikov Gearing: Helical Involute Gearing with Zero Transverse Contact Ratio .....	260
10.2.2	Essence of Novikov Gearing .....	260
10.3	Fundamental Design Parameters of <i>Conformal Gearing</i> .....	266
10.4	Transition from Involute Gearing to Conformal Parallel-Axes Gearing (to Novikov Gearing) .....	267
10.4.1	Boundary <i>N</i> -Circle in Conformal Gearing .....	269
10.4.2	Possible Tooth Geometries in Conformal Gearing .....	271
10.5	Tooth Profile Rolling/Sliding in Conformal Gearing .....	276
10.5.1	Tooth Profile Sliding in Conformal Gearing .....	276
10.5.2	Tooth Profile Rolling in Conformal Gearing .....	279
10.6	Elements of the Kinematics and Geometry in Conformal Gearing .....	280
10.7	Designing of Conformal Gear Pairs .....	282
10.8	Conformal Gearing with Two Pseudo-Paths of Contact .....	284
10.9	Tooth Flank Geometry in Conformal Gearing .....	285
10.10	Configuration of Interacting Tooth Flanks at the Culminating Point .....	288
10.11	Local and Global Contact Geometry of Interacting Tooth Flanks .....	289
10.12	High-Conformal Gearing .....	292
10.12.1	Contact Geometry in High-Conformal Parallel-Axes Gearing .....	292
10.12.2	High-Conformal Parallel-Axes Gearing .....	295
10.13	On the Accuracy Requirements for High-Conformal Parallel-Axes Gearing .....	298
10.14	On the Impossibility of Cutting Gears for Conformal and High-Conformal Gearing in Generating (Continuous-Indexing) Machining Processes .....	303
<b>11.</b>	<b>Noninvolute Gearing .....</b>	<b>307</b>
11.1	Spur Noninvolute Gear Pairs .....	307
11.1.1	Pin Gearing .....	307
11.1.2	Cycloidal Gearing .....	308
11.1.3	Roots Blower .....	310
11.1.4	Spur Rotors of Oil Pumps .....	313
11.2	Peculiarities of Transmission of Rotation by Means of Noninvolute Gearing .....	314
11.2.1	Conditions of Transmission of Rotation by Means of Noninvolute Gearing .....	314
11.2.2	Interaction of Noninvolute Gears with Racks .....	317
11.3	Helical Noninvolute Gear Pairs .....	321
11.3.1	Helical Rotors in Roots Blowers .....	321
11.3.2	Analysis of Infeasibility of <i>Helical Gearing</i> by Wildhaber (US Pat. No. 1,601,750) .....	322

## Section II-B Perfect Gearing: Intersected-Axes Gearing

<b>12.</b>	<b>Perfect Intersected-Axes Gear Pairs .....</b>	<b>329</b>
12.1	Earliest Designs of Intersected-Axes Gearing .....	329



12.2	Kinematics of Intersected-Axes Gearing .....	329
12.3	Base Cones in Intersected-Axes Gearing .....	335
12.3.1	Path of Contact and Instant Line of Action .....	338
12.3.2	Operating Base Pitch Calculation .....	339
12.4	Tooth Flanks of Perfect Intersected-Axes Gear Pairs .....	340
12.4.1	Applied Coordinate Systems and Linear Transformations .....	340
12.4.1.1	Main Reference Systems .....	340
12.4.1.2	Operators of Rolling .....	341
12.4.1.3	Operators of Linear Transformations Associated with the Gear Housing .....	343
12.4.2	Tooth Flank of a Gear in an Intersected-Axes Gear Pair .....	345
12.4.3	Intersected-Axes Gearing with Variable Pressure Angle .....	351
12.5	Tooth Flanks in Perfect Intersected-Axes Gear Pairs .....	351
12.6	Desired Tooth Proportions in Intersected-Axes Gears .....	353
12.6.1	Angular Base Pitch .....	354
12.6.2	Transverse Pressure Angle .....	356
12.6.3	Angular Pitch .....	360
12.6.4	Angular Tooth Thickness and Angular Space Width .....	362
12.6.5	Angular Backlash .....	363
12.6.6	Angular Addendum and Angular Dedendum .....	366
12.6.7	Specification of Design Parameters in Intersected-Axes Gearing .....	367
12.7	<i>Tredgold Approximation</i> .....	370
12.8	Main Features of Perfect Conformal and High-Conformal Intersected-Axes Gearing .....	371
12.8.1	Path of Contact in Conformal/High-Conformal Intersected-Axes Gearing .....	372
12.8.2	Boundary Cones .....	373
12.8.3	Bearing Capacity of High-Conformal Gearing .....	374
12.9	Design Parameters of Conformal/High-Conformal Intersected-Axes Gearing .....	375
<b>13.</b>	<b>Interaction of Tooth Flanks in Perfect Intersected-Axes Gearing .....</b>	<b>381</b>
13.1	Interaction between Tooth Flanks in Perfect Intersected-Axes Gearing .....	381
13.1.1	Pulley-and-Belt Analogy of Intersected-Axes Gear Pair .....	381
13.1.2	Path of Contact .....	381
13.1.3	Zone (Field) of Action in Intersected-Axes Gearing .....	383
13.2	Transmission of a Uniform Rotation by Means of Intersected-Axes Gearing .....	384
13.3	Contact Ratio in Intersected-Axes Gearing .....	387
13.3.1	Transverse Contact Ratio .....	388
13.3.2	Face Contact Ratio .....	390
13.3.3	Total Contact Ratio .....	391
13.4	Contact Motion Characteristics in Intersected-Axes Gearing .....	392
13.4.1	Sliding in Perfect Intersected-Axes Gearing .....	393
13.4.1.1	Descriptive Geometry-Based Solution to the Problem of Determining Sliding in Perfect Intersected-Axes Gearing .....	393
13.4.1.2	Analytical Solution to the Problem of Determining of Sliding in Perfect Intersected-Axes Gearing .....	398
13.4.1.3	Specific Sliding in Perfect Intersected-Axes Gearing .....	403
13.4.1.4	Features of Specific Sliding in Perfect Intersected-Axes Gearing .....	404
13.5	Elements of Dynamics of Perfect Intersected-Axes Gearing .....	405
13.5.1	Principal Assumption Adopted in Load Analysis of Perfect Intersected-Axes Gearing .....	405
13.5.2	Forces of Interaction in Perfect Intersected-Axes Gearing .....	407
13.5.2.1	Resultant Force Acting in Perfect Intersected-Axes Gearing .....	408
13.5.2.2	Forces Acting on the Gear and the Pinion in Perfect Intersected-Axes Gearing .....	410
13.5.2.3	Normal Force Acting on the Gear in Perfect Intersected-Axes Gearing ....	412

13.6	Testing of Perfect Spiral Bevel Gears: Contact Pattern.....	413
13.6.1	Conditions for Testing .....	413
13.6.2	Predicting Contact Geometry in Perfect Spiral Bevel Gearing.....	414

## Section II-C Perfect Gearing: Crossed-Axes Gearing

<b>14.</b>	<b>Perfect Crossed-Axes Gear Pairs: R-Gearing.....</b>	<b>419</b>
14.1	Kinematics of Crossed-Axes Gearing .....	419
14.1.1	Pressure Angle in Crossed-Axes Gearing.....	422
14.1.2	Crossed-Axes Gearing with <i>Constant</i> Transverse Pressure Angle .....	422
14.1.3	Crossed-Axes Gearing with <i>Variable</i> Transverse Pressure Angle.....	423
14.2	Base Cones in Crossed-Axes Gear Pair .....	423
14.3	Tooth Flanks in Perfect Crossed-Axes Gear.....	428
14.3.1	Applied Coordinate Systems and Linear Transformations .....	428
14.3.1.1	Main Reference Systems .....	429
14.3.1.2	Operators of Rolling/Sliding.....	430
14.3.1.3	Operators Associated with Gear Housing .....	432
14.3.1.4	Gear Tooth Flank in Crossed-Axes Gearing.....	433
14.4	Conjugacy of Tooth Flanks of a Gear and a Mating Pinion in R-Gearing .....	442
14.5	Desired Tooth Proportions in Crossed-Axes Gear Pairs .....	444
14.5.1	Operating Angular Base Pitch .....	445
14.5.2	Low-Tooth-Count Crossed-Axes Gears.....	448
14.5.3	Transverse Pressure Angle.....	448
14.5.4	Angular Pitch.....	452
14.5.5	Angular Tooth Thickness and Angular Space Width in the Round Basic Rack .....	453
14.5.6	Angular Addendum and Angular Dedendum of the Round Basic Rack.....	454
14.5.7	Specification of the Design Parameters in Crossed-Axes Gearing .....	458
14.6	Backlash in Crossed-Axes Gearing.....	460
14.7	Possible Analogy of Tredgold Approximation for Crossed-Axes Gearing.....	462
14.8	Main Features of Perfect Conformal and Conformal/High-Conformal Crossed-Axes Gearing .....	462
14.8.1	Path of Contact in High-Conformal Crossed-Axes Gearing .....	463
14.8.2	Boundary <i>N</i> -Cone in Crossed-Axes High-Conformal Gearing .....	463
14.8.3	Bearing Capacity of Crossed-Axes Conformal/High-Conformal Gearing .....	465
14.9	Design Parameters of Conformal/High-Conformal Crossed-Axes Gearing .....	465
<b>15.</b>	<b>Interaction of Tooth Flanks in Perfect Crossed-Axes Gearing.....</b>	<b>471</b>
15.1	Interaction between Tooth Flanks in Perfect Crossed-Axes Gearing.....	471
15.1.1	Pulley-and-Belt Analogy of Crossed-Axes Gear Pair .....	471
15.1.2	Path of Contact .....	471
15.1.3	Zone (Field) of Action in Crossed-Axes Gearing .....	472
15.2	Transmission of a Uniform Rotation by Means of Crossed-Axes Gearing.....	473
15.3	Contact Ratio in Crossed-Axes Gearing .....	476
15.3.1	Transverse Contact Ratio .....	476
15.3.2	Face Contact Ratio.....	476
15.3.3	Total Contact Ratio .....	477
15.4	Contact Motion Characteristics in Crossed-Axes Gearing .....	478
15.4.1	Sliding in Perfect Crossed-Axes Gearing .....	478
15.4.2	Analytical Solution to the Problem of Determining of Sliding in Perfect Crossed-Axes Gearing .....	478

15.4.3	Specific Sliding in Perfect Crossed-Axes Gearing.....	484
15.4.4	Features of Specific Sliding in Perfect Crossed-Axes Gearing .....	485
15.5	Elements of Dynamics of Perfect Crossed-Axes Gearing .....	486
15.5.1	Principal Assumption Adopted in Load Analysis of Perfect Crossed-Axes Gearing .....	486
15.5.2	Forces of Interaction in Perfect Crossed-Axes Gearing .....	489
15.5.2.1	Resultant Force Acting in Perfect Crossed-Axes Gearing .....	489
15.5.2.2	Forces Acting on the Gear and Pinion in Perfect Crossed-Axes Gearing.....	492
15.5.2.3	Normal Force Acting on the Gear in Perfect Crossed-Axes Gearing.....	494
<b>16.</b>	<b>Peculiarities of Perfect Worm Gearing .....</b>	<b>497</b>
16.1	Peculiarities of Worm Gearing with Line Contact between Worm Threads and Worm-Gear Tooth Flanks .....	497
16.1.1	Kinematics of Perfect Worm Gearing.....	497
16.1.2	Base Cones in Perfect Worm Gearing.....	497
16.1.3	Peculiarities of Sliding in the Plane-of-Action Apex in Perfect Worm Gearing.....	500
16.2	Criterion to Distinguish Worm from Gear.....	501
16.3	An Analysis of a Worm Gear-Drive (Pat. No. 257,246, USSR, 1968).....	503
 <b>Part III Perfect Gearing with Point Contact between Tooth Flanks of a Gear and a Mating Pinion</b>		
<b>17.</b>	<b>Kinematics, Geometry, and Design Features of Perfect Gearing with Point Contact between Tooth Flanks of a Gear and a Mating Pinion .....</b>	<b>507</b>
17.1	Examples of Gearings with Point Contact between Tooth Flanks of a Gear and a Mating Pinion.....	507
17.2	Approach to Generating Tooth Flanks in Gearing with Point Contact between Tooth Flanks of a Gear and Mating Pinion .....	509
17.3	Possible Types of Auxiliary Generating Racks.....	511
17.4	Geometry of Tooth Flanks of Perfect Crossed-Axes Gears with Point Contact .....	512
 <b>Part IV Real Gears and Their Application: Perfect Real Gearing</b>		
<b>18.</b>	<b>Perfect Real Gearing: <math>S_{pr}</math>-Gear System .....</b>	<b>519</b>
18.1	Preliminary Considerations.....	519
18.1.1	Root Causes for Real Gears Differing from Perfect Gears .....	519
18.1.2	Applied Coordinate Systems .....	521
18.1.3	Displacements of a Gear Axis of Rotation from Its Desired Configuration.....	522
18.1.4	Closest Distance of Approach between Gear and Mating Pinion Axes of Rotation .....	526
18.2	Tooth Flank Geometry in Perfect Real Gearing: In $S_{pr}$ -Gear System.....	531
18.2.1	Tooth Flank Geometry in Perfect Real Gearing.....	532
18.2.1.1	Adopted Concept Tooth Flank Generation of Gears for $S_{pr}$ -Gear System .....	532
18.2.1.2	Preferred Reference Systems .....	534
18.2.1.3	Derivation of Equation of Tooth Flank in $S_{pr}$ -Gearing .....	535



18.2.1.4	Angular Base Pitch in $S_{pr}$ -Gearing .....	539
18.2.1.5	Features of Interaction of Tooth Flanks in $S_{pr}$ -Gearing.....	541
18.2.2	Possibility of Implementation of the Concept of $S_{pr}$ -Gearing in Design of Two-Degrees-of-Freedom Gearing .....	542
18.2.3	Possibility of Implementation of the Concept of $S_{pr}$ -Gearing in Design of Gear Coupling .....	545
18.2.4	Account for Normal Distribution of Manufacturing Errors in Geometry of Tooth Flanks .....	546
18.3	Possibility of Implementation of the Concept of $S_{pr}$ -Gearing to Gear Systems That Feature Point Contact between Tooth Flanks .....	548
18.4	Correlation among Gear Systems of Various Types .....	549

## Part V $C\Sigma u$ -Variable Gearing

19.	<b>A Novel Concept to Design Perfect Noncircular Gears</b> .....	555
19.1	Fundamentals of Perfect Noncircular Gearing.....	555
19.2	Tooth Flank Generation in Perfect Noncircular Gear Pairs .....	556
19.3	On Inconsistency of Known Methods of Machining Gears for Perfect Noncircular Gear Pairs.....	559

## Part VI Synthesis of Favorable Perfect Gear Pairs

20.	<b>Features of Contact Geometry</b> .....	565
20.1	Meaning of the Term <i>Synthesis of Favorable Gear Pair</i> .....	565
20.2	Dupin Indicatrix .....	566
20.3	Indicatrix of Conformity at Point of Contact of a Gear and Mating Pinion Tooth Flanks .....	567
20.4	A Concept of Synthesis of Favorable Perfect Gear Pairs .....	568

## Part VII Real Gears and Their Application

21.	<b>Generic Gear Shapes</b> .....	573
21.1	Origination of Generic Gear Shape .....	573
21.2	Examples of Gear Pairs Composed of Gears with Various Generic Shapes .....	573
21.3	Evaluation of the Total Number of Possible Generic Gear Shapes.....	575
21.3.1	Possible Profiles of Generic Gear Shape Constructed in Axial Section of a Gear .....	576
21.3.2	Profile of Generic Gear Surface Constructed in Section by Plane at an Angle to Gear Axis .....	584
21.4	Possibility of Classification of Gear Pairs .....	587
21.5	Examples of Implementation of Classification of Gear Pairs .....	588
22.	<b>Approximate Real Gearing</b> .....	593
22.1	Approximate Real Parallel-Axes Gearing.....	594
22.2	Approximate Real Intersected-Axes Gearing .....	596
22.2.1	Root Causes for Inaccuracies of Real Intersected-Axes Gears .....	596
22.2.2	Approximate Real Intersected-Axes Gears .....	597

22.2.2.1	Straight Tooth Bevel Gears.....	597
22.2.2.2	Spiral Bevel Gears.....	600
22.2.2.3	Face Gears.....	602
22.2.3	Generation of Tooth Flanks of Gears for Intersected-Axes Gearing .....	602
22.2.3.1	Generation of Tooth Flanks of Straight Bevel Gears .....	602
22.2.3.2	Generation of Tooth Flanks of Spiral Bevel Gears .....	606
22.2.3.3	Tooth Flanks of Bevel Gears Cut Using Continuous Indexing Method of Gear Machining .....	609
22.2.4	Examples of Approximate Real Intersected-Axes Gear Pairs.....	610
22.3	Approximate Real Crossed-Axes Gearing .....	614
22.4	Worm Gearing .....	618
22.5	Tooth Flank Modification.....	621
22.5.1	Brief Historical Overview of Gear Tooth Flank Modification.....	621
22.5.2	Requirements of Design Parameters of Modified Portions of Tooth Flanks .....	622
22.5.3	Kinds of Tooth Flank Modifications .....	623
22.5.3.1	Tooth Flank Modifications That Restrict the Useable Flank.....	623
22.5.3.2	Transverse Profile Modifications.....	623
22.5.3.3	Flank Line (Helix) Modifications.....	625
22.5.3.4	Flank Face Modifications.....	625
22.5.4	Description of Modifications by Functions .....	626
<b>23.</b>	<b>Local Geometry of Interacting Tooth Flanks of a Gear and a Mating Pinion.....</b>	<b>627</b>
23.1	Local Geometry of Interacting Tooth Flanks in Parallel-Axes Gearing .....	627
23.1.1	Kinematics of Interacting of Tooth Flanks.....	627
23.1.2	Local Geometry of the Interacting Tooth Flanks.....	628
23.2	Local Geometry of Interacting Tooth Flanks in Intersected-Axes Gearing.....	632
23.2.1	Kinematics of Interaction of Tooth Flanks.....	632
23.2.2	Local Geometry of the Interacting Tooth Flanks.....	634
23.3	Local Geometry of Interacting Tooth Flanks in Crossed-Axes Gearing.....	636
23.3.1	Kinematics of Interaction of Tooth Flanks.....	636
23.3.2	Local Geometry of Interacting Tooth Flanks.....	637
23.4	Local Geometry of Interacting Tooth Flanks in High-Conformal Gearing.....	638
23.4.1	Kinematics of Interacting Tooth Flanks.....	639
23.4.2	Geometry of Interacting Tooth Flanks.....	641
<b>24.</b>	<b>Strength of Gear Teeth .....</b>	<b>645</b>
24.1	Contact Strength of <i>Low Tooth Count Gearing</i> .....	645
24.1.1	Adopted Principal Assumptions.....	646
24.1.1.1	Comments on Analytical Description of Local Geometry of Contacting Surfaces Loaded by Normal Force: Hertz Proportional Assumption .....	646
24.1.1.2	Assumption of Equal Torque Share.....	648
24.1.2	Principal Features of Low-Tooth-Count Gears .....	649
24.1.3	Analytical Model for Calculating Contact Stress .....	650
24.1.4	Formula for Calculating <i>Hertz Contact Stress</i> .....	654
24.1.5	Specific Pressure Factor.....	655
24.1.6	Combined Compressive-Shear Stress in Low Tooth Count Gearing .....	655
24.2	Bending Strength of Gear Teeth .....	657
24.2.1	Comments on <i>Lewis's Formula</i> .....	657
24.2.1.1	Cantilever Beam of Equal Strength.....	658
24.2.1.2	Lewis's Formula for the Calculation of Gear Tooth Bending Strength.....	659

24.3	Effective Length of Line of Contact .....	662
24.3.1	Length of a Single Line of Contact in Parallel-Axes Gearing .....	663
24.3.2	Effective Length of Lines of Contact in Parallel-Axes Gearing .....	667
24.3.2.1	Effective Length of Lines of Contact in Spur Parallel-Axes Gearing .....	668
24.3.2.2	Effective Length of Lines of Contact in Helical Parallel-Axes Gearing.....	671
24.4	Loading of Gear Teeth .....	674
24.5	Method for Simulating the Interaction of Gear and Mating Pinion Tooth Flanks .....	678
<b>25.</b>	<b>Gear Tooth Profile Modification: Generating Rack Shift .....</b>	<b>685</b>
25.1	Addendum Modification (Profile Shift).....	685
25.2	Profile Shift Coefficient .....	688
25.3	Gear Tooth Flank Geometry Depending on the Profile Shift Coefficient .....	689
25.4	Basic Equations for a Gear Pair with Addendum Modification .....	690
25.4.1	Principle of Addendum Modification .....	691
25.4.2	External Spur and Helical Gear Pairs.....	691
25.5	Determination of Profile Shift Coefficients: Geometrical Blocking Contours .....	693
<b>26.</b>	<b>Split Torque Transmission Systems.....</b>	<b>697</b>
26.1	Root Cause for Unequal Torque Sharing in a Split Torque Transmission .....	698
26.2	Mobility of Split Torque Transmission Systems .....	700
26.3	Power Density of Gear Transmission Systems.....	702
26.4	Epicyclical Gear Drives .....	703
26.5	Structural Formula for Planetary Gear Drives .....	704
26.6	Correspondence among Angular Velocities of All the Members in a Planetary Gear Drive...	705
26.7	Formulating the Problem of Equal Load Sharing in Planetary Gear Drives: State of the Art..	706
26.7.1	Ordinary Planetary Gear Drives.....	707
26.7.2	Planetary Gear Drives with Flexible Pins.....	707
26.8	Alternative Approach for Equal Torque Sharing in Split Torque Transmission .....	711
26.8.1	Planetary Gear Drive with Elastomeric Load Sharing Device .....	713
26.8.2	Elastic Load Sharing Device .....	714
26.8.2.1	Elastic Properties of Elastic Load Sharing Device.....	714
26.8.2.2	Examples of Implementation of Elastic Load Sharing Devices.....	716
26.9	Main Features of Split Torque Transmission Systems with Preloaded Elastic Load Sharing Devices.....	724
<b>27.</b>	<b>Vector Approach for Kinematic and Dynamic Analysis of Complex Gear Systems.....</b>	<b>725</b>
27.1	Possible Kinds of Images for Rotating Gears .....	725
27.2	Vector Diagrams for Complex Gear Systems .....	727
27.3	Features of Vector Diagrams for Complex Gear Systems with Intersected-Axes and Crossed-Axes Gear Pairs.....	730
27.3.1	Elementary Vector Diagram for Intersected-Axes Gear Pairs.....	730
27.3.2	Elementary Vector Diagram for Crossed-Axes Gear Pair.....	732
<b>28.</b>	<b>Gear Ratio of a Multistage Gear Drive.....</b>	<b>733</b>
28.1	Principal Kinematic Relationships in Multistage Gear Drives .....	733
28.1.1	Range Ratio of Speed Variation for Gear Drives .....	735
28.1.2	Characteristics of Transmission Group .....	735
28.2	Analytical Method for Determining Transmission Ratios .....	735
28.3	Rotational Speed Charts .....	736
28.4	Broken Geometrical Series .....	737
28.5	Minimum Number of Gear Pairs .....	738
28.6	Determining Tooth Number of Gears of Group Transmissions .....	738

<b>29. Accuracy of Gear Teeth</b>	<b>741</b>
29.1 Inspection of Gears for Parallel-Axes Gear Pairs	741
29.2 Inspection of Gears for Intersected-Axes Gear Pairs	748
29.3 Inspection of Gears for Crossed-Axes Gear Pairs	750
29.4 Inspection of the Accuracy of Axial Location in Gears for Crossed-Axes and Intersected-Axes Gear Pairs	751
29.4.1 Mounting Distance	752
29.4.2 Contact Patterns	753
29.4.3 Inspection of the Mounting Distance in Gears for Crossed-Axes and Intersected-Axes Gear Pairs	755
<b>30. Gear Noise and Vibration</b>	<b>757</b>
30.1 Root Causes for Vibration Generation and Noise Excitation	757
30.1.1 Root Cause for Vibration Generation and Noise Excitation in Perfect Gear Pairs	757
30.1.2 Root Cause for Vibration Generation and Noise Excitation in Approximate Gear Pairs	758
30.1.2.1 Violation of the Condition of Contact	758
30.1.2.2 Violation of the Condition of Conjugacy	758
30.1.2.3 Violation of the Equality of the Base Pitches	759
30.2 Transmission Error	763
30.3 Influence of Load Variation on Noise Excitation in a Gear Pair	766
30.3.1 Variation of the Axial and Radial Forces	766
30.3.2 Influence of the Contact Ratio	766
30.4 On the Possibility of Prediction of Noise Excitation in a Gear Pair	767
<b>31. Design Peculiarities of Perfect and Almost Perfect Gears</b>	<b>771</b>
31.1 Design Peculiarities of Gears for $R$ -Gearing	771
31.1.1 Essence of the Kinematics in Crossed-Axes Gearing	771
31.1.2 Base Cones	772
31.1.3 Tooth Flanks in Perfect Crossed-Axes Gears	772
31.2 Permissible Simplification: Design Peculiarities of Gears for $R_{sp}$ -Gearing	776
<b>Appendix A: Elements of Vector Calculus</b>	<b>781</b>
<b>Appendix B: Elements of Differential Geometry of Surfaces</b>	<b>787</b>
<b>Appendix C: Change of Surface Parameters</b>	<b>801</b>
<b>Appendix D: Applied Coordinate Systems and Linear Transformations</b>	<b>803</b>
<b>Appendix E: Contact Geometry of Gear and Mating Pinion Tooth Flanks</b>	<b>829</b>
<b>Appendix F: Closest Distance of Approach between Gear and Mating Pinion Tooth Flanks</b>	<b>851</b>
<b>Appendix G: Engineering Formulae for the Specification of Gear Tooth Flanks</b>	<b>855</b>
<b>Appendix H: On the Inadequacy of the Terms <i>Wildhaber-Novikov Gearing</i> and <i>W-N Gearing</i></b>	<b>859</b>
<b>Conclusion</b>	<b>867</b>

<b>Glossary</b> .....	871
<b>References</b> .....	877
<b>Bibliography</b> .....	883
<b>Index</b> .....	889

---

## Preface

---

Gearing plays a role, usually unseen, in the lives of everyone in the civilized world. Few people know anything about gears, and even fewer understand them. Even practicing engineers, except those who are gear specialists, know little except the rudiments about gears.

A couple dozen more or less serious books have been written on gearing during the last five decades. Numerous monographs titled *Theory of Gearing* have been published. Most texts on theory of gearing target the compilation and systematization of known achievements in the field of gearing. No effort has been undertaken to this end to develop a theory of gearing that covers all known achievements as well as making possible the development of novel kinds of gearing that feature the desired performance (predictive capabilities). A solution to this problem is disclosed by the author in this monograph.

It is likely that Theodore Olivier's *Theory of Gearing* (1842) was the first monograph ever published in the field [81]. To be honest, the monograph by Olivier [81], as well as all other books published to this end, is not a scientific monograph in nature. Practical and theoretical experience are compiled in the published books. A scientific theory should be based on a set of postulates, from which the entire theory is derived. No definitive monograph of this sort in the field of gearing is published to this end.

Previous treatments of the kinematics and geometry of gears use numerous approximations and introduce errors when they are applied to gears with a significant profile mismatch, such as those that have been developed in recent practice. It is therefore timely to reconsider the basic theory of the kinematics and geometry of gears so as to provide a sound basis for the evaluation and development of future designs.

This monograph is written for engineers and researchers who work in the field of gear design, gear production, and application of gears. One of the main goals (purposes) of this monograph is to focus the attention of gear researchers on the development of a *scientific theory of gearing* and to stimulate them to undertake extensive research in this particular field of mechanical engineering. The term *scientific* in this context is understood in the following manner: a concept is postulated and then the entire theory of gearing is derived from the postulated concept. The concept adopted in this monograph incorporates a prespecified configuration of rotation vectors of the gear and the pinion, as well as input torque. The rest of the design parameters of a desired (favorable) gear pair can be derived from the postulated concept. To draw the maximum possible output from what the *kinematics* and *geometry* of gearing are capable of providing us with is among the goals of this monograph.

The theory of gearing is a kind of scientific theory, as all known designs of gear pairs are covered by the theory, and, moreover, all potentially possible designs of gear pairs are predicted by the theory.

The term *scientific theory of gearing* is defined in the following way:

**Definition** The scientific theory of gearing is a self-consistent system of knowledge that is based on, and derived from (or can be derived from), an adopted set of axioms (the fundamental facts that are assumed evident and do not require proof).

The *adopted set of axioms* includes:

1. A rotation vector of the driving shaft.
2. A rotation vector of the driven shaft (that is, a configuration of the two rotation vectors is prespecified).
3. An input/output torque.
4. A criterion to meet when synthesizing a gear pair.

Here and below, the kinematics of a gear pair is a prime input component, as the geometry of the interacting tooth flanks of a gear and a mating pinion can be derived on the premise of a given kinematics of a gear pair. Therefore, the below-discussed theory can be referred to as the kinematic theory of gearing.

All known gear designs are covered by the proposed scientific theory of gearing. Numerous novel designs of gears can be derived using the disclosed theory. For the first time ever, the problem of synthesis of a desired gear pair gets an analytical solution in this monograph.



# Taylor & Francis

Taylor & Francis Group

<http://taylorandfrancis.com>

---

## *Acknowledgments*

---

I would like to share the credit for any research success with my numerous doctoral students with whom I have tested the proposed ideas and applied them in the industry. The contributions of many friends, colleagues, and students are overwhelming in number and cannot be acknowledged individually, and as much as my benefactors have contributed, their kindness and help must go unrecorded.

Special thanks to Mr. Jonathan W. Plant, senior editor, Mechanical, Aerospace, Nuclear & Energy Engineering, for his support of my projects.

My thanks also go to those at CRC Press who took over the final stages of preparing this book and coped with the marketing and sales of the fruit of my efforts.!





# Taylor & Francis

Taylor & Francis Group

<http://taylorandfrancis.com>

---

## Author

---



**Dr. Stephen P. Radzevich** is a professor of mechanical engineering and a professor of manufacturing engineering. He received his MSc in 1976, PhD in 1982, and Dr (Eng)Sc in 1991, all in mechanical engineering. Dr. Radzevich has extensive industrial experience in gear design and manufacture. He has developed numerous software packages dealing with computer-aided design (CAD) and computer-aided machining (CAM) of precise gear finishing for a variety of industrial sponsors. His main research interest is the kinematic geometry of part surface generation, particularly with a focus on precision gear design, high-power-density gear trains, torque share in multiflow gear trains, design of special-purpose gear cutting/finishing tools, and design and machine (finish) of precision gears for low-noise and noiseless transmissions of cars, light trucks, and so on.

Dr. Radzevich has spent over 40 years developing software, hardware, and other processes for gear design and optimization. Besides his work for industry, he trains engineering students at universities and gear engineers in companies.

He has authored and coauthored over 40 monographs, handbooks, and textbooks. The monographs *Generation of Surfaces* (RASTAN, 2001), *Kinematic Geometry of Surface Machining* (CRC Press, 2007, 2nd edition 2014), *CAD/CAM of Sculptured Surfaces on Multi-Axis NC Machine: The DG/K-Based Approach* (M&C Publishers, 2008), *Gear Cutting Tools: Fundamentals of Design and Computation* (CRC Press, 2010, 2017), *Precision Gear Shaving* (Nova Science Publishers, 2010), *Dudley's Handbook of Practical Gear Design and Manufacture* (CRC Press, 2012, 2016), *Geometry of Surfaces: A Practical Guide for Mechanical Engineers* (Wiley, 2013) are among his recently published volumes. He has also authored and coauthored about 350 scientific papers and holds over 250 patents on inventions in the field (United States, Japan, Russia, Europe, Canada, Soviet Union, South Korea, Mexico, Brazil, and others).



# Taylor & Francis

Taylor & Francis Group

<http://taylorandfrancis.com>

# Notation

$A_{pa}$	is the plane-of-action apex in a gear pair
$A_g$	is the gear base cone apex
$A_p$	is the pinion base cone apex
$C$	is the closest distance of approach between a gear axis of rotation, $O_g$ , and a mating pinion axis of rotation, $O_p$ (center-distance)
$Cnf_R(\mathcal{G}/\mathcal{P})$	is the indicatrix of conformity at a point of contact, $K$ , of a gear tooth flank, $\mathcal{G}$ , and a mating pinion tooth flank, $\mathcal{P}$
$C_{1,g}, C_{2,g}$	are the first and the second principal plane sections of a gear tooth flank, $\mathcal{G}$
$\mathbf{Cp}_x(a_x, \varphi_x)$	is the operator of coupled linear transformation along and about the axis, $X$
$\mathbf{Cp}_y(a_y, \varphi_y)$	is the operator of coupled linear transformation along and about the axis, $Y$
$\mathbf{Cp}_z(a_z, \varphi_z)$	is the operator of coupled linear transformation along and about the axis, $Z$
$C_{1,p}, C_{2,p}$	are the first and the second principal plane sections of a mating pinion tooth flank, $\mathcal{P}$
$\mathcal{C}$	is the characteristic line
$E_g, F_g, G_g$	are the fundamental magnitudes of the first order of a gear tooth flank, $\mathcal{G}$
$E_p, F_p, G_p$	are the fundamental magnitudes of the first order of a mating pinion tooth flank, $\mathcal{P}$
$\mathbf{Eu}(\psi, \theta, \varphi)$	is the operator of the <i>Eulerian transformation</i>
$\mathcal{G}$	is the gear tooth flank
$\mathcal{P}$	is the pinion tooth flank
$K$	is the point of contact between the tooth flanks, $\mathcal{G}$ and $\mathcal{P}$ (or a point within a line of contact, $LC$ , between the tooth flanks, $\mathcal{G}$ and $\mathcal{P}$ )
$LA$	is the line of action
$LA_{inst}$	is the instant line of action
$LC$	is the line of contact between the tooth flanks, $\mathcal{G}$ and $\mathcal{P}$
$LC_{des}$	is the line desired of contact between the tooth flanks, $\mathcal{G}$ and $\mathcal{P}$
$L_g, M_g, N_g$	are the fundamental magnitudes of the second order of a gear tooth flank, $\mathcal{G}$
$L_p, M_p, N_p$	are the fundamental magnitudes of the second order of a mating pinion tooth flank, $\mathcal{P}$
$O_g$	is the gear axis of rotation
$O_p$	is the pinion axis of rotation
$PA$	is the plane of action
$P_{ln}$	is the axis of instant rotation
$\mathbf{Rl}_x(\varphi_y, Y)$	is the operator of rolling over a plane ( $Y$ -axis is the axis of rotation, $X$ -axis is the axis of translation)
$\mathbf{Rl}_z(\varphi_y, Y)$	is the operator of rolling over a plane ( $Y$ -axis is the axis of rotation, $Z$ -axis is the axis of translation)
$\mathbf{Rl}_y(\varphi_x, X)$	is the operator of rolling over a plane ( $X$ -axis is the axis of rotation, $Y$ -axis is the axis of translation)
$\mathbf{Rl}_z(\varphi_x, X)$	is the operator of rolling over a plane ( $X$ -axis is the axis of rotation, $Z$ -axis is the axis of translation)
$\mathbf{Rl}_x(\varphi_z, Z)$	is the operator of rolling over a plane ( $Z$ -axis is the axis of rotation, $X$ -axis is the axis of translation)
$\mathbf{Rl}_y(\varphi_z, Z)$	is the operator of rolling over a plane ( $Z$ -axis is the axis of rotation, $Y$ -axis is the axis of translation)
$\mathbf{Rr}_u(\varphi, Z)$	is the operator of rolling of two coordinate systems
$\mathbf{Rs}(A \mapsto B)$	is the operator of the resultant coordinate system transformation, say, from the coordinate system $A$ to the coordinate system $B$
$\mathbf{Rt}(\varphi_x, X)$	is the operator of rotation through an angle $\varphi_x$ about the $X$ -axis
$\mathbf{Rt}(\varphi_y, Y)$	is the operator of rotation through an angle $\varphi_y$ about the $Y$ -axis
$\mathbf{Rt}(\varphi_z, Z)$	is the operator of rotation through an angle $\varphi_z$ about the $Z$ -axis
$R_{1,g}, R_{2,g}$	are the first and second principal radii of curvature at a point of a gear tooth flank, $\mathcal{G}$
$R_{1,T}, R_{2,T}$	are the first and second principal radii of curvature at a point of a mating pinion tooth flank, $\mathcal{P}$

$\mathbf{Sc}_x(\varphi_x, p_x)$	is the operator of screw motion about the X-axis
$\mathbf{Sc}_y(\varphi_y, p_y)$	is the operator of screw motion about the Y-axis
$\mathbf{Sc}_z(\varphi_z, p_z)$	is the operator of screw motion about the Z-axis
$\mathbf{Tr}(a_x, X)$	is the operator of translation at a distance $a_x$ along the X-axis
$\mathbf{Tr}(a_y, Y)$	is the operator of translation at a distance $a_y$ along the Y-axis
$\mathbf{Tr}(a_z, Z)$	is the operator of translation at a distance $a_z$ along the Z-axis
$U_g, V_g$	are the curvilinear (Gaussian) coordinates of a point on a gear tooth flank $\mathcal{G}$
$U_p, V_p$	are the curvilinear (Gaussian) coordinates of a point on a mating pinion tooth flank, $\mathcal{P}$
$\mathbf{U}_g, \mathbf{V}_g$	are the tangent vectors to curvilinear coordinate lines on the work gear tooth flank, $\mathcal{G}$
$\mathbf{U}_p, \mathbf{V}_p$	are the tangent vectors to curvilinear coordinate lines on a mating pinion tooth flank, $\mathcal{P}$
$\mathbf{V}_\Sigma$	is the vector of the resultant motion of a pinion tooth flank, $\mathcal{P}$ , in relation to a tooth flank, $\mathcal{G}$ , of a gear
$k_{1,g}, k_{2,g}$	are the first and second principal curvatures of a gear tooth flank, $\mathcal{G}$
$k_{1,p}, k_{2,p}$	are the first and second principal curvatures of a mating pinion tooth flank, $\mathcal{P}$
$\mathbf{n}_g$	is the unit normal vector at point of a gear tooth flank, $\mathcal{G}$
$\mathbf{n}_p$	is the unit normal vector at point of a mating pinion tooth flank, $\mathcal{P}$
$r_{cnf}$	is the position vector of a point of the indicatrix of conformity, $Cnf_R(\mathcal{G}/\mathcal{P})$
$\mathbf{r}_g$	is the position vector of a point of a gear tooth flank, $\mathcal{G}$
$\mathbf{r}_p$	is the position vector of a point of a pinion tooth flank, $\mathcal{P}$
$\mathbf{t}_{1,g}, \mathbf{t}_{2,g}$	are the unit tangent vectors of principal directions on a gear tooth flank, $\mathcal{G}$
$\mathbf{t}_{1,p}, \mathbf{t}_{2,p}$	are the unit tangent vectors of principal directions on a mating pinion tooth flank, $\mathcal{P}$
$\mathbf{u}_g, \mathbf{v}_g$	are the unit tangent vectors to curvilinear coordinate lines on the work gear tooth flank, $\mathcal{G}$
$\mathbf{u}_p, \mathbf{v}_p$	are the unit tangent vectors to curvilinear coordinate lines on a mating pinion tooth flank, $\mathcal{P}$
$x_g y_g z_g$	is the local Cartesian coordinate system having origin at point of contact of the tooth flanks, $\mathcal{G}$ and $\mathcal{P}$

## Greek Symbols

$\Phi_{1,g}, \Phi_{2,g}$	are the first and second fundamental forms of a gear tooth flank, $\mathcal{G}$
$\Phi_{1,p}, \Phi_{2,p}$	are the first and second fundamental forms of a mating pinion tooth flank, $\mathcal{P}$
$\Sigma$	is the crossed-axis angle
$\Sigma_g$	is the gear cone angle
$\Sigma_p$	is the pinion cone angle
$\varphi_{b.op}$	is the operating base pitch of a gear pair
$\varphi_{b.g}$	is the base pitch of a gear
$\varphi_{b.p}$	is the base pitch of a pinion
$\phi_n$	is the normal pressure angle of a gear tooth
$\phi_t, \phi_{t,\omega}$	is the transfer pressure angle of a gear tooth
$\mu$	is the angle of the tooth flanks, $\mathcal{G}$ and $\mathcal{P}$ , local relative orientation
$\omega_p$	is the rotation of a pinion
$\omega_g$	is the rotation of a gear
$\omega_{pl}$	is the instant rotation of a pinion in relation to a gear

## Subscripts

$cnf$	Conformity
$max$	Maximum
$min$	Minimum
$opt$	Optimal
$g$	Gear
$p$	Pinion

---

# Introduction

---

*There is nothing more practical than a good theory.*

—James C. Maxwell (1831–1879)

This monograph is written for engineers and researchers who work in the field of gear design, gear production, and application of gears.

There are many practical guides for the calculation of the design parameters of gears and gear pairs. This issue is more or less successfully covered the books listed in the “References” and “Bibliography” sections of this monograph. Readers who are interested in performing the calculations of a gear are referred to these sources.

This book aims mostly to outline a possible solution to the problem of synthesis of a gear pair with the most favorable performance. The creation of a gear pair that is capable of reproducing a given motion of a driven member when a motion of a driving member is known is the main goal of the synthesis of gearing. Therefore, in this monograph, a given pair of the rotation vectors,  $\omega_g$  and  $\omega_p$ , and the torque on the input shaft,  $T_{in}$ , are the main inputs for synthesizing gear\* pairs.<sup>†</sup>

In the developed scientific theory of gearing, the following fundamental postulate<sup>‡</sup> is adopted:

**Fundamental Postulate***All the design parameters of a favorable gear pair for a particular application can be derived from a given configuration of the rotation vectors of the driving and driven shafts and on the power being transmitted by the gear pair.*

The kinematics of a gear pair is the starting point for solving the problem of synthesis of a gear pair with the desired performance. The geometry of tooth flanks of the driving and driven members can be derived on the premises of the kinematics of the gear pair. (It is understood here that the kinematics of a gear pair is given.) Ultimately, the best possible set of the design parameters of the gear and the pinion can be derived from the kinematics and geometry of the tooth flanks of the mating gears.

Actually, the main portion of input information for the synthesis of a desired gear pair is limited to the following:

- Input rotation (and torque).
- Configuration of a driven shaft in relation to a driving shaft.
- Desired output rotation and torque.

The rest of the data (between the driving shaft and the driven shaft) should be calculated to ensure the favorable design of a gear pair.

The approach disclosed in the monograph makes possible a solution to the problem of synthesis in compliance with the aforementioned formulation.

Harmonic gear drives are not considered in the book, as harmonic drives are not gear pairs at all. Harmonic gear drives are mechanisms of a different nature than gearing.

I try to refer the reader to related sections of the book in both directions, forward as well as backward.

---

\* James Clerk Maxwell (June 13, 1831—November 5, 1879) was a famous Scottish theoretical physicist.

<sup>†</sup> It should be stressed here that the rotation vectors,  $\omega_g$  and  $\omega_p$ , as well as other rotations to be introduced below, are not vectors in nature. However, when special care is undertaken, rotation vectors,  $\omega_g$  and  $\omega_p$ , can be treated like ordinary vectors.

<sup>‡</sup> It is instructive to point out here on the similarity between the proposed *scientific theory of gearing* and *Euclidean geometry*. The entire Euclidean geometry is derived from the postulated set of a several axioms (the total number of the postulated axioms in Euclidean geometry is still disputed). Any and all scientific theories should possess this property, as Euclidean geometry possesses. The proposed scientific theory of gearing meets this requirement, as it is derived from a set of postulates, outlined in the *fundamental postulate*.

## Historical Background

Since the publication in 1842 of the first book titled *Theory of Gearing* by *Theodore Olivier*, numerous attempts have been undertaken to develop a scientific theory of gearing. Though dozens of books have been published in the field to this end, the problem remains unresolved, and no scientific theory of gearing has been developed so far.

A more detailed historical overview of the developments in this field can be found in [Chapter 1](#): “A Brief Overview of the Evolution of the Scientific Theory of Gearing.”

This book is the first (and only so far) attempt to systematically outline the theory of gearing, starting from very simple things such as rotations of the gear and pinion and ending with the calculation of the design parameters of the desired gear that best fits the prescribed conditions of functioning.

## Importance of the Subject

Gears are used in most mechanisms and machines. Transmittal and transformation of a rotation are the main purpose of gearing. As gearing is extensively used in current practice, even a small improvement to a gear pair is capable of returning significant benefits to the user. This is first of all due to the total number of gears in use, which is enormous.

## Uniqueness of This Publication

This monograph is unique for many reasons. Without going into detail, it is sufficient just to say that a scientific theory of gearing is developed in the monograph for the first time ever. The reader who becomes familiar with the monograph should be able to design the best possible gear pairs for any given application.

## Intended Audience

This monograph is aimed at gear experts from both academia and industry. The book is of critical importance to university students, particularly those studying mechanical and manufacturing engineering. The book could also be interesting to engineers and researchers from other areas of mechanical engineering: aerospace engineering, automobile engineering, and so forth.

## Organization of This Monograph

The monograph is comprised of seven parts (Parts I through VII), and of two separate chapters ([Chapters 1](#) and [11](#)).

To better understand the organization of this book, its structure is schematically illustrated in [Figure I.1](#). As shown in [Figure I.1](#), the book begins with a brief overview of the evolution of the scientific theory of gearing.

In [Chapter 1](#), “A Brief Overview of the Evolution of the Scientific Theory of Gearing,” milestone accomplishments that compose the foundation of the scientific theory of gearing are briefly outlined. The discussion begins with consideration of the earliest designs of gears.

The evolution of gear art falls into three periods, namely the pre-*Eulerian*, Eulerian, and post-Eulerian periods of gear art. The scientific theory of gearing originated in the Eulerian period of gear art. Then, developments in the field of perfect gearings are considered. The contributions by *G. Grant*, *Prof. N. Kolchin*, *Prof. M. Novikov*, *Prof. V. Gavrilenko*, and others are covered in this discussion. Ultimately, a tentative chronology of the evolution of the theory of gearing is established.

Developments in the field of approximate gearings are another consideration in this chapter. Here, *S. Cone*’s double-enveloping worm gearing, approximate bevel gearing, approximate crossed-axes gearing, and face gearing are briefly discussed.

A brief summary of the milestone accomplishments in the theory of gearing achieved by the beginning of the 21st century is provided. The condition of contact of the interacting tooth flanks of a gear and pinion, condition of conjugacy of the interacting tooth flanks of a gear and pinion, and condition of equality of base pitches of the interacting tooth flanks of a gear and pinion are covered in this discussion. The chapter ends with concluding remarks.

The rest of the main body of the monograph is composed of seven parts: Parts I through VII.

The first part of the book is titled “Part I. Fundamentals.” This part of the book comprises four chapters: [Chapters 2](#) through [5](#).

The second chapter of the book is titled “Kinematics of a Gear Pair.” The principal kinematics of a gear pair is discussed in this chapter to the best possible extent. An analysis of transmission motion by means of a gear pair is covered in this chapter. Vector representation of gear pair kinematics in the form of vector diagrams is extensively used for this purpose. For convenience, vector diagrams of three different types of spatial gear pairs are discussed in detail, namely:

1. Vector diagrams of rotary-negative crossed-axes gear pairs.
2. Vector diagrams of rotary-positive crossed-axes gear pairs.
3. Vector diagrams of rotary-zero crossed-axes gear pairs.

In all three cases, the conditions of pure rolling and pure sliding are analyzed. Ultimately, an analytical criterion of types of crossed-axes gear pair is proposed.

Use of the vector diagrams of gear pairs makes possible a scientific classification of all possible types of vector diagrams of gear pairs. Once the classification is developed, a set of complementary vectors to vector diagrams of gear pairs is introduced. They include centerline vectors of a gear pair and axial vectors of a gear pair. This consideration ends with a set of useful kinematic and geometric formulas.

Possible future developments in the theory of gearing are an important output from the analysis undertaken in this chapter of the book.

For convenience of further analysis, three principal planes and three principal reference systems associated with a gear pair are discussed in the third chapter of the book. This chapter is titled “Principal Planes and Principal Reference Systems Associated with a Gear Pair.” Along with a general case of crossed-axes gearing, the reduced cases of intersected-axes gearing and of parallel-axes gearing are both used to illustrate details of the approach. The discussion on principal reference systems associated with a gear pair is complemented with corresponding coordinate systems transformations. Transitions from the gear and pinion reference systems to the main reference system are both described analytically.

In [Chapter 4](#), titled “Conditions for Transmitting a Uniform Rotation Smoothly from a Driving Shaft to a Driven Shaft: Three Fundamental Laws of Gearing,” three fundamental laws of gearing are formulated.

In order to transmit a uniform rotation smoothly from a driving shaft to a driven shaft, all three fundamental laws of gearing must be fulfilled.

To obey the first fundamental law of gearing, proper contact conditions between the gear and mating pinion tooth flanks,  $\mathcal{G}$  and  $\mathcal{P}$ , must be ensured. The Shishkov equation of contact,  $\mathbf{n} \cdot \mathbf{V}_\Sigma = 0$ , is used to analytically describe the conditions of contact of the tooth flanks,  $\mathcal{G}$  and  $\mathcal{P}$ .

The condition of conjugacy between the interacting tooth flanks of a gear and mating pinion,  $\mathcal{G}$  and  $\mathcal{P}$ , is the second fundamental law of gearing. The *pulley-and-belt* analogy of a gear pair is used when this fundamental law of gearing is discussed. An equation of conjugacy,  $\mathbf{p}_{ln} \times \mathbf{V}_m \cdot \mathbf{n}_g = 0$ , of the tooth flanks,  $\mathcal{G}$  and  $\mathcal{P}$ , is derived. The performed analysis makes it possible to formulate the *Camus-Euler-Savary theorem* (CES-theorem). The Camus-Euler-Savary theorem can be viewed as a reduced case of the second fundamental law of gearing. The CES-theorem is valid only for parallel-axes gearing. This theorem is not generalized yet to more general cases of gearing, namely to the cases of intersected-axes or crossed-axes gearing.

Finally, the condition of equal base pitches of a gear and mating pinion is analyzed with respect to parallel-axes gearing. The equality of base pitches is valid only in the case of parallel-axes gearing and is said to be a reduced case of the third fundamental law of gearing. To fulfill the third fundamental law of gearing, the base pitch of a gear, as well as the base pitch of a mating pinion, must both be equal to the operating base pitch of the gear pair.

The permissible variation in the center distance of a parallel-axes gear pair and the actual value of the transverse pressure angle are briefly outlined in the fifth chapter of the book, “A Simplified Approach to Involute Gear Tooth Flank Generation.”

Part II, “Perfect Gearing,” is devoted to the analysis of perfect gearings, and is composed of three sections, namely Section II-A through Section II-C.

Perfect parallel-axes gearings are discussed in Section II-A: “Perfect Gearing: Parallel-Axes Gearing.” This section of the book is composed of five chapters, namely [Chapters 6](#) through [10](#).

Two problems are covered in the discussion in [Chapter 6](#): “Involute Gearing: Kinematics and Geometry”. The principal features of parallel-axes gearing is one of these two problems. The discussion of the first problem



includes, but is not limited to, the analysis of the kinematics, gear ratio, and permissible transverse pressure angle variation in parallel-axes gearing. Tooth flank generation is the second problem discussed in this chapter. The following issues are covered in the consideration: of (a) a desirable line of contact between the tooth flanks of a gear and a mating pinion, (b) the line of action and path of contact in a gear pair, (c) operating base pitch in a gear pair, and (d) general approach to the gear tooth flank of a favorable geometry.

In [Chapter 7](#), “A Simplified Approach for Involute Gear Tooth Flank Generation,” a more detailed analysis of tooth flank generation is performed. A simplified approach for involute gear tooth flank generation is disclosed. For this purpose, generation of an involute tooth profile in a perfect parallel-axes gear pair is considered. The involute gear tooth profile and the tooth flanks of a gear and mating pinion in spur, helical, and circular arc in the lengthwise direction of gear tooth flanks are investigated. Then, possible forms of a gear tooth in the lengthwise direction are considered, and the adopted gear terminology is outlined. Ultimately, the *Euler-Savary equation* is derived.

An alternative approach for the derivation of the equation of the involute tooth flank is discussed. The generating straight line of a spur gear, the length of the involute tooth profile, and generation of the basic rack of a spur gear are covered in this discussion. Both the methods, that is, an analytical approach, as well as the descriptive-geometry-based determination of the straight generating line, are discussed.

Conical involute gears are considered with a focus on the kinematics of conical involute gearing and the geometry of the tooth flanks of a spur and helical conical involute gear. A set of conditions to be fulfilled by a pair of mating gears is formulated in engineering terms.

The discussion in [Chapter 8](#), “Interaction of Tooth Flanks in Parallel-Axes Involute Gearing,” is focused mainly on the interaction between the tooth flanks in parallel-axes spur and helical involute gearing that are capable of transmitting an input uniform rotation smoothly. Special attention is given to the analysis of the contact ratio in parallel-axes involute gearing. The transverse contact ratio, face contact ratio, and total contact ratio in parallel-axes involute gearing are discussed to the best possible extent. In particular, the transverse contact ratio in *low-tooth-count gearing* is given detailed consideration. The impact of elastic deformation of gear teeth on the total contact ratio in gear pairs is briefly outlined.

The main design parameters and their variation within the tooth flank in an external involute gear pair are discussed. In particular, the variation of normal curvature of the gear tooth flank and of the tooth profile angle and helix angle receive detailed investigation. The special point of meshing is discovered, and a location of this point in relation to a gear and mating pinion is determined.

Sliding conditions and specific sliding between gear and mating pinion tooth flanks are discussed in the subsection on contact motion characteristics.

In the discussion of elements of dynamics of perfect parallel-axes gearing, the forces acting in the plane of action and in a transverse section of a perfect parallel-axes involute gear pair are analyzed.

This section of the book ends with a brief consideration of *pinion-gear-to-rack mesh* as a reduced case of an external parallel-axes involute gear pair.

Contact ratio and contact motion characteristics in internal gearing are considered in [Chapter 9](#) “Internal Involute Gearing.” The latter includes sliding conditions and specific sliding in internal gearing. Special attention is given to the analysis of the conditions to be fulfilled by mating gears in internal gear pairs, and a set of engineering formulae for the calculations is outlined. Also, measurement of tooth thickness in internal gears is briefly discussed. Finally, it is shown that *gear couplings* can be viewed as a reduced case of an internal parallel-axes involute gear pair.

In [Chapter 10](#), “High-Conformal Parallel-Axes Gearing,” the kinematics and geometry of tooth flanks in high-conformal parallel-axes gearing are discussed. The consideration begins with a brief overview of conformal gearing with a focus on the origin of high-conformal gearing and power density in high-conformal gearing. It is shown that conformal gearing, that is, *Novikov gearing*, is a reduced case of helical involute gearing with zero length of field of action and zero transverse contact ratio. The essence of Novikov gearing is briefly outlined, and the fundamental design parameters of *conformal gearing* are discussed. This analysis is followed by a discussion on the transition from involute gearing to conformal parallel-axes gearing (Novikov gearing). For this purpose, the boundary *N-circle* in conformal gearing is introduced, and possible tooth geometries in conformal gearing are analyzed. Tooth profile sliding, along with tooth profile rolling in conformal gearing, are covered in a subsection on tooth profile rolling/sliding in conformal gearing. The consideration of the elements of the kinematics and geometry in conformal gearing is followed by the analysis of the design of conformal gear pairs.

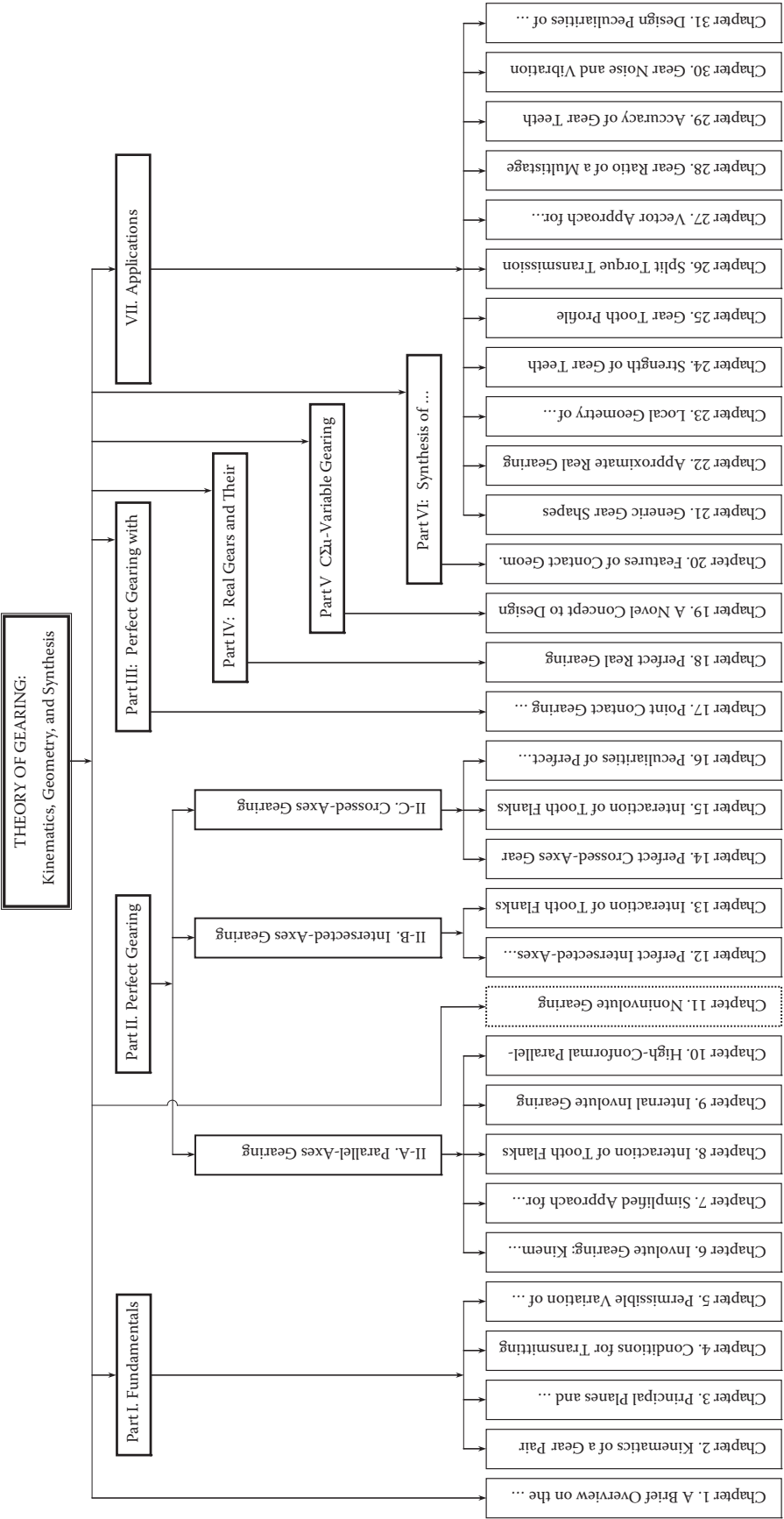


FIGURE I.1  
Organization of the book Theory of Gearing: Kinematics, Geometry, and Synthesis.

A possible way to evolve conventional conformal gearing to conformal gearing with two pseudo-paths of contact is discussed. The consideration of tooth flank geometry in conformal gearing includes an analysis of the configuration of interacting tooth flanks at a culminating point along with the local and global contact geometry of interacting tooth flanks.

Principal features of high-conformal gearing are outlined, and the difference between conformal gearing and *high-conformal gearing* is shown. This discussion is followed by consideration of contact geometry, as well as the accuracy requirements for high-conformal parallel-axes gearing. This chapter of the book ends with a brief discussion of the impossibility of cutting gears for conformal and high-conformal gearing in generating (continuous-indexing) machining processes.

Spur and helical noninvolute parallel-axes gear pairs are discussed in [Chapter 11](#), “Noninvolute Gearing.”\* Pin gearing, cycloidal gearing, lobes of *Roots blowers*, and oil pump rotors are covered in the discussion on spur noninvolute parallel-axes gear pairs. Helical rotors in the design of the lobes of Roots blower rotors, along with an analysis and a proof of infeasibility of *helical gearing* by *Dr. Wildhaber* (US Pat. No. 1,601,750), are covered in the discussion on helical noninvolute parallel-axes gear pairs.

The peculiarities of transmitting a uniform rotation by means of noninvolute gearing are discussed. This discussion includes, but is not limited to, the discussion of conditions of transmission of rotation by means of noninvolute gearing and of interaction of noninvolute gear with a rack.

Perfect intersected-axes gearings are discussed in Section II-B: “Perfect Gearing: Intersected-Axes Gearing.” This section of the book is composed of two chapters, namely [Chapters 12](#) and [13](#).

Perfect intersected-axes gear pairs are discussed in [Chapter 12](#), “Perfect Intersected-Axes Gear Pairs.” The discussion begins with the consideration of the earliest designs of intersected-axes gearing. This discussion follows with analysis of the kinematics and base cones in intersected-axes gearing. The path of contact and instant line of action are considered here. Then, tooth flanks of perfect intersected-axes gear pairs are discussed. For this purpose, a set of reference systems is introduced and discussed in detail, including, but not limited to, intersected-axes gearing with variable pressure angles. This discussion is followed by an analysis of the desired tooth proportions in intersected-axes gears; angular base pitch, transverse pressure angle, angular pitch, angular tooth thickness, angular space width, angular backlash, angular addendum and dedendum, and specification of design parameters in intersected-axes gearing are discussed here. The concept of the *Tredgold approximation* is outlined here.

Perfect conformal and high-conformal intersected-axes gearings receive special attention in this section of the book. The discussion begins with the analysis of the main features of gearing of this particular kind and is followed by a discussion of the path of contact and pseudo-path of contact, boundary cones, and the bearing capacity of high-conformal gearing. This discussion ends with a consideration of the design parameters of conformal and high-conformal intersected-axes gearing.

In [Chapter 13](#), “Interaction of Tooth Flanks in Perfect Intersected-Axes Gearing,” the discussion begins with the analysis of the pulley-and-belt analogy of intersected-axes gear pairs and is followed by the analysis of the path of contact and zone (field) of action in intersected-axes gearing. Then, transmission of a uniform rotation by means of intersected-axes gearing is discussed. Analysis of the transverse contact ratio, face contact ratio, and total contact ratio is performed in the section “Contact Ratio in Intersected-Axes Gearing.” Then, contact motion characteristics in intersected-axes gearing are investigated. For this purpose, sliding in perfect intersected-axes gearing and elements of dynamics of perfect intersected-axes gearing are discussed.

The discussion on sliding between the interacting tooth flanks of a gear and mating pinion includes a descriptive geometry-based solution, as well as an analytical solution to the problem of determination of sliding in perfect intersected-axes gearing. Specific sliding in perfect intersected-axes gearing, along with its features, is also discussed.

In the discussion on the dynamics of perfect intersected-axes gearing, the principal assumption adopted in load analysis of perfect intersected-axes gearing is formulated. Forces of the interaction between the gear teeth are considered.

This chapter ends with a discussion of preliminary testing of perfect spiral bevel gears with a focus on the contact pattern. Conditions of the preliminary testing are outlined, and the parameters of contact geometry in perfect spiral bevel gearing are predicted. The predicted contact geometry has extremely good correlation with the results of the testing.

\* Alternatively, [Chapter 11](#), “Non-Involute Gearing,” can be preceded by [Chapter 5](#), “Permissible Variation of Design Parameters of Pulley-and-Belt Analogy of Parallel-Axes Gearing,” and followed by [Chapter 6](#), “Involute Gearing: Kinematics and Geometry.”

Perfect crossed-axes gearings are discussed in Section II-C: “Perfect Gearing: Crossed-Axes Gearing.” This section of the book is composed of three chapters, namely [Chapters 14](#) through [16](#).

The section of the book opens with [Chapter 14](#), “Perfect Crossed-Axes Gear Pairs: R-Gearing.” The discussion begins with an analysis of the kinematics of crossed-axes gearing. The pressure angle in crossed-axes gearing is specified, and gearings with a *constant* transverse pressure angle, as well as with a variable constant transverse pressure angle, are considered. Then, base cones in crossed-axes gear pairs are constructed.

Numerous reference systems are introduced, aiming at the investigation of tooth flank geometry in perfect crossed-axes gears. Transitions from one reference system to another are described analytically in the form of the operators of linear transformations. This results in an expression for the gear tooth flank in crossed-axes gearing. The condition of conjugacy of tooth flanks of a gear and mating pinion in *R-gearing* is described analytically.

The desired tooth proportions in crossed-axes gear pairs are determined. This includes, but is not limited to:

- Operating angular base pitch.
- Low-tooth-count crossed-axes gears.
- Transverse pressure angle.
- Angular pitch.
- Angular tooth thickness and angular space width in the round basic rack.
- Angular addendum and angular dedendum of the round basic rack.

Possible evolution of the Tredgold approximation toward crossed-axes gearing is briefly outlined.

Special consideration in this chapter of the book is given to the analysis of the main features of perfect conformal and high-conformal crossed-axes gearing. The path of contact, *boundary N-cone*, and bearing capacity of crossed-axes conformal and high-conformal gearings are covered in this discussion. At the end of the chapter, calculation of the design parameters of conformal and high-conformal crossed-axes gearings is considered.

In [Chapter 15](#), “Interaction of Tooth Flanks in Perfect Crossed-Axes Gearing,” the interaction of tooth flanks is discussed. The performed analysis is heavily based on the pulley-and-belt analogy of crossed-axes gear pairs. The path of contact and zone (field) of action in crossed-axes gearing are investigated. This analysis is followed by the consideration of the conditions for transmitting a uniform rotary motion by means of crossed-axes gearing. Then, the contact ratio in crossed-axes gearing is discussed. The transverse contact ratio, face contact ratio, and total contact ratio are covered in this discussion.

Special attention is given to the investigation of contact motion characteristics in crossed-axes gearing. Sliding, specific sliding, and features of specific sliding between the tooth flanks in perfect crossed-axes gearing are investigated.

This chapter of the book ends with a discussion of the elements of dynamics of perfect crossed-axes gearing. A principal assumption adopted in load analysis of perfect crossed-axes gearing is formulated, and forces of interaction in perfect crossed-axes gearing are analyzed. The latter analysis includes, but is not limited to, (a) the resultant force acting in perfect crossed-axes gearing, (b) forces acting on the gear and pinion in perfect crossed-axes gearing, and (c) the normal force acting on the gear in perfect crossed-axes gearing.

Peculiarities of perfect worm gearing are discussed in [Chapter 16](#), “Peculiarities of Perfect Worm Gearing.” The discussion is focused on the features of worm gearing with line contact between worm threads and worm-gear tooth flanks. This is a novel kind of worm gearing not known before. Kinematics, base cones, and the peculiarities of sliding in the plane-of-action apex in perfect worm gearing are covered in this chapter. An analytical criterion to distinguish a worm gear from a helical gear is proposed. The chapter ends with an analysis of a particular design of a worm gear drive [Pat. No. 257,246, USSR, 1968] that is used to demonstrate the importance of the theory of gearing for gear experts.

Part III, “Perfect Gearing with Point Contact between Tooth Flanks of a Gear and a Mating Pinion,” is devoted to the analysis of perfect gearings and is composed of one chapter, namely [Chapter 17](#), “Kinematics, Geometry, and Design Features of Perfect Gearing with Point Contact between Tooth Flanks of a Gear and a Mating Pinion.”

The discussion in this chapter begins with the consideration of examples of gearings with point contact between the tooth flanks of a gear and mating pinion. This discussion is followed by an approach to generating tooth flanks in gearing with point contact between the tooth flanks of a gear and mating pinion. Then, possible

types of auxiliary generating racks are constructed, and the geometry of tooth flanks of perfect crossed-axes gears with point contact is analyzed.

Part III has huge potential for future evolution to be outlined in the future in a few more chapters.

In Part IV, “Real Gears and Their Application,” a novel gear system, the so-called  $S_{pr}$ -gear system is discussed. This part of the book consists of [Chapter 18](#), “Perfect Real Gearing:  $S_{pr}$ -Gear System” In this chapter, perfect real gearing is considered, and a novel design of gearing is proposed. The proposed design of gearing is referred to as an  $S_{pr}$ -gear system. The discussion begins with preliminary considerations and covers (a) root causes for real gears differing from perfect gears, (b) applied coordinate systems, (c) displacements of a gear axis of rotation from its desired configuration, and (d) determination of the closest distance of approach between gear and mating pinion axes of rotation. This analysis is followed by a discussion on tooth flank geometry in perfect real gearing, that is, in gears for an  $S_{pr}$ -gear system. An adopted concept for tooth flank generation of gears for an  $S_{pr}$ -gear system, preferred reference systems, derivation of equations for tooth flanks in  $S_{pr}$ -gearing, angular base pitch in  $S_{pr}$ -gearing, and features of the interaction of tooth flanks in  $S_{pr}$ -gearing are covered in the section on tooth flank geometry in perfect real gearing.

Then, possibilities of implementation of the concept of  $S_{pr}$ -gearing in the design of two-degrees-of-freedom gearing and gear coupling are analyzed.

It is shown that normal distribution of manufacturing errors onto the geometry of tooth flanks can be taken into account when designing gears for an  $S_{pr}$ -gear system. It is also demonstrated that the concept of  $S_{pr}$ -gearing cannot be used in gear systems with point contact between the tooth flanks of a gear and mating pinion, such as in the design of gears for conformal and high-conformal gearing.

The consideration in this section of the book ends with an analysis of a correlation among the gear systems of various types.

Part V, “CΣu–Variable Gearing,” consists of one chapter: [Chapter 19](#), “A Novel Concept to Design Perfect Noncircular Gears.” The discussion begins with an analysis of the fundamentals of perfect noncircular gearing. Then, tooth flank generation in perfect noncircular gear pairs is discussed. The chapter ends with an analysis of the inconsistency of known methods of machining gears for perfect noncircular gear pairs.

Part VI, “Synthesis of Favorable Perfect Gear Pairs,” deals with favorable gear pairs, and is composed of one chapter. In [Chapter 20](#), “Features of Contact Geometry,” the contact geometry between the tooth flanks of a gear and mating pinion is analyzed. The meaning of the term *synthesis of favorable gear pair* is clarified. It is shown how the *Dupin indicatrix* at a point of a gear and pinion tooth flank, as well as the indicatrix of conformity at the point of contact of gear and mating pinion tooth flanks can be employed for solving the problem of synthesizing a favorable gear pair. A concept of synthesis of a favorable perfect gear pair is proposed.

The last part of the book, Part VII: “Real Gears and Their Application,” is composed of 11 chapters ([Chapters 21 through 31](#)).

Generic gear shapes are analyzed in [Chapter 21](#): “Generic Gear Shapes.” The origination of the generic gear shape and examples of gear pairs composed of gears with various generic shapes are covered in this discussion. The total number of possible generic gear shapes is evaluated. The possible profiles of generic gear shapes constructed in the axial section of a gear, as well as the profile of generic gear surface constructed in a section by a plane at an angle to the gear axis, are taken into account in this analysis. The possibility of classification of gear pairs is discussed, and examples of implementation of classification of gear pairs are provided.

[Chapter 22](#), “Approximate Real Gearing,” deals with approximate real gearing. Approximate real parallel-axes gearing, approximate real intersected-axes gearing, and approximate real crossed-axes gearing, including worm gearing, are covered in this discussion. Root causes for inaccuracies of real approximate gears, along with the generation of their tooth flanks, are analyzed. Numerous examples of the gear design and applied methods for tooth flank generation are provided.

Special attention is given to the analysis of gear tooth flank modification. This discussion begins with a brief historical overview of gear tooth flank modification. Then, it is followed by consideration of the requirements to design parameters of modified portions of tooth flanks. Numerous kinds of tooth flank modifications are analyzed. The description of gear tooth flank modifications by functions is briefly outlined.

In [Chapter 23](#), “Local Geometry of Interacting Tooth Flanks of a Gear and a Mating Pinion,” the local geometry of interacting tooth flanks of a gear and a mating pinion is considered. The discussion is followed by an analysis of the local geometry of the interacting tooth flanks in intersected-axes gearing. The kinematics and



local geometry of interacting tooth flanks in intersected-axes gearing are considered. Then, the local geometry of interacting tooth flanks in crossed-axes gearing is investigated. The kinematics and local geometry of interacting tooth flanks in crossed-axes gearing are covered in this discussion. The chapter ends with an analysis of the local geometry of interacting tooth flanks in high-conformal gearing. Again, the discussion is focused on the kinematics and geometry of interacting tooth flanks of high-conformal gearing.

The strength of gear teeth is discussed in [Chapter 24](#), “Strength of Gear Teeth.” The discussion begins with the adopted principal assumptions. The *Hertz proportional assumption* and the *assumption of equal torque share* are the two adopted chapter assumptions. This discussion is followed by the analysis of the principal features of low-tooth-count gears and the development of the analytical model for calculating contact stress. The formula for calculating *Hertz contact stress* is introduced, and the specific pressure factor is discussed. The discussion of gear contact strength ends with the calculation of the combined compressive-shear stress in low-tooth-count gearing.

Then, the bending strength of gear teeth is discussed. For this purpose, the inconsistency of *Lewis’s formula* for the calculation of gear teeth bending strength is discussed.

The effective length of line of contact is discussed in detail, including but not limited to the length of a single line of contact, as well as the effective length of lines of contact in spur and helical parallel-axes gearing. This discussion is followed by an analysis of loading of the gear teeth.

A method for simulating the interaction of gear and mating pinion tooth flanks is disclosed at the end of this chapter.

In [Chapter 25](#), “Gear Tooth Profile Modification: Generating Rack Shift,” gear tooth profile modification generated by means of the basic rack shift is considered. Addendum modification (profile shift), profile shift coefficient, and gear tooth flank geometry depending on the profile shift coefficient are covered. Basic equations for a gear pair with addendum modification are discussed. The principle of addendum modification for external spur and helical gear pairs are also considered. This chapter ends with the determination of profile shift coefficients by means of geometrical blocking contours.

[Chapter 26](#), “Split Torque Transmission Systems,” is devoted to gear transmissions that feature split torque. The root cause of unequal torque sharing in a split torque transmission system, mobility of split torque transmission systems, and *power density* of gear transmission systems are covered in this discussion. This discussion is followed by an analysis of epicyclical gear drives, and the structural formula for planetary gear drives is considered. Then, correspondence among angular velocities of all the members in a planetary gear drive is discussed. Further discussion is focused mainly on formulating the problem of equal load sharing in planetary gear drives, along with consideration of the state of the art in this particular area of gear design. Ordinary planetary gear drives and planetary gear drives with flexible pins are analyzed.

Ultimately, an alternative approach for equal torque sharing in split torque transmission is proposed. This includes, but is not limited to, the planetary gear drive with an elastomeric load sharing device and examples of implementation of the elastic load sharing device. The chapter ends with a discussion of the main features of split torque transmission systems with preloaded elastic load sharing devices.

[Chapter 27](#), “Vector Approach for Kinematic and Dynamic Analysis of Complex Gear Systems,” deals with a vector approach to kinematic and dynamic analysis of complex gear systems. Possible kinds of images for a rotating gear, along with vector diagrams for complex gear systems, are covered in this discussion. Features of vector diagrams for complex gear systems with intersected-axes and crossed-axes gear pairs are disclosed. The elementary vector diagrams for intersected-axes gear pairs and crossed-axes gear pairs are discussed in particular.

In [Chapter 28](#), “Gear Ratio of a Multistage Gear Drive,” discussion begins with the consideration of the principal kinematic relationships in a multistage gear drive. The range ratio of speed variation for gear drives and the characteristics of transmission groups are covered in this discussion. Further, an analytical method for determining transmission ratios is disclosed. The rotational speed chart, broken geometrical series, and minimum required number of gear pairs are discussed. The chapter ends with the determination of the tooth number of gears of group transmissions.

In [Chapter 29](#), “Accuracy of Gear Teeth,” a few novel methods for inspection of gears are briefly discussed. A perfect datum surface is used in each of the considered methods of gear inspection. These make the methods of gear inspection more accurate and more reliable.

There are many sources of vibration generation and excessive noise excitation in a real gear pair. Most of them are analyzed in [Chapter 30](#), “Gear Noise and Vibration.” Kinematical and geometrical factors that affect noise

excitation are briefly discussed. Some physical factors, like a variation of the loading in a gear pair, that allow for a kinematical/geometrical interpretation are also outlined there.

Finally, design peculiarities of perfect and almost perfect gears are discussed in [Chapter 31](#), “Design Peculiarities of Perfect and Almost Perfect Gears.” Features of the design of gears for  $R$ -gearing, as well as for  $R_{sp}$ -gearing, are considered as examples.

There are several appendices in the monograph. All of them are listed immediately below:

Appendix A: Elements of Vector Calculus

Appendix B: Elements of Differential Geometry of Surfaces

Appendix C: Change of Surface Parameters

Appendix D: Applied Coordinate Systems and Linear Transformations

Appendix E: Contact Geometry of Gear and Mating Pinion Tooth Flanks

Appendix F: Closest Distance of Approach between Gear and Mating Pinion Tooth Flanks

Appendix G: Engineering Formulae for the Specification of Gear Tooth Flanks

Appendix H: On the Inadequacy of the Terms *Wildhaber-Novikov Gearing* and *W-N Gearing*

The provided list of titles of the appendices makes clear what the appendices deal with.

The book ends with the conclusion. Here, principal accomplishments are systematically outlined.

This book, which starts with the basics and steadily moves toward an advanced scientific theory of gearing, may help both to refute ill-informed and prejudiced views on the topic, which sometimes even verge on ridicule, and to broaden interest in the science of mechanisms so that its place in our educational institutions and mechanical engineering practice is better recognized.

Much as I wish otherwise, I can hardly hope that this book is entirely free of omissions or mistakes or that it is as clear and unambiguous as it should be. If you have any constructive suggestions, please communicate them to me via e-mail: [radzevich@hotmail.com](mailto:radzevich@hotmail.com).

**Stephen P. Radzevich**  
*Sterling Heights, Michigan*  
*November 24, 2017*

## *A Brief Overview of the Evolution of the Scientific Theory of Gearing\**

Gears are the means by which power is transferred from source to application. Gearing and geared transmissions drive the machines of modern industry. Gears move the wheels and propellers that transport us over the sea, on the land, and in the air. A sizeable section of industry and commerce in today's world depends on gearing for its economy, production, and livelihood.

The art and science of gearing have their roots before the Common Era. Yet many engineers and researchers continue to delve into the areas where improvements are necessary, seeking to quantify, establish, and codify methods to make gears meet the ever-widening needs of advancing technology. It should be stressed here that the scientific theory of gearing is a foundation of design, production, and application of perfect gears and geared mechanisms.

It should be realized here that there are two different considerations when state-of-the-art gearing is discussed. Gear designs and gear manufacture, both based on the common sense of smart handicrafts, constitute one of them. An engineering approach that is based on scientific accomplishments in the theory of gearing is the other one.

Even though gears and gear transmissions have been investigated for a long time, current knowledge of gear theory is poor and completely insufficient. Not much has been contributed to the theory of gearing since the time of *Leonhard Euler* (the middle of the 18th century), who is recognized as the founder of the scientific theory of gearing.

Taking into account the incompleteness and inconsistency of current knowledge in the theory of gearing, an in-depth investigation into gear kinematics and gear geometry has been undertaken by the author. Most of the results of the research that has been carried out are discussed in this monograph. The fundamentals of the scientific theory of gearing are based on key accomplishments in gear kinematics and gear geometry. With that said, it makes sense to begin the discussion with a brief overview of the evolution of the scientific theory of gearing. This will help us to identify what has already been done in the field so far, where we are now, and what to do in the future.

Such an analysis needs to be carried out to credit the right gear researcher with the right accomplishments in the scientific theory of gearing.<sup>†</sup> Unfortunately, in the meantime, numerous achievements in the field of gearing cannot be attributed to the right gear researcher. A gear researcher who has contributed significantly to the theory of gearing deserves to be credited with a corresponding scientific result.

Several achievements in the theory of gearing cannot be credited to the right person. The names of the contributors are missing for: (a) the condition of contact of the tooth flanks,  $\mathcal{G}$  and  $\mathcal{P}$  (may be this accomplishment is not exactly from gearing but from another area of the theory of machines and mechanisms), (b) equal base pitches, and (c) a few more achievements to be mentioned. It is vital to identify these names.

These and other accomplishments are vital to the scientific theory of gearing. It is important to know who was the first to come up with these meaningful results, as well as in what way these results have been accomplished.

The main goal of this chapter, "A Brief Overview of the Evolution of the Scientific Theory of Gearing," is to briefly outline *all* known fundamental accomplishments in the scientific theory of gearing and to credit the right gear researchers with the corresponding scientific achievements in the field; that is, an effort is undertaken in order to associate each of the fundamental accomplishments in the scientific theory of gearing with the name

\* This section of the book is written in the following manner. At the beginning, a brief overview of the pre-Eulerian period of gear art is given. Then, the fundamental accomplishments in the *scientific* theory of gearing are identified, and the name of a corresponding key contributor(s) is associated with each of the accomplishments. As the overall number of *fundamental* accomplishments in the field of the theory of gearing is limited and is not large, the overall number of the founders of the *scientific* theory of gearing is also limited. Though many other researchers (not mentioned in this section of the book) have contributed a lot to the field of gearing, not many of them can be regarded as the *founders* of the *scientific* theory of gearing.

<sup>†</sup> "The beginning of wisdom is to call things by their right names"—a Chinese proverb.



of the corresponding gear researcher who contributed that particular accomplishment. In order to mention all the key researchers in the field and miss none of them, the following approach is adopted.

First, all (with no exclusions) the fundamental accomplishments in the scientific theory of gearing are listed in chronological order.

Second, the right gear researcher's name is assigned to each of the accomplishments; that is, the name of the researcher who was the first to discover or who contributed the most to a particular accomplishment in the scientific theory of gearing. For example, Leonhard Euler (and no other) is credited with the application of the involute of a circle for the gear tooth profile, as he was the first to prove that the involute tooth profile best fits the needs of gear tooth geometry, regardless of the involute of a circle being known\* long before Euler made his discovery in 1760.

In addition to that, a few huge mistakes committed by gear researchers when investigating gears are also mentioned in order to better understand the theory and properly value those scientists who contributed much to the scientific theory of gearing. Mistakes of this type can be referred to as the *key mistakes* in the theory of gearing. Following such an approach, it is helpful to separate the names of the principal contributors to the scientific theory of gearing from those who contributed less to the subject, and, moreover, from those who committed mistakes that significantly affected the evolution of the theory of gearing.

In this section of the book, a brief overview of the evolution of the scientific theory of gearing is presented. The results of the research carried out by the author, and a few papers earlier published by the author [96,122,104] are widely used in this section of the book. Other sources are extensively used as well [16,165]. The consideration begins with ancient gear designs that were created only due to common sense and ends with the modern scientific theory of gearing.

Many sources were previously investigated to make possible the representation of the principal accomplishments in the scientific theory of gearing in chronological order. A limited number of sources were selected for more detailed analysis. These sources are summarized in Table 1.1. The reported analysis is based mostly on the results of the research listed in Table 1.1.

---

## 1.1 Preliminary Remarks

Gears are used to transmit and transform a rotation from an input shaft to an output shaft. Depending on a particular application, gearings have to meet certain additional requirements, that is, high accuracy of the transmission of rotation, high power density,<sup>†</sup> and so forth.

Practical men were able by various empirical means to get gears adequate for their needs, at least until the early 19th century, when the mathematicians' work was translated into practical language. Purely empirical solutions for the form of gear teeth can only be accounted for by the fact that gears operated at *low speeds* and under *small loads*.

The development and investigation of gearings with a constant angular velocity ratio<sup>‡</sup> (that is, gearings for which the equality  $\omega_p/\omega_g = \text{const}$  is valid) is one of the main goals of the scientific theory of gearing [137]. Gearings with a constant angular velocity ratio (or gearings with a prespecified function of the angular velocity ratio) are commonly called *perfect gearings*, *geometrically accurate gearings*, or just *ideal gearings* for simplicity. More generally, the design of gearings with a prescribed function of the angular velocity ratio [that is, (a) noncircular gearings with a constant center distance, (b) noncircular gearings with a variable center distance, (c) gearings with a variable shaft angle, and (d) gearings with a variable center distance and a variable shaft angle simultaneously] is also covered by the scientific theory of gearing.

Many efforts were undertaken in the past by hundreds of researchers aiming at the development of a *theory of gearing*. However, not many of them have really contributed to the theory.

Below, in this section of the book, the evolution of gearing from the earliest times to the present day is concisely discussed, with an emphasis on the theory of gearing. The consideration is mainly focused on the kinematics of gear pairs and the geometry of the interacting tooth surfaces, as well as on some other kinematic and

---

\* The involute of a circle was first proposed by *Philippe de la Hire* in 1696, and it was later in the 18th century when Leonhard Euler proposed the involute curve as a viable tooth profile.

<sup>†</sup> The term *power density* is commonly used as an equivalent to the term *power-to-weight ratio*.

<sup>‡</sup> In more general sense, that is, when noncircular gears are taken into account, use of perfect gearings makes possible an exact function of the prespecified angular velocity ratio.

TABLE 1.1

Main Contributions to the Theory of Gearing

No.	Year	Name of the Key Contributor	Source of Information
1.	1493	da Vinci, Leonardo	da Vinci, Leonardo, <i>The Madrid Codices</i> , Volume 1, 1493, Facsimile Edition of "Codex Madrid 1", original Spanish title: <i>Tratado de Estatica y Mechanica en Italiano</i> , McGraw Hill Book Company, 1974.
2.	1754	Euler, L.	Euler, L., <i>De Optissima Figura Rotatum Dentibus Tribuenda. Supplementum de Figura Dentium Rotatum, Novi Commentarii Academiæ Petropolitanae</i> , 1754/55, 1765.
3.	1841	Willis, R.	Willis, R., <i>Principles of Mechanisms, Designed for the Use of Students in the Universities and for Engineering Students Generally</i> , London, John W. Parker, West Stand, Cambridge: J. & J.J. Deighton, 1841, 446 p. Willis, R., "On the Teeth of Wheels", <i>Trans. Civ. Eng.</i> , Vol. II, 1838.
4.	1842	Olivier, T.	Olivier, T., <i>Théorie Géométrique des Engrenages destinés</i> , Bachelier, Paris 1842, 132 p. [In French].
5.	1861	Reuleaux, F.	Reuleaux, F., <i>The Constructor, a Hand-Book of Machine Design by F. Reuleaux</i> , Authorized translation, complete and unabridged from the 4 <sup>th</sup> enl. German ed. By Henry Harrison Supplee. Philadelphia, H.H. Suplee, 1893, 312 p. [First German edition published in 1861 with title: <i>Der Constructeur. Ein Handbuch zum Gebrauch beim Maschinen-Entwerfen</i> ].
6.	1863	Gibbs, J.W.	Gibbs, J.W., <i>On the Form of the Teeth of Wheels in Spur Gearing</i> , Doctoral Dissertation, Yale University, New Haven, Conn., 1863.
7.	1886	Gochman, H.I.	Gochman, H.I., <i>Theory of Gearing Generalized and Developed Analytically</i> , Odessa, 1886, 229 p. [In Russian].
8.	1887	Grant, G.B.	U.S. Pat. No. 407.437. <i>Machine for Planing Gear Teeth.</i> / G.B. Grant, Filed: January 14, 1887 (serial No. 224,382), Patent issued: July 23, 1889. Grant, G.B., <i>A Treatise on Gear Wheels</i> , 11th Ed., Philadelphia Gear Works, Inc., Philadelphia, 1906, 105 p.
9.	1912	Flanders, R.E.	Flanders, R.E., <i>Bevel Gearing</i> , 4th Ed., Machinery's Reference Series, Number 37, The Industrial Press, 1912, 48 p.
10.	1917	Oberg, E.	Oberg, E., <i>Spur and Bevel Gearing</i> , The Industrial Press, New York, 1917, 274 p.
11.	1935	Dicker, Ya.I.	Dicker, Ya.I., <i>Involute Gearing</i> , Orgametal, Moscow, 1935, 220 p. [In Russian]. Dicker, Ya.I., <i>Internal Gearing: Spur and Helical</i> , Moscow, Orgametal, 1938, 138 pages. [In Russian].
12.	1936	Cormac, P.	Cormac, P., <i>A Treatise on Screws and Worm Gear, Their Mills and Hobs</i> , London, Chapman & Hall, Ltd., 1936, 138p.
13.	1948	Frifeldt, I.A.	Frifeldt, I.A., <i>Continuously Indexing Cutting Tools</i> , Moscow, Mashgiz, 1948, 252 pages. [In Russian].
14.	1948	Shishkov, V.A.	Shishkov, V.A., "Elements of Kinematics of Generating and Conjugating in Gearing", in: <i>Theory and Calculation of Gears</i> , Vol. 6, Leningrad: LONITOMASH, 1948. [In Russian]. Shishkov, V.A., <i>Generation of Surfaces in Continuously Indexing Methods of Machining</i> , Moscow, Mashgiz, 1951, 152 pages. [In Russian].
15.	1948	Wildhaber, E.	Wildhaber, E., <i>Foundations of Meshing of Bevel and Hypoid Gearings</i> , Translated and comments by A.V. Slepak, Moscow, Mashgiz, 1948, 176 pages. [In Russian].—This book is not available in other languages.
16.	1948	Fraifeld, I.A.	Fraifeld, I.A., <i>Cutting Tools that Work on Generating Principle</i> , Moscow, Mashgiz, 1948, 252 pages.
17.	1949	Kolchin, N.I.	Kolchin, N.I., <i>Analytical Calculation of Planar and Spatial Gearings</i> , Moscow-Leningrad, Mashgiz, 1949, 210 pages. [In Russian].
18.	1949	Buckingham, E.	Buckingham, E., <i>Analytical Mechanics of Gears</i> , Dover Publications, Inc., New York, 1988, 546p. (The 1 <sup>st</sup> print - 1949).
19.	1950	Davidov, Ya.S.	Davidov, Ya.S., <i>Non-Involute Gearing</i> , Moscow, Mashgiz, 1950, 179 pages. [In Russian].
20.	1953	Nikolayev, A.F.	Nikolayev, A.F., <i>Kinematical Foundations of the Theory of Spatial Gearing</i> , Doctoral Thesis, Moscow, STANKIN, 1953. [In Russian].
21.	1955	Novikov, M.L.	Novikov, M.L., <i>Fundamental Issues of Geometrical Theory of Point Gear Meshing for Application in Powerful Gear Transmissions</i> , Doctoral Thesis, Moscow, Zhukovsky Air Force Engineering Academy, 1955. [In Russian].

(Continued)

TABLE 1.1 (Continued)

Main Contributions to the Theory of Gearing

No.	Year	Name of the Key Contributor	Source of Information
			Novikov, M.L., <i>Gearing and Cam Mechanisms with Point System of Meshing</i> , Pat. No. 10913 (USSR), Cl. 47, 6. Filed: April 19, 1956. [In Russian].
			Novikov, M.L., <i>Gearing with New Type of Meshing</i> , Moscow, Zhukovsky Air Force Engineering Academy, 1958, 186 pages. [In Russian].
22.	1959	Kudr'avtsev, V.N.	Kudr'avtsev, V.N., <i>Calculation and Design of Novikov Gearing</i> , Leningrad, Military Aviation Academy, 1959, 78 pages. [In Russian].
23.	1960	Litvin, F.L.	Litvin, F.L., <i>Non-Circular Gears</i> , 2nd edition, Moscow-Leningrad, Mashgiz, 1956, 311 pages. [In Russian]. (1st edition: 1950, 218 pages). [In Russian]. Litvin, F.L., <i>Theory of Gearing</i> , 2nd edition, Moscow, Nauka, 1968, 584 pages. (1st edition: 1960). [In Russian]. Litvin, F.L., <i>Theory of Gearing</i> , NASA Reference Publication 1212, AVSCOM Technical Report, 88-C-035, 1989, 470 p. Litvin, F.L., <i>Gear Geometry and Applied Theory</i> , Prentice Hall, Englewood Cliffs, NJ, 1994, 724 p. Litvin, F.L., Fuentes, A., <i>Gear Geometry and Applied Theory</i> , 2nd Edition, Cambridge University Press, Cambridge, UK, 2004, 800 p.
24.	1961	Saari, O.E.	Saari, O.E., <i>Analytical Theory of Gear Tooth Surfaces</i> , Illinois Institute of Technology, 1961, 114 p.
25.	1961	Baxter, M.L., Jr.	Baxter, M.L., Jr., "Basic Geometry and Tooth Contact of Hypoid Gears", <i>Industrial Mathematic</i> , Vol. 11, No. 2, pp. 19–42, 1961. Baxter, Meriwether L. Jr., "Basic Theory of Gear-Tooth Action and Generation". This is the opening chapter of <i>Gear Handbook</i> , 1st Ed., Editor Darle Dudley, McGraw Hill, New York 1962.
26.	1964	Korostel'ev, L.V.	Korostel'ev, L.V., <i>Geometrical and Kinematical Indicators of Bearing Capacity of Spatial Gearing</i> , Doctoral Thesis, Moscow, Stankin, 1964, 48 p. [In Russian].
27.	1968	Dus'ev, I.I. and Vasilyev, V.M.	Dus'ev, I.I. and Vasilyev, V.M., <i>Analytical Theory of Spatial Gearing and its Implementation to Hypoid Gearing</i> , Rostov-on-Don, Book Publishers, 1968, 148 p. [In Russian]. Dus'ev, I.I., <i>Analytical Theory of Spatial Gearing and its Implementation to Hypoid Gearing</i> , Rostov-on-Don, Doctoral Thesis, Novocherkassk, Novocherkassk Polytechnic Institute, 1970. [In Russian].
28.	1968	Lashn'ev, S.I.	Lashn'ev, S.I., <i>Fundamentals of the Theory of Surface Generation by Means of Disk-Type, Rack-Type and Worm-Type Cutting Tools</i> , Doctoral Thesis, Tula, Tula Polytechnic Institute, 1968, 268 pages. [In Russian]. Lashn'ev, S.I., <i>Generation of Gear Tooth Flanks by Means of Rack-Type and Worm-Type Cutting Tools</i> , Moscow, Mashinostroyeniye, 1971, 216 p. [In Russian].
29.	1969	Gavrilenko, V.A.	Gavrilenko, V.A., <i>Fundamentals of Theory of Involute Gearing</i> , Moscow, Mashinostroyeniye, 1969, 432 p. [In Russian].
30.	1969	Chasovnikov, L.D.	Chasovnikov, L.D., <i>Gearing</i> , Moscow, Mashinostroyeniye, 1969, 486 p. [In Russian].
31.	1969	Dyson, A.	Dyson, A., <i>A General Theory of the Kinematics and Geometry of Gears in Three Dimensions</i> , Clarendon Press, Oxford, 1969, 141 p.
32.	1969	Timofeyev, B.P.	Timofeyev, B.P., <i>Synthesis and Analysis of Spiral Bevel Gearing</i> , Doctoral Thesis, Leningrad, Leningrad Polytechnic Institute, 1969. [In Russian].
33.	1971	Merritt, H.E.	Merritt, H.E., <i>Gear Engineering</i> , Putman Publishing, London, New York, Toronto, 1971, 489 p.
34.	1972	Yerikhov, M.L.	Yerichov, M.L., <i>Principles of Systematization, Methods of Analysis, and Problems of Synthesis of Schematics of Gearing</i> , Doctoral Thesis, Khabarovsk, Khabarovsk Polytechnic Institute, 1972, 373 pages. [In Russian].
35.	1972	Pismanik, K.M.	Pismanik, K.M., <i>Theoretical Foundations of Tooth Flank Generation in Bevel and Hypoid Gearing</i> , Doctoral Thesis, Saratov, Saratov Polytechnic Institute, 1972, 408 p. [In Russian]. Pismanik, K.M., <i>Hypoid Gearing</i> , Moscow, Mashinostroyeniye, 1964, 27 p. [In Russian].
36.	1974	Sakharov, G.N.	Sakharov, G.N., <i>Theoretical Issues of Continuously Indexing Cutting Tools</i> , Doctoral Thesis, Moscow, STANKIN, 1974, 320 p. [In Russian]. Sakharov, G.N., <i>Continuously Indexing Cutting Tools</i> , Moscow, Mashinostroyeniye, 1983, 232 p. [In Russian].

(Continued)

TABLE 1.1 (Continued)

Main Contributions to the Theory of Gearing

No.	Year	Name of the Key Contributor	Source of Information
37.	1976	Gul'ayev, K.I.	Gul'ayev, K.I., <i>Theoretical Foundations of Synthesis and Finishing of Bevel Gearing</i> , Doctoral Thesis, Leningrad, 1976. [In Russian].
38.	1977	Lopato, G.A., Segal', M.G.	Lopato, G.A., Kabatov, N.F., Segal', M.G., <i>Spiral Bevel and Hypoid Gearing</i> , 2 <sup>nd</sup> Ed., Moscow, Mashinostroyeniye, 1977, 423 p. [In Russian].
39.	1978	Shtipelman, B.A.	Shtipelman, B.A., <i>Design and Manufacture of Hypoid Gears</i> , John Wiley & Sons, New York, 1978, 394 p.
40.	1979	Henriot, G.	Henriot, G., <i>Traité Théorique et Pratique des Engrenages: Théorie et Technologie</i> , Vol. 1, 6th Ed., Bordas, Paris, 1979, 662 p.
41.	1980	Schulz, V.V.	Schulz, V.V., <i>Geometrical Optimization of Worn Kinematical Pairs</i> , Doctoral Thesis, Kiev, 1980, 32 p. [In Russian].
42.	1985	Goldfarb, V.I.	Goldfarb, V.I., <i>Fundamentals of the Theory of Automated Geometrical Analysis and Synthesis of Generalized Type of Worm Gearing</i> , Doctoral Thesis, Izhevsk, Izhevsk Mechanical Institute, 1985, 432 p. [In Russian].
43.	1987	Colbourne, J. R.	Colbourne, J.R., <i>The Geometry of Involute Gears</i> , New York, Springer-Verlag, 1987, 532 p.
44.	1989	Sizrantsev, V.N.	Sizrantsev, V.N., <i>Synthesis of Cylindrical Gearing with Localized Contact</i> , Doctoral Thesis, Kurgan, Kurgan Polytechnic Institute, 1989, 428 p. [In Russian].
45.	1989	Xuezhu Dong	Dong, X., <i>Theoretical Foundation of Gear Meshing</i> , China Machine Press, Beijing, 1989. [In Chinese]. Dong, X., <i>Design and Modification of Hourglass Worm Drives</i> , China Machine Press, Beijing, 2004. [In Chinese].
46.	1992	Wu, D.R. and Luo, J.S.	Wu, D.R., Luo, J.S., <i>A Geometric Theory of Conjugate Tooth Surfaces</i> , World Scientific Publishing, River Edge, NJ, 1992, 192 p.
47.	1994	Shishov, V.P.	Shishov, V.P., <i>Theory, Mathematical Foundations, and Synthesis of High Power Density Gearing for Industrial Transportation</i> , Doctoral Thesis, East Ukrainian State University, Lugansk, 1994, 580 p. [In Russian].
48.	1994	Wang, X.C.	Wang, X.C., Ghosh, S.K., <i>Advanced Theories of Hypoid Gears</i> , Studies in Applied Mechanics, Vol. 36, Elsevier, Amsterdam, 1994, 341 p.
49.	1995	Vulgakov, E.B.	Vulgakov, E.B., <i>Theory of Involute Gearing</i> , Moscow, Mashinostroyeniye, 1995, 320 p. [In Russian].
50.	1995	Dooner, D.B.	Dooner, D.B., <i>Kinematic Geometry of Gearing</i> , 2nd Ed., John Wiley & Sons, Inc., New York, 2012, 512 p. (Dooner, D.B., Seireg, A.A., <i>The Kinematic Geometry of Gearing. A Concurrent Engineering Approach</i> , 1st Ed., John Wiley & Sons, Inc., NY, 1995, 450 p.).
51.	1999	Sheveleva, G.I.	Sheveleva, G.I., <i>Theory of Surface Generation and of Contact of Moving Bodies</i> , Moscow, STANKIN, 1999, 494 p. [In Russian].
52.	1999	Silich, A.A.	Silich, A.A., <i>Development of Geometrical Theory of Novikov Gearing and Generation of their Tooth Flanks</i> , Doctoral Thesis, Kurgan, Kurgan Polytechnic Institute, 1999, 534 pages. [In Russian].
53.	2000	Dudas, I.	Dudas, I., <i>The Theory and Practice of Worm Gear Drives</i> , London, Penton Press, 2000, 314 p.
54.	2003	Phillips, J.	Phillips, J., <i>General Spatial Involute Gearing</i> , Springer, Berlin Heidelberg, 2003, 498 p.
55.	2005	Pavlov, A.I.	Pavlov, A.I., <i>Modern Theory of Gearing</i> , Kharkov, Kharkov National Automotive State University, 2005, 100 p. [In Russian]. Pavlov, A.I., <i>Synthesis of High Loaded Gearing on the Basis of Linear Gear Meshes with Convex-to-Concave Contact of Tooth Flanks</i> , Doctoral Thesis, East Ukrainian State University, Lugansk, 2009, 42 p. [In Russian].
56.	2007	Krenzer, T.	Krenzer, T., <i>The Bevel Gear</i> , Published October 1, 2007, 252 p.
57.	2008	Radzevich, S.P.	Radzevich, S.P., <i>Theory of Gearing: Kinematics, Geometry, and Synthesis</i> , CRC Press, Boca Raton, Florida, 2012, 743 p. Radzevich, S.P., <i>Gear Cutting Tools: Fundamentals of Design and Computation</i> , Boca Raton Florida, 2010, 754 p. Radzevich, S.P., <i>Geometry of Surfaces: A Practical Guide for Mechanical Engineers</i> , Wiley, 2013, 264 p.

(Continued)

TABLE 1.1 (Continued)

Main Contributions to the Theory of Gearing

No.	Year	Name of the Key Contributor	Source of Information
			Radzevich, S.P., <i>Generation of Surfaces: Kinematic Geometry of Surface Machining</i> , CRC Press, Boca Raton, Florida, 2014, 738 p.
			Radzevich, S.P., <i>High-Conformal Gearing: Kinematics and Geometry</i> , CRC Press, Boca Raton, Florida, 2015, 368 p.
			Radzevich, S.P., <i>Fundamentals of Surface Generation, Monograph</i> , Kiev, Rastan, 2001, 592 p. (In Russian).
			Radzevich, S.P., <i>Differential-Geometric Method of Surface Generation</i> , Dr. Sci. Thesis, Tula, Tula Polytechnic Institute, 1991, 300 pages.
58.	2009	Xuntang, W.	Xuntang, W., <i>Principle of Gearing</i> , Xi'an Jiaotong University, Xi'an, 2009. [In Chinese].
59.	2011	Tsukanov, O.N.	Tsukanov, O.N., <i>Fundamentals of Synthesis of Non-Involute Gearing in Generalized Parameters</i> , Chel'abinsk, South-Ural State University Publishers, 2011, 140 p. [In Russian].
60.	2013	Stadtfeld, H.J.	Stadtfeld, H.J., <i>Gleason Kegelradtechnologie: Ingenieurwissenschaftliche Grundlagen und modernste Herstellungsverfahren für Winkelgetriebe</i> , Renningen, Expert-Verlag, 2013, 491 p.
			Stadtfeld, H.J., <i>Gleason Bevel Gear Technology: The Science of Gear Engineering and Modern Manufacturing Methods for Angular Transmissions</i> , The GLEASON Works, Rochester, New York, 2014, 491 p.

geometric aspects of gears and gearing pairs.\* The following rule is adopted in this section of the book: the principal contributions to the scientific theory of gearing are identified. Then, the names of the scientists who contributed these accomplishments are given. Following this rule, not many scientists are credited with fundamental accomplishments in the field of gearing—only those who were the first to discover a fundamental result in the research in the field.

## 1.2 Earliest Designs of Gears

The earliest account of gears comes from ancient Chinese and Greek literature. Because of the force-multiplying properties of gears, early engineers used them for hoisting heavy loads such as building materials. The mechanical advantage of gears was also used for ship anchor hoists and catapult pretensioning.

At the beginning, transmittal and transformation of a rotation was the main purpose of gearing. The quality of rotation of the output shaft, that is, smoothness of its rotation, was not of importance in the earliest designs of gears. As a result, the gear tooth profile geometry was not considered at all, and pin gears successfully met all the requirements of that time.

The earliest written descriptions of gears are said to have been made by *Aristotle* [16] in the fourth century BC. It has been pointed out that the passage attributed by some to Aristotle, in *Mechanical Problems of Aristotle* (ca. 280 BC), was actually from the writings of his school. In the passage in question, there was no mention of gear teeth on the parallel wheels, and they may just as well have been smooth wheels in frictional contact. Therefore, the attribution of gearing to Aristotle is most likely incorrect. The real beginning of gearing was *probably* with *Archimedes*, who in about 250 BC invented the endless screw turning a toothed wheel, which was used in engines of war. Archimedes also used gears to simulate astronomical ratios. Early forms of the wagon mileage indicator (odometer) and the surveying instrument were *Archimedian*. These devices were *probably* based on thought experiments of *Heron of Alexandria* (ca. 60 AD), who wrote on theoretical mechanics and the basic elements of mechanisms.

Judging from the history books is one thing. Finding hard evidence of actual gears is another. The biggest problem in finding archeological evidence of gears is that early gear materials were not built to last. Gears made during the classical period were probably made of bronze. When bronze tools and mechanical pieces broke, they were simply melted down and refashioned into something else.

\* The evolution of geared mechanisms is out of the scope of this book.

The oldest surviving relic containing gears is the Antikythera\* mechanism, named for the Greek island near which the mechanism was discovered in a sunken ship in 1900. The mechanism is not only the earliest relic of gearing but is also an extremely complex arrangement of epicyclic differential gearing. The mechanism is identified as a calendrical sun and moon computing mechanism and is dated to about 87 BC.

So far,<sup>†</sup> the Antikythera mechanism (Figure 1.1) is the oldest artifact known to consist of gears. An image of the original Antikythera mechanism is shown in Figure 1.1a. Figure 1.1b illustrates the Antikythera mechanism overlapping with the image of its replica. The device has more than 30 gears, although some scientists suggested as many as 72 gears, with teeth formed through equilateral triangles.

Early gears were made of wood with cylindrical pegs for cogs and were often lubricated with animal-fat grease. An example of an old stile gear made of wood is depicted in Figure 1.2. Gears were also used in wind and water wheel machinery for decreasing or increasing the provided rotational speed for application to pumps and other powered machines. An early gear arrangement was used to power textile machinery. The rotational speed of a water or horse-drawn wheel was typically too slow to use, so a set of wooden gears needed to be used to increase the speed to a usable level.

In gearings of old designs (Figures 1.1 and 1.2, and others), no special care was taken on the geometry of the interacting tooth surfaces of the gears. Practical men were able by various empirical means to get gears adequate for their needs, at least until the early 19th century, when mathematicians' work was translated into practical language. Purely empirical solutions for the form of gear teeth can only be accounted for by the fact that gears operated at low speeds and under small loads. No theory of gearing was necessary to design old stile gears, as the rotations were low and there were no constraints on power density of the gearing. Common sense was the only tool used by the smart ancient craftsmen when designing and manufacturing gears.

Accomplishments in the field of gearing and gear art since the earliest times are briefly summarized immediately below:

- Various primitive designs of wooden gears were developed with the purpose to transmit a rotation between two shafts.
- Gears that operate (a) on parallel shafts—that is, parallel-axes gearing; (b) on intersected shafts—that is, intersected-axes gearing; and (c) on crossed shafts—that is, crossed-axes gearing, are known.

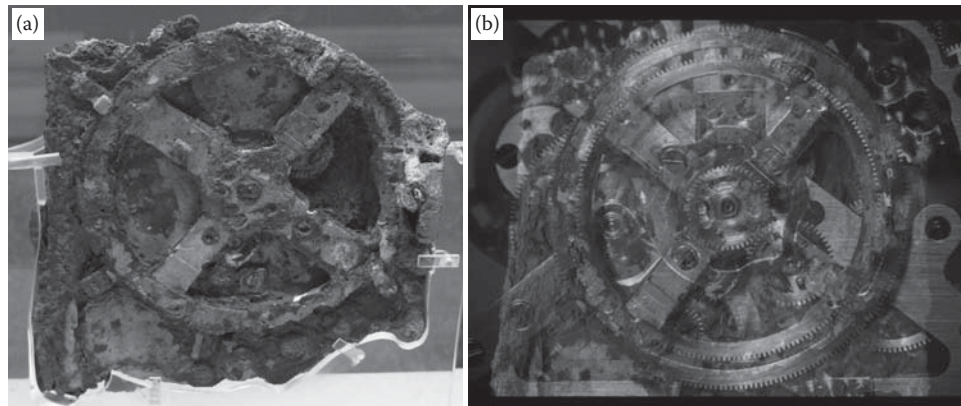


**FIGURE 1.1**

The Antikythera mechanism (100 BC–205 BC).

\* The artifact was recovered in 1900–1901 from the Antikythera shipwreck off the Greek island of Antikythera. Its significance and complexity were not understood until decades later. Believed to have been designed and constructed by Greek scientists, the instrument has been dated either between 150 and 100 BC, or, according to a more recent view, at 205 BC. The complexity grade of this precious example of antique genius was so high that artifacts of a similar complexity and workmanship did not reappear for a millennium and a half, when mechanical astronomical clocks were built in Europe.

<sup>†</sup> The earliest known reference to a gear was around 50 AD in *Hero of Alexandria*, though the *Book of Song* suggests that the south-pointing chariots may have employed differential gears as early as the reign of the Zhou Dynasty (1045–256 BC) of China (Radzevich, S.P., *Dudley's Handbook of Practical Gear Design and Manufacture*, 3rd ed., Boca Raton, FL: CRC Press, 2016, 629 pages.). However, no artifact of a south-pointing chariot has been discovered so far. Today, only designed replicas are known. Therefore, in the meantime, the south-pointing chariot can not be considered a relic of a mechanism with gears.





**FIGURE 1.2**  
Old-style gears made out of wood.

- All the gearings operate at low rotations and transmit a low torque.
- No tooth flank geometry was taken into account, primarily because of the absence of the necessity of doing so: low-power-density wooden gears that operate at low rotations met the current customer requirements of that time.

Old stile gearings are far from capable of being referred to as perfect gearings, as they are not capable of transmitting a rotation smoothly. Geometrically inaccurate gears (those that feature a variable angular velocity ratio) are still used even in the current industry in cases where the rotations are low and the transmitted power is low as well.

---

### 1.3 Pre-Eulerian Period of Gear Art

The art of gearing was carried through the European Dark Ages, appearing in Islamic instruments such as the geared astrolabes that were used to calculate the positions of the celestial bodies. Perhaps the art was relearned by the clock- and instrument-making artisans of 14th-century Europe, or perhaps some crystallizing ideas and mechanisms were imported from the East after the Crusades of the 11th through 13th centuries.

It appears that an English abbot of St. Alban's monastery, born *Richard of Wallingford* in 1330 AD, reinvented the epicyclic gearing concept. He applied it to an astronomical clock that he began to build and that was completed after his death.

A mechanical clock of a slightly later period was conceived by *Giovanni de Dondi* (1348–1364). Diagrams of this clock, which did not use differential gearing, appear in the sketchbooks of *Leonardo da Vinci*, who designed geared mechanisms himself [17]. Numerous designs of gearings are discussed in a famous book by Leonardo da Vinci [17]. In 1967, two of Leonardo da Vinci's manuscripts, lost in the National Library in Madrid since 1830,

were rediscovered [17]. One of the manuscripts, written between 1493 and 1497 and known as *Codex Madrid I* (Figure 1.3) [17], contains 382 pages with some 1600 sketches. Included among this display of da Vinci's artistic skill and engineering ability are his studies of gearing. Among these are tooth profile designs and gearing arrangements that were centuries ahead of their invention.

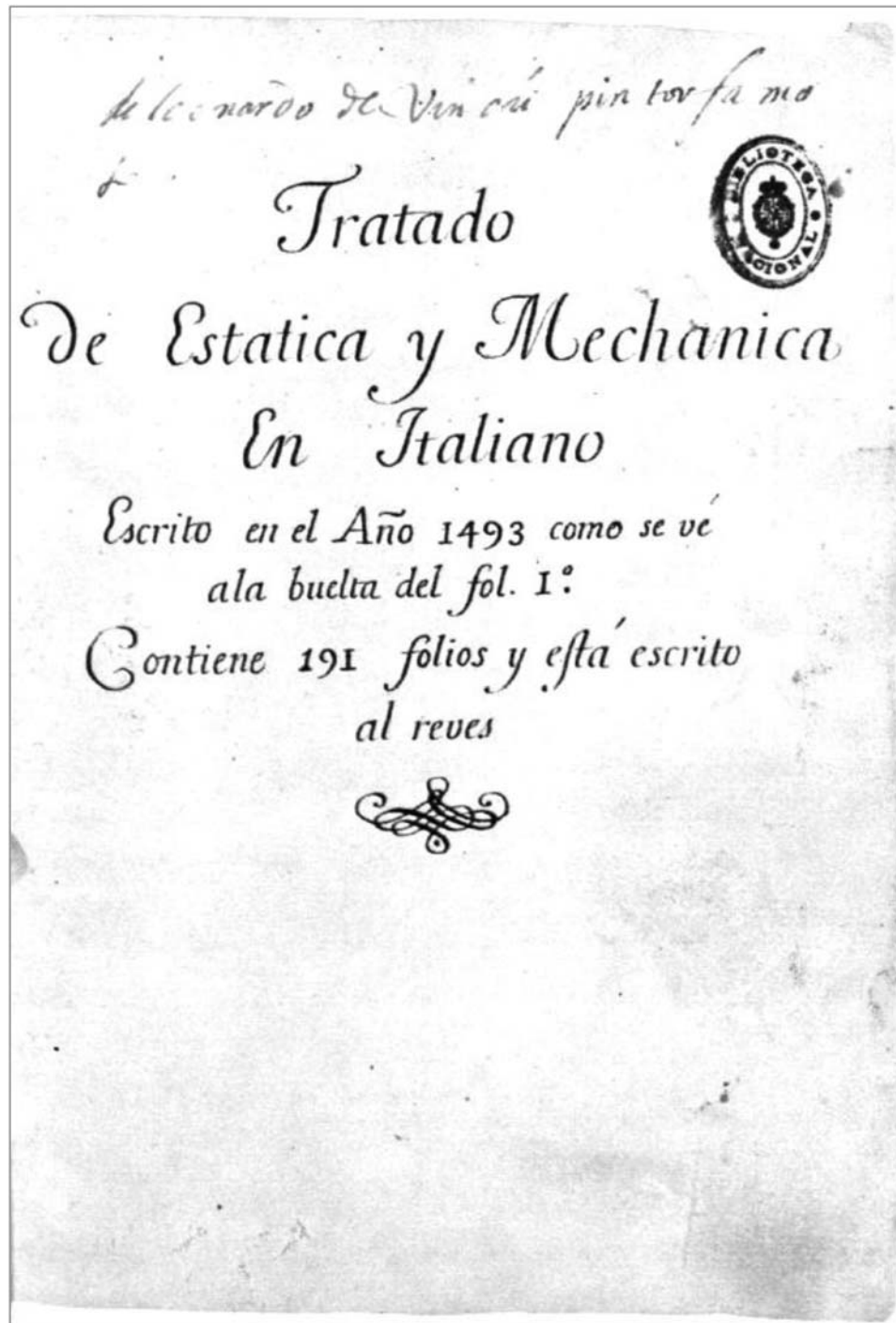


FIGURE 1.3

Title page of the book *The Madrid Codices* by Leonardo da Vinci, 1493. (From da Vinci, L., *The Madrid Codices*, Volume 1, 1493, Facsimile Edition of "Codex Madrid 1", original Spanish title: *Tratado de Estatica y Mechanica en Italiano*, McGraw Hill Book Company, 1974.)



For a long while, the most accurate gears were produced by clockmakers and instrument makers. Questions of exact tooth form, pressure angle, and strength did not enter into the designs of the clockmakers and instrument makers.

Contemporary gears for the uniform transmission of power and rotation are heavily based on the application of mathematical curves discovered by scientists in the 16th and 17th centuries in the design of tooth flanks. In the period 1450–1750, the mathematics of gear-tooth profiles and theories of geared mechanisms became established.

Albrecht Dürer\* is credited with discovering the epicycloidal shape (ca. 1525). The first record of the use of cyclic curves as the tooth profile of a gear is related to Girard Desargues† (Figure 1.4). Desargues's work on gearing is known mostly from the records made by his student Philippe de la Hire.‡ A treaty on epicycloids and their usage in mechanics is discussed in his book [18]. Philippe de la Hire (Figure 1.5) was the first to describe the use of epicycloids for gears that ensured (as he loosely meant) a uniform transmission of rotation. de la Hire considered the involute the best among exterior cycloids, since he recognized that it is the special case in which the generating circle's radius is infinite. He also noted that the involute tooth gives the teeth of the corresponding rack as having straight sides. It took 150 years before this principle found practical application.

The first mathematician to work the theory of gear teeth into a systematic and general theory of mechanism was Charles Etienne Louis Camus.§

Camus (Figure 1.6) was the first [12] who formulated the condition that, in his opinion, has to be fulfilled for a pair of gears to be capable of transmitting rotation smoothly. According to Camus, this condition can be formulated as follows:

*If, in a uniform rotation, power is to be transmitted via a pair of teeth, then the normal to the tooth flanks at the contact point (within the path of contact) must pass through the pitch point.*

Another formulation of that same condition by other researchers is represented in the form:

*If an auxiliary curve is rolling on the pitch circles of circular gears, any point attached to this curve traces conjugate profiles.*



**FIGURE 1.4**  
Girard Desargues (1591–1661).

\* Albrecht Dürer (May 21, 1471–6 April 6, 1528) was a German painter, printmaker, mathematician, engraver, and theorist.

† Girard Desargues (February 21, 1591–September 1661) was a French mathematician and engineer.

‡ Philippe de la Hire (March 18, 1640–April 21, 1718) was a French physicist, astronomer, mathematician, and engineer.

§ Charles Étienne Louis Camus (August 25, 1699–February 2, May 4, 1768) was a French mathematician and mechanician.



**FIGURE 1.5**  
Philippe de La Hire (1640–1718).

This sounds similar to the fundamental theorem of gearing known today (see below in the next section of the book). Camus's principle of gearing is illustrated with a 1733 schematic (Figure 1.7). In this schematic, the path of contact, that is, a curved line segment,  $KBC$ , and the line of action at different angular configurations of the mating gears, that is,  $BC$ ,  $MP$ , and  $RQ$ , do not align to one another.\* The schematic (Figure 1.7) reveals that Camus did not correctly understand the difference between the *path of contact* and between the *line of action*. Therefore, Camus was close to discovering the fundamental theorem of gearing, but did not succeed in doing that. As shown below in this book, for gears that operate on parallel shafts, the only feasible case is when both the path of contact and the line of action are straight lines that align with one another, as observed in involute gearing.

According to some authors, the fundamental theorem of gearing was also known to Leonhard Euler<sup>†</sup> and to Felix Savary.<sup>‡</sup> This statement needs to be verified for correctness and completeness.

Savary is also credited with the so-called *Euler-Savary equation*. A correlation between radii of curvature of the centrodes in a gear pair and the corresponding radii of curvature of the interacting tooth flanks is established by this equation. The Euler-Savary equation is considered in detail in Chapter 7 (see Section 7.1.5, and Figure 7.17).

Camus repeated much of de La Hire's work, although he added many important elements of his own. He gives a detailed analysis of the teeth desirable for the combination of a spur and lantern gear.

Camus did, however, correct de La Hire in that he recognized the fact of sliding of even the epicycloidal teeth, one upon the other, and said that this phenomenon is one of the principal sources of friction and wear in gearing.

The action of engaged teeth relative to the line of centers is discussed, and he points out that the action is best when engagement takes place after the working face of the driving tooth has passed the line of centers, that is, during the receding action.

\* It is instructive to note here that the schematic shown in Figure 1.7 is a kind of mistake because of the following reasons. First, the path of contact is an envelope to consecutive positions of the instant line of action. Therefore, it is not permissible that the line of action,  $BC$ , intersects the path of contact,  $KBC$ . The path of contact must be tangent to the line of action,  $BC$ . Second, when numerous instant lines of contact are through the pitch point,  $C$ , then no enveloping curve (i.e., no path of contact) can be constructed. A few more reasons for the infeasibility of the gearing shown in Figure 1.7 are to be mentioned.

† Leonhard Euler (April 15, 1707–September 18, 1783) was a pioneering Swiss mathematician and physicist.

‡ Felix Savary (October 4, 1797–July, 15, 1841) was a French mathematician and mechanician.



**FIGURE 1.6**  
Charles Camus (1699–1768).

Camus goes on to consider the problem of the minimum number of teeth and that of the proper form for the ends of the teeth. He deals with true bevel gears and uses the rolling-cone principle for their analysis. But he considers only the case of the interaction of a crown and bevel gear.

Camus does not consider the involute tooth at all. Although he analyzes trains of gears, he says nothing of the form of teeth required in a series of three or more gears. This can probably be accounted for by the fact that he had only clockwork in mind. The mills of this era seldom had trains of more than two gears engaged.

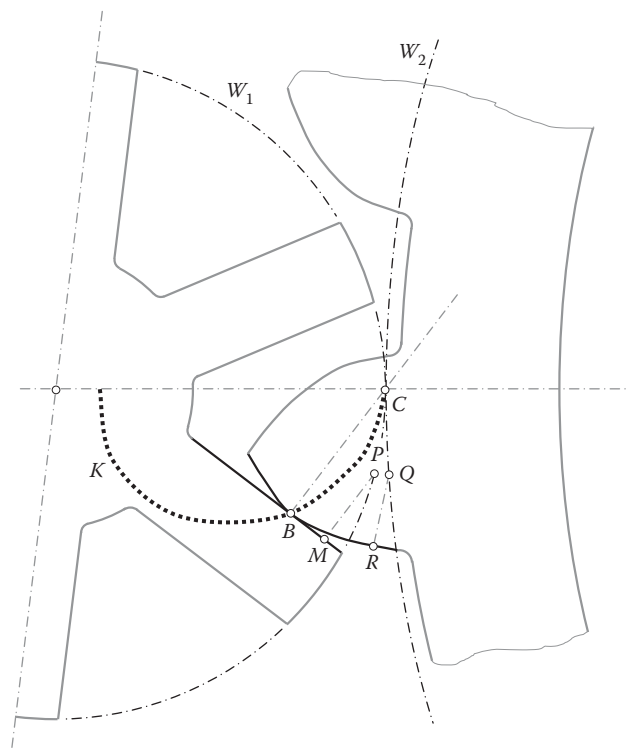


**FIGURE 1.7**  
Illustration of Camus's gearing principle (1733).

Clearly Camus had the basis for a theory of mechanism of gear teeth, but it was not systematically and completely worked out, as in *Willis* [164].

The main accomplishments in the field of gearing in the pre-Eulerian period of time are summarized by Desargues, de la Hire, Camus, and Savary. These accomplishments are briefly outlined below:

- It became clear that performance of a gear pair depends on a specific tooth profile of the mating gears; that is, tooth wear in gearing depends on the actual shape of a gear and mating pinion teeth.
- Mathematicians indicated an interest in a special tooth profile of a gear and a mating pinion that allows the lowest tooth flank wear.
- The epicycloid is investigated as a potential candidate that can be used to shape the gear teeth, and epicycloidal tooth flank geometry was proposed for gearings that operate on parallel shafts.
- It was realized in the pre-Eulerian period of time that a rotation cannot be transmitted smoothly, that is, with a constant angular velocity ratio, if gearings with epicycloid teeth are used.
- The involute of a circle was known at that time. However, there was no understanding that this curve best meets the needs of gearing.

Desargues, de la Hire, and Camus are the main contributors to gear art in the pre-Eulerian period of time.

Although mathematicians began investigating some curves, aiming at their application for the purpose of gearing, no foundations in the theory of gearing originated at this time.

---

#### 1.4 The Origin of the Scientific Theory of Gearing: Eulerian Period of Gear Art

The interest of mathematicians (at the beginning such as Desargues, de La Hire, and Camus, and later on Euler) seems to have come from a desire to increase efficiency and reduce wear in mills of various types where, although the speeds were low, the load was substantial. Indirectly, these problems were associated with the quality of the transmitted rotation, that is, with the smoothness of rotation of the output shaft.

The beginning of the scientific theory of gearing can be traced back to the middle of the 18th century when Leonhard Euler (Figure 1.8) published his famous paper on the geometry of the gear tooth profile [28]. The



**FIGURE 1.8**  
Leonhard Euler (1707–1783).

mathematics of the involute curve and its application to gear teeth were worked out by Euler, a great Swiss mathematician. In this work (Figure 1.9), Euler proved the usefulness of the involute of a circle\* to be used as the shape of gear tooth flanks. In this paper [28], along with his next paper on gearing [29] (Figure 1.10), Euler already shows the grasp and precision of his great mathematical mind. He specifically states the conditions:

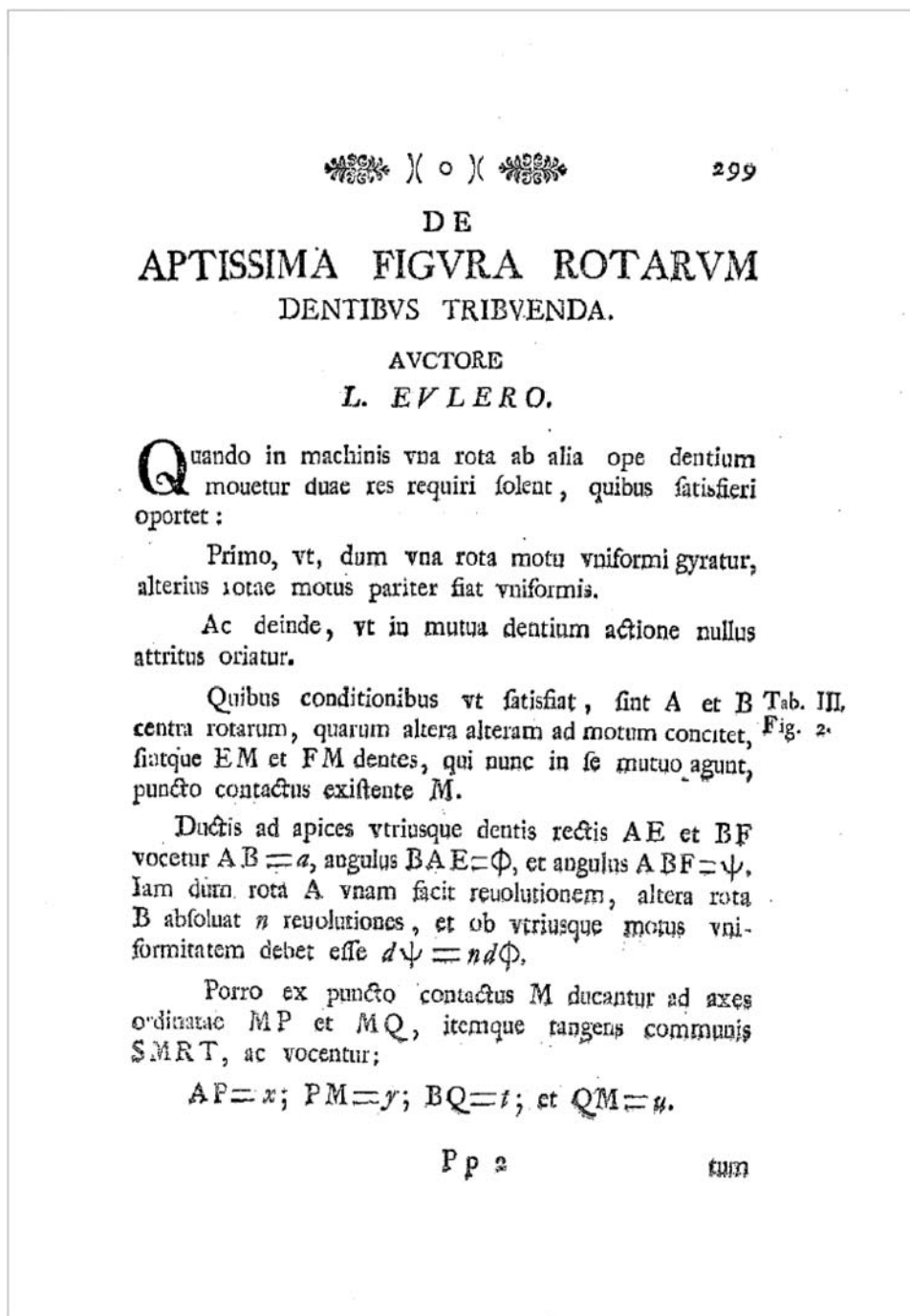


FIGURE 1.9

Title page of the paper by Euler, L., (1754–55), “De Aptissima Figure Rotarum Dentibus Tribuenda” (“On Finding the Best Shape for Gear Teeth”), in: *Academiae Scientiarum Imperiales Petropolitanae, Novi Commentarii*, t. V, pp. 299–316.

\* Invention of the involute tooth profile, which best fits the practical needs of the industry, is commonly credited to Leonhard Euler (1707–1783).



- Uniform rotary motion of both gears
- In the mutual action of the teeth *nullus atritus oriatur* (no interference between the mating tooth flanks; however, a gap between the mating tooth flanks, that is, equality of base pitches of the mating gears, is not considered yet)

The parallel-axes involute gearing with zero axis misalignment/displacement proposed by Euler deserves to be referred to as *Eulerian gearing*, or simply as  $E_u$ -gearing:

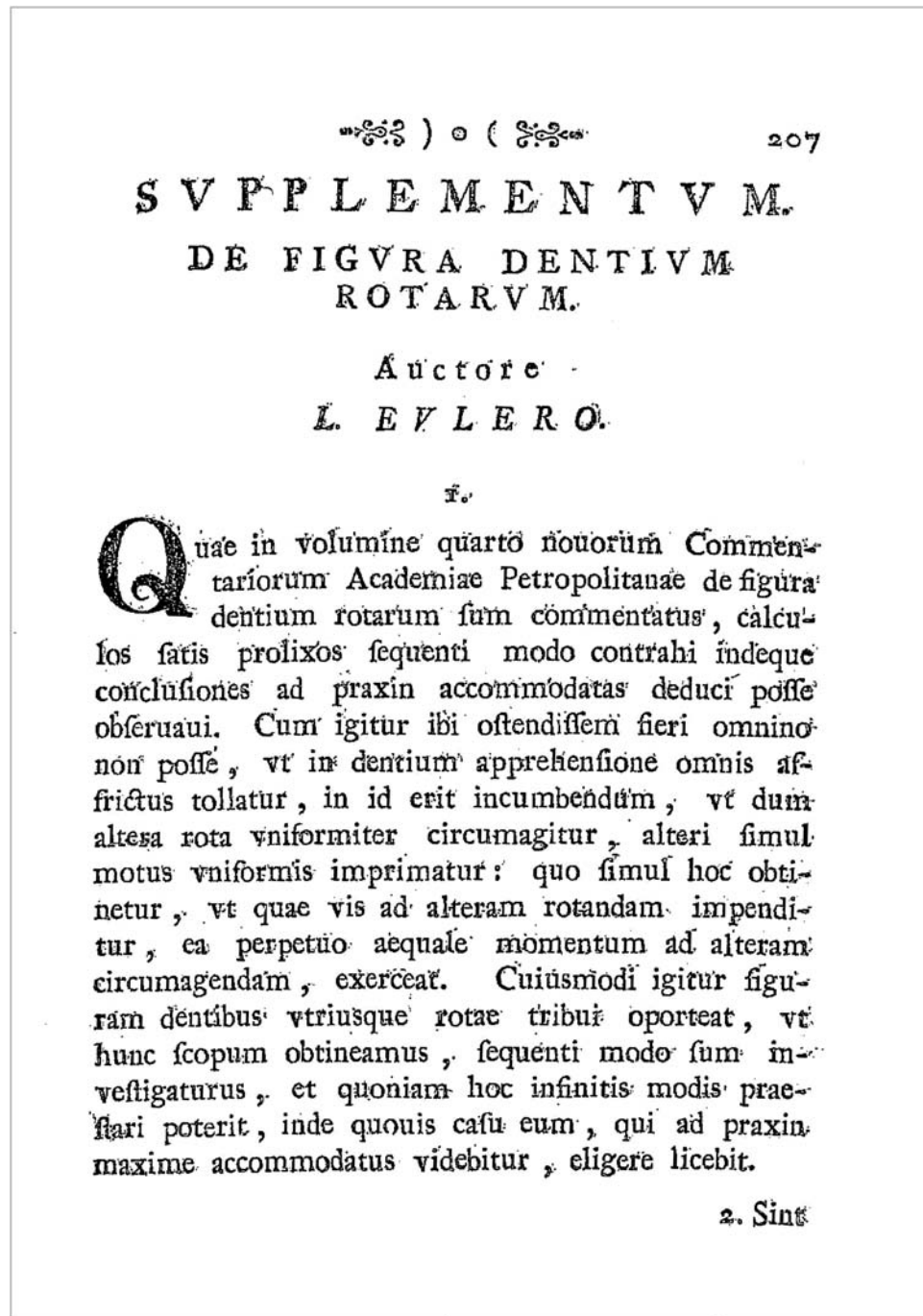


FIGURE 1.10

Title page of the paper by Euler, L., "Supplementum. De figura dentium rotarum." In: *Novi Comm. Acad. Sc. Petropol*, 1767. (Originally published in *Novi Commentarii Academiae Scientiarum Petropolitanae* 11, 1767, pp. 207–231.)

**Definition 1.1**

*Eulerian gearing (or just  $E_u$  gearing, for simplicity) is a kind of parallel-axes involute gearing that features zero axis misalignment/displacement.*

Such terminology can be used at least for scientific purposes, similar to the terms *Newtonian fluid*, *absolutely rigid body*, *absolutely dark body*, and so forth, which are extensively used in science publications.

Although the invention of the involute tooth profile is of critical importance, at the time of Euler, the difference between the line of action and the path of contact in a gear pair was not understood in detail. This is primarily because in the case of a parallel-axes gearing, both the lines, that is, the line of action,  $LA$ , and the path of contact,  $P_c$ , are straight line segments that align with one another. Later on, this inconsistency in interpretation of involute gearing was the root cause of many mistakes when gearings of other designs were proposed and investigated. This is because of the following.

For gearings that operate on parallel shafts, an involute tooth profile is the only tooth geometry under which the tooth flanks: (a) are enveloping to one another and (b) are conjugate to each other (or, in other words, they are reversibly enveloping surfaces, i.e., they are  $R_c$  surfaces, for simplicity [115]). Epicycloid tooth flanks of the mating gears are enveloping to each other, but they are not conjugate to one another—they are not a type of  $R_c$  surfaces.

Euler details the principle of a common tangent. He specifically points out the need for the proper design of gear teeth to avoid friction and wear and indicates this application for clocks. Most clockmakers, however, ignored this, if they ever heard of it. Euler's treatment of gear teeth was very general and was carried out by the application of principles of analytic geometry using both differential and integral calculus. He set up mathematical expressions for gears to move without friction between their teeth (actually for a minimum value of friction). Then, he set up expressions for gears to move with uniform motion. Then, he showed in his famous paper (Euler, 1754–55) that the developed equations can be satisfied only by involute or *epicycloid* teeth.\*

Euler and Savary together devised an analytical method for determining the curvature centers of gear tooth flanks.

The importance of the *law of conjugate action* worked out by Euler (gears designed according to this law have a steady speed ratio) was correctly realized much later.†

For over a century, the invention of the involute tooth profile was not used in practice. The industrial revolution in Britain in the 18th century saw an explosion in the use of metal gearing. A science of gear design and manufacture rapidly developed through the 19th century. The invention and the beginning of the application of steam and gas turbines that operate at high rotations and produce lots of power immediately turned the attention of engineers to involute gearings.

The contribution by Euler is incomplete, as he proposed the involute tooth profile for parallel-axes gear pairs; however, the concept of the *gear/pinion base pitch* (linear base pitch), as well as the concept of the *operating base pitch* (linear operating base pitch) in a parallel-axes gear pair was not known to Euler.

Accomplishments in the field of gearing in the Eulerian time can be briefly summarized as follows:

- It is proven by Euler in the mid-18th century that an involute tooth profile best meets the requirements of parallel-axes gearing.
- It is likely the fundamental theorem of parallel-axes gearing was already known due to Camus, Euler, and Savary.
- There is no evidence that a difference between the line of action,  $LA$ , and the path of contact,  $P_c$ , was recognized at this time, as in cases of parallel-axes gearings, these two lines align with each another.
- No significant accomplishments at that time were made in the area of intersected-axes or crossed-axes gearings.

The invention of the involute tooth profile for parallel-axes gearings is one of the cornerstone accomplishments in the scientific theory of gearing. It is likely this achievement can be referred to as the beginning of the scientific theory of gearing.

\* This indicates that Euler also allows for application of gears with an epicycloid tooth profile for the purpose of transmitting a rotation smoothly, which is incorrect.

† There is no evidence on whether Euler (1760) indicated a difference between the line of action,  $LA$ , and the path of contact,  $P_c$ .

## 1.5 Post-Eulerian Period of Developments in the Field of Gearing

In the 19th century, a profound investigation of mechanisms in general sense was undertaken by Robert Willis\* (Figure 1.11). In his 1841 book [164] titled *Principles of Mechanisms* (Figure 1.12), Willis compiled lectures for his students and knowledge about gears that could be used in practice. In the book [164], gearings were discussed by the author to the best extent possible in his time.

The *fundamental theorem of gearing* is known now mostly due to the book by Willis [164] (Figure 1.13):

### Fundamental Theorem of Gearing (According to Willis)

*The angular velocities of the two pieces are to each other inversely as the segments into which the “line of action” divides the line of centers, or inversely as the perpendiculars from centers of motion upon the line of action.*

This is why, in Eastern Europe, the fundamental theorem of gearing is commonly referred to as the *Willis’s theorem*. However, as this theorem was already known to Camus, Euler and Savary long before Willis, it makes sense to refer to the fundamental theorem of gearing as the *Camus-Euler-Savary fundamental theorem of gearing* (or to the *CES—theorem of gearing*, for simplicity). A contribution by Camus is also covered by the term *CES—theorem of gearing*.

As early as 1842, a monograph by Theodore Olivier† (Figure 1.14) on the theory of gearing [88] was published. This monograph (Figure 1.15) is the first monograph ever to be titled *Geometric Theory of Gearing* (*Théorie Géométrique des Engrenages*). In the monograph, the first and second principles of the generation of enveloping surfaces are proposed. Later on, both these principles received wide usage by gear scientists. Graphical methods developed in descriptive geometry are used by Olivier in this book [88].

In the general case of gear meshing, both the principles proposed by Olivier (1842) are incorrect, as the condition of conjugacy of the interacting surfaces is ignored. Both the principles are valid just in degenerate cases,

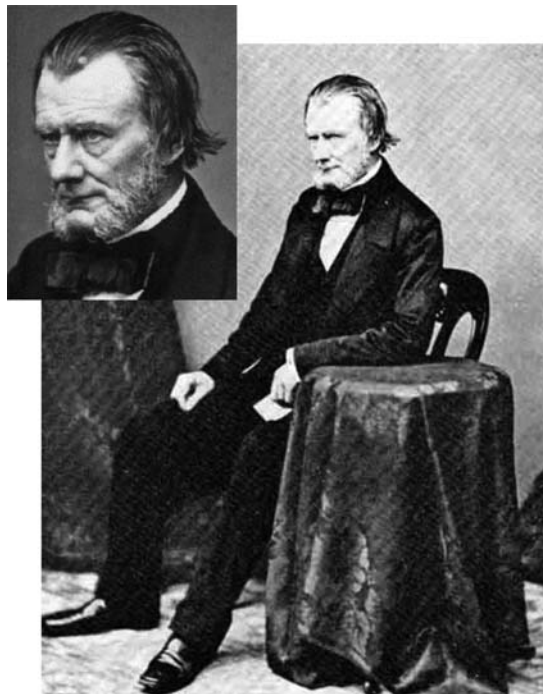


**FIGURE 1.11**  
Reverend Robert Willis (1800–1875).

\* Reverend Robert Willis (February 27, 1800–February 28, 1875), an English academic, was a professor at Cambridge.

† Théodore Olivier (January 21, 1793–August 5, 1853), a French mathematician and engineer.



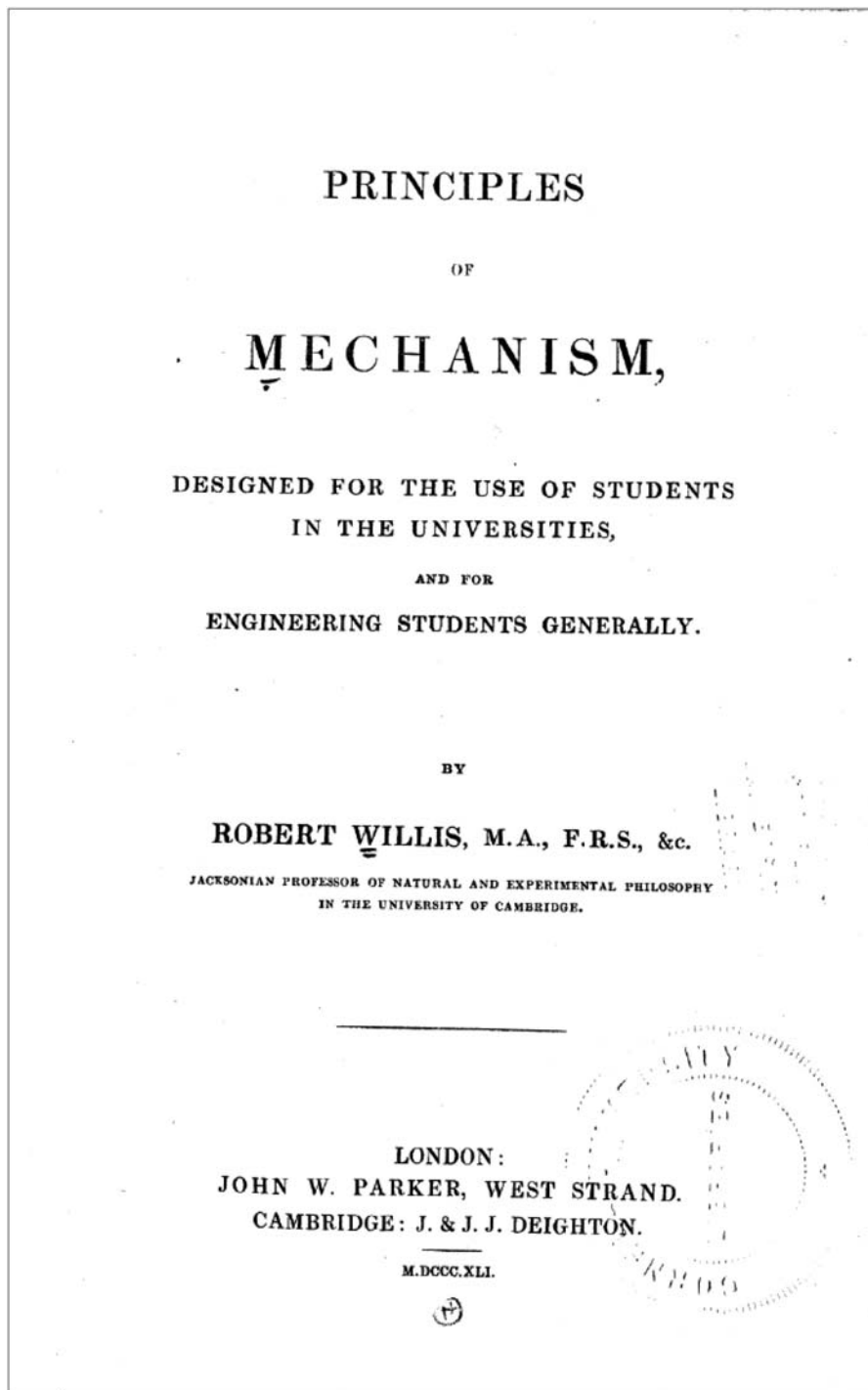


FIGURE 1.12

Title page of the book: Willis, R., *Principles of Mechanisms, Designed for the Use of Students in the Universities and for Engineering Students Generally*, London, John W. Parker, West Stand, Cambridge: J. & J. J. Deighton, 1841, 446 p.

when moving surfaces allow for sliding over themselves in the direction of the enveloping motion. In these reduced cases, the principles by Olivier become useless. Therefore, there is no reason to apply *Olivier principles* for the purpose of generation of conjugate tooth flanks in a gear pair.

Olivier cannot be considered a contributor to the scientific theory of gearing, as his accomplishments are a kind of mistake that has significantly affected further development of the gear science.

38. If the line of direction of the link in link-work, of the common normal to the curves in contact motion, and of the connector in wrapping motion, be severally termed the line of action, we can express the separate propositions which relate to the Velocity Ratio, by saying that the angular velocities of the two pieces are to each other inversely as the segments into which the *line of action* divides the line of centers, or inversely as the perpendiculars from the centers of motion upon the line of action.

I have confined these investigations, for the present,

FIGURE 1.13

The fundamental theorem of gearing as formulated in: Willis, R., *Principles of Mechanisms, Designed For the Use of Students in the Universities and for Engineering Students Generally*, London, John W. Parker, West Stand, Cambridge: J. & J.J. Deighton, 1841, 446 p.



FIGURE 1.14

Théodore Olivier (1793–1853).

In these years (1848), the curved tooth configuration was proposed by A.C. Semple.\* Proposed in the first half of the 19th century, the curved tooth configuration captured the interest of many mechanical engineers and inventors.

The second known monograph on the theory of gearing was published in 1852 by E. Sang [143]. This book, titled *A New General Theory of the Teeth of Wheels*, is nothing more than a collection of the known achievements in the field of gearing. No contribution to the theory of gearing was made by Sang.

In 1886, a new effort to evolve the theory of gearing was undertaken by Chaim Gochman.† In his master's thesis (Figure 1.16), he converted the results earlier obtained by Olivier (who used graphical methods for solving problems in the field of gearing) into the same results obtained using the methods developed in analytical geometry [38]. As claimed on p. 7 in the research by Gochman [38], no new scientific results are contributed by Gochman to those already obtained by Olivier [88]. The interested reader is referred to [122] for details on this research. Taking into account this later conclusion, the accomplishments by Olivier and those by Gochman, below, are considered together.

Olivier in his book [88] (and later on Gochman in his master's thesis [38]) loosely considered the tooth flanks of the gear and the mating pinion only as surfaces enveloping to one another; that is, the requirement of conjugacy of the mating tooth flanks was ignored, which is a huge mistake. Fulfillment of the condition of contact is

\* U.S. Patent No. 5,647, *Rack and Pinion*, Amzi C. Semple, June 27, 1848.

† Chaim I. Gochman (1851–1916), a Russian mechanician (Novorossiysk University, Odessa, now in Ukraine).

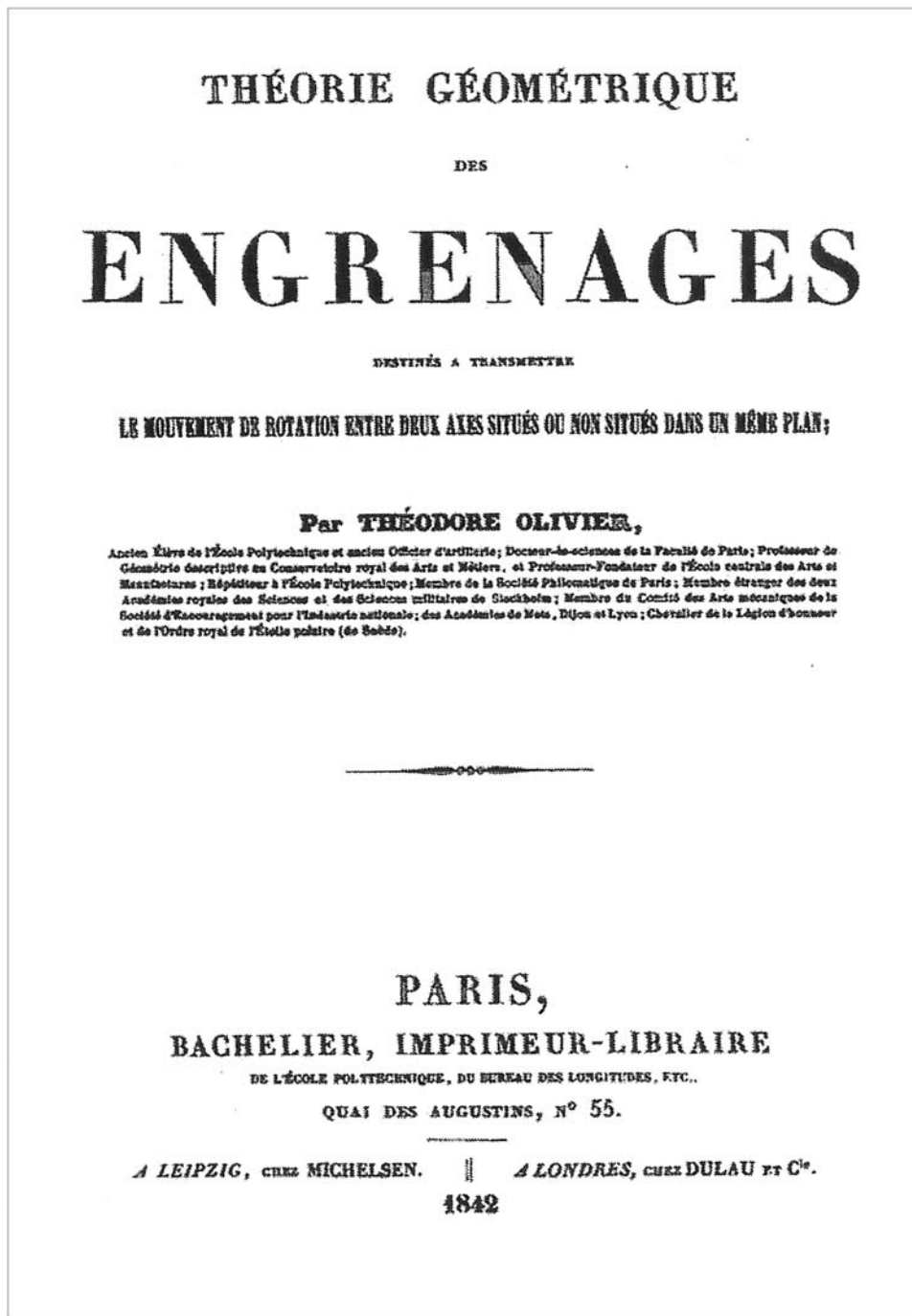


FIGURE 1.15

Title page of the first ever monograph on gearing published by Olivier, T., *Théorie Géométrique des Engrenages destinés*, (Geometric Theory of Gearing), Bachelier, Paris 1842, 118 p.

sufficient only in the cases when *no* rolling motion is observed. Otherwise, this condition needs to be complemented by (a) the condition of conjugacy and (b) the equality of a gear base pitch and its mating pinion base pitch to the operating base pitches of a gear pair [137].

It must be clearly realized that the terms *conjugate surfaces* and *enveloping surfaces* are not equivalent to one another: all conjugate surfaces are enveloping to each other but *not* vice versa; that is, not all enveloping surfaces are conjugate to one another. This mistake is discussed in detail by Professor S. Radzevich [122].

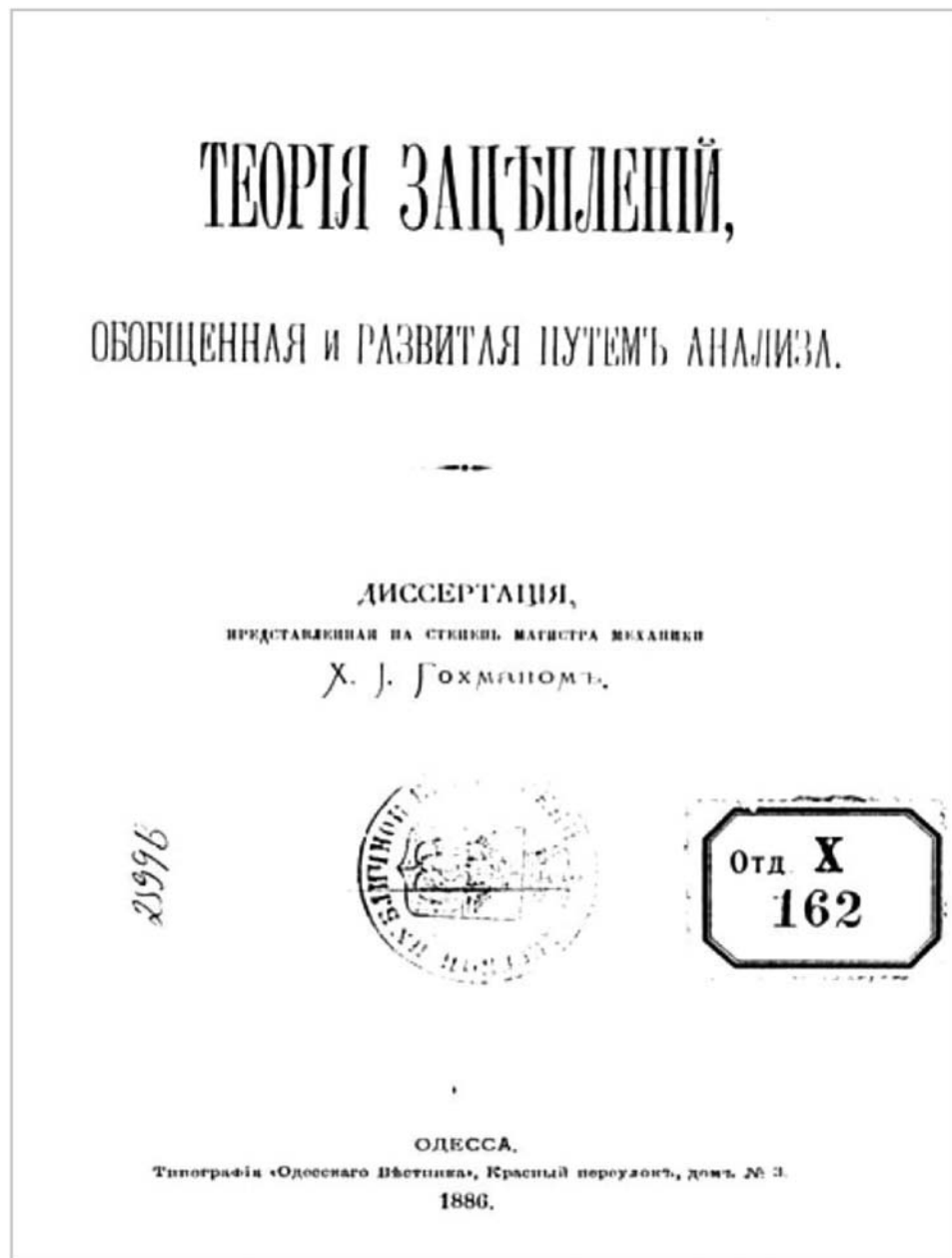


FIGURE 1.16

Title page of Master Thesis by Ch. Gochman: *Theory of Gear Teeth Engagement, Generalized and Developed by Implementation of Mathematical Analysis*, Odessa (Ukraine), 1886, 229 p.

The condition of proper meshing in perfect gearing has been correctly specified by Euler and Savary, and later on by Willis. Camus was also close to the correct understanding of the condition of proper meshing in perfect gearing.

Then, the condition of conjugacy was ignored by Olivier and by *all* of the followers of this approach to the theory of gearing (Gochman, Litvin, and so forth).

Later on, developments in the theory of gearing were significantly affected by the mistake committed by Olivier and later repeated by Gochman. Professor V.A. Shishkov, Professor F.L. Litvin, Professor G.I. Shevel'eva, and many others are among those who followed Olivier's approach.\*

\* It is likely Dr. Fraifeld [34] is among those the most affected (influenced) by the two Olivier principles. Generating (hobbing) of gears for Novikov gearing is another example where ignorance of the condition of conjugacy resulted in insufficient accuracy of the machined gears.

There is no chance of developing a scientific theory of gearing based only on the condition of contact and ignoring:

- a. The condition of conjugacy of the interacting tooth flanks.
- b. The equality of base pitches of a gear and a mating pinion to the operating base pitch of the gear pair, and so forth.

The direction of evolution of the gear theory that strictly follows the *Olivier-Gochman* approach represents the dead end in the evolution of the theory of gearing.

Among the experts in the field of gearing of that period of time, the name of *Thomas Tredgold\** (Figure 1.17) should be mentioned as well. As a gear person, he is mostly known for the approximation of bevel gears (that is, of intersected-axes gears) by appropriate cylindrical gears (that is, by parallel-axes gears) he proposed. The proposed approximation, that is, the so-called *Tredgold approximation*, significantly simplifies the calculation of bevel gearings in engineering practice.

Accomplishments in the field of gearing in the post-Eulerian time can be briefly summarized in the following manner:

- The fundamental theorem of parallel-axes gearing (i.e., the Camus-Euler-Savary fundamental theorem of gearing) is formulated. Later on, this theorem was published in the book by Robert Willis [164], and sometimes is referred to as *Willis fundamental theorem of gearing*, which is incorrect.
- The importance of the *condition of contact* between two interacting tooth, flanks (that is, the *enveloping condition*) is realized; various forms of verbal, as well as analytical, representations of this important condition are known at that time.
- Investigation into intersected-axes and crossed-axes gearings started at this time.
- A huge mistake in the interpretation of the interaction between the tooth flanks of mating gears was committed by Olivier [88] (1842) and repeated by Gochman [38] (1886). All the research in the field of gearing in the years since 1842 through recent years is significantly affected by this mistake.

The fundamental theorem of parallel-axes gearing, and the contact condition (that is, the enveloping condition) can be considered the main contribution to the scientific theory of gearing attained at this time.



**FIGURE 1.17**  
Thomas Tredgold (1788–1829).

\* Thomas Tredgold (August 22, 1788–January 28, 1829), an English engineer and author.

In the period until the end of the 19th century, the development of the tooth flank profile shape was more or less completed for the case of parallel-axes gearing. Since that time, involute gearing has prevailed as the most advantageous shape of the gear tooth flanks.

---

## 1.6 Developments in the Field of Perfect Gearings

Regardless of the unavailability of the scientific theory of gearing until the beginning of the 21st century, gear practitioners on their own have proposed designs of perfect gearings.

### 1.6.1 Grant Bevel Gearing

In this concern, the invention [40] by George Grant\* (Figure 1.18) should be mentioned first of all. Use of the invention [40] allows the generation of perfect bevel gears. This is because in one of the possible applications of the invention, "... the rolling cone is increased in size until its center angle is ninety degrees, and it becomes a plane circle. Its element will form an epicycloidal surface as before, but it is now called an 'involute' surface." (Figure 1.19). Therefore, the bevel gear tooth flanks are generated by the described method adopted to the case of intersected-axes gearing, that is, bevel gearing. This is a significant scientific achievement by Grant in the field of the scientific theory of gearing. Figure 1.20 is a good evidence of perfect tooth flank geometry in a bevel gear, correctly realized by Grant at the end of the 19th century. An elementary device (Figure 1.21) was used in the past to demonstrate the principal features of meshing in a bevel gear pair.

The contribution by Grant is incomplete, as he proposed only a method of generation of tooth flanks of a gear for intersected-axes gear pairs ( $I_a$  gearings). The concept of the *gear/pinion angular base pitch*, as well as the concept of the *operating angular base pitch* of a gear pair, was not known to Grant.



**FIGURE 1.18**  
George Barnard Grant (1849–1917).

---

\* George Barnard Grant (December 21, 1849–August 16, 1917) is considered one of the founders of the gear-cutting industry in the United States (Grant established a gear-cutting machine shop in Charlestown, Massachusetts. When this business expanded, he moved the workshop to Boston, expanded it, and named it the *Grant Gear Works*. From this extremely successful establishment evolved the *Philadelphia Gear Works* and the *Cleveland Gear Works*. George Grant even wrote several very successful books on the subject, for example *A Treatise on Gear Wheels*; *A Handbook on the Teeth of Gears, Their Curves, Properties and Practical Construction*, and so forth).



cone with a circular base; but there are many  
 45 curves that would act as its base without altering the principle of its operation. When the rolling cone is increased in size until its center angle is ninety degrees, it becomes a plane circle. Its element will form an epicycloidal surface as before; but it is now called  
 50 an “involute” surface. The involute surface is a special case of the epicycloidal surface, differing from it principally in the valuable feature that it will allow a variation in the center distance of the shafts of spur-gears, 55 or in the angle between the shafts of bevel-gears, without affecting the uniformity of the motion transmitted.

In the figures, the gear-blank 19 is held by a gear-spindle 20, that is supported by the frame 25 and oscillated by the index-wheel 21. The index-wheel receives a slow feeding motion by means of the pinion 22.

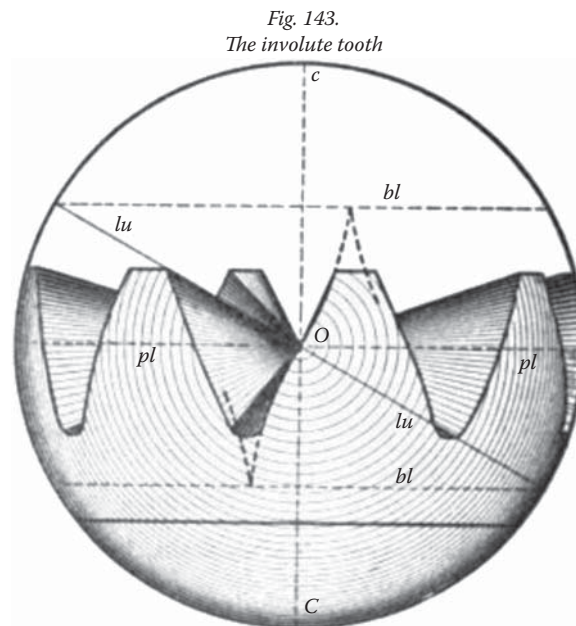
**FIGURE 1.19**

The essential of the G. Grant's invention [U.S. Pat. No. 407.437. *Machine for Planing Gear Teeth*,/G.B. Grant (1887)].

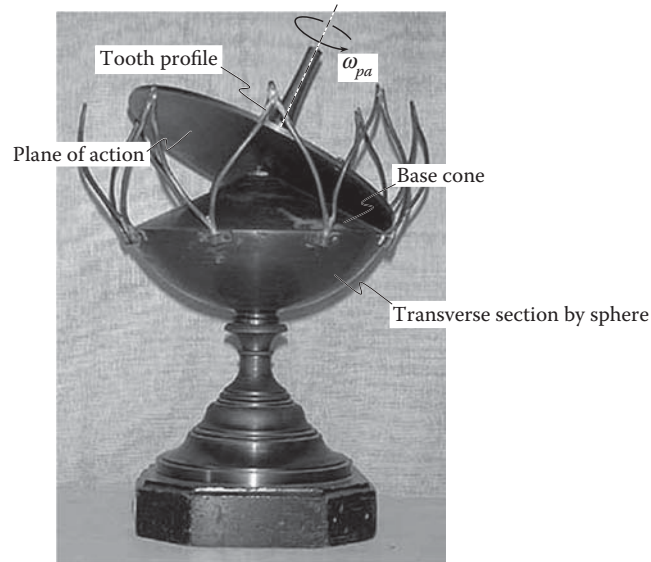
However, Grant was a gear practitioner and not a researcher, and (per the author's personal opinion) he did not properly value his accomplishment, which is of significant importance to the scientific theory of gearing. In addition, in the time of Grant, there was no necessity for more accurate bevel gears compared to those produced by the gear-generating method. Because of this, the invention by Grant was forgotten for over a century.

### 1.6.2 Contribution by Professor N.I. Kolchin

In the mid-20th century, interesting analytical research in gearing (in bevel gearing in particular) was undertaken by Professor N.I. Kolchin of the USSR (Figure 1.22) [56]. Professor Kolchin analytically described the results discovered and known in the public domain before his book was published. However, his contribution

**FIGURE 1.20**

The involute tooth flank in a bevel gear according to G. Grant (see Figure 143 in: Grant, G.B., *A Treatise on Gear Wheels*, 6th ed., Philadelphia Gear Works, Inc., Philadelphia, 1893, 105 p).

**FIGURE 1.21**

Demonstration of principal features of meshing in a bevel gear pair.

to the theory of gearing was important, as a profound mathematical analysis of gears was started from his research [56].

### 1.6.3 Novikov Conformal Gearing

In the late 1940s and at the beginning of the 1950s, an extensive research work in the field of gearing was carried out by Dr. M.L. Novikov\* (Figure 1.23) in Moscow, at the Military Aviation Engineering Academy. Ultimately, a novel design of high-performance gearing was proposed [85,81]. Later on, the results of the research were summarized in the doctoral thesis [82] and a monograph [83] by Novikov (Figure 1.24).

The proposed design of gearing features *concave-to-convex* contact between the interacting tooth flanks of a gear and a mating pinion. The gear designer is free to design the rest of the gear and the pinion tooth profiles.

When Novikov carried out his research in the field of conformal gearing, he loosely assumed that in order to transmit a uniform rotational motion, the gear teeth do not need to have special shapes, such as the involute of a circle. He meant that if a gear is made helical, then the helix itself can ensure uniform angular motion, and tooth profiles can then be chosen with a view to minimizing contact stresses. This is a bit confusing: in order to transmit a rotation smoothly, the mating tooth profiles must be either involute or, in a degenerate case, they can feature the *involute tooth point* geometry.

*Novikov gearing* is a type of helical gearing that has a zero length of the field of action; that is, the equality  $Z_a = 0$  is valid in Novikov gearing (this entails zero transverse contact ratio,  $m_p = 0$ , in Novikov gearing). The equality of the base pitch of the gear and the pinion to the operating base pitch of the gear pair is the principal feature of Novikov gearing that distinguishes it from helical noninvolute gearing of other types.

It is customary to associate Novikov gearing<sup>†</sup> with the patent *Gear Pairs and Cam Mechanisms Having Point System of Meshing* [85]. Evidence can be found in scientific literature revealing the unfamiliarity of the gear community around the world with this original publication [85] on Novikov gearing (see Appendix H for details). As early as 1955, before the invention application was filed, Novikov had defended a doctoral thesis [82] on the subject. The author's familiarity with the practice of defending a doctoral thesis adopted in the former Soviet Union allows an assumption that the concept of Novikov gearing had been proposed in the late 1940s. After Novikov was granted the patent [85], a monograph by him was published (Figure 1.24) [83]. The concept of Novikov gearing is discussed in detail in the two aforementioned valuable sources [82] and [83]. Unfortunately,

\* Mikhail L. Novikov (March 25, 1915–August 19, 1957), a famous Soviet gear researcher.

<sup>†</sup> The first pair of Novikov gearing made of aluminum alloy (a preprototype) was cut on April 25, 1954, by a disk-type mill cutter. For testing, 15 gear pairs were machined in the summer of 1954 by the disk-type milling cutter. Hobs for cutting gears for Novikov gearing were proposed later on by Professor V.N. Kudryavtsev (as early as in 1956).



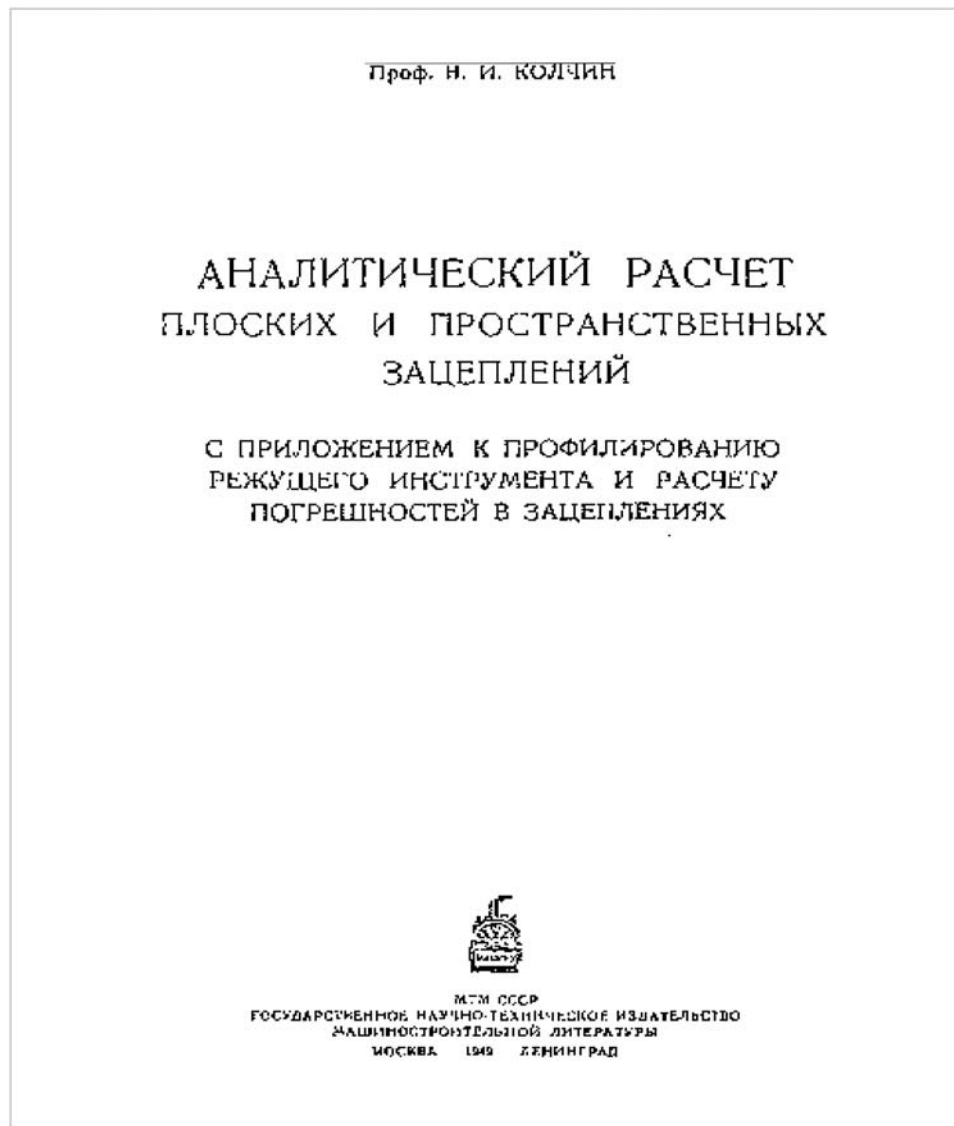


FIGURE 1.22

Title page of a monograph by Dr. Kolchin, N.I., *Analytical Calculation of Planar and Spatial Gearing*, Moscow, Mashgiz, (1949), 210 p.

none of them is quoted by gear experts in Western countries or in the United States. This makes possible a conclusion that gear experts around the world are not familiar with these two valuable sources of information on Novikov gearing.

Formally, the tooth flanks have a circular arc profile. Actually, as was shown later by Radzevich [116], *Novikov conformal gearing* is a reduced type of involute gearing in which the involute tooth profile is shrunk to a point and the rest of the tooth profiles are shaped in the form of a circular arc. Because of this, Novikov conformal gearing is a type of perfect gearing (a reduced type of involute gearing) that is capable of transmitting a rotation smoothly.

#### 1.6.4 Contribution by Professor V.A. Gavrilenko

Extensive research in the field of gearing in the 1930s through 1960s was carried out by Professor V.A. Gavrilenko\* (Figure 1.25). He spent decades on extensive research in the field of gearing, particularly

\* Vladimir A. Gavrilenko (June 21, 1899–June 6, 1977), Doctor of (Engineering) Sciences and Professor of Mechanical Engineering (Bauman State Technical University, Moscow, Russia).



**FIGURE 1.23**  
Dr. Mikhail L. Novikov (1915–1957).

in the geometrical theory of involute gearing. In the author's opinion, the most systematic discussion on involute gearing ever can be found in the monograph by Gavrilenko [36]. Unfortunately, the fundamental monographs by Gavrilenko are not known by most gear experts either in Europe or in the United States.

### 1.6.5 Contribution by Walton Musser

In the late 1950s, *Walton Musser*\* (Figure 1.26) proposed a novel type of transmission, that is, the so-called *harmonic drive*. Although this invention revolutionized the theory of *machines and mechanisms*, harmonic drives are not gear drives in the sense considered in this monograph. This is the only reason harmonic drives are not discussed in this monograph; this kind of transmission is out of the scope of the book.

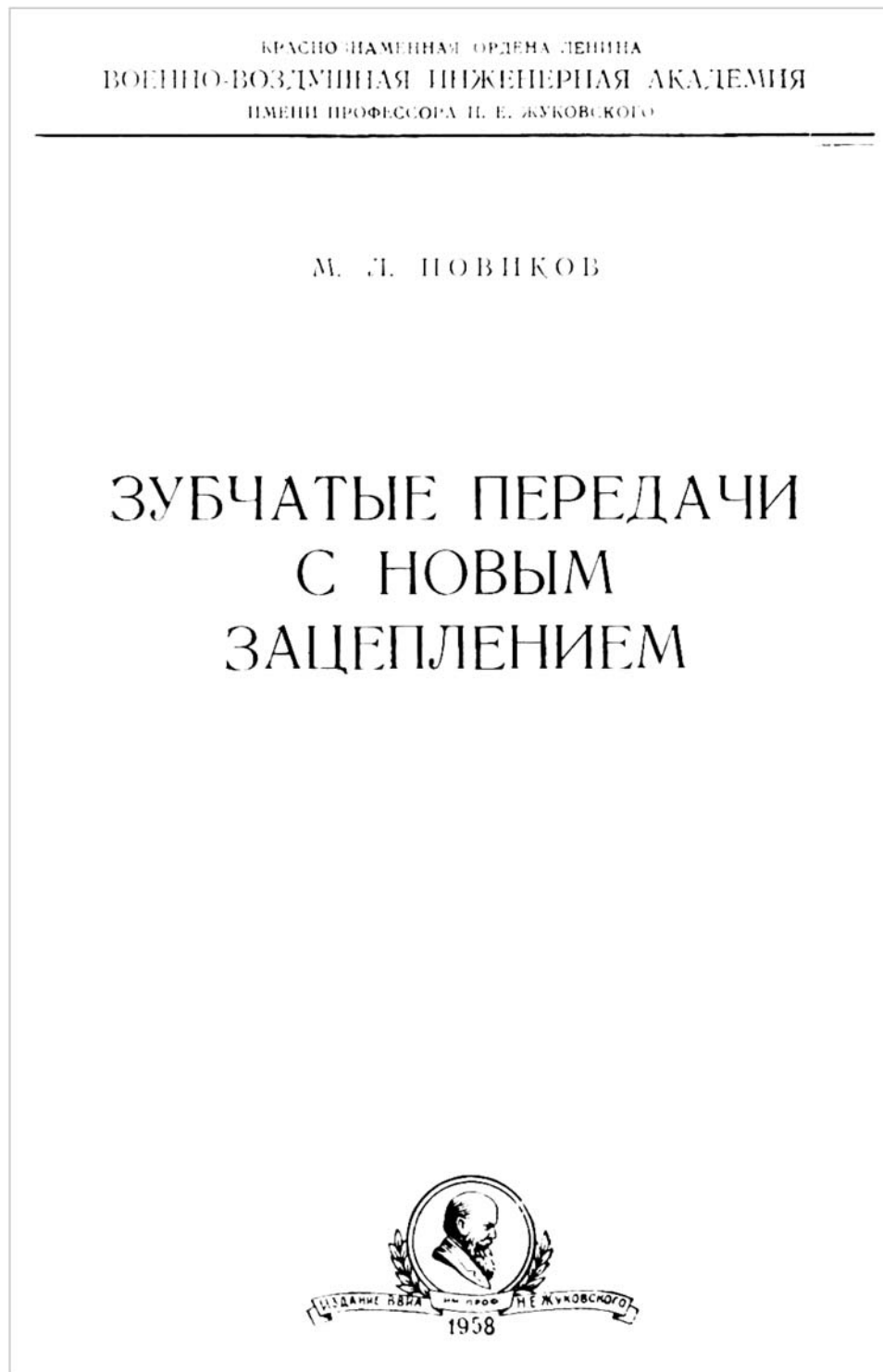
Accomplishments in the field of gearing in that period of time can be briefly summarized as follows:

- A breakthrough invention in the field of intersected-axes gearing was made by Grant. He proposed a *Machine for Planing Gear Teeth* (U.S. Pat. No. 407.437 [149]) that was capable of machining perfect straight bevel gears. The geometry of a straight bevel gear tooth flank (i.e., equivalent to the involute of a circle in cases of parallel-axes gearing) was proposed by Grant for the case of intersected-axes gearing.<sup>†</sup>
- A novel design of conformal gearing was proposed by Novikov [82].

Grant's invention [149] is an important contribution to the theory of gearing. Novikov's invention completely aligns with the well-developed theory of parallel-axes involute gearing, as Novikov conformal gearing is a reduced case of involute gearing.

\* Walton Clarence Musser (April 5, 1909–June 8, 1998), a famous American inventor, is the inventor of the harmonic drive (1957).

<sup>†</sup> Per the author's opinion, Grant did not realize the importance of his invention. In the time of Grant, the industry was fulfilled with the approximate gears available on the market; no interest in precision (and more costly) bevel gears was indicated by the industry at that time.

**FIGURE 1.24**

Title page of Novikov's (1958) monograph, *Gearing with a Novel Kind of Meshing*, 1958. (From Novikov, M.L., *Gearing of Gears with a Novel Type of Teeth Meshing*, Zhukovsky Air Force Engineering Academy, Moscow, 1958, 186 p.)



**FIGURE 1.25**  
Professor Vladimir A. Gavrilenko (1899–1977).

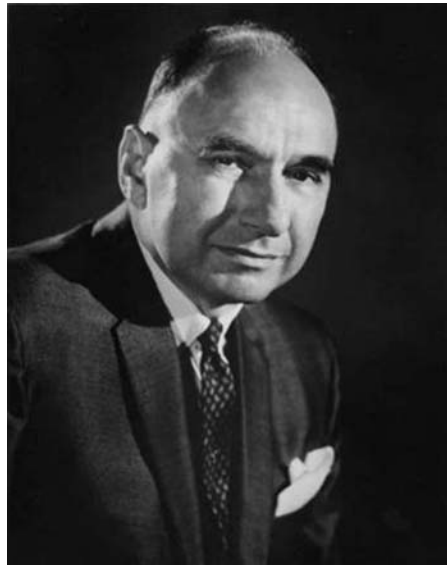


**FIGURE 1.26**  
C. Walton Musser (1909–1998).

---

## 1.7 Tentative Chronology of the Evolution of the Theory of Gearing

Summarizing the above discussion, the benchmark achievements in the theory of gearing are schematically illustrated in [Figure 1.27](#).

Contributions to the field of gearing by Desargues, de la Hire, and Camus constitute the pre-Eulerian period of evolution of the theory of gearing. In the schematic ([Figure 1.27](#)), number 0 is assigned to the pre-Eulerian period evolution of the theory of gearing.

The invention of involute gearing\* by Euler (1760) is a benchmark achievement in the theory of gearing. Per the author's opinion, the origin of the scientific theory of gearing has to be associated with this

---

\* It needs to be stressed here that *involute of a circle* itself was known long before the invention of involute gearing by Euler.

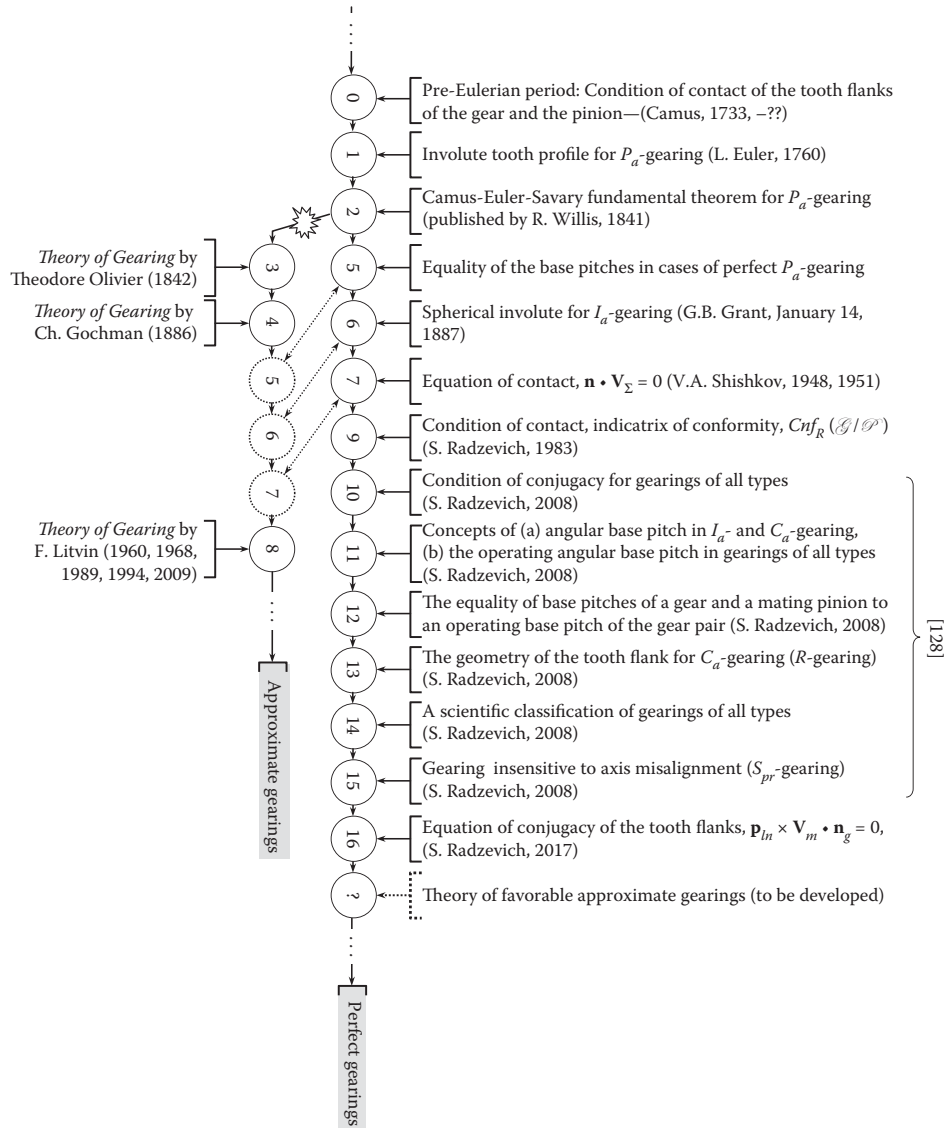


FIGURE 1.27

Principal accomplishments in the scientific theory of gearing.

accomplishment. In the schematic (Figure 1.27), number 1 is assigned to the invention of involute gearing by Euler.

The next step in the development of the theory of gearing was taken by Euler and Savary, who are credited with the fundamental theorem of gearing (along with Camus). Later on, in 1841, this theorem was published in a book by Willis [164]. Number 2 is assigned in the schematic (Figure 1.27) to this achievement in the scientific theory of gearing. The Camus-Euler-Savary fundamental theorem of gearing is valid only for parallel-axes gearings.

In 1842, a huge mistake was committed by Olivier, who proposed his version of the theory of gearing based just on the enveloping condition of conjugacy of the interacting tooth flanks of a gear and a mating pinion. The condition of conjugacy of the tooth flanks is not taken into account by Olivier. This event is labeled as 3 in the schematic (Figure 1.27).

The mistake committed by Olivier [81] (1842) and repeated by Gochman [37] (1886) significantly influenced further fundamental developments in the theory of gearing (4, 8, and others in Figure 1.27).

The accomplishments in the theory of gearing labeled as 5 through 7 are not associated with the necessity of meeting the condition of conjugacy of the interacting tooth flanks and are applicable in both branches,

that is: (a) in the *dead end* of the theory\* (4, 8, and others in Figure 1.27), as well as (b) in the path that leads to the self-consistent scientific theory of gearing [126] (5 through 14, and others in Figure 1.27). No perfect intersected-axes and crossed-axes gearings can be designed following this method. No correct tooth flank modification in parallel-axes gearing is possible—only the trial-and-error method can be used to determine the parameters of the tooth flank modification.

The condition that requires equal base pitches of a gear and its mating pinion (only in cases of parallel-axes gearings) was known for a long time (note the operating base pitch of a gear pair was not known yet). Per the author's estimate, this requirement, that is, item 5 in Figure 1.27, was known since the middle of the 19th century. Unfortunately, in the meantime, it is not possible to identify the name of the gear scientist who should be credited with this significant accomplishment in the scientific theory of gearing.

The spherical involute in perfect bevel gearing (item 6 in Figure 1.27) has been known since 1887.

The *Shishkov equation of contact* (item 7 in Figure 1.27) deserves to be mentioned here, as use of this equation makes possible significant simplifications of the kinematic method of surface generation, especially in cases when both the contact perpendicular,  $\mathbf{n}$ , and the instant linear velocity vector,  $\mathbf{V}_\Sigma$ , can be determined with no derivatives of equations of the tooth flanks,  $\mathcal{G}$  and  $\mathcal{P}$ , as well as the parameters of the kinematics of a gear pair.

Conditions of contact of the interacting tooth flanks,  $\mathcal{G}$  and  $\mathcal{P}$ , are investigated analytically, and an equation of the indicatrix of conformity,  $Cnf_R(\mathcal{G}/\mathcal{P})$ , at the point of contact of tooth flanks of a gear,  $\mathcal{G}$ , and a mating pinion,  $\mathcal{P}$ , (item 9 in Figure 1.27) is derived [86,87,104,109, and others].

Equation of conjugacy:  $\mathbf{p}_{ln} \times \mathbf{V}_m \cdot \mathbf{n}_g = 0$  (item 16 in Figure 1.27) of the interacting tooth flanks,  $\mathcal{G}$  and  $\mathcal{P}$ , is derived by Radzevich (2017).

Then, the accomplishments listed below were contributed by Radzevich in around 2008:

- Condition of conjugacy of the tooth flanks for gear pairs of all types (item 10 in Figure 1.27), including intersected-axes gear pairs and crossed-axes gear pairs.
- The concepts of (a) *base pitch* in intersected-axes gear pairs and crossed-axes gear pairs, and (b) the operating base pitch in gear pairs of all types (item 11 in Figure 1.27).
- The equality of base pitches of a gear and its mating pinion to the operating base pitch in gear pairs of all types (item 12 in Figure 1.27).
- Design of perfect crossed-axes gearing with line contact between the tooth flanks,  $\mathcal{G}$  and  $\mathcal{P}$ , that is, *R* gearing (item 13 in Figure 1.27).
- A scientific classification of vector diagrams of gear pairs of all types (item 14 in Figure 1.27).
- Design of perfect (crossed-axes) gearing insensitive to axis misalignment, that is, *S<sub>pr</sub>*-gearing (item 15 in Figure 1.27).
- Equation of conjugacy:  $\mathbf{p}_{ln} \times \mathbf{V}_m \cdot \mathbf{n}_g = 0$  (item 16 in Figure 1.27) of the interacting tooth flanks,  $\mathcal{G}$  and  $\mathcal{P}$ , derived by Radzevich (2017).

It should be realized that the diagram in Figure 1.27 is tentative. More accomplishments in the scientific theory of gearing and the corresponding gear researchers' names can be added in Figure 1.27 if a more detailed investigation into the evolution of the scientific theory of gearing is undertaken. Only the key (fundamental) achievements in the scientific theory of gearing are included in the diagram (Figure 1.27) in its current stage.

Generally speaking, perfect gear pairs of any type can be designed based on the scientific theory of gearing.

## 1.8 Developments in the Field of Approximate Gearings<sup>†</sup>

To meet the current needs of the industry, practical gear engineers have proposed numerous approximate designs of gearings. Initially when the designs were proposed, it was loosely assumed that each of them was

\* It is the right point to stress here that the dead end in the diagram in Figure 1.27 means that no perfect *I<sub>a</sub>*- and *C<sub>a</sub>*-gearings are possible, no correct tooth flank modification in *P<sub>a</sub>*-gearing is possible, and the trial-and-error method dominates.

<sup>†</sup> For more detailed discussion on the manufacturing of gears for approximate gearing, the interested reader may wish to go to Chapter 1, "Gears: Brief Notes on the History of Methods of Machining Gears and of Design of Gear Cutting Tools," in the book: Radzevich, S.P., *Gear Cutting Tools: Science and Engineering*, CRC Press, Boca Raton, Florida, 2017, 606 pages.

capable of transmitting a rotation smoothly. Unfortunately, it was shown later on that they did not meet all the requirements perfect gears need to meet.

### 1.8.1 Cone Double-Enveloping Worm Gearing

The first rudimentary *double-enveloping* worm gear drive was known since the time of da Vinci [17]. Today, double-enveloping worm gearing was proposed as early as in 1891 by Dr. Friedrich Wilhelm Lorenz\* of Germany. In his invention Lorenz proposed methods to generate the worm and gear of the double-enveloping worm-gear drive, and then he received two patents for this accomplishment. A bit later (around 1920), and independently, a similar double-enveloping worm gearing was proposed by Mr. Samuel Cone† of the United States. Lorenz and Cone understood very well the advantages of the drives they had invented, particularly the increased load capacity due to the higher contact ratio in comparison with that of conventional worm-gear drives. Although the geometry of the Lorenz and Cone drives differs, both types offer this advantage.

Double-enveloping worm gearing is an example of approximate gearing, as it does not meet all the requirements the perfect gears need to meet.

### 1.8.2 Approximate Bevel Gearing

Early accomplishments in the field of bevel gearing are tightly connected with the name of William Gleason‡ (Figure 1.28). In 1874, his invention of the straight bevel gear planer for the production of bevel gears with straight teeth substantially advanced the progress of gear making.

The early part of the 20th century was the beginning of the automotive industry, which required a broader application of bevel gears to transform rotation and power between intersected axes. In the 1920s, automotive industry designers also needed (a) a gear drive to transform motions and power between crossed axes and (b) a lower location for the driving shaft. The Gleason Works engineers met these needs with pioneering developments directed at designing new types of gear drives and the equipment and tools to generate the gears for these drives.

The proposed designs of bevel gears in the current industry are examples of approximate gearing, as they are developed and manufactured based on application of the imaginary straight-sided crown gear (basic crown



**FIGURE 1.28**  
William Gleason (1836–1922).

\* Friedrich Wilhelm Lorenz (1842–1924), doctor of engineering, inventor, and founder of the Lorenz Company.

† Samuel I. Cone (1842–1924), a civilian machinist and draftsman, American inventor of double-enveloping worm gearing.

‡ William Gleason (1836–1922), founder of The Gleason Works, Rochester, NY.



rack). Because of this, today, bevel gears of all types, that is, straight bevel gears, skew bevel gears, spiral bevel gears, and others, both face-milled and face-hobbed, do not meet all the requirements perfect gears need to meet.

### 1.8.3 Approximate Crossed-Axes Gearing

The concept of gearing that operates on crossing shafts can be traced back to the time of da Vinci [17].

The need for more accurate and quieter running gears became obvious with the advent of the automobile. Although the hypoid gear was within our manufacturing capabilities by 1916, it was not used practically until 1926, when it was used in the Packard automobile. The hypoid gear made it possible to lower the drive shaft and gain more usable floor space. By 1937, almost all cars used hypoid-gearred rear axles.

The success with the design, manufacture, and application of the contemporary crossed-axes gearing is credited primarily to two famous gear experts, namely to *Nikola Trbojevich* (also known as *Nicholas Terbo*), and Ernest Wildhaber.

Trbojevich (Figure 1.29), a world-recognized research engineer, mathematician, and inventor, was a nephew and friend of *Nikola Tesla*. *Trbojevich*\* held nearly 200 US and foreign patents, principally in the field of gear design.

Trbojevich's most notable work that brought him international recognition was the invention of the *hypoid gear*. First published in 1923, it was a new type of spiral bevel gear employing previously unexploited mathematical techniques. The hypoid gear is used in the great majority of all cars, trucks, and military vehicles today. Together with Trbojevich's invention of the tools and machines necessary for its manufacture, the hypoid gear became an integral part of the final drive mechanism of automobiles by 1931. Its effect was immediately apparent in that the overall height of rear-drive passenger automobiles was reduced by at least 4 inches.



**FIGURE 1.29**

Nikola John Trbojevich, also known as Nicholas J. Terbo (1886–1973).

\* Nikola John Trbojevich (May 21, 1886–December 2, 1973), also known as Nicholas J. Terbo, a world-recognized research engineer, mathematician, and inventor, held the basic patent for the hypoid gear.



**FIGURE 1.30**  
Ernest Wildhaber (1893–1979).

Wildhaber\* (Figure 1.30) is one of the most famous inventors in the field of gear manufacture and design. He has been granted 279 patents, some of which have a broad application in the gear industry because of his work as an engineering consultant for The Gleason Works. The hypoid gear drive is of the most famous inventions by Dr. Wildhaber. He proposed different pressure angles for the driving and coast tooth sides of a hypoid gear, which allowed him to provide constancy of the tooth top-land.

The proposed designs of crossed-axes gears in the current industry are examples of approximate gearing, as they are developed and manufactured based on application of the imaginary crown gear with a straight-sided profile (basic crown rack). Because of this, current crossed-axes gears of all types, both face-milled and face-hobbed, do not meet all the requirements perfect gears need to meet.

#### 1.8.4 Face Gearing

Face gearing can be viewed as a reduced case either of intersected-axes gearing or of crossed-axes gearing when the pitch cone angle increases to the right angle. All known designs of face gearings, both intersected-axes gearings and crossed-axes gearings, are approximate gearings, as they do not meet all the requirements perfect gears need to meet. The face-cutting technique used to produce these crossed-axes gears supplied by these three companies (The Gleason Works; Klingelnberg-Oerlikon; Yutaka Seimitsu Kogyo, LTD) is based upon an empirical and manufacturing technology that predates World War II.

Accomplishments in the field of gearing in that period of time can be briefly summarized as follows:

- Double-enveloping (approximate) gearing was proposed by Lorenz of Germany (1874) and a bit later (around 1920) by Cone of the United States.
- Design of and methods for machining of approximate hypoid gearing were proposed by Trbojevich, and later on improved by Wildhaber, both of the United States.
- Face gearings are widely used in the design of *Fellow's* gear shaping machines.

The most significant contributions to the field of gearing at that time are made to approximate gearing.

\* Ernest Wildhaber (1893–1979), doctor of engineering, h.c., inventor, and consultant for The Gleason Works.

## 1.9 A Brief Summary of the Principal Accomplishments in the Theory of Gearing Achieved by the Beginning of the 21st Century

It should be stated here from the very beginning that no self-consistent (or potentially self-consistent) scientific theory of gearing had been developed by the beginning of the 21st century (by the year of ~2010).

Among others, a self-consistent scientific theory of gearing must possess two important properties.

First, a self-consistent scientific theory of gearing must cover all known designs of gears and gearings with no exclusion.

Second, a self-consistent scientific theory of gearing must cover all (with no exclusion) yet-unknown designs of gears and gearings; that is, the theory must possess the property to predict novel designs of gears and gearings.

All the books published so far under the title *Theory of Gearing* (starting from the first 1841 book by Olivier [81], and ending with the latest publications in the field—by the year of ~2010) consist of no scientific theory of gearing. These books can not be referred to as a theory of gearing; rather, they are collections of known achievements in the field of gearing, having no ability to predict novel unknown designs of gears and gearings.

No doubt, a scientific theory of gearing is necessary to gear researchers and practical engineers, as it is a powerful tool for the development of novel designs of gears and gearings with a prescribed performance. Such a scientific theory of gearing can be developed now. With that said, it is important to revise the earlier obtained accomplishments in the field of gearing and select those of them that can be useful in the development of the fundamental scientific theory of gearing.

### 1.9.1 Condition of Contact of the Interacting Tooth Flanks of a Gear and Pinion

The condition of contact of the interacting tooth flanks of a gear,  $\mathcal{G}$ , and a mating pinion,  $\mathcal{P}$ , is the first scientific result of fundamental importance that can be used in the foundation of the scientific theory of gearing. The condition of contact is also known as the enveloping condition. The contact condition states that:

#### 1.9.1.1 Condition of Contact

*At every point of contact of the tooth flanks of a gear,  $\mathcal{G}$ , and a mating pinion,  $\mathcal{P}$ , the projection of the relative velocity vector onto the common perpendicular to the interacting tooth flanks is zero.*

The condition of contact of two interacting tooth flanks in a gear pair is known for centuries. Per the author's opinion, this important condition was already known to Camus (1733) [12] or even to Desargues.

Since the time gear scientists started realizing the importance of the condition of contact, the forms of its representation were different. Without going into details of the analysis of this particular problem,\* it should be stressed here that, finally, the condition of contact is represented in the form equal to zero of the dot product of the unit vector of the common perpendicular,  $\mathbf{n}$ , at point of contact of the tooth flanks,  $\mathcal{G}$  and  $\mathcal{P}$ , and the instant velocity vector,  $\mathbf{V}_\Sigma$ , of the resultant relative motion of the tooth flanks,  $\mathcal{G}$  and  $\mathcal{P}$ ; that is:

$$\mathbf{n} \cdot \mathbf{V}_\Sigma = 0 \quad (1.1)$$

In the form of dot product [see Equation 1.1], the condition of contact was proposed by Shishkov in his paper [141]. This equation can be found in his monograph [144] (Figure 1.31), as well as in his later publications.<sup>†</sup>

As shown from the research undertaken by Radzevich [101], Shishkov is the first (not later than 1948) to represent the condition of contact of two smooth regular surfaces in the form of dot product  $\mathbf{n} \cdot \mathbf{V}_\Sigma = 0$  of the unit vector of a common perpendicular,  $\mathbf{n}$ , by the vector of the velocity of the relative motion of the interacting surfaces at a point of their contact.

The equation of contact in the form  $\mathbf{n} \cdot \mathbf{V}_\Sigma = 0$  is known as Shishkov equation of contact [101,126, and others].

The Shishkov equation of contact is a valuable contribution to the scientific theory of gearing.

\* For details, the interested reader is referred to the paper by the author: Radzevich, S.P., "Briefly on the Kinematic Method and on the History of the Equation of Contact in the Form of  $\mathbf{n} \cdot \mathbf{V} = 0$ ," In: *Theory of Mechanisms and Machines*, 2010, No. 1. Vol. 15, pp. 42–51. <http://tmm.spbstu.ru>.

<sup>†</sup> It could happen that the equation of contact,  $\mathbf{n} \cdot \mathbf{V} = 0$ , can be found even in earlier (before 1948) publications by Shishkov—in his earlier papers, PhD thesis, and so forth.

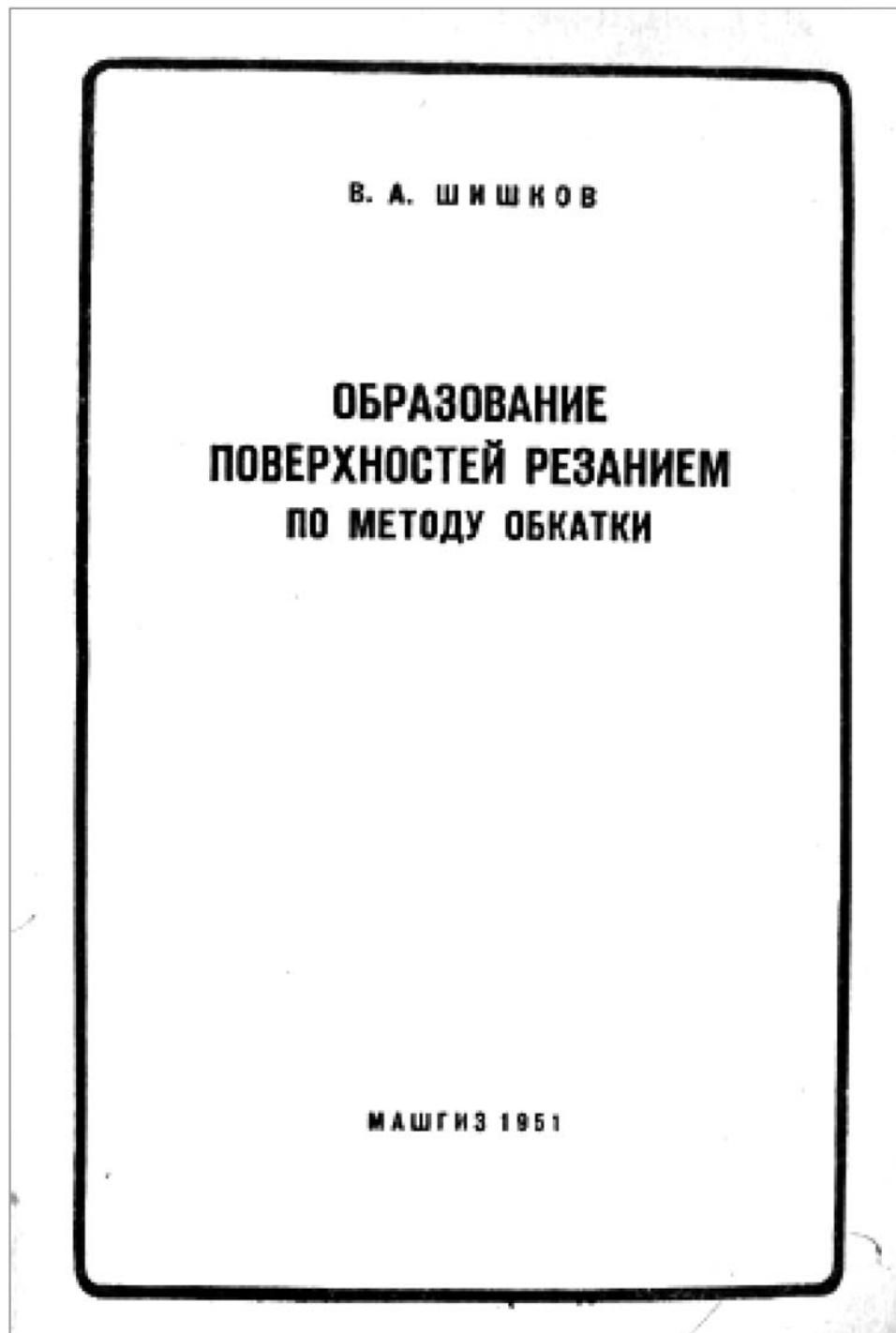


**FIGURE 1.31**

Title page of the monograph (1951) by Prof. V.A. Shishkov. (From Shishkov, V.A., *Generation of Surfaces in Continuous-Indexing Methods of Surface Machining*, Mashgiz, Moscow, 1951, 152 p.)

### **1.9.2 Condition of Conjugacy of the Interacting Tooth Flanks of a Gear and Pinion**

The condition of conjugacy of two interacting tooth profiles of a gear and a mating pinion is a bit tricky. Informally, the condition of conjugacy can be interpreted in the following manner.

Assume that a profile of one member of a gear pair is given. Then, the tooth profile of the mating member of the gear pair can be generated as an envelope to consecutive positions of the first member in its motion in

relation to the second member. Then, assume that the tooth profile of the second member of a gear pair is known, and the tooth profile of the first member of the gear pair is generated as an envelope to consecutive positions of the second member in its motion in relation to the first member. Then, compare the obtained tooth profiles of the first member of the gear pair with its original profile. If they are identical to one another, then the interacting tooth flanks are conjugate to one another. Otherwise, the interacting tooth flanks are not conjugate to one another.

Conjugate tooth profiles/surfaces are also known as reversibly-enveloping profiles/surfaces (or just  $R_e$  profiles/surfaces for simplicity) [112].

For cases of  $P_a$  gearings, the problem of conjugacy of the tooth profiles/flanks was solved by Euler in the 18th century (1760). In his famous work [28], Euler proposed an equation for the involute tooth profiles of a gear and a mating pinion that are conjugate to one another. No special attention is given either to the fulfillment of the condition of contact ( $\mathbf{n} \cdot \mathbf{V}_\Sigma = 0$ ) or to the interacting tooth flanks being conjugate to one another. There is no evidence that Euler himself realized the importance of the condition of conjugacy for the interacting tooth flanks of a gear and a mating pinion. Moreover, amazingly, the solution to the problem of conjugacy of the tooth flanks is not understood in full detail by most of the gear community around the world. Per the author's opinion, the root cause of the poor understanding of necessity of the condition of conjugacy is because of the following.

The condition of conjugacy of interacting surfaces is more robust than the enveloping condition. All conjugate surfaces are enveloping to one another, but not vice versa—not all enveloping surfaces are conjugate.

In an involute gearing (Figure 1.32), the line of action,  $LA$ , and the path of contact,  $P_c$ , align to each other at every point of contact,  $K$ , of the tooth flanks,  $\mathcal{G}$  and  $\mathcal{P}$ , of the gear and the pinion, correspondingly. This is possible as both the line of action,  $LA$ , and the path of contact,  $P_c$ , are straight lines through the pitch point,  $P$ , at the transverse pressure angle,  $\phi_t$ , to a line perpendicular to the center. This feature of involute gearing is the root cause of confusion, as the line of contact and the path of contact are commonly not distinguished from one another in the cases of  $I_a$  gearing, as well as in the cases of  $C_a$  gearing.

To correct the mistake committed by Olivier, and later on followed by Gochman and many other followers, it is necessary to differentiate between the line of action and the path of contact in a gear pair. The Camus-Euler-Savary fundamental theorem of gearing (Figure 1.13) has to be met at every instant of meshing of a gear and a mating pinion.

The CES—fundamental theorem of gearing is a valuable contribution to the scientific theory of gearing.\*

For the first time ever, the condition of conjugacy of a gear,  $\mathcal{G}$ , and a mating pinion's,  $\mathcal{P}$ , tooth flanks is described analytically by Radzevich (2017) in the form of a triple scalar product  $\mathbf{p}_{ln} \times \mathbf{V}_m \cdot \mathbf{n}_g = 0$ .

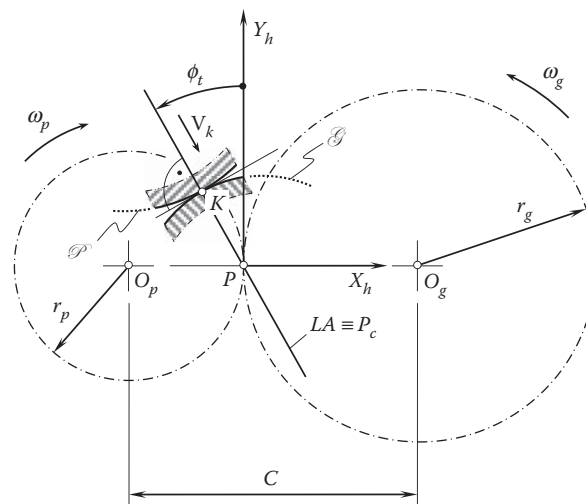


FIGURE 1.32

The line of action,  $LA$ , and the path of contact,  $P_c$ , in an involute gearing.

\* Recall that the CES—fundamental theorem of gearing is proven only for the cases of parallel-axes gearing with zero axis misalignment.

### 1.9.3 Condition of Equality of Base Pitches of the Interacting Tooth Flanks of a Gear and Pinion

In order to transmit a rotation between two shafts, at certain periods of time, more than one pair of teeth need to be engaged in mesh simultaneously. To meet this requirement, the base pitches of the mating gears must be equal to one another. This fundamental requirement\* is known only for cases of perfect parallel-axes gearing with zero axis misalignment.

The *condition of equality of base pitches* of two mating gears is a valuable contribution to the scientific theory of gearing.

Accomplishments in the field of gearing in that period of time can be briefly summarized as follows:

- Shishkov proposed representing the earlier known condition of contact of the interacting tooth flanks of a gear and a mating pinion in the form of dot product,  $\mathbf{n} \cdot \mathbf{V}_\Sigma$ . This equation of contact is a key equation in the kinematic method of surface generation. Commonly, this equation is referred to as the Shishkov equation of contact,  $\mathbf{n} \cdot \mathbf{V}_\Sigma = 0$ .
- The equation of conjugacy:  $\mathbf{p}_m \times \mathbf{V}_m \cdot \mathbf{n}_g = 0$  of the interacting tooth flanks,  $\mathcal{G}$  and  $\mathcal{P}$ , is derived by Radzevich (2017).
- The condition of conjugacy of the interacting tooth flanks of a gear and a mating pinion is not understood, and in most cases, this important condition is ignored. This is a consequence of the mistake committed by Olivier in the 19th century.
- The requirement according to which the base pitches of the mating gear and pinion are construed only in part and only for the case of perfect parallel-axes gearing. The concept of the operating base pitch of a gear pair is not realized at all.

It is likely only a contribution by Shishkov (i.e., the Shishkov equation of contact,  $\mathbf{n} \cdot \mathbf{V}_\Sigma = 0$ ) that can be referred to as a significant contribution to the theory of gearing at that period of time. The equation of conjugacy,  $\mathbf{p}_m \times \mathbf{V}_m \cdot \mathbf{n}_g = 0$  of the interacting tooth flanks,  $\mathcal{G}$  and  $\mathcal{P}$ , is also a significant contribution to the theory of gearing. However, this equation was derived by Radzevich much later (2017).

---

## 1.10 Concluding Remarks

A brief overview of the evolution of the scientific theory of gearing is discussed in this section of the book. Among others, the discussion is aimed to initiate an in-depth investigation in the field of the origins of the scientific theory of gearing.

More gear researchers deserve to be mentioned. However, consideration in this section of the book is limited only to the evolution of the theory of gearing. Therefore, the number of names of researchers is limited only to those who contributed to the kinematics and geometry of gearing.

Comprehensive research on the evolution of the theory of gearing is necessary to undertake in the near future. The research needs to be based on in-depth study of the original scientific works of all principal investigators of the topic. The history of engineering is not less important than the engineering itself. The better we know the past, the better we can predict the future.

---

\* It is the right point to mention here that the author failed in trying to identify the name of a gear researcher who should be credited with this fundamental requirement in the theory of gearing.



# Part I

## Fundamentals

Gears are widely used in the design of many mechanisms and machines in the current industry. Transmission and transformation of an input motion from a driving shaft to a driven shaft is the main goal of using gear pairs. As an example, a gearbox with double-helical gears is depicted in Figure 2.1.

As of today, an enormous amount of practical experience has been accumulated in the designing and manufacturing of gears and gear transmissions. Based on the accumulated experience, it is now possible to design and manufacture gears and gear trains in a wide range of power transmitting applications, rotations of the input and output shafts, and so forth.

In today's design practice, the desired type of a gear pair is commonly given. The design of an actual gear pair goes through a routing procedure that is well established in the industry.

The process of the design of a gear pair begins with an analysis of the kinematics of the gear pair to be designed. This means that the position and orientation of the output shaft in relation to those of the input shaft have to be given. Then, the rotation of the input shaft and the rotation of the output shaft must also be given. Configuration of the input and output shafts in relation to one another, together with a given rotation of the input shaft and desired rotation of the output shaft, make up the so-called *kinematics* of the gear pair. Analysis of the kinematics of a gear pair is always complemented with the analysis of power being transmitted through the gear pair. For this purpose, the input torque also has to be specified.

Based on a given kinematics of a gear pair, the geometry of the teeth flanks of the desired gear pair can be determined. In later phases, physical phenomena in the gear teeth mesh can be taken into account. This includes

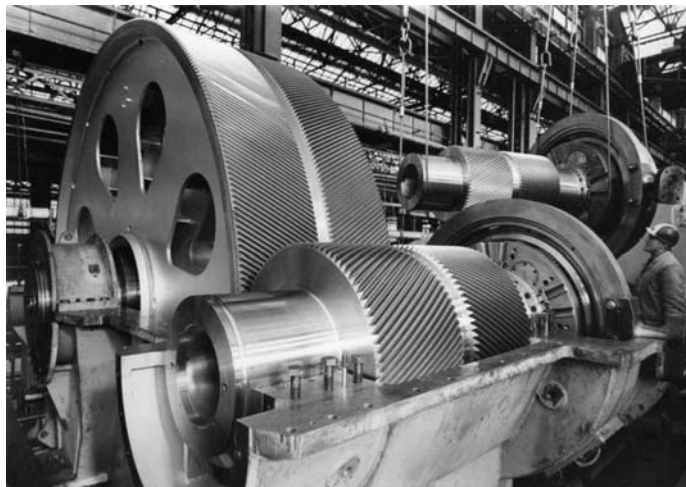


**FIGURE 2.1**  
A gearbox with double-helical gears.



friction between the teeth flanks of mating gears, lubrication of the gear mesh, tooth strength issues, manufacturing errors and axis misalignment, displacements of the tooth flanks under applied load, and so forth.

In summary, one can conclude that the input and output rotations, along with the input torque, are the most critical portion of the input information that is necessary to design a gear pair with a favorable performance. Therefore, a profound investigation of the kinematics of gear pairs is vital for the gear designer.

Here and below, only perfect gear pairs are discussed.

This part of the book is composed of four chapters in total, [Chapters 2](#) through [5](#).

The discussion below begins with the analysis of the kinematics of a gear pair.

# 2

---

## Kinematics of a Gear Pair

---

The main purpose of a gear pair is to transmit and transform a motion from an input shaft to an output shaft. Kinematics of a gear pair includes rotations of the driving and the driven gears about their axes, the instant rotations of the driving and the driven gears in relation to each other, and the sliding of the tooth flanks of the mating gears. Kinematics of a gear pair together with the input torque are the starting point for solving the problem of synthesis of a gear pair that features a desired performance.

---

### 2.1 Transmission of Motion by Means of a Gear Pair

A gear pair is commonly composed of two mating gears that move in relation to each other when a rotation is transmitted from a driving to a driven shaft.\* Although other designs are feasible, it is common practice to mount mating gears on shafts. Examples of commonly used gear pairs are illustrated in Figure 2.2. In Figure 2.2, the input rotation is denoted by  $\omega_{in}$ , and the output rotation is designated as  $\omega_{out}$ .

In this monograph, the following definition is adopted for the term *gear pair*:

#### Definition 2.1

*A gear pair is an elementary mechanism that is used for the purpose of transmitting and transforming a motion (of a rotation) from an input shaft to an output shaft and that is composed of two mating gears (with either line or point contact between the interacting tooth flanks) mounted in a housing.*

In a gear pair, the mating gears perform an instant rotation (instant screw motion) in relation to one another. Such an instant relative motion of the mating gears in a gear pair is a must. This makes possible construction of the plane of action and the path of contact, as well as other elements of gear pair.

Two examples are considered below in this relation.

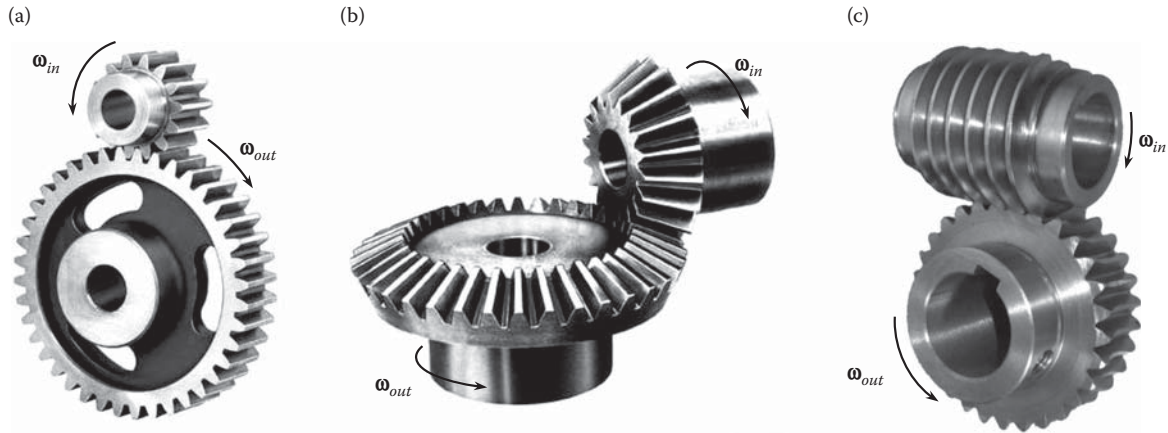
First, consider a *bolt-and-nut* pair. Threads of the bolt and of the nut make *surface-to-surface* contact with each other. With an appropriate value of the helix angle, a rotation of the bolt can be transformed and transmitted to a straight motion of the nut, and vice versa; that is, a rotation of the nut can be transformed and transmitted to a straight motion of the bolt. When the helix angle is zero, then a rotation cannot be transmitted; when the helix angle is a right angle (as in gear coupling), then the translation cannot be transmitted.

Second, consider a *rack-to-rack* pair. Tooth flanks of the racks make surface-to-surface contact with each other. When one of the racks travels straight forward at an angle in relation to another rack, the second one also travels straight forward at an angle in relation to the first rack. In this way, a transformation of the direction of the straight motion occurs. If the first rack travels in a direction parallel to that of the teeth of the second rack, then the tooth flanks of the racks slide over one another—no translation of motion is possible in this case. If the first rack travels in a direction perpendicular to that of the teeth of the second rack, then no transformation of motion is possible in this case.

In the above-discussed examples, that is, the bolt-and-nut pair and *rack-to-rack* pair, both pairs can be construed as a reduced case of a gear pair. However, neither plane of action, nor path of contact, or so forth can be constructed in the case of the considered pairs. The relative motion of the components in both cases is not

---

\* It is the right point to stress here that in contrast to a gear pair, a harmonic drive is composed of more than two components; it is composed of a stator-gear, a flexible gear, and a wave generator. All the components are vital for the design of a harmonic drive. In this monograph, a harmonic drive is not recognized as a gear pair and therefore harmonic drives are not considered in this text.

**FIGURE 2.2**

Examples of: (a) parallel-axes gear pairs, (b) intersected-axes gear pairs, and (c) crossed-axes gear pairs.

a kind of instant rotation (instant screw motion). Therefore, special care must be taken when treating reduced cases of gear pairs, as they often do not possess all the properties that regular gear pairs do.

The purpose of a gear pair is twofold:

- The use of a gear pair makes possible transmission of a motion from an input shaft to an output shaft.
- Motion transformation always occurs when a motion is transmitted (when a motion is transmitted, either the rotation and its direction or just the rotation of the input shaft is altered).

Rotation transformation of another nature can also be observed when transmitting a motion by a gear pair; that is, a rotation can be transformed into a translation and vice versa. Transformation of this kind is observed when a gear is engaged in mesh with a rack. When the rack is driven, the transformation of the rotation into translation occurs; otherwise, when the gear is driven, the translation of the rack is transformed into the rotation of the gear.

A motion can be transmitted between two shafts that are in one of the following relations to each other:

- The axes of rotation are parallel to each other as in parallel-axes gearing (as in  $P_a$ -gearing, for simplicity).
- The axes of rotation intersect each other as in intersected-axes gearing (as in  $I_a$ -gearing, for simplicity).
- The axes of rotation cross each other as in crossed-axes gearing (as in  $C_a$ -gearing, for simplicity).

The third case of crossing axes of rotation of driving and driven shafts ( $C_a$ -gearing) should be construed as the most general one. When the closest distance of approach of the crossing axes is zero, the third case is reduced to the second one; that is, it is reduced to the case of intersecting axes of rotation ( $I_a$ -gearing). On the other hand, if the crossed-axes angle is either zero or equal to  $180^\circ$ , then the third case of crossing axes of rotation is reduced to the first case; that is, it is reduced to the case of parallel axes of rotation ( $P_a$ -gearing).

## 2.2 Vector Representation of Gear Pair Kinematics

The kinematics of a gear pair is based on two rotations. They are:

1. Rotation of a gear about the gear axis of rotation,  $O_g$ , with an angular velocity,  $\omega_g$ .
2. Rotation of a mating pinion about the pinion axis of rotation,  $O_p$ , with an angular velocity,  $\omega_p$ .

The angular velocities,  $\omega_g$  and  $\omega_p$ , are synchronized with one another (commonly, in reduction gear pairs,  $\omega_p/\omega_g = u$ , where  $u$  is the gear ratio. In increasing gear pairs,  $u = \omega_g/\omega_p$ ).

The rotation of a gear can be represented by the rotation vector,  $\omega_g$ , while the rotation of a mating pinion can be represented by the rotation vector,  $\omega_p$ . The rotation vectors,  $\omega_g$  and  $\omega_p$ , are along the corresponding axes of rotation,  $O_g$  and  $O_p$ ; and their magnitudes are equal  $|\omega_g| = \omega_g$ , and  $|\omega_p| = \omega_p$ , correspondingly. The rotation vectors,  $\omega_g$  and  $\omega_p$ , are pointed in a direction defined by the right-hand screw rule.

The instant screw motion of the gear in relation to the pinion, as well as the instant screw motion of the pinion in relation to the gear, can be determined based on the rotation vectors,  $\omega_g$  and  $\omega_p$ , and the actual configuration of the axes,  $O_g$  and  $O_p$ . Making use of the rotation vectors,  $\omega_g$  and  $\omega_p$ , allows for the determination of sliding of the tooth flanks of mating gears. Ultimately, the kinematics of a gear pair can be entirely expressed in terms of the two rotation vectors,  $\omega_g$  and  $\omega_p$  [127,128].

Consider the most general case when the axes of rotation of a gear and its mating pinion are skewed. In this general case, the configuration of the rotation vectors,  $\omega_g$  and  $\omega_p$ , can be expressed in terms of the crossed-axes angle,  $\Sigma$ , and the center distance,  $C$  (i.e., of the closest distance of approach of the crossing axes of rotation,  $O_g$  and  $O_p$ ). The center distance,  $C$ , is measured along the centerline,  $\mathcal{L}$ .

### 2.2.1 Concept of Vector Representation of Gear Pair Kinematics

Referring to Figure 2.3a, consider a crossed-axes gear pair ( $C_a$ -gearing) together with the associated rotation vectors,  $\omega_g$  and  $\omega_p$ . A Cartesian coordinate system,  $XYZ$ , is associated with the crossed-axes gear pair. The rotation vectors,  $\omega_g$  and  $\omega_p$ , of a gear and its mating pinion are at a center distance,  $C$ . The centerdistance,  $C$ , is a straight line segment that is measured along the centerline,  $\mathcal{L}$ , and equals the closest distance of approach between the axes of rotation,  $O_g$  and  $O_p$ , of the gear and its mating pinion. In the particular case under consideration, the crossed-axes angle,  $\Sigma$ , is equal to  $90^\circ$ . The crossed-axes angle,  $\Sigma$ , can also be either acute ( $\Sigma < 90^\circ$ ) or obtuse ( $\Sigma > 90^\circ$ ).

The rotation vectors of a gear,  $\omega_g$ , and its mating pinion,  $\omega_p$ , are in fact sliding vectors (Figure 2.3b). They can be applied at any point within the gear axis,  $O_g$ , and the pinion axis,  $O_p$ , correspondingly. It is convenient to apply the rotation vectors,  $\omega_g$  and  $\omega_p$ , at points of intersection,  $A_g$  and  $A_p$ , of the corresponding axes of rotation,  $O_g$  and  $O_p$ , by the centerline,  $\mathcal{L}$  (i.e., by a line along which the center distance,  $C$ , is measured). As will be

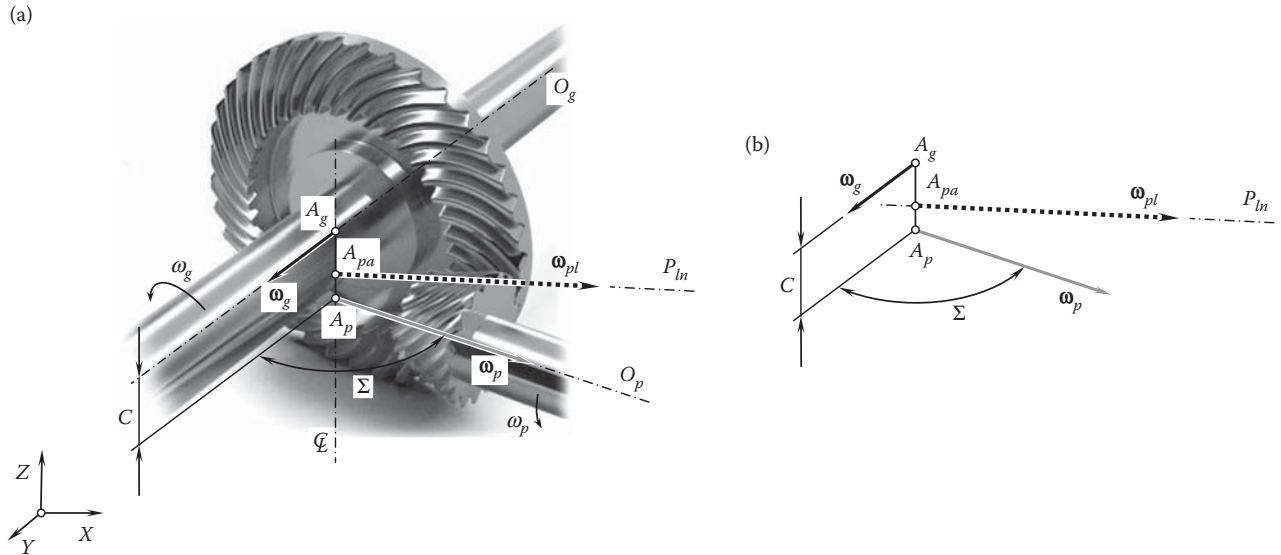


FIGURE 2.3

Kinematics of crossed-axes gearing with a constant tooth ratio,  $u$ : (a) a schematic of the gear pair, and (b) an equivalent vector diagram: the rotation vectors,  $\omega_g$  and  $\omega_p$ , of a  $C_a$ -gearing are at a center distance,  $C$ , from each other, and form a crossed-axes angle,  $\Sigma$ .

\* Angular velocity is considered in this monograph as a vector along the axis of rotation that is pointed in a direction defined by the right-hand screw rule. It is understood here and below that rotations,  $\omega_g$  and  $\omega_p$ , are not vectors in nature. Therefore, special care is required when treating rotations as vectors. In particular, when coordinate system transformation is analytically described by means of matrices, the order of the matrices in the matrix product is predetermined by the order of the elementary coordinate system transformations; that is, the order of the matrices in the matrix product cannot be altered.

shown later in this monograph, points  $A_g$  and  $A_p$  are by nature the apexes of the base cones of a gear and its mating pinion, correspondingly. In a case where the axes of rotation,  $O_g$  and  $O_p$ , intersect one another (i.e., when  $C = 0$ ), it is convenient to apply the rotation vectors,  $\omega_g$  and  $\omega_p$ , at point of intersection of the axes [127,128].

The magnitude of rotation of the gear,  $\omega_g$ , is  $\omega_g = |\omega_g|$ , whereas the magnitude of rotation of the pinion,  $\omega_p$ , is  $\omega_p = |\omega_p|$ . The magnitudes,  $\omega_g$  and  $\omega_p$ , of rotations  $\omega_g$  and  $\omega_p$  are synchronized with each other.

The crossed-axes angle,  $\Sigma$ , is measured between the rotation vectors,  $\omega_g$  and  $\omega_p$ ; that is, the equality\*

$$\Sigma = \angle(\omega_g, \omega_p) \quad (2.1)$$

is observed for a gear pair.

Equation 2.1 immediately yields a formula:

$$\Sigma = \tan^{-1} \frac{|\omega_g \times \omega_p|}{\omega_g \cdot \omega_p} \quad (2.2)$$

for the calculation of the actual value of the crossed-axes angle,  $\Sigma$ .

A more detailed explanation is required in order to make clear the concept of the crossed-axes angle,  $\Sigma$ .

Consider two straight lines,  $L_1$  and  $L_2$ , whose directions are not specified (Figure 2.4a). In the case under consideration, the straight-line segment,  $A_1A_2$ , is the center distance,  $C$ , for the straight lines,  $L_1$  and  $L_2$ . The angular configuration of the straight lines,  $L_1$  and  $L_2$ , can be specified by either the acute angle,  $\Sigma$ , or the obtuse angle,  $\Sigma^*$ . The specifications of the crossed-axes angle of the straight lines,  $L_1$  and  $L_2$ , by means of the angles,  $\Sigma$  and  $\Sigma^*$ , are equivalent to one another as long as the directions of the straight lines,  $L_1$  and  $L_2$ , are not given.

Once the directions of the straight lines,  $L_1$  and  $L_2$ , are specified (e.g., the directions are specified by the unit vectors,  $s_1$  and  $s_2$ , along the straight lines,  $L_1$  and  $L_2$ ), it is easy to see when the crossed-axes angle,  $\Sigma$ , is acute (Figure 2.4b) and when it is obtuse (Figure 2.4c). Thus, no duality in the specification of the crossed-axes angle,  $\Sigma$ , is observed for the rotation vectors,  $\omega_g$  and  $\omega_p$ , of a gear pair.

For a specified pair of rotation vectors,  $\omega_g$  and  $\omega_p$ , the closest distance of approach,  $C$ , between the straight lines,  $L_1$  and  $L_2$ , can be calculated based on the following approach.

In order to obtain the length of the common perpendicular,  $C = A_1A_2$ , to the lines,  $L_1$  and  $L_2$  (see Figure 2.5), the directions of the lines are denoted by the unit vectors,  $s_1$  and  $s_2$ , the position vectors of points  $l_1$  and  $l_2$  by  $r_1(l_1)$  and  $r_2(l_2)$ , and the direction of  $C = \overrightarrow{A_1A_2}$  by the unit vector,  $c$  (unknown).

Then, the following expression can be composed for the calculation of the center distance,  $C$ :

$$C = r_1 + l_1 A_1 s_1 = r_2 + l_2 A_2 s_2 - Cc \quad (2.3)$$

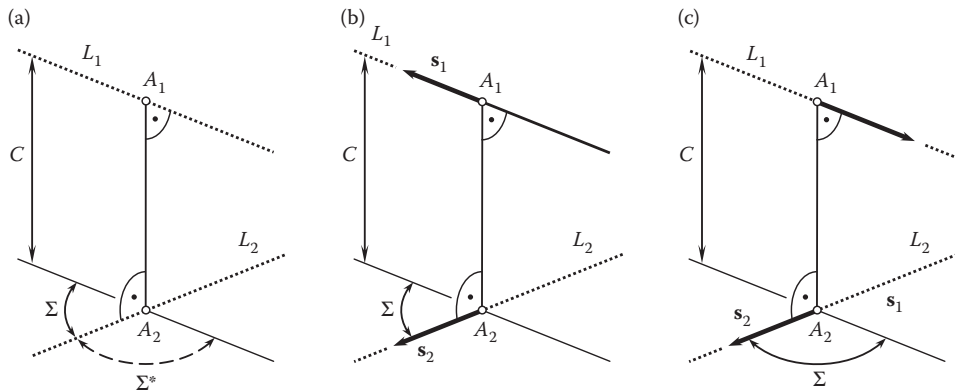


FIGURE 2.4

Definition of the crossed-axes angle,  $\Sigma$ , for a gear pair: the directions of the straight lines,  $L_1$  and  $L_2$ , (a) are not specified, (b) are specified ( $\Sigma < 0^\circ$ ), and (c) are specified ( $\Sigma > 0^\circ$ ).

\* For the reader's convenience, elements of vector calculus are concisely summarized in Appendix A.

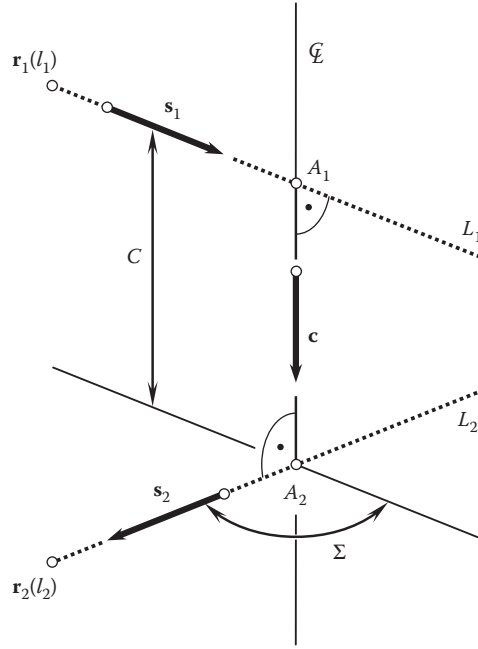


FIGURE 2.5

Determination of the center distance,  $C$ , in a gear pair.

On taking the scalar product of this equation with  $\mathbf{c}$ , we obtain:

$$\mathbf{r}_1 \cdot \mathbf{c} + l_1 A_1 \mathbf{s}_1 \cdot \mathbf{c} = \mathbf{r}_2 \cdot \mathbf{c} + l_2 A_2 \mathbf{s}_2 \cdot \mathbf{c} - C \quad (2.4)$$

However, since the direction,  $\mathbf{C}$ , is perpendicular to  $L_1$  and  $L_2$ , the products,  $\mathbf{s}_1 \cdot \mathbf{c}$  and  $\mathbf{s}_2 \cdot \mathbf{c}$ , are zero, so that:

$$C = (\mathbf{r}_2 - \mathbf{r}_1) \cdot \mathbf{c} \quad (2.5)$$

Moreover, since  $\mathbf{c}$  is perpendicular to  $\mathbf{s}_1$  and  $\mathbf{s}_2$ , it is proportional to  $\mathbf{s}_1 \times \mathbf{s}_2$ . Since the center distance,  $C$ , is to be a length, it must be positive, so that finally:

$$C = \left| \frac{(\mathbf{r}_2 - \mathbf{r}_1) \cdot (\mathbf{s}_1 \times \mathbf{s}_2)}{|\mathbf{s}_1 \times \mathbf{s}_2|} \right| \quad (2.6)$$

The use of the rotation vectors,  $\boldsymbol{\omega}_g$  and  $\boldsymbol{\omega}_p$ , makes possible the construction of the vector of instant rotation,  $\boldsymbol{\omega}_{pl}$  (Figure 2.3b), of the pinion in relation to the gear (or vice versa, the vector of instant rotation of the gear in relation to the pinion). The point of interception of the line of action of the vector of instant rotation,  $\boldsymbol{\omega}_{pl}$ , by the center line,  $\mathcal{L}$ , is designated as  $A_{pa}$ . As will be shown later in this monograph, point  $A_{pa}$  is by nature the apex of the plane of action of the gear pair.

The principle of inversion\* of rotations is used in further analysis below. Two different options are available in this regard:

First, the gear pair can be rotated about the pinion axis of rotation,  $O_p$ , with the rotation vector,  $-\boldsymbol{\omega}_p$ . Under this scenario, the pinion becomes stationary [as:  $\boldsymbol{\omega}_p + (-\boldsymbol{\omega}_p) = 0$ ], and the resultant instantaneous rotation of the gear is equal to the following:

$$\boldsymbol{\omega}_{gp} = (\boldsymbol{\omega}_g - \boldsymbol{\omega}_p) \quad (2.7)$$

\* The process of holding different links of a kinematic chain stationary is known as *inversion*.

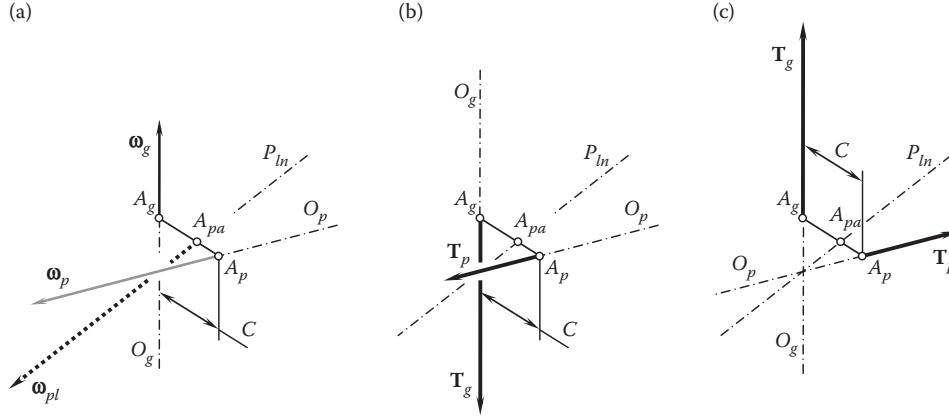


FIGURE 2.6

Vector diagram for the rotations, and two vector diagrams for the torques in a gear pair: (a) vector diagram for the rotations in a crossed-axes gear pair and two vector diagrams for the torques in the same gear pair corresponding to (b) the case of reduction gearing, when the pinion is driving and the gear is driven, and (c) the case of increasing gearing, when the gear is driving and the pinion is driven.

Such a situation corresponds to the case of rotation of the gear in relation to the pinion when the latter is motionless.

Second, the gear pair can be rotated about the gear axis of rotation,  $O_g$ , with the rotation vector,  $-\omega_g$ . Under this scenario, the gear becomes motionless [as:  $\omega_g + (-\omega_g) = 0$ ], and the resultant instantaneous rotation of the pinion is equal to the following:

$$\omega_{pg} = (\omega_p - \omega_g) \quad (2.8)$$

Such a situation corresponds to the case of rotation of the pinion in relation to the gear when the latter is stationary.

Evidently, the rotation vectors,  $\omega_{gp}$  and  $\omega_{pg}$ , are of equal magnitudes and are opposite to each other ( $\omega_{gp} = -\omega_{pg}$ ).

In addition to the vector diagrams for the rotation vectors,  $\omega_g$  and  $\omega_p$ , corresponding vector diagrams can be constructed for torque vectors.

Torque on a gear shaft is denoted by  $T_g$ , and torque on a mating pinion shaft is designated as  $T_p$ . One of the torques (usually the torque,  $T_p$ ) is the input torque, while another one (usually the torque,  $T_g$ ) is the output torque.

An example of vector diagrams for the input and output torques,  $T_g$  and  $T_p$ , is schematically illustrated in Figure 2.6. In Figure 2.6a, a vector diagram for the rotation vectors,  $\omega_g$  and  $\omega_p$ , is shown. Then, a corresponding vector diagram for the input and output torques,  $T_g$  and  $T_p$ , is constructed for the case in which the pinion is driving and the gear is driven (Figure 2.6b). This configuration corresponds to a case of reduction gears. In Figure 2.6c, a vector diagram for the input and output torques,  $T_g$  and  $T_p$ , which is constructed for the case when the gear is driving and the pinion is driven, is shown. This configuration corresponds to a case of increasing gears.

The input torque is always pointed in the same direction as the input rotation vector. The output torque is always pointed in the direction opposite that of the output rotation vector.

Torque diagrams can be constructed for gearings of all types, that is, for gearings that feature crossing axes of rotation, as well as when the axes of rotation of the driving and the driven shafts are either parallel or intersect one another.

### 2.2.2 Vector Diagrams of Three Different Types for Spatial Gear Pairs

Let us suppose that two axes of rotation,  $O_g$  and  $O_p$ , are positioned in space in relation to one another, and the aim is to transmit a rotation and torque between the axes, using for this purpose gears of a certain type. Two



points,  $A_g$  and  $A_p$ , are the points of intersection of the axes of rotation,  $O_g$  and  $O_p$ , by the center line,  $\mathcal{L}$ . Then, the straight-line segment,  $A_gA_p$ , is the center distance,  $C$ .

Depending on the location of the point,  $A_{par}$ , in relation to the end-points,  $A_g$  and  $A_p$ , only three different types of spatial (crossed-axes) gear pairs can be distinguished. They are as follows:

- *Rotary-negative crossed-axes gear pairs*, for which the point,  $A_{par}$ , is located between the end-points,  $A_g$  and  $A_p$ . Gearing of this particular type features a negative gear ratio (i.e.,  $u < 0$ ). The term *rotary-negative crossed-axes gear pairs* is due to  $u < 0$ . In gearing of this type, the direction of the output rotation,  $\omega_{out}$ , is opposite to the direction of the input rotation,  $\omega_{in}$ . In external gearings, the point,  $A_{par}$ , is located between the end-points,  $A_g$  and  $A_p$ . However, internal gearings also may have this design feature.
- *Rotary-positive crossed-axes gear pairs*, for which the point,  $A_{par}$ , is located beyond the end-point,  $A_p$ . Gearing of this particular type features a positive gear ratio (i.e.,  $u > 0$ ). The term *rotary-positive crossed-axes gear pairs* is due to  $u > 0$ . In gearing of this particular type, the direction of the output rotation,  $\omega_{out}$ , is the same as the direction of the input rotation,  $\omega_{in}$ . In internal gearings the point,  $A_{par}$ , is located beyond the end-point  $A_p$ . However, external gearings also may have this design feature.
- *Rotary-zero crossed-axes gear pairs*, for which the point,  $A_{par}$ , is coincident with the end-point  $A_p$ . The term *rotary-zero crossed-axes gear pairs* is because in parallel-axes gearing of this type, the output rotation, that is, the rotation of the gear, is zero (i.e.,  $\omega_g = 0$ ). Rack-type gear pairs of a conventional design feature a zero rotation of the gear (zero rotation of the rack): for a certain rotation of the pinion,  $\omega_p$ , the rotation of the gear (of the rack),  $\omega_g$ , is always zero,  $\omega_g = 0$  (as the rack performs a straight motion). In a more general case of zero crossed-axes gearing, a rotation of the gear is not equal to zero, that is,  $\omega_g \neq 0$ . The gear ratio in zero crossed-axes gear pairs is not zero (i.e.,  $u \neq 0$ ). By convention, the term *rotary-zero crossed-axes gear pairs* is applied to gearings of all types, that is, to parallel-axes gear-to-rack pairs ( $u = 0$ ), intersected-axes gearing ( $u \neq 0$ ), and crossed-axes gearing ( $u \neq 0$ ) as well.

No other types of spatial gear pairs are feasible, and any known or newly designed gear pair in the future falls into one of the three aforementioned types of spatial gear pairs.

Here and below, the proposed terms *rotary-negative crossed-axes gear pairs*, *rotary-positive crossed-axes gear pairs*, and *rotary-zero crossed-axes gear pairs* are used in parallel with the terms *external crossed-axes gear pairs*, *internal crossed-axes gear pairs*, and *rack-type crossed-axes gear pairs*, as the proposed terms and those used in the current practice are not equivalent to one another.

For example, in a case of  $C_a$ -gearing, there exists a corresponding *round rack* (or a *crown gear*). The round rack is the limit case for gearings that either (a) alters the direction of rotation of the driving member (commonly referred to as *external gearing*), or (b) doesn't alter the direction of rotation of the driving member (commonly referred to as *internal gearing*). However, in the first case, the gear may be internal as well, similar to how the gear may be external in the second case.

Moreover, the terminology listed below:

1. *u-positive gearing* (or just  $u^+$ -gearing) when the gear ratio,  $u$ , is of a positive value,  $u > 0$
2. *u-zero gearing* (or just  $u^0$ -gearing) when the gear ratio,  $u$ , is a zero,  $u = 0$
3. *u-negative gearing* (or just  $u^-$ -gearing) when the gear ratio,  $u$ , is of a negative value,  $u < 0$

may also be used in the theory of gearing. Here the gear ratio,  $u$ , equals the ratio of the input rotation to the output rotation.

The actual type of a spatial gear pair, whether rotary-positive, rotary-negative, or rack-type spatial gear pair, depends on:

- a. The magnitudes,  $\omega_g$  and  $\omega_p$ , of the rotations of the gear and the pinion, respectively.
- b. The actual value of the crossed-axes angle,  $\Sigma$ , between the rotation vectors  $\omega_g$  and  $\omega_p$ .
- c. The actual value of the center-distance,  $C$ .

A classification of the vector diagrams of gear pairs of all types can be developed based on the actual values of the parameters ( $\omega_g$  and  $\omega_p$ ,  $\Sigma$ , and  $C$ ) of gear pairs.

It is the right point to stress here that no ultimate decision can be made on whether a gear pair is external or internal based only on a vector diagram of the gear pair.

### 2.2.2.1 Vector Diagrams of Rotary-Negative Crossed-Axes Gear Pairs

A vector diagram that is constructed for a certain combination of the rotation vectors,  $\omega_g$  and  $\omega_p$ , crossed-axes angle,  $\Sigma$ , and center-distance,  $C$ , corresponds to an external spatial gear pair. An example of rotary-negative (commonly external) crossed-axis gear pair (*rotary-negative  $C_a$ -gearing*) is illustrated in Figure 2.7.

Having two rotation vectors,  $\omega_g$  and  $\omega_p$ , specified, the corresponding vector of instant rotation,  $\omega_{pl}$ , of the pinion in relation to the gear ( $\omega_{pl} \equiv \omega_{pg} = -\omega_{gp}$ ) can be constructed. The instant rotation,  $\omega_{pl}$ , is performed about a straight line,  $P_{ln}$ , which is the axis of instant rotation.\*

The vector of instantaneous rotation,  $\omega_{pl}$ , as well as other kinematical parameters of a rotary-negative gear pair, can be determined graphically by implementing the methods developed for this purpose in descriptive geometry. An example of such a construction is illustrated in Figure 2.8.

For the purposes of construction of a vector diagram, a reference system,  $\pi_1\pi_2$ , of two orthogonal planes of projection,  $\pi_1$  and  $\pi_2$ , is implemented (Figure 2.8a). Following the convention adopted in descriptive geometry, the subscript 1 is assigned to projections onto plane  $\pi_1$  of all points, lines, and so forth. Similarly, the subscript 2 is assigned to projections onto plane  $\pi_2$  of all of those same points, lines, and so forth.

The location and orientation of a pair of rotation vectors,  $\omega_g$  and  $\omega_p$ , within the reference system,  $\pi_1\pi_2$ , can be arbitrary. However, for convenience, the rotation vectors,  $\omega_g$  and  $\omega_p$ , are depicted in the reference system,  $\pi_1\pi_2$ , parallel to the horizontal plane of projection,  $\pi_1$ . In this scenario, the crossed-axes angle,  $\Sigma$ , is projected onto plane  $\pi_1$  with no distortion. The centerline,  $\mathcal{L}$ , is projected onto plane  $\pi_1$  into a point. This point is denoted by  $A_{pa}$ .

The principle of inversion of rotations is used again here. Let us assume that a rotation,  $-\omega_g$ , is applied to a gear pair, that is, to the pinion, gear, and housing. The rotation,  $-\omega_g$ , does not affect the relative motion of the gear and the pinion.

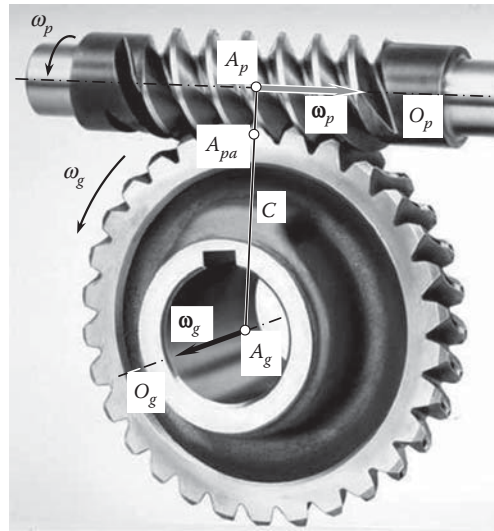


FIGURE 2.7

An example of rotary-negative external crossed-axes gear pair (rotary-negative external  $C_a$ -gearing).

\* It is the right point to explain here the reason the axis of instant rotation of a pinion in relation to its mating gear is designated as  $P_{ln}$ . In the simplest cases of spur and helical gearing, it is a commonly adopted practice to consider the instant motion of a pinion in relation to its mating gear as an instant rotation about the *pitch point*,  $P$ . Actually, the instant rotation of the pinion occurs not about the pitch point,  $P$ , but, instead, about a straight line through the pitch point,  $P$ . This straight line is parallel to the axes of rotation of the gear and the mating pinion. Therefore, it is natural to refer to the axis of instant rotation as to the *pitch line* and to designate such a straight line as  $P_{ln}$ , as it is convenient. However, under such a scenario, the term *pitch line*,  $P_{ln}$  that is used in gear kinematics needs to be distinguished from a similar term *pitch line* that is used, for example, with respect to a rack gear. Here and below through the rest of the book, the term the *pitch line*,  $P_{ln}$  is understood in the sense of the *axis of instant rotation* of a pinion in relation to its mating gear.

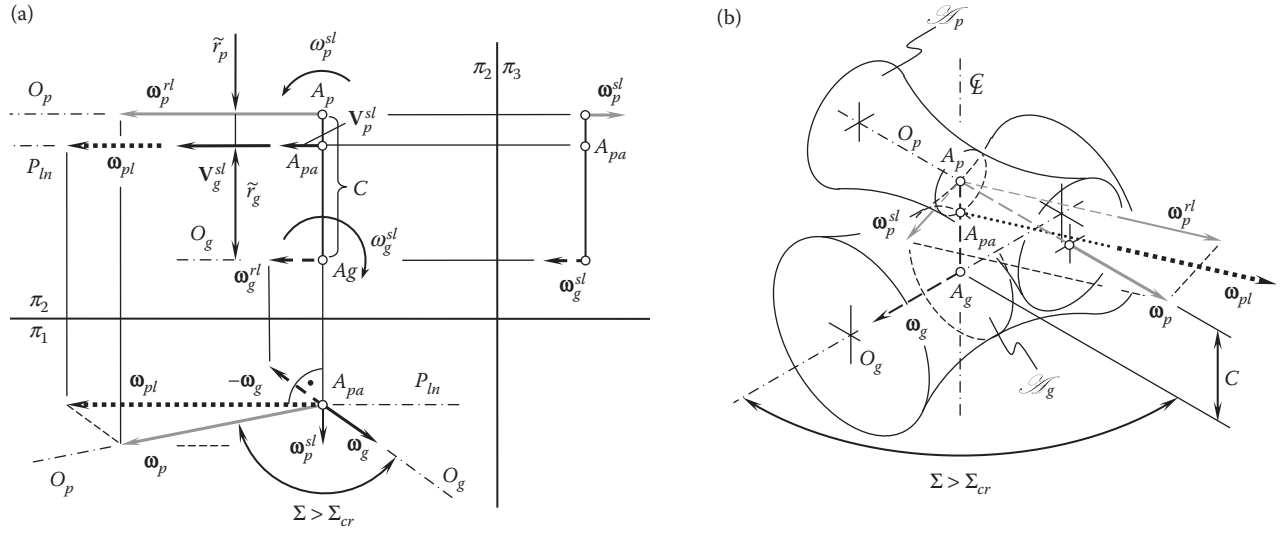


FIGURE 2.8

Vector diagram of a rotary-negative (commonly external) crossed-axes gear pair (rotary-negative  $C_a$ -gearing): (a) the vector diagram for the rotation vectors and (b) an obsolete representation (by means of the axodes) of the kinematics of a gear pair of this type.

Under the additional rotation,  $-\omega_g$ , the gear becomes stationary  $[\omega_g + (-\omega_g) = 0]$ . The rotation of the gear pair housing (denoted by the rotation vector,  $-\omega_g$ ) is opposite to the rotation vector of the gear (denoted by  $\omega_g$ ). Ultimately, the rotation of the pinion is the superposition of two rotations, namely of the rotation vectors,  $\omega_p$  and  $-\omega_g$ . The result of two rotations,  $\omega_p$  and  $-\omega_g$ , is the instant rotation,  $\omega_{pl} = (\omega_p - \omega_g)$ , of the pinion about the pitch line,  $P_{ln}$ .

Within the horizontal plane of projection,  $\pi_1$ , the vector of instant rotation,  $\omega_{pl}$ , can be determined as the vector difference of the rotation vectors,  $\omega_g$  and  $\omega_p$ . Onto the plane of projection,  $\pi_1$ , the vector,  $\omega_{pl}$ , is projected with no distortion since the rotation vectors,  $\omega_g$  and  $\omega_p$ , are parallel to the plane,  $\pi_1$ . The rotation vector,  $\omega_{pl}$ , is applied at point  $A_{pa}$  within the centerline,  $\mathcal{L}$ .

Immediately upon the rotation vector,  $\omega_{pl}$ , being determined, the axis of projection,  $\pi_1/\pi_2$ , can be constructed so that it is parallel to the vector of instant rotation,  $\omega_{pl}$ . Such a configuration of the axis,  $\pi_1/\pi_2$ , is not mandatory; the configuration can be arbitrary. Convenience is the only reason for selecting this particular orientation for the axis of projection,  $\pi_1/\pi_2$ , in relation to the rotation vector,  $\omega_{pl}$ .

#### 2.2.2.1.1 Conditions of Pure Rolling in Rotary-Negative Crossed-Axes Gear Pairs: General Consideration

The shown in Figure 2.8a, the vector diagram of rotary-negative crossed-axes gear pairs is helpful to investigate the conditions of pure rolling (and sliding) in gearings of various types.

Projections of the rotation vectors,  $\omega_g$  and  $\omega_p$ , onto the frontal plane of projections,  $\pi_2$ , are designated as  $\omega_g^{rl}$  and  $\omega_p^{rl}$ , respectively. The components,  $\omega_g^{rl}$  and  $\omega_p^{rl}$ , of the rotation vectors,  $\omega_g$  and  $\omega_p$ , are parallel to the axis of instant rotation,  $P_{ln}$ . These components cause transmission of the rotation between the gear and the pinion. The following equality can be directly derived from Figure 2.8a, [127,128]:

$$\tilde{r}_p \omega_p \cdot \cos \Sigma_p = \tilde{r}_g \omega_g \cdot \cos \Sigma_g \quad (2.9)$$

This equation is valid for the magnitudes,  $\omega_p$ ,  $\omega_g$ , and  $\omega_{pl}$ , of the rotation vectors,  $\omega_g$ ,  $\omega_p$ , and  $\omega_{pl}$ . Here and below, the gear and the pinion cone angle are designated as  $\Sigma_g$  and  $\Sigma_p$ , correspondingly. The ratios,  $\tilde{r}_g/\tilde{r}_p$ ,  $\omega_p/\omega_g$ , and a few more formulas can be directly extracted from Equation 2.9.

Similarly, two more equalities can be directly derived from Figure 2.8a, [127,128]:

$$\tilde{r}_p \omega_{pl} = (\tilde{r}_g + \tilde{r}_p) \omega_g \cdot \cos \Sigma_g \quad (2.10)$$

$$\tilde{r}_g \omega_{pl} = (\tilde{r}_g + \tilde{r}_p) \omega_p \cdot \cos \Sigma_p \quad (2.11)$$

In Equations 2.9 through 2.11, the distance between the apex,  $A_{pa}$ , and the gear axis,  $O_g$ , is designated as  $\tilde{r}_g$  (i.e.,  $\tilde{r}_g = A_g A_{pa}$ ). The distances of the same point,  $A_{pa}$ , from the pinion axis,  $O_p$ , are designated as  $\tilde{r}_p$ , (i.e.,  $\tilde{r}_p = A_p A_{pa}$ ). The distances,  $\tilde{r}_g$  and  $\tilde{r}_p$ , are signed values. For a negative gear pair, both of them are positive (i.e.,  $\tilde{r}_p > 0$  and  $\tilde{r}_g > 0$ ).

Evidently, the equality:

$$\tilde{r}_p + \tilde{r}_g = C \quad (2.12)$$

is valid for a rotary negative external spatial gear pair.

The angles,  $\Sigma_g$  and  $\Sigma_p$ , are the gear and the pinion cone angles, correspondingly. In parallel-axes gearing, these angles equal either zero or  $180^\circ$ . In cases of intersected-axes gearing, the gear and the pinion angles equal the corresponding pitch cone angles; that is, the equalities,  $\Sigma_g = \Gamma$  and  $\Sigma_p = \gamma$ , are observed. No analogies for the cone angles,  $\Sigma_g$  and  $\Sigma_p$ , are available in a case of crossed-axes gearing.

By definition, the cone angles,  $\Sigma_g$  and  $\Sigma_p$ , are specified by the following expressions:

$$\Sigma_g = \angle(\mathbf{w}_g, \mathbf{w}_{pl}) \quad (2.13)$$

$$\Sigma_p = \angle(\mathbf{w}_p, \mathbf{w}_{pl}) \quad (2.14)$$

Equations 2.13 and 2.14 immediately yield the formulas:

$$\Sigma_g = \tan^{-1} \frac{|\mathbf{w}_g \times \mathbf{w}_{pl}|}{\mathbf{w}_g \cdot \mathbf{w}_{pl}} \quad (2.15)$$

$$\Sigma_p = \tan^{-1} \frac{|\mathbf{w}_p \times \mathbf{w}_{pl}|}{\mathbf{w}_p \cdot \mathbf{w}_{pl}} \quad (2.16)$$

for the calculation of the actual values of the gear and pinion cone angles,  $\Sigma_g$  and  $\Sigma_p$ .

Once the rotation vectors,  $\mathbf{w}_g$  and  $\mathbf{w}_p$ , and the crossed-axes angle,  $\Sigma$ , are specified, then it can be easily shown that the gear cone angle,  $\Sigma_g$ , can be calculated from the formula:

$$\sin \Sigma_g = \frac{\omega_p}{\omega_{pl}} \sin \Sigma \quad (2.17)$$

and the pinion cone angle,  $\Sigma_p$ , can be calculated from the formula:

$$\sin \Sigma_p = \frac{\omega_g}{\omega_{pl}} \sin \Sigma \quad (2.18)$$

where the magnitude,  $\omega_{pl}$ , of the relative rotation vector,  $\mathbf{w}_{pl}$ , equals:

$$\omega_{pl} = \sqrt{\omega_g^2 + \omega_p^2 - 2\omega_g\omega_p \cos \Sigma} \quad (2.19)$$

The condition of pure rolling can be employed for the determination of the location of the plane of action apex,  $A_{pa}$ , within the centerline,  $\mathcal{L}$ . In compliance with the condition, the following ratio:

$$\frac{\tilde{r}_g}{\tilde{r}_p} = \frac{\omega_p^{rl}}{\omega_g^{rl}} \quad (2.20)$$

should be fulfilled. Equation 2.20 perfectly correlates to the above Equation 2.9.

In Equation 2.20, the designations  $\omega_g^{rl} = |\omega_g^{rl}|$  and  $\omega_p^{rl} = |\omega_p^{rl}|$  are used (the components,  $\omega_g^{rl}$  and  $\omega_p^{rl}$ , of the rotation vectors,  $\omega_g$  and  $\omega_p$ , cause pure rolling in a gear pair).

Generally speaking, the magnitudes,  $\omega_g^{rl}$  and  $\omega_p^{rl}$ , of the vectors of pure rolling,  $\omega_g^{rl}$  and  $\omega_p^{rl}$ , are not equal to each other. The inequality  $\omega_g^{rl} < \omega_p^{rl}$  is commonly observed. The equality  $\omega_g^{rl} = \omega_p^{rl}$  is observed only in particular cases when the tooth number of a gear,  $N_g$ , and tooth number of its mating pinion,  $N_p$ , are equal to each other (i.e., the equality  $N_g = N_p$  is valid).

From Equation 2.12, the distance  $\tilde{r}_g$  can be expressed in terms of the center distance,  $C$ , and the distance,  $\tilde{r}_p$ :

$$\tilde{r}_g = C - \tilde{r}_p \quad (2.21)$$

Substituting this expression for the distance,  $\tilde{r}_g$ , in Equation 2.20, a formula:

$$\tilde{r}_p = \frac{\omega_g^{rl}}{\omega_p^{rl} + \omega_g^{rl}} \cdot C \quad (2.22)$$

for calculating the distance,  $\tilde{r}_p$ , can be derived.

Further, Equation 2.21 can be used for calculating the distance,  $\tilde{r}_g$ . After substituting Equation 2.22 in Equation 2.21, the equality,  $\tilde{r}_g = C - \tilde{r}_p$ , can be transformed as follows:

$$\tilde{r}_g = \frac{\omega_p^{rl}}{\omega_p^{rl} + \omega_g^{rl}} \cdot C \quad (2.23)$$

For rotary-negative (commonly external) crossed-axes gear pairs, the plane of action apex,  $A_{pa}$ , is located within the centerline between the gear apex,  $A_g$ , and the pinion apex,  $A_p$ .

#### 2.2.2.1.2 Conditions of Pure Sliding in Rotary-Negative Crossed-Axes Gear Pairs: General Consideration

The vector diagram of rotary-negative crossed-axes gear pairs shown in Figure 2.8a is helpful to investigate the conditions of pure sliding in gearings of various types.

In Figure 2.8a, the components,  $\omega_g^{sl}$  and  $\omega_p^{sl}$ , of the rotation vectors,  $\omega_g$  and  $\omega_p$ , are perpendicular to the axis of instant rotation,  $P_{ln}$ . With no distortion, these components are projected onto the frontal plane of projections,  $\pi_3$ . The plane of projections,  $\pi_3$ , is perpendicular to the axis of projections,  $\pi_1/\pi_2$ .

The rotations,  $\omega_g^{sl}$  and  $\omega_p^{sl}$ , cause pure sliding in the direction of the pitch line,  $P_{ln}$ . Magnitudes  $\omega_g^{sl} = |\omega_g^{sl}|$  and  $\omega_p^{sl} = |\omega_p^{sl}|$  of the angular velocities of sliding are equal one another ( $\omega_g^{sl} = \omega_p^{sl}$ ). The rotation vectors of sliding,  $\omega_g^{sl}$  and  $\omega_p^{sl}$ , are pointed in the opposite directions (i.e.,  $\omega_p^{sl} = -\omega_g^{sl}$ ).

Relative sliding in the direction of the pitch line,  $P_{ln}$ , is created by both the gear and the pinion.

The vector of linear velocity of sliding,  $\mathbf{V}_g^{sl}$ , that is created by the gear is equal to:

$$\mathbf{V}_g^{sl} = \tilde{r}_g \cdot \omega_g^{sl} \quad (2.24)$$

Similarly, the vector of linear velocity of sliding,  $\mathbf{V}_p^{sl}$ , that is created by the pinion is equal to:

$$\mathbf{V}_p^{sl} = \tilde{r}_p \cdot \omega_p^{sl} \quad (2.25)$$

The expressions  $|\omega_g^{sl}| = |\omega_p^{sl}|$  and  $\tilde{r}_g \geq \tilde{r}_p$  are valid for a rotary-negative (usually external) crossed-axes gear pairs; then, the component of sliding velocity,  $\mathbf{V}_g^{sl}$ , that is caused by the gear exceeds or is equal to the component of sliding velocity,  $\mathbf{V}_p^{sl}$ , that is caused by the pinion; that is, the inequality  $|\mathbf{V}_g^{sl}| \geq |\mathbf{V}_p^{sl}|$  is always observed.

The directions of the sliding velocity vectors,  $\mathbf{V}_g^{sl}$  and  $\mathbf{V}_p^{sl}$ , in a rotary-negative gear pair are always opposite to each other. The resultant sliding velocity vector,  $\mathbf{V}_{g-p}^{sl}$ , of the gear in relation to the pinion is equal to the difference:

$$\mathbf{V}_{g-p}^{sl} = \mathbf{V}_g^{sl} - \mathbf{V}_p^{sl} \quad (2.26)$$

The resultant sliding velocity vector,  $\mathbf{V}_{p-g}^{sl}$ , of the pinion in relation to the gear is opposite to the sliding velocity vector,  $\mathbf{V}_{g-p}^{sl}$ :

$$\mathbf{V}_{p-g}^{sl} = -\mathbf{V}_{g-p}^{sl} = \mathbf{V}_p^{sl} - \mathbf{V}_g^{sl} \quad (2.27)$$

The magnitude of speed of the resultant sliding in a rotary-negative crossed-axes gear pair can be calculated from the following formula:

$$V_{sc} = V_g^{sl} + V_p^{sl} \quad (2.28)$$

If the component vectors,  $\boldsymbol{\omega}_g^{sl}$  and  $\boldsymbol{\omega}_p^{sl}$ , are of the same magnitude and opposite to each other, then they constitute a *pair of rotation*. An equivalent velocity vector of the translation motion,  $\mathbf{V}_{sc}$ , can be constructed for a given pair of rotations. The velocity vector,  $\mathbf{V}_{sc}$ , is parallel to the vector of instant rotation,  $\boldsymbol{\omega}_{pl}$ . The following formula:

$$V_{sc} = |\mathbf{V}_{sc}| = C \cdot \omega_p \cdot \sin \Sigma_p = C \cdot \omega_g \cdot \sin \Sigma_g \quad (2.29)$$

can be used for calculating the magnitude of the velocity vector,  $\mathbf{V}_{sc}$ .

Ultimately, the resultant instant relative motion of the gear and the pinion is composed of:

- An instantaneous rotation,  $\boldsymbol{\omega}_{pl}$ , about axis of instant rotation,  $P_{ln}$ .
- An instantaneous translation,  $\mathbf{V}_{sc}$ , axis of instant rotation,  $P_{ln}$ .

Superposition of the rotation,  $\boldsymbol{\omega}_{pl}$ , and the translation,  $\mathbf{V}_{sc}$ , results in a screw motion. The parameter of the screw motion is designated as  $p_{sc}$ . The screw parameter,  $p_{sc}$ , is commonly referred to as the *reduced pitch*.

For the calculation of the reduced pitch,  $p_{sc}$ , the following formula is applied [127,128]:

$$p_{sc} = \frac{V_{sc}}{\omega_{pl}} = \frac{C \cdot \omega_p \cdot \sin \Sigma_p}{\omega_{pl}} = \frac{C \cdot \omega_g \cdot \sin \Sigma_g}{\omega_{pl}} \quad (2.30)$$

An expression:

$$\omega_{pl} = \frac{C \cdot \omega_p \cdot \cos \Sigma_p}{\tilde{r}_g} = \frac{C \cdot \omega_g \cdot \cos \Sigma_g}{\tilde{r}_p} \quad (2.31)$$

for the calculation of magnitude of instant rotation can be derived from Equations 2.9 through 2.11.

Therefore, the parameter of a screw motion can be calculated from the following formula:

$$p_{sc} = \tilde{r}_p \cdot \tan \Sigma_g = \tilde{r}_g \cdot \tan \Sigma_p \quad (2.32)$$

This immediately returns the following proportion:\*

$$\frac{\tilde{r}_p}{\tilde{r}_g} = \frac{\tan \Sigma_g}{\tan \Sigma_p} \quad (2.33)$$

The resultant instantaneous motion of the gear and the pinion can be construed as rolling with sliding of two *hyperboloids of one sheet* over each other, as illustrated in [Figure 2.8b](#). (This obsolete approach is known in the literature on gearing.) One of the hyperboloids,  $\mathcal{H}_g$ , is associated with the gear, while the other one,  $\mathcal{H}_p$ , is associated with the pinion. In a particular case, the gear hyperboloid,  $\mathcal{H}_g$ , can be considered stationary. In such a scenario, the instant rotation is performed by the pinion hyperboloid,  $\mathcal{H}_p$ .

\* Note that the radii,  $\tilde{r}_g$  and  $\tilde{r}_p$ , are along the center line,  $\mathcal{L}$ , and not in two different planes perpendicular to the axes of rotation,  $O_g$  and  $O_p$ , of the gear and the mating pinion.

The hyperboloid,  $\mathcal{H}_g$ , which is associated with the gear, is generated by the axis of instant rotation,  $P_{ln}$ , when the axis is rotated about the gear axis,  $O_g$ . Similarly, the hyperboloid,  $\mathcal{H}_p$ , which is associated with the pinion, is generated by the axis of instant rotation,  $P_{ln}$ , when the axis is rotated about the pinion axis,  $O_p$ . The instant rotation occurs about the axis of instant rotation,  $P_{ln}$ . The instant translation is observed in the direction parallel to the axis of instant rotation,  $P_{ln}$ .

As schematically shown in Figure 2.8b, two axodes,  $\mathcal{H}_g$  and  $\mathcal{H}_p$ , contact each other along the axis of instant rotation,  $P_{ln}$ . The vectors, which are used for describing the kinematics of a rotary-negative spatial gear pair (commonly, an external gear pair) are also depicted in Figure 2.8b. It should be mentioned here that the axodes,  $\mathcal{H}_g$  and  $\mathcal{H}_p$ , are shown just for illustrative purposes. The use of axodes for investigation of the kinematics of gearing is known in the literature on gearing and is out of date and an obsolete technique. The use of axodes for the analysis of kinematics of gear pairs has been proven to be inconvenient because axodes cannot be drawn easily and are less informative compared to vector diagrams. More arguments against the application of axodes in the analysis of rotary-negative gear pairs can be mentioned. Because of this, axodes of the gear and the pinion have very limited use in this book. In all possible cases, axodes are replaced with the corresponding vector diagrams, which are more informative and can be drawn easily.

### 2.2.2.2 Vector Diagrams of Rotary-Positive Crossed-Axes Gear Pairs

A vector diagram for a rotary-positive intersected-axes gear pair (commonly, an internal gear pair) is constructed similarly to that for a rotary-negative intersected-axes gear pair (see Figure 2.8). The similarity allows one to focus attention mostly on the peculiarities of the vector diagrams for rotary-positive intersected-axes gear pairs [127,128].

Consider a rotary-positive intersected-axes gear pair for which a set of parameters ( $\omega_g$ ,  $\omega_p$ ,  $\Sigma$ , and  $C$ ) is specified. An example of a vector diagram for a rotary-positive intersected-axes gear pair is shown in Figure 2.9.

The vector diagram (Figure 2.9a) refers to a system of two orthogonal planes of projections,  $\pi_1$  and  $\pi_2$ . The vector of instant rotation,  $\omega_{pl}$ , is constructed as the difference of the rotation vectors,  $\omega_g$  and  $\omega_p$ . In the case under consideration, the equality  $\omega_{pl} = \omega_p - \omega_g$  is valid.

The vector of instant rotation,  $\omega_{pl}$ , is constructed so it is parallel to the plane of projections,  $\pi_1$ . Therefore, the rotation vector,  $\omega_{pl}$ , is projected onto the reference plane,  $\pi_1$ , with no distortions. Similar to the above (see Figure 2.8), those components of the rotation vectors,  $\omega_g$  and  $\omega_p$ , that cause pure rolling of the axodes are designated as  $\omega_g^{rl}$  and  $\omega_p^{rl}$ , correspondingly.

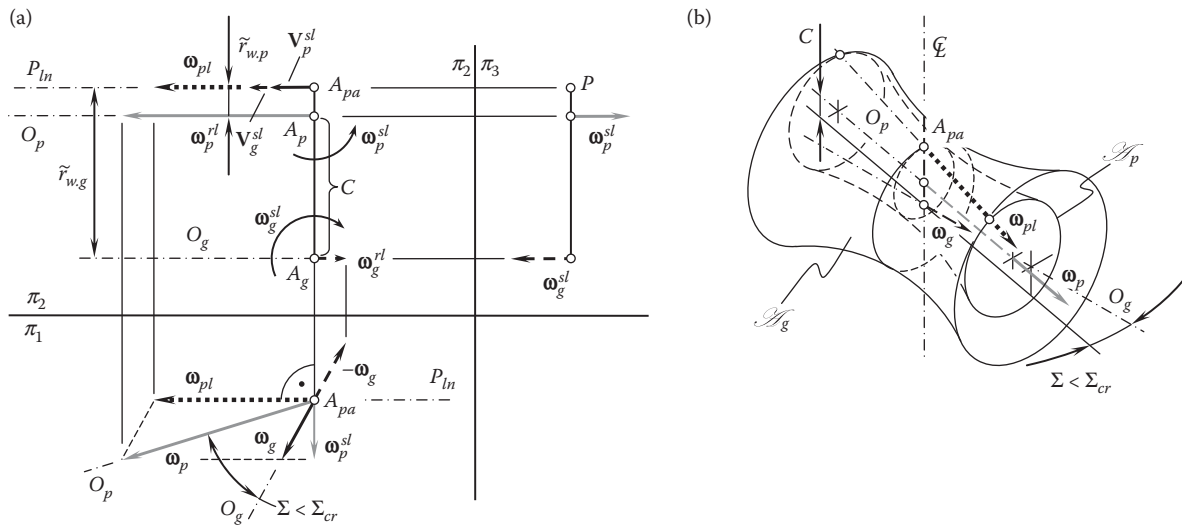


FIGURE 2.9

Vector diagram of a positive (commonly internal) crossed-axis gear pair (positive  $C_a$ -gearing): (a) the vector diagram for the rotation vectors and (b) an obsolete representation (by means of the axodes) of the kinematics of a gear pair of this type.



### 2.2.2.2.1 Conditions of Pure Rolling in Rotary-Positive Crossed-Axes Gear Pairs: General Consideration

For a rotary-positive crossed-axes gear pair, the plane-of-action apex,  $A_{pa}$ , is located outside the center distance,  $C$ . Instead, the pinion axis of rotation,  $O_p$ , intersects the centerline,  $\mathcal{L}$ , at a point that is located between the point,  $A_{pa}$ , and the point of intersection of the centerline,  $\mathcal{L}$ , by the gear axis of rotation,  $O_g$ . Hence, the following equality:

$$-\tilde{r}_p + \tilde{r}_g = C \quad (2.34)$$

is valid for a rotary-positive (commonly an internal) crossed-axes gear pair.

Equation 2.34 allows an expression,  $\tilde{r}_g = C + \tilde{r}_p$ . Making use of this equality and taking into account the conditions of pure rolling of the axodes, the following formulas:

$$\tilde{r}_g = \frac{\omega_p^{rl}}{\omega_p^{rl} - \omega_g^{rl}} \cdot C \quad (2.35)$$

$$\tilde{r}_p = \frac{\omega_g^{rl}}{\omega_p^{rl} - \omega_g^{rl}} \cdot C \quad (2.36)$$

for the calculation of the distances,  $\tilde{r}_g$  and  $\tilde{r}_p$ , can be derived.

### 2.2.2.2.2 Conditions of Pure Sliding in Rotary-Positive Crossed-Axes Gear Pairs: General Consideration

Two others components,  $\omega_g^{sl}$  and  $\omega_p^{sl}$ , of the rotation vectors,  $\omega_g$  and  $\omega_p$ , cause pure sliding along the axis of instant rotation,  $P_{ln}$ . With no distortion, these components are projected onto the frontal plane of projections,  $\pi_3$ . As already shown with respect to a rotary-negative crossed-axes gear pair, the sliding components,  $\omega_g^{sl}$  and  $\omega_p^{sl}$ , of the rotation vectors,  $\omega_g$  and  $\omega_p$ , are of equal magnitude and are opposite each other (i.e.,  $\omega_g^{sl} = -\omega_p^{sl}$ ).

The linear velocity sliding vector that is created by the gear is equal:

$$\mathbf{V}_g^{sl} = r_g \cdot \omega_g^{sl} \quad (2.37)$$

Similarly, the linear velocity sliding vector that is created by the pinion is equal:

$$\mathbf{V}_p^{sl} = r_p \cdot \omega_p^{sl} \quad (2.38)$$

The following expressions:  $|\omega_g^{sl}| = |\omega_p^{sl}|$  and  $r_g \geq r_p$  are valid for a rotary-positive crossed-axes gear pair. Thus, magnitude of the component,  $\mathbf{V}_g^{sl}$ , of the sliding velocity vector caused by the gear exceeds or is equal to the magnitude of the component,  $\mathbf{V}_p^{sl}$ , of the sliding velocity vector caused by the pinion; that is, the inequality  $|\mathbf{V}_g^{sl}| \geq |\mathbf{V}_p^{sl}|$  is always observed.

The sliding velocity vectors,  $\mathbf{V}_g^{sl}$  and  $\mathbf{V}_p^{sl}$ , are always of the same direction. The resultant sliding velocity vector,  $\mathbf{V}_{g-p}^{sl}$ , of the gear in relation to the pinion is equal to the following difference:

$$\mathbf{V}_{p-g}^{sl} = -\mathbf{V}_{g-p}^{sl} = \mathbf{V}_g^{sl} - \mathbf{V}_p^{sl} \quad (2.39)$$

The resultant sliding velocity vector,  $\mathbf{V}_{g-p}^{sl}$ , of the pinion in relation to the gear is opposite to sliding velocity vector  $\mathbf{V}_{p-g}^{sl}$ :

$$\mathbf{V}_{g-p}^{sl} = -\mathbf{V}_{p-g}^{sl} = \mathbf{V}_g^{sl} - \mathbf{V}_p^{sl} \quad (2.40)$$

The magnitude of speed of the resultant sliding in a rotary-positive spatial gear pair (commonly, an internal gear pair) can be calculated from the following formula:

$$V_{sc} = V_g^{sl} + V_p^{sl} \quad (2.41)$$

Similar to that of a rotary-negative crossed-axes gear pair, the components,  $\omega_g^{sl}$  and  $\omega_p^{sl}$ , of the rotation vectors,  $\omega_g$  and  $\omega_p$ , constitute a pair of rotation for a rotary-negative crossed-axes gear pair. The pair of rotation is equivalent to a straight motion. This allows for a formula for the calculation of the magnitude,  $V_{scr}$ , of speed of the resultant sliding similar to Equation 2.29.

Two axodes,  $\mathcal{A}_g$  and  $\mathcal{A}_p$ , of a gear and its mating pinion, along with the corresponding rotation vectors,  $\omega_g$  and  $\omega_p$ , are schematically illustrated in Figure 2.9b (this obsolete approach is known in the literature on gearing). Again, the axodes,  $\mathcal{A}_g$  and  $\mathcal{A}_p$ , are significantly less informative in comparison with the corresponding vector diagrams. It is inconvenient to draw the axodes for illustrative purposes. More arguments against application of axodes in the analysis of rotary-positive spatial gear pairs can be mentioned. Therefore, in further discussions in this chapter, preference is given to vector diagrams (for the rotations) rather than to axodes of a gear and its mating pinion.

### 2.2.2.3 Vector Diagrams of Rotary-Zero Crossed-Axes Gear Pairs

The performed analysis of rotary-negative and rotary-positive crossed-axes gear pairs makes a question reasonable: What is between rotary-positive and rotary-negative crossed-axes gear pairs? It is reasonable to assume that gear pairs with intermediate kinematics, that is, rotary-zero crossed-axes gear pairs can exist. This is greatly similar to the *gear-to-rack* pair for parallel-axes external and internal gear pairs. A crossed-axes gear pair of this nature is referred to as the rotary-zero crossed-axes gear pair or *generalized rack-type crossed-axes gear pair*.

A rotary-zero crossed-axes gear pair can be construed as the reduced (degenerate) case either of a rotary-positive or a rotary-negative crossed-axes gear pair when the gear cone angle is equal to its critical value. In other words, there must exist a rotary-zero crossed-axes gear pair as the limit case either of a rotary-negative (Figure 2.8) or a rotary-positive (Figure 2.9) crossed-axes gear pair.

Without going into a detailed analysis of the vector diagram depicted in Figure 2.7, it can be said that for a rotary-negative crossed-axes gear pair, the gear cone angle,  $\Sigma_g$ , between the rotation vector,  $\omega_g$ , and the vector of instant rotation,  $\omega_{pl}$ :

$$\Sigma_g = \angle(\omega_g, \omega_{pl}) > 90^\circ \quad (2.42)$$

is an obtuse angle (see Figure 2.8).

For a rotary-positive crossed-axes gear pair, the gear cone angle,  $\Sigma_g$ , between the rotation vector,  $\omega_g$ , of the gear and the vector of instant rotation,  $\omega_{pl}$ :

$$\Sigma_g = \angle(\omega_g, \omega_{pl}) < 90^\circ \quad (2.43)$$

is an acute angle (see Figure 2.9).

It is reasonable to question the case where the gear cone angle,  $\Sigma_g$ , between the rotation vector,  $\omega_g$ , of the gear and the vector of instant rotation,  $\omega_{pl}$ , is a right angle (i.e., the rotation vectors,  $\omega_g$  and  $\omega_{pl}$ , are perpendicular to each other:  $\omega_g \perp \omega_{pl}$ ).

The vector diagram of a crossed-axes gear pair for which the equality:

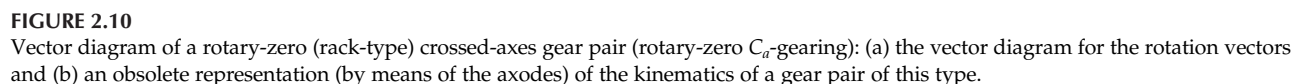
$$\Sigma_g = \angle(\omega_g, \omega_{pl}) = 90^\circ \quad (2.44)$$

is valid is shown in Figure 2.10a.

In the case under consideration, the axode of the gear,  $\mathcal{A}_g$  (a hyperboloid-of-one-sheet) is reduced to a plane that is rotated about an axis perpendicular to the plane. The axode of the pinion,  $\mathcal{A}_p$  (also a hyperboloid-of-one-sheet) is reduced to a cone of revolution. The gear pair, for which the vector diagram is shown in Figure 2.10a, can be interpreted as the case of rolling of the cone of revolution over the rotating plane, as shown in Figure 2.10b. A spatial gear pair featuring this type of kinematics is referred to as a rotary-zero crossed-axes gear pair. (The use of axodes for investigation of the kinematics of gearing is known in the literature on gearing and is out of date and an obsolete technique.)

A critical value,  $\Sigma_{cr}$ , of the crossed-axes angle,  $\Sigma$ , corresponds to a rotary-zero crossed-axes gear pair. In other words, if the condition in Equation 2.44 is fulfilled, then the equality  $\Sigma = \Sigma_{cr}$  is observed.

Within the plane through the centerline,  $\mathcal{L}$ , the linear velocity vector,  $\mathbf{V}_g^{sl}$ , of the sliding in the direction of the axis of instant rotation,  $P_{ln}$ , is created by the component,  $\omega_g^{sl}$ , of the rotation vector,  $\omega_g$ , of the gear. This rotation vector,  $\omega_g^{sl}$ , is contributed by the rotating gear. Although the component,  $\omega_p^{sl}$ , of the rotation vector,  $\omega_p$ , is not



equal to zero (i.e.,  $\omega_p^{sl} \neq 0$ ), the linear velocity,  $\mathbf{V}_p^{sl}$ , is equal to zero ( $\mathbf{V}_p^{sl} = 0$ ). The last equality is possible because the equality  $\tilde{r}_g = C$  is valid for rotary-zero crossed-axes gear pairs (or, in other words, for generalized rack-type crossed-axes gear pairs). As the equality  $\tilde{r}_g = C$  is observed, then the equality  $\tilde{r}_p = 0$  is valid as well. Ultimately, in the case under consideration, the resultant linear velocity,  $V_{scr}$  of the sliding in the direction of the axis of instant rotation,  $P_{ln}$ , is equal to:

$$V_{sc} = V_{\hat{g}}^{sl} \quad (2.45)$$

It must be stressed here that not every case of the rolling of a cone of revolution over the rotating plane corresponds to a rotary-zero crossed-axes gear pair. To be associated with a rotary-zero crossed-axes gear pair, it is critical that the condition in Equation 2.44 be fulfilled in this regard.

The vector diagrams of rotary-zero crossed-axes gear pairs are of particular interest in the designing of gear cutting tools for the machining gears for crossed-axes gear pairs, for example, for machining gears for hypoid and *spiroid* gears and so forth [111,112].

#### 2.2.2.4 Analytical Criterion of Type of Crossed-Axes Gear Pair

Crossed-axes gear pairs of different types are known. The angle that is formed by the rotation vector of a gear,  $\omega_g$ , with the vector,  $\omega_{pl}$ , of instant rotation of the mating pinion in relation to the gear is the root cause for the principal difference between crossed-axes gear pairs of different types, that is, between the rotary-negative, rotary-positive, and rotary-zero crossed-axes gear pairs. These differences are analytically described by Equations 2.43 and 2.44. As shown in Section 1.2.1, the equality:

$$\mathbf{w}_{pl} = \mathbf{w}_p - \mathbf{w}_q \quad (2.46)$$

is observed for a crossed-axes gear pair.

Equations 2.43, 2.44, and 2.46 make possible the representation of the analytical criteria of a type of a crossed-axes gear pair as shown in Table 2.1.

Analytical expressions specifying the criteria for the crossed-axes gear pair are composed on the premise of well-known properties of the dot product of two vectors.

TABLE 2.1

Analytical Criteria of Type of Crossed-Axes Gear Pairs

Type of Crossed-Axes Gear Pairs	Analytical Criterion
Rotary-negative gearing: (external and internal) crossed-axes gear pairs	$\omega_g \cdot (\omega_p - \omega_g) < 0$
Rotary-zero gearing: generalized rack-type crossed-axes gear pairs	$\omega_g \cdot (\omega_p - \omega_g) = 0$
Rotary-positive gearing: (internal and (external) crossed-axes gear pairs	$\omega_g \cdot (\omega_p - \omega_g) > 0$

### 2.3 Classification of Possible Types of Vector Diagrams of Gear Pairs

Possible types of gear pairs can be classified based on the vector representation of gear pair kinematics discussed in Section 2.2. Such a classification is necessary and beneficial for many purposes. The development of all possible types of gears, and then of all possible types of gear pairs, is one of the reasons for the development of the classification.

Crossed-axes gear pairs are considered in this monograph as the most general type of gear pairs. The remaining possible types of gear pairs can be construed as a reduction (simplification) of the corresponding type of the crossed-axes gear pairs.

As stated in Section 2.2, there are only three different types of gear pairs of those featuring crossed axes:

- Rotary-negative crossed-axes gear pairs, in which the input rotation is altered (i.e.,  $\omega_g/\omega_p = -\omega_p/\omega_p$ ) and the gear ratio is negative ( $u < 0$ ).
- Rotary-positive crossed-axes gear pairs, in which the gear rotation remains the same (i.e.,  $\omega_g/\omega_p = \omega_p/\omega_p$ ) and the gear ratio is positive ( $u > 0$ ).
- Rotary-zero crossed-axes gear pairs, in which the gear cone angle,  $\Sigma_g$ , is a right angle (i.e.,  $\Sigma_g = 90^\circ$ ) and rotation of the gear is not zero\* ( $\omega_g \neq 0$ ).

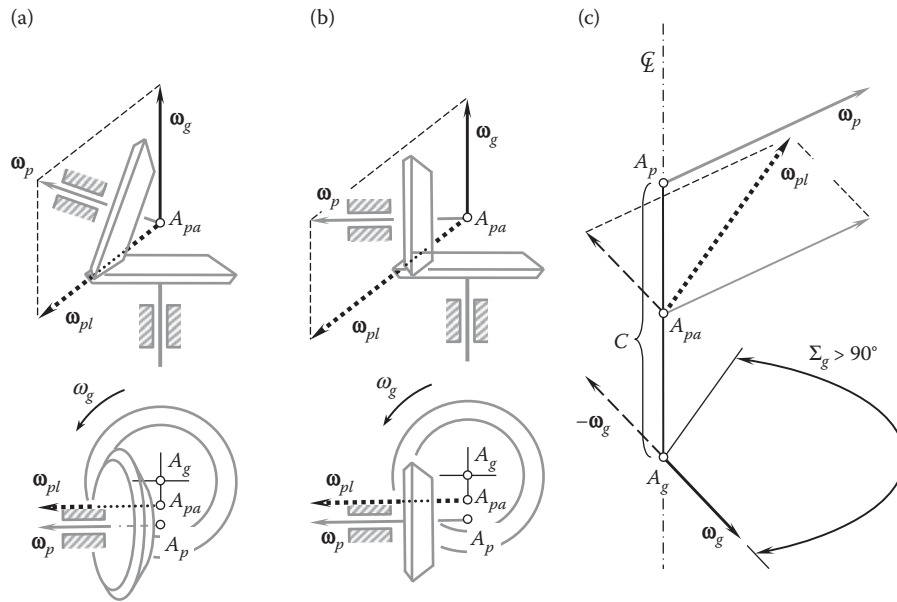
No other types of spatial gear pairs are feasible.

Examples of rotary-negative external crossed-axes gear pairs and their vector representations are schematically illustrated in Figure 2.11. For all types of rotary-negative spatial gear pairs (commonly, external gear pairs), the inequality  $\omega_g \cdot (\omega_p - \omega_g) < 0$  is observed (see Table 2.1). The component,  $\Sigma_g$ , of the crossed-axes angle,  $\Sigma$ , exceeds a right angle (i.e.,  $\Sigma_g > 90^\circ$ ), as illustrated in Figure 2.11. A rotary-negative crossed-axes gear pair can feature a crossed-axes angle,  $\Sigma$ , of various values. In particular, the crossed-axes angle,  $\Sigma$ , can be either acute (i.e.,  $0^\circ < \Sigma < 90^\circ$ , as shown in Figure 2.11a), equal to a right angle,  $\Sigma = 90^\circ$  (Figure 2.11b), or obtuse (i.e.,  $90^\circ < \Sigma < 180^\circ$ ). Vector diagrams for each of three types of rotary-negative crossed-axes gear pairs allow them to be construed as particular cases of the vector diagram shown in Figure 2.11c. In Figure 2.12, a helical gear pair with crossed axes is shown. A helical gear pair is a perfect example of rotary-negative crossed-axes gear pairs.

An example of a rotary-zero crossed-axes gear pair, that is, of a generalized rack-type gear pair, and its vector representation are depicted in Figure 2.13. For gear pairs of this type, the equality  $\omega_g \cdot (\omega_p - \omega_g) = 0$  is always observed (see Table 2.1). The component,  $\Sigma_g$ , of the crossed-axes angle,  $\Sigma$ , is a right angle (i.e.,  $\Sigma_g = 90^\circ$ ), as illustrated in Figure 2.13a. A generalized rack-type crossed-axes gear pair can feature crossed-axes angles of various values. A vector diagram of gear pairs of this type is shown in Figure 2.13b.

A rotary-negative crossed-axes gear pair (commonly, internal gear pair) and its vector representation are schematically shown in Figure 2.14. For all types of rotary-negative crossed-axes gear pairs, the inequality  $\omega_g \cdot (\omega_p - \omega_g) > 0$  is observed (see Table 2.1). The component  $\Sigma_g$  of the crossed-axes angle,  $\Sigma$ , is less than  $90^\circ$  (i.e.,  $\Sigma_g < 90^\circ$ ) as illustrated in Figure 2.14a. A rotary-negative crossed-axes gear pair can feature crossed-axes angles of various values. The vector diagram for a rotary-negative crossed-axes gear pair is shown in Figure 2.14b.

\* The term *rotary-zero crossed-axis gear pair* is because in parallel-axes gearing of this type, the rotation of the gear is zero (that is,  $\omega_g = 0$ ). A *gear-to-rack* gear pair of a conventional design features a zero rotation of the gear: for a certain rotation of the pinion,  $\omega_p$ , the rotation of the gear,  $\omega_g$ , is always zero,  $\omega_g = 0$ . In a more general case of zero crossed-axes gearing, the gear rotation is not zero (that is,  $\omega_g \neq 0$ ). By convention, the term *rotary-zero crossed-axis gear pair* is applied to gearings of all types, that is, to parallel-axes, intersected-axes, and crossed-axes gearings.

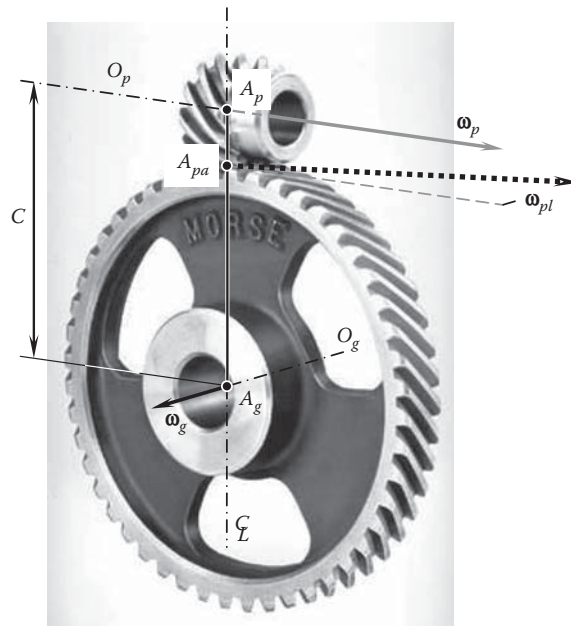
**FIGURE 2.11**

Examples of rotary-negative crossed-axes gear pairs (commonly external gear pairs) and their vector representation with (a) obtuse,  $\Sigma > 90^\circ$  and (b) right,  $\Sigma = 90^\circ$  crossed-axes angle,  $\Sigma$ , and (c) their vector representation.

Three types of crossed-axis gear pairs compose the first stratum of the classification of possible types of vector diagrams of gear pairs (Figure 2.15):

- Rotary-negative crossed-axes gear pairs (Figure 2.11).
- Rotary-zero crossed-axes gear pairs (Figure 2.13).
- Rotary-positive crossed-axes gear pairs (Figure 2.14).

The numbers 1.1, 1.2, and 1.3 are assigned to spatial gear pairs making up the first stratum of the classification.

**FIGURE 2.12**

The rotation vectors,  $\omega_g$ ,  $\omega_p$ , and  $\omega_{pl}$ , associated with a rotary-negative (usually external) crossed-axes gear pair.



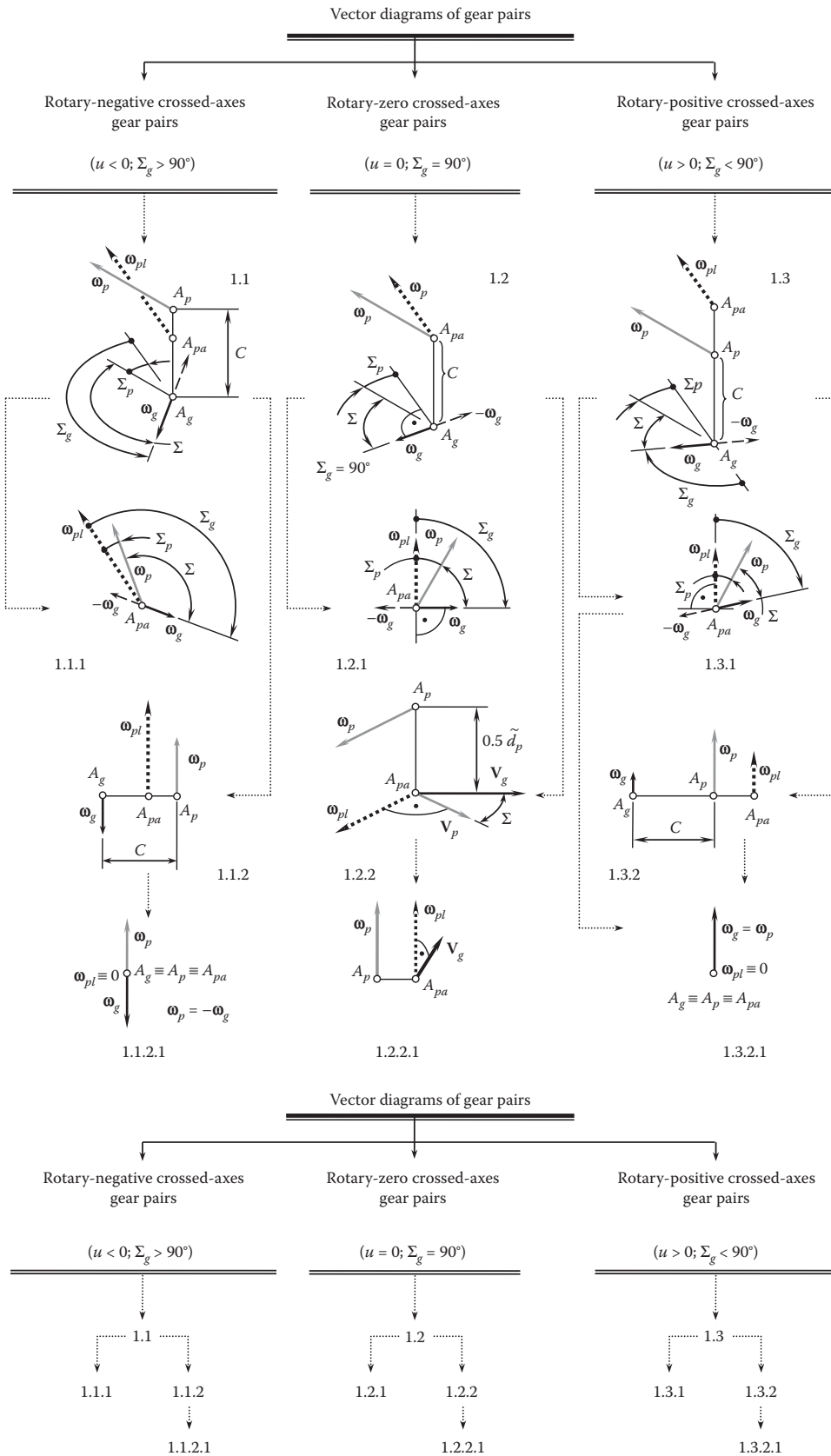


**FIGURE 2.15**  
Classification of possible types of vector diagrams of gear pairs.



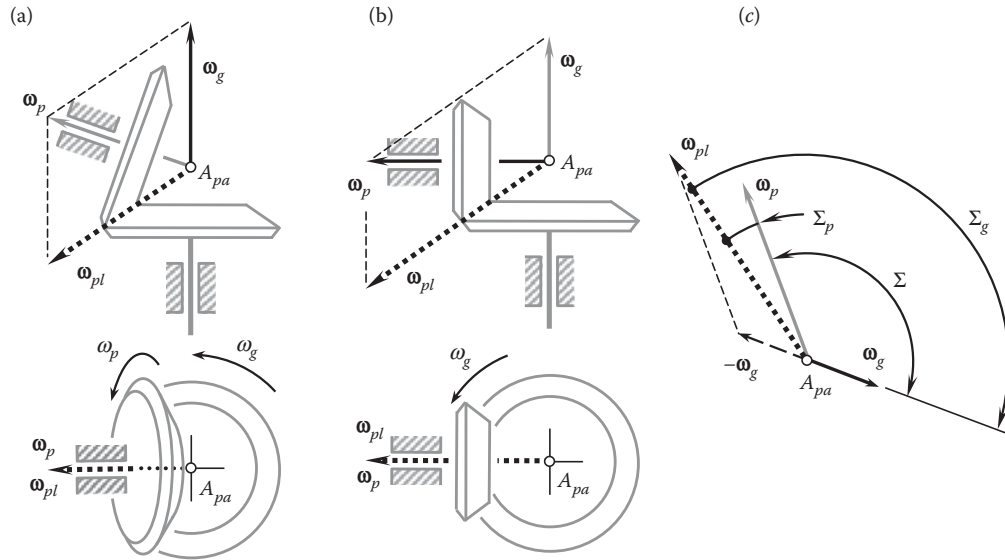


FIGURE 2.16

Examples of rotary-negative intersected-axes gear pairs (commonly external gear pairs) and their vector representation with (a) obtuse,  $\Sigma > 90^\circ$  and (b) right,  $\Sigma = 90^\circ$ , crossed-axes angle,  $\Sigma$ , and (c) the vector representation of the gear pair.

For gear pairs of this type, a sphere that is centered at the point,  $A_{pa}$ , is convenient to be used for the investigation of engagement of the gear teeth. Because of this, intersected-axes gear pairs are loosely referred to as *spherical gear pairs*. The term *spherical* is because the tooth profiles of the gear and pinion in this case are generated on spheres.\* A rotary-negative external intersected-axes gear pair and its vector representation are schematically shown in Figure 2.16. For all rotary-negative intersected-axes gear pairs, the inequality  $\omega_g \cdot (\omega_p - \omega_g) < 0$  is observed (see Table 2.1). The component,  $\Sigma_g$ , of the crossed-axes angle,  $\Sigma$ , exceeds  $90^\circ$  (i.e.,  $\Sigma_g > 90^\circ$ ), as illustrated in Figure 2.16a. Rotary-negative intersected-axes gear pairs can feature crossed-axes angles of various values. In particular, the crossed-axes angle,  $\Sigma$ , can be chosen so as to fulfill the equality  $\Sigma_g = 90^\circ$ , as shown in Figure 2.16b.

The vector diagram for a rotary-negative intersected-axes gear pair is shown in Figure 2.16c. In Figure 2.17, a gear pair with intersected axes of rotation of the gear,  $O_g$ , and the mating pinion,  $O_p$ , is shown, which is a perfect example of rotary-negative gear pairs (usually, external gear pairs) of this particular design.

An example of a rotary-zero intersected-axes gear pair and its vector representation are depicted in Figure 2.18. For gear pairs of this type, the equality  $\omega_g \cdot (\omega_p - \omega_g) = 0$  is always observed (see Table 2.1). The component,  $\Sigma_g$ , of the crossed-axes angle,  $\Sigma$ , is equal to  $90^\circ$  (i.e.,  $\Sigma_g = 90^\circ$ ), as illustrated in Figure 2.18a. A rack-type intersected-axes gear pair can have a crossed-axes angle of various values. An example of a vector diagram of gear pairs of this kind is depicted in Figure 2.18b.

A rotary-positive intersected-axes gear pair and its vector representation are schematically shown in Figure 2.19. For all rotary-positive intersected-axes gear pairs, the inequality  $\omega_g \cdot (\omega_p - \omega_g) > 0$  is observed (see Table 2.1). The component,  $\Sigma_g$ , of the crossed-axes angle,  $\Sigma$ , is less than  $90^\circ$  (i.e.,  $\Sigma_g < 90^\circ$ ), as illustrated in Figure 2.19a. A rotary-positive intersected-axes gear pair can have a crossed-axes angle of various values. A vector diagram for an internal intersected-axes gear pair is shown in Figure 2.19b. Figure 2.20 illustrates a perfect example of an internal intersected-axis gear pair.

Three types of intersected-axes gear pairs, namely

- Rotary-negative intersected-axes gear pairs (Figure 2.16)
- Rotary-zero intersected-axes gear pairs (Figure 2.18)
- Rotary-positive intersected-axes gear pairs (Figure 2.19)

\* The term *spherical gear pair* is incorrect, as gears of other types, for example, crossed-axes gear pairs, are also engaged in mesh on a sphere. Therefore, replacement of the obsolete and widely used term *conical gear pair* with the term *spherical gear pair* is not valid. In order to avoid ambiguities in further discussions, gearing of this type is referred to as *intersected-axes gearing*, or just *I<sub>a</sub>-gearing* for simplicity.

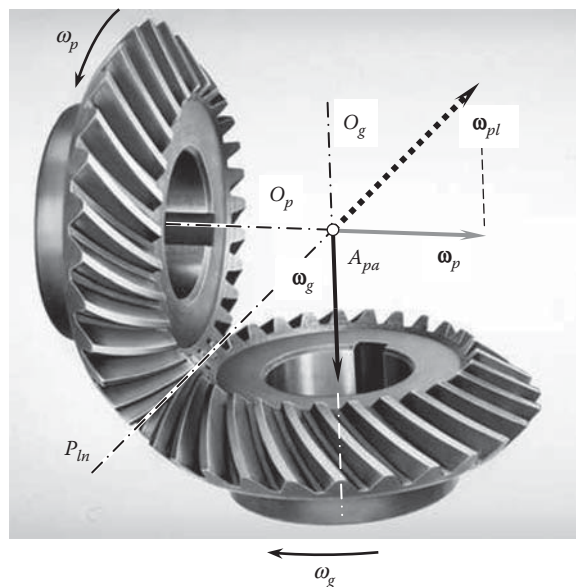


FIGURE 2.17

The rotation vectors,  $\omega_g$ ,  $\omega_p$ , and  $\omega_{pl}$ , associated with a rotary-zero external intersected-axes gear pair.

compose the first row of the second stratum of classification of all possible types of vector diagrams of gear pairs (see Figure 2.15). The numbers 1.1.1, 1.2.1, and 1.3.1 are assigned to intersected-axes gear pairs making up the first row of the second stratum of the classification.

This is followed by the second case in which the gear and pinion axes of rotation are parallel to each other. The shaft angle in these cases is either  $\Sigma = 0^\circ$  or  $\Sigma = 180^\circ$ .

When the equality  $\Sigma = 180^\circ$  is observed, the rotation vectors,  $\omega_g$  and  $\omega_p$ , are pointed in opposite directions. Gear pairs of this type are referred to as *parallel-axes gear pairs*. Sometimes the term *planar gear pair* is used with respect to gearing of this type. The term *planar* is used because the tooth profiles of the gear and the pinion in this case are generated within a plane. The term *parallel-axes gear pair* is preferred, and is recommended for use in scientific publications on theory of gearing. A rotary-negative parallel-axes gear pair and its vector representation are schematically shown in Figure 2.21. For all rotary-negative parallel-axes gear pairs, the inequality  $\omega_g \cdot (\omega_p - \omega_g) < 0$  is observed (see Table 2.1). The vector diagram for a rotary-negative parallel-axes gear pair

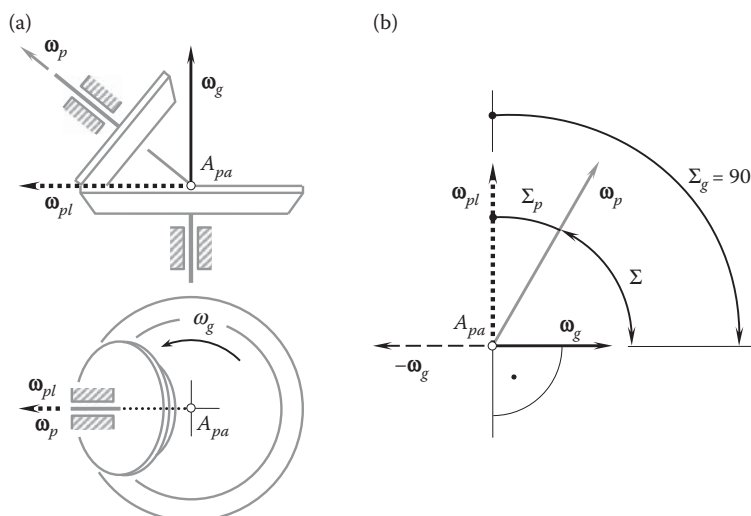
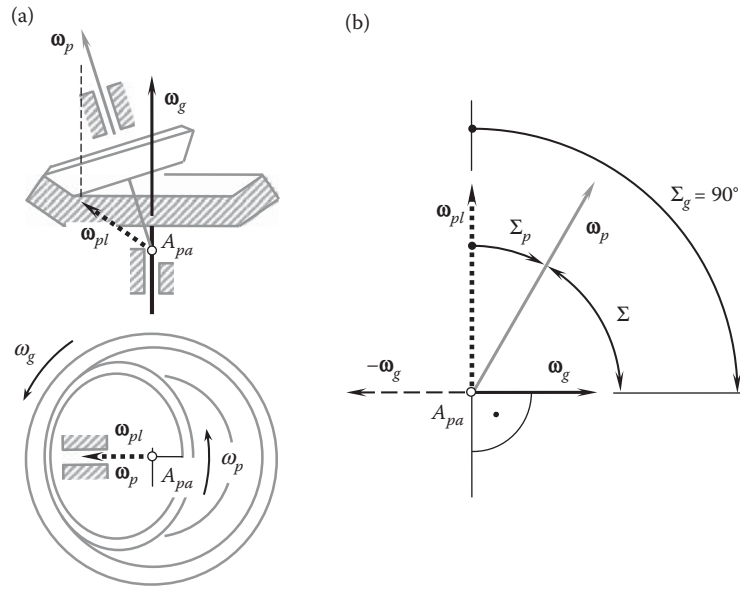


FIGURE 2.18

An example of (a) a rotary-zero intersected-axes gear pair and (b) its vector representation.

**FIGURE 2.19**

An example of rotary-positive intersected-axes gear pair (a) and its vector representation (b).

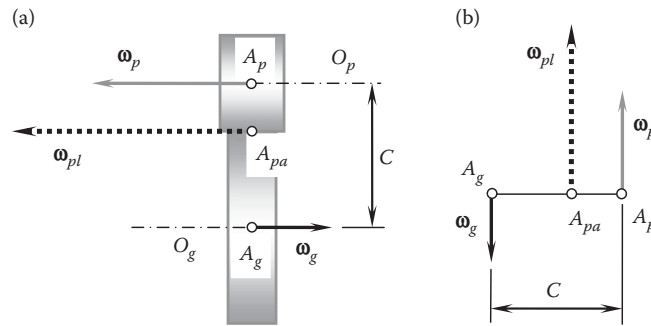
is shown in [Figure 2.21b](#). In [Figure 2.22](#), an external gear pair with parallel axes of rotation of the gear,  $O_g$ , and the pinion,  $O_p$ , is depicted. This is a perfect example of a type of external parallel-axes gear pair (i.e., rotary-negative gear pair).

On the other hand, when the equality  $\Sigma = 0^\circ$  is valid for a parallel-axes gear pair, the rotation vectors,  $\omega_g$  and  $\omega_p$ , are pointed in the same direction, which corresponds to a rotary-positive parallel-axes gear pair. A rotary-positive internal parallel-axes gear pair and its vector representation are schematically shown in [Figure 2.23a](#). For all negative parallel-axes gear pairs, the inequality  $\omega_g \cdot (\omega_p - \omega_g) > 0$  is observed (see [Table 2.1](#)). The vector diagram for a rotary-negative parallel-axes gear pair is shown in [Figure 2.23b](#).

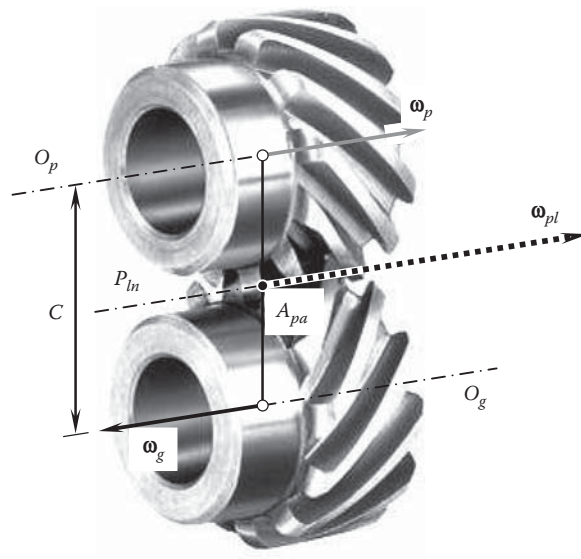
Two types of parallel-axes gear pairs, namely, rotary-negative gear pairs ([Figure 2.21](#)) and rotary-positive parallel-axes gear pairs ([Figure 2.23](#)) compose the second row of the second stratum of the classification of possible types of vector diagrams of gear pairs (see [Figure 2.15](#)). The numbers 1.1.2 and 1.3.2 are assigned to the vector diagrams of parallel-axes gear pairs composing the second row of the second stratum of the classification.

**FIGURE 2.20**

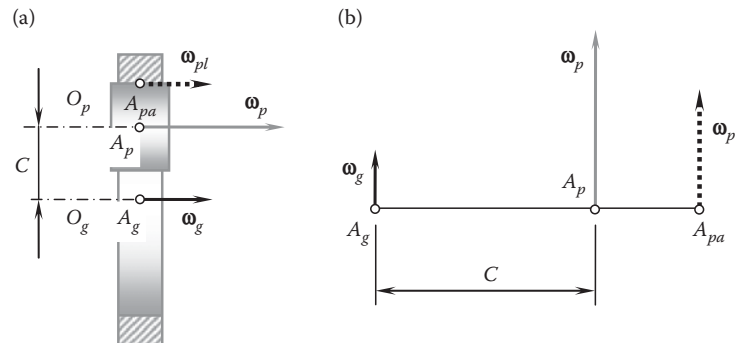
An example of internal straight bevel gear pair.

**FIGURE 2.21**

An example of (a) a rotary-negative parallel-axes gear pair and (b) its vector representation.

**FIGURE 2.22**

The rotation vectors,  $\omega_g$ ,  $\omega_p$ , and  $\omega_{pl}$ , associated with a rotary-negative external parallel-axis gear pair.

**FIGURE 2.23**

An example of (a) a rotary-positive parallel-axes gear pair and (b) its vector representation.

Ultimately, consider a simplified case of a rotary-zero crossed-axes gear pair (Figure 2.13). In extreme cases, the tooth number of the gear can approach infinity. Infinite radius of the gear is the only way to reduce the rotary-zero crossed-axes gear pair when the center distance is not equal to zero (i.e.,  $C \neq 0$ ). In Figure 2.24, a straight rotary-zero crossed-axes gear pair is shown, which corresponds to such a condition. The vectors of linear velocities,  $\mathbf{V}_g$  and  $\mathbf{V}_p$ , are at a crossed-axes angle,  $\Sigma$ , in relation to each other.

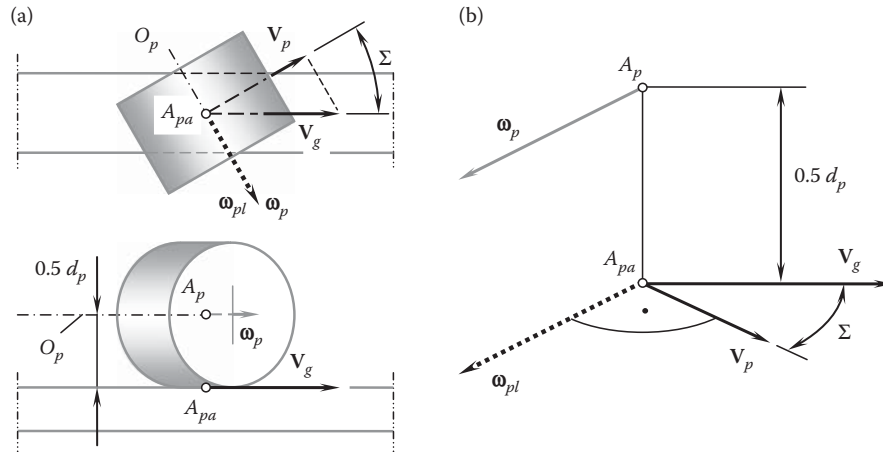


FIGURE 2.24

A rotary-zero crossed-axes rack-type gear pair (a) and its vector representation (b).

Rotary-zero crossed-axes gear pairs of this type (see Figure 2.24) compose the third row of the second stratum of the classification of all possible types of vector diagrams of gear pairs (see Figure 2.15). The number 1.2.2 is assigned to the gear pair that composes the third row of the second stratum of the classification.

In a particular case, say, when the crossed-axes angle is equal to zero ( $\Sigma = 0^\circ$ ), a rotary-zero crossed-axes gear pair reduces to a conventional rotary-zero parallel-axes gear-to-rack gear pair. A gear-to-rack gear pair of this type is shown schematically in Figure 2.25a. The vector diagram for a gear pair of this type is depicted in Figure 2.25b.

The number 1.2.2.1 is assigned to the parallel-axes gear-to-rack gear pair.

The gear-to-rack gear pair shown in Figure 2.26 is a perfect example of a rotary-zero parallel-axes gear pair of this type.

It is instructive to note here that a rotary-zero parallel-axes rack-type gear pair can be obtained as an extreme case of either a rotary-negative parallel-axes gear pair (i.e., of the gear pair 1.1.2), or a rotary-positive parallel-axes gear pair (i.e., of the gear pair 1.3.2) under the condition that the radius of the gear approaches infinity.\* In this case, the corresponding vector diagrams 1.1.2.1 or 1.3.2.1 are formally possible. Gear pairs that correspond to vector diagrams 1.1.2.1 and 1.3.2.1 have not been profoundly investigated yet.†

Finally, another extreme case needs to be mentioned. In a particular case when the rotation vectors,  $\omega_g$  and  $\omega_p$ , are equal to each other (i.e.,  $\omega_g \equiv \omega_p$ ), the rotary-positive parallel-axes gear pair 1.3.2 (see Figure 2.23) reduces to a gear coupling. For a gear coupling, the rotation vector,  $\omega_{pl}$ , is equal to zero ( $\omega_{pl} \equiv 0$ ). The base cones apexes,  $A_g$  and  $A_p$ , are coincident with one another. Because the equality  $\omega_g \equiv \omega_p$  is valid, the diameters,  $d_g$  and  $d_p$ , are both equal to zero (i.e.,  $d_g \equiv d_p \equiv 0$ ). Because of this, the plane of action apex,  $A_{par}$ , is coincident with the base cone apexes,  $A_g$  and  $A_p$  ( $A_g \equiv A_p \equiv A_{par}$ ).

This particular case can also be construed as a reduced case of an internal intersected-axes gear pair featuring a zero intersected-axes angle ( $\Sigma = 0^\circ$ ).

The vector diagram for a gear coupling is depicted in Figure 2.27a. The coupling can be composed of internal and external spur gears with equal tooth numbers, as schematically shown in Figure 2.27b, of a pair of similar bevel gears or of two face gears. The number 1.3.2.1 is assigned to a degenerate gear pair of this kind.

\* More accurately, the radius of the gear sector, and not of the gear, approaches infinity.

† Vector diagrams 1.1.2.1 and 1.3.2.1 correspond to the deeply degenerate designs of gear pairs. Because of this, significant features could be observed when developing tooth flanks for gearings that correspond to vector diagrams 1.1.2.1 and 1.3.2.1. When friction between the interacting tooth flanks of the gear,  $\mathcal{G}$ , and the pinion,  $\mathcal{P}$ , is ignored, the tangential force that transmits the torque from the driving shaft to the driven shaft acts along the common perpendicular,  $\mathbf{n}_g$ , to the interacting tooth flanks,  $\mathcal{G}$  and  $\mathcal{P}$ . The common perpendicular,  $\mathbf{n}_g$ , intersects the pitch line,  $P_{in}$ ; that is, it intersects the line of action of the vector of instant rotation,  $\omega_{pl}$ . In cases of gear pairs that correspond to vector diagrams 1.1.2.1 and 1.3.2.1, all three rotation vectors, that is,  $\omega_g$ ,  $\omega_p$ , and  $\omega_{pl}$ , are along a common straight line,  $P_{in}$ . Once the line of action of the vector,  $\mathbf{n}_g$ , intersects the line of action of the velocity vector,  $\omega_{pl}$ , the arm of tangential force in the gear pair becomes zero. This means that no torque can be transmitted by a gear pair of these particular types of gearings. Gear coupling is not a kind of gearing (no contact ratio can be defined). This discrepancy needs to be thoroughly investigated.

In reality, a gear axis and its mating pinion axis are slightly misaligned. Under such a scenario, no discrepancy is observed, and gear pairs can be designed in accordance with vector diagrams 1.1.2.1 and 1.3.2.1.

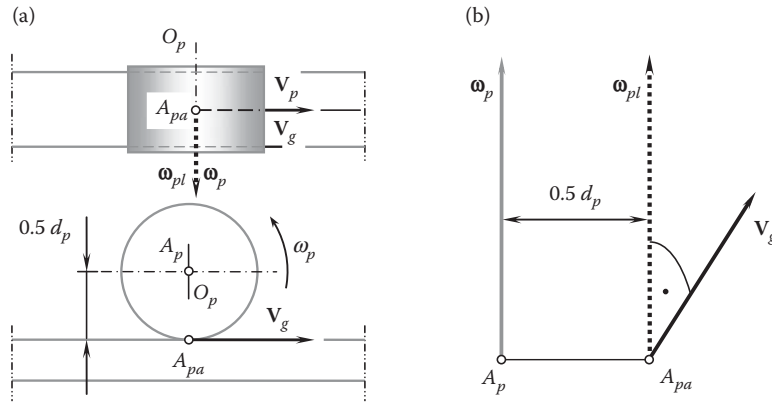


**FIGURE 2.25**  
A rotary-zero parallel-axes gear pair (a) and its vector representation (b).

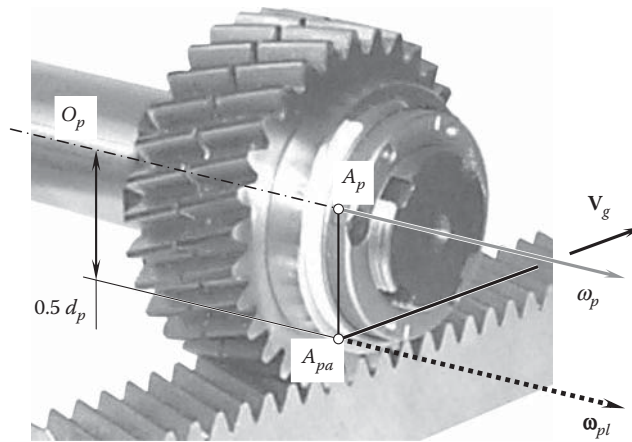


**FIGURE 2.26**  
The rotation vectors,  $\omega_g$ ,  $\omega_p$ , and  $\omega_{pl}$ , associated with a rotary-zero parallel-axes rack-type gear pair.

The third stratum of the classification of all possible types of the vector diagrams of gear pairs (see Figure 2.15) is represented by two types of parallel-axes gear pairs: (1) the rotary-zero gear pair 1.2.2.1 (Figure 2.25) and (2) the gear coupling 1.3.2.1 (Figure 2.27).

The total number of vector diagrams of gear pairs is limited to 11 different types of vector diagrams. Vector diagrams of all possible types of gear pairs are covered by the classification (see Figure 2.15). No vector diagrams of gear pairs outside the classification are feasible. This makes it possible to conclude that the classification shown in Figure 2.15 is complete and self-consistent.

The classification can be used for the investigation of the kinematics and the geometry of gearing of all types, that is, of all known types of gearing, as well as of all types of gearing not known yet and to be developed in the future.

## 2.4 Complementary Vectors to Vector Diagrams of Gear Pairs

In order to make the analytical description of a gear pair easier, it is convenient to introduce a few more vectors to the vector diagrams of gear pairs. Vectors along the centerline, as well as those along the gear and pinion axes of rotations, are of particular importance.

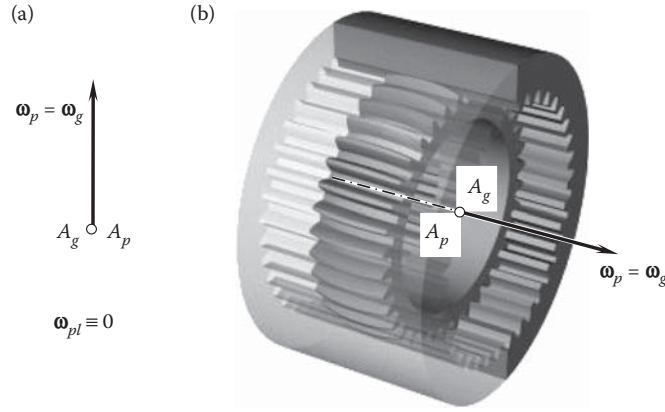


FIGURE 2.27

The vector diagram (a) of a gear coupling (b).

### 2.4.1 Centerline Vectors of a Gear Pair

Referring to Figure 2.28, consider the vector diagram of a gear pair.\* The rotation vectors,  $\omega_g$  and  $\omega_p$ , are apart from each other by a center distance  $C$ .

Two vectors,  $C_g$  and  $C_p$ , are along the centerline,  $\hat{\mathcal{L}}$ . These vectors specify the distances of the axes of rotations of the gear,  $O_g$ , and the pinion,  $O_p$ , from the point,  $A_{pa}$ . The centerline vector,  $C_g$ , can be calculated from the following equation:

$$C_g = -\tilde{r}_g \cdot \mathbf{c} \quad (2.47)$$

Another centerline vector,  $C_p$ , is specified as follows:

$$C_p = \tilde{r}_p \cdot \mathbf{c} \quad (2.48)$$

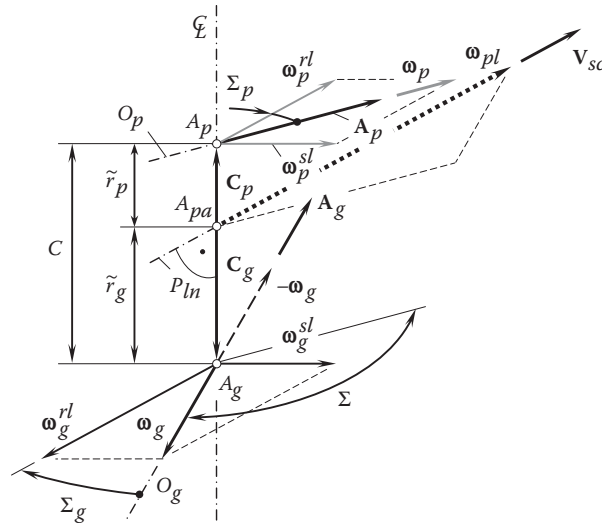
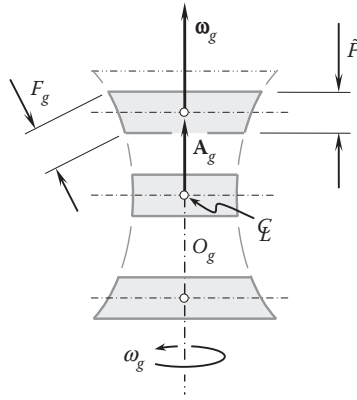


FIGURE 2.28

Complementary vectors to the vector diagram of a gear pair.

\* For gear pairs with varying tooth ratios, for example, for gear pairs composed of noncircular gears, the parameters of the vector diagram,  $\omega_g$ ,  $\omega_p$ ,  $\omega_{pl}$ ,  $C$ ,  $C_g$ ,  $C_p$ ,  $\Sigma$ ,  $\Sigma_g$ ,  $\Sigma_p$ , and others should be considered as corresponding functions of time,  $t$ , or (the same) as the corresponding functions of the angle of rotation of the input shaft, that is, of the angle of rotation either of the gear,  $\varphi_g$ , or the pinion,  $\varphi_p$ . Ultimately, these functions can be represented in a generalized way as  $\omega_g(t)$ ,  $\omega_p(t)$ ,  $\omega_{pl}(t)$ ,  $C(t)$ ,  $C_g(t)$ ,  $C_p(t)$ ,  $\Sigma(t)$ ,  $\Sigma_g(t)$ , and  $\Sigma_p(t)$ . All the parameters are synchronized with each other.



**FIGURE 2.29**

Possible configurations of the gear in relation to the centerline,  $\mathcal{L}$ , in a spatial gear pair specified by the axial vector,  $\mathbf{A}_g$ .

In Equations 2.47 and 2.48,

$\tilde{r}_g$  is the distance of the gear axis of rotation,  $O_g$ , from the axis of instant rotation,  $P_{ln}$ .

$\tilde{r}_p$  is the distance of the pinion axis of rotation,  $O_p$ , from the axis of instant rotation,  $P_{ln}$ .

$\mathbf{c}$  is the unit vector\* along the center line,  $\mathcal{L}$ .

The magnitude of the centerline vector,  $\mathbf{C}_g$ , is always greater in comparison with the magnitude of the centerline vector,  $\mathbf{C}_p$ . Therefore, the inequality  $|\mathbf{C}_g| \geq |\mathbf{C}_p|$  is observed.

### 2.4.2 Axial Vectors of a Gear Pair

Three different locations of a gear in relation to the centerline are distinguished.

*First*, a gear can be located such that the centerline,  $\mathcal{L}$ , goes through the middle of the gear face width, as schematically shown in Figure 2.29. Conventional helical gearing with skew axes of rotation features such a location for the gear and the pinion with respect to the centerline,  $\mathcal{L}$ .

In a more general case, a gear can be located at a certain distance from the centerline,  $\mathcal{L}$ . These shifts in two opposite directions enable two more different locations of a gear in relation to the centerline,  $\mathcal{L}$ .

The *second* configuration features a *positive* shift of the gear in relation to the centerline, that is, to the position *above* the centerline,  $\mathcal{L}$ , in Figure 2.29.

The *third* configuration features a *negative* shift of the gear in relation to the centerline, that is, to the position *below* the centerline,  $\mathcal{L}$ , in Figure 2.29.

A well-known hypoid gear pair is a perfect example of a gear pair with the gear and the pinion shifted in the axial direction of the gear and the pinion, correspondingly.

The actual location of the gear in relation to the centerline is specified by the axial vector,  $\mathbf{A}_g$ , of the gear (and by the corresponding axial vector,  $\mathbf{A}_p$ , of the pinion).

The axial vector,  $\mathbf{A}_g$ , associated with the gear is along the gear axis of rotation,  $O_g$ . This vector is applied at the point of intersection of the gear axis,  $O_g$ , and the centerline (Figure 2.29). The vector,  $\mathbf{A}_g$ , can be expressed in terms of two parameters,  $\mathbf{a}_g$  and  $A_g$ :

$$\mathbf{A}_g = A_g \cdot \mathbf{a}_g \quad (2.49)$$

\* Here and below, when treating *normalized* parameters, it is a must to bear in mind that the original values, that is, a velocity vector,  $\mathbf{V}$ ; a tangent vector,  $\mathbf{T}$ ; a displacement,  $\delta$ ; and so forth, are the vectors with dimensions and therefore cannot be added to one another, as they are of different dimensions. Normalized vectors (a unit speed vector,  $\mathbf{v} = \mathbf{V}/|\mathbf{V}|$ ; a unit tangent vector,  $\mathbf{t} = \mathbf{T}/|\mathbf{T}|$ ; and so forth) can formally be added to one another, as they are dimensionless. The latter can cause mistakes when performing an analysis of gearings.

Here, the distance along the gear axis of rotation,  $O_g$ , from the centerline,  $\mathcal{L}$ , to the middle of the gear face width,  $\tilde{F}_g$ , is denoted as  $A_g$ . The equality  $A_g = |\mathbf{A}_g|$  is observed. The unit vector,  $\mathbf{a}_g$ , is the vector along the rotation vector,  $\boldsymbol{\omega}_g$ , of the gear. The unit vector,  $\mathbf{a}_g$ , is dimensionless. It can be calculated from the following formula:

$$\mathbf{a}_g = \frac{\boldsymbol{\omega}_g}{|\boldsymbol{\omega}_g|} \cdot \text{sgn}(\boldsymbol{\omega}_g \cdot \boldsymbol{\omega}_{pl}) \quad (2.50)$$

The axial vector,  $\mathbf{A}_p$ , associated with the pinion is along the pinion axis of rotation,  $O_p$ . This vector is applied at the point of intersection of the pinion axis,  $O_p$ , by the centerline,  $\mathcal{L}$ . The vector  $\mathbf{A}_p$  can be expressed in terms of two parameters,  $\mathbf{a}_p$  and  $A_p$ :

$$\mathbf{A}_p = A_p \cdot \mathbf{a}_p \quad (2.51)$$

In Equation 2.51, the following are designated:

$A_p$  is the distance along the pinion axis of rotation,  $O_p$ , from the centerline,  $\mathcal{L}$ , to the middle of the face width  $\tilde{F}_p$  of the pinion.

$\mathbf{a}_p$  is the nondimensional unit vector along the rotation vector of the pinion,  $\boldsymbol{\omega}_p$ ; it can be calculated from the formula  $\mathbf{a}_g = \boldsymbol{\omega}_g / |\boldsymbol{\omega}_g|$ .

The multiplier  $\text{sgn}(\boldsymbol{\omega}_g \cdot \boldsymbol{\omega}_{pl})$  in Equation 2.50 allows the accommodation of the unit vector,  $\mathbf{a}_g$ , for both kinds of gear pairs, that is, for negative as well as positive gear pairs.

Once a gear is assumed to be stationary when determining the vector of instant rotation,  $\boldsymbol{\omega}_{pl}$ , then the rotation vectors,  $\boldsymbol{\omega}_p$  and  $\boldsymbol{\omega}_{pl}$ , always form an acute angle. The multiplier  $\text{sgn}(\boldsymbol{\omega}_p \cdot \boldsymbol{\omega}_{pl})$  is always positive; thus, it is not necessary to implement it in Equation 2.51.

The angle between the rotation vectors,  $\boldsymbol{\omega}_g$  and  $\boldsymbol{\omega}_{pl}$ , is obtuse for a rotary-negative gear pair, and it is acute for a rotary-positive gear pair. Because of this, the gear and the pinion of a gear pair are located at the same side of the centerline,  $\mathcal{L}$ , so the axial vectors,  $\mathbf{A}_g$  and  $\mathbf{A}_p$ , should always be acute. This is accounted for by the multiplier,  $\text{sgn}(\boldsymbol{\omega}_g \cdot \boldsymbol{\omega}_{pl})$ .

If magnitude,  $A_g$ , of the vector,  $\mathbf{A}_g$ , is known, then the following formula:

$$r_g = \sqrt{\tilde{r}_g^2 + A_g^2 \cdot \tan^2 \Sigma_g} \quad (2.52)$$

can be implemented for the calculation of pitch radius of the gear,  $r_g$ .

Conversely, if the pitch radius of the gear,  $r_g$ , is given, then for the calculation of the axial shift of the gear, the formula

$$A_g = \frac{\sqrt{r_g^2 - \tilde{r}_g^2}}{\tan \Sigma_g} \quad (2.53)$$

can be used.

Similar to Equations 2.52 and 2.53, the following expressions:

$$r_p = \sqrt{\tilde{r}_p^2 + A_p^2 \cdot \tan^2 \Sigma_p} \quad (2.54)$$

and

$$A_p = \frac{\sqrt{r_p^2 - \tilde{r}_p^2}}{\tan \Sigma_p} \quad (2.55)$$

are valid for calculating the axial shift,  $A_p$ , and pitch radius,  $r_p$ , of a pinion.

\* The width of a gear,  $\tilde{F}_g$ , and the gear face width,  $F_g$ , are not identical in the case under consideration. The width,  $\tilde{F}_g$ , of a cylindrical gear is equal to its face width,  $F_g$ , whereas the width of a conical gear,  $\tilde{F}_g$ , and its face width,  $F_g$ , correlate with each other as  $\tilde{F}_g = F_g \cdot \cos \Gamma$ . Here, the pitch cone angle of the conical gear is denoted by  $\Gamma$ .

It can be easily shown that magnitude,  $A_p$ , of the axial vector,  $\mathbf{A}_p$ , can be expressed in terms of magnitude,  $A_g$ , of the axial vector,  $\mathbf{A}_g$ :

$$A_p = A_g \frac{\cos \Sigma_p}{\cos \Sigma_g} \quad (2.56)$$

Magnitudes,  $A_g$  and  $A_p$ , of the axial vectors,  $\mathbf{A}_g$  and  $\mathbf{A}_p$ , have the same sign. Both are positive (i.e.,  $A_g > 0, A_p > 0$ ), have zero value (i.e.,  $A_g = 0, A_p = 0$ ), or are negative (i.e.,  $A_g < 0, A_p < 0$ ). Consequently, three different locations of a gear in relation to the centerline can be distinguished.

### 2.4.3 Useful Kinematic and Geometric Formulas

The proposed vector diagrams of gear pairs (i.e., vector diagrams for rotations/torques) make it possible to derive numerous auxiliary formulas for calculating the kinematic and geometric parameters of gear pairs.

For calculation of the distances,  $r_g$  and  $r_p$ , of the gear axis of rotation,  $O_g$ , and the pinion axis of rotation,  $O_p$ , from the axis of instant rotation,  $P_{ln}$ , the following approach can be applied: Let us project the rotation vectors,  $\omega_g$ ,  $\omega_p$ , and  $\omega_{pl}$ , onto a plane that is perpendicular to the centerline,  $\Phi$  (see Figure 2.28). The components,  $\omega_g^{rl}$  and  $\omega_g^{sl}$ , of the rotation vector of the gear,  $\omega_g$ , and the components,  $\omega_p^{rl}$  and  $\omega_p^{sl}$ , of the rotation vector of the mating pinion,  $\omega_p$ , are also depicted here. The rolling components,  $\omega_g^{rl}$  and  $\omega_p^{rl}$ , of the rotation vectors,  $\omega_g$  and  $\omega_p$ , are within a plane through the centerline,  $\Phi$ .

The following expression can be derived on the premise of pure rolling in the gear pair:

$$\omega_g^{rl} \cdot \tilde{r}_g = \omega_p^{rl} \cdot \tilde{r}_p \quad (2.57)$$

For the distances,  $r_g$  and  $r_p$ , the following equality is valid:

$$\tilde{r}_g + \tilde{r}_p = C \quad (2.58)$$

If the distances,  $r_g$  and  $r_p$ , are considered signed values, then Equation 2.58 is valid for both negative and positive gear pairs.

The distance,  $r_p$ , can be expressed in terms of the distance,  $r_g$ , and the center distance,  $C$ , as

$$\tilde{r}_p = C - \tilde{r}_g \quad (2.59)$$

Equation 2.59 allows the representation of Equation 2.57 in the following form:

$$\omega_g^{rl} \cdot \tilde{r}_g = \omega_p^{rl} \cdot (C - \tilde{r}_g) \quad (2.60)$$

This immediately returns a formula for the calculation of the distance,  $\tilde{r}_g$ :

$$\tilde{r}_g = \frac{1 + \omega_p - \omega_g}{1 + \omega_p} \cdot C \quad (2.61)$$

Once the distance,  $\tilde{r}_g$ , is determined, for the calculation of the distance  $\tilde{r}_p$ , Equation 2.59 can be implemented. In the case under consideration, Equation 2.59 allows the following formula:

$$\tilde{r}_p = \frac{1 + \omega_g - \omega_p}{1 + \omega_g} \cdot C \quad (2.62)$$

It is the right point to discuss here a few more formulas for the calculation of kinematic and geometric parameters of a gear pair, which directly follow from analysis of Figure 2.28.

The magnitude,  $\omega_{pl}$ , of a vector of instant rotation,  $\omega_{pl}$ , can be calculated from the following equation:

$$\omega_{pl} = \sqrt{(\omega_g^{rl})^2 + (\omega_p^{rl})^2 - 2 \cdot \omega_g^{rl} \cdot \omega_p^{rl} \cdot \cos \Sigma} \quad (2.63)$$

For calculation of the gear angle,  $\Sigma_g$ , between the vectors,  $\omega_g^{rl}$  and  $\omega_{pl}$ , the following equation can be used:

$$\Sigma_g = \frac{1 + \omega_p - \omega_g}{1 + \omega_p} \cdot \Sigma \quad (2.64)$$

Similarly, the pinion angle,  $\Sigma_p$ , between the vectors,  $\omega_p^{rl}$  and  $\omega_{pl}$  can be calculated from the equation:

$$\Sigma_p = \frac{1 + \omega_g - \omega_p}{1 + \omega_g} \cdot \Sigma \quad (2.65)$$

If the angle  $\Sigma_g = 90^\circ$  is entered into Equation 2.64, then the expression:

$$\Sigma_{cr} = \frac{1 + \omega_g}{1 + \omega_g - \omega_p} \cdot \frac{\pi}{2} \quad (2.66)$$

for the calculating of a critical value,  $\Sigma_{cr}$ , of the angle,  $\Sigma$ , between the gear axis of rotation,  $O_g$ , and the pinion axis of rotation,  $O_p$ , can be derived.

---

## 2.5 Possible Future Developments in the Theory of Gearing

Commonly, gearings used in the current industry feature constant fundamental design parameters, such as constant center distance,  $C = \text{const}$ ; crossed-axes angle,  $\Sigma = \text{const}$ ; and gear ratio,  $u = \text{const}$ . All possible types of gear pairs with constant fundamental design parameters are covered by the developed scientific classification of types of vector diagrams of gear pairs illustrated in [Figure 2.15](#). Based on the classification, a gear designer in the industry has the possibility to pick an appropriate kinematics of gearing and then design a corresponding gear pair that best fits particular application requirements. This is a perfect example of how the gear science can govern the practice of gear design and application.

In addition to gear pairs with constant fundamental design parameters (gear pairs of this type may be referred to as *CΣu-constant gear pairs*), gearings of other types are also known. As an example, a noncircular gear pair is depicted in [Figure 2.30](#). Gearings of this particular type feature the gear ratio,  $u$ , that is time dependent; that is,  $u = u(t)$ .

Generally speaking, each of the fundamental design parameters ( $C$ ,  $\Sigma$ , and  $u$ ) can be time dependent. In contrast to *CΣu-constant gear pairs*, gearings with all three variable fundamental design parameters can be referred to as *CΣu-variable gear pairs*. To investigate the possible types and total number of potentially possible gear pairs with variable-in-time fundamental design parameters, the following analysis is performed.

In the analysis, each of the fundamental design parameters of a gear pair is considered as a time-dependent design parameter, that is, as  $C = C(t)$ ,  $\Sigma = \Sigma(t)$ , and  $u = u(t)$ . Gear pairs that feature variables  $C = C(t)$ ,  $\Sigma = \Sigma(t)$ , and  $u = u(t)$  parameters are referred to as *CΣu-variable gear pairs*. For convenience, the numberings of the vector diagrams that are used in the proposed classification of the vector diagrams (see [Figure 2.15](#)) are also used for the analysis of *CΣu-variable gear pairs*.

With that said, various types of vector diagrams of gear pairs with variable fundamental design parameters are distinguished:

1. Vector diagrams with three variable fundamental design parameters ([Figure 2.31](#)):
  - 1.1 Rotary-negative *CΣu-variable gear pairs* (1.1)
  - 1.2 Rotary-zero *CΣu-variable gear pairs* (1.2)
  - 1.3 Rotary-positive *CΣu-variable gear pairs* (1.3)



**FIGURE 2.30**  
Noncircular gearing.

2. Vector diagrams with two variable fundamental design parameters (Figure 2.32):

- 2.1 Rotary-negative  $\Sigma u$ -variable gear pairs:  $C = \text{const} \neq 0$  (1.1)
- 2.2 Rotary-negative  $Cu$ -variable gear pairs:  $\Sigma = \text{const} \neq 0$  (1.1)
- 2.3 Rotary-negative  $C\Sigma$ -variable gear pairs:  $u = \text{const}$  (1.1)
- 2.4 Rotary-zero  $\Sigma u$ -variable gear pairs:  $C = \text{const} \neq 0$  (1.2)
- 2.5 Rotary-zero  $Cu$ -variable gear pairs:  $\Sigma = \text{const} \neq 0$  (1.2)
- 2.6 Rotary-zero  $C\Sigma$ -variable gear pairs:  $u = \text{const}$  (1.2)

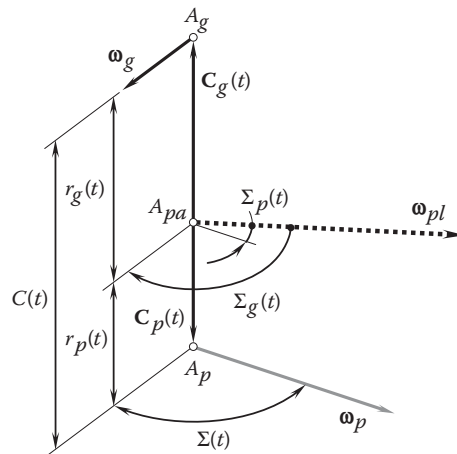


**FIGURE 2.31**  
Vector diagram with three variable fundamental design parameters of a  $C\Sigma u$ -variable gear pair.

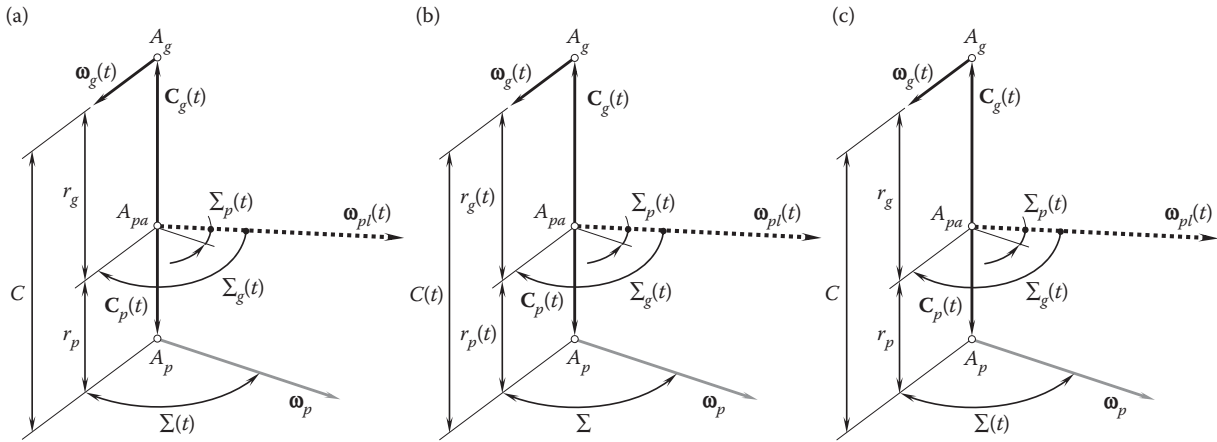


FIGURE 2.32

Vector diagram with two variable fundamental design parameters of (a)  $\Sigma u$ -variable gear pair (or  $C$ -constant gear pair), (b)  $Cu$ -variable gear pair (or  $\Sigma$ -constant gear pair), and (c)  $\Sigma C$ -variable gear pair (or  $u$ -constant gear pair).

- 2.7 Rotary-positive  $\Sigma u$ -variable gear pairs:  $C = \text{const} \neq 0$  (1.3)
- 2.8 Rotary-positive  $Cu$ -variable gear pairs:  $\Sigma = \text{const} \neq 0$  (1.3)
- 2.9 Rotary-positive  $C\Sigma$ -variable gear pairs:  $u = \text{const}$  (1.3)
3. Vector diagrams with two variable fundamental design parameters (Figure 2.33):
  - 3.1 Rotary-negative  $\Sigma u$ -variable gear pairs:  $C = 0$  (1.1.1)
  - 3.2 Rotary-zero  $\Sigma u$ -variable gear pairs:  $C = 0$  (1.2.1)
  - 3.3 Rotary-positive  $\Sigma u$ -variable gear pairs:  $C = 0$  (1.3.1)
4. Vector diagrams with two variable fundamental design parameters (Figure 2.34):
  - 4.1 Rotary-negative  $Cu$ -variable gear pairs:  $\Sigma = 0^\circ$  (1.1.2)
  - 4.2 Rotary-zero  $Cu$ -variable gear pairs:  $\Sigma = \text{const} \neq 0^\circ$  (1.2.2)
  - 4.3 Rotary-positive  $Cu$ -variable gear pairs:  $\Sigma = 180^\circ$  (1.3.2)
5. Vector diagrams with one variable fundamental design parameter (Figure 2.35):
  - 5.1 Rotary-negative  $C$ -variable gear pairs:  $\Sigma = \text{const}$ ,  $u = \text{const}$  (1.1)
  - 5.2 Rotary-negative  $\Sigma$ -variable gear pairs:  $C = \text{const}$ ,  $u = \text{const}$  (1.1)
  - 5.3 Rotary-negative  $u$ -variable gear pairs:  $C = \text{const}$ ,  $\Sigma = \text{const}$  (1.1)
  - 5.4 Rotary-zero  $C$ -variable gear pairs:  $\Sigma = \text{const}$ ,  $u = \text{const}$  (1.2)
  - 5.5 Rotary-zero  $\Sigma$ -variable gear pairs:  $C = \text{const}$ ,  $u = \text{const}$  (1.2)

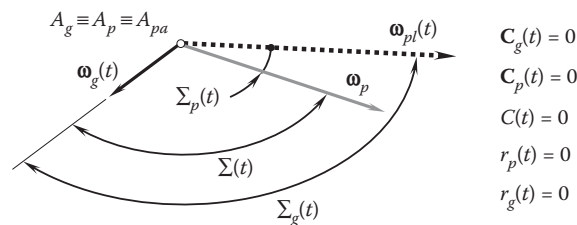


FIGURE 2.33

Vector diagram with two variable fundamental design parameters of  $\Sigma u$ -variable gear pair (or  $C$ -constant gear pair,  $C = 0$ ).

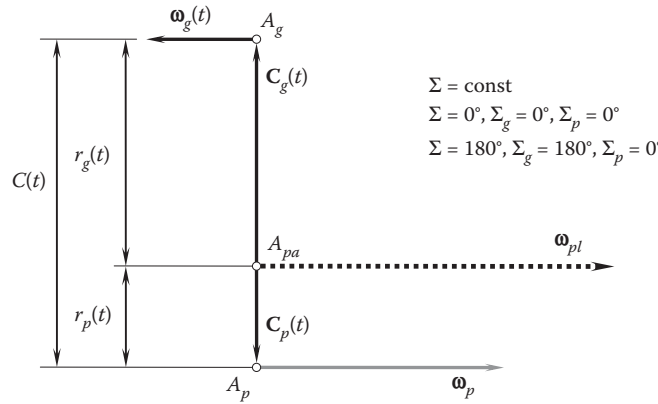


FIGURE 2.34

Vector diagram with three variable fundamental design parameters of a  $Cu$ -variable gear pair (the crossed-axes angle,  $\Sigma$ , is of a constant value,  $\Sigma = \text{const}$ , and can be equal to either  $\Sigma = 0^\circ$  or  $\Sigma = 180^\circ$ ).

5.6 Rotary-zero  $u$ -variable gear pairs:  $C = \text{const}$ ,  $\Sigma = \text{const}$  (1.2)

5.7 Rotary-positive  $C$ -variable gear pairs:  $\Sigma = \text{const}$ ,  $u = \text{const}$  (1.3)

5.8 Rotary-positive  $\Sigma$ -variable gear pairs:  $C = \text{const}$ ,  $u = \text{const}$  (1.3)

5.9 Rotary-positive  $u$ -variable gear pairs:  $C = \text{const}$ ,  $\Sigma = \text{const}$  (1.3)

The  $C$ -variable gear pairs ( $\Sigma$ ,  $u$ -constant gear pairs),  $\Sigma$ -variable gear pairs ( $C$ ,  $u$ -constant gear pairs), and  $u$ -variable gear pairs ( $C$ ,  $\Sigma$ -constant gear pairs) are not feasible in relation to the fundamental design parameters; that is, (a)  $C = \text{var}$ ,  $\Sigma = \text{const}$ ,  $u = \text{const}$ ; (b)  $C = \text{const}$ ,  $\Sigma = \text{var}$ ,  $u = \text{const}$ ; and (c)  $C = \text{const}$ ,  $\Sigma = \text{const}$ ,  $u = \text{var}$  are not compatible.

Vector diagrams with one variable fundamental design parameter that can be derived from the vector diagrams of the types 1.1.1, 1.1.2, 1.2.1, 1.2.2, 1.3.1, 1.3.2, and others are covered by those derived from the vector diagrams of the types 1.1, 1.2, and 1.3 above.

Some additional simplifications can be made to the proposed list of the vector diagrams.

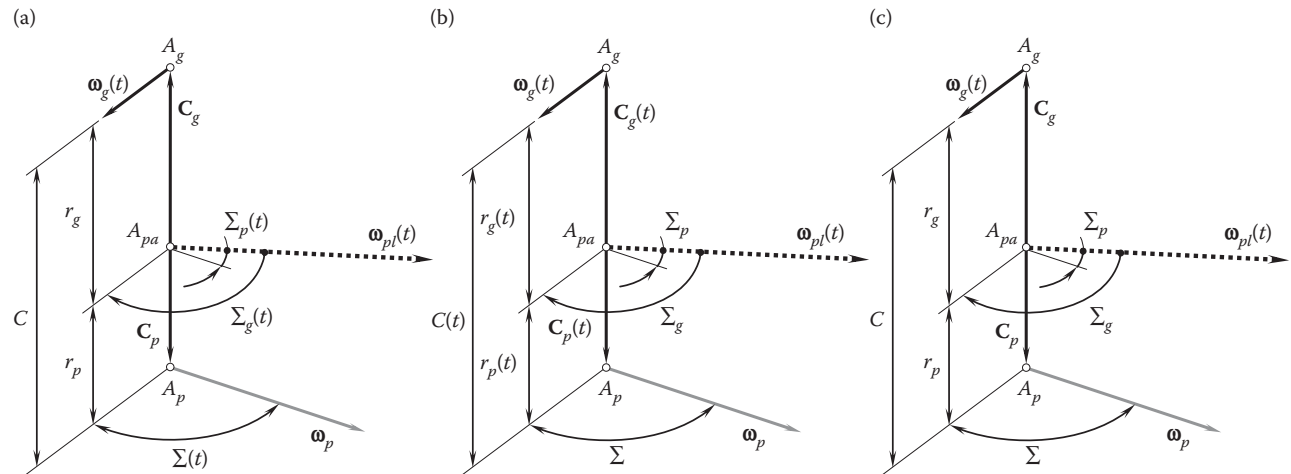


FIGURE 2.35

Vector diagram with one variable fundamental design parameter of (a)  $\Sigma$ -variable gear pair (or  $C, u$ -constant gear pair), (b)  $C$ -variable gear pair (or  $\Sigma, u$ -constant gear pair), and (c)  $u$ -variable gear pair (or  $\Sigma, C$ -constant gear pair)—not feasible.



It is critical that the total number of the vector diagrams listed above is not infinite but instead is limited to a reasonably small number of the vector diagrams (vector diagrams of no other type are feasible). This means that each one of them can be investigated to the best possible extent with the goal of application to design gear pairs.

In *CΣu-variable* gear pairs of all possible types, at every instant of time, that is, for any and all configurations of a gear and its mating pinion, the instant base pitch of a gear, as well as the instant base pitch of the pinion, both have to be equal to the instant operating base pitch of the gear pair—this is a must.

*CΣu-variable* gear pairs of all possible types (i.e., those listed above) is a challenging subject to be investigated in the future.



# Taylor & Francis

Taylor & Francis Group

<http://taylorandfrancis.com>

# 3

---

## *Principal Planes and Principal Reference Systems Associated with a Gear Pair*

---

For a gear pair with a specified set of the design parameters, a corresponding vector diagram for the rotation vectors (as well as for the torques) can be constructed. Several principal directions are associated with a gear pair. These directions are defined by the rotation vectors of a gear and a mating pinion, the instant rotation vector, and the centerline. Use of the principal directions allows for construction of a set of principal planes and principal reference systems associated with a gear pair. By means of the principal planes and principal reference systems, the analysis of gearings of all types can be significantly simplified.

Let us begin the discussion with the consideration of the principal planes associated with a gear pair.

---

### 3.1 Principal Planes Associated with a Gear Pair

Consider a crossed-axes gear pair for which the axes of instant rotation,  $P_{ln}$ , and the centerline,  $\mathfrak{C}$ , are constructed.

A set of three principal planes can be associated with a gear pair.

The *pitch-line plane* (or just  $P_{ln}$ -plane, for simplicity) is the first of three principal planes associated with a crossed-axes gear pair.

#### **Definition 3.1**

*The pitch-line plane is the plane through the axis of instant rotation (the pitch line),  $P_{ln}$ , and the centerline,  $\mathfrak{C}$ , of the gear pair.*

Configuration of the pitch-line plane in relation to the axes of instant rotation,  $P_{ln}$ , and the centerline,  $\mathfrak{C}$ , in a crossed-axes gear pair is schematically shown in [Figure 3.1](#).

The second principal plane associated with a crossed-axes gear pair is the *centerline plane* (or just  $C_{ln}$ -plane, for simplicity).

#### **Definition 3.2**

*The centerline plane is the plane through the centerline,  $\mathfrak{C}$ , of the gear pair perpendicular to the pitch line,  $P_{ln}$ .*

Configuration of the centerline plane in relation to the axis of instant rotation,  $P_{ln}$ , and the centerline,  $\mathfrak{C}$ , in a crossed-axis gear pair is schematically shown in [Figure 3.2](#).

Finally, the *normal plane* (or just  $N_{ln}$ -plane, for simplicity) is the third of three principal planes associated with a crossed-axes gear pair.

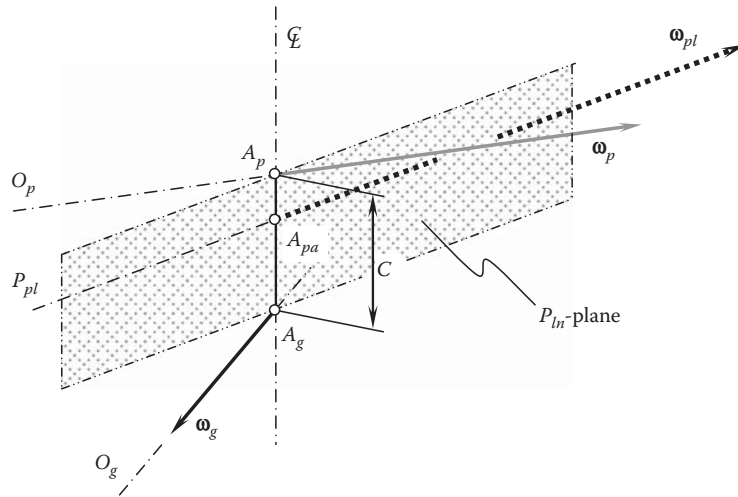
#### **Definition 3.3**

*The normal plane is the plane through the plane-of-action apex,  $A_{pa}$ , perpendicular to the centerline,  $\mathfrak{C}$ , of the gear pair.*

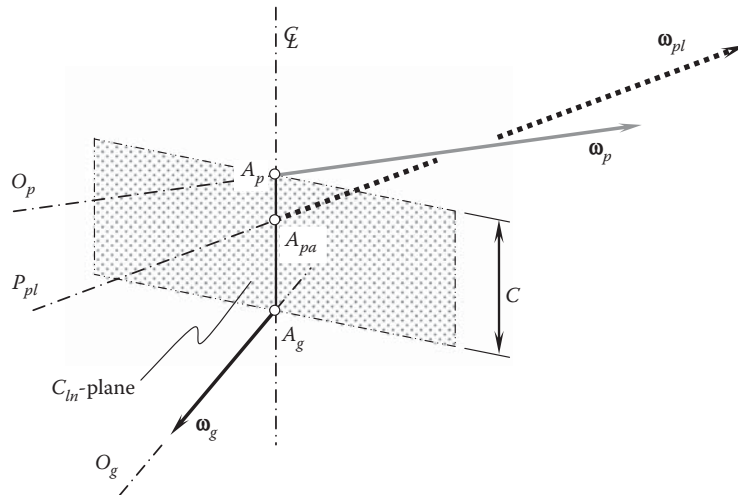
Configuration of the normal plane\* in relation to the axis of instant rotation,  $P_{ln}$ , and the centerline,  $\mathfrak{C}$ , in a crossed-axis gear pair is schematically shown in [Figure 3.3](#).

---

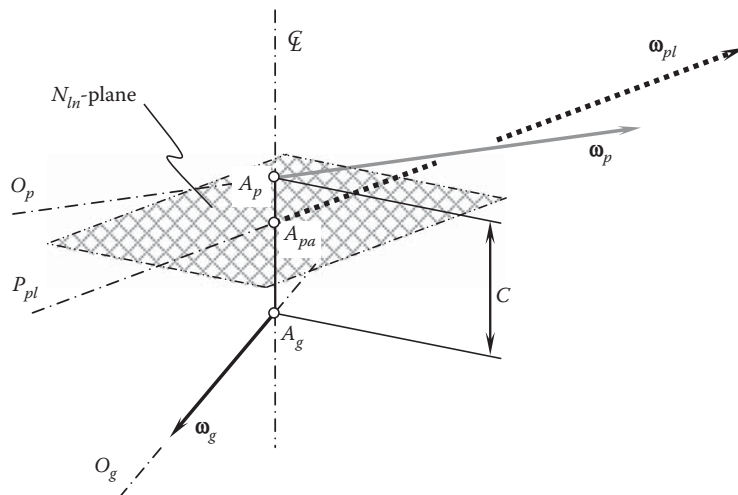
\* Further analysis reveals that, actually, the normal plane, that is, the  $N_{ln}$ -plane, serves as the pitch plane in gearings of all types, that is, in  $C_a$ -,  $I_a$ -, and  $P_a$ -gearings.



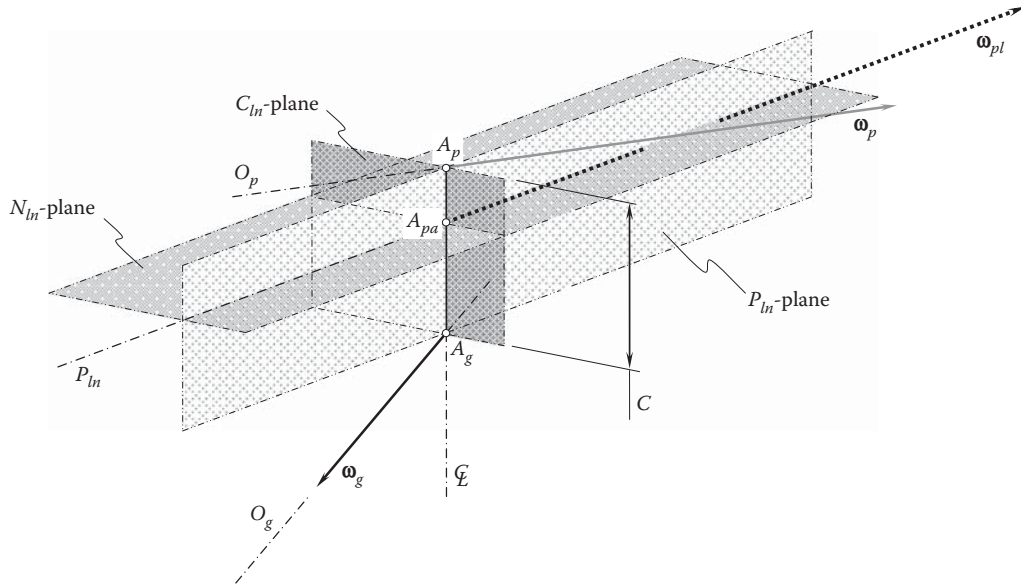
**FIGURE 3.1**  
Principal planes associated with a gear pair: the pitch-line plane (the  $P_{ln}$ -plane).



**FIGURE 3.2**  
Principal planes associated with a gear pair: the centerline plane (the  $C_{ln}$ -plane).



**FIGURE 3.3**  
Principal planes associated with a gear pair: the normal plane (the  $N_{ln}$ -plane).

**FIGURE 3.4**

Principal planes: the pitch-line plane (the  $P_{ln}$ -plane), the centerline plane (the  $C_{ln}$ -plane), and the normal plane (the  $N_{ln}$ -plane) associated with a gear pair.

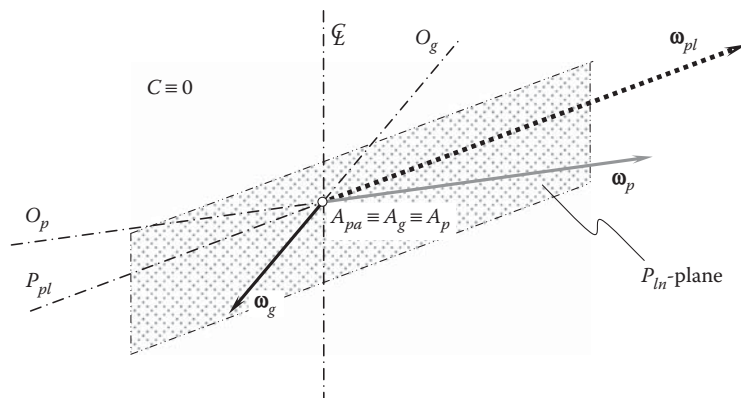
Altogether, the three principal planes are schematically depicted in Figure 3.4. Here, in Figure 3.4 (as well as in Figures 3.1 through 3.3), the principal planes, namely the  $P_{ln}$ -plane,  $C_{ln}$ -plane, and  $N_{ln}$ -plane, are constructed for the most general case of crossed-axes gearing. The definitions for the principal planes are also valid for the reduced cases of gearings that is, for intersected-axes gearing and for parallel-axes gearing as well. However, for the reduced cases of the vector diagrams, simpler specifications of the principal planes can be formulated.

### 3.1.1 Case of Intersected-Axes Gearing

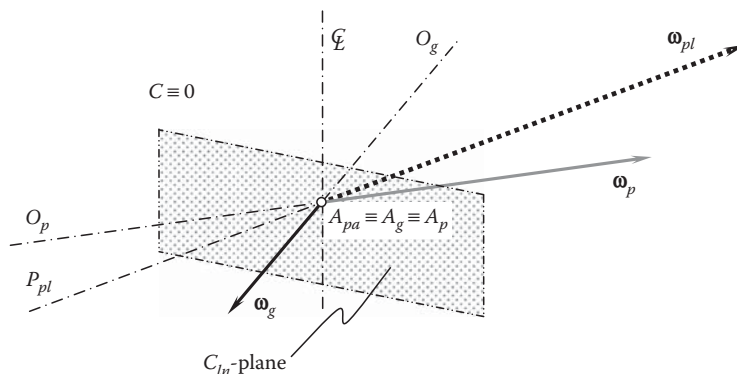
As shown in Figure 3.4, the centerline,  $\mathcal{C}$ , is perpendicular to the axes of rotation of the gear,  $O_g$ , and the pinion,  $O_p$ . This feature is helpful to specify the configuration of the principal planes for intersected-axes gearing.

In the case of intersected-axes gearing, definitions of the principal planes can be reduced to:

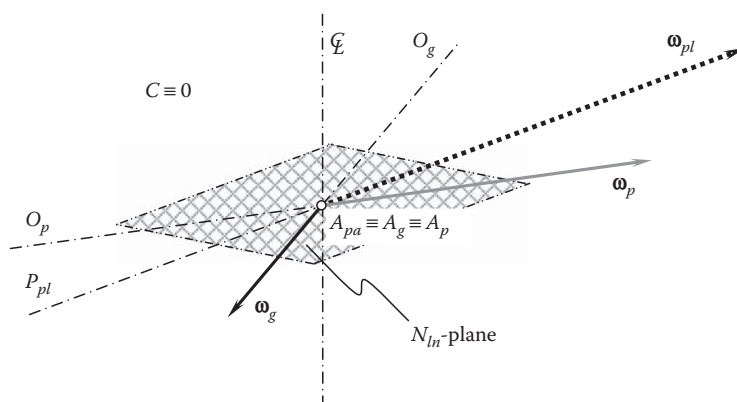
- The  $P_{ln}$ -plane is the plane through the axis of instant rotation,  $P_{ln}$ , and perpendicular to the plane through the axes of rotation,  $O_g$  and  $O_p$ , of the gear and the pinion, as shown in Figure 3.5.

**FIGURE 3.5**

Principal planes associated with an intersected-axes gear pair: the pitch-line plane (the  $P_{ln}$ -plane).

**FIGURE 3.6**

Principal planes associated with an intersected-axes gear pair: the centerline plane (the  $C_{in}$ -plane).

**FIGURE 3.7**

Principal planes associated with an intersected-axes gear pair: the normal plane (the  $N_{in}$ -plane).

- The  $C_{in}$ -plane is the plane perpendicular to the axis of instant rotation,  $P_{in}$ . The centerline plane is also perpendicular to the plane through the axes of rotation,  $O_g$  and  $O_p$ , of the gear and the pinion (Figure 3.6).
- The  $N_{in}$ -plane is the plane through the axes of rotation,  $O_g$  and  $O_p$ , of the gear and the pinion. This is illustrated in Figure 3.7.

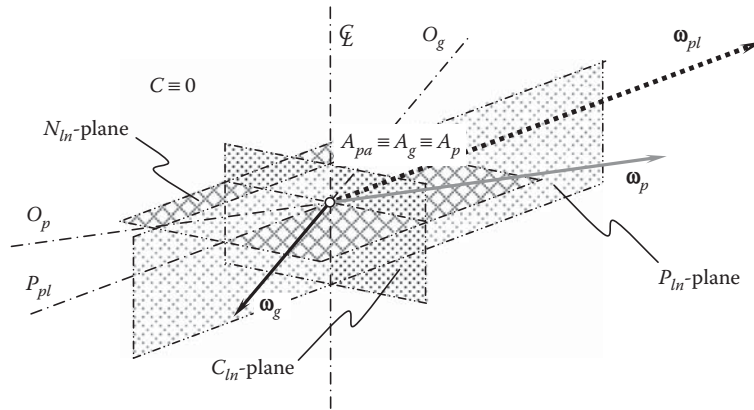
Altogether, the principal planes for intersected-axes gearing are schematically depicted in Figure 3.8.

### 3.1.2 Case of Parallel-Axes Gearing

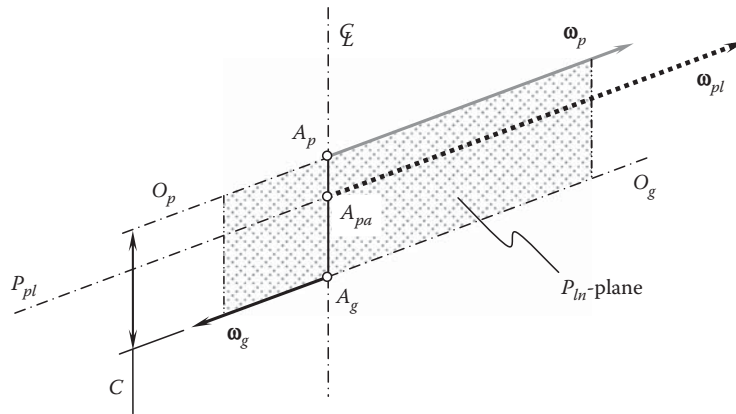
For parallel-axes gearings, the principal planes can be specified in a simplified manner:

- The  $P_{in}$ -plane is the plane through the axis of instant rotation,  $P_{in}$ , and through the axes of rotation,  $O_g$  and  $O_p$ , of the gear and the pinion as shown in Figure 3.9.
- The  $C_{in}$ -plane is the plane through the centerline,  $\mathcal{C}$ , of the gear pair perpendicular to the axis of instant rotation,  $P_{in}$ , as illustrated in Figure 3.10.
- The  $N_{in}$ -plane is the plane perpendicular to the centerline,  $\mathcal{C}$ , of the gear pair. The normal plane is also perpendicular to the plane through the axes of rotation,  $O_g$  and  $O_p$ , of the gear and the pinion (see Figure 3.11).

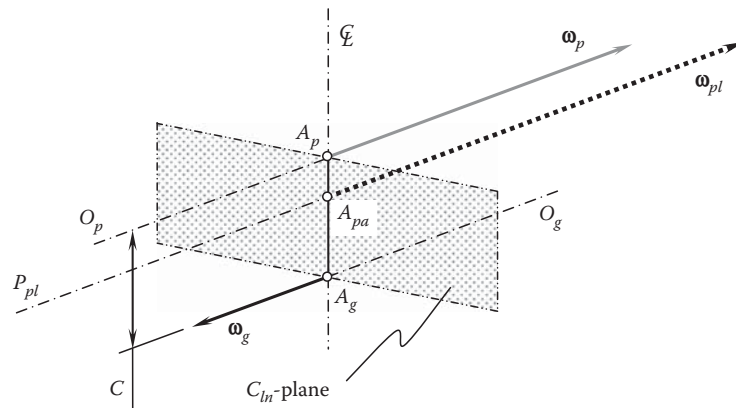
Altogether, the principal planes for parallel-axes gearing are schematically depicted in Figure 3.12. Use of the concept of principal planes simplifies the analysis of gearings of all types.

**FIGURE 3.8**

Principal planes: the pitch-line plane (the  $P_{ln}$ -plane), the centerline plane (the  $C_{ln}$ -plane), and the normal plane (the  $N_{ln}$ -plane) associated with an intersected-axes gear pair.

**FIGURE 3.9**

Principal planes associated with a parallel-axes gear pair: the pitch-line plane (the  $P_{ln}$ -plane).

**FIGURE 3.10**

Principal planes associated with a parallel-axes gear pair: the centerline plane (the  $C_{ln}$ -plane).



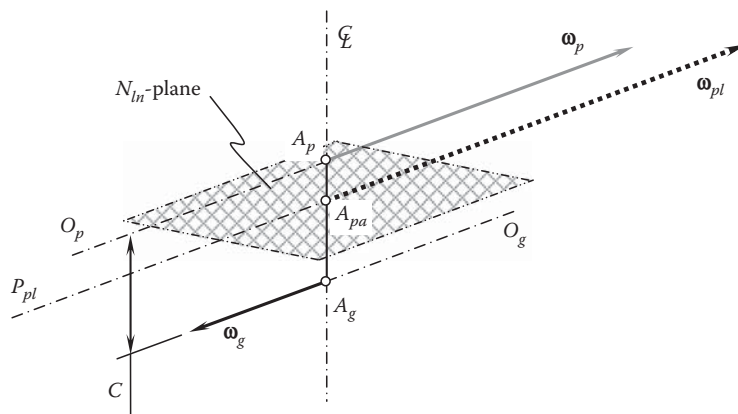


FIGURE 3.11

Principal planes associated with a parallel-axes gear pair: the normal plane (the  $N_{in}$ -plane).

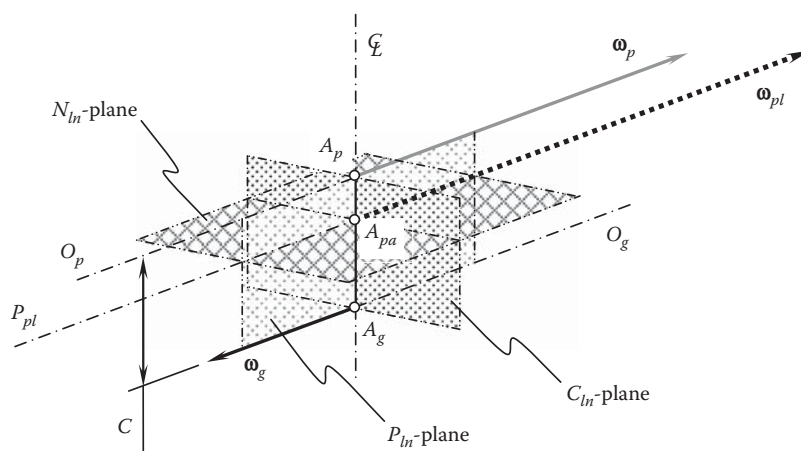


FIGURE 3.12

Principal planes: the pitch-line plane (the  $P_{in}$ -plane), the centerline plane (the  $C_{in}$ -plane), and the normal plane (the  $N_{in}$ -plane) associated with a parallel-axes gear pair.

### 3.2 Principal Reference Systems Associated with a Gear Pair

For the analytical description and investigation of the kinematics of gear pairs and the geometry of the interacting tooth flanks of the gear and a mating pinion, corresponding reference systems are used. Orthogonal *Cartesian* coordinate systems are widely used for these purposes.

Actually, both the kinematics of gearing and the geometry of the gear and the pinion tooth flanks can be analytically described in an arbitrary reference system. It is convenient to choose a reference system whose use allows for the simplest possible analytical expressions for all the elements of the gear pair.

The simplest possible analytical representation of an element of a gear pair can be derived in a specific reference system. These reference systems are associated with the gear pair in a specific manner. The reference systems of these types are referred to as *principal reference systems*.

To determine a set of principal reference systems, consider the vector diagram for an arbitrary gear pair given in Figure 3.13. The rotation vectors,  $\omega_g$  and  $\omega_p$ , of the gear and the pinion are at a certain center distance,  $C$ , and they cross one another. Points,  $A_g$  and  $A_p$ , are points of intersection of the gear axis of rotation,  $O_g$ , and the pinion axis of rotation,  $O_p$ , respectively, with the centerline,  $\zeta$ . The point,  $A_g$ , is referred to as the *gear apex*, and the point,  $A_p$ , is referred to as the *pinion apex*.

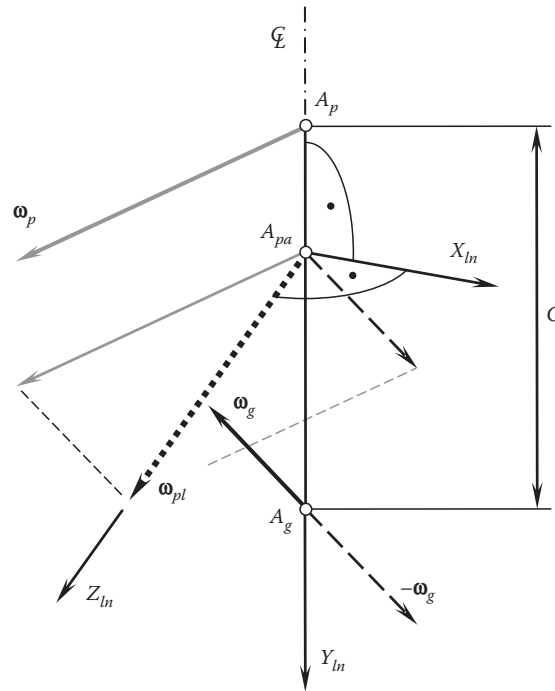


FIGURE 3.13

Principal reference system,  $X_{ln}Y_{ln}Z_{ln}$ , associated with a gear pair.

The vector of instant rotation,  $\omega_{pl}$ , of the pinion in relation to the gear is a vector through the point,  $A_{pa}$ . This point is located within the centerline,  $\mathcal{C}$ . The point,  $A_{pa}$ , is referred to as the *plane-of-action apex*.

The axis of instant rotation,  $P_{ln}$ , is the straight line through the point,  $A_{pa}$ , along the vector of instant rotation,  $\omega_{pl}$ .

Two straight lines through a common point uniquely specify a plane through this point. In the case under consideration, this is the plane through the axis of instant rotation,  $P_{ln}$ , and the centerline,  $\mathcal{C}$ .

The origin of the main reference system,  $X_{ln}Y_{ln}Z_{ln}$ , is coincident with the plane-of-action apex,  $A_{pa}$ . The axes  $X_{ln}$ ,  $Y_{ln}$ , and  $Z_{ln}$  are along the lines of intersection of the principal planes, as illustrated in Figure 3.13: the axis  $Z_{ln}$  is along the vector of instant rotation,  $\omega_{pl}$ ; the axis  $Y_{ln}$  is along the centerline,  $\mathcal{C}$ ; and the  $X_{ln}$ -axis complements the axes  $Y_{ln}$  and  $Z_{ln}$  to a left-hand-oriented Cartesian coordinate system  $X_{ln}Y_{ln}Z_{ln}$ .

(For reduced cases of intersected-axes gearing and of parallel-axes gearing, the main reference system,  $X_{ln}Y_{ln}Z_{ln}$ , is shown in Figures 3.14 and 3.15, respectively.)

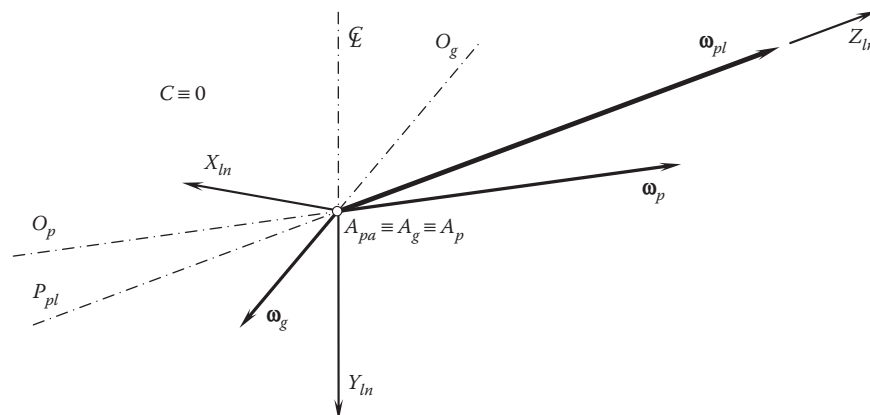
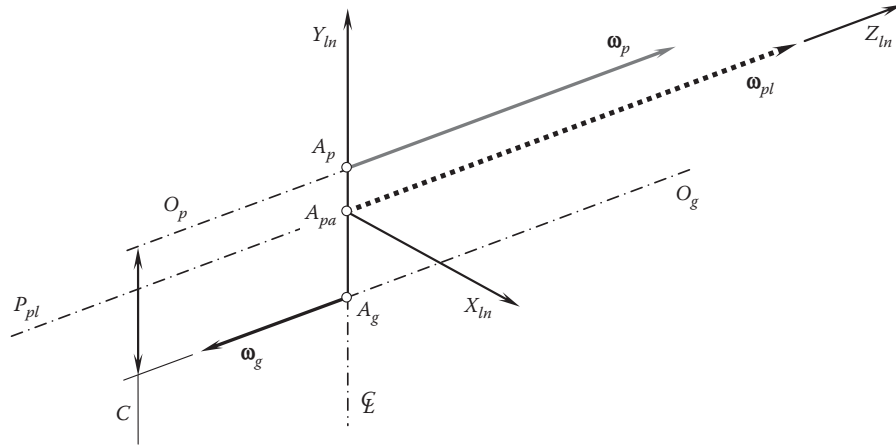


FIGURE 3.14

Principal reference system,  $X_{ln}Y_{ln}Z_{ln}$ , associated with an intersected-axes gear pair.

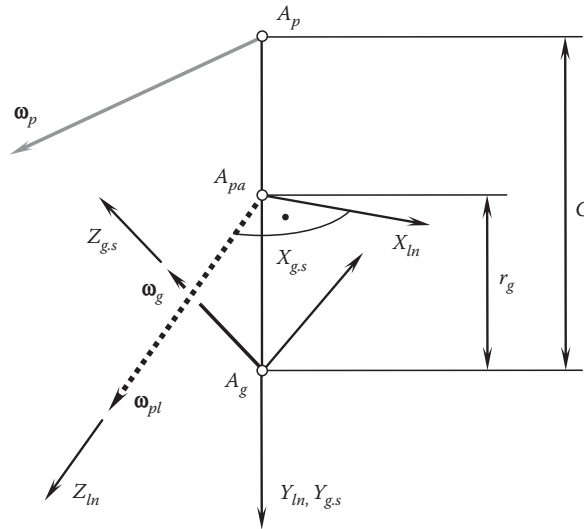
**FIGURE 3.15**

Principal reference system,  $X_{ln}Y_{ln}Z_{ln}$ , associated with a parallel-axes gear pair.

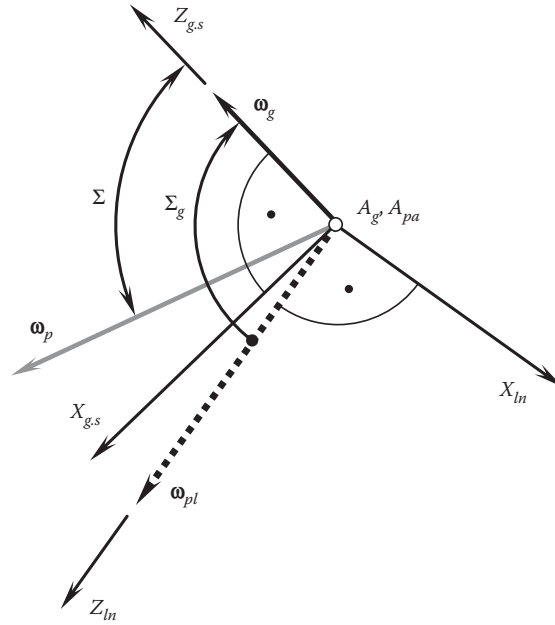
The stationary gear reference system,  $X_{g.s}Y_{g.s}Z_{g.s}$ , is the second reference system associated with the gear pair. The origin of the reference system,  $X_{g.s}Y_{g.s}Z_{g.s}$ , is coincident with the gear apex,  $A_g$ , as shown in Figure 3.16. The axis  $Z_{g.s}$  is along the rotation vector of the gear,  $\omega_g$ ; the axis  $Y_{g.s}$  is along the centerline,  $\mathcal{C}$ ; and the  $X_{g.s}$ -axis complements axes  $Y_{g.s}$  and  $Z_{g.s}$  to a left-hand-oriented Cartesian coordinate system  $X_{g.s}Y_{g.s}Z_{g.s}$ . Actually, the stationary gear reference system,  $X_{g.s}Y_{g.s}Z_{g.s}$ , is turned through the gear cone angle,  $\Sigma_g$ , about the  $Z_{ln}$ -axis of the reference system  $X_{ln}Y_{ln}Z_{ln}$  associated with a gear pair, as illustrated in Figure 3.17.

The gear reference system,  $X_gY_gZ_g$ , is the third reference system associated with the gear pair. The reference system,  $X_gY_gZ_g$ , is rigidly associated with the gear and is rotated together with the gear about its axis of rotation,  $O_g$ . As illustrated in Figure 3.18, the reference systems,  $X_gY_gZ_g$  and  $X_{g.s}Y_{g.s}Z_{g.s}$ , share the common axis  $Z_g \equiv Z_{g.s}$ , and are turned about the  $Z_{g.s}$ -axis through a gear rotation angle,  $\varphi_g$ .

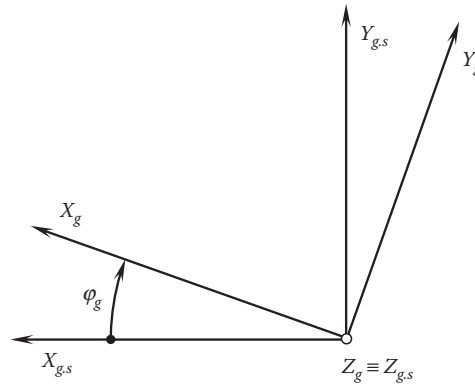
The stationary pinion reference system,  $X_{p.s}Y_{p.s}Z_{p.s}$ , is the fourth reference system associated with the gear pair. The origin of the reference system,  $X_{p.s}Y_{p.s}Z_{p.s}$ , is coincident with the pinion apex,  $A_p$ , as shown in Figure 3.19. The axis  $Z_{p.s}$  is along the rotation vector of the pinion,  $\omega_p$ ; the axis  $Y_{p.s}$  is along the centerline,  $\mathcal{C}$ ; and the  $X_{p.s}$ -axis complements axes  $Y_{p.s}$  and  $Z_{p.s}$  to a left-hand-oriented Cartesian coordinate system,  $X_{p.s}Y_{p.s}Z_{p.s}$ . Actually, the

**FIGURE 3.16**

Configuration of the motionless gear reference systems,  $X_{g.s}Y_{g.s}Z_{g.s}$ , in relation to the principal reference system,  $X_{ln}Y_{ln}Z_{ln}$ , associated with a gear pair.

**FIGURE 3.17**

The gear motionless reference systems,  $X_{g.s}Y_{g.s}Z_{g.s}$ , is turned through the gear cone angle,  $\Sigma_g$ , about  $Z_{ln}$ -axis of the principal reference system,  $X_{ln}Y_{ln}Z_{ln}$ , associated with a gear pair.

**FIGURE 3.18**

Configuration of the gear reference systems,  $X_gY_gZ_g$ , in relation to the motionless gear reference systems,  $X_{g.s}Y_{g.s}Z_{g.s}$ .

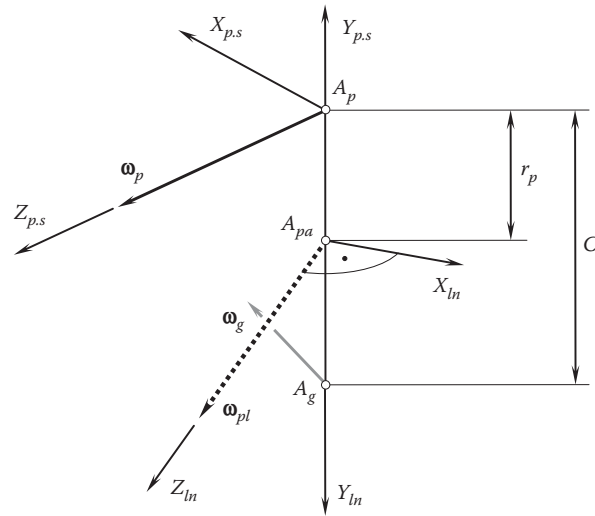
stationary pinion reference system,  $X_{p.s}Y_{p.s}Z_{p.s}$ , is turned through the pinion cone angle,  $\Sigma_p$ , about the  $Z_{ln}$ -axis of the principal reference system,  $X_{ln}Y_{ln}Z_{ln}$ , associated with a gear pair, as illustrated in [Figure 3.20](#).

The pinion reference system,  $X_pY_pZ_p$ , is the fifth reference system associated with the gear pair. The reference system,  $X_pY_pZ_p$ , is rigidly associated with the pinion, and is rotated together with the pinion about its axis of rotation,  $O_p$ . As illustrated in [Figure 3.21](#), the reference systems,  $X_pY_pZ_p$  and  $X_{p.s}Y_{p.s}Z_{p.s}$ , share the common axis  $Z_p \equiv Z_{p.s}$ , and are turned about the  $Z_{p.s}$ -axis through a pinion rotation angle,  $\varphi_p$ .

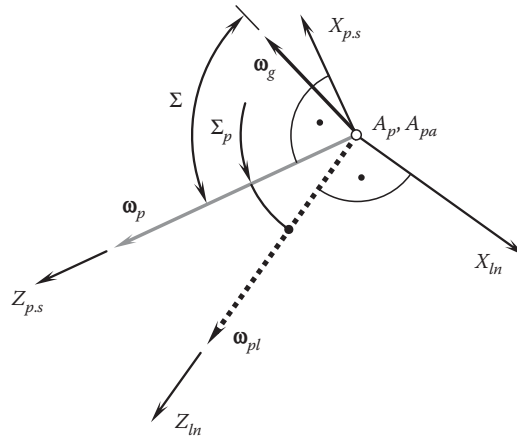
A gear rotation angle,  $\varphi_g$ , in [Figure 3.18](#) and a pinion rotation angle,  $\varphi_p$ , in [Figure 3.21](#) correlate to one another in the following manner:  $\varphi_p = u\varphi_g$ , where  $u$  is the gear ratio of a gear pair.

The introduced five reference systems, namely:

- The main reference system,  $X_{ln}Y_{ln}Z_{ln}$ , associated with the gear pair
- The stationary gear reference system,  $X_{g.s}Y_{g.s}Z_{g.s}$
- The gear reference system,  $X_gY_gZ_g$

**FIGURE 3.19**

Configuration of the motionless pinion reference systems,  $X_{p,s}Y_{p,s}Z_{p,s}$ , in relation to the principal reference system,  $X_{ln}Y_{ln}Z_{ln}$ , associated with a gear pair.

**FIGURE 3.20**

The pinion motionless reference systems,  $X_{p,s}Y_{p,s}Z_{p,s}$ , is turned through the pinion cone angle,  $\Sigma p$ , about the  $Z_{ln}$ -axis of the principal reference system,  $X_{ln}Y_{ln}Z_{ln}$ , associated with a gear pair.

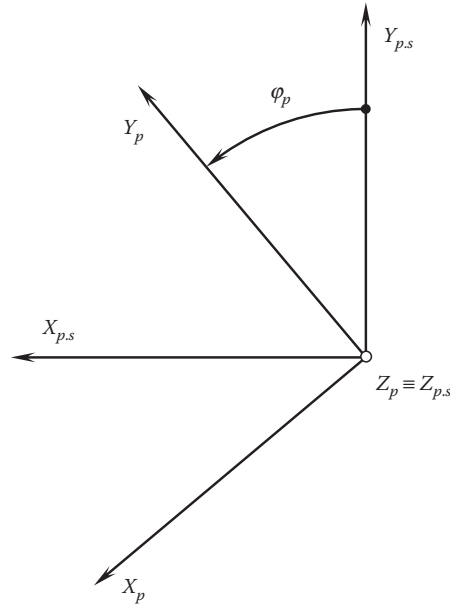
- The stationary pinion reference system,  $X_{p,s}Y_{p,s}Z_{p,s}$
- The pinion reference system,  $X_pY_pZ_p$

are referred to as the principal reference systems associated with a gear pair.

A few more auxiliary reference systems are often used when investigating gear pairs.

### 3.3 Coordinate System Transformations

Multiple reference systems are commonly applied when investigating a gear pair. It is a common practice that one of the coordinate systems be associated with the gear, another with the pinion, and the third reference system with the gear pair housing. In addition, numerous auxiliary (intermediate) reference systems are widely used.

**FIGURE 3.21**

Configuration of the pinion reference systems,  $X_pY_pZ_p$ , in relation to the motionless pinion reference systems  $X_{p,s}Y_{p,s}Z_{p,s}$ .

To investigate the kinematics and the geometry of a gear pair, all the components need to be analytically described in a common reference system. Coordinate system transformations are necessary to represent the entire gearing in a common coordinate system. For this purpose, the operators of elementary coordinate transformations are used (see Appendix D for details).

### 3.3.1 Transition from the Gear Reference System to the Main Reference System

The transition from the gear coordinate system,  $X_gY_gZ_g$ , to the main reference system,  $X_{ln}Y_{ln}Z_{ln}$ , can be performed in three steps.

At the beginning, the gear coordinate system,  $X_gY_gZ_g$ , is turned about its axis,  $Z_g$ , in the counterclockwise direction through a gear rotation angle,  $\varphi_g$  (Figure 3.18). This elementary coordinate system transformation is analytically described by the operator of rotation,  $\mathbf{Rt}(\varphi_g, Z_g)$ :

$$\mathbf{Rt}(\varphi_g, Z_g) = \begin{bmatrix} \cos \varphi_g & \sin \varphi_g & 0 & 0 \\ -\sin \varphi_g & \cos \varphi_g & 0 & 0 \\ 0 & 0 & 1 & 0 \\ 0 & 0 & 0 & 1 \end{bmatrix} \quad (3.1)$$

Second, the stationary gear coordinate system,  $X_{g,s}Y_{g,s}Z_{g,s}$ , is translated at a distance,  $r_g$ , along the axis,  $Y_g$ . In this intermediate position, the coordinate system,  $X_{g,s}Y_{g,s}Z_{g,s}$ , is labeled as  $X_{g,s}^*Y_{g,s}^*Z_{g,s}^*$ . For an analytical description of the transition from the stationary gear coordinate system,  $X_{g,s}Y_{g,s}Z_{g,s}$ , to the intermediate auxiliary coordinate system  $X_{g,s}^*Y_{g,s}^*Z_{g,s}^*$ , the operator of translation,  $\mathbf{Tr}(r_g, Y_{g,s}^*)$ , can be used:

$$\mathbf{Tr}(r_g, Y_{g,s}^*) = \begin{bmatrix} 1 & 0 & 0 & 0 \\ 0 & 1 & 0 & r_g \\ 0 & 0 & 1 & 0 \\ 0 & 0 & 0 & 1 \end{bmatrix} \quad (3.2)$$

Then, the transition from the auxiliary reference system,  $X_{g,s}^*Y_{g,s}^*Z_{g,s}^*$ , to the main reference system,  $X_{ln}Y_{ln}Z_{ln}$ , can be analytically described by the operator of rotation,  $\mathbf{Rt}(\Sigma_g, Y_{g,s}^*)$ , of the coordinate system,  $X_{g,s}Y_{g,s}Z_{g,s}$ ,

about its axis,  $Y_{g.s}$ , in the counterclockwise direction through the gear cone angle,  $\Sigma_g$  (Figure 3.17):

$$\mathbf{Rt}(\Sigma_g, Y_{g.s}) = \begin{bmatrix} \cos \Sigma_g & 0 & \sin \Sigma_g & 0 \\ 0 & 1 & 0 & 0 \\ -\sin \Sigma_g & 0 & \cos \Sigma_g & 0 \\ 0 & 0 & 0 & 1 \end{bmatrix} \quad (3.3)$$

The resultant transition from the gear coordinate system,  $X_g Y_g Z_g$ , to the main reference system,  $X_{ln} Y_{ln} Z_{ln}$ , can be analytically described by the operator of the resultant coordinate system transformation,  $\mathbf{Rs}(g \mapsto ln)$ :

$$\mathbf{Rs}(g \mapsto ln) = \mathbf{Rt}(\Sigma_g, Y_{g.s}) \cdot \mathbf{Tr}(r_g, Y_{ln}) \cdot \mathbf{Rt}(\varphi_g, Z_g) \quad (3.4)$$

For the inverse coordinate system transformation, that is, for transition from the main reference system,  $X_{ln} Y_{ln} Z_{ln}$ , to the gear coordinate system,  $X_g Y_g Z_g$ , the operator of the resultant coordinate system transformation,  $\mathbf{Rs}(ln \mapsto g)$ , can be used:

$$\mathbf{Rs}(ln \mapsto g) = \mathbf{Rs}^{-1}(g \mapsto ln) \quad (3.5)$$

Coupled linear transformations [113,118] can be used to derive the operators  $\mathbf{Rs}(g \mapsto ln)$  and  $\mathbf{Rs}(ln \mapsto g)$  of the resultant coordinate system transformations. Coupled linear transformations combine transformations about and along a coordinate axis.\*

Only rotation is observed in the first step of the coordinate system transformation, that is, the translation is zero. Therefore, in the case under consideration, the coupled operator of the linear transformation,  $\mathbf{Cp}_z(\varphi_g, 0)$ , is identical to the operator of rotation,  $\mathbf{Rt}(\varphi_g, Z_g)$ :

$$\mathbf{Cp}_z(\varphi_g, 0) = \begin{bmatrix} \cos \varphi_g & \sin \varphi_g & 0 & 0 \\ -\sin \varphi_g & \cos \varphi_g & 0 & 0 \\ 0 & 0 & 1 & 0 \\ 0 & 0 & 0 & 1 \end{bmatrix} \quad (3.6)$$

The next two separate linear transformations, that is,  $\mathbf{Tr}(r_g, Y_{ln})$  and  $\mathbf{Rt}(\Sigma_g, Y_{g.s})$ , can be analytically described by the coupled operator of the linear transformation,  $\mathbf{Cp}_y(\Sigma_g, r_g)$ . This operator is equal to:

$$\mathbf{Cp}_y(\Sigma_g, r_g) = \begin{bmatrix} \cos \Sigma_g & 0 & \sin \Sigma_g & 0 \\ 0 & 1 & 0 & r_g \\ -\sin \Sigma_g & 0 & \cos \Sigma_g & 0 \\ 0 & 0 & 0 & 1 \end{bmatrix} \quad (3.7)$$

Ultimately, the resultant transition from the gear coordinate system,  $X_g Y_g Z_g$ , to the main reference system,  $X_{ln} Y_{ln} Z_{ln}$ , can be analytically described by the operator of the resultant coordinate system transformation,  $\mathbf{Rs}(g \mapsto ln)$ :

$$\mathbf{Rs}(g \mapsto ln) = \mathbf{Cp}_y(\Sigma_g, r_g) \cdot \mathbf{Cp}_z(\varphi_g, 0) \quad (3.8)$$

Use of the operators of coupled linear transformations allows a reduction in total number of the operators of elementary coordinate system transformations, which can be reasonable when long chains of consequent coordinate system transformations are necessary to describe analytically.

### 3.3.2 Transition from the Pinion Reference System to the Main Reference System

The transition from the pinion coordinate system,  $X_p Y_p Z_p$ , to the main reference system,  $X_{ln} Y_{ln} Z_{ln}$ , can be performed in the following manner.

At the beginning, the pinion coordinate system,  $X_p Y_p Z_p$ , is turned about its axis,  $Z_p$ , in the clockwise direction through a pinion rotation angle,  $\varphi_p$  (Figure 3.21) to the position of the stationary pinion coordinate system,

\* It is instructive to note here that only the initial and final configurations of a reference system are accounted for by the coupled linear transformation operators. No intermediate configurations of the reference system are described by the coupled linear transformation operators.



$X_{g.s}Y_{g.s}Z_{g.s}$ . This elementary coordinate system transformation is analytically described by the operator of rotation,  $\mathbf{Rt}(\varphi_p, Z_p)$ :

$$\mathbf{Rt}(\varphi_p, Z_p) = \begin{bmatrix} \cos \varphi_p & -\sin \varphi_p & 0 & 0 \\ \sin \varphi_p & \cos \varphi_p & 0 & 0 \\ 0 & 0 & 1 & 0 \\ 0 & 0 & 0 & 1 \end{bmatrix} \quad (3.9)$$

After that, the stationary pinion coordinate system,  $X_{p.s}Y_{p.s}Z_{p.s}$ , is turned about the coordinate axis,  $X_{p.s}$ , through an angle of  $180^\circ$  to a position of the reference system,  $X_{p.s}^*Y_{p.s}^*Z_{p.s}^*$  (Figure 3.20). This linear transformation can be performed by means of the operator,  $\mathbf{Rt}(180^\circ, X_{p.s})$ :

$$\mathbf{Rt}(180^\circ, X_{p.s}) = \begin{bmatrix} 1 & 0 & 0 & 0 \\ 0 & -1 & 0 & 0 \\ 0 & 0 & -1 & 0 \\ 0 & 0 & 0 & 1 \end{bmatrix} \quad (3.10)$$

Then, the intermediate pinion coordinate system,  $X_{p.s}^*Y_{p.s}^*Z_{p.s}^*$ , is translated at a distance  $-r_p$  along the axis,  $Y_{p.s}^*$ . In this intermediate position, the coordinate system,  $X_{p.s}^*Y_{p.s}^*Z_{p.s}^*$ , is labeled as  $X_{p.s}^{**}Y_{p.s}^{**}Z_{p.s}^{**}$ . For analytical description of the transition from the stationary pinion coordinate system,  $X_{p.s}^*Y_{p.s}^*Z_{p.s}^*$ , to the intermediate auxiliary coordinate system,  $X_{p.s}^{**}Y_{p.s}^{**}Z_{p.s}^{**}$ , the operator of translation,  $\mathbf{Tr}(r_p, Y_{p.s}^*)$ , can be used:

$$\mathbf{Tr}(r_p, Y_{p.s}^*) = \begin{bmatrix} 1 & 0 & 0 & 0 \\ 0 & 1 & 0 & -r_p \\ 0 & 0 & 1 & 0 \\ 0 & 0 & 0 & 1 \end{bmatrix} \quad (3.11)$$

Finally, the transition from the auxiliary reference system,  $X_{p.s}^{**}Y_{p.s}^{**}Z_{p.s}^{**}$ , to the main reference system,  $X_{ln}Y_{ln}Z_{ln}$ , can be analytically described by the operator of rotation,  $\mathbf{Rt}(\Sigma_p, Y_{p.s}^{**})$ , of the coordinate system,  $X_{p.s}^*Y_{p.s}^*Z_{p.s}^*$ , about its axis,  $Y_{g.s}$ , in the counterclockwise direction through the angle that equals  $(180^\circ - \Sigma_p)$  (Figure 3.20):

$$\mathbf{Rt}(\Sigma_p, Y_{p.s}^{**}) = \begin{bmatrix} \cos(180^\circ - \Sigma_p) & 0 & \sin(180^\circ - \Sigma_p) & 0 \\ 0 & 1 & 0 & 0 \\ -\sin(180^\circ - \Sigma_p) & 0 & \cos(180^\circ - \Sigma_p) & 0 \\ 0 & 0 & 0 & 1 \end{bmatrix} \quad (3.12)$$

With that said, the resultant transition from the pinion coordinate system,  $X_pY_pZ_p$ , to the main reference system,  $X_{ln}Y_{ln}Z_{ln}$ , can be analytically described by the operator of the resultant coordinate system transformation,  $\mathbf{Rs}(p \mapsto ln)$ :

$$\mathbf{Rs}(p \mapsto ln) = \mathbf{Rt}(\Sigma_p, Y_{p.s}^{**}) \cdot \mathbf{Tr}(r_p, Y_{p.s}^*) \cdot \mathbf{Rt}(180^\circ, X_{p.s}) \cdot \mathbf{Rt}(\varphi_p, Z_p) \quad (3.13)$$

For the inverse coordinate system transformation, that is, for the transition from the main reference system,  $X_{ln}Y_{ln}Z_{ln}$ , to the pinion coordinate system,  $X_pY_pZ_p$ , the operator of the resultant coordinate system transformation,  $\mathbf{Rs}(ln \mapsto p)$ , can be used:

$$\mathbf{Rs}(ln \mapsto p) = \mathbf{Rs}^{-1}(p \mapsto ln) \quad (3.14)$$

Again, coupled linear transformations [113,118] can be used to derive the operators  $\mathbf{Rs}(p \mapsto ln)$  and  $\mathbf{Rs}(ln \mapsto p)$  of the resultant coordinate system transformations. Coupled linear transformations combine transformations about and along a coordinate axis.

Only rotation is observed in the first step of the coordinate system transformation; that is, the translation is zero. Therefore, in the case under consideration, the coupled operator of the linear transformation,  $\mathbf{Cp}_z(\varphi_p, 0)$ ,

is identical to the operator of rotation,  $\mathbf{Rt}(\varphi_p, Z_p)$ :

$$\mathbf{Cp}_z(\varphi_p, 0) = \begin{bmatrix} \cos \varphi_p & -\sin \varphi_p & 0 & 0 \\ \sin \varphi_p & \cos \varphi_p & 0 & 0 \\ 0 & 0 & 1 & 0 \\ 0 & 0 & 0 & 1 \end{bmatrix} \quad (3.15)$$

The transition from the stationary pinion coordinate system,  $X_{p.s}Y_{p.s}Z_{p.s}$ , to a position of the reference system,  $X_{p.s}^*Y_{p.s}^*Z_{p.s}^*$  (Figure 3.20), can be analytically described by means of the operator,  $\mathbf{Cp}_x(180^\circ, 0)$ :

$$\mathbf{Cp}_x(180^\circ, 0) = \begin{bmatrix} 1 & 0 & 0 & 0 \\ 0 & -1 & 0 & 0 \\ 0 & 0 & -1 & 0 \\ 0 & 0 & 0 & 1 \end{bmatrix} \quad (3.16)$$

The next two separate linear transformations  $[\mathbf{Tr}(r_p, Y_{p.s}^*)$  and  $\mathbf{Rt}(\Sigma_p, Y_{p.s}^{**})$ ] can be analytically described by the coupled operator of the linear transformation,  $\mathbf{Cp}_y[(180^\circ - \Sigma_p), -r_p]$ . This operator is equal to:

$$\mathbf{Cp}_y[(180^\circ - \Sigma_p), -r_p] = \begin{bmatrix} \cos(180^\circ - \Sigma_p) & 0 & -\sin(180^\circ - \Sigma_p) & 0 \\ 0 & 1 & 0 & -r_p \\ \sin(180^\circ - \Sigma_p) & 0 & \cos(180^\circ - \Sigma_p) & 0 \\ 0 & 0 & 0 & 1 \end{bmatrix} \quad (3.17)$$

Ultimately, the resultant transition from the pinion coordinate system,  $X_pY_pZ_p$ , to the main reference system,  $X_{ln}Y_{ln}Z_{ln}$ , can be analytically described by the operator of the resultant coordinate system transformation,  $\mathbf{Rs}(p \mapsto ln)$ :

$$\mathbf{Rs}(p \mapsto ln) = \mathbf{Cp}_y[(180^\circ - \Sigma_p), -r_p] \cdot \mathbf{Cp}_x(180^\circ, 0) \cdot \mathbf{Cp}_z(\varphi_p, 0) \quad (3.18)$$

Use of the operators of coupled linear transformations allows a reduction in the total number of the operators of elementary coordinate system transformations, which can be reasonable when long chains of consequent coordinate system transformations are necessary to describe analytically.

The derived operators of coordinate system transformations are also valid for the reduced cases of gearing, that is, for cases of intersected-axes gearing and parallel-axes gearing as well.

As in cases of intersected-axes gearings, the center distance is zero ( $C = 0$ ), then zero values of the pitch radii  $r_g = 0$  and  $r_p = 0$  of the gear and the pinion should be entered into corresponding formula for a coordinate system transformation.

In cases of parallel-axes gearing, the angle  $\Sigma$  is zero ( $\Sigma = 0^\circ$ ) or  $\Sigma = 180^\circ$ . The actual value of the gear cone angle,  $\Sigma_g$ , and the pinion cone angle,  $\Sigma_p$  (either zero or  $180^\circ$ ), depends on whether the actual value of the angle,  $\Sigma$ , is zero ( $\Sigma = 0^\circ$ ) or  $\Sigma = 180^\circ$ .

In a similar manner, any and all coordinate system transformations can be analytically described by means of either the operators of elementary coordinate system transformations, that is, by means of operators of translations,  $\mathbf{Tr}(x_i, X_i)$ , and operators of rotations,  $\mathbf{Rt}(\varphi_{xi}, X_i)$ , or by means of operators of coupled coordinate system transformations,  $\mathbf{Cp}_{xi}(\varphi_{xi}, x_i)$ .

## Conditions for Transmitting a Uniform Rotation Smoothly from a Driving Shaft to a Driven Shaft: Three Fundamental Laws of Gearing

A uniform rotation from a driving shaft to a driven shaft can be transmitted in various manners. In cases when the angular velocity ratio,  $u_\varphi$ , is of a constant value ( $u_\varphi = \omega_{\text{input}}/\omega_{\text{output}} = \text{const}$ ), it is said that the rotation from a driving shaft to a driven shaft is transmitted smoothly. Here, rotation of the input shaft (i.e., rotation of the driving shaft) is designated as  $\omega_{\text{input}}$ , and rotation of the output shaft (i.e., rotation of the driven shaft) is designated as  $\omega_{\text{output}}$ . Perfect gearings feature an angular velocity ratio,  $u_\varphi$ , of a constant value.

Perfect gearings rotate smoothly and produce almost no vibration and zero noise excitation. Approximate gearings feature a variable-in-time angular velocity ratio; that is,  $u_\varphi = u_\varphi(t)$ . Variation of the angular velocity ratio causes vibration generation, excessive noise excitation, excessive tooth flank wear, and so forth.

It is important to identify a set of conditions under which the gear velocity ratio in a gear pair is of a constant value, that is, a set of conditions under which the equality  $u_\varphi = \text{const}$  is valid.

In order to transmit a rotation smoothly, a set of certain conditions have to be fulfilled. In this section of the book, a set of necessary conditions to transmit a uniform rotation smoothly is discussed with regard to parallel-axes gearing ( $P_a$ -gearing). Later on in the subsequent chapters, the equivalent sets of the conditions will be formulated for intersected-axes gearing ( $I_a$ -gearing) and for crossed-axes gearings ( $C_a$ -gearing).

The first three conditions gearings have to obey are referred to as the *fundamental laws of gearing*. These three fundamental laws of gearing are discussed immediately below.

### 4.1 Condition of Contact between Interacting Tooth Flanks: The First Fundamental Law of Gearing

The first fundamental law of gearing to be discussed in this section reflects the condition of contact of tooth flanks of a gear and a mating pinion. The condition of contact of the tooth flanks is the first fundamental condition to be met in gearings of all types, that is, in parallel-axes gearing (as well as in intersected-axes and crossed-axes gearings).

The necessity of alignment of the resultant velocity vector,  $\mathbf{V}_\Sigma$ , to the common tangent at the contact point,  $K$ , of the interacting tooth flanks,  $\mathcal{G}$  and  $\mathcal{P}$ , of a gear and its mating pinion is illustrated by the following example.

Consider a relative motion of the tooth flanks,  $\mathcal{G}$  and  $\mathcal{P}$ , of a gear and mating pinion as illustrated in Figure 4.1. For simplicity, but without loss of generality, normal sections through the contact point of the gear and the mating pinion are depicted there. It is also assumed that the gear tooth flank,  $\mathcal{G}$ , is motionless and the pinion tooth flank,  $\mathcal{P}$ , performs an arbitrary instantaneous motion,  $\mathbf{V}_\Sigma$ , in relation to the gear tooth surface,  $\mathcal{G}$ .

Three different scenarios can be distinguished when the pinion tooth flank,  $\mathcal{P}$ , travels in relation to the gear tooth flank,  $\mathcal{G}$ .

First, an instantaneous motion of point,  $K_a$ , within the pinion tooth flank,  $\mathcal{P}$ , is specified by an instant linear velocity vector,  $\mathbf{V}_\Sigma^a$  (Figure 4.1a). Point  $A$  within the pinion tooth flank,  $\mathcal{P}$ , is chosen so that the projection,  $\text{Pr}_n \mathbf{V}_\Sigma^a$ , of the vector,  $\mathbf{V}_\Sigma^a$ , onto the unit normal vector,  $\mathbf{n}_p^a$ , to the moving surface,  $\mathcal{P}$ , at  $K_a$  is pointed to the interior of the motionless gear tooth flank,  $\mathcal{G}$ ; that is,  $\text{Pr}_n \mathbf{V}_\Sigma^a > 0$ . In the differential vicinity of the point  $K_a$ , this means that the moving pinion tooth flank,  $\mathcal{P}$ , penetrates the motionless gear tooth flank,  $\mathcal{G}$ . A relative motion of this kind is not permissible for the conjugate tooth flanks,  $\mathcal{G}$  and  $\mathcal{P}$ , of a gear and mating pinion.

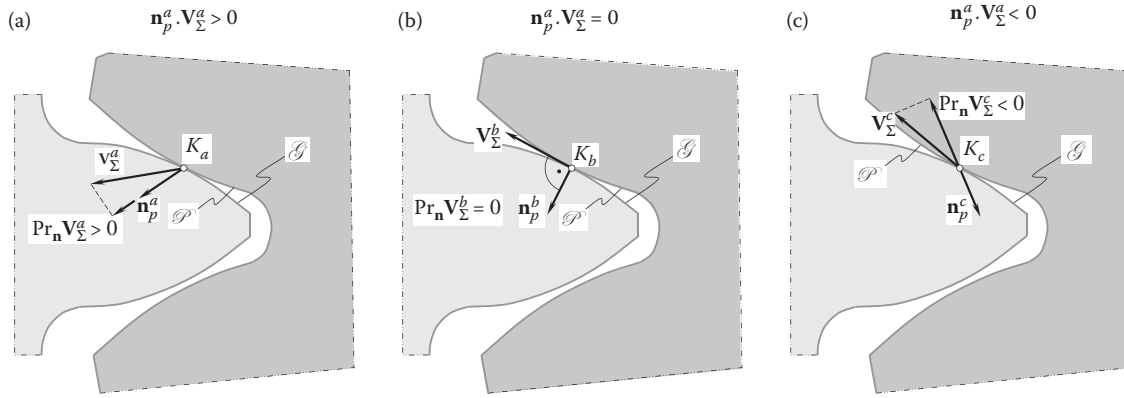


FIGURE 4.1

On the necessity of alignment of the linear velocity vector of resultant relative motion,  $\mathbf{V}_\Sigma$ , to the common tangent to the contacting tooth flanks,  $\mathcal{G}$  and  $\mathcal{P}$ : (a) penetration of the tooth flanks,  $\mathcal{G}$  and  $\mathcal{P}$ ; (b) properly contacted tooth flanks,  $\mathcal{G}$  and  $\mathcal{P}$ ; (c) separation of the tooth flanks,  $\mathcal{G}$  and  $\mathcal{P}$ .

Second, an instantaneous motion of point,  $K_b$ , within the pinion tooth flank,  $\mathcal{P}$ , is specified by an instant linear velocity vector,  $\mathbf{V}_\Sigma^b$  (Figure 4.1b). A point,  $K_b$ , within the pinion tooth flank,  $\mathcal{P}$ , is chosen so that the vector,  $\mathbf{V}_\Sigma^b$ , is perpendicular to the unit normal vector,  $\mathbf{n}_p^b$ ; thus, it is tangential to the gear tooth flank,  $\mathcal{G}$ , at point  $K_b$ . The projection,  $\text{Pr}_n \mathbf{V}_\Sigma^b$ , of the linear velocity vector,  $\mathbf{V}_\Sigma^b$ , onto the unit normal vector,  $\mathbf{n}_p^a$ , to the moving tooth flank,  $\mathcal{P}$ , at  $K_b$  is equal to zero (i.e., an equality  $\text{Pr}_n \mathbf{V}_\Sigma^b = 0$  is valid). In the differential vicinity of point  $K_b$ , this means that the moving pinion tooth flank,  $\mathcal{P}$ , does not penetrate the motionless gear tooth flank,  $\mathcal{G}$ . Instead, the pinion tooth flank,  $\mathcal{P}$ , rolls and slides in relation to the gear tooth flank,  $\mathcal{G}$ . In a particular case, either the rolling component or the sliding component of the resultant relative motion of this kind can be equal to zero. Relative motion of this particular kind is permissible for the conjugate tooth flanks,  $\mathcal{G}$  and  $\mathcal{P}$ . Transmitting a motion from a driving shaft to a driven shaft is possible if and only if a relative motion of this particular kind occurs.

Third, an instantaneous motion of a point,  $K_c$ , within the pinion tooth flank,  $\mathcal{P}$ , is specified by an instantaneous linear velocity vector,  $\mathbf{V}_\Sigma^c$  (Figure 4.1c). A point,  $K_c$ , within the pinion tooth flank,  $\mathcal{P}$ , is chosen so that the projection,  $\text{Pr}_n \mathbf{V}_\Sigma^c$ , of the linear velocity vector,  $\mathbf{V}_\Sigma^c$ , onto the unit normal vector,  $\mathbf{n}_p^c$ , to the moving pinion tooth flank,  $\mathcal{P}$ , at  $K_c$  is pointed outward to the motionless gear tooth flank,  $\mathcal{G}$  (i.e., the equality  $\text{Pr}_n \mathbf{V}_\Sigma^c < 0$  is valid). Therefore, in the differential vicinity of a point,  $K_c$ , the moving pinion tooth flank,  $\mathcal{P}$ , departs from the motionless gear tooth flank,  $\mathcal{G}$ . No motion transmission is possible when a relative motion of this kind occurs.

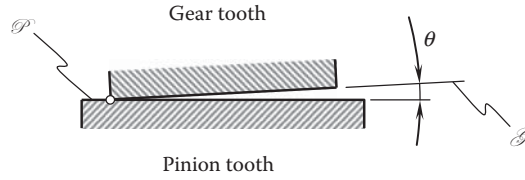
The schematic depicted in Figure 4.1 shows the necessity of the proper alignment of the vector of the linear velocity,  $\mathbf{V}_\Sigma$ , of the resultant relative motion of the tooth flanks,  $\mathcal{G}$  and  $\mathcal{P}$ , to the common tangent to the tooth flanks,  $\mathcal{G}$  and  $\mathcal{P}$ , at every point of their contact. This condition is referred to as the *first fundamental law of gearing*. The first fundamental law of gearing is formulated as follows:

**The first fundamental law of gearing:** *At every point of contact of tooth flanks of a gear and mating pinion, a vector of their instant relative motion has to be perpendicular to the common perpendicular at every instant of time.*

Various forms of analytical representation of the condition of contact of the tooth flanks,  $\mathcal{G}$  and  $\mathcal{P}$ , of a gear and its mating pinion are known.

To derive a convenient analytical representation for the condition of contact of the tooth flanks,  $\mathcal{G}$  and  $\mathcal{P}$ , of the gear and the pinion, let's turn our attention to the following. As shown in Figure 4.1, the dot product of the vectors  $\mathbf{n}_g$  and  $\mathbf{V}_\Sigma$  is:

- Positive ( $\mathbf{n}_p^a \cdot \mathbf{V}_\Sigma^a > 0$ ) in the first case (Figure 4.1a)
- Zero ( $\mathbf{n}_p^b \cdot \mathbf{V}_\Sigma^b = 0$ ) in the second case (Figure 4.1b)
- Negative ( $\mathbf{n}_p^c \cdot \mathbf{V}_\Sigma^c < 0$ ) in the first case (Figure 4.1c)

**FIGURE 4.2**

Example of violation of the condition of contact between a gear tooth profile,  $\mathcal{G}$ , and a mating pinion tooth profile,  $\mathcal{P}$ , in a misaligned parallel-axes gear pair.

The condition of contact between a gear tooth flank,  $\mathcal{G}$ , and a mating pinion tooth flank,  $\mathcal{P}$ , is violated in a misaligned parallel-axes gear pair as schematically illustrated in Figure 4.2. In this particular case, edge contact between the tooth flanks,  $\mathcal{G}$  and  $\mathcal{P}$ , is observed.

The condition of contact of two conjugate tooth flanks of the mating gear teeth can be expressed in the form of a dot product:

$$\mathbf{n}_g \cdot \mathbf{V}_\Sigma = 0 \quad (4.1)$$

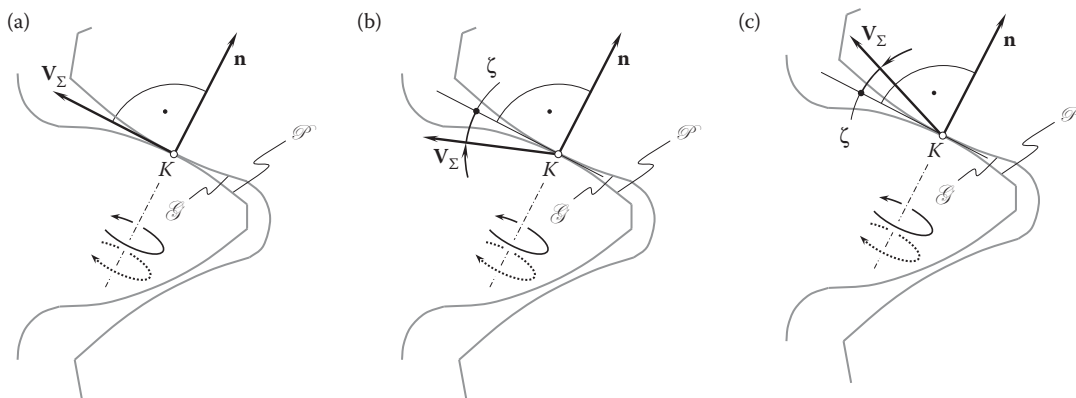
where  $\mathbf{n}_g$  is the unit vector of common perpendicular through the contact point of the tooth flanks,  $\mathcal{G}$  and  $\mathcal{P}$ , of a gear and its mating pinion; and  $\mathbf{V}_\Sigma$  is the linear velocity vector of the resultant instantaneous relative motion of the tooth flanks,  $\mathcal{G}$  and  $\mathcal{P}$ , at contact point  $K$ .

Equation 4.1 reveals that a component of the linear velocity vector,  $\mathbf{V}_\Sigma$ , along the common perpendicular,  $\mathbf{n}_g$ , is equal to zero. Otherwise, either separation or interference of the tooth flanks,  $\mathcal{G}$  and  $\mathcal{P}$ , in the gear pair is observed. Neither separation nor interference of the tooth flanks,  $\mathcal{G}$  and  $\mathcal{P}$ , of a gear and mating pinion is permissible. Therefore, the linear velocity vector,  $\mathbf{V}_\Sigma$ , is either located in a common tangent plane or of a zero value.

Equation 4.1 was proposed by Shishkov as early as 1948, or even earlier [147,148]. Because of this, the equation of contact in the form of Equation 4.1 is commonly referred to as the *Shishkov equation of contact*. The interested reader may wish to go to [104] for details on why Shishkov is credited with the discovery of the equation of contact in the form  $\mathbf{n}_g \cdot \mathbf{V}_\Sigma = 0$ .

The equation of contact in the form  $\mathbf{n}_g \cdot \mathbf{V}_\Sigma = 0$  is practical in cases when the interacting surfaces feature simple geometry and when the resultant relative motion is also simple. The first makes it possible to determine the unit normal vector,  $\mathbf{n}_g$ , without the derivation of the expressions for the derivatives of the equations of the contacting surface with respect to the surface parameters. The second allows the determination of the linear velocity vector,  $\mathbf{V}_\Sigma$ , without derivation of the equation of the moving surface with respect to the parameter of motion. Use of the Shishkov equation of contact in the form  $\mathbf{n}_g \cdot \mathbf{V}_\Sigma = 0$  simplifies the solution to the problem in this particular case. In cases when derivation of the equations of the derivatives for the purposes of determination of the vectors,  $\mathbf{n}_g$  and  $\mathbf{V}_\Sigma$ , cannot be avoided, use of the Shishkov equation of contact in the form  $\mathbf{n}_g \cdot \mathbf{V}_\Sigma = 0$  is less convenient.

The above discussion can be summarized as follows. Permissible instant relative motions of the tooth flanks,  $\mathcal{G}$  and  $\mathcal{P}$ , in a gear pair are illustrated in Figure 4.3. Relative motion of the tooth flanks,  $\mathcal{G}$  and  $\mathcal{P}$ , is not

**FIGURE 4.3**

Permissible (a), and not permissible (b) and (c) instant relative motions in perfect parallel-axes gearing.

permissible along the common perpendicular,  $\mathbf{n}_g$ , and relative motion is allowed in any direction within the common tangent plane through the contact point,  $K$ . It should be pointed out here that a swivel relative motion,  $\pm \varphi_n$ , of the tooth flanks,  $\mathcal{G}$  and  $\mathcal{P}$ , around the axis along the common perpendicular,  $\mathbf{n}_g$ , also meets the requirement specified by Equation 4.1. Not all kinds of the swivel motion of the tooth flanks in Figure 4.3 are permissible. For example, no swivel relative motion is permissible about an axis that either intersects, or crosses a straight line along the common perpendicular,  $\mathbf{n}$ , as the condition of contact,  $\mathbf{n} \cdot \mathbf{V}_\Sigma = 0$ , in these cases is violated.

The swivel motion,  $\pm \varphi_n$ , of the tooth flanks is not necessary to transmit a rotation from the driving shaft to the driven shaft. However, a motion of this nature can be observed in spatial gearing, for example, in  $C_a$ -gearing.

It is necessary to direct the readers' attention to the following. The equation of contact was proposed by Shishkov in the mid of the 20th century (see Equation 4.1). However, the physics of the condition of contact (but not the equation of contact) was properly understood by gear people in the time of da Vinci [17] and even in earlier times.

Fulfillment of the condition of contact of a gear and mating pinion tooth flanks,  $\mathcal{G}$  and  $\mathcal{P}$ , is a necessary but not sufficient condition to transmit a uniform rotation smoothly from the driving shaft to the driven shaft.

The condition of contact of a gear and a mating pinion tooth flanks,  $\mathcal{G}$  and  $\mathcal{P}$ , is the first fundamental law of gearing that all perfect gearings have to fulfill.

## 4.2 Condition of Conjugacy between the Interacting Tooth Flanks: The Second Fundamental Law of Gearing

The second fundamental condition to be discussed in this section is the condition of conjugacy of tooth flanks of a gear and a mating pinion. Conjugacy is a specific property of a gear and a mating pinion tooth flanks (tooth profiles) that roll over one another. This property pertains only to surfaces (to planar curves) that roll over one another.

The condition of conjugacy of the gear and pinion tooth flanks,  $\mathcal{G}$  and  $\mathcal{P}$ , is the second fundamental condition to be fulfilled in perfect gearings of all types. The condition of conjugacy of the gear and pinion tooth flanks is referred to as the *second fundamental law of gearing*. Below in this section, the second fundamental law of gearing is discussed in relation only to perfect parallel-axes gearing. In the later chapters, the second fundamental law of gearing is enhanced to the cases of intersected-axes as well as crossed-axes gearings.

### 4.2.1 Pulley-and-Belt Analogy of a Gear Pair

Let us begin the discussion with a trivial case of transmission of a rotation between two shafts that are parallel to each other. In the simplest case, a rotation from the driving shaft can be transmitted to the driven shaft by means of two disks (pulleys) connected by means of a belt, as schematically illustrated in Figure 4.4. The beginning of the discussion of gearing starting with a *pulley-and-belt* analogy of a gear pair is convenient, especially for readers less experienced with gears and gearings.

The pulleys of diameters,  $d_1$  (driving) and  $d_2$  (driven), are rotated about their axes,  $O_1$  and  $O_2$ , respectively. The axes,  $O_1$  and  $O_2$ , are at a certain center distance,  $C$ , from one another. The pulleys are connected to each other by a belt. The belt is tangent to the pulleys at points  $a$  and  $b$ .

Rotations,  $\omega_1$  and  $\omega_2$ , of the driving and driven pulleys are synchronized with each other so as to meet the following ratio:

$$\frac{\omega_1}{\omega_2} = \frac{d_2}{d_1} \quad (4.2)$$

The linear velocity of the belt,  $V_m$ , can be calculated from the formula:

$$V_m = 0.5 \cdot \omega_1 \cdot d_1 \equiv 0.5 \cdot \omega_2 \cdot d_2 \quad (4.3)$$

Shown in Figure 4.4, the pulley-and-belt mechanism is capable of transmitting a uniform rotation smoothly.

It is the right point to direct the reader's attention here to the three following features of the pulley-and-belt analogy of a gear pair.



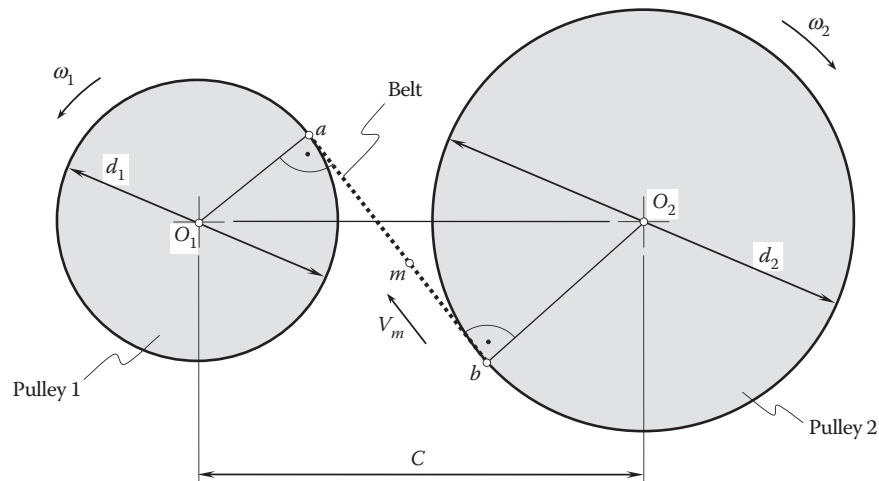


FIGURE 4.4

Schematic of the transmission of a rotation by means of two pulleys connected by a belt.

First, when the pulleys rotate, an arbitrary point,  $m$ , within the portion,  $ab$ , of the belt traces a *straight line* in a motionless reference system associated with the transmission housing. This straight line is the path of point  $m$ . Therefore, in a pulley-and-belt analogy of a gear pair, each point of the belt travels straight forward.\*

Second, when a uniform rotation is transmitted from the driving pulley 1 to the driven pulley 2, the torque is transmitted by a force that acts along the belt, that is, along the straight line,  $ab$ : in a pulley-and-belt mechanism, a force can be transmitted only along the belt. A force acts only along a straight line, and it cannot be transmitted along a curve. Therefore, in a pulley-and-belt analogy of a gear pair, the straight-line segment,  $ab$ , is the *line of action* along which a force that is exerted in the driving pulley is transmitted to the driven pulley.

Third, in a pulley-and-belt analogy of a parallel-axes gear pair, a straight line path of a point,  $m$ , in the belt aligns with the straight line of action along which a force that is exerted in the driving pulley is transmitted to the driven pulley.

It is instructive to note here that the straight-line segment,  $ab$ , at the same time serves both, that is, it serves as the path of point  $m$ , and as the line of action in the pulley-and-belt mechanism (Figure 4.4). Only in parallel-axes gearing are the path of contact and the line of action both straight lines that align with each other. It is critical to distinguish the *path of contact* from the line of action, and never mix these two different entities.

#### 4.2.2 Camus-Euler-Savary theorem for Parallel-Axes Gearing

The performed analysis of transmission of a rotary motion in a pulley-and-belt mechanism is helpful to understand the requirements of the geometry of the tooth flanks in parallel-axes gearing.

The second fundamental condition to be discussed in this section is the condition of conjugacy of tooth flanks of a gear,  $\mathcal{G}$ , and a mating pinion,  $\mathcal{P}$ . The condition of conjugacy of the tooth flanks,  $\mathcal{G}$  and  $\mathcal{P}$ , is the second fundamental law of gearing, which all perfect parallel-axes gearings (as well as  $I_a$ - and  $C_a$ -gearings, discussed later) have to obey. The condition of conjugacy of the tooth flanks,  $\mathcal{G}$  and  $\mathcal{P}$ , in cases of parallel-axes gearing is known as the *Camus-Euler-Savary* fundamental theorem of gearing. This theorem is widely known mostly due to the book published by Willis<sup>†</sup> as early as in 1841 (see Figure 4.5). In Europe, this condition is loosely referred to as the fundamental (main) theorem of gearing, or just as *Willis's theorem* [164].

The fundamental requirements governing the shapes that any pair of conjugate tooth profiles may have in parallel-axes gearing<sup>‡</sup> states:

**The second fundamental law of gearing (in a case of parallel-axes gearing):** *In parallel-axes gearing, in order to transmit a uniform rotary motion from a driving shaft to a driven shaft by means of gear teeth, perpendiculars to the tooth*

\* This statement is valid only with respect to parallel-axes gearing, and it is not valid in cases of intersected- and crossed-axes gearings.

† Robert Willis (27 February 1800 – 28 February 1875), a British engineer; a major contributor to the theory of gear teeth in the 19th century.

‡ For cases of intersected-axes gearing and crossed-axes gearing, this concept is discussed in detail in [137].



38. If the line of direction of the link in link-work, of the common normal to the curves in contact motion, and of the connector in wrapping motion, be severally termed the line of action, we can express the separate propositions which relate to the Velocity Ratio, by saying that the angular velocities of the two pieces are to each other inversely as the segments into which the *line of action* divides the line of centers, or inversely as the perpendiculars from the centers of motion upon the line of action.

I have confined these investigations, for the present,

FIGURE 4.5

The main theorem of gearing (Willis's theorem) as it was originally formulated by Willis on p. 38 in his book: Willis, R., *Principles of Mechanisms, Designed for the Use of Students in the Universities and for Engineering Students Generally*, London, John W. Parker, West Stand, Cambridge: J. & J.J. Deighton, 1841, 446 p.

*flanks of the interacting teeth at all points of their contact must pass through a stationary point located on the line of centers, that is, the pitch point  $P$ ; the pitch point subdivides the center distance reciprocal to the angular velocities of the gear and the pinion.*

In other words, two planar curves are said to be conjugate to one another\* if a contact perpendicular at point of their contact is along a straight line through the pitch point,  $P$ . The center of the instantaneous rotational motion is coincident with the pitch point,  $P$ .

Tooth flanks of a gear,  $\mathcal{G}$ , and a mating pinion,  $\mathcal{P}$ , should be shaped so as to fulfill the requirements of the second fundamental law of gearing. This statement is also often called the *conjugate action law*.

One more consideration needs to be taken into account when discussing conjugate tooth profiles. In the contact point,  $K$ , tooth flanks,  $\mathcal{G}$  and  $\mathcal{P}$ , of a gear and mating pinion slide over one another. Because of the sliding, instant rotation can be performed only about the pitch point,  $P$ , and not about any other point—otherwise, the tooth flanks interfere with each other. When the condition of conjugacy of the tooth flanks,  $\mathcal{G}$  and  $\mathcal{P}$ , is violated, an interference of the gear and the pinion teeth is always observed. The farther the contact point,  $K$ , is located from the pitch point,  $P$ , the more sliding motion is observed, and vice versa.

Refer to Figure 4.6 for more detailed analysis of the conjugate action law. In Figure 4.6, the directions of rotation of the driving and driven gears are reversed compared to those shown in Figure 4.4 as a driven pulley is *pulled* by the belt, while the driven gear is *pushed* by the driving gear.

For properly designed tooth flanks of a gear and mating pinion, the contact point of the tooth flanks,  $\mathcal{G}$  and  $\mathcal{P}$ , traces a straight path of contact,  $P_c$ . When friction is not taken into consideration, a force is acting perpendicular to the common tangent plane,  $t-t$ , to the tooth flanks,  $\mathcal{G}$  and  $\mathcal{P}$ . As long as friction is not accounted for, the acting force is always perpendicular to the tooth flanks,  $\mathcal{G}$  and  $\mathcal{P}$ , at current point of their contact. The straight line of action,  $LA$ , aligns with the straight path of contact,  $P_c$ ; that is, in perfect parallel-axes gearing, the following identity  $LA \equiv P_c$  is observed at every instant of time when the gears rotate. It is critical to bear in mind that the path of contact,  $P_c$ , and the line of action,  $LA$ , are two completely different kinematical entities in the theory of gearing. Therefore, the difference between the line of action,  $LA$ , and the path of contact,  $P_c$ , in  $P_a$ -gearing needs to be firmly realized.

One more example is illustrated in Figure 4.7.

Consider the two tooth profiles,  $\mathcal{G}$  and  $\mathcal{P}$ , that contact one another at a point,  $K$ , as shown in Figure 4.7. The tooth profiles,  $\mathcal{G}$  and  $\mathcal{P}$ , are designed so as to transmit the rotation from the pinion axis of rotation,  $O_p$ , to the gear axis of rotation,  $O_g$ . The axes  $O_g$  and  $O_p$  are at a center distance,  $C$ . The common unit normal vector to the contacting profiles at the contact point,  $K$ , is designated as  $\mathbf{n}_g$ . A straight line that is aligned with the unit

\* It is a wrong practice to define conjugate shapes in the following manner:

**Definition:** A pair of transverse gear tooth profiles is said to be conjugate if a constant angular velocity of one profile produces a constant angular velocity in the meshing profile. Constant output rotation is a consequence of conjugacy of the interacting tooth profiles. The property of conjugacy must be expressed in terms of the kinematics and the geometry of the interacting tooth flanks,  $\mathcal{G}$  and  $\mathcal{P}$ , of a gear and mating pinion.



The point at which the gear tooth profile,  $\mathcal{G}$ , contacts the pinion tooth profile,  $\mathcal{P}$ , is denoted by  $K_g$ . Similarly, the point,  $K_p$ , within the pinion tooth profile,  $\mathcal{P}$ , is specified. At the point of tangency of the tooth profiles, the points,  $K_g$  and  $K_p$ , coincide with the contact point,  $K$ .

The linear velocity vector,  $\mathbf{V}_{K_g}$ , of the point,  $K_g$ , can be expressed in terms of the rotation vector,  $\boldsymbol{\omega}_g$ , of the gear and the position vector,  $\mathbf{r}_{K_g}$ , of the point  $K_g$ ; that is, the equality

$$\mathbf{V}_{K_g} = \boldsymbol{\omega}_g \times \mathbf{r}_{K_g} \quad (4.5)$$

is valid. Similarly, the linear velocity vector,  $\mathbf{V}_{K_p}$ , of the point  $K_p$  can be expressed in terms of the rotation vector,  $\boldsymbol{\omega}_p$ , of the pinion and the position vector,  $\mathbf{r}_{K_p}$ , of the point  $K_p$ ; that is, the equality

$$\mathbf{V}_{K_p} = \boldsymbol{\omega}_p \times \mathbf{r}_{K_p} \quad (4.6)$$

is valid as well. The linear velocity vector,  $\mathbf{V}_\Sigma$ , of the resultant motion of tooth profiles,  $\mathcal{G}$  and  $\mathcal{P}$ , in relation to each other must be aligned with a common tangent to the tooth profiles at  $K$ , or, in other words, it should be perpendicular to the unit normal vector,  $\mathbf{n}_g$ . Therefore, the radius of instant rotation,  $PK$ , is aligned with the normal vector,  $\mathbf{n}_g$ .

Therefore, to be conjugate, common perpendiculars at every point of the line of contact,  $LC$ , between the tooth flanks,  $\mathcal{G}$  and  $\mathcal{P}$ , must pass through the axis of instant screw motion of the surfaces at every instant of time, that is, for any and all possible configurations of the surfaces relative each other.

In most cases, the theoretical analysis of gears and gear pairs is limited to fulfillment only of the *condition of contact* (or, in other words, of the *enveloping condition*) of the interacting tooth flanks of a gear,  $\mathcal{G}$ , and its mating pinion,  $\mathcal{P}$ .

Fulfillment of the condition of contact of the tooth flanks  $\mathcal{G}$  and  $\mathcal{P}$  is necessary but not sufficient to design perfect gears. Conjugacy of the interacting tooth flanks,  $\mathcal{G}$  and  $\mathcal{P}$ , is the other necessary condition to be fulfilled when designing perfect gearing. Use of perfect gears is vital in the design of high-power-density gear transmissions, as well as when the input/output rotations are high.

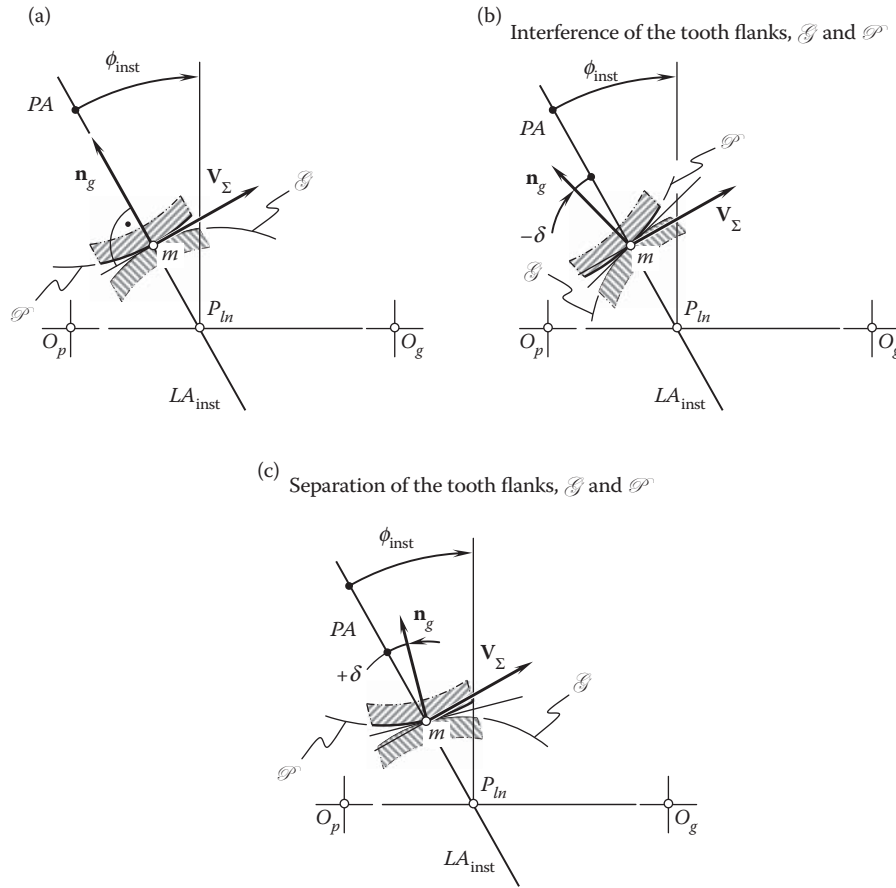
In the current practice, fulfillment of the condition of conjugacy of the interacting tooth flanks of a gear and its mating pinion is commonly limited to the analysis of the simplest case of perfect (with zero axes misalignment) parallel-axes gears, that is, to the case of perfect involute gearing. The condition of conjugacy of the tooth flanks for gears with another tooth flank geometry is not discussed at all.\* Examples can be readily found for gears that feature cycloidal tooth profile, circular-arc tooth profile, and tooth profiles of other tooth flank geometries different from the involute of a circle. Moreover, the condition of conjugacy of the interacting tooth flanks of a gear and its mating pinion is analyzed neither for gears that operate on intersected axes of rotation nor for gears that operate on crossed axes of rotation.

Fulfillment of the condition of conjugacy of the tooth flanks  $\mathcal{G}$  and  $\mathcal{P}$  is necessary but not sufficient to design perfect gears.

The last (but not least) is related to base pitches of a gear and its mating pinion. The equality of the base pitches of a gear and its mating pinion is commonly considered only in the simplest case of perfect (with zero axes misalignment) parallel-axes gears, that is, in the case of perfect involute gearing. The equality of base pitches of the interacting tooth flanks  $\mathcal{G}$  and  $\mathcal{P}$  is analyzed neither for gears that operate on intersected axes of rotation nor for gears that operate on crossed axes of rotation. Moreover, base pitches of the interacting tooth flanks  $\mathcal{G}$  and  $\mathcal{P}$  must be equal to the *operating base pitch* of the gear pair. Unfortunately, so far, the concept of the operating base pitch of a gear pair is not known by most gear experts. Equality of both the base pitches,  $p_{b,g}$  and  $p_{b,p}$ , of the interacting tooth flanks of a gear and its mating pinion to the operating base pitch of a gear pair,  $p_{b,op}$  (i.e.,  $p_{b,g} = p_{b,op}$  and  $p_{b,p} = p_{b,op}$ ), is the third fundamental condition, which gears of all types have to fulfill.

Equality of the base pitches,  $p_{b,g}$  and  $p_{b,p}$ , of a gear and its mating pinion to the operating base pitch of a gear pair,  $p_{b,op}$ , is a necessary and sufficient condition for to design perfect gears.

\* A wrong practice is commonly adopted when analyzing whether the condition of conjugacy of the tooth flanks,  $\mathcal{G}$  and  $\mathcal{P}$ , is fulfilled. The Shishkov equation of contact,  $\mathbf{n} \cdot \mathbf{V}_\Sigma = 0$ , is loosely used for this purpose (here, in the equation,  $\mathbf{n}$  is the unit normal vector to the tooth flanks,  $\mathcal{G}$  and  $\mathcal{P}$ , at point,  $K$ , of their contact, and  $\mathbf{V}_\Sigma$  is the velocity vector of the resultant relative motion of the surfaces,  $\mathcal{G}$  and  $\mathcal{P}$ , at the contact point,  $K$ ). The condition of contact of the tooth flanks,  $\mathcal{G}$  and  $\mathcal{P}$ , and not the condition of conjugacy of the interacting tooth flanks of a gear and its mating pinion, is analytically described by the Shishkov equation of contact. Unfortunately, often, this difference is not recognized at all.

**FIGURE 4.8**

On the derivation of equation of conjugacy,  $\mathbf{p}_{ln} \times \mathbf{V}_m \cdot \mathbf{n}_g = 0$ , of the interacting tooth flanks,  $\mathcal{G}$  and  $\mathcal{P}$ , of a gear and a mating pinion: (a) the condition of conjugacy is fulfilled, (b) the condition of conjugacy is violated: the tooth flanks interfere into one another, and (c) the condition of conjugacy is violated: the tooth flanks separate from one another.

The provided verbal description of the condition of conjugacy of the interacting tooth flanks,  $\mathcal{G}$  and  $\mathcal{P}$ , of a gear and a mating pinion can be complemented with an analytical description. The *equation of conjugacy* (see [Figure 4.8](#)):

$$\mathbf{p}_{ln} \times \mathbf{V}_m \cdot \mathbf{n}_g = 0 \quad (4.7)$$

is derived for this purpose. Here,  $\mathbf{p}_{ln}$  is the unit vector along the axis of instant rotation,  $P_{ln}$ ;  $\mathbf{V}_m$  is the linear velocity vector of point of interest,  $m$ , taken within the instant line of contact,  $LC_{inst}$ , between the interacting tooth flanks,  $\mathcal{G}$  and  $\mathcal{P}$ , of a gear and a mating pinion; and  $\mathbf{n}_g$  is the unit normal vector (common perpendicular) to the gear tooth flank,  $\mathcal{G}$  (to the pinion tooth flank,  $\mathcal{P}$ ), that passes through the point of interest,  $m$ .

As the unit vector,  $\mathbf{p}_{ln}$ , is aligned with the angular velocity vector,  $\boldsymbol{\omega}_{pl}$ , Equation 4.7 can also be represented in the form:

$$\boldsymbol{\omega}_{pl} \times \mathbf{V}_m \cdot \mathbf{n}_g = 0 \quad (4.8)$$

The two vectors, that is,  $\mathbf{p}_{ln}$  and  $\mathbf{V}_m$ , define the plane of action,  $PA$  (as well, as the unit normal vector,  $\mathbf{n}_{pa}$ , to the plane of action,  $PA$ :  $\mathbf{n}_{pa} = \mathbf{p}_{ln} \times \mathbf{V}_m$ ). The unit normal vectors,  $\mathbf{n}_g$  and  $\mathbf{n}_{pa}$ , must be perpendicular to one another. Therefore,  $\mathbf{n}_g \cdot \mathbf{n}_{pa} = 0$ .

Finally, the second fundamental law of gearing analytically can be represented as a set of two equations

$$\begin{cases} \boldsymbol{\omega}_{pl} \times \mathbf{V}_m \cdot \mathbf{n}_g = 0 \\ \mathbf{p}_{ln} \times \mathbf{n}_g \neq 0 \end{cases} \quad (4.9)$$

The equation of conjugacy, Equation 4.7, of a gear tooth flank,  $\mathcal{G}$ , and a mating pinion tooth flank,  $\mathcal{P}$ , requires: to be conjugate, the unit normal vector,  $\mathbf{n}_g$ , must be entirely located within the plane of action,  $PA$ .

A line of action of the unit normal vector,  $\mathbf{n}_g$ , intersects the axis of instant rotation,  $P_{ln}$ , if the condition of conjugacy,  $\mathbf{p}_{ln} \times \mathbf{V}_m \cdot \mathbf{n}_g = 0$ , is fulfilled.

The second fundamental law of gearing is useful when approximate gearing is analyzed. A point of a gear tooth flank,  $\mathcal{G}$ , can be a contact point when the condition of conjugacy is met. For a corresponding angular configuration of a gear and a mating pinion, a point of a pinion tooth flank,  $\mathcal{P}$  that is anticipated to be in contact with the gear tooth flank,  $\mathcal{G}$ , can actually be a contact point when the condition of conjugacy is met. A possibility of contact of the tooth flanks,  $\mathcal{G}$  and  $\mathcal{P}$ , in approximate gearing can be verified by means of comparison of coordinates of the *contact* point on the gear tooth flank,  $\mathcal{G}$ , and that on the pinion tooth flank,  $\mathcal{P}$ . If the coordinates of the points are identical to one another, then a point is a contact point (the unit normal vectors,  $\mathbf{n}_{pl}$  and  $\mathbf{n}_{mr}$ , must be aligned to each other). Otherwise, contact of the tooth flanks,  $\mathcal{G}$  and  $\mathcal{P}$ , at these points is not possible at all.

Fulfillment of the condition of conjugacy is necessary but not sufficient to smoothly transmit a rotation from a driving shaft to a driven shaft by means of a gear pair.

### 4.3 Condition of Equal Base Pitches (in Parallel-Axes Gearing): The Third Fundamental Law of Gearing

Gear teeth are a series of cam surfaces that act on similar surfaces of the mating gear to impart a driving motion. This requires the fulfillment of an additional requirement caused by multiple interacting tooth surfaces in gears.

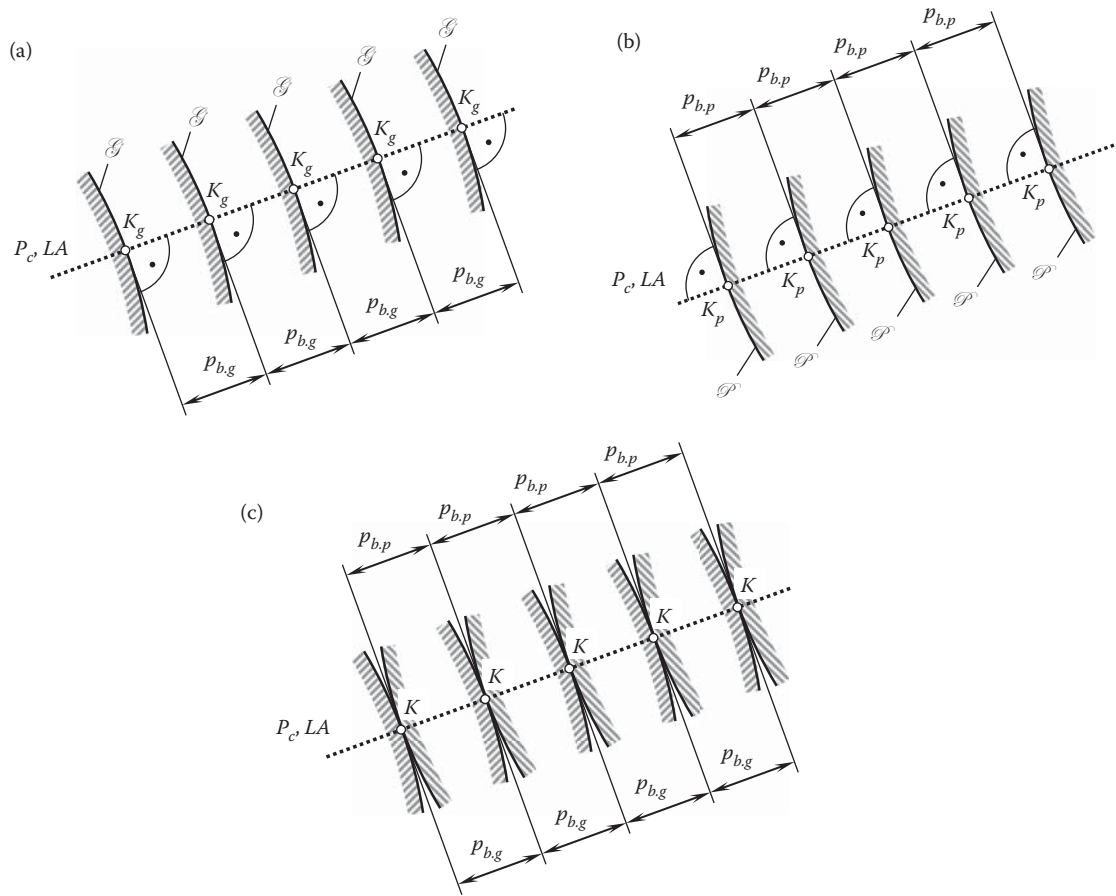
The third fundamental condition to be discussed in this section of the book is the condition that requires equality of base pitches of a gear and a mating pinion. Here, the discussion is limited only to perfect parallel-axes gearing, as this concept is not developed yet to more general cases. More general cases of equality of base pitches in intersected-axes and crossed-axes gearings are considered below in corresponding sections.

In [Figure 4.9](#), local patches of a gear tooth flanks,  $\mathcal{G}$ , are shown. The tooth flanks themselves are not defined yet. Therefore, only small portions of the tooth flanks,  $\mathcal{G}$ , are depicted in [Figure 4.9a](#). All these portions of the tooth flanks of a gear are located in the differential vicinity of points of intersection,  $K_g$ , of the tooth flanks,  $\mathcal{G}$ , by the line of action,  $LA$ . Each tooth flank,  $\mathcal{G}$ , is perpendicular to the line of action,  $LA$ , at points  $K_g$ . All the points,  $K_g$ , are evenly distributed along the line of action. The distance between each pair of neighboring points,  $K_g$ , is equal to the base pitch of the gear,  $p_{b,g}$ .

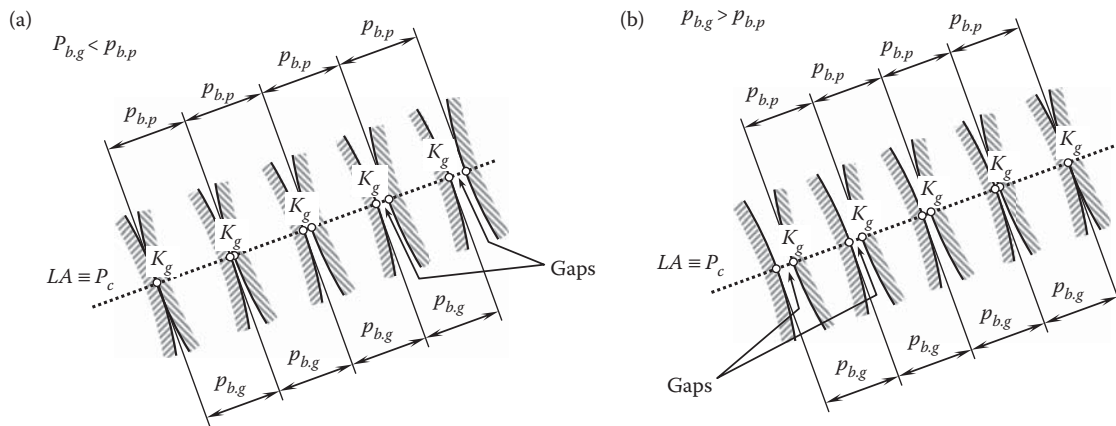
A similar analysis can be performed with respect to the pinion tooth flank,  $\mathcal{P}$ , shown in [Figure 4.9b](#). All these portions of the tooth flanks of a pinion are located in the differential vicinity of points of intersection,  $K_p$ , of the tooth flanks,  $\mathcal{P}$ , by the line of action,  $LA \equiv P_c$ . Each tooth flank,  $\mathcal{P}$ , is perpendicular to the line of action,  $LA$ , at points  $K_p$ . All the points,  $K_p$ , are evenly distributed along the line of action. The distance between each pair of neighboring points,  $K_p$ , is equal to base pitch of the pinion,  $p_{b,p}$ .

When the condition of equal base pitches of a gear,  $p_{b,g}$ , and a mating pinion,  $p_{b,p}$ , is met; that is, when the identity  $p_{b,g} \equiv p_{b,p}$  is fulfilled, then the gear and the pinion can be engaged in mesh, as illustrated in [Figure 4.9c](#). Each gear point,  $K_g$ , coincides with corresponding pinion point,  $K_p$ . Because of this, the gear and the pinion points,  $K_g$  and  $K_p$ , are further designated as the contact point,  $K$ .

As follows from the analysis of [Figure 4.9c](#), it is not a must to keep all the base pitches of a gear,  $p_{b,g}$ , equal to one another or to keep all the base pitches of a mating pinion,  $p_{b,p}$ , also equal to one another. It is critical to keep equality of a gear base pitch to a corresponding pinion base pitch for each pair of teeth engaged in mesh.

**FIGURE 4.9**

On the concept of equal base pitches of a gear and a mating pinion: (a) base pitch in a gear,  $p_{b,g}$ ; (b) base pitch in a pinion,  $p_{b,p}$ ; and (c) equal base pitches in a gear pair,  $p_{b,g} \equiv p_{b,p}$ .

**FIGURE 4.10**

Examples of violation of the condition of equal base pitches: (a) case when the base pitch of a gear,  $p_{b,g}$ , is smaller compared to the base pitch,  $p_{b,p}$ , of a mating pinion ( $p_{b,g} < p_{b,p}$ ); and (b) case when the base pitch of a gear,  $p_{b,g}$ , is larger compared to the base pitch,  $p_{b,p}$ , of a mating pinion ( $p_{b,g} > p_{b,p}$ ); in both cases the gaps are observed.



Physically, this is possible, but limits the gear ratio of a gear pair to an integer number, that is, to 1, 2, 3, and so forth. Such a design of gearing is impractical and is not considered in this book.

When the base pitches of a gear and a mating pinion are not equal to one another ( $p_{b,g} \neq p_{b,p}$ ); for example, the gear base pitch,  $p_{b,g}$ , is smaller compared to the mating pinion base pitch,  $p_{b,p}$ , and the inequality  $p_{b,g} < p_{b,p}$  is valid as shown in Figure 4.10a, only one pair of teeth is engaged in mesh. A gap between the rest pairs of teeth of the gear,  $\mathcal{G}$ , and the pinion,  $\mathcal{P}$ , is observed. No gaps of this sort are permissible in perfect parallel-axes gearing.

In another example illustrated in Figure 4.10b, the gear base pitch,  $p_{b,g}$ , is greater than the mating pinion base pitch,  $p_{b,p}$ , and the inequality  $p_{b,g} > p_{b,p}$  is valid as shown in Figure 4.10b; again, only one pair of teeth is engaged in mesh. A gap between the rest pairs of teeth of the gear,  $\mathcal{G}$ , and the pinion,  $\mathcal{P}$ , is observed. No gaps of this sort are permissible in perfect parallel-axes gearing.

In this second example (Figure 4.10b), the distribution of the gaps is inverse to that shown in Figure 4.10a. This is because the gear and the mating pinion are rigid bodies that physically cannot interfere with one another.

With that said, the third condition to be fulfilled in a perfect parallel-axes gear pair can be formulated in the following manner:

**The third fundamental law of gearing (in parallel-axes gearing):** *In parallel-axes gearing, in order to transmit a uniform rotary motion from a driving shaft to a driven shaft by means of gear teeth, the base pitch of a gear and of a mating pinion must be equal to one another at every instant of time.*

If a discussion is limited just to parallel-axes gearing, the concept of *base pitch* is applicable only to gears with an involute tooth profile, that is, for spur, helical, herring-bone, double-helical, and so forth involute gears. No base pitch can be specified for gears with cycloidal as well as for others with noninvolute tooth profiles. Therefore, when base pitches in a gear and mating pinion are equal ( $p_{b,g} \equiv p_{b,p}$ ), the condition of conjugacy of the tooth flanks  $\mathcal{G}$  and  $\mathcal{P}$  of the gear and the pinion is always fulfilled.

The condition of equal base pitches of the mating tooth flanks of a gear and mating pinion has been known at least since the beginning of the 20th century. Unfortunately, the author failed to identify the name of a gear expert who can be credited with this discovery that is vital for the scientific theory of gearing.

The equality of base pitches of a gear and a mating pinion tooth flanks,  $\mathcal{G}$  and  $\mathcal{P}$ , is the third fundamental law of gearing all perfect gearings have to fulfill.



## Permissible Variation of Design Parameters of Pulley-and-Belt Analogy of Parallel-Axes Gearing

The pulley-and-belt analogy of a parallel-axes gear pair is convenient for the analysis of perfect parallel-axes gearing. There are many similarities in transmitting a rotation by pulley-and-belt and a corresponding gearing.\* Therefore, it is critical to know to what extent this analogy is applicable for the analysis of gearing.

As already discussed above (see Figures 4.4 and 4.6), a pulley-and-belt analogy can be specified in terms of diameters of the pulleys,  $d_1$  and  $d_2$ , and the center distance,  $C$ . Also, the ratio,  $d_2/d_1$ , of diameters of the pulleys needs to be taken into account. The ratio  $d_2/d_1$  is equal to the angular velocity ratio,  $\omega_1/\omega_2$ , of the pulleys and is commonly designated as  $u$ .

Several examples of possible configurations of two pulleys are briefly considered below.

In Figure 5.1, the point of intersection of the belt and the centerline is designated as  $P$ . The point,  $P$ , is a stationary point and does not travel along the centerline,  $\mathcal{C}$ . Because of this, the center distance,  $C$ , is of a constant value. The belt forms an angle,  $\phi_t$ , with respect to the perpendicular through  $P$  to the centerline,  $\mathcal{C}$ . The actual value of the angle,  $\phi_t$ , can be expressed in terms of the center distance,  $C$ , and the diameters,  $d_1$  and  $d_2$ , of the pulleys:

$$\phi_t = \cos^{-1} \left( \frac{d_1 + d_2}{2 \cdot C} \right) \quad (5.1)$$

As the center distance increases ( $C^* > C$ ), the angle  $\phi_t^*$  also increases ( $\phi_t^* > \phi_t$ ), and vice versa, as illustrated in Figure 5.2a. Reducing the center distance results in a corresponding reduction of the angle  $\phi_t$ . Finally, when the center distance  $C^{**} = (d_1 + d_2)/2$ , the angle,  $\phi_t$ , becomes zero (that is,  $\phi_t^{**} = 0^\circ$ ). The last case is schematically illustrated in Figure 5.2b.

Transmission of a rotation between two shafts with parallel axes of rotation,  $O_1$  and  $O_2$ , is also possible when the center distance,  $C$ , is of a negative value (that is,  $C < 0$ ). This particular case is schematically illustrated in Figure 5.3. The pulleys do not physically exist in this particular case; however, the kinematics of the transmission of a rotation can be investigated, assuming that the disks are imaginary (phantom).

The impact of the diameters,  $d_1$  and  $d_2$ , of the pulleys on the actual value of the angle,  $\phi_t$ , can be demonstrated similarly to that as for the impact of the center distance,  $C$ .

For all of these configurations, a corresponding parallel-axes gear pair can be designed. This is because of the following.

First, each of the pulleys of diameters  $d_1$  and  $d_2$  can be construed as the envelopes to consecutive positions of a line along the straight line segment,  $ab$ . As shown below in the further analysis, the line along the straight line segment,  $ab$ , is in nature the line of action,  $LA$ , in the corresponding gear pair. The pulley can be construed as an envelope to consecutive positions of the line of action,  $LA$ , in their motion in relation to a reference associated with the pulley.

Second, consider an arbitrary point within the straight portion of the belt. When the belt-and-pulley mechanism operates, the point traces in a motionless reference system a corresponding pace of contact,  $P_c$ . Evidently, in a case of parallel-axes gearing, the path of contact,  $P_c$ , is a straight line that is aligned with the line of action,  $LA$ . This allows interpretation of the path of contact,  $P_c$ , as an envelope (that is, a reduced case of enveloping) to consecutive positions of the line of action,  $LA$ , when the pulleys rotate.

Another scenario is observed when the rotation from a driving shaft to a driven shaft is transmitted by means of two pulleys, the diameters of which,  $d_1$  and  $d_2$ , are time-dependent; that is,  $d_1 = d_1(t)$  and  $d_2 = d_2(t)$ .

\* The only principal difference between a pulley-and-belt analogy of a gear pair and between the gear pair itself that needs to be taken into consideration at this point is the different direction of the force by means of which the rotation is transmitted. In the pulley-and-belt mechanism, the driving pulley *pulls* the driven pulley, while in the gear pair, the driving gear *pushes* the driven gear.

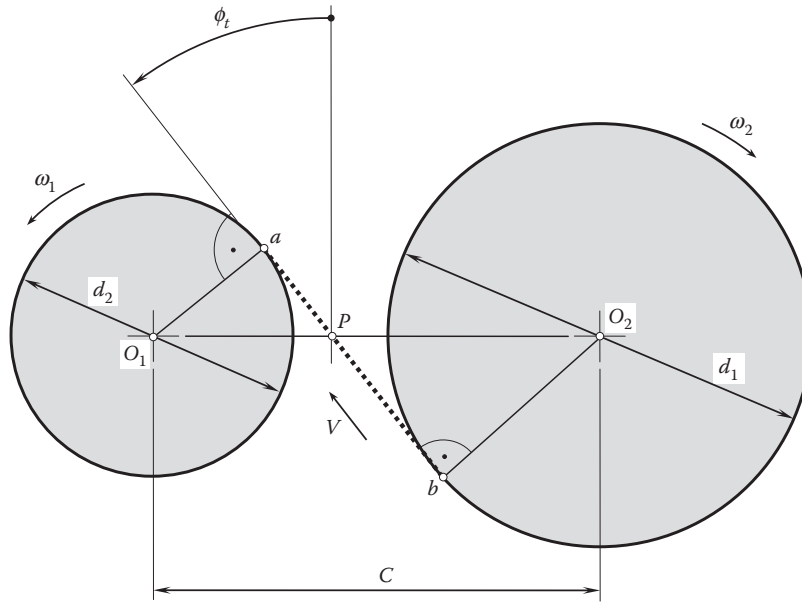


FIGURE 5.1

On the transition from the pulley-and-belt mechanism to a gear pair.

[This feature can also be interpreted as  $d_1 = d_1(\varphi_1)$  and  $d_2 = d_2(\varphi_1)$ , where  $\varphi_1$  and  $\varphi_2$  are the angles of rotation of the pulleys of diameters,  $d_1$  and  $d_2$ , and  $\varphi_2 = \varphi_1 \cdot (d_2/d_1)$ .] The schematic shown in Figure 5.4 corresponds to a case where the belt (the line of action,  $LA$ ) travels back and forth along the center line,  $\mathcal{C}$ .

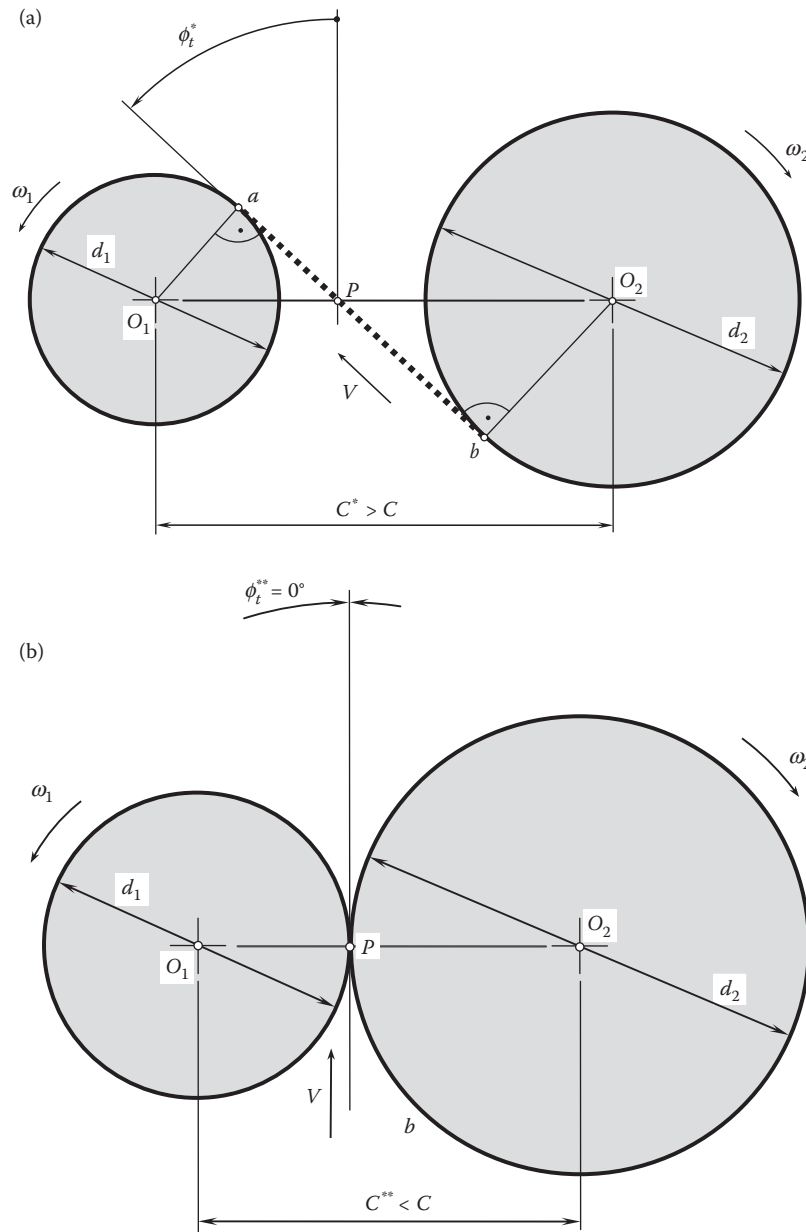
Let us assume that the angle,  $\phi_t$ , is of a constant value ( $\phi_t = \text{const}$ ), although the pitch point,  $P$ , is migrating within the line of centers,  $\mathcal{C}$ , depending on a current value of the rotation angle,  $\varphi_p$ , of the pinion (or the rotation angle,  $\varphi_g$ , of the gear), as schematically illustrated in Figure 5.4. The pitch point,  $P$ , has a certain displacement velocity in a direction parallel to the line of centers,  $\mathcal{C}$ . In such a scenario, for any instantaneous line of action,  $LA_i$ , the instant radii of the pulleys of radii,  $r_{b,g}^{(i)}$  and  $r_{b,p}^{(i)}$  (that is, the base circles for the gear and pinion), can be constructed. The profile of the transverse section of the pulleys (that is, profile of the base curve for gearing) can be specified in terms of instant lines of action,  $LA_{(i-1)}$ ,  $LA_i$ , and  $LA_{(i+1)}$ , and of radii,  $r_{b,p}^{(i-1)}$ ,  $r_{b,p}^{(i)}$ , and  $r_{b,p}^{(i+1)}$  [and  $r_{b,g}^{(i-1)}$ ,  $r_{b,g}^{(i)}$ , and  $r_{b,g}^{(i+1)}$ ], of instant base circles. Such a profile does not exist, as no enveloping curve can be constructed to a family of circles with a common center and of different radii.

It should be pointed out here again that in the case of a constant pressure angle ( $\phi_t = \text{const}$ ) and variable position of the pitch point,  $P$  (see Figure 5.4), no envelope to consecutive positions of instant straight lines of action,  $LA_{(i-1)}$ ,  $LA_i$ , and  $LA_{(i+1)}$ , can be constructed and thus no path of contact,  $P_c$ , is feasible in the case under consideration. Ultimately, no gear tooth profile that is capable of transmitting a rotation from a driving shaft to a driven shaft is feasible. Translation of the instant line of action along the centerline,  $\mathcal{C}$ , is not permissible.

Let us assume a case such that when a pair of pulleys rotate, the angle between the belt and a perpendicular to the center line (that is, the pressure angle,  $\phi_t$ ) are continuously altering, and the line of action,  $LA$ , is always a straight line through the pitch point,  $P$ . Once the pressure angle is continuously altered, then at every instant of time, an instant line of action,  $LA_{\text{inst}}$ , is observed. Considered in a stationary reference system, no envelope to the consecutive positions of the instant lines of action,  $LA_{\text{inst}}$ , is feasible. This means that a path of contact,  $P_c$ , cannot be constructed. Ultimately, no gear tooth profile that is capable of transmitting a rotation from a driving shaft to a driven shaft is feasible. Rotation of the instant line of action about the pitch point,  $P$ , is not permissible.

A similar situation (Figure 5.4) is observed in cases where the instant line of action,  $LA_{\text{inst}}$ , turns about the pitch point,  $P$ , when the gears rotate. When the pitch point,  $P$ , is motionless (Figure 5.5), then no envelope to consecutive positions of the rotating instant line of action,  $LA_i$ , can be constructed. This means that under the condition when the pressure angle,  $\phi_{t,i}$  [that is,  $\phi_{t,i} = \phi_{t,i}(t)$ ], is variable, no gear tooth profile can be generated at all. Pure rotation of the instant line of action,  $LA_i$ , about the pitch point,  $P$ , is not permissible in gearing.

However, when both motions, that is, a rotation of the instant line of action,  $LA_{\text{inst}}$ , about the pitch point,  $P$ , and a translation of the instant line of action,  $LA_{\text{inst}}$ , along the centerline,  $\mathcal{C}$ , are performed simultaneously, the gear teeth of a complex geometry can be generated (Figure 5.6). In the case under consideration, the path of

**FIGURE 5.2**

Impact of the center distance,  $C$ , on the actual value of the angle,  $\phi_t$ .

contact is a planar curve that is enveloping to the family of the instant lines of action,  $LA_i$ . The gear ratio,  $u$ , in Figure 5.6 is time dependent; that is, an equality  $u = u(t)$  is valid [or  $u = u(\varphi_1)$ ].

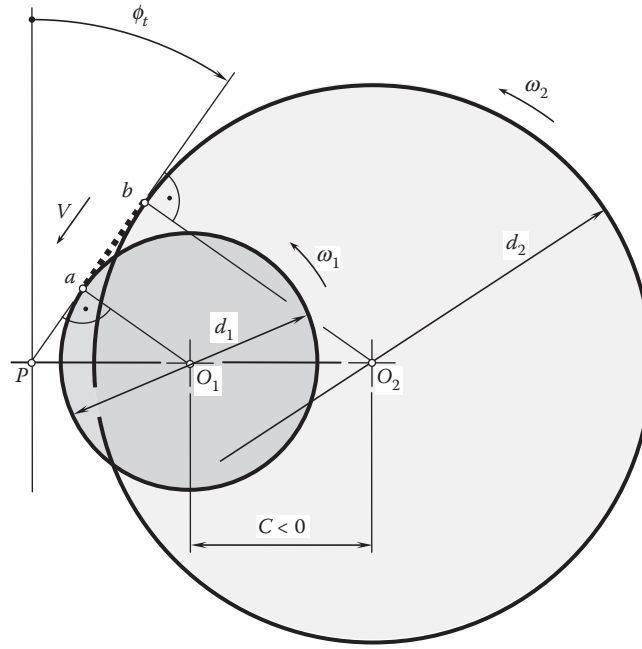
Gears of this type allow a variation of the tangential component of the resultant force of interaction of the teeth in a gear pair.\*

The schematic shown in Figure 5.6 is useful for the investigation and development of noncircular gearings that feature a variable gear ratio,  $u = u(t)$ .

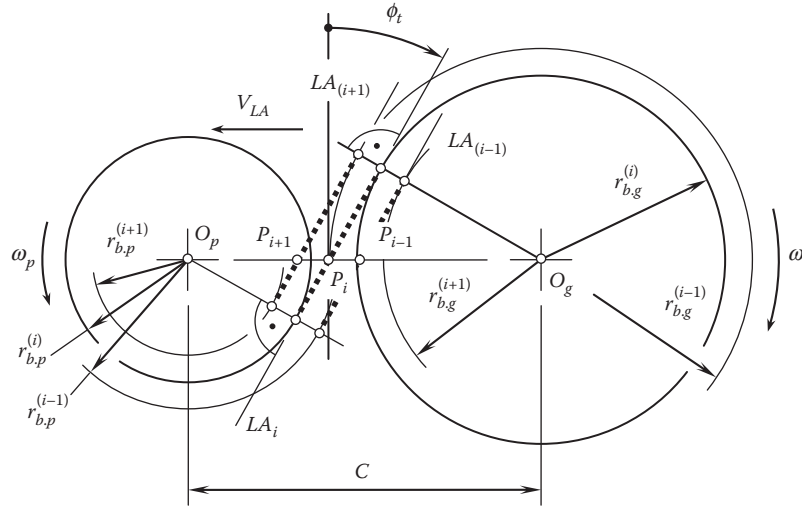
The above discussion can be summarized as follows:

First, formally, pulley diameters, as well as gear pitch diameters, can vary from zero to plus or minus infinity. However, neither a pulley nor a gear of zero diameter is physically feasible. For a particular application, an

\* This concept is used, for example, in the design of a gear pair for fluctuating limited slip automobile differentials (see: U.S. Pat. No. 8,070,640, *Fluctuating Gear Ratio Limited Slip Differential*, S.P. Radzevich, Date: December 6, 2011, Filed: March 12, 2009, Int. Cl. F16H 48/06, F16H 48/20, F16H 57/08, F16H 57/17, U.S. Cl. 475/230).

**FIGURE 5.3**

Schematic of a transmission of rotation between two parallel axes when the center distance is negative ( $C < 0$ ).

**FIGURE 5.4**

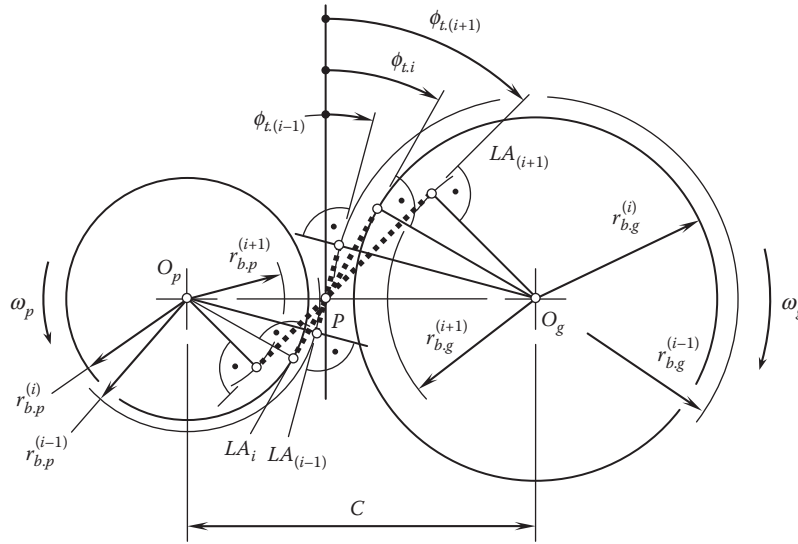
Infesibility of transmitting a rotation when an instant line of action,  $LA$ , travels back and forth along the centerline,  $\mathcal{C}$ :  $\phi_t = \text{Const}$ ,  $r_{b,g} = r_{b,p}$  ( $\varphi_g$ ),  $r_{b,p} = r_{b,p}(\varphi_g)$ .

external pinion of a minimal diameter,  $d_p^{\min}$ , can be manufactured and used (here,  $d_p^{\min}$  has a positive value). Similarly, for a particular application, an internal gear of a minimal diameter,  $d_g^{\min}$ , can be manufactured and used (here,  $d_g^{\min}$  has a negative value). The maximal diameter of a gear approaches infinity,  $d_g^{\min} \rightarrow \infty$ , as observed in a rack gear. Ultimately, the pitch diameter of a gear,  $d_g$ , can vary within the interval:

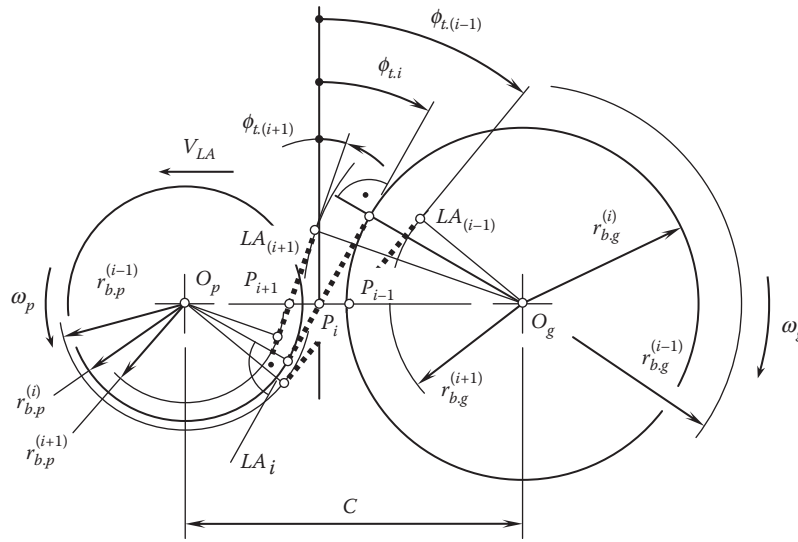
$$d_p^{\min} \leq d_g \leq +\infty \quad (5.2)$$

$$-\infty \leq d_g \leq d_g^{\max} \quad (5.3)$$

The interval for gear pitch diameter,  $d_g^{\min} \leq d_g \leq d_g^{\max}$ , is not feasible for gears.

**FIGURE 5.5**

Inf feasibility of continuous alteration of pressure angle in a parallel-axes gear pair with a constant gear ratio:  $\phi_t = \phi_t(\varphi_g)$ ,  $r_{b,g} = r_{b,g}(\varphi_g)$ ,  $r_{b,p} = r_{b,p}(\varphi_g)$ .

**FIGURE 5.6**

Possibility of transmitting a rotation when an instant line of action travels back and forth along the centerline,  $\mathcal{C}$ , and turns about the pitch point,  $P$ :  $\phi_t = \text{Const}$ ,  $r_{b,g} = r_{b,g}(\varphi_g)$ ,  $r_{b,p} = r_{b,p}(\varphi_g)$ .

Second, formally, the center distance,  $C$ , can vary from  $+\infty$  to  $-\infty$ , including a zero value of  $C$ . Physically, no center distance,  $C$ , of a zero value is feasible.

In external gearing, the shortest permissible center distance is positive and is limited to  $C = 2 \cdot d_p^{\min}/2 = d_p^{\min}$ . Therefore, a permissible interval for positive values of the center distance is as follows:

$$d_p^{\min} \leq C \leq +\infty \quad (5.4)$$

In internal gearing, the shortest permissible center distance is negative and is limited to  $C = (d_g^{\min} - d_p^{\min})/2$ . Therefore, a permissible interval for positive values of the center distance is as follows:

$$-\infty \leq C \leq \frac{d_g^{\min} - d_p^{\min}}{2} \quad (5.5)$$

The interval for the center distance,  $(d_g^{\min} - d_p^{\min})/2 \leq C \leq d_p^{\min}$ , is not feasible for gear pairs.

Third, formally, the pressure angle,  $\phi_t$ , can vary from  $+90^\circ$  to  $-90^\circ$ . Physically, no gear pair is feasible when the pressure angle,  $\phi_t$ , approaches either  $+90^\circ$  or  $-90^\circ$ . Therefore, there exists a maximal permissible value of the positive pressure angle,  $\phi_t^{\max}$ , and the negative pressure angle,  $\phi_t^{\min}$ . A positive pressure angle,  $\phi_t^{\max}$ , is close to  $+90^\circ$ , and a negative pressure angle,  $\phi_t^{\min}$ , is close to  $-90^\circ$ . Ultimately, a permissible interval for the pressure angle,  $\phi_t$ , can be represented in the form:

$$\phi_t^{\min} \leq \phi_t \leq \phi_t^{\max} \quad (5.6)$$

The intervals  $-90^\circ \leq \phi_t \leq \phi_t^{\min}$  and  $\phi_t^{\max} \leq \phi_t \leq +90^\circ$  are not permissible for gear pairs.

## Part II

# Perfect Gearing

Various types of gears are broadly used in the industry to transmit and transform a rotation from a driving shaft to a driven shaft. Transmission and transformation of a rotary motion is the main purpose of early designs of gears. As rotations in the past were low, and the power density was also low, no special care was taken in the accuracy of the transmitted rotation: often, neither input nor output rotation was uniform. Because of this, for a long time, no special efforts were undertaken to optimize gear tooth flank geometry; in early designs of gears, the gear teeth were shaped based mostly on common sense and experience gained by the gear manufacturer. Eventually, it was realized that a special gear tooth flank geometry is required in order to transmit a rotary motion smoothly from a driving shaft to a driven shaft. Gears that feature an appropriate gear tooth flank geometry are capable of transmitting a rotation smoothly; that is, under a steady rotation of the driving shaft, the driven shaft also rotates steadily. This property of gearing can be ignored when the input and output rotary motions are low and the power density through the gear pair is also low. However, this property of gearing becomes more and more vital when the input and output rotations get higher and more power is transmitted by the gear pair.

*Perfect gears* (i.e., *geometrically accurate gears* or *ideal gears*) are capable of transmitting a rotation smoothly. This is due to:

- The tooth flanks of a gear and a mating pinion feature special geometry that meets the requirements outlined in [Chapter 4](#) (“Conditions for Transmitting a Uniform Rotation Smoothly from a Driving Shaft to a Driven Shaft: Three Fundamental Laws of Gearing”) and is discussed in more detail below in this section.
- The axes of rotation of a gear and its mating pinion are perfectly aligned to one another (axis misalignment of both the angular and liner is zero).

Ultimately, these two features of perfect gearings result in the transmission error in perfect gearing always being zero.

The analysis of all three types of perfect gears, that is, of:

- Parallel-axes gearing
- Intersected-axes gearing
- Crossed-axes gearing

is covered in this part of the monograph.

Perfect parallel-axes gear pairs are discussed in the first portion of this section ([Chapters 6](#) through [Chapter 10](#)). This discussion is followed by the analysis of noninvolute gearing\* ([Chapter 11](#)) and of perfect intersected-axes

---

\* Actually, non-involute parallel-axes gearing is not a kind of *perfect* gearing. Non-involute parallel-axes gearing is considered together with the *perfect* gearing just because of the convenience of such a consideration.



gear pairs in the second portion of this section (Chapters 12 and 13). Ultimately, perfect crossed-axes gear pairs are discussed in the third portion of this section (Chapters 14 and 15).

The procedure of designing a perfect gear pair begins with an analysis of the kinematics of the gear pair to be designed. The essence of the approach can be stated as follows:

*Essence of the approach: Given a pair of rotary motions specified, for example, in terms of (a) an input torque,  $T_{\text{input}}$ ; (b) rotation vector of a gear,  $\omega_g$ ; and (c) rotation vector of a pinion,  $\omega_p$ , the rotation vectors,  $\omega_g$  and  $\omega_p$ , are somehow configured in relation to one another. It is required to determine the most favorable geometry of the conjugate tooth flanks of a gear and a mating pinion.*

It is necessary to solve this problem under certain constraints, such as those imposed by specific requirements of a particular gear application. The necessity of meeting the kinematic and geometric requirements induced by the conjugate action of the interacting tooth flanks of the gear and the pinion are of primary importance.

Physical phenomena that occur when two gears are engaged in mesh with one another are taken into consideration in a later stage of the design process. Ultimately,

- The kinematics of meshing
- The geometry of conjugate tooth flanks
- Physical phenomena that occur between the contacting surfaces

all three make up the discussed approach to the problem of designing the most favorable gear pair. Use of the approach enables one to solve the challenging problem of synthesizing the most favorable gear pair for a specified application.

Only the kinematical and geometrical aspects of the problem of designing a perfect gear pair are investigated below.

Three subsections, namely, the subsections II-A, II-B, and II-C, comprise Part II of the monograph.

## Section II-A

# Perfect Gearing: Parallel-Axes Gearing

Gear pairs that operate on parallel axes of rotation of a driving and driven shaft constitute a separate group of gearings that is commonly referred to as *parallel-axes gearing*. Parallel-axes gearing is also often referred to as  $P_a$ -gearing for simplicity. Parallel axes of rotation of a gear and its mating pinion (i.e., the shafts are parallel) is the principal feature of gearing of this particular type. Spur gearing, helical gearing, herring-bone gearing, and so forth are perfect examples of parallel-axes gearing.

A variety of known designs of gear pairs feature parallel axes of rotation of the driven and driving shafts. Parallel-axes gear pairs of each type can be specified by a corresponding vector diagram. Vector representation is the key to proper understanding of the kinematics, as well as the geometry of the conjugate tooth flanks of a gear and its mating pinion in parallel-axes gearing. The geometry of the tooth flanks follows the kinematics. Then, at a later stage, the physical phenomena (tooth flank wear, gear lubricating, contact stress, gear tooth bending strength, and so forth) can be taken into account.

The kinematics of a gear pair (specified in terms of a corresponding vector diagram) is the starting point for solving the problem of designing the most favorable gear pair for a given application, that is, a gear pair with the desired performance. First of all, the configuration of the input shaft in relation to the output shaft has to be given. Then, the input torque must be specified. Finally, the rotation of the driving shaft, as well as the desired rotation of the driven shaft, should be known. This set of input information for solving the problem of designing a desired gear pair is self consistent and is the shortest possible list. None of the aforementioned items can be eliminated from the above-listed set of the input information.

In the discussion given in this part of the book, the reader's attention is focused on the correspondence between the given parameters of kinematics of a gear pair and the desired corresponding geometry of tooth flanks of mating gears.

This section of the book contains [Chapters 6](#) through [10](#).



# Taylor & Francis

Taylor & Francis Group

<http://taylorandfrancis.com>

# 6

## *Involute Gearing: Kinematics and Geometry*

About 80% of gears in total operate on parallel axes of rotation. Involute gearing is the most broadly used type of parallel-axes gearing. An example of an application of involute parallel-axes gearing is shown in [Figure 6.1](#).

The discussion of involute gearing in this chapter begins with an analysis of the specified kinematics of the relative motion of a gear and its mating pinion. Correct transmission and transformation of a steady rotation of an input shaft to a desired rotation of the output shaft is the main purpose of involute gearing. The kinematics of the relative motion of a gear and a mating pinion is a key to understanding parallel-axes gearings of all possible types.

Although this monograph is written mostly for readers who are proficient in the field of gearing and less for beginners in the field, for the reader's convenience, some elementary concepts of the basic of theory of transmission of rotation from an input shaft to an output shaft are briefly considered in this chapter.

### 6.1 Principal Features of Parallel-Axes Gearing

Parallel-axes gearings of various types feature common fundamental components. It is convenient to begin the discussion with an analysis of the kinematics of parallel-axes gearing and to implement for this purpose the vector diagrams of gear pairs introduced earlier (see [Chapter 2](#)).

#### 6.1.1 Kinematics of Parallel-Axes Gearing

A vector diagram of a gear pair is a convenient tool for the investigation of the kinematics of parallel-axes gearing. A vector diagram is composed of two rotation vectors.\* One of the vectors is the rotation vector of the gear. This vector is denoted by  $\omega_g$ . The other is the rotation vector of the pinion. This vector is designated as  $\omega_p$ . Commonly, the rotation vector of the gear,  $\omega_g$ , and the rotation vector of the pinion,  $\omega_p$ , are located apart from each other at a certain distance. This distance is referred to as the *center distance* and is designated as  $C$ .

When the rotation vectors,  $\omega_g$  and  $\omega_p$ , are known, the vector of instantaneous relative rotary motion,  $\omega_{pl}$ , can be constructed. By convention, the vector of instant rotation,  $\omega_{pl}$ , indicates the instant rotation of the pinion in relation to the gear. Under such a scenario, the latter is considered motionless.

The rotation vectors,  $\omega_g$  and  $\omega_p$ , feature directions and certain magnitudes. The magnitudes of the rotation vectors,  $\omega_g$  and  $\omega_p$ , are designated as  $\omega_g = |\omega_g|$  and  $\omega_p = |\omega_p|$ , correspondingly. In parallel-axes gearing, the orientation of the rotation vectors in relation to one another is restricted by the requirement that the vectors should be parallel (see [Chapter 2](#), the first row in [Table 2.1](#)).

While the rotation vectors,  $\omega_g$  and  $\omega_p$ , are parallel, they can be configured in relation to one another in a different manner. Examples are schematically shown in [Figure 6.2](#).

\* Angular velocity is considered in this monograph as a vector along the axis of rotation in a direction defined by the right-hand screw rule. It is understood here and below that rotations,  $\omega_g$  and  $\omega_p$ , are not vectors in nature. Therefore, special care is required when treating rotations as vectors. In particular, when coordinate system transformation is analytically described by means of matrices, the order of the matrices in the matrix product is predetermined by the order of the elementary coordinate system transformations; that is, the order of the matrices in the matrix product cannot be altered.



**FIGURE 6.1**  
Parallel-axes gear pair composed of spur involute gears.

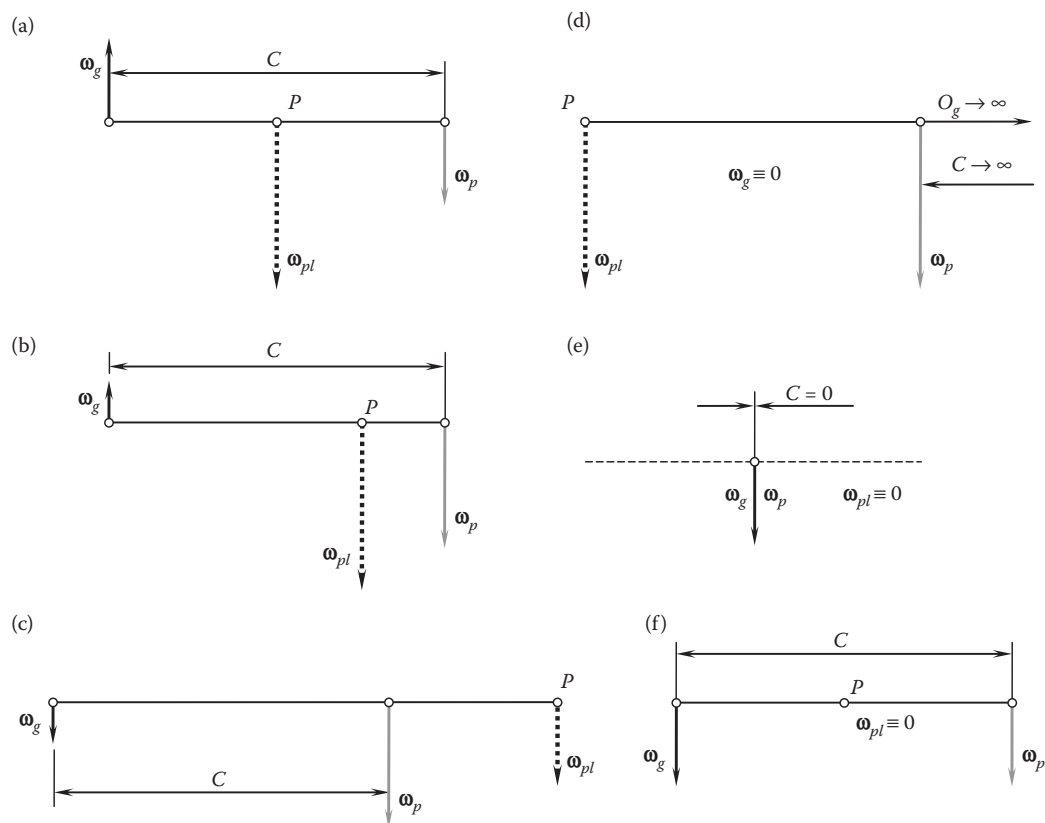


**FIGURE 6.2**  
Possible types of vector diagrams for parallel-axes gear pairs of conventional designs: (a) external rotary-negative gearing with the gear ratio,  $u = -1$ ; (b) external rotary-negative gearing with the gear ratio  $u < 0$ ; (c) internal rotary-positive gearing with the ratio  $u > 0$ ; (d) rotary-zero gear-to-rack pair with the gear ratio  $u = 0$ ; (e) gear coupling with gear the ratio  $u = +1$ ; (f) hypothetical internal rotary-positive gearing with the gear ratio  $u > 0$ .

In a simple case, shown in Figure 6.2a, the rotation vectors,  $\omega_g$  and  $\omega_p$ , are of the same magnitude (i.e.,  $\omega_g = \omega_p$ ) and are pointed in opposite directions. The gear ratio\* in this gear pair is equal to:

$$u = \frac{\omega_p}{\omega_g} = -1 \quad (6.1)$$

The inequality  $\omega_g \leq \omega_p$  is always observed.

The sign “−” in Equation 6.1 is because in external gearings of conventional design, the direction of rotation of the driving shaft is altered to the opposite direction of the driven shaft. This is the reason parallel-axes gearings of this type are referred to as *rotationally negative parallel-axes gearing*. However, as shown below, numerous designs of external parallel-axes gearing can also be a kind of *rotationally positive parallel-axes gearing*, that is, an external parallel-axes gearing with a positive angular velocity ratio,  $\omega_g > \omega_p$ .

The magnitude of the vector of instant rotation,  $\omega_{pl}$ , is double that of the rotation vector of the gear,  $\omega_g$  (or, similarly, of the rotation vector of the pinion,  $\omega_p$ ). The rotation vector,  $\omega_{pl}$ , is parallel to the rotation vectors,  $\omega_g$  and  $\omega_p$ , and it passes through the point,  $P$ , at the middle of the center distance,  $C$ .

In another example (Figure 6.2b), the inequality  $\omega_g < \omega_p$  is observed. The gear ratio in this particular case has a negative value ( $u < 0$ ). The magnitude of the vector of instantaneous rotation,<sup>†</sup>  $\omega_{pl}$ , is equal to the summa of magnitudes of the rotation vectors of the gear,  $\omega_g$ , and the pinion,  $\omega_p$ ; that is, the equality  $\omega_{pl} = \omega_g + \omega_p$  is valid. The rotation vector,  $\omega_{pl}$ , is parallel to the rotation vectors,  $\omega_g$  and  $\omega_p$ . The vector,  $\omega_{pl}$ , passes through the point,  $P$ , within the center distance,  $C$ . The point,  $P$ , is located closer to the rotation vector of the pinion,  $\omega_p$ .

The vector diagrams (see Figures 6.2a and 6.2b) correspond to external gearing of conventional design.

For the same center distance,  $C$ , the rotation vectors,  $\omega_g$  and  $\omega_p$ , of a gear and a mating pinion can be pointed in the same direction, as shown in Figure 6.2c. Because the rotation vectors are of the same direction, the gear ratio of a gear pair of this kind has a positive value ( $u > 0$ ). The magnitude,  $\omega_p$ , of rotation of the pinion always exceeds the magnitude,  $\omega_g$ , of rotation of its mating gear.

The vector diagram shown in Figure 6.2c corresponds to an internal gearing of conventional design.

The magnitude of the vector of instant rotation,  $\omega_{pl}$ , is equal to the difference between the magnitudes of the rotation vectors,  $\omega_g$  and  $\omega_p$ ; that is, the equality  $\omega_{pl} = -\omega_g + \omega_p$  is valid. The rotation vector,  $\omega_{pl}$ , is parallel to the rotation vectors,  $\omega_g$  and  $\omega_p$ , of the gear and the pinion. The vector  $\omega_{pl}$  passes through the point,  $P$ , which is not within the center distance,  $C$ . In internal gearing of conventional design, the point,  $P$ , is located outside the center distance,  $C$ , but on the centerline,  $\mathcal{C}$ .

The actual configuration of the rotation vectors in a vector diagram also depends on the length of the center distance,  $C$ . In the above-considered examples, the center distance is of a finite length. There are no physical constraints to set the center distance of an infinite length ( $C \rightarrow \infty$ ). An example of a vector diagram of a gear pair of this particular type is schematically depicted in Figure 6.2d. A vector diagram of this particular type corresponds to a *pinion-gear-to-rack gearing*. Because the center distance for a *pinion-gear-to-rack* pair is of an infinite length, the gear axis of rotation,  $O_g$ , is remote to infinity. Under such a scenario, the location of the vector of instantaneous rotation,  $\omega_{pl}$ , is specified not in terms of the rotation vectors,  $\omega_g$  and  $\omega_p$ , but in terms of the vectors,  $\mathbf{V}_g$  and  $\omega_p$ , instead. Here, the linear velocity vector of the rack is denoted by  $\mathbf{V}_g$ . The vectors,  $\mathbf{V}_g$  and  $\omega_p$ , are synchronized with one another. The gear ratio in the pinion-gear-to-rack pair (Figure 6.2d) has an infinite value ( $u \rightarrow \infty$ ).

The linear velocity vector,  $\mathbf{V}_g$ , is pointed perpendicular to the rotation vector,  $\omega_p$ , of the pinion and the centerline,  $\mathcal{C}$ .

The vector diagram for a pinion-gear-to-rack gear pair can be considered either as a reduced (limit) case of the vector diagram of an external gear pair (Figure 6.2b), or as a degenerate (limit) case of the vector diagram of an internal gear pair (Figure 6.2c).

\* Commonly, the gear ratio,  $u$ , is the ratio of the larger to the smaller number of teeth in a pair of gears; that is,  $u = N_g/N_p$ , where  $N_g$  and  $N_p$  are tooth numbers of the gear and the pinion, respectively ( $N_g \geq N_p$ ). In the *English* system of symbols, the gear ratio is denoted by  $m_G$ . The gear ratio,  $u$ , can be also expressed in terms of the rotations,  $\omega_g$  and  $\omega_p$ . A formula,  $u = \omega_p/\omega_g$ , can be used for this purpose. Definition of the gear ratio in terms of rotations of the input,  $\omega_{\text{input}}$ , and output,  $\omega_{\text{output}}$ , shafts, that is,  $u = \omega_{\text{input}}/\omega_{\text{output}}$ , is preferred and is adopted in this book.

† In  $P_n$ -gearing, an instantaneous rotation is observed about pitch point,  $P$ . Actually, the instant rotation takes place about an *axis of instant rotation*, that is, about a straight line through the pitch point,  $P$ , that is parallel to the axes of rotation of the gear,  $O_g$ , and its mating pinion,  $O_p$ . It makes sense to refer to the axis of instant rotation as to the *pitch line*,  $P_{\text{lin}}$ . This terminology is adopted below in this book for gearings of all types, that is, for gearings that operate on parallel axes and on intersected axes, as well as on crossed axes of rotation of a gear,  $O_g$ , and its mating pinion,  $O_p$ .

In a particular case under consideration, the rotation vector of the gear,  $\omega_g$ , is zero ( $\omega_g = 0$ ). Formally, a zero vector cannot be parallel to another vector. However, when the center distance approaches infinity, the magnitude of the rotation vector,  $\omega_g$ , becomes smaller and smaller, ultimately approaching zero. The direction of the rotation vector,  $\omega_g$ , remains the same. It is assumed here that the direction of the zero vector,  $\omega_g$ , remains parallel to the rotation vector,  $\omega_p$ .

Theoretically, the length of the center distance,  $C$ , can be set to zero. This case is illustrated in Figure 6.2e. A vector diagram of this type corresponds to a gear coupling. The gear ratio in a gear coupling (Figure 6.2e) is  $u = +1$ .

A vector diagram for a hypothetical internal rotationally positive gearing with gear ratio  $u = +1$  is shown in Figure 6.2f. The feasibility of a gearing that features the vector diagram of this particular type is considered below in this section.

### 6.1.2 Gear Ratio in Parallel-Axes Gearing

The actual type of a gear pair depends, to a great extent, on the magnitude and sign of the angular velocity ratio,  $u$ , in the gear pair. The angular velocity ratio in a parallel-axes gear pair is defined as the ratio of the input rotation,  $\omega_{\text{input}}$ , to the output rotation,  $\omega_{\text{output}}$ ; that is:

$$u = \frac{\omega_{\text{input}}}{\omega_{\text{output}}} \quad (6.2)$$

In reduction gears (i.e., in *gear reducers*), the gear ratio is equal to:

$$u = \frac{\omega_p}{\omega_g} \quad (6.3)$$

In increasing gears (i.e., in *gear increasers*, or *gear multipliers*), the gear ratio is equal to:

$$u = \frac{\omega_g}{\omega_p} \quad (6.4)$$

An external gear pair that is composed of gears with the same tooth number features the gear ratio of  $u = -1$ . A gear ratio in an arbitrary external gear pair of conventional design is within the interval  $-\infty < u < -1$ . A *pinion-gear-to-rack pair* features the gear ratio that approaches infinite value (i.e.,  $u \rightarrow -\infty$ ).

Similarly, in an arbitrary internal gear pair that is composed of gears with the same tooth number, the gear ratio equals  $u = +1$ . A gear ratio within the interval  $+1 < u < +\infty$  corresponds to internal gear pairs of conventional design. Ultimately, a pinion-gear-to-rack pair features a gear ratio that approaches infinity (i.e.,  $u \rightarrow +\infty$ ).

When a discussion is limited only to rotationally negative parallel-axes gearing, the following expressions are valid for the center-distance,  $C$ :

$$C = r_g + r_p \quad (6.5)$$

and for the gear ratio,  $u$ :

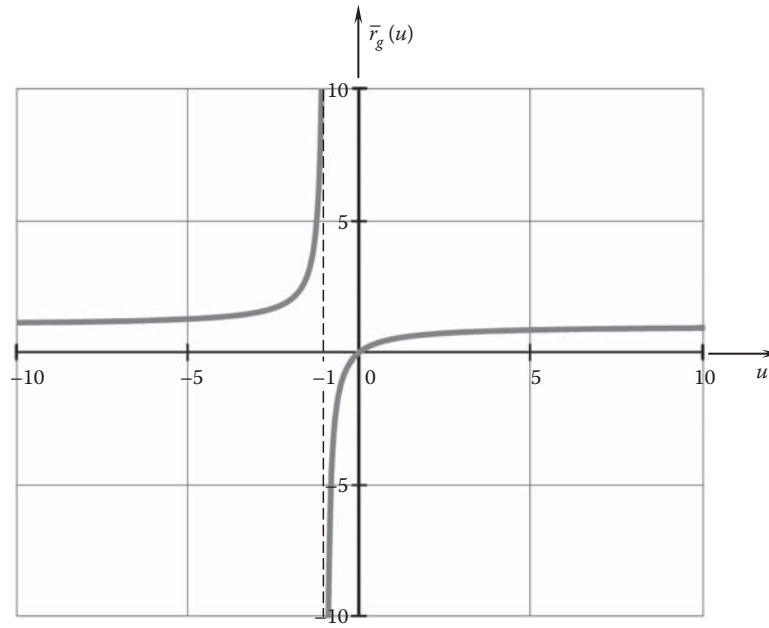
$$u = \frac{r_g}{r_p} \quad (6.6)$$

here, the distance from the gear axis of rotation,  $O_g$ , to point  $P$  is designated as  $r_g$ , and that for the pinion is - designated as  $r_p$ . The distance,  $r_g$ , is a signed value, that is, it has a positive value,  $r_g > 0$  in the case of external parallel-axes gearing and a negative value,  $r_g < 0$ , in the case of internal parallel-axes gearing. The distance,  $r_p$ , is always positive,  $r_p > 0$ . The magnitude,  $|r_g|$ , of the distance,  $r_g$ , is always larger than or equal to the distance,  $r_p$ ; that is, an inequality,  $|r_g| \geq r_p$ , is observed. As becomes clear later on, the distances,  $r_g$  and  $r_p$ , in nature are the pitch radii of a gear and a mating pinion in a gear pair. With this limitation on the distances,  $r_g$  and  $r_p$ , the interval for the center distance,  $C$ , is as follows:  $2r_p \leq C \leq +\infty$  in the case of external parallel-axes gearing and  $-\infty \leq C \leq 0$  in the case of internal parallel-axes gearing.

The discussion on the angular velocity ratio (see Equations 6.2 through 6.4 and Equation 6.6) yields a generalized formula for  $u$ :

$$u = \frac{\omega_p}{\omega_g} = \frac{r_g}{r_p} = \frac{r_{b,g}}{r_{b,p}} \quad (6.7)$$




**FIGURE 6.3**

A function  $\bar{r}_g(u)$  for rotationally negative parallel-axes gearing ( $\bar{r}_g = \bar{r}_g/C$ ).

Here, in Equation 6.7, the radii of the base circles of a gear and a mating pinion are designated as,  $r_{b,g}$  and  $r_{b,p}$ , correspondingly (to be discussed later in this chapter).

Based on the two expressions (Equations 6.5 and 6.6), the following formulas are valid:

$$r_p = C - r_g \quad (6.8)$$

$$u = \frac{r_g}{C - r_g} \quad (6.9)$$

$$u = \frac{\bar{r}_g}{1 - \bar{r}_g} \quad (6.10)$$

where  $\bar{r}_g = r_g/C$ . Ultimately, a formula for the normalized (i.e., normalized\* by the center distance,  $C$ ) pitch radius of the gear,  $\bar{r}_g$ , in rotationally negative parallel-axes gearing can be derived:

$$\bar{r}_g(u) = \frac{u}{u + 1} \quad (6.11)$$

The function  $\bar{r}_g$  vs.  $u$  is plotted in Figure 6.3. A gear pair with the gear ratio  $u = -1$  is not permissible in the case under consideration.

Equation 6.11 returns two critical values for the gear ratio, that is,  $u = -1$  and  $u = 0$  in rotationally negative parallel-axes gearings, as shown in Figure 6.4. As follows from the analysis of Figure 6.3, with these values of the angular velocity ratio, that is,  $u = -1$  and  $u = 0$ , two points,  $A_n$  and  $B_n$ , can be specified in rotationally negative parallel-axes gearings. The first value of the angular velocity ratio means that no rotationally negative gear pair with the gear ratio  $u = -1$  is infeasible (however, this is not a constraint for rotationally positive gear pairs). The second value of the angular velocity ratio means that no rotationally negative gear pair with the gear ratio  $u = 0$  is feasible at all. This feature of rotationally negative parallel-axes gearings is for two reasons. First, for the

\* Here and below, when treating *normalized* parameters, it is a must to bear in mind that the original values, that is, a linear velocity vector,  $\mathbf{V}$ ; a tangent force vector,  $\mathbf{T}$ ; a displacement,  $\delta$ ; and so forth, are the vectors with dimensions and therefore cannot be added to one another, as they have different dimensions. Normalized vectors (a unit linear velocity vector,  $\mathbf{v} = \mathbf{V}/|\mathbf{V}|$ ; a unit tangent force vector,  $\mathbf{t} = \mathbf{T}/|\mathbf{T}|$ ; and so forth) formally can be added to one another, which is incorrect, as they are dimensionless.

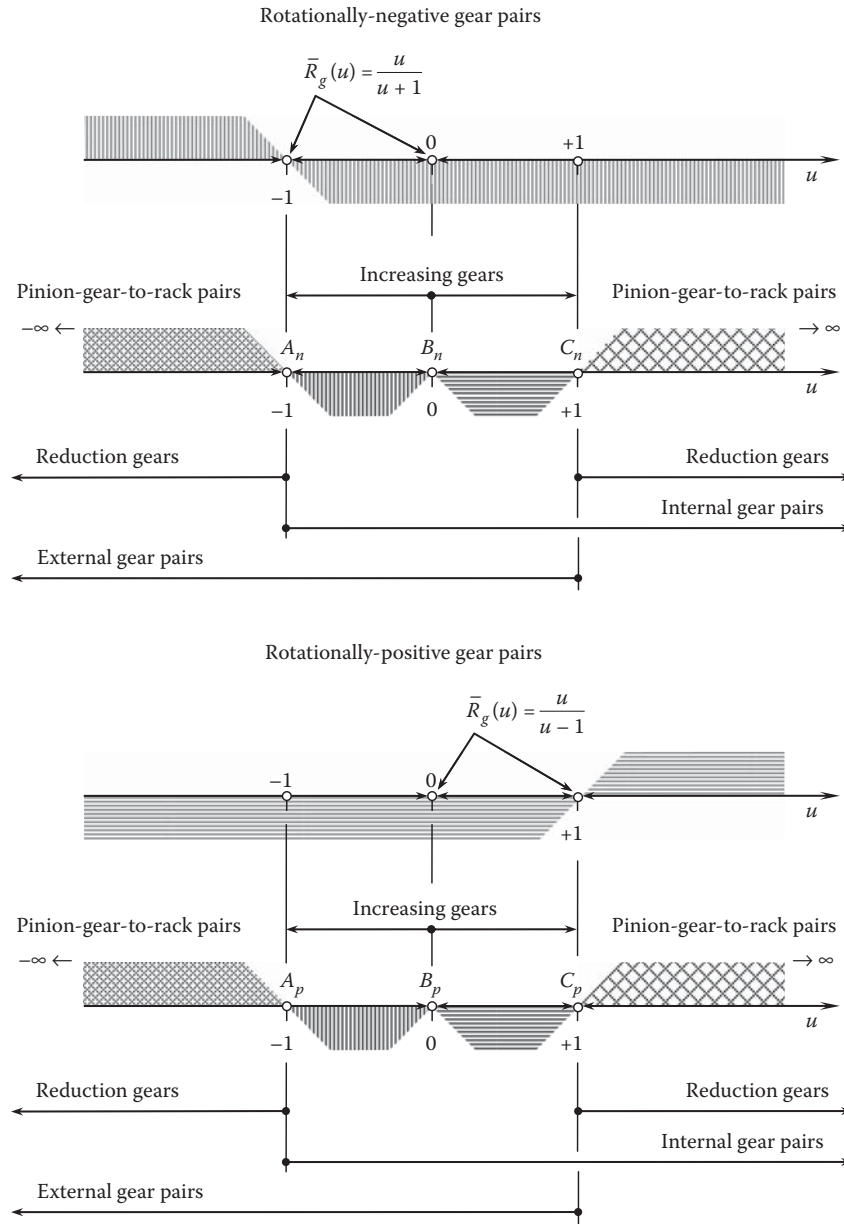


FIGURE 6.4

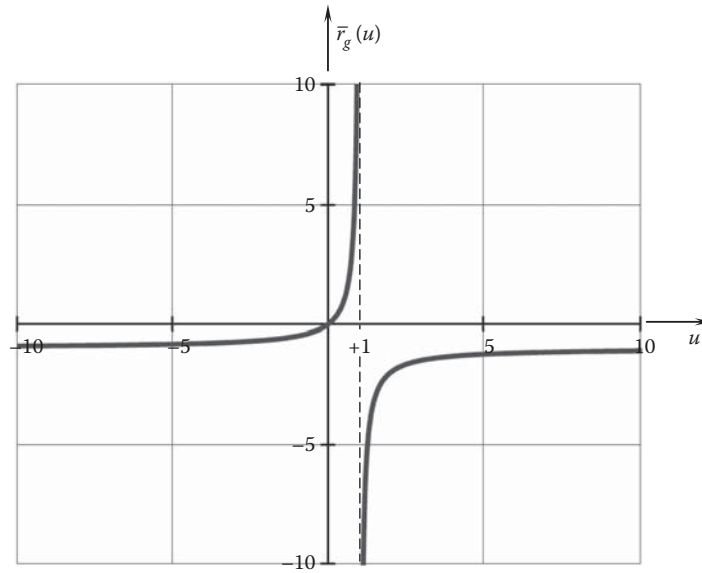
Type of a gear pair depending on the gear ratio  $u$ .

angular velocity ratio  $u = 0$ , the radius  $\bar{r}_g$  needs to be zero (see Equation 6.11), which is physically infeasible—no gear can be designed with a zero radius,  $\bar{r}_g$ . Second, zero angular velocity ratio means that an output rotation of a certain value can be obtained with zero input rotation, which is also infeasible.

Similarly, when a discussion is limited only to rotationally positive parallel-axes gearing, the following expressions are valid for the center distance,  $C$ , and for the angular velocity ratio,  $u$ , namely:

$$C = r_g - r_p \quad (6.12)$$

$$u = \frac{r_g}{r_p} \quad (6.13)$$

**FIGURE 6.5**

A function  $\bar{r}_g(u)$  for rotationally positive parallel-axes gearing ( $\bar{r}_g = \bar{r}_g/C$ ).

These two expressions make possible a formula for the normalized pitch radius of the gear,  $\bar{r}_g$ , in rotationally positive parallel-axes gearing:

$$\bar{r}_g(u) = \frac{u}{u - 1} \quad (6.14)$$

The function  $\bar{r}_g$  vs.  $u$  is plotted in Figure 6.5. A gear pair with the gear ratio  $u = +1$  is not permissible in the case under consideration.

Equation 6.14 returns two critical values for the angular velocity ratio,  $u = 0$  and  $u = +1$ , in rotationally positive parallel-axes gearings (see Figure 6.4). As follows from the analysis of Figure 6.5, with these values of the angular velocity ratio, that is,  $u = 0$  and  $u = +1$ , two points,  $B_p$  and  $C_{pr}$ , can be specified in rotationally positive parallel-axes gearings. The first value of the angular velocity ratio means that no rotationally positive gear pair with the gear ratio  $u = +1$  is infeasible (however, this is not a constraint for rotationally negative gear pairs). The second value of the angular velocity ratio means that no rotationally positive gear pair with the gear  $u = 0$  ratio is infeasible at all. This feature of rotationally positive parallel-axes gearings is for two reasons. First, for the angular velocity ratio  $u = 0$ , the radius,  $\bar{r}_g$ , needs to have a zero value (see Equation 6.11), which is infeasible—no gear can be designed with a zero radius,  $\bar{r}_g$ . Second, a zero angular velocity ratio means that an output rotation of a certain value can be obtained with zero input rotation, which is also infeasible.

Ultimately, in both cases, rotationally negative and rotationally positive parallel-axes gearings, the points,  $A_n$ ,  $B_n$ , and  $B_{pr}$ ,  $C_{pr}$ , can be specified with three values of the angular velocity ratio:  $u = -1$ ,  $u = 0$ , and  $u = +1$ . Only the point  $B_n \equiv B_p$  ( $u = 0$ ) corresponds to a angular velocity pair that is infeasible at all. A gear pair can be designed for the rest of the values of the gear ratio:  $-\infty \leq u < 0$  and  $0 < u \leq +\infty$ .

The correlation between the signed value of the angular velocity ratio,  $u$ , and the type of gearing is schematically illustrated in Figure 6.4.

The schematic shown in Figure 6.4 is constructed in strict formal compliance with Equations 6.11 and 6.14, as well as with the results that are illustrated in Figures 6.3 and 6.5. It should be stressed here that the asymptote  $u = -1$  in Figure 6.3, as well as the asymptote in Figure 6.5, correlate to points  $A_n$  and  $C_{pr}$  in Figure 6.4. Therefore, it is instructive to consider Figures 6.3 through 6.5 together, aligning (in one schematic) the points,  $A_n$  and  $C_{pr}$  with the corresponding asymptotes.

In a rotationally negative gearing, the direction of the input rotation is altered to the opposite direction. Therefore, in a case of rotationally negative gearing (Figure 6.4), gear ratios of reduction gears of a conventional design correspond to the section to the left of the point,  $A_n$  (and the point  $A_p$ ). Gear ratios for increasing gears of a conventional design correspond to the section,  $A_n - B_n$ . Gear pairs with gear ratios that correspond to the section,  $B_n - C_n$ , and those that correspond to the section to the right of the point,  $C_n$ , are not known yet.

A possibility of corresponding novel designs of gear pairs in these sections of the  $u$ -axis needs to be thoroughly investigated. Also, point  $A_n$  corresponds to conventional gearing in which the tooth counts of the gear and pinion are equal to one another. Gearings that correspond to the point,  $C_n$ , are not known yet.

The angular velocity ratio  $u \rightarrow -\infty$  corresponds to a pinion-gear-to-rack pair that is construed as a reduced case of an external gearing when the gear tooth count approaches infinity.

In rotationally positive gearing, the direction of the output rotation is the same as that of the input rotation. Therefore, in the case of rotationally positive gearing (Figure 6.4), the angular velocity ratios of reduction gears of a conventional design correspond to the section to the right of the point,  $C_p$ . Angular velocity ratios for increasing gears of a conventional design correspond to the section,  $B_p - C_p$ . Gear pairs with gear ratios that correspond to the section,  $A_p - B_p$ , and those that correspond to the section to the left of the point,  $A_p$ , are not known yet. A possibility of corresponding novel designs of gear pairs in these sections of the  $u$ -axis needs to be investigated. Also, gearings that correspond to the point,  $C_p$ , are not known yet.

The case of  $u = +1$  corresponds to gear couplings.\*

The angular velocity ratio  $u \rightarrow +\infty$  corresponds to a pinion-gear-to-rack gear pair that is construed as reduced case of an internal gearing when the gear tooth count approaches infinity.

All the gear designs that are formally possible and are outlined in Figure 6.4 need to be investigated to the best possible extent.

### 6.1.3 The Permissible Transverse Pressure Angle Variation

In the *pulley-and-belt* analogy of parallel-axes gearing, the angle that the belt forms with the perpendicular to the centerline,  $\mathcal{C}$ , is of critical importance. In parallel-axes gearing, this angle is commonly referred to as the *transverse pressure angle*, and is designated as  $\phi_t$ .

Commonly, for a particular gear, the transverse pressure angle,  $\phi_t$ , is of a constant value. As discussed in the previous chapter (see Chapter 5), theoretically, this angle,  $\phi_t$ , can be set within the interval  $0^\circ \leq \phi_t \leq 90^\circ$ .

When the transverse pressure angle equals  $\phi_t = 0^\circ$ , the radius of curvature of the gear tooth profile is zero ( $R_g = 0$ ). As the involute tooth profile cannot be extended inward from the base circle, spur gearing is infeasible. Helical gear tooth flanks reduce to helices on the base cylinder. Thus, helical gearing that features a zero transverse pressure angle,  $\phi_t = 0^\circ$ , is impractical. Therefore, the lowest limit of  $\phi_t = 0^\circ$  for the transverse pressure angle,  $\phi_t$ , should be replaced with a certain reasonably small limit,  $[\phi_t]_{\min}$ . Therefore, actually, an inequality  $\phi_t \geq [\phi_t]_{\min}$  is observed.

When the transverse pressure angle equals a right angle,  $\phi_t = 90^\circ$ , there is no tangential force to transmit a torque. Therefore, the highest limit,  $\phi_t = 90^\circ$ , for the transverse pressure angle,  $\phi_t$ , should be replaced with a certain reasonably large limit,  $[\phi_t]_{\max}$ . Therefore, actually, an inequality  $\phi_t \leq [\phi_t]_{\max}$  is observed.

Ultimately, a permissible interval:

$$[\phi_t]_{\min} \leq \phi_t \leq [\phi_t]_{\max} \quad (6.15)$$

can be set for the transverse pressure angle,  $\phi_t$ .

Referring to Figure 6.6, consider a schematic of a parallel-axes external *gear-to-pinion mesh* with an arbitrary value of the transverse pressure angle,  $\phi_t$ . The gear and the pinion rotate about their axes of rotation,  $O_g$  and  $O_p$ , with angular velocities,  $\omega_g$  and  $\omega_p$ , correspondingly. The axes of rotations,  $O_g$  and  $O_p$ , are at a center distance,  $C$ , from one another. The pitch point,  $P$ , is located within the centerline,  $\mathcal{C}$ . The ratio,  $r_g/r_p$ , of the portions,  $r_g$  and  $r_p$ , of the center distance  $C$  is equal to the angular velocity ratio,  $u$ ; that is,  $r_g/r_p = u = \omega_p/\omega_g$ . In perfect parallel-axes gearing, the line of action,  $LA$  (and the path of contact,  $P_c$ ), is at a transverse pressure angle,  $\phi_t$ , in relation to the perpendicular at  $P$  to the centerline,  $\mathcal{C}$ . It is worth stressing here that the line of action,  $LA$ , and the path of

\* It should be noted again that the case of  $u = +1$  corresponds to deeply degenerate designs of gear pairs. Because of this, significant features could be observed when developing tooth flanks for gearings that correspond to the case  $u = +1$ . When the friction between the interacting tooth flanks of a gear,  $\mathcal{G}$ , and its mating pinion,  $\mathcal{P}$ , is ignored, the tangential force that transmits the torque from the driving shaft to the driven shaft acts along the common perpendicular,  $\mathbf{n}_g$ , to the interacting tooth flanks,  $\mathcal{G}$  and  $\mathcal{P}$ . The common perpendicular,  $\mathbf{n}_g$ , intersects the axis of instant rotation,  $P_{in}$ , that is, it intersects the line along which the vector of instant rotation,  $\omega_{pl}$ , acts. In cases of gear pairs that correspond to the case  $u = +1$ , all three rotation vectors, that is,  $\omega_g$ ,  $\omega_p$ , and  $\omega_{pl}$ , are along a common straight line,  $P_{in}$ . Once the line of action of the unit normal vector,  $\mathbf{n}_g$ , intersects the line of action of the angular velocity vector,  $\omega_{pl}$ , the arm of tangential force in the gear pair becomes zero. This means that no torque can be transmitted by a gear pair of these particular types of gearings. This discrepancy needs to be thoroughly investigated. However, when, in a real gear coupling, axis misalignment is taken into account, the gear coupling can be considered a reduced case of gear pairs.

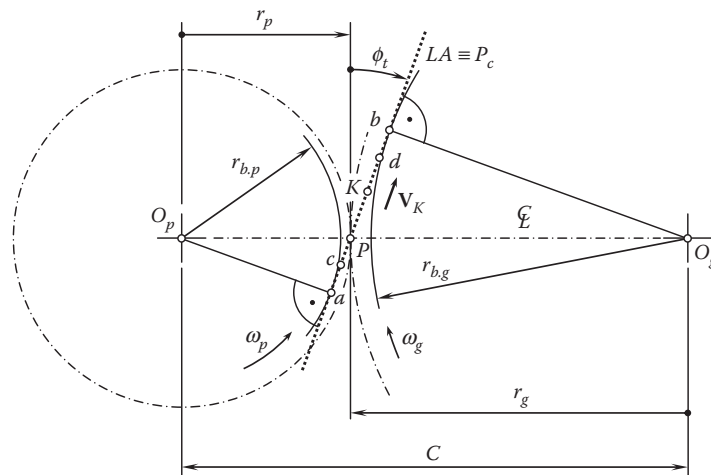


FIGURE 6.6

An external gear-to-pinion mesh with an arbitrary transverse pressure angle,  $\phi_t$ .

contact,  $P_c$ , are two different lines, both through the pitch point,  $P$ . In a reduced case of parallel-axes gearing, these two lines,  $LA$  and  $P_c$ , align with one another. The latter is not observed in more general cases of intersected-axes or crossed-axes gearings.

The portion,  $ab$ , of the line of action,  $LA$ , is an equivalent of the free bunch of the belt in the pulley-and-belt analogy of parallel-axes gearing. The active portion,  $cd$ , of the line of action,  $LA$ , is commonly located within the portion,  $ab$ . However, this is not a constraint, and a gear pair can be designed so the contact point,  $K$ , travels beyond the points,  $a$  and  $b$ . At this point, the actual positions of points  $c$  and  $d$  are not constrained by the location of points  $a$  and  $b$ . Points  $c$  and  $d$  must be located within the line of action,  $LA$ —this is the only constraint taken into account at this point.

When the gears rotate, the contact point,  $K$ , between the tooth flanks of the gear,\*  $\mathcal{G}$ , and the pinion,  $\mathcal{P}$ , travels along the line of action,  $LA \equiv P_c$ , with a constant linear velocity,  $V_K$ , similar to that in the pulley-and-belt analogy of parallel-axes gearing.†

The transverse pressure angle,  $\phi_t$ , in a gear pair can be smaller than that shown in Figure 6.6. A zero pressure angle (Figure 6.7) is the smallest permissible value of the transverse pressure angle. When the transverse pressure angle is zero,  $\phi_t = 0^\circ$ , in this particular case, the following equalities are valid:  $d_{b,g} = d_g$  and  $d_{b,p} = d_p$ .

In a case of the pressure angle,  $\phi_t$ , of a large value, significant alterations to the design parameters of a parallel-axes gear pair are observed.

First, the radii,  $r_{b,g}$  and  $r_{b,p}$ , of the base circles of a gear and a mating pinion get smaller as the transverse pressure angle,  $\phi_t$ , grows larger. Ultimately, at a certain value of the transverse pressure angle,  $\phi_t$ , the base radii,  $r_{b,g}$  and  $r_{b,p}$ , reach their minimum values,  $r_{b,g}^{\min}$  and  $r_{b,p}^{\min}$ , correspondingly. The minimum values,  $r_{b,g}^{\min}$  and  $r_{b,p}^{\min}$ , of the base radii,  $r_{b,g}$  and  $r_{b,p}$ , are the smallest physically possible.

Second, assume that the base radius of the gear,  $r_{b,g}$ , and the base radius of the mating pinion,  $r_{b,p}$ , are equal to their critical values,  $r_{b,g}^{\min}$  and  $r_{b,p}^{\min}$ , or slightly greater. As shown in Figure 6.8, the pitch radii,  $r_g$  and  $r_p$ , of the gear and the mating pinion relate to each other as  $r_g < r_p$ , that is, inversely to that, which is observed in parallel-axes gearing of conventional design ( $r_g > r_p$ ).

Third, the pitch circles of the radii,  $r_g$  and  $r_p$ , correspondingly, contact one another at point,  $P^*$ , and not at the pitch point,  $P$ .

Ultimately, in the internal gear pair shown in Figure 6.8, the rotations,  $\omega_g$  and  $\omega_p$ , of the gear and the mating pinion are opposite one another.

The gear and the pinion tooth flanks interact with one another out of the pitch point; that is, the contact point is never coincident with the pitch point. Because of this, the gearing under consideration is referred to as the *out-of-pitch-point mesh gearing*.

\* It is instructive to point out here that the tooth flanks of a gear,  $\mathcal{G}$ , and a mating pinion,  $\mathcal{P}$ , are not constructed yet.

† The linear velocity,  $V_{K,pc}$ , is commonly specified as a product of the rotation,  $\omega_g$  (or  $\omega_p$ ), by the *pitch radius*,  $r_g$  (or  $r_p$ ); that is,  $V_{K,pc} = \omega_g \cdot r_g = \omega_p \cdot r_p$ . It makes sense to specify the linear velocity,  $V_{K,bc}$ , as a product of the rotations,  $\omega_g$  or  $\omega_p$ , by the *base radius*,  $r_{b,g}$  or  $r_{b,p}$ ; that is,  $V_{K,bc} = \omega_g \cdot r_{b,g} = \omega_p \cdot r_{b,p}$ . The magnitude of the linear velocities correlate to one another as  $V_{K,pc} = V_{K,bc} \cdot \cos \phi_t$ .

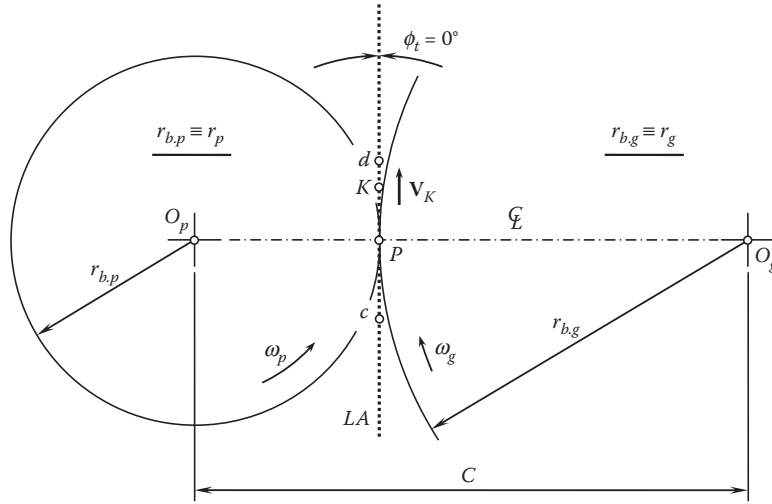


FIGURE 6.7

An external gear-to-pinion mesh with a zero transverse pressure angle,  $\phi_t = 0^\circ$ .

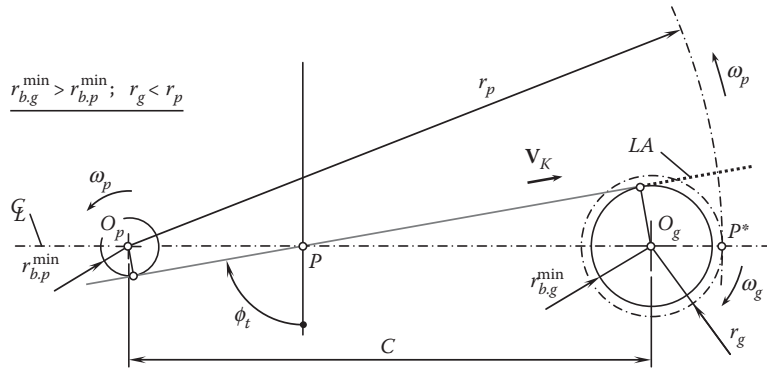


FIGURE 6.8

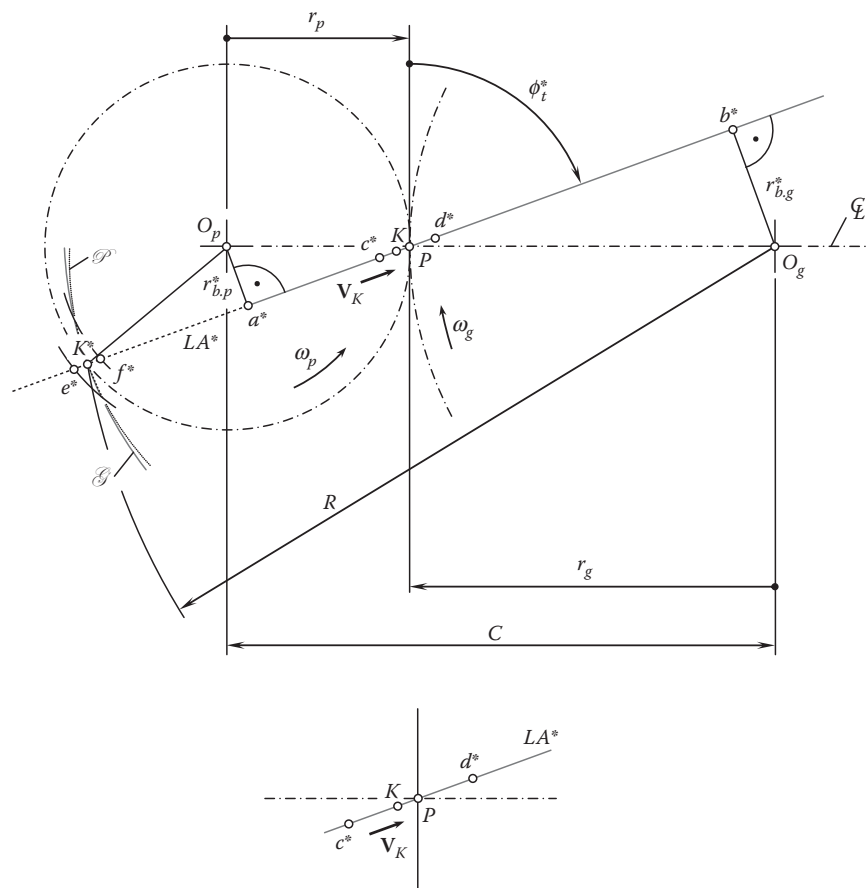
An external gear-to-pinion mesh with a large transverse pressure angle,  $\phi_t$ .

The outlined conditions are necessary but not sufficient to transmit a steady rotation smoothly. This conditions must be complemented by a sufficient total contact ratio in a gear pair. This can be achieved making the teeth of the gear and the mating pinion helical.\*

The transverse pressure angle,  $\phi_t$ , in a gear pair can be of a larger value compared to that shown in Figure 6.6. In Figure 6.9, a schematic of a gear pair with a large pressure angle ( $\phi_t \rightarrow 90^\circ$ ) is depicted. When the transverse pressure angle is large enough, the pinion can be engaged in mesh either with an external or internal gear having that same center distance,  $C$ , in a gear pair. In the first case, the portion,  $c^*d^*$ , of the line of action,  $LA^*$ , is used. In the second case, the portion,  $e^*f^*$ , of the line of action,  $LA^*$ , is used. In both cases, the contact point,  $K$ , travels steadily,  $V_K$ , along the line of action,  $LA^*$ . This means that an internal gear pair could be a *rotationally negative gear pair*. In other words, a change of the direction of the rotation to the opposite direction can be observed not only in external gear pairs, but in internal gear pairs as well.†

\* An active portion of the line of action,  $LA$ , becomes insufficiently short in the gearing under consideration. Therefore, no spur gearing of this type is feasible at all. No pinion-gear-to-rack gearing of this type is feasible. Most of the equations derived for involute gearing are valid for gearing of the type under consideration, as gearing of this type is a reduced case of involute gearing. The concept of this gearing can be enhanced to cases of intersected-axes gearing, as well as crossed-axes gearing.

† A gear pair proposed by Bayazitov and Shitikov [6,149] needs to be mentioned here. An internal gear pair of this type can be rotationally negative, and an external gear pair of this type can be rotationally positive. However, neither the kinematics of the gear pair nor the geometry of gear tooth flanks is correctly specified in the sources [6,149]. A discussion of gearing of this type can also be found in the book [39].



A gear-to-pinion mesh with a large transverse pressure angle,  $\phi_i$ : an external gear-to-pinion mesh within the active portion  $c^*d^*$ , and an internal gear-to-pinion mesh within the active portion  $e^*f^*$  of the line of action,  $LA^*$  (the directions of the rotations,  $\omega_g$  and  $\omega_p$ , remain the same).

$$R = \sqrt{(r_g + r_p)^2 + r_p^2 - 2r_p(r_g + r_p)\cos 2\phi_t} \quad (6.16)$$
$$[\Delta_R] = (C + r_p) - R \quad (6.17)$$
$$[\Delta_R]_{\max} \leq b_p \quad (6.18)$$

\* In addition to the contact point,  $K^*$ , being located far from the contact point,  $K$ , the pitch circles of the gear and its mating pinion remain the same even in cases of large values of the transverse pressure angle,  $\phi_t$ .



The smallest value of the transverse pressure angle,  $\phi_t$ , occurs when the difference,  $[\Delta_R]$ , is of the largest permissible value,  $[\Delta_R]_{\max}$ . With this value of the difference,  $[\Delta_R]_{\max}$ , the minimal permissible value of the transverse pressure angle can be calculated from:

$$[\phi_t]_{\min} = \frac{1}{2} \cos^{-1} \frac{(r_g + r_p)^2 + r_p^2 - (C + r_p - [\Delta_R]_{\max})^2}{2r_p(r_g + r_p)} \quad (6.19)$$

This equation casts into the formula for  $[\phi_t]_{\min}$ :

$$[\phi_t]_{\min} = \frac{1}{2} \cos^{-1} \frac{(u + 1)^2 + 1 - (1 + (C/r_p) - ([\Delta_R]_{\max}/r_p))^2}{2(u + 1)} \quad (6.20)$$

where  $u = r_g/r_p$  is the gear ratio of the gear pair.

Under the assumption that the difference,  $[\Delta_R]$ , equals the pinion module,  $m$ , Equation 6.20 casts into the formula:

$$\phi_{t,m} = \frac{1}{2} \cos^{-1} \frac{(u + 1)^2 + 1 - (1 + (C/r_p) - (m/r_p))^2}{2(u + 1)} \quad (6.21)$$

Use of this formula is helpful for determining favorable values of the angular velocity ratio,  $u$ , at which the rest of the design parameters of the gear pair (especially the transverse pressure angle,  $\phi_t$ ) are also of favorable values.

The determination of the maximum permissible value,  $[\phi_t]_{\max}$ , of the transverse pressure angle,  $\phi_t$ , is discussed above in this chapter. Ultimately, the actual value of the transverse pressure angle,  $\phi_t$ , has to be the interval specified immediately below:

$$[\phi_t]_{\min} \leq \phi_t \leq [\phi_t]_{\max} \quad (6.22)$$

It is clear from the analysis of Equation 6.20 that rotationally negative internal gearing is feasible only when the transverse pressure angle,  $\phi_t$ , is of a large enough value.

An example of a rotationally positive parallel-axes external gear pair is depicted in Figure 6.10. As shown in Figure 6.10, the actual value of the transverse pressure angle,  $\phi_t$ , in this particular design is close to  $\sim 90^\circ$ .

After external rotationally positive and internal rotationally negative gearings are incorporated into the analysis, then a corresponding gear pair can be associated with every point of the  $u$ -axis in Figure 6.4 (except a point  $u = 0$ ). Gear pairs feature gear ratios in the intervals  $-\infty \leq u < 0$  and  $0 < u \leq +\infty$ .

External rotationally positive, as well as internal rotationally negative, gear pairs can be also designed for the cases of gearings that operate on intersecting axes and crossing axes of rotation of a gear and a mating pinion.

As both external rotationally positive and internal rotationally negative gear pairs have no extensive application in the current industry, further attention in this monograph is mostly focused on external rotary-negative and internal rotationally positive gear pairs. The first are commonly referred to as *external gear pairs* and the second as *internal gear pairs*.

In addition to the established intervals for the angular velocity ratio ( $-\infty \leq u < 0$  and  $0 < u \leq +\infty$ ), a possibility of variation of the transverse pressure angle,  $\phi_t$ , needs to be considered here. This is especially of importance in order to avoid any confusion with conclusions drawn from the analysis of Figure 5.5.

The illustration below (Figure 6.11) makes clear the feasibility of variation of the transverse pressure angle,  $\phi_t = \text{var}$ , in a case of parallel-axes gearing.

Three parallel-axes gear pairs, 1, 2, and 3, with the same angular velocity ratio,  $u$ , and equal center distance,  $C$ , but with different radii of base cylinders,  $r_{b,g}^{(1)}$  and  $r_{b,p}^{(1)}$  [ $r_{b,g}^{(2)}$  and  $r_{b,p}^{(2)}$ ;  $r_{b,g}^{(3)}$  and  $r_{b,p}^{(3)}$ ], of a gear and its mating pinion rotate about common axes,  $O_g$  and  $O_p$ , with constant angular velocities,  $\omega_g$  and  $\omega_p$  (where  $u = \omega_p/\omega_g$ ). The face widths of the gears is equal to  $F_{pa}^{(1)}$ ,  $F_{pa}^{(2)}$ , and  $F_{pa}^{(3)}$  correspondingly. As the radii of the base cylinders  $r_{b,g}^{(i)}$  and  $r_{b,p}^{(i)}$  in each pair of gears are different (here,  $i = 1, 2, 3$ ), each pair of gears features a specific value of the transverse pressure angle,  $\phi_{t,1}$ ,  $\phi_{t,2}$ , and  $\phi_{t,3}$ , correspondingly. All the planes of action,  $PA_1$ ,  $PA_2$ , and  $PA_3$ , are the planes through the axis of instant rotation,  $P_{lv}$ , at a corresponding transverse pressure angle,  $\phi_{t,i}$ . In the upper

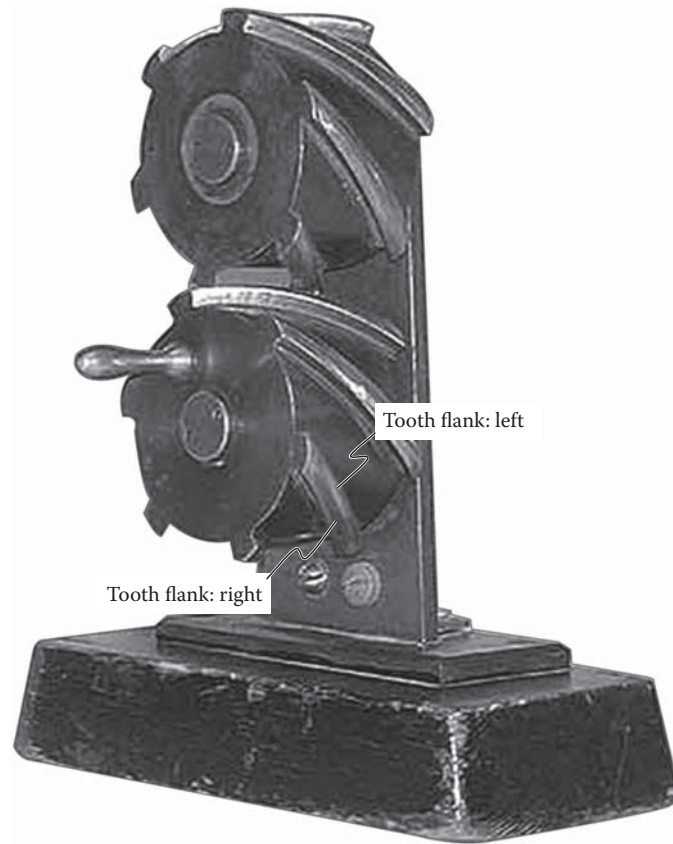


**FIGURE 6.10**  
Rotationally positive external parallel-axes gear pair.

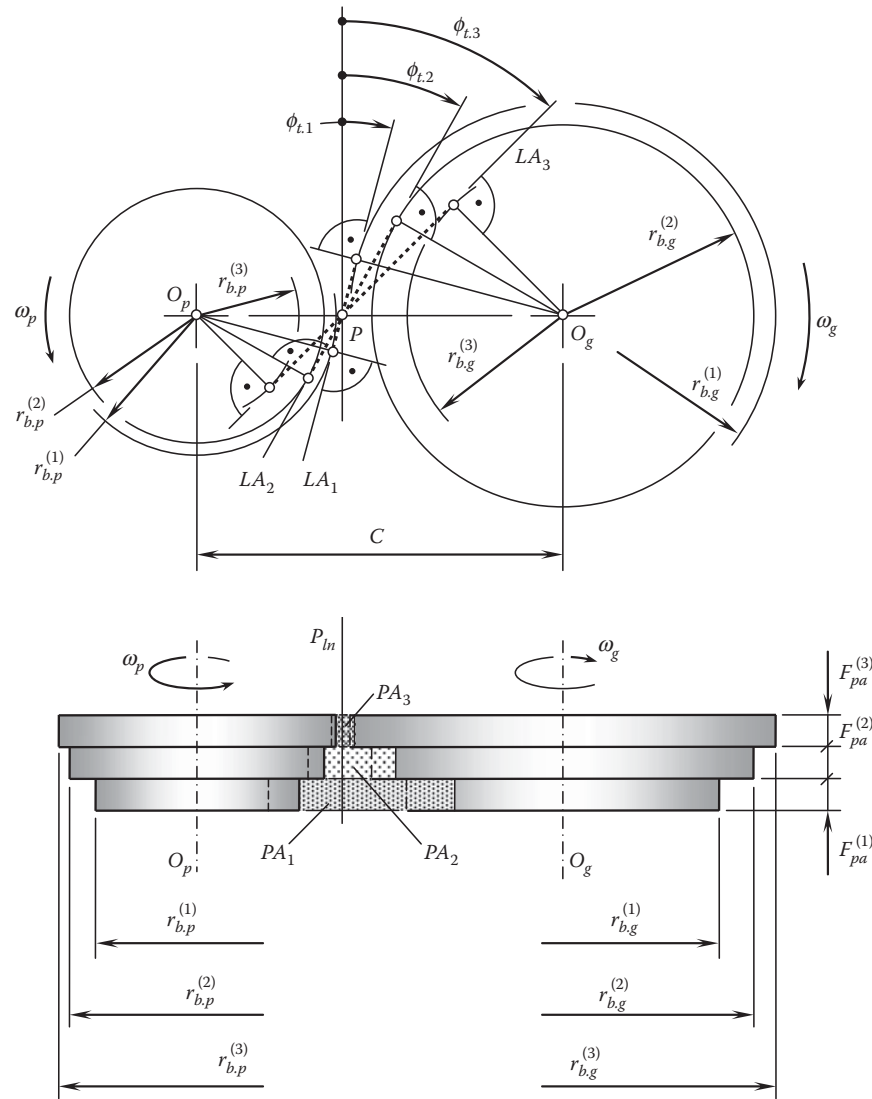
portion of [Figure 6.11](#), the planes of action,  $PA_1$ ,  $PA_2$ , and  $PA_3$ , are projected into the corresponding lines of action,  $LA_1$ ,  $LA_2$ , and  $LA_3$ .

When the gears rotate, the gears in each of the gear pairs 1, 2, and 3 are motionless in relation to one another, as each of the gear pairs features an equal angular velocity ratio,  $u$ . Each of the gears can be subdivided into an infinite number of infinitesimally narrow ( $dF_{pa}$ ) round strips. The transverse pressure angle,  $\phi_t$ , can be set to a different value for each of the strips. In this way, a gear pair with a variable (along the axis of instant rotation,  $P_{ln}$ ) value of the transverse pressure angle,  $\phi_t$ , can be designed.\*

## 6.2 Tooth Flank Generation

In parallel-axes gearing, the tooth flanks of a gear and its mating pinion,  $\mathcal{G}$  and  $\mathcal{P}$ , interact with one another similarly to how the working surfaces in a cam mechanism interact. In order to transmit a uniform rotation smoothly by means of a gear pair, an appropriate geometry of the tooth flanks,  $\mathcal{G}$  and  $\mathcal{P}$ , is required to be reproduced in the gear and in the pinion. To generate the tooth flanks,  $\mathcal{G}$  and  $\mathcal{P}$ , in a *perfect gear pair* (or *geometrically accurate gear pair* or *ideal gear pair*) the discussed in the previous sections, the pulley-and-belt analogy of a gear pair is used. The difference between transmission of rotational motion by a *gear pair* and pulley-and-belt is just the following: in a belt-and-pulley mechanism, the driving pulley *pulls* the driven pulley, while in a gear pair, the driving gear *pushes* the driven gear. With that said, a desirable line of contact between the tooth flanks in the gear pair can be used for the generation of the tooth flanks,  $\mathcal{G}$  and  $\mathcal{P}$ , of a gear and its mating pinion. The

\* This analysis is helpful for understanding of a feasibility of a variable (along the axis of instant rotation,  $P_{ln}$ ) transverse pressure angle,  $\phi_t$ , in cases of intersected-axes gearings, as well as in crossed-axes gearings.

**FIGURE 6.11**

A possibility of a continuous alteration of the transverse pressure angle,  $\phi_t$ , along the axis of instant rotation,  $P_{ln}$ , in a parallel-axes gear pair with a constant gear ratio,  $u$ .

desirable line of contact is a planar curve that is entirely located within the plane of action of the gear pair, that is, within the plane of the belt in a corresponding belt-and-pulley mechanism.\*

### 6.2.1 Desirable Line of Contact between the Tooth Flanks of a Gear and Its Mating Pinion

It is assumed that for the generation of tooth flanks of a gear and its mating pinion, a corresponding vector diagram of the gear pair is constructed. This follows by the construction of a plane of action,  $PA$ :

#### Definition 6.1

The plane of action,  $PA$ , is a plane through the axis of instant rotation,  $P_{ln}$  (or the same through a line along the vector of instant rotation,  $\omega_{pl}$ ), that forms a transverse pressure angle,  $\phi_t$ , with a normal plane ( $N_{ln}$ -plane).

Configuration of the  $N_{ln}$ -plane in relation to other elements of the vector diagram is shown in [Figure 3.11](#).

\* This discussion makes clear why so much attention is given in the previous sections to the detailed consideration of the pulley-and-belt analogy of a gear pair.

### Definition 6.2

*The line of action,  $LA$ , in parallel-axes gearing is an intersection of the plane of action,  $PA$ , by a transverse plane of the gear pair.*

The line of action,  $LA$ , is a straight line that is entirely located within the transverse plane of the gear pair, as it is a line of intersection of the plane of action by the transverse plane of the gear pair.

It is instructive to stress here that the line of action,  $LA$ , is always a straight line, as a force vector of interaction between the gear tooth flanks,  $\mathcal{G}$  and  $\mathcal{P}$ , is along a straight line, and it cannot be a curve.

The plane of action,  $PA$ , can be construed as a family of all the lines of action considered in all possible transverse sections of a gear pair.\* In a particular case, the plane of action can also be construed as a plane that is generated by the line of action,  $LA$ , that travels along the axis of instant rotation,  $P_{ln}$ , and remains parallel to itself.

The plane of action,  $PA$ , is tangent to the base cylinders<sup>†</sup> of a gear and a mating pinion.

### Definition 6.3

*The base cylinder of a gear is a cylinder of revolution that is generated as an envelope to consecutive positions of the plane of action,  $PA$ , in its rotary motion in relation to a reference system associated with the gear when the gears rotate.*

### Definition 6.4

*The base cylinder of a pinion is a cylinder of revolution that is generated as an envelope to consecutive positions of the plane of action,  $PA$ , in its rotary motion in relation to a reference system associated with the pinion when the gears rotate.*

For the generation of tooth flanks of a gear,  $\mathcal{G}$ , and its mating pinion,  $\mathcal{P}$ , a desirable line of contact,  $LC_{des}$ , between the tooth flanks,  $\mathcal{G}$  and  $\mathcal{P}$ , is used. Note: no gear and pinion tooth flanks,  $\mathcal{G}$  and  $\mathcal{P}$ , are generated yet, but a desirable line of their contact,  $LC_{des}$ , is already introduced and is used for the generation of the tooth flanks,  $\mathcal{G}$  and  $\mathcal{P}$ .

### Definition 6.5

*A desirable line of contact,  $LC_{des}$ , between the tooth flanks,  $\mathcal{G}$  and  $\mathcal{P}$ , of a gear and its mating pinion is a planar curve that is entirely located within the plane of action,  $PA$ , and possesses the desired properties that make a favorable design of the gear pair possible.*

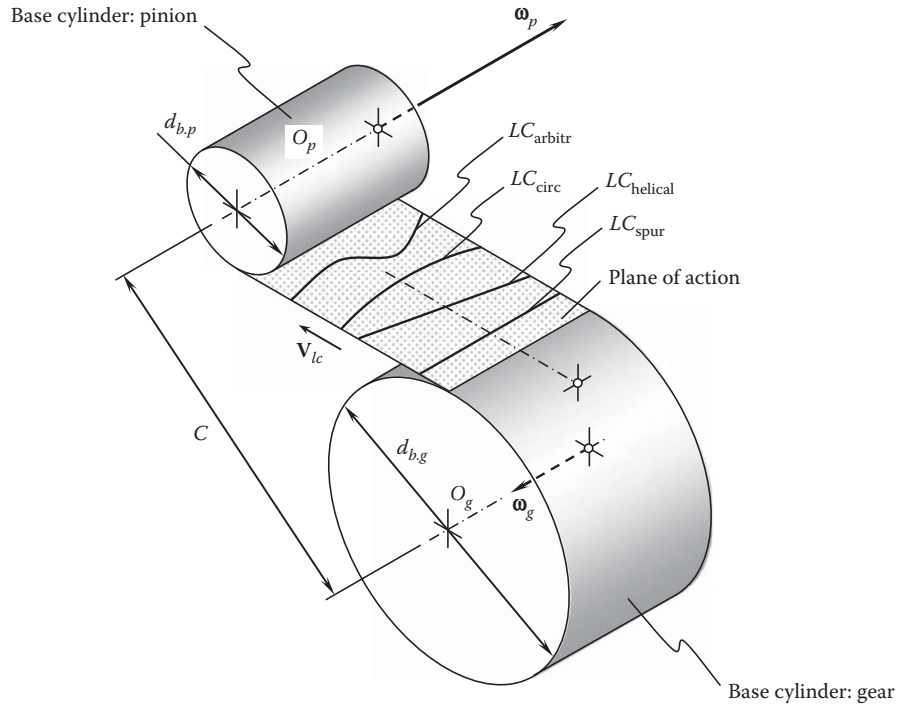
A straight line is commonly used as a desirable line of contact,  $LC_{des}$ , between the tooth flanks of a gear,  $\mathcal{G}$ , and a mating pinion,  $\mathcal{P}$ . The desirable line of contact,  $LC_{des}$ , (or simply *line of contact*,  $LC$ ), is located within the plane of action,  $PA$ . The line of contact is associated with the plane of action. When the plane of action,  $PA$ , unwraps from the base cylinder of the driving member and wraps over the base cylinder of the driven member of the gear pair, the line of contact travels together with the plane of action (and is stationary in relation to the plane of action,  $PA$ ).

The straight line of contact can be parallel to the axis of instant rotation,  $P_{ln}$  (or, the same, parallel to the axes of rotation of both the gear and the mating pinion). Under such a scenario, the tooth flanks of a spur gear and spur pinion are generated by the line of contact,  $LC_{spur}$ , as illustrated in Figure 6.12. When the line of contact,  $LC_{helical}$ , is at a certain angle in relation to the axis of instant rotation,  $P_{ln}$ , the tooth flanks of the helical gear and helical pinion are generated. Actually, any planar curve,  $LC_{arbitr}$ , of a reasonable geometry can be used as a line of contact,  $LC$ , in parallel-axes gearing.

Among other planar curves, a circular arc,  $LC_{circ}$ , can be used as the desirable line of contact in a gear pair that operates on parallel axes of rotation of the gear and the pinion. The tooth flanks of the gear and pinion of such a geometry can be machined either with a face-milling cutter or a face hob. In both cases, the gear-cutting tool to

\* In a more general case of parallel-axes gearing (see Figure 6.11), not a plane of action,  $PA$ , but a *surface of action*,  $SA$  is observed instead. The surface of action,  $SA$ , is a kind of ruled surface through the axis of instant rotation,  $P_{ln}$ .

† Parallel-axes gearing, schematically illustrated in Figure 6.11, features *base surfaces* of the gear and its mating pinion, and not base cylinders. The base surface in the case under consideration is a kind of surface of revolution.

**FIGURE 6.12**

Generation of tooth flank of an involute gear with an arbitrary tooth shape in the lengthwise direction.

be implemented must have a zero profile angle of its teeth. Otherwise (when the profile angle,  $\phi_t$ , of the gear-cutting tool is not equal to zero,  $\phi_t \neq 0$ ), the gear pair cannot be workable at all. The main reason for that is discussed immediately below.

It is important to stress here that neither the geometry of the desired line of contact,  $LC_{des}$ , nor its configuration in relation to the plane of action,  $PA$ , is allowed to alter when generating gear,  $\mathcal{G}$ , and mating pinion,  $\mathcal{P}$ , tooth flanks. This feature of the line of contact,  $LC_{des}$ , needs to be taken into account when developing novel methods of gear cutting, gear inspection, and so forth.

Commonly, practicality is the main constraint on the shape of the desirable line of contact,  $LC_{des}$ , between the tooth flanks,  $\mathcal{G}$  and  $\mathcal{P}$ , of a gear and its mating pinion.

### 6.2.2 Line of Action and Path of Contact in a Gear Pair

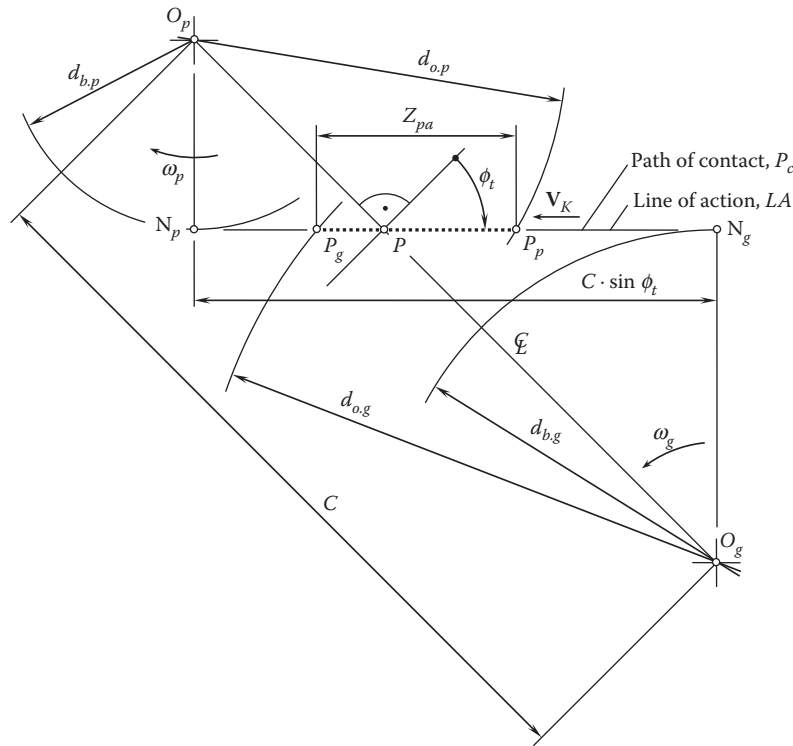
A parallel-axes gearing is schematically shown in Figure 6.13. The gear and pinion rotate about their axes of rotation,  $O_g$  and  $O_p$ , with angular velocities,  $\omega_g$  and  $\omega_p$ , respectively. The axes rotation,  $O_g$  and  $O_p$ , are at a center distance,  $C$ , apart from one another. The base diameter of the gear is designated as  $d_{b,g}$ , and the base diameter of the pinion is designated as  $d_{b,p}$ . The outer diameters of the gear and the pinion are designated as  $d_{o,g}$  and  $d_{o,p}$  correspondingly. In compliance with the pulley-and-belt analogy of a gear pair, the line of action,  $LA$ , between the tooth flanks,  $\mathcal{G}$  and  $\mathcal{P}$ , of a gear and mating pinion is in tangency to both the base circle of the gear and the base circle of the pinion. Points of tangency are labeled as  $N_g$  and  $N_p$ , respectively.

The line of action,  $LA$ , intersects the centerline,  $\mathcal{C}$ , at the pitch point,  $P$ . (The center distance,  $C$ , is a straight line segment of the centerline,  $\mathcal{C}$ .)

Points of intersection,  $P_g$  and  $P_p$ , of the line of action,  $LA$ , by the circles of the outer diameters,  $d_{o,g}$  and  $d_{o,p}$ , are the extreme points of the active portion,  $Z_{pa}$ , of the line of action,  $LA$  (i.e.,  $P_g P_p = Z_{pa}$ ).

A perpendicular through the pitch point,  $P$ , to the centerline,  $\mathcal{C}$ , forms the transverse pressure angle,  $\phi_t$ , with the line of action,  $LA$ .

When the gears rotate, the transverse pressure angle,  $\phi_t$ , has a constant value at every instant of time; that is, it is of a constant value for all configurations of the gear and the pinion in their relation to each other. Therefore, when the gears steadily rotate with the rotations,  $\omega_g$  and  $\omega_p$ , the contact point,  $K$ , between the tooth flanks,  $\mathcal{G}$  and  $\mathcal{P}$ , travels along the straight path of contact,  $P_c$ , with a constant linear velocity,  $V_K$ . When one or both of the


**FIGURE 6.13**

In involute gearing, the line of action,  $LA$ , and the path of contact,  $P_c$ , align with each other.

motions (either the rotations,  $\omega_g$  and  $\omega_p$ , or the translation,  $\mathbf{V}_K$ ) is not steady, the contact point traces a path of contact,  $P_c$ , in the form of a planar curve of a certain geometry and is entirely located in a transverse section of the gear pair. In the latter case, no transmission of a smooth rotation is feasible.

### Definition 6.6

The path of contact,  $P_c$ , in parallel-axes gearing is a planar curve that is traced by the contact point in the motionless transverse section of a gear pair.

The path of contact,  $P_c$ , is entirely located in a corresponding transverse section of the gear pair.

A family of all the paths of contact,  $P_c$ , in a particular gear pair form a *path-of-contact surface*,  $S_c$  (or just *PCS*, for simplicity). When the transverse pressure angle,  $\phi_t$ , is of a constant value ( $\phi_t = \text{const}$ ) within the plane-of-action face width,  $F_{pa}$ , the *path-of-contact surface* is shaped in the form of a plane through the axis of instant rotation,  $P_{ln}$ . When the transverse pressure angle,  $\phi_t$ , varies within the plane-of-action face width,  $F_{pa}$ , a continuous set of the straight-line paths of contact,  $P_c$ , at different transverse pressure angle,  $\phi_t$ , each form the path-of-contact surface in the form of a right angle *helicoid*.

When the path of contact is aligned with the line of action,  $LA$ , the tooth flank geometry generated in this manner is unique. Tooth profiles generated in other manners than that just mentioned are not capable of transmitting an input rotation smoothly.

Consider a schematic diagram of parallel-axes gearing that features a curved path of contact,  $P_c$ , as shown in Figure 6.14. The gear and pinion rotate about their axes of rotation,  $O_g$  and  $O_p$ , with angular velocities,  $\omega_g$  and  $\omega_p$ , correspondingly. The axes,  $O_g$  and  $O_p$ , are at a certain center distance,  $C$ , apart from each another. The pitch point,  $P$ , is at a distance,  $r_g$ , from the gear axis of rotation,  $O_g$ , and at a distance,  $r_p$ , from the pinion axis of rotation,  $O_p$ . The transverse pressure angle at the pitch point,  $P$ , is denoted by  $\phi_t$ .

Let us assume that the gear and its mating pinion rotate so that a curved path of contact,  $P_c$ , is traced by contact point,  $K$ . At every point of the path of contact,  $P_c$ , a corresponding *instant line of action*,  $LA_{\text{inst}}$  can be constructed.

An arbitrary contact point within the path of contact,  $P_c$ , is labeled as  $K^{(i)}$ . When the gear and the mating pinion make contact at point  $K^{(i)}$ , the instant line of action,  $LA_{\text{inst}}^{(i)}$ , is in tangency to the path of contact,  $P_c$ , at  $K^{(i)}$ . This

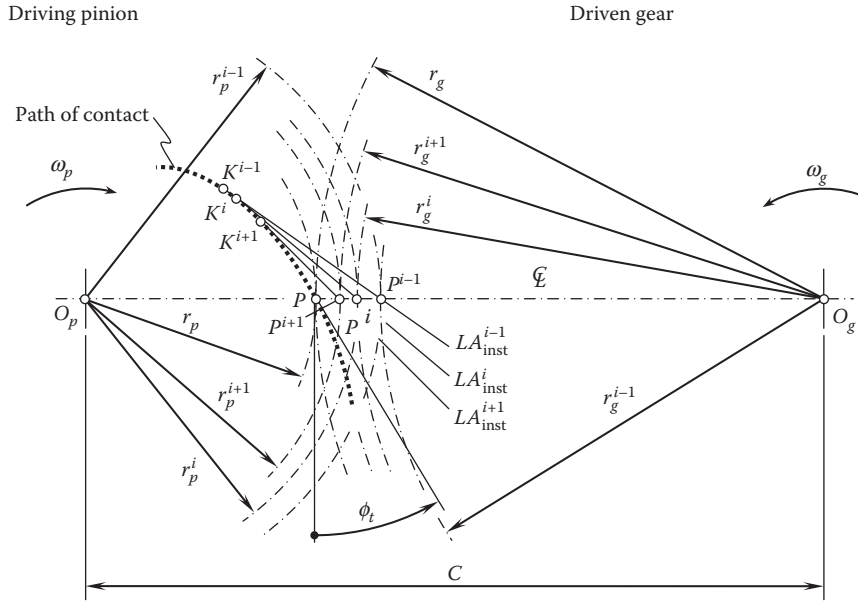


FIGURE 6.14

Schematic diagram of parallel-axes gearing that features a curved path of contact,  $P_c$ .

is because the force of the interaction between the tooth flanks of the driving and the driven gears is along the common perpendicular to the interacting tooth profiles considered in a transverse section of a gear pair, or, the same, the force is along a straight line tangent at contact point  $K^{(i)}$  to the path of contact,\*  $P_c$ .

A few definitions can be drawn up from the above discussion:

#### Definition 6.7

The instant line of action,  $LA_{inst}$ , is a straight line along the common perpendicular,  $\mathbf{n}$ , to the tooth flanks,  $\mathcal{G}$  and  $\mathcal{P}$ , of a gear and a mating pinion at point  $K$  of their contact.

#### Definition 6.8

The instant pitch point,  $P_{inst}$ , is a point of intersection of the centerline,  $\mathcal{C}$ , by the instant line of action,  $LA_{inst}$ .

#### Definition 6.9

The path of contact,  $P_c$ , is a ruled surface composed of consecutive positions of the instant lines of action,  $LA_{inst}$ .

The line of action,  $LA$ , and the path of contact,  $P_c$ , align with each other only in cases of perfect parallel-axes involute gearing.<sup>†</sup>

As the instantaneous line of action,  $LA_{inst}^{(i)}$ , intersects the centerline,  $\mathcal{C}$ , at the instant pitch point,  $P^{(i)}$ , the instant gear ratio,  $u_{inst}^{(i)}$ , at this instant of time can be specified in terms of the instant radii,  $r_g^{(i)}$  and  $r_p^{(i)}$ , of the gear and the mating pinion:

$$u_{inst}^{(i)} = \frac{r_g^{(i)}}{r_p^{(i)}} \quad (6.23)$$

\* It is the right point to stress here that it is incorrect to interpret the line of action,  $LA$ , as a straight line perpendicular to the tooth flanks,  $\mathcal{G}$  and  $\mathcal{P}$ , of a gear and a mating pinion at contact point,  $K$  (nonspur gear pairs). The line of action,  $LA$ , should be considered a line within the transverse section plane that, in the case of  $P_a$ -gearing, is perpendicular to the axes of rotation,  $O_g$  and  $O_p$ , of the gear and the pinion.

† In the rest of the cases of  $P_a$ -gearing (cycloid gear pairs and so forth), as well as in all cases of  $I_a$ -gearing, as well as of  $C_a$ -gearing, (a) the line of action,  $LA$ , does not exist, and (b) the instant line of action,  $LA_{inst}$  and the path of contact,  $P_c$ , do not align with one another.



As the path of contact,  $P_c$ , is not a straight line, the instant pitch point,  $P^{(i)}$ , is not coincident with the nominal pitch point,  $P$ . Therefore, the instant gear ratio (angular velocity ratio, in other words),  $u_{\text{inst}}^{(i)}$ , is not equal to the nominal gear ratio:

$$u_{\text{inst}}^{(i)} \neq u = \frac{r_g}{r_p} \quad (6.24)$$

A similar analysis can be performed for other contact points,  $K^{(i-1)}$  and  $K^{(i+1)}$ , within the path of contact,  $P_c$ . Without going into the details of the analysis, it can be stated that in all the contact points under consideration,  $K^{(i-1)}$ ,  $K^{(i)}$ , and  $K^{(i+1)}$ , the following inequality is valid:

$$u_{\text{inst}}^{(i-1)} \neq u_{\text{inst}}^{(i)} \neq u_{\text{inst}}^{(i+1)} \neq u = \frac{r_g}{r_p} \quad (6.25)$$

It is clear from the above-performed analysis that no smooth transmission of a steady rotation is feasible by means of parallel-axes gearing that features a curved path of contact,  $P_c$ .

A conclusion can be drawn up from the analysis given in [Figure 6.14](#).

### Theorem 6.1

*To transmit a uniform rotary motion from a driving shaft to a driven shaft by means of gear teeth, perpendiculars to the tooth flanks of the interacting teeth at all points of their contact must pass through a stationary point within the centerline of the two shafts.*

This conclusion in nature is the *fundamental theorem of conjugate gear tooth surfaces for parallel-axes gearing with a constant gear ratio* (or *CES-fundamental theorem for parallel-axes gearing*).

Theorem 6.1 immediately follows from the second fundamental law of gearing and obeys the analytical expression:  $\mathbf{p}_m \times \mathbf{V}_m \cdot \mathbf{n}_g = 0$ .

As shown below in this section, only involute gearing features a straight line of action,  $LA$ , and a straight path of contact,  $P_c$ , that align with one another. In other systems of gearing, (a) the line of action,  $LA$ , does not exist; and (b) the instant line of action,  $LA_{\text{inst}}$  (i.e., still a straight line) and the path of contact,  $P_c$  (that could be a planar curve) need to be distinguished from one another.

### 6.2.3 Operating Base Pitch in a Gear Pair

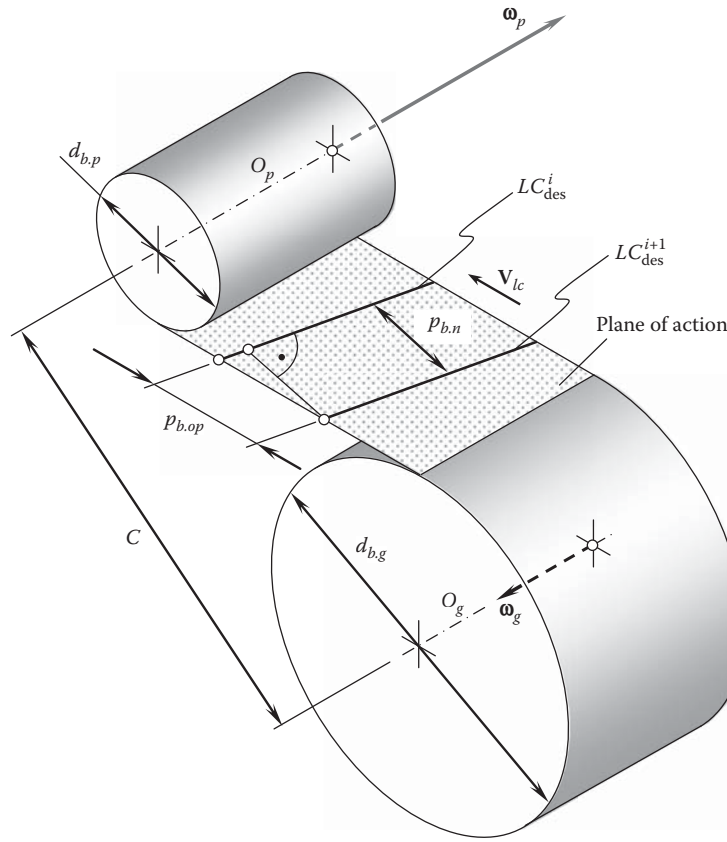
The concept of *base pitch* is introduced to perfect parallel-axes gearing because of the following. When the gears rotate, two (or even more) pairs of teeth can be engaged in mesh at that same time. In order to keep all the gear pairs in contact, the gear teeth, as well as the pinion teeth, must be located at certain distances from one another. Otherwise, only one pair of teeth is engaged in mesh, while a gap will be observed between the other pairs of teeth. This distance is specified by:

- The *operating base pitch* of a gear pair
- The *gear base pitch* for a gear
- The *pinion base pitch* for a mating pinion

Let us consider two neighboring lines of contact in a parallel-axes gear pair as illustrated in [Figure 6.15](#). The axis of rotation of the gear,  $O_g$ , and that of the pinion,  $O_p$ , are parallel to each other and are at a center distance,  $C$ , apart from one another. The base cylinder of a diameter,  $d_{b,g}$ , is associated with the gear. Similarly, the base cylinder of a diameter,  $d_{b,p}$ , is associated with the pinion. The plane of action,  $PA$ , in an external parallel-axes gear pair is tangent to the base cylinders from the opposite sides. The gear and the pinion,  $\omega_g$  and  $\omega_p$ , rotate about their axes of rotation. The magnitudes,  $\omega_g$  and  $\omega_p$ , of the rotations,  $\omega_g$  and  $\omega_p$ , are synchronized with one another reciprocal to the tooth count,  $N_g$  and  $N_p$ , of the gear and the pinion; that is, the ratio:

$$\frac{\omega_g}{\omega_p} = \frac{N_p}{N_g} \quad (6.26)$$

is valid in *perfect* parallel-axes gearing.

**FIGURE 6.15**

Definition of the operating base pitch,  $p_{b,op}$  in perfect parallel-axes gearing.

When the gears rotate, the plane of action is considered a zero-thickness film that is unwrapping from the base cylinder of the gear and wrapping onto the base cylinder of the pinion, or vice versa. In such a motion, the plane of action,  $PA$ , travels with a linear velocity,  $V_{lc}$ . The magnitude,  $V_{lc}$ , of the linear velocity,  $V_{lc}$ , is timed with the rotations,  $\omega_g$  and  $\omega_p$ , so as to ensure rolling with no slippage of the plane of action,  $PA$ , over the base cylinders of the gear and the pinion.

A desirable line of contact,  $LC_{des}^i$ , of the  $i$ th pair of teeth of the gear and the pinion is drawn within the plane of action,  $PA$ . As an example, the desirable line of contact,  $LC_{des}^i$ , is shown for a case of helical involute gearing. In the case under consideration, this straight line segment forms the base helix angle,  $\psi_b$ , with the axis of instant rotation,  $P_{ln}$ , or the same with the axes,  $O_g$  and  $O_p$  (the base helix angle,  $\psi_b$ , is not shown in Figure 6.15).

The desirable line of contact,  $LC_{des}^{i+1}$ , of the adjacent  $(i + 1)$ th pair of teeth of the gear and the pinion is parallel to the straight line,  $LC_{des}^i$  (i.e.,  $LC_{des}^{i+1} \parallel LC_{des}^i$ ), and is also located within the plane of action,  $PA$ .

Measured in a common transverse section of the gear pair, the distance,  $p_{b,op}$ , between two adjacent desirable lines of contact,  $LC_{des}^i$  and  $LC_{des}^{i+1}$ , is referred to as the operating base pitch of the gear pair.\*

### Definition 6.10

The operating base pitch,  $p_{b,op}$ , in a perfect parallel-axes gear pair is a linear distance between each two neighboring desirable lines of contact,  $LC_{des}^i$  and  $LC_{des}^{i+1}$ , measured in a section of the plane of action by a transverse plane.

\* It is also important to stress here that the operating base pitch of a gear pair,  $p_{b,op}$ , is measured in linear units only in cases of perfect parallel-axes gear pairs. In cases of intersected-axes and crossed-axes perfect gearings, the angular operating base pitch of a gear pair,  $\varphi_{b,op}$ , is measured in angular units. Moreover, if the axis misalignment is taken into account, then the angular operating base pitch of a gear pair,  $\varphi_{b,op}$ , is measured in angular units in all cases, that is, in cases of parallel-axes gearings, intersected-axes gearings, and crossed-axes gearings.

Only *conjugate* gear tooth profiles (gear tooth flanks) feature the base pitch. The base pitch cannot be specified for nonconjugate gear tooth profiles (gear tooth flanks); that is, the base pitch cannot be specified for cycloidal gearing and so forth.

The operating base pitch\* of a gear pair is a calculated design parameter of a gear pair. It cannot be measured directly in a gear pair. In a perfect parallel-axes gearing, the operating base pitch of a gear pair is equal to:

$$p_{b.op} = \frac{\pi d_{b.g}}{N_g} \quad (6.27)$$

where  $d_{b.g}$  is the gear base diameter and  $N_g$  is the gear tooth count.

Note, that the operating base pitch in a perfect parallel-axes gear pair is introduced *prior to (!)* the gear and mating pinion tooth flanks,  $\mathcal{G}$  and  $\mathcal{P}$ , being determined.

The operating base pitch of a gear pair can be also expressed in terms of the pinion base diameter,  $d_{b.p}$ , and the pinion tooth count,  $N_p$ ; that is:

$$p_{b.op} = \frac{\pi d_{b.p}}{N_p} \quad (6.28)$$

In a perfect parallel-axes gear pair, the following three identities are observed:

- The base pitch of a gear,  $p_{b.g}$ , is identical to an operating base pitch,  $p_{b.op}$ , of the gear pair (i.e., an identity  $p_{b.g} \equiv p_{b.op}$  is valid).
- The base pitch of a mating pinion,  $p_{b.p}$ , is identical to an operating base pitch,  $p_{b.op}$ , of the gear pair (i.e., an identity  $p_{b.p} \equiv p_{b.op}$  is valid).
- Ultimately, the base pitch of the gear,  $p_{b.g}$ , is identical to base pitch of the pinion,  $p_{b.p}$ , and both of them are identical to the operating base pitch,  $p_{b.op}$ , of the gear pair (i.e., the identity  $p_{b.g} \equiv p_{b.p} \equiv p_{b.op}$  is valid).

Therefore, the condition of equal base pitches in perfect parallel-axes gearing discussed in Section 6.6.2.3 can now be enhanced and formulated as follows:

### Definition 6.11

*Condition of equal base pitches (in perfect parallel-axes gearing): In parallel-axes gearing, in order to transmit a uniform rotary motion from a driving shaft to a driven shaft by means of gear teeth, at every instant of time, the following three conditions must be fulfilled:*

- The base pitch of a gear,  $p_{b.g}$ , must equal the operating base pitch,  $p_{b.op}$ , of the gear pair ( $p_{b.g} \equiv p_{b.op}$ ).
- The base pitch of a mating pinion,  $p_{b.p}$ , must equal the operating base pitch,  $p_{b.op}$ , of the gear pair ( $p_{b.p} \equiv p_{b.op}$ ).
- Both of them,  $p_{b.g}$  and  $p_{b.p}$ , must be identical to the operating base pitch,  $p_{b.op}$ , of the gear pair ( $p_{b.g} \equiv p_{b.p} \equiv p_{b.op}$ ).

It is critical to notice here that the operating base pitch,  $p_{b.op}$ , of the gear pair is constructed (and specified) *prior* to the interacting tooth flanks,  $\mathcal{G}$  and  $\mathcal{P}$ , of the gear and the mating pinion being generated. The use of such an approach gives an opportunity to design gears with favorable geometry of the tooth flanks. For this purpose, the desirable line of contact,  $LC_{des}$ , between the tooth flanks,  $\mathcal{G}$  and  $\mathcal{P}$ , is used to generate the gear and pinion tooth flanks  $\mathcal{G}$  and  $\mathcal{P}$ .

\* It is known that in a case of parallel-axes gearing, the base pitches of a gear and a mating pinion must be equal to one another. However, nothing has been said so far about the operating base pitch in perfect parallel-axes gearings (the concept of the operating base pitch in perfect parallel-axes gear pair is introduced by Radzevich in [136]). Further, neither the concept of the base pitch of the gear and the pinion in the cases of intersected-axes gearings nor in the cases of crossed-axes gearings has been discussed so far in the public domain. Moreover, the concept of the operating base pitch in the cases of intersected-axes and crossed-axes gearings has not been discussed so far in the public domain. Again, the concept of the operating base pitch in intersected-axes and crossed-axes gearings is introduced for the first time by Radzevich in [136].

In cases of parallel-axes gearings that feature a straight desirable line of contact, the distance between every two adjacent lines of contact,  $LC_{des}$ , can also be specified by the *normal base pitch*,  $p_{b.n}$  (see Figure 6.15). The normal base pitch is measured within the plane of action,  $PA$ , perpendicular to the desirable lines of contact,  $LC_{des}^i$  and  $LC_{des}^{i+1}$ . Normal base pitch,  $p_{b.n}$ , can be specified only for parallel-axes gear pairs with a straight desired line of contact,  $LC_{des}$ . Normal base pitch,  $p_{b.n}$ , is an auxiliary design parameter of a gear pair, which is complementary to the base pitch,  $p_{b.g}$ , measured in a transverse plane section of the gear pair.

As long as the line of contact,  $LC_{des}$ , is rigidly connected to the plane of action,  $PA$ , the base pitch of the gear and the base pitch of the mating pinion are equal to one another. Therefore, when two requirements,  $p_{b.g} = p_{b.op}$  and  $p_{b.p} = p_{b.op}$ , are fulfilled, a gear pair of such a design can be workable. In cases of parallel-axes gearing, the identities  $p_{b.g} \equiv p_{b.op}$  and  $p_{b.p} \equiv p_{b.op}$  (or simply  $p_{b.g} \equiv p_{b.p} \equiv p_{b.op}$ ) are met only for *perfect gearing*, that is, for involute gearing. For any and all types of noninvolute gearings, the identity cannot be fulfilled, and, moreover, the base pitch of the gear and the pinion cannot be specified in noninvolute gearings, while the operating base pitch of the gear pair can be easily determined.

#### 6.2.4 Gear Tooth Flank of a Favorable Geometry: General Approach

When a pair of gears rotate, a desirable line of contact,  $LC_{des}$ , travels straight together with the plane of action,  $PA$ . Then, when the plane of action rolls over the base pitch of the gear, the gear tooth flank,  $\mathcal{G}$ , is generated as a family of consecutive positions of the desirable line of contact,  $LC_{des}$ , in its motion in relation to a reference system associated with the gear. Similarly, when the plane of action rolls over the base pitch of the pinion, the pinion tooth flank,  $\mathcal{P}$ , is generated as a family of consecutive positions of the desirable line of contact,  $LC_{des}$ , in its motion in relation to a reference system associated with the gear. Under such a scenario, the actual line of contact,  $LC$ , between the tooth flanks,  $\mathcal{G}$  and  $\mathcal{P}$ , of a gear and a mating pinion is congruent to the desirable line of contact,  $LC_{des}$ , of these surfaces ( $LC \equiv LC_{des}$ ). As an example, the generation of gear and mating pinion tooth flanks,  $\mathcal{G}$  and  $\mathcal{P}$ , is illustrated in Figure 6.16 in the case when the desirable line of contact,  $LC_{des}$ , is a the straight line segment rigidly associated with the  $PA$ .

The general approach to generating tooth flanks,  $\mathcal{G}$  and  $\mathcal{P}$ , of a favorable geometry in a gear pair is based on the consideration of a current configuration of the desirable line of contact,  $LC_{des}$ , in the reference systems

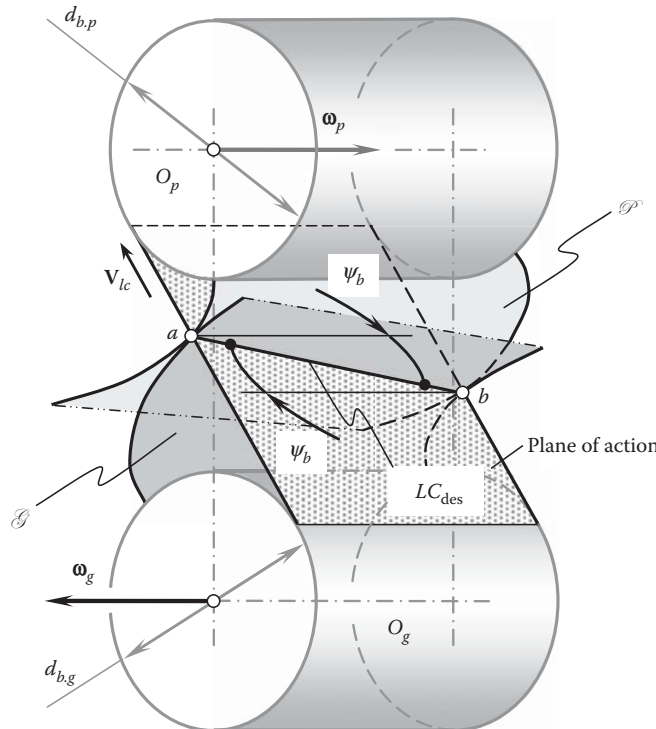
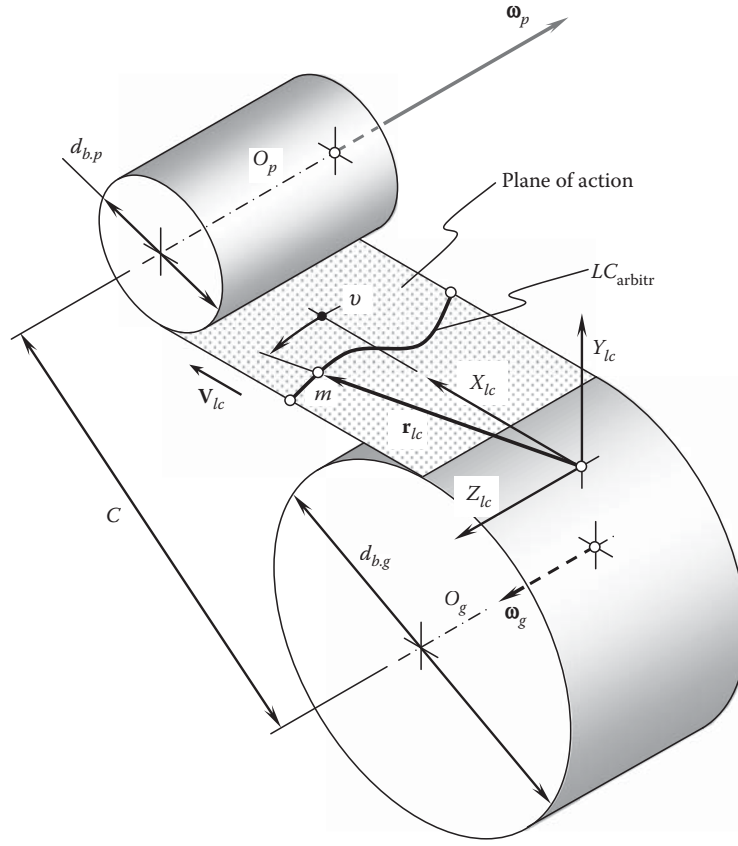


FIGURE 6.16

Generation of screw involute surfaces of the tooth flanks,  $\mathcal{G}$  and  $\mathcal{P}$ , of a pair of helical gears.


**FIGURE 6.17**

Schematics of generation of a tooth flank of a perfect gear for parallel-axes gearing: general approach.

associated with the gear and its mating pinion, correspondingly. The earlier discussed results are helpful in this analysis. Let's begin the consideration with the generation of tooth flanks of a gear and a mating pinion that are generated by a line of contact,  $LC_{arbitr}$ , of an arbitrary geometry.

In a *Cartesian* coordinate system,  $X_{lc}Y_{lc}Z_{lc}$ , associated with the plane of action,  $PA$ , as shown in Figure 6.17, the position vector,  $\mathbf{r}_{lc,arbitr}$ , of a point of interest,  $m$ , within the line of contact,  $LC_{arbitr}$ , allows for matrix representation in a form:

$$\mathbf{r}_{lc,arbitr}(v) = \begin{bmatrix} r_{lc}(v) \cdot \sin v \\ r_{lc}(v) \cdot \cos v \\ 0 \\ 1 \end{bmatrix} \quad (6.29)$$

In Equation 6.29, the distance of point  $m$  within the line of contact,  $LC_{arbitr}$ , from the origin of the coordinate system,  $X_{lc}Y_{lc}Z_{lc}$ , is denoted by  $r_{lc,arbitr} = |\mathbf{r}_{lc,arbitr}|$ , and  $v$  is the angle that the position vector,  $\mathbf{r}_{lc,arbitr}$ , forms with the  $X_{lc}$ -axis. The actual value of the distance,  $r_{lc,arbitr}$ , is a function of the angle,  $v$ ; that is, the equality  $r_{lc,arbitr} = r_{lc,arbitr}(v)$  is valid.

The line of contact,  $LC_{arbitr}$ , travels together with the reference system,  $X_{lc}Y_{lc}Z_{lc}$ , with respect to the stationary Cartesian coordinate system,  $X_{lc}^sY_{lc}^sZ_{lc}^s$  (Figure 6.17). The vector,  $\mathbf{V}_{lc}$ , is the linear velocity vector of such a motion. The distance,  $t$ , that is covered by the reference system,  $X_{lc}Y_{lc}Z_{lc}$ , in its motion with the plane of action,  $PA$ , is measured from the stationary reference system,  $X_{lc}^0Y_{lc}^0Z_{lc}^0$ .

Two more coordinate systems are used for the specification of the tooth flank,  $\mathcal{G}$ , of the gear. The Cartesian coordinate system,  $X_g^sY_g^sZ_g^s$ , is the stationary coordinate system associated with housing of the gear. Ultimately, the Cartesian coordinate system,  $X_gY_gZ_g$ , is associated with the gear itself. This reference system rotates together with the gear.

The tooth flank of the gear,  $\mathcal{G}$ , can be construed as the loci of lines of contact,  $LC_{\text{arbitr}}$ , which are represented in the reference system,  $X_g Y_g Z_g$ . In order to rewrite Equation 6.29 in the coordinate system,  $X_g Y_g Z_g$ , an operator of the resultant coordinate system transformation,  $\mathbf{Rs}(lc \mapsto g)$ , is necessary. The operator,  $\mathbf{Rs}(lc \mapsto g)$ , can be calculated as a product of three corresponding operators of elementary coordinate system transformations:

- The operator of translation,  $\mathbf{Tr}[t(\varphi_g), X_{lc}]$ , from the coordinate system,  $X_{lc} Y_{lc} Z_{lc}$ , to the coordinate system,  $X_{lc}^0 Y_{lc}^0 Z_{lc}^0$
- The operator of translation,  $\mathbf{Tr}(r_{b,g}, Y_{lc}^0)$ , from the coordinate system,  $X_{lc}^0 Y_{lc}^0 Z_{lc}^0$ , to the coordinate system,  $X_g^s Y_g^s Z_g^s$
- The operator of rotation,  $\mathbf{Rt}(\varphi_g, Z_g)$ , of the coordinate system,  $X_g Y_g Z_g$ , in relation to the stationary coordinate system,  $X_g^s Y_g^s Z_g^s$

The operator of translation,  $\mathbf{Tr}[t(\varphi_g), X_{lc}]$ , can be calculated as:

$$\mathbf{Tr}[t(\varphi_g), X_{lc}] = \begin{bmatrix} 1 & 0 & 0 & 0.5 d_{b,g} \varphi_g \\ 0 & 1 & 0 & 0 \\ 0 & 0 & 1 & 0 \\ 0 & 0 & 0 & 1 \end{bmatrix} \quad (6.30)$$

The operator of translation,  $\mathbf{Tr}(r_{b,g}, Y_{lc}^0)$  equals (Figure 6.18):

$$\mathbf{Tr}(r_{b,g}, Y_{lc}^0) = \begin{bmatrix} 1 & 0 & 0 & 0 \\ 0 & 1 & 0 & 0.5 d_{b,g} \\ 0 & 0 & 1 & 0 \\ 0 & 0 & 0 & 1 \end{bmatrix} \quad (6.31)$$

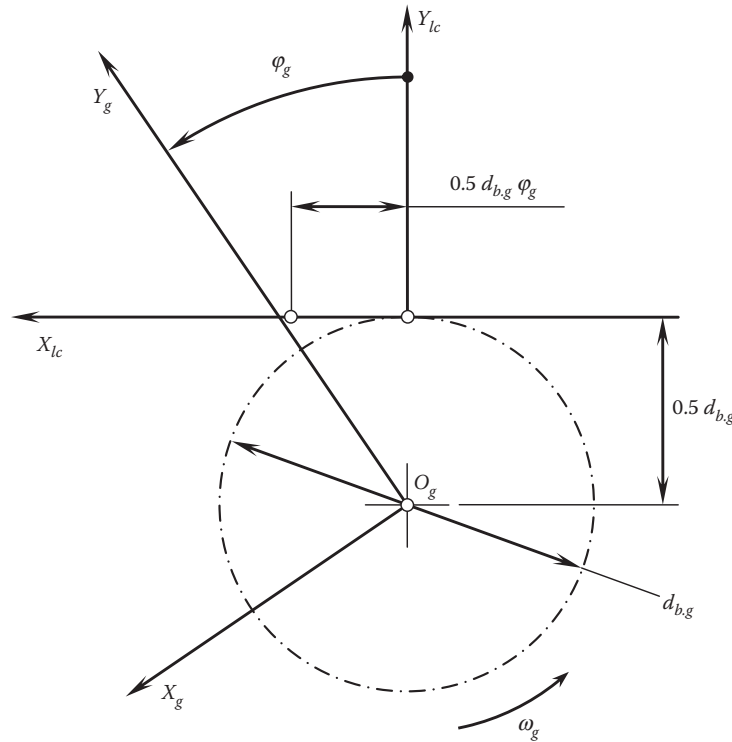


**FIGURE 6.18**  
Schematic of the coordinate systems transformations for parallel-axes gearing.

Ultimately, the following expression can be used for the calculation of the operator of rotation,  $\mathbf{Rt}(\varphi_g, Z_g)$ :

$$\mathbf{Rt}(\varphi_g, Z_g) = \begin{bmatrix} \cos \varphi_g & \sin \varphi_g & 0 & 0 \\ -\sin \varphi_g & \cos \varphi_g & 0 & 0 \\ 0 & 0 & 1 & 0 \\ 0 & 0 & 0 & 1 \end{bmatrix} \quad (6.32)$$

Calculation of operators of translation and rotation is discussed in more detail in Appendix D.

Use of the operators of elementary coordinate system transformations makes it possible to calculate the operator,  $\mathbf{Rs}(lc \mapsto g)$ , of the resultant coordinate system transformation:

$$\mathbf{Rs}(lc \mapsto g) = \mathbf{Rt}(\varphi_g, Z_g) \cdot \mathbf{Tr}(r_{b,g}, Y_{lc}^0) \cdot \mathbf{Tr}[t(\varphi_g), X_{lc}] \quad (6.33)$$

Equation 6.33 together with Equations 6.30 through 6.32 yields an expression for the calculation of the operator,  $\mathbf{Rs}(lc \mapsto g)$ , of the resultant coordinate system transformation:

$$\mathbf{Rs}(lc \mapsto g) = \begin{bmatrix} \cos \varphi_g & \sin \varphi_g & 0 & 0.5 d_{b,g} \varphi_g \\ -\sin \varphi_g & \cos \varphi_g & 0 & 0.5 d_{b,g} \\ 0 & 0 & 1 & 0 \\ 0 & 0 & 0 & 1 \end{bmatrix} \quad (6.34)$$

Rolling of a plane over a cylinder is analytically described by the operators of the resultant coordinate system transformation of the sort (see Equation 6.33). Because of this, they are commonly referred to as the operators of rolling. The operators of rolling are designated as  $\mathbf{Rl}_x(\varphi_g, Z)$ ; that is, in the case under consideration, the equality,  $\mathbf{Rl}_x(\varphi_g, Z) = \mathbf{Rs}(lc \mapsto g)$ , is observed (see Appendix D for details of the operator of rolling).

Once the operator,  $\mathbf{Rs}(lc \mapsto g)$ , of the resultant coordinate system transformation is calculated, the following expression:

$$\mathbf{r}_{g.\text{arbitr}}(v, \varphi_g) = \mathbf{Rl}_x(\varphi_g, Z) \cdot \mathbf{r}_{lc.\text{arbitr}}(v) \quad (6.35)$$

can be used for the analytical description of the position vector of a point,  $\mathbf{r}_{g.\text{arbitr}}$ , of the gear tooth flank,  $\mathcal{G}$ , that features the line of contact,  $LC_{\text{arbitr}}$ , of an arbitrary geometry. Equation 6.35 is valid for parallel-axes gearings of all types, that is:

- External (rotationally positive and rotationally negative) gearings
- Internal (rotationally positive and rotationally negative) gearings
- *Pinion-gear-to-rack* gear pairs

As an example, consider a line of contact that is shaped in the form of a circular arc,<sup>\*</sup>  $LC_{\text{circ}}$ . In a reference system,  $X_{lc}Z_{lc}$  (Figure 6.19a), position vector of a point,  $\mathbf{r}_{lc.\text{circ}}(v)$ , of the line of contact,  $LC_{\text{circ}}$ , in this particular case allows for matrix representation in the form:

$$\mathbf{r}_{lc.\text{circ}}(v) = \begin{bmatrix} r_{lc} \cdot \sin v \\ 0 \\ r_{lc} \cdot \cos v \\ 1 \end{bmatrix} \quad (6.36)$$

<sup>\*</sup> It is likely Semple was the first who suggested the curved tooth configuration (U.S. Patent No. 5,647, *Rack and Pinion*, Amzi C. Semple, June 27, 1848). Proposed in the first half of the 19th century, the curved tooth configuration captured the interest of many mechanical engineers and inventors.



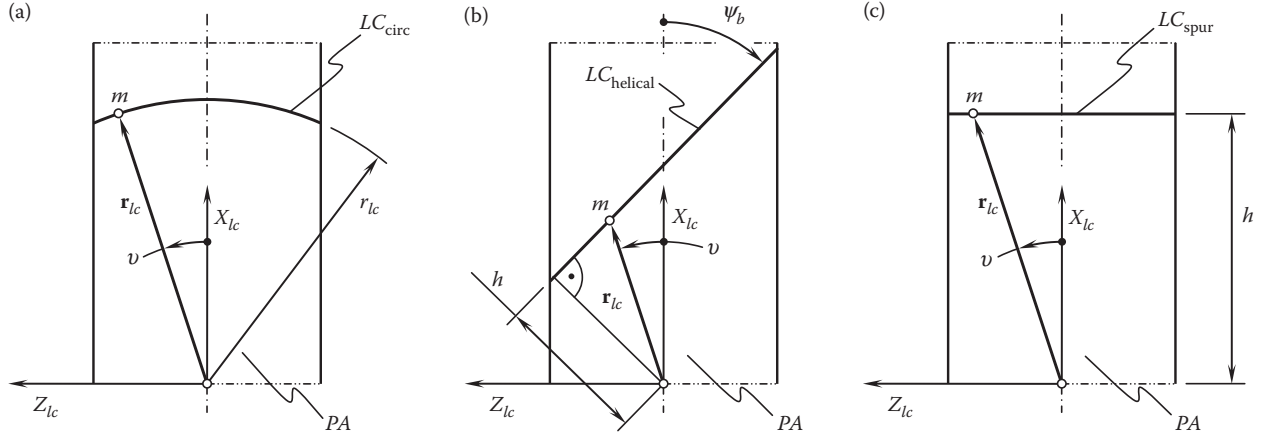


FIGURE 6.19

Desired lines of contact of the tooth flanks,  $\mathcal{G}$  and  $\mathcal{P}$ , of a gear and a mating pinion in a parallel-axes gear pair: (a) a circular arc, (b) an inclined straight line, and (c) a straight line parallel to the gear axis of rotation.

Equation 6.36 together with Equation 6.35 yields an expression for the position vector of a point,  $\mathbf{r}_{g.circ}$ , of the gear tooth flank,  $\mathcal{G}$ , that features the line of contact,  $LC_{circ}$ , in the form of a circular arc:<sup>\*</sup>

$$\mathbf{r}_{g.circ}(v, \varphi_g) = \mathbf{R}\mathbf{l}_x(\varphi_g, Z) \cdot \begin{bmatrix} r_{lc} \cdot \sin v \\ 0 \\ r_{lc} \cdot \cos v \\ 1 \end{bmatrix} = \begin{bmatrix} r_{lc} \cdot \sin v \cdot \cos \varphi_g + 0.5 d_{b,g} \varphi_g \\ -r_{lc} \cdot \sin v \cdot \sin \varphi_g + 0.5 d_{b,g} \\ r_{lc} \cdot \cos v \\ 1 \end{bmatrix} \quad (6.37)$$

In the case of an inclined line of contact,  $LC_{helical}$ , the position vector of a point,  $\mathbf{r}_{l.c.helical}(v)$ , of the line of contact,  $LC_{helical}$ , in this particular case can be analytically described by a column matrix (Figure 6.19b):

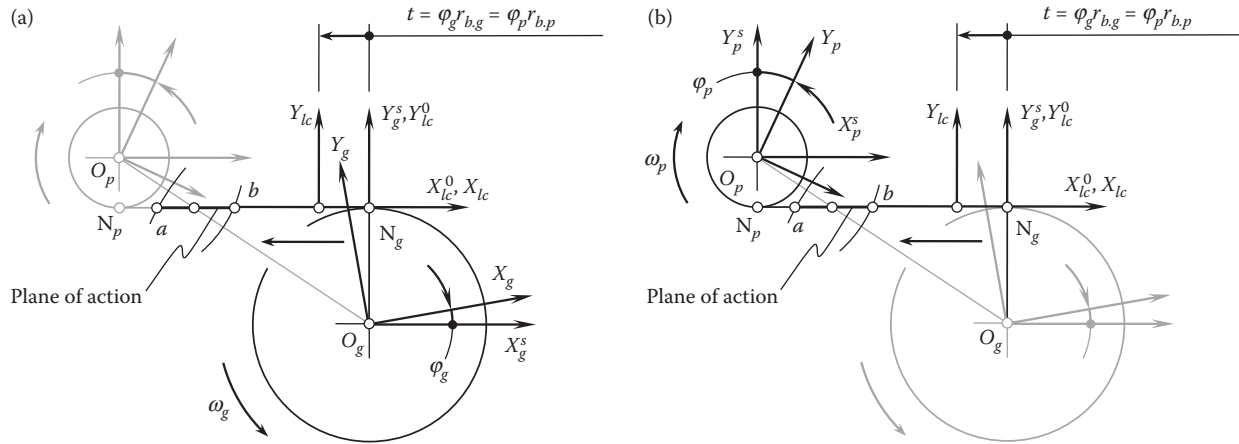
$$\mathbf{r}_{l.c.helical}(v) = \begin{bmatrix} \frac{h}{\cos(\psi_b + v)} \cdot \cos v \\ 0 \\ \frac{h}{\cos(\psi_b + v)} \cdot \sin v \\ 1 \end{bmatrix} \quad (6.38)$$

Here, the base helix angle of the gear is designated as  $\psi_b$ , and  $h$  is the distance of the line of contact,  $LC_{helical}$ , from the origin of the reference system,  $X_{lc}Y_{lc}Z_{lc}$ .

Again, Equation 6.38 together with Equation 6.35 yields an expression for the position vector of a point,  $\mathbf{r}_{g.helical}$ , of the gear tooth flank,  $\mathcal{G}$ , that features the line of contact,  $LC_{helical}$ , in the form of an inclined straight line, that is, of a helical gear:

$$\mathbf{r}_{g.helical}(v, \varphi_g) = \mathbf{R}\mathbf{l}_x(\varphi_g, Z) \cdot \begin{bmatrix} \frac{h}{\cos(\psi_b + v)} \cdot \cos v \\ 0 \\ \frac{h}{\cos(\psi_b + v)} \cdot \sin v \\ 1 \end{bmatrix} = \frac{h}{\cos(\psi_b + v)} \begin{bmatrix} \cos v \cdot \cos \varphi_g + 0.5 d_{b,g} \varphi_g \\ -\cos v \cdot \sin \varphi_g + 0.5 d_{b,g} \\ \sin v \\ 1 \end{bmatrix} \quad (6.39)$$

<sup>\*</sup> In a case when a gear with tooth flanks generated by a circular arc line of contact,  $LC_{circ}$ , is cut by a gear-cutting tool with a nonzero transverse pressure angle ( $\phi_t \neq 0$ ), the condition of equal base pitches is violated.


**FIGURE 6.20**

The coordinate systems applied for the generation of a tooth flank of an involute gear with an arbitrary tooth shape in the lengthwise direction in Figure 6.17: (a) the coordinate systems associated with the gear, and (b) the coordinate systems associated with the mating pinion.

Ultimately, in a case of spur parallel-axes gearing, the desired line of contact,  $LC_{\text{spur}}$ , is parallel to the axis of rotation of the gear,  $O_g$ . In the case of a straight line of contact,  $LC_{\text{spur}}$ , the position vector of a point,  $\mathbf{r}_{lc,\text{spur}}(v)$ , of the line of contact,  $LC_{\text{spur}}$ , in this particular case can be analytically described by a column matrix (Figure 6.19c):

$$\mathbf{r}_{lc,\text{spur}}(v) = \begin{bmatrix} h \\ 0 \\ h \cdot \tan v \\ 1 \end{bmatrix} \quad (6.40)$$

Again, Equation 6.40 together with Equation 6.35 yields an expression for the position vector of a point,  $\mathbf{r}_{lc,\text{spur}}$ , of the gear tooth flank,  $\mathcal{G}$ , that features the line of contact,  $LC_{\text{spur}}$ , in the form of an inclined straight line, that is, of a spur gear (Figure 6.20a):

$$\mathbf{r}_{g,\text{spur}}(v, \varphi_g) = \mathbf{Rl}_x(\varphi_g, Z) \cdot \begin{bmatrix} h \\ 0 \\ h \cdot \tan v \\ 1 \end{bmatrix} = h \cdot \begin{bmatrix} \cos \varphi_g + 0.5 d_{b,g} \varphi_g \\ -\sin \varphi_g + 0.5 d_{b,g} \\ \tan v \\ 1 \end{bmatrix} \quad (6.41)$$

In a similar manner, an expression for the position vector of a point,  $\mathbf{r}_p$ , of the pinion tooth flank,  $\mathcal{P}$ , can be derived. For this purpose, Equation 6.29 should be considered together with the operator,  $\mathbf{Rs}(lc \mapsto p)$ , of the resultant coordinate transformation from the coordinate system,  $X_{lc}Y_{lc}Z_{lc}$ , to the pinion coordinate system,  $X_pY_pZ_p$  (Figure 6.20b). The operator,  $\mathbf{Rs}(lc \mapsto p)$ , can be calculated as a product of operators of elementary coordinate system transformations. For this purpose, a stationary Cartesian coordinate system,  $X_p^sY_p^sZ_p^s$ , and the coordinate system,  $X_pY_pZ_p$ , that is associated with the pinion are used.

An expression for the position vector of a point,  $\mathbf{r}_p$ , of the pinion tooth flank,  $\mathcal{P}$ , can be represented in a form:

$$\mathbf{r}_p(v, \varphi_p) = \mathbf{Rs}(lc \mapsto p) \cdot \mathbf{r}_{lc}(v) \quad (6.42)$$

Gears with tooth flanks,  $\mathcal{G}$  and  $\mathcal{P}$ , designed so to fulfill Equation 6.41, are referred to as the *involute* gears for parallel-axes gear pairs, as the transverse section of the gear tooth flank is an involute of a circle; that is, the involute tooth profile is developed from the base circles of diameters,  $d_{b,g}$  and  $d_{b,p}$ , correspondingly.

The interval of variation of the parameter  $v$  in Equations 6.41 and 6.42 depends on the face width,  $F_{pa}$ , of the gear and on the geometry of the line of contact,  $LC_{arbitr}$ . The interval of variation of the parameter  $\varphi_g$  in Equation 6.41 and the parameter  $\varphi_p$  in Equation 6.42 can be expressed in terms of length  $Z$  of the tooth height of the gear and the geometry of the line of contact,  $LC_{arbitr}$ .

As the tooth flank of a gear,  $\mathcal{G}$ , is generated by a moving line of contact,  $LC$ , use of the theory of enveloping surfaces is not required for the derivation of an equation of the gear tooth flank,  $\mathcal{G}$ .

Gear pairs featuring one of the following lines of contact, that is,  $LC_{spur}$ ,  $LC_{helical}$ ,  $LC_{circ}$ , and  $LC_{arbitr}$ , maintain an operating base pitch,  $p_{b.opr}$ , of a constant value. Therefore, gear pairs of these types are capable of transmitting a smooth rotation from the driving shaft to the driven shaft. Gear pairs of this kind are referred to as *perfect parallel-axes gear pairs* (or *geometrically accurate parallel-axes gear pairs* or *ideal parallel-axes gear pairs*). All of them can be either rotationally positive or rotary negative parallel-axes gear pairs.

## A Simplified Approach for Involute Gear Tooth Flank Generation

The tooth flank of a gear in a perfect parallel-axes gearing is a kind of involute surface. Gears with tooth flanks,  $\mathcal{G}$  and  $\mathcal{P}$ , designed to fulfill Equation 6.35, are referred to as involute gears for parallel-axes gear pairs. The term *involute* is because the transverse section of the gear tooth flank is an involute of a circle; that is, the involute tooth profile is developed from a base circle of a diameter,  $d_{b,g}$ , for a gear and from a base circle of a diameter,  $d_{b,p}$ , for a mating pinion, correspondingly. Once a type of transverse section of a gear tooth flank is known (this is an involute of a circle), simplified approaches can be used for the generation and further analyses of tooth flank geometry of involute gears.

### 7.1 Generation of Involute Tooth Profile in Perfect Parallel-Axes Gear Pair

An involute gear pair is an extensively used type of parallel-axes gearing. Any possible type of parallel-axes gear pair can be specified by one of five possible types of vector diagrams, as illustrated in Figure 6.2. Once the vector diagram of a parallel-axes gear pair is constructed, determination of the involute profile of a gear tooth is the next step in the analysis of parallel-axes gearing.

The uniform rotation of the driving pulley in Figure 7.1 causes the uniform rotation of the driven pulley. This schematic of transmission of a uniform rotary motion is employed for the derivation of an equation of the natural form of a gear tooth profile: tooth flanks of a gear and a mating pinion need to be designed to meet the following requirements:

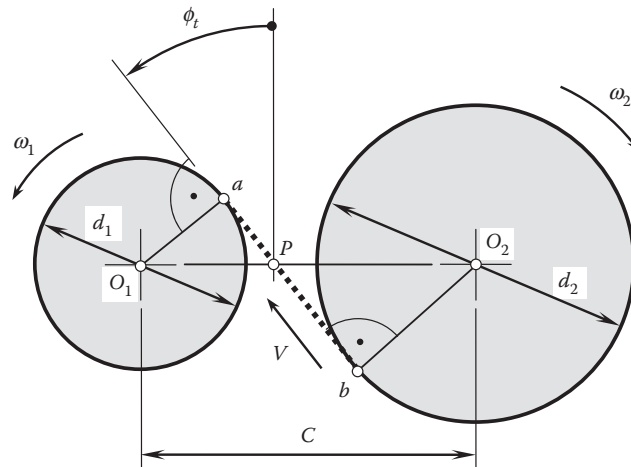
- The contact point between the tooth flanks,  $\mathcal{G}$  and  $\mathcal{P}$ , of a gear and a mating pinion must trace a straight-line segment,  $P_c$  (this is because the belt tightened over the pulleys is always straight and cannot be curved). The straight-line segment,  $P_c$ , aligns with a straight line that intersects the centerline,  $\mathcal{C}$ , at a pitch point,  $P$ .
- The common perpendicular,  $\mathbf{n}_g$ , to the tooth flanks,  $\mathcal{G}$  and  $\mathcal{P}$ , at every contact point,  $K$ , is along a straight line through the point,  $P$ , which in nature is a line of action,  $LA$  (this is because the tooth flanks,  $\mathcal{G}$  and  $\mathcal{P}$ , interact with one another like the working surfaces in a cam mechanism; if the friction is not taken into account, the force of interaction is along the common perpendicular,  $\mathbf{n}_g$ ).
- The pitch point,  $P$ , is motionless; that is, it does not travel along the centerline,  $\mathcal{C}$ , when the gears rotate.
- The distance between contact points for every two neighboring pairs of teeth must be the same value.

With that said, let us investigate a desirable geometry of the interacting tooth flanks,  $\mathcal{G}$  and  $\mathcal{P}$ , in more detail. Often, tooth flank geometry of this type is referred to as *natural form of a gear/pinion tooth flank*.

Gears of a gear pair may have teeth of a particular shape for which a uniform rotation of the input shaft results in a corresponding uniform rotation of the output shaft (i.e., the angular velocity ratio is of a constant value,  $\omega_{input}/\omega_{output} = const$ ). A constant angular velocity ratio,  $\omega_{input}/\omega_{output} = const$ , is a necessary condition for a gear pair to be referred to as the perfect gear pair. The axes of rotation of a gear and a mating pinion in a perfect gear pair are parallel to one another, and no deflections or displacements of the axes in relation to one another are taken into account.

Rotation is transmitted *naturally* by a perfect gear pair.

Consider three *Cartesian* coordinate systems,  $X_1Y_1Z_1$ ,  $X_2Y_2Z_2$ , and  $X_hY_hZ_h$ , as shown in Figure 7.2. The first reference system,  $X_1Y_1Z_1$ , is associated with the first pulley shown (Figure 7.2). This coordinate system rotates with the first pulley. The second reference system,  $X_2Y_2Z_2$ , is associated with the second pulley, and it rotates

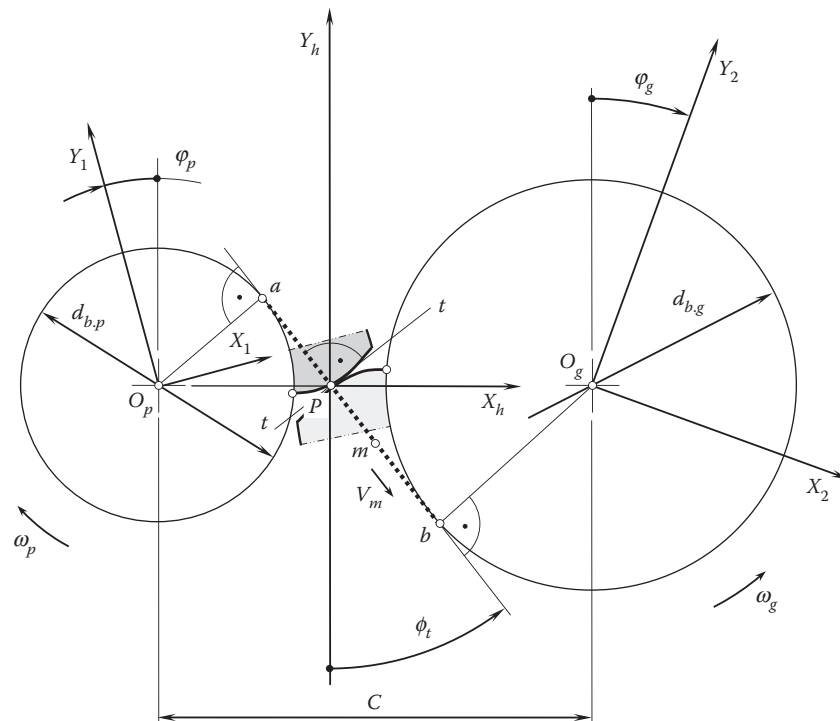
**FIGURE 7.1**

Schematic of the concept of the natural form of a gear tooth profile in perfect parallel-axes gearing.

with this pulley. The third reference system,  $X_h Y_h Z_h$ , is associated with the gear housing. This coordinate system is a stationary coordinate system.

The axis,  $Z_1$ , is aligned with the axis of rotation of the first pulley. This axis is designated as  $O_p$ . The axis,  $Z_2$ , is aligned with the axis of rotation of the second pulley. This axis is designated as  $O_g$ . Finally, the axis,  $Z_h$ , of the stationary reference system,  $X_h Y_h Z_h$ , is the axis through the pitch point,  $P$ . In parallel-axes gearing, this axis is parallel to the axes,  $O_p$  and  $O_g$ ; thus, it is perpendicular to the plane of drawing in Figure 7.2. The axes,  $Z_1$ ,  $Z_2$ , and  $Z_h$ , are not shown in Figure 7.2.

While the pulleys rotate about their axes,  $O_p$  and  $O_g$ , the coordinate systems,  $X_1 Y_1 Z_1$  and  $X_2 Y_2 Z_2$ , turn through corresponding angles,  $\varphi_p$  and  $\varphi_g$ . Once a smooth transmission of a rotation is considered, then the

**FIGURE 7.2**

Conjugate action law: Generation of the natural form of a gear tooth profile in perfect parallel-axes gearing.

angles,  $\varphi_p$  and  $\varphi_g$ , fulfill the following ratio:

$$\varphi_p \cdot r_p = \varphi_g \cdot r_g \quad (7.1)$$

where the radii of the first and the second pulleys are denoted as  $r_p$ , and  $r_g$ , correspondingly (for these radii, the equalities  $r_p = 0.5d_p$  and  $r_g = 0.5d_g$  are valid).

An arbitrary point,  $m$ , within the belt travels together with the belt. The velocity of straight motion of a point,  $m$ , is equal to the linear velocity of the belt,  $V_m$ . A straight line is traced by a point,  $m$ , in the stationary reference system,  $X_h Y_h Z_h$ . The straight line forms a certain angle,  $\phi_t$ , with the perpendicular to the centerline,  $\mathcal{C}$ . The straight line is also tangent to the pulleys. The points of tangency are designated as  $a$  and  $b$  for the first and second pulleys, correspondingly. The straight line is rolling with no slippage over the pulleys of the diameters,  $d_p$  and  $d_g$ . The point of intersection of the straight line with the centerline,  $\mathcal{C}$ , is designated as  $P$ . This point is commonly referred to as the pitch point of a corresponding gear pair.

The motion of a point,  $m$ , can also be observed in the reference system,  $X_1 Y_1 Z_1$ . With respect to this coordinate system, the resultant motion of a point,  $m$ , can be construed as a superposition of a translation with linear velocity,  $V_m$  (see Equation 6.26), and the rotation,  $\omega_1$ . An involute of a circle is traced by point,  $m$ , in the coordinate plane,  $X_1 Y_1$ .

Similarly, the motion of a point,  $m$ , can also be observed in the reference system  $X_2 Y_2 Z_2$ . With respect to this coordinate system,  $X_2 Y_2 Z_2$ , the resultant motion of a point,  $m$ , can be interpreted as a superposition of a translation with the linear velocity,  $V_m$  (see Equation 6.26), and a rotation  $\omega_2$ . Another involute of a circle is traced by a point,  $m$ , in the coordinate plane,  $X_2 Y_2$ .

A point,  $m$ , travels with the belt in a direction predetermined by the straight motion of the belt. The motion of a point,  $m$ , is not feasible in any other direction. In straight motion, a straight path is traced by a point,  $m$ , in a stationary reference system,  $X_h Y_h Z_h$ . In a perfect gear pair, the tooth flanks of the gear and the mating pinion must be designed so as to ensure the path of the contact point is aligned with that same straight path of a point,  $m$ , in the pulley-and-belt mechanism. In parallel-axes gearing, this line is commonly referred to as the path of contact,  $P_c$ .

In a pulley-and-belt mechanism, the force is transmitted along the belt. No other direction of the force is feasible. When, in parallel-axes gearing, friction is not taken into account, the tooth flanks of the gear and the pinion must be designed so as to ensure the line of action of the interacting teeth is aligned with that same straight line along which the force is transmitted in the pulley-and-belt mechanism; that is, it must be directed along the straight portion of the belt. In parallel-axes gearing, this line is commonly referred to as the line of action,  $LA$ . The line of action,  $LA$ , is always a straight line, as no force can be transmitted along a curve.

These two lines, that is, the path of contact,  $P_c$ , and the line of action,  $LA$ , are two different entities. In perfect parallel-axes gearing, these two lines align with each other, which often causes confusion. In parallel-axes gearings of other designs (e.g., in cycloidal parallel-axes gearing), the path of contact,  $P_c$ , and the line of action,  $LA$ , do not align with one another, as the path of contact,  $P_c$ , is a planar curve, while the line of action,  $LA$ , is represented by an infinite number of instant lines of action,  $LA_{inst}$ .

It is the right point to stress here the difference between a pulley-and-belt mechanism and perfect parallel-axes gearing. In a pulley-and-belt mechanism, the straight portion of the belt is terminated by points of tangency,  $a$  and  $b$ , of the belt with the pulleys. In perfect parallel-axes gearing, neither the path of contact,  $P_c$ , nor the line of action,  $LA$ , are terminated by these points. Both the lines,  $P_c$  and  $LA$ , can be extended in both directions beyond the points,  $a$  and  $b$ .

When the gears rotate, the involute profiles traced within the planes,  $X_1 Y_1$  and  $X_2 Y_2$ , roll over one another. It can be shown that no slippage of the involute profiles is observed when the contact point is coincident with the pitch point,  $P$ . However, sliding occurs at all contact points located before and beyond the pitch point,  $P$ .

There is a kinematic requirement for one tooth profile to drive the other at a constant angular velocity ratio ( $\omega_{input}/\omega_{output} = const$ ). It can also be readily understood that a pair of gear profiles contacts each other at different positions as the gears rotate. The locus of all possible contact points for a given pair of tooth profiles, that is, the path of contact,  $P_c$ , is a straight line segment terminated by the extremities of the gear and the pinion teeth.

The three curves involved in the most fundamental part of gear design are as follows:

- Path of contact
- Profile of the gear tooth
- Profile of the pinion tooth

A basic geometric fact\* of great significance is that *given a fixed center distance and speed ratio, any of these curves completely determines the other two*. It is understood here that the necessary conditions of contact of the interacting tooth flanks, as well as the condition of conjugacy of the tooth flanks,  $\mathcal{G}$  and  $\mathcal{P}$ , are met.

Therefore, the three traces obtained in the reference systems,  $X_h Y_h Z_h$ ,  $X_1 Y_1 Z_1$ , and  $X_2 Y_2 Z_2$ , are interdependent. If a trace in one of three coordinate systems is known, then the remaining two traces can be found. This means that the specifications of the traces in the coordinate systems,  $X_h Y_h Z_h$ ,  $X_1 Y_1 Z_1$ , and  $X_2 Y_2 Z_2$ , are equivalent to each other. If necessary, the two tooth profiles of the gear and the mating pinion can be investigated individually, or the geometry of the path of contact,  $P_c$ , can be investigated instead. Once the path of contact,  $P_c$ , is known, conjugate tooth profiles can be easily derived. The last is a routine procedure.

The following can be adopted as a rule:

- The path of contact,  $P_c$ , can be interpreted as the loci of contact points considered in the stationary coordinate system,  $X_h Y_h Z_h$ , associated with the gear housing.
- A gear tooth profile can be construed as the loci of contact points considered in the coordinate system associated with a gear.
- A pinion tooth profile can be interpreted as the loci of contact points considered in the coordinate system associated with a pinion.

It is instructive to note here that in cases of perfect parallel-axes gearing, the path of contact,  $P_c$ , and the line of action,  $LA$ , are congruent to each other. However, it is of critical importance to realize that these two lines are of completely different natures.

In many cases, specification of a gear pair in terms of the shape of the path of contact,  $P_c$ , and not the tooth profiles of the gear and the pinion is proven to be convenient.

Two traces of the point,  $m$ , that are obtained within the coordinate planes,  $X_1 Y_1$  and  $X_2 Y_2$ , are commonly used for designing the tooth profiles of gear pairs. Leonhard Euler<sup>†</sup> (1760) is credited with development of the involute tooth profile for perfect parallel-axes gearing. The involute of a circle, which was proposed by Euler for gear teeth, best fits all cases of parallel-axes gearing with zero axis misalignment, that is, all cases of perfect gearing.

The discussed interpretation of the generation of involute tooth profiles is based on the analogy between two rotating pulleys (see Figure 7.1) and a gear pair (see Figure 7.2). This allows for the conclusion that *an involute of a circle is the locus of a point on a taut cord being unwound from the circumference of a stationary circle*. Alternatively, it is also the locus of a point on a straight line, which rolls with no slippage around the circumference of a stationary circle.

Thus, the interpretation reveals that this method for generating involute tooth profiles can be referred to as the natural way for tooth profile generation.

### 7.1.1 Involute Gear Tooth Profile

Once the kinematics of the generation of an involute curve is understood correctly, an analytical description of this curve can be easily derived.

The equation of involute of a circle can be derived in the following manner (refer to Figure 7.3).

The involute of a circle starts at a point,  $A$ , within the base circle of a radius,  $r_{b,g}$ . The magnitude of the position vector,  $\mathbf{r}_m$ , of an arbitrary point,  $m$ , of the involute curve can be expressed in terms of the base radius,  $r_{b,g}$ , and the central angle  $\varepsilon = \angle(AO_g M)$ . The length of the circular arc,  $\widehat{AB}$ , is equal to the length of the straight line segment,  $AB$ . This is because the straight line rolls with no slippage over the base circle. From  $\triangle BO_g M$ , the following equation can be composed:

$$R_m = r_{b,g} \tan \phi_t \quad (7.2)$$

\* It should be stressed here that this basic geometric fact is valid *only* in cases of perfect gearing (where the interacting tooth flanks are conjugate to one another), and it is *not* applicable in cases of parallel-axes gearings with other geometries of the tooth flanks (where the interacting tooth flanks are not conjugate to one another); for instance, the basic geometry fact is not applicable in cases of parallel-axes gearings with a cycloidal tooth profile, and others.

<sup>†</sup> Leonhard Euler (April 15, 1707–September 18, 1783), a pioneering Swiss mathematician and physicist who spent most of his life in Russia and Germany.



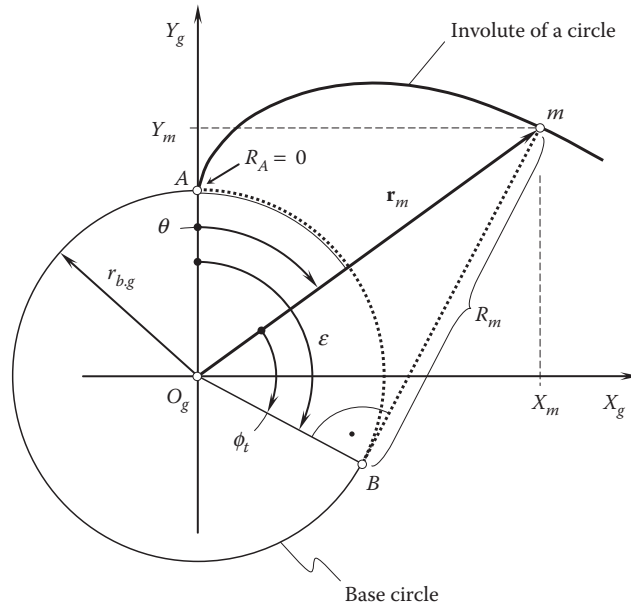


**FIGURE 7.3**  
Involute of a circle.

In Equation 7.2, the profile angle\* of the involute curve is designated as  $\phi_t$ . Because the equality  $R_m = AB$  is valid, the following equality is valid:

$$R_m = r_{b.g} \cdot \varepsilon(\text{rad}) \quad (7.3)$$

The central angle,  $\varepsilon$ , can be represented in the form of the sum:  $\varepsilon = \phi_t + \theta$ . This yields the following formula for  $R_m$ :

$$R_m = r_{b.g} \cdot (\phi_t + \theta) \quad (7.4)$$

Equation 7.2 considered in conjunction with Equation 7.3 results in the following equality:

$$r_{b.g} \tan \phi_t = r_{b.g} \cdot (\phi_t + \theta) \quad (7.5)$$

Ultimately, Equation 7.5 casts into the equation for the involute function:

$$\theta = \text{inv } \phi_t = \tan \phi_t - \phi_t(\text{rad}) \quad (7.6)$$

The involute function,  $\text{inv } \phi_t$ , is significant in the theory of gearing as well as in applications of the theory.

The projection,  $X_m$ , of the position vector,  $\mathbf{r}_m$ , of the point,  $m$ , onto the  $X_g$ -axis can be interpreted as the sum of projections onto the  $X_g$ -axis of the straight line segment,  $O_gB$ , and the straight line segment,  $R_m$ :

$$X_m = r_{b.g} \cos(\varepsilon - 90^\circ) + R_m \sin(\varepsilon - 90^\circ) \quad (7.7)$$

Similarly, the projection,  $Y_m$ , of the position vector,  $\mathbf{r}_m$ , of the point,  $m$ , onto the  $Y_g$ -axis can be interpreted as the sum of projections onto the  $Y_g$ -axis of the same straight line segments,  $O_gB$  and  $R_m$ :

$$Y_m = -r_{b.g} \sin(\varepsilon - 90^\circ) + R_m \cos(\varepsilon - 90^\circ) \quad (7.8)$$

\* The profile angle,  $\phi_t$ , is often referred to as *pressure angle*. Use of the term *pressure angle* with respect to a curve is incorrect. *Pressure* means a kind of interaction between two curves/surfaces. As long as just one involute curve is considered, the term *profile angle* is preferred. The term *pressure angle* is applicable when an interaction of two involute curves is discussed.

Equations 7.7 and 7.8 can be rewritten in a following form:

$$\begin{aligned} \mathbf{r}_m(\phi_t) = & \mathbf{i} \cdot [-r_{b,g} \sin(\phi_t + \text{inv } \phi_t) + r_{b,g}(\phi_t + \text{inv } \phi_t) \cos(\phi_t + \text{inv } \phi_t)] + \\ & + \mathbf{j} \cdot [-r_{b,g} \cos(\phi_t + \text{inv } \phi_t) - r_{b,g}(\phi_t + \text{inv } \phi_t) \sin(\phi_t + \text{inv } \phi_t)] \end{aligned} \quad (7.9)$$

Equation 7.9 describes an involute curve in terms of just two parameters, namely of a radius of the base cylinder,  $r_{b,g}$ , and of the profile angle,  $\phi_t$ .

Equation 7.9 can also be represented in matrix form:

$$\mathbf{r}_m(\phi_t) = \begin{bmatrix} -r_{b,g} \sin(\phi_t + \text{inv } \phi_t) + r_{b,g}(\phi_t + \text{inv } \phi_t) \cos(\phi_t + \text{inv } \phi_t) \\ -r_{b,g} \cos(\phi_t + \text{inv } \phi_t) - r_{b,g}(\phi_t + \text{inv } \phi_t) \sin(\phi_t + \text{inv } \phi_t) \\ 0 \\ 1 \end{bmatrix} \quad (7.10)$$

The representation of an involute curve in this form (see Equation 7.10) is convenient in many applications. Matrix representation of an equation of the involute curve is preferred when multiple coordinate system transformations are performed.

The discussed method for the generation of an involute of a circle is commonly referred to as the *tracing method for generation of an involute of a circle*.

The involute of a circle has an extensive application in the theory of gearing.

### 7.1.2 Tooth Flanks of a Gear and a Mating Pinion

The variety of practical shapes that are possible for gear tooth flanks is limited. Although the physically feasible variety of gear tooth geometries is large enough, commonly used gear tooth forms in their lengthwise direction are limited to just a few forms. Straight, helical, herringbone and double helical, circular, and cycloidal are among them.

The use of modern numerically controlled (NC) machines makes possible the machining of any desired shape of gear tooth flank; application of NC machining is purposely limited to those shapes for which kinematics of machining can be represented as either a single translation/rotation or a superposition of a finite number of translations and rotations (or just a few of them).

An accurate description of a gear tooth flank is of critical importance for many practical applications. An analytical description of gear tooth flanks is preferred from many standpoints.

It is convenient to begin the discussion of a gear tooth flank geometry from the geometry of the tooth flank of a spur involute gear.

#### 7.1.2.1 Spur Involute Gear Tooth Flank

Consider a spur gear with an involute tooth profile (Figure 7.4a). The geometry of the tooth flank of the gear is illustrated in Figure 7.4b. The transverse section of the gear tooth flanks is schematically shown in Figure 7.4c.

In the coordinate system,  $X_g Y_g$ , associated with the gear, the position vector,  $\mathbf{r}_{inv}(V_g)$ , of a point of an involute tooth profile can be represented in the following matrix form:

$$\mathbf{r}_{inv}(V_g) = \begin{bmatrix} r_{b,g} \cdot (\sin V_g - V_g \cdot \cos V_g) \\ r_{b,g} \cdot (\cos V_g + V_g \cdot \sin V_g) \\ 0 \\ 1 \end{bmatrix}, \quad V_g^{(l)} \leq V_g \leq V_g^{(a)} \quad (7.11)$$

In this equation, the values of parameter,  $V_g$ , that correspond to the  $SAP^*$  point of the tooth profile and the point of the tooth profile that is located on the major diameter (EAP) of the gear are designated as  $V_g^{(l)}$  and  $V_g^{(a)}$ , respectively.

\*  $SAP$  stands for *start of active profile* of the gear tooth;  $EAP$  stands for *end of active profile*.

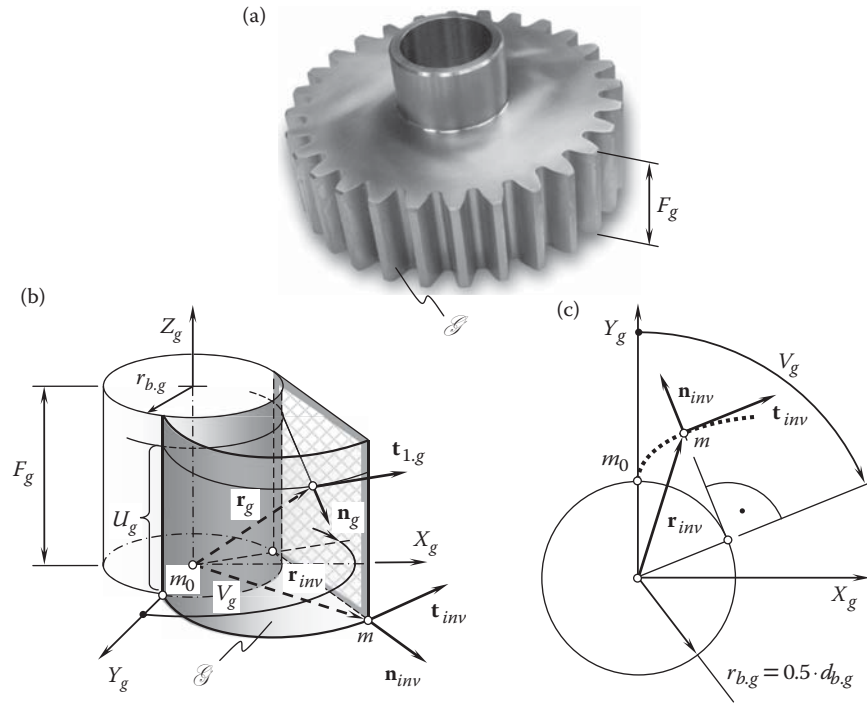


FIGURE 7.4

Geometry of the tooth flank,  $\mathcal{G}$ , of a spur involute gear: (a) a spur gear, (b) a gear tooth flank geometry, and (c) transverse section of the gear tooth flank,  $\mathcal{G}$ .

Once an equation of the transverse section of a gear tooth flank is derived (see Equation 7.11), then the gear tooth flank,  $\mathcal{G}$ , can be generated by means of a *generator line* and a *director line*, as schematically illustrated in Figure 7.5. When a generator line travels along a corresponding director line, the gear tooth flank is generated as a kind of swept surface,  $G$ . In a case of parallel-axes gearing, the generator line is often referred to as the *tooth profile*. Commonly, the terms *tooth profile* (a curve) and the *tooth flank* (a surface) are mostly equivalent. However, this equivalency is valid only in cases of parallel-axes gearing. Use of the term *tooth flank* is preferred rather than the term *tooth profile*, as the term *tooth flank* is more general and is applicable to gears of all types, namely to intersected-axes and crossed-axes gears.

Use of the approach illustrated in Figure 7.5 enables the design of a spur gear. A spur involute gear of  $N_g$  teeth (Figure 7.6) has  $N_g$  left-hand-side tooth flanks and  $N_g$  right-hand-side tooth flanks. All the tooth flanks of a spur

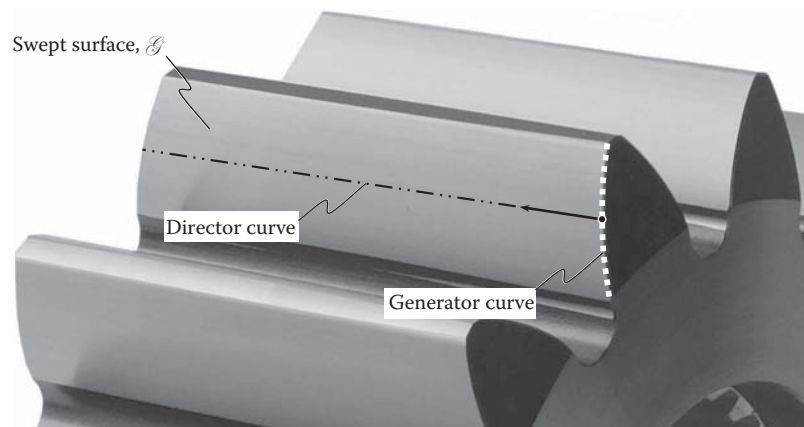


FIGURE 7.5

Tooth flank,  $\mathcal{G}$ , of a spur involute gear generated by means of a *generator curve* and *director curve*.



**FIGURE 7.6**  
Spur involute gear.

gear are terminated by the outside diameter of the gear and by the *SAP* diameter. The tooth flanks of every two neighboring teeth are connected to one another by means of a fillet and a bottom land.

Another example of that same nature is that all the base circles of a gear are of different diameters centering at a common point,  $O_g$ . All the tooth profiles are of involute geometry, but the gear is not a kind of involute gear—no base pitch can be specified for a gear of such a design.

Generally speaking, such an approach for the generation of a gear tooth flank,  $\mathcal{G}$ , is applicable only for parallel-axes gearing. In general cases of intersected-axes, as well as crossed-axes, gearing such an approach is not applicable, as the tooth flanks of a gear do not allow for sliding of the tooth flank over itself (excluding certain types of *two-degrees-of-freedom* gear pairs). More details of this approach for the generation of a gear tooth flank,  $\mathcal{G}$ , are discussed immediately below.

The tooth flank of a spur involute gear,  $\mathcal{G}$ , can be represented as the locus of successive positions of the involute tooth profile,  $\mathbf{r}_{inv}(V_g)$ , that travels straight in the direction of the gear axis,  $Z_g$ . Let us designate the parameter of this motion of the tooth profile as  $U_g$ . Equation 7.11 immediately yields an expression for the position vector,  $\mathbf{r}_g(U_g, V_g)$ , of a point of the tooth flank of a spur involute gear:

$$\mathbf{r}_g(U_g, V_g) = \begin{bmatrix} r_{b,g} \cdot (\sin V_g - V_g \cdot \cos V_g) \\ r_{b,g} \cdot (\cos V_g + V_g \cdot \sin V_g) \\ U_g \\ 1 \end{bmatrix}, \quad \begin{array}{l} V_g^{(l)} \leq V_g \leq V_g^{(a)} \\ 0 \leq U_g \leq B_g \end{array} \quad (7.12)$$

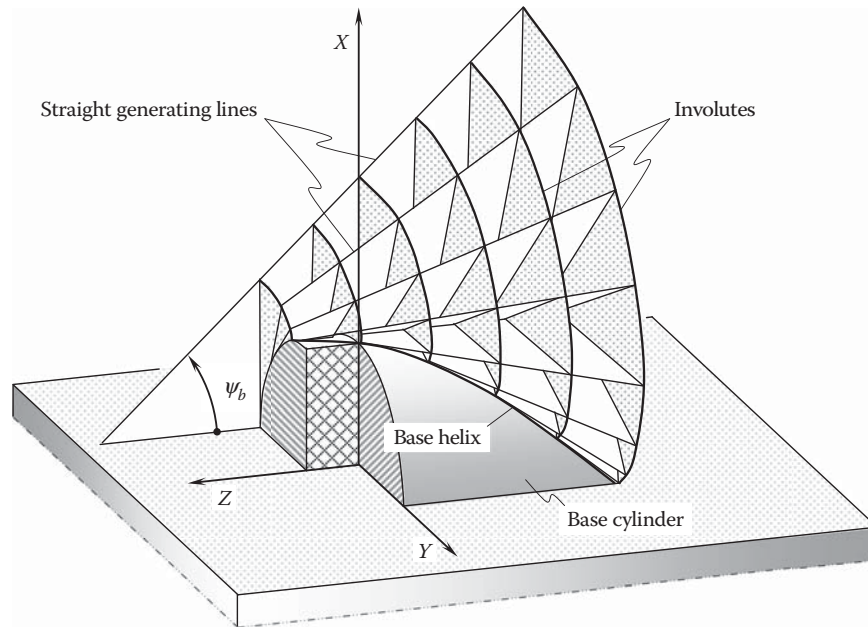
The current value of the parameter  $U_g$  is within the gear face width  $F_g$ ; that is,  $0 \leq U_g \leq F_g$ .

It is easy to see that for the chosen kind of parameterization of the tooth flank,  $\mathcal{G}$ , of a spur involute gear, the identity  $U_g \equiv Z_g$  is observed.

### 7.1.2.2 Helical Involute Gear Tooth Flank

The tooth flanks of helical gears with involute tooth profiles are shaped in the form of a screw involute surface. A possible method for the generation of a screw involute surface by a straight line,  $\mathcal{C}_g$ , rolling with no slipping over the base cylinder of a gear is illustrated in Figure 7.7 [157]. The surface  $\mathcal{G}$  is generated as the loci of successive positions of the straight line,  $\mathcal{C}_g$ , which is the characteristic line.

A screw involute surface,  $\mathcal{G}$ , is generated by a straight line that performs a screw motion in relation to the gear axis,  $O_g$  (Figure 7.8). The generating line is tangent to the helix on the base cylinder of radius,  $r_{b,g}$ . The helix in question is traced on the base cylinder using the point of tangency of the generating straight line,  $\mathcal{C}_g$ , with the

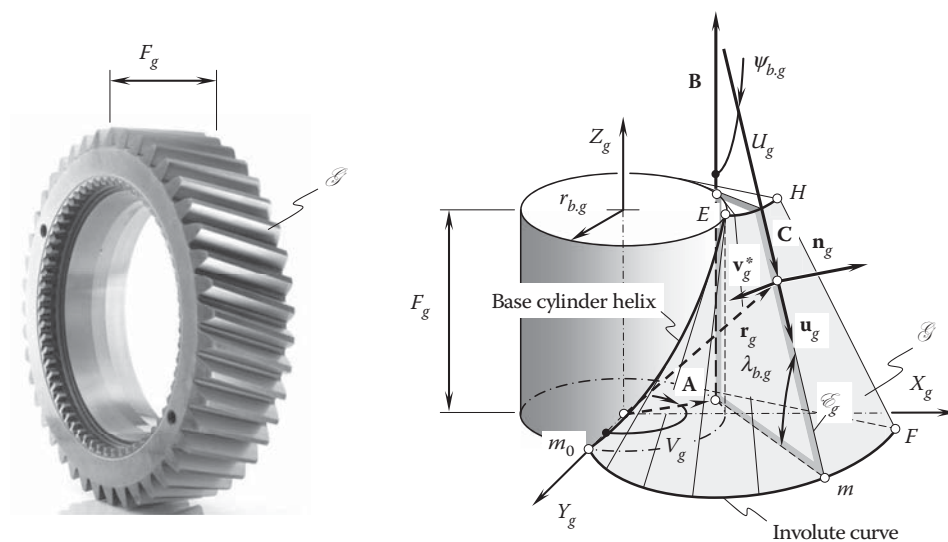
**FIGURE 7.7**

The involute helicoid. (From W.F. Vogel, W.F., *Involutometry and Trigonometry*, Michigan Tool Company, Detroit, MI. Book production by Denham & Co. With permission.)

cylinder. The helix is referred to as the *base helix*. The generating line,  $\mathcal{E}_g$ , forms a base lead angle,  $\lambda_{b,g}$ , with the plane perpendicular to the  $Z_g$ -axis of the Cartesian coordinate system  $X_g Y_g Z_g$ . It must be mentioned here that for the tooth alignment of the mating gears to agree, their *base lead angles must be equal*. A similar statement is valid for base helix angles; that is, for the tooth alignment of the mating gears to agree, the *base helix angles of the mating gears must be equal*.

The position vector,  $\mathbf{r}_g$ , of a point of the screw involute surface can be represented in the form of a sum of three vectors (Figure 7.8):

$$\mathbf{r}_g = \mathbf{A} + \mathbf{B} + \mathbf{C} \quad (7.13)$$

**FIGURE 7.8**

Geometry of tooth flank,  $\mathcal{G}$ , of a helical involute gear. (From Radzevich, S.P., *Differential-Geometrical Method of Part Surface Generation*, DrSc (Eng) thesis. Tula: Tula Polytechnic Institute, 1991, 300 pages.)

Here,  $|\mathbf{A}|$  is the base cylinder radius (i.e., the equality  $|\mathbf{A}| = r_{b,g}$  is observed). The vector,  $\mathbf{A}$ , makes a roll angle,  $V_g$ , with the  $Y_g$ -axis. The axial displacement in the screw motion is given by  $|\mathbf{B}| = p_g \cdot V_g$ , which corresponds to the rotation angle,  $V_g$ ;  $p_g$  designates the *screw parameter* (or the *reduced pitch*, in other terminology) of the tooth flank,  $\mathcal{G}$ . Finally,  $|\mathbf{C}| = U_g$  is the segment of the generating straight line,  $\mathcal{C}_g$ , measured from the tangency point on the base cylinder to the current point on the screw involute surface,  $\mathcal{G}$ .

By projecting three vectors,  $\mathbf{A}$ ,  $\mathbf{B}$ , and  $\mathbf{C}$ , onto the axes of the coordinate system  $X_g Y_g Z_g$ , an equation for the screw involute surface of the gear tooth flank,  $\mathcal{G}$ , becomes possible. After rearranging components and transforming formulas, the equation of the screw involute surface,  $\mathcal{G}$ , can be represented in the following matrix form [101, 74, 110, 111, 113]:

$$\mathbf{r}_g(U_g, V_g) = \begin{bmatrix} r_{b,g} \cos V_g + U_g \cos \lambda_{b,g} \sin V_g \\ r_{b,g} \sin V_g - U_g \sin \lambda_{b,g} \sin V_g \\ r_{b,g} \tan \lambda_{b,g} - U_g \sin \lambda_{b,g} \\ 1 \end{bmatrix} \quad \begin{matrix} V_g^{(l)} \leq V_g \leq V_g^{(a)} \\ 0 \leq U_g \leq [U_g] \end{matrix} \quad (7.14)$$

Here, the maximum allowed value of parameter  $U_g$  is designated as  $[U_g]$ . Actually, the value of the parameter  $[U_g]$  can be expressed in terms of the base diameter,  $d_{b,g} = 2 r_{b,g}$ , of the gear; base lead angle,  $\lambda_{b,g}$ ; and gear face width  $F_g$ .

Use of the approach illustrated in Figure 7.5 enables a design of a helical gear. A helical involute gear of  $N_g$  teeth (Figure 7.9) has  $N_g$  left-hand-side tooth flanks and  $N_g$  right-hand-side tooth flanks. All the tooth flanks of a helical gear are terminated by the outside diameter of the gear and by the *SAP* diameter. The tooth flanks of every two neighboring teeth are connected to one another by means of a fillet and a bottom land.

It can be shown that Equation 7.12 is a particular case of Equation 7.14, and the second can be reduced to the first under the assumption of zero base lead angle (i.e.,  $\lambda_{b,g} = 0^\circ$ ).

With the equation of the lateral tooth surface of a helical involute gear (see Equation 7.14), an analysis of the local topology of the screw involute surface,  $\mathcal{G}$ , can be undertaken.

Equation 7.14 allows the calculation of two tangent vectors,  $\mathbf{U}_g(U_g, V_g)$  and  $\mathbf{V}_g(U_g, V_g)$ , which are tangential to the  $U_g$ - and  $V_g$ -coordinate lines on the surface,  $\mathcal{G}$ . These vectors are correspondingly equal to:

$$\mathbf{U}_g(U_g, V_g) = \frac{\partial \mathbf{r}_g}{\partial U_g}(U_g, V_g) = \begin{bmatrix} \cos \lambda_{b,g} \sin V_g \\ -\cos \lambda_{b,g} \cos V_g \\ -\sin \lambda_{b,g} \\ 1 \end{bmatrix} \quad (7.15)$$



FIGURE 7.9  
Helical involute gear.

$$\mathbf{V}_g(U_g, V_g) = \frac{\partial \mathbf{r}_g}{\partial V_g}(U_g, V_g) = \begin{bmatrix} -r_{b,g} \sin V_g + U_g \cos \lambda_{b,g} \cos V_g \\ r_{b,g} \cos V_g + U_g \cos \lambda_{b,g} \sin V_g \\ r_{b,g} \tan \lambda_{b,g} \\ 1 \end{bmatrix} \quad (7.16)$$

Accordingly, the corresponding unit tangent vectors,  $\mathbf{u}_g$  and  $\mathbf{v}_g$ , are equal to:

$$\mathbf{u}_g(U_g, V_g) = \frac{\mathbf{U}_g}{|\mathbf{U}_g|} \quad (7.17)$$

$$\mathbf{v}_g(U_g, V_g) = \frac{\mathbf{V}_g}{|\mathbf{V}_g|} \quad (7.18)$$

The direction of the tangent to the  $U_g$ -coordinate curve through a given point on the gear tooth flank,  $\mathcal{G}$ , is specified by the unit vector  $\mathbf{u}_g$ . Similarly, the direction of the tangent to the  $V_g$ -coordinate curve through the same point on the surface,  $\mathcal{G}$ , is specified by the unit vector  $\mathbf{v}_g$ .

The calculated vectors,  $\mathbf{U}_g$  and  $\mathbf{V}_g$ , can be used for the calculation of the fundamental magnitudes of the first order of the gear tooth flank,  $\mathcal{G}$ :

$$E_g = \mathbf{U}_g \cdot \mathbf{U}_g, \quad (7.19)$$

$$F_g = \mathbf{U}_g \cdot \mathbf{V}_g \quad (7.20)$$

$$G_g = \mathbf{V}_g \cdot \mathbf{V}_g \quad (7.21)$$

$$H_g = |\mathbf{U}_g \times \mathbf{V}_g| = \sqrt{E_g G_g - F_g^2}, \quad (7.22)$$

For a screw involute surface,  $\mathcal{G}$ , Equations 7.18 through 7.21 return the following expressions:

$$E_g = 1, \quad (7.23)$$

$$F_g = -\frac{r_{b,g}}{\cos \lambda_{b,g}} \quad (7.24)$$

$$G_g = \frac{U_g^2 \cos^4 \lambda_{b,g} + r_{b,g}^2}{\cos^2 \lambda_{b,g}} \quad (7.25)$$

These equations yield an expression for the first fundamental form,  $\Phi_{1,g}$ , of the gear tooth flank,  $\mathcal{G}$ :

$$\Phi_{1,g} \Rightarrow dU_g^2 - 2\frac{r_{b,g}}{\cos \lambda_{b,g}} dU_g dV_g + \frac{U_g^2 \cos^4 \lambda_{b,g} + r_{b,g}^2}{\cos^2 \lambda_{b,g}} dV_g^2 \quad (7.26)$$

The discriminant,  $H_g$  (see Equation 7.22), of the first fundamental form,  $\Phi_{1,g}$ , of the gear tooth flank,  $\mathcal{G}$ , can be calculated from the following formula:

$$H_g = U_g \cos \lambda_{b,g} \quad (7.27)$$



In order to derive an equation for the second fundamental form,  $\Phi_{2,g}$ , of the gear tooth surface,  $\mathcal{G}$ , the second derivatives of the position vector  $\mathbf{r}_g(U_g, V_g)$  with respect to the  $U_g$ - and  $V_g$ -parameters are required. Equations 7.15 and 7.16 for the tangent vectors,  $\mathbf{U}_g$  and  $\mathbf{V}_g$ , respectively, yield expressions for their derivatives with respect to the  $U_g$ - and  $V_g$ -parameters:

$$\frac{\partial \mathbf{U}_g}{\partial U_g}(U_g, V_g) = \begin{bmatrix} 0 \\ 0 \\ 0 \\ 1 \end{bmatrix} \quad (7.28)$$

$$\frac{\partial \mathbf{U}_g}{\partial V_g}(U_g, V_g) = \frac{\partial \mathbf{V}_g}{\partial U_g}(U_g, V_g) = \begin{bmatrix} \cos \lambda_{b,g} \cos V_g \\ \cos \lambda_{b,g} \sin V_g \\ 0 \\ 1 \end{bmatrix} \quad (7.29)$$

$$\frac{\partial \mathbf{V}_g}{\partial V_g}(U_g, V_g) = \begin{bmatrix} -r_{b,g} \cos V_g - U_g \cos \lambda_{b,g} \sin V_g \\ -r_{b,g} \sin V_g + U_g \cos \lambda_{b,g} \cos V_g \\ 0 \\ 1 \end{bmatrix} \quad (7.30)$$

By definition, the fundamental magnitudes of the second order can be represented in the following form:

$$L_g = \frac{\frac{\partial \mathbf{U}_g}{\partial U_g} \times \mathbf{U}_g \cdot \mathbf{V}_g}{H_g} \quad (7.31)$$

$$M_g = \frac{\frac{\partial \mathbf{U}_g}{\partial V_g} \times \mathbf{U}_g \cdot \mathbf{V}_g}{H_g} \quad (7.32)$$

$$N_g = \frac{\frac{\partial \mathbf{V}_g}{\partial V_g} \times \mathbf{U}_g \cdot \mathbf{V}_g}{H_g} \quad (7.33)$$

Equations 7.31 through 7.33 allow the calculation of the set of formulas for computing the second fundamental magnitudes of the helical gear tooth flank,  $\mathcal{G}$ :

$$L_g = 0 \quad (7.34)$$

$$M_g = 0 \quad (7.35)$$

$$N_g = -U_g \sin \lambda_{b,g} \cos \lambda_{b,g} \quad (7.36)$$

The final equation for the calculation of the second fundamental form of the surface,  $\mathcal{G}$ , can be composed as follows:

$$\Phi_{2,g} \Rightarrow -d\mathbf{r}_g \cdot d\mathbf{N}_g = -U_g \sin \lambda_{b,g} \cos \tau \lambda_{b,g} dV_g^2 \quad (7.37)$$

The discriminant,  $T_g$ , of the second fundamental form,  $\Phi_{2,g}$ , of the gear tooth flank,  $\mathcal{G}$ , is as follows:

$$T_g = \sqrt{L_g M_g - N_g^2} = 0 \quad (7.38)$$

Equations 7.26 and 7.37 are utilized when solving a wide variety of geometrical problems pertaining to the design of a gear. For example, they are used for the calculation of the actual value of the radius,  $R_g$ , of normal curvature of the gear tooth flank,  $\mathcal{G}$ ; for this purpose, a simple expression:

$$R_g = \frac{\Phi_{1,g}}{\Phi_{2,g}} \quad (7.39)$$

can be used. Many other parameters of the geometry of the gear tooth flank can be expressed in terms of the first and second fundamental forms,  $\Phi_{1,g}$  and  $\Phi_{2,g}$ , of the gear tooth surface,  $\mathcal{G}$ .

According to the *Bonnet\* theorem*, the specification of the first and second fundamental forms,  $\Phi_{1,g}$  and  $\Phi_{2,g}$ , determines a unique surface  $\mathcal{G}$ , and those two surfaces that have identical first and second fundamental forms must be congruent. Six fundamental magnitudes uniquely determine a surface, except its position and orientation in space. This is often called the *main theorem in surface theory*.

The specification of a gear tooth surface,  $\mathcal{G}$ , by a set of six equations for the calculation of fundamental magnitudes of the first,  $\Phi_{1,g}$ , and second,  $\Phi_{2,g}$ , orders (Table 7.1) is known as the *natural parameterization* of the gear tooth flank,  $\mathcal{G}$ .

The following statements immediately follow from the analysis of Equation 7.14:

- The curvature of the involute profile of the gear tooth flank,  $\mathcal{G}$ , at all points at the base cylinder (i.e., at the start points of the screw involute surface) is equal to infinity, and it is equal to zero at infinity.
- The principal curvatures of the gear tooth flank,  $\mathcal{G}$ , at points within the base helix are equal to  $k_{1,g} \rightarrow \infty$ , and  $k_{2,g} = 0$ , respectively.
- There is an infinite number of points at which the expressions  $k_{1,g} \rightarrow \infty$  and  $k_{2,g} = 0$  are valid.
- The first principal curvature of the gear tooth flank,  $\mathcal{G}$ , is equal to zero ( $k_{1,g} = 0$ ) at points within the straight generating line of the gear tooth surface,  $\mathcal{G}$ , whereas the second principal curvature is equal to infinity ( $k_{2,g} \rightarrow \infty$ ) at points within the base helix.
- The straight generating line (i.e., the straight-line element of the involute surface of the gear tooth flank,  $\mathcal{G}$ ) is tangential to the helix on the base cylinder. Normal vectors to the involute surface—those along the straight-line element of the gear tooth flank,  $\mathcal{G}$ —do not change their orientation; they are located within a common plane.

The aforementioned statements are based on the implementation of formulas (see Equations 7.23 through 7.25 and Equations 7.34 through 7.36) for the calculation of the fundamental magnitudes of the first order,  $\Phi_{1,g}$ , and second order,  $\Phi_{2,g}$ , of the gear tooth flank,  $\mathcal{G}$ .

**TABLE 7.1**

Fundamental Magnitudes of a Screw Involute Surface,  $\mathcal{G}$

Of the First Order, $\Phi_{1,g}$	Of the Second Order, $\Phi_{2,g}$
$E_g = 1$	$L_g = 0$
$F_g = -\frac{r_{b,g}}{\cos \lambda_{b,g}}$	$M_g = 0$
$G_g = \frac{U_g^2 \cos^4 \lambda_{b,g} + r_{b,g}^2}{\cos^2 \lambda_{b,g}}$	$N_g = -U_g \sin \lambda_{b,g} \cos \lambda_{b,g}$

\* Pierre Ossian Bonnet (November 22, 1819–June 22, 1892), a French mathematician.

### 7.1.2.3 Involute Tooth Flank of a Gear with Circular-Arc Teeth in the Lengthwise Direction

A desired line of contact,  $LC_{\text{circ}}$ , between the tooth flanks,  $\mathcal{G}$  and  $\mathcal{P}$ , of a gear and a mating pinion can be shaped in the form of a circular arc of a certain radius,  $R_{lc}$ . The desired line of contact,  $LC_{\text{circ}}$ , is entirely located within the plane of action,  $PA$ , that rolls with no slippage over the base cylinder of the gear (see Figure 6.19).

The position vector of a point,  $\mathbf{r}_g$ , of a gear tooth flank,  $\mathcal{G}$ , with circular-arc teeth in the lengthwise direction can be generated as a locus of consecutive positions of the desired line of contact,  $LC_{\text{circ}}$ , in its motion in relation to a reference system associated with the gear, as schematically illustrated in Figure 7.10, together with the plane of action,  $PA$ . Under such a scenario, the position vector of a point,  $\mathbf{r}_g$ , of a gear tooth flank,  $\mathcal{G}$ , may be construed as the summa of three vectors:

$$\mathbf{r}_g = \mathbf{A} + \mathbf{B} + \mathbf{C} \quad (7.40)$$

Here,  $|\mathbf{A}|$  is the base cylinder radius (i.e., the equality  $|\mathbf{A}| = r_{b,g}$  is observed). Vector  $\mathbf{A}$  makes roll angle,  $V_g$ , with the  $Y_g$ -axis. Axial displacement in the screw motion is given by  $|\mathbf{B}| = p_g \cdot V_g$ , which corresponds to the rotation angle  $V_g$ ;  $p_g$  designates the screw parameter (i.e., the reduced pitch, in other terminology) of the tooth flank,  $\mathcal{G}$ . Finally,  $|\mathbf{C}| = R_{lc}$  is the radius of the desired line of contact,  $LC_{\text{circ}}$ ;  $U_g$  is the angle that the vector  $\mathbf{C}$  forms with the center line of the plane of action,  $PA$ , as shown in Figure 7.10.

By projecting three vectors,  $\mathbf{A}$ ,  $\mathbf{B}$ , and  $\mathbf{C}$ , onto the axes of the coordinate system,  $X_g Y_g Z_g$ , an equation for the circular-arc involute surface of the gear tooth flank,  $\mathcal{G}$ , becomes possible. After rearranging components and transforming formulas, the equation of the circular-arc involute surface,  $\mathcal{G}$ , can be represented in the following matrix form as:

$$\mathbf{r}_g(U_g, V_g) = \begin{bmatrix} r_{b,g} \cos V_g + r_{b,g} V_g \sin V_g + R_{lc} \sin V_g \cos U_g \\ r_{b,g} \sin V_g + r_{b,g} V_g \cos V_g + R_{lc} \cos V_g \cos U_g \\ R_{lc} \sin U_g \\ 1 \end{bmatrix} \quad \begin{matrix} V_g^{(l)} \leq V_g \leq V_g^{(a)} \\ -[U_g] \leq U_g \leq +[U_g] \end{matrix} \quad (7.41)$$

Use of the approach illustrated in Figure 7.5 enables design of an involute gear with circular-arc teeth in the lengthwise direction. An involute gear of such a design with  $N_g$  teeth (Figure 7.11) has  $N_g$  left-hand-side tooth flanks and  $N_g$  right-hand-side tooth flanks. All the tooth flanks of the gear are terminated by the outside diameter of the gear and by the SAP diameter. The tooth flanks of every two neighboring teeth are connected to one another by means of a fillet and a bottom land.

The correct and incorrect approaches used to design a gear with a curved tooth shape in the lengthwise direction are schematically depicted in Figure 7.12.

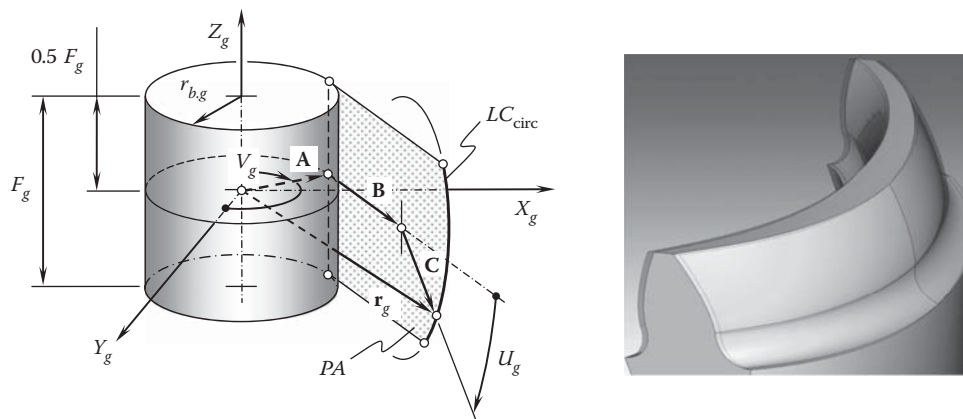
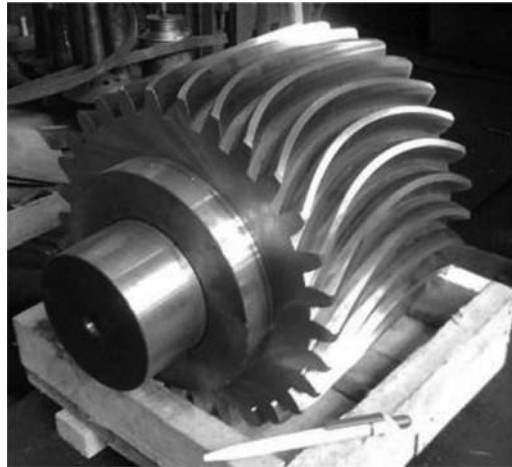


FIGURE 7.10

Geometry of tooth flank,  $\mathcal{G}$ , of an involute gear with circular-arc teeth in the lengthwise direction.



**FIGURE 7.11**  
Gear with circular-arc teeth in their lengthwise direction.

It should be stressed here that a spur gear can be sliced by a family of planes perpendicular to the gear axis, as illustrated in Figure 7.12a. Under such a scenario, the tooth profile for all the slices is the same, and the base pitch of every slice also has the same value.

If the planes of a family are not perpendicular to the gear axis but have another configuration, then the approach under consideration is not suitable for designing gear pairs. For example, a family of radial planes, as shown in Figure 7.12b, cannot be used for transformation of a spur gear into a gear with a circular arc shape in the lengthwise direction. Because the family of planes (Figure 7.12b) is not perpendicular to the gear axis, the base pitch of a slice is different from that of another slice. This consideration reveals that gear pairs with face-milled teeth are inconsistent from a geometrical as well as a kinematical standpoint. Under any circumstances, any and all changes to the geometry of the tooth flanks of a gear and its mating pinion must be *base-pitch preserving*.

Surfaces of both kinds, that is, surfaces specified by Equations 7.12, 7.14, and 7.41, are used in the design of involute gears for parallel-axes gearing. These surfaces are also used as reference surfaces for gears with modified tooth flanks. Here, the term *modification* should be understood in a wider sense: it is not just a tooth profile modification or longitudinal modification (crowning) of a gear tooth flank, but any predesigned deviation of the actual tooth flank from its nominal geometry that is desired for a particular application. Topological modification of a gear tooth flank is a perfect example in this regard.

In a very similar way, an equation for a tooth flank surface can be derived for a gear of any and all designs.

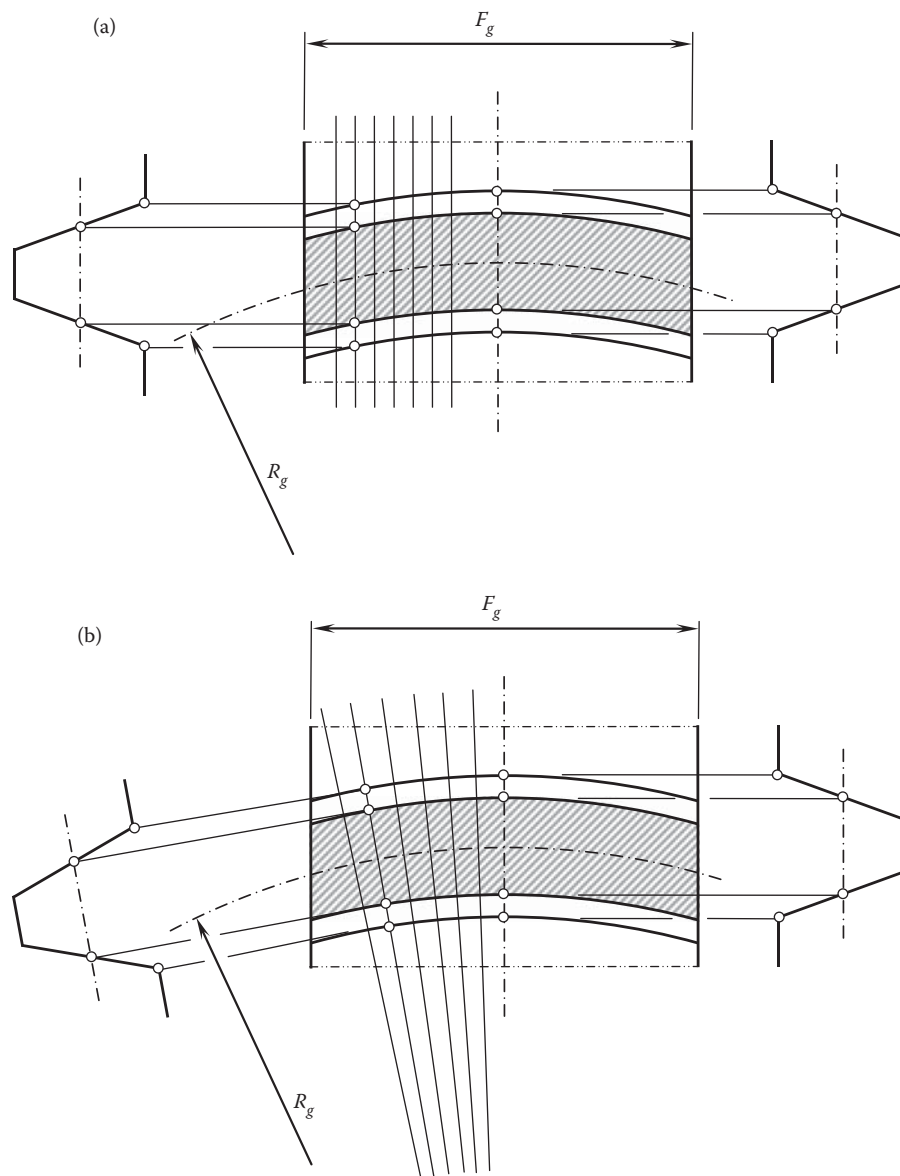
It should be stressed here that for the purpose of transmission of a rotation between two parallel shafts, a gear and a mating pinion's teeth should be shaped in the form of involutes of corresponding circles/cylinders.

### 7.1.3 Possible Form of a Gear Tooth in the Lengthwise Direction

Gears can be designed in such a way as to have various tooth forms in their lengthwise direction. Certain requirements should be fulfilled in order for a particular gear tooth form to be feasible.

In the simplest case of a spur involute gear, the gear teeth are straight and parallel to the gear axis, as schematically shown in Figure 7.13a. A spur gear can be sliced into an infinite number of infinitesimally thin slices by planes perpendicular to the gear axis. The base pitch of the gear teeth for every slice remains the same value. Because of this, a spur gear can be properly meshed with another spur gear.

No change to the base pitch of each slice of the gear occurs if the slices are turned angularly with respect to each other at a certain angular increment. Depending on the direction of the turn of the slices, the spur gear is transformed into a *helical gear* with either a positive or negative helix angle. Right-handed ( $\psi_g > 0^\circ$ ) and left-handed ( $\psi_g < 0^\circ$ ) helical gear teeth are illustrated in Figure 7.13b. In order to balance the axial thrust, two helical gears of opposite hands can be clustered into a *herringbone gear*, as shown in Figure 7.13c. For manufacturing purposes, a gap of a certain width,  $B$ , can be designed between the helical halves of the herring bone gear. Gears of this design are commonly referred to as *double-helical gears* (Figure 7.13d).

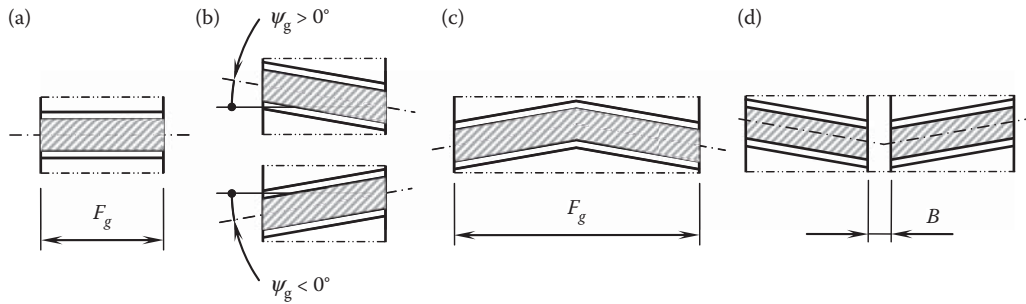
**FIGURE 7.12**

Approaches for designing a gear with curved tooth shape in the lengthwise direction: (a) correct approach, and (b) incorrect approach.

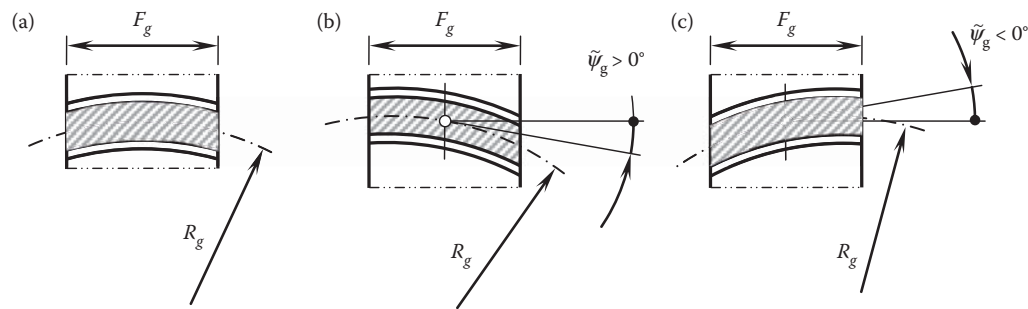
The concept of the transformation of spur gear teeth into helical, herringbone, or double-helical gear teeth can be used to enhance crossed-axis gear pairs as well.\*

No constraints are imposed on the value of the shift of the infinitesimally thin slices of a gear or on the equality of the shifts to each other. In the case of different shifts of adjacent slices, a gear with a circular arc shape in the lengthwise direction can be designed. In Figure 7.14, several possible gear designs are shown. The circular arc gear tooth of radius  $R_g$  can be located either symmetrically (Figure 7.14a) or asymmetrically. Asymmetry in two

\* In the case of a straight bevel gear for an intersected-axis gear pair, the gear tooth profile remains similar (but not identical) in all sections of the gear tooth by a sphere that has its center at the apex of the pitch cone of the bevel gear. The smaller radius of the spherical section, the smaller the gear tooth size, and vice versa. However, not all proportions of the gear tooth depend on the radius of the section by a sphere, and all the proportions remain unchanged. This property allows for the slicing of a bevel gear into an infinite number of infinitesimally thin spherical slices and then shifting the slices in relation to each other. Under a corresponding shift increment, a bevel gear with straight teeth is transformed into a bevel gear with skew teeth. Similar to helical gears, bevel gears can be designed with right-handed ( $\psi_g > 0^\circ$ ) or left-handed ( $\psi_g < 0^\circ$ ) skew teeth. Bevel gears with either herringbone or double-helical teeth are also possible.

**FIGURE 7.13**

Possible forms of gear teeth in the lengthwise direction: (a) spur gear, (b) helical gears, (c) herringbone gears, and (d) double-helical gears.

**FIGURE 7.14**

Possible forms of gear teeth with a circular arc shape in the lengthwise direction: (a) symmetric, (b) asymmetric, shifted left, and (c) asymmetric, shifted right.

opposite directions is possible (Figure 7.14b,c). The case shown in Figure 7.14b resembles a right-handed helical gear ( $\psi_g > 0^\circ$ ), whereas that shown in Figure 7.14c gear resembles a left-handed helical gear ( $\psi_g < 0^\circ$ ).

It should be stressed here that a spur gear can be sliced by a family of planes perpendicular to the gear axis, as illustrated in Figure 7.14a. Under such a scenario, the tooth profile for all the slices remains the same, and the base pitch of every slice also has the same value.

If the planes of a family are not perpendicular to the gear axis but have another configuration, then the approach under consideration is not suitable for designing gear pairs. For example, a family of radial planes, as shown in Figure 7.14b, cannot be used for transformation of a spur gear into a gear with a circular arc shape in the lengthwise direction. Because the family of planes (Figure 7.14b) is not perpendicular to the gear axis, the base pitch of a slice is different from that of another slice. This consideration reveals that gear pairs with face-milled teeth are inconsistent from a geometrical as well as a kinematical standpoint. Under any circumstances, any and all changes to the geometry of the tooth flanks of a gear and its mating pinion must be base-pitch preserving.

The discussed concept of transformation of a spur gear into a gear with a circular arc shape in the lengthwise direction can also be used to enhance intersected-axis gear pairs as well as crossed-axis gear pairs.

Not only spur, but also helical and circular arc gear teeth in their lengthwise direction, can be designed in this way. The combination of either a straight motion with a rotation or of two rotations makes it possible to design gears with teeth shaped in the lengthwise direction as follows: cycloid, epicycloid, hypocycloid, trochoid, epitrochoid, hypotrochoid,\* and involute of a circle. Parallel-axes gear pairs and intersected-axis gear pairs, as well as crossed-axis gear pairs, can be designed in this way.

Making changes to the design of an auxiliary rack is the easiest way to design gears with curved teeth in the lengthwise direction. Once the rack is designed, the teeth of the gear and the pinion can be generated as the

\* Extended cycloids (hypocycloid and hypo-trochoid) are also referred to as *prolate cycloids*. The term *curtate trochoid* is often applied to epicycloids and epitrochoids.

envelopes to consecutive positions of the rack (either a straight rack or a round rack) in its motion with respect to the gear or pinion.

#### 7.1.4 Adopted Gear Terminology

The following terminology is commonly adopted for parallel-axes gearing.

Figure 7.15 shows the names given to the elements that make up a tooth profile. Commonly (but not necessarily), the gear teeth are disposed partly above and partly below the pitch line. The complement profile is made up of the following:

- The *crest*, which is what remains of the original outer surface of the *blank* in which the teeth are cut.
- The *flanks*, which can loosely be described as the part of the profile formed by an involute or another specified curve. The opposed flanks are, for a given direction of drive, the *leading flank* and *trailing flank*.
- The *root curve*, which joins the facing flanks at the bottom of the tooth-space.
- The *tips* are the junctions between the crests and flanks, and lie in the *tip circle*, whence *tip diameter*.
- The terms *addendum* and *dedendum* are used descriptively to refer to those portions of the flank that lie outside and inside the pitch circle, respectively, in a phrase such as “pitted over the dedendum.” They can also mean, dimensionally, the radial distance of the crest above the pitch circle, and the radial distance of the bottom of the tooth-space below the pitch circle, respectively.
- The *active profile* is the portion of the flank profile that makes contact with the profile of a particular mating gear.
- The flanks, described more particularly, have a *nominal profile* defined as the geometrical basis of the tooth design, for example, involute, cycloidal, circular-arc, and others. The active profile may, as designed, depart from the nominal profile by the application of *tip-easing* or *profile modification*.
- The *fillet curve* is the curve that is the prolongation of the flank down to the root. It is of complex form and depends on the form of the cutting or finishing tools.
- The *root* is a term that sometimes means the combined fillet curves that outline the bottom of a tooth-space, as in the phrases “preformed roots” (produced by a separate operation) and “black roots” left untouched during a profile-grinding operation. But when discussing the strength of gear teeth, it means the material of a tooth where it joins the body of the gear.
- *Tip radius* is, obviously enough, a radius replacing an otherwise sharp-cornered tip, as applied to a rack cutter or hob.
- *Tip chamfer* is a chamfer applied to the tip of a tooth while the tooth is being cut in order to prevent a burr from being formed during a subsequent shaving operation.

The disposition of the addendum and dedendum relative to the pitch circle may be varied. This has long been and is still widely termed *correction*. *Addendum modification* and *profile-shift* are other terminologies related to this concern.

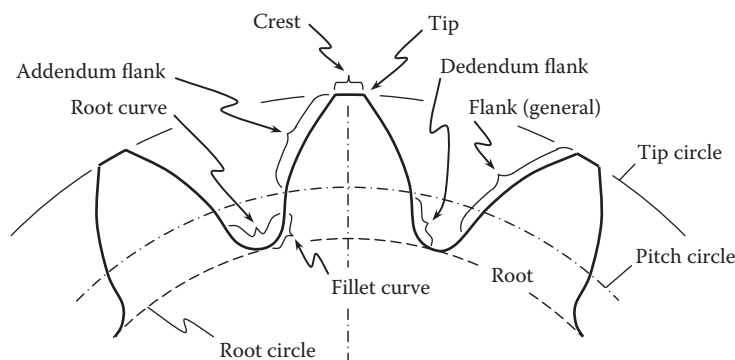
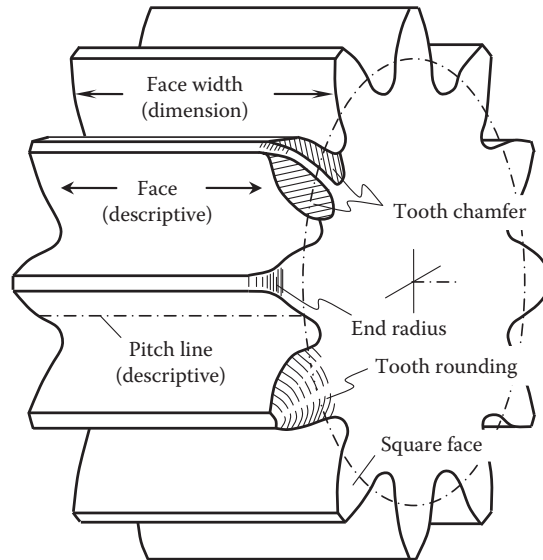


FIGURE 7.15

Tooth profile elements. (Adapted from: Merrit, H.E., *Gear Engineering*, London: Putman Publishers, 1971.)



**FIGURE 7.16**

Lengthwise tooth elements of a spur gear. (Adapted from: Merrit, H.E., *Gear Engineering*, London: Putman Publishers, 1971.)

Lengthwise tooth elements are depicted in [Figure 7.16](#).

- The *face* of a tooth, as a descriptive term, indicates the whole length of the tooth surface, as in the phrase “pitted across the entire face.”
- The *face-width* is the length of the teeth as seen in an axial section. In workshop parlance, it is sometimes shortened to *face* when abbreviating the specified particulars of a gear to, for example, “10 teeth, 4 pitch, 2 in. face.”
- The ends of teeth may be finished with an *end radius* or *end chamfer*. If they slide axially into engagement, *tooth-rounding* or *tooth-chamfering* is applied.

In a spur gear, the nominal tooth surface can be regarded as swept out by a specified profile moved axially. The line of intersection of the profile with the pitch cylinder is referred to, descriptively, as the *pitch line*. In actual manufacture, this straight line may be departed from deliberately, by *crowning*. An accidental departure is a *tooth alignment error*.

In a helical gear, the tooth surface is swept out by a specified profile moved along a helical path. The intersection of the flank with the pitch cylinder is commonly referred to as the *tooth helix*. Deliberate departure from this helix is described as *crowning* in automotive-type gears, and as *helix modification* in large, for example, marine turbine reduction gearing.

In spiral bevel gears, the term corresponding to tooth helix is *tooth spiral*, and corresponding to *combined deliberate departure*, in a mating pair, is *mismatch*.

In the *British Standard Glossary*, the geometrical curve that defines the lengthwise configuration of a tooth on the pitch surface has been named the *tooth trace*. It is a logical omnibus term covering the straight line of spur gears, the helix of helical gears, and the arbitrary curve in spiral bevel gears, but it has not yet become part of general drawing office and workshop vocabulary.

Two methods of generating an involute profile of a gear tooth are considered. According to the first method, an involute tooth profile is traced by a point within a straight line when the line is rolling with no sliding over the base circle of the gear (see [Figure 7.3](#)). In the second method, an involute tooth profile is generated as an envelope to consecutive positions of a straight line that is associated with the pitch line when the pitch line is rolling with no sliding over the pitch circle of the gear. Both methods are used in practice. However, the second method is preferred, mostly due to manufacturing issues. Gear-cutting tools of most practical designs are designed on the premises of the generating rack [112].



The theorem can be proved by means of an equivalent three-bar mechanism,  $O_pABO_g$ , that is superposed over the gear pair under consideration. The radii of curvature of the centrodes,  $r_g$  and  $r_p$ , of the three-bar mechanism are equal to  $r_g = O_gP$  and  $r_p = O_pP$ . The radii of curvature,  $\rho_g$  and  $\rho_p$ , of the conjugate tooth profiles are equal to  $\rho_g = KB$  and  $\rho_p = KA$ , respectively.

In relative motion of the gear and the pinion, the pitch circle of the gear and the pitch circle of the pinion roll without sliding over one another. This relative motion in the gear pair is equivalent to instant relative motion in the three-bar mechanism when the ratio:

$$\frac{\omega_p}{\omega_g} = \frac{O_gP}{O_pP} \quad (7.42)$$

is valid.

Consider the schematic depicted in [Figure 7.17](#) to derive the Euler-Savary equation.\*

The triangles,  $\triangle APE$  and  $\triangle ACO_p$ , are similar to one another. The similarity of the triangles allows for the expression for  $PE$ :

$$PE = O_pC \cdot \frac{AP}{AC} \quad (7.43)$$

Another expression for  $PE$ :

$$PE = O_gD \cdot \frac{BP}{BD} \quad (7.44)$$

can be drawn from the similarity of the triangles,  $\triangle BPE$  and  $\triangle BDO_g$ .

The length of the straight-line segment,  $O_gP$ , is equal to the pitch radius,  $r_g$ , of the gear ( $O_gP = r_g$ ). The length of the straight-line segment,  $O_pP$ , is equal to the pitch radius,  $r_p$ , of the pinion ( $O_pP = r_p$ ). The lengths of the straight-line segments,  $AP$  and  $BP$ , are equal to certain values,  $l_1$  and  $l_2$ .

The following equalities,

$$O_gD = r_g \cos \phi_t \quad (7.45)$$

$$O_pC = r_p \cos \phi_t \quad (7.46)$$

$$AC = l_1 - r_p \sin \phi_t \quad (7.47)$$

$$BD = r_g \sin \phi_t - l_2 \quad (7.48)$$

immediately follow from the consideration of the schematic of [Figure 7.17](#). These expressions for  $O_gD$ ,  $O_pC$ ,  $AC$ , and  $BD$  can be substituted into Equations 7.43 and 7.44:

$$r_p \cdot \frac{l_1}{l_1 - r_p \sin \phi_t} \cos \phi_t = r_g \cdot \frac{l_2}{r_g \sin \phi_t - l_2} \cos \phi_t \quad (7.49)$$

The expression:

$$\frac{1}{r_g} + \frac{1}{r_p} = \left( \frac{1}{l_1} + \frac{1}{l_2} \right) \cdot \sin \phi_t \quad (7.50)$$

immediately follows from Equation 7.49.

\* As cited in: Rosenauer, N., and Willis, A.H., *Kinematics of Mechanisms*, Associated General Publications Pty Ltd., Sydney, Australia, 1953, 395 p.

The lengths,  $l_1$  and  $l_2$ , are equal to the distances from the centers of curvature of the tooth profiles  $\mathcal{G}$  and  $\mathcal{P}$  to the pitch point,  $P$ . As follows from consideration of Figure 7.17, these lengths are equal to:

$$l_1 = AK - KP = \rho_p - x \quad (7.51)$$

$$l_2 = BK + KP = \rho_g + x \quad (7.52)$$

accordingly.

In Equations 7.51 and 7.52, the distance between the point of contact of the conjugate profiles to the pitch point is denoted by  $x$ . This distance is measured along the straight line  $n$  that is aligned with the common perpendicular to the gear,  $\mathcal{G}$ , and the pinion,  $\mathcal{P}$ , tooth profiles.

The Euler-Savary equation:

$$\frac{1}{r_g} + \frac{1}{r_p} = \left( \frac{1}{\rho_g + x} + \frac{1}{\rho_p - x} \right) \cdot \sin \phi_t \quad (7.53)$$

immediately follows from Equation 7.49.

For internal gear pairs, the pitch radius of the gear,  $r_g$ , and the radius,  $\rho_g$ , of curvature of the gear tooth profile have negative values, as they are considered concave.

It is important to mention here that for the purpose of contact stress analysis, the so-called *relative curvature*,  $\rho_{rel}$ , of the contacting tooth profiles is used. For the calculation of relative curvature, the formula:

$$\rho_{rel} = \frac{1}{\frac{1}{\rho_g} + \frac{1}{\rho_p}} = \frac{\rho_g \rho_p}{\rho_g + \rho_p} \quad (7.54)$$

can be used.

In the pitch point,  $P$ ; that is, when  $x = 0$ , Equation 7.53 returns:

$$\rho_{rel} = \frac{\rho_g \rho_p}{\rho_g + \rho_p} \cdot \sin \phi_t \quad (7.55)$$

This means that for a gear pair with a specified center distance,  $C$ , and tooth ratio,  $u$  (when the radii,  $r_g$  and  $r_p$ , of circles are known), the radius of relative curvature,  $\rho_{rel}$ , as well as the rate of contact stress, is predetermined by the pressure angle,  $\phi_t$ .

## 7.2 Alternative Approach for the Derivation of Equation of the Involute Tooth Flank

An alternative approach can be used for the derivation of an equation of the involute gear tooth profile. The relative motion of a straight line that is tangent to the involute profile at a certain point is utilized in this method. For better understanding of the approach, the schematic shown in Figure 7.3 is helpful.

### 7.2.1 Generating the Straight Line of a Spur Gear

Consider a base circle of a radius,  $r_{b.g}$ , shown in Figure 7.18 with the point  $O_g$  as the center. A point,  $P$ , is chosen at a distance,  $r_g$ , from the center,  $O_g$ . The distance,  $r_g$ , exceeds the radius,  $r_{b.g}$ , of the base circle (i.e., the inequality  $r_g \geq r_{b.g}$  is valid). The equality of the radii,  $r_g = r_{b.g}$ , can be observed in degenerate cases only.

The circle of the radius,  $r_g$ , that has the point  $O_g$  as the center is referred to as the *pitch circle*. A straight line that is tangent to the pitch circle is referred to as the *pitch line*. The pitch line is drawn up passing through the point,  $P$ . Thus,  $P$  is referred to as the *pitch point*.

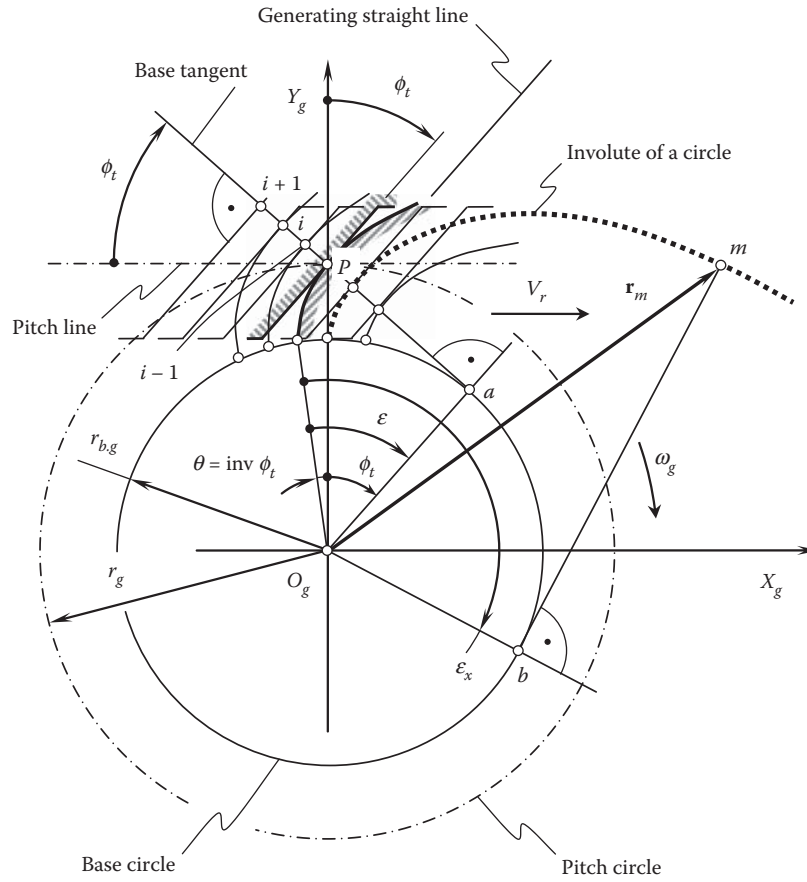


**FIGURE 7.18**  
Generation of an involute profile of a gear tooth by a straight line.

At the pitch point,  $P$ , the base tangent and the pitch line form a certain angle,  $\phi_t$ . The angle,  $\phi_t$ , is referred to as the *profile angle* of the involute curve when just the involute of a circle is considered. The angle,  $\phi_t$ , is referred to as the *pressure angle* when two conjugate profiles are considered.

When the pitch line rolls with no slippage over the pitch circle, the motion of the straight line in relation to the pitch circle can be viewed as the summa of two motions. The straight motion of the pitch line with a linear velocity,  $V_r$ , is one of the two motions. The rotation,  $\omega_g$ , of the pitch circle is the second motion. The linear velocities,  $V_r$ , of the translation and the rotation,  $\omega_g$ , are synchronized with one another to meet the requirement of rolling with no slippage. The requirement of rolling with no slippage can be expressed analytically as:

$$\frac{V_r}{\omega_g} = r_g \quad (7.56)$$

A straight line through the pitch point,  $P$ , forms a transverse pressure angle,  $\phi_t$ , with a perpendicular to the pitch line. When the gear rotates, and when the pitch line rolls with no slippage over the pitch circle, the straight line travels straight together with the pitch line. The motion of the straight line together with the pitch line is equivalent to the motion of the contact point along the base tangent, that is, along the line of action,  $LA$ , as it follows from the analysis of Figure 7.18. As the angle that the straight line forms with the perpendicular to the pitch line is of a constant value,  $\phi_t$ , the straight line is further referred to as the *generating straight line*. This property of the generating straight line is employed below with the aim of generating an involute tooth profile.

The generating straight line travels together with the pitch line, as they are rigidly connected to each other. When traveling, the generating straight line occupies consecutive positions in relation to the pitch circle. At

every position of the generating straight line, the profile angle,  $\phi_t$ , retains the same value. The involute tooth profile can be interpreted as an envelope to consecutive positions of the generating straight line in its motion in relation to the pitch circle. The possibility of generating an involute of a circle as an envelope to consecutive positions of a generating straight line is illustrated below.

Several points,  $i$ , can be chosen within a generating line (base tangent), as is depicted in Figure 7.18 (here,  $i$  is an integer number). When the generating line rolls over the base circle of a radius  $r_{b,g}$ , each point traces a corresponding involute of the circle. All the involutes are offset with respect to one another, or, in other words, the involutes are parallel to each other. The angle that the generating straight line (base tangent) makes with the rolling pitch line is of the same value for all the positions of the generating line. This angle equals  $(90^\circ - \phi_t)$ , where  $\phi_t$  is the profile angle of the involute curve at the pitch point,  $P$ .

The performed descriptive analysis can be complemented by an analytical proof of the possibility of generation of an involute of a circle by means of the moving straight generating line (base tangent) when the straight line is associated with the pitch line. Use of the kinematic method for determining an involute profile as an envelope to the consecutive position of a moving straight line is helpful for this purpose.

The kinematic method is based on implementation of Shishkov equation of contact:

$$\mathbf{n}_g \cdot \mathbf{V}_\Sigma = 0 \quad (7.57)$$

In Equation 7.57, the common perpendicular to the contacting profiles is designated as  $\mathbf{n}_g$ , and the vector of linear velocity of the resultant relative motion of the moving curves is denoted by  $\mathbf{V}_\Sigma$ .

The kinematic method for determination of enveloping curves and surfaces was significantly contributed by Prof. Shishkov in the late 1940s and at the beginning of the 1950s [147,148]. It is preferred to use this method in cases when both the unit common perpendicular,  $\mathbf{n}_g$ , as well as the linear velocity vector,  $\mathbf{V}_\Sigma$ , of the resultant relative motion can be determined with no use of derivatives of the equation of the moving curve with respect to the parameter, which specifies a point within the curve (when the vector,  $\mathbf{n}_g$ , is determining it) and with respect to the parameter of motion (when the linear velocity vector,  $\mathbf{V}_\Sigma$ , is determining it).

The equation of contact is of principal importance for the kinematic method of determining enveloping profiles.

Consider a given involute profile associated with the base circle of a radius  $r_{b,g}$ , as depicted in Figure 7.18. An equation of a profile that is associated with the pitch line when the pitch line is rolling with no slippage over the pitch circle of a radius  $r_g$  needs to be derived.

Referring to Figure 7.18, the position vector of a point,  $\mathbf{r}_m$ , of the involute profile can be described by an equation in vector representation:

$$\mathbf{r}_m(\varepsilon_x) = \mathbf{i} \cdot r_{b,g} [\sin(\varepsilon_x - \theta) - \varepsilon_x \cos(\varepsilon_x - \theta)] + \mathbf{j} \cdot r_{b,g} [\cos(\varepsilon_x - \theta) + \varepsilon_x \sin(\varepsilon_x - \theta)] \quad (7.58)$$

or in a form of matrix:

$$\mathbf{r}_m(\varepsilon_x) = r_{b,g} \cdot \begin{bmatrix} \sin(\varepsilon_x - \theta) - \varepsilon_x \cos(\varepsilon_x - \theta) \\ \cos(\varepsilon_x - \theta) + \varepsilon_x \sin(\varepsilon_x - \theta) \\ 0 \\ 1 \end{bmatrix} \quad (7.59)$$

The parameter,  $\varepsilon_x$ , of the involute curve is shown in Figure 7.18.

When the pitch line rolls with no slippage over the pitch circle, the involute curve occupies different positions in relation to the pitch line. To specify a point within the involute curve in its current configuration with respect to the pitch line, it is necessary to compose the operator  $\mathbf{Rs}(g \mapsto r)$  of the resultant coordinate system transformation. In the particular case under consideration, the operator  $\mathbf{Rs}(g \mapsto r)$  can be represented in the form:

$$\mathbf{Rs}(g \mapsto r) = \begin{bmatrix} -\sin \vartheta & \cos \vartheta & 0 & r_g \vartheta \\ \cos \vartheta & \sin \vartheta & 0 & -r_g \vartheta \\ 0 & 0 & 1 & 0 \\ 0 & 0 & 0 & 1 \end{bmatrix} \quad (7.60)$$

In Equation 7.60, an angle that specifies angular configuration of the involute curve in its current location with respect to the initial location is denoted by  $\vartheta$ .

It should be mentioned here that as long as a two-dimensional problem is considered, the third row and third column in Equation 7.60 can be eliminated. In this way, the  $4 \times 4$  matrix (see Equation 7.60) can be reduced to a corresponding  $3 \times 3$  matrix. The operator of the resultant coordinate system transformation,  $\mathbf{Rs}(g \mapsto r)$ , is written in the form of  $4 \times 4$  matrix only to maintain the uniform style of the coordinate system transformations for two-dimensional cases as well as for three-dimensional (spatial) cases of gear pairs.

For the calculation of the position vector of a point,  $\mathbf{r}_m^r$ , within the involute curve in its current configuration with respect to the pitch line, the expression:

$$\mathbf{r}_m^r(\varepsilon_x, \vartheta) = \mathbf{Rs}(g \mapsto r) \cdot \mathbf{r}_m(\varepsilon_x) \quad (7.61)$$

can be used.

Points that are specified by the position vector  $\mathbf{r}_m^r$  include the points of the enveloping profile to be determined. The position vector of a point of the enveloping profile satisfy both, namely, they satisfy Equation 7.61 as well as the equation of contact,  $\mathbf{n}_g \cdot \mathbf{V}_\Sigma = 0$ . The latter can be used to eliminate the parameter  $\vartheta$  from Equation 7.61.

It makes sense to derive an equation of contact,  $\mathbf{n}_g \cdot \mathbf{V}_\Sigma = 0$ , for a gear tooth profile of an arbitrary shape, as this equation is of importance from a more general viewpoint rather than only for the particular problem under consideration.

Consider an arbitrary tooth profile,  $\mathcal{G}$ , associated with a reference system,  $X_g Y_g$ , as shown in Figure 7.19. In the coordinate system,  $X_g Y_g$ , associated with pitch circle, the unit normal vector,  $\mathbf{n}_g$ , to the tooth profile,  $\mathcal{G}$ , can be described by the following equation:

$$\mathbf{n}_g = \mathbf{i} \cdot \tan(\phi_{t,x} + \vartheta) - \mathbf{j} \quad (7.62)$$

The instant motion of point,  $m$ , within the tooth profile,  $\mathcal{G}$ , is the instant rotation about the pitch point,  $P$ . This immediately allows for an expression for a unit vector,  $\mathbf{v}_\Sigma$ , along the vector of linear velocity,  $\mathbf{V}_\Sigma$ , of the resultant

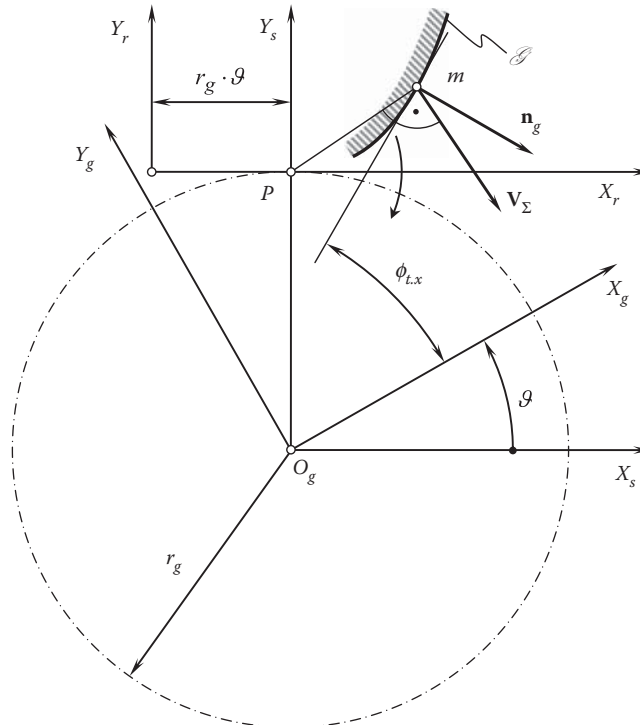


FIGURE 7.19  
Derivation of the equation of the tooth flank,  $\mathcal{G}$ , of an involute spur gear.



relative motion:

$$\mathbf{v}_\Sigma = \mathbf{i} \cdot X_m - \mathbf{j} \cdot Y_m \quad (7.63)$$

In Equation 7.63,  $X_m$  and  $Y_m$  designate the coordinates of the point of interest,  $m$ .

The transition from the coordinate system,  $X_g Y_{g'}$ , associated with pitch circle to the coordinate system,  $X_r Y_r$ , embedded to the pitch line, can be analytically expressed by the operator,  $\mathbf{Rs}(g \mapsto r)$ , of the resultant coordinate system transformation (see Equation 7.60).

With that done, the equation of contact,  $\mathbf{n}_g \cdot \mathbf{V}_\Sigma = 0$ , can be rewritten in the form:

$$\sin(\phi_{t,x} + \vartheta) = \frac{X_g \cos \phi_{t,x} + Y_g \sin \phi_{t,x}}{r_g} \quad (7.64)$$

In a particular case of the involute tooth profile, the equality  $\phi_{t,x} = 90^\circ - (\varepsilon_x - \theta)$  is observed. This expression, considered together with the equation for the involute profile (see Equation 7.58), makes possible a reduction of the equation of contact in the form of Equation 7.64 as:

$$\sin(\phi_{t,x} + \vartheta) = \frac{r_{b,g}}{r_g} = \cos \phi_t \quad (7.65)$$

The last expression immediately returns a formula:

$$\vartheta = \varepsilon_x - \varepsilon_0 = \tan \phi_{t,x} - \tan \phi_t \quad (7.66)$$

for the calculation of the parameter  $\vartheta$ .

The derived equation for the calculation of the angle,  $\vartheta$ , and Equation 7.61 considered together allow for the expression for the position vector of a point of the envelope:

$$\mathbf{r}_m^r(Y_r) = \mathbf{i} \cdot Y_r \cot \phi_t + \mathbf{j} \cdot Y_r \quad (7.67)$$

or in matrix representation:

$$\mathbf{r}_m^r(Y_r) = \begin{bmatrix} Y_r \cot \phi_t \\ Y_r \\ 0 \\ 1 \end{bmatrix} \quad (7.68)$$

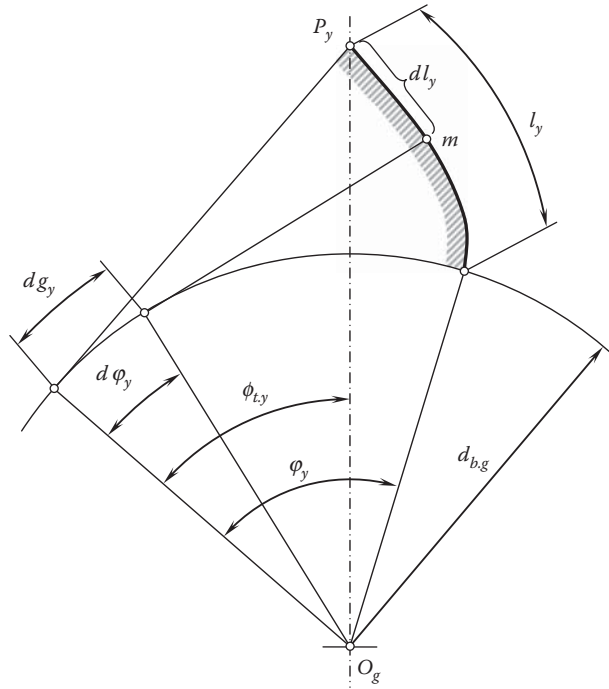
Formally, the position vector of a point,  $\mathbf{r}_m^r$ , of the enveloping profile is a function of the rotation angle,  $\varepsilon_x$ . However, the right side in Equation 7.67 does not depend on  $\varepsilon_x$ . This indicates that rolling of the generating line (base tangent) over the base circle and rolling of the pitch line over the pitch circle are equivalent to one another. Therefore, an involute profile can be generated by a straight line at a constant angle with respect to the pitch line with which it is associated.\*

### 7.2.2 Length of Involute Tooth Profile

It is the right point to consider the arc length of an involute tooth profile, as it is often used in the theory of involute gearing. The arc length of an involute tooth profile can be determined in the following way.

Consider an arc of infinitesimally small length,  $dl_y$ , of the involute tooth profile and the corresponding roll distance,  $dg_y$ , on the base circle, as shown in Figure 7.20.

\* This conclusion is valid only for a case of parallel-axes gearing, and is not valid in cases of intersected-axes or crossed-axes gearings. A crown rack with a straight-sided tooth profile for the cases of intersected-axes and crossed-axes gearings is a kind of approximation.

**FIGURE 7.20**

Relationship between an elemental length of arc,  $dl_y$ , on the involute tooth flank and the corresponding elemental length of arc,  $dg_y$ , on the base circle.

The following relationships are valid:

$$dl_y = r_{b,g} \tan \phi_{t,y} d\phi_y \quad (7.69)$$

$$\tan \phi_{t,y} = \phi_y \quad (7.70)$$

Hence,

$$dl_y = r_{b,g} \phi_y d\phi_y \quad (7.71)$$

The total length of the involute from the base circle to a current point,  $m$ , is equal to  $l_y$ . This length can be obtained by integration between the limits of 0 and  $\phi_y$ :

$$l_y = \int_0^{\phi_y} dl_y = r_{b,g} \int_0^{\phi_y} \phi_y d\phi_y = r_{b,g} \frac{\phi_y^2}{2} \quad (7.72)$$

The length,  $l_{ab}$ , of the involute profile, which is active during the path of contact,  $g_a$ , as shown in [Figure 7.21](#), is obtained below from [Figure 7.20](#).

The length,  $l_{ab}$ , is equal to the difference between the total profile lengths,  $l_a$  and  $l_b$ , at the corresponding points  $a^*$  and  $b^*$ :

$$l_{ab} = l_a - l_b \quad (7.73)$$

$$l_{ab} = \frac{r_{b,g}}{2} (\tan^2 \phi_{t,a} - \tan^2 \phi_{t,b}) \quad (7.74)$$

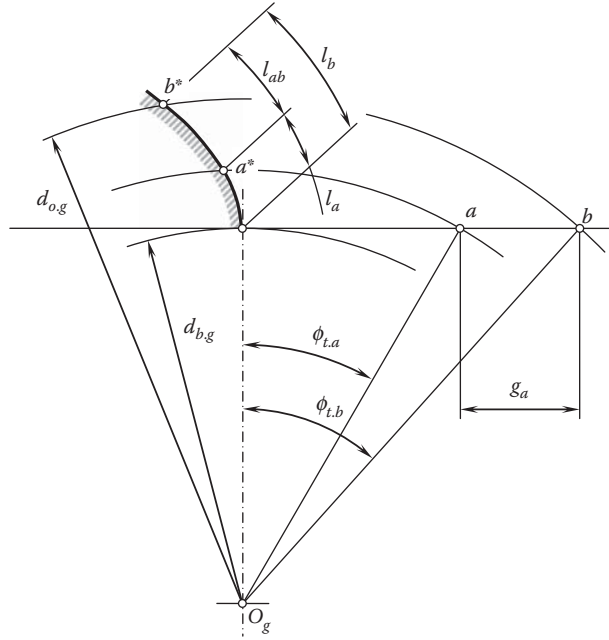


FIGURE 7.21

Relationship between the length of the path of contact,  $g_a$ , and the corresponding (active) length of the involute profile,  $l_{ab}$ .

where:

$$\tan \phi_{t,b} = \tan \phi_{t,a} - \frac{g_a}{r_{b,g}} \quad (7.75)$$

$$\cos \phi_{t,a} = \frac{d_{b,g}}{d_{o,g}} \quad (7.76)$$

and

$$l_{ab} = g_a \left( \tan \phi_{t,a} - \frac{g_a}{d_{b,g}} \right) \quad (7.77)$$

Studying gear teeth sliding is one possible application for the above-derived Equations 7.72 and 7.77.

### 7.2.3 Generating the Basic Rack of a Spur Gear

Generating the basic rack of a spur gear can be accomplished using the straight tooth profile that is specified by Equations 7.67 and 7.68.

The basic rack,  $\mathcal{R}$ , of a spur gear (a generating rack,  $\mathcal{R}$ ), is developed on the premise of the generating straight line (base tangent) (see Equation 7.67). The generating rack,  $\mathcal{R}$ , is shaped in the form shown in Figure 7.21, and it is conjugate to the gear.

The transverse profile angle,  $\phi_t$ , of the generating rack tooth is equal to the profile angle of the gear tooth measured on the pitch diameter. In the most standards issued in industrially developed countries, the specified profile angle equals  $\phi_t = 20^\circ$ . Gears that have a profile angle of  $\phi_t = 14^\circ$  are used in the design of low-noise transmissions. Gears that have a profile angle  $\phi_t = 28^\circ$  are used in the design of heavily loaded gear trains. Gears with profile angles of other values are used as well.

It is common practice to specify the generating rack,  $\mathcal{R}$ , either by module,  $m$ , or by diametral pitch,  $P$ , of the generating rack. For the calculation of the rest of the design parameters (Figure 7.22a), standard formulas are used. These formulas are summarized in Table 7.2.

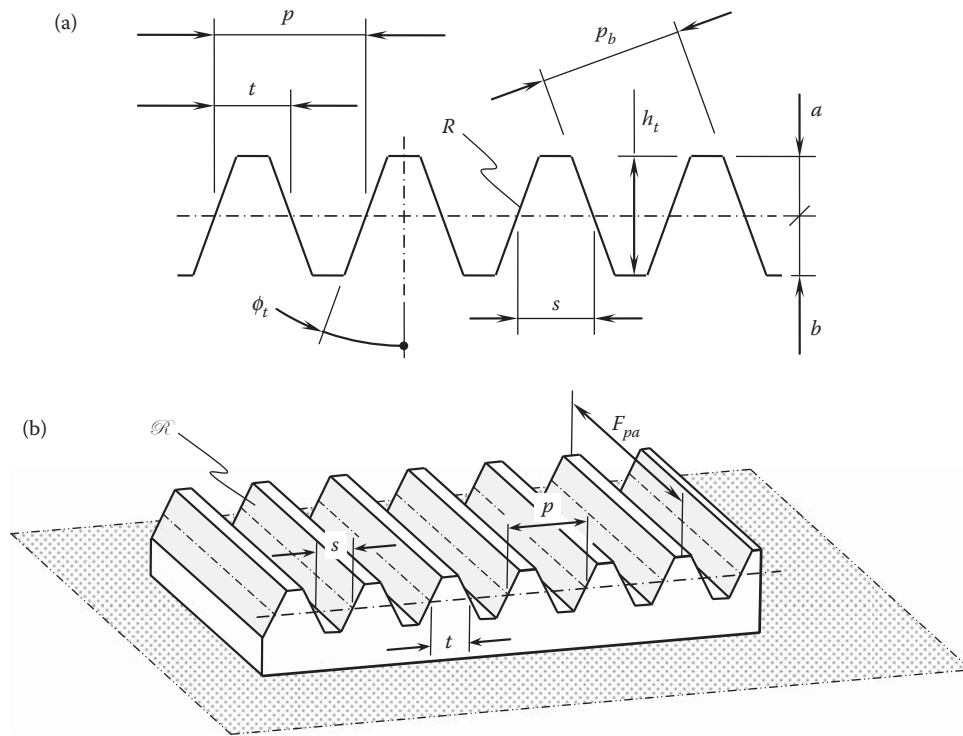


**FIGURE 7.22**  
Generating rack,  $\mathcal{R}$ , of a spur involute gear: (a) the rack profile, and (b) 3D schematic of the rack.

The formula  $m = 25.4/P$  is commonly used for the purpose of the conversion of diametral pitch,  $P$ , to module,  $m$ .

The specified width,  $F_{pa}$ , of a generating rack (Figure 7.22b) is equal to the overlap of a gear face width,  $F_g$ , and a corresponding pinion face width,  $F_p$ .

The basic rack profile is *fundamental* to the specification of involute gears. The tooth profile on the gear, the generating rack profile, and the associate rack by means of which gear-cutting tools are shaped, can all be determined in terms of the basic rack. The relationship between these is discussed below.

**TABLE 7.2**

Design Parameters of a Spur Generating Rack

Design Parameter of the Rack	Metric	English
Normal pitch (mm)	$p = \pi \cdot m$	$p = \frac{\pi}{P}$
Base pitch (mm)	$p_b = \pi \cdot m \cdot \cos \phi$	$p_b = \frac{\pi}{P} \cdot \cos \phi$
Addendum (mm)	$a = m$	$a = \frac{1}{P}$
Dedendum <sup>a</sup> (mm)	$b = 1.25 m$	$b = \frac{1.25}{P}$
Tooth height (mm)	$h_t = a + b = 2.25 m$	$h_t = \frac{2.25}{P}$
Tooth thickness (mm)	$t = \frac{\pi m}{2}$	$t = \frac{\pi}{2P}$
Space width (mm)	$s = \frac{\pi m}{2}$	$s = \frac{\pi}{2P}$

<sup>a</sup> For the calculation of dedendum  $b$  of a small module gear (of a fine pitch gear) the formula  $b = 1.35 m$  (or the equivalent formula  $b = \frac{1.35}{P}$ ) is often used.

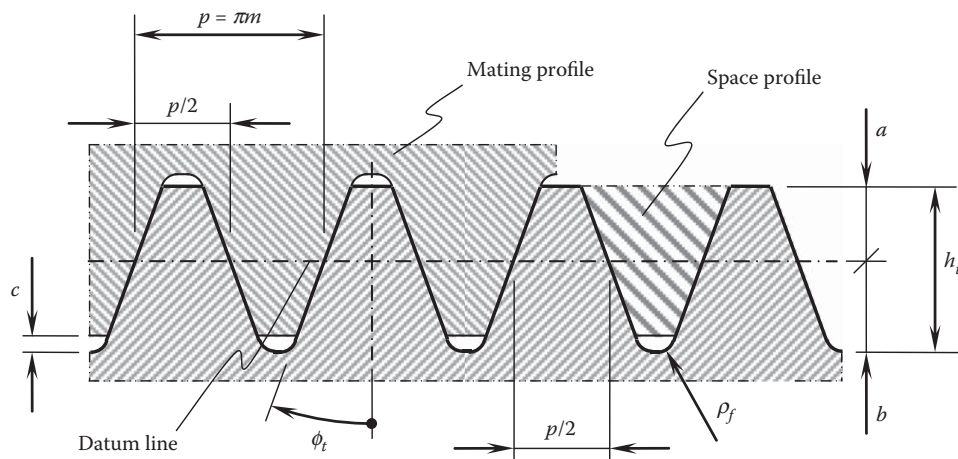


FIGURE 7.23

The correspondence between the generating rack,  $\mathcal{R}$ , and mating rack profiles.

As with a standard rack profile, the tooth thickness is equal to the tooth space width at the profile datum line and hence to half the pitch. Therefore, a gear and a mating gear can be cut with the same gear-cutting tool. The entire dimensions for defining the basic rack profile must be contained in the tooth data.

*The basic rack profile can be viewed as the normal section through the teeth of a basic rack, which corresponds to a gear with number of teeth  $N_g \rightarrow \infty$ , and thus of pitch diameter  $d_g \rightarrow \infty$ .*

The tooth of the basic rack profile is bounded by the tip line at the top and by the parallel root line at the bottom. The fillet between the straight tooth flank and the root line is usually of circular arc form, as shown in Figures 7.23 and 7.24.

The characteristics of the base rack are as follows:

- The basic rack profile with module  $m$  has a pitch  $P = \pi m$ .
- The datum line is the line drawn parallel to the tip and root lines where the tooth thickness is equal to the tooth space width and is equal to half the pitch  $P/2$ .
- The dimensions of the basic rack profile are given relative to the datum line and are quoted as a multiple of the module  $m$ . Dimensions relating to module  $m = 1.0$  are commonly identified by asterisk (\*), that is,  $a^*$ .

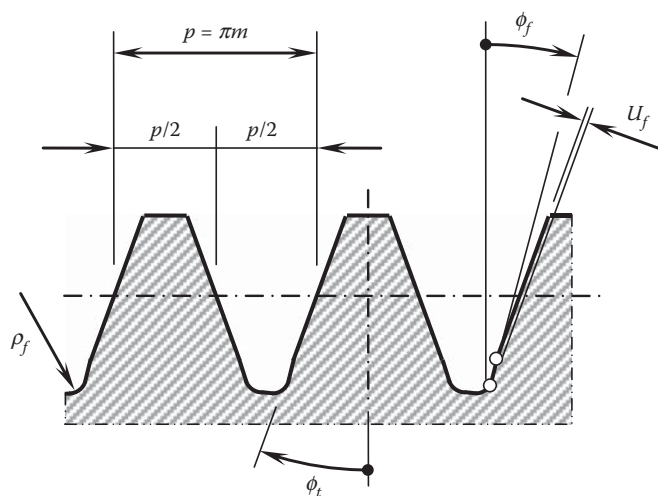


FIGURE 7.24

Basic rack profile with (intentional) fillet undercut.

- The mating rack profile is symmetrical to the basic rack profile about the datum line and is displaced by half a pitch in relation to it.
- The usable parts of the flank are inclined at the profile angle,  $\phi_t$ , to a line normal to the datum line. This angle is the same as the pressure angle,  $\phi_t$  (or  $\phi_n$ ), at the reference cylinder of the gear.
- The tooth depth,  $h_t$ , is divided by the datum line into the addendum,  $a$ , and the dedendum,  $b$ .
- The dedendum,  $b$ , is equal to the summa of the addendum,  $a$ , and the bottom clearance,  $c$ .
- The greatest possible fillet radius,  $\rho_f$ , is determined by the bottom clearance,  $c$ . The condition for this is [74]:

$$\rho_f \leq \left( \frac{\pi m}{4} - b \tan \phi_t \right) \cdot \tan \left( \frac{90^\circ + \phi_t}{2} \right) \quad (7.78)$$

This issue is discussed in more detail in the monograph by Prof. Radzevich [112].

- The basic rack profile with an (intentional) fillet undercut with depth,  $U_f$ , and the profile angle,  $\phi_f$ , which is schematically depicted in Figure 7.24, is used for gears cut by a protuberance gear-cutting tool and finished by grinding.
- The generating rack profile for generating external spur and helical gears is the counterpart of the basic rack profile, that is, the space profile. The true shape of the fillet produced on the gear is a trochoid generated by the tip of the generating rack profile.

Apart from the standard profile angle,  $\phi_t = 20^\circ$ , other profile angles are employed for special applications:

- $\phi_t = 15^\circ$  for certain printing machinery and kinematically exacting gear drives, such as for the movement of telescopes or radar reflectors
- $\phi_t = 17^\circ 30'$  for marine gears with deep teeth where particularly quiet running is required
- $\phi_t = 22^\circ 30'$  and  $\phi_t = 25^\circ$  for cases where the flanks are subjected to externally high contact stresses

Addenda other than the standard  $a = 1 \cdot m$  are used for certain applications:

- $a = 0.75 \cdot m$  for stub teeth for gear of couplings
- $a = 1.25 \cdot m$  for marine gears with deep teeth

Requirements for root forms with an increased bending strength can also be met by:

- $a = 4/3 \cdot m$  for teeth with full fillet root finished by planing with a rack type cutter
- $a = 7/5 \cdot m$  for teeth with full fillet root and intentional fillet undercut (protuberance tool) at the run-out of the grinding allowance finished by grinding (Figure 7.24)

Having calculated the design parameters of a spur rack, the corresponding design parameters of a spur gear with a given tooth number,  $N_g$ , can be calculated as well. Standard equations are used for the calculation of the design parameters of a spur gear. These equations are summarized in Table 7.3.

The involute function,  $\text{inv} \phi_t$ , is used for the purpose of calculating tooth crest width,  $t_o$ , in Table 7.3. The involute function is defined as:

$$\text{inv} \phi_t = \tan \phi_t - \phi_t(\text{rad}) \quad (7.79)$$

For the calculation of profile angle,  $\phi_t$ , expressed in radians, a well-known formula:

$$\phi_t(\text{rad}) = \frac{\pi}{180} \cdot \phi_t^\circ \quad (7.80)$$

is commonly used.

**TABLE 7.3**

Design Parameters of a Spur Gear

Design Parameter of the Gear	Metric	English
Pitch diameter (mm)	$d = mN_g$	$d = \frac{N_g}{P}$
Base diameter (mm)	$d_{b,g} = d_g \cos \phi_t = m N_g \cos \phi_t$	
Base pitch (mm)	$P_b = \frac{\pi d_g}{N_g} \cos \phi_t = p \cos \phi_t$	
Normal tooth thickness (mm)	$t = m \left( \frac{\pi}{2} + 2 \cdot \xi \cdot \tan \phi_t \right)$	$t = \frac{1}{P} \left( \frac{\pi}{2} + 2 \cdot \xi \cdot \tan \phi_t \right)$
Tooth thickness at an arbitrary diameter $d_y$ (mm)	$t_y = d_{g,y} \left( \frac{t}{mN_g} + \text{inv } \phi_t - \text{inv } \phi_{t,y} \right)$	$t_y = d_{g,y} \left( \frac{tP}{N_g} + \text{inv } \phi_t - \text{inv } \phi_{t,y} \right)$
Tooth crest width <sup>a</sup> , mm	$t_o = d_{o,g} \left( \frac{t}{mN_g} + \text{inv } \phi_t - \text{inv } \phi_{t,o} \right)$	$t_o = d_{o,g} \left( \frac{tP}{N_g} + \text{inv } \phi_t - \text{inv } \phi_{t,o} \right)$
Standard outside diameter (mm)	$d_{o,g} = d_g + 2m$	$d_{o,g} = d_g + 2a$
Root diameter (mm)	$d_{f,g} = d_g - 2h_t$	
Circular pitch (mm)	$p = \frac{\pi d_g}{N}$	
Average backlash per gear pair (mm)	$B = 0.040 m$	$B = \frac{0.040}{P}$

<sup>a</sup>Here, the tooth profile angle at the outer diameter,  $d_{o,g}$ , of the gear is designated as  $\phi_{t,o}$ .

Normal tooth thickness,  $t$ , is expressed in terms of the profile shift correction coefficient,  $\xi$ . The profile shift correction coefficient,  $\xi$ , is defined by the formula

$$\xi = \frac{\Delta x}{m} \quad (7.81)$$

In Equation 7.81, the actual value of the tooth profile shift is denoted by  $\Delta x$ .

### 7.2.3.1 Alternative Approach for the Derivation of Equation of Helical Involute Gear Tooth Flank

The discussed approach for the generation of the tooth flank of a spur involute gear by means of a plane that is tangent to the base cylinder can be enhanced for generation of the tooth flank of a helical gear. In the alternative approach for the derivation of the equation of a helical involute gear tooth flank, the tooth flank is generated as an envelope to consecutive positions of a plane that performs a screw motion about the gear axis of rotation.

The tooth flank,  $\mathcal{G}$ , can be generated by a plane,\*  $\mathcal{R}$ , that performs a screw motion about the gear axis. The plane,  $\mathcal{R}$ , makes a certain angle in relation to the gear axis,  $O_g$ . This angle can be specified in terms of the gear transverse profile angle,  $\phi_t$ , and of the plane inclination angle,  $\psi_r$ . It is proven that the angle that the plane,  $\mathcal{R}$ , forms with the gear axis,  $O_g$ , is equal to the base helix angle,  $\psi_{b,g}$ , of the gear. The angle,  $\psi_{b,g}$ , can be calculated from the formula [105]:

$$\psi_{b,g} = \cos^{-1} (\cos \phi_t \cdot \sin \psi_r) \quad (7.82)$$

\* This statement is valid only for a case of parallel-axes gearing, and is not valid in cases of intersected-axes or crossed-axes gearings. A crown rack with a straight-sided tooth profile for the cases of intersected-axes and crossed-axes gearings is a kind of approximation, and cannot be used for the generation of tooth flanks in perfect gearings.



The expression (see Equation 7.76) can be represented in the form:

$$\psi_{b,g} = \cot^{-1} \left( \frac{\cos \phi_t}{\sqrt{\sin^2 \phi_t + \cot^2 \psi_r}} \right) \quad (7.83)$$

which is known from other sources and can be convenient in some applications.

Once the angle between the lateral plane of the rack,  $\mathcal{R}$ , and the gear axis,  $O_g$ , is known, the tooth flank of the helical gear can be determined.

Consider a plane,  $\mathcal{R}$ , that is performing a screw motion, as shown in Figure 7.25. The plane,  $\mathcal{R}$ , makes a certain angle,  $\psi_{b,g}$ , with the  $X_0$ -axis of a Cartesian coordinate system  $X_0Y_0Z_0$ . The reduced pitch,  $p$ , of the screw motion is given. The axis,  $X_0$ , is the axis of the screw motion.

The auxiliary coordinate system,  $X_1Y_1Z_1$ , is rigidly connected to the plane,  $\mathcal{R}$ .

The equation of the plane,  $\mathcal{R}$ , can be represented in the form:

$$Y_1 = X_1 \cdot \tan \psi_{b,g} \quad (7.84)$$

The auxiliary Cartesian coordinate system,  $X_1Y_1Z_1$ , performs a screw motion together with the plane,  $\mathcal{R}$ , in relation to the motionless coordinate system,  $X_0Y_0Z_0$ . In the coordinate system  $X_1Y_1Z_1$ , the unit normal vector,  $\mathbf{n}_r$ , to the plane,  $\mathcal{R}$ , can be analytically expressed as:

$$\mathbf{n}_r = \begin{bmatrix} 1 \\ -\tan \psi_{b,g} \\ 0 \\ 1 \end{bmatrix} \quad (7.85)$$

The position vector,  $\mathbf{r}_r$ , of an arbitrary point,  $m$ , within the plane,  $\mathcal{R}$ , can be expressed by:

$$\mathbf{r}_r = \begin{bmatrix} X_r \\ Y_r \\ Z_r \\ 1 \end{bmatrix} \quad (7.86)$$

where  $X_r$ ,  $Y_r$ , and  $Z_r$  are the Cartesian coordinates of a point of the plane,  $\mathcal{R}$ .

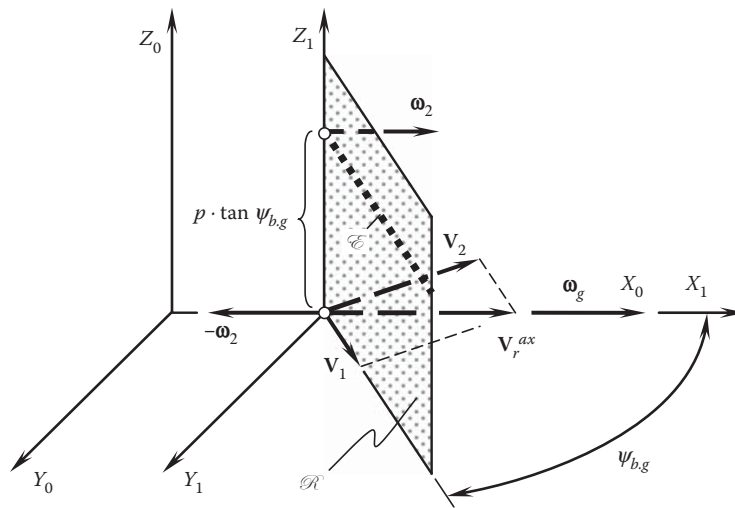


FIGURE 7.25

Generation of a screw involute surface,  $\mathcal{G}$ , as an envelope to consecutive positions of a lateral plane of the rack,  $\mathcal{R}$ , that performs a screw motion.

The resultant speed of the point,  $m$ , in the screw motion of the plane,  $\mathcal{R}$ , can be expressed by the vector  $\mathbf{v}_m$ :

$$\mathbf{v}_m = \mathbf{v} + [\boldsymbol{\omega}_g \times \mathbf{R}] \quad (7.87)$$

where

$\mathbf{v}$  is the linear velocity vector of the translation.

$\boldsymbol{\omega}_g$  is the speed of the rotation.

$\mathbf{R}$  is the position vector of point,  $m$ , with respect to the axis of the screw motion (magnitude of the vector  $\mathbf{R}$  is equal to the distance of point,  $m$ , from the  $X_0$ -axis, and the vector,  $\mathbf{R}$ , is pointed from the axis  $X_0$  to point  $m$ ).

The envelope to consecutive positions of the plane,  $\mathcal{R}$ , that performs a screw motion is identical to the surface that is represented by the loci of consecutive positions of the characteristic line,  $\mathcal{E}$ , that performs the same screw motion as the plane does. The derivation of an equation of the envelope,  $\mathcal{G}$ , to consecutive positions of the plane,  $\mathcal{R}$ , can be significantly simplified if, rather than the screw motion of the plane,  $\mathcal{R}$ , being considered, the screw motion of the characteristic line,  $\mathcal{E}$ , is considered instead.

The direction of the vector,  $\mathbf{v}_m$ , is of importance for determining the characteristic line,  $\mathcal{E}$ , while the magnitude of the vector,  $\mathbf{v}_m$ , is not of interest. Because of this, it can be assumed that the magnitude of the rotation vector,  $\boldsymbol{\omega}_g$ , is  $|\boldsymbol{\omega}_g| = 1$ . Therefore\*

$$\boldsymbol{\omega}_g = \mathbf{i}, \quad (7.88)$$

$$\mathbf{v} = \mathbf{i} \cdot p \quad (7.89)$$

This yields:

$$\mathbf{v}_m = \mathbf{i} \cdot p + \begin{vmatrix} \mathbf{i} & \mathbf{j} & \mathbf{k} \\ 1 & 0 & 0 \\ X_1 & Y_1 & Z_1 \end{vmatrix} \quad (7.90)$$

and

$$\mathbf{v}_m = \mathbf{i} \cdot p - \mathbf{j} \cdot Y_1 + \mathbf{k} \cdot Z_1 \quad (7.91)$$

At any point within the characteristic line,  $\mathcal{E}$ , the dot product of the unit normal vector,  $\mathbf{n}_r$ , and of the linear velocity vector,  $\mathbf{v}_m$ , is equal to:

$$\mathbf{n}_r \cdot \mathbf{v}_m = p \cdot \tan \psi_{b,g} - Z_1 = 0 \quad (7.92)$$

Thus, the equation of contact in this particular case can be represented in the form:

$$Z_1 = p \cdot \tan \psi_{b,g} \quad (7.93)$$

The equation for the position vector of a point,  $\mathbf{r}_e(t)$ , of the characteristic line,  $\mathcal{E}$ ,

$$\mathbf{r}_e(t) = \begin{bmatrix} y \\ t \cdot \tan \psi_{b,g} \\ p \cdot \tan \psi_{b,g} \\ 1 \end{bmatrix} \quad (7.94)$$

is derived on the premises of simultaneous consideration of the equation of contact together with the equation that describes the plane,  $\mathcal{R}$ , in its current configuration with respect to the axis of the screw motion.

\* In reality, the value of the reduced pitch,  $p$ , is given. In this way, the ratio  $|\mathbf{v}|/|\boldsymbol{\omega}| = p$  is specified.

In Equation 7.94,  $\mathbf{r}_e(t)$  designates the position vector of a point of the characteristic line,  $\mathcal{E}$ , and the parameter of motion of the characteristic line,  $\mathcal{E}$ , is denoted as  $t$ .

In the case under consideration, the characteristic line,  $\mathcal{E}$ , is a straight line. This straight line can be viewed as the line of intersection of two planes. The plane,  $\mathcal{R}$ , is the first of two planes. Another plane is parallel to the coordinate plane,  $X_1Z_1$ , and is remote at the distance  $p \cdot \tan \psi_{b.g}$ .

For a specified screw motion, the location of the characteristic line,  $\mathcal{E}$ , within the plane,  $\mathcal{R}$ , in the initial coordinate system,  $X_0Y_0Z_0$ , remains the same.

The angle of rotation of the coordinate system,  $X_1Y_1Z_1$ , about the  $X_0$ -axis is designated as  $\varepsilon$ . The translation of the coordinate system,  $X_1Y_1Z_1$ , in relation to  $X_0Y_0Z_0$  that corresponds to the angle,  $\varepsilon$ , is equal to  $p \cdot \varepsilon$ . This makes possible composing the operator,  $\mathbf{Rs}(1 \rightarrow 0)$ , of the resultant coordinate system transformation:

$$\mathbf{Rs}(1 \rightarrow 0) = \begin{bmatrix} 1 & 0 & 0 & p \cdot \varepsilon \\ 0 & \cos \varepsilon & \sin \varepsilon & 0 \\ 0 & -\sin \varepsilon & \cos \varepsilon & 0 \\ 0 & 0 & 0 & 1 \end{bmatrix} \quad (7.95)$$

In order to analytically represent the enveloping surface,  $\mathcal{G}$ , the equation  $\mathbf{r}_e(t)$  of the characteristic line,  $\mathcal{E}$ , should be considered together with the operator,  $\mathbf{Rs}(1 \rightarrow 0)$ , of the resultant coordinate system transformation:

$$\mathbf{r}_g(X_1, \varepsilon) = \mathbf{Rs}(1 \rightarrow 0) \cdot \mathbf{r}_e(t) = \begin{bmatrix} X_1 + p \cdot \varepsilon \\ X_1 \cdot \tan \psi_{b.g} \cdot \cos \varepsilon + p \cdot \tan \psi_{b.g} \cdot \sin \varepsilon \\ -X_1 \cdot \tan \psi_{b.g} \cdot \sin \varepsilon + p \cdot \tan \psi_{b.g} \cdot \cos \varepsilon \\ 1 \end{bmatrix} \quad (7.96)$$

Consider the intersection of the enveloping surface,  $\mathcal{G}$ , by the plane,  $X_0 = X_1 + p \cdot \varepsilon = 0$ . The last equation allows for an expression,  $X_1 = -p \cdot \varepsilon$ . Therefore,

$$\mathbf{r}_{X_0}(\varepsilon) = \begin{bmatrix} 0 \\ p \cdot \tan \psi_{b.g} \cdot (\sin \varepsilon - p \cdot \varepsilon \cdot \cos \varepsilon) \\ p \cdot \tan \psi_{b.g} \cdot (\cos \varepsilon + p \cdot \varepsilon \cdot \sin \varepsilon) \\ 1 \end{bmatrix} \quad (7.97)$$

The involute of a circle is analytically described by the latter equation.

The radius of the base circle of the involute curve can be expressed by:

$$r_{b.g} = p \cdot \tan \psi_{b.g} \quad (7.98)$$

Therefore, a screw involute surface, that is, a helical involute gear tooth flank,  $\mathcal{G}$ , allows for interpretation in the form of the envelope to consecutive positions of a plane,  $\mathcal{R}$ , that performs a screw motion. The reduced pitch of the screw involute surface is equal to  $p$ , and the radius of the base cylinder is equal to  $r_{b.g} = p \cdot \tan \omega_b$ . The involute screw surface shares common points with the base cylinder. The points are within a helix. The tangent to the helix makes the angle,  $\omega_b$ , with the axis of the screw motion [2,3]:

$$\tan \omega_b = \frac{r_{b.g}}{p} \quad (7.99)$$

From this, one may conclude that  $\tan \omega_b = \tan \psi_{b.g}$  and  $\omega_b = \psi_{b.g}$ . The straight characteristic line,  $\mathcal{E}$ , is tangential to the base helix of the enveloping surface,  $\mathcal{G}$ . This means that if a plane  $A$  is tangential to the base cylinder, then a straight line,  $\mathcal{E}$ , within the plane,  $A$ , makes the angle  $\psi_{b.g}$  with the axis of the screw motion, and if the plane  $A$  rolls without slippage over the base cylinder, then the enveloping surface,  $\mathcal{G}$ , can be represented as a locus of consecutive positions of the straight line,  $\mathcal{E}$ , that rolls without sliding over the base cylinder together with the plane,  $A$ . The enveloping surface is a screw involute surface.

The obtained screw involute surface,  $\mathcal{G}$  (Figure 7.25), is identical to that shown in Figure 7.10 and is analytically described by Equation 7.14.

The above discussion can be summarized with the following theorem:

**Theorem 7.2**

If we screw a plane about an axis fixed in space with pitch,  $p$ , and the axis makes an angle,  $\alpha$ , with the said plane, we describe in space a continuum of planes that successively intersect one another in a continuum of straight lines. These lines sweep out the involute helicoid,  $(a, \alpha)$ , where  $a = p \tan \alpha$ .

It might be correspondingly said that the screw of the plane *sweeps* in the same involute helicoid. The involute helicoid is, in any event, the so-called *envelope* of the continuum of planes.

This is a well-known theorem not found in most books about gearing. It may, however, be found in some books about kinematics [92]. See also page 335 in the book by Dr. Phillips [89].

Another solution to the problem of determining the envelope of a plane that performs a screw motion is given by Cormac [15].

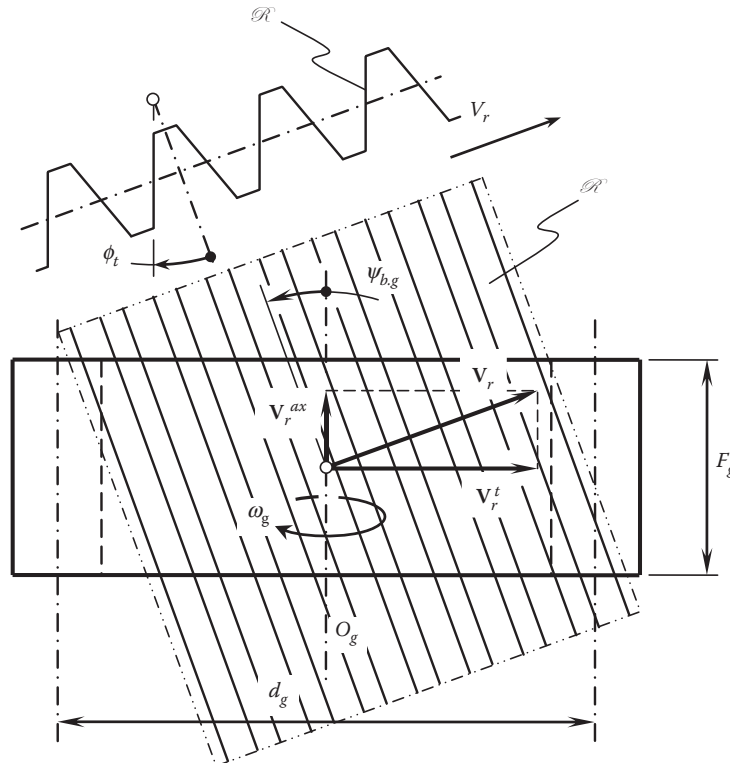
**7.2.3.2 Generating Basic Rack of a Helical Gear**

In the case under consideration, a rack,  $\mathcal{R}$ , is tilted at a certain angle,  $\psi_{b,g}$ , in relation to the axis of rotation of the gear, as shown in Figure 7.26. The rack,  $\mathcal{R}$ , travels in the direction that is specified by the vector,  $\mathbf{V}_r$ . The magnitude,  $V_r$ , of the vector,  $\mathbf{V}_r$ , of the linear velocity is synchronized with a rotation,  $\omega_g$ , of the gear in a timely manner.

The vector of linear velocity,  $\mathbf{V}_r$ , of the translation motion can be decomposed into two components:

$$\mathbf{V}_r = \mathbf{V}_r^t + \mathbf{V}_r^{ax} \quad (7.100)$$

One of the components,  $\mathbf{V}_r^t$ , of the of the linear velocity vector,  $\mathbf{V}_r$ , is in the tangential direction to the pitch cylinder of the gear. This component causes rolling with no sliding of the pitch plane of the rack,  $\mathcal{R}$ , over the pitch cylinder of diameter,  $d_g$ , of the gear.

**FIGURE 7.26**

Generation of the tooth flank,  $\mathcal{G}$ , of a helical gear by a helical rack,  $\mathcal{R}$ .

Another component,  $\mathbf{V}_r^{ax}$ , of the velocity vector,  $\mathbf{V}_r$ , is in the axial direction of the gear. This component, together with the component  $\mathbf{V}_r^t$ , results in a screw motion of the lateral tooth plane of the rack,  $\mathcal{R}$ . The gear axis,  $O_g$ , is the axis of the screw motion of the plane.

The gear tooth flank,  $\mathcal{G}$ , is an envelope to consecutive positions of the lateral plane when the rack,  $\mathcal{R}$ , performs a screw motion about the axis,  $O_g$ .

The helical generating rack,  $\mathcal{R}$ , is commonly specified either by a module,  $m$ , or by the diametral pitch,  $P$ , of the rack. The helix angle,  $\psi$ , of the rack is known. For the calculation of the rest of the design parameters (Figure 7.27), standard formulas are used. The formulas are summarized in Table 7.4.

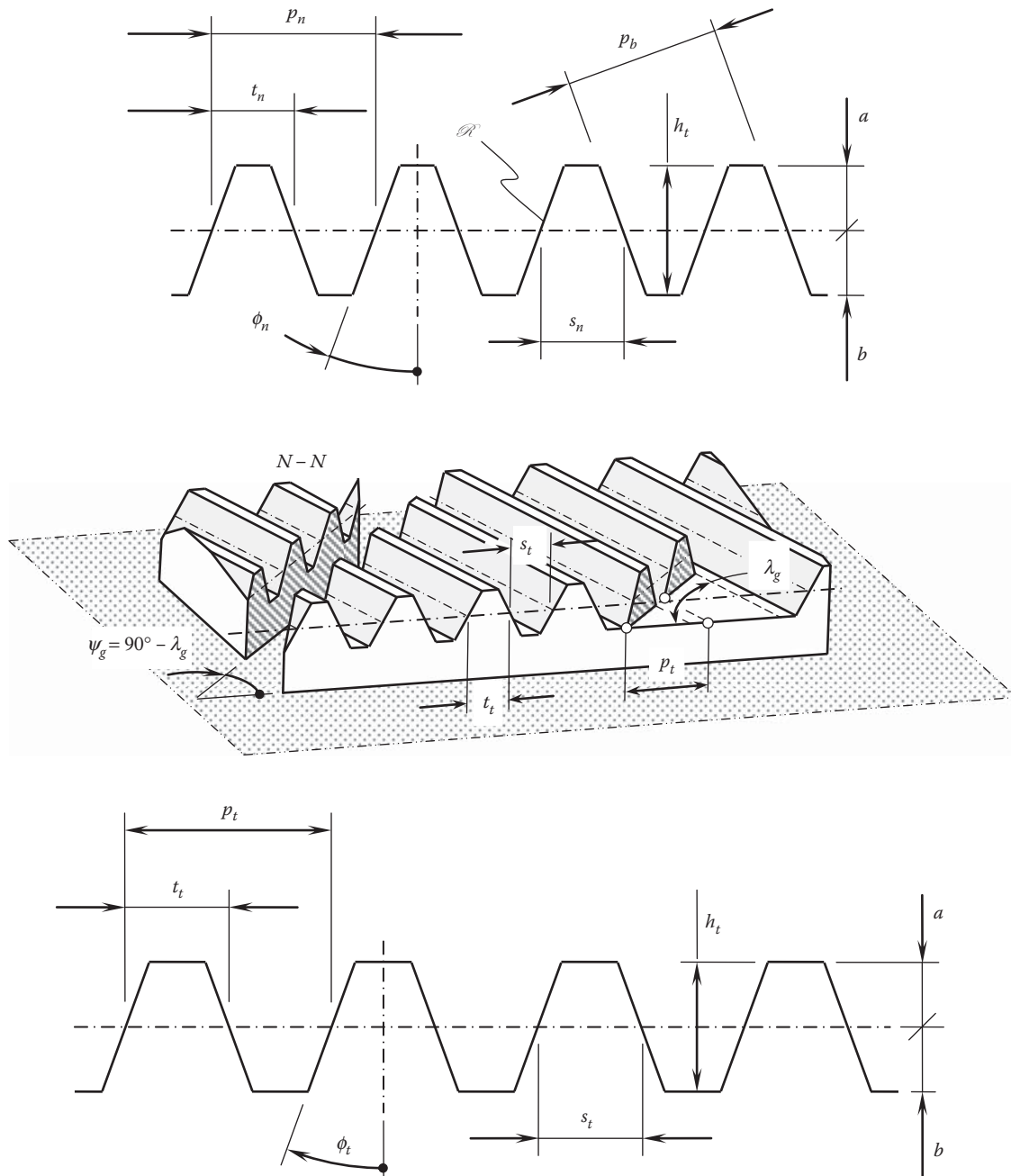


FIGURE 7.27  
Design parameters of a generating rack,  $\mathcal{R}$ , of a helical involute gear.

**TABLE 7.4**

Design Parameters of a Helical Generating Rack

Design Parameter of the Rack	Metric	English
Normal pitch of the rack teeth	$p_n = \pi \cdot m$	$P_n = \frac{\pi}{P}$
Transverse module (mm)	$m_t = \frac{m}{\cos \Psi}$	—
Transverse pitch	—	$p_t = \pi \cdot m_t \frac{\pi m}{\cos \Psi}$
Base pitch (mm)	$P_{b,g} = \pi m \cos \phi_t$	$p_{b,g} = \frac{\pi \cos \phi_t}{P}$
Addendum (mm)	$a = m$	$a = \frac{1}{P}$
Dedendum <sup>a</sup> (mm)	$b = 1.25 m$	$b = \frac{1.25}{P}$
Tooth height (mm)	$h_t = a + b = 2.25 m$	$h_t = \frac{2.25}{P}$
Base pitch (mm)	$p_{b,g} = \pi \cdot m \cdot \cos \phi_t$	$p_{b,g} = \frac{\pi}{P} \cdot \cos \phi_t$
Transverse tooth thickness (mm)	$t_t = \frac{\pi m}{2}$	$t_t = \frac{\pi}{2P}$
Normal tooth thickness (mm)	$t_n = t_t \cos \psi_g$	$t_t = t_t \cos \psi_g$
Transverse space width (mm)	$s_t = \frac{\pi m}{2}$	$s_t = \frac{\pi}{2P}$
Normal space width (mm)	$s_n = s_t \cos \psi_g$	$s_n = s_t \cos \psi_g$
Normal profile angle (deg.)	$\phi_n = \tan^{-1}(\tan \phi_t \cdot \cos \psi_g)$ $\phi_n = \cos^{-1}(\sin \psi_{b,g} \csc \psi_g)$	

<sup>a</sup> For the calculation of dedendum,  $b$ , of a small module gear (of a fine pitch gear) the formula  $b = 1.35 m$  (or the equivalent formula  $b = \frac{1.35}{P}$ ) is often used.

A gear can be generated by specifying only four elements, namely

1. The reference cylinder
2. The basic rack profile (in a normal section)
3. The helix angle
4. The basic rack's position in relation to the generating pitch line, that is, the addendum modification (profile shift)

Having calculated the design parameters of a helical rack, the corresponding design parameters of a helical gear with a given tooth number,  $N_g$ , can be calculated as well. Standard equations are used for the calculation of the design parameters of a helical gear. These equations are summarized in [Table 7.5](#).

Miscellaneous formulas are useful for calculating the gear design parameters are given in [Table 7.6](#).

The circular pitch,  $p$ , and normal circular pitch,  $p_n$ , correlate to diametral pitch,  $P$ , and the normal diametral pitch,  $P_n$ , in compliance with the expression:

$$p_n P_n = p P \quad (7.101)$$

[Figure 7.28](#) shows the development of tooth helices, which then become straight lines. The spacing of these helices on the normal, transverse, and axial planes are the normal,  $p_n$ ; transverse,  $p_t$ ; and axial,  $p_x$ , pitches,

TABLE 7.5

Design Parameters of a Helical Gear

Design Parameter of the Gear	Metric	English
Pitch diameter (mm)	$d_g = mN_g$	$d_g = \frac{N_g}{P_t}$
Outer diameter (mm)	$d_{o,g} = d_g + 2a$	
Reference diameter (mm)	$d_\psi = \frac{mN_g}{\cos \psi_g} = m_t N_g$	$d_\psi = \frac{N_g}{P \cdot \cos \psi_g}$
Standard outside diameter (mm)	$d_{o,g} = d_g + 2m$	$d_{o,g} = d_g + 2a$
Base helix angle (deg)	$\sin \psi_b = \sin \psi_g \cos \phi_t$ $\tan \psi_b = \tan \psi_g \cos \phi_t$	
Transverse profile angle (deg)	$\tan \phi_t = \frac{\tan \phi_n}{\cos \psi_g}$	
	$\sin \phi_t = \frac{\sin \phi_t}{\cos \psi_b}$	
	$\cos \phi_t = \frac{\cos \phi_t \cos \psi_{\partial g}}{\cos \psi_b}$	
Diametral pitch (in)	$P = \frac{N_g}{d_g} = \frac{\pi}{P_t}$	
Normal diametral pitch (in)	$p_n = \frac{N_g}{d_g \cos \psi_g}$	
Transverse diametral pitch (mm)	$P_t = P_n \cos \psi_g$	
Normal circular pitch (mm)	$p_n = \frac{\pi d_g}{N_g} \cos \psi_g$	
Base pitch (mm)	$p_b = \frac{\pi d_g}{N_g} \cos \phi_t = p \cos \phi_t$	
Transverse base pitch (mm)	$p_{bt} = \pi m \frac{\cos \phi_t}{\cos \psi_b}$	$p_{bt} = \frac{\pi \cos \phi_t}{P \cos \psi_b}$
Base diameter (mm)	$d_{b,g} = mN_g \frac{\cos \phi_n}{\cos \psi_b} = d_g \cos \phi_t$	$d_{b,g} = \frac{N_g \cos \phi}{P \cos \psi_b} = d_g \cos \phi_t$
Lead (mm)	$L = \pi d_g \cot \psi = \frac{\pi d_g}{\tan \psi_g}$	
Transverse profile angle at tooth tip (deg)	$\cos \phi_{o,g} = \frac{d_{b,g}}{d_{o,g}}$	
Axial pitch (mm)	$p_x = \frac{\pi d_g}{N_g} \cos \phi_t \cot \psi_b$ $= p_b \cot \psi_b = p \cos \psi_g$	$p_x = \frac{\pi}{P_n \sin \psi} = \frac{p_n}{\sin \psi_g} = \frac{L_g}{N_g}$
Transverse circular pitch (mm)	$p_t = \frac{\pi}{P_t} = \frac{p_n}{\cos \psi_g}$	
Virtual number of teeth	$N_n = \frac{N_g}{\cos^2 \psi_b \cos \psi_g}$	
Normal tooth thickness on reference cylinder (mm)	$t_n = \frac{p_n}{2}$	$t_n = \frac{p_n}{2}$
	$t_n = m \left( \frac{\pi}{2} + 2 \cdot \xi \cdot \tan \phi_t \right)$	$t_n = \frac{1}{P} \left( \frac{\pi}{2} + 2 \cdot \xi \cdot \tan \phi_t \right)$

(Continued)



**TABLE 7.5 (Continued)**

Design Parameters of a Helical Gear

Design Parameter of the Gear	Metric	English
Transverse tooth thickness on reference cylinder (mm)	$t_t = \frac{m}{\cos \psi_g} \left( \frac{\pi}{2} + 2 \cdot \xi \cdot \tan \phi_t \right)$	$t_n = \frac{1}{P \cos \psi_g} \left( \frac{\pi}{2} + 2 \cdot \xi \cdot \tan \phi_t \right)$
Normal base tooth thickness (mm)	$t_{bn} = m N_g \left( \frac{t_n}{m N_g} + \text{inv } \phi_t \right) \cos \phi_t$	$t_{bn} = \frac{N_g}{P} \left( \frac{P t_n}{N_g} + \text{inv } \phi_t \right) \cos \phi_t$
Transverse base tooth thickness (mm)	$t_{bt} = m N_{\partial g} \left( \frac{t_n}{m N_{\partial}} + \text{inv } \phi_t \right) \frac{\cos \phi}{\cos \psi}$	$t_{bt} = \frac{N_g}{P} \left( \frac{t_n P}{N_g} + \text{inv } \phi_t \right) \frac{\cos \phi}{\cos \psi_b}$
Transverse tooth crest width (mm)	$t_{ot} = d_{o,g} \left( \frac{t_n}{m N_g} + \text{inv } \phi_t - \text{inv } \phi_o \right)$	$t_{ot} = d_o \left( \frac{t_n P}{N_g} + \text{inv } \phi_t - \text{inv } \phi_o \right)$
Root diameter (mm)	$d_{f,g} = d_g - 2h_t$	
Normal profile angle (deg)	$\phi_n = \sin^{-1}(\sin \phi \cdot \cos \psi_b)$	
Circular pitch (mm)	$p_t = \frac{\pi d_g}{N_g}$	
Base tangent length <sup>a</sup> (mm)	$W_k = m[(k-0.5)\pi \cos \phi + N_g \cdot \text{inv } \phi_t \cos \phi + 2\xi \sin \phi]$ or $W_k = t_{bn} + p_b(k-1)$	
Average backlash per gear pair (mm)	$B = 0.040 m$	$B = \frac{0.040}{P}$

<sup>a</sup>Tooth number in the span is denoted by  $k$ .**TABLE 7.6**

Miscellaneous Formulas for the Calculation of Design Parameters of a Gear

Helix angle at pitch diameter (deg.)	$\cos \psi_g = \frac{N_g}{P_n d_g}$ $\sin \psi_g = \frac{\pi N_g}{P_n L_g}$
Helix angle at any diameter, $d_{y,g}$ (deg.)	$\tan \psi_{y,g} = \frac{d_{y,g} \tan \psi_g}{d_g}$
Transverse circular pitch at any diameter, $d_{y,g}$ (mm)	$p_{ty} = \frac{\pi d_{y,g}}{N_g}$
Normal profile angle (deg)	$\phi_n = \sin^{-1}(\sin \phi \cos \psi_b)$ $\phi_n = \cos^{-1}(\sin \psi_b \csc \psi_g)$ $\phi_n = \tan^{-1}(\tan \phi_t \cos \psi_g)$
Transverse profile angle at any diameter, $d_{y,g}$ (deg.)	$\phi_{ty} = \cos^{-1} \left( \frac{d_{b,g}}{d_{y,g}} \right)$
Base helix angle (deg.)	$\sin \psi_b = \sin \psi_g \cos \phi_n$ $\cos \psi_b = \frac{\cos \psi_g \cos \phi_n}{\cos \phi_t} = \frac{\sin \phi_n}{\sin \phi_t}$ $\tan \psi_b = \tan \psi_g \cos \phi_t$
Base pitch (mm)	$p_b = \frac{\pi d_{b,g}}{N_g} = p \cos \phi_t$

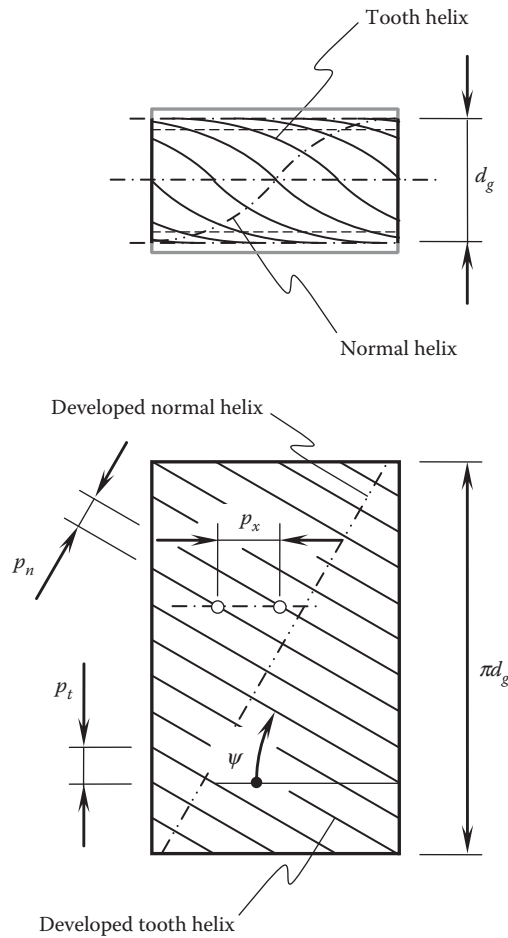


**FIGURE 7.28**  
Definitions of normal,  $p_n$ ; transverse,  $p_t$ ; and axial,  $p_x$ , pitches of a helical gear.

respectively. The diametral pitches corresponding to the normal and transverse measures of linear spacing become the *normal diametral pitch* and *transverse diametral pitch*.

The reciprocals of the normal diametral pitch and transverse diametral pitch are the normal module  $m$  (or  $m_n$ ) and the transverse module,  $m_t$ , respectively, expressed in the same unit of length.

#### 7.2.4 Descriptive-Geometry–Based Determination of the Straight Generating Line

The methods developed in descriptive geometry can be used for the determining of the straight generating line,  $\mathcal{G}$ , as well as the principal design parameters of an involute gear. The descriptive-geometry–based solution to a problem is not as accurate as that derived using analytical methods for solving engineering problems. The main advantage of the descriptive-geometry–based methods is that they are helpful to eliminate rough errors of the analysis. It is strongly recommended to use descriptive-geometry–based methods along with analytical methods (and computer-based methods) for solving engineering problems, problems in gearing in particular.

##### 7.2.4.1 Gear Base Helix Angle $\psi_{b,g}$ : General Approach

For solving the problem of the determining of the gear base helix angle,  $\psi_{b,g}$ , the actual values of the normal profile angle,  $\phi_n$ , as well as of setting angle,  $\zeta_r$ , of the gear rack,  $\mathcal{R}$ , need to be specified. The solution to this problem on the premise of descriptive-geometry–based methods is discussed immediately below.

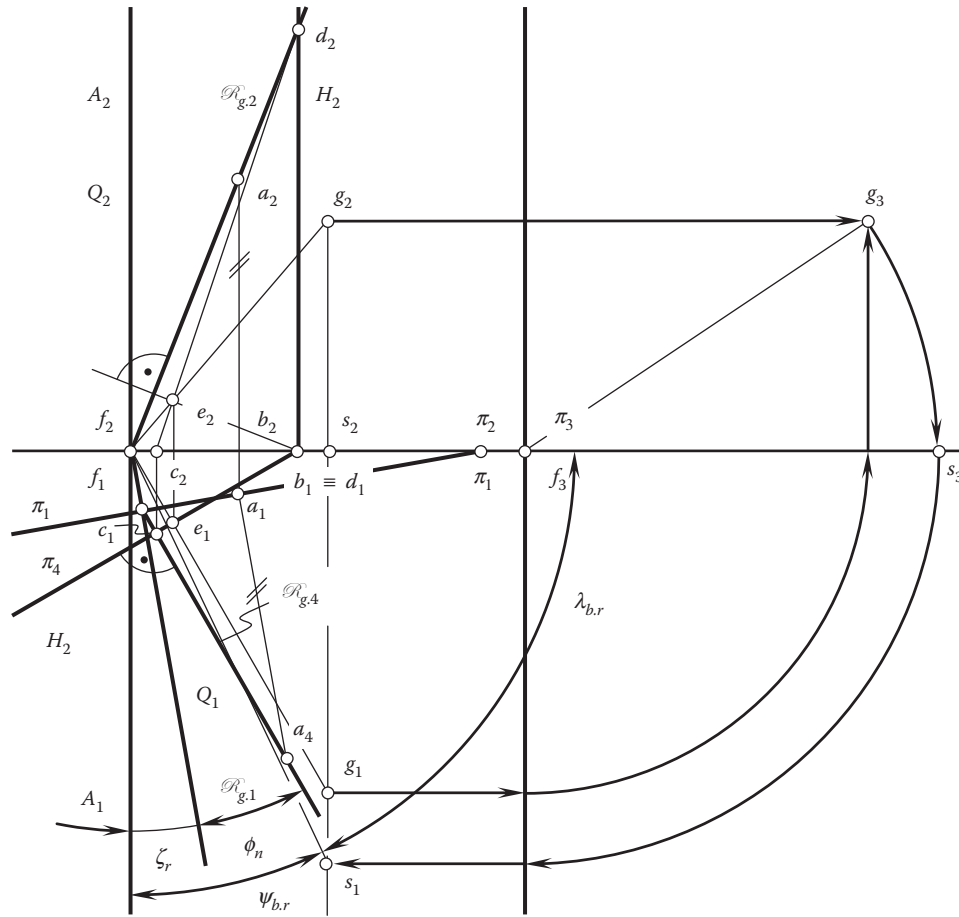


**FIGURE 7.29**  
Determination of the base helix angle,  $\psi_{b,r}$ , of the gear rack.

The base helix angle  $\psi_{b,g}$  can be constructed in a system of planes of projections,  $\pi_1\pi_2\pi_3$ . In a case of necessity, additional auxiliary plane(s) of projections can be constructed as well.

At the beginning, it is necessary to construct the lateral tooth surface of the auxiliary generating rack,  $\mathcal{R}_g$ . A possible method for the construction of the lateral plane of the auxiliary generating rack,  $\mathcal{R}_g$ , is as follows.

Consider an arbitrary plane,  $A$ , that is perpendicular to the axis of projections,  $\pi_1/\pi_2$  (Figure 7.29). The plane,  $A$ , is specified by the traces,  $A_1$  and  $A_2$ , onto the horizontal,  $\pi_1$ , and the vertical,  $\pi_2$ , planes of projections. Next, turn the plane,  $A$ , about the trace,  $A_2$ , through the setting angle,  $\zeta_r$ , of the gear rack to the position,  $Q$ . The plane,  $Q$ , is specified by the traces,  $Q_1$  and  $Q_2$ , the second of which is aligned with the trace,  $A_2$ , of the plane,  $A$ . After that, the plane,  $Q$ , is turned about the trace,  $Q_1$ , through the normal profile angle,  $\phi_n$ , of the gear rack. In this final location, the plane is designated as  $\mathcal{R}_g$ . It is specified by the traces  $\mathcal{R}_{g,1}$  and  $\mathcal{R}_{g,2}$ , respectively.

In order to construct base helix angle,  $\psi_{b,r}$ , for this particular configuration (location and orientation) of the plane,  $\mathcal{R}_g$ , an auxiliary plane of projections,  $\pi_4$ , is constructed so that the axis of projections,  $\pi_1/\pi_4$ , is perpendicular to the trace,  $\mathcal{R}_{g,1}$ .

The base helix angle,  $\psi_{b,r}$ , of the gear rack is the angle that the lateral rack surface,  $\mathcal{R}_g$ , forms with a plane, which is (a) orthogonal to the horizontal plane of projections,  $\pi_1$ , and (b) orthogonal to the trace,  $\mathcal{R}_{g,4}$ . The use of conventional rules—those developed in descriptive geometry—allows for construction of base helix angle,  $\psi_{b,r}$ , of the gear rack, as well as of the base lead angle,  $\lambda_{b,r}$ , of the generating surface of the gear rack. The latter complements the base helix angle,  $\psi_{b,r}$ , to the right angle (Figure 7.29).

The derived descriptive-geometry-based solution to the problem of determining the base helix angle,  $\psi_{b,r}$ , gives an insight into how the expressions for the calculation of the actual value of this angle can be derived analytically. It also serves as a perfect tool for verification of the results of the analytical solution to the problem.

### 7.2.4.2 Base Diameter, $d_{b,g}$ , of an Involute Gear

Let us again begin with the analysis of the property in compliance with which an involute gear tooth flank,  $\mathcal{G}$ , can be represented as an enveloping surface to consecutive positions of the lateral plane of the tooth of the auxiliary generating surface,  $\mathcal{R}_g$ .

Consider the plane,  $\mathcal{R}_g$ , the configuration of which (location and orientation) is specified in a system of planes of projections,  $\pi_1\pi_2\pi_3$ , as shown in Figure 7.30. The plane,  $\mathcal{R}_g$ , performs a translation along the  $\pi_1/\pi_2$ -axis of projections. The velocity of the translation is designated as  $\mathbf{V}_r$ . Simultaneously, the plane,  $\mathcal{R}_g$ , rotates about that same axis,  $\pi_1/\pi_2$ , with an angular velocity,  $\omega_r$ .

The base diameter,  $d_{b,g}$ , of the gear is equal to the shortest distance of approach between the characteristic line,  $\mathcal{E}_r$ , and the axis,  $\pi_1/\pi_2$ , of the screw motion. In order to determine the characteristic line,  $\mathcal{E}_r$ , it is necessary to select those points within the plane,  $\mathcal{R}_g$ , the resultant velocity of which is perpendicular to the normal vector,  $\mathbf{n}_r$ , to the plane,  $\mathcal{R}_g$ , itself. To do that, the velocity vector,  $\mathbf{V}_r$ , of the translation needs to be considered together with linear velocity of the rotation,  $\omega_r$ . Those points within the plane,  $\mathcal{R}_g$ , the resultant velocity,  $\mathbf{V}^\Sigma$ , of which is perpendicular to the normal vector,  $\mathbf{n}_r$ , are the points of the characteristic line,  $\mathcal{E}_r$ . In the case under consideration, the characteristic line,  $\mathcal{E}_r$ , is the straight line at a distance,  $d_{b,g}/2$ , from the axis of rotation,  $\pi_1/\pi_2$ , of the gear-cutting tool. The characteristic line,  $\mathcal{E}_r$ , crosses the axis,  $\pi_1/\pi_2$ , at the base helix angle,  $\psi_{b,r}$ .

The descriptive-geometry-based solution to the problem of determining the base diameter,  $d_{b,g}$ , is represented in Figure 7.30. The derived solution to the problem of determining the base diameter,  $d_{b,g}$ , of the gear provides insight for the derivation of equations for the calculation of the actual value of this diameter.

In both cases (see Figures 7.29 and 7.30), the characteristic straight line,  $\mathcal{E}_r$ , is constructed. An involute gear/pinion tooth flank can be generated by means of the straight line,  $\mathcal{E}_r$ .

Many other design parameters of the generating surface of the gear-cutting tool, as well as the design parameters of the gear-cutting tool itself can be determined using the descriptive-geometry-based method.

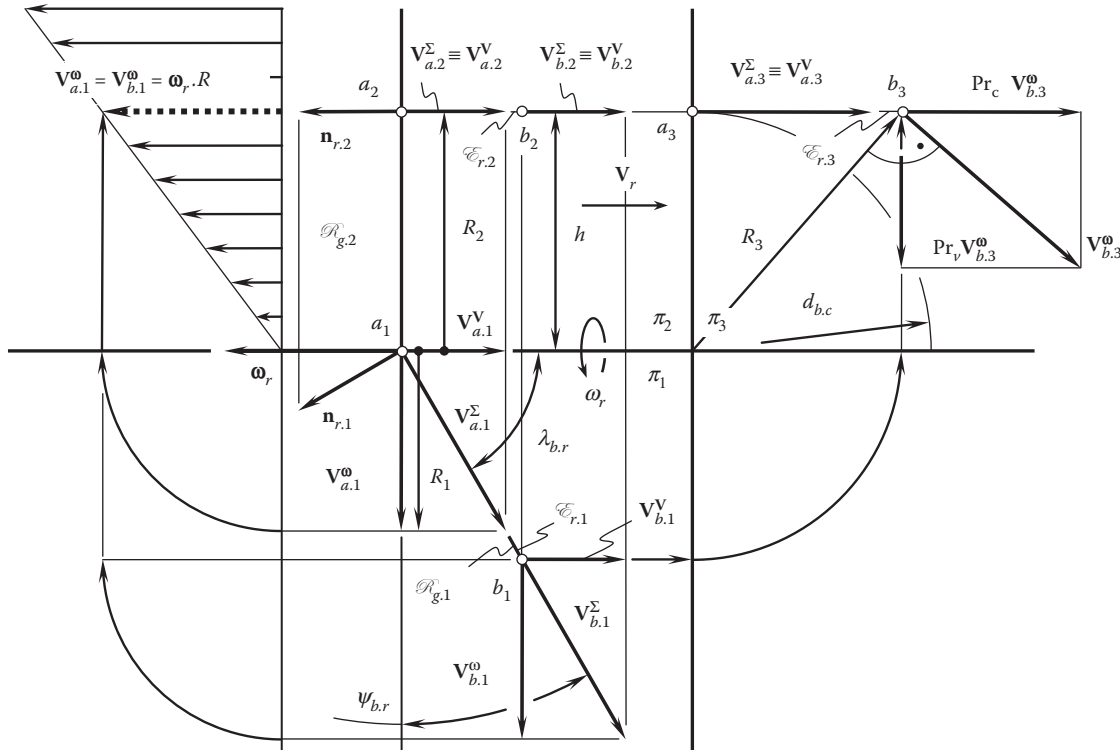


FIGURE 7.30

Determination of base diameter,  $d_{b,g}$ , of an involute gear.

### 7.3 Conical Involute Gears

Cylindrical gears are not the only type of gears used in the design of parallel-axis gear pairs. Conical involute gears are frequently used in antibacklash schemes.

Apart from being frequently used in antibacklash schemes, conical involute gears are also used as reduction, timing, and differential gears. The conical involute gear is also commonly referred to as a *beveloid gear*. A gear of this type is an involute gear with tapered tooth thickness, tapered root, and, in most cases, tapered outside diameter.

#### 7.3.1 Kinematics of Conical Involute Gearing

A close-up of generation of tooth flanks,  $\mathcal{G}$ , of a conical involute gear by means of a generating rack,  $\mathcal{R}$ , is schematically illustrated in Figure 7.31. This is very similar to the generation of the tooth flanks of a spur involute gear. However, instead of being parallel to the axis,  $O_g$ , of the gear, the generating rack,  $\mathcal{R}$ , is inclined to the gear axis,  $O_g$ , at an angle  $\theta$ . The angle,  $\theta$ , is commonly referred to as the *cone angle*.

The gear is rotating about the axis,  $O_g$ , with a certain angular velocity,  $\omega_g$ . The inclined generating rack,  $\mathcal{R}$ , travels tangentially in relation to the gear with a linear velocity,  $V_r$ . Magnitudes,  $\omega_g$  and  $V_r$ , of the angular velocity vector,  $\omega_g$ , and the linear velocity vector,  $V_r$ , respectively, are synchronized with one another ( $V_r = 0.5 \omega_g d_g$ ; here, the pitch diameter of the gear is denoted by  $d_g$ ).

##### 7.3.1.1 Geometry of the Tooth Flanks of a Spur Conical Involute Gear

For the derivation of an equation for the tooth flank,  $\mathcal{G}$ , of a spur conical involute gear, the following reference systems are applied (Figure 7.32).

A Cartesian coordinate system,  $X_n Y_n Z_n$ , is associated with the generating rack,  $\mathcal{R}$ , as shown in Figure 7.32. Another Cartesian coordinate system,  $X_p Y_p Z_p$ , shares the axis,  $X_p \equiv X_n$ , of the coordinate system,  $X_n Y_n Z_n$ . These reference systems are turned in relation to each other about the  $X_p$ -axis through the angle,  $\theta$ .

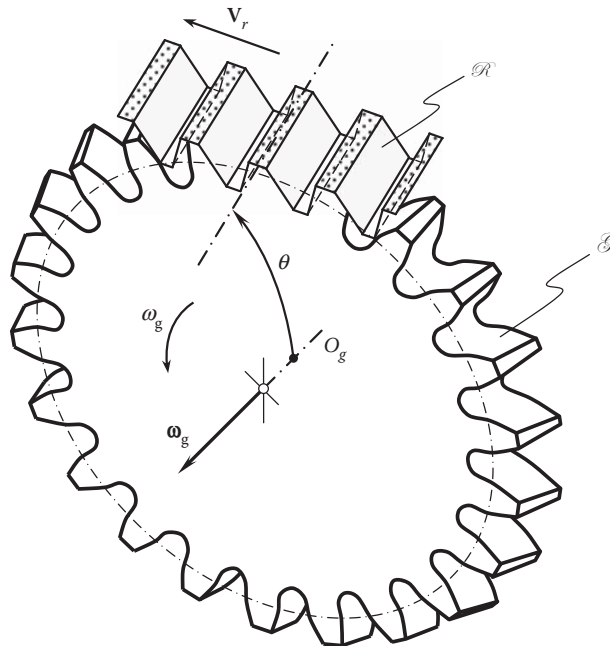


FIGURE 7.31

Close-up of the generating of tooth flanks,  $\mathcal{G}$ , of a conical involute gear by means of a generating rack,  $\mathcal{R}$ .

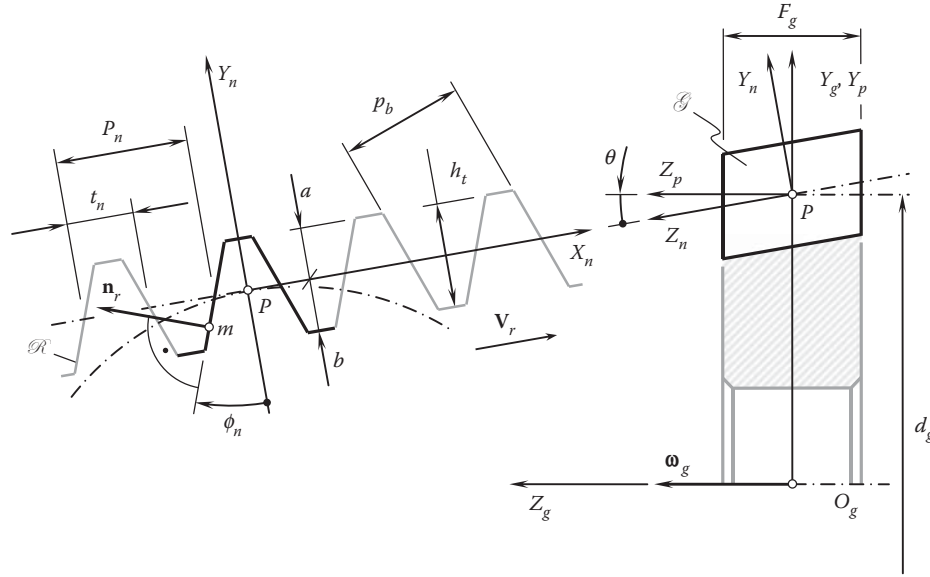


FIGURE 7.32

Applied coordinate systems for the derivation of an equation of tooth flank,  $\mathcal{G}$ , of a spur conical involute gear.

For the analytical description of a transition from the reference system,  $X_n Y_n Z_n$ , to the reference system,  $X_p Y_p Z_p$ , an operator of rotation,  $\mathbf{Rt}(-\theta, Z_n)$ , is used. The operator,  $\mathbf{Rt}(-\theta, Z_n)$ , can be expressed as follows:

$$\mathbf{Rt}(-\theta, Z_n) = \begin{bmatrix} 1 & 0 & 0 & 0 \\ 0 & \cos \theta & -\sin \theta & 0 \\ 0 & \sin \theta & \cos \theta & 0 \\ 0 & 0 & 0 & 1 \end{bmatrix} \quad (7.102)$$

Ultimately, a Cartesian coordinate system,  $X_g Y_g Z_g$ , is associated with the gear itself.

For the analytical description of a transition from the reference system,  $X_p Y_p Z_p$ , to the reference system,  $X_g Y_g Z_g$ , an operator of translation,  $\mathbf{Tr}(0.5 d_g, Y_p)$ , is used. The operator,  $\mathbf{Tr}(0.5 d_g, Y_p)$ , can be expressed in matrix form as follows:

$$\mathbf{Tr}(0.5 d_g, Y_p) = \begin{bmatrix} 1 & 0 & 0 & 0 \\ 0 & 1 & 0 & 0.5 d_g \\ 0 & 0 & 1 & 0 \\ 0 & 0 & 0 & 1 \end{bmatrix} \quad (7.103)$$

An operator of the resultant coordinate system transformation, that is, the operator,  $\mathbf{Rs}(n \mapsto g)$ , of the transition from the reference system,  $X_n Y_n Z_n$ , to the reference system,  $X_g Y_g Z_g$ , can be expressed in terms of the operators,  $\mathbf{Rt}(-\theta, Z_n)$  and  $\mathbf{Tr}(0.5 d_g, Y_p)$ , of elementary coordinate system transformations:

$$\mathbf{Rs}(n \mapsto g) = \mathbf{Tr}(0.5 d_g, Y_p) \cdot \mathbf{Rt}(-\theta, Z_n) = \begin{bmatrix} 1 & 0 & 0 & 0 \\ 0 & \cos \theta & -\sin \theta & 0.5 d_g \\ 0 & \sin \theta & \cos \theta & 0 \\ 0 & 0 & 0 & 1 \end{bmatrix} \quad (7.104)$$

In the reference system,  $X_n Y_n Z_n$ , the position vector of a point,  $\mathbf{r}_r^{(n)}$ , of the left-hand tooth flank of the generating rack,  $\mathcal{R}$ , can be analytically described by the expression:

$$\mathbf{r}_r^{(n)} = -\mathbf{i} \cdot \frac{t_n}{2} + \mathbf{u}_n \cdot U_n = \begin{bmatrix} -\frac{t_n}{2} + U_n \sin \phi_n \\ U_n \cos \phi_n \\ V_n \\ 1 \end{bmatrix} \quad (7.105)$$





of the generating rack,  $\mathcal{R}$ , in such a location and orientation is a function of the angle of rotation,  $\varphi_g$ , of the gear about its axis,  $O_g$ . Then, the Shishkov equation of contact,  $\mathbf{n}_r \cdot \mathbf{v} = 0$ , is used to eliminate the enveloping parameter,  $\varphi_g$ , from the aforementioned equation of the generating rack,  $\mathcal{R}$  (here, the unit normal vector to the tooth flank of the generating rack,  $\mathcal{R}$ , is designated as  $\mathbf{n}_r$ , and the unit vector of the relative motion of the rack,  $\mathcal{R}$ , in relation to the coordinate system,  $X_g Y_g Z_g$ , is denoted by  $\mathbf{v}$ ).

The generating rack,  $\mathcal{R}$ , in its current configuration, as well as the unit vectors,  $\mathbf{n}_r$  and  $\mathbf{v}$ , are necessarily represented in a common reference system associated with the gear, for example, the Cartesian coordinate system,  $X_g Y_g Z_g$ . The auxiliary coordinate systems used for this purpose are depicted in Figure 7.33. The product of corresponding operators of the elementary coordinate system transformations makes it possible to calculate the operator of the resultant coordinate system transformation,  $\mathbf{Rs}(n \mapsto g_r)$ . In the particular case under consideration, the operator,  $\mathbf{Rs}(n \mapsto g_r)$ , analytically describes rolling with no sliding of the coordinate system,  $X_n Y_n Z_n$ , associated with the generating rack,  $\mathcal{R}$ , in relation to the coordinate system,  $X_g Y_g Z_g$ , associated with the gear. Therefore, instead of calculating the operator,  $\mathbf{Rs}(n \mapsto g_r)$ , of the resultant coordinate system transformation, the operator of rolling [110] can be used (Appendix D). The operator of rolling can be expressed in terms of the parameters of relative motion of the generating rack,  $\mathcal{R}$ , and the gear:

$$\mathbf{Rl}_x(\varphi_g, Z) = \begin{bmatrix} \cos \varphi_g & \sin \varphi_g & 0 & 0.5 \varphi_g d_g \cos \varphi_g \\ -\sin \varphi_g & \cos \varphi_g & 0 & 0.5 \varphi_g d_g \sin \varphi_g \\ 0 & 0 & 1 & 0 \\ 0 & 0 & 0 & 1 \end{bmatrix} \quad (7.107)$$

With that said, the position vector of a point,  $\mathbf{r}_r^{(r)}$ , of the generating rack,  $\mathcal{R}$ , in its current configuration can be expressed by the following equation:

$$\mathbf{r}_r^{(r)}(\varphi_g) = \mathbf{Rl}_x(\varphi_g, Z) \cdot \mathbf{r}_r^{(n)} \quad (7.108)$$

Considering Equation 7.108 together with the Shishkov equation of contact,  $\mathbf{n}_r \cdot \mathbf{v} = 0$ , the enveloping parameter,  $\varphi_g$ , can be eliminated from Equation 7.108. In this way, an expression for the position vector of a point of the tooth flank,  $\mathcal{G}$ , of a spur conical involute gear can be derived.

In reality, it often happens that the Shishkov equation of contact,  $\mathbf{n}_r \cdot \mathbf{v} = 0$ , is bulky and inconvenient to be solved with respect to the enveloping parameter,  $\varphi_g$ .

There is another method for the derivation of an expression for the position vector of a point of the tooth flank,  $\mathcal{G}$ , of a spur conical involute gear, which can be used as well.

The gear tooth flank,  $\mathcal{G}$ , is an envelope to consecutive positions of the lateral plane of the generating rack,  $\mathcal{R}$ , when the rack is performing a screw motion about the gear axis,  $O_g$  (Figure 7.34). Therefore, the tooth flank,  $\mathcal{G}$ , can be generated by a plane that is performing a screw motion about the gear axis,  $O_g$ . The lateral plane of the generating rack,  $\mathcal{R}$ , makes a certain angle in relation to the gear axis,  $O_g$ . It is proven by Radzevich [105] that the angle made by the lateral plane of the rack,  $\mathcal{R}$ , with the gear axis,  $O_g$ , is equal to the base helix angle,  $\psi_{b,g}$ , of the gear. The angle  $\psi_{b,g}$  can be expressed in terms of the normal profile angle,  $\phi_n$ , and cone angle,  $\theta$ , of the conical involute gear.

At the beginning, let us express the base helix angle,  $\psi_{b,g}$ , in the form:

$$\tan \psi_{b,g} = \frac{\mathbf{n}_r^{(g)} \cdot \mathbf{k}_g}{|\mathbf{n}_r^{(g)} \times \mathbf{k}_g|} \quad (7.109)$$

where

$\mathbf{n}_r^{(g)}$ : is the unit normal vector to a tooth flank of the generating rack,  $\mathcal{R}$ , which is expressed in the reference system,  $X_g Y_g Z_g$ , associated with the conical involute gear.

$\mathbf{k}_g$  is the unit vector along  $Z_g$ -axis of the reference system,  $X_g Y_g Z_g$ .

From Figure 7.32, the unit normal vector,  $\mathbf{n}_r^{(g)}$ , can be analytically expressed by the following equation:

$$\mathbf{n}_r = \mathbf{Rs}(n \mapsto g) \cdot \mathbf{n}_r^{(g)} = \mathbf{Rs}(n \mapsto g) \cdot \begin{bmatrix} -\cos \phi_n \\ \sin \phi_n \\ 0 \\ 1 \end{bmatrix} = \begin{bmatrix} -\cos \phi_n \\ \sin \phi_n \cos \theta + 0.5 d_g \\ \sin \phi_n \sin \theta \\ 1 \end{bmatrix} \quad (7.110)$$

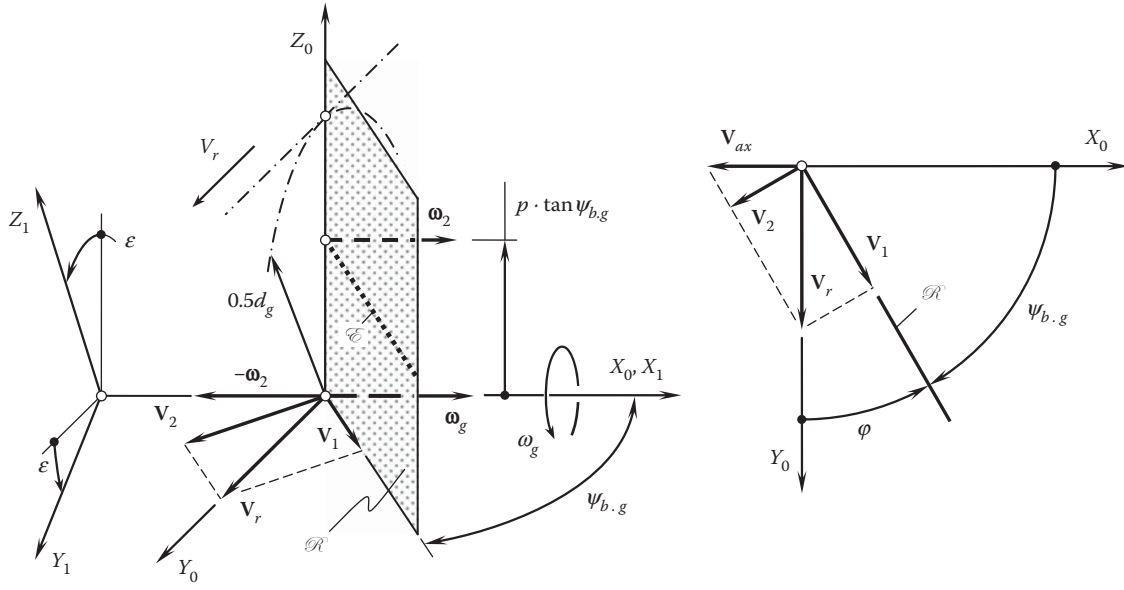


FIGURE 7.34

Generation of a screw involute surface,  $\mathcal{G}$ , as an envelope to consecutive positions of a lateral plane of the rack,  $\mathcal{R}$ , performing a screw motion.

In Equation 7.110, the operator,  $\mathbf{R}_s(n \mapsto g)$ , of the resultant coordinate system transformation is specified by Equation 7.104.

Substituting Equation 7.110 and  $\mathbf{k}_g$  into Equation 7.109, the base helix angle,  $\psi_{b.g}$ , of a conical involute hob can be expressed as follows:

$$\tan \psi_{b.g} = \frac{\sin \phi_n \sin \theta}{\sqrt{1 - \sin^2 \phi_n \sin^2 \theta}} \quad (7.111)$$

Once the angle  $\psi_{b.g}$  is calculated, the tooth flank of a conical involute gear can be described analytically using the following the approach: Consider a plane,  $\mathcal{R}$ , that performs a screw motion, as it is shown in Figure 7.34. The plane,  $\mathcal{R}$ , forms a certain angle,  $\psi_{b.g}$ , with the  $X_0$ -axis of the Cartesian coordinate system,  $X_0Y_0Z_0$ . The axis,  $X_0$ , is the axis of the screw motion.

The screw motion of the plane,  $\mathcal{R}$ , is composed of two elementary motions: (1) the rotation with an angular velocity,  $\omega_g$ , about the  $X_0$ -axis and (2) the translation,  $\mathbf{V}_r$ , along the  $X_0$ -axis is another motion. The magnitudes,  $\omega_g$  and  $V_r$ , of the rotation vector,  $\omega_g$ , and the linear velocity vector,  $\mathbf{V}_r$ , respectively, are synchronized with one another:

$$V_r = 0.5 \omega_g d_g \quad (7.112)$$

Here, the pitch diameter of the gear is denoted by  $d_g$ .

The linear velocity vector,  $\mathbf{V}_r$ , can be expressed as the sum of two vectors:

$$\mathbf{V}_r = \mathbf{V}_1 + \mathbf{V}_2 \quad (7.113)$$

The component,  $\mathbf{V}_1$ , of the translation vector,  $\mathbf{V}_r$ , is within the plane,  $\mathcal{R}$ . This component does not affect the geometry of the enveloping surface,  $\mathcal{G}$ ; thus, the component,  $\mathbf{V}_1$ , can be omitted from further analysis. The component,  $\mathbf{V}_2$ , is perpendicular to the plane,  $\mathcal{R}$ . The geometry of the gear tooth flank strongly depends on the magnitude ( $V_2 = V_r \sin \psi_{b.g}$ ) and direction of this component.

When the plane,  $\mathcal{R}$ , is traveling with the linear velocity vector,  $\mathbf{V}_2$ , speed of the translation,  $V_{ax}$ , of the plane in the direction of the  $X_0$ -axis is given by  $V_{ax} = V_r \tan \psi_{b.g}$ . Therefore, the screw motion of a plane about the  $X_0$ -axis is equivalent to a corresponding screw motion of the characteristic straight line,  $\mathcal{C}$ , about the same  $X_0$ -axis. The

reduced pitch,  $p_{rl}$ , of the screw motion of the plane can be calculated from the following formula:

$$p_{rl} = \frac{V_{ax}}{\omega_g} = \frac{V_r \tan \psi_{b,g}}{\omega_g} \quad (7.114)$$

Consider an auxiliary reference system,  $X_1Y_1Z_1$ , that is rigidly associated with the plane,  $\mathcal{R}$ .

In the Cartesian coordinate system,  $X_1Y_1Z_1$ , an equation of the plane,  $\mathcal{R}$ , can be represented in the form

$$Y_1 = X_1 \cdot \tan \psi_{b,g} \quad (7.115)$$

The coordinate system,  $X_1Y_1Z_1$ , performs the screw motion together with the plane,  $\mathcal{R}$ , in relation to the coordinate system,  $X_0Y_0Z_0$ , which is stationary. In the coordinate system,  $X_1Y_1Z_1$ , the unit normal vector,  $\mathbf{n}_r$ , to the plane,  $\mathcal{R}$ , can be analytically expressed as follows:

$$\mathbf{n}_r = \begin{bmatrix} 1 \\ -\tan \psi_{b,g} \\ 0 \\ 1 \end{bmatrix} \quad (7.116)$$

The position vector,  $\mathbf{r}_r$ , of an arbitrary point,  $m$ , within the plane,  $\mathcal{R}$ , is given by:

$$\mathbf{r}_r = \begin{bmatrix} X_r \\ Y_r \\ Z_r \\ 1 \end{bmatrix} \quad (7.117)$$

The linear velocity of point,  $m$ , in the screw motion of the plane,  $\mathcal{R}$ , can be specified by the vector:

$$\mathbf{v}_m = \mathbf{V}_{ax} + [\boldsymbol{\omega}_g \times \mathbf{R}] \quad (7.118)$$

where:

$\mathbf{V}_{ax}$  is the linear velocity vector of translation motion.

$\boldsymbol{\omega}_g$  is the angular velocity vector of rotation.

$\mathbf{R}$  is the position vector of the point,  $m$ , with respect to the axis of the screw motion (the magnitude of vector,  $\mathbf{R}$ , is equal to the distance of point,  $m$ , from the  $X_0$ -axis, and the vector,  $\mathbf{R}$ , points from the axis  $X_0$  to the point,  $m$ ).

The envelope to consecutive positions of the plane,  $\mathcal{R}$ , that is performing the screw motion is identical to the surface represented by the loci of consecutive positions of the characteristic line,  $\mathcal{C}$ , that is performing the same screw motion as the plane,  $\mathcal{R}$ . The derivation of an equation of the envelope,  $\mathcal{G}$ , to consecutive positions of the plane,  $\mathcal{R}$ , can be significantly simplified if the screw motion of the plane,  $\mathcal{R}$ , is not considered but the screw motion of the characteristic line,  $\mathcal{C}$ , is considered instead.

The direction of the linear velocity vector,  $\mathbf{v}_m$ , is of importance in determining the characteristic line,  $\mathcal{C}$ , whereas the magnitude of vector,  $\mathbf{v}_m$ , is of no interest. Hence, it can be assumed that the magnitude of the rotation vector,  $\boldsymbol{\omega}_g$ , is given as  $|\boldsymbol{\omega}_g| = 1$ . Therefore,

$$\boldsymbol{\omega}_g = \mathbf{i} \quad (7.119)$$

$$\mathbf{V}_{ax} = \mathbf{i} \cdot p_{rl} \quad (7.120)$$

Equations 7.119 and 7.120 yield:

$$\mathbf{v}_m = \mathbf{i} \cdot p_{rl} + \begin{vmatrix} \mathbf{i} & \mathbf{j} & \mathbf{k} \\ 1 & 0 & 0 \\ X_1 & Y_1 & Z_1 \end{vmatrix} \quad (7.121)$$

and

$$\mathbf{v}_m = \mathbf{i} \cdot p_{rl} - \mathbf{j} \cdot Y_1 + \mathbf{k} \cdot Z_1 \quad (7.122)$$

At any point within the characteristic line,  $\mathcal{E}$ , the dot product of the unit normal vector,  $\mathbf{n}_r$ , by the linear velocity vector,  $\mathbf{v}_m$ , is given by the following equation:

$$\mathbf{n}_r \cdot \mathbf{v}_m = p_{rl} \cdot \tan \psi_{b,g} - Z_1 = 0 \quad (7.123)$$

Thus, in this particular case the equation of contact,  $\mathbf{n}_r \cdot \mathbf{v}_m = 0$ , can be represented in the following form:

$$Z_1 = p_{rl} \cdot \tan \psi_{b,g} \quad (7.124)$$

The equation for the position vector of a point,  $\mathbf{r}_e(t)$ , of the characteristic line,  $\mathcal{E}$ ,

$$\mathbf{r}_e(t) = \begin{bmatrix} y \\ t \cdot \tan \psi_{b,g} \\ p_{rl} \cdot \tan \psi_{b,g} \\ 1 \end{bmatrix} \quad (7.125)$$

is derived by simultaneously considering the equation of contact,  $\mathbf{n}_r \cdot \mathbf{v}_m = 0$ , and the equation that describes the plane,  $\mathcal{R}$ , in its current configuration with respect to the axis of screw motion.

In Equation 7.125,  $\mathbf{r}_e(t)$  designates the position vector of a point of the characteristic line,  $\mathcal{E}$ . The parameter of the characteristic line,  $\mathcal{E}$ , is denoted by  $t$ .

In the case under consideration, the characteristic line,  $\mathcal{E}$ , is a straight line of intersection of two planes. The plane,  $\mathcal{R}$ , is the first plane. The second plane is parallel to the coordinate plane,  $X_1Z_1$ , and is remote from the axis of the screw motion at the distance,  $p_{rl} \cdot \tan \psi_{b,g}$ .

For a given screw motion, the location of the characteristic line,  $\mathcal{E}$ , within the plane,  $\mathcal{R}$ , in the initial coordinate system,  $X_0Y_0Z_0$ , remains the same.

The angle of rotation of the coordinate system,  $X_1Y_1Z_1$ , about the  $X_0$ -axis is designated as  $\varepsilon$  (Figure 7.35). The translation of the coordinate system,  $X_1Y_1Z_1$ , in relation to the reference system,  $X_0Y_0Z_0$ , that corresponds to the angle,  $\varepsilon$ , is equal to  $p_{rl} \cdot \varepsilon$ . This makes it possible to find the operator,  $\mathbf{Rs}(1 \rightarrow 0)$ , of the resultant coordinate system transformation, that is, the operator of transition from the coordinate system,  $X_1Y_1Z_1$ , to the coordinate



**FIGURE 7.35**  
A conical involute gear with straight teeth.

system,  $X_0Y_0Z_0$ :

$$\mathbf{Rs}(1 \rightarrow 0) = \begin{bmatrix} 1 & 0 & 0 & p_{rl} \cdot \varepsilon \\ 0 & \cos \varepsilon & \sin \varepsilon & 0 \\ 0 & -\sin \varepsilon & \cos \varepsilon & 0 \\ 0 & 0 & 0 & 1 \end{bmatrix} \quad (7.126)$$

Equation 7.126 for the position vector,  $\mathbf{r}_e(t)$ , of a point of the characteristic line,  $\mathcal{E}$ , considered together with the operator,  $\mathbf{Rs}(1 \rightarrow 0)$ , of the resultant coordinate system transformation, allows an analytical expression for position vector,  $\mathbf{r}_g$ , of a point of the enveloping surface,  $\mathcal{G}$ :

$$\mathbf{r}_g(X_1, \varepsilon) = \begin{bmatrix} X_1 + p_{rl} \cdot \varepsilon \\ X_1 \cdot \tan \psi_{b,g} \cdot \cos \varepsilon + p_{rl} \cdot \tan \psi_{b,g} \cdot \sin \varepsilon \\ -X_1 \cdot \tan \psi_{b,g} \cdot \sin \varepsilon + p_{rl} \cdot \tan \psi_{b,g} \cdot \cos \varepsilon \\ 1 \end{bmatrix} \quad (7.127)$$

Consider a case when the section of the enveloping surface,  $\mathcal{G}$ , is intersected by the plane:

$$X_0 = X_1 + p_{rl} \cdot \varepsilon = 0 \quad (7.128)$$

Equation 7.127 allows the expression  $X_1 = -p \cdot \varepsilon$ . Therefore,

$$\mathbf{r}_{X_0}(\varepsilon) = \begin{bmatrix} 0 \\ p \cdot \tan \psi_{b,g} \cdot (\sin \varepsilon - p \cdot \varepsilon \cdot \cos \varepsilon) \\ p \cdot \tan \psi_{b,g} \cdot (\cos \varepsilon + p \cdot \varepsilon \cdot \sin \varepsilon) \\ 1 \end{bmatrix} \quad (7.129)$$

The involute of a circle is analytically described by Equation 7.129.

The radius of the base circle of the involute curve is as follows:

$$r_{b,g} = p_{rl} \cdot \tan \psi_{b,g} \quad (7.130)$$

Therefore, a screw involute surface allows for interpretation in the form of an envelope to the consecutive positions of a plane,  $\mathcal{R}$ , which is performing a rolling motion. The reduced pitch of the screw involute surface is equal to  $p_{rl}$ , and the radius of the base cylinder is  $r_{b,g} = p_{rl} \cdot \tan \omega_b$ . The involute screw surface shares common points with the base cylinder. The points are within a helix. The tangent to the helix makes an angle,  $\omega_b$ , with the axis of the screw motion [105,113,118]:

$$\tan \omega_b = \frac{r_{b,g}}{p_{rl}} \quad (7.131)$$

From this analysis, one may conclude that  $\tan \omega_b = \tan \psi_{b,g}$  and  $\omega_b = \psi_{b,g}$ . The straight characteristic line,  $\mathcal{E}$ , is tangential to the base helix of the enveloping surface,  $\mathcal{G}$ . This means that if the following conditions are met:

- A plane,  $A$ , is tangential to the base cylinder.
- A straight line,  $\mathcal{E}$ , within the plane,  $A$ , makes an angle,  $\psi_{b,g}$ , with the axis of screw motion.
- The plane,  $A$ , rolls with no sliding over the base cylinder.

then the enveloping surface,  $\mathcal{G}$ , can be represented as the locus of consecutive positions of the straight line,  $\mathcal{E}$ , that rolls without sliding over the base cylinder together with the plane,  $A$ . The enveloping surface is a screw involute surface.

The tooth flanks of opposite sides of the tooth profile of a spur conical involute gear are two screw involute surfaces for which the axial pitches are of the same magnitude and opposite hand.

An example of a conical involute gear that has straight teeth is illustrated in Figure 7.35.

The line of contact,  $LC$ , between the tooth flanks of two spur conical involute gears is a straight line (see Equation 7.125) that is not parallel to the axes of rotations of the gears. The line of contact,  $LC$ , forms a base helix angle,  $\psi_{b,g}$  (see Equation 7.111), with the axes of rotations of the gear and the pinion. Although conical involute gears are of a spur type, the interaction between the tooth flanks of the gear,  $\mathcal{G}$ , and the pinion,  $\mathcal{P}$ , is of the same nature as that of helical gears.



The angle between a lateral plane of the generating rack,  $\mathcal{R}$ , and the axis of rotation,  $O_g$ , of the gear is equal to base helix angle. This angle can be specified as

$$\tan \psi_{b,g} = \frac{\mathbf{n}_r^{(g)} \cdot \mathbf{k}_g}{|\mathbf{n}_r^{(g)} \times \mathbf{k}_g|} \quad (7.132)$$

where

$\mathbf{n}_r^{(g)}$  is the unit normal vector to a tooth flank of the generating rack,  $\mathcal{R}$ , which is expressed in the reference system,  $X_g Y_g Z_g$ , associated with the conical involute gear.

$\mathbf{k}_g$  is the unit vector along the  $Z_g$ -axis of the reference system,  $X_g Y_g Z_g$ .

The unit normal vector,  $\mathbf{n}_r^{(g)}$ , can be expressed in terms of unit the normal vector,  $\mathbf{n}_n^{(g)}$ , and the operator,  $\mathbf{Rs}(n \mapsto g)$ , of the resultant coordinate system transformation.

The unit normal vector,  $\mathbf{n}_n^{(g)}$ , is given in the normal reference system,  $X_n Y_n Z_n$  (see Equation 7.110)

$$\mathbf{n}_n^{(g)} = \begin{bmatrix} -\cos \phi_n \\ \sin \phi_n \\ 0 \\ 1 \end{bmatrix} \quad (7.133)$$

The operator,  $\mathbf{Rs}(n \mapsto g)$ , of the resultant coordinate system transformation can be expressed in terms of operators of elementary coordinate system transformations:

$$\mathbf{Rs}(n \mapsto g) = \mathbf{Tr}(0.5 d_g, Y_p) \cdot \mathbf{Rt}(-\theta, Z_t) \cdot \mathbf{Rt}(\psi_{b,g}, Y_n) \quad (7.134)$$

The operator of translation,  $\mathbf{Tr}(0.5 d_g, Y_p)$ , is determined in Equation 7.134. The operator of rotation,  $\mathbf{Rt}(-\theta, Z_t)$ , is equal to the operator of rotation,  $\mathbf{Rt}(-\theta, Z_n)$ , given by Equation 7.102:

$$\mathbf{Rt}(-\theta, Z_t) = \begin{bmatrix} 1 & 0 & 0 & 0 \\ 0 & \cos \theta & -\sin \theta & 0 \\ 0 & \sin \theta & \cos \theta & 0 \\ 0 & 0 & 0 & 1 \end{bmatrix} \quad (7.135)$$

Finally, the operator of rotation,  $\mathbf{Rt}(\psi_{b,g}, Y_n)$ , can be analytically described as follows:

$$\mathbf{Rt}(\psi_{b,g}, Y_n) = \begin{bmatrix} \cos \psi_{b,g} & 0 & \sin \psi_{b,g} & 0 \\ 0 & 1 & 0 & 0 \\ -\sin \psi_{b,g} & 0 & \cos \psi_{b,g} & 0 \\ 0 & 0 & 0 & 1 \end{bmatrix} \quad (7.136)$$

The aforementioned expressions for operators of elementary coordinate system transformations,  $\mathbf{Tr}(0.5 d_g, Y_p)$ ,  $\mathbf{Rt}(-\theta, Z_n)$ , and  $\mathbf{Rt}(\psi_{b,g}, Y_n)$  allow for an expression

$$\mathbf{Rs}(n \mapsto g) = \begin{bmatrix} \cos \psi_{b,g} & 0 & \sin \psi_{b,g} & 0 \\ \sin \theta \sin \psi_{b,g} & \cos \theta & -\sin \theta \cos \psi_{b,g} & 0.5 d_g \\ -\cos \theta \sin \psi_{b,g} & \sin \theta & \cos \theta \cos \psi_{b,g} & 0 \\ 0 & 0 & 0 & 1 \end{bmatrix} \quad (7.137)$$

for the operator,  $\mathbf{Rs}(n \mapsto g)$ , of the resultant coordinate system transformation for a conical involute gear with helical teeth.



Equation 7.137 allows an expression for the unit normal vector,  $\mathbf{n}_r^{(g)}$ :

$$\mathbf{n}_r^{(g)} = \mathbf{Rs}(n \mapsto g) \cdot \mathbf{n}_n^{(g)} = \begin{bmatrix} -\cos \phi_n \cos \psi_{b.g} \\ \sin \phi_n \cos \theta + 0.5d_{w.g} - \cos \phi_n \sin \theta \sin \psi_{b.g} \\ \sin \phi_n \sin \theta + \cos \phi_n \cos \theta \sin \psi_{b.g} \\ 1 \end{bmatrix} \quad (7.138)$$

In the normal reference system,  $X_n Y_n Z_n$ , the unit vector,  $\mathbf{k}_g$ , along the gear axis of rotation,  $O_g$ , can be expressed as follows:

$$\mathbf{k}_g = \begin{bmatrix} 0 \\ 0 \\ 1 \\ 1 \end{bmatrix} \quad (7.139)$$

Expressions for the unit normal vector,  $\mathbf{n}_r^{(g)}$ , and the unit vector,  $\mathbf{k}_g$ , can be substituted in Equation 7.132. After the necessary formula transformations are completed, an expression for the calculation of the base helix angle,  $\psi_{b.g}$ , is derived:

$$\tan \psi_{b.g} = \frac{\sin \phi_n \sin \theta + \cos \phi_n \cos \theta \sin \psi_{b.g}}{\sqrt{\cos^2 \phi_n \cos^2 \psi_{b.g} + (\sin \phi_n \cos \theta - \cos \phi_n \sin \theta \sin \psi_{b.g})^2}} \quad (7.140)$$

Once the base helix angle,  $\psi_{b.g}$ , is calculated, an expression for the position vector of a point,  $\mathbf{r}_g$ , on the tooth flank of a conical involute gear with helical teeth can be represented in matrix form (see Equation 7.14):

$$\mathbf{r}_g(U_g, V_g) = \begin{bmatrix} r_{b.g} \cos V_g + U_g \cos \lambda_{b.g} \sin V_g \\ r_{b.g} \sin V_g - U_g \sin \lambda_{b.g} \sin V_g \\ r_{b.g} \tan \lambda_{b.g} - U_g \sin \lambda_{b.g} \\ 1 \end{bmatrix} \quad \begin{matrix} V_g^{(l)} \leq V_g \leq V_g^{(a)} \\ 0 \leq U_g \leq [U_g] \end{matrix} \quad (7.141)$$

In Equation 7.133, the base lead angle,  $\lambda_{b.g}$ , is the angle that complements the base pitch angle,  $\psi_{b.g}$ , to  $90^\circ$ ; that is, the equality  $\lambda_{b.g} = 90^\circ - \psi_{b.g}$  is observed.

The tooth flanks of opposite sides of the tooth profile of a conical involute gear that has helical teeth are two screw involute surfaces of different axial pitches. The hand of the axial pitch is commonly the same. However, in particular cases, the pitches can be of opposite hands, and the axial pitch of one of the two flanks can be equal to infinity.

The line of contact,  $LC$ , between the tooth flanks of two conical involute gears that have helical teeth is a straight line that is not parallel to the axes of rotations of the gears. The line of contact,  $LC$ , makes a base pitch angle,  $\psi_{b.g}$  (see Equation 7.140), with the axes of the rotations of the gear and the pinion. The interaction between tooth flanks of the gear,  $\mathcal{G}$ , and the pinion,  $\mathcal{P}$ , is of the same nature as that for helical gears of a conventional design.

## 7.4 Conditions to Be Fulfilled by a Pair of Mating Gears

In order to make the engagement of two gears in mesh feasible, certain geometrical and kinematical conditions have to be fulfilled. The relationships for mating external spur and helical gears are considered.\*

When designing gears, in order to get two involute gears in mesh, it is practical to fulfill the following five geometrical and kinematical conditions.

\* Relationships similar to those considered apply to mating internal gear pairs as well.

*The first condition.* The first condition governing mating involute gears immediately follows from the rope drive analogy illustrated in Figure 7.1. This condition is formulated as follows: *The ratio of the gear and pinion base diameters must be equal to the gear ratio:*

$$\frac{d_{b,g}}{d_{b,p}} = \frac{N_g}{N_p} = u \quad (7.142)$$

Hence:

$$\frac{d_{b,g}}{N_g} = \frac{d_{b,p}}{N_p} \quad \therefore \quad \frac{p_{bt,g}}{\pi} = \frac{p_{bt,p}}{\pi} \quad \therefore \quad p_{bt,g} = p_{bt,p} \quad (7.143)$$

This means that the transverse base pitches of mating gears must be equal.

*The second condition.* For line contact, the base helix angles of a gear and of its mating pinion must be equal:

$$\psi_{b,g} = \psi_{b,p} \quad (7.144)$$

Hence, the second condition can be formulated as follows: *The normal base pitches of the gear and pinion must be equal:*

$$p_{b,g} \equiv p_{b,p} \quad (7.145)$$

Two involute gears having the same base pitch can be engaged in mesh with one another. To make the mesh feasible, equality of base pitches of a gear and its mating pinion is a must.

*The third condition.* For a smooth transition of tooth contact from one pair of teeth to another, there must be, theoretically, at least one point of contact in the zone of action. Because of strength conditions, there is a further requirement in the case of mating helical gears, namely: *All points of contact along the minimum required path of contact should be correspondingly in contact along the contact line over the face width.*

By definition, the transverse contact ratio,  $m_p$ , of a gear pair is equal to:

$$m_p = \frac{\text{Length of path of contact}}{\text{Transverse base pitch } p_t} \quad (7.146)$$

The face contact ratio,  $m_F$  (overlap ratio), of a gear pair is defined as:

$$m_F = \frac{F_{ac} \tan \psi_b}{p_{bt}} \quad (7.147)$$

In Equation 7.147, the active portion of the face width of mating gears is denoted by  $F_{ac}$ .

The total contact ratio,  $m_t$ , of a gear pair is equal to the sum of both:

$$m_t = m_p + m_F \quad (7.148)$$

For any and all gear pairs, satisfaction of the inequality  $m_t > 1$  is a must.

For spur gear pairs,  $m_F = 0$ . Therefore, the inequality  $m_t = m_p > 1$  must be fulfilled for spur gear pairs.

For helical gear pairs,  $m_p > 0$ , and  $m_F > 0$ . Therefore, the inequality  $m_t = m_p + m_F > 1$  must be fulfilled for helical gear pairs.

In order to ensure satisfactory running and loading conditions, it is recommended that (1) transverse contact ratio be somewhat greater than 1, and (2) on helical gears, an overlap ratio that exceeds or is equal to 1 be chosen [74].

*The fourth condition.* Commonly, tooth geometry is calculated for a zero backlash gear pair. At the gear and pinion working pitch cylinders, therefore, the sum of the theoretical transverse tooth thicknesses of the gear,

$t'_{t,g}$ , and pinion,  $t'_{t,p}$ , must be equal to the transverse working pitch,  $p'_t$ :

$$t'_{t,g} + t'_{t,p} = p'_t = \pi \frac{2C}{N_g + N_p} \quad (7.149)$$

*The fifth condition.* The gear and pinion root cylinders must provide an adequate bottom clearance beyond the tip cylinder of the mating gears to avoid interference [74]:

$$d_{o,g} + d_{f,p} + 2C = 2c \quad (7.150)$$

$$d_{o,p} + d_{f,g} + 2C = 2c \quad (7.151)$$

Bottom clearance is denoted here by  $c$ .

To enable two gears to mesh correctly, therefore, the following design parameters of basic tooth data

Number of teeth	$N_g, N_p$
Base diameter	$d_{b,g}, d_{b,p}$
Base helix angle	$\psi_{b,g}, \psi_{b,p}$
Base tooth thickness	$t_{b,g}, t_{b,p}$
Outer diameter	$d_{o,g}, d_{o,p}$
Root diameter	$d_{f,g}, d_{f,p}$

for both individual gears must jointly satisfy the set of the above conditions.

A comprehensive analysis of the geometry and kinematics of involute gearing can be found in the brilliant book by Gavrilenko [37]. This book is especially useful for beginners and for engineers with entry-level experience in gearing.

In a case when the base diameter,  $d_{b,g}$ , of a gear is equal to or larger than the gear start-of-active-profile diameter,  $d_{sap}$ ; that is, when the inequality,  $d_{b,g} \geq d_{sap}$ , is valid, the gear is said to be a *low-tooth-count gear*, or just an *LTC-gear*, for simplicity. In practice, a gear with 18 teeth or fewer is referred to as a low-tooth-count gear. Low-tooth-count gears possess a huge potential for application in the design of *high-power-density gear drives*, or just *HPD-gear drives*, for simplicity. An alternative terminology is used with regards to high-power-density gear drives: they are also called *high power-to-weight-ratio gear pairs*, or just *high PtD-ratio gear pairs*, for simplicity.\*

\* It is the right point to stress here that an increased sliding between the gear tooth flanks and a huge *undercut* of the tooth profiles are the two strong disadvantages of gears with a low tooth count. Two kinds of undercut of a gear tooth profile are distinguished here. The required undercut that is necessary to get a gear engaged in mesh with a mating one is an undercut of the first kind. An undesired undercut when gears are cut by a continuous-indexing (generating) method is an undercut of the second kind. Also, a zero radius of curvature (at the involute tooth profile point on the base circle/cylinder): when this point becomes a contact point, this results in an infinite (theoretically) contact stress (needle-knife).

## Interaction of Tooth Flanks in Parallel-Axes Involute Gearing

In parallel-axes gearing, a power from a driving shaft (a pinion in gear reducers or a gear in gear increasers) is transmitted to a driven shaft (a gear in gear reducers or a pinion in gear increasers) by means of two gears engaged in mesh with one another (Figure 8.1). The involute tooth flanks of a gear and a mating pinion in a parallel-axes gear pair interact with one another when a rotary motion is transmitted by means of a parallel-axes gear pair. Power from a driving shaft to a driven shaft is transmitted across a line of contact between the interacting tooth flanks. A desired line of contact,  $LC_{des.g}$ , that is used for the generating of the tooth flank of a gear, and a desired line of contact,  $LC_{des.p}$ , that is used for the generating of the tooth flank of a mating pinion, align with the line of contact,  $LC$ , in a parallel-axes involute gear pair, that is,  $LC_{des.g} \equiv LC_{des.p} \equiv LC$ .

It is convenient to begin an analysis of interaction of tooth flanks in parallel-axes involute gearing with the analysis of spur parallel-axes involute gearing.

### 8.1 Interaction of Tooth Flanks in Parallel-Axes Spur Involute Gearing

An example of spur parallel-axes gear pair is depicted in Figure 8.2. A schematic that illustrates the interaction of the tooth flanks,  $\mathcal{G}$  and  $\mathcal{P}$ , of a spur gear and its mating pinion in parallel-axes involute gearing is depicted in Figure 8.3. The interaction of the tooth flanks,  $\mathcal{G}$  and  $\mathcal{P}$ , in a spur gear pair is still considered in a tight connection with a corresponding *pulley-and-belt* analogy of a parallel-axes gear pair.

In Figure 8.3, a gear is rotated about its axis of rotation,  $O_g$ . The rotation of the gear is specified by a rotation vector,  $\omega_g$ , of the gear. A mating pinion is rotated about its axis of rotation,  $O_p$ . The rotation of the pinion is specified by a rotation vector,  $\omega_p$ , of the pinion. The axes of rotation,  $O_g$  and  $O_p$ , are parallel to each other, and are at a center distance,  $C$ , from one another.

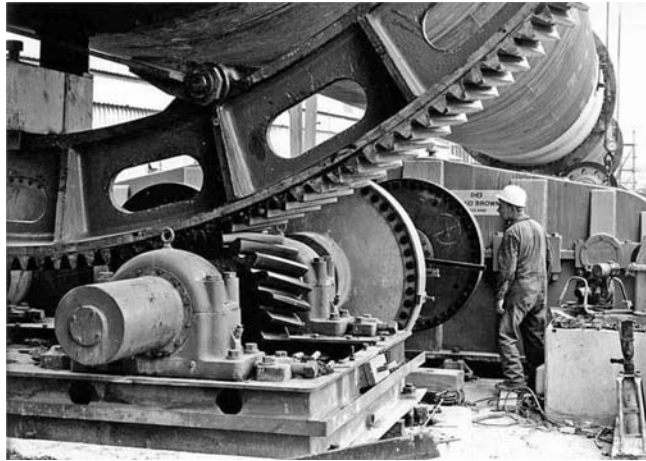
The axis of instant rotation,  $P_{ln}$ , is a straight line that is entirely located within a plane through the axes of rotation,  $O_g$  and  $O_p$ , of a gear and a mating pinion. The axis of instant rotation,  $P_{ln}$ , is parallel to the axes of rotation,  $O_g$  and  $O_p$ .

The line of contact,  $LC$ , in a parallel-axes spur involute gear pair is a straight line parallel to the axis of instant rotation,  $P_{ln}$ . In the particular configuration shown in Figure 8.3, the line of contact,  $LC$ , is aligned with the axis of instant rotation,  $P_{ln}$ .

The plane of action,  $PA$ , in a parallel-axes spur involute gear pair is a plane through the axis of instant rotation,  $P_{ln}$ . The plane of action,  $PA$ , forms a transverse pressure angle,  $\phi_t$ , with a perpendicular to the centerline,  $C$ . The plane of action,  $PA$ , is tangent to the gear base cylinder of a radius,  $r_{b.g}$ , and the plane of action,  $PA$ , is tangent to the pinion base cylinder of a radius,  $r_{b.p}$ . When the gears rotate, the plane of action travels with a liner velocity,  $V_{par}$ , as shown in Figure 8.3.

The straight line segments,  $N_g N_g$  and  $N_p N_p$ , are the lines of tangency of the plane of action,  $PA$ , and the base cylinders of a gear and a mating pinion, correspondingly.

The involute gear,  $\mathcal{G}$  and a mating pinion,  $\mathcal{P}$ , tooth flanks interact with one another within the effective face width,  $F_{par}$ , of the plane of action,  $PA$ . Commonly, a gear is designed so as to make the gear face width,  $F_g$ , smaller than the pinion face width,  $F_p$  (that is, the inequality  $F_g < F_p$  is valid). Under such a scenario, the effective face width,  $F_{par}$ , of the plane of action,  $PA$ , equals the gear face width; thus, an equality  $F_{pa} = F_g$  is observed (Figure 8.4a). Otherwise, when a gear face width,  $F_g$ , is larger than the pinion face width,  $F_p$  (that is, the inequality  $F_g > F_p$  is valid), then the effective face width,  $F_{par}$ , of the plane of action,  $PA$ , equals the pinion face width; thus, the equality  $F_{pa} = F_p$  is observed. In the case of improperly aligned gears, the effective face width,  $F_{par}$ , of the plane of action,  $PA$ , equals the corresponding overlap of the face widths,  $F_g$  and  $F_p$ , of the gear and a mating pinion, as illustrated in Figure 8.4b.

**FIGURE 8.1**

A parallel-axes helical involute gear pair.

With that said, the term *effective face width*,  $F_{pa}$  can be defined as follows:

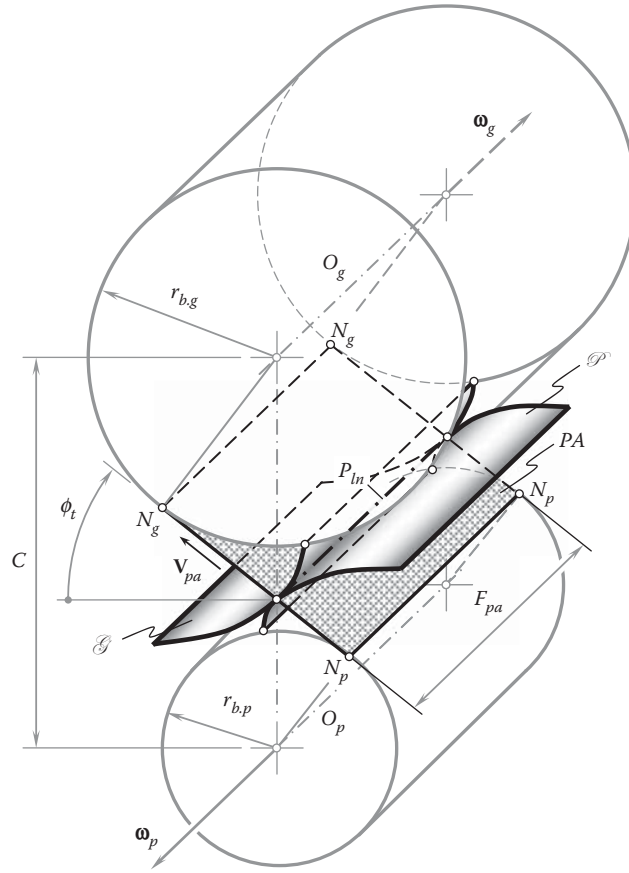
**Definition 8.1**

*The effective face width,  $F_{pa}$ , of a gear pair is a width of the portion of the plane of action,  $PA$ , within which a gear and its mating pinion tooth flanks,  $\mathcal{G}$  and  $\mathcal{P}$ , interact with one another; the effective face width is measured along the axis of instant rotation,  $P_{ln}$ .*

A simple problem of the determination of an effective face width,  $F_{pa}$  (see [Figure 8.4](#)), becomes more complex in special cases of parallel-axes gearing, for example, in the case of the swash plate gear pair depicted in

**FIGURE 8.2**

Spur involute gear pair.

**FIGURE 8.3**

Interaction of gear and mating pinion tooth flanks,  $\mathcal{G}$  and  $\mathcal{P}$ , in a parallel-axes gear pair composed of two spur involute gears.

**Figure 8.5.** The effective face width,  $F_{pa}$ , in the case under consideration is time dependent; that is, it depends on the actual angular configuration of the mating gears.

Another example of a time-dependent face width in a gear is illustrated in **Figure 8.6**. Simple at first glance, this case features the gear face width,  $F_g$ , of a complex geometry: when the gear rotates about its axis, the effective face width alters in time in accordance to a current configuration of the gear in relation to the plane of action,  $PA$ . Considered together with a face width of a mating pinion, the gear face width returns the ultimate effective face width of the gear pair,  $F_{pa}$ .

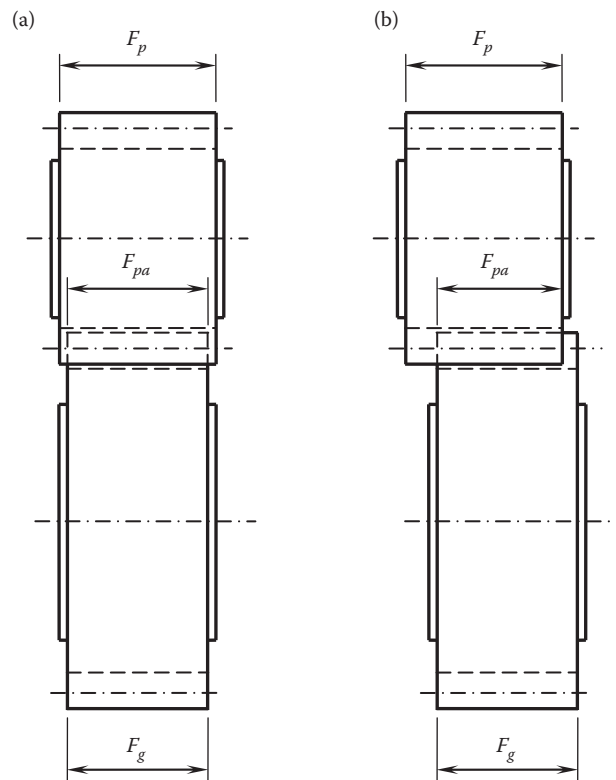
The above Definition 8.1 can be adjusted to cases of variable-in-time instant effective face width,  $F_{pa}^{\text{inst}}$ .

## 8.2 Interaction of Tooth Flanks in Parallel-Axes Helical Involute Gearing

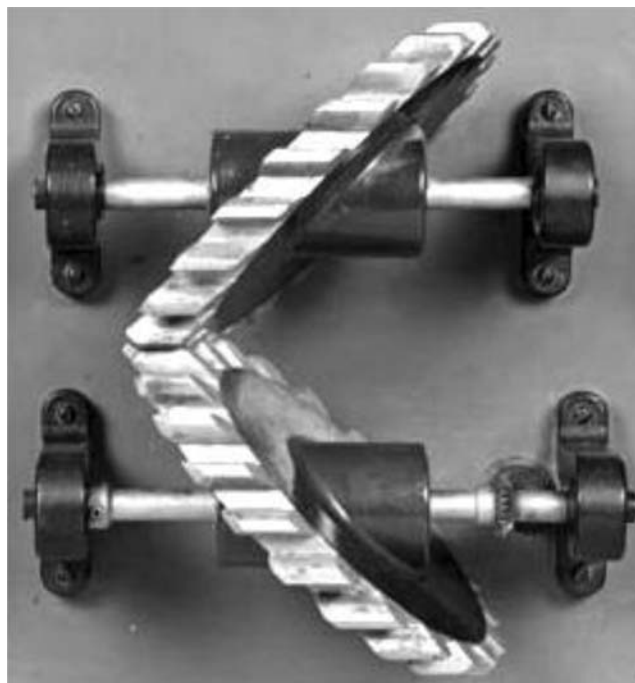
An example of a helical parallel-axes gear pair is depicted in **Figure 8.7**. A schematic that illustrates the interaction of the tooth flanks,  $\mathcal{G}$  and  $\mathcal{P}$ , of a helical gear and its mating pinion in parallel-axes involute gearing is depicted in **Figure 8.8**. The interaction of the tooth flanks,  $\mathcal{G}$  and  $\mathcal{P}$ , in a helical gear pair is still considered in a tight connection with a corresponding pulley-and-belt analogy of a parallel-axes gear pair.

In **Figure 8.8**, a helical gear is rotated about its axis of rotation,  $O_g$ . The rotation of the gear is specified by a rotation vector,  $\omega_g$ , of the gear. A mating helical pinion is rotated about its axis of rotation,  $O_p$ . The rotation of the pinion is specified by a rotation vector,  $\omega_p$ , of the pinion. The axes of rotation,  $O_g$  and  $O_p$ , are parallel to each other and are at a center distance,  $C$ , from one another.

The axis of instant rotation,  $P_{ln}$ , is a straight line that is entirely located within a plane through the axes of rotation,  $O_g$  and  $O_p$ , of a gear and a mating pinion. The axis of instant rotation,  $P_{ln}$ , is parallel to the axes of rotation,  $O_g$  and  $O_p$ .

**FIGURE 8.4**

Gear face width,  $F_g$ ; pinion face width,  $F_p$ ; and effective face width,  $F_{pa}$ , in (a) properly, and (b) improperly aligned gears in a gear pair.

**FIGURE 8.5**

Effective face width,  $F_{pa}$ , in a swash plate gear pair features a complex geometry.



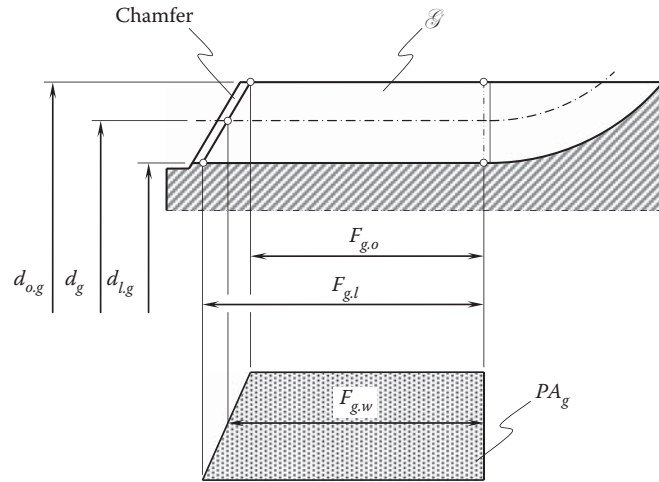


**FIGURE 8.6**  
Gear face width,  $F_g$ , of a complex geometry.



**FIGURE 8.7**  
A gear pair composed of two helical involute gears.

The line of contact,  $LC$ , in a parallel-axes helical involute gear pair is a straight line that forms an angle with the axis of instant rotation,  $P_{ln}$ . This angle is commonly referred to as the *base helix angle*,  $\psi_{b,g}$ . An example of a straight line of contact,  $LC$ , in a parallel-axes helical involute gear pair is shown in Figure 8.8. The helix angle of a gear on the pitch cylinder,  $\psi_g$ , is measured within a common tangent plane in relation to the perpendicular,  $n - n$ , to the axis of instant rotation,  $P_{ln}$ .

The plane of action,  $PA$ , in a parallel-axes helical involute gear pair is a plane through the axis of instant rotation,  $P_{ln}$ . The plane of action,  $PA$ , forms a transverse pressure angle,  $\phi_t$ , with a perpendicular to the centerline,  $\mathcal{C}$ . The plane of action,  $PA$ , is tangent to the gear base cylinder of a radius,  $r_{b,g}$ , and the plane of action,  $PA$ , is tangent to the pinion base cylinder of a radius,  $r_{b,p}$ . When the gears rotate, the plane of action travels with a liner velocity,  $V_{pa}$ , as shown in Figure 8.8.

The straight line segments,  $N_g N_g$  and  $N_p N_p$ , are the lines of tangency of the plane of action,  $PA$ , and the base cylinders of a gear and a mating pinion correspondingly.

Involute tooth flanks a gear,  $\mathcal{G}$ , and a mating pinion,  $\mathcal{P}$ , interact with one another within the effective face width,  $F_{pa}$ , of the plane of action,  $PA$ .

### 8.3 Transmission of a Uniform Rotation by Means of Parallel-Axes Involute Gearing

Parallel-axes involute gearing is capable of transmitting a uniform rotation. Shown in Figure 8.9 is a schematic of a parallel-axes gear pair associated with a corresponding pulley-and-belt analogy. The belt stretched between



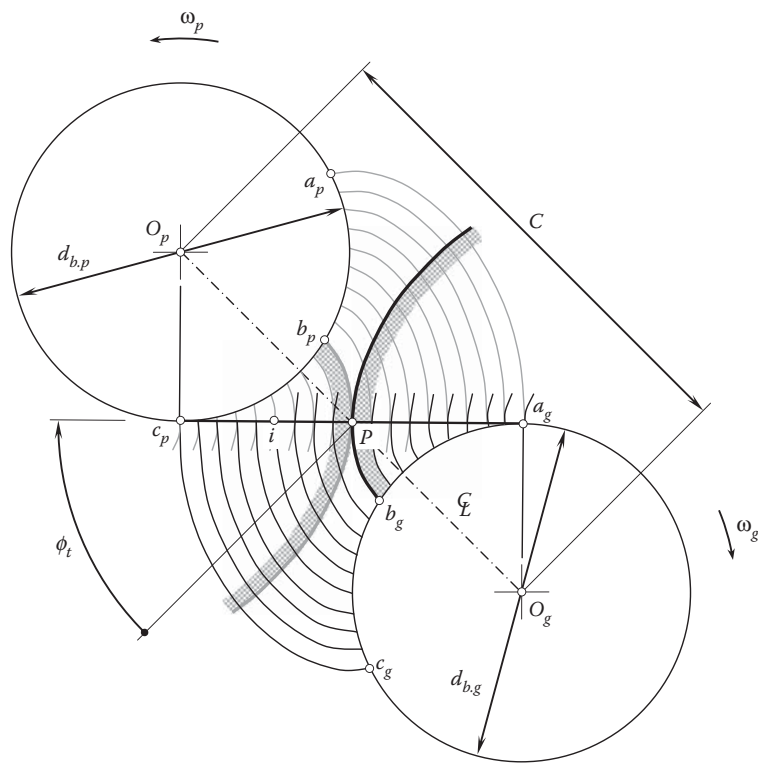


**FIGURE 8.9**  
Interaction of involute profiles in a transverse section of a parallel-axes gear pair.

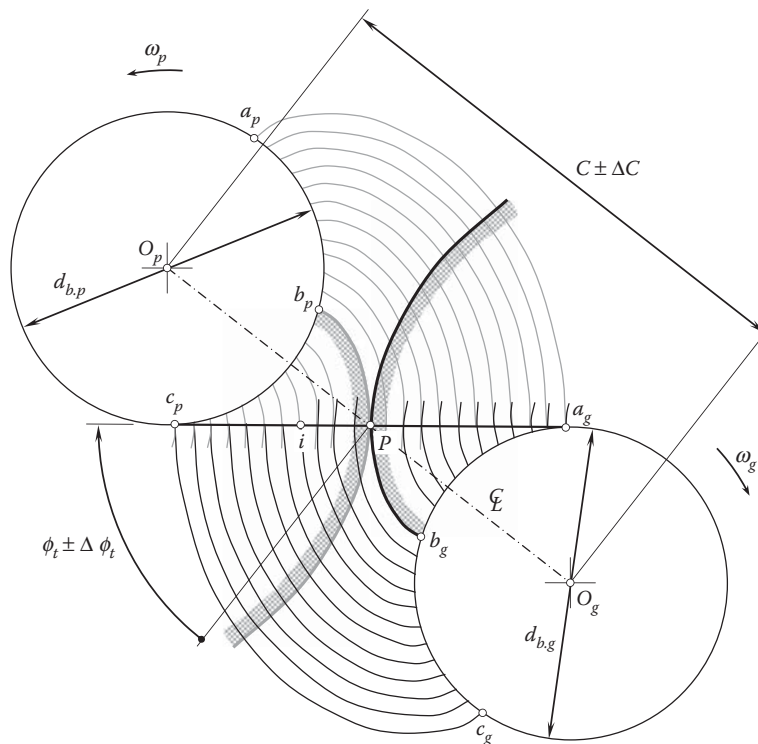


**FIGURE 8.10**  
A schematic on insensitivity of involute gearing to the alteration of center distance.

point,  $P$ , for each regular position of the driving gear at any and all configurations of the mating gears. This statement is in agreement with an important theorem from the study of the kinematics of planar motion, namely the *Arnold-Kennedy instant center theorem*.

## 8.4 Contact Ratio in Parallel-Axes Involute Gearing

Interaction between the tooth flanks of a gear and a mating pinion resembles that in a cam mechanism. In both cases, the working surfaces of a driving member push over the working surfaces of the driven member. The key difference between parallel-axes gearing and cam mechanisms is that in a gear pair, at certain instants of time, two or even more pairs of tooth flanks interact with one another simultaneously. The latter is required by a continuous rotation transmission. For the smooth transition of tooth contact from one pair of teeth to another, there must be one or more pairs of teeth in contact at every instant of time. To transmit a continuous rotation from a driving shaft to a driven shaft, at least one pair of teeth must be engaged in mesh at every instant of time. The transmission of the rotation is interrupted when this condition is violated. The average number of pairs of teeth of a gear and a mating pinion that are engaged in mesh simultaneously is specified by the *total contact ratio*. Commonly, the contact ratio is designated as  $m_t$ .

Three different types of contact ratio are distinguished, that is:

- The *transverse contact ratio*,  $m_p$ , (or *profile contact ratio*)
- The *face contact ratio*,  $m_F$
- The *total contact ratio*,  $m_t$

The total contact ratio,  $m_t$ , in a parallel-axes involute gear pair equals to the summa of the transverse contact ratio,  $m_p$  (or profile contact ratio,  $m_p$ ) and the face contact ratio,  $m_F$ ; that is:

$$m_t = m_p + m_F \quad (8.1)$$

To transmit a continuous rotation from a driving shaft to the driven shaft, the following inequality needs to be observed:

$$m_t \geq 1 \quad (8.2)$$

in addition to the three fundamental conditions just considered.

In order to calculate the total contact ratio,  $m_t$ , in a parallel-axes involute gear pair, both the components,  $m_p$  and  $m_F$ , have to be calculated.

### 8.4.1 Transverse Contact Ratio in Parallel-Axes Involute Gearing

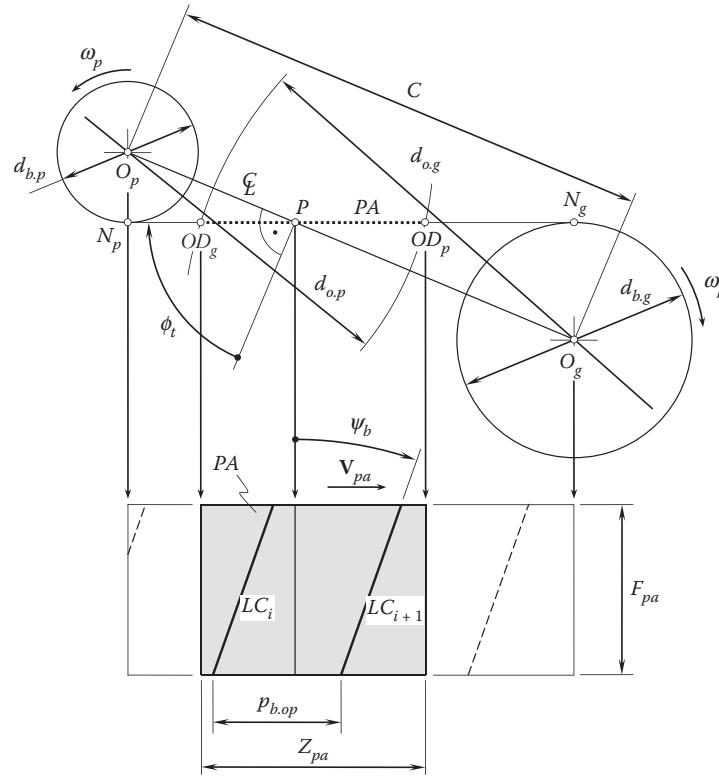
The transverse contact ratio,  $m_p$ , is the contact ratio in a transverse plane. By definition, for involute gears, it is most directly obtained as the ratio of the path of action to the base pitch.

Shown in [Figure 8.11](#) is a schematic of a parallel-axes gear pair associated with a corresponding *pulley-and-belt* analogy. The axis of rotation of the gear,  $O_g$ , and that of the pinion,  $O_p$ , are parallel to each other, and are at a center distance,  $C$ , from one another. The base cylinder of a diameter  $d_{b,g}$  is associated with the gear. Similarly, the base cylinder of a diameter  $d_{b,p}$  is associated with the pinion. The transverse pressure angle in the gear pair is  $\phi_t$ . The plane of action,  $PA$ , in an external parallel-axes gear pair is tangent to the base cylinders from the opposite sides. The gear and the pinion rotate,  $\omega_g$  and  $\omega_p$ , about their axes of rotation,  $O_g$  and  $O_p$ . The magnitudes,  $\omega_g$  and  $\omega_p$ , of the rotation vectors,  $\omega_g$  and  $\omega_p$ , are synchronized with one another reciprocal to the tooth count,  $N_g$  and  $N_p$ , of the gear\* and the pinion; that is, the ratio:

$$\frac{\omega_g}{\omega_p} = \frac{N_p}{N_g} \quad (8.3)$$

is valid in *perfect* parallel-axes gearing.

\* In cases of internal gearing, the tooth count of a gear,  $N_g$ , has a negative value,  $N_g < 0$ .

**FIGURE 8.11**

Definition of the transverse contact ratio,  $m_p$ , in perfect parallel-axes gearing.

When the gears rotate, the plane of action may be considered as a zero-thickness film that is unwrapping from the base cylinder of the gear and wrapping on the base cylinder of the pinion. In such a motion, the plane of action travels with a linear velocity,  $V_{pa}$ . The magnitude,  $V_{pa}$ , of the linear velocity vector,  $V_{pa}$ , is timed with the rotations,  $\omega_g$  and  $\omega_p$ , so as to ensure rolling with no slippage of the plane of action,  $PA$ , over the base cylinders of the gear and the pinion.

A desirable line of contact,  $LC_{des}^i$ , of the  $i$ th pair of teeth of the gear and the pinion is drawn within the plane of action. As an example, the desirable line of contact,  $LC_{des}^i$ , is shown for a case of helical involute gearing. In the case under consideration, this straight line segment forms the base helix angle,  $\psi_b$ , with the axes,  $O_g$  and  $O_p$  (the base helix angle,  $\psi_b$ , is shown in Figure 8.11).

The desirable line of contact,  $LC_{des}^{i+1}$ , of the adjacent  $(i+1)$ th pair of teeth of the gear and the pinion is parallel to the straight line,  $LC_{des}^i$  (i.e.,  $LC_{des}^{i+1} \parallel LC_{des}^i$ ), and is also located within the plane of action,  $PA$ . In a transverse section of a gear pair, the distance between every two adjacent desired lines of contact,  $LC_{des}^i$  and  $LC_{des}^{i+1}$ , equals the operating base pitch,  $p_{b,op}$ , of the gear pair.

The outer cylinders of diameters  $d_{o,g}$  and  $d_{o,p}$  of the gear and the pinion intersect the plane of action,  $PA$ , along two straight lines.

The plane of action,  $PA$ , is terminated by two straight line segments through the endpoints  $N_g$  and  $N_p$  (Figure 8.11). However, the active portion of the plane of action,  $PA$ , is shorter in comparison with the length of the straight line segment,  $N_gN_p$ . The gear teeth do not extend beyond the outer diameter,  $d_{o,g}$ , of the gear. Therefore, a portion of the plane of action beyond the point of intersection,  $OD_g$ , of the plane of action,  $PA$ , by the cylinder of the diameter,  $d_{o,g}$ , is not active. Similarly, the pinion teeth do not extend beyond the outer diameter,  $d_{o,p}$ , of the pinion. Therefore, a portion of the plane of action beyond the point of intersection,  $OD_p$ , of the plane of action,  $PA$ , by the cylinder of the diameter,  $d_{o,p}$ , is not active. Ultimately, the effective portion of the plane of action is terminated by two straight line segments through the endpoints,  $OD_g$  and  $OD_p$ , as shown in Figure 8.11. These two lines form an effective portion of the plane of action in the form of a rectangle. The length of the effective portion of the plane of action is the so-called *length of action*,  $Z_{pa}$ .

**Definition 8.2**

The active portion of the plane of action is a portion of the plane of action,  $PA$ , that is located within the effective face width,  $F_{pa}$ , of a gear pair and bounded by the lines of intersection by the outer surfaces of a gear and its mating pinion.

The active portion of the plane of action is commonly called as the zone of action or contact zone.

The zone of action in involute parallel-axes gears with either spur or helical teeth is a rectangular area in the plane of action bounded by the active portion of the line of action and the active face width. Here and below, the active face width is understood in the sense of the face width common for both the gear and the pinion.

Elementary analysis of the schematic depicted in Figure 8.11 reveals how the length of action,  $Z_{pa}$ , can be expressed in terms of the design parameters of the gear pair.

By definition, the transverse contact ratio,  $m_p$ , in parallel-axes involute gearing equals:

$$m_p = \frac{Z_{pa}}{p_{b.op}} \quad (8.4)$$

Roughly speaking, the transverse contact ratio,  $m_p$ , indicates an average number of pairs of teeth simultaneously engaged in mesh in a particular transverse section of the gear pair.

In the case of spur gearing, the total contact ratio,  $m_t$ , equals the transverse contact ratio,  $m_p$ ; that is, an equality  $m_t = m_p$  is valid for spur gear pairs.

An actual value of transverse contact ratio,  $m_p$ , in a parallel-axes gear pair is in the range of:

$$0 \leq m_p < \infty \quad (8.5)$$

Fulfillment of the condition  $m_t \geq 1$  (see Equations 8.1a and 8.2b) is a must when the inequality (see Equation 8.5) is considered. This means that a permissible interval for the transverse contact ratio,  $m_p$ , also depends on an actual value of the face contact ratio,  $m_F$ .

The following approach can be utilized for the calculation of the length of action,  $Z_{pa}$ .

When two gears are put into mesh with certain center distance,  $C$ , as shown in Figure 8.12, the line tangent to both base cylinders is defined as the *line of action*. The contact starts at a point,  $a$ , where the outside diameter circle of the pinion intersects the line of action,  $LA$  (as well as the path of contact,  $P_c$ ); passes through the pitch point,  $P$ ; and ends at point  $b$ , where the outside diameter of the gear intersects the line of action,  $LA$  (and path of contact,  $P_c$ ). The straight line segment,  $ab$ , of the line of action,  $cd$ , is the active portion of the line of action,  $LA$ . The length of the active portion of the line of action is denoted by  $Z_{pa}$ .

Referring to Figure 8.12, an expression:

$$\rho_g = ad = \frac{1}{2} \sqrt{d_{o.g}^2 - d_{b.g}^2} \quad (8.6)$$

for the calculation of the radius of curvature,  $\rho_g$ , of the gear tooth profile at the outer diameter,  $d_{o.g}$ , of the gear can be derived.

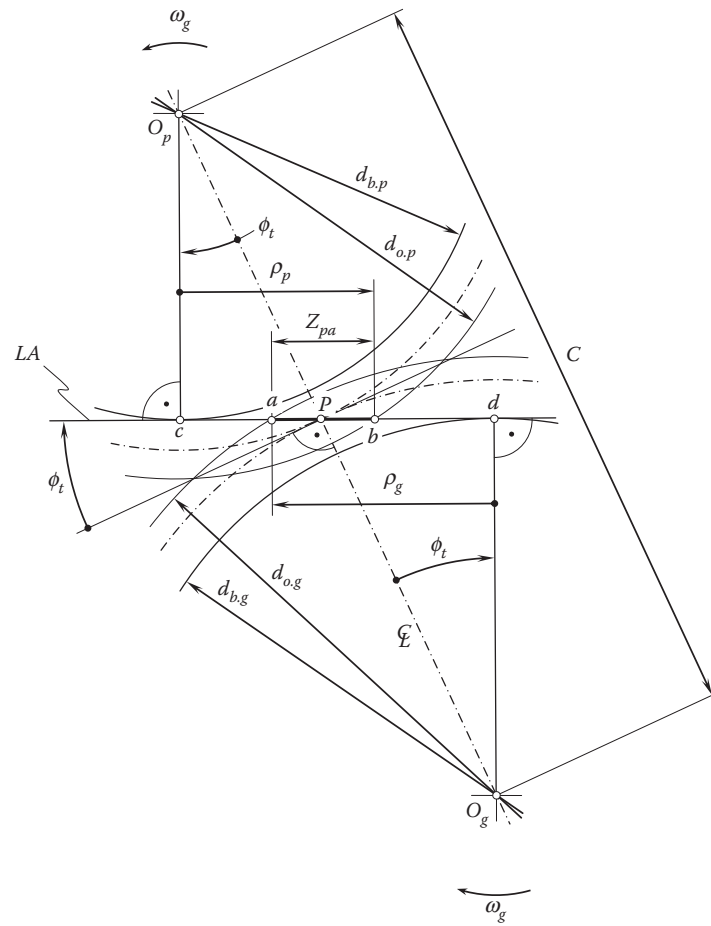
Similarly, an expression:

$$\rho_p = bc = \frac{1}{2} \sqrt{d_{o.p}^2 - d_{b.p}^2} \quad (8.7)$$

for the calculation of the radius of curvature,  $\rho_p$ , of the pinion tooth profile at the outer diameter,  $d_{o.p}$ , of the pinion can be derived as well.

Having calculated the radii of curvature,  $\rho_g$  and  $\rho_p$ , the length,  $Z_{pa}$ , of the active portion of the line of action,  $LA$ , can be calculated from the formula:

$$Z_{pa} = \rho_g + \rho_p - C \sin \phi_t = \frac{1}{2} \left( \sqrt{d_{o.g}^2 - d_{b.g}^2} + \sqrt{d_{o.p}^2 - d_{b.p}^2} - 2C \sin \phi_t \right) \quad (8.8)$$

**FIGURE 8.12**

The line of action,  $LA$ , in an external involute gear pair.

The active portion of the line of action,  $LA$ , can be expressed in terms of two components,  $Z_g$  and  $Z_p$ , that is, as the sum of  $Z_{pa} = Z_g + Z_p$ . The component  $Z_g$  is due to the addendum of the gear,  $a_g$ , and the component  $Z_p$  is due to the addendum of the pinion,  $a_p$ . Usually, the inequality  $Z_g > Z_p$  is observed.

Here, in Equation 8.8, the pressure angle in the transverse plane is denoted by  $\phi_t$ . In the case of spur gears, this angle is equal to the profile angle of the gear and the pinion at the pitch point,  $P$ . In the case of helical gears, the angle,  $\phi$ , is equal to the transverse profile angle,  $\phi_t$ , of the gear and the pinion at the pitch point,  $P$ .

As contacts travel from point  $a$  to point  $b$ , the average number of pairs of teeth moving across  $Z_{pa}$  is defined as the transverse contact ratio (see Equation 8.4).

For a better understanding of what the transverse contact ratio,  $m_p$ , is, a graphical interpretation of  $m_p$  is illustrated in Figure 8.13. When contact point,  $K$ , is within the portion  $ab$  of the plane of action,  $PA$ , then only one pair of teeth is engaged in mesh. When the contact point,  $K$ , is within the portion  $aP_g$  (or  $bP_p$ ) of the plane of action,  $PA$ , one more contact point,  $K$ , is observed within the portion  $bP_p$  (or  $aP_g$ ) of the plane of action,  $PA$ . Therefore, in this case, two pairs of teeth are engaged in mesh. If, for example, the transverse contact ratio is  $m_p = 1.6$ , then the portions  $aP_g$  and  $bP_p$  together occupy 60% of the entire length,  $Z_{par}$ , of the plane of action. In a such a scenario, the portion  $ab$  of the plane of action,  $PA$ , occupies the remaining 40% of the entire length,  $Z_{par}$ , of the plane of action. Thus, for 60% of a meshing cycle, two pairs of teeth are engaged in mesh (these are the so-called *double-tooth contact regions*), and for 40% of a meshing cycle, just one pair of teeth is engaged in mesh. In other words, for 60% of the arc of action (Figure 8.14), two pairs of teeth are engaged in mesh, and for 40% of the arc of action, just one pair of teeth is engaged in mesh (the arc of action is a summa of the arc of approach and the arc of recess). Double-tooth contact regions in a spur parallel-axes involute gear pair are schematically illustrated in Figure 8.15.

The transverse contact ratio,  $m_p$ , can be affected by certain alterations to design parameters in a gear pair. According to Equation 8.4, the actual value of the transverse contact ratio,  $m_p$ , depends on two design



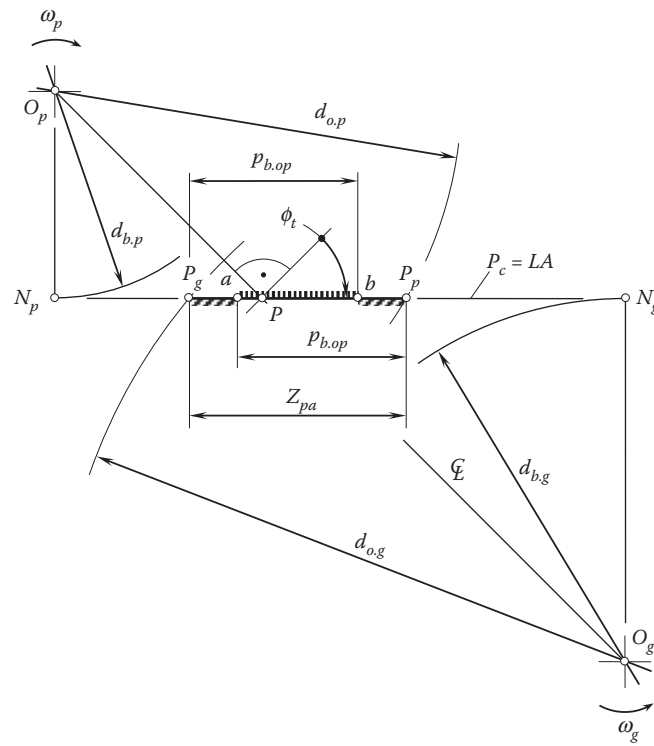


**FIGURE 8.13**  
Graphical interpretation of transverse contact ratio,  $m_p$ .

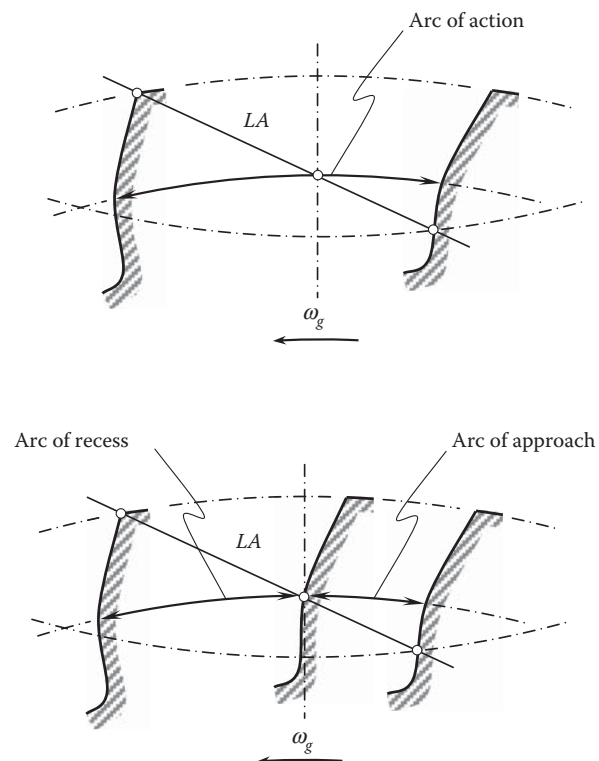


**FIGURE 8.14**  
Arc of action, arc of approach, and arc of recess in a parallel-axes gear pair.

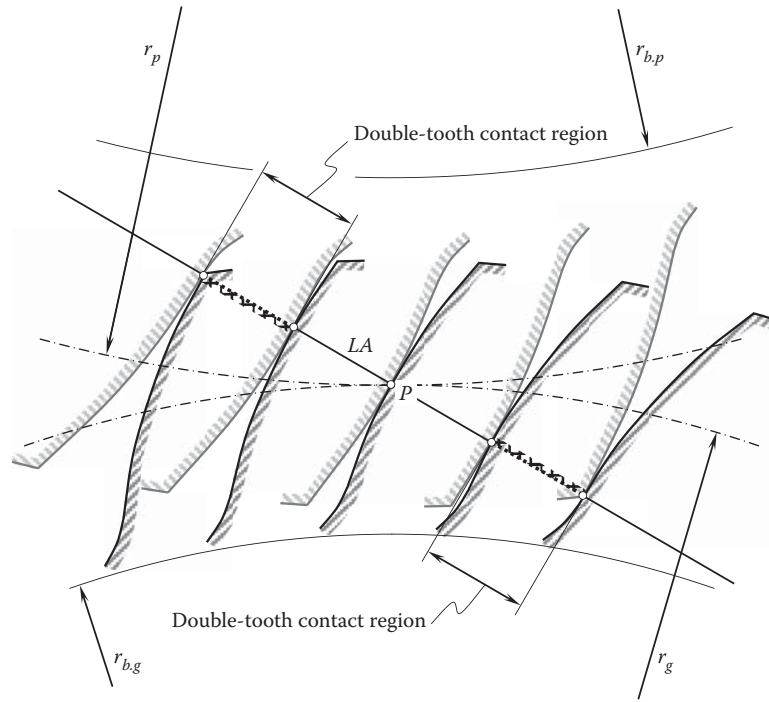


**FIGURE 8.15**  
Double-tooth contact regions in spur parallel-axes involute gear pair.

parameters; that is, it depends on (1) the length,  $Z_{pa}$ , of the path of contact,  $P_c$ , and (2) the operating base pitch,  $p_{b.op}$ , of the gear pair. The accuracy of the operating base pitch,  $p_{b.op}$ , of the gear pair is very high and does not significantly affect the transverse contact ratio,  $m_p$ . The permissible interval of variation of the actual value of the length,  $Z_{pa}$ , of the path of contact,  $P_c$ , is much wider.

For example, in a parallel-axes gear pair, shown in Figure 8.16a, the actual length,  $Z_{pa}$ , of the path of contact,  $P_c$ , can be shortened to a value of  $Z_{pa}^* < Z_{pa}$ . The loss,  $Z_{pa.g}$ , of the length,  $Z_{pa}$ , from the gear side, as well as that of  $Z_{pa.p}$  from the pinion side,  $Z_{pa.p}$  (Figure 8.16b) is caused by the actual location of the start-of-active-profile point, SAP, and the end-of-active-profile point, EAP, as illustrated in Figure 8.16c. The actual values of the design parameters,  $Z_{pa.g}$  and  $Z_{pa.p}$ , can be significantly affected by the shortened addendum, chamfering/rounding of the tip of the gear tooth profile, gear tooth profile undercut, and so forth. Ultimately, this results in the actual value of the transverse contact ratio,  $m_p^*$ , being smaller compared to its nominal value,  $m_p$ ; that is, an inequality  $m_p^* < m_p$  is valid. This can be of critical importance for gear pairs, especially for low-tooth-count gear pairs that feature a total contact ratio,  $m_t$ , close to one.

For spur gears, it is common practice to keep the transverse contact ratio not less than  $m_p \geq 1.2$ .

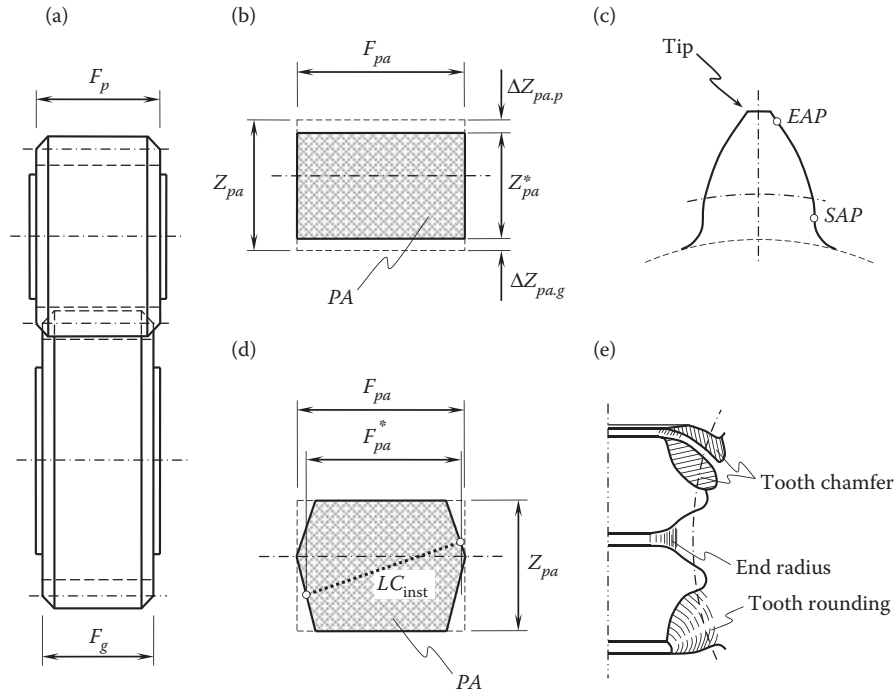
The transverse base pitch,  $p_{b.t}$ , of the helical gear reduces to the base pitch,  $p_b$ , of the spur gear.

#### 8.4.2 Face Contact Ratio in Parallel-Axes Helical Involute Gearing

In the case of helical gearing, in addition to the transverse contact ratio,  $m_p$ , the so-called face contact ratio,  $m_F$ , has to be taken into account when determining the total contact ratio,  $m_t$ , of the gear pair. The face contact ratio,\*  $m_F$ , is the contact ratio in an axial plane, or the ratio of the face width to the axial pitch. By definition, the face contact ratio,  $m_F$ , is defined by the expression (Figure 8.17):

$$m_F = \frac{F_{pa}}{p_x} \quad (8.9)$$

\* The term *face contact ratio* is inconsistent, as no rotation is transmitted across the face of the plane of action,  $PA$ , in a gear pair. Instead, a rotation is transmitted only in transverse section of the plane of action,  $PA$ . The helical teeth of a gear and a mating pinion extend the transverse contact ratio. Therefore, it makes sense to use the terms *transverse contact ratio* and *extension of transverse contact ratio*, instead of *transverse contact ratio* and *face contact ratio*.

**FIGURE 8.16**

Influence of the parameters of the modified plane of action,  $PA$ , on the instant length of the line of contact,  $LC_{inst}$ : (a) parallel-axes gears in mesh; (b) shortened length,  $Z_{pa}^*$ , of the plane of action,  $PA$ ; (c) SAP-point and EAP-point on the gear tooth profile; (d) shortened width,  $F_{pa}^*$ , of the plane of action,  $PA$ ; and (e) corresponding modifications to the gear design.

where:

$F_{pa}$  is the effective face width of the gear pair.

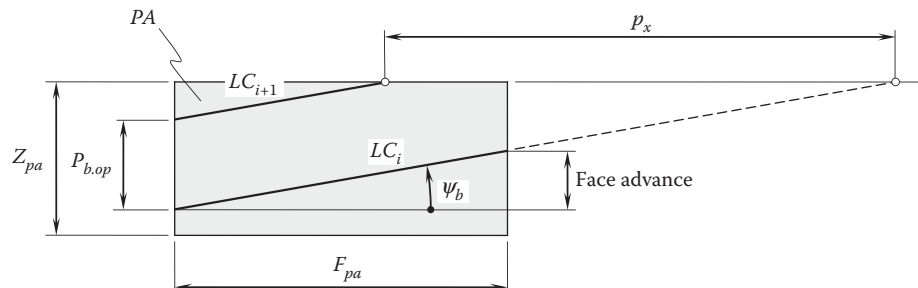
$p_x$  is the axial pitch of the gear teeth.

### Definition 8.3

The axial pitch,  $p_x$ , in a parallel-axes gear pair is equal to the distance between points of intersection of two adjacent desirable lines of contact,  $LC$ , by a straight line parallel to the axis of instant rotation,  $P_{ln}$ .

For spur gearing, the component  $m_F$  is always equal to zero ( $m_F = 0$ ).

The line of contact,  $LC$ , in its axial position with rotation of the gears sweeps out a surface. This surface is referred to as the zone of action (Figure 8.18). Alternatively, the zone of contact can be regarded as the

**FIGURE 8.17**

Definition of the term face contact ratio,  $m_F$  in perfect parallel-axes gearing.

The reduction of the face contact ratio,  $m_F$ , could be critical especially for gears that feature a low tooth count, that is, for *LTC*-gears, and thus a total contact ratio that is close to one.

The total contact ratio,  $m_{tr}$ , is the sum of the transverse contact ratio,  $m_p$ , and the face contact ratio,  $m_F$ . It is calculated from the following formula:

$$m_t = m_p + m_F \quad (8.10)$$

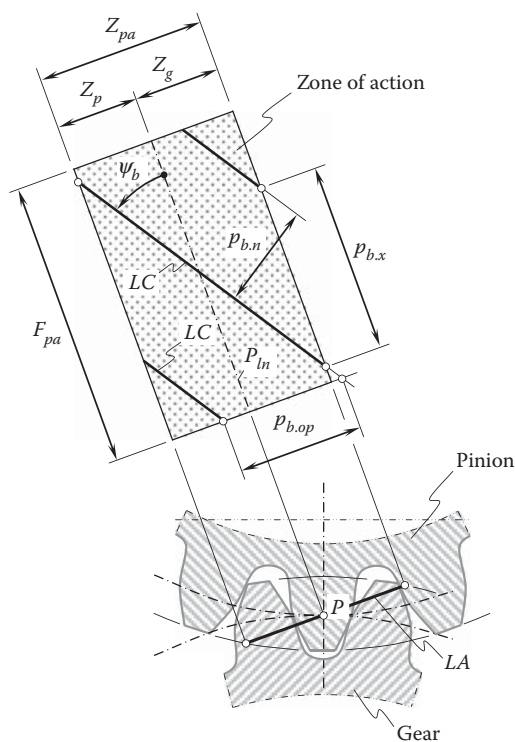


**FIGURE 8.18**  
Zone of action of helical gears.

A gear pair must be designed so to fulfill the inequality  $m_t \geq 1$ .

The axial pitch of a gear teeth,  $p_x$ , can be expressed in terms of the operating base pitch,  $p_{b.op}$ , of the gear pair:

$$p_x = \frac{p_{b.op}}{\tan \psi_b} \quad (8.11)$$

After substituting Equation 8.11 into Equation 8.9, a formula for the calculation of face contact ratio,  $m_F$ , casts into the form:

$$m_F = \frac{F_{pa}}{p_{b.op}} \tan \psi_b \quad (8.12)$$

With this expression for the face contact ratio,  $m_F$ , Equation 8.1 for the total contact ratio,  $m_t$ , can be represented in the form:

$$m_t = \frac{Z_{pa} + F_{pa} \tan \psi_b}{p_{b.op}} \quad (8.13)$$

Equation 8.13 is valid for the calculation of the total contact ratio,  $m_t$ , in both cases, that is, in cases of spur, as well as in cases of helical parallel-axes gear pairs. With Equation 8.13, Equation 8.4 for the transverse contact ratio, and Equation 8.9 for the face contact ratio become unnecessary, and only the term total contact ratio,  $m_t$ , can be used instead of the two terms transverse contact ratio,  $m_p$  and face contact ratio,  $m_F$ . In the case of spur gearing, the base helix angle,  $\psi_b$ , is zero ( $\psi_b = 0^\circ$ ), and Equation 8.13 casts into Equation 8.4.

It is easy to see that Equation 8.13 can be generalized and represented in the form:

$$m_t = \frac{Z_{pa} + Z_{adv}}{p_{b.op}} \quad (8.14)$$

The face advance,  $Z_{adv}$ , is measured between a point of a line of contact,  $LC$ , that is the first to enter the plane of action,  $PA$ , and another point of that same line of contact,  $LC$ , that is the last to enter the plane of action,  $PA$ , when the gears rotate. In the case of parallel-axes helical gear pair, the face advance,  $Z_{adv}$ , is equal to  $Z_{adv} = F_{pa} \tan \psi_b$ . In a more general case, for example, for gears with curved teeth in the lengthwise direction (Figure 8.19), the face advance can also be calculated.

For spur gear pairs, the expression  $m_t \equiv m_p \geq 1$  is valid, as the face contact ratio\* in spur gears is zero (that is,  $m_F = 0$ ).

For conformal and high-conformal gear pairs, for example, in *Novikov gearing*, the face contact ratio should exceed unity (that is,  $m_F \geq 1$ ), whereas the transverse contact ratio is always zero (that is,  $m_p = 0$ ). This is because Novikov gearing features zero length of action,  $Z_{pa}$  (that is, the equality  $Z_{pa} = 0$  is valid in case of conformal and high-conformal gear pairs).

It can be shown that helical gear pairs with a noninvolute tooth profile and nonzero transverse contact ratio ( $m_p \neq 0$ ) are not workable† at all.

Ultimately, only helical gears with an involute tooth profile can be used in the design of gear pairs with contact ratios  $m_p \neq 0$ ,  $m_F \neq 0$ , and  $m_t \geq 1$ .

\* In the case of noninvolute parallel-axes gearing, the contact ratio cannot be specified as the base pitch of a gear,  $p_{b.g}$  ( $=p_{b.op}$ ), and a mating pinion,  $p_{b.p}$  ( $=p_{b.op}$ ). When a noninvolute parallel-axes gear pair is operating, only one pair of teeth is engaged in mesh at every instant of time. This statement can be generalized to the case of noninvolute intersected-axes and crossed-axes gear pairs.

† As follows from analysis of Fig. 2 in U.S. patent No. 1.601.750 (Wildhaber, E., Filed: November 2, 1923, issued in October 5, 1926), the contact point is traveling within the transverse cross-section from a position that is designated as 11 to a position designated as 11'. If the contact point is traveling within the transverse cross-section, then the transverse contact ratio is greater than zero (that is,  $m_p > 0$ ). It can be concluded that, kinematically and geometrically, *helical gearing* (U.S. Pat. No. 1.601.750, Helical Gearing, Wildhaber, E., Date: October 5, 1926, Filed: November 2, 1923) is not workable at all.

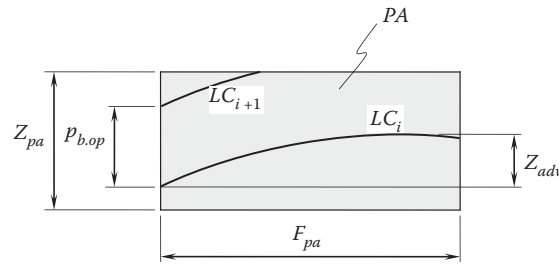


**FIGURE 8.19**  
Definition of the term face advance,  $Z_{adv}$  in perfect parallel-axes gearing.

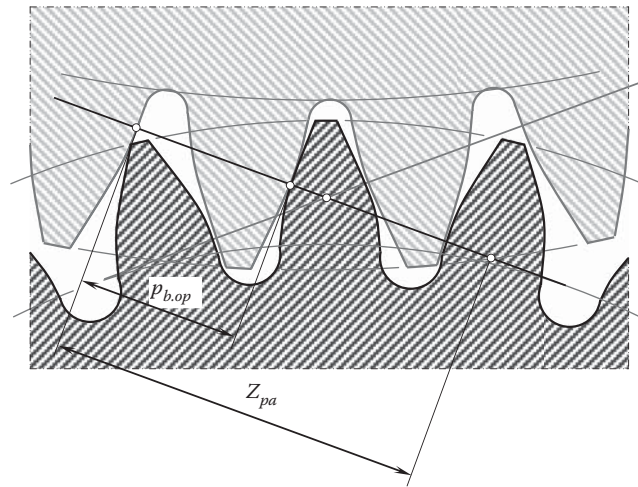


**FIGURE 8.20**  
Schematic of a high-contact-ratio parallel-axes gear pair.

The total contact ratio,  $m_t$ , is an important design parameter of a gear pair for many reasons. As an example, this parameter is used for calculating contact stresses that act between the gear and the pinion tooth flanks. In this last case, the *total length of the line of contact* (or *TLLC* for simplicity) should be taken into account. The total length of the line of contact depends on the actual value of the total contact ratio and is of critical importance, especially for gearing having a low tooth count of the pinion.

Gear pairs that feature a contact ratio greater than 2.0 are commonly referred to as *high-contact-ratio gears*, or just *HCR-gears*, for simplicity. Standard gears have a typical contact ratio of 1.2–1.6. In their most basic form, gears are designed to transmit power, and HCR-gears perform especially well. They are stronger, quieter, and smoother, and they have significantly lower stresses. Also, they normally have lower pressure angles and a greater number of teeth than standard gears.

High-contact-ratio gears always have two or three gear teeth in contact at any one time (Figure 8.20). They never have only one set of teeth in contact; since there are more teeth in contact, the load is spread across more teeth and is therefore reduced. These gears are approximately one-third stronger than standard gears because of the extra sets of gear teeth in contact.

High-contact-ratio gears necessitate higher quality levels due to the required accuracy of the multiple sets of teeth in contact. They are typically more sensitive to manufacturing errors and gear tooth profile modifications.

#### 8.4.4 Transverse Contact Ratio in a Low-Tooth-Count Gear Pair

Parallel-axes gearings with a low tooth count (that is, *LTC-gearings*) are considered below in this section. An example of a helical gear with a low tooth count is illustrated in Figure 8.21. Gears of this particular type are extensively used in the design of gear pumps, as well as in other applications.

Most cut gears with a low tooth count feature an undercut. Because of the undercut, the length of the active portion,  $Z_{pa}$ , of the line of action,  $LA$ , can be specified in terms of the *start-of-active-profile diameters* of the gear and

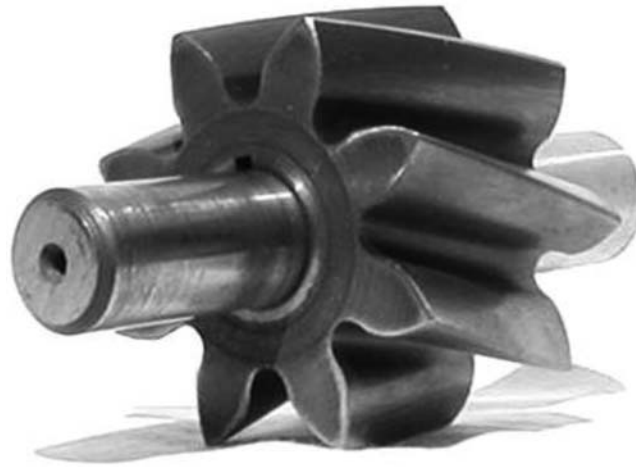


FIGURE 8.21

A gear that features a low tooth count.

the mating pinion, that is, by the diameters,  $d_g^{sap}$  and  $d_p^{sap}$ , correspondingly (Figure 8.22), and not in terms of the outer diameters,  $d_{o,g}$  and  $d_{o,p}$ , of these gears. This narrows the length of the active portion of the line of action,  $LA$ , from  $Z_{pa}^*$  to  $Z_{pa}$ , where  $Z_{pa}^* > Z_{pa}$ . The shorter the length  $Z_{pa}$ , the smaller the transverse contact ratio,  $m_p$ , of the gear pair, and vice versa.

Therefore, another approach for calculation of the transverse contact ratio in *low-tooth-count gearing* needs to be developed.

When hobbing a spur gear with a low tooth count, the generation of the undercut is illustrated in Figure 8.23. It should be noted here that the point,  $m$ , is located on the circle of the start-of-active-profile diameter. This means that this limit point simultaneously satisfies the requirements for the involute tooth profile and the profile of the undercut (as this point is the point of intersection of the involute tooth profile by the undercut profile). The coincidence of the points is the clue to solving the problem under consideration. On the premise of this statement:

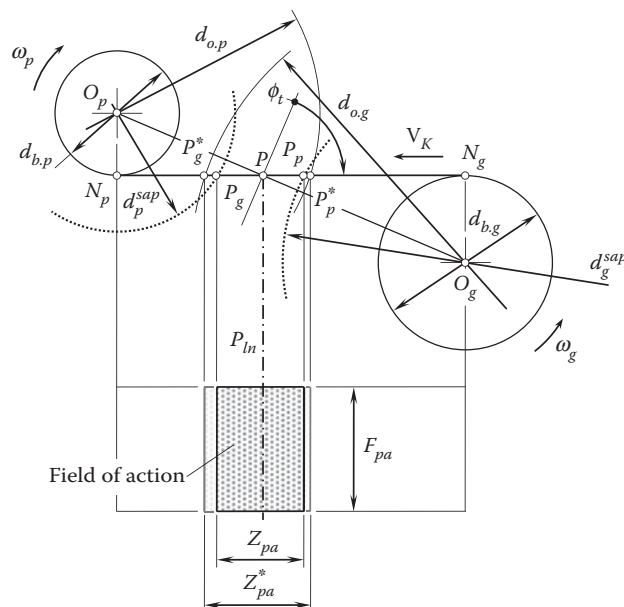
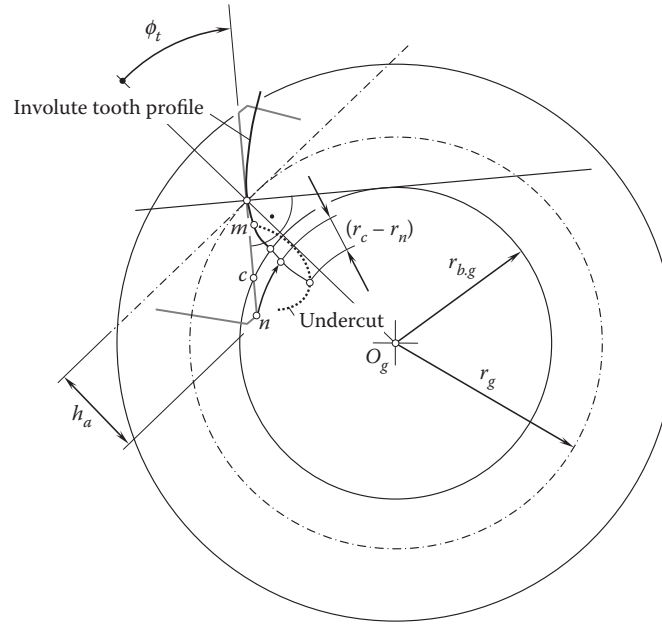


FIGURE 8.22

Field of action in an involute gear pair with a low-tooth-count gear.





**FIGURE 8.23**  
Generation of the undercut in an involute gear.

1. The coordinates of point,  $m$ , are determined, as it is located on the involute tooth profile of the gear/pinion, and the location of the point can be specified by the position vector  $\mathbf{r}_m^{inv}$ .
2. The coordinates of the point,  $m$ , are determined, as it is located on the undercut profile of the gear/pinion, and the location of the point can be specified by the position vector  $\mathbf{r}_m^{uc}$ .

As the coordinates of the point,  $m$ , are specified in terms of two different position vectors,  $\mathbf{r}_m^{inv}$  and  $\mathbf{r}_m^{uc}$ , these position vectors are equal to one another; that is, the identity,  $\mathbf{r}_m^{inv} \equiv \mathbf{r}_m^{uc}$ , is observed. By solving this identity, all the design parameters of the undercut gear tooth profile can be calculated.

The contact ratio,  $m_{p,uc}$ , for an undercut low-tooth-count gearing can be calculated from:

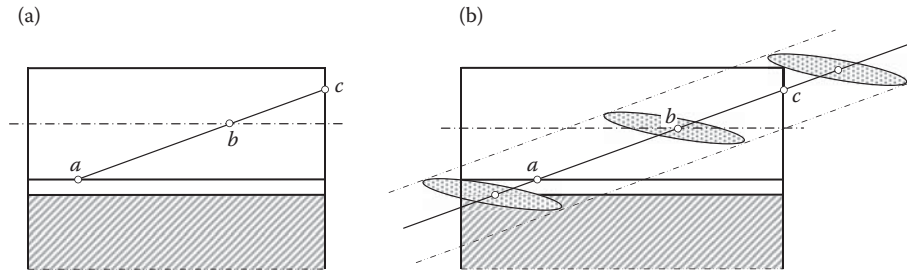
$$m_{p,uc} = \frac{Z_{pa}}{p_{b.op}} \quad (8.15)$$

The inequality,  $m_{p,uc} \leq m_p$ , is always observed.

#### 8.4.5 Impact of the Elastic Deformation on the Total Contact Ratio in Gear Pairs

It should be stressed here that the aforementioned consideration of contact ratios is based on just kinematical and geometrical analysis of a gear pair. When two gears rotate, tooth flanks come into contact at a point,  $a$  (Figure 8.24a). Then, the contact point travels along the path of contact occupying an intermediate position,  $b$ . The contacting tooth flanks get out of contact at a point,  $c$ . The contact ratio depends on the length of the path of contact: the longer the path of contact, the greater the contact ratio, and vice versa. The mechanical properties of the material of which the mating gears are made are not incorporated into the analysis.

In reality, under operating loads, the contact point spreads to an elliptically shaped area of contact. Hence, the tooth flanks get in contact before reaching the point,  $a$ , and they get out of contact beyond the point,  $c$  (Figure 8.24b). This increases the time of meshing of the tooth flanks. Ultimately, the actual contact ratio of the gear pair becomes a bit greater. The significance of an increase in the contact ratio due to the elasticity of the gear material increases for high-conformal gear pairs, as for high-conformal gears, the size of the area of contact is greater.

**FIGURE 8.24**

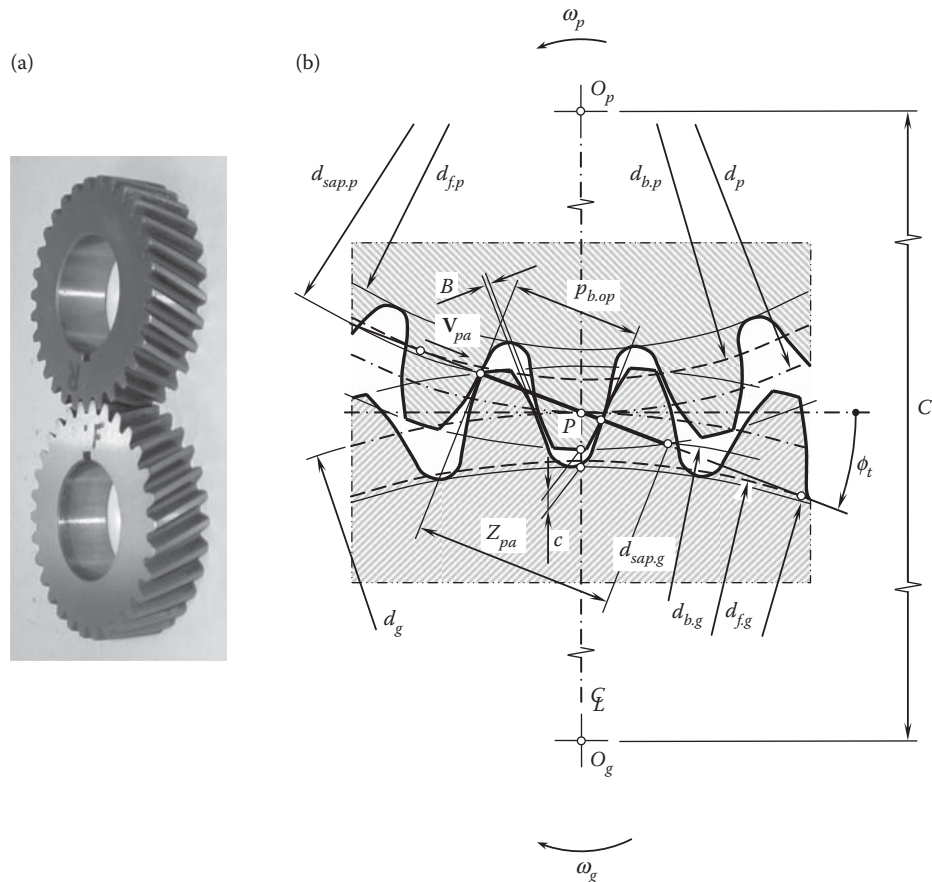
Impact of the elasticity of a gear material on the actual value of the contact ratio of a gear pair: (a) no elastic properties of a gear material are taken into account, and (b) elastic properties of a gear material are taken into account.

## 8.5 External Involute Gear Pair

An external gear pair is composed of two involute gears that feature the same base pitch,  $p_p$ . A close-up view of an external gear pair and its main design parameters are illustrated in Figure 8.25a and b, correspondingly.

### 8.5.1 Main Design Parameters

An external gear pair can be specified by two rotation vectors, namely by a rotation vector of the gear,  $\omega_g$ , and a rotation vector of the pinion,  $\omega_p$ . The rotation vectors,  $\omega_g$  and  $\omega_p$ , are parallel to one another and point in the opposite directions, as schematically shown in Figure 6.2a and b.

**FIGURE 8.25**

Close-up view (a) and the main design parameters (b) of an external involute gear pair.

Listed below are the main design parameters:

$d_{b,g}, d_{b,p}$	are the base diameters of a gear and a mating pinion.
$d_g, d_p$	are the pitch diameters of a gear and a mating pinion.
$d_{f,g}, d_{f,p}$	are the root diameters of a gear and a mating pinion.
$d_{sap,g}, d_{sap,p}$	are the start-of-active-profile diameters of a gear and a mating pinion.
$p_{b,op}$	is the operating base pitch of the gear pair.
$\phi_t$	is the transverse pressure angle of the gear pair.
$Z_{pa}$	is the length of action of the gear pair.
$C$	is the center distance in the gear pair.
$B$	is the backlash.
$c$	is the radial clearance in the gear pair.

These are shown in [Figure 8.25b](#).

The effective backlash,  $B_{pp}$ , is specified within the pitch plane,  $PP$ .

#### Definition 8.4

*The effective backlash,  $B_{pp}$ , in perfect parallel-axes gearing is the distance between a not-interacting tooth flank of a driving member and a tooth-space flank of a driven member measured within the pitch plane in the gear pair.*

The line along which two tooth surfaces are tangent to each other is referred to as the line of contact. The line of contact of tooth flanks is commonly denoted by  $LC$ . In parallel-axes gearing, the line of contact of a screw involute surface,  $\mathcal{G}$ , of a gear tooth and a screw involute surface,  $\mathcal{P}$ , of a pinion tooth is a straight line,  $LC$ .

The configuration of the line of contact,  $LC$ , in relation to the rotation vectors,  $\omega_g$  and  $\omega_p$ , is illustrated in [Figure 8.26](#). The line of contact is entirely located within the plane of action,  $PA$ , which is tangent to the base cylinders of the gear and the pinion. In [Figure 8.26](#), the diameter of the base cylinder of the gear is designated as  $d_{b,g}$ , while the diameter of the base cylinder of the pinion is designated as  $d_{b,p}$ . The line of contact,  $LC$ , crosses the axes of rotations of the gear,  $O_g$ , and the pinion,  $O_p$ , at the same angle,  $\psi_b$ . This is because the axis of rotation of the gear,  $O_g$ , is parallel to the axis of rotation of the pinion,  $O_p$ . The angle,  $\psi_b$ , is commonly referred to as the base helix angle.

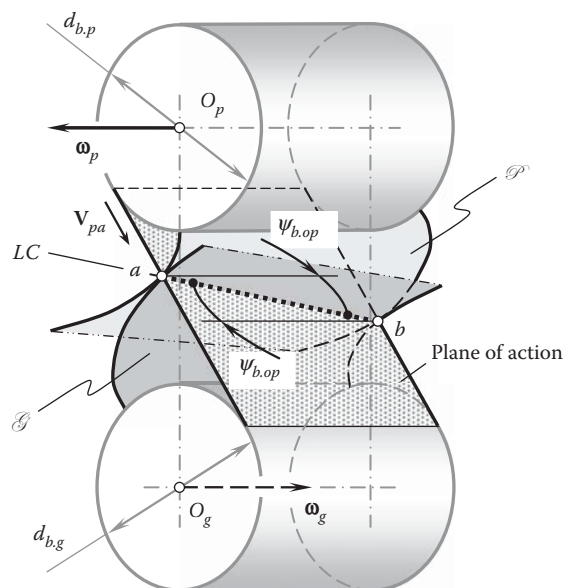


FIGURE 8.26

Interaction of screw involute surfaces,  $\mathcal{G}$  and  $\mathcal{P}$ , of the tooth flanks of a pair of helical gears.

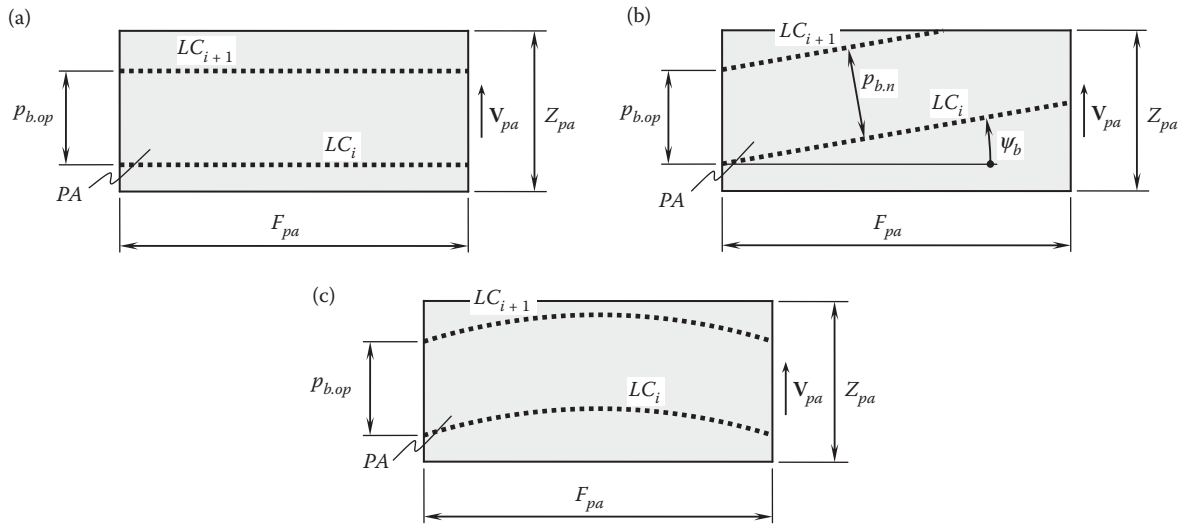


FIGURE 8.27

Operating base pitch,  $p_{b,op}$ , in parallel-axis gearing with (a) straight teeth, (b) helical teeth, and (c) teeth curved in their lengthwise direction.

The angle,  $\psi_b$ , is equal to the base helix angle,  $\psi_{b,g}$ , of the gear and the base helix angle,  $\psi_{b,p}$ , of the pinion. For a spur gear pair, the base helix angle,  $\psi_b$ , is zero; hence, the line of contact is parallel to the axes of rotation of the gear,  $O_g$ , and the pinion,  $O_p$ .

A detailed analysis of the schematic of a parallel-axes gearing shown in Figure 8.26 inspires the introduction of a novel parameter of the gearing.

Consider the active portion of the plane of action,  $PA$ , for parallel-axes gearing (Figure 8.27). The active portion of the plane of action is shaped in the form of a rectangle. The width of the rectangle is equal to the effective face width,  $F_{pa}$ , of the gear set, and the height of the plane of action is equal to  $Z_{pa}$ .

When the driving gear rotates, the line of contact,  $LC$ , travels within the plane of action. The linear velocity vector of the line of contact is denoted by  $V_{pa}$ .

In spur parallel-axes involute gearing (Figure 8.27a), the line of contact in an arbitrary its configuration is designated as  $LC_i$ . Assume that the driving gear is rotated through one tooth. During this time, the line of contact travels within the plane of action at a certain distance,  $p_{b,op}$ . In a new position, the line of contact is designated as  $LC_{i+1}$ . Measured in a common transverse section of the gear pair, the distance,  $p_{b,op}$ , between two adjacent desirable lines of contact,  $LC_{des}^i$  and  $LC_{des}^{i+1}$ , is referred to as the *operating base pitch* of the gear pair\*:

### Definition 8.5

*The operating base pitch in a parallel-axes gearing is a distance measured within the plane of action between corresponding points taken within two lines of contact between two neighboring pairs of teeth.*

The operating base pitch of the gear pair is a calculated design parameter of a gear pair. It cannot be directly measured in a gear pair.

It is important to notice here that the operating base pitch,  $p_{b,op}$ , of the gear pair is determined *before* the interacting tooth flanks,  $\mathcal{G}$  and  $\mathcal{P}$ , of the gear and the mating pinion are generated. The use of such an approach gives an opportunity to design gears with correct geometry of the tooth flanks. For this purpose, the desirable line of contact,  $LC_{des}$ , between the tooth flanks,  $\mathcal{G}$  and  $\mathcal{P}$ , is used to generate the gear and the pinion tooth flanks,  $\mathcal{G}$  and  $\mathcal{P}$ .

When the gears rotate, the desirable line of contact,  $LC_{des}$ , travels together with the plane of action,  $PA$ ; that is, the straight line segment  $LC_{des}$  is rigidly connected with the  $PA$ . When the plane of action rolls over the base

\* It is also important to stress here that the operating base pitch of a gear pair,  $p_{b,op}$ , is measured in linear units only in cases of perfect parallel-axes gear pairs. In cases of intersected-axes and crossed-axes perfect gearings, the operating base pitch of a gear pair,  $\varphi_{b,op}$ , is measured in angular units. Moreover, if axis misalignment is taken into account, then the operating base pitch of a gear pair,  $\varphi_{b,op}$ , is measured in angular units in all cases, that is, in cases of  $P_a$ -gearings,  $I_a$ -gearings, and  $C_a$ -gearings.

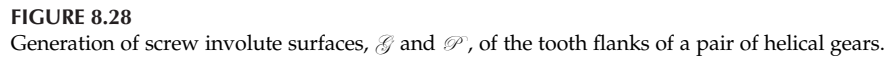


**FIGURE 8.29**  
Base pitch of a gear,  $p_{b,g}$ , (of a pinion,  $p_{b,p}$ ) in perfect involute gear pair.

In the case of  $p_a$ -gearing, the identities  $p_{b,g} \equiv p_{b,op}$  and  $p_{b,p} \equiv p_{b,op}$  (or simply  $p_{b,g} \equiv p_{b,p} \equiv p_{b,op}$ ) are met only for perfect involute gearings. For any and all types of noninvolute gearings, the identity cannot be fulfilled, and, moreover, the base pitch of a gear and a pinion cannot be constructed at all, while the operating base pitch of the gear pair can be easily determined.

The operating base pitch,  $p_{b,op}$ , can be calculated for gear pairs of any and all types. Only *conjugate* gear tooth profiles (gear tooth flanks) feature the base pitch. The base pitch cannot be specified for nonconjugate gear tooth profiles (gear tooth flanks); that is, base pitch of a gear (and of its mating pinion) can be calculated/measured only for *perfect gear pairs*.

The concept of operating base pitch,  $p_{b,op}$ , can be easily enhanced to helical involute parallel-axes gearing, as illustrated in Figure 8.27b. In this particular case, the normal base pitch,  $p_{b,n}$ , of the gear pair, as well as the axial pitch,  $p_x$ , can be expressed in terms of the operating base pitch,  $p_{b,op}$ , and of the base helix angle,  $\psi_b$ .

Ultimately, parallel-axes involute gearing that features teeth curved in their lengthwise direction can also be specified in terms of operating base pitch,  $p_{b,op}$ . This later case is schematically depicted in Figure 8.27c.

In all three cases in Figure 8.27, the operating base pitch in a parallel-axes gearing can be expressed in terms of the base diameters of the gear,  $d_{b,g}$ , and the pinion,  $d_{b,p}$ , and in terms of the tooth numbers of the gear,  $N_g$ , and the pinion,  $N_p$ :

$$p_{b,op} = \frac{\pi d_{b,g}}{N_g} = \frac{\pi d_{b,p}}{N_p} \quad (8.16)$$

The operating base pitch,  $p_{b,op}$ , is measured along the path of contact. The operating base pitch can be calculated for a gear pair independently of the design parameters of the gear and pinion.

For parallel-axes gearing to operate properly, all three base pitches, that is:

- a. Base pitch of a gear,  $p_{b,g}$
- b. Base pitch of a mating pinion,  $p_{b,p}$
- c. Operating base pitch of the gear pair,  $p_{b,op}$

have to be of the same value (that is, the equality  $p_{b,g} = p_{b,p} = p_{b,op}$  has to be observed). Any and all changes to the geometry of the line of contact and to the motion of the line of contact in relation to the plane of action,  $PA$ , have to be *operating base pitch preserved*.

### 8.5.2 Variation of the Tooth Flank Geometry

The geometry of tooth flanks plays an important role for gear pairs. Commonly, tooth flank geometry is specified at the pitch point of a gear pair. The parameters of the geometry of tooth flanks vary within the tooth height of a gear and of a pinion. The variation can be negligibly small for gears that feature a large tooth count; however, it grows more significant for gears with a low tooth count. The lower the tooth count, the more significant the variation.

#### Definition 8.6

*A gear for a parallel-axes gear pair the base diameter,  $d_b$ , equal to or greater than the start-of-active-profile diameter,  $d_{sap}$ , is referred to as a low-tooth-count gear.*

In a design of a low-tooth-count gear\* (or just LTC-gear for simplicity), the inequality  $d_b \geq d_{sap}$  is valid.

The variation of the geometry of the tooth flanks is of critical importance, for example, for gear sets that are used in the design of the automobile differentials, for which the tooth number drops to approximately three to four teeth. It is anticipated that in the immediate future, gear sets with a low tooth count will get much wider application in various industries, as they allow increasing the power density being transmitted by the gear set.

The above discussion reveals the necessity of investigation of the variation of parameters of the geometry of tooth flanks within the tooth height of a gear and of a pinion.

\* The concept of *low-tooth-count gears* can be enhanced for cases of intersected-axes gearing, as well as cases of crossed-axes gearing. The criterion:  $d_b \geq d_{sap}$  that is valid for parallel-axes gearings needs to be replaced with the inequality  $\gamma_b \geq \gamma_{sap}$  that is valid for intersected-axes gears, as well as for cases of crossed-axes gears.

Tooth flank geometry can be specified in terms of (a) radii of normal curvature, or in terms of normal curvatures as the reciprocals to them; (b) profile angle; and (c) helix angle.

### 8.5.2.1 Normal Curvature of the Gear Tooth Flank

The principal curvatures,  $k_{1,g}$  and  $k_{2,g}$ , of a gear tooth flank,  $\mathcal{G}$ , can be calculated as roots of the quadratic equation:

$$\begin{vmatrix} L_g - E_g k_g & M_g - F_g k_g \\ M_g - F_g k_g & N_g - G_g k_g \end{vmatrix} = 0 \quad (8.17)$$

where:

$E_g, F_g, G_g$  are the fundamental magnitudes of the first order of the gear tooth flank,  $\mathcal{G}$ .

$L_g, M_g, N_g$  are the fundamental magnitudes of the second order of the gear tooth flank,  $\mathcal{G}$ .

$k_g$  is the normal curvature at a point of the gear tooth flank,  $\mathcal{G}$ .

$R_g$  is the normal radius of curvature at a point of the gear tooth flank,  $\mathcal{G}$  (the equality  $R_g = k_g^{-1}$  is always observed).

In the case under consideration, that is, for an involute screw surface,  $\mathcal{G}$ , the first principal curvature,  $k_{1,g}$ , is always positive ( $k_{1,g} > 0$ ), while the second principal curvature,  $k_{2,g}$ , always has a zero value ( $k_{2,g} \equiv 0$ ). This immediately yields the conclusion that all points within a screw involute tooth flank,  $\mathcal{G}$ , are points of a parabolic kind. The local geometry of a screw involute tooth flank,  $\mathcal{G}$ , of the gear can also be expressed in terms of the first,  $R_{1,g} = k_{1,g}^{-1}$ , and second,  $R_{2,g} = k_{2,g}^{-1}$ , principal radii of curvature at a point of the surface,  $\mathcal{G}$ .

The first principal radius of curvature,  $R_{1,g}$ , at point within the gear tooth flank,  $\mathcal{G}$ , can be calculated from the known formula [131]:

$$R_{1,p} = \frac{1}{2} \cdot \sqrt{\frac{d_{y,p}^2 - d_{b,p}^2}{1 - \sin^2 \psi \cdot \cos^2 \phi_n}} \quad (8.18)$$

At any point within the screw involute surface,  $\mathcal{G}$ , the second principal radius of curvature,  $R_{2,g}$ , approaches infinity ( $R_{2,p} \rightarrow \infty$ ).

Consider an arbitrary point within the line of action\*  $N_p N_g$  (Figure 8.30). The location of this point can be specified in terms of a variable parameter,  $z$ . The actual value of the parameter,  $z$ , is equal to a portion of the total length,  $Z$ , of the path of contact,  $N_p N_g$ :

$$0 \leq z \leq Z \quad (8.19)$$

The parameter  $z$  is equal to  $z = 0$  at the point  $N_p$ , and it is equal to  $z = Z$  at the point  $N_g$  of the path of contact,  $P_c$ . The smaller the tooth count in the gear,  $N_g$ , the smaller the difference:

$$(C \cdot \sin \phi_t - Z)|_{N_g \rightarrow 0} \rightarrow 0 \quad (8.20)$$

Here, the center distance of the gear pair is denoted by  $C$ . The transverse pressure angle,  $\phi_t$ , can be expressed in terms of the design parameters of the gear:

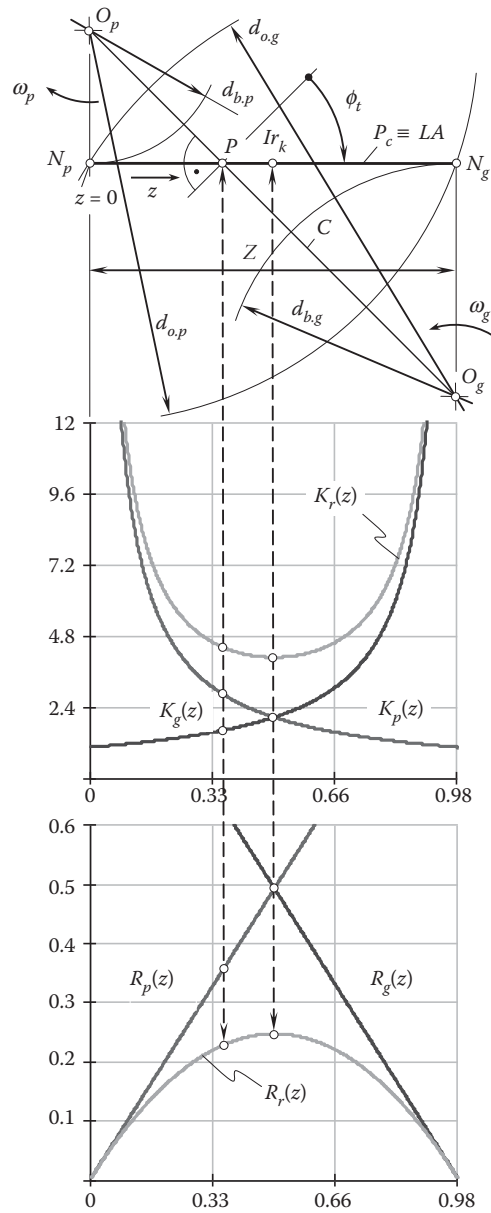
$$\phi_t = \tan^{-1} \left( \frac{\tan \phi_n}{\cos \psi} \right) \quad (8.21)$$

The first principal radius of curvature,  $R_{1,g}$ , at point of the gear tooth flank,  $\mathcal{G}$ , and the first principal radius of curvature,  $R_{1,p}$ , at that same point of the pinion tooth flank,  $\mathcal{P}$ , can be expressed in terms of the parameter,  $z$ , namely in the form of the functions  $R_{1,g} = R_{1,g}(z)$  and  $R_{1,p} = R_{1,p}(z)$ . Substituting the functions  $R_{1,g}(z)$  and  $R_{1,p}(z)$  into the formula for the relative curvature:

$$k_r(z) = \frac{1}{R_{1,g}(z)} + \frac{1}{R_{1,p}(z)} \quad (8.22)$$

\* In the case of parallel-axes gearing, the line of action,  $LA$ , aligns with the path of contact,  $P_c$ .



**FIGURE 8.30**

Change of the elements of local geometry of the interacting tooth flanks of a gear,  $\mathcal{G}$ , and a mating pinion,  $\mathcal{P}$ , within the path of contact,  $P_c$ .

returns the equation:

$$k_r(z) = \frac{\sqrt{1 - \sin^2 \psi \cdot \cos^2 \phi_n}}{z \cdot \left(1 - \frac{z}{C} \cdot \sqrt{1 + \frac{\cos^2 \psi}{\tan^2 \phi_n}}\right)} \quad (8.23)$$

for the calculation of the relative curvature,  $k_r(z)$ , at a current point within the path of contact of the tooth flanks,  $\mathcal{G}$  and  $\mathcal{P}$ .

The radius of relative of curvature,  $R_r(z)$ , is equal to  $R_r(z) = [k_r(z)]^{-1}$ .

For spur involute gears, the curvatures  $k_g$ ,  $k_p$ , and  $k_r$  (or the corresponding radii of curvature  $R_g$ ,  $R_p$ , and  $R_r$ ) are those of the involute tooth profile in the transverse section of the gear tooth flank,  $\mathcal{G}$ .

**TABLE 8.1**

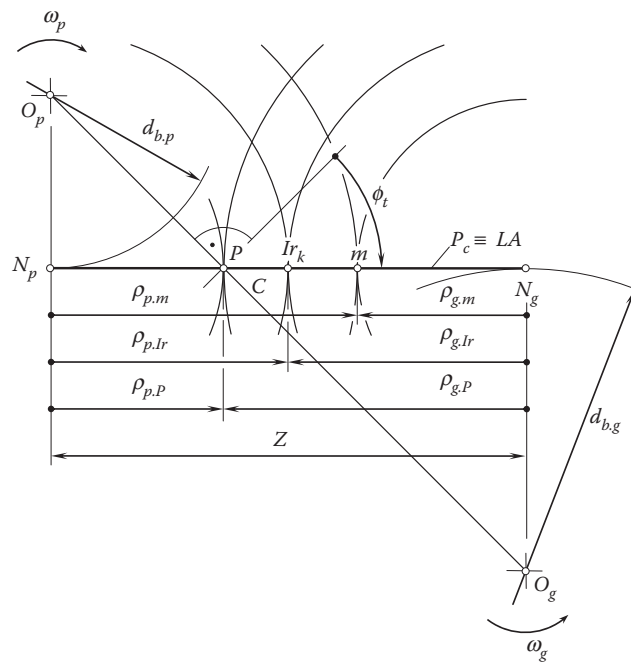
Design Parameters of the Gear Pair for an Automobile Differential

Name of the Parameter	Gear	Pinion
Number of teeth	15	6
Normal profile angle (deg.)	30°	30°
Helix angle (deg.)	40.5526°, RH	40.5526°, LH
Pitch diameter (in)	1.9194	0.7897
Center distance (in)	1.5650	

The change of the curvatures  $k_g \equiv k_g(z)$ ,  $k_p \equiv k_p(z)$ , and  $k_r \equiv k_r(z)$  within the path of contact,  $N_p N_g$ , and those of the corresponding radii of curvatures  $R_g \equiv R_g(z)$ ,  $R_p \equiv R_p(z)$ ,  $R_r \equiv R_r(z)$  are plotted in Figure 8.30. For the computation, the design parameters of the gear pair for an automobile differential (Table 8.1) are used.

The main reason for the variation of the radii of curvature,  $\rho_g$  and  $\rho_p$ , of a gear and mating pinion tooth flanks,  $\mathcal{G}$  and  $\mathcal{P}$ , is illustrated in Figure 8.31. A transverse section of the gear pair is considered as an example. The radii of curvature,  $\rho_g$  and  $\rho_p$ , at the pitch point,  $P$ ;  $Ir_k$ -point; and arbitrary point,  $m$ , all within the path of contact,  $P_c$ , are constructed for the gear,  $\rho_{g,P}$ ,  $\rho_{g,Ir}$ , and  $\rho_{g,m}$ , and for the pinion,  $\rho_{p,P}$ ,  $\rho_{p,Ir}$ , and  $\rho_{p,m}$ . The gear tooth profile radii of curvature,  $\rho_g$ , are centered at point  $N_g$  on the gear base cylinder of a diameter,  $d_{b,g}$ . The pinion tooth profile radii of curvature,  $\rho_p$ , are centered at point  $N_p$  on the pinion base cylinder of a diameter,  $d_{b,p}$ . Circular arcs pass through the points,  $P$ ,  $Ir_k$ , and  $m$ , for the gear (centered at  $N_g$ ), and pinion (centered at  $N_p$ ).

The radii of normal curvature,  $R_g$ , at the point of the gear tooth flank,  $\mathcal{G}$ , and the radii of normal curvature,  $R_p$ , at the point of the pinion tooth flank,  $\mathcal{P}$ , change linearly within the active length of the path of contact,  $P_c$ . The change of normal curvatures,  $k_g$  and  $k_p$ , at point of the gear and pinion tooth flanks follows a hyperbolic function. The relative normal curvature,  $k_r$ , is minimal at a special point of meshing. This point is referred to as the  $Ir_k$ -point of a gear tooth flank. The location of the  $Ir_k$ -point corresponds to the middle of the center distance,  $C$ .

**FIGURE 8.31**

Variation of radii of curvature in a transverse section of the interacting tooth flanks of a gear,  $\mathcal{G}$ , and a mating pinion,  $\mathcal{P}$ , within the path of contact,  $P_c$ .

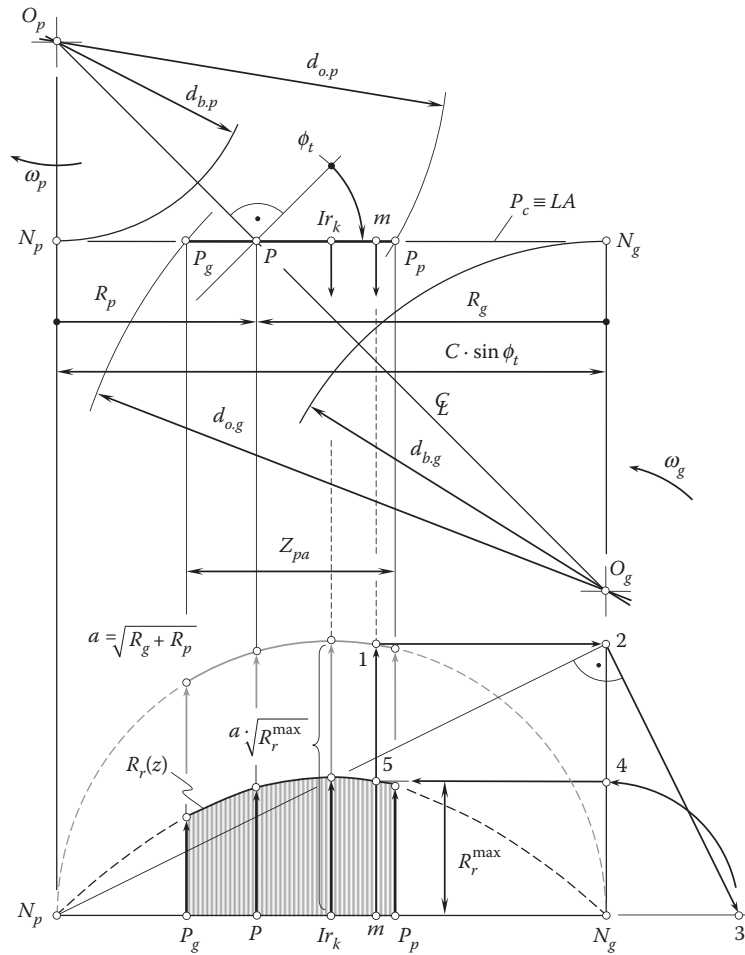


FIGURE 8.32

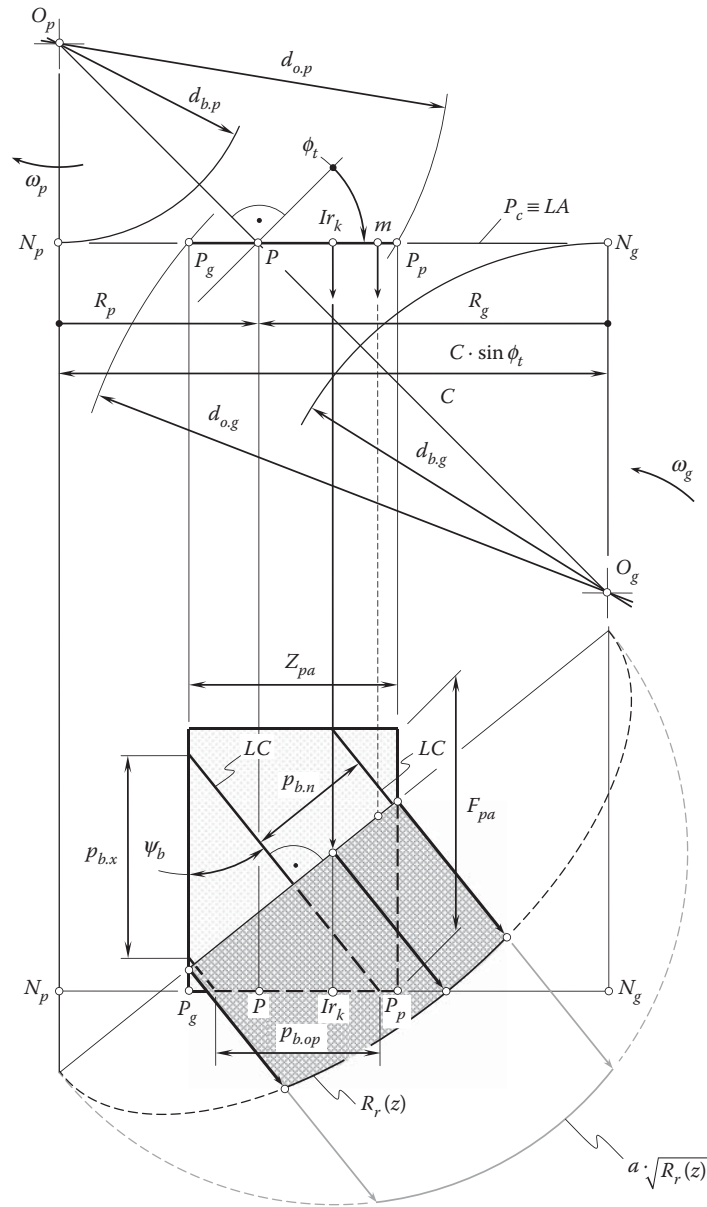
An example of the distribution of the relative radii of normal curvature,  $R_r(z)$ , at contact point of the tooth flanks,  $\mathcal{G}$  and  $\mathcal{P}$ , within the path of contact,  $P_c$ , in a pair of spur gears.

The value of the relative normal curvature,  $k_r$ , increases from the  $Ir_k$ -point in both directions, that is, toward the gear axis of rotation,  $O_g$ , and the pinion axis of rotation,  $O_p$ .

It is necessary to point out here that maximum value of the relative curvature,  $k_r^{\max}$ , occurs at the point of intersection of the outside diameter of a gear,  $d_{o,g}$ , and of the limit diameter of a mating pinion,  $d_{l,p}$ . Similarly, the relative curvature,  $\tilde{k}_r^{\max}$ , reaches its maximum value at the opposite side of the active length of the path of contact, that is, at the point of intersection of the outside diameter of the pinion,  $d_{o,p}$ , and the limit diameter of the gear,  $d_{l,g}$ . However, the inequality  $k_r^{\max} > \tilde{k}_r^{\max}$  is always observed (the equality  $k_r^{\max} = \tilde{k}_r^{\max}$  is observed only in the case when the tooth number of the gear is equal to the tooth number of the pinion and thus the equality  $N_g = N_p$  is valid).

The change of the radius of relative curvature for a gear pair composed of spur gears is illustrated in Figure 8.32. The semicircle constructed with the path of contact,  $N_g N_p$ , as the diameter can be shown to represent, to an appropriate scale, the term  $\sqrt{(R_g + R_p) \cdot R_r}$  (below, the square root  $\sqrt{R_g + R_p}$  is designated as  $a$ ). This is the term by means of which the change in surface stress at the point of contact while it moves from  $P_g$  to  $P_p$  on the path of contact is specified. Near the point  $N_g$ , the product,  $a \cdot \sqrt{R_r}$ , approaches zero. The variation of the relative curvature,  $R_r$ , itself is constructed on the premises of change of the parameter,  $a \cdot \sqrt{R_r}$ , within the straight-line segment,  $P_g P_p$ . The function,  $R_r = R_r(z)$ , is plotted in Figure 8.32. Points of the plot,  $R_r = R_r(z)$ , are constructed using well-known properties of similar right triangles. For an arbitrary point,  $m$ , within the path of contact,  $N_g N_p$ , the sequence of points used for the construction is denoted by 1, 2, 3, 4, and, ultimately, 5 for the point on the plot of the function  $R_r = R_r(z)$ .

The relative curvature,  $R_r$ , reaches its maximum value at the  $Ir_k$ -point. The significance of the  $Ir_k$ -point is becoming clear now.

**FIGURE 8.33**

An example of distribution of the relative radii of normal curvature,  $R_r(z)$ , at contact point of the tooth flanks,  $\mathcal{B}$  and  $\mathcal{P}$ , within the path of contact,  $P_c$ , of a pair of helical gears.

A graph of the function  $R_r = R_r(z)$  similar to that shown in Figure 8.32 for a spur gear pair can be constructed for a gear pair that is composed of helical gears. An example of the function  $R_r = R_r(z)$  of a helical gear pair is depicted in Figure 8.33. For the construction of the plot of the function  $R_r = R_r(z)$ , a straight-line segment perpendicular to the lines of contact,  $LC$ , is used. A semicircle is constructed on this straight-line segment as on the diameter. Further construction is identical to that shown in Figure 8.32 for a spur gear pair.

Variation of the *Hertz contact stress* at the contact points within the line of action is strongly correlated with the function  $k_r \equiv k_r(z)$ .

### 8.5.2.2 Variation of the Tooth Profile Angle and Helix Angle

Change of the tooth profile angle,  $\phi_{n,g}(z)$ , and the helix angle,  $\psi_{y,g}(z)$ , within the active portion of the line of action is commonly negligibly small. However, this change becomes significant for gear pairs that feature low tooth counts.

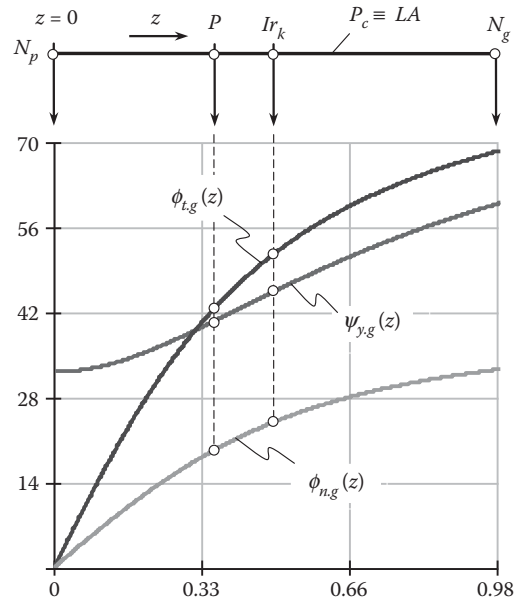


FIGURE 8.34

Variation of the gear normal pressure angle,  $\phi_{n,g}$ ; transverse pressure angle,  $\phi_{t,g}$ ; and helix angle,  $\psi_{y,g}$ , within the active portion of the path of contact,  $P_c$ .

As an example, variations of (1) the normal profile angle,  $\phi_{n,g}(z)$ ; (2) the transverse profile angle,  $\phi_{t,g}(z)$ ; and (3) the helix angle,  $\psi_{y,g}(z)$ , are plotted in Figure 8.34.

### 8.5.3 Special Point of Meshing

It is instructive to point out here that the minimum normal relative curvature,  $k_r^{\min}$  (and the maximum radius of normal curvature,  $R_r^{\max}$ , correspondingly), is observed at the special point,  $I_{r,k}$ , within the path of contact,  $P_c$ . Contact stresses reach their minimum at that point of contact of the gear and the pinion tooth flanks at which the relative curvature is minimal.

The path of contact,  $N_g N_p$ , is subdivided by the point  $I_{r,k}$  on two equal straight-line segments,  $I_{r,k} N_g$  and  $I_{r,k} N_p$ , as illustrated in Figure 8.35. Due to this, the equality  $I_{r,k} N_g = I_{r,k} N_p$  is valid.

The following equations for the calculation of coordinates of the  $I_{r,k}$ -point immediately follow from the analysis of Figure 8.35:

$$r_{I_{r,g}} = \frac{1}{2} \cdot \sqrt{d_{b,g}^2 + C^2 \cdot \sin^2 \phi_t} \quad (8.24)$$

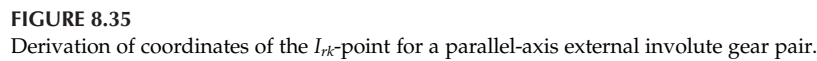
$$r_{I_{r,p}} = \frac{1}{2} \cdot \sqrt{d_{b,p}^2 + C^2 \cdot \sin^2 \phi_t} \quad (8.25)$$

$$\cos v_g = \frac{r_{I_{r,g}}^2 + C^2 - r_{I_{r,p}}^2}{2 \cdot r_{I_{r,g}} \cdot C} \quad (8.26)$$

$$\cos v_p = \frac{r_{I_{r,p}}^2 + C^2 - r_{I_{r,g}}^2}{2 \cdot r_{I_{r,p}} \cdot C} \quad (8.27)$$

$$E_g = r_{I_{r,g}} \cdot \cos v_g \quad (8.28)$$

$$E_p = r_{I_{r,p}} \cdot \cos v_p \quad (8.29)$$



In the case when the design parameters of two gears in mesh are identical, then the point  $Ir_k$  coincides with the pitch point,  $P$ . The more the gear ratio differs from one, the closer the point  $Ir_k$  to the pinion axis,  $O_p$ . The actual location of the point  $Ir_k$  could be of critical importance for gear pairs that feature a low tooth count. When designing a gear pair, it is desired to keep the point  $Ir_k$  as close to the pitch point,  $P$ , as possible (Figure 8.35). Equations 8.24 through 8.29 allow for the calculation of the coordinates of the  $Ir_k$ -point. The desired location of the  $Ir_k$ -point within the active portion of the path of contact,  $P_c$ , is specified by the inequalities  $r_{Ir} \leq 0.5 \cdot d_{o,g}$  and  $r_{Ir} \leq 0.5 \cdot d_{o,p}$ .

The concept of the special point of meshing,  $Ir_k$ , can be enhanced for gear pairs of other kinds, namely, for (1) helical gear pairs, (2) intersected-axes gear pairs, (3) crossed-axes gear pairs, and so forth. For spatial gearing, a three-dimensional  $Ir_k$ -curve is observed instead of the  $Ir_k$  point [124].

Rolling and sliding occur simultaneously between the tooth flanks of two mating gears when transmitting the motion by an external involute parallel-axes gearing. Rolling and sliding are observed at any point of contact within the active portion of the line of contact. The pitch point is the only exception: pure rolling and no sliding occur at the pitch point. Investigation and analysis of sliding and rolling conditions in a gear pair is of importance from an engineering perspective. It enables, for example, determining and reducing friction losses between mating gears.

The velocity vectors at the point of contact between the gear and pinion tooth flanks are schematically shown in Figure 8.36. The contact point,  $m$ , is an arbitrary point within the path of contact,  $P_c$  (or within the active portion of the line of action,  $LA$ ).

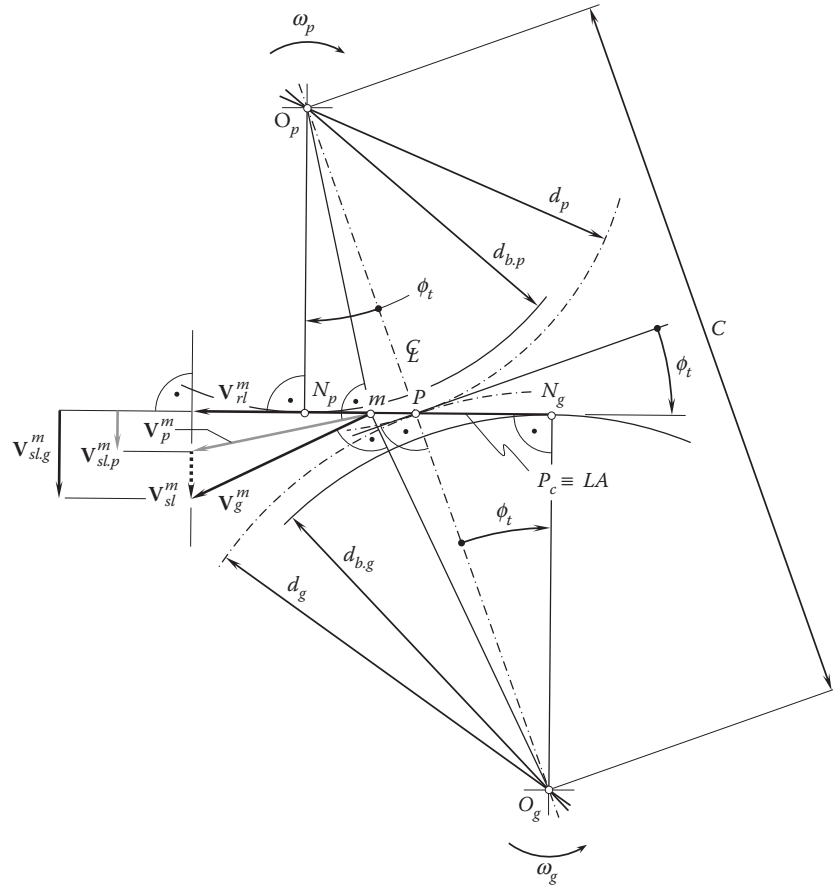


FIGURE 8.36

Tooth profile sliding,  $\mathbf{V}_{sl}$ , at arbitrary point,  $m$ , within the path of contact,  $P_c$ /line of action,  $LA$ , in parallel-axes involute gear pair.

When point  $m$  becomes the contact point,  $K$ , between the tooth flanks,  $\mathcal{G}$  and  $\mathcal{P}$ , the velocity vector,  $\mathbf{V}_g^m$ , of the point  $m$  on the gear tooth flank,  $\mathcal{G}$ , is perpendicular to the straight line segment,  $O_g m$ . Similarly, the velocity vector,  $\mathbf{V}_p^m$ , of the point  $m$  on the pinion tooth flank,  $\mathcal{P}$ , is perpendicular to the straight line segment,  $O_p m$ .

As the contact point  $m$  travels along the path of contact,  $P_c$  (along the line of action,  $LA$ ), neither a gap between the interacting tooth flanks,  $\mathcal{G}$  and  $\mathcal{P}$ , nor the interference of the tooth flanks occurs. Due to this fact, the projections of the velocity vectors,  $\mathbf{V}_g^m$  and  $\mathbf{V}_p^m$ , onto the line of action are equal to each other. The projections are designated as  $\mathbf{V}_{rl}^m$ . This velocity vector results in pure rolling of the gear and of the pinion teeth profiles over one another.

The component,  $\mathbf{V}_{sl.g}^m$ , of the velocity vector,  $\mathbf{V}_g^m$ , is perpendicular to the path of contact,  $P_c$ , (to the line of action,  $LA$ ). The component,  $\mathbf{V}_{sl.p}^m$ , of the velocity vector,  $\mathbf{V}_p^m$ , is also perpendicular to the line of action,  $LA$ . Both the velocity vectors,  $\mathbf{V}_{sl.g}^m$  and  $\mathbf{V}_{sl.p}^m$ , are tangent to the gear teeth profiles at the contact point  $m$ .

The components,  $\mathbf{V}_{sl.g}^m$  and  $\mathbf{V}_{sl.p}^m$ , of the velocity vectors,  $\mathbf{V}_g^m$  and  $\mathbf{V}_p^m$ , are of different magnitudes ( $|\mathbf{V}_{sl.g}^m| \neq |\mathbf{V}_{sl.p}^m|$ ). The sliding velocity vector,  $\mathbf{V}_{sl}^m$ , is equal to the difference  $\mathbf{V}_{sl}^m = \mathbf{V}_{sl.g}^m - \mathbf{V}_{sl.p}^m$ .

The relationships between the velocities in involute gears are governed by the condition occurring at every contact point,  $m$ , within the path of contact,  $P_c$  (the line of action,  $LA$ ). The components,  $\mathbf{V}_{sl.g}^m$  and  $\mathbf{V}_{sl.p}^m$ , are equal to the velocity of the contact point along the path of contact. Otherwise, either separation or penetration between the tooth flanks,  $\mathcal{G}$  and  $\mathcal{P}$ , would be observed.

The similarity of triangles in Figure 8.36 allows for the following expressions:

$$V_{sl.g}^m = |\mathbf{V}_{sl.g}^m| = V_{sl}^m \frac{mN_g}{O_g N_g} \quad (8.30)$$



$$V_{sl,p}^m = |\mathbf{V}_{sl,p}^m| = V_{sl}^m \frac{N_p m}{N_p O_p} \quad (8.31)$$

for magnitudes,  $V_{sl,g}^m$  and  $V_{sl,p}^m$ , of the velocity vectors,  $\mathbf{V}_{sl,g}^m$  and  $\mathbf{V}_{sl,p}^m$ .

At the pitch point,  $P$ , the ratio:

$$\frac{m N_g}{O_g N_g} = \frac{m N_p}{O_p N_p} \quad (8.32)$$

is valid. Due to this, the equality  $V_{sl,g}^m = V_{sl,p}^m$  is valid at the pitch point,  $P$ . This proves that no profile sliding of the tooth flanks,  $\mathcal{G}$  and  $\mathcal{P}$ , can occur in the pitch point,  $P$ .

The magnitude,  $V_{sl}^m$ , of the sliding velocity vector,  $\mathbf{V}_{sl}^m$ , is equal to the difference  $V_{sl}^m = V_{sl,g}^m - V_{sl,p}^m$ .

During an infinitesimally small interval of time, the ratio of the length of the gear and pinion tooth profiles in contact is equal to the ratio of the velocity components,  $V_{sl,g}^m$  and  $V_{sl,p}^m$ . Due to this, at the pitch point,  $P$ , the equality  $V_{sl,g}^m = V_{sl,p}^m$  is valid, and the lengths of the tooth profiles in contact are equal to each other. This corresponds to pure rolling without sliding, which takes place at this point.

In the schematic depicted in Figure 8.37, the velocity vector,  $\mathbf{V}_m$ , of an arbitrary point,  $m$ , of the gear tooth flank,  $\mathcal{G}$ , is perpendicular to the corresponding radius at which the point is located. The velocity vector,  $\mathbf{V}_A^g$ , of the point  $A$  of the gear tooth flank is orthogonal to the radius,  $O_g A$ . The velocity vector,  $\mathbf{V}_A^p$ , of the point  $A$  of the pinion tooth flank is orthogonal to the radius,  $O_p A$ . Projections of velocities of all linear motions of rotation onto the line of action,  $LA$ , are equal to [124]:

$$|\mathbf{V}| = 0.5 \cdot d_{b,p} \cdot \omega_p = 0.5 \cdot d_{b,g} \cdot \omega_g \quad (8.33)$$

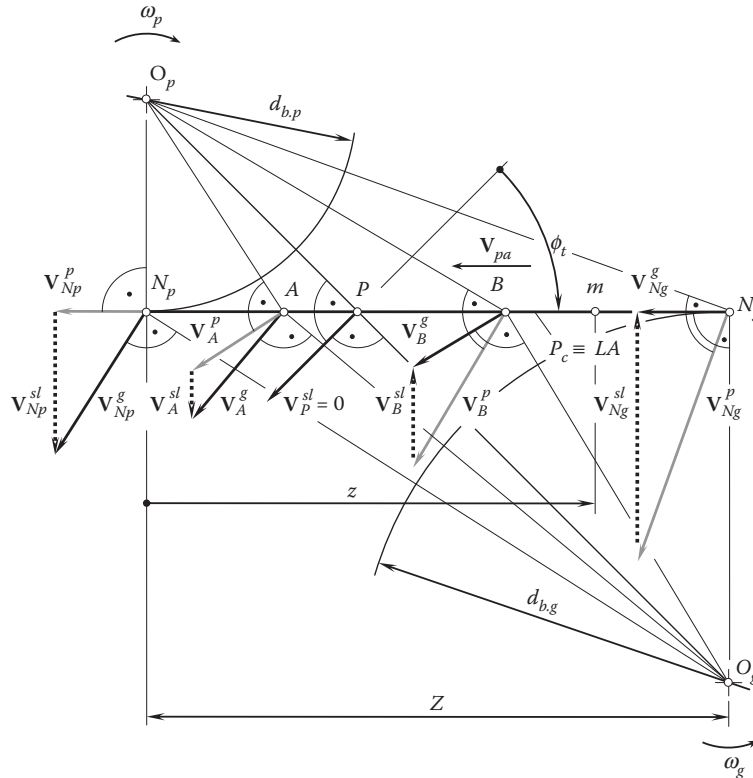
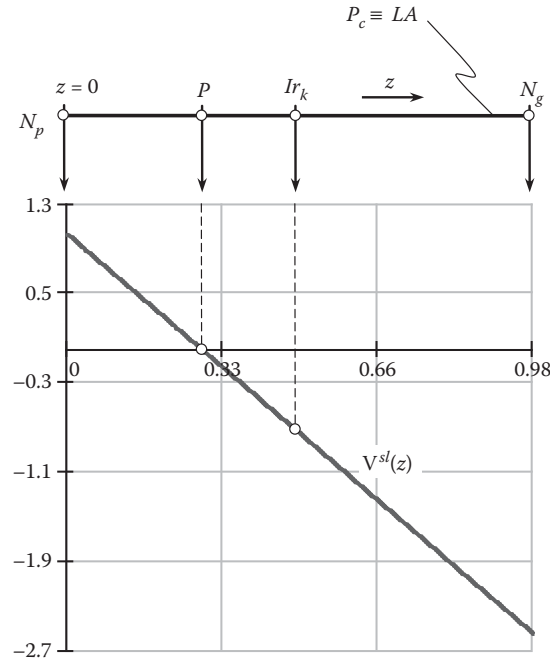


FIGURE 8.37

Kinematics of the relative motion in an external involute gear pair.



**FIGURE 8.38**  
An example of the plot tooth flank sliding vs.  $z$ -parameter.

At an arbitrary contact point, the sliding velocity vector,  $\mathbf{V}_m^{sl}$ , of the gear tooth flank,  $\mathcal{G}$ , in relation to the pinion tooth flank,  $\mathcal{P}$ , is equal to:

$$\mathbf{V}_m^{sl} = \mathbf{V}_m^g - \mathbf{V}_m^p \quad (8.34)$$

At various points within the path of contact,  $P_c$  (within the line of action,  $LA$ ), the relative sliding of the tooth flanks,  $\mathcal{G}$  and  $\mathcal{P}$ , is different. The magnitude of the sliding velocity vector,  $\mathbf{V}_m^{sl}$ , is a function of  $z$ ; that is,  $V^{sl}(z) = |\mathbf{V}^{sl}(z)|$ . The velocity vector,  $\mathbf{V}_m^{sl}$ , of relative sliding is always pointed perpendicularly to the line of action. The equality  $\mathbf{V}_m^{sl} = \mathbf{V}_m^g - \mathbf{V}_m^p$  allows for the following formula for the calculation of the magnitude of the sliding velocity vector:

$$V^{sl}(z) = [Z - (1 - u) \cdot z] \cdot \omega_p \quad (8.35)$$

Here,  $u$  designates the tooth ratio that is equal  $u = d_{b,g}/d_{b,p}$ .

A variation of tooth flank sliding is illustrated in Figure 8.38. The sliding is of a maximum value at the base cylinders, and it is greater for the pinion tooth flank. No sliding is observed at the pitch point,  $P$ . The sliding is of the opposite direction from different sides of the pitch point,  $P$ . For a driving pinion, the sliding is pointed away from the pitch point,  $P$ , while for the driven gear, the sliding is pointed toward the pitch point,  $P$ .

### 8.6.2 Specific Sliding

The impact of the design parameters of a gear and a mating pinion on the sliding conditions is specified by coefficients of specific sliding. For the specification of profile sliding of tooth flanks,  $\mathcal{G}$  and  $\mathcal{P}$ , of a gear and a mating pinion, a unitless parameter is used. This parameter is commonly referred to as *specific sliding* and is denoted by  $\gamma$ . Two different parameters,  $\gamma$ , are distinguished.

First, the slide/roll ratio for the tooth flank,  $\mathcal{G}$ , of a gear:

$$\gamma_g = \frac{V_{sl,g}^m - V_{sl,p}^m}{V_{sl,g}^m} \quad (8.36)$$

The coefficient  $\gamma_g$  is commonly referred to as *specific sliding coefficient of the first order*. Second, the slide/roll ratio for the tooth flank,  $\mathcal{P}$ , of a pinion:

$$\gamma_p = \frac{V_{sl,p}^m - V_{sl,g}^m}{V_{sl,p}^m} \quad (8.37)$$

The coefficient  $\gamma_p$  is commonly referred to as *specific sliding coefficient of the second order*.

The equations (see Equations 8.36 and 8.37) can be expressed in terms of the design parameters of a gear pair:

$$\gamma_g = \left(1 + \frac{1}{u}\right) \frac{Z_{pa,m}}{Z_{pa,m} - Z_{pa,g}} \quad (8.38)$$

$$\gamma_p = \left(1 + \frac{1}{u}\right) \frac{Z_{pa,m}}{Z_{pa,m} + Z_{pa,p}} \quad (8.39)$$

where:

$u$  is the gear ratio of the gear pair.

$Z_{pa,m}$  is the distance of the contact point,  $K$ , from the pitch point,  $P$  (see Figure 8.39).

$Z_{pa,g}$  is the portion of the active part of the plane of action,  $Z_{pa}$ , viewed from the gear side (see Figure 8.39).

$Z_{pa,p}$  is the portion of the active part of the plane of action,  $Z_{pa}$ , viewed from the pinion side (see Figure 8.39).

The impact of only the design parameters of the gear pair is specified by specific sliding coefficients,  $\gamma_g$  and  $\gamma_p$ , of the first and second order; that is, the influence of gear and mating pinion rotations,  $\omega_g$  and  $\omega_p$ , is eliminated.

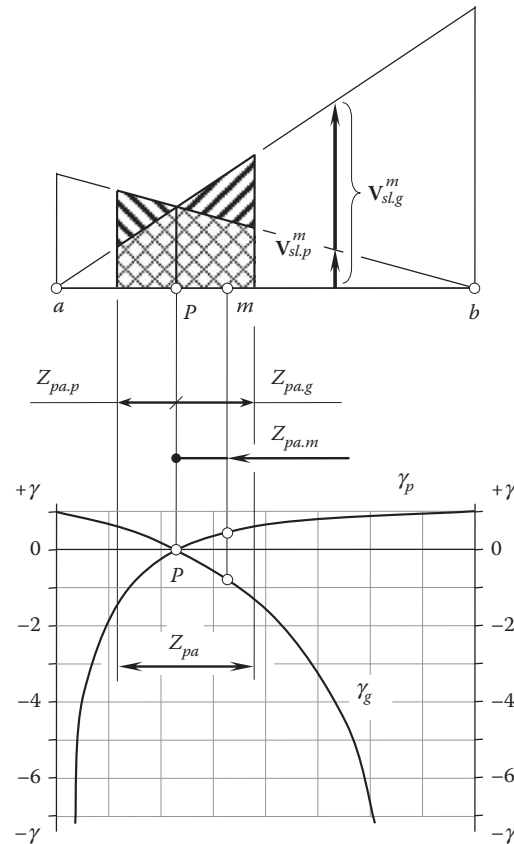


**FIGURE 8.39**  
Specific sliding,  $\gamma$ , of an external involute gear pair.



corresponding output rotation,  $\omega_g = |\omega_g|$ , and torque,  $T_g = |T_g|$ , of an output shaft. The magnitudes of the input torque,  $T_p$ , and output torque,  $T_g$ , correspond to one another as  $T_p = uT_g$ .

When transmitting a rotation by means of a gear pair, the gear and pinion teeth are loaded with a distributed load. The interaction between tooth flanks,  $\mathcal{G}$  and  $\mathcal{P}$ , of the driving and the driven gears is observed along the line(s) of contact,  $LC$ . The distributed force,  $f_t$ , can be determined in the following way.

In Figure 8.40, the input rotation,  $\omega_p$ , is transformed to the corresponding output rotation,  $\omega_g$ . The correlation between an input rotation and an output rotation can be expressed by the following formula:

$$\omega_g = \frac{\omega_p}{u} \quad (8.40)$$

The magnitude,  $F_t = |\mathbf{F}_t|$ , of the acting tangential force,  $\mathbf{F}_t$ , is equal to:

$$F_t = \frac{T_p}{2d_{b,g}} \quad (8.41)$$

where the base diameter of the driving pinion is designated as  $d_{b,p}$ .

The acting tangential force,  $\mathbf{F}_t$ , is evenly distributed,  $f_{t,pa}$ , along the face width,  $F_{pa}$ , of the gear pair. An equation:

$$f_{t,pa} = \frac{F_t}{F_{pa}} \quad (8.42)$$

can be used for the calculation of the distributed load,  $f_{t,pa}$ .

Equation 8.41 is valid for the calculation of a distributed load in spur parallel-axes gear pairs. In a case of helical parallel-axes gearing, the distributed load,  $f_t$ , equals:

$$f_t = \frac{F_t}{F_{pa}} \cos \psi_b \quad (8.43)$$

where the base helix angle is designated as  $\psi_b$ .

At every point of the line of contact,  $LC$ , the distributed load,  $f_t$ , is along a line of action, through the corresponding point.

For the calculation of gear contact strength and bending strength, the normal distributed load,  $f_{t,n}$ , is commonly used:

$$f_{t,n} = \frac{F_t}{F_{pa}} \cos^2 \psi_b \quad (8.44)$$

The lines of action of the normal distributed load,  $f_{t,n}$ , are also entirely located within the plane of action,  $PA$ .

The axial component,  $f_{t,a}$ , of the distributed load causes the axial thrust that is withheld by bearings. For calculation of the axial component,  $f_{t,a}$ , of the distributed load, the following equation can be used:

$$f_{t,a} = \frac{F_t}{2F_{pa}} \sin 2\psi_b \quad (8.45)$$

The axial component,  $f_{t,a}$ , does not transmit the rotation.

Equations 8.42 through 8.45 are valid in cases when gear and mating pinion tooth flanks,  $\mathcal{G}$  and  $\mathcal{P}$ , contact each other along the only line of contact,  $LC$ . As the total contact ratio,  $m_t$ , in a gear pair is always greater than one ( $m_t > 1$ ), in reality, two or even more lines of contact,  $LC_i$ , are observed. Let's consider the load transmission for the cases when the plane of action,  $PA$ , is shaped in the form of a rectangle.

In perfect spur parallel-axes gearing, commonly either one or two lines of contact,  $LC_i$ , are observed. Cases when a gear pair features three and/or more lines of contact,  $LC_i$ , are feasible, but they are not common.

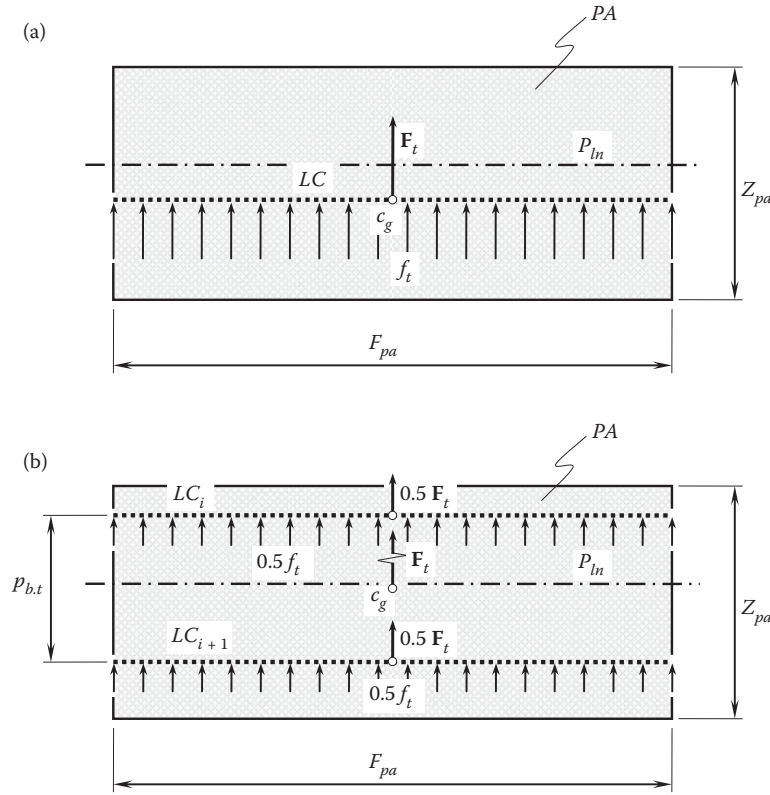


**FIGURE 8.41**  
Lines of contact,  $LC_i$ , in a perfect spur parallel-axes gear pair.

When one pair of the teeth is engaged in mesh, as illustrated in Figure 8.41a, the applied load is evenly distributed along a single line of contact,  $LC$ . The distributed load,  $f_t$ , is calculated from the equation:

$$f_t = \frac{F_t}{F_{pa}} \quad (8.46)$$

The resultant (equivalent) force,  $F_t$ , is applied at a point,  $c_g$ , at the middle of a single line of contact,  $LC$ . The force,  $F_t$ , is along a line of action,  $LA$ , through the point,  $c_g$ .

The distributed load is  $f_t$  (see Equation 8.46), and is used for the calculation of the contact stress, as well as the bending stress in spur parallel-axes gearing for a mating gears configuration when one pair of teeth is engaged in mesh. This mode of the gear teeth loading is the most critical one, as the entire load is withheld by only a pair of interacting teeth of a gear and a mating pinion.

When two (or more) pairs of the teeth are engaged in mesh, as illustrated in Figure 8.41b, the applied load is evenly distributed along the corresponding number of the lines of contact,  $LC_i$ . The distributed load,  $f_t$ , is shared among  $n_\phi$  pairs of teeth engaged in mesh at that same time. The distributed load per a pair of teeth,  $f_{t.n\phi}$ , equals:

$$f_{t.n\phi} = \frac{f_t}{n_\phi} = \frac{F_t}{n_\phi F_{pa}} \quad (8.47)$$

The resultant force,  $F_t$ , is shared among all the lines of contact,  $LC_i$ . The resultant force per a pair of teeth,  $F_{t.n\phi}$ , equals:

$$F_{t.n\phi} = \frac{F_t}{n_\phi} \quad (8.48)$$

All the forces  $F_{t,ni}$  are along a line of action,  $LA$ , through the middle of the lines of contact,  $LC_i$ .

The distributed load is  $f_t$  (see Equation 8.46), used for the calculation of the contact stress, as well as the bending stress in spur parallel-axes gearing for a mating gears configuration when two (or more) pairs of teeth are engaged in mesh.

The resultant (equivalent) force,  $F_t$ , is applied at point  $c_g$ . The point,  $c_g$ , corresponds to the middle of the lines of contact,  $LC_i$ , and between the first,  $LC_i$ , and the last,  $LC_j$ , lines of simultaneous contact. When two lines of contact are observed, point  $c_g$  is located in the middle between the lines of contact. When three lines of contact are observed, point  $c_g$  is located at the center of the second line of contact, and so forth.

Similar to the case of a single line of contact, in cases of multiple lines of contact, the force,  $F_t$ , is along a line of action,  $LA$ , through the point  $c_g$ .

When the gears rotate,  $\omega_g$ , the plane of action,  $PA$ , travels straight,  $V_{pa}$  (Figure 8.42). The arm,  $R_{cg}$ , of the resultant (or equivalent) force,  $F_t$ , with respect to the bearing support remains the same and equals:

$$|R_{cg}| = \sqrt{r_{b,g}^2 + a^2} \quad (8.49)$$

where:

$r_{b,g}$  is the base radius of the gear.

$a$  is the distance of the gear from the bearing support (Figure 8.42).

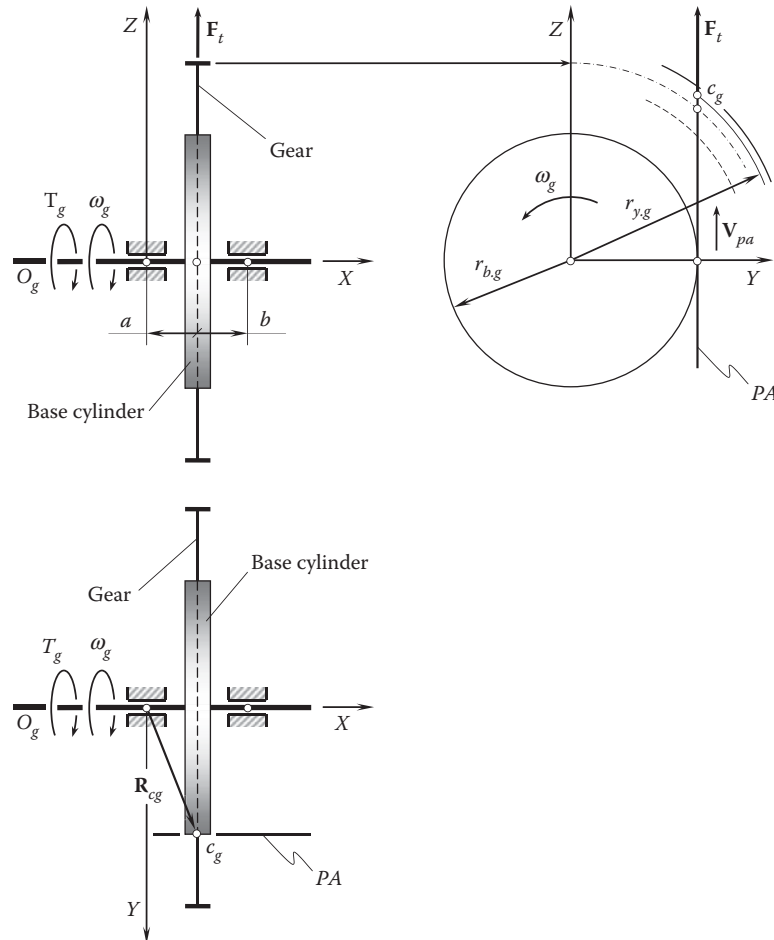


FIGURE 8.42

Bending torque in perfect spur parallel-axes gearing.



The location of the point,  $c_g$ , in the axial direction of the gear is not altered. Thus, the bending moment of the force,  $F_t$ , with respect to the bearing support also remains the same.

Perfect helical parallel-axes gearing represents a more general case of contact between the tooth flanks,  $\mathcal{G}$  and  $\mathcal{P}$ , of a gear and a mating pinion.

In perfect helical parallel-axes gearing, commonly either one or two lines of contact,  $LC_i$ , are observed. Cases when a gear pair features three and/or more lines of contact,  $LC_i$ , are feasible but not common in the current practice. In helical gearings, it is convenient to distinguish two different cases; that is, (a) when all the lines of contact,  $LC$ , are of a full length, and (b) when one or more line(s) of contact is of a reduced length.

When the only pair of the teeth engaged in mesh is as illustrated in Figure 8.43a, the applied load is evenly distributed along a single line of contact,  $LC$ . The distributed load,  $f_t$ , is calculated from the equation:

$$f_t = \frac{F_t}{F_{pa}} \quad (8.50)$$

The resultant (equivalent) force,  $F_t$ , is applied at a point,  $c_g$ , at the middle of a single line of contact,  $LC$ . The force,  $F_t$ , is along a line of action,  $LA$ , through the point,  $c_g$ .

The location of the point,  $c_g$ , where the load,  $F_t$ , is applied is not altered in the axial direction of the gear. Thus, the bending moment of the force,  $F_t$ , with respect to the bearing support also remains the same.

The normal force,  $F_{t,n}$ , is perpendicular to the line of contact,  $LC$ . The component  $F_{t,n}$  of the resultant (equivalent) force,  $F_t$ , is applied at that same point,  $c_g$ , as the load  $F_t$ . The magnitude,  $F_{t,n}$ , of the component,  $F_{t,n}$ , of the resultant (equivalent) force,  $F_t$ , equals:

$$F_{t,n} = F_t \cos \psi_b \quad (8.51)$$

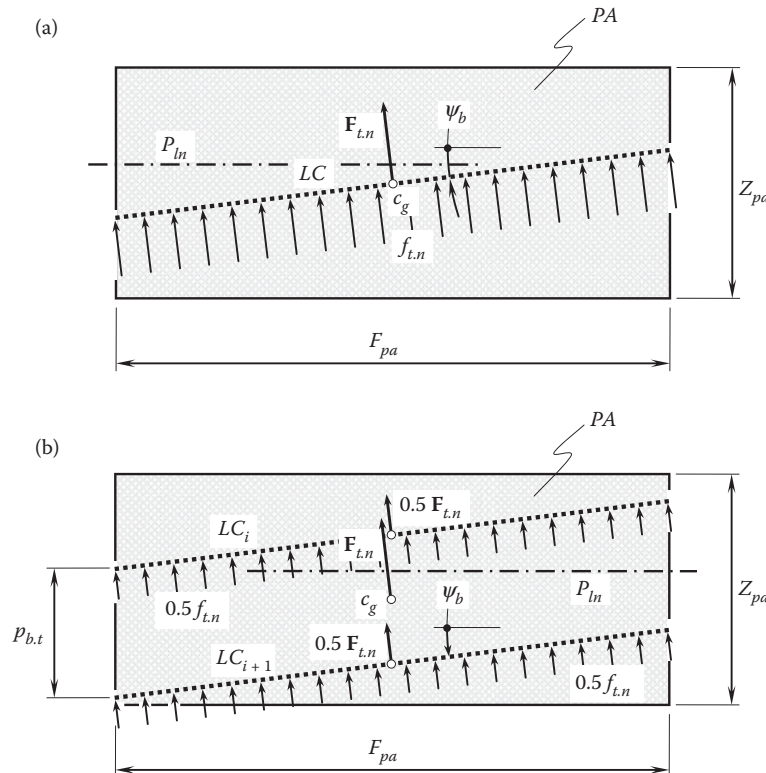


FIGURE 8.43

Lines of contact,  $LC_i$ , of full length in a perfect helical parallel-axes gear pair.

The normal distributed load,  $f_{t,n}$ , can be calculated from the expression:

$$f_{t,n} = \frac{F_t}{F_{pa}} \cos^2 \psi_b \quad (8.52)$$

The normal distributed load is  $f_{t,n}$  (see Equation 8.50), used for the calculation of the contact stress, as well as the bending stress in helical parallel-axes gearing for a mating gears configuration when one pair of teeth is engaged in mesh. This mode of the gear teeth loading is the most critical one, as the entire load is withheld by only a pair of interacting teeth of a gear and a mating pinion.

When two (or more) pairs of the teeth are engaged in mesh, as illustrated in Figure 8.43b, the applied load is evenly distributed along the corresponding number of the lines of contact,  $LC_i$ . The distributed load,  $f_{t,i}$ , is shared among  $n_\phi$  pairs of teeth engaged in mesh at that same time. The distributed load per a pair of teeth,  $f_{t,n\phi}$ , equals:

$$f_{t,n\phi} = \frac{f_{t,i}}{n_\phi} = \frac{F_t}{n_\phi F_{pa}} \quad (8.53)$$

The resultant force,  $F_t$ , is shared among all the lines of contact,  $LC_i$ . The resultant force per a pair of teeth,  $F_{t,n\phi}$ , equals:

$$F_{t,n\phi} = \frac{F_t}{n_\phi} \quad (8.54)$$

The resultant (equivalent) force,  $F_t$  (as well as the resultant [the equivalent] normal force,  $F_{t,n}$ ), is applied at point  $c_g$ . Point  $c_g$  corresponds to the middle of the lines of contact,  $LC_i$ , and between the first,  $LC_i$ , and the last,  $LC_j$ , lines of simultaneous contact. When two lines of contact are observed, point  $c_g$  is located in the middle between the lines of contact. When three lines of contact are observed, point  $c_g$  is located at the center of the second line of contact, and so forth.

Similar to the case of a single line of contact, in cases of multiple lines of contact, the force,  $F_t$ , is along a line of action,  $LA$ , through the point,  $c_g$ .

The normal distributed load,  $f_{t,n}$ , can be calculated from the expression:

$$f_{t,n} = \frac{F_t}{F_{pa}} \cos^2 \psi_b \quad (8.55)$$

The normal distributed load is  $f_{t,n}$  (see Equation 8.46), used for the calculation of the contact stress, as well as the bending stress in helical parallel-axes gearing for a mating gears configuration when two (or more) pairs of teeth are engaged in mesh.

The resultant (equivalent) force,  $F_t$ , is applied at point  $c_g$ . Point  $c_g$  corresponds to the middle of the lines of contact,  $LC_i$ , and between the first,  $LC_i$ , and the last,  $LC_j$ , lines of simultaneous contact. When two lines of contact are observed, then point  $c_g$  is located in the middle between the lines of contact. When three lines of contact are observed, point  $c_g$  is located at the center of the second line of contact, and so forth.

The location of the point,  $c_g$ , where the load,  $F_t$ , is applied is not altered in the axial direction of the gear. Thus, the bending moment of the force,  $F_t$ , with respect to the bearing support also remains the same.

Similar to the case of a single line of contact, in cases of multiple lines of contact, the force,  $F_t$ , is along a line of action,  $LA$ , through the point,  $c_g$ .

The location of the point,  $c_g$ , in the axial direction of the gear is not altered. Thus, the bending moment of the force,  $F_t$ , with respect to the bearing support also remains the same.

Ultimately, one or more lines of contact,  $LC_i$ , can be not of a full length.

As illustrated in Figure 8.44a, the line of contact,  $LC_i$ , is not of a full length, while the next line of contact,  $LC_{i+1}$ , is of a full length (that is, the inequality  $LC_i < LC_{i+1}$  is observed). In the example under consideration, the tangential load,  $F_t$ , is shared between the lines of contact,  $LC_i$  and  $LC_{i+1}$ . The load ( $|F_{t,1}| + |F_{t,2}|$ ) equals (see Figure 8.44a):

$$|F_{t,1}| + |F_{t,2}| = |F_t| \cdot \frac{F_{pa,1}}{F_{pa}} \quad (8.56)$$

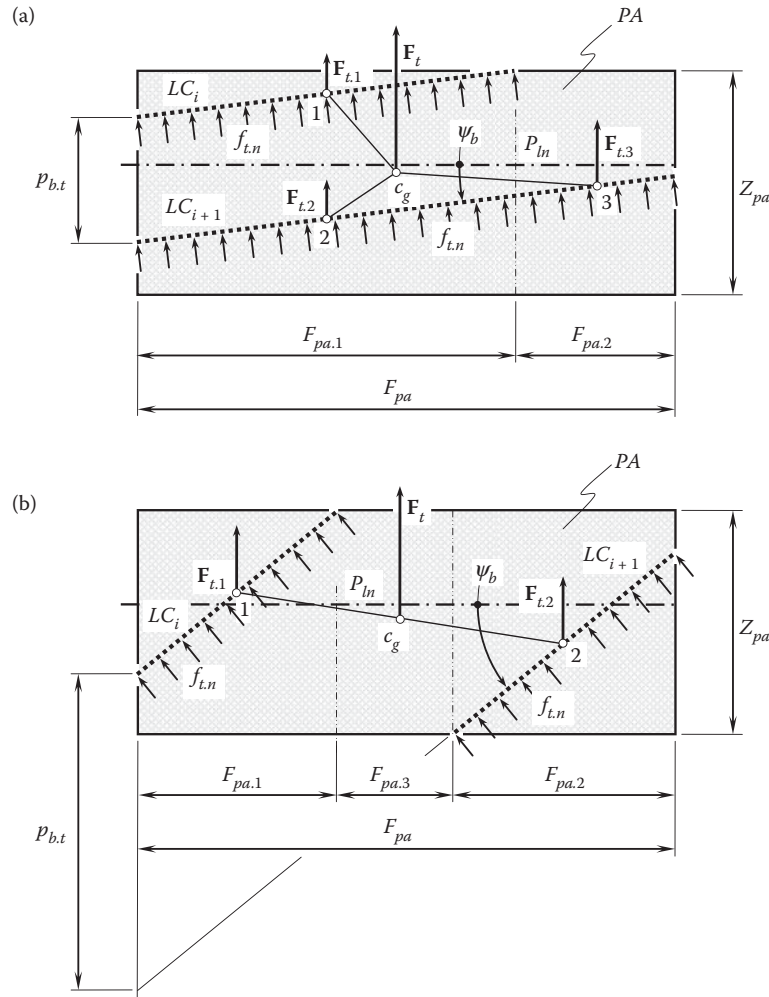


FIGURE 8.44

Lines of contact,  $LC_i$ , not of full length in a perfect helical parallel-axes gear pair.

where:

$$|\mathbf{F}_{t,1}| = |\mathbf{F}_{t,2}| = |\mathbf{F}_t| \cdot \frac{F_{pa,1}}{2 \cdot F_{pa}} \quad (8.57)$$

The loads,  $\mathbf{F}_{t,1}$  and  $\mathbf{F}_{t,2}$ , are applied at points 1 and 2 within the lines of contact. Points 1 and 2 correspond to points within the lines of contact,  $LC_i$  and  $LC_{i+1}$ , at the middle of the portion,  $F_{pa,1}$ , of the face width,  $F_{pa}$ .

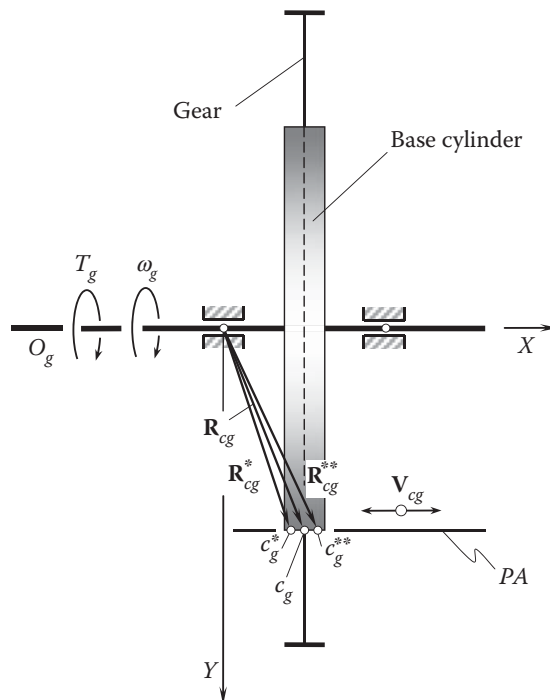
The load  $|\mathbf{F}_{t,3}|$  equals (see Figure 8.44a):

$$|\mathbf{F}_{t,3}| = |\mathbf{F}_t| \cdot \frac{F_{pa,2}}{F_{pa}} \quad (8.58)$$

The load,  $\mathbf{F}_{t,3}$ , is applied at point 3 within the line of contact,  $LC_{i+1}$ . Point 3 corresponds to a point within the line of contact,  $LC_{i+1}$ , at the middle of the portion,  $F_{pa,2}$ , of the face width,  $F_{pa}$ .

The resultant load,  $\mathbf{F}_t$ , is applied at point  $c_g$ . The coordinates of point  $c_g$  can be determined using the principle of the center of gravity, that is, point  $c_g$  is the *center of gravity* of points 1, 2, and 3 with the *weights*  $\mathbf{F}_{t,1}$ ,  $\mathbf{F}_{t,2}$ , and  $\mathbf{F}_{t,3}$ , correspondingly.

As the gears rotate, the lines of contact,  $LC_i$  and  $LC_{i+1}$ , travel together with the plane of action,  $PA$ . The points 1, 2, and 3, as well as point  $c_g$ , migrate within the plane of action,  $PA$ . The migration of point  $c_g$  with a linear velocity,  $\mathbf{V}_{cg}$ , in the axial direction of the gear pair results in a corresponding alteration of the arm,  $\mathbf{R}_{cg}$ , of the resultant



force,  $\mathbf{F}_t$ , in relation to the bearing support of the gear shaft, as schematically illustrated in [Figure 8.45](#). When point  $c_g$  migrates between points  $c_g^*$  and  $c_g^{**}$ , the arm,  $|\mathbf{R}_{c_g}|$ , of the resultant force,  $\mathbf{F}_t$ , changes in the range of:

$$\left| \mathbf{R}_{cg}^* \right| \leq \left| \mathbf{R}_{cg} \right| \leq \left| \mathbf{R}_{cg}^{**} \right| \quad (8.59)$$

Another configuration of the lines of contact,  $LC_i$  and  $LC_{i+1}$ , is illustrated in [Figure 8.44b](#).

As shown in Figure 8.44b, the lines of contact,  $LC_i$  and  $LC_{i+1}$ , are not of full length (that is, the inequality  $LC_i \neq LC_{i+1}$  is observed). In the example under consideration, the tangential load,  $F_t$ , is shared between the lines of contact,  $LC_i$  and  $LC_{i+1}$ . The load,  $F_{t,1}$ , equals (see Figure 8.44b):

$$|\mathbf{F}_{t,1}| = |\mathbf{F}_t| \cdot \frac{F_{pa,1}}{F_{pa,1} + F_{pa,2}} \quad (8.60)$$

The load,  $\mathbf{F}_{t,1}$ , is applied at point 1 within the line of contact,  $LC_i$ . Point 1 is in the middle of the line of contact,  $LC_i$ .

The load,  $|\mathbf{F}_{t.2}|$ , equals (see [Figure 8.44b](#)):

$$|\mathbf{F}_{t,2}| = |\mathbf{F}_t| \cdot \frac{F_{pa,2}}{F_{pa,1} + F_{pa,2}} \quad (8.61)$$

The load,  $\mathbf{F}_{t,2}$ , is applied at point 2 within the line of contact,  $LC_{i+1}$ . Point 2 is in the middle of the line of contact,  $LC_{i+1}$ .

No load is transmitted by the portion,  $F_{pa,3r}$ , of the face width,  $F_{pa}$ , as no lines of contact are located here. This portion of the gear face is excluded from the analysis.

When calculating contact stress in a parallel-axes gear pair, use of the so-called *total length of the lines of contact* is often helpful. Total length of the lines of contact means a summa of the length of all the lines of contact that occur at a specified instant of time.\* When two or more lines of contact do not overlap one another, the importance of the total length of lines of contact is vital: in such a case, an applied load is equally distributed along the TLLC.

The resultant load,  $F_t$ , is applied at point  $c_g$ . The coordinates of point  $c_g$  can be determined using the principle of the center of gravity, that is, point  $c_g$  is the center of *gravity* of the points 1 and 2, having the weights  $F_{t,1}$ , and  $F_{t,2}$ , correspondingly.

As the gears rotate, the lines of contact,  $LC_i$  and  $LC_{i+1}$ , travel together with the plane of action,  $PA$ . The points 1 and 2, as well as the point  $c_g$ , migrate within the plane of action,  $PA$ . The migration of point  $c_g$  with a linear velocity  $V_{cg}$  in the axial direction of the gear pair results in a corresponding alteration of the arm,  $R_{cg}$ , of the resultant force,  $F_t$ , in relation to the bearing support of the gear shaft, as schematically illustrated in Figure 8.44.

When point  $c_g$  migrates between points  $c_g^*$  and  $c_g^{**}$ , the arm,  $|R_{cg}|$ , of the resultant force,  $F_t$ , changes in the range of  $|R_{cg}^*| \leq |R_{cg}| \leq |R_{cg}^{**}|$  (Figure 8.45).

The variation of the magnitude,  $|\Delta R_{cg}|$ , of the arm,  $R_{cg}$ , causes a variable-in-time torque that bends the gear shaft and deforms the gear housing. The variation of the magnitude,  $|\Delta R_{cg}|$ , of the arm,  $R_{cg}$ , can cause an extensive undesirable vibration of the gear housing and extensive noise excitation.

The disclosed approach for determining the loads acting in every pair of teeth in perfect spur and helical parallel-axes gearing can be enhanced to gear pairs with lines of contact of an arbitrary geometry, that is, to gear pairs with lines of contact in the form of arcs of a circle, a spiral curve, and so forth. Generally speaking, for this purpose, the plane-of-action face width,  $F_{par}$ , is subdivided into several segments, and within each of them, either zero, one, two, or so forth lines of contact occur. In the case of a line of contact in a form of a planar curve, the corresponding portion of the plane-of-action face width,  $F_{par}$ , is sliced into an infinite number of infinitesimally narrow slices. The portion of a line(s) of contact within each infinitesimally narrow slice is considered a straight line segment. In such a manner, loading in perfect parallel-axes gear pairs with the lines of contact of an arbitrary geometry can be determined.

### 8.7.2 Forces Acting in a Transverse Section of a Perfect Parallel-Axes Involute Gear Pair

In addition to the forces that act in the plane of action of a perfect parallel-axes gear pair, friction forces act in a transverse section of the gear pair, as schematically illustrated in Figure 8.46.

At an instant of time when two contact points,  $K_1$  and  $K_2$ , are observed, the resultant tangential force,  $F_t$ , is equally shared between the points,  $K_1$  and  $K_2$ ; that is, the forces,  $F_{t,1}$  and  $F_{t,2}$ , are equal to one another. The forces,  $F_{t,1}$  and  $F_{t,2}$ , create the input torque,  $T_p$ .

The friction forces,  $F_{f,1}$  and  $F_{f,2}$ , act perpendicular to the line of action,  $LA$ . As the instant relative motion of the driving gear and the driven pinion is an instant rotation about the pitch point,  $P$ , and the contact points,  $K_1$  and  $K_2$ , are located from the opposite sides of the pitch point, the friction forces,  $F_{f,1}$  and  $F_{f,2}$ , are pointed opposite to each other. The friction forces,  $F_{f,1}$  and  $F_{f,2}$ , are equal:

$$F_{f,1} = \mu \cdot F_{t,1} \quad (8.62)$$

$$F_{f,2} = \mu \cdot F_{t,2} \quad (8.63)$$

Here, the friction coefficient is designated as  $\mu$ .

The friction forces,  $F_{f,1}$  and  $F_{f,2}$ , create a friction torque,  $T_{fr}$ . The friction torque,  $T_{fr}$ , can be calculated as:

$$T_{fr} = F_{f,1} \cdot K_1P + F_{f,2} \cdot K_2P \quad (8.64)$$

\* It is the right point to stress here that gear tooth loading strongly depends on the total length of the line of contact, as well as the contact ratio in the gear pair. The influence of the total length of the line of contact and the contact ratio on gear tooth loading is complex: It could happen that when the pitch helix angle of a gear,  $\psi_g$ , goes up, the total length of the lines of contact goes down; that is, the contact ratio can be greater in this case, but the total length of the line of contact can be shorter. The latter results in a higher contact stress and a higher bending stress in the gear teeth.

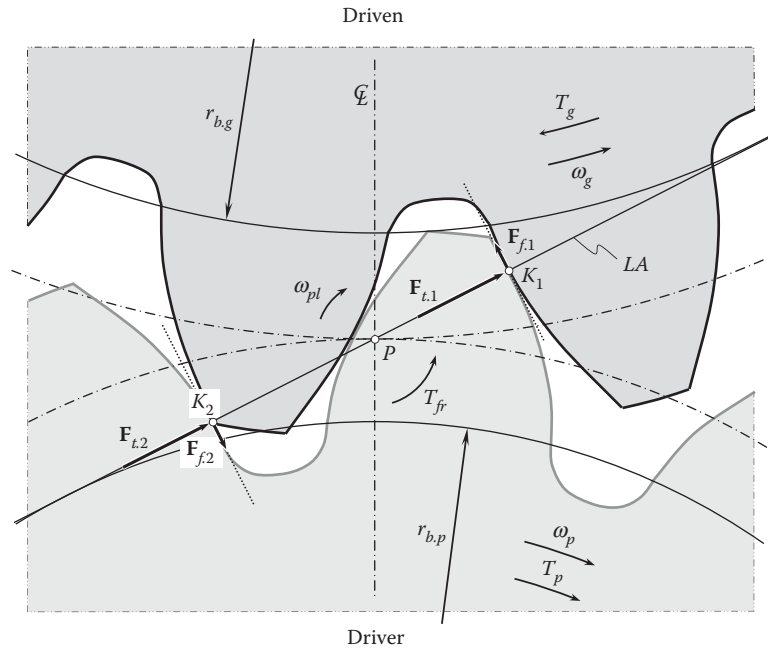


**FIGURE 8.46**  
Forces acting in a transverse section of a perfect parallel-axes involute gear pair.

The friction torque,  $T_{fr}$ , is opposite to the input torque,  $T_p$ .

When the gears rotate, the distances,  $K_1P$  and  $K_2P$ , alter. However, the summa ( $K_1P + K_2P$ ) remains of a constant value. Therefore, in perfect parallel-axes involute gearing, the friction torque,  $T_{fr}$ , also is of a constant value.

### 8.8 Pinion-Gear-to-Rack Mesh as a Reduced Case of External Parallel-Axes Involute Gear Pair

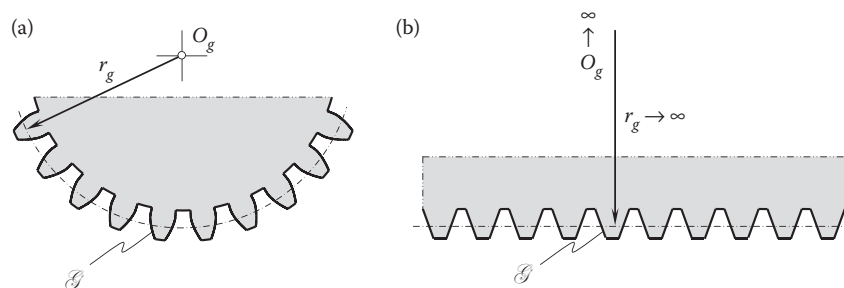
Tooth count in a gears depends on a particular application. There are no physical constraints to designing a gear with an infinite number of teeth. A gear with an infinite tooth count is referred as *rack-gear*, or just *rack*. Mesh of a rack-gear with a pinion-gear is commonly referred to as pinion-gear-to-rack mesh.

An example of a vector diagram for a *pinion-gear-to-rack* gear pair is depicted in Figure 6.2d. The rotation of the gear is equal to zero ( $\omega_g = 0$ ), as the gear has an infinite tooth count. The rotation of the pinion is equal to a certain finite value,  $\omega_p$ . The kinematics of a pinion-gear-to-rack gear pair can be specified in terms of the linear velocity of the rack,  $V_r$ , and rotation of the pinion,  $\omega_p$ .

An involute pinion-gear-to-rack gear pair can be interpreted as the limit case of an external gear pair when the tooth number of the gear approaches infinity ( $N_g \rightarrow \infty$ ). Under such a scenario, the pinion remains the same, while the gear is transformed to the rack. A paradox exists in a pinion-gear-to-rack mesh. The applied technique needs to answer the question *How can you construct a base line for a rack?* in an involute pinion-gear-to-rack gear pair.

Consider a parallel-axis gear pair with a given diametral pitch,  $P$  (or the same with a specified module,  $m$ ), for example, an involute gear sector of a gear of  $N_g = 25$ , as illustrated in Figure 8.47a. The gear sector features 10 teeth ( $N_{gs} = 10$ ). When the gear sector tooth number approaches infinity (that is, when  $N_{gs} \rightarrow \infty$ ), the radius of the pitch circle of the gear,  $r_g$ , approaches infinity as well ( $r_g \rightarrow \infty$ ), and the involute tooth profiles are straightened, as shown in Figure 8.47b. In this way, the gear sector transforms into a rack gear. An example of a pinion-gear-to-rack gear pair is depicted in Figure 8.48. For a rack, the pitch circle is straightened to a straight pitch line. The same is true with respect to the radius of the outer circle,  $r_{o,g}$ , and the radius of the root circle,  $r_f$ . Both of these radii approach infinity, and in the design of a rack, they are straightened to two straight lines, which are parallel to the pitch line.



**FIGURE 8.47**

Interpretation of a rack-gear as a limit case of an external gear: (a) gear with certain tooth count,  $N_g$ , and (b) gear with an infinite tooth count,  $N_g \rightarrow \infty$ .

It is natural to assume that the same is valid with respect to the base circle of the gear, namely when  $N_g \rightarrow \infty$ , then the radius of base circle of the gear,  $r_{b,g}$ , also approaches infinity ( $r_{b,g} \rightarrow \infty$ ). Under such a scenario, the base circle straightens to a corresponding straight base line.

On the other hand, the base circle of a gear is tangent to two straight lines of action,  $LA_1$  and  $LA_2$ , through the pitch point,  $P$ . These two straight lines are perpendicular to opposite sides of the tooth profile of the gear. When the tooth number of the gear approaches infinity ( $N_g \rightarrow \infty$ ), the involute tooth profile of the gear straightens. Therefore, the two above-mentioned straight lines of action,  $LA_1$  and  $LA_2$ , are perpendicular to straight tooth flanks of the rack, as illustrated in [Figure 8.49](#).

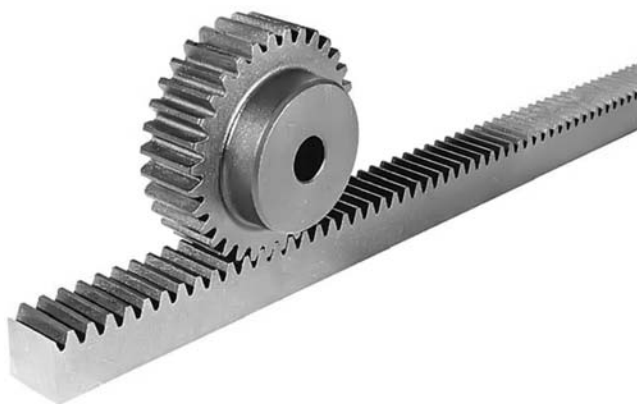
For a rack, the center of the gear,  $O_g$ , approaches infinity ( $O_g \rightarrow \infty$ ). However, the configuration of the straight lines of action,  $LA_1$  and  $LA_2$ , remains the same. Therefore, the straight base line intersects the straight lines of action,  $LA_1$  and  $LA_2$ , regardless of how far the center of the gear,  $O_g$ , is remote from the pitch point,  $P$ .

Ultimately, for a rack, we have, from one side, a straight base line that is parallel to the pitch line, and, from another side, this line must be in tangency to two straight lines of action,  $LA_1$  and  $LA_2$ . No straight line fulfills both these conditions simultaneously. These two requirements conflict with each other. Therefore, the interpretation of a rack-gear as a reduced case of a gear that features an infinite tooth count is not consistent.

In the reduced case of a gear rack, the principal design parameters of involute gear are preserved. Details of the transformation of a gear sector into a rack gear as illustrated in [Figure 8.48](#).

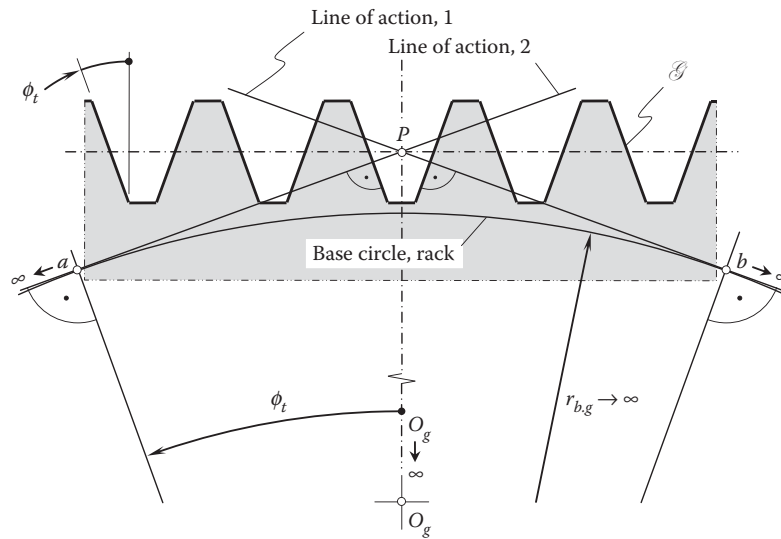
The main design parameters in a transverse section of a pinion-gear-to-rack gear pair are illustrated in [Figure 8.50](#).

Pinion-gear-to-rack gear pairs of two kinds are commonly recognized. They are spur and helical pinion-gear-to-rack gear pairs. The geometry and kinematics of a spur pinion-gear-to-rack pair are schematically illustrated in [Figure 8.51](#).

**FIGURE 8.48**

Pinion-gear-to-rack gear pair.



**FIGURE 8.49**

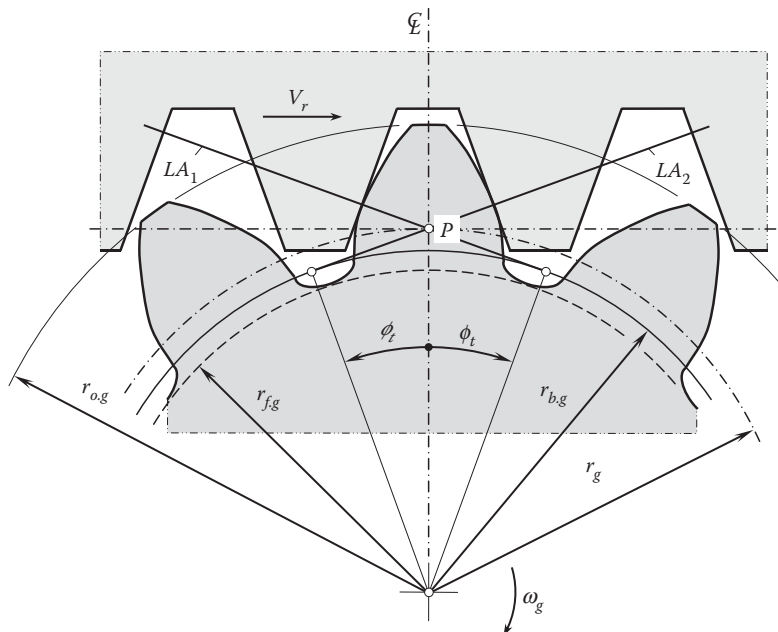
Rack-gear as reduced case of involute gear.

For a spur pinion-gear-to-rack gear pair, the total contact ratio,  $m_t$ , is equal to the transverse (profile) contact ratio,  $m_p$ . For a helical pinion-gear-to-rack gear pair, the total contact ratio,  $m_t$ , is the sum of the transverse contact ratio,  $m_p$ , and the face contact ratio,  $m_F$ .

Because of the greater number of teeth, a pinion-gear-to-rack gear pair features lower profile sliding compared to that in an external gear pair. However, the profile sliding in a pinion-gear-to-rack gear pair exceeds that in an internal gear pair.

Similar to external gear pairs, pinion-gear-to-rack gear pairs can be designed with a certain addendum modification either of the pinion, the rack, or both.

An example of an application of a pinion-gear-to-rack gear pair is illustrated in [Figure 8.48](#).

**FIGURE 8.50**

Main design parameters of a pinion-gear-to-rack gear pair.

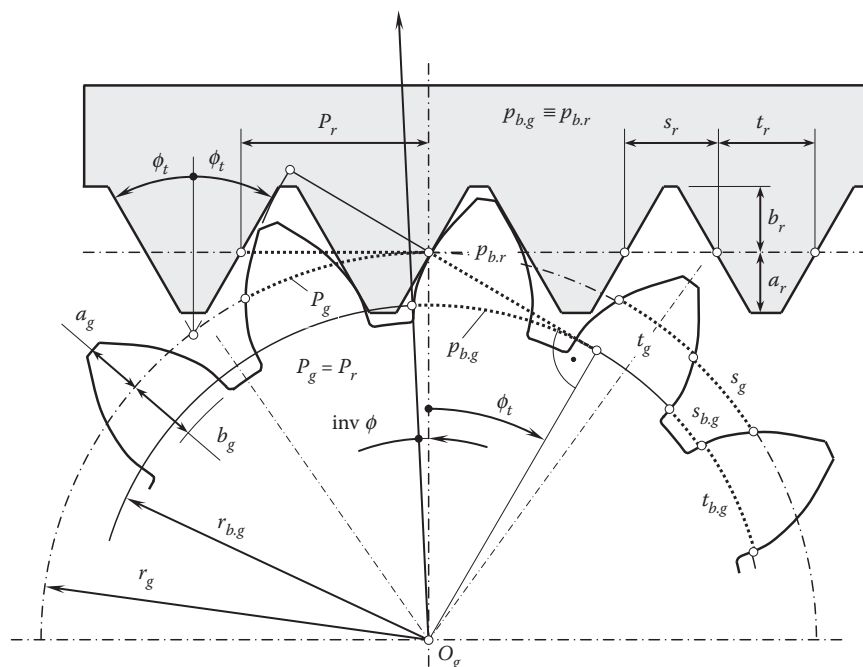


FIGURE 8.51

A spur rack in mesh with a zero backlash gear.

At a point within the line of action,  $LA$ , of a pinion-gear-to-rack gear pair, the difference  $(\rho_g - \rho_p)$  between the radii of curvature is constant, as it is equal to the center distance,  $C$ . Therefore, for a pinion-gear-to-rack gear pair, the point,  $lr_k$ , at which the relative curvature is of minimum value is located far beyond the outer diameter of the pinion ( $lr_k \rightarrow \infty$ ).

The variation intervals for the tooth flank geometry in a pinion-gear-to-rack gear pair are within a smaller range compared to that in external gear pairs, but exceed that in internal gear pairs.

It can be easily shown that that same gear rack can be obtained as a degenerate case of internal parallel-axes involute gearing.

With that said, all the above-discussed results on parallel-axes external involute gearing are still valid for pinion-gear-to-rack mesh.\*

\* The generation of the rack straight tooth profile as an involute tooth profile of the rack base circle is not considered in detail here. The interested reader may wish to go into the problem on his/her own.

# 9

## Internal Involute Gearing

Internal involute gearings are used to transmit a rotation from a driving shaft to the driven shaft when the axes of the rotations are parallel to one another. The vector diagram of an internal gear pair is illustrated in Figure 6.2c. No change to the direction of the rotation is observed in the internal parallel-axis gearing.

An internal gear pair is composed of an external pinion and internal gear. Either a spur or helical pinion is engaged in mesh with an internal gear.

The geometry of the tooth flank of a pinion (Figure 7.4a) is identical to that for an external gear pair.

An example of an internal spur involute gear is illustrated in Figure 9.1. The analytical description of the tooth flanks of an internal gear (see Figure 9.1) is the same as for an external gear. The main difference between an internal gear and an external gear is in the location of the body and void sides of the gear tooth. The tooth flank geometry of an internal gear, including but not limited to, normal curvature, profile angle, and helix angle, as well as others, is similar to that for the corresponding external gear.

An internal parallel-axes gear pair composed of spur involute gears is depicted in Figure 9.2. Internal parallel-axes gear pairs composed of helical involute gears are also extensively used in the current industry. For special applications, internal parallel-axes gear pair composed of herringbone involute gears are designed (Figure 9.3).

Tooth flanks in internal parallel-axes spur and helical gears interact with one another similarly to that of external gear pairs of a corresponding design.

The set of three conditions to fulfill in order to transmit a uniform rotation by means of internal parallel-axes gears is identical to that of external gearings; that is, (1) the condition of contact (*Shishkov equation of contact*), and (2) the condition of conjugacy (*Camus-Euler-Savary theorem*) have to be fulfilled, along with (3) the equality of base pitches of a gear and a mating pinion to the operating base pitch of the gear pair.

An example of application of an internal gear pair is illustrated in Figure 9.4. The design parameters of an internal gear pair are schematically shown in Figure 9.5.

The consideration below is focused on the main features of an internal gearing, while the similarities of internal and external gear pairs are omitted.

### 9.1 Contact Ratio in Internal Gearing

Commonly, the transverse contact ratio, face contact ratio, and total contact ratio in an internal gear pair are distinguished.

The transverse contact ratio,  $m_p$ , is the contact ratio in the transverse plane of the internal gear pair. For involute gears, it is most directly obtained as the ratio of the length of the active portion of the line of action to the base pitch\*.

When two gears are put into mesh with a certain center distance,  $C$ , as shown in Figure 9.6, the line of action is tangent to the base cylinders of the gear,  $d_g$ , and the pinion,  $d_p$ . The contact starts at a point,  $a$ , where the outside diameter circle of the pinion intersects the line of action, passes through the pitch point,  $P$ , and ends at a point,  $b$ , where the outside diameter of the gear intersects the line of action,  $LA$ . The straight-line segment,  $ab$ , of the line of action,  $N_g N_p$ , is the active portion of the line of action,  $LA$ . The length of the active portion of the line of action is denoted by  $Z_{pa}$ .

\* It is incorrect practice to define the term *transverse contact ratio*,  $m_p$ , as the ratio of the angle of action to the angular pitch. Such a definition can be applied to gears with noninvolute tooth profiles, which is incorrect, as in noninvolute gears, only one pair of teeth makes contact at every instant of time.



**FIGURE 9.1**  
An example of an internal spur involute gear.



**FIGURE 9.2**  
An internal parallel-axes gear pair composed of spur involute gears.

Referring to [Figure 9.6](#), an expression:

$$\rho_g = aN_g = \frac{1}{2} \sqrt{d_{o,g}^2 - d_{b,g}^2} \quad (9.1)$$

for the calculation of the radius of curvature,  $\rho_g$ , of the gear tooth profile at the outer diameter,  $d_{o,g}$ , can be derived.



**FIGURE 9.3**  
An internal parallel-axes gear pair composed of herring-bone involute gears.

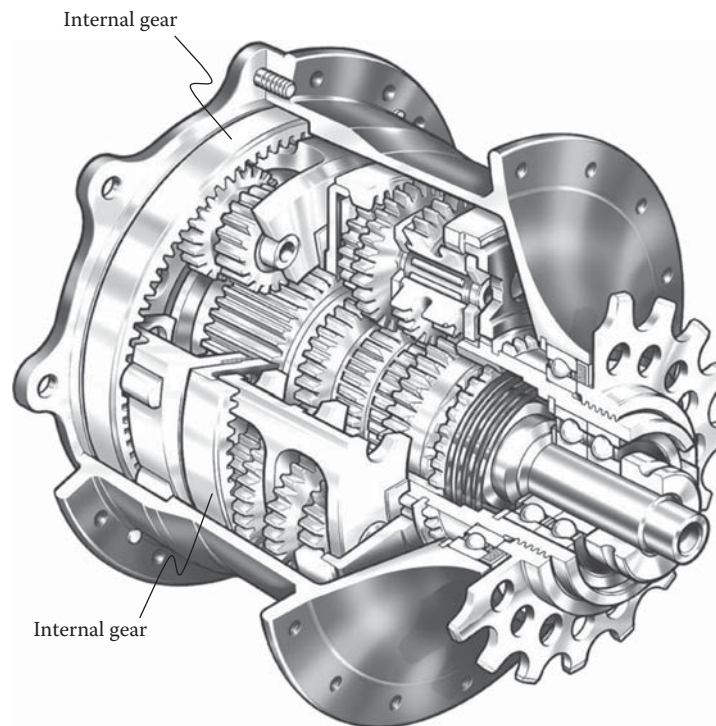


**FIGURE 9.4**  
An example of application of internal gears.

Similarly, an expression:

$$\rho_p = bN_p = \frac{1}{2} \sqrt{d_{o,p}^2 - d_{b,p}^2} \quad (9.2)$$

for the calculation of the radius of curvature,  $\rho_p$ , of the pinion tooth profile at the outer diameter,  $d_{o,p}$ , can be derived as well.

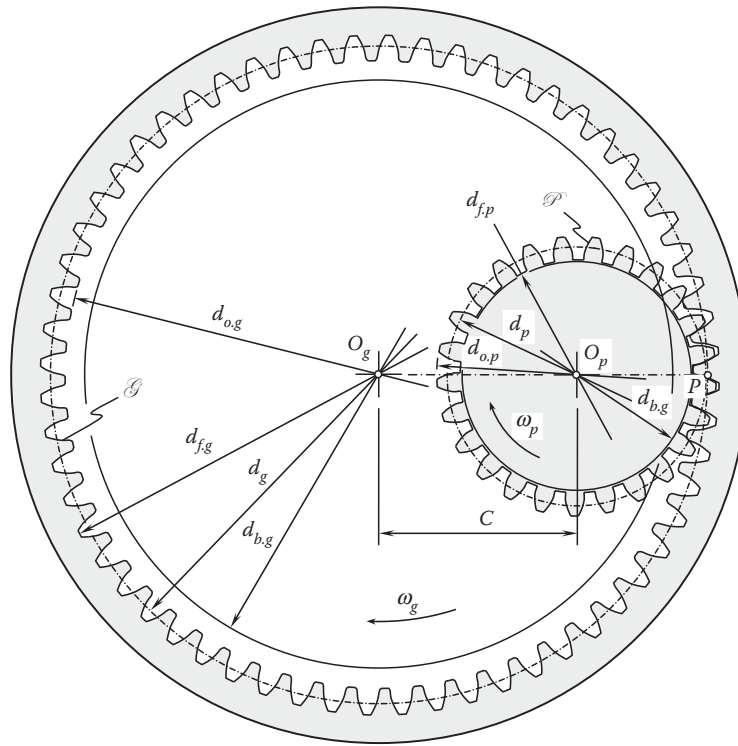


**FIGURE 9.5**  
Design parameters of internal gear pair.

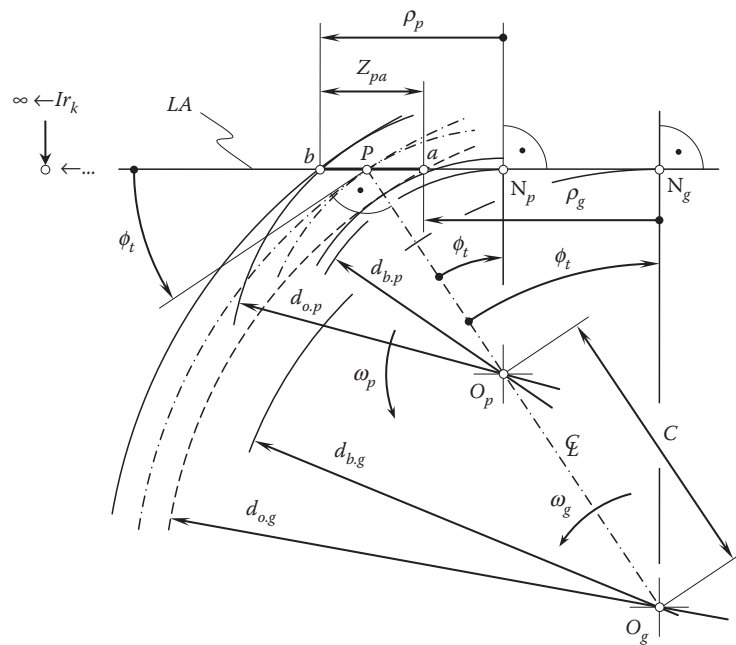


**FIGURE 9.6**  
Line of action,  $LA$ , in an internal involute gear pair.

With the radii of curvature,  $\rho_g$  and  $\rho_p$ , calculated, the length,  $Z_{pa}$ , of the active portion of the line of action can be calculated by the formula:

$$Z_{pa} = \rho_g - \rho_p + C \sin \phi_t = \frac{1}{2} \left( \sqrt{d_{o,g}^2 - d_{b,g}^2} - \sqrt{d_{o,p}^2 - d_{b,p}^2} + 2C \sin \phi_t \right) \quad (9.3)$$

The active portion of the line of action,  $LA$ , can be expressed in terms of two components,  $Z_g$  and  $Z_p$ , that is, as the sum  $Z_{pa} = Z_g + Z_p$ . The component  $Z_g$  is due to the addendum of the gear,  $a_g$ , and the component  $Z_p$  is due to the addendum of the pinion,  $a_p$ . Usually, the inequality  $Z_g > Z_p$  is valid.

In Equation 9.3, the pressure angle in the transverse plane is denoted by  $\phi_t$ . In the case of spur gears, this angle is equal to the profile angle of the gear and the pinion at the pitch point,  $P$ . In the case of helical gears, this angle is equal to the transverse profile angle,  $\phi_t$ , of the gear and the pinion at the pitch point,  $P$ .

It should be mentioned here that for a current point within the line of action,  $LA$ , the difference  $(\rho_g - \rho_p)$  is constant, as it is equal to the center distance,  $C$ . Therefore, for an internal gear pair, the point,  $Ir_k$ , at which the relative curvature is of minimum value is located far beyond the outer diameter of the pinion ( $Ir_k \rightarrow \infty$ ).

As contacts travel from point  $a$  to point  $b$ , the average number of pairs of teeth moving across the zone of action,  $Z_{pa}$ , is defined as the transverse contact ratio:

$$m_p = \frac{Z_{pa}}{p_{b,t}} \quad (9.4)$$

The transverse base pitch,  $p_{b,t}$ , of the helical gear reduces to the base pitch,  $p_b$ , of the spur gear.

The face contact ratio,  $m_F$ , for an internal gear pair is identical to that for an external gear pair (Figure 8.17). It can be defined by the expression:

$$m_F = \frac{F_{pa}}{p_x} \quad (9.5)$$

For spur gear pairs, the component  $m_F$  is equal to zero.

The total contact ratio,  $m_t$ , is the sum of the transverse contact ratio,  $m_p$ , and the face contact ratio,  $m_F$ . It is calculated by the following formula:

$$m_t = m_p + m_F \quad (9.6)$$

It is the right point to stress here that the axial pitch of a gear teeth,  $p_x$ , can be expressed in terms of the operating base pitch,  $p_{b,op}$ , of the gear pair:

$$p_x = \frac{p_{b,op}}{\tan \psi_b} \quad (9.7)$$

After substituting Equation 9.7 into Equation 9.5, a formula for the calculation of face contact ratio,  $m_F$ , casts into the form:

$$m_F = \frac{F_{pa}}{p_{b,op}} \tan \psi_b \quad (9.8)$$

With this expression for the face contact ratio,  $m_F$ , Equation 9.6 for the total contact ratio,  $m_t$ , can be represented in the form:

$$m_t = \frac{Z_{pa} + F_{pa} \tan \psi_b}{p_{b,op}} \quad (9.9)$$

Equation 9.9 is valid for the calculation of the total contact ratio,  $m_t$ , in both cases, that is, in cases of spur, as well as in cases of helical internal parallel-axes gear pairs. With Equation 9.9, Equation 9.4 for the transverse contact ratio and Equation 9.5 for the face contact ratio become unnecessary, and only the term *total contact ratio*,





The component,  $\mathbf{V}_{sl,g}^m$ , of the velocity vector,  $\mathbf{V}_g^m$ , is perpendicular to the line of action,  $LA$ . The component,  $\mathbf{V}_{sl,p}^m$ , of the velocity vector,  $\mathbf{V}_p^m$ , is also perpendicular to the line of action,  $LA$ . Both the velocity vectors,  $\mathbf{V}_{sl,g}^m$  and  $\mathbf{V}_{sl,p}^m$ , are tangent to the gear teeth profiles at the current contact point,  $m$ .

The components,  $\mathbf{V}_{sl,g}^m$  and  $\mathbf{V}_{sl,p}^m$ , are of different magnitudes ( $|\mathbf{V}_{sl,g}^m| \neq |\mathbf{V}_{sl,p}^m|$ ). The sliding velocity vector,  $\mathbf{V}_{sl}^m$ , is equal to the difference:

$$\mathbf{V}_{sl}^m = \mathbf{V}_{sl,g}^m - \mathbf{V}_{sl,p}^m \quad (9.10)$$

The relationships between the velocities on involute gears are governed by the condition occurring at every contact point,  $m$ , within the line of action,  $LA$ . The components,  $\mathbf{V}_{sl,g}^m$  and  $\mathbf{V}_{sl,p}^m$ , are equal to the velocity of the contact point along the path of contact. Otherwise, either separation or penetration between the tooth flanks,  $\mathcal{G}$  and  $\mathcal{P}$ , would be observed.

The similarity of the triangles in Figure 9.7 allows for the following expressions:

$$V_{sl,g}^m = |\mathbf{V}_{sl,g}^m| = V_{sl}^m \frac{N_g m}{N_g O_g} \quad (9.11)$$

$$V_{sl,p}^m = |\mathbf{V}_{sl,p}^m| = V_{sl}^m \frac{N_p m}{N_p O_p} \quad (9.12)$$

for magnitudes  $V_{sl,g}^m$  and  $V_{sl,p}^m$  of the velocity vectors,  $\mathbf{V}_{sl,g}^m$  and  $\mathbf{V}_{sl,p}^m$ .

At the pitch point,  $P$ , the ratio:

$$\frac{N_g m}{N_g O_g} = \frac{N_p m}{N_p O_p} \quad (9.13)$$

is valid. Due to this, the equality  $V_{sl,g}^m = V_{sl,p}^m$  is valid at the pitch point,  $P$ . This proves that no profile sliding of the tooth flanks,  $\mathcal{G}$  and  $\mathcal{P}$ , can occur in the pitch point,  $P$ .

The magnitude,  $V_{sl}^m$ , of the sliding velocity vector,  $\mathbf{V}_{sl}^m$ , is equal to the difference  $V_{sl}^m = V_{sl,g}^m - V_{sl,p}^m$ .

During an infinitesimally small interval of time, the ratio of the length of the gear and pinion tooth profiles in contact is equal to the ratio of the velocity components,  $V_{sl,g}^m$  and  $V_{sl,p}^m$ . Because of this, the equality  $V_{sl,g}^m = V_{sl,p}^m$  is valid at the pitch point,  $P$ , and the length of tooth profiles in contact are equal to each other, which corresponds to pure rolling without sliding taking place at this point.

At an arbitrary contact point, the sliding velocity vector,  $\mathbf{V}_i^{sl}$ , of the gear tooth flank,  $\mathcal{G}$ , in relation to the pinion tooth flank,  $\mathcal{P}$ , is equal to  $\mathbf{V}_i^{sl} = \mathbf{V}_i^g - \mathbf{V}_i^p$ . At different points within the line of action,  $LA$ , the relative sliding of the tooth flanks,  $\mathcal{G}$  and  $\mathcal{P}$ , is different. The magnitude of the sliding velocity vector,  $\mathbf{V}_i^{sl}$ , is a function of  $z$ ; that is,  $V^{sl}(z) = |\mathbf{V}_i^{sl}(z)|$ . The linear velocity vector,  $\mathbf{V}_i^{sl}$ , of relative sliding is always pointed perpendicularly to the line of action. The equality  $\mathbf{V}_i^{sl} = \mathbf{V}_i^g - \mathbf{V}_i^p$  allows for the following formula for the calculation of magnitude of the sliding velocity vector:

$$V^{sl}(z) = [Z_{pa} - (1 - u) \cdot z] \cdot \omega_p \quad (9.14)$$

Here,  $u$  designates the tooth ratio, and it is equal to  $u = d_{b,g}/d_{b,p}$ .

### 9.2.2 Specific Sliding

Specific sliding of the tooth flanks,  $\mathcal{G}$  and  $\mathcal{P}$ , of a gear and a mating pinion for an internal gear pair is defined in a similar manner to that for an external gear pair. Two different parameters,  $\gamma$ , are distinguished.

First, the slide/roll ratio for the tooth flank,  $\mathcal{G}$ , of the gear:

$$\gamma_g = \frac{V_{sl,g}^m - V_{sl,p}^m}{V_{sl,g}^m} \quad (9.15)$$

Second, the slide/roll ratio for the tooth flank,  $\mathcal{P}$ , of the pinion:

$$\gamma_p = \frac{V_{sl,p}^m - V_{sl,g}^m}{V_{sl,p}^m} \quad (9.16)$$

The specific sliding,  $\gamma$ , has a positive value on the addendum portions of the tooth flanks. The parameter  $\gamma$  does not exceed 1. At the pitch point,  $P$ , it is equal to zero, and it is equal to 1 at the base circle of the mating gear.

The specific sliding on the dedendum portion of the tooth flanks has a negative value. It is equal to zero at the pitch point,  $P$ , and it approaches minus infinity at the base circle.

### 9.3 Conditions to Be Fulfilled by Mating Gears in Internal Gear Pair: Engineering Formulae

Usually, the gear addendum modification coefficient,  $\xi_g$ , has to be determined when the pinion addendum modification coefficient,  $\xi_p$ , and the center distance,  $C$ , are given [74]:

$$\phi_t^{op} = \cos^{-1} \left( \frac{d_{b,g} - d_{b,p}}{2C} \right) \quad (9.17)$$

$$(\xi_g - \xi_p) = \frac{N_g - N_p}{2} \cdot \frac{\text{inv } \phi_t^{op} - \text{inv } \phi_t}{\tan \phi} \quad (9.18)$$

$$\xi_g = (\xi_g - \xi_p) + \xi_p \quad (9.19)$$

The following formulae are used for the calculation of the gear diameters:

Reference diameter of the pinion:

$$d_p = \frac{mN_p}{\cos \psi} \quad (9.20)$$

Theoretical pinion root diameter:

$$\tilde{d}_{f,p} = d_p - 2m(h_{f,p}^* - \xi_p) \quad (9.21)$$

Outer diameter of the pinion:

$$d_{o,p} = d_p + 2m(h_{a,p}^* + \xi_p) \quad (9.22)$$

Reference diameter of the gear:

$$d_g = \frac{mN_g}{\cos \psi} \quad (9.23)$$

Apart from the basic rack data, the exact calculation of the theoretical gear root circle diameter,  $\tilde{d}_{f,g}$ , involves the number of cutter teeth,  $N_c$ , and the cutter addendum modification coefficient  $\xi_c$  [74]:

$$\tilde{d}_{f,g} = \frac{d_{b,g} - d_{b,c}}{\cos \phi_{gt}} + \frac{mN_c}{\cos \psi} + 2m(h_{f,p}^* - \xi_c) \quad (9.24)$$

Here, the generation pressure angle,  $\phi_{gt}$ , is calculated from the expression:

$$\text{inv } \phi_{gt} = \text{inv } \phi_t + \frac{2(\xi_g - \xi_c)\tan \phi}{N_g - N_c} \quad (9.25)$$

For the calculation of the approximate value of the gear root diameter, the following expression:

$$d_{f,g} \approx d_g + 2m(h_{f,p}^* + \xi_g) \quad (9.26)$$

is used.

The outer diameter of the gear is calculated from the formula:

$$d_{o,g} = d_g - 2m(h_{a,p}^* - \xi_g) \quad (9.27)$$

The addendum shortening is negative; that is, the tooth depth is increased. It is therefore usually ignored because of tooling considerations.

The theoretical design of internal gears must be checked for cutter interference during their manufacture by a gear shaper cutter. Frequently, addendum shortening on the internal gear and its pinion is required. Only then can the sliding conditions be checked.

For the purposes of obtaining a suitable pinion addendum modification coefficient,  $\xi_p$ , the pinion for an internal gear can be deemed to be mating with a rack with well-matched slide/roll ratios. For this, the tip contact parameters,  $k_{ez}$  and  $k_{az}$ , for the pinion and rack, respectively, must be equal. By varying the pinion addendum modification coefficient,  $\xi_p$ , practically identical values of  $k_{ez}$  and  $k_{az}$  can be obtained from the formulas below.

The subsequent formulae relate to the tooth space of the internal gear so that the addendum modification is positive in the direction away from the center of the gear, as for external gears:

$$k_{ez} = 1 - \frac{\tan \phi_t}{\tan \phi_{o,t}} \quad (9.28)$$

$$k_{az} = \frac{2\cos \psi}{\sin^2 \phi_t} \cdot \frac{1 - \xi_p}{N_p} \quad (9.29)$$

The difference between the addendum modification coefficients of gear and pinion,  $(\xi_g - \xi_p)$ , is then calculated for an internal gear and pinion. The value,  $\xi_g$ , calculated should, if possible, be below the limits quoted below, so that excessive addendum shortening to avoid interference does not become necessary.

Practical, but not absolute limits, for  $\xi_g$  are  $\xi_p \leq \xi_g \leq 1$ .

If  $\xi_g$  does not fall within these limits, then the center distance of the basic data has to be changed.

The inequality  $\xi_p \leq \xi_g$  means that the working pressure angle does not become smaller than the generating pressure angle. The inequality  $\xi_g \leq 1$  means that the reference circle of the gear does not lie beyond the gear teeth.

The values of the profile shift factors,  $\xi_g$  and  $\xi_p$ , now enable the theoretical and still provisional dimensions of the internal gear and pinion to be determined. The subsequent checks for interference may necessitate corrections to these dimensions.

When the dimensions have been finalized, the sliding conditions should be checked as part of the systematic design procedure.

The slide/roll ratios,  $v_g/v_c$ , and the sliding velocities,  $v_g$ , are the criteria selected for the sliding conditions.

The rules quoted below form a part of the systematic design procedure, but are not of great functional significance, as the sliding conditions on internal gears and pinions are not critical:

$$\frac{v_{g1}}{v_{r1}} \leq \frac{v_{g2}}{v_{r2}} \quad (9.30)$$

and

$$v_{g2} \leq v_{g1} \quad (9.31)$$

Equations 9.17 through 9.31 are recommended [74] for use by practical gear engineers.

#### 9.4 Tooth Thickness Measurement in Internal Gears

For the calculation of tooth thickness of an internal gear, measurement between two pins or balls is used. Balls are used for measuring of both spur and helical gears, while pins are used for measuring spur gears only.

The required dimensions between two balls can be calculated in the following way.

The normal space width,  $w_n$ ; ball diameter,  $d_{ball}$ ; and transverse profile angle,  $\phi_m$ , to the center of the ball are used as the input parameters for the calculations. The normal space width is calculated from the equation:

$$w_n = p_n - t_n \quad (9.32)$$

The approximate ball diameter is equal to  $d_{ball} \cong 1.44/P$ . The calculated value of the diameter,  $d_{ball}$ , is then rounded to the nearest standard value.

The transverse profile angle,  $\phi_m$ , to the center of the ball can be calculated from the equation:

$$\text{inv } \phi_m = \text{inv } \phi_t - \frac{d_{ball} - w_n \cos \phi_n}{N_g \cos \phi_n} P_n \quad (9.33)$$

For gears with an even number of teeth, the dimension between two balls,  $D_{Mi}$ , can be expressed by:

$$D_{Mi} = \frac{d_{b.g}}{\cos \phi_m} - d_{ball} \quad (9.34)$$

For gears with odd number of teeth, the dimension between two balls ( $D_{Mi}$ ) can be expressed by:

$$D_{Mi} = \frac{d_{b.g} \cos(90^\circ / N_g)}{\cos \phi_m} - d_{ball} \quad (9.35)$$

Those same formulas are used for the measurements of a spur gear. The only difference is that the transverse profile angle,  $\phi_m$ , and the normal profile angle,  $\phi_n$ , in Equation 9.33, are equal to each other.

#### 9.5 Gear Coupling as a Reduced Case of an Internal Parallel-Axes Involute Gear Pair

When the tooth numbers of an internal gear and pinion are equal to each other, then the internal gear pair is transformed to a gear coupling.

The vector diagram for a gear coupling is depicted in [Figure 6.2e](#). The center distance for a gear coupling is zero ( $C = 0$ ). As the center distance in gear coupling is zero, the pitch radii,  $r_g$  and  $r_p$ , of a gear and a mating pinion also have zero values; that is,  $r_g = 0$  and  $r_p = 0$ . This means that any tooth profile can be used in the design of perfect gear coupling; in the design of gear coupling for joining shafts with zero linear and angular displacements of the shafts. However, the main purpose of gear couplings is to accommodate for axis displacement, as well as for axis misalignment in real mechanisms. Therefore, in cases when gear couplings are used, axis displacement, as well as axis misalignment, always has a nonzero value; thus, the center distance

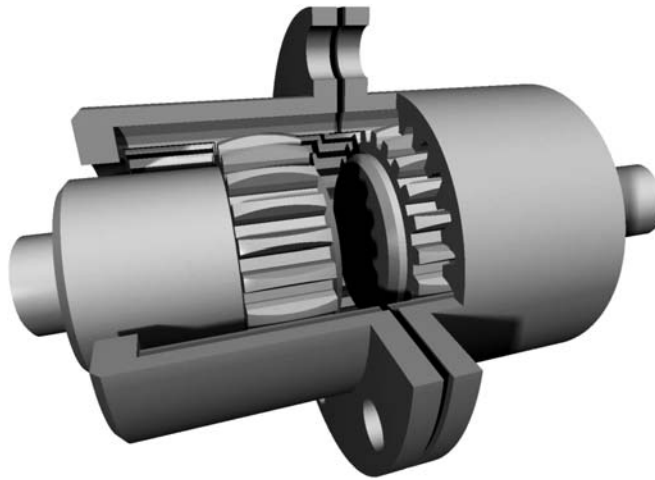


**FIGURE 9.8**  
Gear coupling.

for a gear coupling is not zero ( $C \neq 0$ ). With that said, gear couplings should be considered as a kind of crossed-axes gear pairs.

An example of gear coupling is shown in [Figure 9.8](#).

For the calculation of the design parameters of gear couplings, as well as of involute splines, many of the formulae discussed above can be used.



# Taylor & Francis

Taylor & Francis Group

<http://taylorandfrancis.com>



## High-Conformal Parallel-Axes Gearing

A problem of transmitting a rotation from a driving shaft to a driven shaft with the highest possible power density is a challenging problem that many industries have been faced with for a long while. A solution to such an engineering problem requires application of gear boxes of the smallest possible size that are capable of transmitting the highest possible power. Conformal gearings, especially high-conformal gearings, perfectly fit this requirement. To the best possible extent, both gear systems, that is, conformal and high-conformal gearing, are discussed in the monograph by the author [117]. Here, in this section, the essence of conformal and high-conformal gearings is discussed.

### 10.1 A Brief Overview on Conformal Gearing: State of the Art

Conformal and high-conformal gearings feature *convex-to-concave* contact between the tooth flanks of a gear and a mating pinion. This is true both for external gearings and internal gearings.

#### 10.1.1 The Origin of High-Conformal Gearing

The concept of convex-to-concave contact of the tooth flanks of a gear and a mating pinion can be traced back to the 15th century (1493), when a famous book by da Vinci was published [17]. Initially, long ago, increased contact strength of the gear teeth was the main aspect that initiated developments in the field of conformal gearing.

Conventional (involute) gearing features a *convex-to-convex* contact of the tooth flanks. In conformal gearing, the convex-to-convex contact of the tooth flanks is substituted with a convex-to-concave contact. Due to such a substitution, the contact strength of the gear teeth can be increased proportionally to the increase of the degree of conformity of the interacting gear tooth flanks. It is natural to assume that a decision for the replacement of a convex-to-convex contact with convex-to-concave contact of the gear teeth is based on an observation. For instance, all joints in a human skeleton feature a convex-to-concave contact of the bones, as illustrated in Figure 10.1. None of the bones make convex-to-convex contact.

The earliest design of a gearing with convex-to-concave tooth contact known to the author is discussed in a famous book by da Vinci [17]. The addendum of the gear teeth features convex geometry, while the dedendum is concave [117]. In the pinion, the addendum features a convex tooth profile, and dedendum is also concave. There are a few more illustrations of gearings with convex-to-concave contact of the tooth flanks.

It is not discussed in [17] whether the gearing is spur or helical. However, the gearing is supposed to be a spur gearing, as the invention of helical gearing is credited to *Robert Hooke\**.

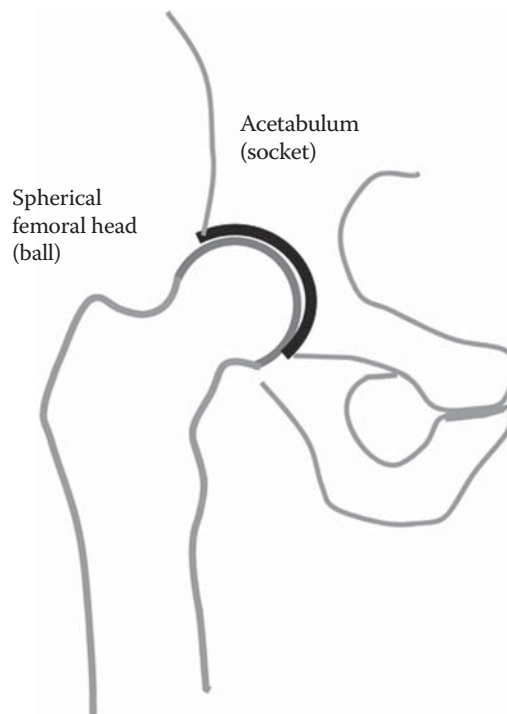
Because of very limited information on the design of the gearing [117], it is almost impossible to accurately evaluate the advantages and disadvantages of this particular ancient design of conformal gearing.

The *Bramley-Moore gearing* (otherwise known as the *Vickers, Bostock, and Bramley gearing*, or just *VBB-gearing*), is another well-known example of gearing with convex-to-concave contact of the gear teeth undertaken in the invention [10].

Toothed gearing proposed by H.J. Schmick [145] relates to the shape and arrangement of the working faces of intermeshing teeth for spur gears for connecting rotating or oscillating bodies.

Helical gearing with a circular arc tooth profile was invented by Wildhaber [161] in the early 1920s. The invention targets an improved power capacity of the gear pair. This gear system is commonly referred to as *Wildhaber gearing*. Wildhaber gearing is a type of approximate gearing, as it is not capable of transmitting a uniform rotation.

\* Robert Hooke (July 28 [O.S. July 18], 1635–March 3, 1703) was an English natural philosopher, architect, and polymath.

**FIGURE 10.1**

*Convex-to-concave* contact of the bones in a human skeleton.

As early as 1956, Novikov proposed conformal helical gearing [85] that later got the name *Novikov gearing*\*. Novikov gearing is a type of perfect gearing, as it is capable of transmitting a uniform rotation.

Novikov gearing and Wildhaber gearing are the most widely known examples of gearing with convex-to-concave contact of the tooth flanks. In Appendix H, the author's comments on the concept of Novikov gearing and on inadequacy of the terms *Wildhaber-Novikov gearing* and *W-N gearing* are presented.

An in-depth analysis of the research carried out and available in the public domain on the *Novikov gear system* is performed by the author. The results of the performed analysis can be found in [117]. The performed research reveals that gear experts all around the globe (including but not limited to Russia, the United States, and China, as well as of the rest of the world) demonstrate no in-depth understanding of the kinematics or geometry of Novikov (conformal) gearing. As a consequence, the kinematics and geometry of *high-conformal gearing* (or just  $H_c$ -gearing, for simplicity) are also not understood properly. It is nonsense that a gear system (Novikov gear system) that was proposed over half a century ago (in the early 1950s) is still not understood by the gear community all around the world. (The Novikov gear system, and especially the proposed later high-conformal gearing [~2008] are both unique gear systems with great potential for the industry.)

Not all gear systems that feature convex-to-concave contact of the tooth flanks are capable of transmitting a rotation smoothly. It is critical to stress from the very beginning that only conformal Novikov gearing is capable of transmitting a rotation smoothly. Gearings of all other types are not capable of transmitting a uniform rotation, as they are approximate gearings.

High-conformal gearing was proposed by Radzevich in around 2010 [137].

### 10.1.2 Power Density in High-Conformal Gearing

It became clear later that use of conformal gear pairs helps to increase the so-called *power density* being transmitted by the gear pair; that is, conformal gearing is capable of transmitting a higher power through a smaller volume occupied by the gear pair.

\* The Novikov gear system is named after Novikov, Dr. Eng. Sc., who was head of a department at the Zhoukovskii Military Aero Academy in Moscow. He developed this particular gear system, but after his death in 1958, it was his colleagues who published his work [83] under his name.

Power density\* is an important consideration in gearing of many designs and applications. The higher the power density of a gear pair, the lighter the gear transmission, and vice versa. A helicopter transmission is a good example of gearing where the highest possible power density is strongly desirable. However, the aerospace industry is not the only industry that needs application of small-size and high-capacity gear transmissions. A gearbox for electric wind power stations is also a good example of this specific type of gearing. Gas consumption of trucks, cars, tractors, and other vehicles strongly depends on the weight of the vehicle; that is, the lighter the vehicle, the less gas consumption, and vice versa. Therefore, use of lighter gearboxes in the automotive industry is also desirable. More examples of the desirable application of lighter gearboxes with higher performance can be found in many industries. *High-power-density gearing*<sup>†</sup> (HPD-gearing for simplicity) is the global target for the future developments in the field of gearing.

The main goal for the development of *conformal* gearing and later high-conformal gearing ( $H_c$ -gearing for simplicity) is to increase the power density transmitted through a gear pair.

Two different ways to increase the power density through a gear pair are recognized.

First, the power density through a gear pair can be increased by means of an increased rotation of the driving member (the pinion). Under such a scenario, the torque applied to the driving member remains the same.

Second, the power density through a gear pair can be increased by means of an increased torque applied to the driving member (the pinion). The rotation of the driving member remains the same under such a scenario.

A combination of the first and the second approaches is possible as well.

Conformal gearing features convex-to-concave contact of the tooth flanks of the gear and the mating pinion. This particular type of contact of the tooth flanks enables an increase in contact strength of the gear and the pinion teeth. It is known that concave-to-convex contact of machine elements is always stronger compared to concave-to-convex contact. Because of this, numerous attempts were undertaken in the past to design gears with convex-to-concave contact of the tooth flanks of the gear and the mating pinion.

In most applications, especially when the input,  $\omega_{in}$ , and the output,  $\omega_{out}$ , rotations are high, use of gearings with a constant angular velocity ratio,<sup>‡</sup>  $u_\omega = \omega_{in}/\omega_{out} = \text{Const}$ , is preferred. Gearings with a constant angular velocity ratio are commonly referred to as *perfect gearings*. Other gearings, whose angular velocity ratio is not constant (that is,  $u_\omega = \text{var}$ , and  $u = \text{Const}$ ), are not capable of transmitting a rotation smoothly. Gearings of this type are referred to as *approximate gearings*. Considered below in this chapter, conformal gearing is capable of transmitting a uniform rotation. Therefore, conformal gearing is a type of perfect gearing. This means that conformal gearing meets the following three requirements:

1. Condition of contact of tooth flanks of a gear,  $\mathcal{G}$ , and a mating pinion,  $\mathcal{P}$ , is fulfilled. It is common practice to specify the condition of contact of two smooth regular surfaces by means of Shishkov's equation of contact,<sup>§</sup>  $\mathbf{n} \cdot \mathbf{V}_\Sigma = 0$ , where  $\mathbf{n}$  designates the unit normal vector of a common perpendicular through point of contact,  $K$ , of the tooth flanks  $\mathcal{G}$  and  $\mathcal{P}$  (this vector is along the line of action,  $LA$ , of the gear pair), and  $\mathbf{V}_\Sigma$  designates vector of the resultant relative motion of the tooth flanks,  $\mathcal{G}$  and  $\mathcal{P}$ , at  $K$  [137].
2. At every instant of time, the line of action,  $LA$ , passes through a point within the instant axis of rotation,  $P_{in}$ , of the pinion relative to the gear (or of the gear relative to the pinion). In cases of parallel-axes gearing, this requirement is specified by *Camus-Euler-Savary theorem*.
3. At every instant of time, the base pitch of a gear is equal to an operating base pitch of the gear pair, and the base pitch of a mating pinion is also equal to the operating base pitch of the gear pair; that is, both of the base pitches (of the gear and of the pinion) are equal to the operating base pitch of the gear pair [137].

\* Here and below, the power density is understood as the ratio of the power being transmitted through a gear pair to the volume occupied by the gear pair.

<sup>†</sup> It is instructive to note here that the broader application of high-power-density gearing in the future will result in the broader use of gears with a low tooth count (*LTC*-gearing, in other words), that is, of gears whose base diameter,  $d_b$ , is equal to or greater than the root diameter,  $d_f$ , and for which the inequality  $d_b \geq d_f$  is observed. Commonly, *LTC*-gears are viewed in a more narrow sense; that is, *LTC*-gears are gears whose tooth count is equal to  $N_g = 12$  or less.

<sup>‡</sup> The difference between the *angular velocity ratio*,  $u_\omega$ , and the *gear ratio*,  $u$ , should be stressed here. The angular velocity ratio is specified as  $u_\omega = \omega_{in}/\omega_{out}$ . The angular velocity ratio has a constant value for perfect gear pairs and is variable for approximate gear pairs. The gear ratio is specified in terms of tooth count of the input,  $N_{in}$ , and the output,  $N_{out}$ , members of the gear pair  $u = N_{in}/N_{out}$ . The gear ratio is always of a constant value, for perfect as well as approximate gearings (except noncircular gearings).

<sup>§</sup> This equation was proposed by Shishkov as early as 1948 (or even earlier) in his paper: Shishkov, V.A., "Elements of Kinematics of Generating and Conjugating in Gearing," in: *Theory and Calculation of Gears*, Vol. 6, Leningrad: Lontomash, 1948. In more detail, this equation is also discussed in the monograph: Shishkov, V.A., *Generation of Surfaces in Continuous-Indexing Methods of Surface Machining*, Moscow, Mashgiz, 1951, 152 pages.

Per the author's opinion, the efforts undertaken in the past to develop conformal gearing need to be discussed in more detail in order to properly evaluate the results obtained in the field so far and to separate the potentially useful achievements of the research in the field from those that are either useless or mistakes. Many ambiguities are observed in interpreting conformal gearing just because of misunderstanding of the kinematics and geometry of this particular type of gearing.

## 10.2 Conformal Gearing

The three fundamental conditions that all perfect gearings need to comply with, discussed in the previous section of the monograph, along with the consideration of the contact ratio in a gear pair (that is, that the total contact ratio,  $m_t$ , always has to be greater than one,  $m_t \geq 1$ ) allow us to proceed with the analysis of the concept of *conformal gearing* (or *C-gearing* for simplicity). Novikov gearing (or *N-gearing* for simplicity) is a perfect example of conformal gearing. Then, the concept of conformal gearing can be evolved to the concept of *high-conformal gearing* (*H<sub>c</sub>-gearing* for simplicity).

It should be noted from the very beginning that conformal gearing, as well as high-conformal gearing, is a reduced case of involute gearing. Because of this, both conformal gearing (that is, Novikov gearing) and *H<sub>c</sub>-gearing* meet the conditions listed in items one through three in the previous section of the book, and both types of gearing feature a total contact ratio greater than one ( $m_t \geq 1$ ).

### 10.2.1 Novikov Gearing: Helical Involute Gearing with Zero Transverse Contact Ratio

Conformal gearing, and Novikov gearing in particular, can be construed as a reduced case of involute gearing that features a zero length,  $Z_{pa}$ , of the path of contact,\*  $P_c$  (that is, in conformal gearing, the equality,  $Z_{pa} = 0$ , is valid). Zero length of the path of contact entails a zero length of the involute profile. Ultimately, only one point of the involute tooth profile remains.† This point is referred to as the *involute tooth point*.

It is customary to associate Novikov gearing\* with the patent *Gear Pairs and Cam Mechanisms Having Point System of Meshing* [85]. Evidence can be found in scientific literature that reveals the unfamiliarity of the gear community around the world with this original publication [85] on Novikov gearing (see Appendix A for details).

### 10.2.2 Essence of Novikov Gearing

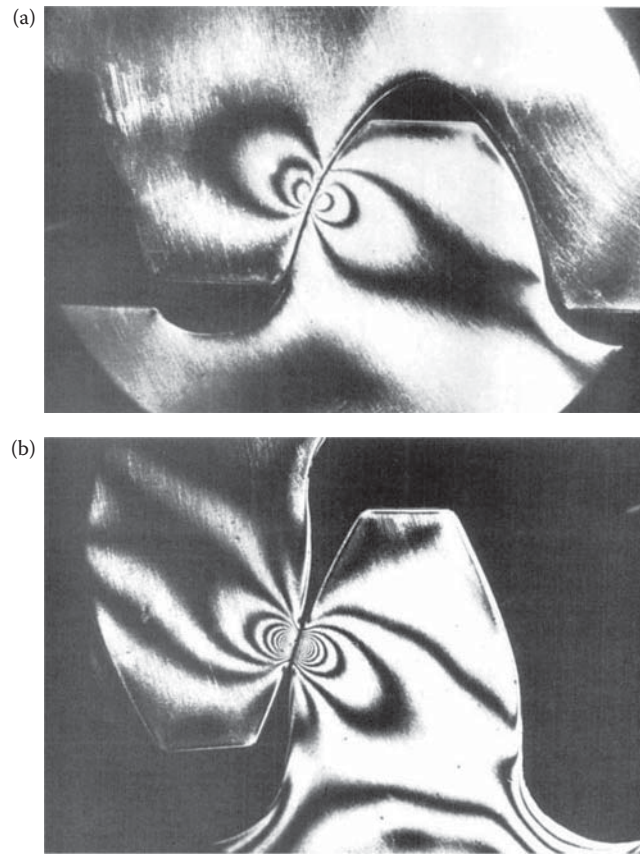
Novikov gearing was developed with the intent to increase the contact strength of the gear teeth. Gearing of this type features higher contact strength due to the favorable curvatures of the interacting tooth flanks. Under equivalent contact stress, similar dimensions, comparable values of the rest of the remaining design parameters, and greater circular forces are permitted by the proposed gearing. (The discussion in this section closely follows that by Novikov [85]). Another factor that contributes to the high load capacity of conformal gears is that they sustain a thicker film of lubricant owing to the rapid rolling of the areas of contact along the helix, which provides vigorous hydrodynamic action.

The shape of the gear teeth designed to transmit power is traditionally based on the involute curve, and all gear tooth profiles in the past have been convex. However, if the mating teeth are *conformal*; that is, one of them

\* In Novikov gearing, the transverse contact ratio,  $m_t$ , has a zero value ( $m_t = 0$ ). Thus, the contact point,  $K$ , in a transverse plane section is motionless, and the path of contact,  $P_c$ , is of a zero length ( $L_{pc} = 0$ ). In *Wildhaber gearing*, the transverse contact ratio cannot be specified. This is because of the following. First, the transverse contact ratio in a parallel-axes gear pair is defined as the ratio  $m_t = Z_{pa}/p_b$ . Second, no base pitch,  $p_b$ , can be specified in Wildhaber gearing. In a transverse plane section of a Wildhaber gear pair, the contact point,  $K$ , travels, and in this way, it traces the path of contact,  $P_c$  (that is,  $L_{pc} \neq 0$ ).

† When Novikov carried out his research in the field of conformal gearing, he loosely assumed that in order to transmit a uniform rotational motion, the gear teeth do not need to have special shapes, such as the involute of a circle. He meant that if a gear is made helical, then the helix itself can ensure uniform angular motion, and tooth profiles can then be chosen with a view to minimizing contact stresses. This is incorrect: in order to transmit a rotation smoothly, the mating tooth profiles must be either involute or, in a degenerate case, they can feature the involute tooth point geometry.

‡ The first pair of Novikov gearing made of aluminum alloy (a preprototype) was cut on April 25, 1954, by a disk-type mill cutter. For testing, 15 gear pairs were machined in the summer of 1954 by a disk-type mill cutter. Hobs for cutting gears for Novikov gearing were proposed later on by Kudryavtsev (as early as 1956).

**FIGURE 10.2**

Comparison of distribution of contact stress: (a) *Novikov gearing*, and (b) *an equivalent involute gearing*.

is convex and the other one concave, stress for a given load can be reduced. Alternatively, a heavier load can be carried for the same amount of stress. The point is made clear by the photographs of photoelastic models shown in Figure 10.2.

Possible geometries of tooth profiles of Novikov gearing are schematically shown in Figure 10.3. In this figure, a section of the tooth flank intersected by a plane perpendicular to the instant axis of relative rotation is shown. The axis passes through the current point of contact of the tooth flanks.

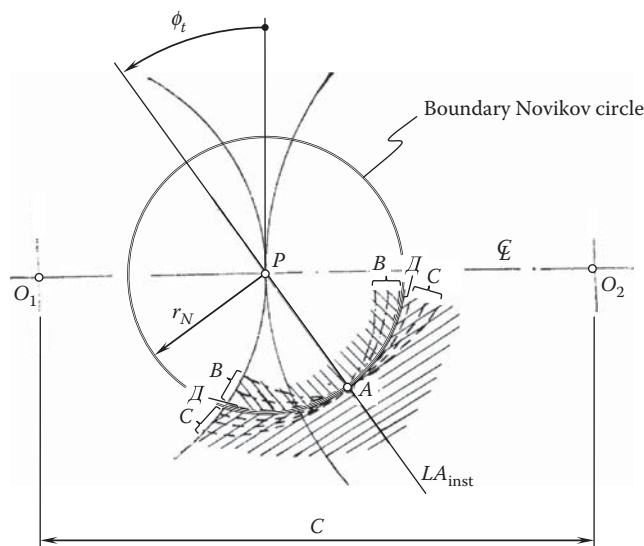
In Figure 10.3, the point of intersection of the planar section by the axis of instant relative rotation is denoted by  $P$ . The points of intersection of the planar section by the axes of the gear and the pinion are designated as  $O_1$  and  $O_2$ . A point,  $A$ , is the point of meshing (in its current location). The line of action is denoted by  $PA$ . Ultimately,  $\mathcal{D}A\mathcal{D}$  (the notations in Figure 10.3 are mostly due to Novikov) is the circle\* centering at the pitch point,  $P$ . The circle corresponds with the limiting case of the tooth profiles (in the case that the profiles are aligned to each other).

Multiple curves denoted by  $BAB$  illustrate examples of possible tooth profiles of one of the mating gears. All the curves denoted by  $BAB$  are arbitrary smooth regular curves, which are located inside the limiting circular arc,  $\mathcal{D}A\mathcal{D}$  (that is, all the arcs,  $BAB$ , are situated within the body side of the limiting tooth flank of one of the gears). All the tooth profiles,  $BAB$ , feature a high degree of conformity to the limiting circular arc,  $\mathcal{D}A\mathcal{D}$ .

Multiple curves denoted by  $CAC$  illustrate examples of possible tooth profiles of the second mating gears. All the curves denoted by  $CAC$  are arbitrary smooth regular curves, which are located outside of the limiting circular arc,  $\mathcal{D}A\mathcal{D}$  (that is, all the arcs denoted by  $CAC$  are located within the body side of the limiting tooth flank of the second of two gears). All the curves,  $CAC$ , feature a high degree of conformity to the circular arc,  $\mathcal{D}A\mathcal{D}$ .

\* The circle of a radius,  $r_N$ , centered at the pitch point,  $P$ , was introduced in recent years by Radzevich [137]. He proposed to refer to this circle as to the *boundary Novikov circle*, or just the *boundary N-circle* in honor of Novikov, the inventor of Novikov gearing. The term *boundary N-circle* was not used by Novikov.



**FIGURE 10.3**

Concept of *Novikov gearing*. (After Professor M.L. Novikov; USSR Pat. No. 109,113, [85]; the boundary *Novikov* circle of a radius,  $r_N$ , was introduced later on by Professor S.P. Radzevich.)

The location and orientation of either the straight path of contact or a smooth curved path of contact is specified in a space in which the location and orientation of the axes of rotations of the gear and the pinion are given. The path of contact is located reasonably close to the axis of instant relative rotation of the gears. Either constant or time-dependent (smoothly varying in time) speed of motion of the point of contact along the path of contact is assigned. A coordinate system is associated with the gear, and a corresponding coordinate system is associated with the pinion. In each of the coordinate systems, the moving contact point traces contact lines. One of the lines is associated with the gear and another is associated with the pinion. Certain smooth regular surfaces through these lines can be used as tooth flanks of the gear and the pinion. The following requirements should be fulfilled so that surfaces can be used as the tooth flanks of Novikov gearing:

- At every location of the point of contact, the tooth flanks should have a common perpendicular through the pitch point,  $P$ ; thus, the requirements of conjugacy of meshing should be satisfied.
- The curvatures of the tooth profiles should correspond to each other.
- No tooth flank interference is allowed within the working portions of the surfaces.

If two surfaces are generated by one of the moving curves,  $BAB$ , and one of the moving curves,  $CAC$ , then the aforementioned requirements are fulfilled and the surfaces can be employed as tooth flanks for Novikov gearing.

Consider a plane through the current contact point, which is perpendicular to the instant axis of relative rotation. Construct two circular arcs centered at points within the straight line through the pitch point and the contact point. The arc centers are located within the line of action and close to the pitch point. The constructed circular arcs can be considered examples of the tooth profiles of the gear and the pinion. The tooth flanks are generated as the loci of tooth profiles constructed for all possible locations of the contact point. The working portion of one of the two tooth flanks is convex, whereas that of another tooth flank is concave (in the direction toward the axis of instant relative rotation). In a particular case, the radii of the tooth profiles can be of the same magnitude and equal to the distance from the contact point to the axis of instant relative rotation. The centers of both profiles in this particular case are situated at the axis of instant relative rotation. Under such a scenario, the point contact is substituted by a special type of *line contact*.<sup>\*</sup> This requires the center distance to be extremely accurate and independent of the conditions of operating of the gear pair, which is impractical. Point contact of

<sup>\*</sup> In the current practice, this type of contact of the tooth flanks of a gear and a mating pinion is referred to as *local line contact* of the tooth flanks,  $\mathcal{G}$  and  $\mathcal{P}$ .

the tooth flanks is preferred when designing tooth profiles. A small difference between the radii of curvature of the tooth profiles is desirable. It should be borne in mind that during the run-in period of time, point contact of gear teeth transforms to the aforementioned line contact of tooth profiles. However, the theoretical point contact of tooth flanks is retained.

Generally speaking, it is not mandatory that tooth profiles have circular arc shapes. Tooth profiles of another geometries (those always passing through the contact point) should be situated (for one gear) within the interior of the above aforementioned circular arc profile,  $\mathcal{AA}\mathcal{A}$ , which centers at a point within the axis of instant relative rotation, as shown in Figure 10.3. For another (mating) gear, the tooth profile should be located outside the circular arc,  $\mathcal{AA}\mathcal{A}$ . Under all circumstances, the centers of curvature of both convex and concave tooth profiles are located within the instant line of action,  $LA_{\text{inst}}$ .

The law of motion of the contact point (that is, speed of the point and its trajectory) should be chosen so as to minimize losses caused by friction and wear. Friction and wear losses are proportional to the relative sliding velocity in the gear mesh. Therefore, it is desirable to reduce the sliding velocity as much as possible. For this purpose, the path of contact should not be too far from the axis of instant relative rotation. On the other hand, it is also not desirable that the path of contact be too close to the axis of instant relative rotation, as this reduces contact strength of the gear tooth flanks. In addition, it is recommended to ensure favorable angles between the common perpendicular (along which the tooth flanks of one of the gears act against the tooth flanks of the other gear) and the axes of rotations of the gears.

Opposite sides of tooth profiles are designed in a manner similar to that just discussed. Tooth thicknesses and tooth pitch are assigned so as to ensure the required bending strength of the teeth.

The face width of the gear or length of the gear teeth should correlate with their pitch so as to ensure the required value of the face contact ratio,  $m_F$ . Gear pairs can feature either one point of contact (when working portions of the tooth flank contact each other at just one point, excluding the phases of teeth reengagement) or multiple contact points (when tooth flanks contact each other at several points simultaneously).

As the transverse contact ratio in conformal, as well as in high-conformal, gearing is zero (that is,  $m_p = 0$ ), a gear pair with a variable transverse profile angle,  $\phi_t = \text{var}$ , within the face width is feasible.

For parallel-axes gear pairs, it is preferable to use a straight line as the path of contact.\* The straight line is parallel to the axes of rotations of the gear and the pinion. The speed of the contact point as it moves along the straight path of contact can be constant. In this particular case, the radii of curvature of the tooth profiles in all sections of the tooth flank by planes are equal. The tooth flanks in this case are regular screw surfaces. Gears featuring tooth flanks of such geometry are easier to manufacture, and they can be cut on machine tools available on the market.

An example of parallel axis gearing with a limiting geometry of tooth profiles is illustrated in Figure 10.3. The point contact of the tooth flanks in this particular case is transformed to the line contact. The curved contact line is situated across the tooth profile. When axial thrust in the gear pair is strongly undesired, herringbone gears can be used instead.

The essence of Novikov gearing outlined above is expressed in terms used by Novikov. A more detailed explanation of the early concept of Novikov gearing can be found in the book by Krasnoschokov et al. [60].

Tooth profiles contact each other only at an instant of time when the tooth profiles of both the gear,  $\mathcal{G}$ , and the pinion,  $\mathcal{P}$ , intersect the line of action,  $LA_{\text{inst}}$ , in a common transverse section. At all times before and after this instant, the tooth profiles,  $\mathcal{G}$  and  $\mathcal{P}$ , do not interact with one another† (Figure 10.4). Because of this, there is no need to design the rest of the tooth profiles of the gear and a mating pinion conjugate to one another—this gives the gear designer lots of freedom when designing the gear teeth geometry. With that said, the tooth profiles can be designed so as to ensure a maximum contact strength of the interacting tooth flanks,  $\mathcal{G}$  and  $\mathcal{P}$ .

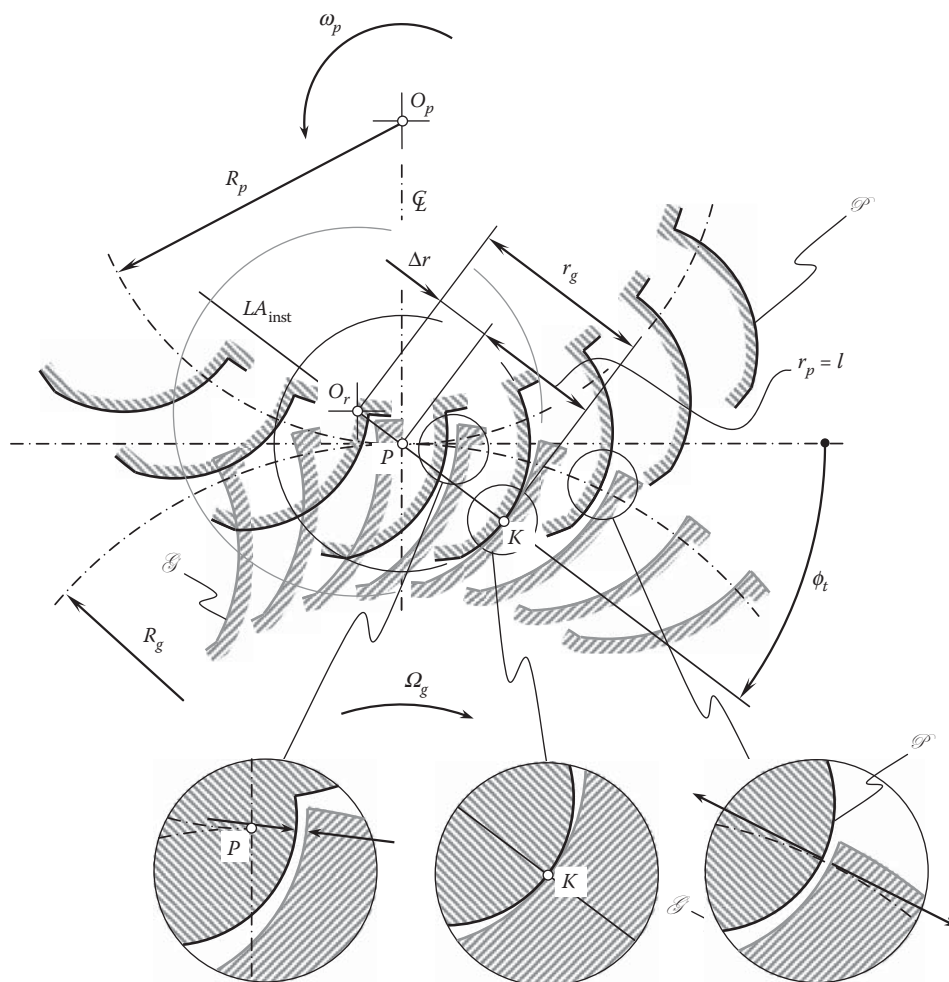
In order to ensure continuous contact between the tooth flanks,  $\mathcal{G}$  and  $\mathcal{P}$ , the teeth of the gear and the pinion are of a helical shape. The path of contact can be located either before or beyond the pitch point,  $P$ . Novikov gears of the first type are commonly referred to as  $N_{\text{by}}$ -gears, whereas those of the second type are referred to as  $N_{\text{bf}}$ -gears.

The discussed method for generating tooth surfaces was proposed by Novikov and is based on the trajectories of the points of contact between the tooth flanks. Novikov used to refer to these trajectories as to the *contact lines*.

\* In the current practice, this straight line is referred to as *pseudo-path of contact*,  $P_{\text{pc}}$ . The path of contact,  $P_c$ , in Novikov gearing is a zero-length straight-line segment of the instant line of action,  $LA_{\text{inst}}$ , at the vicinity of the contact point,  $K$ . When the gears rotate, an infinite number of the instant lines of action,  $LA_{\text{inst}}$ , create an illusion that the contact point,  $K$ , travels along the pseudo-path of contact,  $P_{\text{pc}}$ . Actually, an infinite number of contact points,  $K$ , travel along the corresponding path of contact,  $P_c$ , covering a zero distance in this motion.

† Owing to this, M.J. French proposed [36] referring to this point as *culmination*.





The method for generating tooth flanks proposed by Novikov can be referred to as the *contact lines method*. This method is obsolete and is not used in the current practice of gear design. The point of contact,  $K$ , of the tooth flanks,  $\mathcal{G}$  and  $\mathcal{P}$ , is often referred to as the *point of culmination*.

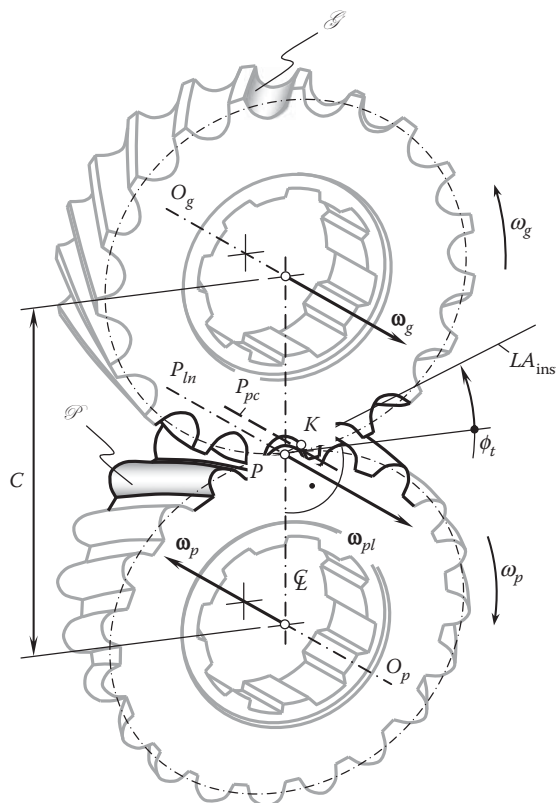
In Novikov gearing, both the pinion and gear are helical. The helices are of opposite hands; that is, one of them is right handed, and the other is left handed. No-spur Novikov gearing is feasible in nature. Because the gears are helical and of opposite hands, the point of contact travels axially along the gears while remaining at the same radial position on both gear and pinion teeth,  $\mathcal{G}$  and  $\mathcal{P}$ . It is therefore fundamental to the operation of the gears that contact occur nominally at a point and the point of contact travel axially across the full face width of the gears during a rotation. It should be stated as a condition of operation of Novikov gearing that for a given profile, tooth surfaces should not interfere before or after culmination when rotated at angular speeds that are in the gear ratio.

The transverse contact ratio,  $m_p$ , of a Novikov gear pair is zero, ( $m_p \equiv 0$ ). The face contact ratio,  $m_F$ , of the gear pair is equal to the total contact ratio ( $m_F = m_t$ ) and is always greater than one, ( $m_F > 1$ ).

In the transverse section of the gear pair, the contact point,  $K$ , is motionless. For parallel-axes configuration, the path of contact,  $P_c$ , is a straight line\* through the contact point,  $K$ . The path of contact,  $P_c$ , is parallel to the axes,  $O_g$  and  $O_p$ , as illustrated in Figure 10.5.

When rotation is transmitted from a driving shaft to a driven shaft, the contact point,  $K$ , travels along the path of contact,  $P_c$  (and it does not travel within the transverse cross section of the gear pair), that is, parallel to the

\* In the current practice, this type of contact of the tooth flanks of a gear and a mating pinion is referred to as *local line contact* of the tooth flanks,  $\mathcal{G}$  and  $\mathcal{P}$ .



axes of rotation,  $O_g$  and  $O_p$ , of the gear and the pinion, accordingly.\* This is because the transverse contact ratio is zero ( $m_p \equiv 0$ ) and the face contact ratio is greater than one ( $m_F > 1$ ), as mentioned earlier in this section.†

The discussed concept of path of contact,  $P_c$ , and of the pseudo-path of contact,  $P_{pc}$ , are also valid with respect to parallel-axes, as well as crossed-axes gearings (see Sections 12.8 and 14.8, correspondingly).

Many gear engineers around the world loosely refer to Novikov gearing as to Wildhaber-Novikov gearing or simply W-N gearing, which is incorrect. *Helical gearing* in accordance with the patent by Wildhaber [161] should be referred to as Wildhaber gearing. *Gearing with Point System of Meshing*, by Novikov [82,83,85] has to be referred to as Novikov gearing. Finally, the terms Wildhaber-Novikov gearing and W-N gearing must be recognized as meaningless terms; both need to be eliminated from the engineering literature. The comparison of Wildhaber gearing and Novikov gearing (see Appendix H for details) makes it possible to realize that the conclusion made by N. Chironis: “Novikov-type gears are similar to those developed by E. Wildhaber in the early 1920s” [14] is incorrect; further, Wildhaber’s statement, “all the characteristics of the Novikov gearing are anticipated by my patent. My gearing never had a real test here, although a pair of gears was made in the 1920s,” as quoted in the work by Chironis [14], is also incorrect. Not all the characteristics of Novikov gearing are known from Wildhaber’s patent [161].

With great respect to the personality and accomplishments of Wildhaber, as well as to most of his contributions, let us assume that Wildhaber had correctly understood the benefits of his invention, helical gearing [161] (1926). Then, being a smart gear expert, why did he not promote the invention to a practical application? Did he have no opportunities to do so? Definitely, he had! According to the author's personal opinion, the gear pair that was manufactured (as Wildhaber mentioned) never worked. The reason for this is clear to us now. Where was Wildhaber for about 30 years, from 1926 to 1956? Why did he wait for the Novikov invention?

It is likely that the unfamiliarity of the gear engineers in Western Europe and the United States with the original publications by Novikov [82,83,85] is the main reason for the incorrect reference to Novikov gearing as Wildhaber-Novikov gearing or W-N gearing. Much evidence to this end can be found in the literature on Novikov gearing; for example, Dyson et al. [27] referred to S.U. Pat. No. 109,750 as the patent on Novikov gearing. In reality, S.U. Pat. No. 109,750 is issued on a *water sprayer* (?), and not on Novikov gearing. The interested reader may wish to investigate this matter on his or her own.



In Equations 10.3 and 10.4, the base diameters,  $d_{b,g}$  and  $d_{b,p}$ , are expressed in terms of the transverse pressure angle,  $\phi_t$ . In parallel-axes Novikov gearing, the transverse pressure angle,  $\phi_t$ , is identical to that in involute parallel-axes gearing.

Because conformal gears feature zero width of the field of action ( $Z_{pa} = 0$ ), the length of the line of contact of their tooth flanks shrinks to zero (that is,  $LC = 0$ ). Although the length of the line of contact is zero, the direction of the line of contact remains the same. Within the plane of action, the line of contact forms a base helix angle,  $\psi_b$ , with the axis of instant rotation,  $P_{ln}$ , of the gear and the pinion.

The base pitch helix angle,  $\psi_b$ , can be calculated from the following formula:

$$\psi_b = \tan^{-1}(\tan \psi \cos \phi_t) \quad (10.5)$$

In Equation 10.5, the pitch helix angle is denoted by  $\psi$ .

The base pitch,  $p_b$ , in the case under consideration is given by:

$$p_b = p_x \sin \psi_b \quad (10.6)$$

where  $p_x$  is the axial pitch of the teeth in conformal gearing.

Finally, the operating base pitch,  $p_{b,op}$ , in conformal gearing can be calculated from the following formula:

$$p_{b,op} = p_x \tan \psi_b \quad (10.7)$$

The similarities between Equation 10.1 through 10.7 and the corresponding set of equations for parallel-axes involute gearing reveal that both gear systems originate from a common concept.

## 10.4 Transition from Involute Gearing to Conformal Parallel-Axes Gearing (to Novikov Gearing)

In parallel-axes perfect involute gearing, the tooth flank of the gear,  $\mathcal{G}$ , and the tooth flank of the pinion,  $\mathcal{P}$ , make contact along the line of contact,  $LC$ . The line of contact is a planar curve of a reasonable geometry that is entirely located within the plane of action,  $PA$ . This could be either a straight line parallel to the axes of rotation of the gear and the pinion, as in spur involute gearing, or a straight line at the base helix angle,  $\psi_b$ , to the axes,  $O_g$  and  $O_p$ , as in helical involute gearing. It also can be a circular arc, an arc of a spiral curve, or a curve of other reasonable geometry. The tooth flanks,  $\mathcal{G}$  and  $\mathcal{P}$ , of the gear and pinion interact with each other only within the active portion of the plane of action. For illustrative purposes, an example of the active portion of the plane of action is depicted in Figure 10.7.

When the gears rotate, contact point  $K$  travels in a transverse section of the gear pair with a linear velocity  $V_K$ .

Referring to Figure 10.7a,  $N_g N_p$  is the total length of the plane of action. In reality, the active portion of the plane of action,  $PA$ , is of a smaller length,  $Z_{pa}$  (Figure 10.7b). This is the length of the straight-line segment,  $P_g P_p$ . Points  $P_g$  and  $P_p$  are the points of intersection of the straight line,  $N_g N_p$ , by the outer circle of the pinion of a radius,  $r_{o,p}$ , and by the outer circle of the gear of a radius,  $r_{o,g}$ , correspondingly. Ultimately, the active portion of the plane of action is a rectangle of  $Z_{pa} \times F_{pa}$ .

In involute helical parallel-axes gearing, the desirable line of contact,  $LC$ , between the tooth flank of a gear,  $\mathcal{G}$ , and a mating pinion,  $\mathcal{P}$  (remember that the tooth flanks,  $\mathcal{G}$  and  $\mathcal{P}$ , are not constructed yet), is a straight-line segment that forms a base helix angle,  $\psi_b$ , with the axis of instant rotation,  $P_{ln}$  (the desirable lines of contact of other geometries are not discussed here).

When the base cylinders of diameters  $d_{b,g}$  and  $d_{b,p}$  rotate, the desirable line of contact,  $LC$ , travels (together with the plane of action,  $PA$ ) in relation to two reference systems. One of the reference systems is associated with the gear, and another is associated with the pinion. In such a motion, the tooth flank of the gear,  $\mathcal{G}$  (as well as the tooth flank of the pinion,  $\mathcal{P}$ ), can be construed as a family of consecutive positions of the desirable line of contact that travels in the corresponding reference system.

In the example illustrated in Figure 10.7b, the active portion,  $ab$ , of the involute tooth profile is specified by the radii of the outer cylinders of the gear and of the pinion,  $r_{o,g}$  and  $r_{o,p}$ , correspondingly. Point  $a$  corresponds to the *start-of-active-profile* point (SAP-point), while point  $b$  corresponds to the *end-of-active-profile* point (EAP-point).

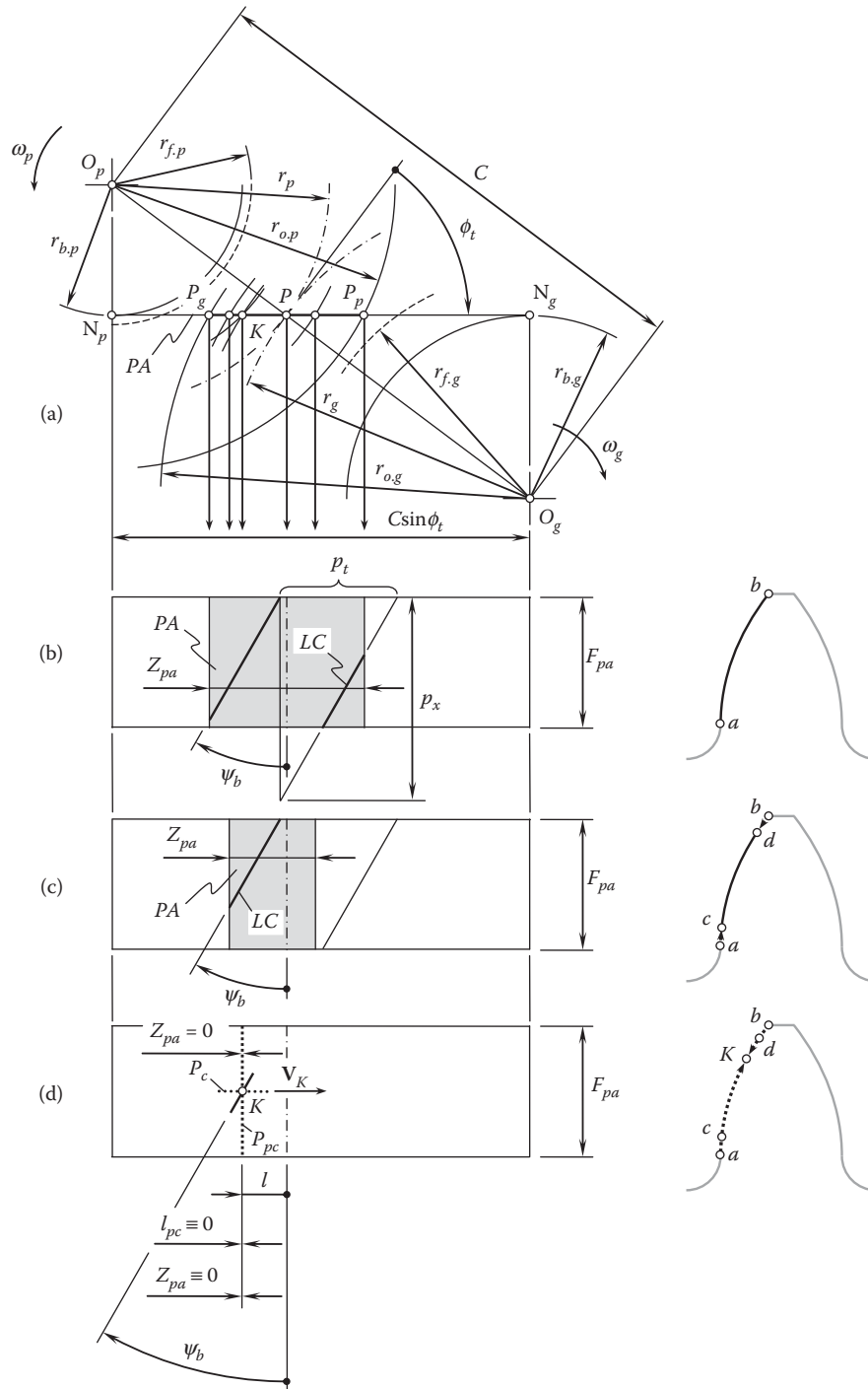


FIGURE 10.7

Elements of a parallel-axes gear pair that features a zero transverse contact ratio ( $m_p = 0$ ).

For both members of a gear pair, that is, for the gear and the pinion, the radius,  $r_{EAP}$ , of the EAP-circle (that is, the end-of-active-profile circle) can be smaller than the outer radius of the gear,  $r_{o,g}$  (or the outer radius of the pinion,  $r_{o,p}$ ), for example, because of chamfering. Under such a scenario (illustrated in Figure 10.7c; the radii,  $r_{EAP}$ , for the gear and the pinion are not labeled there), the active portion of the plane of action gets narrower. The SAP-point,  $c$ , and the EAP-point,  $d$ , become closer to one another: The active portion,  $cd$ , of the involute tooth profile is shorter than that,  $ab$ , in the case illustrated in Figure 10.7b. The remaining portions of the gear teeth profiles are not active and do not come in contact with each other when the gears rotate. Therefore,

the gear designer is free to modify the inactive portions of the gear teeth,  $ac$  and  $bd$ , making them stronger in terms of contact strength.

This gives a certain freedom when selecting the geometry of the nonactive portions,  $ac$  and  $bd$ , of the tooth profile. As these portions of the tooth profile do not interact with one another, the geometry of the segments,  $ac$  and  $bd$ , is not restricted by the conditions of meshing of the tooth profiles (which is a must for the active portion  $cd$ ). All three conditions for perfect gearing, along with the requirement  $m_t \geq 1$ , can be ignored for the non-active portions of the tooth profile of the gear,  $\mathcal{G}$ , and of the pinion, of the gear,  $\mathcal{P}$ .

In the extreme case, the  $EAP$ -circles of the gear and the pinion can pass through a certain point,  $K$ , within the straight-line segment,  $P_g P_p$ . Because of this, the length,  $Z_{pa}$ , of the active portion of the plane of action becomes zero ( $Z_{pa} = 0$ ), and the active portion of the involute tooth profile shrinks to the contact point,  $K$  (proper selection of the distance  $PK = r_N$  is considered below). The nonactive portions,  $aK$  and  $bK$ , of the tooth profile meet each other at the point,  $K$ . These portions are not subject to conditions of meshing of tooth profiles; thus, this gives a certain freedom when selecting the geometry of nonactive portions,  $aK$  and  $bK$ , of the tooth profiles. This particular case of  $P_a$ -gearing is illustrated in Figure 10.7d. The other portions of the gear teeth profiles are not active and do not come in contact with each other when the gears rotate. Therefore, the gear designer is free to modify the inactive portions of the gear teeth,  $aK$  and  $bK$ , making them stronger in terms of contact strength.

As the width of the active portion of the plane of action is zero ( $Z_{pa} = 0$ ), and the involute tooth profile is shrunk to a point, the transverse contact ratio,  $m_p$ , becomes zero. In order to meet the inequality  $m_t \geq 1$ , the following inequality must be satisfied:

$$m_t = m_p + m_F = 0 + m_F = m_F > 0 \quad (10.8)$$

The point system of parallel-axes gearing that is illustrated in Figure 10.7d gives much freedom when designing nonactive portions of tooth profiles of the gear and the pinion, as the geometry of these portions is free of constraints imposed by conditions of meshing of two conjugate tooth profiles. In conformal and high-conformal gearing, this feature is used to increase the contact strength of the gear and the pinion.

The involute gear/pinion tooth profile truncated to contact point,  $K$ , is a degenerate case of the involute tooth profile that conformal and high-conformal gearings feature. This degenerate tooth profile is referred to as the involute tooth point. The rest of the gear and pinion tooth profiles are inactive and do not come in contact with each other when the gears rotate. Therefore, the gear designer is free to modify the inactive portions of the gear teeth, making them stronger in terms of contact strength. The inactive portion of the gear and the pinion tooth profiles can be designed independently of conditions of interaction of tooth profiles.\*

The above discussion reveals that no tooth flank modification is permissible in Novikov gearing. Neither profile modification nor crowning is allowed in Novikov gearing.

It is of importance to stress here that it is an incorrect practice to combine the two gear systems, namely Wildhaber and Novikov gear systems, into a common gear system. This mistake is widespread in the public domain. The two gear systems are incompatible with one another. No Wildhaber/Novikov gearing (or WN-gearing, in other words) is physically feasible at all. The term *Wildhaber/Novikov gearing* (as well as the term *WN-gearing*) is meaningless and cannot be attributed to any gear system. Therefore, any discussion with a person who uses the terms *Wildhaber/Novikov gearing* and/or *WN-gearing* makes no sense,<sup>†</sup> and thus must be terminated immediately, as only poorly proficient gear experts use the terms *Wildhaber/Novikov gearing* and/or *WN-gearing*.

#### 10.4.1 Boundary N-Circle in Conformal Gearing

In parallel-axes gearing, a motion of a pinion in relation to a motionless mating gear is an instant rotation of the pinion about the axis of instant rotation,  $P_{in}$ . Similarly, a motion of the gear in relation to the motionless mating pinion is an instant rotation of the gear about the axis of instant rotation,  $P_{in}$ . It can be seen from that that every contact point,  $K$ , between the tooth flanks of the gear and the pinion,  $\mathcal{G}$  and  $\mathcal{P}$ , traces a circular arc that is centered at the pitch point,  $P$ . One of the circular arcs is associated with the gear, and another is associated with the pinion. Based on this consideration, the concept of the so-called *boundary Novikov circle* was introduced

\* It is a huge mistake to refer to gears for the Novikov gear system as gears with a *circular-arc tooth profile*. Novikov gearing is not a kind of gearing with a *circular-arc tooth profile*, like gears in a Wildhaber gear system are. Novikov gearing is a reduced kind of *involute gearing*. In Novikov gearing, the working involute tooth profile is shrunk to a point. This point is referred to as the involute tooth point.

† Novikov gearing is the only kind of conformal gearing that meets all three fundamental requirements that all kinds of gearing must meet; that is: (1) condition of contact,  $\mathbf{n} \cdot \mathbf{V}_\Sigma = 0$ ; (2) condition of conjugacy; and (3) equality of base pitches of a gear and a mating pinion to the operating base pitch of the gear pair ( $p_{b,g} = p_{b,op}$  and  $p_{b,p} = p_{b,op}$ ). No other kind of conformal gearings meets these three requirements.



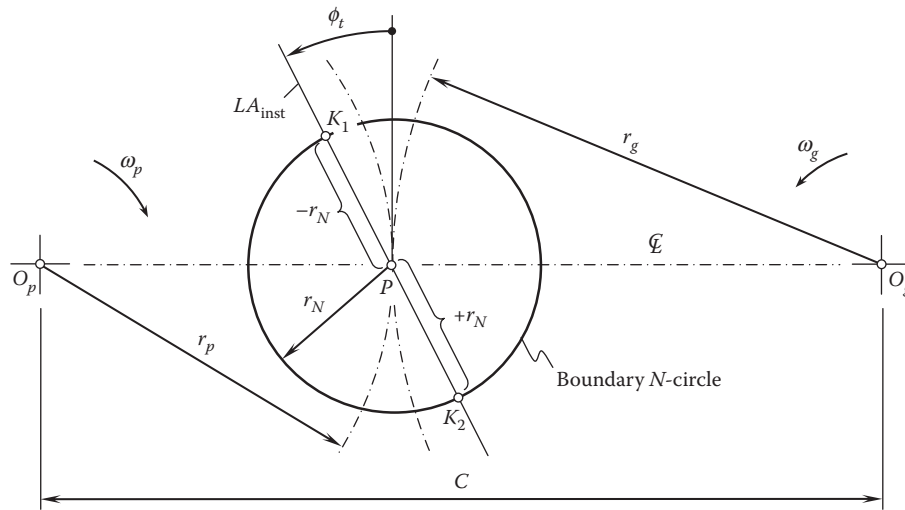


FIGURE 10.8

Boundary  $N$ -circle in a conformal parallel-axes gear pair.

by Radzevich [137]. The boundary Novikov circle is commonly referred to as the *boundary  $N$ -circle*. The procedure of constructing a boundary  $N$ -circle for a conformal gear pair is briefly outlined below.

Consider two axes of rotations of the gear,  $O_g$ , and the pinion,  $O_p$ , in the design of a parallel-axes conformal gear pair, as schematically depicted in Figure 10.8. The axes of rotations,  $O_g$  and  $O_p$ , are at a center distance,  $C$ , from each other. The gear and the pinion are rotated about the axes  $O_g$  and  $O_p$ , and the rotations are labeled as  $\omega_g$  and  $\omega_p$ , respectively. The gear ratio in the conformal gear pair is equal to  $u = \omega_p/\omega_g$ .

The center distance,  $C$ , is subdivided by the point,  $P$ , into two segments,  $O_gP$  and  $O_pP$ . The ratio of the lengths of the straight line segments,  $O_gP$  and  $O_pP$ , is reciprocal to the gear ratio,  $u$ , in the conformal gear pair. If the straight line segments,  $O_gP$  and  $O_pP$ , are the pitch radii ( $O_gP = r_g$  and  $O_pP = r_p$ ) of the conformal gear pair, then the equality  $r_g/r_p = u$  is observed. The point,  $P$ , is the *pitch point* in the conformal gear pair.

The straight instant line of action,\*  $LA_{inst}$ , through the pitch point,  $P$ , is at the transverse pressure angle,  $\phi_t$ , with respect to the perpendicular to the centerline,  $\mathcal{C}$ . Two points, denoted by  $K_1$  and  $K_2$ , are within the straight line,  $LA_{inst}$ , and are displaced at a certain distance,  $\pm r_N$ , from the pitch point,  $P$ . The paths of contact,  $P_{pc}$ , are the two straight line segments along the instant line of action,  $LA_{inst}$ , both of zero length. The pseudo-paths of contact,  $P_{pc}$ , are the two straight lines through the points  $K_1$  and  $K_2$  parallel to the axes,  $O_g$  and  $O_p$ , of the rotations of the gear and the pinion. This distance, that is, the displacement,  $r_N$ , of the pseudo-paths of contact,  $P_{pc}$ , from the pitch point  $P$ , is one of the important geometrical parameters of conformal gearing. The strength of the gear teeth and the performance of the conformal gear pair strongly depend on the actual value of the displacement,  $r_N$ .

The path of contact that is located beyond the pitch point,  $P$  (in the direction of rotation of the gears), features a positive displacement, that is,  $+r_N$ . A conformal gear mesh of this type is referred to as the  $N_{by}$ -mesh of conformal gear pair. The path of contact that is located before the pitch point (in the direction of rotation of the gears) features a negative displacement, that is,  $-r_N$ . A conformal gear mesh of this type is referred to as the  $N_{bf}$ -mesh of conformal gear pair.

In order to avoid violation of the conditions of meshing, as well as targeting wear reduction and a reduction of friction losses, the pseudo-paths of contact,  $P_{pc}$ , are displaced at a reasonably short distance from the axis of instant rotation,  $P_{ln}$ .

Let us imagine that the pinion is motionless; then, the contact point,  $K$ , traces a circle within the corresponding transverse section of the gear pair. The circle is centered at the pitch point,  $P$ . Similarly, the gear can be assumed stationary; then, the contact point,  $K$ , traces a circle within that same transverse section of the gear pair. This

\* The line of action,  $LA$ , in cases of conformal gearing (that is, Novikov gearing), and high-conformal gearing (that is,  $H_c$ -gearing) is referred to as the *instant line of action*,  $LA_{inst}$  because of the following. When the gears rotate, at every instant of time, a motion is transmitted along a path of contact,  $P_{pc}$ , of zero length. At different instants of time, the motion is transmitted along different lines of action. Because of this, an illusion is created that the line of action travels in the axial direction together with the contact point,  $K$ , and that the path of contact is parallel to the axis of instant rotation,  $P_{ln}$ . Instead, not the path of contact,  $P_{pc}$ , but the pseudo-path of contact,  $P_{pc}$ , is created in this way, as every instant line of action is stationary. The projection of the instant line of action onto the transverse plane also remains stationary, as the transverse contact ratio in conformal gearing and  $H_c$ -gearing is zero.



circle is also centered at the pitch point,  $P$ . It is clear from this consideration how the boundary  $N$ -circle of radius  $r_N$  can be constructed.

A transverse section of a conformal gear pair is subdivided by a *boundary  $N$ -circle* of radius  $r_N$  into two areas.\* The area within the interior of the boundary circle of a radius  $r_N$  (including points those within the boundary circle itself) represents the area of feasible shapes of the tooth profiles of one of the mating gears, and the area within the exterior of the boundary circle of the radius  $r_N$  (including points those within the circle itself) represents the area of feasible shapes of tooth profiles of the second mating gear.

The boundary circle of a radius  $r_N$  is referred to as a *boundary Novikov circle in a conformal gear pair* or simply as a *boundary  $N$ -circle*.

### Definition 10.1

*A boundary Novikov circle (or boundary  $N$ -circle for simplicity) is a circle centered at the pitch point of a parallel-axes conformal gearing, the radius of which is equal to a favorable distance of the contact point between the tooth flanks of a gear and a mating pinion from the pitch point of the gear pair.*

It is the right point to stress here that the concept of the boundary  $N$ -circle is helpful for understanding the feasibility of conformal gearing that features *local-line contact* between the tooth flanks of the gear and the mating pinion. In an ideal case, when all the deviations are zero, the tooth flank of the gear,  $\mathcal{G}$ , as well as the tooth flank of the mating pinion,  $\mathcal{P}$ , can both be generated by that same arc of the boundary  $N$ -circle. In other words, an arc of the boundary  $N$ -circle can be used as the tooth profile of the gear, as well as the tooth profile of the pinion in the transverse section of the gear pair.

In practice, a corresponding boundary  $N$ -cylinder can be assigned to any and all parallel-axes conformal gear pairs. The axis of rotation of the boundary  $N$ -cylinder is aligned with the axis of instant rotation,  $P_{lm}$ , of the gear and the pinion,  $\mathcal{G}$  and  $\mathcal{P}$ .

### 10.4.2 Possible Tooth Geometries in Conformal Gearing

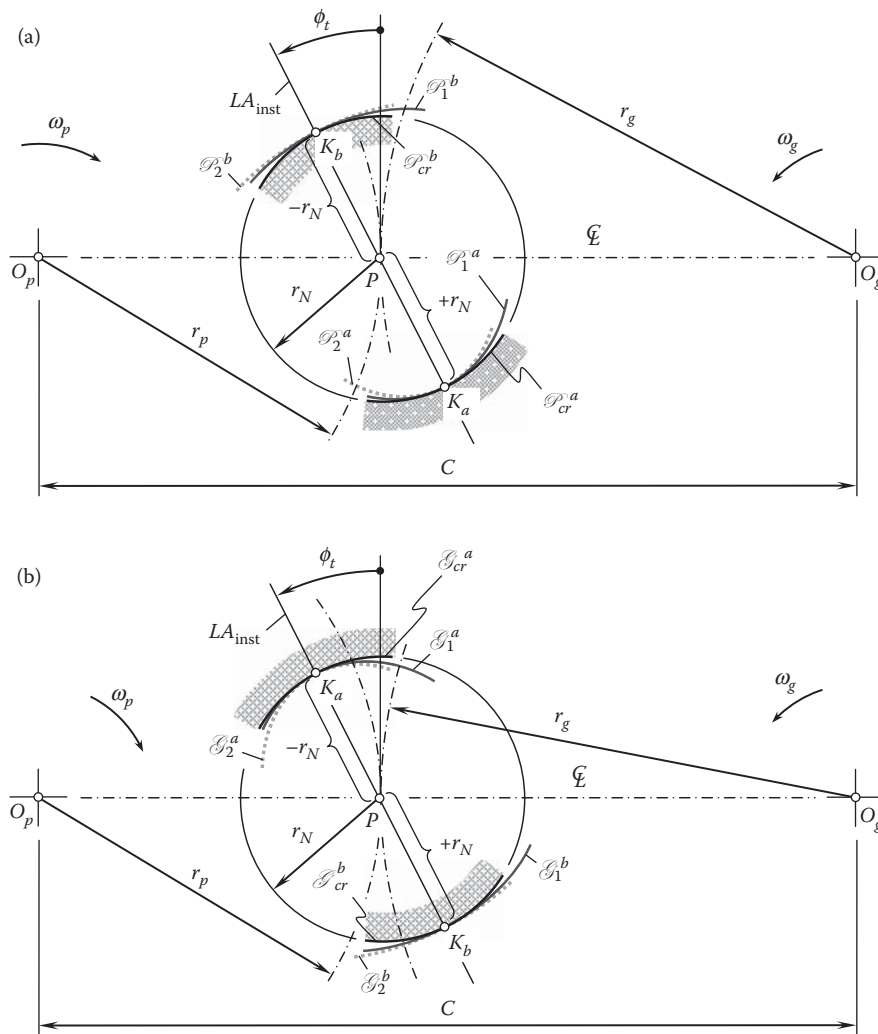
Design of mating tooth profiles for a conformal gear pair begins with the construction of the boundary  $N$ -circle. In Figure 10.9, the boundary  $N$ -circle of a radius  $r_N$  is constructed for the pinion tooth profile (Figure 10.9a), and the mating gear tooth profile (Figure 10.9b) of a conformal gear pair.

The displacement,  $r_N$ , is positive ( $r_N > 0$ ) for the pinion addendum. The tooth profile<sup>†</sup> of the pinion addendum is a convex segment of a smooth regular curve,  $\mathcal{P}_i^a$  ( $i = 1, 2, \dots$ ), through the contact point,  $K_a$ . The radius of curvature,  $R_{\mathcal{P}}$ , of the addendum profile is equal to or less than the radius,  $r_N$ , of the boundary  $N$ -circle ( $R_{\mathcal{P}} \leq r_N$ ). The case of equality  $R_{\mathcal{P}} = r_N$  is the limiting case, which is mostly of theoretical interest. Geometrically, the profile of the pinion addendum can be shaped in the form of a circular arc of radius  $r_N$ . This case of the pinion addendum profile is the limiting one, which is of theoretical interest.

It should be stressed here that none of the feasible profiles,  $\mathcal{P}_i^a$ , of the pinion addendum intersect the boundary  $N$ -circle. The pinion addendum profile is entirely located within the interior of the boundary  $N$ -circle. Therefore, no arc of a smooth regular curve can be used as tooth profile of the pinion addendum. The circular arc, an arc of an ellipse (at one of its apexes), and a cycloidal profile containing its apex are examples of applicable curves for addendum tooth profiles. Spiral curves (involute of a circle, *Archimedean spiral*, logarithmic spiral, and so forth) are examples of smooth regular curves of which no arc can be used in designing a pinion tooth addendum. This is because the radius of curvature of a spiral curve (as well as many other curves) changes uniformly when a point travels along the curve. This is schematically illustrated in Figure 10.10. In Figure 10.10a, an ellipse-arc,  $ab$ , is shown; the ellipse-arc is entirely located within the interior of the boundary  $N$ -circle. The ellipse-arc,  $ab$ , can be selected as the tooth addendum profile of a conformal gear pair. An ellipse-arc,  $cd$  (Figure 10.10a), is entirely located in the exterior of the boundary  $N$ -circle. The ellipse-arc,  $cd$ , can be selected as the tooth dedendum profile of a conformal gear pair. Finally, an ellipse-arc,  $ef$  (Figure 10.10b), intersects the boundary  $N$ -circle. The ellipse-arc,  $ef$ , cannot be used as the tooth profile in a conformal gear pair. The same is valid for all spiral curves.

\* The radius of the boundary Novikov circle is designated as  $r_N$ . The obsolete designation,  $l$ , for this design parameter was used by Novikov for the displacement of the contact point,  $K$ , from the pitch line,  $P_{lm}$ . In reality, the equality  $r_N = |l|$  is always observed.

† Recall that the active portion of the tooth profile in conformal gearing is limited to the so-called *involute point*. The rest of the gear and the pinion tooth profiles are not active; that is, they do not interact with each other. Because of this, there is a certain freedom for the gear designer in selecting the geometry of the inactive portions of the tooth flanks of the gear and the pinion.

**FIGURE 10.9**

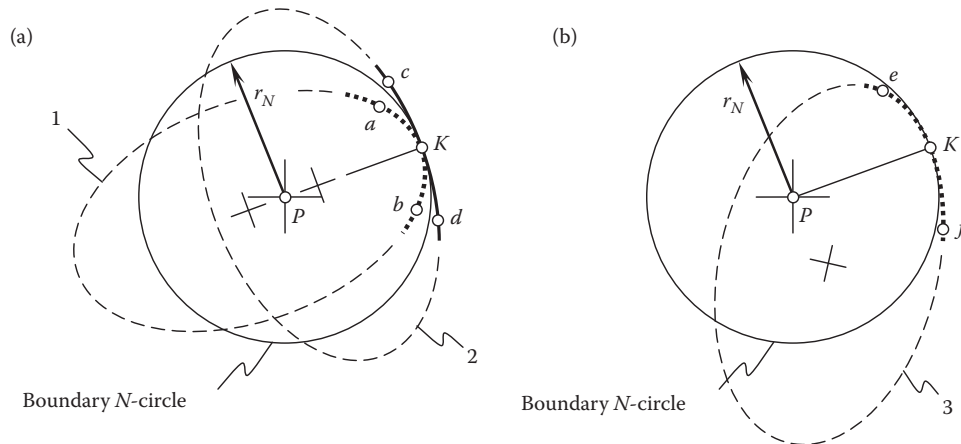
Examples of feasible tooth flank geometries in a conformal gear pair: feasible shapes of the tooth flank of (a) a pinion,  $\mathcal{P}$ , and (b) the mating gear,  $\mathcal{G}$ .

Therefore, at the point of tangency,  $K$ , spiral curves intersect the corresponding boundary  $N$ -circle, which is prohibited. Ultimately, it should be clear that a variety of smooth regular curves can be used in the design of the tooth profile of a conformal gearing. The variety of curves is not limited only to circular arcs.

The displacement,  $r_N$ , is a signed value. It is negative ( $r_N < 0$ ) for the pinion dedendum (see Figure 10.9a). The inactive tooth profile of the pinion dedendum is a concave segment of a smooth regular curve,  $\mathcal{P}_i^b$  ( $i = 1, 2, \dots$ ), through the contact point  $K_b$ . The radius of curvature,  $R_{\mathcal{P}}$ , of the dedendum profile is equal to or greater than the radius,  $r_N$ , of the boundary  $N$ -circle ( $R_{\mathcal{P}} \geq r_N$ ). The case of equality  $R_{\mathcal{P}} = r_N$  is the limiting case, which is mostly of theoretical interest. Geometrically, the profile of the pinion addendum can be shaped in the form of a circular arc of the radius,  $r_N$ . This case of the profile of the pinion addendum is the limiting one and is of theoretical importance.

Constraints that are imposed on the geometry of the inactive tooth profile of the pinion dedendum are similar to those imposed on the geometry of the tooth profile of the pinion addendum. The dedendum profile is entirely located in the exterior of the boundary  $N$ -circle, shares a point with the  $N$ -circle (the contact point,  $K_b$ ), and does not intersect the boundary  $N$ -circle. Not all types of smooth regular curves can be implemented in the design of the pinion tooth dedendum.

An analysis that is similar to the aforementioned one regarding the pinion tooth profile can be performed for the gear tooth profile as well. The analysis is illustrated in Figure 10.9b. The gear tooth addendum,  $\mathcal{G}_i^a$ , is entirely located within the interior of the boundary  $N$ -circle, whereas the gear tooth dedendum,  $\mathcal{G}_i^b$ , is entirely located in

**FIGURE 10.10**

Examples of ellipse-arc tooth profiles for conformal gears: (a) feasible, and (b) not feasible.

the exterior of the boundary  $N$ -circle. Both the profile of the gear tooth addendum,  $\mathcal{G}_i^a$ , and the profile of the gear tooth dedendum,  $\mathcal{G}_i^b$ , share a common point with the boundary  $N$ -circle (the point,  $K_a$ , in the first case and the point,  $K_b$ , in the second). No intersection of tooth profiles,  $\mathcal{G}_i^a$  and  $\mathcal{G}_i^b$ , is permissible within tooth height of the gear and pinion.

The importance of the concept of the boundary  $N$ -circle for gear engineers is as follows: a boundary  $N$ -circle in conformal gear pairs is a constraint imposed on the geometry of the inactive tooth profiles of the gear and the pinion. The gear engineer is free to select an arc of any smooth regular curve of an appropriate geometry to shape the tooth addendum profile if the arc is entirely located within the boundary  $N$ -circle. The gear engineer is also free to select an arc of any smooth regular curve of an appropriate geometry to shape the tooth dedendum profile if the arc is entirely located outside the boundary  $N$ -circle\*.

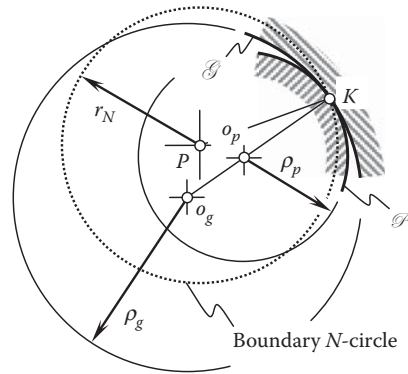
The concept of the boundary  $N$ -circle has proved to be helpful in the theory of conformal gearing (Novikov gearing). As an example, Figure 10.11 illustrates a transverse section of a conformal gear pair. In the case under consideration, the tooth flank of a gear,  $\mathcal{G}$ , makes contact at point,  $K$ , with the tooth flank of the mating pinion,  $\mathcal{P}$ . The inactive circular-arc teeth profiles,  $\mathcal{G}$  and  $\mathcal{P}$ , are centered at the points,  $o_g$  and  $o_p$ , respectively. The centers,  $o_g$  and  $o_p$ , are chosen to fulfill the necessary condition for the magnitudes,  $\rho_g$  and  $\rho_p$ , for the radii of curvature of the teeth profiles,  $\mathcal{G}$  and  $\mathcal{P}$ , at the point of tangency,  $K$  (the inequality  $\rho_g > \rho_p$  is valid). However, as the circular arcs,  $\mathcal{G}$  and  $\mathcal{P}$ , intersect the boundary Novikov circle, the gearing of this particular type is not feasible. In the well-known *Helical Gearing* by Wildhaber [161], an unfavorable configuration of circular-arc teeth profiles is observed. This makes Wildhaber's helical gearing not workable at all.

Another illustration of the infeasibility of helical gearing by Wildhaber (see Figure 10.11) [161] is focused on an incorrect tooth profile orientation in relation to the boundary  $N$ -circle, as well as the instant line of action,  $LA_{inst}$ . An analogy of correct and incorrect tooth profile orientations in involute gearing can be used for the purposes of illustration.

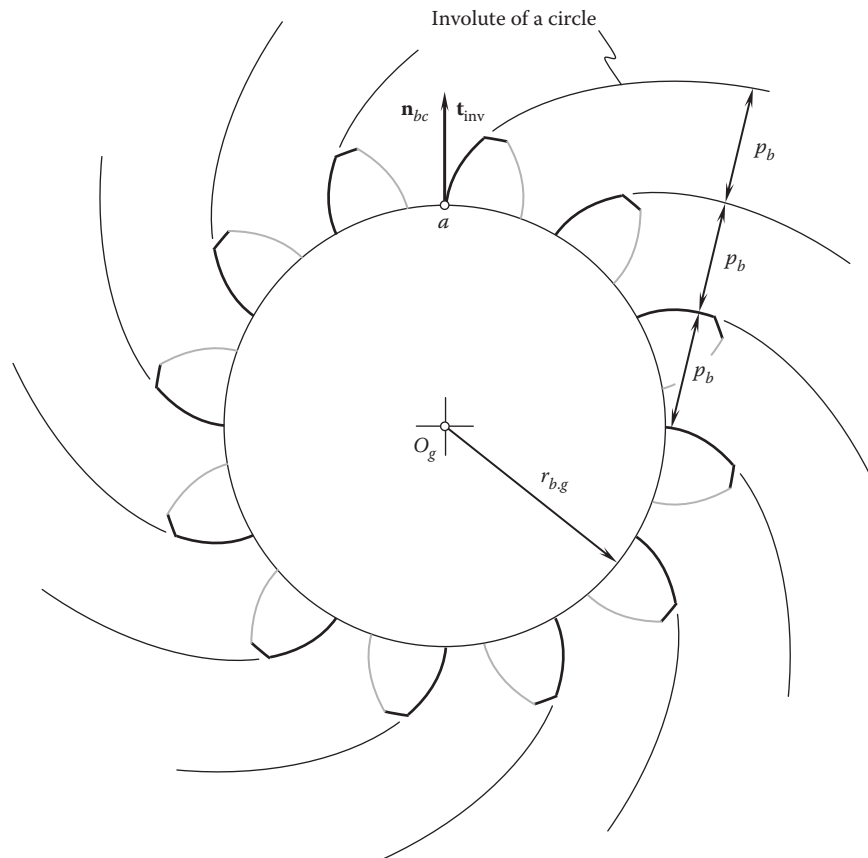
Referring to Figure 10.12, consider a gear that has an involute tooth profile. Point  $a$  within the base circle is the start point of the involute tooth profile. All the involutes are developed from the base circle of a radius  $r_{b,g}$ . Hence, the unit normal vector,  $\mathbf{n}_{bc}$ , to the base circle at point,  $a$ , and the unit tangent vector,  $\mathbf{t}_{inv}$ , to the involute curve at that same point,  $a$ , align with one another. As a result, the base pitch,  $p_b$ , has a constant value for any two adjacent tooth profiles and at any current point within an involute curve. In other words, the base pitch of the involute gear Figure 10.12 is preserved, as all the involutes are developed from a common base circle.

Another example is shown in Figure 10.13. In this particular case, the gear teeth are shaped by means of the same involute curve as in the case shown in Figure 10.12. However, each involute curve is turned through an angle,  $\xi$ , about its corresponding start point of the involute curve. All the shifted involutes are constructed from different base circles of a radius,  $r_{b,g}$ , each. However, each base circle is centered at the point,  $O_g^i$ , that does not coincide with the gear axis,  $O_g$ . Hence, the unit normal vector,  $\mathbf{n}_{bc}$ , to the base circle of the true involute profile at point  $a$  and the unit tangent vector,  $\mathbf{t}_{inv}$ , to the shifted involute curve at the same point,  $a$ , make an angle,  $\xi$ . As a

\* The concept of the boundary  $N$ -circle was introduced around 2008 by Radzevich; Novikov himself did not use the term *boundary N-circle*.

**FIGURE 10.11**

Use of the concept of the boundary  $N$ -circle has proved to be helpful to distinguish whether a circular-arc profile is feasible for a *conformal* gearing, or not.

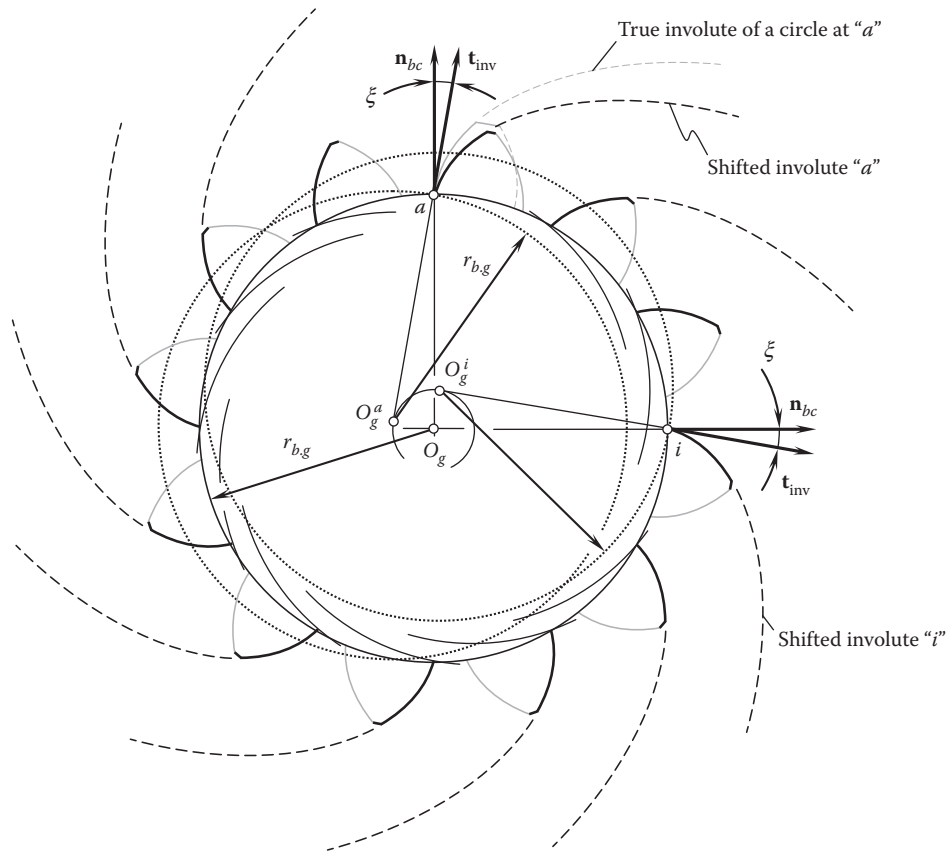
**FIGURE 10.12**

An example of *correct* configuration of involute tooth profiles in relation to the base circle of a gear.

result, the base pitch,  $p_b$ , cannot be specified in the case of the involute gear shown in [Figure 10.13](#). Once the base pitch of the gear cannot be specified, this immediately means the fundamental equality of the base pitch of the gear to the operating base pitch of the gear pair cannot be fulfilled.

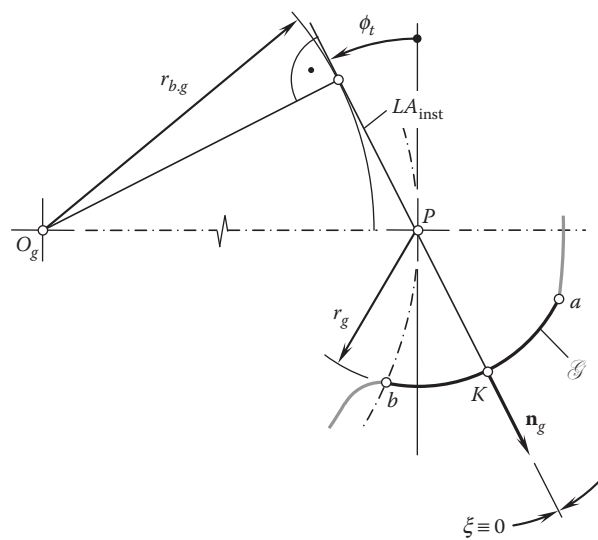
A similar analysis can be performed with respect to gears that feature a circular-arc tooth profile.

In conformal gearing (Novikov gearing), the circular-arc tooth profile,  $ab$ , is centered at point that is situated within the instant line of action,  $LA_{\text{inst}}$ , as illustrated in [Figure 10.14](#). In a particular case, the center of the circular-arc tooth profile,  $ab$ , is coincident with the pitch point,  $P$ . Due to that, the unit normal vector,  $\mathbf{n}_g$ , to the gear tooth profile at the culminating point,  $K$ , aligns with the instant line of action,  $LA_{\text{inst}}$ . The angle,  $\xi$ , that the unit



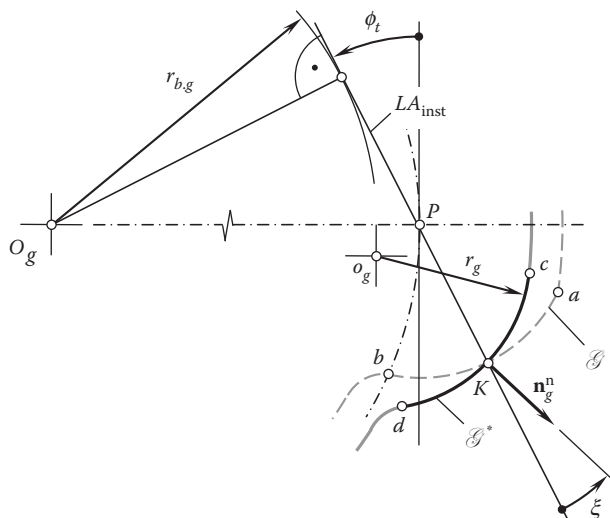
**FIGURE 10.13**

An example of the *incorrect* configuration of involute tooth profiles in relation to the base circle of a gear.



**FIGURE 10.14**

Circular-arc tooth profile in parallel-axes conformal gearing (in *Novikov gearing*): Pat. No. 109,113, (USSR). *Gear Pairs and Cam Mechanisms Having Point System of Meshing*. /M.L. Novikov, National Classification 47h, 6; Filed: April 19, 1956.

**FIGURE 10.15**

Circular-arc tooth profile in helical gearing by Ernst Wildhaber: *Helical Gearing*, US Pat. 1,601,750, E. Wildhaber, Filed: November 2, 1923, Patented: October 5, 1926.

normal vector,  $\mathbf{n}_g$ , forms with the instant line of action,  $LA_{\text{inst}}$ , is zero (that is,  $\xi = 0^\circ$ ). This is a necessary condition that all conformal gearing has to comply with, and, ultimately, the fulfillment of this condition ( $\xi = 0^\circ$ ) makes Novikov gearing workable. The base pitch,  $p_{b,g}$ , in a conformal gearing is measured along the instant line of action,  $LA_{\text{inst}}$ . As the unit normal,  $\mathbf{n}_g$ , is aligned with the instant line of action,  $LA_{\text{inst}}$ , the base pitch can be specified.

In helical gearing with a circular-arc tooth profile proposed by Wildhaber, the circular-arc tooth profile,  $cd$ , is centered at point,  $o_g$ , which is situated outside the instant line of action,  $LA_{\text{inst}}$ , as illustrated in Figure 10.15. Because of that, the unit normal vector,  $\mathbf{n}_g$ , to the gear tooth profile at the point,  $K$ , does not align with the instant line of action,  $LA_{\text{inst}}$ . The angle,  $\xi$ , that the unit normal vector,  $\mathbf{n}_g$ , forms with the instant line of action,  $LA_{\text{inst}}$ , is not of a zero value (that is,  $\xi \neq 0^\circ$ ). Therefore, a necessary condition that all conformal gearing has to comply with ( $\xi = 0^\circ$ ) is violated in helical gearing by Wildhaber. Ultimately, the violation of this condition makes Wildhaber gearing not workable at all. The base pitch in helical gearing with a circular-arc tooth profile proposed by Wildhaber cannot be specified at all.

The difference between the circular-arc tooth profiles illustrated in Figures 10.14 and 10.15 is of the same nature as the difference between the involute gear shown in Figure 10.12 and the gear\* depicted in Figure 10.13.

## 10.5 Tooth Profile Rolling/Sliding in Conformal Gearing

When a pair of parallel-axes gears rotate in mesh, rolling and sliding of the gear and the pinion teeth is always observed.

### 10.5.1 Tooth Profile Sliding in Conformal Gearing

Performance and efficiency of conformal parallel-axes gear pairs depend on friction losses in gearing. Friction losses in conformal gearing strongly depend on tooth profile sliding. Tooth profile sliding affects a permissible location of the culminating point in conformal gearing (Novikov gearing).

The culminating point in conformal parallel-axes gearing is situated within the plane of action,  $PA$ . There is a portion of the plane of action,  $PA$ , within which the culminating point,  $K$ , is situated within the straight-line

\* It must be stressed here that involute gear is referred to as an involute gear not only because its teeth are shaped in the form of the involute of a circle, but also because the base circle of each involute is centered on the gear axis of rotation. Therefore, the gear shown in Figure 10.13 with an involute tooth profile is *not* an involute gear at all.

segment,  $P_g P_p$ . The points,  $P_g$  and  $P_p$ , are the points of interception of line of action by the outer diameter,  $d_{o,g}$ , of the gear, and the outer diameter,  $d_{o,p}$ , of the pinion. The gear and pinion teeth have to be designed so as to ensure a location of the culminating point within this interval,  $P_g P_p$ .

Geometrically, the culminating point,  $K$ , can be situated between the points of tangency,  $N_g$  and  $N_p$ , of the plane of action,  $PA$ , with two base cylinders of diameters,  $d_{b,g}$  and  $d_{b,p}$ , as illustrated in Figure 10.16.

There is a tradeoff between contact stress and the sliding velocity between the tooth flanks when determining the location of the culminating point. The smaller the radius of the boundary  $N$ -circle (that is, when  $r_N \rightarrow 0$ ), the smaller the sliding of tooth flank; however, contact stress in such a scenario increases as the allowed values for the radii of tooth profile curvature of the gear and the pinion decrease ( $\rho_g \rightarrow 0, \rho_p \rightarrow 0$ ). The larger the radius of the boundary  $N$ -circle, the smaller the contact stress; however, the sliding of the tooth flank is larger in this case. Theoretically,  $r_N = 0$  is the smallest possible radius of the boundary  $N$ -circle, and  $r_N = P_g P_p$  is the largest permissible radius of the boundary  $N$ -circle.

In order to make the correct decision regarding the appropriate value of the radius,  $r_N$ , of the boundary  $N$ -circle, both contact stress and the sliding of tooth flanks should be evaluated.

For the calculation of contact stress, the radii of curvature of gear and mating pinion tooth profiles strongly correlate to the radius,  $r_N$ , of the boundary  $N$ -circle. A certain freedom is available for the gear designer when choosing the radius,  $r_N$ .

The sliding of the tooth profile depends on the distance of the culminating point,  $K$ , from the axis of rotation of the gear and the pinion. The radius,  $r_{p,K}$ , at which the culminating point is situated when rotating about the pinion axis of rotation,  $O_p$ , can be calculated from the following expression:

$$r_{p,K} = \sqrt{0.25d_p^2 + r_N^2 - d_p r_N \sin \phi_t} \quad (10.9)$$

A similar formula:

$$r_{g,K} = \sqrt{0.25d_g^2 + r_N^2 - d_g r_N \sin \phi_t} \quad (10.10)$$

is valid for the calculation of the radius,  $r_{g,K}$ , at which the culminating point is situated when the gear pair is rotating about the gear axis of rotation,  $O_g$ .

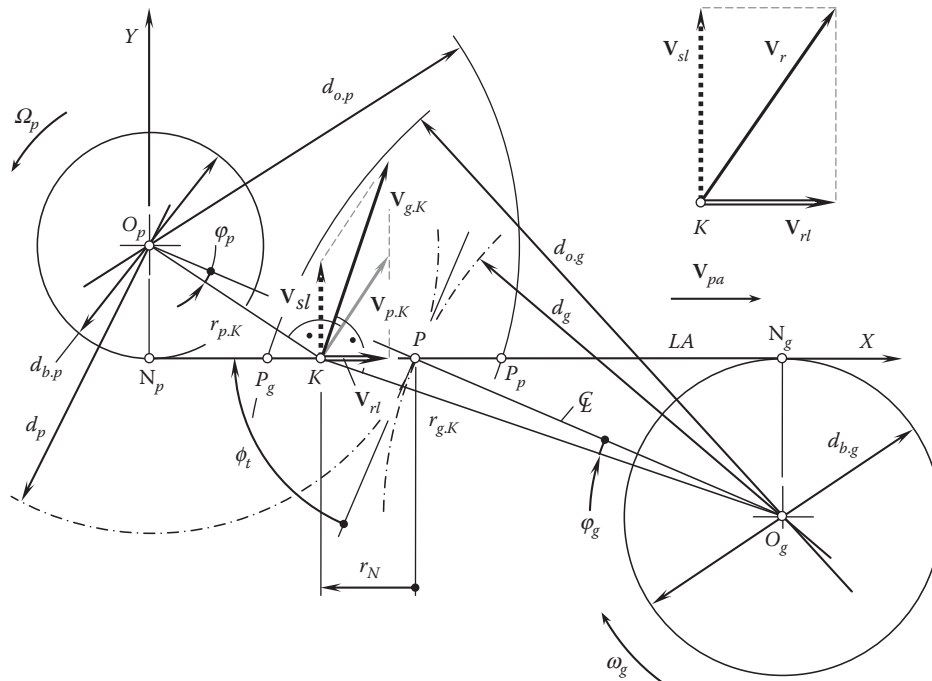


FIGURE 10.16  
Tooth profile sliding in parallel-axes conformal gearing (i.e., in Novikov gearing).



Once the distances,  $r_{g.K}$  and  $r_{p.K}$  (see Equations 10.9 and 10.10), are calculated, then the interval  $P_gP_p$  within which the culminating point,  $K$ , is situated, can be easily determined. For this purpose, the interval,  $P_gP_p$ , is represented in the form of the summa:  $P_gP_p = P_gP + P_pP$  (see Figure 10.16).

Use of the law of cosines with respect to  $\triangle KPO_p$  returns:

$$P_pP = \sqrt{r_p^2 + r_{p.K}^2 - 2r_p r_{p.K} \sin(\psi_p - \phi_t)} \quad (10.11)$$

where the angle  $\psi_p = \angle PO_pP_p$  is calculated from  $\triangle KPO_p$  on the premise of the law of sines:

$$\psi_p = \sin^{-1}\left(\frac{r_p}{r_{p.K}} \cos \phi_t\right) \quad (10.12)$$

Similarly, use of the law of cosines with respect to  $\triangle KPO_g$  returns:

$$P_gP = \sqrt{r_g^2 + r_{g.K}^2 - 2r_g r_{g.K} \sin(\psi_g - \phi_t)} \quad (10.13)$$

where the angle  $\psi_g = \angle PO_gP_g$  is calculated from  $\triangle KPO_g$  on the premise of the law of sines:

$$\psi_g = \sin^{-1}\left(\frac{r_g}{r_{g.K}} \cos \phi_t\right) \quad (10.14)$$

The corresponding calculations can be performed for external rotary-positive conformal gear pairs, as well as internal rotary-negative conformal gear pairs, for which the culminating point,  $K$ , is situated beyond the point,  $N_p$ , of the straight-line segment,  $N_gN_p$ .

For further analysis, it is convenient to express the sliding velocity in a conformal gearing in terms of the radius,  $r_N$ , of the boundary Novikov circle.

Consider a triangle,  $\triangle KPO_p$ , in Figure 10.16. The angle,  $\varphi_p$ , in the triangle,  $\triangle KPO_p$ , can be determined using the cosine law:

$$\varphi_p = \cos^{-1}\left(\frac{r_{p.K}^2 + r_p^2 - r_N^2}{2r_{p.K} r_p}\right) \quad (10.15)$$

In Equation 10.15, the pitch radius of the pinion is designated as  $r_p$ .

An expression similar to Equation 10.15 can be derived for the calculation of the angle,  $\varphi_g$ , in the gear. A simpler approach for calculation of the angle,  $\varphi_g$ , is based on the ratio  $\varphi_p/\varphi_g = u$ , where  $u$  is the gear ratio of the gear pair; that is,  $\varphi_g = \varphi_p/u$ .

With that said, the linear velocity vector,  $\mathbf{V}_{p.K}$ , of the point,  $K$ , in its rotation with the pinion is equal to:

$$\mathbf{V}_{p.K} = \omega_p r_{p.K} [\mathbf{i} \cdot \sin(\phi_t - \varphi_p) + \mathbf{j} \cdot \cos(\phi_t - \varphi_p)] \quad (10.16)$$

Similarly, the linear velocity vector,  $\mathbf{V}_{g.K}$ , of the point,  $K$ , in its rotation with the gear can be represented in the form:

$$\mathbf{V}_{g.K} = u^{-1} \omega_p r_{g.K} [\mathbf{i} \cdot \sin(\phi_t + \varphi_p/u) + \mathbf{j} \cdot \cos(\phi_t + \varphi_p/u)] \quad (10.17)$$

The sliding velocity vector,  $\mathbf{V}_{sl}$ , in conformal gearing can be calculated from the expression:

$$\mathbf{V}_{sl} = \mathbf{V}_{g.K} - \mathbf{V}_{p.K} \quad (10.18)$$

In parallel-axes gearing, the sliding velocity vector,  $\mathbf{V}_{sl}$ , is always perpendicular to the plane of action,  $PA$ .

For the specification of profile sliding of the tooth flanks,  $\mathcal{G}$  and  $\mathcal{P}$ , of the gear and the pinion, a unitless parameter is used. This parameter is commonly referred to as *specific sliding* and is denoted by  $\gamma$ . Two different parameters,  $\gamma$ , are distinguished.

First, the slide/roll ratio for the tooth flank,  $\mathcal{G}$ , of the gear:

$$\gamma_g = \frac{V_{sl,g}^m - V_{sl,p}^m}{V_{sl,g}^m} \quad (10.19)$$

Second, the slide/roll ratio for the tooth flank,  $\mathcal{P}$ , of the pinion:

$$\gamma_p = \frac{V_{sl,p}^m - V_{sl,g}^m}{V_{sl,p}^m} \quad (10.20)$$

The specific sliding,  $\gamma$ , has a positive value on the addendum portions of the tooth flanks. The parameter,  $\gamma$ , does not exceed 1. At the pitch point,  $P$ , it is equal to zero, and it is equal to 1 at the base circle of the mating gear.

The specific sliding on the dedendum portion of the tooth flanks has a negative value. It is equal to zero at the pitch point,  $P$ , and it approaches minus infinity at the base circle.

The parameters,  $V_{sl,g}^m$  and  $V_{sl,p}^m$ , to be entered into Equations 10.19 and 10.20 are already available from Equation 10.16 and 10.17, correspondingly:

$$V_{sl,g}^m = u^{-1} \omega_p r_{g,K} \cos(\phi_t + \varphi_p/u) \quad (10.21)$$

$$V_{sl,p}^m = \omega_p r_{p,K} \cos(\phi_t - \varphi_p) \quad (10.22)$$

Commonly, the specific sliding,  $\gamma$ , is plotted along the line of action as depicted in [Figure 10.17](#). Only the region,  $Z_{pa}$ , within the path of contact comes into effect when investigating the engagement of the gear teeth. In the case of parallel-axes conformal gearing (Novikov gearing), the length of action is zero; that is, the equality  $Z_{pa} = 0$  is valid.

The sliding is of a constant value in conformal as well as in high-conformal gearing; the specific sliding for the gear,  $\gamma_g$ , and the pinion,  $\gamma_p$ , also have constant values [137]. Commonly, in involute gearing, the sliding is different at different points of the tooth profile, and the specific sliding values,  $\gamma_g$  and  $\gamma_p$ , are of a constant value. In involute gearing with a low tooth count, that is, in LTC-gearing, both the sliding and the specific sliding,  $\gamma_g$  and  $\gamma_p$ , are different at different points of the tooth profile.

### 10.5.2 Tooth Profile Rolling in Conformal Gearing

A rotation from a driving shaft to a driven shaft is transmitted by means of rolling motion of the gear and the pinion teeth. The above-derived Equations 10.16 and 10.17 immediately yield the expressions for the linear velocity vector of rolling motion,  $\mathbf{V}_{rl}$ , as the rolling motion vector,  $\mathbf{V}_{rl}$ , is a projection of the linear velocity vectors,  $\mathbf{V}_{g,K}$  and  $\mathbf{V}_{p,K}$ , onto the axis  $X$  (this is because the linear velocity vector of rolling,  $\mathbf{V}_{rl}$ , is perpendicular to the linear velocity vector of rolling,  $\mathbf{V}_{sl}$ , that is,  $\mathbf{V}_{rl} \perp \mathbf{V}_{sl}$ ). Therefore, an expression for the calculation of the linear velocity vector of rolling motion,  $\mathbf{V}_{rl}$ , can be written as:

$$\mathbf{V}_{rl} = \mathbf{i} \cdot \omega_p r_{p,K} \sin(\phi_t - \varphi_p) \quad (10.23)$$

This vector can also be expressed in terms the design parameters and the rotation of the gear:

$$\mathbf{V}_{g,K} = \mathbf{i} \cdot u^{-1} \omega_p r_{g,K} \sin(\phi_t + \varphi_p/u) \quad (10.24)$$

Both expressions return equal numerical values for the linear velocity vector of rolling motion,  $\mathbf{V}_{rl}$ .

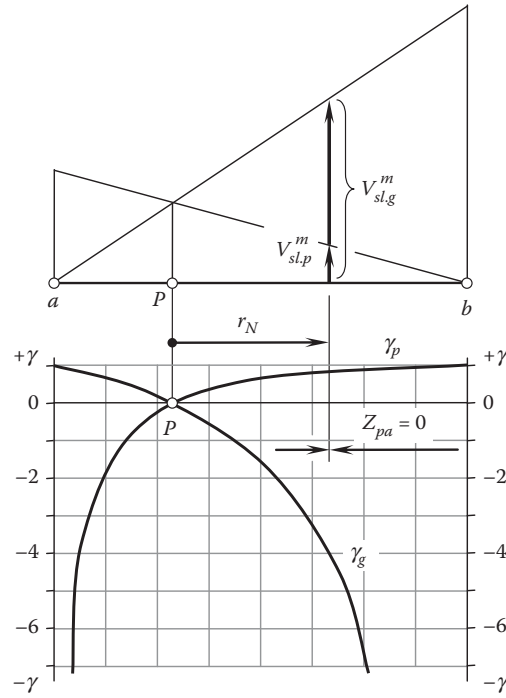


**FIGURE 10.17**  
Specific sliding,  $\gamma$ , in a  $P_a$ -axes conformal gear pair.

The vector,  $\mathbf{V}_r$ , equals the vector summa,  $\mathbf{V}_r = \mathbf{V}_{sl} + \mathbf{V}_{rl}$ , of the linear velocity vectors,  $\mathbf{V}_{sl}$  and  $\mathbf{V}_{rl}$ , of sliding and rolling in a parallel-axes conformal gear pair.

## 10.6 Elements of the Kinematics and Geometry in Conformal Gearing

The kinematics and geometry in conformal gearing differ from those in involute gearing or gearing of other designs.

From [Figure 10.18](#), consider a conformal gear pair that is composed of a driving pinion and a driven gear.

The gear is rotated about the axis,  $O_g$ , and the pinion is rotated about the axis,  $O_p$ . The axes of rotations,  $O_g$  and  $O_p$ , are at a certain center distance,  $\bar{C}$ , from one another. The rotation of the gear,  $\omega_g$ , and the rotation of the pinion,  $\omega_p$ , are synchronized with each other in a timely manner.

The pitch circle of the gear is of a radius,  $R_g$ , and the pitch circle of the pinion is of a radius,  $R_p$ , correspondingly. The pitch circles of radii,  $R_g$  and  $R_p$ , are tangent to one another. The point of tangency of the pitch circles is the pitch point,  $P$ , of the gear pair. An instant line of action,  $LA_{inst}$ , is a straight line through the pitch point,  $P$ , that forms a certain transverse pressure angle,  $\phi_t$ , in relation to the perpendicular to the centerline,  $\mathcal{C}$ , through  $P$ .

The point of contact,  $K$ , of the tooth flanks of the gear,  $\mathcal{G}$ , and the mating pinion,  $\mathcal{P}$ , is a point within the straight line,  $LA_{inst}$ . The farther the contact point,  $K$ , is situated from the pitch point,  $P$ , the more freedom there is in selecting the radii of curvature of the tooth profiles. At the same time, the farther the contact point,  $K$ , is situated from the pitch point,  $P$ , the higher the losses caused by the friction between the tooth flanks,  $\mathcal{G}$  and  $\mathcal{P}$ , and the higher the wear of the tooth flanks. Finally, the actual situation of the contact point,  $K$ , is a trade-off between the two aforementioned factors.

Further, let us assume that the pinion is stationary and the gear performs the instant rotation in relation to the pinion. The axis,  $P_{ln}$ , of the instant rotation,  $\omega_{pl}$ , is the straight line through the pitch point,  $P$ . The axis of the instant rotation,  $P_{ln}$ , is parallel to the axes,  $O_g$  and  $O_p$ , of the rotations,  $\omega_g$  and  $\omega_p$ , of the gear and the pinion. When the pinion is motionless, the contact point,  $K$ , traces a boundary circle of a radius,  $r_N$ , centered at the pitch point,  $P$ .

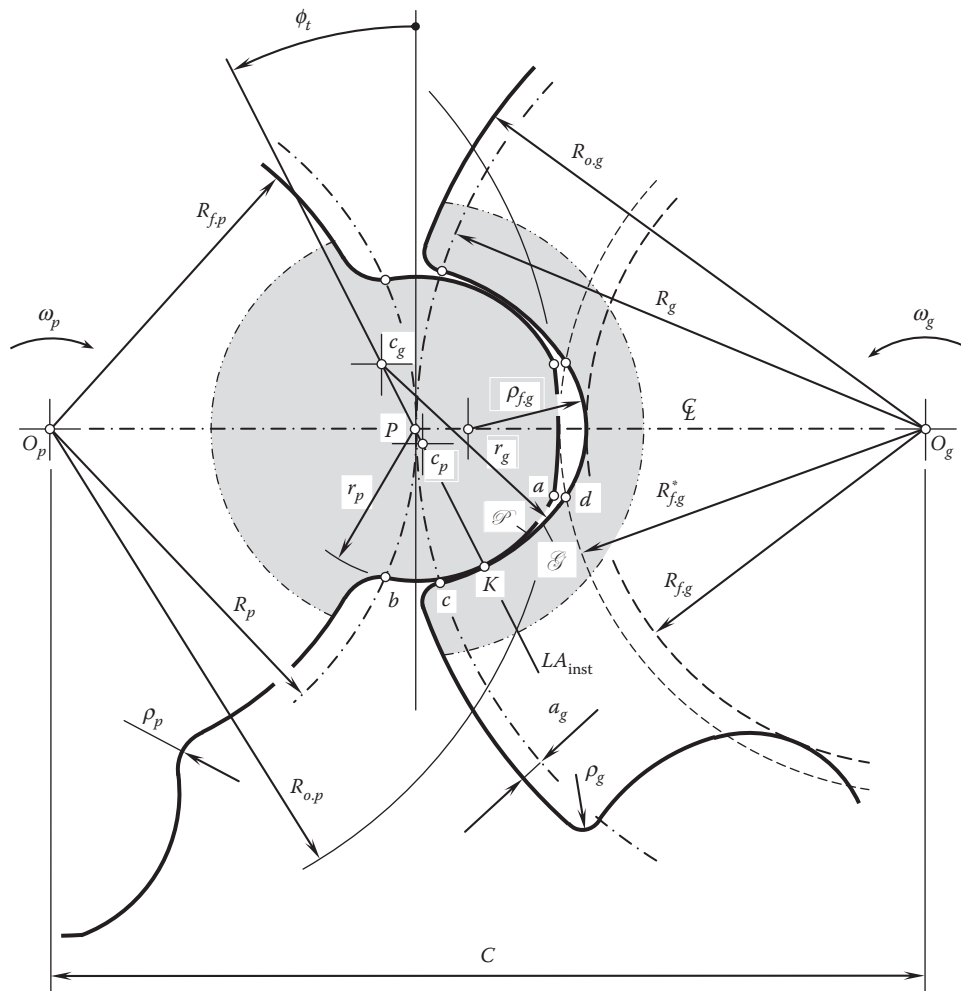


**FIGURE 10.18**  
Kinematics, and tooth flank geometry in a parallel-axes conformal gearing (in Novikov gearing).

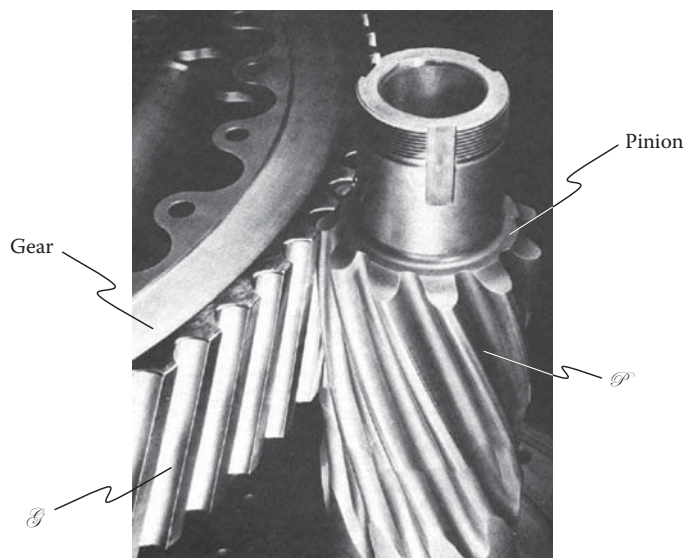
The pinion tooth profile,  $\mathcal{P}$ , can either align with an arc of the boundary circle,  $r_N$ , or it can be relieved inside the bodily side of the pinion tooth. As a consequence, the location of the center of curvature,  $c_p$ , of the convex pinion tooth profile,  $\mathcal{P}$ , within the straight line,  $L_{inst}$ , is limited to just the straight line segment  $PK$ . The pitch point is included in the interval, as shown in Figure 10.18, whereas the contact point,  $K$ , is not.

On the other hand, the location of the center of curvature,  $c_g$ , of the concave gear tooth profile,  $\mathcal{G}$ , within the instant line of action,  $LA_{inst}$ , is limited to the open interval  $P \rightarrow \infty$ . Theoretically, the pitch point,  $P$ , can be included in that interval for  $K$ . However, this is completely impractical, and the center of curvature,  $c_g$ , is situated beyond the pitch point,  $P$ . Hence, the radius of curvature,  $r_p$ , of the convex the pinion tooth profile,  $\mathcal{P}$ , is smaller than the radius of curvature,  $r_g$ , of the concave the gear tooth profile,  $\mathcal{G}$  (that is, the inequality  $r_p < r_g$  is observed).

It should be mentioned here that there are no physical constraints in designing a gear pair that has a convex gear tooth profile and concave pinion tooth profile.

Both the pinion and gear are helical. The helices are of opposite hands; that is, one of them is right handed, and the other is left handed. No spur conformal gearing (that is, Novikov gearing) is feasible at all.

It is fundamental to the operation of the conformal gears that contact occur nominally at a point. At every transverse section of a conformal gear pair, the gear and the pinion tooth flanks,  $\mathcal{G}$  and  $\mathcal{P}$ , interact with one another at a zero time (thus, the length of the path of contact,  $P_c$ , is zero:  $P_c \equiv 0$ ). An instant line of contact,  $LC_{inst}$ , travels together with the plane of action,  $PA$ , in a corresponding transverse section of the gear pair. An instant line of contact,  $LC_{inst}$ , does not travel in the axial direction of the gear pair, as the plane of action does not travel in this direction. Because the gears are helical and of opposite hands, an illusion is created

**FIGURE 10.19**

Close-up of a conformal gear pair (Novikov gear pair) manufactured by Westland Helicopter, Ltd. (After Dyson, A., Evans, H.P., and Snidle, R.W., 1986, "Wildhaber-Novikov Circular Arc Gears: Geometry and Kinematics", *Proceedings of the Royal Society London A* 403: 313-40.)

that the point of contact travels axially along the gears while remaining at the same radial position on both gear and pinion teeth,  $\mathcal{G}$  and  $\mathcal{P}$ . In this *phantom* axial travel of the point across the full face width of the gears during a rotation, a *pseudo-path of contact*,  $P_{pc}$  is generated. It should be stated as a condition of operation of conformal gearing (Novikov gearing) that for a given profile, the tooth surfaces should not interact before or after culmination when rotated at angular speeds that are in the gear ratio.

The transverse contact ratio,  $m_p$ , in a conformal gear pair is zero ( $m_p \equiv 0$ ). The face contact ratio,  $m_F$ , of the gear pair is always greater than one ( $m_F > 1$ ). The equality  $m_F = m_t$  is always observed in conformal gearing (here, the total contact ratio is designated as  $m_t$ ).

In the transverse section of the gear pair, the contact point,  $K$ , is motionless. For parallel-axes configuration, the pseudo-path of contact,  $P_{pc}$ , is a straight line through the culminating point,  $K$ . The pseudo-path of contact,  $P_{pc}$ , is parallel to the axes,  $O_g$  and  $O_p$ , as illustrated in Figure 10.18.

When a rotation is transmitted from a driving shaft to a driven shaft, all the instant contact points,  $K_{inst}$  are stationary. An illusion that the contact point travels along the pseudo-path of contact,  $P_{pc}$ , that is, parallel to the axes of rotation,  $O_g$  and  $O_p$ , of the gear and the pinion is because the gear and pinion tooth flanks,  $\mathcal{G}$  and  $\mathcal{P}$ , contact one another at a plurality of instant contact points,  $K_{inst}$  and because the interacting tooth flanks are helical and of opposite hands. This is only an illusion, and nothing more, as an instant line of contact,  $LC_{inst}$  (an instant contact point,  $K_{inst}$ ), travels together with the plane of action,  $PA$ , in a corresponding transverse section of the gear pair. An instant line of contact,  $LC_{inst}$  does not travel in the axial direction of the gear pair, as the plane of action does not travel in this direction.

A close-up of a conformal gear pair (that is, of a *Novikov gear pair*) is illustrated in Figure 10.19 [27]. This is a *conformal gear pair* (Novikov gear pair) manufactured by Westland Helicopter, Ltd.

## 10.7 Designing of Conformal Gear Pairs

As an example, consider the calculation of design parameters of a Novikov gear pair that has a circular-arc tooth profile following the one proposed by Novikov [82]. The methodology disclosed in this section can be enhanced to conformal gear pairs that have other geometries of the tooth profile in a transverse cross-section of the gear pair.

For the calculation of the design parameters of a Novikov gear pair, the center distance,  $C$ , and the gear ratio,  $u = \omega_p/\omega_g$ , of the gear pair have to be specified.

The radii of the pitch circles of the gear,  $R_g$ , and the pinion,  $R_p$ , can be expressed in terms of the center distance,  $C$ , and the tooth ratio,  $u$ , as follows:

$$R_g = C \cdot \frac{u}{1+u} \quad (10.25)$$

$$R_p = C \cdot \frac{1}{1+u} \quad (10.26)$$

A distance,  $r_N$ , at which the path of contact,  $P_c$ , is away from the pitch point,  $P$ , must be known, as well as the transverse pressure angle,  $\phi_t$ .

The displacement,<sup>\*</sup>  $r_N$ , is the principal design parameter in Novikov gearing. Many of the design parameters of a Novikov gear pair can be expressed in terms of the displacement,  $r_N = KP$ .

For the calculation of the radii of curvature of the tooth profile of the gear,  $r_g$ , and the pinion,  $r_p$ , the following formulas are used:

$$r_g = r_N \cdot (1 + k_{rg}) \quad (10.27)$$

$$r_p = r_N \cdot (1 + k_{rp}) \quad (10.28)$$

The actual value of the factor,  $k_{rp}$ , has to fulfill the inequality  $k_{rp} \geq 0$ . However, it is practical to set the factor,  $k_{rp}$ , equal to zero; then the equality  $r_p = r_N$  is valid. The factor,  $k_{rg}$ , is within the range  $k_{rg} = 0.03 \dots 0.10$ .

The radius of the outside circle of the pinion,  $R_{o,p}$ , is calculated from the following formula:

$$R_{o,p} = R_p + (1 - k_{p0}) \cdot r_N \quad (10.29)$$

The addendum factor,  $k_{p0}$ , of the pinion depends on the pressure angle,  $\phi_t$ ; the absolute dimensions of the gear pair; the accuracy of machining; and the conditions of lubrication. It is common practice to set the pinion addendum factor,  $k_{p0}$ , in the following range:

$$k_{p0} = 0.1 \div 0.2 \quad (10.30)$$

The radius of the root circle of the pinion,  $R_{f,p}$ , can be calculated from the following equation:

$$R_{f,p} = R_p - a_g - \delta \quad (10.31)$$

In Equation 10.31, the following are designated:

$a_g$  is the dedendum of the mating gear [ $a_g = (0.1 \dots 0.2) \cdot r_N$ ].

$\delta$  is the radial clearance in the gear pair ( $\delta = r_N \cdot k_{p0}$ ).

It is practical to set the fillet radius,  $\rho_p$ , in the range  $\rho_p = 0.3 \cdot r_N$ .

The radius of the root circle of the gear,  $R_{f,g}$ , is given as follows:

$$R_{f,g} = C - R_{o,p} \quad (10.32)$$

The radius of the outer circle of the gear,  $R_{o,g}$ , is calculated from the expression

$$R_{o,g} = R_g + a_g \quad (10.33)$$

The corner of the gear tooth addendum should be rounded with radius  $\rho_g$ , which is less than the fillet radius,  $\rho_p$ , of the pinion ( $\rho_g < \rho_p$ ).

\* Recall here that the equality  $l = r_N$  is observed. Here, the parameter  $l$  is the obsolete designation for the radius of the boundary Novikov circle,  $r_N$ .

The following relations among the design parameters of a Novikov gear pair are recommended by Novikov in [82,83]:  $r_p = r_N$ ,  $r_g \leq 1.10 \cdot r_p$ ,  $\rho_p = 0.3 \cdot r_N$ ,  $m_t/r_N = 0.8$ ,  $t_p/t_g = 1.5$ ,  $\phi_t = 30^\circ$ ,  $\lambda = 60 \dots 80^\circ$  ( $\psi = 10 \dots 30^\circ$ ), and circular pitch of the teeth  $p = t_g + t_p + B$ , where backlash  $B = 0.2 \dots 0.4$  mm.

The effective face width of the gear pair is given by:

$$F_{pa} = (1.1 \div 1.2) \cdot p \cdot \tan \lambda \quad (10.34)$$

For a preliminary analysis of Novikov gearing, the following empirical expression returns a practical value for the radius,  $r_N$ , of the boundary  $N$ -circle:

$$r_N = (0.05 \div 0.20) \cdot R_p \quad (10.35)$$

The performance of parallel-axes (Novikov gearing) strongly depends on the following three design parameters of the gears:

- The radius,  $r_N$ , of the boundary  $N$ -circle
- The transverse pressure angle,  $\phi_t$
- The lead angle,  $\lambda$

It should be noticed here one more time that smooth rotation of the driven shaft under a uniform rotation of the driving shaft is possible only if the transverse contact ratio of the Novikov gear pair is always equal to zero ( $m_p \equiv 0$ ) and the face contact ratio is greater than one ( $m_t = m_F > 1$ ).

The application of Novikov gearing ( $N_{by}$ -mesh of Novikov gearing in particular) featuring geometries of the tooth profiles known so far makes it possible to increase the contact strength of the gear teeth up to  $2.0 \div 2.1$  times and the bending strength up to  $1.3 \div 1.5$  times compared to involute helical gearing. Friction losses are up to  $2.0 \div 2.5$  less and tooth wear is  $3 \div 4$  times less in Novikov gearing [60]. All these application data are obtained for Novikov gearings that have hardness of the tooth surfaces up to  $HB$  350. During the years when Novikov gearing was actively being investigated, Novikov gearing with harder tooth flanks was not investigated.

The application of Novikov gearing makes possible the weight reduction of gear boxes (on average) 1.3 times.

Uniform rotation of the shafts in Novikov gearing is attained only due to face overlap of the gear teeth. Geometrically, meshing of gear teeth in a transverse cross-section is instant.

Geometrically, the active portions of the tooth flanks of the gear and the pinion in Novikov gearing are represented by two conjugate helices, that is, by two spatial curves. Under the applied load, these portions spread over helical strips along the helices.

The inactive portions of the tooth flanks are not conjugate to each other. Moreover, they are not envelopes to one another.

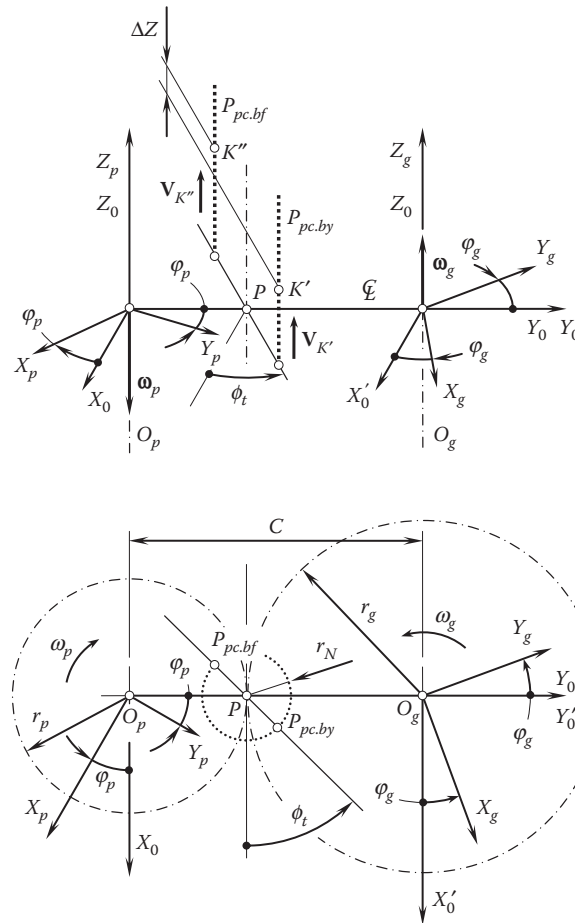
## 10.8 Conformal Gearing with Two Pseudo-Paths of Contact

Conformal gearing that features two pseudo-paths of contact is possible. Such a possibility immediately follows from the analysis of the schematic shown in Figure 10.9.

The possibility of a conformal gear pair that features two contact points,  $K'$  and  $K''$ , simultaneously, inspired R.V. Fed'akin to propose a conformal gearing that features not one pseudo-path of contact,  $P_{pc}$ , as in the original Novikov gear system, but two pseudo-paths of contact instead [31,32]. The invention by Fed'akin is schematically illustrated in Figure 10.20. Two pseudo-paths of contact,  $P_{pc.bf}$  and  $P_{pc.by}$ , are straight lines parallel to the axis of instant rotation of the gears. The pseudo-paths of contact,  $P_{pc.bf}$  and  $P_{pc.by}$ , pass through the points  $K'$  and  $K''$ . They are at distances  $+r_N$  and  $-r_N$  from the pitch point,  $P$ , respectively. As conformal gears are helical, the contact points,  $K'$  and  $K''$ , are displaced in the axial direction in relation to one another at a distance,  $\Delta Z$ . This distance can be calculated from the formula:

$$\Delta Z = 2 \frac{l}{\tan \psi} \quad (10.36)$$



**FIGURE 10.20**

Concept of conformal gear system that features two pseudo-paths of contact, as proposed by R.V. Fed'akin [31], and by R.V. Fed'akin and Chesnokov [32].

The axial displacement of the contact points results in a smoother rotation of the driven shaft of the conformal gear pair.

The average number of contact points between the gear and pinion tooth flanks is doubled in a conformal gear pair of this design.

When designing conformal gears, the gear designer is free to pick a favorable smooth curve to shape the inactive portions of the tooth profile of the gear and of the pinion. An arc of the curve has to be entirely located within the interior of the boundary  $N$ -circle for the tooth addendum, and a corresponding arc of the dedendum must be entirely located within the exterior of the boundary  $N$ -circle of a radius,  $r_N$ .

Use of the concept of Novikov gearing, two pseudo-paths of contact make it possible to design gears with two boundary  $N$ -circles with different radii,  $r_{N,1}$  and  $r_{N,2}$ . One of two boundary  $N$ -circles, that is, a boundary  $N$ -circle of a radius,  $r_{N,1}$ , is used in the design of a convex pinion tooth addendum that contacts a concave gear tooth dedendum. Another boundary  $N$ -circle of a radius,  $r_{N,2}$ , is used in the design of a concave pinion tooth addendum that contacts a convex gear tooth dedendum. Such a design of conformal gearing is not thoroughly investigated yet.

## 10.9 Tooth Flank Geometry in Conformal Gearing

The radii of curvature of the interacting tooth flanks of the gear and pinion in conformal gearing with two pseudo-paths of contact can be determined in the following way: a boundary  $N$ -circle of a certain radius,

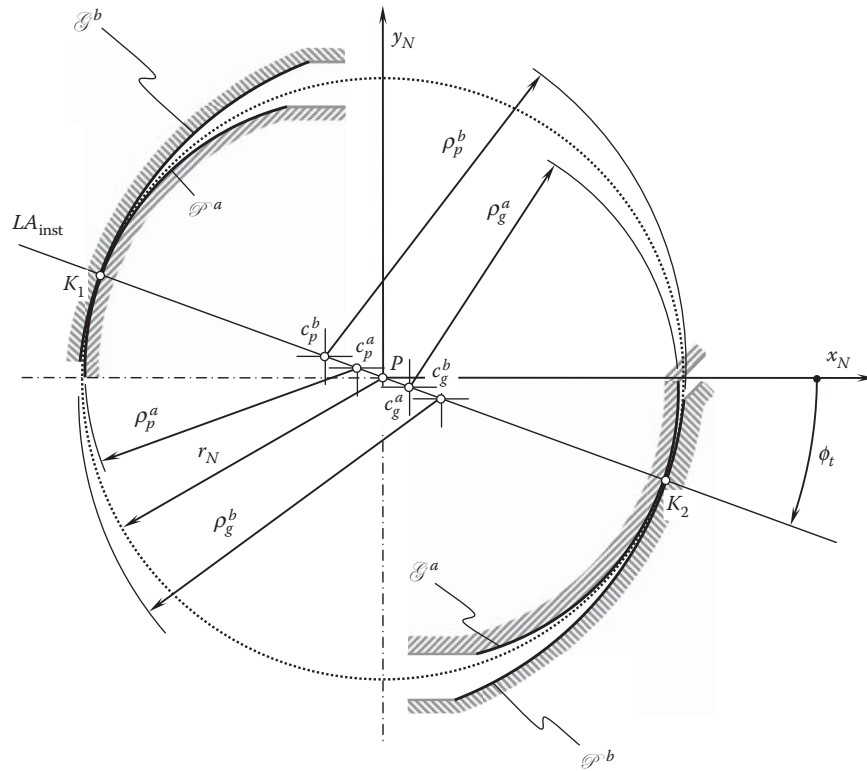


FIGURE 10.21

Tooth profiles  $G^b$  and  $G^a$  — to —  $P^a$  in conformal gearing that features two pseudo-paths of contact through  $K_1$  and  $K_2$ , correspondingly.

$r_N$ , is centered at the pitch point,  $P$ , as illustrated in Figure 10.21. In a local reference system,  $x_N y_N$ , that has the pitch point,  $P$ , as the origin, the position vector,  $\mathbf{r}_N$ , of a point of the boundary  $N$ -circle can be expressed in matrix form as follows:

$$\mathbf{r}_N(\varphi_N) = \begin{bmatrix} r_N \cos \varphi_N \\ r_N \sin \varphi_N \\ 0 \\ 1 \end{bmatrix} \quad (10.37)$$

where  $\varphi_N$  is the angular parameter of the boundary  $N$ -circle of radius  $r_N$ .

The instant line of action,  $LA_{inst}$ , is a straight line through the pitch point,  $P$ . The instant line of action,  $LA_{inst}$ , forms a transverse pressure angle,  $\phi_t$ , with a perpendicular to the centerline,  $\mathcal{C}$ , through the pitch point,  $P$ .

In the particular case under consideration, the addendum of the pinion,  $\mathcal{P}^a$ , is shaped in the form of a circular arc of a radius  $\rho_p^a$ . This circular arc is centered at a point,  $c_p^a$ , within the instant line of action,  $LA_{inst}$ . The radius of curvature,  $\rho_p^a$ , is smaller than the radius,  $r_N$ , of the boundary  $N$ -circle (that is, the inequality  $\rho_p^a < r_N$  is valid). In a local reference system,  $x_N y_N$ , the position vector,  $\mathbf{r}_p^a$ , of a point of the pinion addendum profile can be expressed in matrix form as follows:

$$\mathbf{r}_p^a(\varphi_p^a) = \begin{bmatrix} \rho_p^a \cos \varphi_p^a + (r_N - \rho_p^a) \cos \phi_t \\ \rho_p^a \sin \varphi_p^a - (r_N - \rho_p^a) \sin \phi_t \\ 0 \\ 1 \end{bmatrix} \quad (10.38)$$

In Equation 10.38, the angular parameter of the pinion addendum profile is denoted by  $\varphi_p^a$ .

In the particular case under consideration, the dedendum of the gear,  $\mathcal{G}^b$ , is also shaped in the form of a circular arc, the radius of which is  $\rho_g^b$ . This circular arc is centered at a point,  $c_g^b$ , within the line of action,  $LA$ . The radius of curvature,  $\rho_g^b$ , is larger compared to the radius,  $r_N$ , of the boundary  $N$ -circle (that is, the inequality  $\rho_g^b > r_N$  is observed). In the local reference system,  $x_N y_N$ , the position vector,  $\mathbf{r}_g^b$ , of a point of the gear dedendum profile can be expressed in matrix form as follows:

$$\mathbf{r}_g^b(\varphi_g^b) = \begin{bmatrix} \rho_g^b \cos \varphi_g^b + (r_N - \rho_g^b) \cos \phi_t \\ \rho_g^b \sin \varphi_g^b - (r_N - \rho_g^b) \sin \phi_t \\ 0 \\ 1 \end{bmatrix} \quad (10.39)$$

In Equation 10.39, the angular parameter of the gear dedendum profile is denoted by  $\varphi_g^b$ .

Similar to the way in which Equation 10.38 and 10.39 are derived, the corresponding expressions for the position vectors of a point of the pinion dedendum,  $\mathbf{r}_p^b$ , and the gear addendum,  $\mathbf{r}_g^a$ , can be derived:

$$\mathbf{r}_p^b(\varphi_p^b) = \begin{bmatrix} \rho_p^b \cos \varphi_p^b - (r_N + \rho_p^b) \cos \phi_t \\ \rho_p^b \sin \varphi_p^b + (r_N + \rho_p^b) \sin \phi_t \\ 0 \\ 1 \end{bmatrix} \quad (10.40)$$

$$\mathbf{r}_g^a(\varphi_g^a) = \begin{bmatrix} \rho_g^a \cos \varphi_g^a - (r_N + \rho_g^a) \cos \phi_t \\ \rho_g^a \sin \varphi_g^a + (r_N + \rho_g^a) \sin \phi_t \\ 0 \\ 1 \end{bmatrix} \quad (10.41)$$

In Equations 10.40 and 10.41, the angular parameter of the pinion dedendum and the gear addendum are designated as  $\varphi_p^b$  and  $\varphi_g^a$ , correspondingly.

Once the tooth profiles of the gear and pinion addendum and dedendum are described analytically (see Equations 10.38 through 10.41), equations for the corresponding tooth flanks,  $\mathcal{G}^a$ ,  $\mathcal{G}^b$ ,  $\mathcal{P}^a$ , and  $\mathcal{P}^b$ , can be derived.

For simplicity, but without loss of generality, Equations 10.33 through 10.36 are generalized in the form of a single equation as:

$$\mathbf{r}(\varphi) = \begin{bmatrix} \rho \cos \varphi + A \\ \rho \sin \varphi + B \\ 0 \\ 1 \end{bmatrix} \quad (10.42)$$

where  $\varphi$  is the angular parameter of the circular-arc profile, and the constants  $A$  and  $B$  are the values in terms of which the coordinates of the center of the corresponding point are expressed in a local reference system,  $x_{cr} y_{cr}$ .

The operator,  $\mathbf{Rs}(cr \mapsto fl)$ , of the screw motion of a circular-arc profile (see Equation 10.42) about the  $Z$ -axis can be represented in the form [137]:

$$\mathbf{Rs}(cr \mapsto fl) = \begin{bmatrix} \cos \vartheta & -\sin \vartheta & 0 & 0 \\ \sin \vartheta & \cos \vartheta & 0 & 0 \\ 0 & 0 & 1 & p\vartheta \\ 0 & 0 & 0 & 1 \end{bmatrix} \quad (10.43)$$

where:

$\vartheta$  is the angular parameter of the helical tooth flank (either  $\mathcal{G}^a$ , or  $\mathcal{G}^b$ , or  $\mathcal{P}^a$ , or  $\mathcal{P}^b$ ).

$p$  is the reduced pitch of the corresponding helical tooth flank.



The contact lines on the gear tooth flank,  $\mathcal{G}$ , and the pinion tooth flank,  $\mathcal{P}$ , are helices of opposite hands. If the screw parameter,  $p_p$ , of the pinion tooth flank (reduced pitch of the pinion),  $\mathcal{P}$ , is given, then for the calculation of the screw parameter,  $p_g$ , of the gear tooth flank  $\mathcal{G}$  (reduced pitch of the gear) the expression  $p_g = p_p/u$  can be used. This means that conformal helical gears, which are in point contact, will transform rotation with a constant gear ratio if their screw parameters,  $p_g$  and  $p_p$ , are related as follows:

$$\frac{p_g}{p_p} = \frac{\phi_g}{\phi_p} \quad (10.46)$$

In Equation 10.46,

$$p_g = r_g \tan \lambda_g \quad (10.47)$$

where  $\lambda_g$  is the lead angle and  $r_g$  is the pitch radius of the gear.

Similarly,

$$p_p = r_p \tan \lambda_p \quad (10.48)$$

where  $\lambda_p$  is the lead angle and  $r_p$  is the pitch radius of the pinion.

### 10.11 Local and Global Contact Geometry of Interacting Tooth Flanks

The tooth flanks of the gear and the pinion in a conformal gear pair are assumed to be smooth regular surfaces. The tooth flanks share a common point, which in fact is a point of culmination.

Representation of two contacting tooth flanks,  $\mathcal{G}$  and  $\mathcal{P}$ , in the form of a surface of relative curvature is a practical and widely used kind of surface representation for the purpose of analytically describing the contact geometry of the tooth flanks. An approximation of this kind works perfectly in the differential vicinity of the point of contact. It also covers a greater area around the point of contact of the surfaces in cases when the radii of relative curvature are large enough and significantly exceed the size of the patch of contact. Under such conditions, the contact geometry of the tooth flanks of the gear,  $\mathcal{G}$ , and the pinion,  $\mathcal{P}$ , can be perfectly described by the so-called *ellipse of contact*. Actually, the ellipse of contact is a three-dimensional (3D) curve whose projection onto the tangent plane through the point of contact of the surfaces resembles an ellipse. For a more accurate approximation of the contact geometry of the tooth flanks of the gear,  $\mathcal{G}$ , and of the pinion,  $\mathcal{P}$ , of a conformal gear pair, the methods discussed in Appendix E can be implemented.

Studies of the area of contact and the shape of contact area are commonly based on the assumption that the difference between the profile radii of the tooth flanks,  $\mathcal{G}$  and  $\mathcal{P}$ , is equal to zero.

In the differential vicinity of the point of contact of the tooth flanks,  $\mathcal{G}$  and  $\mathcal{P}$ , the patch of contact is bounded by an ellipse-like curve; that is, this curve can be expressed in terms of second order. However, the radii of relative curvature in the case under consideration are small enough. This is because a convex local patch of the tooth addendum interacts with a saddle-like local patch of the tooth dedendum. The high degree of conformity of the contacting tooth flanks,  $\mathcal{G}$  and  $\mathcal{P}$ , results in small radii of relative curvature. A conclusion can be immediately drawn up from the fact that the outside the differential vicinity of the point of contact boundary curve of the patch of contact between the tooth flanks,  $\mathcal{G}$  and  $\mathcal{P}$ , should differ from what is observed in the differential vicinity of the point of contact when the radii of relative curvature are small. This statement is proved analytically.\*

In a greater area around the point of contact of the tooth flanks of the conformal gears, the terms of the third and higher orders rapidly become important compared with the second-order terms, and they give rise to *banana-shaped* gap contours and the region of potential interference. It is found that a third-order approximation is quite useful in that it gives an analytical expression for the gap, which remains a good approximation of the sufficient distance away from the point of contact so as to provide a good description of these unusual features.

\* It should be pointed out here that because the teeth of gears conform to each other so closely, the conventional *Hertzian second-order equation* may no longer be adequate.

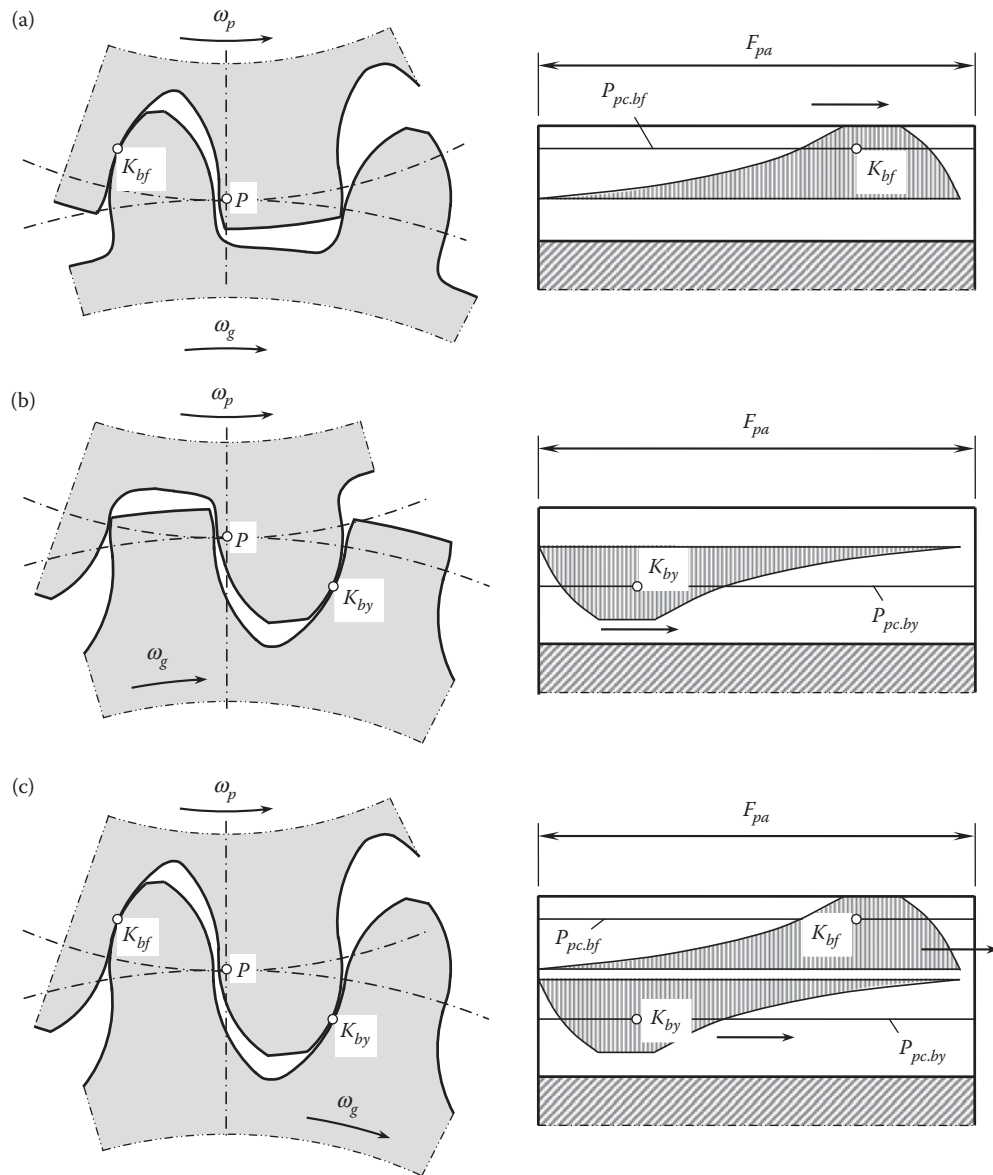


**FIGURE 10.23**  
Contact patches between the teeth flanks in conformal gear pairs.

The qualitative results of the investigation of the contact area of conformal gears are illustrated in [Figure 10.23](#). In [Figure 10.23](#), the shape of the tooth profiles, shapes and configurations of the contact lines, and shapes of the contact areas and directions of their motion are illustrated for conformal gear pairs of various kinds.

In [Figure 10.23a](#), an example of an  $N_{bf}$ -type of conformal gear pair is shown. This type of conformal gear features one pseudo-path of contact,  $P_{pc.bf}$ , which is a straight line parallel to the axis of instant rotation of the gears. The pseudo-path of contact,  $P_{pc.bf}$ , passes through the contact point,  $K_{bf}$ . The pinion features a concave tooth profile. The pinion is driving the gear, which has a convex tooth profile. The contact area between the tooth flanks,  $\mathcal{G}$  and  $\mathcal{P}$ , of the gear and pinion is bounded by a banana-like contour. The wider side of the contact area faces toward the bottom of the gear tooth.

An example of the  $N_{by}$ -type of conformal gear pair is illustrated in [Figure 10.23b](#). Conformal gears of this type also feature one pseudo-path of contact,  $P_{p.by}$ , which is a straight line parallel to the axis of instant rotation of the gears. The pseudo-path of contact,  $P_{p.by}$ , passes through the contact point,  $K_{by}$ . The pinion features a convex tooth profile. The pinion drives the gear, which has a concave tooth profile. The contact area between tooth

flanks,  $\mathcal{G}$  and  $\mathcal{P}$ , of the gear and the pinion is bounded by a banana-like contour. The wider side of the contact area faces toward the top-land of the gear tooth.

The most widely used type of conformal gears features two pseudo-paths of contact,  $P_{c.bf}$  and  $P_{c.by}$  (Figure 10.23c). These pseudo-paths of contact are straight lines parallel to the axis of instant rotation of the gears. The pseudo-path of contact  $P_{c.bf}$  passes through the contact point  $K_{bf}$ , and the pseudo-path of contact  $P_{c.by}$  passes through the contact point  $K_{by}$ . The gear is driven by the pinion. The convex addendum of the gear tooth profile interacts with the concave dedendum of the pinion tooth profile, and the concave dedendum of the gear tooth profile interacts with the convex addendum of the pinion tooth profile. Two contact areas between the tooth flanks of the gear,  $\mathcal{G}$ , and the pinion,  $\mathcal{P}$ , are observed in this particular case. Both of them are bounded by banana-like contours. The wider sides of the contact areas face toward each other, and both face toward the axis of instant rotation of the gears.

The shape and size of the contact area between the tooth flanks of the gear and the pinion are of importance in the stress analysis of conformal gears.

As shown in Figure 10.23, the results of the analytical analysis correlate with results of the corresponding experiments.

Conformal gears with the design parameters of various values, that is, various values of the profile angle,  $\phi_i$ ; pitch helix angle,  $\psi_g$ ; radius,  $r_N$ , of the boundary  $N$ -circle; and mismatch of the radii of profile curvature,  $\Delta r$ , were investigated [60,64]. For the experiments, an experimental rig with a closed load loop was used.

Before beginning the experiments, every conformal gear pair underwent rotation for a run-in period of time. Then the gears were cleaned of the remains of the lubricant and treated by a solution of copper sulfate. Finally, the tooth flanks were coated with a layer of silver just a few micrometers thick. Electrolytic technology was used for this purpose. After preparing them for testing, the gears were placed back in the rig in the same position with respect to each other.

The experiments were carried out under light torque, which was applied to one gear of the gear pair. The other gear remained stationary. Angular vibrations were applied to one of the gears. The angular magnitude of the vibrations was in the range  $\Delta\varphi \leq 15'$ . An increase in size of the contact area did not exceed 5%.

Figure 10.24 is a reproduction of the photograph of the gear of a conformal gear pair that has one pseudo-path of contact and a pitch helix angle  $\psi_g = 30^\circ$ . The banana-shaped contact area is clearly seen from Figure 10.24.

Reduction of the pitch helix angle results in a corresponding increase of the length of the contact area. Examples of various shapes of the contact area for conformal gear pairs that have different pitch helix angles are schematically depicted in Figure 10.25.

The results of research studies similar to the aforementioned ones align with those obtained by other researchers [1,168].

In addition to favorable conditions of contact, conformal gears enable better conditions for lubrication. When the gears rotate, the tooth flanks of the gear and the pinion roll over each other without sliding (or almost without

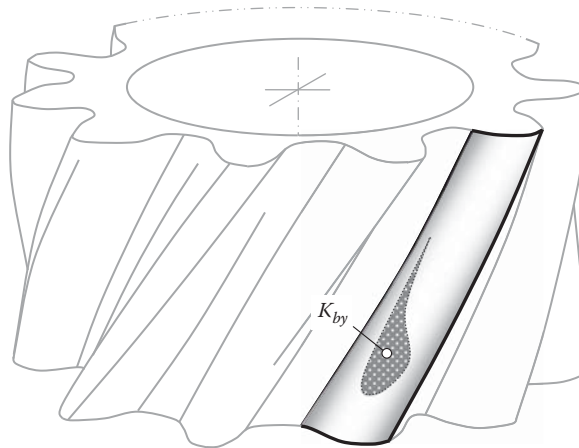
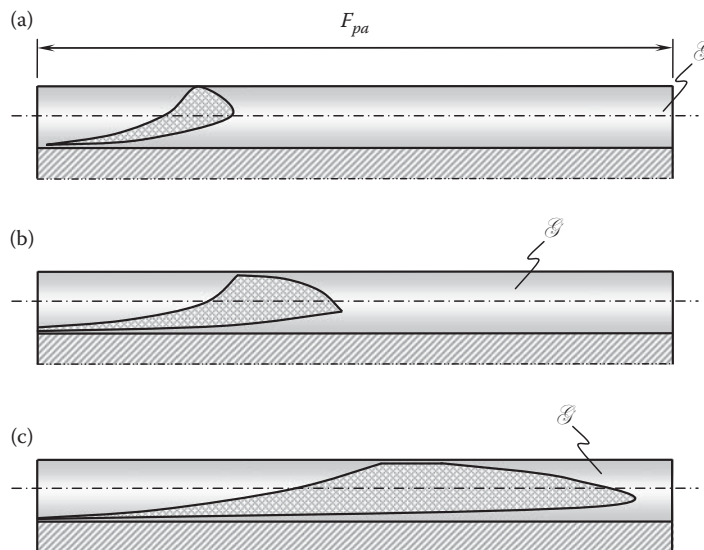


FIGURE 10.24

An example of an experimentally obtained contact pattern between the teeth flanks of a gear,  $\mathcal{G}$ , and a mating pinion,  $\mathcal{P}$ , in conformal gearing. (After Krasnoschokov, N.N., Fed'akin, R.V., and Chesnoschokov, V.A., *Theory of Novikov Gearing*, Moscow: Nauka, 1976.)



**FIGURE 10.25**

Shape of the contact area between the teeth flanks in a conformal gear pair that has pitch helix angles: (a)  $\psi = 30^\circ$ , (b)  $\psi = 20^\circ$ , and (c)  $\psi = 10^\circ$ .

sliding). The speed of the rolling contact point in the rolling motion significantly exceeds the linear speed of rotation of the gears. Hence, the oil film thickness is greater and the conditions of lubrication are significantly better.

## 10.12 High-Conformal Gearing

The power density being transmitted by a gear pair is one of the most critical criteria for the evaluation of quality of a particular gear pair. An increase by all possible means of power density being transmitted through a gear pair is an important consideration in future developments in the theory of gearing, as well as in gear manufacture and applications.

Performance of conformal gear pairs is strongly correlated to the degree of conformity to each other of the gear tooth flank,  $\mathcal{G}$ , and the pinion tooth flank,  $\mathcal{P}$ , at every point of their contact. The more conformal the tooth flanks,  $\mathcal{G}$  and  $\mathcal{P}$ , at points of their contact, the better the performance of the conformal gear pair, and vice versa. This is the main reason conformal gearing (and later high-conformal gearing) has been developed and applied in the industry.

### 10.12.1 Contact Geometry in High-Conformal Parallel-Axes Gearing

General considerations of conformal gearing allow concluding that the substitution of convex-to-convex contact of the tooth flanks of a gear and a mating pinion (as observed in external involute gearing) by their convex-to-concave contact (as observed in conformal gearing) allows an increase of contact strength in conformal gearing. Favorable conditions of contact of the tooth flanks of the gear and the mating pinion are the main anticipated advantage of a conformal gear pair. It can be assumed that the higher the degree of conformity at point of contact of the tooth flanks, the higher the load-carrying capacity of the gear teeth. This immediately entails a corresponding increase in power density through the gear pair, which is of critical importance for the user of the gears. Therefore, the minimum possible mismatch in the curvature of the teeth of the gear and the pinion is strongly desirable.

In reality, the tooth flanks of a gear and a mating pinion in a conformal gear pair are displaced from their desirable positions. The undesirable linear and angular displacements are mostly because of manufacturing errors and mechanical deflections of the gear teeth, shafts, and housing that occur under the applied load because of the thermal extensions of the components and so forth. Conformal and high-conformal gearings are sensitive toward tooth flank displacements.

To accommodate for such displacements, a certain degree of mismatch in the curvature of gear and pinion teeth is necessary. Small mismatches are not capable of accommodating the displacements. However, as the mismatch increases, the contact stresses also increase. A high contact stress may lead to various forms of surface failures such as heavy wear, pitting, or scuffing damage. Therefore, a minimum degree of mismatch in the curvature of the teeth of gear and pinion must be determined in order to make a workable conformal gear pair. Otherwise, one of two scenarios may be observed:

- First, the gear pair is capable of absorbing the inevitable displacements of the tooth flanks, but the degree of conformity of the contacting tooth flanks is not sufficient for a high load-carrying capacity of the gear pair.
- Second, the gear pair features a sufficient degree of conformity of the tooth flanks, but is not capable of accommodating the tooth flank displacements.

In both cases, the gear pair has no chance of being successfully used in practice.

For a better understanding of the *trade-off* between the load-carrying capacity of conformal gearing and its capabilities being reasonably insensitive with respect to the tooth flanks displacement, it is instructive to discuss a following simplified schematic.

At every instant of time, the tooth flanks of a conformal gear pair contact each other at least at one point. When the gears rotate, the point of contact traces a line over each of the two tooth flanks. In reality, these lines are helices of opposite hands and equal axial pitch. As a result, at every contact point,  $K$ , the contact line of the gear,  $CL_g$ , and the contact line of the pinion,  $CL_p$ , share the common tangential straight line,  $t_{CL}$ .

Let us consider a section of the tooth flanks,  $\mathcal{G}$  and  $\mathcal{P}$ , that is intersected by a plane through the contact point,  $K$ . The plane is constructed so as to be perpendicular to the common tangential straight line,  $t_{CL}$ . The constructed section of the tooth flanks is schematically shown in [Figure 10.26](#).

The section of the gear tooth flank is labeled  $\mathcal{G}$ . Within the differential vicinity of the point of contact, the radius of curvature of the curve  $\mathcal{G}$  is labeled  $R_g$ . The radius,  $R_g$ , is negative ( $R_g < 0$ ), as the tooth profile is concave.

The section of the pinion tooth flank before the load is applied is labeled  $\mathcal{P}^*$ . After the load is applied and the pinion tooth flank slightly penetrates the gear tooth flank, the same section,  $\mathcal{P}^*$ , is labeled  $\mathcal{P}$ . It is assumed that within the differential vicinity of the point of contact, the radii of curvature of the curves,  $\mathcal{P}^*$  and  $\mathcal{P}$ , are of the same value,  $R_p$ . The radius of curvature is positive ( $R_p > 0$ ), as the pinion tooth profile is convex.

In the initial position of the tooth profiles,  $\mathcal{G}$  and  $\mathcal{P}$ , the contact point is labeled  $K_g$ . After the load is applied and the tooth flanks interfere with each other, the contact point is labeled  $K_p$ .

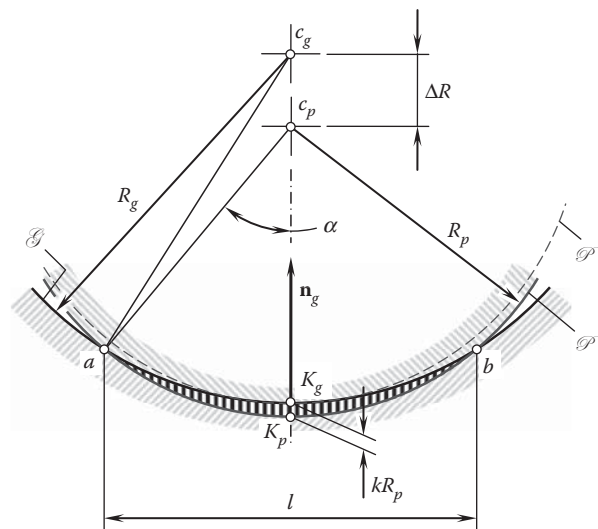


**FIGURE 10.26**

Section of the tooth flanks,  $\mathcal{G}$  and  $\mathcal{P}$ , of a conformal gear pair by a plane through a current point of contact: The plane is perpendicular to the trace of the contact point across the tooth flanks,  $\mathcal{G}$  and  $\mathcal{P}$ .

The tooth profiles,  $\mathcal{G}$  and  $\mathcal{P}$ , intersect each other at two points,  $a$  and  $b$ . The degree of conformity at the point of contact between the tooth profiles of radii  $R_g$  and  $R_p$  is indirectly estimated by the distance,  $l$ . The greater the distance,  $l$ , the higher the degree of conformity of the tooth flanks, and vice versa.

The distance,  $l$ , between points  $a$  and  $b$  can be expressed in terms of the radii of curvature,  $R_g$  and  $R_p$ , and the displacement,  $k$ :

$$l = 2R_p \sin \alpha(R_g, R_p, k) \quad (10.49)$$

For the calculation the angle  $\alpha(R_g, R_p, k)$ , the following formula is derived:

$$\alpha(R_g, R_p, k) = \cos^{-1} \left( \frac{R_p^2 - R_g^2 + (R_p + R_g - kR_p)^2}{2R_p(R_p + R_g - kR_p)} \right) \quad (10.50)$$

Derivation of Equation 10.50 is based on the law of cosines.

The angle  $\alpha$  in Equation 10.49 depends on the radii of curvature,  $R_g$  and  $R_p$ , as well as on the displacement  $k$ , as follows from Equation 10.50.

For convenience of further analysis of the plane section (see Figure 10.26), all the design parameters in Equation 10.50 are normalized by the radius of curvature,  $R_p$ , of the pinion. The normalized design parameters are designated as follows:

$$\frac{R_p}{R_p} = 1 \quad (10.51)$$

$$\frac{R_g}{R_p} = K \quad (10.52)$$

$$\frac{kR_p}{R_p} = k \quad (10.53)$$

The angle  $\alpha$  can be expressed in terms of the normalized design parameters in the following form:

$$\alpha = \cos^{-1} \left( \frac{1 - K^2 + (1 + K - k)^2}{2(1 + K - k)} \right) \quad (10.54)$$

The function  $l = l(k, K)$  is valid for both convex-to-convex, and convex-to-concave contacts of tooth flanks of the gear,  $\mathcal{G}$ , and the pinion,  $\mathcal{P}$ . For high-conformal gearing, only the case of convex-to-concave contacts of tooth flanks is of interest.

In Figure 10.27 is a three-dimensional plot of the function  $l = l(k, K)$  that is constructed for the cases of convex-to-concave contacts of tooth flanks of the gear,  $\mathcal{G}$ , and the pinion,  $\mathcal{P}$ .

Analysis of the 3D-plots allows the following conclusions.

Sections of the surface  $l = l(k, K)$  intersected by planes  $k_i = \text{Const}$  (see Figure 10.27), are represented by curves that have asymptotes. For a particular curve,  $k_i = \text{Const}$ , shown in Figure 10.27 in the bold line, the axis,  $\delta_{\text{cnfr}}$ , and the straight line,  $l = 1$ , are the asymptotes.

The greatest possible degree of mismatch in the curvature of the teeth of a gear and a mating pinion corresponds to the parameter  $K \rightarrow -\infty$ . An interval of changes in the parameter  $K$  starting from  $-\infty$  and going up to approximately  $K = -2$  can conveniently accommodate any desirable displacement of the tooth flanks,  $\mathcal{G}$  and  $\mathcal{P}$ , from their correct location. However, within the interval  $-\infty < K < -2$  of the change of the parameter  $K$ , the increase in the degree of conformity of the tooth profiles,  $\mathcal{G}$  and  $\mathcal{P}$ , is negligibly small. Within this interval of variation of the parameter  $K$ , the load-carrying capacity of a conformal gear pair remains approximately in the same range. Therefore, use of just the convex-to-concave contact of tooth flanks of the gear and pinion

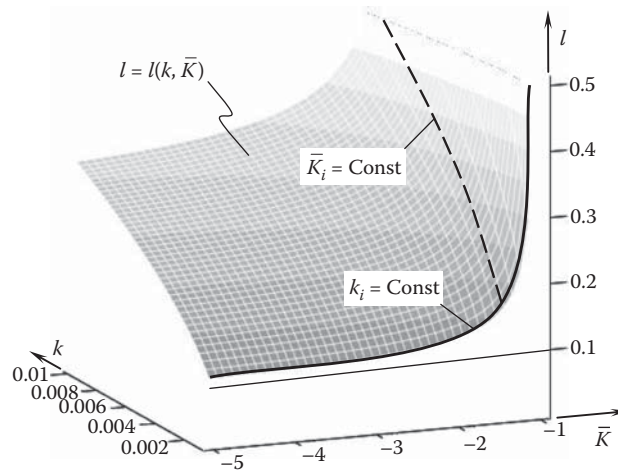


FIGURE 10.27

Three-dimensional plot of the function  $l = l(k, \bar{K})$  constructed for *convex-to-concave* type of contact of the tooth flanks of the gear,  $\mathcal{G}$ , and the pinion,  $\mathcal{P}$ , in a *high-conformal gear pair*.

gives almost no improvement to the load-carrying capacity of a gear pair. For convex-to-concave contact, an additional requirement needs to be met in order to significantly improve the load-carrying capacity of a conformal gear pair.

On the other hand, even a small change in the value of parameter  $K$  within the interval  $-2 < K < -1$  results in a significant increase in the degree of conformity of the teeth profiles,  $\mathcal{G}$  and  $\mathcal{P}$ . This immediately entails a corresponding increase in the load-carrying capacity of the gear pair.

### 10.12.2 High-Conformal Parallel-Axes Gearing

High-conformal gears feature convex-to-concave contacts of the tooth flanks of the gear and the pinion similar to those Novikov gearing\* features. In addition, the degree of conformity at point of contact of the tooth flanks of the gear and the pinion in *high-conformal gearing* exceeds a certain critical value, that is, a threshold.

In the aforementioned example (see Figure 10.27), the value of parameter  $K$  (that is, the value of  $K \approx -2$ ) can be referred to as a critical value, that is,  $K_{cr}$ . This allows one to distinguish between conformal gearing (for which  $-\infty < K < K_{cr}$ ), and high-conformal gearing (for which  $K_{cr} \leq K < -1$ ). Because of the favorable conditions of contact of the tooth flanks, high-conformal gears allow the transmission of higher power density.

Without going into the details of this analysis, it is clear that high-conformal gears require tight tolerances for any possible displacements of the tooth flanks of the gear,  $\mathcal{G}$ , and the pinion,  $\mathcal{P}$ , from their desirable locations and orientations. This relates not just to the tolerances of manufacturing errors, but to any and all possible displacements caused by thermal extension, elastic deflection, and so forth. Otherwise, there could be no future for high-conformal gear systems.

The areas of existence of conformal gearing and high-conformal gearing are schematically illustrated in Figure 10.28.

The performed analysis of the 3D-plot shown in Figure 10.27 can be extended, although the extension is a bit beside the main stream of the scope of the monograph.

\* The concept of Novikov gearing was not understood in detail by the majority of gear experts in the years immediately following Novikov's disclosure. The lack of information on the new gear system was the root cause for this. Later on, after the concept of Novikov gearing was properly disclosed and made available for the use of Western engineers, the principle differences between Novikov gearing [85] and Wildhaber gearing [161] became clear to most gear experts. The essence of Novikov gearing is disclosed in an S.U. patent [85], as well as in Novikov's doctoral thesis [84] and monograph [83], whereas the essence of Wildhaber gearing is disclosed in the U.S. patent [161]. A comparison of the principle features of the Novikov gear system claimed in Novikov's patent [85] and shortly after discussed in Novikov's doctoral thesis [83,84], and the principle features of Wildhaber's gear system claimed in the patent [161] makes it easy to distinguish between the two. Unfortunately, beginners and less experienced gear specialists often make no distinction between the Novikov gear system [85] and the gear system proposed by Wildhaber [161]. Many of them still loosely refer to Novikov gearing as W-N gearing. This term is completely incorrect.

It is instructive to point out here that in order to make the inconsistency of the term W-N gearing clear, one can wish to provide a definition to the term W-N gearing, that is, to formulate what the term W-N gearing stands for. This definition can be compared with that of the Novikov gear system [83–85], as well as the Wildhaber gear system.

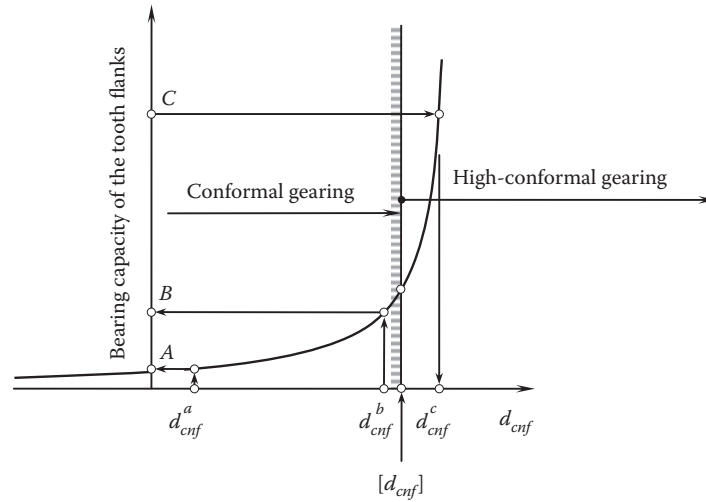


FIGURE 10.28

Impact of degree of conformity,  $d_{cnf}$ , at a current point of contact of a gear tooth flank,  $\mathcal{G}$ , and a mating pinion tooth flank,  $\mathcal{P}$ , onto the bearing capacity of the teeth flanks.

Consider sections of the surface  $l = l(k, K)$  intersected by planes  $K_i = \text{Const}$  (Figure 10.27). An example of such sections is shown by the bold dashed line. For high-conformal gears, parameter  $K_i$  for these lines is within the interval  $K_{cr} \leq K_i < -1$ . The degree of mismatch in the curvature of the teeth in high-conformal gears is smaller compared to that in conformal gears. Without going into the details of this analysis, it is important to point out here that the teeth profiles of high-conformal gears feature convex-to-concave type of contact, and the degree of mismatch in the curvature is small. The aforementioned features allow the conclusion that the Hertz formula is not applicable for the calculation of contact stress in conformal or high-conformal gears.

First, the *Hertz formula* for the calculation of contact stress was derived [43] under an assumption that the dimensions of the contact patch between two contacting surfaces are significantly smaller in comparison with the corresponding radii of curvature of the surface of relative curvature. This requirement is violated by the aforementioned features: a small degree of mismatch in the curvature of the teeth profiles of high-conformal gears results in the sizes of the contact patch becoming comparable with the corresponding radii of curvature of the surface of relative curvature, which is not allowed.

Second, the Hertz formula for the calculation of contact stress was derived [43] for the cases of contact of two bodies of simple geometry. Sphere-to-plane, sphere-to-sphere, and cylinder-to-plane are examples of shapes in relation to which the Hertz formula is valid. Generally speaking, in order to make the Hertz formula valid, the alignment of the principal directions of the contacting surface is a must. At a point of contact, the principal directions of the gear tooth flank are denoted by  $\mathbf{t}_{1,g}$  and  $\mathbf{t}_{2,g}$ . Similarly, at the same point the principal directions of the pinion tooth flank are denoted by  $\mathbf{t}_{1,p}$  and  $\mathbf{t}_{2,p}$ . The Hertz formula is valid in either of the following cases:

- $\mathbf{t}_{1,g}$  is aligned with  $\mathbf{t}_{1,p}$ , and  $\mathbf{t}_{2,g}$  is aligned with  $\mathbf{t}_{2,p}$ .
- $\mathbf{t}_{1,g}$  is aligned with  $\mathbf{t}_{2,p}$ , and  $\mathbf{t}_{2,g}$  is aligned with  $\mathbf{t}_{1,p}$ .

The greater the misalignment of the principal directions, the greater the deviation in the calculated values of contact stress from their actual values, and vice versa.

The active portions of the tooth flanks in high-conformal gears are surfaces that have complex geometry. For these surfaces, the requirement of alignment of the principal directions  $\mathbf{t}_{1,g}$ ,  $\mathbf{t}_{2,g}$  and  $\mathbf{t}_{1,p}$ ,  $\mathbf{t}_{2,p}$  is not fulfilled. This is the second reason the Hertz formula is not valid for the calculation of contact stress between the tooth flanks of high-conformal gears.

Indicatrices of conformity of the kinds  $Cnf_R(\mathcal{G}/\mathcal{P})$  and  $Cnf_k(\mathcal{G}/\mathcal{P})$  are developed for the analytical description of the contact geometry of the interacting tooth flanks,  $\mathcal{G}$  and  $\mathcal{P}$ , of a gear pair (see Appendix E). Characteristic curves of these kinds can be used to construct the contour of the contact patch between two tooth flanks in high-conformal gearing. This can be helpful when solving contact stress problem for gearing of this system.

Based on the aforementioned investigation, high-conformal gearing can be characterized by the following features, each of which is important, and, moreover, all of them are sufficient to refer to this gearing as to high-conformal gearing:

- The transverse contact ratio is identical to zero ( $m_p \equiv 0$ ).
- The total contact ratio,  $m_t$ , is equal to the face contact ratio,  $m_F$ , and is greater than one ( $m_t = m_F > 1$ ).
- The tooth profile of one member of the gear pair is convex, whereas that of the mating gear is concave.
- The convex tooth profile of one member of the gear pair is entirely located within the interior of the boundary  $N$ -circle, whereas the concave tooth profile of the other member of the gear pair is entirely located within the exterior of the boundary  $N$ -circle.
- The difference between the magnitudes of the radii of curvature of the concave tooth profile and the convex tooth profile in the gear pair is equal to or smaller than a specified threshold beyond which the high conformity of the interacting tooth profiles contributes much to the bearing capacity of the gear pair.

The four first listed above features are common for both Novikov gearing and high-conformal gearing. High-conformal gearing differs from Novikov gearing only by the last of the aforementioned features. The difference between the radii of curvature is required in order to make the gear pair capable of absorbing tooth flank displacements due to manufacturing errors, deflections under the operating load, and deflections due to heat extension, as well as all the displacements.

Comparing high-conformal gearing (as well as Novikov gearing) with involute gearing, the following should be noticed:

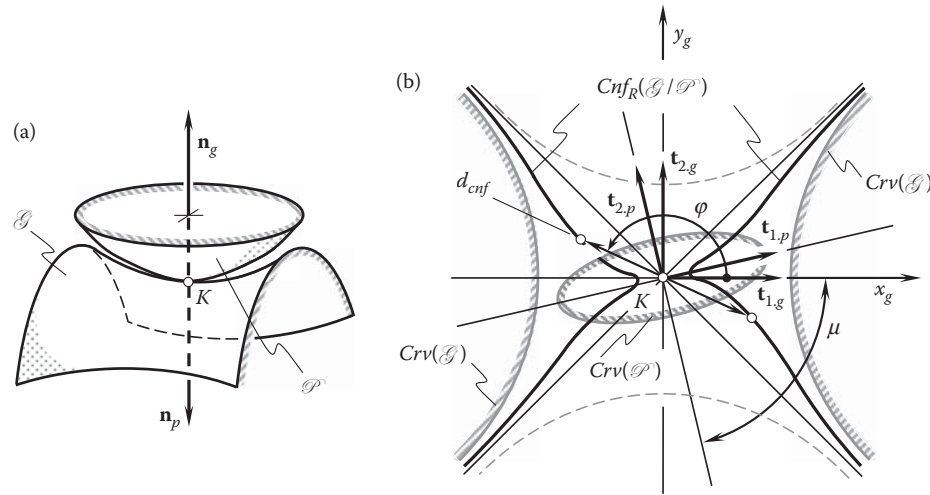
- The spur involute gearing proposed by Euler features a transverse contact ratio,  $m_p$ , greater than one ( $m_p > 1$ ); a zero face contact ratio ( $m_F = 0$ ); and a total contact ratio,  $m_t$ , equal to the transverse contact ratio ( $m_t = m_p > 1$ ). Later, the concept of spur involute gearing was enhanced to include the concept of helical involute gearing that has a face contact ratio greater than zero ( $m_F > 0$ ), and a total contact ratio  $m_t = m_p + m_F > 1$ . (i.e., in involute [Euler] gearing:  $m_p > 1$  and  $m_F = 0$ . Involute gearing can be referred to as *Euler gearing* or just *Eu-gearing* for simplicity.)
- Proposed by Novikov, so-called Novikov gearing (or just  $N$ -gearing for simplicity) features a zero transverse contact ratio ( $m_p \equiv 0$ ); a face contact ratio greater than one ( $m_F > 1$ ); and a total contact ratio,  $m_t$ , equal to the face contact ratio ( $m_t = m_F > 1$ ). Later, the concept of Novikov gearing was enhanced to include the concept of high-conformal gearing that has a degree of conformity at a point of contact of the interacting tooth flanks of the gear and the pinion equal to or smaller than a predetermined threshold (Novikov gearing:  $m_p \equiv 0$  and  $m_F > 1$ ).

As all possible combinations of the values of transverse contact ratio,  $m_p$ , and face contact ratio,  $m_F$ , are covered by either Euler gearing or Novikov gearing, it can be concluded that no new gear system can be developed based on the various combinations of contact ratios.\*

The term high-conformal gearing is broader than the term Novikov gearing. Novikov gearing features a convex-to-concave contact of the tooth flanks of the gear and the pinion, and a particular configuration of the tooth flanks in relation to the line of action under which the transverse contact ratio of a gear pair is identical to zero ( $m_p \equiv 0$ ) and the face contact ratio is always greater than one ( $m_F > 1$ ). In addition, high-conformal gearing features a certain degree of conformity at a point of contact,  $K$ , of the tooth flanks  $\mathcal{G}$  and  $\mathcal{P}$ . The minimum diameter,  $d_{cnf}$ , of the indicatrix of conformity,  $Cnf(\mathcal{G}/\mathcal{P})$ , at a current point of contact,  $K$ , of the tooth flanks,  $\mathcal{G}$  and  $\mathcal{P}$ , can be used as a quantitative measure of the degree of conformity of the interacting tooth flanks. The degree of conformity at point of contact of the tooth flanks of the gear,  $\mathcal{G}$ , and the pinion,  $\mathcal{P}$ , exceeds a threshold beyond which a significant increase in the bearing capacity of the interacting tooth flanks is observed. Schematically, this property of high-conformal gearing is illustrated in [Figure 10.29](#).

\* It is evident that the *Helical Gearing* patent proposed by Wildhaber does not meet the requirements of Euler gearing, nor does it meet the requirements of Novikov gearing. The widely adopted term Wildhaber-Novikov gearing clearly indicates poor understanding of the kinematics and geometry of both Novikov gearing, and of *Helical Gearing* (proposed by Wildhaber). The incorrect terminology must be eliminated from use among proficient gear experts. The invention by Novikov must be referred to as Novikov gearing, and the invention by Wildhaber must be referred to as Wildhaber gearing (or just the *Helical Gearing* patent as proposed by Wildhaber).



**FIGURE 10.29**

An example of the indicatrix of conformity,  $Cnf_R(\mathcal{G}/\mathcal{P})$ , at a point of contact of the tooth flanks,  $\mathcal{G}$  and  $\mathcal{P}$ , of a gear and a mating pinion.

For a certain degree of conformity,  $d_{cnf}^a$ , at point of contact of the tooth flanks,  $\mathcal{G}$  and  $\mathcal{P}$ , the bearing capacity of the tooth surfaces can be evaluated by a number,  $A$ . If the degree of conformity of the tooth flanks of the gear,  $\mathcal{G}$ , and the pinion,  $\mathcal{P}$ , is increased from  $d_{cnf}^a$  to a value of  $d_{cnf}^b$ , an insignificant increase in the bearing capacity of the tooth flanks from number  $A$  to number  $B$  occurs. The increase in bearing capacity is insignificant in the case under consideration, as both degrees of conformity,  $d_{cnf}^a$  and  $d_{cnf}^b$ , are smaller than the threshold  $[d_{cnf}]$  beyond which a significant increase in the bearing capacity of the tooth flanks,  $\mathcal{G}$  and  $\mathcal{P}$ , occurs.

Let us assume that the degree of conformity,  $d_{cnf}^c$ , is greater than the threshold,  $[d_{cnf}]$ . When the inequality  $d_{cnf}^c > [d_{cnf}]$  is valid, the bearing capacity of the tooth flanks of the gear,  $\mathcal{G}$ , and the pinion,  $\mathcal{P}$ , grows fast.

For high-conformal gearing, the inequality  $d_{cnf}^c \geq [d_{cnf}]$  is always observed.

The degree of conformity at the contact point,  $K$ , of a gear,  $\mathcal{G}$ , and its mating pinion,  $\mathcal{P}$ , tooth flanks in internal involute gearing is greater than that in a corresponding external involute gearing. Because of this, with respect to internal parallel-axes gearing, the concept of conformal gearing is not of significant importance, or it can even be useless.

The concept of high-conformal gearing is applicable to internal parallel-axes gearing as well. This becomes possible as the concept gives an opportunity to keep control over the contact geometry between tooth flanks of a gear and its mating pinion, as it helps to achieve (or exceed) the contact geometry required threshold. In conformal gearing, this is not possible.

### 10.13 On the Accuracy Requirements for High-Conformal Parallel-Axes Gearing

As discussed in previous sections, high-conformal gearing features a degree of conformity,  $d_{cnf}$ , at point of contact of the tooth flanks that exceeds a certain critical value,  $[d_{cnf}]$ ; that is, it exceeds a threshold for the degree of conformity ( $d_{cnf} \geq [d_{cnf}]$ ). This condition can be attained if the tolerances for the accuracy of the gear and the pinion are tightened.

In reality, none of the design parameters of a gear pair can be kept with a zero deviation: all of the design parameters of a gear pair are within the corresponding tolerances for the accuracy. For practical needs, it is important to estimate the influence of the variation of the design parameters onto the performance of a high-conformal gear pair.

In a high-conformal gear pair, linear displacements of the gear and the pinion in relation to one another can be expressed in terms of the three components along the axes of a *Cartesian* reference system. The reference system can be associated with the gear pair so as to minimize the total number of the components to be taken into account when calculating the design parameters of the gear and the pinion. If one of the axes is parallel



to the axis of instant rotation,  $P_{ln}$ , and another is along the centerline,  $\mathcal{C}$ , then the total linear displacement of the gear and the pinion in relation to one another is equal to the actual value of variation,  $\Delta C$ , of the center distance,  $C$ .

In Figure 10.30 (see the upper portion of the figure), an ideal high-conformal gear pair is schematically shown. Here, the center distance is equal to a certain value,  $C$ . In reality, because of manufacturing errors, as well as for other reasons, the actual value of the center distance,  $C^*$ , differs from  $C$  (see the upper portion of Figure 10.30). The alteration in the center distance inevitably entails corresponding changes to the diameters,  $d_{g,pc}$  and  $d_{p,pc}$ , of the gear and the pinion at which the path of contact is situated. The actual values of the diameters,  $d_{g,pc}$  and  $d_{p,pc}$ , are labeled as  $d_{g,pc}^*$  and  $d_{p,pc}^*$ , correspondingly.

The operating pressure angle also changes from its nominal value,  $\phi_t$ , to the actual value,  $\phi_t^*$ .

The changes to the center distance and to the pressure angle need to be taken into account when designing a high-conformal gear pair.

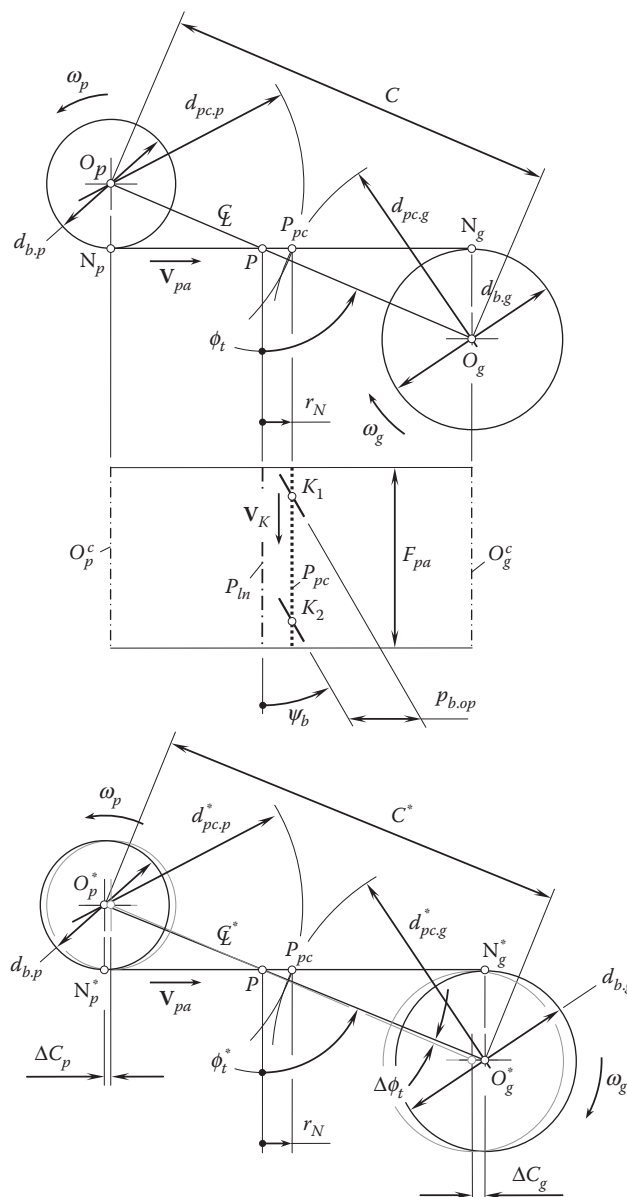


FIGURE 10.30

Variation of the center distance,  $C$ , and the operating pressure angle,  $\phi_t$ , in a real parallel-axes high-conformal gearing.

In the lower portion of Figure 10.30:

$$\frac{PO_p^*}{PO_g^*} = \frac{d_{b,p}}{d_{b,g}} \quad (10.55)$$

and

$$PO_g^* + PO_p^* = C^* \quad (10.56)$$

From these equations, the following expressions can be derived for calculating the parameters  $PO_g^*$  and  $PO_p^*$ :

$$PO_g^* = C^* \frac{d_{b,g}}{d_{b,g} + d_{b,p}} \quad (10.57)$$

$$PO_p^* = C^* \frac{d_{b,p}}{d_{b,g} + d_{b,p}} \quad (10.58)$$

Commonly, the actual value of the center distance,  $C^*$ , is not known. However, the tolerance,  $[\Delta C]$ , is known. Therefore, in the calculations, the actual center distance,  $C^*$ , is substituted with the sum  $C^* = C + [\Delta C]$ . It should be noticed here that the tolerance  $[\Delta C]$  is a signed value. With that said, Equations 10.57 and 10.58 cast into:

$$PO_g^* = (C + [\Delta C]) \cdot \frac{d_{b,g}}{d_{b,g} + d_{b,p}} \quad (10.59)$$

$$PO_p^* = (C + [\Delta C]) \cdot \frac{d_{b,p}}{d_{b,g} + d_{b,p}} \quad (10.60)$$

The calculated values of the parameters,  $PO_g^*$  and  $PO_p^*$ , yield the formula for the calculating of the operating pressure angle,  $\phi_t^*$ :

$$\phi_t^* = \sin^{-1} \frac{d_{b,g}}{PO_g^*} = \sin^{-1} \frac{d_{b,p}}{PO_p^*} \quad (10.61)$$

Equation 10.61 yields the calculation of the design parameters,  $PN_g^*$  and  $PN_p^*$ :

$$PN_g^* = (C + \Delta C) \cdot \frac{d_{b,g}}{d_{b,g} + d_{b,p}} \cos \phi_t^* \quad (10.62)$$

$$PN_p^* = (C + \Delta C) \cdot \frac{d_{b,p}}{d_{b,g} + d_{b,p}} \cos \phi_t^* \quad (10.63)$$

Once the operating pressure angle and the design parameters,  $PN_g^*$  and  $PN_p^*$ , are known, then the diameters,  $d_{pc,g}^*$  and  $d_{pc,p}^*$ , can be calculated from the equations:

$$d_{pc,g}^* = \sqrt{d_{b,g}^2 + 4 \cdot (PN_g^* - r_N)^2} \quad (10.64)$$

$$d_{pc,p}^* = \sqrt{d_{b,p}^2 + 4 \cdot (PN_p^* + r_N)^2} \quad (10.65)$$

A change to the center distance,  $C$ , results in the tooth flanks,  $\mathcal{G}$  and  $\mathcal{P}$ , of the gear and the pinion interacting with one another not by involute tooth points within each of them but instead contacting by points within the tooth profiles that are originally designed with the intent not to be involved in the transmission of the rotation. The conditions of meshing are violated because of this.

As an example, consider the influence of variation of the center distance alteration,  $\Delta C$ , onto the required change of radii of curvature of the gear and the pinion tooth profiles.

Figure 10.31 illustrates a portion of a concave gear tooth profile,  $\mathcal{G}^*$ , in a local vicinity of the involute tooth point. The involute tooth point coincides in Figure 10.31 with the projection of the pseudo-path of contact,  $P_{pc}$ , in the gear pair onto the plane of the drawing in Figure 10.31. The tooth profile,  $\mathcal{G}^*$ , corresponds to a case when the actual center distance,  $C^*$ , in a gear pair is greater than the desirable center distance,  $C$ , at a displacement,  $\Delta C$ . For comparison, the original concave gear tooth profile,  $\mathcal{G}$ , constructed for zero displacement of the gears, is also shown in Figure 10.31.

As the actual linear displacement is commonly unknown, the tolerance,  $[\Delta C]$ , for the displacement is considered instead.

The tolerance,  $[\Delta C]$ , is shared with the corresponding tolerances for the linear displacements,  $[\Delta C_g]$  and  $[\Delta C_p]$ , of the gear and the pinion in the following manner:

$$[\Delta C_g] = [\Delta C] \cdot \frac{d_{b,g}}{d_{b,g} + d_{b,p}} \quad (10.66)$$

$$[\Delta C_p] = [\Delta C] \cdot \frac{d_{b,p}}{d_{b,g} + d_{b,p}} \quad (10.67)$$

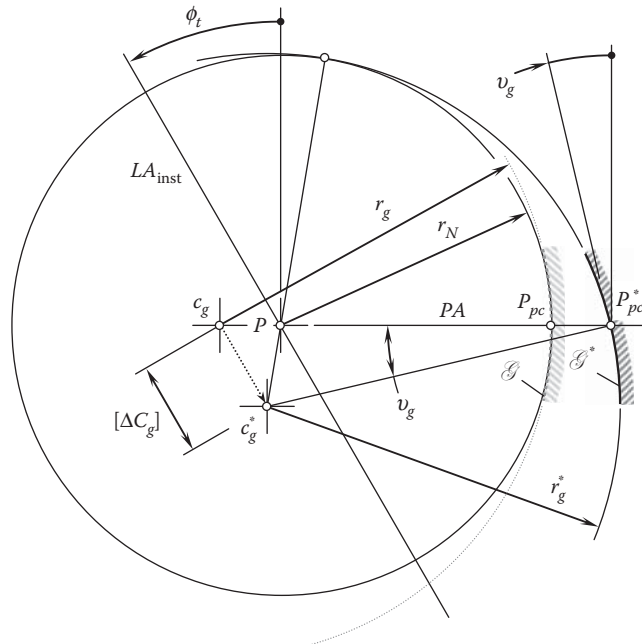


FIGURE 10.31

Configuration of the concave gear tooth profile,  $\mathcal{G}^*$ , in a high-conformal gear pair with an altered center distance,  $[\Delta C]$ .

The components,  $[\Delta C_g]$  and  $[\Delta C_p]$ , of the resultant tolerance,  $[\Delta C]$ , are the signed values. Evidently, the equality:

$$[\Delta C] = [\Delta C_g] + [\Delta C_p] \quad (10.68)$$

is valid.

After the gears are displaced, the gear tooth profile,  $\mathcal{G}^*$ , has to be entirely located outside the boundary  $N$ -circle of a radius  $r_N$ .

The original concave gear tooth profile,  $\mathcal{G}$ , is centered at point  $c_g$ . The radius,  $r_g$ , of this profile is known (here and below, only circular-arc gear tooth profiles are discussed as examples). The radius,  $r_g$ , is greater than the radius,  $r_N$  (that is, the inequality  $r_g > r_N$  is valid).

The concave gear tooth profile,  $\mathcal{G}^*$ , is centered at point  $c_g^*$ . The center,  $c_g^*$ , is displaced parallel to the centerline,  $\mathcal{C}$ , at a distance,  $[\Delta C_g]$ .

As follows from the analysis of Figure 10.31, the minimal permissible radius,  $r_g^*$ , of the concave gear tooth profile,  $\mathcal{G}^*$ , is greater compared to radius,  $r_g$ . The expression can be used for the calculation of the radius  $r_g^*$ :

$$r_g^* = r_g + \sqrt{[\Delta C_g]^2 + (c_g P)^2 - 2[\Delta C_g](c_g P) \sin \phi_t} \quad (10.69)$$

It is clear that the inequality  $r_g^* > r_g$  is valid.

The original concave gear tooth profile,  $\mathcal{G}$ , intersects the plane of action,  $PA$ , at a right angle. This is because the involute tooth point of the gear and the involute tooth point of the pinion make contact at culmination. Due to this, all three condition of meshing are met when the displacement is zero ( $[\Delta C] = 0$ ).

The concave gear tooth profile,  $\mathcal{G}^*$ , intersects the plane of action,  $PA$ , at a certain angle. The angle between the perpendicular to the plane of action,  $PA$ , and the tangent to the profile  $\mathcal{G}^*$  is designated as  $v_g$ . The smaller the angle,  $v_g$ , the better\*.

An equation similar to Equation 10.69 can be derived for the convex pinion tooth profile,  $\mathcal{P}^*$  (Figure 10.32):

$$r_p^* = r_p - \sqrt{[\Delta C_p]^2 + (c_p P)^2 - 2[\Delta C_p](c_p P) \sin \phi_t} \quad (10.70)$$

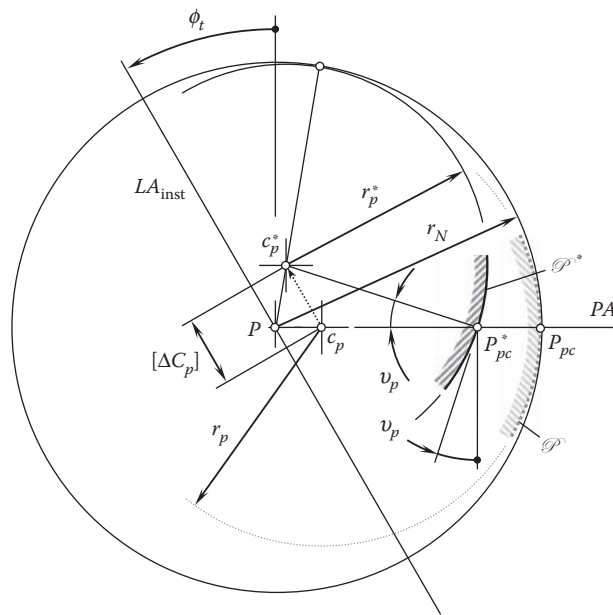
The degree of conformity,  $d_{cnf}^{\min}$ , for real high-conformal gearing needs to be calculated taking into account Equations 10.69 and 10.70. The calculated value of the diameter,  $d_{cnf}^{\min}$ , of the indicatrix of conformity at the point of contact of the tooth flanks,  $\mathcal{G}^*$  and  $\mathcal{P}^*$ , is then compared with the threshold,  $[d_{cnf}^{\min}]$ . If the inequality  $d_{cnf}^{\min} < [d_{cnf}^{\min}]$  is observed, then the gearing can be referred to as high-conformal gearing. Otherwise, that is, when the inequality  $d_{cnf}^{\min} > [d_{cnf}^{\min}]$  is observed, the gearing represents an example of conformal gear pair.

In a case where linear displacement,  $[\Delta C]$ , can take place in both directions, that is,  $[\Delta C^+]$  and  $[\Delta C^-]$ , the analysis needs to be performed for the both values of the displacements,  $[\Delta C^+]$  and  $[\Delta C^-]$ .

In perfect high-conformal gearings (as well as in conformal—Novikov gearings), that is, when the displacement,  $[\Delta C]$ , is zero, then both the angles  $v_g$  and  $v_p$  are zero, and the resultant angle,  $v$ , is also zero. Under such a scenario, all three conditions for proper transmission of a rotation can be fulfilled. All possible efforts need to be undertaken to minimize the angle  $v = v_g + v_p$ , for example, by increasing a radius,  $r_N$ , of the boundary  $N$ -circle. Gearings with a larger radius,  $r_N$ , of the boundary  $N$ -circle are less sensitive to the axes misalignment.

Similarly to the linear displacements of the gears in high-conformal gearing, angular displacements can also be taken into account when designing a high-conformal gear pair. For this analysis, the parallel-axes high-conformal gear needs to be considered as a crossed-axis gear pair having  $[\Delta C]$  as the center distance and  $[\Delta \Sigma]$  as the tolerance for the axis alignment [137]. Both tolerances,  $[\Delta C]$  and  $[\Delta \Sigma]$ , are signed values. This particular problem is more bulky compared to the case when only linear displacements are observed in a gear pair.

\* In involute gearing, when the center distance changes, the contact point between the tooth flanks of the gear and the pinion travels along the involute tooth profiles. Because of the tooth profiles are of involute geometry, this makes involute gearing insensitive to the variation of the center distance. In conformal and in high-conformal gearings, the involute tooth profiles are truncated to the involute point. When the center distance changes, the contact point between the tooth flanks of the gear and the pinion travels along the tooth profiles that are designed so as to not to be engaged in gear mesh. The last makes both conformal and high-conformal gearings sensitive to the variation of the center distance.



The discussion in this section also indirectly confirms that neither profile nor longitudinal modifications are allowed for conformal and high-conformal gears.

It was shown earlier (see [Figure 10.7](#)) that both conformal gearing and high-conformal gearing represent degenerate cases of a corresponding involute gearing. In involute gearing, the line of action,  $LA$ , is a straight line through the pitch point,  $P$ , of the gear pair. This line forms the transverse pressure angle,  $\phi_t$ , with the perpendicular to the centerline,  $\mathcal{C}$ . The path of contact,  $P_c$ , in involute gearing aligns with the line of action,  $LA$ ; that is, the identity  $P_c \equiv LA$  is valid. It is instructive to note here that involute gearing is the only type of parallel-axes gearing for which the identity  $P_c \equiv LA$  is observed. Fulfillment of the condition  $P_c \equiv LA$  makes involute

profiles conjugate to each other. No other shape of the gear teeth allow for the path of contact,  $P_c$ , be congruent to the line of action,  $LA$ . No other shapes of the gear teeth are conjugate to one another in a parallel-axes gearing—gear teeth of other geometries can be enveloping to each other, but not conjugate to one another. From this perspective, involute gearing is a unique kind of gearing.

When either conformal or high-conformal gears rotate, the only point of the gear tooth profile, that is, the involute tooth point of the gear, interacts with the corresponding involute tooth point of the mating pinion. The rest of the tooth profiles of both the gear and the pinion are inactive and do not interact with each other. Moreover, the inactive portions of the gear and the pinion tooth profiles are *not* conjugate to one another. Because of this, a certain freedom is given to the gear designer when designing the inactive portion of the gear and the pinion tooth profiles.

In contrast to the operation of conformal and high-conformal gearing, when machining gears for conformal and high-conformal gear pairs, not point contact of the tooth flanks, is required in the gear machining mesh, as observed in mesh of the tooth flanks  $\mathcal{G}$  and  $\mathcal{P}$ , of the gear and the mating pinion. Instead, line contact between the tooth flanks of the gear,  $\mathcal{G}$ , and of the gear cutting tool,  $\mathcal{T}$ , is required in the gear machining mesh. This means that conjugacy of the tooth profiles,  $\mathcal{G}$  and  $\mathcal{T}$ , is a must when machining gears for conformal and high-conformal gearings. The same is valid with respect to the  $\mathcal{P}$ -to- $\mathcal{T}$  machining mesh.

The required line contact between the tooth flanks of a gear,  $\mathcal{G}$ , and the gear cutting tool,  $\mathcal{T}$ , in the gear-machining mesh causes huge differences in meshing compared to those when high-conformal gears operate.

When a high-conformal gear spins in a gear-machining mesh (Figure 10.33), the gear tooth flank  $\mathcal{G}$ , and the machining surface,  $\mathcal{T}$ , of the gear-cutting tool contact each other along a  $\mathcal{G}$ -to- $\mathcal{T}$  line of contact, that is, along the characteristic line,  $\mathcal{E}$ . The characteristic line,  $\mathcal{E}$ , is a spatial 3D curve that intersects the plane of drawing in Figure 10.33 at a current contact point,  $K_i$ . The instant line of action,  $LA_{inst}$ , at every contact point,  $K_i$ , is along the unit normal vector,  $\mathbf{n}_i$  (Figure 10.34), and therefore is tangent at  $K_i$  to the path of contact. The tangent to the path of contact at  $K_i$  is the instant line of action,  $LA_{inst}$ . The instant line of action,  $LA_{inst}$ , intersects the centerline  $\mathcal{C}$  at a current pitch point  $P_i$ . The instant pitch point,  $P_i$ , subdivides the center distance,  $C$ , into two portions,  $O_g P_i$  and  $O_p P_i$  (that is,  $C = O_g P_i + O_p P_i$ ). The instant ratio  $O_g P_i / O_p P_i$  is reciprocal to the instant gear ratio in the gear machining mesh, that is:

$$\frac{O_g P_i}{O_p P_i} = \frac{\omega_p}{\omega_g} \quad (10.71)$$

where  $\omega_g$  and  $\omega_p$  are the rotations of the gear and the mating pinion, correspondingly.

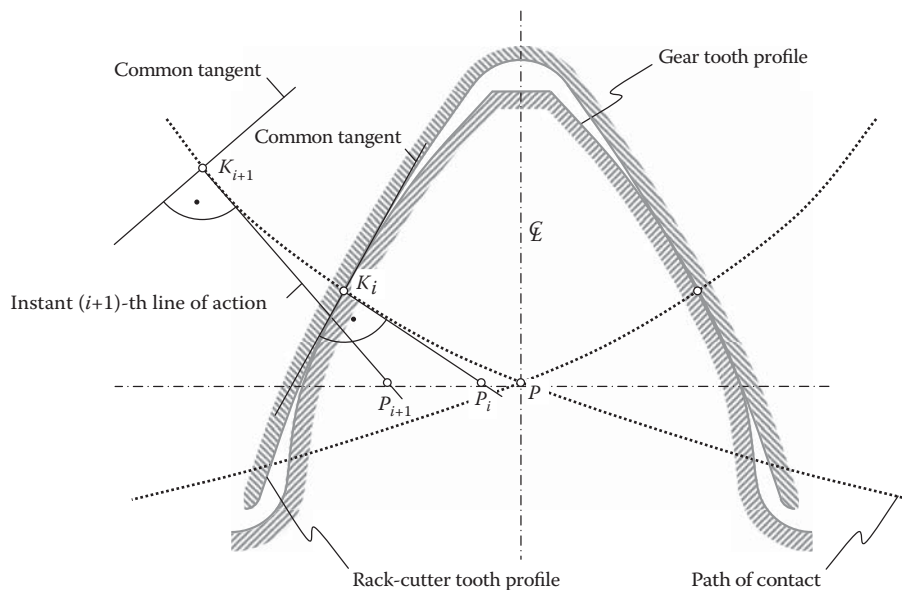


FIGURE 10.33

Instant lines of action,  $LA_{inst}$ , and paths of contact,  $P_c$ , in generating (continuous-indexing) machining processes of gears for conformal and high-conformal gearings.

When the contact point travels along the path of contact, the instant line of action intersects the center distance,  $\mathcal{C}$ , at different points,  $P_i$ . This means, that when the gear and gear-cutting tool rotate in a gear-machining mesh, the rotation of the gear can be steady, while the rotation of the gear-cutting tool must be unsteady. The last is impossible, for example, because there could be two contact points  $K_i$  and  $K_{i+1}$  simultaneously, and, as a consequence, two instant pitch points,  $P_i$  and  $P_{i+1}$ . A rigid body, that is, the gear-cutting tool, cannot spin at two different angular velocities simultaneously.

Another evidence of the impossibility of machining gears for high-conformal gearing in a continuous-indexing gear machining processes is as follows.

Assume that a gear is sliced by planes perpendicular to the gear centerline on an infinite number of zero-thickness slices. As gears for high-conformal gearing are always helical, each slice is turned about the centerline through a certain angle. Because of this, the contact points within each slice are shifted in relation to each other along the path of contact. This immediately results in an instant pitch point,  $P_i$ , for every slice. The orientation of unit normal vectors,  $\mathbf{n}_g$  and  $\mathbf{n}_g^*$ , to the gear tooth flank,  $\mathcal{G}$ , at different points,  $K_i$  and  $K^*$  (see Figure 10.34), within the instant line of contact,  $LC$ , in a continuous-indexing machining processes of gears for conformal and high-conformal gearing is different. The instant lines of action,  $LA_{inst}^i$ , are along the corresponding perpendicular to the gear tooth flank,  $\mathcal{G}$ .

Once there is a plurality of pitch points in the gear machining mesh, machining of a gear for high-conformal gearing in a continuous-indexing gear machining process becomes impossible, and thus the gears cannot be machined in compliance with the blueprint.

Once the entire profile of the gear teeth in Novikov gearing (including inactive portions of the gear teeth), and in high-conformal gearing is noninvolute, this means that profiles of this type cannot be machined in continuous-indexing gear machining process. Tooth profiles of the gear and pinion in Novikov gearing and in high-conformal gearing cannot be generated by the so-called *basic rack*. Violation of both the condition of conjugacy of the tooth profiles and the condition of equality of the base pitches in this case is the main reason for such infeasibility.

The so-called basic rack does not exist in the case of Novikov gearing or the case of high-conformal gearing. Association of a so-called basic rack with gears for Novikov gearing and high-conformal gearing is a huge mistake committed by many gear experts.

The efforts of hundreds of gear experts undertaken so far to improve Novikov gearing and enormous amounts of funds spent on this research were wasted just because the fundamental principles of gearing were ignored when investigating Novikov gearing.

It could be thought that in cases when the active portion of the path of contact in the gear machining mesh is close enough to a straight line, the gear, as well as the pinion tooth flanks,  $\mathcal{G}$  and  $\mathcal{P}$ , can be generated within the tolerance band for the accuracy of the tooth profile. This is correct in general consideration, but is not practical because of the following. The geometry of the path of contact in the gear-machining mesh is strongly correlated to the geometry of the tooth flank of the gear to be machined. The radii of curvature of the gear tooth flank of

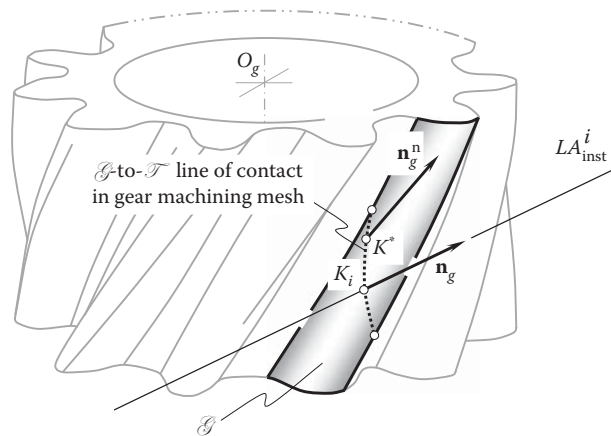


FIGURE 10.34

Orientation of unit normal vectors,  $\mathbf{n}_g$  and  $\mathbf{n}_g^*$ , to the gear tooth flank,  $\mathcal{G}$ , at different points,  $K_i$  and  $K^*$ , of the gear contact line in a generating (continuous-indexing) machining processes of gears for conformal, and high-conformal gearing.



both the gear,  $\mathcal{G}$ , and the pinion,  $\mathcal{P}$ , is close to the radius,  $r_N$ , of the boundary  $N$ -circle. The geometry of the boundary  $N$ -circle is different from that of the involute curve. As a result, the path of contact for a gear tooth profile with a limited mismatch from the boundary  $N$ -circle is different from that of a straight path of contact that occurs for the involute tooth profiles. Therefore, only a wide tolerance band for the gear tooth profile accuracy makes possible an approximation of the actual path of contact in the gear machining by a straight line segment. Wide tolerances for the gear tooth profile accuracy are not applicable for conformal and especially for high-conformal gearings.

It is likely the committed mistakes can be traced back to the publication by Kudriavtsev [62]. Kudriavtsev was the first (1959) who proposed cutting gears for Novikov gearing by means of specially designed gear hobs\*, the so-called *Novikov hobs*.

The infeasibility of correct generation of the tooth profiles of gears for Novikov gearing in generating (continuous-indexing) process of gear machining could be the root cause of insufficient performance of Novikov gearing, especially in cases of case-hardened tooth flanks of the gears. The continuous-indexing process of surface machining is not capable of machining gears with a correct correspondence between the radii of curvature of the convex and concave tooth profiles of the gear and the pinion in a Novikov gear pair.

No generating machining of the gear tooth flanks for Novikov gearing is permissible. Only indexed gear-cutting tools can be used for this purpose. Gears for Novikov gearing, as well as for high-conformal gearing, need to be cut by disk-type milling cutters†, disk-type grinding wheels, and so forth, that is, those used for this purpose form cutters and the indexing processes of surface generation.‡

The bottom line is as follows: no gears for conformal gearing or high-conformal gearing can be finish-cut in generating (continuous-indexing) machining processes.§

\* The acting standards (Russia, China) on Novikov gearing and gear-cutting tools for cutting them are out of critiques for their incorrectness. Gears for Novikov gearing cannot be cut (finish cut) by hobs, shaper cutters, shavers, worm grinding wheels, and others.

† It should be mentioned here that the first pair of Novikov gears made out of aluminum alloy (a preprototype) were cut on April 25, 1954, by means of a disk-type milling cutter [108,109,137]. Fifteen gear pairs for testing purposes were machined in the summer of 1954 by means of a disk-type milling cutter [108,109,137].

‡ It is the right point to stress here that successful accomplishment in machining of gears for Novikov gearing was attained by British gear engineers from Westland Helicopters, Inc. The extremely high-quality gears were finish-ground by means of the disk-type grinding wheel, using the indexing method for this purpose.

§ It can be shown that if special care is undertaken, a convex tooth profile of a pinion can be finish-cut in a generating (continuous-indexing) machining process. A mating concave gear tooth profile cannot be finish-cut in a generating (continuous-indexing) machining process.

# 11

## *Noninvolute Gearing*

Since the very beginning of the practical application of gears, all the gears used by ancient geniuses were gears with noninvolute tooth profiles. Involute gears were invented much later than gears with noninvolute tooth profiles. The kinematics and geometry of noninvolute gearing are of scientific interest and practical importance for gear engineers, as they are broadly used in industry, especially in cases when slow rotations are transmitted.

Prior to discussing in detail the kinematics of noninvolute gear pairs and the geometry of tooth flanks of noninvolute gears, a brief overview of known designs of noninvolute gearing is provided immediately below. The overview begins with a consideration of spur noninvolute gear pairs and is followed by a discussion on helical noninvolute pairs.

### 11.1 Spur Noninvolute Gear Pairs

Various practical applications of spur noninvolute gear pairs are well known. They are used to transmit a rotation from a driving shaft to a driven shaft in various designs of oil pumps, air blowers, and so forth. The tooth profiles of such gears are shaped in the form of cycloids and/or extended epicycloids, round pins, and special-purpose profiles.

In spur noninvolute gear pairs, only one pair of teeth is engaged in mesh at every instant of time. As will become clear from further discussion in this section, this does not mean that the transverse contact ratio in noninvolute gear pair equals one ( $m_p = 1$ ). This is incorrect, as the transverse contact ratio,  $m_p$ , cannot be identified. The face contact ratio,  $m_F$ , in spur noninvolute gear pairs is zero; that is, an equality  $m_F = 0$  is valid.

#### 11.1.1 Pin Gearing

Pin gearing is probably the first kind of noninvolute gearing ever invented. Initially, a small pinion was designed to have pins parallel to the pinion axis of rotation. The pins were evenly distributed circumferentially and assembled between two discs. The discs were rigidly connected to the driving shaft. A large gear had a disc rigidly connected to the driven shaft. The pins were mounted radially around the periphery of the disk with equal space between adjacent pins. A few more modifications of the initial design of pin gearing are also known.

In modern engineering practice, another design of pin gearing is used. The pinion teeth are cylindrical pins, so the teeth profile is a circle. The pinion is designed as an assembly of pins placed between two discs (Figure 11.1). Such a design does not require the generation of the pinion teeth, which is an important advantage of gearing of this particular design. Moreover, in huge pin gearing, the pins can rotate around journals or bearings. This allows for reduction of friction between interacting tooth surfaces, tooth wear, and, ultimately, power losses in the gear pair.

The gear tooth flank is not conjugate to the cylinder surface of the pins. Construction of the path of contact,  $P_c$ , for pin gearing (Figure 11.2) can be found in the work of Prof. Buckingham [11].

Pin gearing of the kind illustrated in Figure 11.1 is considered a particular case of cycloidal gearing. External and internal pin gearing of this particular kind can be designed for the purpose of transmitting a rotation between two parallel shafts.

Watch gears in the design of mechanical watches are probably the most important area of application of pin gearing. However, pin gearing is also broadly used in the design of huge construction and transportation machinery. In these applications, a larger amount of power is transmitted under a very slow rotation of the driving and driven shafts.

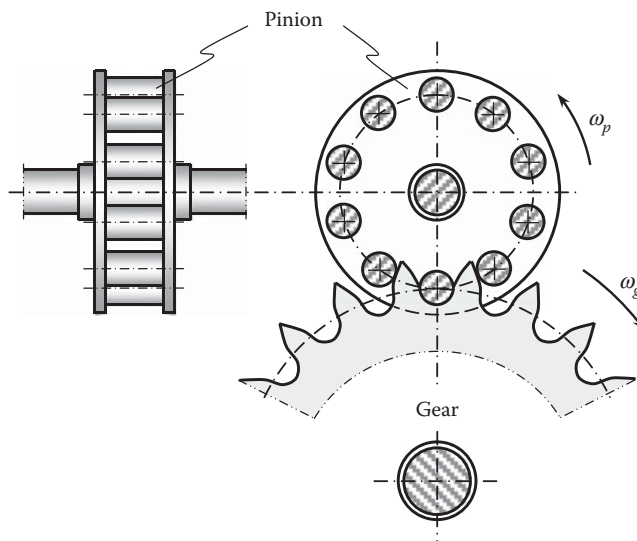


**FIGURE 11.1**  
Schematic of an external pin gearing.

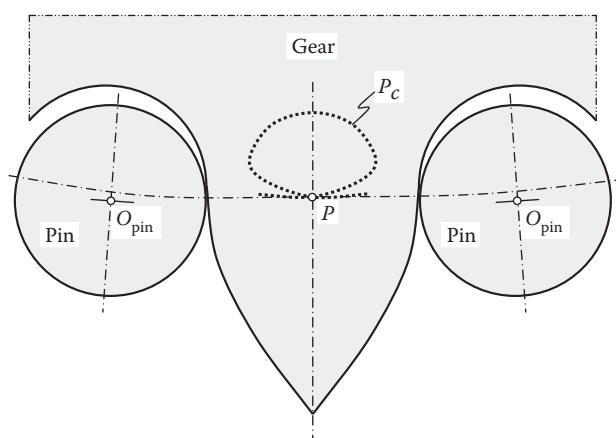


**FIGURE 11.2**  
An example of the path of contact,  $P_c$ , for an internal pin-tooth gear pair (Adapted from Buckingham, E., *Analytical Mechanics of Gears*, New York: Dover Publications, Inc., 1988, first published 1949.)

### 11.1.2 Cycloidal Gearing

Before involute gearing was invented by Euler, cycloidal gearing was the main type of gearing; it received wide application first of all in the design of watch gearings.

The cycloid of a circle is used as a tooth profile in cycloidal gearing. A cycloidal curve is generated as the trajectory of a point of a circle rolling without sliding over another circle (or over a straight line in a reduced case of cycloidal gearing). Henceforth, the difference between ordinary, extended, and shortened cycloids will be given.

An example of cycloidal gearing is schematically shown in [Figure 11.3a](#).

In [Figure 11.3a](#), the center of rotation,  $O_g$ , of the gear, and that of the pinion,  $O_p$ , are at a certain center distance,  $C$ . The rotations of the gear and the pinion are denoted by  $\omega_g$  and  $\omega_p$ , correspondingly. The pitch radius of the gear is designated as  $R_g$ , and that of the pinion is designated as  $R_p$ . The pitch point is denoted by  $P$ .

Two auxiliary centrodes of radii  $r_g$  and  $r_p$  that have centers at  $o_g$  and  $o_p$  are used to generate the addendum and dedendum of the tooth profile of the gear and the pinion.

The generation of the gear tooth profile can be executed in two steps:

First, to generate the gear tooth addendum, consider rolling with no sliding of an auxiliary axode (of a radius,  $r_p$ ) over the gear pitch circle (of a radius,  $R_g$ ). The circles of radii  $r_p$  and  $R_g$  are in external tangency in relation to

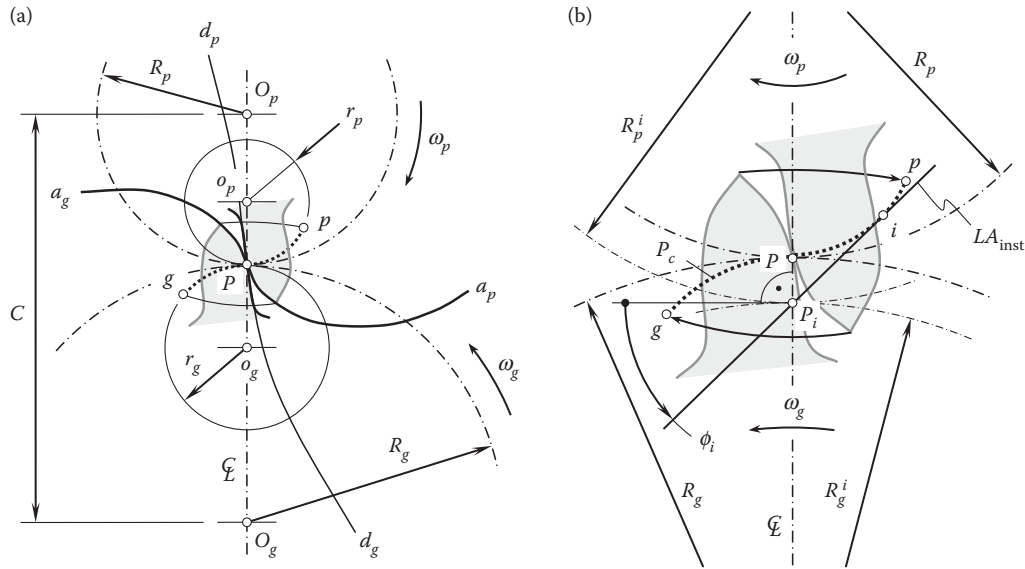


FIGURE 11.3

Schematic of cycloidal gearing: (a) cycloidal tooth profile, and (b) path of contact,  $P_c$ , and the instant line of action,  $LA_{inst}$ , in cycloidal gearing.

one another. The pitch circle of the gear is considered stationary. In such a relative motion, a point of the circle of a radius,  $r_p$ , traces the epicycloid,  $Pa_{g'}$ , within the transverse plane rigidly connected to the gear. A portion of the arc,  $Pa_{g'}$ , is used as the profile of the addendum of the gear tooth.

Second, to generate the gear tooth dedendum, consider rolling with no sliding of an auxiliary axode of a radius,  $r_g$ , over the gear pitch circle of a radius,  $R_g$ . The circles of radii  $r_g$  and  $R_g$  are in internal tangency in relation to one another. The pitch circle of the gear is considered stationary. In such a relative motion, a point of the circle of a radius,  $r_g$ , traces the hypocycloid,  $Pd_{g'}$ , within the transverse plane rigidly connected to the gear. A portion of the arc,  $Pd_{g'}$ , is used as the profile of the dedendum of the gear tooth.

Similar to the generation of the gear tooth profile, the generation of the pinion tooth profile can be executed in two steps as follows:

First, to generate the pinion tooth addendum, consider rolling without sliding of the auxiliary axode of a radius,  $r_g$ , over the pinion pitch circle of a radius,  $R_p$ . The circles of radii  $r_g$  and  $R_p$  are in external tangency in relation to one another. The pitch circle of the pinion is considered stationary. In such a relative motion, a point of the circle of a radius,  $r_g$ , traces the epicycloid,  $Pa_{p'}$ , within the transverse plane rigidly connected to the pinion. A portion of the arc,  $Pa_{p'}$ , is used as the profile of the addendum of the pinion tooth.

Second, to generate the pinion tooth dedendum, consider rolling with no sliding of the auxiliary axode of a radius,  $r_p$ , over the gear pitch circle of a radius  $R_p$ . The circles of radii  $r_p$  and  $R_p$  are in internal tangency in relation to one another. The pitch circle of the pinion is considered stationary. In such a relative motion, a point of the circle of a radius,  $r_p$ , traces the hypocycloid,  $Pd_{p'}$ , within the transverse plane rigidly connected to the gear. A portion of the arc,  $Pd_{p'}$ , is used as the profile of the dedendum of the gear tooth.

The path of contact,  $P_c$ , for a cycloidal gearing\* is a smooth, piecewise curve composed of two circular arcs of radii  $r_g$  and  $r_p$ . These two arcs,  $gP$  and  $pP$ , make up the path of contact,  $gPp$  (Figure 11.3a).

An enlarged view of two teeth in contact for cycloidal gearing is shown in Figure 11.3b. For the driving pinion and the driven gear, the tooth flanks are engaged in contact at the starting point,  $p$ , of the path of contact,  $P_c$ . As the pinion rotates,  $\omega_p$ , the contact point between the tooth flanks travels along the path of contact,  $P_c$ , from point  $p$  to point  $g$ . Point  $g$  is the end point of contact of the tooth flanks. While traveling along the path of contact,  $P_c$ , at a certain configuration of the gears, the contact point passes the pitch point,  $P$ . At every instant of time, the pinion tooth flank acts over the gear tooth flank along the instant line of action,  $LA_{inst}$ , that is, in the direction

\* The path of contact,  $P_c$ , in Figure 11.3 is shown assuming that only one pair of teeth makes contact, and the contact point traces the entire path of contact,  $P_c$ , from point  $p$  to point  $g$ . In reality, in cycloid gear pairs, as well as in noninvolute gear pairs of other designs, at a certain instant of time, the contact between one pair of teeth is terminated by the next pair of teeth that is entered in mesh. The interruption of the contact commonly happens long before the first contact point traverses the entire path of contact,  $P_c$  (from point  $p$  to point  $g$ ). This statement is also valid with respect to every transverse section in a helical noninvolute gear pair.

tangential to the path of contact,  $P_c$ , at the current point,  $i$ , within the path of contact,  $P_c$ . A straight line that is tangent at  $i$  to the path of contact,  $P_c$ , is referred to as the *instant line of action*,  $LA_{inst}$ .

As the path of contact,  $P_c$ , for cycloidal gearing is composed of two circular arcs, a straight line through point  $i$  tangential to  $P_c$  makes a different transverse pressure angle,  $\phi_{t-i}$ , with the perpendicular to the centerline,  $\mathcal{C}$ . Moreover, the location of the current pitch point,  $P_i$ , within the centerline,  $\mathcal{C}$ , can be determined as the point of intersection of the centerline,  $\mathcal{C}$ , by the instant line of action,  $LA_{inst}$ . The instant line action commonly is designated as  $LA_{inst}$ .

Due to the migration of the instant pitch point,  $P_i$ , back and forth along the centerline,  $\mathcal{C}$ , the current values of the pitch radii of the gear,  $R_g^i$ , and the pinion,  $R_p^i$ , differ from their nominal values (the inequalities  $R_g^i \neq R_g$  and  $R_p^i \neq R_p$  are observed). Under the uniform rotation of the driving pinion (when  $\omega_p = \text{const}$ ), and at a constant center distance,  $C$ , the alteration to the pitch radii  $R_g^i$  and  $R_p^i$  of the gear and the pinion causes a variation in the rotation,  $\omega_g$ , of the driven gear. Ultimately, the rotation,  $\omega_g$ , of the gear depends on the angle,  $\varphi_p$ , through which the pinion turns about its axis at a time,  $t$ ; that is, a certain functionality  $\omega_g = \omega_g(\varphi_p)$  is observed for cycloidal gearing. Here,  $\varphi_p = \omega_p t$ .

This consideration allows for an intermediate conclusion:

### Conclusion 11.1

*Cycloidal gearing is not capable of transmitting a uniform rotation smoothly, as the interacting tooth gear flanks are not conjugate to one another.*

This is first of all because in cycloidal gearing, the interacting tooth flanks  $\mathcal{G}$  and  $\mathcal{P}$  are *not conjugate* to one another.

Under a uniform rotation of the driving shaft, the rotation of the driven shaft is not uniform. As the result, cycloidal gearing is used to transmit slow rotations only. When a transmitting rotation is slow, and when the tooth numbers of the gear and the pinion are large enough, the impact of the fluctuation of the driven shaft becomes reasonably small.

It should be mentioned here that cycloidal gear pairs are sensitive to any change in the center distance,  $C$ .

### 11.1.3 Roots Blower

A *Roots blower*\* is another example of a spur gearing that features noninvolute tooth profile. Examples of Roots blowers are shown in [Figure 11.4](#)

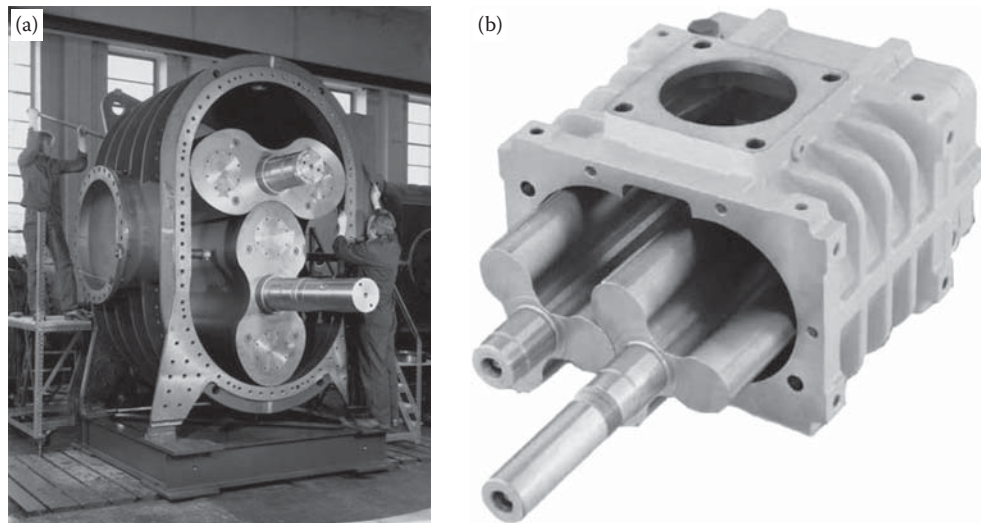


**FIGURE 11.4**  
Roots blowers: (a) two-lobe blower, and (b) three-lobe blower.

\* It is named for the American inventors and brothers Philander and Francis Marion Roots, founders of the Roots Blower Company, Connersville, Indiana, who first patented the basic design in 1860 as an air pump for use in blast furnaces and other industrial applications. In 1900, Gottlieb Daimler included a Roots-style supercharger in a patented engine design, making the Roots-type supercharger the oldest of the various designs now available. Roots blowers are commonly referred to as air blowers or positive displacement (PD) blowers.

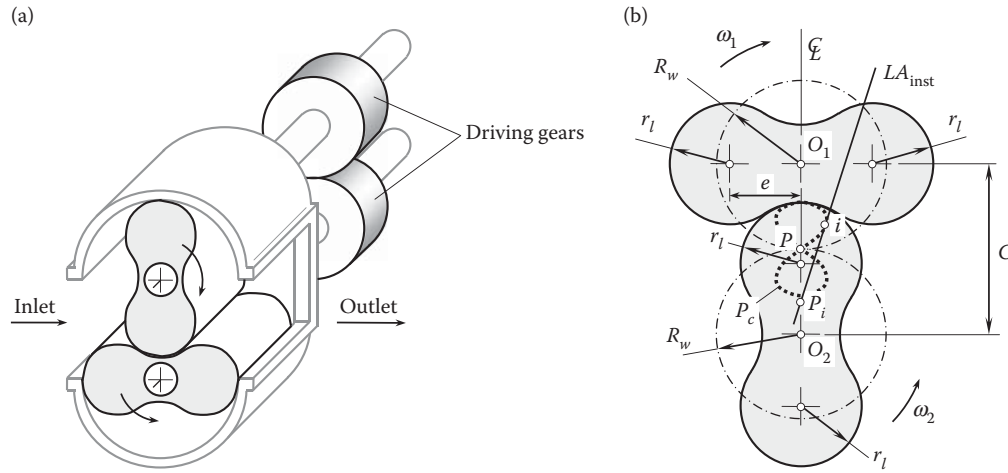


FIGURE 11.5

Two-lobe Roots blower (spur noninvolute gear pair): (a) schematic of the close-up of the blower, and (b) the interacting profiles of the lobes.

Referring to Figure 11.5a, a Roots blower is composed of two rotors. Each rotor has either two or three lobes. The rotors are mounted on shafts and assembled in a housing. The rotors are rotated with angular velocities  $\omega_1$  and  $\omega_2$  about their axes of rotation,  $O_1$  and  $O_2$ . Two driving gears are implemented to synchronize the rotations of the rotors about their axes. The tooth ratio of the driving gear pair is equal to one ( $u = 1$ ). The nominal pitch radius,  $R_w$ , of each rotor is equal to the pitch radius of the driving gear.

The transverse cross-section of the rotors is shaped in the form of four circular arcs of a radius,  $r_l$ , tangential to one another, as shown in Figure 11.5b.

An air discharger for diesel engines is a good example of practical application of Roots blowers.

Two different modes of meshing should be distinguished regarding the Roots blower lobe profiles.

In the first mode, let us assume that the rotors (Figure 11.5) are capable of transmitting a rotation from one shaft to another, or, in other words, let us assume that one of the rotors is the driving member and the another is the driven member of a pair of noninvolute gears represented by two rotors.

The transverse lobe profile of the rotor addendum is a circular arc of a radius,  $r_l$ , centered at a distance,  $e$ , from the axis of rotation of the rotor. The addendum angle of a rotor is equal to  $90^\circ$  for a two-lobe rotor and  $60^\circ$  for a three-lobe rotor.

Following the established practice of designing of Roots blower rotors, the following expression:

$$R_w^2 + e^2 - 2R_w e \cos \nu = r_l^2 \quad (11.1)$$

has to be fulfilled.

In Equation 11.1, the angle  $\nu$  is equal to  $45^\circ$  for two-lobe rotors and  $30^\circ$  for three-lobe rotors. The distance of the center of the circular lobe profile from the axis of rotation of the lobe is designated as  $e$  (see Figure 11.5b).

The position vector of a point,  $\mathbf{r}_1$ , of the rotor addendum can be analytically expressed by the following matrix equation:

$$\mathbf{r}_1(\theta) = \begin{bmatrix} r_l \sin \theta \\ r_l \cos \theta \\ 1 \end{bmatrix} \quad (11.2)$$

For two-lobe rotors, the angular parameter,  $\theta$ , is within an interval:

$$-2 \tan^{-1} \left( \frac{(e + r_l)^2 - R_w}{\sqrt{2} e R_w} \right) \leq \theta \leq 2 \tan^{-1} \left( \frac{(e + r_l)^2 - R_w}{\sqrt{2} e R_w} \right) \quad (11.3)$$



The dedendum of one of the rotors is generated by the addendum of the other one. Equation 11.2 of the lobe addendum allows the equation:

$$\mathbf{r}_2(\theta) = \begin{bmatrix} r_l \sin(\theta - 2\varphi) - e \sin 2\varphi + 2R_w \sin \varphi \\ r_l \sin(\theta - 2\varphi) + e \cos 2\varphi - 2R_w \cos \varphi \\ 1 \end{bmatrix} \quad (11.4)$$

for position vector of a point,  $\mathbf{r}_2$ , of the rotor dedendum.

In Equation 11.4, the current value of the angle of rotation of the rotor,  $\varphi$ , is calculated as the root of the equation of contact:

$$R_w \sin(\theta - \varphi) - e \sin \theta = 0 \quad (11.5)$$

The position vector of a point of the line of action,  $\mathbf{r}_{la}$ , can be expressed in the form of a column matrix:

$$\mathbf{r}_{la}(\theta) = \begin{bmatrix} r_l \sin(\theta - \varphi) - e \sin \varphi \\ r_l \sin(\theta - \varphi) + e \cos \varphi \\ 1 \end{bmatrix} \quad (11.6)$$

The equation of contact for the path of contact,  $P_c$ , can be represented in the following form:

$$R_w \sin(\theta - \varphi) - e \sin \theta = 0 \quad (11.7)$$

It should be stressed here that when the equalities  $e = R_w$  and  $\varphi = 0$  are valid; that is, when the circular arc of a radius,  $R_w$ , is centered at the instantaneous center of rotation,  $P$ , all the perpendiculars to the lobe profile pass through the pitch point,  $P$ , under any value of the angular parameter,  $\theta$ . Therefore, the relation  $e = R_w$  should be avoided when designing rotors for Roots blowers.

The path of contact in [Figure 11.5b](#) is labeled as  $P_c$ . For an arbitrary point,  $i$ , within the path of contact, an instant line of action,  $LA_{inst}$ , that is tangential at  $i$  to the path of contact,  $P_c$ , is constructed. The instant line of action,  $LA_{inst}$ , and the centerline,  $\mathcal{C}$ , intersect each other at the instant pitch point,  $P_i$ . Generally speaking, the instant pitch point,  $P_i$ , is not coincident with the nominal pitch point,  $P$ . Therefore, under a constant center distance,  $C$ , and uniform input rotation,  $\omega_1$ , of a driving rotor, the rotation of the driven rotor,  $\omega_2$ , is not uniform. Moreover, for certain locations of point  $i$  within the path of contact,  $P_c$  (i.e., when the instant line of action,  $LA_{inst}$ , is parallel to the centerline,  $\mathcal{C}$ ), conditions for the transmission of a rotation are especially unfavorable.

Let us consider the second mode. Because of each of the rotors is driven by the individual gear, the rotors are rotated smoothly. However, when driven individually, a gap between the lobe profiles is always observed. A Roots blower is not workable without there being a minimum permissible gap between the lobe profiles. The minimum permissible width of the gap does not have a constant value and depends on actual value of the angle of rotation of the rotors. Once a gap always occurs between the lobes of the rotors, no straight path of contact is observed in the case under consideration ([Figure 11.5b](#)).

It should be mentioned here that the closest distance of approach,  $\delta_{cda}$ , between the working surfaces of the rotors can be calculated. This distance,  $\delta_{cda}$ , depends on the angular orientation of the rotors. As the rotors rotate, the closest distance of approach,  $\delta_{cda}$ , alters from its minimum value,  $\delta_{cda}^{\min}$ , to its maximum value,  $\delta_{cda}^{\max}$ . The inequality  $\delta_{cda}^{\min} \leq \delta_{cda} \leq \delta_{cda}^{\max}$  is valid for Roots blowers that have spur rotors.

This consideration allows for an intermediate conclusion:

## Conclusion 11.2

*Spur rotors of Roots blowers are not capable of transmitting a rotation smoothly, as they are not conjugate to one another.*

Individual rotation of each of the rotors is required for Roots blowers.



### 11.1.4 Spur Rotors of Oil Pumps

Noninvolute rotors are used in design of oil pumps [46]. The pumping mechanism consists of two elements: an inner rotor and an outer rotor. These are schematically shown in Figure 11.6a. The inner element always has one fewer teeth than the outer one. The inner rotor is located off center, and both rotors rotate about their axes of rotation.

During one part of the assembly's rotation cycle, the area between the inner and the outer rotors increases, which creates a vacuum. This vacuum creates suction, and this is where the intake is located. When the area between the rotors decreases, compression occurs. Fluid is pumped during this compression period of time.

A synchronizing involute gear pair axially adjacent to its corresponding rotors usually carries the rotary load, so that the pair of rotors is used solely to create and maintain the typically high pressure differentials between the inlet and outlet ports.

The wheel profiles are either epicycloidal or hypocycloidal. In particular applications, circular arcs are used to shape the lobe profile of the rotors (Figure 11.6a). Minimum tooth clearances are required for handling gases, but curve-linear approximations to epicycloids or hypocycloids usually suffice for handling fluids.

In principle, the interaction on internal spur gears (Figure 11.6) is the same as that for external spur gears. Any of the basic rack forms used for spur gears may be used for internal gears as well. Usually, the form of the basic rack is known.

There are more possible limitations to an internal gear drive than there are for an external gear drive, particularly when the difference between the number of teeth in the internal gear and the number of teeth in the spur pinion is small. Hence, the design of the tooth forms for internal gear drives is more critical and exacting than that for external or spur gear drives.

A secondary action between the teeth of an internal gear drive [11] becomes possible. The most general practical application of an internal gear drive is in pump rotors where the tooth profile of one or both of the two members is formed by continuous curves and where the internal gear has one more tooth than its mating pinion. This secondary action exists mostly between the addendum of the mating gear teeth, whereas the primary action exists between the addendum of one gear tooth and the dedendum of the mating gear tooth.

It can be shown that neither circular arc tooth profiles nor epi- or hypotrochoidal tooth profiles allow the transmission of a uniform rotation from the driving shaft to a driven shaft. Because the pitch point for a (a) circular arc tooth profile, (b) epitrochoidal tooth profile, and (c) hypotrochoidal tooth profile, as well as for many other tooth profile geometries, migrate within a certain portion of the centerline,  $\mathcal{C}$ , rotation of the driven shaft is not uniform.

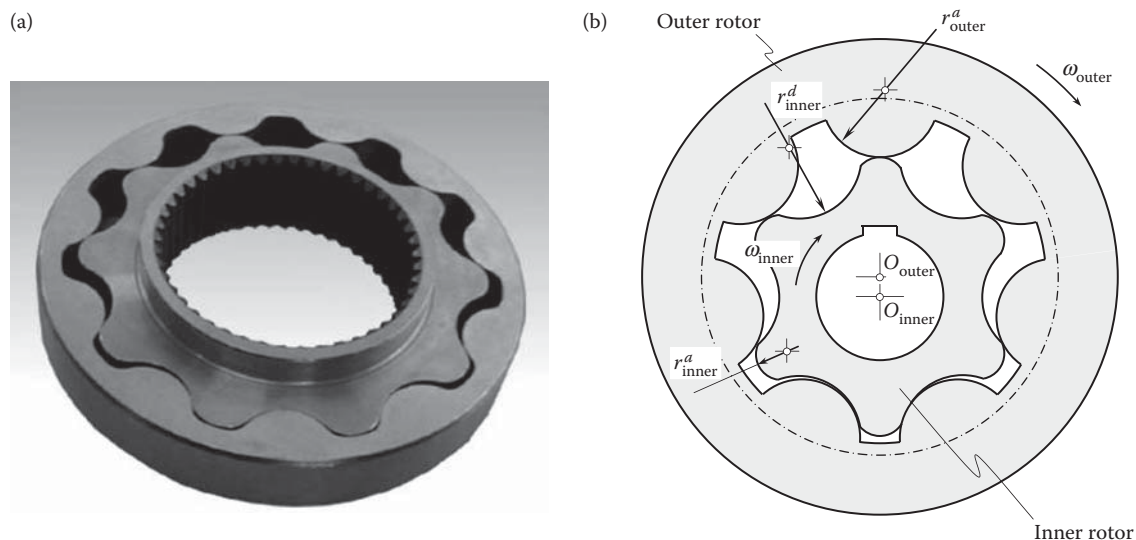


FIGURE 11.6

Oil pump: (a) close-up, and (b) the main design parameters: the radius of the convex circular arc profile of the inner rotor is designated by,  $r_{\text{outer}}^a$ , and the radius of the concave circular arc profile of the outer rotor is designated by  $r_{\text{inner}}^a$ .

This consideration allows an intermediate conclusion:

### Conclusion 11.3

*Spur gears that have a noninvolute tooth profile used in the design of oil pumps are not capable of transmitting a uniform rotation smoothly, as the tooth profiles are not conjugate to one another.*

Practically, a synchronizing involute gear pair is used for resolving the problem of smooth rotation of rotors in the design of oil pumps.

In spur noninvolute gearings of all designs, no base pitch of a gear and a mating pinion can be defined. This is because the desired plane of action,  $PA$ , in spur noninvolute gearings (see the *pulley-and-belt* equivalent for parallel-axes involute gearing), does not intersect the tooth flanks,  $\mathcal{G}$  and  $\mathcal{P}$ , of a gear and a mating pinion at a right angle. Once the base pitch does not exist, the transverse contact ratio in spur noninvolute gearings cannot be defined, and only one pair of teeth is always engaged in mesh.

## 11.2 Peculiarities of Transmission of Rotation by Means of Noninvolute Gearing

Earlier, in [Chapter 4](#), a set of the necessary and sufficient conditions to transmit a uniform rotation smoothly from a driving shaft to a driven shaft by means of involute gearing was outlined. Below, peculiarities of transmission of a rotation by means of noninvolute gearing are discussed.

### 11.2.1 Conditions of Transmission of Rotation by Means of Noninvolute Gearing

To smoothly transmit a uniform rotation of a driving shaft to a driven shaft, the pitch diameters of the driving member and the driven member have to have constant values, and they must not be dependent on the angle of rotation of the driving shaft. Under such a scenario, the pitch point,  $P$ , within the centerline is stationary: the pitch point coincides with the point of tangency of the pitch circles of the gear (of a diameter,  $d_g$ ), and the pinion (of a diameter,  $d_p$ ). Travel of the pitch point within the centerline is not allowed when a rotation of the driven shaft with constant speed is required when the driving shaft rotates steadily.

A noninvolute gear pair features a planar curve as the path of contact,  $P_c$ . At every instance of time, the tooth surface of the driving member acts against the tooth surface of the driven member along an instant line of action,  $LA_{inst}$ . The instant line of action,  $LA_{inst}$ , is tangential to the path of contact,  $P_c$ , at the current instant of time. In order to ensure uniform rotation of the driven shaft, the instant line of action,  $LA_{inst}$ , has to pass through the motionless pitch point,  $P$ . To meet this requirement, it can be assumed that in order to generate a noninvolute tooth profile, the only permissible motion to the instant line of action,  $LA_{inst}$ , to be performed is a rotation about the pitch point,  $P$ , through a certain angle when the contact point,  $K$ , travels along the path of contact,  $P_c$ .

In [Figure 11.7](#), the pitch circles of the gear (of a diameter,  $d_g$ ) and the pinion (of a diameter,  $d_p$ ) share a common point with which the pitch point,  $P$ , is coincident. The axes of rotation of the gear,  $O_g$ , and the pinion,  $O_p$ , are at a certain center distance,  $C$ , apart from each other. The rotations of the gear,  $\omega_g$ , and the pinion,  $\omega_p$ , are synchronized with one another in a timely, proper manner.

At the current instance of time, the tooth flank of the gear,  $\mathcal{G}$ , and its mating pinion,  $\mathcal{P}$ , contact each other at a contact point,  $K$ . The contact point,  $K$ , travels (with a linear velocity vector,  $\mathbf{V}_k$ ) along the instant line of action,  $LA_{inst}$ , when the gears rotate. The magnitude,  $V_k$ , of the linear velocity vector,  $\mathbf{V}_k$ , can be either a constant value or it can be time dependent. The instant line of action,  $LA_{inst}$ , makes a certain transverse pressure angle,  $\phi_{t,inst}$ , in relation to the perpendicular to the centerline,  $\mathcal{C}$ . When the gears rotate, the instant line of action,  $LA_{inst}$ , is free to turn (with an angular velocity,  $\pm \omega_{la}$ ) about the pitch point,  $P$ . No additional straight motion,  $\pm V_{la}$ , of the instant line of action,  $LA_{inst}$ , is allowed in the case under consideration.

When the gears rotate, the contact point,  $K$ , traces:

- The path of contact,  $P_c$ , in a stationary reference system associated with the gear pair housing
- The gear tooth profile,  $\mathcal{G}$ , in a reference system associated with the gear
- The pinion tooth profile,  $\mathcal{P}$ , in a reference system associated with the pinion

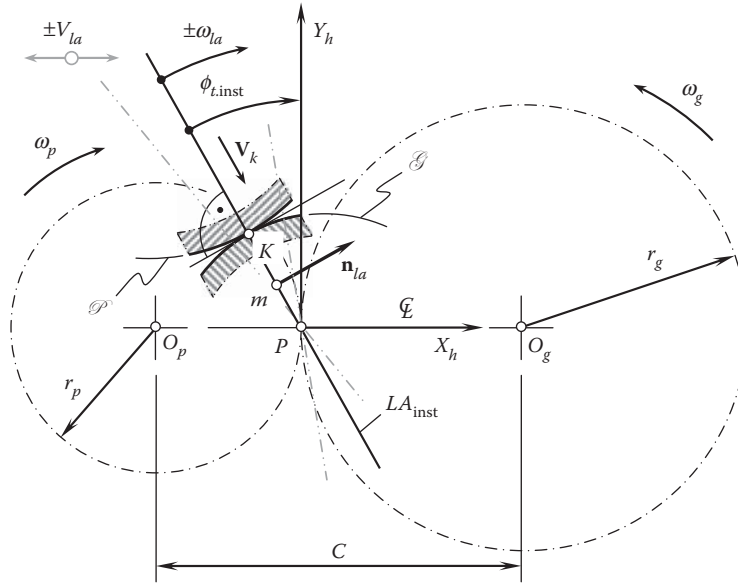


FIGURE 11.7

Permissible kinematics of the instant line of action,  $LA_{inst}$ .

Therefore, it is anticipated that once the path of contact,  $P_c$ , for a noninvolute gear pair is determined, the rest of the design parameters (i.e., tooth profiles,  $\mathcal{G}$  and  $\mathcal{P}$ ) of the gear pair can be derived using routing procedures.

Because the instant line of action,  $LA_{inst}$ , is tangential to the path of contact,  $P_c$ , it can be viewed as an envelope to consecutive positions of  $LA_{inst}$  in its motion in relation to a motionless reference system.

A Cartesian coordinate system,  $X_h Y_h$ , is associated with the gear pair housing. The pitch point,  $P$ , is the origin of the reference system  $X_h Y_h$ .

In the coordinate system  $X_h Y_h$ , the following expression:

$$Y_h = X_h \tan(90^\circ + \phi_{t.inst}) = -X_h \cot \phi_{t.inst} \quad (11.8)$$

can be used for the analytical description of the instant line of action,  $LA_{inst}$ .

The current configuration of the instant line of action,  $LA_{inst}$ , depends on the current value of the transverse pressure angle,  $\phi_{t.inst}$ . Once the parameter  $\phi_{t.inst}$  is eliminated from Equation 11.8, this equation represents the line of action,  $LA$ , itself. The *Shishkov equation of contact*,  $\mathbf{n} \cdot \mathbf{V} = 0$ , can be implemented for the elimination of the angular parameter,  $\phi_{t.inst}$ , from Equation 11.8.

The unit normal vector,  $\mathbf{n}_{la}$ , at a current point,  $m$ , within the instant line of action,  $LA_{inst}$ , can be analytically described as follows:

$$\mathbf{n}_{la} = \mathbf{i} \cos \phi_{t.inst} + \mathbf{j} \sin \phi_{t.inst} \quad (11.9)$$

The linear velocity vector,  $\mathbf{V}_m$ , of the point  $m$  equals:

$$\mathbf{V}_m = \boldsymbol{\omega}_{la} \cdot \mathbf{r}_m \quad (11.10)$$

where the position vector of the point  $m$  is denoted by  $\mathbf{r}_m$ .

The following expression:

$$\mathbf{V}_m = \boldsymbol{\omega}_{la} \cdot \mathbf{r}_m = \boldsymbol{\omega}_{la} \cdot (-\mathbf{i}X_m + \mathbf{j}Y_m) \quad (11.11)$$

can be composed for the linear velocity vector,  $\mathbf{V}_m$ . The velocity vector,  $\mathbf{V}_m$  (not shown in Figure 11.7), is aligned with the unit normal vector,  $\mathbf{n}_{la}$ .

The vectors,  $\mathbf{n}_{la}$  and  $\mathbf{V}_m$ , from Equations 11.9 and 11.11 are substituted in the Shishkov equation of contact,  $\mathbf{n} \cdot \mathbf{V} = 0$ :

$$\mathbf{n}_{la} \cdot \mathbf{V}_m = \omega_{la}(-X_m \cos \phi_{t.inst} + Y_m \sin \phi_{t.inst}) = 0 \quad (11.12)$$

This returns a formula for the function  $-\cot \phi_{t.inst}$ :

$$-\cot \phi_{t.inst} = \frac{Y_h}{X_h} \quad (11.13)$$

After the function  $-\cot \phi_{t.inst}$  from Equation 11.13 is substituted in Equation 11.8, the latter is reduced to an identity,  $1 \equiv 1$ . The identity does not depend on the enveloping parameter,  $\phi_{t.inst}$ . This means that no envelope to consecutive positions of the moving instant line of action,  $LA_{inst}$ , is physically feasible. Therefore, no path of contact,  $P_c$ , as well as no corresponding tooth profiles,  $\mathcal{G}$  and  $\mathcal{P}$ , of a gear and a mating pinion can physically exist for which a noninvolute gear pair is capable of transmitting a rotation smoothly.

In Figure 11.8, an equivalent four-bar mechanism is shown. This mechanism can be used to illustrate the present discussion.

One end of a bar of the equivalent four-bar mechanism is at the pinion center of rotation,  $O_p$ . Let us assume that the length of the bar,  $r_{b.p}$ , can be controlled by a certain linear controller,  $CD_{rp}$ . Also, specified by a certain angle,  $\pm \varphi_p$ , the angular position of the bar is controlled by an angular controller,  $CD_{\varphi p}$  (which is not shown in Figure 11.8).

One end of another bar of the equivalent four-bar mechanism is at the gear center of rotation,  $O_g$ . Let us assume that the length of the bar,  $r_{b.g}$ , can be controlled by a certain linear controller,  $CD_{rg}$ . Specified by a certain angle,  $\mp \varphi_g$ , the angular position of the bar is controlled by a certain angular controller,  $CD_{\varphi g}$  (which is not shown in Figure 11.8). It should be pointed out here that the angles  $\varphi_g$  and  $\varphi_p$  are measured in directions opposite to one another.

The opposite ends of both bars feature slides. The slides are perpendicular to the corresponding bars.

The third bar slides in the direction of the rotation of the driving pinion.

When no changes are observed to the radii,  $r_{b.g}$  and  $r_{b.p}$ , or to the angles,  $\varphi_g$  and  $\varphi_p$ , then the first and second bars remain stationary. Only the third bar slides in the direction of the rotation of the driving pinion. The axis of this bar remains in permanent tangency with both base circles, that is, with the base circle 1 of the pinion and the base circle 2 of the gear in Figure 11.8. No changes to the location of the pitch point,  $P$ , are observed.

This mode of operating of the equivalent four-bar mechanism corresponds to that of parallel-axis gears that have involute tooth profiles in the transverse section. When the pinion rotates with a constant angular velocity,  $\omega_p$ , the gear rotates with a constant angular velocity,  $\omega_g$ .

For any tooth form that differs from the involute form, the lengths of the first bar,  $r_{b.p}$ , and the second bar,  $r_{b.g}$ , are time dependent. The values of the angles,  $\varphi_g$  and  $\varphi_p$ , also alternate in time. All changes to the design parameters and kinematics of the equivalent four-bar mechanism (that is, to the lengths,  $r_{b.g}$  and  $r_{b.p}$ , and the angles,  $\varphi_g$  and  $\varphi_p$ ) meet the requirement that the slides on the ends of the first and second bars allow the third bar to freely slide in the direction of the rotation of the driving pinion. The axis of this bar is in permanent tangency with both

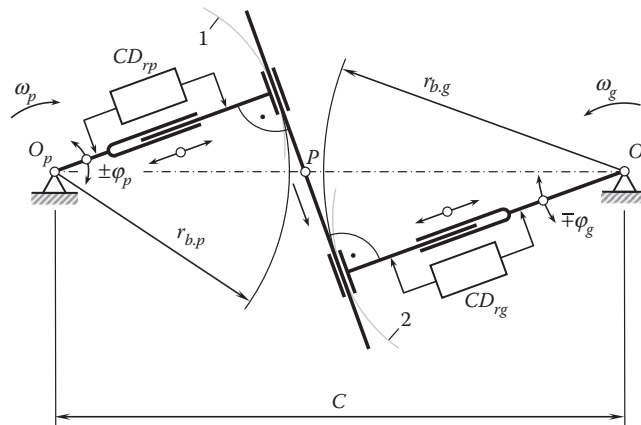


FIGURE 11.8  
An equivalent four-bar mechanism.

base curves, that is, with the base curve 1 of the pinion and the base curve 2 of the gear. The pitch point,  $P$ , travels along the centerline,  $\mathcal{C}$ .

All the motions of the equivalent four-bar mechanism execute for every cycle of meshing of the gear and the pinion teeth.

This mode of operation of the equivalent four-bar mechanism corresponds to parallel-axis gears that feature noninvolute tooth profiles in the transverse section. When the pinion rotates with a constant angular velocity,  $\omega_p$ , then the instant angular velocity of the gear,  $\omega_g$ , is variable and time dependent.

This consideration allows for a conclusion:

#### Conclusion 11.4

*Spur gears that feature noninvolute tooth profiles are not capable of transmitting a uniform rotation smoothly, as their tooth profiles are not conjugate to one another.*

Conclusion 6.4 is of importance for further analysis of helical noninvolute gear pairs. It is also of critical importance for gear-finishing (generating) operations, particularly for the rotary shaving process of spur gears that have noninvolute tooth profiles (e.g., gears for *Novikov gearing*). Regardless of whether the axes of rotation of the work gear and shaving cutter in the rotary shaving process are skewed, the performed two-dimensional analysis makes it clear that noninvolute tooth profiles of spur gears cannot be accurately shaved in nature.

#### 11.2.2 Interaction of Noninvolute Gears with Racks

One more example of the interaction of noninvolute tooth profiles can be found when designing a hob for machining straight-sided splines. The hob design is based on a rack, the teeth of which are engaged in mesh with the splines of the spline shaft. The tooth profile of the rack is commonly generated as an envelope to consecutive positions of the spline profile when the pitch circle of the spline rolls with no sliding over the pitch line associated with the rack.

The determination of the coordinates of points of the tooth profile of a rack conjugate to a spline shaft can be accomplished using the *method of common perpendiculars*. An example of solving a problem of this kind is illustrated in Figure 11.9.

The profile of the spline is associated with a pitch circle of a radius,  $r_{w.sp}$ . The pitch line of the rack to be determined is tangent to the pitch circle of the spline shaft. The point of tangency of the pitch line and the pitch circle,  $r_{w.sp}$ , is the pitch point in the rolling motion of the spline shaft and the rack. The pitch point is designated as  $P$ .

The spline shaft is rotated about its axis of rotation,  $O_{sp}$ . The angular velocity of this rotation is designated as  $\omega_{sp}$ . The rack is associated with the pitch line. The rack travels straight forward together with the pitch line. The linear velocity of the rack is designated as  $V_{rc}$ .

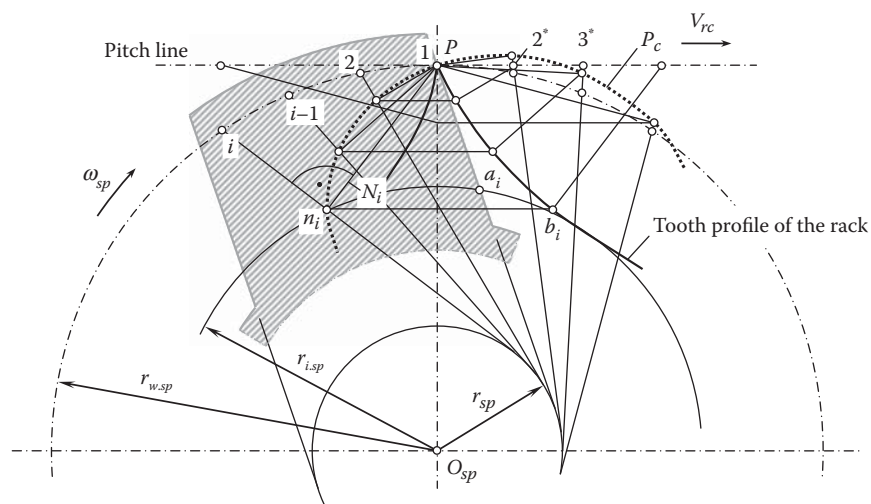


FIGURE 11.9

Generation of a rack tooth profile as an envelope to consecutive positions of the lateral profile of a spline of a straight-sided spline shaft.

Let us assume that at the initial configuration of the pitch circle and the pitch line, the profile of the spline passes through the pitch point,  $P$ . This profile is at a distance,  $r_{sp}$ , from the axis of rotation,  $O_{sp}$ , of the spline shaft. Practically, the straight line profile is tangential to a circle of the radius  $r_{sp}$ . The radius,  $r_{sp}$ , is equal to one-half the spline thickness of the spline shaft.

When the spline shaft rotates, the lateral spline profile is rotated together with the spline shaft. Consequently, the spline shaft lateral profile passes through points  $1, 2, \dots, (i-1), i$ . Point 1 is coincident with the pitch point,  $P$ . The pitch line travels straight forward. In this motion, the pitch point consequently occupies positions  $1^*, 2^*, 3^*, \dots$ . The distances  $1^* - 2^*, 2^* - 3^*, \dots$  between consequent locations of the pitch point are equal to the lengths of the arcs  $\cup 1 - 2, \cup 2 - 3, \dots$  of the pitch circle of the spline shaft. This is because the pitch line of the rack rolls with no sliding over the pitch circle of the spline shaft.

At every chosen location of the lateral profile of the spline, perpendiculars to the profile are constructed so that all of them pass through the pitch point,  $P$ . For example, a perpendicular,  $N_i$ , is normal to the spline profile at its  $i$ th location (see Figure 11.9). Point  $n_i$  is the point of tangency of the lateral profile of the spline and the rack tooth profile.

The plurality of points constructed in this way for various configurations of the lateral spline profile are located within the path of contact,  $P_c$ . In a transverse section by a plane, the path of contact,  $P_c$ , is traced by a contact point in rolling motion of the given spline shaft and the rack to be determined. The path of contact is determined in a stationary reference system.

In a reference system associated with the spline shaft, all the points are located within the lateral spline profile of the spline shaft.

When the spline shaft rotates, points of the lateral profile consequently pass through the path of contact,  $P_c$ . At these instants of time, these points coincide with the corresponding points of the rack tooth profile. If an arbitrary point,  $n_i$ , within the path of contact that corresponds to the point of contact in the  $i$ th location of the lateral profile of the spline returns to the initial position of the spline by means of rotation through the angle of the arc  $Pi$ , then this point occupies the position of the point  $a_i$ .

Similarly, in a reference system associated with the rack, contact points are located within the tooth profile of the rack, which has to be determined.

Let us assume that an arbitrary point,  $n_i$ , within the path of contact,  $P_c$ , is associated with the pitch line,  $P_{lm}$ . In order to determine the location of this point in the initial instant of time, the pitch line together with the point  $n_i$  is moved through a distance that is equal to the arc length  $Pi$  in a direction opposite the direction of straight motion of the rack tooth in its rolling motion. After this transition is complete, point  $n_i$  occupies the position of point  $b_i$ . Point  $b_i$  is located on the tooth profile of the rack. All points of the rack tooth profile are constructed similarly to the way the point  $b_i$  is constructed. By connecting the constructed points by a smooth curve, the rack tooth profile can be determined.

The aforementioned approach for the determination of the tooth profile of a rack that is enveloping to a spline shaft profile is commonly adopted. However, this method is inaccurate in nature—it can be used only for approximate generation of the rack tooth profile. It is assumed here that the generated tooth profile of the rack can generate the spline profile of the straight-sided spline shaft when a problem that is inverse to the original problem is under consideration. This is not correct. As the enveloping profiles are not involutes, no straight-sided spline profile can be generated in the inverse rolling of the rack in relation to spline shafts. In practice, instead of a straight-sided spline profile, a curved profile of the splines is obtained (Figure 11.10).

The aforementioned consideration reveals that the method of common perpendiculars returns a tooth profile of a rack that is an envelope to the spline shaft profile, but not conjugate to it.

The analytical description for a gear tooth flank of appropriate geometry and that for a pinion can be derived solely through the Shishkov equation of contact,  $\mathbf{n} \cdot \mathbf{V} = 0$ . A schematic for the derivation is illustrated in Figure 11.11.

Consider a case when the configuration of the axis of rotation of the gear,  $O_g$ ; the axis of rotation of the pinion,  $O_p$ ; and the pitch point,  $P$ , is given as shown in Figure 11.11. An arbitrary point of contact,  $K_i$ , of the tooth profiles of the gear and the pinion is located within a transverse section by a plane that is perpendicular to the axes of rotations,  $O_g$  and  $O_p$ . For an arbitrary contact point,  $K_i$ , the linear velocity vectors,  $\mathbf{V}_g$  and  $\mathbf{V}_p$ , are constructed. These two linear velocity vectors make possible the construction of the linear velocity vector of sliding,  $\mathbf{V}_{rl}$ , of the tooth flanks in relation to one another. As the gears in mesh have to meet the contact requirement,  $\mathbf{n} \cdot \mathbf{V} = 0$ , the linear velocity vector,  $\mathbf{V}_{K_i}$ , of the contact point has to be perpendicular to the linear velocity vector of relative sliding,  $\mathbf{V}_{rl}$ . The direction of the linear velocity vector,  $\mathbf{V}_{K_i}$ , is through the pitch point,  $P$ . If the linear velocity vector,  $\mathbf{V}_{K_i}$ , is not perpendicular to the linear velocity vector of relative sliding,  $\mathbf{V}_{rl}$ , then a component,  $\mathbf{V}_{int}$ ,



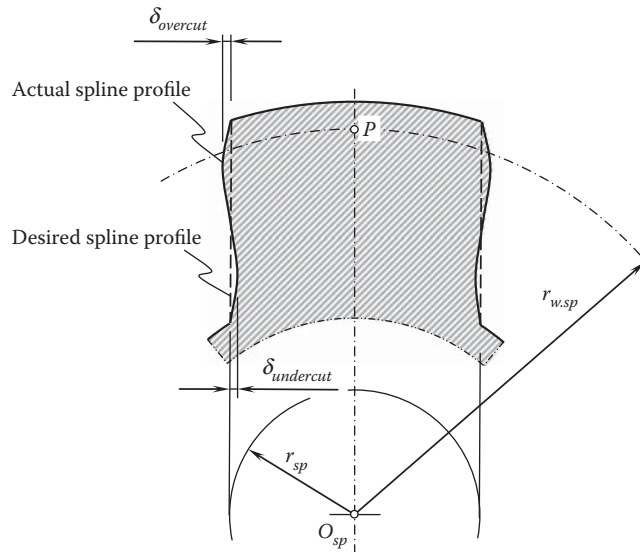


**FIGURE 11.10**  
Deviation of a desired lateral profile of a spline shaft from its actual profile.

of the linear velocity vector,  $\mathbf{V}_{Ki}$ , will either cause interference of the tooth profiles of the mating tooth flanks, or the tooth flanks will depart from one another. Neither interference of the tooth flanks nor their departure is permissible. Moreover, if the linear velocity vector,  $\mathbf{V}_{Ki}$ , is not perpendicular to the vector of relative sliding, this causes the pitch point,  $P$ , to migrate within the centerline,  $\mathcal{C}$ , of the gear pair. This is not permissible, as it causes variation of the angular velocity of the driven shaft.

Once the direction of the linear velocity vector,  $\mathbf{V}_{Ki}$ , is predetermined on the premise of the equation of contact,  $\mathbf{n} \cdot \mathbf{V} = 0$ , the next position of the contact point,  $K_{i+1}$ , is within the straight line through the point,  $P$ , along the linear velocity vector,  $\mathbf{V}_{Ki}$ . Point  $K_{i+1}$  is located at an infinitesimally small distance from point  $K_i$ . Constructed in this way, all the points,  $K_i, K_{i+1}, \dots$ , are within the straight line of action,  $LA$ .

Finally, the use of the Shishkov equation of contact,  $\mathbf{n} \cdot \mathbf{V} = 0$ , makes it possible to determine the desired line of contact,  $LA$ , for a parallel-axis gear pair that is capable of smoothly transmitting a uniform rotation from the driving shaft to the driven shaft. The line of action is represented as the set of contact points  $K_i, K_{i+1}, \dots$  considered in a motionless reference system associated with the gear housing (this line should be a straight line through the pitch point,  $P$ ). This same set of the contact points  $K_i, K_{i+1}$ , considered in a reference system

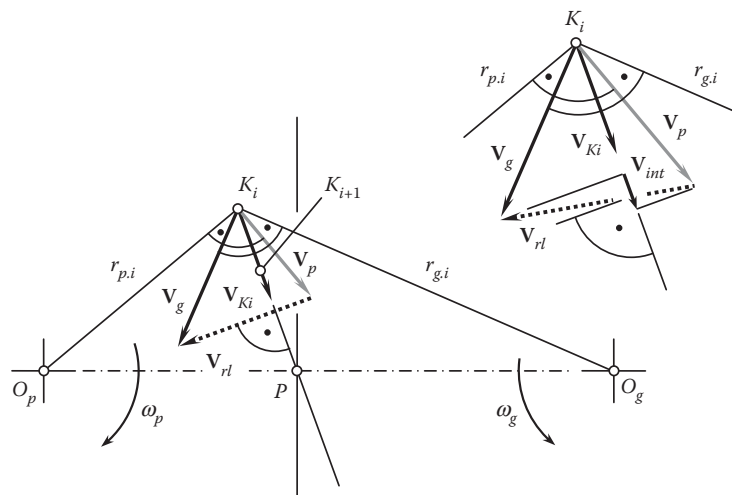


**FIGURE 11.11**  
Kinematics of the contact point of a pair of conjugate tooth profiles.



associated with the gear,  $X_g Y_g Z_g$ , represents the gear tooth flank,  $\mathcal{G}$ . Similarly, this same set of the contact points  $K_i, K_{i+1}, \dots$  considered in a reference system associated with the pinion,  $X_p Y_p Z_p$ , represents the pinion tooth flank,  $\mathcal{P}$ . Only involute tooth profiles meet the requirements imposed by the Shishkov equation of contact,  $\mathbf{n} \cdot \mathbf{V} = 0$ , for spur gearing, and only screw involute tooth flanks meet the requirements imposed by the Shishkov equation of contact,  $\mathbf{n} \cdot \mathbf{V} = 0$ , for helical parallel-axis gears. This statement can be proved analytically. The equation of the involute tooth profile can be derived based solely on the premise of the equation of contact,  $\mathbf{n} \cdot \mathbf{V} = 0$ . Gears of no other geometry are capable of transmitting a smooth rotation from a driving shaft to the driven shaft.

Enveloping profiles and surfaces of all geometries are not suitable for smoothly transmitting a rotation with constant angular velocity of the driven shaft. The only profiles/surfaces that meet this requirement are those that are enveloping to one another in both directions of the generating motion, namely in the direct (in this case, the moving generating profile/surface is generating the generated profile/surface) and the reverse direction of the generating motion (in this second case, the generated profile/surface when moving inversely generates the originally given profile/surface). This makes it possible to formulate a theorem:

### Theorem 11.1

*The only gears capable of transmitting a uniform rotation from a driving shaft to a driven shaft are those for which the tooth flanks envelop each other in both directions of relative motion, that is, in the direction of the gear and pinion, and in the reverse direction of their rotation.*

All conjugate profiles/surfaces meet the theorem, and vice versa: if profiles/surfaces meet the theorem, they are conjugate to one another. Theorem 11.1 is an equivalent of the condition of conjugacy of interacting tooth flanks.

In a case of parallel-axis gearing, only involute tooth profiles (for spur gears) and screw involute surfaces (for helical gearing) are capable of transmitting a uniform rotation. The tooth flanks of no other geometries are capable of transmitting a smooth rotation.

Consider a case in parallel-axis gearing when a tooth profile,  $\mathcal{P}_1$ , is generated as an envelope to consecutive positions of an arbitrary smooth regular tooth profile,  $\mathcal{G}_1$ . When the moving profile,  $\mathcal{G}_1$ , is not of involute shape and the rotations of the driving and driven shafts are at uniform angular velocities,  $\omega_g$  and  $\omega_p$ , respectively, then in the reversed rotation, the tooth profile  $\mathcal{P}_1$  will not generate the initial tooth profile  $\mathcal{G}_1$  but a tooth profile  $\mathcal{G}_2$  of some other geometry. This process can be continued thus: the tooth profile  $\mathcal{P}_{i+1}$  is generated by the tooth profile  $\mathcal{G}_i$ . Then the tooth profile  $\mathcal{G}_{i+1}$  is generated by the tooth profile  $\mathcal{P}_{i+1}$ , and so on. This process could go on endlessly, as the initial tooth profile  $\mathcal{G}_1$  is not involute.

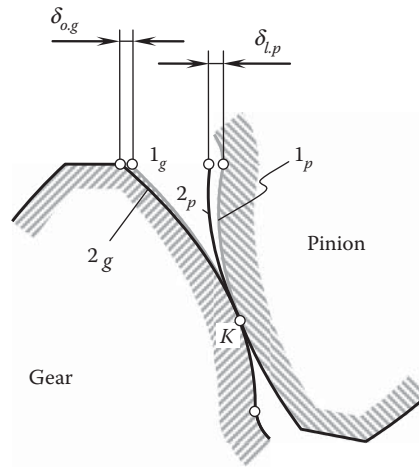
Again, in the case of parallel-axis gearing, only involute tooth profiles,  $\mathcal{G}$  and  $\mathcal{P}$ , are reversibly enveloping (conjugate) in rotation in the direct and inversed directions of the driving and driven shafts. Tooth profiles of no other geometries possess this important property.

One more important result can be taken from Theorem 11.1. When a gear tooth flank deviates at certain value,  $\delta_{o,g}$  (either under the operating load or due to manufacturing errors), from the desired involute shape, this deviation cannot be compensated by a corresponding deviation,  $\delta_{l,p}$ , of the pinion tooth flank, as schematically illustrated in Figure 11.12. With that said, the uselessness of the so-called *ease-off diagrams* that are broadly used by gear experts for graphical interpretation of gear tooth flanks deviations becomes evident.

Although it was used to illustrate for the case of parallel-axis gearing, Theorem 6.1 can be enhanced to illustrate cases of intersected-axes gearing and crossed-axes gearing as well.

The present discussion relates just to one pair of gear teeth engaged in mesh. Further, the requirement of equality of the base pitches of a gear and a mating pinion to the operating base pitch of the gear pair ( $p_{b,g} = p_{b-op}$  and  $p_{b,p} = p_{b-op}$ ) makes it possible to proceed to real gearing that has a certain number of the tooth flanks engaged in mesh simultaneously. This means that the Shishkov equation of contact,  $\mathbf{n} \cdot \mathbf{V} = 0$ , is the first condition to be considered\* in gear kinematics and gear geometry. Ultimately, the entire geometric theory of gearing can be derived on the basis of just three conditions:

\* The importance of the Shishkov equation of contact,  $\mathbf{n} \cdot \mathbf{V} = 0$  in the cases of computer generation of enveloping surfaces should be pointed out here. If an enveloping surface does not exist, then there is no solution to the Shishkov equation of contact,  $\mathbf{n} \cdot \mathbf{V} = 0$ . This clearly indicates that something is wrong either with the geometry of the moving surface or the kinematics of the relative motion of the moving surface. Computer software that is not based on the equation of contact misses inconsistencies of this kind.

**FIGURE 11.12**

Deviations of actual gear,  $2_g$ , and pinion,  $2_p$ , teeth profiles from the corresponding desired involute forms  $1_g$  and  $1_p$  respectively.

- i. The Shishkov equation of contact,  $\mathbf{n} \cdot \mathbf{V} = 0$
- ii. The condition of conjugacy
- iii. The equality of the base pitches,  $p_{b,g} = p_{b-op}$  and  $p_{b,p} = p_{b-op}$

The above discussion can be enhanced to suit gearing of other kinds, that is, intersected-axis gears as well as crossed-axis gearing.

### 11.3 Helical Noninvolute Gear Pairs

Helical gear pairs, those composed of gears that feature noninvolute tooth profiles, deserve a particular mention. Below, a discussion on helical noninvolute gear pairs begins from practical implementation of noninvolute gear pairs.

#### 11.3.1 Helical Rotors in Roots Blowers

Not many applications of noninvolute helical gear pairs can be found in the industry. Helical rotors in Roots blowers are one such rare application.

From Figure 11.13a, a Roots blower is composed of two helical rotors. Each rotor features three lobes. The rotors are mounted on the shafts and assembled in a housing. The rotors are rotated with angular velocities,  $\omega_1$  and  $\omega_2$ , about their axes of rotation,  $O_1$  and  $O_2$ , respectively. The axes of rotation,  $O_1$  and  $O_2$ , are at a certain center distance,  $C$ , from one another. Two driving gears are implemented to rotate the rotors about their axes. The tooth ratio of the driving gear pair equals one ( $u = 1$ ). The nominal pitch radius of each rotor is equal to the pitch radius of the driving gear.

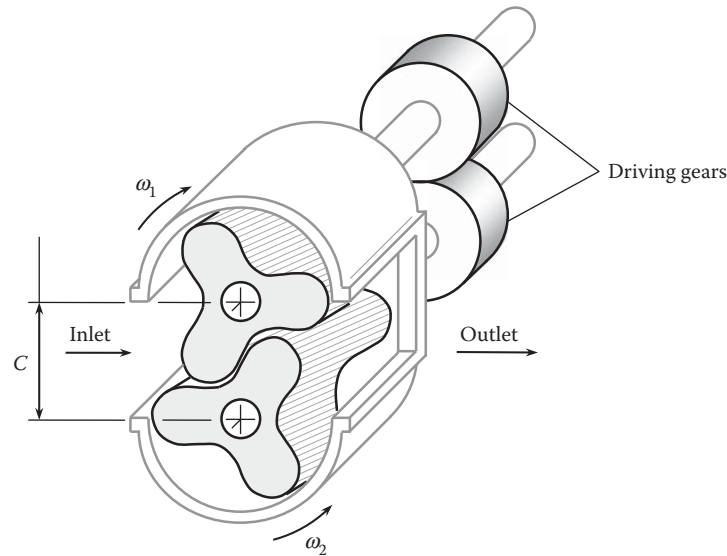
It should be mentioned here that the closest distance of approach,  $\Delta_{cda}$ , between the working surfaces of the helical rotors can be calculated. The distance,  $\Delta_{cda}$ , depends on an angular orientation of the rotors. As the rotors rotate, the distance,  $\Delta_{cda}$ , changes from its minimum value,  $\Delta_{cda}^{\min}$ , to its maximum value,  $\Delta_{cda}^{\max}$ . The inequality  $\Delta_{cda}^{\min} \leq \Delta_{cda} \leq \Delta_{cda}^{\max}$  is valid for Roots blowers that feature helical rotors.

The closest distance of approach,  $\delta_{cda}^{\min}$ , between the working surfaces of spur rotors and that,  $\Delta_{cda}^{\min}$ , between helical rotors of a Roots blower that have helical rotors relate to one another in such a way that the inequality  $\Delta_{cda}^{\min} \geq \delta_{cda}^{\max}$  is observed.

The following statement is proved:

#### Conclusion 11.5

*As only one pair of lobes is always in contact, helical rotors of a Roots blower are not capable of transmitting a uniform rotation.*

**FIGURE 11.13**

A three-lobe Roots blower (helical noninvolute rotors).

Individual rotation of the rotors is a must for Roots blowers with helical rotors.

That same statement is valid with respect to the helical rotors of axial pumps that have a noninvolute profile of the lobes (Figure 11.14), as well as with other helical surfaces that have noninvolute profiles (see Figure 11.15). Therefore, modern designs of blower rotors feature working surfaces in the form of helical involute surfaces, as in the design of a blower depicted in Figure 6.15.

### 11.3.2 Analysis of Infeasibility of Helical Gearing by Wildhaber (US Pat. No. 1,601,750)

The proven infeasibility of helical gearing with noninvolute tooth profiles for transmitting a uniform rotation smoothly makes it reasonable to perform an analysis of feasibility of the well-known helical gearing proposed in 1923 by Wildhaber [40]. Helical Gearing by Wildhaber [40] is a perfect example of helical gearing with a noninvolute tooth profile. The necessity of such an analysis is important because of the following:

1. The analysis can clearly show that Helical Gearing by Wildhaber [40] is infeasible at all to smoothly transmit a uniform rotation from a driving shaft to a driven shaft. This analysis is helpful to less

**FIGURE 11.14**

Features of meshing of two helical noninvolute rotors.

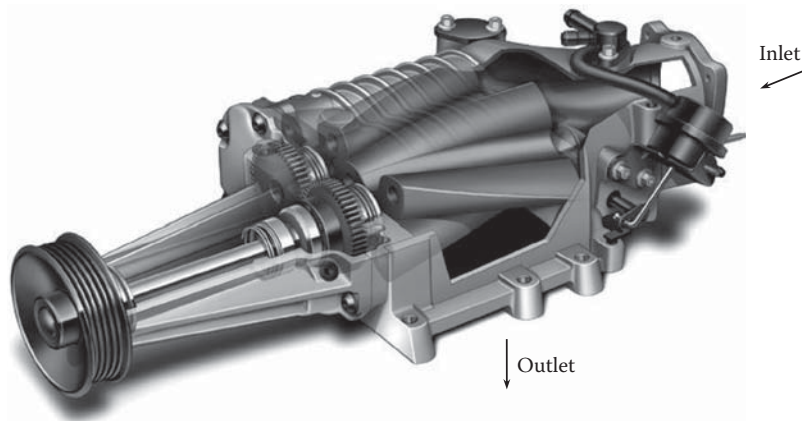


FIGURE 11.15

Example of a blower (super-charger) with screw involute working surfaces of the rotors.

experienced gear experts, those who loosely combine the helical gearing proposed by Wildhaber with conformal gearing proposed later by Novikov [85]. Such a combination of two completely different kinds of gearing results in absolutely meaningless terminology, like *Wildhaber-Novikov gearing* and/or *W-N gearing*.

2. Incorrect interpretation of the kinematics and geometry of helical gearing by Wildhaber [40] (along with that with respect to Novikov gearing) has caused huge confusion in designing and, especially, production of gears for Novikov gearing, as gears for Novikov gearing cannot be finish-cut in a continuous-indexing process of gear machining

A few more reasons for the necessity of such an analysis can be mentioned in addition.

Helical Gearing by Wildhaber [40] is illustrated in Figure 11.16 (for more details, refer to Appendix H).

This invention is related to the tooth shape of gears that run on parallel axes and may be applied to helical gears, such as single helical gears, and double helical gears, or herringbone gears. Providing accurate gearing of a circular arc profile is one of the purposes of helical gearing [40]. No other tooth profiles except the circular arc profile are proposed in this invention.

In Figure 11.16, 1 denotes a helical gear that has teeth, 2, in contact with the teeth, 3, of a mating pinion, 4. As is customary, the helical gearing is analyzed with reference to a normal section, *that is*, line 2 – 2 in the upper part of Figure 11.16, which is normal to the helix of the pitch circle. The lower part in Figure 11.16 illustrates said normal section 2 – 2 for both the pinion, 4, and gear, 1.

As an example, it has been assumed that the tooth profiles, 6, of the gear, 1, are circular arcs of radii, 7, and centers, 8, in the shown normal section. The centers, 8, are situated close to the pitch circle, 9, of the gear. The location of the centers, 8, in relation to the line of action, *LA*, is not specified in the invention. The corresponding teeth of the pinion, 4, are shaped to allow rolling of the pitch circles, 9 and 10, on each other, which is well known to those skilled in the art. So, no freedom in choosing the pinion tooth profile is allowed in the invention.

When the gear tooth, 2, is in the position shown in Figure 11.16 and its center at 8, then it contacts the tooth, 3, at a point, 11, which may be determined by a perpendicular to the tooth, 2, through the point, 12. Point 12 is the contact point between the two pitch circles, 9 and 10. Point 12 is commonly referred to as the *pitch point*. Said perpendicular is, in the present case, the connecting line between the pitch point, 12, and the center, 8, of the tooth profile.

Another position, 2', of the gear tooth and 3' of the corresponding pinion tooth are shown in dotted lines in Figure 11.16. The tooth profiles contact here at a point, 11', which can be determined to be similar to point 11. It is noted that *the contact point has traveled from 11 to 11'* during a small angular motion of the gears.\* A certain path of contact,  $P_c$ , is a curved line through points 11 and 11'. *The contact point has passed practically over the whole active*

\* The ability of the contact point to travel over a tooth profile has been mentioned several times in the patent description (see Appendix H for more details).

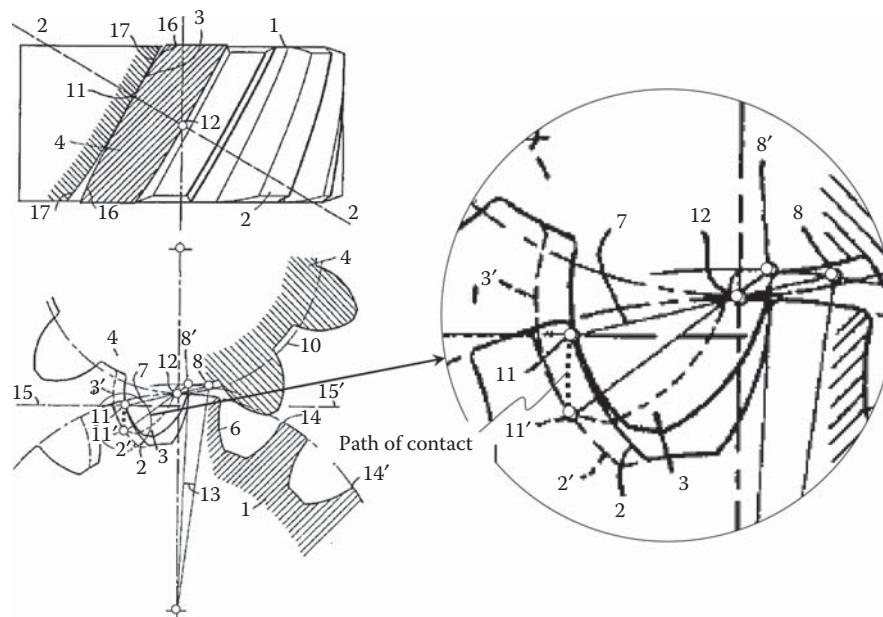


FIGURE 11.16

Schematic of Helical Gearing by Wildhaber. (Wildhaber, E., Helical Gearing. U.S. Pat. No. 1,601,750. Filed: November 2, 1923, published October 5, 1926. [161])

profile during a turning angle, 13, of the gear; this angle corresponds only to a fraction of the normal pitch, 14, that is, 14'. Said normal pitch equals the circular pitch of the shown normal section.

Omitting numerous inconsistencies and discrepancies between the design parameters of the gear pair, it is of critical importance to stress here that traveling of the contact point within a transverse section\* of the gear pair indicates that helical gearing [40] features a path of contact,  $P_c$ , of a certain length,  $L_{pc}$  (that is,  $L_{pc} > 0$ ). If the length,  $L_{pc}$ , of the path of contact,  $P_c$ , is not zero, and the teeth are of a circular arc shape, then the vital requirement of equal base pitches of the gear and the pinion in helical gearing [40] is not fulfilled.

In the invented gearing [40], the contact point between two normal profiles passes over the whole active profile during a turning angle, which corresponds to less than one-half the normal pitch; usually, it is much less than that.

It is then claimed that Wildhaber's helical gearing [40] is capable of ensuring better contact between the teeth of the gear and pinion in a direction perpendicular to the *contact line between two mating teeth*. Therefore, it is expected that the proposed helical gearing features *line contact* (and not *point contact*) between the tooth flanks of the gear and the pinion.

Gearing according to the invention [40] is strictly a gearing for helical teeth. It is not advisable on straight teeth, on account of the explained *short duration of contact between the tooth profiles*. It should be pointed out here that in the invention [40], a short duration of contact and not instantaneous contact between the tooth profiles is anticipated.

The working profiles of the gear are concave and circular, and their *centers are substantially situated on the pitch circle of the gear*. The convex working profiles of the pinion are also of a circular shape. Their radii are substantially the same as the radii of the mating tooth profiles. *The centers of these profiles are similarly situated on pitch circle of the pinion*. Because the centers of the tooth profiles are situated within the corresponding pitch circles, the centers cannot be situated within the line of action,  $LA$  (or the instant line of action,  $LA_{inst}$ ).

More details on inconsistency and discrepancy between the design parameters of Wildhaber's Helical Gearing can be found in Appendix H [136].

The performed analysis reveals that the helical gearing proposed by Wildhaber [40] is a kind of helical gearing that has a noninvolute tooth profile and features the path of contact,  $P_c$ , of a certain length,  $L_{pc}$  (i.e.,  $L_{pc} > 0$ ).

\* If the contact point travels within the normal section, 2 – 2, then the projection of the contact point onto the transverse section travels within the transverse section as well.

According to [Chapter 4](#), gear pairs of this particular type are not capable of transmitting a uniform rotation smoothly.\*

The infeasibility of Wildhaber's helical gearing [40], and the principal features of Novikov gearing (considered in [Chapter 4](#)) make it possible to conclude that these two gearings cannot be combined into a common design of gearing that is often loosely referred to as Wildhaber-Novikov gearing, or WN-gearing. These two gearings must be considered individually and separately from one another.

The consideration in this section can be summarized as follows: neither spur noninvolute gear pairs nor helical noninvolute gear pairs of all known designs (as well as of designs to be developed in the future) are capable of transmitting a uniform rotation smoothly. This is mostly because the condition of conjugacy of the interacting tooth flanks of a gear,  $\mathcal{G}$ , and a mating pinion,  $\mathcal{P}$ , is not fulfilled; thus, base pitches of the gear,  $p_{b-g}$ , and the pinion,  $p_{b-p}$ , do not equal an operating base pitch of the gear pair,  $p_{b-op}$ , as the first two ( $p_{b-g}$  and  $p_{b-p}$ ) do not exist at all.

---

\* It should be noted here that the Wildhaber's Helical Gearing [40] is a kind of mistake. Unfortunately, this invention attracted widespread interest within the gear engineering community. It should be clearly understood that this is a mistake and the invention [40] should be treated as such and nothing more. No doubt, this mistake should be forgiven, as we all make mistakes from time to time. Wildhaber is credited with smart solutions to many complex engineering problems, and his contributions to gear engineering are invaluable.



# Taylor & Francis

Taylor & Francis Group

<http://taylorandfrancis.com>



## Section II-B

# Perfect Gearing: Intersected-Axes Gearing

Gear pairs used for transmission of a rotation between two shafts that have intersecting axes of rotation are referred to as *intersected-axes gear pairs*\* (or just *I<sub>a</sub>-gearing* for simplicity). The geometry of an involute straight bevel gear has been investigated by many authors. Buckingham [11] and Kolchin [56], as well as many others, have contributed much to the investigation of approximate intersected-axes gearing.

Referring to Figure 2.15, intersected-axes gear pairs make up the second stratum in the classification of possible kinds of vector diagrams of gear pairs.

An appropriate vector diagram can be associated with any and all particular kinds of intersected-axes gear pairs. The use of vector diagrams, together with the developed classification of possible types of vector diagrams of gear pairs (see Figure 2.15), allows for a comprehensive analysis of gearing of this kind. All possible types of intersected-axes gear pairs are incorporated into the analysis, and none of them can be missed if the analysis is based on the classification illustrated in Figure 2.15.

This subsection of the monograph consists of two chapters—Chapters 12 and 13.

---

\* Other terminology with regard to intersected-axes gear pairs can be found in the literature. Some authors loosely refer to gears of this particular kind as *conical gear pairs*, *spherical gear pairs*, and others. This is true: meshing of intersected-axes gears can be easily described as meshing on a sphere. However, not only intersected-axes gear pairs feature meshing on a sphere. As discussed below, meshing of crossed-axis gear pairs can also easily be described on a sphere. Therefore, the sphere of meshing is not a sufficient (unique) criterion to refer to intersected-axes gear pairs as spherical gear pairs. *Intersected-axes gear pair* (or just *I<sub>a</sub>-gearing* for simplicity) is the most appropriate terminology with respect to gears of this kind.



# Taylor & Francis

Taylor & Francis Group

<http://taylorandfrancis.com>

## Perfect Intersected-Axes Gear Pairs

Intersected-axes gears have been used in practice for centuries. Numerous designs of intersected-axes gears can be found in da Vinci's famous book *The Madrid Codices* [17]. When motion is to be transmitted between shafts whose axes intersect, some form of bevel gear is applied. Although bevel gears are often made for a shaft angle of  $90^\circ$ , they can be produced for almost any shaft angle.

The discussion of intersected-axes gears begins below from the consideration of the earliest concepts of gear pairs of this particular kind.

### 12.1 Earliest Designs of Intersected-Axes Gearing

The known designs of the earliest intersected-axes gear pairs indicate strong constraints imposed by the gear technology available at that time for the production of gears. This is elaborated on in the following text.

An example of an intersected-axes gear pair is depicted in [Figure 12.1](#). The gear pair is composed of the lantern pinion and the face pin-tooth gear. The pin-tooth face gear has teeth that consist of formed pins. The pinion consists of a number of cylindrical pins equally spaced in a circle that is concentric with the axis of the pinion. These pins are mounted on flanges.

The axes of rotation of the gear,  $O_g$ , and the pinion,  $O_p$ , intersect at a right angle. The ratio of the rotation of the gear,  $\omega_g$ , and the pinion,  $\omega_p$ , is the reciprocal to the ratio of the pin number of the gear,  $N_g$ , and of the pinion,  $N_p$  (i.e., the equality  $\omega_p/\omega_g = N_g/N_p$  is valid).

The rotation vectors,  $\omega_g$  and  $\omega_p$ , are along the axes of rotations,  $O_g$  and  $O_p$ , of the gear and of the pinion, accordingly. The vectors,  $\omega_g$  and  $\omega_p$ , are a kind of sliding vectors. For convenience, they are applied at the point of intersection of the axes of rotations,  $O_g$  and  $O_p$ .

The vector of instant rotation,  $\omega_{pl}$  (i.e., the vector of instant rotation of the pinion in relation to the gear), is along the axis of instant rotation,  $P_{ln}$ . The rotation vector,  $\omega_{pl}$ , is equal to:

$$\omega_{pl} = \omega_p - \omega_g \quad (12.1)$$

The intersected-axes gears shown in [Figure 12.1](#) are used to transmit a rotation from a driving shaft to a driven shaft when the input rotation is slow. The load capacity of such a drive is very low because only point contact can exist between the mating pins or teeth [11]. The working surfaces of the pins are convex. The radius of curvature of the pins is relatively small. Such contacts of the pins feature low bearing capacity.

In the current industry, the bevel gears illustrated in [Figure 12.2](#) are the main type of gearings used to transmit a rotation between two shafts that intersect one another.

### 12.2 Kinematics of Intersected-Axes Gearing

Transmission and transformation of a rotation from a driving shaft to a driven shaft is the main purpose of intersected-axes gears. Both the input and output rotation can be easily represented by means of the corresponding rotation vectors,  $\omega_g$  and  $\omega_p$ . The variety of all possible types of intersected-axes gear pairs is limited to the total number of possible combinations of the rotation vectors,  $\omega_g$  and  $\omega_p$ ; that is, of the rotation vectors (1) of various magnitudes and (2) featuring different shaft angles,  $\Sigma$  [remember that the shaft angle,  $\Sigma$ , is specified as the angle that is formed by the rotation vectors,  $\omega_g$  and  $\omega_p$ ; that is,  $\Sigma = \angle(\omega_g, \omega_p)$ ].

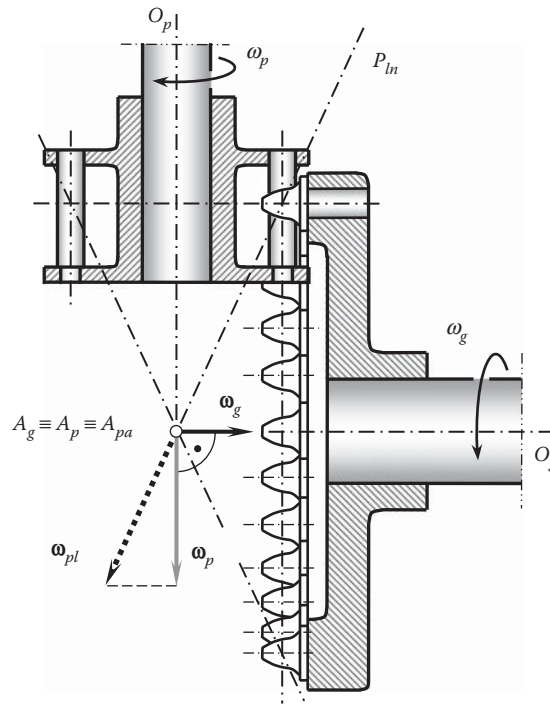


FIGURE 12.1

Intersected-axes gear pair composed of the pin-tooth face gear and the lantern pinion.

The total number of vector diagrams of different kinds of intersected-axes gearing is limited to three when the actual configuration of the rotation vectors,  $\omega_g$  and  $\omega_p$ , of the gear and the pinion in relation to the vector of instant rotation,  $\omega_{pl}$ , is taken into account. These vector diagrams are plotted in Figure 12.3.

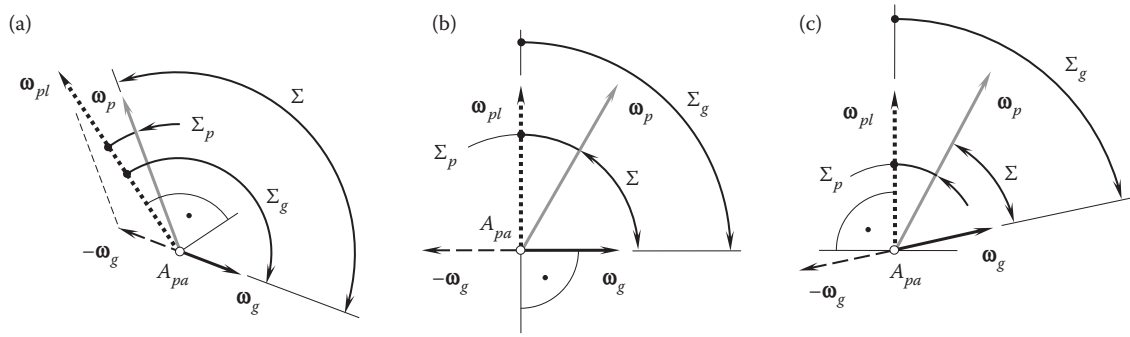
The vector diagram shown in Figure 12.3a features an obtuse angle,  $\Sigma_g$ , between the rotation vector,  $\omega_g$ , of the gear and the vector of instant rotation,  $\omega_{pl}$ . The angle,  $\Sigma_g$ , is commonly referred to as the *gear cone angle*. The gear cone angle,  $\Sigma_g$ , can be expressed in terms of the shaft angle,  $\Sigma$ , and the magnitudes,  $\omega_g$  and  $\omega_p$ , of the rotation vectors,  $\omega_g$  and  $\omega_p$ .

Referring to Figure 12.4, the sides,  $\omega_g$  and  $\omega_p$ , form a crossed-axes angle,  $\Sigma$ , in a triangle vertex,  $A_{pa}$ . All the sides in the triangle can be normalized by  $\omega_p$ . With that said, (a) the length of the side  $\omega_g$  alters to  $\omega_g/\omega_p = u$ , (b) the length of the side  $\omega_p$  alters to  $\omega_p/\omega_p = 1$ , and (c) the length of the side  $\omega_{pl}$  alters to  $\omega_{pl}/\omega_p$ . According to



FIGURE 12.2

Intersected-axes gear pair of conventional design extensively used in the current industry.

**FIGURE 12.3**

The total number of possible types of vector diagrams for intersected-axes gear pairs is limited to three vector diagrams: (a) external  $I_a$  gear pair, (b) pinion-to-round rack  $I_a$  gear pair, and (c) internal  $I_a$  gear pair.

the cosine law, the length of the side  $\omega_{pl}$  alters to  $\omega_{pl}/\omega_p$ , which equals:

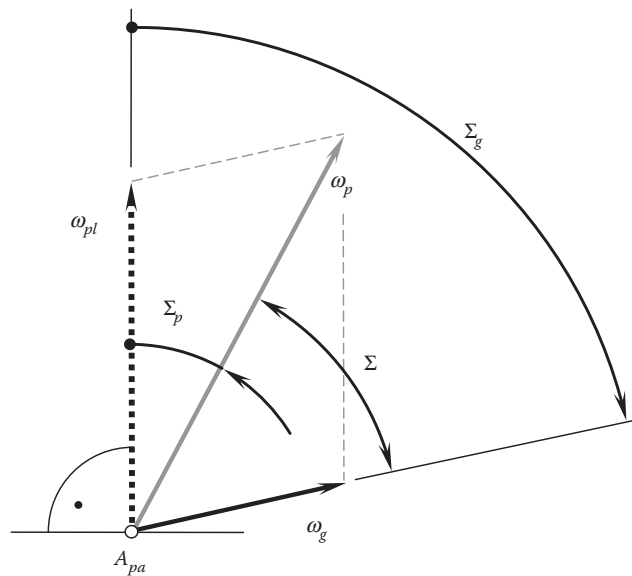
$$\frac{\omega_{pl}}{\omega_p} = \sqrt{1 + u^2 - 2u \cos \Sigma} \quad (12.2)$$

In another triangle in [Figure 12.4](#), the sides  $\omega_p$  and  $\omega_{pl}$  form a *pinion cone angle*,  $\Sigma_p$ , in a triangle vertex,  $A_{pa}$ . Again, all the sides of this second triangle can be normalized by  $\omega_p$ . Then, according to the law of sines, the pinion cone angle,  $\Sigma_p$ , can be calculated as:

$$\sin \Sigma_p = \frac{\omega_{pl}}{\omega_p} \sin \Sigma \quad (12.3)$$

Equation 12.3 yields a formula for the calculation of the pinion cone angle,  $\Sigma_p$ :

$$\Sigma_p = \sin^{-1} \frac{\sin \Sigma}{\sqrt{1 + u^2 - 2u \cos \Sigma}} \quad (12.4)$$

**FIGURE 12.4**

Gear cone angle,  $\Sigma_g$ , and pinion cone angle,  $\Sigma_p$ , in intersected-axes gear pairs.

Ultimately, an equation for the calculation of the gear cone angle,  $\Sigma_g$ , can be derived:

$$\Sigma_g = \Sigma + \sin^{-1} \frac{\sin \Sigma}{\sqrt{1 + u^2 - 2u \cos \Sigma}} \quad (12.5)$$

For a shaft angle of  $90^\circ$ , Equations 12.4 and 12.5 reduce to:

$$\Sigma_p = \sin^{-1} \frac{1}{\sqrt{1 + u^2}} \quad (12.6)$$

$$\Sigma_g = \Sigma + \sin^{-1} \frac{1}{\sqrt{1 + u^2}} \quad (12.7)$$

correspondingly.

The vector diagram shown in [Figure 12.3a](#) corresponds to an external intersected-axes gear pair.

For an external intersected-axes gear pair of this particular kind (namely, when  $\Sigma > 90^\circ$ ), the relation  $\Sigma_g = \angle(\mathbf{w}_g, \mathbf{w}_{pl}) > 90^\circ$  is valid. An equivalent expression is valid for the relation  $\Sigma_g = \angle(\mathbf{w}_g, \mathbf{w}_{pl}) > 90^\circ$ :

$$\mathbf{w}_g \cdot (\mathbf{w}_p - \mathbf{w}_g) < 0 \quad (12.8)$$

or

$$\frac{\mathbf{w}_g \cdot (\mathbf{w}_p - \mathbf{w}_g)}{|\mathbf{w}_g| \cdot |\mathbf{w}_p - \mathbf{w}_g|} = -1 \quad (12.9)$$

Examples of vector diagrams for external intersected-axes gear pairs that have different configurations of the rotation vectors of the gear,  $\mathbf{w}_g$ , and the pinion,  $\mathbf{w}_p$  (and thus feature different shaft angles,  $\Sigma$ ) are depicted in [Figure 12.5](#). The examples ([Figure 12.5](#)) reveal that a configuration of the rotation vector of the gear,  $\mathbf{w}_g$ , in relation to the vector of instant rotation,  $\mathbf{w}_{pl}$ , is critical for the determining whether a gear pair is external, while the relative configuration of the rotation vectors,  $\mathbf{w}_g$  and  $\mathbf{w}_p$ , is of secondary importance.

An analysis of the vector diagrams for intersected-axes gearing ([Figure 12.3](#)) reveals that the rotation vectors,  $\mathbf{w}_g$  and  $\mathbf{w}_p$ , of the gear and pinion are not parallel to the vector of instant rotation,  $\mathbf{w}_{pl}$ . Therefore, axial sliding of the tooth flanks of the gear,  $\mathcal{G}$ , and pinion,  $\mathcal{P}$ , is inevitable in intersected-axes gearing of all kinds. The sliding is caused by the projections of the rotation vectors,  $\mathbf{w}_g$  and  $\mathbf{w}_p$ , onto a perpendicular to the vector of instant rotation,  $\mathbf{w}_{pl}$ .

In a particular case, the rotation vector of the gear,  $\mathbf{w}_g$ , can be orthogonal to the vector of instant rotation,  $\mathbf{w}_{pl}$  [i.e.,  $\Sigma_g = \angle(\mathbf{w}_g, \mathbf{w}_{pl}) = 90^\circ$ ]. An equivalent expression is valid for this formula:

$$\mathbf{w}_g \cdot (\mathbf{w}_p - \mathbf{w}_g) = 0 \quad (12.10)$$

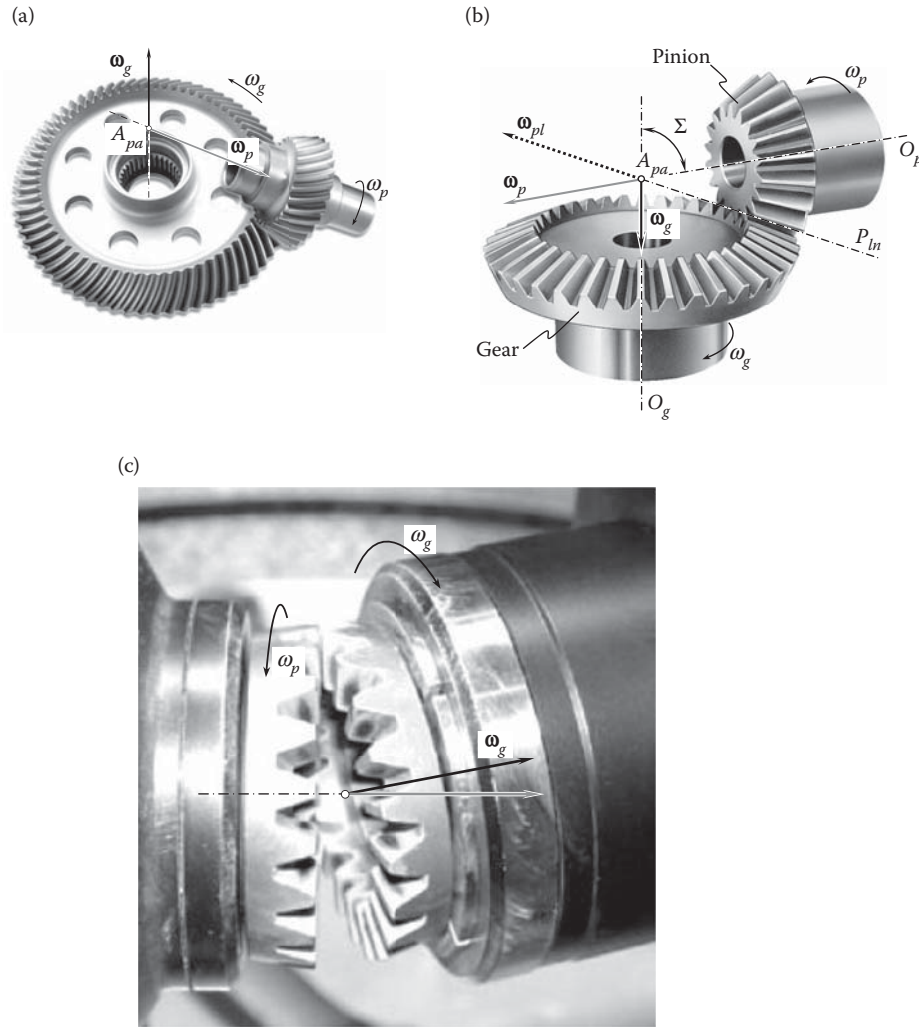
or

$$\frac{\mathbf{w}_g \cdot (\mathbf{w}_p - \mathbf{w}_g)}{|\mathbf{w}_g| \cdot |\mathbf{w}_p - \mathbf{w}_g|} = 0 \quad (12.11)$$

The vector diagram for gear drives of this kind is schematically shown in [Figure 12.3b](#). The vector diagram corresponds to a gear pair composed of a round rack (or face gear) and of a conical pinion.

Ultimately, an intersected-axes gear pair may feature an acute gear cone angle,  $\Sigma_g$ , between the rotation vector,  $\mathbf{w}_g$ , of the gear and the vector of instant rotation,  $\mathbf{w}_{pl}$ , as schematically illustrated in [Figure 12.3c](#). For a gear pair of this particular type, the relation  $\Sigma_g = \angle(\mathbf{w}_g, \mathbf{w}_{pl}) < 90^\circ$  is valid. An equivalent expression is valid for this formula:

$$\mathbf{w}_g \cdot (\mathbf{w}_p - \mathbf{w}_g) > 0 \quad (12.12)$$

**FIGURE 12.5**

External intersected-axes gear pairs that feature different configurations of the rotation vectors of the gear,  $\omega_g$ , and the pinion,  $\omega_p$ : (a) obtuse shaft angle,  $\Sigma > 90^\circ$ , (b) right shaft angle,  $\Sigma = 90^\circ$ , and (c) acute shaft angle,  $\Sigma < 90^\circ$ .

or

$$\frac{\omega_g \cdot (\omega_p - \omega_g)}{|\omega_g| \cdot |\omega_p - \omega_g|} = +1 \quad (12.13)$$

A vector diagram of the kind (Figure 12.3c) corresponds to an internal intersected-axes gear pair.

Internal intersected-axes gear pairs are used in design of nutation drives (Figure 12.6) as well as in other applications.

The analytically expressed conditions (see Equations 12.8 through 12.10), along with Equation 12.12, are summarized in Table 12.1.

Any and all intersected-axes gear pairs fulfill one of three expressions listed in Table 12.1.

In a particular case, the centerlines of the driving shaft and driven shaft intersect each other at a right angle (i.e.,  $\Sigma = 90^\circ$ ). This particular case is the most common in the current practice. Intersected-axes gear pairs of this kind are referred to as *orthogonal intersected-axes gear pairs*. An example of a vector diagram for an orthogonal intersected-axes gear pair is schematically shown in Figure 12.7. In gearing of this kind, the cross-product of the rotation vectors,  $\omega_g$  and  $\omega_p$ , of the gear and the pinion is always equal to zero (i.e.,  $\omega_g \times \omega_p = 0$ ).

An orthogonal intersected-axes gear pair may feature equal tooth numbers of the gear,  $N_g$ , and the pinion,  $N_p$ . When the mating gears are equal in size, and the shafts are positioned at  $\Sigma = 90^\circ$  to each other, the gear pair is referred to as a *miter intersected-axes gear pair*. The vector diagram for miter gears is plotted in Figure 12.8. Not



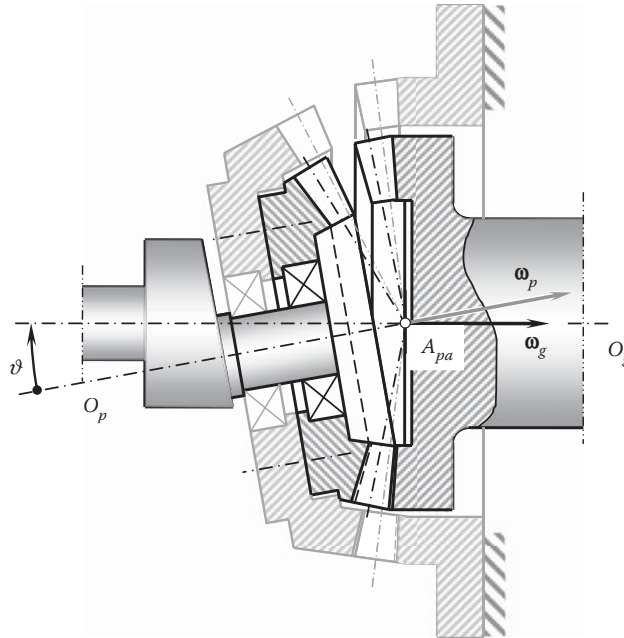


**FIGURE 12.6**  
Implementation of an internal intersected-axes gear pairs in the design of a nutation drive.

**TABLE 12.1**

Analytical Criteria of Type of Intersected-Axes Gearing

Type of Intersected-Axes Gearing	Analytical Criterion [ $C = 0$ and $\Sigma \neq 0$ ]
External intersected-axes gear pair	$\omega_g \cdot (\omega_p - \omega_g) < 0$
Rack-type intersected-axes gear pair	$\omega_g \cdot (\omega_p - \omega_g) = 0$
Internal intersected-axes gear pair	$\omega_g \cdot (\omega_p - \omega_g) > 0$

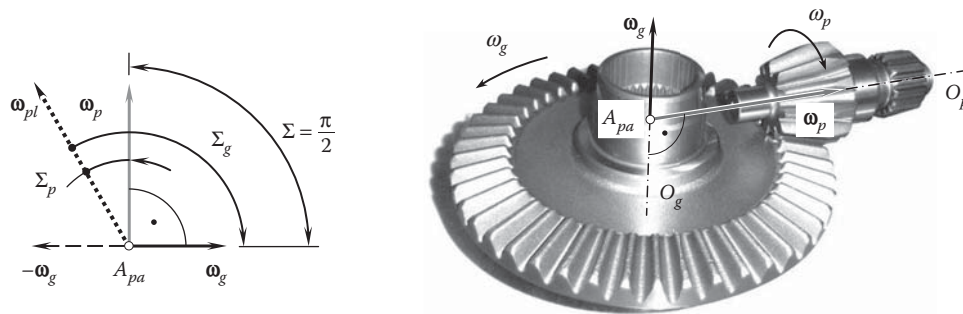


**FIGURE 12.7**  
Vector diagram of an orthogonal intersected-axes gear pair.

only do miter gears meet the requirement  $\omega_g \times \omega_p = 0$ , they also feature rotation vectors,  $\omega_g$  and  $\omega_p$ , of equal magnitudes (i.e.,  $\omega_g = \omega_p$ ).

In a degenerate case, spatial gear pair of the kind 1.2 (see [Figure 2.15](#)) transforms into a *pinion-to-rack gear pair* of the kind 1.2.2. Furthermore, a conventional pinion-to-rack gear pair (see 1.2.2.1 in the classification in [Figure 2.15](#)) can be viewed as a reduced case of an intersected-axes gear pair of the kind 1.2.2. The similarities and differences among gear pairs of different kinds is clearly indicated in the numbering of vector diagrams of every particular case.

An example of a vector diagram for gears of the kind 1.2.2 is shown in [Figure 12.9](#).

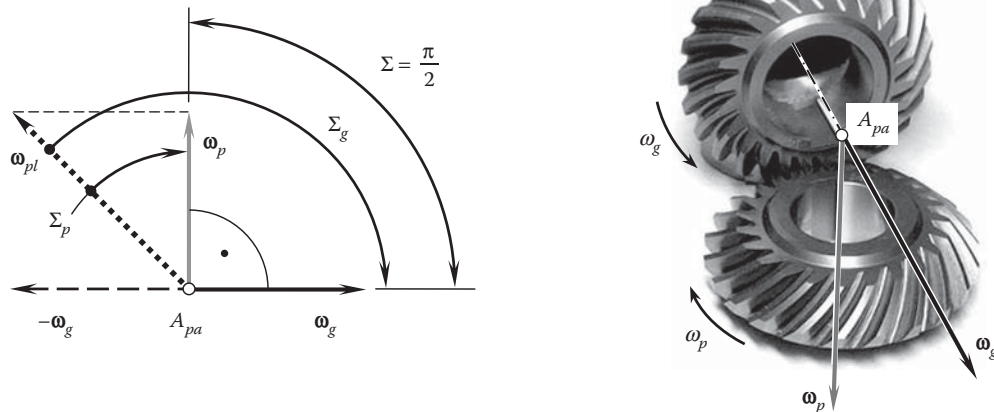


**FIGURE 12.8**  
Vector diagram of a miter gear pair.

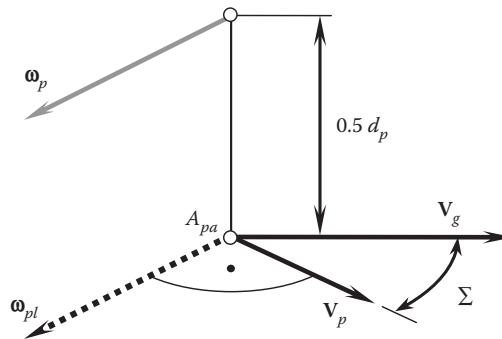


**FIGURE 12.9**  
Vector diagram for a round-rack-to-bevel-gear pair.

It is important to point out here that gears of the kind shown in Figure 12.9 represent that same third stratum of the classification (see Figure 2.15) as gear pairs of the kind in Figure 12.3. However, the gear pairs of these two different kinds represent different branches of the classification (see Figure 2.15).

### 12.3 Base Cones in Intersected-Axes Gearing

Perfect intersected-axes gear pairs are capable of transmitting a uniform rotation from the driving shaft to the driven shaft. From this perspective, perfect intersected-axes gear pairs resemble the previously discussed perfect parallel-axes gear pairs (see the schematic depicted in Figure 8.26). The similarity between these two types of gears can be extended further. Therefore, for convenience, it makes sense to consider perfect intersected-axes gearing in comparison with perfect parallel-axes gearing, as parallel-axes gearing is investigated much more profoundly, and the meshing of the tooth flanks of the gear and pinion in parallel-axes gearing is better understood at this time.

Perfect parallel-axes gear pairs feature two base cylinders, as shown in Figure 8.26. A uniform rotation of the base cylinders allows for an interpretation of parallel-axes gearing as a corresponding *pulley-and-belt* analogy. This is also valid with respect to perfect intersected-axes gear pairs. The base cones are associated with the gear as well as with the pinion of any and all perfect intersected-axes gear pairs. This concept is schematically illustrated in Figure 12.10. An orthogonal intersected-axes gear pair is depicted here solely for illustrative purposes. Without going into THE details of the analysis, it should be stated here that the same approach is applicable with respect to angular bevel gears that have a shaft angle of  $\Sigma \neq 90^\circ$ .

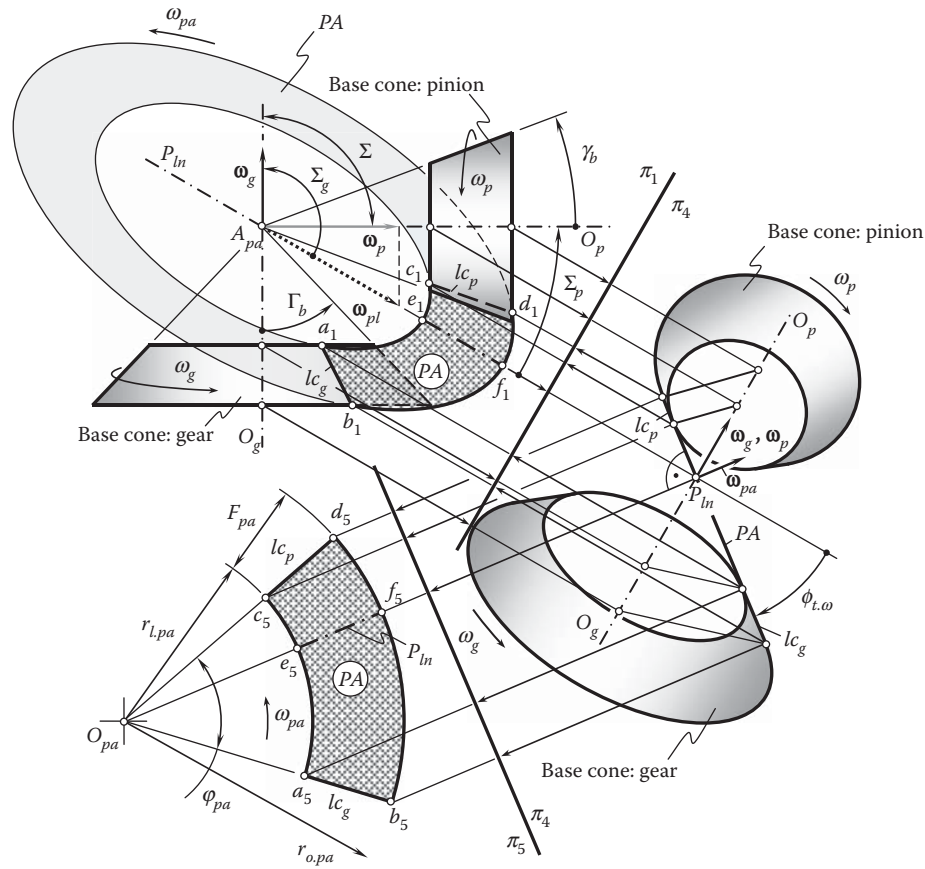


**FIGURE 12.10**  
Base cones and the plane of action,  $PA$ , in an orthogonal intersected-axes gear pair.

The schematic shown in [Figure 12.10](#) is constructed on the premise of the rotation vectors,  $\omega_g$  and  $\omega_p$ , of the gear and the pinion. The gear and the pinion rotate about their axes,  $O_g$  and  $O_p$ , respectively. The rotation vectors,  $\omega_g$  and  $\omega_p$ , allow for the construction of the vector,  $\omega_{pl}$ , of instant relative rotation. The axis of instant rotation,  $P_{ln}$ , is aligned with the rotation vector,  $\omega_{pl}$ .

The gear ratio,  $u$ , in an intersected-axes gear pair can be expressed in terms of the cone angles  $\Sigma_g$  of the gear and  $\Sigma_p$  of the mating pinion (see Equation 2.33):

$$u = \frac{\omega_p}{\omega_g} = \frac{\sin \Gamma_b}{\sin \gamma_b} = \frac{\sin \Sigma_g}{\sin \Sigma_p} \quad (12.14)$$

A few more equations can be used for the calculation of the gear ratio,  $u$ , in an intersected-axes gear pair. From the formula for the calculation of the gear cone angle,  $\Sigma_g$ :

$$\tan \Sigma_g = \frac{\sin \Sigma}{\frac{1}{u} + \cos \Sigma} \quad (12.15)$$

the gear ratio,  $u$ , in an intersected-axes gear pair is calculated as:

$$u = \left( \frac{\sin \Sigma}{\tan \Sigma_g} - \cos \gamma \right)^{-1} = \frac{\tan \Sigma_g}{\sin \Sigma - \cos \Sigma \tan \Sigma_g} \quad (12.16)$$

Similarly, from the formula for the calculation of the pinion cone angle,  $\Sigma_p$ :

$$\tan \Sigma_p = \frac{\sin \Sigma}{u + \cos \Sigma} \quad (12.17)$$

the gear ratio,  $u$ , in an intersected-axes gear pair is calculated as:

$$u = \frac{\sin \Sigma}{\tan \Sigma_p} - \cos \Sigma = \frac{\sin \Sigma - \cos \Sigma \tan \Sigma_p}{\tan \Sigma_p} \quad (12.18)$$

In a case of orthogonal intersected-axes gear pair, Equations 12.15 and 12.17 reduce to:

$$\Sigma_p = \frac{1}{\tan \frac{1}{u}} \quad (12.19)$$

$$\Sigma_p = \frac{1}{\tan u} \quad (12.20)$$

The plane of action,  $PA$ , is a plane through the axis of instant rotation,  $P_{ln}$ . The plane,  $PA$ , is tangent to both base cones, namely to the base cone of the gear and to the base cone of the pinion. The plane of action,  $PA$ , is at a transverse pressure angle,  $\phi_{t.\omega}$ , in relation to a perpendicular to the axis of instant rotation,  $P_{ln}$ , within the plane through the rotation vectors,  $\omega_g$  and  $\omega_p$ . The pressure angle,  $\phi_{t.\omega}$ , is measured within a plane that is perpendicular to the vector of instant rotation,  $\omega_{pl}$ .

The left upper portion of the schematic in Figure 12.10 is plotted within the plane of projections,  $\pi_1$ . Two other planes of projections,  $\pi_2$  and  $\pi_3$ , of a standard set of planes of projections,  $\pi_1\pi_2\pi_3$ , are not used in this particular consideration. Instead, two auxiliary planes of projections, namely the planes  $\pi_4$  and  $\pi_5$ , are used. The axis of projections,  $\pi_1/\pi_4$ , is constructed so as to be perpendicular to the axis of instant rotation,  $P_{ln}$ . The axis of projections,  $\pi_4/\pi_5$ , is constructed so as to be parallel to the trace of the plane of action,  $PA$ , within the plane of projections,  $\pi_4$ .

The plane of action can be imagined as a flexible zero-thickness film that is free to unwrap from and wrap on the base cones. The plane of action is not allowed for any bending about an axis perpendicular to the plane,  $PA$ , itself. Under a uniform rotation of the gears, the motion of the plane of action,  $PA$ , is a pure rotation about the axis,  $O_{pa}$ . The rotation vector,  $\omega_{pa}$ , is along the axis,  $O_{pa}$ , and is perpendicular to the plane of action.

For intersected-axes gear pairs, the plane of action,  $PA$ , can be construed as a round cone that has a  $90^\circ$  cone angle.

The rotation vectors,  $\omega_g$ ,  $\omega_p$ , and  $\omega_{pa}$ , are synchronized with one another in a timely manner:

$$u_{p/pa} = \sin \Sigma_p \quad (12.21)$$

$$u_{pa/g} = \frac{1}{\sin \Sigma_g} \quad (12.22)$$

$$u_{p/g} = u_{p/pa} \cdot u_{pa/g} = \frac{\sin \Sigma_p}{\sin \Sigma_g} \quad (12.23)$$

As the rotations,  $\omega_g$ ,  $\omega_p$ , and  $\omega_{pa}$ , are synchronized with one another, the base cone angles,  $\Gamma_b$  of a gear and  $\gamma_b$  of a mating pinion, can be calculated as:

$$\Gamma_b = \sin^{-1} \frac{\omega_g}{\omega_{pa}} \quad (12.24)$$

$$\gamma_b = \sin^{-1} \frac{\omega_p}{\omega_{pa}} \quad (12.25)$$

From these equations, an expression:

$$\omega_g \sin \gamma_b = \omega_p \sin \Gamma_b \quad (12.26)$$

can be derived.

For intersected-axes gear pairs, the base cone angles,  $\Gamma_b$  and  $\gamma_b$ , vary within the intervals  $0^\circ < \Gamma_b < 180^\circ$  and  $0^\circ < \gamma_b < 180^\circ$ , respectively. So, here and below, all equations are valid for external, rack-type, and internal gear pairs. Formally, the base cone angles,  $\Gamma_b$  and  $\gamma_b$ , can be considered in the narrower intervals, that is, within the intervals  $0^\circ < \Gamma_b < 90^\circ$  and  $0^\circ < \gamma_b < 90^\circ$ , correspondingly. Under such a scenario, the following inequalities are valid for intersected-axes gear pairs of various types:

- Base cone angles have positive values ( $\Gamma_b > 0^\circ$  and  $\gamma_b > 0^\circ$ ) for external gear pairs.
- The base cone angle of the gear is equal to a right angle ( $\Gamma_b = 90^\circ$ ) and  $\gamma_b > 0^\circ$  for rack-type gear pairs.
- Base cone angles of the gear have negative values ( $\Gamma_b < 0^\circ$ ) and  $\gamma_b > 0^\circ$  for internal gear pairs.

It is instructive to note here that only the gear base cone angle,  $\Gamma_b$ , can be up to  $\Gamma_b = 90^\circ$ , and not the pinion base cone angle,  $\gamma_b$ . This is because the gear tooth count,  $N_g$ , by convention is greater than the pinion tooth count,  $N_p$ ; thus, the gear base cone angle,  $\Gamma_b$ , is greater than the pinion base cone angle,  $\gamma_b$  (i.e., the inequality  $\Gamma_b \geq \gamma_b$  is valid).

The face width of the plane of action,  $F_{pa}$ , or, in other words, the working portion of the plane of action,  $PA$ , is located between two circles of radii  $r_{o.pa}$  and  $r_{l.pa}$ . The total portion of the plane of action spans a central angle,  $\varphi_{pa}$ . The angle,  $\varphi_{pa}$ , is measured between the lines of contact,  $lc_g$  and  $lc_p$ , of the plane of action,  $PA$ , and each of the two base cones.

### Conclusion 12.1

*Perfect intersected-axes gear pairs are those capable of transmitting an input uniform rotation smoothly.*

Intersected-axes gear pairs that do not allow for the construction of equivalent base cones and the plane of action,  $PA$ , are referred to as *approximate intersected-axes gear pairs*. The tooth flanks of approximate intersected-axes gear pairs feature geometry for which no equivalent pulley-and-belt mechanism can be designed to replace the gear pair.

### Conclusion 12.2

*Approximate intersected-axes gear pairs are those that are not capable of transmitting an input uniform rotation smoothly.*

Most of the bevel gears produced by the current industry are approximate gears.

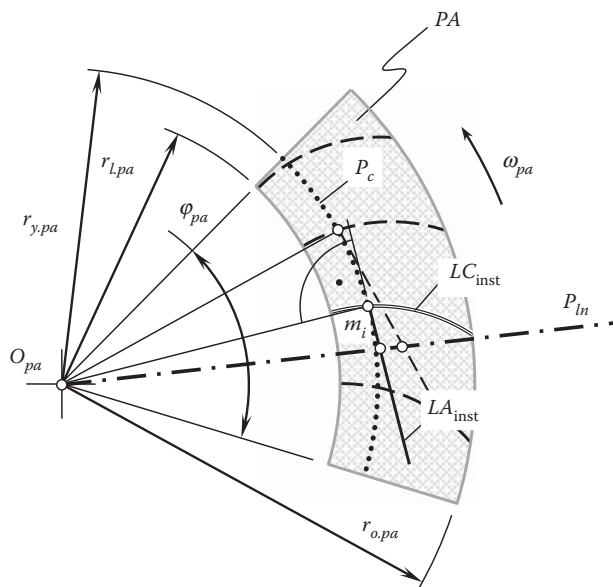
#### 12.3.1 Path of Contact and Instant Line of Action

Consider a plane of action,  $PA$ , in an intersected-axes gear pair, as illustrated in [Figure 12.11](#). When the gears rotate, the plane of action spins about the plane-of-action apex with a certain angular velocity,  $\omega_{pa}$ .

In a random configuration of the gears, an arbitrary point,  $m_i$ , is chosen within the line of contact,  $LC_{inst}$ . When the plane of action,  $PA$ , rotates, the line of contact,  $LC_{inst}$ , travels together with the plane of action. In this motion, each point,  $m_i$ , within the line of contact,  $LC_{inst}$ , traces a circular arc of a radius,  $r_{y.pa}$ . The arc in nature is a path of contact,  $P_c$ , in an intersected-axes gear pair. All the paths of contact are planar curves entirely located within the plane of action,  $PA$ . A family of all the paths of contact,  $P_c$ , can be viewed as the plane of action,  $PA$ .

Neither the geometry of the desired line of contact,  $LC_{des}$ , nor its configuration in relation to the plane of action,  $PA$ , is allowed to be altered when generating a gear,  $\mathcal{G}$ , and a mating pinion,  $\mathcal{P}$ , tooth flanks → gear inspection, gear cutting, and so forth.

At an arbitrary point,  $m_i$ , a straight line tangent to the corresponding path of contact,  $P_c$ , can be constructed. In nature, the straight line is an instant line of action,  $LA_{inst}$ . All the instant lines of action are entirely located within the plane of action, and all of them intersect the axis of instant rotation,  $P_{ln}$ , at a corresponding point. In this way,



the condition of conjugacy of the interacting tooth flanks,  $\mathcal{I}$  and  $\mathcal{P}$ , of a gear and mating pinion in intersected-axes gearing is fulfilled.

### 12.3.2 Operating Base Pitch Calculation

By definition, the operating base pitch,  $\varphi_{b,opr}$  is an angle between two consequent desirable lines of contact,  $LC_{des}^i$  and  $LC_{des}^{i+1}$ , in an intersected-axes gear pair.

$$\varphi_{b.op} = \frac{2\pi}{N_g} \cdot \frac{r_{b.g}}{r_{pa}} \quad (12.27)$$

$$\varphi_{b.op} = \frac{2\pi}{N_p} \cdot \frac{r_{b,p}}{r_{va}} \quad (12.28)$$

The calculated value of the operating base pitch,  $\varphi_{b,op}$  (see Equations 12.27 and 12.28), in an intersected-axes gear pair makes possible calculation of the operating base pitches,  $\varphi_{b,g}$  and  $\varphi_{b,p}$ , of a gear and mating pinion. The base pitches,  $\varphi_{b,g}$  and  $\varphi_{b,p}$ , can be calculated either from the expression:

$$\varphi_{b.op} = 2\pi N_g \sin \Gamma_b \quad (12.29)$$

$$\varphi_{b.op} = 2\pi N_p \sin \gamma_b \quad (12.30)$$

When the gears rotate, a gear/pinion circle of a radius  $r_{b,g}(r_{b,p})$  rolls with no sliding over a circle of a corresponding plane of action radius,  $r_{pa}$ .

## 12.4 Tooth Flanks of Perfect Intersected-Axes Gear Pairs

The conjugate tooth flanks of a gear and a mating pinion in an intersected-axes gear pair are in line contact with one another. The line of contact is entirely located within the plane of action,  $PA$ . As the gears rotate, the line of contact travels with respect to the gear and the pinion, as well as to the gear housing. The tooth flank of the gear,  $\mathcal{G}$ , can be interpreted as loci of successive positions of the line of contact,  $LC$ , in its motion in relation to a reference system associated with the gear. Similarly, the tooth flank of the pinion,  $\mathcal{P}$ , can be viewed as loci of successive positions of that same line of contact,  $LC$ , in its motion in relation to a reference system associated with the pinion. Ultimately, the loci of consecutive positions of that same line of contact,  $LC$ , in its motion in relation to a stationary reference system associated with the gear housing represent the surface of action,  $S_a$ . In a perfect intersected-axes gear pair, the surface of action,  $S_a$ , and the plane of action,  $PA$ , are congruent to each other. However, if a perfect intersected-axes gear pair features different pressure angles,  $\phi_{t,\omega}$ , at different points of the line of contact,  $LC$ , the surface of action,  $S_a$ , differs the plane of action,  $PA$ .

Therefore, once a line of contact,  $LC$ , is determined, the kinematics of an intersected-axes gearing (Figure 12.10) can be employed for the derivation of an analytical representation of the tooth flank of the gear,  $\mathcal{G}$ , and the pinion,  $\mathcal{P}$ . For this purpose, several reference systems need to be introduced.

### 12.4.1 Applied Coordinate Systems and Linear Transformations

Intersected-axes gearing is discussed below, using for this purpose numerous coordinate systems, each of which is convenient for a particular application. For convenience, in addition to the set of main reference systems, numerous intermediate reference systems are introduced below.

#### 12.4.1.1 Main Reference Systems

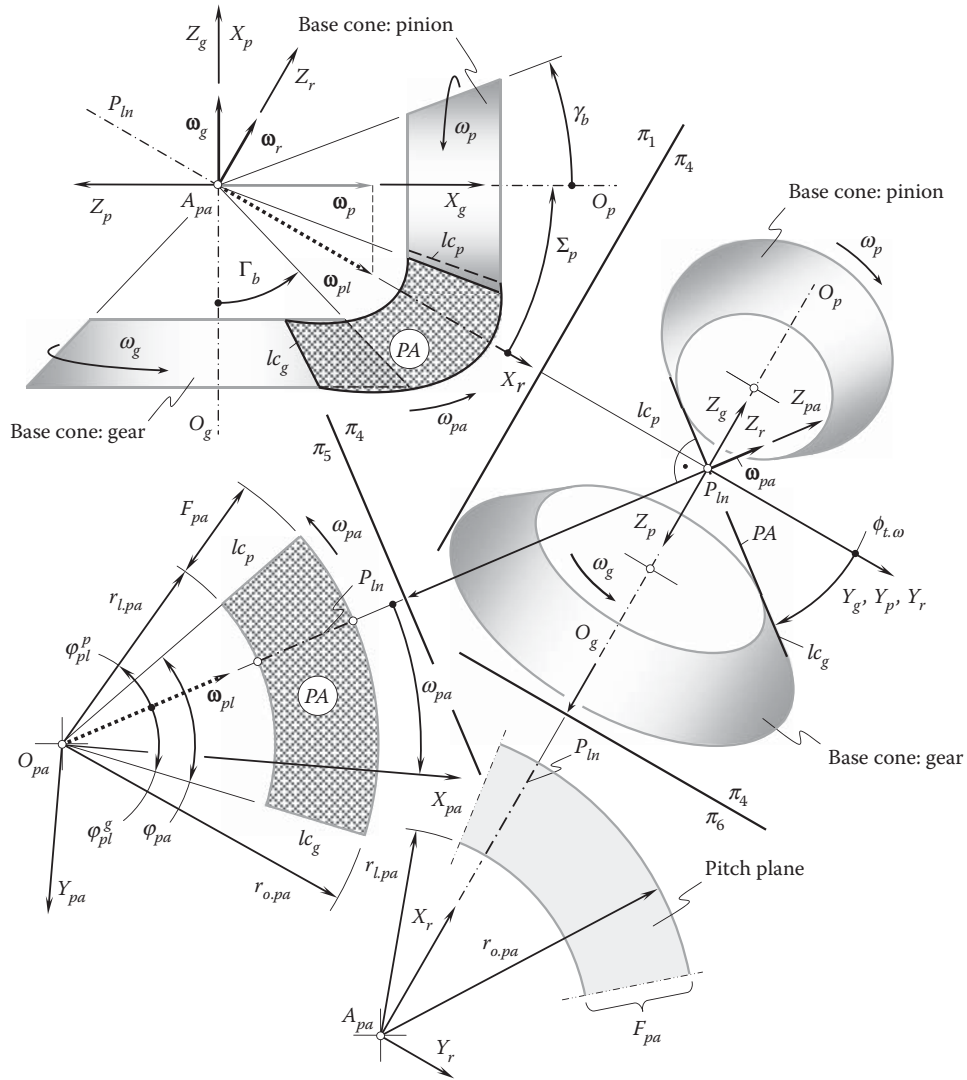
First, a *Cartesian* coordinate system,  $X_g Y_g Z_g$ , is associated with the gear, as shown in Figure 12.12. Second, a *Cartesian* coordinate system,  $X_p Y_p Z_p$ , is associated with the pinion (Figure 12.12). Third, a *Cartesian* coordinate system,  $X_r Y_r Z_r$ , is associated with auxiliary round rack, which is engaged in mesh simultaneously with both the gear and the mating pinion. Fourth, a *Cartesian* coordinate system,  $X_{pa} Y_{pa} Z_{pa}$ , is associated with the plane of action. Finally, a stationary *Cartesian* coordinate system,  $X_h Y_h Z_h$ , is associated with the gear housing. A few more auxiliary reference systems are used below as well.

The origin of the coordinate system  $X_r Y_r Z_r$  coincides with the plane-of-action apex,  $A_{pa}$ . The orientation of the coordinate system,  $X_r Y_r Z_r$ , is defined by the rotation vectors  $\omega_g$ ,  $\omega_p$ , and  $\omega_{pl}$ . The  $X_r$ -axis is aligned with the vector,  $\omega_{pl}$ , of instant rotation. The axis,  $Y_r$ , aligns with the vector defined by the cross product,  $\omega_p \times \omega_g$ . Ultimately, the  $Z_r$ -axis is along the vector that is defined by the triple vector product,  $\omega_p \times \omega_g \times \omega_{pl}$ .

The coordinate system,  $X_{pa} Y_{pa} Z_{pa}$ , shares its origin with the reference system,  $X_r Y_r Z_r$ . The axis,  $X_{pa}$ , is located within the plane of action,  $PA$ . It forms a certain angle,  $\theta_{pa}$ , with the vector of instant rotation,  $\omega_{pl}$ . The  $Y_{pa}$ -axis is also located within the plane of action,  $PA$ , and is perpendicular to the  $X_{pa}$ -axis (here  $\theta_{pa} = \omega_{pa} \cdot t$ , and time is denoted by  $t$ ). Finally, the axis  $Z_{pa}$  makes up the axes  $X_{pa}$  and  $Y_{pa}$  to the left-hand-oriented *Cartesian* coordinate system  $X_{pa} Y_{pa} Z_{pa}$ .

The coordinate system,  $X_{pa} Y_{pa} Z_{pa}$ , is convenient to specify a line of contact,  $LC$ , between the gear tooth flank,  $\mathcal{G}$ , and the pinion tooth flank,  $\mathcal{P}$ , similarly to what has been done with respect to parallel-axes gear pairs (see Figure 6.12 for more details). Then, the representation of the current position of the moving line of contact,  $LC$ , in the reference systems,  $X_g Y_g Z_g$  and  $X_p Y_p Z_p$ , will return analytical expressions for the tooth flanks,  $\mathcal{G}$  and  $\mathcal{P}$ , of the gear and the pinion. Similarly, representation of the current position of the moving line of contact,  $LC$ , in the motionless reference system,  $X_h Y_h Z_h$ , will return an equation for the surface of action.



**FIGURE 12.12**

Reference systems used for the derivation of analytical expressions for a gear tooth flank,  $\mathcal{G}$ , and a mating pinion tooth flank,  $\mathcal{P}$ , in an intersected-axes gearing.

#### 12.4.1.2 Operators of Rolling

For the derivation of an equation of the gear tooth flank,  $\mathcal{G}$ , an operator  $\mathbf{Rs}(PA \mapsto \mathcal{G})$  of the resultant coordinate system transformation needs to be composed. The operator,  $\mathbf{Rs}(PA \mapsto \mathcal{G})$ , can be expressed in terms of the following:

- The operator of rotation,  $\mathbf{Rt}(pa \mapsto pa_0)$ , of the coordinate system,  $X_{pa}Y_{pa}Z_{pa}$  about the  $Z_{pa}$ -axis through a certain angle,  $\theta_{pa}$ . When the axis,  $X_{pa}$ , is aligned to the rotation vector,  $\omega_{pl}$ , then the reference system,  $X_{pa}Y_{pa}Z_{pa}$ , occupies a particular configuration,  $X_{pa}^0Y_{pa}^0Z_{pa}^0$  (the coordinate system,  $X_{pa}^0Y_{pa}^0Z_{pa}^0$ , is not depicted in Figure 12.12). The operator,  $\mathbf{Rt}(pa \mapsto pa_0)$ , can be expressed in the form:

$$\mathbf{Rt}(pa \mapsto pa_0) = \begin{bmatrix} \cos \theta_{pa} & 0 & -\sin \theta_{pa} & 0 \\ 0 & 1 & 0 & 0 \\ \sin \theta_{pa} & 0 & \cos \theta_{pa} & 0 \\ 0 & 0 & 0 & 1 \end{bmatrix} \quad (12.31)$$

- The operator of rotation,  $\mathbf{Rt}(pa_0 \mapsto r)$ , of the coordinate system,  $X_{pa}^0 Y_{pa}^0 Z_{pa}^0$ , about the vector of instant rotation,  $\omega_{pl}$  (through the transverse profile angle,  $\phi_{t,\omega}$ ), is measured within a plane, which is perpendicular to the rotation vector,  $\omega_{pl}$ :

$$\mathbf{Rt}(pa_0 \mapsto r) = \begin{bmatrix} 1 & 0 & 0 & 0 \\ 0 & \cos \phi_{t,\omega} & -\sin \phi_{t,\omega} & 0 \\ 0 & \sin \phi_{t,\omega} & \cos \phi_{t,\omega} & 0 \\ 0 & 0 & 0 & 1 \end{bmatrix} \quad (12.32)$$

- The operator of rotation,  $\mathbf{Rt}(r \mapsto g)$ , of the coordinate system,  $X_r Y_r Z_r$ , about the  $Y_r$ -axis through the angle,  $\angle(\omega_r, \omega_p)$ . Note that the angle,  $\angle(\omega_r, \omega_p)$ , is equal to the angle  $\angle(\omega_p, \omega_{pl}) = \Sigma_p$ . The operator of rotation,  $\mathbf{Rt}(r \mapsto g)$ , can be represented in the form:

$$\mathbf{Rt}(r \mapsto g) = \begin{bmatrix} \cos \Sigma_p & 0 & \sin \Sigma_p & 0 \\ 0 & 1 & 0 & 0 \\ -\sin \Sigma_p & 0 & \cos \Sigma_p & 0 \\ 0 & 0 & 0 & 1 \end{bmatrix} \quad (12.33)$$

The operator,  $\mathbf{Rs}(PA \mapsto \mathcal{G})$ , of the resultant coordinate system transformation is equal to the product:

$$\mathbf{Rs}(PA \mapsto \mathcal{G}) = \mathbf{Rt}(r \mapsto g) \cdot \mathbf{Rt}(pa_0 \mapsto r) \cdot \mathbf{Rt}(pa \mapsto pa_0) \quad (12.34)$$

This operator allows for matrix representation in the form:

$$\begin{aligned} \mathbf{Rs}(PA \mapsto \mathcal{G}) = \\ = \begin{bmatrix} \cos \Sigma_p \cos \theta_{pa} + \sin \Sigma_p \cos \phi_{t,\omega} \sin \theta_{pa} & \sin \Sigma_p \sin \phi_{t,\omega} & \sin \Sigma_p \cos \phi_{t,\omega} \cos \theta_{pa} - \cos \Sigma_p \sin \theta_{pa} & 0 \\ -\sin \phi_{t,\omega} \sin \theta_{pa} & \cos \phi_{t,\omega} & -\sin \phi_{t,\omega} \cos \theta_{pa} & 0 \\ \cos \Sigma_p \cos \phi_{t,\omega} \sin \theta_{pa} - \sin \Sigma_p \cos \theta_{pa} & \cos \Sigma_p \sin \phi_{t,\omega} & \sin \Sigma_p \sin \theta_{pa} + \cos \Sigma_p \cos \phi_{t,\omega} \cos \theta_{pa} & 0 \\ 0 & 0 & 0 & 1 \end{bmatrix} \end{aligned} \quad (12.35)$$

The operator,  $\mathbf{Rs}(PA \mapsto \mathcal{P})$ , of the resultant coordinate system transformation, that is, the operator of transition from the coordinate system,  $X_{pa} Y_{pa} Z_{pa}$ , associated with the plane of action,  $PA$ , to the coordinate system,  $X_p Y_p Z_p$ , associated with the pinion, is equal to the product:

$$\mathbf{Rs}(PA \mapsto \mathcal{P}) = \mathbf{Rt}(r \mapsto p) \cdot \mathbf{Rt}(pa_0 \mapsto r) \cdot \mathbf{Rt}(pa \mapsto pa_0) \quad (12.36)$$

Here, the operator of rotation,  $\mathbf{Rt}(r \mapsto p)$ , can be composed in a similar manner to how the operator  $\mathbf{Rt}(r \mapsto g)$  (see Equation 12.33) is composed. The similarity allows for the following expression for the operator of rotation,  $\mathbf{Rt}(r \mapsto p)$ :

$$\mathbf{Rt}(r \mapsto p) = \begin{bmatrix} \cos \Sigma_g & 0 & \sin \Sigma_g & 0 \\ 0 & 1 & 0 & 0 \\ -\sin \Sigma_g & 0 & \cos \Sigma_g & 0 \\ 0 & 0 & 0 & 1 \end{bmatrix} \quad (12.37)$$

Substituting into Equations 12.36 and 12.37, together with Equations 12.31 and 12.32, returns an expression for the operator of the resultant coordinate system transformation,  $\mathbf{Rs}(PA \mapsto \mathcal{P})$ :

$$\mathbf{Rs}(PA \mapsto \mathcal{P}) = \begin{bmatrix} \cos \Sigma_g \cos \theta_{pa} + \sin \Sigma_g \cos \phi_{t,\omega} \sin \theta_{pa} & \sin \Sigma_g \sin \phi_{t,\omega} & \sin \Sigma_g \cos \phi_{t,\omega} \cos \theta_{pa} - \cos \Sigma_g \sin \theta_{pa} & 0 \\ -\sin \phi_{t,\omega} \sin \theta_{pa} & \cos \phi_{t,\omega} & -\sin \phi_{t,\omega} \cos \theta_{pa} & 0 \\ \cos \Sigma_g \cos \phi_{t,\omega} \sin \theta_{pa} - \sin \Sigma_g \cos \theta_{pa} & \cos \Sigma_g \sin \phi_{t,\omega} & \sin \Sigma_g \sin \theta_{pa} + \cos \Sigma_g \cos \phi_{t,\omega} \cos \theta_{pa} & 0 \\ 0 & 0 & 0 & 1 \end{bmatrix} \quad (12.38)$$

The operators,  $\mathbf{Rs}(PA \mapsto \mathcal{G})$  and  $\mathbf{Rs}(PA \mapsto \mathcal{P})$ , of the resultant coordinate system transformations are a kind of operators of rolling. As they are broadly used in the theory of gearing, for intersected-axes gears in particular, special designations, namely  $\mathbf{Ri}(PA \mapsto \mathcal{G})$  and  $\mathbf{Ri}(PA \mapsto \mathcal{P})$ , can be assigned to each of them:

$$\mathbf{Rs}(PA \mapsto \mathcal{G}) = \mathbf{Ri}(PA \mapsto \mathcal{G}) \quad (12.39)$$

$$\mathbf{Rs}(PA \mapsto \mathcal{P}) = \mathbf{Ri}(PA \mapsto \mathcal{P}) \quad (12.40)$$

As the operators of rolling,  $\mathbf{Ri}(PA \mapsto \mathcal{G})$  and  $\mathbf{Ri}(PA \mapsto \mathcal{P})$ , are known, the operator of rolling,  $\mathbf{Ri}(\mathcal{P} \mapsto \mathcal{G})$ , of the pinion over the gear can be calculated as:

$$\mathbf{Ri}(\mathcal{P} \mapsto \mathcal{G}) = \mathbf{Ri}(PA \mapsto \mathcal{G}) \cdot \mathbf{Ri}^{-1}(PA \mapsto \mathcal{P}) \quad (12.41)$$

Similarly, the operator of rolling,  $\mathbf{Ri}(\mathcal{G} \mapsto \mathcal{P})$ , of the gear over the pinion can be calculated either as reciprocal to the operator,  $\mathbf{Ri}(\mathcal{P} \mapsto \mathcal{G})$ , or the expression:

$$\mathbf{Ri}(\mathcal{G} \mapsto \mathcal{P}) = \mathbf{Ri}^{-1}(\mathcal{P} \mapsto \mathcal{G}) = \mathbf{Ri}(PA \mapsto \mathcal{P}) \cdot \mathbf{Ri}^{-1}(PA \mapsto \mathcal{G}) \quad (12.42)$$

can be used for the calculation of the operator of rolling  $\mathbf{Ri}(\mathcal{G} \mapsto \mathcal{P})$ .

### 12.4.1.3 Operators of Linear Transformations Associated with the Gear Housing

A stationary reference system,  $X_h Y_h Z_{h_r}$ , is associated with a housing of a gear pair. The choice of the coordinate system,  $X_h Y_h Z_{h_r}$ , depends mostly on convenience. In a particular case, either the stationary Cartesian coordinate system,  $X_g^0 Y_g^0 Z_g^0$ , or the stationary Cartesian coordinate system,  $X_p^0 Y_p^0 Z_p^0$ , can be used for this purpose.

The coordinate system,  $X_g^0 Y_g^0 Z_g^0$ , shares a common  $Z_g$ -axis with the coordinate system,  $X_g Y_g Z_g$ , associated with the gear. The coordinate system,  $X_g Y_g Z_g$ , is turned in relation to the motionless coordinate system,  $X_g^0 Y_g^0 Z_g^0$ , through a certain angle,  $\varphi_g$ . Similarly, the system,  $X_p^0 Y_p^0 Z_p^0$ , shares a common  $Z_p$ -axis with the coordinate system,  $X_p Y_p Z_p$ , associated with the pinion. The coordinate system,  $X_p Y_p Z_p$ , is turned in relation to the motionless coordinate system,  $X_p^0 Y_p^0 Z_p^0$ , through a certain angle,  $\varphi_p$ . It is of importance to note here that the rotation angles,  $\varphi_g$  and  $\varphi_p$ , correspond to one another by the expression  $\varphi_p = u\varphi_g$ , and  $u$  designates the tooth ratio of the gear pair.

For external intersected-axes gearing, the rotation angles,  $\varphi_g$  and  $\varphi_p$ , are of opposite signs.

The rotation of the reference system,  $X_g Y_g Z_g$ , about the  $Z_g$ -axis through an angle,  $\varphi_g$ , can be analytically described by the operator of rotation,  $\mathbf{Rt}(\mathcal{G} \mapsto h)$ . This operator can be expressed in the form:

$$\mathbf{Rt}(\mathcal{G} \mapsto h) = \begin{bmatrix} \cos \varphi_g & \sin \varphi_g & 0 & 0 \\ -\sin \varphi_g & \cos \varphi_g & 0 & 0 \\ 0 & 0 & 1 & 0 \\ 0 & 0 & 0 & 1 \end{bmatrix} \quad (12.43)$$

Equation 12.43 allows for an expression for the operator of the resultant coordinate system transformation, that is, for the operator of transition,  $\mathbf{Rs}(pa \mapsto h)$ , from the coordinate system,  $X_{pa}Y_{pa}Z_{pa}$ , associated with the plane of action, to the stationary coordinate system,  $X_hY_hZ_h$ . This operator can be represented as the product:

$$\mathbf{Rs}(pa \mapsto h) = \mathbf{Rt}(\mathcal{G} \mapsto h) \cdot \mathbf{Ri}(PA \mapsto \mathcal{G}) \quad (12.44)$$

or in matrix form:

$$\mathbf{Rs}(pa \mapsto h) = \begin{bmatrix} \cos \varphi_g (\cos \Sigma_p \cos \theta_{pa} + \sin \Sigma_p \cos \phi_{t,\omega} \sin \theta_{pa}) - \sin \varphi_g \sin \phi_{t,\omega} \sin \theta_{pa} & -\sin \varphi_g (\cos \Sigma_p \cos \theta_{pa} + \sin \Sigma_p \cos \phi_{t,\omega} \sin \theta_{pa}) - \cos \varphi_g \sin \phi_{t,\omega} \sin \theta_{pa} & \cos \Sigma_p \cos \phi_{t,\omega} \sin \theta_{pa} - \sin \Sigma_p \cos \theta_{pa} & 0 \\ \sin \varphi_g \cos \phi_{t,\omega} + \sin \Sigma_p \cos \varphi_g \sin \phi_{t,\omega} & -\cos \varphi_g (\cos \Sigma_p \sin \theta_{pa} - \sin \Sigma_p \cos \phi_{t,\omega} \cos \theta_{pa}) - \sin \varphi_g \sin \phi_{t,\omega} \cos \theta_{pa} & 0 & 0 \\ \cos \varphi_g \cos \phi_{t,\omega} - \sin \Sigma_p \sin \varphi_g \sin \phi_{t,\omega} & -\sin \varphi_g (\cos \Sigma_p \sin \theta_{pa} - \sin \Sigma_p \cos \phi_{t,\omega} \cos \theta_{pa}) - \sin \varphi_g \sin \phi_{t,\omega} \cos \theta_{pa} & 0 & 0 \\ \cos \Sigma_p \sin \phi_{t,\omega} & \sin \Sigma_p \sin \theta_{pa} + \cos \Sigma_p \cos \phi_{t,\omega} \cos \theta_{pa} & 0 & 1 \end{bmatrix} \quad (12.45)$$

The rotation of the reference system,  $X_pY_pZ_p$ , about the  $Z_p$ -axis through an angle,  $\varphi_p = -u\varphi_g$ , can be analytically described by the operator of rotation,  $\mathbf{Rt}(\mathcal{P} \mapsto h_p)$ . This operator can be expressed in the form:

$$\mathbf{Rt}(\mathcal{P} \mapsto h_p) = \begin{bmatrix} \cos \varphi_p & \sin \varphi_p & 0 & 0 \\ -\sin \varphi_p & \cos \varphi_p & 0 & 0 \\ 0 & 0 & 1 & 0 \\ 0 & 0 & 0 & 1 \end{bmatrix} \quad (12.46)$$

Equation 12.46 allows for an expression of the operator of the resultant coordinate system transformation, that is, for the operator of transition,  $\mathbf{Rs}(pa \mapsto h_p)$ , from the coordinate system,  $X_{pa}Y_{pa}Z_{pa}$ , associated with the plane of action, to the stationary coordinate system,  $X_{h,p}Y_{h,p}Z_{h,p}$ . This operator can be represented as the product:

$$\mathbf{Rs}(pa \mapsto h_p) = \mathbf{Rt}(\mathcal{G} \mapsto h) \cdot \mathbf{Ri}(PA \mapsto \mathcal{G}) \quad (12.47)$$

or in matrix form:

$$\mathbf{Rs}(pa \mapsto h_p) = \begin{bmatrix} \cos \varphi_p (\cos \Sigma_g \cos \theta_{pa} + \sin \Sigma_g \cos \phi_{t,\omega} \sin \theta_{pa}) - \sin \varphi_p \sin \phi_{t,\omega} \sin \theta_{pa} & -\sin \varphi_p (\cos \Sigma_g \cos \theta_{pa} + \sin \Sigma_g \cos \phi_{t,\omega} \sin \theta_{pa}) - \cos \varphi_p \sin \phi_{t,\omega} \sin \theta_{pa} & \cos \Sigma_g \cos \phi_{t,\omega} \sin \theta_{pa} - \sin \Sigma_g \cos \theta_{pa} & 0 \\ \sin \varphi_p \cos \phi_{t,\omega} + \sin \Sigma_p \cos \varphi_p \sin \phi_{t,\omega} & -\cos \varphi_p (\cos \Sigma_g \sin \theta_{pa} - \sin \Sigma_g \cos \phi_{t,\omega} \cos \theta_{pa}) - \sin \varphi_p \sin \phi_{t,\omega} \cos \theta_{pa} & 0 & 0 \\ \cos \varphi_p \cos \phi_{t,\omega} - \sin \Sigma_p \sin \varphi_p \sin \phi_{t,\omega} & -\sin \varphi_p (\cos \Sigma_g \sin \theta_{pa} - \sin \Sigma_g \cos \phi_{t,\omega} \cos \theta_{pa}) - \sin \varphi_p \sin \phi_{t,\omega} \cos \theta_{pa} & 0 & 0 \\ \cos \Sigma_p \sin \phi_{t,\omega} & \sin \Sigma_g \sin \theta_{pa} + \cos \Sigma_g \cos \phi_{t,\omega} \cos \theta_{pa} & 0 & 1 \end{bmatrix} \quad (12.48)$$

Both reference systems, that is, the coordinate systems,  $X_hY_hZ_h$  and  $X_{h,p}Y_{h,p}Z_{h,p}$ , are stationary reference systems associated with the housing of the gear pair. The relation between these two coordinate systems can be analytically described by the expression:

$$\mathbf{Rs}(h_p \mapsto h) = \mathbf{Rs}(pa \mapsto h) \cdot \mathbf{Rs}^{-1}(pa \mapsto h_p) \quad (12.49)$$

The expressions derived above for the operators of the coordinate system transformations make it possible to express any and all geometrical features (1) of the gear, (2) of the pinion, and (3) of the gear-to-pinion mesh in a common reference system.

#### 12.4.2 Tooth Flank of a Gear in an Intersected-Axes Gear Pair

The tooth flank of a bevel gear allows for interpretation as a locus of consecutive positions of the line of contact,  $LC$ , when the plane of action,  $PA$ , is either wrapping on or unwrapping from the base cone of the gear and is unwrapping or wrapping onto base cone of the pinion.\* For this purpose, the line of contact has to be represented in a reference system associated with the gear.

Any planar curve of a reasonable geometry can be employed as the line of contact,  $LC$ , in an intersected-axes gear pair have to be considered separately.

The shape of the line of contact depends on the geometry of tooth flanks of a gear,  $\mathcal{G}$ , and a mating pinion,  $\mathcal{P}$  (in the lengthwise direction in particular). In any case, the line of contact,  $LC$ , is located within the coordinate plane,  $X_{pa}Y_{pa}$ , of the reference system,  $X_{pa}Y_{pa}Z_{pa}$ , associated with the plane of action, as schematically illustrated in Figure 12.13.

Generally speaking, the position vector of a point,  $\mathbf{r}_{lc}$ , of the line of contact,  $LC$ , can be analytically described by an expression in matrix form:

$$\mathbf{r}_{lc}(v) = \begin{bmatrix} X_{lc}(v) \\ Y_{lc}(v) \\ 0 \\ 1 \end{bmatrix} \quad (12.50)$$

To represent Equation 12.50 of the position vector of a point,  $\mathbf{r}_{lc}$ , of the line of contact,  $LC$ , in the reference system,  $X_gY_gZ_g$ , associated with the gear, the operator of the resultant coordinate system transformation,  $\mathbf{Rs}(PA \mapsto \mathcal{G})$ , can be employed:

$$\mathbf{r}_g(v, \theta_{pa}) = \mathbf{r}_{lc}^g(v, \theta_{pa}) = \mathbf{Rs}(PA \mapsto \mathcal{G}) \cdot \mathbf{r}_{lc}(v) \quad (12.51)$$

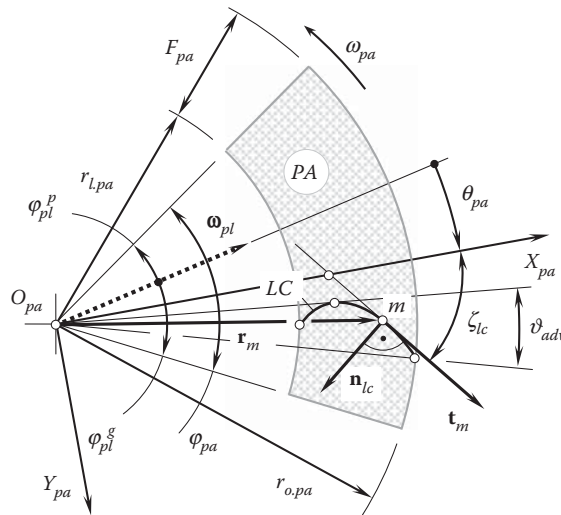


FIGURE 12.13

General case of the line of contact,  $LC$ , between a gear tooth flank,  $\mathcal{G}$ , and a mating pinion tooth flank,  $\mathcal{P}$ , in an intersected-axes gear pair (the line of contact,  $LC$ , is constructed before the tooth flanks,  $\mathcal{G}$  and  $\mathcal{P}$ ).

\* Actually, the proposed approach to generate a gear/pinion tooth flank in intersected-axes gearing can be referred to as a *describing method* for gear/pinion tooth flank generation. It has to be stressed here that generation of an involute curve by (a) a point, that is, in the describing method, and (b) a straight line, that is, in enveloping method, can be equivalent to one another only in a case of parallel-axes gearing, and is valid neither in the case of intersected-axes nor in the case of *crossed-axes* gearings. Only approximate gear/pinion tooth flanks can be generated in the latter two cases of tooth flank generation.

When the axis,  $X_{pa}$ , is along one of the sides of the face advance angle,  $\vartheta_{adv}$ , the central angle,  $\theta_{pa}$ , is within the interval (see Figure 12.12):

$$\varphi_{pl}^p + \vartheta_{adv} \leq \theta_{pa} \leq \varphi_{pl}^s - \vartheta_{adv} \quad (12.52)$$

here, the angles  $\varphi_{pl}^s$  and  $\varphi_{pl}^p$  are of opposite signs. Otherwise, the angles that the  $X_{pa}$ -axis forms with the sides of the face advance angle,  $\vartheta_{adv}$ , should be taken into consideration.

Substituting the position vector,  $\mathbf{r}_{lc}$  (see Equation 12.50) and the operator of the resultant coordinate system transformation,  $\mathbf{R}_s(PA \mapsto \mathcal{G})$  (see Equation 12.35), into Equation 12.51, an expression for the computation of the position vector of a point,  $\mathbf{r}_g$ , of the gear tooth flank,  $\mathcal{G}$ :

$$\mathbf{r}_g(v, \theta_{pa}) = \begin{bmatrix} (\cos \Sigma_p \cos \theta_{pa} + \sin \Sigma_p \cos \phi_{t,\omega} \sin \theta_{pa}) \cdot X(v) + \sin \Sigma_p \sin \phi_{t,\omega} \cdot Y(v) \\ -X(v) \sin \phi_{t,\omega} \sin \theta_{pa} + Y(v) \cos \phi_{t,\omega} \\ -(\sin \Sigma_p \cos \theta_{pa} - \cos \Sigma_p \cos \phi_{t,\omega} \sin \theta_{pa}) \cdot X(v) + \cos \Sigma_p \sin \phi_{t,\omega} \cdot Y(v) \\ 1 \end{bmatrix} \quad (12.53)$$

can be derived.

In a particular case, when the line of contact,  $LC$ , is a straight line segment (Figure 12.14), the position vector of a point,  $\mathbf{r}_{lc}$ , of the line of contact,  $LC$ , is equal to the sum:

$$\mathbf{r}_{lc} = \mathbf{r}_{lc}^0 + \mathbf{r}_{lc}^\lambda \quad (12.54)$$

Here, in Equation 12.54, the vector  $\mathbf{r}_{lc}^0$  is of a constant length,  $\mathbf{r}_{lc}^0 = \mathbf{i} \cdot r_{lc}^0$ , where  $r_{lc}^0 = |\mathbf{r}_{lc}^0|$ . Another component, namely the vector  $\mathbf{r}_{lc}^\lambda$ , can be represented in the form:

$$\mathbf{r}_{lc}^\lambda(\lambda) = \mathbf{i} \cdot \lambda \cos \zeta_{cl} + \mathbf{j} \cdot \lambda \sin \zeta_{cl} \quad (12.55)$$

where:

$\lambda$ : is the length of the vector  $\mathbf{r}_{lc}^\lambda$ .

$\zeta_{cl}$ : is the angle of inclination of the line of contact,  $LC$ , in relation to the  $X_{pa}$ -axis of the coordinate system,  $X_{pa}Y_{pa}Z_{pa}$  (see Figure 12.14).

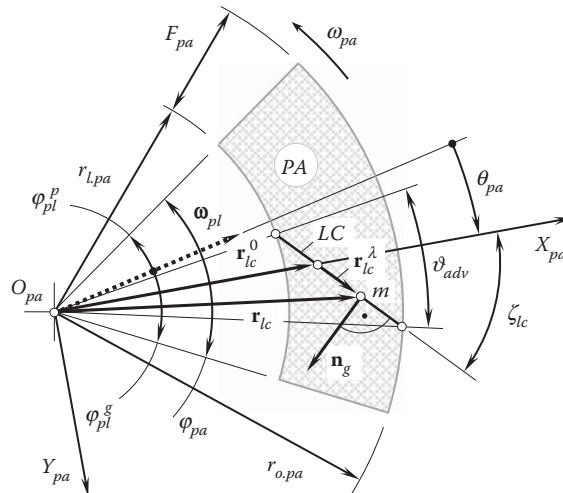


FIGURE 12.14

Line of contact,  $LC$ , between a gear tooth flank,  $\mathcal{G}$ , and a mating pinion tooth flank,  $\mathcal{P}$ , in skew bevel gears.

Ultimately, the position vector of a point,  $\mathbf{r}_{lc}$ , of the line of contact,  $LC$ , allows for matrix representation in the form:

$$\mathbf{r}_{lc}(\lambda) = \begin{bmatrix} r_{lc}^0 + \lambda \cos \zeta_{cl} \\ \lambda \sin \zeta_{cl} \\ 0 \\ 1 \end{bmatrix} \quad (12.56)$$

Equation 12.56 considered together with the operator of the resultant coordinate system transformation,  $\mathbf{Rs}(PA \mapsto \mathcal{G})$  (see Equation 12.35), makes it possible to calculate the position vector of a point,  $\mathbf{r}_g$ , of the tooth flank of a bevel gear,  $\mathcal{G}$ , that features an inclined line of contact:

$$\mathbf{r}_g(v, \theta_{pa}) = \mathbf{r}_{lc}^g(\lambda, \theta_{pa}) = \mathbf{Rs}(PA \mapsto \mathcal{G}) \cdot \mathbf{r}_{lc}(\lambda) \quad (12.57)$$

An expanded form of the expression for the calculation of the position vector,  $\mathbf{r}_{lc}^g$ , can be derived after substitution of the position vector,  $\mathbf{r}_{lc}$  (see Equation 12.56) and  $\mathbf{Rs}(PA \mapsto \mathcal{G})$  (see Equation 12.35) into Equation 12.57:

$$\mathbf{r}_g(\lambda, \theta_{pa}) = \begin{bmatrix} (\cos \Sigma_p \cos \theta_{pa} + \sin \Sigma_p \cos \phi_{t,\omega} \sin \theta_{pa}) \cdot (r_{lc}^0 + \lambda \cos \zeta_{lc}) + \lambda \sin \Sigma_p \sin \phi_{t,\omega} \sin \zeta_{lc} \\ (\lambda \cos \phi_{t,\omega} \sin \zeta_{lc} - \sin \phi_{t,\omega} \sin \theta_{pa}) \cdot (r_{lc}^0 + \lambda \cos \zeta_{lc}) \\ -(\sin \Sigma_p \cos \theta_{pa} - \cos \Sigma_p \cos \phi_{t,\omega} \sin \theta_{pa}) \cdot (r_{lc}^0 + \lambda \cos \zeta_{lc}) + \lambda \cos \Sigma_p \sin \phi_{t,\omega} \sin \zeta_{lc} \\ 1 \end{bmatrix} \quad (12.58)$$

In the particular case of straight bevel gear pair, the line of contact,  $LC$ , is aligned with the  $X_{pa}$ -axis of the Cartesian coordinate system,  $X_{pa}Y_{pa}Z_{pa}$ . This allows representation of the position vector,  $\mathbf{r}_{lc}$ , of a point of the line of contact,  $LC$ , in the form of a column matrix:

$$\mathbf{r}_{lc}(X_{pa}) = \begin{bmatrix} X_{pa} \\ 0 \\ 0 \\ 1 \end{bmatrix} \quad (12.59)$$

An expression for the position vector of a point,  $\mathbf{r}_g$ , of the tooth flank of the straight bevel gear can be defined as the product:

$$\mathbf{r}_g(X_{pa}, \theta_{pa}) = \mathbf{Rs}(PA \mapsto \mathcal{G}) \cdot \mathbf{r}_{lc}(X_{pa}) \quad (12.60)$$

where the operator,  $\mathbf{Rs}(PA \mapsto \mathcal{G})$ , of the resultant coordinate system transformation is given by Equation 12.35.

It is important to stress here that the expression for the position vector of a point,  $\mathbf{r}_g$ , of a gear tooth flank,  $\mathcal{G}$ , as well as a similar expression for a position vector of a point,  $\mathbf{r}_p$ , of a mating pinion tooth flank,  $\mathcal{P}$ , are derived on the premise that both tooth flanks,  $\mathcal{G}$  and  $\mathcal{P}$ , are generated by the moving line of contact,\*  $LC$ , and not as an envelope to consecutive positions of the tooth flank of an auxiliary generating rack,  $\mathcal{R}$ . This eliminates the necessity of implementation of results that are developed in the theory of enveloping surfaces. These results become useless in the case under consideration. In this way, derivation of the necessary equation becomes much easier.

Equation 12.60 allows for an expanded form of the expression for the position vector of a point,  $\mathbf{r}_g$ , of the straight bevel gear tooth flank:

$$\mathbf{r}_g(X_{pa}, \theta_{pa}) = \begin{bmatrix} X_{pa}(\cos \Sigma_p \cos \theta_{pa} + \sin \Sigma_p \cos \phi_{t,\omega} \sin \theta_{pa}) \\ -X_{pa} \sin \phi_{t,\omega} \sin \theta_{pa} \\ -X_{pa}(\sin \Sigma_p \cos \theta_{pa} - \cos \Sigma_p \cos \phi_{t,\omega} \sin \theta_{pa}) \\ 1 \end{bmatrix} \quad (12.61)$$

Gears that have tooth flanks (see Equation 12.61) are often referred to as *involute bevel gears*. However, it is preferred to refer to gears of this particular kind as *perfect gears for intersected-axis gearing*.

\* It is instructive to point out here that the line of contact,  $LC$ , between the tooth flanks,  $\mathcal{G}$  and  $\mathcal{P}$ , is the first to be determined when designing an intersected-axis gear pair. The tooth flanks of a gear,  $\mathcal{G}$ , and a mating pinion,  $\mathcal{P}$ , are determined later on by means of the earlier constructed line of contact,  $LC$ .



Gears for intersected-axes gear pairs that have tooth flank geometry of the discussed type are analogous to involute gearings with parallel axes. Under certain conditions, Equation 12.61 can be reduced to Equation 7.14. Only those gears for intersected-axes gear pairs that feature tooth flank geometry in compliance with Equation 12.61 are capable of transmitting a uniform rotation smoothly.

An analytical expression for the line of contact,  $LC$ , makes possible the calculation of important design parameters of an intersected-axes gearing. Expressions: (1) for the unit normal vector,  $\mathbf{n}_g$ , at a point of interest of the gear tooth flank,  $\mathcal{G}$ ; (2) for the unit normal vector,  $\mathbf{n}_p$ , at a point of interest of the pinion tooth flank,  $\mathcal{P}$ ; and (3) for the unit normal vector,  $\mathbf{n}_r$ , at a point of interest of the tooth flank of an auxiliary generating round rack,  $\mathcal{R}$ , can be derived based on the unit normal vector,  $\mathbf{n}_{lc}$ , to the line of contact,  $LC$ , which is constructed within the plane of action,  $PA$ . For this purpose, an equation for the unit normal vector,  $\mathbf{n}_{lc}$ , should be considered together with the corresponding operators of the coordinate system transformations. The unit normal vector,  $\mathbf{n}_{lc}$ , is a perpendicular to a planar curve. In a general form, the formulas for the unit normal vectors  $\mathbf{n}_g$ ,  $\mathbf{n}_p$ , and  $\mathbf{n}_r$  can be expressed as:

$$\mathbf{n}_g(X_{pa}, \theta_{pa}) = \mathbf{Rs}(PA \mapsto \mathcal{G}) \cdot \mathbf{n}_{lc}(X_{pa}) \quad (12.62)$$

$$\mathbf{n}_p(X_{pa}, \theta_{pa}) = \mathbf{Rs}(PA \mapsto \mathcal{P}) \cdot \mathbf{n}_{lc}(X_{pa}) \quad (12.63)$$

$$\mathbf{n}_r(X_{pa}, \theta_{pa}) = \mathbf{Rs}(PA \mapsto \mathcal{R}) \cdot \mathbf{n}_{lc}(X_{pa}) \quad (12.64)$$

The above-performed analysis allows for the following statement:

### Conclusion 12.3

*In intersected-axes gearing with a constant pressure angle, transmission of a uniform rotation from a driving shaft to a driven shaft is possible if and only if the plane of action is a plane through the axis of instant rotation and is at a constant angle in relation to the plane through the axes of rotation of the gear and the pinion.*

Equation 12.53, as well as Equations 12.58 and 12.61, allows for the calculation of the unit normal vector,  $\mathbf{n}_g$ , to the gear tooth flank,  $\mathcal{G}$ , at any point of interest within the tooth surface,  $\mathcal{G}$ . The unit normal vector,  $\mathbf{n}_g$ , and a straight line along the vector,  $\mathbf{n}_g$ , are used for the calculation of the deviations of a machined gear tooth flank from the tooth flank of the desired geometry.

Knowing the position vector,  $\mathbf{r}_g(v, \theta_{pa})$ , of a point of interest within the gear tooth flank,  $\mathcal{G}$ , the unit normal vector,  $\mathbf{n}_g$ , is calculated as:

$$\mathbf{n}_g(v, \theta_{pa}) = \frac{(\partial \mathbf{r}_g / \partial v) \times (\partial \mathbf{r}_g / \partial \theta_{pa})}{|(\partial \mathbf{r}_g / \partial v) \times (\partial \mathbf{r}_g / \partial \theta_{pa})|} (v, \theta_{pa}) \quad (12.65)$$

Calculation of the derivatives  $(\partial \mathbf{r}_g / \partial v)$  and  $(\partial \mathbf{r}_g / \partial \theta_{pa})$  from Equation 12.53 followed by the formula transformation (see Equation 12.65) is a drilling procedure. The procedure of calculation of the unit normal vector,  $\mathbf{n}_g$ , can be significantly simplified if the vector  $\mathbf{n}_g$  and a straight line along the vector  $\mathbf{n}_g$  are determined in the reference system,  $X_{pa}Y_{pa}Z_{pa}$ , associated with the plane of action (in this reference system, the unit normal vector,  $\mathbf{n}_g$ , is identical to the unit normal vector,  $\mathbf{n}_{lc}$ , to the line of contact,  $LC$ ). Afterward, implementation of the operator,  $\mathbf{Rs}(PA \mapsto \mathcal{G})$ , of the resultant coordinate system transformation (see Equation 12.35) allows for representation of both the unit normal vector,  $\mathbf{n}_{lc}$ , and the straight line along it in the coordinate system  $X_gY_gZ_g$  associated with the gear.

Referring to Figure 12.13, the position vector,  $\mathbf{r}_m$ , of a point of the line of contact,  $LC$ , can be given by an expression of the form:

$$\mathbf{r}_m = \mathbf{i} \cdot X_m + \mathbf{j} \cdot Y_m \quad (12.66)$$

In Equation 12.66, the Cartesian coordinates of the point of interest,  $m$ , are denoted by  $X_m$  and  $Y_m$ , correspondingly.

The unit tangent vector,  $\mathbf{t}_m$ , at point  $m$  can be expressed in the form:

$$\mathbf{t}_m = \mathbf{i} \cdot \cos \zeta_{cl} + \mathbf{j} \cdot \sin \zeta_{cl} \quad (12.67)$$

Consider a case when the line of contact,  $LC$ , is represented in an explicit form as  $Y_{cl} = Y_{cl}(X_{cl})$ . The inclination of the unit tangent vector,  $\mathbf{t}_m$ , in relation to the  $X_g$ -axis (see Equation 12.67) at a point of interest,  $m$ , is specified by an angle,  $\zeta_{cl}$ :

$$\zeta_{cl} = \tan^{-1} \left( \frac{\partial Y_{cl}(X_{cl})}{\partial X_{cl}} \right) \quad (12.68)$$

Once the unit tangent vector,  $\mathbf{t}_m$  (see Equation 12.67), is known, an expression for the unit normal vector,  $\mathbf{n}_{lc}$ , can be represented in vector form:

$$\mathbf{n}_{lc} = -\mathbf{i} \cdot \sin \zeta_{cl} + \mathbf{j} \cdot \cos \zeta_{cl} \quad (12.69)$$

Ultimately, the implementation of Equations 12.66 through 12.69 allows expression of the position vector of a point,  $\mathbf{r}_{n.lc}$ , of a straight line through the point of interest,  $m$ , along the unit vector,  $\mathbf{n}_{lc}$ :

$$\mathbf{r}_{n.lc} = \mathbf{r}_m + \lambda_n \mathbf{n}_{lc} \quad (12.70)$$

or in matrix representation as:

$$\mathbf{r}_{n.lc} = \begin{bmatrix} X_m - \lambda_n \sin \zeta_{lc} \\ Y_m + \lambda_n \cos \zeta_{lc} \\ 0 \\ 1 \end{bmatrix} \quad (12.71)$$

In Equation 12.70,  $\lambda_n$  is the distance of the point of interest,  $m$ , from the end of the position vector,  $\mathbf{r}_m$ .

In the reference system  $X_g Y_g Z_g$ , an expression for the unit normal vector,  $\mathbf{n}_g$ , to the gear tooth flank,  $\mathcal{G}$ , can be derived from the equation:

$$\mathbf{n}_g = \mathbf{Rs}(PA \mapsto \mathcal{G}) \cdot \mathbf{n}_{lc} \quad (12.72)$$

Similarly, an expression for the position vector of a point,  $\mathbf{r}_{n.lc}$ , in the reference system  $X_g Y_g Z_g$  can be derived from the equation:

$$\mathbf{r}_{n.lc}^g = \mathbf{Rs}(PA \mapsto \mathcal{G}) \cdot \mathbf{r}_{n.lc} \quad (12.73)$$

Finally, Equation 12.73 and the operator of the resultant coordinate system transformation,  $\mathbf{Rs}(PA \mapsto \mathcal{G})$  (see Equation 12.35), allow for an equation:

$$\mathbf{r}_{n.lc}^g(\lambda) = \begin{bmatrix} (\cos \Sigma_p \cos \theta_{pa} + \sin \Sigma_p \cos \phi_{t.\omega} \sin \theta_{pa}) \cdot (X_m - \lambda \sin \zeta_{lc}) + \sin \Sigma_p \sin \phi_{t.\omega} (Y_m + \lambda \cos \zeta_{lc}) \\ -\sin \phi_{t.\omega} \sin \theta_{pa} \cdot (X_m - \lambda \sin \zeta_{lc}) + \cos \phi_{t.\omega} (Y_m + \lambda \cos \zeta_{lc}) \\ -(\sin \Sigma_p \cos \theta_{pa} + \cos \Sigma_p \cos \phi_{t.\omega} \sin \theta_{pa}) \cdot (X_m - \lambda \sin \zeta_{lc}) + \cos \Sigma_p \sin \phi_{t.\omega} (Y_m + \lambda \cos \zeta_{lc}) \\ 1 \end{bmatrix} \quad (12.74)$$

for the position vector of a point,  $\mathbf{r}_{n.lc}^g$ , of the tooth flank of the gear,  $\mathcal{G}$ , that features an arbitrary shape in the lengthwise direction.

When a pair of conjugate tooth flanks,  $\mathcal{G}$  and  $\mathcal{P}$ , is generated by means of a desired line of contact,  $LC_{des}$ , an original geometry of the line of contact,  $LC_{des}$ , is not altered when the gears rotate.\* The desired line of contact,  $LC_{des}$ , is a *rigid* planar curve entirely located within the plane of action,  $PA$ . The initially specified configuration of  $LC_{des}$  in relation to the plane of action,  $PA$ , is remained the same.

\* A limited alteration to the geometry of the line of contact,  $LC$ , is observed when the gears are finish-cut either in the face-hobbing process, or in the face-grinding process with the spiral grinding wheel, and so forth. The profile angle,  $\phi_{t.\omega}$ , of the cutting toll (of the face-hob, spiral grinding wheel, and so forth) has a zero value in all cases. A more significant alteration to the geometry of the line of contact,  $LC$ , in perfect bevel gears can be achieved when the gears are cut using NC technology for this purpose. This particular problem is out of the scope of the book, and it is not considered here.

When generating the conjugate tooth flanks,  $\mathcal{G}$  and  $\mathcal{P}$ , for an intersected-axes gear pair by means of the cutter head, envelopes exist; however, these envelopes are not conjugate to one another.

Once an equation of a gear tooth flank is derived, then the variation of the tooth flank geometry can be investigated; that is, the normal curvature of the gear tooth flank can be calculated at an arbitrary point of interest, variation of the tooth profile angle and helix angle can be determined, special points of meshing can be investigated, and so forth.

An equation for an spherical involute tooth profile in intersected-axes gearing can be derived on the premise of Equation 12.74 under the assumption that the coordinates  $X_m$ ,  $Y_m$ , and  $Z_m$  of point of interest,  $m$ , fulfill the requirement:

$$\sqrt{X_m^2 + Y_m^2 + Z_m^2} = R_{sph} \quad (12.75)$$

where  $R_{sph}$  is the radius of a sphere on which the spherical involute tooth profile is constructed.

For a spherical involute ( $I_a$ -gearing) a function  $\text{inv}(\phi_{t,\omega})$  similar to that in  $P_a$ -gearing can be determined.

In a way similar to that just discussed, the unit normal vector,  $\mathbf{n}_g$ , to the gear tooth flank,  $\mathcal{G}$ , as well as the position vector of a point,  $\mathbf{r}_{n,lc}^g$ , of a straight line through a point of interest,  $m$ , in the direction of  $\mathbf{n}_g$  can be calculated for the line of contact,  $LC$ , of any reasonable geometry. An arc of a circle, an arc of a spiral curve, a straight line segment, and so forth are good examples of the line of contact,  $LC$ , in an intersected-axes gear pair.

Depending on the geometry of a chosen line of contact,  $LC$ , a gear tooth flank of a complex geometry can be generated. As an example, Figure 12.15 illustrates a bevel gear that features the line of contact,  $LC$ , shaped in the form of a sine function.

Formulas analogous to the above-discussed equations are valid for a pinion tooth flank,  $\mathcal{P}$ , as well.

The constructed tooth flanks,  $\mathcal{G}$  and  $\mathcal{P}$ , of a gear and a mating pinion meet all three necessary and sufficient conditions that perfect intersected-axes gearing has to meet; that is, they meet the conditions:

- The condition of contact that is analytically expressed by the *Shishkov equation of contact*,  $\mathbf{n} \cdot \mathbf{V}_\Sigma = 0$ .
- The condition of conjugacy (at every instant of time, an instant line of action,  $LA_{inst}$  has to be located within the plane of action,  $PA$ , and must intersect the axis of instant rotation,  $P_{ln}$ , of the gear pair).
- Equality of the angular base pitches,  $\varphi_{b,g} = \varphi_{b,op}$  and  $\varphi_{b,p} = \varphi_{b,op}$  (or in the form  $\varphi_{b,g} = \varphi_{b,op} = \varphi_{b,op}$  for simplicity).

The just-listed conditions that perfect intersected-axes gearing has to meet have to be verified in the order they are listed above. For instance, there is no reason to verify the equality of the angular base pitch if the condition of contact is not fulfilled.



FIGURE 12.15

Bevel gear with tooth flanks generated by means of sine function as the line of contact,  $LC$ .

The derived equations for the gear tooth flank,  $\mathcal{G}$ , as well as for the pinion tooth flank,  $\mathcal{P}$ , can be used as the reference surfaces (datum surfaces) when designing and when machining gears for intersected-axes gearings. Surfaces of this kind are an equivalent to the screw involute surface broadly used as reference surface for parallel-axes gear pairs. The most favorable approximation of the tooth profile of the cutter-heads of conventional design is another possible field of application of the derived equations for a gear and a mating pinion teeth flank.

### 12.4.3 Intersected-Axes Gearing with Variable Pressure Angle

The set of three conditions formulated above that perfect intersected-axes gearings have to fulfill is helpful to realize the possibility of intersected-axes gearing with the transverse pressure angle,  $\phi_{t,\omega} = \text{var}$ , variable within the active portion of the face width,  $F_{pa}$ . The possibility of variation of the transverse pressure angle,  $\phi_{t,\omega}$ , is necessary when solving a problem of synthesizing an intersected-axes gear pair with favorable design parameters, that is, of an intersected-axes gear pair with a desired performance.

In a perfect gear pair, the transverse pressure angle,  $\phi_t$ , is assumed to be of a constant value within a line of contact,  $LC$  (at every contact point). Certain imperfections in approximate gear pairs can be balanced/neutralized by a corresponding variation of the transverse pressure angle,  $\phi_t$ , along the line of contact,  $LC$ .

The plane of action,  $PA$ , can be subdivided into an infinite number of infinitesimally narrow  $dr_{pa}$  round strips. All the strips are through the axis of instant rotation,  $P_{ln}$ . The transverse pressure angle,  $\phi_{t,\omega}$ , can be set to an optimum value for each of the strips; that is, in this way, the transverse profile angle,  $\phi_{t,\omega}$ , is involved in the synthesizing process of the favorable gear pair. In this way, of the plane of action,  $PA$ , in conventional bevel gear design is replaced with the surface of action,  $SA$ . The surface of action,  $SA$ , is a kind of ruled surface.

Gears with a variable pressure angle,  $\phi_{t,\omega}$ , can be cut on a multiaxis NC machine.

---

## 12.5 Tooth Flanks in Perfect Intersected-Axes Gear Pairs

Conjugacy is a specific property of the tooth flanks of a gear,  $\mathcal{G}$ , and a mating pinion,  $\mathcal{P}$ . Only surfaces that roll over one another can feature this unique property. Due to this property, in the rolling motion of a gear and a pinion over one another, the tooth flanks,  $\mathcal{G}$  and  $\mathcal{P}$ , can be viewed as a kind of *reversibly-enveloping surfaces* (or just *R<sub>c</sub>-surfaces* for simplicity) [115]. When a gear and a mating pinion rotate steadily, the gear tooth flank,  $\mathcal{G}$ , can be viewed as an envelope to consecutive positions of the mating pinion tooth flank,  $\mathcal{P}$ . The gear tooth flank,  $\mathcal{G}$ , generated in this way can be used to generate the mating pinion tooth flank. If the tooth flanks,  $\mathcal{G}$  and  $\mathcal{P}$ , are conjugate, then the original pinion tooth flank,  $\mathcal{P}$ , and the pinion tooth flank,  $\mathcal{P}_g$ , generated by the gear tooth flank,  $\mathcal{G}$ , are identical to one another ( $\mathcal{P}_g \equiv \mathcal{P}$ ).

Tooth flanks that do not have many geometries can be referred to as *conjugate surfaces* or *reversibly-enveloping surfaces* [115].

A criterion to be fulfilled by two tooth flanks,  $\mathcal{G}$  and  $\mathcal{P}$ , in order to possess the property of conjugacy can be expressed analytically.

When the gear,  $\mathcal{G}$ , and mating pinion,  $\mathcal{P}$ , tooth flanks interact with one another, straight lines that align to common perpendiculars,  $\mathbf{n}_g$ , through points within a current line of contact,  $LC$ , must always intersect the axis of instant rotation,  $P_{ln}$  (Figure 12.16). The condition of conjugacy must be met at all points of a (desired) line of contact,  $LC_{des}$ , between the interacting tooth flanks,  $\mathcal{G}$  and  $\mathcal{P}$ . This is a key requirement to be fulfilled by conjugate tooth flanks,  $\mathcal{G}$  and  $\mathcal{P}$ , when the gears rotate.

At an arbitrary point,  $m$ , within a desired line of contact,  $LC_{des}$ , an instant line of action,  $LA_{instr}$ , forms an angle with the axis of instant rotation,  $P_{ln}$ . At every instant of time, every instant line of action,  $LA_{instr}$ , intersects the axis of instant rotation,  $P_{ln}$ , at certain point—this is a must for conjugate surfaces.

A component of the instant motion that is parallel to the axis of instant rotation,  $P_{ln}$ , does not affect the conjugate action between the interacting tooth flanks,  $\mathcal{G}$  and  $\mathcal{P}$ . Therefore, this component of the relative motion is not considered here.

The other component of the relative motion is along a straight line through a point,  $P$ , that is located within the axis of instant rotation,  $P_{ln}$ . The conjugate action between the interacting tooth flanks,  $\mathcal{G}$  and  $\mathcal{P}$ , is considered for this component of the relative motion.

Three vectors,  $\mathbf{p}_{ln}$ ,  $\mathbf{V}_m$ , and  $\mathbf{n}_g$ , are constructed in Figure 12.16.

Two of the vectors,  $\mathbf{p}_{ln}$  and  $\mathbf{V}_m$ , are located within the plane of action,  $PA$ .

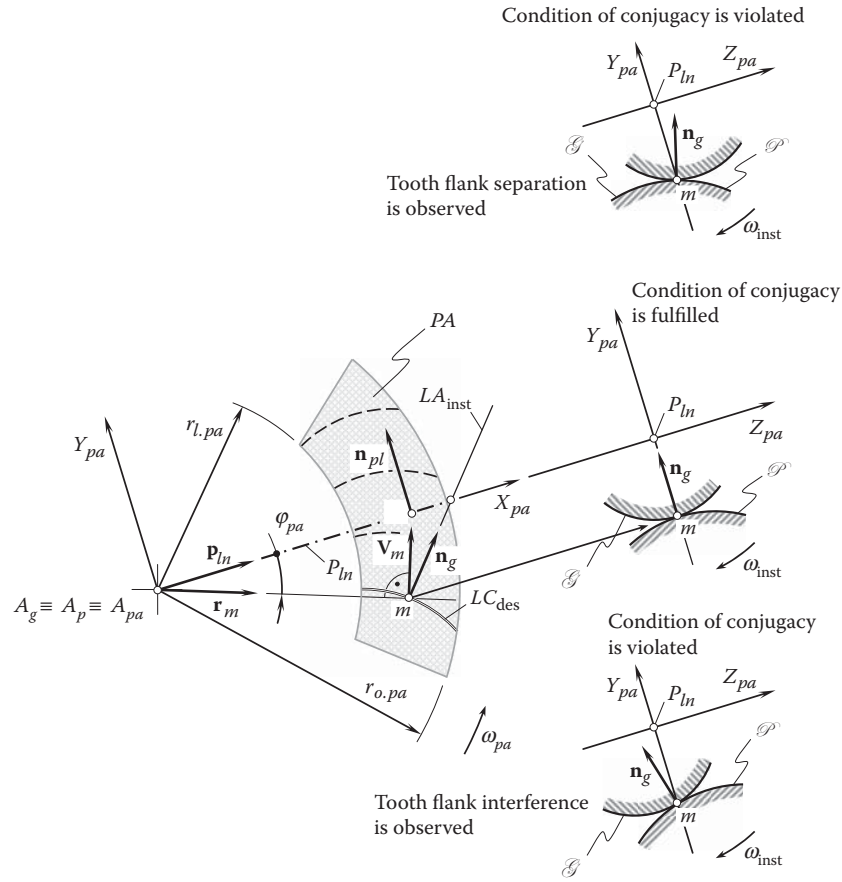


**FIGURE 12.16**  
Condition of conjugacy of gear,  $\mathcal{G}$ , and mating pinion,  $\mathcal{P}$ , tooth flanks in intersected-axes gearing.

The unit vector,  $\mathbf{p}_{ln}$ , is along the axis of instant rotation,  $P_{ln}$ . Therefore, in the plane-of-action Cartesian coordinate system,  $X_{pa}Y_{pa}Z_{pa}$ , it can be analytically represented in a form:

$$\mathbf{p}_{ln} = \mathbf{i} \quad (12.76)$$

The velocity vector,  $\mathbf{V}_m$ , is along an instant line of action,  $LA_{inst}$ . In the plane-of-action Cartesian coordinate system,  $X_{pa}Y_{pa}Z_{pa}$ , this unit vector can be analytically described as:

$$\mathbf{r}_m = \mathbf{i} \sin \varphi_{pa} + \mathbf{j} \cos \varphi_{pa} \quad (12.77)$$

The third unit vector,  $\mathbf{n}_g$ , is perpendicular to the gear tooth flank,  $\mathcal{G}$ . Therefore, it can be calculated from the equation:

$$\mathbf{n}_g = \frac{(\partial \mathbf{r}_g / \partial U_g) \times (\partial \mathbf{r}_g / \partial V_g)}{|(\partial \mathbf{r}_g / \partial U_g) \times (\partial \mathbf{r}_g / \partial V_g)|} \quad (12.78)$$

where:

$\mathbf{r}_g$ : is the position vector of a point of a gear tooth flank,  $\mathcal{G}$ .

$U_g$  and  $V_g$ : are the curvilinear (*Gaussian*) coordinates of a point of a gear tooth flank,  $\mathcal{G}$ .

Gear,  $\mathcal{G}$ , and mating pinion,  $\mathcal{P}$ , tooth flanks are conjugate if a straight line along the unit normal vector,  $\mathbf{n}_g$ , at any point of the line of contact,  $LC$ , intersects the axis of instant rotation,  $P_{ln}$ . To meet this requirement, the unit normal vectors,  $\mathbf{n}_{pl}$  and  $\mathbf{n}_g$ , must be coplanar, and they must not be perpendicular to one another (here, the unit normal vector to the axis of instant rotation,  $P_{ln}$ , is designated as  $\mathbf{n}_{pl}$ . This vector is entirely located within the plane of action,  $PA$ ).

When a gear,  $\mathcal{G}$ , and a mating pinion,  $\mathcal{P}$ , tooth flanks are conjugate, then the three vectors,  $\mathbf{p}_{ln}$ ,  $\mathbf{V}_m$ , and  $\mathbf{n}_g$ , must be coplanar. When the vectors,  $\mathbf{p}_{ln}$ ,  $\mathbf{V}_m$ , and  $\mathbf{n}_g$ , are coplanar, then the triple scalar product,  $\mathbf{p}_{ln} \times \mathbf{V}_m \cdot \mathbf{n}_g$ , is zero; therefore, the equality:

$$\mathbf{p}_{ln} \times \mathbf{V}_m \cdot \mathbf{n}_g = 0 \quad (12.79)$$

is valid. The triple scalar product,  $\mathbf{p}_{ln} \times \mathbf{V}_m \cdot \mathbf{n}_g$ , can be represented in a form of a determinant:

$$\mathbf{p}_{ln} \times \mathbf{V}_m \cdot \mathbf{n}_g = \begin{vmatrix} X_{pl} & Y_{pl} & Z_{pl} \\ V_{m.x} & V_{m.y} & V_{m.z} \\ X_g & Y_g & Z_g \end{vmatrix} = 0 \quad (12.80)$$

The unit vector,  $\mathbf{n}_{pl}$ , is perpendicular to the axis of instant rotation,  $P_{ln}$ . This vector is entirely located within the plane of action,  $PA$ , and is perpendicular to the axis of instant rotation,  $P_{ln}$ . Therefore, in the plane-of-action Cartesian coordinate system,  $X_{pa}Y_{pa}Z_{pa}$ , it can be analytically represented in the form:

$$\mathbf{n}_{pl} = \mathbf{j} \quad (12.81)$$

In addition to Equation 12.80, the condition:

$$\mathbf{n}_{pl} \cdot \mathbf{n}_g \neq 0 \quad (12.82)$$

must also be fulfilled. The parallelism of the directions specified by the unit normal vectors,  $\mathbf{n}_{pl}$  and  $\mathbf{n}_g$ , is eliminated by this condition. No rotation transmission by means of gears is possible when the unit normal vector,  $\mathbf{n}_g$ , is parallel to the axis of instant rotation,  $P_{ln}$ .

An expression:

$$\mathbf{p}_{ln} \times \mathbf{n}_g \neq 0 \quad (12.83)$$

is an alternative representation of the condition specified by Equation 12.82.

Gear,  $\mathcal{G}$ , and mating pinion,  $\mathcal{P}$ , tooth flanks are said to be conjugate if and only if the conditions specified by Equation 12.79 (or Equation 12.80) and Equation 12.82 (or Equation 12.83) are fulfilled for any and all points within the line of contact,  $LC$ , for any possible configurations of the gear and the pinion in relation to one another:

$$\begin{cases} \mathbf{p}_{ln} \times \mathbf{V}_m \cdot \mathbf{n}_g = 0 \\ \mathbf{p}_{ln} \times \mathbf{n}_g \neq 0 \end{cases} \quad (12.84)$$

Equation 12.84 analytically describes the condition of conjugacy of gear,  $\mathcal{G}$ , and mating pinion,  $\mathcal{P}$ , tooth flanks. If the condition is not fulfilled (Figure 12.16), the gear,  $\mathcal{G}$ , and mating pinion,  $\mathcal{P}$ , tooth flanks are not conjugate.

## 12.6 Desired Tooth Proportions in Intersected-Axes Gears

The gear and its mating pinion in an intersected-axes gear pair feature multiple teeth. The teeth are evenly spaced circumferentially. A general form of the equation of a gear tooth flank (see Equation 12.53), as well as Equations 12.58 and 12.61 of particular cases of the gear tooth flank, is necessary, but is not sufficient for the



specification of the tooth shape of the gear or of the pinion. The gear tooth flank,  $\mathcal{G}$ , that is specified by Equation 12.53 has to be properly located in relation to (1) the tooth flank of the opposite side of the gear tooth, and (2) the tooth flanks of the rest of the gear teeth.

The desired tooth proportions for intersected-axes gearings can be established in a way similar to that earlier established for parallel-axes gearings. Following this concept, consider a base cone of a gear for an intersected-axes gear pair. Base cones, along with the configuration of the rotation vectors  $\omega_g$ ,  $\omega_p$ , and  $\omega_{pl}$ , are of critical importance for the determination of the corresponding reference surfaces.

### 12.6.1 Angular Base Pitch

The angular base pitch of a gear,  $\varphi_{b,g}$  (GBP), and angular base pitch of a mating pinion (PBP) are measured within a plane tangent to the base cone of the gear/pinion. The gear/pinion base pitch can be measured directly in the gear and pinion separately. The angular base pitch of a gear,  $\varphi_{b,g}$ , as well as the angular base pitch of a mating pinion,  $\varphi_{b,p}$ , is measured as an angle between the actual lines of intersection of the gear/pinion tooth flanks,  $\mathcal{G}$  and/or  $\mathcal{P}$ , of two neighboring teeth by a plane tangent to the base cone of the gear/pinion. One of the lines of intersection of  $\mathcal{G}/\mathcal{P}$  by the tangent plane may be located either outside the outer diameter or inside the root diameter of the gear/pinion.

In intersected-axes gearing, the operating angular base pitch is an equivalent of the base pitch in parallel-axes gearing. Similarly, the angular distance between every two consequent tooth flanks within the plane of action can be specified in terms of the angular base pitch.

#### Definition 12.1

*The operating angular base pitch in intersected-axes gearing is an angular distance between two consequent tooth flanks measured within a plane that is tangent to the base cone of the gear (the plane of action).*

In intersected-axes gearing, the concept of operating angular base pitch relates to a gear-to-pinion mesh.

To proceed with the analysis of the angular base pitch of a gear in intersected-axes gear pair, it is instructive to recall the following well-known property of two cones that share a common apex and a common generatrix and spin with no slippage about their axis of rotation. If the radii of the bottom circles of the first and the second cones are designated as  $r_1$  and  $r_2$ , then the following equality is valid:

$$r_1 \cdot \varphi_1 = r_2 \cdot \varphi_2 \quad (12.85)$$

where  $\varphi_1$  and  $\varphi_2$  are the angles the cones are turned through.

In intersected-axes gearing, a gear and the plane of action share a common apex and a common generatrix, and they spin about their axes of rotation with no slippage. In the consideration below, the base cone of the gear is designated as  $\Gamma_b$ , and the base cone of the plane of action,  $PA$ , equals a right angle ( $\Gamma_{pa} = 90^\circ$ ).

Consider the intersection of a gear teeth by the plane of action,\* as schematically depicted in Figure 12.17. When the gears rotate, the base cone of the gear rolls with no slippage over the plane of action,  $PA$ . Consider a point within the base cone surface of the gear. The point is remote from the plane-of-action apex,  $A_{pa}$ , at a distance,  $r_{o,pa}$ . The arc distance:

$$\tilde{L}_{b,g} = 2\pi r_{o,pa} \sin \Gamma_b \quad (12.86)$$

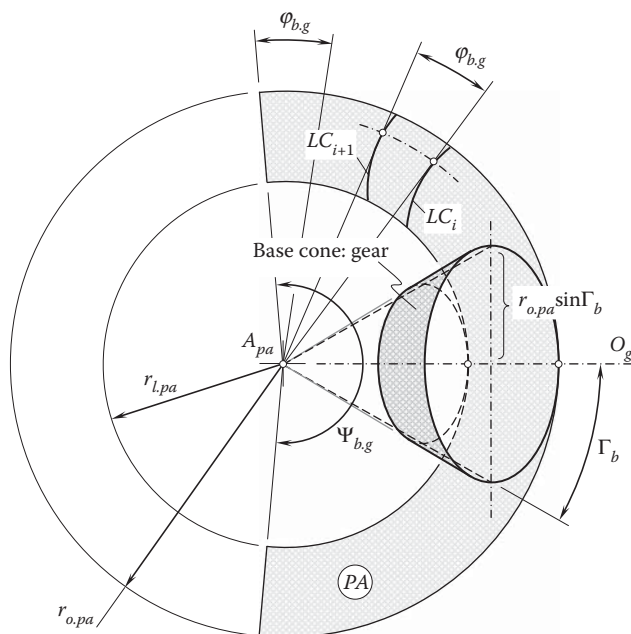
is covered by the point per each rotation of the gear.

Within the plane of action,  $PA$ , a circular arc of the length  $\tilde{L}_{b,g}$  spans over a central angle,  $\Psi_{b,g}$ . The value of the angle,  $\Psi_{b,g}$ , can be calculated as:

$$\Psi_{b,g} = 360^\circ \sin \Gamma_b \quad (12.87)$$

\* Shown in Figures 12.17 and 12.18, the schematic for the determination of a gear angular base pitch,  $\varphi_{b,g}$ , is highly similar to that used for the determination of an operating angular base pitch,  $\varphi_{b,op}$ , of an intersected-axes gear pair.





For a gear with  $N_g$  teeth, a portion,  $\varphi_{b,g}$ , of the central angle,  $\Psi_{b,g}$ , per the gear tooth equals:

The angle,  $\varphi_{b,g}$ , in intersected-axes gearing is an analogue of the base pitch,  $p_b$ , of a gear in parallel-axes gearing. Due to this, the angle,  $\varphi_{b,g}$ , is referred to as the *operating angular base pitch* in intersected-axes gearing, or just as operating base pitch for simplicity.

As illustrated in **Figure 12.18**, for a given gear, the angular base pitch,  $\varphi_{b,g}$ , remains the same value for any and all circles of radii  $r_{x,pa}$ ,  $r_{y,pa}$ , and so on, within the face width,  $F_{pa}$ , of a gear ( $\varphi_{b,p} = \text{const}$ ). The *angular length of contact* is designated in **Figure 12.18** as  $\Phi_{pa}$ . The angular length,  $\Phi_{pa}$ , in intersected-axes gearing is an equivalent of the length of contact,  $Z_{pa}$ , in parallel-axes gearing.

In perfect intersected-axes gearing, all three angular base pitches, namely the operating angular base pitch,  $\phi_{b,op}$ ; the base pitch of the gear,  $\phi_{b,g}$ ; and the base pitch of the pinion,  $\phi_{b,p}$ , are equal to each other:

or

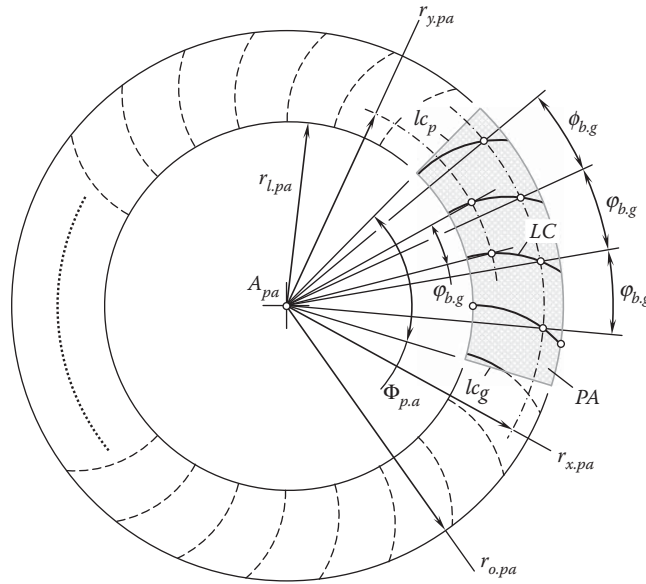
$$\varphi_{b,g} = \varphi_{b,v} = \varphi_{b,ov} \quad (12.90)$$

All the angles,  $\varphi_{b,g}$ ,  $\varphi_{b,p}$ , and  $\varphi_{b,op}$ , share a common apex at the plane-of-action apex,  $A_{pa}$ .

It should be noted here that the tooth number,  $N_{par}$ , within an imaginary plane of action,  $PA$ , is not mandatorily expressed by an integer. It can be expressed by a number with fractions as well.

The angular base pitch can be expressed in terms of linear dimensions. The latter makes sense in cases when the linear dimensions are easier to measure.

Only *conjugate* gear tooth flanks feature the angular base pitch. The angular base pitch cannot be identified for *nonconjugate* gear tooth flanks.

**FIGURE 12.18**

The angular base pitch,  $\phi_{b,g}$ , in a gear for intersected-axes gearing is of a constant value for all the teeth, as well as within the face width of the gear.

A variation of the actual base pitch of the gear/pinion can be measured as the variation of shape and configuration of a line of intersection of a single tooth flank,  $\mathcal{G}/\mathcal{P}$ , when the gear/pinion spins about its axis of rotation.

### 12.6.2 Transverse Pressure Angle

The transverse pressure angle,  $\phi_{t,\omega}$ , is the angle that the plane of action,  $PA$ , forms with the plane that is perpendicular to the plane through the axes of rotation,  $O_g$  and  $O_p$ , of the gear and the mating pinion. The transverse pressure angle,  $\phi_{t,\omega}$ , is measured within a plane that is perpendicular to the axis of instant rotation,  $P_{ln}$  (or the same, i.e., perpendicular to the vector of instant rotation,  $\omega_{pl}$ , similar to that as in parallel-axes gearing). This plane is tangent to the transverse section of the intersected-axes gear pair. The transverse section of the intersected-axes gear pair is a sphere centered at the plane-of-action apex,  $A_{pa}$ , that passes through a point of interest within the axis of instant rotation,  $P_{ln}$ .

Referring to Figure 12.10 (as well as to Figure 12.12), the transverse pressure angle,  $\phi_{t,\omega}$ , can be defined as the angle between the plane of action,  $PA$ , and between a perpendicular,  $\mathbf{n}_{pa}$ , to the plane through the axes of rotations,  $O_g$  and  $O_p$ , of the gear and the pinion.

#### Definition 12.2

*The transverse pressure angle in an intersected-axes gear pair is said to be the angle between the plane of action and a perpendicular,  $\mathbf{n}_{pa}$ , to the plane through the axes of rotation of the gear and the pinion.*

The transverse pressure angle,  $\phi_{t,\omega}$ , can be an independent design parameter of an intersected-axes gear pair. Then, the base cone angles of the gear,  $\Gamma_b$ , and the mating pinion,  $\gamma_b$ , can be expressed in terms of the pressure angle,  $\phi_{t,\omega}$ . Otherwise, the transverse pressure angle,  $\phi_{t,\omega}$ , can be expressed in terms of the base cone angles,  $\Gamma_b$  and  $\gamma_b$ .

The plane of action,  $PA$ , is tangent to the base cone of the gear, as schematically illustrated in Figure 12.18. Therefore, the angle that the plane of action makes with the gear axis of rotation,  $O_g$ , is equal to the base cone angle,  $\Gamma_b$ . Once the angle between the plane of action,  $PA$ , and the gear axis of rotation,  $O_g$ , is known ( $\Gamma_b$ ), then the unit normal vector,  $\mathbf{n}_{pa}$ , to the plane of action,  $PA$ , and the axis,  $O_g$ , form an angle of  $(90^\circ - \Gamma_b)$ .

In the reference system,  $X_r Y_r Z_r$ , the direction of the aforementioned unit normal vector  $\mathbf{n}_{pa}$  can be analytically expressed by the equation:

$$\mathbf{n}_{pa} = \mathbf{j}_r \sin \phi_{t,\omega} + \mathbf{k}_r \cos \phi_{t,\omega} \quad (12.91)$$

To express the base cone angle of the gear,  $\Gamma_b$ , in terms of the transverse pressure angle,  $\phi_{t,\omega}$ , or, conversely, to express the transverse pressure angle,  $\phi_{t,\omega}$ , in terms of the base cone angle of the gear,  $\Gamma_b$ , all the design parameters of the gear pair have to be represented in a common reference system. For this purpose, the use of the Cartesian coordinate system  $X_g Y_g Z_g$  associated with the gear has proven to be convenient. To follow this method, the unit normal vector,  $\mathbf{n}_{pa}$ , has to be represented in the reference system  $X_g Y_g Z_g$ .

The reference systems,  $X_g Y_g Z_g$  and  $X_r Y_r Z_r$ , are turned in relation to one another about the  $Y_r$ -axis through the pinion cone angle,  $\Sigma_p$ . The transition from the coordinate system,  $X_r Y_r Z_r$ , to the coordinate system,  $X_g Y_g Z_g$ , can be analytically described by the operator of rotation,  $\mathbf{Rt}(r \mapsto g)$  (see Equation 12.33). With that said, in the coordinate system,  $X_g Y_g Z_g$ , the direction of the unit normal vector,  $\mathbf{n}_{pa}^g$ , can be analytically described by the expression:

$$\mathbf{n}_{pa}^g = \mathbf{Rt}(r \mapsto g) \cdot \mathbf{n}_{pa} \quad (12.92)$$

Equations 12.33, 12.91, and 12.92 allow for the following expression for the unit normal vector,  $\mathbf{n}_{pa}^g$ :

$$\mathbf{n}_{pa}^g = \begin{bmatrix} \cos \Sigma_p & 0 & \sin \Sigma_p & 0 \\ 0 & 1 & 0 & 0 \\ -\sin \Sigma_p & 0 & \cos \Sigma_p & 0 \\ 0 & 0 & 0 & 1 \end{bmatrix} \cdot \begin{bmatrix} 0 \\ \sin \phi_{t,\omega} \\ \cos \phi_{t,\omega} \\ 1 \end{bmatrix} = \begin{bmatrix} \sin \Sigma_p \cos \phi_{t,\omega} \\ \sin \phi_{t,\omega} \\ \cos \Sigma_p \cos \phi_{t,\omega} \\ 1 \end{bmatrix} \quad (12.93)$$

As the unit vector along the  $O_g$ -axis is equal to  $\mathbf{k}$ , the angle  $\angle(\mathbf{n}_{pa}, \mathbf{k})$  can be calculated as:

$$\angle(\mathbf{n}_{pa}, \mathbf{k}) = \Gamma_b = \cos^{-1} [\mathbf{n}_{pa} \cdot \mathbf{k}] \quad (12.94)$$

which can also be represented in the form:

$$\Gamma_b = \tan^{-1} \left( -\frac{\sqrt{\sin^2 \Sigma_p - \cos^2 \Sigma_p \sin^2 \phi_{t,\omega}}}{\cos \Sigma_p \cos \phi_{t,\omega}} \right) \quad (12.95)$$

The transverse pressure angle,  $\phi_{t,\omega}$ , can be expressed in terms of the base cone angle,  $\Gamma_b$ , of the gear:

$$\phi_{t,\omega} = \cos^{-1} \left( \frac{\cos \Sigma_p}{\cos \Gamma_b} \right) \quad (12.96)$$

An equation similar to Equation 12.95 is valid for the base cone angle of the pinion:

$$\gamma_b = \tan^{-1} \left( -\frac{\sqrt{\sin^2 \Sigma_g - \cos^2 \Sigma_g \sin^2 \phi_{t,\omega}}}{\cos \Sigma_g \cos \phi_{t,\omega}} \right) \quad (12.97)$$

The transverse pressure angle,  $\phi_{t,\omega}$ , can also be expressed in terms of the base cone angle,  $\gamma_b$ , of the pinion:

$$\phi_{t,\omega} = \cos^{-1} \left( \frac{\cos \Sigma_g}{\cos \gamma_b} \right) \quad (12.98)$$

Both the cone angles, namely  $\Sigma_g$  and  $\Sigma_p$ , can be expressed in terms of the rotations of the gear,  $\omega_g$ ; the pinion,  $\omega_p$ ; and the angle  $\Sigma$  between the rotation vectors,  $\boldsymbol{\omega}_g$  and  $\boldsymbol{\omega}_p$ .

When the transverse pressure angle,  $\phi_{t,\omega}$ , is given, the base cone angle of a gear,  $\Gamma_b$ , as well as the base cone angle of its mating pinion,  $\gamma_b$ , can both be expressed in terms of the pressure angle,  $\phi_{t,\omega}$ , the pitch cone angle of the gear,  $\Gamma$ , and the pitch cone angle of the pinion,  $\gamma$ .

As the plane of action,  $PA$ , is tangent with the base cones of the gear and the mating pinion, it makes a transverse pressure angle,  $\phi_{t,\omega}$ , with the pitch plane,  $PP$  (Figure 12.19). An angle that the plane of action,  $PA$ , makes with the axis of rotation of the gear,  $O_g$ , is equal to the base cone angle of the gear,  $\Gamma_b$ . Therefore, the unit normal vector,  $\mathbf{n}_{pa}$ , to the plane of action,  $PA$ , and the axis of rotation,  $O_g$ , make an angle  $(90^\circ - \Gamma_b)$ .

The unit normal vector,  $\mathbf{n}_{pa}$ , to the plane of action,  $PA$ , is specified by Equation 12.91. Referring to Figure 12.20, the unit vector,  $\mathbf{a}$ , along the axis of rotation of the gear,  $O_g$ , can be analytically expressed as:

$$\mathbf{a} = -\mathbf{i} \cos \Gamma + \mathbf{k}, \sin \Gamma \quad (12.99)$$

Once the angle  $\angle(\mathbf{n}_{pa}, \mathbf{a}) = (90^\circ - \Gamma_b)$ , the base cone angle of the gear can be calculated from the formula:

$$\Gamma_b = \tan^{-1} \left( \frac{|\mathbf{n}_{pa} \times \mathbf{a}|}{\mathbf{n}_{pa} \cdot \mathbf{a}} \right) \quad (12.100)$$

The following expression for the calculation of the base cone angle,  $\Gamma_b$ , of a gear:

$$\Gamma_b = \tan^{-1} \left( \frac{\sqrt{\cos^2 \Gamma + \sin^2 \Gamma \cos^2 \phi_{t,\omega}}}{\sin \Gamma \sin \phi_{t,\omega}} \right) \quad (12.101)$$

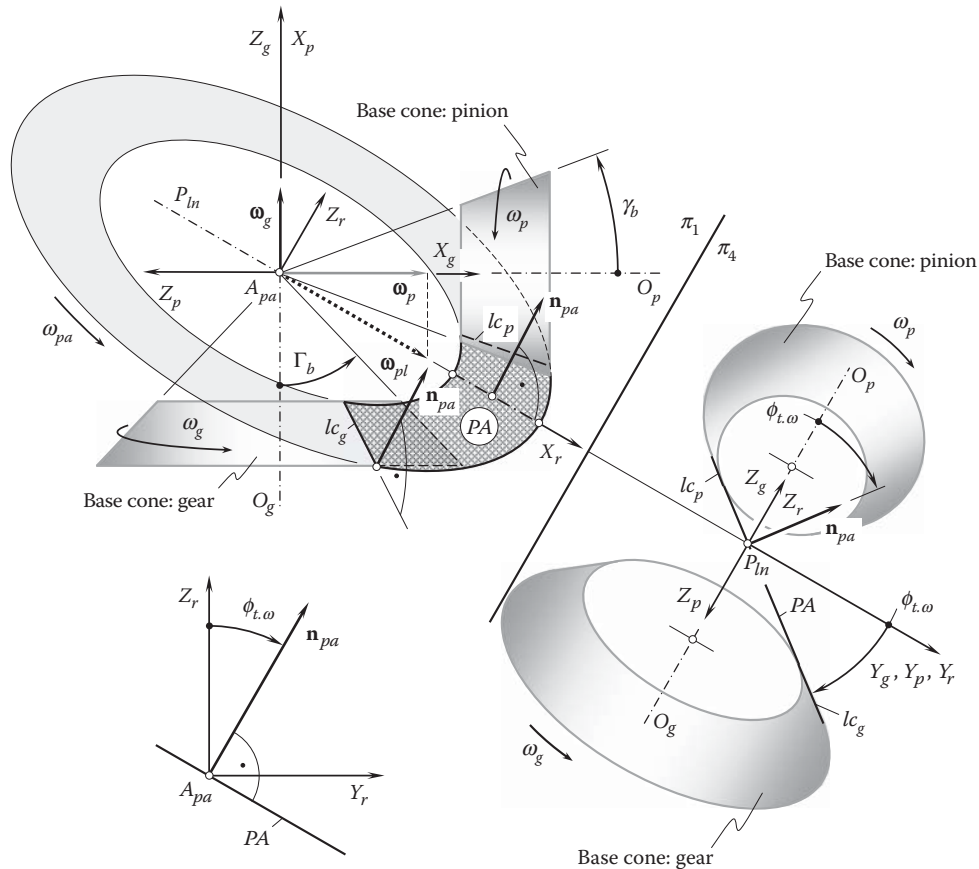
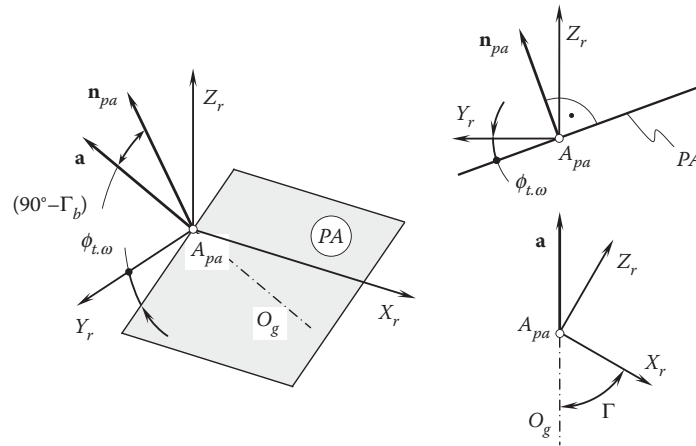


FIGURE 12.19

Specification of the configuration of the plane of action,  $PA$ , in relation to the base cones of a gear and a mating pinion in intersected-axes gear pair.

**FIGURE 12.20**

Relation between the pitch cone angle,  $\Gamma$ , and the base cone angle,  $\Gamma_b$ , of a gear in intersected-axes gearing.

can be derived after substituting the vectors,  $\mathbf{n}_{pa}$  (from Equation 12.91) and  $\mathbf{a}$  (from Equation 12.99) into Equation 12.100.

A similar expression:

$$\gamma_b = \tan^{-1} \left( \frac{\sqrt{\cos^2 \gamma + \sin^2 \gamma \cos^2 \phi_{t,\omega}}}{\sin \gamma \sin \phi_{t,\omega}} \right) \quad (12.102)$$

is valid for the calculation of the base cone angle,  $\gamma_b$ , of a pinion.

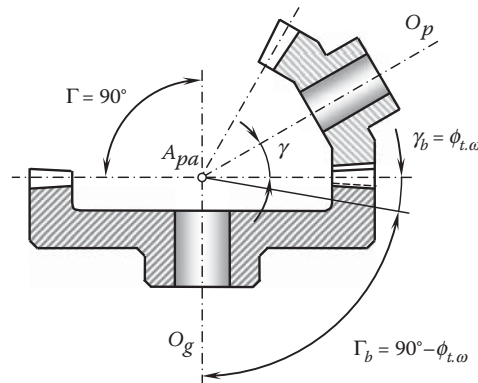
In the particular case when the pitch cone angle of a gear,  $\Gamma$ , is equal to a right angle ( $\Gamma = 90^\circ$ ), the pitch cone becomes a flat surface, and the resulting gear is called a *crown gear*. A crown gear is a bevel gear with a planar pitch surface. The position vector of a point of a crown gear is specified by Equation 12.61 under the assumption that the equality  $\Gamma = 90^\circ$  is valid.

The base cone angle of a crown gear,  $\Gamma_b$ , is equal to  $\Gamma_b = 90^\circ - \phi_{t,\omega}$  (Figure 12.21).

The back cone of a crown gear reduces to a round cylinder. The crown gear is analogous to the basic rack in spur and helical gearing.

For an internal gear, value of the base cone angle,  $\Gamma_b$ , is either within the interval:

$$(90^\circ - \phi_{t,\omega}) < \Gamma_b < 90^\circ \quad (12.103)$$

**FIGURE 12.21**

A crown gear in mesh with a bevel pinion.

or equal to a right angle ( $\Gamma_b = 90^\circ$ ), or within the interval:

$$90^\circ < \Gamma_b < 180^\circ \quad (12.104)$$

This makes it possible to separate internal intersected-axes gears into three types and in this way represent the classification of possible types of vector diagrams of gear pairs (Figure 2.15) in more detail.

### 12.6.3 Angular Pitch

In an intersected-axes gearing, the angular distance between two adjacent tooth flanks measured within the pitch plane is specified by the angular pitch.

#### Definition 12.3

*Angular pitch in intersected-axes gearing is said to be an angular distance between two adjacent tooth flanks of the gear measured within the pitch plane.*

Consider an intersected-axes gear pair, as schematically illustrated in Figure 12.22. An auxiliary round rack can be associated with the gear pair. This auxiliary rack, or, in other words, the *round basic rack*, is analogous to the corresponding auxiliary rack,  $\mathcal{R}$ , associated with a parallel-axes gear pair.

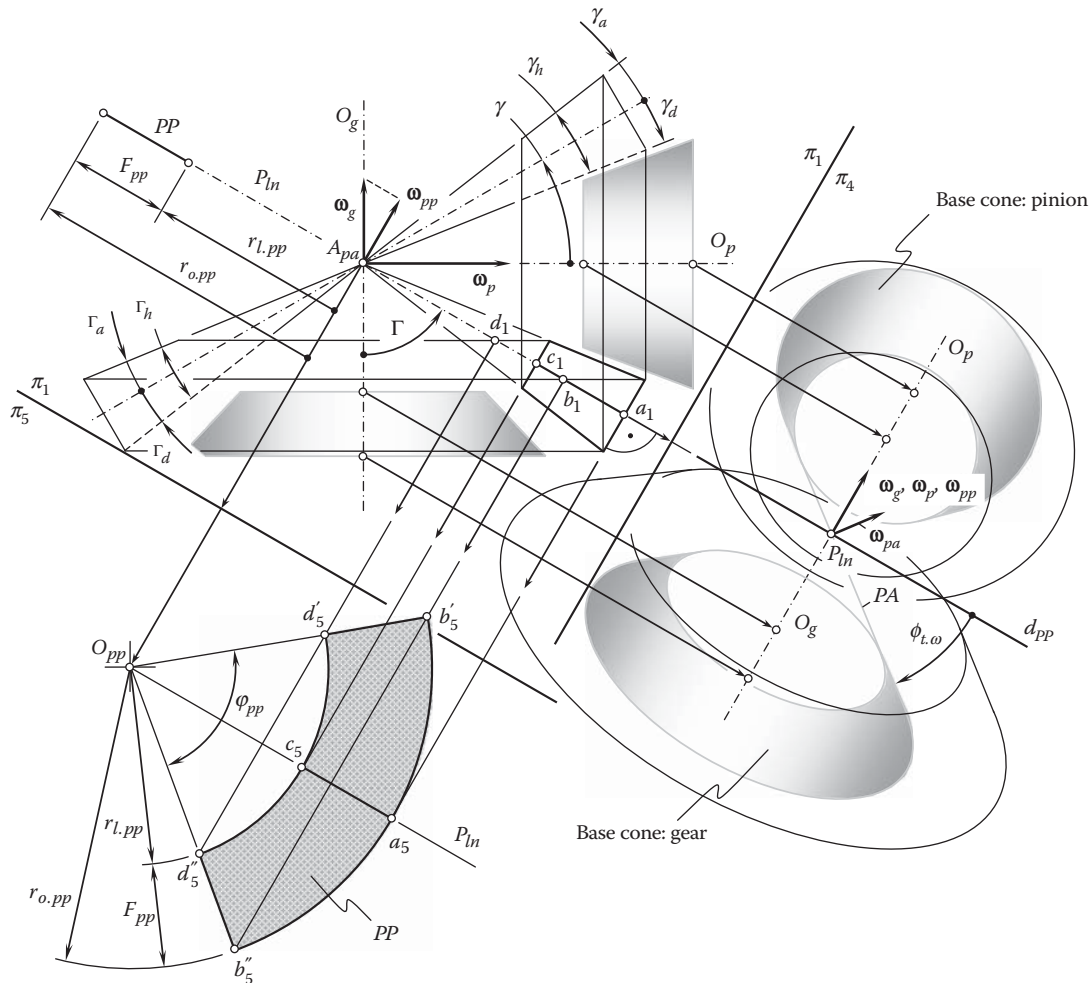


**FIGURE 12.22**  
Pitch cones and the pitch plane in an orthogonal intersected-axes gear pair.

The length of the circular arc  $\cup b'ab''$  is equal to the circumference of the circle at the larger end of the gear:

$$\cup b'ab'' = 2\pi r_{o.pp} \sin \Gamma \quad (12.105)$$

$$\varphi_{n,g} = \frac{360^\circ \cdot \cup b'ab''}{\pi d_{o,pp} N_g} = \frac{360^\circ}{N_g} \cdot \sin \Gamma \quad (12.106)$$

In Equation 12.106, the outer diameter,  $d_{o,pp}$ , of the pitch plane is equal  $d_{o,pp} = 2 r_{o,pp}$ . The angular pitch,  $\phi_{n,g}$ , for a bevel gear is an equivalent to the pitch,  $p$ , for a cylindrical gear.

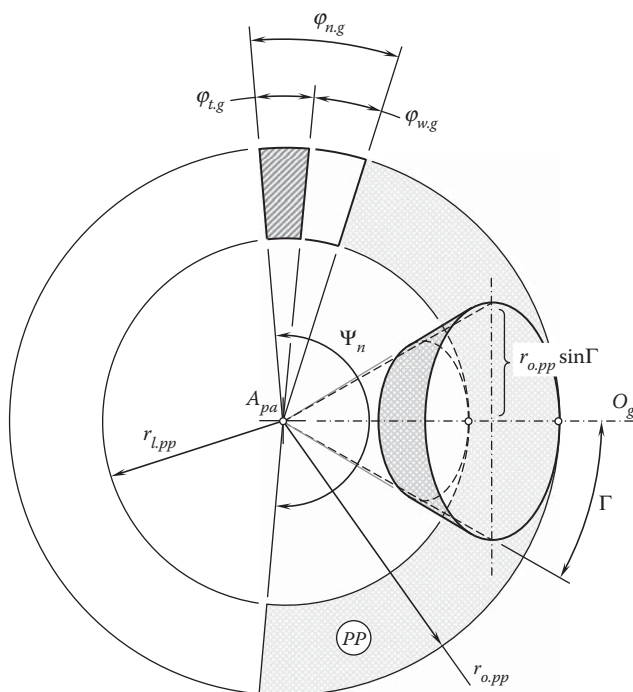


**FIGURE 12.23**  
Definition of the terms, *angular pitch*,  $\phi_{n,s'}$ , *angular tooth thickness*,  $\phi_{t,s'}$ , and *angular space width*,  $\phi_{w,s'}$  of a gear in perfect intersected-axes gearing.



The expression (see Equation 12.106) for the calculation of the angular pitch of the gear,  $\varphi_{n.g}$ , along with the expression (see Equation 12.88) for the calculation of the base angular pitch of the gear,  $\varphi_{b.g}$ , make possible expression of the angular base pitch,  $\varphi_{b.g}$ , in terms of angular pitch,  $\varphi_{n.g}$ . For this purpose, Equations 12.88 and 12.106 can be represented in the forms:

$$N_g = \frac{360^\circ}{\varphi_{b.g}} \cdot \sin \Gamma_b \quad (12.107)$$

$$N_g = \frac{360^\circ}{\varphi_{n.g}} \cdot \sin \Gamma \quad (12.108)$$

correspondingly.

As the left sides of Equations 12.88 and 12.106 are equal to each other, the equality:

$$\frac{360^\circ}{\varphi_{b.g}} \cdot \sin \Gamma_b = \frac{360^\circ}{\varphi_{n.g}} \cdot \sin \Gamma \quad (12.109)$$

is valid.

The expression:

$$\varphi_b = \varphi_{n.g} \frac{\sin \Gamma_b}{\sin \Gamma} \quad (12.110)$$

immediately follows from Equation 12.109.

Depending on the actual value of the angular pitch,  $\varphi_{n.g}$ , *low-tooth-count* intersected-axes gears (*LTC* intersected-axes gears) are recognized. Low-tooth-count intersected-axes gears feature the angular pitch,  $\varphi_{n.g}$ , of a larger value compared to that in gears with a large tooth count. Use of the base cone angle of a gear,  $\Gamma_b$  (of a pinion,  $\gamma_b$ ), and the start-of-active-profile cone angle of the gear,  $\Gamma_{sap}$  (of a pinion,  $\gamma_{sap}$ ), makes possible a numerical criterion to distinguish low-tooth-count intersected-axes gears; that is, for *LTC* intersected-axes gears, the following inequality is valid:

$$\Gamma_b > \Gamma_{sap} \quad (12.111)$$

A similar inequality:

$$\gamma_b > \gamma_{sap} \quad (12.112)$$

is valid with respect to a low-tooth-count intersected-axes pinion.

Low-tooth-count intersected-axes gears feature more significant variation of the most of principal design parameters of the tooth flanks compared to that in gears with a large tooth count.

#### 12.6.4 Angular Tooth Thickness and Angular Space Width

Angular tooth thickness and angular space width in an intersected-axes gearing are equivalent to tooth thickness and space width in parallel-axes gearing. Both the tooth thickness and space width are measured either within the pitch cone of the gear or within the pitch plane, *PP*, of the corresponding round rack of the gear pair.

##### Definition 12.4

*Angular tooth thickness in intersected-axes gearing is said to be the angular distance between the opposite tooth flanks of the gear tooth measured within the pitch plane.*

##### Definition 12.5

*Angular space width in intersected-axes gearing is said to be the angular distance between the opposite tooth flanks of a space between adjacent gear teeth measured within the pitch plane.*

In the tight mesh of an intersected-axes gear pair, the angular tooth thickness,  $\varphi_{t.g}$ , and the angular space width,  $\varphi_{w.g}$ , of a bevel gear together form the angular pitch of the gear,  $\varphi_{N.g}$ :

$$\varphi_{t.g} + \varphi_{w.g} = \varphi_{N.g} \quad (12.113)$$

In practice, backlash between the gear tooth flank,  $\mathcal{G}$ , and the pinion tooth flank,  $\mathcal{P}$ , is required to compensate for heat extension and so forth. The backlash,  $\varphi_{B.n}$ , for a bevel gear should be incorporated into Equation 12.113. Under any circumstances, the equality:

$$\varphi_{B.n} = \varphi_{w.g} - \varphi_{t.g} \quad (12.114)$$

is valid.

As a gear tooth is commonly stronger compared to a mating pinion, it is reasonable to set the angular tooth thickness of the gear:

$$\varphi_{t.g} = \frac{\varphi_{N.g}}{2} - \varphi_{B.n} \quad (12.115)$$

In this case, the angular space width of that same gear can be calculated from:

$$\varphi_{w.g} = \frac{\varphi_{N.g}}{2} \quad (12.116)$$

Similar formulas:

$$\varphi_{t.p} = \frac{\varphi_{N.p}}{2} \quad (12.117)$$

$$\varphi_{w.p} = \frac{\varphi_{N.p}}{2} \quad (12.118)$$

are valid with respect to bevel pinion.

In Equations 12.117 and 12.118, the angular pitch of the pinion,  $\varphi_{N.p}$ , is equal to  $\varphi_{N.p} = \varphi_{N.g}$ . It can also be calculated from the expression:

$$\varphi_{N.p} = \frac{\cup b'ab''}{N_p} = \frac{\pi d_{o.pp}}{N_p} \cdot \sin \gamma \quad (12.119)$$

Other possibilities to distribute the angular pitch,  $\varphi_{N.g}$ , among the three components  $\varphi_{t.g}$ ,  $\varphi_{w.g}$ , and  $\varphi_{B.n}$  are possible for a particular application of an intersected-axes gearing.

### 12.6.5 Angular Backlash

Bevel gears are designed and manufactured to provide a specific amount of backlash—that is, the space between mating gear teeth or the difference in width of the gear tooth and pinion tooth of the mating gear to let the gears mesh without binding and provide space for a film of lubricating oil between the teeth. This prevents overheating and tooth damage. The backlash is necessary for proper operation of the gear pair.

To optimize the performance of any two bevel gears, the gears must be positioned together so that they run smoothly without binding and/or excessive backlash. In the current practice of gear production, unless otherwise specified, the minimum amount of total backlash of a pair of bevel gears is measured at the tightest point of mesh with a dial indicator on a bevel gear testing machine. Unless otherwise specified, backlash is assumed to be normal backlash\* and cannot be measured in the plane of rotation. Backlash is necessary to achieve correct operation of the gears and varies with the size of the tooth and operating conditions. Bevel gears are cut to have a definite amount of backlash when correctly assembled together. But excessive backlash or play, if great

\* A straight line along the so-called *normal backlash* cannot be perpendicular to both the gear tooth flank,  $\mathcal{G}$ , and the pinion tooth flank,  $\mathcal{P}$ , at the same time.

enough, can cause a sudden impulse or shock load in starting or reversing that may cause serious tooth damage. Excessive or insufficient backlash can also result in noise, excessive wear, and damage.

### Definition 12.6

Effective angular backlash,  $\varphi_{B,pa}$ , in perfect intersected-axes gearing is said to be the angular distance between the noninteracting tooth flanks of a driving member and the tooth-space flank of the driven member in a gear pair, measured within the pitch plane.

Consider a phantom crown gear that is engaged in correct mesh with the gear. This crown gear can be referred to as a *crown gear/gear* or simply as  $CG_g$ . The outer diameter of the crown gear is labeled  $r_{o,pp}$ , the inner diameter is labeled  $r_{l,pp}$ , and the pitch diameter is labeled  $r_{pp}$ . The face width,  $F_{pp}$ , of the crown gear is equal to  $F_{pp} = r_{o,pp} - r_{l,pp}$ . The central angle,  $\Psi_{pp}$ , spans the active portion of the crown gear,  $CG_g$ . The axis of rotation of the crown gear,  $CG_g$ , is labeled  $O_{pp}$ . Here, the subscript  $pp$  indicates that the parameters relate to the pitch plane,  $PP$ .

The angular tooth thickness,  $\varphi_{t,g}$ , and the angular space width,  $\varphi_{w,g}$ , in a gear is measured within the pitch plane,  $PP$ , of the crown gear/gear,  $CG_g$ , as shown in Figure 12.24 (a similar schematic is valid for crossed-axes gearing as well). The angular pitch of the gear teeth in Figure 12.24 is labeled  $\varphi_{x,g}$ .

Similarly, consider a phantom crown gear that is engaged in correct mesh with the pinion. This crown gear can be referred to as a *crown gear/pinion* or simply  $CG_p$ . The angular tooth thickness,  $\varphi_{t,p}$ , and the angular space width,  $\varphi_{w,p}$ , of a gear is measured within the pitch plane,  $PP$ , of the crown gear/pinion,  $CG_p$ , (not shown in Figure 12.24). The angular pitch of the pinion teeth is labeled  $\varphi_{x,p}$  (not shown in Figure 12.24).

The angular pitches of the gear,  $\varphi_{x,g}$ , and the pinion,  $\varphi_{x,p}$ , are equal; that is,  $\varphi_{x,g} = \varphi_{x,p} = \varphi_x$ . Therefore, further, the designations for these angular pitches are replaced with  $\varphi_x$ .

When the crown gear,  $CG_g$ , and the crown gear,  $CG_p$ , are engaged in mesh, they are free to turn about the  $O_{pp}$ -axis in relation to one another through a certain angle,  $\varphi_B$ . The angle,  $\varphi_B$ , is referred to as the *angular backlash*. The angular backlash,  $\varphi_B$ , can be calculated as:

$$\varphi_B = \varphi_{w,g} - \varphi_{t,p} \quad (12.120)$$

or as

$$\varphi_B = \varphi_{w,p} - \varphi_{t,g} \quad (12.121)$$

Novel instrumentation can be developed for the direct measurement of the design parameters in a gear ( $\varphi_{t,g}$ ,  $\varphi_{w,g}$ , and  $\varphi_{x,g}$ ), and a pinion ( $\varphi_{t,p}$ ,  $\varphi_{w,p}$ , and  $\varphi_{x,p}$ ). Then, either Equation 12.120 or 12.121 can be used for the calculation of the angular backlash,  $\varphi_B$ .

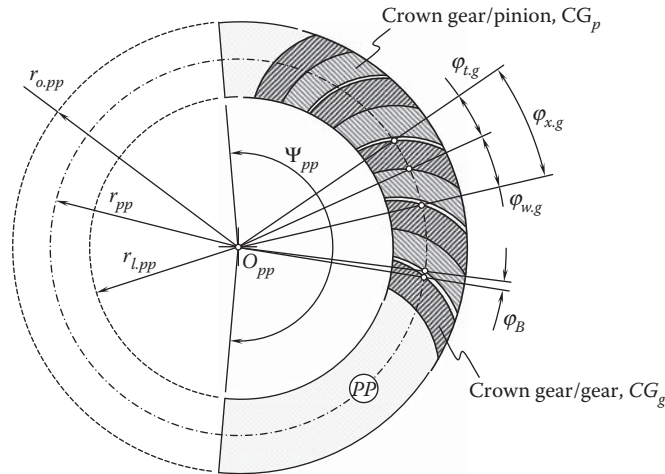


FIGURE 12.24

On definition of the angular tooth thickness,  $\varphi_t$ , angular space width,  $\varphi_w$ , and angular backlash,  $\varphi_B$ , in intersected-axes gearing by means of  $CG_g$ -to- $CG_p$  mesh.

In a bevel gear pair, the backlash is measured at a configuration of a gear and a pinion when *two pairs of teeth are engaged in mesh*.

If the backlash does not fall within the recommended limits, no corrections to the mounting distance are allowed to adjust the backlash. If possible, the tooth thickness can be corrected (reduced) by additional machining. For strength calculations, the normal backlash can be expressed in terms of the backlash in the plane of rotation.

There is a trade-off when setting an actual value of backlash: the backlash must be large enough for operation of the gear pair, and it must be small enough when reversing the rotation.

With the discussed approach, the contact ratio in bevel and hypoid gearing can be accurately calculated (spiral bevel, and others).

#### Conclusion 12.4

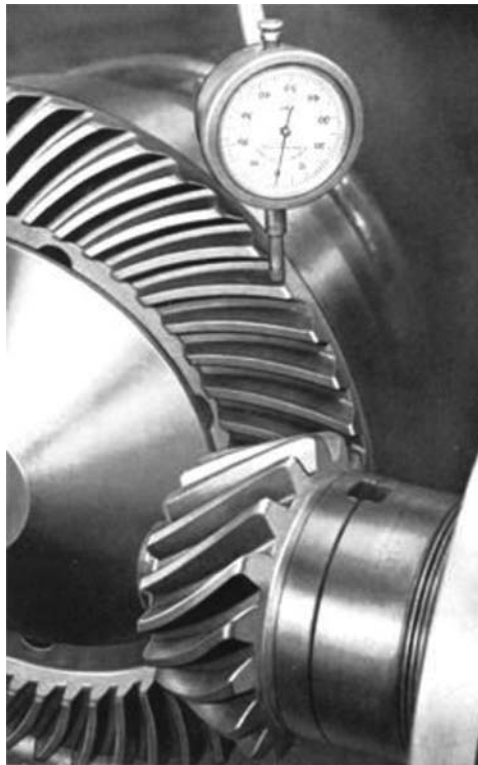
*Backlash in intersected-axes gearing is said to be an angular parameter, and not a linear parameter. Backlash is measured within the pitch plane of the gear pair.*

Conventional techniques can be adapted when inspecting the effective angular backlash,  $\varphi_{B.pa}$ , in perfect intersected-axes gearing (Figure 12.25). If the dial type indicator reading is of a certain value,  $DTI_{\text{reading}}$ , then the angular backlash,  $\varphi_{B.pa}$ , can be calculated as:

$$\varphi_{B.pa} \cong \frac{DTI_{\text{reading}}}{r_{pa.B}}, \text{ rad} \quad (12.122)$$

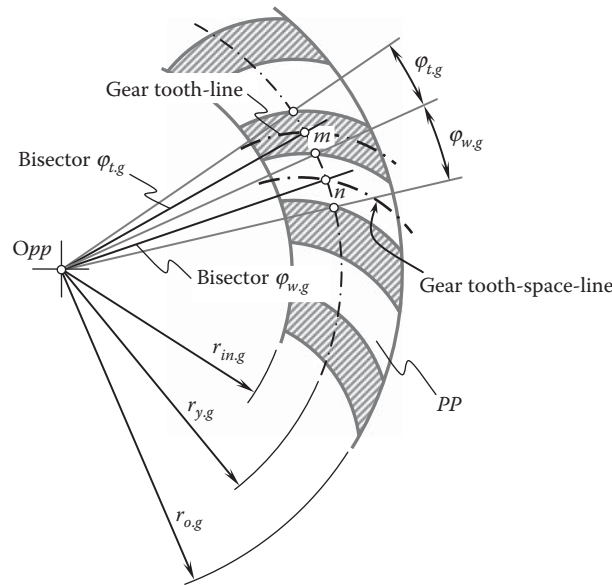
where  $r_{pa.B}$  is the distance from the plane-of-action apex,  $A_{pa}$ , to the section at which the dial type indicator is installed.

The effective angular backlash,  $\varphi_{B.pa}$ , is smaller compared to the angular backlash,  $\varphi_{B.n}$ , measured within the pitch plane,  $PP$ .



**FIGURE 12.25**

Angular backlash,  $\varphi_{B.pa}$ , can be calculated based on the measurement of a linear value of the backlash in compliance with the adopted practice.

**FIGURE 12.26**

On definition of the “gear tooth-line” (“gear tooth-space-line”) in gears for intersected-axes gear pairs (also valid for gears for crossed-axes gear pairs).

The determined values of the angular tooth thickness of a gear,  $\varphi_{t,g}$  (see Equation 12.115), and a mating pinion,  $\varphi_{t,p}$  (see Equation 12.117), as well as the angular space widths of a gear,  $\varphi_{w,g}$  (see Equation 12.116), and a mating pinion,  $\varphi_{w,p}$  (see Equation 12.118) yield the determination of the “gear tooth-line” (and the “gear tooth-space-line”).

The construction of a “gear tooth-line” (and of a “gear tooth-space-line”) is illustrated in Figure 12.26.

In bevel gears with a symmetrical tooth profile, the “tooth-line” can be defined within the pitch plane of the mating crown gear:

#### Definition 12.7

*The gear tooth-line in a bevel gear is a locus of points of intersection of the circles,  $r_{y,g}$  (here  $r_{in,g} \leq r_{y,g} \leq r_{o,g}$ ), by the corresponding bisectors of the angular tooth thicknesses (of the angular spaces widths).*

This definition is also valid with respect to gears that are used in the design of crossed-axes gears.

#### 12.6.6 Angular Addendum and Angular Dedendum

The angular tooth addendum in an intersected-axes gearing is specified by the angular distance between the pitch cone of the gear and the gear top-land cone (outer cone) of the gear.

#### Definition 12.8

*The angular tooth addendum in an intersected-axes gearing is said to be the angular distance between the pitch cone and the outer cone of the gear measured in an axial section of the gear.*

Similarly, the angular dedendum in an intersected-axes gearing is specified by the angular distance between the pitch cone of the gear and the gear bottom-land cone (inner cone) of the gear.

#### Definition 12.9

*The angular tooth dedendum in an intersected-axes gearing is said to be the angular distance between the pitch cone and the inner cone of the gear measured in an axial section of the gear.*

The angular addendum,  $\Gamma_a$ , and angular dedendum,  $\Gamma_d$ , of the gear tooth together specify the angular tooth height,  $\Gamma_h$ , of the gear (Figure 12.22):

$$\Gamma_h = \Gamma_a + \Gamma_d \quad (12.123)$$

For standard bevel gears, the tooth height of a bevel gear is set equal to a module,  $m$ . This makes it possible to calculate the angular addendum,  $\Gamma_a$ , of the gear from the expression:

$$\Gamma_a = \sin^{-1} \left( \frac{m}{r_{o,pp}} \right) \quad (12.124)$$

In such a scenario, the angle,  $\Gamma_a$ , can be viewed as the *angular module*,  $\Gamma_m$  of a gear pair.

Similarly, the angular module,  $\gamma_m$  can be expressed in terms of the design parameters of a bevel pinion.

The dedendum of a standard bevel gear is greater the addendum at a clearance,  $c$ . Therefore, the angular dedendum,  $\Gamma_d$ , of the gear is calculated as follows:

$$\Gamma_d = \sin^{-1} \left( \frac{m + c}{r_{o,pp}} \right) \quad (12.125)$$

The difference,  $\Gamma_c$ , between the angles,  $\Gamma_d$  and  $\Gamma_a$ , can be viewed as the *angular clearance*,  $\Gamma_c$  of a gear pair:

$$\Gamma_c = \Gamma_d - \Gamma_a \quad (12.126)$$

Formulas similar to those aforementioned:

$$\gamma_a = \sin^{-1} \left( \frac{m}{r_{o,pp}} \right) \quad (12.127)$$

$$\gamma_d = \sin^{-1} \left( \frac{m + c}{r_{o,pp}} \right) \quad (12.128)$$

$$\gamma_h = \gamma_a + \gamma_d \quad (12.129)$$

are valid for the calculation of the angular addendum,  $\gamma_a$ , the angular dedendum,  $\gamma_d$ , as well as the angular tooth height,  $\gamma_h$ , of a standard bevel pinion (Figure 12.22).

Similarly, the angular clearance,  $\gamma_c$  can be expressed in terms of the design parameters of a bevel pinion as:

$$\gamma_c = \gamma_d - \gamma_a \quad (12.130)$$

The aforementioned design parameters in intersected-axes gearing correlate to corresponding design parameters in parallel-axes gearing. The correlation between the design parameters is outlined in Table 12.2.

### 12.6.7 Specification of Design Parameters in Intersected-Axes Gearing

Design parameters of an intersected-axes gear that are convenient for investigation and analysis are not always those convenient in gear design and gear manufacturing practice.

The main design parameters of an intersected-axes gearing and elements of the gear tooth are schematically depicted in Figure 12.27.

Additional terms characteristic of intersected-axes gearing are defined in Figure 12.28. Note that a constant clearance is maintained by making the elements of the face cone parallel to the elements of the root cone of the mating gear. This explains why the face cone apex is not coincident with the pitch-cone apex in Figure 12.28. This permits a larger fillet at the small end of the tooth than would otherwise be possible.

TABLE 12.2

Design Parameters in Intersected-Axes Gears and the Corresponding Design Parameters in Parallel-Axes Gears

Design Parameters of Intersected-Axes Gears		Design Parameters of Parallel-Axes Gears	
Term	Designation	Term	Designation
Tooth number	$N_g, N_p$	Tooth number	$N_g, N_p$
Pitch cone angle (gear)	$\Gamma$	Pitch diameter	$d_g, d_p$
Pitch cone angle (pinion)	$\gamma$		
Base pitch angle (gear)	$\Gamma_b$	Base pitch	$P_b$
Base pitch angle (pinion)	$\gamma_b$		
Outer cone angle (gear)	$\Gamma_o$	Outer diameter	$d_{o,g}, d_{o,p}$
Outer cone angle (pinion)	$\gamma_o$		
Root cone (gear)	$\Gamma_f$	Root diameter	$d_{f,g}, d_{f,p}$
Root cone (pinion)	$\gamma_f$		
Transverse pressure angle	$\phi_{t,\omega}$	Transverse pressure angle	$\phi_t$
Angular pitch	$\varphi_n$	Normal circular pitch	$p_n$
Base pitch angle	$\varphi_b$	Base pitch	$p_b$
Angular tooth thickness	$\varphi_t$	Tooth thickness	$t$
Angular space width	$\varphi_w$	Space width	$w$
Angular backlash <sup>a</sup>	$\varphi_B$	Backlash	$B$
Angular addendum (gear)	$\Gamma_a$	Addendum	$a$
Angular addendum (pinion)	$\gamma_a$		
Angular dedendum (gear)	$\Gamma_b$	Dedendum	$b$
Angular dedendum (pinion)	$\gamma_b$		
Angular clearance	$\Gamma_c, \gamma_c$	Clearance	$c$
Angular module	$\Gamma_m, \gamma_m$	Module	$m$

<sup>a</sup> The expressions  $\varphi_n = \varphi_t + \varphi_w$  and  $\varphi_w - \varphi_t = \varphi_B$  are always valid.

It is common practice to specify the design parameters of tooth profile in intersected-axes gearing at the larger end of the gear teeth.

The addendum, and dedendum of a bevel gear are specified on the so-called the *back cone*. The straight generating line of the back cone is perpendicular to the corresponding straight generating line of the pitch cone. The angular addendum,  $\Gamma_a$ , and angular dedendum,  $\Gamma_d$ , can be calculated from the following equations:

$$\Gamma_a = \tan^{-1} \left( \frac{2a \sin \Gamma}{m N_g} \right) \quad (12.131)$$

$$\Gamma_d = \tan^{-1} \left( \frac{2b \sin \Gamma}{m N_g} \right) \quad (12.132)$$

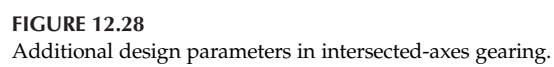
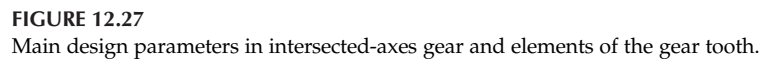
For standard gears for which  $a = m$  and  $b = (1.2 \div 1.3)m$  (here the module of the gear is denoted by  $m$ ), Equations 12.131 and 12.132 can be reduced to:

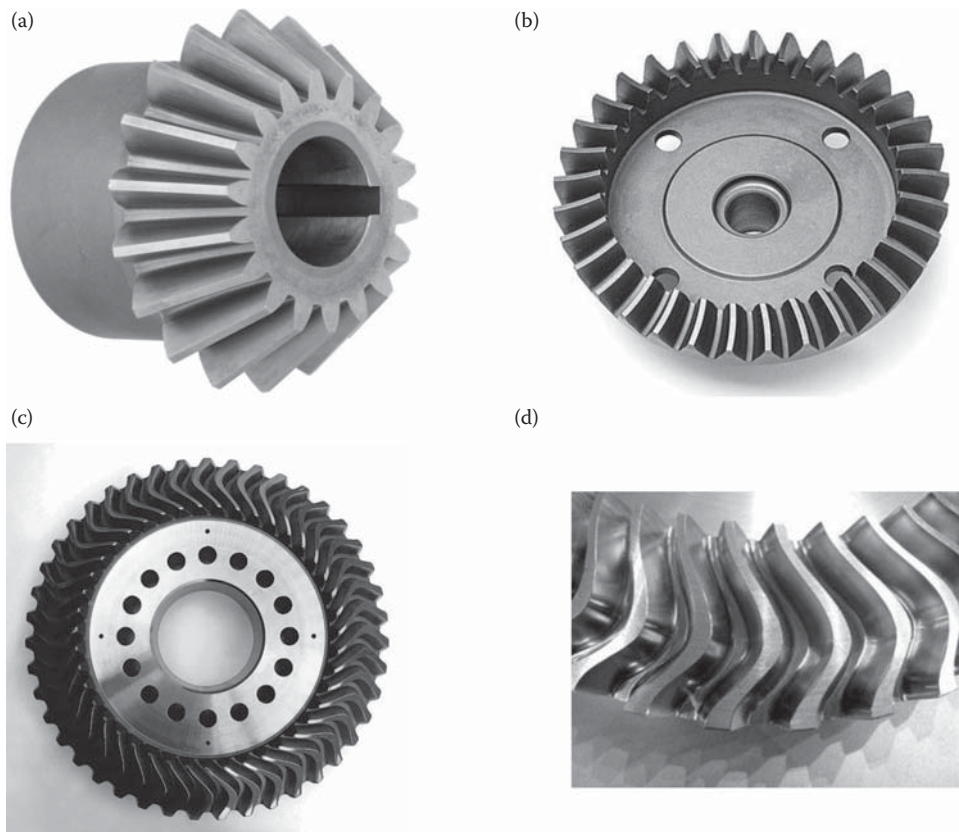
$$\Gamma_a = \tan^{-1} \left( \frac{2 \sin \Gamma}{N_g} \right) \quad (12.133)$$

$$\Gamma_d = \tan^{-1} \left[ \frac{(2.4 \div 2.6) \sin \Gamma}{N_g} \right] \quad (12.134)$$

Equations similar to Equations 12.133 and 12.134 are valid for bevel pinion as well.





**FIGURE 12.29**

Various types of bevel gears used in the current industry in the design of intersected-axes gear pairs: (a) straight bevel gear, (b) spiral bevel gear, (c) S-shaped bevel gear, and (d) teeth of the S-shaped bevel gear.

Practically, most straight-tooth bevel gears manufactured today use the  $\phi_{t,\omega} = 20^\circ$  profile angle.

Various types of bevel gears used in the current industry in intersected-axes gear pairs are illustrated in Figure 12.29.

## 12.7 Tredgold Approximation

Meshing of gears in intersected-axes gearings occurs on a sphere\* of a certain radius, similar to the meshing of gears in parallel-axes gearings that occurs within a plane perpendicular to the axes of rotations of the gears. Projecting bevel gear teeth on the surface of a sphere would indeed be a difficult and time-consuming problem. Fortunately, an approximation is available that reduces the problem to that of ordinary spur gear. This method is called Tredgold's approximation, and as long as the gear has eight or more teeth, it is accurate enough for most practical purposes (see page 88 in [41], and others). It is in almost universal use, and the terminology of bevel gear teeth has evolved around it. Moreover, the method of Tredgold's approximation can further be enhanced for crossed-axes gearing as well.

In using Tredgold's method, a back cone is formed of elements that are perpendicular to the elements of the pitch cone at the large end of the teeth. This is shown in Figure 12.30. The length of a back cone element is called

\* Interpretation of the meshing of intersected-axes gearing as meshing of gears on a sphere mistakenly leads to wrong terminology: intersected-axes gears sometimes are loosely referred to as *spherical gears*. This term is incorrect because meshing in crossed-axes gearing (see below) also occurs on a sphere. Therefore, intersected-axes gears cannot be distinguished from crossed-axes gears as long as gear pairs of both kinds are referred to as spherical gears. The aforementioned ambiguity caused by the term spherical gears can be avoided by using terms such as *intersected-axes gears* ( $I_a$ -gearing for simplicity), and *crossed-axes gears* (or just  $C_a$ -gearing for simplicity). These terms are adopted in this monograph instead of the incorrect term spherical gears.

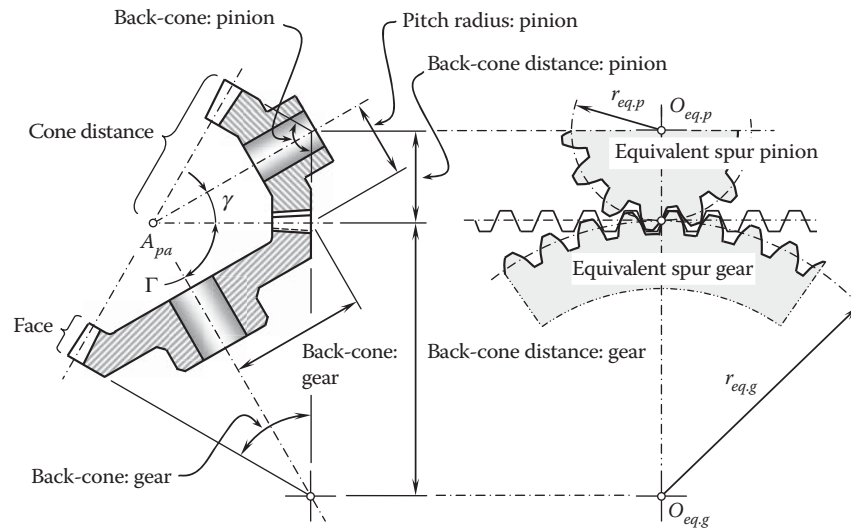


**FIGURE 12.30**  
Tredgold approximation.

the *back-cone radius*. Now, an equivalent spur gear is constructed, whose pitch radius,  $r_{eq}$ , is equal to the back cone radius. Thus, from a pair of bevel gears, we can obtain, using Tredgold's approximation, a pair of equivalent spur gears, which are then used to define the tooth profiles; they can also be used to determine the tooth action and the contact conditions exactly as for ordinary spur gears, and the results will correspond closely to those for bevel gears. From the geometry of Figure 12.30, the equivalent pitch radii are:

$$r_{eq,g} = \frac{r_g}{\cos \Gamma} \quad (12.135)$$

and

$$r_{eq,p} = \frac{r_p}{\cos \gamma} \quad (12.136)$$

The number of teeth on the equivalent spur gear is:

$$N_{eq} = \frac{2\pi r_{eq}}{p} \quad (12.137)$$

where  $p$  is the circular pitch of the bevel gear measured at the large end of the teeth. In the usual case, the equivalent spur gears will not have an integral number of teeth.

It should be pointed out here that the approximation proposed by Tredgold\* for intersected-axes gearing can be evolved to crossed-axes gearing as well.

## 12.8 Main Features of Perfect Conformal and High-Conformal Intersected-Axes Gearing

Conformal and high-conformal intersected-axes gearing can be used for transmitting a rotation from a driving shaft to a driven shaft that intersect each other at a certain angle. Gears of this type are capable of transmitting a uniform rotation from a driving shaft to a driven shaft. So far, conformal and high-conformal intersected-axes gears have no extensive application in the industry. This is mostly because they have not been deeply investigated yet.

\* Thomas Tredgold (August 22, 1788–January 28, 1829)—an English engineer known for his early work on railroad construction.

Perfect conformal/high-conformal intersected-axes gearings feature many similarities with perfect intersected-axes gearings of conventional design, that is, with gearings having line contact between a gear and mating pinion tooth flanks. Because of this, there is no need to consider separately, for example, kinematics of the instantaneous motion in conformal/high-conformal intersected-axes gearing, as it is already discussed in detail in a corresponding section devoted to perfect intersected-axes gearings of conventional design.

Base cones of a gear and mating pinion is the other example of the similarities between conformal/high-conformal intersected-axes gearings and perfect intersected-axes gearings of conventional design.

Sliding between the tooth flanks of a gear and a mating pinion in intersected-axes conformal/high-conformal gearing is a reduced case of the same in perfect intersected-axes gearings of conventional design.

A few more similarities could be mentioned. These similarities, as well as a few others, are omitted from further analysis.

Below, the reader's attention is focused mostly on the main features of perfect conformal/high-conformal intersected-axes gear pairs.

### 12.8.1 Path of Contact in Conformal/High-Conformal Intersected-Axes Gearing

The path of contact in a conformal/high-conformal intersected-axes gear pair is a trace of a contact point when the gears rotate. For better understanding of the kinematics and geometry of conformal/high-conformal gearing, the use of the pulley-and-belt analogy of intersected-axes gear pairs is helpful.

Refer to Figure 12.31 for details on the path of contact in conformal/high-conformal intersected-axes gearing.

The design parameters outer radius,  $r_{o.pa}$ , of the plane of action; inner radius,  $r_{i.pa}$ , of the plane of action; and effective width,  $F_{pa}$ , of the plane of action,  $PA$ , in an intersected-axes conformal/high-conformal gear pair are identical to those in intersected-axes gear pairs of conventional design. The zone of action,  $ZA$ , in intersected-axes conformal/high-conformal gears is shrunk to a straight line, as the angular width of the zone of action,  $ZA$ , is zero ( $\varphi_{pc} = 0^\circ$ ). This straight line forms an angle,  $\Gamma_N$ , with the axis of instant rotation,  $P_{ln}$ .

As the gears rotate, the tooth flanks,  $\mathcal{G}$  and  $\mathcal{P}$ , of a gear and a mating pinion make an instant contact at point,  $K_{inst}$ . The instant line of action,  $LA_{inst}$ , is a straight line through  $K_{inst}$  that is entirely located within the plane of action,  $PA$ . The instant line of action,  $LA_{inst}$ , is perpendicular to the radius,  $A_{pa}K_{inst}$ , and intersects the axis of instant rotation,  $P_{ln}$ , at a corresponding point,  $k_{inst}$ . As the angular width of the zone of action is zero ( $\varphi_{pc} = 0^\circ$ ), the length,  $l_{pc}$ , of the path of contact,  $P_c$ , is also zero ( $l_{pc} = 0$ ).

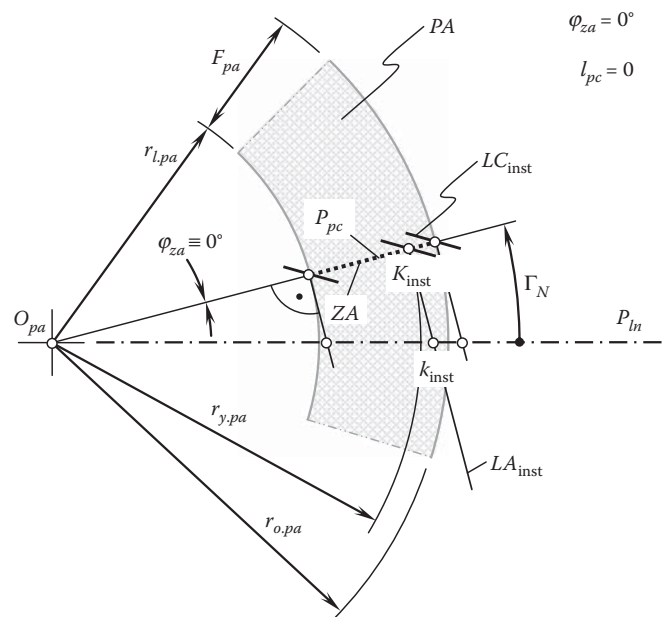


FIGURE 12.31

Path of contact,  $\varphi_{za} = 0^\circ$ , and pseudo-path of contact,  $P_{pc}$ , in intersected-axes conformal/high-conformal gear pair.

The instant line of contact,  $LC_{inst}$ , is a zero-length straight line segment through point,  $K_{inst}$ , that is entirely located within the plane of action,  $PA$ , and is tangent to the gear helix at  $K_{inst}$ .

For different configurations of a gear and mating pinion, the instant contact point,  $K_{inst}$ , occupies different locations along a straight line, which is referred to as the *pseudo-path of contact*,  $P_{pc}$ . *Pseudo* indicates that contact point  $K_{inst}$  does not travel along the straight line,  $P_{pc}$ : the rotation with the plane of action is the only motion that contact point  $K_{inst}$  performs.

### 12.8.2 Boundary Cones

When the gears rotate, a motion of the pinion in relation to the mating gear can be viewed as instant rotation about the axis of instant rotation,  $P_{ln}$ . A boundary  $N$ -circle is traced by the contact point,  $K$ , in such a relative motion. In theory, the radius,  $r_N$ , of the boundary  $N$ -circle is a trade-off between a desirable high contact strength and low friction between the tooth flanks of the gear,  $\mathcal{G}$ , and the pinion,  $\mathcal{P}$ . In practice, run-out of the gear and the pinion, as well as displacements of other types of the tooth flanks,  $\mathcal{G}$  and  $\mathcal{P}$ , in relation to their desirable position should be taken into account.

Since the relative motion of a gear and a mating pinion is an instant rotation,  $\omega_{pl}$ , about the axis of instant rotation,  $P_{ln}$ , the plane perpendicular to the vector of instant rotation,  $\omega_{pl}$ , at an arbitrary point within the axis,  $P_{ln}$ , can be constructed, and the relative motion can be investigated within the normal plane (as illustrated in Figure 12.32).

Within the normal plane, a boundary  $N$ -circle of a radius,  $r_N$ , can be constructed. The center of the boundary  $N$ -circle is coincident with the point of intersection of the axis of instant rotation,  $P_{ln}$ , by the normal plane. The radius,  $r_N$ , of the boundary  $N$ -circle is equal to a desired displacement,  $l$ , of the contact point,  $K$  (either in a positive direction to the position of the point,  $K^+$ , or in a negative direction to the position of the point,  $K^-$ ), from the axis of instant rotation,  $P_{ln}$ , along the instant line of action,  $LA_{inst}$ . The actual value of the displacement,  $l$  (either of a positive value,  $+l$ , or a negative value,  $-l$ ), is a trade-off between the contact strength of the gear teeth and the sliding of the tooth flanks of the gear and the pinion,  $\mathcal{G}$  and  $\mathcal{P}$ , in relation to one another. The larger the distance,  $l$ , the higher the contact strength of the gear teeth and the higher the sliding of the tooth flanks. The smaller the distance,  $l$ , the lower the contact strength of the gear teeth and the lower the sliding of the tooth flanks.

Under the assumptions that  $\Delta l = 0$  and the manufacturing errors are zero, the contact point,  $K$ , is located at the point of intersection of the boundary  $N$ -circle by the instant line of action,  $LA_{inst}$ . At any point within the axis of instant rotation,  $P_{ln}$ , a boundary  $N$ -circle of a certain radius,  $r_N^i$ , can be constructed, and an instant line of action,  $LA_{inst}$ , can be constructed as well. The pressure angle,  $\phi_{t,\omega}^i$ , is not mandatorily of the same value at all the normal transverse sections of the axis,  $P_{ln}$ . The instant line of action,  $LA_{inst}$ , is a line through the axis of instant

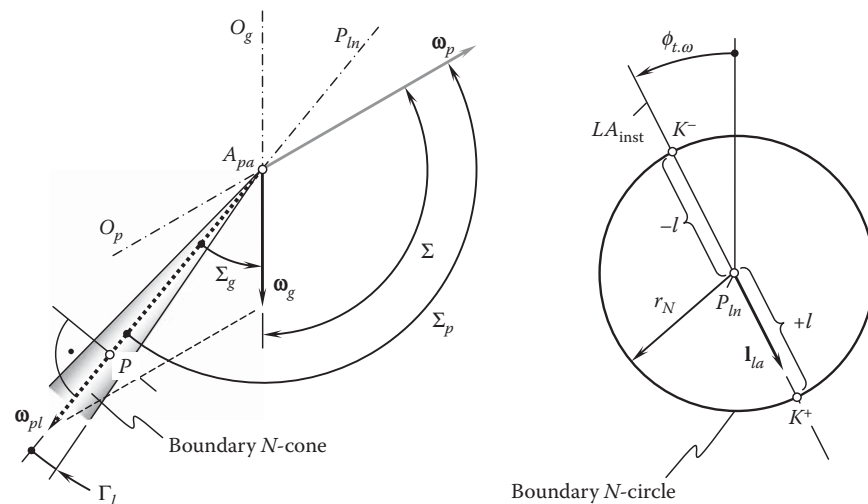


FIGURE 12.32

Configuration of the boundary  $N$ -cone in a conformal/high-conformal intersected-axis gear pair.

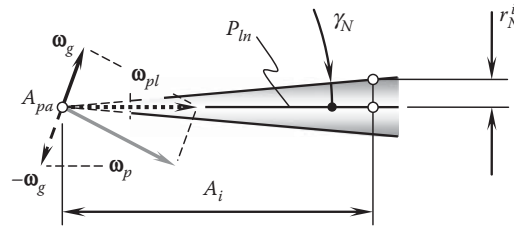


FIGURE 12.33

Boundary cone angle,  $\gamma_N$ , in conformal/high-conformal intersected-axes gearing.

rotation,  $P_{ln}$ . No kinematical and/or geometrical constraints in an intersected-axes conformal/high-conformal gearing are violated in such a consideration.

It is practical to keep the pressure angle,  $\phi_{t,\omega}^i$ , of a certain constant value,  $\phi_{t,\omega}$ , within the active face width,  $F_{par}$ , of the gear pair. Moreover, as a normal section through a point within the axis of instant rotation,  $P_{ln}$ , approaches the apex,  $P_a$ , the radius  $r_N^i$  of the boundary  $N$ -circle gets smaller, accordingly.

Consider a straight line,  $P_{pc}$ , through the contact point,  $K$ , between the tooth flanks,  $\mathcal{G}$  and  $\mathcal{P}$ , of the gear and the pinion and through the common plane-of-action apex,  $A_{pa}$ , as illustrated in Figure 12.32. The pseudo-path of contact,  $P_{pc}$ , forms a boundary cone angle,  $\gamma_N$ , with the axis of instant rotation,  $P_{ln}$ . The boundary cone angle,  $\gamma_N$  (Figure 12.33) can be expressed in terms of (a) the radius,  $r_N^i$ , of the boundary  $N$ -circle at a current point within the axis of instant rotation,  $P_{ln}$ , and (b) the cone distance,  $A_i$ , of that point from the plane-of-action apex,  $A_{pa}$ :

$$\gamma_N = \tan^{-1} \left( \frac{r_N^i}{A_i} \right) \quad (12.138)$$

When rotating about the axis of instant rotation,  $P_{ln}$ , a cone of revolution is generated by this line. This cone of revolution is referred to as the *boundary  $N$ -cone* in an intersected-axes conformal/high-conformal gearing. This makes possible the following definition:

#### Definition 12.10

The boundary Novikov cone (or just  $N$ -cone for simplicity) in intersected-axes conformal/high-conformal gearing is said to be a cone of revolution generated by the pseudo-path of contact,  $P_{pc}$ , in its rotary motion about the axis of instant rotation,  $P_{ln}$ .

The convex tooth flank of one member of a gear pair (primarily the pinion,  $\mathcal{P}$ ) has to be entirely located within the interior of the boundary  $N$ -cone. The concave tooth flank of another member (primarily the gear,  $\mathcal{G}$ ) of the gear pair has to be entirely located outside the interior of the boundary  $N$ -cone.\*

This requirement is of critical importance for intersected-axes conformal/high-conformal gearing.

In a more general case, not a boundary  $N$ -cone, but a boundary  $N$ -surface of revolution should be considered instead.

No rotation is transmitted by an intersected-axes conformal gear pair at the plane-of-action apex  $A_{pa}$ .

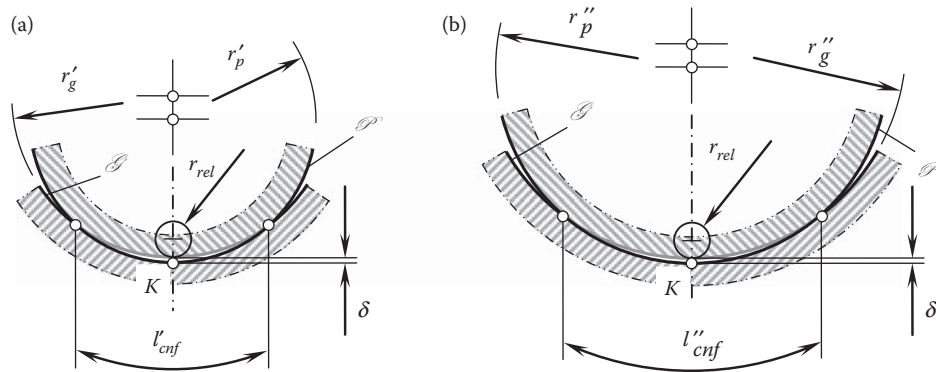
### 12.8.3 Bearing Capacity of High-Conformal Gearing

The influence of an increase in radius,  $r_N$ , of the boundary  $N$ -circle onto a rise of contact strength in high-conformal gearing is schematically illustrated in Figure 12.34, where normal sections of the tooth flanks of a gear and a mating pinion for two high-conformal gear pairs are shown. Both normal sections feature equal radii of relative curvature,  $r_{rel}$ .

In the first case shown in Figure 12.34a, the radius of curvature of the gear tooth profile,  $\mathcal{G}$ , is denoted by  $r'_g$ , while the radius of curvature of the pinion tooth profile,  $\mathcal{P}$ , within that same plane is denoted by  $r'_p$ . The radius

\* The concept of the boundary  $N$ -cone was not known in the time of Novikov. This is a new (circa 2008) concept introduced by Radzevich in intersected-axes conformal/high-conformal gearing.



**FIGURE 12.34**

Impact of the magnitude of the radii of curvature of the gear tooth flank,  $\mathcal{G}$ , and the pinion tooth flank,  $\mathcal{P}$ , on the bearing capacity in gear pairs featuring an equal radius of relative curvature,  $r_{rel}$ .

of relative curvature,  $r_{rel}$ , of the interacting tooth flanks is equal to  $r_{rel} = -r_g' - r_p'$  (as adopted in this monograph, the radii of curvature are signed values: convex profiles feature radii of curvature of positive values, while concave profiles feature radii of curvature of negative values). When a load is applied at a contact point,  $K$ , the tooth flanks,  $\mathcal{G}$  and  $\mathcal{P}$ , approach each other at a certain distance. This distance is designated as  $\delta$ . Under the applied load, the contact point spreads over a certain area of contact. The width of the contact area within the normal plane section in this particular case is designated as  $l_{cnf}'$ .

In the second case, shown in Figure 12.34b, the radius of curvature of the gear tooth profile,  $\mathcal{G}$ , is denoted by  $r_g''$  while the radius of curvature of the pinion tooth profile,  $\mathcal{P}$ , within that same plane is denoted by  $r_p''$ . It should be stressed here that inequalities  $|r_g''| > |r_g'|$  and  $r_p'' > r_p'$  take place in the consideration. The radius of relative curvature,  $r_{rel}$ , of the interacting tooth flanks is equal  $r_{rel} = -r_g'' - r_p''$ . Let us assume that when a load is applied at contact point  $K$ , the tooth flanks  $\mathcal{G}$  and  $\mathcal{P}$  approach each other at the same distance,  $\delta$ , as in the above case (Figure 12.34a). Under the applied load, the contact point spreads over a certain area of contact. The width of the contact area within the normal plane section in this particular case is designated as  $l_{cnf}''$ .

A detailed analysis is unnecessary in order to make it evident that the arc,  $l_{cnf}''$ , is larger compared to the arc,  $l_{cnf}'$ . As the inequality  $l_{cnf}'' > l_{cnf}'$  is valid, it becomes evident that the bearing capacity of a high-conformal intersected-axes gearing depends not only on the relative curvature,  $r_{rel}$ , of the contacting tooth flanks, but also on the magnitudes of the radii of curvature of the tooth flanks,  $\mathcal{G}$  and  $\mathcal{P}$ , at a point of their contact. The larger the magnitudes of the radii,  $r_g$  and  $r_p$ , of normal curvature of the interacting tooth flanks,  $\mathcal{G}$  and  $\mathcal{P}$ , the greater the load capacity of the high-conformal intersected-axes gearing, and vice versa. Ultimately, this makes valid a conclusion:

### Statement 12.1

*High-conformal gearing with larger magnitudes of the radii of normal curvature of the tooth flanks feature a higher load carrying capacity, and vice versa.*

Here is the right point to note that the magnitudes of the radii,  $r_g$  and  $r_p$ , of normal curvature of the interacting tooth flanks,  $\mathcal{G}$  and  $\mathcal{P}$ , strictly correlate to the radius  $r_N$  of the boundary circle in the cross-section of the tooth flanks through the corresponding pitch point. Therefore, high-conformal gearing with the larger radius,  $r_N$ , of the boundary  $N$ -circle features a higher load capacity.

## 12.9 Design Parameters of Conformal/High-Conformal Intersected-Axes Gearing

The rotation vectors of the gear,  $\omega_g$ , and the pinion,  $\omega_p$ , should be given prior to beginning designing a high-conformal intersected-axes gear pair. Once the rotation vectors,  $\omega_g$  and  $\omega_p$ , are known, the vector,  $\omega_{pl}$ , of instant



rotation, as well as the shaft angle,  $\Sigma$ , can be determined. The axes of rotations,  $O_g$ ,  $O_p$ , and  $P_{ln}$ , are the straight lines along the rotation vectors,  $\omega_g$ ,  $\omega_p$ , and  $\omega_{pl}$ , respectively. The known configuration of the axes of rotations,  $O_g$ ,  $O_p$ , and  $P_{ln}$ , makes possible the determination of the tooth ratio,  $u$ , and the pitch cone angles of the gear,  $\Gamma$ , and the pinion,  $\gamma$  [85,137]:

$$\Gamma = -\tan^{-1} \left( \frac{\sin \Sigma}{\omega_p / \omega_g + \cos \Sigma} \right) \quad (12.139)$$

$$\gamma = \tan^{-1} \left( \frac{\sin \Sigma}{\omega_g / \omega_p + \cos \Sigma} \right) \quad (12.140)$$

The design parameters of a high-conformal intersected-axes gear pair can be specified based, to a great extent, on those of parallel-axis gearing. From this perspective, the vector of instant rotation,  $\omega_{pl}$ , and the axis of instant rotation,  $P_{ln}$ , are of critical importance. As the instant motion of the pinion in relation to the mating gear is interpreted as instant rotation about the axis,  $P_{ln}$ , the design parameters of a high-conformal intersected-axes gear pair can be specified within a reference plane through the pitch point,  $P$ . The pitch point,  $P$ , is at a cone distance,  $A$ , from the apex  $A_{pa}$ . The reference plane is perpendicular to the axis of instant rotation,  $P_{ln}$ , as depicted in Figure 12.35.

The calculated values of the pitch cone angles,  $\Gamma$  and  $\gamma$ , along with the given cone distance,  $A$ , make it possible to calculate the pitch diameter of the gear,  $d_g$ , and of the pinion,  $d_p$ :

$$d_g = 2A \cos \Gamma \quad (12.141)$$

$$d_p = 2A \cos \gamma \quad (12.142)$$

The back cone distance of the gear,  $BC_g$ , as well as the back cone distance of the pinion,  $BC_p$ , can be calculated in a way similar to that above:

$$BC_g = 2A \sin \Gamma \quad (12.143)$$

$$BC_p = 2A \sin \gamma \quad (12.144)$$

Once the normal reference plane is constructed, the tooth profile parameters of the gear and the pinion can be specified.

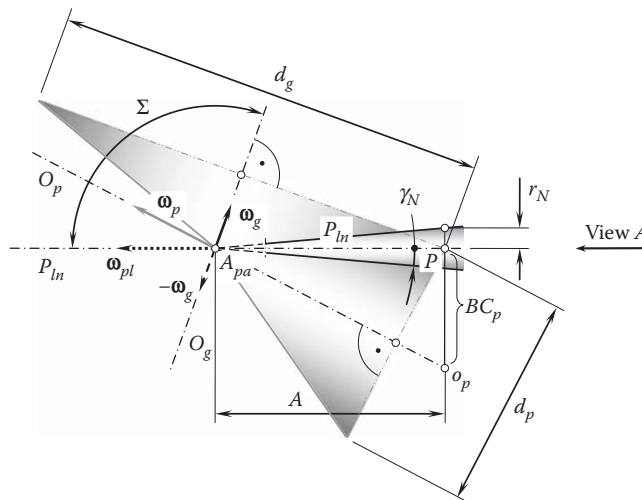


FIGURE 12.35

Configuration of a normal reference plane in relation to the axis of instant rotation,  $P_{ln}$ , and to the pitch cones of a gear and a mating pinion in conformal/high-conformal intersected-axes gearing.

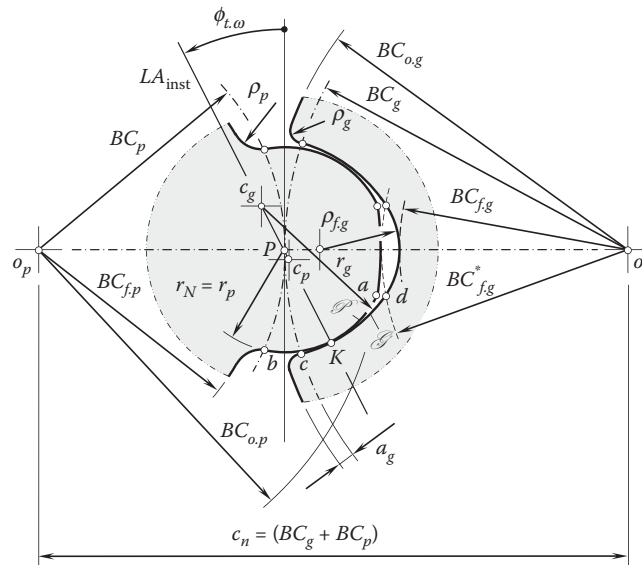


FIGURE 12.36

Geometry of a high-conformal intersected-axes gear pair within the reference plane perpendicular to the pitch line,  $P_{ln}$ .

Referring to Figure 12.36, two points, namely  $o_g$  and  $o_p$ , are in nature the points of intersection of the axes,  $O_g$  and  $O_p$ , by the normal reference plane. The points,  $o_g$  and  $o_p$ , are at a distance  $c_n = (BC_g + BC_p)$  from one another. Two circles of radii,  $BC_g$  and  $BC_p$ , that have the points  $o_g$  and  $o_p$  as the centers are constructed. The circles share a common point, which is the pitch point  $P$ .

An the instant line of action,  $LA_{inst}$ , within the normal reference plane is the line through the pitch point,  $P$ . The line,  $LA_{inst}$ , forms a certain transverse pressure angle,  $\phi_{t,\omega}$ , with the perpendicular to the center distance,  $c_n$ . The point of contact,  $K$ , of the tooth flanks of the gear and pinion is a point within the instant line of action,  $LA_{inst}$ . The further the contact point,  $K$ , is from the pitch point,  $P$ , the more freedom is observed in selecting the radii of curvature of the tooth profiles. At the same time, the further the contact point,  $K$ , from the pitch point,  $P$ , the higher the losses on friction that occur between the tooth flanks and the higher wear of the tooth flanks of the gear and the pinion. Ultimately, the actual location of the contact point,  $K$ , is a kind of trade-off between the two aforementioned factors.

Let us assume that the pinion is stationary and that the gear performs an instant rotation in relation to the pinion. The axis,  $P_{ln}$ , of the instant rotation,  $\omega_{pl}$ , is the straight line through the pitch point,  $P$ . The axis of instant rotation,  $P_{ln}$ , is located within the plane through the axes,  $o_g$  and  $o_p$ , and it goes through the apex,  $A_{pa}$ . When the pinion is motionless, the contact point,  $K$ , traces a boundary circle of radius,  $r_N$ , centered at  $P$ .

The pinion tooth profile,  $\mathcal{P}$ , can either align with the circular arc of the boundary circle,  $r_N$ , or it can be relieved in the bodily side of the pinion tooth. As a consequence, the location of the center of curvature,  $c_p$ , of the convex pinion tooth profile,  $\mathcal{P}$ , within the instant line of action,  $LA_{inst}$ , is limited to the straight line segment,  $PK$ . The pitch point is included in the interval  $[P, K)$  as shown in Figure 12.36, while the contact point,  $K$ , is not.

On the other hand, the location of the center of curvature,  $c_g$ , of the concave gear tooth profile,  $\mathcal{G}$ , within the instant line of action,  $LA_{inst}$ , is limited to the open interval  $P \rightarrow \infty$ . Theoretically, the pitch point,  $P$ , can be included in that interval for  $K$ . However, this is completely impractical, and the center of curvature,  $c_g$ , is actually located beyond the pitch point,  $P$ . Therefore, the radius of curvature,  $r_p$ , of the convex the pinion tooth profile,  $\mathcal{P}$ , is smaller than that,  $r_g$ , of the concave the gear tooth profile,  $\mathcal{G}$  (the inequality  $r_p < r_g$  is observed).

Both the pinion and gear teeth are helical and of opposite hands. Spur high-conformal gearing is not feasible in nature. Because both the gear and the pinion are helical with the helices of the opposite hand, the point of contact will travel along the path of contact,  $P_c$ . It is therefore fundamental to the operating of the gears that contact occur nominally at a point and that the point of contact travel across the full face width of the gears during the rotation. It is clearly a condition of operation that in a given profile, the tooth surfaces should not interfere before or after culmination when rotated at angular speeds that are in the gear ratio.

The transverse contact ratio,  $m_p$ , in a high-conformal gear pair is zero ( $m_p \equiv 0$ ). The face contact ratio,  $m_F$ , of the gear pair is always greater than one ( $m_F > 1$ ). The total contact ratio,  $m_t$ , is equal to the face contact ratio,  $m_F$ ; that is, the identity  $m_t \equiv m_F$  is valid in intersected-axes high-conformal gearing.

When a rotation is transmitted from the driving shaft to the driven shaft, the contact point,  $K$ , travels along the path of contact,  $P_c$  (and it does not travel within the transverse section of the gear pair), that is, within the normal reference plane. This is because  $m_p \equiv 0$  and  $m_F > 1$ , as previously mentioned.

For the calculation of the design parameters of a high-conformal gear pair, the center distance,  $c_n$ , and the tooth ratio,  $u = \omega_p/\omega_g$ , of the gear pair should be given.

The back cone distance of the gear,  $BC_g$ , and the pinion,  $BC_p$ , can be expressed in terms of the center distance,  $c_n$ , and the tooth ratio,  $u$ , as:

$$BC_g = c_n \cdot \frac{u}{1+u} \quad (12.145)$$

$$BC_p = c_n \cdot \frac{1}{1+u} \quad (12.146)$$

A distance,  $l$ , at which the path of contact,  $P_c$ , is remote from the pitch point,  $P$ , must be known, as well as the transverse pressure angle,  $\phi_{t.\omega}$ .

The displacement,  $l$ , is the principal design parameter of a high-conformal gear pair. In terms of the displacement,  $l$ , many of the design parameters of the high-conformal gear pair can be expressed ( $l = KP$ ).

For the calculation of radii of curvature,  $r_g$  and  $r_p$ , of the tooth profiles of the gear and the pinion, respectively, the formulas

$$r_g = l \cdot (1 + k_{rg}) \quad (12.147)$$

$$r_p = l \cdot (1 + k_{rp}) \quad (12.148)$$

are used.

The actual value of the factor,  $k_{rp}$ , should satisfy the inequality  $k_{rp} \geq 0$ . However, as the factor,  $k_{rp}$ , is often set equal to zero, the equality  $r_p = l$  is observed. The factor,  $k_{rg}$ , is within the range  $k_{rg} = 0.03 \dots 0.10$ .

The radius of the outer back cone distance of the pinion,  $BC_{o.p}$ , is calculated from the formula

$$BC_{o.p} = BC_p + (1 - k_{po}) \cdot l \quad (12.149)$$

The addendum factor,  $k_{po}$ , of the pinion depends on the pressure angle,  $\phi_{t.\omega}$ , absolute dimensions of the gear pair, accuracy of machining, and conditions of lubrication. Commonly, the pinion addendum factor,  $k_{po}$ , is set in the range

$$k_{po} = 0.1 \div 0.2 \quad (12.150)$$

The root back cone distance of the pinion,  $BC_{f.p}$ , is calculated from the equation

$$BC_{f.p} = BC_p - a_g - \delta \quad (12.151)$$

where:

$a_g$ : is the dedendum of the mating gear [ $a_g = (0.1 \dots 0.2) \cdot l$ ].

$\delta$ : is the radial clearance in the gear pair ( $\delta = l \cdot k_{po}$ ).

It is practical to set the fillet radius,  $\rho_p$ , in the range of  $\rho_p = 0.3 \cdot l$ .

The root back cone distance of the gear,  $BC_{f.g}$ , is equal to:

$$BC_{f.g} = c_n - BC_{o.p} \quad (12.152)$$

The radius of the outer back cone distance of the gear,  $BC_{o.g}$ , is calculated from the expression

$$BC_{o.g} = BC_g + a_g \quad (12.153)$$

The corner of the gear tooth addendum should be rounded with a radius,  $\rho_g$ , which is less than fillet radius,  $\rho_p$ , of the pinion ( $\rho_g < \rho_p$ ).

The following relation among the design parameters of a high-conformal gear pair have been proved practical:  $r_p = l$ ,  $r_g \leq 1.10 \cdot r_p$ ,  $\rho_p = 0.3 \cdot l$ ,  $m_n/l = 0.8$ ,  $t_p/t_g = 1.5$ ,  $\phi_{t.\omega} = 30^\circ$ ,  $\lambda = 60 \dots 80^\circ$  ( $\psi = 10 \dots 30^\circ$ ), and circular pitch of teeth  $p = t_g + t_p + B$ , where backlash  $B = 0.2 \dots 0.4$  mm.

For the design parameters,  $l$ ,  $p$ ,  $t_g$ ,  $t_p$ ,  $m_n$ , and  $B$ , corresponding angular values can be calculated (Table 12.3).

The effective face width of the gear pair can be calculated as follows:

$$F_{pa} = (1.1 \div 1.2) \cdot p \cdot \tan \lambda \quad (12.154)$$

For a preliminary analysis of high-conformal gearing, an empirical expression

$$l = (0.05 \div 0.20) \cdot BC_p \quad (12.155)$$

returns a practical value for the displacement  $l$ .

**TABLE 12.3**

Design Parameters of Conformal/High-Conformal Intersected-Axis Gearing

Design Parameter	Symbol	Equation
Angular displacement	$\varphi_l$	$\varphi_l = \tan^{-1} \left( \frac{l}{A} \right)$
Angular module	$\varphi_{m.n}$	$\varphi_{m.n} = \tan^{-1} \left( \frac{m_n}{A} \right)$
Angular pitch	$p_\varphi$	$p_\varphi = \tan^{-1} \left( \frac{p}{A} \right)$
Angular tooth thickness, gear	$\varphi_{t.g}$	$\varphi_{t.g} = \tan^{-1} \left( \frac{t_g}{A} \right)$
Angular tooth thickness, pinion	$\varphi_{t.p}$	$\varphi_{t.p} = \tan^{-1} \left( \frac{t_p}{A} \right)$
Angular space width, gear	$\varphi_{w.g}$	$\varphi_{w.g} = \tan^{-1} \left( \frac{w_g}{A} \right)$
Angular space width, pinion	$\varphi_{w.p}$	$\varphi_{w.p} = \tan^{-1} \left( \frac{w_p}{A} \right)$
Angular backlash	$\varphi_B$	$\varphi_B = \tan^{-1} \left( \frac{B}{A} \right)$
Angular addendum, gear	$\varphi_{a.g}$	$\varphi_{a.g} = \tan^{-1} \left( \frac{a_g}{A} \right)$
Angular addendum, pinion	$\varphi_{a.p}$	$\varphi_{a.p} = \tan^{-1} \left( \frac{a_p}{A} \right)$
Angular dedendum, gear	$\varphi_{d.g}$	$\varphi_{d.g} = \tan^{-1} \left( \frac{b_g}{A} \right)$
Angular dedendum, pinion	$\varphi_{d.p}$	$\varphi_{d.p} = \tan^{-1} \left( \frac{b_p}{A} \right)$

The designations:  $a_g$ ,  $b_g$  and  $a_p$ ,  $b_p$  relate to the addendum and dedendum of the gear and the pinion, respectively. These design parameters are measured within the normal reference plane of the high-conformal intersected-axis gear pair.

The functional face width and axial pitch of a high-conformal gear pair depend on each other.

Consider a case when at a uniform rotation of the gear and the pinion, the contact point,  $K$ , travels along the contact line,  $CL$ , at a certain uniform linear speed. As the transverse contact ratio is zero ( $m_p = 0$ ), and the total contact ratio,  $m_t$ , is equal to the face contact ratio,  $m_F$ , the axial pitch,  $p_{cl.g}$ , of the helix on the gear tooth flank,  $\mathcal{G}$ , can be calculated from the formula:

$$p_{cl.g} = \frac{F_{pa}}{m_t} \cdot \cos \Gamma \quad (12.156)$$

A similar expression:

$$p_{cl.p} = \frac{F_{pa}}{m_t} \cdot \cos \gamma \quad (12.157)$$

is valid with respect to the axial pitch,  $p_{cl.p}$ , of the helix on the pinion tooth flank,  $\mathcal{P}$ .

The quality of high-conformal gearing strongly depends on the following design parameters:  $l$ ,  $\phi_{t,\omega}$  and  $\lambda$ .

The tooth flanks,  $\mathcal{G}$  and  $\mathcal{P}$ , interact with one another only at a culminating point,  $K$ , that travels along the pseudo-path of contact,  $P_{pc}$ .

# 13

## *Interaction of Tooth Flanks in Perfect Intersected-Axes Gearing*

Centerlines of the gear shafts that intersect one another are the fundamental feature of intersected-axes gearing. This fundamental feature is reflected even in the name of gearing of this type: *intersected-axes gearing*. Despite the fundamental difference, intersected-axes gearings feature many similarities with gearings of other types, parallel-axes gearings in particular. From this perspective, the interaction of tooth flanks in perfect intersected-axes gearings is discussed below.

### 13.1 Interaction between Tooth Flanks in Perfect Intersected-Axes Gearing

The pulley-and-belt analogy of intersected-axes gear pairs is a convenient and powerful tool to investigate and analyze the transmission of a uniform rotation by means of  $I_a$ -gearing.

#### 13.1.1 Pulley-and-Belt Analogy of Intersected-Axes Gear Pair

Similar to parallel-axes gearing, a pulley-and-belt equivalent can be constructed for an intersected-axes gear pair. As illustrated in Figure 13.1, the base cone of a driving pinion, the base cone of a driven gear, and the plane of action,  $PA$ , compose the pulley-and-belt equivalent of an intersected-axes gear pair. The plane of action,  $PA$ , is viewed as a zero-thickness film that is capable of transmitting a rotary motion; that is, it is free to wrap on the base cone of the driving member and unwrap from the base cone of the driven member of the intersected-axes gear pair. The zero-thickness film cannot be bent about an axis perpendicular the plane of action,  $PA$ .

The rotations: of the base cone of a driving pinion,  $\omega_p$ , the base cone of a driven gear,  $\omega_g$ , and the plane of action,  $\omega_{pa}$ , are synchronized with one another so that no sliding is observed between the interacting surfaces of the base cones and the plane of action,  $PA$ . In the pulley-and-belt equivalent, the driving base cone of the pinion pulls the driven base cone of the gear. In reality, the driving base cone of the pinion pushes the driven base cone of the gear.

When the base cone of the driving member rotates, it pulls the plane of action, and the latter pulls the driven member of the pulley-and-belt equivalent of the intersected-axes gear pair.

It is convenient to use the pulley-and-belt equivalent of the intersected-axes gear pair for the analysis of the path of contact in intersected-axes gearing.

#### 13.1.2 Path of Contact

When a pair of intersected-axes gears rotates, the line of contact,  $LC$ , travels together with the plane of action,  $PA$ . Every point of the line of contact,  $LC$ , traces a corresponding path of contact,  $P_c$ . As the plane of action,  $PA$ , performs a rotary motion about the plane-of-action apex,  $A_{pa}$ , in a stationary reference system associated with the gear pair housing, every path of contact,  $P_c$ , is shaped in the form of a circular arc segment, each of which is centered at the plane-of-action apex,  $A_{pa}$ . Therefore, in intersected-axes gearing, each path of contact,  $P_c$ , is a planar curve (a circular arc segment) that is entirely located within the plane of action,  $PA$ . An instant line of action,  $LA_{inst}$ , is a straight line tangent to the path of contact,  $P_c$ , at every point of it.

In a reference system associated with the gear, the contact point traces a spherical involute on the gear tooth flank,  $\mathcal{G}$ , as illustrated in Figure 13.2. Similarly, in a reference system associated with the pinion, the contact point traces a spherical involute on the pinion tooth flank,  $\mathcal{P}$ . These facts were clearly realized at the end of the 19th century (see Figures 1.20 and 1.21).

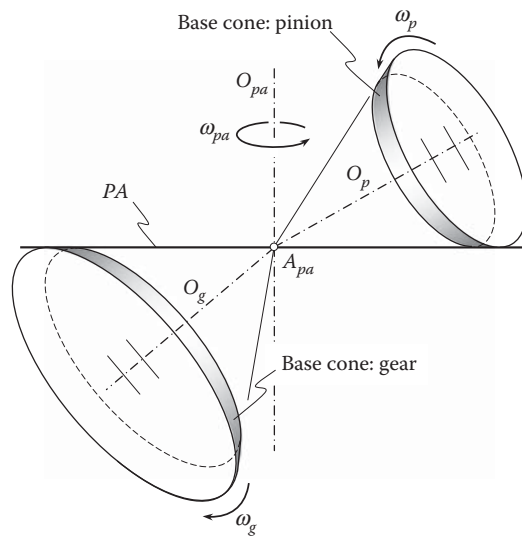


**FIGURE 13.1**  
Pulley-and-belt analogy of intersected-axes gear pair.

A family of paths of contact forms a surface. This surface can be referred to as the *path-of-contact surface*,  $P_{cs}$ . It is evident that in intersected-axes gear pairs with a constant transverse pressure angle ( $\phi_{t,\omega} = \text{const}$ ), the path-of-contact surface,  $P_{cs}$ , is congruent to the plane of action,  $PA$ .

Consider an intersected-axes gear pair that features a transverse pressure angle,  $\phi_{t,\omega}$ , variable within the effective face width,  $F_{pa}$ , of the gear pair (i.e., a case when  $\phi_{t,\omega} = \text{var}$ ). In the case under consideration, the path-of-contact surface,  $P_{cs}$ , is represented by a continuous set of the circular-arc paths of contact,  $P_c$ , that are located in different infinitesimally narrow portions of the plane of action with different transverse pressure angles,  $\phi_{t,\omega}$ , each. The radius of a current circular-arc path of contact,  $P_c$ , can be viewed as a function of the distance of the point on the pitch line,  $P_{ln}$ , from the plane-of-action-apex,  $A_{pa} (\equiv A_g \equiv A_p)$ . The path-of-contact surface,  $P_{cs}$ , is a continuous screw surface generated by the circular arcs of a variable radius.

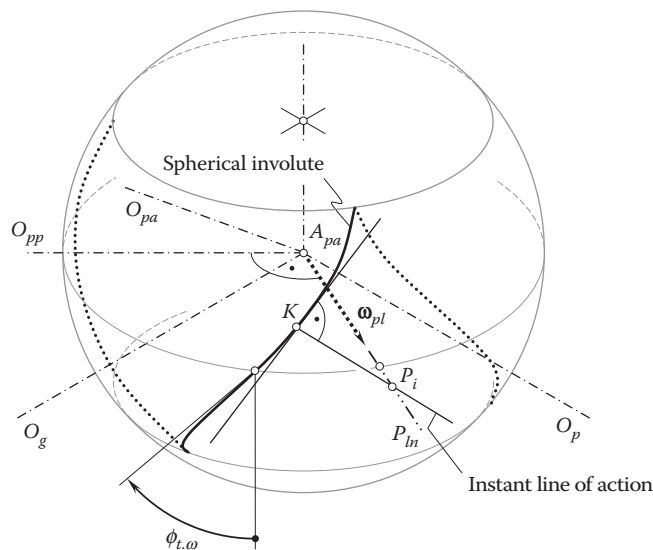


**FIGURE 13.2**  
Trace of contact point in intersected-axes gear pair.



### 13.1.3 Zone (Field) of Action in Intersected-Axes Gearing

It is also convenient to use the pulley-and-belt equivalent of the intersected-axes gear pair for the analysis of the field (zone) of action in intersected-axes gearing.

A bevel gear and a mating pinion interact with one another only within a portion of the plane of action,  $PA$ . This portion of the plane of action is commonly referred to as the *zone (field) of action*,  $ZA$ . In intersected-axes gearing, the field (zone) of action is bounded by the lines of intersection of the plane of action by four boundary lines.

A circular arc of an outer radius,  $r_{o.pa}$ , and a circular arc of a limit radius,  $r_{l.pa}$ , both centered at the plane-of-action apex,  $A_{pa}$ , are the first two boundary lines of the field (zone) of action. The face width,  $F_{pa}$ , of the field (zone) of action,  $ZA$ , is calculated as (Figure 13.3):

$$F_{pa} = r_{o.pa} - r_{l.pa} \quad (13.1)$$

In intersected-axes gearing, the face width,  $F_{pa}$ , of the field (zone) of action,  $ZA$ , equals the width within which the tooth flanks,  $\mathcal{G}$  and  $\mathcal{P}$ , of a gear and mating pinion overlap one another, as illustrated in Figure 13.4.

Two straight lines of intersection,  $kl$  and  $mn$ , of the plane of action,  $PA$ , by the outer cones of the gear, and that of the pinion are the second two boundary lines of the field (zone) of action (Figure 13.3).

Constructed in Figure 13.3, the angle  $\varphi_{pa.z}$  between the straight lines  $kl$  and  $mn$  is referred to as the *angular width of zone of action*. The angular width,  $\varphi_{pa.z}$ , of the zone of action,  $ZA$ , can be expressed in terms of the design parameters of the gear and the mating pinion as:

$$\varphi_{pa.z} = pr_{pa}\Gamma_a + pr_{pa}\gamma_a - \varphi_{pa} \quad (13.2)$$

where:

$\Gamma_a$  is the outer cone angle of the gear.

$\gamma_a$  is the outer cone angle of the pinion.

$\varphi_{pa}$  is the projection onto the plane of action,  $PA$ , of the crossed-axes angle,  $\Sigma$ ; that is,  $\varphi_{pa} = pr_{pa}\Sigma$ .

For reference purposes, the lines of tangency,  $cd$  and  $ab$ , of the base cones of the gear and the mating pinion with the plane of action are shown in Figure 13.3. These straight tangent lines form an angle,  $\varphi_{pa}$ , that is referred to as the *total angular width of plane of action*.

Another approach can be used for the determining of the angular width of the zone of action,  $\varphi_{pa.z}$ .

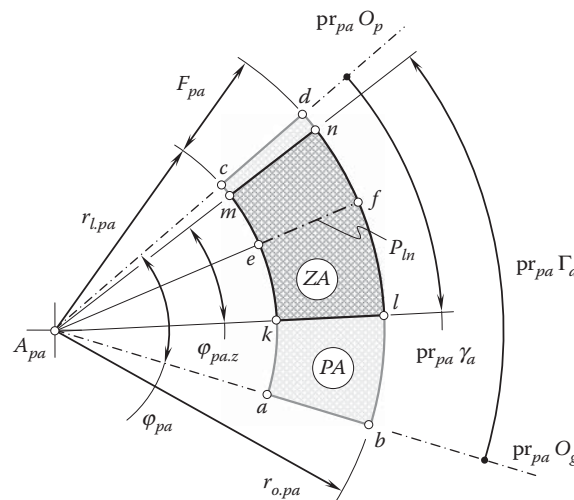
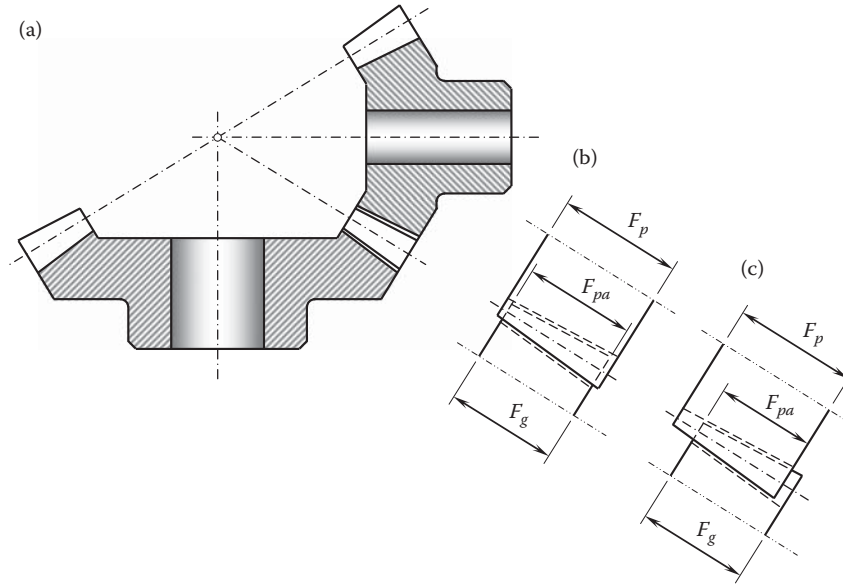


FIGURE 13.3

Zone of action,  $ZA$ , in intersected-axes gearing.

**FIGURE 13.4**

Schematic of an intersected-axes gear pair (a), and effective face width,  $F_{pa}$ , in (b) properly, and (c) improperly aligned gears.

Shown in Figure 13.3, the zone of action,  $ZA$ , features the simplest possible geometry. In reality, the geometry of the zone of action can be more complex. An example of intersected-axes gear pair that features a zone of action,  $ZA$ , of a more complex geometry is illustrated in Figure 13.5.

The geometry of the actual zone of action is a critical consideration when calculating the contact ratio in an intersected-axes gear pair.

### 13.2 Transmission of a Uniform Rotation by Means of Intersected-Axes Gearing

Tooth flanks in a gear for an intersected-axes gear pair can be viewed as a series of cam surfaces that act on similar surfaces of the mating gear to impart a driving motion. In order to transmit a steady input rotation smoothly to the output shaft, three fundamental laws of gearing have to be fulfilled.

The first fundamental law of gearing can be analytically described by the *Shishkov equation of contact*,  $\mathbf{n} \cdot \mathbf{V}_\Sigma = 0$ . Commonly, this condition is met by all perfect intersected-axes gear pairs.

The second fundamental law of gearing requires that interacting tooth flanks of a gear,  $\mathcal{G}$ , and a mating pinion,  $\mathcal{P}$ , be conjugate. With respect to intersected-axes gearing, this condition is discussed in detail, and is analytically described in the previous chapter of the book.

As two (or even more) pairs of teeth make contact at the same time, the fulfillment of an additional condition caused by multiple interacting tooth surfaces in gears is required.

The third fundamental law of gearing that is discussed below in this section is the condition that requires equality of angular base pitches of a gear and a mating pinion to the operating angular base pitch of the gear pair. Here, the discussion is limited to perfect intersected-axes gearing.

A plane of action,  $PA$ , of an intersected-axes gear pair is shown in Figure 13.6a. The plane of action is intersected by a cylinder of revolution of an arbitrary radius,  $r_{y,pa}$ , having the plane-of-action centerline,  $O_{pa}$ , as the axis of rotation. As the angular operating base pitch,  $\varphi_{b,pa}$ , of a gear pair is of a constant value, then the lengths

$$l_{b,pa} = r_{y,pa} \cdot \varphi_{b,pa} \quad (13.3)$$

$$l_{b,g} = r_{y,pa} \cdot \varphi_{b,g} \quad (13.4)$$

$$l_{b,p} = r_{y,pa} \cdot \varphi_{b,p} \quad (13.5)$$

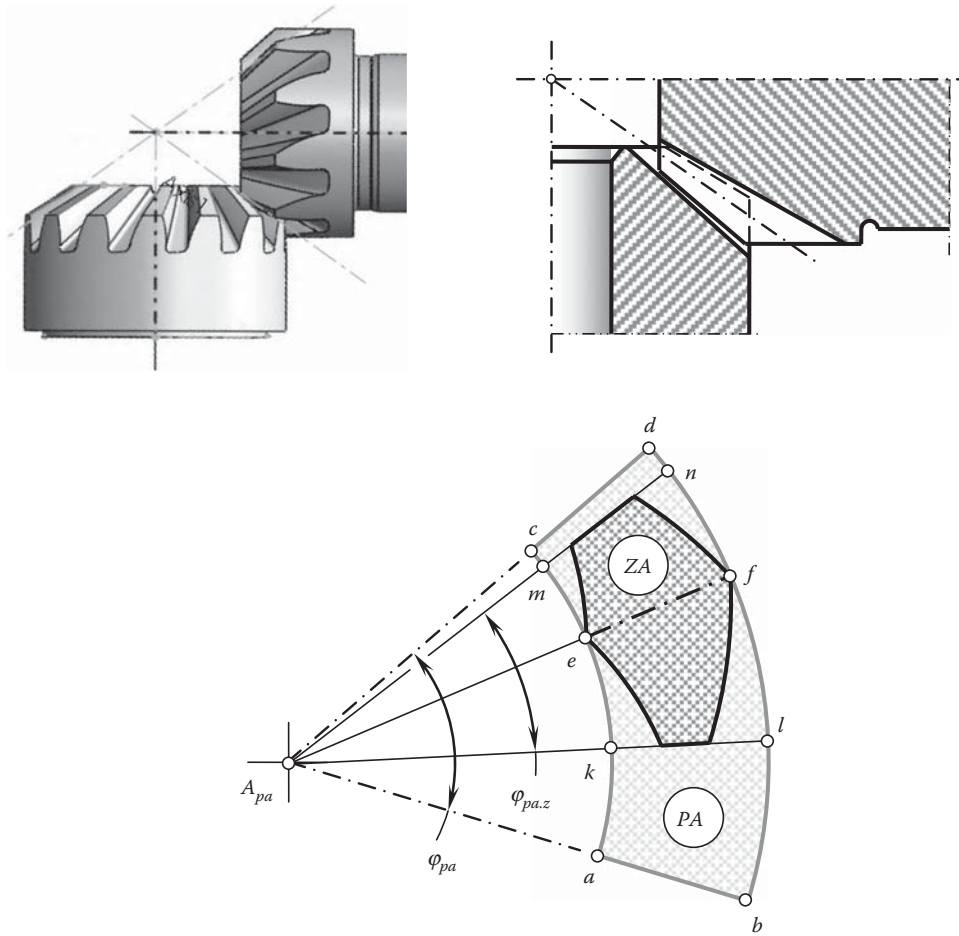


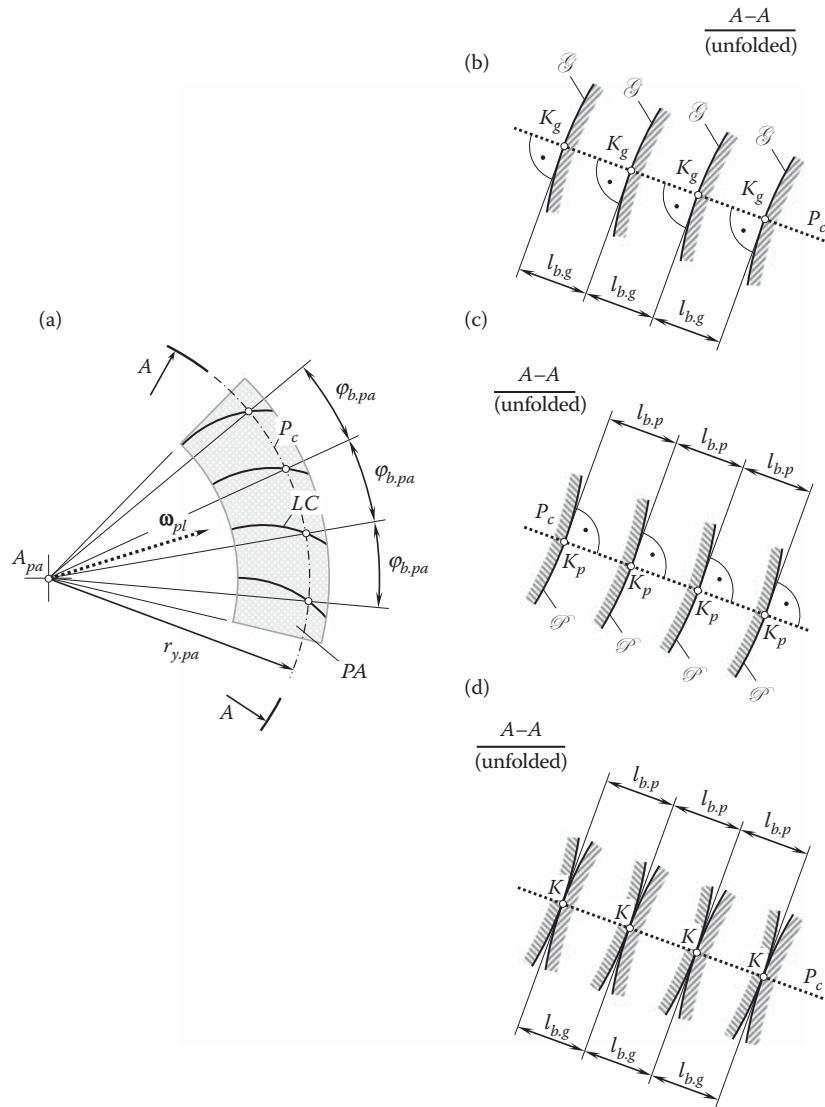
**FIGURE 13.5**  
Intersected-axes gearing that features the zone of action,  $ZA$ , of a complex geometry.

of the circular arcs also are of constant values; that is, in this particular analysis, the angular base pitches  $\varphi_{b.pa}$ ,  $\varphi_{b.g}$ , and  $\varphi_{b.p}$  can be replaced with the lengths  $l_{b.pa}$ ,  $l_{b.g}$ , and  $l_{b.p}$  of the corresponding circular arcs. Once the lengths,  $l_{b.g} = l_{b.pa}$  and  $l_{b.p} = l_{b.pa}$ , are equal, then angular base pitches  $\varphi_{b.g} = \varphi_{b.pa}$  and  $\varphi_{b.p} = \varphi_{b.pa}$  are equal as well.

The unfolded section,  $A - A$ , of the gear tooth flanks,  $\mathcal{G}$ , by the cylinder of revolution is shown in Figure 13.6b, the unfolded section of the pinion tooth flanks,  $\mathcal{P}$ , by the cylinder of revolution is shown in Figure 13.6c, and the unfolded section of the gear intersected-axes gear pair by the cylinder of revolution is shown in Figure 13.6d. Here and below, only local portions of the gear tooth flanks,  $\mathcal{G}$ , are considered. The gear tooth flanks themselves are not defined yet. Therefore, only small portions of the tooth flanks,  $\mathcal{G}$ , are depicted in Figure 13.6b. All these portions of the tooth flanks of a gear are located in the differential vicinity of points of intersection,  $K_g$ , of the tooth flanks,  $\mathcal{G}$ , by the path of contact,  $P_c$ . Each tooth flank,  $\mathcal{G}$ , is perpendicular to the path of contact,  $P_c$ , at points  $K_g$ . All the points,  $K_g$ , are evenly distributed along the path of contact. The distance between each pair of neighboring points,  $K_g$ , is equal to the angular base pitch,  $\varphi_{b.g}$ , of the gear.

A similar analysis can be performed with respect to the pinion tooth flanks,  $\mathcal{P}$ , as shown in Figure 13.6b. All these portions of the tooth flanks of the pinion are located in the differential vicinity of points of intersection,  $K_p$ , of the tooth flanks,  $\mathcal{P}$ , by the path of contact,  $P_c$ . Each the pinion tooth flank,  $\mathcal{P}$ , is perpendicular to the path of contact,  $P_c$ , at points  $K_p$ . All the points,  $K_p$ , are evenly distributed along the path of contact. The distance between each pair of neighboring points,  $K_p$ , is equal to the angular base pitch of the pinion,  $\varphi_{b.p}$ .

When the equality of the angular base pitches of a gear,  $\varphi_{b.g}$ , and a mating pinion,  $\varphi_{b.p}$ , to the operating angular base pitch of the gear pair,  $\varphi_{b.op}$ , is observed; that is, when the identities,  $\varphi_{b.g} \equiv \varphi_{b.op}$  and  $\varphi_{b.p} \equiv \varphi_{b.op}$ , are valid, then the gear and the pinion can be engaged in mesh, as illustrated in Figure 13.6d. Each gear point,  $K_g$ ,

**FIGURE 13.6**

On the concept of equal base pitches in perfect intersected-axes gear pair: (a) plane of action,  $PA$ , and the unfolded section  $A-A$ , (b) of a gear, (c) of a mating pinion, and (d) of the gear pair.

coincides with corresponding pinion point,  $K_p$ . Because of this, the gear and pinion points,  $K_g$  and  $K_p$ , are further designated as contact point  $K$ .

As follows from the analysis of Figure 13.6d, it is not a must to keep all the angular base pitches of a gear,  $\varphi_{b,g}$ , equal to one another or to keep all the angular base pitches of a mating pinion,  $\varphi_{b,p}$ , also equal to one another. It is critical to keep equality of a gear angular base pitch and a mating pinion angular base pitch to the corresponding operating angular base pitch of the gear pair for each pair of teeth engaged in mesh. Physically, this is possible, but limits the gear ratio of a gear pair to integers, that is, to 1, 2, 3, and so forth. Such a design of gearing is impractical and is not considered in this book.

When base pitches of a gear and a mating pinion are not equal to one another ( $\varphi_{b,g} \neq \varphi_{b,p}$ ); for example, the gear base pitch,  $\varphi_{b,g}$ , is smaller compared to the mating pinion base pitch,  $\varphi_{b,p}$ , and the inequality  $\varphi_{b,g} < \varphi_{b,p}$  is valid, as shown in Figure 13.7a, only one pair of teeth is engaged in mesh. A gap between the remaining pairs of teeth of the gear,  $\mathcal{G}$ , and the pinion,  $\mathcal{P}$ , is observed. No gaps of this sort are permissible in perfect intersected-axes gearings.

In another example illustrated in Figure 13.7, the gear angular base pitch,  $\varphi_{b,g}$ , is greater compared to the mating pinion angular base pitch,  $\varphi_{b,p}$ , and the inequality  $\varphi_{b,g} > \varphi_{b,p}$  is valid, as shown in Figure 13.7b, again, only

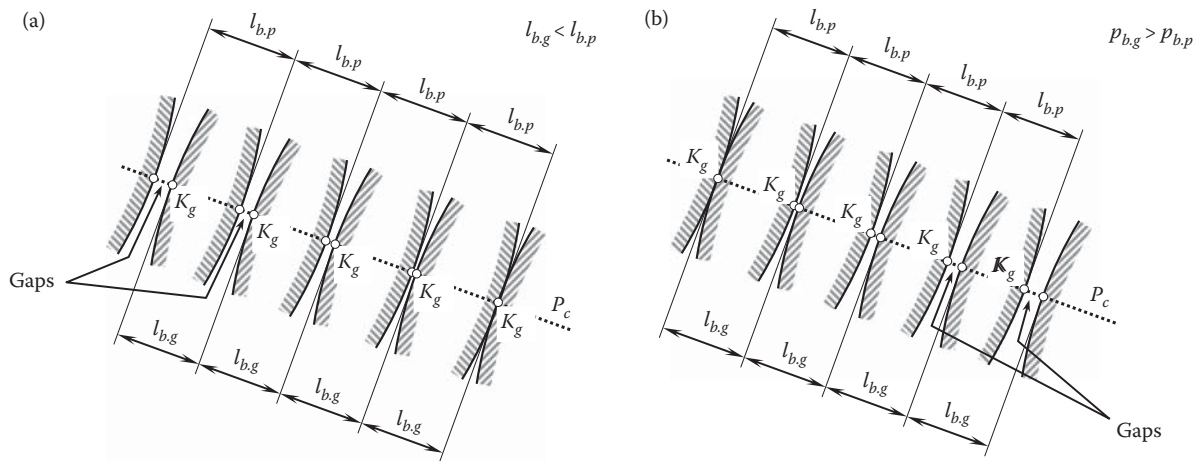


FIGURE 13.7

Examples of violation of the condition of equal angular base pitches in intersected-axes gearing: (a) case when the angular base pitch of a gear,  $\varphi_{b,g}$ , is smaller compared to the angular base pitch,  $\varphi_{b,p}$ , of a mating pinion ( $\varphi_{b,g} < \varphi_{b,p}$ ), and (b) a case when the angular base pitch of a gear,  $\varphi_{b,g}$ , is larger compared to the angular base pitch,  $\varphi_{b,p}$ , of a mating pinion ( $\varphi_{b,g} > \varphi_{b,p}$ ); in both cases, gaps are observed.

one pair of teeth is engaged in mesh. A gap between the remaining pairs of teeth of the gear,  $\mathcal{G}$ , and the pinion,  $\mathcal{P}$ , is observed. No gaps of this sort are permissible in perfect intersected-axes gearing.

In this second example (Figure 13.7b), the distribution of the gaps is inverse to that shown in Figure 13.7a. This is because the gear and the mating pinion are rigid bodies that physically cannot interfere with one another.

Therefore, a uniform rotation can be smoothly transmitted by an intersected-axes gear pair if the following equalities are valid at every instant of time:

$$\varphi_{b,g} \equiv \varphi_{b,op} \quad (13.6)$$

$$\varphi_{b,p} \equiv \varphi_{b,op} \quad (13.7)$$

With that said, the third condition to be fulfilled in a perfect intersected-axes gear pair can be formulated in the following manner:

**The third fundamental law of gearing (in intersected-axes gearing):** *In intersected-axes gearing, in order to transmit a uniform rotary motion from a driving shaft to a driven shaft by means of gear teeth, the angular base pitch of a gear and that of a mating pinion have to be equal to the operating base pitch of the gear pair at every instant of time.*

If a discussion is limited just to intersected-axes gearing, the concept of the *angular base pitch* is applicable only to gear tooth flanks, those generated as loci of corresponding spherical involutes. No angular base pitch can be specified for gears with other tooth flank geometries, such as spiral bevel gears and so forth. Therefore, when angular base pitches in a gear and a mating pinion are equal to the operating angular base pitch of the gear pair (i.e., when the identities  $\varphi_{b,g} \equiv \varphi_{b,op}$  and  $\varphi_{b,p} \equiv \varphi_{b,op}$  are valid), the condition of conjugacy of the tooth flanks,  $\mathcal{G}$  and  $\mathcal{P}$ , is always fulfilled.

The equality of angular base pitches of a gear and a mating pinion to the operating angular base pitch in an intersected-axes gear pair is the third fundamental law of gearing all perfect intersected-axes gearings have to fulfill.

### 13.3 Contact Ratio in Intersected-Axes Gearing

The contact ratio, in general, is the number of angular pitches through which a tooth surface rotates from the beginning to the end of contact.

In practice, the contact ratio, that is, the total contact ratio, is viewed as the summa of the transverse contact ratio (or profile contact ratio),  $m_p$ , and face contact ratio,  $m_F$ . However, such a separation is not a must, as the total contact ratio can be calculated independently of separate calculation of the components  $m_p$  and  $m_F$ .

### 13.3.1 Transverse Contact Ratio

The transverse contact ratio,  $m_p$ , in an intersected-axes gear pair is the contact ratio that is determined within a transverse section of meshing gears. (Recall that a sphere i.e., centering at the plane-of-action apex,  $A_{pa}$ , is a transverse section in intersected-axes gear pair.) The transverse contact ratio is also commonly referred to as the *profile contact ratio*.

The transverse contact ratio,  $m_p$ , in an intersected-axes gear pair can be defined as the ratio of the angle of contact,  $\varphi_{pa.z}$ , to the operating base pitch angle,  $\varphi_{b.op}$ :

$$m_p = \frac{\varphi_{pa.z}}{\varphi_{b.op}} \quad (13.8)$$

The duration of contact of a gear tooth flank,  $\mathcal{G}$ , and a mating pinion tooth flank,  $\mathcal{P}$ , in a particular transverse section of a gear by a sphere is specified by the angle of contact,  $\varphi_{pa.z}$ , in an intersected-axes gear pair. The angle of contact,  $\varphi_{pa.z}$ , is measured within the plane of action,  $PA$ . (The angle,  $\varphi_{pa.z}$ , is an equivalent of the length of contact,  $Z_{pa}$ , in parallel-axes gearing.)

The tooth flank of a gear,  $\mathcal{G}$ , and the tooth flank of a mating pinion,  $\mathcal{P}$ , are engaged in mesh within the angle of contact,  $\varphi_{pa.z}$ . The operating base pitch angle,  $\varphi_{b.op}$  (or the base pitch angle of the gear,  $\varphi_{b.g}$ , or of the pinion,  $\varphi_{b.p}$ ), is specified by Equation 12.110.

Referring to Figure 13.8, the angular width of the zone of action,  $\varphi_{pa.z}$ , can be specified as follows:

$$\varphi_{pa.z} = (\varphi_{pa.g} - \varphi_{pa.p}) - \varphi_{pa} \quad (13.9)$$

The angular width of the zone of action,  $\varphi_{pa.z}$ , depends on two angles. A portion of the angular width of the zone of action,  $\varphi_{pa.z}$ , contributed by the gear is denoted by  $\varphi_{pa.g}$ . Correspondingly, a portion of the angular width of the zone of action,  $\varphi_{pa.z}$ , contributed by the pinion is designated as  $\varphi_{pa.p}$ .

Refer to Figure 13.9 for the calculation of the angular width of the zone of action,  $\varphi_{pa.g}$ .

A unit vector,  $\mathbf{a}$ , is constructed to pass through origin of the *Cartesian* reference system,  $X_g Y_g Z_g$ , associated with the gear. The vector,  $\mathbf{a}$ , is along the straight line of tangency of the base cone of the gear and of the plane of action,  $PA$ . In the coordinate system,  $X_g Y_g Z_g$ , the vector,  $\mathbf{a}$ , can be analytically described by an expression:

$$\mathbf{a} = \mathbf{j} \cdot \sin \Gamma_b + \mathbf{k} \cdot \cos \Gamma_b \quad (13.10)$$

where  $\Gamma_b$  is the base cone angle of the gear.

A unit vector,  $\mathbf{b}$ , through the origin of the coordinate system,  $X_g Y_g Z_g$ , is along the straight line of intersection of the outer cone of the gear by the plane of action,  $PA$ . For composing an expression that analytically describes the vector  $\mathbf{b}$ , the following trick can be applied.

Projection of the vector  $\mathbf{b}$  onto the  $Z_g$ -axis is equal to  $\text{Pr}_z \mathbf{b} = \cos \Gamma_o$  (see Figure 13.9). Here, the outer cone angle of the gear is designated as  $\Gamma_o$ . The projection,  $\text{Pr}_z \mathbf{b}$ , immediately makes it possible to calculate the projection  $\text{Pr}_y \mathbf{b}$  of the vector,  $\mathbf{b}$ , onto the  $Y_g$ -axis. This projection is equal to  $\text{Pr}_y \mathbf{b} = \cos \Gamma_o \tan \Gamma_b$ . Having calculated the projections,  $\text{Pr}_y \mathbf{b}$  and  $\text{Pr}_z \mathbf{b}$ , in the particular case under consideration, the projection  $\text{Pr}_x \mathbf{b}$  of the vector  $\mathbf{b}$  onto the  $X_g$ -axis can be calculated from the equation:

$$\text{Pr}_x \mathbf{b} = \sqrt{1 - \cos^2 \Gamma_o - \cos^2 \Gamma_o \tan^2 \Gamma_b} \quad (13.11)$$

The last expression can be represented in the form:

$$\text{Pr}_x \mathbf{b} = \sqrt{\sin^2 \Gamma_o - \cos^2 \Gamma_o \tan^2 \Gamma_b} \quad (13.12)$$



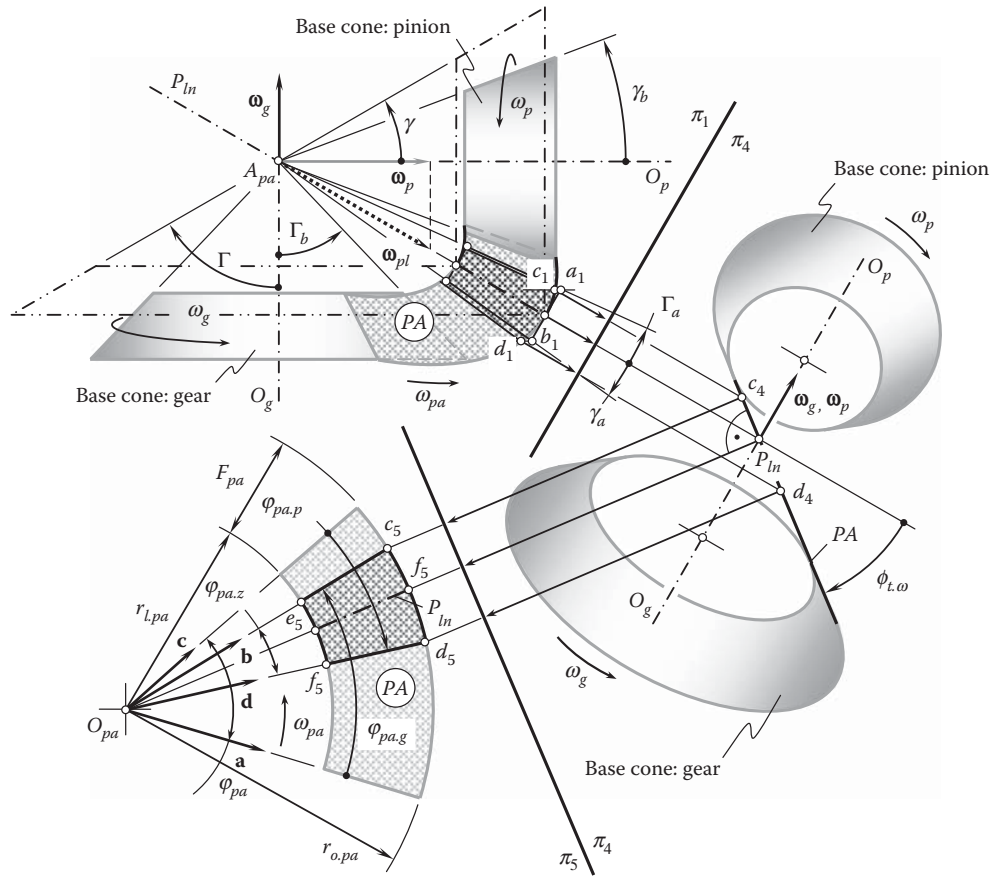


**FIGURE 13.8**  
Active portion,  $\varphi_{pa,z}$ , of the plane of action, PA.

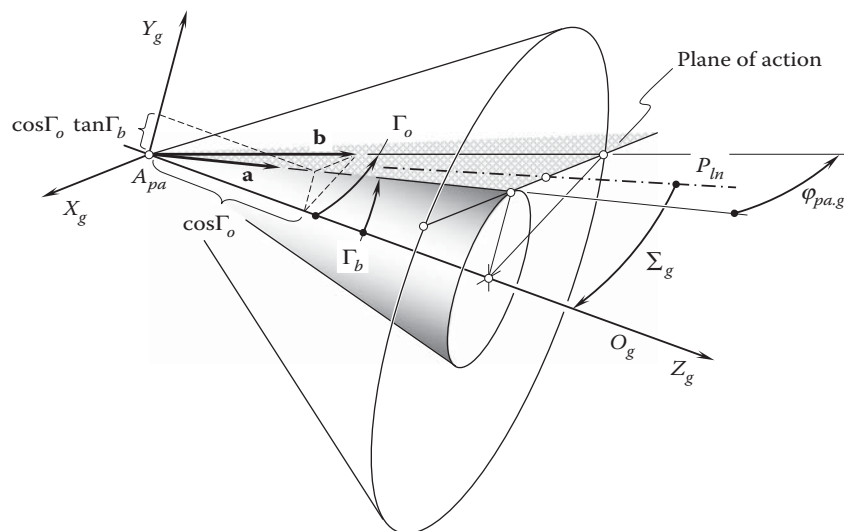


**FIGURE 13.9**  
A schematic for the calculation of the angle,  $\varphi_{pa,g}$ .



Ultimately, the unit vector,  $\mathbf{b}$ , can be analytically expressed as:

$$\mathbf{b} = \mathbf{i} \cdot \sqrt{\sin^2 \Gamma_o - \cos^2 \Gamma_o \tan^2 \Gamma_b} + \mathbf{j} \cdot \cos \Gamma_o \tan \Gamma_b + \mathbf{k} \cdot \cos \Gamma_o \quad (13.13)$$

Having the unit vectors  $\mathbf{a}$  and  $\mathbf{b}$ , an expression:

$$\varphi_{pa.g} = \tan^{-1} \left( \frac{|\mathbf{a} \times \mathbf{b}|}{\mathbf{a} \cdot \mathbf{b}} \right) \quad (13.14)$$

can be used for the calculation of the angle  $\varphi_{pa.g}$ .

After being expanded, Equation 13.14 allows for a formula:

$$\varphi_{pa.g} = \tan^{-1} \left( \sqrt{\sin^2 \Gamma_o + [1 - (\sin \Gamma_b \tan \Gamma_b + \cos \Gamma_b)^2]} \cdot \frac{\cos \Gamma_b}{\cos \Gamma_o} \right) \quad (13.15)$$

for the calculation of the angle  $\varphi_{pa.g}$ .

An equation:

$$\varphi_{pa.p} = \tan^{-1} \left( \sqrt{\sin^2 \gamma_o + [1 - (\sin \gamma_b \tan \gamma_b + \cos \gamma_b)^2]} \cdot \frac{\cos \gamma_b}{\cos \gamma_o} \right) \quad (13.16)$$

that is similar to that above can be derived for the calculation of the angle  $\varphi_{pa.p}$ . Unit vectors  $\mathbf{c}$  and  $\mathbf{d}$  (see Figure 13.8) are used for this purpose.

Here, in Equation 13.16:

$\gamma_o$  is the outer cone angle of the pinion.

$\gamma_b$  is the base cone angle of the pinion.

Equations 12.110, 13.15, and 13.16 are further substituted into Equation 13.9. In this way, the transverse contact ratio for an intersected-axes gearing is calculated:

$$m_p = \frac{\tan^{-1} \left( \sqrt{\sin^2 \Gamma_o + [1 - (\sin \Gamma_b \tan \Gamma_b + \cos \Gamma_b)^2]} \cdot \frac{\cos \Gamma_b}{\cos \Gamma_o} \right)}{\varphi_b} - \frac{\tan^{-1} \left( \sqrt{\sin^2 \gamma_o + [1 - (\sin \gamma_b \tan \gamma_b + \cos \gamma_b)^2]} \cdot \frac{\cos \gamma_b}{\cos \gamma_o} \right) - \varphi_{pa}}{\varphi_b} \quad (13.17)$$

This bulky equation [(13.17)] can be significantly reduced in cases of (a) orthogonal intersected-axes gear pairs, (b) face gear drives, and so forth.

### 13.3.2 Face Contact Ratio

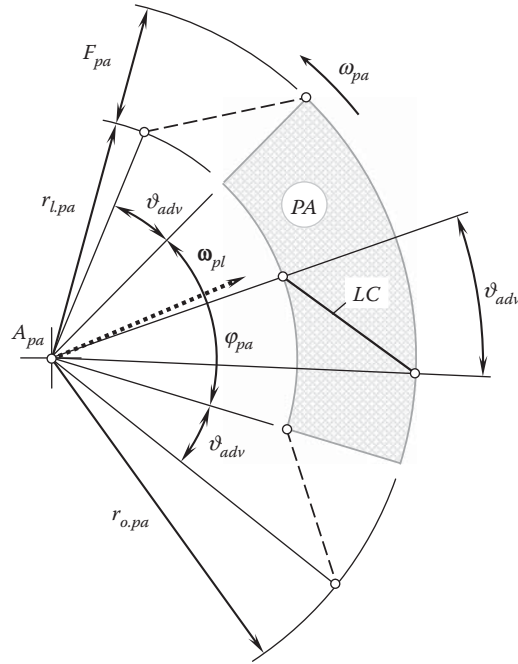
The face contact ratio,  $m_F$ , for an intersected-axes gear pair can be defined as the ratio:

$$m_F = \frac{2 \cdot \vartheta_{adv}}{\varphi_{b.op}} \quad (13.18)$$

of the face advance angle,  $\vartheta_{adv}$  (Figures 12.13 and 12.14), to the operating base pitch angle,  $\varphi_{b.op}$ , of the gear pair.

A more detailed example on construction of the face advance angle,  $\vartheta_{adv}$ , in perfect intersected gearing is illustrated in Figure 13.10.

The actual value of the face advance angle,  $\vartheta_{adv}$ , depends on the geometry of the line of contact,  $LC$ , and its configuration within the plane of action,  $PA$ , in a particular design of intersected-axis gear pair.

**FIGURE 13.10**

On the definition of the advance angle,  $\vartheta_{adv}$ , in perfect intersected-axes gearing.

In a more general case, the outer surfaces of a gear and a mating pinion could be shaped in a form of surfaces of revolution that intersect the plane of action along lines: either along the straight line segments,  $ab$  and  $cd$ , as illustrated in Figure 13.11, or along planar curves. Such a modification to the outer surfaces of a gear and a mating pinion in an intersected-axes gear pair results in an additional gear face advanced angle,  $\vartheta_{adv,g}$ , and pinion advanced angle,  $\vartheta_{adv,p}$ . The face advanced angles,  $\vartheta_{adv,g}$  and  $\vartheta_{adv,p}$ , are signed values, and they have to be taken into account when calculating the face contact ratio,  $m_F$ , in intersected-axes gearing.

### 13.3.3 Total Contact Ratio

The total contact ratio,  $m_t$ , is the sum of the transverse contact ratio,  $m_p$ , and the face contact ratio,  $m_F$ :

$$m_t = m_p + m_F \quad (13.19)$$

In cases of intersected-axes gearing, Equation 13.19 can be represented in a form:

$$m_t = \frac{\varphi_{pa,z} + 2 \cdot \vartheta_{adv}}{\varphi_{b.op}} \quad (13.20)$$

or in a form:

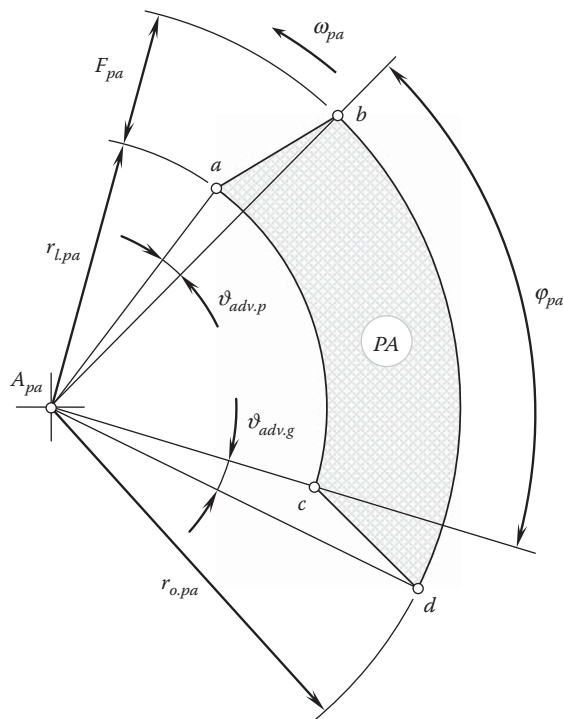
$$m_t = \frac{\varphi_{pa,z} + 2 \cdot \vartheta_{adv} + \vartheta_{adv,g} + \vartheta_{adv,p}}{\varphi_{b.op}} \quad (13.21)$$

In a more general case of intersected-axes gearing.

Equation 13.20 is equivalent to the formula for the calculation of the total contact ratio,  $m_t$ , in parallel-axes gearing. This equation is valid for intersected-axes gearings of all types.

The total contact ratio in intersected-axes gearing is never less than one ( $m_t \geq 1$ ). For spur gearing that has a zero face advance angle,  $\vartheta_{adv}$ , the total contact ratio is  $m_t = m_p \geq 1$ , as the equality  $m_F = 0$  is valid in this particular case. Conversely, for high-conformal gearing, the equality  $m_p = 0$  is valid. Therefore, the total contact ratio for a high-conformal gear pair can be calculated from the expression  $m_t = m_F \geq 1$ .

The above consideration is valid with respect to internal gears used in the design of an intersected-axes gear pair. Because internal intersected-axes gearings are not extensively used in the industry, dies for net forging of

**FIGURE 13.11**

On the definition of the gear advance angle,  $\theta_{adv,g}$ , and the pinion advance angle,  $\theta_{adv,p}$ , in perfect intersected-axes gearing;  $ab$  and  $cd$  are the lines of intersection of the plane of action,  $PA$ , by the outer surfaces of the gear and the pinion, correspondingly.

external bevel gears, electrodes for EDM, and so forth can be calculated by means of the results discussed in this section.

### 13.4 Contact Motion Characteristics in Intersected-Axes Gearing

Originally, there were only two motions in an intersected-axes\* gearing. They are a rotation of the input shaft and a corresponding rotation of the output shaft. These two rotational motions,  $\omega_g$  and  $\omega_p$ , of the gear and the pinion, correspondingly, cause numerous other motions, both rotational and translational, that are observed when the gears rotate. Some of these motions result in sliding of the tooth flanks,  $\mathcal{G}$  and  $\mathcal{P}$ , of the gear and the mating pinion when the gears rotate.

Rolling and sliding take place simultaneously between the tooth flanks of two mating gears when transmitting motion by intersected-axis gearing. Rolling and sliding occur at any point of contact within the active portion of the line of contact. Points within the axis of instant rotation,  $P_{ln}$ , are the exception: pure rolling and no sliding occur in points within the axis of instant rotation,  $P_{ln}$ . Investigation and analysis of sliding and rolling conditions in a gear pair is of importance from an engineering perspective. It enables, for example, determining and reducing friction losses between mating gears.

On the one hand, a sliding motion between the tooth flanks,  $\mathcal{G}$  and  $\mathcal{P}$ , can entail extensive surface wear of the gear teeth. Thus, sliding motion has to be reduced (or even eliminated) in order to improve performance of the gear pair. On the other hand, sliding motion can significantly affect conditions of lubrication in a gear pair. Therefore, in order to improve performance of the gear pair, sliding motion has to be optimized. The latter means that the gears have to be designed so as to provide the most favorable conditions of lubrication of the tooth flanks,  $\mathcal{G}$  and  $\mathcal{P}$ . With that said, the necessity of understanding of conditions of sliding between the tooth flanks,  $\mathcal{G}$  and  $\mathcal{P}$ , becomes clear.

\* The discussion in Section 13.4, *Contact Motion Characteristics*, is valid for both, that is, for intersected-axes gearings with line contact between gear and mating pinion tooth flanks,  $\mathcal{G}$  and  $\mathcal{P}$ , as well as for conformal (Novikov) and high-conformal intersected-axes gearings.

### 13.4.1 Sliding in Perfect Intersected-Axes Gearing

A portion of the relative motion of a gear and a mating pinion cause pure rolling of the pitch cones of the interaction gears, while another portion of the relative motion results in sliding of the tooth flanks of the gear,  $\mathcal{G}$ , and the mating pinion,  $\mathcal{P}$ . For better understanding of the nature of sliding in perfect intersected-axes gearing, use of descriptive geometry-based analysis is recommended.

#### 13.4.1.1 Descriptive Geometry-Based Solution to the Problem of Determining Sliding in Perfect Intersected-Axes Gearing

In order to determine the sliding conditions in intersected-axes gearing, the descriptive geometry-based approach can be used. This approach is illustrated in [Figure 2.8](#). After a zero center distance,  $C$ , is entered, the approach is valid for intersected-axes gearing. Then, the linear velocity vectors of sliding,  $\mathbf{V}_g^{sl}$  and  $\mathbf{V}_p^{sl}$ , of the gear and the mating pinion teeth, correspondingly, can be determined on the premise of the rotation vectors of sliding,  $\boldsymbol{\omega}_g^{sl}$  and  $\boldsymbol{\omega}_p^{sl}$ . Another approach for the determining of the sliding velocity vectors in an intersected-axes gear pair is discussed immediately below.

For the analysis of contact motion characteristics in intersected-axes gear pair, a base cone of a gear, and a base cone of a mating pinion, along with the plane of action,  $PA$ , are depicted in [Figure 13.11](#). An arbitrary point,  $m$ , within the line of contact,  $LC$ , rotates,  $\omega_g$ , together with the gear. The linear velocity vector,  $\mathbf{V}_g$ , is of a length:

$$V_g = |\mathbf{V}_g| = \omega_g \cdot r_{y,g} \quad (13.22)$$

where  $r_{y,g}$  is the distance of point  $m$  from the gear axis of rotation,  $O_g$ .

That same point,  $m$ , within the line of contact,  $LC$ , rotates,  $\omega_p$ , together with the pinion. The linear velocity vector,  $\mathbf{V}_p$ , is of a length:

$$V_p = |\mathbf{V}_p| = \omega_p \cdot r_{y,p} \quad (13.23)$$

where  $r_{y,p}$  is the distance of point  $m$  from the pinion axis of rotation,  $O_p$ .

The actual configurations of the linear velocity vectors,  $\mathbf{V}_g$  and  $\mathbf{V}_p$ , depend on the angular configuration of the gear and the pinion.

The difference  $\mathbf{V}_g - \mathbf{V}_p$  is referred to as the linear velocity vector,  $\mathbf{V}_{rel}$ , of the instant motion of the pinion relative the gear, that is:

$$\mathbf{V}_{rel} = \mathbf{V}_g - \mathbf{V}_p \quad (13.24)$$

Rolling and sliding of the tooth flanks,  $\mathcal{G}$  and  $\mathcal{P}$ , of the gear and the mating pinion are caused by the linear velocity vector,  $\mathbf{V}_{rel}$ .

The sliding velocity vector can be determined graphically by implementing the methods developed in descriptive geometry for this purpose. An example of such a construction is illustrated in [Figure 13.12](#).

For the construction of a sliding velocity vector, a reference system,  $\pi_1\pi_2\pi_3$ , of two orthogonal planes of projection,  $\pi_1$ ,  $\pi_2$ , and  $\pi_3$ , is implemented ([Figure 13.11](#)). Following a convention adopted in descriptive geometry, the subscript "1" is assigned to projections onto plane  $\pi_1$  of all points, lines, and so forth. Similarly, the subscript "2" is assigned to projections onto plane  $\pi_2$  of all the same points, lines, and so forth.

The location and orientation of a pair of rotation vectors,  $\boldsymbol{\omega}_g$  and  $\boldsymbol{\omega}_p$ , within the reference system  $\pi_1\pi_2$  can be arbitrary. However, for convenience, the rotation vectors,  $\boldsymbol{\omega}_g$  and  $\boldsymbol{\omega}_p$ , are depicted in the reference system,  $\pi_1\pi_2$ , parallel to the horizontal plane of projection  $\pi_1$ . In this scenario, the crossed-axes angle,  $\Sigma$ , is projected onto plane  $\pi_1$  with no distortion. The plane-of-action apex point is denoted as  $A_{pa}$ .

The instant rotation vector,  $\boldsymbol{\omega}_{pl}$ , that is, the vector of rotation of the pinion about axis of instant rotation,  $P_{lr}$ , is constructed on the premise of the principle of inversion of rotations.

Immediately upon the rotation vector  $\boldsymbol{\omega}_{pl}$  being determined, the axis of projections  $\pi_1/\pi_2$  can be constructed so that it is parallel to the vector of instant rotation,  $\boldsymbol{\omega}_{pl}$ . Such a configuration of the axis  $\pi_1/\pi_2$  is not mandatory; the configuration can be arbitrary. Convenience is the only reason for selecting this particular orientation for the axis of projections  $\pi_1/\pi_2$  in relation to the rotation vector,  $\boldsymbol{\omega}_{pl}$ .

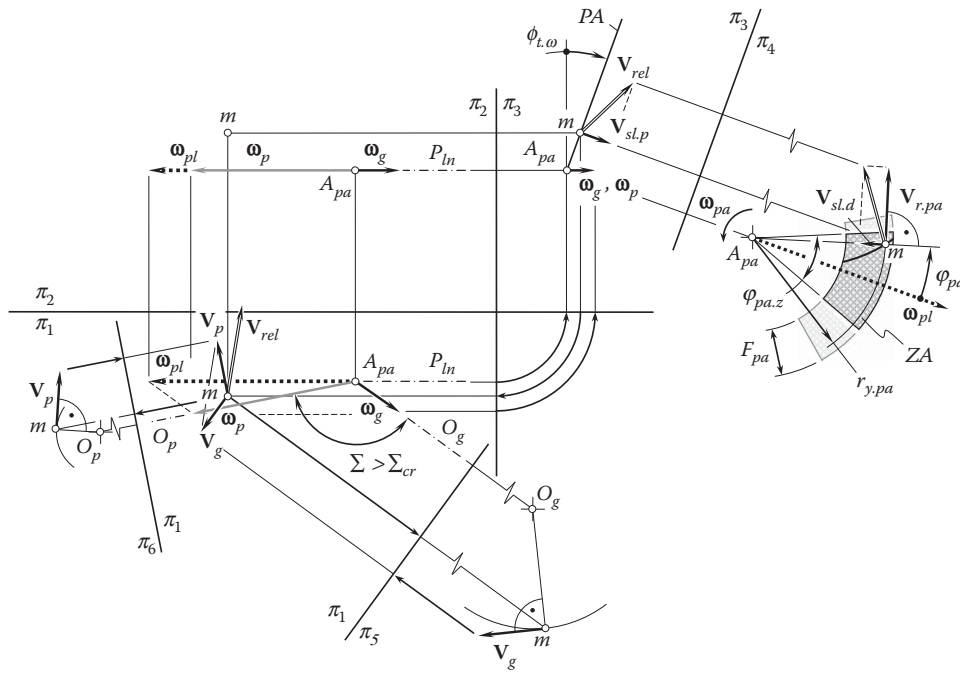


**FIGURE 13.12**  
Sliding in intersected-axes gearing.

Within the plane of projections,  $\pi_3$ , the plane of action,  $PA$ , is a projective plane. In this plane of projections, the plane of action is described as a straight line,  $PA$ , through the plane-of-action apex,  $A_{pa}$ . The trace,  $PA$ , forms the transverse pressure angle,  $\phi_{t,\omega}$ , with the vertical connecting lines.

An additional plane of projections,  $\pi_4$ , is constructed so as to have the axis,  $\pi_3/\pi_4$ , parallel to the trace  $PA$  in the plane of projections,  $\pi_3$ . Due to that, the zone of action,  $ZA$ , is projected onto plane  $\pi_4$  with no distortions.

An arbitrary point,  $m$ , is within the line of contact,  $LC$ . This point is at a distance,  $r_{y,pa}$ , from the plane-of-action apex,  $A_{pa}$ . The linear velocity vectors of sliding are constructed for point  $m$ . Actually, the construction performed for point  $m$  can be performed for any and all points within the zone of action,  $ZA$ .

The projections of point  $m$  onto the rest of the planes of projections, that is, onto the planes of projections  $\pi_1$ ,  $\pi_2$ ,  $\pi_3$ , and others are constructed in compliance with standard procedures established in descriptive geometry.

The linear velocity vector,  $V_g$ , of point  $m$  that is rotated together with the gear is constructed in the auxiliary plane of projections,  $\pi_5$  (Figure 13.13). The axis of projections,  $\pi_1/\pi_5$ , is perpendicular to the angular velocity vector,  $\omega_g$ , of the gear. The linear velocity vector,  $V_g$ , is projected onto the plane of projections,  $\pi_5$ , with no distortions.

The linear velocity vector,  $V_p$ , of point  $m$  that is rotated together with the pinion is constructed in the auxiliary plane of projections,  $\pi_6$  (Figure 13.13). The axis of projections,  $\pi_1/\pi_6$ , is perpendicular to the angular velocity vector,  $\omega_p$ , of the pinion. The linear velocity vector,  $V_p$ , is projected onto the plane of projections,  $\pi_6$ , with no distortions.

The linear velocity vector,  $V_{rel}$ , of the relative motion of the tooth flanks,  $\mathcal{G}$  and  $\mathcal{P}$ , at point  $m$  is constructed in the plane of projections,  $\pi_1$  (Figure 13.13). For this purpose, projections of the linear velocity vectors  $V_g$  and  $V_p$  in the plane of projections,  $\pi_1$ , are constructed. Then, projections of the linear velocity vector,  $V_{rel}$ , of the relative motion onto the remaining planes of projections, that is, onto planes of projections  $\pi_2$ ,  $\pi_3$ , and  $\pi_4$ , are constructed in compliance with standard procedures established in descriptive geometry.\*

Once the linear velocity vector,  $V_{rel}$ , of the relative motion of the tooth flanks,  $\mathcal{G}$  and  $\mathcal{P}$ , at point  $m$  is constructed (Figure 13.13), then this vector is projected onto three perpendicular directions through point  $m$ .

The first direction is within the plane of action,  $PA$ , and is perpendicular to the straight line segment,  $mA_{pa}$ . The projection of the linear velocity vector,  $V_{rel}$ , onto this direction is labeled  $V_{r,pa}$ , as this component of the linear velocity vector,  $V_{rel}$ , causes pure rotation of the plane of action,  $PA$ , about its axis of rotation,  $O_{pa}$ , and pure

\* Note that not all the construction lines are shown in Figure 13.13.

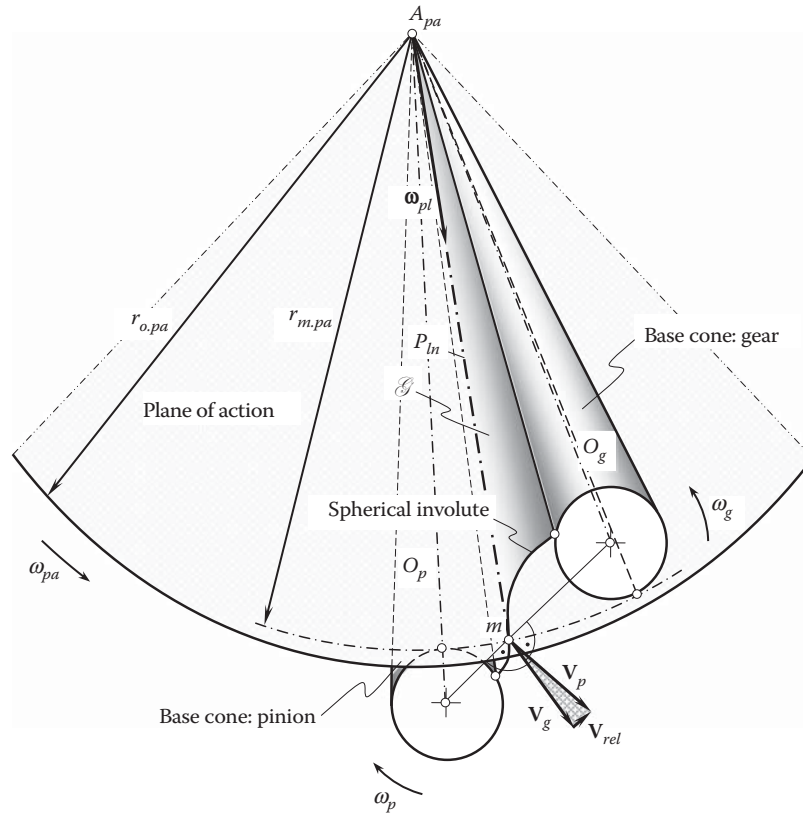


**FIGURE 13.13**  
Contact motion characteristics in intersected-axes gear pairs.

rotation of the gears as well. The magnitude of the linear velocity vector,  $\mathbf{V}_{r.pa}$ , depends on the rotation,  $\omega_{pa}$ , of the plane of action,  $PA$ , and the distance,  $r_{y.pa}$ , of the point of interest,  $m$ , from the plane-of-action apex,  $A_{pa}$ :

$$V_{r.pa} = \omega_{pa} r_{y.pa} \quad (13.25)$$

The second direction is perpendicular to the plane of action,  $PA$ . The projection of the linear velocity vector,  $\mathbf{V}_{rel}$ , onto this direction is labeled  $\mathbf{V}_{sl.pr}$  as this component of the linear velocity vector,  $\mathbf{V}_{rel}$ , causes pure profile sliding of the gear tooth flanks,  $\mathcal{G}$  and  $\mathcal{P}$ .

The third direction is within the plane of action,  $PA$ , and is along the straight line segment,  $mA_{pa}$ . The projection of the linear velocity vector,  $\mathbf{V}_{rel}$ , onto this direction is labeled  $\mathbf{V}_{sl.d}$ , as this component of the linear velocity vector,  $\mathbf{V}_{rel}$ , causes *drag* sliding action. In the case of straight bevel gears, the component,  $\mathbf{V}_{sl.d}$ , causes sliding,  $\mathbf{V}_{sl.l}$ , in the lengthwise direction of the gear teeth. In more general cases of intersected-axes gears, for instance, in cases of skew bevel gears, spiral bevel gears, and so forth, the sliding in the lengthwise direction at the current point,  $m$ , of the gear teeth is tangent to the line of contact of the gear/pinion tooth flanks and is of magnitude (Figure 13.12):

$$V_{sl.l} = \frac{V_{sl.d}}{\cos \varphi_m} \quad (13.26)$$

Here is designated:

$V_{sl.l}$  is the magnitude of the linear velocity vector,  $\mathbf{V}_{sl.l}$ , of sliding in the lengthwise direction of the gear teeth.

$V_{sl.d}$  is the magnitude of the linear velocity vector,  $\mathbf{V}_{sl.d}$ , of drag sliding.

$\varphi_m$  is the actual value of the spiral angle at point  $m$  within the line of contact,  $LC$ , of the gear and pinion teeth

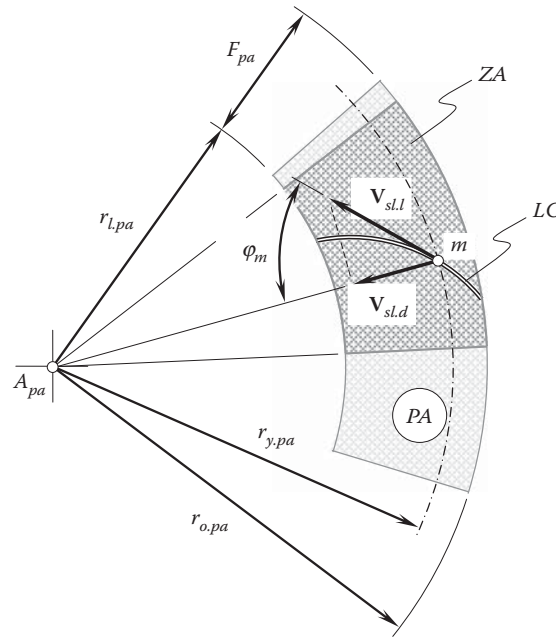


FIGURE 13.14

To the definition of the linear velocity vector,  $\mathbf{V}_{sl,l}$ , of sliding in the lengthwise direction of the gear teeth.

As follows from the analysis of Equation 13.26, sliding in the lengthwise direction of the gear teeth depends on the actual value of the spiral angle at point  $m$  within the line of contact,  $LC$ , of the gear and pinion teeth. This means that the linear velocity vector,  $\mathbf{V}_{sl,l}$ , of sliding in the lengthwise direction of the gear teeth varies along the line of contact,  $LC$ , of the gear and pinion teeth.

Figure 13.13 and Equation 13.26 provide a good opportunity for gear researchers to perform a qualitative analysis of sliding conditions in intersected-axes gearing.

The magnitude of the linear velocity vector of profile sliding,  $\mathbf{V}_{sl,p}$  (Figure 13.14), depends on a distance of the point of interest,  $m$ , from the axis of instant rotation,  $P_{ln}$ . The larger the distance, the larger the magnitude of the linear velocity vector of profile sliding,  $\mathbf{V}_{sl,p}$ , and vice versa. Profile sliding is zero when point  $m$  is within the axis of instant rotation,  $P_{ln}$ . Therefore, pure rolling of the tooth flanks,  $\mathcal{G}$  and  $\mathcal{P}$ , of a gear and a mating pinion occurs along the axis of instant rotation,  $P_{ln}$ .

Constructed at all points of the zone of action,  $ZA$ , the linear velocity vectors of profile sliding form a field of profile sliding in an intersected-axes gear pair, as schematically illustrated in Figure 13.15. The linear velocity vectors of profile sliding through points along the line of contact,  $LC$ , indicate the profile sliding of the tooth flanks,  $\mathcal{G}$  and  $\mathcal{P}$ , for a particular angular configuration of the gear and the mating pinion (not shown in Figure 13.15). The entire field of profile sliding, as well as the linear velocity vectors of profile sliding through points along the line of contact,  $LC$ , can both be transferred to and constructed on either the tooth flank of the gear,  $\mathcal{G}$ , or the tooth flank of the mating pinion,  $\mathcal{P}$ .

Similarly, the magnitude of the linear velocity vector of drag sliding,  $\mathbf{V}_{sl,d}$ , depends on an angular distance,  $\varphi_{m,pa}$ , of the point of interest,  $m$ , from the axis of instant rotation,  $P_{ln}$ . The larger the angular distance,  $\varphi_{m,pa}$ , the larger the magnitude of the linear velocity vector of drag sliding,  $\mathbf{V}_{sl,d}$ , and vice versa. This is because the linear velocity vector of drag sliding,  $\mathbf{V}_{sl,d}$ , equals a projection onto the axis of instant rotation,  $P_{ln}$ , of the linear velocity vector,  $\mathbf{V}_{rel}$ , of the relative motion of the tooth flanks,  $\mathcal{G}$  and  $\mathcal{P}$ , of a gear and a mating pinion.

Drag sliding is zero when point  $m$  is within the axis of instant rotation,  $P_{ln}$ . Therefore, no drag sliding between the tooth flanks,  $\mathcal{G}$  and  $\mathcal{P}$ , of a gear and a mating pinion occurs along the axis of instant rotation,  $P_{ln}$ .

Constructed at all points of the zone of action,  $ZA$ , the linear velocity vectors of drag sliding form a field of drag sliding in an intersected-axes gear pair. The distribution of the linear velocity vectors of drag sliding is quite similar to that shown in Figure 13.15 for the linear velocity vectors of profile sliding. The linear velocity vectors of drag sliding through points along the line of contact,  $LC$ , indicate the drag sliding of the tooth flanks,  $\mathcal{G}$  and  $\mathcal{P}$ , for a particular angular configuration of the gear and the mating pinion.



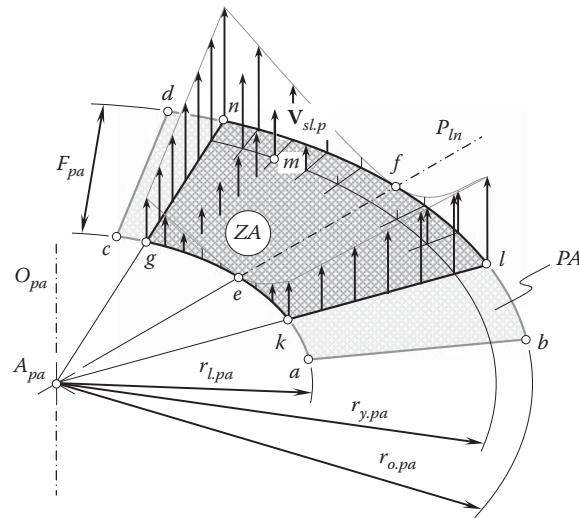


**FIGURE 13.15**  
Field of linear velocity of profile sliding in an intersected-axes gear pair.

The origin of sliding of the teeth flanks,  $\mathcal{G}$  and  $\mathcal{P}$ , in the direction of the axis of instant rotation,  $P_{ln}$ , in intersected-axes gearing is illustrated in Figure 13.16.

When the gears rotate, the plane of action,  $PA$ , is steadily rotated about the plane-of-action apex,  $A_{pa}$ , with an angular velocity,  $w_{pa}$ . In this rotation, the linear velocity vector,  $\mathbf{V}_{m.pa}$ , of an arbitrary point,  $m$ , of the line of contact,  $LC$ , forms a certain angle with the axis of instant rotation,  $P_{ln}$  (this angle equals zero only when point,  $m$ , coincides with point of intersection of the line of contact,  $LC$ , and the axis of instant rotation,  $P_{ln}$ ). The component,  $\mathbf{V}_{m,r}$ , of the linear velocity vector,  $\mathbf{V}_{m.pa}$ , that is perpendicular to the axis,  $P_{ln}$ , causes pure rotation of the driven gear. The component,  $\mathbf{V}_{m,sl}$ , of the linear velocity vector,  $\mathbf{V}_{m.pa}$ , that is parallel to the axis,  $P_{ln}$ , causes sliding of the teeth flanks,  $\mathcal{G}$  and  $\mathcal{P}$ , in the direction of the axis of instant rotation,  $P_{ln}$ .

A similar schematic (see Figure 13.16) is also valid with respect to sliding in crossed-axes gearing.

Total sliding of the tooth flanks,  $\mathcal{G}$  and  $\mathcal{P}$ , in an intersected-axes gear pair can be specified by the linear velocity vector,  $\mathbf{V}_{sl,\Sigma}$ , of total sliding:

$$\mathbf{V}_{sl,\Sigma} = \mathbf{V}_{sl,p} + \mathbf{V}_{sl,l} \quad (13.27)$$

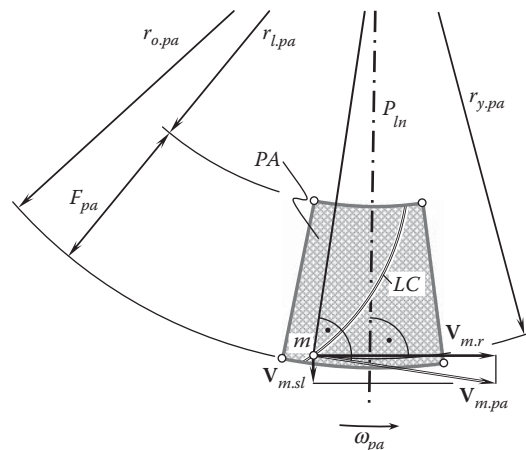


**FIGURE 13.16**  
On the origin of sliding of the teeth flanks,  $\mathcal{G}$  and  $\mathcal{P}$ , in the direction of the axis of instant rotation,  $P_{ln}$ , in intersected-axes gearing.

As the functions of the linear velocity vectors of sliding,  $\mathbf{V}_{sl,p}$  and  $\mathbf{V}_{sl,l}$ , on the parameters of kinematics of a gear pair and the design parameters of a gear and mating pinion are nonlinear, then the superposition of the vectors,  $\mathbf{V}_{sl,p}$  and  $\mathbf{V}_{sl,l}$ , as in Equation 13.27, is valid only in cases when linearization of the functions is permissible. This means that the linear velocity vectors,  $\mathbf{V}_{sl,p}$  and  $\mathbf{V}_{sl,l}$ , depend on parameters of kinematics of a gear pair and the design parameters of a gear and a mating pinion either linearly or nearly linearly.\*

#### 13.4.1.2 Analytical Solution to the Problem of Determining of Sliding in Perfect Intersected-Axes Gearing

The performed descriptive geometry-based solution to the problem of determination of sliding in perfect intersected-axes gearing is helpful for a better understanding of the nature of the problem under consideration, and returns a rough estimate of sliding conditions that occur in intersected-axes gearing. The discussed graphical solution to the problem is also useful for the development of an analytical solution to that same problem. Again, in order to solve the problem analytically, it is necessary to derive equations for the linear velocity vectors,  $\mathbf{V}_{m,g}$  and  $\mathbf{V}_{m,p}$ , of a point of interest,  $m$ , and to represent the derived expressions in a common reference system. A stationary Cartesian coordinate system,  $X_{pa,s}Y_{pa,s}Z_{pa,s}$ , associated with the plane of action,  $PA$ , in the intersected-axes gear pair is especially convenient for solving the problem of determination of sliding in perfect  $I_a$ -gearing.

For the development of an analytical solution to the problem under consideration, operators of linear transformations are extensively used below, as the solution to the problem can be significantly simplified by application of the operators of coordinate system transformations. The chief reason using the operators of linear transformations for the derivation of all the necessary equations is as follows. It is convenient to derive an expression for each of the vectors,  $\mathbf{V}_{m,g}$  and  $\mathbf{V}_{m,p}$ , in a specific reference system and then to represent the derived equation in a reference system that is convenient for further analysis. For instance, it is convenient to determine the linear velocity vector,  $\mathbf{V}_{m,g}$ , in a coordinate system associated with the gear. Similarly, it is convenient to determine the linear velocity vector,  $\mathbf{V}_{m,p}$ , in a coordinate system associated with the pinion. Later, the derived equations for both vectors,  $\mathbf{V}_{m,g}$  and  $\mathbf{V}_{m,p}$ , can be represented in a common reference system. The operators of linear transformations, that is, the operators of translation and the operators of rotation along and about the coordinate axes are very helpful for this purpose.

Relative motion of a driving member, of a driven member in a gear pair, and of the plane of action form the premise on which the corresponding operators of the coordinate system transformations can be derived. When a gear pair is operated, the driving member, the driven member, and the plane of action are rotated in a timely manner; that is, the rotations  $\omega_g$ ,  $\omega_p$  and  $\omega_{pa}$  are synchronized with one another.

As the rotations  $\omega_g$ ,  $\omega_p$ , and  $\omega_{pa}$  are synchronized with one another, the angles of rotation,  $\varphi_{pa}$  and  $\varphi_g$ , of the plane of action and the gear can be expressed in terms of the angle of rotation,  $\varphi_p$ , of the driving pinion, as:

$$\varphi_{pa} = \frac{\varphi_p}{\sin \gamma_b} \quad (13.28)$$

$$\varphi_{pa} = \frac{\varphi_g}{\sin \Gamma_b} \quad (13.29)$$

From these equations, an expression:

$$\varphi_g = \varphi_p \frac{\sin \Gamma_b}{\sin \gamma_b} \quad (13.30)$$

can be derived.

Here, in Equations 13.28 through 13.30, the base cone angles of a gear and a pinion are designated as  $\Gamma_b$  and  $\gamma_b$ , correspondingly.

The relative motion of the members in a gear pair, along with the applied coordinate systems, are schematically shown in [Figure 13.17](#).

\* Another descriptive geometry-based solution to the problem of determination of sliding in perfect intersected-axes gearing with application to high-conformal gearing is discussed in [115]. The applied approach can be used for solving the problem under consideration not only in high-conformal gearings, but in perfect intersected-axes gearing in a more general sense.

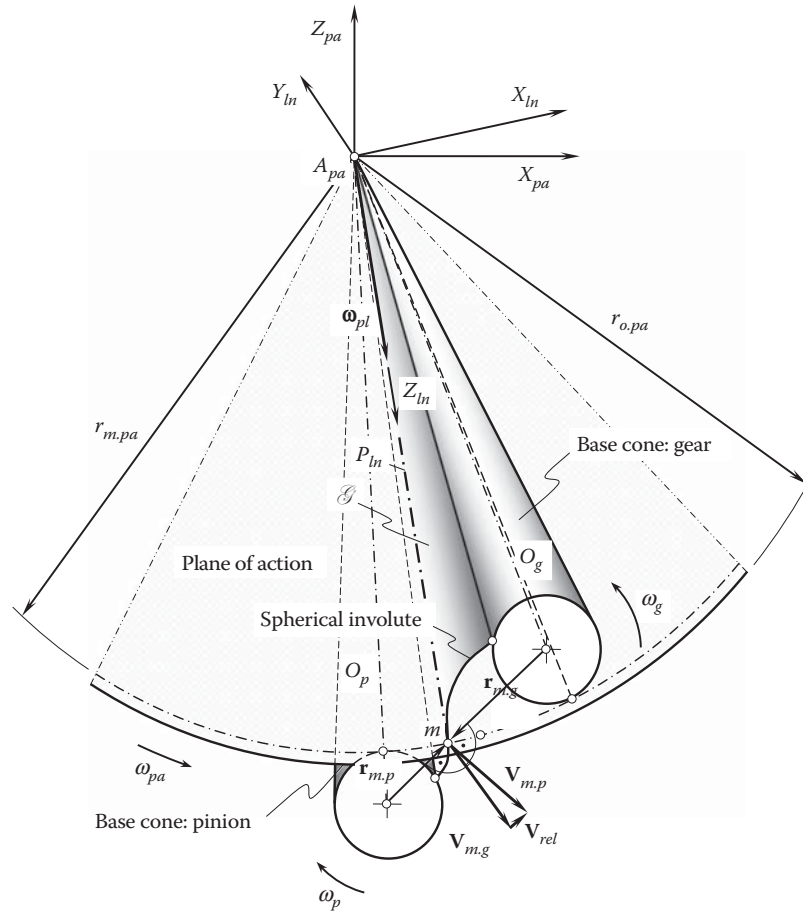


**FIGURE 13.17**  
Reference systems associated with an intersected-axes gear pair.

Assume that the pinion is the driving member and a mating gear the driven member in a gear pair, schematically illustrated in Figure 13.17. To derive a formula for the operator,  $\mathbf{Rs}_{la}(p \rightarrow pa)$ , of transition from the coordinate system,  $X_p Y_p Z_p$ , associated with the driving pinion, to the coordinate system,  $X_{pa} Y_{pa} Z_{pa}$ , associated with the plane of action,  $PA$ , in an intersected-axes gear pair, consider a rotation of a driving pinion (Figure 13.17).

The stationary reference system,  $X_{p.s} Y_{p.s} Z_{p.s}$ , is associated with the gear housing. At the beginning, the axes of the pinion coordinate system,  $X_p Y_p Z_p$ , align with the corresponding axes of the stationary coordinate system,  $X_{p.s} Y_{p.s} Z_{p.s}$ . When the pinion is rotated about the axis,  $O_p$ , through a certain angle,  $\varphi_p$ , the reference system,  $X_p Y_p Z_p$ , is rotated together with the pinion. The transition from the pinion reference system,  $X_p Y_p Z_p$ , to the stationary reference system,  $X_{p.s} Y_{p.s} Z_{p.s}$ , can be analytically described by the operator of rotation,  $\mathbf{Rt}(Z_s, \varphi_p)$ , of the reference system,  $X_p Y_p Z_p$ , through the angle,  $\varphi_p$ , about the axis,  $O_p$ , in the counterclockwise direction.\* In matrix form, this operator can be represented as:

$$\mathbf{Rt}(Z_s, \varphi_p) = \begin{bmatrix} \cos \varphi_p & -\sin \varphi_p & 0 & 0 \\ \sin \varphi_p & \cos \varphi_p & 0 & 0 \\ 0 & 0 & 1 & 0 \\ 0 & 0 & 0 & 1 \end{bmatrix} \quad (13.31)$$

The coordinate system transformation that is analytically described by the operator of rotation,  $\mathbf{Rt}(Z_s, \varphi_p)$ , is followed by the rotation of the reference system,  $X_{p.s} Y_{p.s} Z_{p.s}$ , through the base cone angle,  $\gamma_b$ , of the pinion about

\* Here and below, the direction of rotation of a coordinate system about a coordinate axis is determined looking from the arrowhead of the coordinate axis about which the rotation is performed.

the axis  $Y_{p.s}$ , in the counterclockwise direction. A rotation of this sort can be analytically described by the operator of rotation,  $\mathbf{Rt}(Y_{p.s}, \gamma_b)$ . In matrix form, this operator can be represented as:

$$\mathbf{Rt}(Y_{p.s}, \gamma_b) = \begin{bmatrix} \cos \gamma_b & 0 & -\sin \gamma_b & 0 \\ 0 & 1 & 0 & 0 \\ \sin \gamma_b & 0 & \cos \gamma_b & 0 \\ 0 & 0 & 0 & 1 \end{bmatrix} \quad (13.32)$$

After completion of the rotation of the coordinate system,  $X_{p.s}Y_{p.s}Z_{p.s}$ , about the axis,  $Y_{p.s}$ , through the base cone angle,  $\gamma_b$ , the coordinate system,  $X_{p.s}Y_{p.s}Z_{p.s}$ , occupies the position labeled  $X_{1.s}Y_{1.s}Z_{1.s}$ . The axes of the coordinate system,  $X_{1.s}Y_{1.s}Z_{1.s}$ , and of the stationary coordinate system,  $X_{2.s}Y_{2.s}Z_{2.s}$ , associated with the plane of action,  $PA$ , need to be properly aligned to one another (the reference system,  $X_{1.s}Y_{1.s}Z_{1.s}$ , is not shown in Figure 13.17). To get the axes aligned, an additional rotation of the reference system,  $X_{1.s}Y_{1.s}Z_{1.s}$ , about the axis,  $Z_{p.s}$ , through a right angle has to be performed. An operator,  $\mathbf{Rt}(Z_{p.s}, 90^\circ)$ , of linear transformation that analytically describes this additional rotation can be represented as:

$$\mathbf{Rt}(Z_{p.s}, 90^\circ) = \begin{bmatrix} 0 & 1 & 0 & 0 \\ -1 & 0 & 0 & 0 \\ 0 & 0 & 1 & 0 \\ 0 & 0 & 0 & 1 \end{bmatrix} \quad (13.33)$$

After being turned about the axis,  $Z_{p.s}$ , through a right angle, the coordinate system is designated as  $X_{2.s}Y_{2.s}Z_{2.s}$ .

The next transition is performed from the coordinate system,  $X_{2.s}Y_{2.s}Z_{2.s}$ , to the stationary coordinate system,  $X_{pa.s}Y_{pa.s}Z_{pa.s}$ , associated with the plane of action,  $PA$ . Refer to Figure 13.17 for details on this linear transformation. For the analytical description of the rotation of the reference system,  $X_{2.s}Y_{2.s}Z_{2.s}$ , in the counterclockwise direction about the axis  $Z_{2.s}$  through an angle,  $\sigma_p$ , the operator of rotation,  $\mathbf{Rt}(Z_{2.s}, \sigma_p)$ , is used. In matrix form, this operator can be represented as:

$$\mathbf{Rt}(Z_{2.s}, \sigma_p) = \begin{bmatrix} \cos \sigma_p & \sin \sigma_p & 0 & 0 \\ -\sin \sigma_p & \cos \sigma_p & 0 & 0 \\ 0 & 0 & 1 & 0 \\ 0 & 0 & 0 & 1 \end{bmatrix} \quad (13.34)$$

Here, the projection of the pinion cone angle,  $\Sigma_p$ , onto the plane of action,  $PA$ , is designated as  $\sigma_p$  (i.e., the equality  $\text{Pr}_{pa} \Sigma_p = \sigma_p$  is valid). Referring to Figure 13.9, it can be shown that the angle,  $\sigma_p$ , can be calculated as:

$$\sigma_p = \cos^{-1} \left( \frac{\cos \Sigma_p}{\cos \gamma_b} \right) \quad (13.35)$$

where  $\gamma_b$  is the base cone angle of the pinion.

Finally, the transition is performed from the stationary coordinate system,  $X_{pa.s}Y_{pa.s}Z_{pa.s}$ , associated with the plane of action to the coordinate system,  $X_{pa}Y_{pa}Z_{pa}$ , that is rotated together with the plane of action,  $PA$ . For the analytical description of the rotation of the reference system,  $X_{pa.s}Y_{pa.s}Z_{pa.s}$ , in the clockwise direction about the axis  $Z_{pa.s}$  through an angle,  $\varphi_{pa}$ , the operator of rotation,  $\mathbf{Rt}(Z_{pa.s}, \varphi_{pa})$ , is used. In matrix form, this operator can be represented as:

$$\mathbf{Rt}(Z_{pa.s}, \varphi_{pa}) = \begin{bmatrix} \cos \varphi_{pa} & -\sin \varphi_{pa} & 0 & 0 \\ \sin \varphi_{pa} & \cos \varphi_{pa} & 0 & 0 \\ 0 & 0 & 1 & 0 \\ 0 & 0 & 0 & 1 \end{bmatrix} \quad (13.36)$$

The angle of rotation,  $\varphi_{pa}$ , of the plane of action,  $PA$ , can be expressed in terms of the angle of rotation,  $\varphi_p$ , of the pinion (see Equation 13.28).

For the analytical description of the resultant coordinate system transformation, that is, for the transition from the reference system,  $X_p Y_p Z_p$ , associated with the rotated pinion, to the reference system,  $X_{pa} Y_{pa} Z_{pa}$ , associated with the rotated plane of action,  $PA$ , the operator,  $\mathbf{Rs}_{la}(p \rightarrow pa)$ , of the resultant coordinate system is used. This operator can be expressed in terms of the operators of the elementary linear transformations as:

$$\mathbf{Rs}_{la}(p \rightarrow pa) = \mathbf{Rt}(Z_{2.s}, \varphi_{pa}) \cdot \mathbf{Rt}(Z_{2.s}, \sigma_p) \cdot \mathbf{Rt}(Z_{p.s}, 90^\circ) \cdot \mathbf{Rt}(Y_{p.s}, \gamma_b) \cdot \mathbf{Rt}(Z_s, \varphi_p) \quad (13.37)$$

Note that the order of the multipliers in Equation 13.37 cannot be altered.

For the inverse coordinate system transformation, that is, for the analytical description of the transition from the reference system,  $X_{pa} Y_{pa} Z_{pa}$ , associated with the rotated plane of action,  $PA$ , to the reference system,  $X_p Y_p Z_p$ , associated with the rotated pinion, the operator,  $\mathbf{Rs}_{la}(pa \rightarrow p)$ , of the inverse coordinate system transformation is used. The operator,  $\mathbf{Rs}_{la}(pa \rightarrow p)$ , of this linear transformation can be expressed in terms of the operator,  $\mathbf{Rs}_{la}(p \rightarrow pa)$ , of the direct coordinate system transformation as:

$$\mathbf{Rs}_{la}(pa \rightarrow p) = \mathbf{Rs}_{la}^{-1}(p \rightarrow pa) \quad (13.38)$$

The operators,  $\mathbf{Rs}_{la}(p \rightarrow pa)$  and  $\mathbf{Rs}_{la}(pa \rightarrow p)$ , are not presented here in an exploded form, as both of them are bulky.

In the reference system,  $X_p Y_p Z_p$ , associated with the rotated pinion, the linear velocity vector,  $\mathbf{V}_{m.p}$ , of the point of interest,  $m$ , can be analytically described by a column matrix as:

$$\mathbf{V}_{m.p}|_p = \begin{bmatrix} -r_{b.p} \sin \varphi_p \\ r_{b.p} \cos \varphi_p \\ 0 \\ 1 \end{bmatrix} \quad (13.39)$$

Then the operator of the resultant coordinate system transformation,  $\mathbf{Rs}_{la}(p \rightarrow pa)$ , is used to represent that same linear velocity vector,  $\mathbf{V}_{m.p}$ , in the coordinate system,  $X_{pa} Y_{pa} Z_{pa}$ , associated with the rotated plane of action,  $PA$ :

$$\mathbf{V}_{m.p}|_{pa} = \mathbf{Rs}_{la}(p \rightarrow pa) \cdot \begin{bmatrix} -r_{b.p} \sin \varphi_p \\ r_{b.p} \cos \varphi_p \\ 0 \\ 1 \end{bmatrix} \quad (13.40)$$

A formula for the operator,  $\mathbf{Rs}_{la}(pa \rightarrow g)$ , of the resultant coordinate system transformation, that is, for the analytical description of the transition from the reference system,  $X_{pa} Y_{pa} Z_{pa}$ , associated with the rotated plane of action,  $PA$ , to the reference system,  $X_g Y_g Z_g$ , associated with the rotated gear, can be derived similarly to how Equation 13.37 is derived for the calculation of the operator of linear transformation,  $\mathbf{Rs}_{la}(p \rightarrow pa)$ . The operators,  $\mathbf{Rt}(Z_s, \varphi_g)$ ,  $\mathbf{Rt}(Y_{g.s}, \Gamma_b)$ ,  $\mathbf{Rt}(Z_{g.s}, 90^\circ)$ ,  $\mathbf{Rt}(Z_{3.s}, \sigma_g)$ , and  $\mathbf{Rt}(Z_{3.s}, \varphi_{pa})$ , of the elementary linear transformations are used in this case (Figure 13.17). The above-listed operators of linear transformations are composed similarly to the operators of the linear transformations [i.e.,  $\mathbf{Rt}(Z_s, \varphi_p)$ , Equation 13.31;  $\mathbf{Rt}(Y_{p.s}, \gamma_b)$ , Equation 13.32;  $\mathbf{Rt}(Z_{p.s}, 90^\circ)$ , Equation 13.33;  $\mathbf{Rt}(Z_{2.s}, \sigma_p)$ , Equation 13.34; and  $\mathbf{Rt}(Z_{2.s}, \varphi_{pa})$ , Equation 13.36]:

$$\mathbf{Rt}(Z_s, \varphi_g) = \begin{bmatrix} \cos \varphi_g & \sin \varphi_g & 0 & 0 \\ -\sin \varphi_g & \cos \varphi_g & 0 & 0 \\ 0 & 0 & 1 & 0 \\ 0 & 0 & 0 & 1 \end{bmatrix} \quad (13.41)$$

$$\mathbf{Rt}(Y_{g.s}, \Gamma_b) = \begin{bmatrix} \cos \Gamma_b & 0 & \sin \Gamma_b & 0 \\ 0 & 1 & 0 & 0 \\ -\sin \Gamma_b & 0 & \cos \Gamma_b & 0 \\ 0 & 0 & 0 & 1 \end{bmatrix} \quad (13.42)$$

$$\mathbf{Rt}(Z_{g.s}, 90^\circ) = \begin{bmatrix} 0 & 1 & 0 & 0 \\ -1 & 0 & 0 & 0 \\ 0 & 0 & 1 & 0 \\ 0 & 0 & 0 & 1 \end{bmatrix} \quad (13.43)$$

$$\mathbf{Rt}(Z_{3.s}, \sigma_g) = \begin{bmatrix} \cos \sigma_g & -\sin \sigma_g & 0 & 0 \\ \sin \sigma_g & \cos \sigma_g & 0 & 0 \\ 0 & 0 & 1 & 0 \\ 0 & 0 & 0 & 1 \end{bmatrix} \quad (13.44)$$

$$\mathbf{Rt}(Z_{3.s}, \varphi_{pa}) = \begin{bmatrix} \cos \varphi_{pa} & \sin \varphi_{pa} & 0 & 0 \\ -\sin \varphi_{pa} & \cos \varphi_{pa} & 0 & 0 \\ 0 & 0 & 1 & 0 \\ 0 & 0 & 0 & 1 \end{bmatrix} \quad (13.45)$$

Here, the projection of the gear cone angle,  $\Sigma_g$ , onto the plane of action,  $PA$ , is designated as  $\sigma_g$  (i.e., the equality  $\text{Pr}_{pa} \Sigma_g = \sigma_g$  is valid). Referring to Figure 13.9, it can be shown that the angle,  $\sigma_g$ , can be calculated the following equation:

$$\sigma_g = \cos^{-1} \left( \frac{\cos \Sigma_g}{\cos \Gamma_b} \right) \quad (13.46)$$

where  $\Gamma_b$  is the base cone angle of the gear.

For the analytical description of the resultant coordinate system transformation, that is, for the transition from the reference system,  $X_g Y_g Z_g$ , associated with the rotated pinion, to the reference system,  $X_{pa} Y_{pa} Z_{pa}$ , associated with the rotated plane of action,  $PA$ , the operator,  $\mathbf{Rs}_{la}(g \rightarrow pa)$ , of the resultant coordinate system is used. This operator can be expressed in terms of the operators of the elementary linear transformations as:

$$\mathbf{Rs}_{la}(g \rightarrow pa) = \mathbf{Rt}(Z_{3.s}, \varphi_{pa}) \cdot \mathbf{Rt}(Z_{3.s}, \sigma_g) \cdot \mathbf{Rt}(Z_{g.s}, 90^\circ) \cdot \mathbf{Rt}(Y_{g.s}, \Gamma_b) \cdot \mathbf{Rt}(Z_s, \varphi_g) \quad (13.47)$$

Note that the order of the multipliers in Equation 13.37 cannot be altered.

In the reference system,  $X_g Y_g Z_g$ , associated with the rotated gear, the linear velocity vector,  $\mathbf{V}_{m.g}$ , of the point of interest,  $m$ , can be analytically described by a column matrix as:

$$\mathbf{V}_{m.g}|_g = \begin{bmatrix} -r_{b.g} \sin \varphi_g \\ r_{b.g} \cos \varphi_g \\ 0 \\ 1 \end{bmatrix} \quad (13.48)$$

Then, the operator of the resultant coordinate system transformation,  $\mathbf{Rs}_{la}(g \rightarrow pa)$ , is used to represent that same linear velocity vector,  $\mathbf{V}_{m.g}$ , in the coordinate system,  $X_{pa} Y_{pa} Z_{pa}$ , associated with the rotated plane of action,  $PA$ :

$$\mathbf{V}_{m.g}|_{pa} = \mathbf{Rs}_{la}(g \rightarrow pa) \cdot \begin{bmatrix} -r_{b.g} \sin \varphi_g \\ r_{b.g} \cos \varphi_g \\ 0 \\ 1 \end{bmatrix} \quad (13.49)$$

Consider the relative motion of a point within the line of contact of the tooth flanks,  $\mathcal{G}$  and  $\mathcal{P}$ , of a gear and a mating pinion in an intersected-axes gear pair.

The vector of the relative motion,  $\mathbf{V}_{rel}$ , of the point of interest,  $m$ , within the line of contact,  $LC$ , between the tooth flanks,  $\mathcal{G}$  and  $\mathcal{P}$ , of a gear and a mating pinion in an intersected-axes gear pair equals the difference:

$$\mathbf{V}_{rel} = \mathbf{V}_{m.p}|_{pa} - \mathbf{V}_{m.g}|_{pa} \quad (13.50)$$

where both the linear velocity vectors,  $\mathbf{V}_{m,g}$  and  $\mathbf{V}_{m,p}$ , are represented in a common reference system,  $X_{pa}Y_{pa}Z_{pa}$ , associated with the rotated plane of action,  $PA$ .

In the expanded form, the vector of the relative motion,  $\mathbf{V}_{rel}$ , can be represented in matrix form as:

$$\mathbf{V}_{rel}|_{pa} = \begin{bmatrix} V_{x.rel} \\ V_{y.rel} \\ V_{z.rel} \\ 1 \end{bmatrix} \quad (13.51)$$

The projection,  $V_{y.rel}$ , of the linear velocity vector,  $\mathbf{V}_{rel}$ , onto the axis,  $Y_{pa}$ , causes pure rolling of the gear and mating pinion tooth flanks,  $\mathcal{G}$  and  $\mathcal{P}$ , over each other. Therefore, this component of the linear velocity vector,  $\mathbf{V}_{rel}$ , is labeled below as  $\mathbf{V}_{rol}$ .

The projection,  $V_{z.rel}$ , of the linear velocity vector,  $\mathbf{V}_{rel}$ , onto the axis,  $Z_{pa}$ , causes profile sliding of the gear and mating pinion tooth flanks,  $\mathcal{G}$  and  $\mathcal{P}$ . Therefore, this component of the linear velocity vector,  $\mathbf{V}_{rel}$ , is labeled below as  $\mathbf{V}_{sl,p}$ .

The projection,  $V_{x.rel}$ , of the linear velocity vector,  $\mathbf{V}_{rel}$ , onto the axis,  $X_{pa}$ , causes drag sliding of the gear and mating pinion tooth flanks,  $\mathcal{G}$  and  $\mathcal{P}$ . Therefore, this component of the linear velocity vector,  $\mathbf{V}_{rel}$ , is labeled below as  $\mathbf{V}_{sl,d}$ .

The total sliding,  $\mathbf{V}_{sl}$ , in intersected-axes gearing can be calculated as the sum:

$$\mathbf{V}_{sl} = \mathbf{V}_{sl,p} + \mathbf{V}_{sl,d} \quad (13.52)$$

At different points within the zone of action,  $ZA$ , each of the linear velocity vectors, that is,  $\mathbf{V}_{sl}$ ,  $\mathbf{V}_{sl,p}$ , and  $\mathbf{V}_{sl,d}$ , varies.

A computer code for calculation of all the components,  $\mathbf{V}_{rol}$ ,  $\mathbf{V}_{sl,p}$ , and  $\mathbf{V}_{sl,d}$ , of the linear velocity vector,  $\mathbf{V}_{rel}$ , can be developed on the premise of the equations discussed above in this section. Ultimately, the distribution of the components,  $\mathbf{V}_{rol}$ ,  $\mathbf{V}_{sl,p}$ , and  $\mathbf{V}_{sl,d}$ , within the zone of action,  $ZA$ , in a crossed-axes gear pair can be interpreted graphically.

### 13.4.1.3 Specific Sliding in Perfect Intersected-Axes Gearing

For the specification of sliding of tooth flanks,  $\mathcal{G}$  and  $\mathcal{P}$ , of a gear and mating pinion in an intersected-axes gear pair, a unitless parameter can be used, similar to that in parallel-axes gearing. This sliding parameter can be also referred to as *specific sliding*, as it is common with respect to parallel-axes gearing, and is denoted by  $\gamma_{\Sigma}$ . An actual value of the specific sliding does not depend on a rotation of the input/output shafts, and depends only on the design parameters of the gear and the mating pinion. The latter is important when optimizing the design parameters in intersected-axes gear pairs.

Two different parameters,  $\gamma_{\Sigma}$ , are distinguished.

First, the slide/roll ratio for the tooth flank,  $\mathcal{G}$ , of the gear:

$$\gamma_{\Sigma,g} = \frac{V_{sl,g}^m - V_{sl,p}^m}{V_{sl,g}^m} \quad (13.53)$$

Second, the slide/roll ratio for the tooth flank,  $\mathcal{P}$ , of the pinion:

$$\gamma_{\Sigma,p} = \frac{V_{sl,p}^m - V_{sl,g}^m}{V_{sl,p}^m} \quad (13.54)$$

The sliding velocities,  $V_{sl,g}^m$  and  $V_{sl,p}^m$ , in Equations 13.53 and 13.54 are calculated as explained immediately below.



In the reference system,  $X_{pa}Y_{pa}Z_{pa}$ , associated with the rotated plane of action,  $PA$ , the linear velocity vector,  $\mathbf{V}_{m,g}|_{pa}$  (see Equation 13.49), can be represented in the form:

$$\mathbf{V}_{m,g}|_{pa} = \begin{bmatrix} V_{x.m,g} \\ V_{y.m,g} \\ V_{z.m,g} \\ 1 \end{bmatrix} \quad (13.55)$$

The component,  $V_{z.m,g}$ , contributes to the profile sliding, and the component,  $V_{x.m,g}$ , contributes to the drag sliding in an intersected-axes gear pair (the component,  $V_{y.m,g}$ , contributes to pure rolling of the tooth flanks,  $\mathcal{G}$  and  $\mathcal{P}$ ). The sliding velocity,  $V_{sl,g}^m$  (see Equations 13.53 and 13.54), can be expressed in terms of the velocities,  $V_{x.m,g}$  and  $V_{z.m,g}$ , as:

$$V_{sl,g}^m = \sqrt{V_{x.m,g}^2 + V_{z.m,g}^2} \quad (13.56)$$

Similarly, in the reference system,  $X_{pa}Y_{pa}Z_{pa}$ , associated with the rotated plane of action,  $PA$ , the linear velocity vector,  $\mathbf{V}_{m,p}|_{pa}$  (see Equation 13.40), can be represented in the form:

$$\mathbf{V}_{m,p}|_{pa} = \begin{bmatrix} V_{x.m,p} \\ V_{y.m,p} \\ V_{z.m,p} \\ 1 \end{bmatrix} \quad (13.57)$$

The component,  $V_{z.m,p}$ , contributes to the profile sliding, and the component,  $V_{x.m,p}$ , contributes to the drag sliding in an intersected-axes gear pair (the component,  $V_{y.m,p}$ , contributes to pure rolling of the tooth flanks,  $\mathcal{G}$  and  $\mathcal{P}$ ). The sliding velocity,  $V_{sl,p}^m$  (see Equations 13.53 and 13.54), can be expressed in terms of the velocities,  $V_{x.m,p}$  and  $V_{z.m,p}$ , as:

$$V_{sl,p}^m = \sqrt{V_{x.m,p}^2 + V_{z.m,p}^2} \quad (13.58)$$

The sliding velocities,  $V_{sl,g}^m$  and  $V_{sl,p}^m$  (see Equations 13.56, and 13.58), are entered into Equations 13.53 and 13.54 to calculate the specific roll/slide ratios,  $\gamma_{\Sigma,g}$  and  $\gamma_{\Sigma,p}$ , in intersected-axes gearings.

The specific sliding,  $\gamma_{\Sigma}$ , has a positive value on the addendum portions of the tooth flanks. The parameter,  $\gamma_{\Sigma}$ , does not exceed 1. At points within the axis of instant rotation,  $P_{ln}$ , it is equal to zero, and it is equal to 1 at the base cone of the mating gear.

The specific sliding on the dedendum portion of the tooth flanks has a negative value. It is equal to zero at points within the axis of instant rotation,  $P_{ln}$ , and it approaches minus infinity at the base cone.

The specific rolling/sliding ratios,  $\gamma_{\Sigma,g}$  and  $\gamma_{\Sigma,p}$ , are plotted within the zone of action,  $ZA$ , as only the region,  $ZA$ , plane of action comes into effect when investigating the engagement of the gear teeth.

#### 13.4.1.4 Features of Specific Sliding in Perfect Intersected-Axes Gearing

Sliding conditions in perfect intersected-axes gearing differ from those in parallel-axes gearing. Drag sliding in  $I_a$ -gearing is the main reason for the difference. Therefore, in addition to the specific roll/sliding ratios,  $\gamma_{\Sigma,g}$  and  $\gamma_{\Sigma,p}$  (see Equations 13.53 and 13.54), two more characteristics can be introduced to specify specific sliding in intersected-axes gear pairs.

Specific profile rolling/sliding ratios,  $\gamma_{p,g}$  and  $\gamma_{p,p}$ , are the first of two additional characteristics. These two ratios are specified as:

$$\gamma_{p,g} = \frac{V_{z.m,g} - V_{z.m,p}}{V_{z.m,g}} \quad (13.59)$$

$$\gamma_{p,p} = \frac{V_{z.m,p} - V_{z.m,g}}{V_{z.m,p}} \quad (13.60)$$

Specific drag rolling/sliding ratios,  $\gamma_{d,g}$  and  $\gamma_{d,p}$ , are the second of two additional characteristics. These two ratios are specified as:

$$\gamma_{d,g} = \frac{V_{x.m,g} - V_{x.m,p}}{V_{x.m,g}} \quad (13.61)$$

$$\gamma_{d,p} = \frac{V_{x.m,p} - V_{x.m,g}}{V_{x.m,p}} \quad (13.62)$$

Specific profile roll/slide ratios,  $\gamma_{p,g}$  and  $\gamma_{p,p}$ , and specific drag rolling/sliding ratios,  $\gamma_{d,g}$  and  $\gamma_{d,p}$ , can be helpful in more detailed analysis of sliding conditions in intersected-axes gearings.

It should be mentioned here that gears with a low tooth count are more vulnerable to sliding between the tooth flanks,  $\mathcal{G}$  and  $\mathcal{P}$ , of a gear and mating pinion in intersected-axes gear pairs. They are also more sensitive to the variation of the roll/slide conditions within the zone of action,  $ZA$ .

The performed analysis for sliding conditions in external intersected-axes gearing can be extended to internal intersected-axis gearings, as well as to intersected-axis gearings with a crown gear.

### 13.5 Elements of Dynamics of Perfect Intersected-Axes Gearing

In an intersected-axes gear pair, the input and output shafts are loaded by an input torque and output torque, respectively. As the gears interact with each other, a force of the interaction is exerted from the driving member of the gear pair. An actual value of the force of interaction in intersected-axes gearing, as well as the components of this force, depends on the input torque and the design parameters of the gear and mating pinion. Considering an input torque and an input rotation of constant values (i.e., no acceleration/deceleration is taken into account in the analysis below), it is necessary to determine the forces that act between a gear and mating pinion in an intersected-axes gear pair.\*

#### 13.5.1 Principal Assumption Adopted in Load Analysis of Perfect Intersected-Axes Gearing

When an intersected-axes gear pair operates, the gear and pinion tooth flanks,  $\mathcal{G}$  and  $\mathcal{P}$ , interact with one another at points within the line(s) of contact,  $LC$ . The line(s) of contact is (are) entirely located within the plane of action,  $PA$ . This makes possible a conclusion that the force of interaction between the tooth flanks,  $\mathcal{G}$  and  $\mathcal{P}$ , acts along a straight line that is also located within the plane of action,  $PA$ .

As the line of action of the force is within the plane of action,  $PA$ , then the following assumption seems reasonable in load analysis of perfect intersected-axes gearing.

Referring to Figure 13.18, consider the base cones of a gear and mating pinion, along with the plane of action. The gear rotates,  $\omega_g$ , about its axis of rotation,  $O_g$ , and the pinion rotates,  $\omega_p$ , about its axis of rotation,  $O_p$ , as schematically illustrated in Figure 13.18a. The plane of action,  $PA$ , is in tangency to both the base cones. The plane of action,  $PA$ , rotates,  $\omega_{pa}$ , about its axis of rotation (not shown in Figure 13.18a) that passes through the plane-of-action apex,  $A_{pa}$ . It is instructive to point out here that in contrast to the pulley-and-belt analogy of an intersected-axes gear pair, where the belt pulls the driven member in a gear pair, in reality, the driving gear pushes the driven member in an intersected-axes gearing. In this way, the direction of the rotation,  $\omega_{pa}$ , is specified in Figure 13.18a.

The rotations,  $\omega_g$ ,  $\omega_p$ , and  $\omega_{pa}$ , are synchronized with one another in compliance with Equations 12.24 through 12.26:

$$\frac{\omega_g}{\omega_{pa}} = \sin \Gamma_b \quad (13.63)$$

$$\frac{\omega_p}{\omega_{pa}} = \sin \gamma_b \quad (13.64)$$

\* Friction forces are incorporated into load analysis on later stages.

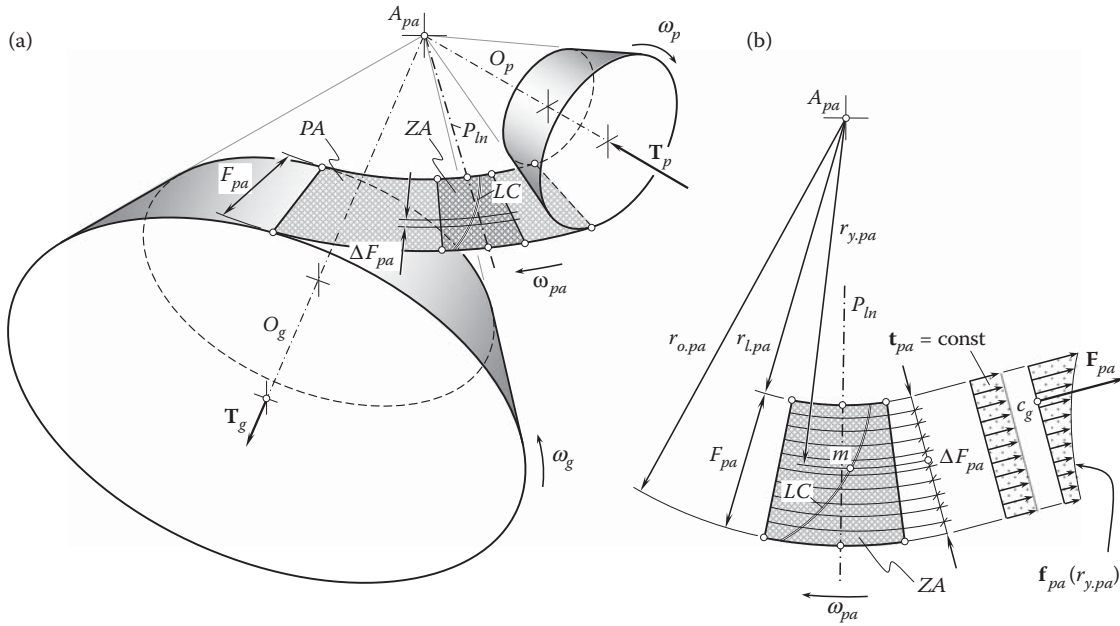


**FIGURE 13.18**  
Forces acting in perfect intersected-axes gear pair.

$$\frac{\omega_g}{\omega_p} = \frac{\sin \Gamma_b}{\sin \gamma_b} \quad (13.65)$$

The input torque,  $T_p$ , is applied to the pinion shaft, and the output torque,  $T_g$ , is applied to the gear shaft. The torque,  $T_{pa}$ , is an *imagined* parameter. This torque is applied to the rotated plane of action,  $PA$ . The magnitudes,  $T_g$ ,  $T_p$ , and  $T_{pa}$ , of the torques,  $T_g$ ,  $T_p$ , and  $T_{pa}$ , correspond to one another inversely to that the rotations,  $\omega_g$ ,  $\omega_p$ , and  $\omega_{pa}$ , are synchronized with one another, that is:

$$\frac{T_g}{T_{pa}} = \frac{1}{\sin \Gamma_b} \quad (13.66)$$

$$\frac{T_p}{T_{pa}} = \frac{1}{\sin \gamma_b} \quad (13.67)$$

$$\frac{T_g}{T_p} = \frac{\sin \gamma_b}{\sin \Gamma_b} \quad (13.68)$$

Interaction between the gear tooth flank,  $\mathcal{G}$ , and a mating pinion tooth flank,  $\mathcal{P}$ , occurs only within the zone of action,  $ZA$ , which is a portion of the plane of action,  $PA$ . The width of the zone of action is designated as  $F_{pa}$ . The width of the zone of action is,  $F_{pa}$ , is calculated as the difference (Figure 13.18b):

$$F_{pa} = r_{o,pa} - r_{l,pa} \quad (13.69)$$

between the outer,  $r_{o,pa}$ , and inner,  $r_{l,pa}$ , radii of the plane of action,  $PA$ .

The interaction between the tooth flanks,  $\mathcal{G}$  and  $\mathcal{P}$ , is observed only along a line(s) of contact,  $LC$  (or portions of the lines of contact), those located only within the zone of action,  $ZA$ . It is common for there to be one or two (and not more than three) lines of contact (portions of the lines of contact) within the zone of action,  $ZA$ , at the same time. In intersected-axes gear pairs of special design, the total number of lines of contact can be greater than three.

A gear and mating pinion in an intersected-axes gear pair can be sliced into a large enough number of slices,  $N_{sl}$ , each of which is perpendicular to the gear axis of rotation,  $O_g$ , and the pinion axis of rotation,  $O_p$ ,

correspondingly. It is convenient to illustrate the slicing of a gear pair using the plane of action,  $PA$ , for this purpose. The thickness of the slices is designated as  $\Delta F_{pa}$ . It can be calculated as:

$$\Delta F_{pa} = \frac{F_{pa}}{N_{sl}} \quad (13.70)$$

In the best-case scenario, the number of slices approaches infinity ( $N_{sl} \rightarrow \infty$ ), and the slice thickness approaches zero ( $\Delta F_{pa} \rightarrow 0$ ). In this latter case, the slice thickness is denoted by  $dF_{pa}$ . It is assumed here and below that the torques transmitted by each of the slices are equal to one another. Considering the plane-of-action torque,  $T_{pa}$ , the following expression:

$$t_{pa} = \frac{T_{pa}}{F_{pa}} = \text{const} \quad (13.71)$$

Equations similar to Equation 13.71, that is:

$$t_g = \frac{T_g}{F_{pa}} = \text{const} \quad (13.72)$$

$$t_p = \frac{T_p}{F_{pa}} = \text{const} \quad (13.73)$$

are valid with respect to the gear, as well as to the mating pinion.

As the torque per unit length,  $t_{pa}$ , has a constant value, and the equality,  $t_{pa}F_{pa} = T_{pa}$ , is valid, then the value of the plane-of-action torque,  $T_{pa}$ , is proportional to the shadowed area in [Figure 13.18b](#).

Equal torque share among the slices is graphically illustrated in [Figure 13.18b](#).

The above discussion makes reasonable the following assumption, which is referred to as the *basic assumption* in the dynamics of intersected-axes gearing:

### Assumption 13.1

*In an intersected-axes gear pair, the torque per unit length,  $t_{pa}$ , is equally shared in the axial direction among an infinite number of infinitesimally thin slices, each of which is perpendicular to the axis of rotation either of the gear, the pinion, or axis of instant rotation.*

A similar assumption has been made with respect to parallel-axes gear pairs (see [Chapter 8](#)).

When gears in an intersected-axes gear pair rotate, an elementary tangential force that is transmitted by each slice alters both; that is, when the rotation angle,  $\varphi_{pa}$ , alters from  $\varphi_{pa}^0$  to  $\varphi_{pa}^i$ , the elementary tangential force,  $t_g$ , alters: (a) its direction, as  $\varphi_{pa}^i - \varphi_{pa}^0 \neq 0$ , as well as (b) its magnitude,  $t_g$ , ( $t_g^i < t_g^0$ , or, more generally,  $t_g^{i-1} < t_g^i < t_g^{i+1}$ )—the latter is because of the variation of the arm:  $r_{b,g}^i > r_{b,g}^0$ .

When the angle,  $\varphi_{pa}^i$ , equals zero ( $\varphi_{pa}^i = 0$ ), the elementary force,  $t_g^0$ , is exactly equal to the tangential force. When the angle,  $\varphi_{pa}^i$ , is not equal to zero ( $\varphi_{pa}^i \neq 0$ ), an axial component is also generated by the elementary force,  $t_g^i$ . There also exists a component of the force,  $t_g^i$ , toward the gear axis of rotation,  $O_g$ , as well as a component along the gear axis of rotation,  $O_g$ . The bearings withhold these components of the resultant force.

The arm,  $\text{arm}^0$ , at  $\varphi_{pa}^i = 0$  equals  $\text{arm}^0 = R_{pa}^i \sin \gamma_{b,g}$ ; an interval for the angle,  $\varphi_{pa}$ , can be expressed in terms of the dimensions of the active portion of the plane of action,  $PA$ .

The arm,  $\text{arm}^i$ , at  $\varphi_{pa}^i \neq 0$  equals  $\text{arm}^i = (A_{pa}A_1) \sin \gamma_{b,g}$ , where  $A_{pa}A_1 = R_{pa}^i / \cos \varphi_{pa}^i$ ; ultimately,  $\text{arm}^i = (R_{pa}^i \sin \gamma_{b,g}) / (\cos \varphi_{pa}^i)$ . This brief analysis needs to be taken into account when performing calculations that pertain to vibration generation and noise excitation in intersected-axes gear pairs.

### 13.5.2 Forces of Interaction in Perfect Intersected-Axes Gearing

The forces that act in a perfect intersected-axes gear pairs are considered below in different reference systems. The analysis begins with a load applied within the plane of action,  $PA$ . Then, the analysis expands to the forces that act on the bearings, gear housing, and so forth.

### 13.5.2.1 Resultant Force Acting in Perfect Intersected-Axes Gearing

In the plane-of-action, torque,  $T_{pa}$ , creates the plane-of-action tangential force,  $F_{pa}$ . The tangential force per unit length,  $f_{pa}$ , can be expressed in terms of the torque per unit length,  $t_{pa}$ , and the distance,  $r_{y.pa}$ , of a particular slice from the plane-of-action point,  $A_{pa}$ , as:

$$f_{pa} = \frac{t_{pa}}{r_{y.pa}} \quad (13.74)$$

It is instructive to point out here that the tangential force per unit length,  $f_{pa}$ , is a function of the distance,  $r_{y.pa}$ , of the point of interest,  $m$ , from the plane-of-action point,  $A_{pa}$ ; that is:

$$f_{pa} = f_{pa}(r_{y.pa}) \quad (13.75)$$

The distribution of the tangential force per unit length,  $f_{pa}(r_{y.pa})$ , in the radial direction of the plane of action is shown in [Figure 13.18b](#).

With the tangential force per unit length,  $f_{pa}$ , determined (see Equation 13.74), the resultant tangential force,  $F_{pa}$ , is calculated as:

$$F_{pa} = F_{pa} \cdot f_{pa} + t_{pa} \int_{r_{l.pa}}^{r_{o.pa}} \frac{1}{r_{y.pa}} dr_{y.pa} = F_{pa} \cdot f_{pa} + t_{pa} \cdot (\ln |r_{o.pa}| - \ln |r_{l.pa}|) \quad (13.76)$$

$$F_{pa} = F_{pa} \cdot f_{pa} + t_{pa} \cdot \ln \left| \frac{r_{o.pa}}{r_{l.pa}} \right| \quad (13.77)$$

Equations similar to Equation 13.77, that is:

$$F_g = F_{pa} \cdot f_g + t_g \cdot \ln \left| \frac{r_{o.pa}}{r_{l.pa}} \right| \quad (13.78)$$

$$F_p = F_{pa} \cdot f_p + t_p \cdot \ln \left| \frac{r_{o.pa}}{r_{l.pa}} \right| \quad (13.79)$$

are valid with respect to the gear as well as the mating pinion.

The resultant force,  $F_{pa}$ , is applied at a point,  $c_g$ , of the line of contact,  $LC$ , that is remote from the plane-of-action apex,  $A_{pa}$ , at a distance,  $r_{cg}$  ([Figure 13.18b](#)).

Transmission of a rotation from a driving shaft to a driven shaft is due to the tangential force,  $F_{pa}$ .

When the gears rotate, friction is observed between the gear tooth flank,  $\mathcal{G}$ , and the pinion tooth flank,  $\mathcal{P}$ . The friction between the compressed gear and pinion tooth flanks,  $\mathcal{G}$  and  $\mathcal{P}$ , is due to the sliding that occurs between tooth flanks,  $\mathcal{G}$  and  $\mathcal{P}$ . As already shown (see the previous section), two types of sliding are distinguished in intersected-axes gear pairs. Profile sliding is the first kind, and drag sliding is the second. Therefore, friction forces of two types need to be recognized, that is, the profile friction force,  $F_{pr}$ , and the friction force in the lengthwise direction,  $F_{dr}$ . These friction forces contribute to the resultant force of the interaction,  $F_{\Sigma}$ , between the gear tooth flank,  $\mathcal{G}$ , and the pinion tooth flank,  $\mathcal{P}$ :

$$F_{\Sigma} = F_{pa} + F_{pr} + F_{dr} \quad (13.80)$$

The component,  $F_{pa}$ , is specified by Equation 13.77.

In the reference system,  $X_{pa}Y_{pa}Z_{pa}$ , associated with the rotated plane of action,  $PA$ , the profile friction force,  $F_{pr}$ , is along the axis  $Z_{pa}$ , as illustrated in [Figure 13.19](#). The actual value of this component equals:

$$F_{pr} = \mu_{pr} \cdot F_{pa} \quad (13.81)$$

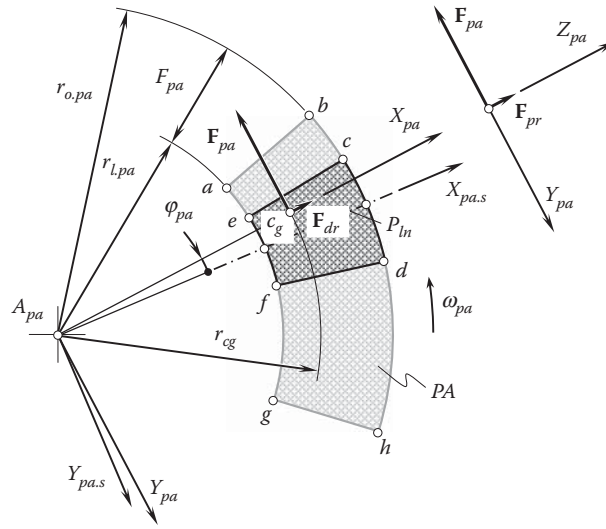


**FIGURE 13.19**  
Tangential force,  $F_{pa}$ , and friction forces,  $F_{pr}$  and  $F_{dr}$ , in intersected-axes gear pair.

Here,  $\mu_{pr}$  designates the coefficient of friction in profile sliding of the gear,  $\mathcal{G}$ , and pinion,  $\mathcal{P}$ , tooth flanks.

In that same reference system,  $X_{pa}Y_{pa}Z_{pa}$ , the friction force in the lengthwise direction,  $F_{dr}$ , is along the axis  $X_{pa}$ . The actual value of this component equals (Figure 13.19):

$$F_{dr} = \mu_{dr} \cdot F_{pa} \quad (13.82)$$

The coefficient of friction in drag sliding of the gear,  $\mathcal{G}$ , and pinion,  $\mathcal{P}$ , tooth flanks is denoted by  $\mu_{dr}$ .

The coefficients of friction,  $\mu_{pr}$  and  $\mu_{dr}$ , can be of different values, as the normal curvatures of the gear and the pinion tooth flanks,  $\mathcal{G}$  and  $\mathcal{P}$ , at point of interest are significantly different in the transverse and lengthwise directions of the tooth flanks,  $\mathcal{G}$  and  $\mathcal{P}$ . Moreover, the conditions of profile sliding and drag sliding are also different. However, when performing preliminary analysis, the coefficients of friction,  $\mu_{pr}$  and  $\mu_{dr}$ , can be considered equal to one another ( $\mu_{pr} = \mu_{dr}$ ).

The total friction force,  $F_{fr,\Sigma}$ , in perfect intersected-axes gearing is calculated as:

$$F_{fr,\Sigma} = F_{pr} + F_{dr} \quad (13.83)$$

The friction forces,  $F_{pr}$  and  $F_{dr}$ , in an intersected-axes gear pair are negligibly small; thus, commonly, they are not taken into account when calculating the design parameters of a gear transmission. Moreover, the friction forces,  $F_{pr}$  and  $F_{dr}$ , do not affect the uniformity of the output rotation in a gear pair, as both  $F_{pr}$  and  $F_{dr}$  are entirely located within a plane that is perpendicular to the plane of action,  $PA$  (i.e., tangent to the gear,  $\mathcal{G}$ , and pinion,  $\mathcal{P}$ , tooth flanks at the point of interest,  $m$ ). Only the component of the resultant force of the interaction,  $F_{\Sigma}$ , that is pointed along the common perpendicular to the tooth flanks,  $\mathcal{G}$  and  $\mathcal{P}$ , causes a rotation of the driven gear in an intersected-axes gear pair.

Different components of the resultant tangential force,  $F_{pa}$ , of the interaction between the tooth flanks,  $\mathcal{G}$  and  $\mathcal{P}$ , of a gear and a mating pinion, along with the forces  $F_g$  and  $F_p$  (see Equations 13.78 and 13.79) that act on the gear and the pinion are entered into equations for the calculation of the bending and contact strength of the gear and the pinion teeth, bearings, housing, shafts, and so forth.

The forces that act on the gear have to be expressed in a stationary coordinate system,  $X_{g,s}Y_{g,s}Z_{g,s}$ , associated with the motionless gear (i.e., associated with the gear pair housing). The operator,  $\mathbf{Rs}_{la}(pa \rightarrow g_s)$ , of the resultant coordinate system transformation can be used for this purpose. The operator,  $\mathbf{Rs}_{la}(pa \rightarrow g_s)$ , can be represented as a product of the operators,  $\mathbf{Rt}(Y_{g,s}, \Gamma_b)$ ,  $\mathbf{Rt}(Z_{g,s}, 90^\circ)$ ,  $\mathbf{Rt}(Z_{g,s}, \sigma_g)$ , and  $\mathbf{Rt}(Z_{3,s}, \varphi_{pa})$ , of the elementary linear transformations as:

$$\mathbf{Rs}_{la}(pa \rightarrow g_s) = \mathbf{Rt}(Y_{g,s}, \Gamma_b) \cdot \mathbf{Rt}(Z_{g,s}, 90^\circ) \cdot \mathbf{Rt}(Z_{3,s}, \sigma_g) \cdot \mathbf{Rt}(Z_{3,s}, \varphi_{pa}) \quad (13.84)$$

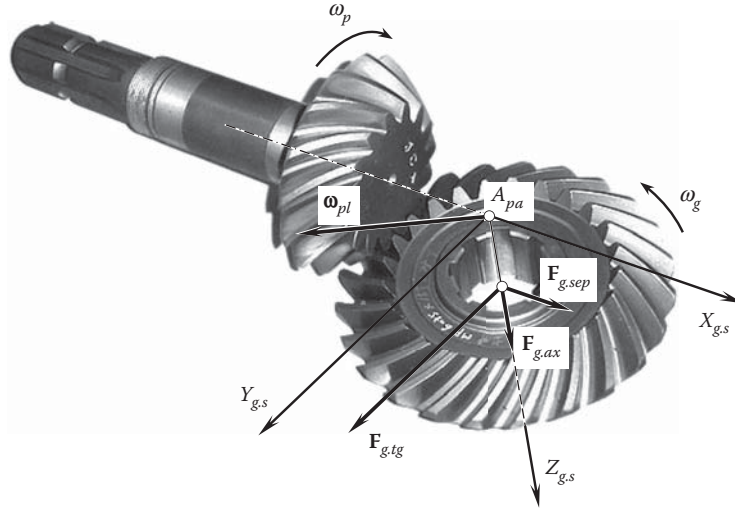


FIGURE 13.20

Forces that act on the gear in perfect intersected-axes gear pair.

After the resultant tangential force,  $\mathbf{F}_{pa}$  (see Equation 13.77), of the interaction between the tooth flanks,  $\mathcal{G}$  and  $\mathcal{P}$ , of a gear and a mating pinion, has been premultiplied by the operator,  $\mathbf{R}_{s_{la}}(pa \rightarrow g_s)$ , of the linear transformation, the resultant force,  $\mathbf{F}_{g,s}$ , that acts over the gear can be represented in the form of a column matrix:

$$\mathbf{F}_{g,s} = \mathbf{R}_{s_{la}}(pa \rightarrow g_s) \cdot \mathbf{F}_{pa} = \begin{bmatrix} F_{x,g,s} \\ F_{y,g,s} \\ F_{z,g,s} \\ 1 \end{bmatrix} \quad (13.85)$$

Referring to Figure 13.20, the components  $F_{x,g,s}$ ,  $F_{y,g,s}$ , and  $F_{z,g,s}$ , of the resultant force,  $\mathbf{F}_{g,s}$ , in Equation 13.85 are equal to the separating force,  $F_{g,sep}$ , the tangential force,  $F_{g,tg}$ , and the axial thrust,  $F_{g,ax}$ , correspondingly; that is, the equalities  $F_{x,g,s} = F_{g,sep}$ ,  $F_{y,g,s} = F_{g,tg}$ , and  $F_{z,g,s} = F_{g,ax}$ , are valid. The forces,  $\mathbf{F}_{g,sep}$ ,  $\mathbf{F}_{g,tg}$ , and  $\mathbf{F}_{g,ax}$ , are entered into the equations for the calculation of the design parameters of a gearbox.

### 13.5.2.2 Forces Acting on the Gear and the Pinion in Perfect Intersected-Axes Gearing

In a reference system,  $X_{pa}Y_{pa}Z_{pa}$ , associated with the rotated plane of action,  $PA$ , an orientation of the force,  $\mathbf{F}_{pa}$  (specified by Equation 13.77), or of the resultant force,  $\mathbf{F}_{\Sigma}$  (specified by Equation 13.80), does not alter when the gears rotate. However, the configuration of the coordinate system,  $X_{pa}Y_{pa}Z_{pa}$ , in relation to a motionless reference system associated with the gear pair housing alters when the gears rotate. Therefore, in a stationary coordinate system,  $X_{g,s}Y_{g,s}Z_{g,s}$ , associated with the motionless gear, Equation 13.85 has to be rewritten as:

$$\mathbf{F}_{g,s}(\varphi_g) = \begin{bmatrix} F_{g,sep}(\varphi_g) \\ F_{g,tg}(\varphi_g) \\ F_{g,ax}(\varphi_g) \\ 1 \end{bmatrix} \quad (13.86)$$

As follows from the analysis of Equation 13.86, the resultant force,  $\mathbf{F}_{g,s}$ , as well as all three components,  $\mathbf{F}_{g,sep}$ ,  $\mathbf{F}_{g,tg}$ , and  $\mathbf{F}_{g,ax}$ , that act over the gear depend on the angle of rotation of the gear; that is, all of them are functions the angle,  $\varphi_g$ , of rotation of the gear:

$$\mathbf{F}_{g,s} = \mathbf{F}_{g,s}(\varphi_g) \quad (13.87)$$

$$\mathbf{F}_{g,sep} = \mathbf{F}_{g,sep}(\varphi_g) \quad (13.88)$$



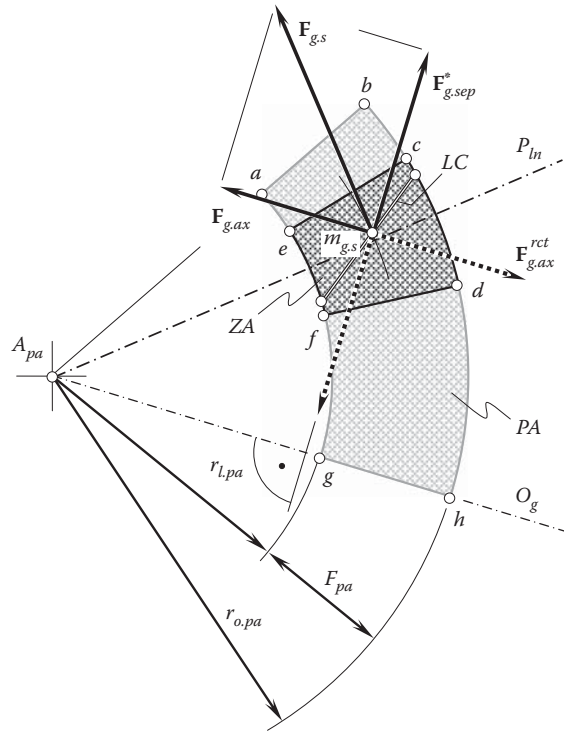


FIGURE 13.21

The axial thrust,  $F_{g,ax}(\varphi_g)$ , and the separating force,  $F_{g,sep}(\varphi_g)$ , as components of resultant force,  $F_{g,s}(\varphi_g)$ , of the interaction of the tooth flanks,  $\mathcal{G}$  and  $\mathcal{P}$ , of a gear and a mating pinion in perfect intersected-axes gear pair.

$$F_{g,tg} = F_{g,tg}(\varphi_g) \quad (13.89)$$

$$F_{g,ax} = F_{g,ax}(\varphi_g) \quad (13.90)$$

The resultant force,  $F_{g,s}(\varphi_g)$ , and the components,  $F_{g,sep}(\varphi_g)$ ,  $F_{g,tg}(\varphi_g)$ , and  $F_{g,ax}(\varphi_g)$ , that depend on the angular parameter,  $\varphi_g$ , are an additional source of vibration generation and noise excitation in intersected-axes gearing. When the gears rotate, the point of intersection of the axis of instant rotation,  $P_{ln}$ , and the instant line of action,  $LA_{instr}$ , must not migrate along the axis of instant rotation,  $P_{ln}$ , or, at least, the distance covered in this migration has to be minimized.

The variation of the forces has to be minimized in order to minimize vibration generation and noise excitation when an intersected-axes gear pair operates.

The variation of the direction of the resultant force,  $F_{g,s}(\varphi_g)$ , of the interaction of the tooth flanks,  $\mathcal{G}$  and  $\mathcal{P}$ , of a gear and a mating pinion is illustrated in Figure 13.21. For an arbitrary configuration of the line of contact,  $LC$ , between the tooth flanks,  $\mathcal{G}$  and  $\mathcal{P}$ , the coordinates of point,  $c_g$ , at which the resultant force,  $F_{g,s}$ , is applied can be determined. The component,  $F_{g,ax}$ , is parallel to the axis of rotation,  $O_g$ , of the gear. The component,  $F_{g,sep}$ , is perpendicular to the axis of rotation,  $O_g$ , of the gear. The magnitude,  $F_{g,sep}^*$ , shown in Figure 13.21 of the force vector,  $F_{g,sep}^*$ , equals  $F_{g,sep}^* = F_{g,sep} / \sin \phi_{t,\omega}$ , where  $\phi_{t,\omega}$  is the transverse pressure angle in the intersected-axes gear pair. (The separating force vector,  $F_{g,sep}$ , is entirely located in the normal  $N_{ln}$ -plane. In the case under consideration, the  $N_{ln}$ -plane is the plane through the axes of rotation,  $O_g$  and  $O_p$ , of the gear and the mating pinion, correspondingly.) As follows from the analysis of the schematic depicted in Figure 13.21, for any configuration of the line of contact,  $LC$ , for which the point,  $c_g$ , is located within the zone of action,  $ZA$ , the forces,  $F_{g,ax}$  and  $F_{g,sep}$ , never equal zero. Thus, the reaction forces,  $F_{g,ax}^{rct}$  and  $F_{g,sep}^{rct}$ , also have nonzero values. As the forces,  $F_{g,ax}^{rct}$  and  $F_{g,sep}^{rct}$ , fluctuate when the gears rotate (see Equations 13.88 and 13.90), excessive vibration generation and noise excitation can be observed when an intersected-axes gear pair operates. The variation of the forces,  $F_{g,ax}^{rct}$  and  $F_{g,sep}^{rct}$ , does not depend on the geometry of the line of contact,  $LC$ . This discussion is also valid in cases when multiple

lines of contact, as well as multiple portions of the lines of contact, are observed in a gear pair of a particular design, as the fluctuation of the forces,  $\mathbf{F}_{g.ax}^{rct}$  and  $\mathbf{F}_{g.sep}^{rct}$ , is inevitable in perfect intersected-axes gear pairs.

An analysis similar to that above can be performed with respect to loading of the pinion in a perfect intersected-axes gear pair.

As follows from the analysis of Equation 13.86, the resultant force,  $\mathbf{F}_{p.s}$ , as well as all three components,  $\mathbf{F}_{p.sep}$ ,  $\mathbf{F}_{p.tg}$ , and  $\mathbf{F}_{p.ax}$ , that act over the pinion depend on the angle of rotation of the pinion; that is, all of them are functions of the angle,  $\varphi_p$ , of rotation of the pinion:

$$\mathbf{F}_{p.s} = \mathbf{F}_{p.s}(\varphi_p) \quad (13.91)$$

$$\mathbf{F}_{p.sep} = \mathbf{F}_{p.sep}(\varphi_p) \quad (13.92)$$

$$\mathbf{F}_{p.tg} = \mathbf{F}_{p.tg}(\varphi_p) \quad (13.93)$$

$$\mathbf{F}_{p.ax} = \mathbf{F}_{p.ax}(\varphi_p) \quad (13.94)$$

The resultant force,  $\mathbf{F}_{p.s}(\varphi_p)$ , and the components,  $\mathbf{F}_{p.sep}(\varphi_p)$ ,  $\mathbf{F}_{p.tg}(\varphi_p)$ , and  $\mathbf{F}_{p.ax}(\varphi_p)$ , that depend on the angular parameter,  $\varphi_p$ , are an additional source of vibration generation and noise excitation in intersected-axes gearing. When the gears rotate, the point of intersection of the axis of instant rotation,  $P_{ln}$ , and the instant line of action,  $LA_{inst}$ , must not migrate along the axis of instant rotation,  $P_{ln}$ , or, at least, the distance covered in this migration has to be minimized.

For any configuration of the line of contact,  $LC$ , for which the point,  $c_{g'}$ , is located within the zone of action,  $ZA$ , the forces,  $\mathbf{F}_{p.ax}$  and  $\mathbf{F}_{p.sep}$ , never equal zero. Thus, the reaction forces,  $\mathbf{F}_{p.ax}^{rct}$  and  $\mathbf{F}_{p.sep}^{rct}$ , also have nonzero values. As the forces,  $\mathbf{F}_{p.ax}^{rct}$  and  $\mathbf{F}_{p.sep}^{rct}$ , fluctuate when the gears rotate, excessive vibration generation and noise excitation can be observed when an intersected-axes gear pair operates. The variation of the forces,  $\mathbf{F}_{p.ax}^{rct}$  and  $\mathbf{F}_{p.sep}^{rct}$ , does not depend on the geometry of the line of contact,  $LC$ . This discussion is also valid in cases when multiple lines of contact, as well as multiple portions of the lines of contact, are observed in a gear pair of a particular design, as the fluctuation of the forces,  $\mathbf{F}_{p.ax}^{rct}$  and  $\mathbf{F}_{p.sep}^{rct}$ , is inevitable in perfect intersected-axes gear pairs.

### 13.5.2.3 Normal Force Acting on the Gear in Perfect Intersected-Axes Gearing

For calculations of gear teeth for contact strength, as well as for contact strength, a component,  $\mathbf{F}_{g.nr}$  of the resultant force,  $\mathbf{F}_{g.s}$ , is entered into the corresponding equations for the calculations. This component is commonly referred to as the *normal force*,  $\mathbf{F}_{g.n}$ . The vector of normal load,  $\mathbf{F}_{g.nr}$  is located within the plane of action,  $PA$ , and is perpendicular to the line of contact,  $LC$ , at point,  $c_{g'}$ , at which the normal load is applied. The magnitude,  $F_{g.nr}$  of the normal force,  $\mathbf{F}_{g.nr}$  can be calculated as:

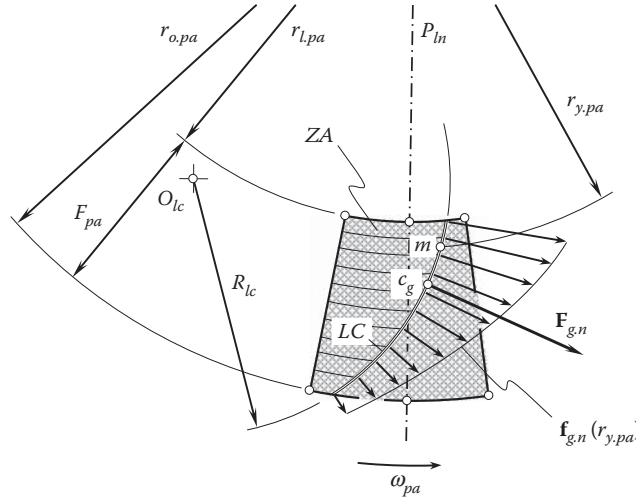
$$F_{g.n} = F_{g.s} \cos \psi_g \quad (13.95)$$

where  $\psi_g$  is the spiral angle of the gear teeth at point,  $c_{g'}$ .

The normal force per unit length,  $\mathbf{f}_{g.nr}$ , is also entirely located within the plane of action,  $PA$ . The normal force per unit length,  $\mathbf{f}_{g.nr}$ , depends on the geometry of a particular line of contact. At every point of the line of contact,  $LC$ , the applied normal load per unit length,  $\mathbf{f}_{g.nr}$ , is perpendicular to the line of contact at that point.

In straight bevel gearings, the normal force per unit length,  $\mathbf{f}_{g.nr}$ , is distributed quite similarly to that shown in [Figure 13.18b](#) for the force per unit length,  $\mathbf{f}_{pa}(r_{y,pa})$ . In skew bevel gearings, the normal force per unit length,  $\mathbf{f}_{g.nr}$ , is distributed similarly to that in straight bevel gearings—all the elementary forces are perpendicular to the line of contact,  $LC$ . The distribution of the normal force per unit length,  $\mathbf{f}_{g.nr}$ , in spiral bevel gearings with a circular-arc line of contact,  $LC$ , of a radius,  $R_{lc}$ , is illustrated in [Figure 13.22](#). In this case, all the elementary forces are along the radius,  $R_{lc}$ , to the corresponding point,  $m$ , within the line of contact,  $LC$ .

In a more general case of perfect intersected-axes gearings, in face-hobbed bevel gears in particular, the following approach can be used to determine the distribution of the normal force per unit length along the line of contact,  $LC$ . First, the unit normal vector,  $\mathbf{n}_{lc}$ , is constructed at every point of the line of contact,  $LC$ . Second, the distribution of the normal load per unit length,  $\mathbf{f}_{g.nr}$ , is constructed as a product of the unit vector,  $\mathbf{n}_{lc}$ , by the function of the distribution of the magnitude,  $f_{g.nr}$ , of the normal load per unit length; that is,  $\mathbf{f}_{g.n} = f_{g.n} \cdot \mathbf{n}_{lc}$ .

**FIGURE 13.22**

Normal force,  $F_{g,n}$ , and normal force per unit length,  $f_{g,n}$ , acting in perfect intersected-axes gear pair.

When two or more lines of contact (or portions of the lines of contact),  $LC_i$ , are observed, then the position vector,  $\mathbf{r}_{cg,\Sigma}$ , of the point,  $c_{g,\Sigma}$ , at which the resultant load,  $F_{g,n,\Sigma}$ , is applied can be calculated as:

$$\mathbf{r}_{cg,\Sigma} = \frac{\sum_i l_{lc,i} \cdot \mathbf{r}_{cg,i}}{\sum_i l_{lc,i}} \quad (13.96)$$

where:

$i$  is the number of a line of contact (or a portion of a line of contact),  $LC_i$ .

$l_{lc,i}$  is the length of a line of contact (or a portion of a line of contact),  $LC_i$ .

$\mathbf{r}_{cg,i}$  is the position vector of a point,  $c_{g,i}$ , of a line of contact (or a portion of a line of contact),  $LC_i$ .

$\sum_i l_{lc,i}$  is the total length,  $TLLC$ , of all the lines of contact,  $l_{lc,i}$ .

The performed analysis of the forces that act in external intersected-axes gearing can also be enhanced to internal intersected-axes gearing, as well as to *pinion-gear-to-rack mesh*, as the latter is a reduced case of external intersected-axes gearing.

## 13.6 Testing of Perfect Spiral Bevel Gears: Contact Pattern

A CAD model of a right-angle spiral bevel gear pair was developed in compliance with the proposed method of designing bevel gears for perfect intersected-axes gear pairs. The accuracy of the developed CAD model has been verified by comparing the sections of the tooth flanks,  $\mathcal{G}$  and  $\mathcal{P}$ , by a plane tangent to the base cone of the gear (and the pinion). In all cases, the interacting tooth flanks,  $\mathcal{G}$  and  $\mathcal{P}$ , of the gear and mating pinion make line contact with each other.

### 13.6.1 Conditions for Testing

A few sets of perfect spiral bevel gears are manufactured for testing purposes [132–134]. A five-axis NC machine was used to cut the tooth flanks of the gear and pinion.

The developed CAD models were used for rapid prototyping and for converting to a G-code for cutting bevel gears of the proposed design\* on a five-axis NC machine (Figure 13.23). When cutting the gears, the radius of

\* Patent pending.



**FIGURE 13.23**  
Spiral bevel gear and a mating pinion cut on a five-axis NC machine.

curvature,  $R_{lc}$ , of the desirable line of contact,  $LC_{des}$ , is set equal to both the convex and concave tooth flanks,  $\mathcal{G}$  and  $\mathcal{P}$ , of the gear and the pinion ( $R_{lc} = 200$  mm). The tolerances for tooth flank accuracy are of the same magnitude,  $\delta$ , but of the opposite sign; that is, the radius  $R_{lc}$  is set equal to  $200^0_{-\delta}$  for the convex tooth flanks  $\mathcal{G}$  and  $\mathcal{P}$ , and equal to  $200^{\delta}_0$  for the concave tooth flanks.

The accuracy of the machined spiral bevel gears was verified by means of the laser scanning of the machined tooth flanks with the consequent comparison of the scanned data with the corresponding points generated by the CAD model. The actual tooth flanks of the gear and the pinion deviate from the desirable tooth flanks,  $\mathcal{G}$  and  $\mathcal{P}$ , less than 0.01 mm.

Before running a contact pattern test, the contact geometry of the bevel gears of the developed design was investigated in comparison to that of a similar gear set cut using Gleason method of gear generating. The comparison is performed based on the developed CAD models.

### 13.6.2 Predicting Contact Geometry in Perfect Spiral Bevel Gearing

When a bevel gear tooth flank is generated following the Gleason method of gear generating, the contact patch (Figure 13.24) is of a nonuniform width that is evident from the analysis of contact patches at a low load (Figure 13.24a), as well as at a high load (Figure 13.24b). The contact patches are considered only within the active face width, that is, where the tooth flanks,  $\mathcal{G}$  and  $\mathcal{P}$ , overlap one another.

These two types of contact patch convince us that geometrically, the gear and pinion tooth flanks make contact at a distinct point, not along a line. Because of the point contact, contact stresses in the vicinity of the contact points always have an increased value.

Point contact between the tooth flanks of bevel gears cut by the Gleason method is the result of violation of the second and third conditions for perfect bevel gear tooth flank generation. The violation of the second and third conditions occurs because the geometry of the tooth flank of the imaginary crown rack that is generated by the cutting edges of the face-milling cutter deviates from that of the desirable imaginary crown rack. In cases of gears with a large tooth count, these deviations are usually small and often can be ignored. In cases of gears with a few teeth, the deviations become much larger and cannot be ignored, especially in cases of precision bevel gears.

In cases of perfect spiral bevel gears, the contact patch is of a uniform width (Figure 13.25). Therefore, the gear and pinion tooth flanks make line contact with each other, and not point contact. The line contact between tooth flanks,  $\mathcal{G}$  and  $\mathcal{P}$ , is observed due to all three conditions for perfect gearings being fulfilled in the case of perfect spiral bevel gearing. Line contact between the tooth flanks,  $\mathcal{G}$  and  $\mathcal{P}$ , results in a uniform loading of the bearing surfaces,  $\mathcal{G}$  and  $\mathcal{P}$ , and in the corresponding reduction of the contact stresses.

When the gear tooth flanks are in line contact, it is anticipated that the contact pattern will spread over the entire tooth flank of the gear and the pinion, as shown in Figure 13.26.

The actual contact pattern in the machined gears (see Figure 13.23) spreads over the entire tooth flank of the gear and the pinion, as shown Figure 13.27 (and as predicted in Figure 13.26). This type of contact pattern is the most favorable, as it makes possible even loading of all portions of the gear and pinion tooth flanks.

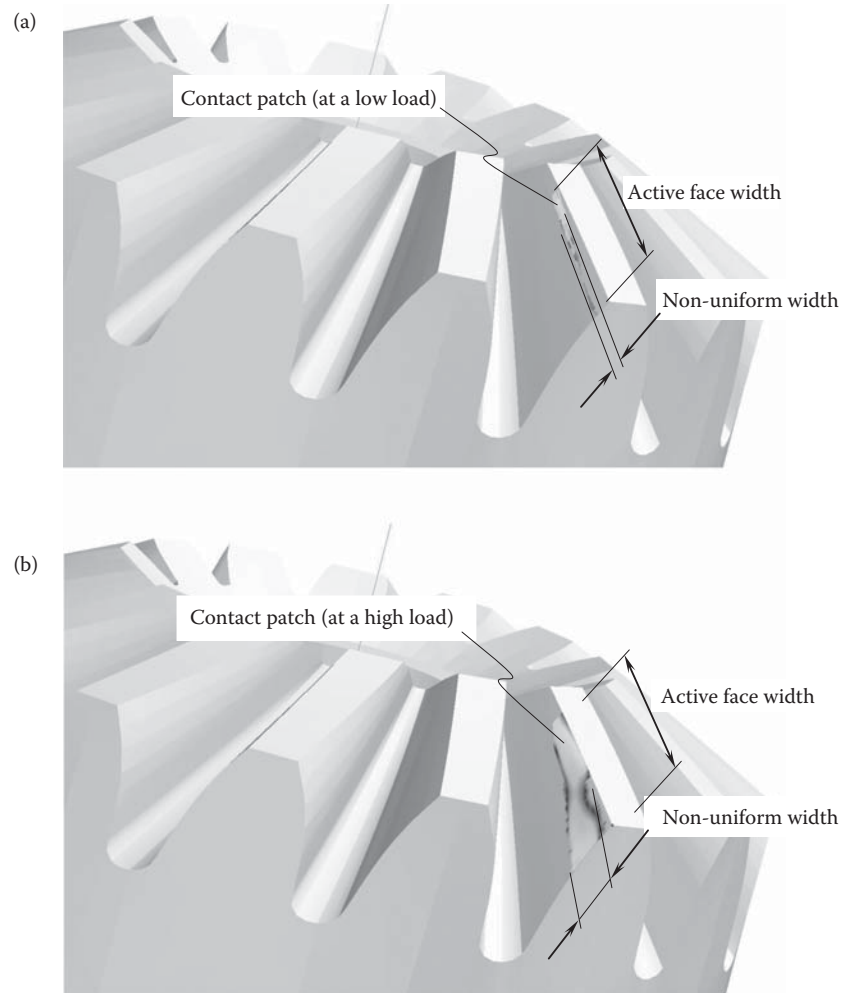


**FIGURE 13.24**  
Contact patch under a low and high load in gears cut by the Gleason method.

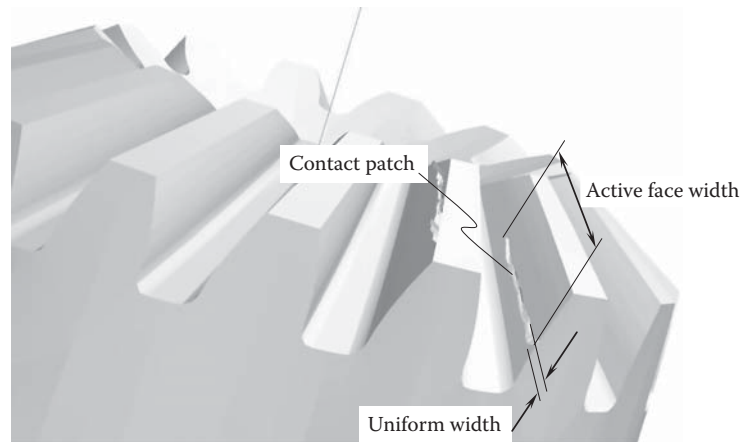


**FIGURE 13.25**  
Contact patch in perfect spiral bevel gears.

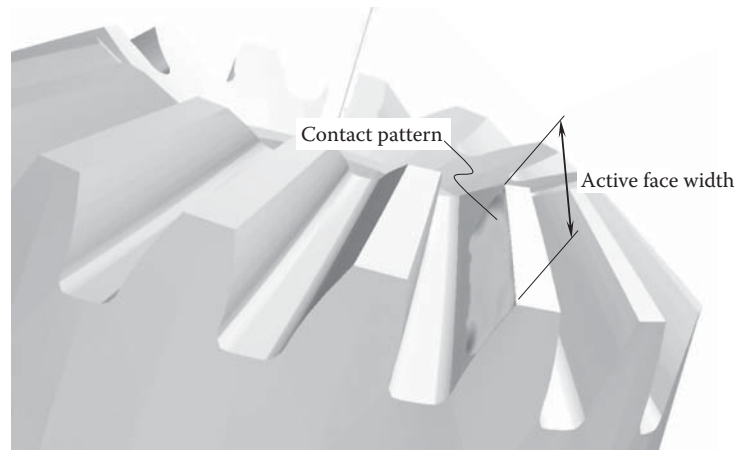


**FIGURE 13.26**  
The anticipated contact pattern in perfect intersected-axes gearing.

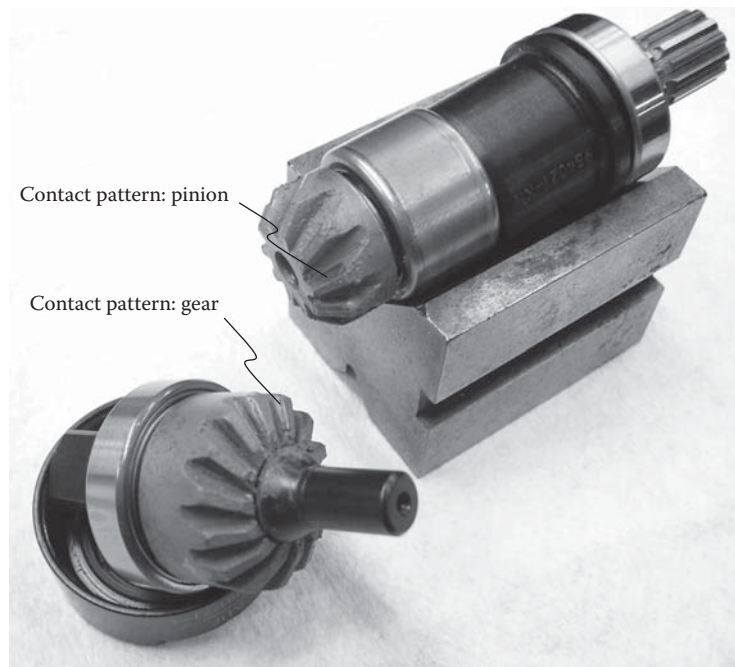


**FIGURE 13.27**  
Contact pattern in perfect spiral bevel gears.

As all three conditions with which perfect gearings have to comply are fulfilled in the discussed design of perfect spiral bevel gears, the tooth flanks of the gear and mating pinion are always in line contact with one another. Line contact of the tooth flanks is favorable, as it allows for a reduction of contact stress. The power density can be increased and the noise excitation can be reduced, and performance of the gear pair as a whole can be significantly improved.

Perfect intersected-axes gear pairs can operate at high rotations. Therefore, gearing of this type can be used as a first stage in a gear train, where rotations are higher but the applied torque is lower. The applied forces are lower when the torque is lower. Ultimately, bearings of a simpler design can be used in an intersected-axes gear pair that operates at lower loads.



## Section II-C

# Perfect Gearing: Crossed-Axes Gearing

Gear pairs used for the transmission of rotation between two shafts that cross the axis of rotation are referred to as *crossed-axes gear pairs*, or simply as  $C_a$ -gearing. Numerous kinds of intersected-axes gearings are extensively used in the current industry. All of them are approximate gearings, as they feature a variable angular velocity ratio,  $u = \omega_{input}/\omega_{output} = \text{var}$ . Amazingly, only approximate  $C_a$ -gears have been investigated so far (Baxter [4,5], Dooner [21,22], Dudas, [23], Dusev and Vasilyev [25], Dyson [26], Klingelnberg [54], Krenzer [61], Litvin [69], Lopato et al. [71], Phillips [89], Pismanik [90], Shevel'ova [146], Shtipelman [150], Stadtfeldt [153,154], Wang and Ghosh [160], Wildhaber [162], Wu and Luo [166], Zak [169], Zhuravlov and Iofis [170], and others). This is mostly because the gears for approximate intersected-axes gear pairs are easier to produce on available gear generators and by means of gear-cutting tools available on the market. No perfect intersected-axes gearings with the desired tooth flank geometry have been investigated so far, as this particular kind of intersected-axes gearing is not developed yet.

Perfect intersected-axes gearings are discussed below in this section.

Referring to [Figure 2.15](#), crossed-axes gear pairs make up the first stratum of the classification of possible kinds of vector diagrams of gear pairs.

Every possible type of crossed-axes gear pairs can be specified by a corresponding vector diagram. Use of the vector diagrams, along with the developed classification of possible types of vector diagrams of gear pairs (see [Figure 2.15](#)), makes possible a comprehensive analysis of gearing of this particular kind. All possible kinds of crossed-axes gear pairs are incorporated into the analysis, and none can be missed if the consideration is based on the classification (see [Figure 2.15](#)).

This subsection of the monograph consists of three chapters—[Chapters 14 through 16](#).





# Taylor & Francis

Taylor & Francis Group

<http://taylorandfrancis.com>

## Perfect Crossed-Axes Gear Pairs: R-Gearing

Early designs of crossed-axes gears can be found in da Vinci's famous book, *The Madrid Codices* [17].

Crossed-axes gears have extensive application in the current industry. When a motion is to be transmitted between two shafts whose axes cross, some form of bevel-like gear is applied, as illustrated in [Figure 14.1](#). Although gears of this kind are often made for a shaft angle of  $90^\circ$ , they can be produced for almost any shaft angle.

### 14.1 Kinematics of Crossed-Axes Gearing

Transmission and transformation of rotation from a driving shaft to a driven shaft is the main purpose of application of crossed-axes gears. Both the input rotation and the output rotation can be easily represented by corresponding rotation vectors,  $\omega_g$  and  $\omega_p$ . The rotation vectors,  $\omega_g$  and  $\omega_p$ , are along straight lines that cross one another. The closest distance of approach between the lines of action of the rotation vectors,  $\omega_g$  and  $\omega_p$ , is denoted by  $C$ . This distance is commonly referred to as the *center distance*,  $C$ . It is convenient to refer to [Figures 2.8](#) and [2.9](#) when investigating perfect crossed-axes gearing.

The variety of all possible types of vector diagrams of crossed-axes gear pairs is limited to the total number of possible combinations of the rotation vectors,  $\omega_g$  and  $\omega_p$ , (a) of various magnitudes and (b) featuring different shaft angles  $\Sigma$  [remember that the shaft angle,  $\Sigma$ , is specified as the angle between the rotation vector,  $\omega_g$ , of a gear and the rotation vector,  $\omega_p$ , of a mating pinion; that is,  $\Sigma = \angle(\omega_g, \omega_p)$ ].

The total number of vector diagrams for different types of crossed-axes gear pairs is limited to just three diagrams when the actual configuration of the rotation vectors,  $\omega_g$  and  $\omega_p$ , of a gear and mating pinion in relation to the vector of instant rotation,  $\omega_{pl}$ , is taken into account. These vector diagrams are depicted in [Figure 14.2](#). Therefore, only three different types of crossed-axes gear pairs are feasible.

The vector diagram shown in [Figure 14.2a](#) features an obtuse gear angle,  $\Sigma_g$ , between the rotation vector,  $\omega_g$ , of the gear and the vector of instant rotation,  $\omega_{pl}$ . The gear angle,  $\Sigma_g$ , can be expressed in terms of the shaft angle,  $\Sigma$ , and the magnitudes,  $\omega_g$  and  $\omega_p$ , of the rotation vectors,  $\omega_g$  and  $\omega_p$ , as:

$$\Sigma_g = \tan^{-1} \left( \frac{\sin \Sigma}{\omega_p / \omega_g + \cos \Sigma} \right) \quad (14.1)$$

For a shaft angle of  $90^\circ$ , Equation 14.1 reduces to:

$$\Sigma_g = \tan^{-1} \left( \frac{\omega_g}{\omega_p} \right) \quad (14.2)$$

The formulae for the calculation of the pinion angle,  $\Sigma_p$ , are similar to Equations 14.1 and 14.2:

$$\Sigma_p = \tan^{-1} \left( \frac{\sin \Sigma}{\omega_g / \omega_p + \cos \Sigma} \right) \quad (14.3)$$



**FIGURE 14.1**  
A crossed-axes gear pair.

and for a right shaft angle, this reduces to:

$$\Sigma_p = \tan^{-1} \left( \frac{\omega_p}{\omega_g} \right) \quad (14.4)$$

For a gear pair of this particular type ( $\Sigma > 90^\circ$ ), the relation  $\Sigma_g = \angle(\omega_g, \omega_{pl}) > 90^\circ$  is valid. This relation can be represented in an equivalent form as:

$$\omega_g \cdot (\omega_p - \omega_g) < 0 \quad (14.5)$$

or

$$\frac{\omega_g \cdot (\omega_p - \omega_g)}{|\omega_g| \cdot |\omega_p - \omega_g|} = -1 \quad (14.6)$$

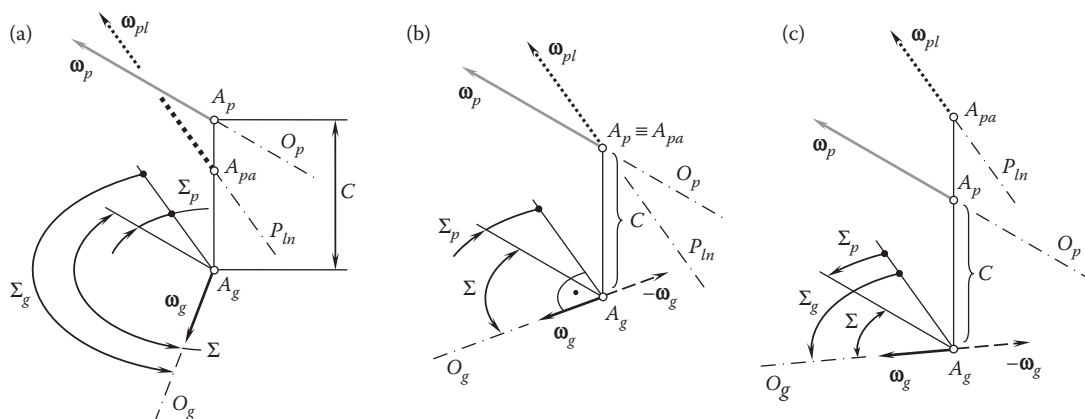


**FIGURE 14.2**  
The total number of possible types of vector diagrams for crossed-axes gear pairs is limited to just three vector diagrams: (a) internal, (b) rack-type, and (c) external gear pairs.

The center distance,  $C$ , can be interpreted as the summa of the pitch radii of the gear,  $r_g$ , and the pinion,  $r_p$ :

$$C = r_g + r_p \quad (14.7)$$

For external crossed-axes gearing of all types, both pitch radii,  $r_g$  and  $r_p$ , are positive (i.e.,  $r_g > 0$ ,  $r_p > 0$ ). The earlier-derived formulas (see Equations 2.61 and 2.62):

$$r_g = \frac{1 + \omega_p - \omega_g}{1 + \omega_p} \cdot C \quad (14.8)$$

$$r_p = \frac{1 + \omega_g - \omega_p}{1 + \omega_g} \cdot C \quad (14.9)$$

can be used for the calculation of the pitch radii,  $r_g$  and  $r_p$ , of the gear and mating pinion, respectively.

The vector diagram (Figure 14.2a) corresponds to an external crossed-axes gearing.

The configuration of the rotation vector of the gear,  $\omega_g$ , in relation to the vector of instant rotation,  $\omega_{pl}$ , is critical for the determination of whether a gear pair is external, while the relative configuration of the rotation vectors,  $\omega_g$  and  $\omega_p$ , is of secondary importance in this consideration.

In a particular case, the rotation vector of the gear,  $\omega_g$ , can be orthogonal to the vector of instant rotation,  $\omega_{pl}$ ; that is,  $\Sigma_g = \angle(\omega_g, \omega_{pl}) = 90^\circ$ . Two equivalent forms of this requirement:

$$\omega_g \cdot (\omega_p - \omega_g) = 0 \quad (14.10)$$

and

$$\frac{\omega_g \cdot (\omega_p - \omega_g)}{|\omega_g| \cdot |\omega_p - \omega_g|} = 1 \quad (14.11)$$

are valid for crossed-axes gearing.\*

Crossed-axes gear pairs for which the condition  $\omega_g \perp \omega_{pl}$  is fulfilled feature pitch radii of the values  $r_g = 0$  and  $r_p = C$ , accordingly (the condition  $C = r_g + r_p$  is still valid).

The vector diagram for gear drives of this particular type is schematically depicted in Figure 14.2b. The vector diagram corresponds to a crossed-axes gear pair composed of a round rack (or a face gear, in other words) and a conical pinion. Crossed-axes gearing of this type is analogous to the aforementioned pinion-to-rack gearing in the case of the parallel axes of the gear and the pinion.

Ultimately, a crossed-axes gear pair may feature an acute angle,  $\Sigma_g$ , between the rotation vector,  $\omega_g$ , of the gear and the vector of instant rotation  $\omega_{pl}$  (Figure 14.2c). For a gear pair of this particular type, the relation  $\Sigma_g = \angle(\omega_g, \omega_{pl}) < 90^\circ$  is valid. The last expression can be represented in the following two forms:

$$\omega_g \cdot (\omega_p - \omega_g) > 0 \quad (14.12)$$

and

$$\frac{\omega_g \cdot (\omega_p - \omega_g)}{|\omega_g| \cdot |\omega_p - \omega_g|} = +1 \quad (14.13)$$

\* While a rotation vector,  $\omega_g$ , can be perpendicular to the vector of instant rotation,  $\omega_{pl} = (\omega_p - \omega_g)$ , the perpendicularity of a rotation vector,  $\omega_p$ , to the vector of instant rotation,  $\omega_{pl}$ , is not considered here, as the magnitude,  $\omega_p$ , of the rotation vector,  $\omega_p$ , is smaller compared to the magnitude,  $\omega_g$ , of the rotation vector,  $\omega_g$ ; that is, the inequality,  $\omega_p < \omega_g$ , is always observed.

TABLE 14.1

Analytical Criteria of Type of Crossed-Axes Gearing

Type of Intersected-Axes Gearing	Analytical Criterion [ $C \neq 0$ and $\Sigma \neq 0$ ]
External crossed-axes gear pair	$\omega_g \cdot (\omega_p - \omega_g) < 0$
Rack-type crossed-axes gear pair	$\omega_g \cdot (\omega_p - \omega_g) = 0$
Internal crossed-axes gear pair	$\omega_g \cdot (\omega_p - \omega_g) > 0$

Crossed-axes gear pairs for which the condition  $\omega_g \perp \omega_{pl}$  is fulfilled feature pitch radii of the values  $r_g < 0$  and  $r_p > 0$  (the condition  $C = r_g + r_p$  is still valid).

A vector diagram of the type (Figure 14.2c) corresponds to internal crossed-axes gearing.

The analytically expressed conditions (see Equations 14.5 through 14.10), along with Equation 14.12, are summarized in Table 14.1.

Any and all crossed-axes gear pairs meet one of three expressions those listed in Table 14.1.

In particular cases, the centerlines of the driving shaft and the driven shaft cross each other at a right angle ( $\Sigma = 90^\circ$ ). This particular case is the most common in practice. Crossed-axes gear pairs of this particular type are referred to as *orthogonal crossed-axes gear pairs*. For gearing of this particular type, the cross-product of the rotation vectors of the gear,  $\omega_g$ , and the pinion,  $\omega_p$ , is always equal to zero ( $\omega_g \times \omega_p = 0$ ).

An orthogonal crossed-axes gear pair may feature equal tooth counts of the gear,  $N_g$ , and the pinion,  $N_p$  (i.e.,  $N_g = N_p$ ). Crossed-axes gearing of this particular type fulfills the requirement  $\omega_g \times \omega_p = 0$ . It is evident that the magnitudes,  $\omega_g$  and  $\omega_p$ , of the rotation vectors,  $\omega_g$  and  $\omega_p$ , in this case are equal ( $\omega_g = \omega_p$ ). Gearings of this particular kind are often referred to as *miter gears*.

#### 14.1.1 Pressure Angle in Crossed-Axes Gearing

The pressure angle is an important design parameter in gearings of all types and in crossed-axes gearing in particular. Performance of a crossed-axes gear pair strongly depends on the actual value of the transverse pressure angle. Accurate specification of the transverse pressure angle is vital when designing crossed-axes gear pairs. This problem becomes even more vital when high power density of a gear transmission is required.

#### 14.1.2 Crossed-Axes Gearing with Constant Transverse Pressure Angle

Crossed-axes gear pairs feature a transverse section that is shaped in the form of a sphere centered at the plane-of-action apex,  $A_{pa}$ . The transverse pressure angle,  $\phi_{t,\omega}$  is specified in the following manner.

First, a plane,  $C_{ln}^*$ , through a point of interest,  $m$ , parallel to the centerline plane,  $C_{ln}$ , is constructed, as illustrated in Figure 14.3. The point,  $m$ , is within the portion of the axis of instant rotation,  $P_{ln}$ , that is located within the face width,  $F_{ap}$ . The plane,  $C_{ln}^*$ , intersects the axes of rotation of the gear and the mating pinion,  $O_g$  and  $O_p$ , at points  $a$  and  $b$ . The straight line is entirely located within the plane,  $C_{ln}^*$ .

Second, a straight line through a point,  $m$ , perpendicular to the straight line segment,  $ab$ , is constructed. This perpendicular is within the plane,  $C_{ln}^*$ .

The actual value of the transverse pressure angle,  $\phi_{t,\omega}$ , is measured within the plane,  $C_{ln}^*$ , between the above-mentioned perpendicular and the pitch-line plane, as shown in Figure 14.3. Note that the pitch-line plane and the plane of action,  $PA$ , are congruent to one another (i.e.,  $P_{ln}$ -plane  $\equiv$  plane of action,  $PA$ ).

When the pressure angle,  $\phi_{t,\omega}$ , alters within the effective face width,  $F_{pa}$ , the *path-of-contact surface*,  $PCS$ , is generated. The path-of-contact surface can be viewed as a continuous set of the circular-arc paths of contact,  $P_c$ , at different pressure angles,  $\phi_{t,\omega}$ . The radius of a current circular-arc path of contact is a *linear* function of the distance of point on the pitch line,  $P_{ln}$ , from the plane-of-action-apex,  $A_{pa}$ . The path-of-contact surface,  $PCS$ , is a continuous screw surface generated by the circular arcs of a variable radius.

As the inclination of straight line segment,  $ab$ , depends on the position of point of interest,  $m$ , the actual value of the transverse pressure angle,  $\phi_{t,\omega}$ , varies along the axis of instant rotation,  $P_{ln}$ . For gears with a large tooth count, this variation can be negligibly small. For gears with a low tooth count (*LTC-gears*), the variation can be significant and should not be ignored.

However, the entire tooth flank of a gear,  $\mathcal{G}$ , and that of a mating pinion,  $\mathcal{P}$ , in both cases is constructed from the corresponding base cones with constant base-cone-angles,  $\Gamma_b$  and  $\gamma_b$ .

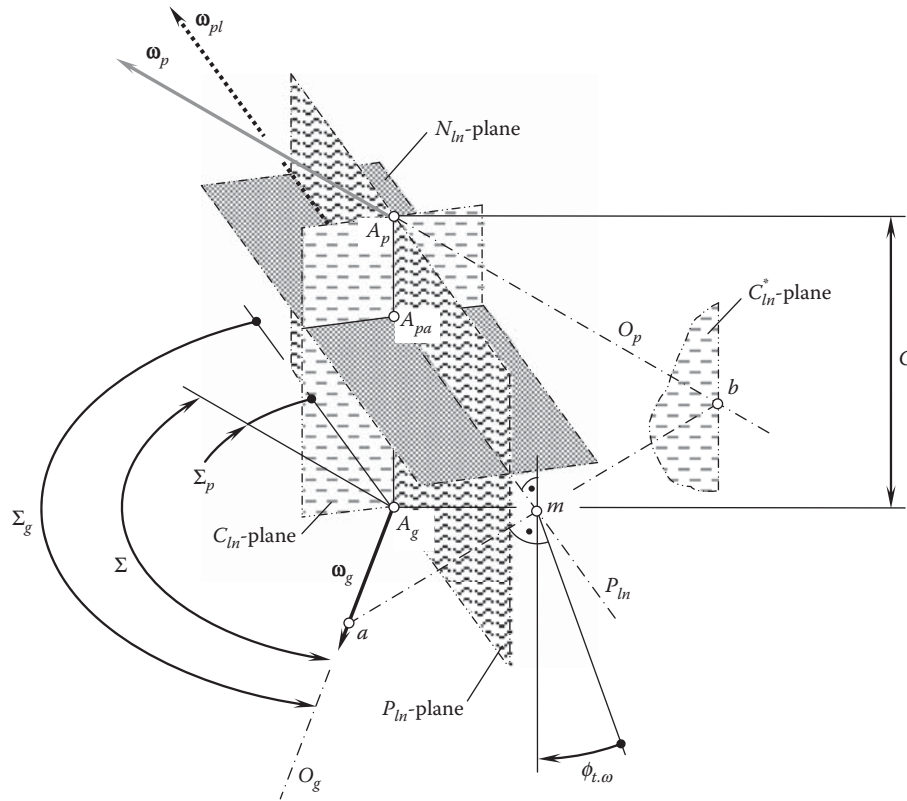


FIGURE 14.3  
Transverse pressure angle,  $\phi_{t,\omega}$ , in a crossed-axes gear pair.

### 14.1.3 Crossed-Axes Gearing with Variable Transverse Pressure Angle

The set of three conditions that perfect crossed-axes gearings have to fulfill, formulated above, is helpful to realize a possibility of  $C_a$ -gearing with the transverse pressure angle,  $\phi_{t,\omega} = \text{var}$  variable within the active portion of the face width,  $F_{pa}$ . The possibility of variation of the transverse pressure angle,  $\phi_{t,\omega}$ , is necessary when solving a problem of synthesizing a crossed-axes gear pair with favorable design parameters, that is, of a crossed-axes gear pair with a desired performance.

The plane of action,  $PA$ , can be subdivided into an infinite number,  $dr_{pa}$ , of infinitesimally narrow round strips. The distance between points  $m_{i-1}$ , and  $m_i$ , as well as between points  $m_i$  and  $m_{i+1}$ , equals  $dr_{pa}$ , as illustrated in Figure 14.4. All the strips are through the axis of instant rotation,  $P_{ln}$ . The transverse pressure angle,  $\phi_{t,\omega}$ , can be set to a favorable value for each of the strips; that is, in this way, the transverse profile angle,  $\phi_{t,\omega}$ , is involved in the synthesizing process of the favorable gear pair. Under such a scenario, the plane of action,  $PA$ , is replaced by the family of narrow strips that form a surface of action,  $SA$ . The surface of action,  $SA$ , is a kind of ruled surface, each straight line of which is a straight line through the axis of instant rotation,  $P_{ln}$ . At every point of the surfaces of action,  $SA$ , the transverse pressure angle,  $\phi_{t,\omega}$ , can have the most favorable value.

In this case, the entire tooth flank of a gear,  $\mathcal{G}$ , and that of a mating pinion,  $\mathcal{P}$ , is constructed from an infinite number of base cones with different base-cone-angles,  $\Gamma_b$  and  $\gamma_b$ , in each round strip of the plane of action,  $PA$ .

Gears with a variable pressure angle,  $\phi_{t,\omega}$ , can be cut on a multiaxis NC machine.

## 14.2 Base Cones in Crossed-Axes Gear Pair

Perfect crossed-axes gear pairs (or, in other words, *geometrically accurate* or *ideal* crossed-axes gear pairs) are capable of transmitting a rotation smoothly. For gearings of this kind, the angular velocity ratio has a constant

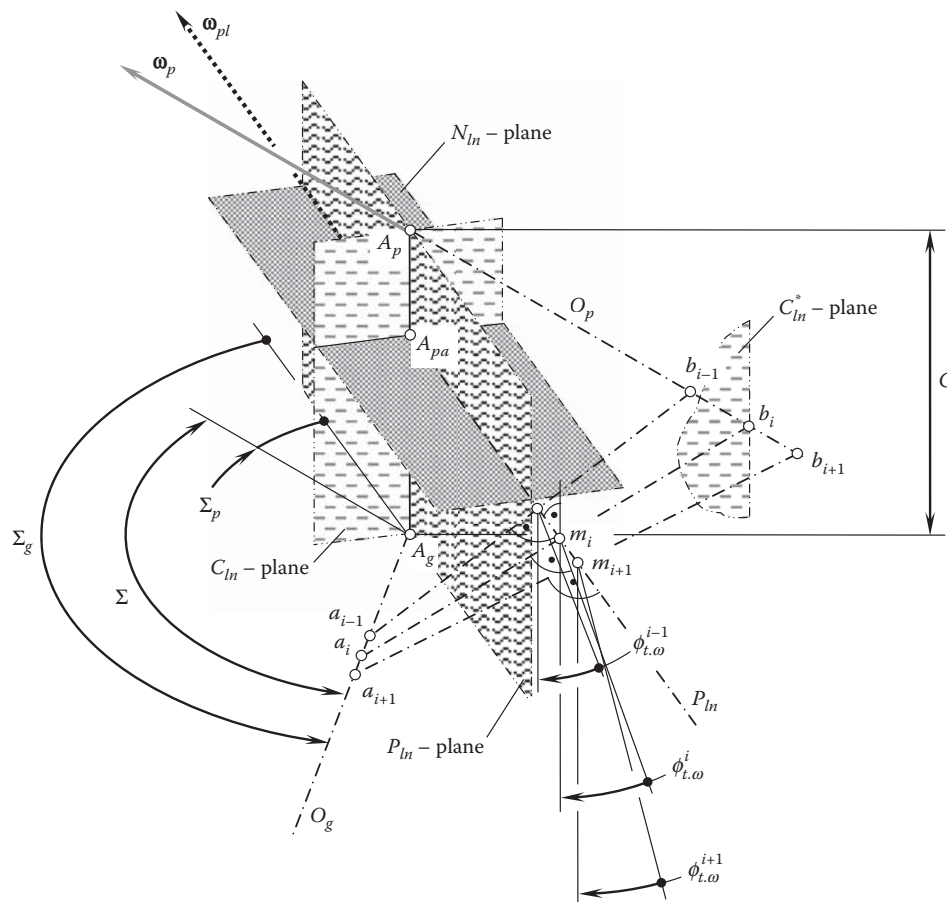


FIGURE 14.4

Variable transverse pressure angle,  $\phi_{t,\omega}$ , in a crossed-axes gear pair.

value,  $\omega_p/\omega_g = \text{const}$ . From this perspective, perfect crossed-axes gear pairs resemble the earlier-discussed perfect parallel-axes gear pairs and perfect crossed-axes gear pairs. This similarity can be extended further; that is, crossed-axes gearings of a particular type can also transmit a uniform rotation from a driving shaft to a driven shaft.

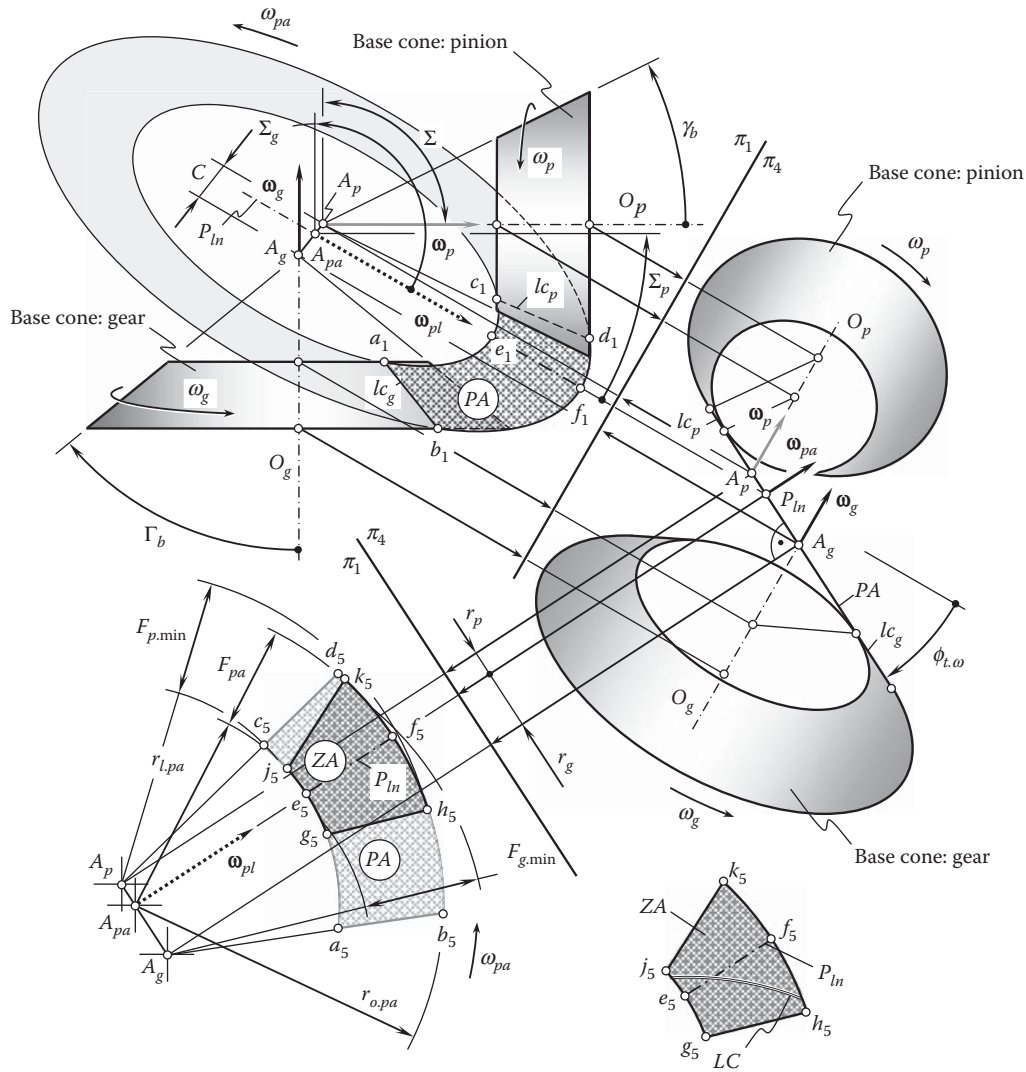
It should be noted here that in a case of crossed axes of rotation of the driving shaft and the driven shaft, there is no freedom in choosing a configuration of the axis of instant rotation,  $P_{ln}$ , in relation to the rotation vectors,  $\omega_g$  and  $\omega_p$ . Once the rotation vectors,  $\omega_g$  and  $\omega_p$ , and their relative location and orientation are specified, the configuration of the axis of instant rotation,  $P_{ln}$ , can be expressed in terms of the rotations,  $\omega_g$  and  $\omega_p$ , and the center distance,  $C$ .

Recall that perfect parallel-axes gear pairs feature two base cylinders (see Figure 8.26). Smooth rotation of the base cylinders allows for an interpretation as a corresponding *pulley-and-belt* mechanism. Then, two base cones\* are associated with the gear and pinion in a crossed-axes gearing (see Figure 12.10). Smooth rotation of the base cones can be interpreted as a pulley-and-belt mechanism with the belt in the form of a round tape. The pulley-and-belt analogy is also valid with respect to perfect crossed-axes gearing.

A base cone can be associated with the gear, and another base cone can be associated with the pinion of any and all perfect crossed-axes gear pairs. This concept is schematically illustrated in Figure 14.5. The axis of rotation of the gear,  $O_g$ , and the axis of rotation of the pinion,  $O_p$ , cross each other at a shaft angle,  $\Sigma$ . The closest distance of approach of the axes of rotations,  $O_g$  and  $O_p$ , is denoted by  $C$ . An orthogonal crossed-axes gear pair is shown here solely for illustrative purposes. Without going into detail on the analysis, it should be stated here that that same approach is applicable with respect to angular bevel gears with a shaft angle  $\Sigma \neq 90^\circ$ , namely either an obtuse or acute shaft angle  $\Sigma$ .

\* A skew base surface that is locally approximated by the base cone. *Locally approximated* means within the infinitesimally narrow strip along the line of contact of the screw surface (of the base cone) and the plane of action, PA.



**FIGURE 14.5**

Base cones; the plane of action,  $PA$ ; and the zone of action,  $ZA$ , in an orthogonal crossed-axes gear pair.

The schematic shown in Figure 14.5 is constructed starting from the rotation vectors,  $\omega_g$  and  $\omega_p$ , of a gear and a mating pinion. The gear and pinion rotate about their axes,  $O_g$  and  $O_p$ , respectively. The rotation vectors,  $\omega_g$  and  $\omega_p$ , allow for the construction of the vector,  $\omega_{pl}$ , of instant relative rotation. The rotation vector,  $\omega_{pl}$ , meets the requirement  $\omega_{pl} = \omega_p - \omega_g$ . The axis of instant rotation,  $P_{ln}$ , is aligned with the vector of instant rotation,  $\omega_{pl}$ .

The vector of instant rotation,  $\omega_{pl}$ , is the vector through the plane-of-action apex,  $A_{pa}$ , within the centerline,  $\mathcal{C}$ . Points of intersection of the centerline,  $\mathcal{C}$ , by the axes of rotations,  $O_g$  and  $O_p$ , are labeled  $A_g$  and  $A_p$ .  $A_g$  is the point of intersection of the centerline,  $\mathcal{C}$ , and the gear axis of rotation,  $O_g$ .  $A_p$  is the point of intersection of the centerline,  $\mathcal{C}$ , and the pinion axis of rotation,  $O_p$ .

The point  $A_{pa}$  is at a certain distance,  $r_g$ , from the axis of rotation,  $O_g$ , of the gear. At that same time, the point  $A_{pa}$  is at a certain distance,  $r_p$ , from the axis of rotation,  $O_p$ , of the pinion. The following expression:

$$r_g + r_p = C \quad (14.14)$$

is valid. Here, in Equation 14.14, the distances  $r_g$  and  $r_p$  are signed values. The distances  $r_g$  and  $r_p$  have positive values ( $r_g > 0$ ,  $r_p > 0$ ) when point  $A_{pa}$  is located within the center distance,  $C$ . When point  $A_{pa}$  is located

outside the center distance,  $C$ , the radius,  $r_g$ , has a negative value ( $r_g < 0$ ), while the distance,  $r_p$ , remains positive ( $r_p > 0$ ).

Use of Equation 2.20:

$$\frac{r_g}{r_p} = \frac{\omega_p^{rl}}{\omega_g^{rl}} \quad (14.15)$$

makes it possible to calculate the distances  $r_g$  and  $r_p$  (see Equations 2.61 and 2.62):

$$r_g = \frac{1 + \omega_p - \omega_g}{1 + \omega_p} \cdot C \quad (14.16)$$

and

$$r_p = \frac{1 + \omega_g - \omega_p}{1 + \omega_g} \cdot C \quad (14.17)$$

For a pair of rotation vectors,  $\omega_g$  and  $\omega_p$ , the ratio  $\tan \Sigma_g / \tan \Sigma_p$  can be calculated (see Eq. 2.33) as\*:

$$\frac{r_p}{r_g} = \frac{\tan \Sigma_g}{\tan \Sigma_p} \quad (14.18)$$

The plane of action,  $PA$ , is a plane through the axis of instant rotation,  $P_{ln}$ . The plane of action,  $PA$ , is in tangency with both base cones, that is, with the base cone of the gear and base cone of the pinion. Due to that, the plane of action,  $PA$ , forms a certain transverse pressure angle,  $\phi_{t,\omega}$ , in relation to a perpendicular to a plane associated with the axis of instant rotation,  $P_{ln}$ . The perpendicular is constructed to the plane through the vector of instant rotation,  $\omega_{pl}$ , and through the centerline,  $\mathfrak{C}$ . The pressure angle,  $\phi_{t,\omega}$ , is measured within a plane that is perpendicular to the axis of instant rotation,  $P_{ln}$ .

The portion of the schematic plotted in the upper-left corner in Figure 14.5 is constructed within the plane of projections,  $\pi_1$ . Two others planes of projections,  $\pi_2$  and  $\pi_3$ , of the standard set of planes of projections,  $\pi_1\pi_2\pi_3$ , are not used in this particular consideration. Therefore, these planes,  $\pi_2$  and  $\pi_3$ , are not shown in Figure 14.5. Instead, two auxiliary planes of projections, namely, planes of projections  $\pi_4$  and  $\pi_5$  are used. The axis of projections,  $\pi_1/\pi_4$ , is constructed so as to be perpendicular to the axis of instant rotation,  $P_{ln}$ . The axis of projections,  $\pi_4/\pi_5$ , is constructed so as to be parallel to the trace of the plane of action,  $PA$ , within the plane of projections,  $\pi_4$ . The plane of action,  $PA$ , is projected with no distortions onto the plane of projections  $\pi_4$ .

The plane of action can be viewed as a flexible zero-thickness film. The film is free to wrap or unwrap from and onto the base cones of the gear and pinion. The plane of action,  $PA$ , is not allowed to be bent about an axis perpendicular to the plane,  $PA$ , itself. Under uniform rotation of the gears, the plane of action,  $PA$ , rotates about the axis,  $O_{pa}$ . The rotation vector,  $\omega_{pa}$ , is along the axis,  $O_{pa}$ . The rotation vector,  $\omega_{pa}$ , is perpendicular to the plane of action,  $PA$ .

As the axis of instant rotation,  $P_{ln}$ , and the axes of rotations of the gear,  $O_g$ , and the pinion,  $O_p$ , cross one another, pure rolling of the base cones of the gear and of the pinion over the pitch plane,  $PA$ , is not observed, but rolling together with sliding of  $PA$  over the base cones is observed instead.

For crossed-axes gearings, the plane of action,  $PA$ , can be understood as a round cone that has a cone angle of  $90^\circ$ . As  $\sin 90^\circ = 1$ , the magnitude,  $\omega_{pa}$ , of the rotation vector,  $\omega_{pa}$ , can be calculated from the formula:

$$\omega_{pa} = \frac{\omega_g}{\sin \Gamma_b} = \frac{\omega_p}{\sin \gamma_b} \quad (14.19)$$

where:

$\omega_g$  is the rotation of the gear.

$\omega_p$  is the rotation of the pinion.

\* Note that the radii,  $r_g$  and  $r_p$ , are along the centerline,  $\mathfrak{C}$ , and not in two different planes perpendicular to the axes of rotation,  $O_g$  and  $O_p$ , of the gear and the mating pinion.

$\Gamma_b$  is the base cone angle of the gear.

$\gamma_b$  is the base cone angle of the pinion.

Equation 14.19 yields a formula for the gear ratio,  $u$ , in crossed-axes gearing:

$$u = \frac{\omega_p}{\omega_g} = \frac{\sin \gamma_b}{\sin \Gamma_b} = \frac{r_g}{r_p} \quad (14.20)$$

For crossed-axes gear pairs, the actual values of base cone angles,  $\Gamma_b$  and  $\gamma_b$ , are within the intervals  $0^\circ < \Gamma_b < 180^\circ$  and  $0^\circ < \gamma_b < (180^\circ - \Gamma_b)$ , correspondingly. Thus, all the equations here and below are valid for (1) external crossed-axes gear pairs, (2) rack-type crossed-axes gear pairs, and (3) internal crossed-axes gear pairs. Formally, the base cone angles,  $\Gamma_b$  and  $\gamma_b$ , can be considered in narrower intervals, that is, within the intervals  $0^\circ < \Gamma_b < 90^\circ$  and  $0^\circ < \gamma_b < 90^\circ$ , correspondingly. Under such a scenario, the following three inequalities are valid for crossed-axes gear pairs of various types:

1. The base cone angles are positive ( $\Gamma_b > 0^\circ$  and  $\gamma_b > 0^\circ$ ) for external gearing.
2. The base cone angle of the gear is equal to a right angle ( $\Gamma_b = 90^\circ$ , while  $\gamma_b > 0^\circ$ ) for rack-type gear pairs.
3. The base cone angle of the gear is negative ( $\Gamma_b < 0^\circ$ , while  $\gamma_b > 0^\circ$ ) for internal crossed-axes gearing.

A desired working portion, or, in other words, *functional portion of the plane of action*,  $PA$ , can be constructed in the following way. Consider a straight-line segment,  $ef$ , within the axis of instant rotation,  $P_{ln}$  (Figure 14.5). When the gears rotate, the straight-line segment,  $ef$ , travels together with the plane of action,  $PA$ . Point  $f$  traces a circular arc of a radius,  $r_{o,pa}$ , while point  $e$  traces a circular arc of a radius,  $r_{l,pa}$ . The face width of the plane of action,  $F_{pa}$ , or, in other words, working (functional) portion of the plane of action, is located between two circles of radii,  $r_{o,pa}$  and  $r_{l,pa}$ . In order to get the desired face width of the plane of action,  $F_{pa}$ , the face width of the gear,  $F_g$ , and the face width of the pinion,  $F_p$ , should have larger values, as shown in Figure 14.5. The appropriate radii of the outer circles,  $r_{o,g}$  and  $r_{o,p}$ , as well as of the inner circles,  $r_{l,g}$  and  $r_{l,p}$ , should have values under which both the face width of the gear,  $F_g$ , and the face width of the pinion,  $F_p$ , overlap the face width,  $F_{pa}$  (the radii,  $r_{o,g}$ ,  $r_{o,p}$ ,  $r_{l,g}$ , and  $r_{l,p}$ , are not labeled in Figure 14.5 because of lack of space). The radii,  $r_{o,g}$  and  $r_{l,g}$ , are centered at the gear apex,  $A_g$ , while the radii,  $r_{o,p}$  and  $r_{l,p}$ , are centered at the pinion apex  $A_p$ . The inequalities,  $F_g > F_{pa}$  and  $F_p > F_{pa}$ , are always valid because the apexes,  $A_g$  and  $A_p$ , are not coincident to one another; thus, sliding in the direction of the axis of instant rotation,  $P_{ln}$ , is inevitable in crossed-axes gearing.

The straight-line segments,  $lc_g$  and  $lc_p$ , are along the corresponding lines of contact between the plane of action,  $PA$ , and between the base cones of the gear and the pinion.

The line segments,  $gh$  and  $lk$ , are the lines of intersection of the plane of action,  $PA$ , by the outer cones of the gear and the mating pinion. The zone of action,  $ZA$ , is bounded by two circular arcs,  $hk$  and  $gj$ , and by the two line segments,  $hg$  and  $kj$ .

When the gears rotate, the entire effective face width of the gear pair,  $F_{pa}$ , has to be overlapped by the gear face width,  $F_g$ , and the pinion face width,  $F_p$ . Therefore, the minimal gear face width,  $F_{g,min}$ , equals the difference between the gear radii,  $r_{o,g}$  and  $r_{l,g}$ , that are centered at the gear apex,  $A_g$  (that is,  $F_{g,min} = r_{o,g} - r_{l,g}$ ). Similarly, the minimal pinion face width,  $F_{p,min}$ , equals the difference between the gear radii,  $r_{o,p}$  and  $r_{l,p}$ , that are centered at the pinion apex,  $A_p$  (i.e.,  $F_{p,min} = r_{o,p} - r_{l,p}$ ).

In reality, crossed-axes gear pairs can be composed of a gear and a pinion with tooth flank geometry for which base cones cannot be constructed. In such a case, the plane of action,  $PA$ , cannot be constructed either. Crossed-axes gear pairs of this type are referred to as *approximate crossed-axes gear pairs*. The tooth flanks of approximate crossed-axes gear pairs feature geometry for which no equivalent pulley-and-belt mechanism can be designed to replace the gear pair.

## Conclusion 14.1

*Perfect crossed-axes gear pairs are those capable of smoothly transmitting a uniform rotation from a driving shaft to a driven shaft.*

### Conclusion 14.2

*Approximate crossed-axes gear pairs are those not capable of smoothly transmitting a uniform rotation from a driving shaft to a driven shaft.*

Approximate crossed-axes gear pairs are not capable of transmitting rotation smoothly. However, approximate gearing is extensively used in practice, as it is much easier to manufacture. Therefore, approximate crossed-axes gear pairs are used in cases when the accuracy requirements are not tight, that is, in cases of low rotation, reasonable constraints on noise excitation, and so forth.

## 14.3 Tooth Flanks in Perfect Crossed-Axes Gear

Conjugate tooth flanks of a gear and a mating pinion in a crossed-axes gear pair are always in line contact with one another. As the gears rotate, the line of contact travels with respect (a) to the gear, (b) to the pinion, and (c) to the gear housing. The tooth flank of the gear,  $\mathcal{G}$ , can be interpreted as a locus of consecutive positions of the line of contact,  $LC$ , in its motion in relation to a reference system associated with the gear. Similarly, the tooth flank of the pinion,  $\mathcal{P}$ , can be viewed as a locus of consecutive positions of that same line of contact,  $LC$ , in its motion in relation to a reference system associated with the pinion. Ultimately, loci of consecutive positions of that same line of contact,  $LC$ , in its motion in relation to a stationary reference system associated with the gearing housing represents the surface of action. Therefore, once the line of contact is known, the kinematics of a crossed-axes gearing (Figure 14.5) can be employed for the derivation of an analytical representation of the tooth flank of a gear,  $\mathcal{G}$ , and a mating pinion,  $\mathcal{P}$ . For this purpose, several reference systems need to be introduced.

### 14.3.1 Applied Coordinate Systems and Linear Transformations

For convenience, several reference systems are introduced. They are associated with the gear, pinion, housing, and so forth, as illustrated in Figure 14.6. Here, a motionless reference system,  $X_{ln}Y_{ln}Z_{ln}$ , of the gear pair and two stationary reference systems,  $X_{g,s}Y_{g,s}Z_{g,s}$  and  $X_{p,s}Y_{p,s}Z_{p,s}$ , of a gear and a mating pinion are shown. A few auxiliary coordinate systems are also used when necessary.

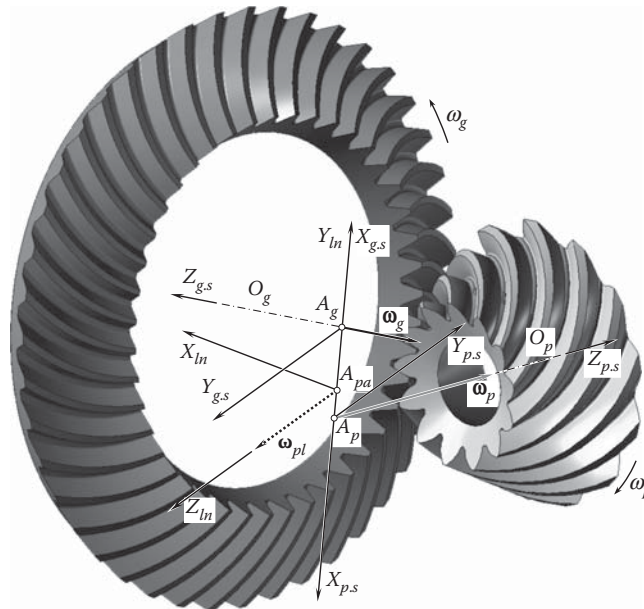


FIGURE 14.6

Motionless reference system,  $X_{ln}Y_{ln}Z_{ln}$ , of a gear pair, and stationary reference systems,  $X_{g,s}Y_{g,s}Z_{g,s}$  and  $X_{p,s}Y_{p,s}Z_{p,s}$ , of the gear and the mating pinion.

### 14.3.1.1 Main Reference Systems

First, a *Cartesian* coordinate system,  $X_g Y_g Z_g$ , is associated with the gear, as shown in Figure 14.7. Second, a Cartesian coordinate system,  $X_p Y_p Z_p$ , is associated with the pinion (see Figure 14.7). Third, a Cartesian coordinate system,  $X_r Y_r Z_r$ , is associated with the auxiliary round rack that is engaged simultaneously with both, namely the gear and the mating pinion. Fourth, a Cartesian coordinate system,  $X_{pa} Y_{pa} Z_{pa}$ , is associated with the plane of action,  $PA$ . Finally, a stationary Cartesian coordinate system,  $X_h Y_h Z_h$ , is associated with the gearing housing. A few more auxiliary reference systems are used below as well.

The origin of the coordinate system,  $X_r Y_r Z_r$ , coincides with the plane-of-action apex,  $A_{pa}$ . The orientation of the coordinate system,  $X_r Y_r Z_r$ , is determined by the rotation vectors,  $\omega_g$ ,  $\omega_p$  and  $\omega_{pl}$ . The  $X_r$ -axis is aligned with the vector,  $\omega_{pl}$ , of instant rotation. The axis  $Y_r$  aligns with the vector defined by the cross-product  $\omega_p \times \omega_g$  of the rotation vectors of the gear and the pinion. Ultimately, the  $Z_r$ -axis is along the vector that is determined by the triple vector product,  $\omega_p \times \omega_g \times \omega_{pl}$ , of the rotation vectors of the gear and the pinion and the vector of instant rotation.

The coordinate system,  $X_{pa} Y_{pa} Z_{pa}$  shares the origin with the reference system,  $X_r Y_r Z_r$ . The axis,  $X_{pa}$  is located within the plane of action,  $PA$ , and forms a certain angle,  $\theta_{pa}$ , with the vector,  $\omega_{pl}$ , of instant rotation. The  $Y_{pa}$ -axis is also within the plane of action,  $PA$ , and is perpendicular to the  $X_{pa}$ -axis (here,  $\theta_{pa} = \omega_{pa} \cdot t$ , and time is denoted

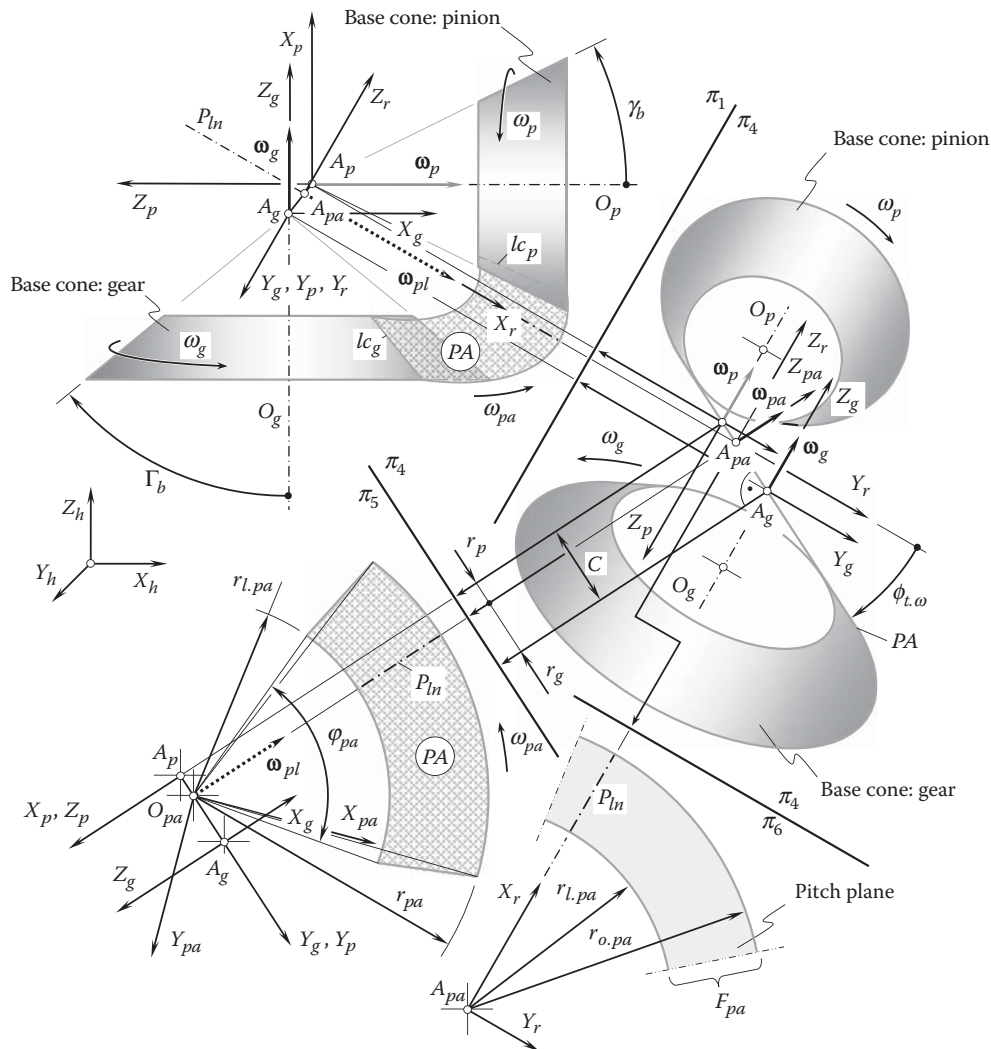


FIGURE 14.7

Reference systems that are used for the derivation of an analytical expression for a gear tooth flank,  $\mathcal{G}$ , and a pinion tooth flank,  $\mathcal{P}$ , in a crossed-axes gear pair.

by  $t$ ). Finally, the axis  $Z_{pa}$  complements the axes,  $X_{pa}$  and  $Y_{pa}$ , to the left-hand-oriented Cartesian coordinate system,  $X_{pa}Y_{pa}Z_{pa}$ .

It is convenient to specify a line of contact,  $LC$ , between the gear tooth flank,  $\mathcal{G}$ , and the mating pinion tooth flank,  $\mathcal{P}$ , in the coordinate system,  $X_{pa}Y_{pa}Z_{pa}$ , similarly to what has been done with respect to parallel-axes gear pairs (see Figure 6.12 for more details). Then, the representation of the current position of the moving line of contact,  $LC$ , in the reference systems,  $X_gY_gZ_g$  and  $X_pY_pZ_p$ , will return analytical expressions for the tooth flanks,  $\mathcal{G}$  and  $\mathcal{P}$ , of the gear and the mating pinion. Similarly, the representation of the current position of the moving line of contact,  $LC$ , in the motionless reference system,  $X_hY_hZ_h$ , will return an equation for the surface of action in crossed-axes gearing.

### 14.3.1.2 Operators of Rolling/Sliding

There are many similarities between the coordinate system transformations that are used in crossed-axes gearing and those used in intersected-axes gearing (see Section 12.4.1).

For the derivation of an equation for the position vector of a point,  $rg$ , of the gear tooth flank,  $\mathcal{G}$ , an operator,  $\mathbf{Rs}(PA \mapsto \mathcal{G})$ , of the resultant coordinate system transformation has to be composed. The operator,  $\mathbf{Rs}(PA \mapsto \mathcal{G})$ , can be expressed in terms of the following operators of linear transformations:

1. The operator of rotation,  $\mathbf{Rt}(pa \mapsto pa_0)$ , of the coordinate system,  $X_{pa}Y_{pa}Z_{pa}$ , about the  $Z_{pa}$ -axis through a certain angle,  $\theta_{pa}$ . When the axis,  $X_{pa}$ , is aligned to the vector of instant rotation,  $\omega_{pl}$ , the reference system,  $X_{pa}Y_{pa}Z_{pa}$ , occupies a particular configuration,  $X_{pa}^0Y_{pa}^0Z_{pa}^0$  (the coordinate system,  $X_{pa}^0Y_{pa}^0Z_{pa}^0$ , is not depicted in Figure 14.7). The operator,  $\mathbf{Rt}(pa \mapsto pa_0)$ , can be expressed in the form:

$$\mathbf{Rt}(pa \mapsto pa_0) = \begin{bmatrix} \cos \theta_{pa} & 0 & -\sin \theta_{pa} & 0 \\ 0 & 1 & 0 & 0 \\ \sin \theta_{pa} & 0 & \cos \theta_{pa} & 0 \\ 0 & 0 & 0 & 1 \end{bmatrix} \quad (14.21)$$

2. The operator of the translation,  $\mathbf{Tr}(-r_g, Y_g)$ , of the reference system,  $X_{pa}^0Y_{pa}^0Z_{pa}^0$ , at a distance,  $-r_g$ , along the centerline,  $P_{a,g}O_{pa}$ , to a position of the coordinate system,  $X_g^0Y_g^0Z_g^0$ .

$$\mathbf{Tr}(-r_g, Y_g) = \begin{bmatrix} 1 & 0 & 0 & 0 \\ 0 & 1 & 0 & -r_g \\ 0 & 0 & 1 & 0 \\ 0 & 0 & 0 & 1 \end{bmatrix} \quad (14.22)$$

3. The operator of rotation,  $\mathbf{Rt}(pa_0 \mapsto r)$ , of the coordinate system,  $X_g^0Y_g^0Z_g^0$ , about the vector of instant rotation,  $\omega_{pl}$ , through the transverse profile angle,  $\phi_{t,\omega}$  (the transverse profile angle,  $\phi_{t,\omega}$ , is measured within a plane, i.e., perpendicular to the vector,  $\omega_{pl}$ ):

$$\mathbf{Rt}(pa_0 \mapsto r) = \begin{bmatrix} 1 & 0 & 0 & 0 \\ 0 & \cos \phi_{t,\omega} & -\sin \phi_{t,\omega} & 0 \\ 0 & \sin \phi_{t,\omega} & \cos \phi_{t,\omega} & 0 \\ 0 & 0 & 0 & 1 \end{bmatrix} \quad (14.23)$$

4. The operator of rotation,  $\mathbf{Rt}(r \mapsto g)$ , of the coordinate system,  $X_rY_rZ_r$ , about the  $Y_r$ -axis through an angle,  $\angle(\omega_r, \omega_p)$ . Note that the angle  $\angle(\omega_r, \omega_p)$  is equal to the angle  $\angle(\omega_p, \omega_{pl}) = \Sigma_p$ . The operator of rotation,  $\mathbf{Rt}(r \mapsto g)$ , can be represented in the form:

$$\mathbf{Rt}(r \mapsto g) = \begin{bmatrix} \cos \Sigma_p & 0 & \sin \Sigma_p & 0 \\ 0 & 1 & 0 & 0 \\ -\sin \Sigma_p & 0 & \cos \Sigma_p & 0 \\ 0 & 0 & 0 & 1 \end{bmatrix} \quad (14.24)$$



The operator,  $\mathbf{Rs}(PA \mapsto \mathcal{G})$ , of the resultant coordinate system transformation is equal to the product:

$$\mathbf{Rs}(PA \mapsto \mathcal{G}) = \mathbf{Rt}(r \mapsto g) \cdot \mathbf{Rt}(pa_0 \mapsto r) \cdot \mathbf{Tr}(-r_{w.g}, Y_g) \cdot \mathbf{Rt}(pa \mapsto pa_0) \quad (14.25)$$

This operator allows for matrix representation in the form:

$$\mathbf{Rs}(PA \mapsto \mathcal{G}) = \begin{bmatrix} \cos \Sigma_p \cos \theta_{pa} + \sin \Sigma_p \cos \phi_{t,\omega} \sin \theta_{pa} & & & & & \\ & -\sin \phi_{t,\omega} \sin \theta_{pa} & & & & \\ \cos \Sigma_p \cos \phi_{t,\omega} \sin \theta_{pa} - \sin \Sigma_p \cos \theta_{pa} & & & & & \\ & 0 & & & & \\ \sin \Sigma_p \sin \phi_{t,\omega} & \sin \Sigma_p \cos \phi_{t,\omega} \cos \theta_{pa} - \cos \Sigma_p \sin \theta_{pa} & -r_g \sin \Sigma_p \sin \phi_{t,\omega} & & & \\ & \cos \phi_{t,\omega} & -\sin \phi_{t,\omega} \cos \theta_{pa} & -r_g \cos \phi_{t,\omega} & & \\ \cos \Sigma_p \sin \phi_{t,\omega} & \sin \Sigma_p \sin \theta_{pa} + \cos \Sigma_p \cos \phi_{t,\omega} \cos \theta_{pa} & -r_g \cos \Sigma_p \sin \phi_{t,\omega} & & & \\ & 0 & 0 & 1 & & \end{bmatrix} \quad (14.26)$$

The operator,  $\mathbf{Rs}(PA \mapsto \mathcal{P})$ , of the resultant coordinate system transformation, that is, the operator of the transition from the coordinate system,  $X_{pa}Y_{pa}Z_{pa}$ , associated with the plane of action,  $PA$ , to the coordinate system,  $X_pY_pZ_p$ , associated with the pinion, is equal to the product:

$$\mathbf{Rs}(PA \mapsto \mathcal{P}) = \mathbf{Rt}(r \mapsto p) \cdot \mathbf{Rt}(pa_0 \mapsto r) \cdot \mathbf{Tr}(r_p, Y_p) \cdot \mathbf{Rt}(pa \mapsto pa_0) \quad (14.27)$$

The operator of rotation,  $\mathbf{Rt}(r \mapsto p)$ , can be composed in a similar manner to that of the operator of rotation,  $\mathbf{Rt}(r \mapsto g)$  (see Equation 14.24). The similarity allows for the following expression for the operator of rotation,  $\mathbf{Rt}(r \mapsto p)$ :

$$\mathbf{Rt}(r \mapsto p) = \begin{bmatrix} \cos \Sigma_g & 0 & \sin \Sigma_g & 0 \\ 0 & 1 & 0 & 0 \\ -\sin \Sigma_g & 0 & \cos \Sigma_g & 0 \\ 0 & 0 & 0 & 1 \end{bmatrix} \quad (14.28)$$

After Equation 11.28, together with Equations 14.21 and 14.23, are substituted into Equation 14.27, this returns an expression for the operator,  $\mathbf{Rs}(PA \mapsto \mathcal{P})$ , of the resultant coordinate system transformation:

$$\mathbf{Rs}(PA \mapsto \mathcal{P}) = \begin{bmatrix} \cos \Sigma_g \cos \theta_{pa} + \sin \Sigma_g \cos \phi_{t,\omega} \sin \theta_{pa} & & & & & \\ & -\sin \phi_{t,\omega} \sin \theta_{pa} & & & & \\ \cos \Sigma_g \cos \phi_{t,\omega} \sin \theta_{pa} - \sin \Sigma_g \cos \theta_{pa} & & & & & \\ & 1 & & & & \\ \sin \Sigma_g \sin \phi_{t,\omega} & \sin \Sigma_g \cos \phi_{t,\omega} \cos \theta_{pa} - \cos \Sigma_g \sin \theta_{pa} & r_p \sin \Sigma_g \sin \phi_{t,\omega} & & & \\ & \cos \phi_{t,\omega} & -\sin \phi_{t,\omega} \cos \theta_{pa} & r_p \cos \phi_{t,\omega} & & \\ \cos \Sigma_g \sin \phi_{t,\omega} & \sin \Sigma_g \sin \theta_{pa} + \cos \Sigma_g \cos \phi_{t,\omega} \cos \theta_{pa} & r_p \cos \Sigma_g \sin \phi_{t,\omega} & & & \\ & 0 & 0 & 1 & & \end{bmatrix} \quad (14.29)$$

The operators,  $\mathbf{Rs}(PA \mapsto \mathcal{G})$  and  $\mathbf{Rs}(PA \mapsto \mathcal{P})$ , are a kind of *operators of rolling/sliding*. The transformation of rolling/sliding is extensively used in the theory of gearing to investigate crossed-axes gearing in particular. With that said, it makes sense to introduce a special designation; for convenience, the operators of the linear



transformations,  $\mathbf{Rc}(PA \mapsto \mathcal{G})$  and  $\mathbf{Rc}(PA \mapsto \mathcal{P})$ , can be designated as:

$$\mathbf{Rs}(PA \mapsto \mathcal{G}) = \mathbf{Rc}(PA \mapsto \mathcal{G}) \quad (14.30)$$

$$\mathbf{Rs}(PA \mapsto \mathcal{P}) = \mathbf{Rc}(PA \mapsto \mathcal{P}) \quad (14.31)$$

As the operators of rolling/sliding,  $\mathbf{Rc}(PA \mapsto \mathcal{G})$  and  $\mathbf{Rc}(PA \mapsto \mathcal{P})$ , are known, the operator of rolling,  $\mathbf{Rc}(\mathcal{P} \mapsto \mathcal{G})$ , of the pinion over the gear can be calculated from the formula:

$$\mathbf{Rc}(\mathcal{P} \mapsto \mathcal{G}) = \mathbf{Rc}(PA \mapsto \mathcal{G}) \cdot \mathbf{Rc}^{-1}(PA \mapsto \mathcal{P}) \quad (14.32)$$

Similarly, the operator of rolling,  $\mathbf{Rc}(\mathcal{G} \mapsto \mathcal{P})$ , of the gear over the pinion can be calculated either as reciprocal to the operator,  $\mathbf{Rc}(\mathcal{P} \mapsto \mathcal{G})$ , or the expression:

$$\mathbf{Rc}(\mathcal{G} \mapsto \mathcal{P}) = \mathbf{Rc}^{-1}(\mathcal{P} \mapsto \mathcal{G}) = \mathbf{Rc}(PA \mapsto \mathcal{P}) \cdot \mathbf{Rc}^{-1}(PA \mapsto \mathcal{G}) \quad (14.33)$$

can be used for the calculation of the operator of rolling,  $\mathbf{Rc}(\mathcal{G} \mapsto \mathcal{P})$ .

#### 14.3.1.3 Operators Associated with Gear Housing

A stationary reference system,  $X_h Y_h Z_h$ , is associated with housing of the gear pair. The choice of the coordinate system,  $X_h Y_h Z_h$ , depends mostly on convenience. In a particular case, either the stationary Cartesian coordinate system,  $X_g^0 Y_g^0 Z_g^0$ , or the stationary Cartesian coordinate system,  $X_p^0 Y_p^0 Z_p^0$ , can be used.

The coordinate system,  $X_g^0 Y_g^0 Z_g^0$ , shares a common  $Z_g$ -axis with the coordinate system,  $X_g Y_g Z_g$ , associated with the gear. The coordinate system,  $X_g Y_g Z_g$ , is turned in relation to the motionless coordinate system,  $X_g^0 Y_g^0 Z_g^0$ , through a certain angle,  $\varphi_g$ .

Similarly, the reference system,  $X_p^0 Y_p^0 Z_p^0$ , shares a common  $Z_p$ -axis with the coordinate system,  $X_p Y_p Z_p$ , associated with the pinion. The coordinate system,  $X_p Y_p Z_p$ , is turned in relation to the motionless coordinate system,  $X_p^0 Y_p^0 Z_p^0$ , through a certain angle,  $\varphi_p$ .

It is important to note here that the rotation angles,  $\varphi_g$  and  $\varphi_p$ , correspond to one another by the relation  $\varphi_p = u \varphi_g$ , and  $u$  designates the tooth ratio of the gear pair. For crossed-axes gearing, the following expression for  $u$ :

$$u = \frac{\omega_p^{rl}}{\omega_g^{rl}} = \frac{\omega_p \cos \Sigma_p}{\omega_g \cos \Sigma_g} \quad (14.34)$$

is valid.

Here, in Equation 14.34, the rolling components of the rotations,  $\omega_g$  and  $\omega_p$ , are designated as  $\omega_g^{rl}$  and  $\omega_p^{rl}$ , correspondingly, and the gear and the pinion angles,  $\Sigma_g$  and  $\Sigma_p$ , are calculated from Equations 2.64 and 2.65:

$$\Sigma_g = \frac{1 - \omega_g + \omega_p}{1 + \omega_p} \Sigma \quad (14.35)$$

$$\Sigma_p = \frac{1 + \omega_g - \omega_p}{1 + \omega_g} \Sigma \quad (14.36)$$

and  $\Sigma$  is the angle between the rotation vectors of the gear,  $\omega_g$ , and the pinion,  $\omega_p$ .

For external crossed-axes gear pairs, the rotation angles,  $\varphi_g$  and  $\varphi_p$ , are of opposite signs, while for internal crossed-axes gearing the rotation angles,  $\varphi_g$  and  $\varphi_p$ , are of the same sign.

The rotation of the reference system,  $X_g Y_g Z_g$ , about the  $Z_g$ -axis through an angle,  $\varphi_g$ , can be analytically described by the operator of rotation,  $\mathbf{Rt}(\mathcal{G} \mapsto h)$ . This operator can be expressed in the form:

$$\mathbf{Rt}(\mathcal{G} \mapsto h) = \begin{bmatrix} \cos \varphi_g & \sin \varphi_g & 0 & 0 \\ -\sin \varphi_g & \cos \varphi_g & 0 & 0 \\ 0 & 0 & 1 & 0 \\ 0 & 0 & 0 & 1 \end{bmatrix} \quad (14.37)$$

Equation 14.37 allows for an expression for the operator of the resultant coordinate system transformation, that is, for the operator of the transition,  $\mathbf{Rs}(pa \mapsto h)$ , from the coordinate system,  $X_{pa} Y_{pa} Z_{pa}$ , associated with the plane of action,  $PA$ , to the stationary coordinate system,  $X_h Y_h Z_h$ . This operator of linear transformation can be represented as the product:

$$\mathbf{Rs}(pa \mapsto h) = \mathbf{Rt}(\mathcal{G} \mapsto h) \cdot \mathbf{Rc}(PA \mapsto \mathcal{G}) \quad (14.38)$$

Equation 14.38 is not represented in matrix form, as it is bulky.

The rotation of the reference system,  $X_p Y_p Z_p$ , about the  $Z_p$ -axis through an angle,  $\varphi_p = -u \varphi_g$ , can be analytically described by the operator of rotation,  $\mathbf{Rt}(\mathcal{P} \mapsto h_p)$ . This operator can be expressed in the form:

$$\mathbf{Rt}(\mathcal{P} \mapsto h_p) = \begin{bmatrix} \cos \varphi_p & \sin \varphi_p & 0 & 0 \\ -\sin \varphi_p & \cos \varphi_p & 0 & 0 \\ 0 & 0 & 1 & 0 \\ 0 & 0 & 0 & 1 \end{bmatrix} \quad (14.39)$$

Equation 14.39 allows for an expression for the operator of the resultant coordinate system transformation, that is, for the operator of transition  $\mathbf{Rs}(pa \mapsto h_p)$  from the coordinate system,  $X_{pa} Y_{pa} Z_{pa}$ , associated with the plane of action,  $PA$ , to the stationary coordinate system,  $X_{h,p} Y_{h,p} Z_{h,p}$ . This operator can be represented as the product:

$$\mathbf{Rs}(pa \mapsto h_p) = \mathbf{Rt}(\mathcal{G} \mapsto h) \cdot \mathbf{Rc}(PA \mapsto \mathcal{G}) \quad (14.40)$$

Equation 14.40 is not represented in matrix form, as it is bulky.

Both reference systems, namely the coordinate systems  $X_h Y_h Z_h$  and  $X_{h,p} Y_{h,p} Z_{h,p}$ , are stationary reference systems somehow associated with the housing of the gear pair. The relation between these two coordinate systems can be analytically described by the expression:

$$\mathbf{Rs}(h_p \mapsto h) = \mathbf{Rs}(pa \mapsto h) \cdot \mathbf{Rs}^{-1}(pa \mapsto h_p) \quad (14.41)$$

The expressions that are derived above for the operators of the coordinate system transformations make it possible to have expressions of any and all geometrical features (a) of a gear, (b) of a mating pinion, and (c) of the gear-to-pinion mesh in a common reference system.

#### 14.3.1.4 Gear Tooth Flank in Crossed-Axes Gearing

The tooth flank of a gear in a crossed-axes gearing allows for its interpretation as a locus of consecutive positions of the line of contact,  $LC$ , when the plane of action,  $PA$ , is either wrapping on or unwrapping from the base cone of the gear. For this purpose, the line of contact in its current configuration should be represented in a reference system associated with the gear.

Any planar curve of reasonable geometry can be employed as the line of contact between the tooth flanks. The geometry of the tooth flanks of the gear,  $\mathcal{G}$ , and the mating pinion,  $\mathcal{P}$ , depends on the shape of the line of contact. Under any circumstances, the line of contact,  $LC$ , is located within the coordinate plane,  $X_{pa} Y_{pa}$ , of the reference system,  $X_{pa} Y_{pa} Z_{pa}$ , associated with the plane of action,  $PA$ , as schematically illustrated in [Figure 14.8](#).

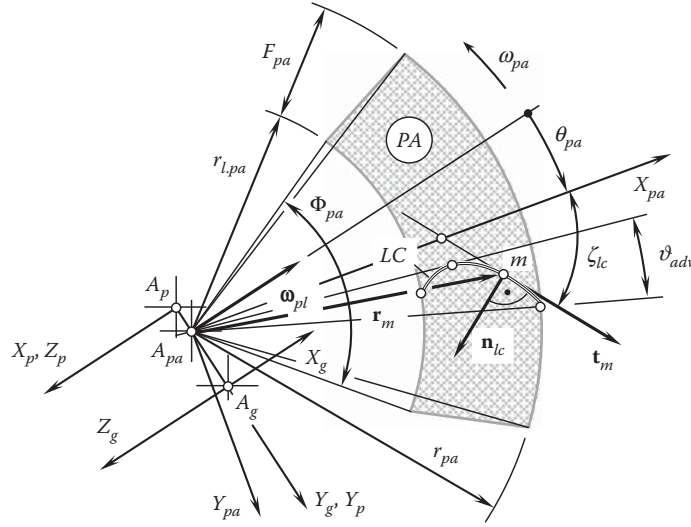


FIGURE 14.8

Line of contact,  $LC$ , between a gear tooth flank,  $\mathcal{G}$ , and a mating pinion tooth flank,  $\mathcal{P}$ , in a crossed-axes gear pair: features of the geometry.

Generally speaking, the position vector of a point,  $\mathbf{r}_{lc}$ , of the line of contact,  $LC$ , can be analytically described by an expression in matrix form:

$$\mathbf{r}_{lc}(v) = \begin{bmatrix} X_{lc}(v) \\ Y_{lc}(v) \\ 0 \\ 1 \end{bmatrix} \quad (14.42)$$

In order to represent Eq. 14.42 for the position vector of a point,  $\mathbf{r}_{lc}$ , of the line of contact,  $LC$ , in the reference system,  $X_g Y_g Z_g$ , the operator of the resultant coordinate system transformation,  $\mathbf{Rs}(PA \mapsto \mathcal{G})$ , can be employed. This makes it possible to have the following expression:

$$\mathbf{r}_g(v, \theta_{pa}) = \mathbf{r}_{lc}^s(v, \theta_{pa}) = \mathbf{Rs}(PA \mapsto \mathcal{G}) \cdot \mathbf{r}_{lc}(v) \quad (14.43)$$

When the axis,  $X_{pa}$ , is pointed along one side of the face advance angle,  $\vartheta_{adv}$ , then the central angle,  $\theta_{pa}$ , is within the domain  $\varphi_{pl}^p + \vartheta_{adv} \leq \theta_{pa} \leq \varphi_{pl}^s - \vartheta_{adv}$  (see Figure 14.7; the angles,  $\varphi_{pl}^s$  and  $\varphi_{pl}^p$ , are of opposite signs). Otherwise, the angles the  $X_{pa}$ -axis forms with the sides of the face advance angle,  $\vartheta_{adv}$ , have to be taken into consideration.

Substituting  $\mathbf{r}_{lc}$  [Equation 14.42 and  $\mathbf{Rs}(PA \mapsto \mathcal{G})$ ; see Equation 14.26] into Equation 14.43, an expression for the calculation of the position vector of a point,  $\mathbf{r}_g$ , of the gear tooth flank,  $\mathcal{G}$ , can be derived:

$$\mathbf{r}_g(v, \theta_{pa}) = \begin{bmatrix} (\cos \Sigma_p \cos \theta_{pa} + \sin \Sigma_p \cos \phi_{t,\omega} \sin \theta_{pa}) \cdot X(v) + \sin \Sigma_p \sin \phi_{t,\omega} \cdot Y(v) + r_p \sin \Sigma_p \sin \phi_{t,\omega} \\ -X(v) \sin \phi_{t,\omega} \sin \theta_{pa} + Y(v) \cos \phi_{t,\omega} + r_p \cos \phi_{t,\omega} \\ -(\sin \Sigma_p \cos \theta_{pa} - \cos \Sigma_p \cos \phi_{t,\omega} \sin \theta_{pa}) \cdot X(v) + \cos \Sigma_p \sin \phi_{t,\omega} \cdot Y(v) + r_p \cos \Sigma_p \sin \phi_{t,\omega} \\ 1 \end{bmatrix} \quad (14.44)$$

A line of intersection of the gear tooth flank (see Equation 14.44) by a sphere of a certain radius centered at the plane-of-action apex,  $A_{pa}$ , is commonly called a *spherical involute*,  $\text{inv}_{\text{sph}}(\phi_{t,\omega})$ . The equation of this curve can be derived from Eq. 14.44 if a radius,  $r_{\text{sph}}$ , of the sphere is entered into this equation.

A comparison of the expression (see Equation 14.44) for the position vector of a point,  $\mathbf{r}_g(v, \theta_{pa})$ , of a gear tooth flank,  $\mathcal{G}$ , for crossed-axes gearing with that for intersected-axes gearing (see Equation 12.53) reveals that they are different. Due to inevitable axial sliding, the desired geometries of the tooth flanks (see Equations 14.44 and 12.53) are not identical. Therefore, the gears that are designed and manufactured for crossed-axes pairs and the

gears that are designed and manufactured for crossed-axes pairs *cannot* be interchangeable. The gears of these two different types cannot make up a perfect gear pair, as theoretically they cannot be engaged in correct mesh. The engagement, if it is possible, can be approximate only.

Similar to parallel-axes gearing (see Figure 6.12), as well as crossed-axes gearing (see Figures 12.13 and 12.14), the lines of contact of various geometries can be used to generate the tooth flanks of a gear and mating pinion in crossed-axes gearing. A few examples are illustrated in Figure 14.9.

Three apexes are recognized in a perfect crossed-axes gear pair. They are: (a) the plane-of-action apex,  $A_{pa}$ ; (b) the gear base cone apex,  $A_g$ ; and (c) the pinion base cone apex,  $A_p$ . (Note: In a perfect crossed-axes gear pair, all three apexes,  $A_{pa}$ ,  $A_g$ , and  $A_p$ , are coincident with one another. Therefore, in a perfect straight bevel gear pair, the line of contact,  $LC$ , is a straight line through the apex,  $A_{pa} \equiv A_g \equiv A_p$ .) In the case of perfect crossed-axes gears, it is not clear which of the apexes,  $A_{pa}$ ,  $A_g$ , and  $A_p$ , has to be used to design a perfect straight gear pair.

In a particular case, a tooth flank of a gear and a mating pinion in a crossed-axes gear pair can be designed so as to keep a straight line of contact,  $LC_{\text{straight}}$ , between the tooth flanks,  $\mathcal{G}$  and  $\mathcal{P}$ , aligned with a straight line through the plane-of-action apex,  $A_{pa}$ . This is schematically illustrated in Figure 14.9a. The gears, the tooth flanks,  $\mathcal{G}$  and  $\mathcal{P}$ , which are generated by means of the line of contact,  $LC_{\text{straight}}$ , are referred to as *pseudo-straight crossed-axes gears* regardless of the tooth flanks,  $\mathcal{G}$  and  $\mathcal{P}$ , of this particular kind of gearing being curved surfaces. The term pseudo-straight crossed-axes gears reflects that the tooth flanks,  $\mathcal{G}$  and  $\mathcal{P}$ , are generated by a straight line through the plane-of-action apex,  $A_{pa}$ . When the gears rotate, at a certain instant of time, the line of contact, in addition, is aligned with the axis of instant rotation,  $P_{ln}$ .

Pseudo-straight crossed-axes gearing features a zero face contact ratio ( $m_F = 0$ ).

Straight line segments that have other configurations within the plane of action,  $PA$ , are of particular interest from the perspective of the tooth flank generation when machining gears. In a particular case, the tooth flanks of a gear and mating pinion in a perfect crossed-axes gear pair can be designed so as to keep the line of contact,  $LC_{\text{spur.g}}$ , between the tooth flanks,  $\mathcal{G}$  and  $\mathcal{P}$ , aligned with a straight line through the gear apex,  $A_g$ . This design is schematically depicted in Figure 14.9b. Both the gear tooth flank,  $\mathcal{G}$ , and the tooth flank,  $\mathcal{P}$ , of the mating pinion generated by means of the line of contact,  $LC_{\text{spur.g}}$ , of such a configuration are not the tooth flanks of straight bevel gears: they are curved surfaces.

Similarly, the tooth flanks of a gear and mating pinion in a crossed-axes gear pair can be designed so as to keep the line of contact,  $LC_{\text{spur.p}}$ , between the tooth flanks,  $\mathcal{G}$  and  $\mathcal{P}$ , aligned with a straight line through the pinion apex,  $A_p$ . This case is schematically shown in Figure 14.9c. Both the gear tooth flank,  $\mathcal{G}$ , and the tooth flank,  $\mathcal{P}$ , of the mating pinion generated by means of the line of contact,  $LC_{\text{spur.p}}$ , of such a configuration are not the tooth flanks of straight bevel gears: they are curved surfaces.

Ultimately, the tooth flanks of a gear and a mating pinion in a crossed-axes gear pair can be generated by an arbitrary straight line,  $LC_{\text{helical}}$ , within the plane of action,  $PA$ . The straight line of contact,  $LC_{\text{helical}}$ , passes neither through the plane-of-action apex,  $A_{pa}$ , nor through the gear apex,  $A_g$ , nor through the pinion apex,  $A_p$ . The configuration of the line of contact for this particular kind of crossed-axes is illustrated in Figure 14.9d. Under such a scenario, the tooth flanks,  $\mathcal{G}$  and  $\mathcal{P}$ , of the gear and the pinion are screw surfaces.

Ultimately, one can conclude from this that no perfect crossed-axes straight bevel gearing is feasible at all.

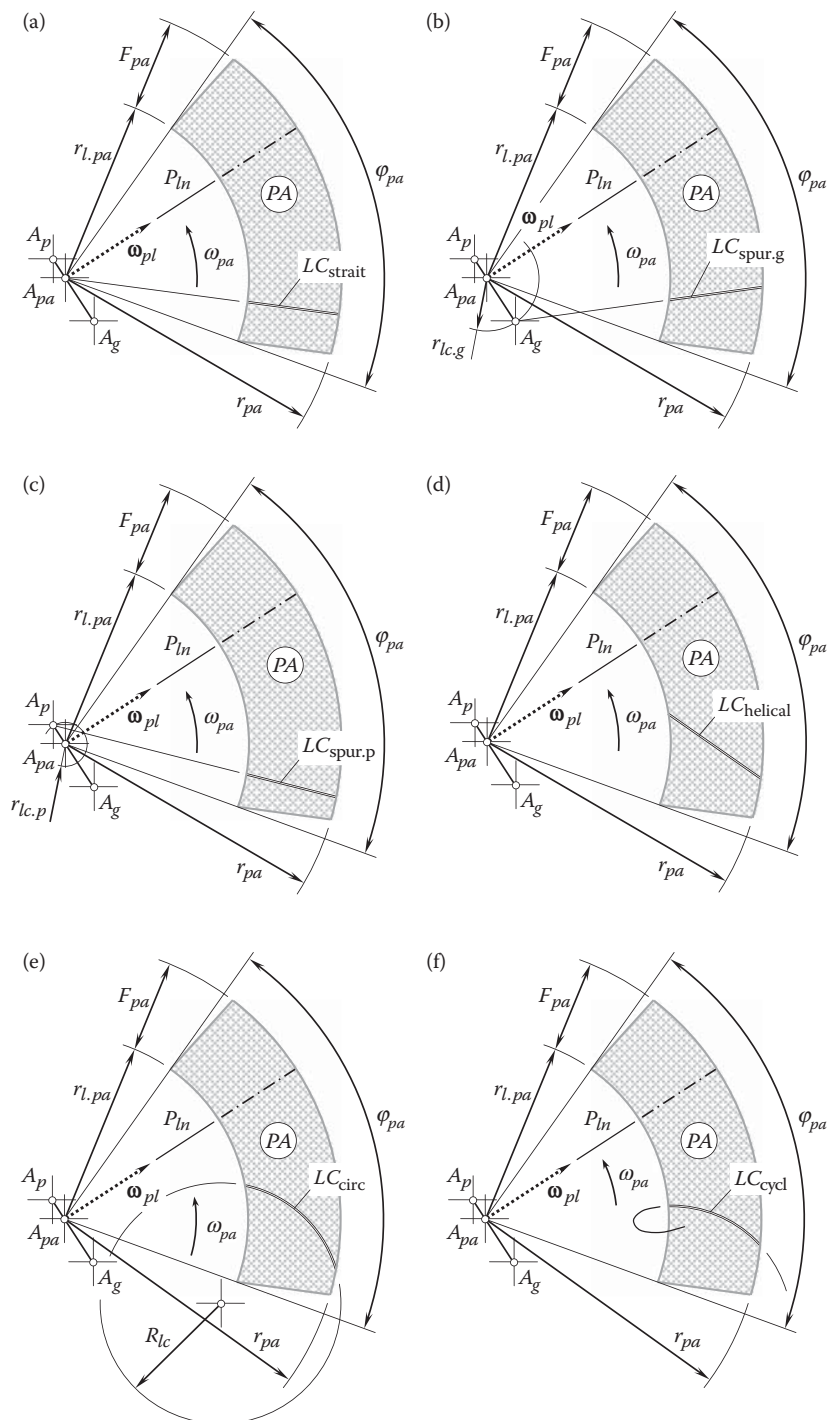
Not only straight lines can be used for the purpose of the generation of the tooth flanks of the gear and pinion in crossed-axes gearing.

Figure 14.9e illustrates a case where a circular arc of a certain radius,  $R_{lc}$ , is used to generate the tooth flanks of a gear and mating pinion in crossed-axes gearing. The arc is centered at a point within the plane of action,  $PA$ , and it is entirely located within the plane,  $PA$ . The tooth flanks,  $\mathcal{G}$  and  $\mathcal{P}$ , of complex geometry are generated by the circular arc. Perfect spiral bevel gears are generated in this way.

One more example of a planar line of contact,  $LC_{\text{cyc}}$ , between the gear tooth flank,  $\mathcal{G}$ , and the pinion tooth flank,  $\mathcal{P}$ , is depicted in Figure 14.9f. The line of contact,  $LC_{\text{cyc}}$ , is entirely located within the plane of action,  $PA$ . Perfect cycloidal bevel gears are generated in this way.

The main advantage of a straight line (see Figures 14.9a through 14.9d), circular arc (see Figure 14.9e), and arc of a cycloidal curve (see Figure 14.9f) is that these lines are easy to reproduce kinematically on a machine tool. The planar curves of other geometries that could be kinematically generated on a machine tool can also be implemented to generate the tooth flanks of a gear and mating pinion in a crossed-axes gear pair. The convenience of the generation of the line of contact,  $LC$ , is of critical importance in this concern. A case of an arbitrary planar line of contact,  $LC$ , is discussed above (see Figure 14.8).

The approach used above for the derivation of an expression for the position vector of a point of the tooth flank generated by means of an arbitrary planar curve (see Equation 14.44) can be used to derive an equation

**FIGURE 14.9**

Examples of possible lines of contact,  $LC$ , between a gear tooth flank,  $\mathcal{G}$ , and a mating pinion tooth flank,  $\mathcal{P}$ , in a perfect crossed-axes gear pair: (a) pseudo-straight crossed-axes gears, (b) straight-gear crossed-axes gears, (c) straight-pinion crossed-axes gears, (d) helical crossed-axes gears, (e) spiral crossed-axes gears, and (f) cycloidal crossed-axes gears.

for the position vector of a point of tooth flanks,  $\mathcal{G}$  and  $\mathcal{P}$ , generated by means of planar curves such as those shown in Figure 14.9.

It is appropriate to stress here the importance of the geometry of the line of contact,  $LC$ , to solve the problem of synthesizing a desired crossed-axes gear pair. The geometry of the line of contact,  $LC$ , is a powerful tool to take control over the geometry of contact of tooth flanks of the gear,  $\mathcal{G}$ , and the pinion,  $\mathcal{P}$ . This means that the

contact geometry of the tooth flanks,  $\mathcal{G}$  and  $\mathcal{P}$  (see Appendix E), is the key for the determining the best possible geometry of the line of contact,  $LC$ , for any particular case of crossed-axes gearing.

In a particular case of a straight line of contact (Figure 14.10), the position vector of a point,  $\mathbf{r}_{lc}$ , of the line of contact,  $LC$ , can be represented as the sum:

$$\mathbf{r}_{lc} = \mathbf{r}_{lc}^0 + \mathbf{r}_{lc}^\lambda \quad (14.45)$$

In Equation 14.45, the vector  $\mathbf{r}_{lc}^0$  is of constant length,  $\mathbf{r}_{lc}^0 = \mathbf{i} \cdot r_{lc}^0$ , where  $r_{lc}^0 = |\mathbf{r}_{lc}^0|$ . Another component of the position vector of a point,  $\mathbf{r}_{lc}$ , namely the vector  $\mathbf{r}_{lc}^\lambda$ , can be represented in the form:

$$\mathbf{r}_{lc}^\lambda(\lambda) = \mathbf{i} \cdot \lambda \cos \zeta_{cl} + \mathbf{j} \cdot \lambda \sin \zeta_{cl} \quad (14.46)$$

where:

$\lambda$  is the magnitude of the vector  $\mathbf{r}_{lc}^\lambda$ .

$\zeta_{cl}$  is the angle of inclination of the line of contact,  $LC$ , in relation to the  $X_{pa}$ -axis of the coordinate system  $X_{pa}Y_{pa}Z_{pa}$  (see Figure 14.10).

Ultimately, the position vector of a point,  $\mathbf{r}_{lc}$ , of the line of contact,  $LC$ , allows for representation in matrix form:

$$\mathbf{r}_{lc}(\lambda) = \begin{bmatrix} r_{lc}^0 + \lambda \cos \zeta_{cl} \\ \lambda \sin \zeta_{cl} \\ 0 \\ 1 \end{bmatrix} \quad (14.47)$$

Equation 14.47 considered together with the operator,  $\mathbf{Rs}(PA \mapsto \mathcal{G})$  (see Equation 14.26), of the resultant coordinate system transformation makes it possible to calculate the position vector of a point,  $\mathbf{r}_g$ , of the tooth flank of a bevel gear that features an inclined line of contact:

$$\mathbf{r}_g(v, \theta_{pa}) = \mathbf{r}_{lc}^g(\lambda, \theta_{pa}) = \mathbf{Rs}(PA \mapsto \mathcal{G}) \cdot \mathbf{r}_{lc}(\lambda) \quad (14.48)$$

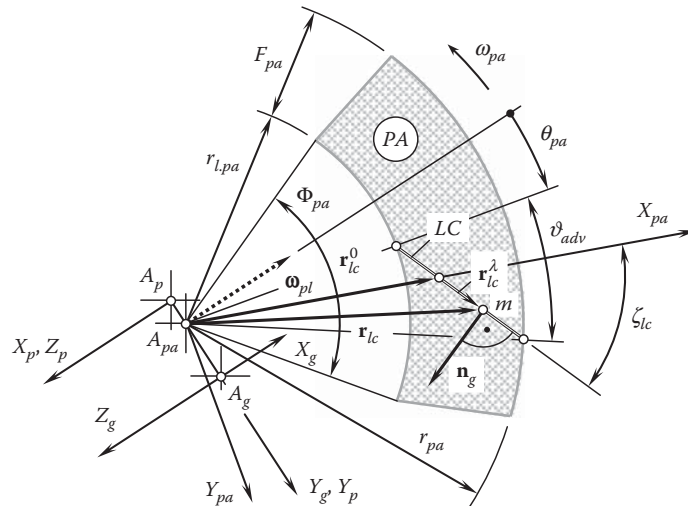


FIGURE 14.10

The line of contact,  $LC$ , between the tooth flank,  $\mathcal{G}$ , of the gear, and the mating pinion,  $\mathcal{P}$ , for a skew crossed-axes gearing.

An expanded form of the expression for the calculation of the position vector of a point of the gear tooth flank,  $\mathbf{r}_{lc}^g$ , can be derived after substituting the position vector,  $\mathbf{r}_{lc}$  (see Equation 14.47), and the operator of the resultant coordinate system transformation,  $\mathbf{Rs}(PA \mapsto \mathcal{G})$  (see Equation 11.26), into Equation 14.48:

$$\mathbf{r}_g(\lambda, \theta_{pa}) = \begin{bmatrix} (\cos \Sigma_p \cos \theta_{pa} + \sin \Sigma_p \cos \phi_{t,\omega} \sin \theta_{pa}) \cdot (r_{lc}^0 + \lambda \cos \zeta_{lc}) + \lambda \sin \Sigma_p \sin \phi_{t,\omega} \sin \zeta_{lc} - r_g \sin \Sigma_p \sin \phi_{t,\omega} \\ (\lambda \cos \phi_{t,\omega} \sin \zeta_{lc} - \sin \phi_{t,\omega} \sin \theta_{pa}) \cdot (r_{lc}^0 + \lambda \cos \zeta_{lc}) - r_g \cos \phi_{t,\omega} \\ -(\sin \Sigma_p \cos \theta_{pa} - \cos \Sigma_p \cos \phi_{t,\omega} \sin \theta_{pa}) \cdot (r_{lc}^0 + \lambda \cos \zeta_{lc}) + \lambda \cos \Sigma_p \sin \phi_{t,\omega} \sin \zeta_{lc} - r_g \cos \Sigma_p \sin \phi_{t,\omega} \\ 1 \end{bmatrix} \quad (14.49)$$

A comparison of Equations 14.49 and 12.53 makes it clear that the tooth flanks of skew conical gears for a crossed-axes gear pair and the tooth flanks of skew gears for an intersected-axes gear pair are surfaces of different geometries. Therefore, gears that are designed and produced for crossed-axes gearing cannot be replaced by gears that are designed and produced for intersected-axes gearing, and vice versa.

In a particular case, the line of contact,  $LC$ , is aligned with the  $X_{pa}$ -axis of the Cartesian coordinate system  $X_{pa}Y_{pa}Z_{pa}$ . This makes it possible to represent the position vector,  $\mathbf{r}_{lc}$ , of a point of the line of contact,  $LC$ , in the form of a column matrix:

$$\mathbf{r}_{lc}(X_{pa}) = \begin{bmatrix} X_{pa} \\ 0 \\ 0 \\ 1 \end{bmatrix} \quad (14.50)$$

An expression for the position vector of a point,  $\mathbf{r}_g$ , of the tooth flank of that geometry can be determined as the product:

$$\mathbf{r}_g(X_{pa}, \theta_{pa}) = \mathbf{Rs}(PA \mapsto \mathcal{G}) \cdot \mathbf{r}_{lc}(X_{pa}) \quad (14.51)$$

where the operator,  $\mathbf{Rs}(PA \mapsto \mathcal{G})$ , of the resultant coordinate system transformation is given by Equation 14.26.

Equation 14.51 allows for an expanded form of the expression for the position vector of a point,  $\mathbf{r}_g$ , of the tooth flank of that geometry:

$$\mathbf{r}_g(X_{pa}, \theta_{pa}) = \begin{bmatrix} X_{pa}(\cos \Sigma_p \cos \theta_{pa} + \sin \Sigma_p \cos \phi_{t,\omega} \sin \theta_{pa}) - r_g \sin \Sigma_p \sin \phi_{t,\omega} \\ -X_{pa} \sin \phi_{t,\omega} \sin \theta_{pa} - r_g \cos \phi_{t,\omega} \\ -X_{pa}(\sin \Sigma_p \cos \theta_{pa} - \cos \Sigma_p \cos \phi_{t,\omega} \sin \theta_{pa}) - r_g \cos \Sigma_p \sin \phi_{t,\omega} \\ 1 \end{bmatrix} \quad (14.52)$$

Expressions for (a) the unit normal vector,  $\mathbf{n}_g$ , to the gear tooth flank,  $\mathcal{G}$ ; (b) the unit normal vector,  $\mathbf{n}_p$ , to the pinion tooth flank,  $\mathcal{P}$ ; and (c) the unit normal vector,  $\mathbf{n}_r$ , to tooth flank of the auxiliary generating round rack,  $\mathcal{R}$ , can be derived based on the unit normal vector,  $\mathbf{n}_{lc}$ , to the line of contact,  $LC$ , which is constructed within the plane of action,  $PA$ . For this purpose, the unit normal vector,  $\mathbf{n}_{lc}$ , has to be considered together with the corresponding operators of the coordinate system transformations. The vector,  $\mathbf{n}_{lc}$ , in nature, is perpendicular to a planar curve. Thus, this perpendicular is entirely located within the plane where the line of contact,  $LC$ , is located.

A conical gear of a crossed-axes gear pair can be engaged in mesh with a corresponding *round rack*,  $\mathcal{R}$  (or *crown gear*,  $\mathcal{R}$ , in other terminology). The geometry of the tooth flanks of the round rack can be determined in a manner similar to that of the gear tooth flank,  $\mathcal{G}$ . The only difference is that the gear cone angle,  $\Sigma_g$ , namely, the angle between the rotation vectors,  $\boldsymbol{\omega}_{pl}$  and  $\boldsymbol{\omega}_g$ , is equal to the right angle ( $\Sigma_g = 90^\circ$ ).

Equation 14.44, as well as Equations 14.49 and 14.52, allow for the calculation of the unit normal vector,  $\mathbf{n}_g$ , to the gear tooth flank,  $\mathcal{G}$ , at every particular case of crossed-axes gears. The unit normal vector,  $\mathbf{n}_g$ , and the



straight line along the vector,  $\mathbf{n}_g$ , are used to calculate deviations of a machined gear tooth flank from the tooth flank of the desired geometry.

Given the position vector of a point,  $\mathbf{r}_g(v, \theta_{pa})$ , of the gear tooth flank,  $\mathcal{G}$ , the unit normal vector,  $\mathbf{n}_g$ , can be calculated from the following well-known formula:

$$\mathbf{n}_g(v, \theta_{pa}) = \frac{\frac{\partial \mathbf{r}_g}{\partial v} \times \frac{\partial \mathbf{r}_g}{\partial \theta_{pa}}}{\left| \frac{\partial \mathbf{r}_g}{\partial v} \times \frac{\partial \mathbf{r}_g}{\partial \theta_{pa}} \right|} (v, \theta_{pa}) \quad (14.53)$$

Calculation of the derivatives  $(\partial \mathbf{r}_g / \partial v)$  and  $(\partial \mathbf{r}_g / \partial \theta_{pa})$  from Equation 14.44, followed by formula transformation (see Equation 14.53) is a drilling procedure. Calculation of the unit normal vector,  $\mathbf{n}_g$ , can be significantly simplified if the vector,  $\mathbf{n}_g$ , and the straight line along the vector,  $\mathbf{n}_g$ , are determined in the reference system  $X_{pa}Y_{pa}Z_{pa}$  (in this reference system, the unit normal vector,  $\mathbf{n}_g$ , is identical to the unit normal vector,  $\mathbf{n}_{lc}$ , to the line of contact,  $LC$ ). Afterward, implementation of the operator,  $\mathbf{Rs}(PA \mapsto \mathcal{G})$ , of the resultant coordinate system transformation (see Equation 14.26) allows for representation of both the unit normal vector,  $\mathbf{n}_{lc}$ , and the straight line along,  $\mathbf{n}_{lc}$ , in the coordinate system,  $X_gY_gZ_g$ , associated with the gear.

Referring to Figure 14.8, the position vector,  $\mathbf{r}_m$ , of a point of the line of contact,  $LC$ , can be given by an expression of the form:

$$\mathbf{r}_m = \mathbf{i} \cdot X_m + \mathbf{j} \cdot Y_m \quad (14.54)$$

In Equation 14.54, the Cartesian coordinates of the point of interest,  $m$ , are denoted by  $X_m$  and  $Y_m$ , respectively.

The unit tangent vector,  $\mathbf{t}_m$ , at  $m$  can be expressed in the form:

$$\mathbf{t}_m = \mathbf{i} \cdot \cos \zeta_{cl} + \mathbf{j} \cdot \sin \zeta_{cl} \quad (14.55)$$

The inclination of the unit tangent vector,  $\mathbf{t}_m$ , in relation to the  $X_g$ -axis (see Equation 14.55) is specified by the angle,  $\zeta_{cl}$ . The angle,  $\zeta_{cl}$ , can be calculated from the formula:

$$\zeta_{cl} = \tan^{-1} \left( \frac{\partial Y_{cl}(X_{cl})}{\partial X_{cl}} \right) \quad (14.56)$$

when the line of contact,  $LC$ , is represented in an explicit form as  $Y_{cl} = Y_{cl}(X_{cl})$ .

Once Equation 14.55 is known, an expression for the calculation of the unit normal vector,  $\mathbf{n}_{lc}$ , can be represented in vector form as:

$$\mathbf{n}_{lc} = -\mathbf{i} \cdot \sin \zeta_{cl} + \mathbf{j} \cdot \cos \zeta_{cl} \quad (14.57)$$

Ultimately, implementation of Equations 14.54 through 14.57 makes it possible to derive an expression for the position vector of a point,  $\mathbf{r}_{n.lc}$ , of a straight line through the point  $m$  along the unit normal vector,  $\mathbf{n}_{lc}$

$$\mathbf{r}_{n.lc} = \mathbf{r}_m + \lambda_n \mathbf{n}_{lc} \quad (14.58)$$

or in matrix form:

$$\mathbf{r}_{n.lc} = \begin{bmatrix} X_m - \lambda_n \sin \zeta_{lc} \\ Y_m + \lambda_n \cos \zeta_{lc} \\ 0 \\ 1 \end{bmatrix} \quad (14.59)$$

In Equations 14.58 and 14.59, the distance of point  $m$  from the end of the position vector,  $\mathbf{r}_m$ , is denoted by  $\lambda_n$ .

In the reference system,  $X_g Y_g Z_g$ , an expression for the unit normal vector,  $\mathbf{n}_g$ , to the gear tooth flank,  $\mathcal{G}$ , can be derived from the equation:

$$\mathbf{n}_g = \mathbf{Rs}(PA \mapsto \mathcal{G}) \cdot \mathbf{n}_{lc} \quad (14.60)$$

Similarly, an expression for the position vector of a point,  $\mathbf{r}_{n.lc}$ , in the reference system,  $X_g Y_g Z_g$ , can be derived from the equation:

$$\mathbf{r}_{n.lc}^g = \mathbf{Rs}(PA \mapsto \mathcal{G}) \cdot \mathbf{r}_{n.lc} \quad (14.61)$$

Finally, Equation 14.61 and the operator  $\mathbf{Rs}(PA \mapsto \mathcal{G})$  (see Equation 14.26) allow for an equation:

$$\begin{aligned} \mathbf{r}_{n.lc}^g(\lambda) &= \begin{bmatrix} (\cos \Sigma_p \cos \theta_{pa} + \sin \Sigma_p \cos \phi_{t.\omega} \sin \theta_{pa}) \cdot (X_m - \lambda \sin \zeta_{lc}) + \sin \Sigma_p \sin \phi_{t.\omega} (Y_m + \lambda \cos \zeta_{lc}) + r_g \sin \Sigma_p \sin \phi_{t.\omega} \\ - \sin \phi_{t.\omega} \sin \theta_{pa} \cdot (X_m - \lambda \sin \zeta_{lc}) + \cos \phi_{t.\omega} (Y_m + \lambda \cos \zeta_{lc}) + r_g \cos \phi_{t.\omega} \\ - (\sin \Sigma_p \cos \theta_{pa} + \cos \Sigma_p \cos \phi_{t.\omega} \sin \theta_{pa}) \cdot (X_m - \lambda \sin \zeta_{lc}) + \cos \Sigma_p \sin \phi_{t.\omega} (Y_m + \lambda \cos \zeta_{lc}) + r_g \cos \Sigma_p \sin \phi_{t.\omega} \\ 1 \end{bmatrix} \end{aligned} \quad (14.62)$$

In a similar manner to that just discussed, the unit normal vector  $\mathbf{n}_g$  to the gear tooth flank,  $\mathcal{G}$ , as well as the position vector of a point,  $\mathbf{r}_{n.lc}^g$ , of a straight line through a point,  $m$ , in the direction of  $\mathbf{n}_g$  can be calculated for a line of contact,  $LC$ , of any reasonable geometry.

Formulas similar to those above can be derived for a pinion tooth flank,  $\mathcal{P}$ , in a crossed-axes gear pair.

The aforementioned approach for the determination of the geometry of the gear tooth flank,  $\mathcal{G}$ , and the pinion tooth flank,  $\mathcal{P}$ , is based on the generation of the tooth flanks in the form of a family of consecutive positions of the line of contact,  $LC$ , that travel together with the plane of action,  $PA$ . This approach does not require specification of the tooth flanks in the form of enveloping surfaces to consecutive positions of the generating basic rack. This means that the proposed method for the generation of the tooth flanks,  $\mathcal{G}$  and  $\mathcal{P}$ , does not require implementation of the elements of the theory of enveloping surfaces. This is a significant advantage of the disclosed method for the generation of tooth flank,  $\mathcal{G}$ , of the gear, and tooth flank,  $\mathcal{P}$ , of the pinion in a crossed-axes gearing.

For correct generation of the tooth flanks,  $\mathcal{G}$  and  $\mathcal{P}$ , the plane of action,  $PA$ , passes through a fixed line known as the *axis of instant rotation*,  $P_{ln}$ . The same requirement is valid with respect to crossed-axes gearing.

The derived equations for the gear tooth flank,  $\mathcal{G}$ , and the pinion tooth flank,  $\mathcal{P}$ , can be used as reference surfaces (datum surfaces) when designing, machining, and inspecting gears for crossed-axes gearings that have line contact of the tooth flanks,  $\mathcal{G}$  and  $\mathcal{P}$ , of the gear and the pinion. Surfaces of this kind are an equivalent to the screw involute surfaces widely used for parallel-axes gear pairs.

Crossed-axes gearings that have tooth flanks of the proposed geometry (which is generated by the line of contact,  $LC$ , traveling together with the plane of action,  $PA$ ) are the most general type of gearings that have line contact of the tooth flanks,  $\mathcal{G}$  and  $\mathcal{P}$ . In a particular case when the center distance is reduced to zero ( $C = 0$ ), the crossed-axes gearing of the proposed geometry simplifies to crossed-axes gearing that have line contact of the tooth flanks. Under another scenario, namely when the crossed-axes angle is equal either



**FIGURE 14.11**  
Spiral bevel pinion for a crossed-axes gear pair.

0 or  $\pi$ , the crossed-axes gearing of the proposed geometry simplifies to parallel-axes gearing that has line contact of the tooth flank.

The desired geometry of contact between the tooth flanks of the gear and pinion in a gearing\* with a line contact between the tooth flanks,  $\mathcal{G}$  and  $\mathcal{P}$ , can be specified at the stage of analysis of the shape and configuration of the line of contact,  $LC$ , within the plane of action,  $PA$ . The indicatrix of conformity,  $Cnf_R(\mathcal{G}/\mathcal{P})$ , at a point of contact between the tooth flanks,  $\mathcal{G}$  and  $\mathcal{P}$ , can be expressed in terms of the shape and configuration of the line of contact. Ultimately, those parameters of the shape and the configuration of the line of contact are selected under which the minimum diameter of the indicatrix of conformity,  $Cnf_R(\mathcal{G}/\mathcal{P})$ , is as small as possible.

When a pair of conjugate tooth flanks,  $\mathcal{G}$  and  $\mathcal{P}$ , is generated by means of a desired line of contact,  $LC_{des}$ , an original geometry of the line of contact,  $LC_{des}$ , is not altered when the gears rotate.† The desired line of contact,  $LC_{des}$ , is a rigid planar curve entirely located within the plane of action,  $PA$ . The initially specified configuration of  $LC_{des}$  in relation to the plane of action,  $PA$ , remains the same.

A sample of spiral bevel pinion for a crossed-axes gear pair is pictured in Figure 14.11.

The crossed-axes gearing for which the tooth flanks of the gear and pinion are generated as loci of consequent positions of the line of contact,  $LC$ , that travels together with the plane of action,  $PA$ , is a novel type of gearing. This novel kind of gearing ensures line contact of the tooth flanks of the gear and of the pinion. This gearing is referred to as the *R-gearing*. *R-gearing* proposed by the author (circa 2008) is the only kind of crossed-axes gearing that features line contact between the tooth flanks,  $\mathcal{G}$  and  $\mathcal{P}$ , of a gear and a mating pinion.‡

\* Crossed-axes gearing with a line contact between the tooth flanks,  $\mathcal{G}$  and  $\mathcal{P}$ , is commonly referred to as *R-gearing*.

† A limited alteration to the geometry of the line of contact,  $LC$ , is observed when the gears are finish-cut, either in the face hobbing process or the in face-grinding process with a spiral grinding wheel, and so forth. The profile angle,  $\phi_{t,av}$  of the cutting toll (of the face hob, spiral grinding wheel, and so forth) has a zero value in all cases. A more significant alteration to the geometry of the line of contact,  $LC$ , in perfect bevel gears can be achieved when the gears are cut using NC technology for this purpose. This particular problem is out of the scope of the book, and it is not considered here.

‡ Many efforts have been undertaken by Phillips targeting the development of a spatial gearing that features line contact between the tooth flanks of a gear and a mating pinion. In the design of spatial gearing proposed by Phillips (2003), both tooth flanks of the gear and pinion are generated by a plane that travels in relation to the axis of rotation,  $O_g$ , of the gear,  $\mathcal{G}$ , and that,  $O_p$ , of the pinion,  $\mathcal{P}$  (when the pinion tooth flank,  $\mathcal{P}$ , is generated). In *R-gearing*, neither the tooth flank of a gear nor of a mating pinion is capable of been generated by a plane. Therefore, it should be concluded that in the spatial gearing proposed by Phillips, the tooth flanks of the mating gears are always in point contact, and they never make line contact. The research on this concern later carried out by Dr. Stachel (2006) to determine a special combination of the design parameters of the gearing under which the tooth flanks make line contact should be qualified as a mistake.

The derived equations for the gear tooth flank,  $\mathcal{G}$ , as well as for the pinion tooth flank,  $\mathcal{P}$ , can be used as the reference surfaces (datum surfaces) when designing, and when machining gears for crossed-axes gearings. Surfaces of this kind are an equivalent to the screw involute surface broadly used as reference surface for parallel-axes gear pairs. The most favorable approximation of the tooth profile of the cutter-heads of conventional design is another possible field of application of the derived equations for a gear and a mating pinion teeth flanks.

The tooth flanks of a gear and a mating pinion in  $R$ -gearing do not allow for *sliding over itself*. The tooth flanks,  $\mathcal{G}$  and  $\mathcal{P}$ , of this particular kind cannot be formed using the generating method of surface generation. However, describing the method of surface generation perfectly fits this purpose.

#### 14.4 Conjugacy of Tooth Flanks of a Gear and a Mating Pinion in $R$ -Gearing

Conjugacy is a specific property of the tooth flanks of a gear,  $\mathcal{G}$ , and a mating pinion,  $\mathcal{P}$ . Only surfaces that roll over one another can feature this unique property. Due to this property, in rolling motion of a gear and a pinion over one another, the tooth flanks,  $\mathcal{G}$  and  $\mathcal{P}$ , can be viewed as a kind of *reversibly-enveloping surfaces* (or just  $R_e$ -surfaces for simplicity) [115].

In crossed-axes gearing, when a gear and a mating pinion rotate steadily, the gear tooth flank,  $\mathcal{G}$ , can be viewed as an envelope to consecutive positions of the mating pinion tooth flank,  $\mathcal{P}$ . The gear tooth flank,  $\mathcal{G}$ , generated in this way can be used to generate the mating pinion tooth flank. If the tooth flanks,  $\mathcal{G}$  and  $\mathcal{P}$ , are conjugate, then the original pinion tooth flank,  $\mathcal{P}$ , and the pinion tooth flank,  $\mathcal{P}_g$ , generated by the gear tooth flank,  $\mathcal{G}$ , are identical to one another ( $\mathcal{P}_g \equiv \mathcal{P}$ ).

Tooth flanks not of many geometries can be referred to as conjugate surfaces or reversibly-enveloping surfaces. [115]

A criterion to be fulfilled by two tooth flanks,  $\mathcal{G}$  and  $\mathcal{P}$ , of a crossed-axes gear pair in order to possess the property of conjugacy can be expressed analytically.

When gear,  $\mathcal{G}$ , and mating pinion,  $\mathcal{P}$ , tooth flanks interact with one another, straight lines that align to common perpendiculars,  $\mathbf{n}_g$ , through points within a current line of contact,  $LC$ , must always intersect the axis of instant rotation,  $P_{ln}$ . The condition of conjugacy must be met at all points of a (desired) line of contact,  $LC_{des}$ , between the interacting tooth flanks,  $\mathcal{G}$  and  $\mathcal{P}$ . This is a key requirement to be fulfilled by conjugate tooth flanks,  $\mathcal{G}$  and  $\mathcal{P}$ , when the gears rotate.

At an arbitrary point,  $m$ , within a desired line of contact,  $LC_{des}$ , an instant line of action,  $LA_{inst}$ , forms an angle with the axis of instant rotation,  $P_{ln}$ . At every instant of time, every instant line of action,  $LA_{inst}$ , intersects the axis of instant rotation,  $P_{ln}$ , of a gear, and mating pinion tooth flanks,  $\mathcal{G}$  and  $\mathcal{P}$ ; this is a must for conjugate tooth flanks.

A component of the instant motion that is parallel to the axis of instant rotation,  $P_{ln}$ , does not affect the conjugate action between the interacting tooth flanks,  $\mathcal{G}$  and  $\mathcal{P}$ . Therefore, this component of the relative motion is not considered here.

The other component of the relative motion is along a straight line through a point,  $P$ , that is located within the axis of instant rotation,  $P_{ln}$ . The conjugate action between the interacting tooth flanks,  $\mathcal{G}$  and  $\mathcal{P}$ , is considered for this component of the relative motion.

Three vectors,  $\mathbf{p}_{ln}$ ,  $\mathbf{V}_m$ , and  $\mathbf{n}_g$ , are constructed in Figure 14.12.

Two of the vectors,  $\mathbf{p}_{ln}$  and  $\mathbf{V}_m$ , are located within the plane of action,  $PA$ .

The unit vector,  $\mathbf{p}_{ln}$ , is along the axis of instant rotation,  $P_{ln}$ . Therefore, in the plane-of-action Cartesian coordinate system,  $X_{pa}Y_{pa}Z_{pa}$ , it can be analytically represented in a form:

$$\mathbf{p}_{ln} = \mathbf{i} \quad (14.63)$$

The velocity vector,  $\mathbf{V}_m$ , is along an instant line of action,  $LA_{inst}$ , through the point of interest,  $m$ . In the plane-of-action Cartesian coordinate system,  $X_{pa}Y_{pa}Z_{pa}$ , the velocity vector,  $\mathbf{V}_m$ , can be analytically described as:

$$\mathbf{V}_m = \mathbf{i} \cdot V_m \sin \varphi_{pa} + \mathbf{j} \cdot V_m \cos \varphi_{pa} \quad (14.64)$$

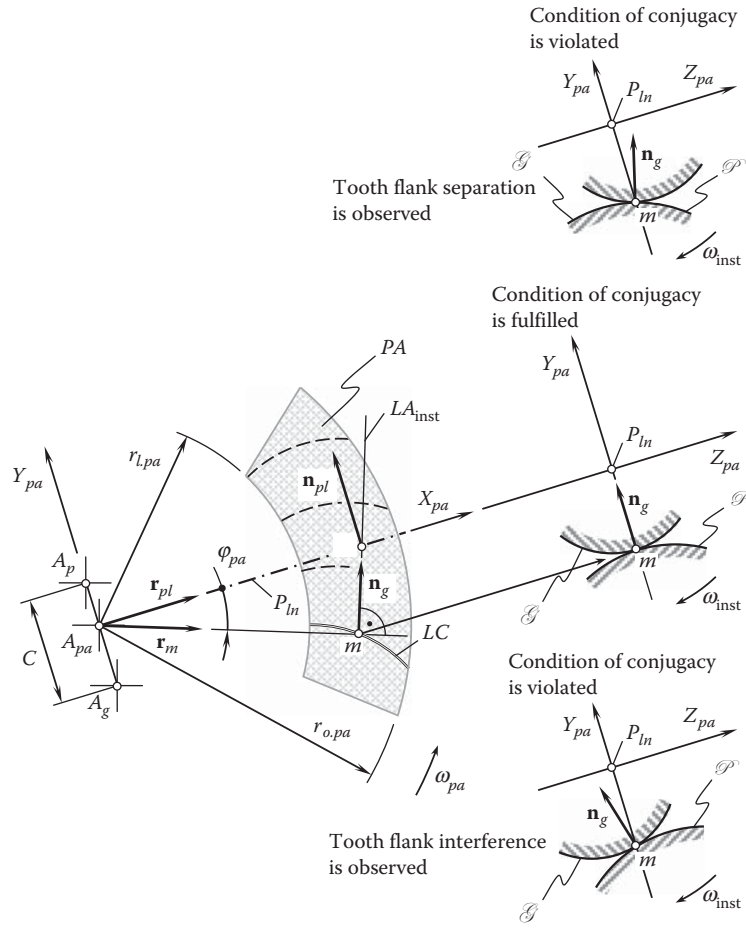


FIGURE 14.12

Condition of conjugacy of a gear,  $\mathcal{G}$ , and a mating pinion,  $\mathcal{P}$ , tooth flanks in crossed-axes gearing.

The magnitude,  $V_m$ , of the linear velocity vector,  $\mathbf{V}_m$ , is omitted from the further analysis, as it does not affect the direction of the vector,  $\mathbf{V}_m$ .

The third unit vector,  $\mathbf{n}_g$ , is perpendicular to the gear tooth flank,  $\mathcal{G}$ . Therefore, it can be calculated from the equation:

$$\mathbf{n}_g = \frac{\frac{\partial \mathbf{r}_g}{\partial U_g} \times \frac{\partial \mathbf{r}_g}{\partial V_g}}{\left| \frac{\partial \mathbf{r}_g}{\partial U_g} \times \frac{\partial \mathbf{r}_g}{\partial V_g} \right|} \quad (14.65)$$

where:

$\mathbf{r}_g$  is the position vector of a point of a gear tooth flank,  $\mathcal{G}$ .

$U_g$  and  $V_g$  are the curvilinear (Gaussian) coordinates of a point of a gear tooth flank,  $\mathcal{G}$ .

A gear,  $\mathcal{G}$ , and mating pinion,  $\mathcal{P}$ , tooth flanks are conjugate if a straight line along the unit normal vector,  $\mathbf{n}_g$ , intersects the axis of instant rotation,  $P_{ln}$ , at any point of the line of contact,  $LC$ . To meet this requirement, the unit normal vectors,  $\mathbf{n}_{pl}$  and  $\mathbf{n}_g$ , must be coplanar, and they must not be perpendicular to one another (here, the unit normal vector to the axis of instant rotation,  $P_{ln}$ , is designated as  $\mathbf{n}_{pl}$ . This vector is entirely located within the plane of action,  $PA$ ).

When gear,  $\mathcal{G}$ , and mating pinion,  $\mathcal{P}$ , tooth flanks are conjugate, then the three unit vectors,  $\mathbf{p}_{ln}$ ,  $\mathbf{V}_m$ , and  $\mathbf{n}_g$ , must be coplanar. The unit vectors,  $\mathbf{p}_{ln}$ ,  $\mathbf{V}_m$ , and  $\mathbf{n}_g$ , are coplanar if and only if the triple scalar product,  $\mathbf{p}_{ln} \times \mathbf{V}_m \cdot \mathbf{n}_g$ , is zero; that is, if the equality:

$$\mathbf{p}_{ln} \times \mathbf{V}_m \cdot \mathbf{n}_g = 0 \quad (14.66)$$

is valid. The triple scalar product,  $\mathbf{p}_{ln} \times \mathbf{V}_m \cdot \mathbf{n}_g$ , can be represented in a form of a determinant:

$$\mathbf{p}_{ln} \times \mathbf{V}_m \cdot \mathbf{n}_g = \begin{vmatrix} X_{pl} & Y_{pl} & Z_{pl} \\ V_{x.m} & V_{y.m} & V_{z.m} \\ X_g & Y_g & Z_g \end{vmatrix} = 0 \quad (14.67)$$

The unit vector,  $\mathbf{n}_{pl}$ , is entirely located within the plane of action,  $PA$ , and is perpendicular to the axis of instant rotation,  $P_{ln}$ . Therefore, in the plane-of-action Cartesian coordinate system,  $X_{pa}Y_{pa}Z_{pa}$ , it can be analytically represented in a form:

$$\mathbf{n}_{pl} = \mathbf{j} \quad (14.68)$$

In addition to Equation 14.67, the condition:

$$\mathbf{n}_{pl} \cdot \mathbf{n}_g \neq 0 \quad (14.69)$$

must also be fulfilled. The parallelism of the directions specified by the unit normal vectors,  $\mathbf{n}_{pl}$  and  $\mathbf{n}_g$ , is eliminated by this condition. No rotation transmission by means of gears is possible when the unit normal vector,  $\mathbf{n}_g$ , is parallel to the axis of instant rotation,  $P_{ln}$ .

An expression:

$$\mathbf{p}_{ln} \times \mathbf{n}_g \neq 0 \quad (14.70)$$

is an alternative representation of the condition specified by Equation 14.69.

Gear,  $\mathcal{G}$ , and mating pinion,  $\mathcal{P}$ , tooth flanks are said to be conjugate if and only if the conditions specified by Equation 14.66 (or Equation 14.67) and Equation 14.69 (or Equation 14.70), are fulfilled for any and all points within the line of contact,  $LC$ , for any possible configurations of the gear and the pinion in relation to one another.

$$\begin{cases} \mathbf{p}_{ln} \times \mathbf{V}_m \cdot \mathbf{n}_g = 0 \\ \mathbf{p}_{ln} \times \mathbf{n}_g \neq 0 \end{cases} \quad (14.71)$$

Equation 14.71 analytically describes the condition of conjugacy of gear,  $\mathcal{G}$ , and mating pinion,  $\mathcal{P}$ , tooth flanks.

The above discussion can be summarized and represented as:

**The second fundamental law of gearing (general case):** "In crossed-axes gearing, in order to transmit a uniform rotary motion from a driving shaft to a driven shaft by means of gear teeth, perpendicular to the tooth flanks of the interacting teeth at all points of their contact must intersect the axis of instant rotation.

All perfect gearings obey the second fundamental law of gearing.

## 14.5 Desired Tooth Proportions in Crossed-Axes Gear Pairs

A gear and a mating pinion in a crossed-axes gear pair have a plurality of teeth. The teeth are evenly spaced circumferentially. The general form of the equation of a gear tooth flank (see Equation 14.44), as well as Equations 14.49 and 14.52, of particular cases of the gear tooth flank,  $\mathcal{G}$ , are convenient for research purposes.

However, these equations are not sufficient for the specification of the tooth shape either of the gear or the pinion for engineering purposes. In the last case, the gear tooth flank,  $\mathcal{G}$ , specified by Equation 14.44 should be properly located in relation to the tooth flank of the opposite side of the gear tooth, as well as the tooth flanks of the rest of the gear teeth.

The desired tooth proportions in crossed-axes gearing can be established in a way similar to how the desired tooth proportions are established in parallel-axes gearing, as well as how they are established in crossed-axes gearing. Following this concept, let us begin from the base cone of a gear in a crossed-axes gear pair.

### 14.5.1 Operating Angular Base Pitch

The angular distance between two adjacent desirable lines of contact,  $LC_{\text{des}}^i$  and  $LC_{\text{des}}^{i+1}$ , of gear and mating pinion tooth flanks,  $\mathcal{G}$  and  $\mathcal{P}$ , in a crossed-axes gear pair is specified by the operating angular base pitch,  $\varphi_{b,op}$  of the gear pair. The *operating angular base pitch*,  $\varphi_{b,op}$  is a design parameter of critical importance for gear engineers.

In a crossed-axes gear pair, the operating angular base pitch is an equivalent to the operating base pitch in a parallel-axes gearing and the operating angular base pitch in a crossed-axes gearing. Based on these similarities, the angular distance between every two consequent tooth profiles within the plane of action,  $PA$ , is specified by the operating angular base pitch in a crossed-axes gearing.

#### Definition 14.1

The *operating base pitch*,  $\varphi_{b,op}$ , in crossed-axes gearing is an angular distance between every two adjacent desired lines of contact,  $LC_{\text{des}}^i$  and  $LC_{\text{des}}^{i+1}$ ; the angle,  $\varphi_{b,op}$ , is measured within the plane of action,  $PA$ , and is centered at the plane-of-action apex,  $A_{pa}$ .

In a certain sense, the operating angular base pitch in a crossed-axes gear pair is an equivalent of the angular module,  $\gamma_m$ , of the gear pair.

Consider a gear and the plane of action,  $PA$ , as schematically illustrated in Figure 14.13. When the gears rotate, the base cone of the gear rolls over the plane of action,  $PA$ .

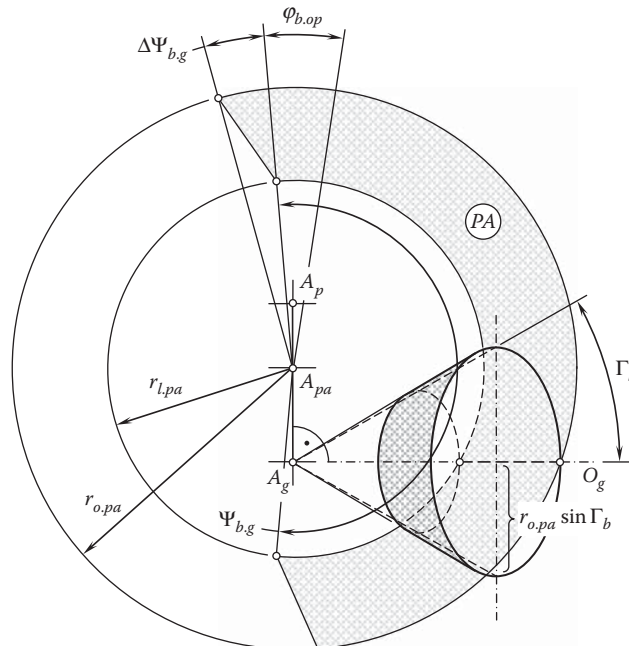


FIGURE 14.13

Definition of the term *operating angular base pitch*,  $\varphi_{b,op}$ , in perfect crossed-axes gearing.



Consider a point within the surface of the base cone of a gear. The point is remote from the base cone apex,  $A_g$ , at a distance  $r_{o.pa}$ . The arc distance:

$$\tilde{L}_{b.g} = 2\pi r_{o.pa} \sin \Gamma_b \quad (14.72)$$

is covered by the point per each rotation of the gear.

Within the plane of action,  $PA$ , a circular arc of the length  $\tilde{L}_{b.g}$  spans over a central angle,  $\Psi_{b.g}$ . The value of the angle,  $\Psi_{b.g}$ , can be calculated from the formula:

$$\Psi_{b.g} = 360^\circ \sin \Gamma_b \quad (14.73)$$

For a gear with  $N_g$  teeth, a portion,  $\varphi_{b.op}$ , of the central angle,  $\Psi_{b.g}$ , per gear tooth is equal to:\*

$$\varphi_{b.op} = \frac{\Psi_{b.g}}{N_g} = \frac{360^\circ}{N_g} \sin \Gamma_b \quad (14.74)$$

The angle,  $\varphi_{b.op}$ , in crossed-axes gearing is analogous to the operating base pitch,  $p_{b.op}$ , in parallel-axes gearing. Due to this, the angle,  $\varphi_{b.op}$ , is referred to as the operating angular base pitch in a crossed-axes gear pair.

As illustrated in Figure 14.14, for a specified gear, the operating angular base pitch,  $\varphi_{b.op}$ , remains the same for any and all circles of radii  $r_{x.pa}$ ,  $r_{y.pa}$ , and so forth, within the face width,  $F_{pa}$ , of the gear ( $\varphi_{b.op} = \text{const}$ ).

It should be noted here that the tooth number,  $N_{pa}$ , within the imaginary plane of action,  $PA$ , is not mandatorily expressed by an integer number. It can be expressed by a number with fractions as well. This is feasible, as the plane of action,  $PA$ , as well as entities associated with the plane, do not exist physically.

The operating angular base pitch,  $\varphi_b$  can be expressed in terms of linear dimensions. The latter makes sense in cases when the linear dimensions are easier to measure.

The operating angular base pitch,  $\varphi_{b.op}$ , is measured within the plane of action,  $PA$ , of the gear pair. The operating angular base pitch is a calculated design parameter in a crossed-axes gear pair; that is, it cannot be measured directly.

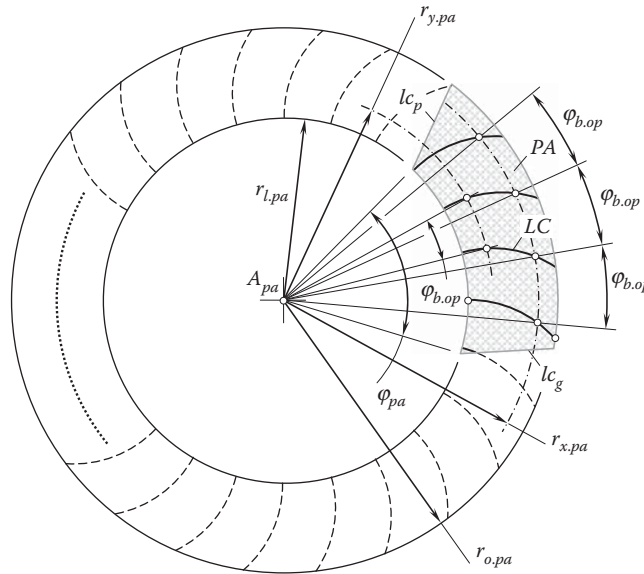


FIGURE 14.14

The operating angular base pitch,  $\varphi_{b.op}$ , for crossed-axes gears has a constant value for all the teeth, as well as within the face width of the gear.

\* The angular normal module,  $m_{\gamma.pa}$ , is equivalent to the angular base pitch,  $\varphi_{b.op}$ , as:  $m_{\gamma.pa} = (360^\circ / N_{pa}) = (2\pi / N_{pa})$ .

The angular base pitch of a gear,  $\varphi_{b,g}$  (as well as that of a mating pinion,  $\varphi_{b,p}$ ), is measured within a plane tangent to the base cone of the gear. The gear angular base pitch can be measured directly in the gear and pinion separately. The angular base pitch is measured within the tangent plane as an angle between the actual lines of intersection of the gear and pinion tooth flanks,  $\mathcal{G}$  and/or  $\mathcal{P}$ , of two adjacent teeth. One of the lines of intersection of the gear and pinion tooth flanks,  $\mathcal{G}$  and/or  $\mathcal{P}$ , by the plane of action,  $PA$ , may be located either outside the outer cone or inside the root cone either of the gear or the pinion.

A variation of the actual value of the angular base pitch of a gear (and mating pinion) can be measured as the variation of the configuration and the geometry of the line of intersection of a single tooth flank,  $\mathcal{G}$  (or a single tooth flank  $\mathcal{P}$ ), when the gear (or pinion) turns about its axis of rotation.

The apex for the measurement of a gear (and mating pinion) angular base pitch,  $\varphi_{b,g}$  (and  $\varphi_{b,p}$ ), in crossed-axes gearing coincides with the plane-of-action apex,  $A_{pa}$ , and not with the gear base cone apex,  $A_g$  (and the pinion base cone apex,  $A_p$ ).

The operating base pitch can be determined following the routine outlined immediately below:

1. Consider rolling of the base cone of the gear (or pinion) over the plane of action,  $PA$ . The base cone contacts the plane of action along a straight line.
2. When rolling, sliding between the base cone and the plane of action along the line of contact is observed; however, the angular velocity ratio is not affected by the sliding.
3. The sliding is observed along the axis of instant rotation,  $P_{ln}$ .
4. No sliding is observed in the direction perpendicular to the axis of instant rotation,  $P_{ln}$ , that is, in the tangential direction to the base cones.
5. Consider the roll angle of a value  $2\pi/N_g$  (or  $2\pi/N_p$ ).
6. When the base cone of the gear (or pinion) turns about its axis through the angle  $2\pi/N_g$  (or  $2\pi/N_p$ ), the base cone turns about the plane-of-action apex,  $A_{pa}$ , through the operating base pitch angle,  $\varphi_{b,op}$ .
7. Once the angle of rotation of the gear (or pinion) is known— $2\pi/N_g$  (or  $2\pi/N_p$ ), then the equation:

$$u = \frac{r_g}{r_p} = \frac{\tan \Sigma_g}{\tan \Sigma_p} \quad (14.75)$$

can be used to calculate the operating angular base pitch,  $\varphi_{b,op}$ .

The operating angular base pitch,  $\varphi_{b,op}$  can be specified for of any and all crossed-axes gear pairs, while the angular base pitches,  $\varphi_{b,g}$  and  $\varphi_{b,p}$ , of a gear and its mating pinion can be specified only in cases of conjugate tooth flanks,  $\mathcal{G}$  and  $\mathcal{P}$ , and not for arbitrary tooth flanks.

The operating angular base pitch,  $\varphi_{b,op}$  can be calculated from the following formula:

$$\varphi_{b,op} = \frac{2\pi}{N_g} \sin \Gamma_b = \frac{2\pi}{N_p} \sin \gamma_b \quad (14.76)$$

$$\frac{N_g}{N_p} = u \quad (14.77)$$

$$N_g = u \cdot N_p \quad (14.78)$$

$$\varphi_{b,op} = \frac{2\pi}{u \cdot N_p} \sin \Gamma_b = \frac{2\pi}{N_p} \sin \gamma_b \quad (14.79)$$

The operating angular base pitch,  $\varphi_{b,op}$  can be construed as a vector associated with the gear pair,  $\vec{\varphi}_{b,op}$ , with the gear,  $\vec{\varphi}_{b,g}$ , and the mating pinion,  $\vec{\varphi}_{b,p}$ . The vectors  $\vec{\varphi}_{b,op}$ ,  $\vec{\varphi}_{b,g}$ , and  $\vec{\varphi}_{b,p}$  are along the corresponding axes of rotation:

- $O_{pa}$ , of the plane of action,  $PA$
- $O_g$ , of the gear
- $O_p$ , of the pinion

The magnitude of each of the vectors,  $\vec{\varphi}_{b.op}$ ,  $\vec{\varphi}_{b.g}$ , and,  $\vec{\varphi}_{b.p}$ , is proportional to the corresponding angular base pitch.

In the case of crossed-axes gearing,

- The vector,  $\vec{\varphi}_{b.op}$ , is applied at the plane-of-action-apex,  $A_{pa}$ , and is pointed along the axis  $O_{pa}$ .
- The vector,  $\vec{\varphi}_{b.g}$ , is a vector of the length,  $|\vec{\varphi}_{b.g}|$ , and is applied perpendicular to a plane that is tangent to the base cone of the gear; the line along which the vector  $\vec{\varphi}_{b.g}$  acts is at a distance,  $r_g$ , from the plane-of-action-apex,  $A_{pa}$ , measured along the perpendicular to the axis  $O_{pa}$ .
- The vector,  $\vec{\varphi}_{b.p}$ , is a vector of the length,  $|\vec{\varphi}_{b.p}|$ , and is applied perpendicular to a plane that is tangent to the base cone of the pinion; the line along which the vector  $\vec{\varphi}_{b.p}$  acts is at a distance,  $r_p$ , from the plane-of-action-apex,  $A_{pa}$ , measured along the perpendicular to the axis  $O_{pa}$ .

The corresponding tolerances in vector notation can be assigned to each of the base pitches.

#### 14.5.2 Low-Tooth-Count Crossed-Axes Gears

Depending on the actual value of the angular pitch,  $\varphi_b$ , low-tooth-count crossed-axes gears (*LTC* crossed-axes gears) are recognized. Low-tooth-count crossed-axes gears feature the angular pitch,  $\varphi_b$ , of a larger value compared to that in gears with a large tooth count. Use of the base cone angle of a gear,  $\Gamma_b$  (of a pinion,  $\gamma_b$ ), and the start-of-active-profile cone angle of the gear,  $\Gamma_{sap}$  (of a pinion,  $\gamma_{sap}$ ), makes possible a numerical criterion to distinguish low-tooth-count crossed-axes gears; that is, for *LTC* crossed-axes gears, the following inequality is valid:

$$\Gamma_b > \Gamma_{sap} \quad (14.80)$$

A similar inequality:

$$\gamma_b > \gamma_{sap} \quad (14.81)$$

is valid with respect to a low-tooth-count crossed-axes pinion.

Low-tooth-count crossed-axes gears feature more significant variation of the most of the principal design parameters of the tooth flanks compared to that in gears with a large tooth count.

#### 14.5.3 Transverse Pressure Angle

The transverse pressure angle,  $\phi_{t.\omega}$ , is measured within a plane that is perpendicular to the axis of instant rotation,  $P_{ln}$  (or it is measured within a plane that is perpendicular to the vector of instant rotation,  $\omega_{pl}$ ). Referring to [Figure 14.5](#) (as well as to [Figure 14.7](#)), the transverse pressure angle,  $\phi_{t.\omega}$ , is the angle between a perpendicular to the plane of action,  $PA$ , and a perpendicular to the plane through the vector of instant rotation,  $\omega_{pl}$ , and the line along the closest distance of approach of the axes of rotations,  $O_g$  and  $O_p$ , of the gear and the pinion.

#### Definition 14.2

*The transverse pressure angle in crossed-axes gearing is the angle between a perpendicular to the plane of action and a perpendicular to the plane through the vector of instant rotation and the centerline of the axes of rotation of the gear and the pinion. The transverse pressure angle is measured within a plane that is perpendicular to the axis of instant rotation.*

The transverse pressure angle,  $\phi_{t.\omega}$ , can be considered an independent design parameter in a crossed-axes gear pair. Then, the base cone angles of the gear,  $\Gamma_b$ , and the pinion,  $\gamma_b$ , can be expressed in terms of the transverse pressure angle  $\phi_{t.\omega}$ . Otherwise, the transverse pressure angle,  $\phi_{t.\omega}$ , can be expressed in terms of the base cone angles,  $\Gamma_b$  and  $\gamma_b$ .

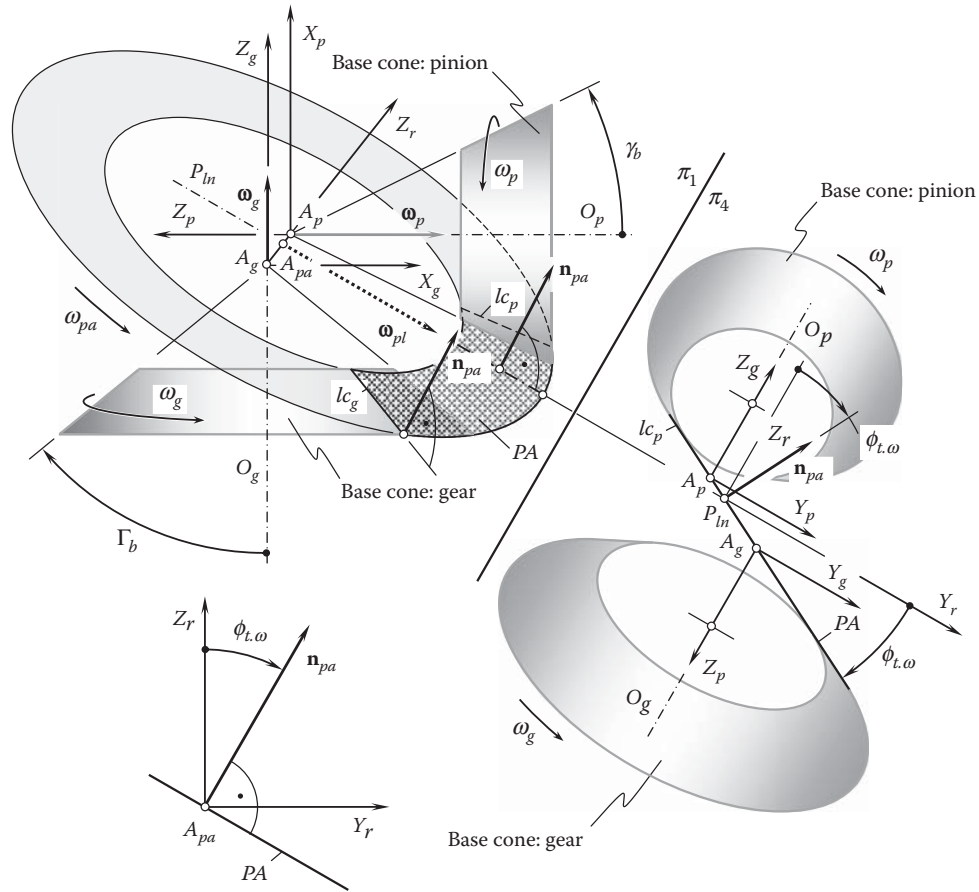


FIGURE 14.15

Specification of the configuration of the plane of action,  $PA$ , in relation to the base cone of the gear in a crossed-axes gear pair.

The plane of action,  $PA$ , is tangential to the base cone of the gear, as schematically illustrated in Figure 14.15. Therefore, the angle that the plane of action,  $PA$ , forms with the gear axis of rotation,  $O_g$ , is equal to the base cone angle,  $\Gamma_b$ . Once the angle between the plane of action,  $PA$ , and the axis,  $O_g$ , is known ( $\Gamma_b$ ), the unit normal vector,  $\mathbf{n}_{pa}$ , to the plane of action,  $PA$ , is equal to  $(90^\circ - \Gamma_b)$ .

In the reference system,  $X_r Y_r Z_r$ , the direction of the aforementioned unit normal vector,  $\mathbf{n}_{pa}$ , can be analytically expressed by the equation:

$$\mathbf{n}_{pa} = \mathbf{j}_r \sin \phi_{t,\omega} + \mathbf{k}_r \cos \phi_{t,\omega} \quad (14.82)$$

To express the base cone angle of the gear,  $\Gamma_b$ , in terms of the transverse pressure angle,  $\phi_{t,\omega}$ , or, conversely, to express the transverse pressure angle,  $\phi_{t,\omega}$ , in terms of the base cone angle of the gear,  $\Gamma_b$ , all the elements should be represented in a common reference system. Using the Cartesian coordinate system,  $X_g Y_g Z_g$ , associated with the gear is convenient for the purpose of calculating the base cone angle. To do so, the unit normal vector,  $\mathbf{n}_{pa}$ , should be represented in the reference system,  $X_g Y_g Z_g$ .

The reference systems,  $X_g Y_g Z_g$  and  $X_r Y_r Z_r$ , are turned in relation to one another about the  $Y_r$ -axis through the pinion angle  $\Sigma_p$ . Transition from the coordinate system,  $X_r Y_r Z_r$ , to the coordinate system,  $X_g Y_g Z_g$ , can be analytically described by the operator of rotation,  $\mathbf{Rt}(r \mapsto g)$  (see Equation 14.24). With that said, in the coordinate system,  $X_g Y_g Z_g$ , the direction of the unit normal vector,  $\mathbf{n}_{pa}$ , can be analytically described by the expression:

$$\mathbf{n}_{pa}^g = \mathbf{Rt}(r \mapsto g) \cdot \mathbf{n}_{pa} \quad (14.83)$$

Equations 14.24, 14.82, and 14.83 allow for the following expression for the vector  $\mathbf{n}_{pa}^g$ :

$$\mathbf{n}_{pa}^g = \begin{bmatrix} \cos \Sigma_p & 0 & \sin \Sigma_p & 0 \\ 0 & 1 & 0 & 0 \\ -\sin \Sigma_p & 0 & \cos \Sigma_p & 0 \\ 0 & 0 & 0 & 1 \end{bmatrix} \cdot \begin{bmatrix} 0 \\ \sin \phi_{t,\omega} \\ \cos \phi_{t,\omega} \\ 1 \end{bmatrix} = \begin{bmatrix} \sin \Sigma_p \cos \phi_{t,\omega} \\ \sin \phi_{t,\omega} \\ \cos \Sigma_p \cos \phi_{t,\omega} \\ 1 \end{bmatrix} \quad (14.84)$$

As the unit vector along the  $O_g$ -axis is equal to  $-\mathbf{k}$ , the angle  $\angle(\mathbf{n}_{pa}^g, -\mathbf{k})$  can be calculated from the formula:

$$\angle(\mathbf{n}_{pa}^g, -\mathbf{k}) = \Gamma_b = \cos^{-1}[\mathbf{n}_{pa}^g \cdot (-\mathbf{k})] \quad (14.85)$$

This formula can also be represented in the form:

$$\Gamma_b = \tan^{-1} \left( -\frac{\sqrt{\sin^2 \Sigma_p - \cos^2 \Sigma_p \sin^2 \phi_{t,\omega}}}{\cos \Sigma_p \cos \phi_{t,\omega}} \right) \quad (14.86)$$

The transverse profile angle,  $\phi_{t,\omega}$ , can be expressed in terms of the base cone angle,  $\Gamma_b$ , of the gear:

$$\phi_{t,\omega} = \cos^{-1} \left( \frac{\cos \Sigma_p}{\cos \Gamma_b} \right) \quad (14.87)$$

An equation similar to Equation 14.86 is valid for the base cone angle of the pinion:

$$\gamma_b = \tan^{-1} \left( -\frac{\sqrt{\sin^2 \Sigma_g - \cos^2 \Sigma_g \sin^2 \phi_{t,\omega}}}{\cos \Sigma_g \cos \phi_{t,\omega}} \right) \quad (14.88)$$

The transverse pressure angle,  $\phi_{t,\omega}$ , can also be expressed in terms of the base cone angle,  $\gamma_b$ , of the pinion:

$$\phi_{t,\omega} = \cos^{-1} \left( \frac{\cos \Sigma_g}{\cos \gamma_b} \right) \quad (14.89)$$

Both cone angles, namely  $\Sigma_g$  and  $\Sigma_p$ , can be expressed in terms of the rotations of the gear,  $\omega_g$ ; the pinion,  $\omega_p$ ; and the angle,  $\Sigma$ , between the rotation vectors,  $\boldsymbol{\omega}_g$  and  $\boldsymbol{\omega}_p$  (see Eqs. 14.1 and 14.3).

In the case where the transverse pressure angle,  $\phi_{t,\omega}$ , is given, the base cone angle of a gear,  $\Gamma_b$ , as well as the base cone angle of a mating pinion,  $\gamma_b$ , can both be expressed in terms of the transverse pressure angle,  $\phi_{t,\omega}$ , of the pitch cone angle of the gear,  $\Gamma$ , and pinion,  $\gamma$ .

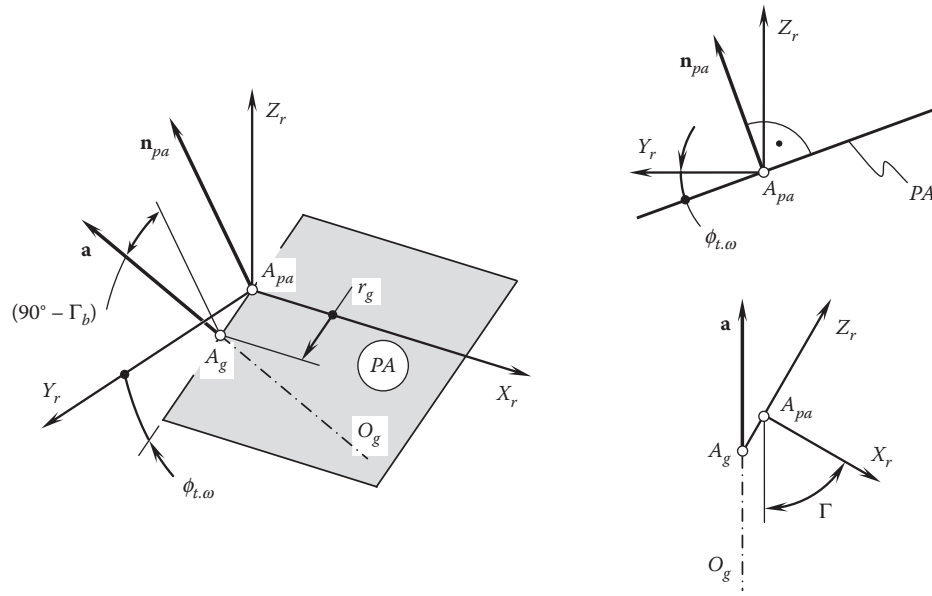
As the plane of action,  $PA$ , is in tangency with base cones of the gear and the pinion, it makes the transverse pressure angle,  $\phi_{t,\omega}$ , with the pitch plane,  $PP$  (see Figure 14.15). An angle that the plane of action,  $PA$ , makes with the axis of rotation of the gear,  $O_g$ , is equal to the base cone angle of the gear,  $\Gamma_b$ . Therefore, the unit normal vector,  $\mathbf{n}_{pa}$ , to the plane of action,  $PA$ , and the axis of rotation,  $O_g$ , make an angle  $(90^\circ - \Gamma_b)$ .

The unit normal vector,  $\mathbf{n}_{pa}$ , to the plane of action,  $PA$ , is specified by Equation 14.82. Referring to Figure 14.16, the unit vector,  $\mathbf{a}$ , along the axis of rotation of the gear,  $O_g$ , can be analytically expressed as

$$\mathbf{a} = -\mathbf{i} \cdot r_g \cos \Gamma + \mathbf{k}_r \cdot \sin \Gamma \quad (14.90)$$

Once the equality  $\angle(\mathbf{n}_{pa}, \mathbf{a}) = (90^\circ - \Gamma_b)$  is valid, the base cone angle of the gear can be calculated from the formula:

$$\Gamma_b = \tan^{-1} \left( \frac{|\mathbf{n}_{pa} \times \mathbf{a}|}{\mathbf{n}_{pa} \cdot \mathbf{a}} \right) \quad (14.91)$$

**FIGURE 14.16**

The relationship between the pitch cone angle,  $\Gamma$ , and the base cone angle,  $\Gamma_b$ , of a gear in a crossed-axes gearing.

The following expression for the calculation of the base cone angle,  $\Gamma_b$ , in a gear:

$$\Gamma_b = \tan^{-1} \left( \frac{\sqrt{\cos^2 \Gamma + \sin^2 \Gamma \cos^2 \phi_{t,\omega}}}{\sin \Gamma \sin \phi_{t,\omega}} \right) \quad (14.92)$$

can be derived after substituting the vectors  $\mathbf{n}_{pa}$  (from Equation 14.82) and  $\mathbf{a}$  (from Equation 14.90) into Equation 14.91.

A similar expression:

$$\gamma_b = \tan^{-1} \left( \frac{\sqrt{\cos^2 \gamma + \sin^2 \gamma \cos^2 \phi_{t,\omega}}}{\sin \gamma \sin \phi_{t,\omega}} \right) \quad (14.93)$$

is valid for the calculation of the base cone angle,  $\gamma_b$ , in a pinion.

In a particular case, when the pitch cone angle in a gear,  $\Gamma$ , is set equal to a right angle ( $\Gamma = 90^\circ$ ), the pitch cone becomes a flat surface and the resulting gear is commonly called a *crown gear*. So, a crown gear is a bevel gear with a planar pitch surface. The position vector of a point of a crown gear is specified by Eq. 14.52 under the assumption that the equality  $\Gamma = 90^\circ$  is valid.

The base cone angle of a crown gear,  $\Gamma_b$ , is equal to  $\Gamma_b = 90^\circ - \phi_{t,\omega}$  (similar to that in crossed-axes gearing, as schematically shown in Figure 12.21).

The back cone in a crown gear is degenerated to a round cylinder. The crown gear is an analogous to the basic rack in spur and helical gears.

For an internal gearing, the value of the base cone angle,  $\Gamma_b$ , (a) is either within the interval  $(90^\circ - \phi_{t,\omega}) < \Gamma_b < 90^\circ$ , (b) it is equal to a right angle ( $\Gamma_b = 90^\circ$ ), or (c) it is within the interval  $90^\circ < \Gamma_b < 180^\circ$ . This makes it possible to distinguish internal crossed-axes gears of three different types, and in this way to represent the classification of types of vector diagrams of gear pairs (see Figure 2.15) in more detail.





instant rotation,  $P_{ln}$ . Evidently, the rotation vector,  $\omega_{pp}$ , is perpendicular to the vector of instant rotation,  $\omega_{pl}$ . Due to lack of space, the last is not shown in Figure 14.17.

The outer radius,  $r_{o,pp}$ , of the working portion of the pitch plane is equal to the cone distance of the gear pair, while the inner radius,  $r_{i,pp}$ , is smaller than  $r_{o,pp}$  by the face width,  $F_{pp}$ , of the pitch plane.

An equation for the calculation of the angular pitch of the gear,  $\varphi_{n,g}$ , in a crossed-axes gearing can be derived similarly to an equation for the calculation of angular pitch of the gear,  $\varphi_{n,g}$ , in a crossed-axes gears (see Equation 14.88):

$$\varphi_{n,g} = \frac{360^\circ}{N_g} \cdot \frac{\sin \Gamma}{\cos \Sigma_g} \quad (14.94)$$

In Equation 14.94, the diameter,  $d_{o,pp}$ , is equal to  $d_{o,pp} = 2 r_{o,pp}$ .

The difference between Equations 12.106 and 14.94 is that the rolling component,  $\omega_g^{rl}$ , of the rotation vector of the gear,  $\omega_g$ , is taken into account. The sliding component,  $\omega_g^{sl}$ , does not cause rolling motion.

The expression (see Equation 14.94) for the calculation of the angular pitch of the gear,  $\varphi_{n,g}$ , along with the expression (see Equation 14.74) for the calculation of the base angular pitch of the gear,  $\varphi_b$ , makes possible an expression:

$$\varphi_b = \varphi_{n,g} \frac{\sin \Gamma_b}{\sin \Gamma} \quad (14.95)$$

for the angular base pitch,  $\varphi_b$ , in terms of the angular pitch,  $\varphi_{n,g}$ .

In perfect crossed-axes gearing, the angular base pitch of the gear,  $\varphi_{b,g}$ , is equal to the angular base pitch of the pinion,  $\varphi_{b,p}$ , and both of them are equal to the operating base pitch,  $\varphi_{b,op}$ , of the gear pair.

#### 14.5.5 Angular Tooth Thickness and Angular Space Width in the Round Basic Rack

Angular tooth thickness and angular space width in the round basic rack in a crossed-axes gear pair are the equivalents to tooth thickness and space width in parallel-axes gears. Both tooth thickness and space width are measured within the pitch plane, PP, of the corresponding round rack of the gear pair.

The determined values of the angular tooth thickness of a gear,  $\varphi_{t,g}$ , and a mating pinion,  $\varphi_{t,p}$ , as well as the angular space widths of a gear,  $\varphi_{w,g}$ , and a mating pinion,  $\varphi_{w,p}$ , yield the determination of the "gear tooth-line" (and the "gear tooth-space-line") in crossed-axes gearing. Definition 12.7 for intersected-axes gearing (see Section 12.6.5) is also valid with respect to gears that are used in the design of crossed-axes gears.

##### Definition 14.4

*The angular tooth thickness in a crossed-axes gear pair is the angular distance between opposite tooth flanks of the gear tooth measured within the pitch plane.*

##### Definition 14.5

*The angular space width in a crossed-axes gear pair is the angular distance between opposite tooth flanks of space between adjacent gear teeth measured within the pitch plane.*

As a gear tooth is commonly stronger compared to that of a mating pinion, it is reasonable to set the angular tooth thickness of the gear equal:

$$\varphi_{t,g} = \frac{\varphi_{N,g}}{2} - \varphi_{B,n} \quad (14.96)$$

In this case, the angular space width of that same gear can be calculated from:

$$\varphi_{w,g} = \frac{\varphi_{N,g}}{2} \quad (14.97)$$

Formulas similar to those above are valid with respect to the pinion.

As the gears in crossed-axes gearings interact with one another within the plane of action, the effective angular backlash,  $\varphi_{B.pa}$ , is specified within the plane of action,  $PA$ , and not within the pitch plane,  $PP$ .

#### 14.5.6 Angular Addendum and Angular Dedendum of the Round Basic Rack

For the specification of the angular tooth addendum, as well as of the angular tooth dedendum in a crossed-axes gearing, the outer surface and the surface of the bottom lands have to be determined. The pitch surface of the gear is used for the specification of these two surfaces.

The pitch surface of the gear,  $W_g$ , can be interpreted as the loci of consecutive positions of the axis of instant rotation,  $P_{ln}$ , in its rotation about the gear axis of rotation,  $O_g$ . As the straight line,  $P_{ln}$ , does not intersect the axis,  $O_g$ , but instead crosses the axis,  $O_g$ , the pitch surface of the gear is shaped in the form of a hyperboloid of one sheet and not in the form of a cone of revolution. The generation of the pitch surface,  $W_g$ , of the gear is illustrated in Figure 14.18.

The position vector of a point,  $\mathbf{w}_g$ , of the pitch surface,  $W_g$ , can be represented in the form of the summa of three vectors, namely of the vectors  $\mathbf{R}$ ,  $\mathbf{B}_{z.g}$ , and  $\mathbf{C}$ :

$$\mathbf{w}_g = \mathbf{R} + \mathbf{B}_{z.g} + \mathbf{C} \quad (14.98)$$

The vectors  $\mathbf{R}$ ,  $\mathbf{B}_{z.g}$ , and  $\mathbf{C}$  can be expressed in terms of their projections onto the axes of the coordinate system,  $X_g Y_g Z_g$ , as:

$$\mathbf{R} = \mathbf{i} \cdot r_g \cos \varphi_g + \mathbf{j} \cdot r_g \sin \varphi_g \quad (14.99)$$

$$\mathbf{B}_{z.g} = k B_{z.g} \quad (14.100)$$

$$\mathbf{C} = -\mathbf{i} B_{z.g} \tan \Sigma_g \sin \varphi_g + \mathbf{j} B_{z.g} \tan \Sigma_g \cos \varphi_g \quad (14.101)$$

The Gaussian parameters,  $\varphi_g$  and  $B_{z.g}$ , of the pitch surface,  $W_g$ , are schematically shown in Figures 14.18 and 14.19.

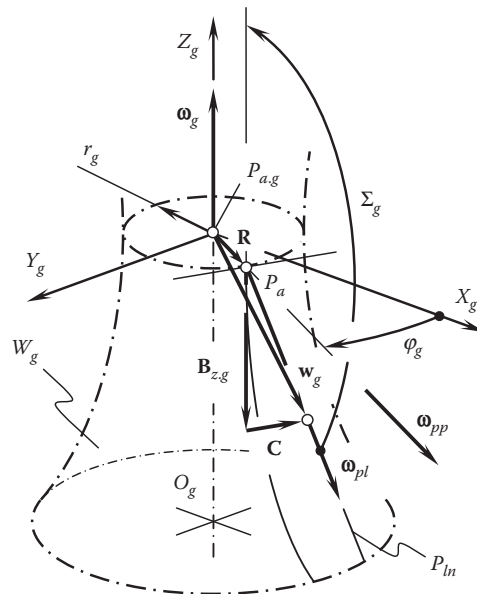
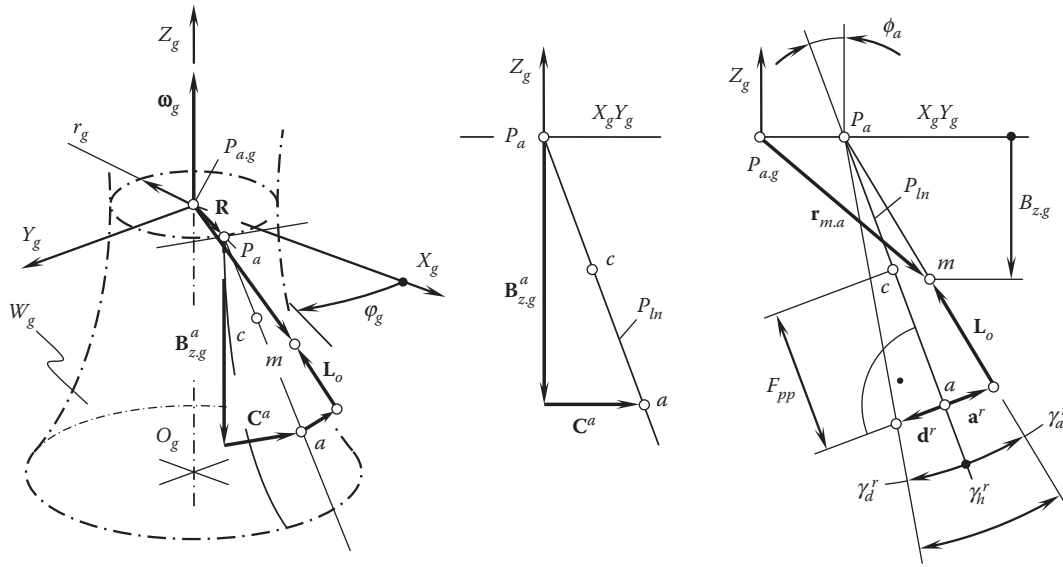


FIGURE 14.18

The generation of the pitch surface,  $W_g$ , of the gear in a crossed-axes gearing.



**FIGURE 14.19**  
Generation of the outer surface of the gear in a crossed-axes gearing.

Equations 14.98 through 14.101 make it possible to have an expression for the position vector of a point,  $\mathbf{w}_g$ , of the pitch surface,  $W_g$ , in terms of the Gaussian parameters,  $\varphi_g$  and  $B_{z,g}$ , as:

$$\mathbf{w}_g(\varphi_g, B_{z,g}) = \begin{bmatrix} r_g \cos \varphi_g - B_{z,g} \tan \Sigma_g \sin \varphi_g \\ r_g \sin \varphi_g + B_{z,g} \tan \Sigma_g \cos \varphi_g \\ B_{z,g} \\ 1 \end{bmatrix} \quad (14.102)$$

The pitch surface,  $W_g$ , is shaped in the form of a surface of revolution, which is commonly referred to as the *hyperboloid of one sheet*.

The pitch surface,  $W_g$  (see Equation 14.102), is convenient to use as a reference surface.

An equation:

$$\mathbf{w}_p(\varphi_p, B_{z,p}) = \begin{bmatrix} r_p \cos \varphi_p + B_{z,p} \tan \Sigma_p \sin \varphi_p \\ r_p \sin \varphi_p - B_{z,p} \tan \Sigma_p \cos \varphi_p \\ B_{z,p} \\ 1 \end{bmatrix} \quad (14.103)$$

similar to Equation 14.102 can be derived for the position vector of a point,  $\mathbf{w}_p$ , of the pitch surface,  $W_p$ , of the mating pinion in a crossed-axes gear pair.

The *angular tooth addendum*, as well as the *angular tooth dedendum*, in a crossed-axes gear pair can be specified in relation to the round basic rack of the gear pair. This allows for two more definitions to be introduced:

#### Definition 14.7

The *angular tooth addendum*,  $\gamma_a^r$ , in a crossed-axes gear pair is the angular distance measured between the pitch plane and the outer cone of the round basic rack of the gear pair.

Similar to this, the angular dedendum in a crossed-axes gearing is specified by the angular distance between the pitch plane of the gear and the gear bottom-land cone (inner cone of the gear).

**Definition 14.8**

The angular tooth dedendum,  $\gamma_a^r$ , in a crossed-axes gear pair is the angular distance measured between the pitch plane and the inner cone of the round basic rack of the gear pair.

For the specification of both the angular tooth addendum and the angular tooth dedendum in a crossed-axes gear pair, the use of expressions for the outer surface (top land) of the gear and the inner surface (bottom land) of the gear is convenient.

An analytical expression for the position vector of a point,  $\mathbf{r}_{m,a}$ , of the outer surface of the gear in a crossed-axes gearing can be derived using the vector approach.

Referring to Figure 14.19 and using the pitch surface,  $W_g$ , as the reference surface, the position vector of a point,  $\mathbf{r}_{m,a}$ , of the outer surface of the gear in a crossed-axes gearing can be represented as the vector summa:

$$\mathbf{r}_{m,a} = \mathbf{w}_p + \mathbf{a}^r + \mathbf{L}_o \quad (14.104)$$

The vector,  $\mathbf{w}_p$ , is specified by Equation 14.102.

The tooth addendum at the periphery of the round basic rack is specified by the vector,  $\mathbf{a}^r$ . The vector,  $\mathbf{a}^r$ , is perpendicular to the pitch surface,  $W_g$ , and the magnitude of the vector,  $\mathbf{a}^r$ , is equal to the tooth dedendum at the point  $a$ . The vector,  $\mathbf{a}^r$ , can be expressed in terms of design parameters of the gear:

$$\mathbf{a}^r = -i\mathbf{a}^r \cos \Sigma_g \cos \varphi_g - \mathbf{j}\mathbf{a}^r \cos \Sigma_g \sin \varphi_g + \mathbf{k}\mathbf{a}^r \sin \Sigma_g \quad (14.105)$$

In Equation 14.105, the magnitude of the vector,  $\mathbf{a}^r$ , is denoted by  $a^r$ , ( $a^r = |\mathbf{a}^r|$ ).

The vector,  $\mathbf{L}_o$ , is along a straight generating line of the outer surface of the gear. The distance of the point of interest,  $m$ , from the periphery of the round basic rack is equal to the magnitude of the vector,  $\mathbf{L}_o$  ( $L_o = |\mathbf{L}_o|$ ). For the calculation of the vector,  $\mathbf{L}_o$ , the following expression:

$$\mathbf{L}_o = iL_o \cos(\Sigma_g + \gamma_a^r) \cos \varphi_g + \mathbf{j}L_o \cos(\Sigma_g + \gamma_a^r) \sin \varphi_g + \mathbf{k} \left[ B_{z,g}^a - a^r \sin \Sigma_g - L_o \sin(\Sigma_g + \gamma_a^r) \right] \quad (14.106)$$

is derived.

In Equation 14.106, the length of the vector,  $\mathbf{L}_o$ , is designated as  $L_o$  ( $L_o = |\mathbf{L}_o|$ ). The distance,  $L_o$ , can be calculated from the formula:

$$L_o = \frac{B_{z,g}^a - a^r \sin \Sigma_g - B_{z,g}}{\cos(\Sigma_g + \gamma_a^r)} \quad (14.107)$$

Having calculated the vectors,  $\mathbf{w}_p$ ,  $\mathbf{a}^r$ , and  $\mathbf{L}_o$  (see Equations 14.102, 14.103, and 14.107), the position vector of a point,  $\mathbf{r}_{m,a}$ , of the outer surface of the gear in a crossed-axes gearing can be analytically described by a matrix equation in the form:

$$\mathbf{r}_{m,a}(\varphi_g, L_o) = \begin{bmatrix} r_g \cos \varphi_g - B_{z,g} \tan \Sigma_g \sin \varphi_g - a^r \cos \Sigma_g \cos \varphi_g + L_o \cos(\Sigma_g + \gamma_a^r) \cos \varphi_g \\ r_g \sin \varphi_g + B_{z,g} \tan \Sigma_g \cos \varphi_g - a^r \cos \Sigma_g \sin \varphi_g + L_o \cos(\Sigma_g + \gamma_a^r) \sin \varphi_g \\ B_{z,g} + a^r \sin \Sigma_g + B_{z,g}^a - a^r \sin \Sigma_g - L_o \sin(\Sigma_g + \gamma_a^r) \\ 1 \end{bmatrix} \quad (14.108)$$

Referring to Figure 14.19 and using the pitch surface,  $W_g$ , as the reference surface, the position vector of a point,  $\mathbf{r}_{m,a}$ , of the inner surface of the gear in a crossed-axes gearing can be represented as a vector summa:

$$\mathbf{r}_{m,a} = \mathbf{w}_p - \mathbf{d}^r + \mathbf{L}_o \quad (14.109)$$

The vector,  $\mathbf{w}_p$ , is specified by Equation 14.102.

The tooth dedendum at the periphery of the round basic rack is specified by the vector,  $\mathbf{d}^r$ . The vector,  $\mathbf{d}^r$ , is perpendicular to the pitch surface,  $W_g$ , and the magnitude of this vector is equal to the tooth dedendum at the point  $a$ . The vector,  $\mathbf{d}^r$ , can be expressed in terms of the design parameters of the gear:

$$\mathbf{d}^r = \mathbf{i}d^r \cos \Sigma_g \cos \varphi_g + \mathbf{j}d^r \cos \Sigma_g \sin \varphi_g - \mathbf{k}d^r \sin \Sigma_g \quad (14.110)$$

In Equation 14.110, the magnitude of the vector,  $\mathbf{d}^r$ , is designated as  $d^r$ , ( $d^r = |\mathbf{d}^r|$ ).

Ultimately, Eq. 14.106 can be used for the calculation of the vector,  $\mathbf{L}_o$ .

Having calculated the vectors  $\mathbf{w}_p$ ,  $\mathbf{d}^r$ , and  $\mathbf{L}_o$  (see Equations 14.102, 14.110, and 14.107), the position vector of a point,  $\mathbf{r}_{m,d}$ , of the inner surface of the gear in a crossed-axes gearing can be analytically described by a matrix equation in the form:

$$\mathbf{r}_{m,d}(\varphi_g, L_o) = \begin{bmatrix} r_g \cos \varphi_g - B_{z,g} \tan \Sigma_g \sin \varphi_g + d^r \cos \Sigma_g \cos \varphi_g + L_o \cos(\Sigma_g + \gamma_a^r) \cos \varphi_g \\ r_g \sin \varphi_g + B_{z,g} \tan \Sigma_g \cos \varphi_g + d^r \cos \Sigma_g \sin \varphi_g + L_o \cos(\Sigma_g + \gamma_a^r) \sin \varphi_g \\ B_{z,g} - d^r \sin \Sigma_g + B_{z,g}^a - a^r \sin \Sigma_g - L_o \sin(\Sigma_g + \gamma_a^r) \\ 1 \end{bmatrix} \quad (14.111)$$

In a similar manner, corresponding expressions for the outer surface and inner surface of a pinion in a crossed-axes gear pair can be derived as well.

Once the outside and inner surfaces of a gear are described analytically (see Equations 14.108 and 14.111), they can be approximated by corresponding cone surfaces. This is practical from a manufacturing standpoint. In most cases, the apexes of the outer and inner surfaces are displaced in the axial direction of the gear at a certain distance. The displacement,  $\Delta A$ , depends on the kind of approximation of the hyperboloid of one sheet by a cone surface.

It should be pointed out here that the aforementioned approximation is not a must, and both the gear and the pinion can be manufactured with these surfaces shaped in the form of hyperboloid of one sheet.

The angular addendum,  $\Gamma_a$ , and the angular dedendum,  $\Gamma_d$ , of the gear tooth together specify the angular tooth height,  $\Gamma_h$ , of the gear (Figure 14.20) in a crossed-axes gearing:

$$\Gamma_h = \Gamma_a + \Gamma_d \quad (14.112)$$

For standard gears, the tooth height of a round basic rack is set equal to the module  $m$ . This makes it possible to calculate the angular addendum,  $\Gamma_a$ , of the gear:

$$\Gamma_a = \sin^{-1} \left( \frac{m}{r_{o,pp}} \right) \quad (14.113)$$

The dedendum of a standard gear is greater than the addendum at clearance  $c$ . Therefore, the angular dedendum,  $\Gamma_d$ , of the gear can be calculated as follows:

$$\Gamma_d = \sin^{-1} \left( \frac{m + c}{r_{o,pp}} \right) \quad (14.114)$$

Formulae similar to those aforementioned:

$$\gamma_a = \sin^{-1} \left( \frac{m}{r_{o,pp}} \right) \quad (14.115)$$



TABLE 14.2

Design Parameters of Crossed-Axes Gears and Their Corresponding Design Parameters of Parallel-Axes Gears

Design Parameters of Crossed-Axes Gearing		Design Parameters of Parallel-Axes Gearing	
Term	Designation	Term	Designation
Tooth number	$N_g, N_p$	Tooth number	$N_g, N_p$
Pitch cone angle (gear)	$\Gamma$	Pitch diameter	$d_g, d_p$
Pitch cone angle (pinion)	$\gamma$		
Base pitch angle (gear)	$\Gamma_b$	Base pitch	$p_b$
Base pitch angle (pinion)	$\gamma_b$		
Outer cone angle (gear)	$\Gamma_o$	Outer diameter	$d_{o,g}, d_{o,p}$
Outer cone angle (pinion)	$\gamma_o$		
Root cone (gear)	$\Gamma_f$	Root diameter	$d_{f,g}, d_{f,p}$
Root cone (pinion)	$\gamma_f$		
Normal profile angle	$\phi_n$	Normal profile angle	$\phi_n$
Angular pitch	$\varphi_n$	Normal circular pitch	$p_n$
Base pitch angle	$\varphi_b$	Base pitch	$p_b$
Angular tooth thickness	$\varphi_t$	Tooth thickness	$t$
Angular space width	$\varphi_w$	Space width	$w$
Angular backlash <sup>a</sup>	$\varphi_B$	Backlash	$B$
Angular addendum (gear)	$\Gamma_a$	Addendum	$a$
Angular addendum (pinion)	$\gamma_a$		
Angular dedendum (gear)	$\Gamma_b$	Dedendum	$b$
Angular dedendum (pinion)	$\gamma_b$		

<sup>a</sup> The expressions  $\varphi_n = \varphi_t + \varphi_w$  and  $\varphi_w - \varphi_t = \varphi_B$  are always valid.

pitch cone. The angular addendum,  $\Gamma_a$ , and angular dedendum,  $\Gamma_d$ , can be calculated from equations:

$$\Gamma_a = \tan^{-1} \left( \frac{2a \sin \Gamma}{m N_g} \right) \quad (14.119)$$

$$\Gamma_d = \tan^{-1} \left( \frac{2b \sin \Gamma}{m N_g} \right) \quad (14.120)$$

For standard gears for which  $a = m$  and  $b = (1.2 \div 1.3)m$  (here, the module of the gear is denoted by  $m$ ) Equations 14.119 and 14.120 are reduced to:

$$\Gamma_a = \tan^{-1} \left( \frac{2 \sin \Gamma}{N_g} \right) \quad (14.121)$$

$$\Gamma_d = \tan^{-1} \left[ \frac{(2.4 \div 2.6) \sin \Gamma}{N_g} \right] \quad (14.122)$$

Equations similar to the above Equations 14.121 through 14.122 are also valid for a bevel pinion. It is instructive to point out here that once one of three elements below:

- The path of contact
- The gear tooth flank geometry
- The mating pinion tooth flank geometry



is known, then the two others are predetermined by the known one. Only perfect gears feature this unique property.

Perfect crossed-axes gear pairs can operate at high RPM, as they feature equal base pitches: the gear base pitch,  $p_{b,g}$ , and the pinion base pitch,  $p_{b,p}$ , both are equal to the operating base pitch,  $p_{b,op}$ , of the gear pair, (i.e., the following two equalities,  $p_{b,g} = p_{b,op}$  and  $p_{b,p} = p_{b,op}$ , are valid in perfect conformal/high-conformal gear pairs). Therefore, gearing of this type can be used in first stages in gear trains, where forces and torque are low.

## 14.6 Backlash in Crossed-Axes Gearing

Gears for crossed-axes gear pairs are designed and manufactured to provide a specific amount of backlash—that is, the space between mating gear teeth or the difference in width of the gear tooth and pinion tooth of the mating gear to let the gears mesh without binding and to provide space for a film of lubricating oil between the teeth. This prevents overheating and tooth damage. The backlash is necessary for proper operation of the gear pair.

To optimize the performance of gears in any crossed-axes gearing, the gears must be positioned together so that they run smoothly without binding and/or excessive backlash. In the current practice of gear production, unless otherwise specified, the minimum amount of total backlash of a pair of gears in crossed-axes gearing is measured at the tightest point of mesh with a dial indicator on a bevel gear testing machine. Unless otherwise specified, backlash is assumed to be normal backlash\* and cannot be measured in the plane of rotation. Backlash is necessary to achieve correct operation of the gears and varies with the size of the tooth and operating conditions. Gears for crossed-axes gear pairs are cut to have a definite amount of backlash when correctly assembled together. But excessive backlash or play, if great enough, can cause a sudden impulse or shock load in starting or reversing that may cause serious tooth damage. Excessive or insufficient backlash can also result in noise, excessive wear, and damage.

Numerous inconsistencies are observed in the definition and interpretation of backlash in crossed-axes gearings. To avoid the above-discussed inconsistencies in the definition of backlash in crossed-axes gearings, the backlash in crossed-axes gearing can be defined in the following manner.

Consider a phantom crown gear that is engaged in correct mesh with the gear. This crown gear can be referred to as a *crown gear/gear*, or simply as  $CG_g$ . The outer diameter of the crown gear is labeled as  $r_{o,pp}$ ; the inner diameter is labeled as  $r_{l,pp}$ ; and the pitch diameter is labeled as  $r_{pp}$ . The face width,  $F_{pp}$ , of the crown gear is equal to  $F_{pp} = r_{o,pp} - r_{l,pp}$ . The central angle  $\Psi_{pp}$  spans the active portion of the crown gear,  $CG_g$ . The axis of rotation of the crown gear,  $CG_g$ , is labeled as  $O_{pp}$ . Here, the subscript  $pp$  indicates that the parameters relate to the pitch plane,  $PP$ .

The angular tooth thickness,  $\varphi_{t,g}$ , and the angular space width,  $\varphi_{w,g}$ , in a gear is measured within the pitch plane,  $PP$ , of the crown gear/gear,  $CG_g$ , as shown in Figure 14.21. The angular pitch of the gear teeth in Figure 14.21 is labeled as  $\varphi_{x,g}$ .

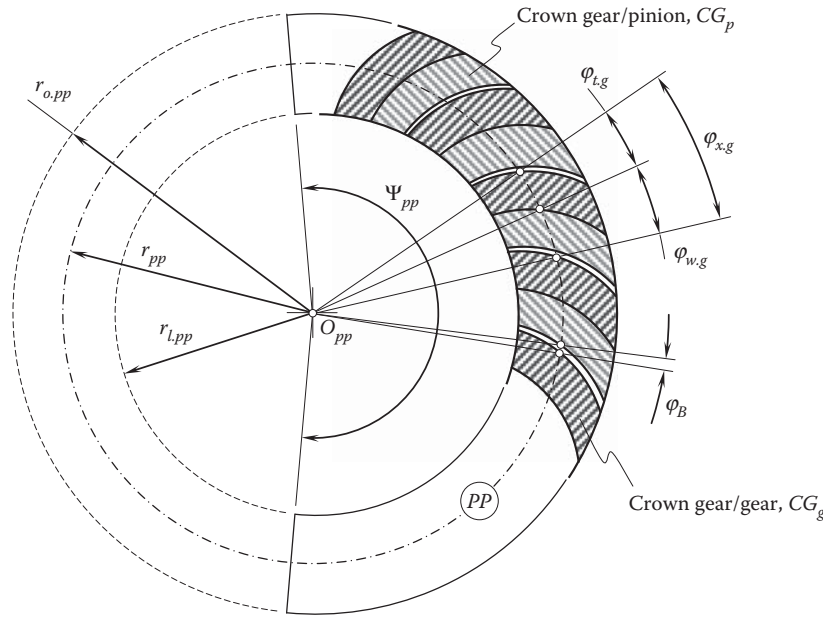
Similarly, consider a phantom crown gear that is engaged in correct mesh with the pinion. This crown gear can be referred to as a *crown gear/pinion* or simply as  $CG_p$ . The angular tooth thickness,  $\varphi_{t,p}$ , and the angular space width,  $\varphi_{w,p}$ , of a gear is measured within the pitch plane,  $PP$ , of the crown gear/pinion,  $CG_p$  (not shown in Figure 14.21). The angular pitch of the pinion teeth is labeled as  $\varphi_{x,p}$  (not shown in Figure 14.21).

The angular pitches of the gear,  $\varphi_{x,g}$ , and the pinion,  $\varphi_{x,p}$ , are equal; that is, the equality  $\varphi_{x,g} = \varphi_{x,p} = \varphi_x$ . Therefore, further, the designations for these angular pitches are replaced with  $\varphi_x$ .

### Definition 14.9

*The effective angular backlash,  $\varphi_{B,pa}$ , in perfect crossed-axes gearing is said to be a distance between the noninteracting tooth flank of a driving member and the tooth-space flank of the driven member in a gear pair, measured within the plane of action.*

\* A straight line along which the so-called *normal backlash* cannot be perpendicular to both the gear tooth flank,  $\mathcal{G}$ , and the pinion tooth flank,  $\mathcal{P}$ , at the same time.

**FIGURE 14.21**

On definition of the: (a) angular tooth thickness,  $\varphi_{t,i}$ , (b) angular space width,  $\varphi_{w,i}$ , and (c) angular backlash,  $\varphi_B$ , in crossed-axes gearing by means of  $CG_g$ -to- $CG_p$  mesh.

When the crown gear,  $CG_g$ , and the crown gear,  $CG_p$ , are engaged in mesh, they are free to turn about the  $O_{pp}$ -axis in relation to one another through a certain angle,  $\varphi_B$ . The angle,  $\varphi_B$ , is referred to as the angular backlash. The angular backlash,  $\varphi_B$ , can be calculated as:

$$\varphi_B = \varphi_{w,g} - \varphi_{t,p} \quad (14.123)$$

or as

$$\varphi_B = \varphi_{w,p} - \varphi_{t,g} \quad (14.124)$$

### Conclusion 14.3

*Backlash in crossed-axes gearing is an angular parameter, and not a linear parameter. Backlash is measured within the pitch plane of the gear pair.*

Novel instrumentation can be developed for the direct measurement of the design parameters in a gear ( $\varphi_{t,g}$ ,  $\varphi_{w,g}$ , and  $\varphi_{x,g}$ ), and a pinion ( $\varphi_{t,p}$ ,  $\varphi_{w,p}$ , and  $\varphi_{x,p}$ ). Then, either Equation 14.123 or 14.124 can be used for the calculation of the angular backlash,  $\varphi_B$ .

In a crossed-axes gear pair, the backlash is measured at a configuration of a gear and a pinion when *two pairs of teeth are engaged in mesh*.

If the backlash does not fall within the recommended limits, no corrections to the mounting distance are allowed to adjust the backlash. If possible, the tooth thickness can be corrected (reduced) by additional machining. For strength calculations, the normal backlash can be expressed in terms of the backlash in the plane of rotation.

There is a trade-off when setting an actual value of backlash: the backlash must be large enough for operating of the gear pair, and it must be small enough when reversing the rotation.

### 14.7 Possible Analogy of Tredgold Approximation for Crossed-Axes Gearing

Meshing of crossed-axes gears occurs on a sphere of certain radius, similar to the way that meshing of parallel-axes gears occurs within a plane perpendicular to the axes of rotations of the gears. The sphere is centered at a point,  $A_{pa}$ , within the instant axis of rotation,  $P_{ln}$ . At that same time, the sphere is centered at a point within the centerline,  $\mathcal{C}$ , between the axis of rotation of the gear,  $O_g$ , and the pinion,  $O_p$ . The *Tredgold method* can be adjusted for the purposes of crossed-axes gearing.

By using the Tredgold method, a back cone is formed of elements that are perpendicular to the axis of instant rotation,  $P_{ln}$ , at the large end of the teeth. The length of a back cone element is called the back-cone radius. Now, an equivalent spur gear is constructed, whose pitch radius,  $r_{eq}$ , is equal to the back cone radius. Thus, from a pair of crossed-axes gears, we can obtain a pair of equivalent spur gears using the approximation, which are then used to define the tooth profiles; they can also be used to determine the tooth action and the contact conditions exactly as for ordinary spur gears, and the results will correspond closely to those for the crossed gears. The equivalent pitch radii are:

$$r_{eq.g} = \frac{r_g}{\cos \Gamma} \quad (14.125)$$

and

$$r_{eq.p} = \frac{r_p}{\cos \gamma} \quad (14.126)$$

The number of teeth on the equivalent spur gear is:

$$N_{eq} = \frac{2\pi r_{eq}}{p} \quad (14.127)$$

where  $p$  is the circular pitch of the crossed-axes gear measured at the large end of the teeth. In the usual case, the equivalent spur gears will not have an integral number of teeth.

### 14.8 Main Features of Perfect Conformal and Conformal/High-Conformal Crossed-Axes Gearing

Conformal and high-conformal crossed-axes gearing can be used for transmitting a rotation from a driving shaft to a driven shaft that cross each other at a certain angle. Gears of this type are capable of transmitting a uniform rotation from a driving shaft to a driven shaft. So far, conformal and high-conformal crossed-axes gears have no application in the industry. This is mostly because they have not been profoundly investigated yet. A very limited amount of research has been carried out so far on this particular kind of gearing. A few papers by Dr. Roslivker [139,140] are to be mentioned in this concern.

Perfect conformal/high-conformal crossed-axes gearings feature many similarities with perfect crossed-axes gearings of conventional design, that is, with gearings having line contact between a gear and a mating pinion tooth flanks. Because of this, there is no need to consider separately, for example, kinematics of the instantaneous motion in conformal/high-conformal crossed-axes gearing, as it is already discussed in detail in a corresponding section devoted to perfect crossed-axes gearings of conventional design.

Base cones of a gear and of a mating pinion are the other example of the similarities between conformal/high-conformal crossed-axes gearings and perfect crossed-axes gearings of conventional design.

Sliding between the tooth flanks of a gear and a mating pinion in crossed-axes conformal/high-conformal gearing is a reduced case of that in perfect crossed-axes gearings of conventional design.

A few more similarities can be mentioned. These similarities, as well as a few others, are omitted from further analysis.

Below, the reader's attention is directed mostly to the main features of perfect conformal/high-conformal crossed-axes gear pairs.

#### 14.8.1 Path of Contact in High-Conformal Crossed-Axes Gearing

The path of contact in a high-conformal crossed-axes gear pair is a trace of the contact point when the gears rotate. The path of contact,  $P_c$ , is commonly considered in a stationary reference system associated with the gear housing.

As the relative motion of the gear and the pinion is an instant rotation,  $\omega_{pl}$ , about the axis of instant rotation,  $P_{ln}$ , a plane perpendicular to the rotation vector,  $\omega_{pl}$ , at an arbitrary point,  $P$ , within  $P_{ln}$  can be constructed. The relative motion of the gear and the pinion can be investigated within the normal plane (Figure 14.22).

Within the normal plane, a boundary  $N$ -circle can be constructed. The center of the boundary  $N$ -circle is coincident with the point of intersection of the axis of instant rotation,  $P_{ln}$ , by the normal plane. The radius,  $r_N$ , of the boundary  $N$ -circle is equal to a desired displacement,  $l$ , of the contact point,  $K$ , from the pitch point along the instant line of action,  $LA_{inst}$ . Displacements that are both positive,  $+l$ , and negative,  $-l$ , are feasible. Therefore, two contact points,  $K^+$  and  $K^-$ , are potentially possible.

The magnitude of the desired displacement,  $l$ , is a trade-off between the contact strength of the gear teeth and sliding between the tooth flanks,  $\mathcal{G}$  and  $\mathcal{P}$ , of the gear and pinion in relation to one another. The larger the displacement,  $l$ , the higher the contact strength of the gear teeth and the higher the sliding between the tooth flanks. The smaller the distance,  $l$ , the lower the contact strength of the gear teeth and the lower the sliding between the tooth flanks.

#### 14.8.2 Boundary $N$ -Cone in Crossed-Axes High-Conformal Gearing

A boundary  $N$ -cone in crossed-axes high-conformal gearing can be constructed in a manner similar to that of a boundary  $N$ -cone in intersected-axes high-conformal gearing.

When the gears rotate, the motion of the pinion in relation to the gear can be construed as instant rotation about the axis of instant rotation,  $P_{ln}$ . A boundary  $N$ -circle is traced by the contact point,  $K$ , in such a relative motion. In theory, the radius,  $r_N$ , of the boundary  $N$ -circle is a trade-off between the desired high contact strength of the interacting tooth flanks and low friction between the tooth flanks of the gear,  $\mathcal{G}$ , and the pinion,  $\mathcal{P}$ . In practice, run-out of the gear and pinion should be taken into account.

Under the assumption that  $\Delta l = 0$  and the manufacturing errors are zero, the point of contact,  $K$ , is located at the point of intersection of the boundary  $N$ -circle by the instant line of action,  $LA_{inst}$ . At any point within the axis

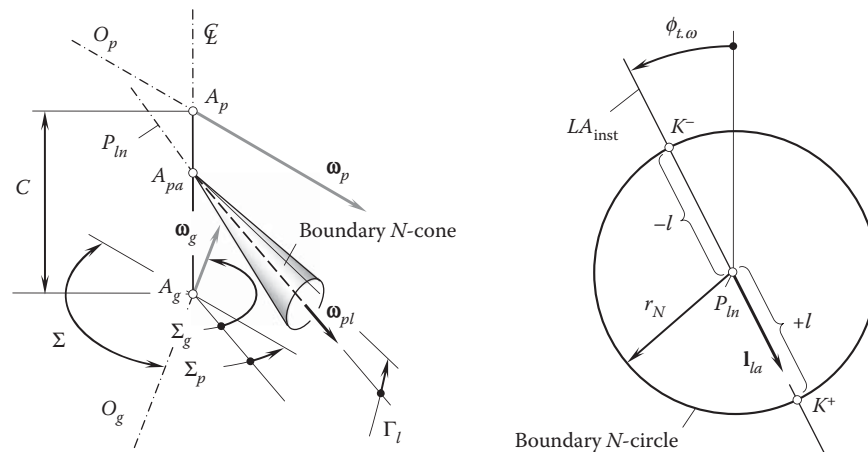


FIGURE 14.22 Configuration of the boundary  $N$ -cone in high-conformal crossed-axes gearing.

of instant rotation,  $P_{ln}$ , a boundary  $N$ -circle of a certain radius,  $r_N^i$ , can be constructed, and a line of action,  $L_{inst}^i$ , can be constructed as well. The pressure angle,  $\phi_{t,\omega}^i$ , is not mandatorily of the same value at all normal sections of the axis,  $P_{ln}$ . The instant line of action,  $LA_{inst}$ , is a line through a point within the pitch line,  $P_{ln}$ . The path of contact,  $P_c$ , is a zero-length straight line segment that is aligned with the instant line of action,  $L_{inst}^i$ . No kinematical and/or geometrical constraints are violated under such a consideration.

In practice, it is reasonable to keep the pressure angle,  $\phi_{t,\omega}^i$ , of a certain constant value,  $\phi_{t,\omega}$ , within the active face width of the gear pair. Moreover, as a normal section through a point within the axis,  $P_{ln}$ , approaches the apex,  $A_{pa}$ , the radius  $r_N^i$  of the boundary  $N$ -circle gets smaller. In this way, the pseudo-path of contact,  $P_{pc}$ , is the straight line through all the contact points,  $K^i$ . The pseudo-path of contact,  $P_{pc}$ , passes through the apex,  $A_{pa}$ . When the pseudo-path of contact,  $P_{pc}$ , is rotated about the axis of instant rotation, the boundary  $N$ -cone is generated as a locus of consecutive positions of the pseudo-path of contact,  $P_{pc}$ , in its rotation in relation to the axis,  $P_{ln}$ .

#### Definition 14.10

The boundary  $N$ -cone in crossed-axes conformal/high-conformal gearing is said to be a cone of revolution that is generated by rotation of the pseudo-path of contact,  $P_{pc}$ , about the axis of instant rotation,  $P_{ln}$ .

The apex of the boundary  $N$ -cone coincides with the plane-of-action apex,  $A_{pa}$ .

It is natural to assume that the concave tooth flank (primarily of the gear,  $\mathcal{G}$ ) is located outward from the boundary  $N$ -cone, while the convex tooth flank (primarily of the pinion,  $\mathcal{P}$ ) is located within the interior of the boundary  $N$ -cone. However, as the apex,  $A_{pa}$ , is not coincident either with the gear base cone apex,  $A_g$ , or with the pinion base cone apex,  $A_p$ , the boundary  $N$ -cone is not the only constraint in the geometry of the tooth flanks,  $\mathcal{G}$  and  $\mathcal{P}$ . The envelopes to consecutive positions of the boundary  $N$ -cone in their instant screw motion are used for this purpose instead. For the gear tooth flank, the constraint is generated when the boundary  $N$ -cone is rotated about the gear axis of rotation,  $O_g$ . Similarly, for the pinion tooth flank, the constraint is generated when the boundary  $N$ -cone is rotated about the pinion axis of rotation,  $O_p$ . Ultimately, the convex tooth flank of one member of the gear pair must be entirely located with the interior of the corresponding enveloping surface, while the concave tooth flank of another member of the gear pair must be entirely located outside the interior of the corresponding enveloping surface.

The boundary cone angle,  $\Gamma_l$  (Figure 14.23), can be specified in terms (1) of the radius,  $r_N^i$ , of the boundary  $N$ -circle at an arbitrary point within the axis of instant rotation,  $P_{ln}$ , and (2) of the cone distance,  $A_i$ , of that point from the apex,  $A_{pa}$ :

$$\Gamma_l = \tan^{-1} \left( \frac{r_N^i}{A_i} \right) \quad (14.128)$$

In general, a boundary  $N$ -surface should be considered. The boundary  $N$ -surface is a kind of *Archimedean* screw surface. This is possible geometrically under the assumption that manufacturing errors are zero. In practice, a boundary  $N$ -cone is a reasonable approximation to the screw boundary  $N$ -surface.

No rotation is transmitted by a crossed-axes conformal gear pair at the plane-of-action apex,  $A_{pa}$ .

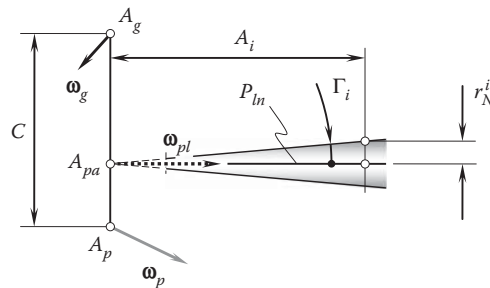


FIGURE 14.23

The boundary  $N$ -cone angle and the cone angle,  $\Gamma_l$ , in a conformal/high-conformal crossed-axes gearing.

### 14.8.3 Bearing Capacity of Crossed-Axes Conformal/High-Conformal Gearing

The influence of an increase in radius,  $r_N$ , of the boundary  $N$ -circle on the rise of contact strength in a crossed-axes conformal/high-conformal gear pair overall resembles that for the cases of parallel-axes and intersected-axes high-conformal gearing.

The aforementioned conclusion on the bearing capacity of intersected-axes high-conformal gearing is also valid with respect to the bearing capacity of crossed-axes conformal/high-conformal gearing.

The bearing capacity of a conformal/high-conformal crossed-axes gearing depends not only on the relative curvature,  $r_{rel}$ , of the interacting tooth flanks, but also on the magnitudes of the radii of curvature of the tooth flanks,  $\mathcal{G}$  and  $\mathcal{P}$ , at a point of their contact. The larger the magnitudes of the radii,  $r_g$  and  $r_p$ , of normal curvature of the interacting tooth flanks,  $\mathcal{G}$  and  $\mathcal{P}$ , the larger the load capacity of the conformal/high-conformal crossed-axes gearing, and vice versa.\* In other words:

#### Statement 14.1

*Conformal/high-conformal crossed-axes gearing with larger magnitudes of radii of curvature of the tooth flanks feature higher load-carrying capacity.*

As can be concluded from Statement 14.1 [117], conformal/high-conformal crossed-axes gearing with a larger radius,  $r_N$ , of the boundary  $N$ -circle feature higher load carrying capacity.

## 14.9 Design Parameters of Conformal/High-Conformal Crossed-Axes Gearing

The design of a conformal/high-conformal crossed-axes gear pair begins with the determination of the rotation vectors of the gear,  $\omega_g$ , and the pinion,  $\omega_p$ , in a certain reference system. Once the rotation vectors,  $\omega_g$  and  $\omega_p$ , are known, the vector,  $\omega_{pl}$ , of instant rotation, as well as the shaft angle,  $\Sigma$ , can be determined. The axes of rotations,  $O_g$ ,  $O_p$ , and  $P_{ln}$ , are the straight lines along the rotation vectors  $\omega_g$ ,  $\omega_p$ , and  $\omega_{pl}$ , respectively. Then, the known configuration of the axes of rotations,  $O_g$ ,  $O_p$ , and  $P_{ln}$ , makes it possible to determine the tooth ratio,  $u$ , and pitch cone angles,  $\Gamma$ , of the gear and the pinion,  $\gamma$ :

$$\Gamma = -\tan^{-1} \left( \frac{\sin \Sigma}{\omega_p/\omega_g + \cos \Sigma} \right) \quad (14.129)$$

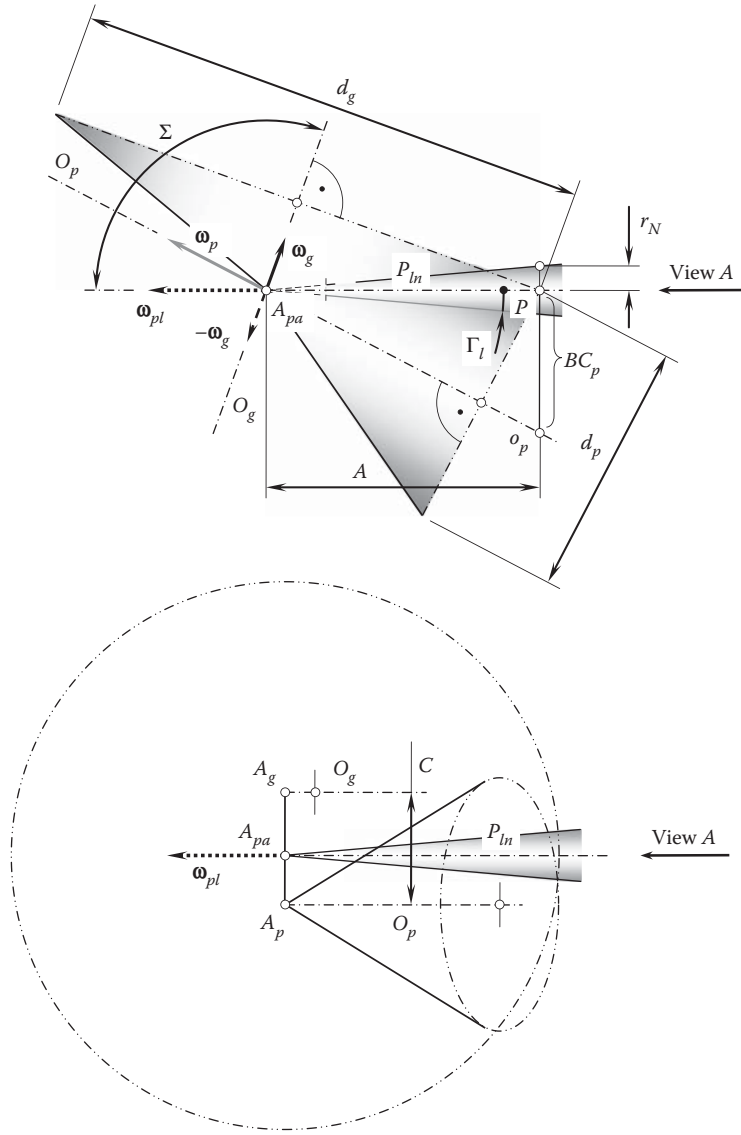
$$\gamma = \tan^{-1} \left( \frac{\sin \Sigma}{\omega_g/\omega_p + \cos \Sigma} \right) \quad (14.130)$$

The design parameters of a conformal/high-conformal crossed-axes gear pair can be specified based, to a great extent, on those for conformal/high-conformal intersected-axis gears. From this perspective, the vector of instant rotation,  $\omega_{pl}$ , and the axis of instant rotation,  $P_{ln}$ , are of critical importance. As the instant motion of a pinion in relation to the mating gear is interpreted as instant rotation about the axis,  $P_{ln}$ , the design parameters of a conformal/high-conformal crossed-axes gear pair can be specified within a reference plane through the pitch point,  $P$ . The pitch point,  $P$ , is at a cone distance,  $A$ , from the apex  $A_{pa}$ . The reference plane is perpendicular to the axis of instant rotation,  $P_{ln}$ , as schematically depicted in Figure 14.24.

The calculated values of the pitch angles,  $\Gamma$  and  $\gamma$ , along with the given cone distance,  $A$ , make it possible to calculate the pitch diameter of the gear,  $d_g$ , and of the pinion,  $d_p$ :

$$d_g = 2A \cos \Gamma \quad (14.131)$$

\* It is the right point to note here that the magnitudes of the radii,  $r_g$  and  $r_p$ , of curvature of the interacting tooth flanks,  $\mathcal{G}$  and  $\mathcal{P}$ , strictly correlate to the radius,  $r_N$ , of the boundary circle in the cross-section of the tooth flanks through the corresponding point within the axis of instant rotation,  $P_{ln}$ .

**FIGURE 14.24**

Configuration of a normal reference plane in relation to the axis of instant rotation,  $P_{in}$ , and the base cones of the gear and the pinion in a conformal/high-conformal crossed-axes gear pair.

$$d_p = 2A \cos \gamma \quad (14.132)$$

The back cone distance of the gear,  $BC_g$ , as well as the back cone distance of the pinion,  $BC_p$ , can be calculated in a similar manner to that above:

$$BC_g = 2A \sin \Gamma \quad (14.133)$$

$$BC_p = 2A \sin \gamma \quad (14.134)$$

Once the normal reference plane is constructed, the tooth profile parameters of the gear and the pinion can be specified within the reference plane.

Referring to [Figure 14.25](#), two points, namely,  $o_g$  and  $o_p$ , are in nature the points of intersection of the axes,  $O_g$  and  $O_p$ , by the normal reference plane. The points are at the distance  $c_n = (BC_g + BC_p)$  from one another. Two



circles of radii,  $BC_g$  and  $BC_p$ , that have the points  $o_g$  and  $o_p$  as the centers are constructed. The circles share a common point, which is the pitch point,  $P$ .

A straight instant line of action,  $LA_{inst}$  within the normal reference plane is the line through the pitch point,  $P$ . The instant line of action,  $LA_{inst}$  forms a certain transverse pressure angle,  $\phi_{t,\omega}$ , with the perpendicular to the center-distance,  $c_n$ . The contact point,  $K$ , between the tooth flanks of the gear,  $\mathcal{G}$ , and the mating pinion,  $\mathcal{P}$ , is a point within the straight line  $LA_{inst}$ . The further the contact point,  $K$ , is located from the pitch point,  $P$ , the greater the freedom in selecting the radii of curvature of the tooth flanks. At that same time, the further the contact point,  $K$ , from the pitch point,  $P$ , the higher the losses in friction between the tooth flanks and wear of the tooth flanks of the gear and the pinion. Ultimately, the actual location of the contact point,  $K$ , is a trade-off between the two above-mentioned factors.

Let us assume that the pinion is stationary and the gear is performing the instant rotation in relation to the pinion. The axis,  $P_{ln}$ , of the instant rotation,  $\omega_{pl}$ , is the straight line through the pitch point,  $P$ . The axis of instant rotation,  $P_{ln}$ , goes through the apex,  $A_{pa}$ . When the pinion is motionless, the contact point,  $K$ , traces a boundary circle of a radius,  $r_N$ , centered at  $P$ .

In the normal cross-section, the pinion tooth profile,  $\mathcal{P}$ , can either align with a circular arc of the boundary circle,  $r_N$ , or it can be relieved in the bodily side of the pinion tooth. As a consequence, the location of the center of curvature,  $c_p$ , of the convex pinion tooth profile,  $\mathcal{P}$ , within the straight line of action,  $LA_{inst}$ , is limited to the straight line segment,  $PK$ . The pitch point is included into the interval,  $[P, K)$ , as shown in Figure 14.25, while the contact point,  $K$ , is not.

On the other hand, the location of the center of curvature,  $c_g$ , of the concave gear tooth profile,  $\mathcal{G}$ , within the straight line of action,  $LA_{inst}$  is limited to the open interval  $P \rightarrow \infty$ . Theoretically, the pitch point,  $P$ , can be included in that interval for,  $K$ . However, this is completely impractical, and actually the center of curvature,  $c_g$ , is located beyond the pitch point,  $P$ . Due to this, the radius of curvature,  $r_p$ , of the convex pinion tooth profile,  $\mathcal{P}$ , is smaller than that,  $r_g$ , of the concave gear tooth profile,  $\mathcal{G}$  (the inequality  $r_p < r_g$  is always observed).

Both the pinion teeth and the gear teeth are helical and of opposite hands. No spur conformal/high-conformal gearing is feasible in nature. It is fundamental to the operating of the gears that contact occur nominally at a point and that the length,  $l_{pc}$ , of the path of contact,  $P_c$ , in every transverse section of the gear pair have a zero length; that is,  $l_{pc} = 0$ . It is clearly a condition of operation that in a given profile, the tooth surfaces should not interfere before or after culmination when rotated at angular speeds that are in the gear ratio. Because both the gear and the pinion are helical and of opposite hands, an illusion is created that the point of contact is traveling across the full face width of the gears during rotation, which is incorrect. The so-called pseudo-path of contact,  $P_{pc}$ , and not the path of contact,  $P_c$ , is created in such a motion.

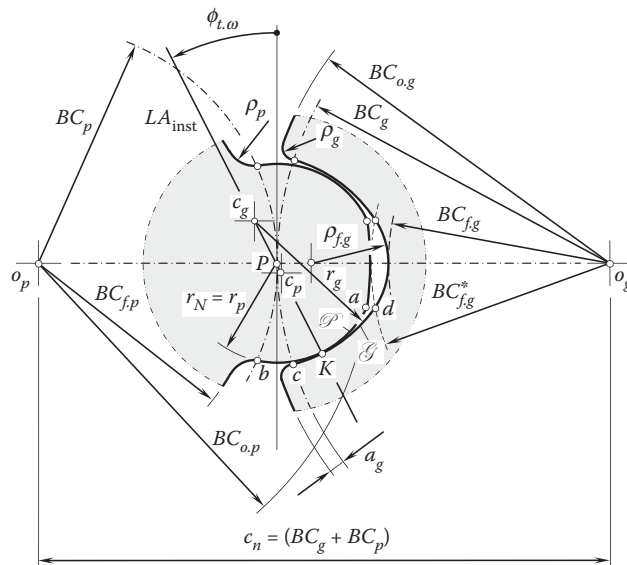


FIGURE 14.25

Geometry of a conformal/high-conformal crossed-axes gear pair within the normal reference plane.

The transverse contact ratio,  $m_p$ , in a conformal/high-conformal crossed-axes gear pair is zero ( $m_p \equiv 0$ ). The face contact ratio,  $m_F$ , is equal to the total contact ratio,  $m_t$ , of the gear pair, and is always greater than one ( $m_F = m_t > 1$ ).

To calculate the design parameters of a conformal/high-conformal crossed-axes gear pair, the center distance,  $c_n$ , and the tooth ratio,  $u = \omega_p/\omega_g$ , of the gear pair have to be specified.

The back cone distance of the gear,  $BC_g$ , and the pinion,  $BC_p$ , can be expressed in terms of the center distance,  $c_n$ , and the tooth ratio,  $u$ :

$$BC_g = c_n \cdot \frac{u}{1+u} \quad (14.135)$$

$$BC_p = c_n \cdot \frac{1}{1+u} \quad (14.136)$$

The displacement,  $l$ , at which the pseudo-path of contact,  $P_{pc}$ , is remote from the pitch point,  $P$ , must be known, as well as the transverse pressure angle,  $\phi_{t,\omega}$ .

The displacement,  $l$ , is the principal design parameter of a conformal/high-conformal crossed-axes gear pair. Many of the design parameters of the conformal/high-conformal gear pair can be expressed in terms of the displacement ( $l = KP$ ).

For the calculation of the radii of curvature,  $r_g$  and  $r_p$ , of tooth profiles of the gear and the pinion, respectively, the formulas:

$$r_g = l \cdot (1 + k_{rg}) \quad (14.137)$$

$$r_p = l \cdot (1 + k_{rp}) \quad (14.138)$$

can be used.

The actual value of the factor  $k_{rp}$  has to satisfy the inequality  $k_{rp} \geq 0$ . However, when the factor  $k_{rp}$  can be set equal to zero, the equality  $r_p = l$  is observed. The factor  $k_{rg}$  is within the range  $k_{rg} = 0.03 \dots 0.10$ .

The radius of the outer back cone distance of the pinion,  $BC_{o,p}$ , is calculated from the formula

$$BC_{o,p} = BC_p + (1 - k_{po}) \cdot l \quad (14.139)$$

The addendum factor,  $k_{po}$ , of the pinion depends on (1) the pressure angle,  $\phi_{t,\omega}$ ; (2) absolute dimensions of the gear pair; (3) the accuracy of machining; and (4) the conditions of lubrication. The pinion addendum factor,  $k_{po}$ , can be set in the range

$$k_{po} = 0.1 \div 0.2 \quad (14.140)$$

The root back cone distance of the pinion,  $BC_{f,p}$ , can be calculated from the equation

$$BC_{f,p} = BC_p - a_g - \delta \quad (14.141)$$

where:

$a_g$  is the dedendum of the mating gear [ $a_g = (0.1 \dots 0.2) \cdot l$ ].

$\delta$  is the radial clearance in the gear pair ( $\delta = l \cdot k_{po}$ ).

The fillet radius,  $\rho_p$ , is practical to set in the range of  $\rho_p = 0.3 \cdot l$ .

The root back cone distance of the gear,  $BC_{f,g}$ , is equal to:

$$BC_{f,g} = c_n - BC_{o,p} \quad (14.142)$$

The radius of the outer back cone distance of the gear,  $BC_{o.g}$ , is calculated from the expression:

$$BC_{o.g} = BC_g + a_g \quad (14.143)$$

The corner of the gear tooth addendum should be rounded with the radius,  $\rho_g$ , which is less than the fillet radius,  $\rho_p$ , of the pinion ( $\rho_g < \rho_p$ ).

The following relations among the design parameters in a conformal/high-conformal crossed-axes gear pair are anticipated to be practical (as the first approximation):

$$r_p = l, \quad (14.144)$$

$$r_g \leq 1.10 \cdot r_p, \quad (14.145)$$

$$\rho_p = 0.3 \cdot l, \quad (14.146)$$

$$m_n/l = 0.8, \quad (14.147)$$

$$t_p/t_g = 1.5, \quad (14.148)$$

$$\phi_{t.\omega} = 30^\circ, \quad (14.149)$$

$$\lambda = 60 \dots 80^\circ (\psi = 10 \dots 30^\circ), \quad (14.150)$$

circular pitch of teeth  $p = t_g + t_p + B$ , where backlash  $B = 0.2 \dots 0.4$  mm.

For the design parameters  $l$ ,  $p$ ,  $t_g$ ,  $t_p$ ,  $m_n$ , and  $B$ , the corresponding angular values can be calculated (Table 14.3).

The effective face width of the gear pair can be calculated as follows:

$$F_{pa} = (1.1 \div 1.2) \cdot p \cdot \tan \lambda \quad (14.151)$$

For preliminary analysis of conformal/high-conformal crossed-axes gearing, an empirical expression:

$$l = (0.05 \div 0.20) \cdot BC_p \quad (14.152)$$

returns a value for the displacement,  $l$ , that could be practical.

The functional face width and axial pitch of a conformal/high-conformal gear pair depend on each other.

Consider a case with a uniform rotation of the gear and pinion. Because the transverse contact ratio is zero ( $m_p = 0$ ), and the total contact ratio,  $m_t$ , is equal to the face contact ratio,  $m_F$ , the axial pitch  $p_{cl.g}$  of the helix on the gear tooth flank,  $\mathcal{G}$ , can be calculated from the formula:

$$p_{cl.g} = \frac{F_{pa}}{m_t} \cdot \cos \Gamma \quad (14.153)$$

A similar expression:

$$p_{cl.p} = \frac{F_{pa}}{m_t} \cdot \cos \gamma \quad (14.154)$$

is valid with respect to the axial pitch,  $p_{cl.p}$ , of the helix on the pinion tooth flank,  $\mathcal{P}$ .

**TABLE 14.3**

Design Parameters of Conformal/High-Conformal Crossed-Axes Gearing

The Design Parameter	Symbol	Equation
Angular displacement	$\varphi_l$	$\varphi_l = \tan^{-1}\left(\frac{l}{A}\right)$
Angular module	$\varphi_{m,n}$	$\varphi_{m,n} = \tan^{-1}\left(\frac{m_n}{A}\right)$
Angular pitch	$P_\varphi$	$p_\varphi = \tan^{-1}\left(\frac{P}{A}\right)$
Angular tooth thickness (gear)	$\varphi_{t,g}$	$\varphi_{t,g} = \tan^{-1}\left(\frac{t_g}{A}\right)$
Angular tooth thickness (pinion)	$\varphi_{t,p}$	$\varphi_{t,p} = \tan^{-1}\left(\frac{t_p}{A}\right)$
Angular space width (gear)	$\varphi_{w,g}$	$\varphi_{w,g} = \tan^{-1}\left(\frac{w_g}{A}\right)$
Angular space width (pinion)	$\varphi_{w,p}$	$\varphi_{w,p} = \tan^{-1}\left(\frac{w_p}{A}\right)$
Angular backlash	$\varphi_B$	$\varphi_B = \tan^{-1}\left(\frac{B}{A}\right)$
Angular addendum (gear)	$\varphi_{a,g}$	$\varphi_{a,g} = \tan^{-1}\left(\frac{a_g}{A}\right)$
Angular addendum (pinion)	$\varphi_{a,p}$	$\varphi_{a,p} = \tan^{-1}\left(\frac{a_p}{A}\right)$
Angular dedendum (gear)	$\varphi_{d,g}$	$\varphi_{d,g} = \tan^{-1}\left(\frac{b_g}{A}\right)$
Angular dedendum (pinion)	$\varphi_{d,p}$	$\varphi_{d,p} = \tan^{-1}\left(\frac{b_p}{A}\right)$

Note: The following designations:  $a_g$ ,  $b_g$  and  $a_p$ ,  $b_p$  relate to the addendum and dedendum of the gear and pinion, respectively. These design parameters are measured within the normal reference plane in the conformal/high-conformal crossed-axes gear pair.

The quality of conformal/high-conformal gearing strongly depends first of all on the following design parameters:  $l$ ,  $\phi_{t,\omega}$ , and  $\lambda$ .

The tooth flanks of the gear,  $\mathcal{G}$ , and the pinion,  $\mathcal{P}$ , of conformal/high-conformal crossed-axes gearing are not conjugate surfaces; moreover, they are not envelopes to one another.

Conformal/high-conformal crossed-axes gearing is not been profoundly investigated yet. This gearing has received only episodic application, as no practical guide to design of this gearing has been developed yet.

When designing conformal/high-conformal crossed-axes gear pairs, it is desired to accommodate the actual values of the design parameters for potential linear displacements, as well as for potential angular displacements. Under an arbitrary combination of elementary displacements (linear, and angular), the contact point alters its location within the transverse section so as to retain the gear set being conformal/high-conformal. The condition of high conformity has to be met at all locations of contact point, that is, under any and all displacements of the gear and its mating pinion.

## *Interaction of Tooth Flanks in Perfect Crossed-Axes Gearing*

Centerlines of the gear shafts that cross one another are the fundamental feature of crossed-axes gearing. This fundamental feature is reflected even in the name of gearing of this type: *crossed-axes gearing*. Despite the fundamental difference, crossed-axes gearings feature many similarities with gearings of other types, with parallel-axes gearings, as well as with crossed-axes gearings. From this perspective, the interaction of tooth flanks in perfect crossed-axes gearings is discussed below.

### 15.1 Interaction between Tooth Flanks in Perfect Crossed-Axes Gearing

The pulley-and-belt analogy of crossed-axes gear pairs is a convenient and powerful tool to investigate and analyze the transmission of a uniform rotation by means of  $C_a$ -gearing.

#### 15.1.1 Pulley-and-Belt Analogy of Crossed-Axes Gear Pair

Similar to parallel-axes gearing, as well as to crossed-axes gearing, a pulley-and-belt equivalent can be constructed for a crossed-axes gear pair. As illustrated in [Figure 14.5](#), the base cone of a driving pinion, the base cone of a driven gear, and the plane of action,  $PA$ , make up the pulley-and-belt equivalent of an crossed-axes gear pair. The plane of action,  $PA$ , is viewed as a zero-thickness film that is capable of transmitting a rotary motion. The zero-thickness film is free to wrap on the base cone of the driving member and unwrap from the base cone of the driven member of the crossed-axes gear pair. The zero-thickness film cannot be bent about an axis perpendicular to the plane of action,  $PA$ .

The rotations of the base cone of a driving pinion,  $\omega_p$ , the base cone of a driven gear,  $\omega_g$ , and the plane of action,  $\omega_{pa}$ , are synchronized with one another so that no sliding is observed between the interacting surfaces of the base cones and the plane of action,  $PA$ , in the tangential direction of the base cones. In the pulley-and-belt equivalent, the driving base cone of the pinion pulls the driven base cone of the gear. In reality, the driving base cone of the pinion pushes the driven base cone of the gear.

When the base cone of the driving member rotates, it pulls the plane of action, and the latter pulls the driven member of the pulley-and-belt equivalent of the crossed-axes gear pair.

The pulley-and-belt equivalent of the crossed-axes gear pair is convenient when investigating the path of contact in crossed-axes gearing.

#### 15.1.2 Path of Contact

When a pair of crossed-axes gears rotates, the line of contact,  $LC$ , between the tooth flanks,  $\mathcal{G}$  and  $\mathcal{P}$ , of the gear and the mating pinion travels together with the plane of action,  $PA$ . Every point of the line of contact,  $LC$ , traces a corresponding path of contact,  $P_c$ . As the plane of action,  $PA$ , performs a rotary motion about the plane-of-action apex,  $A_{pa}$ , in a stationary reference system associated with the gear pair housing, every path of contact,  $P_c$ , is shaped in the form of a circular arc segment, each of which is centered at the plane-of-action apex,  $A_{pa}$ . Therefore, in crossed-axes gearing, each path of contact,  $P_c$ , is a planar curve (a circular arc segment) that is entirely located within the plane of action,  $PA$ . An instant line of action,  $LA_{inst}$ , is a straight line tangent to the path of contact,  $P_c$ , at every point of it.

In a reference system associated with the gear, the contact point traces a spherical involute on the gear tooth flank,  $\mathcal{G}$ . Similarly, in a reference system associated with the pinion, the contact point traces a spherical involute on the pinion tooth flank,  $\mathcal{P}$ .

A family of paths of contact forms a surface. This surface can be referred to as the *path-of-contact surface*,  $P_{cs}$ . It is evident that in crossed-axes gear pairs with a constant transverse pressure angle ( $\phi_{t,\omega} = \text{const}$ ), the path-of-contact surface,  $P_{cs}$ , is congruent to the plane of action,  $PA$ .

Consider a crossed-axes gear pair that features a transverse pressure angle,  $\phi_{t,\omega}$ , variable within the effective face width,  $F_{par}$ , of the gear pair (that is, a case when  $\phi_{t,\omega} = \text{var}$ ). In the case under consideration, the path-of-contact surface,  $P_{cs}$ , is represented by a continuous set of the circular-arc paths of contact,  $P_c$ , that are located in different infinitesimally narrow portions of the plane of action with different transverse pressure angles,  $\phi_{t,\omega}$ , each. The radius of a current circular-arc path of contact,  $P_c$ , can be viewed as a function of the distance of the point on the pitch line,  $P_{ln}$ , from the plane-of-action-apex,  $A_{pa}$ . The path-of-contact surface,  $P_{cs}$ , is a continuous (screw) surface generated by the circular arcs of a variable radius.

### 15.1.3 Zone (Field) of Action in Crossed-Axes Gearing

It is also convenient to use the pulley-and-belt equivalent of the crossed-axes gear pair for analysis of the field (zone) of action in crossed-axes gearing.

A bevel gear and mating pinion interact with one another only within a portion of the plane of action,  $PA$ . This portion of the plane of action is commonly referred to as the field (zone) of action,  $ZA$ . In crossed-axes gearing, the field (zone) of action is bounded by four boundary lines entirely located in the plane of action,  $PA$ .

A circular arc of an outer radius,  $r_{o,pa}$ , and a circular arc of a limit radius,  $r_{l,pa}$ , both centered at the plane-of-action apex,  $A_{pa}$ , are the first two boundary lines of the field (zone) of action. The face width,  $F_{pa}$ , of the field (zone) of action,  $ZA$ , is calculated as:

$$F_{pa} = r_{o,pa} - r_{l,pa} \quad (15.1)$$

In crossed-axes gearing, the face width,  $F_{pa}$ , of the field (zone) of action,  $ZA$ , equals the width within which the tooth flanks,  $\mathcal{G}$  and  $\mathcal{P}$ , of a gear and a mating pinion overlap one another.

Two lines of intersection,  $kl$  and  $mn$ , of the plane of action,  $PA$ , by the outer cones of the gear and that of the pinion are the second two boundary lines of the field (zone) of action (Figure 15.1). When the apex of the outer cone in the gear/pinion is coincident with the base cone apex, the field of action is bounded by two straight line segments, that is, by the lines of intersection of the outer cones of the gear/pinion by the plane of action,  $PA$ . Commonly, the lines,  $kl$  and  $mn$ , are slightly convex. Commonly, they can be replaced by two straight line segments,  $kl$  and  $mn$ .

Constructed in Figure 15.1, the angle  $\varphi_{za}$  between the lines  $kl$  and  $mn$  is referred to as the *angular width of zone of action*. The angular width,  $\varphi_{za}$ , of the zone of action,  $ZA$ , can be expressed in terms of the design parameters of the gear and the mating pinion. For reference purposes, the lines of tangency,  $cd$  and  $ab$ , of the base cones of the

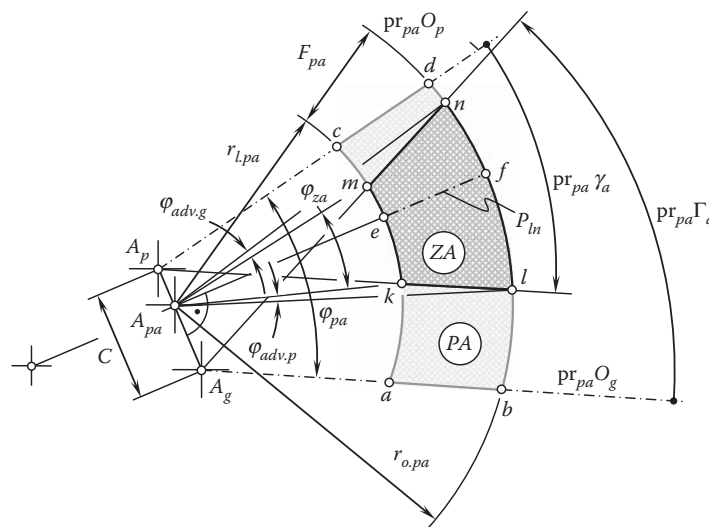


FIGURE 15.1  
Zone of action,  $ZA$ , in crossed-axes gearing.

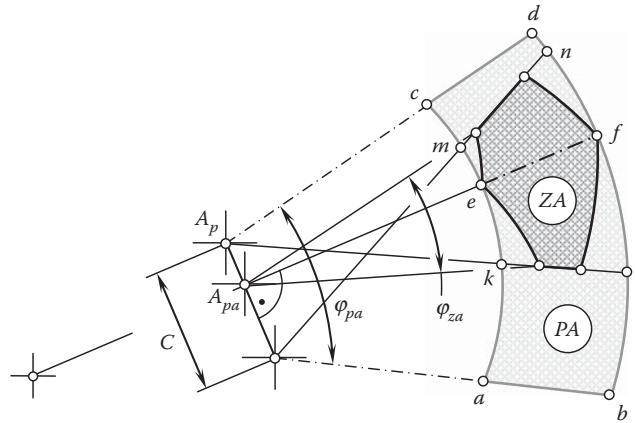


FIGURE 15.2

Crossed-axes gearing that features the zone of action,  $ZA$ , of a complex geometry.

gear and mating pinion with the plane of action are shown in Figure 15.1. These straight tangent lines form an angle,  $\varphi_{pa}$ , that is referred to as the *total angular width of plane of action*.

Another approach can be used for the determining of the angular width of the zone of action,  $\varphi_{pa.z}$ .

Shown in Figure 15.1, the zone of action,  $ZA$ , features the simplest possible geometry. In reality, the geometry of the zone of action can be more complex. An example of a crossed-axes gear pair that features a zone of action,  $ZA$ , of a more complex geometry is illustrated in Figure 15.2.

In crossed-axes gearing (in worm gearing in particular) the zone of action,  $ZA$ , is not mandatorily shaped in the form of a round strip. Depending on the actual shape of the outer surfaces of both the gears in mesh, the zone of action can be bounded by lines of a more complex geometry.

The lines of contact of the plane of action,  $PA$ , with the both base cones remain the same—they are straight line segments.

The geometry of the actual zone of action,  $ZA$ , is a critical consideration when calculating the contact ratio in a crossed-axes gear pair.

## 15.2 Transmission of a Uniform Rotation by Means of Crossed-Axes Gearing

Tooth flanks in a gear for a crossed-axes gear pair can be viewed as a series of cam surfaces that act on similar surfaces of the mating gear to impart a driving motion. In order to smoothly transmit a steady input rotation to the output shaft, three fundamental laws of gearing have to be fulfilled.

First, the condition of contact,  $\mathbf{n} \cdot \mathbf{V}_\Sigma = 0$ , between two interacting tooth flanks,  $\mathcal{G}$  and  $\mathcal{P}$ , of a gear and a mating pinion has to be fulfilled when transmitting a uniform rotation by means of crossed-axes gearing.

Second, the interacting tooth flanks,  $\mathcal{G}$  and  $\mathcal{P}$ , of a gear and a mating pinion have to be conjugate to one another at any and all angular configurations of the gear and the pinion when the gears rotate. This means that the common perpendicular through any and all points within the line of contact intersect the axis of instant rotation,  $P_{in}$  in the gear pair.

The third fundamental condition that is discussed below is the condition that requires equality of angular base pitches of a gear and a mating pinion to the operating angular base pitch of the gear pair. As two (or even more) pairs of teeth make contact at the same time, the fulfillment of an additional condition caused by multiple interacting tooth surfaces in gears is necessary. Here, the discussion is limited to perfect crossed-axes gearing.

A plane of action,  $PA$ , of an crossed-axes gear pair is shown in Figure 15.3a. The plane of action is intersected by a cylinder of revolution of an arbitrary radius,  $r_{y.pa}$ , having the plane-of-action centerline,  $O_{pa}$ , as its axis of rotation. As the angular operating base pitch,  $\varphi_{b.pa}$ , of a gear pair is of a constant value, then the lengths

$$l_{b.pa} = r_{y.pa} \cdot \varphi_{b.pa} \quad (15.2)$$



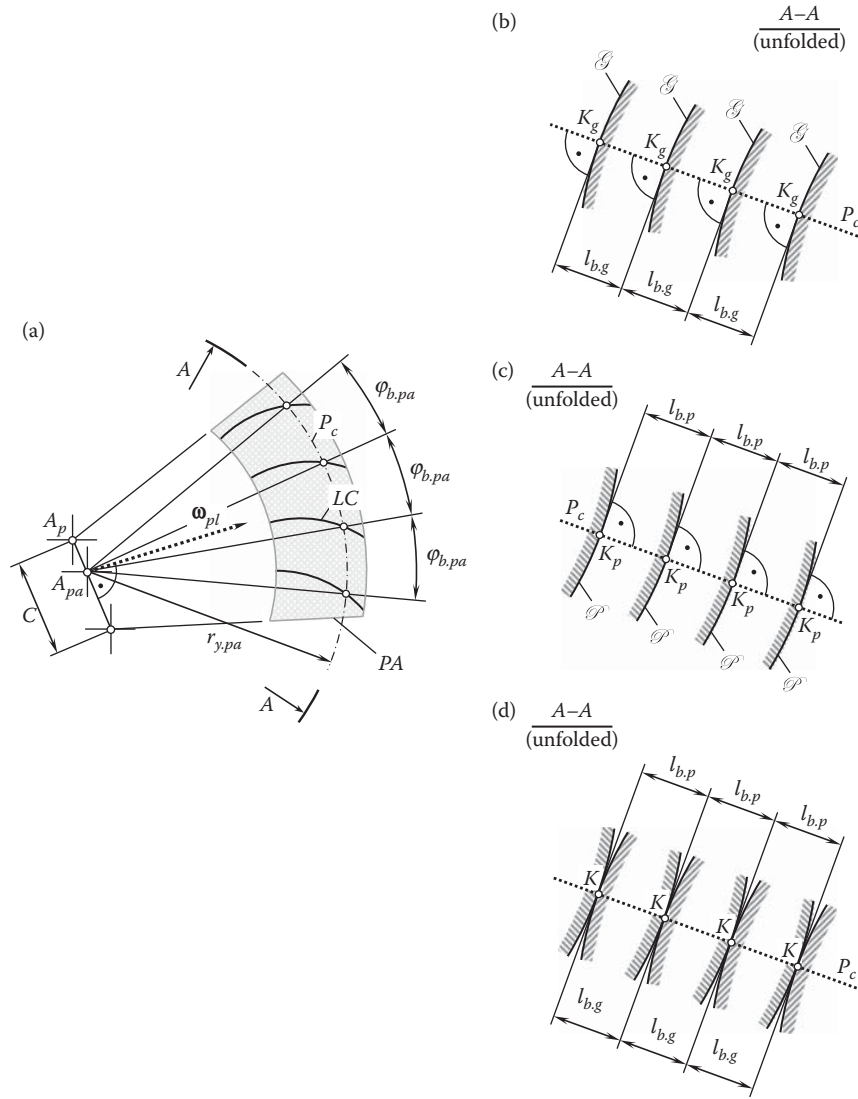


FIGURE 15.3

On the concept of equal base pitches in a perfect crossed-axes gear pair: (a) plane of action,  $PA$ , and the unfolded section  $A-A$ ; (b) of a gear; (c) of a mating pinion; and (d) of the gear pair.

$$l_{b,g} = r_{y.pa} \cdot \varphi_{b,g} \quad (15.3)$$

$$l_{b,p} = r_{y.pa} \cdot \varphi_{b,p} \quad (15.4)$$

of the circular arcs also have constant values; that is, in this particular analysis, the angular base pitches  $\varphi_{b.pa}$ ,  $\varphi_{b,g}$ , and  $\varphi_{b,p}$  can be replaced with the lengths  $l_{b.pa}$ ,  $l_{b,g}$ , and  $l_{b,p}$  of the corresponding circular arcs. Once the lengths,  $l_{b,g} = l_{b.pa}$  and  $l_{b,p} = l_{b.pa}$ , are equal, then the angular base pitches,  $\varphi_{b,g} = \varphi_{b.pa}$  and  $\varphi_{b,p} = \varphi_{b.pa}$ , are equal as well.

The unfolded section,  $A-A$ , of the gear tooth flanks,  $\mathcal{G}$ , by the cylinder of revolution is shown in Figure 15.3b; the unfolded section of the pinion tooth flanks,  $\mathcal{P}$ , by the cylinder of revolution is shown in Figure 15.3c; and the unfolded section of the gear crossed-axes gear pair by the cylinder of revolution is shown in Figure 15.3d. Here and below, only local portions of the gear tooth flanks,  $\mathcal{G}$ , are considered. The gear tooth flanks themselves are not defined yet. Therefore, only small portions of the tooth flanks,  $\mathcal{G}$ , are depicted in Figure 15.3b. All these portions of the tooth flanks of a gear are located in the differential vicinity of points of intersection,  $K_g$ , of the tooth flanks,  $\mathcal{G}$ , by the path of contact,  $P_c$ . Each tooth flank,  $\mathcal{G}$ , is perpendicular to the path of contact,  $P_c$ , at points  $K_g$ . All points  $K_g$  are evenly distributed along the path of contact. The distance between each pair of neighboring points,  $K_g$ , is equal to the angular base pitch,  $\varphi_{b,g}$ , of the gear.

An analysis similar to that above can be performed with respect to the pinion tooth flanks,  $\mathcal{P}$ , as shown in Figure 15.3b. All these portions of the tooth flanks of the pinion are located in the differential vicinity of points of intersection,  $K_p$ , of the tooth flanks,  $\mathcal{P}$ , by the path of contact,  $P_c$ . Each pinion tooth flank,  $\mathcal{P}$ , is perpendicular to the path of contact,  $P_c$ , at points  $K_p$ . All points  $K_p$  are evenly distributed along the path of contact. The distance between each pair of neighboring points,  $K_p$ , is equal to the angular base pitch of the pinion,  $\varphi_{b,p}$ .

When the equality of the angular base pitches of a gear,  $\varphi_{b,g}$ , and a mating pinion,  $\varphi_{b,p}$ , to the operating angular base pitch of the gear pair,  $\varphi_{b,op}$ , is observed; that is, when the identities,  $\varphi_{b,g} \equiv \varphi_{b,op}$  and  $\varphi_{b,p} \equiv \varphi_{b,op}$ , are valid, then the gear and the pinion can be engaged in mesh as illustrated in Figure 15.3d. Each gear point,  $K_g$ , coincides with corresponding pinion point,  $K_p$ . Because of this, the gear and pinion points,  $K_g$  and  $K_p$ , further are designated as the contact point,  $K$ .

As follows from the analysis of Figure 15.3d, it is not a must to keep all the angular base pitches of a gear,  $\varphi_{b,g}$ , equal to one another or to keep all the angular base pitches of a mating pinion,  $\varphi_{b,p}$ , also equal to one another. It is critical to keep equality of a gear angular base pitch and a mating pinion angular base pitch to the corresponding operating angular base pitch of the gear pair for each pair of teeth engaged in mesh. Physically, this is possible, but it limits the gear ratio of a gear pair to integers, that is, to 1, 2, 3, and so forth. Such a design of gearing is impractical and is not considered in this book.

When base pitches of a gear and a mating pinion are not equal to one another ( $\varphi_{b,g} \neq \varphi_{b,p}$ ); for example, the gear base pitch,  $\varphi_{b,g}$ , is smaller compared to the mating pinion base pitch,  $\varphi_{b,p}$ , and the inequality  $\varphi_{b,g} < \varphi_{b,p}$  is valid, as shown in Figure 15.4a, only one pair of teeth is engaged in mesh. A gap between the other pairs of teeth of the gear,  $\mathcal{G}$ , and the pinion,  $\mathcal{P}$ , is observed. No gaps of this sort are permissible in perfect crossed-axes gearings.

In another example illustrated in Figure 15.4, the gear angular base pitch,  $\varphi_{b,g}$ , is greater compared to the mating pinion angular base pitch,  $\varphi_{b,p}$ , and the inequality  $\varphi_{b,g} > \varphi_{b,p}$  is valid as shown in Figure 15.4b; again, only one pair of teeth is engaged in mesh. A gap between the remaining pairs of teeth of the gear,  $\mathcal{G}$ , and the pinion,  $\mathcal{P}$ , is observed. No gaps of this sort are permissible in perfect crossed-axes gearing.

In this second example (see Figure 15.4b), the distribution of the gaps is inverse to that shown in Figure 15.4a. This is because the gear and mating pinion are rigid bodies that physically cannot interfere with one another.

Therefore, a uniform rotation can be smoothly transmitted by an crossed-axes gear pair if the following equalities are valid at every instant of time:

$$\varphi_{b,g} \equiv \varphi_{b,op} \quad (15.5)$$

$$\varphi_{b,p} \equiv \varphi_{b,op} \quad (15.6)$$

With that said, the third condition to be fulfilled in a perfect crossed-axes gear pair can be formulated in the following manner:

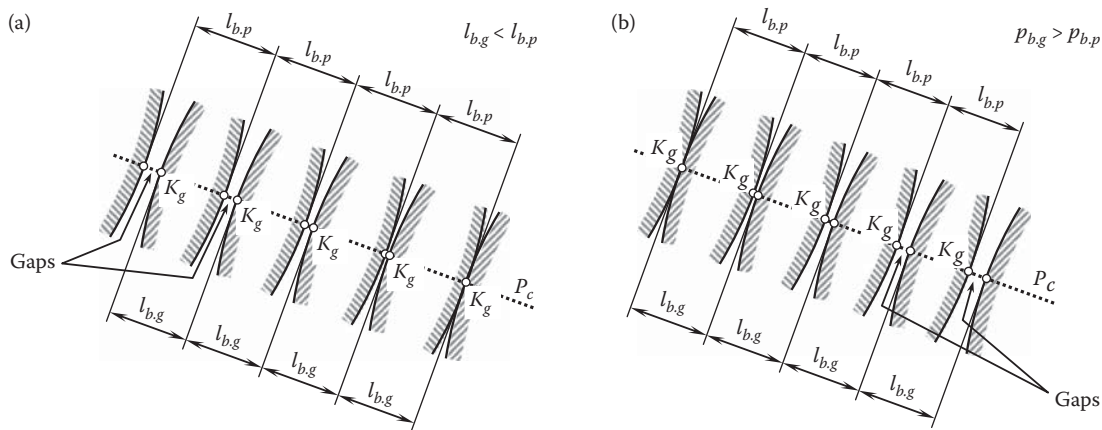


FIGURE 15.4

Examples of violations of the condition of equal angular base pitches in crossed-axes gearing: (a) case when the angular base pitch of a gear,  $\varphi_{b,g}$ , is smaller compared to the angular base pitch,  $\varphi_{b,p}$ , of a mating pinion ( $\varphi_{b,g} < \varphi_{b,p}$ ), and (b) case when the angular base pitch of a gear,  $\varphi_{b,g}$ , is larger compared to the angular base pitch,  $\varphi_{b,p}$ , of a mating pinion ( $\varphi_{b,g} > \varphi_{b,p}$ ); in both cases, gaps are observed.

*The third fundamental law of gearing (in crossed-axes gearing):* “In crossed-axes gearing, in order to transmit a uniform rotary motion from a driving shaft to a driven shaft by means of gear teeth, the angular base pitch of a gear and that of a mating pinion have to be equal to the operating base pitch of the gear pair at every instant of time.”

Only *conjugate* gear tooth flanks feature base pitch. Base pitch cannot be specified for nonconjugate gear tooth flanks. Therefore, only conjugate tooth flanks of a gear and a mating pinion can fulfill the *third fundamental law of gearing (in crossed-axes gearing)*.

If a discussion is limited just to crossed-axes gearing, the concept of the *angular base pitch* is applicable only to gear tooth flanks generated as loci of corresponding spherical involutes. No angular base pitch can be specified for gears with other tooth flanks geometries, such as spiral bevel gears and so forth. Therefore, when angular base pitches in a gear and a mating pinion are equal to the operating angular base pitch of the gear pair (that is, when the identities  $\varphi_{b,g} \equiv \varphi_{b,op}$  and  $\varphi_{b,p} \equiv \varphi_{b,op}$  are valid), the condition of conjugacy of the tooth flanks,  $\mathcal{G}$  and  $\mathcal{P}$ , is always fulfilled.

The equality of angular base pitches of a gear and mating pinion to the operating angular base pitch in a crossed-axes gear pair is the third fundamental law of gearing all perfect crossed-axes gearings have to fulfill.

### 15.3 Contact Ratio in Crossed-Axes Gearing

The contact ratio, in general, is the number of angular pitches through which a tooth surface rotates from the beginning to the end of contact.

In practice, the contact ratio, that is, the total contact ratio,  $m_t$ , is viewed as summa of transverse contact ratio (or profile contact ratio),  $m_p$ , and face contact ratio,  $m_F$ . However, such a separation is not a must, as the total contact ratio,  $m_t$ , can be calculated independently of separate calculation of the components  $m_p$  and  $m_F$ .

#### 15.3.1 Transverse Contact Ratio

The transverse (profile) contact ratio,  $m_p$ , in a crossed-axes gear pair is the contact ratio that is determined within a transverse section of meshing gears. (Recall that a sphere that is centering at the plane-of-action apex,  $A_{pa}$ , is a transverse section in crossed-axes gear pair.) The transverse contact ratio is also commonly referred to as the *profile contact ratio*.

The transverse contact ratio,  $m_p$ , in a crossed-axes gear pair can be defined as the ratio of the angular width,  $\varphi_{za}$ , of the zone of action,  $ZA$ , to the operating base pitch angle,  $\varphi_{b,op}$ :

$$m_p = \frac{\varphi_{za}}{\varphi_{b,op}} \quad (15.7)$$

The duration of contact of a gear tooth flank,  $\mathcal{G}$ , and a mating pinion tooth flank,  $\mathcal{P}$ , in a particular transverse section of a gear by a sphere is specified by the angular width of the zone of action,  $\varphi_{za}$ , in a crossed-axes gear pair. The angular width of the zone of action,  $\varphi_{za}$ , is measured within the plane of action,  $PA$ , and spans over a circular arc of full face width,  $F_{pa}$ . (The angle,  $\varphi_{za}$ , is an equivalent of the length of contact,  $Z_{pa}$ , in parallel-axes gearing).

The tooth flank of a gear,  $\mathcal{G}$ , and the tooth flank of a mating pinion,  $\mathcal{P}$ , are engaged in mesh within the angular width of the zone of action,  $\varphi_{za}$ .

#### 15.3.2 Face Contact Ratio

The face contact ratio,  $m_F$ , in a crossed-axes gear pair can be defined as the ratio:

$$m_F = \frac{\vartheta_{adv}}{\varphi_b} \quad (15.8)$$

of the advance angle,  $\vartheta_{adv}$ , to the angular base pitch,  $\varphi_b$ .

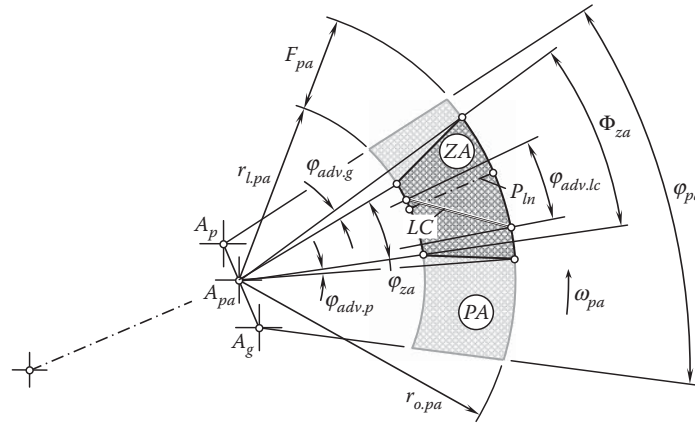


**FIGURE 15.5**  
Angular width,  $\Phi_{z\alpha}$ , of the zone of action,  $ZA$ , in crossed-axes gear pair.

Referring to [Figure 15.5](#), the advance angle,  $\vartheta_{adv}$ , can be specified as follows:

$$\vartheta_{adv} = \varphi_{adv.g} + \varphi_{adv.p} + \varphi_{adv.lc} \quad (15.9)$$

All the angles,  $\varphi_{adv.g}$ ,  $\varphi_{adv.p}$ , and  $\varphi_{adv.lc}$ , are shown in [Figure 15.5](#).

The actual value of the face advance angle,  $\vartheta_{adv}$ , depends on the geometry of the line of contact,  $LC$ , and its configuration within the plane of action,  $PA$ , in a particular design of crossed-axes gear pair.

### 15.3.3 Total Contact Ratio

The total contact ratio,  $m_t$ , is the sum of the transverse contact ratio,  $m_p$ , and the face contact ratio,  $m_F$ :

$$m_t = m_p + m_F \quad (15.10)$$

The total contact ratio,  $m_t$ , in an crossed-axes gear pair can be also defined as the ratio of the total angular width,  $\Phi_{z\alpha}$ , of the zone of action,  $ZA$ , to the operating base pitch angle,  $\varphi_{b.op}$ :

$$m_t = \frac{\Phi_{z\alpha}}{\varphi_{b.op}} \quad (15.11)$$

Referring to [Figure 15.5](#), the total angular width,  $\Phi_{z\alpha}$ , of the zone of action,  $ZA$ , can be specified as follows:

$$\Phi_{z\alpha} = \varphi_{z\alpha} + \varphi_{adv.g} + \varphi_{adv.p} \quad (15.12)$$

All the angles,  $\varphi_{z\alpha}$ ,  $\varphi_{adv.g}$ , and  $\varphi_{adv.p}$ , are shown in [Figure 15.5](#).

Equation 15.12 is an equivalent to the corresponding formulas for the calculation of the total contact ratio,  $m_t$ , in parallel-axes gearing and to the formula for the calculation of the total contact ratio,  $m_t$ , in crossed-axes gearing. This equation is valid for crossed-axes gearings of all types.

The total contact ratio in crossed-axes gear pair is always greater than one ( $m_t \geq 1$ ). For a gearing that features a zero face advance angle,  $\vartheta_{adv}$ , the total contact ratio,  $m_t = m_p \geq 1$ , as the equality,  $m_F = 0$ , is valid in this particular case. Conversely, for high-conformal gears, the equality  $m_p = 0$  is valid. Therefore, the total contact ratio for a high-conformal gear pair can be calculated based on the equality  $m_t = m_F \geq 1$ .

Commonly, the higher the input rotation, the higher the contact ratio, and higher accuracy of the gears is required. In high power density gear transmissions, a high contact ratio is desired, as this is a load-sharing factor that increases the number of pairs of teeth that make contact simultaneously.

The above discussion is valid with respect to internal gears used in the design of a crossed-axes gear pair. Though internal crossed-axes gearings are not extensively used in the industry, dies for net forging of external bevel gears, electrodes for electric-discharging-machining (EDM), and so forth can be calculated by means of the results discussed in this section of the book.

## 15.4 Contact Motion Characteristics in Crossed-Axes Gearing

Two main motions are observed in crossed-axes\* gearing. They are a rotation of the input shaft and a corresponding rotation of the output shaft. These two rotational motions,  $\omega_g$  and  $\omega_p$ , of a gear and mating pinion, correspondingly, cause numerous other motions, both rotational and translational, that are observed when the gears rotate. Some of these motions result in sliding of the tooth flanks,  $\mathcal{G}$  and  $\mathcal{P}$ , of the gear and the mating pinion when the gears rotate.

Rolling and sliding take place simultaneously between the tooth flanks of two mating gears when transmitting a motion by intersected-axis gearing. Rolling and sliding occur at any point of contact within the active portion of the line of contact. Rolling and sliding occur in crossed-axes gearing even at points within the axis of instant rotation,  $P_{ln}$ . Investigation and analysis of sliding and rolling conditions in a gear pair is of importance from an engineering perspective. It enables, for example, determining and reducing friction losses between mating gears.

On the one hand, sliding motion between the tooth flanks,  $\mathcal{G}$  and  $\mathcal{P}$ , can entail extensive surface wear of the gear teeth. Thus, sliding motion has to be reduced (or even eliminated) in order to improve performance of the gear pair. On the other hand, sliding motion can significantly affect conditions of lubrication in a gear pair. Therefore, in order to improve performance of the gear pair, sliding motion has to be optimized. The latter means that gears have to be designed so as to provide the most favorable conditions of lubrication of the tooth flanks,  $\mathcal{G}$  and  $\mathcal{P}$ . With that said, the necessity of understanding conditions of sliding between the tooth flanks,  $\mathcal{G}$  and  $\mathcal{P}$ , becomes clear.

### 15.4.1 Sliding in Perfect Crossed-Axes Gearing

Not many efforts have been undertaken so far to investigate sliding in crossed-axes gearing. Only a few publications on this concern deserve to be mentioned. Publications by Dusev [24], Dusev and Vasiliyev [25], Klingelnberg [54,50], Korostelev [54], and others are among them. Only approximate crossed-axes gearings are investigated in the publications available in the public domain.

A portion of the relative motion of a gear and a mating pinion causes pure rolling of the pitch cones of the interaction gears, while another portion of the relative motion results in sliding of the tooth flanks of the gear,  $\mathcal{G}$ , and the mating pinion,  $\mathcal{P}$ . For better understanding of the nature of sliding in perfect crossed-axes gearing, a detailed investigation of teeth sliding must be carried out. This analysis can be performed either using descriptive geometry-based methods or analytical methods. Below, preference is given to analytical investigation of sliding in perfect crossed-axes gearing.<sup>†</sup>

### 15.4.2 Analytical Solution to the Problem of Determining of Sliding in Perfect Crossed-Axes Gearing

There are numerous similarities between perfect crossed-axes gearing and perfect intersected-axes gearing. From the perspective of the analysis below, it is critical to turn the reader's attention to sliding between gear and mating pinion tooth flanks,  $\mathcal{G}$  and  $\mathcal{P}$ , considered in a local reference system associated with the plane of action,  $PA$ . Considered locally, the sliding between the tooth flanks in both cases is similar. The differences in the analysis appear when a configuration of the axes of rotation,  $O_g$  and  $O_p$ , of the gear and the pinion in crossed-axes gearing is taken into account, as this configuration differs from that in intersected-axes gearing.

\* The discussion in section 13.4, "Contact Motion Characteristics," is valid for both, that is, for crossed-axes gearings with line contact between a gear and a mating pinion tooth flanks,  $\mathcal{G}$  and  $\mathcal{P}$ , as well as for conformal (Novikov gearing) and high-conformal crossed-axes gearings.

† A descriptive geometry-based solution to the problem of sliding in crossed-axes gearing is not discussed here, as it requires illustrations that are too large to be convenient in a book.

To accommodate for the different configuration of the axes of rotation,  $O_g$  and  $O_p$ , of the gear and the pinion in crossed-axes gearing and that in intersected-axes gearing, the operators of the resultant linear transformations,  $\mathbf{Rs}_{la}(p \rightarrow pa)$  and  $\mathbf{Rs}_{ca}(p \rightarrow pa)$ , in a case of intersected-axes gearing (see Equation 13.37) and in a case of crossed-axes gearing (the operator of linear transformation is derived below in this section of the book), correspondingly, are used.

In order to solve the problem of determination of sliding in perfect crossed-axes gearing, it is necessary to derive equations for the linear velocity vectors,  $\mathbf{V}_{m,g}$  and  $\mathbf{V}_{m,p}$ , of a point of interest,  $m$ , within the line of contact,  $LC$ , between the tooth flanks,  $\mathcal{G}$  and  $\mathcal{P}$ , and to represent the derived expressions in a common reference system. A stationary Cartesian coordinate system,  $X_{pa.s}Y_{pa.s}Z_{pa.s}$ , associated with the plane of action,  $PA$ , in the crossed-axes gear pair is especially convenient for solving the problem of determining sliding in perfect  $C_a$ -gearing.

For the development of an analytical solution to the problem under consideration, operators of linear transformations are extensively used below, as the solution to the problem can be significantly simplified by application of the operators of coordinate system transformations. The chief reason the operators of linear transformations are used for the derivation of all the necessary equations is as follows. It is convenient to derive an expression for each of the linear vectors,  $\mathbf{V}_{m,g}$  and  $\mathbf{V}_{m,p}$ , in a specific reference system and then to represent the derived equation in a common reference system that is convenient for further analysis. For instance, it is convenient to determine the linear velocity vector,  $\mathbf{V}_{m,g}$ , in a coordinate system associated with the gear. Similarly, it is convenient to determine the linear velocity vector,  $\mathbf{V}_{m,p}$ , in a coordinate system associated with the pinion. Later on, the derived equations for both the vectors,  $\mathbf{V}_{m,g}$  and  $\mathbf{V}_{m,p}$ , can be represented in a common reference system. Use of the operators of linear transformations, that is, the operators of translation and the operators of rotation, along and about the coordinate axes is very helpful for this purpose.

The relative motion of a driving member and a driven member in a gear pair, as well as of the plane of action, forms the premise on which the corresponding operators of the coordinate system transformations can be derived. When a gear pair is operated, the driving member, the driven member, and the plane of action are rotated in a timely manner; that is, the rotations,  $\omega_g$ ,  $\omega_p$  and  $\omega_{pa}$ , are synchronized with one another.

Numerous similarities between the discussed derivation of the equation for sliding in intersected-axes gearing (see Chapter 13) and that in crossed-axes gearing are employed below.

The stationary reference system,  $X_{p.s}Y_{p.s}Z_{p.s}$ , is associated with the gear housing. At the beginning, the axes of the pinion coordinate system,  $X_pY_pZ_p$ , align to the corresponding axes of the stationary coordinate system,  $X_{p.s}Y_{p.s}Z_{p.s}$ . When the pinion is rotated about the axis,  $O_p$ , through a certain angle,  $\varphi_p$ , the reference system,  $X_pY_pZ_p$ , is rotated together with the pinion. The transition from the pinion reference system,  $X_pY_pZ_p$ , to the stationary reference system,  $X_{p.s}Y_{p.s}Z_{p.s}$ , can be analytically described by the operator of rotation,  $\mathbf{Rt}(Z_s, \varphi_p)$ , of the reference system,  $X_pY_pZ_p$ , through the angle,  $\varphi_p$ , about the axis,  $O_p$ , in the counterclockwise direction.\* In matrix form, this operator can be represented as:

$$\mathbf{Rt}(Z_s, \varphi_p) = \begin{bmatrix} \cos \varphi_p & -\sin \varphi_p & 0 & 0 \\ \sin \varphi_p & \cos \varphi_p & 0 & 0 \\ 0 & 0 & 1 & 0 \\ 0 & 0 & 0 & 1 \end{bmatrix} \quad (15.13)$$

The coordinate system transformation that is analytically described by the operator of rotation,  $\mathbf{Rt}(Z_s, \varphi_p)$ , is followed by the rotation of the reference system,  $X_{p.s}Y_{p.s}Z_{p.s}$ , through the base cone angle,  $\gamma_b$ , of the pinion about the axis  $Y_{p.s}$ , in the counterclockwise direction. The rotation of this sort can be analytically described by the operator of rotation,  $\mathbf{Rt}(Y_{p.s}, \gamma_b)$ . In matrix form, this operator can be represented as:

$$\mathbf{Rt}(Y_{p.s}, \gamma_b) = \begin{bmatrix} \cos \gamma_b & 0 & -\sin \gamma_b & 0 \\ 0 & 1 & 0 & 0 \\ \sin \gamma_b & 0 & \cos \gamma_b & 0 \\ 0 & 0 & 0 & 1 \end{bmatrix} \quad (15.14)$$

\* Here and below, the direction of rotation of a coordinate system about a coordinate axis is determined looking from the arrowhead of the coordinate axis about which the rotation is performed.



After the rotation of the coordinate system,  $X_{p.s}Y_{p.s}Z_{p.s}$ , about the axis,  $Y_{p.s}$ , through the base cone angle,  $\gamma_b$ , is completed, the coordinate system,  $X_{p.s}Y_{p.s}Z_{p.s}$ , occupies the position that is labeled  $X_{1.s}Y_{1.s}Z_{1.s}$ . The axes of the coordinate system,  $X_{1.s}Y_{1.s}Z_{1.s}$ , and the stationary coordinate system,  $X_{2.s}Y_{2.s}Z_{2.s}$ , associated with the plane of action,  $PA$ , have to be properly aligned to one another. To get the axes aligned, an additional rotation of the reference system,  $X_{1.s}Y_{1.s}Z_{1.s}$ , about the axis,  $Z_{p.s}$ , through a right angle have to be performed. An operator,  $\mathbf{Rt}(Z_{p.s}, 90^\circ)$ , of linear transformation that analytically describes this additional rotation can be represented as:

$$\mathbf{Rt}(Z_{p.s}, 90^\circ) = \begin{bmatrix} 0 & 1 & 0 & 0 \\ -1 & 0 & 0 & 0 \\ 0 & 0 & 1 & 0 \\ 0 & 0 & 0 & 1 \end{bmatrix} \quad (15.15)$$

After being turned about the axis,  $Z_{p.s}$ , through a right angle, the coordinate system is designated as  $X_{2.s}Y_{2.s}Z_{2.s}$ .

Then, as the pinion base cone apex,  $A_p$ , is not coincident with the plane-of-action apex,  $A_{pa}$ , the origin of the reference system,  $X_{2.s}Y_{2.s}Z_{2.s}$ , has to be translated from  $A_p$  to  $A_{pa}$ . This linear transformation can be analytically described by an operator of transition in the form of a matrix:

$$\mathbf{Tr}(Y_{p.s}, -r_p) = \begin{bmatrix} 1 & 0 & 0 & 0 \\ 0 & 1 & 0 & -r_p \\ 0 & 0 & 1 & 0 \\ 0 & 0 & 0 & 1 \end{bmatrix} \quad (15.16)$$

The next transition is performed from the coordinate system,  $X_{2.s}Y_{2.s}Z_{2.s}$ , to the stationary coordinate system,  $X_{pa.s}Y_{pa.s}Z_{pa.s}$ , associated with the plane of action,  $PA$ . For the analytical description of the rotation of the reference system,  $X_{2.s}Y_{2.s}Z_{2.s}$ , in the counterclockwise direction about the axis  $Z_{2.s}$  through an angle,  $\sigma_p$ , the operator of rotation,  $\mathbf{Rt}(Z_{2.s}, \sigma_p)$ , is used. In matrix form, this operator can be represented as:

$$\mathbf{Rt}(Z_{2.s}, \sigma_p) = \begin{bmatrix} \cos \sigma_p & \sin \sigma_p & 0 & 0 \\ -\sin \sigma_p & \cos \sigma_p & 0 & 0 \\ 0 & 0 & 1 & 0 \\ 0 & 0 & 0 & 1 \end{bmatrix} \quad (15.17)$$

Here, the projection of the pinion cone angle,  $\Sigma_p$ , onto the plane of action,  $PA$ , is designated as  $\sigma_p$  (that is, the equality  $\Pr_{pa} \Sigma_p = \sigma_p$  is valid). It can be shown that the angle,  $\sigma_p$ , can be calculated as:

$$\sigma_p = \cos^{-1} \left( \frac{\cos \Sigma_p}{\cos \gamma_b} \right) \quad (15.18)$$

where  $\gamma_b$  is the base cone angle of the pinion.

Finally, the transition is performed from the stationary coordinate system,  $X_{pa.s}Y_{pa.s}Z_{pa.s}$ , associated with the plane of action to the coordinate system,  $X_{pa}Y_{pa}Z_{pa}$ , that is rotated together with the plane of action,  $PA$ . For the analytical description of the rotation of the reference system,  $X_{pa.s}Y_{pa.s}Z_{pa.s}$ , in the clockwise direction about the axis  $Z_{pa.s}$  through an angle,  $\varphi_{pa}$ , the operator of rotation,  $\mathbf{Rt}(Z_{pa.s}, \varphi_{pa})$ , is used. In matrix form, this operator can be represented as:

$$\mathbf{Rt}(Z_{2.s}, \varphi_{pa}) = \begin{bmatrix} \cos \varphi_{pa} & -\sin \varphi_{pa} & 0 & 0 \\ \sin \varphi_{pa} & \cos \varphi_{pa} & 0 & 0 \\ 0 & 0 & 1 & 0 \\ 0 & 0 & 0 & 1 \end{bmatrix} \quad (15.19)$$



The angle of rotation,  $\varphi_{pa}$ , of the plane of action,  $PA$ , can be expressed in terms of the angle of rotation,  $\varphi_p$ , of the pinion.

For the analytical description of the resultant coordinate system transformation, that is, for the transition from the reference system,  $X_p Y_p Z_p$ , associated with the rotated pinion, to the reference system,  $X_{pa} Y_{pa} Z_{pa}$ , associated with the rotated plane of action,  $PA$ , the operator,  $\mathbf{Rs}_{Ca}(p \rightarrow pa)$ , of the resultant coordinate system is used. This operator can be expressed in terms of the operators of the elementary linear transformations as:\*

$$\mathbf{Rs}_{Ca}(p \rightarrow pa) = \mathbf{Rt}(Z_{2.s}, \varphi_{pa}) \cdot \mathbf{Rt}(Z_{2.s}, \sigma_p) \cdot \mathbf{Tr}(Y_{p.s}, -r_p) \cdot \mathbf{Rt}(Z_{p.s}, 90^\circ) \cdot \mathbf{Rt}(Y_{p.s}, \gamma_b) \cdot \mathbf{Rt}(Z_s, \varphi_p) \quad (15.20)$$

Note that the order of the multipliers in Equation 15.20 cannot be altered.

For the inverse coordinate system transformation, that is, for the analytical description of the transition from the reference system,  $X_{pa} Y_{pa} Z_{pa}$ , associated with the rotated plane of action,  $PA$ , to the reference system,  $X_p Y_p Z_p$ , associated with the rotated pinion, the operator,  $\mathbf{Rs}_{Ca}(pa \rightarrow p)$ , of the inverse coordinate system transformation is used. The operator,  $\mathbf{Rs}_{Ca}(pa \rightarrow p)$ , of this linear transformation can be expressed in terms of the operator,  $\mathbf{Rs}_{Ca}(p \rightarrow pa)$ , of the direct coordinate system transformation as:

$$\mathbf{Rs}_{Ca}(pa \rightarrow p) = \mathbf{Rs}_{Ca}^{-1}(p \rightarrow pa) \quad (15.21)$$

The operators,  $\mathbf{Rs}_{Ca}(p \rightarrow pa)$  and  $\mathbf{Rs}_{Ca}(pa \rightarrow p)$ , are not presented here in an exploded form, as both of them are bulky.

In the reference system,  $X_p Y_p Z_p$ , associated with the rotated pinion the linear velocity vector,  $\mathbf{V}_{m.p}$ , of point of interest,  $m$ , can be analytically described by a column matrix as:

$$\mathbf{V}_{m.p}|_p = \begin{bmatrix} -r_{b.p} \sin \varphi_p \\ r_{b.p} \cos \varphi_p \\ 0 \\ 1 \end{bmatrix} \quad (15.22)$$

Then, the operator of the resultant coordinate system transformation,  $\mathbf{Rs}_{Ca}(p \rightarrow pa)$ , is used to represent that same linear velocity vector,  $\mathbf{V}_{m.p}$ , in the coordinate system,  $X_{pa} Y_{pa} Z_{pa}$ , associated with the rotated plane of action,  $PA$ :

$$\mathbf{V}_{m.p}|_{pa} = \mathbf{Rs}_{Ca}(p \rightarrow pa) \cdot \begin{bmatrix} -r_{b.p} \sin \varphi_p \\ r_{b.p} \cos \varphi_p \\ 0 \\ 1 \end{bmatrix} \quad (15.23)$$

A formula for the operator,  $\mathbf{Rs}_{Ca}(pa \rightarrow g)$ , of the resultant coordinate system transformation, that is, for the analytical description of the transition from the reference system,  $X_{pa} Y_{pa} Z_{pa}$ , associated with the rotated plane of action,  $PA$ , to the reference system,  $X_g Y_g Z_g$ , associated with the rotated gear, can be derived similarly to how Equation 15.20 is derived for the calculation of the operator of linear transformation,  $\mathbf{Rs}_{Ca}(p \rightarrow pa)$ . The operators,  $\mathbf{Rt}(Z_s, \varphi_g)$ ,  $\mathbf{Rt}(Y_{g.s}, \Gamma_b)$ ,  $\mathbf{Tr}(Y_{p.s}, r_g)$ ,  $\mathbf{Rt}(Z_{g.s}, 90^\circ)$ ,  $\mathbf{Rt}(Z_{3.s}, \sigma_g)$ , and  $\mathbf{Rt}(Z_{3.s}, \varphi_{pa})$ , of the elementary linear transformations are used in this case. The above-listed operators of linear transformations are composed similarly to how the operators of the linear transformations [that is,  $\mathbf{Rt}(Z_s, \varphi_p)$ , Equation 15.13;  $\mathbf{Rt}(Y_{p.s}, \gamma_b)$ , Equation 15.14;  $\mathbf{Tr}(Y_{p.s}, r_g)$ , Equation 15.16;  $\mathbf{Rt}(Z_{p.s}, 90^\circ)$ , Equation 15.15;  $\mathbf{Rt}(Z_{2.s}, \sigma_p)$ , Equation 15.17; and  $\mathbf{Rt}(Z_{2.s}, \varphi_{pa})$ ,

\* It is important to stress here the difference between the operator of the resultant coordinate system transformation,  $\mathbf{Rs}_{Ca}(p \rightarrow pa)$ , in the case of crossed-axes gearing, and the similar operator of the resultant coordinate system transformation,  $\mathbf{Rs}_{la}(p \rightarrow pa)$ , in the case of intersected-axes gearing (see Equation 13.37).

Equation 15.19] are composed:

$$\mathbf{Rt}(Z_s, \varphi_g) = \begin{bmatrix} \cos \varphi_g & \sin \varphi_g & 0 & 0 \\ -\sin \varphi_g & \cos \varphi_g & 0 & 0 \\ 0 & 0 & 1 & 0 \\ 0 & 0 & 0 & 1 \end{bmatrix} \quad (15.24)$$

$$\mathbf{Rt}(Y_{g.s}, \Gamma_b) = \begin{bmatrix} \cos \Gamma_b & 0 & \sin \Gamma_b & 0 \\ 0 & 1 & 0 & 0 \\ -\sin \Gamma_b & 0 & \cos \Gamma_b & 0 \\ 0 & 0 & 0 & 1 \end{bmatrix} \quad (15.25)$$

$$\mathbf{Rt}(Z_{g.s}, 90^\circ) = \begin{bmatrix} 0 & 1 & 0 & 0 \\ -1 & 0 & 0 & 0 \\ 0 & 0 & 1 & 0 \\ 0 & 0 & 0 & 1 \end{bmatrix} \quad (15.26)$$

$$\mathbf{Tr}(Y_{g.s}, r_g) = \begin{bmatrix} 1 & 0 & 0 & 0 \\ 0 & 1 & 0 & r_g \\ 0 & 0 & 1 & 0 \\ 0 & 0 & 0 & 1 \end{bmatrix} \quad (15.27)$$

$$\mathbf{Rt}(Z_{3.s}, \sigma_g) = \begin{bmatrix} \cos \sigma_g & -\sin \sigma_g & 0 & 0 \\ \sin \sigma_g & \cos \sigma_g & 0 & 0 \\ 0 & 0 & 1 & 0 \\ 0 & 0 & 0 & 1 \end{bmatrix} \quad (15.28)$$

$$\mathbf{Rt}(Z_{3.s}, \varphi_{pa}) = \begin{bmatrix} \cos \varphi_{pa} & \sin \varphi_{pa} & 0 & 0 \\ -\sin \varphi_{pa} & \cos \varphi_{pa} & 0 & 0 \\ 0 & 0 & 1 & 0 \\ 0 & 0 & 0 & 1 \end{bmatrix} \quad (15.29)$$

Here, the projection of the gear cone angle,  $\Sigma_g$ , onto the plane of action,  $PA$ , is designated as  $\sigma_g$  (that is, the equality  $\text{Pr}_{pa} \Sigma_g = \sigma_g$  is valid). It can be shown that the angle,  $\sigma_g$ , can be calculated the following equation:

$$\sigma_g = \cos^{-1} \left( \frac{\cos \Sigma_g}{\cos \Gamma_b} \right) \quad (15.30)$$

where  $\Gamma_b$  is the base cone angle of the gear.

For the analytical description of the resultant coordinate system transformation, that is, for the transition from the reference system,  $X_g Y_g Z_g$ , associated with the rotated pinion, to the reference system,  $X_{pa} Y_{pa} Z_{pa}$ , associated with the rotated plane of action,  $PA$ , the operator,  $\mathbf{Rs}_{Ca}(g \rightarrow pa)$ , of the resultant coordinate system is used. This operator can be expressed in terms of the operators of the elementary linear transformations as:

$$\mathbf{Rs}_{Ca}(g \rightarrow pa) = \mathbf{Rt}(Z_{3.s}, \varphi_{pa}) \cdot \mathbf{Tr}(Y_{g.s}, r_g) \cdot \mathbf{Rt}(Z_{3.s}, \sigma_g) \cdot \mathbf{Rt}(Z_{g.s}, 90^\circ) \cdot \mathbf{Rt}(Y_{g.s}, \Gamma_b) \cdot \mathbf{Rt}(Z_s, \varphi_g) \quad (15.31)$$

Note that the order of the multipliers in Equation 15.31 cannot be altered.

In the reference system,  $X_g Y_g Z_g$ , associated with the rotated gear the linear velocity vector,  $\mathbf{V}_{m.g}$ , of point of interest,  $m$ , can be analytically described by a column matrix as:

$$\mathbf{V}_{m.g}|_g = \begin{bmatrix} -r_{b.g} \sin \varphi_g \\ r_{b.g} \cos \varphi_g \\ 0 \\ 1 \end{bmatrix} \quad (15.32)$$

Then, the operator of the resultant coordinate system transformation,  $\mathbf{Rs}_{Ca}(g \rightarrow pa)$ , is used to represent that same linear velocity vector,  $\mathbf{V}_{m,g}$ , in the coordinate system,  $X_{pa}Y_{pa}Z_{pa}$ , associated with the rotated plane of action,  $PA$ :

$$\mathbf{V}_{m,g}|_{pa} = \mathbf{Rs}_{Ca}(g \rightarrow pa) \cdot \begin{bmatrix} -r_{b,g} \sin \varphi_g \\ r_{b,g} \cos \varphi_g \\ 0 \\ 1 \end{bmatrix} \quad (15.33)$$

Consider the relative motion of a point within the line of contact of the tooth flanks,  $\mathcal{G}$  and  $\mathcal{P}$ , of a gear and a mating pinion in an crossed-axes gear pair.

The vector of the relative motion,  $\mathbf{V}_{rel}$ , of the point of interest,  $m$ , within the line of contact,  $LC$ , between the tooth flanks,  $\mathcal{G}$  and  $\mathcal{P}$ , of a gear and a mating pinion in an crossed-axes gear pair equals the difference:

$$\mathbf{V}_{rel} = \mathbf{V}_{m,p}|_{pa} - \mathbf{V}_{m,g}|_{pa} \quad (15.34)$$

where both the linear velocity vectors,  $\mathbf{V}_{m,g}$  and  $\mathbf{V}_{m,p}$ , are represented in a common reference system,  $X_{pa}Y_{pa}Z_{pa}$ , associated with the rotated plane of action,  $PA$ .

These velocities,  $\mathbf{V}_{m,g}$  and  $\mathbf{V}_{m,p}$ , decisively affect the lubrication and friction parameters on the mating flanks and hence influence the load capacity and efficiency of the bevel gear set.

In the expended form, the vector of the relative motion,  $\mathbf{V}_{rel}$ , can be represented in matrix form as:

$$\mathbf{V}_{rel}|_{pa} = \begin{bmatrix} V_{x,rel} \\ V_{y,rel} \\ V_{z,rel} \\ 1 \end{bmatrix} \quad (15.35)$$

The projection,  $V_{y,rel}$ , of the linear velocity vector,  $\mathbf{V}_{rel}$ , onto the axis,  $Y_{pa}$ , causes pure rolling of the gear and mating pinion tooth flanks,  $\mathcal{G}$  and  $\mathcal{P}$ , over each other. Therefore, this component of the linear velocity vector,  $\mathbf{V}_{rel}$ , is labeled below as  $\mathbf{V}_{rol}$ .

The projection,  $V_{z,rel}$ , of the linear velocity vector,  $\mathbf{V}_{rel}$ , onto the axis,  $Z_{pa}$ , causes profile sliding of the gear and mating pinion tooth flanks,  $\mathcal{G}$  and  $\mathcal{P}$ . Therefore, this component of the linear velocity vector,  $\mathbf{V}_{rel}$ , is labeled below as  $\mathbf{V}_{sl,p}$ .

The projection,  $V_{x,rel}$ , of the linear velocity vector,  $\mathbf{V}_{rel}$ , onto the axis,  $X_{pa}$ , causes drag sliding of the gear and mating pinion tooth flanks,  $\mathcal{G}$  and  $\mathcal{P}$ . Therefore, this component of the linear velocity vector,  $\mathbf{V}_{rel}$ , is labeled below as  $\mathbf{V}_{sl,d}$ .

The total sliding,  $\mathbf{V}_{sl}$ , in crossed-axes gearing can be calculated as the sum:

$$\mathbf{V}_{sl} = \mathbf{V}_{sl,p} + \mathbf{V}_{sl,d} \quad (15.36)$$

At different points within the zone of action,  $ZA$ , each of the linear velocity vectors, that is,  $\mathbf{V}_{sl}$ ,  $\mathbf{V}_{sl,p}$ , and  $\mathbf{V}_{sl,d}$ , varies.

Computer code for the calculation of all the components,  $\mathbf{V}_{rol}$ ,  $\mathbf{V}_{sl,p}$ , and  $\mathbf{V}_{sl,d}$ , of the linear velocity vector,  $\mathbf{V}_{rel}$ , can be developed on the premise of the equations discussed above. Ultimately, the distribution of the components,  $\mathbf{V}_{rol}$ ,  $\mathbf{V}_{sl,p}$ , and  $\mathbf{V}_{sl,d}$ , within the zone of action,  $ZA$ , in a crossed-axes gear pair can be interpreted graphically.

The origin of sliding of the teeth flanks,  $\mathcal{G}$  and  $\mathcal{P}$ , in the direction of the axis of instant rotation,  $P_{ln}$ , in crossed-axes gearing is illustrated in [Figure 15.6](#).

When the gears rotate, the plane of action,  $PA$ , is steadily rotated about the plane-of-action apex,  $A_{pa}$ , with an angular velocity,  $\omega_{pa}$ . In this rotation, the linear velocity vector,  $\mathbf{V}_{m,pa}$ , of an arbitrary point,  $m$ , of the line of contact,  $LC$ , forms a certain angle with the axis of instant rotation,  $P_{ln}$  (this angle equals zero only when point,  $m$ , coincides with point of intersection of the line of contact,  $LC$ , and the axis of instant rotation,  $P_{ln}$ ). The component,  $\mathbf{V}_{m,r}$ , of the linear velocity vector,  $\mathbf{V}_{m,pa}$ , that is perpendicular to the axis,  $P_{ln}$ , causes pure rotation of the

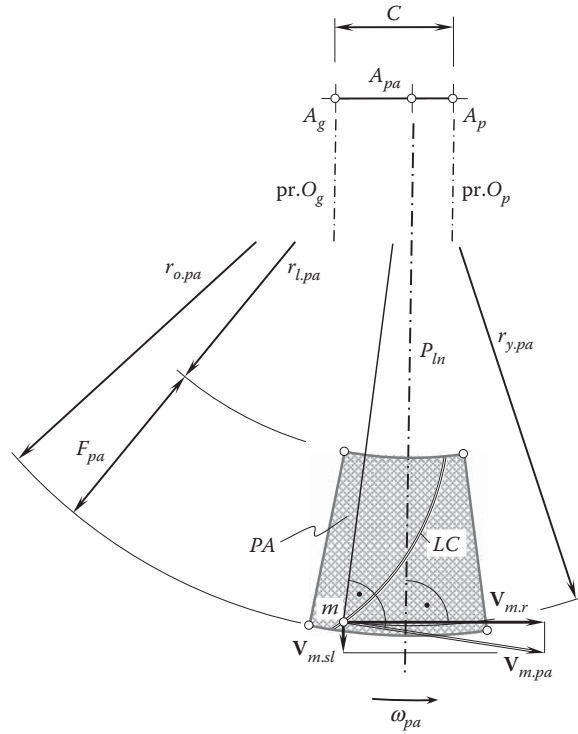


FIGURE 15.6

On the origin of sliding of the teeth flanks,  $\mathcal{G}$  and  $\mathcal{P}$ , in the direction of the axis of instant rotation,  $P_{ln}$ , in crossed-axes gearing.

driven gear. The component,  $V_{m.sl}$ , of the linear velocity vector,  $V_{m.pa}$ , that is parallel to the axis,  $P_{ln}$ , causes sliding of the teeth flanks,  $\mathcal{G}$  and  $\mathcal{P}$ , in the direction of the axis of instant rotation,  $P_{ln}$ .

A similar schematic (see Figure 15.6) is also valid with respect to sliding in intersected-axes gearing (see Section 13.4).

### 15.4.3 Specific Sliding in Perfect Crossed-Axes Gearing

For the specification of sliding of tooth flanks,  $\mathcal{G}$  and  $\mathcal{P}$ , of a gear and a mating pinion in a crossed-axes gear pair, a dimensionless parameter can be used similar to that in parallel-axes gearing, as well as in intersected-axes gearing. This sliding parameter can be also referred to as *specific sliding*, as it is common with respect to parallel-axes gearing and intersected-axes gearing, and it is denoted by  $\gamma_{\Sigma}$ . The actual value of the specific sliding does not depend on a rotation of the input/output shafts, and depends only on the design parameters of the gear and the mating pinion. The latter is important when optimizing design parameters in crossed-axes gear pairs.

Two different parameters,  $\gamma_{\Sigma}$ , are distinguished.

First, the slide/roll ratio for the tooth flank,  $\mathcal{G}$ , of the gear:

$$\gamma_{\Sigma,g} = \frac{V_{sl,g}^m - V_{sl,p}^m}{V_{sl,g}^m} \quad (15.37)$$

Second, the slide/roll ratio for the tooth flank,  $\mathcal{P}$ , of the pinion:

$$\gamma_{\Sigma,p} = \frac{V_{sl,p}^m - V_{sl,g}^m}{V_{sl,p}^m} \quad (15.38)$$

The sliding velocities,  $V_{sl,g}^m$  and  $V_{sl,p}^m$ , in Equations 15.37 and 15.38 are calculated as explained immediately below.

In the reference system,  $X_{pa}Y_{pa}Z_{pa}$ , associated with the rotated plane of action,  $PA$ , the linear velocity vector,  $\mathbf{V}_{m,g}|_{pa}$  (see Equation 15.33), can be represented in the form:

$$\mathbf{V}_{m,g}|_{pa} = \begin{bmatrix} V_{x.m,g} \\ V_{y.m,g} \\ V_{z.m,g} \\ 1 \end{bmatrix} \quad (15.39)$$

The component,  $V_{z.m,g}$ , contributes to the profile sliding, and the component,  $V_{x.m,g}$ , contributes to the drag sliding in the crossed-axes gear pair (the component,  $V_{y.m,g}$ , contributes to pure rolling of the tooth flanks,  $\mathcal{G}$  and  $\mathcal{P}$ ). The sliding velocity,  $V_{sl,g}^m$  (see Equations 15.37 and 15.38), can be expressed in terms of the velocities,  $V_{x.m,g}$  and  $V_{z.m,g}$ , as:

$$V_{sl,g}^m = \sqrt{V_{x.m,g}^2 + V_{z.m,g}^2} \quad (15.40)$$

Similarly, in the reference system,  $X_{pa}Y_{pa}Z_{pa}$ , associated with the rotated plane of action,  $PA$ , the linear velocity vector,  $\mathbf{V}_{m,p}|_{pa}$ , can be represented in the form:

$$\mathbf{V}_{m,p}|_{pa} = \begin{bmatrix} V_{x.m,p} \\ V_{y.m,p} \\ V_{z.m,p} \\ 1 \end{bmatrix} \quad (15.41)$$

The component,  $V_{z.m,p}$ , contributes to the profile sliding, and the component,  $V_{x.m,p}$ , contributes to sliding along the gear tooth in the crossed-axes gear pair (the component,  $V_{y.m,p}$ , contributes to pure rolling of the tooth flanks,  $\mathcal{G}$  and  $\mathcal{P}$ ). The sliding velocity,  $V_{sl,p}^m$ , can be expressed in terms of the velocities,  $V_{x.m,p}$  and  $V_{z.m,p}$ , as:

$$V_{sl,p}^m = \sqrt{V_{x.m,p}^2 + V_{z.m,p}^2} \quad (15.42)$$

The sliding velocities,  $V_{sl,g}^m$  and  $V_{sl,p}^m$  (see Equations 15.40, and 15.42), are entered into:

$$\gamma_{\Sigma,g} = \frac{V_{sl,g}^m - V_{sl,p}^m}{V_{sl,g}^m} \quad (15.43)$$

$$\gamma_{\Sigma,p} = \frac{V_{sl,p}^m - V_{sl,g}^m}{V_{sl,p}^m} \quad (15.44)$$

to calculate the specific roll/slide ratios,  $\gamma_{\Sigma,g}$  and  $\gamma_{\Sigma,p}$ , in crossed-axes gearings.

The specific sliding,  $\gamma_{\Sigma}$ , has a positive value on the addendum portions of the tooth flanks. The parameter,  $\gamma_{\Sigma}$ , does not exceed 1. At points within the axis of instant rotation,  $P_{ln}$ , it is equal to zero, and it is equal to 1 at the base cone of the mating gear.

The specific sliding on the dedendum portion of the tooth flanks has a negative value. It is equal to zero at points within the axis of instant rotation,  $P_{ln}$ , and it approaches minus infinity at the base cone.

The specific rolling/sliding ratios,  $\gamma_{\Sigma,g}$  and  $\gamma_{\Sigma,p}$ , are plotted within the zone of action,  $ZA$ , as only the region,  $ZA$ , plane of action comes into effect when investigating the engagement of the gear teeth.

#### 15.4.4 Features of Specific Sliding in Perfect Crossed-Axes Gearing

Sliding conditions in perfect crossed-axes gearing feature sliding in the lengthwise direction of gear teeth. Therefore, in addition to the specific roll/slide ratios,  $\gamma_{\Sigma,g}$  and  $\gamma_{\Sigma,p}$  (see Equations 15.43 and 15.44), two more characteristics can be introduced to specify specific sliding in crossed-axes gear pairs.

Specific profile rolling/sliding ratios,  $\gamma_{p,g}$  and  $\gamma_{p,p}$ , are the first of two additional characteristics. These two ratios are specified as:

$$\gamma_{p,g} = \frac{V_{z.m,g} - V_{z.m,p}}{V_{z.m,g}} \quad (15.45)$$

$$\gamma_{p,p} = \frac{V_{z.m,p} - V_{z.m,g}}{V_{z.m,p}} \quad (15.46)$$

Specific rolling/sliding ratios,  $\gamma_{d,g}$  and  $\gamma_{d,p}$ , for the sliding in the lengthwise direction of the gear teeth are the second of two additional characteristics. These two ratios are specified as:

$$\gamma_{d,g} = \frac{V_{x.m,g} - V_{x.m,p}}{V_{x.m,g}} \quad (15.47)$$

$$\gamma_{d,p} = \frac{V_{x.m,p} - V_{x.m,g}}{V_{x.m,p}} \quad (15.48)$$

Specific profile roll/slide ratios,  $\gamma_{p,g}$  and  $\gamma_{p,p}$ , and specific drag rolling/sliding ratios,  $\gamma_{d,g}$  and  $\gamma_{d,p}$ , can be helpful in more detailed analysis of sliding conditions in crossed-axes gearings.

It should be mentioned here that gears with a low tooth count are more vulnerable to sliding between the tooth flanks,  $\mathcal{G}$  and  $\mathcal{P}$ , of a gear and a mating pinion in crossed-axes gear pairs. They are also more sensitive to the variation of the roll/slide conditions within the zone of action,  $ZA$ .

The performed analysis for sliding conditions in external crossed-axes gearing can be extended to internal intersected-axis gearings, as well as to intersected-axis gearings with a crown gear.

The disclosed approach for the calculation of the sliding parameters in perfect crossed-axes gearing is also applicable to calculating the sliding parameters in conformal and high-conformal gearing. The main feature here is that the angular face width in a gear pair is zero.

## 15.5 Elements of Dynamics of Perfect Crossed-Axes Gearing

In a crossed-axes gear pair, the input shaft and output shaft are loaded by an input torque and output torque, correspondingly. As the gears interact with each other, a force of the interaction is exerted from the driving member of the gear pair. An actual value of the force of interaction in crossed-axes gearing, as well as the components of this force, depends on the input torque and on the design parameters of the gear and the mating pinion. Considering an input torque and an input rotation of constant values (that is, no acceleration/deceleration is taken into account in the analysis performed below), it is necessary to determine the forces that act between a gear and a mating pinion in an crossed-axes gear pair.\*

### 15.5.1 Principal Assumption Adopted in Load Analysis of Perfect Crossed-Axes Gearing

When a crossed-axes gear pair operates, the gear and the pinion tooth flanks,  $\mathcal{G}$  and  $\mathcal{P}$ , interact with one another at points within the line(s) of contact,  $LC$ . The line(s) of contact is entirely located within the plane of action,  $PA$ . This makes possible a conclusion that the force of interaction between the tooth flanks,  $\mathcal{G}$  and  $\mathcal{P}$ , acts along a straight line that is also located within the plane of action,  $PA$ .

As the line of action of the force is within the plane of action,  $PA$ , then the following assumption seems reasonable in load analysis of perfect crossed-axes gearing.

Referring to Figure 15.7, consider the base cones of a gear and a mating pinion, along with the plane of action. The gear rotates,  $\omega_g$ , about its axis of rotation,  $O_g$ , and the pinion rotates,  $\omega_p$ , about its axis of rotation,  $O_p$ , as schematically illustrated in Figure 15.7. The plane of action,  $PA$ , is in tangency to both the base cones. The plane

\* Friction forces are incorporated into the load analysis at later stages.

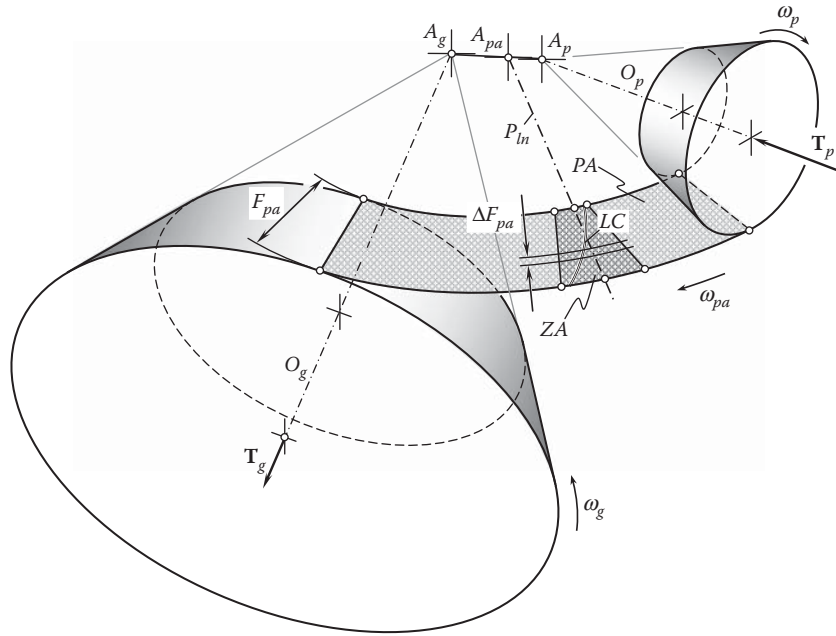


**FIGURE 15.7**  
Calculation of the forces acting in a perfect crossed-axes gear pair.

of action,  $PA$ , rotates,  $\omega_{pa}$ , about its axis of rotation (not shown in Figure 15.7) that passes through the plane-of-action apex,  $A_{pa}$ . It is instructive to point out here that in contrast to the *pulley-and-belt* analogy of a crossed-axes gear pair, where the belt *pulls* the driven member in a gear pair; in reality, the driving gear *pushes* the driven member in a crossed-axes gearing. In this way, the direction of the rotation,  $\omega_{pa}$ , is specified in Figure 15.7.

The rotations,  $\omega_g$ ,  $\omega_p$ , and  $\omega_{pa}$ , are synchronized with one another in compliance with the equations:

$$\frac{\omega_g}{\omega_{pa}} = \sin \Gamma_b \quad (15.49)$$

$$\frac{\omega_p}{\omega_{pa}} = \sin \gamma_b \quad (15.50)$$

$$\frac{\omega_g}{\omega_p} = \frac{\sin \Gamma_b}{\sin \gamma_b} \quad (15.51)$$

The input torque,  $T_p$ , is applied to the pinion shaft, and the output torque,  $T_g$ , is applied to the gear shaft. The torque,  $T_{pa}$ , is an *imagined* parameter. This torque is applied to the rotated plane of action,  $PA$ . The magnitudes,  $T_g$ ,  $T_p$ , and  $T_{pa}$ , of the torques,  $T_g$ ,  $T_p$ , and  $T_{pa}$ , correspond to one another inversely so that the rotations,  $\omega_g$ ,  $\omega_p$ , and  $\omega_{pa}$ , are synchronized with one another; that is:

$$\frac{T_g}{T_{pa}} = \frac{1}{\sin \Gamma_b} \quad (15.52)$$

$$\frac{T_p}{T_{pa}} = \frac{1}{\sin \gamma_b} \quad (15.53)$$

$$\frac{T_g}{T_p} = \frac{\sin \gamma_b}{\sin \Gamma_b} \quad (15.54)$$





Equations similar to Equation 13.71; that is:

$$t_g = \frac{T_g}{F_{pa}} = \text{const} \quad (15.58)$$

$$t_p = \frac{T_p}{F_{pa}} = \text{const} \quad (15.59)$$

are valid with respect to the gear as well as the mating pinion.

As the torque per unit length,  $t_{pa}$ , has a constant value, and the equality,  $t_{pa}F_{pa} = T_{pa}$ , is valid, then the value of the plane-of-action torque,  $T_{pa}$ , is proportional to the shadowed area in [Figure 15.8](#).

Equal torque share among the slices is graphically illustrated in [Figure 15.8](#).

In order to transmit a given power, it is always desired to design and implement gearboxes of the smallest possible size. From this perspective, the active portion of the line of contact,  $LC$ , should begin from the apex  $A_{pa}$  of the plane of action,  $PA$ . Evidently, the line of contact of such a geometry is far from practical, as the maximum contact and bending strength of the gear teeth are restricted by physical properties of the material the gear and pinion are made of.

Calculation of the design parameters of the favorable portion of the line of contact is based on the assumption that the power being transmitting by a gear pair is equally shared within active portion of the gear pair face width. With that said, under torque of a constant value, the smaller diameter of a gear/pinion, the larger the force, and vice versa. Therefore, a practical value of the smallest feasible diameter of the gear/pinion is limited by the yield contact and bending stress in the gear tooth.

The above discussion makes reasonable the following assumption that is referred to as the basic assumption in dynamics of crossed-axes gearing:

### Assumption 13.1

*In a crossed-axes gear pair, the torque per unit length,  $t_{pa}$ , is equally shared in the radial direction among an infinite number of infinitesimally thin slides, each of which is perpendicular to the axis of rotation either of the plane of action or the pinion.*

A similar assumption has been made with respect to parallel-axes gear pairs (see [Chapter 8](#)), as well as with respect to intersected-axes gearing (see [Chapter 13](#)).

## 15.5.2 Forces of Interaction in Perfect Crossed-Axes Gearing

The forces that act in a perfect crossed-axes gear pair are considered below in different reference systems. The analysis begins with load applied within the plane of action,  $PA$ . Then, the analysis is expanded to the forces that act on the bearings, gear housing, and so forth.

### 15.5.2.1 Resultant Force Acting in Perfect Crossed-Axes Gearing

In the plane-of-action torque,  $T_{pa}$ , creates the plane-of-action tangential force,  $F_{pa}$ . The tangential force per unit length,  $f_{pa}$ , can be expressed in terms of the torque per unit length,  $t_{pa}$ , and the distance,  $r_{y.pa}$ , of a particular slice from the plane-of-action point,  $A_{pa}$ , as:

$$f_{pa} = \frac{t_{pa}}{r_{y.pa}} \quad (15.60)$$

It is instructive to point out here that the tangential force per unit length,  $f_{pa}$ , is a function of the distance,  $r_{y.pa}$ , of the point of interest,  $m$ , from the plane-of-action point,  $A_{pa}$ ; that is:

$$f_{pa} = f_{pa}(r_{y.pa}) \quad (15.61)$$

The distribution of the tangential force per unit length,  $\mathbf{f}_{pa}(r_{y,pa})$ , in the radial direction of the plane of action is shown in [Figure 15.8](#).

With the tangential force per unit length,  $\mathbf{f}_{pa}$ , determined (see Equation 15.60), the resultant tangential force,  $\mathbf{F}_{pa}$ , is calculated as:

$$\mathbf{F}_{pa} = F_{pa} \cdot \mathbf{f}_{pa} + \mathbf{t}_{pa} \int_{r_{l,pa}}^{r_{o,pa}} \frac{1}{r_{y,pa}} dr_{y,pa} = F_{pa} \cdot \mathbf{f}_{pa} + \mathbf{t}_{pa} \cdot (\ln |r_{o,pa}| - \ln |r_{l,pa}|) \quad (15.62)$$

$$\mathbf{F}_{pa} = F_{pa} \cdot \mathbf{f}_{pa} + \mathbf{t}_{pa} \cdot \ln \left| \frac{r_{o,pa}}{r_{l,pa}} \right| \quad (15.63)$$

Equations similar to Equation 15.49, that is:

$$\mathbf{F}_g = F_{pa} \cdot \mathbf{f}_g + \mathbf{t}_g \cdot \ln \left| \frac{r_{o,pa}}{r_{l,pa}} \right| \quad (15.64)$$

$$\mathbf{F}_p = F_{pa} \cdot \mathbf{f}_p + \mathbf{t}_p \cdot \ln \left| \frac{r_{o,pa}}{r_{l,pa}} \right| \quad (15.65)$$

are valid with respect to the gear as well as the mating pinion.

The resultant force,  $\mathbf{F}_{pa}$ , is applied at a point,  $c_g$ , of the line of contact,  $LC$ , that is remote from the plane-of-action apex,  $A_{pa}$ , at a distance,  $r_{cg}$  (see [Figure 15.8](#)).

Transmission of a rotation from a driving shaft to a driven shaft is due to the tangential force,  $\mathbf{F}_{pa}$ .

When the gears rotate, friction is observed between the gear tooth flank,  $\mathcal{G}$ , and the pinion tooth flank,  $\mathcal{P}$ . The friction between the compressed the gear and the pinion tooth flanks,  $\mathcal{G}$  and  $\mathcal{P}$ , is due to the sliding that occurs between tooth flanks,  $\mathcal{G}$  and  $\mathcal{P}$ . As already shown above (see the previous section), two types of sliding are distinguished in crossed-axes gear pairs. The profile sliding is the first kind, and the sliding in the lengthwise direction of the gear teeth is the second kind. Therefore, friction forces of two types need to be recognized, that is, the profile friction force,  $\mathbf{F}_{pr}$ , and the friction force in the lengthwise direction,  $\mathbf{F}_{dr}$ . These friction forces contribute to the resultant force of the interaction,  $\mathbf{F}_{\Sigma}$ , between the gear tooth flank,  $\mathcal{G}$ , and the pinion tooth flank,  $\mathcal{P}$ :

$$\mathbf{F}_{\Sigma} = \mathbf{F}_{pa} + \mathbf{F}_{pr} + \mathbf{F}_{dr} \quad (15.66)$$

The component,  $\mathbf{F}_{pa}$ , is specified by Equation 15.63.

In the reference system,  $X_{pa}Y_{pa}Z_{pa}$ , associated with the rotated plane of action,  $PA$ , the profile friction force,  $\mathbf{F}_{pr}$ , is along the axis  $Z_{pa}$ , as illustrated in [Figure 15.9](#). The actual value of this component equals:

$$\mathbf{F}_{pr} = \mu_{pr} \cdot \mathbf{F}_{pa} \quad (15.67)$$

Here,  $\mu_{pr}$  designates the coefficient of friction in profile sliding of the gear,  $\mathcal{G}$ , and the pinion,  $\mathcal{P}$ , tooth flanks.

In that same reference system,  $X_{pa}Y_{pa}Z_{pa}$ , the friction force in the lengthwise direction,  $\mathbf{F}_{dr}$ , is along the axis  $X_{pa}$ . The actual value of this component equals (see [Figure 15.9](#)):

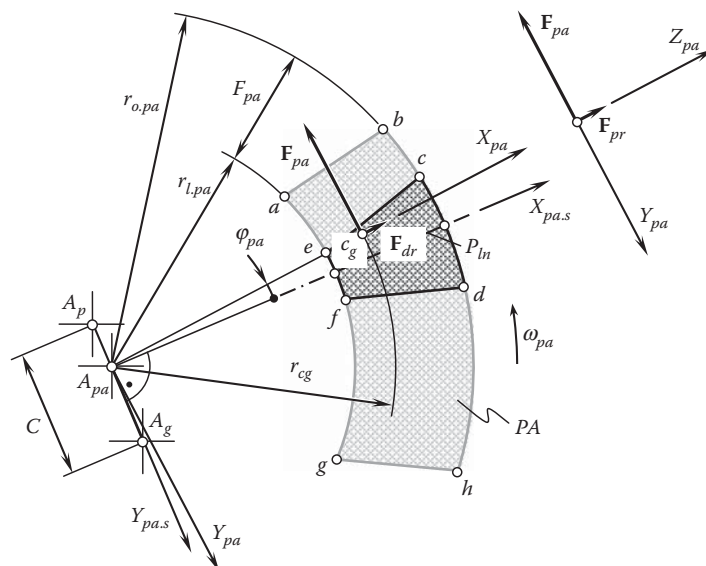
$$\mathbf{F}_{dr} = \mu_{dr} \cdot \mathbf{F}_{pa} \quad (15.68)$$

The coefficient of friction in *drag* sliding of the gear,  $\mathcal{G}$ , and the pinion,  $\mathcal{P}$ , tooth flanks is denoted by  $\mu_{dr}$ .

The coefficients of friction,  $\mu_{pr}$  and  $\mu_{dr}$ , can be of different values, as the normal curvatures of the gear and pinion tooth flanks,  $\mathcal{G}$  and  $\mathcal{P}$ , at point of interest are significantly different in the transverse and lengthwise directions of the tooth flanks  $\mathcal{G}$  and  $\mathcal{P}$ . Moreover, the conditions of profile sliding and sliding in the lengthwise direction of the gear teeth are also different. However, when performing preliminary analysis, the coefficients of friction,  $\mu_{pr}$  and  $\mu_{dr}$ , can be considered equal to one another ( $\mu_{pr} = \mu_{dr}$ ).

Total friction force,  $\mathbf{F}_{fr,\Sigma}$ , in perfect crossed-axes gearing is calculated as:

$$\mathbf{F}_{fr,\Sigma} = \mathbf{F}_{pr} + \mathbf{F}_{dr} \quad (15.69)$$



The friction forces,  $\mathbf{F}_{pr}$  and  $\mathbf{F}_{dr}$ , in a crossed-axes gear pair are negligibly small, and thus are commonly not taken into account when calculating the design parameters of a gear transmission. Moreover, the friction forces,  $\mathbf{F}_{pr}$  and  $\mathbf{F}_{dr}$ , do not affect the uniformity of the output rotation in a gear pair, as both  $\mathbf{F}_{pr}$  and  $\mathbf{F}_{dr}$  are entirely located within a plane that is perpendicular to the plane of action,  $PA$  (and that is tangent to the gear,  $\mathcal{G}$ , and the pinion,  $\mathcal{P}$ , tooth flanks at point of interest,  $m$ ). Only the component of the resultant force of the interaction,  $\mathbf{F}_{\Sigma}$ , that is pointed along the common perpendicular to the tooth flanks,  $\mathcal{G}$  and  $\mathcal{P}$ , causes a rotation of the driven gear in an crossed-axes gear pair.

The forces that act on the gear have to be expressed in a stationary coordinate system,  $X_{g,s}Y_{g,s}Z_{g,s}$ , associated with the motionless gear (that is, associated with the gear pair housing). The operator,  $\mathbf{Rs}_{Ca}(pa \rightarrow g_s)$ , of the resultant coordinate system transformation can be used for this purpose. The operator,  $\mathbf{Rs}_{Ca}(pa \rightarrow g_s)$ , can be represented as a product of the operators,  $\mathbf{Rt}(Y_{g,s}, \Gamma_b)$ ,  $\mathbf{Rt}(Z_{g,s}, 90^\circ)$ ,  $\mathbf{Rt}(Z_{g,s}, \sigma_g)$ ,  $\mathbf{Tr}(Y_{3,s}, r_g)$ , and  $\mathbf{Rt}(Z_{3,s}, \varphi_{pa})$ , of the elementary linear transformations as:

After the resultant tangential force,  $\mathbf{F}_{pa}$  (see Equation 15.63), of the interaction between the tooth flanks,  $\mathcal{G}$  and  $\mathcal{P}$ , of a gear and a mating pinion, has been premultiplied by the operator,  $\mathbf{Rs}_{Ca}(pa \rightarrow g_s)$ , of the linear transformation, the resultant force,  $\mathbf{F}_{g,s}$ , that acts over the gear can be represented in the form of a column matrix:

The components  $F_{x.g.s}$ ,  $F_{y.g.s}$ , and  $F_{z.g.s}$  of the resultant force,  $\mathbf{F}_{g.s}$ , in Equation 15.71 are equal to the separating force,  $F_{g.sep}$ ; the tangential force,  $F_{g.tg}$ ; and the axial thrust,  $F_{g.ax}$ , correspondingly; that is, the equalities  $F_{x.g.s} = F_{g.sep}$ ,  $F_{y.g.s} = F_{g.tg}$ , and  $F_{z.g.s} = F_{g.ax}$  are valid. The forces,  $\mathbf{F}_{g.sep}$ ,  $\mathbf{F}_{g.tg}$ , and  $\mathbf{F}_{g.ax}$ , are entered into the equations for the calculation of the design parameters of a gearbox.

### 15.5.2.2 Forces Acting on the Gear and Pinion in Perfect Crossed-Axes Gearing

In a reference system,  $X_{pa}Y_{pa}Z_{pa}$ , associated with the rotated plane of action,  $PA$ , an orientation of the force,  $\mathbf{F}_{pa}$  (that is specified by Equation 15.63), or of the resultant force,  $\mathbf{F}_\Sigma$  (that is specified by Equation 15.66), does not alter when the gears rotate. However, the configuration of the coordinate system,  $X_{pa}Y_{pa}Z_{pa}$ , in relation to a motionless reference system associated with the gear pair housing alters when the gears rotate. Therefore, in a stationary coordinate system,  $X_{g.s}Y_{g.s}Z_{g.s}$ , associated with the motionless gear, Equation 15.71 has to be rewritten in a form as:

$$\mathbf{F}_{g.s}(\varphi_g) = \begin{bmatrix} F_{g.sep}(\varphi_g) \\ F_{g.tg}(\varphi_g) \\ F_{g.ax}(\varphi_g) \\ 1 \end{bmatrix} \quad (15.72)$$

As follows from the analysis of Equation 15.72, the resultant force,  $\mathbf{F}_{g.s}$ , as well as all three components,  $\mathbf{F}_{g.sep}$ ,  $\mathbf{F}_{g.tg}$ , and  $\mathbf{F}_{g.ax}$ , that act over the gear depend on the angle of rotation of the gear; that is, all of them are functions of the angle,  $\varphi_g$ , of rotation of the gear:

$$\mathbf{F}_{g.s} = \mathbf{F}_{g.s}(\varphi_g) \quad (15.73)$$

$$\mathbf{F}_{g.sep} = \mathbf{F}_{g.sep}(\varphi_g) \quad (15.74)$$

$$\mathbf{F}_{g.tg} = \mathbf{F}_{g.tg}(\varphi_g) \quad (15.75)$$

$$\mathbf{F}_{g.ax} = \mathbf{F}_{g.ax}(\varphi_g) \quad (15.76)$$

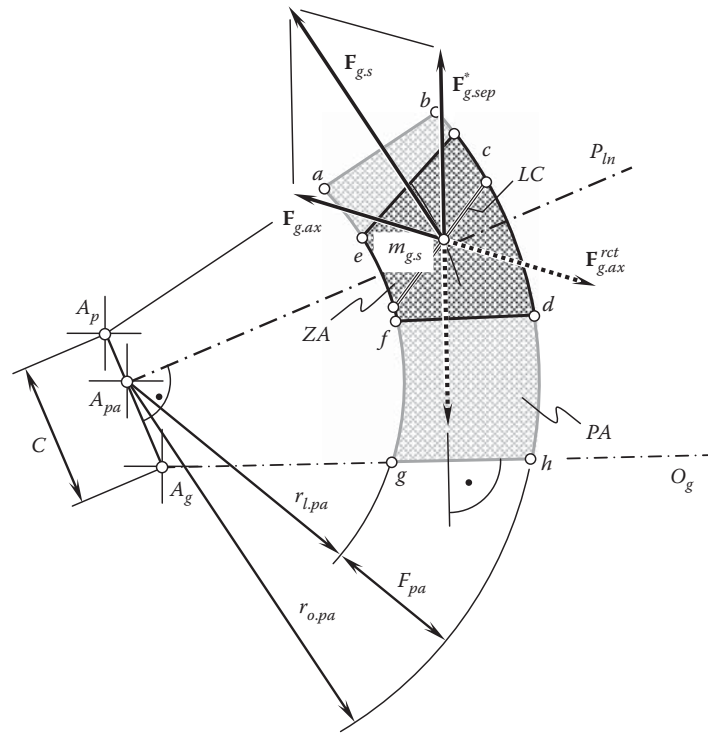
The resultant force,  $\mathbf{F}_{g.s}(\varphi_g)$ , and the components,  $\mathbf{F}_{g.sep}(\varphi_g)$ ,  $\mathbf{F}_{g.tg}(\varphi_g)$ , and  $\mathbf{F}_{g.ax}(\varphi_g)$ , that depend on the angular parameter,  $\varphi_g$ , are an additional source of vibration generation and noise excitation in crossed-axes gearing. When the gears rotate, the point of intersection of the axis of instant rotation,  $P_{ln}$ , and the instant line of action,  $LA_{inst}$ , must not migrate along the axis of instant rotation,  $P_{ln}$ , or, at least, the distance covered in this migration has to be minimized.

The variation of the forces has to be minimized in order to minimize vibration generation and noise excitation when a crossed-axes gear pair operates.

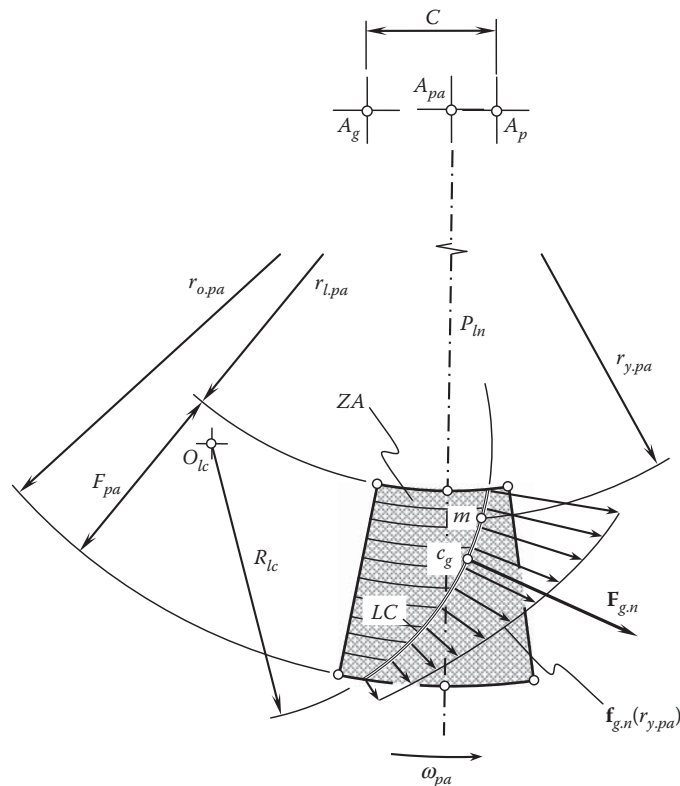
The variation of the direction of the resultant force,  $\mathbf{F}_{g.s}(\varphi_g)$ , of the interaction of the tooth flanks,  $\mathcal{G}$  and  $\mathcal{P}$ , of a gear and a mating pinion is illustrated in Figure 15.10. For an arbitrary configuration of the line of contact,  $LC$ , between the tooth flanks,  $\mathcal{G}$  and  $\mathcal{P}$ , coordinates of point  $c_g$  at which the resultant force,  $\mathbf{F}_{g.s}$ , is applied can be determined. The component  $\mathbf{F}_{g.ax}$  is parallel to the axis of rotation,  $O_g$ , of the gear. The component  $\mathbf{F}_{g.sep}$  is perpendicular to the axis of rotation,  $O_g$ , of the gear. The magnitude,  $F_{g.sep}^*$ , of the force vector,  $\mathbf{F}_{g.sep}^*$ , shown in Figure 15.11 equals  $F_{g.sep}^* = F_{g.sep} / \sin \phi_{t.o}$ , where  $\phi_{t.o}$  is the transverse pressure angle in the crossed-axes gear pair. (The separating force vector,  $\mathbf{F}_{g.sep}$ , is entirely located in the normal  $N_{ln}$ -plane. In the case under consideration, the  $N_{ln}$ -plane is the plane through the axes of rotation,  $O_g$  and  $O_p$ , of the gear and mating pinion, correspondingly.) As follows from the analysis of the schematic depicted in Figure 15.11, for any configuration of the line of contact,  $LC$ , for which the point,  $c_g$ , is located within the zone of action,  $ZA$ , the forces,  $\mathbf{F}_{g.ax}$  and  $\mathbf{F}_{g.sep}$ , never equal zero. Thus, the reaction forces,  $\mathbf{F}_{g.ax}^{rct}$  and  $\mathbf{F}_{g.sep}^{rct}$ , also have nonzero values. As the forces,  $\mathbf{F}_{g.ax}^{rct}$  and  $\mathbf{F}_{g.sep}^{rct}$ , fluctuate when the gears rotate (see Equation 15.74 and 15.76), excessive vibration generation and noise excitation can be observed when a crossed-axes gear pair operates. The variation of the forces,  $\mathbf{F}_{g.ax}^{rct}$  and  $\mathbf{F}_{g.sep}^{rct}$ , does not depend on the geometry of the line of contact,  $LC$ . This discussion is also valid in cases when multiple lines of contact, as well as multiple portions of the lines of contact, are observed in a gear pair of a particular design, as the fluctuation of the forces,  $\mathbf{F}_{g.ax}^{rct}$  and  $\mathbf{F}_{g.sep}^{rct}$ , is inevitable in perfect crossed-axes gear pairs.

An analysis similar to that above can be performed with respect to loading of the pinion in a perfect crossed-axes gear pair.

As follows from the analysis of Equation 15.72, the resultant force,  $\mathbf{F}_{p.s}$ , as well as all three components,  $\mathbf{F}_{p.sep}$ ,  $\mathbf{F}_{p.tg}$ , and  $\mathbf{F}_{p.ax}$ , that act over the pinion depend on the angle of rotation of the pinion; that is, all of them

**FIGURE 15.10**

The axial thrust,  $F_{g.ax}(\varphi_g)$ , and the separating force,  $F_{g.sep}(\varphi_g)$ , as components of the resultant force,  $F_{g.s}(\varphi_g)$ , of the interaction of the tooth flanks,  $\mathcal{G}$  and  $\mathcal{P}$ , of a gear and mating pinion in a perfect intersected-axes gear pair.

**FIGURE 15.11**

Normal force,  $F_{g.n}$ , and normal force per unit length,  $f_{g.n}$ , acting in a perfect crossed-axes gear pair.

are functions of the angle,  $\varphi_p$ , of rotation of the pinion:

$$\mathbf{F}_{p.s} = \mathbf{F}_{p.s}(\varphi_p) \quad (15.77)$$

$$\mathbf{F}_{p.sep} = \mathbf{F}_{p.sep}(\varphi_p) \quad (15.78)$$

$$\mathbf{F}_{p.tg} = \mathbf{F}_{p.tg}(\varphi_p) \quad (15.79)$$

$$\mathbf{F}_{p.ax} = \mathbf{F}_{p.ax}(\varphi_p) \quad (15.80)$$

The resultant force,  $\mathbf{F}_{p.s}(\varphi_p)$ , and the components,  $\mathbf{F}_{p.sep}(\varphi_p)$ ,  $\mathbf{F}_{p.tg}(\varphi_p)$ , and  $\mathbf{F}_{p.ax}(\varphi_p)$ , that depend on the angular parameter,  $\varphi_p$ , are an additional source of vibration generation and noise excitation in crossed-axes gearing. When the gears rotate, the point of intersection of the axis of instant rotation,  $P_{ln}$ , and the instant line of action,  $LA_{inst}$ , must not migrate along the axis of instant rotation,  $P_{ln}$ , or, at least, the distance covered in this migration has to be minimized.

For any configuration of the line of contact,  $LC$ , for which the point  $c_g$  is located within the zone of action,  $ZA$ , the forces,  $\mathbf{F}_{p.ax}$  and  $\mathbf{F}_{p.sep}$ , never equal zero. Thus, the reaction forces,  $\mathbf{F}_{p.ax}^{rct}$  and  $\mathbf{F}_{p.sep}^{rct}$ , also have nonzero values. As the forces,  $\mathbf{F}_{p.ax}^{rct}$  and  $\mathbf{F}_{p.sep}^{rct}$ , fluctuate when the gears rotate, excessive vibration generation and noise excitation can be observed when a crossed-axes gear pair operates. The variation of the forces,  $\mathbf{F}_{p.ax}^{rct}$  and  $\mathbf{F}_{p.sep}^{rct}$ , does not depend on the geometry of the line of contact,  $LC$ . This discussion is also valid in cases when multiple lines of contact, as well as multiple portions of the lines of contact, are observed in a gear pair of a particular design, as the fluctuation of the forces,  $\mathbf{F}_{p.ax}^{rct}$  and  $\mathbf{F}_{p.sep}^{rct}$ , is inevitable in perfect crossed-axes gear pairs.

### 15.5.2.3 Normal Force Acting on the Gear in Perfect Crossed-Axes Gearing

For the calculations of gear teeth for contact strength, as well as for contact strength, a component,  $\mathbf{F}_{g.n}$ , of the resultant force,  $\mathbf{F}_{g.s}$ , is entered into the corresponding equations for the calculations. This component is commonly referred to as the *normal force*,  $\mathbf{F}_{g.n}$ . The vector of normal load,  $\mathbf{F}_{g.n}$ , is located within the plane of action,  $PA$ , and is perpendicular to the line of contact,  $LC$ , at point  $c_g$ , at which the normal load is applied. The magnitude,  $F_{g.n}$ , of the normal force,  $\mathbf{F}_{g.n}$ , can be calculated as:

$$F_{g.n} = F_{g.s} \cos \psi_g \quad (15.81)$$

where  $\psi_g$  is the spiral angle of the gear teeth at point  $c_g$ .

The normal force per unit length,  $\mathbf{f}_{g.n}$ , is also entirely located within the plane of action,  $PA$ . The normal force per unit length,  $\mathbf{f}_{g.n}$ , depends on the geometry of a particular line of contact. At every point of the line of contact,  $LC$ , the applied normal load per unit length,  $\mathbf{f}_{g.n}$ , is perpendicular to the line of contact at that point.

In straight bevel gearings, the normal force per unit length,  $\mathbf{f}_{g.n}$ , is distributed quite similarly to that shown in Figure 15.8 for the force per unit length,  $\mathbf{f}_{pa}(r_{y.pa})$ . In skew crossed-axes gearings, the normal force per unit length,  $\mathbf{f}_{g.n}$ , is distributed similarly to that in straight bevel gearings—all the elementary forces are perpendicular to the line of contact,  $LC$ . The distribution of the normal force per unit length,  $\mathbf{f}_{g.n}$ , in spiral bevel gearings with a circular-arc line of contact,  $LC$ , of a radius,  $R_{lc}$ , is illustrated in Figure 15.11. In this case, all the elementary forces are along the radius,  $R_{lc}$ , to the corresponding point,  $m$ , within the line of contact,  $LC$ .

In a more general case of perfect crossed-axes gearings, in face-hobbed bevel gears in particular, the following approach can be used to determine the distribution of the normal force per unit length along the line of contact,  $LC$ . First, the unit normal vector,  $\mathbf{n}_{lc}$ , is constructed at every point of the line of contact,  $LC$ . Second, the distribution of the normal load per unit length,  $\mathbf{f}_{g.n}$ , is constructed as a product of the unit vector,  $\mathbf{n}_{lc}$ , by the function of the distribution of the magnitude,  $f_{g.n}$ , of the normal load per unit length; that is,  $\mathbf{f}_{g.n} = f_{g.n} \cdot \mathbf{n}_{lc}$ .



When two or more lines of contact (or portions of the lines of contact),  $LC_i$ , are observed, then the position vector,  $\mathbf{r}_{cg.\Sigma}$ , of the point,  $c_{g.\Sigma}$ , at which the resultant load,  $\mathbf{F}_{g.n.\Sigma}$ , is applied can be calculated as:

$$\mathbf{r}_{cg.\Sigma} = \frac{\sum_i l_{lc.i} \cdot \mathbf{r}_{cg.i}}{\sum_i l_{lc.i}} \quad (15.82)$$

where:

$i$  is the number of a line of contact (or a portion of a line of contact),  $LC_i$ .

$l_{lc.i}$  is the length of a line of contact (or a portion of a line of contact),  $LC_i$ .

$\mathbf{r}_{cg.i}$  is the position vector of a point,  $c_{g.i}$ , of a line of contact (or a portion of a line of contact),  $LC_i$ .

$\sum_i l_{lc.i}$  is the total length,  $TLLC$ , of all the lines of contact,  $l_{lc.i}$ .

The variation of the direction of the resultant force of the interaction of the tooth flanks,  $\mathcal{G}$  and  $\mathcal{P}$ , can be minimized by means of a proper geometry of the desired line of contact,  $LC_{des}$ . When the gears rotate, the point of intersection of the axis of instant rotation,  $P_{ln}$ , and the line along the resultant force of interaction of the tooth flanks,  $\mathcal{G}$  and  $\mathcal{P}$ , must not migrate along the  $P_{ln}$ , or, at least, the distance of this migration has to be minimized. In this way, vibration generation and noise excitation can be minimized.

The performed analysis of the forces that act in external crossed-axes gearings can also be extended to internal crossed-axes gearing, as well as to *pinion-gear-to-rack mesh*, as the latter is a reduced case of external crossed-axes gearing.

The disclosed approach for the calculation of the elements of dynamics in perfect crossed-axes gearing is also applicable for calculating the elements of dynamics in conformal and high-conformal gearing. The main feature here is that the angular face width in a gear pair is zero.



# Taylor & Francis

Taylor & Francis Group

<http://taylorandfrancis.com>

# 16

## *Peculiarities of Perfect Worm Gearing*

Worm gearing is a type of crossed-axes gearing that features a low tooth count of the pinion and a high gear ratio. In conventional worm-gear pairs (Figure 16.1), the tooth count of the pinion (which is called the *worm*) is in the range of one to three. Worm-gear pairs with a larger number of starts,\* that is, with four starts and more, are also used in the current industry (Figure 16.2). When the number of starts of a worm is two or more, the worm is referred to as a *multiple-start worm*.

Commonly, the crossed-axes angle,  $\Sigma$ , in worm gearing is equal to a right angle (see Figure 16.1); however, this is not a must. Worm gearings with either an acute,  $\Sigma < 90^\circ$ , or obtuse,  $\Sigma > 90^\circ$ , crossed-axes angle are possible as well.

Most worm gearings are external. Gear pairs that feature mesh of a worm with a crown gear are used in the industry. Worm-gear pairs of this type are an equivalent of the *rack-gear-to-pinion* gear pair in parallel-axes gearing. An example of a worm gear pair with a crown worm gear and a conical worm is illustrated in Figure 16.3. Internal worm gearing (Figure 16.4) has not been deeply investigated yet.

Worm gearings of all known types feature point contact between the worm threads and the worm-gear tooth flanks. Only perfect worm-gear pairs feature line contact between the worm threads,  $\mathcal{P}$ , and the worm-gear tooth flanks,  $\mathcal{G}$ . Peculiarities of perfect worm gearing with line contact between the worm threads and the worm-gear tooth flanks are briefly outlined below.

### 16.1 Peculiarities of Worm Gearing with Line Contact between Worm Threads and Worm-Gear Tooth Flanks

A higher bearing capacity and a higher power density are the two main advantages of perfect worm gearing over worm gearings of other known designs that feature point contact between the worm threads and the worm-gear tooth flanks. These two features, along with a few others, are due to the worm threads,  $\mathcal{P}$ , and the worm-gear tooth flanks,  $\mathcal{G}$ , making line contact with one another, and thus having an increased area of contact between the interacting surfaces of the worm and the worm gear.

#### 16.1.1 Kinematics of Perfect Worm Gearing

Perfect worm gearing is a particular kind of crossed-axes gearing. Therefore, the kinematics of perfect worm gearing is quite similar to that in the earlier-discussed perfect crossed-axes gearing. The difference is chiefly due to a higher gear ratio in worm gearing compared to that in crossed-axes gearings of other designs. Once the rotation vectors of a worm gear,  $\omega_g$ , and a mating worm,  $\omega_p$ , are specified, the rest of the elements of the corresponding vector diagram, that is, the pitch-line plane ( $P_{ln}$ -plane), the centerline plane ( $C_{ln}$ -plane), the normal plane ( $N_{ln}$ -plane), the plane of action,  $PA$ , the base cones, and so forth, can be constructed identically to how they are constructed for a crossed-axes gear pair of conventional design.

#### 16.1.2 Base Cones in Perfect Worm Gearing

The base cones in a perfect worm gear pair can be viewed as enveloping surfaces to consecutive positions of the plane of action,  $PA$ , when the plane of action is rotated either about the worm-gear axis of rotation,  $O_g$ , or about the worm axis of rotation,  $O_p$ . The base cones are tangent to the plane of action from the opposite sides of the  $PA$ .

\* In worm gearing, the *starts* are often loosely called *threads*. The number of starts in worm gearing is equivalent to the number of *teeth* in gearings of other types.



**FIGURE 16.1**  
Worm gear pair with a single-start worm.

The configuration of the rotation vectors,  $\omega_s$ ,  $\omega_p$ , and  $\omega_{pl}$ , of the base cones is illustrated in [Figure 16.5](#). More detailed information on the configuration of the plane of action,  $PA$ , and base cones in a perfect worm gear pair is shown in [Figure 16.6](#). The plane of action,  $PA$ , is shaped in the form of a portion of the plane bounded by a circle centered at the plane-of-action apex,  $A_{pa}$ . The radius of the outer circle is designated as  $r_{o.pa}$ . The inner radius,  $r_{i.pa}$ , of the plane of action is zero ( $r_{i.pa} = 0$ ). Therefore, the effective width,  $F_{pa}$ , of the plane of action,  $PA$ , equals the outer radius of the plane of action; that is, the equality,  $F_{pa} = r_{o.pa}$ , is valid.

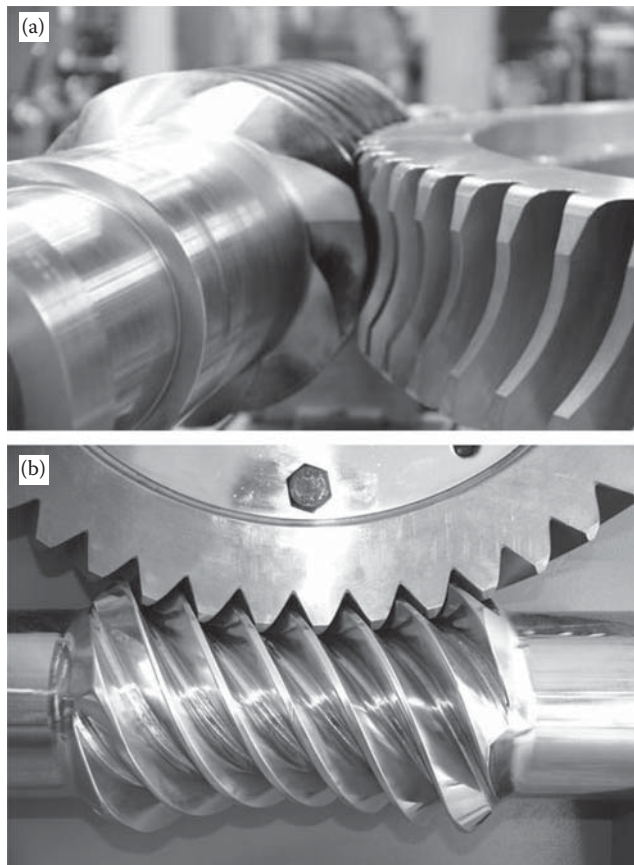


**FIGURE 16.2**  
Worm gear pairs with a multiple-start worms: (a) with a cylindrical multiple-start worm, (b) with a double-enveloping multiple-start worm.

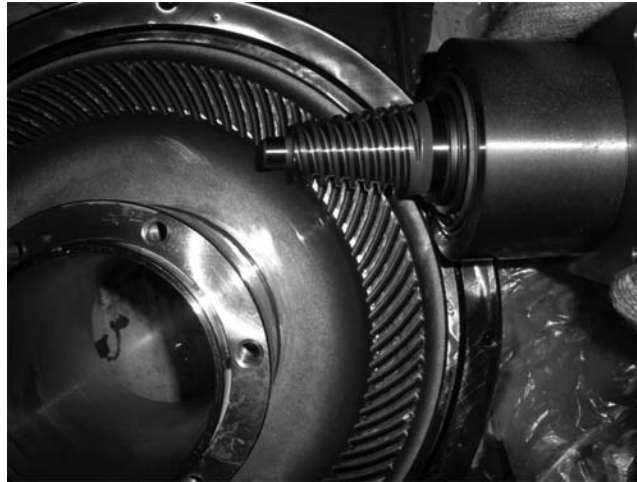


**FIGURE 16.3**  
Worm gear pair with a crown worm gear and a conical worm.

Worm gearing with line contact between the worm threads,  $\mathcal{P}$ , and the worm-gear tooth flanks,  $\mathcal{J}$ , features two base cones for the worm and two base cones for the worm-gear.

The worm-gear is split into two portions by a plane through the centerline,  $\mathcal{C}$ , perpendicular to the worm-gear axis of rotation,  $O_g$ . The tooth flanks,  $\mathcal{J}$ , of one of the two portions of the worm-gear are generated from one of the base cones. The tooth flanks,  $\mathcal{J}$ , of the other portion of the worm-gear are generated from the other base cone.

The same is true with respect to the worm. The worm is split into two portions by a plane through the centerline,  $\mathcal{C}$ , perpendicular to the worm axis of rotation,  $O_p$ . The worm threads,  $\mathcal{P}$ , of one of the two portions of the worm are generated from one of the base cones. The worm threads,  $\mathcal{P}$ , of the other portion of the worm are generated from the other base cone.

In order to generate the tooth flanks,  $\mathcal{J}$ , of the worm-gear, as well as the threads,  $\mathcal{P}$ , of the mating worm, the desired line of contact,  $LC_{des}$ , has to pass through the plane-of-action apex,  $A_{par}$  of the worm gear pair.

As the kinematics in perfect worm gearing, the plane of action, and the base cones are similar to those in crossed-axes gearing, ultimately, all the equations derived above for perfect crossed-axes gearing are valid with respect to perfect worm gearing.

Perfect worm gear pairs of all designs, those illustrated in [Figure 16.7](#), as well as others not shown in [Figure 16.7](#), can be designed using the approach adopted for the design of *R*-gearing.



**FIGURE 16.4**  
Internal worm gear pairs.

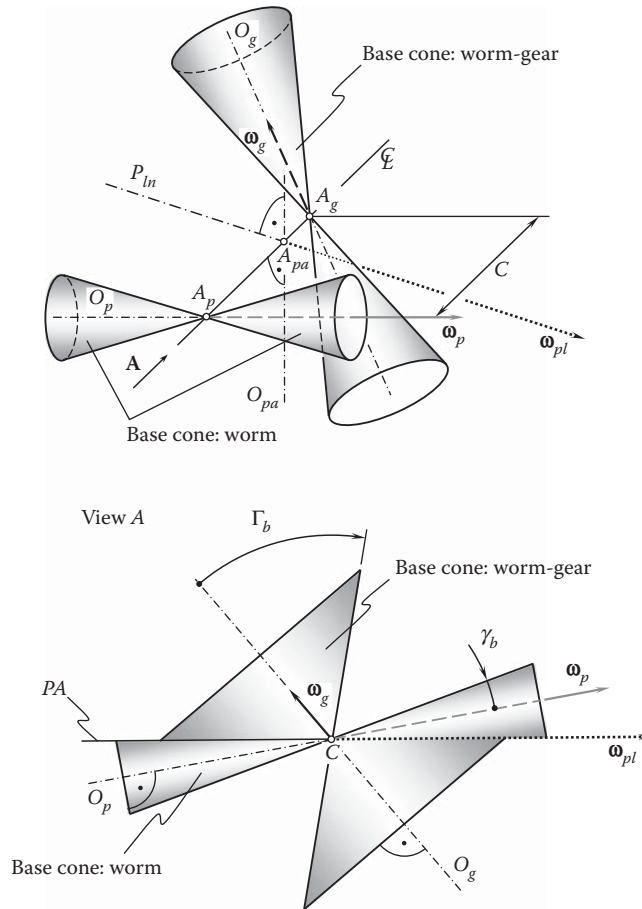


FIGURE 16.5

Configuration of the rotation vectors,  $\omega_g$ ,  $\omega_p$ , and  $\omega_{pl}$ , and base cones in a perfect worm gear pair.

### 16.1.3 Peculiarities of Sliding in the Plane-of-Action Apex in Perfect Worm Gearing

Sliding between the tooth flanks,  $\mathcal{G}$ , of the worm-gear and the threads,  $\mathcal{P}$ , of the mating worm in perfect worm gearing follows the rules established above with respect to crossed-axes gearing in a more general sense (see Chapter 15). The main feature of worm gearing from this perspective is the sliding in the vicinity of the plane-of-action apex,  $A_{pa}$ .

As the inner radius of the plane of action in the plane-of-action apex,  $A_{pa}$ , has a zero value ( $r_{l,pa} = 0$ ), no rolling ( $\omega_g^{rl} = 0$ ,  $\omega_p^{rl} = 0$ ) and only axial sliding ( $\omega_g^{sl} \neq 0$ ,  $\omega_p^{sl} \neq 0$ ) is observed in the vicinity of the plane-of-action apex,  $A_{pa}$ , in worm gearing (see Figure 2.9 in Chapter 2). Therefore, unfavorable conditions of interaction between the tooth flanks,  $\mathcal{G}$ , of a worm-gear and the threads,  $\mathcal{P}$ , of a mating worm are observed in the vicinity of the plane-of-action apex,  $A_{pa}$ , in perfect worm gearing.

Not much research has been undertaken so far to investigate the sliding conditions in the vicinity of the plane-of-action apex,  $A_{pa}$ , in worm gearing. The paper by Korstel'ov [55] is one of a few of them.

No rolling motion can be added to the contact area in the vicinity of the apex,  $A_{pa}$ , where the velocity of the rolling motion is either zero or of a negligibly small value. Therefore, the area that features unfavorable conditions of interaction between the tooth flanks,  $\mathcal{G}$ , of the worm-gear and the threads,  $\mathcal{P}$ , of the mating worm in perfect worm gearing has to be eliminated from contact.

The parameters of the favorable and unfavorable areas in the interior of which the conditions of interaction between the tooth flanks,  $\mathcal{G}$ , of the worm-gear and the threads,  $\mathcal{P}$ , of the mating worm can be specified in terms of the ratio  $\omega_p^{sl}/\omega_p^{rl}$ . Within the plane of action,  $PA$ , the smallest possible area around the plane-of action apex,  $A_{pa}$ , in the interior of which conditions of interaction are unfavorable can be determined. The corresponding areas on the tooth flanks,  $\mathcal{G}$ , of the worm-gear can be relieved to eliminate them from interaction with the threads,  $\mathcal{P}$ , of the mating worm.

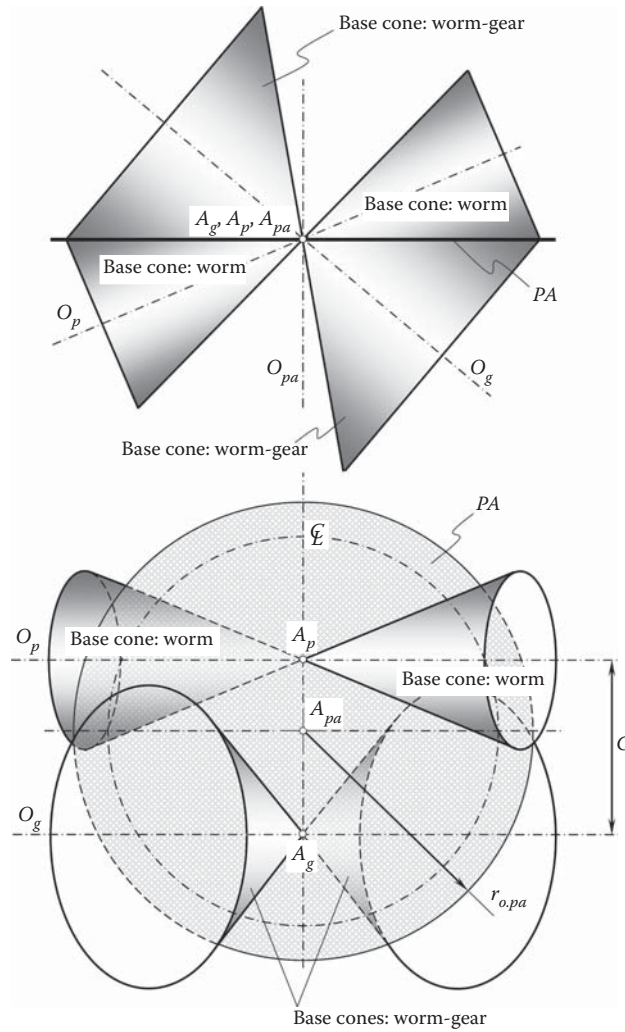


**FIGURE 16.6**  
Configuration of the plane of action,  $PA$ , and base cones in a perfect worm gear pair.

## 16.2 Criterion to Distinguish Worm from Gear

The number of starts in a worm and the number of teeth in a gear are equivalent to one another. Because of that, both are denoted by  $N_p$ .

Depending on a particular application, the number of starts in a worm is within the interval  $N_p = 1 \div 5$ . Sometimes the number of starts can exceed this number ( $N_p > 5$ ).

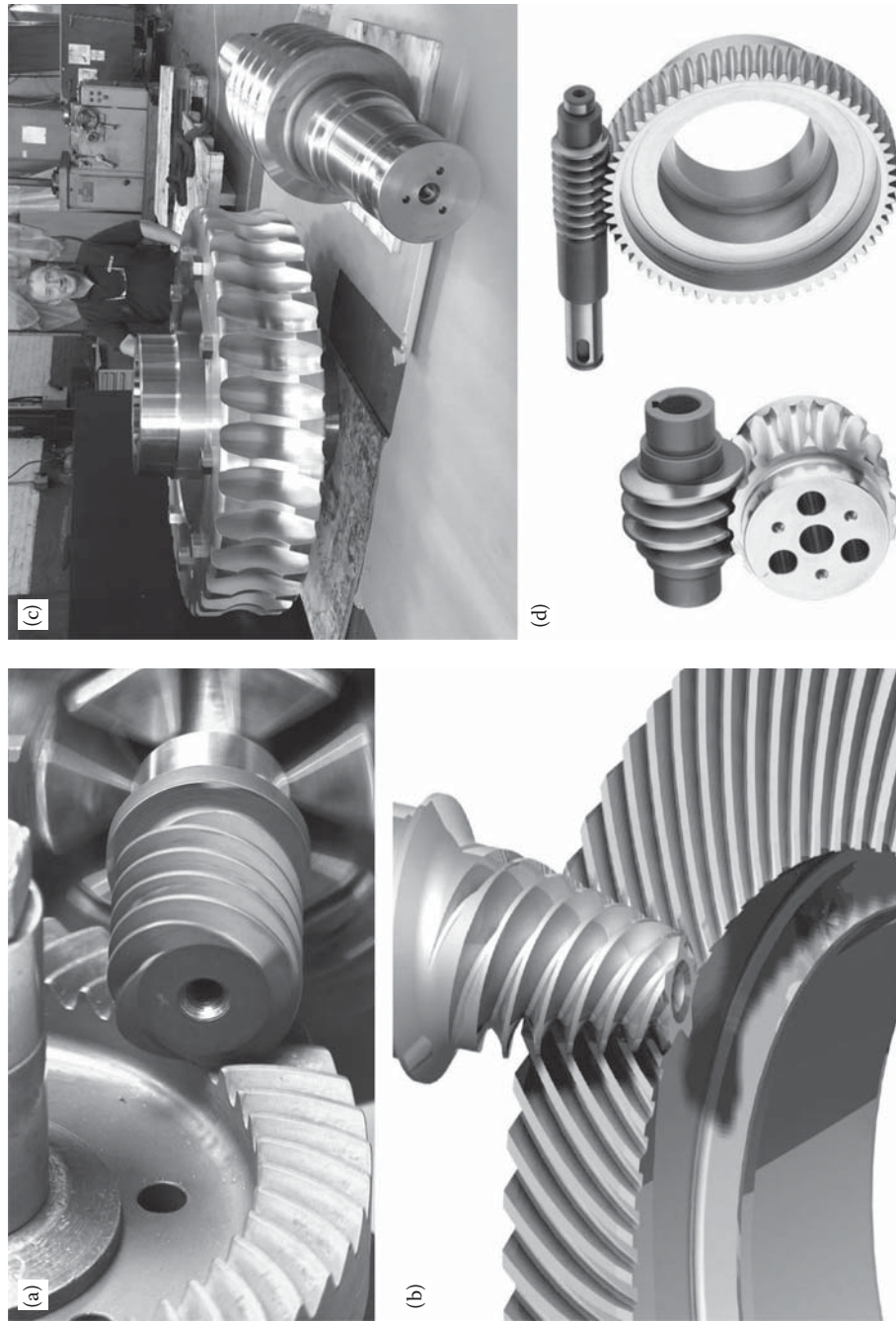
Similarly, depending on a particular application, the number of teeth in a low-tooth-count gear can be as small as  $N_p = 3$ . Sometimes the number of teeth can be even smaller ( $N_p < 3$ ).

With that said, it is important to establish a quantitative criterion to distinguish a worm from a low-tooth-count gear. Use of a plane of action,  $PA$ , zone of action,  $ZA$ , and tooth contact ratio,  $m_t$ , can be helpful when solving this particular problem.

It is proposed here to distinguish a worm from a low-tooth-count gear in the following way. A thread of each worm start features at least two points of contact with the worm-gear teeth; that is, within the zone of action,  $ZA$ , at every start of a multiple-start worm, the worm thread,  $\mathcal{P}$ , contacts the worm-gear teeth,  $\mathcal{G}$ , at two or more points. This immediately returns a simple expression:

$$\text{Worm: } \frac{m_t}{N_p} \geq 1 \quad (16.1)$$



**FIGURE 16.7**

Various kinds of worm gear pairs: (a) face worm gear with a cylindrical worm, (b) face worm gear with a double-enveloping and a cylindrical worm of equal capacity: with a double-enveloping and a cylindrical worm.

to distinguish a worm from a low-tooth-count gear. Consequently, for low-tooth-count gears, the expression:

$$\text{Low-tooth-count gear: } \frac{m_t}{N_p} < 1 \quad (16.2)$$

is valid.

For worm gearing with transverse pressure angle,  $\phi_{t.w} = 20^\circ$ , Equation 16.1 indicates that worms can feature either one start or two starts only ( $N_p = 1, 2$ ).

If it seems that a worm may feature, for example, up to five starts, then the expression (see Equation 16.1) can be modified and represented in the form:

$$\text{Worm: } \frac{m_t + 3.5}{N_p} \geq 1 \quad (16.3)$$

Modifications to Equation 16.1 of other types can also be discussed.

### 16.3 An Analysis of a Worm Gear-Drive (Pat. No. 257,246, USSR, 1968)

Below, some of the capabilities of the developed approach to designing perfect *R*-gearing and perfect worm gearing in particular are demonstrated. A worm gear drive according to USSR Pat. No. 257,246 [85] is used for this purpose as an illustrative example. The invention [85] is chosen because it is convenient to demonstrate the capabilities of the developed approach. It is also instructive to know how poor understanding of the theory of gearing can result in a plurality of engineering mistakes (see [85], as well as many other patents of this sort, especially committed by the followers of Korostel'ov).

The complex geometry of double-enveloping worm-gear drives, specific conditions of lubrication, and formation of the worm-gear tooth surface inspired many researchers to develop analytical aspects of the meshing of the worm and the worm-gear tooth surface. Novel designs of worm gearing were also proposed. At least one of them deserves to be discussed in detail.

As early as in 1968, Korostel'ov of the Soviet Union invented a worm-gear drive that features (as claimed) unique conditions of lubrication of the interacting tooth flanks of the worm gear and the worm threads [85]. According to the invention (Figure 16.8): "Tooth flanks of the worm-gear and threads of the worm make line contact with one another at every instant of time. In axial section of the worm thread surface, profile of the worm threads is composed of two segments. One of the segments is either a straight line segment or a segment of a smooth curve with a large radius of curvature. This portion of the thread profile is tangential to another segment, which is shaped either in the form of a circular arc, or in the form of a smooth curve with small deviations from the circular arc. This second portion of the thread profile corresponds to the addendum. Face width of the worm-gear exceeds width of the zone of action. No undercut is allowed to the worm-gear tooth profile. Pitch point in the worm-gear drive is shifted toward the worm axis of rotation and is located outside the outer diameter of the worm-gear.

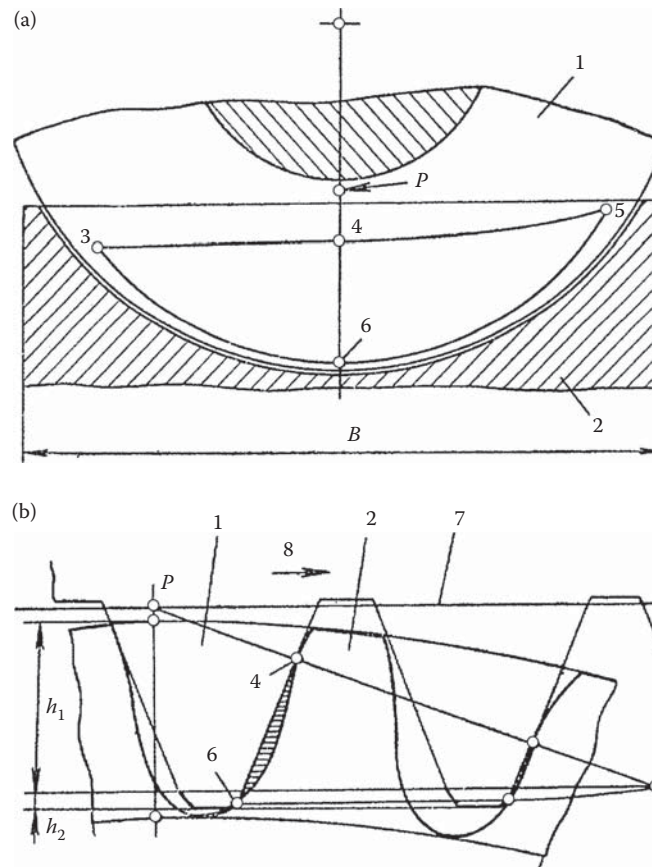
In this case, the line of contact between worm-gear tooth flanks and worm threads is shaped in the form of a closed contour. The lubricant is trapped in the area within the line of contact bounded by worm-gear tooth flanks and worm threads. The lubricant becomes the third body by means of which the torque is transmitted from the worm shaft to the worm-gear shaft.

Contact stresses are reduced due to the even distribution of the contact load within the interior of the line of contact.

A worm-gear drive features increased efficiency, as the interacting surfaces of the worm gear and the worm interact through a lubricant, which is squeezed out of the contact area as the worm rotates; as a result, the trapped volume of the lubricant becomes smaller.

The proposed design of a worm-gear drive is illustrated in Figure 16.8. In Figure 16.8a, a section of the worm-gear drive by a plane perpendicular to the worm axis of rotation is schematically depicted. Similarly, a section of the worm-gear drive by a plane perpendicular to the worm-gear axis of rotation is depicted in Figure 16.8b.

The worm-gear drive is composed of a worm (1 in Figure 16.8) and the worm-gear (2 in the figure).

**FIGURE 16.8**

A worm-gear drive proposed by Korostel'ov as early as 1968 [85]: (a) a worm engaged in mesh with a worm-gear, and (b) a volume with a lubricant locked between the worm threads and the tooth flanks of the worm-gear.

The line 3-4-5-6-3 represents a projection onto the plane of Figure 16.8a of the closed line of contact. The axial profile of the worm is composed of two portions. The first portion has a height,  $h_1$ , shaped in the form of a straight line segment (or a smooth curve that has a large radius of curvature). The second portion has a height,  $h_2$ , shaped in the form of a circular arc (or a smooth curve that has a reasonably small deviation from the circular arc profile). The two portions of the worm thread profile are in tangency with each other.

The tooth profile of the worm-gear (2 in Figure 16.8) is conjugate to the thread profile of the worm (1 in the figure). Such profiles of the worm and the worm-gear make it possible to trap the lubricant in the hatched volume.

The pitch point,  $P$ , in the worm-gear drive is shifted toward the worm axis of rotation and is located outside the outer diameter of the worm-gear in order to reduce the volume of lubricant. In this case, the zone of engagement is located outside the pitch cylinder of the worm. The pitch line (denoted 7 in Figure 16.8) is a straight line through the pitch point,  $P$ .

When the worm is rotating, thread profiles are traveling in the direction of the arrow denoted by 8 in Figure 16.8. The volume of the trapped lubricant becomes smaller. The lubricant under such conditions is squeezed out of the line of contact."

A worm gearing according to Korostel'ov's invention [85] is not workable at all. This is because neither the tooth flanks of a worm-gear nor the threads of a mating worm can be generated by a closed line of contact that is located within the plane of action. Moreover, it is not feasible to keep the volume with lubricant isolated from the environment. Violation of the three fundamental laws of gearing is the root cause for this mistake. Unfortunately, the worm-gear drive shown in Figure 16.8 [85] is an example of an engineering mistake. Lack of knowledge in the theory of gearing caused this mistake, as well as many other mistakes of a similar nature, committed by the followers of Korostel'ov.

## Part III

# Perfect Gearing with Point Contact between Tooth Flanks of a Gear and a Mating Pinion

The vector diagrams of gear pairs considered so far and the corresponding kinds of gear pairs do not cover all possible types of gearing. This does not mean that the classification of possible types of vector diagrams, shown in [Figure 2.15](#), is inconsistent. No, the classification is still consistent. All possible types of vector diagrams for gearing that feature *line contact* between the interacting tooth flanks are covered by the classification. However, there is another large group of gear pairs that feature *point contact* between the interacting tooth flanks. Point contact between the tooth flanks of a gear and a mating pinion is achieved due to implementation of the additional auxiliary generating surface to generate the tooth flanks of a gear and mating pinion. For this purpose, in addition to the rotation vectors that make up a corresponding vector diagram, gearing with point contacts between the tooth flanks also features vector(s) of an additional relative motion of the gear and the pinion. It should be stressed here that even with an additional motion, gearing of the type under consideration remains *perfect gearing*. Due to the features of contact, gearings of this particular type are referred to as *gearings with point contact between the tooth flanks of a gear and a mating pinion*.

Part III of the book consists of [Chapter 17](#). Room for a few more chapters is left, as this part of the book has the potential for growth in the future.



# Taylor & Francis

Taylor & Francis Group

<http://taylorandfrancis.com>

## *Kinematics, Geometry, and Design Features of Perfect Gearing with Point Contact between Tooth Flanks of a Gear and a Mating Pinion*

Potentially, the total number of possible types of gearings with point contact between the tooth flanks of a gear and a mating pinion is large. In order to consider all the possible types of gearings of this type, one may wish to employ the classification of possible types of vector diagrams of gearing (see [Figure 2.15](#)). Using this classification, it is possible to investigate what kind of additional motion, if any, could be added to each of the vector diagrams in order to come up with the concept of a corresponding gearing with point contact between tooth flanks of a gear and a mating pinion. This particular problem is out the scope of the monograph. The goal is to illustrate a possibility of designing gearings of the type under consideration that are already used in the industry, as well as those that potentially may be useful in practice.

### **17.1 Examples of Gearings with Point Contact between Tooth Flanks of a Gear and a Mating Pinion**

It is clear, even without a comprehensive investigation of the vector diagrams, that the total number of possible vector diagrams of gearings with point contact between tooth flanks of a gear and a mating pinion, as well as the total number of possible gearings of the type under consideration, is large enough. Not all of them are used in practice; however, a few of them have relatively broad practical applications.

Skew-axes gearing that is composed of two helical involute gears is a perfect example of gearing with point contact between tooth flanks of a gear and a mating pinion that is used in practice. An example of skew-axes gearing is illustrated in [Figure 17.1](#).

In gearing of this design, the axis of rotation of the gear and the axis of rotation of the mating pinion are crossed at a certain crossed-axes angle. The crossed-axes angle can be either acute, obtuse, or equal to a right angle. In the particular example under consideration, the axes of rotation of the gear and pinion are crossed at a right angle. The axes of rotation of the gear and mating pinion are separated from one another at a certain center distance. Commonly, the pinion is the driving member of the gear pair, while the gear is the driven member of the gear pair.

The vector diagram of the gearing shown in [Figure 17.1](#) is illustrated in [Figure 17.2](#). As in the case of gearing with line contact between tooth flanks,  $\mathcal{G}$  and  $\mathcal{P}$ , of a gear and a mating pinion, the vector diagram is composed of the rotation vector of the gear,  $\omega_g$ ; the rotation vector of the pinion,  $\omega_p$ ; and the vector of instant rotation,  $\omega_{pl}$ , of the pinion in relation to the gear. The rotation vectors,  $\omega_g$  and  $\omega_p$ , are at a certain center distance,  $C$ . The crossed-axes angle,  $\Sigma$ , is equal to  $90^\circ$  (that is,  $\Sigma = 90^\circ$ ).

In addition to the vectors just mentioned, gearing with point contact between tooth flanks of a gear and a mating pinion also features either a linear motion,  $\mathbf{V}_g$ , along the gear axis of rotation,  $O_g$ ; a linear motion,  $\mathbf{V}_p$ , along the pinion axis of rotation,  $O_p$ ; or both  $\mathbf{V}_g$  and  $\mathbf{V}_p$  simultaneously. The vectors of translation,  $\mathbf{V}_g$  and  $\mathbf{V}_p$ , are independent vectors. Both linear velocity vectors,  $\mathbf{V}_g$  and  $\mathbf{V}_p$ , can be pointed out either along the corresponding rotation vectors,  $\omega_g$  or  $\omega_p$ , or oppositely in the directions of the rotation vectors,  $\omega_g$  or  $\omega_p$ .

The length of the path along the axes,  $O_g$  and  $O_p$ , is limited by the face width of the gear,  $F_g$ , and the face width of the pinion,  $F_p$ . The linear velocity vector of the relative motion,  $\mathbf{V}_r = \mathbf{V}_p - \mathbf{V}_g$  (that is, the motion of the pinion in relation to the gear), is always perpendicular to the centerline,  $\mathcal{C}$ , along the closest distance of approach between the axes,  $O_g$  and  $O_p$ . In other words, the vector,  $\mathbf{V}_r$ , is always within the plane that is perpendicular to the centerline, that is, within the  $N_{ln}$  - plane.

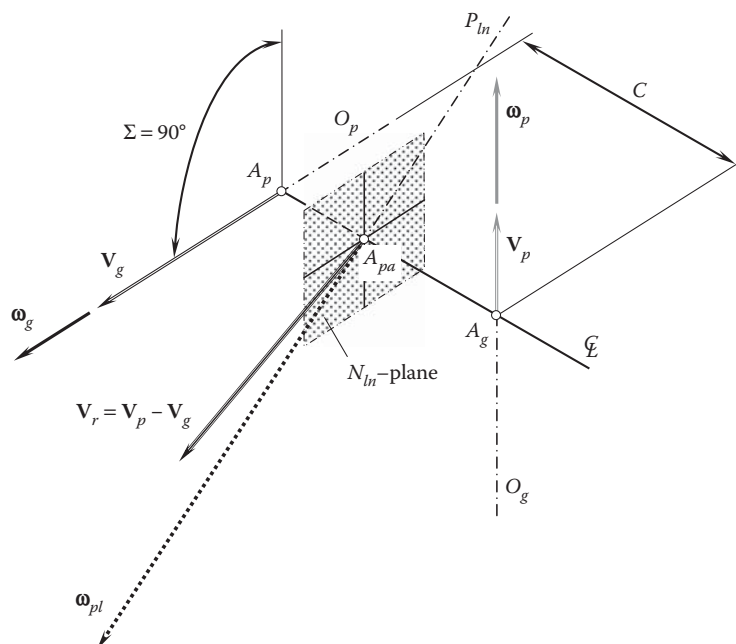


**FIGURE 17.1**

An example of skew axis gearing composed of two helical involute gears.

Worm gearing composed of an involute worm that is engaged in mesh with an involute gear (either a spur involute gear or a helical involute gear) is another good example of gearing with point contact between tooth flanks of a gear and a mating pinion. A schematic of gearing composed of a cylindrical involute worm that is engaged in mesh with a cylindrical involute helical gear is illustrated in Figure 17.3. Worm gearing of this type does not need more detailed discussion, as it is similar to that shown in Figure 17.1.

In a practical case, skew-axes involute gearing (see Figure 17.2) and worm involute gearing (see Figure 17.3) are the only two kinds of gearing with point contact between tooth flanks of a gear and a mating pinion used in the industry. The tooth flanks in both cases are generated following the first *Olivier principle* of generation of enveloping surfaces, that is, on the premise of two relative motions. Both of these gearings potentially incorporate an additional linear relative motion. The additional linear motion can be controlled independently of the rotations,  $\omega_g$  and  $\omega_p$ .

**FIGURE 17.2**

A vector diagram for the skew-axes gearing shown in Figure 17.1.



**FIGURE 17.3**

An example of a gear pair composed of a cylindrical involute worm and a helical involute gear.

## 17.2 Approach to Generating Tooth Flanks in Gearing with Point Contact between Tooth Flanks of a Gear and Mating Pinion

The tooth flank geometry of all the aforementioned possible gear pairs covered by the classification illustrated in Figure 2.15 in Chapter 2 are determined in compliance with the second Olivier principle [88] of the generation of enveloping surfaces.\* As a consequence of the implementation of this principle, the tooth flanks of the gear,  $\mathcal{G}$ , and the pinion,  $\mathcal{P}$ , are the surfaces enveloping to one another. Therefore, the tooth flanks  $\mathcal{G}$  and  $\mathcal{P}$  are in line contact with one another: when engaged in mesh, the tooth flanks  $\mathcal{G}$  and  $\mathcal{P}$  share a common characteristic line,  $\mathcal{E}$ .

Tooth flank geometry can be determined on the premise of the corresponding vector diagram of a perfect gear pair with point contact between tooth flanks of a gear and a mating pinion. Shown in Figure 17.4 is a vector diagram of a perfect external crossed-axes gear pair<sup>†</sup> constructed on the premise of the rotation vectors,  $\omega_g$  and  $\omega_p$ , of a gear and a mating pinion. The gear base-cone apex,  $A_g$ , is located within the centerline,  $\mathcal{C}$ . The actual location of the base-cone apex,  $A_g$ , is specified by the gear centerline vector,  $\mathbf{C}_g$ . Similarly, the pinion base-cone apex,  $A_p$ , is also located within the centerline,  $\mathcal{C}$ . The actual location of the base-cone apex,  $A_p$ , is specified by the pinion centerline vector,  $\mathbf{C}_p$ .

Points  $A_g$  and  $A_p$  at which the rotation vectors,  $\omega_g$  and  $\omega_p$ , are applied are at a center distance,  $C$ . The rotation vectors  $\omega_g$  and  $\omega_p$  form the crossed-axes angle,  $\Sigma$ . The rotation vector  $\omega_{pl}$  is along the axis of instant rotation,  $P_{ln}$ .

The gear tooth flank,  $\mathcal{G}$ , and the pinion tooth flank,  $\mathcal{P}$ , of a perfect external crossed-axes gear pair with line contact between the tooth flanks  $\mathcal{G}$  and  $\mathcal{P}$  can be constructed (see Chapter 14) on the premise of the vector diagram just discussed.

The vector diagram is complemented by an additional rotation,  $\omega_{r,p}$ , aiming to generate the tooth flanks of an auxiliary generating rack,  $\mathcal{R}$ . The rotation vector,  $\omega_{r,p}$ , is applied at point  $A_{r,p}$ . Point  $A_{r,p}$  is located within the centerline,  $\mathcal{C}$ . The actual location of the point,  $A_{r,p}$ , is specified by the rack centerline vector,  $\mathbf{C}_{r,p}$ . The vector  $\mathbf{C}_{r,p}$  originates at the plane-of-action apex,  $A_{pa}$ . In the case under consideration, the centerline vector,  $\mathbf{C}_{r,p}$ , is greater

\* Perfect gears with point contact also can be designed using the describing method, that is, using for this purpose a desired line of contact,  $LC_{des}$ .

<sup>†</sup> A similar analysis can be also performed with respect to perfect crossed-axes gear pairs, both internal gear pairs and rack-type gear pairs (see Figure 2.15).

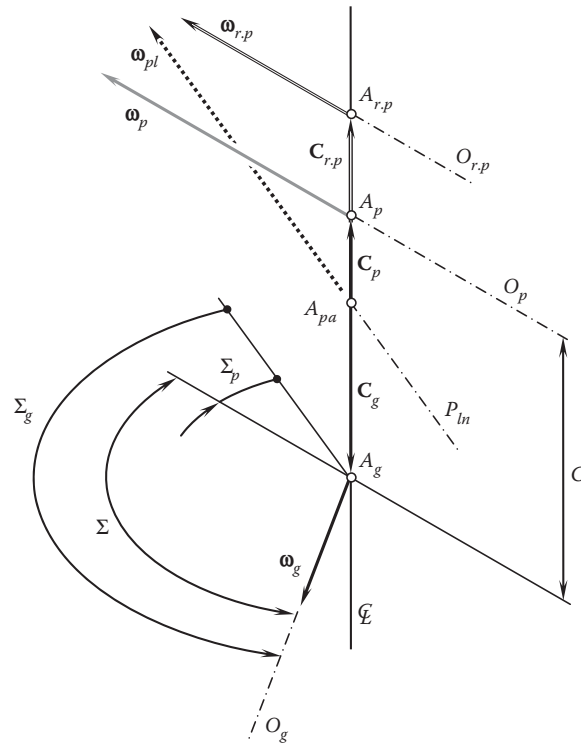


FIGURE 17.4

Vector diagram for the case of generation of an external crossed-axes gear pair with point contact between the tooth flanks,  $\mathcal{G}$  and  $\mathcal{P}$ , of a gear and a mating pinion

compared to the pinion centerline vector,  $\mathbf{C}_p$ ; that is, the inequality  $\mathbf{C}_{r,p} > \mathbf{C}_p$  is valid ( $\mathbf{C}_{r,p} = |\mathbf{C}_{r,p}| \leq \infty$ ). Otherwise, interference between the pinion and auxiliary generating rack is inevitable.

The rotation vector,  $\boldsymbol{\omega}_{r,p}$ , is parallel to the rotation vector,  $\boldsymbol{\omega}_p$ , of the pinion. If this requirement is violated, then the angular base pitch of the generated auxiliary rack cannot be equal to the operating base pitch of the gear pair: only base pitch-preserving alterations to the vector diagram are permissible.

When the equality  $\mathbf{C}_{r,p} = \infty$  is valid, then the complementary rotation,  $\boldsymbol{\omega}_{r,p}$ , reduces to a corresponding translation,  $\mathbf{V}_{r,p}$ . Thus, only rotations and translations are considered complementary motions when designing gearing with point contact between tooth flanks of a gear and a mating pinion.

The complementary rotation,  $\omega_{r,p}$ , is synchronized with the initial rotations,  $\omega_g$  and  $\omega_p$ , as well as with the rest of the design parameters of the gear pair.

When generating an auxiliary generating rack,  $\mathcal{R}$ , all three fundamental requirements [that is, (a) the condition of contact; (b) the condition of conjugacy; and (c) the condition of equality of the three base pitches:  $\varphi_{b,op} = \varphi_{b,g}$ ,  $\varphi_{b,op} = \varphi_{b,p}$ , or  $\varphi_{b,op} = \varphi_{b,g} = \varphi_{b,p}$ ] have to be fulfilled.

The auxiliary generating surface,  $\mathcal{R}$ , is generated as an enveloping surface to consecutive positions of the pinion tooth flanks,  $\mathcal{P}$ , generated above for the case of the gear pair with line contact between the tooth flanks,  $\mathcal{G}$  and  $\mathcal{P}$ . Note that the condition of conjugacy of the tooth flanks,  $\mathcal{P}$  and  $\mathcal{R}$ , of the pinion and the generating rack is still a must: at every instant of time, the straight line along the common perpendicular through contact point has to intersect the axis of instant rotation,  $P_{ln}$ . If the tooth flanks of the pinion,  $\mathcal{P}$ , and the auxiliary generating rack,  $\mathcal{R}$ , are not conjugate, then the auxiliary generating rack,  $\mathcal{R}$ , is not appropriate for a particular application.

Neither kinematical nor geometrical constraints are imposed onto the tooth flank geometry to be generated following the first Olivier principle [88] of enveloping surface generation. In accordance with the first Olivier principle, an auxiliary generating surface,  $\mathcal{R}$ , is used as an intermediate (an auxiliary) enveloping surface. The auxiliary generating surface,  $\mathcal{R}$ , is an envelope to both to the gear tooth flank,  $\mathcal{G}$ , as well as the pinion tooth flank,  $\mathcal{P}$ . Commonly, a characteristic line,  $\mathcal{E}_{r,g}$ , in the  $\mathcal{G}$ -to- $\mathcal{R}$  mesh, and a characteristic line,  $\mathcal{E}_{r,p}$ , in the  $\mathcal{P}$ -to- $\mathcal{R}$  mesh, do not

align with one another.\* Instead, these two lines intersect each other at a point. In the  $\mathcal{G}$ -to- $\mathcal{P}$  mesh, the point of intersection in nature is a point of contact,  $K$ , of the gear tooth flank,  $\mathcal{G}$ , and the mating pinion tooth flank,  $\mathcal{P}$ .

The use of the first Olivier principle makes it possible to determine the tooth flank geometry for any and all possible types of gear kinematics covered by the classification in Figure 2.15. However, for the cases (a) of parallel-axes gearing, as well as (b) intersected-axes gearing, implementation of the first Olivier principle results in tooth flank geometries that are degenerate to those already considered in the previous chapters. This is mostly because in cases (a) and (b), the characteristic lines,  $\mathcal{E}_{r,g}$  and  $\mathcal{E}_{r,p}$ , do not intersect each other: they either align with one another or are parallel to each other. Implementation of the first Olivier principle makes possible the derivation of novel types of tooth flank geometries only in cases of crossed-axes gearing.†

The geometry of the tooth flank of a gear,  $\mathcal{G}$ , and a mating pinion,  $\mathcal{P}$ , depends on the design parameters of the auxiliary generating rack,  $\mathcal{R}$ , and the parameters of its motion in relation to the reference systems,  $X_g Y_g Z_g$  and  $X_p Y_p Z_p$ , associated with the gear and the pinion, respectively.

Gearing of the type under consideration always features point contact between the tooth flank of a gear and a mating pinion. This requires tighter accuracy tolerance when producing gearing of this kind.

### 17.3 Possible Types of Auxiliary Generating Racks

Once the tooth flanks of the gear and pinion are generated in compliance with the first Olivier principle of surface generation, the geometry of the generating (auxiliary) surface in gearing with point contact between tooth flanks of a gear and a mating pinion needs to be investigated in more detail.

A gear tooth flank,  $\mathcal{G}$ , as well as a mating pinion tooth flank,  $\mathcal{P}$ , in a geometrically accurate crossed-axes gearing of this particular type can be interpreted as envelopes to consecutive positions of the auxiliary generating rack,  $\mathcal{R}$ , in its motion relative to a reference system associated with the gear and pinion, respectively. A straight generating rack,  $\mathcal{R}$ , is commonly used for this purpose. However, auxiliary racks of other geometries can be used for the generation of tooth flanks of the gear,  $\mathcal{G}$ , and the pinion,  $\mathcal{P}$ , as well. Feasible motions of the auxiliary generating surface,  $\mathcal{R}$ , in relation to the reference system,  $X_g Y_g Z_g$ , associated with the gear strongly depend on the geometry of the actual surface,  $\mathcal{R}$ .

In the simplest case, the auxiliary rack is shaped in the form of a straight rack,  $\mathcal{R}$ , that features a symmetrical tooth profile, as depicted in Figure 17.5a. In the case of straight rack,  $\mathcal{R}$ , the equality  $C_{r,p} = \infty$  is valid. A straight auxiliary rack that has an asymmetrical tooth profile is also known. A rack of this particular type is schematically shown in Figure 17.5b.

An auxiliary generating rack,  $\mathcal{R}$ , can be shaped in the form of a round rack,  $\mathcal{R}$ , with an involute tooth profile. Round racks of convex and concave types are possible, as shown in Figure 17.5c and d, respectively. The radius of the pitch cylinder,  $R_{r,p}$ , of the auxiliary rack,  $\mathcal{R}$ , is negative ( $R_{r,p} < 0$ ) in the first case (Figure 17.5c), and it is positive ( $R_{r,p} > 0$ ) in the second case (Figure 17.5d).

The round rack,  $\mathcal{R}$ , performs a rotation,  $\omega_{r,p}$ , about an axis of rotation,  $O_{r,p}$ , of the rack,  $\mathcal{R}$ . Superposition of the rotation of the round rack,  $\omega_{r,p}$ , with the rotation of the gear,  $\omega_g$ , results in a complex relative motion of the auxiliary rack,  $\mathcal{R}$ , about the axis of rotation,  $O_g$ , of the gear. The resultant motion,  $\omega_{scr} = \omega_p + \omega_{r,p}$ , is feasible when the rotations,  $\omega_{r,p}$  and  $\omega_g$ , are synchronized with each other in a timely manner. Appropriate portions of

\* Alignment of the characteristic lines,  $\mathcal{E}_{gr}$  and  $\mathcal{E}_{pr}$ , occurs in cases when the axes of rotation of the gear and pinion are either parallel to one another or intersect each other.

† In the case of gearing that features line contact between the tooth flanks,  $\mathcal{G}$  and  $\mathcal{P}$ , the second Olivier principle is employed for the generation of the tooth flanks of the gear and the pinion. In the case of gearing that features point contact between the tooth flanks,  $\mathcal{G}$  and  $\mathcal{P}$ , the first Olivier principle is employed for the generation of the tooth flanks of a gear and a mating pinion. Gearings that feature two (or more) auxiliary racks,  $\mathcal{R}_1$ ,  $\mathcal{R}_2$ , is impractical because of the following.

First, in a case of gearing with line contact between the tooth flanks,  $\mathcal{G}$  and  $\mathcal{P}$ , the gear tooth flank,  $\mathcal{G}$ , and the mating pinion tooth flank,  $\mathcal{P}$ , are in line contact with each other. The characteristic line,  $\mathcal{E}$ , is the line along which the tooth flanks,  $\mathcal{G}$  and  $\mathcal{P}$ , interact with one another.

Second, in a case of gearing with point contact between the tooth flanks,  $\mathcal{G}$  and  $\mathcal{P}$ , the gear tooth flank,  $\mathcal{G}$ , and the pinion tooth flank,  $\mathcal{P}$ , make point contact with each other at every instant of time. The point of contact,  $K$ , of the tooth flanks,  $\mathcal{G}$  and  $\mathcal{P}$ , is in nature the point of intersection of the gear,  $\mathcal{E}_{gr}$ , and pinion,  $\mathcal{E}_{pr}$ , characteristic lines.

Third, in a case of gearing two (or more) auxiliary racks,  $\mathcal{R}_1$ ,  $\mathcal{R}_2$ , the gear tooth flank,  $\mathcal{G}$ , and the pinion tooth flank,  $\mathcal{P}$ , should be designed so as to maintain point contact with each other, as well as with all the auxiliary racks,  $\mathcal{R}_i$ , at that same contact point,  $K$ . As in this particular case, three (or more) characteristic lines,  $\mathcal{E}_i$ , intersecting at a common point,  $K$ , must be ensured at every instant of time, making gearings with two (or more) auxiliary racks,  $\mathcal{R}_1$ ,  $\mathcal{R}_2$ , impractical.

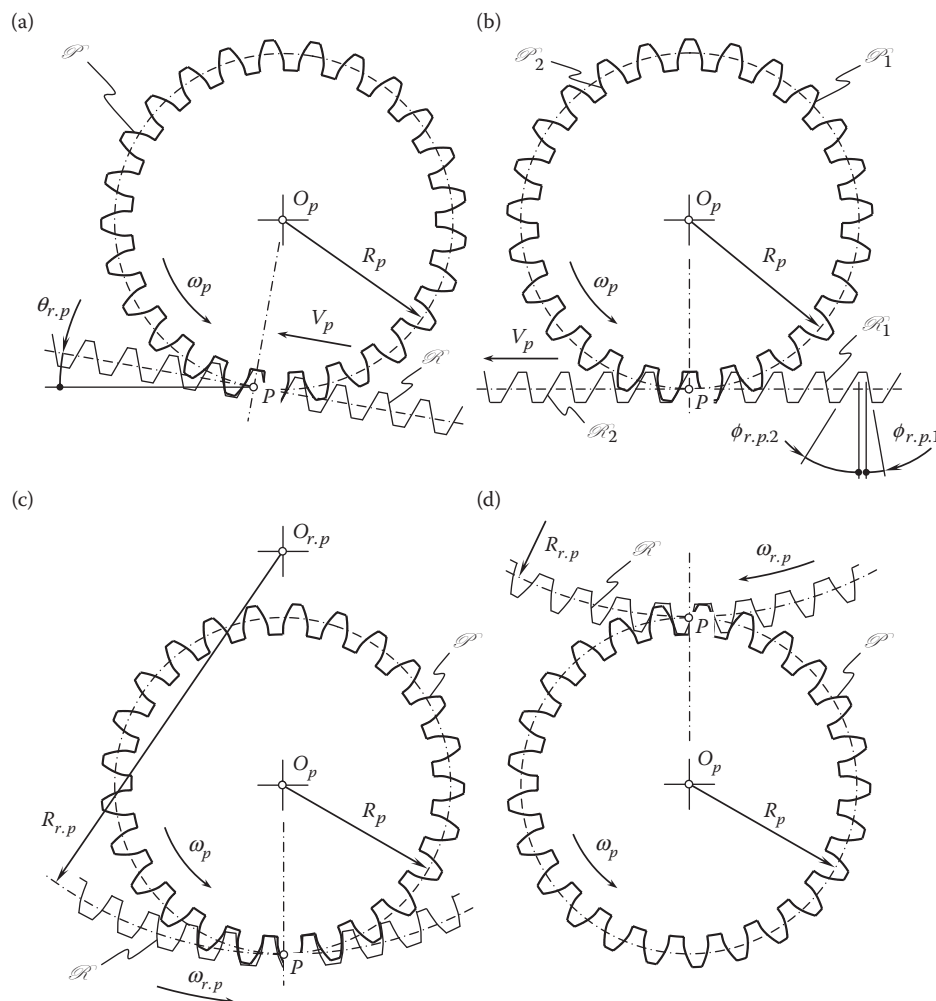


FIGURE 17.5

Examples of possible types of auxiliary generating surfaces,  $\mathcal{R}$ : (a) a straight inclined rack,  $\mathcal{R}$ ; (b) a straight rack,  $\mathcal{R}$ , with asymmetrical tooth profile; (c) a concave round rack,  $\mathcal{R}$ ; and (d) a convex round rack,  $\mathcal{R}$ .

the circular sectors can be employed as the auxiliary generating surfaces of gear-cutting tools for machining gears for gearing with point contact between tooth flanks of a gear and a mating pinion of this particular kind [111,112].

## 17.4 Geometry of Tooth Flanks of Perfect Crossed-Axes Gears with Point Contact

Consider an auxiliary straight rack,  $\mathcal{R}$ , of symmetrical tooth profile, as shown in Figure 17.5a. Let us assume that the rack,  $\mathcal{R}$ , performs a straight motion in a direction that is parallel to the pitch plane of the auxiliary rack. The straight motion of the auxiliary generating rack,  $\mathcal{R}$ , is superimposed with a rotation,  $\omega_g$ , of the gear. The resultant screw motion of the rack,  $\mathcal{R}$ , about the axis of rotation,  $O_g$ , of the gear is feasible in this particular case. The tooth flank of the gear,  $\mathcal{G}$ , is generated as an envelope to consecutive positions of the auxiliary rack,  $\mathcal{R}$ , that perform a screw motion with the gear axis,  $O_g$ , as the axis. Accordingly, the pinion tooth flank,  $\mathcal{P}$ , is generated as an envelope to consecutive positions of the auxiliary rack,  $\mathcal{R}$ , that performs the screw motion with the pinion axis,  $O_p$ , as the axis.

The tooth flanks of a gear,  $\mathcal{G}$ , and a mating pinion,  $\mathcal{P}$ , generated in this way belong to a skew-axes helical gearing (see Figure 17.6). Skew-axes gears are used in practice to transmit a rotation from a driving shaft to

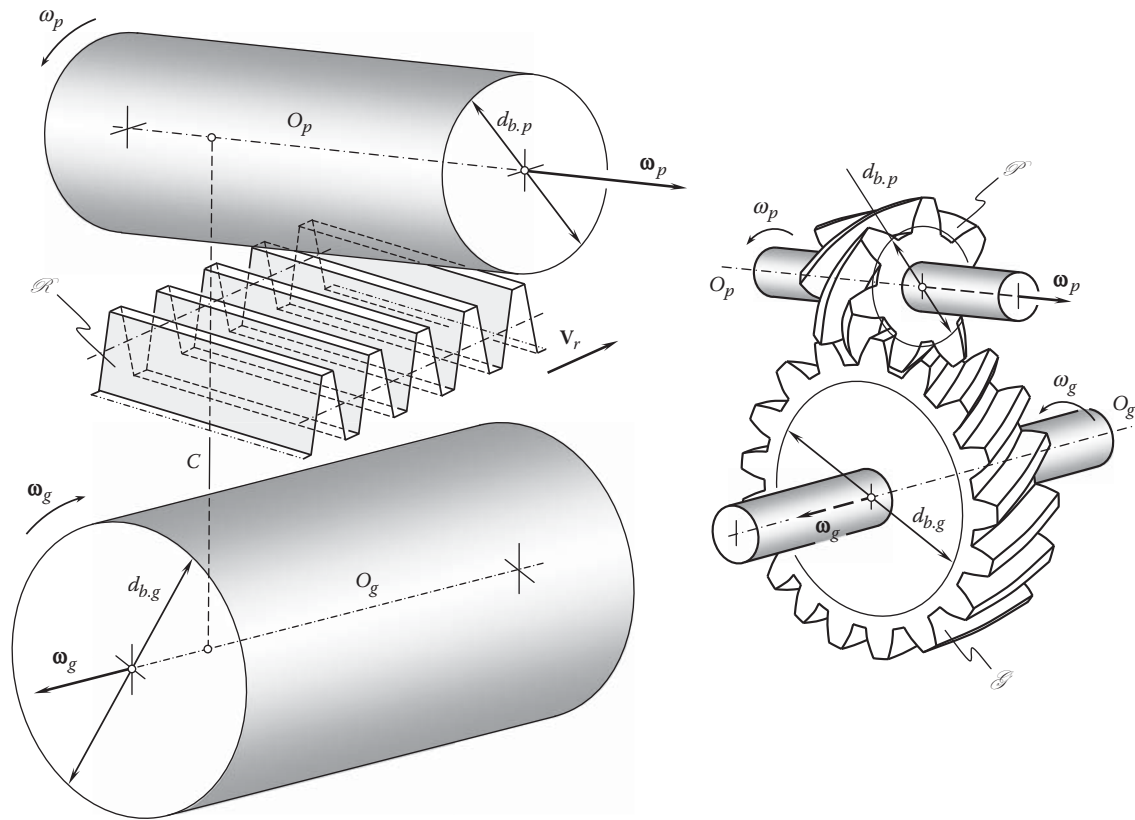


FIGURE 17.6

The generation of the tooth flanks,  $\mathcal{G}$  and  $\mathcal{P}$ , of a geometrically accurate crossed-axes gears by means of a straight auxiliary rack,  $\mathcal{R}$ .

a driven shaft, the axes of which cross one another. The use of gearing of this particular type makes sense only in cases when the power density to be transmitted is reasonably low. This is mostly because the gear and the pinion tooth flanks are in point contact. The bearing capacity of gearing that features point contact of the tooth flanks is relatively low.\*

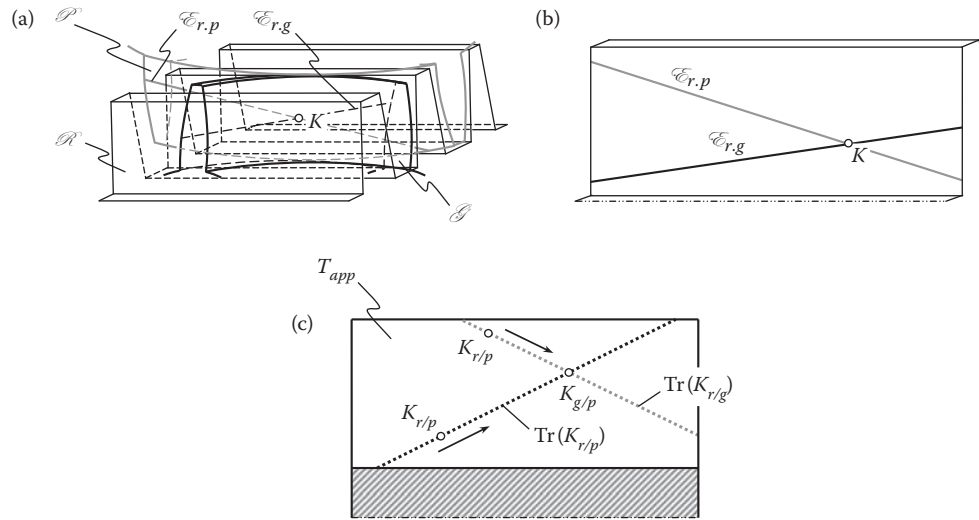
A characteristic line,  $\mathcal{E}_{r,g}$ , in the gear-to-rack mesh ( $\mathcal{G}$ -to- $\mathcal{R}$ -mesh) is a straight line. The straight line,  $\mathcal{E}_{r,g}$ , is located within the lateral tooth surface of the auxiliary rack,  $\mathcal{R}$  (see Figure 17.7a). The characteristic line,  $\mathcal{E}_{r,g}$ , is tangential to the base helix of the gear. Similarly, a characteristic line,  $\mathcal{E}_{r,p}$ , in the pinion-to-rack mesh ( $\mathcal{P}$ -to- $\mathcal{R}$ -mesh) is also a straight line. This straight line,  $\mathcal{E}_{r,p}$ , is located within the lateral tooth surface of the auxiliary rack,  $\mathcal{R}$ . The characteristic line,  $\mathcal{E}_{r,p}$ , is tangential to the base helix of the pinion.

The characteristic lines,  $\mathcal{E}_{r,g}$  and  $\mathcal{E}_{r,p}$ , intersect each other at a certain point, as schematically illustrated in Figure 17.7a and b. The point of intersection, in nature, is a point of contact,  $K$ , of the tooth flanks,  $\mathcal{G}$  and  $\mathcal{P}$ , of the gear and the pinion at a current instant of time. As the straight lines,  $\mathcal{E}_{r,g}$  and  $\mathcal{E}_{r,p}$ , intersect each other at a distinct point, the tooth flanks,  $\mathcal{G}$  and  $\mathcal{P}$ , of the gear and pinion are always in point contact.†

Similar to a skew-axes helical gearing, a gear pair composed of a helical involute gear that is engaged in mesh with an involute worm can be designed as well. Two options are available in this particular case.

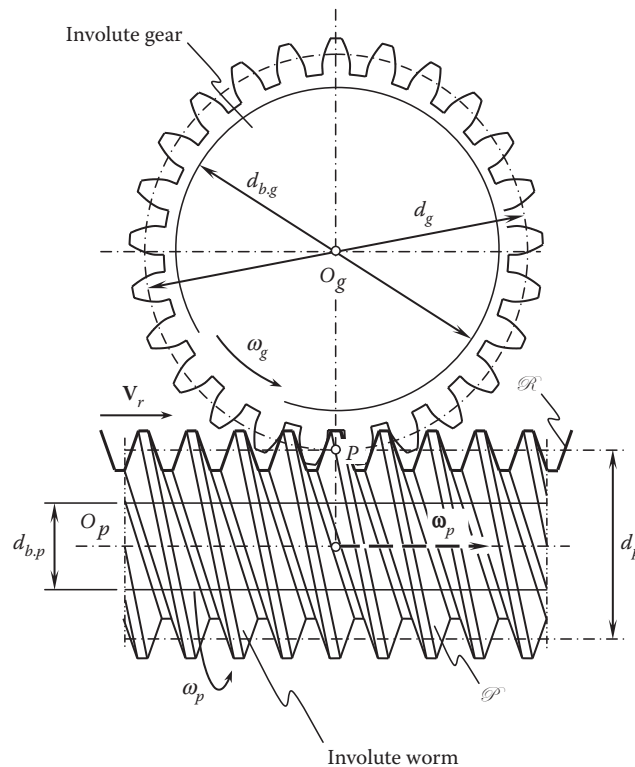
\* As there are not many examples of perfect gearing with point contact between tooth flanks of a gear and a mating pinion, and gearing of this type is poorly investigated, it is the right point to mention here the so-called *helipoid gearing* (see Wu, L.-L., Liu, C.-C., Tsay, C.-B., "Mathematical Model and Surface Deviation of Helipoid Gears Cut by Shaper Cutter", *ASME J Mechanical Design*, Volume 125, Issue 2, June 2003, pp. 351–355). Helipoid gearing can be viewed as an approximate gearing with point contact between tooth flanks of a gear and a mating pinion, as the base pitches of the shaper cutter are not equal to the operating angular base pitch of a helipoid gear pair [168].

† It is likely only crossed-axes gearing is of interest when designing perfect gearing with point contact between tooth flanks of a gear and a mating pinion, as only in this case do the characteristic lines,  $\mathcal{E}_{gr}$  and  $\mathcal{E}_{pr}$ , intersect one another. In crossed-axes gearing, as well as in parallel-axes gearing, the characteristic lines,  $\mathcal{E}_{gr}$  and  $\mathcal{E}_{pr}$ , do not intersect one another; therefore, no perfect gearing with point contact between tooth flanks of a gear and a mating pinion can be designed either in a case of  $I_a$  – axis gearing or in a case of  $P_a$  – axis gearing.

**FIGURE 17.7**

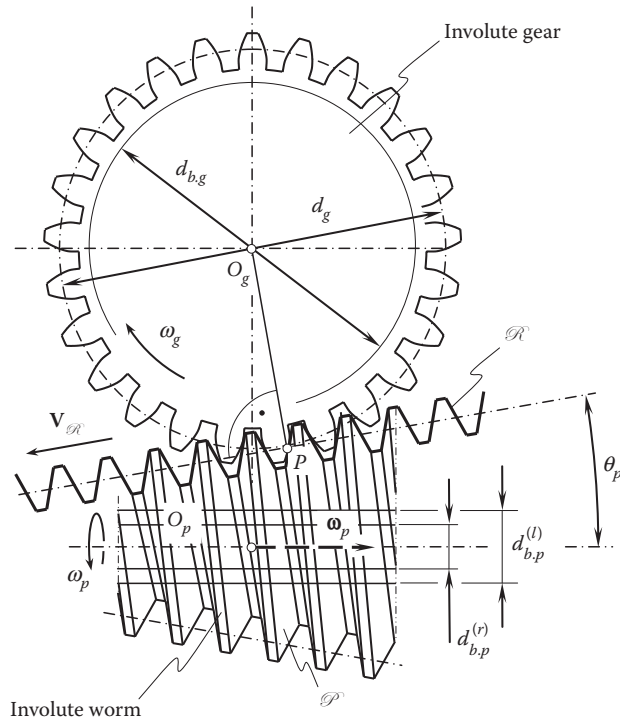
A characteristic line,  $\mathcal{E}_{r,g}$ , in the gear-to-rack mesh ( $\mathcal{G}$ -to- $\mathcal{R}$ -mesh), and a characteristic line,  $\mathcal{E}_{r,p}$ , in the pinion-to-rack mesh ( $\mathcal{P}$ -to- $\mathcal{R}$ -mesh) intersect each other at current point of contact,  $K$ , of the tooth flanks,  $\mathcal{G}$  and  $\mathcal{R}$ : (a) close-up; (b) the intersection of the characteristics,  $\mathcal{E}_{r,g}$  and  $\mathcal{E}_{r,p}$ , at contact point,  $K$ ; and (c) traces of contact,  $\text{Tr}(K_{r/g})$  and  $\text{Tr}(K_{r/p})$ , of contact points,  $K_{r/g}$  and  $K_{r/p}$ , on the auxiliary rack tooth flank,  $T_{app}$ .

First, when the axis of rotation of the worm is parallel to the pitch plane of the auxiliary rack,  $\mathcal{R}$ , a worm of cylindrical type is generated by the rack,  $\mathcal{R}$ , as schematically shown in Figure 17.8. Gearing of that type is geometrically accurate; however, the power density being transmitted is low, as the tooth flanks of the gear and threads of the worm are not in line contact, but rather in point contact. Worm gear pairs of this design have limited application in the industry.

**FIGURE 17.8**

A geometrically accurate crossed-axes worm gearing composed of a helical involute gear and a cylindrical involute worm.

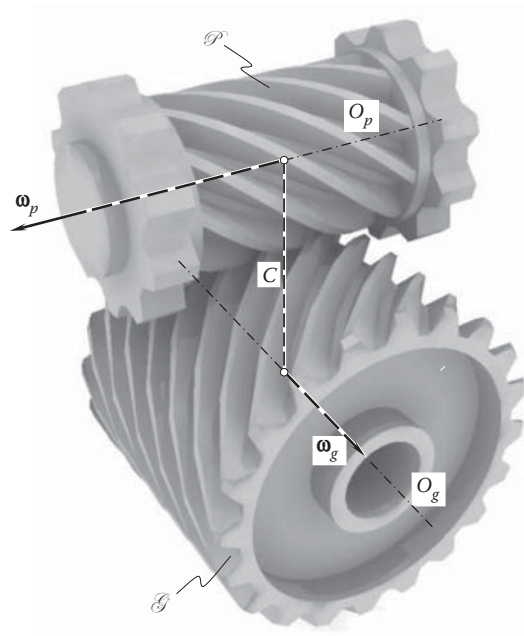


**FIGURE 17.9**

A geometrically accurate crossed-axes worm gearing composed of a helical involute gear and a conical involute worm.

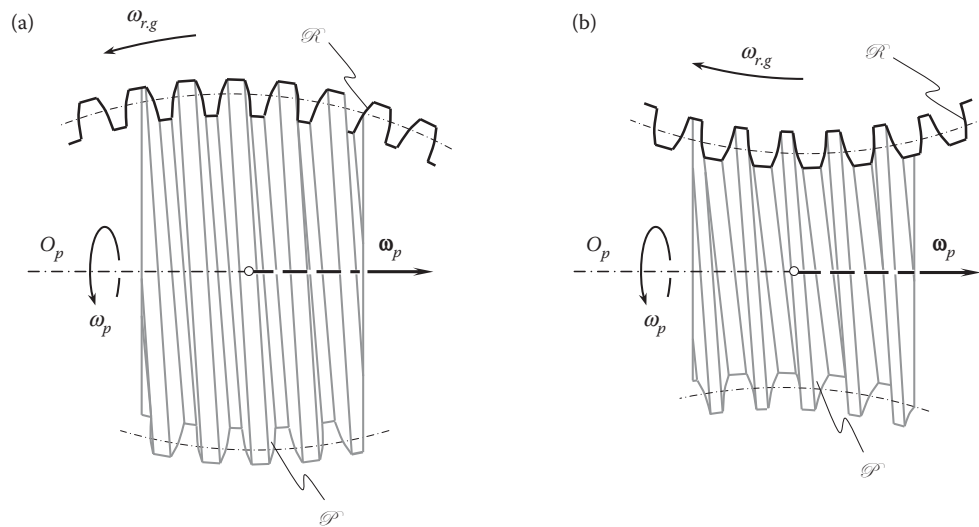
In the manner just discussed, an inner cylindrical worm can be generated.

Second, when the axis of rotation of the worm is at a certain angle,  $\theta_p$ , in relation to the pitch plane of the auxiliary rack,  $\mathcal{R}$ , a worm of conical type is generated by the rack,  $\mathcal{R}$ , as schematically depicted in Figure 17.9. Gearing of this type is also geometrically accurate; however, the power density being transmitted is low, as tooth flanks of the gear and threads of the worm are not in line contact, but rather in point contact.

**FIGURE 17.10**

External geometrically accurate crossed-axes gear set featuring point contact of the tooth flanks of the gear,  $\mathcal{G}$ , and the pinion,  $\mathcal{P}$ .



**FIGURE 17.11**

External worms generated by means of (a) convex, and (b) concave auxiliary generating racks,  $\mathcal{R}$ .

In the manner just discussed, an inner conical worm can be generated.

An example of the implementation of geometrically accurate crossed-axes gearing that features point contacts of the tooth flanks of the gear,  $\mathcal{G}$ , and the pinion,  $\mathcal{P}$ , is illustrated in Figure 17.10.

Auxiliary racks of other geometries can be used for generation of the tooth flanks of the gear and pinion of a perfect intersected-axes gearing with point contact between the tooth flanks of a gear and mating pinion. As an example, Figure 17.11 illustrates possible types of external worms, the threads of which are generated by means of a convex round auxiliary rack,  $\mathcal{R}$  (see Figure 17.11a) and by means of a concave round auxiliary rack,  $\mathcal{R}$  (see Figure 17.11b).

*General spatial involute gearing*, to the best possible extent investigated by Phillips [89] is a perfect example of gearing with point contact between tooth flanks of a gear and a mating pinion.

Internal worms, as well as internal gears for perfect crossed-axes gearing with point contact between the tooth flanks,  $\mathcal{G}$  and  $\mathcal{P}$ , are feasible as well. However, because of high sliding velocity between the tooth flanks, gear meshes of these kinds are of interest mostly for designing gear-cutting tools [111,112] and not for gearing itself.

So far perfect gearing with point contact between tooth flanks of a gear and a mating pinion has been poorly investigated. There is much room for an extensive research in this particular area of gearing.

The discussion in this chapter can be summarized as follows:

- Examples of perfect gearings with point contact between tooth flanks of a gear and a mating pinion are briefly discussed
- An approach to generating tooth flanks in perfect gearing with point contact between tooth flanks of a gear and a mating pinion is outlined
- Possible types of auxiliary generating racks are considered
- The geometry of tooth flanks of perfect crossed-axes gears with point contact is discussed

A better understanding of the kinematics, geometry, and interaction between tooth flanks can help identify appropriate areas of application of perfect gearing with point contact between tooth flanks of a gear and a mating pinion.

## Part IV

# Real Gears and Their Application: Perfect Real Gearing

The gears and gear pairs discussed in the previous sections of the monograph do not exist physically. They are a kind of abstraction. However, abstractions of this kind are helpful for in-depth understanding of gear tooth flank geometry, the kinematics of teeth flanks meshing, and gear operations in general. Although there are many similarities between the two, real gears differ from perfect gearing for many reasons.

Real gearing, which consists of some aspects of application of gears, including but not limited to gear trains, planetary gearing, and so on, along with a novel concept for the calculation of the contact and bending strength of gear teeth, especially the teeth of gears featuring a low tooth count (the so-called *low-tooth-count gears*, or just *LTC-gears* for simplicity), are covered in this part of the monograph.

All the sections deal with gears that feature linear and angular displacements in relation to one another. The nature of the displacements is of secondary importance. This could be manufacturing errors, deflections under operating load, thermal distortions, and so forth.

Part IV of the book consists of [Chapter 18](#). Room for a few more chapters is left, as this part of the book has the potential for growth in the future.



# Taylor & Francis

Taylor & Francis Group

<http://taylorandfrancis.com>

## Perfect Real Gearing: $S_{pr}$ -Gear System

Perfect real gears feature tooth flank geometry that is determined to provide the gears with the capability to be *insensitive* to any and all displacements of reasonable values of the tooth flanks from their nominal disposition. With tooth flank geometries of this kind, the displacements are simply absorbed due to the specific shape of the tooth flanks. This makes it possible to reduce the accuracy requirements to the gear, keep accuracy tolerances wider, and thus use less accurate and cheaper gears instead of more precise and costly gears. Considered below in this chapter, the gear system (or just  $S_{pr}$ -gearing for simplicity) is developed to accommodate manufacturing errors, as well as other displacements of the tooth flanks from their desired location and orientation. Also,  $S_{pr}$ -gearings are capable of accommodating displacements of the tooth flanks under operating loads.

### 18.1 Preliminary Considerations

In order to derive equations for the tooth flanks of the perfect real gears, it is necessary to have an in-depth understanding of all root causes of the high sensitivity of gearing to tooth flank displacements under operating loads, and so forth.

#### 18.1.1 Root Causes for Real Gears Differing from Perfect Gears

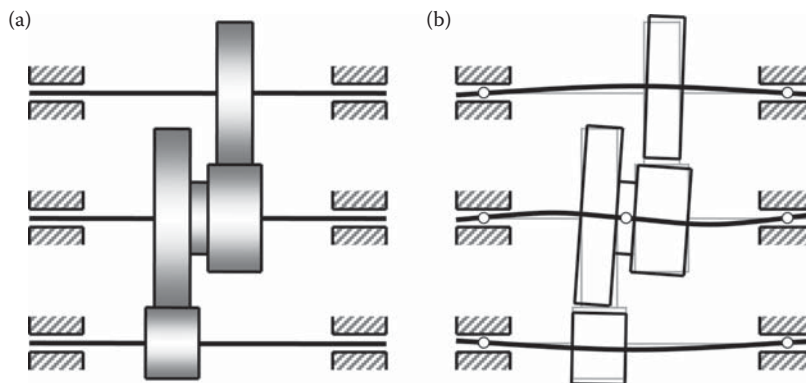
The design parameters of a perfect gear pair are exactly equal to their desirable (calculated) values. In reality, however, gear pairs undergo bending under loads. Overheating may result in heat distortion of gears, shafts, and housing. The shafts of a gear and mating pinion are displaced from their desirable positions by manufacturing and mounting errors, as well as by the flexibility of housing, and so forth. Finally, it can be concluded that under a load and when manufacturing errors occur, the initial configuration of the rotation vectors of a gear and a mating pinion tends to change.

Shown in Figure 18.1, an example illustrates the parallel axes of rotation of the gears in the ideal case (Figure 18.1a) and the misaligned axes of rotation of each gear under the operating load (Figure 18.1b). It should be noted here that the neutral and initially straight centerline of the shafts in Figure 18.1a becomes a spatial three-dimensional, curved centerline under the load applied (Figure 18.1b).

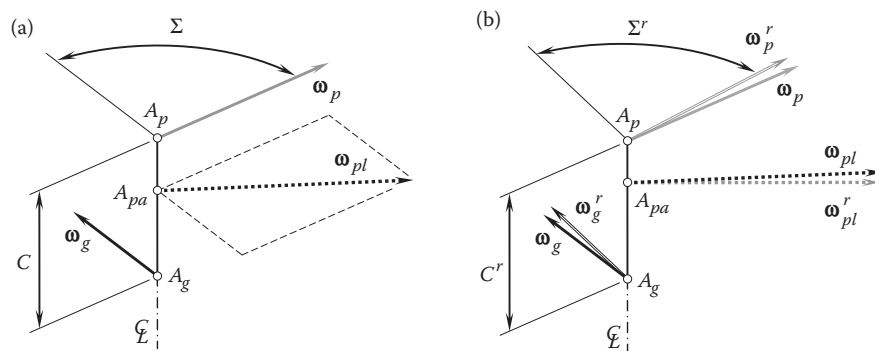
The deviations of the shaft bearings from their nominal configuration due to manufacturing errors and deflections under the load should be recognized as the potential root cause of the axis misalignment. Larger deviations result in larger axis misalignments, and vice versa. Longer shafts are less sensitive to the displacements of this kind. However, the stiffness of longer shafts is lower than that of short shafts. For a particular case, a favorable combination of the allowed bearing displacements and the shaft length can be determined. This issue could be of critical importance for high-power-density gearboxes, for which the shafts should be of the shortest possible length. The shorter the shafts, the tighter the tolerances on bearing displacements.

It is clear from the aforementioned brief discussion that, in reality, the axes of rotations of gears are displaced from their desirable positions. The actual root causes of axis displacements are not of critical importance in further analysis and therefore can often be omitted. In this monograph, the root causes of axis displacement are not investigated; instead, the values of the displacements themselves are investigated. However, the actual configuration of the axis of rotation of a gear in relation to the desired configuration is of critical importance and investigated in detail. Use of vector diagrams is convenient for such an analysis.

Shown in Figure 18.2a, a vector diagram is constructed for an arbitrary perfect crossed-axes gear pair. The vector diagram is composed of the rotation vector of the gear,  $\omega_g$ , and the rotation vector of the pinion,  $\omega_p$ . The closest distance of approach of the lines of action of the rotation vectors,  $\omega_g$  and  $\omega_p$ , is designated as  $C$ .

**FIGURE 18.1**

An example of the root cause of axis misalignment in parallel-axes gearing: (a) perfect alignment of the gears, and (b) a case of gear misalignment under the operating load.

**FIGURE 18.2**

Vector diagrams for (a) a perfect crossed-axes gear pair, and (b) for a corresponding real (loaded) crossed-axes gear pair.

An angle,  $\Sigma = \angle(\omega_g, \omega_p)$ , is formed by the rotation vectors,  $\omega_g$  and  $\omega_p$ . The angle,  $\Sigma$ , is the crossed-axes angle in the gear pair. The vector of instant rotation,  $\omega_{pl}$ , is constructed so as to fulfill the condition  $\omega_{pl} = \omega_p - \omega_g$ . The rotation vector,  $\omega_{pl}$ , is a vector through the plane-of-action apex,  $A_{pa}$ . This point is located within the centerline,  $\mathcal{C}$ , between the lines of action of the rotation vectors,  $\omega_g$  and  $\omega_p$ . The location of the apex,  $A_{pa}$ , within the centerline,  $\mathcal{C}$ , depends on the magnitudes,  $\omega_g$  and  $\omega_p$ , of the rotation vectors,  $\omega_g$  and  $\omega_p$ .

In reality, the vector diagram for that same gear pair (see Figure 18.2b) differs from that constructed for perfect gearing (see Figure 18.2a). The configuration of the real rotation vectors,  $\omega_g^r$  and  $\omega_p^r$ , deviates from the desirable configuration of the rotation vectors,  $\omega_g$  and  $\omega_p$ . The deviation of the rotation vector,  $\omega_g^r$ , from its desired location and orientation, which is specified by the rotation vector,  $\omega_g$ , as well as the deviation of the rotation vector,  $\omega_p^r$ , from its desired location and orientation, which is specified by the rotation vector,  $\omega_p$ , entail a deviation of the real vector of instant rotation,  $\omega_{pl}^r$ , from that,  $\omega_{pl}$ , in the perfect gearing. However, when the *relative motion* of the gear and pinion is considered, the rotation vector,  $\omega_{pl}^r$ , can be ignored.

The center distance and the crossed-axes angle are also affected by the aforementioned deviations in the location and orientation of the rotation vectors,  $\omega_g^r$  and  $\omega_p^r$ . The center distance in real gearing is designated as  $C^r$ , and the crossed-axes angle is denoted by  $\Sigma^r$ , correspondingly.

Because the vector diagram for real gearing (see Figure 18.2b) differs from that for perfect gearing (see Figure 18.2a), this results in different operating condition for the real gears. The larger the deviation of the rotation vectors,  $\omega_g^r$  and  $\omega_p^r$ , from their ideal configuration ( $\omega_g$  and  $\omega_p$ ), the larger the difference between the actual performance of the gears and its expected parameters.\*

\* Numerous efforts were undertaken in the past to make gears insensitive (or at least less sensitive) to displacements of the real tooth flanks of the gear and mating pinion from their desired configuration resulting from axis misalignment. Inventions by Wildhaber (U.S. Pat. No. 1.816.273, *Gearing*, Filed: June 18, 1928, patented: July 28, 1931; and U.S. Pat. No. 1.934.754, *Method and Means for Forming Gears*, Filed: March 23, 1931, patented: November 14, 1933) are two of many examples of such the efforts. It should be stressed here that the problem

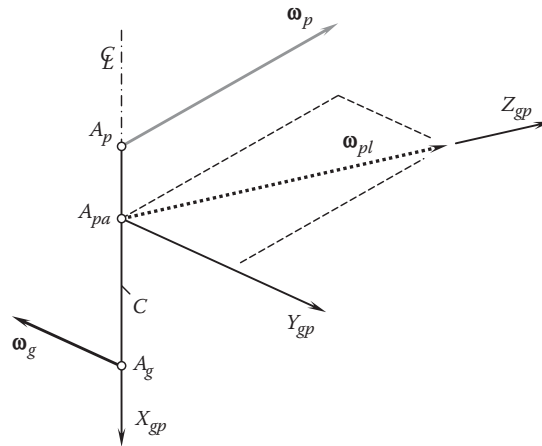


FIGURE 18.3  
Applied reference systems.

### 18.1.2 Applied Coordinate Systems

Several reference systems are introduced in this section for investigating the displacements of the tooth flanks in real gearing in relation to those in the corresponding perfect gearing.

Consider the vector diagram constructed for an arbitrary crossed-axes gear pair, as illustrated in Figure 18.3.

First, a left-hand-oriented Cartesian coordinate system,  $X_g Y_g Z_g$ , is associated with the gear. The  $Z_g$ -axis of this reference system is aligned with the rotation vector,  $\omega_g$ , of the gear. The axis is pointed in the same direction as the rotation vector,  $\omega_g$ .

Second, a left-hand-oriented Cartesian coordinate system,  $X_p Y_p Z_p$ , is associated with the pinion. Axis  $Z_p$  of the reference system,  $X_p Y_p Z_p$ , is aligned with the rotation vector,  $\omega_p$ , of the pinion. The axis is pointed in the same direction as the rotation vector,  $\omega_p$ .

Third, a stationary left-hand-oriented Cartesian coordinate system,  $X_{gp} Y_{gp} Z_{gp}$ , is associated with the gear pair.

The origin of the reference system,  $X_{gp} Y_{gp} Z_{gp}$ , is placed in the plane-of-action apex,  $A_{pa}$ , within the centerline,  $\mathcal{C}$ .

Axis  $Z_{gp}$  of the coordinate system,  $X_{gp} Y_{gp} Z_{gp}$ , is aligned with the vector of instant rotation,  $\omega_{pl}$ . This axis is pointed in the same direction as the rotation vector,  $\omega_{pl}$ . Axis  $X_{gp}$  is along the centerline,  $\mathcal{C}$ . This axis is pointed from the origin toward the gear reference system,  $X_g Y_g Z_g$ . Finally, the  $Y_{gp}$ -axis complements the first two axes to the left-hand-oriented Cartesian coordinate system,  $X_{gp} Y_{gp} Z_{gp}$ .

The axes,  $X_g$  and  $X_p$ , of the corresponding reference systems,  $X_g Y_g Z_g$  and  $X_p Y_p Z_p$ , are aligned with the centerline,  $\mathcal{C}$ . These axes ( $X_g$  and  $X_p$ ) are pointed in the same direction as the axis  $X_{gp}$ .

Immediately after the construction of the reference systems is completed, the corresponding operators of the coordinate systems transformation have to be composed. Following routing practice (see Appendix D), the operator,  $\mathbf{Rs}(g \mapsto gp)$ , of the transition from the coordinates system,  $X_g Y_g Z_g$ , associated with the gear to the coordinate system,  $X_{gp} Y_{gp} Z_{gp}$ , can be composed. Similarly, the operator  $\mathbf{Rs}(p \mapsto gp)$  of the transition from the coordinate system,  $X_p Y_p Z_p$ , associated with the pinion to the coordinate system,  $X_{gp} Y_{gp} Z_{gp}$ , can be composed. Use of the operators of the resultant coordinate system transformations,  $\mathbf{Rs}(g \mapsto gp)$  and  $\mathbf{Rs}(p \mapsto gp)$ , makes it possible to represent the gear axis of rotation,  $O_g^r$ , and the pinion axis of rotation,  $O_p^r$ , in the common reference system,  $X_{gp} Y_{gp} Z_{gp}$ , which is associated with the vector of instant rotation,  $\omega_{pl}$ , and the centerline,  $\mathcal{C}$ .

If necessary, the operators  $\mathbf{Rs}(g \mapsto gp)$  and  $\mathbf{Rs}(p \mapsto gp)$  can also be used for direct transition from the gear reference system,  $X_g Y_g Z_g$ , to the pinion reference system,  $X_p Y_p Z_p$ :

$$\mathbf{Rs}(g \mapsto p) = \mathbf{Rs}^{-1}(p \mapsto gp) \cdot \mathbf{Rs}(g \mapsto gp) \quad (18.1)$$

under consideration could not be solved in Wildhaber's time, as the concept of the *angular base pitch* was not known to Wildhaber or other gear experts. The concept of the angular base pitch was introduced much later (at around 2008) by Radzevich [137]. The newly introduced concept of the angular base pitch turns the problem of designing gears that are not sensitive to axis misalignment into a solvable one. The  $S_{pr}$ -gearing proposed by the author is the solution to the problem under consideration.

or in the inverse direction,

$$\mathbf{Rs}(p \mapsto g) = \mathbf{Rs}^{-1}(g \mapsto p) = \mathbf{Rs}^{-1}(g \mapsto gp) \cdot \mathbf{Rs}(p \mapsto gp) \quad (18.2)$$

Use of operators of coordinate system transformations is helpful in solving the problem under consideration.

### 18.1.3 Displacements of a Gear Axis of Rotation from Its Desired Configuration

Once the reference systems are constructed, the resultant deviation of a gear axis of rotation in real gearing from its desired configuration can be expressed in terms of six elementary displacements, that is, in terms of three linear displacements and three angular displacements.

The elementary linear displacements,  $\delta_{gx}$ ,  $\delta_{gy}$ , and  $\delta_{gz}$ , are the linear displacements along the corresponding axes of the reference system,  $X_g Y_g Z_g$ , associated with the gear (Figure 18.4a). The elementary linear displacements,  $\delta_{gx}$ ,  $\delta_{gy}$ , and  $\delta_{gz}$ , are positive when measured in the positive direction of the corresponding coordinate axis and negative when measured in the corresponding opposite direction. The resultant linear displacement,  $\delta_g$ , of the gear axis of rotation,  $O_g$ , can be expressed in terms of the elementary linear displacements by the following column matrix:

$$[\vec{\delta}_g] = \mathbf{i}\delta_{gx} + \mathbf{j}\delta_{gy} + \mathbf{k}\delta_{gz} = \begin{bmatrix} \delta_{gx} \\ \delta_{gy} \\ \delta_{gz} \\ 1 \end{bmatrix} \quad (18.3)$$

The elementary angular displacements,  $\varphi_{gx}$ ,  $\varphi_{gy}$ , and  $\varphi_{gz}$ , are angular displacements about the corresponding axes of the reference system,  $X_g Y_g Z_g$ , associated with the gear (see Figure 18.4b). The elementary angular displacements,  $\varphi_{gx}$ ,  $\varphi_{gy}$ , and  $\varphi_{gz}$ , are positive when the corresponding rotation vector of the elementary displacement is pointed in the positive direction of the corresponding coordinate axis. The elementary angular displacements,  $\varphi_{gx}$ ,  $\varphi_{gy}$ , and  $\varphi_{gz}$ , are negative when the elementary rotation vector of the elementary displacement is pointed in the opposite direction. The resultant angular displacement,  $\vec{\varphi}_g$ , of the gear axis of rotation,  $O_g$ , cannot be expressed in vector form as:

$$[\vec{\varphi}_g] \neq \mathbf{i}\varphi_{gx} + \mathbf{j}\varphi_{gy} + \mathbf{k}\varphi_{gz} \quad (18.4)$$

as rotations are not vectors in nature.

To calculate the resultant angular displacement,  $\vec{\varphi}_g$ , of the gear axis of rotation,  $O_g$ , in real gearing from its configuration in perfect gearing,  $O_g^r$ , the following approach is adopted below.

A unit vector,  $\mathbf{a}_g$ , is along the gear axis of rotation,  $O_g$ . The vector,  $\mathbf{a}_g$ , can be expressed in terms of the axial vector,  $\mathbf{A}_g$ , of the gear, shown in Figure 2.28 (see Chapter 2):

$$\mathbf{a}_g = \frac{\mathbf{A}_g}{|\mathbf{A}_g|} \quad (18.5)$$

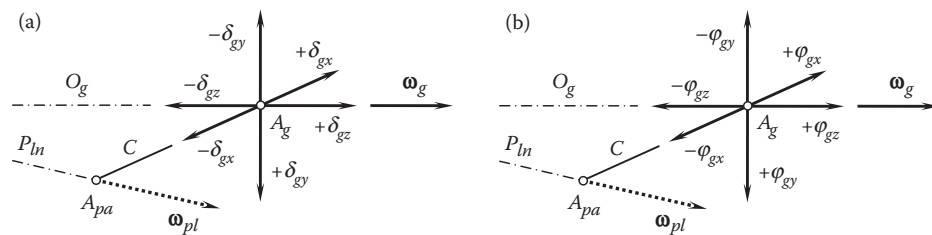


FIGURE 18.4

Displacements of the gear axis of rotation,  $O_g$ , in relation to the vector of instant rotation,  $\omega_{pl}$ : (a) linear displacements, and (b) angular displacements.



The unit vector,  $\mathbf{a}_g$ , is along the axis,  $Z_g$ , of the reference system,  $X_g Y_g Z_g$ , associated with the perfect gear pair. Therefore:

$$\mathbf{a}_g = \mathbf{k}_g \quad (18.6)$$

After being displaced through the angular displacement,  $\vec{\varphi}_g$ , the unit vector,  $\mathbf{a}_g^r$ , in the real gear pair equals:

$$\mathbf{a}_g^r = \mathbf{Rs}(p_{rf} \rightarrow r_{eal}) \cdot \mathbf{a}_g \quad (18.7)$$

The resultant angular displacement,  $\vec{\varphi}_g$ , of the gear axis of rotation,  $O_g$ , can be expressed as:

$$\varphi_g = \tan^{-1} \frac{\mathbf{a}_g \cdot \mathbf{a}_g^r}{|\mathbf{a}_g \times \mathbf{a}_g^r|} \quad (18.8)$$

In Equation 18.7, the operator,  $\mathbf{Rs}(p_{rf} \rightarrow r_{eal})$ , of the resultant coordinate system transformation is calculated as the product:

$$\mathbf{Rs}(p_{rf} \rightarrow r_{eal}) = \mathbf{Rt}(\varphi_{gz}, \hat{Z}_g) \cdot \mathbf{Rt}(\varphi_{gy}, \tilde{Y}_g) \cdot \mathbf{Rt}(\varphi_{gx}, X_g) \quad (18.9)$$

The operator,  $\mathbf{Rt}(\varphi_{gx}, X_g)$ , of the elementary coordinate system transformation can be analytically described in matrix form as:

$$\mathbf{Rt}(\varphi_{gx}, X_g) = \begin{bmatrix} 1 & 0 & 0 & 0 \\ 0 & \cos \varphi_{gx} & -\sin \varphi_{gx} & 0 \\ 0 & \sin \varphi_{gx} & \cos \varphi_{gx} & 0 \\ 0 & 0 & 0 & 1 \end{bmatrix} \quad (18.10)$$

In this case, it takes advantage of the fact that all the angular displacements,  $\varphi_{gx}$ ,  $\varphi_{gy}$ , and  $\varphi_{gz}$ , have small values. Taking into account that, for angles of a small value, an equality  $\sin \varphi_{gx} \cong \tan \varphi_{gx} \cong \varphi_{gx}$  is valid (here, the angle,  $\varphi_{gx}$ , is expressed in radians), Equation 18.10 is reduced to:

$$\mathbf{Rt}(\varphi_{gx}, X_g) = \begin{bmatrix} 1 & 0 & 0 & 0 \\ 0 & \sqrt{1 - \varphi_{gx}^2} & -\varphi_{gx} & 0 \\ 0 & \varphi_{gx} & \sqrt{1 - \varphi_{gx}^2} & 0 \\ 0 & 0 & 0 & 1 \end{bmatrix} \quad (18.11)$$

The operator,  $\mathbf{Rt}(\varphi_{gy}, \tilde{Y}_g)$ , of the elementary coordinate system transformation can be analytically described in matrix form as:

$$\mathbf{Rt}(\varphi_{gy}, \tilde{Y}_g) = \begin{bmatrix} \sqrt{1 - \tilde{\varphi}_{gy}^2} & 0 & -\tilde{\varphi}_{gy} & 0 \\ 0 & 1 & 0 & 0 \\ \tilde{\varphi}_{gy} & 0 & \sqrt{1 - \tilde{\varphi}_{gy}^2} & 0 \\ 0 & 0 & 0 & 1 \end{bmatrix} \quad (18.12)$$

Because the axis,  $\tilde{Y}_g$ , of the intermediate reference system,  $\tilde{X}_g \tilde{Y}_g \tilde{Z}_g$ , does not align with the coordinate axis,  $Y_g$ , of the original reference system,  $X_g Y_g Z_g$ , the angular displacements,  $\tilde{\varphi}_{gy}$  and  $\varphi_{gy}$ , are not equal to one another (that is, the inequality,  $\tilde{\varphi}_{gy} \neq \varphi_{gy}$ , is valid). However, the angular displacements,  $\tilde{\varphi}_{gy}$ , can be expressed in terms of the angular displacements,  $\varphi_{gx}$  and  $\varphi_{gy}$ .

The operator,  $\mathbf{Rt}(\varphi_{gz}, \hat{Z}_g)$ , of the elementary coordinate system transformation can be expressed in matrix form as:

$$\mathbf{Rt}(\varphi_{gz}, \hat{Z}_g) = \begin{bmatrix} \sqrt{1 - \hat{\varphi}_{gz}^2} & -\hat{\varphi}_{gz} & 0 & 0 \\ \hat{\varphi}_{gz} & \sqrt{1 - \hat{\varphi}_{gz}^2} & 0 & 0 \\ 0 & 0 & 0 & 0 \\ 0 & 0 & 0 & 1 \end{bmatrix} \quad (18.13)$$

Because the axis,  $\hat{Z}_g$ , of the intermediate reference system,  $\hat{X}_g \hat{Y}_g \hat{Z}_g$ , does not align with the coordinate axis,  $Z_g$ , of the original reference system,  $X_g Y_g Z_g$ , the angular displacements,  $\hat{\varphi}_{gz}$  and  $\varphi_{gz}$ , are not equal to one another (that is, the inequality,  $\hat{\varphi}_{gz} \neq \varphi_{gz}$ , is valid). However, the angular displacements,  $\hat{\varphi}_{gz}$ , can be expressed in terms of the angular displacements,  $\varphi_{gx}$ ,  $\varphi_{gy}$ , and  $\varphi_{gz}$ .

In a particular case(s), certain elementary displacement,  $\delta_{gx}$ ,  $\delta_{gy}$ ,  $\delta_{gz}$ , and  $\varphi_{gx}$ ,  $\varphi_{gy}$ ,  $\varphi_{gz}$ , do not affect the accuracy of the gear pair. For example, in a parallel-axes gearing, an axial linear displacement of a gear and a mating pinion in relation to one another, as well as angular displacements of a gear and a mating pinion about the axes of their rotation, do not affect the accuracy of the gear pair. Such elementary displacements have to be eliminated from further analysis.

The resultant displacement of the axis of rotation,  $O_p^r$ , of a mating pinion in real gearing from its desired configuration,  $O_p$ , can also be expressed in terms of six displacements, that is, of three linear displacements and three angular displacements similar to the displacement of the gear axis of rotation:

$$[\vec{\delta}_p] = \mathbf{i}\delta_{px} + \mathbf{j}\delta_{py} + \mathbf{k}\delta_{pz} = \begin{bmatrix} \delta_{px} \\ \delta_{py} \\ \delta_{pz} \\ 1 \end{bmatrix} \quad (18.14)$$

$$\varphi_p = \tan^{-1} \frac{\mathbf{a}_p \cdot \mathbf{a}_p^r}{|\mathbf{a}_p \times \mathbf{a}_p^r|} \quad (18.15)$$

where the unit vectors,  $\mathbf{a}_p$  and  $\mathbf{a}_p^r$ , are along the axis of rotation,  $O_p$ , of a perfect gearing, and along the axis of rotation,  $O_p^r$ , in the corresponding real gearing, correspondingly.

It should be pointed out here that although the configurations of the rotation vectors,  $\omega_g^r$ ,  $\omega_p^r$ , and  $\omega_{pl}^r$ , in real gearing are different from those ( $\omega_g$ ,  $\omega_{pl}$ , and  $\omega_p$ ) in perfect gears, the tooth ratio of the gear pair ( $u = \omega_p/\omega_g$ ) remains the same. Therefore, the actual configuration of the rotation vectors,  $\omega_g^r$  and  $\omega_{pl}^r$ , and the actual configuration of the rotation vectors,  $\omega_p^r$  and  $\omega_{pl}^r$ , correlate with each other so as to keep the tooth ratio a constant value ( $u = \text{const}$ ).

It can be shown that the aforementioned correlation between pairs of the rotation vectors ( $\omega_g$ ,  $\omega_{pl}$ , and  $\omega_p$ ,  $\omega_{pl}$ ) in perfect gearing and pairs of rotation vectors ( $\omega_g^r$ ,  $\omega_{pl}^r$  and  $\omega_p^r$ ,  $\omega_{pl}^r$ ) in real gearing, due to the equality  $u = \text{const}$ , results in negligibly small deviations of the vector of instant rotation,  $\omega_{pl}^r$ , from its desired configuration, which is specified by the vector of instant rotation,  $\omega_{pl}$ . Thus, it can be assumed that when the location and orientation of the rotation vectors,  $\omega_g$  and  $\omega_p$ , change to  $\omega_g^r$  and  $\omega_p^r$ , the initial location and orientation of the rotation vector,  $\omega_{pl}$ , remains the same\* ( $\omega_{pl} \approx \omega_{pl}^r$ ).

The actual values of neither the elementary linear displacements ( $\delta_{gx}$ ,  $\delta_{gy}$ ,  $\delta_{gz}$  and  $\delta_{px}$ ,  $\delta_{py}$ ) nor the elementary angular displacements ( $\varphi_{gx}$ ,  $\varphi_{gy}$ ,  $\varphi_{gz}$  and  $\varphi_{px}$ ,  $\varphi_{py}$ ,  $\varphi_{pz}$ ), are known. This is the first reason elementary displacements are inconvenient when treated mathematically. The second reason is that a real gear pair has to be capable of accommodating the elementary displacements of various actual values, from the smallest possible to the largest permissible. This issue can be easily resolved if the elementary displacements are replaced by their corresponding tolerances. In this chapter, the *tolerance* is understood in the sense of the largest permissible displacement. The tolerance for a linear displacement,  $\delta_{gx}$ , is designated as  $\{\delta_{gx}\}$ . The linear displacement,  $\delta_{gx}$ , and its corresponding tolerance,  $\{\delta_{gx}\}$ , relate to each other in the following manner:  $\delta_{gx} \leq \{\delta_{gx}\}$ . Similarly, the

\* When the relative motion of the gear and the pinion is considered, the rotation vector,  $\omega_{pl}^r$ , can be ignored.

angular displacement,  $\varphi_{gx}$ , and its corresponding tolerance,  $\{\varphi_{gx}\}$ , relate to each other in the following manner:  $\varphi_{gx} \leq \{\varphi_{gx}\}$ . The same relation is valid with respect to the rest of the elementary displacements, both linear and angular.

For the tolerances, equations similar to Equations 18.3 through 18.15 are valid. For the gear axis of rotation, an equation for the linear displacement can be represented in the following form:

$$[\vec{\delta}_g] = \mathbf{i}\{\delta_{gx}\} + \mathbf{j}\{\delta_{gy}\} + \mathbf{k}\{\delta_{gz}\} = \begin{bmatrix} \{\delta_{gx}\} \\ \{\delta_{gy}\} \\ \{\delta_{gz}\} \\ 1 \end{bmatrix} \quad (18.16)$$

For the angular displacement,  $\{\varphi_g\}$ , Equation 18.8 still valid:

$$\{\varphi_g\} = \tan^{-1} \frac{\mathbf{a}_g \cdot \mathbf{a}_g^r}{|\mathbf{a}_g \times \mathbf{a}_g^r|} \quad (18.17)$$

except the unit vectors,  $\mathbf{a}_g$  and  $\mathbf{a}_g^r$ , along the gear axes of rotation,  $O_g$  and  $O_g^r$ , have to be expressed in terms of the angular tolerances,  $\varphi_{gx}$ ,  $\varphi_{gy}$ , and  $\varphi_{gz}$ .

Similarly, for the pinion axis of rotation, the following equations are valid:

$$[\vec{\delta}_p] = \mathbf{i}\{\delta_{px}\} + \mathbf{j}\{\delta_{py}\} + \mathbf{k}\{\delta_{pz}\} = \begin{bmatrix} \{\delta_{px}\} \\ \{\delta_{py}\} \\ \{\delta_{pz}\} \\ 1 \end{bmatrix} \quad (18.18)$$

$$\{\varphi_p\} = \tan^{-1} \frac{\mathbf{a}_p \cdot \mathbf{a}_p^r}{|\mathbf{a}_p \times \mathbf{a}_p^r|} \quad (18.19)$$

where the unit vectors,  $\mathbf{a}_p$  and  $\mathbf{a}_p^r$ , along the pinion axes of rotation,  $O_p$  and  $O_p^r$ , have to be expressed in terms of the angular tolerances,  $\varphi_{px}$ ,  $\varphi_{py}$ , and  $\varphi_{pz}$ .

Ultimately, the total linear displacement,  $\{\vec{\delta}_\Sigma\}$ , of the gear and the pinion in real gearing is calculated as the difference:

$$\{\vec{\delta}_\Sigma\} = \{\vec{\delta}_g\} - \{\vec{\delta}_p\} \quad (18.20)$$

Similarly, the total angular displacement,  $\{\varphi_\Sigma\}$ , of the gear and the pinion in real gearing is calculated from the expression:

$$\{\varphi_\Sigma\} = \tan^{-1} \frac{\mathbf{a}_g^r \cdot \mathbf{a}_p^r}{|\mathbf{a}_g^r \times \mathbf{a}_p^r|} \quad (18.21)$$

Here, the linear displacements,  $[\delta_g]$  and  $[\delta_p]$ , as well as the corresponding tolerances,  $[\{\delta_g\}]$  and  $[\{\delta_p\}]$ , of the displacements are treated as vectors. This is true with respect to all the linear displacements and the corresponding tolerances for these displacements. The same is not valid with respect to the angular displacements,  $[\varphi_g]$  and  $[\varphi_p]$ , or the corresponding tolerances,  $[\{\varphi_g\}]$  and  $[\{\varphi_p\}]$ . This is because the angular displacements,  $[\varphi_g]$  and  $[\varphi_p]$ , and the angular tolerances,  $[\{\varphi_g\}]$  and  $[\{\varphi_p\}]$ , are not vectors in nature. Therefore, care is required when treating the rotations as vectors.

It should be pointed out here that not all the aforementioned elementary displacements, both linear displacements ( $[\delta_g]$  and  $[\delta_p]$ ) and angular displacements ( $[\varphi_g]$  and  $[\varphi_p]$ ), are critical for a particular configuration of the axes of rotation of a gear and a mating pinion. This makes it possible to reduce the total number of the elementary displacements (or the total number of the tolerances,  $[\{\delta_g\}]$ ,  $[\{\delta_p\}]$ , and  $[\{\varphi_g\}]$ ,  $[\{\varphi_p\}]$ ) for the elementary displacements,  $[\delta_g]$ ,  $[\delta_p]$  and  $[\varphi_g]$ ,  $[\varphi_p]$ , respectively to be taken into account in a particular analysis.

For example, only two elementary displacements are of critical importance in parallel-axes gearing. The intersected-axes angular deviation,  $\theta_{ins}$ , is one of them, and the crossed-axes angular deviation,  $\theta_{crs}$ , is another. The

impact of the remaining elementary displacements on the performance of a parallel-axes gear pair is negligibly small, and in many cases it can be omitted from analysis. The tolerances for the elementary displacements,  $\theta_{ins}$  and  $\theta_{crs}$ , are designated as  $\{\theta_{ins}\}$  and  $\{\theta_{crs}\}$ , respectively ( $\theta_{ins} \leq \{\theta_{ins}\}$ ,  $\theta_{crs} \leq \{\theta_{crs}\}$ ).

#### 18.1.4 Closest Distance of Approach between Gear and Mating Pinion Axes of Rotation

Elementary displacements alter the initial relative orientation of a gear and a mating pinion in a real gear pair. The location of the closest distance of approach (the centerline) between the gear axis of rotation,  $O_g$ , and the pinion axis of rotation,  $O_p$ , alters in particular. Changes to the configuration of the axes,  $O_g$  and  $O_p$ , significantly depend on the actual mounting of the gear and mating pinion.

As illustrated in Figure 18.5a, even in a simple case of parallel-axes gear pair, when the distances to the bearings at the left,  $l_l$ , and right,  $l_r$ , sides are equal to one another ( $l_l = l_r$ ), the shape of the neutral centerlines of the gear and mating pinion shafts (Figure 18.5b) differently from that (Figure 18.5d) when the distances to the bearings at left,  $l_l$ , and right,  $l_r$ , sides are not equal to one another ( $l_l \neq l_r$ ), as illustrated in Figure 18.5c. Moreover, in the second case, a certain inclination at an angle,  $\Delta\Sigma$ , between the gear and mating pinion is observed.\* The deformed real gearings under operating load can be substituted with equivalent *displaced* gearings.

An example of an overhung bevel pinion is schematically shown in Figure 18.6. The pinion is rotated about the axis,  $O_p$ . The pinion shaft is subject to bending under the separating load,  $P_{sep}$ . Due to the load,  $P_{sep}$ , the neutral centerline of the pinion shaft is curved. A straight line,  $O_p^r$ , tangential to the curved centerline at point,  $f$  (here, the point,  $f$ , is chosen at the middle of the face width of the pinion) is referred to as the actual axis of rotation of the pinion,  $O_p^r$ , in real gearing. The point of intersection of the centerline,  $O_p$ , by the straight tangent line,  $O_p^r$ , is the plane-of-action apex,  $A_{pa}$ , in the real gearing.† The centerlines,  $O_p^r$  and  $O_p$ , form an acute angle,  $\Delta\Sigma$ .

A similar actual axis of rotation,  $O_g^r$ , can be determined for the mating gear. Finally, the closest distance of approach,  $C^r$ , between the axes of rotation,  $O_g^r$  and  $O_p^r$ , of the gear and pinion can be expressed in terms of the design parameters of the gear pair and of the load,  $P_{sep}$ .

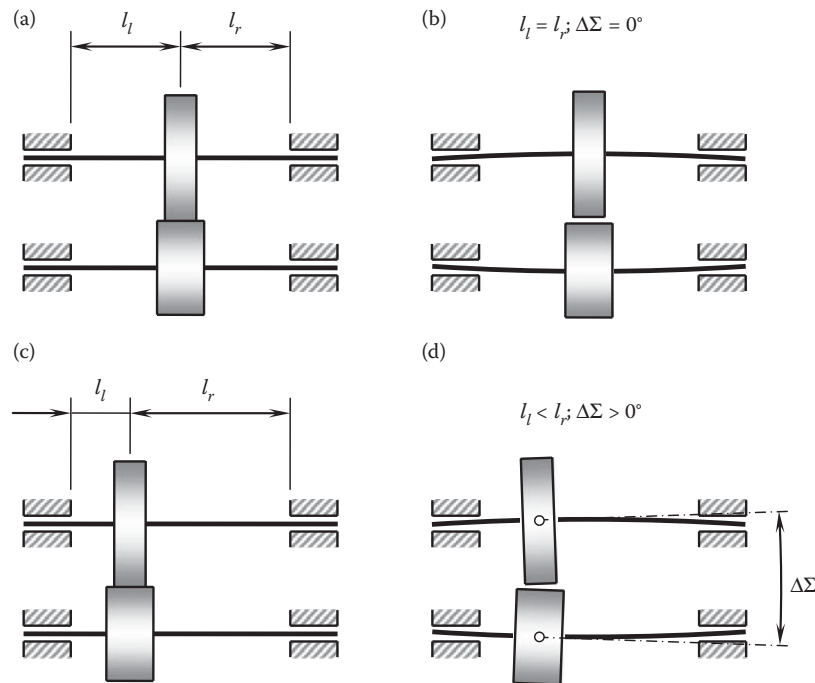
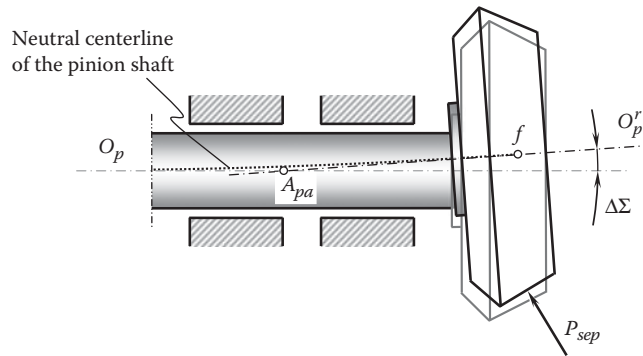


FIGURE 18.5

Design features and shaft deflections in real parallel-axes gearing: (a) symmetrical gear pair,  $l_l = l_r$ , and (b) gear and pinion shaft deflections; (c) asymmetrical gear pair,  $l_l \neq l_r$ , and (d) gear and pinion shaft deflections.

\* More accurately, the neutral centerlines of a gear and a pinion shaft are spatial curves.

† More accurately, the neutral centerline of the pinion shaft is a spatial curve, and the plane-of-action apex,  $A_{pa}$ , is located within the centerline,  $\mathcal{C}$ .

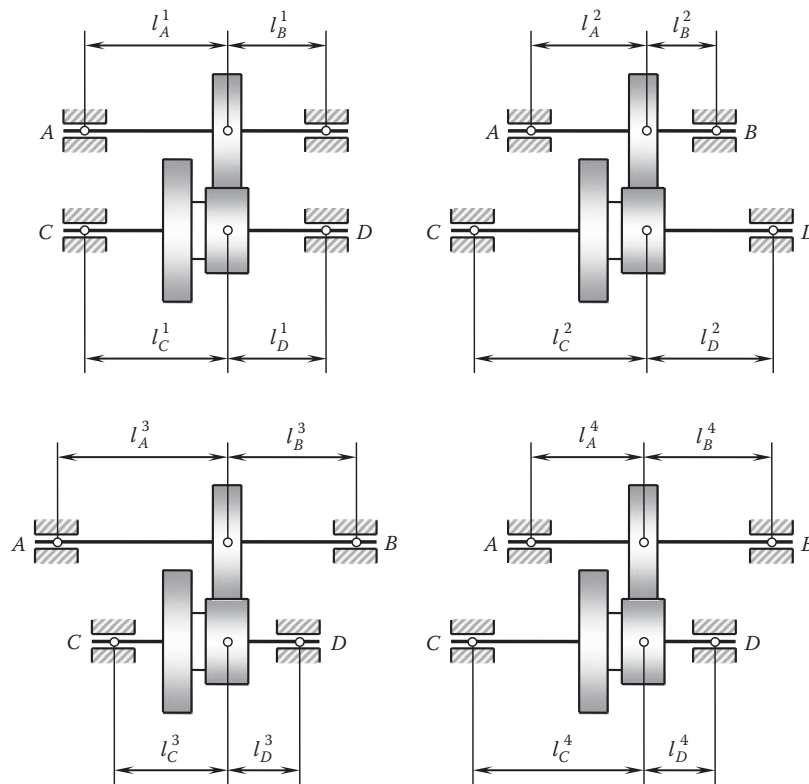
**FIGURE 18.6**

Shaft deflection in overhung bevel pinion under the separating force,  $P_{sep}$ .

The centerline,  $\mathcal{C}$ , between the axes of rotation,  $O_g^r$  and  $O_p^r$ , is located at a certain distance from the point,  $f$ . This distance, denoted by  $l_{CDA}$ , is referred to as the *closest distance of approach* between the gear and pinion axes,  $O_g^r$  and  $O_p^r$ , respectively. The value of the distance,  $l_{CDA}$ , strongly depends on the deflection of the pinion shaft. Either the actual distance,  $l_{CDA}$ , or tolerance for the value of this distance,  $\{l_{CDA}\}$ , is required to be known.

Shafts of straddle-mounted gears are less subject to deflections under an applied load. Examples are illustrated in Figure 18.7 with parallel-axes gearing. The angular displacements,  $\theta_{ins}$  and  $\theta_{crs}$ , depend on both linear displacements of bearings at the shaft ends  $A$ ,  $B$ ,  $C$  and  $D$ , and configuration of the bearings in relation to the gears themselves. The distance,  $l_{CDA}$ , of the centerline in relation to the middle of a gear strongly depends on the actual values of the design parameters  $l_A^i$ ,  $l_B^i$ ,  $l_C^i$ , and  $l_D^i$  of the gearbox (here,  $i = 1, 2, 3, 4$ ).

The geometry of the tooth flanks of perfect real gears depends on the location of the centerline along  $c^r$  in relation to the tooth flanks of a gear,  $\mathcal{G}$ , and a mating pinion,  $\mathcal{P}$ . It is desired to have the closest distance of approach

**FIGURE 18.7**

Various configurations of straddle-mounted parallel-axes gearing.

of the gear axis of rotation,  $O_g$ , and the pinion axis of rotation,  $O_p$ , pass through the middle of the face width of the gear and the pinion. In this particular case, the tooth flanks are symmetrical in the lengthwise direction, which makes assembly of the gearboxes easier. Otherwise, when gear and pinion teeth are asymmetrical, it is necessary to distinguish two ends of a gear (of a mating pinion) from each other.

The aforementioned point is true with respect to intersected-axes gearing, as well as with respect to crossed-axes gearing.

As an example, consider a straddle-mounted shaft of the worm of a worm gearing, as shown in Figure 18.8. The configuration of the axis of rotation,  $O_g$ , of the gear can be specified in terms of the coordinates of the shaft bearings,  $A$  and  $B$ , given in a certain stationary (motionless) reference system,  $X_s Y_s Z_s$ . Thus, the position vectors,  $\mathbf{r}_A$  and  $\mathbf{r}_B$ , of the points,  $A$  and  $B$ , within the axis of rotation,  $O_g$ , are known. The position vector of a point of the gear axis of rotation,  $O_g$ , is designated as  $\mathbf{r}_{O_g}$ . As points within the axis  $O_g$  are considered, the following expression is valid:

$$(\mathbf{r}_{O_g} - \mathbf{r}_A) \times (\mathbf{r}_B - \mathbf{r}_A) = 0 \quad (18.22)$$

This expression casts into an equation for the position vector  $\mathbf{r}_{O_g}$ :

$$\mathbf{r}_{O_g}(\lambda^*) = \mathbf{r}_A + \lambda^*(\mathbf{r}_B - \mathbf{r}_A) \quad (18.23)$$

The difference,  $(\mathbf{r}_B - \mathbf{r}_A)$ , can be expressed in terms of the unit vector,  $\mathbf{u}_g$ , along the axis of rotation,  $O_g$ , of the gear:

$$(\mathbf{r}_B - \mathbf{r}_A) = \lambda^{**} \mathbf{u}_g \quad (18.24)$$

This yields a simplified equation for the position vector,  $\mathbf{r}_{O_g}$ :

$$\mathbf{r}_{O_g}(\lambda) = \mathbf{r}_A + \lambda \mathbf{u}_g \quad (18.25)$$

where the equality,  $\lambda = \lambda^* \cdot \lambda^{**}$ , is valid.

An ideal configuration of the axis of rotation of the gear,  $O_g$ , is described by Equation 18.23. In real gearing, the bearings,  $A$  and  $B$ , are displaced from their desired positions. The vectors,  $\delta_A$  and  $\delta_B$ , of the actual deviations are usually not known. However, the tolerances,  $\{\delta_A\}$  and  $\{\delta_B\}$ , for the displacements,  $\delta_A$  and  $\delta_B$ , are commonly assigned by the gear designer and therefore are considered known parameters of the gear set. Taking into

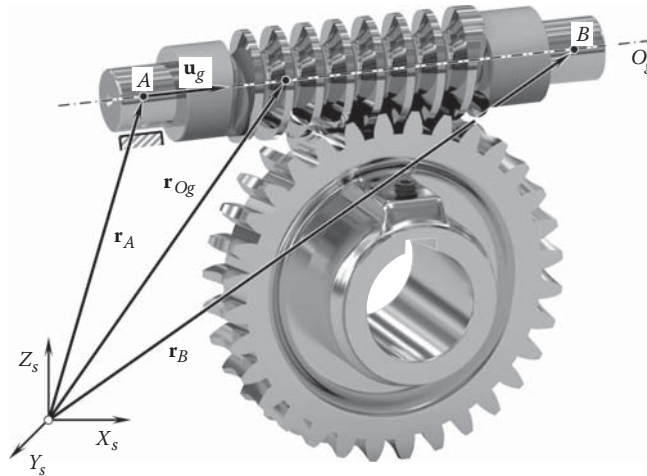


FIGURE 18.8

Actual configuration of straddle-mounted shaft of a worm.

account the tolerances,  $\{\delta_A\}$  and  $\{\delta_B\}$ , an expression for the position vector of a point,  $\mathbf{r}_{O_g}^r$ , for real configuration of the axis of rotation,  $O_g^r$ , of the gear can be expressed in the following form:

$$\mathbf{r}_{O_g}^r(\lambda_g^r) = \mathbf{r}_A + \{\delta_A\} + \lambda_g^r[(\mathbf{r}_B + \{\delta_B\}) - (\mathbf{r}_A + \{\delta_A\})] \quad (18.26)$$

In Equation 18.26, the parameter of the axis of rotation,  $O_g^r$ , is designated as  $\lambda_g^r$ .

An equation similar to Equation 18.26 can be derived for the position vector of a point,  $\mathbf{r}_{O_p}^r$ , for a real configuration of the axis of rotation,  $O_p^r$ , of the mating pinion:

$$\mathbf{r}_{O_p}^r(\lambda_p^r) = \mathbf{r}_C + \{\delta_C\} + \lambda_p^r[(\mathbf{r}_D + \{\delta_D\}) - (\mathbf{r}_C + \{\delta_C\})] \quad (18.27)$$

In Equation 18.27, an ideal configuration of the bearings,  $C$  and  $D$ , of the pinion is specified by the position vectors,  $\mathbf{r}_C$  and  $\mathbf{r}_D$ . The tolerances for the actual displacements,  $\delta_C$  and  $\delta_D$ , of the bearings,  $C$  and  $D$ , are denoted by  $\{\delta_C\}$  and  $\{\delta_D\}$ , respectively. The parameter of the axis of rotation,  $O_p^r$ , is designated as  $\lambda_p^r$ .

Once the expressions for the position vectors,  $\mathbf{r}_{O_g}^r$  and  $\mathbf{r}_{O_p}^r$ , are derived (see Equations 18.26 and 18.27), the closest distance of approach between the axes of rotation,  $O_g^r$  and  $O_p^r$ , in the real gear pair can be determined. For this purpose, it is convenient to represent Equation 18.26 in the following form:

$$\mathbf{r}_{O_g}^r(\lambda_g^r) = \mathbf{r}_{og}^0 + \lambda_g^r \mathbf{u}_g \quad (18.28)$$

Similarly, Equation 18.27 can be rewritten in the following form:

$$\mathbf{r}_{O_p}^r(\lambda_p^r) = \mathbf{r}_{op}^0 + \lambda_p^r \mathbf{v}_p \quad (18.29)$$

The center distance between the axes of rotation,  $O_g^r$  and  $O_p^r$ , is designated as  $C^r$  (as shown in Figure 18.9). In the general case of crossed-axes gearing, the center distance,  $C^r$ , is a function of the form:

$$C^r = C^r(C, \Sigma, \{\delta\}, \{\varphi\}) \quad (18.30)$$

where  $\{\delta\}$  and  $\{\varphi\}$  are the tolerances for the resultant linear displacement and angular displacement, respectively. These tolerances can be expressed in terms of the tolerances for elementary linear displacements, that is,  $\{\delta\} = \{\delta_g\} + \{\delta_p\}$ , and in terms of tolerances for elementary angular displacements, that is,  $\{\varphi\} = \{\varphi\}(\{\varphi_g\}, \{\varphi_p\})$ . The unit vector aligned with the center distance,  $C^r$ , is denoted by  $\mathbf{c}^r$ .

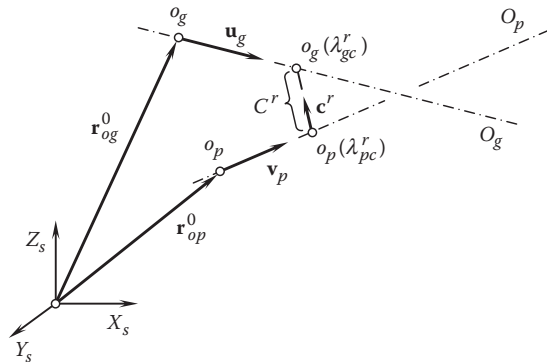


FIGURE 18.9

Calculation of the resultant displacement along the center distance for perfect real parallel-axes gearing.



The distance,  $\mathbf{d}$ , between two arbitrary points in the axes  $O_g^r$  and  $O_p^r$  can be calculated from the following equation:

$$\mathbf{d}(\lambda_g^r, \lambda_p^r) = \mathbf{r}_{O_g^r}(\lambda_g^r) - \mathbf{r}_{O_p^r}(\lambda_p^r) \quad (18.31)$$

It is necessary to find the distance,  $\mathbf{d}(\lambda_g^r, \lambda_p^r)$ , that has a minimum length for all  $\lambda_g^r$  and  $\lambda_p^r$ . This distance corresponds to the closest distance of approach,  $C^r$ , between the gear axis of rotation,  $O_g^r$ , and the pinion axis of rotation,  $O_p^r$ , (that is,  $|\mathbf{d}^{\min}| = C^r$ ).

The two axes of rotation, that is,  $O_g^r$  and  $O_p^r$ , are closest to one another at unique points, that is,  $o_g(\lambda_{gc}^r)$  and  $o_p(\lambda_{pc}^r)$ , for which the distance  $\mathbf{d}(\lambda_g^r, \lambda_p^r)$  attains its minimum length. The subscript  $c$  indicates here that a corresponding parameter is relevant to the center distance. Also, if the axes,  $O_g^r$  and  $O_p^r$ , are not parallel (which is a trivial case), then the straight line segment,  $\mathbf{d}(\lambda_g^r, \lambda_p^r) = \mathbf{r}_{og} - \mathbf{r}_{op}$ , joining the closest points,  $o_g(\lambda_{gc}^r)$  and  $o_p(\lambda_{pc}^r)$ , is uniquely perpendicular to both axes at the same time. No other straight line segment between the axes,  $O_g^r$  and  $O_p^r$ , possesses this property. That is, the vector,  $\mathbf{d}_c = \mathbf{d}(\lambda_{gc}^r, \lambda_{pc}^r)$ , is uniquely perpendicular to the line direction vectors,  $\mathbf{u}_g$  and  $\mathbf{v}_p$ . This is equivalent to the vector,  $\mathbf{d}_c$ , and satisfies the following two equations simultaneously:

$$\mathbf{u}_g \cdot \mathbf{d}_c = 0 \quad (18.32)$$

$$\mathbf{v}_p \cdot \mathbf{d}_c = 0 \quad (18.33)$$

These two equations can be solved by substituting

$$\mathbf{d}_c = \mathbf{r}_{og}(\lambda_{gc}^r) - \mathbf{r}_{op}(\lambda_{pc}^r) = \mathbf{d}_0 + \lambda_{gc}^r \mathbf{u}_g - \lambda_{pc}^r \mathbf{v}_p \quad (18.34)$$

into each to get simultaneous linear equations:

$$(\mathbf{u}_g \cdot \mathbf{u}_g)\lambda_{gc}^r - (\mathbf{u}_g \cdot \mathbf{v}_p)\lambda_{pc}^r = -\mathbf{u}_g \cdot \mathbf{d}_0 \quad (18.35)$$

$$(\mathbf{v}_p \cdot \mathbf{u}_g)\lambda_{gc}^r - (\mathbf{v}_p \cdot \mathbf{v}_p)\lambda_{pc}^r = -\mathbf{v}_p \cdot \mathbf{d}_0 \quad (18.36)$$

In Equations 18.34 through 18.36,  $\mathbf{d}_0 = \mathbf{r}_{og}^0 - \mathbf{r}_{op}^0$  is the distance between two known points; in our case, it is the distance between the points  $o_g$  and  $o_p$ .

Then, from  $\mathbf{u}_g \cdot \mathbf{u}_g = a$ ,  $\mathbf{u}_g \cdot \mathbf{v}_p = b$ ,  $\mathbf{v}_p \cdot \mathbf{v}_p = c$ ,  $\mathbf{u}_g \cdot \mathbf{d}_0 = d$ , and  $\mathbf{v}_p \cdot \mathbf{d}_0 = e$ , the solution to Equations 18.35 and 18.36 with respect to  $\lambda_{gc}^r$  and  $\lambda_{pc}^r$  can be represented as follows:

$$\lambda_{gc}^r = \frac{be - cd}{ac - b^2} \quad (18.37)$$

$$\lambda_{pc}^r = \frac{ae - bd}{ac - b^2} \quad (18.38)$$

In these equations, the denominator  $ac - b^2$  is nonzero. Note that the following expression is always nonnegative:

$$ac - b^2 = |\mathbf{u}_g|^2 |\mathbf{v}_p|^2 - (|\mathbf{u}_g| |\mathbf{v}_p| \cos \theta)^2 = (|\mathbf{u}_g| |\mathbf{v}_p| \sin \theta)^2 \geq 0 \quad (18.39)$$

When the equality  $ac - b^2 = 0$  is valid, the two equations are dependent; the two axes,  $O_g^r$  and  $O_p^r$ , are parallel to one another; and the distance between the axes is a constant value. We can solve for this parallel distance of separation by fixing the value of one parameter and using either equation to solve the other. Selecting  $\lambda_{gc}^r = 0$ , we get  $\lambda_{pc}^r = d/b = e/c$ .

Once the solution for  $\lambda_{gc}^r$  and  $\lambda_{pc}^r$  (see Equations 18.37 and 18.38) is determined, the coordinates of the two points,  $o_g(\lambda_{gc}^r)$  and  $o_p(\lambda_{pc}^r)$ , are determined as well. The axes of rotation,  $O_g^r$  and  $O_p^r$ , are closest to one another at these two points,  $o_g(\lambda_{gc}^r)$  and  $o_p(\lambda_{pc}^r)$ . Then, the distance between the points is given as follows:

$$C^r(C, \Sigma, \{\delta\}, \{\varphi\}) = |\mathbf{d}^{\min}| = \left| (\mathbf{r}_{og}^0 - \mathbf{r}_{op}^0) + \frac{(be - cd)\mathbf{u}_g - (ae - bd)\mathbf{v}_p}{ac - b^2} \right| \quad (18.40)$$

In the general case of crossed-axes gearing, the crossed-axes angle,  $\Sigma^r$ , between the axes of rotation,  $O_g^r$  and  $O_p^r$ , is a function of the form  $\Sigma^r = \Sigma^r(C, \Sigma, \{\delta\}, \{\varphi\})$ . It can be calculated from the following expression:

$$\Sigma^r(C, \Sigma, \{\delta\}, \{\varphi\}) = \tan^{-1} \left( \frac{|\mathbf{u}_g \times \mathbf{v}_p|}{\mathbf{u}_g \cdot \mathbf{v}_p} \right) \quad (18.41)$$

For convenience in calculating the distance,  $l_{CDA}$ , the points,  $o_g$  and  $o_p$ , can be chosen at the middle of the face width of a gear and mating pinion, respectively.\*

## 18.2 Tooth Flank Geometry in Perfect Real Gearing: In $S_{pr}$ -Gear System

One of the major differences between real gearing and its corresponding perfect gearing is that in the former, the configuration of the axes of rotation of the gear and mating pinion is different from that in the latter. This is because the configuration of the axes of rotation of the gear and mating pinion in perfect gearing is exactly specified, while in real gearing, the configuration depends on the deviation of the actual configuration of the axes of rotation from the desired configuration, and is mostly indefinite. Although the deviation of the actual configuration of the axes of rotation from the desired configuration in real gearing can be expressed in terms of linear and angular displacements, the actual values of both the linear and angular displacements are not known. However, the actual displacements can be substituted with the corresponding tolerances for accuracy in axes configuration.

The desired tooth flank geometry in real gearing is determined on the premises of equality of the base pitch of a gear and that of a mating pinion to the operating base pitch of the gear pair. The equality of base pitches ( $\varphi_{b,g} = \varphi_{b,op}$  and  $\varphi_{b,p} = \varphi_{b,op}$ ) is the fundamental principle in the design of perfect real gearing.†

The equality of the base pitches has to be complemented with those for the following distances:

- From the gear base-cone-apex,  $A_g$ , to the middle of the effective face width,  $F_{pa}$
- From the pinion base-cone-apex,  $A_p$ , to the middle of the effective face width,  $F_{pa}$
- From the plane-of-action-apex,  $A_{pa}$ , to the middle of the effective face width,  $F_{pa}$

All these distances have correlate to one another. The correlation can be expressed in terms of the design parameters of the gear pair.

All three apexes,  $A_g$ ,  $A_p$ , and  $A_{pa}$ , are always located within a common straight line, that is, within the centerline,  $\mathcal{C}$ .

As shown below in this chapter, in desirable real gearing (that is, in  $S_{pr}$ -gear systems), the tooth flank of one member of a gear pair rolls over the tooth flank of a mating member, similar to that in perfect gearing of a corresponding design. In this way, a uniform rotation from the driving shaft is transmitted to the driven shaft smoothly with zero transmission error. The tooth flank of a gear,  $\mathcal{G}$ , and that of the mating pinion,  $\mathcal{P}$ , make point contact at every instant of time. The degree of conformity of the tooth flanks,  $\mathcal{G}$  and  $\mathcal{P}$ , of the gear

\* CAD/CAM tools and finite-element analysis (FEA) can be used to evaluate the anticipated displacements and deformations in a gear drive under an operating load.

† The three conditions for existence of perfect gearing, that is, (a) the condition of contact between the tooth flanks, (b) the condition of conjugacy, and (c) the equality of three base pitches, have to be fulfilled within the effective face width,  $F_{pa}$ , of a perfect gear pair. In the case where face widths of a gear,  $F_g$ , and that of a mating pinion,  $F_p$ , do not overlap one another, the effective face width,  $F_{pa}$ , is either zero or has a negative value ( $F_{pa} \leq 0$ ), which is not permissible, as no physical contact between the tooth flanks,  $\mathcal{G}$  and  $\mathcal{P}$ , is observed in this case.

and the pinion has the highest attainable value at every contact point,  $K$ . The path of contact point on both tooth flanks,  $\mathcal{G}$  and  $\mathcal{P}$ , is a spatial curve. The location of the path of contact within the tooth flanks  $\mathcal{G}$  and  $\mathcal{P}$  depends on the actual values of misalignment of the axes of rotation,  $O_g^r$  and  $O_p^r$ , of the gear and pinion. The larger the axis misalignment, the more the path of contact shifts toward one end of the gear pair. However, under no circumstances does the path of contact intersect either end of the gear and the pinion, as it is determined for the case of the maximum allowed axis misalignment, which does not exceed the specified tolerance for axis misalignment.

In theory, three different types of perfect gearings are distinguished:

1. Parallel-axes gearing ( $P_a$ -gearing)
2. Intersected-axes gearing ( $I_a$ -gearing)
3. Crossed-axes gearing ( $C_a$ -gearing)

In reality, because of axis misalignment (which is inevitable), neither parallel-axes gearing nor intersected-axes gearing is physically possible. Gearing of any and all designs is a kind of crossed-axes gearing. Therefore, the discussion below begins with crossed-axes gearing.

### 18.2.1 Tooth Flank Geometry in Perfect Real Gearing

In gears for  $S_{pr}$ -gear systems, the tooth flank geometry is derived so as to ensure smooth transmission of a uniform rotation from a driving shaft to a driven shaft. Taken as a whole, the tooth flanks,  $\mathcal{G}$  and  $\mathcal{P}$ , of a gear and mating pinion are neither enveloping nor conjugate to one another. However, because of point contact between the tooth flanks  $\mathcal{G}$  and  $\mathcal{P}$ , at every instant of time, (a) a straight line along the contact perpendicular,  $\mathbf{n}_g$ , always intersects the axis of instant rotation,  $P_{ln}$ , and (b) instant values of base pitches of both the gear and mating pinion are equal to the instant value of the operating base pitch of the gear pair.

For convenience, particular reference systems are preferred to be used when deriving equations for the gear,  $\mathcal{G}$ , and the mating pinion,  $\mathcal{P}$ , tooth flanks, correspondingly.

#### 18.2.1.1 Adopted Concept Tooth Flank Generation of Gears for $S_{pr}$ -Gear System

In all cases, perfect real gear pairs are subject to similar inaccuracies as gearings of other designs. Because of manufacturing errors, inaccuracies in the mounting distance, deflections under applied loads, and so forth, the tooth flanks of perfect real gears are displaced from their desired location, and their actual orientation is different from the desired orientation. Perfect real gearing has to be designed so as to make gearing of this type insensitive to manufacturing errors as well as axis misalignment.

Tooth flanks in perfect real gearing are generated by a line of contact,\*  $LC$ , that is specified under an assumption that all the displacements, both linear and angular, are zero. Specified this way, the tooth flanks in a gear for an  $S_{pr}$ -gear system is identical to that in the  $R$ -gearing discussed above (see Chapter 14). Then, an impact of the displacements onto the geometry of gear and mating pinion tooth flanks in  $S_{pr}$ -gearing is incorporated.

For this purpose, when the gears rotate, the line of contact,  $LC$ , is considered to rotate together with the plane of action,  $PA$ . The current configuration of the line of contact in relation to the plane of action remains the same. However, the configurations of the line of contact in relation to the reference systems,  $X_gY_gZ_g$  and  $X_pY_pZ_p$ , associated with the gear and mating pinion depend on the actual values of axis misalignment in the gear pair. Axis misalignment in the gear pair is kept within the prespecified tolerances for the accuracy of axis misalignment.

All possible configurations of the plane of action,  $PA$ , in relation to the reference systems,  $X_gY_gZ_g$  and  $X_pY_pZ_p$ , are taken into account. The plane of action,  $PA$ , is rotated about the axis,  $O_{pa}$ , under all possible values of the deviations, both linear and angular, in terms of which the axis misalignment can be expressed. All possible configurations of the line of contact,  $LC$ , in relation to the reference systems,  $X_gY_gZ_g$  and  $X_pY_pZ_p$ , are considered in this way. Ultimately, a gear tooth flank,  $\mathcal{G}$ , is generated in a reference system,  $X_gY_gZ_g$ , associated with the gear as a locus of the line of contact,  $LC$ . Similarly, a mating pinion tooth flank,  $\mathcal{P}$ , is generated in a reference system,  $X_pY_pZ_p$ , associated with the pinion as a locus of that same line of contact,  $LC$ . Regardless of the tooth flanks,  $\mathcal{G}$  and  $\mathcal{P}$ , of a gear and a mating pinion being generated by that same line of contact,  $LC$ , the tooth flanks,  $\mathcal{G}$  and

\* It should be stressed from the very beginning that, as contact ratio in a gear pair is always greater than one, no changes to the geometry of the line of contact,  $LC$ , are permissible. Once the geometry of the line of contact is specified for a certain pair of the gear teeth, this geometry should remain the same when the gears rotate. Otherwise, the equality between the base pitches of a gear and a mating pinion in the gear pair cannot be kept.

$\mathcal{P}$ , in  $S_{pr}$ -gearing are always in point contact with one another. The degree of conformity at the point of contact between the tooth flanks  $\mathcal{G}$  and  $\mathcal{P}$  in  $S_{pr}$ -gearing is always the highest possible.

The concept adopted for tooth flank generation of gears in  $S_{pr}$ -gear systems can be viewed in an alternative manner.

Consider the plane of action,  $PA$ , for example, in a perfect parallel-axes gear pair, as schematically depicted in Figure 18.10.  $F_{pa}$  is the effective face width of the gear pair. Construct a desired line of contact,  $LC_{des}$ , in the nominal configuration of the axes of rotation,  $O_g$  and  $O_p$ , of a gear and mating pinion. After that, two extremal configurations of the desired line of contact,  $LC_{des}$ , are constructed. One of them is for the maximal positive and the other for the extreme negative deviation of the desired line of contact,  $LC_{des}$ , from its nominal configuration. All three desired lines of contact are located within the plane of action,  $PA$ .

The plane of action,  $PA$ , can be sliced into an infinite number of slices, each of which is perpendicular to the gear axis of rotation,  $O_g$ , of the gear. The width of each elementary slice is designated as  $\Delta F_{pa}$ .

For the slices,  $\Delta F_{pa}$ , at both ends of the face width,  $F_{pa}$ , the elementary lines of contact,  $lc_g$  and  $lc_p$ , for the gear and mating pinion are constructed for a perfect crossed-axes gear pair having maximal linear,  $\{\delta_g\}$  and  $\{\delta_p\}$ , and angular,  $\{\varphi_g\}$  and  $\{\varphi_p\}$ , displacements of the gear,  $O_g$ , and pinion,  $O_p$  axes of rotation from their nominal configuration in relation to the plane of action,  $PA$  (see Equations 18.16 and 18.17 for the calculation of the displacements,  $\{\delta_g\}$  and  $\{\varphi_g\}$ , and Equations 18.18 and 18.19 for the calculation of the displacements,  $\{\delta_p\}$  and  $\{\varphi_p\}$ ). The displacements,  $\{\delta_g\}$  and  $\{\varphi_g\}$ , in nature are the tolerances for the elementary displacements,  $[\delta_g]$  and  $[\varphi_g]$ , respectively.

For the slice,  $\Delta F_{pa}$ , at the middle of the face width,  $F_{pa}$ , the elementary lines of contact,  $lc_g$  and  $lc_p$ , are constructed for a perfect crossed-axes gear pair with zero linear,  $\{\delta_g\}$  and  $\{\delta_p\}$ , and angular,  $\{\varphi_g\}$  and  $\{\varphi_p\}$ , displacements of the gear,  $O_g$ , and pinion,  $O_p$ , axes of rotation from their nominal configuration in relation to the plane of action,  $PA$ .

For the rest of the slices,  $\Delta F_{pa}$ , between the middle slice and the slices at the both ends of the face width,  $F_{pa}$ , the elementary lines of contact,  $lc_g$  and  $lc_p$ , are constructed for a perfect crossed-axes gear pair having intermediate values of the linear,  $\{\delta_g\}$  and  $\{\delta_p\}$ , and angular,  $\{\varphi_g\}$  and  $\{\varphi_p\}$ , displacements of the gear,  $O_g$ , and pinion,  $O_p$ , axis of rotation from their nominal configuration in relation to the plane of action,  $PA$ .

It is the right point to stress here that the instant plane-of-action apex,  $A_{pa}$ , as well as the instant base cone apexes,  $A_g$  and  $A_p$ , of a gear and a mating pinion occupy different locations for different slices. The central point,  $P$ , remains stationary. There is a certain freedom for the gear designer to choose functions of the distribution of the elementary displacements,  $[\delta_g]$ ,  $[\varphi_g]$  and  $[\delta_p]$ ,  $[\varphi_p]$ , within the face width,  $F_{pa}$ .

Two curves,  $a_gPc_g$  and  $a_pPc_p$ , are the enveloping curves to the family of the elementary lines of contact,  $lc_g$  and  $lc_p$ .

The tooth flanks,  $\mathcal{G}$  and  $\mathcal{P}$ , of a gear and a mating pinion are generated by two curves,  $a_gPc_g$  and  $a_pPc_p$ , one of which is constructed for the gear, and the other of which is constructed for the pinion.

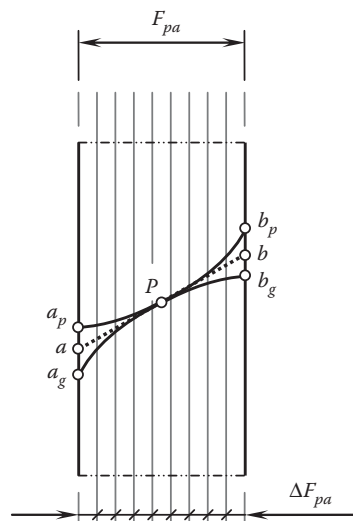


FIGURE 18.10

On the adopted concept for tooth flank generation in gears for  $S_{pr}$ -gear system.

### 18.2.1.2 Preferred Reference Systems

Prior to deriving an equation for the gear tooth flank,  $\mathcal{G}$ , and its mating pinion tooth flank,  $\mathcal{P}$ , the tolerance,  $\{C\}$ , for the center distance,  $C$ ; the tolerance,  $\{\Sigma\}$ , for the crossed-axes angle,  $\Sigma$ ; and the tolerance,  $\{A\}$ , for the axial location of the gear in the direction of the gear axial vector,  $\mathbf{A}_g$  (see Figure 2.28 in Chapter 2) have to be specified.

The actual value of the center distance,  $C$ , is within the interval:

$$C - \{C_-\} \leq C \leq C + \{C^+\} \quad (18.42)$$

where  $\{C^+\}$  is the upper and  $\{C_-\}$  the lower maximum permissible deviations of the center distance,  $C$ .

The actual value of the crossed-axes angle,  $\Sigma$ , is within the interval:

$$\Sigma - \{\Sigma_-\} \leq \Sigma \leq \Sigma + \{\Sigma^+\} \quad (18.43)$$

where  $\{\Sigma^+\}$  is the upper and  $\{\Sigma_-\}$  the lower maximum allowed deviations of the crossed-axes angle,  $\Sigma$ .

The actual value of the axial distance,  $A$ , is within the interval:

$$A - \{A_-\} \leq A \leq A + \{A^+\} \quad (18.44)$$

where  $\{A^+\}$  is the upper and  $\{A_-\}$  the lower maximum allowed deviations in the direction of the gear axial vector,  $\mathbf{A}_g$ .

A convenient reference system can be determined in a few steps illustrated in Figure 18.11.

First, for a nominal configuration of the rotation vectors in  $S_{pr}$ -gearing, all the elements of the corresponding vector diagram are predetermined by configuration of the rotation vectors,  $\boldsymbol{\omega}_g$  and  $\boldsymbol{\omega}_p$ , as illustrated in Figure 18.10a. The vector diagram can be constructed in an arbitrary reference system: a reference system,  $X_h Y_h Z_h$ , associated with the housing of the gear pair, in particular.

Second, in a perfect real gear pair, all the elements of the vector diagram are displaced from their nominal locations and orientations, as shown in Figure 18.10b. None of the angular velocity vectors in a perfect real gear pair,  $\boldsymbol{\omega}_g^r$ ,  $\boldsymbol{\omega}_p^r$ , and  $\boldsymbol{\omega}_{pl}^r$ , align with the corresponding angular velocity vectors,  $\boldsymbol{\omega}_g$ ,  $\boldsymbol{\omega}_p$ , and  $\boldsymbol{\omega}_{pl}$ , constructed for their nominal configuration. Moreover, the gear base cone apex,  $A_g^r$ , the pinion base cone apex,  $A_p^r$ , and the

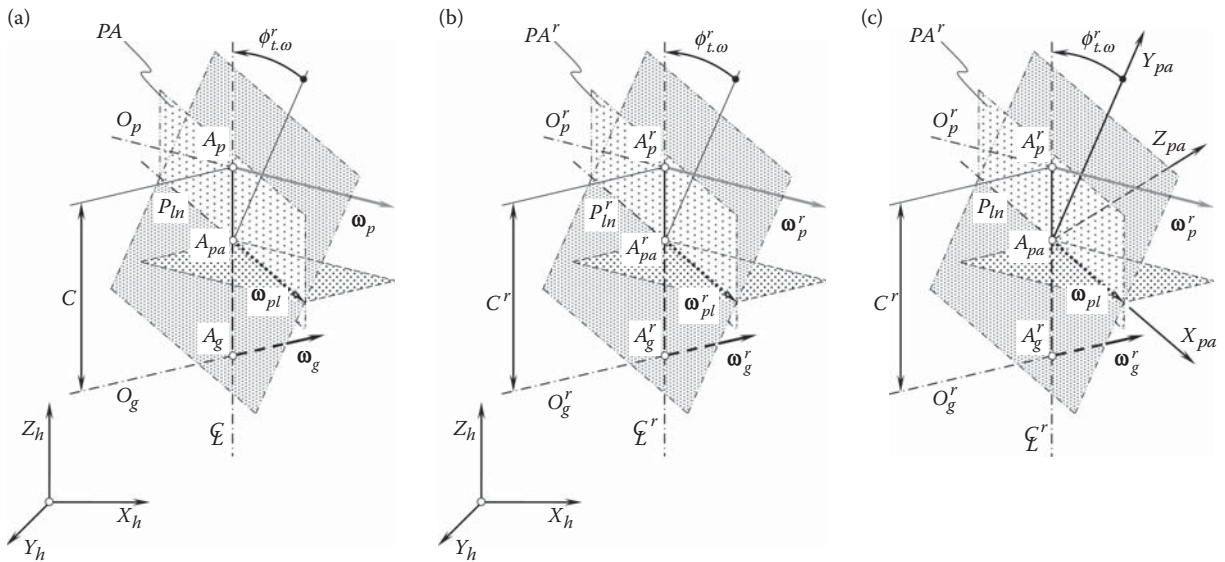


FIGURE 18.11

Vector diagrams constructed for crossed-axes gear pairs: (a) perfect gear pair, (b) perfect real gear pair (in a motionless reference system associated with the gear pair housing), and (c) perfect real gear pair (in a reference system associated with the plane of action,  $PA$ , of the gear pair).

plane-of-action apex,  $A_{pa}^r$ , are all displaced from their nominal positions, labeled as  $A_g$ ,  $A_p$ , and  $A_{pa}$ . Ultimately, the center distance,  $C^r$ ; the crossed-axes angle,  $\Sigma^r$ ; and the pressure angle,  $\phi_{t,\omega}^r$ , in a perfect real gear pair differ from those,  $C$ ,  $\Sigma$ , and  $\phi_{t,\omega}$ , constructed for their nominal configuration. Permissible deviations of all the displacements in a perfect real gear pair in relation to their nominal values are limited by:

- The tolerance,  $\{C\}$ , on the accuracy of the center distance,  $C$
- The tolerance,  $\{\Sigma\}$ , on the accuracy of the crossed-axes angle,  $\Sigma$
- The tolerance,  $\{A\}$ , on the accuracy of the gear axial distance,  $A$

The displacements could be more visible in a case where both vector diagrams in Figure 18.10a and b are constructed together so as to overlap one another. However, as the displacements are of small values, the overlapped vector diagrams are not shown in Figure 18.10.

Third, a reference system,  $X_{pa}Y_{pa}Z_{pa}$ , can be associated with the plane of action,  $PA$ . The reference system originates at the plane-of-action apex,  $A_{pa}$ , and the axis,  $X_{pa}$ , is pointed along the vector of instant rotation,  $\omega_{pl}$ , as illustrated in Figure 18.10c. In this case, an advantage can be gained from the fact that the configurations of the following elements of the vector diagram, that is (a) of the plane-of-action apex,  $A_{pa}$ ; (b) of the vector of instant rotation,  $\omega_{pl}$ ; and (c) of the centerline,  $\mathcal{C}$ , are not altered under the manufacturing errors or the displacements caused by other reasons. Ultimately, in the case under consideration, the plane of action,  $PA$ , becomes stationary.

Fourth, it is assumed below that when a gear displaces from its nominal position and orientation, the position of the middle,  $f$ , of the effective face width,  $F_{pa}$ , is not altered within the axis of instant rotation,  $P_{ln}$ , and remains the same. This point can be chosen as the origin of a Cartesian reference system,  $X_fY_fZ_f$ , associated with the plane of action,  $PA$ , as illustrated in Figure 18.12. The reference system,  $X_fY_fZ_f$ , is shifted along the axis,  $X_{pa}$ , with respect to the reference system,  $X_{pa}Y_{pa}Z_{pa}$ , at a distance,  $r_{w,pa}$ , and turned about this axis through the transverse pressure angle,  $\phi_{t,\omega}$ .

The reference system,  $X_fY_fZ_f$ , is adopted below as a motionless reference system. It does not alter its configuration with respect to the gear housing when the gear displaces from its nominal location and orientation because of manufacturing errors, under an operating load, because of heat extension of the gear housing or the rest of the components of the gear transmission, and so forth.

### 18.2.1.3 Derivation of Equation of Tooth Flank in $S_{pr}$ -Gearing

The tooth flanks of a gear and mating pinion in  $S_{pr}$ -gearing are generated by a line of contact,  $LC$ , between the tooth flanks,  $\mathcal{G}$  and  $\mathcal{P}$ . Though the tooth flanks are not generated yet, a desired line of contact can be constructed at this point. The line of contact,  $LC$ , is a planar curve that is entirely located within the plane of action,  $PA$ . When generating the tooth flanks, the desired line of contact travels together with the plane of action,  $PA$ .

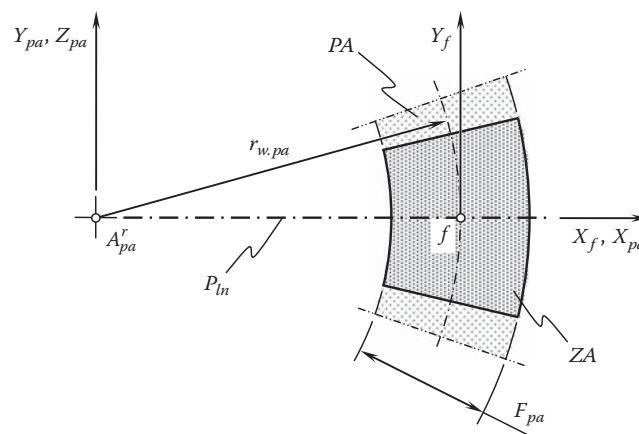


FIGURE 18.12

The Cartesian reference system,  $X_fY_fZ_f$ , associated with the plane of action,  $PA$ , and originating at the middle,  $f$ , of the effective face width,  $F_{pa}$ .



In the reference system,  $X_f Y_f Z_f$ , associated with the plane of action,  $PA$ , the position vector of a point,  $\mathbf{r}_{lc}^{pa}$ , of the desired line of contact,  $LC$ , can be analytically described in matrix form as:

$$\mathbf{r}_{lc}^{pa}(r_{pa}) = \begin{bmatrix} X_{lc}^{pa}(r_{pa}) \\ Y_{lc}^{pa}(r_{pa}) \\ 0 \\ 1 \end{bmatrix} \quad (18.45)$$

Here, in Equation 18.45,  $r_{pa}$  designates a current value of the distance at which point,  $f$ , is remote from a current plane-of-action apex,  $A_{pa}^{r,cur}$ . For a specified gear pair, the distance,  $r_{pa}$ , is within the interval:

$$r_{w.pa} - \{\Delta r_{pa}^{(-)}\} \leq r_{pa} \leq r_{w.pa} + \{\Delta r_{pa}^{(+)}\} \quad (18.46)$$

The tolerances,  $\{\Delta r_{pa}^{(-)}\}$  and  $\{\Delta r_{pa}^{(+)}\}$ , for the accuracy of the distance,  $r_{pa}$ , are shown in Figure 18.13.

Considered in the reference system,  $X_f Y_f Z_f$ , the line of contact,  $LC$ , remains stationary when the distance,  $r_{pa}$ , changes from its minimum value,  $r_{w.pa} - \{\Delta r_{pa}^{(-)}\}$ , to its maximum value,  $r_{w.pa} + \{\Delta r_{pa}^{(+)}\}$ . However, a current location of the plane-of-action apex,  $A_{pa}^{r,cur}$ , travels within the interval specified by Equation 18.46, that is, between the extremal positions,  $A_{pa}^{r,min}$  and  $A_{pa}^{r,max}$ . An operator,  $\mathbf{Rs}(f \mapsto pa)$ , of the resultant coordinate system transformation can be used for the analytical description of the transition from the Cartesian coordinate system,  $X_f Y_f Z_f$ , to the reference system,  $X_{pa} Y_{pa} Z_{pa}$ , associated with the plane of action,  $PA$ :

$$\mathbf{Rs}(f \mapsto pa) = \begin{bmatrix} 1 & 0 & 0 & 0 \\ 0 & \cos \phi_{t,\omega} & \sin \phi_{t,\omega} & 0 \\ 0 & -\sin \phi_{t,\omega} & \cos \phi_{t,\omega} & -r_{pa} \\ 0 & 0 & 0 & 1 \end{bmatrix} \quad (18.47)$$

It is of critical importance to stress here that the operator,  $\mathbf{Rs}(f \mapsto pa)$ , of the resultant coordinate system transformation is a function of a current value of the distance,  $r_{pa}$ .

Further, the operator,  $\mathbf{Rs}(PA \mapsto \mathcal{G})$ , of the resultant coordinate system transformation can be used for the analytical description of the transition from the Cartesian coordinate system,  $X_{pa} Y_{pa} Z_{pa}$ , associated with the plane of action,  $PA$ , to the Cartesian coordinate system,  $X_g Y_g Z_g$ , associated with the gear. Again, in the case of  $S_{pr}$ -gearing, the operator,  $\mathbf{Rs}(PA \mapsto \mathcal{G})$ , of the resultant coordinate system transformation is a function of a current value of the distance,  $r_{pa}$ .

With that said, for the analytical description of the transition from the Cartesian coordinate system,  $X_f Y_f Z_f$ , to the coordinate system,  $X_g Y_g Z_g$ , associated with the gear, the operator,  $\mathbf{Rs}(f \mapsto \mathcal{G})$ , of the resultant coordinate

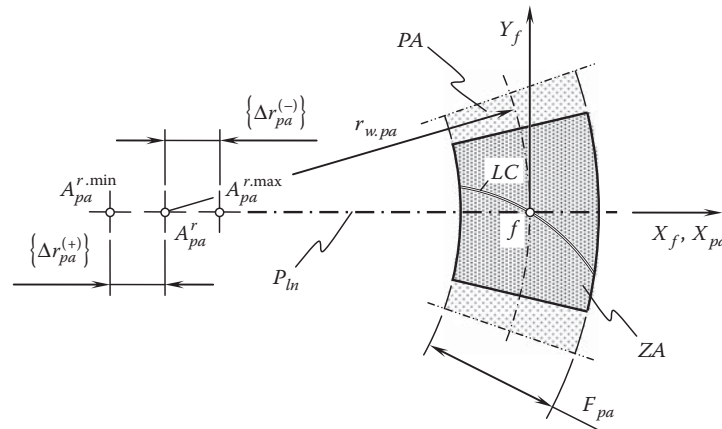


FIGURE 18.13

Line of contact,  $LC$ , between the interacting tooth flanks,  $\mathcal{G}$  and  $\mathcal{P}$ , and tolerances,  $\{\Delta r_{pa}^{(-)}\}$  and  $\{\Delta r_{pa}^{(+)}\}$ , for the accuracy of the distance,  $r_{pa}$ .



system transformation can be used. The operator,  $\mathbf{Rs}(f \mapsto \mathcal{G})$ , equals the product:

$$\begin{aligned}\mathbf{Rs}(f \mapsto \mathcal{G}) &= \mathbf{Rs}(PA \mapsto \mathcal{G}) \cdot \mathbf{Rs}(f \rightarrow pa) \\ &= \mathbf{Rt}(r \mapsto g) \cdot \mathbf{Rt}(pa_0 \mapsto r) \cdot \mathbf{Tr}(-r_{w.g}, Y_g) \cdot \mathbf{Rt}(pa \mapsto pa_0) \cdot \mathbf{Rs}(f \rightarrow pa)\end{aligned}\quad (18.48)$$

Once the operators,  $\mathbf{Rs}(f \rightarrow pa)$  and  $\mathbf{Rs}(PA \mapsto \mathcal{G})$ , are functions of a current value of the distance,  $r_{pa}$ , the operator,  $\mathbf{Rs}(f \mapsto \mathcal{G})$ , is also a function of this design parameter of the gear pair. Below, this function is expressed in terms of the parameter,  $X_f|_{A_{pa}^{inst}}$ , which is the X-coordinate of the plane-of-action apex,  $A_{pa}^{inst}$ .

For the analytical description of a gear tooth flank,  $\mathcal{G}$ , in  $S_{pr}$ -gearing, an equation can be used:

$$\mathbf{r}_g^r(r_{pa}, \varphi_p, X_f|_{A_{pa}^{inst}}) = \mathbf{Rs}(f \mapsto \mathcal{G}) \cdot \mathbf{r}_{lc}^{pa}(r_{pa}) \quad (18.49)$$

The gear tooth flank,  $\mathcal{G}$ , in  $S_{pr}$ -gearing is a surface of three independent parameters. An instant value of the radius,  $r_{pa}$ , of the point of the line of contact,  $LC$ , is the first parameter. An instant value of the angle,  $\varphi_p$ , through which the input shaft is turned about the pinion axis of rotation,  $O_p$ , is the second parameter [the operator,  $\mathbf{Rs}(f \mapsto \mathcal{G})$ , of the resultant coordinate system transformation is a function of the angle,  $\varphi_p$ ], while the coordinate,  $X_f|_{A_{pa}^{inst}}$ , of the instant plane-of-action apex,  $A_{pa}^{inst}$ , is the third parameter.

Similarly, for a pinion tooth flank,  $\mathcal{P}$ , a corresponding equation is derived:\*

$$\mathbf{r}_p^r(r_{pa}, \varphi_p, X_f|_{A_{pa}^{inst}}) = \mathbf{Rs}(f \mapsto \mathcal{P}) \cdot \mathbf{r}_{lc}^{pa}(r_{pa}) \quad (18.50)$$

Here, the operator,  $\mathbf{Rs}(f \mapsto \mathcal{P})$ , of the transition from the reference system,  $X_f Y_f Z_f$ , associated with the plane of action,  $PA$ , to the coordinate system,  $X_p Y_p Z_p$ , associated with the pinion, equals the product:

$$\begin{aligned}\mathbf{Rs}(f \mapsto \mathcal{P}) &= \mathbf{Rs}(PA \mapsto \mathcal{P}) \cdot \mathbf{Rs}(f \rightarrow pa) \\ &= \mathbf{Rt}(r \mapsto p) \cdot \mathbf{Rt}(pa_0 \mapsto r) \cdot \mathbf{Tr}(r_p, Y_p) \cdot \mathbf{Rt}(pa \mapsto pa_0) \cdot \mathbf{Rs}(f \rightarrow pa)\end{aligned}\quad (18.51)$$

The pinion tooth flank,  $\mathcal{P}$ , in  $S_{pr}$ -gearing is also a surface with three independent parameters. An instant value of the radius,  $r_{pa}$ , of the point of the line of contact,  $LC$ , is the first parameter. An instant value of the angle,  $\varphi_p$ , through which the input shaft is turned about the pinion axis of rotation,  $O_p$ , is the second parameter [the operator,  $\mathbf{Rs}(f \mapsto \mathcal{P})$ , of the resultant coordinate system transformation is a function of the angle,  $\varphi_p$ ], while the coordinate,  $X_f|_{A_{pa}^{inst}}$ , of the instant plane-of-action apex,  $A_{pa}^{inst}$ , is the third parameter.

Three independent parameters,  $r_{pa}$ ,  $\varphi_p$ , and  $X_f|_{A_{pa}^{inst}}$ , are excessive for the determination of a surface, in both cases, that is, for a gear tooth flank,  $\mathcal{G}$ , as well as for a mating pinion tooth flank,  $\mathcal{P}$ , as a surface is a space of two dimensions. An advantage can be gained from the available plurality of independent parameters by setting a favorable functional correlation between two of them, that is, between the parameters  $\varphi_p$  and  $X_f|_{A_{pa}^{inst}}$ . The function  $X_f|_{A_{pa}^{inst}} = X_f|_{A_{pa}^{inst}}(\varphi_p)$  has to be of a kind that guarantees the tooth flanks,  $\mathcal{G}$  and  $\mathcal{P}$ , are smooth regular surfaces. Once two of three independent parameters somehow correlate to one another, then the tooth flanks,  $\mathcal{G}$  and  $\mathcal{P}$ , become functions of two independent parameters. Below in this chapter, an example of such a functional correlation,  $X_f|_{A_{pa}^{inst}} = X_f|_{A_{pa}^{inst}}(\varphi_p)$ , between two of three independent parameters is considered.

The operator of the resultant coordinate system transformation,  $\mathbf{Rs}(PA \mapsto \mathcal{P})$ , that is, the operator of the transition from the reference system,  $X_{pa} Y_{pa} Z_{pa}$ , associated with the plane of action,  $PA$ , to the Cartesian coordinate system,  $X_p Y_p Z_p$ , associated with the pinion, needs to be composed.

The operator of the resultant coordinate system transformation,  $\mathbf{Rs}(f \mapsto \mathcal{P})$ , as well as the operators,  $\mathbf{Rs}(f \rightarrow pa)$  and  $\mathbf{Rs}(PA \mapsto \mathcal{G})$ , are functions of a current value of the distance,  $r_{pa}$ .

\* Another approach to the derivation of equations for the position vectors of a point,  $\mathbf{r}_g$  and  $\mathbf{r}_p$ , of gear,  $\mathcal{G}$ , and mating pinion,  $\mathcal{P}$ , tooth flanks in  $S_{pr}$ -gearing is disclosed on pages 427 through page 435 in the first edition of this monograph [137].

The distance,  $r_{pa}$ , can be expressed in terms of elementary linear displacements,  $\delta_{gx}$ ,  $\delta_{gy}$ , and  $\delta_{gz}$ , and elementary angular displacements,  $\varphi_{gx}$ ,  $\varphi_{gy}$ , and  $\varphi_{gz}$ , of a gear, together with elementary linear displacements,  $\delta_{px}$ ,  $\delta_{py}$ , and  $\delta_{pz}$ , and elementary angular displacements,  $\varphi_{px}$ ,  $\varphi_{py}$ , and  $\varphi_{pz}$ , of a mating pinion.

In  $S_{pr}$ -gearing, when the gears rotate, tooth flanks,  $\mathcal{G}$  and  $\mathcal{P}$ , of a gear and a mating pinion, correspondingly, are generated as loci of consecutive positions of a “pseudo-line of contact,  $LC_{psv}$ .” In the best-case scenario, a “pseudo-line of contact,  $LC_{psv}$ ” is of a favorable geometry. When a gear pair operates, the tooth flanks,  $\mathcal{G}$  and  $\mathcal{P}$ , of a gear and a mating pinion, make point contact, and not line contact. The contact geometry at every contact point,  $K$ , in this case is “near-favorable,” as the “pseudo-line of contact,  $LC_{psv}$ ” geometry is determined meaning line contact of the tooth flanks,  $\mathcal{G}$  and  $\mathcal{P}$ , and not point contact between them.

In  $S_{pr}$ -gearing, at the beginning, favorable contact geometry between the tooth flanks,  $\mathcal{G}$  and  $\mathcal{P}$ , is determined at every point of contact,  $K$ , of the teeth flanks (within the active portion of the face width,  $F_{pa}$ ). After that, the “pseudo-line of contact,  $LC_{psv}$ ” can be determined (if necessary) as a planar curve (that is entirely located within the plane of action,  $PA$ ) that is tangent to the direction of extremum degree of conformity of the tooth flanks at every contact point,  $K$ .

The disclosed approach for generating gear,  $\mathcal{G}$ , and mating pinion,  $\mathcal{P}$ , tooth flanks can be qualitatively summarized in the following way. Consider that the plane-of-action apex,  $A_{pa}^{r,cur}$ , at its initial location coincides with the point,  $A_{pa}^{r,min}$ . For such a configuration of the axes of rotation,  $O_g$  and  $O_p$ , of a gear and a mating pinion, the tooth flanks,  $\mathcal{G}_{min}$  and  $\mathcal{P}_{min}$ , of an  $R$ -gearing can be generated as disclosed above (see Chapter 14). Then the apex,  $A_{pa}^{r,cur}$ , is shifted toward the plane-of-action apex,  $A_{pa}^{r,max}$ , at a reasonably small distance (or at an infinitesimally short distance). As the operators of the resultant coordinate systems transformation are functions of a current value of the distance,  $r_{pa}$ , the initial configuration of the axes of rotation,  $O_g$  and  $O_p$ , is altered under such a shift. A novel  $R$ -gearing can be generated for a new configuration of the axes of rotation,  $O_g$  and  $O_p$ . Gradually shifting the apex,  $A_{pa}^{r,max}$ , toward the plane-of-action apex,  $A_{pa}^{r,max}$ , a set of tooth flanks,  $\mathcal{G}_{cur}$  and  $\mathcal{P}_{cur}$ , of different  $R$ -gearings can be generated. Finally, when the plane-of-action apex,  $A_{pa}^{r,cur}$ , at its current location coincides with the point,  $A_{pa}^{r,max}$ , the tooth flanks,  $\mathcal{G}_{max}$  and  $\mathcal{P}_{max}$ , are generated.

The tooth flanks of a gear in  $S_{pr}$ -gearing are the enveloping surfaces to all the intermediate gear tooth flanks,  $\mathcal{G}_{min}$ ,  $\mathcal{G}_{cur}$ , ..., and  $\mathcal{G}_{max}$ . Similarly, the tooth flanks of a pinion in  $S_{pr}$ -gearing are the enveloping surfaces to all the intermediate pinion tooth flanks,  $\mathcal{P}_{min}$ ,  $\mathcal{P}_{cur}$ , ..., and  $\mathcal{P}_{max}$ . Under any and all permissible configurations of the axes of rotation,  $O_g$  and  $O_p$ , of a gear and a mating pinion, the interacting tooth flanks of a gear and a mating pinion in  $S_{pr}$ -gearing make point contact.

A detailed analysis of Equation 18.49 for the position vector of a point,  $\mathbf{r}_g^r$ , of a tooth flank,  $\mathcal{G}_r$ , in  $S_{pr}$ -gearing, as well as the similar Equation 18.50 for the position vector of a point,  $\mathbf{r}_p^r$ , of a mating pinion tooth flank,  $\mathcal{P}_r$ , in  $S_{pr}$ -gearing reveal that alterations (in comparison to perfect gearing) should be made to the tooth flanks of both members engaged in mesh. It is not allowed to keep one of the members with the original perfect geometry of the tooth flanks and compensate for the required changes with the mating member of the gear pair. Making changes to the geometry of the tooth flanks of both members of the gear pair is necessary because in  $S_{pr}$ -gearing, the geometry of the tooth flanks,  $\mathcal{G}_r$  and  $\mathcal{P}_r$ , is predetermined by a given configuration of the rotation vectors,  $\boldsymbol{\omega}_g$  and  $\boldsymbol{\omega}_p$ , of the gear and the pinion.

The tooth flanks of a gear and mating pinion in  $S_{pr}$ -gearing are always in point contact. However, the degree of conformity\* of the interacting tooth flanks of the gear and mating pinion is always of the highest possible value.

The derived equations (see Equations 18.49 and 18.50) for the tooth flanks,  $\mathcal{G}$  and  $\mathcal{P}$ , of a gear and a mating pinion in  $S_{pr}$ -gearing can be used for design of both gear and mating pinion tooth flanks, as well as reference surfaces in inspection of gear and mating pinion tooth flanks. Implementation of the proposed geometry of tooth flanks in  $S_{pr}$ -gearing as a datum surface for the purposes of gear inspection and for measuring deviations of an approximate gear due to *design* errors, as well as *manufacturing* errors, is an additional advantage of this novel kind of gearing.

The geometry of tooth flanks in  $S_{pr}$ -gearing is the target when designing real gears. Later on, the determined most favorable tooth flank geometry can be approximated by surfaces convenient for machining/finishing of the gears.

\* A high degree of conformity between the tooth flanks,  $\mathcal{G}$  and  $\mathcal{P}$ , of a gear and mating pinion in  $S_{pr}$ -gearing is of critical importance, as the contact strength of the gear and mating pinion tooth flanks strongly depends on the degree of conformity: the higher the degree of conformity, the higher contact strength of the interacting teeth, and vice versa.

The tooth flank in  $S_{pr}$ -gearing is also used as the *reference surface* for any and all desired tooth flank modifications. Once the desired tooth flanks of a gear and mating pinion in  $S_{pr}$ -gearing are specified in terms of the linear and angular displacement, design parameters of the gear set, and so forth, then it can be approximated by a corresponding surface that is convenient for machining. This returns a practical kind of gear tooth flank modification: not a profile modification or a lead modification, but a modification of the entire tooth flank of a gear and mating pinion.

It is instructive to stress here the important difference between *conjugate* tooth surfaces,  $\mathcal{G}$  and  $\mathcal{P}$ , in  $S_{pr}$ -gearing and those in gearings of other types: parallel-axes gearings, intersected-axes gearings, and crossed-axes gearings. In the latter cases, gear and mating pinion tooth flanks,  $\mathcal{G}$  and  $\mathcal{P}$ , are conjugate\* to one another and are in line contact with each other. In  $S_{pr}$ -gearing, the condition of conjugacy is also fulfilled; however, the tooth flanks,  $\mathcal{G}$  and  $\mathcal{P}$ , make *point contact* (and not *line contact*) with one another. It is proposed to refer to conjugacy of this sort as *conjugacy of higher order* of the tooth flanks,  $\mathcal{G}$  and  $\mathcal{P}$ , of a gear and mating pinion.

#### 18.2.1.4 Angular Base Pitch in $S_{pr}$ -Gearing

In  $S_{pr}$ -gearing, at every instant of time, the angular base pitch of a gear,  $\varphi_{b,g}^{\text{inst}}$ , and angular base pitch of a mating pinion,  $\varphi_{b,p}^{\text{inst}}$ , are both equal to the instant value of the angular operating base pitch,  $\varphi_{b,op}^{\text{inst}}$ , of the gear pair† (that is, the equalities‡  $\varphi_{b,g}^{\text{inst}} = \varphi_{b,op}^{\text{inst}}$  and  $\varphi_{b,p}^{\text{inst}} = \varphi_{b,op}^{\text{inst}}$  are valid). These two equalities have to be fulfilled within the effective face width,  $F_{pa}$ , of a gear pair. Only under such conditions can a pure rotation be transmitted from a driving shaft to a driven shaft by means of  $S_{pr}$ -gearing.

The actual values of the instant angular base pitches in  $S_{pr}$ -gearing vary depending on the actual configuration of the rotation vectors,  $\omega_g$  and  $\omega_p$ . Current configuration of the rotation vectors,  $\omega_g$  and  $\omega_p$ , varies either in time as a function of the gear pair loading or for different gear pairs of the same design. Current deviations of the rotation vectors,  $\omega_g$  and  $\omega_p$ , from their desired configuration are not known. However, the corresponding tolerances,  $\{\Delta\varphi_{b,g}^{\text{inst}}\}$ ,  $\{\Delta\varphi_{b,p}^{\text{inst}}\}$ , and  $\{\Delta\varphi_{b,op}^{\text{inst}}\}$ , for the accuracy of the configuration of the rotation vectors,  $\omega_g$  and  $\omega_p$ , can be set up. Further the tolerances,  $\{\Delta\varphi_{b,g}^{\text{inst}}\}$ ,  $\{\Delta\varphi_{b,p}^{\text{inst}}\}$ , and  $\{\Delta\varphi_{b,op}^{\text{inst}}\}$ , the actual values of which are known, are handled instead of the deviations,  $\Delta\varphi_{b,g}^{\text{inst}}$ ,  $\Delta\varphi_{b,p}^{\text{inst}}$ , and  $\Delta\varphi_{b,op}^{\text{inst}}$ , the actual values of which are unknown.§

Shown in Figure 18.14 is an operating angular base pitch,  $\varphi_{b,op}^r$ , constructed for a nominal configuration of the rotation vectors,  $\omega_g$  and  $\omega_p$ , in an  $S_{pr}$ -gearing. The plane-of-action pitch circle of a radius,  $r_{w,pa}$ , is intersected by the sides of the angle,  $\varphi_{b,op}^r$ , at points,  $a$  and  $b$ ; that is, the points  $a$  and  $b$  are at an angular distance,  $\varphi_{b,op}^r$ , from one another. One of the three design parameters,  $\varphi_{b,op}$ ,  $r_{w,pa}$ , and  $ab$ , can be expressed in terms of the other two. Moreover, the linear distance,  $ab$ , also can be calculated:

$$ab = 2r_{w,pa} \sin \frac{\varphi_{b,op}^r}{2} \quad (18.52)$$

For a gear pair with the displaced tooth flanks,  $\mathcal{G}$  and  $\mathcal{P}$ , the actual values of the design parameters,  $\varphi_{b,op}$  and  $r_{pa}^{\text{inst}}$ , alter, while the linear distance,  $ab$ , remains the same value ( $ab = \text{const}$ ). For a specified value of the distance,

\* It is the right point to note here that the term *conjugate surfaces* is often used incorrectly. Commonly, a surface that is an envelope to another surface that travels in space is referred to as a *conjugate surface*—this is a mistake, as fulfillment of the enveloping condition,  $\mathbf{n} \cdot \mathbf{V}_\Sigma = 0$ , is necessary but not sufficient to generate conjugate surfaces. Therefore, the term *reversibly-enveloping surfaces* (or just *R<sub>e</sub>-surfaces* for simplicity) [115] can be considered an alternative to the term *conjugate surface* in all three types of gearing, that is, in parallel-axes gearing, intersected-axes gearing, and crossed-axes gearing.

† In  $S_{pr}$ -gearing, the necessary condition of contact ( $\mathbf{n} \cdot \mathbf{V}_\Sigma = 0$ ), and the necessary condition of conjugacy of the tooth flanks,  $\mathcal{G}$  and  $\mathcal{P}$ , of a gear and mating pinion are fulfilled, as both tooth flanks,  $\mathcal{G}$  and  $\mathcal{P}$ , are generated by means of a desired line of contact,  $LC$ , that is entirely located within and travels with the instant plane of action,  $PA$ , of the gear pair.

‡ Reminder: The necessity of consideration of the concept of *operating base pitch* is because of the following. When a gear and mating pinion in an  $S_{pr}$ -gear pair are disengaged from mesh, the angular base pitches,  $\varphi_{b,g}$  and  $\varphi_{b,p}$ , of both remain the same value. However, the gears cannot be engaged in proper mesh with one another when an actual configuration of the gears axes of rotation,  $O_g$  and  $O_p$ , is out of the interval that is specified for a particular  $S_{pr}$ -gear pair. This is because the actual value of the operating angular base pitch alters, as it depends on the actual configuration of the gear and pinion in relation to each other, including the location in relation to the centerline.

§ An  $S_{pr}$ -gear system is developed so as to accommodate a variable operating angular base pitch caused by variation of the displacements and deflections under a variable operating load of the shafts, housing, gear and pinion teeth, and so forth.



center distance,  $C$ , and the length of the axial vector,  $A$ . The geometry of the traces of contact point,  $K$ , on the gear,  $\mathcal{G}$ , and mating pinion,  $\mathcal{P}$ , tooth flanks, as well as the parameters of the actual portion of the active tooth flanks,  $\mathcal{G}$  and  $\mathcal{P}$ , depends on the actual values of the deviations  $\Delta C$  and  $\Delta A$ .

### 18.2.1.5 Features of Interaction of Tooth Flanks in $S_{pr}$ -Gearing

A few features of interaction of tooth flanks,  $\mathcal{G}$  and  $\mathcal{P}$ , of a gear and mating pinion, correspondingly, are briefly discussed immediately below. The reader's attention is focused on the path of the contact point over the tooth flanks,  $\mathcal{G}$  and  $\mathcal{P}$ , and features of geometry of contact between the tooth flanks,  $\mathcal{G}$  and  $\mathcal{P}$ .

*Trace of contact point on tooth flanks.* As an example, the location and orientation of the trace of contact point,  $tr$ , within the tooth flank of a spur  $S_{pr}$ -gearing is schematically shown in Figure 18.15. In a case of zero axis misalignment, the trace of contact point on the left flank,  $tr_l^0$ , of the gear tooth, as well as on the right flank,  $tr_r^0$ , of the gear tooth goes through the middle of the face of the gear (see Figure 18.15b). In a case where positive axis misalignment is observed, the trace of contact points for the left,  $tr_l^+$ , and right,  $tr_r^+$ , sides of the gear tooth are shifted oppositely toward the ends of the gear, as schematically illustrated in Figure 18.15a. Similarly, negative axis misalignment results in the trace of contact point for the left,  $tr_l^-$ , and right,  $tr_r^-$ , sides of the gear tooth being shifted oppositely toward the opposite ends of the gear, as illustrated in Figure 18.15c. The schematics shown in Figure 18.15 pertain to  $S_{pr}$ -gearing that features constant-in-time values of all the displacements. When the displacements alter in time, then paths of contact of a more complex geometry are observed.

*Features of the contact geometry between the tooth flanks.* When perfect parallel-axes gears rotate, the plane of action is unwrapping from one base cylinder and wrapping onto the other base cylinder of mating gears, as schematically shown in Figure 8.26 (see Chapter 8). This schematic is valid as long as the axes of rotations of the gear,  $O_g$ , and its pinion,  $O_p$ , are parallel to one another. In reality, the axes of rotation,  $O_g^r$  and  $O_p^r$ , of a gear and mating pinion are not parallel to each other. At every instant of time, the axes of rotation,  $\hat{O}_g^r$  and  $\hat{O}_p^r$ , cross one another at a certain crossed-axes angle instead. The value of the crossed-axes angle depends on the current parameters of axis misalignment. Therefore, for desirable parallel-axes real gearing, a schematic based on crossing rotation vectors,  $\omega_g^r$  and  $\omega_p^r$ , of the gear and pinion should be applied instead of that for parallel-axes gearing.

Because of axis misalignment, parallel-axes gearing is actually a type of spatial gearing that features a distance of closest approach of the axes of a gear and mating pinion, as well as a crossed-axes angle. In reality, the closest distance of approach of the axes is approximately equal to the distance between parallel axes of the gear and pinion, and the actual value of the crossed-axes angle is close to either  $180^\circ$  (in external gearing) or  $0^\circ$  (in internal gearing).

In any case, the line contact in a perfect gear pair is substituted by point contact in its corresponding  $S_{pr}$ -gearing. The degree of conformity of the tooth flanks of the gear,  $\mathcal{G}_r$ , and the pinion,  $\mathcal{P}_r$ , at every point of their contact is of the maximum possible degree. No other systems of gearing of feature a degree of conformity of the tooth flanks of gears as high as that in  $S_{pr}$ -gearing. The last is of critical importance from the standpoint of

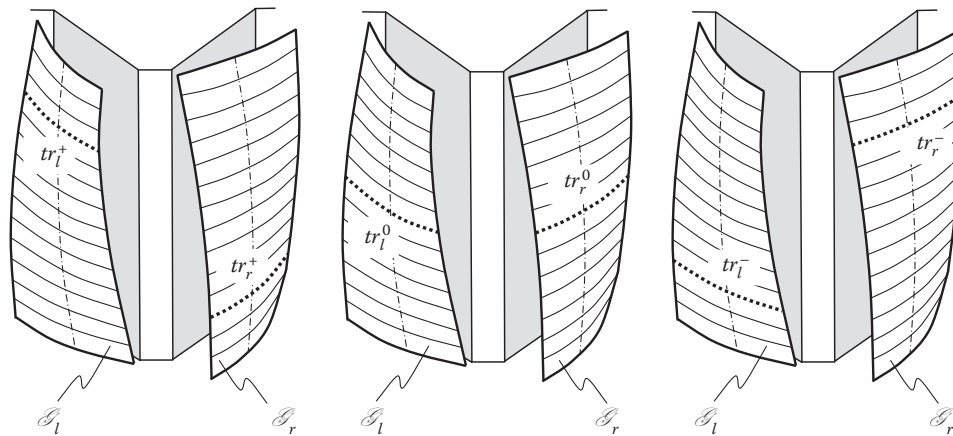


FIGURE 18.15

Traces of contact point,  $tr$ , on tooth flanks of  $S_{pr}$ -gear depending on an actual value of the axis misalignment: (a) positive axis misalignment, (b) zero axis misalignment, and (c) negative axis misalignment.



reduction of contact stress, as well as of increase in the wear resistance of the interacting tooth flanks of the gear and pinion.

Tooth flanks in  $S_{pr}$ -gearing always make point contact. The actual location and configuration of the trace of contact point,  $PC$ , depends on the actual value of the axis misalignment. As the tooth flanks of a gear,  $\mathcal{G}_r$ , and a mating pinion,  $\mathcal{P}_r$ , are always in point contact with one another, they do not envelop each other. However, under any reasonable axis misalignment, the instant base pitch of a gear,  $\varphi_{b,g}^{inst}$ , is equal to the instant base pitch of a mating pinion,  $\varphi_{b,p}^{inst}$ , and both of them are equal to the instant operating base pitch,  $\varphi_{b,op}^{inst}$ , of the gear pair:

$$\varphi_{b,g}^{inst} = \varphi_{b,op}^{inst} \quad (18.55)$$

$$\varphi_{b,p}^{inst} = \varphi_{b,op}^{inst} \quad (18.56)$$

The proposed geometry of tooth flanks in  $S_{pr}$ -gearing is derived to accommodate axes misalignment of all three components of linear displacements and all three components of angular displacements. This makes  $S_{pr}$ -gearing insensitive to axis misalignment within their reasonable range). The proposed gear system (that is,  $S_{pr}$ -gearing) is the only kind of self-adjustable gearing. No other kind of gearing can accommodate axis misalignment.

The geometry of the tooth flanks of intersected-axes  $S_{pr}$ -gearing is derived to accommodate axis misalignment of all three components of both the linear and angular displacements. This makes  $S_{pr}$ -gearing insensitive to axis misalignment. Gearing of the proposed design is the only kind of self-adjustable gearing possible at all. This significant advantage is achieved due to equality of the angular base pitches of a gear and a mating pinion to the operating base pitch of the gear pair at every instant of time. No transmission error is observed when, at every instant of time, the base pitches of a gear and mating pinion are equal to the operating base pitch of the gear pair. Ultimately, by means of  $S_{pr}$ -gears, a uniform rotation can be smoothly transmitted from a driving shaft to a driven shaft with no vibration generation or noise excitation.

The concept of the *path-of-contact surface*,  $P_{cs}$ , can be easily enhanced to  $S_{pr}$ -gearing: the path-of-contact surface,  $P_{cs}$ , is a continuous set of the circular-arc paths of contact,  $P_c$ , at different transverse pressure angles,  $\phi_{t,\omega}$ . The radius of a current circular-arc path of contact is a *nonlinear* function of the distance of the point on the pitch line,  $P_{ln}$ , from the plane-of-action-apex,  $A_{pa}$  ( $\neq A_g \neq A_p$ ). The path-of-contact surface,  $P_{cs}$ , is a continuous screw surface of variable transverse pressure angles,  $\phi_{t,\omega}$ , and variable pitch (along the axis of instant rotation,  $P_{ln}$ ).

### 18.2.2 Possibility of Implementation of the Concept of $S_{pr}$ -Gearing in Design of Two-Degrees-of-Freedom Gearing

Gears commonly used in the industry feature one degree of freedom. The input rotation is the only independent mobility in gear pairs of conventional design. For particular applications, additional mobility in a gear pair is desired. Gear pairs of this particular kind are referred to as *two-degrees-of-freedom gearings*, or just *2DOF-gearings* for simplicity, as they feature two mobilities. The rotation of the input shaft is one of two mobilities, and the motion by means of which the angle between gear and mating pinion axes of rotation alters is the other. Other kinds of two-degrees-of-freedom gearings that feature a combination of a translational and rotational motion are possible as well.

Two-degrees-of-freedom gearings have been investigated since the beginning of 1960s [152], or even earlier. They can be used in the design of *constant velocity joints*, or just CV-joints for simplicity. Robot arms are another area of potential application of  $S_{pr}$ -gearing.

In the example shown in Figure 18.16, a bevel gear coupling is composed of three bevel gears. Use of an  $S_{pr}$ -gear system makes possible a replacement of a gear joint with three bevel gears, with a gear joint having two  $S_{pr}$  gears, as illustrated in Figure 18.17.

The developed classification of possible kinds of the vector diagrams of gear pairs (see Figure 2.15) is helpful in the development of novel kinds of two-degrees-of-freedom gearings.

When developing a vector diagram for 2DOF-gearings, either a vector of linear or angular motion can be added to each of the vector diagrams shown in Figure 2.15. Then, each of the vector diagrams is investigated for whether a two-degrees-of freedom gear pair can be constructed on the premise of an enhance vector diagram. The vector diagrams of the gear pairs are those on the premise of which a corresponding two-degrees-of freedom gear pair can be constructed.

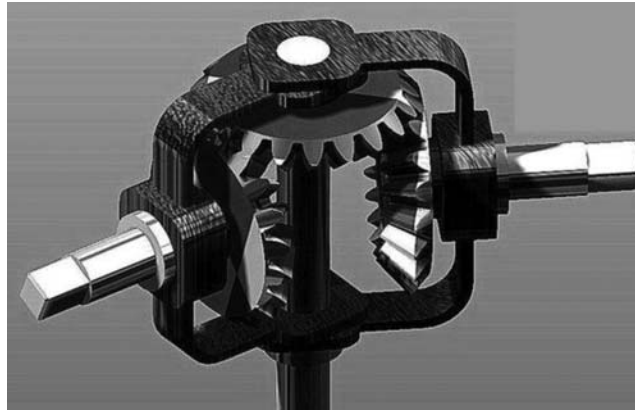


**FIGURE 18.16**  
Bevel gear coupling.



**FIGURE 18.17**  
Gear joint composed of two gears.

As an example, a vector diagram for intersected-axes two-degrees-of-freedom gear pair is constructed in [Figure 18.18](#). Originally a vector diagram is constructed for a conventional intersected-axes gear pair using the rotation vectors,  $\omega_g$  and  $\omega_p$ , of a gear and a mating pinion for this purpose. In the example under consideration, it is adopted that the magnitudes,  $\omega_g$  and  $\omega_p$ , of the rotation vectors,  $\omega_g$  and  $\omega_p$ , are equal to one another (that is, an equality,  $\omega_g = \omega_p$ , is valid). The rotation vectors,  $\omega_g$  and  $\omega_p$ , form the intersected-axes angle,  $\Sigma$ . Then, a vector of instant rotation,  $\omega_{pl}$ , is constructed (recall that the vector of instant rotation,  $\omega_{pl}$ , equals  $\omega_{pl} = \omega_p - \omega_g$ ). The axial vectors,  $A_g$ , of a gear and mating pinion,  $A_p$ , are along the straight lines of action of the rotation vectors,  $\omega_g$  and  $\omega_p$ . The axial vector,  $A_{pl} = A_g + A_p$ , is along the line of action of the vector of instant rotation,  $\omega_{pl}$ . The midpoint,  $f$ , of the face width,  $F_{pa}$ , in a gear pair is located within the line of action of the axial vector,  $A_{pl}$ .

The complementary instant rotation,  $\omega_{rol}$ , of the gear and mating pinion is perpendicular to the plane through the rotation vectors,  $\omega_g$  and  $\omega_p$ . The complementary rotation,  $\omega_{rol}$ , is an independent parameter of the kinematics of the gear pair. It is anticipated that the magnitude,  $\omega_{rol}$ , of the rotation vector,  $\omega_{rol}$ , will be smaller compared to that of the rotation vectors,  $\omega_g$  and  $\omega_p$ .

With the vector diagram constructed (see [Figure 18.18](#)), a detailed design of the intersected-axes two-degrees-of-freedom gear pair can be developed.

A schematic of an intersected-axes two-degrees-of-freedom gear pair is illustrated in [Figure 18.19](#).

The rotation vectors,  $\omega_g$  and  $\omega_p$ , of a gear and a mating pinion form an intersected-axes angle,  $\Sigma$ , that varies in time; that is,  $\Sigma = \Sigma(t)$ . The gear is rotated about its axis of rotation,  $O_g$ , with an angular velocity,  $\omega_g$ . The mating pinion is rotated about its axis of rotation,  $O_p$ , with an angular velocity,  $\omega_p$ . The axes of rotations,  $O_g$  and  $O_p$ , intersect one another at the plane-of-action apex,  $A_{pa}^{inst}$ .



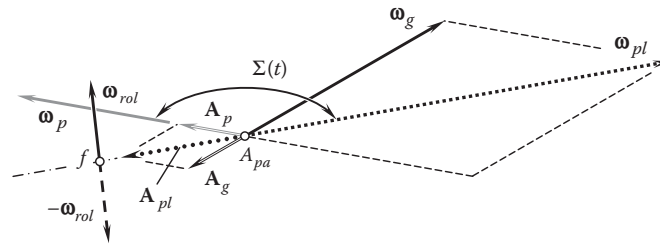


FIGURE 18.18

An example of a vector diagram constructed for an intersected-axes two-degrees-of-freedom gear pair.

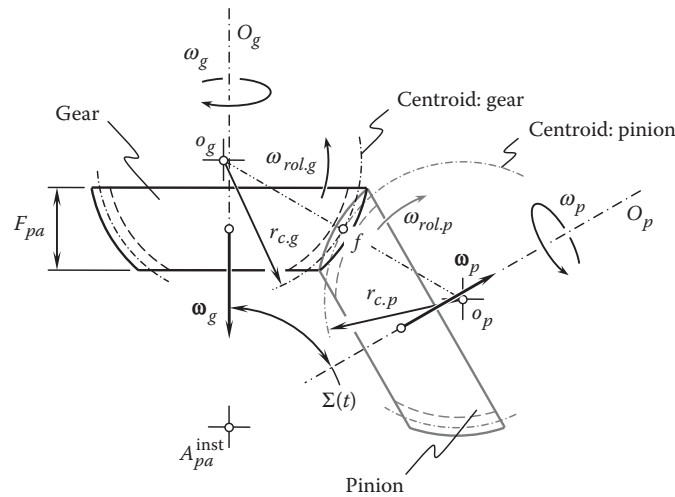


FIGURE 18.19

Schematic of perfect intersected-axes two-degrees-of-freedom gear pair.

In order to perform the complementary instant rotation,  $\omega_{rot}$ , the gear and pinion roll over one another. For this purpose, the gear and pinion rotate with angular velocities,  $\omega_{rot.g}$  and  $\omega_{rot.p}$ , correspondingly, about the centers,  $o_g$  and  $o_p$ . The midpoint,  $f$ , of the face width,  $F_{pa}$ , in the gear pair is located within a straight line through  $o_g$  and  $o_p$ .

When performing these rotations, the circular arc of a radius,  $r_{c.g}$ , associated with the gear rolls over the circular arc of a radius,  $r_{c.p}$ , associated with the pinion. The circular arcs are centered at  $o_g$  and  $o_p$ . The circular arcs of the radii,  $r_{c.g}$  and  $r_{c.p}$ , are the centroids in the rolling motion of the gear and the pinion. As the rolling motions,  $\omega_{rot.g}$  and  $\omega_{rot.p}$ , progress, the actual value of the intersected-axes angle,  $\Sigma(t)$ , varies.

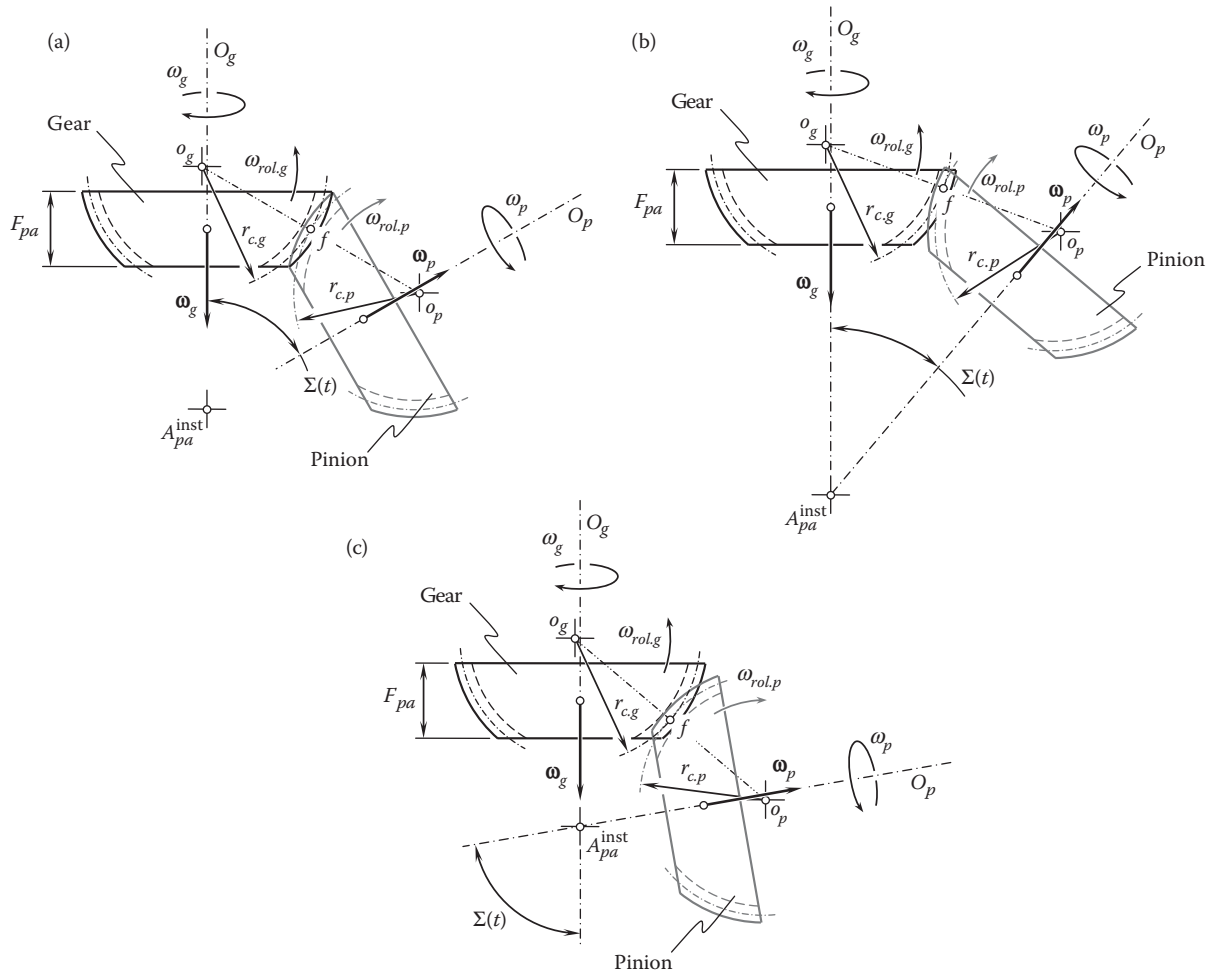
The variation of the intersected-axes angle,  $\Sigma(t)$ , is illustrated in Figure 18.20.

In the schematic shown in Figure 18.20a, a nominal configuration of a gear and a mating pinion in an intersected-axes two-degrees-of-freedom gear pair is depicted. As the rolling motions,  $\omega_{rot.g}$  and  $\omega_{rot.p}$ , progress, the actual value of the intersected-axes angle,  $\Sigma(t)$ , can be reduced, as illustrated in Figure 18.20b, or it can be increased, as shown in Figure 18.20c.

Shown in Figure 18.20, an intersected-axes two-degrees-of-freedom gear pair is capable of transmitting a uniform rotation smoothly from a driven shaft to a driven shaft. This is because the tooth flanks,  $\mathcal{G}$  and  $\mathcal{P}$ , of the gear and its mating pinion: (a) make proper contact with one another ( $\mathbf{n} \cdot \mathbf{v}_\Sigma = 0$ ); (b) are conjugate to one another; and (c) at every instant of time, the angular base pitch of a gear,  $\phi_{b.g}$ , equals the operating angular base pitch of the gear pair,  $\phi_{b.op}$ , and the angular base pitch of a mating pinion,  $\phi_{b.p}$ , also equals the operating angular base pitch of the gear pair,  $\phi_{b.op}$ ; that is, the equalities,  $\phi_{b.g} = \phi_{b.op}$  and  $\phi_{b.p} = \phi_{b.op}$ , are valid.

A two-degrees-of-freedom gear pair is designed in a way similar to how real gear pairs are designed. The only difference is that the tolerance for the accuracy of the crossed-axes angle,  $\Sigma$ , is substituted with a required interval of variation of the angle formed by the axes of rotation of a gear and a mating pinion.

The gear ratio in two-degrees-of-freedom gear pairs has a constant value ( $u = \text{const}$ ).

**FIGURE 18.20**

Different configurations of a gear and a mating pinion in intersected-axes two-degrees-of-freedom gear pair: (a) nominal configuration; (b) configuration with a reduced crossed-axes angle,  $\Sigma(t)$ ; and (c) configuration with a reduced crossed-axes angle,  $\Sigma(t)$ .

The developed classification of possible kinds of vector diagrams of gear pairs (see Figure 2.15) can be evolved if two-degrees-of-freedom gear pairs are taken into account.

### 18.2.3 Possibility of Implementation of the Concept of $S_{pr}$ -Gearing in Design of Gear Coupling

Gear coupling (see Figure 18.21) can be viewed as being composed of two internal gear pairs featuring a tooth ratio  $u = 1$ . A gear mesh of this particular type can be viewed as degenerate case of parallel-axes gearing. In a gear coupling, one spur gear is connected to a driving shaft, and the other is connected to a driven shaft. Both spur gears interact either with a common internal spur gear or two individual internal spur gears that share the common body of the gear.

When the linear and angular displacements of the axes of rotation of the input and output shafts are zero, the tooth profile in a gear coupling is not important (from the standpoint of gear meshing), and it can be of an arbitrary reasonable geometry. However, gear couplings are used in cases where the linear and angular displacements of the axes of rotation of the input and output shafts have nonzero values. If the linear and the angular displacements are taken into account, the tooth flank geometry becomes of critical importance. For gear couplings operating at high rotations, the geometry of the tooth flanks has to be determined based on the concept of  $S_{pr}$ -gearing.

In the ideal case when no axis misalignment occurs, the rotation vector,  $\omega_g$ , of the internal gear in a gear coupling is identical to the rotation vector,  $\omega_p$ , of the external gear in the gear coupling ( $\omega_g \equiv \omega_p$ ). As illustrated in

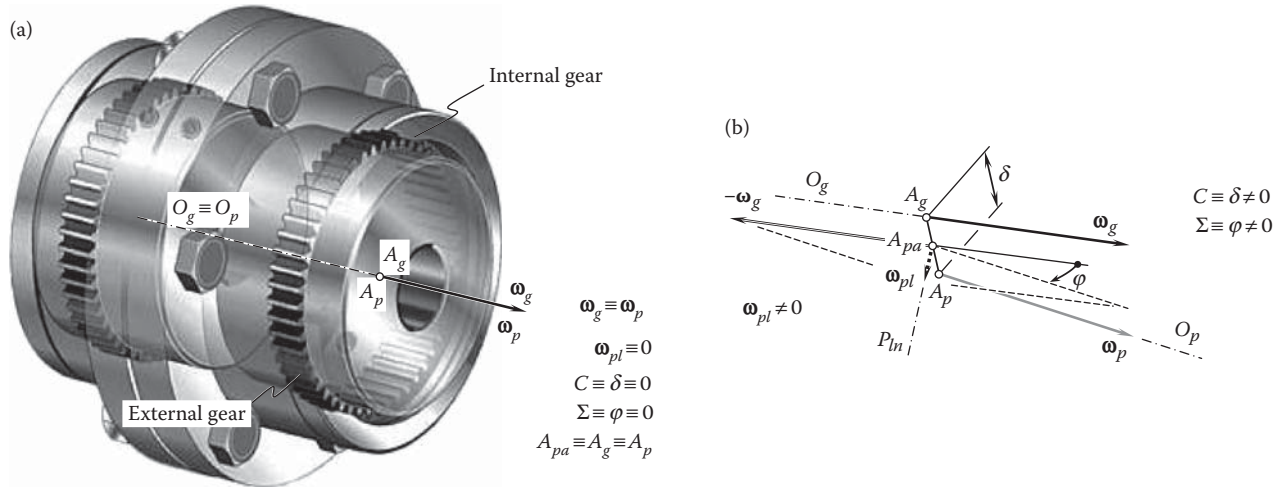


FIGURE 18.21

Implementation of the concept of  $S_{pr}$ -gearing in the design of a gear coupling (a) close-up view of a gear coupling, and (b) the vector diagram constructed for gear coupling.

Figure 18.21a, the crossed-axes angle is zero ( $\Sigma = 0$ ) and the closest distance of approach,  $C$ , between the gear axis,  $O_g$ , and the pinion axis,  $O_p$ , is also zero ( $C \equiv 0$ ). The gear apex,  $A_g$ , and the pinion apex,  $A_p$ , are snapped together into a common point,  $A_{pa}$ . In such a scenario, the gear coupling designer is free to select any reasonable tooth flank geometry for the gear and the pinion. In this particular case, the tooth flank geometry does not affect vibration generation and noise excitation by the gear coupling.

In reality, the axes of rotation,  $O_g$  and  $O_p$ , of the internal and external gears, respectively, in a gear coupling do not align to one another. A certain linear,  $\delta$ , and angular,  $\varphi$ , displacement is inevitable (see Figure 18.21b). With that said, gear coupling can be interpreted as a crossed-axes gear pair that has a center distance,  $C = \delta$ , and a crossed-axes angle  $\Sigma = \varphi$ . The rotation vector,  $\omega_g$ , of the internal gear no longer aligns with the rotation vector,  $\omega_p$ , of the external gear. Therefore, a certain rotation of the external gear in relation to the internal gear is observed. This relative rotation can be expressed in terms of the vector of instant rotation,  $\omega_{pl} = \omega_p - \omega_g$ . If the rotation,  $\omega_{pl}$ , is observed ( $\omega_{pl} \neq 0$ ), then it makes sense to implement the concept of  $S_{pr}$ -gearing in the design of internal and external gears of a gear coupling in order to avoid vibration generation and noise excitation when the gear coupling operates at high rotations.

A gear coupling designed utilizing the concept of  $S_{pr}$ -gearing can feature only one external gear and one internal gear. This means that with  $S_{pr}$ -gearing, it is sufficient to have only two components, not three.

#### 18.2.4 Account for Normal Distribution of Manufacturing Errors in Geometry of Tooth Flanks

In real gearing, the tooth flanks of a gear and mating pinion can both be viewed as a kind of smooth regular surface. A surface is a two-dimensional space and thus can be analytically expressed in terms of two parameters. As shown earlier (see Section 18.2.1.3), the position vector of a point,  $\mathbf{r}_g^r$ , of a gear tooth flank,  $\mathcal{G}_r$ , as well as the position vector of a point,  $\mathbf{r}_p^r$ , of a pinion tooth flank,  $\mathcal{P}_r$ , are expressed in terms of three parameters, that is,  $r_{pa}$ ,  $\varphi_{pr}$ , and  $X_f$  (see Equations 18.49 and 18.50). An excessive independent parameter in the equations for position vectors of a point,  $\mathbf{r}_g^r$  and  $\mathbf{r}_p^r$ , can be used to develop favorable designs of gear,  $\mathcal{G}_r$ , and mating pinion,  $\mathcal{P}_r$ , tooth flanks in  $S_{pr}$ -gearing.

There is a certain freedom in varying the design parameters of the tooth flanks of the gear,  $\mathcal{G}_r$  and pinion,  $\mathcal{P}_r$ , within the intervals  $-0.5 F_{pa} \leq f_{pa} \leq 0$  and  $0 \leq f_{pa} \leq +0.5 F_{pa}$ . It is reasonable to assume that zero axis misalignment occurs at a midpoint of the effective face width,  $F_{pa}$ . Transition from zero axis misalignment at the midpoint to maximum axis misalignment at one end of the gear and maximum axis misalignment at the opposite end of the gear follows a certain function. This makes it possible to synchronize permissible linear and angular displacements in the  $S_{pr}$  gear pair. Use of Gauss's (normal) distribution of manufacturing errors sounds attractive from this perspective. The instant values of the design parameters,  $r_{pa}$  and  $X_f$ , in  $S_{pr}$ -gearing may correlate to one another so as to follow Gauss's distribution. When a gear and a mating pinion in  $S_{pr}$ -gearing are designed this way, for smaller instant values of axis misalignment (the probability of which is higher),

the contact point is mainly located in the vicinity of the midpoint of the effective face width,  $F_{pa}$ . For larger instant values of axis misalignment (the probability of which is lower), the contact point is mainly located at the ends of the effective face width,  $F_{pa}$ .

As manufacturing errors perfectly follow normal distribution, the implementation of Gauss's distribution formula for the derivation of an equation for position vectors of points  $\mathbf{r}_g^r$  and  $\mathbf{r}_p^r$  for tooth flanks  $\mathcal{G}_r$  and  $\mathcal{P}_r$  becomes reasonable (see Figure 18.22):

$$\varphi_{\mu,\sigma}(X) = \frac{1}{\sqrt{2\pi\sigma^2}} e^{-\frac{(X-\mu)^2}{2\sigma^2}} \quad (18.57)$$

In Equation 18.57, the parameter  $\mu$  is the mean (location of the peak) and  $\sigma^2$  variance (the measure of the width) of the distribution.

It is reasonable to assume that the actual values of the design parameters  $r_{pa}$  and  $X_f$  correlate to one another following Gauss's distribution formula (see Equation 18.57):

$$\frac{\partial X_f}{\partial r_{pa}}(r_{pa}) = \frac{1}{\sqrt{2\pi\sigma^2}} e^{-\frac{(r_{pa} - r_{w,pa})^2}{2\sigma^2}} \quad (18.58)$$

The generation of the tooth flank of a gear,  $\mathcal{G}_r$ , and its mating pinion,  $\mathcal{P}_r$ , in  $S_{pr}$ -gearing, generated in accordance with Equation 18.58, could be of practical importance, as the manufacturing errors, as well as the errors and displacements of other nature, follow Gauss's distribution formula with high accuracy.

Once one of the design parameters,  $r_{pa}$  and  $X_f$ , in  $S_{pr}$ -gearing is expressed in terms of one; that is, when a function,  $X_f = X_f(r_{pa})$ , is established, then the position vectors of a point,  $\mathbf{r}_g^r$  and  $\mathbf{r}_p^r$ , of the tooth flank of a gear,  $\mathcal{G}_r$ , and its mating pinion,  $\mathcal{P}_r$ , are expressed in terms of two (not three) design parameters, as required for any and all smooth regular surfaces.

Figure 18.23 is helpful for a better understanding of the normal distribution of manufacturing errors onto the geometry of tooth flanks of a gear and mating pinion in  $S_{pr}$ -gearing. In Figure 18.10, all the slices are of equal thickness,  $\Delta F_{pa}$ . In the case illustrated in Figure 18.23, the thickness,  $\Delta F_{pa}^{(i)}$ , of each  $i$ th slice strictly follows the Gaussian distribution.

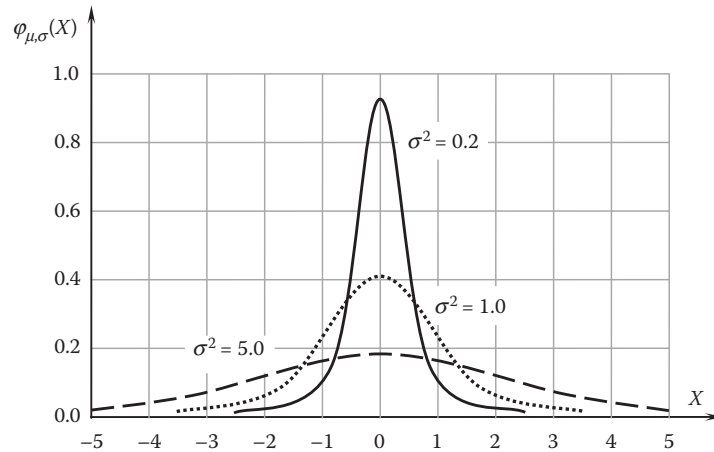


**FIGURE 18.22**  
Probability density function ( $\mu = 0$ ).

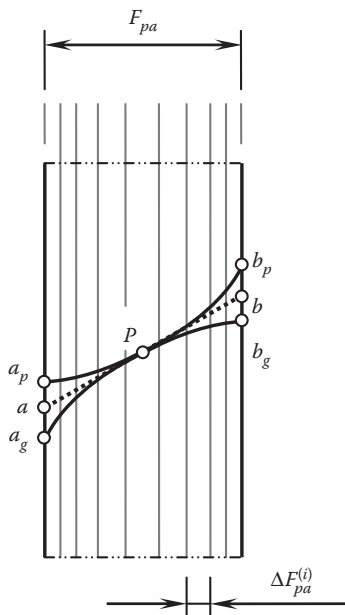


FIGURE 18.23

On accounting for normal distribution of manufacturing errors in the geometry of tooth flanks.

### 18.3 Possibility of Implementation of the Concept of $S_{pr}$ -Gearing to Gear Systems That Feature Point Contact between Tooth Flanks

Gear systems that feature point contact of tooth flanks of the gear and pinion, and high-conformal gears in particular, are more sensitive to axis misalignment, and they require tighter tolerances on the actual configuration of the axis of rotation of a gear in relation to the axis of rotation of a mating pinion. It is of interest to investigate whether the disclosed approach for the generation of tooth flanks of desirable real gearing, that is, of  $S_{pr}$ -gearing, can be enhanced to gearing that features point contact of tooth flanks.

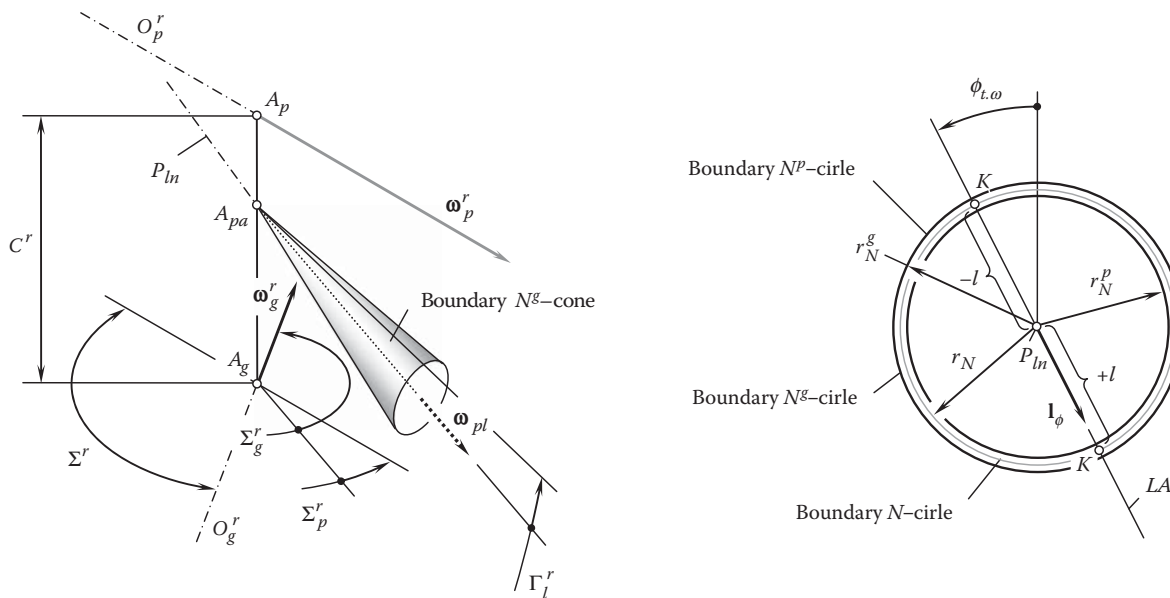
The profile contact ratio,  $m_p$ , for any  $S_{pr}$ -gearing is greater than zero ( $m_p > 0$ ). For spur  $S_{pr}$ -gearing, the inequality  $m_p = m_t > 1$  is always observed. For helical  $S_{pr}$ -gearing, the inequality  $m_t = m_p + m_F > 1$  is valid. Here, the face contact ratio is designated as  $m_F$ , and the total contact ratio is denoted by  $m_t$ . High-conformal gears of all types feature  $m_p = 0$  and  $m_t = m_F > 1$ .

The generation of tooth flanks for desirable real high-conformal gears is based on the principle of generation of tooth flanks for perfect crossed-axes high-conformal gears. Two of the most unfavorable cases should be considered there.

First, the boundary  $N^p$ -circle is constructed for the midpoint of the effective face width,  $F_{pa}$ , of the gear. For the construction, the original configuration of the rotation vectors,  $\omega_g$ ,  $\omega_p$  and  $\omega_{pl}$ , is used. This set of the rotation vectors is complemented by the zero tolerance vector,  $\{\varphi\}$ , for the angular displacement, and the minimum tolerance vector,  $\{\delta\}$ , for the linear displacement. For such a configuration of the rotation vectors, the limiting radius,  $r_N^p$ , is derived. The radius of curvature of the convex tooth profile does not exceed  $r_N^p$  (see Figure 18.24).

Second, the boundary  $N^g$ -circle is constructed for both ends of the gear. For the construction, the original configuration of the rotation vectors,  $\omega_g$ ,  $\omega_p$  and  $\omega_{pl}$ , is used. This set of rotation vectors is complemented by the maximum tolerance vector,  $\{\varphi\}$ , for the angular displacement and the maximum tolerance vector,  $\{\delta\}$ , for the linear displacement. For such a configuration of the rotation vectors, the limiting radius,  $r_N^g$ , is derived. The radius of curvature of the concave tooth profile exceeds the value of  $r_N^g$  (see Figure 18.24).

A performed analysis of Figure 18.24 makes a conclusion possible. In gearing that has line contact between the tooth flanks of a gear and a mating pinion, the line contact can be substituted with point contact in order to make the gearing insensitive to axis misalignment. The gear designer sacrifices the line contact for point contact. In gearing that features point contact, there is nothing to sacrifice—the gear and mating pinion tooth flanks are



already in point contact. This makes possible a conclusion: *No changes to the tooth flank geometry are permissible in gearing that features point contact between the tooth flanks.*

The perfect and desirable real gear systems discussed so far correlate to each other in a way illustrated in [Table 18.1](#).

- Perfect gear pairs
- Perfect real gear pairs
- Real (approximate) gear pairs

Ideal gears are capable of transmitting a smooth rotation from a driving shaft to a driven shaft.

$S_{pr}$ -gears are capable of transmitting a smooth rotation from a driving shaft to a driven shaft.

**TABLE 18.1**  
Desired Geometries for Tooth Flanks of Gear Pairs with  $m_p > 0$  (Correlation among Gear Systems of Various Types)

Configuration of the Axes of Rotation	Perfect Gear Pairs	Perfect Real Gear Pairs	Real (Approximate) Gearing
Parallel-axes gearing ( $P_r$ -gearing)	Involute of a circle tooth profile <sup>a</sup> used in spur, helical, herringbone, and double-helical gears. ( $p_{b,g} \equiv p_{b,p}$ )	Parallel-axes $S_{pr}$ -gearing <sup>c</sup> used in spur, helical, herringbone, double-helical, and cycloidal gears, as well as any other geometries in the lengthwise direction of the gear teeth. ( $\varphi_{b,g} = \varphi_{b,opr}$ , $\varphi_{b,p} = \varphi_{b,op}$ )	Gears with a noninvolute tooth profile, circular-arc tooth flank geometry in the lengthwise direction of the gear tooth cut by milling cutter, and so forth. ( $p_{b,g} \neq p_{b,opr}$ , $p_{b,p} \neq p_{b,op}$ )
Intersected-axes gearing ( $I_r$ -gearing)	Involute flank developed from a base cone of the gear <sup>b</sup> used in straight-tooth bevel gears. ( $\varphi_{b,g} = \varphi_{b,p}$ )	Intersected-axes $S_{pr}$ -gearing <sup>c</sup> used in bevel, skew bevel, spiral bevel gears, as well as in any other geometries in the lengthwise direction of the gear teeth. ( $\varphi_{b,g} = \varphi_{b,opr}$ , $\varphi_{b,p} = \varphi_{b,op}$ )	Bevel gears, spiral bevel gears, and so forth cut on gear generators with a cutting tool with a nonzero profile angle ( $\phi_c > 0^\circ$ ). ( $\varphi_{b,g} = \varphi_{b,opr}$ , $\varphi_{b,p} = \varphi_{b,op}$ )
Crossed-axes gearing ( $C_r$ -gearing)	Crossed-axes $R$ -gearing <sup>c</sup> used for various tooth flank geometries in the lengthwise direction of the gear teeth. ( $\varphi_{b,g} = \varphi_{b,p}$ )	Crossed-axes $S_{pr}$ -gearing <sup>c</sup> used in hypoid and worm gears, and so forth. ( $\varphi_{b,g} = \varphi_{b,opr}$ , $\varphi_{b,p} = \varphi_{b,op}$ )	Hypoid gearing; <i>spiroid</i> gearing; double enveloping worm gears, ZA -, ZC -, ZN - worm gearing; and so forth. ( $\varphi_{b,g} = \varphi_{b,opr}$ , $\varphi_{b,p} = \varphi_{b,op}$ )

<sup>a</sup> Proposed by Leonhard Euler in 1760.

<sup>b</sup> This was known to George Grant (see U.S. Pat. No. 407,437 of July 23, 1889; this patent is granted to him for a gear cutting machine). However, it should be stressed here that the concept of the angular base pitch was not known to Grant. The concept of the angular base pitch was introduced later by Radzevich.

<sup>c</sup> Proposed by Radzevich in 2008.



Real (approximate) gearing features tooth flank geometry of a gear and pinion that deviates from the geometry in perfect gearing, as well as  $S_{pr}$ -gearing. In real (approximate) gearing, the tooth flanks of the gear and its mating pinion always make point contact with one another. The coordinates of the contact point are not predictable. The degree of conformity of the interacting tooth flanks is commonly out of control.

Real (approximate) gears are not capable of transmitting a smooth rotation from a driving shaft to a driven shaft.

Vector diagrams for all possible types of perfect gear pairs are classified in Figure 2.15. For every vector diagram, a corresponding gear pair can be designed. For a specified configuration of the rotation vectors of the gear,  $\omega_g$ , and the pinion,  $\omega_p$ , and for a given rotation and torque on the input shaft, a unique desired gear pair can be synthesized.

Similarly (see Chapter 2, Figure 2.15), a classification of vector diagrams can be developed for the case of desired real gearing, that is,  $S_{pr}$ -gearing. Again, for a specified configuration of the rotation vectors of the gear,  $\omega_g$ , and the pinion,  $\omega_p$ , and for a given rotation and torque on the input shaft, a unique desired gear pair can be synthesized. In this last case, permissible misalignment of the gear and the pinion has to be specified.

Finally, no classification of real (approximate) gearing can be developed, as the number of possible kinds of gears of this kind is endless. For a specified configuration of the rotation vectors of the gear,  $\omega_g$ , and the pinion,  $\omega_p$ , multiple real (approximate) gear pairs can be designed.

The discussion in this chapter of the book can be summarized as follows:

- Root causes for how real gears differ from perfect gears are identified. For convenience of analysis, different reference systems are used, and the transition from one of the coordinate systems to another is analytically described by the corresponding operators of the coordinate system transformation.
- Displacements of a gear axis of rotation from its desired configuration are discussed and described analytically. For this purpose, the closest distance of approach between gear and mating pinion axes of rotation is determined.
- Tooth flank geometry in perfect real gearing is determined. The gearing of the proposed design is referred to as  $S_{pr}$ -gearing. For this purpose, the adopted concept for tooth flank generation is formulated and preferred reference systems are identified. Equations for the position vectors of a point,  $\mathbf{r}_g$  and  $\mathbf{r}_p$ , of a gear tooth flank,  $\mathcal{G}_r$ , and a mating pinion tooth flank,  $\mathcal{P}_r$ , are derived. Angular base pitch in  $S_{pr}$ -gearing is specified, and features of interaction of the tooth flanks are discussed.
- Possibilities of implementation of the concept of  $S_{pr}$ -gearing in the design of two-degrees-of-freedom gearing, as well as in the design of gear coupling, are discussed. It is proposed to take into account the normal distribution of manufacturing errors in geometry of the tooth flanks  $\mathcal{G}_r$  and  $\mathcal{P}_r$ .
- It is shown that the concept of  $S_{pr}$ -gearing cannot be applied to gear systems that feature point contact between the tooth flanks: in conformal gearing (that is, in *Novikov gearing*), as well as in high-conformal gearing.
- Correlation among gear systems of various types is outlined.

An in-depth understanding of the kinematics, geometry, and interaction between tooth flanks can help to identify appropriate areas of application of perfect gearing with point contact between the tooth flanks of a gear and a mating pinion.



# Taylor & Francis

Taylor & Francis Group

<http://taylorandfrancis.com>

## Part V

# $C\Sigma u$ – Variable Gearing

Gear pairs discussed in previous chapters feature fundamental design parameters center distance,  $C$ ; crossed-axes angle,  $\Sigma$ ; and gear ratio,  $u$ , of certain constant values. It is proposed to refer to gears of this kind as  $C\Sigma u$  – *constant gear pairs*. Generally speaking, each of the fundamental design parameters ( $C$ ,  $\Sigma$ , and  $u$ ) can be a function of the actual value of the angle of rotation of the driving gear. In contrast to  $C\Sigma u$  – constant gear pairs, gearings with all three variable fundamental design parameters can be referred to as  $C\Sigma u$  – *variable gear pairs*. To investigate the possible types and potential capabilities of  $C\Sigma u$  – variable gear pairs, corresponding analysis is performed in this section.

In addition, all kinds of gear pairs, that is, parallel-axes gear pairs, intersected-axes gear pairs, and crossed-axes gear pairs, are covered by  $C\Sigma u$  – variable gear pairs, but below, only noncircular gears are discussed as an example of more general  $C\Sigma u$  – variable gear pairs. First of all, this is because of lack of knowledge and experience with  $C\Sigma u$  – variable gear pairs of other kinds.

$C\Sigma u$  – variable gearing has huge potential for researchers. This part has just one chapter. This chapter is an illustration of the capabilities of  $C\Sigma u$  – variable gearing. Each particular kind of  $C\Sigma u$  – variable gear pairs deserves to be considered in a separate chapter. The chapter is titled “A Novel Concept to Design Perfect Noncircular Gears.” It aims to outline a novel concept to design perfect noncircular gear pairs, and in this way to illustrate the inconsistencies of the known approach to designing and manufacturing noncircular gears, as well as the advantages of the proposed novel approach. Noncircular gears are used here just as an example to demonstrate the capabilities of the approach disclosed here.

Room for a few more chapters is left, as this part of the book has the potential for growth in the future.



# Taylor & Francis

Taylor & Francis Group

<http://taylorandfrancis.com>

## A Novel Concept to Design Perfect Noncircular Gears

The idea of noncircular gears originates from the precursors of engineering thought. Gears of this kind were sketched by da Vinci. In the current industry, they have found application in many mechanical devices (Figure 19.1). In the past, many efforts to investigate noncircular gears were undertaken by *Franz Reuleaux*. The recent accomplishments in the field are summarized in [70]. This book overall is a refinement of the earlier published book on the topic [67,68]. A contribution to the field by Dooner [21,22] also needs to be acknowledged.

The current literature pertaining to the design and manufacture of noncircular gears is less developed than that on gearings of other designs.

Many gear experts noted the lack of exact methods of generation of noncircular gears, and efforts were first focused on the development of methods based on the meshing of generating tools with master gears.

Use of the known methods of generation of tooth flanks in noncircular gears returns sufficient results as long as no tight tolerances on the accuracy of the output rotation are imposed: noncircular gears are used in the design of toys and so forth. No sufficient output can be received if these methods are used for gears applied in the design of precise mechanisms.

The salient theme of this book is to present a single kinematic/geometric theory of noncircular gearing to transmit power (motion and torque) from a driving shaft to a driven shaft. The end result is a novel approach in the theory of meshing of noncircular gears. This approach is valid for (a) external gear pairs, (b) internal gear pairs, and (c) gear-to-rack gear pairs.

### 19.1 Fundamentals of Perfect Noncircular Gearing

Noncircular gear pairs are designed and manufactured solely with the goal of transmitting a power (motion and torque) from a driving gear to a driven gear with a prespecified function of the gear ratio, that is,  $u = u(\varphi_{\text{input}})$ . Actually, gear pairs of this particular kind can be viewed either as  $u$  – variable gear pairs or  $C\Sigma$  – constant gear pairs, where either an equality,  $\Sigma = 0^\circ$ , or an equality,  $\Sigma = 180^\circ$ , is valid.

Shown in Figure 2.31 (see Chapter 2), the generalized vector diagram in the case of noncircular gearing reduces to that illustrated in Figure 19.2.

With the vector diagram constructed, an actual design of a noncircular gear pair is developed in strict compliance with the three fundamental laws of gearing. This means that at every instant of time, the following requirements are fulfilled in a perfect noncircular gear pair, which is a must:

- The condition of contact of the interacting tooth flanks,  $\mathcal{G}$  and  $\mathcal{P}$ , of a gear and a mating pinion, that is, the equality  $\mathbf{n} \cdot \mathbf{v}_\Sigma = 0$  is valid.
- The condition of conjugacy of the interacting tooth flanks,  $\mathcal{G}$  and  $\mathcal{P}$ —at every instant of time, the contact perpendicular,  $\mathbf{n}$ , is along a straight line through the pitch point,  $P$ , in its current location in relation to the axes,  $O_g$  and  $O_p$ , of the gear and the mating pinion.
- Instant values of the angular base pitches of a gear and a mating pinion have to be equal to the corresponding instant value of the operating base pitch of the gear pair.

If a noncircular gear pair is designed so as to fulfill all three mandatory requirements, then the angular velocity ratio:

$$u(\varphi_{\text{input}}) = \frac{\omega_p}{\omega_g(\varphi_{\text{input}})} \quad (19.1)$$



**FIGURE 19.1**  
Noncircular gear pair with a constant center distance.

exactly corresponds to a predesigned function, a smooth input rotation is transmitted smoothly, and no fluctuation in the output rotation occurs. This can be adopted as a definition to the term *perfect noncircular gear pair*.

## 19.2 Tooth Flank Generation in Perfect Noncircular Gear Pairs

The generation of tooth flanks of a gear and mating pinion in a perfect noncircular gear pair is executed on the premise of the vector diagram of the gear pair and strictly follows all three fundamental requirements with which perfect gearings of all kinds have to comply. These requirements are listed in a previous section.

The principal features of the generation of tooth flanks in perfect noncircular gearing are briefly outlined below. In parallel, the reader's attention here is pointed toward the weaknesses of the commonly adopted practice of generation of tooth flanks in noncircular gearing.

The principle of the generation of tooth flanks,  $\mathcal{G}$  and  $\mathcal{P}$ , of a gear and a mating pinion by means of a desired line of contact,  $LC_{des}$ , that is associated with the plane of action,  $PA$ , can be enhanced for generation of the tooth flanks of gears for noncircular gearing.

In the case of parallel-axes gearing ( $P_a$ -gearing): an *instant* location ( $r_g$ ,  $r_p$ , and  $P$ ), an instant orientation ( $\phi_t \rightarrow d_{b,g}$ , and  $d_{b,p}$ ), and the instant speed,  $V/\omega$ , of the plane of action,  $PA$ , are specified. At every instant of time, the

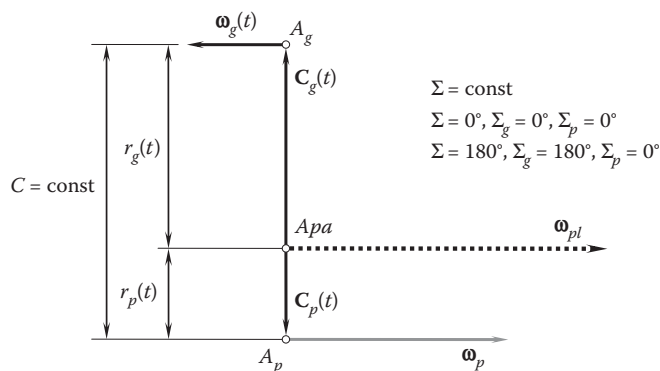
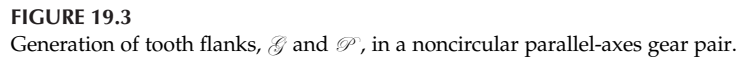


**FIGURE 19.2**  
Vector diagram constructed for an external noncircular gear pair:  $u$  – variable gear pair (the crossed-axes angle,  $\Sigma$ , is of a constant value,  $\Sigma = \text{const}$ , and can be equal either to  $\Sigma = 0^\circ$  or  $\Sigma = 180^\circ$ ).



Consider a parallel-axes noncircular gear pair that features a variable center distance,\*  $C(\varphi_p)$ . Here, the angle of rotation of the driver (of the pinion) is designated as  $\varphi_p$ . The gears rotate about their axes of rotation,  $O_g$  and  $O_p$ , with variable-in-time rotations,  $\omega_g(\varphi_p)$  and  $\omega_p(\varphi_p)$ , correspondingly. A functionality:

\* A case of a noncircular gear pair with constant center distance,  $C = \text{const}$ , can be viewed as a reduced case of a noncircular gear pair that features a variable center distance,  $C(\varphi_v)$ .



When the gears rotate, the center distance,  $C(\varphi_p)$ , varies  $[V_{o,p}(\varphi_p)$  and  $V_{o,g}(\varphi_p)]$  in the range of:

$$C_{\min} \leq C(\varphi_p) \leq C_{\max} \quad (19.4)$$

The instant pitch point,  $P_i$ , that corresponds to the input rotation angle  $\varphi_p = \varphi_p^i$ , is considered motionless. The distance,  $r_g$ , between an instant location of the gear axis of rotation,  $O_g$ , and the pitch point,  $P_i$ , and the distance,  $r_p$ , between an instant location of the pinion axis of rotation,  $O_p$ , and the pitch point,  $P_i$ , are both variable in time; that is,  $r_g = r_g(\varphi_p)$  and  $r_p = r_p(\varphi_p)$ .

The instant line of action,  $LA_{\text{inst}}$ , is a straight line segment that forms an instant pressure angle,  $\phi_{\text{inst}}$ , with respect to a perpendicular to the centerline,  $\mathcal{C}$ , through the instant pitch point,  $P_i$ . As the pitch point,  $P_i$ , is motionless, when the gears rotate, the axes of rotation,  $O_g$  and  $O_p$ , travel back and forth along the centerline,  $\mathcal{C} [V_{o,p}(\varphi_p)$  and  $V_{o,g}(\varphi_p)]$ . The configurations  $O_g^{i-1}, O_g^i, O_g^{i+1}$  and  $O_p^{i-1}, O_p^i, O_p^{i+1}$  of the centers of rotations are examples of the current locations of the gear axis of rotation,  $O_g$ , and the pinion axis of rotation,  $O_p$ , correspondingly.

For a current configuration of the gears, it is assumed that both the instant center distance,  $C_{\text{inst}}$ , and the instant pressure angle,  $\phi_{\text{inst}}$ , as well as the instant pitch radii  $r_g(\varphi_p)$  and  $r_p(\varphi_p)$ , are specified. The angles  $\phi_{i-1}$ ,  $\phi_i$ , and  $\phi_{i+1}$  are examples of the instant pressure angle,  $\phi_{\text{inst}}$ . When the gears rotate, the instant line of action,  $LA_{\text{inst}}$ , occupies different locations and orientations relative to the centerline,  $\mathcal{C}$ , and the pitch points,  $P_{i-1}$ ,  $P_i$ , and  $P_{i+1}$ . The instant lines of action,  $LA_{\text{inst}}^{i-1}$ ,  $LA_{\text{inst}}^i$ , and  $LA_{\text{inst}}^{i+1}$ , are straight lines through the corresponding instant pitch points,  $P_{i-1}$ ,  $P_i$ ,  $P_{i+1}$ , and so forth. The instant lines of action,  $LA_{\text{inst}}^{i-1}$ ,  $LA_{\text{inst}}^i$ , and  $LA_{\text{inst}}^{i+1}$ , are examples of current configurations of the instant line of action,  $LA_{\text{inst}}$ , when the gears rotate. When the gears rotate, the path of contact,  $P_c$ , is generated as an envelope to consecutive positions of the instant line of action,  $LA_{\text{inst}}$ , that is, a family of straight lines.

The path of contact,  $P_c$ , is considered in a stationary reference system,  $X_h Y_h Z_h$ , associated with the gear housing. In cases of parallel-axes noncircular gearing, the path of contact,  $P_c$ , is a planar curve that is entirely located within a plane perpendicular to the axes of rotation,  $O_g$  and  $O_p$ .

For generating the base curves in noncircular gears: (a) the pitch point is traveling up and down along the centerline,  $\mathcal{C}$ , and (b) the transverse pressure angle is altering accordingly. The base curve of the gear,  $BC_g$ , is an envelope to consecutive positions of the instant line of action,  $LA_{\text{inst}}$ , when the gears rotate. The base curve of the gear,  $BC_g$ , is considered in a reference system,  $X_g Y_g Z_g$ , associated with the gear. Similarly, the base curve of the pinion,  $BC_p$ , is an envelope to consecutive positions of the instant line of action,  $LA_{\text{inst}}$ , when the gears rotate. The base curve of the pinion,  $BC_p$ , is considered in a reference system,  $X_p Y_p Z_p$ , associated with the pinion.\*

The gear tooth profile,  $\mathcal{G}$ , is the trace of the contact point,  $K$ , between the tooth flanks of the gear and pinion when the gears rotate. The gear tooth profile is specified in the reference system,  $X_g Y_g Z_g$ , associated with the gear. Similarly, the pinion tooth profile,  $\mathcal{P}$ , is the trace of the contact point,  $K$ , between the tooth flanks,  $\mathcal{G}$  and  $\mathcal{P}$ , of the gear and pinion when the gears rotate. The pinion tooth profile is specified in the reference system,  $X_p Y_p Z_p$ , associated with the pinion.

For generation of the tooth flanks,  $\mathcal{G}$  and  $\mathcal{P}$ , of a gear and mating pinion in a noncircular gear pair, a desired line of contact,  $LC_{\text{des}}$ , is used. The desired line of contact,  $LC_{\text{des}}$ , is entirely located within the plane of action,  $PA$ , and travels together with the plane of action (see Figure 6.12 and others). Depending on the geometry and the actual configuration of the desired line of contact,  $LC_{\text{des}}$ , gears of different kinds are generated, that is, spur gears, helical gears, and so forth.

The desired rotation of the driven shaft can be expressed in terms of the instant configurations of the instant line of action. Then, the desired tooth profiles have to interact with one another along the same instant line of action,  $LA_{\text{inst}}$ , that is tangent to the base curves at the corresponding instant of time.

The instant pitch circles of the diameters,  $d_g^{\text{inst}}$  and  $d_p^{\text{inst}}$ , correspondingly, pass through the instant pitch point,  $P_{\text{inst}}$ , and they center at the corresponding instant centers of rotations,  $O_g^{\text{inst}}$  and  $O_p^{\text{inst}}$ .

A local segment of the gear tooth flank,  $\mathcal{G}$ , and the pinion tooth flank,  $\mathcal{P}$ , can be specified in terms of the instant contact point,  $K$ , and the corresponding centers of rotation,  $O_g^{\text{inst}}$  and  $O_p^{\text{inst}}$ .

\* Actually, the base curves,  $BC_g$  and  $BC_p$ , are directors of the two base cylinders, each of which is associated with a gear and a mating pinion. The base cylinders are cylinders in general sense of this term, and are not cylinders of revolution.

† In the current practice, it is common to construct pitch lines associated with the gear and mating pinion as an equivalent of the pitch circles in conventional parallel-axes gearing. The pitch lines are also commonly referred to as the *centrodes*. By definition, centrodes are the two lines in contact that roll over one another *with no sliding* between them. In noncircular gear pairs, the pitch lines/centrodes cannot roll over one another with no sliding between them. Actually, the pitch lines of a gear and mating pinion are useless, as they are neither conjugate nor enveloping to one another, which is a must when the gears rotate.

All the instant lines of action,  $LA_{inst}$ , that is,  $LA_{inst}^{i-1}$ ,  $LA_{inst}^i$ ,  $LA_{inst}^{i+1}$ , and so forth, have to intersect the centerline,  $\mathcal{L}$ . None of the instant lines of action,  $LA_{inst}$ , are allowed to pass either through the instant axis of rotation,  $O_g^{inst}$ , of the gear, or the instant axis of rotation,  $O_p^{inst}$ , of the pinion.

The curved line segment of the path of contact,  $P_c$ , that corresponds to the input rotation, under which the center distance increases from the minimal value of  $C_{min}$  to the maximal value of  $C_{max}$ , and then back and forth from the maximal value of  $C_{max}$  to the minimal value of  $C_{min}$ ; that is, through the input rotation angle per lobe (the active portion of the path of contact,  $P_c$ ) is divided on a certain number of arc segments, the total number of which equals the tooth count per lobe. All the arc segments of the active portion of the path of contact,  $P_c$ , overlap one another. This is an equivalent of the contact ratio in conventional parallel-axes involute gearing. The tooth flanks of the gear and mating pinion are generated by a contact point that travels within a corresponding arc segment of the active portion of the path of contact,  $P_c$ . There is no need to construct a pitch curve. Actually, the latter, that is, the *pitch curve*, is meaningless, and a kind of nonsense. The pitch curves for each lobe of the gear and the mating pinion have to be conjugate to one another. Otherwise, two curves that are associated with the gear and mating pinion cannot serve as the pitch curves for the gear and pinion.

The endpoints of the arc segments of the active portion of the path of contact,  $P_c$ , are located within the corresponding outer curve (top-lands) and root curve (bottom-lands) of the gear and mating pinion, correspondingly.

### 19.3 On Inconsistency of Known Methods of Machining Gears for Perfect Noncircular Gear Pairs

In the current industry, gears for noncircular gear pairs are machined in compliance with the continuous generating method (molding generating method). The tooth flanks of a gear and mating pinion in this case are generated as envelopes to consecutive positions of cutting edges of the gear-cutting tool. Shown in Figure 19.4, the gear-shaping process perfectly fits the needs of machining of noncircular gears. This is illustrated in Figure 19.5, where the hobbing operation of a gear for a noncircular gear pair is depicted. A gear generator of a special design is used on the operation. Shown in Figure 19.6, noncircular gears of other designs (Figure 19.7) can also be hobbled by standard hobs.

Only approximate gears for noncircular gear pairs can be cut this way, as the fundamental conditions (condition of contact, condition of conjugacy, and equality of base pitches of a gear to be cut and the hob to the operating base pitch in the gear hobbing process) all the gear meshes have to comply with are violated in the gear machining mesh.



**FIGURE 19.4**  
Shaping a noncircular gear by the gear shaper.

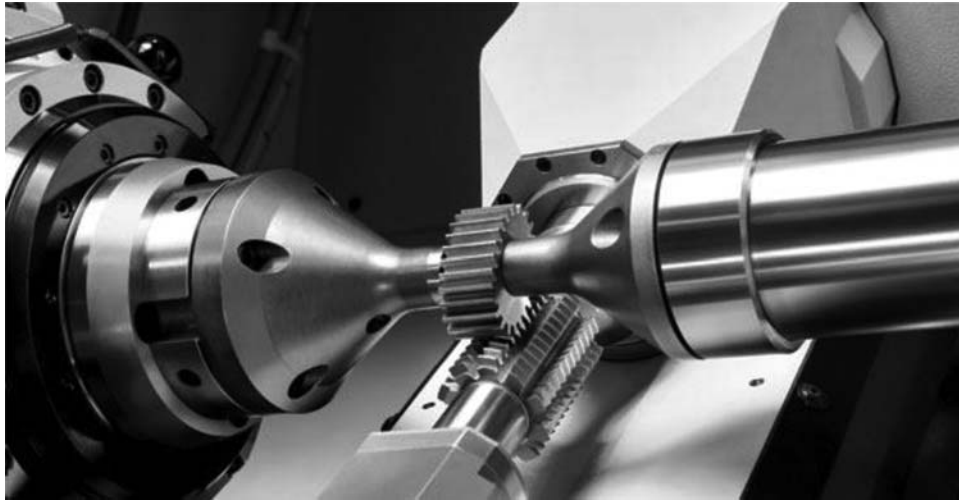


**FIGURE 19.5**  
Hobbing a gear for a noncircular gear pair.



**FIGURE 19.6**  
Elliptical gear for a noncircular gear pair.

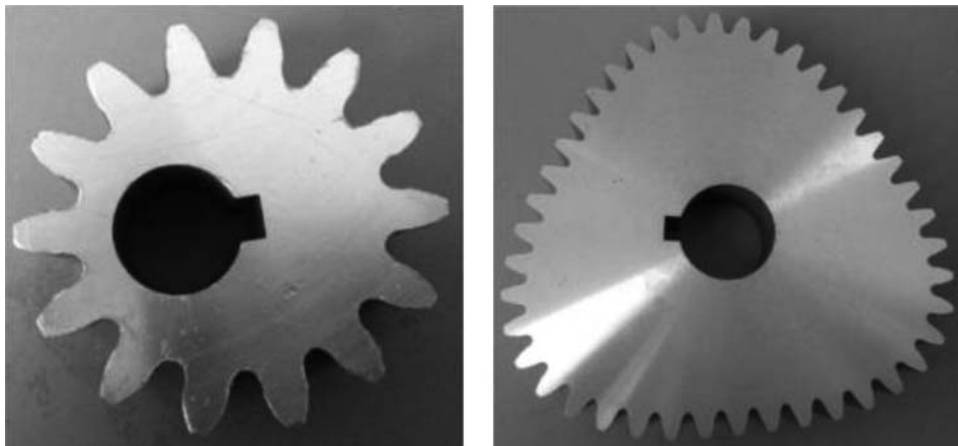


**FIGURE 19.7**  
Noncircular gears for a parallel-axes gear pair.

The above discussion in this chapter can be summarized as follows:

- No pitch surfaces can be used to design noncircular gears for *perfect noncircular gear pairs*.
- Neither involute shaper cutters nor straight-sided rack cutters/hobs can be used to cut gears for perfect noncircular gear pairs. Only approximate noncircular gears can be cut by the shaper cutter or the straight-sided rack/hob cutter.
- The generating (molding) principle of cutting perfect noncircular gears is impractical in the production of noncircular gears for perfect noncircular gear pairs.
- When the tooth flanks in noncircular gears are generated, the instant line of action,  $LA_{inst}$ , has to perform two motions simultaneously: it has to travel straight and spin about the instant pitch point simultaneously. This also means that noncircular gears cannot be designed with a constant transverse pressure angle,  $\phi_t$ .
- The describing principle is applicable generate the tooth flank geometry and cutting noncircular gears for perfect noncircular gear pairs.

More detailed analysis of the generation of tooth flanks of a gear and a mating pinion in a noncircular gear pairs needs to be developed. However, the analysis to be developed has to comply with all the concepts discussed in this section.

In this section, perfect noncircular gears are considered just as an example of perfect  $C\Sigma u$  – variable gearing. The other kinds of perfect  $C\Sigma u$  – variable gearing (see Section 2.5) can be investigated similarly to how perfect noncircular gearings are investigated.



# Taylor & Francis

Taylor & Francis Group

<http://taylorandfrancis.com>

## Part VI

# Synthesis of Favorable Perfect Gear Pairs

The main purpose of gears is to transmit and transform power (a rotation and torque) for a specified configuration of the axes of rotation of a gear and a mating pinion, a given gear ratio, and so forth.

Perfect gears of all kinds, that is, parallel-axes gear pairs, intersected-axes gear pairs, and crossed-axes gear pairs can be designed now based on the theoretical approach outlined in previous chapters. Of course, it is always desired to design, produce, and use gear pairs with the most favorable performance. This is a challenging problem for gear experts.

A gear pair with the most favorable design parameters can be synthesized. To synthesize a favorable gear pair, an appropriate criterion is required. Contact and bending strength of the gear teeth, wear resistance of the gear tooth flanks, condition of lubrication of the interacting teeth surfaces, elasto-hydro-dynamic lubrication (EHD-lubrication), and so forth can be used to develop a criterion in compliance with which a gear pair can be synthesized. It is the right point to call to the reader's attention here that all the above-listed requirements the synthesized gear pair has to comply with depend on the conditions of contact between the interacting tooth flanks, and , of a gear and a mating pinion.

This section of the book is composed of one chapter. The chapter is titled "Features of Contact Geometry." It aims to outline a novel approach for analytical description of the contact geometry of the interaction tooth flanks, and , of a gear and a mating pinion, and to illustrate in this way the possibility of synthesis of perfect gear pairs with favorable performance, using for this purpose a possible minimum of input information.

Room for a few more chapters is left, as this part of the book has the potential for growth in the future.



# Taylor & Francis

Taylor & Francis Group

<http://taylorandfrancis.com>



## Features of Contact Geometry

The investigation of the contact geometry of curves and surfaces can be traced back to the 18th century. The study of the contact of curves and surfaces was undertaken in considerable detail by J.L. Lagrange\* in his *Theorie des Fonctions Analytiques* (1797) [65] and by A.L. Cauchy† in his *Leçons sur les Applications du Calcul Infinitésimal à la Géométrie* (1826) [13]. Later, in the 20th century, an investigation in the realm of contact geometry of curves and surfaces was undertaken by J. Favard‡ in his *Course de Géométrie Différentielle Locale* (1957) [30]. A few more names of researchers who have contributed to the subject could be mentioned.

### 20.1 Meaning of the Term *Synthesis of Favorable Gear Pair*

A gear pair contains two mating gears mounted in a gear housing.§ Although other designs are feasible, it is common practice to mount the mating gears on shafts.

The purpose of a gear pair is twofold:

- The use of a gear pair makes possible the transmission of power (that is, a rotation and torque) from an input shaft to an output shaft.
- Transformation always occurs when power is transmitted. Either the direction/orientation or just the rotation of the output motion is altered when a motion is transmitted by a gear pair.

In design practice, the desired gear pair can be given, or the designer is free to select a gear pair. In the first case, the design of an actual gear pair goes through a routine procedure that is well established in the industry. In the second case, the designer has an opportunity to synthesize a gear pair with favorable performance.

It is important to stress here the principal difference between the concept of synthesis of a favorable gear pair and *optimization of a gear pair*.

The term *optimization of a gear pair* means the determination of an optimal (in a certain prespecified sense) set of design parameters of an object/process whose structure is known; the structure does not undergo any changes after the object/process is optimized. Optimization targets the determination (that is, calculation) of a set of input parameters under which a given criterion of the optimization can be achieved. The structure of the object/process after optimization remains the same as before optimization.

In the case of optimization of a gear pair design, a circular arc can be prespecified as a desired line of contact,  $LC_{des}$ . A solution to the problem of optimization returns an optimal value of the radius,  $[R_{lc}]_{opt}$ , of the desired line of contact,  $LC_{des}$ , and an optimal configuration of the desired line of contact,  $LC_{des}$ , in relation to the plane of action,  $PA$ .

Crossed-axes gear pairs are convenient to illustrate the difference between synthesis and optimization.

Consider synthesizing a crossed-axes gear pair with a variable transverse profile angle,  $\phi_{t,\omega}$ , across the effective portion of the face width,  $F_{pa}$ . No input information is available about a desired line of contact,  $LC_{des}$ , in this case. All the parameters of the geometry of the desired line of contact,  $LC_{des}$ , are derived as the output in the synthesizing process. This is impossible in the process of optimization, when a structure of the desired line of contact,  $LC_{des}$ , has to be specified. More examples of this type can be provided.

\* Joseph-Louis Lagrange (January 25, 1736–April 10, 1813), an Italian-born (born Giuseppe Lodovico (Luigi) Lagrangia) famous French mathematician and mechanician.

† Augustin-Louis Cauchy (August 21, 1789–May 23, 1857), a famous French mathematician.

‡ Jean Favard (August 28, 1902–January 21, 1965), a French mathematician.

§ In contrast to a gear pair, a harmonic gear drive is composed of more than two components; it is composed of a stator-gear, a flexible gear, and a wave generator. All the components are vital for the design of a harmonic gear drive. In this monograph, a harmonic gear drive is not viewed as a gear pair; therefore, harmonic drives are not considered.

The term *synthesis of a favorable gear pair* means determining both a desired structure and a desired set (in a certain sense) of parameters of an object/process. In synthesizing, the structure of the object/process is not predetermined. Moreover, usually, the structure of the object/process is unknown. The desired structure of the object/process must be determined simultaneously with the parameters that ensure its desired functioning.

The synthesized object/process is always the best possible in a certain sense, whereas the optimized one could be the best among others of that same structure, which is not the same.

Despite numerous attempts made so far to solve the problem of synthesizing a gear pair with the desired properties, the problem remains unsolved. It is unsolved on the kinematic/geometric level and, moreover, it is not yet solved on a higher level. Physical phenomena (those observed when a gear pair is functioning) are incorporated in higher-level synthesis.

Regarding gear pairs, synthesis begins from given motion requirements and proceeds to determining the type and design parameters of a desired gear pair.

The development of the best possible design of a gear pair that is capable of transmitting and/or transforming a rotation from a driving shaft to the driven shaft is the main goal of synthesis of a favorable gear pair. Therefore, for a given configuration of the input and output shafts, the problem of synthesizing a favorable gear pair can be solved if:

- Rotations of the input shaft and the output shaft are specified
- Torque in the input shaft is known

In a case of synthesizing a gear pair design, the geometry of a desired line of contact,  $LC_{des}$ , is not prespecified. A solution to the problem of synthesizing of a gear pair design returns a desired line of contact,  $LC_{des}$ , of a novel favorable geometry, as well as the best possible configuration of the desired line of contact,  $LC_{des}$ , in relation to the plane of action,  $PA$ . Then, the calculated  $LC_{des}$  can be approximated either by a circular arc or an arc of a curve of other geometry.

In a general case, two rotations about skew axes are specified. One of the rotations is the input rotation, whereas the other is the output rotation. The input torque is known. It is required to determine the set of design parameters of a desired gear pair for transmitting rotation from the input shaft to the output shaft.

Here, the term *favorable gear pair* should be specified in engineering terms.\*

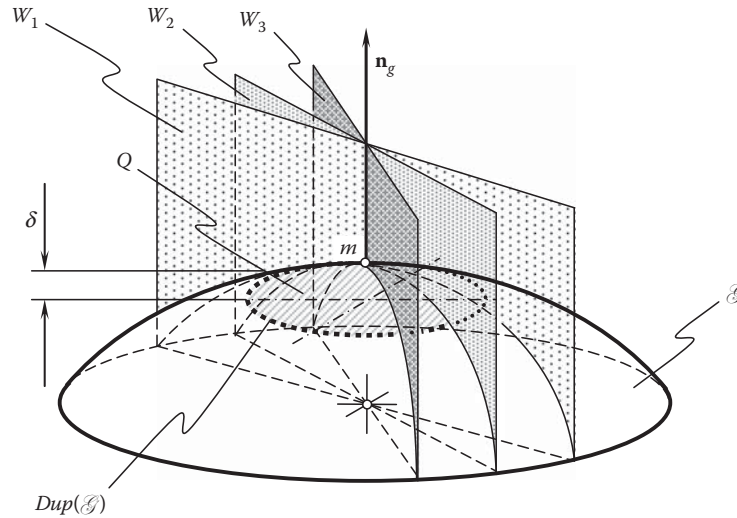
## 20.2 Dupin Indicatrix

At any point of a smooth regular gear tooth flank,  $\mathcal{G}$  (as well as at any point of a smooth regular pinion tooth flank,  $\mathcal{P}$ ) a corresponding *Dupin indicatrix* can be constructed. The Dupin indicatrix,  $Dup(\mathcal{G})$ , at a point of a gear tooth flank,  $\mathcal{G}$ , as well as the Dupin indicatrix,  $Dup(\mathcal{P})$ , at a point of the mating pinion tooth flank,  $\mathcal{P}$ , are planar characteristic curves of the second order. They are used for graphical interpretation of the distribution of normal curvatures of a surface in the differential vicinity of a surface point.

The Dupin indicatrix at a point of gear,  $\mathcal{G}$ , and a mating pinion,  $\mathcal{P}$ , tooth flanks are of critical importance in the theory of gearing and when synthesizing a gear pair with the most favorable performance. Generation of this planar characteristic curve is illustrated with a diagram shown in Figure 20.1.

A plane,  $W$ , through the unit normal vector,  $\mathbf{n}_g$ , to the gear tooth flank,  $\mathcal{G}$ , at an arbitrary point,  $m$ , rotates about  $\mathbf{n}_g$ . When rotating, the plane occupies consecutive positions  $W_1$ ,  $W_2$ ,  $W_3$ , and others. The radii of normal curvature of the line of intersection of the gear tooth flank,  $\mathcal{G}$ , by the normal planes  $W_1$ ,  $W_2$ ,  $W_3$  are equal to  $R_{g,1}$ ,  $R_{g,2}$ ,  $R_{g,3}$ , and so forth. The tooth flank,  $\mathcal{G}$ , is intersected by a plane  $Q$ . The plane  $Q$  is orthogonal to the unit normal vector,  $\mathbf{n}_g$ . This plane is at a certain small distance,  $\delta$ , from the point  $m$ . When the distance,  $\delta$ , approaches zero ( $\delta \rightarrow 0$ ), and when the scale of the line of intersection of the part surface gear tooth flank face,  $\mathcal{G}$ , by the plane,  $Q$ , approaches infinity, then the line of intersection of the gear tooth flank,  $\mathcal{G}$ , by the plane,  $Q$ , approaches the planar characteristic curve that is commonly referred to as the Dupin indicatrix,  $Dup(\mathcal{G})$  at a point of a smooth regular gear tooth flank,  $\mathcal{G}$ .

\* This interpretation of the problem of synthesis of a favorable gear pair significantly differs from what is commonly understood by the term *synthesizing a gear pair*. In order to distinguish the proposed interpretation of the problem from what is known from other sources, this interpretation of the problem of synthesizing can be referred to as *S<sub>pr</sub>-synthesis of a desired gear pair*.

**FIGURE 20.1**

The Dupin indicatrix at a point of a smooth regular gear tooth flank,  $\mathcal{G}$ .

An equation for the Dupin indicatrix,  $Dup(\mathcal{G})$ , can be represented in the form:

$$k_{1,g} x_g^2 + k_{2,g} y_g^2 = 1 \quad (20.1)$$

Here, the principal curvatures at a point of a gear tooth flank,  $\mathcal{G}$ , are designated as,  $k_{1,g}$  and  $k_{2,g}$ , correspondingly.

Equation 20.1 describes a particular case of the Dupin indicatrix, which is represented in *Darboux frame*.

The interested reader may wish to go to Appendix E for details on the Dupin indicatrix,  $Dup(\mathcal{G})$  and  $Dup(\mathcal{P})$ , at a point of gear,  $\mathcal{G}$ , and mating pinion,  $\mathcal{P}$ , tooth flanks.

### 20.3 Indicatrix of Conformity at Point of Contact of a Gear and Mating Pinion Tooth Flanks

A quantitative measure of degree of conformity at a point of contact between a gear tooth flank,  $\mathcal{G}$ , and a mating pinion tooth flank,  $\mathcal{P}$ , is concisely outlined below.

Quantitatively, the degree of conformity at a point of contact of a surface  $\mathcal{P}$  to another surface  $\mathcal{G}$  can be expressed in terms of difference between the corresponding radii of normal curvature of the contacting surfaces. The discussed quantitative measure of degree of conformity of the tooth flanks,  $\mathcal{G}$  and  $\mathcal{P}$ , is based on implementation of Dupin indicatrices,  $Dup(\mathcal{G})$  and  $Dup(\mathcal{P})$ , constructed at a point of contact of the tooth flanks,  $\mathcal{G}$  and  $\mathcal{P}$ .

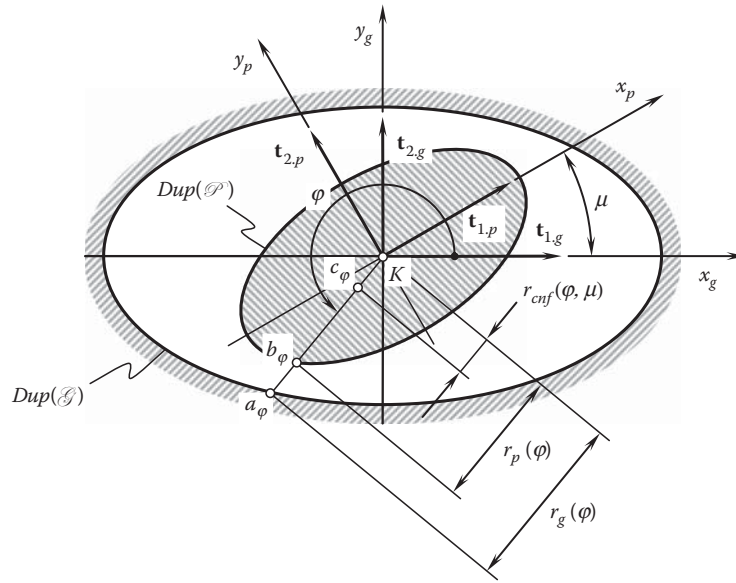
The Dupin indicatrix,  $Dup(\mathcal{G})$ , indicates the distribution of radii of normal curvature at a point of a gear tooth flank,  $\mathcal{G}$ , as shown, for example, for a concave elliptic patch of the tooth flank,  $\mathcal{G}$  (Figure 20.2).

An equation of the indicatrix of conformity  $Cnf_R(\mathcal{G}/\mathcal{P})$  at a point of contact of a gear tooth flank,  $\mathcal{G}$ , and a mating pinion tooth flank,  $\mathcal{P}$ , is postulated with the following structure:\*

$$Cnf_R\left(\frac{\mathcal{G}}{\mathcal{P}}\right) \Rightarrow r_{cnf}(\varphi, \mu) = r_g(\varphi) \operatorname{sgn} R_g(\varphi) + r_p(\varphi, \mu) \operatorname{sgn} R_p(\varphi, \mu) \quad (20.2)$$

\* The equation of this characteristic curve is known from:

- Pat. No.1249787, USSR, *A Method of Sculptured Part Surface Machining on a Multi-Axis NC Machine*, S.P. Radzevich, B23C 3/16, Filed: December 27, 1984, [94], and (in hidden form) from:
- Pat. No.1185749, USSR, *A Method of Sculptured Part Surface Machining on a Multi-Axis NC Machine*, S.P. Radzevich, B23C 3/16, Filed: October 24, 1983, [93].

**FIGURE 20.2**

The derivation of an equation of the indicatrix of conformity,  $Cnf_R(\mathcal{G}/\mathcal{P})$ , at a point of contact of a tooth flank,  $\mathcal{G}$ , and of a mating pinion tooth flank,  $\mathcal{P}$ , that are in the first order of tangency.

Because of the location of a point  $a_\varphi$  of the Dupin indicatrix,  $Dup(\mathcal{G})$ , at a point of the part surface,  $\mathcal{G}$ , is defined by the position vector  $r_p(\varphi)$ , and the location of a point  $b_\varphi$  of the Dupin indicatrix,  $Dup(\mathcal{P})$ , at a point of generating surface,  $\mathcal{P}$ , of the cutting tool is defined by the position vector  $r_T(\varphi, \mu)$ , then the location of a point  $c_\varphi$  (see Figure 20.2) of the indicatrix of conformity  $Cnf_R(\mathcal{G}/\mathcal{P})$  at a point of contact  $K$  of the surfaces  $\mathcal{G}$  and  $\mathcal{P}$  is defined by the position vector  $r_{cnf}(\varphi, \mu)$ . Therefore, the equality  $r_{cnf}(\varphi, \mu) = Kc_\varphi$  is observed, and the length of the straight line segment  $Kc_\varphi$  is equal to the distance  $a_\varphi b_\varphi$ .

Here, in Equation 20.2 is designated:

$r_g = \sqrt{|R_g|}$  is the position vector of a point of the Dupin indicatrix of the gear tooth flank,  $\mathcal{G}$ , at point,  $K$ , of contact with mating pinion tooth flank,  $\mathcal{P}$ .

$R_g$  is the normal radius of curvature of the gear tooth flank,  $\mathcal{G}$ , at point,  $K$ , of contact with mating pinion tooth flank,  $\mathcal{P}$ .

$r_p = \sqrt{|R_p|}$  is the position vector of a point of the Dupin indicatrix of the pinion tooth flank,  $\mathcal{P}$ , at a point,  $K$ , of contact with mating gear tooth flank,  $\mathcal{G}$ .

$R_p$  is the normal radius of curvature of the pinion tooth flank,  $\mathcal{P}$ , at point,  $K$ , of contact with mating gear tooth flank,  $\mathcal{G}$ .

The maximal and minimal degrees of conformity at the point of contact of tooth flanks,  $\mathcal{G}$  and  $\mathcal{P}$ , as well as the orientation of the normal planes within which the maximal and minimal degree of conformity are specified can be calculated by means of the indicatrix of conformity,  $Cnf_R(\mathcal{G}/\mathcal{P})$ .

The interested reader may wish to go to Appendix E for details on indicatrix of conformity,  $Cnf_R(\mathcal{G}/\mathcal{P})$ , at the point of contact of a gear tooth flank,  $\mathcal{G}$ , and a mating pinion tooth flank,  $\mathcal{P}$ .

## 20.4 A Concept of Synthesis of Favorable Perfect Gear Pairs

As the contact geometry at a point of contact between the tooth flanks of a gear and mating pinion,  $\mathcal{G}$  and  $\mathcal{P}$ , can be precisely described analytically by means of the indicatrix of conformity,  $Cnf_R(\mathcal{G}/\mathcal{P})$ , then this characteristic curve can be utilized for solving the problem of synthesis of favorable perfect gear pairs.

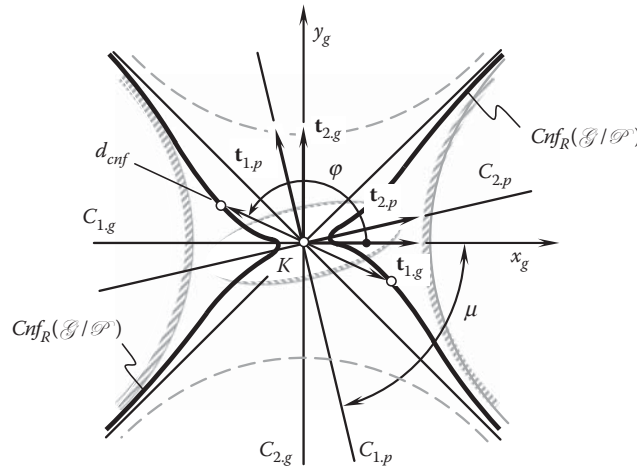


FIGURE 20.3

Indicatrix of conformity,  $Cnf_R(\mathcal{G}/\mathcal{P})$ , at point of contact,  $K$ , of a smooth regular saddle-like gear tooth flank,  $\mathcal{G}$ , and a mating pinion convex tooth flank,  $\mathcal{P}$  (the tooth flanks,  $\mathcal{G}$  and  $\mathcal{P}$ , are in the first order of tangency).

At a contact point,  $K$ , within a desired line of contact,  $LC_{des}$ , between a saddle-like gear tooth flank,  $\mathcal{G}$ , and a convex mating pinion tooth flank,  $\mathcal{P}$ , the indicatrix of conformity,  $Cnf_R(\mathcal{G}/\mathcal{P})$  is constructed, as illustrated in Figure 20.3. The equation of the indicatrix of conformity returns the following information about the interacting tooth flanks,  $\mathcal{G}$  and  $\mathcal{P}$ , at contact point,  $K$ :

- Configuration of the principal directions,  $\mathbf{t}_{1,g}$  and  $\mathbf{t}_{2,g}$ , on the gear tooth flank,  $\mathcal{G}$ , in relation to the linear velocity vector,  $\mathbf{V}_\Sigma$ , of their relative motion (Figure 20.4).
- The principal radii of curvature,  $R_{1,g}$  and  $R_{2,g}$ , in the sections of the gear tooth flank,  $\mathcal{G}$ , by the first,  $C_{1,g}$ , and second,  $C_{2,g}$ , principal planes.
- Configuration of the principal directions,  $\mathbf{t}_{1,p}$  and  $\mathbf{t}_{2,p}$ , on the pinion tooth flank,  $\mathcal{P}$ , in relation to the linear velocity vector,  $\mathbf{V}_\Sigma$ , of their relative motion.
- The principal radii of curvature,  $R_{1,p}$  and  $R_{2,p}$ , in the sections of the pinion tooth flank,  $\mathcal{P}$ , by the first,  $C_{1,p}$ , and second,  $C_{2,p}$ , principal planes.
- The angle,  $\mu$ , of local relative orientation of the tooth flanks,  $\mathcal{G}$  and  $\mathcal{P}$ , in relation to one another.
- A current,  $d_{cnf}$  (and the minimum,  $d_{cnf}^{\min} = 0$ ), diameters of the indicatrix of conformity,  $Cnf_R(\mathcal{G}/\mathcal{P})$ .
- A direction of the maximal,  $\mathbf{t}_{\max}$ , and minimal,  $\mathbf{t}_{\min}$ , degree of conformity of the tooth flanks at a point within a line of their contact.

All the output data are expressed in terms of the design parameters of the gear pair and in terms of parameters of the kinematics of the relative motion of the gear and the pinion (these parameters are considered variable at this point).

The active portion of the axis of instant rotation,  $P_{ln}$ , can be divided into a certain number,  $N_{ln}$ , of straight line segments of length  $a_{ln}$ . The value of the transverse pressure angle,  $\phi_{t,\omega}$ , can be different at each straight line segment of length  $a_{ln}$ . For each  $a_{ln}$ , a corresponding narrow plane of action,  $PA_a$ , can be constructed. When the number,  $N_{ln}$ , approaches infinity ( $N_{ln} \rightarrow \infty$ ), and the length,  $a_{ln}$ , approaches zero ( $a_{ln} \rightarrow 0$ ), then a smooth ruled surface of action,  $SA$ , can be constructed.\* Such an alteration of the transverse pressure angle,  $\phi_{t,\omega}$ , can be incorporated in the process of synthesizing of synthesis of a favorable gear pair.

A desired parameter,  $P_s$ , the extremum of which is required to be attained when synthesizing the gear pair, has to be expressed as a function of a radius,  $r_{cnf}$ , of the indicatrix of conformity,  $P_s = P_s(r_{cnf})$ .

\* Continuous and smooth alteration of both parameters,  $N_{ln}$  and  $a_{ln}$ , is assumed in this consideration.

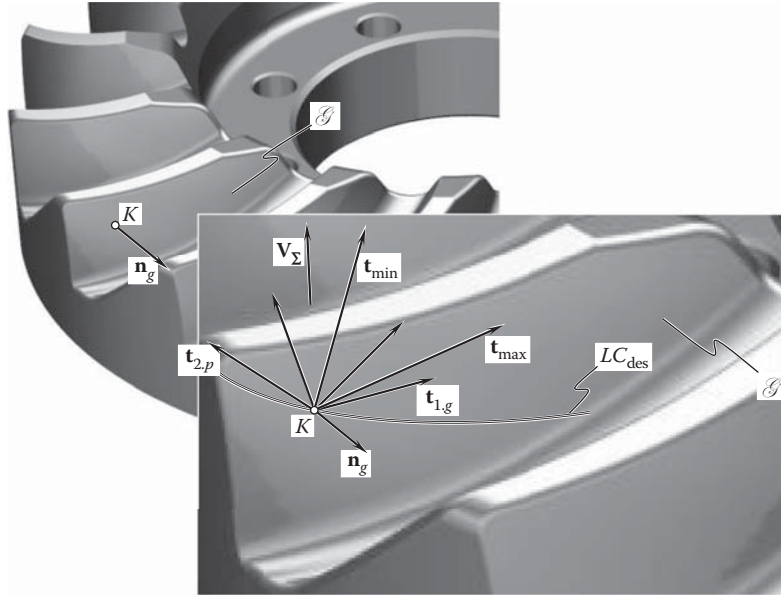


FIGURE 20.4

Contact geometry at point,  $K$ , of contact between the tooth flanks,  $\mathcal{G}$  and  $\mathcal{P}$ , of a gear and a mating pinion.

A solution to the set of equations:

$$\frac{\partial P_s}{\partial \varphi}(\varphi, \mu, R_g, R_p, \dots) = 0 \quad (20.3)$$

$$\frac{\partial P_s}{\partial \mu}(\varphi, \mu, R_g, R_p, \dots) = 0 \quad (20.4)$$

$$\frac{\partial P_s}{\partial R_g}(\varphi, \mu, R_g, R_p, \dots) = 0 \quad (20.5)$$

$$\frac{\partial P_s}{\partial R_p}(\varphi, \mu, R_g, R_p, \dots) = 0 \quad (20.6)$$

along with the derivatives with respect to the other parameters of a gear pair returns a set of the design parameters of the gear pair and the parameters of the kinematics of the relative motion of the gear and the pinion. Where appropriate, the solution to the set of Equations 20.3 through 20.6 has to comply with permissible intervals for the design parameters, for example, for the transverse pressure angle,  $5^\circ \leq \phi_{t,\omega} \leq 35^\circ$ , pitch helix angle,  $-40^\circ \leq \psi \leq 40^\circ$ , and so forth.

Conclusions that can be drawn from the discussion in this section are briefly outlined immediately below:

- The problem of synthesis of perfect gear pairs with favorable performance is challenging. This problem can be solved analytically.
- Implementation of analytical description of contact geometry of tooth flanks of a gear and mating pinion is a promising approach to solving the problem of synthesis of perfect gear pairs with favorable performance.
- It is proposed to develop a solution to the problem of synthesis of perfect gear pairs with favorable performance on the premise of the indicatrix of conformity,  $Cnf_R(\mathcal{G}/\mathcal{P})$ , constructed at a point of contact between the tooth flanks,  $\mathcal{G}$  and  $\mathcal{P}$ , of a gear and mating pinion.
- A gear pair of any kind, that is, parallel-axes gear pairs, intersected-axes gear pairs, crossed-axes gear pairs, and  $S_{pr}$ -gearings, can be synthesized using the disclosed approach.

The proposed method of synthesis of perfect gear pairs with favorable performance needs to evolve and become convenient for practical implementation, for example, in the development of corresponding software.

## Part VII

# Real Gears and Their Application

This section of the book is composed of [Chapters 21](#) through [Chapter 31](#). This section of the book deals with numerous areas of application of gears and gear pairs of all kinds. The consideration is mostly (but not only) focused on illustration of novel results in the theory of gearing outlined in this monograph.





# Taylor & Francis

Taylor & Francis Group

<http://taylorandfrancis.com>

---

## *Generic Gear Shapes*

---

When two rotation vectors associated with an input and output shaft are specified, gears of various geometries can be used to transmit and transform a rotation from the driving shaft to the driven shaft. Skew-axes helical gears, worm gearing, and others are used to transmit and transform a rotation from an input shaft to an output shaft, the axes of which cross each other at a crossed-axes angle.

Gears that feature various generic shapes can be used to transmit and transform a given rotation. This makes it possible to conclude that the vector diagram of a gear pair is necessary but not sufficient for identifying the actual type of a gear pair. In this regard, the generic shape of gears of which a gear pair is composed is of importance. If the generic gear shape is incorporated into consideration, this makes it possible to further develop a classification of possible types of gear pairs. An orderly classification of gear pairs and a classification of gears themselves is a desirable preliminary to the study of gears in general. It is a challenging problem to develop a scientific classification of gear pairs. In general engineering practice, names have been given to most of the numerous types of gear members and gear combinations. However, these names, although generally accepted and used, are sometimes indefinite and ambiguous. In some cases, it is hard to find a sufficient number of names to distinguish between variants that deserve some recognition of their individuality; in others, the same gear operating in different ways may have different names. The problem of classification, moreover, yields different results according to the direction from which it is approached. By treating gears according to the character of their teeth, one system of grouping emerges; by considering the relative position of the shafts they connect, another system is possible; and from the point of view of the real nature of tooth action, a third grouping is possible.

In this chapter, an attempt to classify gear pairs based on their associated vector diagrams is undertaken.

---

### **21.1 Origination of Generic Gear Shape**

Gears used in the design of various machines and mechanisms are somehow machined on machine tools. Nowadays, machine tools, especially numerical control (NC) machines, are capable of performing any desired motion of the cutting tool in relation to the workpiece. This makes it possible to machine a gear that has any desired tooth flank geometry. Using any desired motion of the cutting tool with respect to the work gear is not a common practice in machining gears, especially machining gears in high-volume production industries.

Motions performed by the gear-cutting tool in relation to a work gear are either a translation, a rotation, or a combination of translations and rotations [111,112]. This is because translation and rotation are the two elementary motions that can be easily performed on a machine tool. If a relative motion of a gear-cutting tool is limited either to a translation, a rotation, or a combination of a few translations and rotations, then all possible types of gears and gear pairs can be identified and consequently investigated.

Let us proceed with a discussion of possible generic shapes of gears machined on conventional machine tools for gear production.

---

### **21.2 Examples of Gear Pairs Composed of Gears with Various Generic Shapes**

Various designs of gears can be developed for the purpose of connecting parallel shafts.

In spur and helical involute gears, teeth are generated from a basic rack whose pitch plane rolls over the pitch cylinder of the gear; further, the teeth of the basic rack are symmetrical with respect to the pitch plane, or they have, in the case of corrected gears, a plane of symmetry parallel to the pitch plane [76,77].

There is a possible departure from these conditions that leads to a type of gear that has valuable but little-explored possibilities; to this type is given the name, for want of a better one, *conical involute gears*. The principle underlying generation and action of gears of this type may be approached in the following way.

Suppose that a spur gear is generated by the rack planing process, which is carried out in the usual way except that the direction of reciprocation of the rack cutter, instead of being parallel to the axis of the gear, is inclined, as shown in Figure 21.1. Since the work gear is rolled in the same way as for a normal spur gear, it still has a pitch cylinder that rolls with the real pitch plane, represented by  $W$ , of the basic rack,  $\mathcal{R}$ , although the plane of symmetry of the teeth of the basic rack is now inclined at an angle,  $\theta$ , to the axis of the work gear. Moreover, on all transverse planes, such as  $aO$ ,  $bO$ , the inclination of the profiles of the rack teeth is the same and is equal to  $\phi_t$ , whereas the intersection of the pitch plane,  $W$ , with any basic rack tooth gives a straight line representing a tooth spiral on the developed pitch cylinder. Hence the teeth generated by the basic rack,  $\mathcal{R}$ , are involute helicoids. On sections such as  $aO$  and  $bO$ , the profiles,  $a_1$  and  $b_1$ , are involutes to the same base circle of diameter,  $d_{bg}$ , and really represent the profiles of spur gears with different degrees of correction.

Figure 21.2a shows a pair of cylindrical gears of pitch diameters,  $d_g$  and  $d_p$ , connecting parallel shafts. The same shafts might be connected, with the same result, by a pair of conical involute gears, shown in Figure 21.2b. The pitch diameters,  $d_g$  and  $d_p$ , are the diameters of the pitch cylinders when the gears are rolled

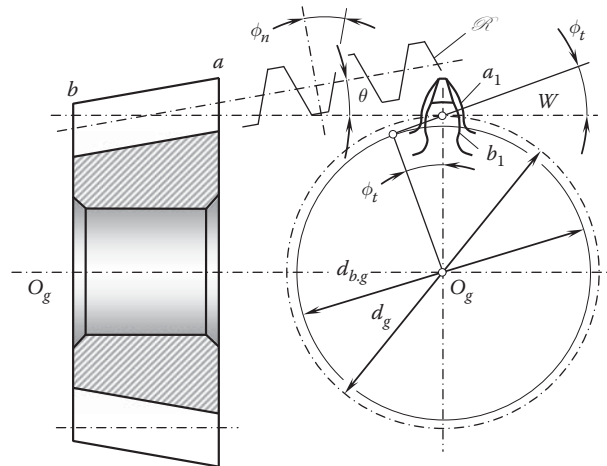


FIGURE 21.1

Generation of a conical involute gear. (From Merritt, H.E. 1971, *Gear Engineering*, London: Putman Publishing) [76].

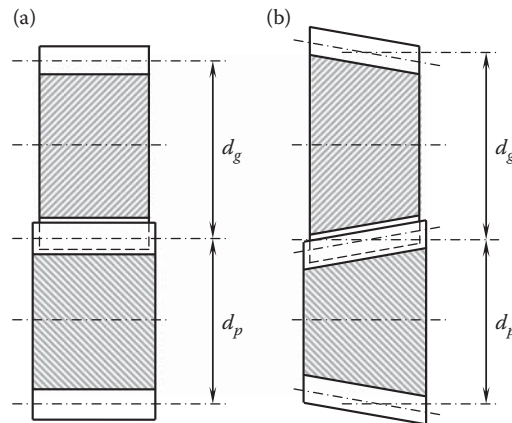
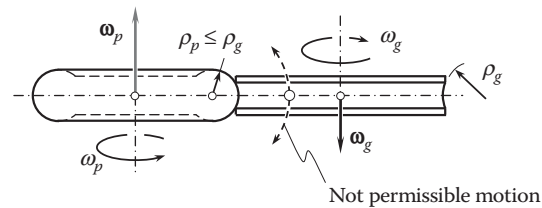


FIGURE 21.2

Derivation and example of application of a conical involute gear [76]: (a) conventional cylindrical gear pair, and (b) conical involute gear pair. (From Merritt, H.E. 1971, *Gear Engineering*, London: Putman Publishing.)

**FIGURE 21.3**

Toroidal involute gears for connecting parallel shafts.

with the inclined basic rack,  $\mathcal{R}$ , and the only condition is that the pitch cone angle,  $\theta$ , must be the same for both gears. If the teeth are also generated with a spiral, the spiral angles of generation,  $\psi_g$  and  $\psi_p$ , must be equal and opposite.

In comparison with the conventional cylindrical gear pair shown in Figure 21.2a, a conical involute gear pair (see Figure 21.2b) has the same pitch diameter of the gear,  $d_g$ , and pinion,  $d_p$ . Neither the pitch surfaces nor the axodes of the gear pair (see Figure 21.2b) feature conical shapes. A conical shape is the generic gear shape of conical involute gears.

In this and other applications described below in this chapter, the angular velocity ratio is (theoretically) constant and independent of the axial position of either gear within the practical limits. Axial adjustment of either gear relative to the other will, however, alter the backlash, and may in fact provide a useful means of doing this [76,77].

A few more examples to this end can be found in [9]. Internal gear pairs similar to the aforementioned (see Figure 21.2) can also be designed.

A pinion and gear can be machined when both members of the gear pair feature a toroidal generic gear shape. Toroidal involute gears of this design are schematically illustrated in Figure 21.3. Gears with such a geometry can be generated by a hob fed along a circular arc path in relation to a work gear. The radius of the gear contour,  $\rho_g$ , in this case is equal to or exceeds the corresponding radius,  $\rho_p$ , of the pinion contour ( $\rho_g \geq \rho_p$ ). Gear pairs with a toroidal generic shape allow for axial adjustment of the gear and the pinion in relation to each other. When the inequality  $\rho_g > \rho_p$  is observed, the gear pair features a tooth flank geometry that can be viewed as equivalent to tooth modification in the lengthwise direction.

It is often loosely claimed that gear pairs that feature toroidal generic shapes have an additional degree of freedom, meaning that the gear can spin relative to the pinion in both directions shown by means of the dashed arrow. This is not correct, as this *motion* is not permissible at all (see comments to Figure 18.19 in Chapter 18).

Again, internal gear pairs similar to the aforementioned (see Figure 21.3) can also be designed.

The discussed examples make clear the difference between the generic gear shape and the pitch surfaces, as well as between the corresponding axodes. Neither the cone in a conical involute gear (see Figure 21.2) nor the torus surface in a toroidal gear pair (see Figure 21.3) is equivalent to an axode or a pitch surface.

It must be stressed here that an approach that is based on the elements of vector algebra can be implemented for the analytical description of the generic gear shape in all practical cases. Vector representation of generic gear shapes is convenient for many reasons, which are discussed below in Section 21.3.

### 21.3 Evaluation of the Total Number of Possible Generic Gear Shapes

Once all possible types of gear design are limited to those gears for which generic shapes are generated either by a straight line segment or by a circular arc, the following two actions are possible:

1. Identification of all possible types of gears
2. Development of a classification of possible types of the generic gear shapes

This classification is of importance for the purpose of designing gear pairs that feature the most favorable design parameters.

### 21.3.1 Possible Profiles of Generic Gear Shape Constructed in Axial Section of a Gear

From Figure 21.4, consider a generic gear shape designed for a spatial gear pair.

If no constraints are imposed, the ideal generic gear surface can be interpreted as the loci of consecutive positions of the axis of instant rotation,  $P_{ln}$ , when the axis is rotated about the gear axis,  $O_g$ . In this way, the generic gear surface is shaped in the form of a hyperboloid of revolution of one sheet. Two hyperbolas appear in the section of this surface by a plane through the gear axis of rotation,  $O_g$ .

An expression for the analytical description of a generic gear surface can be derived in the following way: consider a generic gear surface that is referred to a Cartesian coordinate system,  $X_g^a Y_g^a Z_g^a$ , as shown in Figure 21.4. The position vector,  $\mathbf{r}_g^a$ , of an arbitrary point,  $m$ , of the generic gear surface can be considered as the summa of two components, that is,

$$\mathbf{r}_g^a = \mathbf{R}_g^a + \mathbf{L}_g^a \quad (21.1)$$

In the reference system,  $X_g^a Y_g^a Z_g^a$ , one of the components,  $\mathbf{R}_g^a$  (see Figure 21.4), can be analytically represented as:

$$\mathbf{R}_g^a = \mathbf{i} \cdot \tilde{r}_g \cos \phi_g^a + \mathbf{j} \cdot \tilde{r}_g \sin \phi_g^a \quad (21.2)$$

where:

$\tilde{r}_g$  is the radius of the throat of the generic gear surface (the radius,  $\tilde{r}_g$ , is measured in the coordinate plane,  $X_g^a Y_g^a$ ).

$\phi_g^a$  is the angular parameter of the generic gear surface.

For an analytical description of another component,  $\mathbf{L}_g^a$ , of the position vector,  $\mathbf{r}_g^a$ , the following expression can be used:

$$\mathbf{L}_g^a = -\mathbf{i} \cdot z_g^a \tan \Sigma_g \sin \phi_g^a + \mathbf{j} \cdot z_g^a \tan \Sigma_g \cos \phi_g^a + \mathbf{k} \cdot z_g^a \quad (21.3)$$

The angular parameter,  $\phi_g^a$ , of the generic gear surface, is the first Gaussian parameter of the generic gear surface.

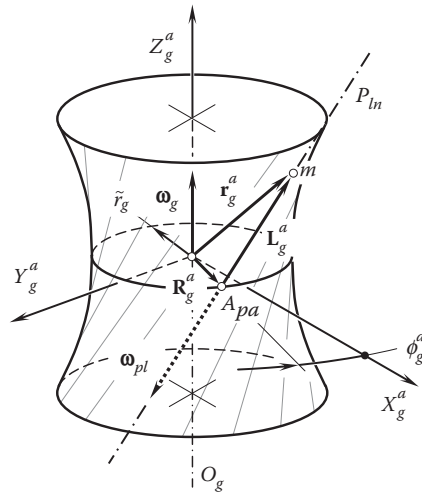


FIGURE 21.4

Analytical description of a gear generic surface.

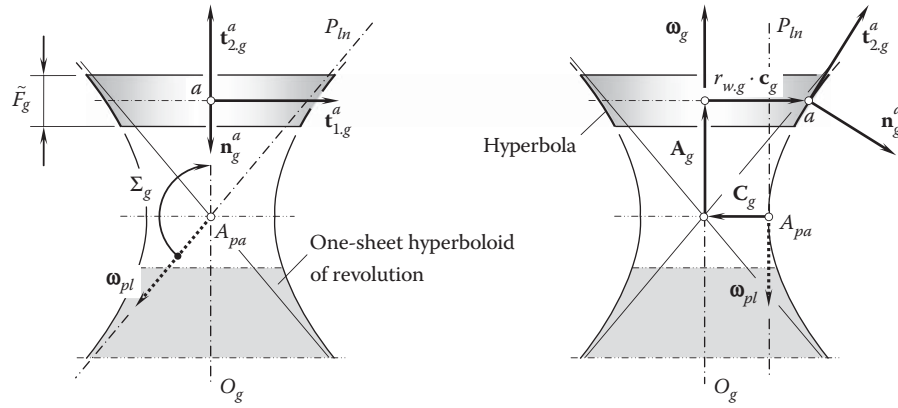


FIGURE 21.5

Darboux frame,  $\mathbf{n}_g^a, \mathbf{t}_{1,g}^a, \mathbf{t}_{2,g}^a$ , associated with the desired generic surface of a gear.

Equations 21.2 and 21.3 allow for the derivation of an expression:

$$\mathbf{r}_g^a(\phi_g^a, z_g^a) = \begin{bmatrix} \tilde{r}_g \cos \phi_g^a - z_g^a \tan \Sigma_g \sin \phi_g^a \\ \tilde{r}_g \sin \phi_g^a + z_g^a \tan \Sigma_g \cos \phi_g^a \\ z_g^a \\ 1 \end{bmatrix} \quad (21.4)$$

for the position vector,  $\mathbf{r}_g^a$ , of an arbitrary point,  $m$ , of the generic gear surface.

In Equation 21.4, another Gaussian parameter of the generic gear surface, denoted by  $z_g^a$ , and  $\Sigma_g$  designates the angle that the rotation vector of the gear,  $\omega_g$ , makes with the vector,  $\omega_{pl}$  of instant rotation [ $\Sigma_g = \angle(\omega_g, \omega_{pl})$ ].

The rotation vector of the gear,  $\omega_g$ , is along the gear axis of rotation,  $O_g$ . The vector,  $\omega_g$ , is applied at the throat of the generic gear surface. The vector of instant rotation,  $\omega_{pl}$ , is along the axis of instant rotation,  $P_{ln}$ . This vector is applied at the plane of action apex,  $A_{pa}$ .

The face width of the gear is denoted by  $\tilde{F}_g$ . The location of the middle section of the generic gear surface is specified by the vectors  $\mathbf{C}_g$ ,  $\mathbf{A}_g$ , and  $r_{w,g} \cdot \mathbf{c}_g$ , as shown in Figure 21.5.

A local reference system is associated with the generic gear surface. The origin of the reference system is at a point,  $a$ , within the axial profile of the generic gear surface. The origin,  $a$ , is at the middle of the width,  $\tilde{F}_g$ . In the particular case under consideration, a *Darboux\** frame is used as the reference system. Three unit vectors,  $\mathbf{n}_g^a$ ,  $\mathbf{t}_{1,g}^a$ , and  $\mathbf{t}_{2,g}^a$  make up the Darboux frame.

The vector,  $\mathbf{n}_g^a$ , is a unit normal vector to the generic gear surface at the point,  $a$ . The  $\Phi_T$  equation:

$$\mathbf{n}_g^a = \mathbf{u}_g \cdot \mathbf{v}_g \quad (21.5)$$

can be used for the calculation of the unit normal vector,  $\mathbf{n}_g^a$ .

In Equation 21.5, the unit tangent vectors to the generic gear surface at  $a$  are designated as  $\mathbf{u}_g$  and  $\mathbf{v}_g$ . The unit vectors,  $\mathbf{u}_g$  and  $\mathbf{v}_g$ , are dimensionless. They are given as follows:

$$\mathbf{u}_g = \frac{\mathbf{U}_g}{|\mathbf{U}_g|} \quad (21.6)$$

$$\mathbf{v}_g = \frac{\mathbf{V}_g}{|\mathbf{V}_g|} \quad (21.7)$$

respectively.

\* Jean-Gaston Darboux (August 14, 1842–February 23, 1917), a French mathematician.

In Equations 21.6 and 21.7, the tangent vectors,  $\mathbf{U}_g$  and  $\mathbf{V}_g$ , are given by  $\mathbf{U}_g = \partial \mathbf{r}_g^s / \partial U_g$  and  $\mathbf{V}_g = \partial \mathbf{r}_g^s / \partial V_g$ , respectively, and the vector,  $\mathbf{r}_g^s$ , is the position vector of a point of the generic gear surface. The Gaussian parameters of the generic gear surface are denoted by  $U_g$  and  $V_g$ .

The unit normal vector,  $\mathbf{n}_g^a$ , is a dimensionless parameter, as it is expressed in terms of the dimensionless unit tangent vectors,  $\mathbf{u}_g$  and  $\mathbf{v}_g$  (see Equation 21.5).

Labeling of the principal directions depends upon the curvature of the generic gear surface. The principal direction featuring a greater curvature,  $k_{1,g}^a$  (and thus a smaller radius of curvature,  $R_{1,g}^a$ ), is labeled as  $\mathbf{t}_{1,g}^a$ . The principal direction featuring a smaller curvature,  $k_{2,g}^a$  (and thus a greater radius of curvature,  $R_{2,g}^a$ ) is labeled as  $\mathbf{t}_{2,g}^a$  [111,112] (here, the curvatures, as well as the corresponding radii of curvature, are signed values. They are positive in the case of convex section by a normal plane, and they are negative when the section is concave). As the equality  $R_1 = k_1^{-1}$  is valid by definition, the inequalities,  $k_{1,g}^a > k_{2,g}^a$  and  $R_{1,g}^a < R_{2,g}^a$ , are always valid.\* In umbilical points on a surface, when all the radii of normal curvature are of a constant value ( $R_g^a = \text{const}$ ), the Darboux frame does not exist. In this reduced case, a limit case of the Darboux frame when  $R_{1,g}^a$  approaches infinity (that is,  $R_{1,g}^a \rightarrow \infty$ ) is used instead of the trihedron,  $\mathbf{n}_g^a \mathbf{t}_{1,g}^a \mathbf{t}_{2,g}^a$ .

The unit tangent vectors,  $\mathbf{t}_{1,g}^a$  and  $\mathbf{t}_{2,g}^a$ , are the principal vectors at point within the generic gear surface. The first and second principal directions of the gear generic surface are specified by the tangent vectors,  $\mathbf{t}_{1,g}^a$  and  $\mathbf{t}_{2,g}^a$ . The vector,  $\mathbf{t}_{1,g}^a$ , is tangential to the section of the generic surface by a transverse plane through the point,  $a$ , as this section is convex. The first principal direction is specified by the unit tangent vector,  $\mathbf{t}_{1,g}^a$ . The vector,  $\mathbf{t}_{2,g}^a$ , is tangential to the cross-section of the generic surface by axial plane through the point,  $a$ , as this section is concave. The second principal direction is specified by the unit tangent vector,  $\mathbf{t}_{2,g}^a$ .

The unit tangent vectors,  $\mathbf{t}_{1,g}^a$  and  $\mathbf{t}_{2,g}^a$ , are specified by the expressions:

$$\mathbf{t}_{1,g}^a = \frac{\mathbf{T}_{1,g}^a}{|\mathbf{T}_{1,g}^a|} \quad (21.8)$$

$$\mathbf{t}_{2,g}^a = \frac{\mathbf{T}_{2,g}^a}{|\mathbf{T}_{2,g}^a|} \quad (21.9)$$

where  $\mathbf{T}_{1,g}^a$  and  $\mathbf{T}_{2,g}^a$  are the vectors of the first and second principal directions of the generic gear surface. Known methods [118,119] are used for the calculation of the unit tangent vectors,  $\mathbf{t}_{1,g}^a$  and  $\mathbf{t}_{2,g}^a$ .

Once the unit vectors,  $\mathbf{n}_g^a$ ,  $\mathbf{t}_{1,g}^a$  and  $\mathbf{t}_{2,g}^a$ , are mutually orthogonal and two of them (that is,  $\mathbf{t}_{1,g}^a$  and  $\mathbf{t}_{2,g}^a$ ) are along principal directions on the generic gear surface, they make up a trihedron that is commonly referred to as a Darboux frame.

As shown in Figure 21.5, the generic gear surface has a favorable geometry, as it is generated by the axis,  $P_{lm}$ , when the axis is given a rotation about the gear axis of rotation,  $O_g$ . Unfortunately, a generic gear surface of this geometry is impractical, mostly because it is inconvenient for manufacturing purposes. Generic gear surfaces of a simplified geometry are commonly used instead of the one depicted in Figure 21.5.

It is proven that all possible elementary motions of a gear-cutting tool in relation to a work gear are limited to just translations, rotations, and feasible combinations of translations and rotations. Once this concept is adopted, all possible shapes of generic gear surfaces can be identified. The Darboux frame,  $\mathbf{n}_g^a \mathbf{t}_{1,g}^a \mathbf{t}_{2,g}^a$ , is helpful to this end.

Consider the generic surface of a gear that is machined by a gear-cutting tool, which is performing a straight motion relative to the work gear. No physical constraints are imposed on the machining of the gear in this way. The parameters of the straight motion are assigned so as to make a trajectory of the straight motion of the gear-cutting tool tangential at the point,  $a$ , to the hyperbola, as schematically illustrated in Figure 21.6. In the case under consideration, the desired hyperbolic profile of the generic gear surface is replaced with the straight line segment that is tangential to the hyperbola at  $a$ . The straight line segment is at an angle,  $\varphi_g^a$ , relative to the gear axis of rotation,  $O_g$ . The angle,  $\varphi_g^a$ , can be expressed in terms of the first derivative of an equation of the hyperbola calculated at the point,  $a$ . The actual form of an equation for the calculating the angle,  $\varphi_g^a$ , depends on the parameterization of the equation of the hyperbolic axial profile of the desired generic gear surface.

\* Remember that the algebraic values of the radii of principal curvatures,  $R_{1,g}^a$  and  $R_{2,g}^a$ , relate to each other as  $R_{2,g}^a > R_{1,g}^a$ . In the case of umbilical points, all radii of normal curvature are equal. As a result, the principal directions,  $\mathbf{t}_{1,g}^a$  and  $\mathbf{t}_{2,g}^a$  (and, consequently, the principal radii of curvature,  $R_{1,g}^a$  and  $R_{2,g}^a$ ), are not identified for umbilical points on a generic gear surface.



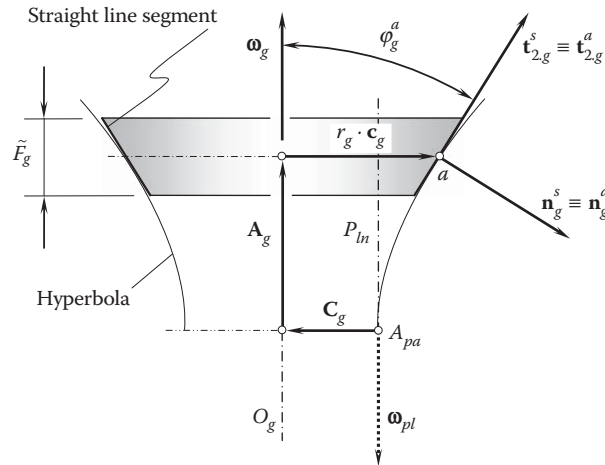


FIGURE 21.6

Axial profile of a generic gear surface approximated by a straight line segment tangential at point,  $a$ , to hyperbola.

The approximation of the hyperbolic arc segment by the straight line segment results in zero curvature of the generic gear surface in the second principal direction ( $k_{2,g}^a = 0$ ). The first principal curvature,  $k_{1,g}^a$ , can be determined using the *Mensnier\** theorem:

$$k_{1,g}^a = \frac{\cos [\angle(\mathbf{c}_g, \mathbf{n}_g^a)]}{r_{w,g}} \quad (21.10)$$

As the straight-line axial profile is tangential at  $a$  to the hyperbola, no changes to the orientation of the axial profile are observed. As a result, the Darboux frame,  $\mathbf{n}_g^s \mathbf{t}_{1,g}^s \mathbf{t}_{2,g}^s$ , associated with the approximated generic gear surface is identical to the trihedron  $\mathbf{n}_g^a \mathbf{t}_{1,g}^a \mathbf{t}_{2,g}^a$  associated with the desired generic gear surface.

Crossed-axes gears of a conventional design, *hypoid gearing* in particular, feature generic gear surfaces that have the geometry illustrated in Figure 21.6.

Consider a generic gear shape that is machined by a gear-cutting tool, which is performing a rotary motion relative to the work gear. Again, no physical constraints are imposed on machining of the gear in this way.

Two different methods of cutting the gear can be distinguished in this case.

First, the parameters of the rotary motion are assigned so as to make the trajectory of the rotary motion of the gear-cutting tool tangential at point  $a$  to the hyperbola, as schematically illustrated in Figure 21.7. In the case under consideration, the desired hyperbolic profile of the generic gear surface is replaced with a circular arc segment that is tangential to the hyperbola at  $a$ . The approximation of the hyperbolic arc segment by the circular arc segment results in a positive curvature of the axial cross-section of the generic gear surface. The direction at which the normal curvature is greater is labeled as  $\mathbf{t}_{1,g}^s$ . The normal curvature in this direction is labeled as  $k_{1,g}^s$ . The direction at which the normal curvature has a smaller value is labeled as  $\mathbf{t}_{2,g}^s$ . The normal curvature in this direction is labeled as  $k_{2,g}^s$ . Ultimately, either the two identities  $\mathbf{t}_{1,g}^s \equiv \mathbf{t}_{1,g}^a$  and  $\mathbf{t}_{2,g}^s \equiv \mathbf{t}_{2,g}^a$  (as depicted in Figure 21.7) or the inverse identities,  $\mathbf{t}_{1,g}^s \equiv \mathbf{t}_{2,g}^a$  and  $\mathbf{t}_{2,g}^s \equiv \mathbf{t}_{1,g}^a$  are valid. In this way, the generic gear surface is affected by the kinematics of the gear-machining process. Consequently, kinematics affects the labeling of the unit vectors of which the Darboux frame is composed.

Because the circular arc axial profile is tangential at point  $a$  to the hyperbola, no changes to the orientation of the axial profile are observed. As a result, the Darboux frame,  $\mathbf{n}_g^s \mathbf{t}_{1,g}^s \mathbf{t}_{2,g}^s$ , associated with the approximated generic gear surface is identical to that,  $\mathbf{n}_g^a \mathbf{t}_{1,g}^a \mathbf{t}_{2,g}^a$ , associated with the desired generic gear surface.

Second, the parameters of the rotary motion are assigned so as to make the trajectory of the rotary motion of the gear-cutting tool tangential at point  $a$  to the hyperbola, as schematically illustrated in Figure 21.8. In the case under consideration, the desired hyperbolic profile of the generic gear surface is replaced with a circular arc segment that is tangential to the hyperbola at point,  $a$ . The approximation of the hyperbolic arc segment by the

\* Jean Baptist Marie Charles de la Place Mensnier (June 19, 1754–June 17, 1793), a French mathematician.

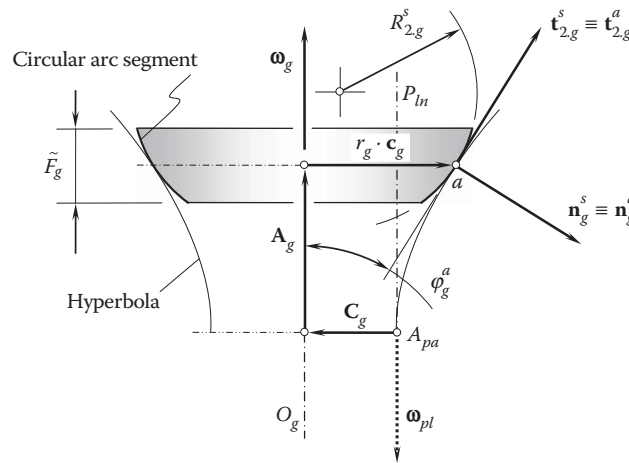


FIGURE 21.7

Axial profile of the generic surface of a gear approximated by a convex circular arc tangential at a point,  $a$ , to hyperbola.

circular arc segment results in a negative curvature of the axial cross-section of the generic gear surface. The identities  $\mathbf{t}_{1g}^s \equiv \mathbf{t}_{2g}^a$  and  $\mathbf{t}_{2g}^s \equiv \mathbf{t}_{1g}^a$  are valid in the case under consideration, as illustrated in Figure 21.8.

Because the circular arc axial profile is tangential at  $a$  to the hyperbola, no changes to the orientation of the axial profile are observed. As a result, the Darboux frame,  $\mathbf{n}_g^s \mathbf{t}_{1g}^s \mathbf{t}_{2g}^s$ , associated with the approximated generic gear surface is similar to the  $\mathbf{n}_g^a \mathbf{t}_{1g}^a \mathbf{t}_{2g}^a$  associated with the desired generic gear surface.

Gears that have circular arc axial profiles of the generic gear surface (see Figures 21.7 and 21.8) do not have wide application in the industry yet.

Methods to cut gears on both machine tools and gear generators are not limited to those in which the actual and desired axial profiles of generic gear surface are in tangency to each other at a certain point. The profiles can intersect each other at a certain angle.

The straight line segment of an actual axial profile of the generic gear surface can be tilted at an angle,  $\vartheta_g^s$ , as schematically shown in Figure 21.9. The angle,  $\vartheta_g^s$ , measured in the counterclockwise direction, is considered positive. The orientation of the Darboux frame,  $\mathbf{n}_g^s \mathbf{t}_{1g}^s \mathbf{t}_{2g}^s$ , of the actual generic gear surface in relation to the Darboux frame,  $\mathbf{n}_g^a \mathbf{t}_{1g}^a \mathbf{t}_{2g}^a$ , of the desired generic gear surface is specified by the angle,  $\vartheta_g^s$ . The trihedron,  $\mathbf{n}_g^s \mathbf{t}_{1g}^s \mathbf{t}_{2g}^s$ , is turned about the unit vector,  $\mathbf{t}_{1g}^a$ , in a counterclockwise direction through the angle,  $\vartheta_g^s$  (see Figure 21.9a).

The value of angle,  $\vartheta_g^s$ , is within the interval  $0^\circ < \vartheta_g^s < \phi_g^a + 90^\circ$ . In a particular case, the value of the angle,  $\vartheta_g^s$ , can be chosen as equal to the angle,  $\phi_g^a$ , at which the tangent to the hyperbola is tilted relative to the gear axis of

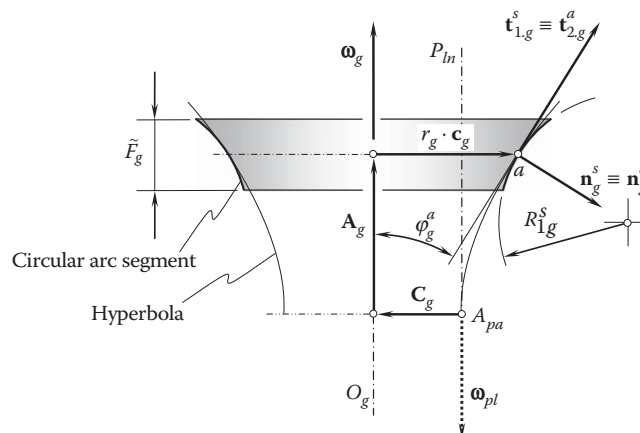
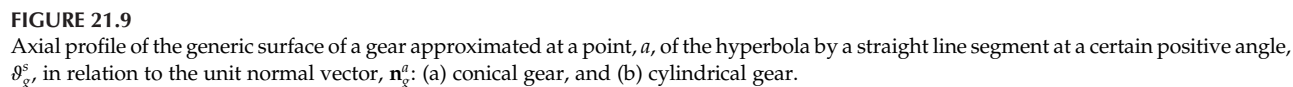


FIGURE 21.8

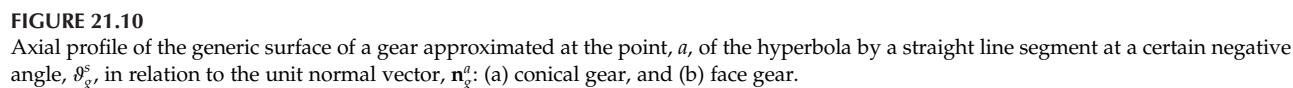
Axial profile of the generic surface of a gear approximated by a concave circular arc tangential at a point,  $a$ , to hyperbola.



Similarly, the straight line segment of an actual axial profile of the generic gear surface can be tilted at an angle,  $\vartheta_{g'}^s$ , in the opposite direction, as schematically shown in [Figure 21.10](#). The angle,  $\vartheta_{g'}^s$ , in this case is negative. The trihedron,  $\mathbf{n}_g^s \mathbf{t}_{1-g}^s \mathbf{t}_{2-g'}^s$ , is turned about the unit vector,  $\mathbf{t}_{1-g}^s$ , in a clockwise direction through the angle,  $\vartheta_{g'}^s$  (see [Figure 21.10a](#)).

Gears that feature an axial profile of the generic gear surface in the form of straight line segments tilted at a certain angle,  $\vartheta_g^s$  (see [Figures 21.9](#) and [21.10](#)), are used in the design of special-purpose gear trains.

Similar to gears that have an inclined straight line profile (see Figures 21.9 and 21.10), a circular arc axial profile of generic gear surfaces can also be tilted at either a positive or negative angle,  $\vartheta_g^s$ , relative to the unit normal vector,  $\mathbf{n}_{g'}^a$ , to the desired generic gear surface.



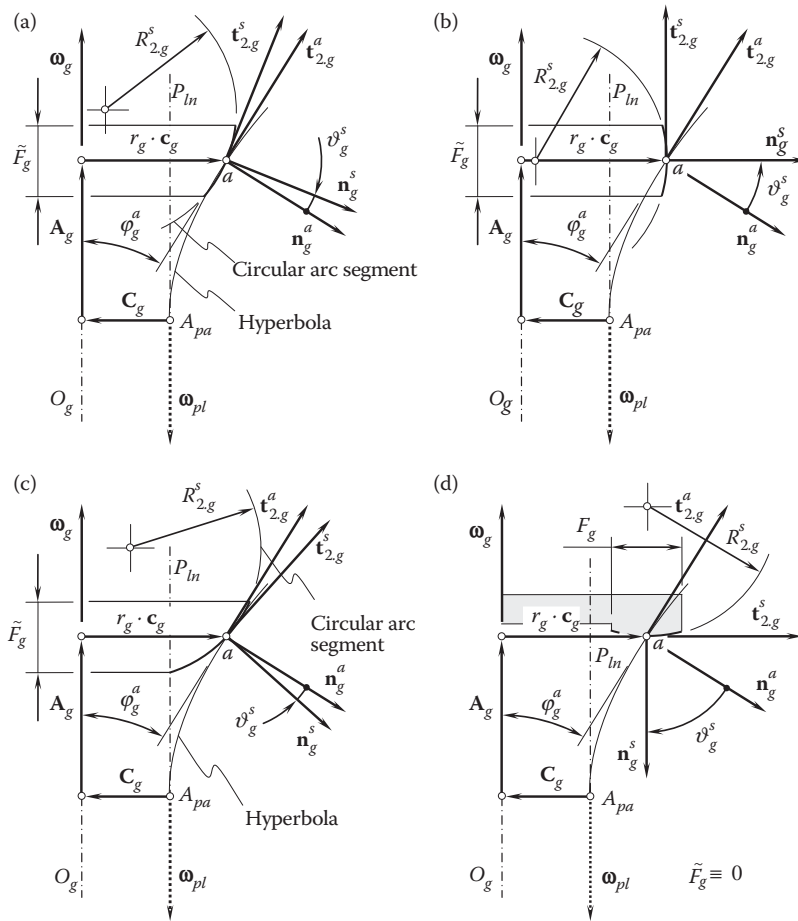


FIGURE 21.11

Axial profile of the generic surface of a gear approximated by a convex circular arc at a certain angle,  $\vartheta_g^s$ , in relation to the unit normal vector,  $\mathbf{n}_g^a$ , at the point,  $a$ , to the hyperbola.

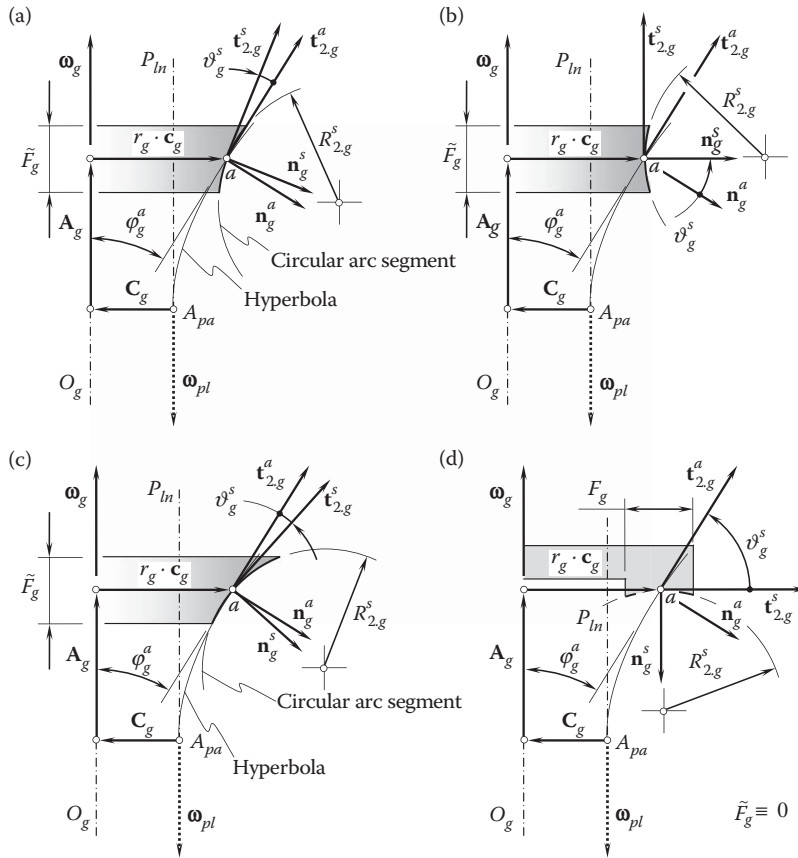
Results of the analysis for convex circular arc axial profiles inclined at a certain angle,  $\vartheta_g^s$ , in relation to the unit normal vector,  $\mathbf{n}_g^a$ , at the point,  $a$ , to the hyperbola are illustrated in Figure 21.11.

When an angle,  $\vartheta_g^s$ , is positive (see Figure 21.11a), the Darboux frame,  $\mathbf{n}_g^s \mathbf{t}_{1,g}^s \mathbf{t}_{2,g}^s$ , of the actual generic gear surface in relation to the Darboux frame,  $\mathbf{n}_g^a \mathbf{t}_{1,g}^a \mathbf{t}_{2,g}^a$ , of the desired generic gear surface is turned about the unit vector,  $\mathbf{t}_{1,g}^a$ , in a counterclockwise direction through the angle,  $\vartheta_g^s$ . The value of an angle,  $\vartheta_g^s$ , is within the interval  $0^\circ < \vartheta_g^s < \varphi_g^a + 90^\circ$ . In a particular case, the value of an angle,  $\vartheta_g^s$ , can be chosen as equal to the angle,  $\varphi_g^a$ , at which the tangent to the hyperbola is tilted relative to the gear axis of rotation,  $O_g$ , as shown in Figure 21.11b. A torus-like gear for a spatial gear pair is machined under such conditions. The outer portion of the torus serves in this case as the generic gear surface.

When the angle,  $\vartheta_g^s$ , is negative (Figure 21.11c), the Darboux frame,  $\mathbf{n}_g^s \mathbf{t}_{1,g}^s \mathbf{t}_{2,g}^s$ , of the actual generic gear surface in relation to the Darboux frame,  $\mathbf{n}_g^a \mathbf{t}_{1,g}^a \mathbf{t}_{2,g}^a$ , of the desired generic gear surface is turned about the unit vector,  $\mathbf{t}_{1,g}^a$ , in a clockwise direction through the angle,  $\vartheta_g^s$ . The value of the angle,  $\vartheta_g^s$ , is within the interval  $-(\varphi_g^a + 90^\circ) < \vartheta_g^s < 0^\circ$ . In a particular case, the value of the angle,  $\vartheta_g^s$ , can be chosen as equal to  $\vartheta_g^s = 90^\circ - \varphi_g^a$ , at which the tangent to the hyperbola is tilted relative to the gear axis of rotation,  $O_g$ , as shown in Figure 21.11d. A torus-like face gear for a spatial gear pair is machined under such conditions.

Results of the analysis for a concave circular arc axial profile that is inclined at a certain angle,  $\vartheta_g^s$ , in relation to the unit normal vector,  $\mathbf{n}_g^a$ , at the point,  $a$ , to the hyperbola are illustrated in Figure 21.12.

When the angle,  $\vartheta_g^s$ , is positive (see Figure 21.12a), the Darboux frame,  $\mathbf{n}_g^s \mathbf{t}_{1,g}^s \mathbf{t}_{2,g}^s$ , of the actual generic gear surface in relation to the Darboux frame,  $\mathbf{n}_g^a \mathbf{t}_{1,g}^a \mathbf{t}_{2,g}^a$ , of the desired generic gear surface is turned about the unit vector,  $\mathbf{t}_{1,g}^a$ , in a counterclockwise direction through the angle,  $\vartheta_g^s$ . The value of the angle,  $\vartheta_g^s$ , is within the interval  $0^\circ < \vartheta_g^s < \varphi_g^a + 90^\circ$ . In a particular case, the value of the angle,  $\vartheta_g^s$ , can be chosen as equal to the angle,  $\varphi_g^a$ . In

**FIGURE 21.12**

Axial profile of the generic surface of a gear approximated by a concave circular arc at a certain angle,  $\vartheta_g^s$ , in relation to the unit normal vector,  $\mathbf{n}_g^a$ , at the point,  $a$ , to the hyperbola. Parts (a) and (d) are discussed in the text.

this case, the equality  $\vartheta_g^s = \varphi_g^a$  is observed. The angle,  $\varphi_g^a$ , is the angle at which the tangent to the hyperbola is tilted relative to the gear axis of rotation,  $O_g$ , as shown in Figure 21.12b. A torus-like gear for a spatial gear pair is machined under such conditions. The inner portion of the torus serves in this case as the generic gear surface.

When the angle  $\vartheta_g^s$  is negative (Figure 21.12c), the Darboux frame,  $\mathbf{n}_g^s \mathbf{t}_{1g}^s \mathbf{t}_{2g}^s$ , of the actual generic gear surface in relation to the Darboux frame,  $\mathbf{n}_g^a \mathbf{t}_{1g}^a \mathbf{t}_{2g}^a$ , of the desired generic gear surface is turned about the unit vector,  $\mathbf{t}_{1g}^a$ , in a clockwise direction through the angle,  $\vartheta_g^s$ . The actual value of the angle,  $\vartheta_g^s$ , is within the interval  $-(\varphi_g^a + 90^\circ) < \vartheta_g^s < 0^\circ$ . In a particular case, the value of the angle,  $\vartheta_g^s$ , can be set as  $\vartheta_g^s = 90^\circ - \varphi_g^a$ , at which the tangent to the hyperbola is tilted relative to the gear axis of rotation,  $O_g$ , as shown in Figure 21.12d. A torus-like face gear for a spatial gear pair is machined under such conditions.

In addition to the possible generic gear surfaces shown in Figures 21.5 through 21.12, a few more generic gear surfaces can be derived under the assumption that the axial vector,  $\mathbf{A}_g$ , is equal to zero (that is,  $\mathbf{A}_g = 0$ ). Examples of such generic gear surfaces are schematically illustrated in Figure 21.13.

The total number of generic gear surfaces in this case is limited to six different kinds from three surfaces.

First, the straight line segment can be either tangential to the hyperbola at point  $a$  (see Figure 21.13a) or inclined to it at a certain angle,  $\vartheta_g^s$  (see Figure 21.13b). From the perspective of the design of the gear, it makes no difference whether the angle,  $\vartheta_g^s$ , is positive or negative.

Second, the convex circular arc profile also can be either tangential to the hyperbola at point  $a$  (see Figure 21.13c) or inclined to it at a certain angle,  $\vartheta_g^s$  (see Figure 21.13d). From the perspective of the design of the gear, it makes no difference whether the angle,  $\vartheta_g^s$ , is positive or negative.

Third, this statement is also true with respect to a concave circular arc profile, which also can be either tangential to the hyperbola at point  $a$  (see Figure 21.13e) or inclined to it at a certain angle,  $\vartheta_g^s$  (see Figure 21.13f).

An intermediate conclusion can be drawn from this discussion: the total number of possible generic gear surfaces of the considered geometry is a finite value and is limited to 27 generic gear surface profiles. They are

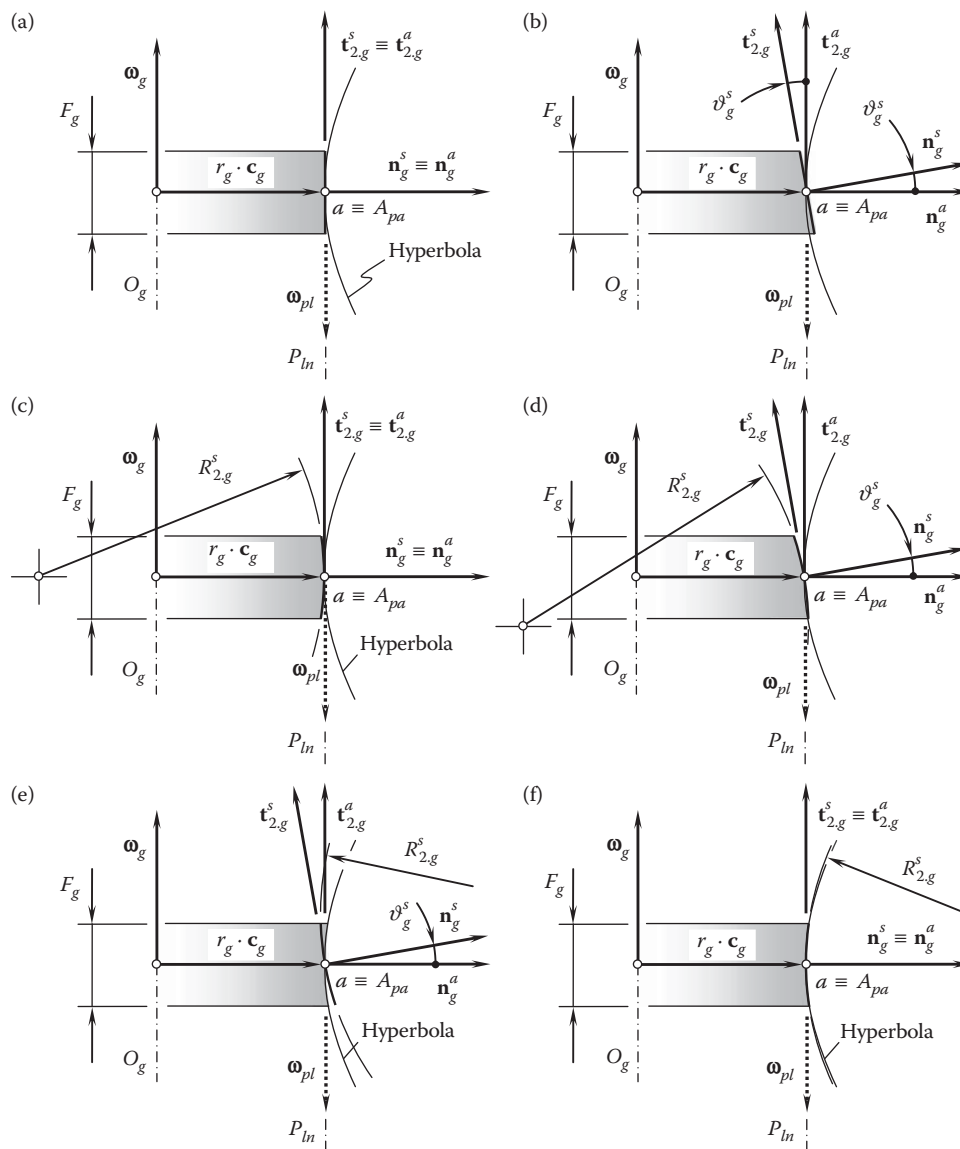


FIGURE 21.13

Generic shapes of the gears that feature zero axial vectors ( $\mathbf{A}_g = 0$ ). Parts (a) through (f) are discussed in the text.

constructed in the axial cross-section of the gears. In addition to the ideal generic gear surfaces (see Figure 21.5), three more generic gear surfaces can be drawn up from Figures 21.6 through 21.8. Then, analysis of Figures 21.9 and 21.10 returns four generic gear surfaces: two of them feature an arbitrary angle,  $\vartheta_g^s$ , and two more feature a specific value of the angle,  $\vartheta_g^s$ , that is, either  $\vartheta_g^s = \varphi_g^a$  in the first case, or  $\vartheta_g^s = 90^\circ - \varphi_g^a$  in the second case. Similarly, four generic gear surfaces can be drawn from the analysis of Figures 21.11 and 21.12. Three more generic gear surfaces of face gears can be obtained similar to those illustrated in Figures 21.10b, 21.11d and 21.12d. The geometry of generic gear surfaces of these types is evident; therefore, it is not illustrated in the figures. Ultimately, nine more generic gear surfaces are drawn up from Figure 21.13.

Therefore, there exists an opportunity to investigate all possible designs of gears machined on conventional machine tools as well as on gear generators of conventional design.

### 21.3.2 Profile of Generic Gear Surface Constructed in Section by Plane at an Angle to Gear Axis

Possible generic gear surfaces discussed earlier in this monograph are constructed in the section of the gear by a plane through the gear axis of rotation. More opportunities in this area are available if sections by a plane at an

angle to the gear axis of rotation are considered. A plane at an angle to the gear axis is referred to as the *inclined cross-section* of the gear.

The axial section of a gear by a plane is a convenient reference for the specification of the configuration of an inclined section of the gear.

The axial section of a gear is specified as a section by a plane through the gear axis of rotation,  $O_g$ . An equivalent specification of an axial cross-section of the approximate gear can be given in terms of the unit tangent vectors,  $\mathbf{t}_{1,g}^a$  and  $\mathbf{t}_{2,g}^a$ , of the principal directions on the perfect (desired) generic gear surface, as illustrated in Figure 21.14a.

It is convenient to specify an inclined plane section of a gear in terms of the unit tangent vectors,  $\mathbf{t}_{1,g}^s$  and  $\mathbf{t}_{2,g}^s$ , of the principal directions on the actual generic gear surface. The inclined cross-section is a plane through the unit tangent vectors,  $\mathbf{t}_{1,g}^s$  and  $\mathbf{t}_{2,g}^s$ .

At a point,  $a$ , configuration of the Darboux frame,  $\mathbf{n}_g^s \mathbf{t}_{1,g}^s \mathbf{t}_{2,g}^s$ , of the actual generic gear surface with respect to the Darboux frame,  $\mathbf{n}_g^a \mathbf{t}_{1,g}^a \mathbf{t}_{2,g}^a$ , of the perfect generic gear surface can be specified by an angle,  $\nu_g^s$ . The trihedron  $\mathbf{n}_g^s \mathbf{t}_{1,g}^s \mathbf{t}_{2,g}^s$  is turned about the common unit normal vector,  $\mathbf{n}_g^a \equiv \mathbf{n}_g^s$ , through the angle,  $\nu_g^s$ , in the clockwise direction looking from the end of the vector,  $\mathbf{n}_g^a$  (see Figure 21.14a). In a particular case when the equality  $\nu_g^s = 0^\circ$  is valid, an inclined plane section reduces to the aforementioned axial plane section. When the angle,  $\nu_g^s$ , is not equal to zero ( $\nu_g^s \neq 0^\circ$ ), three different cases can be distinguished. Before proceeding with this issue, it is necessary to point out the following observation: as the unit normal vector,  $\mathbf{n}_g^a$ , in the general case is not perpendicular to the gear axis of rotation,  $O_g$  [the angle between the vector,  $\mathbf{n}_g^a$ , and the gear axis,  $O_g$ , is given by  $\angle(\mathbf{n}_g^a, O_g) = 90^\circ - \varphi_g^a$ ], the projection,  $\theta_g^s$ , of the angle,  $\nu_g^s$ , onto the plane through the gear axis of rotation,  $O_g$ , perpendicular to the axial plane section is not equal to the angle,  $\nu_g^s$ , itself ( $\theta_g^s \neq \nu_g^s$ ). However, the angles,  $\nu_g^s$  and  $\theta_g^s$ , correlate to each other. The correlation is of importance in further discussion. It can be established in the following way.

The angle,  $\theta_g^s$ , can be defined as the angle that is formed by the unit tangent vector,  $\mathbf{t}_{2,g}^s$ , and the gear axis of rotation,  $O_g$ . In a local reference system,  $x_s y_s z_s$ , that has the axes along the unit vectors,  $\mathbf{n}_g^s$ ,  $-\mathbf{t}_{1,g}^s$ , and  $\mathbf{t}_{2,g}^s$ , the unit tangent vector,  $\mathbf{t}_{2,g}^s$ , can be expressed as  $\mathbf{t}_{2,g}^s = \mathbf{k}_s$ . The directions of axes of this reference system are specified by the *Darboux trihedron*,  $\mathbf{n}_g^s \mathbf{t}_{1,g}^s \mathbf{t}_{2,g}^s$ , as shown in Figure 21.14. In the Cartesian coordinate system,  $X_g Y_g Z_g$ , associated with the gear, the direction of the gear axis,  $O_g$ , can be specified by the unit vector,  $\mathbf{k}_g$ . In order to calculate the value of the angle,  $\theta_g^s$ , both vectors,  $\mathbf{t}_{2,g}^s$  and  $\mathbf{k}_g$ , have to be represented in a common reference system. Let us represent the vector,  $\mathbf{t}_{2,g}^s$ , in the coordinate system,  $X_g Y_g Z_g$ . For this purpose, a local coordinate system,  $x_s y_s z_s$ , that has its origin at point  $a$  is used. The unit tangent vector, together with the coordinate system,  $x_s y_s z_s$ , has to be turned about the axis,  $x_s$  [about the unit normal vector  $\mathbf{n}_g^s$  ( $\equiv \mathbf{n}_g^a$ )] through the angle,  $\nu_g^s$ . The operator of rotation,  $\text{Rt}(\nu_g^s, \mathbf{n}_g^a)$ , is used for the analytical description of this

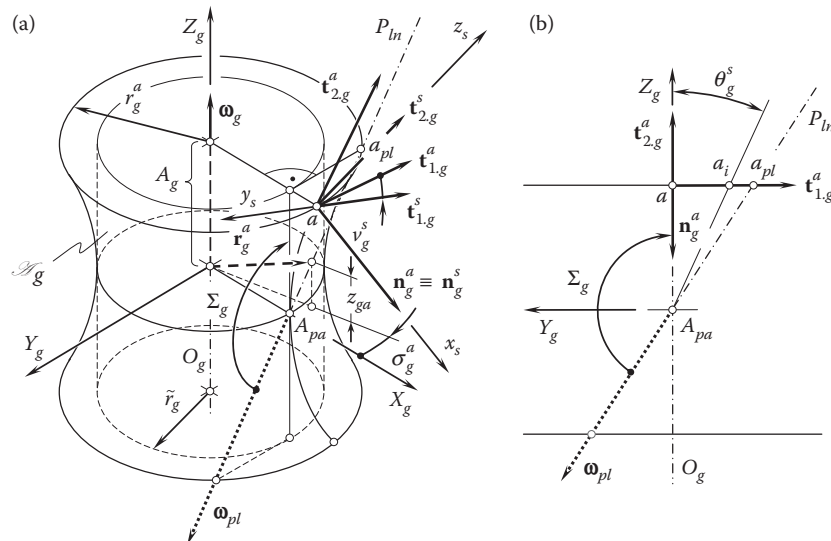


FIGURE 21.14

Possible configurations of the characteristic cross-section of a generic gear surface. Parts (a) and (b) are discussed in the text.



coordinate system transformation:

$$\mathbf{Rt}(v_g^s, \mathbf{n}_g^a) = \begin{bmatrix} 1 & 0 & 0 & 0 \\ 0 & \cos v_g^s & \sin v_g^s & 0 \\ 0 & -\sin v_g^s & \cos v_g^s & 0 \\ 0 & 0 & 0 & 1 \end{bmatrix} \quad (21.11)$$

In this new position of the local reference system,  $x_s y_s z_s$ , the unit vectors,  $\mathbf{n}_g^s$ ,  $\mathbf{t}_{1.g}^s$ , and  $\mathbf{t}_{2.g}^s$ , align with corresponding unit vectors of the Darboux frame,  $\mathbf{n}_g^a$ ,  $\mathbf{t}_{1.g}^a$ ,  $\mathbf{t}_{2.g}^a$ .

Then, it is necessary to turn the Darboux frame,  $\mathbf{n}_g^a$ ,  $\mathbf{t}_{1.g}^a$ ,  $\mathbf{t}_{2.g}^a$ , about the  $y_s$ -axis (about the unit tangent vector,  $\mathbf{t}_{1.g}^a$ ) through the angle,  $\varphi_g^a$  (see Figure 21.6). The operator of the rotation,  $\mathbf{Rt}(\varphi_g^a, \mathbf{t}_{1.g}^a)$ , is used for the analytical description of this coordinate system transformation:

$$\mathbf{Rt}(\varphi_g^a, \mathbf{t}_{1.g}^a) = \begin{bmatrix} \cos \varphi_g^a & 0 & -\sin \varphi_g^a & 0 \\ 0 & 1 & 0 & 0 \\ \sin \varphi_g^a & 0 & \cos \varphi_g^a & 0 \\ 0 & 0 & 0 & 1 \end{bmatrix} \quad (21.12)$$

The operator,  $\mathbf{Rs}(s \mapsto g)$ , of the resultant coordinate system transformation is calculated as the product of the operators of rotation,  $\mathbf{Rt}(v_g^s, \mathbf{n}_g^a)$  and  $\mathbf{Rt}(\varphi_g^a, \mathbf{t}_{1.g}^a)$ :

$$\mathbf{Rs}(s \mapsto g) = \mathbf{Rt}(\varphi_g^a, \mathbf{t}_{1.g}^a) \cdot \mathbf{Rt}(v_g^s, \mathbf{n}_g^a) \quad (21.13)$$

It should be noted here that the order of multipliers in Equation 21.13 is of importance and cannot be altered. Once the operator,  $\mathbf{Rs}(s \mapsto g)$ , of the resultant coordinate system transformation is calculated, the expression:

$$\mathbf{t}_{2.g}^{s(g)} = \mathbf{Rs}(s \mapsto g) \cdot \mathbf{t}_{2.g}^s \quad (21.14)$$

can be used for the analytical description of the unit tangent vector,  $\mathbf{t}_{2.g}^s$ , in the reference system,  $X_g Y_g Z_g$ .

The use of the expression for the unit tangent vector,  $\mathbf{t}_{2.g}^{s(g)}$  (see Equation 21.14), makes calculation of the angle  $\theta_g^s$  possible:

$$\theta_g^s = \tan^{-1} \left( \frac{|\mathbf{t}_{2.g}^{s(g)} \times \mathbf{k}_g|}{\mathbf{t}_{2.g}^{s(g)} \cdot \mathbf{k}_g} \right) \quad (21.15)$$

Equations 21.12 through 21.15 allow for derivation of an expression:

$$\theta_g^s = \cos^{-1} [\cos \varphi_g^a \cdot \cos v_g^s] \quad (21.16)$$

for calculating the angle,  $\theta_g^s$ .

When the angle,  $v_g^s$ , is:

$$v_g^s = \cos^{-1} \left[ \frac{\cos \Sigma_g}{\cos \varphi_g^a} \right] \quad (21.17)$$

the unit tangent vector,  $\mathbf{t}_{2.g}^s$ , is aligned with the axis of instant rotation,  $P_{ln}$ . The actual value of the angle,  $\theta_g^s$  (see Figure 21.14b), in this particular case is equal to  $\Sigma_g$ .

Four different configurations of the inclined plane section of a gear are distinguished, depending on the actual value of the angle,  $\theta_g^s$ .

First, the angle,  $\theta_g^s$ , can be equal to zero. When the equality  $\theta_g^s = 0^\circ$  is valid, the inclined plane section reduces to the axial plane section of the gear.

Second, the actual value of the angle  $\theta_g^s$  can be within the interval  $0^\circ < \theta_g^s < 180^\circ - \Sigma_g$ . For convenience, the difference  $(180^\circ - \Sigma_g)$  is denoted as  $[\theta_g^s]$ . It can be shown that the rotation of the inclined plane section about the  $x_s$ -axis through an angle,  $\nu_g^s$ , is equivalent to its rotation about the centerline through a corresponding angle,  $\theta_g^s$ . This is because the perfect generic gear surface is a surface of revolution. Surfaces of revolution allow for sliding over themselves. Therefore, the parameters of rotation of an inclined plane section about the centerline can be expressed in terms of the parameters of rotation of the same inclined plane section about the unit normal vector,  $\mathbf{n}_g^a \equiv \mathbf{n}_g^s$ , and vice versa. Under such an interpretation, point  $a$  is not considered; point,  $a_i$ , can be considered instead (see Figure 21.14b).

Third, the actual value of the angle,  $\theta_g^s$ , can be equal to its critical value,  $[\theta_g^s]$ . When the equality  $\theta_g^s = [\theta_g^s]$  is observed, the unit tangent vector,  $\mathbf{t}_{2,g}^{s(g)}$ , is aligned with the vector of instant rotation,  $\boldsymbol{\omega}_{pl}$ . In this particular case, point  $a$  is not considered; point  $a_{pl}$  is considered instead (see Figure 21.14b).

Fourth, the actual value of the angle,  $\theta_g^s$ , can exceed its critical value,  $[\theta_g^s]$ ; thus, the inequality  $\theta_g^s > [\theta_g^s]$  is valid. The corresponding point,  $a_j$  (not shown in Figure 21.14b), in this particular case is located beyond point  $a_{pl}$ .

Taking into account that the first case ( $\theta_g^s = 0^\circ$ ) returns 26 possible generic gear surfaces, one of which is the perfect generic gear surface, the total number of possible generic gear surfaces is limited to just 105. Some of the generic gear surfaces resemble each other. However, even for generic gear surfaces with a similar appearance, the conditions of generation of tooth flanks could be different. Therefore, all of the generic gear surfaces should be carefully investigated individually.

The following three important conclusions can be drawn from this discussion:

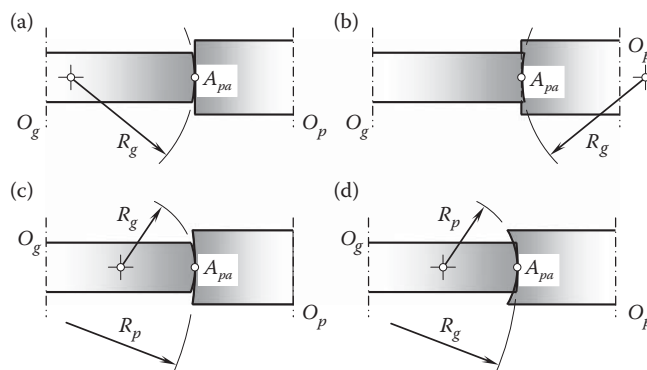
1. The total number of feasible generic gear surfaces is not infinite but a finite number. This means that it is possible to count and investigate all possible designs of gears machined on conventional gear generators.
2. Gears with any of the generic gear shapes are convenient for machining, as only rotations and translations are required to reproduce the required motion of the gear-cutting tool in relation to the work gear.
3. An appropriate area of application can be found for all the gears briefly discussed in this section of the monograph.

The above discussion is helpful to systemize possible geometries of generic gear surfaces.

## 21.4 Possibility of Classification of Gear Pairs

Once the total number of possible generic gear surfaces is limited to just 105, it is possible to combine the surfaces by two and in this way obtain all possible gear pairs. It can be proved that the total number of such combinations does not exceed  $105^2$ . Not all of them are physically possible. For example, no parallel-axes gear pair can be designed using two generic gear surfaces with concave axial profiles. Because interference of generic gear surfaces in this case is inevitable, gear pairs of this particular type cannot be designed. A few examples of feasible and infeasible combinations of gears by two are schematically shown in Figure 21.15. A gear with a convex axial profile and a pinion with a straight axial profile is a possible combination of gears. A gear pair of this type can exist physically (see Figure 21.15a). In contrast, a gear with a concave axial profile and a pinion with a straight axial profile does not constitute a possible combination of gears. A gear pair of this type cannot exist physically (see Figure 21.15b). A similar behavior is observed with a gear and a pinion that have convex and concave axial profiles, respectively, as illustrated in Figure 21.15c and d. In order to come up with a feasible combination of gears forming a gear pair, the magnitude of the radius of curvature of the concave profile,  $R_p$ , should exceed the radius of curvature,  $R_g$ , as shown in Figure 21.15c. Otherwise, when the inequality  $R_p < R_g$  is observed, a gear pair of this geometry becomes infeasible (Figure 21.15d). More examples to this end can be provided.

It can be assumed from this simple example that the total number of possible gear pairs is significantly less than  $105^2$ .

**FIGURE 21.15**

Combinations of two generic surfaces: (a) and (c) feasible, and (b) and (d) infeasible combinations.

In order to evaluate the maximum number of possible gear pairs, it is useful to recall that 105 possible types of the generic surfaces are composed of one perfect generic surface, 26 generic surfaces with a convex axial profile, 26 generic surfaces with a straight axial profile, and 26 generic surfaces with a concave axial profile.

Generic surfaces of a gear featuring a convex axial profile can be properly combined with all 105 generic surfaces of the pinion. Therefore, the total number of combinations of this particular type is limited to  $26 \cdot 105 = 2730$  combinations.

Generic surfaces of a gear featuring a straight axial profile can be properly combined with all 70 generic surfaces of the pinion. Therefore, the total number of combinations of this particular type is limited to  $26 \cdot 70 = 1820$  combinations.

Finally, generic surfaces of a gear featuring a concave axial profile can be properly combined with all 70 generic surfaces of the pinion. Therefore, the total number of combinations of this particular type is limited to  $26 \cdot 35 = 910$  combinations.

Because 2730, 1820, and 910 are finite numbers, the total number of possible combinations of generic gear surfaces is also a limited number. This number does not exceed 5460 combinations. Evidently, not all of them can exist physically. After a detailed investigation of all the possible combinations is carried out, it is possible to see that the total number of practical types of gear pairs is significantly under the precalculated number of 5460 combinations.

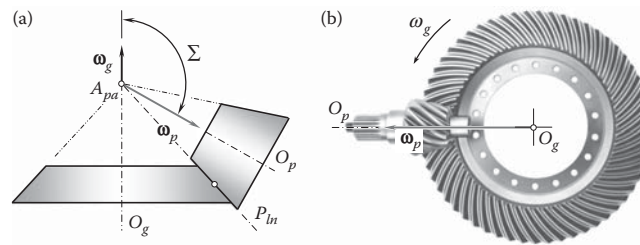
The total number of possible types of gear pairs to be determined should be considered together with the possible types of vector diagrams of gear pairs (see [Chapter 2, Figure 2.15](#)). All possible types of gear pairs can be investigated. This is because the total number of possible types of gear pairs is equal to a finite number and not an infinite number.

Use of the aforementioned technique makes it possible to investigate all possible types of gear pairs. No gear pair will be missed under such an investigation. Novel designs of gear pairs can be discovered as the output of such an investigation.

## 21.5 Examples of Implementation of Classification of Gear Pairs

Once the number of possible combinations of generic gear surfaces by two is found to be finite, it is possible to individually consider every possible combination of the generic surfaces by two and identify an appropriate area of application for each particular combination. A few illustrative examples in this regard are considered in this section.

The desired generic gear surfaces of a gear pair featuring intersecting axes of the gear and the pinion are represented with two cones that have a common apex. The perfect generic gear surfaces for the case of an external gear pair are schematically shown in [Figure 21.16a](#). The generic gear surfaces contact each other along a straight line that is aligned with the axis of instant rotation,  $P_{ln}$ . The axis of rotation of the gear,  $O_g$ ; axis of rotation of the pinion,  $O_p$ ; and axis of instant rotation,  $P_{ln}$ , intersect at a common point, which is coincident with the apexes.

**FIGURE 21.16**

Desired generic surfaces of an external gear pair featuring intersecting axes of rotation of the gear and the pinion.

In [Figure 21.16](#), a trivial case of interacting of generic gear surfaces in gear pairs is shown. Many types of external conical gear pairs can be designed on the premise of this particular combination of generic gear surfaces. One of many possible examples is illustrated in [Figure 21.16b](#).

Internal gear pairs as well as rack-type gear pairs that have intersecting axes of a gear and a mating pinion also feature the desired generic gear surfaces, which are shaped in the form of cones. The apexes of the cones are snapped together. For internal gear pairs, a generic gear surface is represented with a surface of an internal cone of revolution, as depicted in [Figure 21.17a](#). The generic gear surface of the pinion is represented with a surface of an external cone of revolution.

In a particular case, the pitch angle of a gear can reach  $90^\circ$ . Under such a scenario, the gear degenerates into a flat gear, as schematically shown in [Figure 21.17b](#). A gear of this kind is commonly referred to as a *round rack* (or a *crown gear* in other terminology). The apex of the round rack is always snapped together with the apex of the pinion.

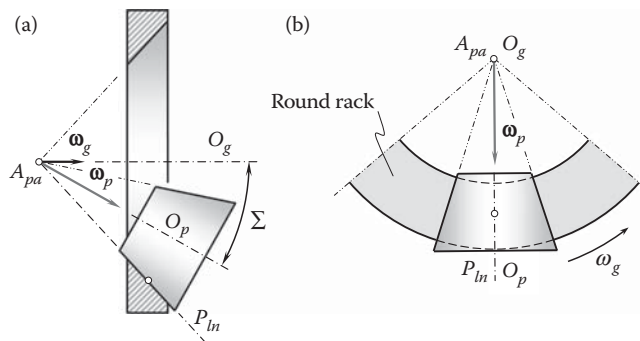
Gear pairs designed on the basis of perfect generic gear surfaces, as schematically shown in [Figure 21.17](#), have limited application in practice. One reason for this is the lack of comprehensive investigation of generic gear surfaces of these kinds.

A gear and pinion can be designed and machined in such a way that the actual generic gear surfaces of each of them differ from the perfect shape. In cases like these, the apex of the gear, pinion, or both, is off the axis of instant rotation,  $P_{ln}$ .

Two examples of generic gear surfaces of external gear pairs that have intersecting axes of the gear and the pinion are shown in [Figure 21.18](#).

A gear pair may feature generic surfaces shaped in the form of external cones of revolution. When cone angles of the cones of revolution differ from the cone angle for the perfect generic gear surfaces, as illustrated in [Figure 21.18a](#), the apex of the gear is off the axis of instant rotation,  $P_{ln}$ . Ultimately, a conical gear pair can be designed on the basis of the actual generic gear surfaces of this kind. Gear pairs of this kind do not have wide application in the current practice.

In a particular case, a gear pair can be designed in such a way that the generating straight line segment of the actual generic gear surface of the pinion is parallel to the pinion axis of rotation,  $O_p$  (see [Figure 21.18b](#)). Under such a scenario, the actual generic gear surface of the pinion is not a cone of revolution; it is shaped

**FIGURE 21.17**

Desired generic surfaces of gear pairs with intersecting axes of rotation of the gear and the pinion: (a) an internal gear pair and (b) a rack-type gear pair.

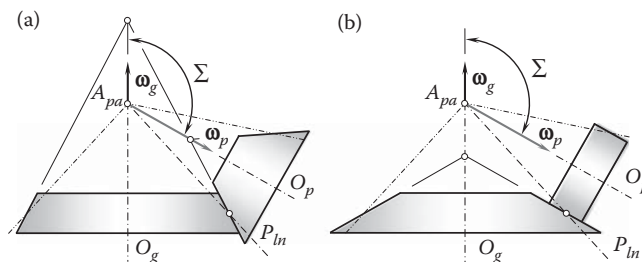


FIGURE 21.18

Two examples of generic surfaces of external gear pairs featuring intersecting axes of rotation of the gear and the pinion and with straight-line axial profiles.

in the form of a cylinder of revolution instead. Gear pairs composed of an external conical gear and a mating cylindrical pinion are used, for example, in the design of helicopter transmissions; they also have numerous other applications.

In both cases shown in Figure 21.18, the gears are referred to as *external crown gears*.

A gear pair can be designed and machined in such a way that the actual generic gear surface of the gear is shaped in the form of an internal cone of revolution (Figure 21.19). Many similarities can be found between external (see Figure 21.18) and internal gear pairs of these two kinds. Again, in a particular case, the actual generic gear surface of the pinion is not a cone of revolution but is shaped in the form of a cylinder of revolution instead. Gear pairs composed of an internal conical gear and a mating cylindrical pinion have limited application in industry. Gear pairs of this kind are not investigated yet, and their area of potential application has not been properly identified so far.

In the cases shown in Figure 21.19a and b, gears are referred to as *internal crown gears*.

Ultimately, the generic cone of a gear of a gear pair that has intersecting axes of rotation of the gear and pinion can be degenerated into plane that is rotated about the gear axis of rotation,  $O_g$ . Two examples of generic gear surfaces of this type are schematically shown in Figure 21.20a,b. In a particular case, when the pitch radius of the gear approaches infinity, the gear is transformed into a straight rack (see Figure 21.20c). Gear pairs of this kind have not been investigated yet, and their area of potential application is not properly identified so far.

In all cases illustrated in Figure 21.20, the gear is referred to as *rack-type crown gear*. Rack-type gear pairs have the following two features: (1) the pitch plane of the gear is the plane through the centerline, and (2) the apex of the pitch cone of the pinion is located within the centerline.

Based on the developed classification of vector diagrams of gear pairs and the concept of generic gear surfaces, all known gear drives can be developed. For example, advanced gear drives such as spiroid gearing [141], helicon gearing [142], and others can be developed using the proposed approach. Moreover, many novel gearings can be developed using the proposed approach.

Use of the discussed approach makes it possible to cover all known designs of gear pairs, as well as all novel potentially possible designs of gear pairs, many of which have potential areas of implementation still to be identified. As the approach is based on the broad application of vector representation of gear pairs, the use of axodes

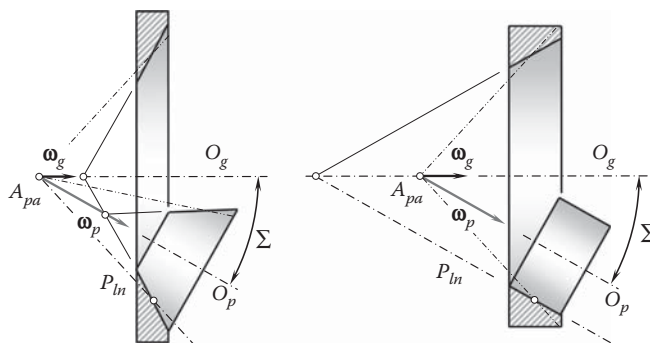
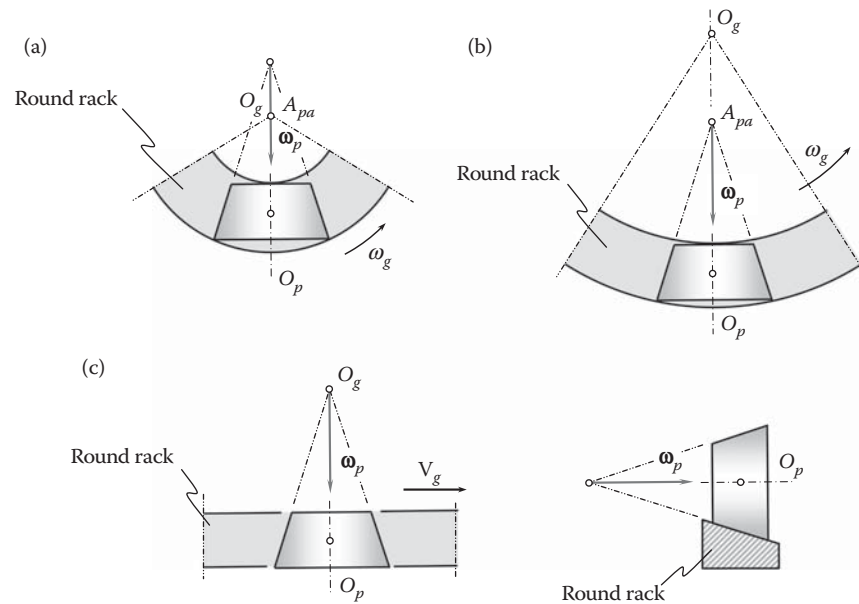


FIGURE 21.19

Two examples of generic surfaces of internal gear pairs featuring intersecting axes of rotation of the gear and the pinion and with straight-line axial profiles.

**FIGURE 21.20**

Examples of the generic surfaces of rack-type crown gear pairs featuring intersecting axes of rotation of the gear and the pinion and with straight-line axial profiles.

and operating pitch surfaces in many cases becomes useless. However, pitch surfaces relevant to the corresponding gear-machining process are still useful.

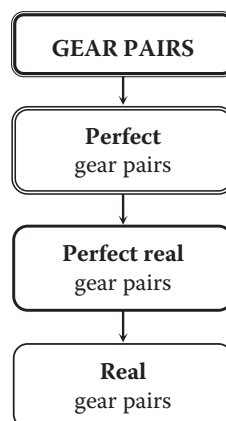
The discussion on classification can be ended with a generalized classification of possible gear pairs, which is schematically depicted in [Figure 21.21](#).

Based on the classification of possible types of vector diagrams (see [Chapter 2, Figure 2.15](#)), a certain number of gear pairs can be developed for each vector diagram. The gear pairs differ from one another by the geometry of the tooth flanks in the lengthwise direction. All these gear pairs are referred to as *perfect gear pairs*.

Taking into account possible displacements of the tooth flanks of the gear and pinion, a certain number of  $S_{pr}$ -gear pairs can be developed. The number of possible  $S_{pr}$ -gear pairs is equal to the number of ideal gear pairs. Gear pairs of this kind can also be referred to as *desired real gear pairs*.

Ultimately, a certain number of *real gear pairs* can be developed based on a corresponding desired gear pair. The total number of real gear pairs significantly exceeds the total number of desired real gear pairs.

The discussion in this chapter illustrates the possibility of developing a scientific classification of all possible gearings. It is clear now that the classification can be represented in detail based on the results of the analysis discussed in this monograph.

**FIGURE 21.21**

A generalized classification of a possible kind of gear pairs.



# Taylor & Francis

Taylor & Francis Group

<http://taylorandfrancis.com>



## Approximate Real Gearing

Approximate real gears have been known for a long time. Amazingly, most of the efforts of gear experts all around the world so far have not focused on improvements in the design of and production methods for perfect gears (or real perfect gears). Instead, all the efforts have focused on improvements in the design of and production methods for approximate real gears. This is true with respect to:

- Parallel-axes gearings with modified tooth flanks of a gear and a mating pinion
- Intersected-axes gearings, either with gears that feature modified tooth flanks of a gear and a mating pinion or without the modification of the tooth flanks
- Crossed-axes gearings, either with gears that feature modified tooth flanks of a gear and a mating pinion or without the modification of the tooth flanks

Easier methods and means for manufacturing approximate real gears are the main reason for their broad application in the current industry. Gears for parallel-axes gearings can be produced accurately with very small deviations of the desired tooth flanks from a true involute profile.\* In cases of intersected-axes and crossed-axes gearings, the situation is not as clear as in the case of gears for parallel-axes gearings.

Manufacturing methods of gears for intersected-axes, as well as for crossed-axes approximate real gearings, are based on a design of the gear-cutting tool for machining gear teeth. Gear and mating pinion tooth flanks,  $\mathcal{G}_{r.app}$  and  $\mathcal{P}_{r.app}$ , are generated as enveloping surfaces to consecutive positions of the generating surface,  $T$ , of the gear-cutting tool in its motion in relation to a reference system, which a machined gear is associated with. As a result, only the condition of contact,  $\mathbf{n} \cdot \mathbf{v}_\Sigma = 0$ , is fulfilled in approximate real gearings, as the gear and pinion tooth flanks,  $\mathcal{G}_{r.app}$  and  $\mathcal{P}_{r.app}$ , are enveloping to one another. The condition of conjugacy of the interacting tooth flanks,  $\mathcal{G}_{r.app}$  and  $\mathcal{P}_{r.app}$ , is not fulfilled; thus, the fundamental law of gearing in approximate real gearing is violated. Moreover, the condition of equality of base pitches of a gear and mating pinion to the operating base pitch of the gear pair† is not met in approximate real gearings.

Gear-cutting tools for machining approximate real gears, as well as the methods of machining gears of this particular type are discussed in detail in the monograph [111,112] by Radzevich. The consideration in this monograph is limited to a discussion of examples of real approximate gearings that illustrate the violation of:

- The fundamental law of gearing (gear,  $\mathcal{G}_{r.app}$ , and mating pinion,  $\mathcal{P}_{r.app}$ , tooth flanks are not conjugate to one another)
- The requirement of equality of the angular base pitches of a gear and a mating pinion to the operating angular base pitch of the gear pair ( $\varphi_{b.g} = \varphi_{b.op}$  and  $\varphi_{b.p} = \varphi_{b.op}$ )

Because of the low accuracy of real approximate gears, their application is limited to cases of transmitting relatively low rotations of the input and output shafts by means of gears with a large tooth count.

\* Gears with a large tooth count for parallel-axes gearings that operate at low rotation are commonly designed and manufactured with a straight tooth profile instead of true involute tooth profile. Parallel-axes approximate real gearings of this particular kind are permissible, as the deviation of the straight-line tooth profile from the true involute profile in case of gears with a large tooth count is negligibly small and often can be ignored.

† It is instructive to stress here that in both intersected-axes and crossed-axes approximate real gearings, only the operating angular base pitch of a gear pair,  $\varphi_{b.op}$ , can be specified. Neither the angular base pitch of a gear,  $\varphi_{b.g}$ , nor the angular base pitch of a mating pinion,  $\varphi_{b.p}$ , can be specified in intersected-axes and crossed-axes approximate real gearings, as the plane of action,  $PA$ , in these cases intersects the tooth flanks,  $\mathcal{G}_{r.app}$  and  $\mathcal{P}_{r.app}$ , along the lines, at points of which common perpendiculars to the tooth flanks do not lie in a common plane. Thus, no common normal plane can be constructed in cases of intersected-axes and crossed-axes approximate real gearings. As the angular base pitches,  $\varphi_{b.g}$  and  $\varphi_{b.p}$ , do not exist, the equalities,  $\varphi_{b.g} = \varphi_{b.op}$  and  $\varphi_{b.p} = \varphi_{b.op}$ , cannot be fulfilled in cases of intersected-axes and crossed-axes approximate real gearings.

## 22.1 Approximate Real Parallel-Axes Gearing

It has been well known since the time of Euler (1707–1783) that only gears that have involute tooth profiles are capable of transmitting smooth rotation from driving shafts to driven shafts. Gears that have tooth profiles of other geometries different from involute tooth profile are not capable of transmitting rotations smoothly.

Noninvolute gearings are viewed as an example of real approximate parallel-axes gearings (see Table 18.1). Pin gears, gears that have cycloidal tooth profiles, lobe profiles in the design of *Roots blowers*, and so forth represent perfect examples of approximate real parallel-axes gearing. In all the cases mentioned, as well as in numerous other cases, the tooth flanks,  $\mathcal{G}_{r.app}$  and  $\mathcal{P}_{r.app}$ , of a gear and mating pinion are not conjugate to one another, and the condition of equal base pitches cannot be fulfilled, as the base pitches of a gear and of a mating pinion do not exist.

One more example of approximate real parallel-axes gearing to be considered is related to parallel-axes gears cut by either a face milling cutter or face hob.

As schematically illustrated in Figure 22.1 [111,112], the tooth flanks of a gear are generated by two face milling cutters. In this method, the face milling cutters rotate with angular velocity,  $\omega_c$ , about their axes, and

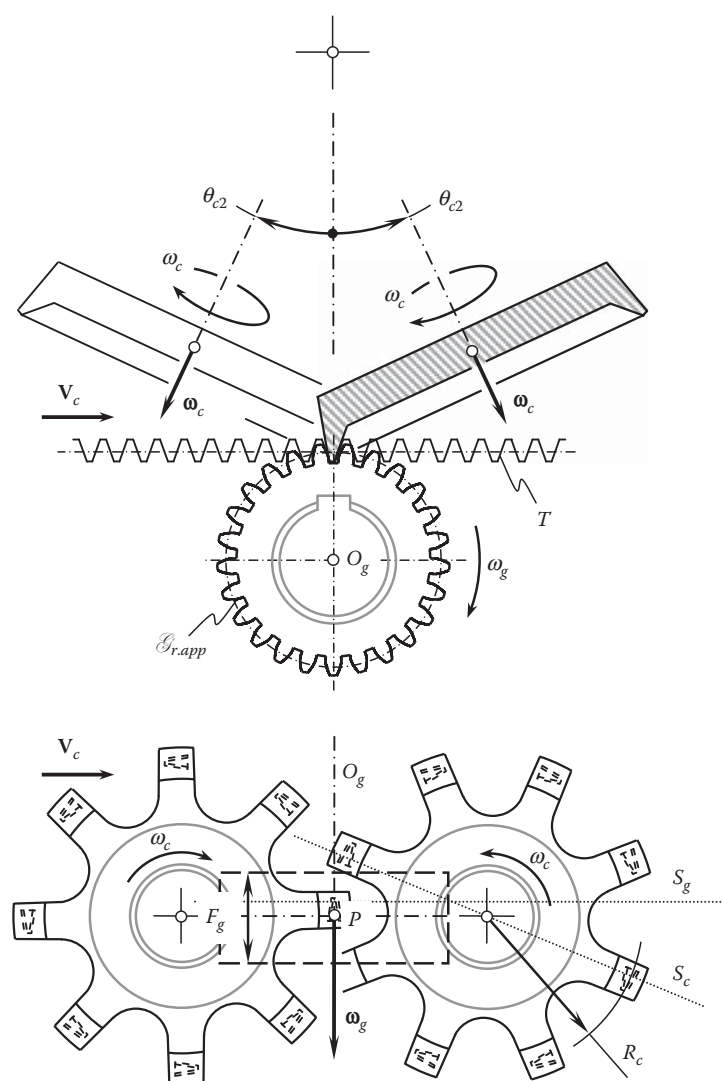


FIGURE 22.1

Generation of tooth flanks,  $\mathcal{G}_{r.app}$ , of a real approximate gear by two tilted face milling cutters. (Adopted from: Radzevich, S.P., *Gear Cutting Tools: Fundamentals of Design and Computation*, CRC Press, Boca Raton FL, 2010, 786 p.; Radzevich, S.P., *Gear Cutting Tools: Science and Engineering*, 2nd Ed., CRC Press, Boca Raton, FL, 2017, 606 p. [111,112].)

travel straight forward with velocity,  $V_c$ , tangentially to the gear pitch circle. The rotation,  $\omega_g$ , and translation,  $V_c$ , of the gear blank are synchronized with one another in a timely manner.

The axes of rotation of the face milling cutters intersect each other at a certain angle,  $2 \cdot \theta_{c2}$ . The angle  $\theta_{c2}$  is within the interval  $0^\circ \leq \theta_{c2} \leq \phi_n$  (in a particular case of gear machining, the axes of rotation of the cutting tools can be parallel to each other). The angle  $\phi_n$  is the normal profile angle.

A parallel-axes approximate real gear pair with arc-shaped teeth in a lengthwise direction is shown in Figure 22.2.

The machined gear must have a constant base pitch,  $p_{b,g}$ , in all sections,  $S_g$ , perpendicular to the gear axis of rotation,  $O_g$ . For this purpose, in all the sections by the planes,  $S_g$ , the face milling cutter has to have the same base pitch,  $p_{b,c}$  (that is,  $p_{b,g} = p_{b,c}$ ). However, the base pitch of the face milling cutter,  $p_{b,c}$ , is not of a constant value in the sections by planes,  $S_g$ ; however, it is of constant value in the sections by axial planes,  $S_c$ , instead. The sections,  $S_c$ , pass through the axis of rotation of the face milling cutter. Generally speaking, the planes denoted by  $S_g$  and  $S_c$ , are not congruent to one another, except in one particular configuration. Therefore, the cut gear has different values of the base pitch,  $p_{b,g}$ , in different sections by the planes,  $S_g$ . As a result, gears generated in accordance with the method shown in Figure 22.1 are approximate real parallel-axes gears. The larger the face width,  $F_g$ , of the gear, the larger the deviations of its base pitch of the gear,  $p_{b,g}$ , from the desired value. Similarly, the smaller the radius,  $R_c$ , of the face milling cutter, the larger the deviations of the base pitch of the gear,  $p_{b,g}$ , from the desired value, and vice versa.

More examples of approximate real parallel-axes gearing are known. In all cases, gears are referred to as *approximate real gears* mostly because either the tooth profile of the gear is not involute or the tooth flanks are improperly generated in a lengthwise direction.

An example of the application of parallel-axes approximate real gears that have circular arc teeth in a lengthwise direction is illustrated in Figure 22.3.

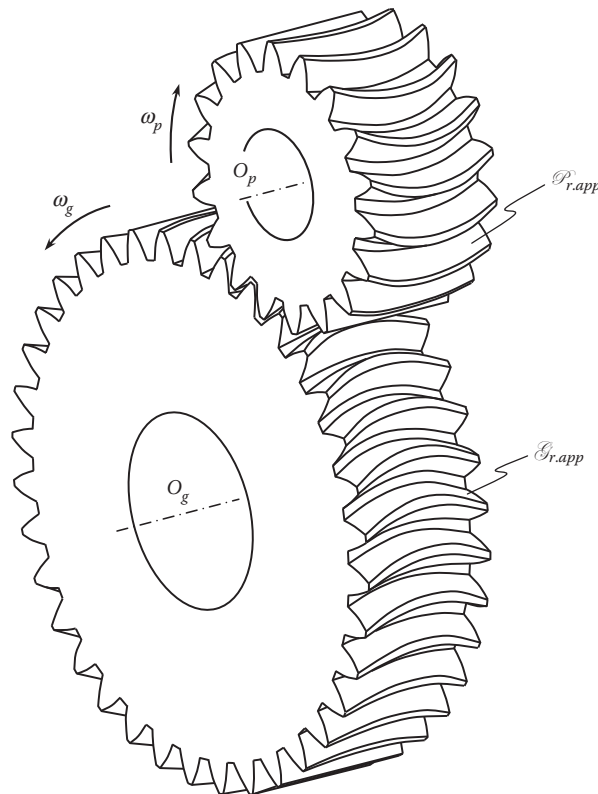


FIGURE 22.2

A gear pair that has circular arc teeth in the lengthwise direction: an example of real approximate parallel-axes gearing.



FIGURE 22.3

An example of the application of parallel-axes approximate real gears that have circular arc teeth in the lengthwise direction.

## 22.2 Approximate Real Intersected-Axes Gearing

The application of approximate real intersected-axes gearing can be traced back to when the first intersected-axes pin gears were used. Since then, many significant improvements to the geometry of the interacting tooth surfaces of gears of this type have been made.

### 22.2.1 Root Causes for Inaccuracies of Real Intersected-Axes Gears

Approximate real intersected-axes gears (see Table 18.1) are broadly used in the industry today, as in most cases they sufficiently meet the requirements for their performance and production. Intersected-axes gearing of this type will be in use for a long time in applications with low input/output rotations, low vibration generation and noise excitation requirements, and a relatively low power density transmitted through the gearboxes. The last requirement is mostly due to the shape, location, and orientation of the contact pattern between the tooth flanks of the mating gears.

Two main reasons can be noted for designing, production, and application of approximate real intersected-axes gears in the current industry.

First, the tooth flank geometry of perfect real intersected-axes gearing,  $\mathcal{G}_r$ , is not considered when determining the geometry of the generating surface,  $T$ , of the gear-cutting tool for machining gears for approximate real intersected-axes gearings. Instead, for user convenience, the desired generating surface,  $T$ , of the gear-cutting tool is commonly replaced by a surface,  $T_{appr}$ , of simpler geometry. Such a substitution of the desired generating surface,  $T$ , of the gear-cutting tool with a chosen (approximate) surface,  $T_{appr}$ , is equivalent to replacement of a straight-sided generating rack for machining involute parallel-axes gears with a generating rack of another geometry. Evidently, the replacement entails the deviation of the machined tooth flanks from desired tooth flanks of the gear and pinion. The deviation of the actual gear tooth flank,  $\mathcal{G}_{r,appr}$ , from the desired tooth flank,  $\mathcal{G}_r$ , is associated with the deviation of the surface,  $T_r$ , from the surface  $T$ , and is inevitable in this case. As a result, real intersected-axes gearing is an approximate one almost in all practical cases of implementation. Approximate gears are not capable of transmitting a rotation smoothly.

Second, for the purpose of transmitting a uniform rotation from a driving shaft to a driven shaft, intersected-axes gears that have various generic shapes are used. The actual kind of the generic shape of a gear depends on

an adopted method of gear cutting. Because of this, the machined tooth flanks,  $\mathcal{G}_{r.app}$  and  $\mathcal{P}_{r.app}$ , are neither conjugate to one another nor feature equal angular base pitches (the angular base pitches are not specified in bevel gears for approximate intersected-axis gearings). Thus, gearings of these kinds are not capable of transmitting a rotation smoothly. This is one more reason why gears for approximate intersected-axis gearings are referred to as *approximate real intersected-axis gears*.

The smaller the deviations of the actual generating surface,  $T_{app}$ , of a gear-cutting tool of a specified design from the desirable generating surface,  $T$ , of the gear-cutting tool, the smaller the deviation of the actual machined gear tooth flank,  $\mathcal{G}_{r.app}$ , from the desired tooth flank,  $\mathcal{G}_r$ , and vice versa. The smaller the deviation of the tooth flank,  $\mathcal{G}_{r.app}$ , from the desired tooth flank,  $\mathcal{G}_r$ , the smoother the rotation that can be transmitted from a driving shaft to a driven shaft.

It should be pointed out here that because approximate real intersected-axis gears are a kind of approximation of corresponding perfect real intersected-axis gears, the latter should be used as a datum surface when determining the accuracy of the former, that is, when measuring both *design deviations* and *manufacturing errors*. The geometry of perfect real intersected-axis gears is required to be known for inspection purposes.

### 22.2.2 Approximate Real Intersected-Axes Gears

Gears that feature various geometries in the lengthwise direction of the gear teeth are used to transmit a rotation between two shafts with intersected axes of rotation. Straight tooth bevel gears, skew tooth bevel gears, spiral bevel gears (those cut by a face mill cutter, as well as by a face hob), straight teeth face gears, helical teeth face gears, and others can be mentioned as examples of approximate real intersected-axis gears.

#### 22.2.2.1 Straight Tooth Bevel Gears

Depending on the manufacturing methods used in gear production, multiple types of straight tooth bevel gears are recognized.

A straight tooth bevel gear cut in a continuous-indexing method of gear cutting is shown in [Figure 22.4](#). A straight-sided generating round rack,  $T_{app}$ , is used for the generation of gear tooth flanks,  $\mathcal{G}_{r.app}$ . The generating rack,  $T_{app}$ , is used as an approximate generating surface of the gear-cutting tool. The tooth flanks of the rack are shaped in the form of planes.

In the gear machining process, both the work gear and the generating round rack are continuously rotated about their axes of rotation at uniform angular velocities. The desired tooth flank,  $T$ , of the virtual generating rack has to be shaped in the form of an involute surface developed from the base cone of the gear-cutting tool. Only in this case, the generating rack,  $T$ , and the cut gear,  $\mathcal{G}_r$ , are capable of transmitting a rotation smoothly with constant angular velocities.



FIGURE 22.4

A straight bevel gear cut by the continuous-indexing method of gear generation.

The actual tooth flank,  $T_{app}$ , of the virtual generating rack (a plane) differs from the desired tooth flank,  $T$  (an involute surface). In reality, the tooth flank of the generating rack (a plane,  $T_{app}$ ), and the tooth flank of the machined gear,  $\mathcal{G}_{r.app}$ , are not conjugate to one another. Moreover, the angular base pitch cannot be specified either for the actual generating rack,  $T_{app}$ , or for the tooth flank,  $\mathcal{G}_{r.app}$ , of the machined gear. Therefore, the mandatory condition to be met,  $\varphi_{b.g} = \varphi_{b.c}$ , cannot be even discussed, as the angular base pitches,  $\varphi_{b.c}$ , and  $\varphi_{b.g}$ , of the gear and generating rack are not specified at all.

As a result, a gear pair composed of a gear and a pinion both cut by the continuous-indexing method of gear cutting is not capable of transmitting a uniform rotation smoothly. Gears of this type can be used only in low-rotation applications. At higher rotations, gears of this kind generate excessive vibration and are subject to noise excitation.

All bevel-gear generating machines operate on the so-called *octoid gear system*, and not on the involute as is generally supposed. In the octoid gear system, a crown gear with plane tooth flanks is used to generate gear,  $\mathcal{G}_{r.app}$ , and mating pinion,  $\mathcal{P}_{r.app}$ , tooth flanks. The path of contact,  $P_c$  (loosely called the *line of action*, from which the tooth derives its name), is the peculiar *figure-eight* curve, which is at right angles to the tooth curves of the crown line and tangential to the polar circles, to which the great circle crown odontoids are also tangential, as shown in Figure 22.5a.

The cutting edge of the tool being straight, no change is required while it is in motion, except in its position, and that is accomplished by giving it a motion in such a direction that its corner moves in the radial line of the corner of the bottom of the tooth space.

The octoid gear system, together with an ingenious machine for planning it, was invented by Hugo Bilgram.\* Following George Grant†: “This tooth owes its existence to the fact that it is the only known tooth, and probably the only possible tooth, that can be practically formed by the molding planning process.”

As illustrated in Figure 22.5b, in octoid gear systems, the trace of contact point, that is, the path of contact,  $P_c$ , is a spatial curve. At an arbitrary point,  $m$ , within the path of contact,  $P_c$ , a straight tangent line can be constructed. In nature, this straight tangent line is the instant line of action,  $LA_{inst}$ . In order to generate conjugate tooth flanks,  $\mathcal{G}_r$  and  $P_r$ , of a gear and a mating pinion, at any and all configurations of the gear and the mating pinion, the instant line of action,  $LA_{inst}$ , has to intersect the axis of instant rotation,  $P_{ln}$ , in the gear pair. In Figure 22.5b, the instant line of action,  $LA_{inst}$ , has to pass through the plane-of-action apex,  $A_{pa}$ . Instead, it does not go through the plane-of-action apex,  $A_{pa}$ . Because of this, the tooth flank,  $T_{app}$ , of the generating

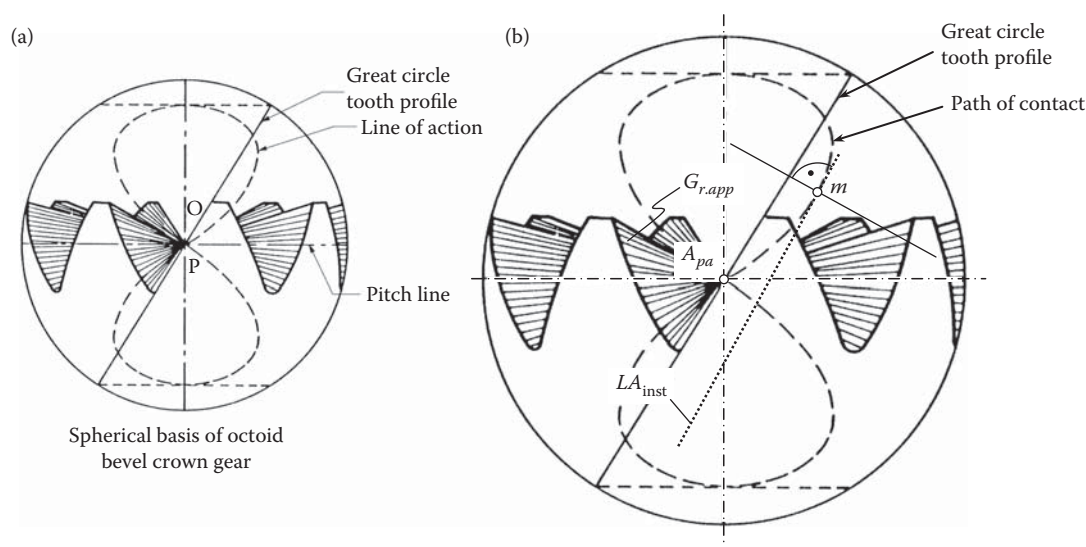


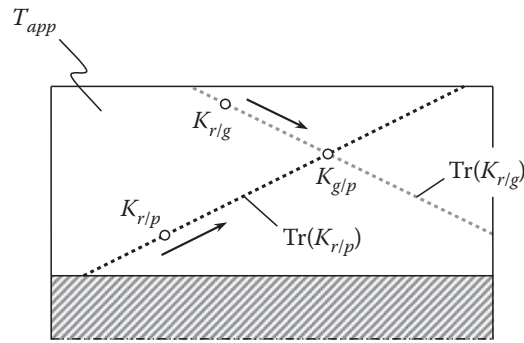
FIGURE 22.5

The difference between the path of contact,  $P_c$ , and the *instant line of action*,  $LA_{inst}$  in approximate real intersected-axes gearing: (a) original commonly adopted image, and (b) modified and updated image.

\* Hugo Bilgram (January 13, 1847–August 27, 1932), a famous American (German-born) gear engineer.

† George Grant (December 21, 1849–August 16, 1917), a famous American gear engineer.



**FIGURE 22.6**

Traces of contact,  $\text{Tr}(K_{r/g})$  and  $\text{Tr}(K_{r/p})$ , of contact points,  $K_{r/g}$  and  $K_{r/p}$ , on the auxiliary rack tooth flank,  $T_{app}$ .

rack, and the tooth flank,  $\mathcal{G}_{r.app}$ , of the machined bevel gear are not conjugate to one another. Thus, bevel gears of this particular kind are not capable of transmitting an input uniform rotation smoothly.

The violation of the condition of conjugacy of the tooth flanks,  $\mathcal{G}_{r.app}$  and  $\mathcal{P}_{r.app}$ , is illustrated by means of a schematic depicted in Figure 22.6.

As the tooth flanks,  $T_{app}$  and  $\mathcal{G}_{r.app}$ , of the generating rack and of the machined gear are not conjugate to one another, they contact each other at a point. The contact point is designated as  $K_{r/g}$ . When the gears rotate, the contact point,  $K_{r/g}$ , traces a trace,  $\text{Tr}(K_{r/g})$ , over the generating rack,  $T_{app}$ . Similarly, as the tooth flanks,  $T_{app}$  and  $\mathcal{P}_{r.app}$ , of the generating rack and of the machined pinion are not conjugate to one another, they contact each other at a point. The contact point is designated as  $K_{r/p}$ . When the gears rotate, the contact point,  $K_{r/p}$ , traces a trace,  $\text{Tr}(K_{r/p})$ , over the generating rack,  $T_{app}$ .

Generally speaking, the contact points,  $K_{r/g}$  and  $K_{r/p}$ , do not coincide with one another (the contact points,  $K_{r/g}$  and  $K_{r/p}$ , can be coincident only in a degenerate case. In Figure 22.6, the common contact point in this case is designated as  $K_{g/p}$ ). Therefore, at every instant of time, a gap between the tooth flanks,  $\mathcal{G}_{r.app}$  and  $\mathcal{P}_{r.app}$ , should be observed.\* As the gears are loaded by a torque being transmitted, no gap between the tooth flanks,  $\mathcal{G}_{r.app}$  and  $\mathcal{P}_{r.app}$ , occurs. Instead, a transmission error in the gear pair is observed. The actual value of the transmission error can be expressed in terms of the gap between the tooth flanks,  $\mathcal{G}_{r.app}$  and  $\mathcal{P}_{r.app}$ .

Manufacturing errors can be a root cause for low accuracy of the gears in intersected-axes gear pairs. Such a problem arises, for example, in high-volume production of forged gears.

Forged straight tooth bevel gears (Figure 22.7) are used in not critical applications. Actually, gears of this type can be manufactured with any desired geometry of the tooth flanks, as the geometry of the gear tooth flank

**FIGURE 22.7**

Forged straight bevel gear.

\* No gap between the tooth flanks of a gear and a mating pinion is observed when a rotation is transmitted by means of perfect bevel gears. In a case of perfect bevel gear pair, the tooth flanks,  $T$  and  $\mathcal{G}_r$ , of the generating rack and machined gear tooth flank are conjugate to one another. They contact each other along a line,  $E_{r/g}$ , that is entirely located within the tooth flank of the generating rack. Similarly, in a case of a perfect bevel gear pair, the tooth flanks,  $T$  and  $P_r$ , of the generating rack and machined pinion tooth flank are conjugate to one another. They contact each other along a line,  $E_{r/p}$ , that is entirely located within the tooth flank of the generating rack. Both of the just-mentioned lines of contact,  $E_{r/g}$  and  $E_{r/p}$ , intersect one another, as both are located within the tooth flank of the generating rack (degenerate cases of configuration of the lines of contact,  $E_{r/g}$  and  $E_{r/p}$ , are not considered here). This means in perfect intersected-axes gear pairs, there always exists at least one point of contact. Ultimately, the gear pair is capable of transmitting an input uniform rotation smoothly.





**FIGURE 22.8**  
Net forged straight bevel gear.

entirely depends on the geometry of dies used in the production process of forged gears. Practically, however, forged straight bevel gears feature the same geometry of the tooth flanks as that for cut straight bevel gears (see [Figure 22.4](#)). Therefore, in addition to manufacturing errors, violation of the condition of conjugacy, along with nonexistence of the angular base pitches,  $\varphi_{b.g}$  and  $\varphi_{b.p}$ , in a gear and a mating pinion are observed.

An important advantage of forging technology is that it allows the production of straight bevel gears that have a web at the inner end of the gear tooth ([Figure 22.8](#)), at the outer end, or both. Gear teeth that have a web are stronger and capable of transmitting larger torque.

#### 22.2.2.2 Spiral Bevel Gears

Bevel gears for approximate real intersected-axes gear pairs can be designed so as to have curved teeth in their lengthwise direction. Three major types of curved teeth are used today:

- Spiral bevel gears cut by face mill cutters
- Bevel gears that have teeth shaped in the form of circle cycloids, which are cut by face hobs
- Bevel gears that have teeth shaped in the form of circle involute in their longitudinal direction, which are cut by conical hobs

A face-milled spiral bevel gear is depicted in [Figure 22.9](#). Fine-pitch and medium-pitch bevel gears are produced used face-milled process.

The tooth flanks,  $\mathcal{G}_{r.app}$  and  $\mathcal{P}_{r.app}$ , of bevel gears of this particular type are generated by means of straight-sided generating round racks that feature the teeth shaped in the form of circular arcs in their lengthwise direction. In the gear-machining process, both the work gear and the generating round rack are continuously rotating about their axes of rotation at uniform angular velocities. The tooth flank of the generating rack,  $T_{app}$ , and the generated tooth flank of the machined gear make line contact with one another.

Because the geometry of the actual generating rack,  $T_{app}$ , differs from that for a perfect generating rack,  $T$ , the tooth flanks,  $\mathcal{G}_{r.app}$  and  $\mathcal{P}_{r.app}$ , of a gear and its mating pinion are not conjugate to one another, and the requirement of equal angular base pitches is not met, as the angular base pitches do not exist. As a result, spiral bevel gears transmit a rotation with a certain transmission error, the actual value of which can be precalculated based on the set of design parameters of the spiral bevel gear and the cutting head used to machine the gear. Transmission errors of this particular kind are inevitable when spiral bevel gears are used to transmit a rotation between two shafts intersecting one another.



**FIGURE 22.9**  
Face-milled spiral bevel gear.

Large coarse-pitch spiral bevel gears, for example, the ones shown in [Figure 22.10](#), are commonly machined on multiaxis numerically controlled machines. End-type mill cutters are used in this process. This makes it possible to machine gear tooth flanks of any desired geometry. However, in practice, the tooth flanks of large coarse-pitch spiral bevel gears are designed so as to have a tooth flank geometry similar to that of small- and medium-pitch spiral bevel gears. The tooth flanks,  $\mathcal{G}_{r.app}$  and  $\mathcal{P}_{r.app}$ , of a gear and mating pinion are not conjugate to one another. Moreover, the requirement of equal angular base pitches is not met, as the angular base pitches do not exist in bevel gears manufactured this way.

Bevel gears having teeth shaped in the form of cycloid of a circle (gears cut by face hobs) and bevel gears that have teeth shaped in the form of the involute of a circle in their longitudinal direction (cut by conical hobs, the so-called *palloid system*) have many similarities with conventional spiral bevel gears. In particular, the tooth flanks,  $\mathcal{G}_{r.app}$  and  $\mathcal{P}_{r.app}$ , of a gear and a mating pinion cut this way are not conjugate to one another, and the requirement of equal angular base pitches is not met. As a result, bevel gears of this particular kind are



**FIGURE 22.10**  
Large size coarse-pitch spiral bevel gear.



**FIGURE 22.11**  
Forged face gear.

capable of transmitting a rotation with a certain transmission error, the actual value of which can be expressed in terms of the set of design parameters of the spiral bevel gear and the cutting-tool used to machine the gear.

Noise excitation always occurs when high rotations are transmitted by spiral bevel gears. Improper location and orientation of the contact pattern is another bottleneck for bevel gears that have curved teeth in their longitudinal direction.

### 22.2.2.3 Face Gears

Face gearing (or *pseudo-bevel gearing* in other terminology) is also used to transmit a rotation between two shafts, the axes of which intersect one another. A face gear set consists of a face gear in combination with a spur, helical, or conical pinion. The shaft angle is commonly equal to  $90^\circ$ . However, face gear sets can be designed so as to have other values of the shaft angle.

Shown in [Figure 22.11](#), a face gear has a planar pitch surface and a planar root surface, both of which are perpendicular to the axis of rotation of the gear.

The spur pinion is commonly a duplicate of the shaper cutter used to cut the face gear, except, of course, for the additional clearance at the tips of the cutter teeth. The face width of the teeth on the face gear has to be made quite short; otherwise the top land will become pointed at the larger diameter of the gear.

Possible types of gears used to transmit a rotation between shafts that feature intersected axes of rotation are not limited to the aforementioned ones. Many novel types of gearing can be designed based on various combinations of generic shapes of gears (see [Chapter 21](#)). Gearing composed of internal bevel gears are included as well.

### 22.2.3 Generation of Tooth Flanks of Gears for Intersected-Axes Gearing

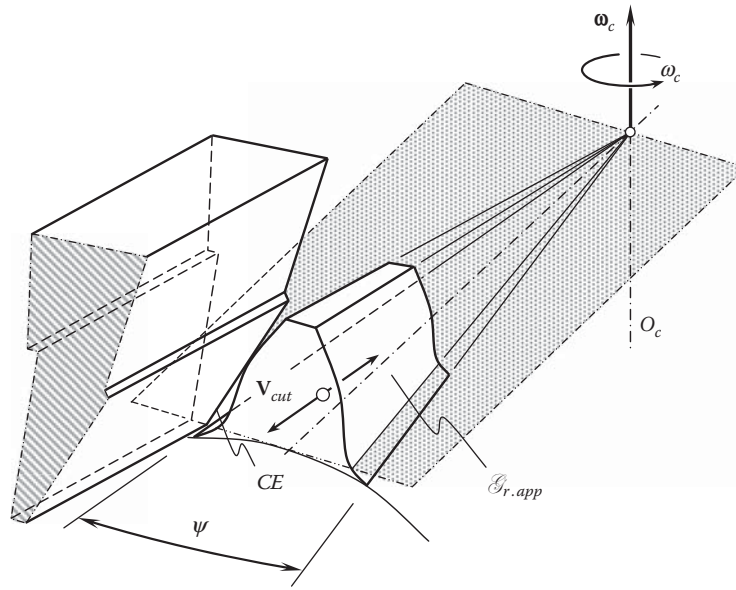
The approximate generating surface of a gear-cutting tool,  $T_{app}$ , is reproduced by the cutting edges of the tool when machining straight bevel gears. The tooth flanks of an approximate generating surface,  $T_{app}$ , are shaped in the form of a plane surface in the cases of machining both straight bevel gears of conventional design and straight bevel gears with offset teeth.

The straight cutting edge of the gear-cutting tool is the simplest shape of the cutting edge to be used for the purpose of reproduction of the plane,  $T_{app}$ . The straight motion of the cutting edge is the easiest motion to reproduce. The straight motion is performed in a direction parallel to the plane,  $T_{app}$ .

#### 22.2.3.1 Generation of Tooth Flanks of Straight Bevel Gears

Reciprocation of the straight cutting edge,  $CE$ , toward the axis of rotation,  $O_c$ , of the generation surface,  $T_{app}$ , as shown in [Figure 22.12](#), is the most practical way of reproducing the approximate generating surface,  $T_{app}$ , of the gear-cutting tool.\* In such a scenario, the plane,  $T_{app}$ , is reproduced as the loci of consequent positions of the straight cutting edge,  $CE$ , when it is reciprocating toward the axis,  $O_c$ , of rotation,  $\omega_c$ .

\* Other directions of the reciprocation motion,  $V_{cut}$ , are also theoretically possible. Commonly, they are less practical.

**FIGURE 22.12**

Generation of the plane,  $T_{app}$ , by a straight cutting edge,  $CE$ , moving toward the axis of rotation,  $O_c$ , of the gear-cutting tool.

Principles governing the generation of bevel gears are analogous to those governing the generation of spur and helical gears, with the difference that whereas spur and helical gears are generated by tools that represent the teeth of the basic rack, cutters used for bevel gear generation represent the teeth of the straight-sided basic crown wheel. The straight-sided base crown wheel is commonly called the *generating surface of the gear-cutting tool*. The motions that result in the generation of gears are therefore those of rolling pitch cones instead of rolling pitch cylinders.

The cutters themselves must be given a form and a motion, which cause them to sweep out the surface of the basic crown wheel,  $T_{app}$ , and the work gear is then given, relative to the cutters, the rolling motion the finished gear would have when engaging with the crown wheel that the cutters represent. Two distinct cases arise:

1. Each of a pair of gears (both of which are to be generated) is conjugate to the same side of the surface of the imaginary crown wheel (which must therefore be symmetrical).
2. Mating gears are conjugate to opposite sides of the same basic crown wheel.

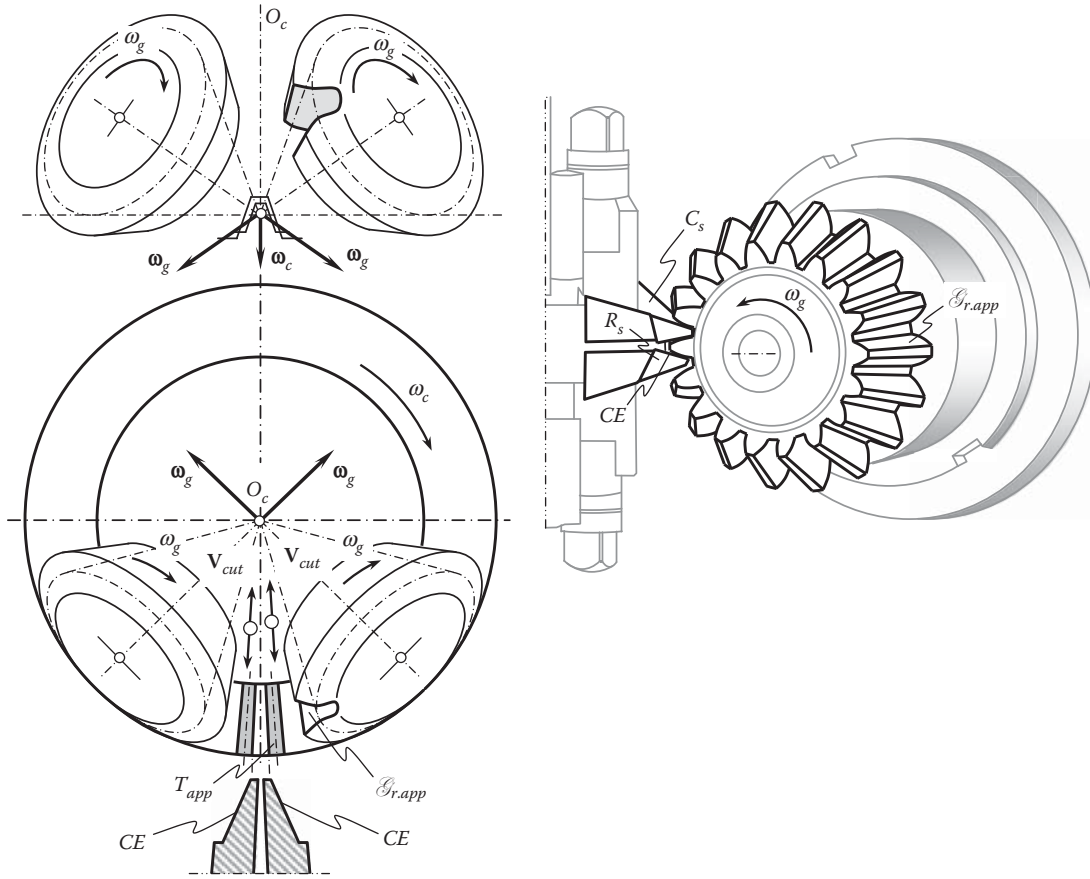
The first case finds application in the cutting of bevel gears that have straight (and *uncorrected*) teeth and the second in the cutting of spiral bevel gears. Considering the generation of either pair of gears individually, however, both cases reduce to the same thing, the only difference being in the setting of the cutters.

Figure 22.13 illustrates the process diagrammatically for the case of straight bevel gears. Two cutters that have straight-side cutting edges,  $CE$ , are arranged to reciprocate with velocity,  $V_{cut}$ , along radial lines, sweeping out the surfaces,  $T_{app}$ , of the teeth of the imaginary crown wheel that has its center at  $O_c$ . The cutting edge,  $CE$ , is understood as the line of intersection of the rake surface,  $R_s$ , and the clearance surface,  $C_s$ , of the gear-cutting tool.

The position vector of a point,  $\mathbf{r}_{Ta}$ , of the lateral plane,  $T_{app}$ , of the generating surface of the gear-cutting tool can be expressed in terms of two Gaussian parameters,  $u$  and  $\theta$ :

$$\mathbf{r}_{Ta}(u, \theta) = \begin{bmatrix} u \cos \theta \\ 0 \\ u \sin \theta \\ 1 \end{bmatrix} \quad (22.1)$$

In order to derive an equation for the family of lateral planes,  $T_{app}$ , when the generating surface of the gear-cutting tool is rolling over the pitch cone of the gear to be cut, two operators of the coordinate system transformation have to be derived.



**FIGURE 22.13**  
Diagrammatic representation of straight bevel gear generation.

The first,  $\mathbf{Rt}(\phi, Z_t)$ , is the operator of rotation through the pressure angle,  $\phi$ . This rotation is performed about the  $Z_t$ -axis of a Cartesian coordinate system,  $X_t Y_t Z_t$ , which is associated with the tooth flank,  $T_{app}$ , of the generating surface of the gear-cutting tool. The operator,  $\mathbf{Rt}(\phi, Z_t)$ , can be represented in matrix form as follows:

$$\mathbf{Rt}(\phi, Z_t) = \begin{bmatrix} \cos \phi & \sin \phi & 0 & 0 \\ -\sin \phi & \cos \phi & 0 & 0 \\ 0 & 0 & 1 & 0 \\ 0 & 0 & 0 & 1 \end{bmatrix} \quad (22.2)$$

The second operator,  $\mathbf{Rt}(\psi, X_T)$ , is the operator of rotation through a current angle  $\psi$ . This rotation is performed about the  $X_T$ -axis of a Cartesian coordinate system,  $X_T Y_T Z_T$ , which is associated with the generating surface,  $T_{app}$ , of the gear-cutting tool. The following expression:

$$\mathbf{Rt}(\psi, X_T) = \begin{bmatrix} 1 & 0 & 0 & 0 \\ 0 & \cos \psi & \sin \psi & 0 \\ 0 & -\sin \psi & \cos \psi & 0 \\ 0 & 0 & 0 & 1 \end{bmatrix} \quad (22.3)$$

is derived for the operator,  $\mathbf{Rt}(\psi, X_T)$ , of the coordinate system transformation.

The operator of the resultant coordinate system transformation,  $\mathbf{Rs}(t \mapsto T)$ , that is, the operator of the transition from the reference system,  $X_t Y_t Z_t$ , to the reference system,  $X_T Y_T Z_T$ , can be expressed in the form of a product:

$$\mathbf{Rs}(t \mapsto T) = \mathbf{Rt}(\psi, X_T) \cdot \mathbf{Rt}(\phi, Z_t) \quad (22.4)$$

This allows the following expression for the operator of the resultant coordinate system transformation:

$$\mathbf{Rs}(t \mapsto T) = \begin{bmatrix} \cos \phi & \sin \phi & 0 & 0 \\ -\sin \phi \cos \psi & \cos \phi \cos \psi & \sin \psi & 0 \\ \sin \phi \sin \psi & -\cos \phi \sin \psi & \cos \psi & 0 \\ 0 & 0 & 0 & 1 \end{bmatrix} \quad (22.5)$$

The position vector of a point,  $\mathbf{r}_{Tf}$ , of the family of lateral planes,  $T_{app}$ , when the generating surface of the gear-cutting tool is rolling over pitch cone of the gear to be cut, can be analytically represented in the following form:

$$\mathbf{r}_{Tf}(u, \theta, \psi) = \mathbf{Rs}(t \mapsto T) \cdot \mathbf{r}_{Ta}(u, \theta) \quad (22.6)$$

where the subscript  $Tf$  refers to the family of lateral planes  $T_{app}$ .

Equation 22.6 casts into:

$$\mathbf{r}_{Tf}(u, \theta, \psi) = \begin{bmatrix} u \cos \phi \cos \theta \\ u (-\sin \phi \cos \theta \cos \psi + \sin \theta \sin \psi) \\ u (\sin \phi \cos \theta \sin \psi + \sin \theta \cos \psi) \\ 1 \end{bmatrix} \quad (22.7)$$

In the reference system  $X_t Y_t Z_t$ , the unit normal vector to the plane,  $T_{app}$ , is along the  $Y_t$ -axis. Therefore, in the reference system,  $X_T Y_T Z_T$ , it can be analytically described as follows:

$$\mathbf{n}_T(\phi, \psi) = \begin{bmatrix} \sin \phi \\ \cos \phi \cos \psi \\ -\cos \phi \sin \psi \\ 0 \end{bmatrix} \quad (22.8)$$

Once the expressions for the position vector,  $\mathbf{r}_{Tf}$  (see Equation 22.7), as well as for the unit normal vector,  $\mathbf{n}_T$ , (see Equation 22.8), are derived, the *Shishkov equation of contact*,  $\mathbf{n} \cdot \mathbf{V}_\Sigma = 0$ , can be represented in the following form:

$$\cot \theta - \frac{\sin \phi \sin \psi + \tan \delta_k \cos \phi}{\cos \psi} = 0 \quad (22.9)$$

In Equation 22.9, the angle  $\delta_k$  is used to specify the velocity vector,  $\mathbf{V}_\Sigma$ .

Equation 22.9 is used to express the angle,  $\psi$ , in terms of the parameters,  $\phi$ ,  $\theta$ ,  $\psi$ , and  $\delta_k$ . Then the derived expression for the angle,  $\psi$ , is substituted in Equation 22.7. The position vector of a point,  $\mathbf{r}_g = \mathbf{r}_g(u, \theta)$ , of the gear tooth flank,  $\mathcal{G}_{r.app}$ , can be obtained after the angular parameter,  $\psi$ , is eliminated from Equation 22.7.

The tooth flank,  $T_{app}$ , of the generating surface of the gear-cutting tool and the flank,  $\mathcal{G}_{r.app}$ , of the generated straight tooth bevel gear are not conjugate to one another. Bevel gears generated using this method are not capable of transmitting a rotation smoothly. This restricts the area of application of straight tooth bevel gears to low-rotation applications.

The work gear is arranged with its axis,  $O_g$ , passing through the axis,  $O_c$ , and its pitch cone in contact with the pitch plane of the crown wheel,  $T_{app}$ . It is then given a rotation,  $\omega_g$ , about its own axis, together with a rotation of the axis bodily about the axis,  $O_c$ , of the crown wheel,  $T_{app}$ , which are related so that the pitch cone of the work gear rolls over the pitch plane of the crown wheel. In passing through the zone where the cutters operate, therefore, material is removed and the result is a generated tooth flank,  $\mathcal{G}_a$ . The generated tooth flank,  $\mathcal{G}_a$ , is not conjugate with the tooth flank of the basic crown wheel. It may be observed that in practice the component motions are rearranged as a matter of convenience, the work gear and the cutter head each with only rotational motion about their respective axes.

When cutting straight bevel gears, especially those that have a low tooth count, the problem of tooth under-cutting becomes critical. This issue is discussed in detail in the monograph by Radzevich [111,112].



### 22.2.3.2 Generation of Tooth Flanks of Spiral Bevel Gears

Spiral bevel gears are cut by face mill cutters. The rotation vector,  $\omega_{cut}$ , of the face mill cutter is pointed in such a direction that it is parallel to the axis of rotation,  $O_c$ , of the generating surface of the cutting tool, as shown in Figure 22.14. In this way, bevel gears that have spiral teeth with a certain spiral angle,  $\psi_g$ , are produced. Although suitable spiral angles lie in the range of  $\psi_g = 15^\circ \dots 35^\circ$ , they are usually chosen in the range of  $\psi_g = 30^\circ \dots 35^\circ$  to provide adequate overlap, and it is normal practice to make spiral bevel gears with about 35% overlap.

When machining a spiral bevel gear, the cutter rotates about its axis with a certain angular velocity,  $\omega_{cut}$ . The work gear and the generating surface,  $T_{app}$ , roll over each other. For this purpose, rotations of the work gear,  $\omega_g$ , and the generating surface of the gear-cutting tool,  $\omega_c$ , are synchronized with each other in a timely manner.

In the method of generating curved tooth bevel gears, the tooth spirals take the form of circular arcs. Straight-sided cutting tools represent the flanks of the basic crown wheel teeth, and the combined motions of the generating cutter and the work gear sweep out the surface of the imaginary crown wheel teeth (round rack teeth). The generation of the tooth profiles is obtained by giving the work gear a rolling motion relative to the cutter, similar to what the finished gear would have when engaging with the crown wheel.

The tool holder is rotated to cause a cutting action while the work gear slowly rotates with the tool holder. The rotation of the work gear with respect to the tool holder causes a generating action to occur. After one tooth space is finished, the machine goes through an indexing motion to bring the cutter into the next tooth slot.

Pinions are cut as the reverse of wheels insofar as they are assumed to engage with the opposite side of the basic crown wheel surface. In practice, the axes of the generating cutter and the work gear are not inclined at the theoretical angle; the axes are arranged to accommodate the tapering depth of the tooth and also to provide deflection allowance in the tooth spirals.

During operation, the cutter is given a rotation speed and feed rate suitable for the material of the work gear and is fed to the full depth required while the cutter and work gear roll together. A copious supply of cutting

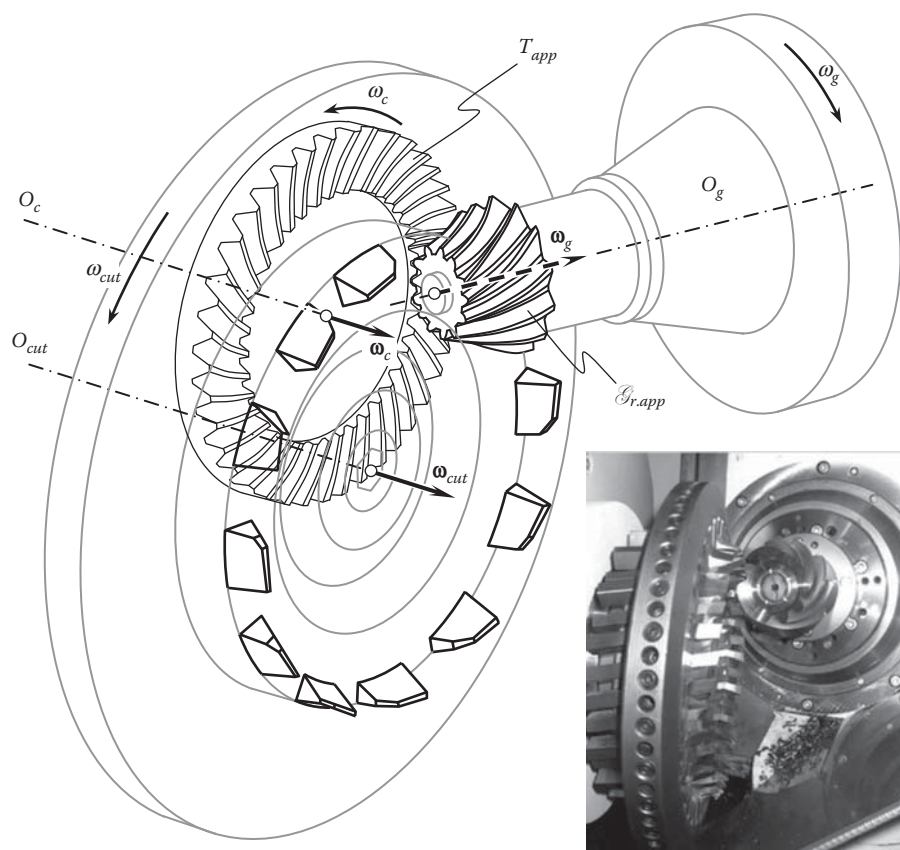


FIGURE 22.14

Representation of the generating surface,  $T_{app}$ , of the face mill cutter.



Gears that demand high quality are always provided with fully generated teeth on both the wheel and pinion.

**FIGURE 22.15**  
Diagrammatic arrangement of spiral bevel gear generation.

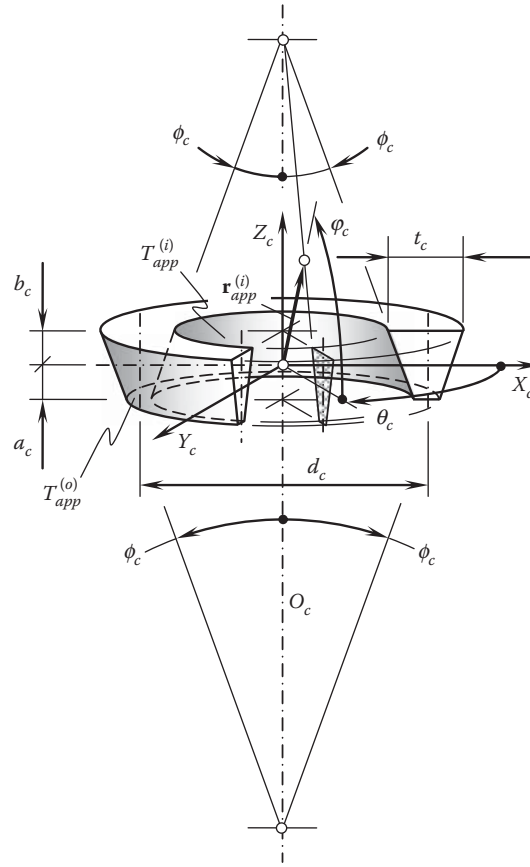


**FIGURE 22.16**  
Design parameters of the generating surface,  $T_{app}$ , of the face mill cutter.

For machining of bevel gears with circular arc teeth, the generating surface of the cutting tool is chosen in the form of two cones of revolution that have a common axis of rotation (Figure 22.16). The equation of the generating surface,  $T_{app}$ , can be derived from Figure 22.16.

The position vector of a point,  $\mathbf{r}_{app}^{(i)}$ , for the inner portion,  $T_{app}^{(i)}$ , of the generating surface can be expressed in the following form:

$$\mathbf{r}_{app}^{(i)}(\varphi_c, \theta_c) = \frac{(d_c - t_c)}{2} \cdot \begin{bmatrix} \cos \varphi_c \cdot \cos \theta_c \\ \cos \varphi_c \cdot \sin \theta_c \\ \sin \varphi_c \\ 1 \end{bmatrix} \cdot \frac{\cos \phi_c}{\cos(\varphi_c - \phi_c)} \quad (22.14)$$

Similarly, for the outer portion,  $T_{app}^{(o)}$ , of the generating surface for the position vector of a point,  $\mathbf{r}_{app}^{(o)}$ , the following formula can be derived:

$$\mathbf{r}_{app}^{(o)}(\varphi_c, \theta_c) = \frac{(d_c + t_c)}{2} \cdot \begin{bmatrix} \cos \varphi_c \cdot \cos \theta_c \\ \cos \varphi_c \cdot \sin \theta_c \\ -\sin \varphi_c \\ 1 \end{bmatrix} \cdot \frac{\cos \phi_c}{\cos(\varphi_c - \phi_c)} \quad (22.15)$$

The lateral cutting edges,  $CE$ , of the face mill cutter are located within the surfaces  $T_{app}^{(i)}$  and  $T_{app}^{(o)}$  (Equations 22.14 and 22.15). In this way, straight-sided cutting tools represent the flanks of the basic crown wheel teeth.

The rolling motion of the face mill cutter in relation to the work gear (Figure 22.17) is the same as in the case of cutting straight tooth bevel gears (see Equation 22.5). Therefore, the position vector of a point,  $\mathbf{r}_{app.f}^{(o)}$ , of a family of surfaces,  $T_{app}^{(o)}$ , in the rolling motion of the face milling cutter can be calculated as the dot product of the

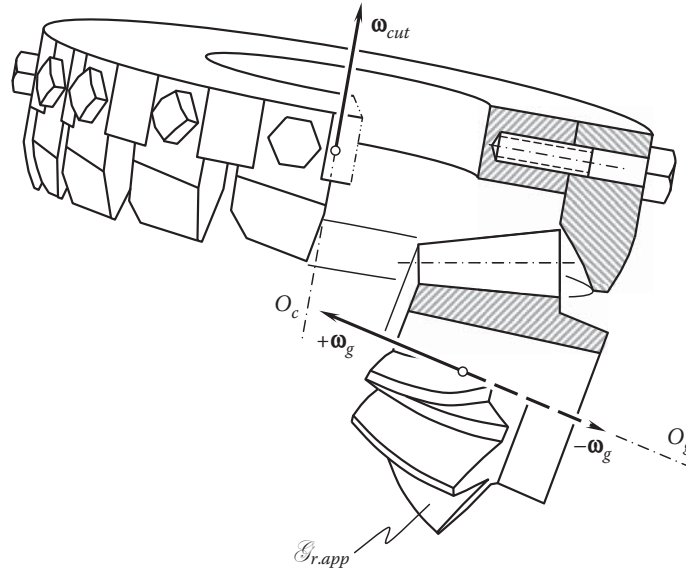


FIGURE 22.17

Rolling motion of the face-mill cutter when cutting a spiral bevel gear.

position vector of a point,  $\mathbf{r}_{app}^{(o)}$  (see Equation 22.15) and the operator of the resultant coordinate system transformation,  $\mathbf{Rs}(t \mapsto T)$  (see Equation 22.5):

$$\mathbf{r}_{app,f}^{(o)}(\varphi_c, \theta_c, \psi) = \mathbf{Rs}(t \mapsto T) \cdot \mathbf{r}_{app}^{(o)}(\varphi_c, \theta_c) \quad (22.16)$$

The enveloping parameter,  $\psi$ , can be eliminated from Equation 22.16 if this equation is considered together with the Shishkov equation of contact,  $\mathbf{n} \cdot \mathbf{V}_\Sigma = 0$ . Ultimately, this returns an equation for tooth flank,  $\mathcal{G}_{r.app}$ , of the spiral bevel gear cut by a face mill cutter.

Spiral bevel gears cut by face mill cutters that have straight-sided tooth profiles are not capable of transmitting a rotation smoothly. They are subject to noise excitation when the rotation exceeds a certain limit value. This is because in the gear-machining mesh, the gear tooth flank,  $\mathcal{G}_{r.app}$ , and the generating surface tooth flank,  $T_{app}$ , are not conjugate to one another, and neither features the angular base pitches. Therefore, the mandatory condition of equal operating base pitches of a gear and a mating pinion to the operating angular base pitch of the gear pair is not fulfilled.

When cutting spiral bevel gears, especially those that feature a low tooth count, the problem of tooth under-cutting becomes critical. This issue is discussed in detail in the monograph by Radzevich [111,112].

### 22.2.3.3 Tooth Flanks of Bevel Gears Cut Using Continuous Indexing Method of Gear Machining

Two continuously indexing methods of cutting bevel gears are used today:

1. Face hobbing of bevel gears: Bevel gears that have teeth shaped in the form of a cycloid in their lengthwise direction are cut by this method.
2. Hobbing of gears for palliod system by means of conical hobs: Using this method, bevel gear teeth are shaped in the form of an involute curve in their lengthwise direction.

In both cases, the generating surface of the gear-cutting tool,  $T_{app}$ , features a straight-sided tooth profile. The tooth flanks,  $\mathcal{G}_{r.app}$ , of the gear to be machined are generated as envelopes to consecutive positions of the generating surface,  $T_{app}$ , when the pitch cone that is associated with the gear-cutting tool rolls with no slippage over the pitch cone of the work gear. Except for the rolling motion, tooth flanks generation by the continuous indexing methods of machining of bevel gears are very similar to that by the indexing methods of bevel gear machining. This makes it possible to conclude immediately that bevel gears that have curvilinear teeth in their lengthwise direction cut by face hobs with straight-sided tooth profiles, as well as gears for palliod systems,

**FIGURE 22.18**

Approximate real intersected-axes gear pair composed of forged straight bevel gear and pinion.

are not capable of transmitting a smooth rotation from a driving shaft to a driven shaft. They are subject to noise excitation when the rotation exceeds a certain limit value. This is because in the gear-machining mesh, the gear tooth flank,  $\mathcal{G}_{r,app}$ , and the generating surface tooth flank,  $T_{app}$ , are not conjugate to one another, and neither features the angular base pitches. Therefore, the mandatory condition of equal operating base pitches of a gear and a mating pinion to the operating angular base pitch of the gear pair is not fulfilled.

When cutting bevel gears with curvilinear teeth, especially those with low tooth count, the problem of tooth undercutting becomes critical. This issue is discussed in detail in the monograph by Radzevich [111,112].

#### 22.2.4 Examples of Approximate Real Intersected-Axes Gear Pairs

Various approximate real intersected-axes gears are used to transmit a rotation from a driving shaft to a driven shaft. For low-rotation applications, forged approximate real intersected-axes gear pairs are used. An example of a gear pair of this type composed of a straight bevel gear and pinion is illustrated in Figure 22.18.

Gear pairs of high accuracies are composed of cut straight bevel gears (Figure 22.19). Commonly, the planing method of gear cutting is used to produce gears for these purposes.

For certain applications, approximate real intersected-axes gearing featuring small shaft angles is used. An example is illustrated in Figure 22.20.

**FIGURE 22.19**

Approximate real intersected-axes gear pair composed of cut straight bevel gear and pinion.



**FIGURE 22.20**  
Approximate real intersected-axes gear pair featuring a small shaft angle.

In the past, approximate real intersected-axes gear pairs composed of a cast herringbone gear and a pinion were used ([Figure 22.21](#)). Because of the poor accuracy of cast gears, gearing of this type is used in noncritical applications featuring low rotation of the input and output shafts.

Spiral bevel gear pairs represent the most broadly used type of gears with curvilinear teeth. Examples of orthogonal spiral bevel gear pairs that have tooth ratios  $u = 1$  and  $u > 1$  are illustrated in [Figure 22.22](#). It is not mandatory that the axes of rotation of a gear and the mating pinion in a spiral bevel gear pair be orthogonal to each other. An example of a nonorthogonal spiral bevel gear pair is shown in [Figure 22.23](#).

Spiral bevel gear pairs are broadly used in automobile applications ([Figure 22.24](#)). For special applications, large-size spiral bevel gears are used ([Figure 22.25](#)).

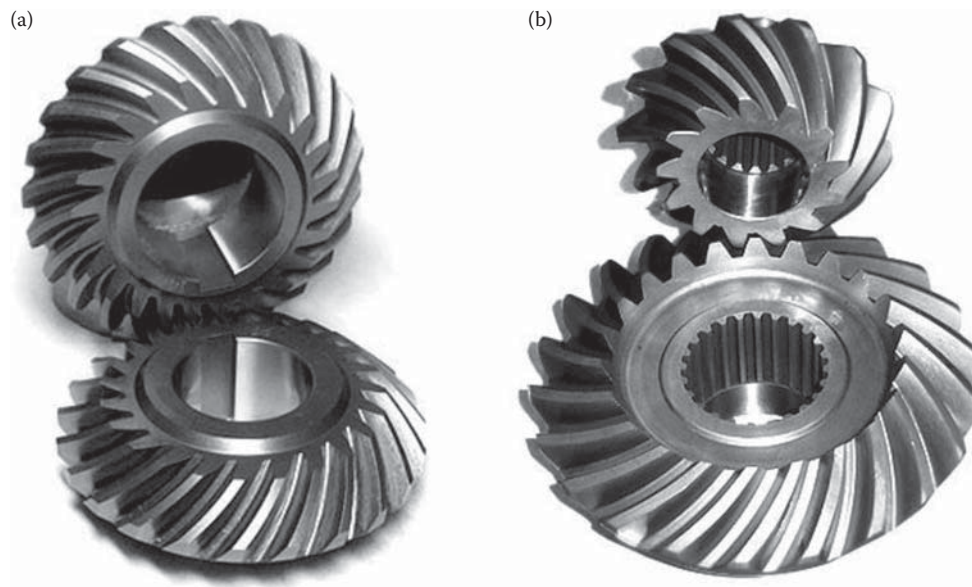
Both orthogonal and nonorthogonal spiral bevel gears cut by the gear-cutting tool that features a straight-sided generating round rack are examples of approximate real intersected-axes gearing.

Face gears represent another type of approximate real intersected-axes gearing.

A spur involute pinion can be engaged in mesh with a face gear that has an appropriate geometry of the tooth flanks, as depicted in [Figure 22.26](#). A gear pair of this kind is insensitive to the axial displacements of the pinion. Moreover, that same pinion can be engaged in mesh with a face gear as well as with straight bevel gears that have different number of teeth and pitch cone angles, including mesh with a spur gear ([Figure 22.27](#)).



**FIGURE 22.21**  
Approximate real intersected-axes gear pair composed of cast herringbone gear and pinion.

**FIGURE 22.22**

Examples of approximate real crossed-axes gear pairs: orthogonal spiral bevel gear pairs that have tooth ratios (a)  $u = 1$ , and (b)  $u > 1$ .

**FIGURE 22.23**

Nonorthogonal spiral bevel gear pair.

**FIGURE 22.24**

Spiral bevel gear pair for automobile application.





**FIGURE 22.25**  
Large-size spiral bevel gear pair.



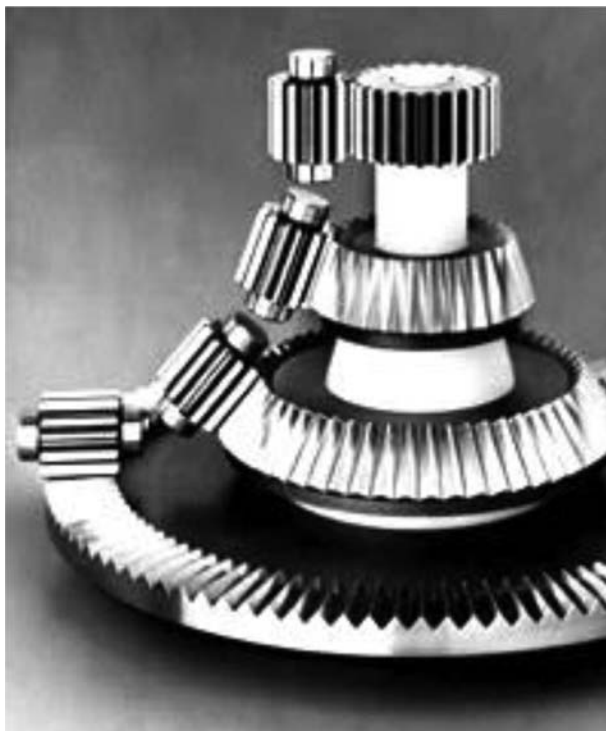
**FIGURE 22.26**  
Example of a spur face gear pair.

Similarly, face gearing can be composed of a helical involute pinion and a face gear that has the appropriate geometry of tooth flanks, as shown in [Figure 22.28](#).

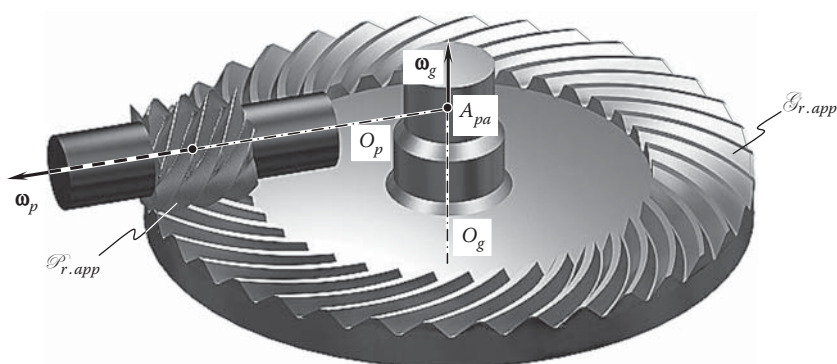
In face gearing, the gear tooth flank,  $\mathcal{G}_{r.app}$ , and pinion flank,  $\mathcal{P}_{r.app}$ , are not conjugate to one another, and do not feature the angular base pitches. Therefore, the mandatory condition of equal operating base pitches of a gear and a mating pinion to the operating angular base pitch of the gear pair is not fulfilled. This is mainly for two reasons:

1. The tooth flanks of the face gear and the mating pinion are generated by straight-sided racks; that is, a round rack for the side gear and a straight rack for the mating pinion. As a result, the tooth flanks of the face gear and the mating pinion make point contact. This limits the power capacity of face gear drives.
2. The tooth flanks of the face gear and the mating pinion are generated from base surfaces, which are different from the surfaces in mesh of the face gear and the pinion.



**FIGURE 22.27**

Meshing of spur pinion with straight bevel gears that feature different pitch cone angles.

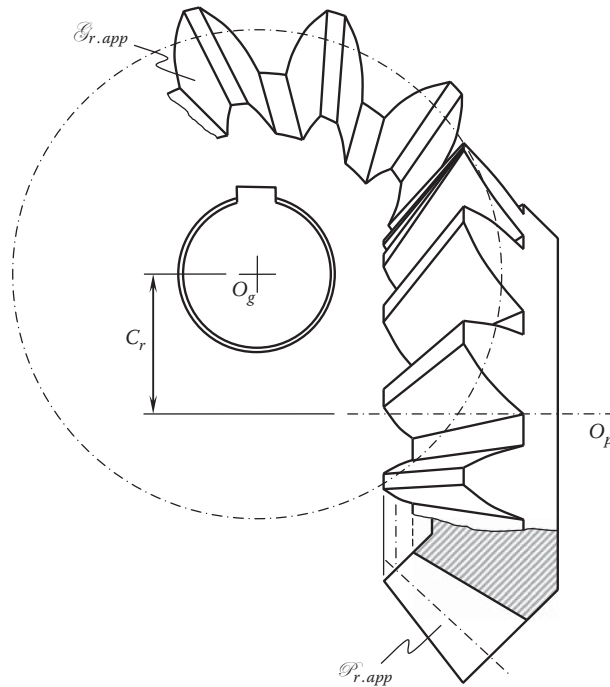
**FIGURE 22.28**

An approximate real intersected-axes gearing composed of a face gear and a helical involute pinion.

Therefore, face gearing is not capable of transmitting a rotation smoothly without vibration and noise excitation. These disadvantages of face gearing become more severe when the tooth numbers of the face gear and the mating pinion become smaller.

### 22.3 Approximate Real Crossed-Axes Gearing

Crossed-axes gear pairs represent a group of approximate real crossed-axes gearing (see [Chapter 18, Table 18.1](#)). Manufacturing processes used in the production of gears for crossed-axes gear pairs are much the same as those

**FIGURE 22.29**

Crossed-axes gear pair composed of skew tooth gear and pinion.

used in production of gears for approximate real intersected-axes gearing. The tooth flanks of a gear and a mating pinion are commonly generated with gear-cutting tools that have a straight-sided generating rack.

The nonzero axis offset,  $C_r$ , is a principal difference between crossed-axes gearing and intersected-axes gearing (Figure 22.29).

Gears that have either skew teeth (as shown in Figure 22.29) or circular arc teeth (as shown in Figure 22.30) are used in crossed-axes gearing. The axes of rotation of a gear and mating pinion in most crossed-axes gear pairs used in the industry cross at right angles to each other. Crossed-axes gears of this kind are referred to as *orthogonal crossed-axes gearings*. In special applications, crossed-axes gears that have nonorthogonal axes of rotation are also used (Figure 22.31).

The concept of *octoid gearing* can be also used in the case of crossed-axes gears. A conical gear of a crossed-axes gear pair can be engaged in mesh with a corresponding *round rack*,  $\mathcal{R}$ . The tooth flanks of the round rack (the crown gear, in other words) have an octoidal profile (Figure 22.32). The tooth profile

**FIGURE 22.30**

Crossed-axes gear pair composed of circular arc bevel gear and pinion.



**FIGURE 22.31**  
Nonorthogonal crossed-axes gear pair.

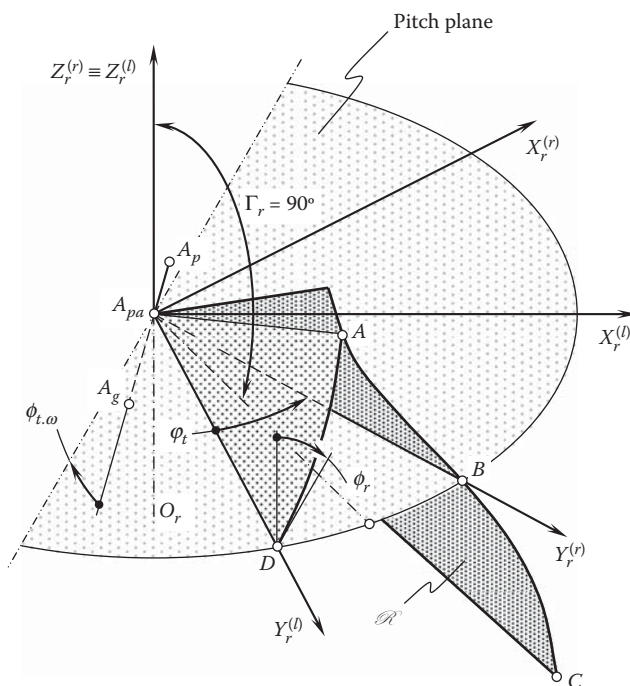


**FIGURE 22.32**  
Geometry of the tooth flank of the basic rack,  $\mathcal{R}$ , for a crossed-axes gear pair.

of this type is often viewed as an involute curve constructed on a sphere of a corresponding diameter. Tooth profiles of this kind feature a point of inflection. The tooth profile,  $ABC$ , of the right side of the tooth profile initially is given in a reference system  $X_r^{(r)}Y_r^{(r)}Z_r^{(r)}$ . Similarly, the tooth profile,  $AD$ , of the opposite side (the left side) is specified in a Cartesian coordinate system  $X_g^{(l)}Y_g^{(l)}Z_g^{(l)}$ . The coordinate systems  $X_r^{(r)}Y_r^{(r)}Z_r^{(r)}$  and  $X_g^{(l)}Y_g^{(l)}Z_g^{(l)}$  are turned in relation to one another about the  $Z_r$ -axis through the tooth thickness angle,  $\phi_t$ , of the generating rack,  $\mathcal{R}$ .

A crossed-axes gear pair for which the tooth flanks of the gear and pinion are generated by an octoidal profile is not capable of transmitting a smooth rotation from a driving shaft to a driven shaft (at a uniform angular velocity of rotation of both the gear and the pinion).

Approximate real crossed-axes gear pairs composed of a face gear and the mating cylindrical pinion (either a spur pinion, as shown in Figure 22.33, or a helical pinion, as shown in Figure 22.34) are used in special applications.

Violation of the condition of conjugacy of the tooth flanks,  $\mathcal{G}_{r.app}$  and  $\mathcal{P}_{r.app}$ , of a gear and a mating pinion, along with indefinite angular base pitches of the gear and the pinion, are the main reasons real crossed-axes gearing of the discussed kind can be only approximate. Crossed-axes gears of this kind are not capable of transmitting a rotation smoothly from a driving shaft to a driven shaft.



**FIGURE 22.33**  
Face gear pair that has offset axes of rotation of the face gear and the spur pinion.



**FIGURE 22.34**  
Face gear pair that has offset axes of rotation of the face gear and the helical pinion.

## 22.4 Worm Gearing

Worm gearing represents another group of real crossed-axes gear pairs (see [Chapter 18, Table 18.1](#)).

It makes sense to start the discussion on worm gearing from similarities between worm gearing and crossed-axes gearing that is composed of helical involute gears.

Consider a crossed-axes gear pair that is composed of two helical involute gears (see [Chapter 13, Figure 13.19](#)), and a worm gearing that is composed of an involute gear and an involute worm shown in [Figure 22.35](#). The number of teeth of the pinion is the only difference between these two types of gearing, which are shown in [Figure 13.19](#) and [Figure 22.35](#), respectively. The worm gear can be either spur or helical. Worm gear pair features either a single start or a multistart worm. However, the number of starts of the worm,  $N_w$ , is less than the tooth number of a pinion,  $N_p$ , in a crossed-axes gear pair that is composed of two helical involute gears ( $N_w < N_p$ ).

Point contact between the interacting tooth flanks of a worm gear,  $\mathcal{G}_{r.app}$ , and the threads of the worm,  $\mathcal{P}_{r.app}$ , limits the power capacity of the worm-gear drive, as well as the power density transmitted by the worm gear pair.

In the worm gearing of the discussed design, the condition of conjugacy of the tooth flanks of a worm gear,  $\mathcal{G}_{r.app}$ , and the threads of the worm,  $\mathcal{P}_{r.app}$ , is fulfilled. It is also can be shown that at every instant of time, the angular base pitch of the worm gear,  $\varphi_{b.g}$ , and the angular base pitch of the worm,  $\varphi_{b.p}$ , are equal to the operating base pitch,  $\varphi_{b.op}$ , of the gear pair. As a result, worm gearing is capable of transmitting a rotation smoothly.

Instead of an involute worm, a worm of another design is often used in the current practice. The involute worm can be replaced with an *Archimedean worm*, a convolute worm, or a worm of another design. Such a replacement is required mostly due to manufacturing issues. Worms of designs that are easy in production can be used to replace the desired involute worm.

By targeting an increase of power density being transmitted through a gearbox, a single enveloping type of worm gearing has been developed. Worm gearing of this type features a cylindrical worm. The worm can be either a single-start worm, as illustrated in [Figure 22.36a](#), or a multiple-start worm, for example, a four-start worm as, shown in [Figure 22.36b](#).

Designing a double-enveloping worm gearing is the next step to be undertaken in order to improve the power density transmitted by the worm drive. Actually, this worm gearing has been known since the time of da Vinci ([Figure 22.37](#)) [17] or even earlier. However, no discussion on worm thread geometry can be found in work by da Vinci [17].

Significant improvements in the design of double-enveloping worm gearing were proposed by Lorenz and Cone. The invention of the double-enveloping worm-gear drive ([Figure 22.38](#)) is a breathtaking story centering on two dramatic individuals, Lorenz and Cone.

Worm-gear drives of all known designs (except the worm-gear drive composed of an involute gear and an involute worm) are *approximate* worm-gear drives. This is because the geometries of worm-gear teeth, as well as the geometries of worm threads, deviate from the desired geometries. As a result, the tooth flanks of a worm gear and the threads of a mating worm are not conjugate to one another. Moreover, no angular base

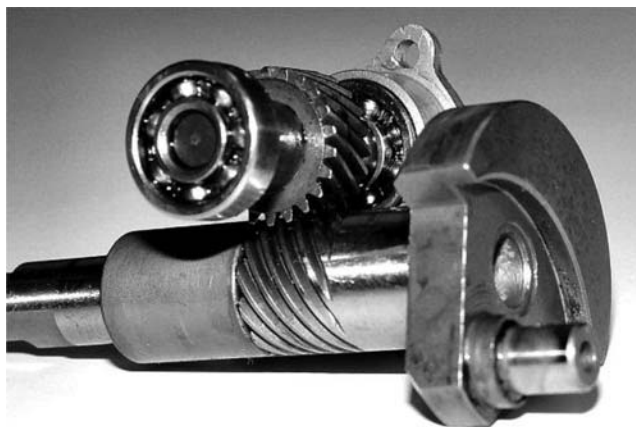
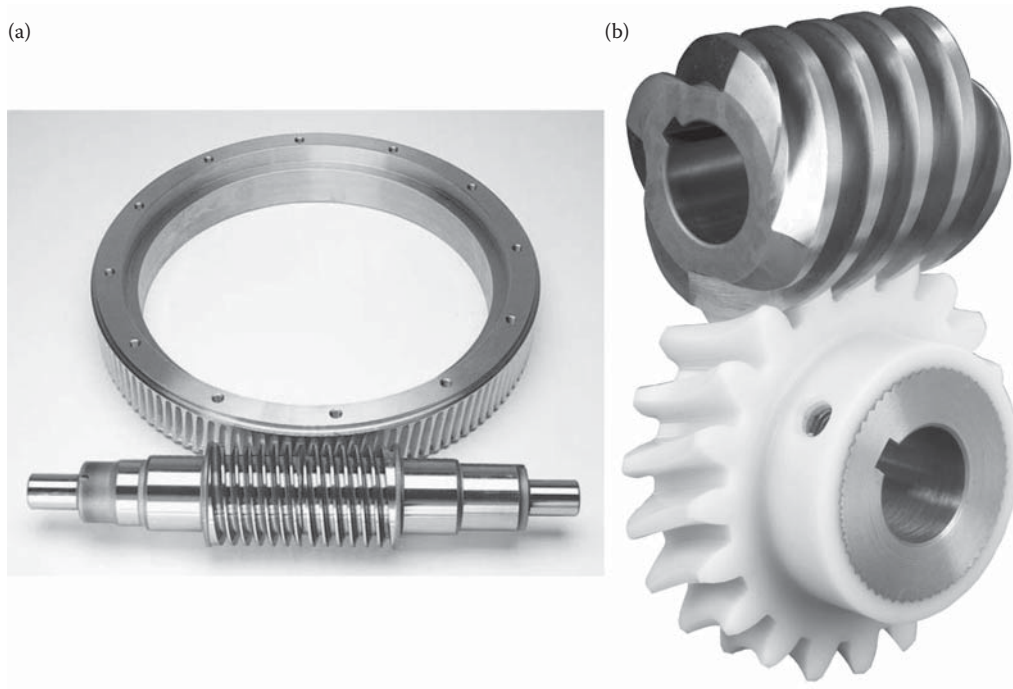


FIGURE 22.35

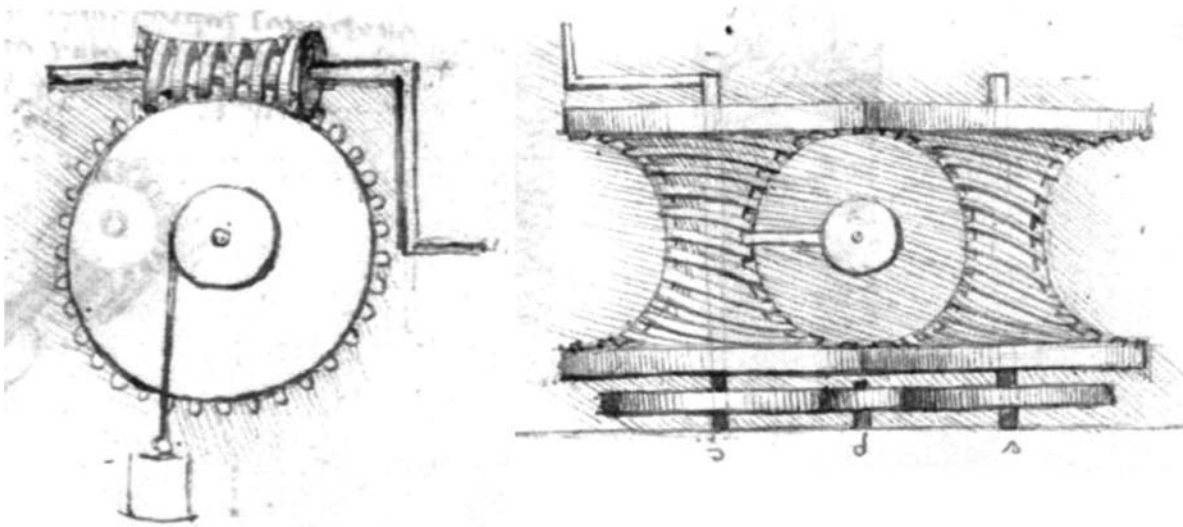
Worm gear pair that is composed of an involute helical gear and an involute worm.



**FIGURE 22.36**

Examples of worm gearing featuring a cylindrical worm: (a) a single-start worm and (b) a four-start worm.

pitch can be specified in the design the worm gear and worm. Therefore, the fundamental requirements all gear pairs have to comply with ( $\phi_{b,g} = \phi_{b,op}$ , and  $\phi_{b,p} = \phi_{b,op}$ ) cannot be fulfilled. Because of this, real worm gearing can only be approximate. It is not capable of transmitting a smooth rotation from a driving shaft to a driven shaft. In order to eliminate the root cause of vibration generation and noise excitation, worm-gear tooth flanks, as well as mating worm threads, should be developed from the base cones, as schematically illustrated in Figure 22.39. Worm gearing featuring geometry of the interacting surface developed from the base cones of the worm gear and worm (see Figure 22.39) corresponds to *R-gearing*. Only worm gearing of this particular type features line contact between the tooth flanks of a worm gear and the threads of the mating worm.

**FIGURE 22.37**

Double-enveloping worm gearing from the book by da Vinci, *The Madrid Codices*, Volume 1, 1493, Facsimile Edition of *Codex Madrid 1*, original Spanish title: *Tratado de Estatica y Mechanica en Italiano*, McGraw Hill Book Company, 1974.



**FIGURE 22.38**  
Double-enveloping worm-gear drive.

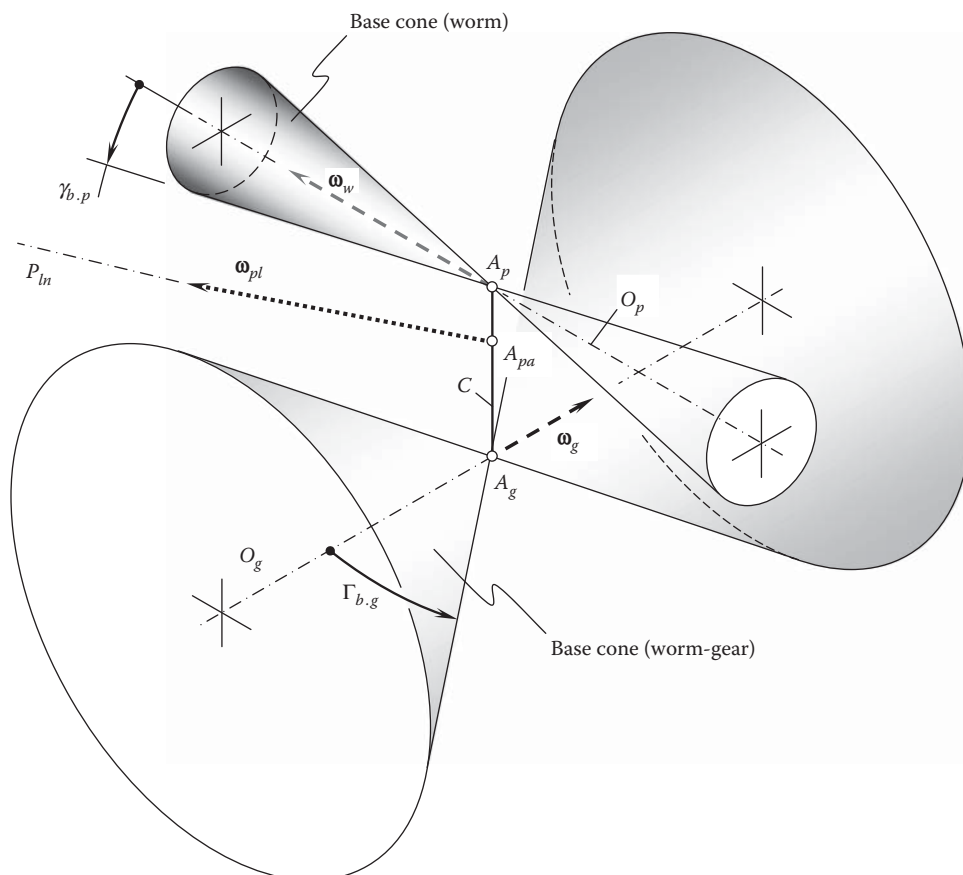


**FIGURE 22.39**  
Configuration of base cones of a worm gear and mating worm.



In order to make worm gearing capable of accommodating manufacturing errors, as well as deflections under operating loads, heat extension, and so on, it is necessary to enhance worm gearing of the kind *R*-gearing to worm gearing of the kind *S<sub>pr</sub>-gearing*. Worm gearing of the type *S<sub>pr</sub>-gearing* features point contact between the tooth flanks,  $\mathcal{G}_r$  and  $\mathcal{P}_r$ , of a worm gear and the threads of the mating worm. However, the degree of conformity of the interacting surfaces of the worm gear teeth and the worm threads retains the highest possible value. This ensures higher contact strength of worm gearing of the kind *S<sub>pr</sub>-gearing*, as well as the highest possible power density transmitted by the worm-gear drive. Numerous other advantages can be discussed for worm gear pairs of the kind *S<sub>pr</sub>-gearing*.

Internal approximate intersected-axes and crossed-axes gears are not used to transmit a rotation from a driving shaft to a driven shaft. Gears of these designs can be of interest when designing dies for net forging of gears, electrodes for EDM of gears, and so forth.

## 22.5 Tooth Flank Modification

The tooth flanks of real gears differ from those of perfect gears for many reasons. Deviations of tooth flanks of real gears from those of perfect gears, as well as axis misalignment, are among the root causes of vibration generation and noise excitation when a gear drive operates.

In order to make real gears less sensitive to axis misalignment, in practice, the interacting surfaces of the mating gear teeth are often subject to modifications. Tooth flank modification is also performed to accommodate manufacturing errors, which are inevitable in production of gears.

### 22.5.1 Brief Historical Overview of Gear Tooth Flank Modification

The idea of gear tooth flank modification can be traced back to the second half of the 20th century. H. Walker [159] was among the first to point out the importance of tooth flank corrections for spur gears. The concept of a gear tooth addendum modification is illustrated in Figure 22.40.

Initially, tooth flank modification targeted the accommodation of gear tooth deflection under loads. Since the time of Walker [159], the key problem in gear tooth flank modification was how to get precise deflections, including load tooth elastic deformations and shaft deflections, and how to distribute the load evenly along the contact lines.

Eventually, the concept of spur gear tooth flank modification was applied to helical gears.

In addition to the modification of a gear tooth addendum, modification of the gear tooth dedendum, crown modification, and topological modification of gear tooth flanks were proposed.

Extensive research in the field of gear tooth flank modification was carried out by Kolchin of the USSR. The results of this research are discussed in his monograph [56] (Figure 1.22). The influence of axis misalignment on

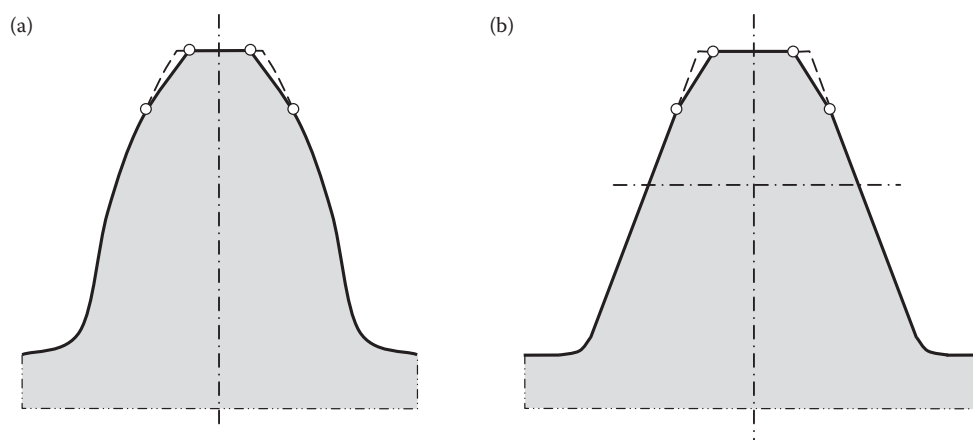


FIGURE 22.40

Concept of tooth addendum modification: (a) modified tooth addendum of an involute gear, and (b) of a basic rack.

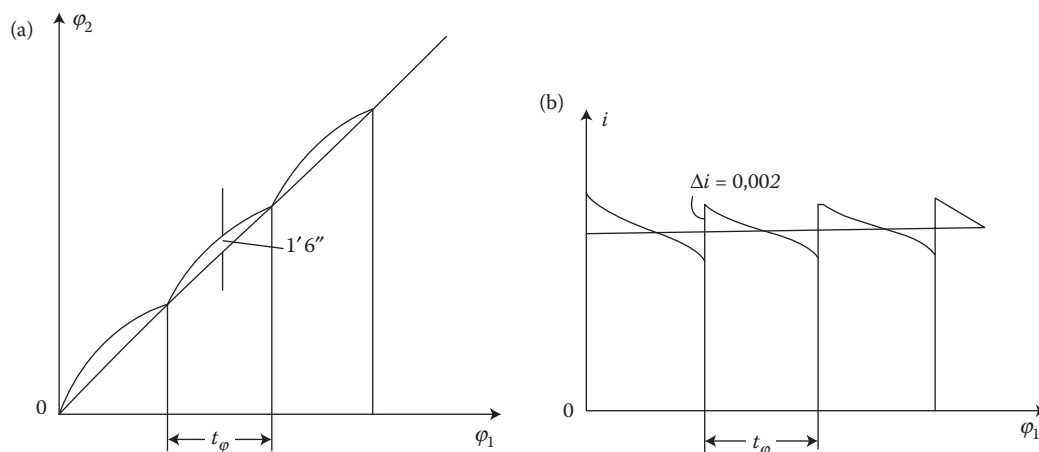


FIGURE 22.41

(a) Angle of rotation,  $\varphi_2$ , of a driven shaft versus angle of rotation,  $\varphi_1$ , of the driving shaft and (b) Gear ratio,  $i$ , versus angle of rotation,  $\varphi_1$ , of the driving shaft. (From Figure 119 on page 191 and Figure 118 on page 189 in Kolchin, N.I., *Analytical Calculation of Planar and Spatial Gearing*, Mashgiz, Moscow, 1949, 210 p. [56])

the smoothness of the rotation of the driven shaft was investigated. Some of the results obtained by Kolchin are illustrated in Figure 22.41. Numerical examples provided by Kolchin reveal that transmission errors in the range of  $1'6''$  (see Figure 22.41a), as well as deviations of the gear ratio in the range of 0.442% (see Figure 22.41b), are realistic values that cannot be ignored when designing transmission gear drives for critical applications.

### 22.5.2 Requirements of Design Parameters of Modified Portions of Tooth Flanks

The design parameters of modified portions of the tooth flanks of a gear and mating pinion must be determined so as to minimize the deviation of the real tooth flanks from perfect tooth flanks. The perfect tooth flank of an involute gear (Figure 22.42) is used as a datum surface when designing gears with modified tooth flank geometry. Under any circumstances, the difference between the base pitches of modified portions of the interacting surfaces of a gear and mating pinion should be as small as possible. Ideally, the base pitch,  $\varphi_{b,g}^m$ , of the modified portion of the gear tooth flank has to be equal to the base pitch,  $\varphi_{b,p}^m$ , of the modified portion of the mating pinion tooth flank.

Modification of the tooth flanks of gears of all types should be considered an approximation of the corresponding  $S_{pr}$ -gearing by modified tooth flanks. The smaller the deviations of the modified tooth flank from the tooth flank of the corresponding  $S_{pr}$ -gearing, the better. Once the geometry of the tooth flank of an  $S_{pr}$ -gearing is determined, the design parameters of any and all types of tooth flank modification can be derived targeting a reasonable adjustment of an existing tooth flank geometry, which bridges it as close as possible

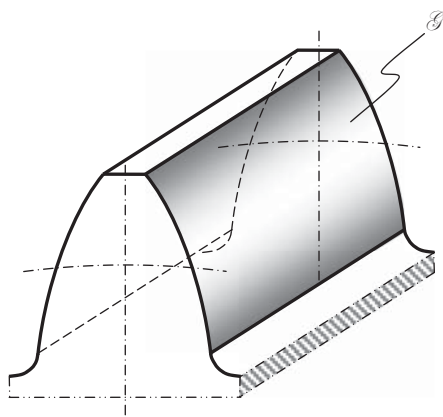


FIGURE 22.42

Involute gear tooth flank,  $\mathcal{I}$ , as a datum surface.

to the tooth flank geometry of the corresponding  $S_{pr}$ -gear. Actually, the geometry of the tooth flanks in  $S_{pr}$ -gearing is the target for all possible tooth flank modifications.

Evidently, not only tooth flanks of one member of the gear pair have to be modified. Instead, tooth flanks of both mating gears should be modified, maintaining the equality of the base pitches ( $\varphi_{b,g} = \varphi_{b,op}$  and  $\varphi_{b,p} = \varphi_{b,op}$ ). The requirement is a must for proper designing of a gear pair.

The best-known method so far for tooth flank modification [75] took into account variations of torque being transmitting by a gear drive. However, even in this case, the proposed method of tooth flank modification should be considered a kind of approximation to the tooth flanks of  $S_{pr}$ -gearing by smooth regular tooth flanks, the design parameters of which can be expressed in terms of the applied load.

The following conclusion can be drawn based on the discussion in this section of the book:

Almost all kinds of gears manufactured in the current industry are a kind of approximate real gearing. In the meantime, no perfect intersected-axes or perfect crossed-axes gearings are commonly used. The condition of conjugacy of the interacting tooth flanks of a gear and mating pinion is not fulfilled when the gears are designed, manufactured, and used in the industry. Moreover, intersected-axes and crossed-axes approximate real gears do not feature such an important design parameter as the *angular base pitch*. Because of this, the required condition of equality of angular base pitches of a gear and mating pinion to the operating base pitch of the gear pair cannot be fulfilled in intersected-axes or crossed-axes approximate real gears. In certain cases (straight bevel gears cut by disk-type mill cutters) even the condition of contact ( $\mathbf{n} \cdot \mathbf{v}_\Sigma = 0$ ) between the tooth flanks,  $\mathcal{G}_{r,app}$  and  $\mathcal{P}_{r,app}$ , is also violated.

Lack of knowledge of the kinematics and geometry of perfect intersected-axes and crossed-axes gearings is the primary root cause of insufficient accuracy of gears of these particular types.

### 22.5.3 Kinds of Tooth Flank Modifications

Tooth flank modifications are desired alterations to the tooth flank face compared with the main geometry shown in Figure 22.42. Superimposing nominal modifications on the main geometry produces the nominal tooth flank. The modifications can be defined in characteristic profiles of the tooth flank or in relation to the flank face. Modification depths are always given in the transverse section and normal to the involute of the main geometry.

#### 22.5.3.1 Tooth Flank Modifications That Restrict the Useable Flank

Modification of tooth flank geometry is extensively used in the industry to improve the performance of all parallel-axes gear pairs. Numerous kinds of tooth flank geometry are developed to this end. *Trial and error* is the main tool when doing such an analysis.

*Prefinish flank undercut*: Prefinish (root) relief is a planned, generated undercut (that is, using a protuberance tool) of the transverse profile of a tooth flank in the area of the root. The magnitude of the relief,  $q_{Fs}$ , is the greatest distance between the root rounding and the involute imagined as extended to the base circle (Figure 22.43a). Below this, the datum is a line from the involute origin to the gear center.

*Tip corner chamfering, tip corner rounding*: Tip corner chamfering and tip corner rounding are reliefs of the transverse profile that restrict the usable area of the tooth flank. Tip corner chamfering is the chamfer arising through removal of the tip corner. In the case of tip corner rounding, this corner is radiused in the normal plane. The radial height,  $h_k$ , and the residual tooth thickness at the tip,  $s_{ak}$ , are given as the dimensions of this modification (Figure 22.43a) and are different for chamfering and rounding.

#### 22.5.3.2 Transverse Profile Modifications

In the following,  $L_{AE}$  is used\* to define the roll length for compatibility with ISO 1328-1. The length,  $L_{AE}$ , is an equivalent to length of path of contact,  $g_a$ .

*Tip and root relief*: Tip and root reliefs (Figure 22.43b) are the continuously increasing reliefs of the transverse profile of the main geometry from defined points in each case (diameter, length of roll, roll angle) in the direction of the tip or root (mostly involute).

*Transverse profile slope modification,  $C_{Ha}$* : This is similarly defined as tip or root relief, except that  $C_{Ha}$  extends over the whole width of the face (Figure 22.43c).

\* DIN ISO 21771:2014-08, Gears—Cylindrical Involute Gears and Gear Pairs: Concepts and Geometry (ISO 21771:2007), English translation of DIN ISO 21771:2014-08.

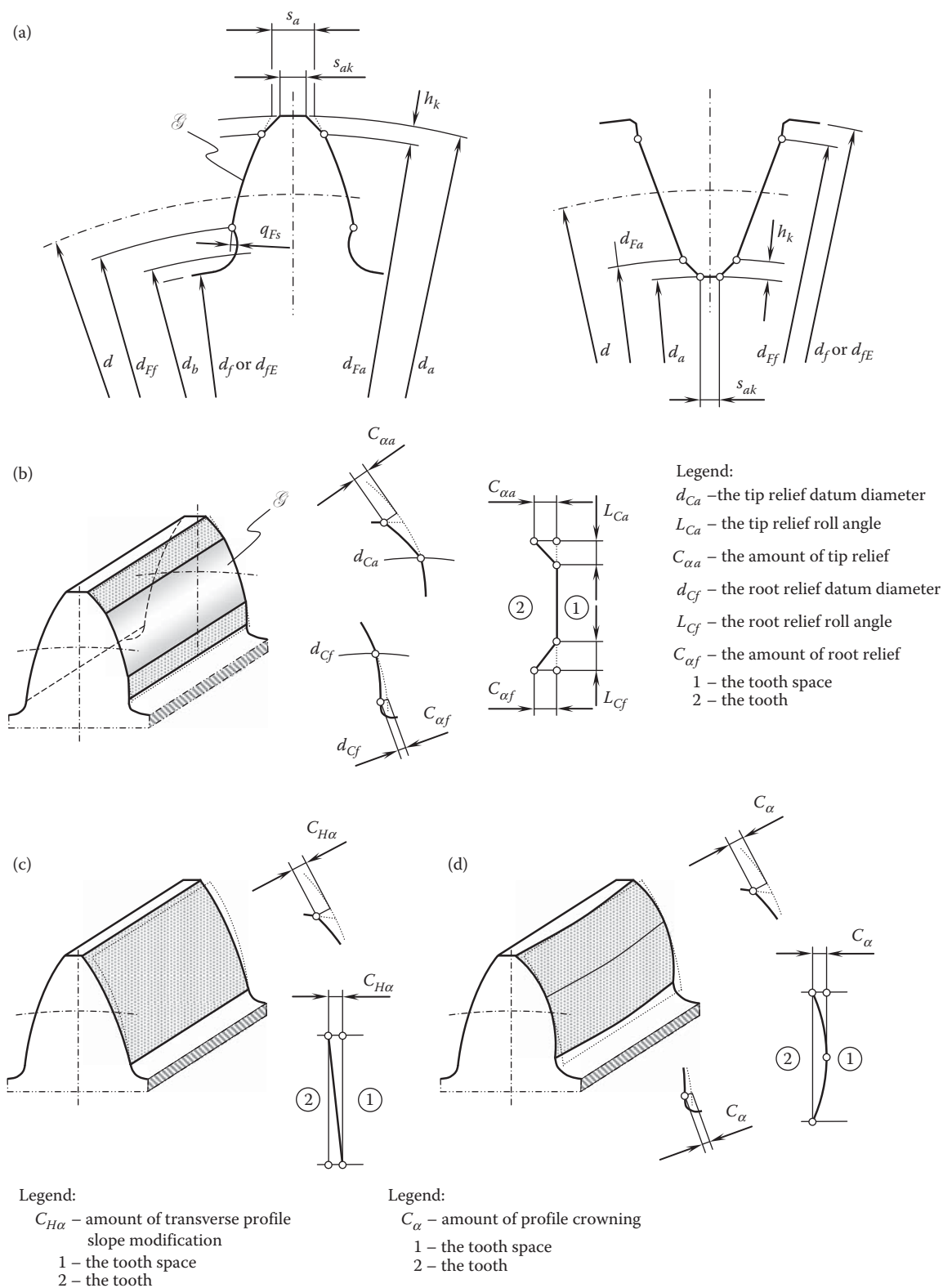


FIGURE 22.43

Kinds of tooth flank modification of an involute gear for parallel-axes gearing: (a) spur cylindrical gear with undercut and tip chamfering, (b) tip and root relief, (c) transverse profile slope modification, and (d) profile crowning.

(Continued)

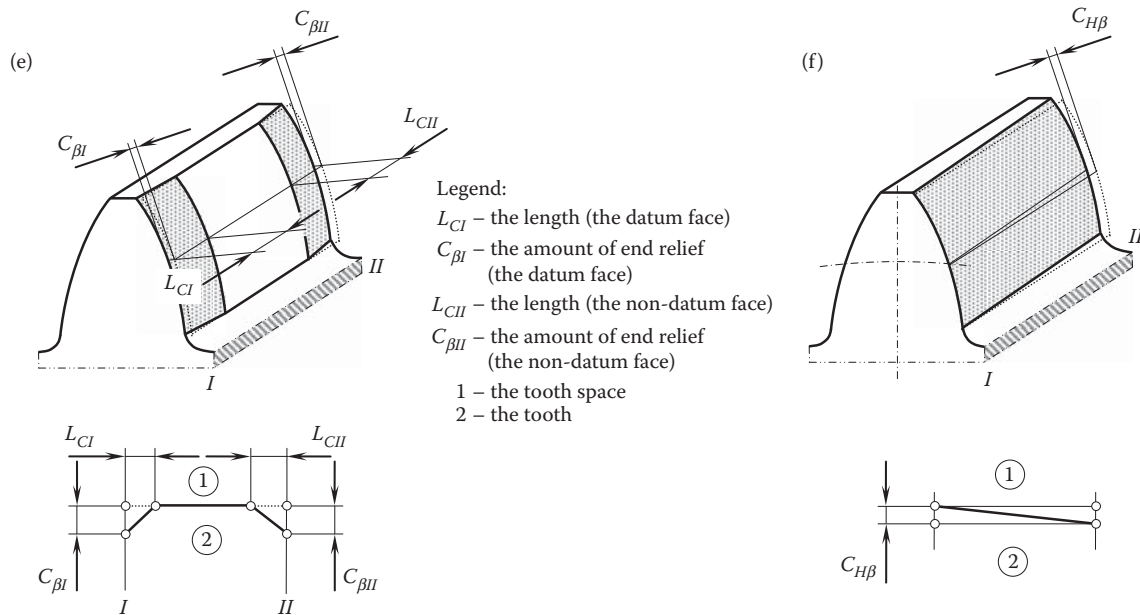


FIGURE 22.43 (Continued)

Kinds of tooth flank modification of an involute gear for parallel-axes gearing: (e) flank line end relief and (f) flank line slope modification.

*Profile crowning (barreling),  $C_{\alpha}$* : Profile crowning is the continuously increasing relief of the transverse profile from a common defined point of the main geometry (diameter, length of roll, roll angle) in the direction of the tip and root of the gear teeth (Figure 22.43d).

Profile crowning is generally defined with respect to the center of the length of roll of the usable flank and has a parabolic form passing through the points defined by  $C_{\alpha}$ .

### 22.5.3.3 Flank Line (Helix) Modifications

Modification of the flank line of a gear tooth gives the gear designer an additional opportunity to improve the performance of a gear pair.

*Flank line end relief*: Flank line end reliefs (Figure 22.43e) are continuously increasing reliefs of the flank line from defined points of the main geometry in each case in the direction of the datum faces (linear or parabolic).

*Flank line (helix) slope modification,  $C_{H\beta}$* : This is similarly defined as end relief, but  $L_{CI}$  or  $L_{CII}$  extends across the whole face width (Figure 22.43f). It is not necessarily linear.

*Flank line (helix) crowning,  $C_{\beta}$* : Flank line crowning (Figure 22.44a) is the continuously increasing relief of the flank line from a common defined point of the main geometry symmetrically in the direction of both ends of the tooth (arc-shaped or parabolic).

### 22.5.3.4 Flank Face Modifications

More complex alterations to gear tooth flank geometry are also used in practice. Examples can be readily found in production of gears for low-noise gear pairs.

*Topographical modifications*: The desired deviation from the unmodified involute helicoid (Figure 22.44b) is determined in relation to each point of intersection on a grid laid over the tooth flank of the main geometry.

*Triangular end relief*: Triangular end reliefs are continuously increased reliefs of the tooth flanks generally perpendicular to the generators of the main geometry (along the lines of contact) from a defined roll angle in the direction of the start or end of the roll on the tooth flanks. See Figure 22.44c for details.

*Flank twist*: Twist is an effect on a flank described as a rotation of the transverse profile along a helix. There is a distinction between twist of the transverse profile,  $S_{\alpha}$ , and of the flank line,  $S_{\beta}$ . If not otherwise defined, it changes linearly from the beginning to the end of the usable flank. The sign of the flank twist is very important. A right-handed twist is commonly considered a positive twist. Accordingly, a left-handed twist is commonly considered a negative twist (see Figure 22.44d for details).

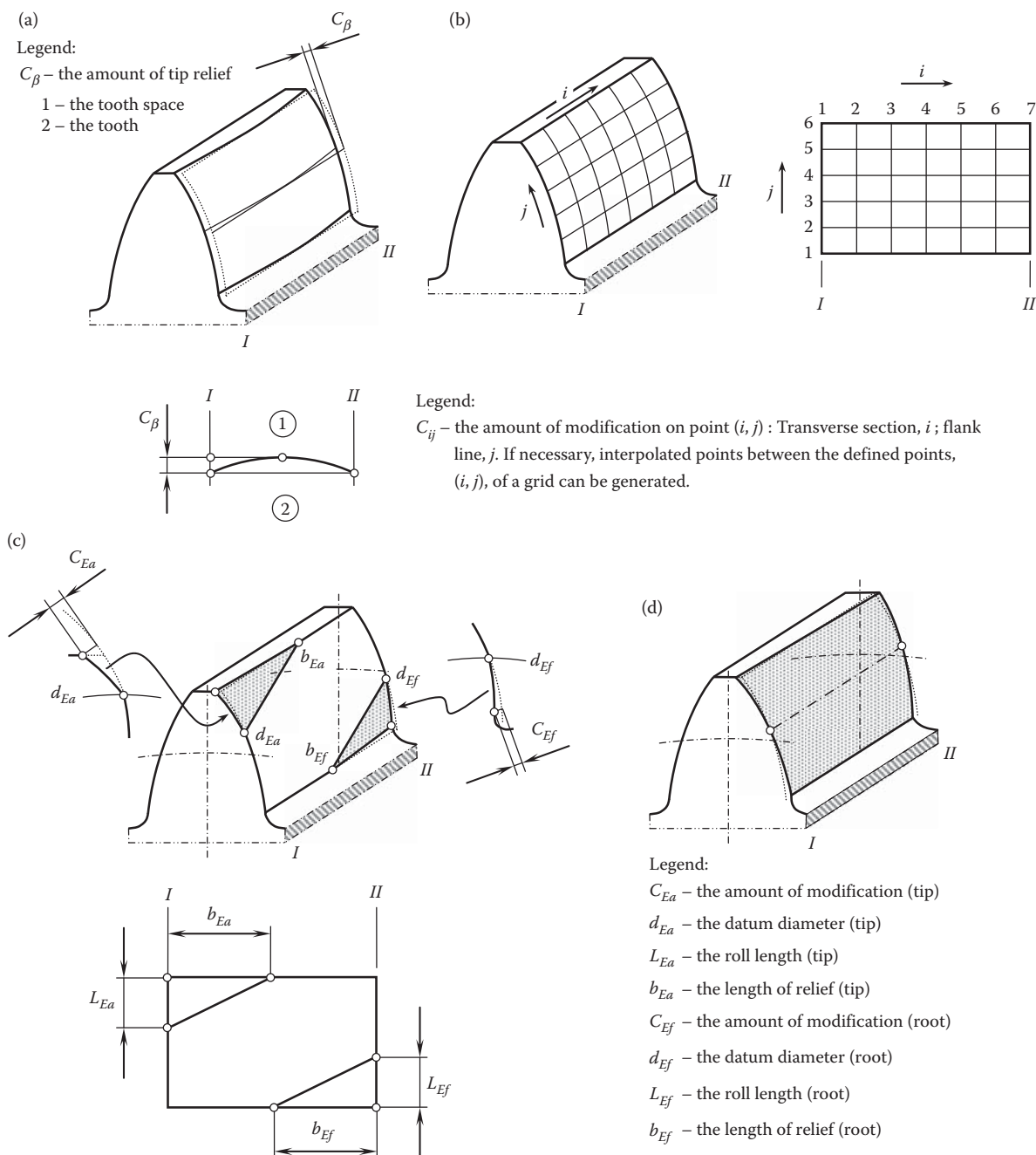


FIGURE 22.44

Involute gear tooth flank modifications: (a) flank line crowning, (b) topographical/topological modification, (c) triangular end relief, and (d) flank twist.

#### 22.5.4 Description of Modifications by Functions

Modifications of the profile can be given as functions of the diameter or the corresponding roll distances or angles and modifications of the flank lines as functions of the axial distance from the start of the usable face width in the direction of the nondatum face. The combination of both functional relationships describes the modification of the whole flank surface.

Graphically, it is usual to show tooth surface modifications as deviations from the exact involute helicoid with respect to roll length for radial deviations (as in Figure 22.43b) and position across the tooth width for axial deviations (as in Figure 22.43e).



## *Local Geometry of Interacting Tooth Flanks of a Gear and a Mating Pinion*

Interacting tooth flanks of a gear and a mating pinion feature a complex geometry. It is a challenging problem to investigate contact geometry of the tooth flanks of a complex geometry. An advantage is that in nature, only small local patches in the differential vicinity of the contact point of the tooth flanks interact with one another. Therefore, there is no need to involve the entire interacting tooth flanks in the analysis. It is sufficient to consider only corresponding local patches of the interacting tooth flanks, which are of much simpler geometry and can be locally approximated by surfaces of the second order.

Three principal configurations of gear shafts are distinguished. They are:

1. Parallel-axes gearing
2. Intersected-axes gearing
3. Crossed-axes gearing

The local geometry of the interacting tooth flanks of mating gears is considered following this sequence of gear types.

### **23.1 Local Geometry of Interacting Tooth Flanks in Parallel-Axes Gearing**

The interaction of tooth flanks in parallel-axes gearing is considered in the following section for the case of external meshing of the gear and mating pinion. Then, the obtained results of the analysis can be enhanced to the case of internal meshing of the gear and mating pinion.

#### **23.1.1 Kinematics of Interacting of Tooth Flanks**

The interaction of the tooth flanks of the gear and mating pinion in parallel-axes gearing is schematically illustrated in [Figure 23.1](#). The plane of action,  $PA$ , is tangent to base cylinders of a gear and a mating pinion. The base cylinder of the gear is of diameter  $d_{b,g}$  and the base cylinder of the pinion is of diameter  $d_{b,p}$ .

The rotation vector of the gear,  $\omega_g$ , and the rotation vector of the pinion,  $\omega_p$ , are pointed opposite one another. The magnitudes,  $\omega_g$  and  $\omega_p$ , of the rotation vectors,  $\omega_g$  and  $\omega_p$ , are in inverse proportion to the diameters of the base cylinders. The rotation vectors,  $\omega_g$  and  $\omega_p$ , are at a certain center distance,  $C$ , from one another.

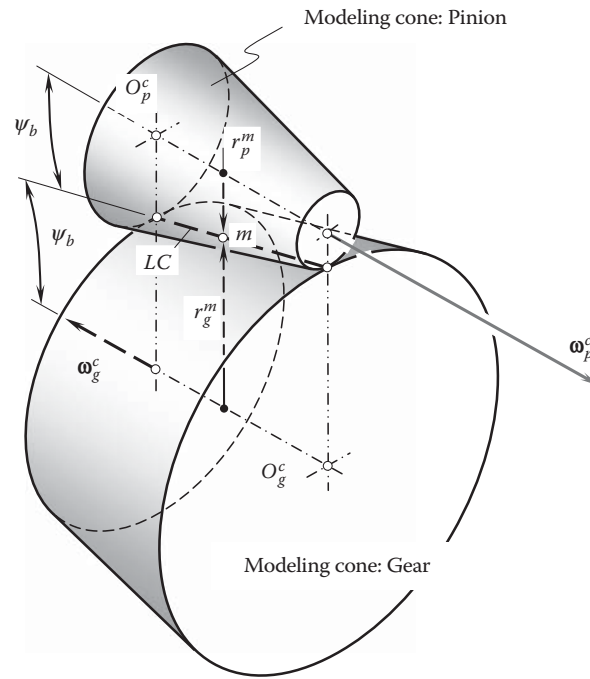
A straight line of contact,  $LC$ , of the gear and the pinion teeth is entirely located within the plane of action. The line of contact forms a base helix angle,  $\psi_b$ , with the axis of rotation of the gear,  $O_g$ , and the axis of rotation,  $O_p$ , of the pinion (because of lack of space, the base helix angle,  $\psi_b$ , is not shown in [Figure 23.1](#)). In the case of a spur gear, the base helix angle equals zero ( $\psi_b = 0^\circ$ ).

The plane of action,  $PA$ , can be construed as a zero-thickness film. When the gears rotate, the film is unwrapped from the driving pinion base cylinder of diameter  $d_{b,p}$  and it is wrapped onto the driven gear base cylinder of diameter  $d_{b,g}$ . In the case of gear increasers, the film is unwrapped from the driving gear base cylinder of diameter  $d_{b,g}$  and it is wrapped onto the driven pinion base cylinder of diameter  $d_{b,p}$ .

The line of contact,  $LC$ , travels together with the plane of action,  $PA$ , in relation to the reference systems associated with the gear and pinion. An arbitrary point,  $m$ , within the line of contact,  $LC$ , traces an involute profile of the gear tooth in a reference system associated with the gear, and it traces another involute profile of the pinion tooth in a reference system associated with the pinion.





**FIGURE 23.2**

Modeling cones of a gear tooth flank,  $\mathcal{G}$ , and a mating pinion tooth flank,  $\mathcal{P}$ , in an external parallel-axes gearing.

In the case of spur gears, the line of contact,  $LC$ , is a line that is parallel to the axes of rotation of the gear,  $O_g$ , and the pinion,  $O_p$ . In this particular case, the modeling cones reduce to corresponding modeling cylinders.

If either a circular arc, an arc of a cycloid, or an arc of an arbitrary planar curve is used to generate the gear and pinion tooth flanks,  $\mathcal{G}$  and  $\mathcal{P}$ , as illustrated in Figure 23.3, then, locally, in the differential vicinity of point  $m$ , within the line of contact, the line of contact,  $LC$ , can be represented by a straight line segment,  $ab$ , that is tangent to the line of contact,  $LC$ , at  $m$ . Therefore, in the case under consideration, the gear and pinion tooth flanks can be locally represented by the surfaces of truncated cones.

The schematic depicted in Figure 23.1 is convenient for the investigation of gear drives composed of spur and helical gears, as well as gears that have either a circular-arc or cycloidal longitudinal tooth shape. It is also applicable for analysis of parallel-axes gearing with other geometries in the lengthwise direction of the gear teeth.

View A of Figure 23.1 is convenient for the analysis of the design features of parallel-axes gear drives.

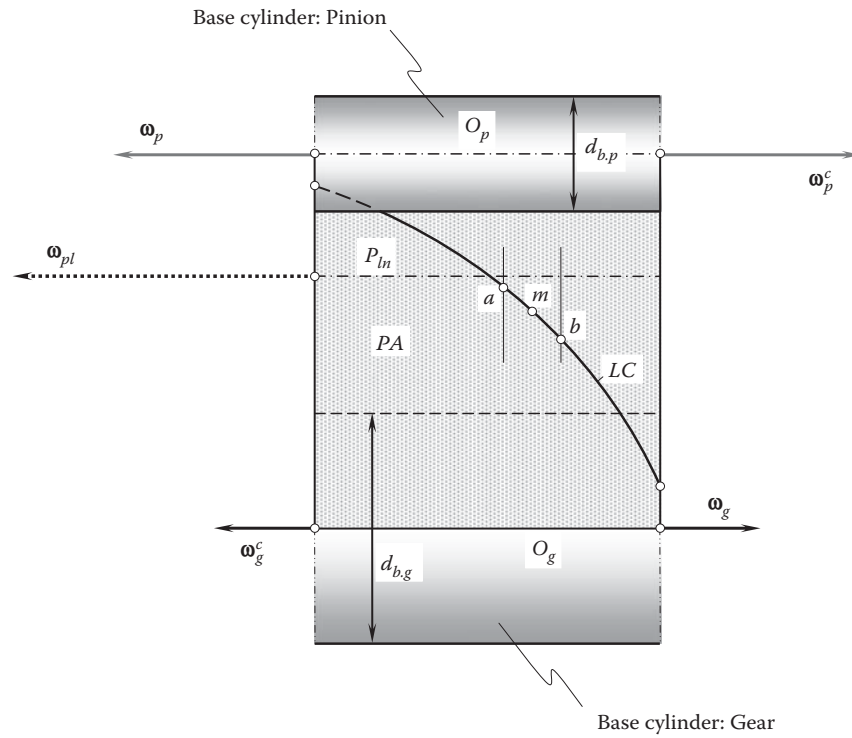
Figure 23.4 gives a clear understanding of:

1. How the modeling cones are configured in relation to the interacting tooth flanks,  $\mathcal{G}$  and  $\mathcal{P}$ , of a gear and a mating pinion
2. How the axes of instant rotations,  $O_g^c$  and  $O_p^c$ , are configured in relation to the axes of rotation,  $O_g$  and  $O_p$ , of the gear and the pinion
3. How the vectors of instant rotations,  $\omega_g^c$  and  $\omega_p^c$ , are configured with respect to the rotation vectors,  $\omega_g$  and  $\omega_p$ , of the gear and the pinion [124]

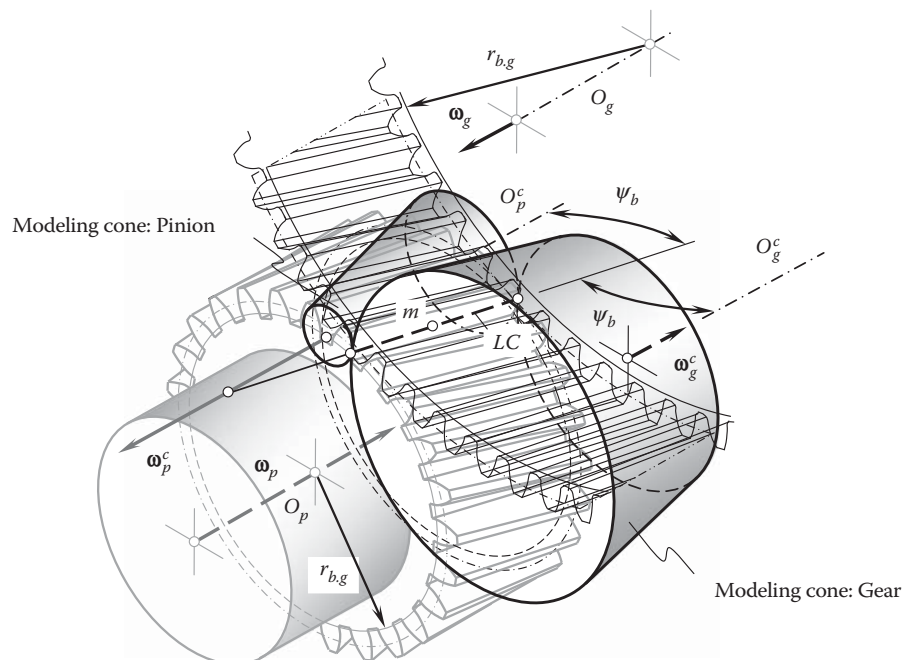
In the particular case of spur gears, the configuration of the modeling cylinders,  $G^c$  and  $P^c$ , in relation to the gear tooth flank,  $\mathcal{G}$ , and the pinion tooth flank,  $\mathcal{P}$ , is schematically depicted in Figure 23.5.

In the case of internal gearing, the modeling cone of the ring gear,  $G^c$ , is shaped in the form of an internal truncated cone of revolution, as shown in Figure 23.6.

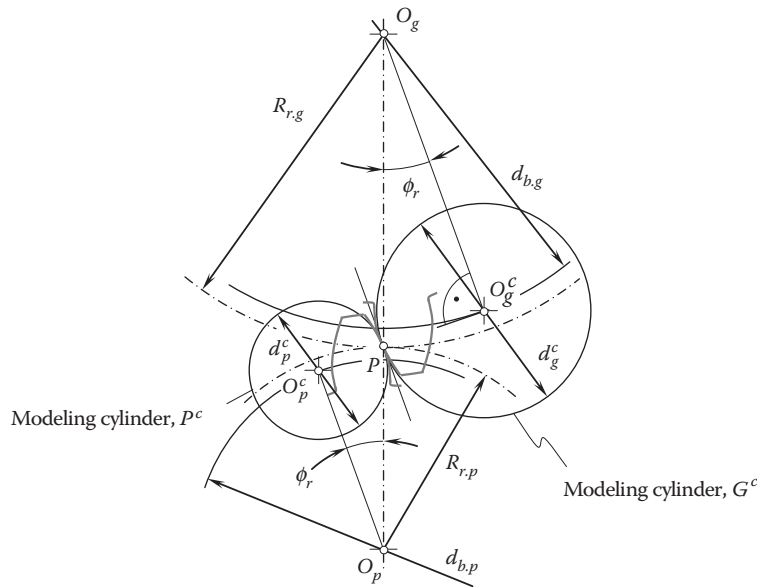
It should be pointed out here how the radii of curvature of the modeling cones,  $G^c$  and  $P^c$ , for an internal gearing are different than those of an external gearing. The modeling cones shown in Figure 23.6 reveal that when a point travels along the line of contact from left to right, the radii of curvature of both modeling cones get larger. Thus, the relative curvature of the modeling cones for internal gearing within the line of contact alters

**FIGURE 23.3**

Determination of the parameters of the desired local geometry of the interacting tooth flanks of the gear,  $\mathcal{G}$ , and the pinion,  $\mathcal{P}$ , generated by a curved line of contact,  $LC$ .

**FIGURE 23.4**

Configuration of the modeling cones with respect to a gear and a mating pinion in parallel-axes gearing.

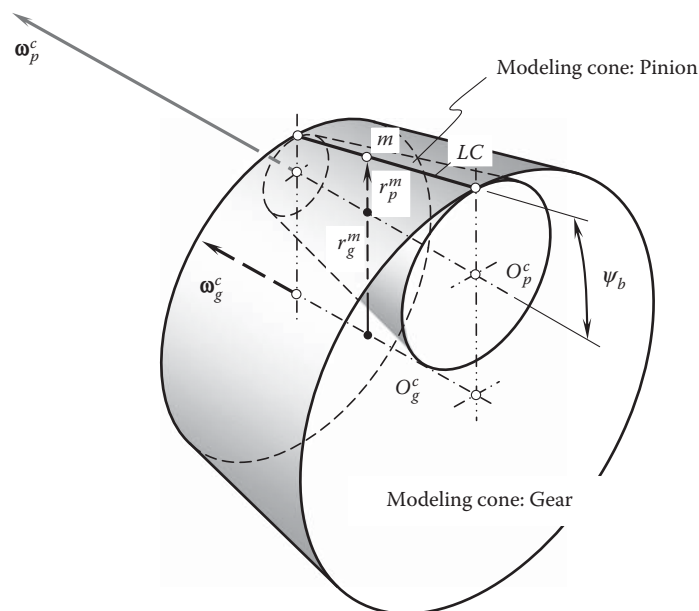
**FIGURE 23.5**

Configuration of the modeling cylinders,  $G^c$  and  $P^c$ , in relation to the interacting tooth flanks,  $\mathcal{G}$  and  $\mathcal{P}$ , of a spur gear and a mating pinion.

slightly. For external gearing (see Figure 23.2), in contrast, when a point travels along the line of contact from left to right, the radius of curvature of the modeling cone for the gear gets larger, while that for the pinion gets smaller. This results in an extensive change of relative curvature of the modeling cones for external gearing within the line of contact,  $LC$ .

The aforementioned can be summarized in the form of two significant advantages of internal parallel-axes gearing over external parallel-axes gearing:

- The contact of the convex tooth flank of a pinion with the concave tooth flank of a mating gear in internal gearing is more favorable than the contact of two convex tooth flanks of a gear and a mating pinion for external gearing.

**FIGURE 23.6**

Modeling cones,  $G^c$  and  $P^c$ , of the gear tooth flank and the pinion tooth flank for an internal parallel-axes gearing.

- The alteration of the relative curvature within the line of contact for an internal parallel-axes gear pair is more favorable than that for external parallel-axes gearing.

An arbitrary point,  $m$ , within the line of contact,  $LC$ , is at a certain distance,  $r_g^m$ , from the axis of instant rotation about the gear and at a distance,  $r_p^m$ , from the axis of instant rotation about the pinion. Both the axes,  $O_g^c$  and  $O_p^c$ , of instant rotations,  $\omega_g^c$  and  $\omega_p^c$ , are naturally the lines of tangency between the plane of action,  $PA$ , and the base cylinders of the gear and the pinion.

The distances,  $r_g^m$  and  $r_p^m$ , can be expressed in terms of the base diameters,  $d_{b,g}$  and  $d_{b,p}$ , of the gear and pinion and in terms of the distances,  $r_{m,g}$  and  $r_{m,p}$ , of an arbitrary point,  $m$ , from the axes of rotation of the gear,  $O_g$ , and the pinion,  $O_p$ , respectively. For the calculation, the following formulae can be used:

$$r_g^m = \sqrt{0.25 d_{m,g}^2 - r_{b,g}^2} \quad (23.1)$$

$$r_p^m = \sqrt{0.25 d_{m,p}^2 - r_{b,p}^2} \quad (23.2)$$

The values of the radii,  $r_g^m$  and  $r_p^m$ , calculated from Equations 23.1 and 23.2 are used further to calculate the normal radii of curvature of the modeling cones. The *Mensnier formula* is used in this case. The normal radii of curvature in nature are the first principal radii of curvature at a point of the tooth flanks (the second principal radii of curvature have a zero value). A distance,  $C^c$ , between the axes of rotation of the modeling cones,  $O_g^c$  and  $O_p^c$ , is equal to:

$$C^c = C \sin \phi_t \quad (23.3)$$

The height,  $h^c$ , of both truncated cones can be calculated from the equation:

$$h^c = L_{lc} \cos \psi_b \quad (23.4)$$

where  $L_{lc}$  is the length of the line of contact,  $LC$ .

Modeling cones for low-tooth-count gears are represented with a full cone of revolution, not with a truncated cone. The apex of the cone of revolution is within the surface of the base cylinder of the gear.

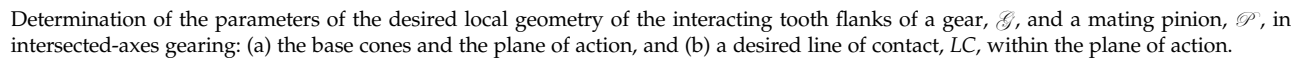
## 23.2 Local Geometry of Interacting Tooth Flanks in Intersected-Axes Gearing

External intersected-axes gearing is chosen for the analysis of the interaction of the tooth flanks in intersected-axes gearing. Then, the results of the analysis obtained for external gearing can be enhanced to other intersected-axes gearings as well.

### 23.2.1 Kinematics of Interaction of Tooth Flanks

The interaction of tooth flanks in intersected-axes gearing is schematically illustrated in [Figure 23.7](#). The gear rotates about its axis of rotation,  $O_g$ , at a uniform angular velocity,  $\omega_g$ . The rotation vector of the gear is designated as  $\omega_g$ . The mating pinion rotates about its axis of rotation,  $O_p$ , at a uniform angular velocity,  $\omega_p$ . The rotation vector of the pinion is designated as  $\omega_p$ . The vector of instant rotation,  $\omega_{pl}$ , of the gear and the pinion is a vector within the plane through the rotation vectors,  $\omega_g$  and  $\omega_p$ . The rotation vector,  $\omega_{pl}$ , passes through the point of intersection,  $A_{par}$ , of straight lines along the rotation vectors,  $\omega_g$  and  $\omega_p$ . The axis of instant rotation,  $P_{ln}$ , is aligned with the vector,  $\omega_{pl}$ .

The plane of action,  $PA$ , is a plane through the vector of instant rotation,  $\omega_{pl}$ , of the gear and the pinion. It forms a certain angle in relation to the plane through the rotation vectors,  $\omega_g$  and  $\omega_p$ . This angle is equal to  $(90^\circ - \phi_{\omega,t})$ , where  $\phi_{\omega,t}$  denotes the transverse pressure angle measured within a plane that is perpendicular



The motion of the desired line of contact,  $LC$ , in relation to the base cones can be interpreted as an instant rotation about a straight line of tangency (a) between the base cone of the gear and the plane of action and (b) between the base cone of the pinion and the plane of action. In Figure 23.7, the axis of instant rotation of the desired line of contact,  $LC$ , in relation to the base cone of the gear is designated as  $O_g^c$ . The vector of instant rotation is designated as  $\omega_g^c$ . Similarly, the axis of instant rotation of the line of contact,  $LC$ , in relation to the base cone of the pinion is designated as  $O_p^c$ . The vector of instant rotation is designated as  $\omega_p^c$ .

\* Remember that the tooth flanks,  $\mathcal{G}$  and  $\mathcal{P}$ , of a gear and mating pinion are not generated yet. Therefore, only the desired line of contact,  $LC$ , can be discussed, as the actual line of contact does not exist at this step of the analysis.



It should be pointed out here that all the rotation vectors,  $\omega_g^c$ ,  $\omega_p^c$ ,  $\omega_{pl}$ , and  $\omega_{pa}$ , are the vectors through a common point that in nature is the plane-of-action apex,  $A_{pa}$ .

Ultimately, the instant kinematics of intersected-axes gearing is represented by two rotations,  $\omega_g^c$  and  $\omega_p^c$ , of the desired line of contact,  $LC$ , about the axes of instant rotations,  $O_g^c$  and  $O_p^c$ .

### 23.2.2 Local Geometry of the Interacting Tooth Flanks

The generation of the local geometry of the interacting tooth flanks of the gear and pinion is illustrated in Figure 23.7. At every instant of time, the tooth flanks of the gear,  $\mathcal{G}$ , and pinion,  $\mathcal{P}$ , are generated by the desired line of contact,  $LC$ , that is rigidly connected to the plane of action,  $PA$ , and travels together with the plane of action.

Two surfaces generated by the desired line of contact in its instant rotations about the axes of instant rotation,  $O_g^c$  and  $O_p^c$ , can be employed as the surfaces, which model the actual tooth flanks of the gear and pinion at every instant of time.

The desired line of contact,  $LC$ , in the form of a straight line segment can be used as an example for generating the modeling surfaces. The desired line of contact,  $LC$ , is at a base helix angle,  $\psi_b$ , in relation to the axis of instant rotation.

In the instant rotation,  $\omega_g^c$ , a cone of revolution is generated by the rotating line of contact,  $LC$ . The axis of instant rotation,  $O_g^c$ , is the axis of the modeling cone of revolution (Figure 23.8). The cone angle of the cone of revolution is designated as  $\psi_g^c$ . Similarly, in the instant rotation,  $\omega_p^c$ , another cone of revolution is generated by the rotating line of contact,  $LC$ . The axis of instant rotation,  $O_p^c$ , is the axis of this modeling cone of revolution (see Figure 23.8). The cone angle of the cone of revolution is designated as  $\psi_p^c$ . The cone angles,  $\psi_g^c$  and  $\psi_p^c$ , can be expressed in terms of the base cone angle,  $\psi_b$ , and the angles that specify the current angular location of the line of contact,  $LC$ , within the plane of action,  $PA$ .

In the case of straight bevel gears, the cone angle of the modeling cones is equal to the base helix angle,  $\psi_b$ .

When either a circular arc, an arc of a cycloid, or an arc of an arbitrary planar curve is used as the desired line of contact for the generation of the gear and pinion tooth flanks, then, *locally*, in the differential vicinity of a point within the desired line of contact, the line  $LC$  can be represented by a straight line segment that is tangent to

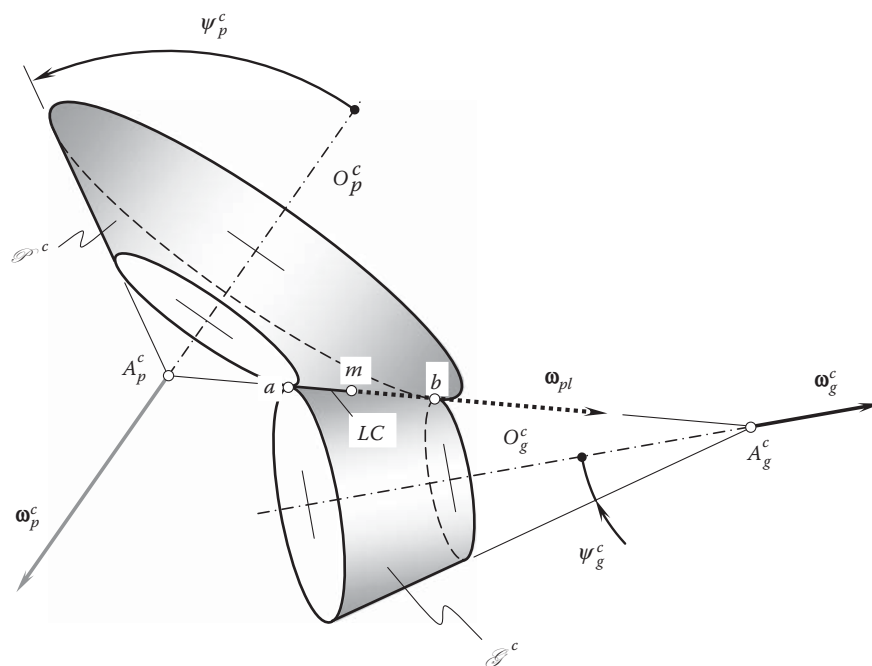
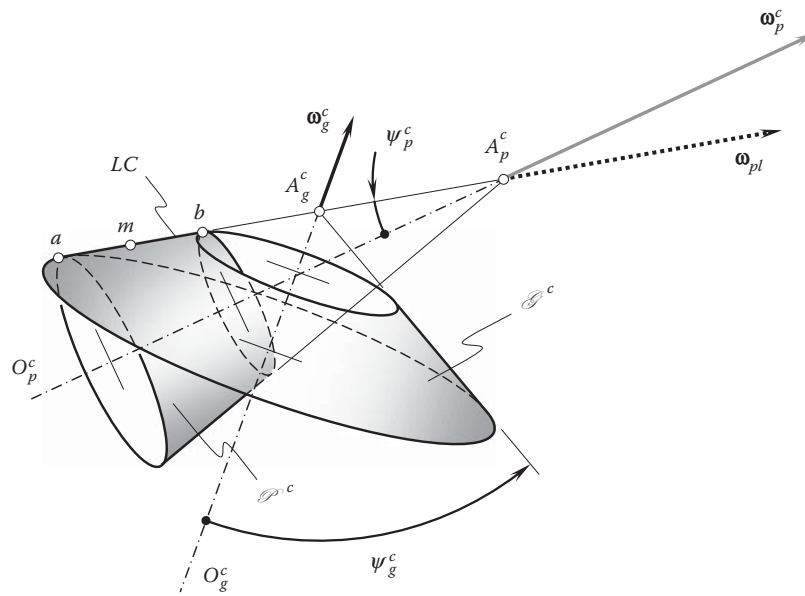


FIGURE 23.8

Modeling cones,  $\mathcal{G}^c$  and  $\mathcal{P}^c$ , of the gear tooth flank,  $\mathcal{G}$ , and the pinion tooth flank,  $\mathcal{P}$ , in an external intersected-axes gearing.





**FIGURE 23.9** Modeling cones,  $\mathcal{G}^c$  and  $\mathcal{P}^c$ , of the gear tooth flank,  $\mathcal{G}$ , and the pinion tooth flank,  $\mathcal{P}$ , in an internal intersected-axes gearing.

the desired line of contact,  $LC$ . Therefore, in this particular case, the gear and pinion tooth flanks can be locally represented by surfaces of truncated cones.

The schematic shown in Figure 23.7 is convenient for the investigation of gear drives composed of straight bevel gears, spiral bevel gears, and gears that have a cycloidal longitudinal tooth shape. It is always applicable for the analysis of intersected-axes gearing with other geometries in the lengthwise direction of the gear teeth.

For internal intersected-axes gearing, the modeling cone of the gear is shaped in the form of an internal cone of revolution (as shown in Figure 23.9), similar to that schematically illustrated in Figure 23.6.

It is instructive to point out here the manner in which the radii of curvature of the modeling cones for internal gearing are altered in comparison to those for external gearing. The modeling cones reveal that when a point travels along the line of contact from one end to the opposite end of the modeling cones, the radii of curvature of both modeling cones get either larger or smaller. Thus, the relative curvature of the modeling cones for internal intersected-axes gearing within the line of contact alters slightly. For an external gearing (see Figure 23.8), in contrast, when a point travels along the line of contact from one end to the opposite end of the modeling cones, the radius of curvature of one member gets larger, while that for the mating member gets smaller. This results in an extensive change of relative curvature of the modeling cones for external gearing within the line of contact of the tooth flanks.

The aforementioned can be summarized in the form of two important advantages of internal gearing over external gearing:

- The contact of the convex tooth flank of the pinion with the concave tooth flank of the gear in internal gearing is more favorable than the contact of two convex tooth flanks of the gear and pinion for external gearing.
- The alteration of the relative curvature within the line of contact for internal gearing is preferable to that for external gearing.

The dimensions of the modeling cones for external and internal intersected-axes gearing (the radii of curvature, the cone angle, and so forth), as well as the configuration of the modeling cones in relation to each other, can be expressed in terms of the design parameters of the gear pair to be modeled.



The synchronization of the rotations makes it possible to construe the plane of action,  $PA$ , as a portion of a round strip of zero-thickness film. This strip is absolutely flexible, and when the gear pair operates, the round strip of zero-thickness film is free to unwrap from one of the base cones and wrap over the other base cone.

A straight desired line of contact,  $LC$ , between the tooth flanks of the gear and mating pinion is located within the plane of action,  $PA$ . The desired line of contact is at a base helix angle,  $\psi_b$ , with respect to the axis of instant rotation,  $P_{in}$ . In the case of *straight* crossed-axes gearing, the base helix angle is equal to zero ( $\psi_b = 0^\circ$ ). It should be pointed out here that in this case ( $\psi_b = 0^\circ$ ), both the gear and pinion feature spiral teeth.

When the plane of action,  $PA$ , rotates ( $\omega_{pa}$ ), the desired line of contact,  $LC$ , travels together with the plane of action. In such a motion in relation to a reference system associated with the gear, the gear tooth flank,  $\mathcal{G}$ , can be represented as the loci of consecutive positions of the desired line of contact,  $LC$ , represented in that reference system. Similarly, in such a motion in relation to a reference system associated with the pinion, the pinion tooth flank,  $\mathcal{P}$ , can be represented as the loci of successive positions of the desired line of contact,  $LC$ , represented in that reference system.

An arbitrary point,  $m$ , taken within the desired line of contact,  $LC$ , traces a curve that is entirely located on the gear tooth flank,  $\mathcal{G}$ . That same point,  $m$ , traces the corresponding curve that is entirely located on the pinion tooth flank,  $\mathcal{P}$ . These two spatial curves are conjugate to each other, as both of them are generated by a point that is located within the plane of action.

The motion of the desired line of contact,  $LC$ , in relation to the base cones can be interpreted as the instant rotation about a straight line of tangency between the base cone of the gear and the plane of action, and between the base cone of the pinion and the plane of action. In Figure 23.10, the axis of instant rotation of the line of contact,  $LC$ , in relation to the base cone of the gear is designated as  $O_g^c$ . The vector of instant rotation is designated as  $\omega_g^c$ . Similarly, the axis of instant rotation of the line of contact,  $LC$ , in relation to the base cone of the pinion is designated as  $O_p^c$ . The vector of instant rotation is designated as  $\omega_p^c$ .

It should be pointed out here that all the rotation vectors,  $\omega_g^c$ ,  $\omega_p^c$ ,  $\omega_{pl}$ , and  $\omega_{pa}$ , are not the vectors through a common point,  $A_{pa}$ , that is, through the plane-of-action apex,  $A_{pa}$ . This causes sliding of the modeling cones along the line of their contact. Noncoincidence of the apexes  $A_g^c$ ,  $A_p^c$ , and  $A_{pa}$  is the root cause of so-called *axial sliding*.

Ultimately, the instant kinematics of crossed-axes gearing is represented by two rotations,  $\omega_g^c$  and  $\omega_p^c$ , of the line of contact,  $LC$ , about the axes of instant rotations,  $O_g^c$  and  $O_p^c$ , along with relative sliding of the modeling cones along the common generating line.

### 23.3.2 Local Geometry of Interacting Tooth Flanks

Generating the local geometry of the interacting tooth flanks of the gear and pinion is illustrated in Figure 23.10. At every instant of time, the tooth flanks of the gear,  $\mathcal{G}$ , and those of the pinion,  $\mathcal{P}$ , are generated by the line of contact,  $LC$ , that travels together with the plane of action,  $PA$ .

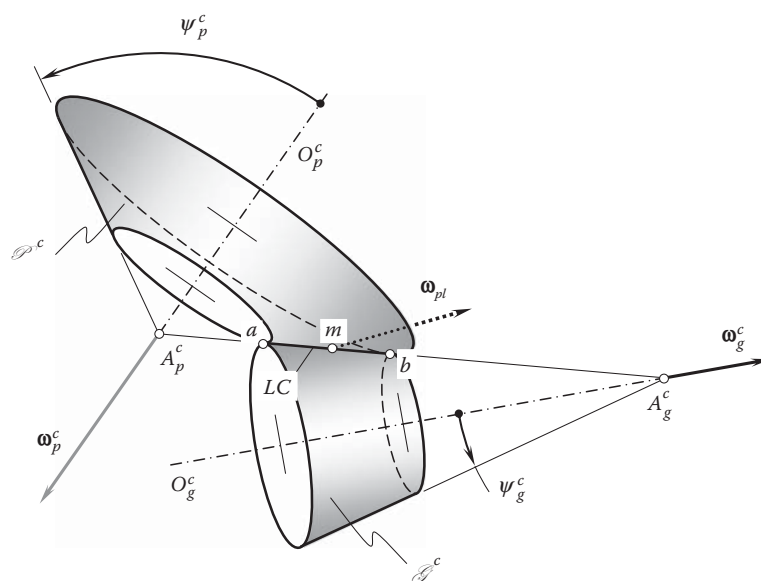
Two surfaces generated by the desired line of contact in its instant rotations about the axes of instant rotation,  $O_g^c$  and  $O_p^c$ , can be employed as surfaces that model the actual tooth flanks of the gear and pinion at every instant of time.

The line of contact,  $LC$ , in the form of a straight line segment can be used as an example for generating the modeling surfaces. The line of contact,  $LC$ , is at a base helix angle,  $\psi_b$ , in relation to the axis of instant rotation.

In the instant rotation,  $\omega_g^c$ , a cone of revolution is generated by the rotating line contact,  $LC$ . The axis of instant rotation,  $O_g^c$ , is the axis of the modeling cone of revolution (Figure 23.11). The cone angle of the cone of revolution is designated as  $\psi_g^c$ . Similarly, in the instant rotation,  $\omega_p^c$ , another cone of revolution is generated by the rotating line of contact,  $LC$ . The axis of instant rotation,  $O_p^c$ , is the axis of this modeling cone of revolution (see Figure 23.11). The cone angle of the cone of revolution is designated as  $\psi_p^c$ . The cone angles,  $\psi_g^c$  and  $\psi_p^c$ , can be expressed in terms of the base cone angle,  $\psi_b$ , and the angles that specify the current angular location of the line of contact,  $LC$ , within the plane of action,  $PA$ .

In the case of straight crossed-axes gearing, the cone angle of the modeling cones is equal to the base helix angle,  $\psi_b$ .

When either a circular arc, an arc of a cycloid, or an arc of an arbitrary planar curve is used as the line of contact for the generation of the gear and the pinion tooth flank, then, *locally*, in the differential vicinity of a point within the line of contact, the line  $LC$  can be represented by a straight line segment that is tangential to the line of contact,  $LC$ . Therefore, in this particular case, the gear and pinion tooth flanks can be locally represented by the surfaces of truncated cones.

**FIGURE 23.11**

Modeling cones,  $\mathcal{G}^c$  and  $\mathcal{P}^c$ , of the gear tooth flank,  $\mathcal{G}$ , and the pinion tooth flank,  $\mathcal{P}$ , in an external crossed-axes gearing.

The schematic shown in [Figure 23.11](#) is convenient for the investigation of gear drives composed of gears with various longitudinal tooth shapes. It is always applicable for the analysis of crossed-axes gears that have other geometries in lengthwise direction of the gear teeth.

For internal intersected-axes gearing, the modeling cone of the gear is shaped in the form of an internal cone of revolution similar to that schematically illustrated in [Figure 23.6](#) for parallel-axes gearing and in [Figure 23.9](#) for intersected-axes gearing.

The following two statements are valid for crossed-axes gearing:

- The contact of the convex tooth flank of the pinion with the concave tooth flank of the gear in internal gearing is more favorable than the contact of two convex tooth flanks of the gear and the pinion for external gearing.
- The alteration of the relative curvature within the line of contact for internal gearing is preferable to that in external gearing.

These two statements are equivalent to the above-formulated statements that are valid for parallel-axes gearing and intersected-axes gearing.

The dimensions of the modeling cones for external and internal intersected-axes gearing (the radii of curvature, the cone angle, and so forth), as well as the configuration of the modeling cones in relation to each other, can be expressed in terms of the design parameters of the gear pair to be modeled.

### 23.4 Local Geometry of Interacting Tooth Flanks in High-Conformal Gearing\*

High-conformal gearing can be interpreted as a particular case of involute gearing when the height of the field of action approaches zero and, as a result, the profile contact ratio is equal to zero. There are many similarities between high-conformal gearing and the above-considered gearings.

\* It is instructive to stress here one more time that conformal gearing, as well as high-conformal gearing, can be viewed as a reduced case of involute gearing (see [Chapter 10](#) for details).

### 23.4.1 Kinematics of Interacting Tooth Flanks

A parallel-axes high-conformal gear pair is considered as an example for the analysis of the kinematics of the interacting tooth flanks in high-conformal gears.

Consider two rotation vectors,  $\omega_g$  and  $\omega_p$ . The rotation vectors are parallel to each other and are apart from one another at a center distance,  $C$ .

When the pressure angle is known, for a given pair of the rotation vectors of the gear,  $\omega_g$ , and the pinion,  $\omega_p$ , two base cylinders of diameters  $d_{b,g}$  and  $d_{b,p}$  can be constructed for a high-conformal gear pair. The plane of action,  $PA$ , is in tangency with both base cylinders, as schematically depicted in Figure 23.12.

The base cylinders in a high-conformal gear pair are useful for the interpretation of the gear pair in terms of a pulley-and-belt model. Rotation from the driving shaft is transmitted to the driven shaft by forces acting within the plane of action. This makes it reasonable to consider the interaction of the tooth flanks of the gear and pinion in a plane of action. Due to this, the tooth profiles of the gear and pinion in the section by the plane of action are of critical importance for evaluating the power capacity of a high-conformal gear drive.

The vector of instant rotation of the plane of action in relation to the gear is designated as  $\omega_g^c$ . This rotation vector is along the line of tangency between the plane of action and the gear base cylinder of diameter,  $d_{b,g}$ . Similarly, the vector of instant rotation of the plane of action in relation to the pinion is designated as  $\omega_p^c$ . This rotation vector is along the line of tangency between the plane of action and the pinion base cylinder of diameter,  $d_{b,p}$ .

A plane through the axis of rotation of the gear,  $O_g$ , the axis of rotation of the pinion,  $O_p$ , and the plane of action,  $PA$ , intersect one another. The straight line of intersection of the aforementioned planes is the pitch line,  $P_{ln}$ .

The height,  $Z_{pa}$ , of the field of action in a high-conformal gear pair is equal to zero ( $Z_{pa} = 0$ ).

The path of contact,  $P_c$ , in high-conformal gearing is always of a zero length, as the length of the active portion of the line of action is zero ( $Z_{pa} = 0$ ). However, the plurality of zero-length paths of contact,  $P_c$ , forms the so-called *pseudo-path of contact*,  $P_{pc}$ .

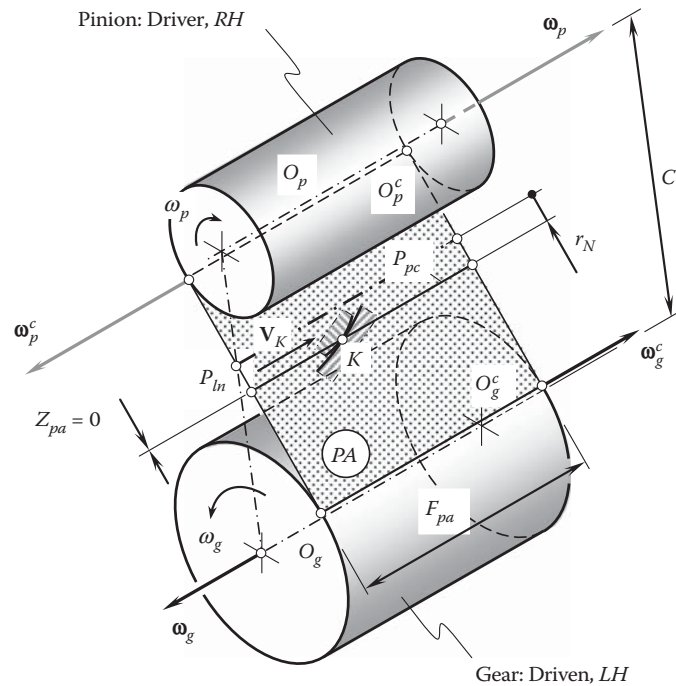


FIGURE 23.12

Determination of the parameters of the desired local geometry of the interacting tooth flanks of a gear,  $\mathcal{G}$ , and a mating pinion,  $\mathcal{P}$ , in parallel-axes high-conformal gearing.



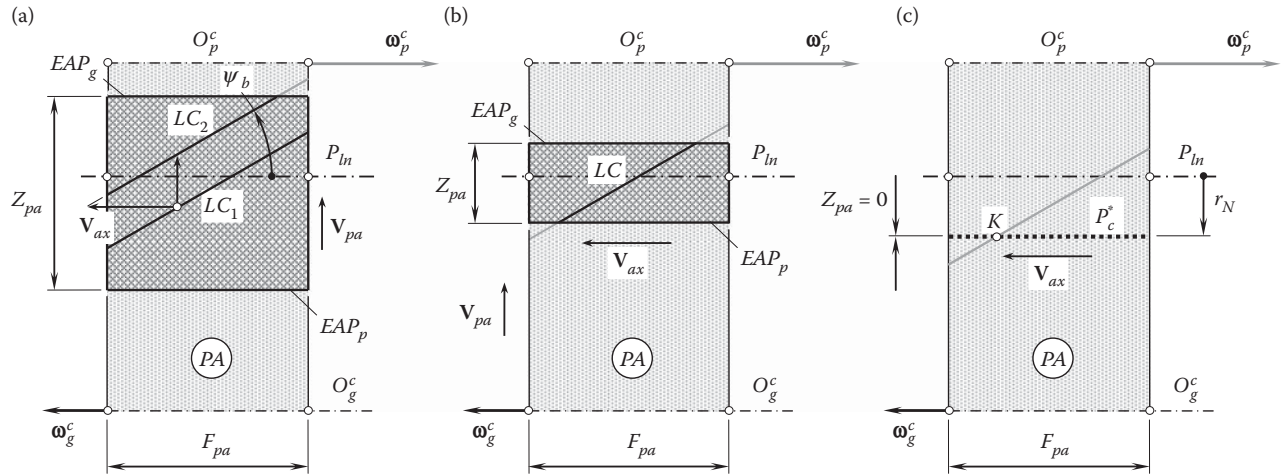


FIGURE 23.13

Traveling of the line of contact,  $LC$ , in parallel-axes gearing: (a) high-transverse-contact-ratio gear pair, (b) regular transverse contact ratio gear pair, and (c) high-conformal gearing.

The pseudo-path of contact,  $P_{pc}$ , is parallel to the pitch line,  $P_{ln}$ , and is located at a distance,  $r_N$ , from the axis of instant rotation,  $P_{ln}$ . When a high-conformal gear pair operates, the point of contact,  $K$ , of the tooth flanks travels,  $V_K$ , along the pseudo-path of contact,  $P_{pc}$ .

Since the height of the field of action in high-conformal gearing is equal to zero ( $Z_{pa} = 0$ ), this makes it possible to design the gear and pinion tooth flanks so as to make their contact the convex-to-concave kind.

High-conformal gears allow for interpretation in terms of involute gears.

First, let us consider a straight line,  $LC$ , within the plane of action,  $PA$ , that makes a base helix angle,  $\psi_b$ , with both rotation vectors,  $\omega_g$  and  $\omega_p$ . When the gears operate, the line of contact travels together with the plane of action from the position labeled as  $LC_1$  to a certain position labeled as  $LC_2$  (Figure 23.13a). As long as the line,  $LC$ , is a straight line, that is traveling ( $V_{pa}$ ) with the plane of action,  $PA$ , this motion is equivalent to the travel of the straight line,  $LC$ , along the pitch line,  $P_{ln}$ , (see Figure 23.13b). The speed of this motion is designated as  $V_{ax}$ . It is clear that the magnitudes,  $V_{pa}$  and  $V_{ax}$ , of the velocity vectors,  $V_{pa}$  and  $V_{ax}$ , correspond to one another in accordance with the formula  $V_{ax} = V_{pa} / \tan \psi_b$ .

The following analogy can be useful in particular cases.

A cylinder of revolution can be generated when the pseudo-path of contact,  $P_{pc}$ , is rotated about the axis of rotation,  $O_g$ , of the gear. The line of intersection of the gear tooth flank by the cylinder is a helix. The point of contact,  $K$ , can be construed as the point of intersection of the cylinder by the plane of action,  $PA$ . A similar consideration is valid with respect to the pinion. When the gears operate, the helix rotates. Due to this, the contact point,  $K$ , travels along the pseudo-path of contact,  $P_{pc}$ .

When the height,  $Z$ , of the field of action becomes smaller, as illustrated in Figure 23.13b, the motion of the straight line segment in the axial direction becomes more evident. In the limit case ( $Z_{pa} = 0$ ), only axial motion,  $V_{ax}$ , of the  $LC$  remains. When the equality  $Z_{pa} = 0$  is observed (Figure 23.13c), the straight line segment,  $LC$ , is of zero length; however, the inclination angle,  $\psi_b$ , is preserved. Due to this, the base pitch,  $p_b$ , can be calculated for a high-conformal gear pair. This can be identical to the calculation for a corresponding involute gearing done in the following manner:

- The axial pitch,  $p_x$ , of a high-conformal gear can be calculated from the formula:

$$p_x = \frac{\pi d_g}{N_g \tan \psi} \quad (23.8)$$

- The base helix angle,  $\psi_b$ , for a high-conformal gearing is:

$$\psi_b = \tan^{-1} (\tan \psi \tan \phi_t) \quad (23.9)$$

- With the axial pitch,  $p_x$ , and the base helix angle,  $\psi_b$ , known, the base pitch,  $p_b$ , for a parallel-axes high-conformal gearing is calculated from the expression:

$$p_b = p_x \sin \psi_b \quad (23.10)$$

In Equation 23.8 through 23.10:

$d_g$  is the pitch diameter of a high-conformal gear.

$N_g$  is the tooth number of a high-conformal gear.

$\phi_t$  is the transverse pressure angle.

Calculations similar to those above are also valid with respect to a high-conformal pinion.

The above consideration is true not only for external parallel-axes high-conformal gears, but for external high-conformal gears of all other kinds (intersected-axes gearing, crossed-axes gearing), as well as for internal gearing.

### 23.4.2 Geometry of Interacting Tooth Flanks

The tooth flanks of the gear and pinion in a high-conformal gear pair make point contact at every instant of time as the involute tooth profiles of the gear and the pinion are reduced to the so-called *involute tooth points*. Due to this, the geometry of the interacting tooth flanks is *local* in nature. The tooth flanks of the gear and mating pinion before and beyond the involute tooth point in the gear and pinion are not conjugate to each other.

Taking advantage of this, local patches of the gear tooth flank, as well as of the pinion tooth flank, are designed to give the highest possible bearing capacity of the gear pair. Because of this, a convex shape is given to tooth profiles in the transverse section of one member of the gear pair, and a corresponding concave shape is given to tooth profiles of another member of the gear pair.

Consider the high-conformal gear pair schematically shown in Figure 23.14. The rotation vector,  $\omega_g$ , of the gear and the rotation vector,  $\omega_p$ , of the pinion are along the corresponding axes of rotation,  $O_g$  and  $O_p$ . When the gears rotate, the contact point,  $K$ , travels along the pseudo-path of contact,  $P_{pc}$ . A point on the gear tooth that makes contact with the pinion tooth is labeled  $K_g$ . Accordingly, a point on the pinion tooth that makes contact with the gear tooth is labeled  $K_p$ . At a certain instant of time, the points  $K_g$  and  $K_p$  coincide with one another. In such a position, they are labeled as a common contact point,  $K$ .

Because the point,  $K_g$ , is located within the concave tooth profile of the gear, the local surface patch in the differential vicinity of the point,  $K_g$ , is the saddle type. Three unit vectors are associated with the point,  $K_g$ . They are  $\mathbf{u}_g$ ,  $\mathbf{v}_g$ , and  $\mathbf{n}_g$ . The unit vector,  $\mathbf{u}_g$ , is tangential to the  $U_g$ -coordinate line on the gear tooth surface,  $\mathcal{G}$ . The unit vector,  $\mathbf{v}_g$ , is tangential to the  $V_g$ -coordinate line on the gear tooth surface,  $\mathcal{G}$ . Ultimately, the unit vector,  $\mathbf{n}_g$ , is perpendicular at  $K_g$  to the gear tooth surface,  $\mathcal{G}$ . The vectors,  $\mathbf{u}_g$  and  $\mathbf{v}_g$ , are equal to  $\mathbf{u}_g = \mathbf{U}_g/|\mathbf{U}_g|$  and  $\mathbf{v}_g = \mathbf{V}_g/|\mathbf{V}_g|$ , respectively. For a gear tooth surface,  $\mathcal{G}$ , specified by the position vector of a point  $\mathbf{r}_g = \mathbf{r}_g(U_g, V_g)$ , the vectors,  $\mathbf{U}_g$  and  $\mathbf{V}_g$ , are calculated from the formulas  $\mathbf{U}_g = \partial \mathbf{r}_g / \partial U_g$  and  $\mathbf{V}_g = \partial \mathbf{r}_g / \partial V_g$ , where  $U_g$  and  $V_g$  represent curvilinear (Gaussian) coordinate lines on the gear tooth surface,  $\mathcal{G}$ .

The normal unit vector,  $\mathbf{n}_g$ , is pointed out from the body side to the void side of the gear tooth, as illustrated in Figure 23.14. The normal unit vector,  $\mathbf{n}_g$ , is equal to  $\mathbf{n}_g = \mathbf{u}_g \times \mathbf{v}_g$ . In particular cases, an inverse cross-product,  $\mathbf{n}_g = \mathbf{v}_g \times \mathbf{u}_g$ , is used for the calculation of the unit normal vector,  $\mathbf{n}_g$ . This depends on which of two curvilinear coordinate lines is labeled as the  $U_g$ -coordinate line and which is labeled as the  $V_g$ -coordinate line.

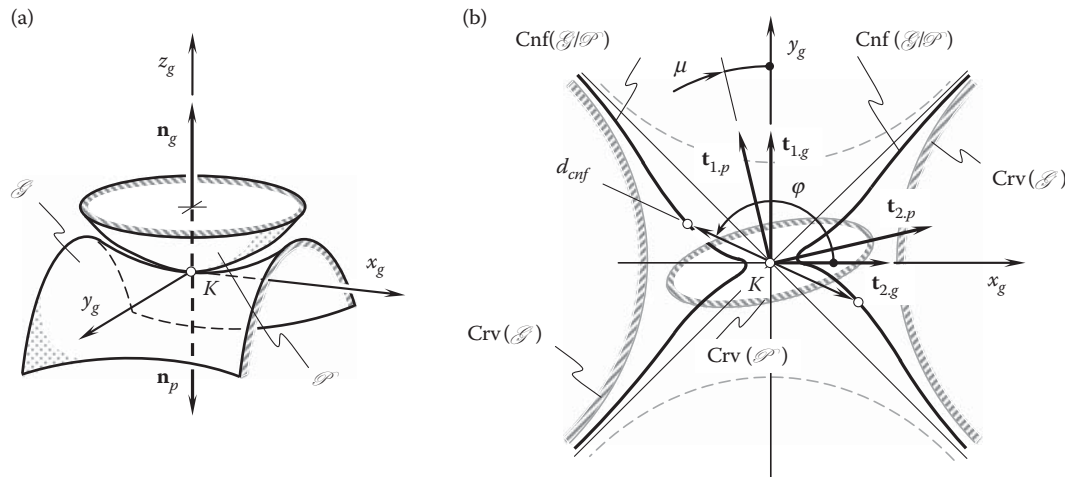
The unit vectors  $\mathbf{u}_g$ ,  $\mathbf{v}_g$ , and  $\mathbf{n}_g$ , are used to construct a local Cartesian coordinate system,  $x_g y_g z_g$ . In the case of the unit vectors,  $\mathbf{u}_g$  and  $\mathbf{v}_g$ , aligning with the principal directions,  $\mathbf{t}_{1,g}$  and  $\mathbf{t}_{2,g}$ , on the surface,  $\mathcal{G}$ , the axes  $x_g$ ,  $y_g$ , and  $z_g$  align with the corresponding unit vectors,  $\mathbf{u}_g$ ,  $\mathbf{v}_g$ , and  $\mathbf{n}_g$ . For other configurations of the unit vectors,  $\mathbf{u}_g$ ,  $\mathbf{v}_g$ , and  $\mathbf{n}_g$ , a known technique can be used to construct the local Cartesian coordinate system,  $x_g y_g z_g$  [113,118].

The unit vectors,  $\mathbf{u}_p$ ,  $\mathbf{v}_p$ , and  $\mathbf{n}_p$ , on the pinion tooth surface,  $\mathcal{P}$ , at point  $K_p$  are constructed in a manner similar to that the set of unit vectors,  $\mathbf{u}_g$ ,  $\mathbf{v}_g$ , and  $\mathbf{n}_g$ , for the gear tooth surface,  $\mathcal{G}$ .

The local geometry of the tooth surfaces,  $\mathcal{G}$  and  $\mathcal{P}$ , in the differential vicinity of the corresponding points,  $K_g$  and  $K_p$ , is expressed in terms of the curvature indicatrices,  $\text{Crv}(\mathcal{G})$  and  $\text{Crv}(\mathcal{P})$ , which are constructed at the point,  $K_g$ , for the surface,  $\mathcal{G}$ , and at the point,  $K_p$ , for the surface,  $\mathcal{P}$ . It should be pointed out here that the





**FIGURE 23.15**

Configuration of the local patches of the tooth flanks of a gear,  $\mathcal{G}$ , a mating pinion,  $\mathcal{P}$ , and a corresponding indicatrix of conformity,  $\text{Cnf}(\mathcal{G}/\mathcal{P})$ , at the contact point,  $K$ , of the two smooth regular surfaces,  $\mathcal{G}$  and  $\mathcal{P}$ : (a) schematic of the surface contact, and (b) corresponding indicatrix of conformity,  $\text{Cnf}(\mathcal{G}/\mathcal{P})$ .

both surfaces,  $\mathcal{G}$  and  $\mathcal{P}$ , need to be represented in a common reference system. The left-hand-oriented Cartesian coordinate system,  $x_g y_g z_g$ , is used for this purpose.

For the case under consideration, the indicatrix of conformity,\*  $\text{Cnf}(\mathcal{G}/\mathcal{P})$ , of the tooth surfaces,  $\mathcal{G}$  and  $\mathcal{P}$ , at the contact point  $K$  is constructed.† This characteristic curve (see Figure 23.15b) reveals that the contacting surfaces,  $\mathcal{G}$  and  $\mathcal{P}$ , are turned in relation to each other at an angle,  $\mu$ , of the surface's local relative orientation. The angle of orientation,  $\mu$ , is measured between the corresponding principal directions on the contacting surfaces at  $K$ , that is, between the first principal directions,  $\mathbf{t}_{1,g}$  and  $\mathbf{t}_{1,p}$ , or between the second principal directions,  $\mathbf{t}_{2,g}$  and  $\mathbf{t}_{2,p}$ . The minimum diameter,  $d_{cnf}^{\min}$ , of the indicatrix of conformity,  $\text{Cnf}(\mathcal{G}/\mathcal{P})$ , is of small value. The higher the degree of conformity of the tooth surfaces,  $\mathcal{G}$  and  $\mathcal{P}$ , the smaller the diameter,  $d_{cnf}^{\min}$ , of the indicatrix of conformity,  $\text{Cnf}(\mathcal{G}/\mathcal{P})$ , and vice versa.

The local geometry of contact of a gear,  $\mathcal{G}$ , and a mating pinion,  $\mathcal{P}$ , tooth flank considered in this chapter can be used to investigate contact strength of the gear teeth; the conditions of lubrication of the tooth flanks,  $\mathcal{G}$  and  $\mathcal{P}$ ; gear tooth wear, and so forth.

\* The concept of the indicatrix of conformity at a point of contact of two smooth regular surfaces was proposed by the author in the late 1970s/early 1980s. It has been disclosed in two publications [93] and [94]. Later, this concept received wide application in many publications, including but not limited to, [107,113,118,136], as well as in many others.

† For completeness of the analysis, the curvature indicatrices,  $\text{Crv}(\mathcal{G})$  and  $\text{Crv}(\mathcal{P})$ , at a point of the tooth surfaces,  $\mathcal{G}$  and  $\mathcal{P}$ , are indicated in Figure 19.15 as well.



# Taylor & Francis

Taylor & Francis Group

<http://taylorandfrancis.com>

## Strength of Gear Teeth

Strength of gear teeth is an important consideration. When a pair of gears operate, an operating load causes stresses in the gear teeth, as well as in the gear body. Quantitatively, the stresses in the gear teeth are illustrated in [Figure 24.1](#).

Contact and bending strength of gear teeth are the two of most important indicators of performance of a gear pair. New accomplishments in the theory of gearing are helpful in the development of gear pairs with better performance. All types of gear tooth failures depend on contact stress, as well as on bending stress in the gear teeth.

The results of the research derived from the disclosed theory of gearing have tremendous potential. They can be applied for solving a plurality of problems targeting improvement of power density, lowering vibration generation and noise excitation, and so on. A few areas of implementation of the developed theory of gearing are discussed below as examples. Much room is available for researchers and engineers in this field of mechanical engineering.

### 24.1 Contact Strength of Low Tooth Count Gearing\*

Today's involute gears carry far more power with greater reliability than was once thought possible. Improvements in the material and lubrication and more precise manufacture, which is made possible by modern equipment, are mainly responsible for this. Still, the search for greater strength goes on, as indicated by continuing test programs at many laboratories. As further progress from these standard approaches becomes increasingly difficult, it is worthwhile to look into better load distribution in parallel-axes gears.

Gears fail by pitting and wear as well as by tooth breakage. For the prediction of gear-tooth strength and calculating stresses within the gear-tooth body, an adequate load distribution model is required.

As discussed in [Chapter 2](#), the results of the analysis of the instant kinematics of relative motion of the interacting tooth flanks of a gear and a mating pinion,  $\mathcal{G}$  and  $\mathcal{P}$ , respectively, as well as those pertaining to local geometry of the surfaces, are of critical importance in many practical applications. The calculation of the contact strength of gear teeth is one of the examples of the potential areas of application of the aforementioned results of the research.

The contact strength of gear teeth depends on two factors:

1. The geometry of the contacting surfaces in the differential vicinity of the point of contact
2. The applied normal load at the point of contact

Once the local geometry of the interacting tooth flanks of a gear and a mating pinion is determined, and the applied normal force is specified, the contact stress can be calculated by the following technique.

An accurate model of load distribution within the line of tooth contact for gears, especially for gears that have low tooth counts,<sup>†</sup> is discussed below. Gears with low tooth counts are commonly referred to as low tooth count gears (or just *LTC-gears* for simplicity).

\* Considered in this section of the book, low-tooth-count gears can be viewed as a more general case compared to gears with a large tooth count. The results of calculation of contact strength obtained for low tooth count gears are valid for gears with a large tooth count as well, and not vice versa.

† Gears that feature a root diameter smaller than the base diameter are referred to as low-tooth-count gears. In a more narrow sense, low-tooth-count gears are those having 15 teeth or fewer. This definition can be enhanced to the cases of intersected-axes and crossed-axes gearings as well.

It should be stressed here that the results of the research obtained for *LTC-gears* still valid for gears for which the root diameter is greater than the base diameter ( $d_{f,g} > d_{b,g}$ ).

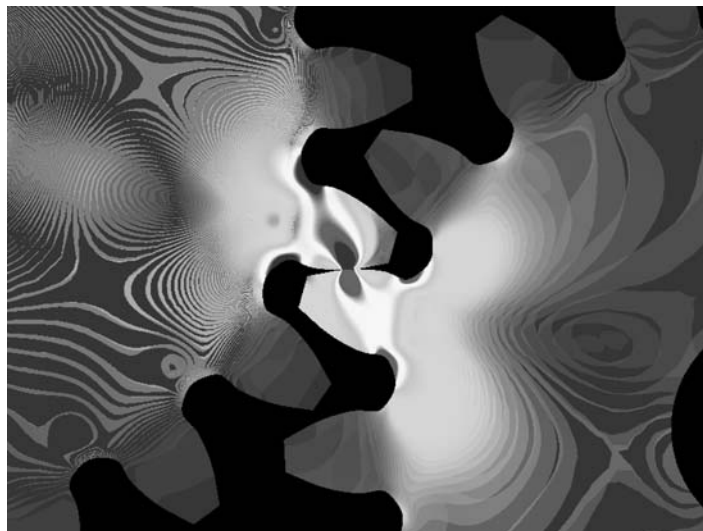


**FIGURE 24.1**  
Stresses in the gear teeth under the operating load.

### 24.1.1 Adopted Principal Assumptions

Several assumptions are adopted for developing a load distribution model. First, it is assumed that mating gears are precise and their axes of rotation are aligned to each other. This assumption pertains to gearing of all kinds, that is, parallel-axes gearing, intersected-axes gearing, and crossed-axes gearing.

It is reasonable to begin the discussion on adopted assumptions with the assumptions made by the founder of contact mechanics of materials, the German physicist Heinrich Hertz.\*

#### 24.1.1.1 Comments on Analytical Description of Local Geometry of Contacting Surfaces Loaded by Normal Force: Hertz Proportional Assumption

The investigation of the geometry of interacting surfaces under an applied normal load can be traced back to the fundamental research undertaken by Hertz on the contact of solid elastic bodies [43].

Between 1886 and 1889, Hertz published two articles on what became known as the field of contact mechanics of materials. His work basically summarizes how two axisymmetric objects placed in contact behave under loading. The developed theory is based on Hertz's observation of elliptical Newton rings formed by placing a glass sphere upon a lens; this led him to assume that the pressure exerted by the sphere follows an elliptical distribution.

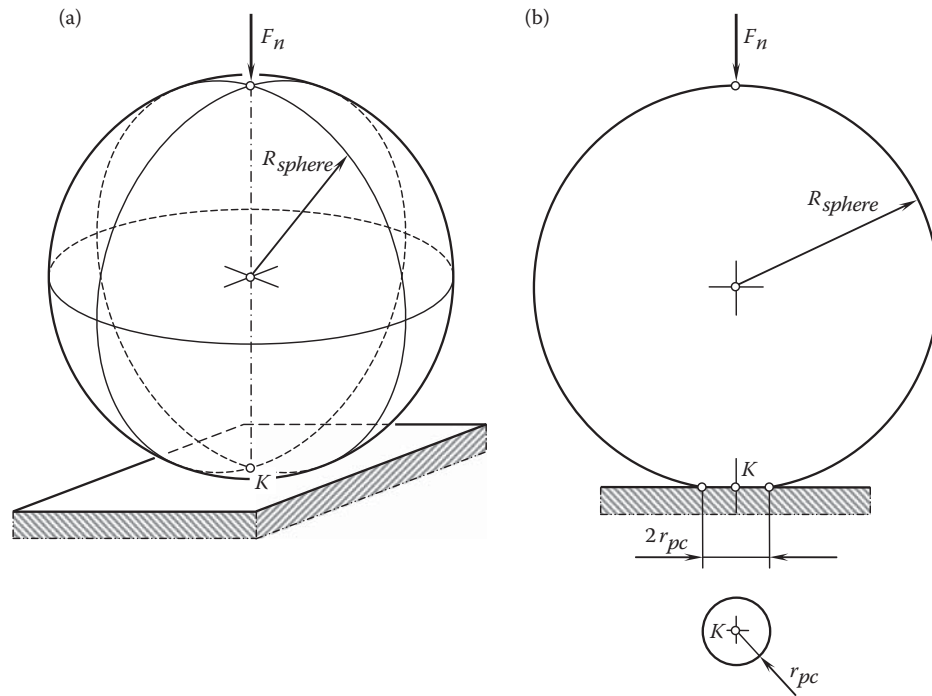
The interaction of an elastic sphere and a plane is schematically illustrated in Figure 24.2a. The initial contact of the sphere of a certain radius,  $R_{\text{sphere}}$ , and the plane can be assumed at point,  $K$ . After a normal load,  $F_n$ , is applied, the contact point,  $K$ , spreads to a round contact patch of radius  $r_{pc}$ , as schematically illustrated in Figure 24.2b.

The contact of surfaces of simple geometry (Hertz) has been incorrectly adapted to cases of contact of surfaces with complex geometries.

It is of critical importance to stress here two features of the theory developed by Hertz.

First, the theory developed by Hertz is based on the assumption that the radius,  $r_{pc}$ , of the *contact patch* (or the *bearing contact*) is much smaller compared to the radius of the sphere,  $R_{\text{sphere}}$ . The theory returns reasonable results of the calculation of contact stress if the radius,  $r_{pc}$ , is 10 (or more) times smaller than the radius of the sphere,  $R_{\text{sphere}}$ . If the inequality  $R_{\text{sphere}} \gg r_{pc}$  is not fulfilled, then the Hertz theory is not valid. This feature of the Hertz theory is often ignored, which is not correct.

\* Heinrich Rudolf Hertz (February 22, 1857–January 1, 1894), a famous German physicist.

**FIGURE 24.2**

Interaction of a sphere of a radius,  $R_{\text{sphere}}$ , and a plane under a normal load,  $F_n$ : (a) geometrical model, and (b) account for elastic deformation of the sphere.

### Assumption 24.1

*Dimensions of the bearing contact are much smaller in comparison to the corresponding radii of curvature of the contacting elastic bodies.*

A conclusion that can be immediately made from that statement is as follows: special care is required to be undertaken when applying the Hertz theory for the calculation of contact stress in the case of contact of elastic bodies bounded by *convex* and *concave* surfaces, as in this particular case, the inequality  $R_{\text{sphere}} \gg r_{pc}$  is commonly violated.

Second, Hertz considered the interaction of two elastic bodies that have simple geometries of contacting surfaces. A plane, spheres of various radii, and so on are commonly used in the research carried out by Hertz. It should be pointed out here that for surfaces of such simple geometries, the principal directions at the point of contact,  $K$ , are either not identified (as observed for a sphere and a plane) or congruent to one another. For surfaces of such simple geometries, the concept of the surface of relative curvature is applicable.

In the simplest case of contact of a plane and a sphere (Figure 24.3a), the radius of the sphere,  $R_{\text{sphere}}$ , is sufficient for an analytical description of the contact geometry of the *sphere-to-plane* contact. No radius of relative curvature,  $R_{rl}$ , is necessary in this simplest case of the surfaces in contact, as the two radii,  $R_{\text{sphere}}$  and  $R_{rl}$ , are identical to one another ( $R_{\text{sphere}} \equiv R_{rl}$ ). The results of the analytical description of the contact geometry of a sphere-to-plane contact can be enhanced to suit similar problems when two bodies with more complex geometries come into contact, for example, the contact of two spheres of different radii. For this purpose, the radius of relative curvature can be taken into consideration. In the case of contact depicted in Figure 24.3a, two points,  $a$  and  $b$ , are taken at a reasonably short distance,  $r$ , from a straight line through the contact point,  $K$ . The straight line is perpendicular to the plane. Points  $a$  and  $b$  are at a certain distance,  $\delta_{ab}$ , from one another.

In the case of contact of two spheres,  $A$  and  $B$ , of the radii,  $R_{\text{sphere}}^{(A)}$  and  $R_{\text{sphere}}^{(B)}$ , respectively (Figure 24.3b), two points,  $c$  and  $d$ , are taken into consideration. These two points are equivalent to points  $a$  and  $b$  in the aforementioned case of contact of a sphere and a plane. The distance,  $\delta_{cd}$  (not shown in Figure 24.3b), between points  $c$  and  $d$  significantly exceeds the distance,  $\delta_{ab}$ . A surface of relative curvature of a radius,  $R_{rl}$ , for spheres  $A$  and  $B$  is designed so as to ensure equality of the distances  $\delta_{ad}$  and  $\delta_{ab}$  in the case depicted in Figure 24.3a. If the equality

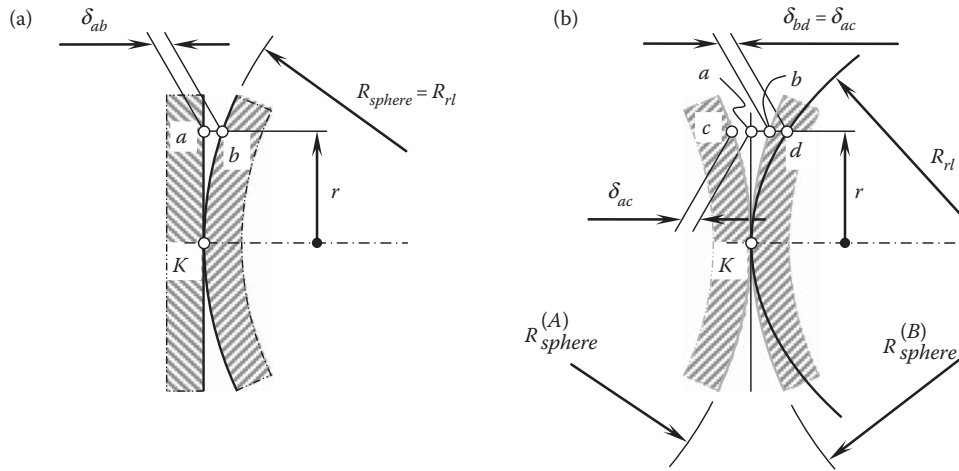


FIGURE 24.3

Definition of relative curvature,  $R_{rl}$ , at a contact point,  $K$ , of two smooth regular surfaces, 1 and 2, in cases of (a) sphere-to-plane contact, and (b) convex sphere-to-sphere contact.

$\delta_{ad} = \delta_{ab}$  is fulfilled, then the problem of contact of the two spheres of radii,  $R_{sphere}^{(A)}$  and  $R_{sphere}^{(B)}$  (see Figure 24.3b), can be substituted with the equivalent problem of contact of a plane and a sphere (see Figure 24.3a).

In order to construct a surface of relative curvature, the following manipulations with the radii of curvatures need to be performed.

The contact geometry of two surfaces can be expressed in terms of curvature of the sphere. For a sphere of a radius  $R_{sphere}$ , its curvature is expressed by a parameter that is inverse to the radius of the sphere, that is,  $k_{sphere} = R_{sphere}^{-1}$ .

In order to apply the obtained results to the case of contact of two elastic bodies bounded by two spheres,  $A$  and  $B$ , a concept of the surface of relative curvature is introduced. At any normal section through the contact point,  $K$ , of the bodies bounded by two spheres of the radii,  $R_{sphere}^{(A)}$  and  $R_{sphere}^{(B)}$  (with the normal curvatures,  $k_A$  and  $k_B$ , respectively), the normal curvature,  $k_r$ , of the surface of relative curvature can be calculated from the following formula:

$$k_r = k_A + k_B \quad (24.1)$$

This formula is derived under the assumption that the deviation,  $\delta_{ad}$ , of the surface of relative curvature from the plane in the case depicted in Figure 24.3b is equal to the deviation,  $\delta_{ab}$ , of the sphere from the plane, as illustrated in Figure 24.3a. The equality,  $\delta_{ad} = \delta_{ab}$ , is fulfilled when the deviations,  $\delta_{bd}$  and  $\delta_{ac}$ , are equal ( $\delta_{bd} = \delta_{ac}$ ). Such an equality ( $\delta_{ad} = \delta_{ab}$ ) is reasonable if and only if the inequality  $R_{sphere} \gg r_{pc}$  is valid. Otherwise, the application of the Hertz theory is invalid.

The contact of elastic bodies bounded by surfaces that have more complex geometries was not investigated by Hertz.

Once this discussion is understood, one can proceed with further analysis of the calculation of the contact strength of the teeth.

#### 24.1.1.2 Assumption of Equal Torque Share

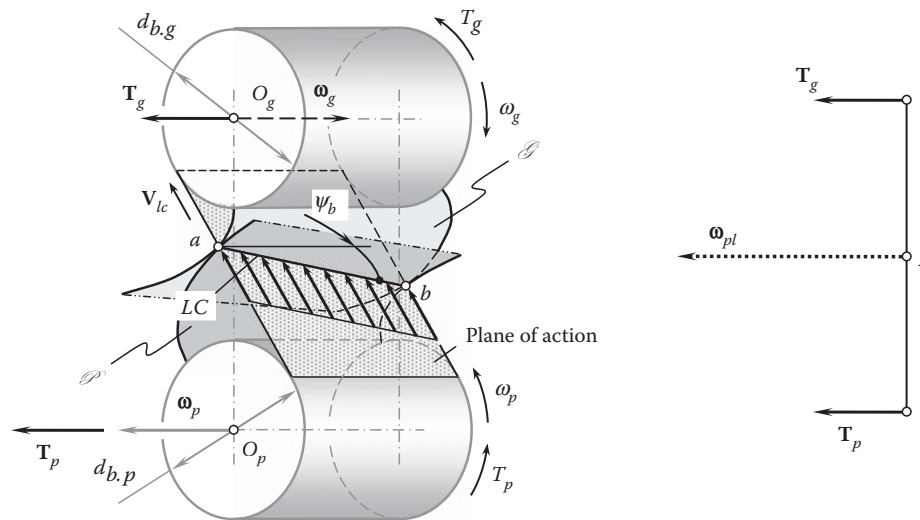
For the purpose of analysis, as well as for the purpose of designing power gearing, the use of vectors is commonly convenient. In this particular case, the earlier-discussed vector diagrams composed of rotation vectors can be complemented with vector diagrams composed of vectors of torques (see Chapter 2).

Power transmitted by a gear pair can be represented in terms of two parameters, that is, in terms of:

1. Rotation of the driving and driven shafts,  $\omega_p$  and  $\omega_g$ , respectively
2. Torques,  $T_g$  and  $T_p$ , applied to the driving and driven shafts, respectively, as shown in Figure 24.4

Tooth flank interaction of a gear and mating pinion teeth occurs under a load. The load is represented by normal forces and friction forces. Forces of interaction between the gear and pinion teeth are within the plane of



**FIGURE 24.4**

Torque vectors,  $T_g$  and  $T_p$ , associated with a gear and a mating pinion.

action,  $PA$ . As the plane of action is in tangency with both base cylinders, the tangential load is distributed equally along the line of contact,  $LC$ , that passes through points,  $a$  and  $b$ .

The values of the forces of interaction are necessary for performing strength and stress analysis of the gears. The required forces can be expressed in terms of the torques acting on the input and output shafts and in terms of the design parameters of the gears. Ultimately, contact stresses, as well as bending stresses, can be calculated for a given gear pair.

The following assumption is adopted in the analysis below:

#### Assumption 24.2

*Torque being transmitted by a pair of gears from the driving shaft to the driven shaft is distributed evenly within the active face width of the interacting gears.*

The active face width,  $F_{pa}$ , means either the effective face width (the overlapped portion of face widths of the gear and the pinion) or a portion of the effective face width within the lengths of the line of contact at a given instant of time.

The correctness of the assumption immediately follows from an equilibrium analysis of each gear of the gear pair, which considers them as solid bodies, and an equilibrium analysis of each slice of the mating gears.

Consider a gear with a certain active face width,  $F_{pa}$  (Figure 24.5a). The gear can be sliced by planes perpendicular to the gear axis,  $O_g$ , into multiple slices. Each slice is of a thickness,  $\Delta F_{pa}$  (Figure 24.5b). Actually, the thickness,  $\Delta F_{pa}$ , can approach zero when the number of slices,  $n_s$ , approaches infinity. In the limiting case ( $\Delta F_{pa} \rightarrow 0$  when  $n_s \rightarrow \infty$ ), the thickness of slices is designated as  $dF_{pa}$ . In compliance with the aforementioned assumption, equal torque is transmitted by each slice.

For the slices featuring two (or more) portions of lines of contact, the equality of torques acting on neighboring slices is maintained; however, the forces become twice as small. This is because within a slice, torque is equally shared between two (or more) portions of the line of contact.

It should be stressed here that the torque is shared equally within the effective face width and not within the line(s) of contact.

The adopted Assumption 24.2 makes possible the development of an accurate loading model of gear teeth. This concept can be expanded to gearing with intersected axes as well as gearing that has crossing axes of rotation.

#### 24.1.2 Principal Features of Low-Tooth-Count Gears

This section of the chapter focuses on the development of a load distribution model for involute gears that have a low tooth count.

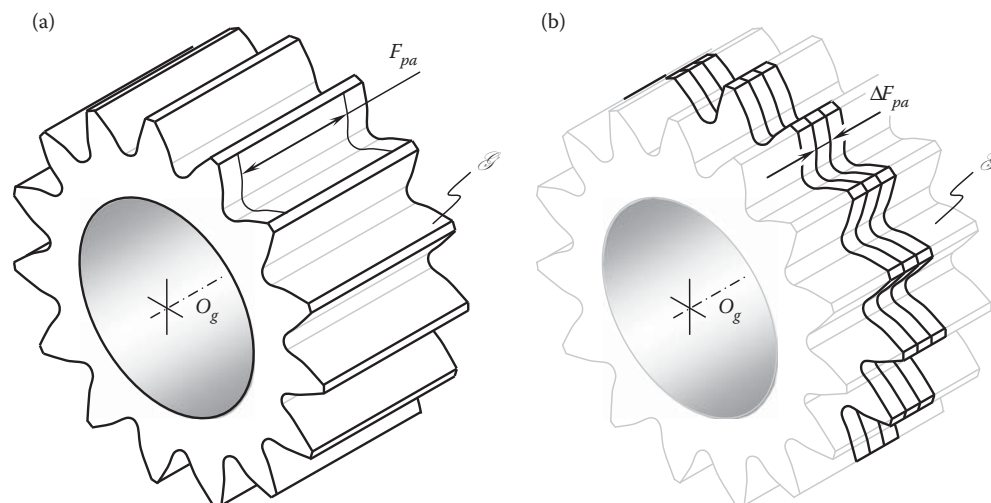


FIGURE 24.5

Torque share within the active face width,  $F_{par}$  of a gear pair: (a) effective face width,  $F_{par}$  and (b) slicing of a gear.

Low-tooth-count gears feature a rapidly diminishing radius of curvature of the involute curve in the vicinity of the base circle. At the base circle, the radius of curvature becomes zero. The contact stresses (Hertz stresses) between gear teeth become larger as the radii of curvature become smaller; in fact, at the base circle, the stress is theoretically infinite.\* Hence, involute gears should never be designed for contact at or near the base circle. Good design can usually minimize this drawback of the involute geometry; nevertheless, in many highly optimized designs, especially designs that have a small number of teeth, contact stress is still the principal limitation on load capacity.

A basic geometric fact of great significance for consideration is that given a fixed center distance and speed ratio, any one of the curves (pinion tooth profile, gear tooth profile, and path of contact) completely determines the other two.† Thus, it is possible to find mathematical relationships between tooth curvatures from given properties of the path of contact.

For an involute system, the path of contact is a straight line and the relative curvature for each of its mating gears near their base circle approaches infinity. Since a large relative curvature indicates a high probability of surface failure, one can readily understand that an involute gear is weak near its base circle. The weakness problem of involute gears is emphasized even more when one considers that for involute gears that have relatively few teeth (less than about 16), the teeth are undercut near their base circle.

A pair of spur or helical gears in mesh makes line contact, and the curvature of the mating surfaces at points along the lines of contact differs according to the relative dimensions of the gear concerned and varies with each phase of contact. In the case of external gears, contact is *convex-to-convex*, whereas for internal gears, it is *convex-to-concave*. It is commonly supposed that the nature of tooth contact is analogous to that of two cylinders, the diameters of which are dependent on the conditions prevailing at any given point of contact on the line of action. Such an assumption is valid only for gears with a large number of teeth. Gears that have a low tooth count should be modeled by corresponding cones of revolution.

### 24.1.3 Analytical Model for Calculating Contact Stress

The corresponding radii of normal curvature of the gear tooth flank,  $\rho_{n,g}$ , and the pinion tooth flank,  $\rho_{n,p}$ , are measured within the plane that is perpendicular to the line of contact. At the point of intersection within the line of contact,  $LC$ , the radii of normal curvature,  $\rho_{n,g}$  and  $\rho_{n,p}$ , are equal to the lengths of the straight-line segments connecting the line of contact and the axis of rotation of the corresponding equivalent cones.

The straight-line generators of the cone surfaces,  $C_g$  and  $C_p$ , align with the corresponding straight-line generators,  $\mathcal{E}_g$  and  $\mathcal{E}_p$ , of the involute screw surfaces,  $\mathcal{G}$  and  $\mathcal{P}$ , of the gear and pinion, respectively. The normal

\* The adopted Assumption 24.2 eliminates infinite contact stress on the base cylinder of the gear. For tooth profile points of this kind, the Hertz formula for the calculation of contact stresses is not valid.

† It should be stressed here that this statement is valid only for involute gears and invalid in case of gears with different tooth geometries.

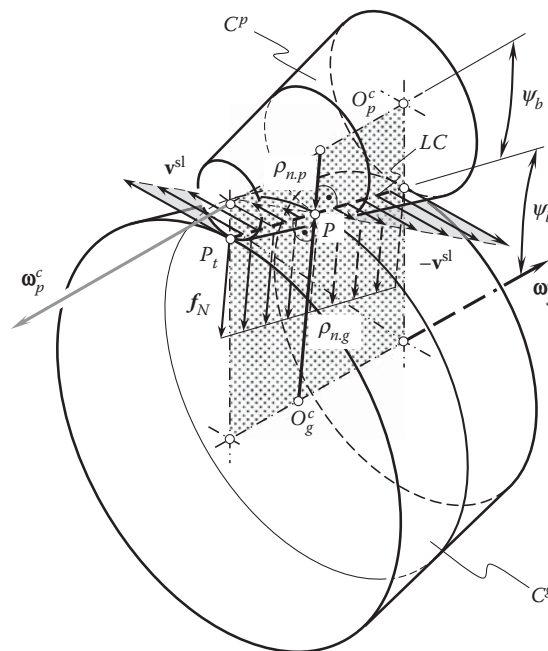


FIGURE 24.6

Interaction of modeling cones of revolution under load.

curvatures of the cone surfaces,  $C_g$  and  $C_p$ , are equal to the corresponding normal curvatures of the tooth flanks,  $\mathcal{G}$  and  $\mathcal{P}$ . Along the straight-line generators, the cones of revolution,  $C_g$  and  $C_p$ , are identical to the corresponding tooth surfaces,  $\mathcal{G}$  and  $\mathcal{P}$ , up to members of the second order. Thus, implementation of the *DG/K*-based\* method of surface generation for the derivation of equations for the calculation of geometry of the cones of revolution,  $C_g$  and  $C_p$ , makes sense.

The equivalent cones of revolution,  $C_g$  and  $C_p$ , are loaded by the distributed load,  $f_N$ , which is perpendicular to the line of contact of the equivalent cones. Under the distributed load,  $f_N$ , the equivalent cones of revolution,  $C_g$  and  $C_p$ , are rotating about their axes, as illustrated in Figure 24.6. The rotations of the equivalent cones are designated as  $\omega_g^c$  and  $\omega_p^c$ , respectively. Denoted by  $V^{sl}$ , the relative sliding of the cone surfaces  $C_g$  and  $C_p$  is observed under such a rotation of the equivalent cones.

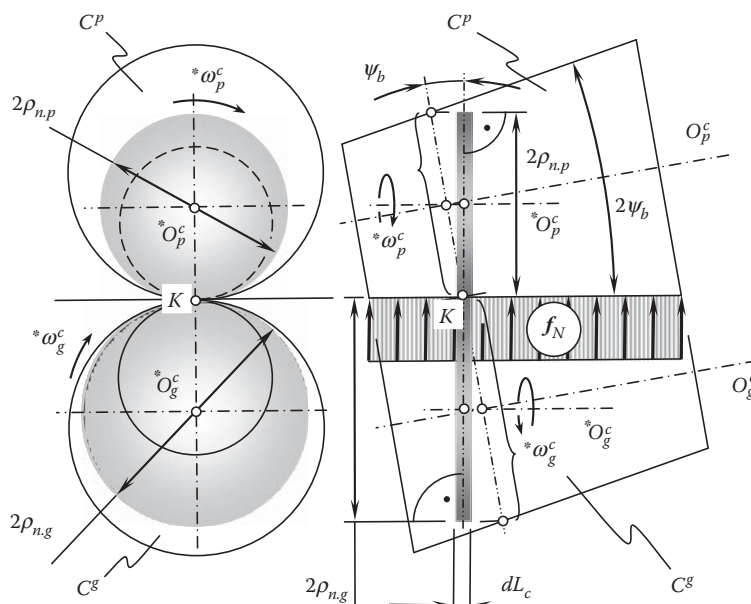
It follows from this discussion that the total length of the line of contact is an important consideration for tooth failure analysis in *LTC*-gearing. The longer the total line of contact,  $LC_\Sigma$ , the lower the load per unit length of the line of contact, and vice versa.

The distribution of the tangential load,  $f_t$ , within the line of contact,  $LC$ , is linear. Moreover, the distributed load,  $f_t$ , is of a constant value. The normal component of the distributed load,  $f_N$ , can be expressed in terms of the tangential load,  $f_t$ , and of the base helix angle  $\psi_b$ :

$$f_N = f_t \cos \psi_b \quad (24.2)$$

For further analysis, both the equivalent cones of revolution,  $C_g$  and  $C_p$ , can be sliced on an infinite number of infinitely thin  $dL_c$  cylinders, as shown in Figure 24.7. The axes of rotation of the infinitesimally thin cylinders of the gear,  $O_g^c$ , and the pinion,  $O_p^c$ , are within the plane of action, and they are parallel to the line to tooth contact. The radii of the cylinders are equal to the first principal radii of curvature of the screw involute tooth flanks,  $\mathcal{G}$  and  $\mathcal{P}$ , or they are equal to the first principal radii of curvature of the equivalent cones of revolution,  $C_g$  and  $C_p$ .

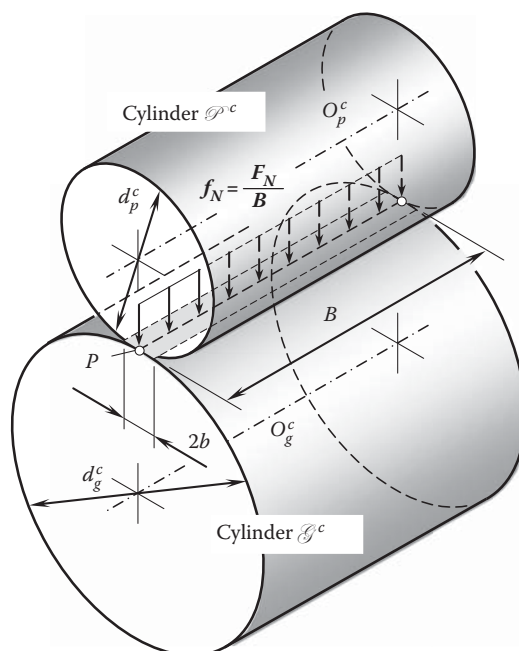
\* The *DG/K*-based method of surface generation is based on fundamental results obtained in the differential geometry of surfaces and on kinematics of multiparametric motion of a rigid body in the E3 space. This method was developed by the author and is disclosed in: Radzevich, S.P., *Differential-Geometric Method of Surface Generation*, DrSc thesis. Tula, Tula Polytechnic Institute, 1991, 300p [107]. The interested reader can refer to the following monograph: Radzevich, S.P., *Kinematic Geometry of Surface Machining*, CRC Press, Boca Raton, Florida, 2007, 536p. [113,118]. Second edition: Radzevich, S.P., *Generation of Surfaces: Kinematic Geometry of Surface Machining*, CRC Press, Boca Raton, Florida, 2014, 738p.

**FIGURE 24.7**

Local substitution of the equivalent cones of revolution,  $C^g$  and  $C^p$ , with the infinitesimally thin,  $dL_c$ , cylinders.

For calculating the normal radii of curvature of the gear,  $\rho_{n,g}$ , and that of the pinion,  $\rho_{n,p}$ , use of the *Meusnier equation* is helpful [107,113,118].

It should be mentioned here that in the case of large tooth counts, the modeling cones degenerate to corresponding modeling cylinders. This load distribution model is illustrated in Figure 24.8. Local substitution of the screw involute surfaces with infinitesimally thin cylinders is applicable for both gears that have a low number of teeth and gears with a regular tooth number. In cases of large tooth counts, the gear teeth are loaded as schematically illustrated in Figure 24.9.

**FIGURE 24.8**

Local approximation of the screw involute tooth flanks,  $\mathcal{G}$  and  $\mathcal{P}$ , with the equivalent cylinders of revolution,  $\mathcal{G}^c$  and  $\mathcal{P}^c$ .

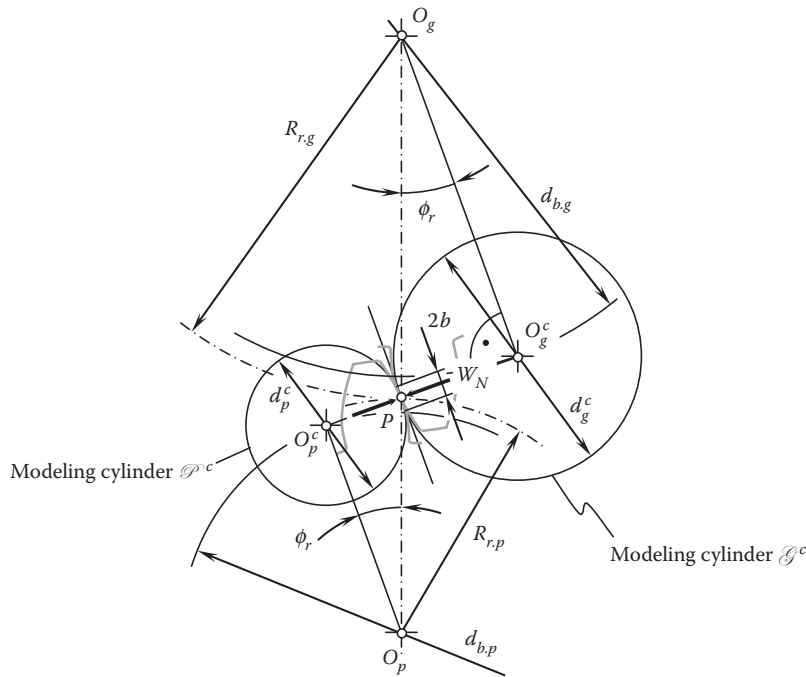


**FIGURE 24.9**  
Load distribution model in parallel-axes gearing (a reduced case).

The proposed load distribution model is used in computer code for the computation of the distribution of contact stresses within the path of contact. An example of the computation of the distribution of maximal contact stresses within the path of contact is shown in [Figure 24.10](#).

In [Figure 24.10](#), zones A and C are the zones within which the Hertz assumption is not valid. Thus, the Hertz formula is valid only for points within a zone, B, where Assumption 21.1 is fulfilled.

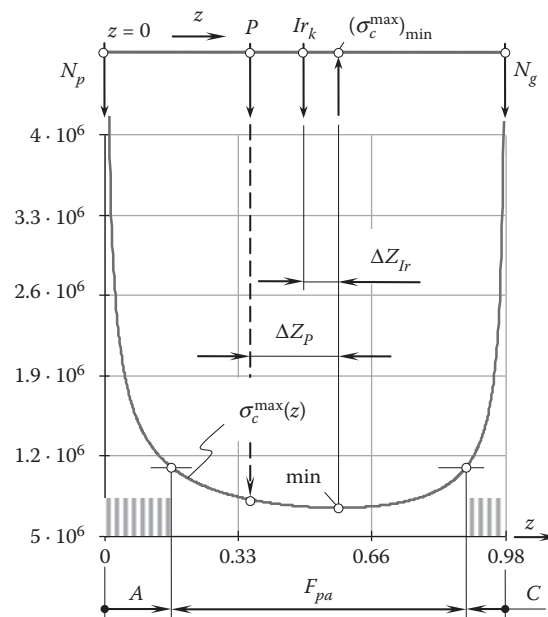


**FIGURE 24.10**  
An example of the computation of the distribution of Hertz contact within the line of contact in a low tooth count gear pair.

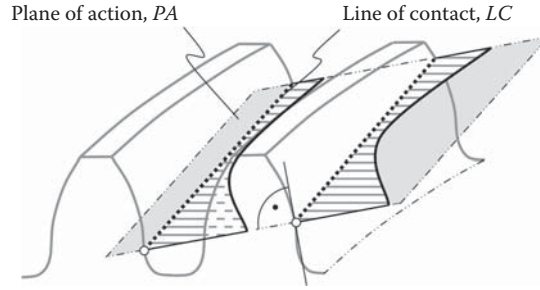


FIGURE 24.11

Distribution of Hertz contact stress within the line of contact,  $LC$ , in a low-tooth-count gearing.

The distribution curve,  $\sigma_c^{\max}(z)$ , has an asymmetric geometry. The point at which the minimum contact stresses,  $(\sigma_c^{\max})_{\min}$ , are observed is shifted from the pinion toward the gear at a certain distance,  $\Delta Z_{lr}$ . This point is at a distance,  $\Delta Z_P$ , from the pitch point,  $P$ . The shift,  $\Delta Z_{lr}$ , is caused by the normal force per unit length of the path of contact,  $f_N(z)$ , which varies within the path of contact. For conventional gear drives, this variation of the component,  $f_N(z)$ , is negligibly small. Therefore, for conventional gear drives, the shift  $\Delta Z_{lr} \cong 0$ .

For a gear drive that features a low number of teeth, the distribution of maximum contact stresses within the line of contact,  $LC$ , is illustrated in Figure 24.11.

For a gear drive that has a large number of teeth and a reasonable value of the gear ratio, the distribution curve reduces almost to a straight line. In this case, the distribution line is almost straight and almost parallel to the line of contact. This means that the load distribution model for parallel-axes gearing (Figures 24.6 and 24.7) is valid for both low-tooth-count gear drives and gear drives with regular tooth numbers. The load distribution model for parallel-axes gearing (Figure 24.8) is applicable only for gear drives that have regular tooth numbers, and it is not applicable for low-tooth-count gear drives.

Similarly, the model of contact loads of parallel-axes gear drives can be constructed for cases of intersected-axes gearing as well as crossed-axes gears.

#### 24.1.4 Formula for Calculating Hertz Contact Stress

The pitting-resistant formula is based on *Hertz contact stress equation* for cylinders with parallel axes (see Figure 24.9). The load applied to the cylinder is the load normal to the tooth flank, and the length of contact is the minimum total length of lines of contact in the contact zone of the gear set. The radii of the cylinders are the radii of curvature of the teeth at the point of contact for the mating pair of gears. Depending on the face gear ratio of the gear set, this point can be the mean diameter of the pinion or the lowest point of single-tooth contact on the pinion. Additional rating factors are also added to the basic equation to adjust the stress due to factors peculiar to gearing. Starting with the general *Hertz equation*:

$$s_c = \frac{2W}{\pi bL} \quad (24.3)$$

$$b = \sqrt{\frac{2W}{\pi L} \cdot \frac{\frac{1 - \mu_1^2}{E_1} + \frac{1 - \mu_2^2}{E_2}}{\frac{1}{d_1} + \frac{1}{d_2}}} \quad (24.4)$$

where:

$s_c$  is the maximum stress of parallel axis cylinders.

$W$  is the contact load normal to the cylinders.

$b$  is the semiwidth of contact between cylinders, in.

$L$  is the length of contact between cylinders, in.

$\mu_1, \mu_2$  are the *Poisson's ratio* of material of cylinders 1 and 2.

$E_1, E_2$  are the modulus of elasticity of material of cylinders 1 and 2.

$d_1, d_2$  are the diameter of cylinders 1 and 2.



### 24.1.5 Specific Pressure Factor

The specific pressure factor,  $\gamma$ , is of critical importance when performing calculation of gear teeth on contact strength. By definition, the specific pressure factor equals:

$$\gamma = \frac{m}{\rho_{rel}} \quad (24.5)$$

where module is designated as  $m$ , and relative curvature is denoted by  $\rho_{rel}$ .

It is convenient to represent Equation 24.5 in the form:

$$\gamma = \frac{mC}{\rho_g(C/\cos \phi_t - \rho_g) \cos \phi_t} \quad (24.6)$$

Here, the center distance is designated as  $C$ , the transverse pressure angle is denoted by  $\phi_t$ , and the radius of curvature of the gear is designated as  $\rho_g$ .

### 24.1.6 Combined Compressive-Shear Stress in Low Tooth Count Gearing

The following stresses are present in the region of a contact band: in the center of the band, there is a point of maximal compressive stress. Directly underneath this point, there is a maximal subsurface shear stress. Approximately, the depth to the point of maximum shear stress is a little less than one-third the width of the band of contact.

The gear-tooth surfaces move across each other with a combination of rolling and sliding motions. The sliding motions plus friction tend to cause additional surface stresses. Just ahead of the band of contact, there is a narrow band of compression. Just behind the band of contact, there is a narrow region of tensile stresses. A bit of metal on the surface of a gear tooth goes through a cycle of compression and tension each time a mating gear tooth passes over it. There may also be rupturing of the metal due to subsurface shear stresses.

Generally, interaction between the gear and pinion tooth surfaces in low-tooth-count gearing can be considered rolling and sliding of elastically dissimilar cylinders. For further analysis, the aforementioned model of tooth loading (see Figure 24.6) can be implemented. For this purpose, the zone of contact of the surfaces,  $\mathcal{G}$  and  $\mathcal{P}$  (Figure 24.12a), is considered the contact of two cylinders loaded by a normal force,  $W_N$ , and a shear force,  $Q$ . It is assumed that the shear force,  $Q$ , is sufficient to cause sliding of the contacting surfaces.

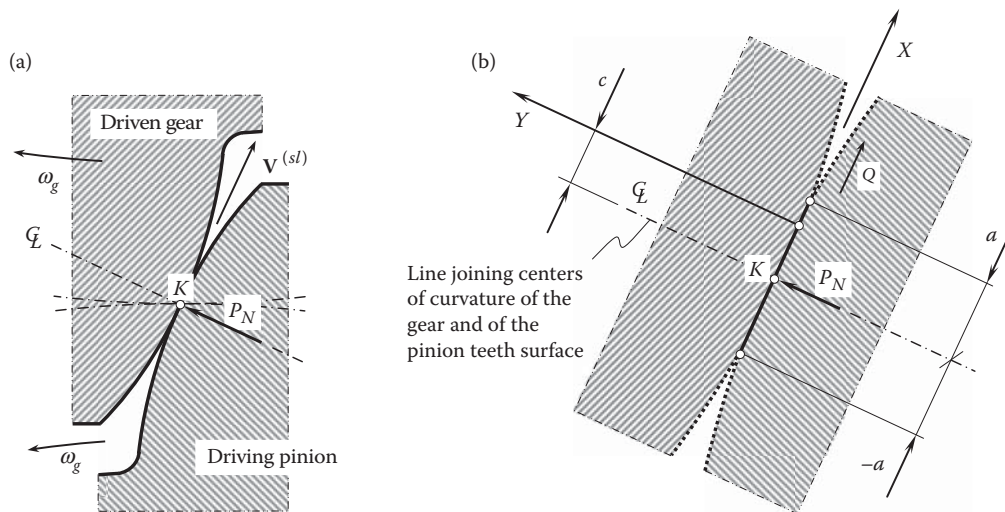


FIGURE 24.12

Contacting of two cylinders loaded by a normal load,  $P_N$ , and shear force,  $Q$ , which is sufficient to cause sliding: (a) schematic of the loading by the normal force,  $P_N$ , and (b) shear force,  $Q$ , in contact.



Shear traction, whether arising from sliding friction or other sources, cause a vertical displacement of the surface of the components [47]. However, since the shear traction distribution is mutual, the  $y$ -direction displacements will also be the same if the materials are the same. Hence, the integral equation reduces, as the influence of the shear and direct tractions may be treated separately, and such problems are said to be uncoupled. The effect of sliding of two cylinders is to induce a shear traction distribution that is limited everywhere by friction; that is, if the *Coulomb* friction law is assumed, which indicates that the friction force is proportional to the normal force and independent of speed, we have:

$$\frac{|q(x)|}{f} = -p(x) = p_0 \sqrt{1 - (x/a)^2} \quad (24.7)$$

where  $f$  designates the coefficient of friction.

However, if the contacting bodies are dissimilar, there is a coupling effect. It must still be true that the shear stress is everywhere limited by friction, that is:

$$q(x) = -f \cdot p(x) \quad (24.8)$$

We do not expect the contact patch to be positioned on the line joining the centers of the cylinders:

$$\frac{1}{\pi} \int_{-a}^a \frac{p(\xi) \cdot d\xi}{x - \xi} + \beta \cdot f \cdot p(x) = \frac{-k(x - c)}{A} \quad (24.9)$$

This is a *Cauchy* singular integral equation of the second kind, which can be solved directly. The tangential offset,  $c$ , is found from the consistent condition:

$$\int_{-a}^a \frac{(x - c) \cdot dx}{(a - x)^m (a + x)^{1-m}} \quad (24.10)$$

These equations can be more conveniently treated if rewritten as follows [49]:

$$p_0 = \frac{P \cdot \sin(m\pi)}{2 \cdot \pi \cdot a \cdot m \cdot (1 - m)} \quad (24.11)$$

$$a^2 = \frac{P \cdot A}{2 \cdot \pi \cdot m \cdot (1 - m) \cdot k} \quad (24.12)$$

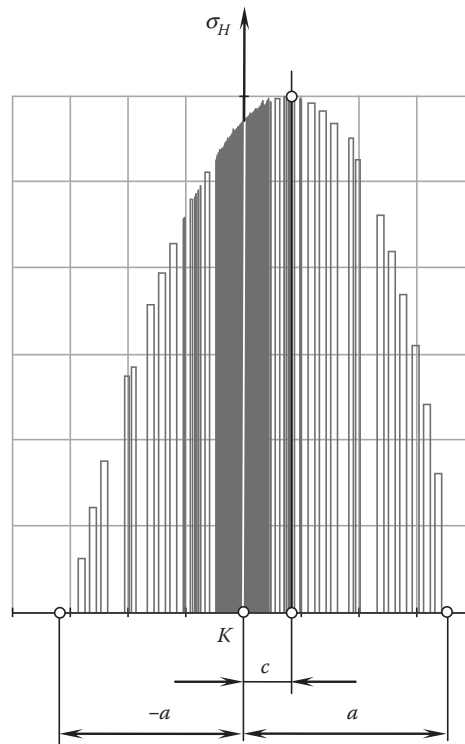
$$\frac{p(s) \cdot a}{P} = -\frac{\sin(m\pi)}{2 \cdot \pi \cdot m \cdot (1 - m)} \cdot (1 - s)^m (1 + s)^{1-m} \quad (24.13)$$

The aforementioned equations are expressed in terms of the parameters of the contact zone shown in Figure 24.12.

In practice, the actual value of parameter  $|\beta|$  rarely exceeds  $|\beta| = 0.4$ ; hence, if the maximal value of  $f$  is about  $f = 0.6$ , then  $m$  lies in the range  $m = 0.46 \div 0.54$ . The difference from the Hertz solution to the problem is therefore small and confident to the very near surface.

Using the aforementioned equations, computer code is worked out for the computation of both contact stresses and the combined compression and shear stresses (C/S-stresses). A qualitative example of the analysis is shown in Figure 24.13. Here, the distribution of the combined C/S-stresses across the band of contact is depicted. Figure 24.13 reveals that due to gear-tooth sliding, the stress distribution curve assumes an asymmetrical shape.

Use of the discussed method also yields computation of just contact stresses. For this purpose, it is required to enter the load  $Q = 0$  in the aforementioned equations. The results of such computations perfectly correlate with the results of computations obtained using the method of computation of contact stresses (in accordance with the Hertz approach).

**FIGURE 24.13**

Qualitative example of the combined compression and shear stresses (C/S – stresses) distribution across the band of contact.

The preliminary analysis indicates that the difference between the combined C/S-stresses and contact stresses for a conventional gear drive is negligibly small in most cases. However, for *LTC*-gearing, shear stresses could add significantly to the resultant C/S-stresses. The performed computations show that the difference between the combined C/S-stresses and contact stresses reaches up to 15%. This result indicates that for *LTC*-gearing, shear stresses should be taken into consideration.

## 24.2 Bending Strength of Gear Teeth

The strength of gear teeth and bending strength, in particular, are of critical importance for all power gear trains. Gear teeth must be strong enough to hold the applied loads. In order to design gears properly, it is necessary to know how stress in the gear tooth body can be calculated. The calculation of the bending strength of a gear tooth is a very complicated engineering problem.

### 24.2.1 Comments on Lewis's Formula

Many attempts have been undertaken to develop a practical method to calculate of the bending stress in a gear tooth loaded by torque that is being transmitted by the gear pair. Almost all attempts fall into one of two categories.

The first is based on the application of conventional equations that are developed in the *strength of materials*. Lewis's formula is the best-known way to make calculations of this sort.

The second is based on application of the finite-element method.

Without going into details of implementation of FEM software for the computation of bending stress in a gear tooth, let us briefly outline the main reason conventional equations developed in strength of materials are not valid for the calculation of bending stress in a gear tooth.

As most of the equations that are derived for engineering purposes, conventional formulas for the calculation of bending stress in a cantilever beam are derived under *Saint Venant's principle*.\*

Some comments on the calculation of bending stress in gear teeth are briefly outlined in the next section.

#### 24.2.1.1 Cantilever Beam of Equal Strength

There are many similarities between the loading of a gear tooth and loading of a cantilever beam. These similarities inspired gear engineers to implement the results developed for a cantilever beam for calculating the bending strength of a gear tooth.

Consider a cantilever beam that is loaded by a bending force,  $P$ . A schematic of this loading is illustrated in Figure 24.14a. The cantilever beam is of a certain length,  $l$ .

Let us assume that the beam is of equal bending strength. For cantilever beams of this particular kind, the maximum bending stress,  $\sigma_{\max}$ , at every cross-section is equal to the yield stress,  $[\sigma]$ :

$$\sigma_{\max} = \frac{|M(x)|}{W(x)} = [\sigma] \quad (24.14)$$

where:

$M(x)$  is the applied torque [ $M(x) = P x$ ].

$P$  is the load applied at the end of the cantilever beam.

$x$  is the distance from the end of the cantilever beam to a point of interest within length,  $l$ , of the beam.

$W(x)$  is the section moduli of the cross-sectional area at the distance  $x$  from the end of the cantilever beam.

An equation for the calculation of the dimensions of a cross-section of the equal strength beam immediately follows from Equation 24.14:

$$W(x) = \frac{M(x)}{[\sigma]} \quad (24.15)$$

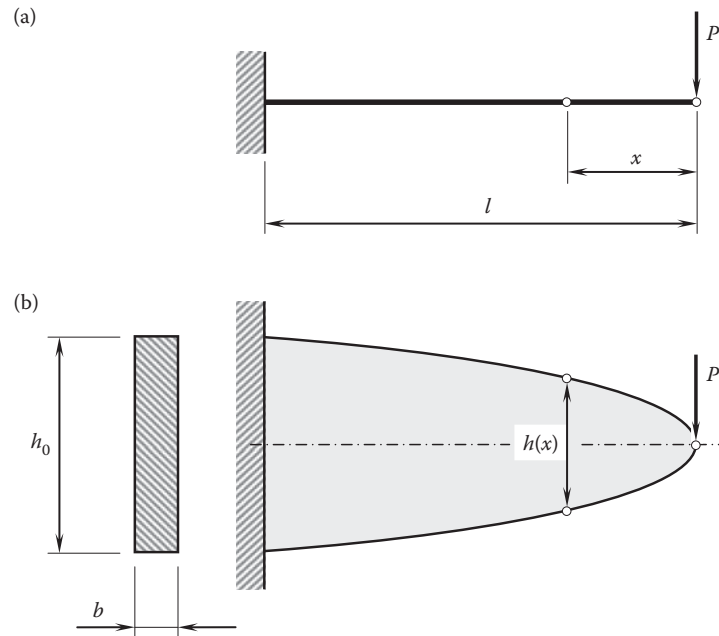


FIGURE 24.14

Geometry of an equally strong cantilever beam: (a) schematic of a cantilever beam, and (b) parabolic shape of the lengthwise section of the rectangular cantilever beam.

\* Saint-Venant's principle, named after the French elasticity theorist Adhémar Jean Claude Barré de Saint-Venant, can be stated as saying that: "the difference between the effects of two different but statically equivalent loads becomes very small at sufficiently large distances from load." Occasionally, Saint-Venant's principle is also called Saint-Venant's assumption.

It is assumed that the cantilever beam has a rectangular cross-section. The width,  $b$ , of the cross-section is constant within the length,  $l$ , of the cantilever beam. The height,  $h$ , of the cantilever beam is variable,  $h = h(x)$ , within the length,  $l$ , of the cantilever beam.

With that said, Equation 24.15 can be rewritten in the form:

$$W(x) = \frac{b h^2(x)}{6} \quad (24.16)$$

In the case under consideration, the equality  $|M(x)| = P x$  is valid. Therefore,

$$\frac{b h^2(x)}{6} = \frac{P x}{[\sigma]} \quad (24.17)$$

Equation 24.17 casts into an expression for  $h(x)$ :

$$h(x) = \sqrt{\frac{6 P}{b [\sigma]}} \cdot \sqrt{x} \quad (24.18)$$

This equation can also be represented in an equivalent form:

$$x = \frac{b [\sigma]}{6 P} \cdot h_x^2 \quad (24.19)$$

As follows from Equation 24.18, the height,  $h(x)$ , of the equal strength cantilever beam follows a parabolic function (Figure 24.14b). It should be mentioned here that for the calculation of maximum height,  $h_0$ , the following formula can be used:

$$h_0 = \sqrt{\frac{6 P}{b [\sigma]}} \cdot \sqrt{l} \quad (24.20)$$

The derived Equation 24.19 for an equal strength cantilever beam is used for the calculation of the bending strength of a gear tooth.

#### 24.2.1.2 Lewis's Formula for the Calculation of Gear Tooth Bending Strength

Being concerned with the necessity of performing the calculation of the bending stress of a gear tooth, in the late 1890s, Lewis proposed [66] a corresponding formula. To derive the formula, Lewis inscribed a parabola into the gear tooth shape (Figure 24.15), then calculated stress in the gear teeth for the cantilever beam for the inscribed parabolic shape instead of calculating the actual gear tooth shape.

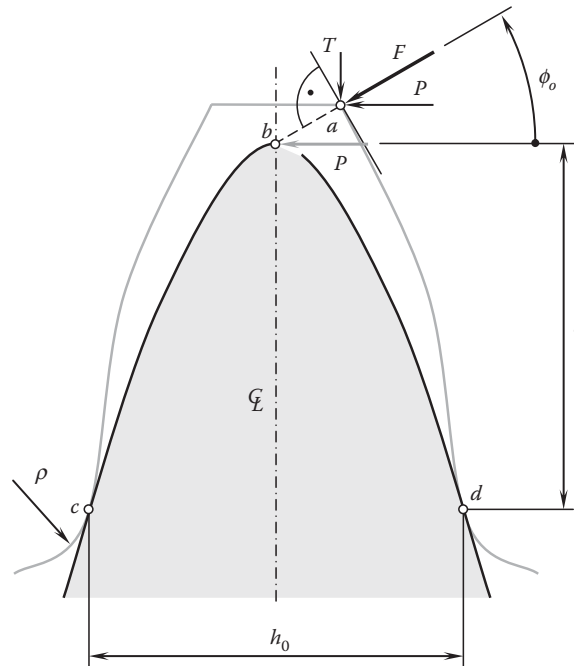
In the worst-case scenario of gear tooth loading, the force,  $F$ , is applied at the tooth tip, namely, at point  $a$ . At point  $a$ , the force,  $F$ , can be decomposed into two components. The tangential component of the force,  $F$ , is labeled as  $P$ . This component can be expressed in terms of the force,  $F$ , and the pressure angle,  $\phi_o$ , measured at a major diameter of the gear:  $P = F \cos \phi_o$ . The radial component,  $T$ , can be calculated from the expression  $T = F \sin \phi_o$ .

The line of action of the applied force,  $F$ , intersects the centerline,  $\mathcal{C}$ , of the gear tooth shape at a certain point,  $b$ . The component,  $P$ , of the force,  $F$ , is applied at this point,  $b$ .

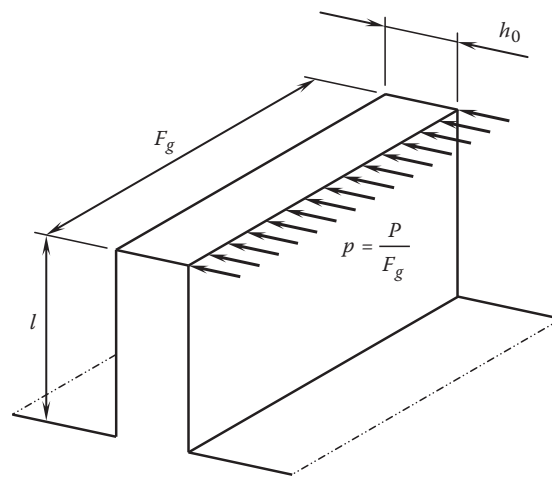
Then, a parabola is inscribed into the gear tooth shape. The apex of the parabola is located at point,  $b$ . The parabola makes tangency with the gear tooth shape at certain points,  $c$  and  $d$ . Once points  $b$ ,  $c$  and  $d$  are determined, the dimensions,  $h_0$  and  $l$ , are considered known design parameters.

Use of the inscribed parabola makes it possible to calculate the bending stress for a cantilever beam of known geometry and design parameters instead of calculating the stress for an indefinite case with unknown parameters,  $h_0$  and  $l$ , for the original shape of the gear tooth. The maximum stress is equal to:

$$\sigma_{\max} = \frac{|M(x)|}{W(x)} \quad (24.21)$$

**FIGURE 24.15**

A parabola inscribed into a gear tooth shape.

**FIGURE 24.16**

An equivalent cantilever beam used as the replacement for the actual shape of the gear tooth.

Calculations are performed for an equivalent cantilever beam, shown in [Figure 24.16](#). The distributed applied load is  $p = P/F_g$ , where face width of the gear is denoted by  $F_g$ . It should be pointed out here that such a schematic for the loading of the gear tooth is not equivalent to the actual loading of the gear tooth. For example, the radial component,  $T$ , is not incorporated into the schematic of the gear tooth loading shown in [Figure 24.16](#). Ignoring the load,  $T$ , is not allowed when accurate calculations need to be performed.

However, the root cause of poor accuracy of calculations is that Saint Venant's\* principle (1855) is violated in the loading model that is used for derivation of Lewis's formula. This is illustrated in [Figure 24.17](#).

\* Adhémar Jean Claude Barré de Saint-Venant (August 23, 1797–January 6 [January 22 ??], 1886), a French mathematician and mechanician.

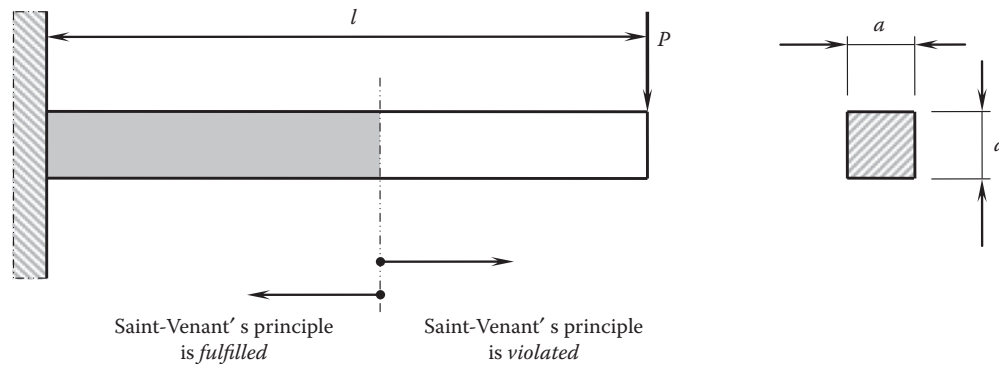


**FIGURE 24.17**  
Explanation of Saint-Venant's principle.

In [Figure 24.17](#), a cantilever beam is shown. The cantilever beam is loaded by a bending force,  $P$ . The distribution of the actual stress in the cantilever beam under the applied load strongly depends on the clamping of the beam, any changes of its shape and dimensions, and so on. The calculated stress within the body of the cantilever beam correlates with the actual stress at a distance from the place of clamping that exceeds three to five, and not less than one, characteristic dimensions, that is, maximal dimensions of the cross-section of the cantilever beam. For example, the cantilever beam shown in [Figure 24.17](#) has a squared cross-section of size  $a \times a$ . The influence of clamping on the distribution of stress is negligibly small and can be ignored at a certain critical distance,  $l_{cr} = (3 \dots 5) a$ . Within the length  $0 \leq l \leq l_{cr}$ , Saint Venant's principle is violated. This makes it impossible to have an accurate calculation of stress using elementary formulas derived in strength of materials.

With respect to gear teeth, the length,  $l_{cr}$ , should exceed  $l_{cr} = (3 \dots 5) F_g$  (or at least  $l_{cr} = F_g$ ), where  $F_g$  designates the face width of the gear.

The discussion on the correctness of implementation of Saint Venant's principle to calculation of bending stress in gear teeth can also be illustrated by the following example.

The so-called effect of stress concentration is due to violation of Saint Venant's principle. Stress concentration is observed in the cross-sections at which the shape and dimensions of a specimen are changed. The larger the changes of the shape and dimensions, the higher the rise of stress levels.

The distribution of bending stress within the body of a cantilever beam is illustrated in [Figure 24.18](#).

No stress increase is observed in cross-sections for which Saint Venant's principle is fulfilled. An example of such a cross-section is depicted in [Figure 24.18a](#). This cross-section is located beyond the critical length,  $l_{cr}$ . Therefore, the bending stress for this cross-section can be calculated from Equation 24.21.

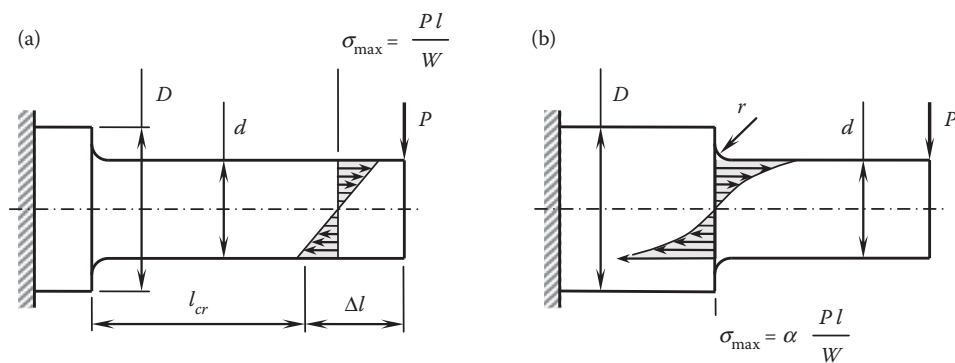


**FIGURE 24.18**  
Distribution of stress within the body of a cantilever beam in a case when (a) Saint-Venant's principle is fulfilled, and (b) Saint-Venant's principle is violated.

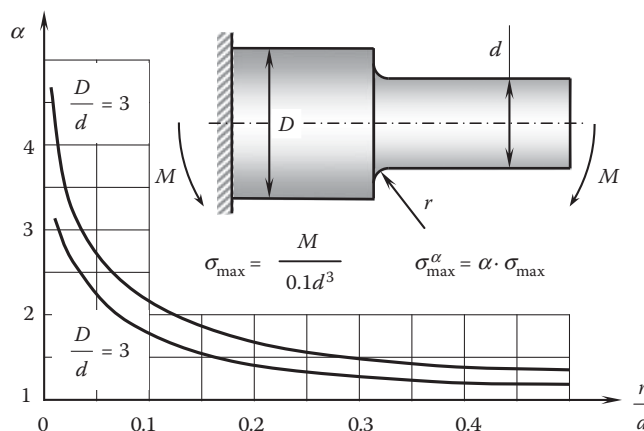


FIGURE 24.19

Impact of a stress raiser onto maximum stress within the body of a cantilever beam.

In a cross-section that is closer to the place where a change of shape is observed (Figure 24.18b), for calculation of bending stress, the following expression can be used:

$$\sigma_{\max}^{\alpha} = \alpha \sigma_{\max} \quad (24.22)$$

In Equation 24.22, the theoretical coefficient of stress concentration is designated as  $\alpha$ .

The value of the coefficient,  $\alpha$ , depends on the ratio of the diameters,  $D$  and  $d$ , of the neighboring portions of the specimen, as well as on the radius,  $r$ , of the blend. Methods that are developed in the theory of elasticity are used for calculating the stress concentration factor,  $r$ .

An example of the function,  $\alpha = \alpha\left(r, \frac{d}{D}\right)$ , is illustrated in Figure 24.19. This example reveals that the use of mathematical expressions developed in the elementary strength of materials is not capable of returning an accurate value for the bending stress.

The shape of a gear tooth has a complex geometry. No elementary formulas from the strength of materials are capable of returning results of the calculations that properly correlate with the actual bending stress within the tooth body of a gear.

No sufficient analytical solution to the problem has been proposed yet.

### 24.3 Effective Length of Line of Contact

The main purpose of power gears is to transmit torque from the input shaft to the output shaft of the gear pair. Transmission of torque from the driven pinion to the driving gear is observed when the gear teeth interact with one another. The interacting tooth flanks of the gear and pinion are commonly in line contact. Physically, the power is transmitted through a narrow strip of the tooth surfaces contact. This strip is along the line(s) of contact,  $LC$ , between the gear tooth flank,  $\mathcal{G}$ , and the pinion tooth flank,  $\mathcal{P}$ . The longer the line of contact,  $LC$ , the more power can be transmitted by the gear pair. This clearly shows the importance of the longer line of contact between the tooth flanks of a gear and a mating pinion.

The length of the line of contact is a critical consideration of the designer of a gear pair. Three different types of the lengths of the line of contact,  $LC$ , are considered:

1. The maximum length of a single line of contact,  $l_{LC}$
2. The total length of the lines of contact,  $l_{LC}^t$
3. The effective length of the lines of contact,  $l_{LC}^e$

Let us begin the consideration from the simplest case of the length of a single line of contact.



### 24.3.1 Length of a Single Line of Contact in Parallel-Axes Gearing

The length,  $l_{LC}$ , of a single line of contact can be expressed in terms of design parameters of the gear and pinion.

For spur gears, the maximum length of a single line of contact,  $l_{LC}$ , is always equal to the effective face width,  $F_{pa}$ , of the gear pair. The equality  $l_{LC} = F_{pa}$  is illustrated in Figure 24.20a. Here, the *effective face width* is understood in the sense of the lengths of the gear face width,  $F_g$ , and the pinion face width,  $F_p$ , which overlap one another. The tooth flanks of the gear,  $\mathcal{G}$ , and pinion,  $\mathcal{P}$ , contact one another within the entire effective face width,  $F_{pa}$ .

In the case of gears that have relatively small base helix angles,  $\psi_b$ , that is, when the inequality:

$$\psi_b \leq \tan^{-1}\left(\frac{Z}{F^e}\right) \quad (24.23)$$

is valid, the maximum length of a single line of contact,  $l_{LC}$ , can be calculated from the expression:

$$l_{LC} = \frac{F^e}{\cos \psi_b} \quad (24.24)$$

This case is illustrated in Figure 24.20b.

When the base helix,  $\psi_b$ , exceeds the value given by Equation 24.23:

$$\psi_b \geq \tan^{-1}\left(\frac{Z}{F^e}\right) \quad (24.25)$$

the equation:

$$l_{LC} = \frac{Z}{\sin \psi_b} \quad (24.26)$$

can be used for the calculation of the maximum length of a single line of contact,  $l_{LC}$ . This case is schematically shown in Figure 24.20c.

Consider an external parallel-axes gearing that is schematically depicted in Figure 24.21. The axis of rotation,  $O_g$ , of the gear and the axis of rotation,  $O_p$ , of the pinion are at a center distance,  $C$ . The radius of the base cylinder of the gear is designated as  $r_{b,g}$ , and the radius of the base cylinder of the pinion is labeled as  $r_{b,p}$ . The plane of action,  $PA$ , is in tangency to both the base cylinders. The lines of the tangency,  $O_g^c$  and  $O_p^c$ , are, in nature, the axes of rotation of the modeling cones of the gear tooth flank,  $\mathcal{G}$ , and the pinion tooth flank,  $\mathcal{P}$ .

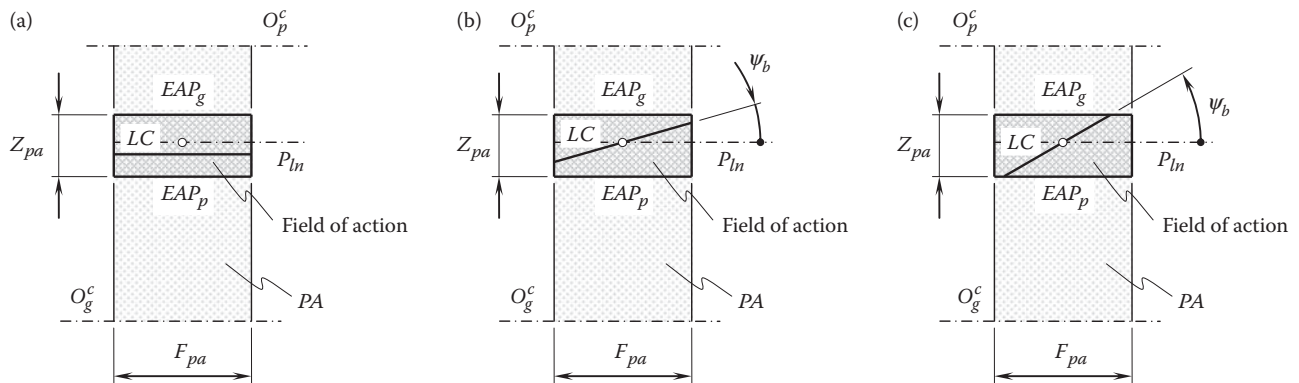
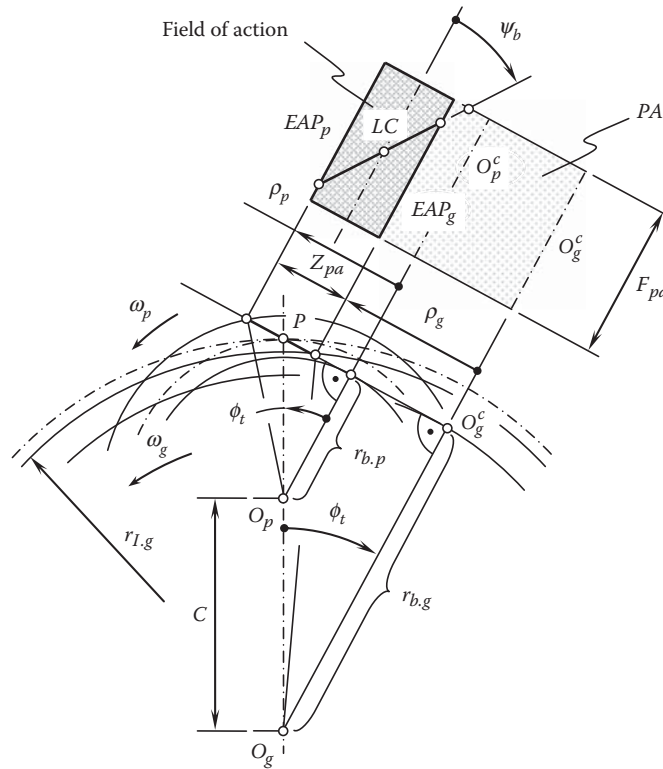


FIGURE 24.20

Maximum length of a single line of contact,  $LC$ , (a) for spur gears, (b) for helical gears with  $\psi_b \leq \tan^{-1}\left(\frac{Z}{F_{pa}}\right)$ , and (c) for helical gears with  $\psi_b \geq \tan^{-1}\left(\frac{Z}{F_{pa}}\right)$ .





**FIGURE 24.22**  
Line of contact,  $LC$ , in an internal parallel-axis gearing.

Substituting Equations 24.29 and 24.30 into Equation 24.28, an expression for the calculation of width,  $Z$ , of the field of action can be derived:

$$Z_{pa} = \sqrt{r_{o,g}^2 - r_{b,g}^2} + \sqrt{r_{o,p}^2 - r_{b,p}^2} - C \sin \phi_t \quad (24.31)$$

Then, Equation 24.31 can be substituted into Equation 24.27. This returns an expression for the calculation of the maximum length of a single line of contact:

$$l_{LC} = \frac{\sqrt{r_{o,g}^2 - r_{b,g}^2} + \sqrt{r_{o,p}^2 - r_{b,p}^2} - C \sin \phi_t}{\sin \psi_b} \quad (24.32)$$

A schematic for the internal parallel-axes gearing that is shown in Figure 24.22 makes it possible to derive an equivalent equation for calculation of the width,  $Z$ , of the field of action:

$$Z = \sqrt{r_{o,p}^2 - r_{b,p}^2} - \sqrt{r_{l,g}^2 - r_{b,g}^2} + C \sin \phi_t \quad (24.33)$$

Then, this result can be substituted into Equation 24.27. Ultimately, an expression for  $l_{LC}$  can be obtained:

$$l_{LC} = \frac{\sqrt{r_{o,p}^2 - r_{b,p}^2} - \sqrt{r_{l,g}^2 - r_{b,g}^2} + C \sin \phi_t}{\sin \psi_b} \quad (24.34)$$

In a similar manner, the corresponding expressions for the calculation of the maximum length of a single line of contact can be derived for cases of intersected-axes gearing as well as crossed-axes gearing.

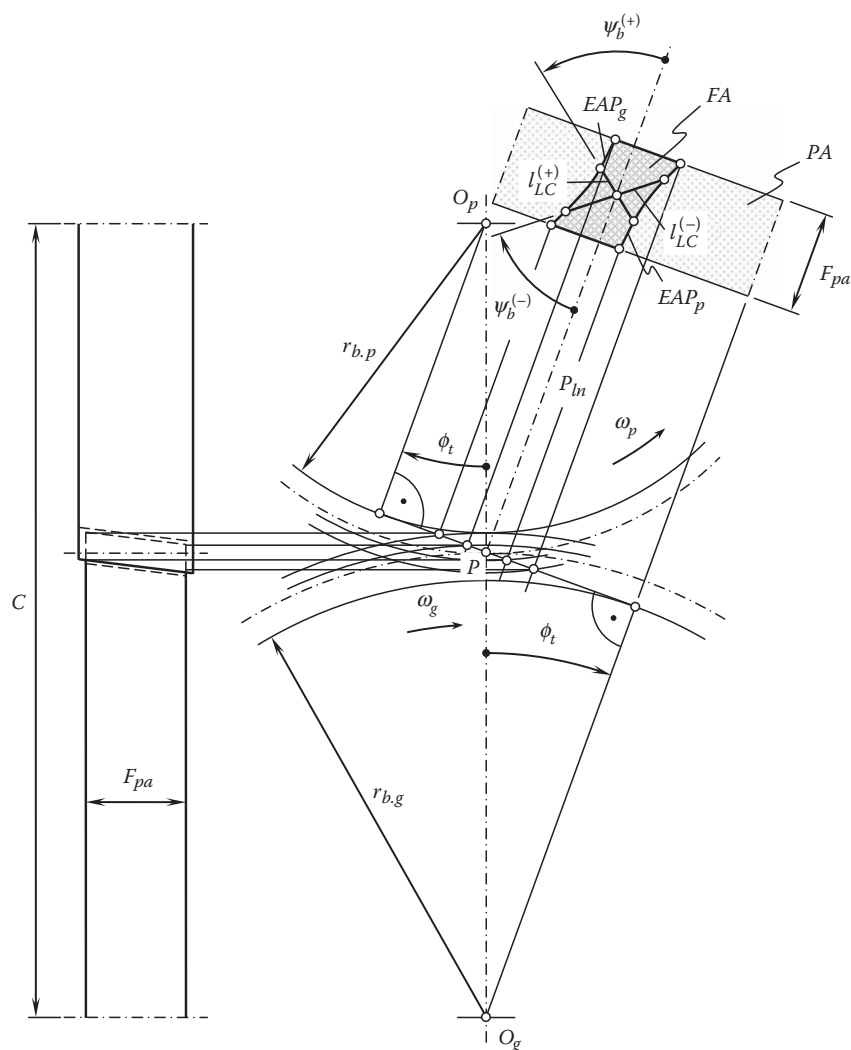


FIGURE 24.23

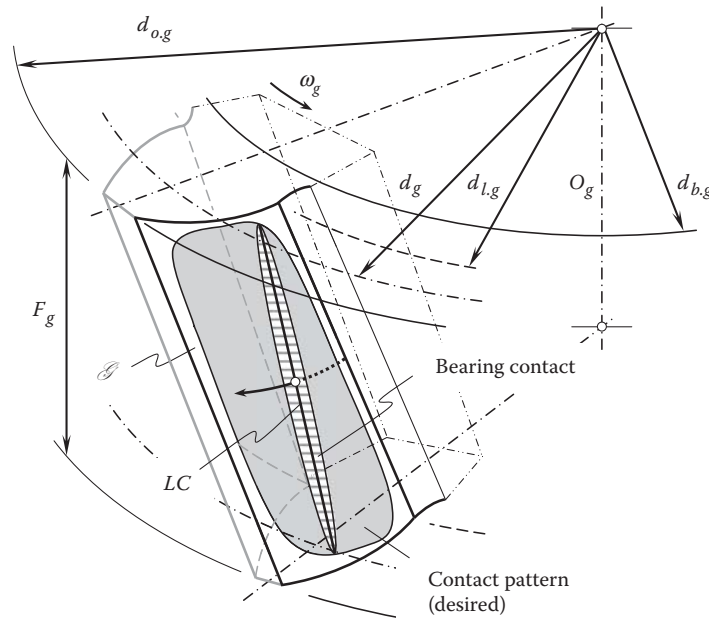
Impact of the geometry of the boundary curves,  $EAP_g$  and  $EAP_p$ , on the maximum length of a single line of contact,  $LC$ .

As noted previously, the maximum length of a single line of contact depends on the configuration of two lines,  $EAP_g$  and  $EAP_p$ . This means that changes to the shape as well as to the configuration of these two lines entail corresponding changes to the maximum length of a single line of contact,  $l_{LC}$ .

As an example, consider a parallel-axes gear pair composed of two helical involute gears that have the outside surface of the gear tooth shaped in the form of a cone of revolution.\* The gear pair is schematically illustrated in Figure 24.23. Because the plane of action,  $PA$ , is still tangent to the base cylinders and does not make a plane through the axis of rotation of the gear,  $O_g$ , and pinion,  $O_p$ , the borders  $EAP_g$  and  $EAP_p$  of the field of action,  $FA$ , are shaped in the form of two segments of a hyperbola. For a gear pair with a base helix angle of a certain value,  $\psi_b$ , the maximum length of the single line of contact is equal to a certain value,  $l_{LC}$ . However, if the gear pair is designed so as to have a base helix angle of that same value but the opposite sign (i.e., of the opposite hand of the helix), this immediately allows for a significant increase of the maximum length of the single line of contact (from  $l_{LC}^{(+)}$  to  $l_{LC}^{(-)}$ ). The gear pair that has a longer line of contact,  $LC$ , is capable of transmitting a higher power and features a higher power density. The latter is of critical importance for many applications.

Another example that illustrates the impact of changes to the design of a gear tooth flank on the maximum length,  $l_{LC}$ , of a single line of contact,  $LC$ , is illustrated in Figure 24.24.

\* Parallel-axes gearing of this particular kind is considered in more detail in Chapter 7 (see Figures 7.32 through 7.37, for example).

**FIGURE 24.24**

An example of a desired contact pattern on the tooth flanks of an involute gear.

The portions of tooth flanks of a gear that are close to the edges at both ends of the gear face are weaker compared to those within the interior of the tooth flanks. In order to avoid tooth breakage, it is often recommended to relieve the tooth flanks at both ends of the gear face. A similar relief is often made at the edges close to the top land of the gear teeth. For pinions that have lower tooth counts, the radius of curvature of the tooth flanks at points close to the bottom land is commonly small. It is often desired to eliminate these portions of the tooth flanks from interaction with conjugate tooth flanks of the mating gear. Tip relieving of the mating gear teeth allows for elimination of this area of the pinion tooth flank from interaction with the mating gear tooth. Ultimately, the desired contact pattern is shaped in the form of a closed loop, as schematically depicted in Figure 24.24.

Under an applied load, the contact line,  $LC$ , spreads to a form of narrow, ellipse-like bearing contact area. When the bearing contact area travels across the gear tooth flank, the corresponding contact pattern is covered by the bearing contact area.

With that said, relieving the gear tooth flanks, as shown in Figure 24.24, entails corresponding changes to the geometry and parameters of the field of action. Schematically, these changes are illustrated in Figure 24.25. Depending on the design parameters of the tooth flank relief, fields of action of different geometries 1, 2, 3, 4, and so on are obtained. The maximum length,  $l_{LC}$ , of a single line of contact,  $LC$ , depends on the actual shape and design parameters of the boundary of the field of action. In the case of the first field of action, the maximum length,  $l_{LC}^{(1)}$ , of a single line of contact,  $LC$ , is smaller compared to that in the second,  $l_{LC}^{(2)}$ ; third,  $l_{LC}^{(3)}$ ; and fourth,  $l_{LC}^{(4)}$ , cases (the lengths  $l_{LC}^{(2)}$  and  $l_{LC}^{(3)}$  are not shown in Figure 24.25).

Again, the longer the single line of contact, the better, as it makes possible a corresponding reduction in the contact load acting on the gear and the pinion teeth.

### 24.3.2 Effective Length of Lines of Contact in Parallel-Axes Gearing

When a gear pair is operating, the line of contact,  $LC$ , under the operating load spreads to a narrow strip of bearing contact, which is commonly shaped in the form of a long ellipse-like curve. The longer axis of the ellipse-like curve is equal to the length of a single line of contact. The length of the shorter axis depends on (1) the radii of curvature of the gear tooth flank and the pinion tooth flank, (2) the elastic properties of a material that the gear and the pinion are made of, and (3) the applied load. For a given gear pair that transmits torque of a specified value, the contact stress varies in time. The contact stress at a current instant of time depends on the angular

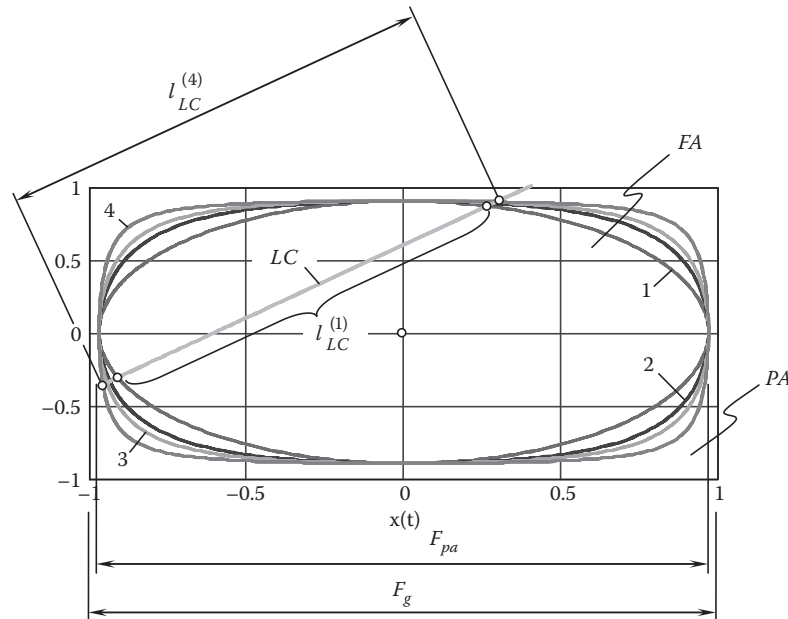


FIGURE 24.25

The maximum length,  $l_{LC}^{(i)}$ , of a single line of contact,  $LC$ , versus the design parameters of the relief of tooth flank edges.

orientation of the pinion in relation to the gear. This means that the maximum contact stress is observed at a certain instant of time, or, in other words, at a certain angular configuration of the pinion in relation to the gear.

#### 24.3.2.1 Effective Length of Lines of Contact in Spur Parallel-Axes Gearing

Again, let us consider the effective length of the lines of contact for the case of a parallel-axes spur gear.

When a gear pair is operated, either one or two pairs of teeth are in contact at a certain instant of time (for high contact ratio gearing, the number of pairs of teeth in contact simultaneously is equal to two, and it could be even higher).

In cases when only one pair of teeth is in contact, all the power is transmitted through a single bearing contact. This case is schematically illustrated in Figure 24.26. The contact stress depends only on the current location of the line of contact,  $LC$ , within the field of action,  $FA$ . The closer the line of contact is located to the bottom land of the pinion (closer to the  $EAP_g$  in Figure 24.26), the higher the contact stress developed (see Figure 24.10 for details). When the line of contact is close to the bottom land of the gear (closer to the  $EAP_p$  in Figure 24.26),

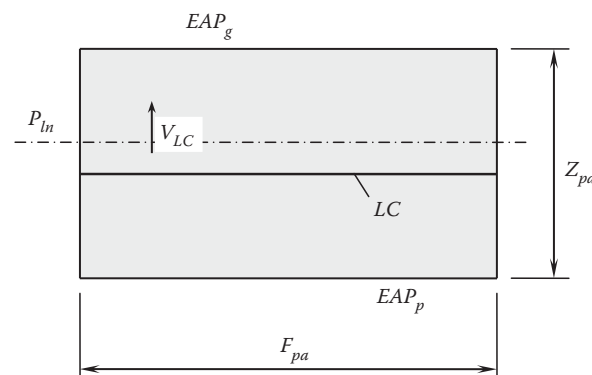


FIGURE 24.26

Configuration of the line of contact,  $LC$ , in a spur parallel-axes gearing at an instant of time that corresponds to contact of one pair of teeth of the gear and the pinion.

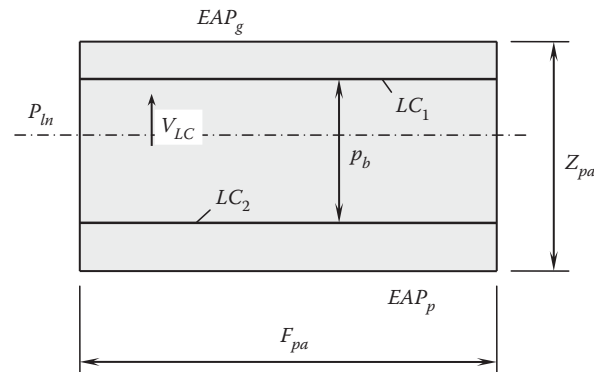


FIGURE 24.27

Configuration of the lines of contact,  $LC_1$  and  $LC_2$ , in a spur parallel-axes gearing at an instant of time that corresponds to contact of two pairs of teeth of the gear and the pinion.

the contact stress also increases. However, this rise is not that significant, as the relative curvature at the bottom land of the gear is a bit greater than the relative curvature at the bottom land of the pinion (see Figure 24.10).

The contact ratio of a gear pair is always greater than one. As a consequence, at a certain instant of time (for a certain angular configuration of the pinion in relation to the gear), the gear and pinion teeth contact one another not along one line of contact, but along two lines of contact instead. This is in part due to the fact that when the gears rotate, the line of contact,  $LC$ , travels within the field of action,  $FA$ , with a certain linear velocity,  $V_{LC}$ . Schematically, this case is illustrated in Figure 24.27. The lines of contact are labeled  $LC_1$  and  $LC_2$ . They are at a distance from each other, and this distance is equal to the base pitch,  $p_b$ , of the gear pair.

As two lines of contact are observed, the applied load is equally shared between the lines  $LC_1$  and  $LC_2$ .

The contact stress depends only on the current location of the lines of contact,  $LC_1$  and  $LC_2$ , within the field of action,  $FA$ . The closer the line of contact,  $LC_1$ , is located to the bottom land of the pinion (closer to the  $EAP_g$  in Figure 24.27), the higher the contact stress developed (see Figure 24.10 for details). When the line of contact,  $LC_2$ , is close to the bottom land of the gear (closer to the  $EAP_p$  in Figure 24.27) contact stress also increases. However, this rise is not that significant, as the relative curvature at the bottom land of the gear is greater than the relative curvature at the bottom land of the pinion (see Figure 24.10).

In cases of two or more lines of contact, the total length,  $l_{LC}^t$ , of the lines of contact,  $LC_i$ , is doubled (tripled, quadrupled, etc.). This makes it possible to have a corresponding reduction of contact stress as the applied load is shared along a longer (total) line of contact, which is evident. However, a length of line of contact that should be used for calculation of contact stress is not equal to the total length,  $l_{LC}^t$ , of the lines of contact. For this purpose, an effective length,  $l_{LC}^e$ , of the lines of contact should be entered into an expression for the calculation of contact stress.

When two or more lines of contact are observed, the total length,  $l_{LC}^t$ , of the lines of contact,  $LC_i$ , can be expressed by the following formula:

$$l_{LC}^t = l_{LC} \cdot [\text{trunc}(m_t) + 1] \quad (24.35)$$

In Equation 24.35, the  $\text{trunc}(m_t)$  function returns a number truncated to an integer portion of contact ratio,  $m_t$ .

For gearings that have contact ratio in the range of  $1 \leq m_t < 2$ ,  $\text{trunc}(m_t) = 1$ . Similarly, for gears with contact ratio in the range of  $2 \leq m_t < 3$ ,  $\text{trunc}(m_t) = 2$ , and so on.

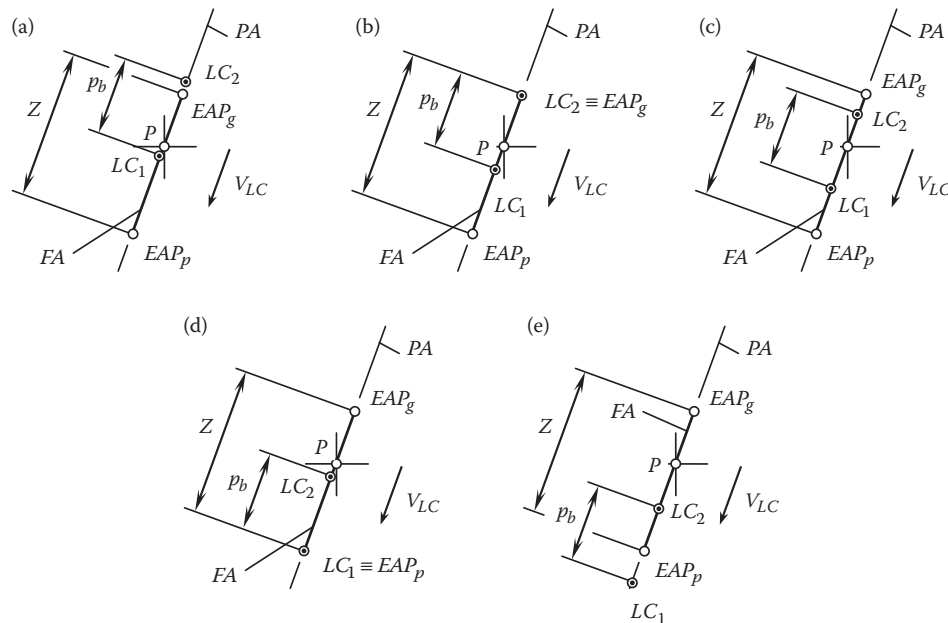
However, along with an increase of the length of the line of contact, a corresponding reduction of the applied load per unit length is observed. Therefore, for the calculation of maximum contact stress, the applied load per unit length should be divided by  $\text{trunc}(m_t)$ . Ultimately, this returns an effective length,  $l_{LC}^e$ , of the lines of contact,  $LC_i$ , for the case of spur gearing:

$$l_{LC}^e = l_{LC} \cdot \text{trunc}(m_t) \quad (24.36)$$

Figure 24.28a illustrates an example of the function,  $l_{LC}^t = l_{LC}^t(\varphi_g)$ , for parallel-axes gearing with a contact ratio in the range of  $1 \leq m_t < 2$ . A similar example of the function,  $l_{LC}^e = l_{LC}^e(\varphi_g)$ , for parallel-axes gearing with a





**FIGURE 24.30**

Progression of the two lines of contact,  $LC_1$  and  $LC_2$ , through the field of action,  $FA$ . Parts (a) through (e) are discussed in the text.

problem reduces to a determination of an instant of time of single-line-of-contact meshing, when the line of contact occupies the closest possible location in relation to the bottom land of the pinion.

Consider the progression of the two lines of contact,  $LC_1$  and  $LC_2$ , through the field of action,  $FA$ , as schematically depicted in Figure 24.30.

At a certain instant of time, the gear tooth flank,  $\mathcal{G}$ , and the pinion tooth flank,  $\mathcal{P}$ , contact one another along just one line of contact,  $LC_1$ . This relative orientation of the gear and pinion is schematically illustrated in Figure 24.30a. The second potential line of contact,  $LC_2$ , is at a distance,  $p_b$ , from the first line of contact,  $LC_1$ . The second line of contact,  $LC_2$ , is located within the plane of action,  $PA$ , but not within the field of action,  $FA$ .

When the gears rotate, the lines of contact,  $LC_1$  and  $LC_2$ , travel within the plane of action. The speed of this motion is denoted by  $V_{LC}$ . At a certain instant of time, the second line of contact,  $LC_2$ , reaches the line  $EAP_g$ . Starting from this instant of time, two lines of contact,  $LC_1$  and  $LC_2$ , are observed (see Figure 24.30b). In this particular configuration of the gear and the pinion, the distance from the line of contact,  $LC_2$ , to the bottom land of the pinion is the closest possible.

While the rotation progresses, both lines of contact continue traveling within the field of action and occupy a location shown in Figure 24.30c.

At the final stage of double-line-of-contact meshing (see Figure 24.30d), the first line of contact,  $LC_1$ , occupies a position within the field of action at which it is closest to the bottom land of the gear. For this configuration, the line of contact,  $LC_1$ , is aligned with the line  $EAP_p$ .

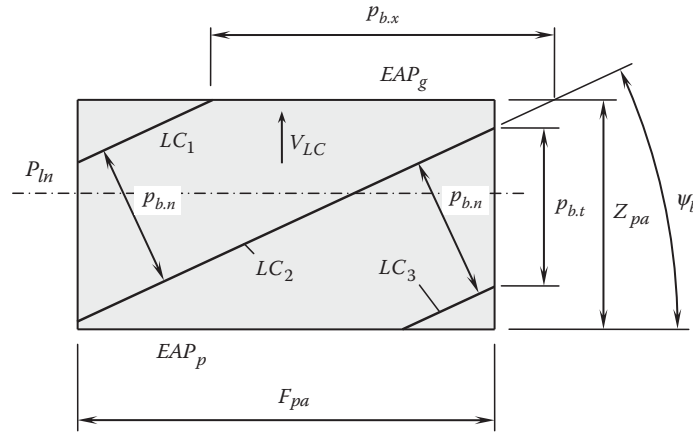
Under further rotation of the gears, the gear tooth flanks,  $\mathcal{G}$ , and pinion tooth flanks,  $\mathcal{P}$ , again contact one another along just one line of contact,  $LC_2$  (see Figure 24.30e). The first line of contact is located outside the field of action,  $FA$ .

As is clear from the above consideration, the calculation of contact stress should be performed for a relative orientation of the gear and pinion for which the first line of contact,  $LC_1$ , aligns with the line  $EAP_g$ . This particular configuration of the gear and pinion is the most critical from the contact stress standpoint.

### 24.3.2.2 Effective Length of Lines of Contact in Helical Parallel-Axes Gearing

The effective length of the lines of contact is of critical importance for the calculation of contact stress in helical involute gearing, as well as in gearing of all other kinds, namely, in intersected-axes and crossed-axes gearing.

The field of action for an involute helical parallel-axes gearing is schematically depicted in Figure 24.31. The configuration shown in Figure 24.31 corresponds to a case when three lines of contact,  $LC_1$ ,  $LC_2$ , and  $LC_3$ , are

**FIGURE 24.31**

Configuration of the lines of contact,  $LC_1$ ,  $LC_2$ , and  $LC_3$  in a helical parallel-axis gearing at an instant of time that corresponds to contact of three pairs of teeth of the gear and the pinion.

observed. The lines of contact,  $LC_i$  (here the number of a line of contact is denoted by  $i$ ;  $i = 1, 2, 3, \dots$  is an integer number), are parallel to each other and are apart from one another at a distance equal to the normal base pitch,  $p_{b,n}$ . The relative configuration of the lines of contact,  $LC_i$ , can be expressed either in terms of the transverse base pitch,  $p_{b,t}$ , or the axial base pitch,  $p_{b,x}$ . This is because the following relations are valid (see Figure 24.31):

$$p_{b,t} = \frac{p_{b,n}}{\cos \psi_b} \quad (24.37)$$

$$p_{b,x} = \frac{p_{b,n}}{\sin \psi_b} \quad (24.38)$$

As in helical gearing, the gear teeth are at the base helix angle,  $\psi_b$ , in relation to the gear axis of rotation,  $O_g$ ; therefore, all the lines of contact,  $LC_i$ , are at the angle  $\psi_b$  with respect to the axis  $O_g$ . Due to this, the total contact ratio,  $m_t$ , of the helical gear is greater when compared to that in a spur gear with design parameters similar to those in helical gearing.

The lines of contact,  $LC_1$ ,  $LC_2$ , and  $LC_3$ , are of certain lengths,  $l_{LC}^{(1)}$ ,  $l_{LC}^{(2)}$ , and  $l_{LC}^{(3)}$ , (or, briefly, of a certain length  $l_{LC}^{(i)}$ ). The total length,  $l_{LC}^t$ , of the lines of contact at a given instant of time is equal to:

$$l_{LC}^t = l_{LC}^{(1)} + l_{LC}^{(2)} + l_{LC}^{(3)} = \sum_{i=1}^n l_{LC}^{(i)} \quad (24.39)$$

In Equation 24.39, the total number of lines of the action is designated as  $n$ .

For a specified instant of time, the length,  $l_{LC}^{(i)}$ , of each line of contact,  $LC_i$ , can be expressed in terms of effective face width,  $F^e$ ; width of the field of action,  $Z$ ; the base pitch,  $p_b$ ; and the base helix angle,  $\psi_b$ . It is evident that the length,  $l_{LC}^{(i)}$ , is a time-dependent parameter; that is, the actual value of the length,  $l_{LC}^{(i)}$ , is a function of the current value of angle of rotation of the gear,  $\varphi_g$ :

$$l_{LC}^{(i)} = l_{LC}^{(i)}(\varphi_g) \quad (24.40)$$

Ultimately, the total length,  $l_{LC}^t$ , of the lines of contact is also a time-dependent parameter; that is, the actual value of the length,  $l_{LC}^t$ , is a function of the current value of angle of rotation of the gear,  $\varphi_g$ :

$$l_{LC}^t = l_{LC}^t(\varphi_g) \quad (24.41)$$

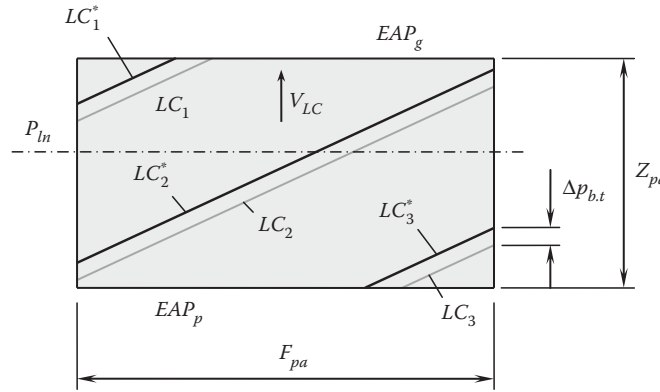


FIGURE 24.32

Variation in time of the length of a single line of contact.

The dependence of the total length,  $l_{LC}^t$ , of the lines of contact from the angle of rotation of the gear,  $\varphi_g$ , is illustrated in Figure 24.32.

At a certain initial configuration of the gear in relation to the mating pinion, three lines of contact,  $LC_1$ ,  $LC_2$ , and  $LC_3$ , are observed. The length of each line of contact is equal to  $l_{LC}^{(1)}$ ,  $l_{LC}^{(2)}$ , and  $l_{LC}^{(3)}$ , respectively.

When the gears rotate, all the lines of contact,  $l_{LC}^{(i)}$ , travel together with the plane of action,  $PA$ . Let us assume that the lines of contact travel from positions labeled  $LC_1$ ,  $LC_2$ , and  $LC_3$  to corresponding positions designated as  $LC_1^*$ ,  $LC_2^*$ , and  $LC_3^*$ . In the new position, the lines of contact are of lengths  $l_{LC}^{(1)*}$ ,  $l_{LC}^{(2)*}$ , and  $l_{LC}^{(3)*}$ , respectively.

The active portions of the lines of contact are located within the field of action,  $FA$ . When the lines of action,  $l_{LC}^{(i)}$ , travel at a certain distance,  $\Delta p_t$ , the length of each line of action changes from  $l_{LC}^{(i)}$  to  $l_{LC}^{(i)*}$ . Consequently, the total length,  $l_{LC}^t$ , of the lines of contact also changes.

The effective length of the lines of contact,  $l_{LC}^e$ , is used for the calculation of contact stress. Referring to Figure 24.33, consider a field of action,  $FA$ , with three lines of contact,  $LC_1$ ,  $LC_2$  and  $LC_3$ .

The gear pair can be sliced by numerous planes perpendicular to the axis of rotation of the gear. Certain section planes intersect just one line of contact (line of contact  $LC_2$  in Figure 24.33). Other section planes within the length,  $\Delta p_x$ , intersect two lines of contact (lines of contact  $LC_1$  and  $LC_2$  in Figure 24.33). Within portions of the field of action, where two (or more) lines of contact overlap one another ( $\Delta p_x$ ), the torque being transmitted is shared equally between the lines of contact. Thus, the nominal load,  $P_{nom}$ , in a section with one line of contact is equally shared between two lines of contact in a section with two lines of contact (see Figure 24.33). Due to this, the effective length of the lines of contact,  $l_{LC}^e$ , is shorter compared to that for the total length,  $l_{LC}^t$ , of lines of contact. As the length,  $l_{LC}^e$ , is shorter compared to the length,  $l_{LC}^t$ , the calculated value of contact stress is higher.

It can be shown that for helical gearing, the effective length of the lines of contact,  $l_{LC}^e$ , depends on the actual value of the angle of rotation of the gear,  $\varphi_g$ :

$$l_{LC}^e = l_{LC}^e(\varphi_g) \quad (24.42)$$

The effective length of the lines of contact,  $l_{LC}^e$ , can be calculated in the following way.

Different portions of the lines of contact can be distinguished. First, some portions of the lines of contact do not overlap with each other. Portions of this particular kind can be designated as  $LC_{0,o}^{(i)}$ . Then, a certain number of portions of the lines of contact can overlap with one another just once. Portions of this kind are designated as  $LC_{1,o}^{(i)}$ . Similarly, a certain number of portions of the lines of contact can overlap with one another twice. Portions of this kind are designated as  $LC_{2,o}^{(i)}$ , and so on.

With that said, the effective length of the lines of contact,  $l_{LC}^e$ , is equal to the total length of the portions,  $LC_{0,o}^{(i)}$ , times 1, plus the total length of the portions,  $LC_{1,o}^{(i)}$ , times 1/2, plus the total length of the portions,  $LC_{2,o}^{(i)}$ , times 1/3 and so on.

For the calculation of the effective length of the lines of contact,  $l_{LC}^e$ , it is convenient to develop corresponding computer codes.



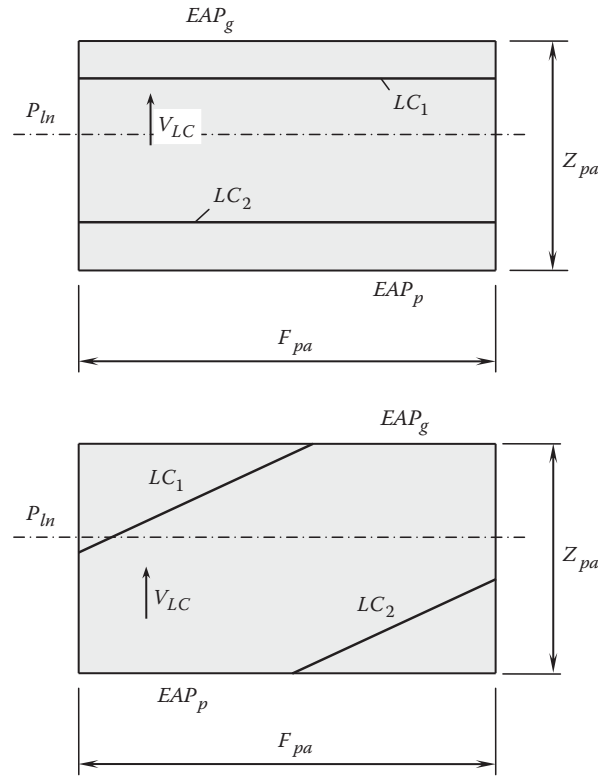


**FIGURE 24.34**  
Different bearing capacities of spur and helical gearing with equal contact ratios.

by the entire active face width of the gear,  $F_{pa}$ . The load per unit length of the face width,  $\mathbf{p}_F^t$ , can be expressed in terms of the torque on the driving shaft,  $\mathbf{T}_p$ ; the base diameter of the pinion,  $d_{b,p}$ ; and the effective face width,  $F_{pa}$ :

$$p_F^t = 2 \frac{T_p}{d_{b,p} F_{pa}} \quad (24.43)$$

where the equalities  $p_F^t = |\mathbf{p}_F^t|$  and  $T_p = |\mathbf{T}_p|$  are observed.

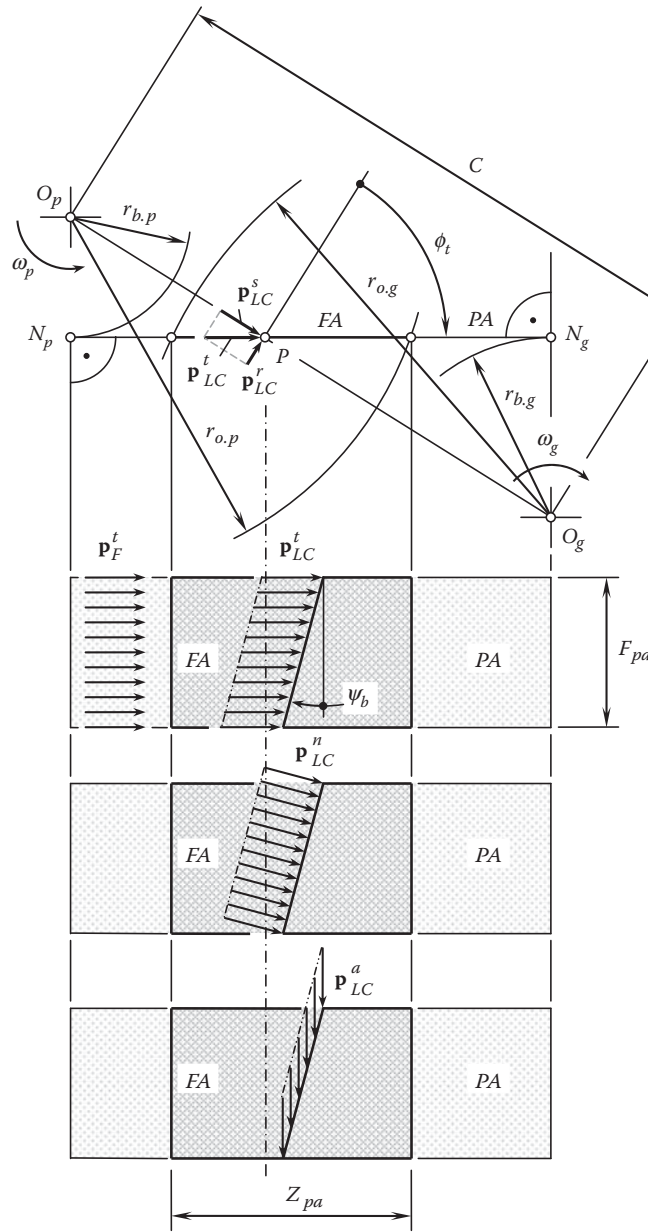
The load is evenly distributed within the line of contact,  $LC$  (consider a simplified case when the entire power is transmitted through the load bearing along a single line of contact,  $LC$ ). The load per unit length of the effective length of lines of contact,  $\mathbf{p}_{LC}^t$ , can be expressed in terms of the torque on the driving shaft,  $\mathbf{T}_p$ ; the base diameter of the pinion,  $d_{b,p}$ ; and the length,  $l_{LC}^e$ , of the line of contact:

$$p_{LC}^t = |\mathbf{p}_{LC}^t| = 2 \frac{T_p}{d_{b,p} l_{LC}^e} \quad (24.44)$$

The effective length of the lines of contact,  $l_{LC}^e$ , should be entered into Equation 24.15 for the calculation of the load,  $\mathbf{p}_{LC}^t$ , per unit length of the line of contact. In cases of single line of contact, the effective length of the lines of contact,  $l_{LC}^e$ , is equal to the length of the line of contact,  $l_{LC}$ .

The load per unit length of the line of contact,  $\mathbf{p}_{LC}^n$ , that causes contact stress is perpendicular to the gear tooth flank. This load can be expressed in terms of the load  $\mathbf{p}_{LC}^t$ , and the base helix angle,  $\psi_b$ :

$$p_{LC}^n = |\mathbf{p}_{LC}^n| = 2 \frac{T_p}{d_{b,p} l_{LC}^e} \cos \psi_b \quad (24.45)$$

**FIGURE 24.35**

Components of the distributed force of interaction of the gear tooth flank,  $\mathcal{G}$ , and the pinion tooth flank,  $\mathcal{P}$ , in a helical parallel-axes gear pair.

Ultimately, an expression for the calculation of one more load that acts within the plane of action can be derived from Figure 24.35. This load,  $p_{LC}^a$ , acts in the axial direction of the gears:

$$p_{LC}^a = |\mathbf{p}_{LC}^a| = 2 \frac{T_p}{d_{b,p} l_{LC}^e} \sin \psi_b \quad (24.46)$$

The separating load per unit length of the line of contact,  $\mathbf{p}_{LC}^s$ , acts within the plane through the axis of rotation of the gear,  $O_g$ , and the pinion,  $O_p$ . This load can be calculated from the expression:

$$p_{LC}^s = |\mathbf{p}_{LC}^s| = 2 \frac{T_p}{d_{b,p} l_{LC}^e} \sin \phi_t \quad (24.47)$$



The component,  $\mathbf{p}_{LC}^r$ , acts in the direction perpendicular to the plane through the axes,  $O_g$  and  $O_p$ . For the calculation of this component, an expression is derived:

$$p_{LC}^r = |\mathbf{p}_{LC}^r| = 2 \frac{T_p}{d_{b,p} l_{LC}^e} \cos \phi_t \quad (24.48)$$

Equations 24.43 through 24.48 are valid for parallel-axes gearing of all kinds: spur, helical, herringbone, circular-arc, and so on. These equations can be enhanced for cases of real gearing that have point contact of the gear and pinion tooth flanks.

The components  $\mathbf{p}_{LC}^t$ ,  $\mathbf{p}_{LC}^n$ ,  $\mathbf{p}_{LC}^a$ ,  $\mathbf{p}_{LC}^s$ , and  $\mathbf{p}_{LC}^r$  in Equations 24.44 through 24.48 are expressed in terms of the base diameter of the pinion,  $d_{b,p}$ , and the base helix angle,  $\psi_b$ . For the needs of practical (engineering) calculations, it is preferable to express all of these components in terms of design parameters of the pinion.

First, the base diameter of the pinion can be calculated from the formula:

$$d_{b,p} = d_p \cos \phi_{t,p} \quad (24.49)$$

The transverse profile angle,  $\phi_t$ , can be expressed in terms of the normal pressure angle,  $\phi_n$ , and the pitch helix angle,  $\psi$ :

$$\tan \phi_t = \frac{\tan \phi_n}{\cos \psi} \quad (24.50)$$

The last two equations allow for the following expression to calculate the pinion base diameter:

$$d_{b,p} = d_p \cdot \sqrt{1 - \sin^2 \phi_n \sin^2 \psi} \quad (24.51)$$

Then, the base helix angle,  $\psi_b$ , can be expressed in terms of the pitch helix angle,  $\psi$ , and the normal pressure angle,  $\phi_n$ :

$$\psi_b = \sin^{-1} (\cos \phi_n \sin \psi) \quad (24.52)$$

After substituting these expressions for  $d_{b,p}$  and for  $\psi_b$  into Equations 24.44 through 24.48, the equations cast into:

$$p_{LC}^t = 2 \frac{T_p}{d_{b,p} l_{LC}^e} \quad (24.53)$$

$$p_{LC}^n = 2 \frac{T_p}{d_{b,p} l_{LC}^e} \sqrt{1 - \cos^2 \phi_n \sin^2 \psi} \quad (24.54)$$

$$p_{LC}^a = 2 \frac{T_p}{d_{b,p} l_{LC}^e} \cos \phi_n \sin \psi \quad (24.55)$$

$$p_{LC}^s = 2 \frac{T_p}{d_{b,p} l_{LC}^e} \cdot \frac{\tan \phi_n}{\sqrt{\cos^2 \psi + \tan^2 \phi_n}} \quad (24.56)$$

$$p_{LC}^r = 2 \frac{T_p}{d_{b,p} l_{LC}^e} \cdot \frac{\cos \psi}{\sqrt{\cos^2 \psi + \tan^2 \phi_n}} \quad (24.57)$$

Equations 24.53 through 24.57 return the average values of gear tooth loading. They are valid for gears that have relatively large tooth counts.

For gears that have large tooth counts, the variation of the design parameters of the gear and pinion tooth flanks within the tooth height is negligibly small and thus can be neglected. For low-tooth-count gearing, the variation of the design parameters of the gear and pinion tooth flanks cannot be ignored, as this variation causes significant changes to the geometry of the tooth flanks. Therefore, it is necessary to take into account a variation of the gear tooth loading within the tooth height. For this purpose, the diameter,  $d_{y,p}$ , of the location of a current point,  $m$ , within the line of contact should be considered a variable parameter. Then, the helix angle,  $\psi_y$ , on a cylinder of the diameter,  $d_{y,p}$ , can be calculated from:

$$\psi_y(d_{y,p}) = \tan^{-1} \left( \frac{d_{y,p}}{d_{b,p}} \tan \psi \right) \quad (24.58)$$

Equation:

$$d_{b,p}(d_{y,p}) = d_{y,p} \sqrt{1 - \sin^2 \phi_n \sin^2 \psi} \quad (24.59)$$

for the base diameter,  $d_{b,p}$ , and Equation 24.58 for the helix angle,  $\psi_y$ , make it possible to have a set of equations for the calculation of loading for low-tooth-count gearing:

$$p_{LC}^t = 2 \frac{T_p}{d_{b,p} l_{LC}^e} \quad (24.60)$$

$$p_{LC}^n(d_{y,p}) = 2 \frac{T_p \sqrt{1 - \cos^2 \phi_n \sin^2 \psi(d_{y,p})}}{d_{y,p} \sqrt{1 - \sin^2 \phi_n \sin^2 \psi} l_{LC}^e} \quad (24.61)$$

$$p_{LC}^a(d_{y,p}) = 2 \frac{T_p \cos \phi_n \sin \psi(d_{y,p})}{d_{y,p} l_{LC}^e \sqrt{1 - \sin^2 \phi_n \sin^2 \psi}} \quad (24.62)$$

$$p_{LC}^s(d_{y,p}) = 2 \frac{T_p \tan \phi_n}{d_{y,p} l_{LC}^e \sqrt{(1 - \sin^2 \phi_n \sin^2 \psi) \cdot [\cos^2 \psi(d_{y,p}) + \tan^2 \phi_n]}} \quad (24.63)$$

$$p_{LC}^r(d_{y,p}) = 2 \frac{T_p \cos \psi}{d_{y,p} l_{LC}^e \sqrt{(1 - \sin^2 \phi_n \sin^2 \psi) \cdot [\cos^2 \psi(d_{y,p}) + \tan^2 \phi_n]}} \quad (24.64)$$

It should be pointed out here that for the calculation of gear tooth strength, the component  $\mathbf{p}_{LC}^n$  is the most critical.

The performed analysis is of critical importance for the purposes of calculation of a gear tooth loading when performing contact stress and strength, as well as bending strength and stress calculations.

This analysis can be enhanced to gearing of other kinds, that is, to intersected-axes gearing, as well as crossed-axes gearing.

## 24.5 Method for Simulating the Interaction of Gear and Mating Pinion Tooth Flanks

A method for simulating the interaction of gear and mating pinion tooth flanks is developed based on the method\* proposed by Radzevich for the experimental simulation of machining of a sculptured surface on a multiaxis NC machine [95,98,119]. The method of simulation is illustrated in Figure 24.36.

\* Pat. No.1449246 (USSR). *A Method of Experimental Simulation of Machining a Sculptured Part Surface on a Multi-Axis NC Machine*. S.P. Radzevich. Filed: February 17, 1987, Int. Cl. B 23 C, 3/16.

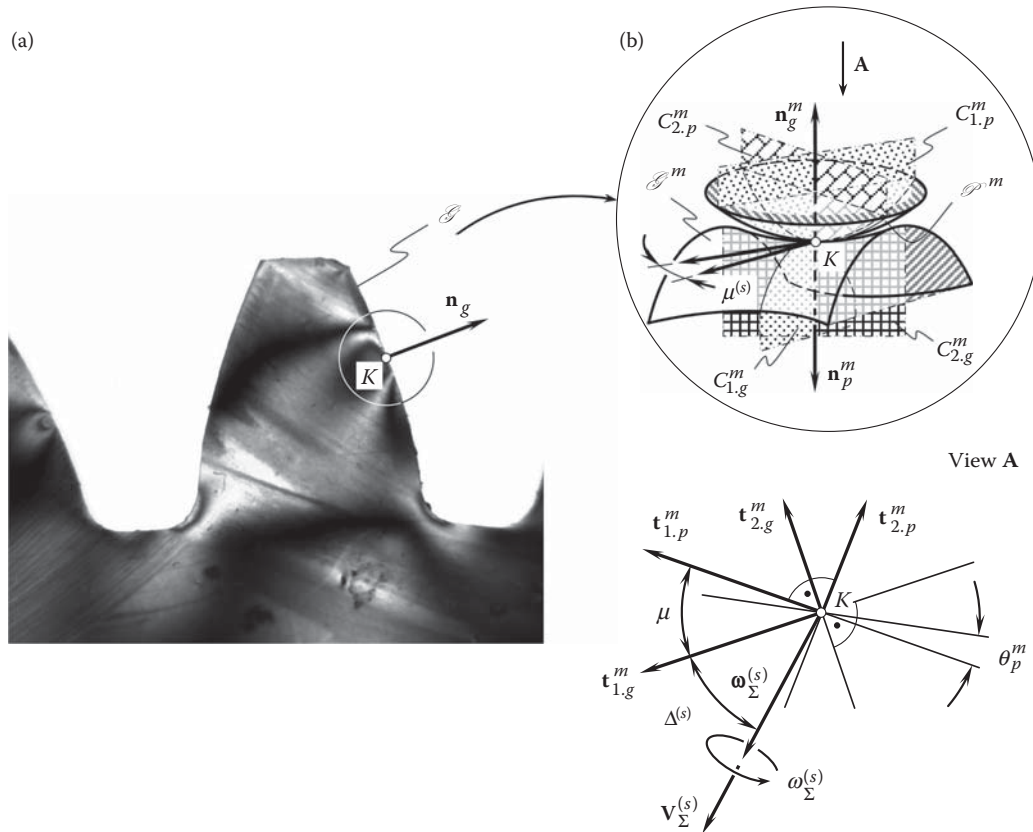


FIGURE 24.36

Schematic of the method for the simulation of the interaction of a gear tooth flank,  $\mathcal{G}$ , and the mating pinion tooth flank,  $\mathcal{P}$ . Parts (a) and (b) are discussed in the text.

As an example of implementation of the method of simulation, consider a gear tooth flank,  $\mathcal{G}$  (see Figure 24.36a), that interacts with the pinion tooth flank,  $\mathcal{P}$  (not shown in Figure 24.36a).

The method of simulation of the interaction of the gear and pinion tooth flanks,  $\mathcal{G}$  and  $\mathcal{P}$ , is carried out with the equivalent models,  $\mathcal{G}^m$ , of the gear tooth flank and the pinion tooth flank,  $\mathcal{P}^m$  (see Figure 24.36b).

The local topology of the surfaces,  $\mathcal{G}^m$  and  $\mathcal{P}^m$ , can be uniquely specified by two parameters, the mean curvature,  $\tilde{M}_{g(p)}$ , and the Gaussian curvature,  $\tilde{G}_{g(p)}$ , at the point of contact of the tooth flanks,  $\mathcal{G}$  and  $\mathcal{P}$ . As there are only two parameters of local topology, the variety of kinds of modeling surfaces,  $\mathcal{G}^m$  and  $\mathcal{P}^m$ , is limited to only [107,113,118].

The surface,  $\mathcal{G}^m$ , as well as the surface,  $\mathcal{P}^m$ , is a quadric surface. Both surfaces,  $\mathcal{G}^m$  and  $\mathcal{P}^m$ , make tangency at a point,  $K$ . The local geometry of the tangency of the surfaces,  $\mathcal{G}^m$  and  $\mathcal{P}^m$ , is identical to that of the gear tooth flank,  $\mathcal{G}$ , and the pinion tooth flank,  $\mathcal{P}$ , respectively. Due to this, the unit tangent vectors,  $\mathbf{t}_{1,g}^{(m)}$  and  $\mathbf{t}_{2,g}^{(m)}$ , of the principal directions on the quadric surface,  $\mathcal{G}^m$ , align with the corresponding unit tangent vectors,  $\mathbf{t}_{1,g}$  and  $\mathbf{t}_{2,g}$ , of the gear tooth flank,  $\mathcal{G}$ . Moreover, the principal radii of curvature,  $R_{1,g}^{(m)}$  and  $R_{2,g}^{(m)}$ , of the quadric surface,  $\mathcal{G}^m$ , at every contact point,  $K$ , are equal to the corresponding principal radii of curvature,  $R_{1,g}$  and  $R_{2,g}$ , of the gear tooth flank,  $\mathcal{G}$  (that is, the identities  $R_{1,g}^{(m)} \equiv R_{1,g}$  and  $R_{2,g}^{(m)} \equiv R_{2,g}$  are observed). Due to this, Euler's formula yields the conclusion that in the differential vicinity of a contact point,  $K$ , the surfaces  $\mathcal{G}^m$  and  $\mathcal{G}$  are locally congruent to each other up to the members of the second order.

A similar statement is valid for the quadric surface,  $\mathcal{P}^m$ , that is used for the local simulation of the pinion tooth flank,  $\mathcal{P}$ . At a point of contact,  $K$ , the unit tangent vectors,  $\mathbf{t}_{1,p}^{(m)}$  and  $\mathbf{t}_{2,p}^{(m)}$ , of the principal directions on the quadric surface,  $\mathcal{P}^m$ , align with the corresponding unit vectors,  $\mathbf{t}_{1,p}$  and  $\mathbf{t}_{2,p}$ , of the pinion tooth flank,  $\mathcal{P}$ . The principal radii of curvature,  $R_{1,p}^{(m)}$  and  $R_{2,p}^{(m)}$ , of the quadric surface,  $\mathcal{P}^m$ , are also equal to the corresponding principal radii of curvature,  $R_{1,p}$  and  $R_{2,p}$ , of the surface,  $\mathcal{P}$  (that is, the identities  $R_{1,p}^{(m)} \equiv R_{1,p}$  and  $R_{2,p}^{(m)} \equiv R_{2,p}$  are observed). Therefore, in the differential vicinity of every contact point  $K$ , the surfaces  $\mathcal{P}^m$  and  $\mathcal{P}$  are locally congruent to each other up to the members of the second order.

For the orthogonally  $(U_g, V_g)$ -parameterized gear tooth flank,  $\mathcal{G}$ , the ratio  $\partial U_g / \partial V_g$  determines the value of  $\tan \xi_g$ . Here, the angle that the unit vectors,  $\mathbf{t}_{1,g}$  and  $\mathbf{t}_{2,g}$ , of the principal directions form with the coordinate  $U_g$ - and  $V_g$ -lines on the gear tooth flank,  $\mathcal{G}$ , is designated as angle,  $\xi_g$ . Usually, parameterization of the surface,  $\mathcal{G}$ , is not orthogonal. In such a case, the angle  $\tan \xi_g$  (not shown in Figure 24.36b) can be calculated from the formula [107,113,118]:

$$\sin \xi_g = \frac{\partial V_g}{\partial U_g} \left[ \left( \frac{\partial V_g}{\partial U_g} \right)^2 - 2 \frac{\partial V_g}{\partial U_g} \cos \omega_g + 1 \right]^{-\frac{1}{2}} \quad (24.65)$$

For the orthogonally  $(U_p, V_p)$ -parameterized pinion tooth flank,  $\mathcal{P}$ , the ratio  $\partial U_p / \partial V_p$  determines the value of  $\tan \xi_p$ . Here, the angle that the unit vectors,  $\mathbf{t}_{1,p}$  and  $\mathbf{t}_{2,p}$ , of the principal directions form with the coordinate  $U_p$ - and  $V_p$ -lines on the pinion tooth flank,  $\mathcal{P}$ , is designated as an angle,  $\xi_p$ . Usually, parameterization of the pinion tooth surface,  $\mathcal{P}$ , is not orthogonal. In such a case, angle  $\tan \xi_p$  (not shown on Figure 24.36b) can be calculated from the formula [107,113,118]:

$$\sin \xi_p = \frac{\partial V_p}{\partial U_p} \left[ \left( \frac{\partial V_p}{\partial U_p} \right)^2 - 2 \frac{\partial V_p}{\partial U_p} \cos \omega_p + 1 \right]^{-\frac{1}{2}} \quad (24.66)$$

The quadric surfaces,  $\mathcal{G}^m$  and  $\mathcal{P}^m$ , are turned about the unit normal vector,  $\mathbf{n}_g^{(m)}$ , relative to each other through an angle,  $\mu^{(s)}$ . The angle,  $\mu^{(s)}$ , is the angle of the local relative orientation of the modeling surfaces  $\mathcal{G}^m$  and  $\mathcal{P}^m$ . The angle,  $\mu^{(s)}$ , is identical to the angle,  $\mu$ , of the local relative orientation of the actual gear and pinion tooth surfaces,  $\mathcal{G}$  and  $\mathcal{P}$  (that is,  $\mu^{(s)} \equiv \mu$ ). Angle  $\mu$  is the angle that makes the first,  $\mathbf{t}_{1,g}$  and  $\mathbf{t}_{1,p}$ , (or the second,  $\mathbf{t}_{2,g}$  and  $\mathbf{t}_{2,p}$ ) principal directions of the tooth flanks,  $\mathcal{G}$  and  $\mathcal{P}$ , at the point of contact [107,113,118]:

$$\mu^{(s)} \equiv \mu = \tan^{-1} \frac{|\mathbf{t}_{1,g} \times \mathbf{t}_{1,p}|}{\mathbf{t}_{1,g} \cdot \mathbf{t}_{1,p}} \equiv \tan^{-1} \frac{|\mathbf{t}_{2,g} \times \mathbf{t}_{2,p}|}{\mathbf{t}_{2,g} \cdot \mathbf{t}_{2,p}} \quad (24.67)$$

The local relative orientation of the quadric surfaces,  $\mathcal{G}^m$  and  $\mathcal{P}^m$ , in the differential vicinity of the point,  $K$ , is identical to the local relative orientation of the actual tooth surfaces,  $\mathcal{G}$  and  $\mathcal{P}$ .

The trajectory of a point,  $m$ , within the line of contact,  $LC$ , relative to the gear tooth flank,  $\mathcal{G}$ , can be represented as a vector sum of the motions that the surfaces,  $\mathcal{G}$  and  $\mathcal{P}$ , perform in the mesh.

When simulating the meshing of gear and its mating pinion tooth flanks, the quadric surfaces,  $\mathcal{G}^m$  and  $\mathcal{P}^m$ , perform the relative motion with respect to one another.

The instant relative motion of the tooth flanks,  $\mathcal{G}$  and  $\mathcal{P}$ , in meshing can be represented as an instant screw motion. Therefore, when simulating the mesh, the modeling quadric surfaces,  $\mathcal{G}^m$  and  $\mathcal{P}^m$ , perform rotation with the resultant angular velocity,  $\boldsymbol{\omega}_\Sigma^{(s)}$ , in addition to the resultant linear motion,  $\mathbf{V}_\Sigma^{(s)}$ .

While simulating, the resultant relative motion,  $\mathbf{V}_\Sigma^{(s)}$ , of the modeling surfaces,  $\mathcal{G}^m$  and  $\mathcal{P}^m$ , is identical to that,  $\mathbf{V}_\Sigma$ , of the actual gear tooth flank,  $\mathcal{G}$ , and the pinion tooth flank,  $\mathcal{P}$  (that is,  $\mathbf{V}_\Sigma^{(s)} \equiv \mathbf{V}_\Sigma$ ). For this purpose, the angle,  $\Delta^{(s)}$ , that the vector,  $\mathbf{V}_\Sigma^{(s)}$ , forms with the unit tangent vector,  $\mathbf{t}_{1,g}^{(m)}$ , of the first principal direction on the quadric surface,  $\mathcal{G}^m$ , is identical to the similar angle,  $\Delta$ , that the vector,  $\mathbf{V}_\Sigma$ , makes with the unit tangent vector,  $\mathbf{t}_{1,g}$ , of the first principal direction on the gear tooth flank,  $\mathcal{G}$  (that is,  $\Delta^{(s)} \equiv \Delta$ ).

The instant relative screw motion of the modeling quadric surfaces,  $\mathcal{G}^m$  and  $\mathcal{P}^m$ , is identical to that of the gear tooth flank,  $\mathcal{G}$ , and the pinion tooth flank,  $\mathcal{P}$ .

At every contact point,  $K$ , implementation of the method of experimental simulation (see Figure 24.36) ensures local identity to each other of all geometrical and kinematical parameters of a gear mesh to be modeled [95]:

- Of the quadric surface,  $\mathcal{G}^m$ , and the actual gear tooth flank surface,  $\mathcal{G}$
- Of the quadric surface,  $\mathcal{P}^m$ , and the actual pinion tooth flank,  $\mathcal{P}$
- The relative local orientation of the quadric surfaces,  $\mathcal{G}^m$  and  $\mathcal{P}^m$ , and the relative local orientation of the actual tooth flanks,  $\mathcal{G}$  and  $\mathcal{P}$

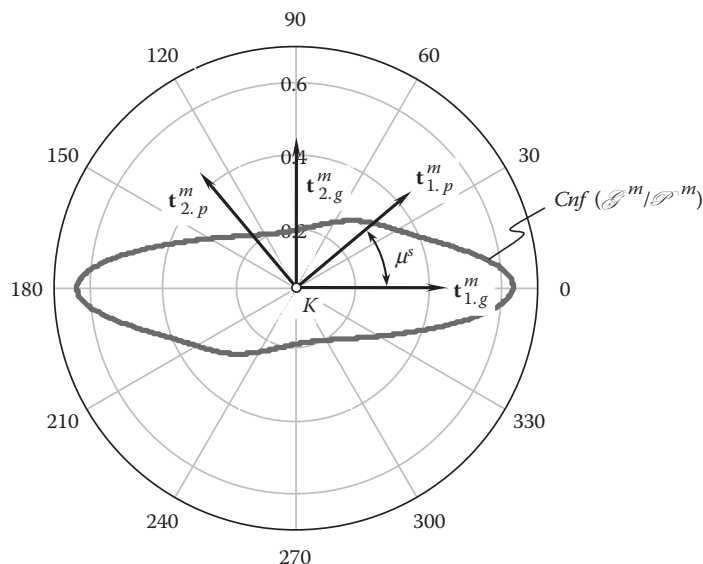


FIGURE 24.37

Indicatrix of conformity,  $Cnf(\mathcal{G}^m/\mathcal{P}^m)$ , at a point of contact of the modeling surfaces,  $\mathcal{G}^m$  and  $\mathcal{P}^m$ , is identical to the indicatrix of conformity,  $Cnf(\mathcal{G}/\mathcal{P})$ , at a corresponding point of contact of the gear tooth flank,  $\mathcal{G}$ , and the pinion tooth flank,  $\mathcal{P}$  [ $Cnf(\mathcal{G}^m/\mathcal{P}^m) \equiv Cnf(\mathcal{G}/\mathcal{P})$ ].

- The instant relative motion while simulating and the instant relative motion in mesh (that is, the kinematics of meshing remains the same)

Shown in Figure 24.37, the indicatrix of conformity,  $Cnf(\mathcal{G}/\mathcal{P})$ , at a point of contact of the gear tooth flank,  $\mathcal{G}$ , and the pinion tooth flank,  $\mathcal{P}$ , and the indicatrix of conformity  $Cnf(\mathcal{G}^m/\mathcal{P}^m)$  for the models,  $\mathcal{G}^m$  and  $\mathcal{P}^m$ , are identical to one another.

Ultimately, this results in high accuracy of the method of simulation of interaction of the gear tooth flank and the mating pinion tooth flank.

When simulating meshing of a gear and pinion, it is preferred to perform not the instant relative motions of the modeling quadrics,  $\mathcal{G}^m$  and  $\mathcal{P}^m$ , but a continuous relative motion instead. Implementation of continuous motions leads to a significant simplification of the procedure of simulation. In order to perform the desired continuous relative motion of the modeling quadrics,  $\mathcal{G}^m$  and  $\mathcal{P}^m$ , use of the surfaces that allow for sliding *over itself* is helpful. A screw surface of constant pitch,  $p = \text{Const}$ , is the most general case of the surfaces,  $\mathcal{G}^m$  and  $\mathcal{P}^m$ , that allow for sliding over itself.

While a screw surface travels along and rotates about its axis with the same parameter of the screw motion as the instant screw parameter of the screw surface itself, the enveloping surface to consecutive positions of the screw surface is congruent to the screw surface itself. Particular cases of surfaces that allow for sliding *over themselves* [surfaces of revolution (for which  $p = 0$ ), surfaces of translation (for which  $p = \infty$ )] are considered in [107,113,118]. Cylinders of revolution, spherical surfaces, and the plane represent examples of the simplest and completely degenerated surfaces that allow for sliding over themselves.

For the simulation of gear meshing, it is convenient to use a screw with external surface,  $\mathcal{G}^m$ , and either a convex or concave thread profile (see Figure 24.38). The application of such a screw enables the simulation of both convex and saddle-like local patches of given tooth flanks,  $\mathcal{G}$ .

For the simulation of concave and saddle-like local patches of a given pinion tooth flank,  $\mathcal{G}$ , a screw with an internal surface,  $\mathcal{G}^m$ , and either convex or concave thread profile can be used (see Figure 24.39).

In both cases (see Figures 24.38 and 24.39), the screw might be either single- or multithreaded, as well as single- or multistarted.

In order to provide the required parameters of the topology of the modeling surface,  $\mathcal{G}^m$ , that is, the parameters  $R_{1.g}^{(m)} \equiv R_{1.g}$ ,  $R_{2.g}^{(m)} \equiv R_{2.g}$ , the required radii of principal curvature of the surface,  $\mathcal{P}^m$ , that is, the parameters  $R_{1.p}^{(m)} \equiv R_{1.p}$ ,  $R_{2.p}^{(m)} \equiv R_{2.p}$ , and their local relative orientation, that is, the angle,  $\mu^{(s)} \equiv \mu$ , of the local relative



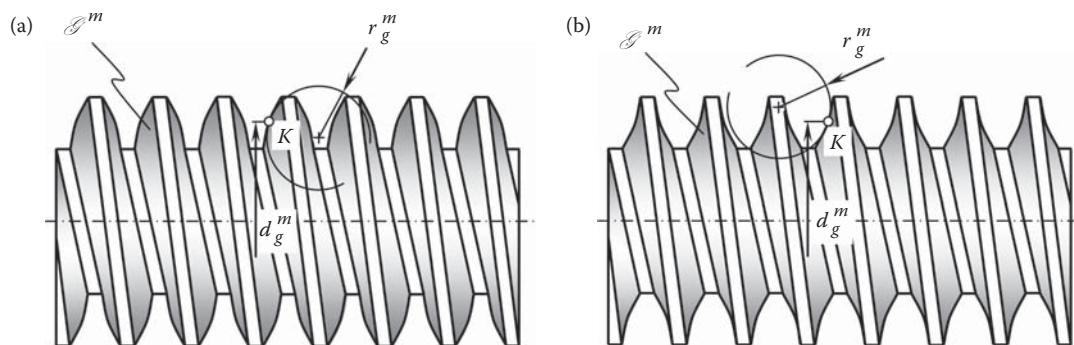


FIGURE 24.38

An external screw with convex (a) and saddle-like (b) local patches of quadric surface,  $\mathcal{G}^m$ , for the experimental simulation of the interaction of a gear tooth flank,  $\mathcal{G}$ , and the mating pinion tooth flank,  $\mathcal{P}$ . Parts (a) and (b) are discussed in the text.

orientation of the modeling surfaces,  $\mathcal{G}^m$  and  $\mathcal{P}^m$ , the parameters  $d_g^{(m)}$ , and  $r_g^{(m)}$  of the design of the screw have to be calculated in a proper way. For this purpose, the *Meusnier formula* and the *Euler formula* can be used.

The Meusnier formula establishes the correspondence between a radius of normal curvature,  $R_g$ , at a point of a modeling surface,  $\mathcal{G}$  (or a modeling surface  $\mathcal{P}$ ), through a certain direction,  $\mathbf{t}_g$ , on the surface, and between the radius of curvature,  $R_g^{(\theta)}$ , of the surface,  $\mathcal{G}$  (or a surface  $\mathcal{P}$ ), through that same direction,  $\mathbf{t}_g$ , on the surface, which is inclined to the normal plane section at a known angle,  $\vartheta_g$ . Commonly, the Meusnier formula is represented in the form:

$$R_g^{(\theta)} = R_g \cdot \cos \vartheta_g \quad (24.68)$$

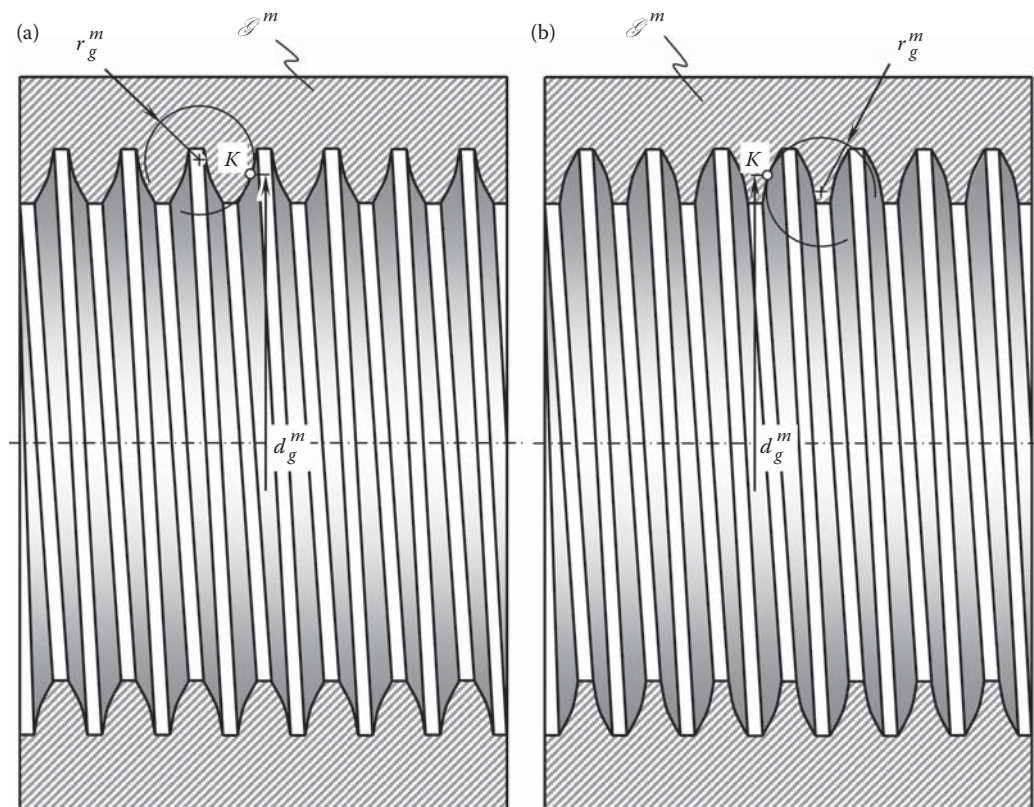
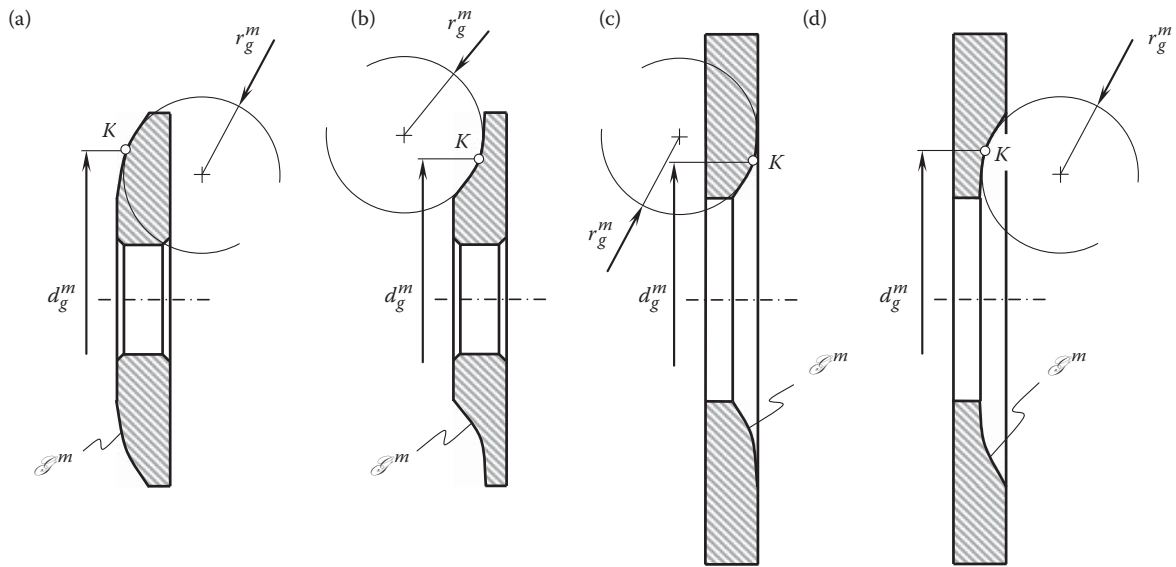


FIGURE 24.39

An internal screw with convex (a) and saddle-like (b) local patches of quadric surface,  $\mathcal{G}^m$ , for the experimental simulation of the interaction of a gear tooth flank,  $\mathcal{G}$ , and the mating pinion tooth flank,  $\mathcal{P}$ . Parts (a) and (b) are discussed in the text.

**FIGURE 24.40**

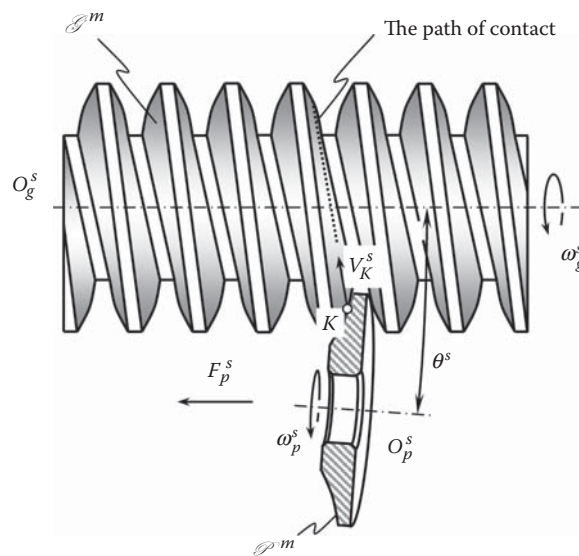
External (a), (b) and internal (c), (d) surfaces of revolution with (a) convex, (b) and (c) saddle-like, and (d) concave local patches of the quadric surface,  $\mathcal{P}^m$ , for the experimental simulation of meshing of a gear tooth flank,  $\mathcal{G}$ , and the mating pinion tooth flank,  $\mathcal{P}$ . Parts (a) through (d) are discussed in the text.

Equation 24.69:

$$k_g = k_{1,g} \cos^2 \varphi + k_{2,g} \sin^2 \varphi \quad (24.69)$$

represents a conventional form of the Euler formula.

For the purposes of simulation, it is much more convenient to model the surface,  $\mathcal{P}^m$ , with an external or internal surface of revolution that has either a convex or concave axial profile (see Figure 24.40). The same formulas can be used for calculating the parameters,  $d_p^{(m)}$  and  $r_p^{(m)}$ , of design of the cutting tool in order to provide the identities  $R_{1,p}^{(m)} \equiv R_{1,p}$ , and  $R_{2,p}^{(m)} \equiv R_{2,p}$ .

**FIGURE 24.41**

Schematic of simulation of interaction of a convex local patch of a gear tooth flank,  $\mathcal{G}$ , with the saddle-like local patch of the mating pinion tooth flank,  $\mathcal{P}$ .



The implementation of the screw surfaces,  $\mathcal{G}^m$  (see Figures 24.38 and 24.39), and the surfaces of revolution (see Figure 24.40) allows one to reach the desired kind of topology of the simulating surfaces,  $\mathcal{G}$  and  $\mathcal{P}$ .

Figure 24.41 illustrates the schematic of an example of implementation of the disclosed method of simulation [95]. The particular case (see Figure 24.41) of interacting of a convex local patch of the gear tooth flank,  $\mathcal{G}$ , with the saddle-like local patch of the pinion tooth flank,  $\mathcal{P}$ , is simulated with the external worm with a convex profile of threads that interact with the specimen with a concave axial profile. The design parameters of the worm, as well as the design parameters of the specimen, are precalculated in tight correlation with the corresponding design parameters of the actual gear tooth surface,  $\mathcal{G}$ , and the actual pinion tooth surface,  $\mathcal{P}$ , of the tool. The rotation of the worm and specimen are timed in order to make the resultant motion of the modeling surfaces,  $\mathcal{G}^m$  and  $\mathcal{P}^m$ , identical to the relative motion of the surfaces in the gear pair to be simulated.

In the case when one or both modeling quadric surfaces,  $\mathcal{G}^m$  and  $\mathcal{P}^m$ , allow for sliding *over itself*, manufacturing of the specimens for the simulation is simplified. At the same time, use of the modeling quadric surfaces,  $\mathcal{G}^m$  and  $\mathcal{P}^m$ , that allow for sliding over itself results in the ability of the two instant relative motions of the surfaces,  $\mathcal{G}^m$  and  $\mathcal{P}^m$ , to be substituted with the continuous motion of their surfaces. The latter is much more convenient for the simulation and enables more precise and reliable experiment results. Ultimately, this allows for an accurate simulation of the interaction of a gear tooth flank,  $\mathcal{G}$ , and the mating pinion tooth flank,  $\mathcal{P}$ .

The discussed method of simulation can also be used in stress analysis, solving lubricating problems, and so forth.

Numerous examples of how the contact between two tooth flanks,  $\mathcal{G}$  and  $\mathcal{P}$ , of a complex geometry can be substituted with equivalent contact of surface of much simpler geometry are discussed in this section of the book. This makes clear the importance of the discussion in Chapter 23.

## Gear Tooth Profile Modification: Generating Rack Shift

It is common practice to generate tooth flanks in spur and helical involute gears by means of a straight-sided *generating rack* (*basic rack*, in other words). The interaction of the basic rack and the gear is observed when the gears are cut on gear hobbers or gear shaping machines, or in generating grinding by means of a worm grinding wheel, and so forth.

When cutting spur and helical gears, the basic rack can be set up either to a nominal position in relation to the gear or it can be shifted from the nominal configuration. In the second case, the displacement of the basic rack can be pointed either inward or outward relative to the gear to be generated. Commonly, the amount of the basic rack shift is specified by the *profile shift coefficient*.

### 25.1 Addendum Modification (Profile Shift)

When gears are produced by a generating process, the datum line of the basic rack profile need not necessarily form a tangent to the reference circle. The gear tooth form can be altered by shifting the datum line from the tangential position. The involute shape of the tooth profile is retained, and the effect is merely to use parts further from or closer to the origin of the same involute. The radial displacement from the tangential position is termed the *addendum modification*. The displacement is considered positive when in the direction outward from the center of the gear and negative when in the direction toward the center of the gear (this also applies to internal spur and helical gears). The effect of addendum modification on the tooth form is shown in [Figure 25.1](#).

The load-carrying capacity of the teeth without addendum modification in [Figure 25.1a](#) can be improved by the positive addendum modification shown in [Figure 25.1b](#).

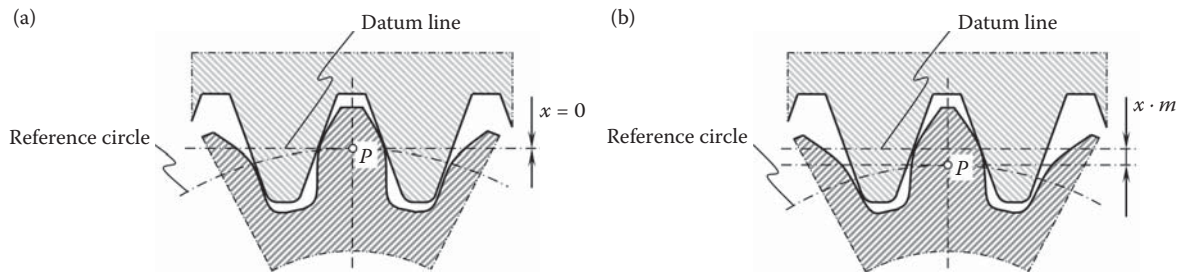
The positive/negative displacement of the basic rack makes possible:

- An increase of contact strength of gear/pinion teeth
- An increase of bending strength of gear/pinion teeth
- A reduction of profile sliding
- Inscription of a gear pair into a specified center distance
- Elimination (or to reduction) of a gear/pinion undercut
- An increase of the contact ratio

An extremely large addendum modification results in an unsuitable tooth form with pointed teeth.

The tooth form is affected by the addendum modification. The following characteristics of a generated tooth form are particularly significant for its load capacity:

- The profile angle,  $\phi_t$ , because of the relationship between the mean radius of curvature of the tooth flanks and the contact load capacity
- The tooth root thickness, because of the relationship between the modulus of the section and the bending strength at the root of the tooth
- The fillet radius at the critical point for bending, as at this point, a rapid change in the cross-section results in stress concentration
- The crest width, as excessive shear stress at the tip is undesirable, particularly in surface-hardened gears

**FIGURE 25.1**

The effect of addendum modification on the generated tooth profile of the gear: (a) zero profile shift, and (b) positive profile shift.

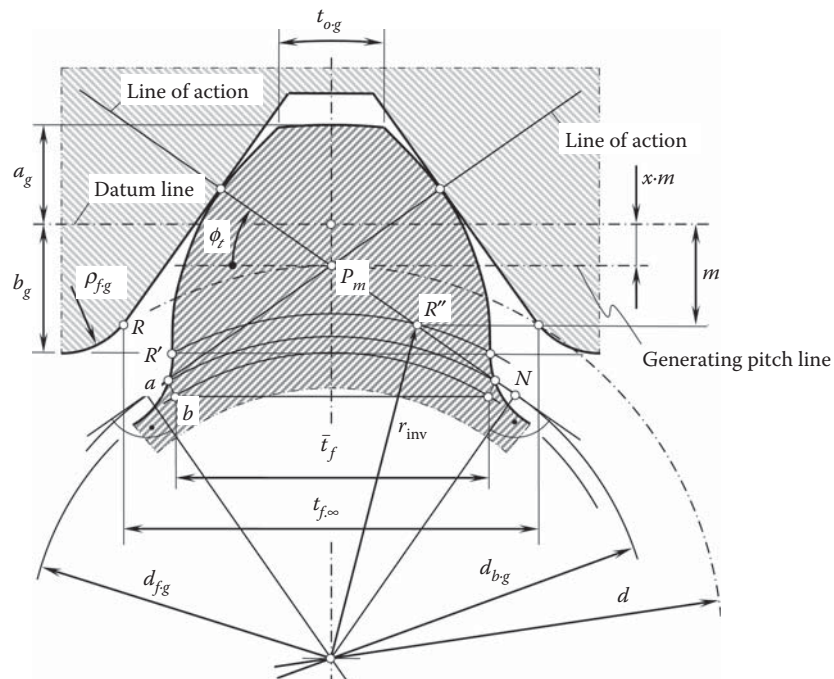
Two tooth profile zones have to be distinguished: the involute zone and the root fillet. The fillet form is affected greatly by the choice of the basic rack profile. While the tooth depth has to be increased slightly where the fillet forms a continuous, semicircular arc, the tooth root thickness and the fillet radius are improved significantly; therefore, the bending strength can be affected greatly by addendum modification.

Some simplifying assumptions have to be made in the mathematical analysis of the effect of addendum modification on the tooth root thickness:

1. The normal tooth form of a helical gear is deemed equivalent to that of a spur gear with a virtual number of teeth,  $N_{eq}$ , where:

$$N_{eq} = \frac{N}{\cos^2 \psi_b \cos \psi} \quad (25.1)$$

2. The tooth root thickness is taken to be the length,  $\bar{t}_f$ , of the chord on the root circle between the points of intersection with the tangents to the lowest points on the left- and right-hand involute flank profiles, as shown in Figure 25.2.

**FIGURE 25.2**

An involute gear tooth form generated by the rack.

A generating rack profile and a tooth generated thereby are shown in Figure 25.2. The pitch point when machining the gear is denoted by  $P_m$ . When in the course of generating the tooth, the generating rack profile rolls to the right on reference circle  $d$  from the position shown and the gear being cut carries out a corresponding clockwise rotation, the right point,  $R''$ , on the line of action will be reached where the lowest point,  $R$ , of the straight generating rack flanks comes into engagement and cuts the bottom point,  $R'$ , on the involute. This point at the beginning of the involute profile has the radius  $r_{\text{inv}}$ . The fillet begins at this point on the gear and is in the form of trochoids.

For the trochoidal fillet to blend tangentially with the involute, the point,  $R''$ , on the line of action must lie above point,  $N$ . The point,  $N$ , here is the point of intersection between the line of action and a line drawn normal to it through the fillet trochoids that no longer blends tangentially with the involute, but intersects and shortens it.

The chord,  $\bar{t}_f$ , at the root of the tooth shown in Figure 25.2 is governed by the geometry of the involute and is related to the number of teeth,  $N_{eq}$ , and the addendum modification,  $x$ . To measure the chord,  $\bar{t}_f$ , the hypothetical straight line root profile through points  $a$  and  $b$  is constructed. The largest possible chord dimension,  $t_{f,\infty}$ , is obtained with a rack tooth.

The performed analysis is used for determining a favorable value of the profile shift for a specified gear pair. To enable tooth forms to be compared, curves for various root thickness ratios,  $K_f$ ,

$$K_f = \frac{\bar{t}_f}{t_{f,\infty}} \quad (25.2)$$

can be constructed. In Figure 25.3, the root thickness ratio,  $K_f$ , curves are plotted in relation to the number of teeth and their addendum modification coefficient.

This is the first method for determining a favorable value of the generating profile shift.

The curves  $K_f = K_f(N_g)$  correlate to those shown in Figure 10.9 (see page 239 in [111]) and in Figure 10.11 (see page 183 in [112]).

Diagrams similar to that shown in Figure 25.3 can be constructed for various values of the transverse profile angle,  $\phi_t$ .

The bottom left region of the diagram is the cutter interference zone. The region of greater specific tooth thickness is reached rapidly by positive addendum modification. As a rough guideline, it can be assumed that below the root thickness ratio  $K_f \approx 0.7$ , poor tooth forms are obtained, which may even lead to meshing interference [74]. With extreme profile modifications, the limit of the feasible crest width of the tooth is reached;  $t_o^*$  is the crest width for a unit module.

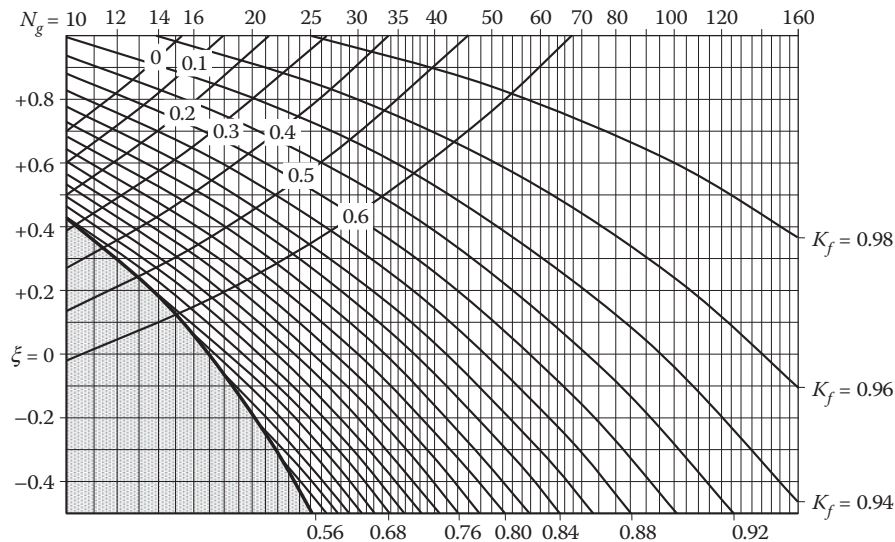


FIGURE 25.3

Effect of the addendum modification coefficient,  $x$ , on the root thickness ratio,  $K_f$ , and the crest width,  $t_o^*$ , for  $\phi_t = 20^\circ$ ,  $a_a^* = 1.0$ ,  $b_f^* = 1.25$ , and  $\rho_{f,\text{max}}^*$ .

## 25.2 Profile Shift Coefficient

Meshing of the gear cutting tool with the gear to be machined in the process of gear machining is commonly referred to as *gear machining meshing*.

Three different types of gear generating processes are distinguished depending on the configuration of the gear-cutting tool in relation to the work (Figure 25.4):

- The pitch line of the gear-cutting tool is tangent to the pitch circle of the gear being machined (Figure 25.4a).
- The pitch line of the gear-cutting tool has no common points with the pitch circle of the gear being machined (Figure 25.4b).
- The pitch line of the gear-cutting tool intersects the pitch circle of the gear being machined (Figure 25.4c).

In the first case (Figure 25.4a), the so-called *zero setup* of the gear-cutting tool is observed. The gear is generated with no profile shift (or, in other words, with zero profile shift):

$$\chi = xm = 0 \quad (25.3)$$

$$x = 0 \quad (25.4)$$

Here,  $\chi$  is the total profile shift,  $x$  is the profile shift coefficient, and  $m$  is module of the gear to be machined. The gear tooth thickness,  $s$ , is equal to the space width,  $w$ ; that is:

$$s = 0.5 \pi m \quad (25.5)$$

In the second case (Figure 25.4b), the so-called *positive setup* of the gear-cutting tool is observed. The gear is generated with a positive profile shift:

$$\chi = xm > 0 \quad (25.6)$$

$$x > 0 \quad (25.7)$$

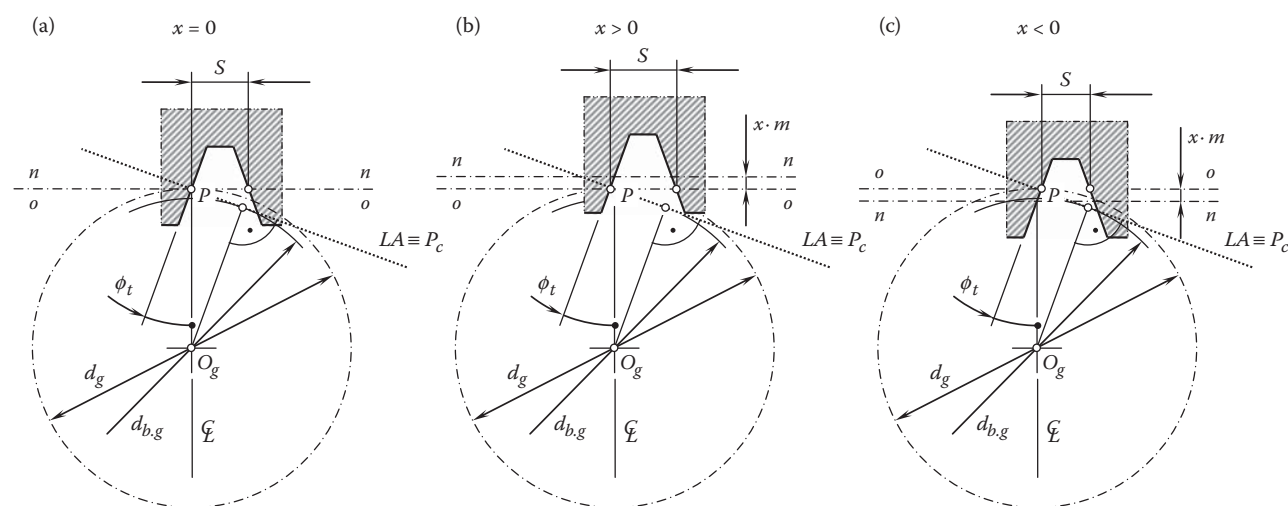


FIGURE 25.4

Generation of an involute gear tooth profile with different values of the profile shift coefficient,  $x$ : (a) zero,  $x = 0$ , (b) positive,  $x > 0$ , and (c) negative,  $x < 0$ .

The gear tooth thickness,  $s$ , is greater compared to the space width,  $w$ , [Figure 25.4b](#):

$$s = 0.5 \pi m + 2 x m \tan \phi_t \quad (25.8)$$

Therefore, tooth thickness in a gear with a positive profile shift is greater than that in a gear with zero profile shift. It is also clear that in a gear with a positive profile shift, tooth thickness is greater compared to the space width.

In the third case ([Figure 25.4c](#)), the so-called *negative setup* of the gear-cutting tool is observed. The gear is generated with a negative profile shift:

$$\chi = xm < 0 \quad (25.9)$$

$$x < 0 \quad (25.10)$$

The gear tooth thickness,  $s$ , is smaller compared to the space width,  $w$ , [Figure 25.4c](#):

$$s = 0.5 \pi m - 2 x m \tan \phi_t \quad (25.11)$$

Therefore, tooth thickness in a gear with a negative profile shift is smaller than that in a gear with zero profile shift. It is also clear that in a gear with a negative profile shift, tooth thickness is smaller compared to the space width.

Under any circumstances, regardless of the actual value of the gear tooth profile shift, the tooth flanks of gears that have an equal module and pressure angle remain conjugate to one another. The radii of the base circles (cylinders) remain the same. According to [Figure 25.4](#), they can be calculated from the following formulas:

$$r_b = r \cos \phi_t \quad (25.12)$$

$$r_b = 0.5 m z \cos \phi_t \quad (25.13)$$

Equations 25.12 and 25.13 make possible a conclusion that only the tooth thickness (as well as the space width) is affected by the tooth profile shift. Also, an active portion of the tooth profile depends on the actual value of gear tooth profile shift.

The profile shift factor can be calculated according to a formula proposed by *Robert Errichello*:

$$x_1 = \frac{x_\Sigma}{u + 1} + \frac{u - 1}{3u} \quad (\text{for speed reducers}) \quad (25.14)$$

$$x_1 = \frac{x_\Sigma}{u + 1} \quad (\text{for speed increasers}) \quad (25.15)$$

This is the second method for determining a favorable value of the generating profile shift.

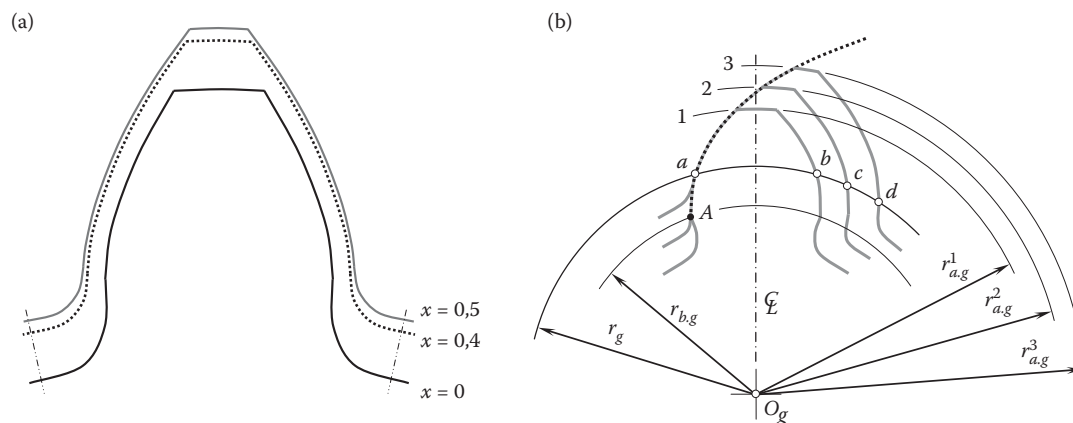
The use of gears with appropriate profile shift coefficients allows the design of gearboxes with improved performance.

---

### 25.3 Gear Tooth Flank Geometry Depending on the Profile Shift Coefficient

The profiles of three teeth of a gear with the same tooth count and with a different gear tooth profile shift coefficient are shown in [Figure 25.5a](#). As follows from the analysis of [Figure 25.5a](#), the gear tooth profile shift



**FIGURE 25.5**

The involute tooth profile geometry depending on an actual value of the profile shift coefficient,  $x$  (a), and alignment of the modified teeth profiles with a common involute curve (b).

coefficients  $x_1$ ,  $x_2$ , and  $x_3$  relate to one another in the following manner:

$$x_3 > x_2 > x_1 \quad (25.16)$$

As the pitch radii in all cases under consideration are of the same value, then an increase in the gear tooth profile shift coefficient results in a corresponding increase of the gear tooth thickness; that is,  $s_3 > s_2 > s_1$ , where  $s_1 = \widehat{ab}$ ,  $s_2 = \widehat{ac}$ , and  $s_3 = \widehat{ad}$  (see Figure 25.5a). The outer radii as well as the fillet radii of the gear also become larger in size. The gear teeth get thicker at the fillet diameter and thinner at the outer diameter. Ultimately, the gear tooth bending strength is improved.

On the other hand, the base circles of a gear retain the same radii. Therefore, that same involute profile is used as an operating profile of the gear teeth. However, depending on the actual value of the gear tooth profile shift coefficient, different portions of that same involute are used to form the gear tooth profile. Referring to Figure 25.5b, the larger the actual value of the gear tooth profile shift coefficient, the farther the working portion of the involute tooth profile from the base (that is, from point  $A$ ). This immediately entails a corresponding increase in the radius of curvature of the gear tooth profile and a corresponding decrease of the contact stress (Hertz equation).

Use of the gear tooth profile shift makes it possible to design gears with various arc segments of that same involute curve: the actual portion of the involute tooth profile of that same involute curve depends on the actual value of the profile shift coefficient, either  $x_1$  or  $x_2$ .

Finally, the tooth profile shift coefficient in a gear and its mating pinion is a powerful tool that can be used in designing gear pairs with a favorable performance.

## 25.4 Basic Equations for a Gear Pair with Addendum Modification

For a long while, simple rules of thumb were applied to gear design geometry, before it was realized that more latitude could be applied to the tooth form. Although the basic rack profile still usually forms the basis because of gear cutter standardization, it was already recognized in the pioneering days of gear generation that the reference circle only has significance in gear production, not for the running geometry of mating gears.

Dr. Max Maag\* contributed significantly to this development by systematically working out guidelines for obtaining strong tooth forms from a multitude of gear designs for various gear ratios, giving rise to a system now known as the MAAG-tooth system [74].

\* Max Maag (February 7, 1883–February 16, 1960), a Swiss engineer; Doctor of Engineering, h.c.; inventor; and founder of the MAAG Company.



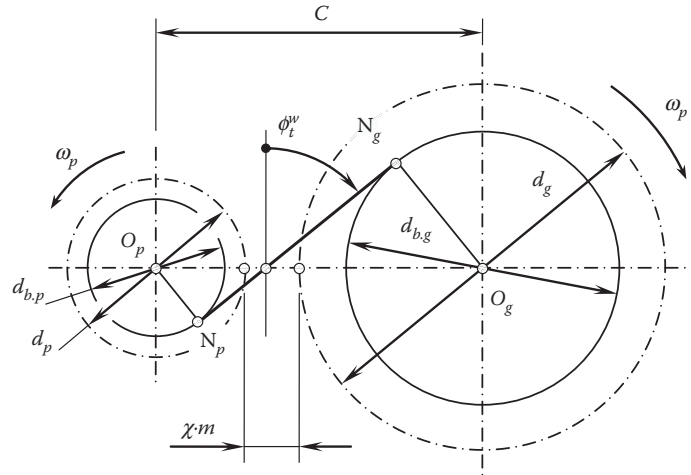


FIGURE 25.6

An external involute gear pair with a center distance modification,  $\chi \cdot m$ .

### 25.4.1 Principle of Addendum Modification

If the sum of the addendum modification coefficients ( $\xi_g + \xi_p$ ) is not zero, then the center distance is not equal to the sum of radii of the reference circle. The working (operating) pressure angle,  $\phi_t^w$ , then differs from the generating transverse pressure angle,  $\phi_t$ . The amount by which the center distance deviates from the sum of radii of the reference circles is known as the center distance modification,  $\chi \cdot m$ . The working pressure angle,  $\phi_t^w$  (see Figure 25.6), is given by the formula [74]:

$$\chi \cdot m = C - \frac{d_g + d_p}{2} = \frac{d_g + d_p}{2} \left( \frac{\cos \phi_t}{\cos \phi_t^w} - 1 \right) \quad (25.17)$$

For mating external spur and helical gears, the center distance modification is always smaller than the sum of the addendum modifications. An addendum shortening of  $k \cdot m$  is therefore necessary to maintain the basic rack profile bottom clearance,  $c_p$  [74]:

$$k \cdot m = \frac{m(N_g + N_p)}{2} \left[ \frac{\text{inv } \phi_t^w - \text{inv } \phi_t}{\tan \phi} - \frac{1}{\cos \psi} \left( \frac{\cos \phi_t}{\cos \phi_t^w} - 1 \right) \right] \quad (25.18)$$

This is the third method for determining a favorable value of the generating profile shift.

The geometrical relationship of involute teeth was exploited in the MAAG-tooth system by choosing relatively large addendum modifications with consequent addendum shortening large enough to avoid excessively pointed teeth. This has resulted in tooth forms with typically high bending strength.

### 25.4.2 External Spur and Helical Gear Pairs

Once the design parameters of each of the two mating gears are given (Table 25.1), there still remains the choice of the center distance,  $C$ , which need not necessarily equal the reference center distance,  $C_d = (d_g + d_p)/2$ , but can be modified by addendum modification subject to the dimensional criteria.

Two of the following three variables must always be specified to fix the tooth geometry. The third variable then follows from the other two (Table 25.2).

An unconstrained choice of the center distance,  $C$  (that is, rounded-off center distance for standardized gear boxes), within the aforementioned dimensional criteria for the sum of the addendum modification coefficients becomes possible with a closely graduated series of formulas.

**TABLE 25.1**

Given Design Parameters of a Gear Pair

Pressure angle (transverse)	$\phi_t$
Module	$m$
Number of the gear teeth	$N_g$
Number of the pinion teeth	$N_p$
Addendum of basic rack profile per unit module, $m = 1$	$h_{aP}^*$
Dedendum of basic rack profile per unit module, $m = 1$	$h_{fP}^*$
Pitch helix angle	$\psi$

**TABLE 25.2**

Design Parameters of a Gear Pair to Be Determined

Addendum modification coefficient of the gear	$\xi_g$
Addendum modification coefficient of the pinion	$\xi_p$
Center distance (hence, indirectly $\xi_g + \xi_p$ )	$C$

First, when the pinion addendum modification coefficient,  $\xi_p$ , and the center distance,  $C$ , are given, the gear addendum modification coefficient,  $\xi_g$ , can be calculated using the following formulas [74]:

$$\cos \phi_t^w = \frac{d_{b,g} + d_{b,p}}{2C} \quad (25.19)$$

$$\xi_g + \xi_p = \frac{N_g + N_p}{2} \cdot \frac{\text{inv } \phi_t^w - \text{inv } \phi_t}{\tan \phi} \quad (25.20)$$

$$\xi_g = (\xi_g + \xi_p) - \xi_p \quad (25.21)$$

Second, when the pinion and gear addendum modification coefficients ( $\xi_g$  and  $\xi_p$ ) are given, the center distance,  $C$ , can be calculated using the following formulas [74]:

$$\text{inv } \phi_t^w = \text{inv } \phi_t + \frac{2(\xi_g + \xi_p) \tan \phi}{N_g + N_p} \quad (25.22)$$

$$C = \frac{d_{b,g} + d_{b,p}}{2 \cos \phi_t^w} \quad (25.23)$$

Third, when the gear addendum modification coefficient,  $\xi_g$ , and center distance,  $C$ , are given, the pinion addendum modification coefficient,  $\xi_p$ , can be calculated using the following formulas [74]:

$$\cos \phi_t^w = \frac{d_{b,g} + d_{b,p}}{2C} \quad (25.24)$$

$$\xi_g + \xi_p = \frac{N_g + N_p}{2} \cdot \frac{\text{inv } \phi_t^w - \text{inv } \phi_t}{\tan \phi} \quad (25.25)$$

$$\xi_p = (\xi_g + \xi_p) - \xi_g \quad (25.26)$$

Miscellaneous formulas are summarized in [Table 25.3](#).

TABLE 25.3

Gear Diameters

Gear reference diameter	$d_g = \frac{m N_g}{\cos \psi}$
Theoretical gear root diameter	$d_{f,g}^* = d_g - 2m(h_{fp}^* - \xi_g)$
Outside diameter of the gear <sup>a</sup>	$d_{C,g} = d_g + 2m(h_{ap}^* + \xi_g) - 2km$
Pinion reference diameter	$d_p = \frac{m N_p}{\cos \psi}$
Theoretical pinion root diameter (neglecting the backlash)	$d_{f,p}^* = d_p - 2m(h_{fp}^* - \xi_p)$
Outside diameter of the gear <sup>a</sup>	$d_{C,p} = d_p + 2m(h_{ap}^* + \xi_p) - 2km$

<sup>a</sup> Here,  $k \cdot m$  is the addendum shortening.

The formulas above allow for the calculation of the design parameters of spur and helical gears, as well as the design parameters of parallel-axis gear pairs.

## 25.5 Determination of Profile Shift Coefficients: Geometrical Blocking Contours

The determination of the gear tooth profile shift coefficients is targeted to ensure:

- Absence of gear tooth undercutting ( $x_1 \geq x_{1,\min}$ ,  $x_2 \geq x_{2,\min}$ )
- Absence of gear tooth pointing ( $x_1 \leq x_{1,\max}$ ,  $x_2 \leq x_{2,\max}$ )
- Continuous engagement of the gear teeth in mesh ( $m_p \geq m_{p,\min}$ )

This means that there exists a certain permissible interval for the tooth profile shift coefficients of a gear and its mating pinion:

$$x_{1,\min} \leq x_1 \leq x_{1,\max} \quad (25.27)$$

$$x_{2,\min} \leq x_2 \leq x_{2,\max} \quad (25.28)$$

The relationship between the design parameters of a gear pair and its performance and the actual values of the profile shift coefficients  $x_1$  and  $x_2$  can be graphically illustrated in a Cartesian coordinate system,  $x_1 x_2$  (see [Figure 25.7](#)) by means of planar curves constructed for every combination of the tooth count in the gear,  $N_g$ , and its mating pinion,  $N_p$ . Each point of the Cartesian coordinate plane,  $x_1 x_2$ , corresponds to a gear pair with a certain values of the profile shift coefficients,  $x_1$  and  $x_2$ . The origin of the coordinate system,  $x_1 x_2$ , corresponds to a so-called *gear pair* that features the profile shift coefficients,  $x_1$  and  $x_2$ , of a zero value, that is,  $x_1 = 0$  and  $x_2 = 0$ . Point *A* corresponds to a *positive gear pair* for which  $x_1 > 0$  and  $x_2 > 0$ . Point *B* corresponds to a *negative gear pair* for which  $x_1 < 0$  and  $x_2 < 0$ .

A straight line that forms a  $45^\circ$  angle with the  $x_1$ -axis corresponds to a certain value of the total profile shift coefficient  $x_\Sigma = x_1 + x_2$ , and thus with a specific value of pressure angle,  $\phi_w$ . A straight line through the origin of the coordinate system,  $x_1 x_2$ , corresponds to the so-called *equally shifted gear pairs* that feature a zero total profile shift coefficient  $x_\Sigma = 0$ . Gear pairs with a positive  $x_\Sigma > 0$  (and thus with an increased pressure angle,  $\phi_w > \phi$ ), correspond to points of the coordinate system,  $x_1 x_2$ , that are located above the straight line  $x_\Sigma = 0$ . Gear pairs with a negative  $x_\Sigma < 0$  (and thus with a reduced pressure angle,  $\phi_w < \phi$ ), correspond to points of the coordinate plane,  $x_1 x_2$ , that are located below the straight line  $x_\Sigma = 0$ .

Not all the points of the coordinate plane,  $x_1 x_2$ , correspond to a workable gear pair. Tooth profile interference, reduction of the total contact ratio ( $m_t < 1$ ), tooth pointing, tooth profile undercut, and so forth can be observed for a certain combinations of the profile shift coefficients,  $x_1$  and  $x_2$ . In the coordinate system,  $x_1 x_2$ , the limiting

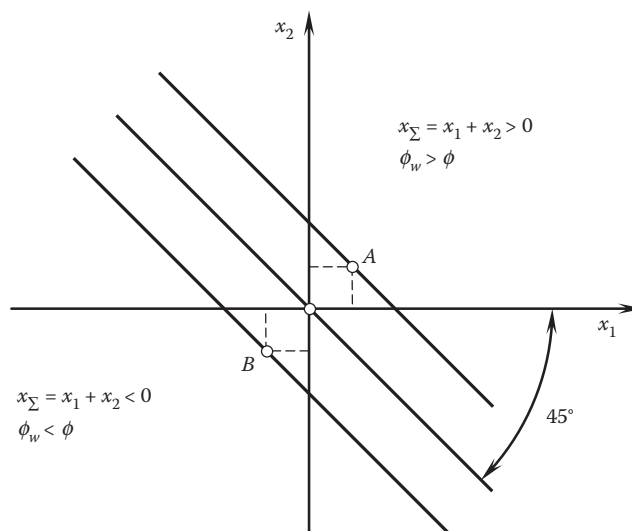


**FIGURE 25.7**  
Cartesian  $x_1x_2$  coordinate plane.

values of each of these factors can be graphically interpreted by means of a corresponding planar curve. The areas of permissible and not permissible values of the profile shift coefficients,  $x_1$  and  $x_2$ , are separated from one another by such a curve. A permissible area of the profile shift coefficients,  $x_1$  and  $x_2$ , is bounded within the coordinate plane,  $x_1x_2$ , by a set of graphs constructed for the limiting values of the design parameters of a gear pair. The contour constructed in this manner is commonly referred to as the *geometric blocking contour* of a gear pair.\* An example of a blocking contour for a gear pair with the tooth counts  $N_g = 28$  and  $N_p = 20$  is depicted in Figure 25.8. The hatching lines indicate the impermissible area for the profile shift coefficients,  $x_1$  and  $x_2$ .

In Figure 25.8, the geometric blocking contour is bounded by the following lines:

1. The line of zero interference within the gear tooth dedendum
2. The line of undercut of the pinion tooth profile
3. The line of the limiting contact ratio
4. The line of zero interference within the pinion tooth dedendum
5. The line of undercut of the gear tooth profile
6. The line of pointing of the pinion tooth profile

Gear pairs that correspond to zone A in Figure 25.8 feature the interaction of the gear and pinion tooth profiles from both sides of the pitch point; gear pairs that correspond to zone B in Figure 25.8 feature the interaction of the gear and pinion tooth profiles only from one side of the pitch point.

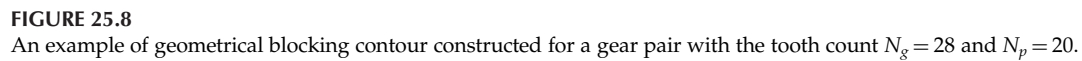
The lines that form a blocking contour are the undisputable boundaries of an area within the coordinate plane,  $x_1x_2$ , outside of which no workable gear pair is feasible. Additional lines can be traced inside a blocking contour, that is, the lines that correspond to certain values of parameters of a gear pair:

1.  $\alpha$  and  $\delta$  are the lines of equal tooth bending strength ( $\alpha$ —when the pinion is driving, and  $\delta$ —when the pinion is driving).
2.  $m_t = 1, 2$  is the recommended value of the tooth contact ratio.

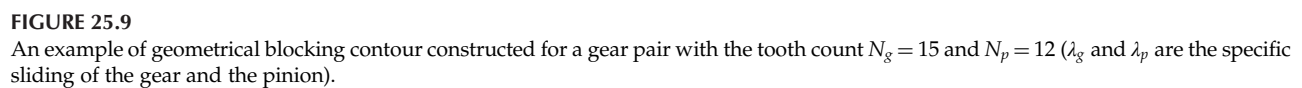
\* Engineer M.B. Groman is credited for the idea of the so-called *geometrical blocking contours*. He was the first to propose the concept of the geometrical blocking contours in his 1952 and 1955 papers:

Groman, N.B., "On Blocking Contours for Involute Gearing," *Vestnik Mashinostroyeniya*, 1952, No. 12, pages 12–17.

Groman, M.B., "On Selection of Profile Corrections for Gear Transmissions," *Vestnik Mashinostroyeniya*, 1955, No. 2, pages 3–13.



An area of the permissible values of the profile shift coefficients,  $x_1$  and  $x_2$ , is shown in black. At the left side and the bottom, this area is bounded by the condition of absence of undercut of the gear teeth ( $x_1 = x_{1.\min}$  and  $x_2 = x_{2.\min}$ ). At the right side, this area is bounded by the condition of continuous engagement of the gear teeth



in mesh ( $m_p \geq m_{p,\min}$ ). An analysis of [Figure 25.9](#) shows that the conditions of the gear and pinion tooth pointing ( $s_{a,1} = 0$  and  $s_{a,2} = 0$ ) are out of the permissible area of variation of the profile shift coefficients,  $x_1$  and  $x_2$ . This reveals that for a spur gear pair with the tooth count  $N_g = 15$  and  $N_p = 12$ , the limitation on  $m_p \geq m_{p,\min}$  is more severe compared to that on gear/pinion tooth pointing.

In grey dashed lines (see [Figure 25.9](#)), an enhanced area for the permissible values of the profile shift coefficients,  $x_1$  and  $x_2$ , is shown. An enhanced area for the coefficients  $x_1$  and  $x_2$  has a limited application.

A set of iso-lines of favorable values of the parameters of performance of the gear pair are traced within the area of the permissible values of the profile shift coefficients,  $x_1$  and  $x_2$ . The iso-lines are helpful for proper selection of the coefficients  $x_1$  and  $x_2$ .

The method that is based on geometrical blocking contours is the fourth method for the determination of a favorable value of the generating profile shift.

Geometrical blocking contours are a powerful tool for designing perfect parallel-axes gear pairs. The concept of geometrical blocking contours can be extended to the area of intersected-axes gear pairs, as well as to the area of crossed-axes gear pairs.

## *Split Torque Transmission Systems*

The conventional gear drive, for example, a parallel-axes gear drive, suits most purposes well and is the most economical method of reducing speeds and increasing torques, or vice versa. The approach starts running into problems when size and weight are critical or when wheels start becoming too large for easy manufacture. If we consider torques of the order of 1 MN m that are needed for 6000 kW at 60 rpm, we can estimate the wheel size for a 5 m to 1 m final reduction. The standard rule of thumb allows us about  $100 \text{ N mm}^{-1}$  per mm module; so, assuming a 20 mm module gives a wheel face width of about 450 mm and a diameter of 2.25 m. This is not a problem, but if the torque increases, we rapidly reach the point where sizes are too large for manufacture and satisfactory heat treatment, especially as the required thickness of the carburized case also increases [151]. The solution is to split the power between two pinions so that loadings per unit face width remain the same, but the torque is doubled. A further stage in this approach is to split the power among four pinions to give a roughly quadruple increase in torque without significant increase in size. This fits well if there is a double turbine power drive, which is often required for reliability [151].

An epicyclic gearing system is particularly well suited for achieving a high-reduction ratio in a relatively small, power-dense package.

A close-up of a planetary gear set with five planetary pinions is depicted in Figure 26.1a. A cutaway view of a planetary gearbox is shown in Figure 26.1b. Planetary gearboxes can be of a huge sizes, as in wind-power gear transmissions (see Figure 26.2), and of very high level of complexity (see Figures 26.3 and 26.4, a planetary gear set with multiple planetary pinions in every path of power from a driving member to a driven member).

Bevel gears can be used in the design of split torque transmission systems. As an example, a planetary gear set composed of bevel gears is shown in Figure 26.5, and a bevel gear set in the design of a split torque transmission system with six power paths is illustrated in Figure 26.6. More examples in this area will be provided.

The basic principles of epicyclic gearing are well established, and historically the epicyclic gear has been used almost as long as the simpler forms of gears, which comprise a single pinion and wheel. Basically, an epicyclic gear consists of three co-axial torque-carrying members, which, quite arbitrarily, can be input, output, or stationary reaction members:

- A sun gear, which has external teeth
- An annulus gear, which is a ring that has teeth on its inner surface
- A planetary carrier, which supports the bearing spindles of a number of identical planetary pinions that have external teeth

Planetary pinions are engaged in mesh with both the sun gear and the annulus.

As with any type of power transmission system, the engineer is faced with many analytical challenges during the design phase to ensure a highly reliable power train is obtained. In the case of an epicyclic gearing system, this challenge is particularly difficult due to the complex interaction of revolving and rotation components as they transmit power.

As no set of gears can ever be made to absolute precision, each of the individual gear teeth will have geometrical variations. To achieve the desired gains with power splitting, it is absolutely essential that equal power flow through each mesh in parallel. As manufacturing tolerances, eccentricities, and casing distortions, as well as displacements under operating load, are inevitable, equal power sharing needs to be ensured by certain means.

Manufacturing errors and deflections of the components are the root causes for excessive mobility in a split gear drive. Excessive mobility makes equal torque sharing among all the power paths in the split gear drive impossible.



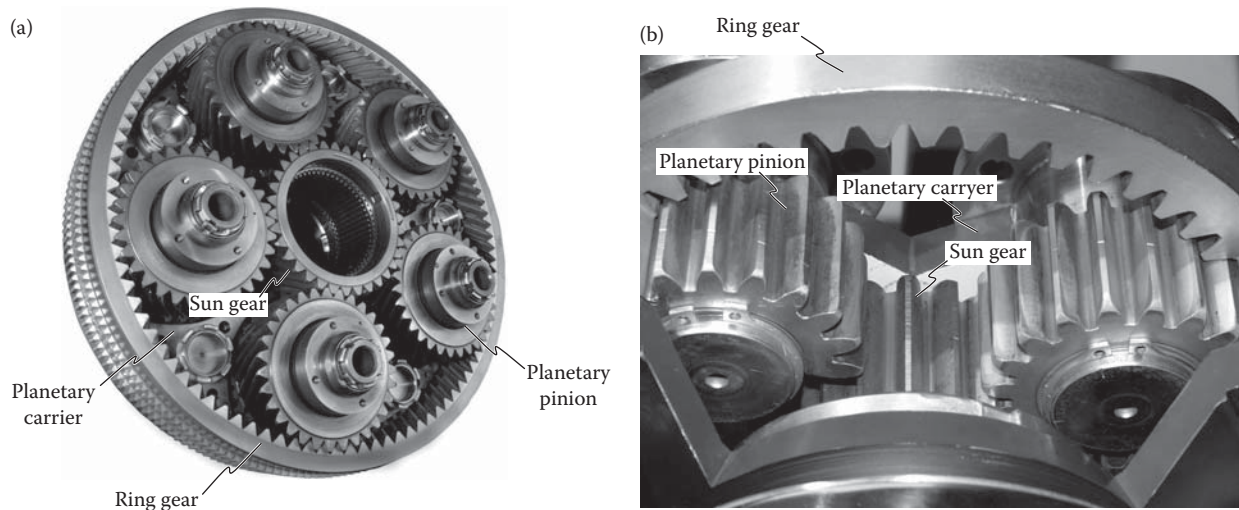


**FIGURE 26.1**  
Close-up view (a), and cutaway view (b), of a planetary gear drive.

### 26.1 Root Cause for Unequal Torque Sharing in a Split Torque Transmission

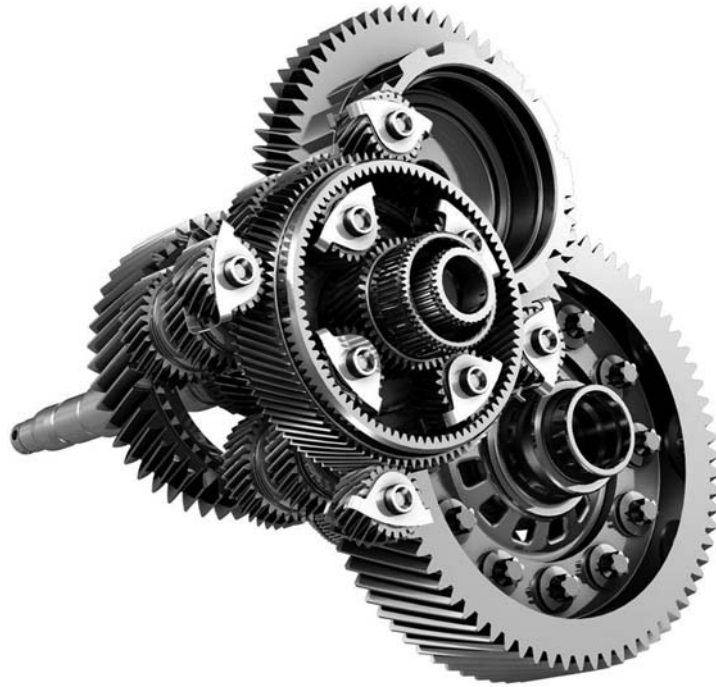
Gear drives with torque sharing mesh multiple gears simultaneously so that there are errors in machining and assembly, deflections under a load, and so on, that can cause load imbalances between them. Such load imbalances reduce transmission efficiency and durability, so high-precision manufacturing and uniform load distribution mechanisms are required.

Displacements of gears due to manufacturing errors and so on result in disengagement out of mesh in each power flow except one of the gears, which has a minimal displacement.

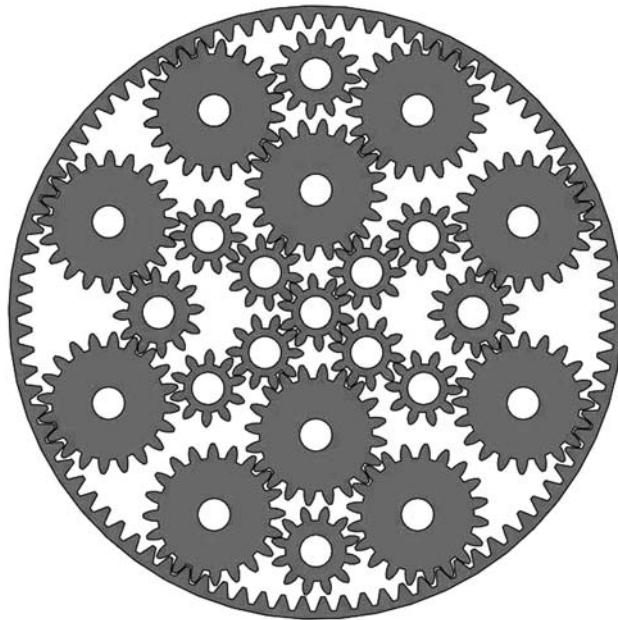
As an example, [Figure 26.7](#) shows a planetary gearbox that has three planetary pinions. It can be assumed that the axes of the sun gear,  $O_{sg}$ ; the ring gear,  $O_{rg}$ ; and the planetary carrier,  $O_c$ , are aligned to each other. Due to manufacturing errors, a deviation of the actual configuration of the planetary pinion axes of rotation from their desired locations is always observed.



**FIGURE 26.2**  
A huge-size planetary gear set for a wind-power transmission.

**FIGURE 26.3**

A split torque transmission system of a high level of complexity.

**FIGURE 26.4**

A planetary gear set with multiple planetary pinions in every path of power from a driving member to a driven member.

A radial displacement,  $\delta r_c$ , and an angular displacement,  $\delta \phi_c$ , are the two major contributors to the resultant displacement of the planetary pinion axis of rotation from its desired configuration,  $O_p$ , to the actual configuration,  $O_p^*$ . Ultimately, the displacements,  $\delta r_c$ ,  $\delta \phi_c$ , and others are the root cause for the low power density of the gearbox: when the ring gear is engaged in mesh with all the planetary pinions at plurality of points,  $K_{rg,p}$ , the sun gear is engaged in mesh with the planetary pinion only at one point,  $K_{sg,p}$ , and at other similar locations, the sun gear is disengaged from mesh with rest of the planetary pinions.

**FIGURE 26.5**

A planetary gear set can be composed of bevel gears.

**FIGURE 26.6**

Bevel gears in the design of a split torque transmission system with six power paths.

In order to achieve a high-power density (or, in other words, the *power-to-weight ratio*), all the pinions should be engaged in mesh, and all of them should be loaded equally. Multiflow gear drives feature an excessive mobility of members. The highest possible power density can be attained if the mobility of the gear drive is equal to one. Load-equalizing means of various designs are used to minimize the mobility of a gear drive and make it equal to one [137,138].

---

## 26.2 Mobility of Split Torque Transmission Systems

The mobility of a split torque transmission system can be calculated based on the principles used to determine the mobility of other mechanisms. A structural formula is used for this purpose. The structural formula is based on *classes of kinematical pairs*.

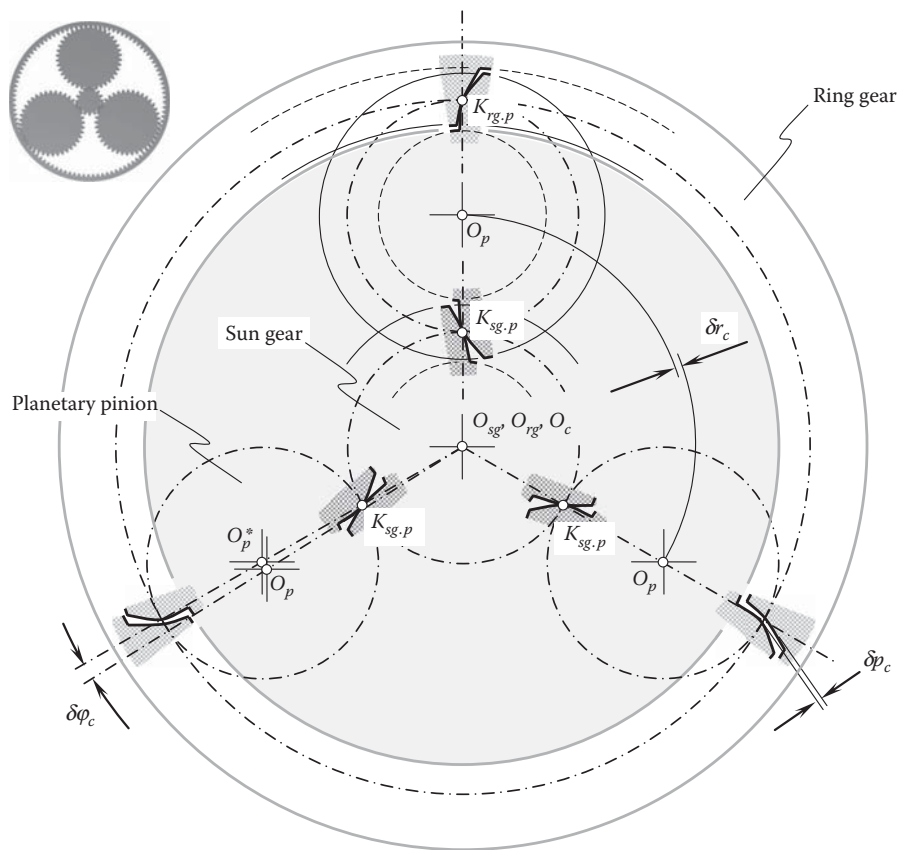


FIGURE 26.7

Deviation of the actual configuration of the planetary pinion axis of rotation,  $O_p^*$ , from its desired configuration,  $O_p$ .

A class of a kinematical pair is defined as the number of constraints imposed by a given kinematical pair. The constraints of a kinematical pair are thus the constraints on a linear displacement along a given axis or an angular displacement about the same axis.

The necessity of transmitting a force in a kinematical pair between its links is implied by a linear displacement, whereas the necessity of transmitting a torque between the links in the kinematical pair is implied by an angular displacement. Therefore, the notion of *kinematic constraint* in a structure has as its counterparts the notions of *transmitted forces* or *transmitted torques* in dynamics.

Let the total number of movable links in a mechanism be designated as  $n$ . The mechanism is said to have  $6n$  degrees of freedom (each link itself is free to move along three axes of an orthogonal Cartesian coordinate system and to rotate about the same axes). In order to determine mobility of this mechanism, the total number of degrees of freedom ( $6n$ ) should be deducted by constraints imposed by the kinematical pairs.

The number,  $p_i$ , of kinematical pairs of the  $i$ th class or order imposes  $i p_i$  constraints in total. Thus, all the kinematical pairs impose  $\sum_{i=1}^5 i p_i$  constraints. However, not all the constraints should be subtracted from  $6n$ . This is because redundant constraints duplicate other constraints without reducing the mobility of the mechanism. Let us denote the total number of redundant constraints by  $q$ . The mobility,  $w$ , of a mechanism can be calculated from the following formula.\*

$$w = 6n - \left( \sum_{i=1}^5 i p_i - q \right) \quad (26.1)$$

In a slightly different form, this formula was proposed by Prof. A.P. Malishev.<sup>†</sup>

\* Commonly, this formula is called either *Chebyshev-Grübler-Kutzbach criterion*, or *Kutzbach criterion for mobility*.

† This formula sometimes is also called the *Somov-Malishev formula*.

Ultimately, Equation 26.1 allows for an expression for  $q$ :

$$q = w - 6n + \sum_{i=1}^{i=5} i p_i \quad (26.2)$$

In expanded form, Equation 26.2 is given as follows:

$$q = w - 6n + 5p_1 + 4p_2 + 3p_3 + 2p_4 + p_5 \quad (26.3)$$

The *Malishev equation* can also be derived based on expressions used for the evaluation of both external and internal loads (within kinematical pairs) acting in a mechanism.

In a statically determined mechanism, the number of equations of equilibrium of the links is sufficient for evaluation of loads. In mechanisms with redundant constraints, they have to be complemented by equations of deformation of the links, housing, and so on. The number of the aforementioned equations is equal to the number of redundant constraints.

For planar mechanisms, the Malishev equation reduces to:

$$w = 3n + 2p_1 + p_2 \quad (26.4)$$

Equation 26.4 is commonly referred to as the *Chebichev formula*.

Although Equation 26.4 is derived for cases of planar mechanisms, it is also valid for certain cases of spatial mechanisms featuring kinematical pairs only of classes  $p_1$  and  $p_2$ .

---

### 26.3 Power Density of Gear Transmission Systems

The power density of a gear transmission system is an important consideration. The higher the power density, the more advanced the gear transmission system of a particular design. The aerospace and automotive industries, as well as many other industries, are targeting designing gear transmissions that feature the highest possible power density.

Conventionally, the term power density is defined either as a ratio of power being transmitted by a gear transmission to a volume occupied by the gear transmission or as a ratio of power being transmitted by a gear transmission to the gear transmission weight. In the second case, the term *power-to-weight ratio* is commonly employed. Sometimes the term *specific power* is used as well.\*

Power being transmitted by a gear pair is always known. There is an uncertainty when determining the volume occupied by a gear transmission. The weight of a gear transmission can be easily determined. Therefore, the definition of the term *power density*,  $P_d$ , as a ratio of power being transmitted by a gear transmission to the gear transmission weight is preferred. In this book, the term power density is viewed as the power-to-weight ratio:

$$P_d = \frac{P}{W} \quad (26.5)$$

where the power being transmitted by a gear transmission is designated as  $P$ , and the gear transmission weight is denoted by  $W$ .

---

\* The terms *volume power density* and *volume specific power* are also occasionally used.



The power,  $P$ , being transmitted by a gear transmission always has a nonzero value,  $P \geq 0$ . The weight,  $W$ , of a gear transmission always has a positive value,  $W > 0$ . Therefore, the power density,  $P_d$  is always nonzero:

$$P_d \geq \frac{\geq 0}{> 0} = \geq 0 \quad (26.6)$$

In a reference system, the *power-power density-weight system* (or just *P-  $P_d$ - W-reference system* for simplicity), a point corresponds to every known design of a gear transmission. A cloud of points is formed in the *P-  $P_d$ - W-reference system* in this way. From the top, the cloud of points is bounded by a surface,  $P_d^{\max}$ . Similarly, from the bottom, the cloud of points can be bounded by a surface,  $P_d^{\min}$ . Such a 3D plot can be useful for the gear designer, for example, to determine trends in the gear transmission industry, and so forth.

When two or more gear transmissions of different designs that transmit equal torque (or reasonably different torques), and equal rotation (or reasonably different rotations), the criterion power density,  $P_d$  works perfectly for comparison purposes. If two or more gear transmissions of different designs transmit significantly different torques and significantly different rotations, another criterion needs to be proposed to compare the gear transmissions. It is realized here that with that same power being transmitted, design of a *low rotation and high torque* gear pair and that of a *high rotation and low torque* gear pair are significantly different.

The criterion to be developed must be expressed in terms of the torques, as well as of the rotations to be transmitted.

## 26.4 Epicyclical Gear Drives

*Epicyclical gear drive* is another term often used for *planetary gear drive*. Pedantically, the term *planetary gear* is used to describe all such gears, whereas the more commonly used *epicyclical gear* is correct only for a stationary annulus; if the planet carrier is stationary, it is a star gear. When a gear is used in an infinitely variable drive as a method of adding speeds, all three members (sun, annulus, and planet carrier) are rotating.

In epicyclic gear drives, the axes of rotation of the planetary pinions are installed in a component commonly referred to as a *carrier*. Usually, there are three or more planetary pinions, which are engaged in mesh with the central sun gear. The planetary pinions rotate about the sun gear.

While being engaged in mesh with the sun gear, all the planetary pinions are also engaged in mesh with an internal gear. The last is commonly referred to as a *ring gear*.

The number of planetary pinions in a planetary gear drive depends on the required gear ratio. The higher the required gear ratio, the smaller number of the planetary gears, and vice versa. This is because a higher contact ratio requires implementation of the planetary pinions of a larger size; thus, due to lack of room, the feasible number of planetary pinions is restricted. In common practice, a correlation between the total gear ratio,  $u$ , and the permissible number of the planetary pinions is established as follows:

Total gear ratio ( $u$ )	Permissible number of planetary pinions
12.0	3
5.2	4
3.4	5
2.7	6
2.2	7
2.0	8

The power share among the planetary pinions makes possible a more compact gear drive design. In other words, planetary gear drives are capable of a *higher power density*\* compared to gear drives of other designs. This advantage is more evident in cases where very high torques are transmitted at medium and low rotations.

\* Or, in other words, a *higher power-to-weight ratio*.

In planetary gear drives, manufacturing errors can never be reduced to zero. High manufacturing accuracy is required. Thus, it is necessary to specify the maximum allowed geometric variations, also called tolerances, which are often defined as the difference between the maximum and minimum allowed backlashes of a gear mesh.

As the torque grows, the deflections of the planet gear teeth, planet pins, and sun and ring gear teeth engaged with that planet also grow. When the sum of those deflections closes the gap of any given planet, the planet begins to share the load, although not equally. Load sharing is proportional to the displacement of each planet's center of rotation from its original position. Planets that are not yet loaded will (obviously) not displace.

As the displacement of planetary pinion grows, the gaps of other planets close, and they begin to share load in proportion to the displacement of each, again unequally.

Load sharing among the planetary pinions requires that all planetary pinions be engaged, and this requires that the planets that were earlier engaged be displaced enough to allow the other planets to engage.

Some methods utilized in practice to improve the load sharing are listed as follows:

- High accuracy of all members
- Increased precision of carrier elements that locate planetary pinions
- Matching planet gear sets by tooth thickness
- Improving tooth alignment of compound planetary pinions by using matched sets of planetary pinions (compound epicyclics only)
- Oil film thickness variation due to changes in oil flow and loads in journal bearings
- Allowing radial float of one or more elements
- Elastic deformation of the ring or sun gear or both
- Reducing tooth stiffness
- Elastic deformation of planetary pinion shafts
- Elastic deformation of planetary pinion carrier
- Eccentric planetary pinion shafts with a load-responsive rotation device
- Load-sensitive displacement of a journal-bearing oil film
- Load-sensitive consumption of planetary pinion shaft material when utilized as a journal bearing
- Improved gear and shaft alignment
- Reduced shaft runout
- Improved bearing quality and alignment (true position of bearing location in carrier)
- Improved assembly (location) of carrier if the carrier is split axially
- Improved compliance of components (gears, shafts, bearings, housing)
- Improved dynamics (operating speed vs. resonant frequencies)

Additional factors can affect bearing capabilities, because as designs are scaled up, mesh forces and hence bearing loads tend to rise proportionally to the size squared, whereas the capacity of rolling bearings rises more slowly, and the permitted speeds decrease.

Planetary pinions are very inaccessible and very highly loaded, so they present the most difficult problems in cooling. For high-power gears, it is normal to have the planet carrier stationary, as this makes introducing large quantities of cooling oil required much easier.

These and other methods attempt to reduce load imbalance by either reducing position variation due to manufacturing allowances or allowing the movement of elements in response to a load imbalance.

---

## 26.5 Structural Formula for Planetary Gear Drives

Planetary gear drives feature the following properties:

- a. Each of them is composed of a certain number of *elementary planetary gear drives* (see [Figure 26.8](#)). The elementary gear drives cannot be subdivided into more elementary consistent mechanisms.



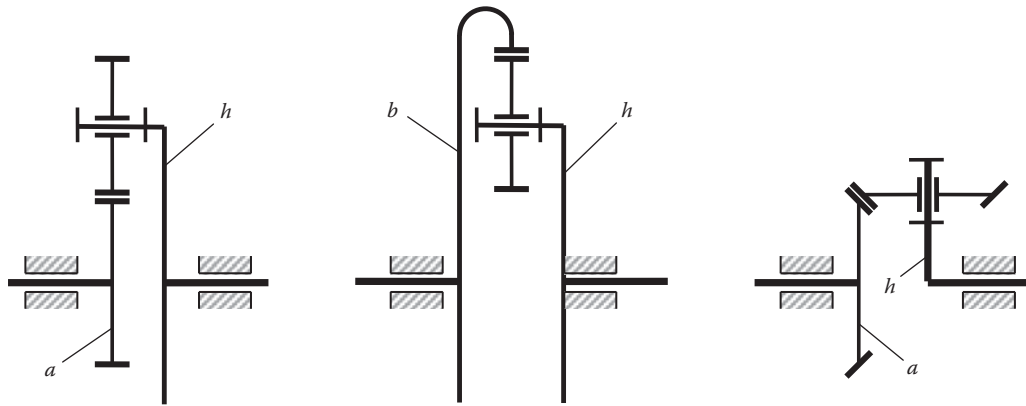


**FIGURE 26.8**  
Elementary planetary gear drives.

- b. The carrier (member  $h$ ) of any elementary gear drive either has a stationary-in-space axis of rotation, or it is motionless.
- c. The angular velocities of the three main members, that is,  $a$ ,  $b$ , and  $h$ , correlate to one another in accordance with the following formula:

$$i^h = \frac{\omega_a - \omega_h}{\omega_b - \omega_h} \quad (26.7)$$

The members of a planetary gear drive that have motionless axes of rotation are referred to as the *main members*. The total number of main members in a planetary gear drive is designated as  $n_0$ .

The number of degrees of freedom in a planetary gear drive can be calculated from Equation 26.4.

Assuming in Equation 26.4  $p_1 = n$ , one can obtain the following equation [63]:

$$w = n - p_2 \quad (26.8)$$

In planetary gear drives, the equality  $n = n_0 + k$  is valid (here,  $k$  is the number of planetary pinions).

The number of higher kinematical pairs is equal to the number,  $p_z$ , of meshes, that is,  $p_z = 2k$ . These result in a formula for calculating the total number of degrees of freedom in a planetary gear drive:

$$w = n_0 - k \quad (26.9)$$

It can be shown that the total number of unbalanced degrees of freedom for a planetary gear drive can be calculated as:

$$w_{unbalanced} = k - 1 \quad (26.10)$$

The problem of evenly loading planetary pinions can be interpreted as a particular case of the more general problem of self-alignment of mechanisms [138].

## 26.6 Correspondence among Angular Velocities of All the Members in a Planetary Gear Drive

A corresponding subscript is added to symbols that relate to rotations of a member of a planetary gear drive. For example, the angular velocity of a member,  $b$ , is denoted by  $\omega_b$ .

The gear ratio is the ratio of angular velocities of the rotating members. The gear ratio is designated as  $u$ . Two subscripts are added to  $u$ , which are related to the rotating members. The first subscript is that of angular velocity in the numerator, whereas the second subscript is that in the denominator. For example, for members  $a$  and  $b$ :

$$u_{ab} = \frac{\omega_a}{\omega_b} \quad (26.11)$$

$$u_{ba} = \frac{\omega_b}{\omega_a} \quad (26.12)$$

In the case of parallel axes of rotations, the gear ratio is positive if the rotations are in the same direction (this can be clearly shown by means of a corresponding vector diagram). Otherwise, when the rotations are in opposite directions, the tooth ratio is of a negative value.

In addition, a superscript can be used in certain cases. The superscript indicates a member in relation to which the rotations are considered. For example, if members  $A$ ,  $B$ , and  $C$  are rotating with angular velocities  $\omega_A$ ,  $\omega_B$ , and  $\omega_C$ , respectively, then the rotations of the members  $A$  and  $B$  in relation to the member  $C$  are equal to  $(\omega_A - \omega_C)$  and  $(\omega_B - \omega_C)$ ; that is,

$$\frac{(\omega_A - \omega_C)}{(\omega_B - \omega_C)} = u_{AB}^C \quad (26.13)$$

Similarly, for a planetary gear drive

$$\frac{(\omega_a - \omega_c)}{(\omega_b - \omega_c)} = u_{ab}^c \quad (26.14)$$

If one of the central gears is stationary, a superscript indicates the stationary member. For example, if a central gear  $b$  is motionless, then:

$$\frac{\omega_a}{\omega_h} = u_{ah}^b \quad (26.15)$$

or

$$\frac{\omega_h}{\omega_a} = u_{ha}^b = \frac{1}{u_{ah}^b} \quad (26.16)$$

The tooth ratio  $u_{ah}^b$  for central gears when the carrier is motionless is commonly referred to as a *tooth ratio with motionless carrier*.

Conventional rules are used for the calculation of the tooth ratio:

$$u_{ah}^b = \frac{\omega_a}{\omega_b} = \pm \frac{(r_w)_b}{(r_w)_a} = \pm \frac{z_b}{z_a} \quad (26.17)$$

Other forms of representation of Equations 26.11 through 26.17 are known as well.

---

## 26.7 Formulating the Problem of Equal Load Sharing in Planetary Gear Drives: State of the Art

Numerous designs of planetary gear drives have been developed so far. This section briefly reviews some of the conceptual achievements in solving the problem of equal load sharing in planetary gear drives.

### 26.7.1 Ordinary Planetary Gear Drives

Ordinary planetary gear drives enable the achievement a substantial reduction of the dimensions and weight of the gear drive, particularly when the number of planetary pinions is large enough. However, this is true only under the condition when the *transmitted load is equally shared among all the planetary pinions*. This requires the implementation of equalizing mechanisms, which are incorporated into the design of the gear drive. Whether a design of the equalizing mechanism is appropriate can be checked by counting the number of redundant constraints. The appropriate equalizing mechanism should be statically determined. For this purpose, conventional expressions derived for planar mechanisms can be used.

The equalizing mechanism of the simplest design is the one that has two planetary pinions (see Figure 26.9). The carrier is made floating [138]. It is connected to the driven shaft by two arms. The arms are parallel to the line connecting the centers of the planetary pinions. Parallelism of the lines should be ensured, as the radial displacement of the center of a planetary pinion does not influence the movement of other members, whereas a tangential displacement does. This displacement should be permitted by the equalizing mechanism.

With two planetary pinions, the equalizing mechanism should not be mounted on the sun gear or the supporting or ring gear. Otherwise, the aforementioned direction of the arms will not be attained.

The mobility of the planetary gear drive in the case under consideration is equal to two ( $w = 2$ ). The second mobility is brought by the rotation of the carrier about both the pairs  $III_4$  and  $III_4$  in Figure 26.9. This mobility is harmful. It should be eliminated by implementation of corresponding abutments. With  $n = 7$ ,  $p_v = 4$ ,  $p_{iii} = 4$ , and  $p_{ii} = 4$ ,

$$q = 2 - 6 \cdot 7 + 5 \cdot 4 + 3 \cdot 4 + 2 \cdot 4 = 0 \quad (26.18)$$

The discussed approach is applicable for both planetary gearboxes of conventional design, that is, with spur and helical gears, and planetary gearboxes with bevel gears (see Figure 26.5).

Numerous alternative approaches are known that target an almost equal load sharing among the planetary pinions by means of eliminating of the excessive mobility of the gear drive.

### 26.7.2 Planetary Gear Drives with Flexible Pins

The application of gearboxes with flexible pins is based on the ideas of the British inventor *Ray Hicks* proposed in 1969–1970 [45]. In 1964, Hicks developed a method of providing load sharing between the planetary pinions of

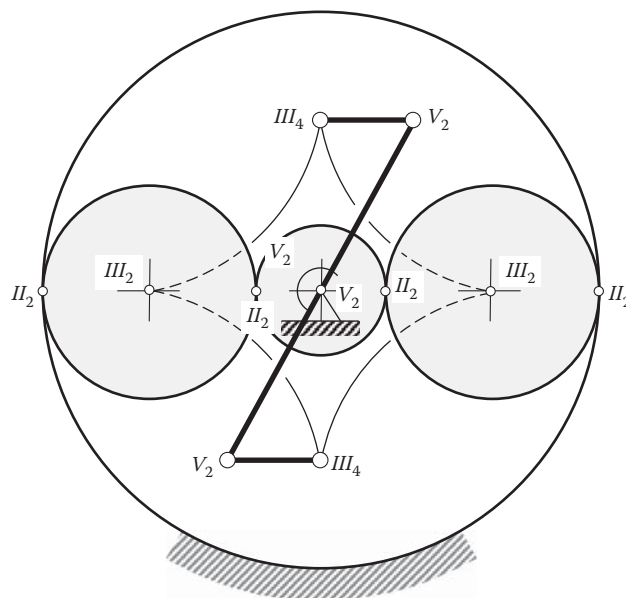


**FIGURE 26.9**  
Equalizing mechanism of a planetary gear drive that has two planetary pinions.

an epicyclic gearbox: the flexible pin, which has been applied to a large variety of industrial, aerospace, and marine gearboxes from 1964 onward.

Epicyclic gear systems have typically been equipped with straddle-mounted planetary pinions with pins supported on the input and output sides of the carrier. The torsional windup of the carrier, position accuracy of the pins, machining tolerances of the planetary gear system components, and bearing clearances can all contribute to poor load sharing among planetary pinions as well as misaligned gear contacts in the deflected state. The double-cantilevered flexible pin concept to achieve better load sharing and gear contact patterns among a multiplicity of planetary pinions has been used to improve reliability in advanced gear drives for many years. This has resulted in a compliant epicyclic system that improves power density in the gear length direction because the probability of achieving a properly centered gear contact is increased.

In the traditional epicyclic gearing system, where the distance between planetary pinion centerlines is specified by the design to be within a fixed range, it is widely recognized that the load sharing is not equal among the planetary gear meshes. Similarly, stress is distributed variably at mesh points. Load sharing and stress distribution at each mesh point are heavily influenced by global design configuration, backlash tolerance, component design tolerances, manufacturing accuracy, component deflection, and thermal distortion. The earlier-discussed Figure 26.7 shows in exaggerated form that contact is made at the mesh point  $K_{sg,p}$  of the planetary pinion before any contact is made at the mesh points of the other planets (it is assumed that the ring gear makes contact with all the pinions at points  $K_{rg,p}$ ). In a rigid system, this condition imposes unbalanced loading among the planetary pinions.

Use of a flexible pin eliminates the need for straddle mounting and thereby enables the maximum possible number of planetary pinions to be used subject to tip-to-tip clearance for any particular gear ratio. The number of planetary pinions varies with the ratio between the annulus and sun gear tooth numbers.

Load sharing is achieved by ensuring that deflection of the planetary pinion spindle under its normal load is considerably greater than the manufacturing errors that cause maldistribution; that is, if one planetary pinion tends to take more load than the others, it will deflect until the others take their share.

The original Hicks invention is shown in Figure 26.10 as a fragmentary and diagrammatic part-sectional elevation of an epicyclic gear with flexure, greatly enlarged for illustration. Referring to Figure 26.10, which illustrates the invention diagrammatically, the epicyclic gear broadly comprises a sun wheel 10, an annulus gear ring 11, and a plurality of planetary pinions 12, which mesh with both sun and annulus. The planets are supported on spindles 13, fast with a carrier 14. The effect of the gear depends upon whether the sun,

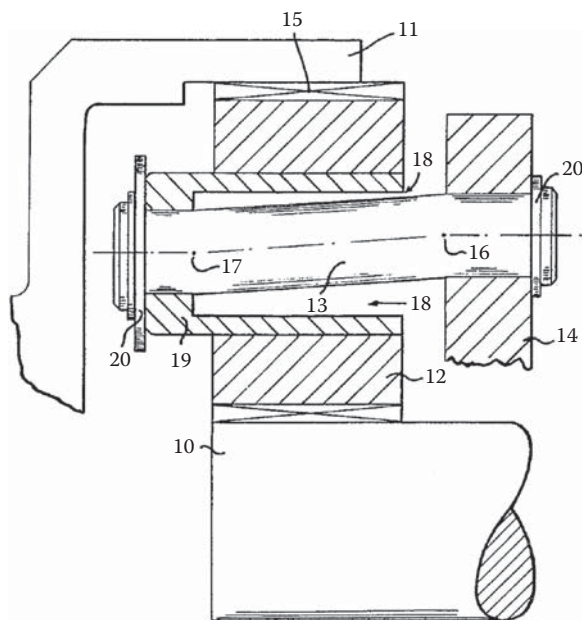


**FIGURE 26.10**

A fragmentary and diagrammatic part-sectional elevation of an epicyclic gear with flexure grossly exaggerated. (After Hicks, R.J., *Load Equalizing Means for Planetary Pinions*. U.S. Pat. 3,303,713. February 14, 1967, Filed: February 8, 1965 [44].)

annulus, or carrier is the input or output and which of these three is fixed either permanently or optionally. In any event, the center 15 of the planet teeth, measured axially, is at an equal distance from points 16 and 17, which lie in planes contacting the point of emergence of spindle 13 from the carrier and planet, respectively. Thus, the couples will be equal, as previously explained.

Similarly, the planet does not skew when misaligned; rather, it deflects the shaft (see Figure 26.10) until each planet is equally loaded; the annular gap 18 permits this. (It is understood that, in practice, the deflection involved is relatively slight.)

The planet 12 may sit directly on spindle 13, or, as shown in Figure 26.10, may seat and be journaled on a sleeve 19 that provides the gap. In this case, the sleeve is fast with the spindle. The spindle is a press or shrink-fit in the carrier 14 and possibly in the sleeve 19, but a system of c-clips 20 is also used as a precaution against damage through fit relaxation.

The use of flexible pins eliminates the need for straddle mounting and so allows the maximum possible number of planetary pinions to be used, subject to tip-to-tip clearance for any particular gear ratio. The number of planetary pinions varies with the ratio between the annulus and sun gear tooth numbers.

Load sharing is achieved by ensuring that deflection of the planetary pinion spindle under its normal load is considerably greater than the manufacturing errors that cause misallocation. Put another way, if one planetary pinion tends to take more load than the others, it will deflect until the others assume their share.

Figure 26.11a shows a typical planet gear supported by a planet spindle mounted on a flexible pin cantilevered from a simple carrier plate. The two ends of the pin are fitted to the carrier plate and the spindle, whereas the latter is counterbored to allow the pin to deflect freely.

Figure 26.11b shows that a uniform tooth load, where the centroid is symmetrical with the tooth length of the flexible pin, exerts equal and opposite moments on the built-in ends so that they remain parallel during deflection.

Figure 26.11c shows that a point load concentrated on either end of the tooth face produces a relative angular deflection of that end, with respect to the other, which is six times the finite deflection that occurs when it is loaded at the center.

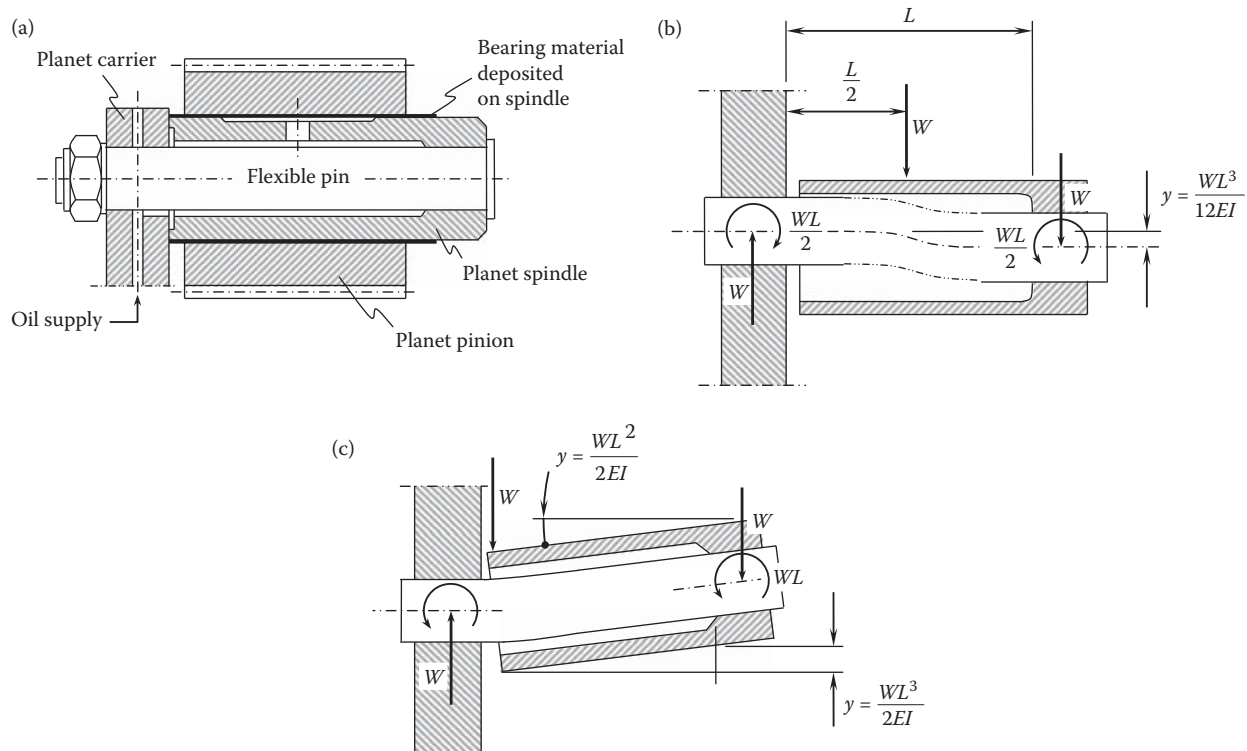


**FIGURE 26.11**

Compact orbital gear's flexible pin: (a) planet pinion rotates on a flexibly mounted spindle, (b) planet spindle is loaded at center, and (c) planet spindle loaded at end.  $W$  is applied load,  $L$  is the length of the flex-pin, and  $E$  is the Young's modulus of elasticity. (From Hicks, R.J., *Proceedings of the Institution of Mechanical Engineers*, 1969–1970, Vol. 184, No. Pt. 30, pp. 85–94 [45].)

The deflections shown are theoretical values, which assume that the built-in portions of the pin at either end are supported so rigidly that they have zero slopes. However, static tests have shown that elastic deflections in the joints between the spindle and carrier plane give complementary finite slopes such that the effective flexibility of the pin is more than doubled without affecting the parallel movement of the spindle.

With the proportions shown, the relative rigidity of the spindle is such that its own cantilever deflection in terms of the total is so small that it has virtually no effect on tooth load distribution. If a thinner planet spindle is used with a significant flexibility, it is possible to compensate for this by reducing the length of the counterbore.

An important feature of the design is that because the planet spindle and flexible pin are coaxial, it is capable of deflection about two axes, which makes it virtually self-aligning. This means that the pin is influenced by radial as well as tangential tooth loads, and it is able to compensate for helix errors of different magnitudes or sense at the sun and annulus mesh points. It is therefore capable of compensating for torsional deflection of the sun gear, which takes place in gearboxes of large tooth ratios. If the resultant load of the sun and annulus mesh points is not in the same plane as the midpoint of the unsupported portion of the flexible pin, there are two restoring effects:

1. The offset tangential load tips the spindle in the tangential plane in a manner that tends to offset the respective load points an equal amount to either side of the midpoint of the pin.
2. The radial couple resulting from the offset radial loads tilts the spindle in the radial plane until the residual couple is reduced to an amount compatible with the angular flexibility of the spindle assembly.

In short, there is a complex movement in two planes as the spindle takes up a position of minimum strain energy. This complex movement is in fact beneficial, since it promotes a slight crowing effect as a result of the skewed or nonparallel axes.

If, on the other hand, the planetary pinion is cross-cornered so that the resultant tangential load is in the same plane as the midpoint of the pin, there is still a radial tilting couple to provide a restoring action.

When a gearbox has a rotating planet carrier, additional radial loads and deflections are imposed on the flexible pin assembly due to the centrifugal weights of the planetary pinion, spindle, and pin.

The flexible pin eliminates the need for straddle mounting and therefore enables the maximum possible number of planetary pinions to be used subject to tip-to-tip clearance for any particular epicyclic ratio. Load sharing is achieved by ensuring that deflection of the planet spindle under its normal load is considerably greater than the manufacturing errors that cause maldistribution; that is, if one planet tends to take more load than the others, it will deflect until the others take their share.

Simply put, the flexible pin is designed to use high deflections to provide uniform tooth loads between planetary pinions and across sun-to-planet and planet-to-annulus tooth face widths. An added benefit of producing equal loads across tooth contact face widths is the occurrence of equal loading along the planetary pinion bearings, which is the most critical element of a high-capacity low-speed epicyclic gear.

Conversely, the industrial design of the epicyclic gear requires high carrier rigidity relative to the gear tooth stiffness, which is impractical and leads to maldistribution of load across the teeth and bearing, leading to premature failure.

Because a supporting shaft of the planet gear has a flexible double cantilever construction (flexible pin system), a planetary pinion that receives more load moves in parallel due to sagging of the pinion, so that all the planetary pinions receive equal load. Consequently, an excellent equal sharing effect is shown in such cases, and the whole system is of a smaller size.

Due to the flexible pin system, the shock-absorbing effect for torque variation of a prime mover or a load is expected.

If the load is distributed evenly among the tooth faces, it is the same as when a concentrated load is applied to the center; the pins flex as double cantilever beams, and parallelism relative to other planetary pinions is not lost. If there is any error in relative positioning between flexible pins due to errors in machining or assembly, the planetary pinion positioned here receives more load than the others and the flexible pin supporting that gear flexes further to absorb the error. Thus, the uniform load distribution mechanism keeps load distribution even.

If an eccentric load is applied to the left end of a tooth face, the flexible pin flexes as shown in [Figure 26.11c](#) and the load on the right side of the tooth face increases, mitigating the eccentric distribution of the load across the



width of the tooth. The effect of gear tooth trace errors, gear casing deformation, misalignment, and other problems can be absorbed and mitigated.

However, for just about all equipment types, economics dictates the need for increased power density and improved reliability. A common approach is to attempt to build in more planets, thereby reducing forces and stresses at each mesh point. But, as planets are added, so is uncertainty about just how much power each planet is transmitting.

Instead of fixing the angular positions of the planetary pinions, the flexible pins were designed so that they deflect independently in a circumferential direction, which ultimately helps equalize the force distribution among the planets while transmitting torque at various levels. This feature is henceforth referred to as *torsional compliancy*.

Torsional compliancy is achieved by applying the double-cantilevered-beam design that is illustrated in [Figure 26.7](#). Simply stated, when two tangential forces are applied to the flex-pin pinion, the angular deflection caused by the bending of the pin cantilevered from a carrier wall can be offset in the opposite direction by the angular deflection caused by bending of the sleeve cantilevered from the other end of the pin. If sections of the pin and sleeve are carefully designed with that goal in mind, deflection at each gear contact follows a circumferential translation, which means the axis of the gear contact does not tip from side-to-side angular positioning inaccuracy or lead from torsional windup of the carrier.

Flexible pins have been designed in various types of equipment, and the designs have typically included assembly of separable components including gears, pins, mounting sleeves, backing plates, cap screws, and various type of rolling element bearing races and bushings.

Such a design achieves the objective of creating a torsionally compliant system. Additionally, since gears are less prone to be tipped off axis because the single-sided planetary carrier can no longer wind up, it can be argued that gear contacts have a much higher probability of remaining centered at all meshes. It follows, then, that the flexible pin permits the designer to specify narrower gears and still avoid stress concentration at the ends of the face. Power density is therefore improved in the axial direction.

An elastic deformation of the flex-pin allows for overcoming manufacturing errors, displacements under operating load, and so forth. The elastic deformation must be large enough to accommodate manufacturing errors and the like, yet not exceed a particular given value. When zero torque is applied to the driving member of the planetary gearbox, no force is exerted from the flex-pin and no deformation of the flex-pin is observed. When the maximum torque is applied, maximum force is exerted from the flex-pin and maximum deformation of the flex-pin occurs. Because only elastic deformations of the flex-pin are considered valid (see *Young's law*), the loaded diagram is represented by a linear function (see [Figure 26.12](#)). Huge displacements,  $y$ , of the flex-pin are necessary to attain the operating load that acts against the flex-pin. It is best to keep the displacements,  $y$ , as small as possible; however, they need to be sufficient to address the manufacturing errors and the like.

A substantial improvement can be realized if one takes advantage of modern bearing technology and advances the entire design to the next level, which is full integration of the gear with the outer races of the bearings and full integration of the sleeve with the inner races of the bearings. This advancement is the *integral flex-pin bearing*, and it is illustrated in [Figure 26.13](#). This approach to design and construction of the flexible pin arrangement provides an increased opportunity to add power density to an epicyclic gear drive in the axial and radial directions. The beam strength of the sleeve and gear are increased from the integration of bearing components allowing downsizing, especially in the radial direction.

Many other designs of planetary gear drives are based on application of the concept of flexible pins for the purpose of equalizing load sharing among pinions.

The overview of known designs of gear trains with splits of power flow given in this section reveals the complexity of equal power sharing in gear trains of this specific kind.

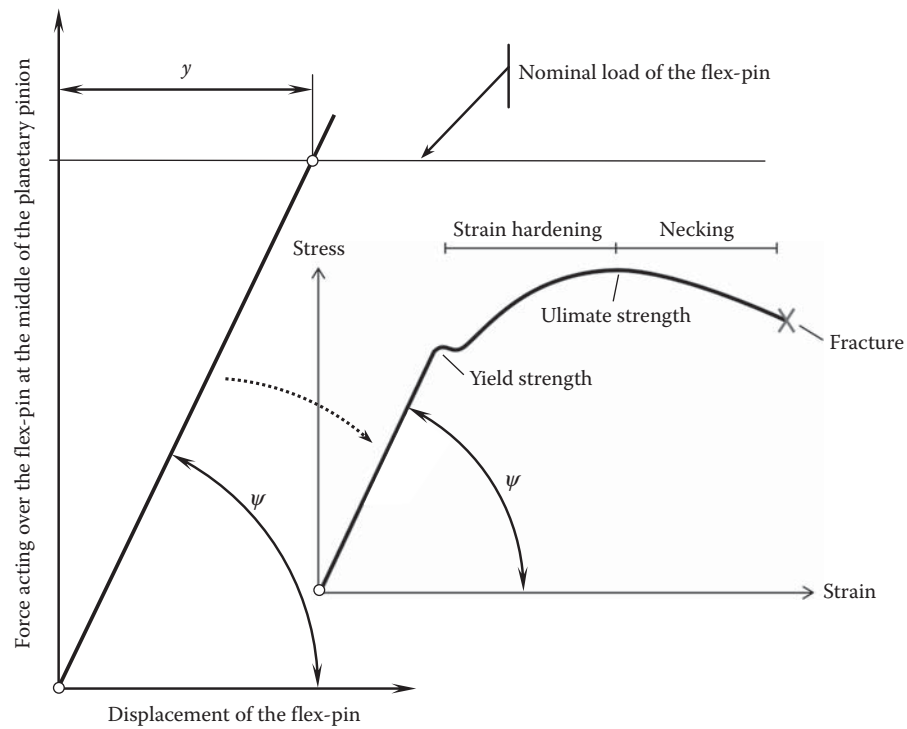
The flex-pin concept was presented here in order to make a correct comparison of this concept with the concept of the elastic load sharing device.

---

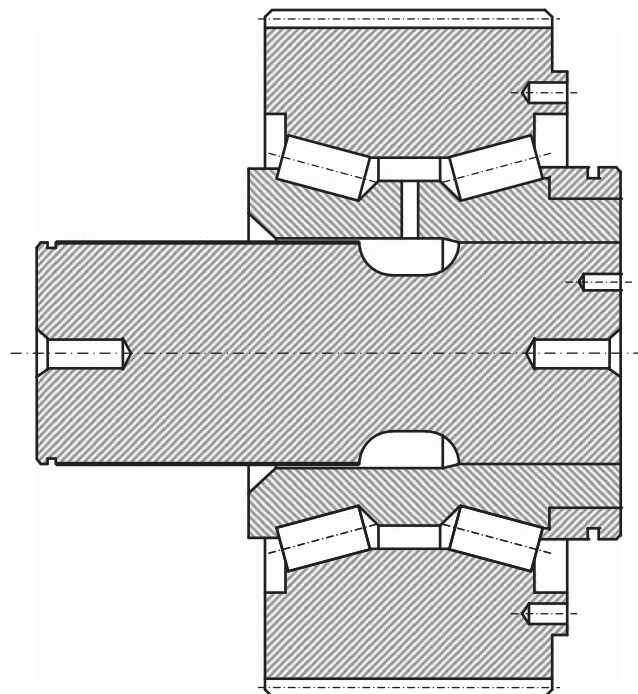
## 26.8 Alternative Approach for Equal Torque Sharing in Split Torque Transmission

Elimination (or at least substantial reduction) of the total number of redundant constraints is a straightforward way of equalizing load sharing in planetary gear drives as well as in gear drives of other kinds that also feature



**FIGURE 26.12**

Stress-strain diagram for the flex-pin. (Hicks, R.J., *Load Equalizing Means for Planetary Pinions*. U.S. Pat. 3.303.713. February 14, 1967, Filed: February 8, 1965 [44].)

**FIGURE 26.13**

Cross-sectional view of an integrated flex-pin bearing.

split torque. Simpler methods for reasonably equal torque sharing in multifold gear trains have been developed as well. Neither an increase in the complexity of the design of the gear train nor significant weight increase of the gearbox occurs when these methods of load equalizing are applied.

The basic problem in all epicyclic gearing is ensuring equal load sharing among the multitude of mesh points. For example, the *Stoeckicht* system (circa 1940) solves this problem by making the annulus ring flexible while allowing it and the sun gear to float without bearings so that they are supported by their respective mesh points.

Alternatively, designers have applied a number of novel designs with various levels of success to build epicyclic gearing systems that help to distribute load among the planetary pinions more evenly, thereby increasing the power density. In general, such improvements use components in the gear train that are elastically compliant and intended to compensate for clearance variations without imparting any negative operating characteristics, including:

- Flexible ring gears have been applied, but the effectiveness of this approach is not universal because radial deflections of the ring gear are not sufficient to compensate for clearance (backlash) variations present at the various mesh points.
- Floating ring gear system (used in some off-highway applications).
- Floating sun gear.
- Floating planet carrier.
- Double-helical gear with floating members.
- Floating planetary pinion, also called a flexible pin or abbreviated to *flex-pin*.

In the remaining sections of this chapter, application of elastic absorbers of manufacturing errors in the design of split torque gear trains is discussed. The focus is particularly on various designs of planetary gear drives, which present perfect examples of gear trains with split torque.

### 26.8.1 Planetary Gear Drive with Elastomeric Load Sharing Device

Application of an elastomeric load sharing device in the design of split torque transmission systems is illustrated in Figure 26.14. The core (essence) of the invention is briefly outlined below.

There are three major objectives of this invention. To provide a simplified load sharing device that provides substantially equal torque distribution between the load paths of a split power transmission system is one of

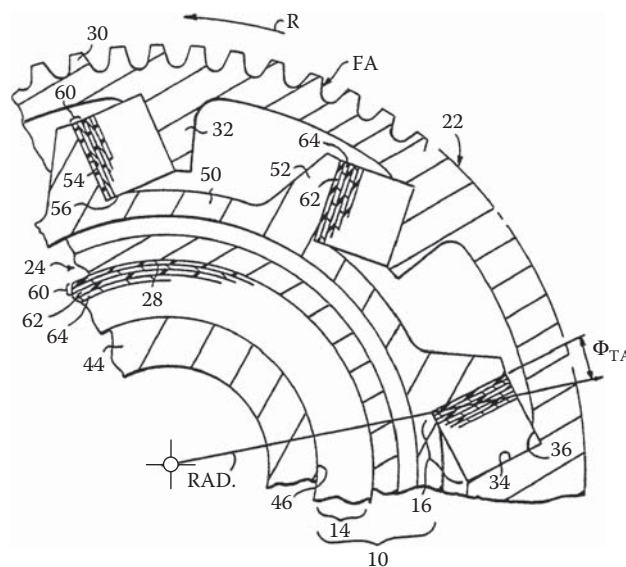


FIGURE 26.14

Concept of the elastomeric load sharing device. (Adapted from Isabelle, C.J., Kish, J.G., Stone, R.A., *Elastomeric Load Sharing Device*. U.S. Pat. No. 5,113,713. Filed: February 11, 1991, Date of Patent: May 19, 1992, Int. Cl.5 F16H 55/18, U.S. Cl. 74/410, 74/411, 74/440 [171].)

them. To provide a load sharing device that reduces the weight and complexity of a split power transmission system is the other objective. Yet another objective of the present invention is to provide a load sharing device that enhances the overall reliability of a split power transmission system.

An elastomeric load sharing device,\* interposed in combination between a driven gear and a central drive shaft to facilitate balanced torque distribution in split power transmission systems, includes a cylindrical elastomeric bearing and a plurality of elastomeric bearing pads. The elastomeric bearing and bearing pads make up one or more layers, each including elastomer with a metal backing strip secured thereto. The elastomeric bearing is configured to have a high radial stiffness and low torsional stiffness and is operative to radially center the driven gear and minimize torque transfer through the elastomeric bearing. The bearing pads are configured to have a low radial and torsional stiffness and high axial stiffness and are operative to compressively transmit torque from the driven gear to the drive shaft. The elastomeric load sharing device has spring rates that compensate for mechanical deviations in the gear train assembly to provide balanced torque distribution between complementary load paths of split power transmission systems.

The angular tilt of the bearing pads with respect to a radial line is generally between about 10 degrees and about 20 degrees.

An elastomeric material having excellent high-temperature properties and resistance to gearbox and hydraulic oils is used in the design of the elastomeric load sharing device. A metal backing strip is secured to said elastomeric material.

Elastomeric bearing pads are sufficiently compliant to accommodate a predetermined circumferential displacement facilitate balanced torque distribution.

An elastomeric torsional isolator can be preloaded† by a compressive load. Compressive preloading of the elastomeric torsional isolator provides a high normal force between the upper and lower rims and the spur gear for frictionally transmitted torque across the elastomeric torsional isolator from the spur gear to the annular flange gear.

Split torque designs can offer significant advantages over traditional planetary designs for helicopter transmissions. However, they have two unique properties, gap and phase differences, that result in the risk of unequal load sharing. Various methods have been proposed to eliminate the effect of gap and promote load sharing to a certain extent.

## 26.8.2 Elastic Load Sharing Device

In order to make a split torque transmission system nearly insensitive to manufacturing errors as well as to displacements of other natures, elastic load sharing devices (ELSDs) can be used. When designing a multiflow gear train, many considerations should be taken into account.

### 26.8.2.1 Elastic Properties of Elastic Load Sharing Device

The capability of an elastic load sharing device to accommodate for manufacturing errors strongly depends on spring characteristics. The following types of spring characteristics are known. They are listed immediately below (as illustrated in Figure 26.15):

1. Progressive
2. Linear
3. Degressive
4. Substantially constant
5. Progressive with knee

\* U.S. Pat. No. 5,113,713, "Elastomeric Load Sharing Device", /C.J. Isabelle, J.G. Kish, R.A. Stone, Int. Cl.<sup>5</sup> F16H 55/18, U.S. Cl. 74/410, 74/411, 74/440, Filed: February 11, 1991, Date of Patent: May 19, 1992.

† The necessity of a preloading of the elastomeric torsional isolator is just mentioned in the text body of the patent, and it is *not* listed among the claims of the invention. Moreover, the preload is not specified, and, per the invention, it could have either a negligibly small value or an extremely high value: both cases are impractical. Only a specific preloading is useful, and can be helpful to attain the objective of the invention. Considering the thickness of the elastomeric torsional isolator, no sufficient preloading of the elastomeric torsional isolator is physically possible—a large elastic deformation of the elastomeric torsional isolator is required.

In addition, the elastomeric torsional isolators are located at an angle 10° to 20° to a radial direction of the gear train—a radial direction for the elastomeric torsional isolator is preferred. One more feature: the split torque transmission system (U.S. Pat. No. 5,113,713) is not reversible.

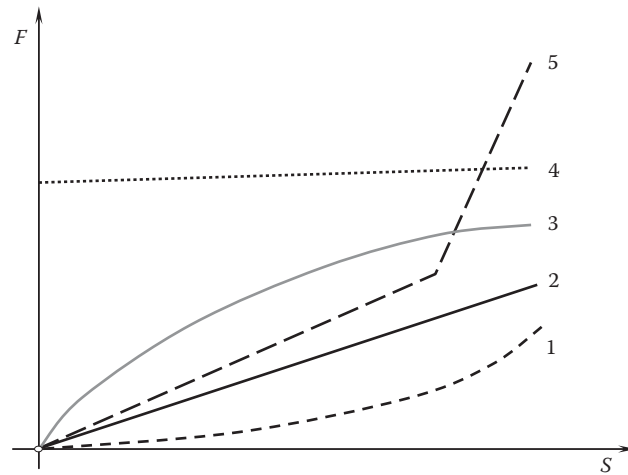


FIGURE 26.15

Spring characteristics: (1) progressive, (2) linear, (3) degressive, (4) substantially constant, (5) progressive with knee.

For implementation in the design of split torque transmission system, materials with the spring characteristics substantially constant (4) and degressive (3) are preferred. However, for most materials used in the production of gears and gear units, the relationship between the applied load and the displacement caused by the load is linear (2).

Significant improvement in the load-carrying capacity of a gear train with split torque can be attained by improvement in the design of the preloaded elastic load sharing device.\*

A deformation of the elastic load sharing device allows accommodation of manufacturing errors, displacements under operating load, and so forth. The elastic deformation must be large enough to accommodate manufacturing errors and the like, yet not exceed a particular given value. When zero torque is applied to the driving member of the planetary gearbox, no force is exerted from the elastic component and no deformation of the elastic component is observed. When the maximum torque is applied, maximum force is exerted from the elastic component and maximum deformation of the elastic component occurs. Because only elastic deformations of the elastic component are considered valid (see Young's law), the loaded diagram is represented by a linear function (see Figure 26.12). Huge displacements,  $y$ , of the elastic component are necessary to attain the operating load that acts against the elastic component. It is best to keep the displacements,  $y$ , as small as possible; however, they need to be sufficient to address manufacturing errors and the like.

The flex-pin concept was presented here in order to make a correct comparison of this concept with the concept of elastic load sharing devices.†

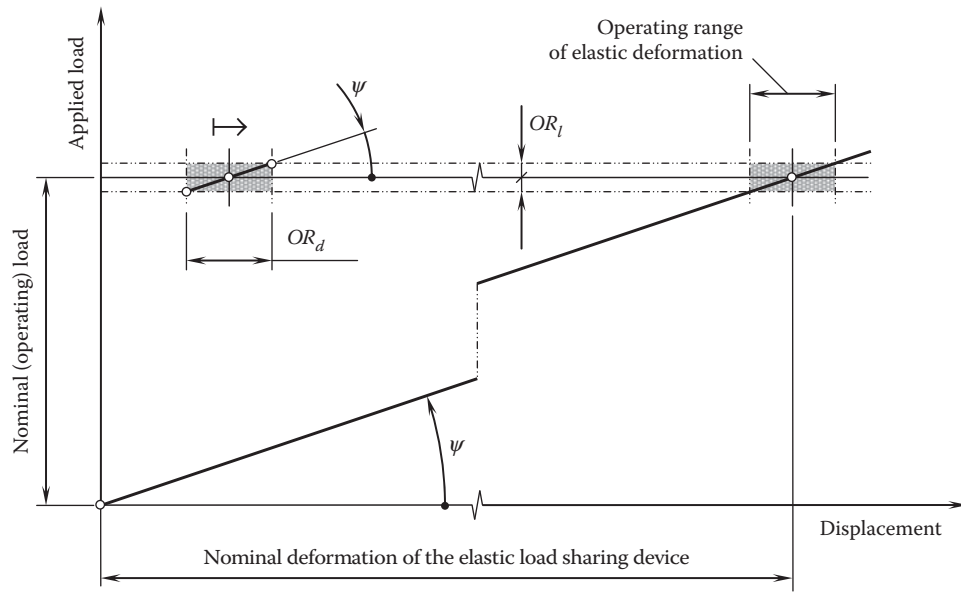
If the preloaded elastic load sharing device is loaded by a precalculated value of the load, the actual displacement of the pinions does not exceed the allowed displacement tolerance.

Consider a planetary gearbox for which the permissible range of variation of load share among the planetary pinions is equal to  $\pm OR_l$  (see Figure 26.16, upper left). The operating range of the elastic deformation,  $OR_d$ , of the elastic load sharing device needs to be the smallest possible; however, it must also be large enough to allow for accommodation of manufacturing errors and planetary pinion displacement under operating load. The two ranges,  $\pm OR_l$  and  $OR_d$  specify a rectangle. In Figure 26.16, a diagonal of this rectangle forms an angle,  $\psi$ , with the horizontal axis *applied load*. The desirable stiffness,  $c$ , of the elastic load sharing device must be equal to (or less than):

$$c \leq \tan \psi \quad (26.19)$$

\* The concept of the preload elastic absorber (PEA) has been proposed by the author as early as 2000 while with New Venture Gear, Inc., Syracuse, NY, USA.

† The term *load sharing device* is used here and below, not the more general term *power sharing device*, because the applied load, and not the transmitted power (or rotation), is used to keep control over the actual configuration of the components in the split torque transmission system.

**FIGURE 26.16**

Determination of the principal design parameters of the elastic load sharing device. (After Dr. S.P. Radzevich, circa 2000, *New Venture Gear*, Syracuse, NY.)

Once the stiffness,  $c$ , is determined, a straight line through the origin of the coordinate system *applied load—displacement* can then be traced. This line is at the angle  $\psi$  with respect to the horizontal axis displacement. The point of interception of the constructed straight line and the straight line of the nominal (operating) load,  $NL_{op}$ , specifies the desirable predeformation of the elastic load sharing device (see Figure 26.16).

The elastic load sharing device in (a) in a not-deformed stage, (b) in a preloaded stage, and (c) in a fully loaded stage is shown in Figure 26.17.

The predeformation,  $PD_{ea}$ , of the elastic load sharing device is calculated as:

$$PD_{ea} = (NL_{op} - OR_l) \cdot \cot \psi \quad (26.20)$$

Calculation of the design parameters of the elastic load sharing device is based on two parameters, that is, on the design parameters  $\pm OR_l$  and  $OR_d$ .

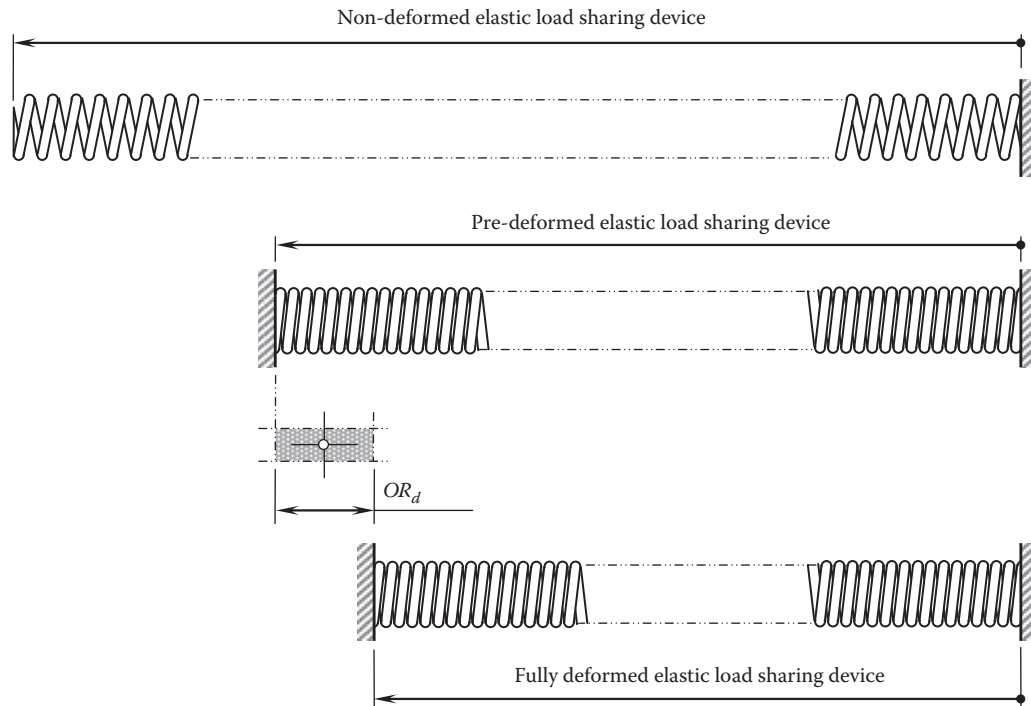
If the preloaded elastic absorber is loaded by a precalculated value, the actual displacements of the pinions do not exceed the prescribed tolerance for the displacement of the pinions. Practically, this can be done, for example, in the manner discussed immediately below.

### 26.8.2.2 Examples of Implementation of Elastic Load Sharing Devices

In some transmission systems, in particular helicopter transmission systems, there is a need to split the power (torque) developed by the engine system so that two or more load paths are provided for transfer of power to an output member. Such split power configurations reduce the tooth loading of the gear train assemblies making up the respective load paths while concomitantly providing redundant paths for torque transmission. Should one gear assembly, that is, load path, become inoperative, torque will be transmitted through the remaining gear assembly, thereby ensuring continued operation of the transmission system.

An example of application of an elastic load sharing device in the design of a planetary gearbox is discussed below; however, it also can be used in any other design of split torque transmission system.

Because of split torque, planetary gearboxes can feature significantly higher power density compared to that in gear transmissions of traditional design. This is true when the torque being transmitted is equally shared among all the planetary pinions. To attain the highest possible power density (strongly desired!), the accuracy requirements to machining the components of the planetary gearbox are high, and the tolerances for the accuracy of the components of the gearbox are tight enough. The tighter the tolerances, the higher the production costs, and vice versa.

**FIGURE 26.17**

Elastic load sharing device: nondeformed, predeformed, and fully deformed. (After Dr. S.P. Radzevich, circa 2000, *New Venture Gear*, Syracuse, NY.)

Epicyclical gear systems have typically been equipped with straddle-mounted planetary pinions with pins supported on the input and output sides of the carrier. The torsional wind-up of the carrier, position accuracy of the pins, machining tolerances of the planetary gear system components, and bearings clearances all can contribute to poor load sharing among the planet pinions, as well as misaligned gear contacts in the deflected state. In epicyclical gearing systems of traditional design—that is, where the distance between planetary pinion centerlines is specified by the design to be within a fixed range—it is widely recognized that load sharing is not evenly distributed among planetary gear meshes. Furthermore, stress, too, is distributed invariably at mesh points. Load sharing and stress distribution at each mesh point are heavily influenced by global design configuration, component design tolerances, manufacturing accuracy, component deflection, and thermal distortion (see Figure 26.7).

Consider a planetary gearbox for which the permissible range of variation of load sharing among the planetary pinions is equal to  $\pm OR_l$  (see Figure 26.16). The operating range of the deformation,  $OR_d$ , of the elastic load sharing device has to be a smallest possible.

The concept of application of the elastic load sharing device is illustrated in Figure 26.18, where a schematic of a possible design of a planetary gearbox with almost equal load sharing among the planetary pinions is shown. The sun gear and ring gear are mounted in the gear housing. The gear housing is stationary. A few planetary pinions (1 through 5 in Figure 26.18) are evenly distributed in the space formed by the sun gear and ring gear. When the sun gear rotates, the torque and rotation are transmitted to the ring gear by means of the planetary pinions.

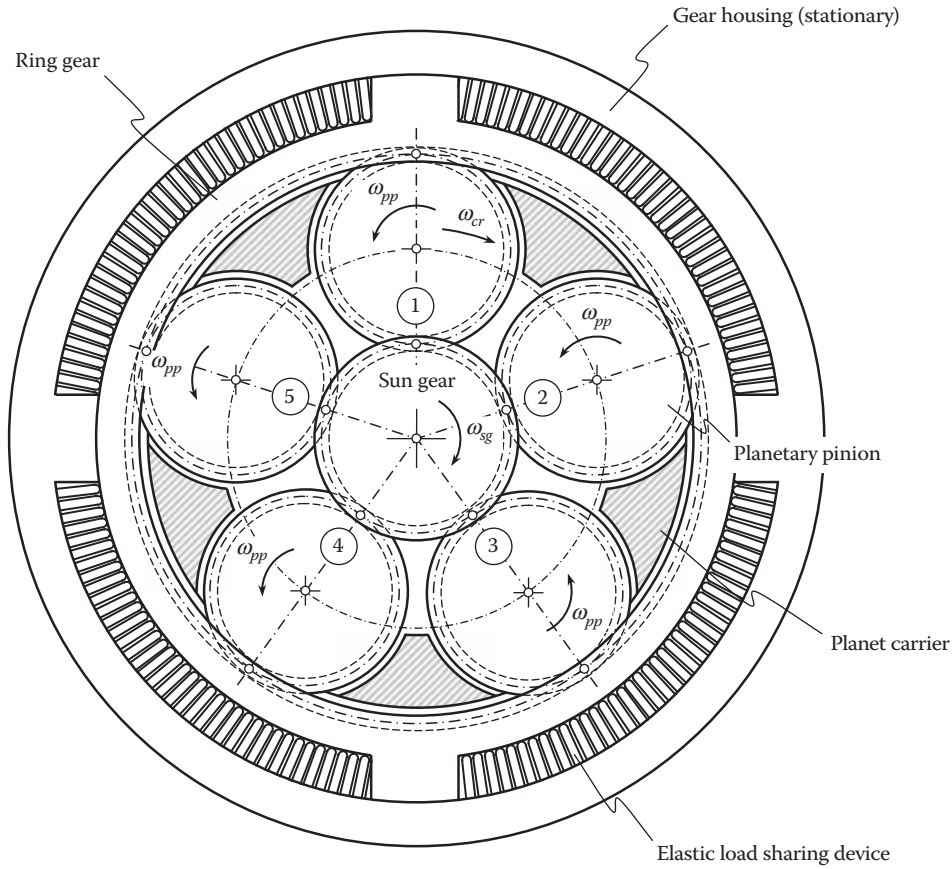
The ring gear is mounted to have a possibility to turn about its axis through a certain small angle. In the particular case under consideration, the elastic load sharing devices are placed between the gear housing and the ring gear. Therefore, the ring gear and gear housing interact with one another through the elastic load sharing device.

Various designs of the elastic load sharing device can be used in the design of the planetary gearbox. Shown in Figure 26.19, these can be rectangular springs, one or a few round springs of conventional design, a piece of elastic material with appropriate properties, and so forth.

There can be either one or several elastic load sharing devices. Depending on the available room, elastic load sharing devices can be mounted from one or both ends of the gear set. Also, in case of necessity, elastic load sharing devices can be mounted from around the gear set and from both ends of the gear set.

When the power (that is, a rotation and torque) are transmitted, at the beginning, only one planetary pinion is engaged in tight mesh with both the sun gear and the ring gear. The rest of the planetary pinions are either



**FIGURE 26.18**

Springs as elastic load sharing device in the design of a planetary gearbox with almost equal load sharing among the planetary pinions.

underloaded, or they can even be idle. When the applied load ramps up, the ring gear slightly turns about its axis in relation to the gear housing. Because there are two pitch points for each of the planetary pinions (one of them is in mesh with the sun gear and another is in mesh with the ring gear), the second planetary pinion is engaged in mesh with the ring gear, and so forth, up to a configuration when all the planetary pinions are engaged in mesh with the ring gear. The difference in load sharing among all the planetary pinions is small and is always within a prespecified interval, for example, within the interval  $\pm 5\%$ .

Assume that a split torque transmission system (a planetary gearbox) consists of  $n_{pp}$  planetary pinions (and a corresponding number of the *elastic load sharing device*). The maximum torque being transmitted equals  $T_{\max}$ . The design parameter of the elastic load sharing device,  $OR_d$ , is specified. A permissible deviation of the torque been transmitted by the split torque transmission from the given torque specified for the transmission must not exceed a certain value,  $t_{\text{var}}$ , %.

This is illustrated in more detail in [Figure 26.20](#). Commonly, all the planetary pinions are loaded randomly, as shown in [Figure 26.20a](#). When the split torque transmission operates, the pinion with a largest displacement is the first to interact with the elastic load sharing device. As this pinion interacts with the ring gear and sun gear at the same time, it pushes the elastic load sharing device. However, no additional planetary pinion is engaged if the exerted torque is less than the torque per one planetary pinion

$$t_p = \frac{T_{\text{nom}} - NL_{op}}{n_{pp}} \quad (26.21)$$

or:

$$t_p = \frac{T_{\text{nom}} - 0.5 \cdot NL_{op}}{n_{pp}} \quad (26.22)$$



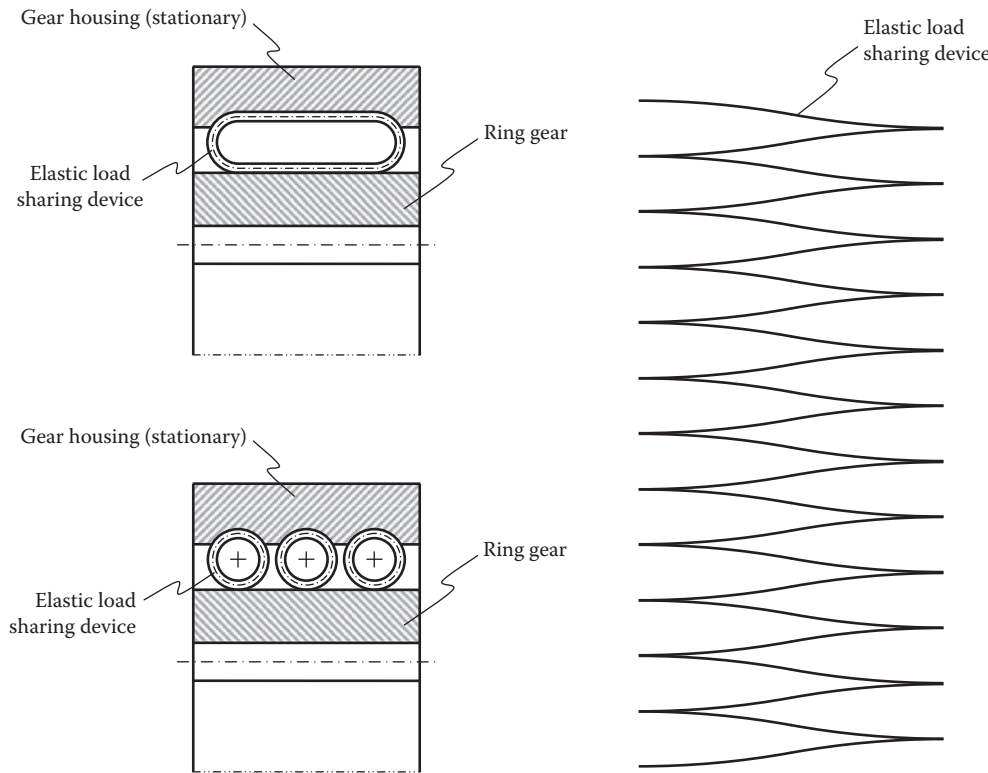


**FIGURE 26.19**  
Possible designs of elastic load sharing devices.

Once the inequality:

$$t_p > \frac{T_{nom} - NL_{op}}{n_{pp}} \quad (26.23)$$

is observed, then the next planetary pinion is engaged in the interaction with the ring gear. At a certain time, two planetary pinions push the ring gear, and in this way engage one more planetary pinion in mesh. Then, the next planetary pinion is engaged in the interaction with the ring gear, and so forth until all the planetary pinions are involved in the interaction with the ring gear.

In the best-case scenario, all the planetary pinions are fully loaded except one that is loaded to the minimum level (see Figure 26.20b). The load capacity of the planetary gear set is maximal in this case. Finally, in the

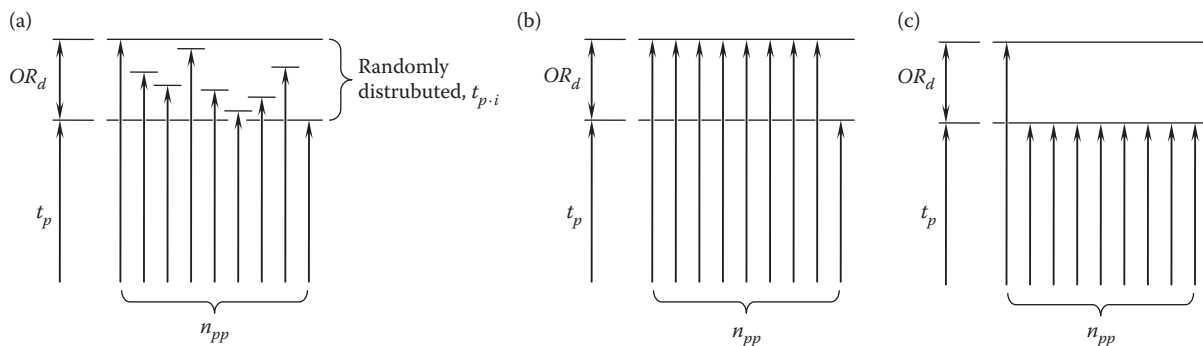


**FIGURE 26.20**  
Kinds of loading of the planetary pinions when an elastic load sharing device is used: (a) randomly loaded planetary pinions, (b) maximal, and (c) minimal load capacity of the gear set.

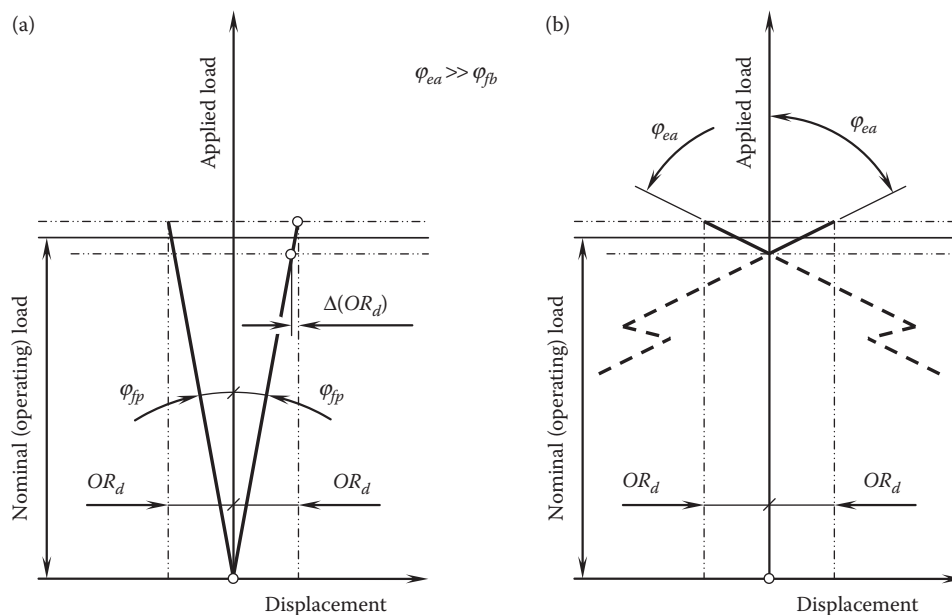


FIGURE 26.21

Comparison of the “load vs. displacement” diagrams for the flex-pin approach (a) and for the elastic load sharing device (b).

worst-case scenario, all the planetary pinions are loaded to the minimal level except one that is loaded to the maximum level (see Figure 26.20c). The load capacity of the planetary gear set is minimal in this case.

Use of the schematic shown in Figure 26.16 for determining the required preloading of the elastic load sharing device is illustrated in Figure 26.17.

An advantage of the preloaded elastic load sharing device over the unloaded elastic component in the design of a planetary gearbox is illustrated in Figure 26.21. The preloading of the elastic load sharing device along with a reduced slope of the characteristic curve together make possible an accurate adjustment of the split torque transmission system to a load variation in the gear transmission.

In the worst-case scenario of load sharing among planetary pinions in a split torque transmission system, only one of  $n_{pp}$  planetary pinions is loaded the most heavily, while the rest withhold the lowest permissible torque. Remember that all the loads per planetary pinion are within the allowed band of variation,  $k$ .

The calculations reveal that in the worst-case scenario for a planetary gearbox—eight planetary pinions ( $n_{pp} = 8$ ) and the allowed variation of the load per planet pinion  $k = 0.1$ —the deviation of the transmitted load from the desired value does not exceed 8.75%. Thus, for a planetary gear drive with three planetary pinions ( $n_{pp} = 3$ ) and the allowed variation of the load per planet pinion  $k = 0.05$ , the deviation of the transmitted load from the desired value does not exceed 3.33%. The actual deviations are less than those calculated for the worst-case scenario.

The planetary gearbox with the elastic load sharing device of the proposed design is reversible; that is, a rotation can be transmitted in both directions of rotation of the input shaft. No radial load is exerted when the elastic load sharing device of the proposed design is used.

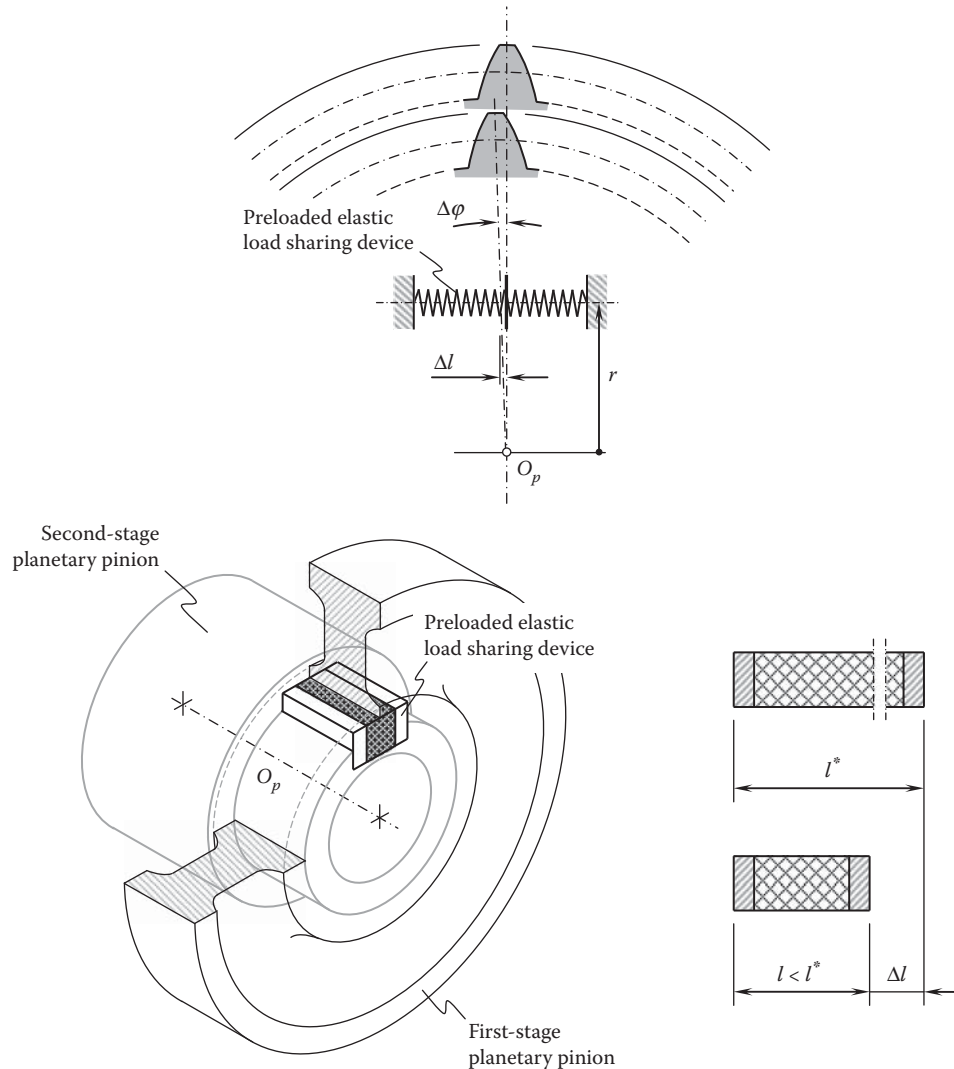
If the preloaded elastic load sharing device is loaded by a precalculated value, the actual displacement of the pinions does not exceed the allowed displacement tolerance.

Another example of application of an elastic load sharing device in the design of a two-stage planetary reducer is shown in Figure 26.22. The preloaded elastic load sharing device is placed here between the first-stage planetary pinion and the second-stage planetary pinion.\*

In a two-stage planetary reducer, the preloaded elastic load sharing device can be mounted between the first-stage planetary pinion and the second-stage planetary pinion† (see Figures 26.21 and 26.22). It is common practice to hob both planetary pinions of the cluster planetary pinion. For this purpose, it is convenient to assemble

\* Radzevich, S.P., *A Planetary Reducer*, Invention disclosure, filed to New Venture Gear, Inc., Patent Office (Syracuse, NY) on October 30, 2001, patent pending.

† Radzevich, S.P., *A Planetary Reducer*, Invention disclosure, filed to New Venture Gear, Inc., Patent Office (Syracuse, NY) on October 30, 2001, patent pending.

**FIGURE 26.22**

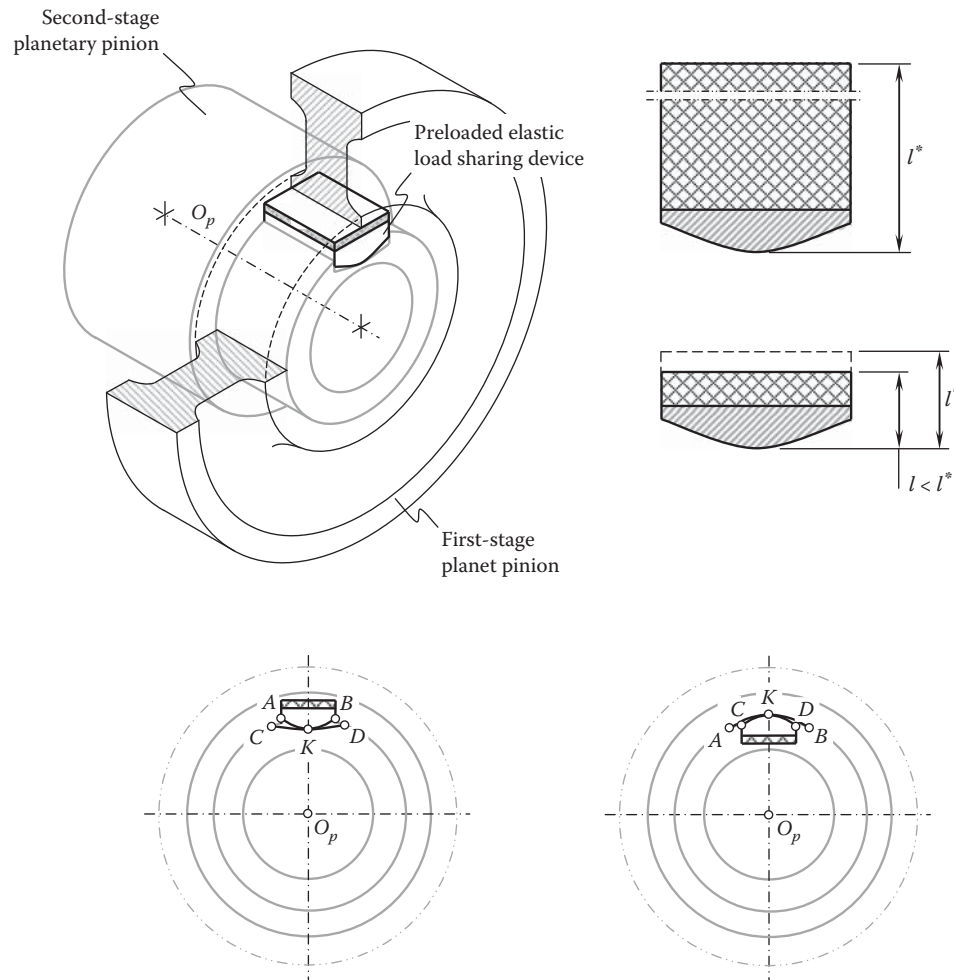
Application of a preloaded elastic absorber of manufacturing errors in the design of a cluster planet pinion. (As proposed by Dr. S.P. Radzevich around 2000.)

the cluster planetary pinion comprising two planetary pinions. However, note that proper phasing of the pieces in relation to one another while assembling the cluster planetary pinion is critical; misphasing errors with planetary pinions can be catastrophic. The preloaded elastic load sharing device is installed between the two planetary pinions of the cluster planetary pinion (see Figure 26.21 and 26.22).

For equal torque sharing among the planetary pinions, the misphasing  $\Delta\varphi$  must be zero. As the misphasing  $\Delta\varphi$  cannot be eliminated, it must be absorbed. For this purpose, it is necessary to introduce an additional degree of freedom for one of the planetary pinions in relation to another and, in this way, to make the planetary pinions self-aligning. Self-alignment of the planetary pinions can be ensured by implementation of the preloaded elastic load sharing device. An angular displacement,  $\Delta\varphi$ , to be absorbed by the elastic absorber can be eliminated when the linear displacement,  $\Delta l$ , is equal to:

$$\Delta l = \Delta\varphi \cdot r \cdot \frac{\pi}{180^\circ} \quad (26.24)$$

In Equation 26.24, the radial location of the preloaded elastic absorber is specified by the distance  $r$ . Deformation,  $\Delta l$ , of an elastic body under load usually (but not necessarily) relates to the applied load,  $T$ , linearly or (at

**FIGURE 26.23**

A cluster pinion gear with a preloaded elastic load sharing device. (As proposed by Dr. S.P. Radzevich around 2000.)

least) almost linearly,  $\Delta = c \cdot T$  ( $c$  is a proportionality factor equal to the rigidity of the preloaded elastic absorber). In such a case, the angle,  $\phi$ , can be calculated from the formula:

$$\phi = \tan^{-1}(c) \quad (26.25)$$

In the general case, when  $c \neq \text{const}$ , the current value of  $c$  is equal to  $c = \frac{dT}{d(\Delta l)}$ .

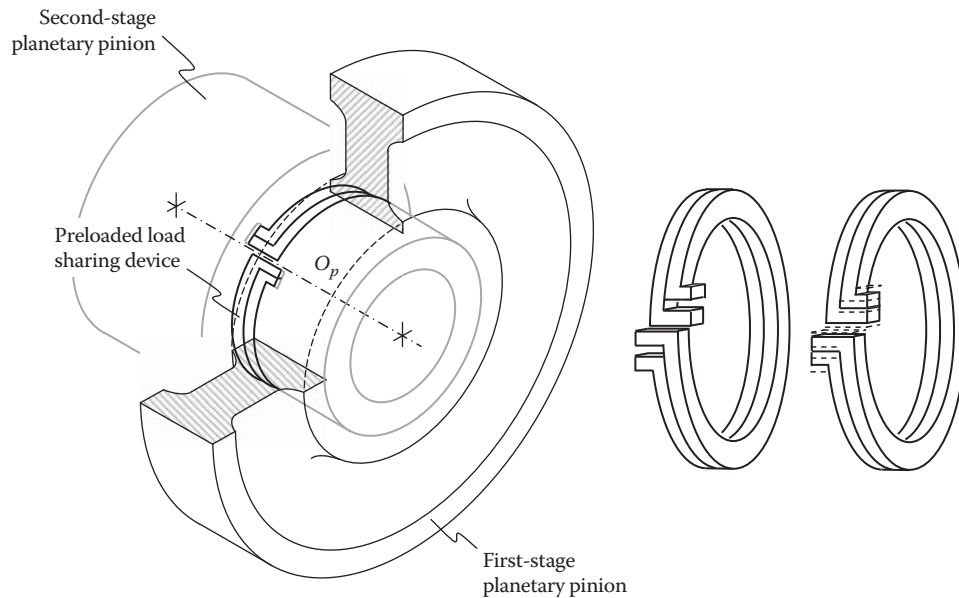
The variation interval for the applied load should be known for the calculation of the design parameter of the preloaded elastic load sharing device.

Another example of application of the preloaded elastic load sharing device in the design of a cluster pinion gear\* is shown in Figure 26.23.

In the example under consideration, the first-stage planetary pinion is assembled with the second-stage planetary pinion.

The preloaded elastic load sharing device must be elastic to accommodate for the misphasing error, and it should be rigid enough to transmit power from the first-stage planetary pinion to the second-stage planetary pinion.

\* Radzevich, S.P., *A Gear Train*, Invention disclosure, filed to New Venture Gear, Inc. Patent Office (Syracuse, NY) on November 30, 2001, patent pending.

**FIGURE 26.24**

An example of implementation of an elastic load sharing device in the design of a split torque transmission system. (As proposed by Dr. S.P. Radzevich around 2000.)

The elastic load sharing device is composed of two plates made of steel, separated from each other by, for example, either elastomer or a spring of a known design.

The preloaded elastic load sharing device is capable of accommodating a large misphasing error. The profiles *AB* and *CD* function as a cam mechanism, which allows the planets to find for themselves their proper relative orientation. Both profiles, that is, *AB* and *CD*, have to be determined in such a way as to incorporate friction; the inclination of the profiles must exceed the angle of friction.

Gear transmission with split torque\* features a preloaded elastic load sharing device, which is composed of two round springs (see Figure 26.24). The round springs are preloaded in opposite directions.

The elastic load sharing device in Figure 26.24 operates in a way similar to the aforementioned elastic absorbers.

Note: It should be stressed here that the elastic load sharing device can be applied in the design of split torque transmission systems (including, but not limited to, planetary gearboxes) of any and all types and sizes: small, medium, and large size.

The advantage of the elastic load sharing device over the flex-pin concept is clearly illustrated in Figure 26.21. When the flex-pin concept is used, only a small fraction,  $\Delta(OR_d)$ , is used to overcome the unfavorable displacement of the planetary pinions under operating load (see Figure 26.21a). This is because the flex-pins are not preloaded and therefore the stiffness angle  $\varphi_{fp}$  is relatively small. When the concept of the elastic load sharing device is used, the entire  $OR_d$  is used to accommodate for the unfavorable displacement of planetary pinions under operating load (see Figure 26.21b). As such, the stiffness angle  $\varphi_{ea}$  is significant. Typically, the inequality  $\varphi_{ea} \gg \varphi_{fp}$  is always observed. This advantage of the elastic load sharing device is significant in that it enables a higher power density for transmission through the planetary gearbox. Evidently, the presented concept of the elastic load sharing device can be used for the improvement of power density in split torque transmission systems of any and all designs.

Numerous other examples of the implementation of the preloaded elastic load sharing device are also known.

Use of the concept of elastic load sharing devices allows a significant improvement in power density being transmitted through the planetary gearbox. Elastic load sharing devices can be applied in the design of split torque transmission systems of any type.

\* Radzevich, S.P., *A Gear Transmission*, Invention disclosure, filed to New Venture Gear, Inc. Patent Office (Syracuse, NY) on December 30, 2001, patent pending.

## 26.9 Main Features of Split Torque Transmission Systems with Preloaded Elastic Load Sharing Devices

There is a variety of forms of application of the concept of *preloaded elastic load sharing devices*. Application of all of them makes possible a significant increase in power density.

In the design of a split torque transmission system, for example, a planetary gearbox, the following are true:

- All the planetary pinions are preloaded with the torque,  $t_p$ , which is equal to  $t_p = T_{nom}/n_{pp}$ , where  $T_{nom}$  denotes the total torque transmitted by the gearbox, and  $n_{pp}$  denotes the number of planetary pinions.
- Elastic deformation of the load sharing device under preloading should be of a precalculated value. Further elastic deformation of the elastic load sharing device (within the displacements corresponding to the manufacturing errors to be absorbed) does not significantly affect the loading of the planetary pinions.
- With the application of preloaded elastic load sharing devices, no tight tolerances are required in many dimensions.
- With a preloaded elastic load sharing device, the axes of rotation of all the planetary pinions are not deflected (as with flexible pins), and they remain straight and parallel to each other under the load.

The lower the stiffness of the elastic load sharing device, the lower the difference in operating loading of each of the planetary pinions.

Split torque transmission systems are briefly discussed in this section. The problem of equal (or almost equal) load sharing among all the paths of power flow (among all the planetary pinions) is addressed. The root cause of uneven load sharing is outlined. Numerous approaches to equalize load sharing among the planetary pinions in a planetary gearbox are reported.

## Vector Approach for Kinematic and Dynamic Analysis of Complex Gear Systems

Application of the earlier-discussed rotation vectors of a gear and its mating pinion, that is, of the vector diagrams of a gear pair (see [Chapter 2](#)), can be enhanced and used for the kinematic and dynamic analysis of complex gear systems, as well as to design complex gear systems with desirable performance.

The principal steps of a vector approach for kinematic and dynamic analysis of complex gear systems are briefly outlined below. The disclosed method is applicable for the analysis of all kinds of complex gear systems with parallel axes of rotation of the gears and pinions, including but not limited to single-stage and multistage planetary gear systems in particular. The vector diagram of an intersected-axes gear pair is constructed. The disclosed approach can be enhanced to crossed-axes gear pairs as well.

### 27.1 Possible Kinds of Images for Rotating Gears

Different ways can be employed to graphically depict a rotating gear. An image of a rotating gear (see [Figure 27.1a](#)) can be used in certain applications. A rotating gear can be depicted by means of its axis of rotation,  $O_g$ , and a circular arc with an arrow at one end (see [Figure 27.1b](#)). The arrow indicates the direction of the rotation of the gear. The axis of rotation,  $O_g$ , and an arrowed circular arc can be complemented with a corresponding rotation vector,  $\omega_g$  (see [Figure 27.1c](#)). The rotation vector,  $\omega_g$ , is along the gear axis  $O_g$ , and is applied at an arbitrary point within the gear axis, as the rotation vector,  $\omega_g$ , is a kind of sliding vector. The *right-hand rule* can be used for the determination of the direction of the rotation vector,  $\omega_g$ . The rotation vector,  $\omega_g$ , of a gear itself is sufficient to specify a rotating gear (see [Figure 27.1d](#)).

A consideration similar to that discussed above is valid with respect to a gear that is rotated in the opposite direction. The latter is illustrated in [Figures 27.1e](#) through [27.1g](#).

For the purposes of kinematic and dynamic analysis of complex gear systems, vector representation of a rotating gear (see [Figures 27.1d](#) and [27.1g](#)) is advantageous over other possible types of graphical representation of a rotating gear. Therefore, in the analysis below, a rotating gear (see [Figure 27.2a](#)) is depicted by means of the rotation vector,  $\omega_g$ , as illustrated in [Figure 27.2b](#).

In addition to the rotation vector,  $\omega_g$ , a complementary torque vector,  $T_g$ , can be assigned. The torque vector,  $T_g$ , is along the gear axis  $O_g$ . The torque vector,  $T_g$ , is applied at an arbitrary point within the gear axis, as the torque vector,  $T_g$ , is a kind of sliding vector. It is convenient to apply the torque vector,  $T_g$ , at a point at which the rotation vector,  $\omega_g$ , is applied.

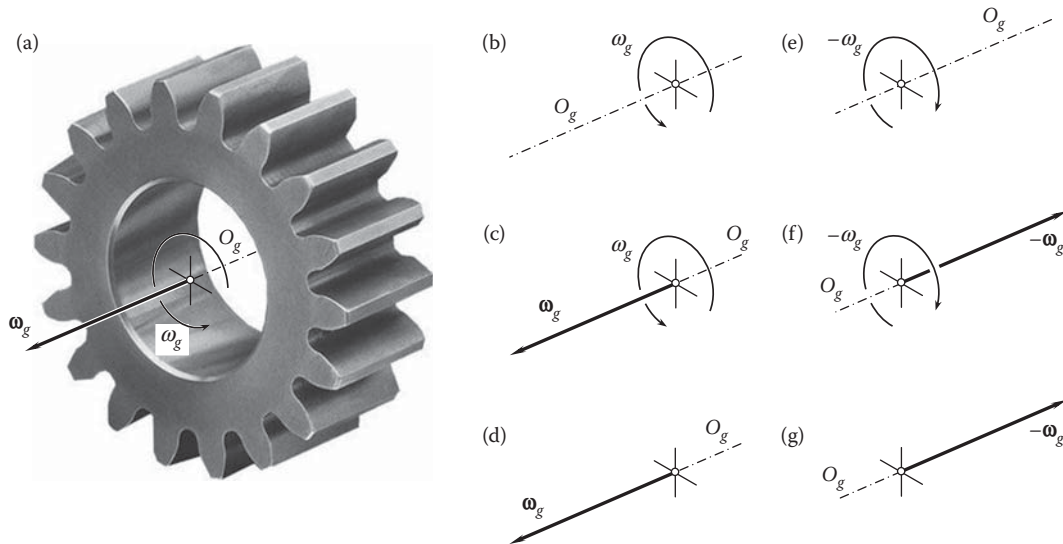
Two different cases of the torque vector,  $T_g$ , are distinguished.

First, for a driving gear in a gear pair, shown in [Figure 27.3a](#), the torque vector,  $T_g$ , is pointed at the direction the rotation vector,  $\omega_g$ , is pointed to (see [Figure 27.3b](#)).

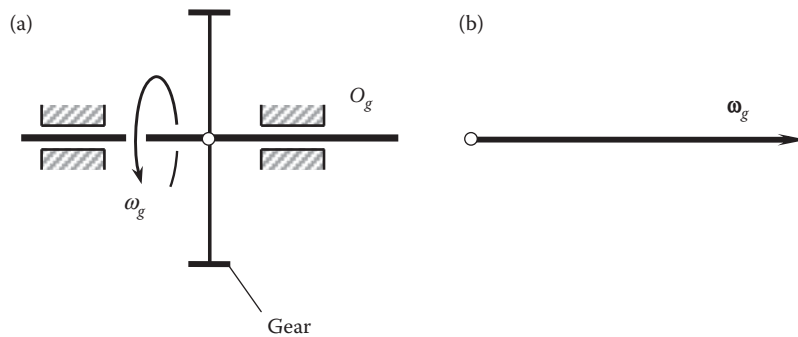
Second, for a driven gear in a gear pair, shown in [Figure 27.4a](#), the torque vector,  $T_g$ , is pointed at the direction that is opposite to the one the rotation vector,  $\omega_g$ , is pointed to (see [Figure 27.4b](#)).

Therefore, in a driving gear, the rotation vector,  $\omega_g$ , and the torque vector,  $T_g$ , are always of the same direction, and in a driven pair, the rotation vector,  $\omega_g$ , and the torque vector,  $T_g$ , are always of the opposite direction to each other. An illustrative example of this rule is illustrated in [Figure 27.5](#), where an elementary gear drive is schematically shown. The gear pair is composed of two gears, 1 and 2. Gear 1 is rotating about the axis  $O_I$ . Accordingly, gear 2 is rotating about the axis  $O_{II}$ . Gear 1 is the driving component of the gear pair, while the gear 2 is driven. The rotation vector  $\omega_1$  of the driving gear 1, and input torque vector,  $T_1$ , are pointed in the same direction. For an external gear pair, rotation vector,  $\omega_2$ , of the driven gear 2 is pointed oppositely to the rotation vector,  $\omega_1$ . For an internal gear pair, the rotation vectors,  $\omega_1$  and  $\omega_2$ , are pointed in the same direction.

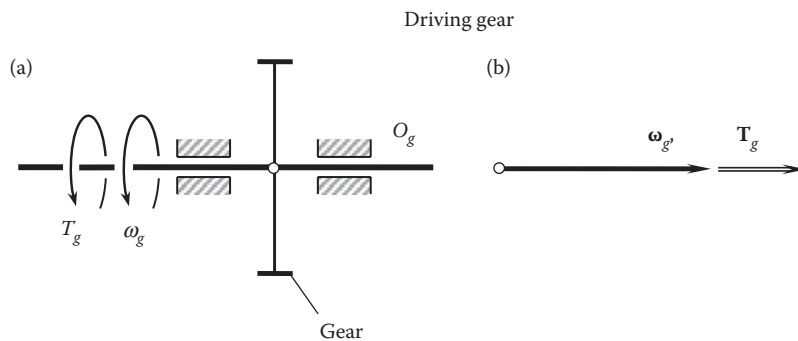


**FIGURE 27.1**

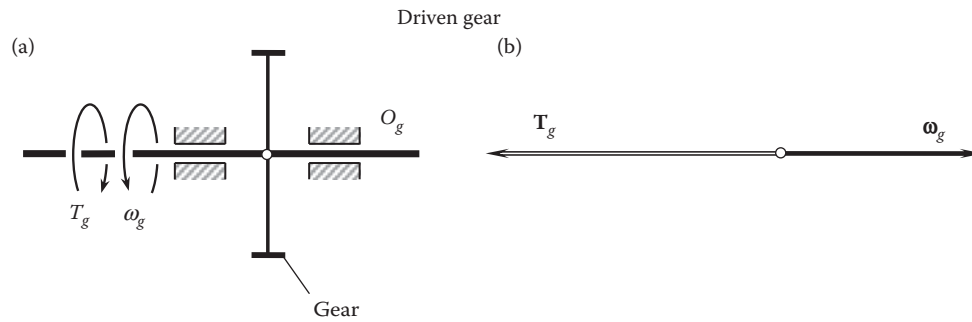
Possible images for a rotating gear: (a) rotating gear, (b) direction of rotation of a gear, (c) direction of rotation of a gear and rotation vector of a gear, (d) rotation vector of a gear; (e) through (g) are equivalents for oppositely directed cases in (b) through (d).

**FIGURE 27.2**

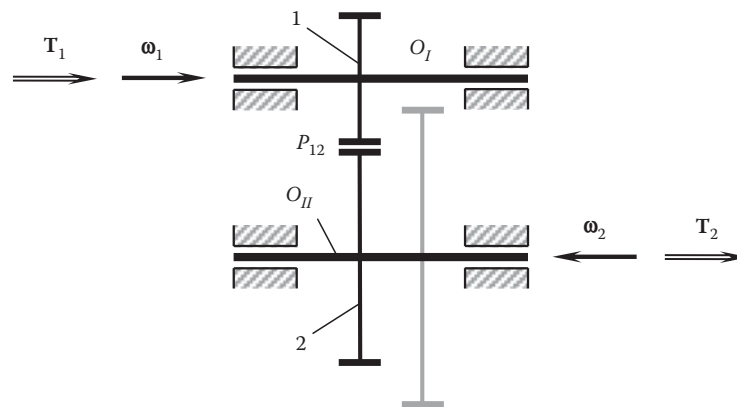
Schematic of a rotating,  $\omega_g$ , gear (a), and the corresponding rotation vector,  $\omega_g$ , associated with the gear (b).

**FIGURE 27.3**

Schematic of a rotating,  $\omega_g$ , gear with the applied input torque,  $T_g$  (a), and the corresponding rotation vector,  $\omega_g$ , and input torque vector,  $T_g$ , associated with the *driving* gear (b).

**FIGURE 27.4**

Schematic of a rotating,  $\omega_g$ , gear with the applied input torque,  $T_g$  (a), and the corresponding rotation vector,  $\omega_g$ , and input torque vector,  $T_g$ , associated with the *driven* gear (b).

**FIGURE 27.5**

Rotation vectors,  $\omega_1$  and  $\omega_2$ , and torque vectors,  $T_1$  and  $T_2$ , at input shaft 1 and output shaft 2 of a gear pair.

The output torque vector,  $T_2$  (the torque vector at the driven gear 2), is pointed oppositely to the rotation vector,  $\omega_2$ , of the second gear.

The above consideration can be interpreted as a kind of qualitative analysis of the kinematics and of dynamics of a gear pair with parallel axes of rotation of the gear and its mating pinion.

## 27.2 Vector Diagrams for Complex Gear Systems

Once the concept of the gear rotation vector,  $\omega$ , and torque vector,  $T$ , is understood, this allows us to proceed with the analysis of the kinematics and of dynamics of a gear pair and perform the analysis in terms of the vectors,  $\omega$  and  $T$ , for each of the elementary gear pairs.

For the kinematic and dynamic analysis of complex gear systems, vector representation of rotations of a driving and driven gear of a gear pair, as well as vector representation of torque vectors of the driving and the driven gears of a gear pair, are convenient.

A quantitative kinematic and dynamic analysis of an external gear pair is illustrated in [Figure 27.6](#).

The driving gear 1 is rotated about its axis,  $I$ , with an angular velocity,  $\omega_1$ . The rotation vector,  $\omega_1$ , of the driving gear 1 in [Figure 27.6](#) is depicted along the axis,  $I$ . The applied torque vector,  $T_1$ , is also along the gear axis of rotation,  $I$ . The input vectors,  $\omega_1$  and  $T_1$ , are one-sided to one another.

The driving gear 1 is engaged in mesh with a driven gear 2.  $P_{12}$  is the pitch point of the gear 1-to-gear 2 mesh.

The driven gear 2 is rotated about its axis,  $II$ , with a certain angular velocity,  $\omega_2$ . The rotation vector,  $\omega_2$ , of the driven gear is along the axis,  $II$ . The magnitude,  $\omega_2$ , of the rotation vector,  $\omega_2$ , is to be determined. The output

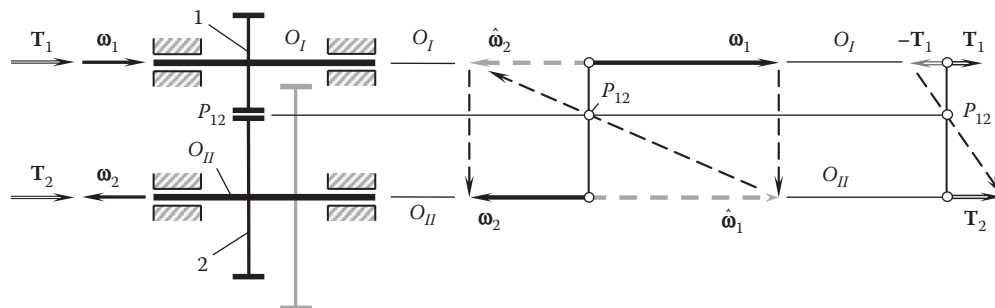


FIGURE 27.6

Elements of a quantitative kinematic and dynamic analysis of an external gear pair.

torque vector,  $\mathbf{T}_2$ , is also along the gear axis of rotation,  $II$ . The magnitude,  $T_2$ , of the torque vector,  $\mathbf{T}_2$ , is to be determined. In external gearings, the output vectors,  $\omega_2$  and  $\mathbf{T}_2$ , are reciprocal to one another.

A straight line through the origin of the rotation vector,  $\omega_1$ , is constructed in Figure 27.6. Every point within this straight line features zero rotation. Therefore, the constructed straight line is referred to as the *reference line*. Evidently, the pitch point,  $P_{12}$ , is located within the reference line. The actual location of the pitch point,  $P_{12}$ , in the vector diagram of the gear pair is defined as the intersection of the horizontal straight line through the pitch point,  $P_{12}$ , in the kinematic scheme of the gear pair (see the left-hand portion of Figure 27.6) by the reference line (see the right-hand portion of Figure 27.6).

The rotation vector,  $\omega_2$ , of the driven gear, and the output torque vector,  $\mathbf{T}_2$ , are constructed so as to meet the conventional requirements external gearing obeys:

$$\omega_1 \cdot r_1 = \omega_2 \cdot r_2 \quad (27.1)$$

Here, in Equation 27.1,  $r_1$  and  $r_2$  designate radii of pitch circles of the driving gear 1 and driven gear 2, accordingly ( $r_1 + r_2 = C$ , and  $C$  is the center distance between the axes,  $O_I$  and  $O_{II}$ ).

As the ratios,  $\omega_1/\omega_2$  and  $r_1/r_2$ , are reciprocal to one another, two auxiliary rotation vectors,  $\hat{\omega}_1$  and  $\hat{\omega}_2$ , are used to construct the rotation vector,  $\omega_2$ . The rotation vector,  $\hat{\omega}_1$ , is along the driven gear axis of rotation,  $O_{II}$ , and the rotation vector,  $\hat{\omega}_2$ , is along the driving gear axis of rotation,  $O_I$ . The magnitude of the auxiliary rotation vector,  $\hat{\omega}_1$ , is equal to the magnitude of the rotation vector,  $\omega_1$ ; that is, the equality  $|\hat{\omega}_1| = |\omega_1|$  is valid. Use of Equation 27.1 allows for a construction (see Figure 27.6) by means of which the magnitude of the output rotation vector,  $\omega_2$ , is determined.

There is no need to use an auxiliary torque vector,  $\hat{\mathbf{T}}_2$ , to construct the output torque vector,  $\mathbf{T}_2$ , as the ratios  $|\mathbf{T}_1|/|\mathbf{T}_2|$  and  $r_1/r_2$  are one-sided to one another (see Figure 27.6). The determination of the output torque vector,  $\mathbf{T}_2$ , is clear from the schematic shown in Figure 27.6 (at the right-hand side).

More complex gear drives can also be analyzed using the approach outlined above. As an example, Figure 27.7 illustrates a gear drive composed of several gear pairs. The gear drive consists of two external gear pairs 1-2 and 3-4, and one internal gear pair 5-6. The gears rotate about the axes  $O_I$ ,  $O_{II}$ ,  $O_{III}$ , and  $O_{IV}$ . Points  $P_{12}$ ,  $P_{34}$ , and  $P_{56}$  are the pitch points in the gear pairs 1-2, 3-4, and 5-6, correspondingly. The rotation,  $\omega_1$ , of the driving gear, and the input torque,  $\mathbf{T}_1$ , are given. It is necessary to determine the rest of the rotation vectors  $\omega_2$ ,  $\omega_3$ ,  $\omega_4$ ,  $\omega_5$ , and  $\omega_6$ , and torques  $\mathbf{T}_2$ ,  $\mathbf{T}_3$ ,  $\mathbf{T}_4$ ,  $\mathbf{T}_5$ , and  $\mathbf{T}_6$ .

The discussed approach (see Figure 27.6) is consequently used for each of the gear pairs 1-2, 3-4, and 5-6. The results of the kinematic and dynamic analysis of the gear drive are presented in Figure 27.7. It is of importance to stress here that in an internal gear pair, the directions of the rotation vectors,  $\omega_5$  and  $\omega_6$ , are the same; that is, in an internal gear pair, the direction of rotation of the driven gear in comparison with rotation of the driving gear remains the same.

The kinematic and dynamic analysis of a planetary gearbox can be performed in a similar manner.

In Figure 27.8, a schematic of a planetary gearbox and the results of its kinematic analysis are shown. In this design, the central sun gear 1 is a driving component, and the carrier is the driven component of the gearbox. The ring gear 4 is stationary. The sun gear 1 is rotated about its axis,  $O_I$ . The rotation of the sun gear is the input rotation,  $\omega_1$ . Sun gear 1 is engaged in mesh with planet gear 2 that is a part of the cluster planet gear 2/3.  $P_{12}$  is the pitch point of the sun gear-to-planet gear 1 mesh. The cluster planet gear 2/3 is rotated by the carrier about the

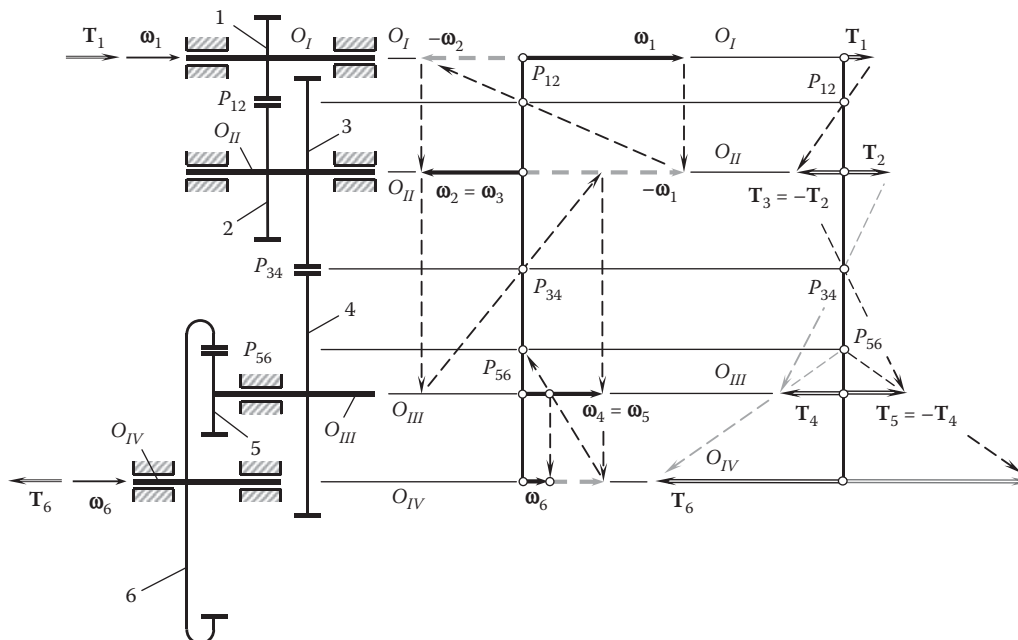


FIGURE 27.7

Results of kinematic and dynamic analysis performed for a complex gear drive shown at left.

axis,  $O_{II}$ . The carrier is rotated about its axis,  $O_{cr}$ . Planet gear 3 is engaged in mesh with stationary ring-gear, 4.  $P_{34}$  is the pitch point of sun gear 1-to-planet gear mesh.

When constructing the vector diagram for the rotation vectors, the axes of rotation,  $O_I$  and  $O_{II}$ , as well as the pitch points,  $P_{12}$  and  $P_{34}$ , are constructed within the reference line. When the input rotation vector,  $\omega_1$ , is given, the set of points,  $O_I$ ,  $O_{II}$ ,  $P_{12}$ , and  $P_{34}$ , is the key to constructing the vector diagram for the rotation vectors,  $\omega_1$ ,  $\omega_2$ ,  $\omega_3$ ,  $\omega_4$ , and  $\omega_{cr}$  (see Figure 27.8).

Similarly, the dynamic analysis of the planetary gearbox can be performed. The input torque,  $T_1$ , and the set of points,  $O_I$ ,  $O_{II}$ ,  $P_{12}$ , and  $P_{34}$ , within the reference line is the key to constructing the vector diagram for the torque vectors,  $T_1$ ,  $T_2$ ,  $T_3$ ,  $T_4$ , and  $T_{cr}$  (see Figure 27.9).

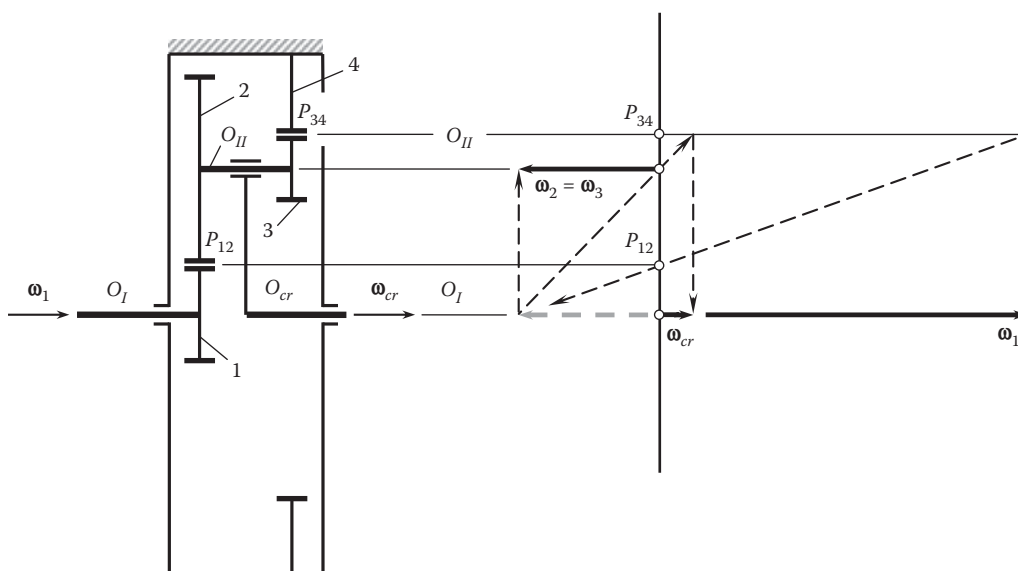
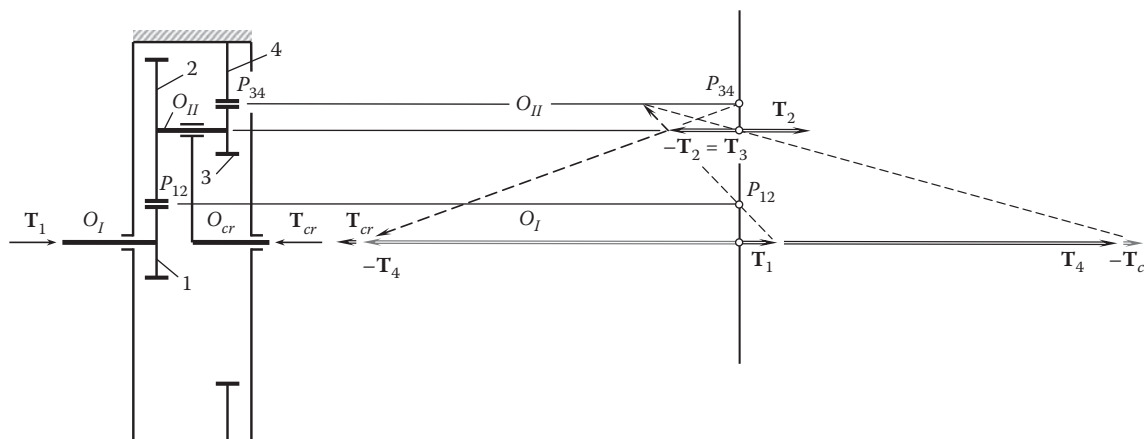


FIGURE 27.8

Results of kinematic analysis performed for a planetary gearbox shown at left.



**FIGURE 27.9**  
Results of dynamic analysis performed for a planetary gearbox shown at left.

The discussed approach can be also used for the kinematic and dynamic analysis of multistage (two and more stages) planetary gearboxes.

## 27.3 Features of Vector Diagrams for Complex Gear Systems with Intersected-Axes and Crossed-Axes Gear Pairs

Vector diagrams are developed in this book for gear pairs of all possible kinds, that is, for parallel-axes, intersected-axes, and crossed-axes gear pairs. As was already discussed, vector diagrams are constructed based on the rotation vectors of a driving and a driven gear. For a complex gear system, a corresponding vector diagram can be constructed based on the gear diagrams of corresponding gear pairs. The vector diagrams of this sort are constructed based on the rotation vector of the driving gear and the design parameters of the gear train: the rotation vector of the driven gear is the output of this analysis. Such a feature of vector diagrams was already discussed in this section with respect to parallel-axes gearings. Now, intersected-axes and crossed axes gearings need to be involved in the analysis of complex gear systems.

### 27.3.1 Elementary Vector Diagram for Intersected-Axes Gear Pairs

External and internal intersected-axes gear pairs are schematically shown in [Figure 27.10](#).

Construction of the vector diagram for an external elementary intersected-axes gear pair is schematically illustrated in [Figure 27.11](#). Two bevel gears are engaged in mesh with one another. Input gear 1 is steadily rotated about its axis,  $I$ , with an angular velocity,  $\omega_{in}$ . The input rotation of driving gear 1 is also illustrated by the rotation vector,  $\omega_{in}$ . The rotation vector,  $\omega_{in}$ , is along the gear axis of rotation,  $I$ . Output gear 2 is steadily rotated about its axis,  $II$ , with an angular velocity,  $\omega_{out}$ . The output rotation of driven gear 2 is also illustrated by the rotation vector,  $\omega_{out}$ . The rotation vector,  $\omega_{out}$ , is along the gear axis of rotation,  $II$ . In the particular example under consideration, axes  $I$  and  $II$  of the rotations form a right angle. The pitch cone angle of the driven gear is labeled  $\Gamma$ . The plane-of-action apex of the intersected-axes gear pair, the point of intersection of the axes  $I$  and  $II$ , is labeled  $A_{pa}^{12}$ .

In the example under consideration, it is necessary to determine the output rotation vector,  $\omega_{out}$ , considering the input rotation vector,  $\omega_{in}$ , and the design parameters of the intersected-axes gear pair known.

To construct the rotation vector,  $\omega_{out}$ , a rotation vector,  $-\omega_{in}$ , is constructed. The rotation vector,  $-\omega_{in}$ , is originated at the plane-of-action apex,  $A_{pa}^{12}$ . Then a circular arc of a radius,  $|\omega_{out}|$ , that is centered at  $A_{pa}^{12}$  is constructed. The point of intersection of the circular arc with the generating straight line of the pitch cone of the gear is projected onto the horizontal line. Then, this point is transferred to the vertical straight line, as shown in [Figure 27.11](#) by an arrowed circular arc segment. Ultimately, the output rotation vector,  $\omega_{out}$ , is constructed.

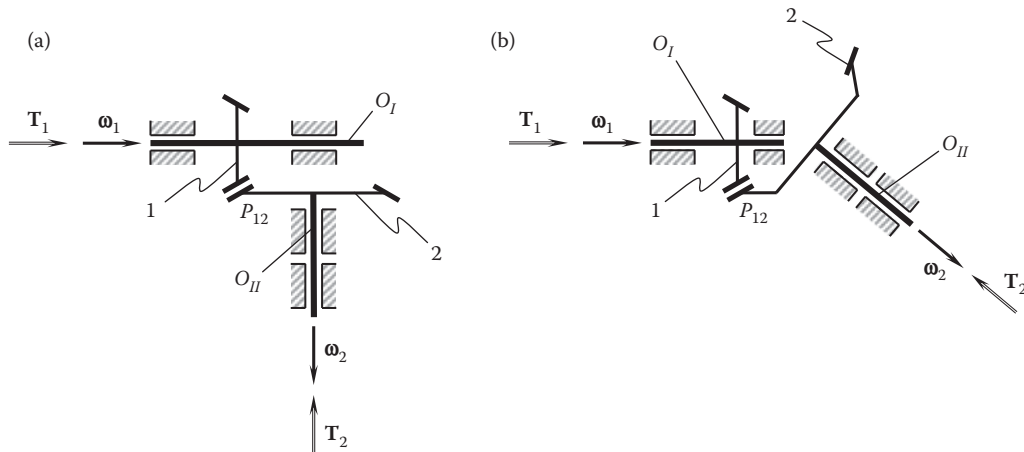


**FIGURE 27.10**  
Schematic of (a) external, and (b) internal intersected-axes gear pairs.

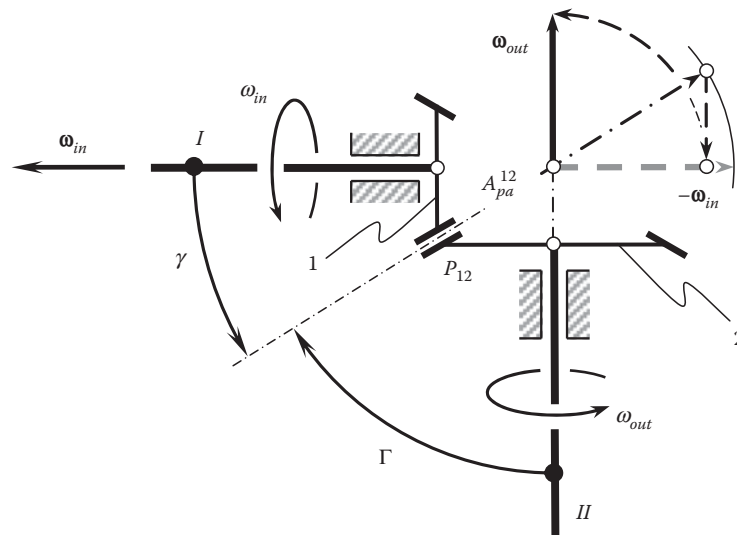


**FIGURE 27.11**  
Vector diagram for an external intersected-axes gear pair.

The performed analysis is based on the definition of the gear ratio,  $u$ , in an intersected-axes gear pair; that is:

$$u = \frac{\sin \gamma}{\sin \Gamma} \quad (27.2)$$

where  $\gamma$  is the pitch cone angle of the driving gear.

The obtained results of the analysis can be used for the kinematic analysis of a complex gear pair schematically shown in Figure 27.12a. The gearbox is composed of a parallel-axes gear pair and an intersected-axes gear pair. The plane-of-action apex,  $A_{pa}^{12}$ , in Figure 27.12a is at a distance,  $L$ , from driven gear 2. The kinematic analysis of the parallel-axes gear is similar to that shown in Figure 27.6. The kinematic analysis of the intersected-axes gear is similar to that shown in Figure 27.12. In Figure 27.12b, the plane-of-action apex,  $A_{pa}^{12}$ , is at a distance,  $L$ , from driven gear 2. Here, the distance,  $L$ , can be scaled. Further dynamic analysis of the complex gear pair (see Figure 27.12) is a routine procedure.

The discussed approach can be used for the purpose of kinematic and dynamic analysis of complex gear trains composed of parallel-axes and intersected-axes gear pairs.

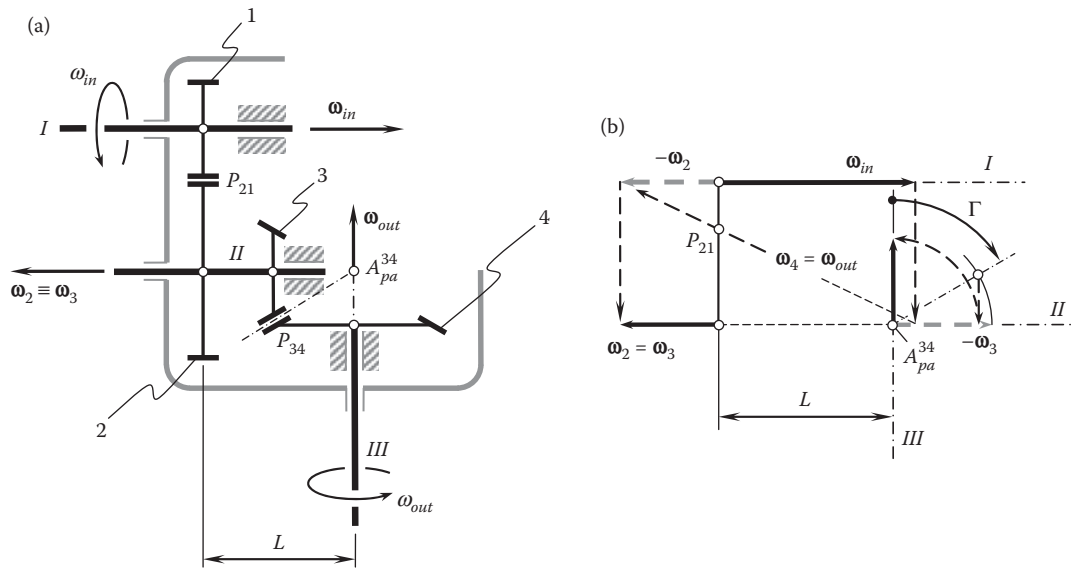


FIGURE 27.12

The vector diagram for a gear train that consists of a bevel gear pair: (a) schematic of the gearbox, and (b) the vector diagram for the rotations.

### 27.3.2 Elementary Vector Diagram for Crossed-Axes Gear Pair

Two projections of a vector diagram can be constructed for a crossed-axes gear pair. A vector diagram for  $P_a$ -gearing is used to construct one of the projections (onto a plane perpendicular to the centerline,  $\mathcal{C}$ ;  $N_{ln}$ -plane). A vector diagram for  $I_a$ -gearing is used to construct the other projection (onto the  $P_{ln}$ -plane).

Prior to constructing the elementary vector diagrams for a crossed-axes gear pair, it is instructive to note that the gear ratio in a crossed-axes gear pair can be specified either as a ratio of pitch radii,  $r_g$  and  $r_p$ , of the gear and pinion, or as a ratio of sines of the cone angles of the gear and pinion,  $\Sigma_g$  and  $\Sigma_p$  correspondingly.

In the first case, when the gear ratio is  $u = r_g/r_p$ , the analysis is performed within the pitch-line plane (see Figure 3.4). This analysis is similar to that illustrated in Figure 27.6. The projections of the input and output rotation vectors,  $\text{pr}_{pln} \omega_{in}$  and  $\text{pr}_{pln} \omega_{out}$ , onto the  $P_{ln}$ -plane are considered instead of the actual rotation vectors  $\omega_{in}$  and  $\omega_{out}$ . The rest of the steps are similar to those shown in Figure 27.6. In addition to kinematic analysis, dynamic analysis can be performed as well.

In the second case, when the gear ratio is  $u = \sin \Sigma_p / \sin \Sigma_g$ , the analysis is performed within the normal plane (see Figure 3.4). This analysis is similar to that illustrated in Figure 27.11. The projections of the input and output rotation vectors,  $\omega_{in}$  and  $\omega_{out}$ , onto the  $N_{ln}$ -plane are considered (these projections are identical to the actual rotation vectors,  $\omega_{in}$  and  $\omega_{out}$ ). The gear and pinion cone angles,  $\Sigma_g$  and  $\Sigma_p$ , are equal to the pitch cone angles,  $\Gamma$  and  $\gamma$ , correspondingly. The rest of the steps are similar to those shown in Figure 27.11. In addition to kinematic analysis, dynamic analysis can be performed as well.

The concept of vector diagrams can be expanded to rotations with acceleration/deceleration. This is of particular importance in dynamic analysis of a gear drive, calculation of forces, and so forth. The velocities of rolling and sliding of the interacting tooth flanks of a gear and its mating pinion can also be determined by means of vector diagrams.

The discussion in this chapter can be summarized as follows. Vector diagrams are an efficient tool for investigating gear pairs as well as complex gearboxes. The vector diagrams of gear transmission are convenient in the cases when the diagram can be plotted as a 2D graph. In cases of 3D, vector diagrams are less convenient, and there is no evidence (in the public domain) of their application (practicality).

This tool (the vector diagrams) is convenient if 2D schematics are valid; 3D plots can be constructed, but they are inconvenient.



## *Gear Ratio of a Multistage Gear Drive*

The gear ratio of a gear pair, as discussed in [Chapter 2](#), is uniquely determined by the rotation vectors of the input shaft (commonly of the pinion,  $\omega_p$ ) and the output shaft (commonly of the gear,  $\omega_g$ ). A multistage gear drive is composed of two or more gear pairs. The gear ratio of a whole multistage gear drive can also be specified in terms of the rotation vectors of the input shaft,  $\omega_{in}$ , and the output shaft,  $\omega_{out}$ .

An example of a simple two-stage gear train composed of helical gears is shown in [Figure 28.1](#). Gear trains of this kind are typical for industrial applications. A multistage gear drive that has three to five stages is common for industrial gearboxes as well as for other applications. More complex gear trains (more than five stages in total) are used as well.

Another example of a gear train is illustrated in [Figure 28.2](#). This is a multistage gear train capable of a changeable gear ratio between the input and the output shafts. The actual value of the gear ratio of the gear train (see [Figure 28.2](#)) depends on which of gear pairs is engaged in mesh.

A gear train can be composed either of gear pairs of the same type (that is, all the gear pairs in a gear train are cylindrical parallel-axes gear pairs), or it can be composed of gear pairs of different types. For example, a gear train can be composed either of (1) bevel and cylindrical gear pairs, (2) a worm gear pair and a cylindrical gear pair, or (3) a hypoid gear pair and a cylindrical gear pair, and so forth. In the first case, the entire gear ratio is evenly distributed among all the stages of the gear train. In the rest of the cases, additional investigation is necessary, as losses of power in gear pairs of different kinds are also different, regardless of certain correlations among the range of losses.

In a gear drive with favorable performance, the gear ratios of each gear pair should correlate to one another. If the gear ratio of a gear pair is too small, then a larger number of gear pairs is required to provide the required gear ratio of the whole gear train. If the gear ratio of a gear pair is excessive, then larger losses of the power being transmitted are observed. Neither the first nor the second is desired. A multistage gear drive of a favorable design must have a reasonable number of stages, and the gear ratio in each stage must be as close to the favorable value as possible. Otherwise, the design parameters of the whole gear drive can be far from the optimal values.

### **28.1 Principal Kinematic Relationships in Multistage Gear Drives**

Multistage gear drives of two different kinds are distinguished below.

In gear drives of the first kind, all the gear pairs are engaged in mesh simultaneously. The total gear ratio of the gear drive of this kind is of a constant value. The gear ratio cannot be changed. Gear drives of this kind are used in applications when both (1) the given input rotation and (2) the desired output rotation are of a constant values.

In gear drives of the second kind, only one gear on each shaft is engaged in mesh with a gear on another shaft. The total gear ratio of the gear drive of this kind can be changed. The actual value of the gear ratio depends on which of the gears on each shaft is engaged in mesh with a mating gear on another shaft. Gear drives of this kind are used in applications when the given input rotation is of a constant value, while several desired rotations of the output shaft are required.

Multistage gear drives of the second kind represent more gearings of a more general kind. Therefore, it makes sense to begin the discussion from gear drives of the second kind. Then the obtained results can be reduced to simpler cases of multistage gear drives of the first kind.

A multistage gear drive should provide a gradation of rotations of the output shaft in a geometrical series with a selected progression ratio and given maximum,  $\omega_{out}^{max}$  (or  $n_{out}^{max}$ ), and minimum,  $\omega_{out}^{min}$  (or  $n_{out}^{min}$ ), speeds. Methods for solving problems of this kind are based on kinematic calculations [33].

**FIGURE 28.1**

A two-stage gear train with split torque composed of helical gears (Note: torque is split on each stage).

Any regularity in the series of rotational speeds,  $\omega_{out}^i$ , is the result of a similar regularity in the series of tooth ratios,  $u^j$ , in the multistage gear drive.

In cases when rotational speeds of the output shaft are obtained by means of gear pairs of the only kind, that is, by making engagements between sets of simple gear pairs arranged on two shafts, any series of rotational speeds of the output shaft can be achieved by selecting a corresponding series of tooth ratios for the gear pairs.

However, in cases when different rotational speeds are obtained by consecutive engagement of gear pairs, only a geometrical series of the rotational speeds can be set up. This method of speed changing requires a

**FIGURE 28.2**

A multistage gear train.

minimum number of gear pairs to ensure the required number of rotations of the output shaft as well as the required range of rotations of the output shaft.

### 28.1.1 Range Ratio of Speed Variation for Gear Drives

The total gear ratio,  $u_{gd}$ , of a multistage gear drive is equal to the product of gear ratios of all the gear pairs that make up the gear drive:

$$u_{gd} = \prod_{i=1}^n u_{gd}^i \quad (28.1)$$

In Equation 28.1, the superscript  $j$  is assigned to a current gear pair ( $j = 1, 2, \dots, n$  is an integer number), and the total number of gear pairs in the multistage gear drive is denoted by  $n$ .

Equation 28.1 is valid for the calculation of the maximum total gear ratio,  $u_{gd}^{\max}$ , in the range, as well as for the calculation of the minimum total gear ratio,  $u_{gd}^{\min}$ .

Following from Equation 28.1, the range ratio of the gear drive can be calculated from the formula:

$$R_{gd} = \frac{u_{gd}^{\max}}{u_{gd}^{\min}} = \prod_{j=1}^n R_{gd}^j \quad (28.2)$$

where  $R_{gd}^j = \frac{u_j^{\max}}{u_j^{\min}}$  is the range of gear ratios for each gear pair.

### 28.1.2 Characteristics of Transmission Group

The progression ratio of a series of gear ratios in a transmission group can be expressed in the form:

$$\varphi_n = \varphi^x \quad (28.3)$$

where the exponent  $x$  is referred to as *characteristic of the group*.

The characteristic of a group is equal to the number of speed steps for the whole complex of transmission groups kinematically preceding a given group.

The general setup equation for group transmission can be written as:

$$u_1:u_2:u_3: \dots :u_n = 1:\varphi^x:\varphi^{2x}: \dots :\varphi^{(n-1)x} \quad (28.4)$$

Equation 28.4 can be used for finding ratios of all the transmissions in a group in cases when the ratio,  $u$ , of one transmission is known.

## 28.2 Analytical Method for Determining Transmission Ratios

All standard rotational speed series are covered by the finest series, for which  $\varphi = 1.06$ . The standard gear ratio of any gear drive in the gearbox, in general, can be expressed as:

$$u_{st} = 1.06^{\pm E} \quad (28.5)$$

where  $E$  is an integer.

The values  $\varphi = 1.26$  and  $\varphi = 1.41$  are other examples of practical values for the parameter  $\varphi$ .

Many calculations of the kinematics of multistage gear drives can be simplified in cases when all the gear ratios are expressed in terms of the progression ratio,  $\varphi$ , of the series of rotational speeds of the output shaft being designed.

The minimum gear ratio is commonly limited to  $u_{\min} = 0.25$ . The maximum gear ratio for spur gearing is equal to  $u_{\max} = 2.0$  and  $u_{\max} = 2.5$  for helical gearing. These recommended values for  $u_{\min}$  and for  $u_{\max}$  make it possible to avoid excessively large diameters of the driven gear and a consequent increase in the overall radial dimensions of the gearbox. The aforementioned values of the gear ratio allow for minimization of power losses in the gearbox.

Thus, the limiting maximum range ratio in a two-shaft transmission group is equal to:

$$R^{\max} = \frac{u_{\max}}{u_{\min}} = 8 \quad (28.6)$$

Again, this value for  $R^{\max}$  is a reasonable recommendation.

### 28.3 Rotational Speed Charts

Rotational speed charts are used to determine the actual values of gear ratios for all the gearing in the gearbox and to determine the rotational speed of all shafts. This can be done on the premises of the kinematic diagram of the gearbox. Each shaft of the gearbox is depicted by a vertical straight line in the chart. Horizontal straight lines are spaced at equal intervals. The intervals are proportional to the value of  $\log \varphi$ . They are labeled with all the rotational speeds of the corresponding shaft within the limits from the minimum to the maximum rotational speed.

A gear pair that is engaged in mesh at a definite speed of the driving shaft,  $I$ , and the driven shaft,  $II$ , is shown in the chart by rays connecting the points of the shaft lines representing this speed, as schematically illustrated in Figure 28.3.

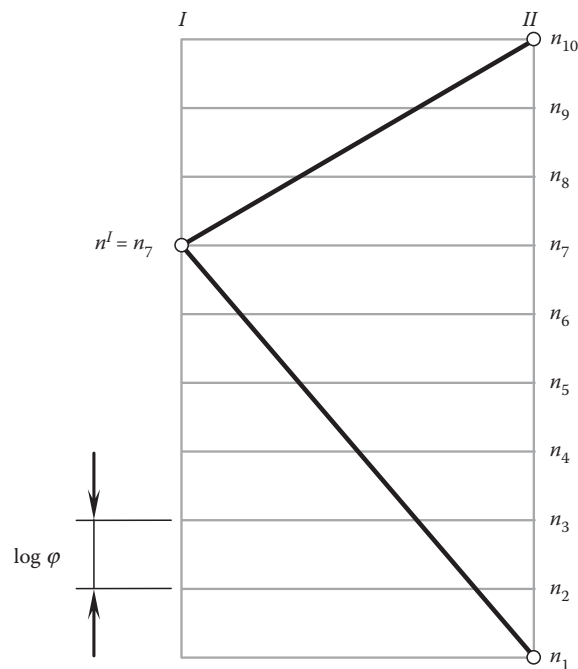


FIGURE 28.3

An example of rotational speed chart for a gear pair ( $\varphi = 1.26$ ).

The gear ratio is expressed in the form  $\varphi^m$ , where  $m$  is the number of intervals between the horizontal lines spanned by the corresponding ray.

If the rotational speeds are written from the bottom to the top in increasing order of magnitude, for a speed (increase) gear pair, that is, for  $u > 1$ , and  $m > 0$ , the ray is inclined upward (in the direction from the driving shaft to the driven shaft). In the cases of reduction gear pairs, that is, when  $u < 1$ , and  $m < 0$ , the ray is inclined downward. For a gear pair for which  $u = 1$ , the exponent  $m = 0$  and the ray is horizontal. Thus, for the transmission engaged in the mesh at  $n^I = n_7$  and  $n^{II} = n_{10}$ , the ray is inclined upward and spans three intervals so that the gear ratio is:

$$u^{I/II} = \frac{n_{10}}{n_7} = \varphi^3 \quad (28.7)$$

In the gear pair engaged in mesh at  $n^I = n_7$  and  $n^{II} = n_1$ , the ray spans six intervals and is inclined downward. Thus, the gear ratio in this case is equal to:

$$u^{I/II} = \frac{n_1}{n_7} = \frac{1}{\varphi^6} \quad (28.8)$$

The speed chart shown in [Figure 28.3](#) is constructed for the progression ratio,  $\varphi = 1.26 (= \sqrt[3]{2})$ .

The analytical method for kinematic calculations is employed for research purposes as well as for tentative calculations in studying various possible versions of the gearbox.

## 28.4 Broken Geometrical Series

The academic A. Gadolin\* proposed a geometrical series of spindle rotational speeds for machine tools on the basis of equal probability of operation at all spindle speed steps within the whole range of variation. To adopt a spindle drive mainly for the machining of medium-sized work (in terms of the capacity of the given machine tool), and taking into consideration the possibility of handing over work near limiting sizes (maximum and minimum) for machining in machine tools of adjacent sizes in the same size range, a broken geometrical series is employed with a progression ratio  $\varphi_1$  for middle speeds and  $\varphi_2 > \varphi_1^2$  for extreme speed steps in the range of speed variation. This reduces the total number of speed steps and the number of gear pairs (in comparison to a normal uniform structure). It also simplifies the construction and makes it possible to increase the range ratio of the spindle drive without changing the limiting gear ratios and without introducing a multiplier device [33].

The concept is illustrated with an example that is schematically shown in [Figure 28.4](#).

The multistage gear train is in wide use in the automotive industry and many other industries. Usually, the resultant gear ratio,  $u_\Sigma$ , in the multistage gear train is distributed equally among all the stages; that is, the gear ratio,  $u_1$ , in the first stage of the multistage gear train is equal to the gear ratio,  $u_2$  in the second stage ( $u_1 = u_2$ ). The gear ratio,  $u_2$ , of the second stage is equal to the gear ratio,  $u_3$ , of the third stage ( $u_2 = u_3$ ), and so on ( $\dots = u_{i-1} = u_i = u_{i+1} = \dots$ ). Equal distribution of the resultant gear ratio,  $u_\Sigma$ , among all stages of multistage gear trains causes high power losses when the gear train operates.

In order to reduce losses of power in the multistage gear train, it is necessary to distribute the resultant gear ratio,  $u_\Sigma$ , unequally. The gear ratio,  $u_1^*$ , in the first stage of the multistage gear train must be the smallest one. The gear ratio,  $u_2^*$ , of the second stage of the multistage gear train must exceed the gear ratio,  $u_1^*$ , of the first stage and has to be smaller than the gear ratio,  $u_3^*$ , of the third stage, and so on.

[Figure 28.4](#) illustrates how the resultant gear ratio,  $u_\Sigma$ , has to be distributed among all stages of the multistage gear train.

\* Axel Wilhelm Gadolin (June 12, 1828–December 15, 1892), a Finnish-born Russian mechanician.

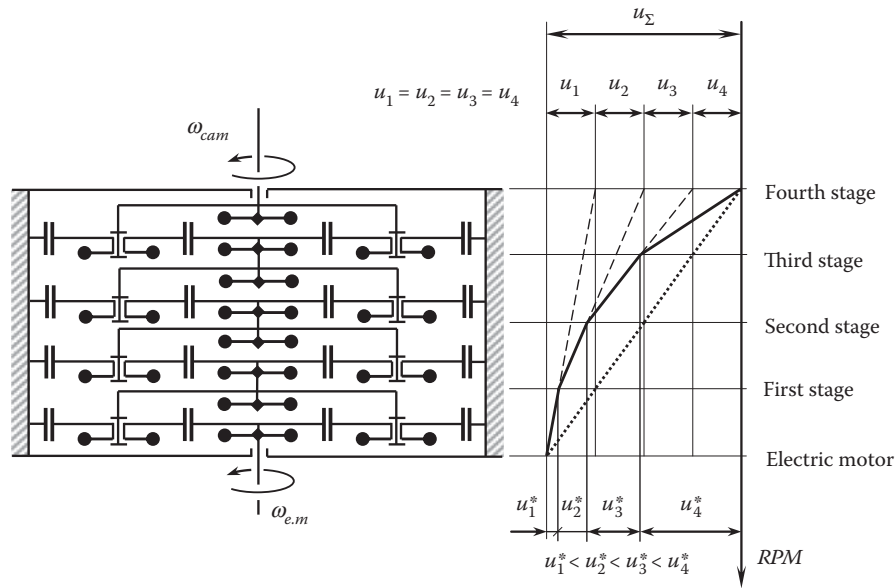


FIGURE 28.4

An example of a multistage gear train with properly distributed tooth ratios (Dr. Radzevich, S.P., circa 2000, New Venture Gear, Syracuse, NY.)

## 28.5 Minimum Number of Gear Pairs

The total number of gear pairs in the groups:

$$S_p = p_a + p_b + p_c + \dots + p_r \quad (28.9)$$

that are required to obtain a specified number of speed steps  $z = p_a p_b p_c \dots p_r$  is minimum if:

$$p_a = p_b = p_c = \dots = p_r = \sqrt[m]{z} = p \quad (28.10)$$

It can be shown that when the number of transmission groups,  $m$ , is not specified, the minimum number of transmissions can be obtained under the condition that either  $p = 2$  or  $p = 3$ . Thus, it proves expedient to have either two or three transmissions in each group, since  $2 + 2 = 2 \times 2 = 4$ ,  $p = 4$  as well.

These are actually the numbers of transmission that are employed for gearing with sliding cluster gears when the number of gears is twice the number of transmissions. This condition does not hold true for interchangeable gears, where the same pair of gears can be interchanged.

The application of a broken geometrical series considerably reduces the number of transmissions required.

## 28.6 Determining Tooth Number of Gears of Group Transmissions

In cases where the center distance is maintained at a constant value and all the gears of a group are of the same module,

$$N_\Sigma = N_g^j + N_p^j = \text{const} \quad (28.11)$$

where:

$N_\Sigma$  is the sum of tooth numbers of the meshing gears.

$N_g^j$  and  $N_p^j$  are the tooth numbers, respectively, of driven and of driving gears.

$j$  is the integer number ( $j = 1, 2, 3, \dots, p$ ).

By definition,

$$u_j = \frac{N_g^j}{N_p^j} \quad (28.12)$$

Combining these two equations, one can obtain:

$$N_p^j = \frac{u_j}{u_j + 1} N_\Sigma \quad (28.13)$$

$$N_g^j = \frac{1}{u_j + 1} N_\Sigma \quad (28.14)$$

When the sum of the tooth numbers of the meshing gears,  $N_\Sigma$ , is given, Equations 28.13 and 28.14 can be used for the calculation of the tooth numbers of all the gears in the group. The method of the least common multiplier is commonly used for such a purpose.

In cases when  $u_j = \frac{N_g^j}{N_p^j} = \frac{a_j}{b_j}$ , where  $a_j$  and  $b_j$  are mutually prime numbers, Equations 28.13 and 28.14 can be rewritten in the form

$$N_p^j = \frac{a_j}{a_j + b_j} N_\Sigma \quad (28.15)$$

$$N_g^j = \frac{b_j}{a_j + b_j} N_\Sigma \quad (28.16)$$

Hence, when the tooth numbers of driven and driving gears,  $N_g^j$  and  $N_p^j$ , are integer numbers, the sum of the tooth numbers of the meshing gears,  $N_\Sigma$ , should be a multiplier of the sum  $a_j + b_j$ .

Vector diagrams of gear pairs can be implemented for solving the problem of calculation of favorable gear ratios for multistage gear drives. Implementation of vector diagrams also appears promising for solving gear-related kinematical problems of other sorts as well. Gear trains with favorable performance can be *synthesized* by means of vector diagrams of gear pairs.

Gear ratios of multistage gear drives are a poorly investigated part of the theory of gearing. More efforts are required to be undertaken in the future to get things clear.





# Taylor & Francis

Taylor & Francis Group

<http://taylorandfrancis.com>

## Accuracy of Gear Teeth

Accuracy of gear teeth is an important consideration when designing and manufacturing gears. Even perfectly designed gears feature manufacturing errors of certain values; therefore, the actual tooth flanks,  $\mathcal{G}_r$  and  $\mathcal{P}_r$ , of a gear and mating pinion deviate from their desired geometries,  $\mathcal{G}$  and  $\mathcal{P}$ . For inspection purposes, tooth flanks,  $\mathcal{G}$  and  $\mathcal{P}$ , of perfect gears are used as the datum surfaces. It is of critical importance to use the perfect tooth flanks,  $\mathcal{G}$  and  $\mathcal{P}$ , as the corresponding datum surfaces. Otherwise, no reliable results of the inspection can be obtained. In the current practice of inspection of gears for intersected-axes and crossed-axes gearings, no perfect tooth flanks,  $\mathcal{G}$  and  $\mathcal{P}$ , are used as the datum surfaces. Instead, approximate surfaces are used for inspection purposes, which is incorrect, especially in cases when gears with low tooth counts are inspected.

Modern computer measuring machines (CMMs) and gear measuring machines (GMMs) are capable of taking measurements when inspecting the accuracy of a surface of an arbitrary geometry. When inspecting the accuracy of gears, features of the tooth flank geometry can be taken into account. The latter is helpful to simplify the method of the inspection, improve the accuracy of the inspection, and make the results of the inspection reliable.

In this section, the reader's attention is focused mostly on the features of the tooth flank,  $\mathcal{G}$  and  $\mathcal{P}$ , geometry that can be taken into account when developing methods of and means for inspection of the accuracy of real gears.

### 29.1 Inspection of Gears for Parallel-Axes Gear Pairs

Perfect gears for parallel-axes gear pairs are shaped in a form of a screw involute surface,  $\mathcal{G}$ . The screw involute surface is reduced to a surface of an involute cylinder in the case of spur gears. The derivation of the geometry of a tooth flank,  $\mathcal{G}$ , of a helical involute gear is illustrated in Figure 7.9. Here, in Figure 29.1, important features of the geometry of the screw involute surface are discussed.

A conventional method of inspection of the accuracy of the involute gear tooth profile is based on the kinematical properties of the involute of a circle. The method is illustrated in Figure 29.2. For the inspection, the axis of the stylus of the indicator of dial type is set tangential to the base cylinder of a base radius,  $r_{b,g}$ , of the involute gear to be inspected. Then the gear and dial type indicator are given relative motion so the axis of the indicator of dial type rolls with no slippage over the base circle of radius  $r_{b,g}$ . The required relative motion can be a superposition of a rotation,  $\omega_g$ , of the gear about its axis of rotation,  $O_g$ , and a translation either of the gear or the stylus along the stylus axis, as shown in Figure 29.2. The gear travels straight with a linear velocity,  $V_g$ . The rotation and translation velocities,  $\omega_g$  and  $V_g$ , are synchronized with one another to ensure rolling with no slippage of the stylus axis over the base circle. If the stylus travels straight, then the direction of the translation,  $V_s$ , is reciprocal to the translation of the gear,  $V_g$ .

In the relative motion, the stylus point traces a true involute profile in a reference system associated with the gear. When inspecting an involute gear, the stylus follows the gear tooth profile. If the arrow of the dial type indicator does not change its position; that is, readings are *zero*, this means that the gear tooth profile has high accuracy (with zero deviation from the true involute profile). If the arrow of the dial type indicator changes position; that is, readings are *nonzero*, this means that the gear tooth profile deviates from the true involute profile. In this second case, a decision has to be made about whether the deviations are reasonably small and all within the tolerance band for the specified gear, or the deviations of the involute tooth profile are unacceptably large, and the gear is not machined in compliance with the blueprint.

After the accuracy of the involute tooth profile is inspected, then the accuracy of the helix angle is inspected. Common methods of and means for the inspection of the accuracy of the helix angle are used in this case.

The features of the involute gear tooth flank geometry are used in another method for the inspection of the accuracy of involute gear tooth flanks. The method is discussed immediately below.

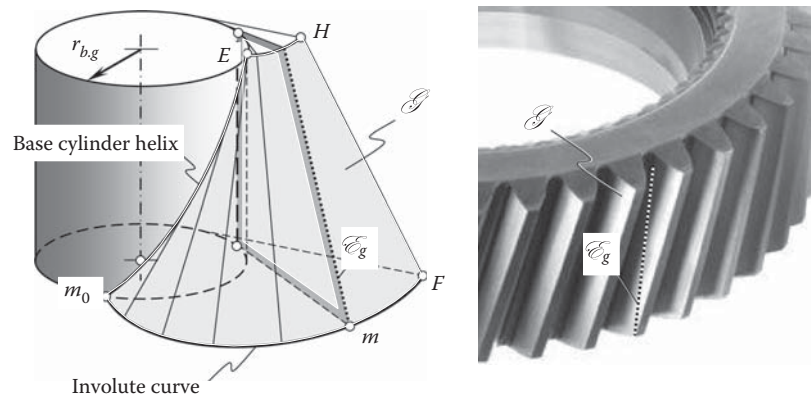


**FIGURE 29.1**  
Features of the geometry of tooth flank,  $\mathcal{G}$ , of a helical involute gear.

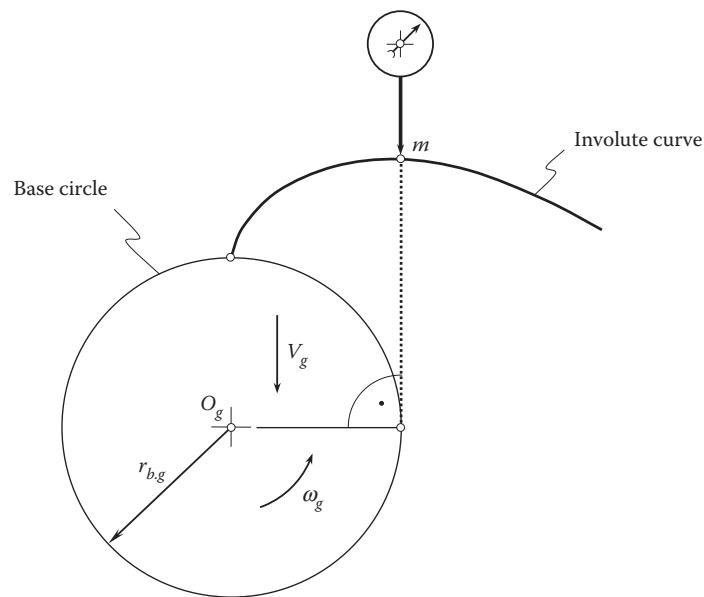


**FIGURE 29.2**  
Schematic of a method of inspection of the accuracy of the involute gear tooth profile.

In a normal section of a screw involute surface by a plane, the line of intersection is a straight line. This means that a screw involute surface can be generated by a straight line,  $\mathcal{E}_g$ , that performs a corresponding screw motion about the axis of the screw involute surface. In such a motion, the straight line,  $\mathcal{E}_g$ , is tangent to the base helix of the screw involute surface (Figure 29.1).

The method of inspection of an involute gear tooth flank is illustrated in Figure 29.3. The straight line,  $\mathcal{E}_g$ , is entirely located on the screw involute surface,  $\mathcal{G}$ . The stylus of the dial type indicator is traced along the straight generator,  $\mathcal{E}_g$ , of the gear tooth flank,  $\mathcal{G}$ . In the case of a perfect screw involute surface,  $\mathcal{G}$ , the readings of the dial type indicator are zero. If the actual gear tooth flank deviates from the perfect screw involute surface,  $\mathcal{G}$ , the readings of the dial type indicator are nonzero. The smaller the readings of the dial type indicator, the smaller the deviations of the actual gear tooth flank from the perfect screw involute surface,  $\mathcal{G}$ . After the straightness and a proper configuration of one straight line on the gear tooth flank is performed, the gear is indexed, and the straightness and a proper configuration of the other straight line on the gear tooth flank are performed. The meaning of the term *indexed* in this particular case becomes clear from Figure 7.8.

One more method of inspection of involute gears is based on the following consideration.

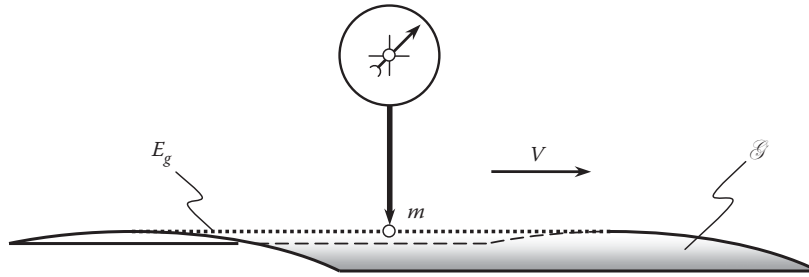


**FIGURE 29.3**  
Schematic of a method of inspection of the accuracy of the involute gear tooth flank.

The normal sectional view of the auxiliary generating rack,  $\mathcal{R}_g$  (of the basic rack), is depicted in Figure 29.4 with respect to the helical involute gear. An elementary trigonometrical analysis immediately returns an equation:

$$M_n = d_{b,g} \frac{\tan \phi_t}{\sin \psi_{b,g}} \quad (29.1)$$

for the span measurement,  $M_n$ .

In Equation 29.18:

$d_{b,g}$  is the base diameter of the helical gear.

$\phi_t$  is the transverse profile angle at the pitch diameter of the gear.

$\psi_{b,g}$  is the base helix angle of the gear.

The base tangent length is the distance between two parallel planes tangential to two opposite tooth flanks, that is, a left-hand and a right-hand flank. It is an indirect measure of the tooth thickness. This makes use of the property of the involute by which the points of intersection of a tangent to the base circle with a right- and left-hand involute flank are equidistant irrespective of the position of the tangent. In the case of the opposed involutes forming a tooth, this constant distance is the transverse base tooth thickness,  $s_b$ , and is equal to the length of the arc between the origins of the involutes on the base circle, as illustrated in Figure 29.5.

The involute helicoid flanks on a helical tooth have the same properties. The parallel planes tangential to the tooth flanks are at an angle,  $\psi_b$ , to the axis of the gear, and the distance between them is  $s_{bn}$ . In practice, the measurement has to be carried out over tooth flanks spanning a number,  $k$ , of teeth instead of a single tooth as shown in Figure 29.6. The number  $k$  depends on the tooth geometry, that is, on the pressure angle, number of teeth, and addendum modification coefficient.

The base tangent length,  $W_k$  (the subscript  $k$  after  $W$  specifies the number of teeth between the flanks measured), on spur or helical gears is composed of the normal base tooth thickness,  $s_b$ , and a number of normal base pitches,  $p_b$ . The number of teeth included in the measurement should be chosen so that there is some latitude in the position in which the measuring instrument can be applied to the flanks.

This characteristic is also true for helical gears.

Calculation of the base tangent length,  $W_k$ :

1. The tooth thickness measured along the arc of the reference cylinder on the spur and helical gears is:

$$S_n = m \left( \frac{\pi}{2} + 2x \tan \phi \right) \quad (29.2)$$

2. The base tooth thickness measured along the arc of the base cylinder is on:

**Spur gears:**

$$s_b = N m \cos \phi \left( \frac{S_n}{N m} + \text{inv} \phi \right) \quad (29.3)$$



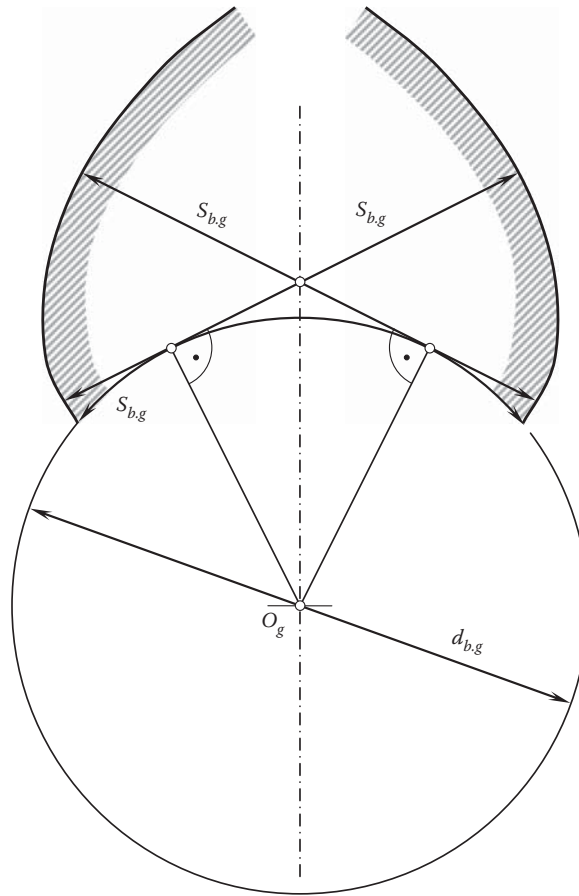


**FIGURE 29.5**  
Equidistant base thickness of an involute tooth.

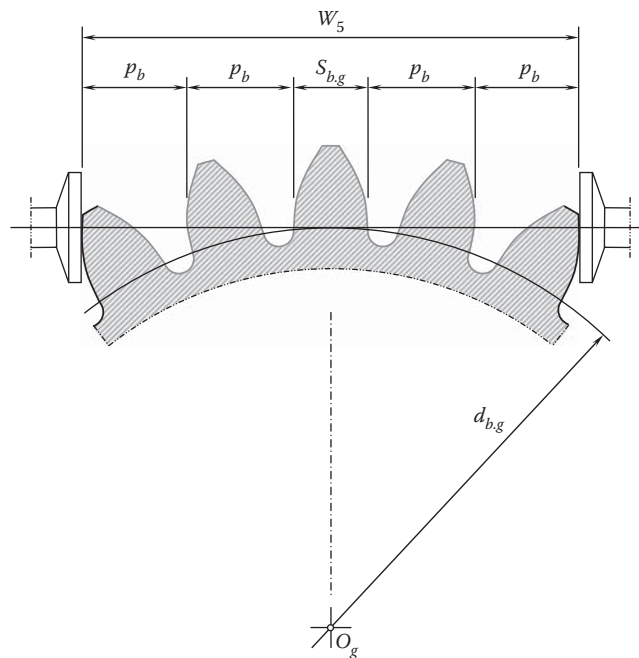


**FIGURE 29.6**  
Base tangent length,  $W_k$ , on a spur gear.

The combined formula for the base tangent length,  $W_k$ , is therefore as follows:

$$W_k = m[(k - 0.5)\pi \cos \phi + N \operatorname{inv} \phi_t \cos \phi + 2x \sin \phi] \quad (29.7)$$

The number of teeth,  $k$ , can be calculated from the following formulas:

$$k = \frac{S_x - W_1}{\pi m \cos \phi} + 1 \quad (29.8)$$

(rounding off the calculated value from Equation 29.8 to the nearest integer).

$$S_x = \frac{d_b \tan \phi_x}{\cos \psi_b} \quad (29.9)$$

$$\cos \phi_x = \frac{d_b}{d_o - 2m} \quad (29.10)$$

$$W_1 = m\left(\frac{\pi}{2} \cos \phi + N \operatorname{inv} \phi_t \cos \phi + 2x \sin \phi\right) \quad (29.11)$$

The above formulae apply to external spur and helical gears and also to the tooth space profile of internal spur and helical gears, although the base tangent length on such gears only has a largely theoretical significance.

On internal gears, the tooth thickness is measured by taking measurements between balls.

On external gears, the *actual base tangent length*,  $AW_k$ , is less than the theoretical dimension,  $W_k$ , for zero backlash by the amount of the normal backlash allowance,  $\Delta j_n$ . On internal gears, the base tangent length is increased by the amount of the backlash allowance. Therefore, the base tangent length is:

**On external gears:**

$$AW_k = W_k - \Delta j_n \quad (29.12)$$

**On internal gears:**

$$AW_k = W_k + \Delta j_n \quad (29.13)$$

The tooth thickness of a gear can also be inspected based on the discussed features (see [Figure 29.4](#)) of the geometry of an involute helical gear. Two approaches are used for determining the tooth thickness of an involute gear. One of them is based on span measurement over two or more gear teeth. The other is based on measurement over ball/pins.

When the span measurement,  $M_n$ , over two or more gear teeth is given, the following approach can be used for the calculation of circular tooth thickness,  $t_n$ , of the helical gear.

The dimension,  $M_t$ , in the transverse section that corresponds to the span measurement,  $M_n$ , of the helical gear ([Figure 29.7](#)) can be calculated from the formula:

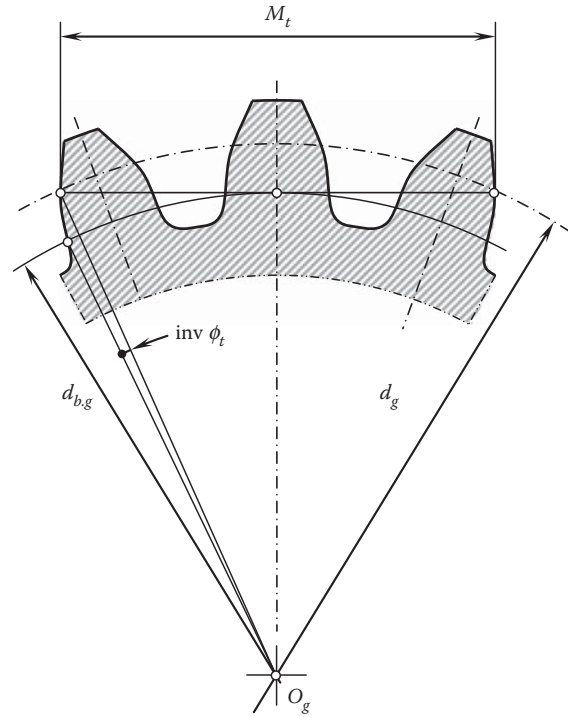
$$M_t = \frac{M_n}{\cos \psi_b} = M_n \frac{\sin \phi_t}{\sin \phi_n} \quad (29.14)$$

The calculated value of the dimension,  $M_t$ , allows for the calculation of the transverse circular tooth thickness,  $t_t$ , at the pitch diameter of the gear:

$$t_t = d \left( \frac{M_t}{d_b} - \frac{\pi N_s}{N_g} - \operatorname{inv} \phi_t \right) \quad (29.15)$$

where  $N_s$  is the number of tooth spaces.



**FIGURE 29.7**

Span measurement,  $M_t$ , over two or more teeth in transverse cross-section of a helical gear.

Ultimately, for the calculation of normal circular tooth thickness,  $t_n$ , the formula:

$$t_n = t_t \cos \psi \quad (29.16)$$

is used.

The number of teeth in a span can be calculated from the approximate formula:

$$k_w = \frac{N_g}{\cos^3 \psi} \cdot \frac{\phi_t}{180^\circ} + 0.5 \quad (29.17)$$

where  $\beta$  is the pitch helix angle of the gear.

Following another approach, either balls or pins are implemented for the measurement of the tooth thickness of a spur gear. For the measurement of a helical gear tooth thickness, balls are commonly used.

When the dimension over two balls or pins is given, the following approach can be used for the calculation of the circular tooth thickness,  $t_n$ , of the helical gear.

For the calculations, the normal width of space between teeth is used as an input parameter. The normal space width,  $w_n$ , is equal to  $w_n = p_n - t_n$ .

The measurements are performed with the help of balls of a certain standard diameter. For a given gear, the approximate diameter of the ball is approximately:

$$d_{ball} \cong 1.728/P_n \quad (29.18)$$

Then, the calculated value of the diameter,  $d_{ball}$ , is rounded to the nearest standard value.

The transverse profile angle,  $\phi_m$ , to the center of the ball/pin is calculated from the equation:

$$\text{inv } \phi_m = \text{inv } \phi_t + \frac{d_{ball} - w_n \cos \phi_n}{N_g \cos \phi_n} P_n \quad (29.19)$$

With the input parameters,  $w_n$ ,  $d_{ball}$ , and  $\phi_m$ , calculated, the dimension over two balls,  $D_{Me}$ , for a gear with an even tooth number can be calculated from the formula:

$$D_{Me} = \frac{d_{b.g}}{\cos \phi_m} + d_{ball} \quad (29.20)$$

For gears with an odd number of teeth, the dimension over two balls is equal to:

$$D_{Me} = \frac{d_{b.g} \cos(90^\circ/N_g)}{\cos \phi_m} + d_{ball} \quad (29.21)$$

The same formulas are used for the measurement of a spur gear. The only difference is that the transverse profile angle,  $\phi_t$ , and the normal profile angle,  $\phi_n$ , in Equation 29.19 are equal to each other.

## 29.2 Inspection of Gears for Intersected-Axes Gear Pairs

The current practice of the inspection of gears for intersected-axes gear pairs is inconsistent. The approximate datum surface that is used for inspection purposes is the main reason for that. The datum surface is not conjugate to the gear being inspected, as it is generated as an enveloping surface to consecutive positions of the crown rack in its motion in relation to the gear being inspected. This is especially clear when gears with a low tooth count are inspected—in this case, the inconsistency of the known method for the inspection of gears is more evident. As the datum surface itself deviates from the perfect datum surface, the output of the gear inspection cannot be precise.

For the inspection of gears for intersected-axes gear pairs, methods of and means for inspection that are based on the features of the tooth flank geometry can be developed.

For the inspection of bevel gears, a novel method is proposed. The determination of how much an actual tooth flank of a bevel gear deviates from the nominal (desired) tooth flank geometry is the main goal of the gear inspection. The smaller the deviation, the more accurate the bevel gear, vice versa.

Selection of a proper reference surface for the inspection of bevel gears for intersected-axes gearing is of critical importance, especially in cases of inspection of bevel gears with a low tooth count (12 teeth and lower).

In the current practice, a tooth flank of a crown gear is used for reference purposes. The tooth flank of a crown gear is simulated by the cutting blades of the gear-cutting tool when machining the gear. When the pitch plane of a crown gear rolls with no sliding over the pitch cone of the bevel gear being inspected, the desired tooth flank of the bevel gear is generated as an envelope to consecutive positions of the tooth flank of the crown gear. This enveloping surface serves as the reference surface when inspecting bevel gears.

Similarly, the tooth flank of a crown gear is simulated by the corresponding motions of the stylus when inspecting the gear. When inspecting a bevel gear, the pitch plane of a crown gear rolls with no sliding over the pitch cone of the bevel gear being inspected. The anticipated tooth flank of the bevel gear is generated as an envelope to consecutive positions of the tooth flank of the crown gear.

In known methods of inspection of bevel gears for intersected-axes gearing, the stylus travels over the tooth flank to be inspected so that it is always at the kinematically generated anticipated (desired) tooth flank of the bevel gear. The tooth flank of an actual gear being inspected deviates from the tooth flank of the desired geometry. This deviation causes corresponding displacements of the stylus. In this way, a tooth flank of a bevel gear is inspected.

An improper reference surface is the main disadvantage of the known methods of inspection of bevel gears for intersected-axes gearing. This disadvantage is mostly because the implemented reference surface is not a kind of conjugate surface. Because of this, the results of the measurements do not correctly reflect the actual accuracy of the bevel gear. Ultimately, accurate gears can be evaluated as being of poor quality, and, inversely, poor-quality gears can be mistakenly evaluated as accurate gears.

In the method for inspection of gears for intersected-axes gear pairs, the problem of increasing the accuracy of the inspection is solved by means of implementation of the correct reference surface, that is, a kind of conjugate surface.

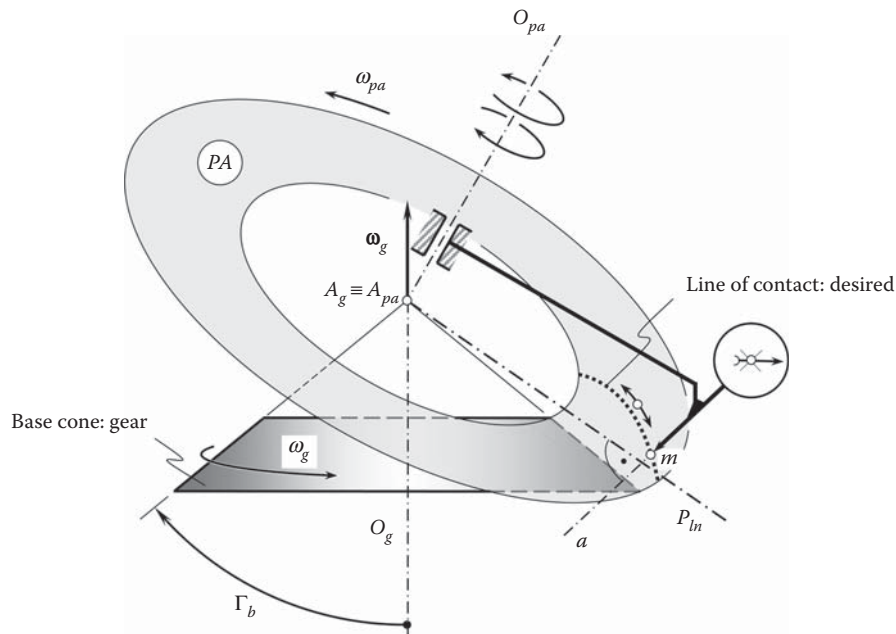


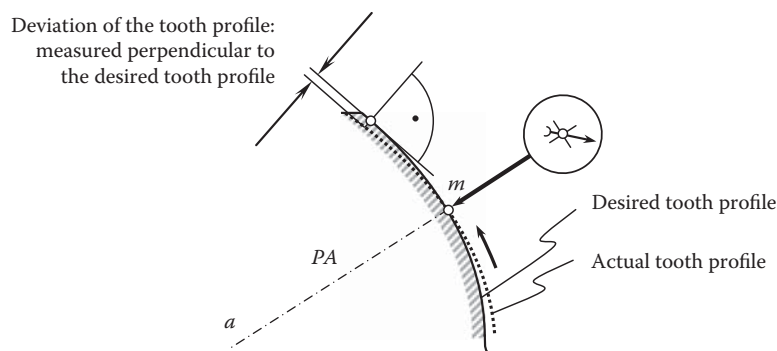
**FIGURE 29.8**  
Kinematics of a method of inspection of a gear for an intersected-axes gear pair.

To proceed with the development of the method of inspection of bevel gears for intersected-axes gearing, the base cone of the gear to be inspected and the plane of action have to be constructed.

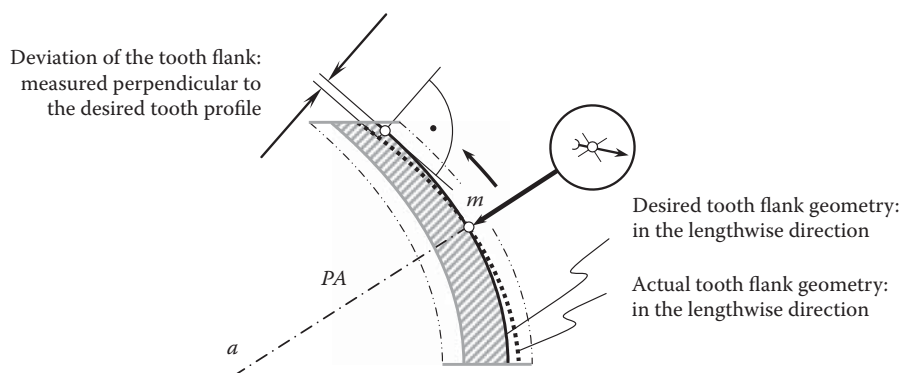
When inspecting a bevel gear (see Figure 29.8), the relative motion of the gear to be inspected and the plane of action are performed. The gear is rotated about its axis of rotation,  $O_g$ . The plane of action,  $PA$ , is rotated about its axis of rotation,  $O_{pa}$ . The rotations,  $\omega_g$  and  $\omega_{pa}$ , are synchronized with one another.

When inspecting a bevel gear tooth profile (Figure 29.9), the rotations,  $\omega_g$  and  $\omega_{pa}$ , are synchronized so as to keep the stylus at a current point  $m$  on the desired bevel gear tooth flank. The point,  $m$ , is within the plane of action,  $PA$ . The line  $a - a$  along which the deviation is measured is within the plane of action,  $PA$ , and it is perpendicular to the bevel gear tooth flank at the point,  $m$ . The stylus tip is motionless in relation to the plane of action,  $PA$ , when inspecting the profile error of the bevel gear tooth flank.

When inspecting tooth flank geometry of a bevel gear in the lengthwise direction (see Figure 29.10), the stylus tip travels along the line of intersection of the desired tooth flank by the plane of action,  $PA$ . At the current point,  $m$ , the line  $a - a$  along which the deviation is measured is within the plane of action,  $PA$ , and perpendicular to the bevel gear tooth flank at the point,  $m$ .



**FIGURE 29.9**  
Inspection of the accuracy of the tooth profile in a gear for an intersected-axes gear pair.

**FIGURE 29.10**

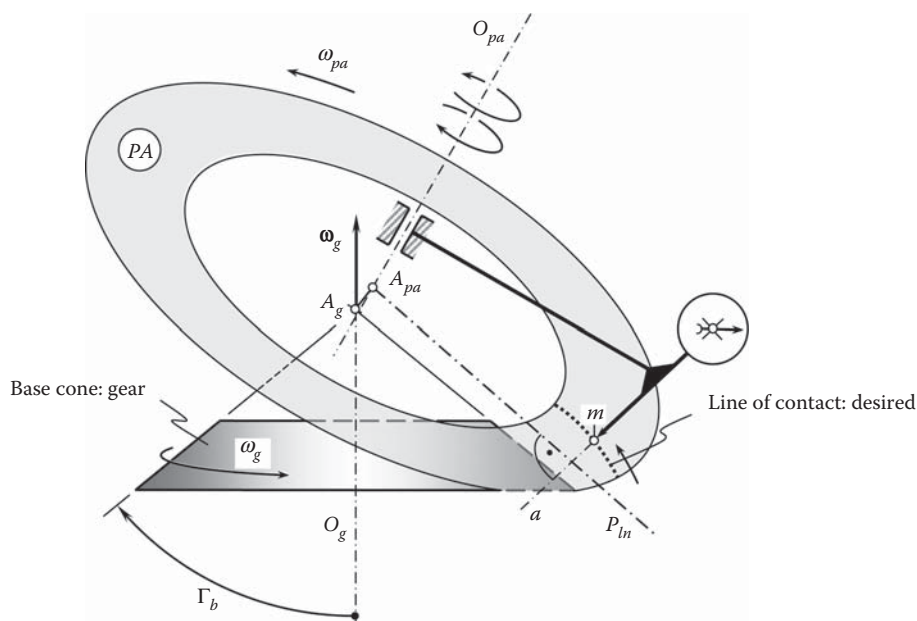
Inspection of the accuracy in the lengthwise direction in a gear for an intersected-axes gear pair.

### 29.3 Inspection of Gears for Crossed-Axes Gear Pairs

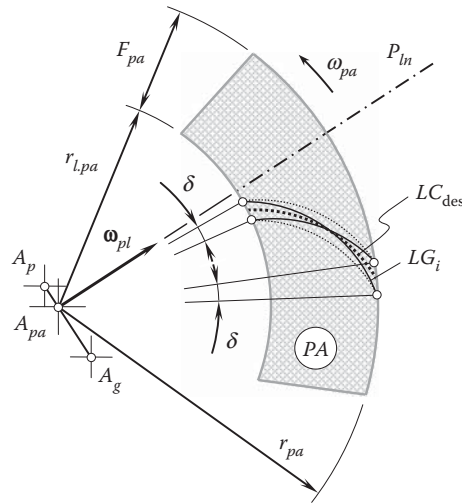
The methods of inspection of gears for crossed-axes gear pairs used in the current practice are inconsistent. The approximate datum surface that is used for inspection purposes is the main reason for that. The datum surface is not conjugate to the gear being inspected, as it is generated as an enveloping surface to consecutive positions of the crown rack in its motion in relation to the gear being inspected. This is especially clear when gears with a low tooth count are inspected—in this case, the inconsistency of the known method for inspecting gears is more evident. As the datum surface itself deviates from the perfect datum surface, the output of the gear inspection cannot be precise.

When inspecting a gear for an intersected-axes gear pair (see Figure 29.11), the relative motion of the gear to be inspected and the plane of action are performed. The gear is rotated about its axis of rotation,  $O_g$ . The plane of action,  $PA$ , is rotated about its axis of rotation,  $O_{pa}$ . The rotations,  $\omega_g$  and  $\omega_{pa}$ , are synchronized with one another.

Inspection of a gear tooth profile of a gear for a crossed-axes gear pair is similar to that of a gear for an intersected-axes gear pair. When inspecting a gear tooth profile (see Figure 29.9), the rotations,  $\omega_g$  and  $\omega_{pa}$  are

**FIGURE 29.11**

Kinematics of a method of inspection of a gear for a crossed-axes gear pair.

**FIGURE 29.12**

Deviation of tooth flank of approximate gear from tooth flank,  $\mathcal{G}$ , of a corresponding perfect gear.

synchronized so as to keep the stylus at a current point,  $m$ , on the desired bevel gear tooth flank. The axes,  $O_g$  and  $O_{pa}$ , are at a certain distance from one another when inspecting crossed gears. The rotations,  $\omega_g$  and  $\omega_{pa}$ , are synchronized with one another in a timely manner to keep the stylus at a current point,  $m$ , on the desired bevel gear tooth flank.

The point,  $m$ , is within the plane of action,  $PA$ . The line,  $a$ , along which the deviation is measured, is within the plane of action,  $PA$ , and is perpendicular to the gear tooth flank at point  $m$ . The stylus tip is motionless in relation to the plane of action,  $PA$ , when inspecting the profile error of the bevel gear tooth flank.

When inspecting the tooth flank geometry of a gear in the lengthwise direction (see Figure 29.10), the stylus tip travels along the line of intersection of the desired tooth flank by the plane of action,  $PA$ . At a current point,  $m$ , the line,  $a$ , along which the deviation is measured, is within the plane of action,  $PA$ , and perpendicular to the bevel gear tooth flank at the point,  $m$ .

In the course of inspection of a gear for a real crossed-axes gear pair, the tooth flank of the gear,  $\mathcal{G}$ , is intersected by the plane of action,  $PA$ , along a line of intersection. In Figure 29.12, the line of intersection through an arbitrary point within the tooth flank is labeled as  $LG_i$ . When the gear is rotated simultaneously with the plane of action,  $PA$ , the geometry of the line of intersection,  $LG_i$ , of the approximate gear alters. A plurality of the lines of intersection,  $LG_i$ , on the approximate gear tooth flank generated during the meshing cycle of a pair of teeth is located within a bend of an angular width,  $\delta$ , in the plane of action,  $PA$ . The angular deviation,  $\delta_i$ , at a current configuration of the gear in relation to the plane of action,  $PA$ , can be physically measured in a gear/pinion. The current value of the angular deviation,  $\delta_i$ , can be also calculated.

In a similar manner, the variation of the angular base pitch in a gear can be inspected.

## 29.4 Inspection of the Accuracy of Axial Location in Gears for Crossed-Axes and Intersected-Axes Gear Pairs

The performance of intersected-axes and crossed-axes gear pairs strongly depends on the accuracy of the axial location of the gears. Precision gearings are especially sensitive to the accuracy of the mounting of the gears in the gear housing.

Mounting distance in gears for intersected-axes and crossed-axes gear pairs is a design parameter that is inconvenient for inspection. The base cone apex of the gear does not exist physically. This is the root cause of inconveniences when inspecting the accuracy of the mounting distance. Therefore, indirect methods for the inspection of the accuracy of the mounting distance are used in practice.

Inspection of the contact pattern and mounting distance are the two main approaches for inspection of the correctness of the axial location of the gears in intersected-axes and crossed-axes gear pairs.

### 29.4.1 Mounting Distance

To operate properly, gears in intersected-axes and crossed-axes gear pairs must be properly configured in relation to one another.

First, let's clarify what the term *mounting distance* stands for.

- First, and most critical, by means of mounting distances, the location of tooth flanks in the axial direction of a gear and a mating pinion are specified in relation to the centerlines in the gear housing. The apex point of a tooth flank of both the gear,  $A_{fg}$ , and the pinion,  $A_{fp}$ , must coincide either with the point of intersection of the centerlines in the gear housing (for  $I_a$ -gearings) or with the *pitch plane/plane of action* apex (for  $C_a$ -gearings). The pitch plane apex is commonly designated as  $A_{pp}$ , and the plane of action apex is commonly designated as  $A_{pa}$ . These two conditions can be expressed as follows:  $A_{fg} \equiv A_{pp} \equiv A_{pa}$  and  $A_{fp} \equiv A_{pp} \equiv A_{pa}$
- Second, the pitch cone apex of a gear,  $A_g$  (and mating pinion,  $A_p$ ) must coincide with the apex point of a tooth flank of both the gear,  $A_{fg}$ , and pinion,  $A_{fp}$ . These two conditions can be expressed as follows:  $A_g \equiv A_{fg}$  and  $A_p \equiv A_{fp}$
- Third, the base cone apex of a gear,  $A_{bg}$  (and mating pinion,  $A_{bp}$ ) must coincide with the apex point of a tooth flank of both the gear,  $A_{fg}$ , and the pinion,  $A_{fp}$ . These two conditions can be expressed as follows:  $A_{bg} \equiv A_{fg}$  and  $A_{bp} \equiv A_{fp}$
- Fourth, there are two outer cones. One of them is for the gear and the other is for the mating pinion. There are also two root cones. Again, one of them is for the gear and the other is for the mating pinion. Neither outer cones nor root cones directly affect the actual value of the mounting distance. However, these cones need to be mentioned here, as in the current practice, outer cones are commonly used when determining the mounting distance.

In a precision gear pair, it is recommended to inspect the mounting distance at a nominal operating load and the preloaded bearings.

Theoretically, in an intersected-axes gear pair, a gear base cone apex,  $A_g$ ; a mating pinion base cone apex,  $A_p$ ; and the plane-of-action apex,  $A_{par}$ , must be snapped together, as schematically illustrated in Figure 29.13a. In reality, in order to transmit power, gears need to be supported. For this purpose, a gear housing (see Figure 29.13b) is used. The gear housing features a corresponding number of bores that are used to support gear shafts in the housing. A centerline of a bore for the gear shaft is labeled as  $O_{hg}$ . Correspondingly, a centerline of a bore for the pinion shaft is designated by  $O_{hp}$ . The centerlines,  $O_{hg}$  and  $O_{hp}$ , intersect at point  $A_h$ . Strong constraints on the configuration of the gear and its mating pinion in the gear housing are imposed by this point,  $A_h$ .

The gear must be configured in the gear housing so as to keep the gear axis of rotation,  $O_g$ , aligned with the axis,  $O_{hg}$ , in the gear housing (that is,  $O_g \equiv O_{hg}$ ), as illustrated in Figure 29.13c. The gear base cone apex,  $A_g$ , must be coincident with the point,  $A_h$ , of intersection of the centerlines,  $O_{hg}$  and  $O_{hp}$  (that is,  $A_g \equiv A_h$ ). Then, the rest of the important components, that is, bearings, shims, fasteners, and so forth, are put together so as to keep the gear mounting distance,  $MD_g$ , to the blueprint. The gear mounting distance,  $MD_g$ , is measured between the gear back face and the corresponding gear housing face, as shown in Figure 29.13d.

Similarly, the pinion must be configured in the gear housing so as to keep the pinion axis of rotation,  $O_p$ , aligned with the axis,  $O_{hp}$  (that is,  $O_p \equiv O_{hp}$ ), in the gear housing, as illustrated in Figure 29.13e. The pinion base cone apex,  $A_p$ , must be coincident with the point,  $A_h$ , of intersection of the centerlines,  $O_{hg}$  and  $O_{hp}$  (that is,  $A_p \equiv A_h$ ). Then, the rest of the important components, that is, bearings, shims, fasteners, and so forth, are put together so as to keep the pinion mounting distance,  $MD_p$ , to the blueprint. The pinion mounting distance,  $MD_p$ , is measured between the pinion back face and the corresponding gear housing face, as shown in Figure 29.13f.

Finally, once the gear and pinion are properly mounted in the gear housing, their axes are aligned to the centerlines of the corresponding bores in the gear housing (that is,  $O_g \equiv O_{hg}$  and  $O_p \equiv O_{hp}$ ), and the apexes,  $A_g$ ,  $A_p$ , and  $A_{par}$  are all snapped together with the point of intersection,  $A_h$ , of the centerlines,  $O_{hg}$  and  $O_{hp}$  in the gear housing, as schematically illustrated in Figure 29.13g.

The discussed approach can be easily adapted to the case of crossed-axes gear pairs.



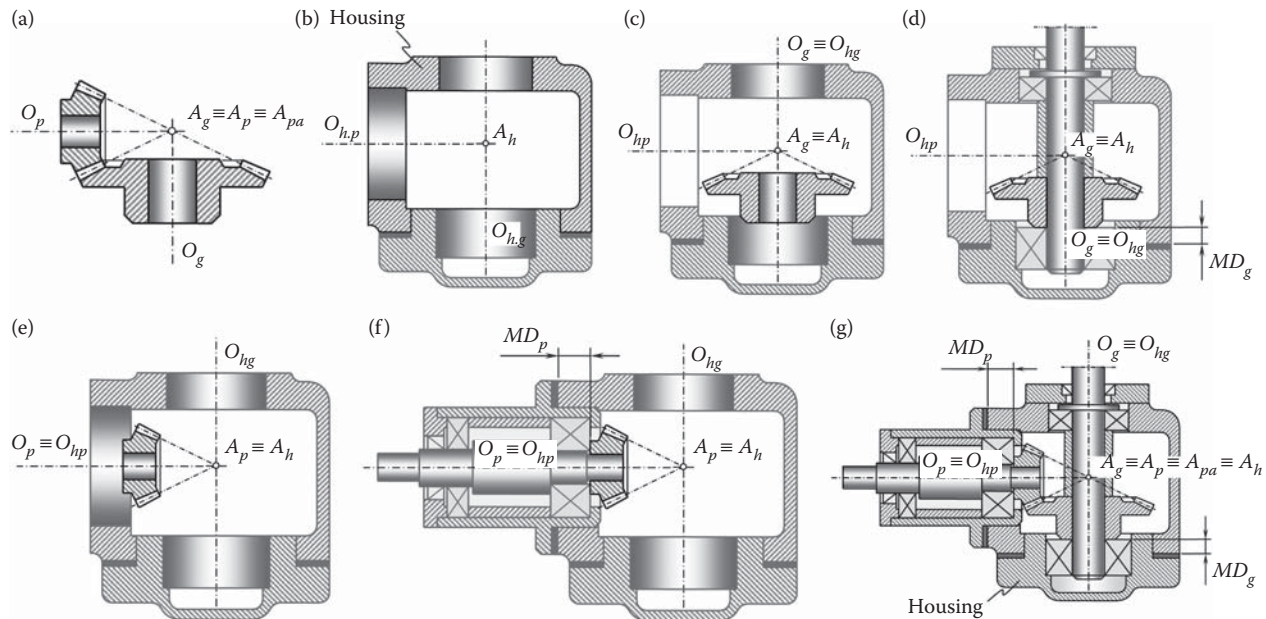


**FIGURE 29.13**  
Schematic of mounting bevel gears in the housing.

An important conclusion can be drawn from the above discussion: *no* axial shift of the gears from the point of intersection,  $A_h$ , of the centerlines,  $O_{hg}$  and  $O_{hp}$ , in the gear housing is allowed in intersected-axes or crossed-axes gearings (see Figure 29.14). This is an incorrect practice to adjust for the backlash in intersected-axes and crossed-axes gearings by means of an *inward-outward* axial shift of the gears.

### 29.4.2 Contact Patterns

Gears in intersected-axes and crossed-axes gear pairs must be assembled in a specific way to ensure smooth running and a favorable load distribution between gears. To attain this goal, a contact pattern between the interacting tooth flanks of a gear and a mating pinion is commonly used.

The contact pattern is a critical attribute of any and all bevel/hypoid gear design. An example of a contact pattern is depicted in Figure 29.15. For this purpose, the gear teeth are covered by a stain and roll over one another in a tight mesh, as illustrated in Figure 29.16.

Simply stated, the contact pattern is the area in which the gear teeth come into contact as they engage and disengage during their rotation. When a gear is installed in a gearbox and is powering the designated

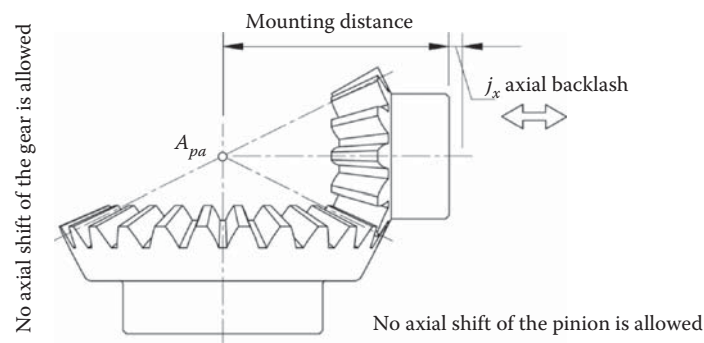


**FIGURE 29.14**  
The wrong practice to adjust for the backlash in intersected-axes and crossed-axes gearings by means of “inward-outward” axial shift of the gears: *no* axial shift of the gears from the point of intersection,  $A_h$ , of the centerlines,  $O_{hg}$  and  $O_{hp}$ , in the gear housing, is allowed in  $I_a$ -axes or  $C_a$ -gearings.



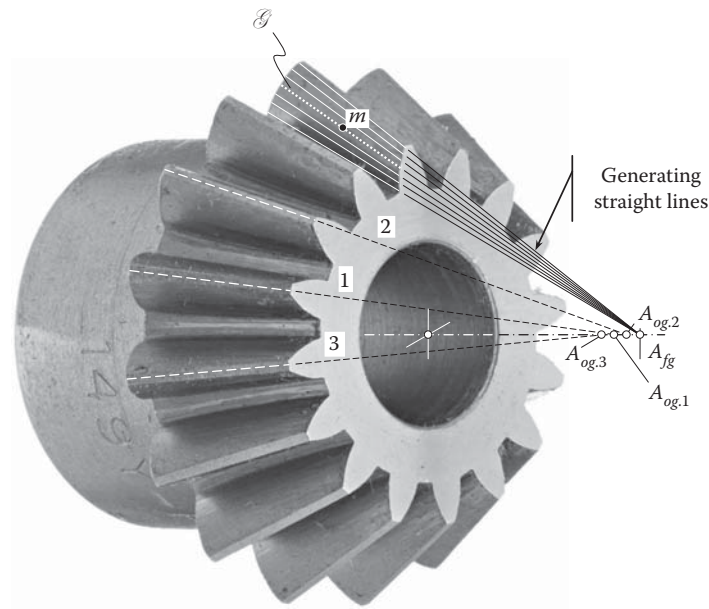
**FIGURE 29.15**

An example of acceptable shape and configuration of the contact pattern under a low load.

application, there are varying degrees of pressure—or load—on the gear teeth. These pressures are influenced by box deflections, bearing movement, and temperature changes. When the gear teeth are subjected to these variables, the contact pattern will change. There is a general rule of thumb stating that the heavier the load, the larger the contact pattern, and vice versa. For a gear to perform properly under operating load, the contact pattern must be of a certain shape and at a certain location. Typically, an ideal tooth contact pattern under load should encompass the bulk of the tooth surface while avoiding any contact with the edges of the tooth flank. So far, the contact pattern is more a *qualitative* rather than a *quantitative* indicator of gear pair quality.

**FIGURE 29.16**

Two gears with the teeth covered by stain roll over each other in tight mesh to get a favorable shape, size, and configuration of the contact pattern.

**FIGURE 29.17**

On the definition of the tooth flank apex,  $A_{fg}$ , in intersected-axes and crossed-axes gearings.

The permissible variation in contact pattern location, orientation, and shape can be used to calculate the tolerances for design parameters of a gear pair.\* Unfortunately, in the current gear practice, contact pattern is a qualitative and not quantitative measure of gear pair quality.

Instead of contact pattern analysis, the tooth flank geometry, along with the actual value of the mounting distance, should be measured. No contact pattern analysis is necessary if the gears for intersected-axes/crossed-axes gear pairs are machined and assembled according to a properly designed blueprint.

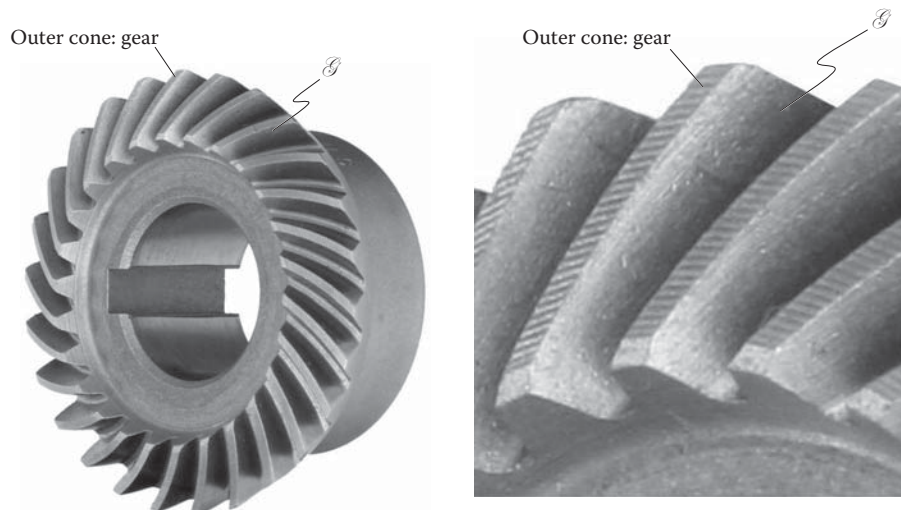
### 29.4.3 Inspection of the Mounting Distance in Gears for Crossed-Axes and Intersected-Axes Gear Pairs

Mounting distance is a vital design parameter for intersected-axes gearings, as well as for crossed-axes gearings. The specification, inspection, and tolerancing of the mounting distance are challenging to understand by practical gear engineers.

To make things clear, it is necessary to outline to the best possible extent what the term *mounting distance* stands for. As an example, consider a tooth flank of a straight bevel gear,<sup>†</sup> as illustrated in Figure 29.17. The tooth flank of the gear,  $\mathcal{G}$ , can be construed as a family of straight lines through each point of the gear tooth profile and the gear tooth flank apex,  $A_{fg}$  (the gear tooth flank apex,  $A_{fg}$ , is equivalent to the gear base cone apex,  $A_{bg}$ ). Only the gear tooth flank apex,  $A_{fg}$ , should be used for the specification and inspection of the mounting distance,  $MD$ . Commonly, the outer cone apex of the gear,  $A_{og,1}$ , is inward in relation to the gear tooth flank apex,  $A_{fg}$ , as shown for straight generating line 1 in Figure 29.17. However, this is not a must, as the gear outer cone apex,  $A_{og,2}$ , can be located outward, or the gear outer cone apex,  $A_{og,3}$ , can be located inward in relation to the apex,  $A_{og,1}$ , as illustrated in Figure 29.17 for straight generating lines 2 and 3 of the outer cone of the gear. The actual location of the gear outer cone apex ( $A_{og,1}$ ,  $A_{og,2}$ , or  $A_{og,3}$ ) does not affect the conditions of meshing of the gear,  $\mathcal{G}$ , and pinion,  $\mathcal{P}$ , tooth flanks. The conditions of meshing of the gear,  $\mathcal{G}$ , and pinion,  $\mathcal{P}$ , tooth flanks depends only on the actual location of the gear/pinion tooth flank apex,  $A_{fg}$ . Therefore, the tolerance for the mounting distance (the mounting distance is measured in relation to the gear tooth flank apex,  $A_{fg}$ ) is tight,

\* Overall, the contact pattern is a subjective (not objective) parameter. Neither the dimensions and orientation nor the tolerances for the dimensions and orientation of the contact pattern can be assigned (or be directly measured on the shop floor). The contact pattern is an insufficiently engineered parameter of quality of a gear pair. The contact pattern is *not* measurable; that is, it *cannot* be reliably measured by means that are commonly available on the shop floor. It is desired to substitute the contact pattern with another reliably measurable design parameter of a gear pair. The mounting distance is a promising candidate for that.

<sup>†</sup> This concept can be easily extended to bevel gears of any and all other types.

**FIGURE 29.18**

The outer cone surface of a gear for intersected-axes and crossed-axes gear pairs can be used as a datum surface for the inspection of the mounting distance if the cone surface is finish-cut in one setup with the gear tooth flank,  $\mathcal{G}$ .

while the configuration of the apex of the outer cone of the gear,  $A_{og}$ , is a free dimension with no specified tolerance.

Depending on the accuracy of the setup parameters when cutting straight bevel gears, the axial position of the tooth flank,  $\mathcal{G}$ , can be changed. After being assembled, the gear tooth flank apex,  $A_{fg}$ , must be coincident with the centerlines in the gearbox housing. Therefore, the mounting distance of a gear is the distance from the gear tooth flank apex,  $A_{fg}$ , to the common reference surface of the gear. A similar definition is valid with respect to the mounting distance of a pinion.

Then, the crown is not geometrically associated with the gear tooth flank,  $\mathcal{G}$ . An analysis of Figure 29.18 reveals that, depending on the accuracy of the setup parameters when machining straight bevel gears, the axial position of the tooth flank,  $\mathcal{G}$ , and the gear tooth flank apex,  $A_{fg}$ , can be variable.

Gear tooth flanks in intersected-axes and crossed-axes gearings must be correctly specified in relation to the common reference surface. For this purpose, an arbitrary point,  $m$ , either within the tooth flank or within an extension of this surface can be used. The tooth flank apex,  $A_{fg}$  (see Figure 29.17), is convenient to be used for this purpose. It is a wrong practice to use the wedge,  $E$ , and the dimension,  $F$  (see Figure 29.18), to specify the mounting distance in bevel/hypoid gearing.

Direct measurements of the mounting distance\* are necessary. This can be done, for example, by means of laser scanning of the machined tooth flank and creating CAD model of the actual tooth flanks on-site. Comparison of two CAD models, that is, of the desirable and actual tooth flanks, returns an exact number of the mounting distance in a machined bevel/hypoid gear. Simpler methods and means for the direct inspection of the actual mounting distance in intersected-axes and crossed-axes gearings can be developed.

Reliable methods for the calculation of the tolerances for the mounting distance in intersected-axes and crossed-axes gearings need to be developed. The tooth flank of a gear can be used for the inspection of the accuracy of the mounting distance. The problem in question can be resolved if an alternative equivalent surface can be used for the inspection. The outer cone surface of a gear to be inspected can be used for the inspection of the accuracy of the mounting distance if this surface is finish-cut in one setup with finish machining of the tooth flanks of the gear. This can be done either if full profile cutters are used in the design of the cutter heads or an additional one or two cutters are mounted on the cutter head of the conventional design.

\* *Important:* In addition to the mounting distance, in  $C_n$  - gearings, one more design parameter must be inspected. This is the angle that a gear/pinion axis of rotation forms with the centerline,  $\angle$ . A tolerance for this angle needs to be specified, and the actual deviation of the angle from its required value needs to be inspected. An appropriate tolerance for the center distance is required to be set up.

Noise and vibration excitation are annoying problems. These problems have been exacerbated due to the continuous reduction in sounds from other systems noise exciters, such as engines and so forth. All of them are theoretically preventable. Unfortunately, gear noise prevention methods can be costly, both in terms of equipment and labor. The reduction of gear noise/vibration excitation is a complex engineering problem.

### 30.1 Root Causes for Vibration Generation and Noise Excitation

Many factors, such as transmission errors, tooth impacts, mesh stiffness variations, force axial shuttling, friction, air, and lubricant entrapment, cause gear noise and vibration. Only factors that cause noise and vibration in the gear mesh are considered in this chapter.

In the analysis of root causes for vibration generation and noise excitation, it is reasonable to begin from the consideration of perfect gear pairs. Later on, the obtained results of the discussion can be applied to approximate gear pairs as well.

#### 30.1.1 Root Cause for Vibration Generation and Noise Excitation in Perfect Gear Pairs

Perfect gear pairs of all kinds, that is, parallel-axes, intersected-axes, and crossed-axes gear pairs, meet all three fundamental conditions that gearings have to fulfill. These conditions are as follows (see [Chapter 4](#)):

- Condition of contact of the interacting tooth flanks,  $\mathcal{G}$  and  $\mathcal{P}$ , of a gear and a mating pinion. This condition is commonly expressed by the *Shishkov equation of contact*,  $\mathbf{n} \cdot \mathbf{V}_\Sigma = 0$ .
- Condition of conjugacy of the interacting tooth flanks,  $\mathcal{G}$  and  $\mathcal{P}$ , of a gear and a mating pinion—at every point within the line of contact, the unit normal vector,  $\mathbf{n}$ , of a common perpendicular is along a straight line that intersects the axis of instant rotation,  $P_{ln}$ , in the gear pair.
- Condition in which the angular base pitch of a gear,  $\varphi_{b,g}$ , and that of a mating pinion,  $\varphi_{b,p}$ , are both equal to the operating angular base pitch of the gear pair,  $\varphi_{b,op}$ ; that is, the equalities  $\varphi_{b,g} = \varphi_{b,op}$  and  $\varphi_{b,p} = \varphi_{b,op}$  are valid for any configuration of the gear and mating pinion in relation to each other.

In perfect gear pairs, all three fundamental conditions are fulfilled. It seems at first glance that there is no reason for vibration generation and noise excitation in perfect gear pairs. Unfortunately, this is not correct.

In: (a) parallel-axes helical gearing, (b) intersected-axes gearing, and (c) crossed-axes gearing, variation of the *axial* component and *radial* component of the resultant force of the interaction between gear mating pinion tooth flanks is observed. Therefore, even in a case of perfect gearings (a) and (b), noise excitation and vibration generation become inevitable.

In perfect intersected-axes and crossed-axes gear pairs, forces that act in the gear mesh vary in time. This is true first of all with respect to the axial component, as well as the radial component of the resultant force. The tangential component that causes transmission of the rotation also contributes to vibration and noise generation. However, this contribution is not as significant as a contribution by the axial and radial components.

The variation in time of the axial component of the resultant force, as well as the radial component of the resultant force, are both transmitted to the gear housing, and so forth.

### 30.1.2 Root Cause for Vibration Generation and Noise Excitation in Approximate Gear Pairs

The three fundamental conditions that gearings have to fulfill are violated in approximate gearings, that is, in parallel-axes, intersected-axes, and crossed-axes gear pairs.

#### 30.1.2.1 Violation of the Condition of Contact

In compliance with the condition of contact between the tooth flanks,  $\mathcal{G}$  and  $\mathcal{P}$ , of a gear and a mating pinion, a common perpendicular,  $\mathbf{n}$ , to the interacting tooth flanks,  $\mathcal{G}$  and  $\mathcal{P}$ , is always orthogonal to the linear velocity vector,  $\mathbf{V}_K$ , of the resultant relative motion of the tooth flanks. Analytically, this condition is described by the Shishkov equation of contact,  $\mathbf{n} \cdot \mathbf{V}_K = 0$ .

The condition of contact is commonly violated in cases of so-called “edge contact” of the interacting tooth flanks,  $\mathcal{G}$  and  $\mathcal{P}$ , of a gear and mating pinion.

The condition of contact is fulfilled in most cases of approximate gearings, as gear,  $\mathcal{G}$ , and mating pinion,  $\mathcal{P}$ , tooth flanks in approximate gearings are smooth surfaces having appropriate principal radii of curvature. Commonly, fulfillment of the condition of contact causes no problem when designing perfect gears. However, this could be a huge problem when designing approximate gears.

#### 30.1.2.2 Violation of the Condition of Conjugacy

In approximate gearings, the condition of conjugacy of the tooth flanks,  $\mathcal{G}$  and  $\mathcal{P}$ , of a gear and a mating pinion is often violated.

Referring to Figure 30.1, consider the interaction between the local patches of gear and mating pinion tooth profiles,  $\mathcal{G}$  and  $\mathcal{P}$ . The local patches are within the differential vicinity of the contact point,  $K$ .

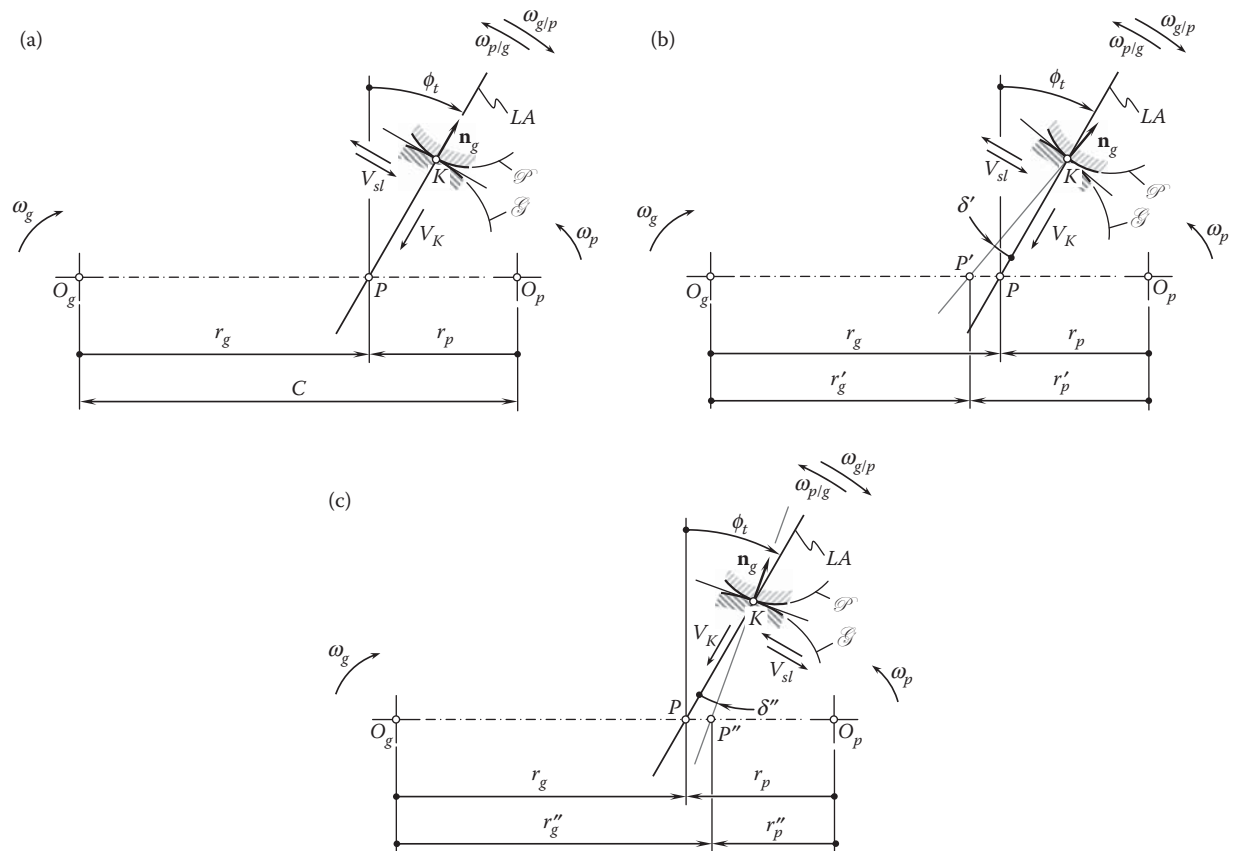


FIGURE 30.1

Condition of conjugacy of the interacting tooth flanks of a gear,  $\mathcal{G}$ , and mating pinion,  $\mathcal{P}$ : (a) the condition of conjugacy is fulfilled; (b) the condition of conjugacy is violated: the tooth flanks,  $\mathcal{G}$  and  $\mathcal{P}$ , are turned clockwise through an angle,  $\delta'$ ; and (c) the condition of conjugacy is violated: the tooth flanks,  $\mathcal{G}$  and  $\mathcal{P}$ , are turned counterclockwise through an angle,  $\delta''$ .



In the case of perfect gearing (see Figure 30.1a), a gear and mating pinion rotate,  $\omega_g$  and  $\omega_p$ , about their axes of rotation,  $O_g$  and  $O_p$ . The axes,  $O_g$  and  $O_p$ , are at a center distance,  $C$ , from one another. The pitch point,  $P$ , is located within the centerline,  $\mathcal{C}$ . The ratio,  $r_g/r_p$ , of the distances,  $r_g$  and  $r_p$ , of the pitch point,  $P$ , from the axes of rotation,  $O_g$  and  $O_p$ , is reciprocal to the ratio,  $\omega_p/\omega_g$ , of the rotations of the gear and mating pinion.

The line of action,  $LA$ , is a straight line through the pitch point,  $P$ . The line of action,  $LA$ , forms a transverse pressure angle,  $\phi_t$ , with a perpendicular to the centerline,  $\mathcal{C}$ , through the pitch point,  $P$ .

When the gears rotate, the contact point,  $K$ , travels along the line of action,  $LA$ , with a linear velocity,  $V_K$ . The tooth flanks,  $\mathcal{G}$  and  $\mathcal{P}$ , slide over one another. The linear velocity of sliding is labeled  $V_{sl}$ .

When the gear is considered stationary, the instant motion of a gear and mating pinion in relation to one another can be viewed as an instant rotation,  $\omega_{p/g}$ , about the pitch point,  $P$ , of the pinion in relation to the gear. Otherwise, when the pinion is considered stationary, the instant motion of a gear and mating pinion in relation to one another can be viewed as an instant rotation,  $\omega_{g/p}$ , about the pitch point,  $P$ , of the gear in relation to the pinion.

It is critical to stress here that in Figure 30.1a, the common perpendicular vector,  $\mathbf{n}_g$ , is along the line of action,  $LA$ . This reveals that the gear and mating pinion tooth profiles,  $\mathcal{G}$  and  $\mathcal{P}$ , are designed properly, and the condition of conjugacy of the interacting tooth profiles,  $\mathcal{G}$  and  $\mathcal{P}$ , is fulfilled.

Let's proceed to the analysis of the case shown in Figure 30.1b. In the case in question, the gear and mating pinion tooth profiles,  $\mathcal{G}$  and  $\mathcal{P}$ , are designed so that the common perpendicular vector,  $\mathbf{n}_g$ , is turned about the contact point,  $K$ , clockwise through an angle,  $\delta'$ . A straight line along the unit vector,  $\mathbf{n}_g$ , intersects the centerline,  $\mathcal{C}$ , at point,  $P'$  (instant pitch point). The ratio,  $r'_g/r'_p$ , of the distances,  $r'_g$  and  $r'_p$ , of the instant pitch point,  $P'$ , from the axes of rotation,  $O_g$  and  $O_p$ , is not reciprocal to the ratio,  $\omega_p/\omega_g$ , of the rotations of the gear and mating pinion. The gears tend to rotate about the instant pitch point,  $P'$ , and not about the pitch point,  $P$ . None of the instant rotations ( $\omega_{p/g}$  or  $\omega_{g/p}$ ) are feasible. This reveals that the gear and mating pinion tooth profiles,  $\mathcal{G}$  and  $\mathcal{P}$ , are designed improperly, and the condition of conjugacy of the interacting tooth profiles,  $\mathcal{G}$  and  $\mathcal{P}$ , is violated.

Finally, let's analyze the case shown in Figure 30.1c. In the case under consideration, the gear and mating pinion tooth profiles,  $\mathcal{G}$  and  $\mathcal{P}$ , are designed so that the common perpendicular vector,  $\mathbf{n}_g$ , is turned about the contact point,  $K$ , counterclockwise through an angle,  $\delta''$ . A straight line along the unit vector,  $\mathbf{n}_g$ , intersects the centerline,  $\mathcal{C}$ , at point  $P''$  (instant pitch point). The ratio,  $r''_g/r''_p$ , of the distances,  $r''_g$  and  $r''_p$ , of the instant pitch point,  $P''$ , from the axes of rotation,  $O_g$  and  $O_p$ , is not reciprocal to the ratio,  $\omega_p/\omega_g$ , of the rotations of the gear and mating pinion. The gears tend to rotate about the instant pitch point,  $P'$ , and not about the pitch point,  $P$ . None of the instant rotations ( $\omega_{p/g}$  or  $\omega_{g/p}$ ) are feasible. This reveals that the gear and mating pinion tooth profiles,  $\mathcal{G}$  and  $\mathcal{P}$ , are designed improperly, and the condition of conjugacy of the interacting tooth profiles,  $\mathcal{G}$  and  $\mathcal{P}$ , is violated.

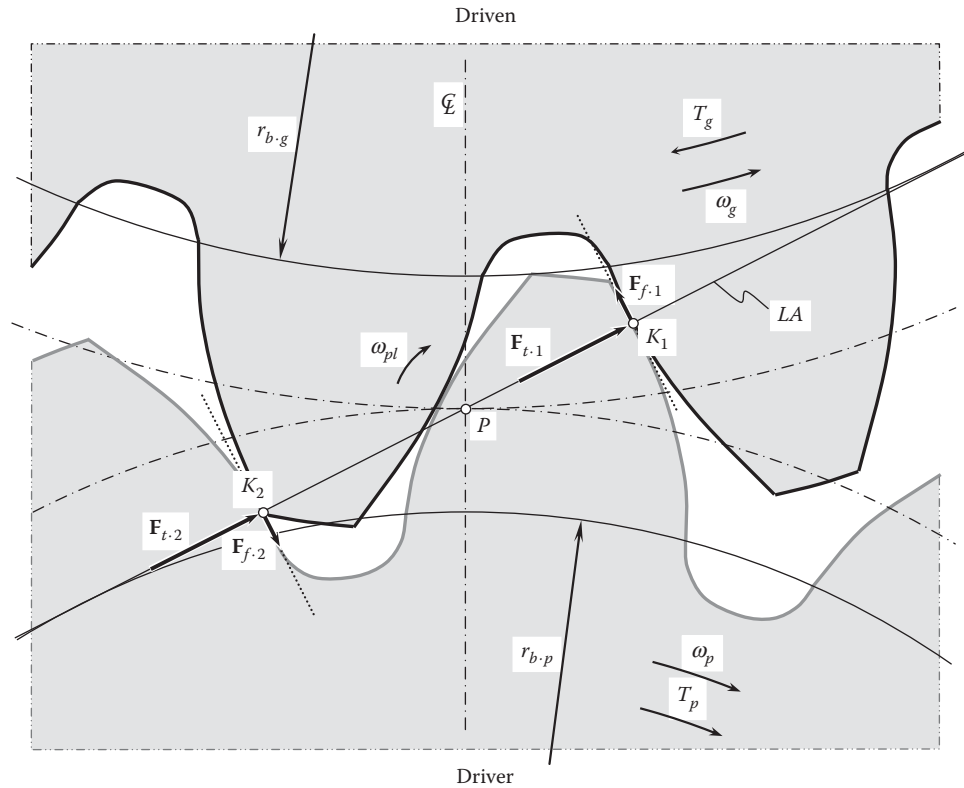
As the line along the unit normal vector,  $\mathbf{n}_g$ , of a common perpendicular does not go through the pitch point,  $P$ , the actual instant pitch point,  $P$ ,  $P'$ , and  $P''$ , migrates up and down along the centerline,  $\mathcal{C}$ ; therefore, vibration generation and noise excitation increase when the gears transmit power.

When friction between a gear tooth flank,  $\mathcal{G}$ , and a mating pinion tooth flank,  $\mathcal{P}$ , is taken into account, the friction forces alter the actual direction of a straight line along which the resultant force of the interaction is pointed, as illustrated in Figure 30.2. The normal forces,  $F_{t,1}$  and  $F_{t,2}$ , are along the line of action,  $LA$ . The line of action,  $LA$ , is a straight line through the pitch point,  $P$ . The friction forces,  $F_{f,1}$  and  $F_{f,2}$ , are entirely located within the common tangent plane, and they are perpendicular to the corresponding normal forces,  $F_{t,1}$  and  $F_{t,2}$ . As the inequalities  $F_{f,1} \neq 0$  and  $F_{f,2} \neq 0$  are valid, then the resultant force of interaction,  $F_{\Sigma}$ , does not align with the line of action,  $LA$ , or with the instant line of action,  $LA_{inst}$ . As the resultant force,  $F_{\Sigma}$ , is no longer along a line through the pitch point,  $P$ , an instant pitch point,  $P_{inst}$ , is created.

The resultant force is along a straight line that is not through the pitch point,  $P$ . The latter, along with the variation of the normal forces,  $F_{t,1}$  and  $F_{t,2}$ , and friction forces  $F_{f,1}$  and  $F_{f,2}$ , depending on an actual configuration of the gear and pinion in relation to one another (see Figure 30.2), is a potential root cause of excessive noise excitation. The better the lubrication, the lower the noise excitation, and vice versa. When performing the analysis, the process of vibration generation and noise excitation can be expressed in terms of the torques,  $T_{f,1}$  and  $T_{f,2}$ , created by the friction forces,  $F_{f,1}$  and  $F_{f,2}$ , as well as in terms of the resultant torque,  $T_{f,\Sigma}$ , that is created by the resultant friction force,  $F_{f,\Sigma} = F_{f,1} + F_{f,2}$ .

### 30.1.2.3 Violation of the Equality of the Base Pitches

In approximate gearings, either the base pitch of a gear, the base pitch of a mating pinion, or both are not equal to the operating base pitch of the gear pair. Moreover, often, the base pitch either of a gear, a mating pinion, or both cannot be specified at all. The operating base pitch of a gear pair can always be calculated.

**FIGURE 30.2**

The direction of the resultant force,  $\mathbf{F}_\Sigma$ , in a gear mesh can be affected by the friction forces,  $\mathbf{F}_{f,1}$  and  $\mathbf{F}_{f,2}$ .

The base pitch variation is a root cause for vibration generation and excessive noise excitation. The parameters of noise excitation can be expressed in terms of the variation of the base pitch when the gears rotate. Thus, the noise frequency must correlate to the base pitch variation.

Base pitch variation is caused by one of the following factors (or a combination of these factors), namely:

1. The deviation of the gear tooth flank geometry in relation to the desired geometry
2. The displacement, both linear and angular, of the gear tooth flank in relation to the axis of rotation of the gear/pinion (of the gear/pinion body)
3. Axis misalignment

The actual value of the base pitch variation can be expressed in terms of these three elementary components.

Deviations of the tooth flank geometry from its desired geometry, as well as the displacement of the tooth flanks from their desired location and orientation, are measured from the nominal tooth flank geometry, location, and orientation specified by the gear blueprint. Under such a scenario, the base pitches of the gear and mating pinion and the operating base pitch are equal to those specified by the gear pair blueprint.

Without loss of generality, to illustrate the approach employed for the analysis of base pitch deviations and their impact on the noise excitation in a gear pair, consider a simplified example. A parallel-axis helical gear pair is schematically depicted in Figure 30.3. The gear pair features zero axis misalignment. The gear and pinion are rotated about their axes of rotation,  $O_g$  and  $O_p$ , correspondingly. The angular velocities,  $\omega_g$  and  $\omega_p$ , are synchronized with one another to keep valid the ratio:

$$\frac{\omega_p}{\omega_g} = \frac{N_g}{N_p} \quad (30.1)$$

Here, in Equation 30.1, the tooth numbers of the gear and pinion are designated as  $N_g$  and  $N_p$ , correspondingly.



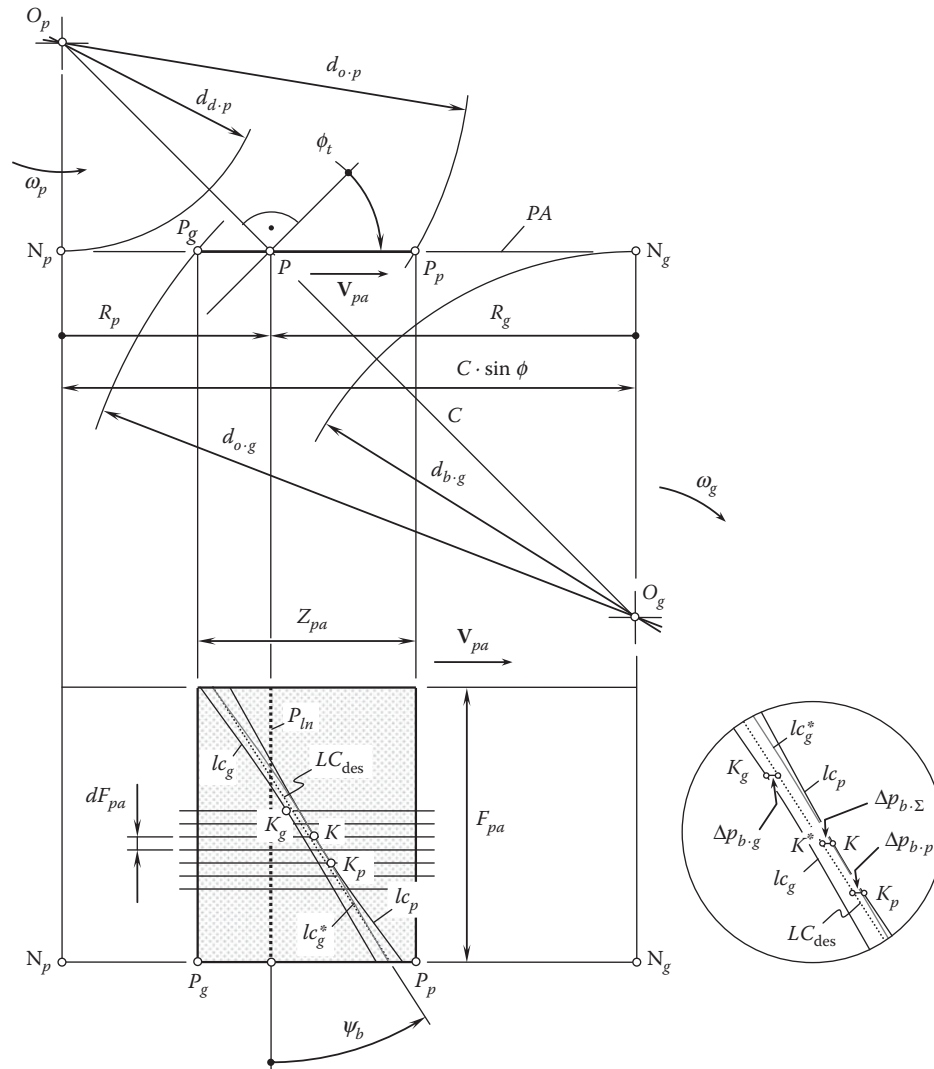


FIGURE 30.3

Details of the concept used for the analysis of the deviations: of the base pitch,  $\Delta p_{b,g}$ , in a gear; the base pitch,  $\Delta p_{b,p}$ , in a mating pinion; and the operating base pitch,  $\Delta p_{b,\Sigma}$ , in a gear pair.

The axes of rotation,  $O_g$  and  $O_p$ , of the gear and pinion are at a certain center distance,  $C$ , from each other. The transverse pressure angle is denoted by  $\phi_t$ .

The plane of action,  $PA$ , is tangent from opposite sides to the base cylinders of diameters,  $d_{b,g}$  and  $d_{b,p}$ , of the gear and pinion, correspondingly. The width of the zone of action,  $ZA$ , equals  $F_{pa}$ , and the length is equal to  $Z_{pa}$ . The desired line of contact,  $LC_{des}$ , forms a base helix angle,  $\phi_t$ , with the axis of instant rotation,  $P_{ln}$ . The tooth flanks,  $\mathcal{G}$  and  $\mathcal{P}$ , of the perfect gears are intersected by the plane of action,  $PA$ , along the desired line of contact,  $LC_{des}$ .

The tooth flanks,  $\mathcal{G}_a$  and  $\mathcal{P}_a$ , of the actual gear and mating pinion deviate from their desired geometries,  $\mathcal{G}$  and  $\mathcal{P}$ . Therefore, the gear tooth flank,  $\mathcal{G}_a$ , is intersected by the plane of action,  $PA$ , along the gear line of contact,  $lc_g$ . The line of intersection,  $lc_g$ , does not align with the desired line of contact,  $LC_{des}$ . Similarly, the pinion tooth flank,  $\mathcal{P}_a$ , is intersected by the plane of action,  $PA$ , along the pinion line of contact,  $lc_p$ . The line of intersection,  $lc_p$ , also does not align with the desired line of contact,  $LC_{des}$ . Evidently, the lines of intersection,  $lc_g$  and  $lc_p$ , do not align with the desired line of contact,  $LC_{des}$ .

The plane of action,  $PA$ , is sliced by an infinite number of planes, all of which are perpendicular to the axis of instant rotation,  $P_{ln}$ . The planes are at an infinitesimally short distance,  $dF_{pa}$ , from one another. Within every slice, the gear line of contact,  $lc_g$ , deviates from the desired line of contact,  $LC_{des}$ , at a distance,  $\Delta p_{b,g}$ . At a point,  $K_g$ , the deviation,  $\Delta p_{b,g}$ , is of a minimal value. Similarly, within every slice, the pinion line of contact,  $lc_p$ , deviates

from the desired line of contact,  $LC_{des}$ , at a distance,  $\Delta p_{b,p}$ . At a point,  $K_p$ , the deviation,  $\Delta p_{b,p}$ , is of a minimal value. In fact, the deviations,  $\Delta p_{b,g}$  and  $\Delta p_{b,p}$ , are equal to the deviations of the linear base pitches,  $p_{b,g}$  and  $p_{b,p}$ , of the gear and mating pinion from the operating linear base pitch,  $p_{b,op}$ , of the gear pair. As is clear from the above discussion, base pitch deviations are caused by deviations in tooth flank geometries,  $\mathcal{G}_a$  and  $\mathcal{P}_a$ , of the gear and mating pinion from their desired geometries,  $\mathcal{G}$  and  $\mathcal{P}$ .

Theoretically, the tooth flanks,  $\mathcal{G}$  and  $\mathcal{P}$ , are at certain distance from one another, but in reality, they contact each another at a point, as both the driving pinion and driven gear are loaded by an operating torque. As the gears are loaded, there is no gap between the gear line of contact,  $lc_g$ , and the pinion line of contact,  $lc_p$ . The gear line of contact,  $lc_g$ , travels toward the pinion line of contact,  $lc_p$ . In a shifted position, the line,  $lc_g$ , is labeled as  $lc_g^*$ . These two lines of contact have a common point; that is, they share contact point  $K$ . The distance covered by the pinion line of contact,  $lc_p$ , to get in contact with the gear line of contact,  $lc_g$ , depends on the actual values of the deviations,  $\Delta p_{b,g}$  and  $\Delta p_{b,p}$ . This distance is the operating base pitch error. In a case where the minimal deviations are observed in a common slice, the total deviation of the base pitches,  $\Delta p_{b,\Sigma}$ , is equal to the sum of the instant deviations,\*  $\Delta p_{b,g}$  and  $\Delta p_{b,p}$ ; that is:

$$\Delta p_{b,\Sigma} = \Delta p_{b,g} + \Delta p_{b,p} \quad (30.2)$$

Commonly, minimal deviations,  $\Delta p_{b,g}$  and  $\Delta p_{b,p}$ , are observed in different slices. Therefore, the total deviation of the base pitches,  $\Delta p_{b,\Sigma}$ , is calculated as:

$$\Delta p_{b,\Sigma} = a(\varphi_p) \cdot \Delta p_{b,g} + b(\varphi_p) \cdot \Delta p_{b,p} \quad (30.3)$$

Here, in Equation 30.3, the multipliers,  $a(\varphi_p)$  and  $b(\varphi_p)$ , are functions of the angular configuration of the input shaft, that is, of the angular configuration of the pinion.

The instant value of the total deviation of the base pitch,  $\Delta p_{b,\Sigma}$ , is within the interval:

$$\Delta p_{b,g} - b\Delta p_{b,p} \leq \Delta p_{b,\Sigma} \leq \Delta p_{b,g} + b\Delta p_{b,p} \quad (30.4)$$

This idea of relative displacement (in micrometers) as the cause of a force variation and hence vibration is unusual, since traditionally, an external force such as an out-of-balance rotating component or vibration of the supporting ground is excited to produce a vibration. In gearing, relative displacement between the mating gears generates forces between the teeth and subsequent vibrations through the system.

Once the deviations of the base pitch are measured in both the gear and mating pinion, then each of the components of the total deviation of the base pitch,  $\Delta p_{b,\Sigma}$ , can be corrected so as to keep the base pitches,  $p_{b,g}$  and  $p_{b,p}$ , equal to the operating base pitch,  $p_{b,op}$ . This is important, as it makes clear how much deviations in the tooth flank geometry in a gear and mating pinion contribute to the total deviation in the base pitch. Moreover, it becomes clear if the components, either the gear or pinion, need more improvement to reduce the operating base pitch variation.

Here and below, it is assumed that the total deviation of the base pitches,  $\Delta p_{b,\Sigma}$ , is specified at every instant of time.<sup>†</sup> Moreover, for convenience of the analysis below, it is also assumed that the deviation,  $\Delta p_{b,\Sigma}$ , is always observed in that same slice, and the contact point,  $K$ , does not migrate within the face of the gear pair.

The model of a parallel-axis gear pair simplified in such a way is used below for the purpose of demonstrating one of the root causes of vibration generation and noise excitation in approximate gear pairs.

The variation in the current value of the base pitch causes a corresponding transmission error,  $\Delta\varphi = \Delta\varphi(\varphi_p)$ .

It is necessary to stress here that not all source of noise excitation in a gear pair can be eliminated by means of alterations of the gear design. When gears in a gear pair rotate, point at which the resultant force is applied migrates along the line of action,  $LA$ , and within the face width,  $F_{pa}$ . The variation of the axial component of the resultant force causes vibrations of the housing (panel, membrane, and so forth). Noise caused by the migration of the point of application of the resultant force (axial component of the resultant force) cannot be eliminated by means of an alteration of the gear design.

\* The instant values of the deviations,  $\Delta p_{b,g}$  and  $\Delta p_{b,p}$ , commonly are not known. However, calculations can be performed for the tolerances,  $[\Delta p_{b,g}]$  and  $[\Delta p_{b,p}]$ , for the corresponding deviations.

<sup>†</sup> It is realized here that the actual values of the deviations,  $\delta p_{b,g}$  and  $\delta p_{b,p}$ , are never known. However, corresponding tolerances,  $[\delta p_{b,g}]$  and  $[\delta p_{b,p}]$ , can be set for each of the deviations. In many cases, it is more convenient solving problems using the tolerances for the deviations rather than the actual values of the deviations.

### 30.2 Transmission Error

Gear noise is caused, to a great extent, by the dynamic phenomena in tooth meshing. It can be characterized by transmission error, which is the root cause for vibration generation and noise excitation.

Transmission errors are the most important factor in the generation of gear noise. Transmission errors are errors between the gear teeth. They can be defined in the following way: imagine that the input gear is being driven at an absolutely steady angular velocity. It is hoped that the output gear is rotating at a steady angular velocity as well. Any variation from this steady velocity gives a variation from the correct position of the output, and this is the *transmission error*, which will subsequently generate vibration and noise excitation. More formally:

#### Definition 30.1

*Transmission error is the difference between the angular position that the output shaft of a drive would occupy if the drive were perfect and the actual position of the output.*

In practical terms, the successive angular positions of the output, where the output should be, can be taken. These can be subtracted from the measured output positions to give the error in position. Measurements are made by measuring angular displacements, so the answers appear initially in units of seconds of arc [151].

By definition:

$$TE(t) = r_{b,g}\theta_g(t) - r_{b,p}\theta_p(t) \quad (30.5)$$

where  $r_{b,g}$  and  $r_{b,p}$  are the base pitch radii, and the angles,  $\theta_g(t)$  and  $\theta_p(t)$ , are the angles of rotation of the gear and mating pinion, correspondingly.

When no transmission error occurs and the input shaft rotates steadily [ $\omega_p(t) = \text{const}$ ], the output shaft also rotates steadily [ $\omega_g^{des}(t) = \text{const}$ ], as schematically illustrated in Figure 30.4a. Under the influence of transmission errors, the output shaft does not rotate steadily [ $\omega_g(t) \neq \text{const}$ ]. The period of oscillation of the output shaft is designated as  $C_m$ .

The transmission error for an ideal gear train is almost a linear function of time. It can be represented in the form of a function,  $\varphi_g = (N_g/N_p) \cdot \varphi_p$ . Here,  $N_g$  and  $N_p$  are the number of teeth of the gear and pinion, and  $\varphi_g$  and  $\varphi_p$  are the rotation angles of the gear and the pinion. Due to axis misalignment, the transmission function becomes piecewise almost linearly with the period of the cycle of meshing,  $C_m$ , of a pair of teeth. Due to the jump of the angular velocity at the junction of cycles (see Figure 30.4a) [126], the acceleration approaches an infinitely large value. This causes vibration generation and noise excitation.

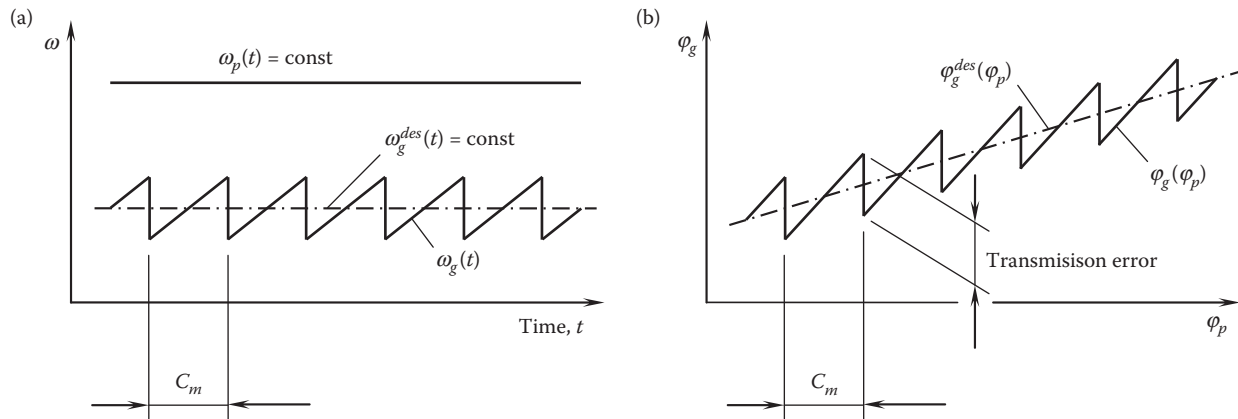


FIGURE 30.4

Rotation of a driver,  $\omega_p(t)$ , and desired,  $\omega_g^{des}(t)$ , and real,  $\omega_g(t)$ , rotations of the driven functions vs. time,  $t$  (a), and desired,  $\varphi_g^{des}(\varphi_p)$ , and real,  $\varphi_g(\varphi_p)$ , transmission functions (b). (Adapted from Radzevich, S.P., *International Journal of Vehicle Noise and Vibration*, Vol. 2, No. 4, pp. 283–291, 2006 [126].)

A desired gear transmission function,  $\varphi_g^{des}(\varphi_p) = a \cdot \varphi_p$ , is a linear function of the angle of rotation of the input shaft,  $\varphi_p$ . Here, the factor  $a = \tan(u_t)$ . The actual gear transmission function,  $\varphi_g = \varphi_g(\varphi_p)$ , can be represented in the form of a piecewise function, as shown in Figure 30.4b.

A steady rotation of the driving pinion cannot be transmitted by the gear pair smoothly to the driven gear if the total deviation of the base pitch,  $\Delta p_{b,\Sigma}$ , is not zero ( $\Delta p_{b,\Sigma} \neq 0$ ). The base pitch error,  $\Delta p_{b,\Sigma}$ , causes a transmission error,  $\Delta\varphi$ . The transmission error,  $\Delta\varphi$ , can be expressed in terms of the total deviation of the base pitch,  $\Delta p_{b,\Sigma}$ .

Refer to Figure 30.5 to express an instant value of the transmission error,  $\Delta\varphi$ , in terms of the total deviation of the base pitch,  $\Delta p_{b,\Sigma}$ .

In the case of a perfect parallel-axes gear pair, the contact point,  $K$ , occupies a certain position within the line of action,  $LA$ . For a specified value of the angle of rotation of the gear,  $\varphi_g$ , the distance,  $PK$ , traveled by the contact point together with the plane of action,  $PA$ , can be determined from  $\Delta PKO_g$ :

$$PK = r_g \frac{\sin \varphi_g}{\cos(\varphi_g - \phi_t)} \quad (30.6)$$

where:

$r_g$  is the radius of the pitch circle of the gear.

$\phi_t$  is the transverse pressure angle in the gear pair.

To derive Equation 30.6, the sine rule was applied to  $\Delta PKO_g$ .

In reality, because the base pitch error is not equal to zero, the gears make contact not at point,  $K$ , but at point  $K^*$  instead. The distance between the points  $K$  and  $K^*$  equals the total deviation of the base pitch,  $\Delta p_{b,\Sigma}$ ; that is, an equality  $KK^* = \Delta p_{b,\Sigma}$  is valid. The deviation,  $\Delta p_{b,\Sigma}$ , is calculated from Equation 30.3.

An additional rotation through an angle,  $\Delta\varphi$ , is caused by the deviation of  $\Delta p_{b,\Sigma}$ . In nature, this additional rotation is equal to the instant value of the transmission error.

In order to determine the angle,  $\Delta\varphi$ , it is necessary to determine the distance,  $K^*O_g$ . This distance can be determined from  $\Delta PK^*O_g$ :

$$K^*O_g = r_g \sqrt{1 + \frac{\sin^2 \varphi_g}{\cos^2(\varphi_g - \phi_t)} - 2 \frac{\sin \varphi_g}{\cos(\varphi_g - \phi_t)} \sin \phi_t} \quad (30.7)$$

To derive Equation 30.7, the cosine rule was applied to  $\Delta PK^*O_g$ .

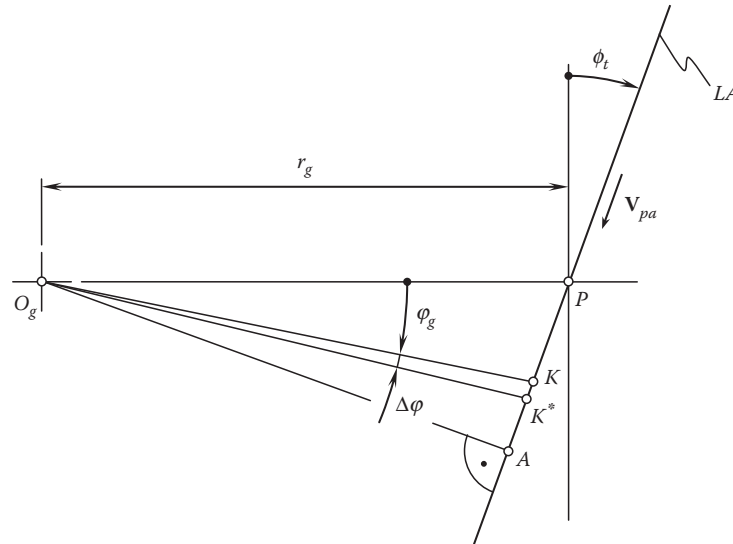


FIGURE 30.5

A schematic for the calculation of the instant value of the transmission error,  $\Delta\varphi$ , in a parallel-axes gear pair.

Then, the rule of sine is applied to  $\Delta PK^* O_g$ :

$$\sin(\varphi_g + \Delta\varphi) = \frac{r_g \sin \varphi_g + \Delta p_{b,\Sigma} \cos(\varphi_g - \phi_t)}{\underbrace{K^* O_g \cos(\varphi_g - \phi_t)}_A} \cos \phi_t \quad (30.8)$$

Ultimately, the angle,  $\Delta\varphi$ , equals:

$$\Delta\varphi = \sin^{-1}(a) - \varphi_g \quad (30.9)$$

For the determination of the distance,  $KO_g$ , another approach can be used. It can be written from  $\Delta PO_g$  that:

$$O_g A = r_g \cos \phi_t \quad (30.10)$$

$$AP = r_g \sin \phi_t \quad (30.11)$$

and then from  $\Delta AKO_g$ :

$$AK = r_g \left( \sin \phi_t - \frac{\sin \varphi_g}{\sin(\varphi_g - \phi_t)} \right) \quad (30.12)$$

Equations 30.10 through 30.12 make possible an expression for the calculation of the distance,  $KO_g$ :

$$KO_g = r_g \frac{\sqrt{[\cos(\varphi_g - \phi_t) - 2 \sin \phi_t \sin \varphi_g] \cos(\varphi_g - \phi_t)}}{\cos(\varphi_g - \phi_t)} \quad (30.13)$$

The determined distance,  $KO_g$  (see Equation 30.13), is used for the derivation of Equation 30.9.

The approach applied for the derivation of Equation 30.9 can also be used for the calculation of the components,  $\Delta\varphi_g$  and  $\Delta\varphi_p$ , of the transmission error,  $\Delta\varphi$ . The components,  $\Delta\varphi_g$  and  $\Delta\varphi_p$ , are contributed by the gear and pinion, correspondingly.

Another approach can be used for the derivation of Equation 30.9. The transmission error,  $\Delta\varphi$ , can be expressed in terms of the total deviation of the base pitch,  $\Delta p_{b,\Sigma}$ , and the base diameters of a gear and mating pinion in a gear pair.

As the driving pinion rotates steadily, and the distance,  $KK^*$ , is specified, then this distance is equivalent to an additional rotation of the driving pinion through an angle,  $\Delta\varphi_p$ :

$$\Delta\varphi_p = \frac{KK^*}{r_{b,p}} \quad (30.14)$$

Taking into account that  $\Delta\varphi_g = \Delta\varphi_p/u$  (here  $u$  is the gear ratio of the gear pair), Equation 30.14 immediately returns an expression for the angular deviation,  $\Delta\varphi$ :

$$\Delta\varphi = \Delta\varphi_p = \frac{\Delta p_{b,\Sigma}}{u \cdot r_{b,p}} \quad (30.15)$$

In this case, there is no need to determine the deviation,  $\Delta\varphi$ , using the rule of sine for this purpose.

The rotation of the gear through an angle,  $\Delta\varphi$ , causes an additional rotation of the gear. This additional rotation can be represented by the rotation vector,  $\omega_{bpv}(\varphi_g)$ . The rotation vector,  $\omega_{bpv}(\varphi_g)$ , is referred to as the *base pitch variation rotation*,  $\omega_{bpv}(\varphi_g)$ .

The resultant rotation vector of the gear is:

$$\mathbf{\omega}_\Sigma(\varphi_g) = \mathbf{\omega}_g + \mathbf{\omega}_{bpv}(\varphi_g) \quad (30.16)$$

The transmission error is an integral parameter of accuracy of the gear pair. When only a transmission error is specified, it is not clear what has to be done to keep the base pitches equal, that is, whether a gear or mating pinion has to be corrected, and to what extent.

It seems ridiculous that a 1-mm module (25 DP) gear less than an inch in diameter will have roughly the same transmission error as a 25-mm module (1 DP) gear of 3 m diameter of the same quality, but this is surprisingly close to what happens in practice. This unexpected constant size of errors is liable to cause problems in the future with the current trend toward micromechanics. If a gear tooth is only 20  $\mu\text{m}$  tall, the base pitch is about 20  $\mu\text{m}$ , but errors of 2  $\mu\text{m}$  in pitch or profile are still likely with corresponding transmission errors, so that a speed variation of 10% becomes possible.

### 30.3 Influence of Load Variation on Noise Excitation in a Gear Pair

Unfortunately, transmission errors are not the only cause of vibration generation and noise excitation. A variation of the instant (equivalent) force, that is, of its magnitude; coordinates of a point where the force is applied (especially in gears that feature a low tooth count); and the orientation, are root causes of vibration generation and noise excitation. The variation of the loading is transmitted to the housing, which works like panels, and so forth.

Helical gears, for example, are subjected to variation of the force between the gears. They are sensitive to force variation in particular.

#### 30.3.1 Variation of the Axial and Radial Forces

Consider a gear pair that has a nominal contact ratio of  $m_t$ . At a particular instant of time, the lengths of the theoretical lines of contact get the two extreme positions schematically depicted in [Figure 30.6](#).

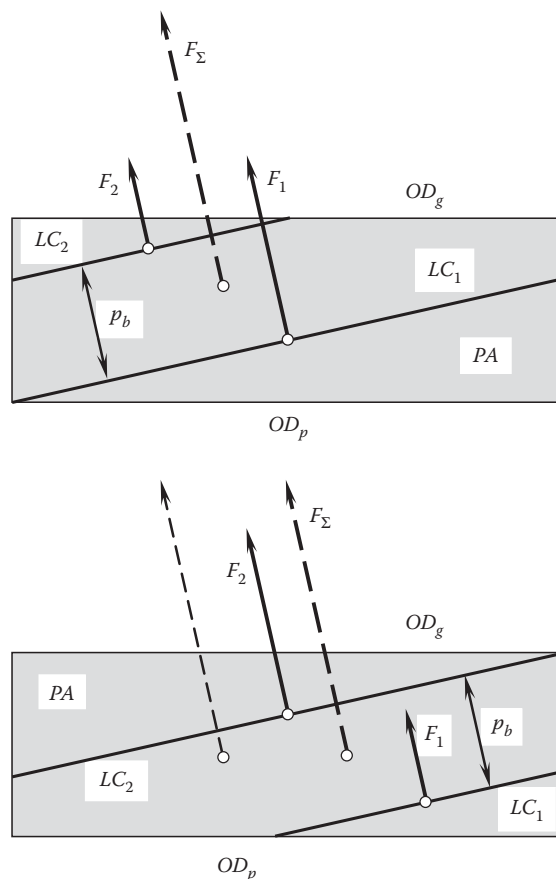
These show the plane of action for the worst case with a correct face width of an axial pitch and a small helix angle. In the case under consideration, any end relief effects or tip relief effects are ignored. A constant loading along the contact line is assumed. Practical teeth tend to give slightly larger effects.

The extreme position of the center of action of the resultant force is determined by taking moments about one end and is approximately  $[(m_t - 1)^2 + 1]/2m_t$  from one end. This has a minimum when the total contact ratio,  $m_t$ , is equal to  $\sqrt{2}$  and the center of force oscillates about 0.086 of the face width on either side of the center of the face.

There is a corresponding radial force variation at the bearing housings on the order of 8% of the mean value when the gears are well supported by close shafts or less if the supporting shafts are long [\[151\]](#).

#### 30.3.2 Influence of the Contact Ratio

The influence of the contact ratio on the gear transmission function,  $\varphi_g = \varphi_g(\varphi_p)$ , is more or less clear as long as the consideration relates to an elementary gear drive (that is, to a gear-to-pinion mesh) with a contact ratio exactly equal to  $u_t = 1$  ([Figure 30.7](#)). However, in reality, the contact ratio is greater than one ( $u_t > 1$ ). Because of this, during certain periods of meshing, not one but more pairs of teeth are engaged in mesh simultaneously. Generally speaking, the piecewise linear functions of transmission errors for distinct pairs of contacting teeth do not coincide with each other. The cycle of meshing,  $c_m^{(i)}$ , for the  $i$ th pair of teeth is shifted in relation to the previous/consequent cycle of meshing,  $c_m^{(i\pm 1)}$ , in the direction of the  $\varphi_g$ -axis at a certain distance,  $\Delta C_m$ . The actual value of the shift,  $\Delta C_m$ , depends on the actual value of the contact ratio,  $u_t$ . The transmission functions,  $Tr_f^{(i)}$  and  $Tr_f^{(i\pm 1)}$ , make it possible to compose the resultant transmission function,  $Tr_f^{(\Sigma)}$ , for the elementary gear drive that has a total contact ratio  $u_t > 1$ . In the same way, the resultant transmission function,  $Tr_f^{(\Sigma)}$ , can be composed (see [Figure 30.7](#)) for any actual value of contact ratio that exceeds  $u_t > 2$  [\[126\]](#).

**FIGURE 30.6**

Extreme positions of the lines of contact,  $LC$ , in the plane of action,  $PA$ , showing how the forces at the centers of each section of the line of contact give a resultant force whose position varies.

Figure 30.7 shows that for the case when the contact ratio is greater than one,  $u_t > 1$ , the resultant transmission function,  $Tr_f^{(\Sigma)}$ , significantly differs from that for the case when the equality  $u_t = 1$  is valid. The situation gets more severe when there are no common multipliers in the gear and pinion tooth numbers,  $N_g$  and  $N_p$  [126].

The impact of transmission errors on noise excitation is commonly considered from the geometrical and kinematical points of view. No tooth flank wear is incorporated into the analysis.

The most reliable way to reduce noise excitation is to ensure equality of the operating base pitch of a gear to the operating base pitch of a mating pinion, and keep both of them equal to the operating base pitch of the gear pair. Once the base pitches are equal to one another, the gear mesh generates no vibration and produces no noise excitation.

### 30.4 On the Possibility of Prediction of Noise Excitation in a Gear Pair

The problem of analytical prediction of noise excitation in a gear pair falls into three levels/iterations (parallel-axes gearing is considered below as an example for all three iterations):

- *The first level of iteration:* The geometry and configuration of a desired line of contact,  $LC_{des}$ , are specified within the plane of action,  $PA$ . When the gears rotate, the transverse pressure angle,  $\phi_t$ , in the gear pair retains a constant value. Because of variation of the tooth flank geometry of a gear,  $\mathcal{G}$ , and mating



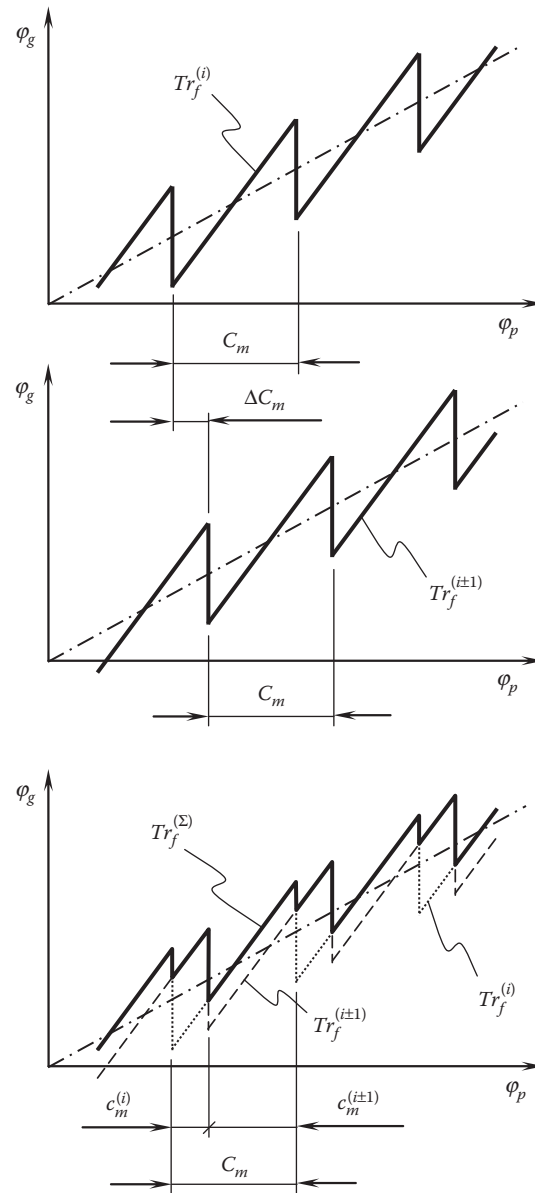


FIGURE 30.7

Transmission function as a superposition of a linear function,  $\varphi_g^{des}(\varphi_p)$ , and piecewise linear functions for the case when the total contact ratio  $m_t > 1$ . (Adapted from Radzevich S.P., *International Journal of Vehicle Noise and Vibration* Vol. 2, No. 4, pp. 283–291, 2006 [126].)

pinion,  $\mathcal{P}$ , the lines of intersection,  $LC_g$  and  $LC_p$ , of the tooth flanks,  $\mathcal{G}$  and  $\mathcal{P}$ , by the plane of action,  $PA$ , differ from the desired line of contact,  $LC_{des}$ . The lines,  $LC_g$  and  $LC_{des}$ , and the lines,  $LC_p$  and  $LC_{des}$ , make contact at points,  $K_g$  and  $K_p$ , correspondingly. As considered in this section, a gap exists between the lines of intersection,  $LC_g$  and  $LC_p$ . The gap equals the closest distance of approach between the lines of intersection,  $LC_g$  and  $LC_p$ , and in nature is equal to the variation of the base pitch in a gear,  $\Delta p_{b,g}$ , and mating pinion,  $\Delta p_{b,p}$ ; that is, the gap equals the algebraic summa ( $\Delta p_{b,g} + \Delta p_{b,p}$ ).

Physically, the gap cannot exist, as the gears transmit a load. Zero gap is observed between the gear,  $\mathcal{G}$ , and mating pinion,  $\mathcal{P}$ , tooth flanks when the gears transmit power.

As the input shaft rotates steadily with a constant angular velocity,  $\omega_p$ , then the driven shaft must make an additional turn through an angle,  $\Delta\varphi_g$ , to bridge the gap. The angle,  $\Delta\varphi_g$ , can be expressed in terms of the distance,  $\Delta p_{b,g} + \Delta p_{b,p}$ , and in terms of the parameters of configuration of the lines of intersection,  $LC_g$  and  $LC_p$ , by the plane of action,  $PA$ .

The variation,  $\Delta p_{b,g} + \Delta p_{b,p}$ , of the base pitch is the root cause of excessive noise excitation in a gear pair. An analysis like that above can be performed for intersected-axes gear pairs, as well as for crossed-axes gear pairs.

### Conclusion 30.1

*The deviations measured within the plane of action, PA, contribute the most to variation of the base pitch, as well as to the transmission error.*

- *The second level of iteration:* It is assumed in the first level of iteration that the condition of conjugacy of the transverse sections of a gear and mating pinion is fulfilled for all points within the line of intersection,  $LC_g$ , and all the corresponding points within the line of intersection,  $LC_p$ . For more accurate calculations, the points at which the condition of conjugacy of the gear and mating pinion transverse tooth profiles should be considered within spatial curves both for the gear and the pinion.

As the input shaft rotates steadily with a constant angular velocity,  $\omega_p$ , then the driven shaft must make an additional turn through an angle,  $\Delta\phi_g$ , to bridge the gap. The angle,  $\Delta\phi_g$ , can be expressed in terms of the distance ( $\Delta p_{b,g} + \Delta p_{b,p}$ ) and in terms of the parameters of configuration of the lines of intersection,  $LC_g$  and  $LC_p$ , by the plane of action, PA.

The variation ( $\Delta p_{b,g} + \Delta p_{b,p}$ ) of the base pitch is the root cause of excessive noise excitation in a gear pair. An analysis like the above can be performed for intersected-axes gear pairs, as well as for crossed-axes gear pairs.

### Conclusion 30.2

*The deviations perpendicular to the plane of action, PA, contribute less to the variation of the base pitch, as well as to the transmission error (projections onto the plane of action, PA).*

- *The third level of iteration:* Finally, as the desired line of contact,  $LC_{des}$ , travels together with the plane of action, PA, the actual value of the transverse pressure angle,  $\phi_t$ , could vary depending on the actual angular configuration of the gear and pinion in relation to one another.

As the input shaft rotates steadily with a constant angular velocity,  $\omega_p$ , then the driven shaft must make an additional turn through an angle,  $\Delta\phi_g$ , to bridge the gap. The angle,  $\Delta\phi_g$ , can be expressed in terms of the distance,  $\Delta p_{b,g} + \Delta p_{b,p}$ , and in terms of the parameters of configuration of the lines of intersection,  $LC_g$  and  $LC_p$ , by the plane of action, PA.

The variation,  $\Delta p_{b,g} + \Delta p_{b,p}$ , of the base pitch is the root cause of excessive noise excitation in a gear pair. An analysis like the above can be performed for intersected-axes gear pairs, as well as for crossed-axes gear pairs.

### Conclusion 30.3

*The deviations perpendicular to the plane of action, PA, contribute less to the variation of the base pitch, as well as to the transmission error (projections onto the plane of action, PA).*

Lots of room is available for further developments in this particular area of gearing.



# Taylor & Francis

Taylor & Francis Group

<http://taylorandfrancis.com>

## *Design Peculiarities of Perfect and Almost Perfect Gears*

This chapter deals with perfect and almost perfect gear pairs. Manufacture of gears for perfect and almost perfect gear pairs is almost the same as that for conventional gear pairs. Finishing gear and mating pinion tooth flanks is the only principal feature in production of gears for perfect and almost perfect gearings different from that for conventional gearings. Below, this feature is illustrated by a few examples in finishing gears for crossed-axes perfect and almost perfect gearings.

### 31.1 Design Peculiarities of Gears for *R*-Gearing

In order to develop a crossed-axes gearing with the desirable properties, the kinematics of  $C_a$ -gearing is thoroughly investigated. It is shown that the tooth flanks of the gear and mating pinion can be generated as loci of the desirable line of their contact considered in corresponding reference systems associated with the gear and pinion. Crossed-axes gearing of the proposed design\* is referred to as *R*-gearing. *R*-gearing is the only type of perfect crossed-axes gearing with a line contact between the tooth flanks of a gear and mating pinion. Parallel-axes involute gearing (Euler, 1760) and intersected-axes gearing with spherical involute tooth flank geometry (Grant, 1889) represent reduced cases of *R*-gearing. The shaft angle is either zero or  $\Sigma = 180^\circ$  in the first case. In the second case, the center distance is zero. The ability to transmit a rotation smoothly along with a high-power density are the two main advantages of *R*-gearing.

#### 31.1.1 Essence of the Kinematics in Crossed-Axes Gearing

The kinematics and geometry of perfect crossed-axes gearing (or just  $C_a$ -gearing for simplicity) with a line contact between the tooth flanks of the gear,  $\mathcal{G}$ , and mating pinion,  $\mathcal{P}$ , is discussed immediately below.

Transmission and transformation of a rotation from a driving shaft to a driven shaft is the main purpose of implementation of crossed-axes gears. Both the input rotation and the output rotation can be easily represented by corresponding rotation vectors,<sup>†</sup>  $\omega_g$  and  $\omega_p$  (Figure 31.1). The rotation vectors,  $\omega_g$  and  $\omega_p$ , are along the gear and the pinion center lines,  $O_g$  and  $O_p$ .

A vector,  $\omega_{pl} = \omega_p - \omega_g$ , analytically describes the instant rotation of the pinion in relation to the motionless gear. The axis of instant rotation,  $P_{lr}$ , is along the vector,  $\omega_{pl}$ .

A gear cone angle,  $\Sigma_g$ , is formed by the rotation vectors,  $\omega_g$  and  $\omega_{pl}$ . This angle equals:

$$\Sigma_g = \angle(\omega_g, \omega_{pl}) \quad (31.1)$$

A mating pinion cone angle,  $\Sigma_p$ , is formed by the rotation vectors,  $\omega_p$  and  $\omega_{pl}$ . This angle equals:

$$\Sigma_p = \angle(\omega_p, \omega_{pl}) \quad (31.2)$$

A crossed-axes angle,  $\Sigma$ , is formed by the rotation vectors,  $\omega_g$  and  $\omega_p$ . This angle equals:

$$\Sigma = \angle(\omega_g, \omega_p) \quad (31.3)$$

\* Patent pending.

<sup>†</sup> It is instructive to note here that rotations are not vectors in nature. Therefore, special care needs to be undertaken when treating rotations as vectors.

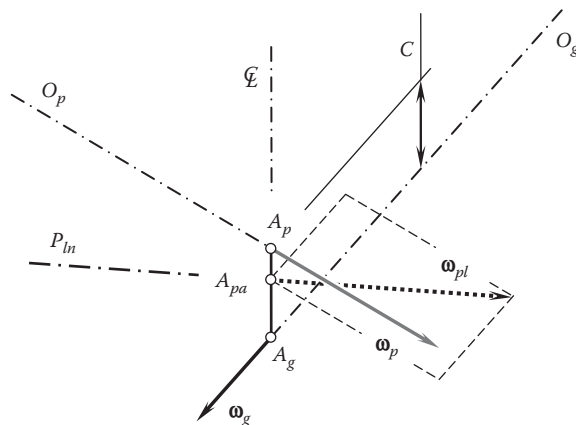


FIGURE 31.1

Kinematics of a crossed-axes gear pair.

The actual values of the angles,  $\Sigma_g$ ,  $\Sigma_p$  and  $\Sigma$ , are predetermined by the magnitudes and the actual configuration of the rotation vectors,  $\omega_g$  and  $\omega_p$ .

### 31.1.2 Base Cones

A *pulley-and-belt* analogy can be constructed for a crossed-axes gearing. For this purpose, two base cones are associated with the gear and pinion. This concept is schematically illustrated in Figure 31.2. The schematic shown in Figure 31.2 is constructed starting from the rotation vectors,  $\omega_g$  and  $\omega_p$ , of the gear and pinion.

The vector of instant rotation,  $\omega_{pl}$ , is the vector through an apex,  $A_{pa}$ , within the center distance,  $C$ . The endpoints of the straight line segment,  $C$ , are labeled as  $A_g$  and  $A_p$ .  $A_g$  is the point of intersection of the centerline,  $\mathcal{L}$ , and the gear axis of rotation,  $O_g$ .  $A_p$  is the point of intersection of the centerline,  $\mathcal{L}$ , and the pinion axis of rotation,  $O_p$ .

The plane-of-action apex,  $A_{pa}$ , is at a distance,  $r_g$ , from the axis of rotation,  $O_g$ . At that same time, the point,  $A_{pa}$ , is at a distance,  $r_p$ , from the axis of rotation,  $O_p$ . The following expression,  $r_g + r_p = C$ , is true where the radii  $r_g$  and  $r_p$  are signed values.

The plane of action,  $PA$ , is a plane through the axis of instant rotation,  $P_{ln}$ . Let us assume that the plane of action rotates about the gear axis of rotation,  $O_g$ . The base cone of the gear is an envelope to consecutive positions of  $PA$  in such a rotation. Similarly, the base cone of the pinion is constructed.

The plane of action,  $PA$ , is in tangency with the base cones of the gear and the pinion. Due to that, the plane of action,  $PA$ , makes a certain transverse pressure angle,  $\phi_{t,\omega}$ , in relation to the  $P_{ln}$ -plane. The pressure angle,  $\phi_{t,\omega}$ , is measured within the  $C_{ln}$ -plane.

The plane of action can be viewed as a flexible zero-thickness film. The film is free to wrap on and unwrap from the base cones of the gear and the pinion. The plane of action,  $PA$ , is not allowed to bend about an axis perpendicular to the plane,  $PA$ .

As the axis of instant rotation,  $P_{ln}$ , and the axes of rotations of the gear,  $O_g$ , and the pinion,  $O_p$ , cross one another, the pure rolling of the base cones of the gear and pinion over the pitch plane,  $PA$ , is not observed. Instead, rolling together with sliding of  $PA$  over the base cones is observed.

### 31.1.3 Tooth Flanks in Perfect Crossed-Axes Gears

The conjugate tooth flanks\* of a gear and mating pinion in a crossed-axes gear pair are in line contact with one another. As the gears rotate, the line of contact travels with respect to several reference systems associated with: (a) the gear, (b) the pinion, and (c) the housing. The tooth flank of the gear,  $G$ , can be construed as loci of consecutive positions of the desirable line of contact,  $LC_{des}$ , in its motion in relation to the reference system,  $X_gY_gZ_g$ , associated with the gear. Similarly, the tooth flank of the pinion,  $P$ , can be represented as loci of consecutive positions of that same line of contact,  $LC_{des}$ , in its motion in relation to the reference system,  $X_pY_pZ_p$ , associated

\* Reversibly-enveloping surfaces (or just  $R_e$ -surfaces for simplicity) is the other term for conjugate tooth flanks [115].

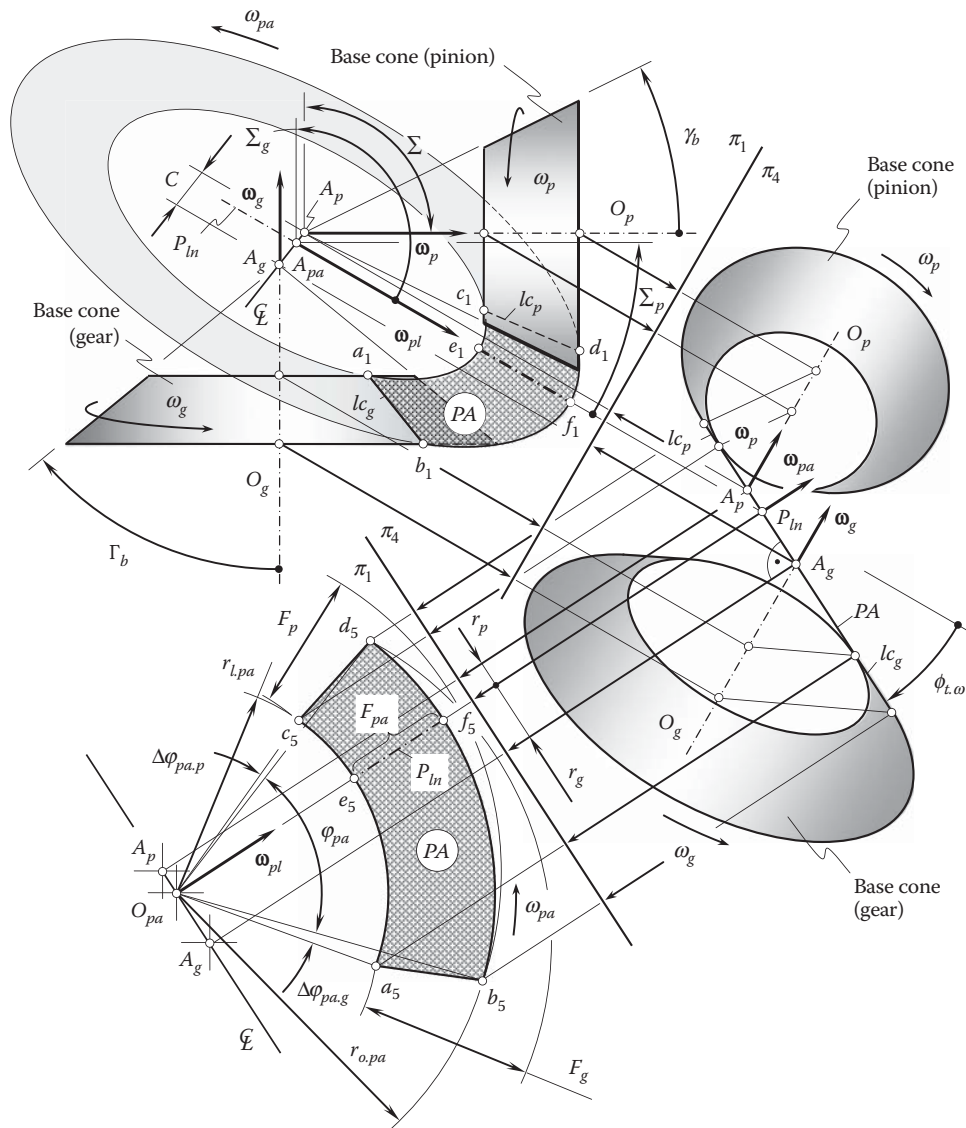


FIGURE 31.2

Base cones and the plane of action,  $PA$ , in an orthogonal crossed-axis gear pair.

with the pinion. Ultimately, loci of consecutive positions of that same line of contact,  $\varphi_{lc}$ , in its motion in relation to a stationary reference system associated with the housing,  $X_h Y_h Z_h$ , represent the surface of action. Therefore, once the line of contact is known, the kinematics of a crossed-axes gearing (see Figure 31.2) can be employed for the derivation of an analytical representation of the tooth flank of the gear,  $G$ , and the pinion,  $P$ . For this purpose, several auxiliary reference systems are commonly used. A Cartesian coordinate system,  $X_r Y_r Z_r$ , associated with the plane of action (see Figure 31.3) is one of the auxiliary reference systems.

In a local Cartesian reference system,  $x_{lc} y_{lc} z_{lc}$ , associated with the plane of action,  $PA$ , and centered at the center,  $O_{lc}$ , of the circular arc of the radius  $R_{lc}$ , the position vector of a point,  $\mathbf{r}_{des}^{(lc)}$ , of the desirable line of contact,  $LC_{des}$ , can be analytically described by an expression in the form (see Figure 31.4):

$$\mathbf{r}_{des}^{(lc)}(\varphi_{lc}) = \begin{bmatrix} R_{lc} \cos \varphi_{lc} \\ R_{lc} \sin \varphi_{lc} \\ 0 \\ 1 \end{bmatrix} \quad (31.4)$$

where  $\varphi_{lc}$  is the angular parameter of the desired line of contact,  $LC_{des}$ .

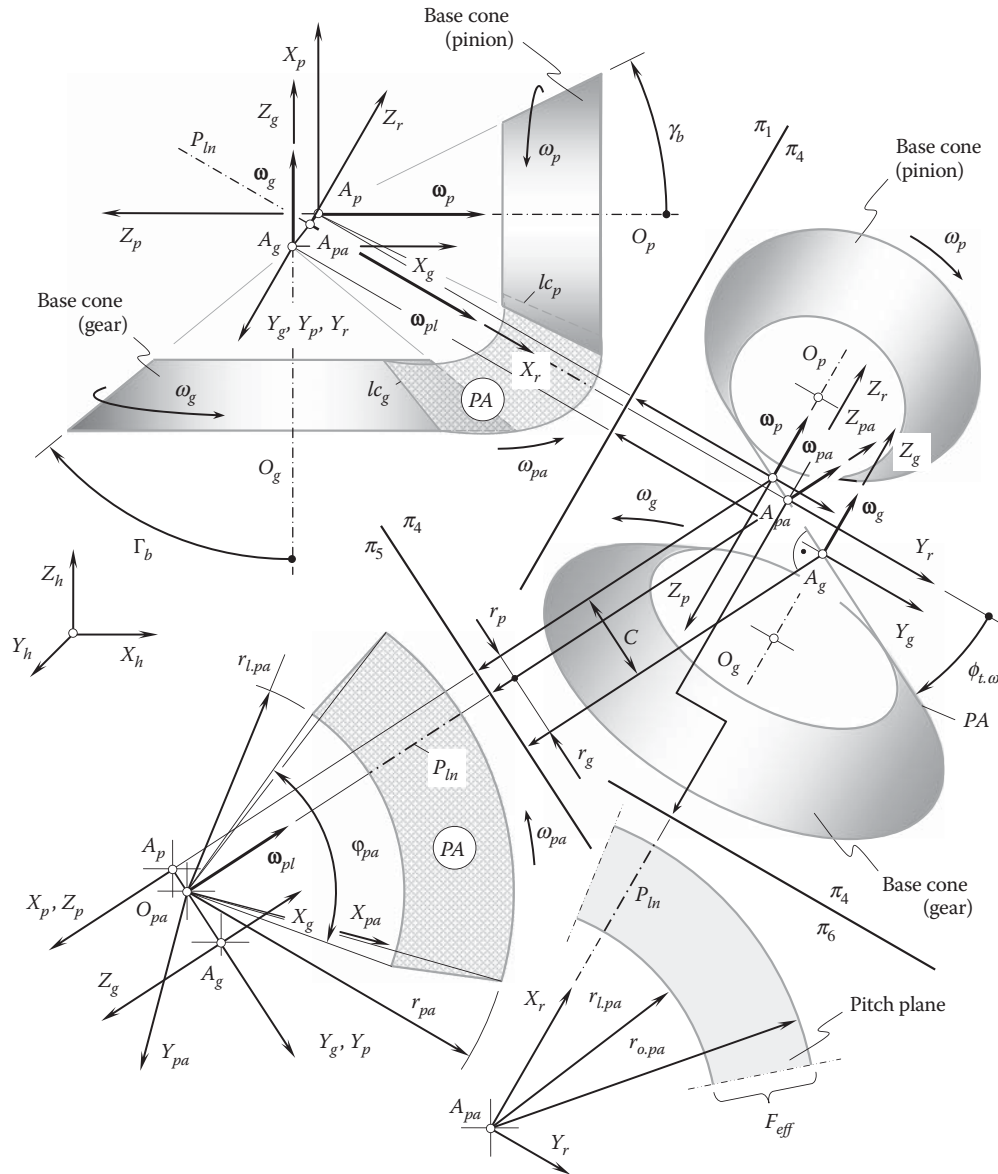


FIGURE 31.3

Reference systems that are used for the derivation of an analytical expression for a gear tooth flank,  $\mathcal{G}$ , and a pinion tooth flank,  $\mathcal{P}$ , for a crossed-axis gear pair.

In a reference system  $X_{pa}Y_{pa}Z_{pa}$ , the position vector of a point,  $\mathbf{r}_{des}^{(pa)}$ , of the desirable line of contact,  $LC_{des}$ , can be analytically described by an equation:

$$\mathbf{r}_{des}^{(pa)}(\varphi_{lc}) = \underbrace{\text{Tr}[(r_{w,pa} - R_{lc} \sin \psi_{lc}), X] \cdot \text{Tr}(R_{lc} \cos \psi_{lc}, Y)}_{\mathbf{Rs}(lc \mapsto pa)} \cdot \mathbf{r}_{des}^{(lc)}(\varphi_{lc}) \quad (31.5)$$

where  $\text{Tr}[(r_{w,pa} - R_{lc} \sin \psi_{lc}), X]$  and  $\text{Tr}(R_{lc} \cos \psi_{lc}, Y)$  are the standard operators of the translations along the coordinate axes  $X$  and  $Y$ , correspondingly. Standard formulae (see Appendix D) are used for the calculation of these operators. The interested reader may wish to try composing the operators of translation as well as the operators of rotation,  $\mathbf{Rt}(\varphi \mapsto X)$ , used below on his/her own.  $\mathbf{Rs}(lc \mapsto pa)$  is the operator of the resultant coordinate system transformation, that is, the operator of the transition from  $x_{lc}y_{lc}z_{lc}$  to  $X_{pa}Y_{pa}Z_{pa}$ .



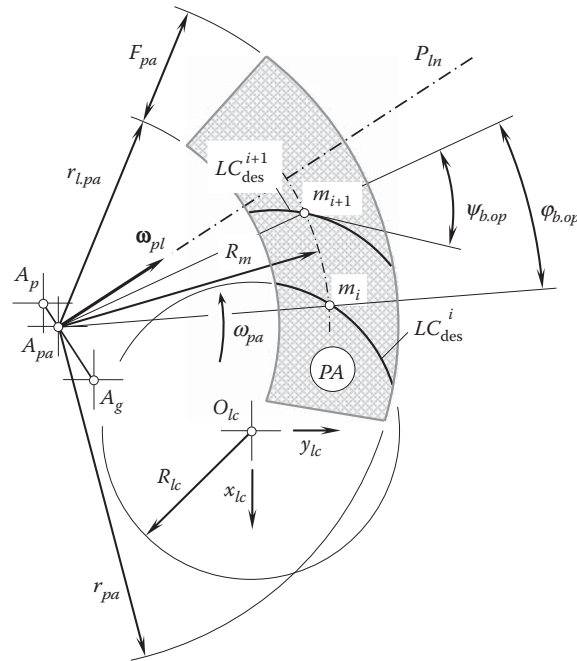


FIGURE 31.4

Configuration of the desirable line of contact,  $LC_{des}$ , in the form of an arc of a circle within the plane of action,  $PA$ , in a crossed-axes gear pair.

Ultimately, it can be shown that in the reference system,  $X_{pa}Y_{pa}Z_{pa}$ , associated with the plane of action, the position vector of a point,  $\mathbf{r}_{des}^{(pa)}$ , can be written in the form:

$$\mathbf{r}_{des}^{(pa)}(\varphi_{lc}) = \mathbf{Rs}(lc \mapsto pa) \cdot \mathbf{r}_{des}^{(lc)}(\varphi_{lc}) = \begin{bmatrix} R_{lc} \cos \varphi_{lc} + r_{w.pa} + R_{lc} \sin \psi_{lc} \\ R_{lc} \sin \varphi_{lc} - R_{lc} \cos \psi_{lc} \\ 0 \\ 1 \end{bmatrix} \quad (31.6)$$

When the gears rotate, the desirable line of contact,  $LC_{des}$ , travels with respect to a reference system,  $X_gY_gZ_g$ , associated with the gear. Simultaneously,  $LC_{des}$  travels with respect to a reference system,  $X_pY_pZ_p$ , associated with the pinion. Therefore, the gear tooth flank,  $\mathcal{G}$ , can be viewed as loci of consecutive positions of the line of contact,  $LC_{des}$ , in the reference system,  $X_gY_gZ_g$ . Similarly, the pinion tooth flank,  $\mathcal{P}$ , can be viewed as loci of consecutive positions of the line of contact,  $LC_{des}$ , in the reference system  $X_pY_pZ_p$ . To derive equations for the position vectors of a point of the gear tooth flank,  $\mathbf{r}_g$ , and the pinion tooth flank,  $\mathbf{r}_p$ , the operators,  $\mathbf{Rs}(pa \mapsto g)$  and  $\mathbf{Rs}(pa \mapsto p)$ , of transition from the reference system  $X_{pa}Y_{pa}Z_{pa}$  to the reference systems  $X_gY_gZ_g$  and  $X_pY_pZ_p$  are used:

$$\mathbf{r}_g(\varphi_{lc}, \varphi_g) = \mathbf{Rs}(pa \mapsto g) \cdot \mathbf{r}_{des}^{(lc)}(\varphi_{lc}) \quad (31.7)$$

$$\mathbf{r}_p(\varphi_{lc}, \varphi_p) = \mathbf{Rs}(pa \mapsto p) \cdot \mathbf{r}_{des}^{(lc)}(\varphi_{lc}) \quad (31.8)$$

The operator of the resultant coordinate system transformation,  $\mathbf{Rs}(pa \mapsto g)$ , is a function of the angle of rotation of the gear,  $\varphi_g$ , and the angular parameter  $\varphi_{lc}$ . The operator of the resultant coordinate system transformation,  $\mathbf{Rs}(pa \mapsto p)$ , is a function of the angle of rotation of the pinion,  $\varphi_p$ , and the angular parameter  $\varphi_{lc}$ .

Paths of contact,  $P_c$ , are circular arcs through points of the desirable line of contact,  $LC_{des}$ . All the paths of contact are within the plane of action,  $PA$ , and are centered at the plane-of-action apex,  $A_{pa}$ . It can be construed that paths of contact lie on spheres,\* all of which are centered at the plane-of-action apex,  $A_{pa}$ .

\* Because the paths of contact in crossed-axes gearings lie on spheres, crossed-axes gearings can be called *spherical gearings*. This causes confusion because engagement in mesh in intersected-axes gearings is also observed on spheres. Therefore, the terms *intersected-axes gearing* and *crossed-axes gearing* are preferred to the ambiguous term *spherical gearing*.

At every instant of time, the instant line of action,  $LA_{inst}$ , is a straight line tangent to the path of contact at its corresponding point. All the instant lines of action intersect the pitch line,  $P_{ln}$ . In this way, the condition of conjugacy is met.

The discussed approach for the determination of the geometry of the gear tooth flank,  $\mathcal{G}$ , and the pinion tooth flank,  $\mathcal{P}$ , is based on the generation of the tooth flanks in the form of a family of consecutive positions of the line of contact,  $LC$ , that travels together with the plane of action,  $PA$ . This approach does not require in specification of the tooth flanks in the form of enveloping surfaces to consecutive positions of the generating basic rack. This means that the proposed method for the generation of the tooth flanks,  $\mathcal{G}$  and  $\mathcal{P}$ , does not require implementation of the elements of the theory of enveloping surfaces. This is a significant advantage of the disclosed method for the generation of tooth flank,  $\mathcal{G}$ , of the gear and tooth flank,  $\mathcal{P}$ , of the pinion in an intersected-axes gearing.

The derived equations for the gear tooth flank,  $\mathcal{G}$ , as well as for the pinion tooth flank,  $\mathcal{P}$ , can be used as reference surfaces (datum surfaces) when (a) designing, (b) machining, and (c) inspecting gears for a crossed-axes gearing that have *line contact* of the tooth flanks,  $\mathcal{G}$  and  $\mathcal{P}$ , of the gear and pinion. They are constructed on the premise of the describing (and not enveloping) principle of surface generation.

Crossed-axes gearings that have tooth flanks of the proposed geometry are the most general type of gearing that features line contact between the tooth flanks,  $\mathcal{G}$  and  $\mathcal{P}$ . In a particular case, when the center distance is reduced to zero ( $C = 0$ ), the  $C_a$ -gearing of the proposed geometry simplifies to  $I_a$ -gearing that has line contact of the tooth flanks. Under another scenario, that is, when the crossed-axes angle is equal either 0 or  $\pi$ , the  $C_a$ -gearing of the proposed geometry simplifies to  $P_a$ -gearing that features line contact of the tooth flanks.

The desirable geometry of contact of tooth flanks of the gear and pinion,  $\mathcal{G}$  and  $\mathcal{P}$ , in  $R$ -gearing can be specified in the stage of analysis of the shape and configuration of the line of contact,  $LC$ , within the plane of action,  $PA$ . The indicatrix of conformity,  $Cnf_R(\mathcal{G}/\mathcal{P})$ , at a point of contact of the tooth flanks,  $\mathcal{G}$  and  $\mathcal{P}$  (see Appendix E), can be expressed in terms of the shape and configuration of the line of contact. Ultimately, those parameters of the shape and configuration of the line of contact are selected under which the minimum diameter of the indicatrix of conformity,  $Cnf_R(\mathcal{G}/\mathcal{P})$ , is as small as possible.

Crossed-axes gearing, for which the tooth flanks of the gear and pinion are generated as loci of consequent positions of the line of contact,  $LC$ , that travels together with the plane of action,  $PA$ , is a novel type of gearing. This novel type of gearing ensures line contact of the tooth flanks of the gear and pinion. This gearing is referred to as  $R$ -gearing.

### 31.2 Permissible Simplification: Design Peculiarities of Gears for $R_{sp}$ -Gearing

A novel design\* of precision gears insensitive to axis misalignment (as well as other sources of linear and angular displacement of tooth flanks,  $\mathcal{G}$  and  $\mathcal{P}$ , of a gear and mating pinion from their desired configuration) is disclosed below [135].

For the derivation of an equation of the tooth flanks,  $\mathcal{G}$  and  $\mathcal{P}$ , an equation of the line of contact,  $LC$ , is used. Initially, this equation is commonly given in a reference system,  $X_{lc}Y_{lc}Z_{lc}$ , associated with the plane of action,  $PA$ . In order to convert the equation of the line of contact,  $LC$ , to a corresponding equation of the gear tooth flank,  $\mathcal{G}$ , as well as to a corresponding equation of the pinion tooth flank,  $\mathcal{P}$ , operators of coordinate system transformation are used. To compose the required operators of the coordinate system transformation,  $\mathbf{Rs}(LC \rightarrow \mathcal{G})$  and  $\mathbf{Rs}(LC \rightarrow \mathcal{P})$ , the schematic depicted in Figure 31.5 is helpful.

Then, position vector  $\mathbf{r}_g$  of a point of the gear tooth flank,  $\mathcal{G}$ , can be expressed by the equation:

$$\mathbf{r}_g = \mathbf{Rs}(LC \rightarrow \mathcal{G}) \cdot \mathbf{r}_{lc} \quad (31.9)$$

\*  $R_{sp}$ -Gearing Insensitive to Axes Misalignment and Other Displacement and Methods of Producing Gears. S.P. Radzevich, International Application Number PCT/US 038753, International Filing Date: May 20, 2014, International Publication Number 2014/189903 A1, Int. Pat. Classification F16H 1/26 (2006.01), Priority Data: 13/900,946, May 23, 2013, 34 pages.

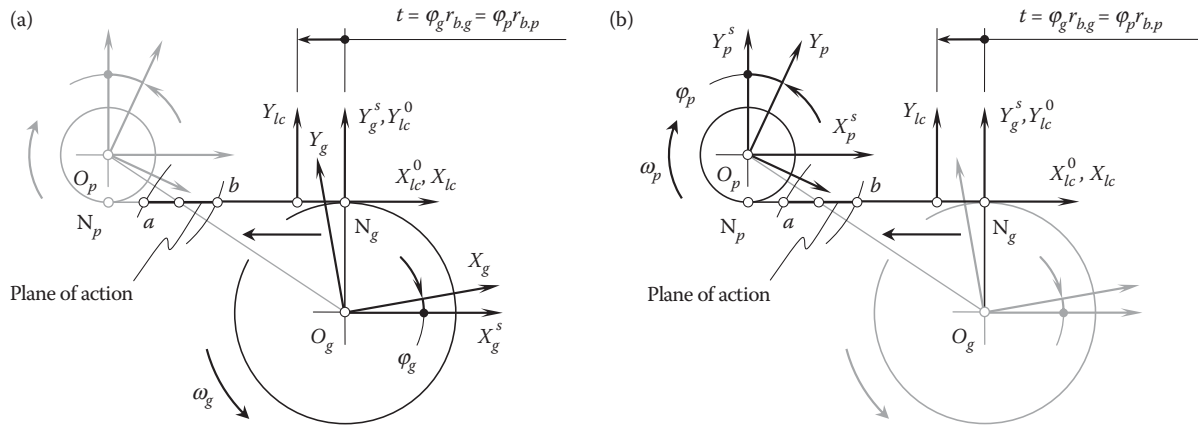


FIGURE 31.5

Applied reference systems associated with a gear (a), and with a mating pinion (b).

Similarly, position vector  $\mathbf{r}_p$  of a point of the pinion tooth flank,  $\mathcal{P}$ , can be expressed by the equation:

$$\mathbf{r}_p = \mathbf{Rs}(LC \rightarrow \mathcal{P}) \cdot \mathbf{r}_{lc} \quad (31.10)$$

Composing operators of the coordinate system transformation is a routine procedure (see Appendix D).

The matrices  $\mathbf{Rs}(LC \rightarrow \mathcal{G})$  and  $\mathbf{Rs}(LC \rightarrow \mathcal{P})$  of the resultant coordinate system transformation can be composed as product of certain number of the operators  $\mathbf{Tr}(a_x, X)$ ,  $\mathbf{Tr}(a_y, Y)$ ,  $\mathbf{Tr}(a_z, Z)$ , and  $\mathbf{Rt}(\varphi_x, X)$ ,  $\mathbf{Rt}(\varphi_y, Y)$ ,  $\mathbf{Rt}(\varphi_z, Z)$  of elementary coordinate system transformation.

For the analytical description of translation along the coordinate axes, the operators of translation,  $\mathbf{Tr}(a_x, X)$ ,  $\mathbf{Tr}(a_y, Y)$ , and  $\mathbf{Tr}(a_z, Z)$ , are used. The operators yield matrix representations in the form:

$$\mathbf{Tr}(a_x, X) = \begin{bmatrix} 1 & 0 & 0 & a_x \\ 0 & 1 & 0 & 0 \\ 0 & 0 & 1 & 0 \\ 0 & 0 & 0 & 1 \end{bmatrix} \quad (31.11)$$

$$\mathbf{Tr}(a_y, Y) = \begin{bmatrix} 1 & 0 & 0 & 0 \\ 0 & 1 & 0 & a_y \\ 0 & 0 & 1 & 0 \\ 0 & 0 & 0 & 1 \end{bmatrix} \quad (31.12)$$

$$\mathbf{Tr}(a_z, Z) = \begin{bmatrix} 1 & 0 & 0 & 0 \\ 0 & 1 & 0 & 0 \\ 0 & 0 & 1 & a_z \\ 0 & 0 & 0 & 1 \end{bmatrix} \quad (31.13)$$

in which  $a_x$ ,  $a_y$ , and  $a_z$ , are signed values that denote distances of translations along corresponding axes.

For the analytical description of the rotation about the coordinate axes, the operators of rotation  $\mathbf{Rt}(\varphi_x, X)$ ,  $\mathbf{Rt}(\varphi_y, Y)$ , and  $\mathbf{Rt}(\varphi_z, Z)$ , are used. The operators yield representation in the form of the homogenous matrices:

$$\mathbf{Rt}(\varphi_x, X) = \begin{bmatrix} 1 & 0 & 0 & 0 \\ 0 & \cos \varphi_x & \sin \varphi_x & 0 \\ 0 & -\sin \varphi_x & \cos \varphi_x & 0 \\ 0 & 0 & 0 & 1 \end{bmatrix} \quad (31.14)$$

$$\mathbf{Rt}(\varphi_y, Y) = \begin{bmatrix} \cos \varphi_y & 0 & -\sin \varphi_y & 0 \\ 0 & 1 & 0 & 0 \\ \sin \varphi_y & 0 & \cos \varphi_y & 0 \\ 0 & 0 & 0 & 1 \end{bmatrix} \quad (31.15)$$

$$\mathbf{Rt}(\varphi_z, Z) = \begin{bmatrix} \cos \varphi_z & \sin \varphi_z & 0 & 0 \\ -\sin \varphi_z & \cos \varphi_z & 0 & 0 \\ 0 & 0 & 1 & 0 \\ 0 & 0 & 0 & 1 \end{bmatrix} \quad (31.16)$$

Here,  $\varphi_x$ ,  $\varphi_y$ , and  $\varphi_z$  are signed values that denote angles of rotation about a corresponding axis:  $\varphi_x$  is an angle of rotation around the X-axis (pitch);  $\varphi_y$  is an angle of rotation around the Y-axis (roll); and  $\varphi_z$  is an angle of rotation around the Z-axis (yaw). Further details on the coordinate system transformations are not discussed, but are well within the skill level of one of ordinary skill in the art.

Manufacturing errors and elastic deformation of the shafts, housing, bearings, and so forth are the main contributors to the resultant linear and angular displacements of the tooth flanks  $\mathcal{G}$  and  $\mathcal{P}$  in real parallel-axes gearing. Gearing of the proposed design is capable of compensating for all of these displacements.

Let's consider an impact of the resultant linear/angular displacements of the tooth flanks,  $\mathcal{G}$  and  $\mathcal{P}$ , in real parallel-axes-gearing on the actual deviation of base pitch from its nominal value. The resultant displacement can be decomposed into two components. One of the components is within the plane of action,  $PA$ , while the other is in the direction orthogonal to  $PA$ .

Refer to Figure 31.6. This schematic illustrates the case when the deviation,  $\delta_{n,g}$ , is within the plane of action,  $PA$ . Due to this displacement,  $\delta_{n,g}$ , the resultant displacement,  $\delta_{n,g}^n$ , in the direction perpendicular to the tooth profile is identical to  $\delta_{n,g}$ , and the identity  $\delta_{n,g}^n \equiv \delta_{n,g}$  is valid.

On the other hand (see Figure 31.7), a deviation of that same value,  $\delta_{\tau,g}$ , but in the direction tangential to the gear/pinion tooth flank, results in a much smaller deviation  $\delta_{\tau,g}^n$ :

$$\delta_{\tau,g}^n = r_\delta - \sqrt{r_\delta^2 - \delta_{\tau,g}^2} \quad (31.17)$$

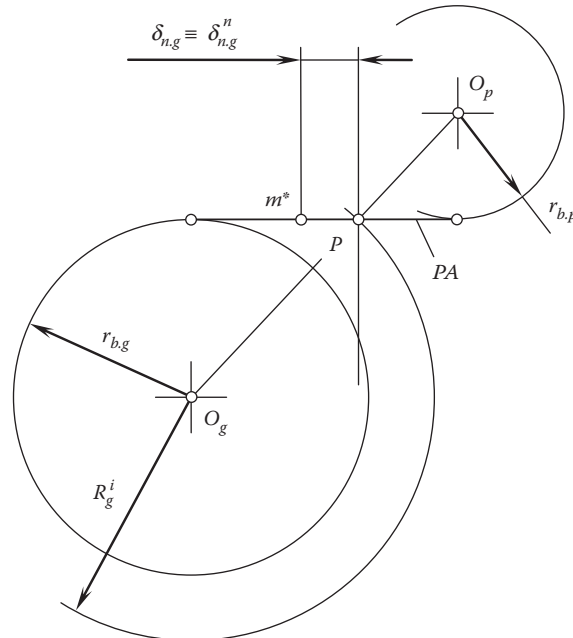
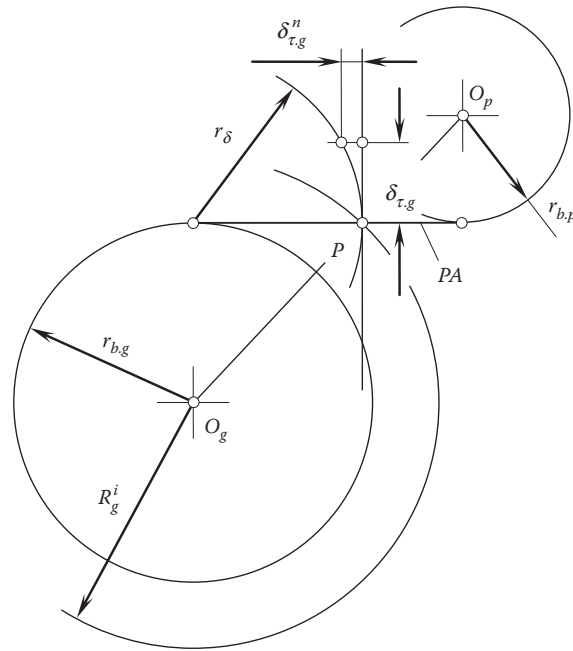


FIGURE 31.6

The deviation,  $\delta_{n,g}$ , is within the plane of action,  $PA$ .

**FIGURE 31.7**

The deviation,  $\delta_{\tau,g}$ , is in the direction tangential to the gear/pinion tooth flank.

This means that the component,  $\delta_{n,g}$ , in the direction within the plane of action,  $PA$ , is the major contributor to actual variation of the base pitch.

In the gearing of the proposed design ( $R_{sp}$ -gearing) the negligibly small component,  $\delta_{\tau,g}^n$  (see Equation 31.17), of the resultant deviation is omitted. As a consequence, the proposed  $R_{sp}$ -gearing features several advantages over known designs of gearing.

The geometry of the tooth flanks of the gear and pinion in  $R_{sp}$ -gearing is capable of accommodating various values of axis misalignment. In this way, the base pitch of the gear is always equal to the operating base pitch,  $\phi_b^{op}$ , of the gear pair. Similarly, base pitch of the pinion is always equal to the operating base pitch,  $\phi_b^{op}$ , of the gear pair. Ultimately, base pitches of the gear and mating pinion are *always* equal to one another (and to the operating base pitch as well).

The line of contact may be any planar curve that is entirely within the plane of action. The geometry of the line of contact may be chosen based on manufacturing considerations, for example, a line of contact that ensures a low-cost manufacturing technique can be utilized might be preferred.

The geometry of the line of contact is not limited to straight line segments, circular arc segments, and cycloid arc segments. Any planar curve that is located entirely within the plane of action may be utilized for the purpose of producing a worm gear set with reduced noise and vibration characteristics and an increased loading capacity.



# Taylor & Francis

Taylor & Francis Group

<http://taylorandfrancis.com>

---

## Appendix A: Elements of Vector Calculus

---

The *vector*, the key to all theory of part surface generation, is a triple real number (in most computer languages, these are usually called *floating-point numbers*) and is noted in a **bold** typeface, that is, **A** or **a**.

Care must be taken to differentiate between two types of vectors:

- **Position vector:** A position vector runs from the origin of the coordinates (0, 0, 0) to a point (X, Y, Z), and its length gives the distance of the point from the origin. Its components are given by (X, Y, Z). The essential concept to understand about a position vector is that it is anchored to specific coordinates (points in space). The set of points that are used to describe the shape of all part surfaces can be thought of as position vectors.
- **Direction vector:** A direction vector differs from a position vector in that it is *not* anchored to specific coordinates. Frequently, direction vectors are used in a form where they have unit length; in this case, they are said to be *normalized*. The most common application of a direction vector in the theory of part surface generation is to specify the orientation of a surface or ray direction. For this, we use a direction vector at right angles (*normal*) and pointing away from the part surface. Such normal vectors are also the key in many calculations in the theory of part surface generation.

Vector calculus is a powerful tool for solving many of the geometrical and kinematical problems that pertain to the design and generation of part surfaces. In this book, *vectors* are understood as quantities that have magnitude and direction and obey the law of addition.

---

### A.1 Fundamental Properties of Vectors

The distance-and-direction interpretation suggests a powerful way to visualize a vector: as a directed line segment or arrow. The length of the arrow (at some predetermined scale) represents the magnitude of the vector, and the orientation of the segment and placement of the arrowhead (at one end of the segment or the other) represent its direction.

Vectors possess certain properties, the set of which is commonly interpreted as the set of fundamental properties of vectors.

#### A.1.1 Addition

Given two vectors **a** and **b**, their sum (**a** + **b**) is graphically defined by joining the tail of **b** to the head of **a**. Then, the line from the tail of **a** to the head of **b** is the sum **c** = (**a** + **b**).

#### A.1.2 Equality

Two vectors are equal when they have the same magnitude and direction. Position of the vectors is unimportant for equality.

#### A.1.3 Negation

The vector **-a** has the same magnitude as **a** but the opposite direction.

#### A.1.4 Subtraction

From the properties of *addition* and *negation*, the following **a** - **b** = **a** + (**-b**) can be defined.



### A.1.5 Scalar Multiplication

The vector  $k\mathbf{a}$  has the same direction as  $\mathbf{a}$ , with a magnitude  $k$  times that of  $\mathbf{a}$ .  $k$  is called a scalar, as it changes the scale of the vector  $\mathbf{a}$ .

## A.2 Mathematical Operations over Vectors

The following rules and mathematical operations can be determined from the above-listed fundamental properties of vectors.

### A.2.1 Components of Vectors

Let's assume that a set of three vectors  $\mathbf{a}$ ,  $\mathbf{b}$ ,  $\mathbf{c}$  and two scalars,  $k$  and  $t$ , are given. Then, vector addition and scalar multiplication have the following properties:

$$\mathbf{a} + \mathbf{b} = \mathbf{b} + \mathbf{a} \quad (\text{A.1})$$

$$\mathbf{a} + (\mathbf{b} + \mathbf{c}) = (\mathbf{a} + \mathbf{b}) + \mathbf{c} \quad (\text{A.2})$$

$$k(t\mathbf{a}) = kt\mathbf{a} \quad (\text{A.3})$$

$$(k + t)\mathbf{a} = k\mathbf{a} + t\mathbf{a} \quad (\text{A.4})$$

$$k(\mathbf{a} + \mathbf{b}) = k\mathbf{a} + k\mathbf{b} \quad (\text{A.5})$$

The magnitude  $a$  of a vector  $\mathbf{a}$  is:

$$a = |\mathbf{a}| = \sqrt{a_x^2 + a_y^2 + a_z^2} \quad (\text{A.6})$$

where  $a_x$ ,  $a_y$ , and  $a_z$  are the scalar components of  $\mathbf{a}$ .

A unit vector  $\bar{\mathbf{a}}$  in the direction of a vector  $\mathbf{a}$  is:

$$\bar{\mathbf{a}} = \frac{\mathbf{a}}{|\mathbf{a}|} = \frac{\mathbf{a}}{a} \quad (\text{A.7})$$

The components  $\bar{a}_x$ ,  $\bar{a}_y$ , and  $\bar{a}_z$  of a unit vector  $\bar{\mathbf{a}}$  are also the direction cosines of the vector  $\bar{\mathbf{a}}$ :

$$\cos \alpha = \bar{a}_x \quad (\text{A.8})$$

$$\cos \beta = \bar{a}_y \quad (\text{A.9})$$

$$\cos \gamma = \bar{a}_z \quad (\text{A.10})$$

It is common practice to denote the components  $\bar{a}_x$ ,  $\bar{a}_y$ , and  $\bar{a}_z$  by  $l$ ,  $m$ , and  $n$  accordingly.

### A.2.2 Scalar Product (or Dot Product)

For the *scalar product* (or *dot product*) of two vectors, the formula:

$$\mathbf{a} \cdot \mathbf{b} = a_x b_x + a_y b_y + a_z b_z = |\mathbf{a}| |\mathbf{b}| \cos \angle(\mathbf{a}, \mathbf{b}) \quad (\text{A.11})$$

is commonly used for the calculation of the scalar product of two vectors,  $\mathbf{a}$  and  $\mathbf{b}$ .

Equation A.11 can also be represented in the form:

$$\mathbf{a} \cdot \mathbf{b} = [\mathbf{a}]^T \cdot [\mathbf{b}] = [a_x \ a_y \ a_z] \cdot \begin{bmatrix} b_x \\ b_y \\ b_z \end{bmatrix} \quad (\text{A.12})$$

The angle  $\angle(\mathbf{a}, \mathbf{b})$  between two vectors,  $\mathbf{a}$  and  $\mathbf{b}$ , is calculated from:

$$\angle(\mathbf{a}, \mathbf{b}) = \cos^{-1} \left( \frac{\mathbf{a} \cdot \mathbf{b}}{|\mathbf{a}||\mathbf{b}|} \right) \quad (\text{A.13})$$

The scalar product of two vectors,  $\mathbf{a}$  and  $\mathbf{b}$ , features the following properties:

$$\mathbf{a} \cdot \mathbf{a} = |\mathbf{a}|^2 \quad (\text{A.14})$$

$$\mathbf{a} \cdot \mathbf{b} = \mathbf{b} \cdot \mathbf{a} \quad (\text{A.15})$$

$$\mathbf{a} \cdot (\mathbf{b} + \mathbf{c}) = \mathbf{b} \cdot \mathbf{a} + \mathbf{b} \cdot \mathbf{c} \quad (\text{A.16})$$

$$(k\mathbf{a}) \cdot \mathbf{b} = \mathbf{a} \cdot (k\mathbf{b}) = k(\mathbf{a} \cdot \mathbf{b}) \quad (\text{A.17})$$

If  $\mathbf{a}$  is perpendicular to  $\mathbf{b}$ , then:

$$\mathbf{a} \cdot \mathbf{b} = 0 \quad (\text{A.18})$$

### A.2.3 Vector Product (or Cross Product)

The vector product of two vectors can be calculated from the formula:

$$\mathbf{a} \times \mathbf{b} = (a_y b_z - a_z b_y) \mathbf{i} + (a_z b_x - a_x b_z) \mathbf{j} + (a_x b_y - a_y b_x) \mathbf{k} \quad (\text{A.19})$$

Here, in Equation A.19,  $\mathbf{i}$ ,  $\mathbf{j}$ , and  $\mathbf{k}$  are unit vectors in the  $X$ ,  $Y$ , and  $Z$  directions of the reference system  $XYZ$ , in which the vectors  $\mathbf{a}$  and  $\mathbf{b}$  are specified.

The vector product possesses the following property: in the case  $\mathbf{a} \times \mathbf{b} = \mathbf{c}$ , then the vector  $\mathbf{c}$  is perpendicular to a plane through the vectors  $\mathbf{a}$  and  $\mathbf{b}$ .

The vector product of two vectors,  $\mathbf{a}$  and  $\mathbf{b}$ , features the following properties:

$$\mathbf{a} \times \mathbf{b} = \begin{vmatrix} \mathbf{i} & \mathbf{j} & \mathbf{k} \\ a_x & a_y & a_z \\ b_x & b_y & b_z \end{vmatrix} \quad (\text{A.20})$$

$$\mathbf{a} \times \mathbf{b} = |\mathbf{a}||\mathbf{b}|\mathbf{n} \sin \angle(\mathbf{a}, \mathbf{b}) \quad (\text{A.21})$$

where the unit normal vector to the plane through the vectors  $\mathbf{a}$  and  $\mathbf{b}$  is denoted by  $\mathbf{n}$ :

$$|\mathbf{a} \times \mathbf{b}| = |\mathbf{a}||\mathbf{b}| \sin \angle(\mathbf{a}, \mathbf{b}) \quad (\text{A.22})$$

Coordinates of the vector product  $\mathbf{a} \times \mathbf{b}$  can also be expressed in the form:

$$|\mathbf{a} \times \mathbf{b}| = \begin{bmatrix} 0 & -a_z & a_y \\ a_z & 0 & -a_x \\ -a_y & a_x & 0 \end{bmatrix} \cdot \begin{bmatrix} b_x \\ b_y \\ b_z \end{bmatrix} = \begin{bmatrix} -a_z b_y + a_y b_z \\ -a_x b_z + a_z b_x \\ -a_y b_x + a_x b_y \end{bmatrix} \quad (\text{A.23})$$

$$\mathbf{a} \times \mathbf{b} = -\mathbf{b} \times \mathbf{a} \quad (\text{A.24})$$

$$\mathbf{a} \times (\mathbf{b} + \mathbf{c}) = \mathbf{a} \times \mathbf{b} + \mathbf{a} \times \mathbf{c} \quad (\text{A.25})$$

$$(k\mathbf{a}) \times \mathbf{b} = \mathbf{a} \times (k\mathbf{b}) = k(\mathbf{a} \times \mathbf{b}) \quad (\text{A.26})$$

$$\mathbf{i} \times \mathbf{j} = \mathbf{k}, \mathbf{j} \times \mathbf{k} = \mathbf{i}, \mathbf{k} \times \mathbf{i} = \mathbf{j} \quad (\text{A.27})$$

If  $\mathbf{a}$  is parallel to  $\mathbf{b}$ , then:

$$\mathbf{a} \times \mathbf{b} = 0 \quad (\text{A.28})$$

#### A.2.4 Triple Scalar Product of Three Vectors

The product  $(\mathbf{a} \times \mathbf{b}) \cdot \mathbf{c}$  is commonly referred to as the *triple scalar product* of three vectors,  $\mathbf{a}$ ,  $\mathbf{b}$ , and  $\mathbf{c}$ .

The triple scalar product of three vectors,  $\mathbf{a}$ ,  $\mathbf{b}$ , and  $\mathbf{c}$ , features the following properties:

$$(\mathbf{a} \times \mathbf{b}) \cdot \mathbf{c} = (\mathbf{b} \times \mathbf{c}) \cdot \mathbf{a} = (\mathbf{c} \times \mathbf{a}) \cdot \mathbf{b} \quad (\text{A.29})$$

$$(\mathbf{b} \times \mathbf{c}) \cdot \mathbf{a} = \mathbf{a} \cdot (\mathbf{b} \times \mathbf{c}) \quad (\text{A.30})$$

$$(\mathbf{a} \times \mathbf{b}) \cdot \mathbf{c} = \mathbf{a} \cdot (\mathbf{b} \times \mathbf{c}) \quad (\text{A.31})$$

$$\mathbf{a} \cdot (\mathbf{b} \times \mathbf{c}) = \begin{vmatrix} a_x & a_y & a_z \\ b_x & b_y & b_z \\ c_x & c_y & c_z \end{vmatrix} \quad (\text{A.32})$$

#### A.2.5 Triple Vector Product of Three Vectors

The product  $(\mathbf{a} \times \mathbf{b}) \times \mathbf{c}$  is commonly referred to as the *triple vector product* of three vectors,  $\mathbf{a}$ ,  $\mathbf{b}$ , and  $\mathbf{c}$ .

The product  $(\mathbf{a} \times \mathbf{b}) \times \mathbf{c}$  can be evaluated by two vector products. However, it also can be evaluated in a more simple way by use of the identity:

$$(\mathbf{a} \times \mathbf{b}) \times \mathbf{c} = (\mathbf{a} \cdot \mathbf{c})\mathbf{b} - (\mathbf{b} \cdot \mathbf{c})\mathbf{a} \quad (\text{A.33})$$

It should be mentioned here that, in general, the triple vector products,  $(\mathbf{a} \times \mathbf{b}) \times \mathbf{c}$  and  $\mathbf{a} \times (\mathbf{b} \times \mathbf{c})$ , are not equal:

$$(\mathbf{a} \times \mathbf{b}) \times \mathbf{c} \neq \mathbf{a} \times (\mathbf{b} \times \mathbf{c}) \quad (\text{A.34})$$

Analytical interpretation of many problems and results in the field of geometry of surfaces becomes much simpler when vector calculus is used.

### A.2.6 Lagrange Equation for Vectors

For the purposes of calculation of the mixed product of vectors,  $\mathbf{a}$  and  $\mathbf{b}$ , an equation:

$$(\mathbf{a} \times \mathbf{b}) \cdot (\mathbf{a} \times \mathbf{b}) = (\mathbf{a} \cdot \mathbf{a})(\mathbf{b} \cdot \mathbf{b}) - (\mathbf{a} \cdot \mathbf{b})^2 \quad (\text{A.35})$$

can be used.

Equation A.35 is due to *Lagrange*.\*

---

## A.3 On Similarity and Difference between Vectors and Matrices

A vector,  $\mathbf{a}$ , is commonly represented in the form:

$$\mathbf{a} = ia + jb + kc \quad (\text{A.36})$$

That same vector,  $\mathbf{a}$ , allows for matrix representation in one of the following forms:

$$\mathbf{a} = \begin{bmatrix} a \\ b \\ c \end{bmatrix} \quad (\text{A.37})$$

$$\mathbf{a} = \begin{bmatrix} a \\ b \\ c \\ 1 \end{bmatrix} \quad (\text{A.38})$$

$$\mathbf{a} = \begin{bmatrix} 1 & 0 & 0 & a \\ 0 & 1 & 0 & b \\ 0 & 0 & 1 & c \\ 0 & 0 & 0 & 1 \end{bmatrix} \quad (\text{A.39})$$

Operations over vectors in matrix representation (see the form Equation A.39) are preferred, as multiple coordinate system transformations are often required.

Vectors obey the commutative law; that is, the equalities  $\mathbf{a} \times \mathbf{b} = \mathbf{b} \times \mathbf{a}$  and  $\mathbf{a} \cdot \mathbf{b} = \mathbf{b} \cdot \mathbf{a}$  are valid for vectors. This is not always applicable to matrices.

Two kinds of products are valid for vectors, that is, the dot product ( $\mathbf{a} \cdot \mathbf{b}$ ), and cross product ( $\mathbf{a} \times \mathbf{b}$ ) of vectors, which are not valid with respect to matrices.

---

\* Joseph-Louis Lagrange (January 25, 1736-April 10, 1813), a famous French mathematician, astronomer, and mechanician.



# Taylor & Francis

Taylor & Francis Group

<http://taylorandfrancis.com>

## Appendix B: Elements of Differential Geometry of Surfaces

Discussion in this book is focused primarily on the elements of the theory of gear-cutting tool design.

The gear and pinion tooth flanks and their motion in space in relation to one another are analytically described in a reference system. An orthogonal *Cartesian*<sup>\*</sup> reference system is a major kind of reference system that is commonly used for this purpose. Mutually perpendicular coordinate axes of a Cartesian coordinate system are conventionally labeled as  $X$ ,  $Y$ , and  $Z$ .

In a Cartesian reference system, the axes can be oriented in either a left- or right-handed sense. A right-handed Cartesian reference system is preferred, and all algorithms and formulae used in this book assume a right-handed convention.

A coordinate system provides a numerical frame of reference for the three-dimensional space in which the theory is developed. Two coordinate systems are particularly useful to us: the ubiquitous Cartesian ( $XYZ$ ) rectilinear system and the spherical polar ( $r, \theta, \varphi$ ) or angular system. Cartesian coordinate systems are the most commonly used, but angular coordinates are often helpful as well.

### B.1 Specification of a Gear Tooth Flank

A gear tooth flank could be uniquely determined by two independent variables. Therefore, we give a gear tooth flank  $\mathcal{G}$  (see Figure B.1) in most cases by expressing its rectangular coordinates,  $X_g$ ,  $Y_g$ , and  $Z_g$ , as functions of two *Gaussian*<sup>†</sup> coordinates,  $U_g$  and  $V_g$ , in a certain closed interval<sup>‡</sup>:

$$\mathcal{G} \Rightarrow \mathbf{r}_g = \mathbf{r}_g(U_g, V_g) = \begin{bmatrix} X_g(U_g, V_g) \\ Y_g(U_g, V_g) \\ Z_g(U_g, V_g) \\ 1 \end{bmatrix} \quad (\text{B.1})$$

$$U_{1,g} \leq U_g \leq U_{2,g}; \quad V_{1,g} \leq V_g \leq V_{2,g}$$

where:

$\mathbf{r}_g$ : is the position vector of a point of the gear tooth flank,  $\mathcal{G}$ .

$U_g$  and  $V_g$ : are curvilinear coordinates (Gaussian coordinates) of the gear tooth flank,  $\mathcal{G}$ .

$X_g, Y_g, Z_g$ : are Cartesian coordinates of the point of the gear tooth flank,  $\mathcal{G}$ .

$U_{1,g}, U_{2,g}$ : are the boundary values of the closed interval of the  $U_g$ -parameter.

$V_{1,g}, V_{2,g}$ : are the boundary values of the closed interval of the  $V_g$ -parameter.

The parameters,  $U_g$  and  $V_g$ , must enter Equation B.1 independently, which means that the matrix:

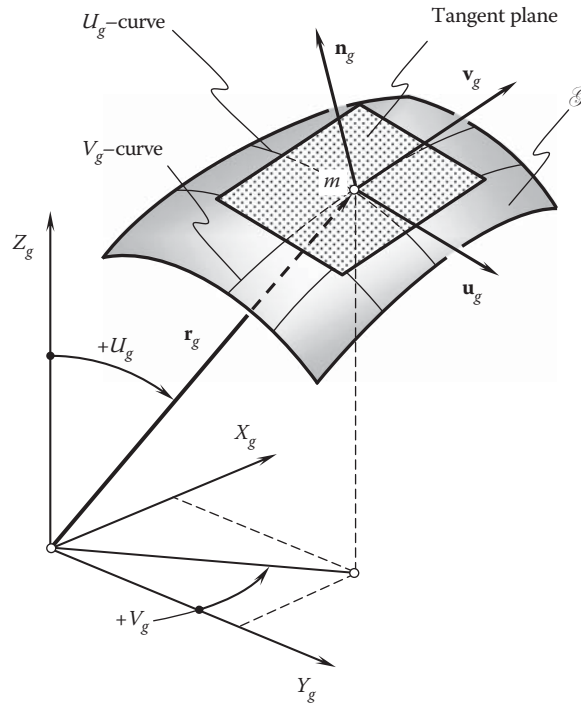
$$\mathbf{M} = \begin{bmatrix} \frac{\partial X_g}{\partial U_g} & \frac{\partial Y_g}{\partial U_g} & \frac{\partial Z_g}{\partial U_g} \\ \frac{\partial X_g}{\partial V_g} & \frac{\partial Y_g}{\partial V_g} & \frac{\partial Z_g}{\partial V_g} \end{bmatrix} \quad (\text{B.2})$$

has a rank of 2.

<sup>\*</sup> René Descartes (March 31, 1596–February 11, 1650; Latinized form: Renatus Cartesius), a French mathematician, philosopher, and writer.

<sup>†</sup> Johann Carl Friedrich Gauss (April 30, 1777–February 23, 1855)—a famous German mathematician and physical scientist.

<sup>‡</sup> All equations that are valid for the gear tooth flank,  $\mathcal{G}$ , are also valid for the pinion tooth flank,  $\mathcal{P}$ .

**FIGURE B.1**

Principal parameters of local topology of a gear tooth flank,  $\mathcal{G}$ .

Positions where the rank is 1 or 0 are singular points; when the rank at all points is 1, then Equation B.1 represents a curve.

Other methods of surface specification are known as well. Specification of a gear tooth flank by

- An equation in explicit form
- An equation in implicit form
- A set of parametric equations

are among the methods of surface specification most frequently used in practice.

It is assumed here and below that for any given kind of gear tooth flank,  $\mathcal{G}$ , the specification can be converted either into the vector form or into the matrix form of its specification, as follows from Equation B.1.

## B.2 Tangent Vectors and Tangent Plane; Unit Normal Vector

The following notation is proven to be convenient in the consideration below.

The first derivatives of  $\mathbf{r}_g$  with respect to Gaussian coordinates  $U_g$  and  $V_g$  are designated as:

$$\frac{\partial \mathbf{r}_g}{\partial U_g} = \mathbf{U}_g \quad (\text{B.3})$$

$$\frac{\partial \mathbf{r}_p}{\partial V_p} = \mathbf{V}_p \quad (\text{B.4})$$



and for the unit tangent vectors:

$$\mathbf{u}_g = \frac{\mathbf{U}_g}{|\mathbf{U}_g|} \quad (\text{B.5})$$

$$\mathbf{v}_g = \frac{\mathbf{V}_g}{|\mathbf{V}_g|} \quad (\text{B.6})$$

correspondingly.\*

The direction of the tangent line to the  $U_g$ -coordinate line through a given point  $m$  on the gear tooth flank,  $\mathcal{G}$ , is specified by the unit tangent vector  $\mathbf{u}_g$  (as well as by the tangent vector  $\mathbf{U}_g$ ). Similarly, the direction of the tangent line to the  $V_g$ -coordinate line through that same point  $m$  on a gear tooth flank  $\mathcal{G}$  is specified by the unit tangent vector  $\mathbf{v}_g$  (as well as by the tangent vector  $\mathbf{V}_g$ ).

The significance of the unit tangent vectors,  $\mathbf{u}_g$  and  $\mathbf{v}_g$ , becomes evident from the following considerations.

First, unit tangent vectors  $\mathbf{u}_g$  and  $\mathbf{v}_g$  yield an equation of the tangent plane to a gear tooth flank  $\mathcal{G}$  at a specified point  $m$ :

$$\text{Tangent plane} \Rightarrow \begin{bmatrix} [\mathbf{r}_{i,p} - \mathbf{r}_g^m] \\ \mathbf{u}_g \\ \mathbf{v}_g \\ 1 \end{bmatrix} = 0 \quad (\text{B.7})$$

where:

$\mathbf{r}_{i,p}$ : is the position vector of a point of the tangent plane to a gear tooth flank  $\mathcal{G}$  at a specified point  $m$ .

$\mathbf{r}_g^m$ : is the position vector of the point  $m$  on a gear tooth flank  $\mathcal{G}$ .

Second, tangent vectors yield an equation of the perpendicular  $\mathbf{N}_g$  and the unit normal vector  $\mathbf{n}_g$  to a gear tooth flank  $\mathcal{G}$  at a given point  $m$ :

$$\mathbf{N}_g = \mathbf{U}_g \times \mathbf{V}_g \quad (\text{B.8})$$

and

$$\mathbf{n}_g = \frac{\mathbf{N}_g}{|\mathbf{N}_g|} = \frac{\mathbf{U}_g \times \mathbf{V}_g}{|\mathbf{U}_g \times \mathbf{V}_g|} = \mathbf{u}_g \times \mathbf{v}_g \quad (\text{B.9})$$

When the order of the multipliers in Equations B.8 and B.9 is chosen properly, then the unit normal vector  $\mathbf{n}_g$  (as well as the normal vector  $\mathbf{N}_g$ ) is pointed outward of the bodily side of the surface  $\mathcal{G}$ .

### B.3 Local Frame

Two unit tangent vectors,  $\mathbf{u}_g$  and  $\mathbf{v}_g$ , along with the unit normal vector  $\mathbf{n}_g$  make up a local frame,  $\mathbf{u}_g, \mathbf{v}_g, \mathbf{n}_g$ , having the origin at a current point  $m$  on a gear tooth flank  $\mathcal{G}$ . Unit tangent vector  $\mathbf{u}_g$  is perpendicular to the unit normal vector  $\mathbf{n}_g$  (that is,  $\mathbf{u}_g \perp \mathbf{n}_g$ ), and unit tangent vector  $\mathbf{v}_g$  is also perpendicular to the unit normal vector  $\mathbf{n}_g$  (that is,  $\mathbf{v}_g \perp \mathbf{n}_g$ ). Speaking generally, the unit tangent vectors  $\mathbf{u}_g$  and  $\mathbf{v}_g$  are not perpendicular to one another; they form a certain angle,  $\omega_g$ . In order to construct an orthogonal local frame, either the unit tangent vector  $\mathbf{u}_g$  in the local frame ( $\mathbf{u}_g, \mathbf{v}_g, \mathbf{n}_g$ ) must be substituted with a unit tangent vector,  $\mathbf{u}_g^*$ , or the unit tangent vector  $\mathbf{v}_g$  in

\* It is the right point to underline here that the unit tangent vectors  $\mathbf{u}_p$  and  $\mathbf{v}_p$  are dimensionless values, as follows from Equations B.5 and B.6.

that same local frame ( $\mathbf{u}_g, \mathbf{v}_g, \mathbf{n}_g$ ) must be substituted with a unit tangent vector,  $\mathbf{v}_g^*$ . For the calculation of the newly introduced unit tangent vectors,  $\mathbf{u}_g^*$  and  $\mathbf{v}_g^*$ , the following equations can be used:

$$\mathbf{u}_g^* = \mathbf{u}_g \times \mathbf{n}_g \quad (\text{B.10})$$

$$\mathbf{v}_g^* = \mathbf{v}_g \times \mathbf{n}_g \quad (\text{B.11})$$

It is convenient to choose an order of the multipliers in Equations B.10 and B.11 that preserves the orientation (the hand) of the original local frame ( $\mathbf{u}_g, \mathbf{v}_g, \mathbf{n}_g$ ); that is, if the original local frame ( $\mathbf{u}_g, \mathbf{v}_g, \mathbf{n}_g$ ) is right-hand-oriented, then the newly constructed local frame [either the local frame ( $\mathbf{u}_g^*, \mathbf{v}_g, \mathbf{n}_g$ ) or the local frame ( $\mathbf{u}_g^*, \mathbf{v}_g^*, \mathbf{n}_g$ )] should also be a right-hand-oriented local frame, and vice versa.

It should be pointed out here that another possibility to construct an orthogonal local frame is also available. Local frames of this kind are commonly referred to as *Darboux\* frames*, and are briefly considered below in this section.

Unit tangent vectors  $\mathbf{u}_g$  and  $\mathbf{v}_g$  to a surface  $\mathcal{G}$  at a point  $m$  are of critical importance when solving practical problems in the field of gearing. This statement is proven by numerous examples shown below.

#### B.4 Fundamental Forms of a Surface

Consider two other important issues concerning the gear tooth flank geometry—both relate to intrinsic geometry in the differential vicinity of a current surface point  $m$ .

*First fundamental form of a surface.* The first issue is the so-called the *first fundamental form*,  $\Phi_{1,g}$  of a gear tooth flank  $\mathcal{G}$ . The metric properties of a gear tooth flank  $\mathcal{G}$  are described by the first fundamental form,  $\Phi_{1,g}$ , of the surface. Usually, the first fundamental form,  $\Phi_{1,g}$ , is represented as the quadratic form:

$$\Phi_{1,g} \Rightarrow ds_g^2 = E_g dU_g^2 + 2F_g dU_g dV_g + G_g dV_g^2 \quad (\text{B.12})$$

Here, in Equation B.12:

$s_g$ : is the linear element on a gear tooth flank  $\mathcal{G}$  ( $s_g$  is equal to the length of a segment of a certain curve on a gear tooth flank  $\mathcal{G}$ ).

$E_g, F_g, G_g$ : are fundamental magnitudes of the first order at a surface point.

Equation B.12 for the first fundamental form,  $\Phi_{1,g}$ , is known from many advanced sources. In the theory of gearing, another form of analytical representation of the first fundamental form,  $\Phi_{1,g}$ , is proven to be useful:

$$\Phi_{1,g} \Rightarrow ds_g^2 = [dU_g \quad dV_g \quad 0 \quad 0] \cdot \begin{bmatrix} E_g & F_g & 0 & 0 \\ F_g & G_g & 0 & 0 \\ 0 & 0 & 1 & 0 \\ 0 & 0 & 0 & 1 \end{bmatrix} \cdot \begin{bmatrix} dU_g \\ dV_g \\ 0 \\ 0 \end{bmatrix} \quad (\text{B.13})$$

This kind of analytical representation of the first fundamental form,  $\Phi_{1,p}$ , is proposed by Radzevich [107, 119].

The practical advantage of Equation B.13 is that it can easily be incorporated into computer programs when multiple coordinate system transformations are used. The last is vital for the theory of gearing.

\* Jean Gaston Darboux (August 14, 1842–February 23, 1917), a French mathematician.

Fundamental magnitudes of the first order,  $E_g$ ,  $F_g$ ,  $G_g$ , can be calculated from the set of the following equations:

$$E_g = \mathbf{U}_g \cdot \mathbf{U}_g \quad (\text{B.14})$$

$$F_g = \mathbf{U}_g \cdot \mathbf{V}_g \quad (\text{B.15})$$

$$G_g = \mathbf{V}_g \cdot \mathbf{V}_g \quad (\text{B.16})$$

Equations B.14 through B.16 can be represented in an expended form:

$$E_g = \frac{\partial \mathbf{r}_g}{\partial U_g} \cdot \frac{\partial \mathbf{r}_g}{\partial U_g} = \frac{\partial X_g}{\partial U_g} \cdot \frac{\partial X_g}{\partial U_g} + \frac{\partial Y_g}{\partial U_g} \cdot \frac{\partial Y_g}{\partial U_g} + \frac{\partial Z_g}{\partial U_g} \cdot \frac{\partial Z_g}{\partial U_g} \quad (\text{B.17})$$

$$F_g = \frac{\partial \mathbf{r}_g}{\partial U_g} \cdot \frac{\partial \mathbf{r}_g}{\partial V_g} = \frac{\partial X_g}{\partial U_g} \cdot \frac{\partial X_g}{\partial V_g} + \frac{\partial Y_g}{\partial U_g} \cdot \frac{\partial Y_g}{\partial V_g} + \frac{\partial Z_g}{\partial U_g} \cdot \frac{\partial Z_g}{\partial V_g} \quad (\text{B.18})$$

$$G_g = \frac{\partial \mathbf{r}_g}{\partial V_g} \cdot \frac{\partial \mathbf{r}_g}{\partial V_g} = \frac{\partial X_g}{\partial V_g} \cdot \frac{\partial X_g}{\partial V_g} + \frac{\partial Y_g}{\partial V_g} \cdot \frac{\partial Y_g}{\partial V_g} + \frac{\partial Z_g}{\partial V_g} \cdot \frac{\partial Z_g}{\partial V_g} \quad (\text{B.19})$$

Fundamental magnitudes of the first order,  $E_g$ ,  $F_g$ ,  $G_g$ , are functions of the  $U_g$ - and  $V_g$ -coordinates of a point of a gear tooth flank,  $\mathcal{G}$ . In general form, these relationships can be represented in the form:

$$E_g = E_g(U_g, V_g) \quad (\text{B.20})$$

$$F_g = F_g(U_g, V_g) \quad (\text{B.21})$$

$$G_g = G_g(U_g, V_g) \quad (\text{B.22})$$

It is important to point out here that fundamental magnitudes  $E_g$  and  $G_g$  are always positive (that is,  $E_g > 0$ ,  $G_g > 0$ ), and the fundamental magnitude  $F_g$  can equal zero ( $F_g \geq 0$ ). This means the first fundamental form,  $\Phi_{1.g}$ , at a point of a gear tooth flank,  $\mathcal{G}$ , is always positively defined ( $\Phi_{1.g} \geq 0$ ), and it cannot have a negative value.

By use of the first fundamental form,  $\Phi_{1.g}$ , the following major parameters of geometry of a gear tooth flank  $\mathcal{G}$  can be calculated:

1. Length of a curve-line segment on a gear tooth flank,  $\mathcal{G}$
2. Square of a gear tooth flank,  $\mathcal{G}$ , portion that is bounded by a closed curve on the surface
3. Angle between any two directions on a gear tooth flank  $\mathcal{G}$

The length,  $s_g$ , of a curve-line segment:

$$U_g = U_g(t) \quad (\text{B.23})$$

$$V_g = V_g(t) \quad (\text{B.24})$$

on a gear tooth flank,  $\mathcal{G}$ , is given by the equation:

$$s_g = \int_{t_0}^t \sqrt{E_g \left( \frac{dU_g}{dt} \right)^2 + 2F_g \frac{dU_g}{dt} \frac{dV_g}{dt} + G_g \left( \frac{dV_g}{dt} \right)^2} dt \quad (\text{B.25})$$

$$t_0 \leq t \leq t_1$$

For calculation of a square,  $\mathcal{S}_g$ , of a gear tooth flank,  $\mathcal{G}$ , patch  $\Sigma$ , which is bounded by a closed curve on the surface  $\mathcal{G}$ , the following equation can be used:

$$\mathcal{S}_g = \iint_{\Sigma} \sqrt{E_g G_g - F_g^2} dU_g dV_g \quad (\text{B.26})$$

Ultimately, the value of the angle,  $\omega_g$ , between two given directions through a certain point  $m$  on a gear tooth flank,  $\mathcal{G}$ , can be calculated from one of the equations below:

$$\cos \omega_g = \frac{F_g}{\sqrt{E_g G_g}} \quad (\text{B.27})$$

$$\sin \omega_g = \frac{H_g}{\sqrt{E_g G_g}} \quad (\text{B.28})$$

$$\tan \omega_g = \frac{H_g}{F_g} \quad (\text{B.29})$$

For the calculation of the discriminant,  $H_g$ , of the first fundamental form,  $\Phi_{1.g}$ , the following equation can be used:

$$H_g = \sqrt{E_g G_g - F_g^2} \quad (\text{B.30})$$

It is assumed here that the discriminant  $H_g$  is always nonnegative—that is,  $H_g = +\sqrt{E_g G_g - F_g^2}$ .

The first fundamental form,  $\Phi_{1.g}$ , represents the length of a curve-line segment; thus, it is always nonnegative—that is, the inequality  $\Phi_{1.g} \geq 0$  is always valid.

The first fundamental form,  $\Phi_{1.g}$ , remains the same when the surface is banding. This is another important feature of the first fundamental form  $\Phi_{1.g}$ .

*Second fundamental form of a surface.* The *second fundamental form*,  $\Phi_{2.g}$  of a gear tooth flank,  $\mathcal{G}$ , is another of the two above-mentioned issues. The second fundamental form  $\Phi_{2.g}$  describes the curvature of a smooth regular surface  $\mathcal{G}$ .

Consider a point,  $K$ , on a smooth regular part surface,  $\mathcal{G}$  (Figure B.2). The location of the point  $K$  is specified by two coordinates,  $U_g$  and  $V_g$ . A line through point  $K$  is entirely located within the surface,  $\mathcal{G}$ . A nearby point  $m$  is located within the line through point  $K$ . The location of point  $m$  is specified by the coordinates  $U_g + dU_g$  and  $V_g + dV_g$ , as it is infinitesimally close to point  $K$ . The closest distance of approach of point  $m$  to the tangent plane through point  $K$  is expressed by the second fundamental form,  $\Phi_{2.g}$ . The torsion of the curve  $Km$  is ignored. Therefore, the distance  $a$  is assumed to be equal to zero ( $a = 0$ ).

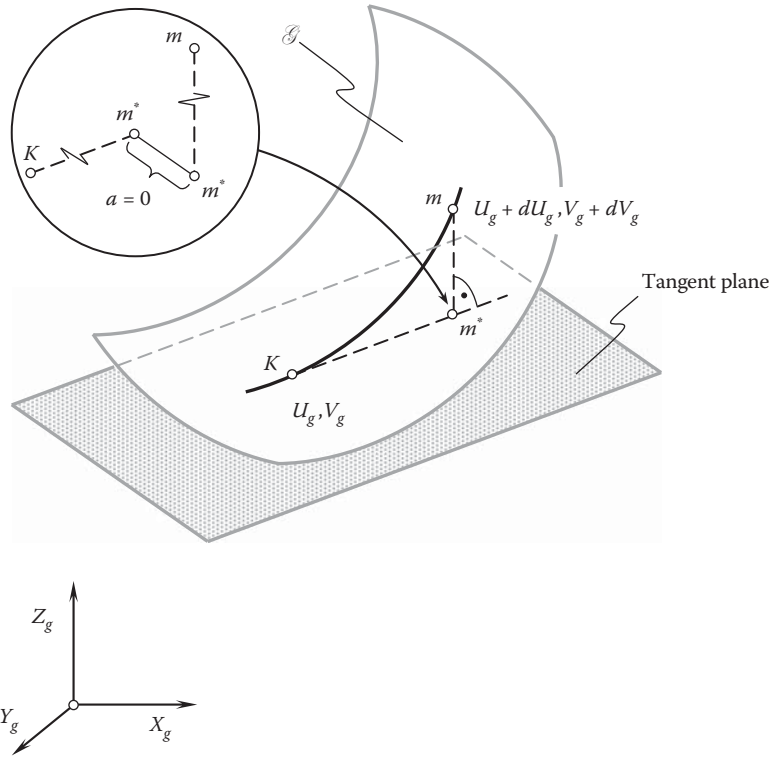
The second fundamental form,  $\Phi_{2.g}$ , describes the curvature of a smooth, regular part surface,  $\mathcal{G}$ . Usually, it is represented as the quadratic form (Figure B.2):

$$\Phi_{2.g} \Rightarrow -d\mathbf{r}_g \cdot d\mathbf{n}_g = L_g dU_g^2 + 2M_g dU_g dV_g + N_g dV_g^2 \quad (\text{B.31})$$

Equation B.31 is known from many advanced sources.

In the theory of gearing, another analytical representation of the second fundamental form,  $\Phi_{2.g}$ , is proven to be useful:

$$\Phi_{2.g} \Rightarrow [dU_g \ dV_g \ 0 \ 0] \cdot \begin{bmatrix} L_g & M_g & 0 & 0 \\ M_g & N_g & 0 & 0 \\ 0 & 0 & 1 & 0 \\ 0 & 0 & 0 & 1 \end{bmatrix} \cdot \begin{bmatrix} dU_g \\ dV_g \\ 0 \\ 0 \end{bmatrix} \quad (\text{B.32})$$

**FIGURE B.2**

On the definition of second fundamental form,  $\Phi_{2,g}$ , at a point of a smooth gear tooth flank,  $\mathcal{G}$ .

This analytical representation of the second fundamental form,  $\Phi_{2,p}$ , is proposed by Radzevich [107,119].

Similar to Equation B.13, the practical advantage of Equation B.32 is that it can easily be incorporated into computer programs when multiple coordinate system transformations are used. The last is vital for the theory of gearing.

In Equation B.32, the parameters  $L_g$ ,  $M_g$ , and  $N_g$  designate fundamental magnitudes of the second order.

By definition, fundamental magnitudes of the second order are equal to:

$$L_g = -\mathbf{U}_g \cdot \frac{\partial \mathbf{n}_g}{\partial U_g} = \mathbf{n}_g \cdot \frac{\partial \mathbf{U}_g}{\partial U_g} \quad (\text{B.33})$$

$$M_g = -\frac{1}{2} \left( \mathbf{U}_g \cdot \frac{\partial \mathbf{n}_g}{\partial V_g} + \mathbf{V}_g \cdot \frac{\partial \mathbf{n}_g}{\partial U_g} \right) = \mathbf{n}_g \cdot \frac{\partial \mathbf{U}_g}{\partial V_g} = \mathbf{n}_g \cdot \frac{\partial \mathbf{V}_g}{\partial U_g} \quad (\text{B.34})$$

$$N_g = -\mathbf{V}_g \cdot \frac{\partial \mathbf{n}_g}{\partial V_g} = \mathbf{n}_g \cdot \frac{\partial \mathbf{V}_g}{\partial V_g} \quad (\text{B.35})$$

For the calculation of the fundamental magnitudes of the second order of a smooth regular gear tooth flank,  $\mathcal{G}$ , the following equations can be used:

$$L_g = \frac{\frac{\partial \mathbf{U}_g}{\partial U_g} \times \mathbf{U}_g \cdot \mathbf{V}_g}{\sqrt{E_g G_g - F_g^2}} \quad (\text{B.36})$$

$$M_g = \frac{\frac{\partial \mathbf{U}_g}{\partial V_g} \times \mathbf{U}_g \cdot \mathbf{V}_g}{\sqrt{E_g G_g - F_g^2}} = \frac{\frac{\partial \mathbf{V}_g}{\partial U_g} \times \mathbf{U}_g \cdot \mathbf{V}_g}{\sqrt{E_g G_g - F_g^2}} \quad (\text{B.37})$$

$$N_g = \frac{\frac{\partial \mathbf{V}_g}{\partial V_g} \times \mathbf{U}_g \cdot \mathbf{V}_g}{\sqrt{E_g G_g - F_g^2}} \quad (\text{B.38})$$

Equations B.36 through B.38 can be represented in an expanded form:

$$L_g = \frac{\begin{vmatrix} \frac{\partial^2 X_g}{\partial U_g^2} & \frac{\partial^2 Y_g}{\partial U_g^2} & \frac{\partial^2 Z_g}{\partial U_g^2} \\ \frac{\partial X_g}{\partial U_g} & \frac{\partial Y_g}{\partial U_g} & \frac{\partial Z_g}{\partial U_g} \\ \frac{\partial X_g}{\partial V_g} & \frac{\partial Y_g}{\partial V_g} & \frac{\partial Z_g}{\partial V_g} \end{vmatrix}}{\sqrt{E_g G_g - F_g^2}} \quad (\text{B.39})$$

$$M_g = \frac{\begin{vmatrix} \frac{\partial^2 X_g}{\partial U_g \partial V_g} & \frac{\partial^2 Y_g}{\partial U_g \partial V_g} & \frac{\partial^2 Z_g}{\partial U_g \partial V_g} \\ \frac{\partial X_g}{\partial U_g} & \frac{\partial Y_g}{\partial U_g} & \frac{\partial Z_g}{\partial U_g} \\ \frac{\partial X_g}{\partial V_g} & \frac{\partial Y_g}{\partial V_g} & \frac{\partial Z_g}{\partial V_g} \end{vmatrix}}{\sqrt{E_g G_g - F_g^2}} \quad (\text{B.40})$$

$$N_g = \frac{\begin{vmatrix} \frac{\partial^2 X_g}{\partial V_g^2} & \frac{\partial^2 Y_g}{\partial V_g^2} & \frac{\partial^2 Z_g}{\partial V_g^2} \\ \frac{\partial X_g}{\partial U_g} & \frac{\partial Y_g}{\partial U_g} & \frac{\partial Z_g}{\partial U_g} \\ \frac{\partial X_g}{\partial V_g} & \frac{\partial Y_g}{\partial V_g} & \frac{\partial Z_g}{\partial V_g} \end{vmatrix}}{\sqrt{E_g G_g - F_g^2}} \quad (\text{B.41})$$

Fundamental magnitudes of the second order,  $L_g, M_g, N_g$ , are also functions of the  $U_g$ - and  $V_g$ -coordinates of a point of a gear tooth flank,  $\mathcal{G}$ . In general form, these relationships can be represented in the form:

$$L_g = L_g(U_g, V_g) \quad (\text{B.42})$$

$$M_g = M_g(U_g, V_g) \quad (\text{B.43})$$

$$N_g = N_g(U_g, V_g) \quad (\text{B.44})$$

The discriminant,  $T_g$ , of the second fundamental form,  $\Phi_{2,g}$ , can be calculated from the following equation:

$$T_g = \sqrt{L_g N_g - M_g^2} \quad (\text{B.45})$$

We now come to the theorem, which is essential justification for considering the differential geometry of surfaces in connection with the six fundamental magnitudes. It was proven (1867) first by Bonnet\* [8] and may be enunciated as follows:

### Theorem B.1

When six fundamental magnitudes,  $E_g, F_g, G_g$  and  $L_g, M_g, N_g$ , are given, and they fulfill the Gauss characteristic equation and the two Mainardi†-Codazzi‡ relations, they determine a gear tooth flank  $\mathcal{G}$  uniquely as to its position and orientation in space.

This theorem is commonly referred to as the *main theorem in the theory of surface* or simply as the *Bonnet theorem*. According to the main theorem, two surfaces that have identical first and second fundamental forms must be either congruent or symmetrical to one another.

By the use of six fundamental magnitudes, all parameters of local geometry of a given part surface can be calculated.

## B.5 Principal Directions on a Gear Tooth Flank

The direction of vectors of principal directions,  $\mathbf{T}_{1,g}$  and  $\mathbf{T}_{2,g}$  at a point on a gear tooth flank,  $\mathcal{G}$ , can be specified in terms of the ratio  $dU_g/dV_g$ . For the vectors of the first,  $\mathbf{T}_{1,g}$ , and second,  $\mathbf{T}_{2,g}$ , principal directions at point  $m$  of a smooth, regular part surface,  $\mathcal{G}$ , the corresponding values of the ratio  $dU_g/dV_g$  are calculated as roots of the quadratic equation:

$$\begin{vmatrix} E_g dU_g + F_g dV_g & F_g dU_g + G_g dV_g \\ L_g dU_g + M_g dV_g & M_g dU_g + N_g dV_g \end{vmatrix} = 0 \quad (\text{B.46})$$

The first principal plane section,  $C_{1,g}$ , is perpendicular to a gear tooth flank,  $\mathcal{G}$ , at a current surface point,  $m$ , and passes through the vector of the first principal direction,  $\mathbf{T}_{1,g}$ . The second principal plane section,  $C_{2,g}$ , is orthogonal to a gear tooth flank,  $\mathcal{G}$ , at a current surface point,  $m$ , and passes through the vector of the second principal direction,  $\mathbf{T}_{2,g}$ .

The principal directions,  $\mathbf{T}_{1,g}$  and  $\mathbf{T}_{2,g}$ , can be identified at any and all points of a smooth, regular gear tooth flank,  $\mathcal{G}$ , except umbilic points and flatten points of the surface. At umbilic points of a surface, as well as at flattened points, the principal directions cannot be identified.

In the theory of gearing, it is often preferred not to use the vectors  $\mathbf{T}_{1,g}$  and  $\mathbf{T}_{2,g}$  of the principal directions, but instead to use the unit vectors,  $\mathbf{t}_{1,g}$  and  $\mathbf{t}_{2,g}$ , of the principal directions. The unit tangent vectors,  $\mathbf{t}_{1,g}$  and  $\mathbf{t}_{2,g}$ , are calculated from the equations:

$$\mathbf{t}_{1,g} = \frac{\mathbf{T}_{1,g}}{|\mathbf{T}_{1,g}|} \quad (\text{B.47})$$

$$\mathbf{t}_{2,g} = \frac{\mathbf{T}_{2,g}}{|\mathbf{T}_{2,g}|} \quad (\text{B.48})$$

correspondingly.

\* Pierre Ossian Bonnet (December 22, 1819–June 22, 1892), a French mathematician.

† Gaspare Mainardi (June 27, 1800–March 9, 1879)—an Italian mathematician.

‡ Delfino Codazzi (March 7, 1824–July 21, 1873)—an Italian mathematician.



Unit tangent vectors  $\mathbf{t}_{1,g}$  and  $\mathbf{t}_{2,g}$  of principal directions at a point  $m$  on a gear tooth flank  $\mathcal{G}$ , along with the unit normal vector,  $\mathbf{n}_g$ , at that same point,  $m$ , make up an orthogonal local frame  $(\mathbf{t}_{1,g}, \mathbf{t}_{2,g}, \mathbf{n}_g)$ . All three unit vectors,  $\mathbf{t}_{1,g}$ ,  $\mathbf{t}_{2,g}$ , and  $\mathbf{n}_g$ , are mutually perpendicular to one another. The local frame  $(\mathbf{t}_{1,g}, \mathbf{t}_{2,g}, \mathbf{n}_g)$  is commonly referred to as a *Darboux frame*.

## B.6 Curvatures at a Point of a Part Surface

The first,  $R_{1,g}$ , and second,  $R_{2,g}$ , principal radii of curvature at a point of a gear tooth flank,  $\mathcal{G}$ , are measured within the first and second principal plane sections,  $C_{1,g}$  and  $C_{2,g}$ , accordingly. For the calculation of values of the principal radii of curvature, the following equation is commonly used:

$$R_g^2 - \frac{E_g N_g - 2F_g M_g + G_g L_g}{T_g} R_g + \frac{H_g}{T_g} = 0 \quad (\text{B.49})$$

Remember that algebraic values of the radii of principal curvature,  $R_{1,g}$  and  $R_{2,g}$ , relate to one another as  $R_{2,g} > R_{1,g}$ . In particular cases, at umbilic points on a gear tooth flank,  $\mathcal{G}$ , no principal curvatures can be identified, as all normal curvatures of the tooth surface,  $\mathcal{G}$ , at an umbilic point are equal to one another.

Another two important parameters of the local topology of a gear tooth flank  $\mathcal{G}$  are:

- Mean curvature,  $\mathcal{M}_g$
- Intrinsic (Gaussian or full) curvature,  $\mathcal{G}_g$

For the calculation of the curvatures  $\mathcal{M}_g$  and  $\mathcal{G}_g$ , the following equations are commonly used:

$$\mathcal{M}_g = \frac{k_{1,g} + k_{2,g}}{2} = \frac{E_g N_g - 2F_g M_g + G_g L_g}{2 \cdot (E_g G_g - F_g^2)} \quad (\text{B.50})$$

$$\mathcal{G}_g = k_{1,g} \cdot k_{2,g} = \frac{L_g N_g - M_g^2}{E_g G_g - F_g^2} \quad (\text{B.51})$$

The expressions for the mean curvature,  $\mathcal{M}_g$ , and the Gaussian curvature,  $\mathcal{G}_g$ :

$$\mathcal{M}_g = \frac{k_{1,g} + k_{2,g}}{2} \quad (\text{B.52})$$

$$\mathcal{G}_g = k_{1,g} \cdot k_{2,g} \quad (\text{B.53})$$

considered together yield a quadratic equation with respect to principal curvatures  $k_{1,g}$  and  $k_{2,g}$ :

$$k_g^2 - 2 \mathcal{M}_g k_g + \mathcal{G}_g = 0 \quad (\text{B.54})$$

The following formulae

$$k_{1,g} = \mathcal{M}_g + \sqrt{\mathcal{M}_g^2 - \mathcal{G}_g} \quad (\text{B.55})$$

$$k_{2,g} = \mathcal{M}_g - \sqrt{\mathcal{M}_g^2 - \mathcal{G}_g} \quad (\text{B.56})$$

are the solutions to Equation B.54.

Here, in Equations B.55 and B.56, the first principal curvature of a gear tooth flank,  $\mathcal{G}$ , at a current point,  $m$ , is designated as  $k_{1,g}$ , and  $k_{2,g}$  designates the second principal curvature of a gear tooth flank,  $\mathcal{G}$ , at that same point,  $m$ .

The principal curvatures,  $k_{1,g}$  and  $k_{2,g}$ , are the reciprocals to the corresponding principal radii of curvature,  $R_{1,g}$  and  $R_{2,g}$ :

$$k_{1,g} = \frac{1}{R_{1,g}} \quad (\text{B.57})$$

$$k_{2,g} = \frac{1}{R_{2,g}} \quad (\text{B.58})$$

The first principal curvature,  $k_{1,g}$ , is always larger than the second principal curvature,  $k_{2,g}$ , of a gear tooth flank,  $\mathcal{G}$ , at a current point,  $m$ —that is, the inequality:

$$k_{1,g} > k_{2,g} \quad (\text{B.59})$$

is always valid.

This brief consideration of major elements of part surface geometry makes possible the introduction of two of the definitions that are of critical importance for further discussion.

As already mentioned earlier in this section, it was proven by Bonnet [8] that the specification of the first and second fundamental forms determines a unique surface if the *Gauss characteristic equation* and the *Mainardi-Codazzi relations of compatibility* are satisfied and those two surfaces that have identical first and the second fundamental forms are congruent.\* Six fundamental magnitudes determine a surface uniquely, except as to position and orientation in space.

Specification of a surface in terms of the first and second fundamental forms is usually called the *natural kind* of surface representation. In general form, this kind of part surface representation can be expressed by a set of two equations:

$$\left. \begin{array}{l} \text{Natural form of a} \\ \text{surface } \mathcal{G} \text{ representation} \end{array} \right| \Rightarrow \mathcal{G} = \mathcal{G}(\Phi_{1,g}, \Phi_{2,g}) \left\{ \begin{array}{l} \Phi_{1,g} = \Phi_{1,g}(E_g, F_g, G_g) \\ \Phi_{2,g} = \Phi_{2,g}(E_g, F_g, G_g, L_g, M_g, N_g) \end{array} \right. \quad (\text{B.60})$$

Equation B.60 can be derived from Equation B.1. A given gear tooth flank  $\mathcal{G}$  can be expressed in both forms, that is, either by Equation B.19 or by Equation B.1.

---

## B.7 Illustrative Example

Consider an example of how an analytical representation of a surface in a Cartesian reference system can be converted into the natural representation of that same surface [113].

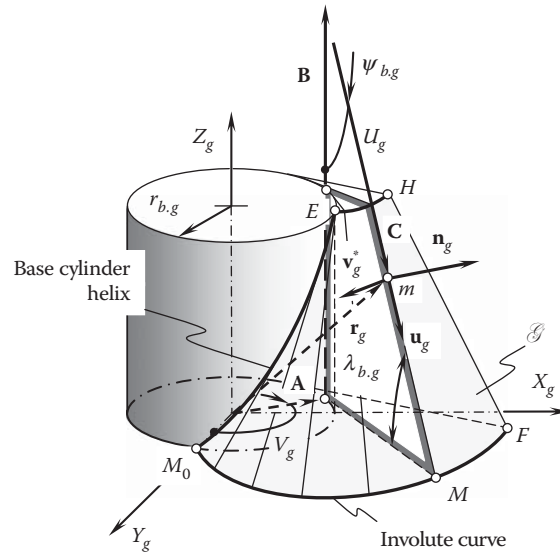
A Cartesian coordinate system,  $X_g Y_g Z_g$ , is associated with a gear tooth flank,  $\mathcal{G}$ , as schematically shown in Figure B.3.

The position vector of a point,  $\mathbf{r}_g$ , of the gear tooth flank,  $\mathcal{G}$ , can be represented as the summa of three vectors:

$$\mathbf{r}_g = \mathbf{A} + \mathbf{B} + \mathbf{C} \quad (\text{B.61})$$

---

\* Two surfaces with identical first and second fundamental forms might also be symmetrical. Refer to the literature: Koenderink, J.J., *Solid Shape*, MIT Press, Cambridge, MA, 1990, 699 p.—on differential geometry of surfaces for details about this specific issue.

**FIGURE B.3**

Derivation of the natural form of representation of a gear tooth flank,  $\mathcal{G}$ .

Each of the vectors,  $\mathbf{A}$ ,  $\mathbf{B}$ , and  $\mathbf{C}$ , can be expressed in terms of projections onto the axes of the reference system  $X_g Y_g Z_g$ . Then, Equation B.61 casts into the equation

$$\mathbf{r}_g(U_g, V_g) = \begin{bmatrix} r_{b,g} \cos V_g + U_g \cos \tau_{b,g} \sin V_g \\ r_{b,g} \sin V_g - U_g \sin \tau_{b,g} \sin V_g \\ r_{b,g} \tan \tau_{b,g} - U_g \sin \tau_{b,g} \\ 1 \end{bmatrix} \quad (\text{B.62})$$

This yields the calculation of two tangent vectors,  $\mathbf{U}_g(U_g, V_g)$  and  $\mathbf{V}_g(U_g, V_g)$ , which are correspondingly equal:

$$\mathbf{U}_g(U_g, V_g) = \begin{bmatrix} \cos \tau_{b,g} \sin V_g \\ -\cos \tau_{b,g} \cos V_g \\ -\sin \tau_{b,g} \\ 0 \end{bmatrix} \quad (\text{B.63})$$

$$\mathbf{V}_g(U_g, V_g) = \begin{bmatrix} -r_{b,g} \sin V_g + U_g \cos \tau_{b,g} \cos V_g \\ r_{b,g} \cos V_g + U_g \cos \tau_{b,g} \sin V_g \\ r_{b,g} \tan \tau_{b,g} \\ 0 \end{bmatrix} \quad (\text{B.64})$$

Substituting the derived vectors,  $\mathbf{U}_g$  and  $\mathbf{V}_g$ , into Equation B.14, one can come up with formulae for the calculation of the fundamental magnitudes of the first order:

$$E_g = 1 \quad (\text{B.65})$$

$$F_g = -\frac{r_{b,g}}{\cos \tau_{b,g}} \quad (\text{B.66})$$

$$G_g = \frac{U_g^2 \cos^4 \tau_{b,g} + r_{b,g}^2}{\cos^2 \tau_{b,g}} \quad (\text{B.67})$$

These expressions can be substituted directly into Equation B.12 for the first fundamental form,  $\Phi_{1,g}$ , of the gear tooth flank,  $\mathcal{G}$ :

$$\Phi_{1,g} \Rightarrow dU_g^2 - 2 \frac{r_{b,g}}{\cos \tau_{b,g}} dU_g dV_g + \frac{U_g^2 \cos^4 \tau_{b,g} + r_{b,g}^2}{\cos^2 \tau_{b,g}} dV_g^2 \quad (\text{B.68})$$

The derived expressions for the fundamental magnitudes,  $E_g$ ,  $F_g$ , and  $G_g$  (see Equations B.65 through B.67), can also be substituted into Equation B.13. In this way, a corresponding matrix representation of the first fundamental form,  $\Phi_{1,g}$ , of the gear tooth flank,  $\mathcal{G}$ , can be calculated. The interested reader may wish to complete these formulae on his or her own.

The discriminant,  $H_g$ , of the first fundamental form of the gear tooth flank,  $\mathcal{G}$ , can be calculated from the expression:

$$H_g = U_g \cos \tau_{b,g} \quad (\text{B.69})$$

In order to derive an equation for the second fundamental form,  $\Phi_{2,g}$ , of the gear tooth flank,  $\mathcal{G}$ , the second derivatives of the position vector of a point,  $\mathbf{r}_g(U_g, V_g)$ , with respect to the  $U_g$ - and  $V_g$ - parameters are necessary. The above-derived equations for the tangent vectors  $\mathbf{U}_g$  and  $\mathbf{V}_g$  (see Equations B.63 and B.64) make possible the following expressions for the derivatives under consideration:

$$\frac{\partial \mathbf{U}_g}{\partial U_g} = \begin{bmatrix} 0 \\ 0 \\ 0 \\ 1 \end{bmatrix} \quad (\text{B.70})$$

$$\frac{\partial \mathbf{U}_g}{\partial V_g} \equiv \frac{\partial \mathbf{V}_g}{\partial U_g} = \begin{bmatrix} \cos \tau_{b,g} \cos V_g \\ \cos \tau_{b,g} \sin V_g \\ 0 \\ 1 \end{bmatrix} \quad (\text{B.71})$$

$$\frac{\partial \mathbf{V}_g}{\partial V_g} = \begin{bmatrix} -r_{b,g} \cos V_g - U_g \cos \tau_{b,g} \sin V_g \\ -r_{b,g} \sin V_g + U_g \cos \tau_{b,g} \cos V_g \\ 0 \\ 1 \end{bmatrix} \quad (\text{B.72})$$

Further, substitute these expressions (see Equations B.70 through B.72) into Equations B.36 through B.38. After the necessary formulae transformations are complete, then Equations B.36 through B.38 cast into the set of formulae for the calculation of the fundamental magnitudes of the second order of the gear tooth flank,  $\mathcal{G}$ . This set of formulae is as follows:

$$L_g = 0 \quad (\text{B.73})$$

$$M_g = 0 \quad (\text{B.74})$$

$$N_g = -U_g \sin \tau_{b,g} \cos \tau_{b,g} \quad (\text{B.75})$$

Further, after substituting Equations B.73 through B.75 into Equation B.31, an equation for the calculation of the second fundamental form of the gear tooth flank,  $\mathcal{G}$ , can be represented in the form:

$$\Phi_{2,g} \Rightarrow -d\mathbf{r}_g \cdot d\mathbf{N}_g = -U_g \sin \tau_{b,g} \cos \tau_{b,g} dV_g^2 \quad (\text{B.76})$$

Similar to Equation B.68, the derived expressions for the fundamental magnitudes,  $L_g$ ,  $M_g$ , and  $N_g$ , of the second order can be substituted into Equation B.32 for the second fundamental form,  $\Phi_{2,g}$ . In this way, a corresponding matrix representation of the second fundamental form,  $\Phi_{2,g}$ , of the surface,  $\mathcal{G}$ , can be derived. The interested reader may wish to complete this formulae transformation on his or her own.

**TABLE B.1**

Fundamental Magnitudes of the First and Second Order of the Gear Tooth Flank,  $\mathcal{G}$

$E_g = 1$	$L_g = 0$
$F_g = -\frac{r_{b,g}}{\cos \tau_{b,g}}$	$M_g = 0$
$G_g = \frac{U_g^2 \cos^4 \tau_{b,g} + r_{b,g}^2}{\cos^2 \tau_{b,g}}$	$N_g = -U_g \sin \tau_{b,g} \cos \tau_{b,g}$

For the calculation of the discriminant,  $T_g$ , of the second fundamental form,  $\Phi_{2,g}$ , of the gear tooth flank,  $\mathcal{G}$ , the following expression can be used:

$$T_g = U_g \sin \tau_{b,g} \cos \tau_{b,g} \quad (\text{B.77})$$

The natural representation of the gear tooth flank,  $\mathcal{G}$ , can be expressed in terms of the set of six equations for the calculation of the fundamental magnitudes of the first,  $E_g, F_g, G_g$ , and second,  $L_g, M_g$  and  $N_g$  (Table B.1), fundamental forms.

All major elements of local geometry of the gear tooth flank,  $\mathcal{G}$ , can be calculated based on the fundamental magnitudes,  $E_g, F_g, G_g$ , of the first,  $\Phi_{1,g}$ , and  $L_g, M_g, N_g$  of the second,  $\Phi_{2,g}$ , fundamental forms. The location and orientation of the gear tooth flank,  $\mathcal{G}$ , are the two parameters that remain indefinite.

Once a part surface is represented in natural form—that is, it is expressed in terms of six fundamental magnitudes of the first and second order—then further calculation of parameters of a gear tooth flank,  $\mathcal{G}$ , becomes much easier. In order to demonstrate the significant simplification of the calculation of the parameters of a gear tooth flank,  $\mathcal{G}$ , several useful equations are presented below as examples.

## B.8 A Few More Useful Equations

Many calculations of parameters of geometry can be significantly simplified by use of the first and second fundamental forms of a smooth, regular part surface,  $\mathcal{G}$ .

1. For calculation of the value of the radius,  $R_g$ , of normal curvature within a normal plane section through a current point,  $m$ , on a gear tooth flank,  $\mathcal{G}$ , and in a given direction, the following equation can be used:

$$R_g = \frac{\Phi_{1,g}}{\Phi_{2,g}} \quad (\text{B.78})$$

2. The *Euler formula* for the calculation of normal curvature,  $k_{\theta,g}$ , at a point,  $m$ , in a direction that is specified by the angle  $\theta$  can be represented as follows:

$$k_{\theta,g} = k_{1,g} \cos^2 \theta + k_{2,g} \sin^2 \theta \quad (\text{B.79})$$

Here, in Equation B.79,  $\theta$  is the angle that the normal plane section,  $C_g$ , makes with the first principal plane section,  $C_{1,g}$ . In other words,  $\theta = \angle(\mathbf{t}_g, \mathbf{t}_{1,g})$ ; here,  $\mathbf{t}_g$  designates the unit tangent vector within the normal plane section  $C_g$ .

Equation B.79 is also a good illustration of significant simplification of the calculations when fundamental magnitudes,  $E_g, F_g, G_g$ , of the first and  $L_g, M_g, N_g$  of the second order are used.

In order to get a profound understanding of the differential geometry of surfaces, the interested reader may wish to go to advanced monographs in the field. Systematic discussion of the topic is available from many sources. The author would like to turn the reader's attention to books by do Carmo, Eisenhart, Stuik, and others.

## Appendix C: Change of Surface Parameters

When designing a form-cutting tool, it is often necessary to treat two or more surfaces simultaneously. For example, the cutting edge of the cutting tool can be considered the line of intersection of the generating surface,  $T$ , of the form-cutting tool by the rake surface,  $R_s$ . The equation of the cutting edge can't be derived on the premises of equations of the surfaces  $T$  and  $R_s$  as long as the initial parameterization of the surfaces is improper.

When two surfaces,  $\mathbf{r}_i$  and  $\mathbf{r}_j$ , have necessarily been treated simultaneously, then it is required that they not only be represented in a common reference system, the  $U_i$ - and  $V_i$ -parameters of one of the surfaces,  $\mathbf{r}_i = \mathbf{r}_i(U_i, V_i)$ , have to be synchronized with the corresponding  $U_j$ - and  $V_j$ -parameters of another surface,  $\mathbf{r}_j = \mathbf{r}_j(U_j, V_j)$ . The procedure of changing surface parameters is used for this purpose. Use of the procedure allows representation of one of the surfaces, for example, of the surface  $\mathbf{r}_j = \mathbf{r}_j(U_j, V_j)$  in terms of the  $U_i$ - and  $V_i$ -parameters, say, as  $\mathbf{r}_j = \mathbf{r}_j(U_i, V_i)$ .

If the parameterization of a surface is transformed by the equations  $U^* = U^*(U, V)$  and  $V^* = V^*(U, V)$ , we obtain the new derivatives:

$$\frac{\partial \mathbf{r}}{\partial U^*} = \frac{\partial \mathbf{r}}{\partial U} \cdot \frac{\partial U}{\partial U^*} + \frac{\partial \mathbf{r}}{\partial V} \cdot \frac{\partial V}{\partial U^*} \quad (\text{C.1})$$

$$\frac{\partial \mathbf{r}}{\partial V^*} = \frac{\partial \mathbf{r}}{\partial U} \cdot \frac{\partial U}{\partial V^*} + \frac{\partial \mathbf{r}}{\partial V} \cdot \frac{\partial V}{\partial V^*} \quad (\text{C.2})$$

so that:

$$\mathbf{A}^* = \left[ \frac{\partial \mathbf{r}}{\partial U^*} \mid \frac{\partial \mathbf{r}}{\partial V^*} \right] = \mathbf{A} \cdot \mathbf{J} \quad (\text{C.3})$$

where:

$$\mathbf{J} = \begin{bmatrix} \frac{\partial U}{\partial U^*} & \frac{\partial U}{\partial V^*} \\ \frac{\partial V}{\partial U^*} & \frac{\partial V}{\partial V^*} \end{bmatrix} \quad (\text{C.4})$$

is called the *Jacobian matrix* of the transformation.

It can be shown that the new fundamental matrix,  $\mathbf{G}^*$ , is given by:

$$\mathbf{G}^* = \mathbf{A}^{*T} \mathbf{A}^* = \mathbf{J}^T \mathbf{A}^T \mathbf{A} \mathbf{J} = \mathbf{J}^T \mathbf{G} \mathbf{J} \quad (\text{C.5})$$

From this equation, we see by the properties of determinants that  $|\mathbf{G}^*| = |\mathbf{J}|^2 |\mathbf{G}|$ . Using this result and Equation C.2, we can show that the unit surface normal,  $\mathbf{n}$ , is invariant under the transformation, as we would expect.

The transformation of the second fundamental matrix can similarly be shown to be given by:

$$\mathbf{D}^* = \mathbf{J}^T \mathbf{D} \mathbf{J} \quad (\text{C.6})$$

by differentiating Equation C.2 and using the invariance of  $\mathbf{n}$  from Equations C.5 and C.6, it can be shown that the principal curvatures and directions are invariant under the transformation.

We conclude that the unit normal vector,  $\mathbf{n}$ , and the principal directions and curvatures are independent of the parameters used and are therefore geometric properties of the surface itself. They should be continuous if the surface is to be tangent and the curvature continuous.



# Taylor & Francis

Taylor & Francis Group

<http://taylorandfrancis.com>



---

## Appendix D: Applied Coordinate Systems and Linear Transformations

---

Consequent coordinate system transformations can be easily described analytically with the implementation of matrices. The use of matrices for coordinate system transformation\* can be traced back to the mid-1940s† when Mozhayev‡ began describing coordinate system transformations by means of matrices.

Below, coordinate system transformation is briefly discussed from the standpoint of its implementation in the theory of gearing.

---

### D.1 Coordinate System Transformation

Homogeneous coordinates utilize a mathematical trick to embed three-dimensional coordinates and transformations into a four-dimensional matrix format. As a result, inversions or combinations of linear transformations are simplified to inversions or multiplication of the corresponding matrices.

#### D.1.1 Homogeneous Coordinate Vectors

Instead of representing each point,  $\mathbf{r}(x, y, z)$ , in three-dimensional space with a single three-dimensional vector,

$$\mathbf{r} = \begin{bmatrix} x \\ y \\ z \end{bmatrix} \quad (\text{D.1})$$

homogeneous coordinates allow each point,  $\mathbf{r}(x, y, z)$ , to be represented by any of an infinite number of four-dimensional vectors:

$$\mathbf{r} = \begin{bmatrix} T \cdot x \\ T \cdot y \\ T \cdot z \\ T \end{bmatrix} \quad (\text{D.2})$$

The three-dimensional vector corresponding to any four-dimensional vector can be calculated by dividing the first three elements by the fourth, and a four-dimensional vector corresponding to any three-dimensional vector can be created by simply adding a fourth element and setting it equal to one.

#### D.1.2 Homogeneous Coordinate Transformation Matrices of the Dimension $4 \times 4$

Homogeneous coordinate transformation matrices operate on four-dimensional homogeneous vector representations of traditional three-dimensional coordinate locations. Any three-dimensional linear transformation (translation, rotation, and so forth) can be represented by a  $4 \times 4$  homogeneous coordinate transformation matrix. In fact, because of the redundant representation of three-space in a homogeneous coordinate system,

---

\* Matrices were introduced into mathematics by A. Cayley in 1857. They provide a compact and flexible notation particularly useful in dealing with linear transformations, and they present an organized method for the solution of systems of linear differential equations.

† Application of matrices for the purposes of analytical representation of coordinate system transformation should be credited to Dr. S.S. Mozhayev (Mozhayev, S.S., *General Theory of Cutting Tools*, Doctoral Thesis, Leningrad, Leningrad Polytechnic Institute, 1951, 295 p.). Dr. S.S. Mozhayev began using matrices for this purpose in the mid-1940s. Later on, a matrix approach for coordinate system transformation was used by Denavit and Hartenberg [13], as well as by many other researchers.

‡ S.S. Mozhayev is a Soviet scientist mostly known for his accomplishments in the theory of cutting tool design.

an infinite number of different  $4 \times 4$  homogeneous coordinate transformation matrices are available to perform any given linear transformation. This redundancy can be eliminated to provide a unique representation by dividing all elements of a  $4 \times 4$  homogeneous transformation matrix by the last element (which will become equal to one). This means that a  $4 \times 4$  homogeneous transformation matrix can incorporate as many as 15 independent parameters. The generic format representation of a homogeneous transformation equation for mapping the three-dimensional coordinate  $(x_1, y_1, z_1)$  to the three-dimensional coordinate  $(x_2, y_2, z_2)$  is:

$$\begin{bmatrix} T^* \cdot x_2 \\ T^* \cdot y_2 \\ T^* \cdot z_2 \\ T^* \end{bmatrix} = \begin{bmatrix} T^* \cdot a & T^* \cdot b & T^* \cdot c & T^* \cdot d \\ T^* \cdot e & T^* \cdot f & T^* \cdot g & T^* \cdot h \\ T^* \cdot i & T^* \cdot j & T^* \cdot k & T^* \cdot m \\ T^* \cdot n & T^* \cdot p & T^* \cdot q & T^* \end{bmatrix} \cdot \begin{bmatrix} T \cdot x_2 \\ T \cdot y_2 \\ T \cdot z_2 \\ T \end{bmatrix} \quad (D.3)$$

If any two matrices or vectors of this equation are known, the third matrix (or vector) can be calculated, and then the redundant  $T$  element in the solution can be eliminated by dividing all elements of the matrix by the last element.

Various transformation models can be used to constrain the form of the matrix to transformations with fewer degrees of freedom.

### D.1.3 Translations

Translation of a coordinate system is one of the major linear transformations used in the theory of part surface generation. Translations of the coordinate system  $X_2Y_2Z_2$  along axes of the coordinate system  $X_1Y_1Z_1$  are depicted in Figure D.1. Translations can be analytically described by the homogeneous transformation matrix of dimension  $4 \times 4$ .

For an analytical description of translation along coordinate axes, the operators of translation  $\text{Tr}(a_x, X)$ ,  $\text{Tr}(a_y, Y)$ , and  $\text{Tr}(a_z, Z)$  are used. These operators yield matrix representation in the form:

$$\text{Tr}(a_x, X) = \begin{bmatrix} 1 & 0 & 0 & a_x \\ 0 & 1 & 0 & 0 \\ 0 & 0 & 1 & 0 \\ 0 & 0 & 0 & 1 \end{bmatrix} \quad (D.4)$$

$$\text{Tr}(a_y, Y) = \begin{bmatrix} 1 & 0 & 0 & 0 \\ 0 & 1 & 0 & a_y \\ 0 & 0 & 1 & 0 \\ 0 & 0 & 0 & 1 \end{bmatrix} \quad (D.5)$$

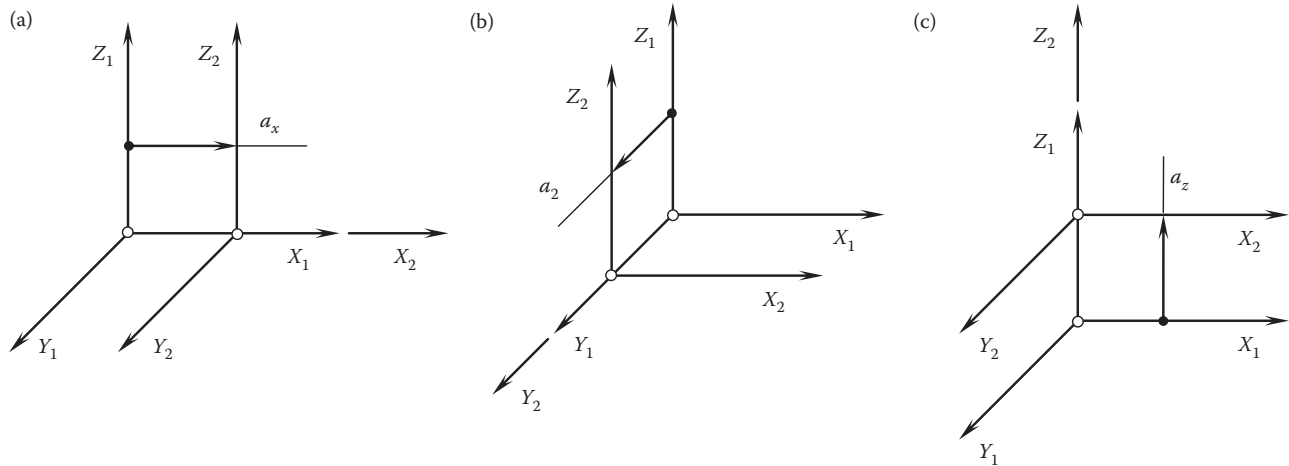


FIGURE D.1

Analytical description of the operators of translation,  $\text{Tr}(a_x, X)$ ,  $\text{Tr}(a_y, Y)$ ,  $\text{Tr}(a_z, Z)$ , along the coordinate axes of a Cartesian reference system,  $XYZ$ .

$$\mathbf{Tr}(a_z, Z) = \begin{bmatrix} 1 & 0 & 0 & 0 \\ 0 & 1 & 0 & 0 \\ 0 & 0 & 1 & a_z \\ 0 & 0 & 0 & 1 \end{bmatrix} \quad (\text{D.6})$$

Here, in Equations D.4 through D.6, the parameters  $a_x$ ,  $a_y$ , and  $a_z$  are signed values that denote the distance of translation along the corresponding axis.

Consider two coordinate systems,  $X_1Y_1Z_1$  and  $X_2Y_2Z_2$ , displaced along the  $X_1$ -axis at a distance  $a_x$ , as schematically depicted in Figure D.1a. A point,  $m$ , in the reference system  $X_2Y_2Z_2$  is given by the position vector  $\mathbf{r}_2(m)$ . In the coordinate system,  $X_1Y_1Z_1$ , that same point,  $m$ , can be specified by the position vector  $\mathbf{r}_1(m)$ . Then, the position vector  $\mathbf{r}_1(m)$  can be expressed in terms of the position vector  $\mathbf{r}_2(m)$  by the equation:

$$\mathbf{r}_1(m) = \mathbf{Tr}(a_x, X) \cdot \mathbf{r}_2(m) \quad (\text{D.7})$$

Equations similar to Equation D.7 are valid for the operators  $\mathbf{Tr}(a_y, Y)$  and  $\mathbf{Tr}(a_z, Z)$  of the coordinate system transformation. The later is schematically illustrated in Figures D.1b and c.

Use of the operators of translation,  $\mathbf{Tr}(a_x, X)$ ,  $\mathbf{Tr}(a_y, Y)$ , and  $\mathbf{Tr}(a_z, Z)$ , makes possible an introduction of an operator  $\mathbf{Tr}(a, \mathbf{A})$  of a combined transformation. Suppose that point  $p$  on a rigid body goes through a translation describing a straight line from point  $p_1$  to point  $p_2$  with a change of coordinates of  $(a_x, a_y, a_z)$ . This motion of the point,  $p$ , can be analytically described with a resultant translation operator,  $\mathbf{Tr}(a, \mathbf{A})$ :

$$\mathbf{Tr}(a, \mathbf{A}) = \begin{bmatrix} 1 & 0 & 0 & a_x \\ 0 & 1 & 0 & a_y \\ 0 & 0 & 1 & a_z \\ 0 & 0 & 0 & 1 \end{bmatrix} \quad (\text{D.8})$$

The operator,  $\mathbf{Tr}(a, \mathbf{A})$ , of the resultant coordinate system transformation can be interpreted as the operator of translation along an arbitrary axis having the vector  $\mathbf{A}$  as the direct vector.

An analytical description of translation of the coordinate system  $X_1Y_1Z_1$  in direction of an arbitrary vector,  $\mathbf{A}$ , to the position of  $X_2Y_2Z_2$  can be composed from Figure D.2. The operator of translation,  $\mathbf{Tr}(a, \mathbf{A})$ , of that particular kind can be expressed in terms of the operators  $\mathbf{Tr}(a_x, X)$ ,  $\mathbf{Tr}(a_y, Y)$ , and  $\mathbf{Tr}(a_z, Z)$  of elementary translations:

$$\mathbf{Tr}(a, \mathbf{A}) = \mathbf{Tr}(a_z, Z) \cdot \mathbf{Tr}(a_y, Y) \cdot \mathbf{Tr}(a_x, X) \quad (\text{D.9})$$

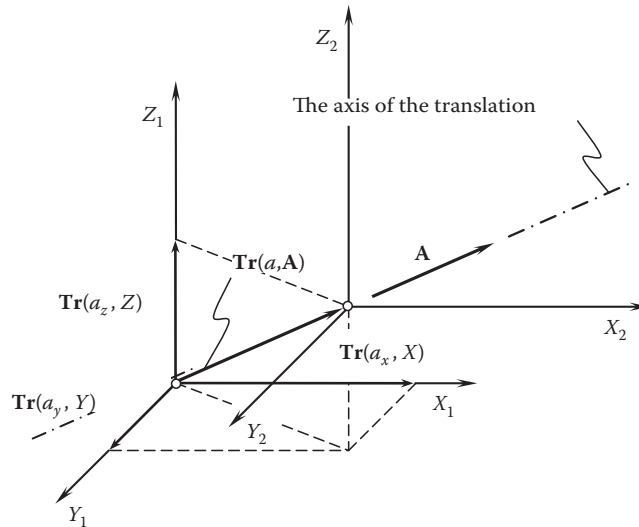


FIGURE D.2

Analytical description of an operator,  $\mathbf{Tr}(a, \mathbf{A})$ , of translation along an arbitrary axis (vector  $\mathbf{A}$  is the direct vector of the axis).

Evidently, the axis along the vector  $\mathbf{A}$  is always the axis through the origins of both reference systems  $X_1Y_1Z_1$  and  $X_2Y_2Z_2$ .

Any and all coordinate system transformations that do not change the orientation of a geometrical object are referred to as *orientation-preserving transformations*, or *direct transformations*. Therefore, transformation of translation is an example of a direct transformation.

#### D.1.4 Rotation about a Coordinate Axis

Rotation of a coordinate system about a coordinate axis is another major linear transformation used in the theory of part surface generation. A rotation is specified by an axis of rotation and the angle of the rotation. It is a fairly simple trigonometric calculation to obtain a transformation matrix for a rotation about one of the coordinate axes.

Possible rotations of the coordinate system  $X_2Y_2Z_2$  about the axis of the coordinate system  $X_1Y_1Z_1$  are illustrated in Figure D.3.

For analytical description of rotation about a coordinate axis, the operators of rotation,  $\mathbf{Rt}(\varphi_x, X_1)$ ,  $\mathbf{Rt}(\varphi_y, Y_1)$ , and  $\mathbf{Rt}(\varphi_z, Z_1)$ , are used. These operators of linear transformations yield representation in the form of homogeneous matrices:

$$\mathbf{Rt}(\varphi_x, X_1) = \begin{bmatrix} 1 & 0 & 0 & 0 \\ 0 & \cos \varphi_x & \sin \varphi_x & 0 \\ 0 & -\sin \varphi_x & \cos \varphi_x & 0 \\ 0 & 0 & 0 & 1 \end{bmatrix} \quad (\text{D.10})$$

$$\mathbf{Rt}(\varphi_y, Y_1) = \begin{bmatrix} \cos \varphi_y & 0 & \sin \varphi_y & 0 \\ 0 & 1 & 0 & 0 \\ -\sin \varphi_y & 0 & \cos \varphi_y & 0 \\ 0 & 0 & 0 & 1 \end{bmatrix} \quad (\text{D.11})$$

$$\mathbf{Rt}(\varphi_z, Z_1) = \begin{bmatrix} \cos \varphi_z & \sin \varphi_z & 0 & 0 \\ -\sin \varphi_z & \cos \varphi_z & 0 & 0 \\ 0 & 0 & 1 & 0 \\ 0 & 0 & 0 & 1 \end{bmatrix} \quad (\text{D.12})$$

Here,  $\varphi_x$ ,  $\varphi_y$ , and  $\varphi_z$  are signed values that denote the corresponding angles of rotation about a corresponding coordinate axis:  $\varphi_x$  is the angle of rotation around the  $X_1$ -axis (pitch) of the *Cartesian* coordinate system  $X_1Y_1Z_1$ ,  $\varphi_y$  is the angle of rotation around the  $Y_1$ -axis (roll), and  $\varphi_z$  is the angle of rotation around the  $Z_1$ -axis (yaw) of that same Cartesian reference system  $X_1Y_1Z_1$ .

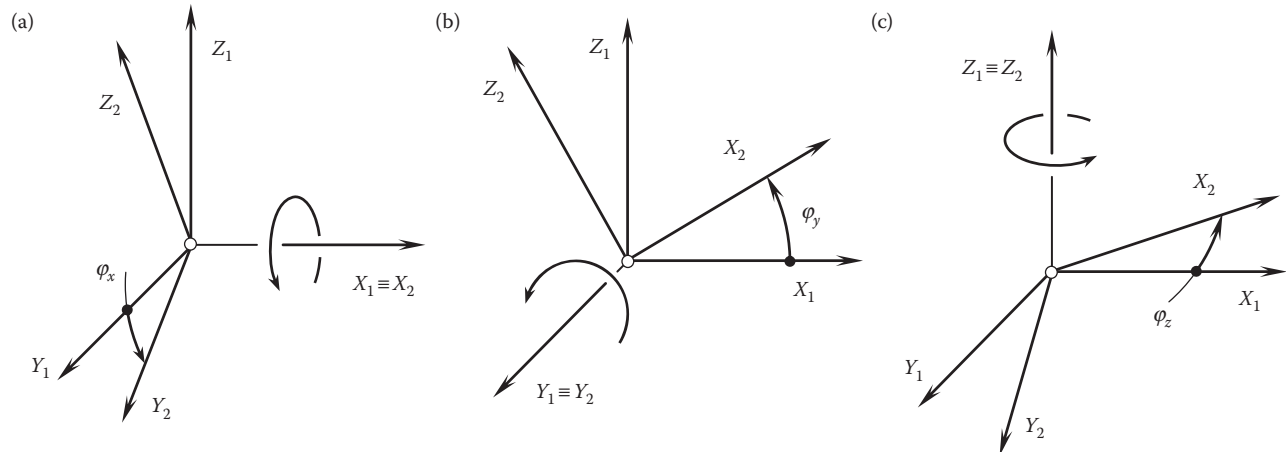


FIGURE D.3

Analytical description of the operators of rotation,  $\mathbf{Rt}(\varphi_x, X)$ ,  $\mathbf{Rt}(\varphi_y, Y)$ , and  $\mathbf{Rt}(\varphi_z, Z)$ , about a coordinate axis of a reference system,  $X_1Y_1Z_1$ .

Rotation about a coordinate axis is illustrated in [Figure D.3](#).

Consider two coordinate systems,  $X_1Y_1Z_1$  and  $X_2Y_2Z_2$ , which are turned about the  $X_1$ -axis through an angle,  $\varphi_x$ , as shown in [Figure D.3a](#). In the reference system,  $X_2Y_2Z_2$ , a point  $m$  is given by a position vector,  $\mathbf{r}_2(m)$ . In the coordinate system,  $X_1Y_1Z_1$ , that same point,  $m$ , can be specified by the position vector  $\mathbf{r}_1(m)$ . Then, the position vector  $\mathbf{r}_1(m)$  can be expressed in terms of the position vector  $\mathbf{r}_2(m)$  by the equation:

$$\mathbf{r}_1(m) = \mathbf{Rt}(\varphi_x, X) \cdot \mathbf{r}_2(m) \quad (\text{D.13})$$

Equations similar to Equation D.13 are also valid for other operators,  $\mathbf{Rt}(\varphi_y, Y)$  and  $\mathbf{Rt}(\varphi_z, Z)$ , of the coordinate system transformation. These elementary coordinate system transformations are schematically illustrated in [Figures D.3b and c](#) accordingly.

### D.1.5 Rotation about an Arbitrary Axis through the Origin

When a rotation is to be performed around an arbitrary vector based at the origin, the transformation matrix must be assembled from a combination of rotations about the Cartesian coordinate.

Two different approaches for analytical description of a rotation about an arbitrary axis through the origin are discussed below.

#### D.1.5.1 Conventional Approach

Analytical description of rotation of the coordinate system,  $X_1Y_1Z_1$ , about an arbitrary axis through the origin to the position of a reference system,  $X_2Y_2Z_2$ , is illustrated in [Figure D.4](#). It is assumed here that the rotation is performed about the axis having a vector  $\mathbf{A}_0$  as the direction vector. The operator,  $\mathbf{Rt}(\varphi_A, \mathbf{A}_0)$ , of rotation of that kind can be expressed in terms of the operators  $\mathbf{Rt}(\varphi_x, X)$ ,  $\mathbf{Rt}(\varphi_y, Y)$ , and  $\mathbf{Rt}(\varphi_z, Z)$  of elementary rotations:

$$\mathbf{Rt}(\varphi_A, \mathbf{A}_0) = \mathbf{Rt}(\varphi_z, Z) \cdot \mathbf{Rt}(\varphi_y, Y) \cdot \mathbf{Rt}(\varphi_x, X) \quad (\text{D.14})$$

Evidently, the axis of rotation (a straight line along the vector  $\mathbf{A}_0$ ) is always an axis through the origin. The operators of translation and rotation also yield linear transformations of other kinds.

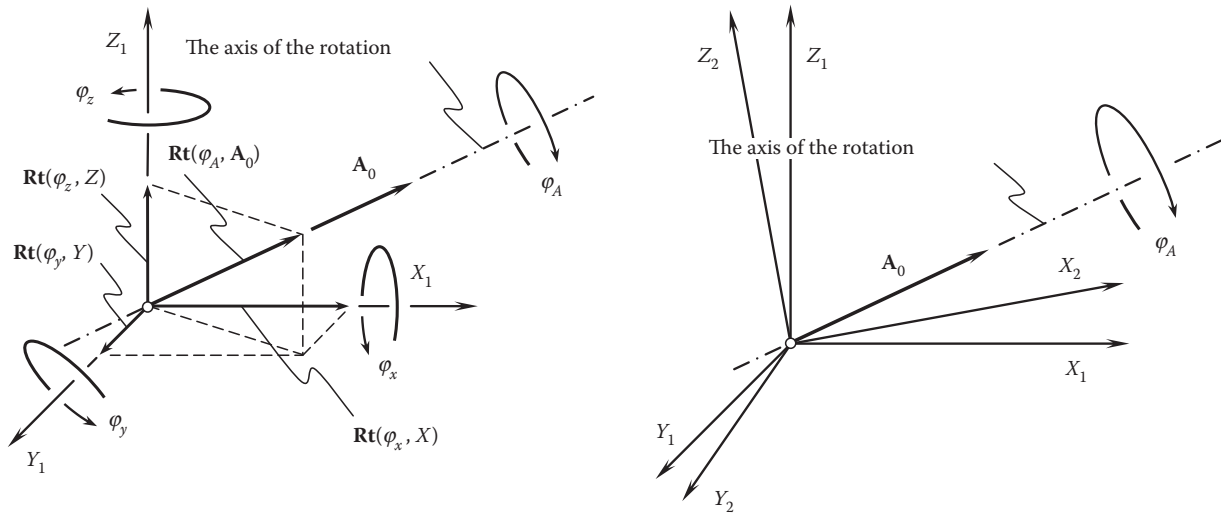


**FIGURE D.4**

Analytical description of the operator,  $\mathbf{Rt}(\varphi_A, \mathbf{A})$ , of rotation about an arbitrary axis through the origin of a Cartesian coordinate system,  $X_1Y_1Z_1$  (the vector  $\mathbf{A}$  is the directing vector of the axis of rotation).

### D.1.5.2 Eulerian Transformation

Eulerian transformation is a well-known kind of linear transformation used widely in mechanical engineering. This kind of linear transformation is analytically described by the operator  $\mathbf{Eu}(\psi, \theta, \varphi)$  of Eulerian\* transformation.

The operator  $\mathbf{Eu}(\psi, \theta, \varphi)$  is expressed in terms of three Euler angles (or Eulerian angles),  $\psi$ ,  $\theta$ , and  $\varphi$ . Configuration of an orthogonal Cartesian coordinate system,  $X_1Y_1Z_1$ , in relation to another orthogonal Cartesian coordinate system,  $X_2Y_2Z_2$ , is defined by the Euler angles  $\psi$ ,  $\theta$ , and  $\varphi$ . These angles are shown in Figure D.5.

The line of intersection of the coordinate plane,  $X_1Y_1$ , of the first reference system by the coordinate plane,  $X_2Y_2$ , of the second reference system is commonly referred to as *line of nodes*. In Figure D.5, the line  $OK$  is the line of nodes. It is assumed here and below that the line of nodes,  $OK$ , and the axes  $Z_1$  and  $Z_2$  form a frame of that same orientation as the reference systems  $X_1Y_1Z_1$  and  $X_2Y_2Z_2$  do.

The Euler angle  $\varphi$  is referred to as the *angle of pure rotation*. This angle is measured between the  $X_1$ -axis and the line of nodes,  $OK$ . The angle of pure rotation,  $\varphi$ , is measured within the coordinate plane,  $X_1Y_1$ , in the direction of shortest rotation from the axis  $X_1$  to the axis  $Y_1$ .

The Euler angle  $\theta$  is referred to as the *angle of nutation*. The angle of nutation,  $\theta$ , is measured between the axes  $Z_1$  and  $Z_2$ . The actual value of this angle never exceeds  $180^\circ$ .

The Euler angle  $\psi$  is referred to as the *angle of precession*. The angle of precession,  $\psi$ , is measured in the coordinate plane  $X_2Y_2$ . This is the angle between the line of nodes,  $OK$ , and the  $X_2$ -axis. The direction of the shortest rotation from the axis  $X_2$  to the axis  $Y_2$  is the direction in which the angle of precession is measured.

In the case where the angle of nutation is either  $\theta = 0^\circ$  or  $\theta = 180^\circ$ , then the Euler angles are not defined.

The operator  $\mathbf{Eu}(\psi, \theta, \varphi)$  of Eulerian transformation allows for the following matrix representation:

$$\mathbf{Eu}(\psi, \theta, \varphi) = \begin{bmatrix} -\sin \psi \cos \theta \sin \varphi + \cos \psi \cos \varphi & \cos \psi \cos \theta \sin \varphi + \sin \psi \cos \varphi & \sin \theta \sin \varphi & 0 \\ -\sin \psi \cos \theta \cos \varphi - \cos \psi \sin \varphi & \cos \psi \cos \theta \cos \varphi - \sin \psi \sin \varphi & \sin \theta \cos \varphi & 0 \\ \sin \theta \sin \varphi & -\cos \psi \cos \theta & \cos \theta & 0 \\ 0 & 0 & 0 & 1 \end{bmatrix} \quad (\text{D.15})$$

It is important to stress here the difference between the operator,  $\mathbf{Eu}(\psi, \theta, \varphi)$ , of Eulerian transformation and the operator,  $\mathbf{Rt}(\psi_A, \mathbf{A}_0)$ , of rotation about an arbitrary axis through the origin.

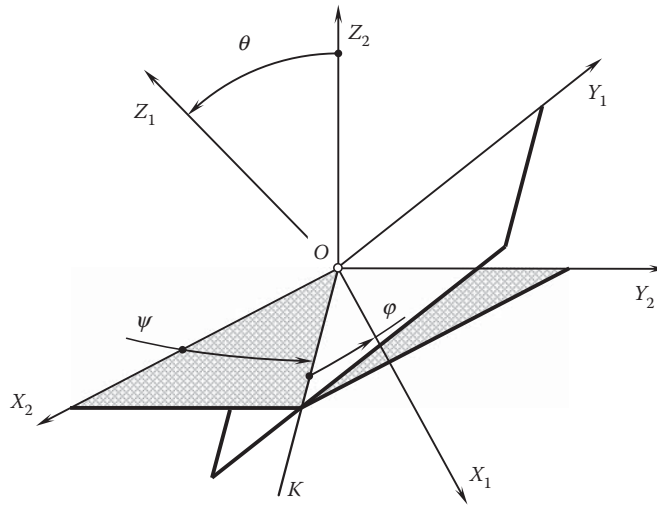


FIGURE D.5  
Euler angles.

\* Leonhard Euler (April 15, 1707–September 18, 1783), a famous Swiss mathematician and physicist who spent most of his life in Russia and Germany.

The operator,  $\mathbf{Rt}(\psi_A, \mathbf{A})$ , of rotation about an arbitrary axis through the origin can result in the same final orientation of the coordinate system  $X_2Y_2Z_2$  in relation to the coordinate system  $X_1Y_1Z_1$  as the operator,  $\mathbf{Eu}(\psi, \theta, \varphi)$ , of Eulerian transformation does. However, the operators of linear transformation,  $\mathbf{Rt}(\psi_A, \mathbf{A}_0)$  and  $\mathbf{Eu}(\psi, \theta, \varphi)$ , are operators of a completely different nature. They can result in identical coordinate system transformation, but they are not equal to one another.

#### D.1.6 Rotation about an Arbitrary Axis Not through the Origin

The transformation corresponding to the rotation of an angle,  $\varphi$ , around an arbitrary vector not through the origin cannot readily be written in a form similar to the rotation matrices about the coordinate axes.

The desired transformation matrix is obtained by combining a sequence of elementary translation and rotation matrices. (Once a single  $4 \times 4$  matrix has been obtained representing the composite transformations, it can be used in the same way as any other transformation matrix.)

Rotation of the coordinate system,  $X_1Y_1Z_1$ , to a configuration that the coordinate system,  $X_2Y_2Z_2$ , possesses can be performed about a corresponding axis that features an arbitrary configuration in space (see Figure D.6). The vector  $\mathbf{A}$  is the direction vector of the axis of the rotation. The axis of rotation is not a line through the origin.

The operator of linear transformation of this particular kind,  $\mathbf{Rt}(\psi_A, \mathbf{A})$ , can be expressed in terms of the operator  $\mathbf{Tr}(a, \mathbf{A})$  of translation along and of operator,  $\mathbf{Rt}(\psi_A, \mathbf{A}_0)$ , of rotation about an arbitrary axis through the origin:

$$\mathbf{Rt}(\varphi_A, \mathbf{A}) = \mathbf{Tr}(-b, \mathbf{B}^*) \cdot \mathbf{Rt}(\varphi_A, \mathbf{A}_0) \cdot \mathbf{Tr}(b, \mathbf{B}) \quad (\text{D.16})$$

In Equation D.16:

$\mathbf{Tr}(b, \mathbf{B})$ : is the operator of translation along the shortest distance of approach of the axis of rotation and origin of the coordinate system.

$\mathbf{Tr}(-b, \mathbf{B}^*)$ : is the operator of translation in the direction opposite to the translation,  $\mathbf{Tr}(b, \mathbf{B})$ , after the rotation,  $\mathbf{Rt}(\psi_A, \mathbf{A})$ , is completed.

In order to determine the shortest distance of approach,  $B$ , of the axis of rotation (i.e., the axis along the directing vector  $\mathbf{B}$ ) and origin of the coordinate system, consider the axis ( $\mathbf{B}$ ) through two given points,  $\mathbf{r}_{B.1}$  and  $\mathbf{r}_{B.2}$ .

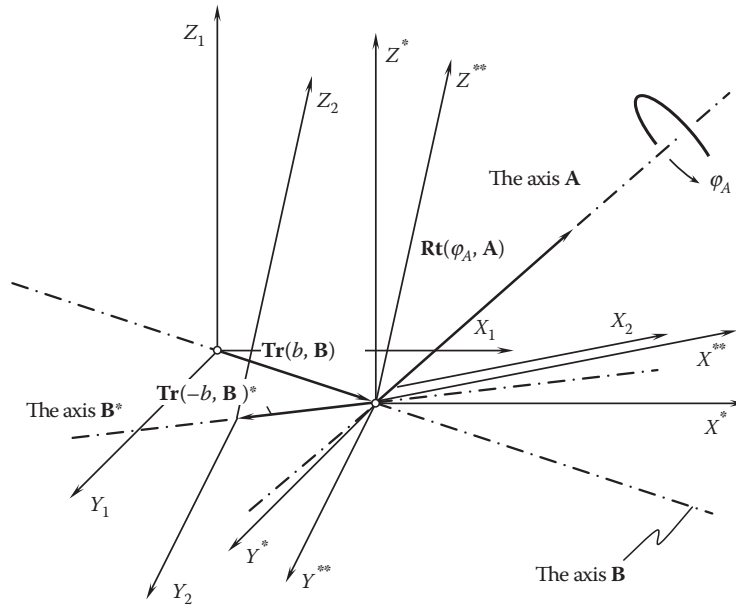


FIGURE D.6

Analytical description of the operator,  $\mathbf{Rt}(\varphi_A, \mathbf{A})$ , of rotation about an arbitrary axis not through the origin (vector  $\mathbf{A}$  is the direct vector of the axis of the rotation).



The shortest distance between a certain point,  $\mathbf{r}_0$ , and the straight line through the points  $\mathbf{r}_{B,1}$  and  $\mathbf{r}_{B,2}$  can be calculated from the following formula:

$$B = \frac{|(\mathbf{r}_2 - \mathbf{r}_1) \times (\mathbf{r}_1 - \mathbf{r}_0)|}{|\mathbf{r}_2 - \mathbf{r}_1|} \quad (\text{D.17})$$

For the origin of the coordinate system, the equality  $\mathbf{r}_0 = 0$  is observed. Then,

$$B = |\mathbf{r}_1| \cdot \sin \angle [\mathbf{r}_1, (\mathbf{r}_2 - \mathbf{r}_1)] \quad (\text{D.18})$$

Matrix representation of the operators of translation,  $\mathbf{Tr}(a_x, X)$ ,  $\mathbf{Tr}(a_y, Y)$ ,  $\mathbf{Tr}(a_z, Z)$ , along the coordinate axes, together with the operators of rotation,  $\mathbf{Rt}(\varphi_x, X)$ ,  $\mathbf{Rt}(\varphi_y, Y)$ ,  $\mathbf{Rt}(\varphi_z, Z)$ , about the coordinate axes is convenient for implementation in the theory of part surface generation. Moreover, use of the operators is the simplest possible way to analytically describe the linear transformations.

### D.1.7 Resultant Coordinate System Transformation

The operators of translation,  $\mathbf{Tr}(a_x, X)$ ,  $\mathbf{Tr}(a_y, Y)$ , and  $\mathbf{Tr}(a_z, Z)$ , together with the operators of rotation,  $\mathbf{Rt}(\varphi_x, X)$ ,  $\mathbf{Rt}(\varphi_y, Y)$ , and  $\mathbf{Rt}(\varphi_z, Z)$ , are used for the purpose of composing the operator,  $\mathbf{Rs}(1 \mapsto 2)$ , of the resultant coordinate system transformation. The transition from the initial Cartesian reference system,  $X_1Y_1Z_1$ , to the other Cartesian reference system,  $X_2Y_2Z_2$ , is analytically described by the operator,  $\mathbf{Rs}(1 \mapsto 2)$ , of the resultant coordinate system transformation.

For example, the expression:

$$\mathbf{Rs}(1 \mapsto 5) = \mathbf{Tr}(a_x, X) \cdot \mathbf{Rt}(\varphi_z, Z) \cdot \mathbf{Rt}(\varphi_x, X) \cdot \mathbf{Tr}(a_y, Y) \quad (\text{D.19})$$

indicates that the transition from coordinate system  $X_1Y_1Z_1$  to coordinate system  $X_5Y_5Z_5$  is executed in the following four steps (see Figure D.7):

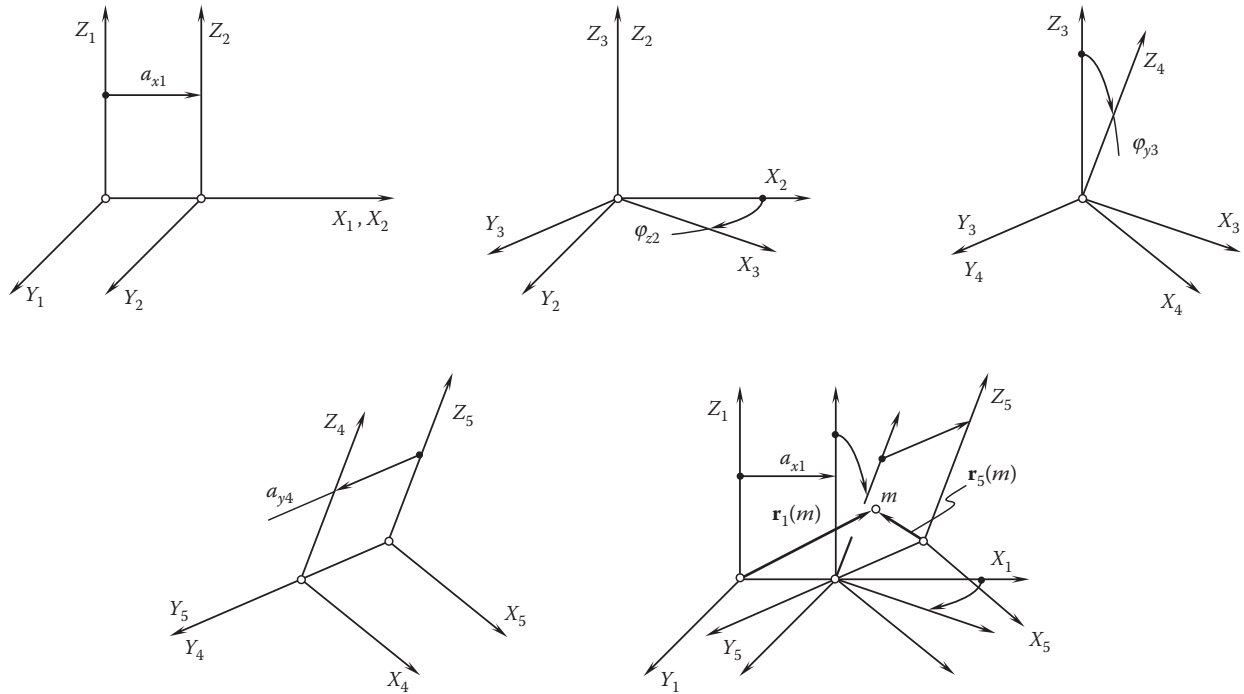


FIGURE D.7

An example of the resultant coordinate system transformation, analytically expressed by the operator  $\mathbf{Rs}(1 \mapsto 5)$ .

- Translation,  $\mathbf{Tr}(a_y, Y)$ , followed by
- Rotation,  $\mathbf{Rt}(\varphi_x, X)$ , followed by
- Second rotation,  $\mathbf{Rt}(\varphi_z, Z)$ , finally followed by
- Translation,  $\mathbf{Tr}(a_x, X)$

Ultimately, the equality:

$$\mathbf{r}_1(m) = \mathbf{Rs}(1 \mapsto 5) \cdot \mathbf{r}_5(m) \quad (\text{D.20})$$

is valid.

When the operator,  $\mathbf{Rs}(1 \mapsto t)$ , of the resultant coordinate system transformation is specified, then the transition in the opposite direction can be performed by means of the operator,  $\mathbf{Rs}(t \mapsto 1)$ , of the inverse coordinate system transformation. The following equality can be easily proven:

$$\mathbf{Rs}(t \mapsto 1) = \mathbf{Rs}^{-1}(1 \mapsto t) \quad (\text{D.21})$$

In the above example illustrated in [Figure D.7](#), the operator,  $\mathbf{Rs}(5 \mapsto 1)$ , of the inverse resultant coordinate system transformation can be expressed in terms of the operator,  $\mathbf{Rs}(1 \mapsto 5)$ , of the direct resultant coordinate system transformation. Following Equation D.21, one can come up with the equation:

$$\mathbf{Rs}(5 \mapsto 1) = \mathbf{Rs}^{-1}(1 \mapsto 5) \quad (\text{D.22})$$

It is easy to show that the operator,  $\mathbf{Rs}(1 \mapsto t)$ , of the resultant coordinate system transformation allows for representation in the following form:

$$\mathbf{Rs}(1 \mapsto t) = \mathbf{Tr}(a, A) \cdot \mathbf{Eu}(\psi, \theta, \varphi) \quad (\text{D.23})$$

The linear transformation,  $\mathbf{Rs}(1 \mapsto t)$  (see Equation D.23), can also be expressed in terms of rotation about an axis,  $\mathbf{Rt}(\varphi_A, A)$ , not through the origin (see Equation D.16).

## D.2 Complex Coordinate System Transformation

In particular cases of complex coordinate system transformations that are repeatedly used in practice, special-purpose operators of coordinate system transformation can be composed of elementary operators of translation and operators of rotation.

### D.2.1 Linear Transformation Describing a Screw Motion about a Coordinate Axis

Operators for analytical description of screw motion about an axis of the Cartesian coordinate system are a particular case of the operators of the resultant coordinate system transformation.

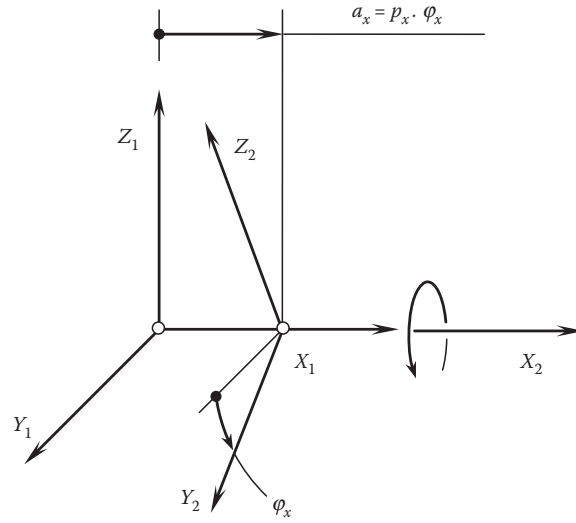
By definition (see [Figure D.8](#)), the operator,  $\mathbf{Sc}_x(\varphi_x, p_x)$ , of a screw motion about X-axis of the Cartesian coordinate system XYZ is equal to:

$$\mathbf{Sc}_x(\varphi_x, p_x) = \mathbf{Rt}(\varphi_x, X) \cdot \mathbf{Tr}(a_x, X) \quad (\text{D.24})$$

After substitution of the operator of translation,  $\mathbf{Tr}(a_x, X)$  (see Equations 3.4 through 3.6), and the operator of rotation,  $\mathbf{Rt}(\varphi_x, X)$  (see Equation D.10), Equation D.24 casts into the expression:

$$\mathbf{Sc}_x(\varphi_x, p_x) = \begin{bmatrix} 1 & 0 & 0 & p_x \cdot \varphi_x \\ 0 & \cos \varphi_x & \sin \varphi_x & 0 \\ 0 & -\sin \varphi_x & \cos \varphi_x & 0 \\ 0 & 0 & 0 & 1 \end{bmatrix} \quad (\text{D.25})$$

for the calculation of the operator of the screw motion,  $\mathbf{Sc}_x(\varphi_x, p_x)$ , about the X-axis.

**FIGURE D.8**

On analytical description of the operator of screw motion,  $\mathbf{Sc}_x(\varphi_x, p_x)$ .

The operators of screw motions,  $\mathbf{Sc}_y(\varphi_y, p_y)$  and  $\mathbf{Sc}_z(\varphi_z, p_z)$ , about the Y- and Z-axes, correspondingly, are defined in a way similar to how the operator of the screw motion,  $\mathbf{Sc}_x(\varphi_x, p_x)$ , is defined:

$$\mathbf{Sc}_y(\varphi_y, p_y) = \mathbf{Rt}(\varphi_y, Y) \cdot \mathbf{Tr}(a_y, Y) \quad (\text{D.26})$$

$$\mathbf{Sc}_z(\varphi_z, p_z) = \mathbf{Rt}(\varphi_z, Z) \cdot \mathbf{Tr}(a_z, Z) \quad (\text{D.27})$$

Using Equations D.5 and D.6 together with Equations D.11 and D.12, one can come up with the expressions:

$$\mathbf{Sc}_y(\varphi_y, p_y) = \begin{bmatrix} \cos \varphi_y & 0 & -\sin \varphi_y & 0 \\ 0 & 1 & 0 & p_y \cdot \varphi_y \\ \sin \varphi_y & 0 & \cos \varphi_y & 0 \\ 0 & 0 & 0 & 1 \end{bmatrix} \quad (\text{D.28})$$

$$\mathbf{Sc}_z(\varphi_z, p_z) = \begin{bmatrix} \cos \varphi_z & \sin \varphi_z & 0 & 0 \\ -\sin \varphi_z & \cos \varphi_z & 0 & 0 \\ 0 & 0 & 1 & p_z \cdot \varphi_z \\ 0 & 0 & 0 & 1 \end{bmatrix} \quad (\text{D.29})$$

for the calculation of the operators of the screw motion,  $\mathbf{Sc}_y(\varphi_y, p_y)$  and  $\mathbf{Sc}_z(\varphi_z, p_z)$ , about the Y- and Z-axes.

Screw motions about a coordinate axis, as well as screw surfaces, are common in the theory of part surface generation. This makes it practical to use the operators of the screw motion,  $\mathbf{Sc}_x(\varphi_x, p_x)$ ,  $\mathbf{Sc}_y(\varphi_y, p_y)$ , and  $\mathbf{Sc}_z(\varphi_z, p_z)$ , in the theory of part surface generation.

In case of necessity, an operator of the screw motion about an arbitrary axis either through the origin of the coordinate system or not through the origin of the coordinate system can be derived following the method similar to that used for the derivation of the operators  $\mathbf{Sc}_x(\varphi_x, p_x)$ ,  $\mathbf{Sc}_y(\varphi_y, p_y)$ , and  $\mathbf{Sc}_z(\varphi_z, p_z)$ .

### D.2.2 Linear Transformation Describing Rolling Motion of a Coordinate System

One more practical combination of a rotation and translation is often used in the theory of part surface generation.

Consider a Cartesian coordinate system,  $X_1Y_1Z_1$  (see Figure D.9). The coordinate system,  $X_1Y_1Z_1$ , is traveling in the direction of the  $X_1$ -axis. The velocity of the translation is denoted by  $V$ . The coordinate system,  $X_1Y_1Z_1$ , is

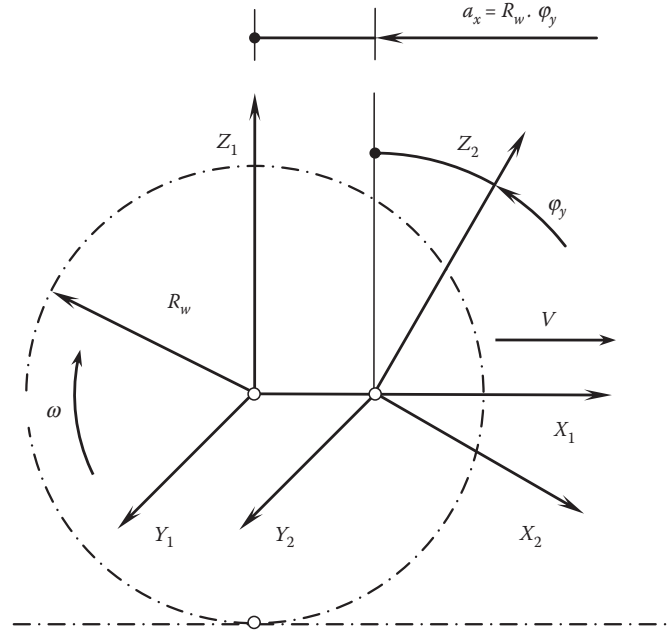


**FIGURE D.9**  
Illustration of the transformation of rolling,  $\mathbf{Rl}_x(\varphi_y, Y)$ , of a coordinate system.

rotating about its  $Y_1$ -axis simultaneously with the translation. The speed of the rotation is denoted as  $\omega$ . Assume that the ratio  $V/\omega$  is constant. Under such a scenario, the resultant motion of the reference system,  $X_1Y_1Z_1$ , to its arbitrary position,  $X_2Y_2Z_2$ , allows interpretation in the form of rolling with no sliding of a cylinder of radius,  $R_w$ , over the plane. The plane is parallel to the coordinate  $X_1Y_1$ -plane, and it is remote from it at the distance  $R_w$ . For the calculation of the radius of the rolling cylinder, the expression  $R_w = V/\omega$  can be used.

Because rolling of the cylinder of a radius,  $R_w$ , over the plane is performed with no sliding, a certain correspondence between the translation and rotation of the coordinate system is established. When the coordinate system turns through a certain angle,  $\varphi_y$ , then the translation of origin of the coordinate system along the  $X_1$ -axis is equal to  $a_x = \varphi_y \cdot R_w$ .

Transition from the coordinate system,  $X_1Y_1Z_1$ , to the coordinate system,  $X_2Y_2Z_2$ , can be analytically described by the operator of the resultant coordinate system transformation,  $\mathbf{Rs}(1 \mapsto 2)$ .  $\mathbf{Rs}(1 \mapsto 2)$  is equal to:

$$\mathbf{Rs}(1 \mapsto 2) = \mathbf{Rt}(\varphi_y, Y_1) \cdot \mathbf{Tr}(a_x, X_1) \quad (\text{D.30})$$

Here,  $\mathbf{Tr}(a_x, X_1)$  designates the operator of the translation along the  $X_1$ -axis, and  $\mathbf{Rt}(\varphi_y, Y_1)$  is the operator of the rotation about the  $Y_1$ -axis.

The operator of the resultant coordinate system transformation of this kind (see Equation D.30) is referred to as the *operator of rolling motion over a plane*.

When the translation is performed along the  $X_1$ -axis and the rotation is performed about the  $Y_1$ -axis, the operator of rolling is denoted as  $\mathbf{Rl}_x(\varphi_y, Y)$ . In this particular case, the equality  $\mathbf{Rl}_x(\varphi_y, Y) = \mathbf{Rs}(1 \mapsto 2)$  (see Equation D.30) is valid. Based on this equality, the operator of rolling over a plane,  $\mathbf{Rl}_x(\varphi_y, Y)$ , can be calculated from the equation:

$$\mathbf{Rl}_x(\varphi_y, Y) = \begin{bmatrix} \cos \varphi_y & 0 & -\sin \varphi_y & a_x \cdot \cos \varphi_y \\ 0 & 1 & 0 & 0 \\ \sin \varphi_y & 0 & \cos \varphi_y & a_x \cdot \sin \varphi_y \\ 0 & 0 & 0 & 1 \end{bmatrix} \quad (\text{D.31})$$

While rotation remains about the  $Y_1$ -axis, the translation can be performed not along the  $X_1$ -axis, but along the  $Z_1$ -axis instead. For rolling of this kind, the operator of rolling is equal to:

$$\mathbf{Rl}_z(\varphi_y, Y) = \begin{bmatrix} \cos \varphi_y & 0 & -\sin \varphi_y & -a_z \cdot \sin \varphi_y \\ 0 & 1 & 0 & 0 \\ \sin \varphi_y & 0 & \cos \varphi_y & a_z \cdot \cos \varphi_y \\ 0 & 0 & 0 & 1 \end{bmatrix} \quad (\text{D.32})$$

For cases when the rotation is performed about the  $X_1$ -axis, the corresponding operators of rolling are as follows:

$$\mathbf{Rl}_y(\varphi_x, X) = \begin{bmatrix} 1 & 0 & 0 & 0 \\ 0 & \cos \varphi_x & \sin \varphi_x & a_y \cdot \cos \varphi_x \\ 0 & -\sin \varphi_x & \cos \varphi_x & -a_y \cdot \sin \varphi_x \\ 0 & 0 & 0 & 1 \end{bmatrix} \quad (\text{D.33})$$

for the case of rolling along the  $Y_1$ -axis and

$$\mathbf{Rl}_z(\varphi_x, X) = \begin{bmatrix} 1 & 0 & 0 & 0 \\ 0 & \cos \varphi_x & \sin \varphi_x & a_z \cdot \sin \varphi_x \\ 0 & -\sin \varphi_x & \cos \varphi_x & a_z \cdot \cos \varphi_x \\ 0 & 0 & 0 & 1 \end{bmatrix} \quad (\text{D.34})$$

for the case of rolling along the  $Z_1$ -axis.

Similar expressions can be derived for the case of rotation about the  $Z_1$ -axis:

$$\mathbf{Rl}_x(\varphi_z, Z) = \begin{bmatrix} \cos \varphi_z & \sin \varphi_z & 0 & a_x \cdot \cos \varphi_z \\ -\sin \varphi_z & \cos \varphi_z & 0 & a_x \cdot \sin \varphi_z \\ 0 & 0 & 1 & 0 \\ 0 & 0 & 0 & 1 \end{bmatrix} \quad (\text{D.35})$$

$$\mathbf{Rl}_y(\varphi_z, Z) = \begin{bmatrix} \cos \varphi_z & \sin \varphi_z & 0 & a_y \cdot \sin \varphi_z \\ -\sin \varphi_z & \cos \varphi_z & 0 & a_y \cdot \cos \varphi_z \\ 0 & 0 & 1 & 0 \\ 0 & 0 & 0 & 1 \end{bmatrix} \quad (\text{D.36})$$

Use of the operators of rolling (Equations D.31 through D.36) significantly simplifies analytical description of coordinate system transformations.

### D.2.3 Linear Transformation Describing Rolling of Two Coordinate Systems

In the theory of part surface generation, combinations of two rotations about parallel axes are of particular interest.

As an example, consider two Cartesian coordinate systems,  $X_1Y_1Z_1$  and  $X_2Y_2Z_2$ , shown in [Figure D.10](#). The coordinate systems,  $X_1Y_1Z_1$  and  $X_2Y_2Z_2$ , are rotated about their axes,  $Z_1$  and  $Z_2$ . The axes of the rotations are parallel to each other ( $Z_1 \parallel Z_2$ ). The rotations,  $\omega_1$  and  $\omega_2$ , of the coordinate systems can be interpreted so that a circle of a certain radius,  $R_1$ , that is associated with the coordinates system,  $X_1Y_1Z_1$ , rolls with no sliding over a circle of the corresponding radius,  $R_2$ , that is associated with the coordinate system  $X_2Y_2Z_2$ . When the center distance  $C$  is known, then radii,  $R_1$  and  $R_2$ , of the circles (i.e., of centrodes) can be expressed in terms

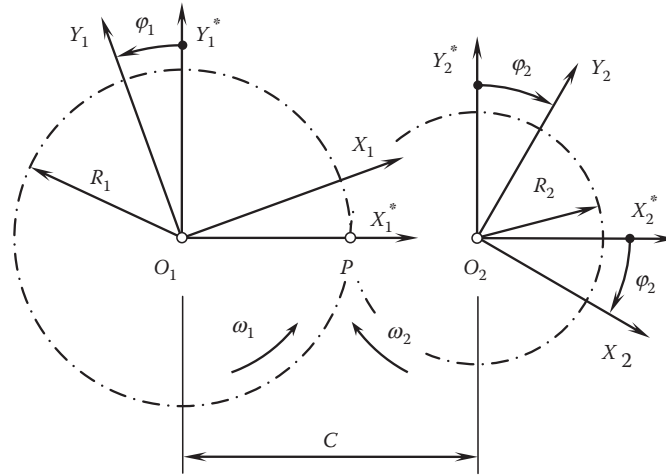


FIGURE D.10

On derivation of the operator of rolling,  $\mathbf{Rr}_u(\varphi_1, Z_1)$ , of two coordinate systems.

of the center distance,  $C$ , and of the given rotations,  $\omega_1$  and  $\omega_2$ . For the calculations, the following formulae:

$$R_1 = C \cdot \frac{1}{1+u} \quad (\text{D.37})$$

$$R_2 = C \cdot \frac{u}{1+u} \quad (\text{D.38})$$

can be used. Here, the ratio  $\omega_1/\omega_2$  is denoted by  $u$ .

In the initial configuration, the  $X_1$ - and  $X_2$ -axis align to each other. The  $Y_1$ - and  $Y_2$ -axis are parallel to each other. As shown in Figure D.10, the initial configuration of the coordinate systems,  $X_1Y_1Z_1$  and  $X_2Y_2Z_2$ , is labeled as  $X_1^*Y_1^*Z_1^*$  and  $X_2^*Y_2^*Z_2^*$ .

When the coordinate system,  $X_1Y_1Z_1$ , turns through a certain angle,  $\varphi_1$ , then the coordinate system,  $X_2Y_2Z_2$ , turns through the corresponding angle,  $\varphi_2$ . When the angle  $\varphi_1$  is known, then the corresponding angle,  $\varphi_2$ , is equal to  $\varphi_2 = \varphi_1/u$ .

Transition from the coordinate system,  $X_2Y_2Z_2$ , to the coordinate system,  $X_1Y_1Z_1$ , can be analytically described by the operator of the resultant coordinate system transformation,  $\mathbf{Rs}(1 \mapsto 2)$ . In the case under consideration, the operator,  $\mathbf{Rs}(1 \mapsto 2)$ , can be expressed in terms of the operators of the elementary coordinate system transformations:

$$\mathbf{Rs}(1 \mapsto 2) = \mathbf{Rt}(\varphi_1, Z_1) \cdot \mathbf{Rt}(\varphi_1/u, Z_1) \cdot \mathbf{Tr}(-C, X_1) \quad (\text{D.39})$$

Other equivalent combinations of the operators of elementary coordinate system transformations can result in that same operator,  $\mathbf{Rs}(1 \mapsto 2)$ , of the resultant coordinate system transformation. The interested reader may wish to exercise on his or her own deriving the equivalent expressions for the operator,  $\mathbf{Rs}(1 \mapsto 2)$ .

The operators of the resultant coordinate system transformations of this kind (see Equation D.39) are referred to as the *operators of rolling motion over a cylinder*.

When rotations are performed around the  $Z_1$ - and  $Z_2$ -axis, the operator of rolling motion over a cylinder is designated as  $\mathbf{Rr}_u(\varphi_1, Z_1)$ . In this particular case, the equality  $\mathbf{Rr}_u(\varphi_1, Z_1) = \mathbf{Rs}(1 \mapsto 2)$  (see Equation D.39) is valid. Based on this equality, the operator of rolling,  $\mathbf{Rr}_u(\varphi_1, Z_1)$ , over a cylinder can be calculated from the equation:

$$\mathbf{Rr}_u(\varphi_1, Z_1) = \begin{bmatrix} \cos\left(\varphi_1 \cdot \frac{u+1}{u}\right) & \sin\left(\varphi_1 \cdot \frac{u+1}{u}\right) & 0 & -C \\ -\sin\left(\varphi_1 \cdot \frac{u+1}{u}\right) & \cos\left(\varphi_1 \cdot \frac{u+1}{u}\right) & 0 & 0 \\ 0 & 0 & 1 & 0 \\ 0 & 0 & 0 & 1 \end{bmatrix} \quad (\text{D.40})$$

For the inverse transformation, the inverse operator of rolling of two coordinate systems,  $\mathbf{Rr}_u(\varphi_2, Z_2)$ , can be used. It is equal to  $\mathbf{Rr}_u(\varphi_2, Z_2) = \mathbf{Rr}_u^{-1}(\varphi_1, Z_1)$ . In terms of the operators of the elementary coordinate system transformations, the operator,  $\mathbf{Rr}_u(\varphi_2, Z_2)$ , can be expressed as follows:

$$\mathbf{Rr}_u(\varphi_2, Z_2) = \mathbf{Rt}(\varphi_1/u, Z_2) \cdot \mathbf{Rt}(\varphi_1, Z_2) \cdot \mathbf{Tr}(C, X_1) \quad (\text{D.41})$$

Other equivalent combinations of the operators of elementary coordinate system transformations can result in the same operator,  $\mathbf{Rr}_u(\varphi_2, Z_2)$ , of the resultant coordinate system transformation. The interested reader may wish to exercise on his or her own deriving the equivalent expressions for the operator  $\mathbf{Rr}_u(\varphi_2, Z_2)$ .

For the calculation of the operator of rolling of two coordinate systems,  $\mathbf{Rr}_u(\varphi_2, Z_2)$ , the equation:

$$\mathbf{Rr}_u(\varphi_2, Z_2) = \begin{bmatrix} \cos\left(\varphi_1 \cdot \frac{u+1}{u}\right) & -\sin\left(\varphi_1 \cdot \frac{u+1}{u}\right) & 0 & C \\ \sin\left(\varphi_1 \cdot \frac{u+1}{u}\right) & \cos\left(\varphi_1 \cdot \frac{u+1}{u}\right) & 0 & 0 \\ 0 & 0 & 1 & 0 \\ 0 & 0 & 0 & 1 \end{bmatrix} \quad (\text{D.42})$$

can be used.

Similar to how the expression (see Equation D.40) is derived for the calculation of the operator of rolling,  $\mathbf{Rr}_u(\varphi_1, Z_1)$ , around the  $Z_1$ - and  $Z_2$ -axis, corresponding formulae can be derived for the calculation of the operators of rolling,  $\mathbf{Rr}_u(\varphi_1, X_1)$  and  $\mathbf{Rr}_u(\varphi_1, Y_1)$ , about parallel axes  $X_1$  and  $X_2$ , as well as about parallel axes  $Y_1$  and  $Y_2$ .

Use of the operators of rolling about two axes,  $\mathbf{Rr}_u(\varphi_1, X_1)$ ,  $\mathbf{Rr}_u(\varphi_1, Y_1)$ , and  $\mathbf{Rr}_u(\varphi_1, Z_1)$ , substantially simplifies analytical description of coordinate system transformations.

#### D.2.4 Coupled Linear Transformation

It is the right point to note here that a translation,  $\mathbf{Tr}(a_x, X)$ , along the  $X$ -axis of a Cartesian reference system,  $XYZ$ , and a rotation,  $\mathbf{Rt}(\varphi_x, X)$ , about the axis  $X$  of that same coordinate system,  $XYZ$ , obey the commutative law; that is, these two coordinate system transformations can equally be performed in a different order. It makes no difference whether the translation,  $\mathbf{Tr}(a_x, X)$ , is initially performed, then followed by the rotation,  $\mathbf{Rt}(\varphi_x, X)$ , or the rotation,  $\mathbf{Rt}(\varphi_x, X)$ , is initially performed, then followed by the translation,  $\mathbf{Tr}(a_x, X)$ . This is because the dot products  $\mathbf{Rt}(\varphi_x, X) \cdot \mathbf{Tr}(a_x, X)$  and  $\mathbf{Tr}(a_x, X) \cdot \mathbf{Rt}(\varphi_x, X)$  are identical to one another:

$$\mathbf{Rt}(\varphi_x, X) \cdot \mathbf{Tr}(a_x, X) \equiv \mathbf{Tr}(a_x, X) \cdot \mathbf{Rt}(\varphi_x, X) \quad (\text{D.43})$$

This means that translation from the coordinate system,  $X_1Y_1Z_1$ , to the intermediate coordinate system,  $X^*Y^*Z^*$ , followed by the rotation from the coordinate system,  $X^*Y^*Z^*$ , to the final coordinate system,  $X_2Y_2Z_2$ , produces the same reference,  $X_2Y_2Z_2$ , as in a case when the rotation from the coordinate system,  $X_1Y_1Z_1$ , to the intermediate coordinate system,  $X^*Y^*Z^*$ , is followed by the translation from the coordinate system,  $X^*Y^*Z^*$ , to the final coordinate system,  $X_2Y_2Z_2$ .

The validity of Equation D.43 is illustrated in [Figure D.11](#). The translation,  $\mathbf{Tr}(a_x, X)$ , that is followed by the rotation,  $\mathbf{Rt}(\varphi_x, X)$ , as shown in [Figure D.11a](#), is equivalent to the rotation,  $\mathbf{Rt}(\varphi_x, X)$ , that is followed by the translation,  $\mathbf{Tr}(a_x, X)$  as shown in [Figure D.11b](#).

Therefore, the two linear transformations,  $\mathbf{Tr}(a_x, X)$  and  $\mathbf{Rt}(\varphi_x, X)$ , can be coupled into a linear transformation:

$$\mathbf{Cp}_x(a_x, \varphi_x) = \mathbf{Rt}(\varphi_x, X) \cdot \mathbf{Tr}(a_x, X) \equiv \mathbf{Tr}(a_x, X) \cdot \mathbf{Rt}(\varphi_x, X) \quad (\text{D.44})$$

The operator of linear transformation,  $\mathbf{Cp}_x(a_x, \varphi_x)$ , can be expressed in matrix form (see [Figure D.12a](#)):

$$\mathbf{Cp}_x(a_x, \varphi_x) = \begin{bmatrix} 1 & 0 & 0 & a_x \\ 0 & \cos \varphi_x & \sin \varphi_x & 0 \\ 0 & -\sin \varphi_x & \cos \varphi_x & 0 \\ 0 & 0 & 0 & 1 \end{bmatrix} \quad (\text{D.45})$$



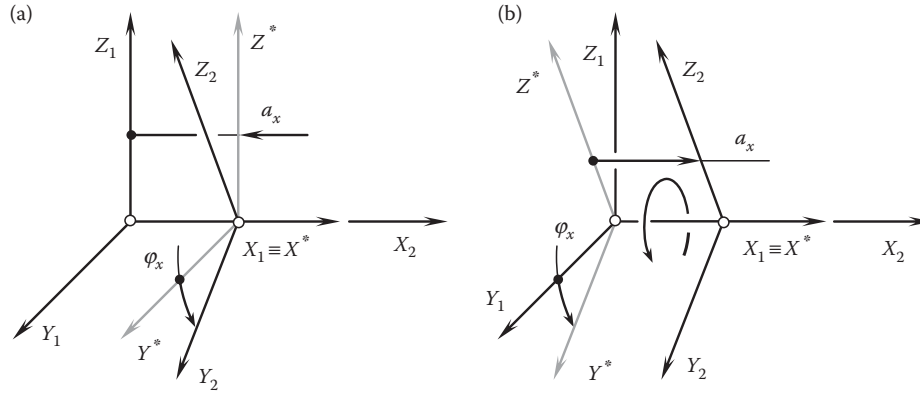


FIGURE D.11

On the equivalency of the linear transformations,  $\mathbf{Rt}(\varphi_x, X) \cdot \mathbf{Tr}(a_x, X)$  and  $\mathbf{Tr}(a_x, X) \cdot \mathbf{Rt}(\varphi_x, X)$ , in the operator,  $\mathbf{Cp}_x(a_x, \varphi_x)$ , of coupled linear transformation of a Cartesian reference system,  $XYZ$ .

This expression is composed based on Equation D.4 for the linear transformation,  $\mathbf{Tr}(a_x, X)$ , and in Equation D.10, which describes the linear transformation,  $\mathbf{Rt}(\varphi_x, X)$ .

Two reduced cases of operator of the linear transformation,  $\mathbf{Cp}_x(a_x, \varphi_x)$ , are distinguished.

First, it could happen that in a particular case, the component,  $a_x$ , of the translation is zero; that is  $a_x = 0$ . Under such a scenario, the operator of linear transformation,  $\mathbf{Cp}_x(a_x, \varphi_x)$ , reduces to the operator of rotation,  $\mathbf{Rt}(\varphi_x, X)$ , and the equality  $\mathbf{Cp}_x(a_x, \varphi_x) = \mathbf{Rt}(\varphi_x, X)$  is observed in the case under consideration.

Second, it could happen that in a particular case, the component,  $\varphi_x$ , of the rotation is zero; that is  $\varphi_x = 0^\circ$ . Under such a scenario, the operator of linear transformation,  $\mathbf{Cp}_x(a_x, \varphi_x)$ , reduces to the operator of translation,  $\mathbf{Tr}(a_x, X)$ , and the equality  $\mathbf{Cp}_x(a_x, \varphi_x) = \mathbf{Tr}(a_x, X)$  is observed in the case under consideration.

The above is valid with respect to translations and rotations along and about the  $Y$  and  $Z$  axes of a Cartesian reference system,  $XYZ$ . The corresponding coupled operators,  $\mathbf{Cp}_y(a_y, \varphi_y)$  and  $\mathbf{Cp}_z(a_z, \varphi_z)$ , for linear transformations of these kinds can also be composed (see Figure D.12b, c):

$$\mathbf{Cp}_y(a_y, \varphi_y) = \begin{bmatrix} \cos \varphi_y & 0 & \sin \varphi_y & 0 \\ 0 & 1 & 0 & a_y \\ -\sin \varphi_y & 0 & \cos \varphi_y & 0 \\ 0 & 0 & 0 & 1 \end{bmatrix} \quad (\text{D.46})$$

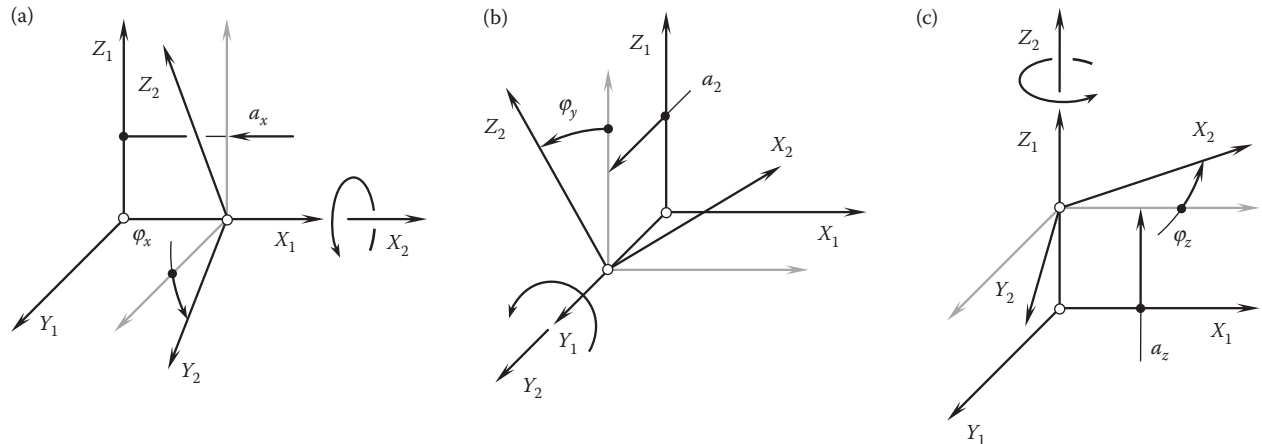


FIGURE D.12

Analytical description of the operators,  $\mathbf{Cp}_x(a_x, \varphi_x)$ ,  $\mathbf{Cp}_y(a_y, \varphi_y)$ , and  $\mathbf{Cp}_z(a_z, \varphi_z)$ , of linear transformation of a Cartesian reference system,  $XYZ$ .

$$\mathbf{Cp}_z(a_z, \varphi_z) = \begin{bmatrix} \cos \varphi_z & \sin \varphi_z & 0 & 0 \\ -\sin \varphi_z & \cos \varphi_z & 0 & 0 \\ 0 & 0 & 1 & a_z \\ 0 & 0 & 0 & 1 \end{bmatrix} \quad (\text{D.47})$$

In the operators of linear transformation,  $\mathbf{Cp}_x(a_x, \varphi_x)$ ,  $\mathbf{Cp}_y(a_y, \varphi_y)$ , and  $\mathbf{Cp}_z(a_z, \varphi_z)$ , values of the translations,  $a_x$ ,  $a_y$ , and  $a_z$ , as well as values of the rotations,  $\varphi_x$ ,  $\varphi_y$ , and  $\varphi_z$ , are finite values (and not continuous). The linear and angular displacements do not correlate to one another in time; thus, they are not screws. They are just a kind of coupled transformation, that is, of translation along and a rotation about a coordinate axis of a Cartesian reference system.

Introduction of the operators of linear transformation,  $\mathbf{Cp}_x(a_x, \varphi_x)$ ,  $\mathbf{Cp}_y(a_y, \varphi_y)$ , and  $\mathbf{Cp}_z(a_z, \varphi_z)$ , makes linear transformations, easier as all the operators of the linear transformations become uniform.

The operators of linear transformation,  $\mathbf{Cp}_x(a_x, \varphi_x)$ ,  $\mathbf{Cp}_y(a_y, \varphi_y)$ , and  $\mathbf{Cp}_z(a_z, \varphi_z)$ , do not obey the commutative law. This is because rotations are not vectors in nature. Therefore, special care should be undertaken when treating rotations as vectors—when implementing coupled operators of linear transformations in particular.

The operators of coupled linear transformations,  $\mathbf{Cp}_x(a_x, \varphi_x)$ ,  $\mathbf{Cp}_y(a_y, \varphi_y)$ , and  $\mathbf{Cp}_z(a_z, \varphi_z)$  (see Equations D.45 through D.47), can be used for the purpose of analytical description of a resultant coordinate system transformation. Under such a scenario, the operator,  $\mathbf{Rs}(1 \mapsto t)$ , of a resultant coordinate system transformation can be expressed in terms of all the operators,  $\mathbf{Cp}_x(a_x, \varphi_x)$ ,  $\mathbf{Cp}_y(a_y, \varphi_y)$ , and  $\mathbf{Cp}_z(a_z, \varphi_z)$ , by the following expression:

$$\mathbf{Rs}(1 \mapsto t) = \prod_{\substack{i=1 \\ j=x,y,z}}^{t-1} \mathbf{Cp}_j^i(a_j^i, \varphi_j^i) \quad (\text{D.48})$$

In Equation D.48, only operators of coupled linear transformations are used.

### D.2.5 An Example of Nonorthogonal Linear Transformation

Consider a nonorthogonal reference system,  $X_1Y_1Z_1$ , having certain angle,  $\omega_1$ , between axes  $X_1$  and  $Y_1$ . Axis  $Z_1$  is perpendicular to the coordinate plane,  $X_1Y_1$ . Another reference system,  $X_2Y_2Z_2$ , is identical to the first coordinate system,  $X_1Y_1Z_1$ , and is turned about the  $Z_1$ -axis through a certain angle,  $\varphi$ . Transition from the reference system,  $X_1Y_1Z_1$ , to the reference system,  $X_2Y_2Z_2$ , can be analytically described by the operator of linear transformation:

$$\mathbf{Rt}_\omega(1 \rightarrow 2) = \begin{bmatrix} \frac{\sin(\omega_1 + \varphi)}{\sin \omega_1} & \frac{\sin \varphi}{\sin \omega_1} & 0 & 0 \\ -\frac{\sin \varphi}{\sin \omega_1} & \frac{\sin(\omega_1 - \varphi)}{\sin \omega_1} & 0 & 0 \\ 0 & 0 & 1 & 0 \\ 0 & 0 & 0 & 1 \end{bmatrix} \quad (\text{D.49})$$

In order to distinguish the operator of rotation in the orthogonal linear transformation,  $\mathbf{Rt}(1 \rightarrow 2)$ , from the similar operator of rotation in a nonorthogonal linear transformation,  $\mathbf{Rt}_\omega(1 \rightarrow 2)$ , the subscript  $\omega$  is assigned to the last.

When  $\omega = 90^\circ$ , Equation D.49 casts into Equation D.12.

### D.2.6 Conversion of a Coordinate System Hand

Application of the matrix method of coordinate system transformation presumes that both of the reference systems,  $i$  and  $(i \pm 1)$ , are of the same hand. This means that it is assumed from the very beginning that both of them are either right-hand- or left-hand-oriented Cartesian coordinate systems. In the event the coordinate systems  $i$  and  $(i \pm 1)$  are of opposite hands, say, one of them is a right-hand-oriented coordinate system while

the other is left-hand-oriented, then one of them must be converted into the oppositely oriented Cartesian coordinate system.

For the conversion of a left-hand-oriented Cartesian coordinate system into a right-hand-oriented coordinate system or vice versa, the operators of reflection are commonly used.

In order to change the direction of the  $X_i$  axis of the initial coordinate system,  $i$ , to the opposite direction [in this case, in the new coordinate system,  $(i \pm 1)$ , the equalities  $X_{i\pm 1} = -X_i$ ,  $Y_{i\pm 1} \equiv Y_i$  and  $Z_{i\pm 1} \equiv Z_i$  are observed], the operator of reflection,  $\mathbf{Rf}_x(Y_i Z_i)$ , can be applied. The operator of reflection yields representation in matrix form:

$$\mathbf{Rf}_x(Y_i Z_i) = \begin{bmatrix} -1 & 0 & 0 & 0 \\ 0 & 1 & 0 & 0 \\ 0 & 0 & 1 & 0 \\ 0 & 0 & 0 & 1 \end{bmatrix} \quad (\text{D.50})$$

Similarly, implementation of the operators of reflection,  $\mathbf{Rf}_y(X_i Z_i)$  and  $\mathbf{Rf}_z(X_i Y_i)$ , change the directions of the  $Y_i$  and  $Z_i$  axes to opposite directions. The operators of reflection,  $\mathbf{Rf}_y(X_i Z_i)$  and  $\mathbf{Rf}_z(X_i Y_i)$ , can be expressed analytically in the form:

$$\mathbf{Rf}_y(X_i Z_i) = \begin{bmatrix} 1 & 0 & 0 & 0 \\ 0 & -1 & 0 & 0 \\ 0 & 0 & 1 & 0 \\ 0 & 0 & 0 & 1 \end{bmatrix} \quad (\text{D.51})$$

$$\mathbf{Rf}_z(X_i Y_i) = \begin{bmatrix} 1 & 0 & 0 & 0 \\ 0 & 1 & 0 & 0 \\ 0 & 0 & -1 & 0 \\ 0 & 0 & 0 & 1 \end{bmatrix} \quad (\text{D.52})$$

A linear transformation that reverses the direction of the coordinate axis is an *opposite transformation*. Transformation of reflection is an example of an *orientation-reversing transformation*.

### D.3 Useful Equations

The sequence of the successive rotations can vary depending on the intention of the researcher. Several special types of successive rotations are known, including Eulerian transformation, *Cardanian transformation*, two kinds of *Euler-Krylov transformations*, and so forth. The sequence of the successive rotations can be chosen from a total of 12 different combinations. Even though Cardanian transformation is different from Eulerian transformation in terms of the combination of the rotations, they both use a similar approach to calculate the orientation angles.

#### D.3.1 Roll-Pitch-Yaw-Transformation

A series of rotations can be performed in the order *roll matrix*, ( $R$ ), by *pitch matrix* ( $P$ ), and finally by *yaw matrix* ( $Y$ ). Linear transformation of this kind is commonly referred to as *RPY-transformation*. The resultant transformation of this kind can be represented by the homogenous coordinate transformation matrix:

$$\text{RPY}(\varphi_x, \varphi_y, \varphi_z) = \begin{bmatrix} \cos \varphi_y \cos \varphi_z + \sin \varphi_x \sin \varphi_y \sin \varphi_z & \cos \varphi_y \sin \varphi_z - \sin \varphi_x \sin \varphi_y \cos \varphi_z & \cos \varphi_x \sin \varphi_y & 0 \\ -\cos \varphi_x \sin \varphi_z & \cos \varphi_x \cos \varphi_z & \sin \varphi_x & 0 \\ \sin \varphi_x \cos \varphi_y \sin \varphi_z - \sin \varphi_y \cos \varphi_z & -\sin \varphi_x \cos \varphi_y \cos \varphi_z - \cos \varphi_y \sin \varphi_z & \cos \varphi_x \cos \varphi_y & 0 \\ 0 & 0 & 0 & 1 \end{bmatrix} \quad (\text{D.53})$$

RPY-transformation can be used for solving problems in the field of part surface generation.

### D.3.2 Operator of Rotation about an Axis in Space

A spatial rotation operator for the rotational transformation of a point about a unit axis,  $\mathbf{a}_0(\cos \alpha, \cos \beta, \cos \gamma)$ , passing through the origin of the coordinate system can be described as follows, with  $\mathbf{a}_0 = \mathbf{A}_0/|\mathbf{A}_0|$  designating the unit vector along the axis of rotation,  $\mathbf{A}_0$ .

Suppose the angle of rotation of the point about  $\mathbf{a}_0$  is  $\theta$ ; the *rotation operator* is expressed by:

$$\mathbf{Rt}(\theta, \mathbf{a}_0) = \begin{bmatrix} (1-\cos \theta)\cos^2 \alpha + \cos \theta & (1-\cos \theta)\cos \alpha \cos \beta - \sin \theta \cos \gamma & & & \\ (1-\cos \theta)\cos \alpha \cos \beta + \sin \theta \cos \gamma & (1-\cos \theta)\cos^2 \beta + \cos \theta & & & \\ (1-\cos \theta)\cos \alpha \cos \gamma - \sin \theta \cos \beta & (1-\cos \theta)\cos \beta \cos \gamma + \sin \theta \cos \alpha & & & \\ 0 & 0 & & & \\ (1-\cos \theta)\cos \alpha \cos \gamma + \sin \theta \cos \beta & 0 & & & \\ (1-\cos \theta)\cos \beta \cos \gamma - \sin \theta \cos \alpha & 0 & & & \\ (1-\cos \theta)\cos^2 \gamma + \cos \theta & 0 & & & \\ 0 & 0 & & & 1 \end{bmatrix} \quad (\text{D.54})$$

The solution to a problem in the field of part surface generation can be significantly simplified by implementation of the rotational operator,  $\mathbf{Rt}(\theta, \mathbf{a}_0)$  (see Equation D.54).

### D.3.3 Combined Linear Transformation

Suppose a point,  $p$ , on a rigid body rotates with an angular displacement,  $\theta$ , about an axis along a unit vector,  $\mathbf{a}_0$ , passing through the origin of the coordinate system at first, then followed by a translation at a distance,  $B$ , in the direction of a unit vector,  $\mathbf{b}$ . The linear transformation of this kind can be analytically described by the homogenous matrix

$$\mathbf{Rt}(\theta_{\mathbf{a}_0}, B_{\mathbf{b}}) = \begin{bmatrix} (1-\cos \theta)\cos^2 \alpha + \cos \theta & (1-\cos \theta)\cos \alpha \cos \beta - \sin \theta \cos \gamma & & & \\ (1-\cos \theta)\cos \alpha \cos \beta + \sin \theta \cos \gamma & (1-\cos \theta)\cos^2 \beta + \cos \theta & & & \\ (1-\cos \theta)\cos \alpha \cos \gamma - \sin \theta \cos \beta & (1-\cos \theta)\cos \beta \cos \gamma + \sin \theta \cos \alpha & & & \\ 0 & 0 & & & \\ (1-\cos \theta)\cos \alpha \cos \gamma + \sin \theta \cos \beta & B \cos \alpha & & & \\ (1-\cos \theta)\cos \beta \cos \gamma - \sin \theta \cos \alpha & B \cos \beta & & & \\ (1-\cos \theta)\cos^2 \gamma + \cos \theta & B \cos \gamma & & & \\ 0 & 0 & & & 1 \end{bmatrix} \quad (\text{D.55})$$

More operators of particular linear transformations can be found in the literature.

## D.4 Chains of Consequent Linear Transformations and a Closed Loop of Consequent Coordinate Systems Transformations

Consequent coordinate system transformations form chains (circuits) of linear transformations. The elementary chain of coordinate system transformation is composed of two consequent transformations. Chains of linear transformations play an important role in the theory of part surface generation.

Two different kinds of chains of consequent coordinate system transformations are distinguished.

*First*, transition from the coordinate system,  $X_g Y_g Z_g$ , associated with the gear tooth flank,  $\mathcal{G}$ , to the local Cartesian coordinate system,  $x_g y_g z_g$ , with the origin at a point,  $K$ , of contact of the gear tooth flank,  $\mathcal{G}$ , and pinion tooth flank,  $\mathcal{P}$ . This linear transformation is also made up of numerous operators of intermediate coordinate

system transformations ( $X_{in}Y_{in}Z_{in}$ ). It forms a chain of direct consequent coordinate system transformations, illustrated in Figure D.13a.

The local coordinate system,  $x_gy_gz_g$ , is associated with the gear tooth flank,  $\mathcal{G}$ . The operator,  $\mathbf{Rs}(\mathcal{G} \rightarrow K_g)$ , of the resultant coordinate system transformation for a direct chain of linear transformations can be composed using for this purpose a certain number of operators of translation (see Equations D.4 through D.6) and a corresponding number of the operators of rotation (see Equations D.10 through D.12).

*Second* is transition from the coordinate system,  $X_gY_gZ_g$ , to the local Cartesian coordinate system,  $x_py_pz_p$ , with the origin at a point,  $K$ , of contact of the tooth flanks,  $\mathcal{G}$  and  $\mathcal{P}$ . The local coordinate system,  $x_py_pz_p$ , is associated with the pinion tooth flank,  $\mathcal{P}$ . This linear transformation is also made up of numerous intermediate coordinate system transformations ( $X_jY_jZ_j$ ), for example, transitions from the coordinate system,  $X_hY_hZ_h$ , associated with gear housing, to numerous intermediate coordinate systems,  $X_iY_iZ_i$ . The linear transformation of this kind forms a chain of inverse consequent coordinate system transformations, shown in Figure D.13b. The operator,  $\mathbf{Rs}(\mathcal{G} \rightarrow K_p)$ , of the resultant coordinate system transformations for the inverse chain of transformations can be composed using for this purpose a certain number of the operators of translation (see Equations D.4 through D.6) and a corresponding number of the operators of rotation (see Equations D.10 through D.12).

Chains of direct and reverse consequent coordinate system transformations together with the operator of transition from the local coordinate system,  $x_py_pz_p$ , to the local coordinate system,  $x_gy_gz_g$ , form a closed loop (closed circuit) of the consequent coordinate system transformations depicted in Figure D.13c.

If a closed loop of the consequent coordinate system transformations is complete, implementation of a certain number of the operators of translation (see Equations D.4 through D.6) and a corresponding number of the operators of rotation (see Equations D.10 through D.12) returns a result that is identical to the input data. This means that analytical description of a meshing process specified in the original coordinate system remains the same after implementation of the operator of the resultant coordinate system transformations. This condition is the necessary and sufficient condition for the existence of a closed loop of consequent coordinate system transformations.

Implementation of the chains, as well as of the closed loops, of consequent coordinate system transformations makes it possible to consider the meshing process of the tooth flanks,  $\mathcal{G}$  and  $\mathcal{P}$ , in any and all reference systems that make up the loop. Therefore, for consideration of a particular problem of part surface generation, the most convenient reference system can be chosen.

In order to complete the construction of a closed loop of consequent coordinate system transformations, an operator of transformation from the local coordinate system,  $x_py_pz_p$ , to the local coordinate system,  $x_gy_gz_g$ , must be composed. Usually, the local reference systems,  $x_gy_gz_g$  and  $x_py_pz_p$ , are a kind of semiorthogonal coordinate systems. This means that the axis,  $z_p$ , is always orthogonal to the coordinate plane,  $x_gy_g$ , while the axes,  $x_g$  and  $y_g$ , can be either orthogonal or not orthogonal to each other. The same is valid with respect to the local coordinate system,  $x_py_pz_p$ .

Two possible ways to perform the required transformation of the local reference systems,  $x_gy_gz_g$  and  $x_py_pz_p$ , are considered below.

Following the first way, the operator,  $\mathbf{Rt}_\omega(p \rightarrow g)$ , of the linear transformation of the semiorthogonal coordinate systems (see Figure D.14) must be composed. The operator,  $\mathbf{Rt}_\omega(p \rightarrow g)$ , can be represented in the form of

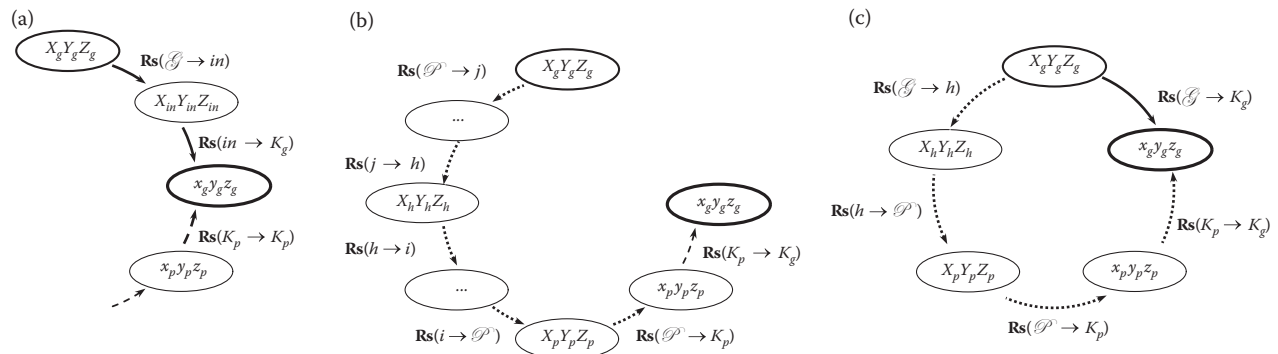


FIGURE D.13

An example of direct chain (a), reverse chain (b), and closed loop (c) of consequent coordinate system transformations.

the homogenous matrix:

$$\mathbf{Rt}_\omega(p \rightarrow g) = \begin{bmatrix} \frac{\sin(\omega_p + \alpha)}{\sin \omega_p} & -\frac{\sin(\omega_g - \omega_p - \alpha)}{\sin \omega_p} & 0 & 0 \\ -\frac{\sin \alpha}{\sin \omega_p} & \frac{\sin(\omega_g - \alpha)}{\sin \omega_p} & 0 & 0 \\ 0 & 0 & -1 & 0 \\ 0 & 0 & 0 & 1 \end{bmatrix} \quad (\text{D.56})$$

where

$\omega_g$ : is the angle that makes  $U_g$  and  $V_g$  coordinate lines on the gear tooth flank,  $\mathcal{G}$ .

$\omega_p$ : is the angle that makes  $U_p$  and  $V_p$  coordinate lines on the pinion tooth flank,  $\mathcal{P}$ .

$\alpha$ : is the angle that makes the axes,  $x_g$  and  $x_p$ , of the local coordinate systems,  $x_g y_g z_g$  and  $x_p y_p z_p$ .

The auxiliary angle,  $\beta$ , in Figure D.14 is equal to  $\beta = \omega_T + \alpha$ .

The inverse coordinate system transformation, that is, the transformation from the local coordinate system,  $x_g y_g z_g$ , to the local coordinate system,  $x_p y_p z_p$ , can be analytically described by the operator,  $\mathbf{Rt}_\omega(g \rightarrow p)$ , of the inverse coordinate system transformation. The operator,  $\mathbf{Rt}_\omega(g \rightarrow p)$ , can be represented in the form of the homogenous matrix:

$$\mathbf{Rt}_\omega(g \rightarrow p) = \begin{bmatrix} \frac{\sin(\omega_g - \alpha)}{\sin \omega_g} & \frac{\sin(\omega_g - \omega_p - \alpha)}{\sin \omega_g} & 0 & 0 \\ \frac{\sin \alpha}{\sin \omega_g} & \frac{\sin(\omega_p + \alpha)}{\sin \omega_g} & 0 & 0 \\ 0 & 0 & -1 & 0 \\ 0 & 0 & 0 & 1 \end{bmatrix} \quad (\text{D.57})$$

Following the second method of transformation of the local coordinate systems, the auxiliary orthogonal local coordinate system must be constructed.

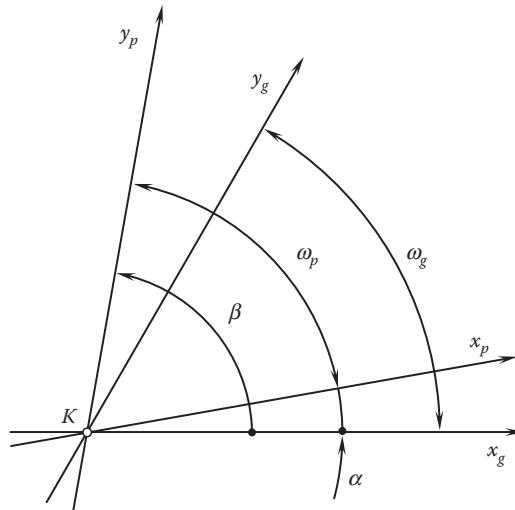


FIGURE D.14

Local coordinate systems,  $x_g y_g z_g$  and  $x_p y_p z_p$ , with the origin at contact point,  $K$ .

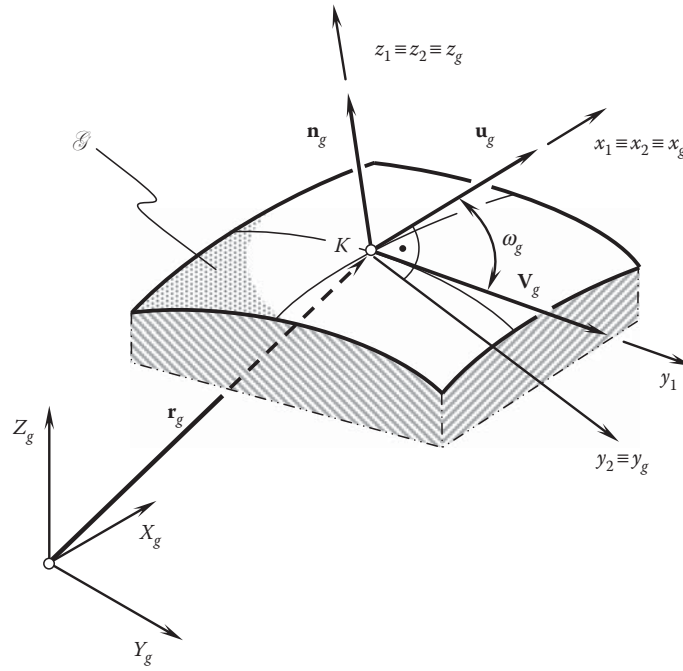


FIGURE D.15

Local coordinate system,  $x_g y_g z_g$ , associated with the gear tooth flank,  $\mathcal{G}$ .

Let's consider an approach according to which a closed loop (closed circuit) of the consequent coordinate system transformations can be composed.

In order to construct an orthogonal normalized basis of the coordinate system,  $x_g y_g z_g$ , an intermediate coordinate system,  $x_1 y_1 z_1$ , is used. Axis  $x_1$  of the coordinate system,  $x_1 y_1 z_1$ , is pointed out along the unit vector,  $\mathbf{u}_g$ , that is tangent to the  $U_g$ -coordinate curve (see Figure D.15). Axis  $y_1$  is directed along vector  $\mathbf{v}_g$  that is tangent to the  $V_g$ -coordinate line on the gear tooth flank,  $G$ . The axis,  $z_1$ , aligns with unit normal vector,  $\mathbf{n}_g$ , and is pointed outward from the gear tooth body.

For a gear tooth flank,  $\mathcal{G}$ , having orthogonal parameterization (for which  $F_g = 0$  and therefore  $\omega_g = \pi/2$ ), analytical description of coordinate system transformations is significantly simpler. Further simplification of the coordinate system transformation is possible when the coordinate  $U_g$ - and  $V_g$ -lines are congruent to the lines of curvature on the part surface,  $\mathcal{G}$ . Under such a scenario, the local coordinate system is represented by a *Darboux frame*.

In order to construct a Darboux frame, principal directions on the gear tooth flank,  $\mathcal{G}$ , must be calculated. Determination of the unit tangent vectors,  $\mathbf{t}_{1,g}$  and  $\mathbf{t}_{2,g}$ , of the principal directions on the gear tooth flank,  $\mathcal{G}$ , is considered in Appendix B.

In the common tangent plane, orientation of the unit vector,  $\mathbf{t}_{1,g}$ , of the first principal direction on the gear tooth flank,  $\mathcal{G}$ , can be uniquely specified by the included angle,  $\xi_{1,g}$ , that the unit vector,  $\mathbf{t}_{1,g}$ , forms with the  $U_g$ -coordinate curve. This angle depends on both the gear tooth flank,  $\mathcal{G}$ , geometry and parameterization. Depicted in Figure D.16 is the relationship between the tangent vectors,  $\mathbf{U}_g$  and  $\mathbf{V}_g$ , and the included angle,  $\xi_{1,g}$ . From the law of sines,

$$\frac{\sqrt{G_g}}{\sin \xi_{1,g}} = \frac{\sqrt{E_g}}{\sin [\pi - \xi_{1,g} - (\pi - \omega_g)]} = \frac{\sqrt{F_g}}{\sin(\omega_g - \xi_{1,g})} \quad (\text{D.58})$$

Here,  $\omega_g = \cos^{-1}(F_g / \sqrt{E_g G_g})$ .



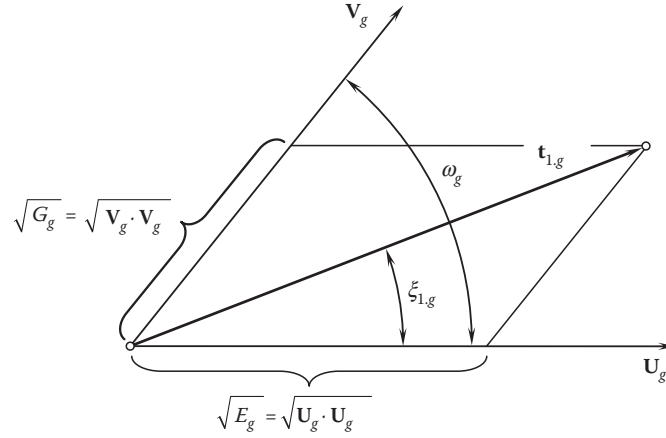


FIGURE D.16

Differential relationships between the tangent vectors,  $\mathbf{U}_g$  and  $\mathbf{V}_g$ , the fundamental magnitudes of the first order, the included angle,  $\xi_{1,g}$ , and the direction of the unit vector  $\mathbf{t}_{1,g}$  of the first principal direction.

Solving the expression above for the included angle,  $\xi_{1,g}$ , results in:

$$\xi_{1,g} = \tan^{-1} \frac{\sqrt{E_g G_g - F_g^2}}{E_g + F_g} \quad (\text{D.59})$$

Another possible method of constructing the orthogonal local basis of the local Cartesian coordinate system,  $x_p y_p z_p$ , is based on the following consideration.

Consider an arbitrary nonorthogonal and not normalized basis,  $\mathbf{x}_1 \mathbf{x}_2 \mathbf{x}_3$  (see Figure D.17a). Let's construct an orthogonal and normalized basis based on the initial given basis,  $\mathbf{x}_1 \mathbf{x}_2 \mathbf{x}_3$ .

The cross-product of any two of three vectors,  $\mathbf{x}_1, \mathbf{x}_2, \mathbf{x}_3$ , for example, the cross-product of the vectors  $\mathbf{x}_1 \times \mathbf{x}_2$ , determines a new vector,  $\mathbf{x}_4$  (see Figure D.17b). Evidently, the vector,  $\mathbf{x}_4$ , is orthogonal to the coordinate plane,  $\mathbf{x}_1 \mathbf{x}_2$ . Then, use the calculated vector,  $\mathbf{x}_4$ , and one of the two original vectors,  $\mathbf{x}_1$  or  $\mathbf{x}_2$ , for instance, the vector  $\mathbf{x}_2$ . This yields calculation of a new vector,  $\mathbf{x}_5 = \mathbf{x}_4 \times \mathbf{x}_2$  (see Figure D.17c). The calculated basis,  $\mathbf{x}_1 \mathbf{x}_4 \mathbf{x}_5$ , is orthogonal. In order to convert it into a normalized basis, each of the vectors,  $\mathbf{x}_1$ ,  $\mathbf{x}_2$ , and  $\mathbf{x}_5$  must be divided by its magnitude:

$$\mathbf{e}_1 = \frac{\mathbf{x}_1}{|\mathbf{x}_1|} \quad (\text{D.60})$$

$$\mathbf{e}_4 = \frac{\mathbf{x}_4}{|\mathbf{x}_4|} \quad (\text{D.61})$$

$$\mathbf{e}_5 = \frac{\mathbf{x}_5}{|\mathbf{x}_5|} \quad (\text{D.62})$$

The resultant basis,  $\mathbf{e}_1 \mathbf{e}_4 \mathbf{e}_5$  (see Figure D.17d), is always orthogonal and always normalized.

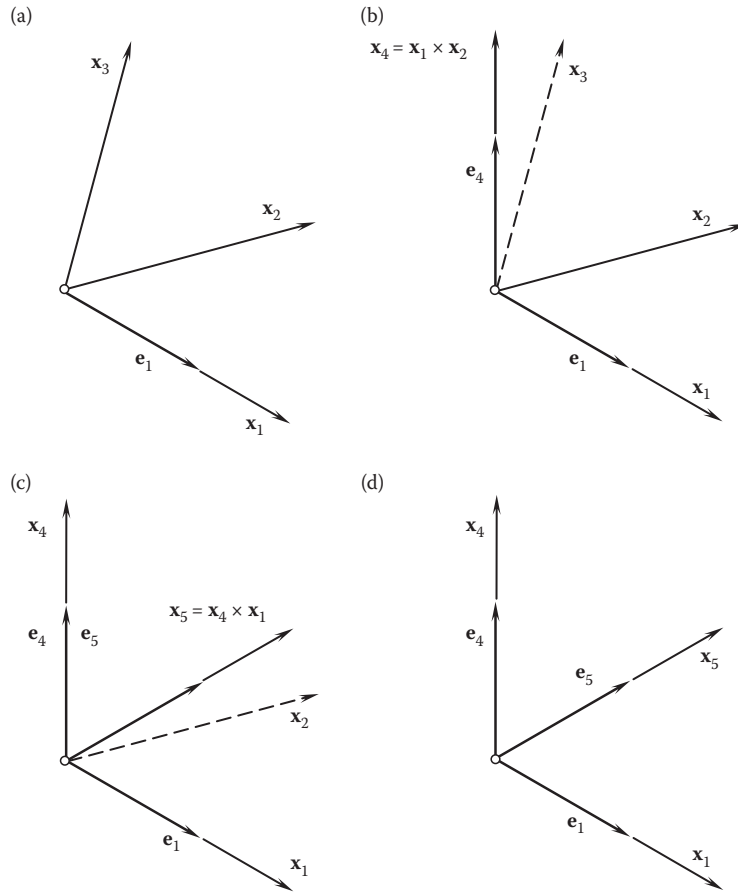
In order to complete the analytical description of a closed loop of consequent coordinate system transformations, it is necessary to compose the operator,  $\mathbf{Rs}(K_p \rightarrow K_g)$ , of transformation from the local reference system,  $x_p y_p z_p$ , to the local reference system,  $x_g y_g z_g$  (see Figure D.13c).

In the case under consideration, the axes,  $z_g$  and  $z_p$ , align with the common unit normal vector,  $\mathbf{n}_g$ . The axis,  $z_g$ , is pointed out from the body side to the void side of the gear tooth flank,  $\mathcal{G}$ . The axis,  $z_g$ , is pointed oppositely. Due to that, the following equality is observed:

$$\mathbf{Rs}(K_p \rightarrow K_g) = \mathbf{Rt}(\varphi_z, z_p) \quad (\text{D.63})$$

The inverse coordinate system transformation can be analytically described by the operator:

$$\mathbf{Rs}(K_g \rightarrow K_p) = \mathbf{Rs}^{-1}(K_p \rightarrow K_g) = \mathbf{Rt}(-\varphi_z, z_p) \quad (\text{D.64})$$

**FIGURE D.17**

A normalized and orthogonally parameterized basis,  $\mathbf{e}_1\mathbf{e}_4\mathbf{e}_5$ , that is constructed from an arbitrary basis,  $\mathbf{x}_1\mathbf{x}_2\mathbf{x}_3$ .

Implementation of the discussed results allows for:

- Representation of the gear tooth flank,  $\mathcal{G}$ , and the pinion tooth flank,  $\mathcal{P}$ , of the form-cutting tool, as well as their relative motion in a common coordinate system
- Consideration meshing of the gear tooth flank,  $\mathcal{G}$ , in any desired coordinate systems that is a component of the chain and/or the closed loop of consequent coordinate system transformations

Transition from one coordinate system to another can be performed in both of two feasible directions, say, the direct as well as inverse direction.

## D.5 Impact of Coordinate System Transformations on Fundamental Forms of the Surface

Every coordinate system transformation results in a corresponding change to the equation of the gear,  $\mathcal{G}$ , and/or pinion,  $\mathcal{P}$ , tooth flank. Because of this, it is often necessary to recalculate coefficients of the first,  $\Phi_{1,g'}$  and second,  $\Phi_{2,g'}$  fundamental forms of the gear tooth flank,  $G$  (as many times as the coordinate system transformation is performed). This routine and time-consuming operation can be eliminated if the operators of coordinate system transformations are used directly with the fundamental forms,  $\Phi_{1,g}$  and  $\Phi_{2,g}$ .

After being calculated in an initial reference system, the fundamental magnitudes,  $E_g$ ,  $F_g$ , and  $G_g$ , of the first,  $\Phi_{1,g'}$ , and the fundamental magnitudes,  $L_g$ ,  $M_g$ , and  $N_g$ , of the second,  $\Phi_{2,g'}$  fundamental forms can be

determined in any new coordinate system using for this purpose the operators of translation and rotation and the resultant coordinate system transformation [107]. Transformation of such a kind of the fundamental magnitudes,  $\Phi_{1,g}$  and  $\Phi_{2,g}$ , becomes possible due to implementation of a formula that can be found immediately below.

Let's consider a gear tooth flank,  $\mathcal{G}$ , that is given by the equation  $\mathbf{r}_g = \mathbf{r}_g(U_g, V_g)$ , where  $(U_g, V_g) \in G$ .

For the analysis below, it is convenient to use the equation of the first fundamental form,  $\Phi_{1,g}$ , of the gear tooth flank,  $G$ , represented in matrix form:

$$[\Phi_{1,g}] = [dU_g \quad dV_g \quad 0 \quad 0] \cdot \begin{bmatrix} E_g & F_g & 0 & 0 \\ F_g & G_g & 0 & 0 \\ 0 & 0 & 1 & 0 \\ 0 & 0 & 0 & 1 \end{bmatrix} \cdot \begin{bmatrix} dU_g \\ dV_g \\ 0 \\ 0 \end{bmatrix} \quad (\text{D.65})$$

Similarly, the equation of the second fundamental form,  $\Phi_{2,g}$ , of the gear tooth flank,  $\mathcal{G}$ , can be given by:

$$[\Phi_{2,g}] = [dU_g \quad dV_g \quad 0 \quad 0] \cdot \begin{bmatrix} L_g & M_g & 0 & 0 \\ M_g & N_g & 0 & 0 \\ 0 & 0 & 1 & 0 \\ 0 & 0 & 0 & 1 \end{bmatrix} \cdot \begin{bmatrix} dU_g \\ dV_g \\ 0 \\ 0 \end{bmatrix} \quad (\text{D.66})$$

The coordinate system transformation that is performed by the operator of linear transformation,  $\mathbf{Rs}(1 \rightarrow 2)$ , transfers the equation  $\mathbf{r}_g = \mathbf{r}_g(U_g, V_g)$  of the gear tooth flank,  $\mathcal{G}$ , initially given in  $X_1Y_1Z_1$ , to the equation  $\mathbf{r}_g^* = \mathbf{r}_g^*(U_g^*, V_g^*)$  of that same gear tooth flank,  $\mathcal{G}$ , in a new coordinate system,  $X_2Y_2Z_2$ . It is clear that  $\mathbf{r}_g \neq \mathbf{r}_g^*$ . In the new coordinate system, the gear tooth flank,  $\mathcal{G}$ , is analytically described by the following expression:

$$\mathbf{r}_g^*(U_g^*, V_g^*) = \mathbf{Rs}(1 \rightarrow 2) \cdot \mathbf{r}_g(U_g, V_g) \quad (\text{D.67})$$

The operator of the resultant coordinate system transformation,  $\mathbf{Rs}(1 \rightarrow 2)$ , casts the column matrices of variables in Equations D.65 and D.66 to the form:

$$[dU_g^* \quad dV_g^* \quad 0 \quad 0]^T = \mathbf{Rs}(1 \rightarrow 2) \cdot [dU_g \quad dV_g \quad 0 \quad 0]^T. \quad (\text{D.68})$$

Substitution of Equation D.68 into Equations D.65 and D.66 makes possible the expressions for the fundamental forms,  $\Phi_{1,g}^*$  and  $\Phi_{2,g}^*$ , in the new coordinate system:

$$[\Phi_{1,g}^*] = [\mathbf{Rs}(1 \rightarrow 2) \cdot [dU_g \quad dV_g \quad 0 \quad 0]^T]^T \cdot [\Phi_{1,g}] \cdot \mathbf{Rs}(1 \rightarrow 2) \cdot [dU_g \quad dV_g \quad 0 \quad 0]^T \quad (\text{D.69})$$

$$[\Phi_{2,g}^*] = [\mathbf{Rs}(1 \rightarrow 2) \cdot [dU_g \quad dV_g \quad 0 \quad 0]^T]^T \cdot [\Phi_{2,g}] \cdot \mathbf{Rs}(1 \rightarrow 2) \cdot [dU_g \quad dV_g \quad 0 \quad 0]^T \quad (\text{D.70})$$

The following equation is valid for multiplication:

$$[\mathbf{Rs}(1 \rightarrow 2) \cdot [dU_g \quad dV_g \quad 0 \quad 0]^T]^T = \mathbf{Rs}^T(1 \rightarrow 2) \cdot [dU_g \quad dV_g \quad 0 \quad 0] \quad (\text{D.71})$$

Therefore,

$$[\Phi_{1,g}^*] = [dU_g \quad dV_g \quad 0 \quad 0]^T \cdot \{\mathbf{Rs}^T(1 \rightarrow 2) \cdot [\Phi_{1,g}] \cdot \mathbf{Rs}(1 \rightarrow 2)\} \cdot [dU_g \quad dV_g \quad 0 \quad 0] \quad (\text{D.72})$$

$$[\Phi_{2,g}^*] = [dU_g \quad dV_g \quad 0 \quad 0]^T \cdot \{\mathbf{Rs}^T(1 \rightarrow 2) \cdot [\Phi_{2,g}] \cdot \mathbf{Rs}(1 \rightarrow 2)\} \cdot [dU_g \quad dV_g \quad 0 \quad 0] \quad (\text{D.73})$$

It can be easily shown that the matrices,  $[\Phi_{1,g}^*]$  and  $[\Phi_{2,g}^*]$ , in Equations D.72 and D.73 represent quadratic forms with respect to  $dU_g$  and  $dV_g$ .

The operator of transformation,  $\mathbf{Rs}(1 \rightarrow 2)$ , of the gear tooth flank,  $\mathcal{G}$ , having the first,  $\Phi_{1,g}$ , and second,  $\Phi_{2,g}$ , fundamental forms from the initial coordinate system,  $X_1Y_1Z_1$ , to the new coordinate system,  $X_2Y_2Z_2$ , means that in the new coordinate system, the corresponding fundamental forms are expressed in the form:

$$[\Phi_{1,g}^*] = \mathbf{Rs}^T(1 \rightarrow 2) \cdot [\Phi_{1,g}] \cdot \mathbf{Rs}(1 \rightarrow 2) \quad (\text{D.74})$$

$$[\Phi_{2,g}^*] = \mathbf{Rs}^T(1 \rightarrow 2) \cdot [\Phi_{2,g}] \cdot \mathbf{Rs}(1 \rightarrow 2) \quad (\text{D.75})$$

Equations D.74 and D.75 reveal that after the coordinate system transformation is completed, the first,  $\Phi_{1,g}^*$ , and second,  $\Phi_{2,g}^*$ , fundamental forms of the gear tooth flank,  $\mathcal{G}$ , in the coordinate system,  $X_2Y_2Z_2$ , are expressed in terms of the first,  $\Phi_{1,g}$ , and second,  $\Phi_{2,g}$ , fundamental forms initially represented in the coordinate system,  $X_1Y_1Z_1$ . In order to do that, the corresponding fundamental form (either  $\Phi_{1,g}$  or  $\Phi_{2,g}$ ) must be premultiplied by  $\mathbf{Rs}(1 \rightarrow 2)$  and then postmultiplied by  $\mathbf{Rs}^T(1 \rightarrow 2)$ .

Implementation of Equations D.74 and D.75 significantly simplifies formulae transformations.

Equations similar to those above (Equations D.74 and D.75) are valid with respect to the pinion tooth flank,  $\mathcal{P}$ .

In the case of use of the third,  $\Phi_{3,g}$ , and fourth,  $\Phi_{4,g}$ , fundamental forms, their coefficients can be expressed in terms of the fundamental magnitudes of the first and second order.



# Taylor & Francis

Taylor & Francis Group

<http://taylorandfrancis.com>

---

## Appendix E: Contact Geometry of Gear and Mating Pinion Tooth Flanks

---

In the theory of gearing, the kinematics of gearing is considered the prime element of the gear pair. Other important elements of gearing, namely:

- a. The shape and geometry of the gear tooth flank,  $\mathcal{G}$
- b. The shape and geometry of the mating pinion tooth flank,  $\mathcal{P}$  (as well as numerous others)

are considered the secondary elements of gearing. This does not mean that the importance of the secondary elements is lower than that of the primary element. This is incorrect. This just means that the most favorable parameters of the secondary elements can be expressed in terms of the parameters of the prime element. Ultimately, the entire gear pair can be synthesized on the premise just of the prime element—that is, on the premise of the desirable kinematics of the gear pair. In other words, having just the desirable kinematics of the gear pair to be designed, it is possible to synthesize the rest of the design parameters of the gear pair. Only the kinematics of gearing is used for the purposes of synthesizing of the best possible gear pair for transmitting the input rotation and torque.

In order to solve the problem of synthesizing the most favorable gear pair, an appropriate analytical description of contact geometry of the gear tooth flank,  $\mathcal{G}$ , and mating pinion tooth flank,  $\mathcal{P}$ , is required. The problem of analytical description of contact geometry between two smooth regular surfaces in the first order of tangency is a sophisticated one.

Investigation of contact geometry of curves and surfaces can be traced back to the 18th century. The study of the contact of curves and surfaces was undertaken in considerable detail by Lagrange\* in his *Theorie des Fonctions Analytiques* (1797) [65], and Cauchy† in his *Leçons sur les Applications du Calcul Infinitésimal à la Géométrie* (1826) [13]. Later on, in the 20th century, an investigation in the realm of contact geometry of curves and surfaces was undertaken by Favard‡ in his *Cours de Géométrie Différentielle Locale* (1957) [30]. A few more names of researchers in the field could be mentioned.

The results of the research obtained in the field of contact geometry of two smooth regular surfaces are widely used in the theory of gearing. The problem of synthesizing of the most favorable gear pair can be solved on the premise of the analysis of topology of the contacting surfaces in differential vicinity of the point of their contact.

Various methods for analytical description of contact geometry between two smooth regular surfaces have been developed by now. An overview of the methods can be found in a monograph by Radzevich [120]. The latest achievements in the field are discussed in the papers [107,120,121] and in the monograph [137].

A detailed analysis of known methods of analytical description of the geometry of contact between two smooth regular surfaces uncovered the poor capability of known methods for solving problems in the field of designing efficient gear pairs. Therefore, an accurate method for analytical description of contact geometry between two smooth regular surfaces,  $\mathcal{G}$  and  $\mathcal{P}$ , in the first order of tangency that fits the needs of the theory of gearing is necessary. Such a method is worked out in this appendix.

It is convenient to begin the discussion starting from analytical description of local relative orientation of the gear tooth flank,  $\mathcal{G}$ , and mating pinion tooth flank,  $\mathcal{P}$ . The proposed analytical description is relevant to the differential vicinity of the point of contact,  $K$ , of the tooth flanks,  $\mathcal{G}$  and  $\mathcal{P}$ .

---

\* Joseph-Louis Lagrange (January 25, 1736–April 10, 1813)—an Italian-born (born Giuseppe Lodovico (Luigi) Lagrangia) famous French mathematician and mechanician.

† Augustin-Louis Cauchy (August 21, 1789–May 23, 1857)—a famous French mathematician.

‡ Jean Favard (August 28, 1902–January 21, 1965)—a French mathematician.

### E.1 Local Relative Orientation at a Point of Contact of Gear and Mating Pinion Tooth Flanks

When the gears rotate, a gear tooth flank,  $\mathcal{G}$ , and mating pinion tooth flank,  $\mathcal{P}$ , are in permanent tangency with one another. Locally, the contacting surfaces,  $\mathcal{G}$  and  $\mathcal{P}$ , can be approximated by the corresponding quadrics, as schematically illustrated in Figure E.1. The requirement to be permanently in tangency to each other imposes a kind of restriction on the relative configuration (location and orientation) of the tooth flanks,  $\mathcal{G}$  and  $\mathcal{P}$ , and on their instant relative motion.

In the theory of gearing, a quantitative measure of relative orientation of the gear tooth flank,  $\mathcal{G}$ , and mating pinion tooth flank,  $\mathcal{P}$ , is established [107].

Relative orientation at a point of contact of the gear tooth flank,  $\mathcal{G}$ , and mating pinion tooth flank,  $\mathcal{P}$ , is specified by the angle,  $\mu$ , of local\* relative orientation of the surfaces. By definition, the angle  $\mu$  is equal to the angle that the unit tangent vector,  $\mathbf{t}_{1,g}$ , of the first principal direction of the gear tooth flank,  $\mathcal{G}$ , forms with the unit tangent vector,  $\mathbf{t}_{1,p}$ , of the first principal direction of the mating pinion tooth flank,  $\mathcal{P}$ . That same angle,  $\mu$ , can also be determined as the angle that makes the unit tangent vectors,  $\mathbf{t}_{2,g}$  and  $\mathbf{t}_{2,p}$ , of the second principal directions of the surfaces,  $\mathcal{G}$  and  $\mathcal{P}$ , at the contact point,  $K$ . This immediately yields equations for the calculation of the angle,  $\mu$ :

$$\sin \mu = |\mathbf{t}_{1,g} \times \mathbf{t}_{1,p}| = |\mathbf{t}_{2,g} \times \mathbf{t}_{2,p}|, \quad (\text{E.1})$$

$$\cos \mu = \mathbf{t}_{1,g} \cdot \mathbf{t}_{1,p} = \mathbf{t}_{2,g} \cdot \mathbf{t}_{2,p}, \quad (\text{E.2})$$

$$\tan \mu = \frac{|\mathbf{t}_{1,g} \times \mathbf{t}_{1,p}|}{\mathbf{t}_{1,g} \cdot \mathbf{t}_{1,p}} \equiv \frac{|\mathbf{t}_{2,g} \times \mathbf{t}_{2,p}|}{\mathbf{t}_{2,g} \cdot \mathbf{t}_{2,p}} \quad (\text{E.3})$$

where

$\mathbf{t}_{1,g}$ ,  $\mathbf{t}_{2,g}$  are the unit vectors of the principal directions on the gear tooth flank,  $\mathcal{G}$ , measured at the contact point,  $K$ .

$\mathbf{t}_{1,p}$ ,  $\mathbf{t}_{2,p}$  are the unit vectors of the principal directions on the mating pinion tooth flank,  $\mathcal{P}$ , at that same contact point,  $K$ , of the tooth flanks,  $\mathcal{G}$  and  $\mathcal{P}$ .

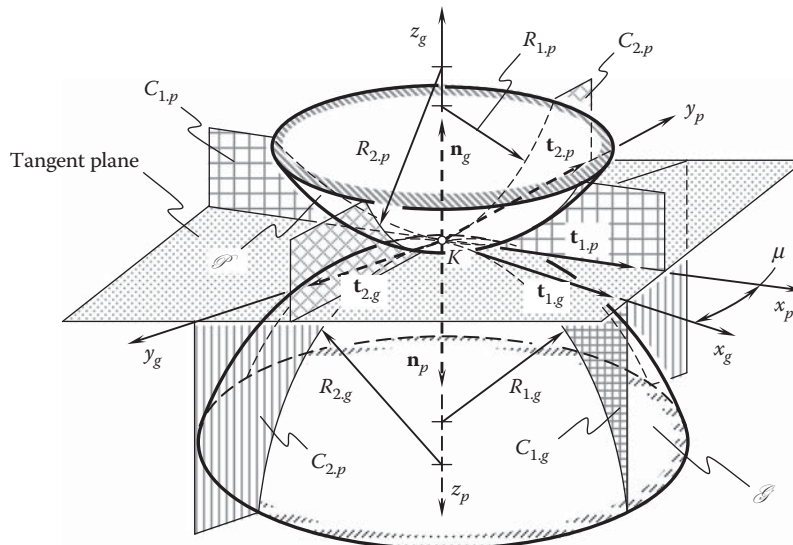


FIGURE E.1

Local configuration of two quadrics tangent to a gear tooth flank,  $\mathcal{G}$ , and a mating pinion tooth flank,  $\mathcal{P}$ , at a point,  $K$ , of their contact. (After Radzevich, S.P., *Theory of Gearing: Kinematics, Geometry, and Synthesis*, CRC Press, Boca Raton, FL, 2012, 760 p.)

\* The surface orientation is *local* in nature because it relates only to the differential vicinity of the point,  $K$ , of contact of the tooth flanks,  $\mathcal{G}$  and  $\mathcal{P}$ .



The directions of the unit tangent vectors,  $\mathbf{t}_{1,g}$  and  $\mathbf{t}_{2,g}$ , of the principal directions on the gear tooth flank,  $\mathcal{G}$  (as well as the directions of the unit tangent vectors  $\mathbf{t}_{1,p}$  and  $\mathbf{t}_{2,p}$  of the principal directions on the pinion tooth flank,  $\mathcal{P}$ ) can be specified in terms of the ratio  $dU_g/dV_g$  (or the ratio  $dU_p/dV_p$  in the case of the pinion tooth flank,  $\mathcal{P}$ ). The corresponding values of the ratio,  $dU_{g(p)}/dV_{g(p)}$ , are calculated as roots of the quadratic equation:

$$\begin{vmatrix} E_{g(p)} \frac{dU_{g(p)}}{dV_{g(p)}} + F_{g(p)} & F_{g(p)} \frac{dU_{g(p)}}{dV_{g(p)}} + G_{g(p)} \\ L_{g(p)} \frac{dU_{g(p)}}{dV_{g(p)}} + M_{g(p)} & M_{g(p)} \frac{dU_{g(p)}}{dV_{g(p)}} + N_{g(p)} \end{vmatrix} = 0 \quad (\text{E.4})$$

In the case of point contact of the surfaces,  $\mathcal{G}$  and  $\mathcal{P}$ , an actual value of the angle,  $\mu$ , is calculated at the contact point,  $K$ . If the tooth flanks,  $\mathcal{G}$  and  $\mathcal{P}$ , are in line contact, then actual value of the angle,  $\mu$ , can be calculated at every point within the line of contact.\* The line of contact of the tooth flanks,  $\mathcal{G}$  and  $\mathcal{P}$ , is commonly referred to as the *characteristic line*,  $\mathcal{E}$ , or just as the *characteristic*,  $\mathcal{E}$  for simplicity.

Determination of the angle,  $\mu$ , of local relative orientation of the tooth flanks,  $\mathcal{G}$  and  $\mathcal{P}$ , of a gear and mating pinion is illustrated in Figure E.1.

In order to calculate an actual value of the angle,  $\mu$ , of local relative orientation of the tooth flanks,  $\mathcal{G}$  and  $\mathcal{P}$ , the unit vectors of the principal directions,  $\mathbf{t}_{1,g}$  and  $\mathbf{t}_{1,p}$ , are employed.

Consider the tooth flanks,  $\mathcal{G}$  and  $\mathcal{P}$ , in point contact, which are represented in a common reference system. The surfaces make contact at a point,  $K$ . For further analysis, an equation of the common tangent plane to the tooth flanks,  $\mathcal{G}$  and  $\mathcal{P}$ , at the contact point,  $K$ , is necessary (see Figures E.1 and E.2).

$$(\mathbf{r}_{tp} - \mathbf{r}_K) \cdot \mathbf{u}_g \cdot \mathbf{v}_g = 0 \quad (\text{E.5})$$

where

$\mathbf{r}_{tp}$  is the position vector of a point of the common tangent plane.

$\mathbf{r}_K$  is the position vector of the contact point,  $K$ .

$\mathbf{u}_g$  and  $\mathbf{v}_g$  are unit vectors that are tangent to the  $U_g$ - and  $V_g$ -coordinate lines on the gear tooth flank,  $\mathcal{G}$  at the contact point,  $K$ .

The angle,  $\omega_g$ , is the angle that is formed by the unit vectors,  $\mathbf{u}_g$  and  $\mathbf{v}_g$ . The actual value of the angle,  $\omega_g$ , can be calculated from one of the following equations [137]:

$$\sin \omega_g = \frac{\sqrt{E_g G_g - F_g^2}}{\sqrt{E_g G_g}} \quad (\text{E.6})$$

$$\cos \omega_g = \frac{F_g}{\sqrt{E_g G_g}} \quad (\text{E.7})$$

$$\tan \omega_g = \frac{\sqrt{E_g G_g - F_g^2}}{F_g} \quad (\text{E.8})$$

Equations similar to Equations E.6 through E.8 are also valid for the calculation of the angle,  $\omega_p$ , at a point on the pinion tooth flank,  $\mathcal{P}$ .

Tangent directions,  $\mathbf{u}_g$  and  $\mathbf{v}_g$  to the  $U_g$ - and  $V_g$ -coordinate lines at a point on the gear tooth flank,  $\mathcal{G}$ , as well as tangent directions,  $\mathbf{u}_p$  and  $\mathbf{v}_p$  to the  $U_p$ - and  $V_p$ -coordinates at a point on the pinion tooth flank,  $\mathcal{P}$ , are specified

\* It is worth pointing out here that in a case of line contact, the relative orientation of two surfaces,  $\mathcal{G}$  and  $\mathcal{P}$ , is predetermined in *global* sense. However, the actual value of the angle,  $\mu$ , of the surfaces' local relative orientation at different points of the characteristic,  $\mathcal{E}$ , is different.



The equation for the calculation of the actual value of the angle,  $\xi_g$ , allows for another representation. Following the chain rule,  $d\mathbf{r}_g$  can be represented in the form:

$$d\mathbf{r}_g = \mathbf{U}_g dU_g + \mathbf{V}_g dV_g \quad (\text{E.14})$$

By definition,  $\tan \xi_g = \frac{\sin \xi_g}{\cos \xi_g}$ . The functions,  $\sin \xi_g$  and  $\cos \xi_g$ , yield representation as:

$$\sin \xi_g = \frac{|\mathbf{U}_g \times d\mathbf{r}_g|}{|\mathbf{U}_g| \cdot |d\mathbf{r}_g|} \quad (\text{E.15})$$

$$\cos \xi_g = \frac{\mathbf{U}_g \cdot d\mathbf{r}_g}{|\mathbf{U}_g| \cdot |d\mathbf{r}_g|} \quad (\text{E.16})$$

The last expressions yield:

$$\tan \xi_g = \frac{\sin \xi_g}{\cos \xi_g} = \frac{|\mathbf{U}_g \times d\mathbf{r}_g|}{\mathbf{U}_g \cdot d\mathbf{r}_g} = \frac{|\mathbf{U}_g \times d\mathbf{r}_g|}{\mathbf{U}_g \cdot (\mathbf{U}_g dU_g + \mathbf{V}_g dV_g)} = \frac{|\mathbf{U}_g \times d\mathbf{r}_g| \cdot dV_g}{\mathbf{U}_g \cdot \mathbf{U}_g dU_g + \mathbf{U}_g \cdot \mathbf{V}_g dV_g} \quad (\text{E.17})$$

By definition:

$$\mathbf{U}_g \cdot \mathbf{U}_g = E_g \quad (\text{E.18})$$

$$\mathbf{U}_g \cdot \mathbf{V}_g = F_g \quad (\text{E.19})$$

$$|\mathbf{U}_g \times \mathbf{V}_g| = \sqrt{E_g G_g - F_g^2} \quad (\text{E.20})$$

Equations E.14 through E.20 yield the formula:

$$\tan \xi_g = \frac{\sqrt{E_g G_g - F_g^2}}{\eta_g \cdot E_g + F_g} \quad (\text{E.21})$$

for the calculation of actual value of the angle,  $\xi_g$ .

Equations similar to those above (Equations E.11 and E.21) are also valid for the calculation of the actual value of the angle,  $\xi_p$ , that the first principal direction,  $\mathbf{t}_{1,p}$ , at a point on the pinion tooth flank,  $\mathcal{P}$ , forms with the unit tangent vector,  $\mathbf{u}_p$ .

The performed analysis makes possible the following equations for the calculation of the unit vectors of the principal directions,  $\mathbf{t}_{1,g}$  and  $\mathbf{t}_{2,g}$ :

$$\mathbf{t}_{1,g} = \mathbf{Rt}(\xi_g, \mathbf{n}_g) \cdot \mathbf{u}_g \quad (\text{E.22})$$

$$\mathbf{t}_{2,g} = \mathbf{Rt}\left[\left(\xi_g + \frac{\pi}{2}\right), \mathbf{n}_g\right] \cdot \mathbf{u}_g \quad (\text{E.23})$$

for the gear tooth flank,  $\mathcal{G}$ , and similar equations for the calculation of the unit vectors of the principal directions,  $\mathbf{t}_{1,p}$  and  $\mathbf{t}_{2,p}$ :

$$\mathbf{t}_{1,p} = \mathbf{Rt}(\xi_p, \mathbf{n}_g) \cdot \mathbf{u}_p \quad (\text{E.24})$$

$$\mathbf{t}_{2,p} = \mathbf{Rt}\left[\left(\xi_p + \frac{\pi}{2}\right), \mathbf{n}_g\right] \cdot \mathbf{u}_p \quad (\text{E.25})$$

for the pinion tooth flank,  $\mathcal{P}$ .

Equation D.16 for the operator of rotation,  $\mathbf{Rt}(\varphi_A, A_0)$ , through an angle,  $\varphi_A$ , about an axis,  $A_0$ , is employed for the calculation of the operators of rotation in Equations E.22 through E.25.

## E.2 Second-Order Analysis: Planar Characteristic Images

For a more accurate analytical description of the contact geometry of the gear tooth flank,  $\mathcal{G}$ , and the pinion tooth flank,  $\mathcal{P}$ , consideration of the second-order parameters is necessary. The second-order analysis incorporates elements of both the first-order and second-order analysis. For performing second-order analysis, familiarity with the *Dupin indicatrix* is highly desirable.\* The Dupin indicatrix is a perfect starting point for consideration of second-order analysis.

### E.2.1 Preliminary Remarks: Dupin Indicatrix

At any point of a smooth regular gear tooth flank,  $\mathcal{G}$  (as well as at any point of a smooth regular pinion tooth flank,  $\mathcal{P}$ ), corresponding Dupin indicatrices can be constructed. The Dupin indicatrix,  $\text{Dup}(\mathcal{G})$ , at a point of a gear tooth flank,  $\mathcal{G}$ , and the Dupin indicatrix,  $\text{Dup}(\mathcal{P})$ , at a point of the pinion tooth flank,  $\mathcal{P}$ , are planar characteristic curves of the second order. They are used for graphical interpretation of the distribution of normal radii of curvature of a surface in the differential vicinity of a surface point.

Dupin indicatrices at a point of the tooth flank,  $\mathcal{G}$  (as well as at a point of the tooth flank,  $\mathcal{P}$ ) are of critical importance in the theory of gearing. Generation of this planar characteristic curve is illustrated with a diagram shown in Figure E.3.

A plane,  $W$ , through the unit normal vector,  $\mathbf{n}_g$ , to the gear tooth flank,  $\mathcal{G}$ , at a point,  $m$ , is rotating about the unit normal vector,  $\mathbf{n}_g$ . While rotating, the plane occupies consecutive positions,  $W_1, W_2, W_3$ , and others. The radii of normal curvature of the line of intersection of the gear tooth flank,  $\mathcal{G}$ , by normal planes,  $W_1, W_2, W_3$ , are equal to  $R_{g,1}, R_{g,2}, R_{g,3}$ , and so forth. The gear tooth flank,  $\mathcal{G}$ , is intersected by a plane,  $Q$ . The plane,  $Q$ , is orthogonal to the unit normal vector,  $\mathbf{n}_g$ . This plane is at a certain small distance,  $\delta$ , from the point,  $m$ . When the distance,  $\delta$ , approaches zero ( $\delta \rightarrow 0$ ), and when the scale of the line of intersection of the gear tooth flank,  $\mathcal{G}$ , by the plane,  $Q$ , approaches infinity, then the line of intersection of the gear surface,  $\mathcal{G}$ , by the plane,  $Q$  approaches the planar characteristic curve that is commonly referred to as the Dupin indicatrix,  $\text{Dup}(\mathcal{G})$ .

In differential geometry of surfaces, a surface is construed as a zero-thickness film. Because of this, Dupin indicatrices of the following five different types are distinguished in the differential geometry of surfaces (see Figure E.4):

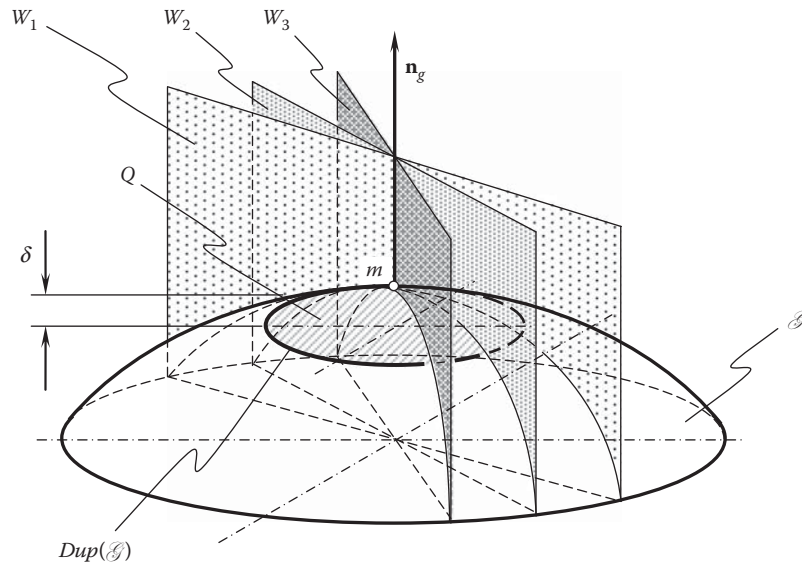
- Elliptic (Figure E.4a)
- Umbilic (Figure E.4b)
- Parabolic (Figure E.4c)
- Hyperbolic (Figure E.4d)
- Minimal (Figure E.4e).

The Dupin indicatrix for a plane local surface patch doesn't exist. In the case of planes, all points of the Dupin indicatrix are remote to infinity.

For local surface patches having negative full curvature ( $\mathcal{G}_g < 0$ ), phantom branches (i.e., branches that are not intersected by a plane perpendicular to the unit normal vector,  $\mathbf{n}_g$ , to the gear tooth flank,  $\mathcal{G}$ , at a point,  $m$ ) of the characteristic curve,  $\text{Dup}(\mathcal{G})$ , are shown in dashed lines in Figure E.4d and e.

An easy way to derive an equation of the characteristic curve,  $\text{Dup}(\mathcal{G})$ , is discussed immediately below.

\* Fransua Pier Charles Dupin (October 6, 1784–January 18, 1873)—a French mathematician.

**FIGURE E.3**

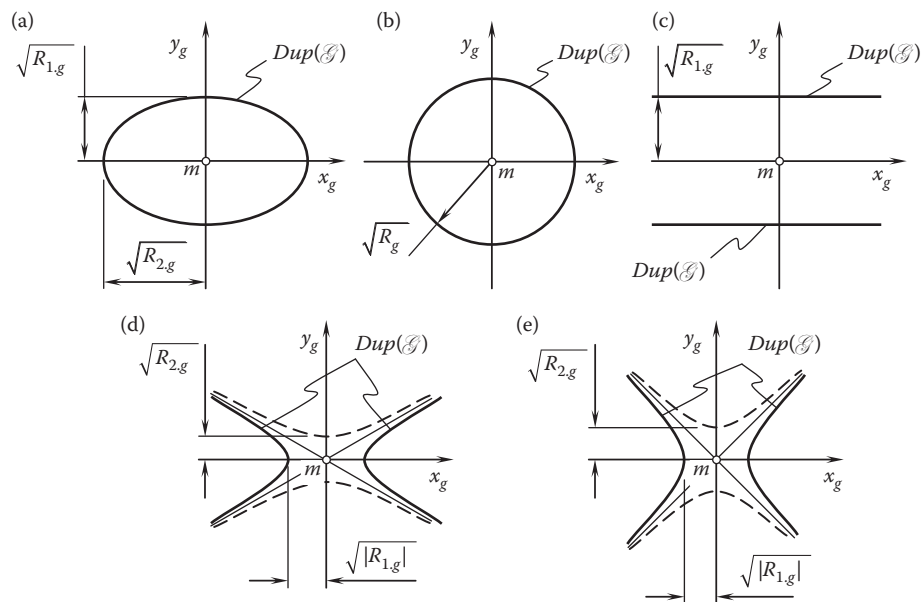
Dupin indicatrix at a point of a smooth regular gear tooth flank,  $\mathcal{G}$ .

The Euler formula:

$$k_{1,g} \cos^2 \varphi + k_{2,g} \sin^2 \varphi = k_g \quad (\text{E.26})$$

yields representation in the form:

$$\frac{k_{1,g}}{k_g} \cos^2 \varphi + \frac{k_{2,g}}{k_g} \sin^2 \varphi = 1 \quad (\text{E.27})$$

**FIGURE E.4**

Five different types of Dupin indicatrices,  $\text{Dup}(\mathcal{G})$ , at a point,  $m$ , of a smooth regular gear tooth flank,  $\mathcal{G}$ .

Transition from polar coordinates to *Cartesian coordinates* can be performed using well-known formulas:

$$x_g = \rho \cos \varphi \quad (\text{E.28})$$

$$y_g = \rho \sin \varphi \quad (\text{E.29})$$

These formulas make possible the following expressions for  $\cos^2 \varphi = x_g^2 / \rho^2$  and  $\sin^2 \varphi = y_g^2 / \rho^2$ . After substituting the last formulas into Equation E.27, one can come up with the equation:

$$\frac{k_{1.g}}{k_g} \cdot \frac{x_g^2}{\rho^2} + \frac{k_{2.g}}{k_g} \cdot \frac{y_g^2}{\rho^2} = 1. \quad (\text{E.30})$$

It is convenient to designate  $\rho = \sqrt{k_g^{-1}}$ . The principal curvatures,  $k_{1.g}$  and  $k_{2.g}$ , are the roots of the quadratic equation:

$$\begin{vmatrix} L_g - E_g k_g & M_g - F_g k_g \\ M_g - F_g k_g & N_g - G_g k_g \end{vmatrix} = 0 \quad (\text{E.31})$$

Substituting the calculated values of the principal curvatures,  $k_{1.g}$  and  $k_{2.g}$ , into Equation E.30, and after performing necessary formulae transformations, an equation\* for the Dupin indicatrix,  $Dup(\mathcal{G})$  can be represented in the form:

$$k_{1.g} x_g^2 + k_{2.g} y_g^2 = 1 \quad (\text{E.32})$$

Equation E.32 describes a particular case of the Dupin indicatrix, which is represented in *Darboux frame*.<sup>†</sup>

The general form of equation of Dupin indicatrix at a point,  $m$ , of a gear tooth flank,  $\mathcal{G}$ , is often represented as:

$$Dup(\mathcal{G}) \Rightarrow \frac{L_g}{E_g} x_g^2 + \frac{2M_g}{\sqrt{E_g G_g}} x_g y_g + \frac{N_g}{G_g} y_g^2 = 1 \quad (\text{E.33})$$

In Equation E.33, the characteristic curve,  $Dup(\mathcal{G})$ , is expressed in terms of the fundamental magnitudes,  $E_g$ ,  $F_g$ , and  $G_g$  of the first,  $\Phi_{1.g}$ , and in terms of the fundamental magnitudes,  $L_g$ ,  $M_g$ , and  $N_g$  of the second order,  $\Phi_{2.g}$ , at a point of the gear tooth flank,  $\mathcal{G}$ .

## E.2.2 Matrix Representation of Equation of Dupin Indicatrix at Point of a Gear Tooth Flank

Like any other quadratic form, the equation of the Dupin indicatrix of the gear tooth flank,  $\mathcal{G}$ , can be represented in matrix form:

$$Dup(\mathcal{G}) \Rightarrow \begin{bmatrix} x_g & y_g & 0 & 0 \end{bmatrix} \cdot \begin{bmatrix} \frac{L_g}{E_g} & \frac{2M_g}{\sqrt{E_g G_g}} & 0 & 0 \\ \frac{2M_g}{\sqrt{E_g G_g}} & \frac{N_g}{G_g} & 0 & 0 \\ 0 & 0 & \mp 1 & 0 \\ 0 & 0 & 0 & 1 \end{bmatrix} \cdot \begin{bmatrix} x_g \\ y_g \\ 0 \\ 0 \end{bmatrix} = \pm 1 \quad (\text{E.34})$$

\* The same equation of the Dupin indicatrix could be derived in another way. Coxeter [49] considers a pair of conics obtained by expanding an equation in Monge's form  $z = z(x, y)$  in a MacLaurin series:

$$z = z(0, 0) + z_1 x + z_2 y + \frac{1}{2} (z_{11} x_1^2 + 2z_{12} xy + z_{22} y^2) + \dots = \frac{1}{2} (b_{11} x^2 + 2b_{12} xy + b_{22} y^2).$$

† This gives the equation  $(b_{11} x^2 + 2b_{12} xy + b_{22} y^2) = \pm 1$  of the Dupin indicatrix.

<sup>†</sup> Jean Gaston Darboux (August 13, 1842–February 23, 1917), a French mathematician.

In the Darboux frame, this equation reduces to:

$$Dup(\mathcal{G}) \Rightarrow \begin{bmatrix} x_g & y_g & 0 & 0 \end{bmatrix} \cdot \begin{bmatrix} L_g & M_g & 0 & 0 \\ M_g & N_g & 0 & 0 \\ 0 & 0 & \mp 1 & 0 \\ 0 & 0 & 0 & 1 \end{bmatrix} \cdot \begin{bmatrix} x_g \\ y_g \\ 0 \\ 0 \end{bmatrix} = \pm 1 \quad (\text{E.35})$$

It is convenient to implement matrix representation of the equation of the Dupin indicatrix (see above), for instance, when investigating spatial gearings, that is, crossed-axes gearings, when multiple coordinate system transformations are required.

The equation of the Dupin indicatrix can be represented in the form:

$$r_{Dup}(\varphi) = \sqrt{|R_g(\varphi)|} \cdot \text{sgn } \Phi_{2,g}^{-1} \quad (\text{E.36})$$

The last equation reveals that the position vector of a point of the Dupin indicatrix,  $Dup(\mathcal{G})$ , in any direction is equal to the square root of the radius of curvature in that same direction.\*

### E.3 Degree of Conformity at Point of Contact of Gear and Mating Pinion Tooth Flanks in the First Order of Tangency

For an accurate analytical description of the contact geometry of the gear and mating pinion tooth flanks in the first order of tangency, a higher-order analysis must be done.

The method of a higher order analysis discussed below targets the development of an analytical description of a degree of conformity of the pinion tooth flank,  $\mathcal{P}$ , to the gear tooth flank,  $\mathcal{G}$ , at a current point,  $K$  of their contact. The higher the degree of conformity of the tooth flanks,  $\mathcal{G}$  and  $\mathcal{P}$ , the closer these surfaces to each other in the differential vicinity of the point,  $K$ . This qualitative (*intuitive*) definition of degree of conformity of two smooth regular surfaces needs a corresponding quantitative measure.

#### E.3.1 Preliminary Remarks

Implementation of the resultant deviation,  $l_{cnf}$  (see Figure E.5), [137] of two smooth regular surfaces in contact for the analytical description of the contact geometry of two surfaces in contact is a type of straightforward solution to the problem under consideration. This approach is proven to be computationally ineffective. However, the approach gives insight into how an effective method for solving the problem under consideration can be developed.

As seen in Figure E.5, three geometrical parameters are interrelated when a deviation of a surface from the tangent plane is considered in differential vicinity of a surface point. They are:

- The measure of the deviation,  $m_g m_g^*$ , of a gear tooth flank,  $\mathcal{G}$ , from the tangent plane,  $l_{cnf}$
- The distance,  $K m_g^*$ , of a current point,  $m_g$ , from the contact point,  $K$
- The radius of normal curvature  $R_g$  of the gear tooth flank,  $\mathcal{G}$ , at the contact point,  $K$

As a consequence of this relationship among the parameters,  $m_g m_g^*$ ,  $K m_g^*$ , and  $R_g$ , any one of them can be used for the purposes of quantitative evaluation of degree of conformity of the contacting tooth flanks,  $\mathcal{G}$  and  $\mathcal{P}$ , of

\* Similar to the Dupin indicatrix,  $Dup(\mathcal{G})$ , a planar characteristic curve of another type can be introduced. The equation of this characteristic curve can be postulated in the form:  $r_{Dup,k}(\varphi) = \sqrt{|k_g(\varphi)|} \cdot \text{sgn } \Phi_{2,g}^{-1}$ . Application of curvature indicatrix in the form  $r_{Dup,k}(\varphi)$  makes it possible to avoid uncertainty in cases of plane surfaces. For plane surfaces, the characteristic curve,  $Dup(\mathcal{G})$ , does not exist, while  $r_{Dup,k}(\varphi)$  exists. It shrinks to the point,  $m$ , on the gear tooth flank,  $\mathcal{G}$ .



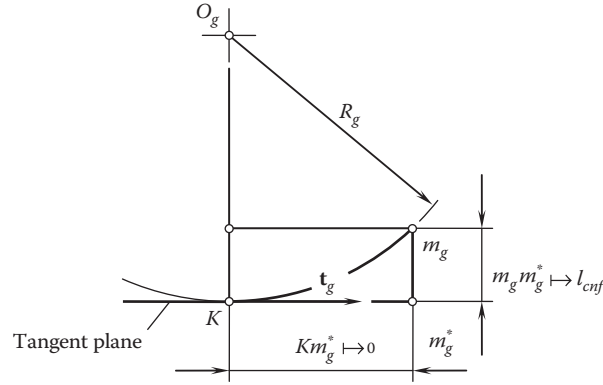


FIGURE E.5

On transition from the resultant deviation,  $l_{cnf}$ , of two tooth flanks to the indicatrix of conformity,  $C_{nf}(\mathcal{G}|\mathcal{P})$ , at a contact point,  $K$ , between smooth regular tooth flanks,  $\mathcal{G}$  and  $\mathcal{P}$ .

the gear and mating pinion. As follows from Figure E.5:

$$m_g m_g^* = R_g - \sqrt{R_g^2 - (K m_g^*)^2} \Big|_{m_g \rightarrow K} \mapsto l_{cnf} \quad (\text{E.37})$$

Inversely, for the radius of normal curvature,  $R_g$ , at a point of the gear tooth flank,  $\mathcal{G}$ , the following expression is valid:

$$R_g = \frac{(m_g m_g^*)^2 + (K m_g^*)^2}{2 \cdot m_g m_g^*} \quad (\text{E.38})$$

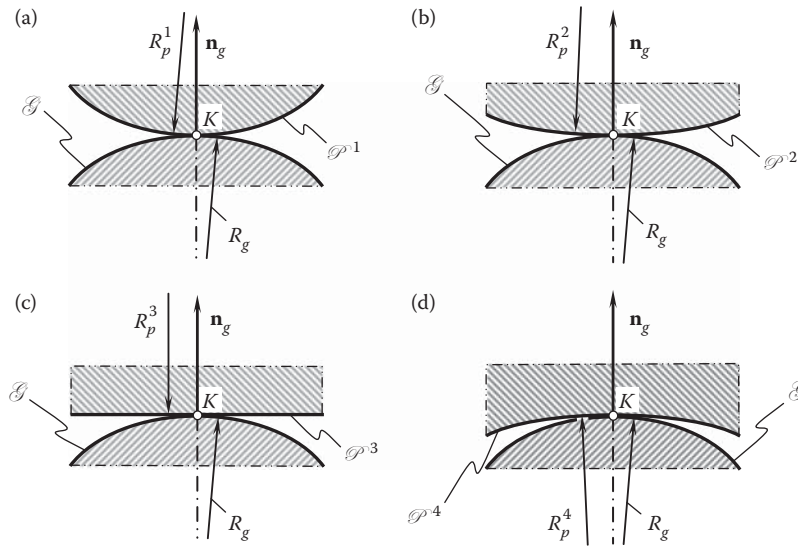
Ultimately, one may conclude that any legitimate analytical function of normal radii of curvature,  $R_g$  and  $R_p$ , at a point of contact of the gear tooth flank,  $\mathcal{G}$ , and pinion tooth flank,  $\mathcal{P}$ , can be used for this particular purpose.

Consider two smooth regular tooth flanks,  $\mathcal{G}$  and  $\mathcal{P}$ , in the first order of tangency that make contact at a point,  $K$ . The degree of conformity of the tooth flanks,  $\mathcal{G}$  and  $\mathcal{P}$ , can be construed as a function of radii of normal curvature,  $R_g$  and  $R_p$ , of the contacting surfaces. The radii of normal curvature,  $R_g$  and  $R_p$ , of the tooth flanks,  $\mathcal{G}$  and  $\mathcal{P}$ , are taken in a common normal plane section through the point,  $K$ . For a specified radius of normal curvature,  $R_g$ , of the tooth flank,  $\mathcal{G}$ , the degree of conformity of the tooth flanks depends upon the corresponding value of radius of normal curvature,  $R_p$ , of the pinion tooth flank,  $\mathcal{P}$ .

In most cases of gear meshing, the degree of conformity at a point of contact of the tooth flanks,  $\mathcal{G}$  and  $\mathcal{P}$ , is not constant and changes as coordinates of the contact point change. The degree of the surfaces' conformity to one another depends on orientation of the normal plane section through the contact point,  $K$ , and changes as the normal plane section turns about the common perpendicular,  $\mathbf{n}_g$ . This statement immediately follows from the above conclusion that degree of conformity at a point of contact of the tooth flanks,  $\mathcal{G}$  and  $\mathcal{P}$ , yields interpretation in terms of radii of normal curvature,  $R_g$  and  $R_p$ .

The change of degree of conformity of a gear tooth flank,  $\mathcal{G}$ , and mating pinion tooth flank,  $\mathcal{P}$ , due to turning of the normal plane section about the common perpendicular,  $\mathbf{n}_g$ , is illustrated in Figure E.6. Here, in Figure E.6, just two-dimensional examples are shown, for which that same normal plane section of the gear tooth flank,  $\mathcal{G}$ , makes contact with different plane sections,  $\mathcal{P}^i$ , of the pinion tooth flank,  $\mathcal{P}$ .

In the example shown in Figure E.6a, the radius of normal curvature,  $R_p^1$ , of the convex plane section,  $\mathcal{P}^1$ , of the pinion tooth flank,  $\mathcal{P}$ , is positive ( $R_p^1 > 0$ ). The convex normal plane section of the pinion tooth flank,  $\mathcal{P}$ , makes contact with the convex normal plane section ( $R_g > 0$ ) of a gear tooth flank,  $\mathcal{G}$ . The degree of conformity of the pinion tooth flank,  $\mathcal{P}$ , to the gear tooth flank,  $\mathcal{G}$ , in Figure E.6a is relatively low, as both the contacting surfaces are convex.

**FIGURE E.6**

Sections of two smooth regular tooth flanks,  $\mathcal{G}$  and  $\mathcal{P}$ , in contact by a plane through the common perpendicular,  $\mathbf{n}_g$ .

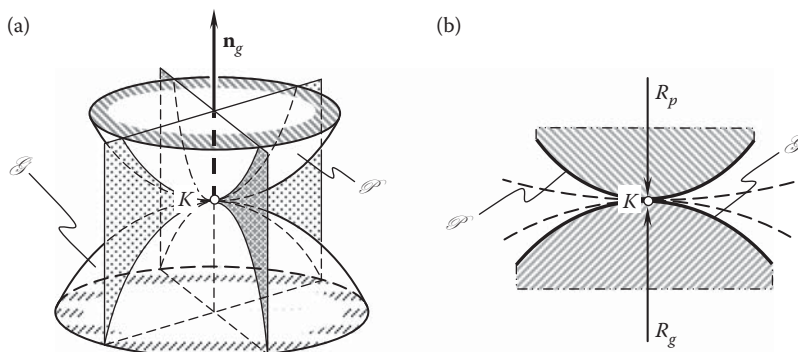
Another example is shown in Figure E.6b. The radius of normal curvature,  $R_p^2$ , of the convex plane section,  $\mathcal{P}^2$ , of the pinion tooth flank,  $\mathcal{P}$ , is also positive ( $R_p^2 > 0$ ). However, its value exceeds the value,  $R_p^1$ , of the radius of normal curvature in the first example ( $R_p^2 > R_p^1$ ). This results in a degree of conformity of the pinion tooth flank,  $\mathcal{P}$ , to the gear tooth flank,  $\mathcal{G}$  (Figure E.6b), that is greater compared to that shown in Figure E.6a.

In the next example, depicted in Figure E.6c, the normal plane section  $\mathcal{P}^3$  of the pinion tooth flank,  $\mathcal{P}$ , is represented with locally flattened section. The radius of normal curvature,  $R_p^3$ , of the flattened plane section,  $\mathcal{P}^3$ , approaches infinity ( $R_p^3 \rightarrow \infty$ ). Thus, the inequality,  $R_p^3 > R_p^2 > R_p^1$ , is valid. Therefore, the degree of conformity of the pinion tooth flank,  $\mathcal{P}$ , to the gear tooth flank,  $\mathcal{G}$  in Figure E.6c, is also greater.

Finally, for a concave normal plane section,  $\mathcal{P}^4$ , of the pinion tooth flank,  $\mathcal{P}$ , that is illustrated in Figure E.6d, the radius of normal curvature,  $R_p^4$ , has a negative value ( $R_p^4 < 0$ ). In this case, the degree of conformity of the pinion tooth flank,  $\mathcal{P}$ , to the gear tooth flank,  $\mathcal{G}$ , is the greatest of four examples considered in Figure E.6.

The examples shown in Figure E.6 qualitatively illustrate what is known intuitively regarding the different degrees of conformity of two smooth regular surfaces in the first order of tangency. Intuitively, one can realize that in the examples shown in Figure E.6a–d, the degree of conformity at a point of contact of two tooth flanks,  $\mathcal{G}$  and  $\mathcal{P}$ , is gradually increased.

A similar observation is made for a given pair of tooth flanks,  $\mathcal{G}$  and  $\mathcal{P}$ , when different sections of the surfaces by a plane surface through the common perpendicular,  $\mathbf{n}_g$ , are considered (see Figure E.7a). When rotating the plane section about the common perpendicular,  $\mathbf{n}_g$ , it can be observed that the degree of conformity of the gear and pinion tooth flanks,  $\mathcal{G}$  and  $\mathcal{P}$ , is different in different configurations of the cross-sectional plane (see Figure E.7b).

**FIGURE E.7**

Analytical description of contact geometry of two smooth regular tooth flanks,  $\mathcal{G}$  and  $\mathcal{P}$ , of a gear and mating pinion.

The above examples provide an intuitive understanding of what the degree of conformity at a point of contact of two smooth regular tooth flanks,  $\mathcal{G}$  and  $\mathcal{P}$ , means. The examples cannot be employed directly for the purpose of quantitatively evaluating the degree of conformity at a point of contact of two smooth regular tooth flanks,  $\mathcal{G}$  and  $\mathcal{P}$ . The next necessary step is to introduce an appropriate quantitative evaluation of the degree of conformity of two smooth regular surfaces in the first order of tangency. In other words, how can a certain degree of conformity of two smooth regular surfaces be described analytically?

### E.3.2 Indicatrix of Conformity at Point of Contact of Gear and Mating Pinion Tooth Flanks

This section aims to introduce of a quantitative measure of degree of conformity at a point of contact between two smooth regular surfaces. The degree of conformity at a point of contact of two tooth flanks,  $\mathcal{G}$  and  $\mathcal{P}$ , indicates how the pinion tooth flank,  $\mathcal{P}$ , is close to the gear tooth flank,  $\mathcal{G}$ , in differential vicinity of a point,  $K$ , of their contact, say, how much the surface,  $\mathcal{P}$ , is *congruent* to the surface,  $\mathcal{G}$ , in the differential vicinity of the contact point,  $K$ . This particular type of congruency between the contacting surfaces,  $\mathcal{G}$  and  $\mathcal{P}$ , can also be construed as the *local congruency* of the contacting surfaces.

Quantitatively, the degree of conformity at a point of contact of a smooth regular surface,  $\mathcal{P}$ , to another surface,  $\mathcal{G}$ , can be expressed in terms of the difference between the corresponding radii of normal curvature of the contacting surfaces. In order to develop a quantitative measure of the degree of conformity of the tooth flanks,  $\mathcal{G}$  and  $\mathcal{P}$ , it is convenient to implement Dupin indicatrices,  $Dup(\mathcal{G})$  and  $Dup(\mathcal{P})$ , constructed at a point of contact of the gear tooth flank,  $\mathcal{G}$ , and pinion tooth flank,  $\mathcal{P}$ , respectively.

It is natural to assume that a smaller difference between the normal curvatures of the surfaces,  $\mathcal{G}$  and  $\mathcal{P}$ , in a common cross-section by a plane through the common normal vector,  $\mathbf{n}_g$ , results in a greater degree of conformity at a point of contact of the tooth flanks,  $\mathcal{G}$  and  $\mathcal{P}$ .

The Dupin indicatrix,  $Dup(\mathcal{G})$ , indicates the distribution of radii of normal curvature at a point of the gear tooth flank,  $\mathcal{G}$ , as shown, for example, for a concave elliptical patch of the surface,  $\mathcal{G}$  (see Figure E.8). For a gear tooth flank,  $\mathcal{G}$ , the equation of this characteristic curve in polar coordinates can be represented in the form:

$$Dup(\mathcal{G}) \Rightarrow r_g(\varphi_g) = \sqrt{|R_g(\varphi_g)|} \quad (\text{E.39})$$

where

$r_g$  is the position vector of a point of the Dupin indicatrix,  $Dup(\mathcal{G})$  at a point of the gear tooth flank,  $\mathcal{G}$ .

$\varphi_g$  is the polar angle of the indicatrix,  $Dup(\mathcal{G})$ .

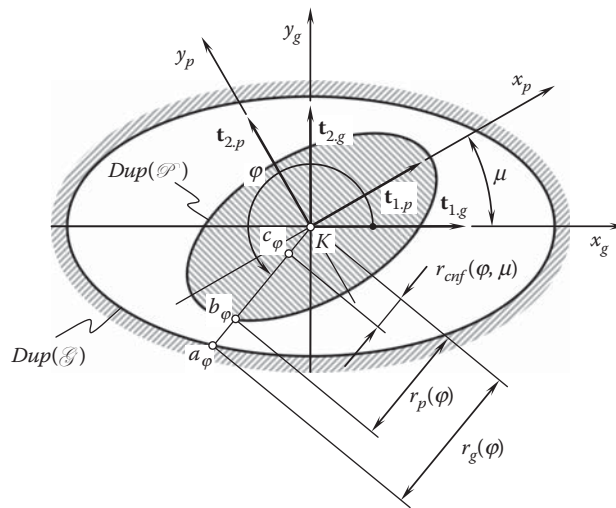


FIGURE E.8

Derivation of equation of indicatrix of conformity,  $Cnf_K(\mathcal{G}/\mathcal{P})$ , at a point of contact of a smooth regular gear tooth flank,  $\mathcal{G}$ , and the mating pinion tooth flank,  $\mathcal{P}$ , that are in the first order of tangency.

The similar is true with respect to the Dupin indicatrix,  $Dup(\mathcal{G})$ , at a point of the pinion tooth flank,  $\mathcal{P}$ , as shown, for instance, for a convex elliptical patch of the pinion tooth flank,  $\mathcal{P}$  (see Figure E.8). The equation of this characteristic curve in polar coordinates can be represented in the form:

$$Dup(\mathcal{P}) \Rightarrow r_p(\varphi_p) = \sqrt{|R_p(\varphi_p)|} \quad (E.40)$$

where

$r_p$  is the position vector of a point of the Dupin indicatrix,  $Dup(\mathcal{G})$  at a point of the pinion tooth flank,  $\mathcal{P}$ .

$\varphi_p$  is the polar angle of the indicatrix,  $Dup(\mathcal{P})$ .

In the coordinate plane,  $x_g y_{g'}$  of the local reference system,  $x_g y_g z_{g'}$ , the equalities,  $\varphi_g = \varphi$  and  $\varphi_p = \varphi + \mu$ , are valid. Therefore, in the coordinate plane,  $x_g y_g$ , Equations E.39 and E.40 cast into:

$$Dup(\mathcal{G}) \Rightarrow r_g(\varphi) = \sqrt{|R_g(\varphi)|} \quad (E.41)$$

$$Dup(\mathcal{P}) \Rightarrow r_p(\varphi, \mu) = \sqrt{|R_p(\varphi, \mu)|} \quad (E.42)$$

When the degree of conformity at a point of contact to the gear tooth flank,  $\mathcal{G}$ , is greater, then the difference between the functions  $r_g(\varphi)$  and  $r_p(\varphi, \mu)$  becomes smaller, and vice versa. The last makes valid the following conclusion:

### Conclusion E.1

The distance between the corresponding\* points of the Dupin indicatrices,  $Dup(\mathcal{G})$  and  $Dup(\mathcal{P})$ , constructed at a point of contact of a gear tooth flank,  $\mathcal{G}$ , and mating pinion tooth flank,  $\mathcal{P}$ , can be employed for the purpose of indication of the degree of conformity at a point of contact of the gear tooth flank,  $\mathcal{G}$ , and the pinion tooth flank,  $\mathcal{P}$ , at the contact point,  $K$ .

The equation of the *indicatrix of conformity*,  $Cnf_R(\mathcal{G}/\mathcal{P})$ , at a point of contact of a gear tooth flank,  $\mathcal{G}$ , and mating pinion tooth flank,  $\mathcal{P}$ , is defined with the following structure:

$$\begin{aligned} Cnf_R(\mathcal{G}/\mathcal{P}) \Rightarrow r_{cnf}(\varphi, \mu) &= \sqrt{|R_g(\varphi)|} \operatorname{sgn} R_g(\varphi) + \sqrt{|R_p(\varphi, \mu)|} \operatorname{sgn} R_p(\varphi, \mu) \\ &= r_g(\varphi) \operatorname{sgn} R_g(\varphi) + r_p(\varphi, \mu) \operatorname{sgn} R_p(\varphi, \mu) \end{aligned} \quad (E.43)$$

Because the location of a point,  $a_\varphi$ , of the Dupin indicatrix,  $Dup(\mathcal{G})$ , at a point of the gear tooth flank,  $\mathcal{G}$ , is specified by the position vector,  $r_g(\varphi)$ , and the location of a point,  $b_\varphi$ , of the Dupin indicatrix,  $Dup(\mathcal{P})$ , at a point of the pinion tooth flank,  $\mathcal{P}$ , is specified by the position vector,  $r_p(\varphi, \mu)$ , then the location of a point,  $c_\varphi$  (see Figure E.8), of the indicatrix of conformity,  $Cnf_R(\mathcal{G}/\mathcal{P})$ , at a point of contact,  $K$ , of the tooth flanks,  $\mathcal{G}$  and  $\mathcal{P}$ , is specified by the position vector,  $r_{cnf}(\varphi, \mu)$ . Therefore, the equality  $r_{cnf}(\varphi, \mu) = Kc_\varphi$  is observed, and the length of the straight line segment,  $Kc_\varphi$ , is equal to the distance,  $a_\varphi b_\varphi$ .

Here, in Equation E.43:

$r_g = \sqrt{|R_g|}$  is the position vector of a point of the Dupin indicatrix of the gear tooth flank,  $\mathcal{G}$ , at a point  $K$  of contact with the pinion tooth flank,  $\mathcal{P}$ .

$r_p = \sqrt{|R_p|}$  is the position vector of a corresponding point of the Dupin indicatrix of the pinion tooth flank,  $\mathcal{P}$ .

Here, in Equation E.43, the multipliers  $\operatorname{sgn} R_g(\varphi)$  and  $\operatorname{sgn} R_p(\varphi, \mu)$  are assigned to each of the functions,  $r_g(\varphi) = \sqrt{|R_g(\varphi)|}$  and  $r_p(\varphi, \mu) = \sqrt{|R_p(\varphi, \mu)|}$ , accordingly, just to maintain the corresponding signs of the functions, that is, to keep the same sign the radii of normal curvature,  $R_g(\varphi)$  and  $R_p(\varphi, \mu)$ , have.

\* Corresponding points of the Dupin indicatrices,  $Dup(\mathcal{G})$  and  $Dup(\mathcal{P})$ , share the same straight line through the contact point,  $K$ , of the tooth flanks,  $\mathcal{G}$  and  $\mathcal{P}$ , and are located at the same side of the point,  $K$ .

Ultimately, one can conclude that the position vector,  $r_{cnf}$ , of a point of the indicatrix of conformity,  $Cnf_R(\mathcal{G}/\mathcal{P})$ , can be expressed in terms of position vectors,  $r_g$  and  $r_p$ , of the Dupin indicatrices,  $Dup(\mathcal{G})$  and  $Dup(\mathcal{P})$ .

For the calculation of a current value of the radius of normal curvature,  $R_g(\varphi)$ , at a point of the gear tooth flank,  $\mathcal{G}$ , the equality:

$$R_g(\varphi) = \frac{\Phi_{1,g}}{\Phi_{2,g}} \quad (\text{E.44})$$

can be used.

Similarly, for the calculation of the current value of the radius of normal curvature,  $R_p(\varphi, \mu)$ , at a point of the pinion tooth flank,  $\mathcal{P}$ , the equality:

$$R_p(\varphi, \mu) = \frac{\Phi_{1,p}}{\Phi_{2,p}} \quad (\text{E.45})$$

can be employed.

Use of the angle,  $\mu$ , of local relative orientation of the tooth flanks,  $\mathcal{G}$  and  $\mathcal{P}$ , indicates that the radii of normal curvature,  $R_g(\varphi)$  and  $R_p(\varphi, \mu)$ , are taken in a common normal plane section through the contact point,  $K$ .

Further, it is well known that the inequalities,  $\Phi_{1,g} \geq 0$  and  $\Phi_{1,p} \geq 0$ , are always valid. Therefore, Equation E.43 can be rewritten in the following form:

$$r_{cnf} = r_g(\varphi) \operatorname{sgn} \Phi_{2,g}^{-1} + r_p(\varphi, \mu) \operatorname{sgn} \Phi_{2,p}^{-1} \quad (\text{E.46})$$

For the derivation of an equation of the indicatrix of conformity,  $Cnf_R(\mathcal{G}/\mathcal{P})$ , it is convenient to use the Euler equation for normal radius of curvature,  $R_g(\varphi)$ , at a point of the gear tooth flank,  $\mathcal{G}$  [137]:

$$R_g(\varphi) = \frac{R_{1,g} \cdot R_{2,g}}{R_{1,g} \cdot \sin^2 \varphi + R_{2,g} \cdot \cos^2 \varphi} \quad (\text{E.47})$$

Here, the radii of principal curvature,  $R_{1,g}$  and  $R_{2,g}$ , are the roots of the quadratic equation:

$$\begin{vmatrix} L_g \cdot R_g - E_g & M_g \cdot R_g - F_g \\ M_g \cdot R_g - F_g & N_g \cdot R_g - G_g \end{vmatrix} = 0 \quad (\text{E.48})$$

Recall that the inequality,  $R_{1,g} < R_{2,g}$ , is always observed.

Equations E.47 and E.48 allow for expression of the radius of normal curvature,  $R_g(\varphi)$ , at a point of the gear tooth flank,  $\mathcal{G}$ , in terms of the fundamental magnitudes of the first order,  $E_g$ ,  $F_g$ , and  $G_g$ , and the fundamental magnitudes of the second order,  $L_g$ ,  $M_g$ , and  $N_g$ .

A similar consideration is applicable for the pinion tooth flank,  $\mathcal{P}$ . Omitting routing analysis, one can conclude that the radius of normal curvature,  $R_p(\varphi, \mu)$ , at a point of the pinion tooth flank,  $\mathcal{P}$ , can be expressed in terms of the fundamental magnitudes of the first order,  $E_p$ ,  $F_p$ , and  $G_p$ , and the fundamental magnitudes of the second order,  $L_p$ ,  $M_p$ , and  $N_p$ .

Finally, on the premise of the above-performed analysis, the following equation for the indicatrix of conformity,  $Cnf_R(\mathcal{G}/\mathcal{P})$ , at a point of contact of the tooth flanks,  $\mathcal{G}$  and  $\mathcal{P}$ , can be derived:

$$\begin{aligned} r_{cnf}(\varphi, \mu) = & \sqrt{\left| \frac{E_g G_g}{L_g G_g \cos^2 \varphi - M_g \sqrt{E_g G_g} \sin 2\varphi + N_g E_g \sin^2 \varphi} \right|} \operatorname{sgn} \Phi_{2,g}^{-1} \\ & + \sqrt{\left| \frac{E_p G_p}{L_p G_p \cos^2(\varphi + \mu) - M_p \sqrt{E_p G_p} \sin 2(\varphi + \mu) + N_p E_p \sin^2(\varphi + \mu)} \right|} \operatorname{sgn} \Phi_{2,p}^{-1} \end{aligned} \quad (\text{E.49})$$

Equation E.49 of the characteristic curve\*  $Cnf_R(P/T)$  has been known since the late 1970s, and is published in [94] and (in a hidden form) in [93].

Analysis of Equation E.49 reveals that the indicatrix of conformity,  $Cnf_R(\mathcal{G}/\mathcal{P})$ , at a point of contact of a gear tooth flank,  $\mathcal{G}$ , and mating pinion tooth flank,  $\mathcal{P}$ , is represented by a planar centro-symmetrical curve of the fourth order. In particular cases, this characteristic curve possess also a property of mirror symmetry. Mirror symmetry of the indicatrix of conformity is observed, for example, when the angle,  $\mu$ , of local relative orientation of the tooth flanks,  $\mathcal{G}$  and  $\mathcal{P}$ , is  $\mu = \pm \pi \cdot n/2$ , where  $n$  designates an integer.

It is important to notice here that even for the most general case of gearing, position vector of a point,  $r_{cnf}(\varphi, \mu)$ , of the indicatrix of conformity,  $Cnf_R(\mathcal{G}/\mathcal{P})$ , are not dependent on the fundamental magnitudes,  $F_g$  and  $F_p$ . The independence of the indicatrix of conformity,  $Cnf_R(\mathcal{G}/\mathcal{P})$ , of the fundamental magnitudes,  $F_g$  and  $F_p$ , is because of the following.

The coordinate angle,  $\omega_g$ , at a point of the gear tooth flank,  $\mathcal{G}$ , can be calculated from the formula:

$$\omega_g = \arccos \frac{F_g}{\sqrt{E_g G_g}} \quad (\text{E.50})$$

It is natural that the position vector,  $r_{cnf}(\varphi, \mu)$ , of a point of the indicatrix of conformity,  $Cnf_R(\mathcal{G}/\mathcal{P})$ , is not a function of the coordinate angle,  $\omega_g$ . Although the position vector,  $r_{cnf}(\varphi, \mu)$ , depends on the fundamental magnitudes,  $E_g$ ,  $G_g$  and  $E_p$ ,  $G_p$ , the above analysis makes it clear why the position vector,  $r_{cnf}(\varphi, \mu)$ , does not depend upon the fundamental magnitudes  $F_g$  and  $F_p$ .

Two illustrative examples of the indicatrix of conformity,  $Cnf_R(\mathcal{G}/\mathcal{P})$ , at a point of contact of a gear tooth flank,  $\mathcal{G}$ , and mating pinion tooth flank,  $\mathcal{P}$ , are shown in Figure E.9. The first example (see Figure E.9a) relates to cases of contact of a saddle-like local patch of the tooth surface,  $\mathcal{G}$ , and a convex elliptic-like local patch of the tooth surface,  $\mathcal{P}$ . The second (see Figure E.9b) is for the case of contact of a convex parabolic-like local patch of the tooth surface,  $\mathcal{G}$ , and a convex elliptic-like local patch of the tooth,  $\mathcal{P}$ . For both cases (see Figure E.9), the corresponding curvature indicatrices,<sup>†</sup>  $Crv(\mathcal{G})$  and  $Crv(\mathcal{P})$ , at the point of contact of the tooth flanks,  $\mathcal{G}$  and  $\mathcal{P}$ , are depicted in Figure E.9 as well. The imaginary (phantom) branches of the Dupin indicatrix,  $Dup(\mathcal{G})$  (not labeled in Figure E.9a), for the saddle-like local patch of the gear tooth flank,  $\mathcal{G}$ , are shown as dashed lines (see Figure E.9a).

A gear tooth flank,  $\mathcal{G}$ , and pinion tooth flank,  $\mathcal{P}$ , can make contact geometrically; however, physical conditions of their contact could be violated. Violation of the physical condition of contact results in the bodies bounded by the contacting surfaces,  $\mathcal{G}$  and  $\mathcal{P}$ , interfering with one another. Implementation of the indicatrix of conformity,  $Cnf_R(\mathcal{G}/\mathcal{P})$ , immediately uncovers the surface interference, if there is any. Three illustrative examples of the violation of the physical condition of contact are illustrated in Figure E.10. When correspondence between the radii of normal curvature of the contacting tooth flanks,  $\mathcal{G}$  and  $\mathcal{P}$ , is inappropriate, then the indicatrix of conformity,  $Cnf_R(\mathcal{G}/\mathcal{P})$ , either intersects itself (see Figure E.10a), or all of its diameters become negative (see Figure E.10b,c).

Another interpretation of the satisfaction and violation of the physical condition of contact of two smooth regular tooth flanks,  $\mathcal{G}$  and  $\mathcal{P}$ , is illustrated in Figure E.11. The condition of physical contact is fulfilled when all diameters of the indicatrix of conformity,  $Cnf_R(\mathcal{G}/\mathcal{P})$ , are positive. In this case, the gear tooth flank,  $\mathcal{G}$ , and mating pinion tooth flank,  $\mathcal{P}$ , may contact one another like two rigid bodies do. An example of the indicatrix of conformity,  $Cnf_R(\mathcal{G}/\mathcal{P})$ , for such a case is depicted in Figure E.11a. In cases when this planar characteristic curve has negative diameters, as schematically shown in Figure E.11b, physical contact between the tooth flanks,  $\mathcal{G}$  and  $\mathcal{P}$ , is infeasible.

The value of the current diameter,<sup>‡</sup>  $d_{cnf}$ , of the indicatrix of conformity,  $Cnf_R(\mathcal{G}/\mathcal{P})$ , indicates the degree of conformity of the gear tooth flank,  $\mathcal{G}$ , and mating pinion tooth flank,  $\mathcal{P}$ , to each other in a corresponding

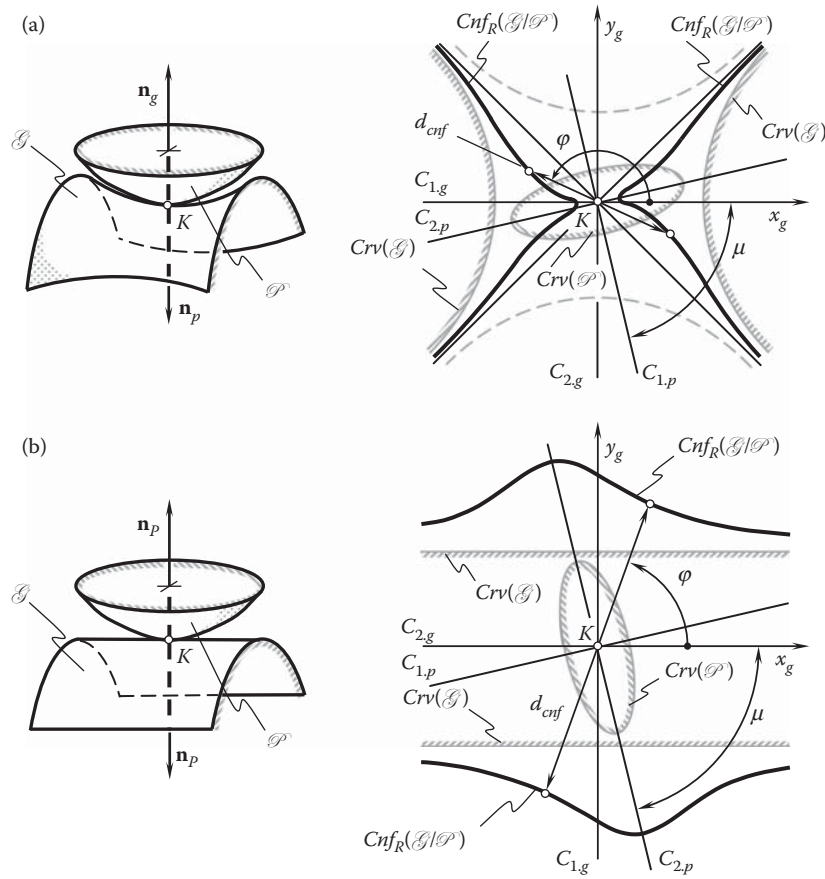
\* The equation of this characteristic curve is known from:

a. Pat. No.1249787, USSR, *A Method of Sculptured Part Surface Machining on a Multi-Axis NC Machine*, S.P. Radzevich, B23C 3/16, Filed: December 27, 1984, [94], and (in hidden form) from:  
b. Pat. No.1185749, USSR, *A Method of Sculptured Part Surface Machining on a Multi-Axis NC Machine*, S.P. Radzevich, B23C 3/16, Filed: October 24, 1983, [93].

<sup>†</sup> See [137] for details on the curvature indicatrices,  $Crv(\mathcal{G})$  and  $Crv(\mathcal{P})$ .

<sup>‡</sup> The diameter of a centro-symmetrical curve can be defined as a distance between two points of the curve, measured along the corresponding straight line through the center of symmetry of the curve.



**FIGURE E.9**

Examples of indicatrix of conformity,  $Cnf_R(\mathcal{G}/\mathcal{P})$ , at a point of contact,  $K$ , of a smooth regular gear tooth flank,  $\mathcal{G}$ , and mating pinion tooth flank,  $\mathcal{P}$ , in the first order of tangency.

cross-section of the surfaces by normal plane through the common perpendicular. The orientation of the normal plane section with respect to the tooth flanks,  $\mathcal{G}$  and  $\mathcal{P}$ , is specified by the corresponding central angle,  $\varphi$ .

For the orthogonally parameterized gear tooth flank,  $\mathcal{G}$ , and mating pinion tooth flank,  $\mathcal{P}$ , the equation of the Dupin indicatrices,  $Dup(\mathcal{G})$  and  $Dup(\mathcal{P})$ , simplifies to:

$$L_g x_g^2 + 2M_g x_g y_g + N_g y_g^2 = \pm 1 \quad (\text{E.51})$$

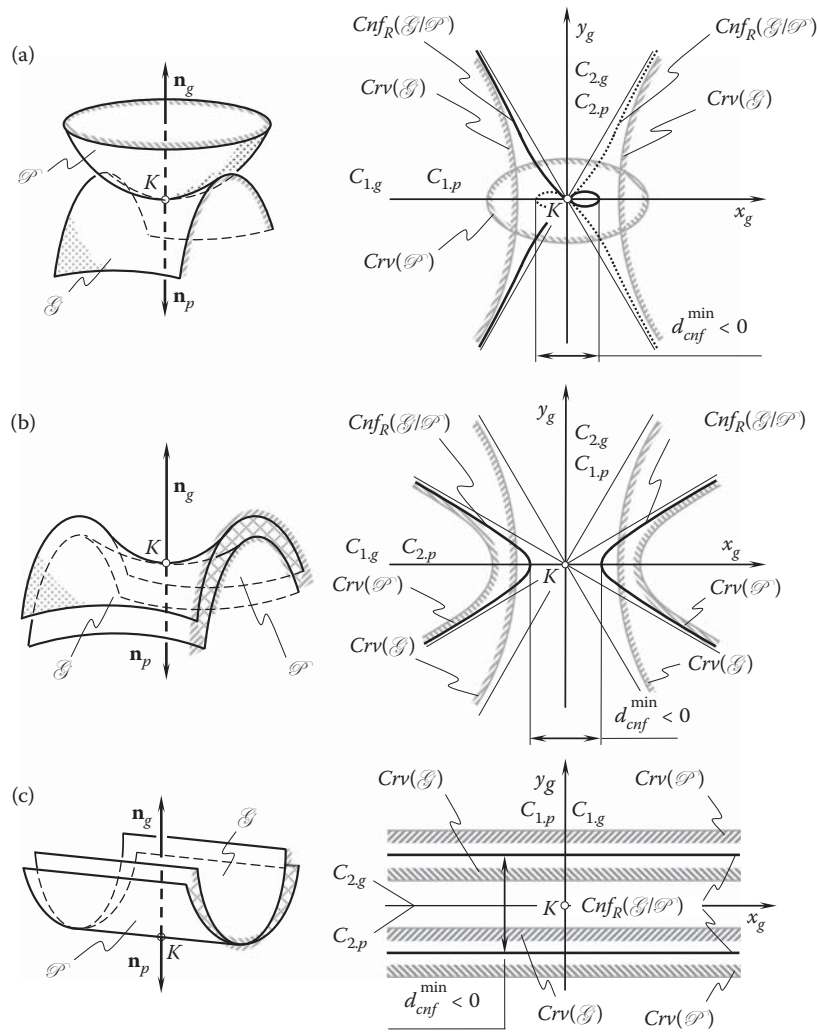
$$L_p x_p^2 + 2M_p x_p y_p + N_p y_p^2 = \pm 1 \quad (\text{E.52})$$

After being represented in a common reference system, the use of Equations E.51 and E.52 makes possible a simplified equation of the indicatrix of conformity,  $Cnf_R(\mathcal{G}/\mathcal{P})$ , at a point of contact of the tooth flanks,  $\mathcal{G}$  and  $\mathcal{P}$ :

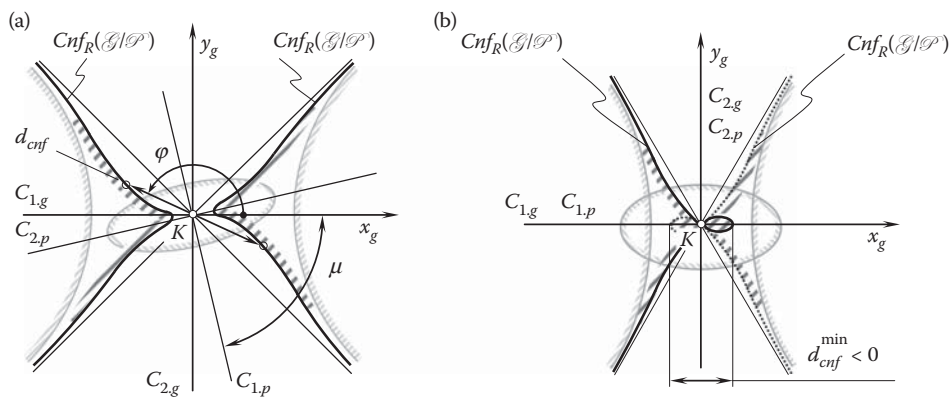
$$r_{cnf}(\varphi, \mu) = (L_g \cos^2 \varphi - M_g \sin 2\varphi + N_g \sin^2 \varphi)^{-0.5} \text{sgn } \Phi_{2,g}^{-1} + [L_p \cos^2 (\varphi + \mu) - M_p \sin 2(\varphi + \mu) + N_p \sin^2 (\varphi + \mu)]^{-0.5} \text{sgn } \Phi_{p,T}^{-1} \quad (\text{E.53})$$

Equation E.53 is valid for the orthogonally parameterized tooth flanks,  $\mathcal{G}$  and  $\mathcal{P}$ .



**FIGURE E.10**

Examples of violation of physical condition of contact of a smooth regular gear tooth flank,  $\mathcal{G}$ , and mating pinion tooth flank,  $\mathcal{P}$ .

**FIGURE E.11**

Another interpretation of satisfaction (a) and of violation (b) of the condition of physical contact of a smooth regular gear tooth flank,  $\mathcal{G}$ , and the mating pinion tooth flank,  $\mathcal{P}$ .

### E.3.3 Directions of Extremum Degree of Conformity at Point of Contact of Gear and Mating Pinion Tooth Flanks

The directions along which the degree of conformity at a point of contact of a gear tooth flank,  $\mathcal{G}$ , and mating pinion tooth flank,  $\mathcal{P}$ , is extremum—that is, the degree of conformity reaches either its maximal or minimal value—are of prime importance for engineering applications. This issue is especially important for synthesizing a favorable gear pair.

The directions of the extremal degree of conformity of the contacting smooth regular tooth flanks,  $\mathcal{G}$  and  $\mathcal{P}$ , that is, the directions pointed along the extremal diameters,  $d_{cnf}^{\min}$  and  $d_{cnf}^{\max}$ , of the indicatrix of conformity,  $Cnf_R(\mathcal{G}/\mathcal{P})$ , can be found from the equation of the indicatrix of conformity,  $Cnf_R(\mathcal{G}/\mathcal{P})$ . For the reader's convenience, the equation of this characteristic curve is transformed and is represented in the form:

$$r_{cnf}(\varphi, \mu) = \sqrt{|r_{1,g}\cos^2\varphi + r_{2,g}\sin^2\varphi|\operatorname{sgn}\Phi_{2,g}^{-1}} + \sqrt{|r_{1,p}\cos^2(\varphi + \mu) + r_{2,p}\sin^2(\varphi + \mu)|\operatorname{sgn}\Phi_{2,p}^{-1}} \quad (\text{E.54})$$

Two directions within the common tangent plane are specified by the angles,  $\varphi_{\min}$  and  $\varphi_{\max}$ . These directions feature an extremum degree of conformity of the pinion tooth flank,  $\mathcal{P}$ , to the gear tooth flank,  $\mathcal{G}$ . Actually, the angles are the roots of the equation:

$$\frac{\partial}{\partial\varphi} r_{cnf}(\varphi, \mu) = 0. \quad (\text{E.55})$$

It can be easily proved that in the general case of contact of two smooth regular tooth flanks,  $\mathcal{G}$  and  $\mathcal{P}$ , the difference between the angles,  $\varphi_{\min}$  and  $\varphi_{\max}$ , is not equal to  $0.5\pi$ . This means that the equality

$$\varphi_{\min} - \varphi_{\max} = \pm 0.5\pi n \quad (\text{E.56})$$

is not always observed, and in most cases the relationship:

$$\varphi_{\min} - \varphi_{\max} \neq \pm 0.5\pi n \quad (\text{E.57})$$

is valid (here  $n$  is an integer number). The condition (see Equation E.56):  $\varphi_{\min} = \varphi_{\max} \pm 0.5\pi n$  is fulfilled only in cases when the angle,  $\mu$ , of local relative orientation of the contacting surfaces,  $\mathcal{G}$  and  $\mathcal{P}$ , is equal to  $\mu = \pm 0.5\pi n$  and thus the principal directions,  $\mathbf{t}_{1,g}$  and  $\mathbf{t}_{2,g}$ , of the gear tooth flank,  $\mathcal{G}$ , and the principal directions,  $\mathbf{t}_{1,p}$  and  $\mathbf{t}_{2,p}$ , of the mating pinion tooth flank,  $\mathcal{P}$ , either aligned to each other or directed oppositely.

This enables one to make the following statement:

#### Statement E.1

In the general case of contact of two smooth regular tooth flanks, the directions along which the degree of conformity of the tooth flanks,  $\mathcal{G}$  and  $\mathcal{P}$ , is extremal are not orthogonal to one another.

This statement is important for engineering applications.

The solution to the equation,  $\partial r_{rel}(\varphi)/\partial\varphi = 0$ , returns two extremal angles,  $\varphi_{\min}$  and  $\varphi_{\max} = \varphi_{\min} + 90^\circ$  [here  $r_{rel}(\varphi)$  denotes the position vector of a point of the Dupin indicatrix at the point of the surface of relative curvature]. Equation E.55 allows for two solutions,  $\varphi_{\min}^*$  and  $\varphi_{\max}^*$ . Therefore, the extremal difference:

$$\Delta\varphi_{\min} = \varphi_{\min} - \varphi_{\min}^* \quad (\text{E.58})$$

as well as the extremal difference:

$$\Delta\varphi_{\max} = \varphi_{\max} - \varphi_{\max}^* \quad (\text{E.59})$$

can be easily calculated.

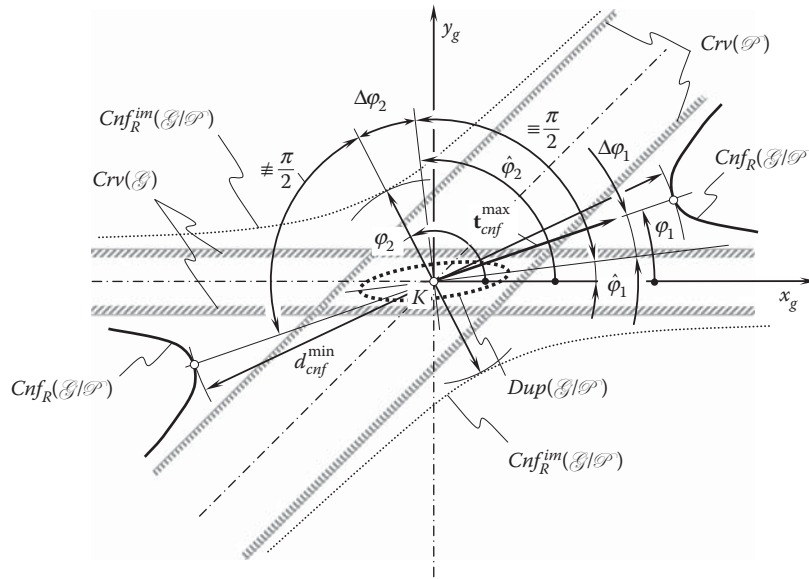


FIGURE E.12

Example 5.1: Determination of the optimum instant kinematics for a gear-shaving operation.

Generally speaking, neither the extremal difference,  $\Delta\varphi_{\min}$ , nor the extremal difference,  $\Delta\varphi_{\max}$ , is equal to zero. They are equal to zero only in particular cases, say, when the angle,  $\mu$ , of local relative orientation of the surfaces,  $\mathcal{G}$  and  $\mathcal{P}$ , fulfills the relationship  $\mu = \pm 0.5\pi n$ .

Let us consider an example that illustrates Statement E.1.

*Example.* As an illustrative example, let us describe analytically the contact geometry of two convex parabolic patches of the contacting tooth flanks,  $\mathcal{G}$  and  $\mathcal{P}$  (see Figure E.12). The example pertains to finishing a helical involute gear by a disk-type shaving cutter. In the example under consideration, the design parameters of the gear and the shaving cutter, along with the specified gear and shaving cutter configuration, yield the following numerical data for the calculation. At the point,  $K$ , of the tooth flank contact, principal curvatures of the gear tooth flank,  $\mathcal{G}$ , are  $k_{1,g} = 4 \text{ mm}^{-1}$  and  $k_{2,g} = 0$ . The principal curvatures of the mating pinion tooth flank,  $\mathcal{P}$ , are  $k_{1,p} = 1 \text{ mm}^{-1}$  and  $k_{2,p} = 0$ . The angle,  $\mu$ , of local relative orientation of the tooth flanks,  $\mathcal{G}$  and  $\mathcal{P}$ , is  $\mu = 45^\circ$ .

Two approaches can be implemented for the analytical description of the contact geometry of the tooth flanks,  $\mathcal{G}$  and  $\mathcal{P}$ . The first is based on implementation of the Dupin indicatrix of the surface of relative curvature. The second is based on application of the indicatrix of conformity,  $Cnf_R(\mathcal{G}/\mathcal{P})$ , constructed at a contact point,  $K$ , of the interacting tooth flanks,  $\mathcal{G}$  and  $\mathcal{P}$ .

*The first approach.* In the case under consideration, normal curvature,  $k_R$ , of the surface of relative curvature,  $R$ , can be analytically expressed as:

$$k_R = k_{1,g} \cos^2 \varphi - k_{1,p} \cos^2 (\varphi + \mu) \quad (\text{E.60})$$

Therefore, the following equality:

$$\frac{\partial k_R}{\partial \varphi} = -2k_{1,g} \sin \varphi \cos \varphi + 2k_{1,p} \sin (\varphi + \mu) \cos (\varphi + \mu) = 0 \quad (\text{E.61})$$

is valid for the directions of the extremum degree of conformity of the tooth flanks,  $\mathcal{G}$  and  $\mathcal{P}$ , at every point of their contact.

For the directions of the extremal degree of conformity at the point of contact of the gear tooth flank,  $\mathcal{G}$ , and mating pinion tooth flank,  $\mathcal{P}$ , Equation E.61 yields calculation of the extremal values,  $\varphi_{\min} = 7^\circ$  and  $\varphi_{\max} = \varphi_{\min} + 90^\circ = 97^\circ$ , of the angles,  $\varphi_{\min}$  and  $\varphi_{\max}$ .

The direction that is specified by the angle,  $\varphi_{\min} = 7^\circ$ , indicates the direction of the minimal diameter of the Dupin indicatrix of the surface of relative curvature. That same direction corresponds to the maximal degree

of conformity at the point of contact of the tooth flanks,  $\mathcal{G}$  and  $\mathcal{P}$ . Another direction that is specified by the angle,  $\varphi_{\max} = 97^\circ$ , indicates the direction of the minimum degree of conformity of the contacting tooth flanks,  $\mathcal{G}$  and  $\mathcal{P}$ , at that same contact point.

*The second approach.* For the case under consideration, the use of Equation E.49 of the indicatrix of conformity,  $Cnf_R(\mathcal{G}/\mathcal{P})$ , at a point of contact of the gear tooth flank,  $\mathcal{G}$ , and mating pinion tooth flank,  $\mathcal{P}$ , makes possible the calculation of the extremal angles,  $\varphi_{\min}^* = 19^\circ$  and  $\varphi_{\max}^* = 118^\circ$ .

Imaginary branches of the indicatrix of conformity,  $Cnf_R(\mathcal{G}/\mathcal{P})$ , at the point of contact of the tooth flanks,  $\mathcal{G}$  and  $\mathcal{P}$ , in Figure E.12 are depicted with dashed lines.

It is important to direct the reader's attention here to two issues.

First, the extremal angles,  $\varphi_{\min}$  and  $\varphi_{\max}$ , that are calculated using the first approach are not equal to the corresponding extremal angles,  $\varphi_{\min}^*$  and  $\varphi_{\max}^*$ , that are calculated using the second approach. The relationships,  $\varphi_{\min} \neq \varphi_{\min}^*$  and  $\varphi_{\max} \neq \varphi_{\max}^*$ , are generally observed.

Second, the difference,  $\Delta\varphi^*$ , between the extremal angles,  $\varphi_{\min}^*$  and  $\varphi_{\max}^*$ , is not equal to half of  $\pi$ . Therefore, the relationship,  $\varphi_{\max}^* - \varphi_{\min}^* \neq 90^\circ$ , between the extremal angles,  $\varphi_{\min}^*$  and  $\varphi_{\max}^*$ , is observed. In the general case of contact of two sculptured surfaces, the directions of the extremal degree of conformity of the gear tooth flank,  $\mathcal{G}$ , and mating pinion tooth flank,  $\mathcal{P}$ , are not orthogonal to one another.

The discussed example reveals that in general cases of contact of two smooth regular tooth flanks, the indicatrix of conformity,  $Cnf_R(\mathcal{G}/\mathcal{P})$ , can be implemented for the purpose of accurate analytical description of the contact geometry of the surfaces. The Dupin indicatrix of the surface of relative curvature can be implemented for this purpose only in particular cases of the surface,  $\mathcal{G}$  and  $\mathcal{P}$ , relative orientation. Application of the Dupin indicatrix of the surface of relative curvature enables only approximate analytical description of the geometry of contact of the surfaces. The Dupin indicatrix of the surface of relative curvature could be equivalent to the indicatrix of conformity only in degenerate cases of contact of the surfaces. Advantages of the indicatrix of conformity over the Dupin indicatrix of the surface of relative curvature are because the characteristic curve,  $Cnf_R(\mathcal{G}/\mathcal{P})$ , is a curve of the fourth order.

### E.3.4 Important Properties of Indicatrix of Conformity $Cnf_R(\mathcal{G}/\mathcal{P})$ at Point of Contact of Gear and Mating Pinion Tooth Flanks

The performed analysis of Equation E.49 of the indicatrix of conformity,  $Cnf_R(\mathcal{G}/\mathcal{P})$ , at a point of contact of gear and mating pinion tooth flanks reveals that this characteristic curve possesses the following important properties.

1. The indicatrix of conformity,  $Cnf_R(\mathcal{G}/\mathcal{P})$ , at a point of contact of the tooth flanks,  $\mathcal{G}$  and  $\mathcal{P}$ , is a planar characteristic curve of the fourth order. It possesses the property of central symmetry and, in particular cases, also possesses the property of mirror symmetry.
2. The indicatrix of conformity,  $Cnf_R(\mathcal{G}/\mathcal{P})$ , is closely related to the surface,  $\mathcal{G}$  and  $\mathcal{P}$ , second fundamental forms,  $\Phi_{2,g}$  and  $\Phi_{2,p}$ . This characteristic curve is invariant with respect to the kind of parameterization of the tooth flanks,  $\mathcal{G}$  and  $\mathcal{P}$ , but its equation does change. A change in the surface,  $\mathcal{G}$  and  $\mathcal{P}$ , parameterization leads to the equation of the indicatrix of conformity,  $Cnf_R(\mathcal{G}/\mathcal{P})$ , also changing, while the shape and parameters of this characteristic curve remained unchanged.
3. The characteristic curve,  $Cnf_R(\mathcal{G}/\mathcal{P})$ , is independent of the actual value of the coordinate angle,  $\omega_g$ , that forms the coordinate lines,  $U_g$  and  $V_g$ , on the gear tooth flank,  $\mathcal{G}$ . It is also independent of the actual value of the coordinate angle,  $\omega_p$ , that forms the coordinate lines,  $U_p$  and  $V_p$ , on the mating pinion tooth flank,  $\mathcal{P}$ . However, parameters of the indicatrix of conformity,  $Cnf_R(\mathcal{G}/\mathcal{P})$ , depend upon the angle,  $\mu$ , of the local relative orientation of the tooth flanks,  $\mathcal{G}$  and  $\mathcal{P}$ . Therefore, for a given pair of tooth flanks,  $\mathcal{G}$  and  $\mathcal{P}$ , the degree of conformity of the surface varies correspondingly with variation of the angle,  $\mu$ , while the pinion tooth flank,  $\mathcal{P}$ , is spinning around the unit vector of the common perpendicular.

More properties of the indicatrix of conformity,  $Cnf_R(\mathcal{G}/\mathcal{P})$ , at a point of contact of a gear tooth flank,  $\mathcal{G}$ , and mating pinion tooth flank,  $\mathcal{P}$ , can be outlined.

### E.3.5 Converse Indicatrix of Conformity at Point of Contact of Gear and Mating Pinion Tooth Flanks in the First Order of Tangency

For the Dupin indicatrix,  $Dup(\mathcal{G}/\mathcal{P})$ , at a point of the surface of relative curvature,  $\mathcal{R}$ , there exists a corresponding inverse Dupin indicatrix,  $Dup_k(\mathcal{G}/\mathcal{P})$ . Similarly, for the indicatrix of conformity,  $Cnf_R(\mathcal{G}/\mathcal{P})$ , at a point of contact of the tooth flanks,  $\mathcal{G}$  and  $\mathcal{P}$ , there exists a corresponding converse indicatrix of conformity,  $Cnf_k(\mathcal{G}/\mathcal{P})$ . This characteristic curve can be expressed directly in terms of the surface,  $\mathcal{G}$  and  $\mathcal{P}$ , normal curvatures,  $k_g$  and  $k_p$ :

$$Cnf_k(G/P) \Rightarrow r_{cnf}^{cnv}(\varphi, \mu) = \sqrt{|k_g(\varphi)|} \cdot \text{sgn } \Phi_{2,g}^{-1} - \sqrt{|k_p(\varphi, \mu)|} \cdot \text{sgn } \Phi_{2,p}^{-1} \quad (\text{E.62})$$

For derivation of an equation of the *converse indicatrix of conformity*,  $Cnf_k(\mathcal{G}/\mathcal{P})$ , the Euler formula for a surface normal curvature is used in the following representation:

$$k_g(\varphi) = k_{1,g} \cos^2 \varphi + k_{2,g} \sin^2 \varphi \quad (\text{E.63})$$

$$k_p(\varphi, \mu) = k_{1,p} \cos^2(\varphi + \mu) + k_{2,p} \sin^2(\varphi + \mu) \quad (\text{E.64})$$

Here, in Equations E.63 and E.64, the principal curvatures of the gear tooth flank,  $\mathcal{G}$ , are designated as  $k_{1,g}$  and  $k_{2,g}$ , while  $k_{1,p}$  and  $k_{2,p}$  designate the principal curvatures of the mating pinion tooth flank,  $\mathcal{P}$ .

After substituting Equations E.63 and E.64 into Equation E.62, one can come up with the equation:

$$r_{cnf}^{cnv}(\varphi, \mu) = \sqrt{|k_{1,g} \cos^2 \varphi + k_{2,g} \sin^2 \varphi|} \text{sgn } \Phi_{2,g}^{-1} - \sqrt{|k_{1,p} \cos^2(\varphi + \mu) + k_{2,p} \sin^2(\varphi + \mu)|} \text{sgn } \Phi_{2,p}^{-1} \quad (\text{E.65})$$

for the converse indicatrix of conformity,  $Cnf_k(\mathcal{G}/\mathcal{P})$ , at a point of contact of the tooth flanks  $\mathcal{G}$  and  $\mathcal{P}$  in the first order of tangency.

Here, in Equation E.65, principal curvatures,  $k_{1,g}$ ,  $k_{2,g}$  and  $k_{1,p}$ ,  $k_{2,p}$ , can be expressed in terms of the corresponding fundamental magnitudes  $E_g$ ,  $F_g$ , and  $G_g$  of the first and  $L_g$ ,  $M_g$ , and  $N_g$  of the second order of the gear tooth flank  $\mathcal{G}$ , and in terms of the corresponding fundamental magnitudes  $E_p$ ,  $F_p$ , and  $G_p$  of the first and  $L_p$ ,  $M_p$ , and  $N_p$  of the second order of the mating pinion tooth flank  $\mathcal{P}$ . Following this method, Equation E.65 of the converse indicatrix of conformity,  $Cnf_k(\mathcal{G}/\mathcal{P})$ , can be cast to a form similar to Equation E.49 of the ordinary indicatrix of conformity,  $Cnf_R(\mathcal{G}/\mathcal{P})$ , at a point of contact of the tooth flanks,  $\mathcal{G}$  and  $\mathcal{P}$ .

It can be shown that, similarly to the indicatrix of conformity,  $Cnf_R(\mathcal{G}/\mathcal{P})$ , the characteristic curve  $Cnf_k(\mathcal{G}/\mathcal{P})$  also possesses the property of central symmetry. In particular cases of surface contact, it also possesses the property of mirror symmetry. The directions of the extremal degree conformity of the gear tooth flank,  $\mathcal{G}$ , and mating pinion tooth flank,  $\mathcal{P}$ , are orthogonal to one another only in degenerate cases of the surfaces contact.

Equation E.65 of the converse indicatrix of conformity,  $Cnf_k(\mathcal{G}/\mathcal{P})$ , is convenient for implementation when:

- Either the gear tooth flank  $\mathcal{G}$ , or
- The mating pinion tooth flank  $\mathcal{P}$ , or
- Both

feature point(s) or line(s) of inflection. In the point(s) or (line[s]) of inflection, the radii of normal curvature,  $R_{g(p)}$  of the surface,  $\mathcal{G}$  and  $\mathcal{P}$ , are equal to infinity. Points/lines of inflection cause indefiniteness when calculating the position vector,  $r_{cnf}(\varphi, \mu)$ , of a point of the characteristic curve,  $Cnf_R(\mathcal{G}/\mathcal{P})$ . Equation E.65 of the converse indicatrix of conformity,  $Cnf_k(\mathcal{G}/\mathcal{P})$ , is free of the disadvantages of this kind and therefore is recommended for practical applications.



# Taylor & Francis

Taylor & Francis Group

<http://taylorandfrancis.com>

## Appendix F: Closest Distance of Approach between Gear and Mating Pinion Tooth Flanks

Generally, the problem of the calculation of the closest distance of approach between two smooth regular surfaces is sophisticated and challenging. Per the author's knowledge, no general solution to the problem of calculation of the closest distance of approach between two smooth regular surfaces is available in the public domain. For the purpose of calculation of the deviation,  $\delta_g$ , of the actual gear tooth flank,  $\mathcal{G}_{ac}$ , with respect to the desired (nominal) gear tooth flank,  $\mathcal{G}_{nom}$ , the problem under consideration can be reduced to the problem of computation of the closest distance of approach between two torus surfaces,  $Tr_g$  and  $Tr_p$ .

Consider a gear tooth flank,  $\mathcal{G}$ , and mating pinion tooth flank,  $\mathcal{P}$ , that are initially given in a common coordinate system,  $X_h Y_h Z_h$ , associated with the gear housing, as illustrated in Figure F.1. The tooth flanks,  $\mathcal{G}$  and  $\mathcal{P}$ , are locally approximated by portions of torus surfaces,  $Tr_g$  and  $Tr_p$ , respectively. Again, not all points of the torus surfaces,  $Tr_g$  and  $Tr_p$ , can be used for the local approximation of the gear and pinion tooth flanks,  $\mathcal{G}$  and  $\mathcal{P}$ . Only points that are located either within the biggest or smallest meridian of the torus surface are employed for this purpose.

The points,  $K_g$  and  $K_p^*$ , are chosen as the first-guess points on the torus surfaces,  $Tr_g$  and  $Tr_p$ . For the analysis below, it is convenient to relabel the points,  $K_g$  and  $K_p^*$ , to  $g_i$  and  $p_i$ , accordingly.

For a given configuration of the torus surfaces,  $Tr_g$  and  $Tr_p$ , the closest distance of approach between these surfaces can be used as a first approximation of the closest distance of approach between the original gear and pinion tooth flanks,  $\mathcal{G}$  and  $\mathcal{P}$ .

The closest distance of approach between the torus surfaces,  $Tr_g$  and  $Tr_p$ , is measured along the common perpendicular to these surfaces. The following equations can be composed on the premises of this property of the closest distance of approach.

The unit normal vector,  $\mathbf{n}_{Tr,g}$ , to the torus surface,  $Tr_g$ , is located within a plane through the axis of rotation of the surface,  $Tr_g$ . In the coordinate system,  $X_{tr,g} Y_{tr,g} Z_{tr,g}$ , that is associated with the torus surface,  $Tr_p$ , the equation of a plane through the axis of rotation of the torus surface,  $Tr_g$ , can be expressed in the form [20,107,110,136]:

$$[\mathbf{r}_{tg} - \mathbf{r}_{tr,g}^{(0)}] \times \mathbf{k}_{tr,g} \times \mathbf{R}_{tr,g} = 0 \quad (\text{F.1})$$

where:

$\mathbf{r}_{tg}$ : is the position vector of the point of the plane through the axis of rotation of the torus,  $Tr_g$ .

$\mathbf{r}_{tr,g}^{(0)}$ : is the position vector of the point within the plane,  $\mathbf{r}_{tg}$  (it is assumed below that this point coincides with the origin of the coordinate system,  $X_{tr,g} Y_{tr,g} Z_{tr,g}$ ).

$\mathbf{k}_{tr,g}$ : is the unit vector of the  $Z_{tr,g}$ -axis.

Equation F.1 is expressed in terms of the radius,  $\mathbf{R}_{tr,g}$ . This indicates that the set of all planes through the fixed  $Z_{tr,g}$ -axis forms a pencil of planes. The equation of the pencil of planes,  $\mathbf{r}_{tg}$ , in the common coordinate system,  $X_h Y_h Z_h$ , can be represented in the form:

$$\mathbf{r}_{tg}(Z_{tr,g}, V_{tr,g}, \theta_{tr,g}) = \mathbf{Rs}(Tr_g \mapsto h) \cdot \begin{bmatrix} V_{tr,g} \cdot \cos \theta_{tr,g} \\ V_{tr,g} \cdot \sin \theta_{tr,g} \\ Z_{tr,g} \\ 1 \end{bmatrix} \quad (\text{F.2})$$



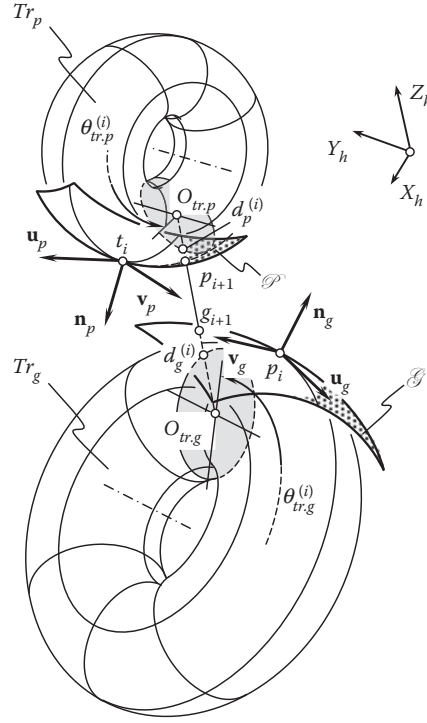


FIGURE F.1

Computation of the closest distance of approach of a gear tooth flank,  $\mathcal{G}$ , and mating pinion tooth flank,  $\mathcal{P}$ .

The unit normal vector,  $\mathbf{n}_{Tr,p}$ , to the torus surface,  $Tr_p$ , is located within a plane through the axis of rotation of the surface,  $Tr_p$ . In the coordinate system,  $X_{tr,p}Y_{tr,p}Z_{tr,p}$ , that is associated with the surface,  $Tr_p$ , the equation of a plane through the axis of rotation of the torus surface,  $Tr_p$ , can be represented in the form:

$$[\mathbf{r}_{tp} - \mathbf{r}_{tr,p}^{(0)}] \times \mathbf{k}_{tr,p} \times \mathbf{R}_{tr,p} = 0 \quad (\text{F.3})$$

where:

$\mathbf{r}_{tp}$ : is the position vector of the point of the plane through the torus,  $Tr_p$ , axis of rotation.

$\mathbf{r}_{tr,p}^{(0)}$ : is the position vector of the point within the plane,  $\mathbf{r}_{tp}$  (it is assumed below that this point coincides with the origin of the coordinate system,  $X_{tr,p}Y_{tr,p}Z_{tr,p}$ ).

$\mathbf{k}_{tr,p}$ : is the unit vector of the  $Z_{tr,p}$ -axis.

Equation F.3 is expressed in terms of the radius,  $\mathbf{R}_{tr,p}$ . This indicates that the set of all planes through the fixed  $Z_{tr,p}$ -axis forms a pencil of planes. The equation of this pencil of planes,  $\mathbf{r}_{tp}$ , in the common coordinate system,  $X_hY_hZ_h$ , can be represented in the form:

$$\mathbf{r}_{tp}(Z_{tr,p}, V_{tr,p}, \theta_{tr,p}) = \mathbf{Rs}(Tr_p \mapsto h) \cdot \begin{bmatrix} V_{tr,p} \cdot \cos \theta_{tr,p} \\ V_{tr,p} \cdot \sin \theta_{tr,p} \\ Z_{tr,p} \\ 1 \end{bmatrix} \quad (\text{F.4})$$

A straight line through the points,  $d_g^{(i)}$  and  $d_p^{(i)}$ , along which the shortest distance of approach,  $d_{gp}^{\min}$ , of the torus surfaces,  $Tr_g$  and  $Tr_p$ , is measured is the line of intersection of the planes,  $\mathbf{r}_{tg}$  and  $\mathbf{r}_{tp}$ . Therefore, this line,  $d_{gp}^{\min}$ , must be aligned with both unit normal vectors,  $\mathbf{n}_{tr,g}$  and  $\mathbf{n}_{tr,p}$ .

In the coordinate system,  $X_h Y_h Z_h$ , the equation for the unit normal vector,  $\mathbf{n}_{tr,g}$ , to the torus surface,  $Tr_g$ , yields representation in matrix form:

$$\mathbf{n}_{tr,g} = \mathbf{Rs}(Tr_g \mapsto h) \cdot \begin{bmatrix} (C_{tr,g} + \cos \varphi_{tr,g}) \cdot \cos \varphi_{tr,g} \cdot \cos \theta_{tr,g} \\ (C_{tr,g} + \cos \varphi_{tr,g}) \cdot \cos \varphi_{tr,g} \cdot \sin \theta_{tr,g} \\ (C_{tr,g} + \cos \varphi_{tr,g}) \cdot \sin \varphi_{tr,g} \\ 1 \end{bmatrix} \quad (\text{F.5})$$

where  $C_{tr,g}$  designates the parameter  $C_{tr,g} = 1 - \frac{R_{2,g}}{R_{1,g}}$ .

Similarly, in the coordinate system,  $X_h Y_h Z_h$ , the equation for the unit normal vector,  $\mathbf{n}_{tr,p}$ , to the torus surface,  $Tr_p$ , yields matrix representation in the form:

$$\mathbf{n}_{tr,p} = \mathbf{Rs}(Tr_p \mapsto h) \cdot \begin{bmatrix} (C_{tr,p} + \cos \varphi_{tr,p}) \cdot \cos \varphi_{tr,p} \cdot \cos \theta_{tr,p} \\ (C_{tr,p} + \cos \varphi_{tr,p}) \cdot \cos \varphi_{tr,p} \cdot \sin \theta_{tr,p} \\ (C_{tr,p} + \cos \varphi_{tr,p}) \cdot \sin \varphi_{tr,p} \\ 1 \end{bmatrix} \quad (\text{F.6})$$

where  $C_{tr,p}$  designates the parameter  $C_{tr,p} = 1 - \frac{R_{2,p}}{R_{1,p}}$ .

Evidently, the points  $O_{tr,g}$ ,  $O_{tr,p}$ ,  $d_g^{(i)}$ , and  $d_p^{(i)}$  (see Figure F.1) are located within the straight line through the centers,  $O_{tr,g}$  and  $O_{tr,p}$ . The position vector,  $\mathbf{r}_{cd}$ , of this straight line can be calculated from the equation:

$$(\mathbf{r}_{cd} - \mathbf{r}_{cg}) \times (\mathbf{r}_{cp} - \mathbf{r}_{cg}) = 0 \quad (\text{F.7})$$

where:

$\mathbf{r}_{cg}$ : is the position vector of a point on the circle of a radius,  $R_{tr,g}$ .

$\mathbf{r}_{cp}$ : is the position vector of a point on the circle of a radius,  $R_{tr,p}$ .

It is necessary that the straight line,  $\mathbf{r}_{cd}$ , be along the unit normal vectors,  $\mathbf{n}_{tg}$  and  $\mathbf{n}_{tp}$ , to the torus surfaces,  $Tr_g$  and  $Tr_p$ .

Considered together, Equations F.2, F.4, and F.7 make possible the calculation of the closest distance of approach between the torus surfaces,  $Tr_g$  and  $Tr_p$ . Then, the straight line,  $d_{gp}^{\min}$ , intersects the part surface,  $\mathcal{G}$ , and the generating surface,  $\mathcal{P}$ , of the form-cutting tool at the points,  $g_{i+1}$  and  $p_{i+1}$ , correspondingly. The points,  $g_{i+1}$  and  $p_{i+1}$ , serve as the second guess to the closest distance of approach between the surfaces,  $\mathcal{G}$  and  $\mathcal{P}$ .

The cycle of recursive calculations is repeated as many times as necessary for making the deviation of the calculation of the closest distance of approach between the surfaces,  $\mathcal{G}$  and  $\mathcal{P}$ , smaller than the maximal permissible value.

There is an alternative approach for the calculation of the closest distance of approach between two torus surfaces. The direction of the unit normal vector to an offset surface to  $Tr_g$  is identical to the direction of the unit normal vector,  $\mathbf{n}_{tr,g}$ , to the torus surface,  $Tr_g$ . This statement is also valid for the unit normal vector,  $\mathbf{n}_{tr,p}$ , to the torus surface,  $Tr_p$ . This property of the unit normal vectors,  $\mathbf{n}_{tr,g}$  and  $\mathbf{n}_{tr,p}$ , can be used for the modification of the method of calculation of the closest distance of approach between two torus surfaces.

The equation of the circle of radius  $R_{tr,g}$  yields the matrix representation:

$$\mathbf{r}_{cg}(\theta_{tr,g}) = \mathbf{Rs}(\mathcal{G} \mapsto h) \cdot \begin{bmatrix} R_{tr,g} \cdot \cos \theta_{tr,g} \\ R_{tr,g} \cdot \sin \theta_{tr,g} \\ 0 \\ 1 \end{bmatrix} \quad (\text{F.8})$$

The equation of the circle of radius  $R_{tr,p}$  can be analytically described in a similar way:

$$\mathbf{r}_{cp}(\theta_{tr,p}) = \mathbf{Rs}(\mathcal{P} \mapsto h) \cdot \begin{bmatrix} R_{tr,p} \cdot \cos \theta_{tr,p} \\ R_{tr,p} \cdot \sin \theta_{tr,p} \\ 0 \\ 1 \end{bmatrix} \quad (\text{F.9})$$

The distance,  $d_{gp}$ , between two arbitrary points on the circles,  $\mathbf{r}_{cg}(\theta_{tr,g})$  and  $\mathbf{r}_{cp}(\theta_{tr,p})$ , equals:

$$d_{gp}(\theta_{tr,g}, \theta_{tr,p}) = |\mathbf{r}_{cg}(\theta_{tr,g}) - \mathbf{r}_{cp}(\theta_{tr,p})| \quad (\text{F.10})$$

The distance,  $d_{gp}$ , is minimal for a specific (optimal) combination of the parameters,  $\theta_{tr,g}$  and  $\theta_{tr,p}$ . The favorable values of the parameters  $\theta_{tr,g}$  and  $\theta_{tr,p}$  can be calculated on the solution of the set of two equations:

$$\frac{\partial}{\partial \theta_{tr,g}} \mathbf{r}_{cg}(\theta_{tr,g}) = 0 \quad (\text{F.11})$$

$$\frac{\partial}{\partial \theta_{tr,p}} \mathbf{r}_{cp}(\theta_{tr,p}) = 0 \quad (\text{F.12})$$

On solution of Equations F.11 and F.12, the optimal values,  $\theta_{tr,g}^{(opt)}$  and  $\theta_{tr,p}^{(opt)}$ , can be determined. These angles specify the direction of the closest distance of approach of the torus surfaces,  $Tr_g$  and  $Tr_p$ .

Following this method, the three-dimensional problem of calculation of the closest distance of approach of two torus surfaces is reduced to the problem of calculation of the closest distance between two circles. Under a certain scenario, the last approach could possess an advantage over the previous approach.

Convergence of the disclosed algorithms for the computation of the closest distance of approach between two smooth regular surfaces is illustrated in Figure F.2. The computation procedure is convergent regardless of the actual location of the first guess points on the surfaces,  $\mathcal{G}$  and  $\mathcal{P}$ .

It is instructive to draw attention here to the similarities between the disclosed iterative method for the computation of the closest distance of approach between two smooth regular surfaces and *Newton-Raphson's method*, the iterative method of chords, and so forth. Many similarities can be found in this comparison.

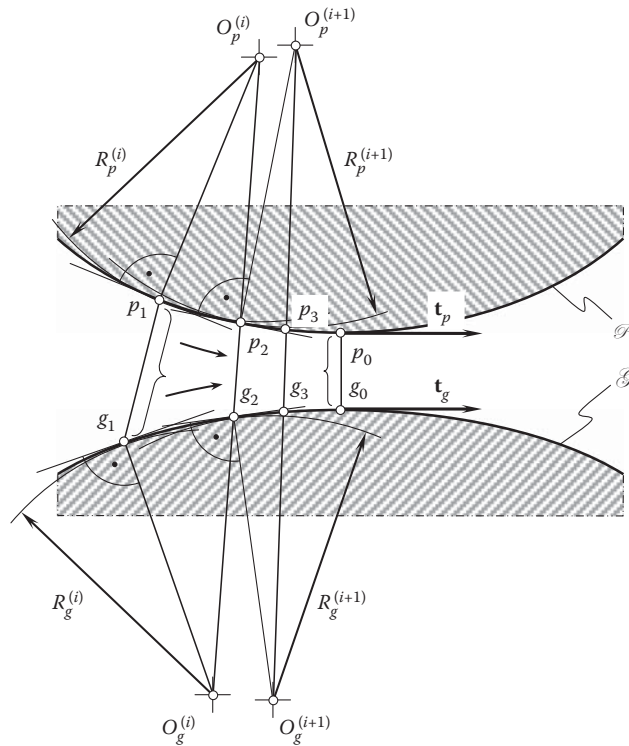


FIGURE F.2

Convergence of the methods of computation of the closest distance of approach of a gear tooth flank,  $\mathcal{G}$ , and mating pinion tooth flank,  $\mathcal{P}$ .

## Appendix G: Engineering Formulae for the Specification of Gear Tooth Flanks

The engineering representation of gear tooth flanks can be converted into scientific representation and vice versa. For the conversion, it is convenient to use the so-called *fundamental gear equations* listed below (Table G.1). More useful equations can be found in many advanced sources.

**TABLE G.1**

Fundamental Gear Equations

Name of the Parameter	Formulae
Transverse diametral pitch, $P_t$	$P_t = P_n \cos \psi$
Pitch diameter, $D$	$D = \frac{N}{P_t}$
Standard addendum, $a$	$a = \frac{1}{P_n}$
Outside diameter, $D_o$	$D_o = D + 2 \cdot a$
Transverse pressure angle, $\phi_t$	$\tan \phi_t = \frac{\tan \phi_n}{\cos \psi}$
Base diameter, $d_b$	$d_b = D \cdot \cos \phi_t$
Lead, $L$	$L = \pi \cdot D \cdot \cot \psi = \frac{\pi \cdot D}{\tan \psi}$ $L = \pi \cdot d_b \cdot \cos \psi_b$
Normal circular pitch, $p_n$	$p_n = \frac{\pi}{P_n}, \quad p_n = \frac{\pi \cdot D \cdot \cos \psi}{N}$
Standard normal circular thickness, $t_n$	$t_n = \frac{p_n}{2}, \quad t_n = t \cdot \cos \psi$
Axial pitch, $p_x$	$p_x = \frac{\pi}{P_n \cdot \sin \psi} = \frac{p_n}{\sin \psi} = \frac{L}{N}$
Transverse circular pitch, $p_t$	$p_t = \frac{\pi}{P_t} = \frac{p_n}{\cos \psi}$
Helix angle, when the given center distance is standard, $\psi$	$\cos \psi = \frac{N_p + N_g}{2 \cdot p_n \cdot C}$
Operating pitch diameter (pinion), $D_{rp}$ , with nonstandard center distance, $C$	$D_{rp} = \frac{2 \cdot C \cdot N_p}{N_p + N_g}$
Operating pressure angle, $\phi_{rt}$ , with nonstandard center distance, $C$	$\sin \phi_{rt} = \frac{d_{bp} + d_{bg}}{2 \cdot C}$
Normal diametral pitch, $P_n$	$P_n = P_t \cdot \sec \psi$
Helix angle, $\psi$	$\cos \psi = \frac{N}{D \cdot P_n}, \quad \sin \psi = \frac{\pi \cdot N}{P_n \cdot L}$
Helix angle, $\psi_y$ , at any diameter, $d_y$	$\tan \psi_y = \frac{d_y}{d_1} \cdot \tan \psi_1$

(Continued)

**TABLE G.1 (Continued)**

Fundamental Gear Equations

Name of the Parameter	Formulae
Transverse circular pitch, $p_{t2}$ , at any diameter, $d_y$	$p_{t2} = \frac{\pi \cdot d_y}{N}$
Involute function of pressure angle	$\text{inv } \phi = \tan \phi - \widehat{\phi}$
Normal pressure angle, $\phi_n$	$\tan \phi_n = \tan \phi_t \cdot \cos \psi$ $\sin \phi_n = \sin \phi \cdot \cos \psi_b$ $\cos \phi_n = \sin \psi_b \cdot \csc \psi$
Transverse pressure angle, $\phi_{ty}$ , at any diameter, $d_y$	$\cos \phi_{ty} = \frac{d_b}{d_y}$
Base helix angle, $\psi_b$	$\cos \psi_b = \frac{\cos \psi \cdot \cos \phi_n}{\cos \phi_t} = \frac{\sin \phi_n}{\sin \phi_t}$ $\sin \psi_b = \sin \psi \cdot \cos \phi_n$ $\tan \psi_b = \tan \psi \cdot \cos \phi_t$
Base pitch, $p_b$ (here, $\rho$ designates radius of profile curvature)	$p_b = \frac{\pi \cdot d_b}{N} = \frac{\pi \cdot D \cdot \cos \phi_t}{N} = \rho \cdot \cos \phi_t$

**TABLE G.2**

Formulae for the Conversion from Pitch System to Metric System

Name of the Parameter	English (Inches)	Metric (Millimeters)
Pitch diameter, $D$	$D = \frac{N}{P}$	$D = m \cdot N$
Addendum, $a$	$a = \frac{1}{P}$	$a = m$
Standard outside diameter, $D_o$	$D_o = D + 2 \cdot a$	$D_o = D + 2 \cdot m$
Base diameter, $d_b$	$d_b = D \cdot \cos \phi$	
Circular pitch, $p$	$p = \frac{\pi}{P}$	$p = \pi \cdot m$
Standard circular tooth thickness, $t$	$t = \frac{p}{2}$	
Average backlash per pair, $B$	$B = \frac{.040}{P}$	$B = .040 \cdot m$

Formulae used for the conversion from the English (pitch) system to the metric system are summarized below (Table G.2).

The formula  $P = \frac{25.4}{m}$  is used to express diametral pitch,  $P$ , in terms of module  $m$ . The expression:

$$m = \frac{25.4}{P} \quad (\text{G.1})$$

is used for the inverse conversion. For the correspondence between millimeters and inches, the ratio:

$$\text{Millimeters (mm)} = \frac{\text{Inches}}{.03937} = 25.4 \text{ Inches} \quad (\text{G.2})$$

$$\text{Inches} = .03937 \text{ mm} = \frac{\text{mm}}{25.4} \quad (\text{G.3})$$

is valid.

A brief analysis of the types of gears used in the industry, together with the analysis of the local topology of gear tooth flanks to be machined, is necessary for the design of gear-cutting tools, especially gear-cutting tools for machining/finishing precision gears.



# Taylor & Francis

Taylor & Francis Group

<http://taylorandfrancis.com>



---

## Appendix H: On the Inadequacy of the Terms Wildhaber-Novikov Gearing and W-N Gearing

---

Wildhaber helical gearing [161] and Novikov gearing [85] are briefly discussed below, aiming to illustrate the inadequacy of the terms *Wildhaber-Novikov gearing* and *W-N gearing*. As follows from the discussion, helical gearing proposed by Wildhaber must be referred to as *Wildhaber helical gearing* or the like. Helical gearing proposed by Novikov must be referred to as *Novikov gearing* or the like. The extensively used terms *Wildhaber-Novikov gearing* and *W-N gearing* are meaningless and are commonly used by people with poor knowledge.

---

### H.1 Wildhaber Helical Gearing

Helical gearing with a circular arc tooth profile [161] targets an improved power capacity of the gear pair. The invention relates to the tooth shape of gears that run on parallel axes and may be applied to helical gears, such as single and double helical gears or herringbone gears.

The purpose of the invention is threefold:

1. To provide helical gearing with an improved tooth contact, so as to lessen surface stresses and wear
2. To provide helical gearing, which is capable of rapid and accurate production and may be ground without difficulty, if so desired
3. To provide accurate gearing of circular tooth profiles

The invention is illustratively exemplified in the accompanying drawings, in which [Figure H.1a](#) is a side elevational view of the proposed gear, showing parts thereof in section; [Figure H.1d](#) is a normal sectional view of [Figure H.1a](#), taken on lines 2–2 of the latter figure; [Figure H.1g](#) is a side elevational view of a pair of gears constructed in accordance with the invention; [Figure H.1h](#) is a sectional view taken through a pair of gears; [Figure H.1b](#) and [c](#) are sectional views of milling cutters used in the manufacture of gears of the proposed design; [Figure H.1e](#) and [f](#) are elevational views of corresponding tools of rack shape to be used in reciprocating machines for cutting helical gears in accordance with the invention; [Figure H.1k](#) and [l](#) are side elevational views of the improved gear, showing a pair of grinding wheels in different operating positions, the wheels being set to grind opposite tooth surfaces; [Figure H.1m](#) is a view of a gear taken in normal section and showing the grinding wheels in the operation position; [Figure H.1n](#) is a view of a mate pinion showing the grinding wheels in the operation position; [Figure H.1o](#) is a view of the modified form of gear made in accordance with the invention; [Figure H.1j](#) is a sectional view taken through an internal gear and its pinion; [Figure H.1](#) is a normal section through helical teeth of a composite outline constructed from the invention; [Figure H.1p](#) is a view of a reciprocating tool of rack shape in the operating position; and [Figure H.1r](#) is a view of a modified type of reciprocating tool in position to start a cut on a herringbone gear.

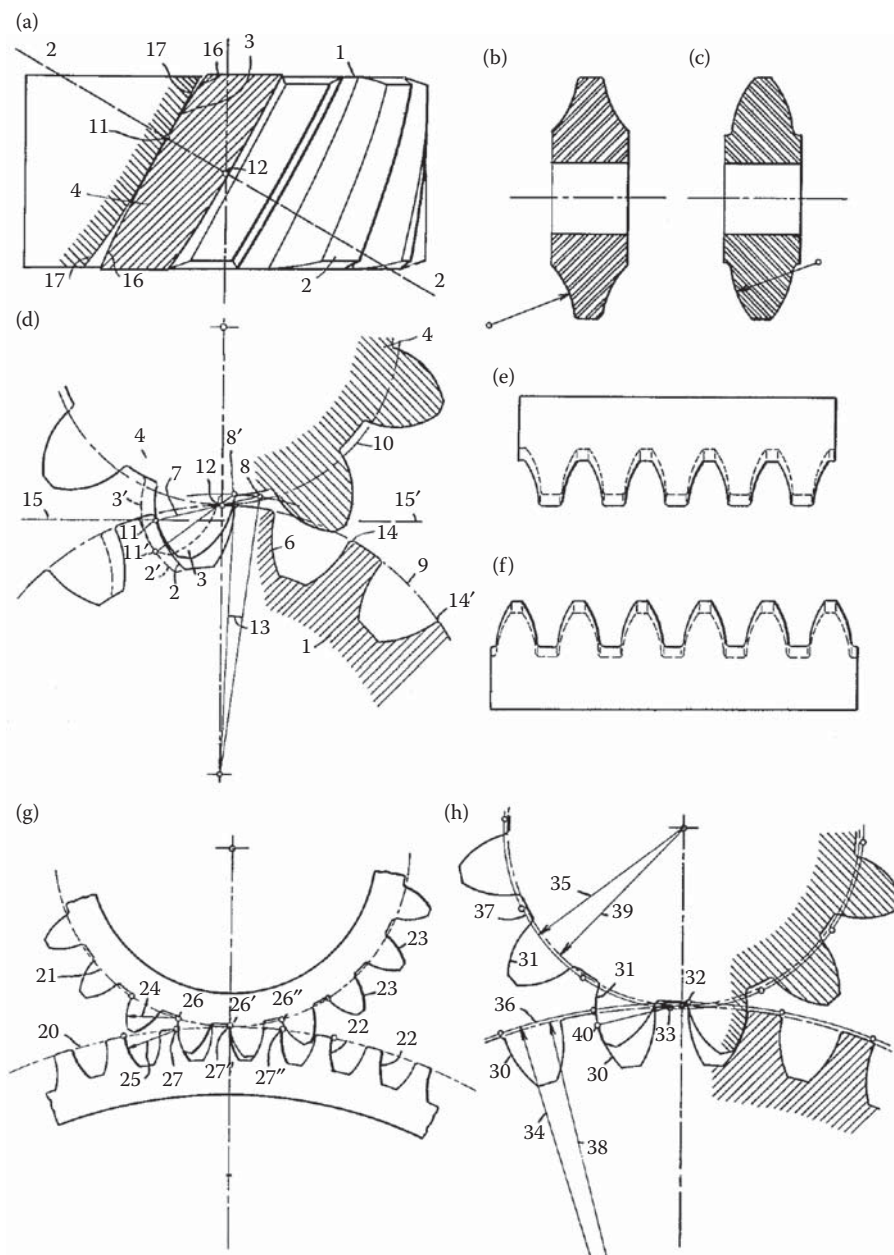
Referring to the drawings, and particularly to [Figure H.1a](#) and [d](#), 1 denotes a helical gear having teeth 2 in contact with the teeth 3 of a mating pinion 4. In order to clearly illustrate the degree of contact between the teeth of the gear and pinion, tooth 4 is shown in section in [Figure H.1a](#).

It is customary to analyze helical gearing with reference to a normal section, that is, line 2–2 of [Figure H.1a](#), line 2–2 being normal to the helix of the pitch circle. [Figure H.1d](#) illustrates said normal section 2–2 for both pinion 4 and gear 1.

It has been assumed as an example that the tooth profiles 6 of gear 1 are circular arcs of radii 7 and centers 8 in the normal section shown. Centers 8 are situated close to the pitch circle 9 of the gear.\* The corresponding teeth

---

\* Centers 8 need to be situated along the line of action,  $LA$ : that is a must. Otherwise, the condition of contact ( $\mathbf{n} \cdot \mathbf{V}_2 = 0$ ) is violated.

**FIGURE H.1**

Helical gearing. (After E. Wildhaber, US Patent 1,601,750, Patented: October 5, 1926, Filed: November 2, 1923.)

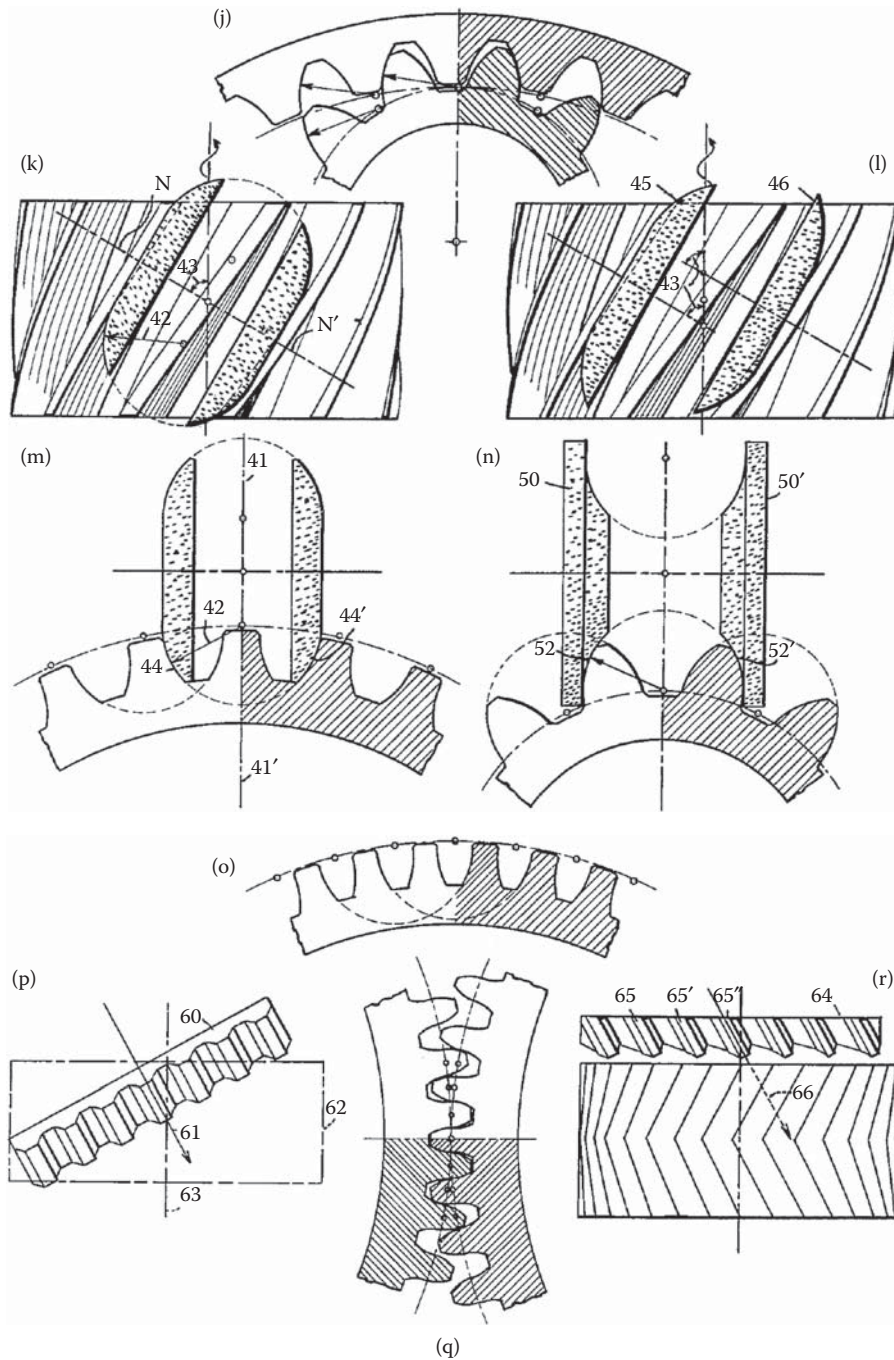
(Continued)

of pinion 4 are so shaped as to allow rolling of pitch circles 9 and 10 on each other, as is well known to those skilled in the art.

When gear tooth 2 is in the position shown in Figure H.1a and d, and its center is at 8, then it contacts tooth 3 at point 11, which may be determined by a perpendicular to tooth 2 through point 12, point 12 being the contact point between the two pitch circles 9 and 10. The said perpendicular is, in the present case, the connecting line between point 12 and center 8 of the tooth profile.

Another position 2' of the gear tooth and 3' of the corresponding pinion tooth are shown in dotted lines in Figure H.1d. The tooth profiles contact here at a point 11', which can be determined like point 11. It can be seen that the contact point has traveled from 11 to 11' during a small angular motion of the gears.\* The contact

\* Once the contact point has traveled from 11 to 11' during a small angular motion of the gears, this immediately reveals that the transverse contact ratio,  $m_p$ , in Wildhaber helical gearing is greater than 0; that is,  $m_p > 0$ , which is not permissible.

**FIGURE H.1 (Continued)**

Helical gearing. (After E. Wildhaber, US Patent 1,601,750, Patented: October 5, 1926, Filed: November 2, 1923.)

point has passed practically over the whole active profile during a turning angle  $13$  of the gear, which corresponds to only a fraction of the normal pitch  $14$ ,  $14'$ . Said normal pitch equals the circle pitch of the normal section shown.

In gearing now in use, however, the tooth outline and tooth proportions are selected so that the contact of corresponding normal profiles lasts for an angle, which, as a rule, corresponds to more than one full pitch.

In gearing according to the invention, the contact point between two normal profiles passes over the whole active profile during a turning angle, which corresponds to less than one-half the normal pitch, and usually much less than that.

Gearing designed according to the invention allows the teeth to come into better contact with each other, inasmuch as the tooth surfaces remain much closer to each other in a direction perpendicular to the contact line between two mating gears. This is illustrated by a section taken in the direction of lines 15, 15' of [Figure H.1d](#). In [Figure H.1a](#), lateral profile 16 of tooth 3 and profile 17 of tooth 2 of said section are shown to contact at point 11 and remain close to each other for their whole length. The same holds true for other sections taken parallel to section 15, 15'.

Close contact between teeth is well known to reduce wear and improve the efficiency of the gears.

Although a circular arc is shown as the normal tooth profile of gear 1, in [Figure H.1d](#), it can be understood that this is not the only shape to affect the stated purpose of increasing the speed at which the contact point travels over the tooth profile of a normal section. As a rule, however, the shape can be approximated by a circle whose center is close to the pitch center.

The gearing according to the present invention is strictly for helical teeth. It would not be advisable on straight teeth because of the explained short duration of contact between tooth profiles. This would cause intermittent action, whereas on helical gears, similar parts of the teeth are always in contact because of the twisted nature of the tooth surfaces.

[Figure H.1g](#) may be considered a view taken in the direction of the axes of a pair of gears. The tooth profiles are the circles in a section perpendicular to the axes. The gear is provided with helical teeth, with working faces below pitch circle 20, while the pinion teeth have working faces above pitch circle 21 only. Working profiles 22 of the gear are concave and circular, and their centers are substantially situated on pitch circle 20. Convex working profiles 23 of the pinion are also of circular shape. Their radii 24 are substantially the same as radii 25 of the mate profiles. Centers 26, 26', 26'' are similarly situated on pitch circle 21. Profile centers 27, 27', 27'' of pitch circle 20 and profile centers 26, 26', 26'' of pitch circle 21 correspond to each other. They coincide during mesh, which takes place on the whole tooth profile at once.

[Figure H.1g](#) may also be considered a section perpendicular to helical teeth, and then shows normal tooth profiles.

[Figure H.1h](#) shows a refinement of the preferred embodiments of the invention. It is a normal section through the helical teeth, but can also be considered a section perpendicular to the axes. Corresponding profiles 30 and 31 are circular, as in [Figure H.1g](#), but in this case, the radius of concave circular profile 30 is made a trifle larger than the radius of convex circular profile 31. Consequently profile centers 32 and 33 do not exactly coincide during the mesh. Radii 34 and 35 of circles 36 and 37, constituted by profile centers 32 and 33, respectively, are not accurately identical to pitch radii 38 and 39 of the two gears. The sum of radii 34 and 35 is a trifle larger than the sum of the pitch radii. Radii 34 and 35 are selected so that the main tooth pressure runs about in a direction 33, 40.

The slight difference of the radii of profiles 30 and 31 facilitates the tooth contact and allows for small errors in making and assembling.

[Figure H.1b](#) and [c](#) show a pair of milling cutters for milling gear teeth. The cutter may be applied in the usual manner, their axes being inclined in correspondence with the tooth inclination, that is, with the helix angle of teeth. It can be found that the cutters should be inclined for an angle a trifle smaller than the helix angle in the pitch circle to produce the most accurate results.

In [Figure H.1e](#) and [f](#), a pair of rack-shaped cutters is shown.\* These cutters are for use in a reciprocating machine. The teeth of these tools are relieved inwardly, in the usual manner, as evident by the dotted lines.

The convex grinding wheels shown in [Figure H.1k](#) are illustrated in their operating positions in a view that is taken perpendicular to the axis of the gear blank as well as to the axis of the grinding wheels, that is, a view along the gear radii 41, 41' of [Figure H.1m](#). The wheels that are to produce concave circular teeth profiles in a normal section are of convex circular profiles, the radius 42 being the same as the radius of the concave circular profile. The grinding wheels are inclined for angle 43, which equals the helix angle of the teeth in the pitch circle. The wheels grind along their profiles indicated in dotted lines 44 and 44', which are located in a normal section. As shown in [Figure H.1k](#), the two grinding wheels are coaxially arranged with respect to each other.

The device shown in [Figure H.1l](#) corresponds to that shown in [Figure H.1k](#), with the exception that grinding wheels 45 and 46 are not coaxially arranged. Although the arrangement shown in [Figure H.1k](#) imposes certain restrictions on the tooth design, it is frequently preferred. The arrangement of [Figure H.1l](#) is advantageous when grinding wheels are not free to run out, for instance, when they must clear against a shoulder or in the case of herringbone teeth.

\* Conformal gears cannot be cut by rack cutters, and, more generally, cannot be machined in any gear-generating process.



Referring particularly to [Figure H.1m](#), a normal section is illustrated and taken along lines N, N' of [Figure H.1k](#). In this view, the axis of the coaxially arranged grinding wheels is situated in said normal section. The wheels grind along profiles 44 and 44' of the normal section shown, while the blank performs a translator motion in the direction of its axis and, in timed relation thereto, a turning motion about its axis. In other words, the blank is screwed past the grinding wheels.

[Figure H.1n](#) discloses a normal section through the teeth of the mating gear or pinion. Grinding wheels 50 and 50' are provided with concave circular profiles 52 and 52' with which they grind the convex gear teeth.

It can be understood that milling cutters might be used instead of the grinding wheels shown in [Figure H.1k through n](#), and also that grinding wheels of the shape shown in [Figure H.1b and c](#) might be used, if so desired.

The teeth ground according to [Figure H.1k](#), m and n are preferably designed so that the centers of opposite tooth arcs 44 and 44', 52 and 52', respectively, in [Figure H.1n](#) coincide. In [Figure H.1m](#) and [n](#), the tooth arcs of every third tooth side have a common center.

The tooth arcs of every fifth tooth side have a common center in the normal section shown in [Figure H.1o](#).

In [Figure H.1m](#), the common center of opposite tooth arcs of alternate teeth is situated on the centerline of the intermediate tooth. The corresponding pinion shows convex circular profiles, of which opposite tooth sides of adjacent teeth have common centers in the middle of the intermediate tooth space.

The normal section shown in [Figure H.1j](#) shows an internal gear and its mate pinion constructed in accordance with the concave tooth profiles. In external gears, preference is similarly given to providing the larger gears with concave tooth profiles.

The normal section through a pair of helical gears shown in [Figure H.1q](#) discloses opposite tooth profiles, the addendum being convex and the dedendum concave.

A rack-shaped planing tool is illustrated in the operating position in [Figure H.1p](#). Tools of this kind are shown in another view in [Figure H.1e and f](#). Reciprocatory tool 60 moves in direction 61 at an inclination equal to the helix angle of the teeth. Gear 62, with its axis 63, is shown in dotted and dashed lines. In order to cut the proper tooth shape, gear blank 62, after every cut, is slightly fed in a rolling generating motion with respect to a rack embodied by tool 60.

Another reciprocatory tool 64 is shown in [Figure H.1r](#), the tool in this case being provided with stepped teeth 65, 65', 65'', which allow it to clear shoulders and herringbone teeth. The tool moves in direction 66 of the helical teeth, which it cuts.

Other ways of producing gearing according to the invention, that is, hobbing, planing with a pinion cutter, rolling and casting, may be contemplated, but it is not deemed necessary at this time to give a detailed explanation of the mechanisms used in connection therewith.

Briefly stated, the invention consists of providing helical gearing of such a profile that tooth contact passes rapidly over the normal profile of teeth. This has been found to result in close contact between helical mate teeth. In a direction at right angles to the contact line, the mate teeth recede from each other only slightly and thus provide a tooth contact that is not very far from surface contact.

It is claimed\* Wildhaber gearing features a nonzero transverse contact ratio ( $m_p > 0$ ) and a nonzero face contact ratio  $m_F > 0$ . The total contact ratio,  $m_t$ , is greater than one ( $m_t \equiv m_p + m_F > 1$ ).

Wildhaber gearing (see [Figure H.1](#)) does not meet the condition of contact. The condition of conjugacy of the tooth flanks and the condition of equality of the base pitches of the gear and pinion to the operating base pitch are not fulfilled in this design of gearing. This immediately yields a conclusion that Wildhaber gearing is not workable at all.

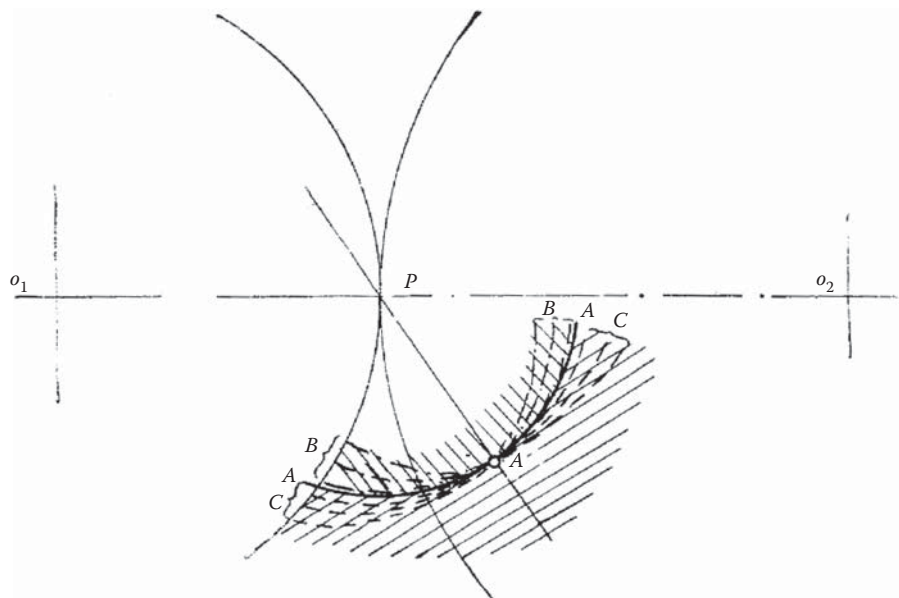
The invention by Wildhaber is explained to the best possible extent in [116,117].

## H.2 Novikov Gearing

Novikov gearing [85] is an example of conformal helical gearing. For a long while, Novikov's patent (S.U. Patent No. 109,113 of 1956) was not available to most gear experts.

Known designs of gearing, those featuring the point system of meshing, feature low contact strength and are not widely used in practice.

\* Wildhaber, E., *Helical Gearing*, US Patent 1,601,750, Patented: October 5, 1926, Filed: November 2, 1923.

**FIGURE H.2**

Helical gearing. (After Dr. M. Novikov, Pat. No. 109,113, (USSR). *Gear Pairs and Cam Mechanisms Having Point System of Meshing*. /National Classification 47h, 6; Filed: April 19, 1956, published in Bull. of Inventions No. 10, 1957.)

The contact strength of known designs of gearing with a line system of meshing, including the widely used involute gearing, is limited.

The proposed gearing\* [85] features higher contact strength due to favorable curvatures of the interacting tooth flanks. Under equivalent contact stress, similar dimensions, and comparable remaining design parameters, greater circular forces are permissible by the proposed gearing. Lower sensitivity to manufacturing errors and deflections under the load are the other advantages of the proposed gearing.

The proposed gearing can be designed either with parallel, intersecting, or crossing axes of rotations of the gears. External gearing as well as internal gearing of the proposed system of meshing is possible. The tooth ratio of the proposed gearing can be either of a constant value or it can be variable and time dependent. The proposed concept of gearing can be utilized in the design of cam mechanisms.

In Figure H.2, possible tooth profiles in the cross-section of tooth flanks by a plane that is perpendicular to the instant axis of relative rotation through the current point of contact are illustrated.

Here, the point of intersection of the planar cross-section by the axis of instant relative rotation is denoted by  $P$ .

$O_1$  and  $O_2$  are the points of intersection of the planar cross-section by the axes of the gear and the pinion.

$A$  is the point of meshing (in its current location).

$PA$  denotes the line of action.

$\Delta A \Delta$  is the circle centered at point  $P$  that corresponds to the limit case of the tooth profiles (in the case where the profiles are aligned to each other).

Several curves,  $BAB$ , represent examples of the tooth profiles of one of the mating gears. The curves,  $BAB$ , are arbitrary smooth curves, which are located inside the circular arc,  $\Delta A \Delta$  (that is, the arcs are located within the body side of the limit tooth flank of one of the gears). The curves,  $BAB$ , are located close to the circular arc,  $\Delta A \Delta$ , and they feature a high degree of conformity to the circular arc.

Several curves,  $CAC$ , represent examples of the tooth profiles of the second of the mating gears. The curves,  $CAC$ , are arbitrary smooth curves that are located outside the circular arc,  $\Delta A \Delta$  (that is, the arcs are located within the body side of the limit tooth flank of another two gears). The curves,  $CAC$ , are also located close to the circular arc,  $\Delta A \Delta$ , and they feature a high degree of conformity to the circular arc.

\* Pat. No. 109,113, (USSR). *Gear Pairs and Cam Mechanisms Having Point System of Meshing*. M.L. Novikov, National Classification 47h, 6; Filed: April 19, 1956, published in Bull. of Inventions No. 10, 1957.

The entity of the invention is disclosed below in detail.

The location and orientation either of a straight path of contact or a smooth curved path of contact are specified in that space in which the location and orientation of the axes of rotation of the gear and pinion are given. The path of contact is located reasonably close to the axis of instant relative rotation of the gears. Either constant or time-dependent (smoothly varying in time) speed of motion of the contact point along the path of contact is assigned. A coordinate system is associated with the gear, and a corresponding coordinate system is associated with the pinion. In the coordinate systems, the moving contact point traces the so-called contact lines.\* One of the paths of contact is associated with the gear and the other is associated with the pinion. Certain smooth regular surfaces through the pseudo-paths of contact can be used as the tooth flanks of the gear and pinion. The following requirements should be fulfilled in order for the surfaces to be used as the tooth flanks:

- At every location of the contact point, the tooth flanks should have a common perpendicular; thus, the requirements of the main theorem of meshing should be satisfied.
- The curvatures of the tooth profiles should correspond to each other.
- No tooth flank interference occurs within the working portions of the surfaces.

The proposed tooth flanks fulfill the above-listed requirements and allow for high contact strength of the gear teeth.

Consider a plane through the current contact point that is perpendicular to the instant axis of relative rotation. Then, two circular arcs are constructed. The circular arcs are centered at points within the straight line through the pitch point and contact point. The arc centers are located close to the pitch point. The constructed circular arcs can be considered an example of the tooth profiles of the gear and pinion. The tooth flanks are generated as loci of the tooth profiles constructed for all possible locations of the contact point. The working portion of one of two tooth flanks is convex, while the working portion of the other tooth flank is concave (in the direction toward the axis of instant relative rotation). In a particular case, the radii of tooth profiles could be of the same magnitude and equal to the distance from the contact point to the axis of instant relative rotation. The centers of both profiles in this particular case are located at the axis of instant relative rotation. Under such a scenario, point meshing reduces to a special line meshing. This would require extremely high accuracy of the center distance and independence of it from operation conditions, which is impractical. Point meshing is preferred when designing tooth profiles. A small difference between the radii of curvature of the tooth profiles is desirable. It should be kept in mind that during the run-in period of time, point meshing of the gear teeth will transform to the above-mentioned local line meshing of the tooth profiles. However, the theoretical point contact of the tooth flanks will be retained.

Tooth profiles can differ from the circular arcs. However, the tooth profiles of other geometries (those always passing through the contact point) should be located (for one gear) within the interior of the above-mentioned circular arc profile that centers at the point within the axis of instant relative rotation, as shown in [Figure H.2](#). For another gear, the tooth profile should be located outside the circular arc.

The law of motion of the contact point (that is, the speed of the point and its trajectory) should be chosen so as to minimize friction and wear losses. Friction and wear losses are proportional to the relative sliding velocity in the gear mesh. Therefore, it is desirable to reduce the sliding velocity as much as possible. For this purpose, the path of contact should be located not far from the axis of instant relative rotation. On the other hand, a location of the path of contact too close to the axis of instant relative rotation is also not desirable, as that reduces the contact strength of the gear tooth flanks. In addition, it is recommended to ensure favorable angles between the common perpendicular (along which the tooth flanks of one of the gears act against the tooth flanks of the other) and between the axes of rotation of the gears.

The opposite sides of tooth profiles are designed in a manner similar to that just discussed. Tooth thicknesses and angular pitch are assigned to ensure the required bending tooth strength.

The face width of the gear or length of the gear teeth should correlate to their pitch to ensure the required value of the face contact ratio. Gear pairs can feature either one point of contact (when working portions of the tooth flank contact each other just at one point, excluding the phases of tooth re-engagement), or they can feature multiple contact points when the tooth flanks contact each other at several points simultaneously.

\* *Contact line* is a term used by Novikov. Actually, the *contact line* is the *pseudo-path of contact*.



For parallel-axes gear pairs, it is preferred to use a straight line as the path of contact, parallel to the axes of rotations of the gear and pinion. The speed of the contact point along the straight path of contact can have a constant value. In this particular case, the radii of curvature of the tooth profiles in all cross-sections by planes are equal to each other. Tooth flanks in this case are regular screw surfaces. Gears that feature tooth flanks of such a geometry are easy to manufacture, and they can be cut on machine tools available on the market.

An example of parallel-axes gearing with limited geometry of tooth profiles is illustrated in [Figure H.2](#). Point contact of the tooth flanks in this particular case is transformed almost to line contact of the tooth flanks. The curved contact line is located across the tooth profile. When axial thrust in the gear pair is strongly undesirable, herringbone gears can be used instead.

Novikov gearing (see [Figure H.2](#)) meets the condition of contact, the condition of conjugacy of the tooth surfaces, and the condition of equality of the base pitches of the gear and pinion to the operating base pitch. Novikov gearing is a type of perfect gearing.\* Novikov gearing is the only feasible type of gearing with point contact of the tooth flanks that is capable of transmitting a rotation smoothly. As is clear now, Novikov gearing is a reduced type of involute gearing.

The invention by Novikov is explained to the best possible extent in [\[116,117\]](#). There [\[116,117\]](#), the author's comments on the concept of Novikov gearing and the inadequacy of the terms *Wildhaber-Novikov gearing* and *W-N gearing* are presented.

---

\* It needs to be noted here that Wildhaber did not recognize the difference between Novikov gearing and the helical gearing he proposed [\[161\]](#). This conclusion immediately follows from Wildhaber's statement: "I may say also that it gives me satisfaction to see the original concept vindicated through the Russian reinvention and effort and through subsequent efforts and articles." This statement from Wildhaber can be found on p. 949 in a paper by T. Allan ("Some Aspects of the Design and Performance of Wildhaber-Novikov Gearing," *Proc. Inst. Mech. Engrs, Part I*, Vol. 179, No 30, 1964/1965, pp. 931–954; see the *Communications* section in the paper by T. Allan). Other evidence in this area is also known.

---

## Conclusion

---

The principal accomplishments and new results obtained in this monograph are briefly outlined below.

Aiming at the development of a scientific theory of gearing, this research begins with a brief scientific overview in the area of gearing. For this purpose, all the fundamental accomplishments in the field are listed in chronological order, and a corresponding name of a scientist/engineer is assigned to each of the fundamental accomplishments. For example, Leonhard Euler is credited for the application of the involute tooth profile in gears for parallel-axes gear pairs; Charles Camus, Leonhard Euler, and Felix Savary are credited with the formulation of the main theorem of parallel-axes gearing (the so-called *CES*-theorem), and so forth. The above-listed names of gear scientists illustrate positive contributions to the scientific theory of gearing. There are also a few names of gear scientists who committed huge mistakes that negatively affected the evolution of the gear art. Theodore Olivier, Chaim Gochman, and a few more names are mentioned in this area.

Use of such an approach for analysis of the fundamental contributions is helpful to separate the fundamental accomplishments in the theory of gearing, along with the appropriate names of the researchers associated with these accomplishments, from the names of other scientists/engineers who did not contribute to the fundamentals of the scientific theory of gearing.

The total number of fundamental accomplishments in gearing is limited. Therefore, the total number of names of scientists/engineers who really contributed to the fundamentals of the scientific theory of gearing is also limited.

The kinematics of a gear pair is discussed to the best possible extent. Vector diagrams of gear pairs are extensively used for this purpose. Rotationally positive, rotationally negative, and rotationally zero gear pairs are distinguished in this research, and an analytical criterion of all types of gear pairs is proposed.

The use of vector diagrams of gear pairs makes possible a scientific classification of all possible types of vector diagrams. Upon development of the classification, a set of complementary vectors to vector diagrams of gear pairs is introduced.

Possible future developments in the theory of gearing are an important output from the above-mentioned analysis.

For convenience of further analysis of gears and gear pairs, a set of the principal planes and reference systems associated with a gear pair are introduced.

Then, conditions to transmit a uniform rotation smoothly from a driving shaft to a driven shaft are formulated in the form of three fundamental laws of gearing. These three fundamental laws of gearing can briefly be stated as: (1) condition of contact, (2) condition of conjugacy, and (3) the condition that requires base pitches of a gear and a mating pinion to be equal to the operating base pitch of the gear pair.

The Shishkov equation of contact,  $\mathbf{n} \cdot \mathbf{V}_\Sigma = 0$  (Prof. Shishkov, late 1940s), is adopted for analytical description of the first fundamental law of gearing.

The equation of conjugacy,  $\mathbf{p}_{ln} \times \mathbf{V}_m \cdot \mathbf{n}_g = 0$  (Prof. Radzevich, 2017), is adopted for analytical description of the second fundamental law of gearing.

The equalities  $\varphi_{b,g} = \varphi_{b,op}$  and  $\varphi_{b,p} = \varphi_{b,op}$  (Prof. Radzevich, 2008), is adopted for analytical description of the third fundamental law of gearing.

In perfect gear pairs, all three fundamental laws of gearing are met; if one or more fundamental law(s) of gearing is violated, no smooth transmission of a uniform rotation from an input shaft to an output shaft is possible at all.

Kinematics and geometry of parallel-axes gearing are discussed. Analysis of the kinematics, gear ratio, and a variation of the permissible transverse pressure angle in parallel-axes gearing are covered in this discussion. Gear pairs with gear ratios in the range of  $-\infty \leq u \leq +\infty$  are considered.

A desirable line of contact between the tooth flanks of a gear and mating pinion, the line of action, and the path of contact in a gear pair are analyzed. The concept of the operating base pitch in a gear pair is introduced.

Special attention is given to the analysis of the contact ratio in parallel-axes involute gearing. The transverse contact ratio, face contact ratio, and total contact ratio in parallel-axes involute gearing are discussed to the best possible extent. In particular, the transverse contact ratio in low-tooth-count gearing receives detailed consideration.

Sliding conditions and specific sliding between gear and mating pinion tooth flanks in both external and internal parallel-axes gearing are discussed in detail, along with the forces acting in the plane of action and in a transverse section of a perfect parallel-axes involute gear pair.

In addition, conformal and high-conformal parallel-axes gearings are discussed. It is shown that conformal gearing (Novikov gearing, in other words) and high-conformal parallel-axes gearing represent reduced cases of parallel-axes involute gearing that feature a zero-length line of action, zero-length path of contact, and a certain length of the pseudo-path of contact. The principal features of high-conformal gearing are outlined, and the difference between conformal gearing and high-conformal gearing is shown. The impossibility of cutting gears for conformal and high-conformal gearing in the generating (continuous-indexing) machining processes is illustrated in detail.

It is proven that no perfect helical gear pairs with a noninvolute tooth profile [Roots blower, rotors for oil pumps, and *Helical Gearing* by Dr. Wildhaber (US Pat. No. 1,601,750)] is possible at all.

For the analysis of intersected-axes gearing, a pulley-and-belt analogy of intersected-axes gear pairs is constructed. The path of contact and the instant line of action are investigated by means of the pulley-and-belt analogy of intersected-axes gear pairs. Equations for the tooth flanks of gear pairs are derived.

It is shown that most of the desired tooth proportions in intersected-axes gear pairs are angular and not linear design parameters, that is, the angular base pitch, angular pitch, angular tooth thickness, angular space width, angular backlash, angular addendum, angular dedendum, and so forth.

Perfect conformal and high-conformal intersected-axes gearing receive particular attention. The path of contact and pseudo-path of contact, boundary cones, and bearing capacity of high-conformal gearing are covered in this discussion. The design parameters of conformal/high-conformal intersected-axes gearing are discussed as well.

The pulley-and-belt analogy of intersected-axes gear pair is employed for analysis of the path of contact and the zone (field) of action in intersected-axes gearing. Conditions to transmit a uniform rotation by means of intersected-axes gearing are covered in this discussion, along with analysis of the transverse contact ratio, face contact ratio, and total contact ratio. Sliding of the tooth flanks and elements of the dynamics of perfect intersected-axes gearing are investigated. The principal assumption adopted in load analysis of perfect intersected-axes gearing is formulated.

The kinematics of crossed-axes gearing is investigated. The pressure angle and the base cones in crossed-axes gear pairs are constructed. Ultimately, this results in an expression for the gear tooth flank in perfect crossed-axes gearing. Perfect crossed-axes gearing of this kind is referred to as *R*-gearing. The condition of conjugacy of tooth flanks of a gear and a mating pinion in *R*-gearing are described analytically.

It is shown that most of the desired tooth proportions in crossed-axes gear pairs are angular and not linear design parameters, that is, the angular base pitch, angular pitch, angular tooth thickness, angular space width, angular backlash, angular addendum, angular dedendum, and so forth.

Special consideration is given to the analysis of the main features of perfect conformal and high-conformal crossed-axes gearing. The path of contact, pseudo-path of contact, boundary N-cone, and bearing capacity of crossed-axes conformal/high-conformal gearing, along with the calculation of the design parameters of conformal/high-conformal crossed-axes gearing, are covered in this discussion.

The pulley-and-belt analogy of crossed-axes gear pairs is employed for the investigation of tooth flanks in perfect crossed-axes gearing. The path of contact and the zone (field) are investigated, and the conditions for transmitting a uniform rotary motion by means of crossed-axes gearing are analyzed. The contact ratio in crossed-axes gearing is discussed. The transverse contact ratio, face contact ratio, and total contact ratio are covered in this discussion.

Sliding, specific sliding, and features of specific sliding between the tooth flanks are investigated, along with elements of dynamics of perfect crossed-axes gearing.

A principal assumption adopted in the load analysis of perfect crossed-axes gearing is formulated, and forces of interaction in perfect crossed-axes gearing are analyzed.

The peculiarities of perfect worm gearing are discussed, with focus on worm gearing with line contact between the worm threads and worm-gear tooth flanks being a particular kind of crossed-axes gearing, considered earlier in this book. The kinematics, base cones, and peculiarities of sliding in the plane-of-action apex in perfect worm gearing are covered in this discussion. An analytical criterion to distinguish a worm gear from a helical gear is proposed.

The discussion of perfect gearing with point contact between the tooth flanks of a gear and mating pinion covers examples of gearings with the point contact, and follows the approach to generate tooth flanks in gearing with point contact between tooth flanks of a gear and mating pinion.

A novel kind of crossed-axes gearing that is insensitive to axis misalignment is proposed. The proposed design of gearing is referred to as the  $S_{pr}$ -gear system. Finally, a correlation among gear systems of various types is outlined.

A novel approach to designing perfect noncircular gears is proposed.

An approach for synthesizing perfect gear pairs is proposed. The meaning of the term *synthesis of favorable gear pairs* is clarified. A concept of synthesis of a favorable perfect gear pair is proposed.

Generic gear shapes are analyzed to the best possible extent. The origins of the generic gear shape and examples of gear pairs composed of gears with various generic shapes are covered in this discussion. The total number of possible generic gear shapes is evaluated. A possibility of classification of gear pairs is discussed, and examples of implementation of classification of gear pairs are provided.

The local geometry of interacting tooth flanks of a gear and mating pinion is considered. The kinematics and local geometry of the interacting tooth flanks are discussed. This discussion is followed by the analysis of local geometry of the interacting tooth flanks in gearings of all kinds.

Various aspect of gear tooth strength are analyzed. The Hertz proportional assumption and the assumption of equal torque share are the two assumptions adopted in this analysis. The importance of the Saint-Venant principle (or Saint-Venant assumption) in the bending strength of gear teeth is mentioned.

The gear tooth profile modification generated by means of the basic rack shift is considered. Addendum modification (profile shift), profile shift coefficient, and gear tooth flank geometry depending on the profile shift coefficient are covered.

The root cause of unequal torque sharing in a split torque transmission system, mobility of split torque transmission systems, and power density of gear transmission systems are analyzed. Ultimately, a novel approach for equal torque sharing in a split torque transmission is proposed. This includes, but is not limited to, the planetary gear drive with an elastomeric load sharing device and examples of the implementation of the elastic load sharing device. The main features of split torque transmission systems with preloaded elastic load sharing devices are outlined.

A vector approach for the kinematic and dynamic analysis of complex gear systems is briefly outlined.

A few novel methods for gear inspection are briefly discussed. A perfect datum surface is used in each of the considered methods of gear inspection. These makes the methods of gear inspection more accurate and the readings more reliable.

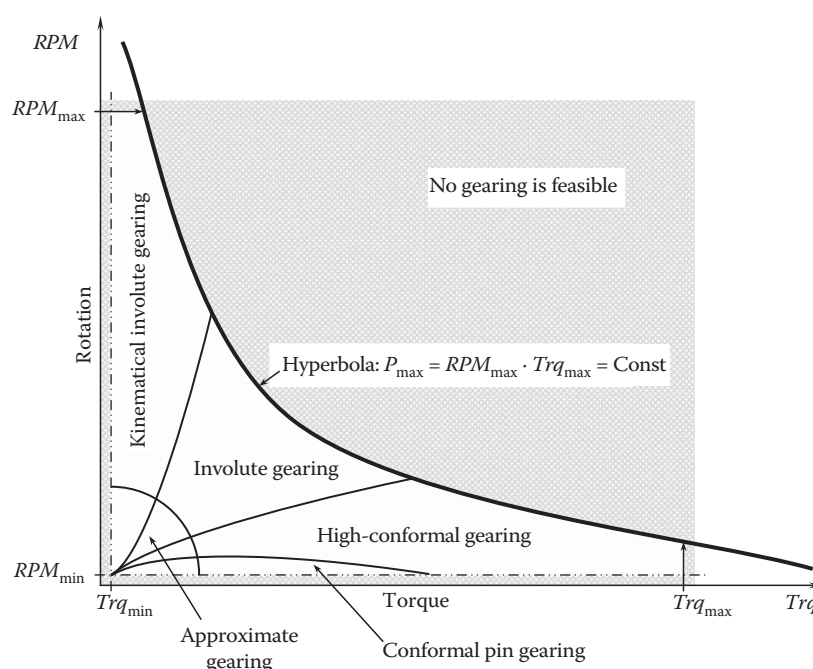


FIGURE 1

Areas of different kinds of gearing.

The kinematical and the geometrical factors that affect noise excitation in gearings are briefly discussed. Some physical factors, like a variation of the loading in a gear pair, that allow for a kinematical/geometrical interpretation are also outlined.

Design peculiarities of perfect and almost perfect gears are discussed. Features of the design of gears for  $R$ -gearing, as well as for  $R_{sp}$ -gearing, are considered as examples.

The obtained results of the research are applicable to gearings of all kinds operating under various conditions (Figure 1). Here, in Figure 1, the area where gears can be used for the transmission of a motion is constructed. Gearings can be used for transmission of rotation in the range of the lowest rotation,  $RPM_{min}$ , to a certain highest rotation,  $RPM_{max}$ . A range for a torque being transmitting is designated as  $Trq_{min}$  for a minimal torque and  $Trq_{max}$  for a maximal torque. The highest power,  $P_{max}$ , that can be transmitted by a gear pair is:

$$P_{max} = RPM_{max} \cdot Trq_{max}$$

Considering  $P_{max} = \text{Const}$ , a boundary hyperbola can be constructed in the reference system,  $RPM/Trq$ .

Transmission of a rotation from a driving shaft to a driven shaft by means of a gear pair is possible only inside the area shown in Figure 1. Areas of preferable applications of gear pairs of different types are also shown. The schematic shown in Figure 1 is qualitative (not quantitative) and intuitive.

---

## Glossary

---

Here we list alphabetically the most commonly used terms in gearing. Most newly introduced terms are also listed below.

**Active profile:** Part of the tooth profile that experiences contact during the mesh cycle.

**Addendum:** In parallel-axes gearing, the addendum of a gear tooth is the radial distance from the nominal pitch circle to the top of the tooth (or, in other words, the portion of the gear tooth above the reference pitch surface). This concept can be extended to gearing of all other kinds.

**Addendum (chordal):** The *chordal addendum* is used for the purpose of setting a gear tooth vernier to measure the tooth thickness, which is the chord length subtended by the two flanks of a gear tooth at the nominal pitch circle. This must be calculated from the known circular tooth thickness. The distance from the chord to the top of the tooth is known as the *chordal addendum*.

**Addendum angle:** In a bevel gear, this is the angle between elements of the pitch cone and the face cone.

**Addendum modification:** A displacement of nominal addendum profile in the radial direction of the gear.

**Angular base pitch:** This is an angle measured within the plane of action. The apex of the angle is coincident to the plane-of-action apex,  $A_{pa}$ . The sides of the angle are through the corresponding points of intersection of two adjacent tooth flanks of the gear.

**Angular pitch:** This is the angle subtended by the circular pitch, usually expressed in radians.

**Apex to back:** In a bevel gear, this is the distance from the apex of the pitch cone to a locating surface at the back of the gear.

**Approximate gearing:** A means by which a rotation of the driving shaft at a *uniform angular velocity* is transmitted to the corresponding rotation of the driven shaft *not* at a *uniform angular velocity*. The tooth flanks of the gear and of the mating pinion in approximate gearing are shaped so that the three fundamental laws of gearing are not fulfilled.

**Arc of action:** The angular displacement of the input defined by the mesh cycle. It can also be understood as the arc on the pitch circle through which a tooth profile moves from the beginning to the end of contact with a mating tooth profile.

**Arc of approach:** The arc on the pitch circle through which a tooth profile moves from the beginning of its contact with a mating tooth profile until it reaches the pitch point.

**Arc of recess:** The arc on the pitch circle through which a tooth profile moves from contact with a mating tooth profile at the pitch point until contact ends.

**Axial pitch:** The pitch measured in the axial direction in helical gears. It is therefore the normal circular pitch divided by the sine of the helix angle.

**Axial runout:** Also known as *wobble*, this is the runout of the gear in the axial direction, measured at just below the root circle. It is expressed as a *total indicator reading*.

**Axis misalignment factor:** A design parameter in an  $S_{pr}$ -gear system by means of which a desired line of contact is transformed to the base line of the gear and the base line of the pinion.

**Axis of instant rotation:** The straight line through the plane-of-action apex along the vector of instant rotation; also referred to as the *pitch line*.

**Axodes:** A pair of ruled surfaces that roll and slide upon one another in a special way so there is no relative sliding perpendicular to the generators of the ruled surfaces; an obsolete term with limited usage (not recommended for use in the *theory of gearing*).

**Back angle:** In a bevel gear, this is the angle between an element of the back cone and the plane of rotation. It is usually equal to the pitch angle.

**Back angle:** The elements of the back cone of a bevel gear extend from the outside diameter of the gear blank to its axis and are perpendicular to the elements of the pitch cone.

**Back cone distance:** The distance along an element of the back cone from its apex to the pitch circle.

**Backlash:** The amount by which the tooth space of one gear exceeds the tooth width of its mating gear.

**Base angular pitch:** The angular distance between two adjacent lines of contact of the tooth flanks of the gear and pinion in intersected-axes and crossed-axes gearing. This design parameter is measured within the plane of action of the gear pair.

**Base circle:** In parallel-axes gearing, the circle from which involute tooth profiles are developed.

**Base diameter:** In parallel-axes gearing, the diameter of the base circle of an involute gear.

**Base helix angle:** The angle of crossing of the straight generating line of a screw involute tooth surface with the gear axis of rotation.

**Base pitch:** This is the pitch, in inches or millimeters, measured along the circumference of the base circle or along the *line of action*. It is therefore the circumference of the base pitch divided by the number of teeth. It is the same if measured along the line of action because the corresponding profiles of involute gear teeth are parallel curves, and the base pitch is the constant distance between them along the common normal in the direction of rotation, which, by definition, is the line of action.

**Boundary N-circle:** In *Novikov* and parallel-axis *high-conformal gearing*, this is the circle that subdivides a transverse section of the gearing into two portions. The convex tooth profile of one member of the gearing must be entirely located within the interior of the boundary N-circle, while the concave tooth profile of the other member of the gearing must be entirely located within the exterior of the boundary N-circle.\* To be more precise, the concept of the *boundary N-circle* should be referred to as the *boundary N-cylinder*.

**Boundary N-cone:** In intersected-axes as well as in crossed-axes *high-conformal gearing*, this is the cone that subdivides the space into two portions. The convex tooth flank of one member of the gear pair must be entirely located within the interior of the *boundary N-cone*, while the concave tooth flank of the other member of the gear pair must be entirely located within the exterior of the *boundary N-cone*.†

**Boundary N-cylinder:** See *Boundary N-circle*.

**Bottom land:** This is the surface at the bottom of a tooth space that adjoins the fillets. For full fillet teeth, there is no bottom land as such.

**Cartesian coordinate system:** A reference system composed of three mutually perpendicular straight axes through the common origin. Determination of the location of a point in a *Cartesian* coordinate system is based on the distances along the coordinate axes. Commonly, the axes are labeled X, Y, and Z. Often, either a subscript or superscript is added to designation of the reference system XYZ.

**Centerline:** The straight line that is perpendicular to the two axes of rotation.

**Centrode:** A line of intersection between axodes and their corresponding transverse planes. The term *centrode* is applicable to parallel axes gearing; an obsolete term with limited usage (not recommended for use in *theory of gearing*).

**Center distance:** In parallel-axes gearing, this is the distance between the axes of rotation of two gears in mesh with each other on parallel shafts. It is measured along the mutual perpendicular to the shafts, called the *line of centers*. In the case of crossed-axes gearing (skew axis helical gearing, worm gearing, crossed-axes gearing, and so forth), the center distance is equal to the closest approach of two axes of rotation crossing in space. In the particular case of crossed-axes gearing, the center distance is often referred to as the *offset*.

**Characteristic line:** A limit configuration of the line of intersection of a moving surface that occupies two distinct positions when the distance between the surfaces in these positions approaches zero. In the limit case, a characteristic line aligns with the line of tangency of the moving surface and the envelope to consecutive positions of the moving surface. In other words, this is the curve of intersection of a single surface as defined by two distinct configurations.

**Chordal thickness:** The length of the chord subtended by the two flanks of a gear tooth, usually at the nominal pitch circle diameter.

**Circular pitch:** The distance between the corresponding profiles of two adjacent teeth as measured along the pitch circle. It is therefore the circumference of the pitch circle divided by the number of teeth.

**Circular tooth thickness:** The length of the arc between the two flanks of a gear tooth, usually at the nominal pitch circle diameter.

**Clearance:** A measure of the amount of space that exists between the tip of one gear tooth and the tooth-space bottom of the mating gear.

**Cone distance:** In a bevel gear, the distance from the base of its cone to the cone's apex.

**Conjugate:** A term used to describe gear tooth forms that properly mate with each other. More generally, *conjugate* stands for reciprocally related and interchangeable as to properties, as two points, lines, and so

\* The concept of the *boundary N-circle* was introduced around 2008 by Dr. S.P. Radzevich. Dr. M.L. Novikov himself didn't use the concept of the *boundary circle*.

† The concept of the *boundary N-cone* was introduced around 2008 by Dr. S.P. Radzevich. This concept was not known to Dr. M.L. Novikov.



- on. When gear and mating pinion tooth flanks,  $\mathcal{G}$  and  $\mathcal{P}$ , interact with one another, the common perpendicular intersects the axis of instant rotation if the tooth flanks,  $\mathcal{G}$  and  $\mathcal{P}$ , are conjugate to one another, and does not intersect the axis of instant rotation if the tooth flanks,  $\mathcal{G}$  and  $\mathcal{P}$ , are not conjugate to one another.
- Contact ratio:** The measure of the average number of pairs of teeth in contact during the mesh cycle. In parallel-axes gearing, it is equal to the length of the *arc of action* divided by the *base pitch*.
- Crowned teeth:** Crowned teeth are often specified for spur, helical, and straight-tooth bevel gears. They are thicker at or near the center of the tooth face than at the ends of the teeth. Crowning is accomplished by crown hobbing, shaving, or grinding. The purpose of crowning is to minimize the chance of end bearing of the teeth when there is misalignment in assembly, distortion from heat treating, or deflection under load. The amount of crowning is commonly in the neighborhood of 0.0003" per inch of face (0.0006" change in tooth thickness per inch of face). Crowned gears are examples of *approximate gears*.
- Darboux frame:** In the differential geometry of surfaces, this is a local moving *Cartesian* reference system constructed on a surface. The origin of the *Darboux frame* is at a current point of interest on the surface. The axes of the *Darboux frame* are along three unit vectors, that is, along the unit normal vector to the surface and two unit tangent vectors along the principal directions on the gear tooth flank. The *Darboux frame* is analogous to the *Frenet-Serret* frame as applied to surface geometry. A *Darboux frame* exists at any non-umbilic point of a surface. It is named after the French mathematician *Jean Gaston Darboux*.
- Dedendum:** The dedendum of a gear tooth is the radial distance from the nominal pitch circle to its root circle. In other words, this is a portion of the gear tooth below the reference pitch surface.
- Dedendum angle:** In a bevel gear, this is the angle between elements of the root cone and pitch cone.
- Degree of conformity:** A qualitative parameter to evaluate how close the tooth flank of one member of a gear pair is to the tooth flank of another member of the gear pair in the differential vicinity of a point of their contact (or at a point within the line of contact of the tooth flanks).
- Desired line of contact:** In an  $S_{pr}$ -gear system, the line of contact of tooth flanks of the gear and pinion under zero parameters of axis misalignment.
- Diametral pitch:** In spur gearing and transversal pitch helical gearing, this is the number of teeth per inch of pitch diameter.
- Effective length of the lines of contact:** A portion of the total length of the line(s) of contact within which the driving gear is acting against the driven gear.
- Effective radius of curvature:** A measure of the relative distance between two planar curves in tangency expressed in terms of the radius of curvature of each curve.
- Evolute:** A locus of the centers of curvature for a planar curve.
- Face width:** The length between two ends of a gear. It is equal to the tooth length of spur gearing. In helical or herringbone gearing, it is equal to the length of the teeth multiplied by the cosine of the helix angle.
- Field of action:** A portion of the plane of action bounded by two lines of intersection of outer surfaces of the gear and pinion, and by two lines specified in terms of the effective face width of the gear pair (it is also often called the *zone of action*).
- Fillet:** A part of the tooth profile below the active region.
- Fillet radius:** The radius of an arc approximating the root fillet curve.
- Gear apex:** In a crossed-axes gear pair, this is a point of intersection of the gear axis of rotation with the centerline.
- Gear ratio:** The ratio between the instantaneous displacement of the output and input. It is also known as the *speed ratio*, which is the number of teeth in the driven member (usually the larger, or the gear) divided by the number of teeth in the driver (usually the smaller, or the pinion).
- Gear tooth-line:** In a gear for intersected-axes, as well as for crossed-axes gear pair, the gear tooth-line (the gear space-width-line) is a locus of points of intersection of all the circles with a radius in between the radius of the outer circle, and the radius of the inner circle of the gear, by the corresponding bisectors of the angular tooth thicknesses (of the angular spaces widths).
- Generalized rack-type gear pair:** A crossed-axes gearing for which the vector of instant rotation is perpendicular to the gear axis of rotation.
- Generic gear shape:** A shape of a gear generated in cases when the pitch line in the gear machining process does not align with the axis of instant rotation in the gear pair.
- Generic gear surface:** A surface of revolution generated by the pitch line (in the gear machining process) about the gear axis of rotation.

- Geometrically accurate (*ideal* or *perfect*) gearing:** A parallel-axes, intersected-axes, and/or crossed-axes gearing that is capable of transmitting a uniform rotation of the driving shaft to a uniform rotation of the driven shaft.
- Heel:** The thickest end of a bevel gear tooth.
- Helix angle:** In helical and herringbone gears, this is the angle between the gear teeth and the axis of rotation of the gear. The orientation of the basic rack in relation to the gear axis of rotation is specified by the helix angle. Commonly, the helix angle is measured at the pitch circle.
- Hunting ratio:** A particular tooth ratio of a gear pair. This phenomenon used to describe two toothed bodies in mesh where the ratio of number of teeth cannot be reduced using a common integer. If the hunting ratio exists between two toothed bodies in mesh, each tooth of one body meshes with each tooth of the other body.
- Ideal gearing:** A gearing that has zero linear and angular displacements of the axes of rotations from their nominal configuration. *Ideal gearing* is commonly referred to as *geometrically accurate gearing* or *perfect gearing*.
- Indicatrix of conformity:** A planar centrosymmetrical characteristic curve of the fourth order that is used for the analytical description of the geometry of contact of the gear tooth flank and pinion tooth flank. In particular cases, the indicatrix of conformity also possesses the property of mirror symmetry.
- Instant line of action:** Instant line of action is a straight line that is tangent to the path of contact at point of interest.
- Involute:** A curve traced by a point on a flexible band as it is wrapped on/unwrapped from another curve (the evolute).
- Lead:** The axial advance of a helix for one complete turn, as in the treads of cylindrical worms and the teeth of helical gears.
- Lead angle:** The angle between any helix and plane of rotation. It is the complement to the helix angle and used for convenience in worms and hobs. It is understood to be at the standard pitch diameter.
- Length of action:** The distance along the *line of action* that a tooth moves from the beginning to the end of contact with its mating tooth.
- Line of action:** The straight line that is tangential to the base circles of two mating gears. Its intersection with the centerline of the two base circles defines the *pitch point*. The line of action is the path the teeth follow while in contact.
- Line of contact:** A line within which a gear tooth flank,  $\mathcal{G}$ , and mating pinion tooth flank,  $\mathcal{P}$ , share common points.
- Long-and-short addendum:** This term is used to describe modified gear teeth in which the pinion teeth are cut on an oversized blank and the gear teeth are cut on a blank that is undersized by the same amount. This design is usually specified when an oversized pinion is necessary to avoid *undercut* and a standard center distance must be maintained.
- Low-tooth-count gear:** A gear that has a base diameter,  $d_{b,g}$ , equal to or greater than the limit diameter,  $d_{l,g}$ , of the gear; that is, the inequality  $d_{b,g} \geq d_{l,g}$  is valid with respect to *low-tooth-count gearing*. (*LTC-gearing* is another term used for gears of this particular kind.)
- Master gear:** Used in checking a production gear in a composite action inspection test by rolling the master with the production gear in tight mesh (spring loaded) and measuring the variation in centers. Usually, the master gear is hardened, has ground teeth, and is produced to a high degree of accuracy.
- Mesh cycle:** The time length defined as the instance when two teeth come into contact until they are separated. The mesh cycle also yields interpretation in terms of angles of rotation or the length the contact point travels through.
- Module (of a gear):** The design parameter used for specifying the size of gear teeth using ISO standards. The module is specified as the ratio of the pitch diameter in millimeters to the number of teeth. The module is reciprocal of diametral pitch.
- Mounting distance:** In bevel gearing, this is the distance from the crossing point of the axes of two bevel gears in mesh with each other to a locating surface of each. It is used in assembling bevel gearing.
- Noninvolute gearing:** In parallel-axes gearing, noninvolute gearing is composed of gears that have noninvolute tooth profiles. Noninvolute gearing is an example of *approximate gearing*.
- Normal pressure angle:** The pressure angle that is measured within a plane perpendicular to the axis of instant rotation of the gear and the pinion.

- Number of teeth or threads:** The number of teeth or threads contained in the whole circumference of the pitch circle.
- Operating base pitch:** The angular distance between corresponding points within two lines of intersection of the tooth flanks of two neighboring teeth by the plane of action (measured within the plane of action,  $PA$ , in degrees/radians). The configuration of the plane of action,  $PA$ , is specified in terms of axis misalignment and the actual displacement of the interacting tooth flanks. In ideal parallel-axes gearing, operating base pitch is a linear dimension.
- Path of contact:** Path of contact is a locus of contact points considered in a stationary reference system associated with the gear housing.
- $P_a$ -gearing:** Gearing featuring axes of rotation of the gear and pinion parallel to one another (parallel-axes gearing).
- Pinion:** The smaller of two gears in mesh.
- Pinion apex:** In a crossed-axes gear pair, a point of intersection of the pinion axis of rotation with the centerline.
- Pitch:** A measure of tooth spacing and size.
- Pitch circle:** Circle through the pitch point that is centered on the gear/pinion axis of rotation (other definitions for the *pitch circle* are also known).
- Pitch diameter:** Pitch nominal diameter is the diameter of the pitch circle of a gear. The nominal pitch circles of two gears in mesh at standard centers will be tangent to each other. The operating pitch circles of two gears when meshing at greater than standard centers, as when the pinion is oversized, will be greater than the nominal pitch circles, and now they will be tangential to each other.
- Pitch line:** Straight line through the pitch point that is perpendicular to the centerline (other definitions for the *pitch line* are also known).
- Pitch point:** Point of intersection of the centerline by the line of action in a parallel-axes gearing. *Pitch point* can also be specified as the point of tangency of two pitch circles or the pitch circle and the pitch line, and is located on the line of centers (other definitions for the *pitch point* are also known).
- Pitch surfaces:** A pair of ruled surfaces that roll and slide upon one another and are used as a reference when designing direct-contact mechanisms for spatial motion. In general, pitch surfaces are different from axodes.
- Plane of action:** The plane tangential to the base surfaces of two gears in mesh. It is perpendicular to the tooth flanks of two gears in mesh.
- Plane-of-action apex:** In a crossed-axes gear pair, this is a point of intersection of the axis of instant rotation with the centerline.
- $P_{in}$ -plane:** In a crossed-axes gear pair, this is the plane through the centerline and axis of instant rotation of the gear and pinion. For intersected-axes gearing, as well as for parallel-axes gearing, the  $P_{in}$ -plane can also be defined as the plane through the axis of rotation of the gear and pinion.
- Point of contact:** Any point at which two tooth flanks touch each other.
- Power density:** The ratio of the amount of power transmitted to the weight of the gear pair (also known as the amount of power transmitted unit volume of the gearbox).
- Pressure angle:** The included angle between the line of action and the plane tangential to two reference pitch surfaces where the line of action intersects. This angle is defined in terms of the transverse, axial, and normal pressure angles.
- Profile angle:** The angle that makes a tangent to the gear tooth profile and centerline of the gear tooth.
- Pseudo-path of contact:** In *conformal* and *high-conformal gearing*, a line along which the contact point *pseudo-travels*.
- Rack:** A toothed wheel whose pitch radius is infinite, pitch circle is a straight line, and tooth number is infinite.
- R-gearing:** A perfect crossed-axes gearing that features *line contact* between the tooth flanks of a gear and mating pinion. No other kind of crossed-axes gearing has *line contact* between the tooth flanks of a gear and mating pinion.
- Rotation vector:** A pseudo-vector along an axis of rotation that has a magnitude equal to the rotation about the axis. The direction of the rotation vector depends on the direction of the rotation. Commonly, the rotation vector is designated as  $\omega$ . The magnitude of the rotation vector is commonly denoted by  $\omega$ . Therefore, the equality  $\omega = |\omega|$  is valid. The rotation vector of a gear is designated as  $\omega_g$ , the rotation vector of the mating pinion is designated as  $\omega_p$ , and the rotation vector of the plane of action is designated as  $\omega_{pa}$ .
- Runout:** Phenomenon describing the variation in pitch surface that results from nonzero eccentricity. There is a difference between the desired location of the axis of rotation and its actual location. It is measured in

- the radial direction, and the amount of runout is the difference between the highest and lowest reading in  $360^\circ$ . For gear teeth, runout is usually checked by placing a pin in tooth spaces and rolling past a dial indicator or by rolling with a master gear.
- Shaft angle:** The angle between the axes of two nonparallel gear shafts.
- Spacing:** A general term to describe the accuracy with which teeth are spaced around the gear.
- Span measure:** The measurement of the distance across several teeth of gears too large to use pin measurements. The measurement is made along a line tangent to the base circle. It is used to determine tooth thickness and spacing accuracy. For such measurements, a *span measuring tool* is used, set to touch the flanks of teeth at the ends of each span at or near the middle of the tooth height. A span measure tool will usually be set by a vernier and will be equipped with a dial indicator to indicate any deviation from the theoretical chord length.
- Spiral angle:** The angle between the tooth and an element of the pitch cone in a spiral bevel gear. It is usually understood to be at the mean cone distance.
- Throat diameter:** The diameter of the addendum circle at the center of the face of a cylindrical or double-enveloping worm gear.
- Throat form radius:** The radius of the throat of a cylindrical or double-enveloping worm gear in an axial plane. It is normally generated by the worm gear hob, which is a topping hob, and will be slightly larger than the minor radius of the mating worm.
- Tip radius:** The radius between the outside and side cutting edges of hobs and other gear-cutting tools.
- Tip relief:** An arbitrary modification of the tooth profile near the tip of the teeth to minimize or eliminate tip interference.
- Toe:** In a bevel gear or pinion, the thinnest end of a tooth.
- Tolerance:** The amount by which a specific dimension is permitted to vary. It is usually expressed as the difference between the maximum and minimum limits allowed.
- Top land:** The width, or thickness, of a gear tooth measured at its maximum (for external gears) or minimum (for internal gears) diameter.
- Transmission function:** The ratio between the instantaneous position of the output and that of the input.
- Undercut:** A condition during gear fabrication involving a generation process where auxiliary material is removed as a result of the relative motion between the cutter and the gear blank. For pinions with small numbers of teeth, the cutting tool will cut away that portion of the involute that is near and below the base circle. This cut-away portion is called *undercut*, and it increases as the number of teeth becomes lower.
- Vector of instant rotation:** A pseudo-vector along the axis of instant rotation either of a pinion in relation to the gear or the gear in relation to the pinion. The direction of the vector of instant rotation depends on the direction of rotation of the gear and the pinion. The vector of instant rotation is designated as  $\omega_{pt}$ .
- Whole depth:** The distance from the top land of a gear tooth to its root. In parallel-axes gearing, full depth is the distance between the top land and bottom land of a gear tooth. It is equal to half the difference between the outside diameter and root diameter of a gear.
- Winding relationship:** A manufacturing specification between the coordinates used to parameterize the cutter and those used to parameterize the desired gear.
- Working depth:** The depth at which gear teeth are engaged.
- Zone of action:** The portion of the plane of action within which the tooth flanks of the gear and pinion interact with one another (it is often called *field of action*).

## References

1. An'ishchenko, V.V., Koval'enko, G.D., "Investigation of Contact Stress in Novikov Gears Using Photo-Elastic Approach," *Novikov Gearing*, Vol. I, TsINTIAM, Moscow, 1964.
2. Ball, R.S., *A Treatise on the Theory of Screws*, Cambridge University Press, Cambridge, UK, 1900, 544 p.
3. Ball, R.S., *The Theory of Screws*, Hodges & Foster, Dublin, 1876.
4. Baxter, M.L., Jr., "Basic Geometry and Tooth Contact of Hypoid Gears," *Industrial Mathematics*, Vol. 11, No. 2, pp. 19–42, 1961.
5. Baxter, M.L., Jr., "Basic Theory of Gear-Tooth Action and Generation," in: D. Dudley (ed.) *Gear Handbook*, 1st Ed., McGraw Hill, New York, 1962.
6. Bayazitov, N., *Helical Gears with a New Type of Gearing*, PhD Thesis, Kazan, Kazan Technological & Chemical Institute, 1964.
7. Böehm, W., "Differential Geometry II," pp. 367–383, in: *Curves and Surfaces for Computer Aided Geometric Design. A Practical Guide*, 2nd Ed., Academic Press, Inc., Boston, 1990, 444 p.
8. Bonnet, P.O., *Journ. Ec. Polytech*, Vol. xiii, p. 31, 1867.
9. Börner, J., Humm, K., Joachim, F., "Development of Conical Involute Gears (Beveloids) for Vehicle Transmissions," *Gear Technology Magazine*, Vol. November/December, pp. 28–35, 2005.
10. Bostock, F.J., Bramley-Moore, S., *Improvements in and Relating to Gear Teeth*. Great Britain Pat. No. 186,436. October 2, 1922. Filed July 2, 1921, No. 18,014/21.
11. Buckingham, E., *Analytical Mechanics of Gears*, Dover Publications, Inc., New York, 1988, 546 p. (First published in 1949.)
12. Camus, C.-É.-L., "Sur la figure des dents des rouës, et des ai les des pignons, pour rendre les horloges plus parfaites," 1733.
13. Cauchy, A.L., *Leçons sur les Applications du Calcul Infinitésimal à la Geometrie*, Imprimerie Royale, Paris, 1826.
14. Chironis, N., "Design of Novikov Gears," pp. 124–135, in: N.P. Hironis (ed.) *Gear Design and Application*, McGraw-Hill Company, New York, 1967, 374 p.
15. Cormac, P., *A Treatise on Screws and Worm Gear, Their Mills and Hobs*, Chapman & Hall, Ltd., London, 1936, 138 p.
16. Coy, J.J., Townsend, D.P., Zaretsky, E.V., *Gearing*, NASA Reference Publication 1152, AVSCOM, Technical Report 84-C-15, 1985, 76 p.
17. da Vinci, L., *The Madrid Codices*, Volume 1, 1493, Facsimile Edition of "Codex Madrid 1," original Spanish title: *Tratado de Estatica y Mechanica en Italiano*, McGraw Hill Book Company, 1974.
18. de la Hire, P., *Mémoires de Mathématique et de Physique*, Impr. Royale, Paris, 1694.
19. Denavit, J., Hartenberg, R.S., "A Kinematics Notation for Lower-Pair Mechanisms Based on Matrices," *ASME Journal of Applied Mechanics*, Vol. 77, pp. 215–221, 1955.
20. do Carmo, M.P., *Differential Geometry of Curves and Surfaces*, Prentice-Hall, Englewood Cliffs, NJ, 1976, 503 p.
21. Dooner, D.B., *Kinematic Geometry of Gearing*, 2nd Ed., John Wiley & Sons, Inc., New York, 2012, 512 p.
22. Dooner, D.B., Seireg, A.A., *The Kinematic Geometry of Gearing. A Concurrent Engineering Approach*, John Wiley & Sons, Inc., New York, 1995, 450 p.
23. Dudas, I., *The Theory and Practice of Worm Gear Drives*, Penton Press, London, 2000, 314 p.
24. Dusev, I.I., "Sliding between Enveloping Gear Teeth Surfaces in Spatial Gearing," *Proceedings of the Universities, Mechanical Engineering*, 1968, No. 4, pp. 15–18.
25. Dusev, I.I., Vasilyev, V.M., *Analytical Theory of Spatial Gearings and Its Application to Investigation of Hypoid Gearing*, Rostov-on-Don Book Publishers, Rostov-on-Don, Russia 1968, 148 p.
26. Dyson, A., *A General Theory of the Kinematics and Geometry of Gears in Three Dimensions*, Clarendon Press, Oxford, UK, 1969, 141 p.
27. Dyson, A., Evans, H.P., Snidle, R.W., "Wildhaber-Novikov Circular Arc Gears: Geometry and Kinematics," *Proceedings of the Royal Society of London A*, Vol. 403, pp. 313–340, 1986.
28. Euler, L., "De Aptissima Figure Rotarum Dentibus Tribuenda" ("On Finding the Best Shape for Gear Teeth"), *Academiae Scientiarum Imperiales Petropolitae, Novi Commentarii*, Vol. 1754–55, No. t. V, pp. 299–316, 1760.
29. Euler L. "Supplementum. De Figura Dentium Rotarum," *Novi Commentarii adacemiae Petropolitanae*, Vol. 11, pp. 207–231, 1767.
30. Favard, J., *Course de Géométrie Différentielle Locale*, Gauthier-Villars, Paris, 1957, viii+553 p.
31. Fed'akin, R.V., *Investigation of Strength of Circular-Arc Gear Teeth*, PhD Thesis, Moscow, Zhukovsky Air Force Engineering Academy, 1955.

32. Fed'akin, R.V., Chesnokov, V.A., *Gearing Featuring Point System of Meshing and Having Multiple Lines of Action*. Pat. No. 182,462, USSR, National Cl. 47 h, 6, Filed: November 20, 1963, published in B.I. No. 7, 1966.
33. Fedot'onok, A.A., *Kinematic Structure of Machine Tools*, Mashinostroyeniye, Moscow, 1970, 403 p.
34. Fisher, G. (ed.), *Mathematical Models*, Friedrich Vieweg & Sohn, Braunschweig/Wiesbaden, Germany, 1986.
35. Fraifeld, I.A., *Cutting Tools That Work on Generating Principle*, Mashgiz, Moscow, 1948, 252 p.
36. French, M.J., "Conformity of Circular-Arc Gears," *Journal of Mechanical Engineering Science*, Vol. 7, No. 2, 1965, pp. 220–223.
37. Gavrilenko, V.A., *Fundamentals of the Theory of Involute Gearing*, Mashinostroyeniye, Moscow, 1969, 432 p.
38. Gochman, Ch.I., *Theory of Gear Teeth Engagement, Generalized and Developed by Implementation of Mathematical Analysis*, Odessa, Ukraine, 1886, 229 p.
39. Golovin, A.A., Tarabarin, V.B., *Russian Models from the Mechanisms Collection of Bauman University*, History of Mechanism and Machine Science 5, Springer, Berlin, 2008, 238 p.
40. Grant, G.B., *Machine for Planing Gear Teeth*. U.S. Pat. No. 407,437. Filed: January 14, 1887 (serial No. 224,382), Patent issued: July 23, 1889.
41. Grant, G.B., *A Treatise on Gear Wheels*, 6th Ed., Philadelphia Gear Works, Inc., Philadelphia, 1893, 105 p.
42. Gray, A., "Plücker's Conoid," pp. 435–437, in: *Modern Differential Geometry of Curves and Surfaces with Mathematics*, 2nd Ed., CRC Press, Boca Raton, FL, 1997.
43. Hertz, H., "Über die Berührung Fester Elastischer Körper (The Contact of Solid Elastic Bodies)," *Journal für die Reine und Angewandte Mathematik (Journal for Pure and Applied Mathematic)*, Berlin, 1881, pp. 156–171, 1896; *Über die Berührung Fester Elastischer Körper und Über die Härte (The Contact of Solid Elastic Bodies and Their Harnesses)*, Berlin, 1882; Reprinted in: H.Hertz, *Gesammelte Werke (Collected Works)*, Vol. 1, pp. 155–173 and pp. 174–196, Leipzig, 1895, or the English translation: *Miscellaneous Papers*, translated by D.E. Jones and G.A. Schott), pp. 146–162, 163–183, London: McMillan and Co., Ltd.
44. Hicks, R.J., *Load Equalizing Means for Planetary Pinions*. U.S. Pat. 3,303,713. February 14, 1967, Filed: February 8, 1965.
45. Hicks, R.J., "Experience with Compact Orbital Gears in Service," *Proceedings of the Institution of Mechanical Engineers*, 1969–1970, Vol. 184, No. Pt. 30, pp. 85–94.
46. Hill, M., *Kinematics of Gerotors*, 2nd Ed., The Peter Reilly Company, Philadelphia, 1927, 44 p.
47. Hills, D.A., Nowell, D., Sackfield, A., *Mechanics of Elastic Contact*, Butterworth-Heinemann Ltd., Oxford, UK, 1993, 496 p.
48. Hills, D.A., Sackfield, A., "Sliding Contact between Dissimilar Elastic Cylinders," *Journal of Tribology*, Vol. 10, pp. 372–378, 1988.
49. [http://www.math.hmc.edu/faculty/gu/curves\\_and\\_surfaces/surfaces/plucker.html](http://www.math.hmc.edu/faculty/gu/curves_and_surfaces/surfaces/plucker.html)
50. <http://www.mathcurve.com/surfaces/plucker/plucker.shtml>
51. Jeffreys, H., *Cartesian Tensors*, Cambridge University Press, Cambridge, UK, 1961, 93 p.
52. Kimura, K., Ainoura, M., *Hobbing Cutter*. U.S. Pat. No. 3,786,719 (AZUMI), 1974.
53. Klingelnberg, J. (Hrsg.), *Kegelräder: Grundlagen, Anwendungen*, Springer, Berlin, 2008 edition, 381 p.
54. Klingelnberg, J. (ed.), *Bevel Gear: Fundamentals and Applications*, Springer-Verlag GmbH, Berlin, 2016, 328 p.
55. Koenderink, J.J., *Solid Shape*, MIT Press, Cambridge, MA, 1990, 699 p.
56. Kolchin, N.I., *Analytical Calculation of Planar and Spatial Gearing*, Mashgiz, Moscow, 1949, 210 p.
57. Korostelev, L.V., "Kinematical Indicators of Bearing Capacity in Spatial Gearing," *Proceedings of the Universities, Mechanical Engineering*, 1964, No. 10, pp. 5–15.
58. Korostelev, L.V., "Peculiarities of Meshing in the Pole of Worm Gearing," *Mashinovedeniye*, No. 2, 1967, 5 p.
59. Korostel'ov, L.V., *A Worm-Gear Drive*. Pat. No. 257,246, USSR. Filed: October 25, 1968, Int. Cl. F 16h.
60. Krasnoschokov, N.N., Fed'akin, R.V., Chesnokov, V.A., *Theory of Novikov Gearing*, Nauka, Moscow, 1976, 173 p.
61. Krenzer, T., *The Bevel Gear*, Published October 1, 2007, 252 p.
62. Kudriavtsev, V.N., *Calculation and Design of Novikov Gearing*, Leningrad Mozhaiskii Military Aviation Academy, Leningrad, Russia, 1959, 78 p.
63. Kudryavtsev, V.N. et al., *Planetary Gear Drives*, Mashinostroyeniye, Leningrad, Russia, 1977, 536 p.
64. Kul'ikov, G.V., Fed'yakin, R.V., Chesnokov, V.A., "An Investigation of Contact Strength of Novikov Gears," in: *Novikov Gearing*, Vol. II, Zhukovsky Air Force Engineering Academy, Moscow, 1962.
65. Lagrange, J.L., *Théorie des Fonctions Analytiques*, Impr. De la République, prairial an V, Paris, 1797, 277 p.
66. Lewis, W., "Investigation of the Strength of Gear Teeth," *Proc. of the Engineers Club*, Philadelphia, PA, pp. 16–23, 1893.
67. Litvin, F.L., *Noncircular Gears*, Mashgiz, Moscow, 1950, 218 p.
68. Litvin, F.L., *Noncircular Gears*, 2nd Ed., Mashgiz, Moscow, 1956, 311 p.
69. Litvin, F.L., Fuentes, A., *Gear Geometry and Applied Theory*, 2nd Ed., Cambridge University Press, Cambridge, UK, 2004, 800 p.
70. Litvin, F.L., Fuentes-Anzar, A., Gonzalez-Perez, I., Hayasaka, K., *Noncircular Gears: Design and Generation*, Cambridge University Press, New York, 2009, 204 p.

71. Lopato, G.A., Kabatov, N.F., Segal, M.G., *Spiral Bevel and Hypoid Gearing*, 2nd Ed., Mashinostroyeniye, Moscow, 1977, 423 p.
72. Lowe, P.G., "A Note on Surface Geometry with Special Reference to Twist," *Mathematical Proceedings of the Cambridge Philosophical Society*, Vol. 87, pp. 481–487, 1980.
73. Lowe, P.G., *Basic Principles of Plate Theory*, Surrey University, Surrey, UK, 1982.
74. MAAG Gear Book: *Calculation and Practice of Gears, Gear Drives, Toothed Couplings and Synchronous Clutch Couplings*, MAAG Gear Company, Ltd., Zurich, Switzerland, 1990, 440 p.
75. Maki, H., *Gear with Modified Tooth Surface and Gear Tooth Surface Modification Method*. U.S. Pat. No. 6,112,611. Filed: May 18, 1998, Int. Cl. B23F 9/00, B23F 19/00.
76. Merritt, H.E., *Gear Engineering*, Putman Publishing, London, 1971, 489 p.
77. Michalec, G.W., *Precision Gearing: Theory and Practice*, John Wiley & Sons, Inc., New York, 1966, 620 p.
78. Miron, R., "Observatii a Supra Unor Formule din Geometria Varietatiilor Neonolome  $E_3^2$ ," *Bulletinul Institutului Politehnic din Iasi*, 1958.
79. Mozhayev, S.S., *Analytical Theory of Twist Drills*, Mashgiz, Moscow, 1948, 136 p.
80. Mozhayev, S.S., *A Generalized Theory of Cutting Tools*, Doctoral Thesis, Leningrad, Leningrad Polytechnic Institute, 1953, 295 p.
81. Nieman, G., "Novikov Gear System and Other Special Gear Systems for High Load Carrying Capacity," *VDI, Berichte*, p. 47, 1961.
82. Novikov, M.L., *Fundamentals of Geometric Theory of Gearing with Point Meshing for High Power Density Transmissions*, Doctoral Thesis, Moscow, Military Aviation Engineering Academy (MAEA), 1955.
83. Novikov, M.L., *Gearing of Gears with a Novel Type of Teeth Meshing*, Zhukovsky Air Force Engineering Academy, Moscow, 1958, 186 p.
84. Novikov, M.L., *The Principles of the Geometric Theory of Point Meshing of Gearing for the Purpose of Transmitting of High Power*, Doctoral Thesis, Moscow, Zhukovsky Air Force Engineering Academy, 1955.
85. Novikov, M.L., *Gear Pairs and Cam Mechanisms Having Point System of Meshing*. Pat. No. 109,113, USSR. National Classification 47h, 6; Filed: April 19, 1956, published in Bull. of Inventions No.10, 1957.
86. Nutbourn, A.W., "A Circle Diagram for Local Differential Geometry," in: J. Gregory (ed.) *Mathematics of Surfaces*, Conference Proceedings, Institute of Mathematics and Its Application, 1984, Oxford University Press, Oxford, UK, 1986.
87. Nutbourn, A.W., Martin, R.R., *Differential Geometry Applied to Curve and Surface Design*, Vol. 1: *Foundations*, Ellis Horwood Ltd. Publishers, Chichester, UK, 1988, 282 p.
88. Olivier, T., *Théorie Géométrique des Engrenages destinés à transmettre le mouvement de rotation entre deux axes ou non situés dans un même plan*, (Geometric Theory of Gearing), Bachelier, Paris, 1842, 118 p.
89. Phillips, J., *General Spatial Involute Gearing*, Springer, New York, 2003, 498 p.
90. Pismanik, K.M., *Hypoid Gearing*, Mashinostroyeniye, Moscow, 1964, 227 p.
91. Plücker, J., "On a New Geometry of Space," *Proceedings of the Royal Society of London A*, Vol. 155, pp. 725–791, 1865.
92. Prudhomme, R., Lemasson, G., *Cinématique*, École Nationale Supérieure d'Arts et Métiers, École d'Ingénieurs, Paris, 1906, 1955.
93. Radzevich, S.P., *A Method of Sculptured Surface Machining on Multi-Axis NC Machine*. Pat. No. 1,185,749, USSR. Int. Cl. B23c 3/16, Filed: October 24, 1983.
94. Radzevich, S.P., *A Method of Sculptured Surface Machining on Multi-Axis NC Machine*. Pat. No. 1,249,787, USSR. Int. Cl. B23c 3/16, Filed: December 27, 1984.
95. Radzevich, S.P., *A Method of Experimental Simulation of Machining of a Sculptured Surface on Multi-Axis NC Machine*. Pat. No. 1,449,246, USSR. Int. Cl. B 23 C, 3/16, Filed: February 17, 1987.
96. Radzevich, S.P., "A Brief Overview on the Evolution of the Scientific Theory of Gearing: A Preliminary Discussion." Proceedings of International Conference on Gears 2015, October 5–7, 2015, Technische Universität München (TUM), Garching, Germany, 2015, pp. 1035–1046.
97. Radzevich, S.P., *A Method for Designing of the Optimal Form-Cutting-Tool for Machining of a Given Sculptured Surface on Multi-Axis NC Machine*. Pat. No. 4242296/08 (USSR), Filed: March 31, 1987.
98. Radzevich, S.P., "A Novel Method for Mathematical Modeling of a Form-Cutting-Tool of the Optimum Design," *Applied Mathematical Modeling*, Vol. 31, pp. 2639–2654, 2007.
99. Radzevich, S.P., *A Parallel-Axes Involute Gearing*, Invention disclosure PDS 10-PPD-161, submitted to Eaton Patent on February 9, 2010.
100. Radzevich, S.P., "A Possibility of Application of Plücker's Conoid for Mathematical Modeling of Contact of Two Smooth Regular Surfaces in the First Order of Tangency," *Mathematical and Computer Modeling*, Vol. 42, pp. 999–1022, 2004.
101. Radzevich, S.P., "About Hob Idle Distance in Gear Hobbing Operation," *ASME Journal of Mechanical Design*, Vol. 124, pp. 772–786, 2002.



102. Radzevich, S.P., *CAD/CAM of Sculptured Surfaces on Multi-Axis NC Machine: The DG/K-Based Approach*, M&C Publishers, San Rafael, CA, 2008, 114 p.
103. Radzevich, S.P., *Classification of Surfaces*, Monograph, Kiev, Ukraine, No. 1440-Yk88, 1988, 185 p.
104. Radzevich, S.P., "Concisely on Kinematic Method and about History of the Equation of Contact in the Form  $\mathbf{n} \cdot \mathbf{V} = 0$ ," *Theory of Mechanisms and Machines* 8, Vol. 1, No. 15, pp. 42–51, 2010.
105. Radzevich, S.P., *Design and Investigation of Skiving Hobs for Finishing of Hardened Gears*, PhD Thesis, Kiev, Kiev Polytechnic Institute, 1982, 298 p.
106. Radzevich, S.P., "Design of Shaving Cutter for Plunge Shaving a Topologically Modified Involute Pinion," *ASME Journal of Mechanical Design*, Vol. 125, pp. 632–639, 2003.
107. Radzevich, S.P., *Differential-Geometric Method of Surface Generation*, Dr. Sci. Thesis, Tula, Tula Polytechnic Institute, 1991, 300 p.
108. Radzevich, S.P., *Dudley's Handbook of Practical Gear Design and Manufacture*, 2nd Ed., CRC Press, Boca Raton, FL, 2012, 896 p.
109. Radzevich, S.P., *Dudley's Handbook of Practical Gear Design and Manufacture*, 3rd Ed., CRC Press, Boca Raton, FL, 2016, 629 p.
110. Radzevich, S.P., *Fundamentals of Surface Generation*, Monograph, Rastan, Kiev, 2001, 592 p.
111. Radzevich, S.P., *Gear Cutting Tools: Fundamentals of Design and Computation*, CRC Press, Boca Raton FL, 2010, 786 p.
112. Radzevich, S.P., *Gear Cutting Tools: Science and Engineering*, 2nd Ed., CRC Press, Boca Raton, FL, 2017, 606 p.
113. Radzevich, S.P., *Generation of Surfaces: Kinematic Geometry of Surface Machining*, CRC Press, Boca Raton, FL, 2014, 747 p.
114. Radzevich, S.P., "Generating Surfaces of Worm-Type Gear Cutting Tools," pp. 64–78, in: S.N. Medveditskov (ed.) *Advance Processes in Production Technology*, VolgPI, Volgograd, Russia, 1985.
115. Radzevich, S.P., *Geometry of Surfaces: A Practical Guide for Mechanical Engineers*, Wiley, Chichester, UK, 2013, 264 p.
116. Radzevich, S.P., "High-Conformal Gearing: A new look at the concept of Novikov gearing," *Proceedings of International Conference on Gears 2015*, October 5–7, 2015, Technische Universität München (TUM), Garching, Germany, 2015, pp. 457–470.
117. Radzevich, S.P., *High-Conformal Gearing: Kinematics and Geometry*, CRC Press, Boca Raton, FL, 2015, 368 p.
118. Radzevich, S.P., *Kinematic Geometry of Surface Machining*, CRC Press, Boca Raton, FL, 2007, 508 p.
119. Radzevich, S.P., "Mathematical Modeling of Contact of Two Surfaces in the First Order of Tangency," *Mathematical and Computer Modeling*, Vol. 39, No. 9–10, pp. 1083–1112, 2004.
120. Radzevich, S.P., *Methods for Investigation of the Conditions of Contact of Surfaces*, Monograph, Kiev, UkrNIINTI, No. 759–Uk88, 1987, 103 p.
121. Radzevich, S.P., "On Analytical Description of the Geometry of Contact of Surfaces in Highest Kinematic Pairs," *Theory for Mechanisms and Machines*, St. Petersburg Polytechnic Institute, Vol. 3, No. 5, pp. 3–14, 2005.
122. Radzevich, S.P., "On Master Thesis: Gochman, Ch.I., Theory of Gear Teeth Engagement, Generalized and Developed by Implementation of Mathematical Analysis," *Theory of Mechanisms and Machines*, Vol. 17, No. 1, pp. 33–43, 2011. [http://tmm.spbstu.ru/01\\_2011.html](http://tmm.spbstu.ru/01_2011.html)
123. Radzevich, S.P., "On the Priority of Dr. M.L. Novikov in the Development of Novikov Gearing," *Theory of Mechanisms and Machines*, <http://tmm.spbstu.ru> (In press).
124. Radzevich, S.P., "On Tooth Failure Analysis in Small-Teeth-Number Gearing: An Analytical Approach," 2006 Fall Technical Meeting, October 22–24, 2006, Grosvenor Resort, Orlando, FL, AGMA Paper 06FTM11 2006, 22 p.
125. Radzevich, S.P., "Possible Kinds of the Vector Diagrams of Gear Pairs," *Theory of Mechanisms and Machines*, Vol. 7, No. 2, 2009, pp. 10–18.
126. Radzevich, S.P., "Technological Methods for Noise/Vibration Reduction in Driveline/Transmission of Truck and All-Wheel-Drive Vehicles," *International Journal of Vehicle Noise and Vibration*, Vol. 2, No. 4, pp. 283–291, 2006.
127. Radzevich, S.P., "Vector Representation of Gear Pairs. Part I," *Theory of Mechanisms and Machines*, Vol. 6, No. 2, 2008, pp. 74–81.
128. Radzevich, S.P., "Vector Representation of Gear Pairs. Part II," *Theory of Mechanisms and Machines*, Vol. 7, No. 1, 2009, pp. 17–26.
129. Radzevich, S.P. et al., "Gear Train with Split Torque," Patent Application Publication, Pub. No.: US 2010/0261568 A1, Pub. Date: October 14, 2010, Int. Cl. F16H 48/06, F16H 1/16, U.S. Cl. 475/226; 74/425, Filed: April 14, 2009. (Patent pending).
130. Radzevich, S.P. et al., "A Gear Set for X-Locker Differential," Patent Application Publication, Pub. No.: US 2010/0323840 A1, U.S. Cl. 475/220, Filed: June 17, 2009. (Patent pending).
131. Radzevich, S.P., Goodman, E.D., Palaguta, V.A., "Tooth Surface Fundamental Forms in Gear Technology," *University of Niš, the Scientific Journal Facta Universitatis, Series: Mechanical Engineering*, Vol. 1, No. 5, 1998, pp. 515–525.
132. Radzevich, S.P., Irigireddy, V., Vijayakar, S.M., Stewart, J., Warner, T.P., "Preliminary Results of Testing of Low-Tooth-Count Bevel Gears of a Novel Design. Part 1," *Gear Solutions*, pp. 25–26, 2014.

133. Radzevich, S.P., Irigireddy, V., Vijayakar, S.M., Stewart, J., Warner, T.P., "Preliminary Results of Testing of Low-Tooth-Count Bevel Gears of a Novel Design. Part 2," *Gear Solutions*, pp. 20–21, 2014.
134. Radzevich, S.P., Irigireddy, V., Vijayakar, S.M., Stewart, J., Warner, T.P., "Preliminary Results of Testing of Low-Tooth-Count Bevel Gears of a Novel Design. Part 3," *Gear Solutions*, pp. 20–23, 2015.
135. Radzevich, S.P., *R<sub>sp</sub> – Gearing Insensitive to Axes Misalignment and other Displacement, and Methods of Producing Gears*, International Application Number PCT/US 038753, International Filing Date: May 20, 2014, International Publication Number 2014/189903 A1, Int. Pat. Classification F16H 1/26 (2006.01), Priority Data: 13/900,946, May 23, 2013, 34 p.
136. Radzevich, S.P., *Sculptured Surface Machining on Multi-Axis NC Machine*, Monograph, Vishcha Schola, Kiev, 1991, 192 p.
137. Radzevich, S.P., *Theory of Gearing: Kinematics, Geometry, and Synthesis*, CRC Press, Boca Raton, FL, 2012, 760 p.
138. Reshetov, L.N., *Self-Aligning Mechanisms*, Translated from Russian by L.M. Sachs, Mir Publishers, Moscow, 1982, 582 p. (Russian edition: Moscow, Mashinostroyeniye, 1979.)
139. Roslivker, Ye.G., "Hyperboloid Novikov Gearing," pp. 87–112, in: *Novikov Gearings*, Vol. 3, Zhukovskii Military Aviation Academy Publishers, Moscow, 1964.
140. Roslivker, Ye.G., "Investigation of Hyperboloid and Bevel Novikov Gearing," pp. 5–85, in: *Novikov Gearings*, Vol. 3, Manufacturing Research Institute Publishers, Rostov-on-Don, Russia, 1964.
141. Saari, O.E., *Speed-Reduction Gearing*. U.S. Pat. No. 2,696,125. Cl. 74-459.5, Filed: July 12, 1954.
142. Saari, O.E., *Skew Axis Gearing*. U.S. Pat. No. 2,954,704. Cl. 74-466, Filed: April 10, 1957.
143. Sang, E., *A New General Theory of the Teeth of Wheels*, A&C Black, North Bridge, Edinburgh, 1852, 257 p.
144. Savary, F., *Journal de Mathematique*, 1845.
145. Schmick, H.J., *Toothed Gearing*. U.S. Pat. No. 1,425,144, Patented: August 8, 1922, Filed: June 30, 1921, Serial No. 481,561.
146. Shevel'ova, G.I., *Theory of Surface Generation and of Contact of Moving Bodies*, Mosstankin, Moscow, 1999, 494 p.
147. Shishkov, V.A., "Elements of the Kinematics of Generating, and the Conjugation in Gearing," in: *Theory and Computation of Gears*, Vol. 6, LONITOMASH, Leningrad, 1948.
148. Shishkov, V.A., *Generation of Surfaces in Continuous-Indexing Methods of Surface Machining*, Mashgiz, Moscow, 1951, 152 p.
149. Shitikov, B.V., Bayazitov, N.A., *A Helical Gearing*. Pat. No. 163857, USSR. Int. Cl. F06h, Filed: February 25, 1963, Published: July 22, 1964.
150. Shtipelman, B.A., *Design and Manufacture of Hypoid Gears*, John Wiley & Sons, New York, 1978, 394 p.
151. Smith, J.D., *Gear Noise and Vibration*, 2nd Ed., Marcel Dekker Inc., New York, 2003, 318 p.
152. Soldatkin, Ye.P., "Gearings with Variable Angle between the Gear and Pinion Axes of Rotation," *Vestnik Mashinostroyeniya*, No. 7, 1962. [Солдаткин Е.П., "Зубчатые передачи с переменным углом между осями," *Вестник машиностроения*, 1962, №7].
153. Stadtfeld, H.J., *Gleason Bevel Gear Technology: Basics of Gear Engineering and Modern Manufacturing Methods for Angular Transmissions*, The Gleason Works, Rochester, NY, 2014, 503 p.
154. Stadtfeld, H.J., *Gleason Kegelradtechnologie: Ingenieurwissenschaftliche Grundlagen und modernste Herstellungsverfahren für Winkelgetriebe*, Expert-Verlag, Renningen, Germany, 2013, 491 p.
155. Struik, D.J., *Lectures on Classical Differential Geometry*, 2nd Ed., Addison-Wesley Publishing Company Inc., Boston, 1961, 232 p.
156. Vaisman, I., "Unele Observatii Privind Suprafetele si Varietatile Neonolome din  $S_3$  Euclidian," *Mathematica, Academia R.P.R., Filiala Iasi, Studii si Cercetari Stiintifice*, Vol. 10, No. 1, 195–?.
157. Vogel, W.F., *Involutometry and Trigonometry*, Michigan Tool Company, Book production by Denham & Co., Detroit, Michigan, U.S.A., 1945, 321 p.
158. von Seggern, D., *CRC Standard Curves and Surfaces*, CRC Press, Boca Raton, FL, 1993, 288 p.
159. Walker, H., "Gear Tooth Deflection and Profile Modification," *Engineer*, Vol. 166, pp. 434–436, 1938; Walker, H., "Gear Tooth Deflection and Profile Modification," *The Engineer*, August 1940, Vol. 170, p. 102.
160. Wang, X.C., Ghosh, S.K., "Advanced Theories of Hypoid Gears," in: *Studies in Applied Mechanics*, Vol. 36, Elsevier, Amsterdam, 1994, 341 p.
161. Wildhaber, E., *Helical Gearing*. U.S. Pat. No. 1,601,750. Filed: November 2, 1923, published October 5, 1926.
162. Wildhaber, E., *Foundations of Meshing of Bevel and Hypoid Gearings*, A collection of journal papers translated from English and comments by A.V. Slepak, Mashgiz, Moscow, 1948, 176 p (In Russian).
163. Willis, R., "On the Teeth of Wheels," *Trans. Civ. Eng.*, Vol. II, 1838.
164. Willis, R., *Principles of Mechanisms, Designed for the Use of Students in the Universities and for Engineering Students Generally*, John W. Parker, West Stand, London, 1841, 446 p.
165. Woodbury, R.S., *History of the Gear-Cutting. A Historical Study in Geometry and Machine*, MIT Press, Cambridge, MA, 1958, 135 p.
166. Wu, D.R., Luo, J.S., *A Geometric Theory of Conjugate Tooth Surfaces*, World Scientific Publishing, River Edge, NJ, 1992, 192 p.

167. Wu, L.-L., Liu, C.-C., Tsay, C.-B., "Mathematical Model and Surface Deviation of Helipoid Gears Cut by Shaper Cutter," *ASME J Mechanical Design*, Vol. 125, No. 2, pp. 351–355, 2003.
168. Yakovl'ev, A.S., Pecheniy, V.I., "An Experimental Investigation of the Load Distribution within the Patch of Contact in Novikov Gears," in: *Reliability and Quality of Gearing*, Vol. 18-67-36, NIINFORMT'AZhMASH, Moscow, 1967.
169. Zak, P.S., *Hypoid Gearing*, Mashinostroyeniye, Moscow, 1962, 256 p.
170. Zhuravl'ov, G.A., Iofis, R.B., *Hypoid Gearing, Problems and Evolution*, Rostov State University Publishers, Rostov, Russia, 1978, 160 p.
171. Isabelle, C.J., Kish, J.G., Stone, R.A., *Elastomeric Load Sharing Device*. U.S. Pat. No. 5,113,713. Filed: February 11, 1991, Date of Patent: May 19, 1992, Int. Cl.5 F16H 55/18, U.S. Cl. 74/410, 74/411, 74/440.

---

## Bibliography

---

- Adams, C.E., *Plastics Gearing: Selection and Application*, Marcel Dekker, Inc., New York, 1986, 384 p.
- Addomine, M., Figliolini, G., Pennestri, E., "A Landmark in the History of Non-Circular Gears Design: The Mechanical Masterpiece of Dondi's astrarium," *Mechanism and Machine Theory*, Vol. 122, pp. 219–232, April 2018.
- Airy, G.B., "On the Forms of the Teeth of Wheels," *Cambridge Philosophical Society*, Vol. II, p. 277, 1825.
- Alexandrov, V.M., Romalis, B.L., *Contact Problems in Engineering*, Mashinostroyeniye, Moscow, 1986, 174 p.
- Allan, T., "Some Aspects of the Design and Performance of Wildhaber-Novikov Gearing," *Proceedings of the Institution of Mechanical Engineers*, Vol. 179, No. 1, pp. 931–954, June 1964.
- Argyris, J., Litvin, F.L., Peng, A., Stadtfeld, H.J., "Axes of Meshing and Their Application in Theory of Gearing," *Computer Methods in Applied Mechanics and Engineering*, Vol. 163, No. 1–4, pp. 293–310, September 1998.
- Asbridge, S.S., *American Machinist*, December 1910, p. 1211.
- Astridge, D.G. et al., "Tribology of High Conformity Gears," *Proceedings of the Institution of Mechanical Engineers*, 1987, pp. 819–825.
- Babichev, D.T., Lagutin, S.A., Barmina, N.A., "Overview of the Works of the Russian School of Theory of and the Geometry of Gear Meshing. Part 1. Origins of the Theory of Gearing, and its Heyday Time in 1935–1975," *Theory of Mechanisms and Machines*, Vol. 14, No. 3(31), pp. 101–134, 2016.
- Babichev, D.T., Lagutin, S.A., Barmina, N.A., "Overview of the Works of the Russian School of Theory and the Geometry of Gearing. Part 2. Development of the Classical Theory of Gearing and Establishment of the Theory of Real Gearing in 1976–2000," *Theory of Mechanisms and Machines*, Vol. 15, No. 3(35), pp. 86–119, 2017.
- Babichev, D.T., Volkov, A.E., "History of Evolution of the Theory of Gearing," *Journal of Scientific and Technological Development*, Vol. 5, No. 93, pp. 25–42, 2015.
- Baldayev, V.P., *Novikov Gearing: Kinematics and Wear Calculations*, LAP LAMBERT Academic Publishing, Saarbruchen, 2015, 68 p.
- Bazhin, A.A., *Gear Cutting Tools*, ONTI NKTP, Moscow, 1935, 112 p.
- Bernoulli, J., *Opera Omnia*, Lausanne and Generva, t. III, "Lect. Hospitalii," XXII, 1742, p. 454.
- Bian, W.S.R.Z., *Concise Course of the Meshing Theory of Gearing*, University Press, 1991.
- Bilgram, H., U.S. Patent No. 749,683 of January 12, 1904.
- Bodmer, J.G., "On the Pitch of Spur and Bevel Wheels and the Shape of the Teeth of Worm Wheels and Worms Working into Each Other," listed in: *Min. and Proc. Inst. Civil Engineers*, Vol. II, p. 32, 1843.
- Brown, U.S. Patent No. 45,294 of November 29, 1864.
- Buchanan, R., *An Essay on the Teeth of Wheels*, Edinburg, 1808, 164 p.
- Buchanan, R., *Treatise on Millwork*, 3rd Ed., London, 1841, pp. 83–172.
- Buckingham, E., *Analytical Mechanics of Gears*, Dover Publications, Inc., New York, 1988, 546 p.
- Buckingham, E., Ryffel, H.H., *Design of Worm and Spiral Gears: A Manual for the Design and Manufacture of All-Redress-Action Worm and Spiral Gear Drives*, The Industrial Press, New York, 1960, 450 p.
- Camus, C.É.L., "Sur la Figure des Dents des Roues et des Ailes des Pignons," 1733, in: *Histoires et Mémoires de l'Académie des Sciences*, Paris, and later included in his *Cours de Mathématique*, Paris, 1766. Books X and XI were translated as *Teeth of Wheels* by John Issac Hawkins, London, 1806.
- Candee, A.H., *Introduction to the Kinematic Geometry of Gear Teeth*, Chilton Co., Book Division, Philadelphia, 1961, 204 p.
- Cardano, G., *De Rerum Varietate*, Basel, 1557, pp. 263–372.
- Chasovnikov, L.D., *Gear Transmissions*, Mashinostroyeniye, Moscow, 1969, 486 p.
- Chironis, N.P. (ed.), *Gear Design and Application*, McGraw-Hill, New York, 1967, 374 p.
- Colbourne, J.R., *The Geometry of Involute Gears*, Springer-Verlag, New York, 1987, 532 p.
- Crosher, W.P., *Design and Application of the Worm Gear*, ASME Press, New York, 2002, 256 p.
- Cusanus, N., *Opera*, Paris, Vol. II, 1451, pp. 33–59.
- Daryani, P.H., *The Art of Gear Fabrication*, Industrial Press, Inc., New York, 2001, 208 p.
- Davidov, Ya.S., *Non-Involute Gearing*, Mashgiz, Moscow, 1950, 179 p.
- Davis, J.R. (ed.), *Gear Materials, Properties, and Manufacture*, ASM Press, Materials Park, OH, 2005, 339 p.
- Drago, R.J., *Fundamentals of Gear Design*, Butterworths, Boston, 1988, 560 p.
- Dooner, D.B., Seireg, A.A., *The Kinematic Geometry of Gearing. A Concurrent Engineering Approach*, John Wiley & Sons, Inc., NY, 1995, 450 p.
- Dowd, A.A., *Spiral and Worm Gearing*, Lightning Source, Inc., Tennessee, USA, 2001, 288 p.
- Dudley, D.W., *Practical Gear Design*, McGraw-Hill, New York, 1954.

- Dudley, D.W., *Zahnräder-Berechnung, Entwurf und Herstellung nach Amerikanischen Erfahrungen*, Springer-Verlag, Berlin, 1961.
- Dudley, D.W., *Gear Handbook: The Design, Manufacture, and Application of Gears*, McGraw-Hill, New York, 1962.
- Dudley, D.W., *The Evolution of the Gear Art*, AGMA, Washington DC, 1969, 93 p.
- Dudley, D.W., *Handbook of Practical Gear Design*, McGraw-Hill, Inc., New York, 1984.
- Dudley, D.W., *Handbook of Practical Gear Design*, CRC Press, Boca Raton, Florida, 1994, 688 p.
- Dürer, A., *Unterweysung der Messung mit dem Zirckel und Richtscheyt*, 1525, pp. 6–17.
- Eberhardt, H.J., "Influence of the Automobile on Gear Cutting and Gear Cutting Machinery," *Meeting Am. Soc. Mech. Eng.*, May 26–27, 1921, partially reprinted in: *Mechanical Engineering*, August 1921.
- Ewert, R.H., *Gears and Gear Manufacture: The Fundamentals*, Springer, 1997, 324 p.
- Fairbairn, W., *Treatise of Mills and Millwork*, London, 1864.
- Fed'akin, R.V., *On Selection of Teeth Shape having Circular Profile*, NMS No. 13-14, VVIA, Moscow, 1957, pp. 63–94.
- Fed'akin, R.V., Chesnokov, V.A., "Novikov Gearing," *Vestnik Mashinostroyeniya*, No. 4, 1958, pp. 3–11.
- Fed'akin, R.V., Chesnokov, V.A., *A Gear Drive*, SU Pat. 735855, Int. Cl. F 16 h 1/18, Filed: June 28, 1967, Patented: 1980.
- Fed'akin, R.V., Chesnokov, V.A., *Calculation of Novikov Gearing*, VVIA, Moscow, 1982, 114 p.
- Ferguson, J., *Ferguson's Lectures on Select Subjects*, New Ed., With additions by David Brewster (ed.), 2nd edition, Bell & Bradfute, Edinburgh, 1806, pp. 210–226.
- Field, J.V., Wright, M.T., "The Early History of Mathematical Gearing," *Endeavour*, Vol. 9, No. 4, pp. 198–203, 1985.
- Figliolini, G., Stachel, H., Angeles, J., "On Martin Disteli's Main Achievements in Spatial Gearing: Disteli's Diagram," *Proceedings of EuCoMeS, European Conference on Mechanism Science*, February 21–26, 2006, Obergurgl (Austria), 2006, 12 p.
- Figliolini, G., Stachel, H., Angeles, J., "On the Synthesis of Spatial Cycloidal Gears," manuscript, 10 p.
- Flanders, R.E., *Bevel Gearing*, 4th Ed., *Machinery's Reference Series*, Number 37, The Industrial Press, New York, 1912, 48 p.
- Flanders, R.E., *American Machinist*, December 1910, p. 1064.
- Flanders, R.E., "Interchangeable Involute Gear Tooth Systems," *Journal of American Society of Mechanical Engineers*, December 1908, pp. 1501–1520.
- Flanders, R.E., *Machinery*, p. 369, January 1911.
- Flanders, R.E., *Machinery*, p. 659, March 1911.
- Flanders, R.E., *Machinery*, p. 798, June 1911.
- French, M.J., "Gear Conformity and Local Capacity," *Proceedings of the Institution of Mechanical Engineers, Part I*, Vol. 180, No. 43, June 1965, pp. 1013–1024.
- Gibbs, J.W., *On the Form of the Teeth of Wheels in Spur Gearing*, Doctoral dissertation, Yale University, New Haven, CT, 1863 [A copy of the dissertation is available from Engineering Library at Michigan State University].
- Gochman, H.I., *Theory of Gearing Generalized and Developed Analytically*, Odessa, 1886, 229 p.
- Gol'dfarb, V.I., *Fundamentals of Theory of Computer Aided Geometric Analysis and Synthesis of General Kind of Worm Gearing*, Doctoral thesis, Moscow Aviation Institute, Moscow, 1986, 48 p.
- Grant, G.B., *Handbook of the Teeth of Gears*, Boston, 1885.
- Grant, G.B., *Machinery*, p. 813, June 1911.
- Grant, G.B., *Odontics, or the Theory and Practice of the Teeth of Gears*, Lexington, Massachusetts, 1891.
- Groman, N.B., "On Blocking Contours for Involute Gearing," *Vestnik Mashinostroyeniya*, No. 12, pp. 12–17, 1952.
- Groman, M.B., "On Selection of Profile Corrections for Gear Transmissions," *Vestnik Mashinostroyeniya*, No. 2, pp. 3–13, 1955.
- Gul'ayev, K.I., *Theoretical Foundations of Synthesis and of Finishing of Bevel Gearing*, Doctoral thesis, Leningrad, 1976, 48 p.
- Hawkins, J.I., *Teeth of Wheels*, London, 1806.
- Herrmann, G., "Die Zahnflächen und ihre automatische Erzeugung," p. 61, in: *Vr. Der V. Beförderung des Gewerbflusses im Preussen*, Berlin, 1877.
- Hertz, H., "On Contact of Solid Elastic Bodies and on Hardness," *Journal of Mathematics*, Vol. 92, pp. 156–171, 1881.
- Hooke, R., *Lectiones Cutlerianae*, London, No. 2, "Animadversions on Helvius 'Machina Coelecteds'," 1679, pp. 70–72 and Figs. 20 and 21 (the date of 1666 is Hooke's).
- Howes, M.A.H. (Consulting Editor), *Source Book on Gear Design, Technology and Performance*, A Comprehensive Collection of Outstanding Articles from the Periodical and Reference Literature, American Society for Metals, Metals Park, Ohio 44073, 1980, 417 p [Compiled by Howes, M.A.H., Director, Metals Research, IIT Research Institute.].
- Hunt, K.H., *Kinematic Geometry of Mechanisms*, Clarendon Press, Oxford, 1978, 465 p.
- Imison, J., *Mechanical Power*, London, 1787.
- Itkis, M.Ya., *Cylindrical Novikov Gearing: Calculation of Geometrical Parameters*, Local Book Publisher, Volgograd, 1973, 312 p.
- Ivanov, M.N., *Harmonic Drives*, Visshaya Shkola, Moscow, 1981, 160 p.
- Johnson, D.C., *Novikov Gears (Gear Teeth with Circular Arc Profile)*, Published 1959 by Engineering. [IID Numbers: Open Library, OL20877712M].
- Johnson, D.C., *Gear Teeth with Circular Arc Profiles: The Novikov Gearing System*, Engineering, London, 1960.
- Kabatov, N.F., Lopato, G.A., *Spiral Conical Gearing*, Mashinostroyeniye, Moscow, 1966, 299 p.

- Kaestner, A.G., "De Dentibus Rotarum," 1781, in: *Commentationes Societatis Regiae Scientiarum Gottingensis, Classis Mathematicae*, t. IV, pp. 3–25.
- Kaestner, A.G., "De Dentibus Rotarum," t. 5, 1782, p. 3.
- Kalashnikov, S.N. et al. (eds), *Production of Gears. Handbook*, Mashinostroyeniye, Moscow, 1990, 463 p.
- Kis'el'ev, S.S., *Methods for Design of Series of External Gear Drives*, ITMO-State University, St. Petersburg, 2007, 112 p.
- Kird'ashev, Yu.N., *Closed Gearing of Differential Kind*, Mashinostroyeniye, Leningrad, 1969, 176 p.
- Kirichenko, A.F., *Theory, Calculation, and Analysis of 3D Bending Stress of Gear Teeth*, Doctoral thesis, Moscow, 1991, 32 p.
- Kirichenko, A.F., *Further Development of the Theory of Gearing for the Purposes of Power Drives*, Mashinoznavstvo, L'viv, 2003.
- Korostel'ev, L.V., *Geometrical and Kinematical Criteria of Bearing Capacity of Spatial Gearing*, Doctoral thesis, STANKIN, Moscow, 1964, 48 p.
- Korotkin, V.I., Kharitonov, Yu.D., *Novikov Gearing*, Rostov State University Publishers, Rostov-on-Don, 1991, 208 p.
- Korotkin, V.I., Onishkov, N.P., Kharitonov, Yu.D., *Novikov Gearing: Achievements and the Development*, Mashinostroyeniye-1, Moscow, 2007, 384 p.
- Korotkin, V.I., Onishkov, N.P., Kharitonov, Yu.D., *Novikov Gearing: Achievements and Development*, Nova Science Publishers, Inc., New York, 2011, 249 p.
- Kreynes, M.A., Rozovskii, M.S., *Gear Drives (Selection of Optimal Schematic)*, Nauka, Moscow, 1972, 427 p.
- Kudr'avtsev, V.N., *Gear Transmissions*, Mashgiz, Moscow-Leningrad, 1957, 264 p.
- Kudr'avtsev, V.N., *Planetary Gear Transmissions*, 2nd Ed., Mashinostroyeniye, Leningrad, 1966, 308 p.
- Kudr'avtsev, V.N., Derzhavets, Yu.A., Glukhar'ev, E.G., *Design and Calculation of Gear Reducers*, Mashinostroyeniye, Leningrad, 1971, 328 p.
- Kudr'avtsev, V.N. et al., in: V.N. Kudr'avtsev, Yu.N. Kird'ashev (eds), *Planetary Gear Transmissions, Handbook*, Mashinostroyeniye, Leningrad, 1977a, 536 p.
- Kudr'avtsev, V.N. et al., in: V.N. Kudr'avtsev, Yu.A. Derzhavets (eds), *Strength and Reliability of Gear Transmissions, Handbook*, Mashinostroyeniye, Leningrad, 1977b, 240 p.
- Kudr'avtsev, V.N., Kuz'min, I.S., Filippenko, A.L., *Calculation and Design of Gear Reducers*, Polytechnica, St. Petersburg, 1993, 448 p.
- Kutzbach, K., "Grundlagen und meure Fortschritte des Zahnradzengung," in: *Z.V.D.I.*, 1924, pp. 913, 1076, 1105.
- Lagutin, S.A., Barmina, N.A., "Prof. F.L. Litvin: Contribution to the Formation of the Russian School of the Theory of Gearing," in: V. Goldfarb, Barmina (eds), *Theory and Practice of Gearing and Transmissions*, Mechanisms and Machine Science 34, Springer International Publishing, Switzerland, pp. 19–36, 2016.
- Leibniz, G.W.F., *Societati Regiae Scientiarum, Miscellanea Berolinensia*, Berlin, Vol. I, "Tentamen Natura et Remediis Resistentiarum," 1710, p. 315. [Leibnitz does not give any date; he only says that it was done while Römer was at the Royal Observatory in Paris].
- Lewis, W., "Interchangeable Involute Gearing," *American Machinist*, pp. 307–314, 1909.
- Lewis, W., "Interchangeable Involute Gearing," *Journal of American Society of Mechanical Engineers*, October 1910, p. 1631.
- Lewis, E.J., *Machinery*, p. 569, April 1911.
- Litvin, F.L., *Non-Circular Gears*, Mashgiz, Moscow-Leningrad, 1950, 218 p.
- Litvin, F.L., *Non-Circular Gears*, 2nd Ed., Mashgiz, Moscow-Leningrad, 1956, 311 p.
- Litvin, F.L., *Theory of Gearing*, Nauka, Moscow, 1960.
- Litvin, F.L., *Cylindrical Worm Gearing of New Kinds*, Mashgiz, Moscow, 1962, 103 p.
- Litvin, F.L., *Theory of Gearing*, 2nd Ed., Nauka, Moscow, 1968, 548 p.
- Litvin, F.L., *Theory of Gearing*, NASA Reference Publication 1212, AVSCOM Technical Report, 88-C-035, 1989, 470 p.
- Litvin, F.L., *Gear Geometry and Applied Theory*, Prentice Hall, Englewood Cliffs, NJ, 1994, 724 p.
- Litvin, F.L., *Development of Gear Technology and Theory of Gearing*, NASA Reference Publication 1406, ARL-TR-1500, 1997, 114 p.
- Logue, C.H., *American Machinist*, October 1907, pp. 573–575.
- Lopato, G.A., Kabatov, N.F., Segal', M.G., *Spiral Bevel and Hypoid Gearing*, 2nd Ed., Mashinostroyeniye, Moscow, 1977, 423 p.
- L'ukshin, V.S., *Theory of Screw Surfaces: For the Purposes of Design of Cutting Tools*, Mashinostroyeniye, Moscow, 1968, 372 p.
- Lynwander, P., *Gear Drive Systems: Design and Application*, Marcel Dekker, New York, 1983, 415 p.
- MAAG Gear Book. *Calculation and Manufacture of Gears and Gear Drives for Designers and Works Engineers*, MAAG Gear-Wheel Company Ltd., Zurich/Switzerland, 1963, 576 p.
- MAAG-Teschchenbuch, 2nd Ed., MAAG Gear-Wheel Company Ltd., Zurich/Switzerland, 1985, 727 p.
- Maitra, G.M., *Handbook of Gear Design*, 2nd Ed., Tata McGraw-Hill Publishing Company Limited, New Delhi, 1994, (First edition, 1989), (Fifth reprint, 2001), 534 p.
- Marc, L., *Investigation of the Conformal Gear for Helicopter Power Transmission*, Boeing Co., Morton, PA, Vertol Div., June 1964, 136 p.
- Matschoss, C., *Geschichte des Zahnrades*, Berlin, 1940, p. 68.
- Mozhayev, S.S., *Analytical Theory of Twist Drills*, Moscow-Leningrad, 1948, 136 p.
- Nikolayev, A.F., *Kinematic Foundation of the Theory of Spatial Gearing*, Doctoral thesis, Mosstankin, Moscow, 1953.

- Oberg, E., *Spur and Bevel Gearing*, The Industrial Press, New York, 1917, 274 p.
- Olivier, T., *Théorie Géométrique des Engrenages destinés à transmettre le mouvement de rotation entre deux axes ou non situés dans un même plan*, Bulletin de la soc d'Encouragement etc., Vol. xxviii, 1839, p. 430.
- Onishchenko, V.P., *Prediction of Duration of Power Gearing Based on Modeling of the Teeth Wear*, Zeszyty Naukowe Politechniki Śląskiej, Mechanika, z. 131, Gliwice, 1999, 200 p.
- Pappi, *Math. Col. Commandini, Bononiae*, lib. XIII, p. 461 and prop. 24, 1660, p. 480.
- Pascal, B., *Oeuvres*, La Haye, t. V., 1779, pp. 135–275.
- Pavl'enko, A.V., Fed'akin, R.V., Chesnokov, V.A., *Novikov Gearing*, Technika, Kiev, 1978, 144 p.
- Pavlov, A.I., *Modern Theory of Gearing*, KhNADU, Kharkov, 2005, 100 p.
- Pismanik, K.M., *Theoretical Foundations of Grinding of Bevel and Hypoid Gearing*, Doctoral thesis, Saratov Polytechnic Institute, 1972, 408 p.
- Popov, A.P., *Gearing with Point Contact of the Teeth Flanks*, ATOLL, Nikolayev, 2011, 700 p.
- Porvatov, N.A., Panin, G.F., *Use of Novikov Gearing in Construction and Road Building Machinery*, Defense Technical Information Center, 1973, 7 p.
- Radzevich, S.P., "An Examination of High-Conformal Gearing," *Gear Solutions*, pp. 31–39, February 2018.
- Radzevich, S.P., "Three Fundamental Laws of Gearing: for Gear Design and Gear Production," in: *Complex Ensure of Quality of Manufacturing Processes and Systems*, VIII International Scientific Conference, May 10–13, 2018, Chernihiv, Ukraine, pp. 17–18.
- Ramsden, J., *Description of an Engine for Dividing Mathematical Instruments*, London, 1777.
- Reuleaux, F., *Lehrbuch der Kinematik*, Braunschweig, 1875.
- Reuleaux, F., *The Constructor, a Hand-Book of Machine Design by F. Reuleaux*, Authorized translation, complete and unabridged from the 4th enl. German ed. By Henry Harrison Suplee. Philadelphia, H.H. Suplee, 1893, 312 p. [First German edition published in 1861 with title: *Der Constructeur. Ein Handbuch zum Gebrauch beim Maschinen-Entwerfen*].
- Rudenko, N.F., *Planetary Gearing: Theory, Application, Calculation and Desing*, 3rd Ed., Mashgiz, Moscow, 1947.
- Rudenko, V.N., *Planetary and Harmonic Drives*, Mashinostroyeniye, Moscow, 1980, 148 p.
- Sakharov, G.N., *Generating Cutting Tools*, Moscow, 1983, 232 p.
- Sakharov, G.N., *Issues on the Theory of Generating Cutting Tools*, Dissertation Dr(Eng)Sci, Stankin, Moscow, 1974, 320 p.
- Sang, E., in: *Trans. Roy. Scot. Soc. Arts.*, 1837.
- Sang, E., *New General Theory of the Teeth of Wheels*, Edinburgh, 1852.
- Schultz, V.V., *Geometrical Optimization of Wearing Kinematic Pairs*, Doctoral thesis, Kiev, 1980, 32 p.
- Schultz, V.V., *Shape of Natural Wear of Machine Parts and Tools*, Mashinostroyeniye, Leningrad, 1990, 208 p.
- Sevr'uk, V.N., *Theory of Circular-Screw Surfaces in Design of Novikov Gearing*, KhPU Publishers, Kharkov, 1952, 167 p.
- Shelomov, V.B., *Properties of Structure of Planetary Gear Boxes*, Nestor, St. Petersburg, 2004, 206 p.
- Shishov, V.P., *Theory, Mathematical Support and Synthesis of Power Gearing for the Needs of Industrial Transportation*, Doctoral thesis, Vostochnoukrainskiy University, Lugansk, 1994, 580 p.
- Shishov, V.P., Nosko, P.L., Fil', P.V., *Theoretical Foundation of Synthesis of Gearing*, Vostochnoukrainskiy University, Lugansk, 2006, 408 p.
- Shotter, B.A., "The Lynx Transmission and Conformal Gearing," SAE Paper 781041, Aerospace Meeting, November 27–30, 1978, Town & Country, San Diego, 7 p. ISSN 0148-7191.
- Silich, A.A., *Development of a Geometric Theory for Design of Novikov Gearing and for Finishing the Gear Teeth*, Doctoral thesis, Kurgan Polytechnic Institute, Kurgan, 1999, 534 p.
- Smith, J.D., *Gears and Their Vibration, A Basic Approach to Understanding Gear Noise*, The Macmillan Press Ltd., Cambridge, England, 1983.
- Smith, J.D., *Gear Noise and Vibration*, Marcel Dekker Inc., New York, 1999.
- Snesar'ev, G.A., *Theoretical Foundations of Series of Gear Reducers*, Doctoral thesis, MVTU, Moscow, 1980, 32 p.
- Stachel, H., "Spatial Involute Gearing—A New Type of Skew Gears," manuscript, 6 p.
- Stadtfeld, H.J., *Handbook of Bevel and Hypoid Gears*, R.I.T., Rochester, NY, 1993, 251 p.
- Stadtfeld, H.J., *Gleason Bevel Gear Technology*, The Gleason Works, Division of Gleason Corporation, Rochester, NY, 1995, 202 p.
- Stadtfeld, H.J., *Advanced Bevel Gear Technology*, Edition 2000, The Gleason Works, Division of Gleason Corporation, Rochester, NY, 2000, 343 p.
- Stadtfeld, H.J., *Gear Encyclopedia*, 2008 Edition, The Gleason Works, Division of Gleason Corporation, Rochester, NY, 2008, 462 p.
- Stribeck, R., "Berechnung der Zahnräder," in *Z.V.D.I.*, 1894, p. 1182.
- Sukhorukov, Yu.N., *Modification of Cylindrical Involute Gears. Handbook*, Technika, Kiev, 1992, 197 p.
- Sushko, Yu.A., *Graphs of Gear Drives*, Mashinostroyeniye, Leningrad, 1983, 216 p.
- Taiz, B.A., *Gear Accuracy and Inspection*, Mashinostroyeniye, Moscow, 1972, 368 p.
- TCA: *Tooth Contact Analysis. Formulas and Calculation Procedure*, The Gleason Works, Rochester, NY, 1964.
- Tkachenko, V.A., *Design of Planetary Gear Drives*, KhGU Publishers, Kharkov, 1991, 182 p.



- Tkachenko, V.A., *Planetary Gear Drives: Optimal Design*, KhAI Publishers, Kharkov, 2003, 446 p.
- Townsend, D.P., *Dudley's Gear Handbook. The Design, Manufacture, and Application of Gears*, 2nd Ed., McGraw Hill, Inc., NY, 1992, 1111 p.
- Tredgold, T., *Practical Essay on the Strength of Cast Iron*, London, 1822, pp. 85–86.
- Understanding Tooth Contact Analysis*, The Gleason Works, Rochester, NY, 1981.
- Volkov, A.E., Babichev, D.T., "History of Gearing Theory Development," 25th Working Meeting of IFToMM Permanent Commission for Standardization of Terminology on MMS, June 23–29, 2014, Saint-Petersburg, Russia, pp. 71–102.
- Volkov, A.E., Medved'ev, V.I., *Computation of Spiral Bevel Gearing for Design and Manufacturing Purposes*, MGTU "Stankin," Moscow, 2007, 151 p.
- Vulgakov, E.B., *Theory of Involute Gearing*, Mashinostroyeniye, Moscow, 1995, 320 p.
- Walker, H., "Gear Tooth Deflection and Profile Modification," *Engineer*, Vol. 166, pp. 434–436, 1938.
- Walker, H., "Gear Tooth Deflection and Profile Modification," *The Engineer*, Vol. 170, p. 102, August 1940.
- Watson, H.J., *Modern Gear Production*, Pergamon Press, New York, 1970, 359 p.
- Wells, C.F., Shotter, B.A., "The Development of 'Circarc' Gearing," *AEI Engineering*, March/April, 1962.
- Wildhaber, E., "Gear Tooth Curvature Treated Simply," *American Machinist*, Vol. 89, No. 18, August 30, 1945a.
- Wildhaber, E., "Basic Relations of Bevel Gears," *American Machinist*, Vol. 89, No. 20, September 7, 1945b.
- Wildhaber, E., "Relative Curvature Controls Gear Tooth Surface Strength," *American Machinist*, Vol. 89, No. 21, October 11, 1945c.
- Wildhaber, E., "Special Analysis of Gear Mesh Clarifies Curvature Conditions," *American Machinist*, Vol. 89, No. 22, October 25, 1945d.
- Wildhaber, E., "Basic Relationship of Hypoid Gears," *American Machinist*, Vol. 90, No. 4, February 14, 1946a.
- Wildhaber, E., "Basic Relationship of Hypoid Gears – II," *American Machinist*, Vol. 90, No. 5, February 28, 1946b.
- Wildhaber, E., "Basic Relationship of Hypoid Gears – III," *American Machinist*, Vol. 90, No. 6, March 14, 1946c.
- Wildhaber, E., "Tooth Contact," *American Machinist*, Vol. 90, No. 12, June 6, 1946d.
- Wildhaber, E., "Conjugate Tooth Surfaces," *American Machinist*, Vol. 90, No. 13, June 20, 1946e.
- Wildhaber, E., "Gear Tooth Sliding," *American Machinist*, Vol. 90, No. 15, July 18, 1946f.
- Wildhaber, E., "Skew Hypoid Gears," *American Machinist*, Vol. 90, No. 16, August 1, 1946g.
- Wildhaber, E., "Design for Duplex Cutting," *American Machinist*, Vol. 90, No. 17, August 15, 1946h.
- Wildhaber, E., "Surface Curvature," *Product Engineering*, May, 1956.
- Wildhaber, E., *Fundamentals of Bevel and Hypoid Gearing*, Translated from English by A.V. Slepak, Mashgiz, Moscow, 176 p.
- Winter, H., Looman, J., "Tools for Making Helical Circular Arc Spur Gears," *VDI Berichte*, No. 47, 1961.
- Winter, H., Stölzle, K., Placzek, T., *Topological Tooth Modifications and Contact Patterns of Spur and Helical Gears*, AGMA Paper 89FTM6, AGMA, Alexandria, VA, 1989, 10 p.
- White, J., *Mémoire*, Paris, 1812.
- Worm Gearing*, Machinery's Reference Series, Number 1, 4th Ed., The Industrial Press, New York, 1910, 48 p.
- Yelisseyev, Yu.S. (ed.), *Production of Gears for Jet Engines*, Mashinostroyeniye, Moscow, 2001, 493 p.
- Yerikhov, M.L., *Principles of Systematization, Methods of Analysis and Problems of Synthesis of Gearing*, Doctoral thesis, Leningrad Polytechnic Institute, 1972, 48 p.
- Young, T., *Lectures on Natural Philosophy and the Mechanical Arts*, London, Vol. I, 1807, p. 175, and plate 15.
- Zablonskii, K.I., *Gearing: The Load Share in Gear Mesh*, Tekhnika, Kiev, 1977, 298 p.



# Taylor & Francis

Taylor & Francis Group

<http://taylorandfrancis.com>

# Index

**Note:** Page numbers with “f” refer to figures. Page numbers with “t” refer to tables.

## A

Active profile, 158  
 Addendum, 158, 178  
 Addendum angle, 311, 366–367, 454–458, 458f  
 Addendum modification, 158, 178, 685–687, 686f, 687f, 690–693, 691f  
*Analytical Calculation of Planar and Spatial Gearing*, 3t, 26f  
 Angular base pitch, 23, 350, 354–356, 355f, 385–387, 386f, 387f  
 Angular pitch, 360–364, 361f  
 Antikythera mechanism, 7–8, 7f  
 Apex, 44–45, 50–54  
 Approximate real gearings; *see also* Real gearings  
   bevel gears in, 597–602  
   continuous-indexing processes, 609–610  
   crossed-axes gearing, 614–617, 615f–617f  
   developments in, 31–34, 593  
   examples of, 610–614, 610f–614f  
   face gearing, 602, 602f  
   inaccuracies of, 596–597  
   intersected-axes gearings, 596–614  
   parallel-axes gearings, 594–596, 595f, 596f  
   spiral bevel gears, 600–602, 601f, 606–609, 606f–609f  
   straight tooth bevel gears, 597–600, 597f–600f, 602–605, 603f, 604f, 610f  
   tooth flanks in, 594–595, 594f, 595f, 598f, 599f  
   tooth modifications, 621–626, 621f–622f, 624f–626f  
   undercut in, 623–624, 624f  
   worm gearing, 618–621, 618f–620f  
 Arc of action, 207, 208f  
 Arc of approach, 207, 208f  
 Arc of recess, 207, 208f  
 Archimedes, 6  
 Aristotle, 6  
 Automobile differentials, 220, 223, 223t  
 Axial pitch, 191–194, 209–210  
 Axis misalignment, 15–16, 31, 37f, 38–40

Axis of instant rotation, 42–56, 68–83, 98–100, 124–132, 197–201, 261–271  
 Axodes, 49, 53–56  
**B**  
 Back cone distance, 369f, 371f, 376–379  
 Backlash, 460–461, 461f  
 Base angular pitch, 362, 453  
 Base circle, 104, 117, 120–121  
 Base cones  
   in crossed-axes gearing, 423–428, 425f, 772, 773f  
   in intersected-axes gearing, 335–339, 336f, 358–359, 358f, 360f  
   in worm gearing, 497–499, 500f, 501f  
 Base cylinder, 120, 124, 127–132, 128f, 266f  
 Base diameter, 128–133, 183, 183f  
 Base helix angle, 132, 138, 172, 177–196, 201–217  
 Base lead angle, 149–150, 194  
 Base pitches  
   in crossed-axes gearing, 473–476, 474f, 475f  
   of gears, 1, 15–16, 20–25, 30–31, 38, 75, 98–102, 101f  
   in intersected-axes gearing, 339–340, 354–356, 355f  
   in involute gearing, 131–134, 132f, 138f, 140, 217–219, 218f, 219f  
   in Novikov gearing, 266–267, 266f  
   in real gearings, 539–541, 540f  
   violation of equality of, 759–762, 761f  
 Bending torque, 235–239, 235f, 239f  
 Bevel gear coupling, 542, 543f  
 Bevel gear pairs  
   in approximate real gearings, 32–33, 597–602, 597f–599f  
   developments in, 23–24, 25f  
   face gearing, 602, 602f  
   in intersected-axes gearing, 335–338, 335f, 345–351, 346f, 350f, 359, 361–370, 370f, 597–602  
   spiral bevel gears, 413–416, 414f–416f, 600–602, 601f, 606–610, 606f–610f  
   straight tooth bevel gears, 62–64, 63f, 597–600, 597f–600f, 602–605, 603f, 604f

Bottom land, 148, 150, 154, 366–369, 369f, 454–456, 667–671  
 Boundary Novikov circle, 261–262, 262f, 269–274, 270f, 277–278, 283–291, 297, 302, 306, 373–375, 463–465  
 Boundary Novikov cone, 373–375, 373f, 463–465, 463f, 464f, 549f  
**C**  
 Calculus, elements of, 781–785  
 Camus, Charles, 10–13, 12f, 21, 29, 35, 867  
 Camus-Euler-Savary theorem, 17–19, 22, 30, 37, 95–100, 245, 259, 867  
 Cartesian coordinate system, 43, 82–84, 135–142, 872  
 Centerline plane, 77–79, 78f–82f  
 CΣu-variable gearing, 71–75, 72f, 73f, 553–561  
 Characteristic curve, 296, 566–568  
 Characteristic line, 148–149, 174–175, 183, 189–192  
 Circular arc, 26, 98, 127, 137–138  
 Circular pitch, 178–180  
 Complementary vectors, 66–71, 67f, 68f  
 Complex gear systems, 725–732, 728f, 729f; *see also* Gear systems  
 Condition of conjugacy, 36–37, 94–100, 97f, 351–352, 352f, 758–759, 758f, 760f  
 Condition of contact, 1, 19–22, 35–38, 91–94, 93f, 758  
 Cone, Samuel, 32, 34  
 Conformal gearing, 257–306; *see also* High-conformal gearing  
 Conformity, degree of, 837–839, 838f, 839f, 846–848, 847f  
 Conformity, extremum degree of, 846–848  
 Conformity, indicatrix of, 840–844, 840f, 844f, 845f, 848–849  
 Conical involute gears  
   geometry of, 184–194  
   kinematics of, 184–194  
   with straight teeth, 190–191, 190f  
   tooth flanks and, 184–194, 184f  
 Conjugacy, condition of, 36–37, 94–100, 97f, 351–352, 352f, 758–759, 758f, 760f

- Conjugate action, 16, 96–97, 97f, 110, 141–142, 142f, 351, 442
- Contact, condition of, 1, 19–22, 35–38, 91–94, 93f, 758
- Contact geometry; *see also* **Geometry**
  - degree of conformity, 837–839, 838f, 839f, 846–848, 847f
  - Dupin indicatrix, 834–837, 835f
  - extremum degree of conformity, 846–848
  - features of, 565–570
  - of gear and mating pinion, 829–849
  - indicatrix of conformity, 840–844, 840f, 844f, 845f, 848–849
  - local orientations, 830–834, 830f, 832f
  - planar characteristics, 834–837
  - of tooth flanks, 35–38, 565–570, 570f, 829–849
- Contact motion
  - in crossed-axes gearing, 478–486
  - in intersected-axes gearing, 392–405, 394f, 395f
  - of mating pairs, 227–232, 229f
- Contact ratio
  - in crossed-axes gearing, 476–478
  - in helical gears, 209–217, 210f, 260–265, 261f
  - in high-conformal gearing, 260–265, 261f, 267–268, 268f
  - in internal involute gearing, 245–250, 246f, 247f
  - in intersected-axes gearing, 387–392, 389f, 391f, 392f
  - in involute gearing, 209–217, 210f
  - in mating gear pairs, 194–196
  - in noise excitation, 766–767, 767f, 768f
  - in parallel-axes gearing, 204–216, 205f, 208f, 213f
- Convex-to-concave contact, 257–259, 258f, 294–297, 295f, 301–303, 301f, 303f, 640, 640f
- Coordinate systems
  - arbitrary axis and, 807–810, 807f, 809f
  - Cartesian system, 43, 82–84, 135–142
  - chains of linear transformations and, 820–825, 821f
  - closed loop coordinate system, 820–825, 821f
  - complex coordinate systems, 811–819
  - consequent coordinate system transformations and, 820–825, 821f
  - conversion of, 818–819
  - coupled linear transformations, 816–818, 817f
  - for crossed-axes gearing, 428–442, 478–486
  - Eulerian transformation and, 808, 808f
  - examples of, 804f, 805f, 810f
  - homogeneous coordinate transformations, 803–804
  - homogeneous coordinate vectors, 803
  - for intersected-axes gearing, 340–345
  - linear transformations and, 803–827
  - local coordinate system, 822–823, 822f, 823f
  - nonorthogonal linear transformation and, 818, 824–825, 825f
  - for parallel-axes gearing, 135–139, 136f, 226–227, 227f
  - for real gearings, 521–526, 534–538
  - rolling motion and, 812–814, 813f
  - rolling of two systems, 814–816, 815f
  - rotation of coordinate axis, 806–807, 806f
  - schematics of, 136f
  - screw motion and, 811–814, 814f
  - tangent vectors and, 823–824, 824f
  - for tooth flanks, 135–139, 136f, 139f, 185f
  - transformations and, 803–827
  - translations and, 804–806, 804f, 805f
  - useful equations for, 819–820
- Crossed-axes angle, 42–44, 43f, 44f, 45f, 47–61, 53f, 58f, 61f, 64–65, 65f, 71, 74
- Crossed-axes gearing
  - analytical criterion of, 56–57, 57t, 422t
  - angular addendum in, 454–458, 458f
  - angular base pitch of, 445–448, 445f, 446f, 452
  - angular dedendum in, 454–458, 458f
  - angular tooth thickness in, 453–454, 461f
  - approximate real gearings, 614–617
  - backlash in, 460–461, 461f
  - base cones in, 423–428, 425f, 772, 773f
  - base pitches in, 473–476, 474f, 475f
  - bearing capacity of, 465
  - boundary cones in, 463–465, 463f, 464f
  - concept of, 33–34
  - contact motion in, 478–486
  - contact ratio in, 476–478
  - coordinate systems for, 428–442, 478–486
  - crossed-axes worm gearing, 514–515, 514f, 515f
  - design parameters of, 458–460, 459t, 465–471, 470t
  - design peculiarities of, 771–776
  - diagrams of, 420f
  - dynamics of, 486–495
  - elements of, 486–495
  - examples of, 53f, 56f, 57–66, 58f–59f, 61f–64f, 420f
  - forces acting in, 486–495, 487f, 488f, 491f, 493f
  - gear housing and, 432–433
  - gear tooth accuracy, 750–756, 750f–751f
  - high-conformal crossed-axes, 462–465
  - kinematics of, 419–422, 771–772, 772f
  - line of contact in, 434f, 436f, 437f, 774–775, 775f
  - linear transformations for, 428–442
  - load analysis of, 486–495
  - low tooth count in, 448
  - nonorthogonal crossed-axes, 615, 616f
  - operators associated with, 432–433
  - orthogonal crossed-axes, 422–425, 425f, 452, 452f, 615
  - path of contact in, 463, 471–472
  - perfect crossed-axes gearing, 417–495
  - pitch surfaces in, 452–453, 452f, 454f, 455f
  - plane of action in, 449–450, 449f, 773–774, 774f, 775f
  - possible types of, 57–66, 58f, 60f
  - pressure angle in, 422–423
  - pulley-and-belt analogy of, 471, 772
  - real crossed-axes gearing, 520f
  - reference plane in, 465–467, 466f, 467f
  - reference systems for, 429–430, 429f, 478–486, 773, 774f
  - rolling conditions in, 430–432
  - round basic rack and, 452–457
  - sliding conditions in, 430–432, 478–486, 484f
  - spiral bevel pinion for, 437f, 441–442
  - tooth flanks in, 428–436, 434f, 436f, 437–443, 443f, 471–495, 512–513, 513f, 636–638, 636f, 638f, 772
  - tooth proportions in, 444–445
  - transmission of rotation, 473–474
  - transverse pressure angle in, 422–423, 423f, 424f, 448–451
  - Tredgold approximation for, 462
  - vector diagrams for, 730–732
  - zone of action of, 472–473, 472f, 473f, 477f
- Crown gear, 47, 159, 359–366, 359f
- Curvatures of surfaces, 796–797
- Cu-variable gear, 71–74, 74f
- Cycloidal gearing, 308–310, 309f

**D**

Da Vinci, Leonardo, 3t, 8–9  
 Darboux, Jean-Gaston, 577, 790, 836  
 Darboux frame, 567, 577–586, 790, 823, 836–837  
 De Dondi, Giovanni, 8  
 De La Hire, Philippe, 10–11, 11f, 13, 29  
 Dedendum, 158, 366–367, 454–458, 458f  
 Dedendum angle, 454–458, 458f  
 Degree of conformity, 837–839, 838f, 839f, 846–848, 847f  
 Degree of conformity, extremum, 846–848  
 Deliberate departure, 159  
 Desargues, Girard, 10, 10f, 13, 29, 35  
 Design peculiarities  
   of almost perfect gears, 771–779  
   of crossed-axes gearing, 771–776  
   of perfect gears, 771–779  
   for real gearings, 776–779  
 Desired gear pair, 39, 111, 542, 551, 565–566, 591, 764; *see also* Gear pairs  
 Desired line of contact, 128, 134, 138–139, 154; *see also* Line of contact  
 Double-helical gears, 39, 39f  
 Double-tooth contact regions, 207–209, 209f  
 Driven shaft, rotation of, 91–102  
 Dupin indicatrix, 566–568, 567f, 642, 834–849, 835f  
 Dürer, Albrecht, 10

**E**

Elastic deformation, 215–216, 216f  
 Elastic load sharing devices, 713–724, 713f, 715f–723f  
 Elastomeric load sharing device, 713–714, 713f  
 End chamfer, 159  
 End radius, 159  
 Epicyclical gear drives, 703–704, 707, 708f, 710–713, 717  
 Equal base pitches, 1, 31, 100–102, 101f, 133–134, 324, 386, 460, 474f  
 Equation of contact  
   in approximate real gearings, 605, 609  
   gear noise and, 757–758  
   interacting tooth flanks and, 31, 35–36, 38, 93–94, 98  
   in intersected-axes gearing, 350, 384  
   in involute gearing, 164–166, 165f, 174, 187, 245, 259  
   in noninvolute gearing, 312–321  
 Euler, Leonhard, 1, 11, 13–17, 13f, 21, 29, 37, 594

Eulerian gearing, 15–16, 297  
 Eulerian transformation, 808, 808f  
 Euler-Savary equation, 11, 17, 160–162, 160f

**F**

Face advance, 210f, 212–213, 213f  
 Face contact ratio, 209–210, 210f, 476–477  
 Face gearing, 34  
 Face of tooth, 159  
 Face width, 159, 197–199, 200f, 201f  
 Favorable gear pair; *see also* Gear pairs  
   conformity of, 567–568, 568f, 569f  
   designing, 110–111, 563–570  
   Dupin indicatrix of, 566–568, 567f  
   meaning of, 565–567  
   optimization of, 565–566  
   point contact of, 567–570, 568f–570f  
   synthesis of, 110, 351, 423, 563–570, 829, 846, 869  
   tooth flanks in, 566–570  
 Field of action, 25, 214f, 266–267, 383, 472–473, 472f, 473f, 477f  
 Fillet, 148, 150, 154, 170–171, 170f  
 Fillet curves, 158, 158f  
 Fillet radius, 171, 283, 378–379, 468–469, 685–686, 690  
 Fillet undercut, 170–171, 170f  
 Fundamental theorem of gearing, 17–19, 18f, 19f

**G**

Gavrilenko, Vladimir A., 4t, 26–27, 29f  
 Gear apex, 51, 82–84, 427, 435, 546, 589  
 Gear art, 1, 7–14  
 Gear cone angle, 330, 331f  
 Gear coupling, 254–255, 255f  
 Gear coupling design concepts, 545–546, 546f  
 Gear drives  
   characteristics of, 735–739  
   epicyclical gear drives, 703–704, 707, 708f, 710–713, 717  
   examples of, 734f, 738f  
   gear pairs in, 738–739  
   gear ratios of, 733–739, 738f  
   gear transmission systems, 702–703  
   multistage gear drives, 733–739  
   planetary gear drives, 698f–701f, 704–711, 705f, 707f, 709f, 713–723, 718f–722f  
   power density of, 702–703  
   rotational speeds, 736–737, 736f  
   speed variation for, 735–737  
   transmission characteristics, 735–739  
   transmission ratios, 735–736

Gear housing, 432–433

Gear noise

  causes of, 757–769  
   equation of contact and, 757–758  
   vibration and, 757–769  
 Gear pairs; *see also* specific gear pairs  
   axial vectors of, 68–70  
   bolt-and-nut pair, 41  
   definition of, 41–42  
   design parameters of, 223, 223t, 245–250, 248f, 691–692, 692t  
   desired gear pair, 39, 111, 542, 551, 565–566, 591, 764  
   dynamic analysis of, 725–732, 728f, 729f, 730f  
   elastic deformation in, 215–216, 216f  
   examples of, 41–42, 42f, 43f, 53f, 56f, 57–66, 58f–59f, 61f–64f  
   favorable gear pairs, 110–111, 563–570  
   field of action in, 213–214, 214f  
   formulas for, 70–71  
   fundamentals of, 39–75  
   gear diameters, 690, 693t  
   internal involute gearing, 246f, 247f, 248f  
   kinematic analysis of, 725–732, 728f, 729f  
   kinematics of, 39–75, 43f, 867–870  
   low tooth count, 213–214, 214f, 448, 645–646, 649–650, 655–657  
   in multistage gear drives, 738–739  
   parallel-axes gearing and, 141–196  
   perfect gear pairs, 549–551, 550t  
   planes associated with, 77–90  
   possible types of, 57–66, 58f, 60f  
   pulley-and-belt analogy of, 94–95, 95f, 103–111, 104f–107f  
   rack-to-rack pair, 41–42  
   reference systems for, 77–90, 83f  
   transmission of motion by, 41–42  
   types of, 869–870, 869f  
   undercut in, 211–215, 215f, 693–695  
   vector complements to, 66–71  
   vector representation of, 42–75  
 Gear ratios  
   of multistage gear drives, 733–739, 738f  
   in parallel-axes gearing, 116–123, 118f, 204–216  
 Gear shapes  
   axial sections, 576–584, 579f–585f, 590f–591f  
   classification of, 587–591  
   cross-section of, 584–586, 585f  
   examples of, 573–591, 574f–577f, 579f–585f, 588f–591f  
   generic shapes, 573–591, 588f–591f  
   possible number of, 575–580

- Gear systems  
 analysis of, 725–732  
 complex gear systems, 725–732, 728f, 729f  
 with crossed-axes gearing, 730–732  
 dynamic analysis of, 725–732, 728f, 729f, 730f  
 with intersected-axes gearing, 730–732, 731f, 732f  
 kinematic analysis of, 725–732, 728f, 729f  
 rotating gear images, 725–726, 726f, 727f  
 $S_{pr}$ -gear system, 519–551, 776–777  
 vector approach for, 725–732  
 vector diagrams for, 727–728
- Gear teeth; *see also* **Tooth flanks**  
 accuracy of, 741–756, 742f–745f, 747f, 749f–751f  
 bending strength of, 657–662  
 cantilever beam and, 658–662, 658f, 660f–662f  
 contact patterns, 753–755, 754f  
 engineering formulae for, 855–857, 855t–856t  
 features of, 649–650  
 Hertz contact stress equation, 654  
 Hertz proportional assumption, 646–648, 653f, 654f  
 interactions of, 646–648, 647f–652f, 655f  
 Lewis's formula, 657–660, 660f  
 line of contact in, 662–674  
 load analysis of, 652f, 674–678, 675f, 676f  
 mounting distance of, 752–753, 753f, 755f, 756f  
 Saint Venant's principle, 658–661, 661f  
 simulating gear and pinion, 678–684, 679f, 681f–683f  
 specific pressure factor, 655  
 strength of, 645–684  
 stresses in, 645–646, 646f, 650–657, 657f
- Gear tooth line, 366, 366f, 453
- Gear tooth profile; *see also* **Tooth flanks**  
 accuracy of teeth, 741–756, 742f–745f, 747f, 749f–751f  
 addendum modification, 685–687, 686f, 687f, 690–693, 691f  
 contact patterns, 753–755, 754f  
 elements of, 158, 158f, 159f  
 generation of, 141–161  
 geometrical blocking contours, 693–696, 694f, 695f  
 geometry of, 13–16, 14f, 15f  
 helix angle and, 225–226, 226f  
 involute gearing and, 141–196  
 length of, 166–168, 167f, 168f  
 in lengthwise direction, 154–158, 156f, 157f, 159f  
 modifications of, 685–696  
 mounting distance of, 752–753, 753f, 755f, 756f  
 parallel-axes gearing and, 141–196, 142f  
 profile shift coefficient, 688–690, 688f, 690f, 693–696, 694f, 695f  
 rack shift and, 685–696  
 sliding angle of, 227–232, 228f, 231f  
 sliding conditions in, 250–252, 250f  
 strength of teeth, 645–684
- Gear transmission systems, 702–703
- Gearbox, 39, 39f, 259
- Gearing, theory of, 1–38; *see also* **Theory of gearing**
- Gearing principle, 11, 12f
- Gearing with a Novel Kind of Meshing*, 28f
- Gearings  
 accomplishments with, 29–31, 30f, 35–38  
 approximate gearings, 31–34  
 art of, 1, 7–14  
 background of, xxviii, 1–29  
 concluding remarks on, 867–870  
 crossed-axes gearing, 33–34, 417–470  
 design parameters of, 103–111  
 developments in, 6–8, 13–34  
 explanation of, xxvii, 1–6  
 fundamentals of, 17–19, 39–75  
 geometrically accurate gearings, 2, 109, 125, 140, 423–424, 511–516, 513f–515f  
 glossary of terms, 871–876  
 history of, xxviii, 1–29  
 ideal gearings, 2  
 intersected-axes gearing, 327, 329–416  
 introduction to, xxviii–xxx  
 involute gearing, 113–140  
 laws of, 91–102, 131, 384–387, 444, 476, 593, 867  
 overview of, 1–38  
 parallel-axes gearing, 103–111, 113–140  
 perfect gearing, 2–3, 23–29, 113–148  
 post-Eulerian period of, 17–22  
 pre-Eulerian period of, 8–14  
 theory of, 1–38
- Gears  
 apex of, 51, 82–84, 427, 435, 546, 589  
 base pitches of, 1, 15–16, 20–25, 30–31, 38, 75, 98–102, 101f, 131–134, 132f, 138f, 140  
 complex gear systems, 725–732, 728f, 729f  
 contact geometry of, 829–849  
 design of, 6–8  
 design peculiarities of, 771–779  
 distance of approach for, 851–854, 852f, 854f  
 early designs of, 6–8  
 face width of, 197–199, 200f, 201f  
 gear joint, 542, 543f  
 gear-to-pinion mesh, 120–123, 121f–123f, 345, 354, 433, 766  
 generic shapes of, 573–591, 574f–577f, 579f–585f, 588f–591f  
 low-tooth-count gear, 196, 209–215, 214f, 220, 448, 501–503, 645–646, 649–650, 655–657  
 master gear, 555  
 mating pinion and, 146–155, 505–516, 627–643, 776–779, 777f, 779f, 829–854  
 old-style gears, 7–8, 8f  
 point contact of, 505–516  
 shapes of, 573–591, 574f–577f, 579f–585f, 588f–591f  
 simulating gear and pinion, 678–684, 679f, 681f–683f  
 strength of, 645–684  
 terminology of, 158–160  
 tooth flanks and, 505–516, 627–643, 829–854  
 Gear-to-pinion mesh, 120–123, 121f–123f, 345, 354, 433, 766  
 Gear-to-rack mesh, 413, 495, 513–514, 514f  
*Generation of Surfaces in Continuous-Indexing Methods of Surface Machining*, 3t, 36f  
*Geometric Theory of Gearing (Théorie Géométrique des Engrenages)*, 3t, 17–20, 20f  
 Geometrical blocking contours, 693–696, 694f, 695f  
 Geometrically accurate gearings, 2, 109, 125, 140, 423–424, 511–516, 513f, 514f, 515f; *see also* **Gearings**
- Geometry  
 of conical involute gears, 184–194  
 contact geometry, 565–570, 829–849  
 elements of, 787–800  
 features of, 565–570  
 of gear tooth profile, 13–16, 14f, 15f  
 in high-conformal gearing, 280–286, 281f, 286f, 290–295, 290f–293f, 376–377, 376f, 377f  
 in intersected-axes gearing, 376–377, 376f, 377f  
 in involute gearing, 113–140  
 kinematics and, 113–140, 507–516, 867–870  
 of surfaces, 787–800



- of tooth flanks, 134–140, 134f, 147f, 148–149, 149f, 154, 154f, 184–194, 220–223, 222f, 289–295, 290f–293f, 512–513, 546–547, 550t, 627–643, 787–788, 788f
- Gleason, William, 32–34, 32f
- Glossary, 871–876
- Gochman, Chaim, 3t, 19, 21–22, 30, 37, 867
- Grant, George Barnard, 3t, 23–24, 23f
- H**
- Helical gears
  - bending torque in, 235–239, 235f, 239f
  - contact ratio in, 209–217, 210f, 260–265, 261f
  - design parameters of, 178t, 179t, 180t
  - determining angle of, 181–182, 182f
  - equation of, 172–176
  - examples of, 508f, 509
  - formulas for, 179–180, 180t
  - gearbox with, 39, 39f
  - generating basic rack of, 176–182, 176f, 177f, 178t, 192f
  - helix angle, 225–226, 226f
  - involute gearing and, 134–135, 134f, 148–154, 149f, 150f, 159
  - line of contact in, 663, 663f
  - load distribution in, 232–240, 232f
  - noninvolute gearing and, 321–325, 322f, 323f, 324f
  - Novikov gearing and, 863–866, 864f
  - parallel-axes gearing and, 199–202, 201f, 202f
  - pitch of, 180–181, 181f
  - tooth flanks and, 198f, 199–202, 201f, 202f
  - tooth profile angle, 225–226, 226f
  - Wildhaber-Novikov gearing and, 859–866, 860f, 861f
  - zone of action of, 206–211, 211f
- Helix angle, 41, 132, 138, 155, 172, 177–196, 201
- Helix modification, 159
- Heron of Alexandria, 6
- Hertz, Heinrich, 646–648
- Hertz contact stress equation, 654
- Hertz proportional assumption, 646–648, 653f, 654f
- High-conformal crossed-axes, 462–465; *see also* Crossed-axes gearing
- High-conformal gearing
  - accuracy for, 298–306, 299f, 301f, 303f
  - bearing capacity of, 374–375, 375f, 465
  - boundary cones in, 373–375, 373f, 374f
  - close-up of, 282f
  - contact ratio in, 260–265, 261f, 267–268, 268f
  - continuous-indexing processes, 303–306, 304f, 305f
  - convex-to-concave contact of, 257–259, 258f, 294–297, 295f, 301–303, 301f, 303f, 640, 640f
  - degree of conformity, 295–298, 296f, 298f
  - design parameters of, 266–267, 266f, 282–284, 282f, 375–380, 376f, 379t, 465–471, 470t
  - geometry in, 280–286, 281f, 286f, 290–295, 290f–293f, 376–377, 376f, 377f
  - kinematics of, 280–282, 281f, 282f
  - linear velocity vector in, 279–280, 280f
  - machining processes in, 303–306, 304f, 305f
  - origin of, 257–258
  - parallel-axes gearing and, 257–306
  - path of contact in, 372–373, 372f
  - point of culmination, 264, 288–292, 288f
  - power density in, 258–260
  - pseudo-path of contact, 263–267, 265f, 270, 283–291, 285f, 301, 372–374, 372f, 380
  - reference plane in, 465–467, 466f, 467f
  - sliding conditions in, 276–280, 277f, 280f
  - tooth flanks in, 269–274, 272f–276f, 285–288, 286f, 289–292, 290f–292f, 639f–643f, 640–644
  - tooth profile rolling, 279–280
  - transitions in, 267–276
- High-conformal intersected-axes, 371–380; *see also* Intersected-axes gearing
- Hyperboloids, 52–55, 454–457, 576–577
- Hypoid gear, 33–34, 56, 68, 365, 579, 733, 753, 756
- I**
- Ideal gearings, 2; *see also* Geometrically accurate gearings
- Indicatrix of conformity, 840–844, 840f, 844f, 845f, 848–849
- Instant line of action; *see also* Line of action
  - condition of contact and, 91–92
  - description of, 11
  - in high-conformal gearing, 274–276, 280–281
  - in involute gearing, 129–130
  - in parallel-axes gearing, 104–107, 106f, 107f, 232f
- Internal involute gearing; *see also* Involute gearing
  - contact ratio in, 245–250, 246f, 247f
  - design parameters of, 245–250, 248f
  - examples of, 246f, 247f
  - gear coupling in, 254–255, 255f
  - mating gears in, 252–255
  - sliding conditions in, 250–252, 250f
  - tooth thickness in, 254
- Intersected-axes gearing
  - analytical criterion of, 334t
  - angular addendum in, 366–367
  - angular backlash in, 363–366, 365f
  - angular base pitch of, 354–356, 355f, 385–387, 386f, 387f
  - angular dedendum in, 366–367
  - angular pitch of, 360–364, 361f
  - approximate real gearings, 596–614
  - base cones in, 335–339, 336f, 358–359, 358f, 360f
  - base pitches in, 339–340, 354–356, 355f
  - bearing capacity of, 374–375, 375f
  - bevel gears in, 335–338, 345–351, 346f, 350f, 359, 361–370, 370f, 597–602
  - boundary cones in, 373–375, 373f, 374f
  - case of, 79–80, 80f, 81f
  - cone angle, 330, 331f
  - contact motion in, 392–405, 394f, 395f
  - contact pattern in, 413–416, 415f, 416f
  - contact ratio in, 387–392, 389f, 391f, 392f
  - coordinate systems for, 340–345, 398–410
  - crown gear, 359–366, 359f
  - design parameters of, 367–370, 368t, 369f, 375–380, 376f, 379t
  - designs of, 329–335, 330f
  - diagrams of, 330f, 331f, 334f
  - dynamics of, 405–416
  - early designs of, 329
  - elements of, 405–416
  - equal base pitch of, 385–387, 386f, 387f
  - face width of, 383–384, 384f
  - forces acting in, 405–413, 406f, 409f, 410f, 411f, 413f
  - gear tooth accuracy, 748–750, 749f–750f
  - gear tooth line in, 366, 366f
  - geometry of, 376–377, 376f, 377f



- Intersected-axes gearing (*Continued*)  
 high-conformal intersected-axes,  
   371–380  
 inaccuracies of, 596–597  
 kinematics of, 329–335, 330f  
 line of action in, 338–339, 339f  
 line of contact in, 345–346, 345f, 346f,  
   350f  
 linear transformations for,  
   340–345  
 linear velocity vector in, 393–398,  
   396f, 397f, 401–404  
 load analysis of, 405–413  
 miter intersected-axes, 333–334, 335f  
 nutation drives and, 333, 334f  
 operating base pitches in, 339–340  
 orthogonal intersected-axes,  
   333–337, 334f, 336f, 360f, 390  
 path of contact in, 338–339, 339f,  
   372–373, 372f, 381–382, 382f  
 perfect gear pairs, 327, 329–416  
 pitch cone angle in, 358–359, 358f,  
   359f, 360f  
 plane of action in, 357, 358f, 383–386,  
   386f, 389f  
 pressure angle in, 340, 348, 351  
 pulley-and-belt analogy of, 381–382,  
   382f  
 reference systems for, 82–84, 83f,  
   398–410, 399f  
 rolling conditions in, 341–345  
 rotation vectors of, 329–337, 333f,  
   340–342  
 round basic rack and, 360–361  
 round rack-to-bevel gears, 334–335,  
   335f  
 sliding conditions in, 393–394, 394f,  
   397f, 403–405  
 spiral bevel gears and, 413–416, 414f,  
   415f, 416f  
 tooth flanks in, 340–364, 341f, 345f,  
   350f, 381–416, 602–610,  
   632–635, 633f–635f  
 tooth thickness in, 362–363, 364f  
 transverse pressure angle in,  
   356–360, 356f  
 Tredgold approximation, 370–371,  
   371f  
 vector diagrams for, 730–732, 731f,  
   732f  
 zone of action of, 383–384,  
   383f, 385f
- Involute gearing  
 base diameter of, 183, 183f  
 of circle, 144–146, 145f  
 concept of, 11, 15–16, 23–27,  
   37, 37f  
 conical involute gears, 184–194  
 contact ratio in, 209–217, 210f  
 design parameters of, 216–217, 216f  
 double-tooth contact regions in,  
   207–209, 209f  
 examples of, 508f, 509  
 external gear pair, 216–227, 216f  
 face contact ratio in, 209–210, 210f  
 gear tooth profile, 141–196  
 geometry and, 113–140  
 helical gears and, 148–154,  
   149f, 150f  
 internal involute gearing, 245–255  
 invention of, 29–30  
 kinematics of, 113–140  
 line of action in, 37, 37f, 207f  
 line of contact in, 666, 667f  
 noninvolute gearing, 307–325  
 parallel-axes gearing and,  
   113–148, 197–244, 199f,  
   201f, 203f  
 path of contact in, 37, 37f  
 pinion-gear-to-rack mesh, 241–244,  
   242f, 243f  
 screw involute surface, 134–135,  
   134f, 148–153, 153t, 173–175,  
   173f, 217–219, 217f, 219f  
 sliding angle of, 227–232, 228f, 231f  
 spur involute gears, 111, 114f,  
   120–122, 127–128, 146–148,  
   147f, 148f  
 theory of, 24f, 25–27  
 tooth flank generation, 141–196  
 tooth flank interaction, 197–244
- K**
- Kinematics  
 of complex gear systems, 725–732,  
   728f, 729f  
 of conical involute gears, 184–194  
 of crossed-axes gearing, 419–422,  
   771–772, 772f  
 fundamentals of, 39–75  
 of gear pairs, 39–75, 43f, 725–732,  
   728f, 729f, 867–870  
 geometry and, 113–140, 507–516,  
   867–870  
 in high-conformal gearing, 280–282,  
   281f, 282f  
 of intersected-axes gearing, 329–335,  
   330f  
 involute gearing and, 113–140  
 of multistage gear drives, 733–735  
 of noninvolute gearing, 315–319,  
   315f, 319f  
 of parallel-axes gearing, 113–116  
 of rotation vectors, 42–75  
 of tooth flanks, 125–140, 627–628,  
   632–634, 636–637, 639–641  
 vector approach for, 725–732
- vector representation of, 42–75  
 of worm gearing, 497  
 Kolchin, N. I., 3t, 24–26, 621–622
- L**
- Laws of gearing, 91–102, 131, 384–387,  
   444, 476, 593, 867  
 Lead angle, 149–150, 194, 284, 289  
 Leading flank, 158  
 Length of action, 205–206, 212, 217, 279  
 Lewis's formula, 657–660  
 Line of action; *see also* Geometrically  
   accurate gearings  
   description of, 11–17  
   instant line of action, 11, 91–92, 99,  
     104–107, 106f, 107f, 129–130,  
     232f, 274–276, 280–281  
   in intersected-axes gearing, 338–339,  
     339f  
   in involute gearing, 37, 37f, 127–131,  
     129f, 207f  
 Line of contact  
   in crossed-axes gearing, 434f, 436f,  
     437f, 774–775, 775f  
   desired line of contact, 128, 134,  
     138–139, 154  
   equation of contact and, 98–99  
   in gear teeth, 662–674  
   in helical gears, 663, 663f  
   for intersected-axes gearing,  
     345–346, 345f, 346f, 350f  
   in involute gearing, 37, 125–128,  
     138–139, 138f, 666, 667f  
   in parallel-axes gearing, 232–240,  
     234f, 238f, 662–674, 663f–666f,  
     668f–674f  
   in real gearings, 536–538, 536f,  
     548–549, 549f  
   in worm gearing, 497–500  
 Linear transformations  
   coordinate systems and, 803–827  
   for crossed-axes gearing, 428–442  
   for intersected-axes gearing, 340–345  
 Linear velocity vector, 91–92, 92f  
 Litvin, F. L., 4t, 21  
 Local frame, 789–790  
 Lorenz, Friedrich Wilhelm, 32, 34  
 Low-tooth-count gear, 196, 209–215,  
   214f, 220, 448, 501–503,  
   645–646, 649–650, 655–657
- M**
- Madrid Codices, The*, 3t, 9f, 329, 419, 619f  
 Master gear, 555; *see also* Gears  
 Mating gear pairs; *see also* Gear pairs  
   contact motion of, 227–232, 229f  
   contact ratio of, 194–196

- internal involute gearing, 252–255
- tooth flanks and, 197–199, 199f
- tooth thickness in, 254
- Mating pinion; *see also* Pinion
  - contact geometry of, 829–849
  - distance of approach for, 851–854, 852f, 854f
  - gears and, 505–516, 508f, 627–643, 776–779, 777f, 779f, 829–854
  - point contact of, 505–516
  - simulating gear and pinion, 678–684, 679f, 681f–683f
  - tooth flanks and, 36–37, 565–570, 570f, 627–643, 829–854
- Mechanical Problems of Aristotle*, 6
- Mesh cycle; *see also* Gear pairs
- Meshing point, 223, 226–227, 261, 864
- Mismatch, 159
- Mounting distance, 365, 369f, 461, 532, 751–756, 753f, 756f
- Multistage gear drives; *see also* Gear drives
  - characteristics of, 735–739
  - examples of, 734f, 738f
  - gear pairs in, 738–739
  - gear ratios of, 733–739, 738f
  - of helical gears, 733, 734f
  - kinematics of, 733–735
  - rotational speeds, 736–737, 736f
  - transmission characteristics, 735–739
  - transmission ratios, 735–736
- Musser, C. Walton, 27, 29f
  
- N**
- New General Theory of the Teeth of Wheels*, 19
- Noise excitation
  - causes of, 757–769
  - contact ratio in, 766–767, 767f, 768f
  - load variation on, 766–767
  - prediction of, 767–769
  - vibration and, 757–769
- Nominal profile, 158
- Noncircular gears
  - design concepts, 555–561
  - developments in, 71–72, 72f
  - diagrams of, 556f, 557f
  - elliptical gears, 560f
  - examples of, 556f, 559f, 560f
  - fundamentals of, 555–556
  - gear shapers, 559f, 561
  - machining processes in, 559–561, 559f, 560f
- Noninvolute gearing; *see also* Involute gearing
  - four-bar mechanism, 316–317, 316f
  - helical gears and, 321–325, 322f, 323f, 324f
  - interaction with racks, 317–318, 317f
  - kinematics of, 315–319, 315f, 319f
  - linear velocity vector in, 314–319
  - rotation and, 314–321, 315f
  - spline shafts and, 317–319, 317f, 319f
  - spur noninvolute gears, 307–325
- Normal plane, 77–79, 78f–82f
- Normal pressure angle, 226, 677
- Novikov, Mikhail L., 3t–5t, 25–28, 27f, 260, 859
- Novikov gearing, 25–26, 212, 258–261, 261f–262f, 262–270, 264f–266f, 273–284, 295–297, 302–306, 323–325, 859–866; *see also* Wildhaber-Novikov gearing
- Nutation, angle of, 808
- Nutation drives, 333, 334f
  
- O**
- Oil pumps, 313–314, 313f
- Olivier, Théodore, 3t, 17–22, 19f, 30, 35, 37–38, 867
- Operating base pitches
  - of gears, 1, 15–16, 20–25, 30–31, 38, 75, 98–102, 101f
  - in intersected-axes gearing, 339–340
  - in involute gearing, 131–134, 132f, 138f, 140, 217–219, 218f
  - in Novikov gearing, 266–267, 266f
  - in real gearings, 539–541, 540f
  
- P**
- Parallel-axes gearing
  - approximate real gearings, 594–596, 595f, 596f
  - arcs in, 207, 208f
  - base diameter of, 128–129, 133
  - base pitches in, 100–102, 217–219, 218f, 219f
  - bending torque in, 235–239, 235f, 239f
  - Camus-Euler-Savary theorem for, 95–100
  - case of, 80–82, 81f, 82f
  - conformal gearing, 257–306
  - contact ratio in, 204–216, 205f, 208f, 213f
  - coordinate systems for, 135–139, 136f, 226–227, 227f
  - design parameters of, 103–111
  - face advance in, 210f, 212–213, 213f
  - features of, 113–125, 114f, 117f, 119f
  - forces acting in, 240–241, 241f
  - gear axis displacement, 524–526, 526f, 529f
  - gear ratio in, 116–123, 118f, 204–216
  - gear tooth accuracy, 741–748, 742f–745f, 747f
  - helical gears and, 199–202, 201f, 202f
  - high-conformal gearing, 257–306
  - involute gearing and, 113–148, 197–244, 199f, 201f, 203f
  - kinematics of, 113–116
  - line of contact in, 232–240, 234f, 238f, 662–674, 663f–666f, 668f–674f
  - load distribution in, 232–240, 232f
  - permissible motions in, 91–94, 93f
  - pinion-gear-to-rack mesh, 241–244, 242f, 243f
  - pulley-and-belt analogy, 94–95, 95f, 103–111, 104f–107f, 120–121
  - real parallel-axes gearing, 526–527, 526f, 529f
  - reference systems for, 82–84, 84f
  - rotationally positive gear pair, 123–125, 125f
  - spur involute gears, 111, 114f, 120–122
  - straddle-mounted gearing, 527–528, 527f
  - terminology of, 158–160
  - tooth flanks in, 197–244, 198f, 627–632, 628f–631f
  - transverse pressure angle variation, 120–129, 121f–123f, 126f
- Path of contact
  - in crossed-axes gearing, 463, 471–472
  - description of, 10–16
  - in intersected-axes gearing, 338–339, 339f, 381–382, 382f
  - in involute gearing, 37, 37f, 126–131, 129f, 130f, 138f
  - in spur involute gears, 163–168, 168f
- Perfect gearings
  - developments in, 23–29
  - explanation of, 2–3
  - parallel-axes gearing, 113–148
  - perfect crossed-axes gearing, 417–495
  - perfect real gearings, 519–551, 550t
  - tooth flanks in, 772–776
- Perfect parallel-axes gear pairs
  - base cones in, 335, 424
  - base pitches in, 217–219, 218f
  - bending torque in, 240
  - dynamics of, 232–241
  - elements of, 232–241
  - forces acting in, 240–241, 241f
  - gear tooth profile and, 141–142, 142f
  - geometrical blocking contours, 696
  - geometrically accurate gearings, 109–110
  - tooth flanks and, 132, 132f, 135f, 140
- Perfect real gearing, 519–551, 550t; *see also* Real gearings

- Perfect worm gearing, 497–504; *see also* Worm gearing
- Pin gearing, 307–308, 308f
- Pinion; *see also* Mating pinion
- apex of, 51, 82–84, 427, 435, 546, 589
  - contact geometry of, 829–849
  - distance of approach for, 851–854, 852f, 854f
  - gears and, 146–155, 505–516, 627–643, 829–854
  - gear-to-pinion mesh, 120–123, 121f–123f, 345, 354, 433, 766
  - point contact of, 505–516
  - tooth flanks and, 36–37, 627–643, 829–854
- Pinion apex, 51, 82–84, 427, 435, 546, 589
- Pinion reference system, 88–90
- Pinion-gear-to-rack mesh, 241–244, 242f–244f
- Pitch circle, 10, 121–123, 162
- Pitch diameter, 105–106, 168–170, 184, 188
- Pitch line, 48–51, 65, 159
- Pitch point, 10–11, 37, 48, 96–97, 104, 120–121, 162
- Pitch surfaces, 159, 359, 451–457, 452f, 454f
- Pitch-line plane, 77–79, 78f–82f
- Plane of action
- apex of, 45, 50–51, 65, 77, 83, 338–340, 354–356
  - in crossed-axes gearing, 449–450, 449f, 773–774, 774f, 775f
  - in involute gearing, 126–127
  - in real gearings, 535–538, 535f, 778–779, 778f
  - in worm gearing, 497–501, 501f
- Planes
- associated with gear pairs, 77–90
  - centerline plane, 77–79, 78f–82f
  - normal plane, 77–79, 78f–82f
  - pitch-line plane, 77–79, 78f–82f
- Planetary gear drives, 698f–701f, 704–711, 705f, 707f, 709f, 713–723, 718f–722f
- Point of contact
- design features of, 507–516
  - of favorable gear pair, 567–570, 568f–570f
  - of gears and pinions, 505–516
  - of tooth flanks, 505–516, 515f, 548–549
- Point of culmination, 264, 288–292, 288f
- Point of meshing, 223, 226–227, 261, 864
- Power density, 258–260
- Pressure angle
- in crossed-axes gearing, 34, 422–423, 423f, 424f, 448–451
  - description of, 10
  - in intersected-axes gearing, 356–360, 356f
  - in involute gearing, 37
  - in parallel-axes gearing, 104–108, 120–129, 121f–123f, 126f
- Principles of Mechanisms*, 3t, 17–19, 18f, 19f, 96f
- Profile angle, 128, 145–146, 163–187
- Profile modification, 158
- Profile shift, 158
- Pseudo-path of contact, 263–267, 265f, 270, 283–291, 285f, 301, 372–374, 372f, 380
- Pulley-and-belt analogy
- in crossed-axes gearing, 471, 772
  - in intersected-axes gearing, 381–382, 382f
  - in parallel-axes gearing, 94–95, 95f, 103–111, 104f–107f, 120–121
- ## R
- Rack, 10, 32–34, 41–42, 47–48
- Rack shift
- addendum modification, 685–687, 686f, 687f, 690–693, 691f
  - gear tooth modifications, 685–696
  - generating, 685–696
  - profile shift coefficient, 688–690, 688f, 690f, 693–696, 694f, 695f
- Radzevich, S. P., 5t, 6t, 20, 26, 35, 37, 38
- Real gearings
- angular base pitch in, 539–541
  - applications of, 571–626
  - approximate real gearings, 31–34, 593–626
  - auxiliary generating surfaces, 516f
  - base pitches in, 539–541, 540f
  - bevel gear coupling, 542, 543f
  - constant velocity joints, 542
  - coordinate systems for, 521–526, 534–538
  - design features of, 526–531, 526f
  - design peculiarities for, 776–779
  - gear axis displacement, 522–526, 522f, 529f
  - gear axis distance of approach, 526–531
  - gear coupling design concepts, 545–546, 546f
  - gear joint, 542, 543f
  - line of contact in, 536–538, 536f, 548–549, 549f
  - operating base pitches in, 539–541, 540f
  - overhung bevel pinion, 526, 527f
  - perfect real gearings, 519–551, 550t
  - plane of action in, 535–538, 535f, 778–779, 778f
  - real crossed-axes gearing, 519–520, 520f
  - reference systems for, 521–526, 521f, 534–538, 534f, 535f
  - shaft deflection in, 526, 527f
  - $S_{pr}$ -gear system and, 519–551, 776–777
  - straddle-mounted gearing, 527–528, 527f, 528f
  - tooth flanks in, 531–533, 533f, 534–551, 550t
  - two-degrees-of-freedom gearing, 542–545, 544f, 545f
  - types of, 549–551, 550t
  - vector diagrams, 520f
- Reference systems
- for crossed-axes gearing, 478–486, 773, 774f
  - for gear pairs, 77–90, 83f, 84f
  - motionless reference system, 84–87, 84f–87f
  - for real gearings, 521–526, 521f, 534–538, 534f
- R-gearing, 419–470; *see also* Crossed-axes gearing
- Richard of Wallingford, 8
- Root, 158
- Root curve, 158, 559
- Roots blower, 310–312, 310f, 311f, 321–322, 322f, 323f, 594
- Rotating gears, 725–730, 726f, 727f
- Rotation, transmission of
- in crossed-axes gearing, 417, 473–476
  - description of, 2, 10
  - to driven shaft, 91–102
  - in involute gearing, 125–126, 131
  - in noninvolute gearing, 314–321, 315f
  - in parallel-axes gearing, 104f–107f, 108–111, 201–204
- Rotation vectors
- of complex gear systems, 725–732, 728f, 729f
  - diagrams of, 43f, 46f, 48f–49f, 53f, 56f, 58f, 62f, 64f–66f
  - of intersected-axes gearing, 329–337, 333f, 340–342
  - kinematics of, 42–75
- Rotational speeds, 736–737, 736f
- ## S
- Saint Venant's principle, 658–661, 661f
- Sang, E., 19
- Savary, Felix, 11, 13, 16–17, 21, 30, 867
- Screw involute surface
- generation of, 187–188, 188f

- in involute gearing, 134–135, 134f, 148–153, 153t, 173–175, 173f, 217–219, 217f, 219f
  - in parallel-axes gearing, 217–219, 217f, 219f
  - Semple, Amzi C., 19
  - Shaft angle, 2, 62, 329–335, 333f, 419–424, 602, 610–611, 611f
  - Shevel'eva, G. I., 5t, 21
  - Shishkov, V. A., 3t, 21, 31, 35–36, 38, 93–94, 98, 164
  - Skew-axes gearing, 508f, 508–509
  - Span measurement, 743–747, 744f, 747f
  - Spatial gear pairs, 46–51, 53–58, 68, 68f, 334, 576–583; *see also* Crossed-axes gearing
  - Spiral angle, 395–396, 412, 494, 575, 606–607
  - Spiral bevel gears, 413–416, 414f–416f, 600–602, 601f, 606–610, 606f–610f; *see also* Bevel gear pairs
  - Spiral bevel pinion, 437f, 441–442
  - Split torque transmission systems
    - elastic load sharing devices, 713–724, 713f, 715f–723f
    - elastomeric load sharing device, 713–714, 713f
    - epicyclical gear drives, 703–704, 707–710, 708f, 711–713, 717
    - examples of, 698f, 699f, 700f
    - features of, 724
    - gear ratio, 703–704
    - gear transmission systems, 702–703
    - load sharing devices, 713–724
    - mobility of, 700–702
    - planetary gear drives, 698f–701f, 704–711, 705f, 707f, 709f, 713–723, 718f–722f
    - power density, 702–703
    - preloaded elastic sharing devices, 714–716, 720–724, 721f, 722f
    - torque sharing in, 698–700, 711–724, 712f, 713f
  - $S_{pr}$ -gear system, 519–551, 776–777; *see also* Real gearings
  - Spur involute gears; *see also* Involute gearing
    - design parameters of, 169t, 172t
    - generating basic rack of, 168–181, 169t, 170f
    - generating straight line of, 162–166, 163f, 181–183
    - line of contact in, 663, 663f
    - parallel-axes gearing and, 111, 114f, 120–122
    - tooth flanks and, 127–128, 146–148, 147f, 148f, 162–166, 169f, 172–176, 197–198, 198f
    - undercut in, 170–171, 170f, 196
  - Spur noninvolute gears, 307–325; *see also* Noninvolute gearing
  - Straight line, generating, 162–166, 163f, 181–183
  - Surfaces; *see also* Screw involute surface
    - change of parameters for, 801
    - coordinate system transformations and, 825–827
    - curvatures of, 796–797
    - differential geometry of, 787–800
    - forms of, 790–795, 793f
    - geometry of, 787–800
    - parameters of, 801–802
- T**
- Tangent plane, 788–789
  - Tangent vectors, 788–789, 823–824, 824f
  - Terbo, Nicholas, 33–34, 33f
  - Terms, glossary of, 871–876
  - Tesla, Nikola, 33
  - Theory of Gear Teeth Engagement*, 21f
  - Theory of gearing; *see also* Gearings; *see also* Gears
    - accomplishments in twenty-first century, 29–31, 30f, 35–38
    - chronology of evolution, 29–31
    - concluding remarks on, 867–870
    - contributors to, 2, 3t–6t
    - developments in, 6–8, 13–34
    - evolution of, 1–38
    - explanation of, 1–6
    - future developments in, 71–75
    - introduction to, xxviii–xxx
    - origin of, 13–16
    - overview of, 1–38
  - Tip chamfer, 158
  - Tip circle, 158
  - Tip diameter, 158
  - Tip radius, 158
  - Tip relief, 667, 766
  - Tip-easing modification, 158
  - Tolerances, 295, 298–306, 414
  - Tooth alignment error, 159
  - Tooth face, 159
  - Tooth flanks; *see also* Gear teeth; *see also* Gear tooth profile
    - in approximate real gearings, 594–595, 594f, 595f, 598f, 599f, 602–610
    - auxiliary generating surfaces, 510–513, 512f, 513f, 514–516
    - base pitches in, 131–134, 138f, 140
  - circular-arc teeth, 154–158
  - conical involute gears and, 184–194, 184f
  - conjugacy between, 36–37, 94–100, 97f, 99f, 442–443, 443f
  - contact geometry of, 35–38, 565–570, 570f, 829–849
  - contact of, 35–38, 91–94, 98, 128f, 131–140, 138f, 164–166, 165f, 187–191, 245, 259, 312–321, 321f, 350, 384, 605, 609, 757–758, 829–849
  - coordinate systems for, 135–139, 136f, 139f, 185f
  - in crossed-axes gearing, 428–441, 434f, 436f, 442–445, 443f, 453–454, 471–495, 512–513, 513f, 636–638, 636f, 638f, 772
  - curvature and, 221–226, 223f, 224f, 225f
  - degree of conformity of, 837–838, 838f, 846–848, 847f
  - design features of, 507–516, 627–643
  - distance of approach for, 851–854, 852f, 854f
  - double-tooth contact regions in, 207–209, 209f
  - Dupin indicatrix of, 834–837, 835f
  - engineering formulae for, 855–857, 855t–856t
  - equation of, 162–182, 165f
  - examples of, 797–799, 798f
  - extremum degree of conformity, 846–848
  - in favorable gear pair, 566–570
  - of gear and pinion, 36–37, 146–155, 565–570, 570f, 627–643, 829–854
  - gear-to-rack mesh, 513–514, 514f
  - generating basic rack of, 176–182, 177f, 186f
  - generation of, 135–139, 135f, 139f, 141–176, 176f, 178–196, 186f, 192f, 509–512, 510f, 512f, 532–533, 533f, 556–559, 602–610
  - geometry of, 134–140, 134f, 147f, 148–149, 149f, 154, 154f, 184–194, 220–223, 222f, 289–295, 290f–293f, 512–513, 546–547, 550t, 627–643, 787–788, 788f
  - helical gears and, 148–154, 149f, 150f, 198f, 199–202, 201f, 202f
  - in high-conformal gearing, 269–274, 272f–276f, 285–288, 286f, 289–292, 290f–292f, 639f–643f, 640–644

- Tooth flanks (*Continued*)  
 indicatrix of conformity, 840–844, 840f, 844f, 845f, 848–849  
 interaction of, 35–38, 91–100, 148–154, 197–244, 263–264, 264f, 288–292, 381–416, 471–495, 541–542, 627–643, 646–648, 647f–652f, 655f  
 interference of, 93, 96, 99f  
 in internal gears, 254, 364f  
 in intersected-axes gearing, 340–364, 341f, 345f, 350f, 352f, 381–416, 602–610, 632–635, 633f–635f  
 in involute gearing, 147–154, 197–244  
 kinematics of, 125–140, 627–628, 632–634, 636–637, 639–641  
 local orientation for, 830–834, 830f, 832f  
 low tooth count, 213–214, 214f, 448, 645–646, 649–650, 655–657  
 magnitudes of, 795–800, 800t  
 manufacturing errors in, 546–547, 547f, 548f  
 of mating gear pairs, 197–199, 199f  
 modifications of, 621–626, 621f–622f, 624f–626f  
 in noncircular gears, 556–559  
 in parallel-axes gearing, 197–244, 198f, 627–632, 628f–631f  
 in perfect crossed-axes gearing, 772–776  
 in perfect parallel-axes gear pairs, 381–416  
 plot tooth flank, 230, 230f  
 point contact of, 505–516, 515f, 548–549  
 point of culmination, 264, 288–292, 288f  
 principal directions on, 795–796  
 in real gears, 531–533, 533f, 534–551, 550t  
 rolling conditions in, 279–280  
 schematics of, 134f, 135f, 136f  
 separation of, 92f, 93, 99f  
 simulating gear and pinion, 678–684, 679f, 681f–683f  
 sliding angle of, 227–232, 228f, 231f  
 sliding conditions in, 250–252, 250f, 276–280, 277f, 280f  
 spur involute gears and, 127–128, 146–148, 147f, 148f, 169f, 172–176, 197–199, 198f  
 strength of, 645–684  
 tooth thickness of, 254, 362–363, 364f, 453–454  
 Tooth helix, 159  
 Tooth spiral, 159  
 Tooth trace, 159  
 Tooth-chamfering, 159  
 Tooth-rounding, 159  
 Top land, 34, 291, 366, 369f, 456, 559, 667  
 Trailing flank, 158  
 Transmission  
   characteristics of, 735–739  
   error in, 763–766, 763f, 764f  
   of motion, 41–42  
   of rotation, 2, 10, 91–102, 104f–107f, 108–111, 125–126, 131, 201–204, 314–321, 315f, 417, 473–476, 870  
   split torque transmissions, 697–724  
 Transmission function, 763–767, 763f, 768f  
 Transverse contact ratio, 476  
 Transverse pressure angle variation;  
   *see also* Pressure angle  
   in crossed-axes gearing, 422–423, 423f, 424f, 448–451  
   in intersected-axes gearing, 356–360, 356f  
   in parallel-axes gearing, 120–129, 121f–123f, 126f  
 Trbojevič, Nikola John, 33–34, 33f  
*Treatise on Gear Wheels, A*, 3t, 23, 24f  
 Tredgold, Thomas, 22–23, 22f  
 Tredgold approximation, 22, 370–371, 371f, 462  
 Two-degrees-of-freedom gearing, 542–545, 544f, 545f
- U
- Undercut  
   in approximate real gearings, 623–624, 624f  
   face contact ratio and, 209  
   in gear pairs, 211–215, 215f, 693–695  
   spiral bevel gears and, 605–610  
   in spur involute gears, 170–171, 170f, 196  
 Unit normal vector  
   crossed-axes gearing and, 438–450  
   high-conformal gearing and, 304–305, 305f  
   intersected-axes gearing and, 348–358  
   tangent vectors and, 788–789  
   tooth flanks and, 91–100, 173–174, 187–193  
 Unit tangent vector  
   gear pairs and, 68, 577–579, 585–587  
   gear ratios and, 117  
   intersected-axes gearing and, 348–349  
   relative orientation and, 830–833  
   tangent plane and, 788–796  
   tooth flanks and, 151, 273, 288, 678–680, 830–833  
 Unit vector, 35, 44, 68–70, 99, 151, 165, 186–189, 193–194
- V
- Vector calculus, elements of, 781–785  
 Vector of instant rotation, 45, 48–55, 69–70, 113–115, 120, 126–127, 329–332  
 Vectors, properties of, 781–785  
 Vibration causes, 757–769
- W
- Wildhaber, Ernest, 33–34, 34f, 859  
 Wildhaber-Novikov (W-N) gearing, 258, 265, 269, 297, 323–325, 859–866; *see also* Novikov gearing  
 Willis, Robert, 3t, 17–19, 17f, 21–22, 96  
 Worm gearing  
   analysis of, 503–504, 504f  
   approximate real gearings, 618–621  
   base cones in, 497–499, 500f, 501f  
   conical worm gear, 497–498, 499f  
   crossed-axes worm gearing, 514–515, 514f, 515f  
   crown worm gear, 497–498, 499f  
   distinguishing, 501–503  
   double-enveloping gear, 498f, 502f, 503, 618, 619f, 620f  
   examples of, 498f, 502f, 509  
   internal worm gears, 497–498, 499f  
   kinematics of, 497  
   line of contact in, 497–500  
   multiple-start worms, 497, 498f  
   peculiarities of, 497–504  
   perfect worm gearing, 497–504  
   plane of action in, 497–501, 501f  
   rotation vectors of, 497–498, 500f  
   single-start worm, 497, 498f  
   sliding conditions in, 500–501  
   straddle-mounted gearing, 528, 528f  
   tooth profile of, 503–504, 504f  
   worm threads and, 497–504
- Z
- Zone of action  
   in crossed-axes gearing, 472–473, 472f, 473f, 477f  
   of helical gears, 206–211, 211f  
   in intersected-axes gearing, 383–384, 383f, 385f  
   in involute gearing, 195, 206–211